Ferrofluid Spin-up Flows From Uniform and Non-uniform Rotating Magnetic Fields

by

Shahriar Rohinton Khushrushahi

B.S. Electrical Engineering
Georgia Institute of Technology
Atlanta, GA, 2003

M.S. Electrical Engineering and Computer Science
Massachusetts Institute of Technology
Cambridge, MA, 2005

SUBMITTED TO THE DEPARTMENT OF ELECTRICAL ENGINEERING AND COMPUTER SCIENCE IN PARTIAL FULFILLMENT OF THE REQUIREMENTS FOR THE DEGREE OF

DOCTORATE OF PHILOSOPHY
AT THE
MASSACHUSETTS INSTITUTE OF TECHNOLOGY

JUNE 2010

Signature of Author: _____
Department of Electrical Engineering and Computer Science
May 20, 2010

Certified by: _____
Markus Zahn
Professor of Electrical Engineering and Computer Science
Thesis Supervisor

Accepted by: _____
Terry P. Orlando
Professor of Electrical Engineering and Computer Science
Chairman, Department Committee on Graduate Students

Ferrofluid Spin-up Flows From Uniform and Non-uniform Rotating Magnetic Fields

by

Shahriar Rohinton Khushrushahi

Submitted to the Department of Electrical Engineering and Computer Science on May 20, 2010 in Partial Fulfillment of the Requirements for the Degree of Doctor of Philosophy in Electrical Engineering and Computer Science

ABSTRACT

When ferrofluid in a cylindrical container is subjected to a rotating azimuthally directed magnetic field, the fluid "spins up" into an almost rigid-body rotation where ferrofluid nanoparticles have both a linear and an angular "spin" velocity. Flow observations are often limited to the ferrofluid free surface due to the opaque nature of the ferrofluid and the surface flow can spin-up in the same or opposite directions to the direction of the rotating field. The mechanisms governing this flow have been attributed to surface driven flows that depend on the shape of the meniscus formed by the free surface. However, bulk flow experiments using ultrasound velocimetry show that even in the presence of a stationary cover, bulk ferrofluid flows would result when a rotating magnetic field was applied. The mechanisms explaining the bulk flows have been attributed by some authors to being a result of spin diffusion theory while others believe that non-uniform magnetic properties drive the flow, with both theories being rigorously explored in this thesis.

This thesis applies ferrohydrodynamic analysis to extended fluid flow equations driven by magnetization forces and torques on the ferrofluid, Maxwell's equations relating magnetization, magnetic field and ferrofluid flow, and a Langevin magnetization relaxation constitutive law including the effects of fluid linear and spin velocities.

Some key concepts investigated in this analysis are: (1) Ferrofluid filled cylindrical vessels of finite height placed within a uniform magnetic field result in non-uniform magnetic fields inside the ferrofluid due to demagnetization effects that can drive the flow; (2) A spherical vessel of ferrofluid in a uniform magnetic field has a resulting uniform magnetic field unless there is a spatial variation of magnetic properties, induced in this thesis by an external source of non-uniform magnetic field from a current carrying coil or a permanent magnet; and (3) COMSOL Multiphysics spin-diffusion modeling shows that spin viscosity can also initiate a flow due to spin-velocity boundary conditions which can hinder magnetic nanoparticle rotation near a wall or allow particles to roll along a wall due to flow vorticity.

Ferrofluid spin-up flows were investigated that take into account demagnetizing effects associated with the shape of the container. The experiments conducted in this thesis involve using a sphere of ferrofluid in a uniform rotating field since a sphere has uniform and equal demagnetizing factors in all three Cartesian directions. The uniform rotating magnetic field is generated by two orthogonally placed spherical coils, known as "fluxballs" that generate a

uniform magnetic field in the horizontal and vertical directions inside the fluxballs and a dipole field outside. By driving the coils with sinusoidal signals that are out of phase in time by 90 degrees a uniform rotating field is generated inside the test chamber containing the sphere of ferrofluid. The test sphere of ferrofluid is placed at the center of the larger surrounding "fluxball" machine.

Negligible flows are measured within the ferrofluid filled sphere using ultrasound velocimetry in the "fluxball" machine with a uniform rotating magnetic field. COMSOL simulations using non-zero values of spin-viscosity, with a zero spin-velocity boundary condition at the outer wall, predict measureable flow while simulations setting spin-viscosity to zero result in negligible flow. Previously published values of spin-viscosity measured in cylindrical vessels are much larger than values allowed by kinetic theory because the flows, from which they were determined, are actually due to the demagnetizing field effects and not due to spin-diffusion. Experiments were also performed by partially filling the test sphere with ferrofluid but only 2/3 full, resulting in significant flows due to non-uniform magnetic fields from spatially dependent demagnetizing factors and possibly free surface effects.

Ultrasound velocimetry measurements were also performed with a small permanent magnet or a DC/AC excited small coil on top of the ferrofluid filled test sphere, causing a non-uniform DC or AC magnetic field within the ferrofluid filled test sphere in addition to the uniform rotating magnetic field imposed by the fluxball coils. With an imposed non-uniform magnetic field component from magnet or coil, complex measureable flows with strong vortices are obtained. Formation of vortices is also confirmed in COMSOL simulations of an infinitely long cylinder subjected to a uniform rotating field and the field from an infinitely long permanent magnet.

These measurements demonstrate that a non-uniform magnetic field or a non-uniform distribution of magnetic properties drive the flow. The spin-up ferrofluid flow in a rotating uniform externally applied field is highly dependent on the shape of the container due to demagnetizing effects. These demagnetizing effects in a finite-height ferrofluid filled cylindrical container create a non-uniform field inside the ferrofluid that drives the flow and is the cause for previously observed flows in the classic cylindrical spin-up flow experiments. COMSOL Multiphysics simulations applied to a cylinder of infinite height filled with ferrofluid show that spin-diffusion theory cannot be the dominant mechanism for spin-up flows as fitting the COMSOL analysis to measurements result in unphysically large values of spin viscosity. The unphysically large values of spin viscosity are obtained by attributing spin-up flow to be due to spin-diffusion alone rather than the correct non-uniform magnetic field effects.

In conclusion, this thesis, through experimental results and numerical simulations, proves that non-uniform magnetic properties within the ferrofluid and not spin-diffusion theory is the driving mechanism for the measured flow.

Thesis Supervisor: Markus Zahn
Title: Professor

ACKNOWLEDGEMENTS

My time at MIT has been a hard one, and at many times I felt that I would fall short of fulfilling my dream of getting my PhD from MIT. But my dream has been realized and I owe a lot to many people who have helped me achieve it over these years.

I would like to thank my advisor, Prof. Markus Zahn for being an excellent mentor to me. His level of rigor and care in research, writing and teaching are something I will never forget and will always aspire towards in my life.

I would like to thank my committee members Prof. Jeffrey Lang and Prof. Jacopo Buongiorno for all their guidance and suggestions that have made my thesis something I am very proud of.

I would like to thank Prof. Terry Orlando for helping me find Prof. Zahn, when I was switching labs, and always being concerned about my well being.

I would also like to thank my friends in the Zahn Lab - Ben Cannon, George Hwang, Hsin-Fu Huang and Xuewei Zhang and the rest of the LEES lab for their good company and help.

I'd like to thank Xiaowei He (Tony) for coming in after work to help me and Id like to also thank Wayne Ryan for all his expertise in designing and building the parts required for my experiments. I would also like to thank Prof. Gwan Soo Park for all his help with my experiments.

To all my friends who have been my family all these years. The list is a long one but I would like to thank in particular Kayvan Zainabadi, Emmanuel Abbe and Alex Tsankov. We have shared some great times that I will look back at them very fondly.

I'd like to thank Victor Lelyveld for being there for me, Joshua Alper, Marie-Eve Aubin-Tam, Kate Brown, Aaron Santos, Sunho Park from my masters lab. I'd like to thank Tarek Shazly, and Mike Feldstein for their great company over these years. To any of my friends that I have missed, my sincerest apologies but all of you have been an important part of my life and I am very grateful.

I would like to thank Stefanie Heizmann for being there for me during the darkest chapter of my graduate life here. I was still happy because of you even though around me there was very little reason to be.

To my good friend Sara Mahdavi who has been my buddy all these years, thank you for keeping me company especially on the loneliest day of the week - Sunday.

To my aunt Shaheen Kayani, thank you for taking care of me all these years and showing me a good time on breaks.

Lastly, Id like to thank my parents, Homa Goshtasb and Rohinton Khushrushahi, and my sister Noushin. If it werent for you and the support over the years, I would have not made it. Thank you for giving me everything I ever wanted in life and supporting me in every endeavor I have undertaken.

In loving memory of my late grandmother,

Shirin Rostam Hormuzdiyari (Goshtasb)

شیرین رستم هرمزدیاری (گشتاسب)

Table of Contents

Table of Figures

magnet that is 10 times stronger than the strength of the rotating field. The blue circle which represents a weak field, due to near complete cancellation of the rotating magnetic field and the field due to the permanent magnet, can be clearly seen to rotate in an arc near the top of the sphere. The red region represents the strong field that saturates the EFH1 with a normalized saturation magnetization of $\overline{\mathbf{M}} = 4.2$. Non-uniform distribution of the magnetization also contributes to the generation of non-zero velocity flows..... 352

Figure 7-9. Position of region of weak field is dependent on the strength of the permanent magnet, a stronger magnet creates a blue region further away from the top of the cylinder than a weaker magnet. Top Left: For a permanent magnet that is 10 times stronger than the strength of the rotating field, position of the center of the blue circle is at 0.885. Top Right: For a permanent magnet that is 10 times stronger than the strength of the rotating field, position of the center of the blue circle is at 0.739. Bottom: For a permanent magnet that is 40 times stronger than the strength of the rotating field, position of the center of the blue circle is at 0.536. 353

Figure 7-10. Distribution of torque (surface plot) and streamlines of magnetic field as a function of time for MSGW11 filled cylinder with a permanent magnet 20 times stronger than the strength of the counter-clockwise rotating field. Torque distribution can clearly be seen to have regions of torque reversal as seen at $\Omega t = \frac{3\pi}{4}$. The shape of the streamlines of magnetic field inside the cylinder are affected by the torque as shown with arrows. 355

Figure 7-11. Distribution of magnitude of spin velocity ω (surface plot) and streamlines of magnetic field as a function of time for MSGW11 filled cylinder with a permanent magnet 20 times stronger than the strength of the counter-clockwise rotating field. Spin-velocity can clearly

List of Tables

Chapter 1. Introduction to Ferrofluid Spin-up Flow Phenomena

1.1. Background

Ferrofluids are stable colloidal suspensions of single domain magnetic nanoparticles in a carrier fluid like oil or water. The nanoparticles are usually ferro- or ferrimagnetic particles with typical diameters of order 10 nm coated with a surfactant layer of 1 to 2 nm as seen in Figure 1-1. Their small size allows them to be easily dispersed by Brownian motion and prevents them from agglomerating under gravity, while their surfactant layer prevents them from sticking to each other from van der Waals attraction forces. Ferrofluids exhibit superparamagnetic behavior and the nanoparticles typically make up to 10% of the total fluid volume.

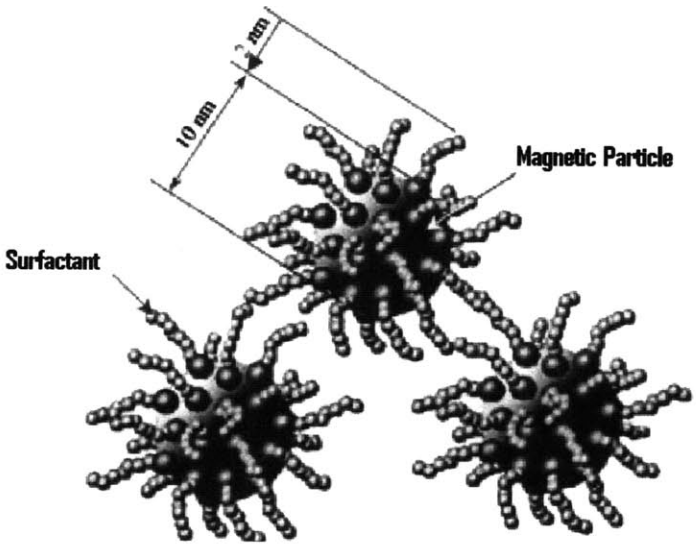

Figure 1-1. 10 nm diameter magnetic nanoparticles coated with 2 nm surfactant. Image taken from [1].

In the presence of DC, AC and rotating magnetic fields, ferrofluids exhibit a rich set of behavior that has led to many thousands of application patents [2, 3]. They are used for improved heat transfer in loud speakers [1], as liquid-rotary-shaft seals on disk drives [4], as inertia dampers in stepper motors [4] and in the development of microfluidic pumps driven by rotating/alternating magnetic fields [5-8]. Ferrofluids are also increasingly being used in medical applications including targeted destruction of tumors [9], drug delivery devices [10], in-vivo monitoring of chemical activity in the brain [11] and as enhanced contrast agents for MRI [12].

1.2. Spin-up Mechanisms in Ferrofluid Literature

Spin-up flow is the term given to describe the process in which a fluid in a container reaches a state of rotation due to a rotating uniform or non-uniform magnetic field. In the case of spin-up flow of ferrofluid in a stationary cylindrical container, ferrofluid flow is set into rigid-body-like motion driven by a uniform rotating magnetic field. The mechanism governing the spin-up flow of ferrofluids in rotating fields has been a topic of interest since its first experiment in 1967 by Rosensweig and Moskowitz [13]. The various mechanisms for spin-up flow will be discussed in this section.

1.2.1. Surface Driven Flows

Historically, such rigid-body observations were made only on the rotating free surface since velocity distributions in the bulk of the ferrofluid could not be easily measured, using streak path techniques or other optical methods, due to the opacity of the ferrofluids. Brown and Horsnell [14] observed for low applied fields that the fluid would co-rotate with the field while counter-rotation would occur for high applied magnetic fields. Kagan [15] and Calugaru [16]

observed the opposite behavior of counter-rotation at low fields and co-rotation at higher applied fields. These authors however, used micron-sized concentrated suspensions of particles and non-uniform magnetic fields.

Rosensweig [17] showed that for ferrofluids in uniform rotating magnetic fields, magnetic surface shear stresses caused by the shape of the meniscus at the free surface drive surface flow. A perfectly flat surface would not rotate, while a concave and convex shaped meniscus creates flow that counter-rotates and co-rotates respectively to the magnetic field rotational direction. Additionally, Rosensweig [17] observed that the angular rotational rate of the free surface increased with a decrease in the internal diameter of the cylindrical container, contrary to expected results in viscous flows. These observations led Rosensweig [17] to conclude that "surface stress rather than volumetric stress is responsible for the spin-up phenomenon" and that surface flows entrain the bulk fluid layers below.

For this theory to hold, a ferrofluid filled cylinder with no free surface would not have any surface shear stresses and never result in any spin-up flow. Experiments done by Chaves [18, 19], Elborai [20] and He [21], using ultrasound velocimetry, were able to show that in a ferrofluid container without a free surface there is a bulk flow that co-rotates with the rotating magnetic field direction. In experiments with the presence of a free surface, the surface flow would confirm Rosensweig's theory [17] but the flow would be opposite to the co-rotating bulk flow in the case of a concave shaped meniscus. The mechanisms explaining the driving force behind these bulk flow spin-up flow experiments have been attributed to two different theories, described in the next sections, which until this thesis no single theory has been proven to be solely responsible.

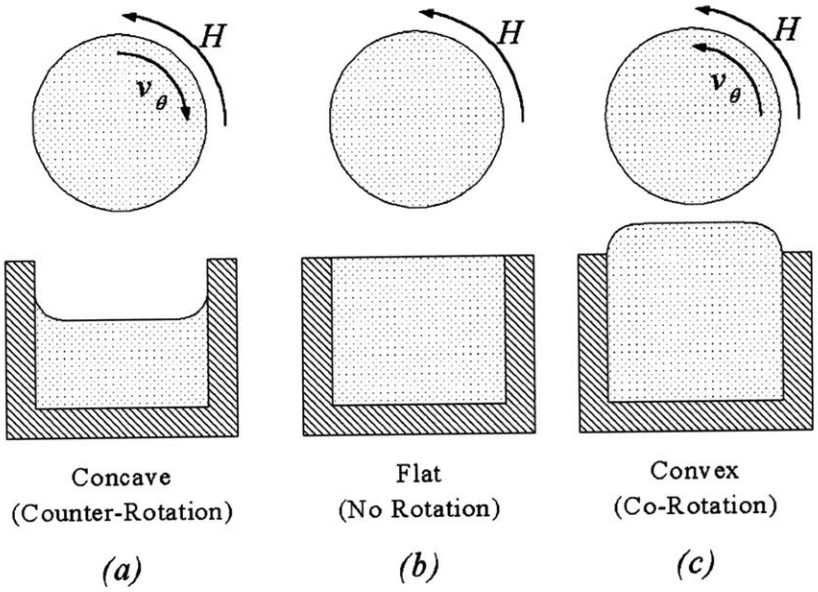

Figure 1-2. Experimental observations of driven ferrofluid free-surface flow. A) Concave shaped free-surface results in fluid counter-rotating with respect to magnetic field. B) Flat surface results in no discernible motion, c) Convex shaped free-surface results in fluid surface co-rotating with magnetic field [17, 22]. This image taken from [23].

1.2.2. Spin Diffusion Theory

When a ferrofluid is subjected to a magnetic field the nanoparticles try to align their internal dipole moments in the direction of the field. However, this alignment is impeded by two processes: rotational Brownian motion and Néel redistribution of sub-particle magnetic domains. As a result, these delays lead to a lag between the magnetization $\mathbf{M}$ and the applied field $\mathbf{H}$ such that they are not collinear. This creates a body-torque density, given by $\mu_0 \mathbf{M} \times \mathbf{H}$, which results in spinning nanoparticles dragging the fluid around it and converting some of its internal angular momentum to the angular momentum of the fluid. In effect, the particle's 'spin' diffuses to the external fluid and this process is known as "spin-diffusion".

Chaves [18, 19], Elborai [20] and He [21] account for the bulk ferrofluid flows to the spin-diffusion theory initially proposed by Zaitsev and Shliomis [24]. The spin diffusion theory confirms the results obtained by Moskowitz and Rosensweig [13], in that the fluid rotates in near rigid-body motion right up to a thin boundary layer (about 10% of cylinder radius) near the solid wall surface [25]. It assumes that the magnetic field throughout the ferrofluid region is uniform with uniform magnetization of the ferrofluid. This results in a magnetic body force of exactly zero and a uniform magnetic body couple.

Zaitsev and Shliomis [24] analytically determine using the phenomenological structured continuum theory [26-28] which includes the effects of body couples, which have antisymmetric stresses representing the short-range transport of spin. This short-range transport of internal angular momentum would only result in macroscopic motion if there were a non-uniform distribution of spin cancellation that depends on particle/wall interactions. Their results were used to estimate the magnitude of the phenomenological spin-viscosity coefficient η' of the commonly accepted constitutive form of the couple stress pseudodyadic.

Kaloni [29] also uses spin-diffusion but attributes the experimental observation of Rosensweig [17] to a shear stress dependent slip boundary condition [30] on the translational velocity coupled with a spin-slip boundary condition [31]. Kaloni, however, fails to make definite predictions on the magnitude and direction of spin-up flows under experimental conditions.

There are several problems with spin-diffusion theory. One such discrepancy is the value of spin-viscosity, determined by Zaitsev and Shliomis [24], who predict an angular velocity of 5-6 orders of magnitude less than that obtained experimentally [2, 32]. As a result many authors consider the effect of spin-diffusion to be negligible [32-35]. But the analysis of Zaitsev and

Shliomis [24] lacks the $(\boldsymbol{\omega}\times\mathbf{M})$ and the $(\mathbf{v}\bullet\nabla\mathbf{M})$ in their magnetic relaxation equation. The importance of these terms has been previously shown in works by Zahn and co-workers [20, 21, 36-39].

1.2.3. Spatial Non-Uniformities in Magnetic Field

Shliomis [34] states that the assumption of a uniform magnetic field throughout the ferrofluid is incorrect and attributes the spin-up flow to the inherent non-uniform field generated within the ferrofluid due to the demagnetizing effects of the finite height cylinder. Geometry of the material body plays a vital role when it is subjected to an external uniform magnetic field. If a material body of irregular shape is subjected to an external uniform field, the magnetic field inside the body is no longer uniform in direction and magnitude throughout the body. The magnetic field inside an ellipsoidal body's axis is given by

$$\mathbf{H}_{internal} = \mathbf{H}_{external} - N\mathbf{M} \tag{1.1}$$

where the internal magnetic field $\mathbf{H}_{internal}$ [A/m] and magnetization $\mathbf{M}$ [A/m] inside the material are uniform if the external magnetic field, $\mathbf{H}_{external}$ [A/m] is also uniform where N represents the demagnetizing factor.

Demagnetizing factors in the three perpendicular directions for external magnetic fields in the x, y and z directions obey the following relation.

$$N_x + N_y + N_z = 1 \tag{1.2}$$

For the internal magnetic field to be uniform for an external uniform magnetic field the shape of the body must be ellipsoidal such as that of a sphere, a prolate or oblate spheroid, or an infinitely long cylinder. The demagnetizing factor N for an oblate spheroid is derived in [40] and can be written as

$$N_x = N_y = \frac{1}{2}\left[\frac{m^2}{\left(m^2-1\right)^{\frac{3}{2}}}\arcsin\frac{\sqrt{m^2-1}}{m} - \frac{1}{m^2-1}\right] \tag{1.3}$$

$$N_z = \frac{m^2}{m^2-1}\left[1 - \frac{1}{\sqrt{m^2-1}}\left(\arcsin\left(\frac{\sqrt{m^2-1}}{m}\right)\right)\right] \tag{1.4}$$

and for a prolate ellipsoid

$$N_x = \frac{1}{m^2-1}\left[\frac{m}{2\sqrt{m^2-1}}\ln\left(\frac{m+\sqrt{m^2-1}}{m-\sqrt{m^2-1}}\right) - 1\right] \tag{1.5}$$

$$N_y = N_z = \frac{m}{2\left(m^2-1\right)}\left[m - \frac{1}{2\sqrt{m^2-1}}\ln\left(\frac{m+\sqrt{m^2-1}}{m-\sqrt{m^2-1}}\right)\right] \tag{1.6}$$

where m is the ratio of major to minor axis.

Figure 1-3 is a plot of demagnetizing factor N_x (shown as $\frac{L}{4\pi}$) as a function of the three equatorial axes (a, b and c corresponding to x, y and z) including the prolate (b=c) and oblate (a=b) spheroid cases. Figure 1-3 also confirms the demagnetizing factor N_x of a sphere (where all equatorial axes are equal a=b=c resulting in equal demagnetizing factors as follows [41])

$$N_x = N_y = N_z = \frac{1}{3} \tag{1.7}$$

Demagnetizing factors for non-ellipsoidal bodies are only an approximation and represent an average of the internal field. In the case of a right-circular cylinder, as seen in Figure 1-4, with

radius r and length $2nr$, where n is a non-dimensional length to diameter ratio, simple and approximate demagnetizing factors in different directions can be given by the following equations [42].

$$N_x = N_y = \frac{\frac{2n}{\sqrt{\pi}}}{2\left(\frac{2n}{\sqrt{\pi}}\right)+1} \tag{1.8}$$

$$N_z = \frac{1}{2\left(\frac{2n}{\sqrt{\pi}}\right)+1} \tag{1.9}$$

These directional demagnetizing factors applied to an infinitely long cylinder ($n \to \infty$) would have uniform internal magnetic fields with N_x=N_y=1/2 and N_z=0. Table 1-1 is a list of demagnetizing factors for uniformly magnetized bodies.

Direction of Magnetization M	**Demagnetizing Factor *N* (SI)**
Sphere, any direction	1/3
Prolate Spheroid, long axis	<1/3
Prolate Spheroid, short axis	>1/3
Needle (∞ long cylinder), axial **M**	≈0
Needle (∞ long cylinder), transverse **M**	≈1/2
Thin disc or sheet, in-plane **M**	≈0
Thin disc or sheet, transverse **M**	≈1

Table 1-1. Table of demagnetizing factors for uniformly magnetized bodies.

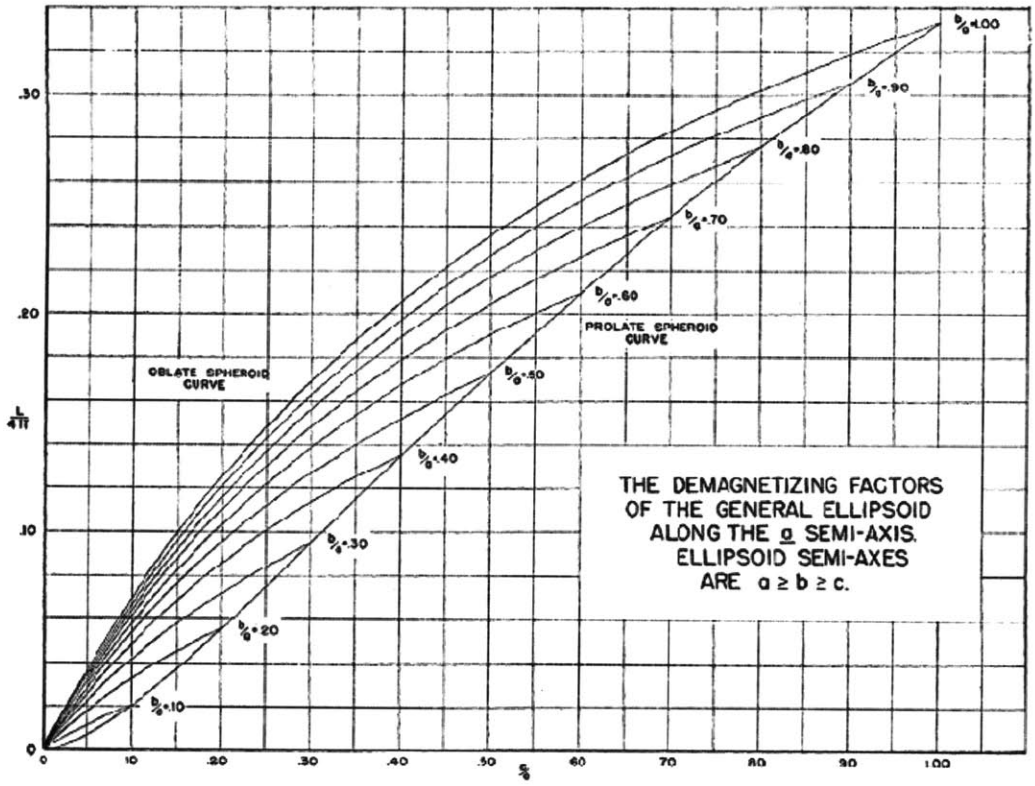

Figure 1-3. Demagnetizing factor along the major axis (N_x) of a general ellipsoid [40].

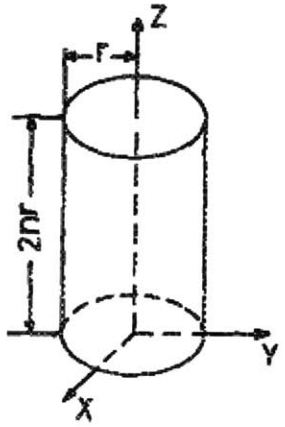

Figure 1-4. Right-circular cylinder. Image taken from [42].

The notion that ferrofluid spin-up flows are a result of field non-uniformities is also described by Glazov [32, 35, 43]. Glazov attributes the spin-up flow due to higher-order spatial harmonics that occur due to non-idealities in the stator winding distribution, in particular, slot effects. Glazov concludes that no flow should occur in the absence of the higher-order harmonics, in the two-pole stator winding source of applied magnetic field, and all observations of spin-up flow are due to imperfections in the experimental apparatus. Jenkins's analysis [44] agrees with Glazov's work in that there should be no rotating flow. However, Glazov's analysis fails to explain the experimentally observed counter-rotation of the fluid motion with respect to rotating magnetic field direction at the free surface [17].

1.2.4. Non-Uniform Magnetic Properties Driving Flow

Shliomis [34] states that another possible reason for spin-up flow is the non-uniformity of magnetic permeability due to radial temperature gradients produced by viscous dissipation in the microeddies created around the rotating particles. Pshenichnikov [33] states that such forces play a dominant role in strong fields or high frequencies and account for measured flows when there are no free surfaces. Pshenichnikov analytically predicts counter-rotation of fluid with respect to rotational field direction for frequencies below 16 kHz and states that experimental data obtained in [45, 46] support this conclusion about the significant role played by internal heat sources in the generation of flows. Pshenichnikov [33] extends this analysis by conducting an experiment where a spatial non-uniformity in the magnetic susceptibility is created by placing a permanent magnet under a thin cuvette filled with ferrofluid where flows are generated rotating counter to the direction of the rotating magnetic field. Pshenichnikov [33, 47] states that for low frequencies

and weak field, energy dissipation is minimal and surface driven flows are the main cause of spin-up flows.

Pshenichnikov in [45] states that the non-uniformity of the field due to demagnetizing effects is not sufficient to produce the rotational flow and that the flow has to have been a result of non-isothermal distribution of the dissipation energy resulting in flow that is counter to the direction of the rotating field. This contradicts the observations of Chaves [18, 19], Elborai [20] and He [21] where bulk flows were found to co-rotate with the magnetic field direction.

1.2.5. Overview of Thesis

The objective of this thesis is to determine whether spin-diffusion theory or non-uniformities in the magnetic field drive the spin-up flow. Ultrasound velocimetry experiments conducted in a spherical container of ferrofluid, driven by uniform fields generated in a spherical 'fluxball' machine, ensure a uniform rotating magnetic field within the ferrofluid volume. These results will be bolstered by simulations of spin-up flow done using COMSOL Multiphysics 3.5a. Through these rigorous experiments and simulations, the conclusions of this thesis determine that non-uniform magnetic fields and non-uniform magnetic properties within the ferrofluid are the governing mechanisms for spin-up flow. The thesis is structured as follows:

Chapter 2 summarizes the physical, magnetic and rheological properties of the ferrofluids used in the experiments. It also describes the system of governing ferrohydrodynamic equations used this thesis.

Chapter 3 theoretically solves for ferrofluid flows in a planar geometry under the influence of an AC and DC magnetic field. Results are obtained using Mathematica and COMSOL which corroborate results of Zahn and co-workers [21, 36-38].

Chapter 4 describes the classic spin-up experiments in cylindrical geometry done by Chaves [18, 19], He [21] and Elborai [20] using the non-invasive ultrasound velocimetry technique. Results by Chaves [19] are simulated with COMSOL Multiphysics using spin-diffusion theory. Corrections to other authors' works are also given.

Chapter 5 presents the spherical apparatus and design of the setup used by this thesis to generate and control the uniform rotating magnetic field of the fluxball coils. Several tests are performed and documented to ensure that the magnetic field generated is uniform and parts were designed to ensure accurate measurement of velocity profiles within a sphere of ferrofluid.

Chapter 6 presents the results of the experiments with negligible fluid flows in the sphere of ferrofluid driven by the rotating field of the fluxball machine. Through further COMSOL simulations and experimental results in a uniform field, flows generated due to spin-diffusion are shown to be negligible. The spin-viscosity values used by other authors [19-21] are shown to be overstated, by many orders of magnitude to account for the demagnetizing fields of a finite height cylinder, through a theoretical determination of spin-viscosity. Experiments are performed where a non-uniform field is introduced to a sphere of ferrofluid concentric to the spherical fluxball machine, by using a solenoidal coil or a permanent magnet placed on top of the ferrofluid filled sphere and the resulting measureable flows are analyzed. Experiments of measureable flow, due to non-uniform demagnetizing effects, are obtained using both a 2/3 full sphere of ferrofluid and a finite height cylinder in a uniform rotating magnetic field. This chapter confirms that non-uniform distribution of magnetic properties within the ferrofluid drives any measureable flow and the effects of spin-diffusion are negligible. This determines the reason for the discrepancy between experimentally fitted and theoretically derived values for spin viscosity

to be due to demagnetizing effects associated with the shape of the container that were previously ignored for short cylinders of ferrofluid.

Chapter 7 presents COMSOL simulations of flow in an infinitely long cylinder in the presence of a non-uniform field, generated as a result of a permanent magnet and a uniform rotating field, with spin-viscosity η'=0. COMSOL was not able to solve for the three dimensional flows within a sphere but was able to solve two dimensional flows in infinite height cylinders, both cases perturbed by non-uniform fields from a permanent magnet and a uniform rotating field. These cylindrical simulations are not representative of the experiments in the spherical geometry but the results obtained have many of the same characteristics.

Chapter 8 summarizes the accomplishments and contributions of this thesis and also lists some topics of interest for future work.

Appendices that follow document the COMSOL Multiphysics®, Mathematica® and LabVIEW® code used in this thesis. It also documents all the designs of the parts built and used in this thesis as well as all the data taken from all the experiments conducted.

Bibliography

[1] S. Odenbach, "Ferrofluids--magnetically controlled suspensions," *Colloids and Surfaces A: Physicochemical and Engineering Aspects,* vol. 217, pp. 171-178, 2003.

[2] R. E. Rosensweig, *Ferrohydrodynamics*: Dover Publications, 1997.

[3] B.M. Berkovskii and V.G.Bashtovoi, *Magnetic Fluids and Applications Handbook.* New York, Wallingford (UK): Begell house, Inc, 1996.

[4] K. Raj and R. J. Boulton, "Ferrofluids -- Properties and applications," *Materials & Design,* vol. 8, pp. 233-236.

[5] R. Pérez-Castillejos, *et al.*, "The use of ferrofluids in micromechanics," *Sensors and Actuators A: Physical,* vol. 84, pp. 176-180, 2000.

[6] H. Hartshorne, *et al.*, "Ferrofluid-based microchip pump and valve," *Sensors and Actuators B: Chemical,* vol. 99, pp. 592-600, 2004.

[7] A. Menz, *et al.*, "Fluidic components based on ferrofluids," in *Microtechnologies in Medicine and Biology, 1st Annual International, Conference On. 2000*, 2000, pp. 302-306.

[8] L. Mao and H. Koser, "An Integrated, High Flow Rate MEMS Ferrofluid Pump," in *Proc. of 9th International Conference on Miniaturized Systems for Chemistry and Life Sciences (μTAS)*, Boston, MA, 2005.

[9] D. K. Kim, *et al.*, "Energy absorption of superparamagnetic iron oxide nanoparticles by microwave irradiation," Jacksonville, Florida (USA), 2005, pp. 10J510-3.

[10] A. M. Derfus, *et al.*, "Remotely Triggered Release from Magnetic Nanoparticles," vol. 19, pp. 3932-3936, 2007.

[11] D. K. Kim, *et al.*, "Characterization and MRI study of surfactant-coated superparamagnetic nanoparticles administered into the rat brain," *Journal of Magnetism and Magnetic Materials,* vol. 225, pp. 256-261, 2001.

[12] P. J. Cantillon-Murphy, "On the dynamics of magnetic fluids in magnetic resonance imaging," Ph. D., Dept. of Electrical Engineering and Computer Science., Massachusetts Institute of Technology, 2008.

[13] R. Moskowitz and R. E. Rosensweig, "Nonmechanical torque-driven flow of a ferromagnetic fluid by an electromagnetic field," *Appl. Phys. Lett., 11: 301-3 (Nov. 15, 1967).* 1967.

[14] R. Brown and T. S. Horsnell, "The Wrong Way Round," *Electrical Review,* vol. 183, 1969.

[15] I. Y. Kagan, *et al.*, "Flow of a dielectric ferromagnetic suspension in a rotating magnetic field," *Magnetohydrodynamics,* vol. 9, pp. 258-261, 1973.

[16] G. H. Calugaru, *et al.*, "A new aspect of the movement of ferrofluids in a rotating magnetic field," *Rev. Roum. Phys.,* vol. 21, p. 439, 1976.

[17] R.E.Rosensweig, *et al.*, "Magnetic Fluid Motion in Rotating Field," *Journal of Magnetism and Magnetic Materials,* vol. 85, pp. 171-180, 1990.

[18] A. Chaves, *et al.*, "Bulk Flow in Ferrofluids in a Uniform Rotating Magnetic Field," *Physical Review Letters,* vol. 96, pp. 194501-4, 2006.

[19] A. Chaves, *et al.*, "Spin-up flow of ferrofluids: Asymptotic theory and experimental measurements," vol. 20, p. 053102, 2008.

[20] S. Elborai, "Ferrofluid surface and volume flows in uniform rotating magnetic fields," Ph.D thesis, Dept of Electrical Engineering and Computer Science, Massachusetts Institute of Technology, Cambridge, MA, 2006.

[21] X. He, "Ferrohydrodynamic flows in uniform and non-uniform rotating magnetic fields," Ph.D thesis, Dept of Electrical Engineering and Computer Science, Massachusetts Institute of Technology, Cambridge, MA, 2006.

[22] R. E. Rosensweig and R. J. Johnston, "Aspects of Magnetic Fluid Flow with Nonequilibrium Magnetization," in *Continuum Mechanics and Its Applications*, G. A. C. Graham and S. K. Malik, Eds., ed: Hemisphere Pub. Corp., 1989.

[23] C. Rinaldi, "Continuum modeling of polarizable systems," Ph.D, Dept. of Chemical Engineering., Massachusetts Institute of Technology, Cambridge, MA, 2002.

[24] V. M. Zaitsev and M. I. Shliomis, "Entrainment of ferromagnetic suspension by a rotating field," *Journal of Applied Mechanics and Technical Physics,* vol. 10, pp. 696-700, 1969.

[25] R. E. Rosensweig and R. J. Johnston, "Aspects of Magnetic Fluid Flow with Nonequilibrium Magnetization," in *Continuum Mechanics and Its Applications*, G. A. C. Graham and S. K. Malik, Eds., ed: Hemisphere Pub. Corp., 1989, pp. 707-729.

[26] J. S. Dahler and L. E. Scriven, "Angular Momentum of Continua," *Nature,* vol. 192, pp. 36-37, 1961.

[27] J. S. Dahler and L. E. Scriven, "Theory of Structured Continua. I. General Consideration of Angular Momentum and Polarization," *Proceedings of the Royal Society of London. Series A, Mathematical and Physical Sciences,* vol. 275, pp. 504-527, 1963.

[28] D. W. Condiff and J. S. Dahler, "Fluid Mechanical Aspects of Antisymmetric Stress," *Physics of Fluids,* vol. 7, pp. 842-854, 1964.

[29] P. N. Kaloni, "Some remarks on the boundary-conditions for magnetic fluids," *Int. J. Eng. Sci,* vol. 20, p. 1451, 1992.

[30] P. Brunn, "The velocity slip of polar fluids," *Rheol. Acta.,* vol. 14, p. 1039, 1975.

[31] E. L. Aero, *et al.*, "Asymmetric hydromechanics," *J. LUMIN,* vol. 29, p. 333, 1965.

[32] O. A. Glazov, "Motion of a ferrosuspension in rotating magnetic fields," *Magnetohydrodynamics,* vol. 11, pp. 140-145, 1975.

[33] A. Pshenichnikov, *et al.*, "On the rotational effect in nonuniform magnetic fluids," *Magnetohydrodynamics,* vol. 36, pp. 275-281, 2000.

[34] M. I. Shliomis, *et al.*, "Ferrohydrodynamics: An essay on the progress of ideas," *Chem. Eng. Comm.,* vol. 67, pp. 275 - 290, 1988.

[35] O. A. Glazov, "Role of higher harmonics in ferrosuspension motion in a rotating magnetic field," *Magnetohydrodynamics,* vol. 11, pp. 434-438, 1975.

[36] M. Zahn and D. R. Greer, "Ferrohydrodynamic pumping in spatially uniform sinusoidally time-varying magnetic fields," *Journal of Magnetism and Magnetic Materials,* vol. 149, pp. 165-173, 1995.

[37] M. Zahn and L. Pioch, "Ferrofluid flows in AC and traveling wave magnetic fields with effective positive, zero or negative dynamic viscosity," *J. Magn. Magn. Mater.,* vol. 201, p. 144, 1999.

[38] L. L. V. Pioch, "Ferrofluid flow & spin profiles for positive and negative effective viscosities," M. Eng., Dept. of Electrical Engineering and Computer Science, Massachusetts Institute of Technology, 1997.

[39] C. Rinaldi and M. Zahn, "Effects of spin viscosity on ferrofluid flow profiles in alternating and rotating magnetic fields," *Phys. Fluids,* vol. 14, p. 2847, 2002.
[40] J. A. Osborn, "Demagnetizing Factors of the General Ellipsoid," *Physical Review,* vol. 67, p. 351, 1945.
[41] R. Skomski, *et al.*, "Effective Demagnetizing Factors of Complicated Particle Mixtures," *Magnetics, IEEE Transactions on,* vol. 43, pp. 2956-2958, 2007.
[42] M. Sato and Y. Ishii, "Simple and approximate expressions of demagnetizing factors of uniformly magnetized rectangular rod and cylinder," vol. 66, ed: AIP, 1989, pp. 983-985.
[43] O.A.Glazov, "Velocity profiles for magnetic fluids in rotating magnetic fields," *Magn. Gidrodinamkia,* vol. 18, 1982.
[44] J. T. Jenkins, "Some simple flows of a para-magnetic fluid," *Journal de Physique,* vol. 32, pp. 931-938, 1971.
[45] A. V. Lebedev and A. F. Pshenichnikov, "Motion of a magnetic fluid in a rotating magnetic field," *Magnetohydrodynamics,* vol. 27, pp. 4-8, 1991.
[46] A. V. Lebedev, *et al.*, *Bull. Acad. Sci. USSR Phys. Ser.*, vol. 55, p. 14, 1991.
[47] A. Pshenichnikov and A. Lebedev, "Tangential stresses on the magnetic fluid boundary and rotational effect," *Magnetohydrodynamics,* vol. 36, pp. 254-263, 2000.

Chapter 2. Governing Equations and Ferrofluid Properties

This chapter summarizes the measured physical properties of two commercial ferrofluids used extensively in experiments and simulations reported in this thesis. The values used were taken from a combination of measurements made by Elborai, He and Franklin and reported in their respective theses [1-3].

In addition, this chapter will outline the governing ferrohydrodynamic equations used in this thesis. These include Maxwell's equations, the magnetic relaxation constitutive relation and the fluid mechanical conservation of linear and angular momentum equations. These equations describe ferrofluid behavior in static, oscillating and rotating uniform and non-uniform magnetic fields.

2.1. Governing Equations

2.1.1. Maxwell's Equations

The ferrohydrodynamic experiments are usually conducted at low frequencies, typically less than a few MHz, and at non-relativistic velocities allowing for the analysis to be considered in the magnetoquasistatic limit (MQS). In this limit, the displacement current density term is ignored and Ampere's law reduces to

$$\nabla \times \mathbf{H} = \mathbf{J} + \cancel{\frac{\partial \mathbf{D}}{\partial t}} = 0 \tag{2.1}$$

where **H** [A/m] is the magnetic field and the volume current density source **J** [A/m^3] can be set to zero since the ferrofluid is non-conductive. The irrotational magnetic field can then be represented as a gradient of a magnetic scalar potential ψ [A] as

$$\mathbf{H} = -\nabla \psi \tag{2.2}$$

Gauss's law for the magnetic flux density is given by

$$\nabla \bullet \mathbf{B} = 0 \tag{2.3}$$

where the magnetic flux density **B** [T] has a constitutive relation with respect to magnetic field and magnetization **M** [A/m] of a material given as

$$\mathbf{B} = \mu_0 (\mathbf{H} + \mathbf{M}) \tag{2.4}$$

where $\mu_0 = 4\pi \times 10^{-7}$ [H/m] is the magnetic permeability of free space. Combining equations (2.2)-(2.4) yields a Poisson's equation, in terms of scalar potential and magnetization, with an effective magnetic volume charge density of $-\mu_0 \nabla \bullet \mathbf{M}$.

$$\nabla^2 \psi = \nabla \bullet \mathbf{M} \tag{2.5}$$

2.1.2. Fluid Mechanics Equations

The fluid mechanics equations governing ferrohydrodynamics are conservation of linear and angular momentum equations [4]. The conservation of linear momentum equation is

$$\rho \left[\frac{\partial \mathbf{v}}{\partial t} + (\mathbf{v} \bullet \nabla) \mathbf{v} \right] = -\nabla p' + 2\zeta \nabla \times \boldsymbol{\omega} + (\zeta + \eta) \nabla^2 \mathbf{v} + (\eta + \lambda - \zeta) \nabla (\nabla \bullet \mathbf{v}) + \mathbf{F} \tag{2.6}$$

where ρ [kg/m^3] is the ferrofluid mass density, p' [N/m^2] is the dynamic pressure including gravity effects where $p' = p - \rho(\mathbf{r}\bullet\mathbf{g})$ and $\mathbf{g}$ [m/s^2] is the gravitational acceleration and $\mathbf{r}$ [m] is the position vector with respect to an arbitrary origin. $\mathbf{F}$ [N/m^3] is the Kelvin body force density given as $\mathbf{F} = \mu_0(\mathbf{M}\bullet\nabla)\mathbf{H}$, $\boldsymbol{\omega}$ [1/s] is the spin velocity, η [Ns/m^2] is the dynamic viscosity of the ferrofluid, λ [Ns/m^2] the bulk viscosity and ζ [Ns/m^2] is the vortex viscosity approximately equal to $\zeta = \frac{3}{2}\eta\phi_{vol}$ for small volume fraction ϕ_{vol} of magnetic nanoparticles [4, 5].

The conservation of angular momentum equation is given as follows [4]

$$I\left[\frac{\partial\boldsymbol{\omega}}{\partial t} + (\mathbf{v}\bullet\nabla)\boldsymbol{\omega}\right] = \mathbf{T} + 2\zeta(\nabla\times\mathbf{v} - 2\boldsymbol{\omega}) + (\eta' + \lambda')\nabla(\nabla\bullet\boldsymbol{\omega}) + \eta'\nabla^2\boldsymbol{\omega} \tag{2.7}$$

where I [kg/m] is the moment of inertia density, η' [Ns] is the shear coefficient of spin viscosity, λ' [Ns] is the bulk coefficient of spin viscosity and $\mathbf{T}$ [N/m^2] is the magnetic torque density given by $\mathbf{T} = \mu_0(\mathbf{M}\times\mathbf{H})$.

The ferrofluid is considered to be an incompressible fluid where the conservation of mass equation given by

$$\frac{\partial\rho}{\partial t} + \nabla\bullet(\rho\mathbf{v}) = 0 \tag{2.8}$$

reduces to the necessary condition

$$\nabla\bullet\mathbf{v} = 0 \tag{2.9}$$

since ρ =constant.

For analyses done in this thesis, the spin velocity is only in the z direction perpendicular to the x-y plane of the rotating field so that

$$\nabla \cdot \boldsymbol{\omega} = 0 \tag{2.10}$$

where it is assumed that the spin velocity is z directed and does not depend on z. This simplifies Eq (2.7) as the next to last term is zero.

2.1.3. Magnetic Relaxation Equation

When a ferrofluid is subject to a magnetic field, the individual nanoparticles try to align their dipole moment to the applied field and the whole fluid eventually 'relaxes' into being magnetized in that direction. The two processes that dominate this relaxation process are Brownian relaxation, where the particle physically rotates against the viscous drag force of the fluid, and Néel relaxation which is characterized by the movement of the nanoparticle's magnetic moment relative to the crystal axis. These two processes can be explained by a graphic [1] shown in Figure 2-1.

The characteristic relaxation times associated with both relaxation mechanisms are given in (2.11) and (2.12) where K = 23000-100000 [J/m^3] (for magnetite) [6] represents the anisotropy constant of the magnetic domains and depends on the size of magnetic nanoparticles, $f_0 = 10^9$ [Hz] (for magnetite) as the frequency constant for Néel relaxation, η_0 [Ns/m^2] is the dynamic viscosity of the carrier fluid, k =1.38x10^{-23} [J/K] is Boltzmann's constant and T [K] the temperature in Kelvin.

$$\tau_B = \frac{3V_B\eta_0}{kT} \quad \text{Brownian relaxation time} \tag{2.11}$$

$$\tau_N = \frac{1}{f_0} e^{\frac{KV_N}{kT}} \quad \text{Néel relaxation time} \tag{2.12}$$

The two particle volumes V_B and V_N for spherical particles are given by

$$V_B = \frac{4}{3}\pi(R+\delta)^3 \text{ Brownian particle volume} \tag{2.13}$$

$$V_N = \frac{4}{3}\pi R^3 \text{ Néel particle volume} \tag{2.14}$$

where δ [m] represents the thickness of the surfactant layer surrounding the spherical magnetic nanoparticle and R [m] the radius of the magnetic nanoparticle. Typical relaxation times for Brownian and Néel relaxations are on the order of 10^{-5} – 10^{-9} seconds [4] and depends on the radius of the nanoparticles.

The combined effect of both relaxation times can be expressed by the following equation for the effective time constant τ_{eff} .

$$\frac{1}{\tau_{eff}} = \frac{1}{\tau_B} + \frac{1}{\tau_N} \tag{2.15}$$

The smaller of the two time constants dominates the physical relaxation process, with Néel relaxation dominating τ_{eff} for small particles and Brownian relaxation dominating τ_{eff} for larger particles. A plot of the relaxation times as a function of particle diameter is given in Figure 2-2 [1].

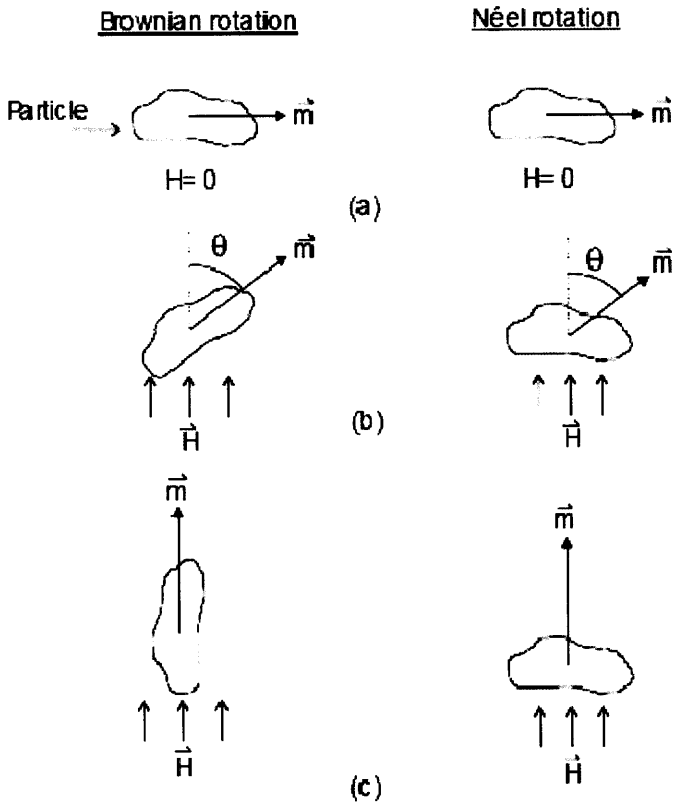

Figure 2-1. Brownian and Néel relaxation illustrated here with non-spherical particles taken from [1]. A) Particles have their magnetic moment aligned horizontally in the presence of no applied field. B) Magnetic moment relaxes at angle θ to the vertically applied magnetic field. For Brownian relaxation the whole particle turns to angle θ, whereas Néel relaxation only results in the moment turning with respect to the crystal axis. C) In the steady state the magnetic moment is aligned with the applied field resulting in complete rotation of particle by Brownian relaxation and only magnetic moment rotation in Néel relaxation.

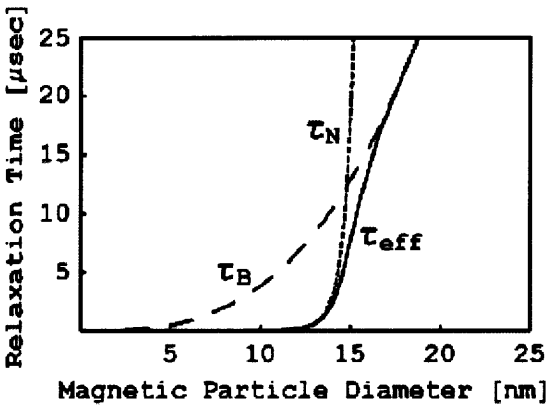

Figure 2-2. Brownian, Néel and effective relaxation times are illustrated in this plot as a function of spherical particle diameter. This plot corresponds to EFH1 hydrocarbon-based ferrofluid, with the following parameters, ρ =1169 kg/m^3, η_0 =10 cP, K = 23000 J/m^3 for magnetite, f_0=10^9 Hz and T=300K. Brownian plot assumes zero surfactant thickness δ=0 [1] .

In addition to the particle relaxation times, the ferrofluid magnetization as a whole relaxes depending on translational and spin velocity. The ferrofluid magnetic relaxation equation used in this thesis is the one derived by Shliomis [5] and is given by

$$\frac{\partial \mathbf{M}}{\partial t} + (\mathbf{v}\cdot\nabla)\mathbf{M} + \mathbf{M}(\nabla\cdot\mathbf{v}) = \boldsymbol{\omega}\times\mathbf{M} - \frac{1}{\tau_{eff}}(\mathbf{M}-\mathbf{M}_{eq}) \tag{2.16}$$

where τ_{eff} [s] is the effective relaxation time constant, $\mathbf{v}$ [m/s] the translational velocity, $\boldsymbol{\omega}$ [1/s] the spin velocity and $\mathbf{M_{eq}}$ [A/m] the equilibrium magnetization. This relaxation equation is used in this thesis for alternating and rotating magnetic fields, of angular frequency Ω, where $\Omega\tau_{eff} << 1$. The ferrofluids used in this thesis have a maximum $\tau_{eff} \approx 10^{-5}$s and the maximum experimental rotational frequency used is 95 Hz resulting in a valid regime of operation since the maximum $\Omega\tau_{eff} \approx 0.006$.

The equilibrium magnetization $\mathbf{M}_{eq}$ for a monodisperse ferrofluid is given by the Langevin equation $L(\alpha)$ [4]

$$\mathbf{M}_{eq} = M_s L(\alpha)\frac{\mathbf{H}}{H} = M_s\left(\coth(\alpha) - \frac{1}{\alpha}\right)\frac{\mathbf{H}}{H} \tag{2.17}$$

$$\alpha = \frac{M_d V_p \mu_0 H}{kT}, M_s = \phi_{vol} M_d$$

where M_s [A/m] is the saturation magnetization, ϕ_{vol} [%] is the volume fraction of magnetic particles in the ferrofluid, M_d = 446 kA/m [A/m] is the domain magnetization for magnetite [4], V_p [m^3] is the magnetic core volume per particle, μ_0 [H/m] is the magnetic permeability of free space, H [A/m] is the magnetic field magnitude within the particle, k =1.38x10^{-23} [J/K] is Boltzmann's constant and T [K] the temperature in Kelvin.

Equations (2.5), (2.6), (2.7) & (2.16) with assumptions in (2.9) and (2.10) govern the ferrohydrodynamic behavior of isothermal ferrofluids.

2.2. Properties of Ferrofluids Used In This Thesis

2.2.1. Magnetic Properties and Particle Size

The magnetization curves of the two Ferrotec® ferrofluids used in this thesis, oil-based EFH1 and water based MSGW11, were measured by Elborai [2], Franklin [1] and He [3] using an ADE Technologies Model 880 Digital Measurement Systems (DMS) Vibrating Sample Magnetometer (VSM). These plots can be seen in Figure 2-3 and Figure 2-4 respectively. These figures have values of magnetization $\boldsymbol{M}$ and field intensity $\boldsymbol{H}$ reported as $\mu_0 M$ and $\mu_0 H$ with units of Gauss. The saturation magnetization for the different ferrofluids also determines the volume fraction of the particles in the different ferrofluids given by

$$\phi_{vol} = \frac{\mu_0 M_s}{\mu_0 M_d} \tag{2.18}$$

The low-field limit of the Langevin curve describes a linear relation between magnetization $\boldsymbol{M}$ and applied field $\boldsymbol{H}$ and is given by slope of the magnetization curve corresponding to the magnetic susceptibility χ. The Langevin curves of Figure 2-3 and Figure 2-4 do not have enough precision in the low field to accurately determine the slope. Elborai [2] and He [3] separately measured the low field linear regions of the magnetization curve for EFH1 and MSGW11 as shown in Figure 2-5 and Figure 2-6. The values of magnetic susceptibility χ were then determined through a linear least squares fit of the linear region data.

Values for saturation magnetization, magnetic susceptibility and volume fraction for MSGW11 and EFH1 are listed in Table 2-3.

The minimum and maximum particle size diameters for MSGW11 and EFH1 were estimated using the data from the linear and saturation portions of the magnetization curves. The high field asymptote of the Langevin equation is given as

$$\lim_{\alpha>>1} L(\alpha) \approx \left(1-\frac{1}{\alpha}\right) = \left(1-\frac{6}{\pi}\frac{kT}{\mu_0 M_d H d_{min}^{\ 3}}\right) \tag{2.19}$$

where d_{min} is the minimum diameter of the assumed spherical shaped particles. The low field asymptote of the Langevin equation is given by (2.20) where d_{max} is the maximum diameter of the assumed spherical shaped particles.

$$\lim_{\alpha<<1} L(\alpha) \approx \frac{\alpha}{3} = \frac{\pi\mu_0 M_d H d_{max}^3}{18kT} = \frac{\chi H}{M_s} \tag{2.20}$$

Elborai [2] and He [3] also use TEM images to determine the particle size for MSGW11 but not for EFH1 due to incomplete evaporation of the oil-based ferrofluid. Franklin [1] also determines an average particle diameter by using a non-linear best least-squares fit to the experimental data. The range of particle size diameters for both these techniques along with Franklin's [1] average particle sizes are tabulated for MSGW11 and EFH1 in Table 2-1. Franklin's average particle sizes are used in this thesis and are tabulated in Table 2-3.

Ferrofluid	**Estimated particle diameter (VSM) [nm]**	**Estimated particle diameter (TEM) [nm]**	**Franklin's [1] Average particle diameter [nm]**
MSGW11	5.5-12.4	6.3-27.6 (mean) 9.4±3.4 (STD)	7.9
EFH1	6.9-13.3	-	10.6

Table 2-1. Estimated particle diameters for MSGW11 and EFH1 ferrofluids by Elborai [2], Franklin [1] and He [3] using VSM measurements. Elborai [2] and He [3] also made measurements of particle size using TEM. Franklin's [1] average particle diameter is also listed.

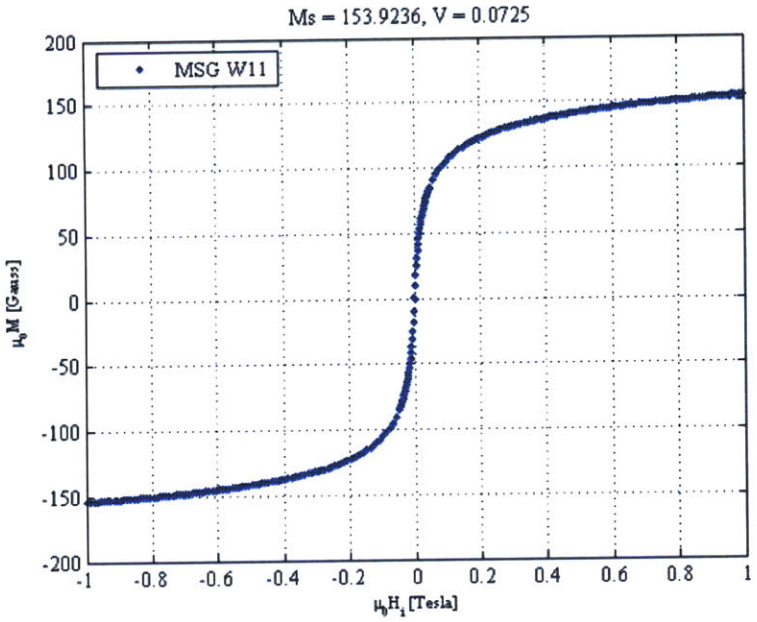

Figure 2-3. Magnetization curve for MSGW11, measured by Elborai [2] and He [3], used in this thesis. A saturation magnetization of ≈ 154 Gauss is measured.

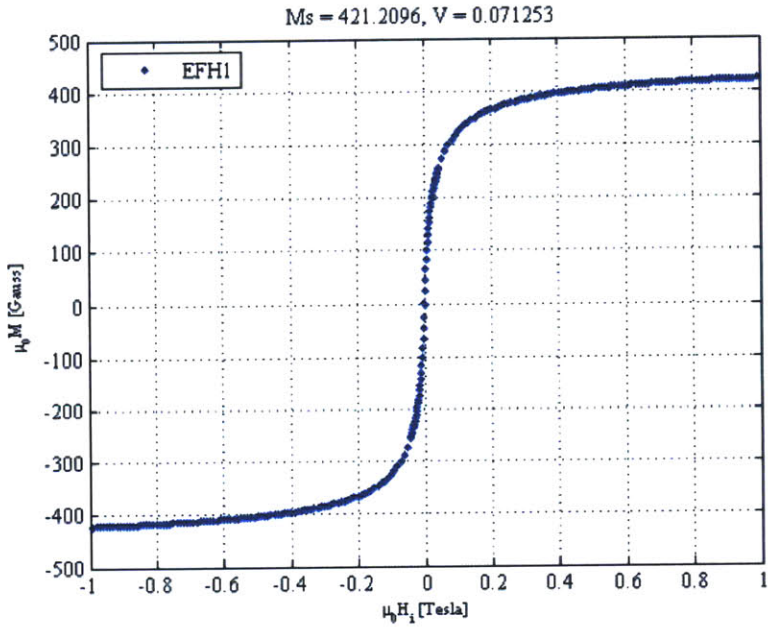

Figure 2-4. Magnetization curve for EFH1, measured by Elborai [2] and He [3], used in this thesis. A saturation magnetization of ≈ 421 Gauss is measured.

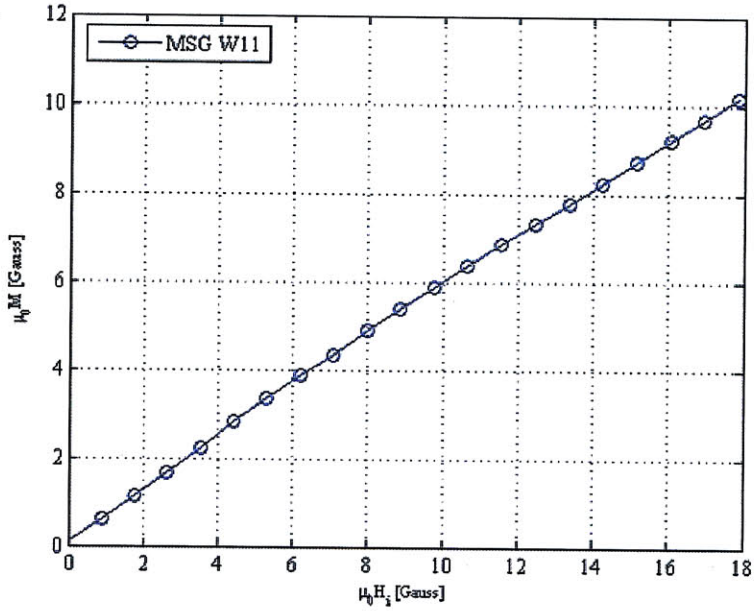

Figure 2-5. Measured linear magnetization at low applied fields by Elborai [2] and He [3] for MSGW11. $\chi \approx 0.56$.

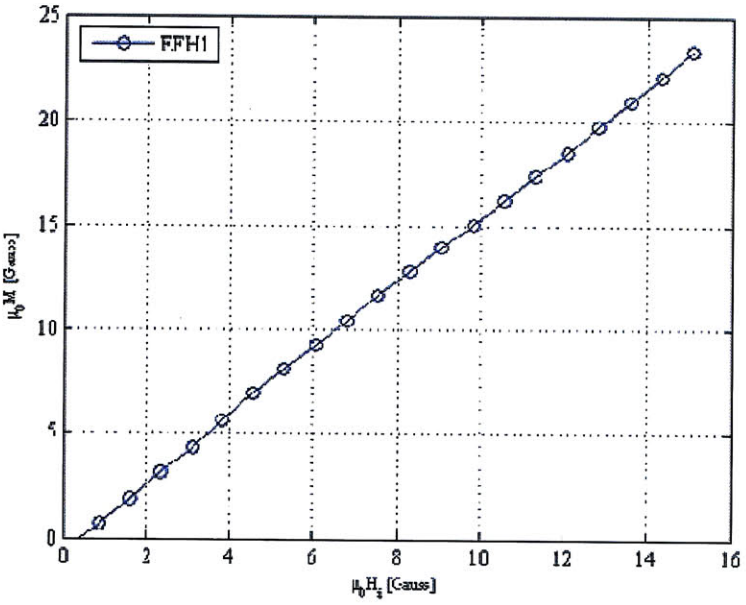

Figure 2-6. Measured linear magnetization at low applied fields by Elborai [2] and He [3] for EFH1. $\chi \approx 1.59$.

2.2.2. Relaxation Times and Spin-viscosity

Knowledge of the size of the particles allows for the calculation of the Brownian and Néel relaxation times in (2.11) and (2.12). He [3] calculates the Brownian and Néel relaxation times using particle sizes from both the VSM and TEM measurements. For Brownian relaxation times a surfactant layer of thickness $\delta=2\ nm$ is assumed and for Néel relaxation, the anisotropy constant K=78000 J/m^3 is assumed for a 12.6 nm particle [3, 6]. He [3] and Elborai [2] also calculate the values of τ_{eff} and η' from their experimental results for MSGW11. The values of τ_{eff} are in close agreement with the values calculated using the VSM particle size and are tabulated in Table 2-2.

The values of τ_{eff} and η' for MSGW11 used in this thesis are the average of the experimentally derived τ_{eff} and η' obtained by Elborai [2] and He [3]. There are no experimentally reported values of τ_{eff} and η' for EFH1, the τ_{eff} used is the average of the τ_{eff} values calculated using VSM and are tabulated in Table 2-3.

Ferrofluid	**Calculated τ_B [μs][3]**	**Calculated τ_N [s][3]**	**Calculated τ_{eff} [μs][3]**	**Experimental τ_{eff} [μs]**	**Experimental η' [kg m/s]**
MSGW11	0.66-3.38 (VSM) 0.84-24.2 (TEM)	5.16×10^{-9}-0.147 (VSM) 1.18×10^{-8}-1.91×10^{81} (TEM)	0.0051-3.38 (VSM) 0.012-24.2 (TEM)	$1.57\times10^{-5}\pm1.43\times10^{-5}$ [3] $1.2\times10^{-5}\pm1.18\times10^{-5}$ [2]	$6.4\times10^{-9}\pm5.4\times10^{-9}$ [3] $3.15\times10^{-9}\pm1.13\times10^{-9}$ [2]
EFH1	3.57-14.28 (VSM)	2.56×10^{-8}-12.0 (VSM)	0.025-14.3 (VSM)	-	-

Table 2-2. Table of calculated and experimentally determined values of relaxation times and spin -viscosity for ferrofluids, MSGW11 and EFH1, based on magnetic nanoparticle sizes listed in Table 2-1 for VSM and TEM measurements.

2.2.3. Viscosity and Mass Density

The values for the viscosity and mass density for the two ferrofluids, MSGW11 and EFH1, were taken from Elborai's and He's theses [2, 3]. The mass density was determined by filling a container of calibrated volume with each ferrofluid, measuring the difference in weight between the full and empty container and dividing the mass value by the volume of the container. The viscosity measurement was made by Elborai and He using the CSL500 rheometer from TA instruments configured in a Couette cell geometry [2, 3].

2.2.4. Speed of Sound Measurement

Precise knowledge of the speed of sound in the sample fluid is necessary to accurately interpret ultrasound reflections. Signal Processing Corporation's DOP 2000 comes with a speed of sound measuring device as seen in Figure 2-7. A schematic cross-section of it, shown in Figure 2-8, contains a micrometer screw gauge at one end and an ultrasound probe at the other. By turning the micrometer the distance between the face of the ultrasound probe and the reflecting face of the micrometer is changed. The Signal Processing program measures the differential change in the time taken for an ultrasound echo signal to propagate over a distance that is incrementally changed by adjusting the micrometer, giving the speed of sound in the sample fluid. The values measured are similar to those measured by Elborai and He in their theses [2, 3] and are tabulated in Table 2-3.

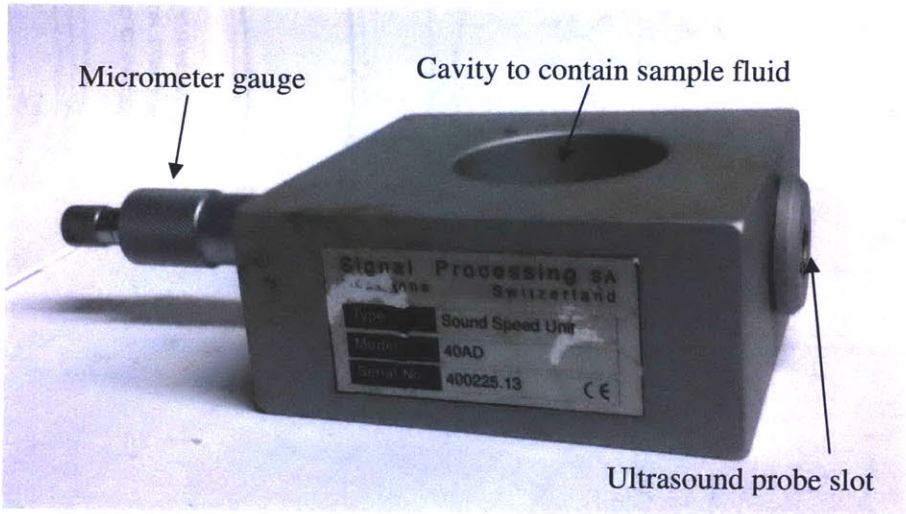

Figure 2-7. Picture of Signal Processing's speed of sound measuring device.

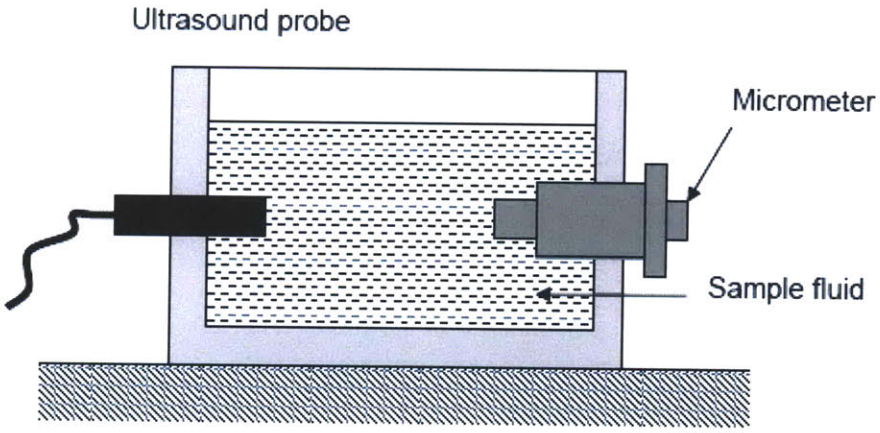

Figure 2-8. Schematic cross-section of speed of sound measuring device by Signal Processing Corporation [3].

Ferrofluid	Mass Density [kg/m^3]	Viscosity η [cP]	Vortex Viscosity ζ [cP] $\zeta=1.5\eta\varphi$	Saturation Magnetization $\mu_0 M_s$ [G]	Magnetic Susceptibility χ	Volume fraction % vol. $\phi_{vol}=\frac{\mu_0 M_s}{\mu_0 M_d}$	Average particle diameter d_{avg} (nm)	Speed of sound [m/s]	τ_{eff} [μs]	η' [kg m/s]
MSGW11	1200	2.02	0.83×10^{-4}	153.9	0.56	2.75	7.9	1439 [2, 3], 1487 [SK]	13.9	4.78×10^{-9}
EFH1	1221	7.27	8.2×10^{-4}	421.2	1.59	7.52	10.6	1116 [2, 3], 1116 [SK]	7.16	-

Table 2-3. Values for the mechanical, physical and magnetic properties for the two ferrofluids (MSGW11 and EFH1) used in this thesis. Most of these values were taken from measurements by Elborai and He documented in their theses [2, 3]. The speed of sound measurement was made by the author of this thesis and is denoted by his initials [SK].

Bibliography

[1] T. A. Franklin, "Ferrofluid Flow Phenomena," Masters of Science, Dept. of Electrical Engineering and Computer Science, MIT, Cambridge, MA, 2003.

[2] S. Elborai, "Ferrofluid surface and volume flows in uniform rotating magnetic fields," Ph.D thesis, Dept of Electrical Engineering and Computer Science, Massachusetts Institute of Technology, Cambridge, MA, 2006.

[3] X. He, "Ferrohydrodynamic flows in uniform and non-uniform rotating magnetic fields," Ph.D thesis, Dept of Electrical Engineering and Computer Science, Massachusetts Institute of Technology, Cambridge, MA, 2006.

[4] R. E. Rosensweig, *Ferrohydrodynamics*: Dover Publications, 1997.

[5] M. I. Shliomis, "Effective viscosity of magnetic suspensions," *Soviet Physics JETP,* vol. 34, pp. 1291-1294, 1972.

[6] A.-F. Lehlooh, *et al.*, "On the particle size dependence of the magnetic anisotropy energy constant," *Physica B: Condensed Matter,* vol. 321, pp. 159-162, 2002.

Chapter 3. Ferrofluid Flows in Planar Geometry

The application of magnetic fields to ferrofluids tends to orient the magnetic moments of the constituting magnetic particles in the direction of the applied field with resistance to free rotation of the particles from fluid viscosity or magnetic crystalline anisotropy. Hydrodynamic forces and Brownian and Néel relaxation effects contribute to the antisymmetric stress between the magnetic particle and the carrier fluid, affecting the effective magnetoviscosity of the magnetic fluid.

This chapter derives the effective magnetoviscosity for planar-Couette magnetic fluid flow, with an applied uniform AC magnetic field transverse to the duct axis, using Shliomis's first magnetization relaxation equation with zero spin-viscosity coefficients $(\lambda' = \eta' = 0)$ in Eq. 2.7.

The case of planar Poiseuille flow stressed by magnetic fields similar to that described by Zahn [1] and Pioch [2-4] is also replicated using Mathematica® and COMSOL Multiphysics® 3.5a with $(\eta' \neq 0)$ and without spin-viscosity $(\eta' = 0)$. The results of Zahn [1] are extended to include the physical vortex viscosity ζ [Ns/m^2], equal to $\zeta = \frac{3}{2}\eta\phi_{vol}$ for dilute suspensions, where η [Ns/m^2] is the dynamic viscosity of the fluid, and ϕ_{vol} is the volume fraction of magnetic nanoparticles [5, 6].

3.1. Planar Geometry Setup

The planar geometry used in this chapter is shown in Figure 3-1. To impose the horizontal tangential field H_z, ±y directed surface currents on the x=0 and x=d planes are required. The uniform AC magnetic flux density B_x is imposed by an external permanent magnet or electromagnet as shown in Figure 3-2b.

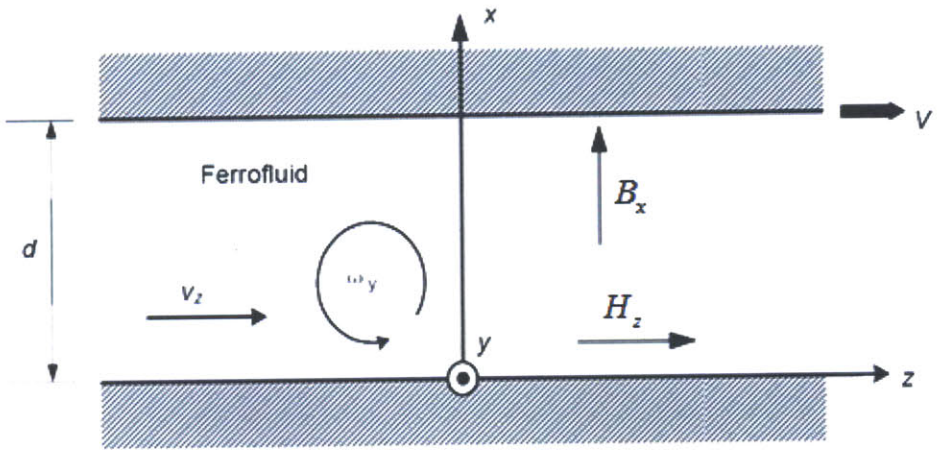

Figure 3-1. Planar ferrofluid layer between rigid walls. Planar Couette flow is generated by moving the surface at x=d at a velocity V. It is magnetically stressed by a uniform x directed AC magnetic flux density B_x, or by a uniform z directed tangential AC magnetic field H_z. Image taken and modified from [7].

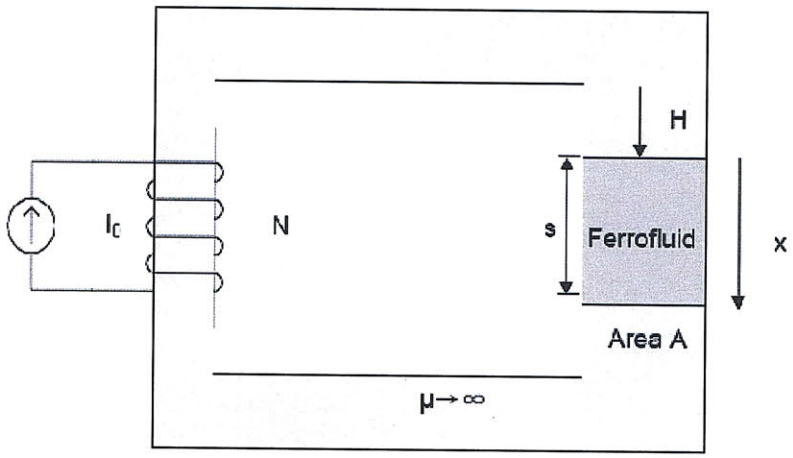

(a)

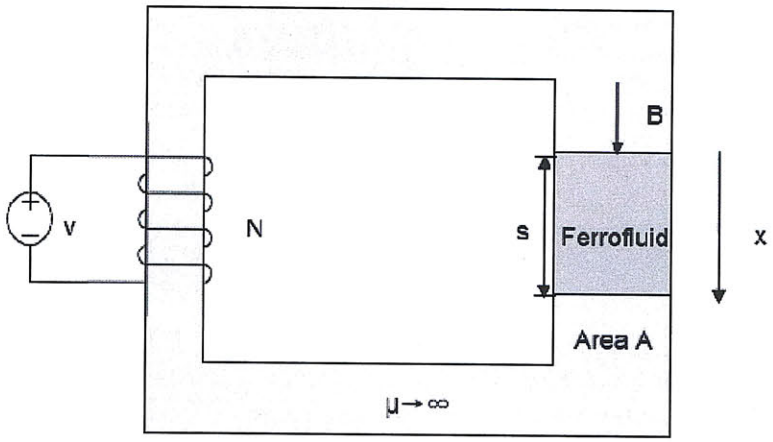

(b)

Figure 3-2. (a) An imposed current i will impose a magnetic field $\mathbf{H} = \frac{Ni}{s}\mathbf{i}_x$ in the ferrofluid. (b) An imposed voltage source $v(t) = \frac{d\lambda}{dt}$ will impose a flux $\frac{\lambda}{N}$ in the magnetic circuit, that will result in a flux density $\mathbf{B}$ that is spatially uniform in the ferrofluid given by $\mathbf{B} = \frac{\lambda}{NA}\mathbf{i}_x$ for planar Couette flow. Image taken and modified from [7].

3.2. Governing Equations

The governing equations outlined here are explained in detail in Chapter 2.

1) Maxwell's Equations: Ampere's Law

$$\nabla \times \mathbf{H} = \mathbf{J} \tag{3.1}$$

Since the ferrofluid in Figure 3-1 is a current free region $\mathbf{J} = 0$, (3.1) results in H_y and H_z being constant in the ferrofluid volume, assuming that $\mathbf{H}$ only varies with the x coordinate

$$\nabla \times \mathbf{H} = 0 \rightarrow \frac{dH_z}{dx} = \frac{dH_y}{dx} = 0 \rightarrow H_y, H_z = constant \tag{3.2}$$

Maxwell's Equations: Gauss's Law for Magnetic Flux Density

$$\nabla \bullet \mathbf{B} = 0 \tag{3.3}$$

Similarly (3.3) results in a spatially uniform B_x in the ferrofluid volume

$$\nabla \bullet \mathbf{B} = 0 \rightarrow \frac{dB_x}{dx} = 0 \rightarrow B_x = constant \tag{3.4}$$

The three other coupled equations are the two fluid mechanics conservation of linear and angular momentum equations and the magnetic relaxation equation given below.

2) Conservation of Linear Momentum

$$\rho\left[\frac{\partial \mathbf{v}}{\partial t} + (\mathbf{v} \bullet \nabla)\mathbf{v}\right] = -\nabla p' + 2\zeta \nabla \times \boldsymbol{\omega} + (\zeta + \eta)\nabla^2 \mathbf{v} + \mu_0 (\mathbf{M} \bullet \nabla)\mathbf{H} \tag{3.5}$$

3) Conservation of Angular Momentum

$$I\left[\frac{\partial \boldsymbol{\omega}}{\partial t} + (\mathbf{v} \bullet \nabla)\boldsymbol{\omega}\right] = \mu_0 \mathbf{M} \times \mathbf{H} + 2\zeta(\nabla \times \mathbf{v} - 2\boldsymbol{\omega}) + \eta' \nabla^2 \boldsymbol{\omega} \tag{3.6}$$

4) Magnetic Relaxation Equation

$$\frac{\partial \mathbf{M}}{\partial t} + (\mathbf{v} \bullet \nabla)\mathbf{M} = \boldsymbol{\omega} \times \mathbf{M} - \frac{1}{\tau_{eff}}(\mathbf{M} - \mathbf{M}_{eq}) \tag{3.7}$$

3.2.1. Assumptions

In addition to the assumptions of incompressible flow $(\nabla \bullet \mathbf{v} = 0)$ and no divergence of spin velocity $\boldsymbol{\omega}$ $(\nabla \bullet \boldsymbol{\omega} = 0)$, the fluid's equilibrium magnetization ($\mathbf{M_{eq}}$) is assumed to be given by a linear relationship with respect to the magnetic field $\mathbf{H}$ with χ the magnetic susceptibility.

$$\mathbf{M}_{eq} = \chi \mathbf{H} \tag{3.8}$$

By ensuring that the gap d is sufficiently small, the imposed magnetic field, H_z or magnetic flux density B_x , do not depend on the y and z coordinates for the geometry shown in Figure 3-1. The imposed horizontal magnetic field H_z is generated by surface currents, in the y direction on x=0 and x=d planes, that extend beyond the volume of ferrofluid such that the fringing fields at the ends are ignored. As a result, the imposed magnetic field and flux sources only depend on x.

The flow velocity $\mathbf{v}$ and spin velocity $\boldsymbol{\omega}$ are of the form

$$\mathbf{v} = v_z(x)\mathbf{i_z}, \boldsymbol{\omega} = \omega_y(x)\mathbf{i_y} \tag{3.9}$$

associated with planar Couette flow. The pressure term given in (3.5) is given by

$$p' = p - \rho(\mathbf{r} \bullet \mathbf{g}) \tag{3.10}$$

where $\mathbf{r}$ [m] is a position vector with respect to the origin, p is the applied pressure and $\mathbf{g}$ [m/s^2], the gravitational acceleration. In the planar case of Figure 3-1, the gravitational field is given as $-g\mathbf{i_x}$. Eq. (3.10) can then be written as

$$p' = p + \rho g x \tag{3.11}$$

The AC magnetization, flux density and field can be written in phasor form as given as

$$\mathbf{M} = \mathrm{Re}[\hat{\mathbf{M}} e^{j\Omega t}], \mathbf{B} = \mathrm{Re}[\hat{\mathbf{B}} e^{j\Omega t}], \mathbf{H} = \mathrm{Re}[\hat{\mathbf{H}} e^{j\Omega t}] \tag{3.12}$$

where the small hat symbol above the variables represents the complex amplitude of the individual magnetization, flux density and magnetic field, and Ω represents the AC radian frequency of operation.

Steady state flow is assumed as the fluid responds to the time average component of both the force and torque density terms in (3.15) and (3.16). These are given as

$$<\mathbf{F}>=\frac{\mu_0}{2}\mathrm{Re}\left[\left(\hat{\mathbf{M}}\bullet\nabla\right)\hat{\mathbf{H}}^*\right] \tag{3.13}$$

and

$$<\mathbf{T}>=\frac{\mu_0}{2}\mathrm{Re}\left[\hat{\mathbf{M}}\times\hat{\mathbf{H}}^*\right] \tag{3.14}$$

where the delimiters < > denote time average values and * represents the complex conjugate.

The flow is also assumed to be viscous dominated, setting the inertial terms in Eqs (3.5)-(3.6) to 0, resulting in

$$0=-\nabla p'+2\zeta\nabla\times\boldsymbol{\omega}+\left(\zeta+\eta\right)\nabla^2\mathbf{v}+<\mathbf{F}> \tag{3.15}$$

$$0=<\mathbf{T}>+2\zeta\left(\nabla\times\mathbf{v}-2\boldsymbol{\omega}\right)+\eta'\nabla^2\boldsymbol{\omega} \tag{3.16}$$

3.2.2. General Solution for Planar Couette Flow With Imposed AC B_x Field Only with Zero Spin-Viscosity ($\eta'=0$)

The only imposed flux density is B_x therefore

$$\hat{H}_z = \hat{H}_y = 0 \tag{3.17}$$

and using Gauss's law for the magnetic flux density

$$\mathbf{B} = \mu_0 (\mathbf{M} + \mathbf{H}) \tag{3.18}$$

$H_x(x)$ can be determined to be

$$H_x(x) = \frac{B_x}{\mu_0} - M_x(x) \tag{3.19}$$

The force density terms in (3.15), in different Cartesian directions, can be calculated to be

$$\begin{aligned} < F_x > &= \frac{1}{2}\mathrm{Re}\left[\mu_0 \hat{M}_x^{\,*} \frac{d}{dx}\left(\frac{\hat{B}_x}{\mu_0} - \hat{M}_x\right)\right] = \frac{1}{2}\mathrm{Re}\left[\mu_0 \hat{M}_x^{\,*} \frac{d}{dx}\left(-\hat{M}_x\right)\right] \\ < F_x > &= -\frac{\mu_0}{4}\left[\hat{M}_x^{*} \frac{d\hat{M}_x}{dx} + \hat{M}_x \frac{d\hat{M}_x^{*}}{dx}\right] = \frac{-\mu_0}{4}\frac{d}{dx}\left(\hat{M}_x^{*}\hat{M}_x\right) = -\frac{d}{dx}\left(\frac{1}{4}\mu_0 \left|\hat{M}_x^{2}\right|\right) \end{aligned} \tag{3.20}$$

$$< F_y > = < F_z > = 0 \tag{3.21}$$

Expanding (3.15) for all three Cartesian directions gives

$$\mathbf{x}: \quad 0 = -\frac{\partial p'}{\partial x} + < F_x > \tag{3.22}$$

$$\mathbf{y}: \quad 0 = -\cancel{\frac{\partial p'}{\partial y}} + \cancel{< F_y >} \tag{3.23}$$

$$\mathbf{z}: \quad 0 = -\cancel{\frac{\partial p'}{\partial z}} + \cancel{< F_z >} + 2\zeta\left(\frac{d\omega_y}{dx}\right) + (\zeta + \eta)\frac{d^2 v_z}{dx^2} \tag{3.24}$$

where $\frac{\partial}{\partial y}=\frac{\partial}{\partial z}=0$ and $p'=p+\rho gx$

The applied magnetic flux density $\mathbf{B_x}$ increases the pressure in the x direction in (3.22) and is given by p''

$$0=-\frac{\partial p'}{\partial x}+<F_x>=-\frac{\partial}{\partial x}\left(p+\rho gx+\frac{1}{4}\mu_0\left|\hat{M}_x^2\right|\right)=-\frac{\partial p''}{\partial x} \tag{3.25}$$

Integrating (3.24) with respect to x gives

$$\begin{aligned}&\mathbf{z}:\quad 0=2\zeta\omega_y+(\zeta+\eta)\frac{dv_z}{dx}+C_1\\&\rightarrow\frac{dv_z}{dx}=\frac{-2\zeta\omega_y}{\zeta+\eta}+C_2,\quad C_2=-\frac{C_1}{\zeta+\eta}\end{aligned} \tag{3.26}$$

with constants C_1 and C_2. With zero spin-viscosity ($\eta'=0$), equation (3.16) results in

$$0=<\mathbf{T}>+2\zeta(\nabla\times\mathbf{v}-2\boldsymbol{\omega}) \tag{3.27}$$

which reduces to

$$<T_y>-2\zeta\left(\frac{dv_z}{dx}+2\omega_y\right)=0 \tag{3.28}$$

Substituting (3.26) in (3.28) results in (3.29) with constant C_3.

$$\begin{aligned}&<T_y>-2\zeta\left(\frac{-2\zeta\omega_y}{\zeta+\eta}+2\omega_y+C_2\right)=0\\&\rightarrow<T_y>-\frac{4\zeta\eta}{\zeta+\eta}\omega_y=C_3,\quad C_3=2\zeta C_2\end{aligned} \tag{3.29}$$

For (3.29) to be valid for all x, $<T_y>$ and ω_y have to be constants and not functions of x.

Using (3.19) in (3.7) with (3.12) results in magnetization components given as

$$\hat{M}_x=\frac{\chi_0\left[(j\Omega\tau+1)\hat{B}_x\right]}{\mu_0\left[(\omega_y\tau)^2+(j\Omega\tau+1)(j\Omega\tau+1+\chi_0)\right]} \tag{3.30}$$

$$\hat{M}_z = \frac{-\chi_0\left[\omega_y\tau\hat{B}_x\right]}{\mu_0\left[\left(\omega_y\tau\right)^2+(j\Omega\tau+1)(j\Omega\tau+1+\chi_0)\right]} \tag{3.31}$$

Integrating (3.28) gives the solution for the flow velocity of the form

$$v_z(x) = \left(\frac{<T_y>}{2\zeta} - 2\omega_y\right)x + C \tag{3.32}$$

Using the boundary conditions associated with planar Couette flow

$$\begin{aligned} &v_z(x=0)=0 \rightarrow \text{C=0} \\ &\text{v}_z(x=d)=V \rightarrow \left(\frac{<T_y>}{2\zeta} - 2\omega_y\right) = \frac{V}{d} \end{aligned} \tag{3.33}$$

The resulting flow and spin velocities can then be given as

$$v_z(x) = \frac{Vx}{d} \tag{3.34}$$

$$\omega_y = \frac{<T_y>}{4\zeta} - \frac{V}{2d} \tag{3.35}$$

The time averaged magnetic torque density in the y direction is given by

$$<T_y> = \frac{\mu_0}{2}\text{Re}[\hat{M}_z\hat{H}_x^*] = \frac{\mu_0}{2}\text{Re}[\hat{M}_z\frac{\hat{B}_x^*}{\mu_0} - \hat{M}_z\hat{M}_x^*] \tag{3.36}$$

$$<T_y> = \frac{-\hat{B}_x^2\tau\chi_0\omega_y\left(1-(\Omega\tau)^2+\left(\omega_y\tau\right)^2\right)}{2\mu_0\left(\left(1+\chi_0+\left(\omega_y\tau\right)^2\right)^2+(\Omega\tau)^2\left(2+\chi_0(2+\chi_0)-2\left(\omega_y\tau\right)^2+(\Omega\tau)^2\right)\right)} \tag{3.37}$$

Substituting (3.37) in (3.28) with $\frac{dv_z}{dx} = \frac{V}{d}$ gives

$$\frac{V}{d} + 2\omega_y + \frac{-\hat{B}_x^2\tau\chi_0\omega_y\left(1-(\Omega\tau)^2+\left(\omega_y\tau\right)^2\right)}{2\mu_0\left(\left(1+\chi_0+\left(\omega_y\tau\right)^2\right)^2+(\Omega\tau)^2\left(2+\chi_0(2+\chi_0)-2\left(\omega_y\tau\right)^2+(\Omega\tau)^2\right)\right)} = 0 \tag{3.38}$$

Using the following substitutions in (3.38)

$$r = \frac{1}{2} + \frac{\omega_y d}{V} \tag{3.39}$$

$$V_{new} = \frac{V\tau}{d} \tag{3.40}$$

$$P = \frac{\left|\hat{B}_x\right|^2 \tau\chi_0}{8\zeta\mu_0} \tag{3.41}$$

results in a fifth order equation in r

$$r + \frac{P\left(r-\frac{1}{2}\right)\left(1-(\Omega\tau)^2 + V_{new}^2\left(r-\frac{1}{2}\right)^2\right)}{V_{new}\left((\Omega\tau)^4 + (\Omega\tau)^2\left(2+\chi_0(2+\chi_0) - 2V_{new}^2\left(r-\frac{1}{2}\right)^2\right) + \left(1+\chi_0+V_{new}^2\left(r-\frac{1}{2}\right)^2\right)^2\right)} = 0 \tag{3.42}$$

which can be solved for P as

$$P = -\frac{r\left(\tau^4\Omega^4 + \left(1+\left(-\frac{1}{2}+r\right)^2 V_{new}^{\ 2} + \chi_0\right)^2 + \tau^2\Omega^2\left(2-2\left(-\frac{1}{2}+r\right)^2 V_{new}^{\ 2} + \chi_0(2+\chi_0)\right)\right)}{\left(-\frac{1}{2}+r\right)\left(1+\left(-\frac{1}{2}+r\right)^2 V_{new}^{\ 2} - \tau^2\Omega^2\right)} \tag{3.43}$$

He [7], in his thesis, defines r the same way as defined in (3.39) and proves r is related to the effective viscosity $\Delta\eta$ by

$$r = \frac{\Delta\eta}{2\zeta} \tag{3.44}$$

He [7] also defines a parameter P_B which is related to P for all non-zero frequencies as

$$P_B = \frac{\chi_0\left|\hat{B}_x\right|^2\tau}{\mu_0 4\zeta(1+\chi_0)^2} = \frac{2}{(1+\chi_0)^2}P \tag{3.45}$$

The derivation in this section assumes non-zero frequencies resulting in a time-averaged torque density in Eq. (3.14) that is half as large as the DC torque density

$$\mathbf{T} = \mu_0 (\mathbf{M} \times \mathbf{H}) \tag{3.46}$$

This causes $P_B|_{DC} = 2P_B|_{AC}$ to be double of what it should be so that for the DC case, P_B defined by He [7] is given as

$$P_B|_{DC} = \frac{P}{(1+\chi_0)^2} \tag{3.47}$$

Using He's value of $\chi_0 = 1.55$ (for EFH1), with values of V_{new} from his thesis, a plot of P_B as a function of $2r$ for the DC case $(\Omega\tau = 0)$ can be seen in Figure 3-3. Figure 3-3 is identical to He's plot, from his thesis [7], shown in Figure 3-4.

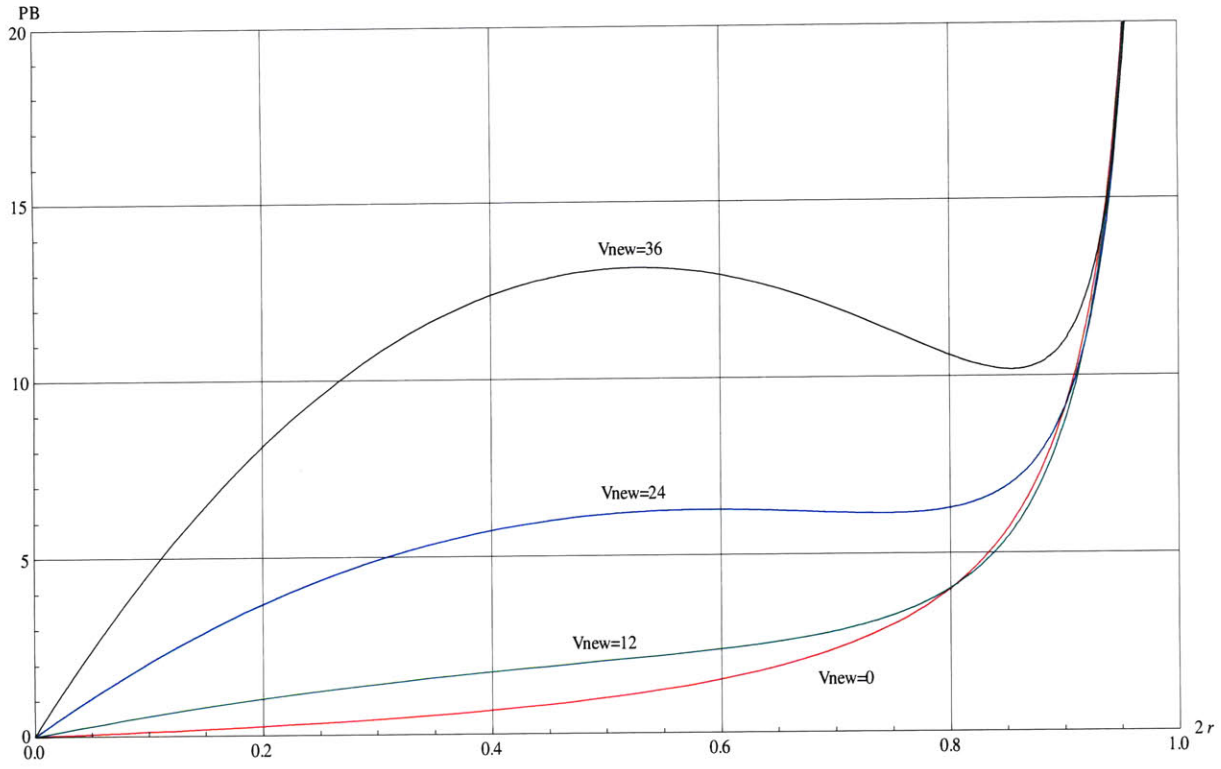

Figure 3-3. Solutions for the change in non-dimensional magnetoviscosity $2r = \frac{\Delta\eta}{\zeta}$ for planar Couette flow versus magnetic flux density parameter P_B for various values of V_{new} with an imposed DC B_x field for EFH1 using Eq. (3.47) for $P_B\big|_{DC}$ as a function of $2r = \frac{\Delta\eta}{\zeta}$.

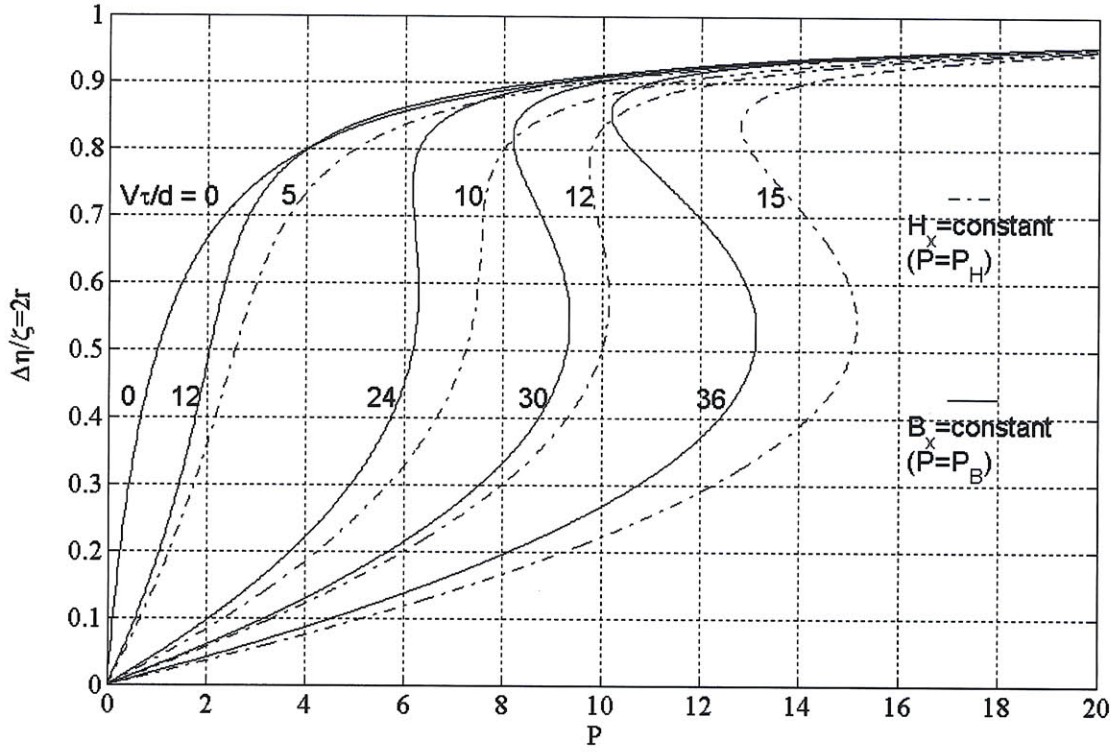

Figure 3-4. He's [7] solution for the change in magnetoviscosity for planar Couette flow as a function of $P=P_B$ with an imposed DC B_x and or $P=P_H$ for an imposed H_x field for various values of $V_{new} = \frac{V\tau}{d}$ with EFH1. The imposed H_x can be generated using a current source as seen in Figure 3-2 (a) . Results are identical to Figure 3-3 for imposed B_x.

The fifth order equation in (3.42) can have five real roots, three real and two imaginary roots, or one real and four imaginary roots to the equation depending on values of P_B and V_{new}. This is illustrated in Figure 3-3 and Figure 3-4 where for certain values of applied magnetic field and flow parameters P_B and V_{new} there are either one (one real and four imaginary roots) or three (three real and two imaginary roots) possible solutions for $\Delta\eta$. The three possible solutions include both stable and unstable multiple values for $\Delta\eta$. This behavior is also seen in plots of P_B as a function of $2r$, at four different values for V_{new} (V_{new}=0 (red), 12 (green), 24

(blue), 36 (black)), at different normalized frequencies $\Omega\tau = 0.2, 0.4, 0.6, 0.8, 1.0$ given in Figure 3-5 to Figure 3-9. The Mathematica® code for generating these plots are given in Appendix A.

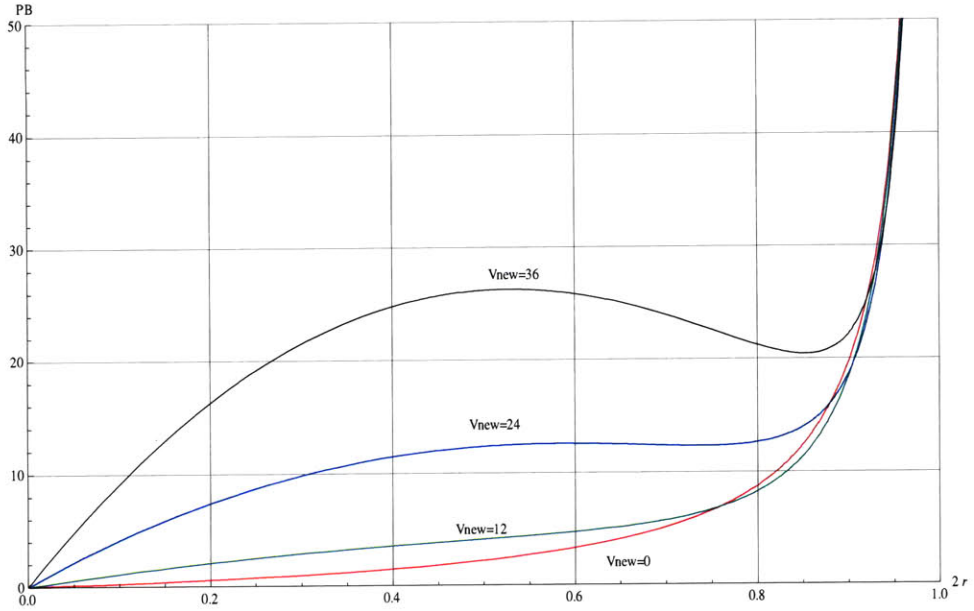

Figure 3-5. Solutions for the change in magnetoviscosity for planar Couette flow versus magnetic flux density parameter P_B for various values of V_{new} with an imposed AC B_x field, for EFH1 using Eq. (3.45) as a function of $2r = \dfrac{\Delta\eta}{\zeta}$, at a normalized frequency of $\Omega\tau = 0.2$.

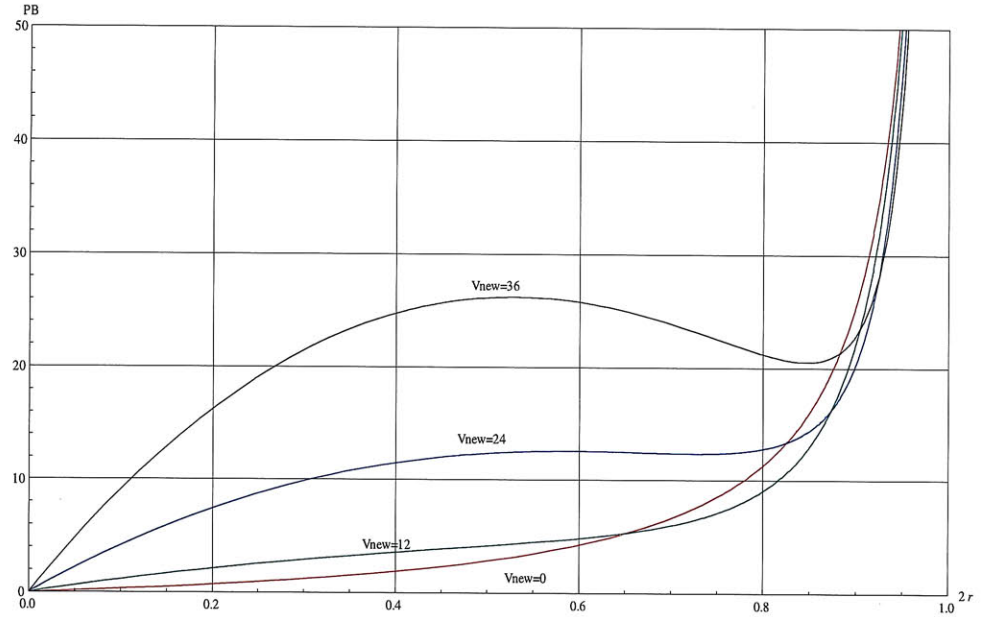

Figure 3-6. Solutions for the change in magnetoviscosity for planar Couette flow versus magnetic flux density parameter P_B for various values of V_{new} with an imposed AC B_x field, for EFH1 using Eq. (3.45) as a function of $2r = \dfrac{\Delta\eta}{\zeta}$, at a normalized frequency of $\Omega\tau = 0.4$.

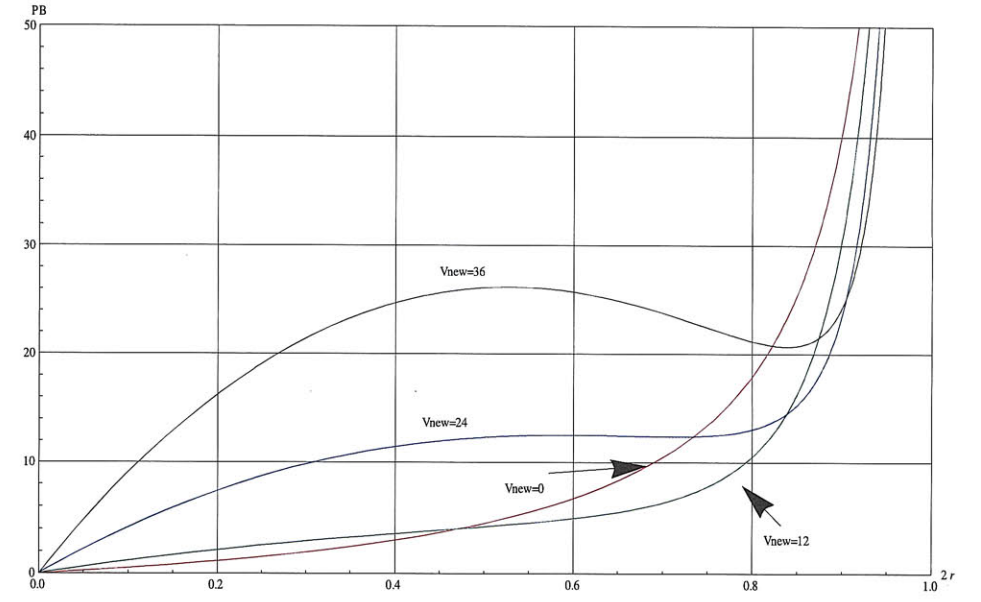

Figure 3-7. Solutions for the change in magnetoviscosity for planar Couette flow versus magnetic flux density parameter P_B for various values of V_{new} with an imposed AC B_x field, for EFH1 using Eq. (3.45) as a function of $2r = \dfrac{\Delta\eta}{\zeta}$, at a normalized frequency of $\Omega\tau = 0.6$.

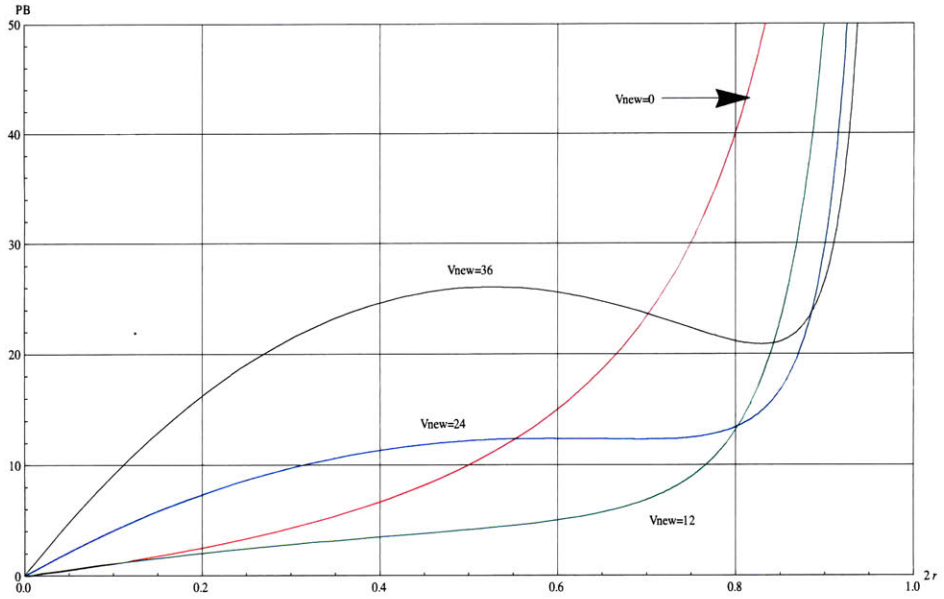

Figure 3-8. Solutions for the change in magnetoviscosity for planar Couette flow versus magnetic flux density parameter P_B for various values of V_{new} with an imposed AC B_x field, for EFH1 using Eq. (3.45) as a function of $2r = \dfrac{\Delta\eta}{\zeta}$, at a normalized frequency of $\Omega\tau = 0.8$.

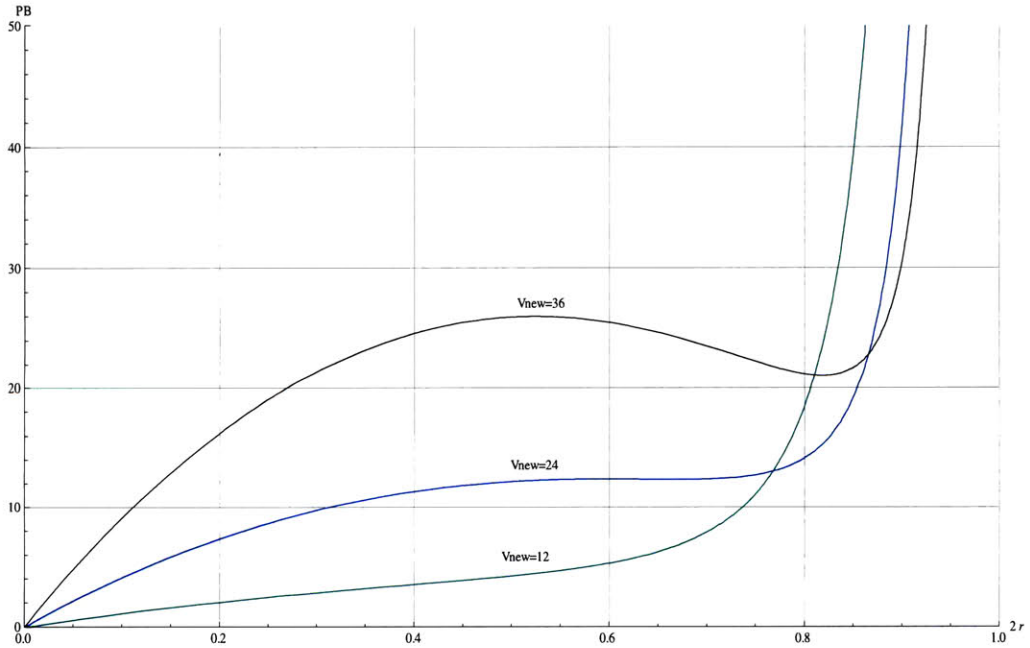

Figure 3-9. Solutions for the change in magnetoviscosity for planar Couette flow versus magnetic flux density parameter P_B for various values of V_{new} with an imposed AC B_x field, for EFH1 using Eq. (3.45) as a function of $2r = \dfrac{\Delta\eta}{\zeta}$, at a normalized frequency of $\Omega\tau = 1.0$.

3.2.3. General Solution for Planar Couette Flow With Imposed AC H_z Field Only with Zero Spin-Viscosity ($\eta'=0$)

The only imposed flux density is H_z therefore

$$\hat{B}_x = \hat{H}_y = 0 \tag{3.48}$$

The zero imposed flux density however, using Gauss's law for the magnetic flux density

$$\mathbf{B} = \mu_0 (\mathbf{M} + \mathbf{H}) \tag{3.49}$$

still generates an x directed magnetic field in the fluid $H_x(x)$ and with $B_x = 0$

$$H_x(x) = -M_x(x) \tag{3.50}$$

The force density terms in (3.15), in different Cartesian directions, can be calculated to be

$$\begin{aligned} < F_x > &= \frac{1}{2}\mathrm{Re}\left[\mu_0 \hat{M}_x \frac{d}{dx}\left(\hat{H}_x^*\right)\right] = \frac{1}{2}\mathrm{Re}\left[\mu_0 \hat{M}_x \frac{d}{dx}\left(-\hat{M}_x^*\right)\right] \\ < F_x > &= -\frac{\mu_0}{4}\left[\hat{M}_x^* \frac{d\hat{M}_x}{dx} + \hat{M}_x \frac{d\hat{M}_x^*}{dx}\right] = \frac{-\mu_0}{4}\frac{d}{dx}\left(\hat{M}_x^* \hat{M}_x\right) = -\frac{d}{dx}\left(\frac{1}{4}\mu_0 \left|\hat{M}_x^2\right|\right) \end{aligned} \tag{3.51}$$

$$< F_y > = 0, < F_z > = \frac{1}{2}\mathrm{Re}\left[\mu_0 \hat{M}_x \frac{d\hat{H}_z^*}{dx}\right] = 0 \tag{3.52}$$

Expanding (3.15) for all three Cartesian directions gives

$$\mathbf{x}: \quad 0 = -\frac{\partial p'}{\partial x} + < F_x > \tag{3.53}$$

$$\mathbf{y}: \quad 0 = -\cancel{\frac{\partial p'}{\partial y}} + \cancel{< F_y >} \tag{3.54}$$

$$\mathbf{z}: \quad 0 = -\cancel{\frac{\partial p'}{\partial z}} + \cancel{< F_z >} + 2\zeta\left(\frac{d\omega_y}{dx}\right) + (\zeta + \eta)\frac{d^2 v_z}{dx^2} \tag{3.55}$$

where $\frac{\partial}{\partial y}=\frac{\partial}{\partial z}=0$ and $p'=p+\rho gx$

The x directed magnetic field results in an increase in x directed pressure and is given by p''

$$0=-\frac{\partial p'}{\partial x}+<F_x>=-\frac{\partial}{\partial x}\left(p+\rho gx+\frac{1}{4}\mu_0\left|\hat{M}_x^2\right|\right)=-\frac{\partial p''}{\partial x} \tag{3.56}$$

Integrating (3.55) with respect to x gives

$$\begin{aligned}&\mathbf{z}:\quad 0=2\zeta\omega_y+(\zeta+\eta)\frac{dv_z}{dx}+C_1\\&\rightarrow\frac{dv_z}{dx}=\frac{-2\zeta\omega_y}{\zeta+\eta}+C_2,\quad C_2=-\frac{C_1}{\zeta+\eta}\end{aligned} \tag{3.57}$$

with constants C_1 and C_2. With zero spin-viscosity ($\eta'=0$), equation (3.16) results in

$$0=<\mathbf{T}>+2\zeta(\nabla\times\mathbf{v}-2\boldsymbol{\omega}) \tag{3.58}$$

which reduces to

$$<T_y>-2\zeta\left(\frac{dv_z}{dx}+2\omega_y\right)=0 \tag{3.59}$$

Substituting (3.57) in (3.59) results in (3.60) with constant C_3.

$$\begin{aligned}&<T_y>-2\zeta\left(\frac{-2\zeta\omega_y}{\zeta+\eta}+2\omega_y+C_2\right)=0\\&\rightarrow<T_y>-\frac{4\zeta\eta}{\zeta+\eta}\omega_y=C_3,\quad C_3=2\zeta C_2\end{aligned} \tag{3.60}$$

For (3.60) to be valid for all x, $<T_y>$ and ω_y have to be constants and not functions of x.

Using (3.50) in (3.7) with (3.12) results in magnetization components given as

$$\hat{M}_x=\frac{\chi_0\left[(\omega_y\tau)\hat{H}_z\right]}{\left[(\omega_y\tau)^2+(j\Omega\tau+1)(j\Omega\tau+1+\chi_0)\right]} \tag{3.61}$$

$$\hat{M}_z = \frac{\chi_0\left[\left(j\Omega\tau+1+\chi_0\right)\hat{H}_z\right]}{\mu_0\left[\left(\omega_y\tau\right)^2+\left(j\Omega\tau+1\right)\left(j\Omega\tau+1+\chi_0\right)\right]} \tag{3.62}$$

and the resulting flow and spin velocities can be determined, similar to Eqs (3.32)-(3.35), as

$$v_z(x) = \frac{Vx}{d} \tag{3.63}$$

$$\omega_y = \frac{<T_y>}{4\zeta} - \frac{V}{2d} \tag{3.64}$$

The time averaged magnetic torque density in the y direction is given by

$$<T_y> = \frac{\mu_0}{2}\mathrm{Re}[-\hat{M}_x\hat{H}_z^* + \hat{M}_z\hat{H}_x^*] = -\frac{\mu_0}{2}\mathrm{Re}[\hat{M}_x\hat{H}_z^* + \hat{M}_z\hat{M}_x^*] \tag{3.65}$$

$$<T_y> = \frac{-\hat{H}_z^2\tau\chi_0\omega_y\left(\left(1+\chi_0\right)^2-\left(\Omega\tau\right)^2+\left(\omega_y\tau\right)^2\right)}{2\left(\left(1+\chi_0+\left(\omega_y\tau\right)^2\right)^2+\left(\Omega\tau\right)^2\left(2+\chi_0\left(2+\chi_0\right)-2\left(\omega_y\tau\right)^2+\left(\Omega\tau\right)^2\right)\right)} \tag{3.66}$$

Substituting (3.37) in (3.28) with $\frac{dv_z}{dx} = \frac{V}{d}$ gives

$$\frac{V}{d} + 2\omega_y + \frac{-\mu_0\hat{H}_z^2\tau\chi_0\omega_y\left(\left(1+\chi_0\right)^2-\left(\Omega\tau\right)^2+\left(\omega_y\tau\right)^2\right)}{4\zeta\left(\left(1+\chi_0+\left(\omega_y\tau\right)^2\right)^2+\left(\Omega\tau\right)^2\left(2+\chi_0\left(2+\chi_0\right)-2\left(\omega_y\tau\right)^2+\left(\Omega\tau\right)^2\right)\right)} = 0 \tag{3.67}$$

Using the following substitutions in (3.38)

$$r = \frac{1}{2} + \frac{\omega_y d}{V} \tag{3.68}$$

$$V_{new} = \frac{V\tau}{d} \tag{3.69}$$

$$P_H = \frac{\mu_0\left|\hat{H}_z\right|^2\tau\chi_0}{4\zeta} \tag{3.70}$$

results in a fifth order equation in r

$$r+\frac{\mathrm{P}_H\left(-\frac{1}{2}+r\right)\left(\left(-\frac{1}{2}+r\right)^2 \mathrm{V}_{new}{}^2-\tau^2\Omega^2+(1+\chi_0)^2\right)}{2\left(\tau^4\Omega^4+\left(1+\left(-\frac{1}{2}+r\right)^2 \mathrm{V}_{new}{}^2+\chi_0\right)^2+\tau^2\Omega^2\left(2-2\left(-\frac{1}{2}+r\right)^2 \mathrm{V}_{new}{}^2+\chi_0(2+\chi_0)\right)\right)}=0 \quad (3.71)$$

which can be solved for P_H as

$$P_H=-\frac{2r(\tau^4\Omega^4+(1+(-\frac{1}{2}+r)^2 V_{new}{}^2+\chi_0)^2+\tau^2\Omega^2(2-2(-\frac{1}{2}+r)^2 V_{new}{}^2+\chi_0(2+\chi_0)))}{(-\frac{1}{2}+r)((-\frac{1}{2}+r)^2 V_{new}{}^2-\tau^2\Omega^2+(1+\chi_0)^2)} \quad (3.72)$$

where r is defined the same way as defined in (3.39) and is equivalent to the change in viscosity term in (3.44).

The derivation in this section assumes non-zero frequencies resulting in a time-averaged torque density in Eq. (3.14) that is half as large as the DC torque density given in (3.46). For the DC case P_H is given as

$$P_H\big|_{DC}=\frac{P_H}{2} \quad (3.73)$$

Using EFH1's value of $\chi_0=1.55$, a plot of P_H as a function of $2r$ for the DC case ($\Omega\tau=0$) with V_{new}=[0 (red), 4 (green), 8 (blue) and 12 (black)] can be seen in Figure 3-10.

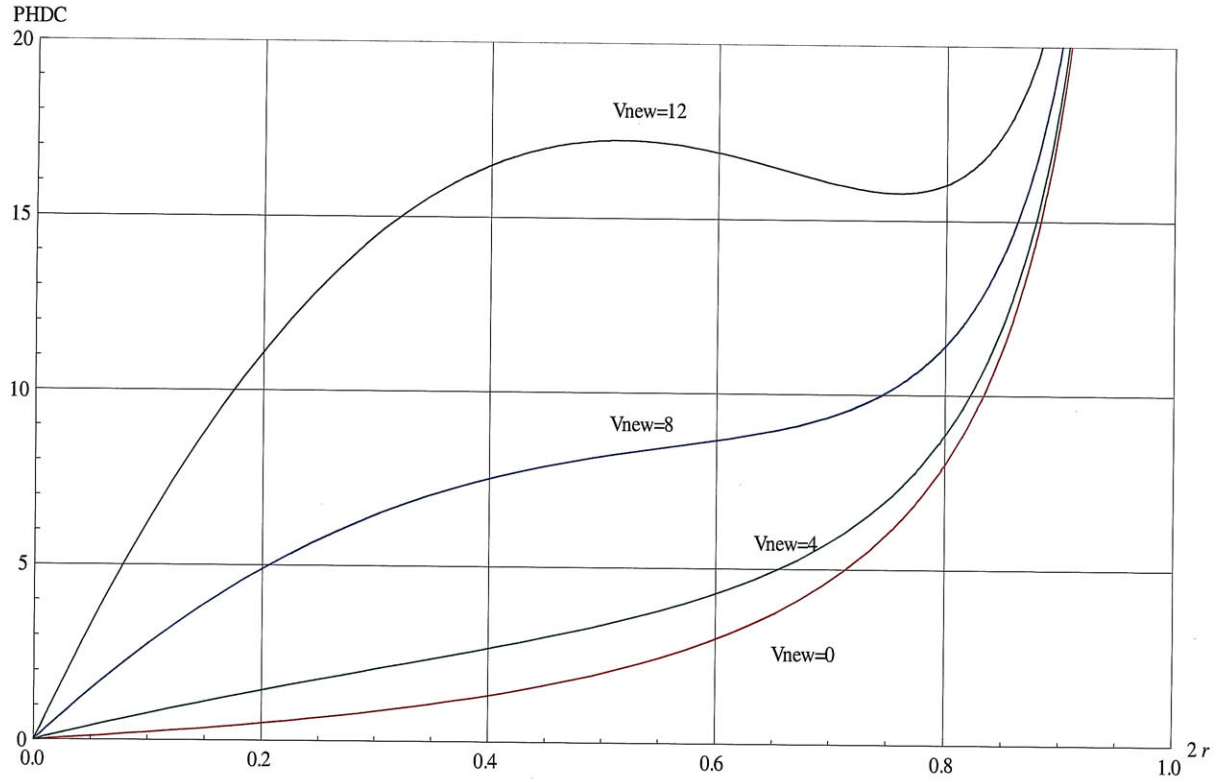

Figure 3-10. Solutions for the change in magnetoviscosity for planar Couette flow versus magnetic field intensity parameter P_H for various values of V_{new} with an imposed DC H_z field, for EFH1 using Eq. (3.73) as a function of $2r = \dfrac{\Delta\eta}{\zeta}$.

The fifth order equation in (3.71) could have for some values of P_H and V_{new} either five real roots, three real and two imaginary roots or one real and four imaginary roots to the equation. This is illustrated in Figure 3-10 where for certain values of applied magnetic field and flow parameters P_H and V_{new} there are either one (one real and four imaginary roots) or three (three real and two imaginary roots) possible solutions for $\Delta\eta$. The three possible solutions include both stable and unstable multiple values for $\Delta\eta$. This behavior is also seen in plots of P_H as a function of $2r$, at four different values for V_{new} (V_{new}=0 (red), 4 (green), 8 (blue), 12 (black)), at different normalized frequencies $\Omega\tau = 0.2, 0.4, 1.0$ given in Figure 3-11 - Figure 3-13 respectively. The Mathematica® code for generating these plots are given in Appendix A.

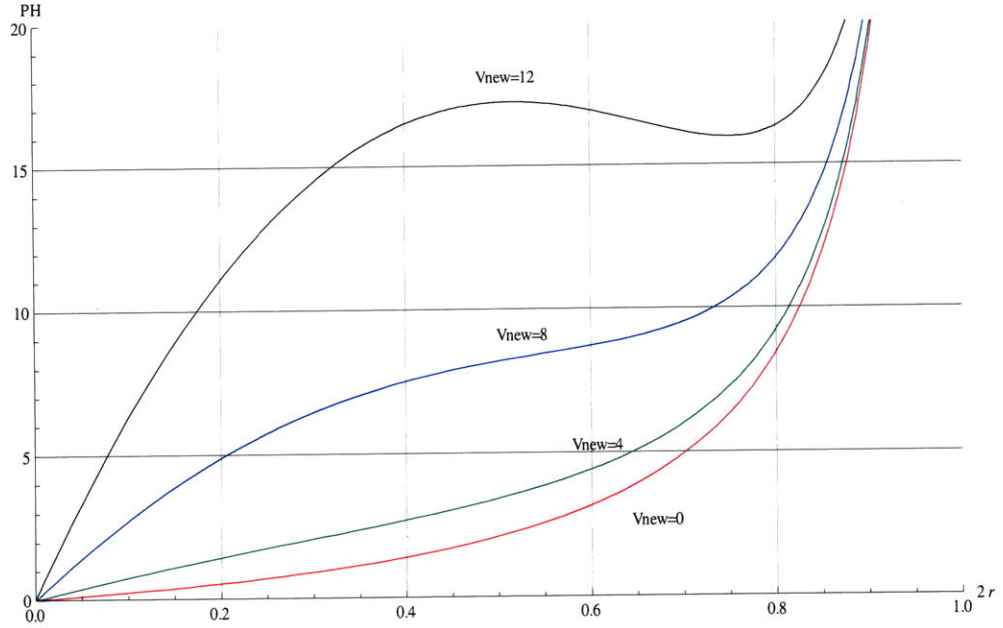

Figure 3-11. Solutions for the change in magnetoviscosity for planar Couette flow versus magnetic field intensity parameter P_H for various values of V_{new} with an imposed AC H_z field, for EFH1 with normalized frequency of $\Omega\tau = 0.2$ using Eq. (3.72) as a function of $2r = \frac{\Delta\eta}{\zeta}$.

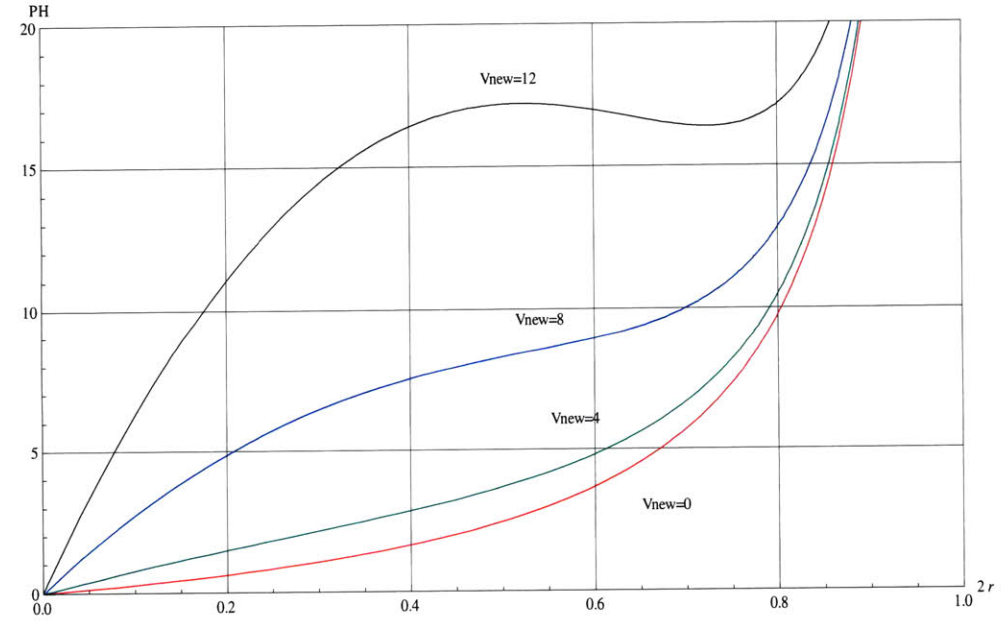

Figure 3-12. Solutions for the change in magnetoviscosity for planar Couette flow versus magnetic field intensity parameter P_H for various values of V_{new} with an imposed AC H_z field, for EFH1 with normalized frequency of $\Omega\tau = 0.4$ using Eq. (3.72) as a function of $2r = \frac{\Delta\eta}{\zeta}$.

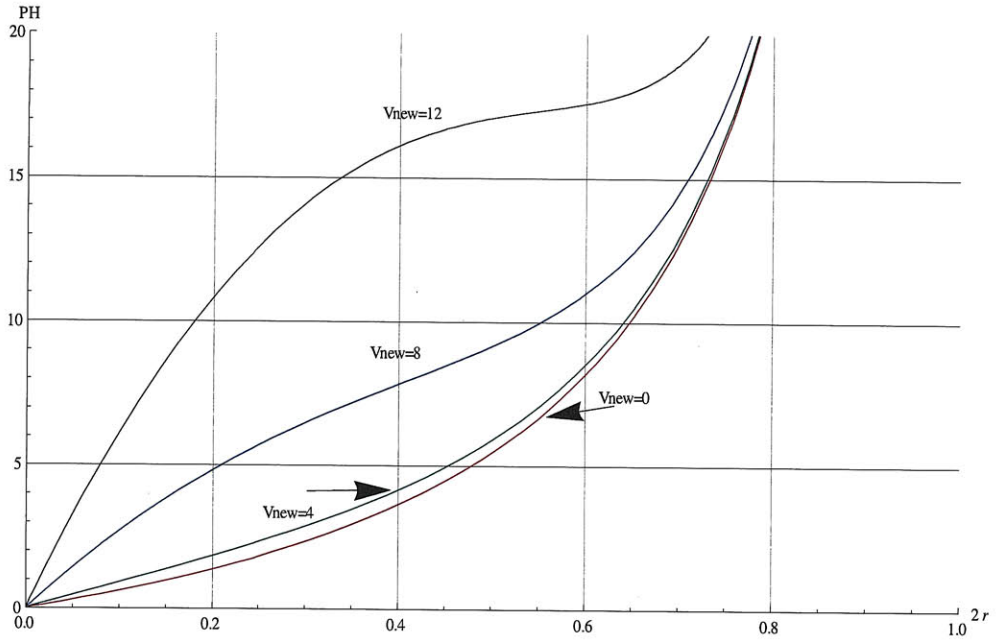

Figure 3-13. Solutions for the change in magnetoviscosity for planar Couette flow versus magnetic field intensity parameter P_H for various values of V_{new} with an imposed AC H_z field, for EFH1 with normalized frequency of $\Omega\tau = 1.0$ using Eq. (3.72) as a function of $2r = \frac{\Delta\eta}{\zeta}$.

3.2.4. Numerical Simulations of Planar Poiseuille Flow

Zahn and Greer, in their paper [1], derive coupled linear and angular momentum conservation equations for planar Poiseuille flow with imposed magnetic flux density B_x and magnetic field H_z with the same geometry setup as Figure 3-1. The parameters are expressed in dimensionless form indicated by tildes, given in (3.74) with time normalized to the magnetic relaxation time τ, space normalized to the duct spacing d, and magnetic field quantities normalized to a nominal magnetic field strength H_0.

$$\begin{aligned}&\tilde{\Omega}=\Omega\tau,\tilde{\mathbf{H}}=\frac{\hat{\mathbf{H}}}{H_0},\tilde{\mathbf{M}}=\frac{\hat{\mathbf{M}}}{H_0},\tilde{\mathbf{B}}=\frac{\hat{\mathbf{B}}}{\mu_0 H_0},\tilde{x}=\frac{x}{d},\tilde{v}_z=\frac{v_z\tau}{d},\tilde{\omega}_y=\omega_y\tau,\\&\tilde{T}_y=\frac{T_y}{\mu_0 H_0^2},\tilde{\eta}=\frac{2\eta}{\mu_0 H_0^2\tau},\tilde{\eta}'=\frac{\eta'}{\mu_0 H_0^2\tau d^2},\tilde{\zeta}=\frac{2\zeta}{\mu_0 H_0^2\tau},\frac{\partial\tilde{p}'}{\partial\tilde{z}}=\frac{d}{\mu_0 H_0^2}\frac{\partial p'}{\partial z}\end{aligned} \tag{3.74}$$

The coupled dimensionless flow and spin velocity equations that are solved are given as

$$0=-\frac{\partial\tilde{p}'}{\partial\tilde{z}}+\tilde{\zeta}\left(\frac{d\tilde{\omega}_y}{d\tilde{x}}\right)+\frac{1}{2}\left(\tilde{\zeta}+\tilde{\eta}\right)\frac{d^2\tilde{v}_z}{d\tilde{x}^2} \tag{3.75}$$

$$<\tilde{T}_y>-\tilde{\zeta}\left(\frac{d\tilde{v}_z}{d\tilde{x}}+2\tilde{\omega}_y\right)+\tilde{\eta}'\frac{d^2\tilde{\omega}_y}{d\tilde{x}^2}=0 \tag{3.76}$$

with magnetization derived in [1] as

$$\tilde{M}_x=\frac{\chi_0\left[\tilde{\omega}_y\tilde{H}_z+\left(j\tilde{\Omega}+1\right)\tilde{B}_x\right]}{\left[\tilde{\omega}_y^{\,2}+\left(j\tilde{\Omega}+1\right)\left(j\tilde{\Omega}+1+\chi_0\right)\right]} \tag{3.77}$$

$$\tilde{M}_z=\frac{\chi_0\left[\left(j\tilde{\Omega}+1+\chi_0\right)\tilde{H}_z-\tilde{B}_x\tilde{\omega}_y\right]}{\left[\tilde{\omega}_y^2+\left(j\tilde{\Omega}+1\right)\left(j\tilde{\Omega}+1+\chi_0\right)\right]} \tag{3.78}$$

and torque calculated to be

$$<\tilde{T}_y>=\frac{1}{2}\mathrm{Re}\left[\tilde{M}_z\tilde{B}_x^*-\tilde{M}_x^*\left(\tilde{H}_z+\tilde{M}_z\right)\right] \tag{3.79}$$

and is given by a complicated equation, Eq. (33), in [1]. Zahn [1] simplifies the expression by linearizing the torque in the limit of small $\tilde{\omega}_y$ and is given by the form

$$\lim_{\tilde{\omega}_y << 1} < \tilde{T}_y >= \tilde{T}_0 + \alpha \tilde{\omega}_y \tag{3.80}$$

where $\tilde{T}_0$ and α are given as

$$\tilde{T}_0 = -\frac{\chi_0 \operatorname{Re}\left[\left[\chi_0 \tilde{\Omega}^2 + j\tilde{\Omega}\left(\tilde{\Omega}^2 + 1 + \chi_0\right)\right]\left[\tilde{H}_z \tilde{B}_x^{\,*}\right]\right]}{\left[1 + \chi_0 + \tilde{\Omega}^2\right]^2 + \chi_0^2 \tilde{\Omega}^2} \tag{3.81}$$

$$\alpha = \frac{\chi_0}{2} \frac{\left[\left|\tilde{B}_x\right|^2 \left(\tilde{\Omega}^2 - 1\right) + \left|\tilde{H}_z\right|^2 \left[\tilde{\Omega}^2 - \left(1 + \chi_0\right)^2\right]\right]}{\left[1 + \chi_0 + \tilde{\Omega}^2\right]^2 + \chi_0^2 \tilde{\Omega}^2} \tag{3.82}$$

Equations (3.75)-(3.76) along with the complete torque expression, given by Eq. (3.79), were simultaneously solved using Mathematica® and COMSOL Multiphysics® 3.5a. For (3.75) the no slip boundary condition was implemented on the flow velocity while for (3.76), the boundary condition on spin velocity was set to 0 if $\tilde{\eta}' \neq 0$, otherwise no boundary condition was implemented on spin velocity if $\tilde{\eta}' = 0$. These boundary conditions for $\tilde{\eta}' \neq 0$ are

$$\begin{aligned} \tilde{v}_z(\tilde{x} = 0) &= 0 \quad \tilde{\omega}_y(\tilde{x} = 0) = 0 \\ \tilde{v}_z(\tilde{x} = 1) &= 0 \quad \tilde{\omega}_y(\tilde{x} = 1) = 0 \end{aligned} \tag{3.83}$$

The results were also compared to the linearized torque expression in Eq. (3.80). The Mathematica® code implemented the *shooting method* to solve for the boundary value problem while COMSOL® used the finite element method. The code to generate these results are given in Appendix A.

3.2.4.1. Zero Spin-viscosity Cases ($\eta'=0$)

The results of Zahn and Greer [1] were first replicated with parameters taken from their paper such as $\chi_0 = 1, \tilde{\eta} = 1, \tilde{\zeta} = 1, \frac{\partial \tilde{p}'}{\partial \tilde{z}} = 0.00001$. The value for the vortex viscosity $\tilde{\zeta}$ is set equal to the dynamic viscosity $\tilde{\zeta} = \tilde{\eta}$ and was used to verify the results obtained in the paper [1] as given in Figure 3-14. The results obtained are identical to that of Figure 3-14. The value for the vortex viscosity is not physical since it should be equal to $\tilde{\zeta} = \frac{3}{2}\tilde{\eta}\phi_{vol}$ [6], and this case is considered in 3.2.4.4.

Figure 3-15 and Figure 3-16 are results of normalized flow and spin velocities as a function of normalized distance $\tilde{x}$ with an imposed normalized magnetic flux density $\tilde{B}_x = 1$. The results of Mathematica® and COMSOL® are in good agreement with each other. Figure 3-17 and Figure 3-18 are results of normalized flow and spin velocities with an imposed normalized magnetic field $\tilde{H}_z = 1$ with good agreement between COMSOL® and Mathematica®. The linearized torque in both these cases gives similar results to that obtained by using the complete torque equation.

Figure 3-19 and Figure 3-20 are for the case of an imposed rotating field with $\tilde{B}_x = 1$ and $\tilde{H}_z = i$. In this case, the linearized torque equation gives results that are slightly different from using the complete torque equation, however, if the field magnitude is increased such that $\tilde{B}_x = 10$ and $\tilde{H}_z = i$ as seen in Figure 3-21 and Figure 3-22, the difference between the results using the complete and linearized torque equation can be clearly seen.

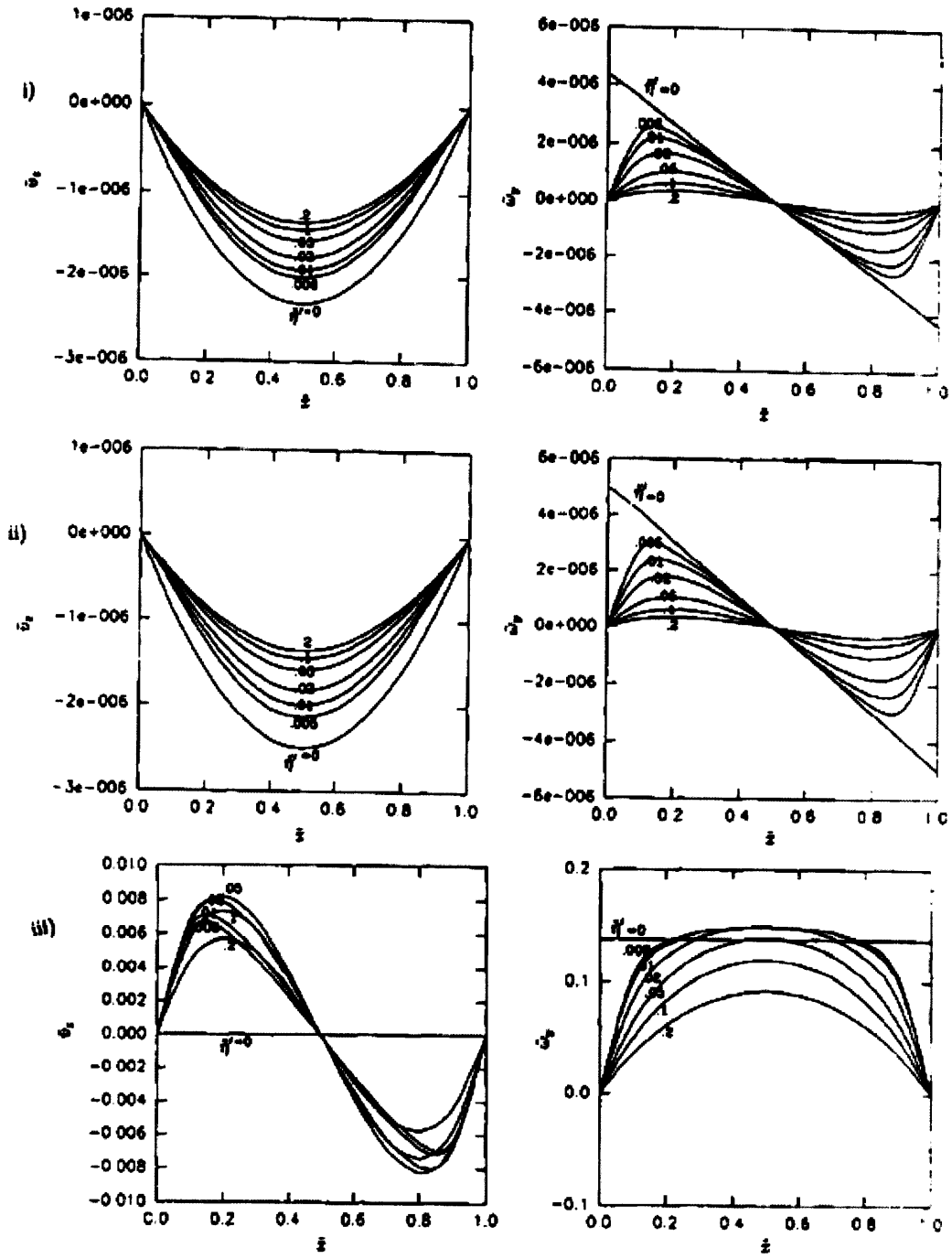

Figure 3-14. Dimensionless flow velocity $\tilde{v}_z(\tilde{x})$ and spin velocity $\tilde{\omega}_y(\tilde{x})$ versus position $\tilde{x}$ with $\chi_0 = 1, \tilde{\eta} = 1, \tilde{\zeta} = 1, \frac{\partial \tilde{p}'}{\partial \tilde{z}} = 0.00001, \tilde{\Omega} = 1$ for various values of dimensionless spin viscosity $\tilde{\eta}'$ with (i) tangential magnetic field ($\hat{H}_z = H_0, \hat{B}_x = 0$); (ii) perpendicular magnetic field ($\hat{H}_z = 0, \hat{B}_x = \mu_0 H_0$); and (iii) rotating magnetic field ($\hat{H}_z = iH_0, \hat{B}_x = \mu_0 H_0$) taken from [1].

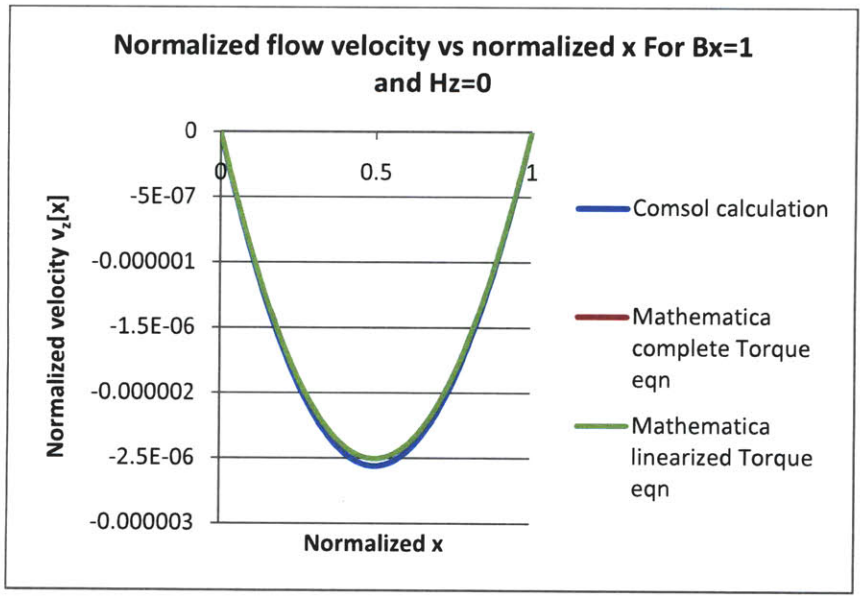

Figure 3-15. Normalized flow velocity $\tilde{v}_z(\tilde{x})$ for an imposed normalized magnetic flux density $\tilde{B}_x = 1$ with zero spin-viscosity condition ($\tilde{\eta}' = 0$) and $\chi_0 = 1, \tilde{\eta} = 1, \tilde{\zeta} = 1, \frac{\partial \tilde{p}'}{\partial \tilde{z}} = 0.00001, \tilde{\Omega} = 1$. The linearized torque and complete torque implementations in Mathematica give identical results with their curves overlapping.

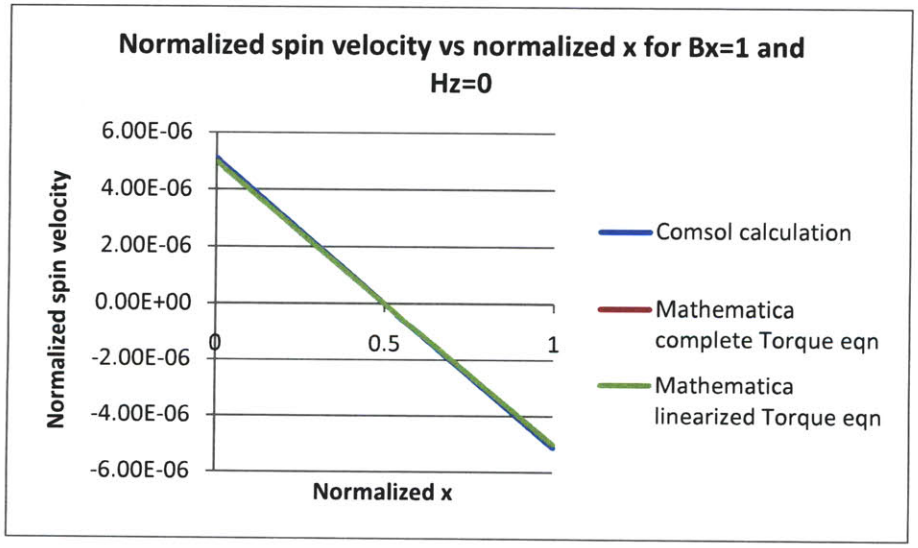

Figure 3-16. Normalized spin velocity $\tilde{\omega}_y(\tilde{x})$ for an imposed normalized magnetic flux density $\tilde{B}_x = 1$ with zero spin-viscosity condition ($\tilde{\eta}' = 0$) and $\chi_0 = 1, \tilde{\eta} = 1, \tilde{\zeta} = 1, \frac{\partial \tilde{p}'}{\partial \tilde{z}} = 0.00001, \tilde{\Omega} = 1$. The linearized torque and complete torque implementations in Mathematica give identical results with their curves overlapping.

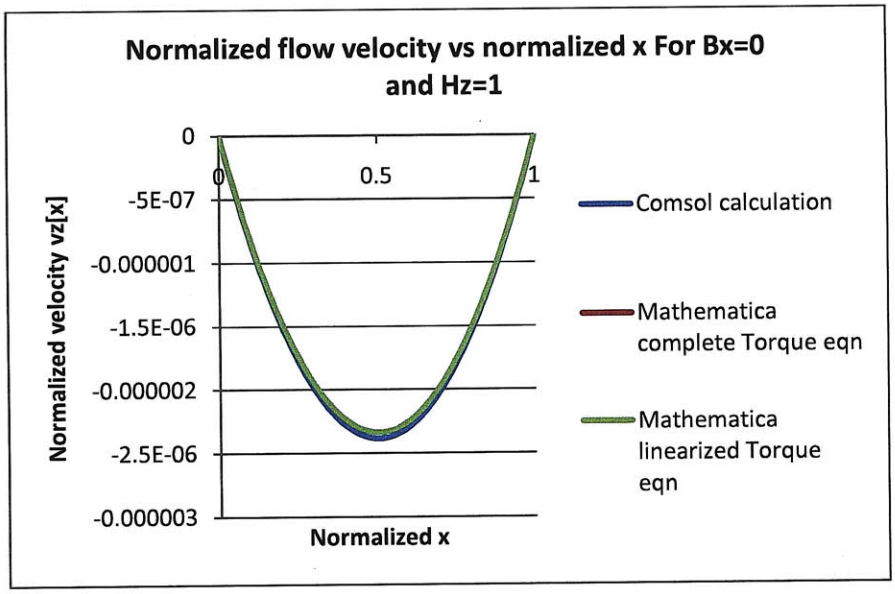

Figure 3-17. Normalized flow velocity $\tilde{v}_z(\tilde{x})$ for an imposed normalized magnetic field $\tilde{H}_z = 1$ with zero spin-viscosity condition $(\tilde{\eta}' = 0)$ and $\chi_0 = 1, \tilde{\eta} = 1, \tilde{\zeta} = 1, \frac{\partial \tilde{p}'}{\partial \tilde{z}} = 0.00001, \tilde{\Omega} = 1$. The linearized torque and complete torque implementations in Mathematica give identical results with their curves overlapping.

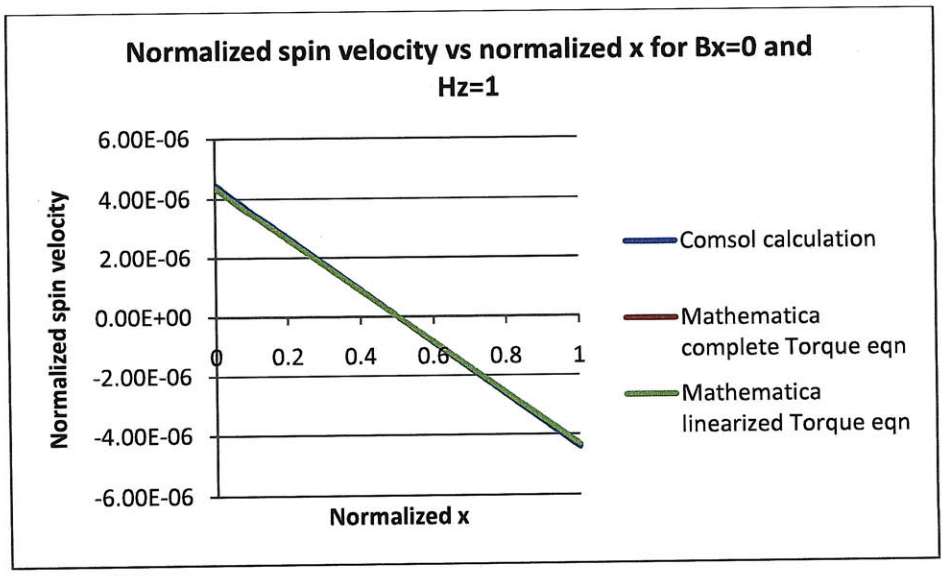

Figure 3-18. Normalized spin velocity $\tilde{\omega}_y(\tilde{x})$ for an imposed normalized magnetic flux density $\tilde{H}_z = 1$ with zero spin-viscosity condition $(\tilde{\eta}' = 0)$ and $\chi_0 = 1, \tilde{\eta} = 1, \tilde{\zeta} = 1, \frac{\partial \tilde{p}'}{\partial \tilde{z}} = 0.00001, \tilde{\Omega} = 1$. The linearized torque and complete torque implementations in Mathematica give identical results with their curves overlapping.

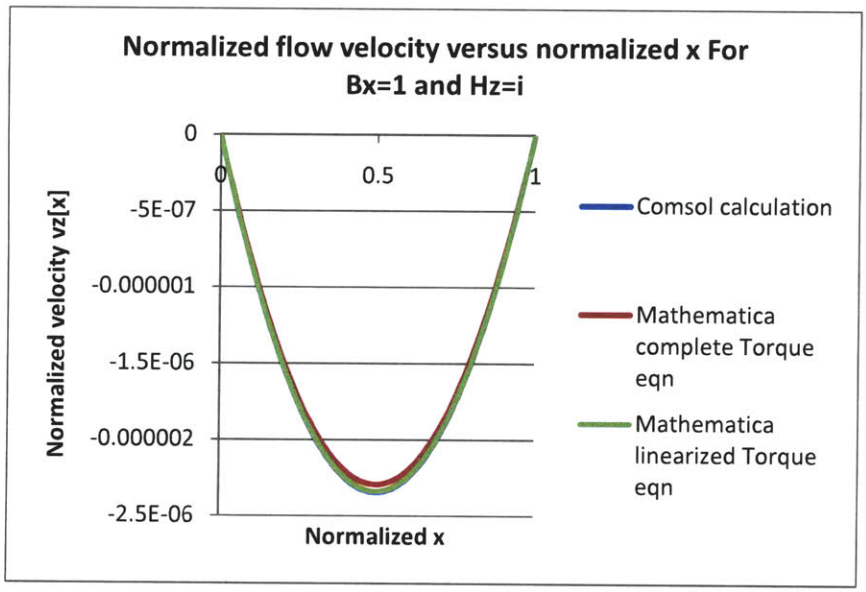

Figure 3-19. Normalized flow velocity $\tilde{v}_z(\tilde{x})$ for an imposed rotating normalized rotating field with $\tilde{B}_x = 1, \tilde{H}_z = i$ and zero spin-viscosity condition $(\tilde{\eta}' = 0)$ and $\chi_0 = 1, \tilde{\eta} = 1, \tilde{\zeta} = 1, \frac{\partial \tilde{p}'}{\partial \tilde{z}} = 0.00001, \tilde{\Omega} = 1$. There is a slight deviation between the results using the linearized torque equation and the complete torque equation.

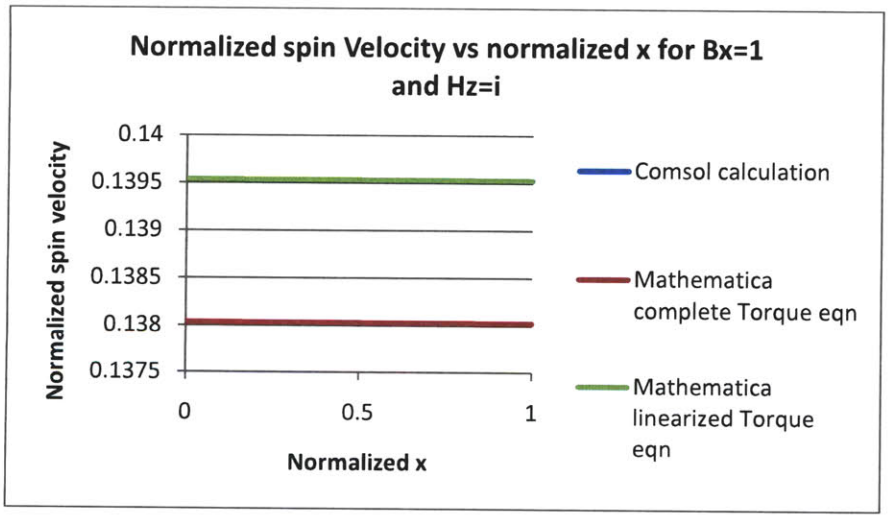

Figure 3-20. Normalized spin velocity $\tilde{\omega}_y(\tilde{x})$ for an imposed normalized rotating field with $\tilde{B}_x = 1, \tilde{H}_z = i$ and zero spin-viscosity condition $(\tilde{\eta}' = 0)$ and $\chi_0 = 1, \tilde{\eta} = 1, \tilde{\zeta} = 1, \tilde{\Omega} = 1$ $\frac{\partial \tilde{p}'}{\partial \tilde{z}} = 0.00001$. There is a slight deviation between the results using the linearized torque equation and the complete torque equation.

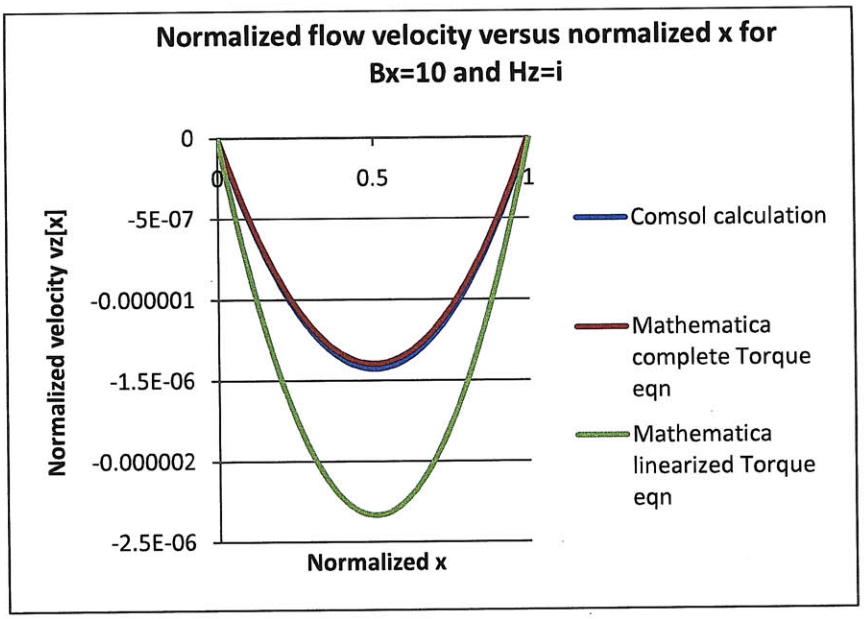

Figure 3-21. Normalized flow velocity $\tilde{v}_z(\tilde{x})$ for an imposed rotating normalized rotating field with $\tilde{B}_x = 10, \tilde{H}_z = i$ and zero spin-viscosity condition $(\tilde{\eta}' = 0)$ and $\chi_0 = 1, \tilde{\eta} = 1, \tilde{\zeta} = 1, \tilde{\Omega} = 1$ $\frac{\partial \tilde{p}'}{\partial \tilde{z}} = 0.00001$. The linearized torque equation gives a significantly different result than the solution obtained with the complete torque equation.

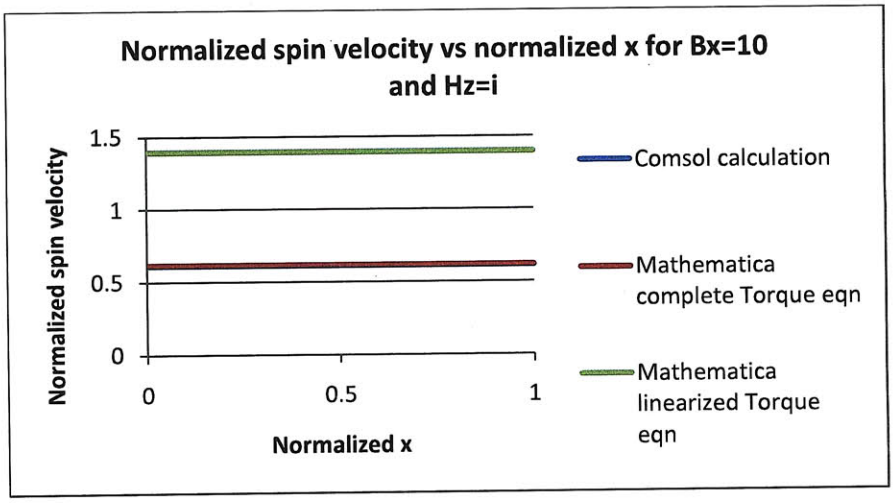

Figure 3-22. Normalized spin velocity $\tilde{\omega}_y(\tilde{x})$ for an imposed normalized rotating field with $\tilde{B}_x = 10, \tilde{H}_z = i$ and zero spin-viscosity condition $(\tilde{\eta}' = 0)$ and $\chi_0 = 1, \tilde{\eta} = 1, \tilde{\zeta} = 1, \tilde{\Omega} = 1$ $\frac{\partial \tilde{p}'}{\partial \tilde{z}} = 0.00001$. There is a significant difference between the results using the linearized torque equation and the complete torque equation.

3.2.4.2. Non-Zero Spin-viscosity Cases ($\eta' \neq 0$)

Similar to the zero spin-viscosity cases, the results of non-zero spin viscosity were first replicated with parameters taken from Zahn and Greer [1], such as $\chi_0 = 1, \tilde{\eta} = 1, \tilde{\zeta} = 1, \frac{\partial \tilde{p}'}{\partial \tilde{z}} = 0.00001$, with the value for the vortex viscosity $\tilde{\zeta} = \tilde{\eta}$ which gives results identical to that of Zahn and Greer [1] as given in the plots of Figure 3-14. The value of the vortex viscosity is not physical since it should be equal to $\tilde{\zeta} = \frac{3}{2}\tilde{\eta}\phi_{vol}$ [6] and this case is explored in 3.2.4.4.

Figure 3-23 and Figure 3-24 are plots of the normalized flow and spin velocities for a rotating imposed field $\tilde{B}_x = 0.1, \tilde{H}_z = 0.1i$ with $\tilde{\eta}' = 0.01$. There is good agreement between the results of using the linearized and complete torque expressions. The COMSOL results have kinks in the plot due to the meshing algorithm of the program. These results were obtained with a triangular mesh. By changing the mesh to a quadrilateral mesh, the kinks vanish but convergence is hard to obtain for stronger imposed normalized fields. The quadrilateral mesh results are shown in Figure 3-25 and Figure 3-26.

Similarly, Figure 3-27 and Figure 3-28 are plots of the normalized flow and spin velocities for a rotating imposed field $\tilde{B}_x = 1, \tilde{H}_z = i$ with $\tilde{\eta}' = 0.01$ with a triangular mesh. Figure 3-29 and Figure 3-30 are flow profiles obtained with an imposed magnetic flux density $\tilde{B}_x = 1, \tilde{H}_z = 0$ while Figure 3-31 and Figure 3-32 are flow profiles obtained with an imposed magnetic field $\tilde{B}_x = 0, \tilde{H}_z = 1$. In all cases, COMSOL simulations were performed with a triangular mesh.

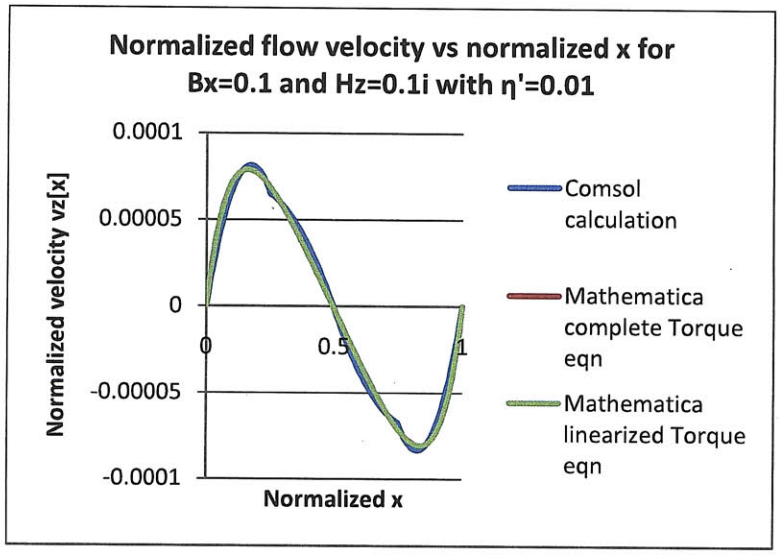

Figure 3-23. Normalized flow velocity $\tilde{v}_z(\tilde{x})$ for an imposed rotating normalized rotating field with $\tilde{B}_x = 0.1, \tilde{H}_z = 0.1i$ with normalized spin-viscosity condition $\tilde{\eta}' = 0.01$ and $\chi_0 = 1, \tilde{\eta} = 1,$ $\tilde{\zeta} = 1, \frac{\partial \tilde{p}'}{\partial \tilde{z}} = 0.00001, \tilde{\Omega} = 1$. The linearized torque and complete torque implementations in Mathematica give identical results with their curves overlapping.

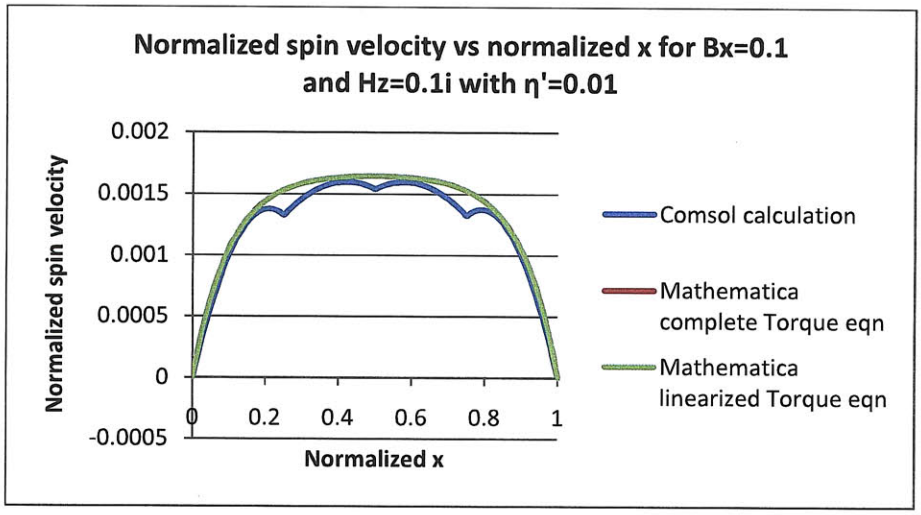

Figure 3-24. Normalized spin velocity $\tilde{\omega}_y(\tilde{x})$ for an imposed rotating normalized rotating field with $\tilde{B}_x = 0.1, \tilde{H}_z = 0.1i$ and normalized spin-viscosity condition $\tilde{\eta}' = 0.01$ with $\chi_0 = 1, \tilde{\eta} = 1,$ $\tilde{\zeta} = 1, \frac{\partial \tilde{p}'}{\partial \tilde{z}} = 0.00001, \tilde{\Omega} = 1$. The COMSOL calculation has kinks in it due to the shape of the triangular mesh elements used in the meshing. The linearized torque and complete torque implementations in Mathematica give identical results with their curves overlapping.

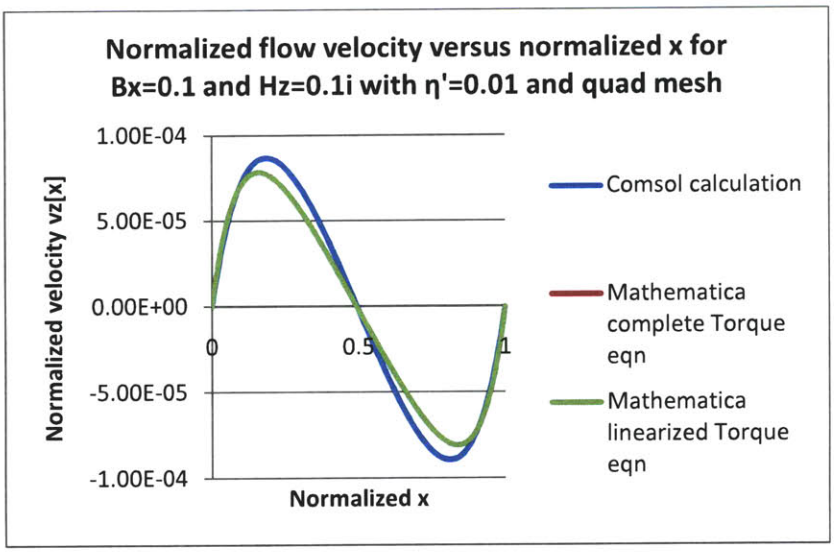

Figure 3-25. Normalized flow velocity $\tilde{v}_z(\tilde{x})$ for an imposed rotating normalized rotating field with $\tilde{B}_x = 0.1, \tilde{H}_z = 0.1i$ with normalized spin-viscosity condition $\tilde{\eta}' = 0.01$ and $\chi_0 = 1, \tilde{\eta} = 1,$ $\tilde{\zeta} = 1, \frac{\partial \tilde{p}'}{\partial \tilde{z}} = 0.00001, \tilde{\Omega} = 1$. The mesh uses quadrilateral elements instead of triangular elements removing the kinks in the graph.

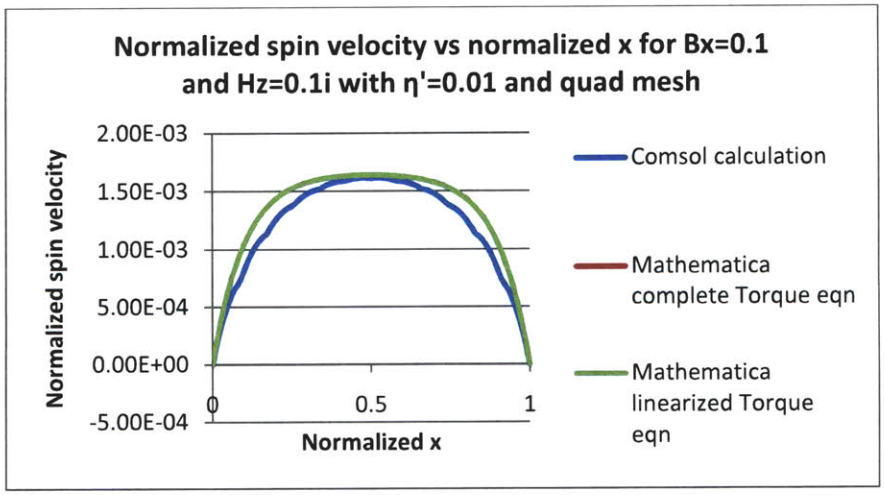

Figure 3-26. Normalized spin velocity $\tilde{\omega}_y(\tilde{x})$ for an imposed rotating normalized rotating field with $\tilde{B}_x = 0.1, \tilde{H}_z = 0.1i$ and normalized spin-viscosity condition $\tilde{\eta}' = 0.01$ with $\chi_0 = 1, \tilde{\eta} = 1,$ $\tilde{\zeta} = 1, \frac{\partial \tilde{p}'}{\partial \tilde{z}} = 0.00001, \tilde{\Omega} = 1$. The mesh uses quad elements instead of triangular elements removing the kinks in the graph.

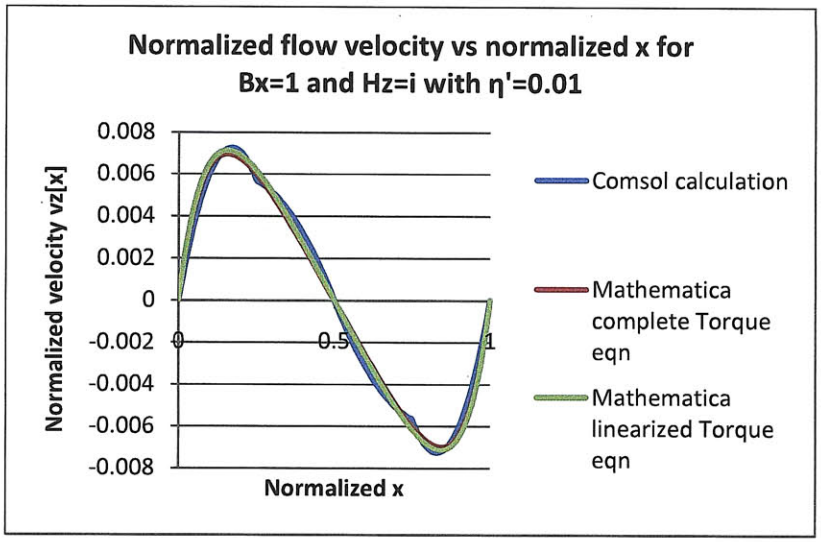

Figure 3-27. Normalized flow velocity $\tilde{v}_z(\tilde{x})$ for an imposed rotating normalized rotating field with $\tilde{B}_x = 1, \tilde{H}_z = i$ and normalized spin-viscosity condition $\tilde{\eta}' = 0.01$ with $\chi_0 = 1, \tilde{\eta} = 1,$ $\tilde{\zeta} = 1, \frac{\partial \tilde{p}'}{\partial \tilde{z}} = 0.00001, \tilde{\Omega} = 1$. The linearized torque and complete torque implementations in Mathematica give identical results with their curves overlapping.

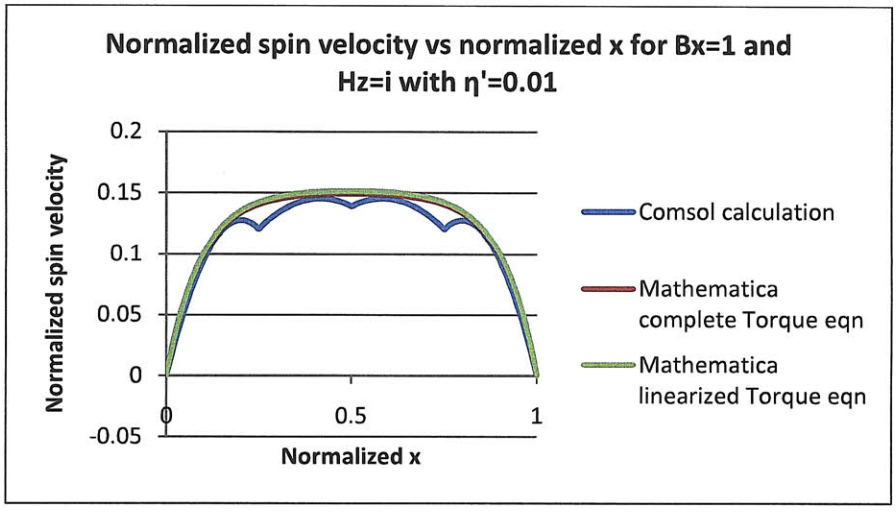

Figure 3-28. Normalized spin velocity $\tilde{\omega}_y(\tilde{x})$ for an imposed rotating normalized rotating field with $\tilde{B}_x = 0.1, \tilde{H}_z = 0.1i$ and normalized spin-viscosity condition $\tilde{\eta}' = 0.01$ with $\chi_0 = 1, \tilde{\eta} = 1,$ $\tilde{\zeta} = 1, \frac{\partial \tilde{p}'}{\partial \tilde{z}} = 0.00001, \tilde{\Omega} = 1$. The COMSOL calculation has kinks in it due to the shape of the triangular mesh elements used in the meshing affecting the results. The linearized torque and complete torque implementations in Mathematica give identical results with their curves overlapping.

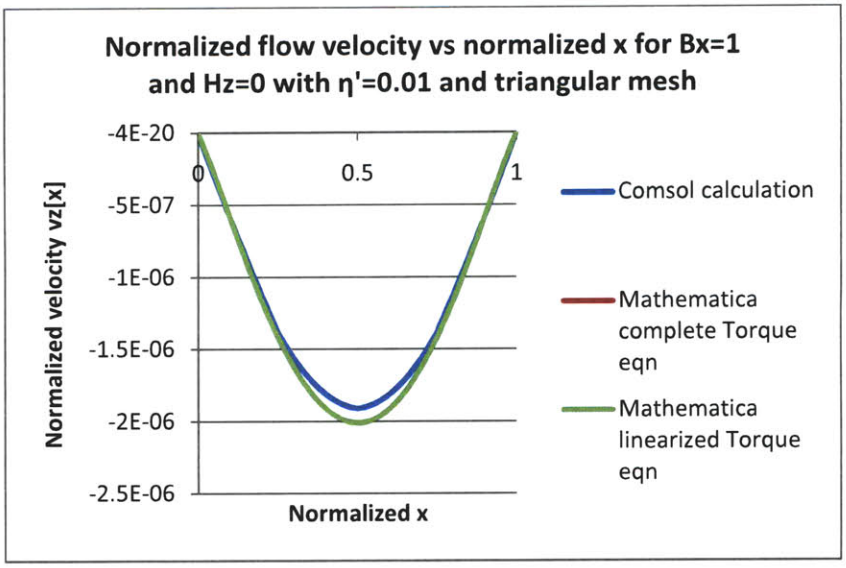

Figure 3-29. Normalized flow velocity $\tilde{v}_z(\tilde{x})$ for an imposed normalized magnetic flux density with $\tilde{B}_x = 1, \tilde{H}_z = 0$ and normalized spin-viscosity condition $\tilde{\eta}' = 0.01$ with $\chi_0 = 1, \tilde{\eta} = 1,$ $\tilde{\zeta} = 1, \frac{\partial \tilde{p}'}{\partial \tilde{z}} = 0.00001, \tilde{\Omega} = 1$. The linearized torque and complete torque implementations in Mathematica give identical results with their curves overlapping.

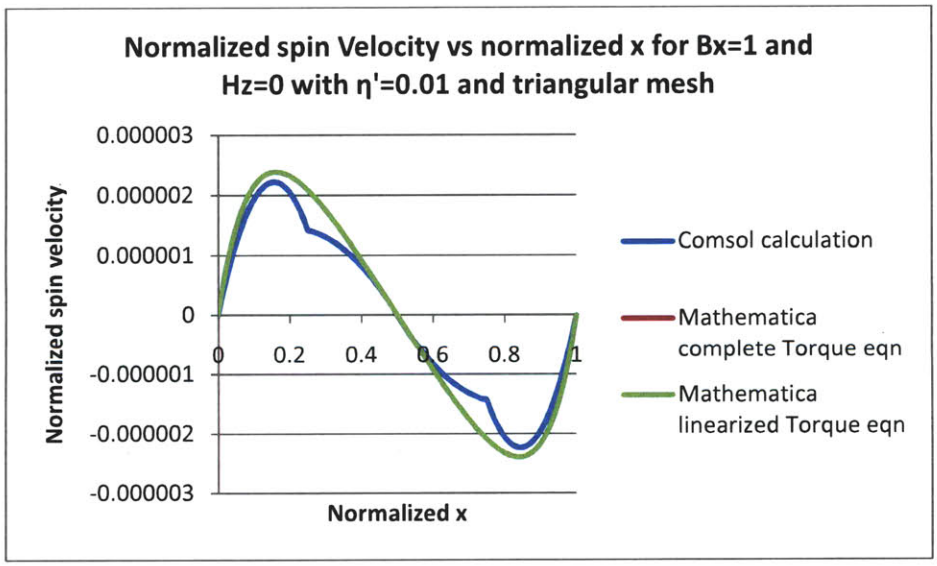

Figure 3-30. Normalized spin velocity $\tilde{\omega}_y(\tilde{x})$ for an imposed normalized magnetic flux density with $\tilde{B}_x = 1, \tilde{H}_z = 0$ and normalized spin-viscosity condition $\tilde{\eta}' = 0.01$ with $\chi_0 = 1, \tilde{\eta} = 1,$ $\tilde{\zeta} = 1, \frac{\partial \tilde{p}'}{\partial \tilde{z}} = 0.00001, \tilde{\Omega} = 1$. The linearized torque and complete torque implementations in Mathematica give identical results with their curves overlapping.

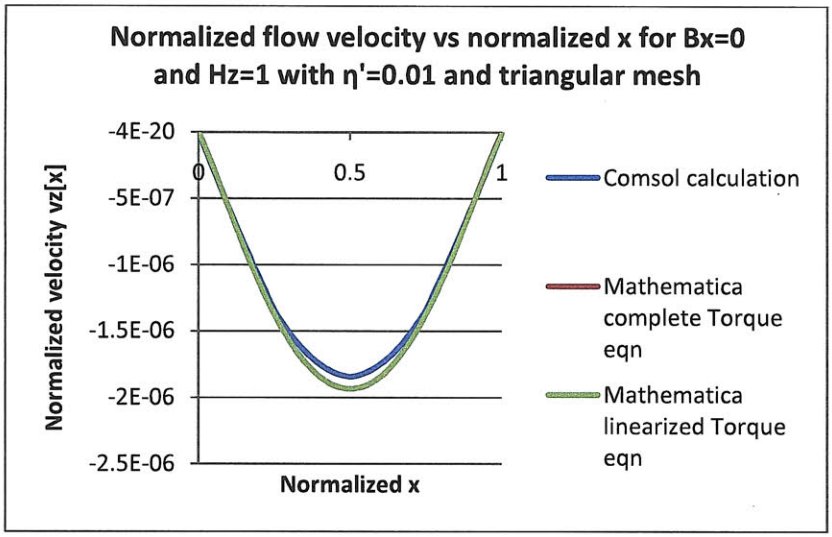

Figure 3-31. Normalized flow velocity $\tilde{v}_z(\tilde{x})$ for an imposed normalized magnetic field with $\tilde{B}_x = 0, \tilde{H}_z = 1$ and normalized spin-viscosity condition $\tilde{\eta}' = 0.01$ with $\chi_0 = 1, \tilde{\eta} = 1,$ $\tilde{\zeta} = 1, \frac{\partial \tilde{p}'}{\partial \tilde{z}} = 0.00001, \tilde{\Omega} = 1$. The linearized torque and complete torque implementations in Mathematica give identical results with their curves overlapping.

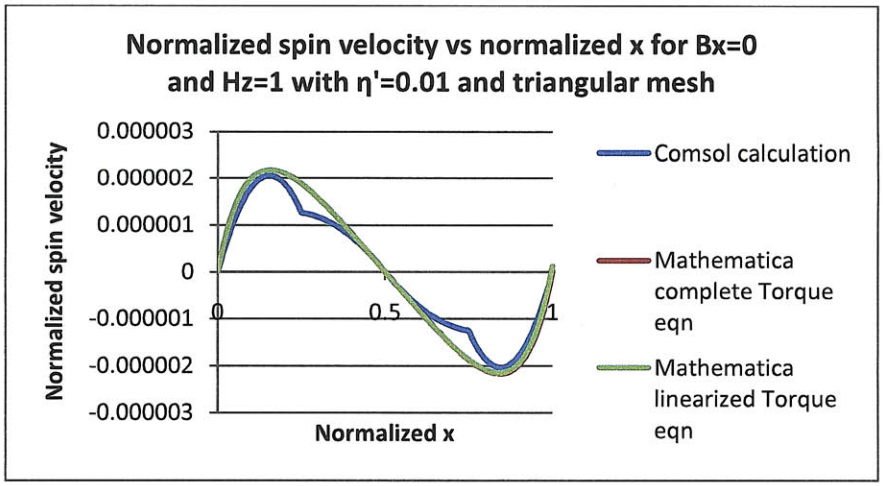

Figure 3-32. Normalized spin velocity $\tilde{\omega}_y(\tilde{x})$ for an imposed normalized magnetic field with $\tilde{B}_x = 0, \tilde{H}_z = 1$ and normalized spin-viscosity condition $\tilde{\eta}' = 0.01$ with $\chi_0 = 1, \tilde{\eta} = 1,$ $\tilde{\zeta} = 1, \frac{\partial \tilde{p}'}{\partial \tilde{z}} = 0.00001, \tilde{\Omega} = 1$. The linearized torque and complete torque implementations in Mathematica give identical results with their curves overlapping.

3.2.4.3. Comparison with Pioch's results [2, 3]

Pioch, in her analytical results [2-4], obtained kinks in her distribution of flow and spin velocities with certain parameters. Figure 3-33 and Figure 3-34 are flow and spin velocity profiles obtained using zero spin-viscosity $\tilde{\eta}' = 0$ with parameters $\chi_0 = 1, \tilde{\eta} = \tilde{\zeta}, \frac{\partial \tilde{p}'}{\partial \tilde{z}} = 1, \tilde{\Omega} = 5$. Even though the value of vortex viscosity $\tilde{\zeta}$ is not physical and is simply set to the dynamic viscosity of the fluid, the presence of sharp kinks can be independently verified using Mathematica® and COMSOL Multiphysics® code that is documented in Appendix A.

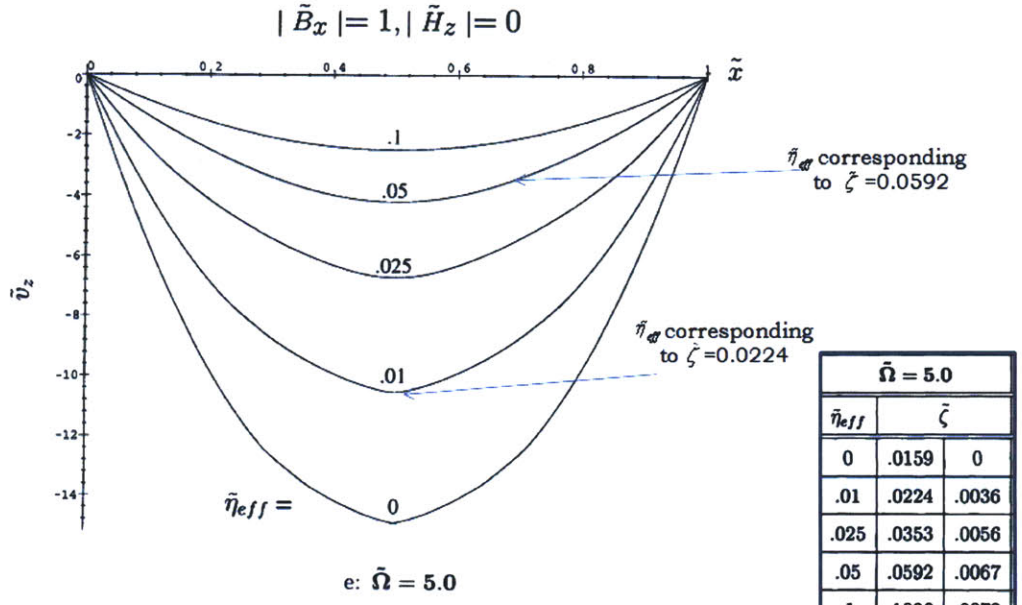

$\tilde{\Omega} = 5.0$		
$\tilde{\eta}_{eff}$	$\tilde{\zeta}$	
0	.0159	0
.01	.0224	.0036
.025	.0353	.0056
.05	.0592	.0067
.1	.1086	.0073

Figure 3-33. Pioch's [2] planar Poiseuille velocity flow $\tilde{v}_z(\tilde{x})$ distribution stressed with a perpendicular magnetic field at normalized frequency $\tilde{\Omega} = 5$ for different values of effective viscosity $\tilde{\eta}_{eff}$ corresponding to different values of vortex viscosity $\tilde{\zeta}$. Other parameters are $\chi_0 = 1, \tilde{\eta} = \tilde{\zeta}, \frac{\partial \tilde{p}'}{\partial \tilde{z}} = 1$.

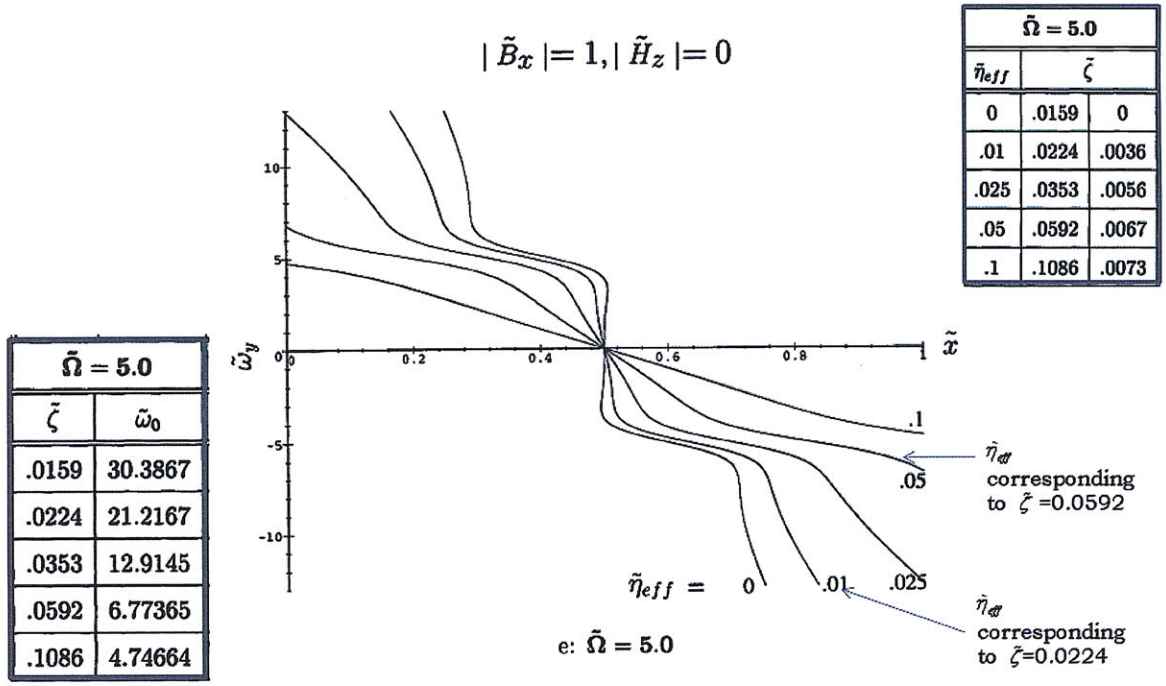

Figure 3-34. Pioch's [2] planar Poiseuille spin velocity $\tilde{\omega}_y(\tilde{x})$ distribution stressed with a perpendicular magnetic field at normalized frequency $\tilde{\Omega}=5$ for different values of effective viscosity $\tilde{\eta}_{eff}$ corresponding to different values of vortex viscosity $\tilde{\zeta}$. Other parameters are $\chi_0=1, \tilde{\eta}=\tilde{\zeta}, \frac{\partial \tilde{p}'}{\partial \tilde{z}}=1$.

Figure 3-35 and Figure 3-36 are Mathematica and COMSOL implementations using Pioch's parameters of $\chi_0=1, \tilde{\eta}=\tilde{\zeta}=0.0592, \frac{\partial \tilde{p}'}{\partial \tilde{z}}=1, \tilde{\Omega}=5$ for an imposed magnetic flux density $\tilde{B}_x=1, \tilde{H}_z=0$. The spin velocity plot of Figure 3-36 has a similar kink pattern as that obtained by Pioch in Figure 3-34.

Figure 3-37 and Figure 3-38 are Mathematica simulations of flow and spin velocity distributions with Pioch's parameters of $\chi_0=1, \tilde{\eta}=\tilde{\zeta}=0.0224, \frac{\partial \tilde{p}'}{\partial \tilde{z}}=1, \tilde{\Omega}=5$ for an imposed magnetic flux density $\tilde{B}_x=1, \tilde{H}_z=0$. The kinks in the flow and spin velocity distributions are identical to that obtained by Pioch in Figure 3-33 and Figure 3-34.

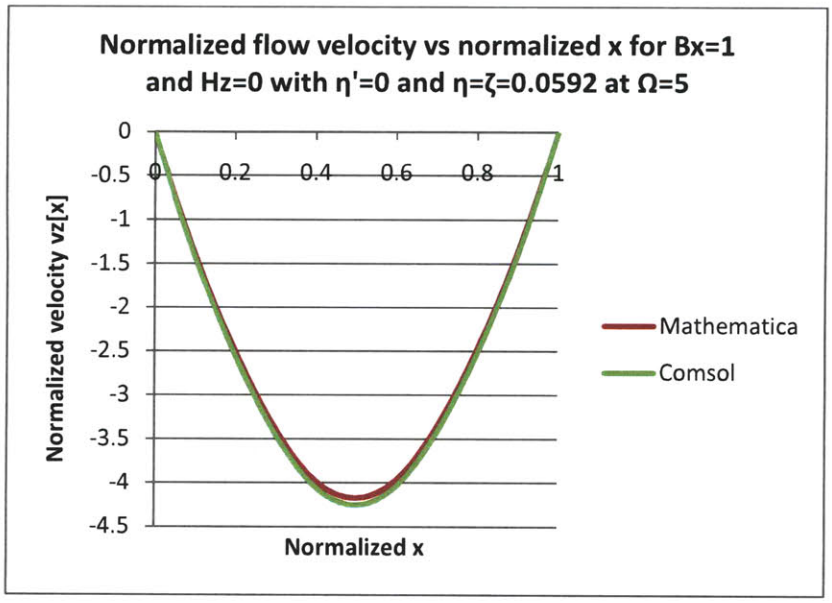

Figure 3-35. Normalized flow velocity $\tilde{v}_z(\tilde{x})$ for an imposed normalized magnetic field with $\tilde{B}_x = 1, \tilde{H}_z = 0$ and zero spin-viscosity condition with Pioch's parameters given as $\chi_0 = 1, \tilde{\eta} = \tilde{\zeta} = 0.0592, \frac{\partial \tilde{p}'}{\partial \tilde{z}} = 1, \tilde{\Omega} = 5$ corresponding to $\tilde{\zeta} = 0.0592$ in Figure 3-33. There is good agreement between the Mathematica and COMSOL simulations.

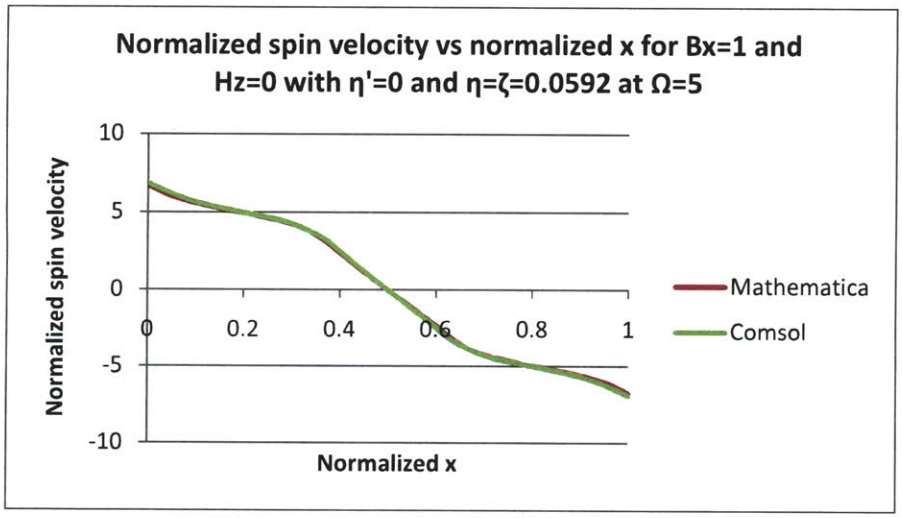

Figure 3-36. Normalized spin velocity $\tilde{\omega}_y(\tilde{x})$ as a function of $\tilde{x}$ distance for an imposed normalized magnetic field with $\tilde{B}_x = 1, \tilde{H}_z = 0$ and zero spin-viscosity condition with Pioch's parameters given as $\chi_0 = 1, \tilde{\eta} = \tilde{\zeta} = 0.0592, \frac{\partial \tilde{p}'}{\partial \tilde{z}} = 1, \tilde{\Omega} = 5$ corresponding to $\tilde{\zeta} = 0.0592$ in Figure 3-34. Kinks as observed in Figure 3-34 are replicated in Mathematica and COMSOL.

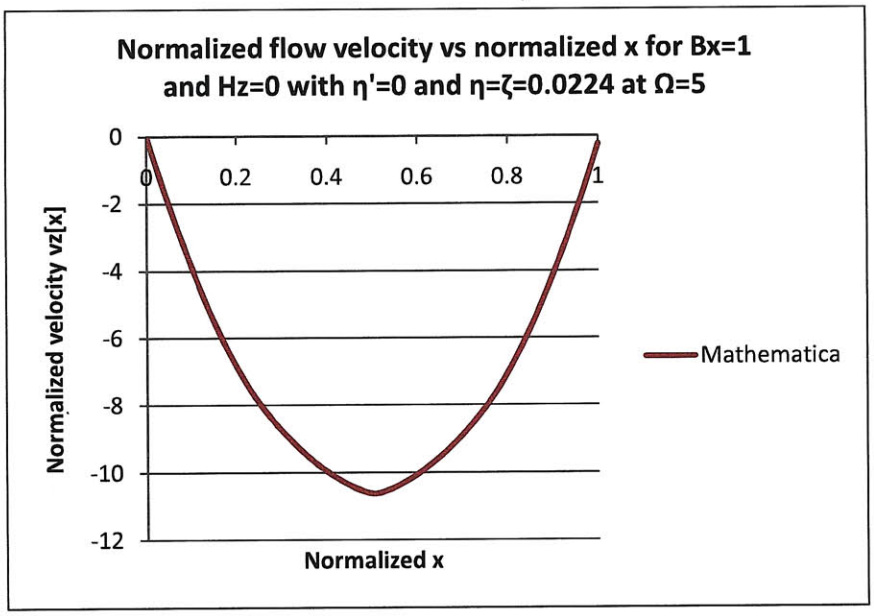

Figure 3-37. Normalized flow velocity $\tilde{v}_z(\tilde{x})$ for an imposed normalized magnetic field with $\tilde{B}_x = 1, \tilde{H}_z = 0$ and zero spin-viscosity condition with $\chi_0 = 1, \tilde{\eta} = \tilde{\zeta} = 0.0224, \frac{\partial \tilde{p}'}{\partial \tilde{z}} = 1, \tilde{\Omega} = 5$. The kink in the velocity at $\tilde{x} = 0.5$ is identical to that obtained by Pioch in Figure 3-33 with $\tilde{\zeta} = 0.0224$.

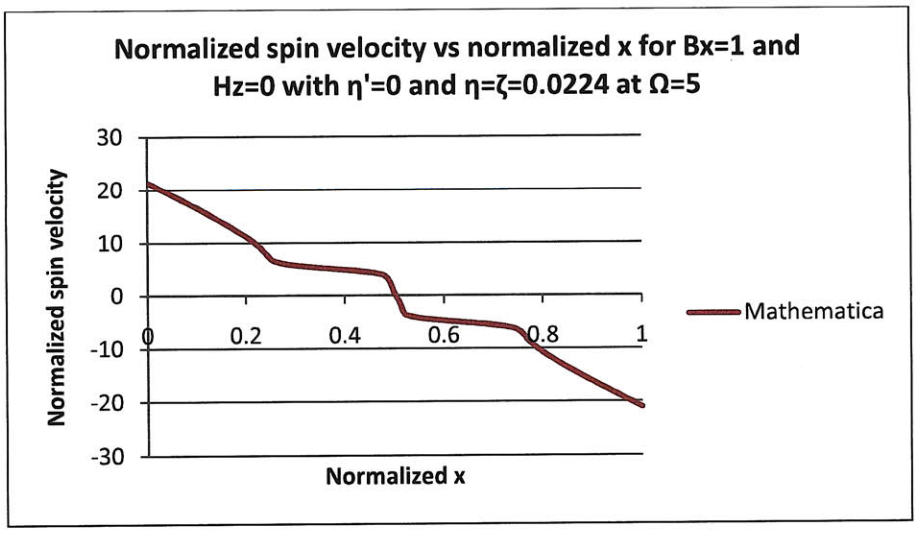

Figure 3-38. Normalized spin velocity $\tilde{\omega}_y(\tilde{x})$ for an imposed normalized magnetic field with $\tilde{B}_x = 1, \tilde{H}_z = 0$ and zero spin-viscosity condition with $\chi_0 = 1, \tilde{\eta} = \tilde{\zeta} = 0.0224, \frac{\partial \tilde{p}'}{\partial \tilde{z}} = 1, \tilde{\Omega} = 5$ .The kinks in the spin velocity are identical to that obtained by Pioch in Figure 3-34 with $\tilde{\zeta} = 0.0224$..

3.2.4.4. Simulations Using Physical Values For Vortex Viscosity $\tilde{\zeta}$ With Non-Zero Spin-viscosity $\tilde{\eta}' \neq 0$

The results of Zahn [1] and Pioch [2, 3] used values of vortex viscosity $\tilde{\zeta}$ that were non-physical ($\tilde{\zeta} = \tilde{\eta}$). Vortex viscosity $\tilde{\zeta}$ is given by the following relationship [6]

$$\tilde{\zeta} = \frac{3}{2}\tilde{\eta}\phi_{vol} \tag{3.84}$$

where $\tilde{\eta}$ is the normalized dynamic viscosity and ϕ_{vol} is the volume fraction of the magnetic nanoparticles.

Assuming a typical volume fraction of 10% for ferrofluids, Mathematica® simulations were done using values given $\chi_0 = 1, \tilde{\eta} = 1, \tilde{\zeta} = 0.15, \frac{\partial \tilde{p}'}{\partial \tilde{z}} = 0.00001, \tilde{\Omega} = 1, \tilde{\eta}' = 0.01$.

Figure 3-39 and Figure 3-40 are Mathematica® plots of normalized flow and spin velocity distributions for an imposed perpendicular magnetic flux density ($\tilde{B}_x = 1$) while Figure 3-41 and Figure 3-42 are plots for an imposed tangential magnetic field ($\tilde{H}_z = 1$). In both these cases there is good agreement between using the complete and linearized torque expressions.

Figure 3-43 and Figure 3-44 are Mathematica® plots of normalized flow and spin velocity distributions for an imposed rotating magnetic field $\tilde{B}_x = 1, \tilde{H}_z = i$ with observable deviations between the results using the complete and linearized torque expressions.

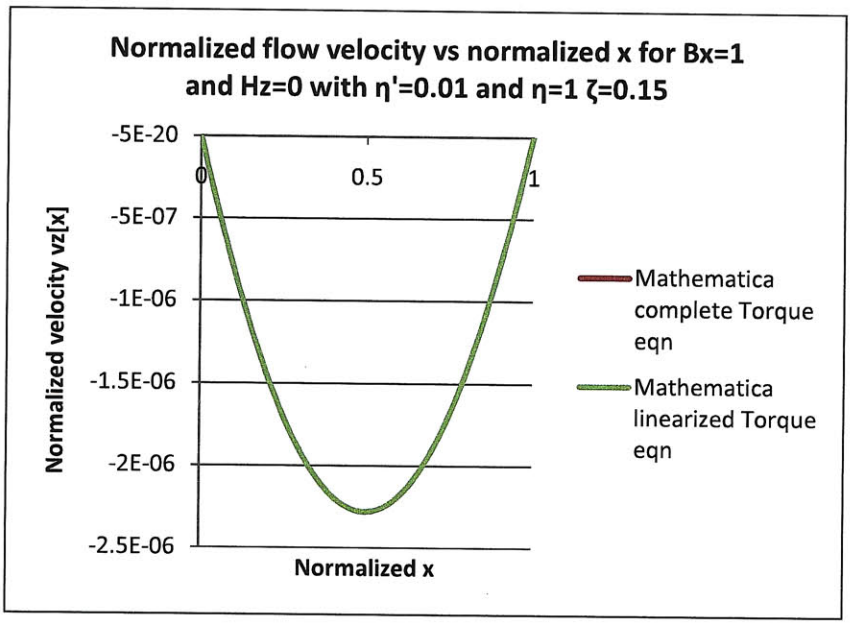

Figure 3-39. Normalized flow velocity $\tilde{v}_z(\tilde{x})$ for an imposed normalized magnetic field with $\tilde{B}_x = 1, \tilde{H}_z = 0$ with $\chi_0 = 1, \tilde{\eta} = 1, \tilde{\zeta} = 0.15, \frac{\partial \tilde{p}'}{\partial \tilde{z}} = 0.00001, \tilde{\Omega} = 1, \tilde{\eta}' = 0.01$. The results obtained with the complete torque equation and the linearized torque equation are in good agreement with their curves overlapping each other.

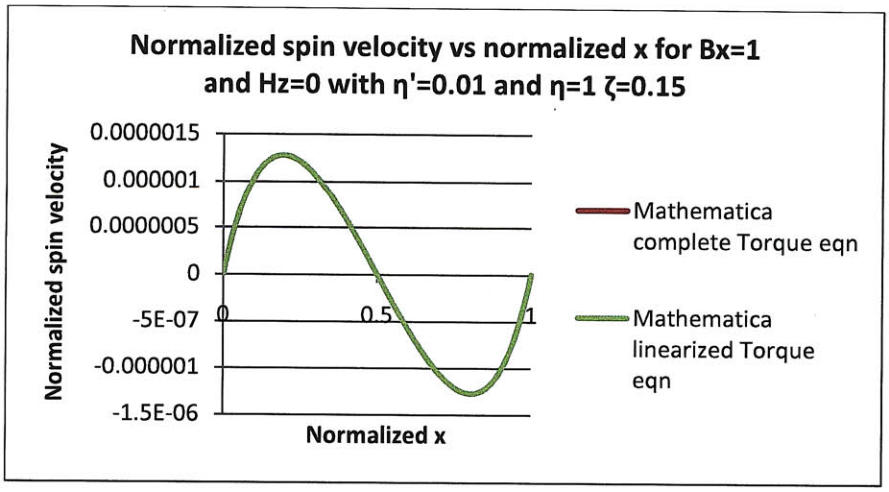

Figure 3-40. Normalized spin velocity $\tilde{\omega}_y(\tilde{x})$ for an imposed normalized magnetic field with $\tilde{B}_x = 1, \tilde{H}_z = 0$ with $\chi_0 = 1, \tilde{\eta} = 1, \tilde{\zeta} = 0.15, \frac{\partial \tilde{p}'}{\partial \tilde{z}} = 0.00001, \tilde{\Omega} = 1, \tilde{\eta}' = 0.01$. The results obtained with the complete torque equation and the linearized torque equation are in good agreement with their curves overlapping each other.

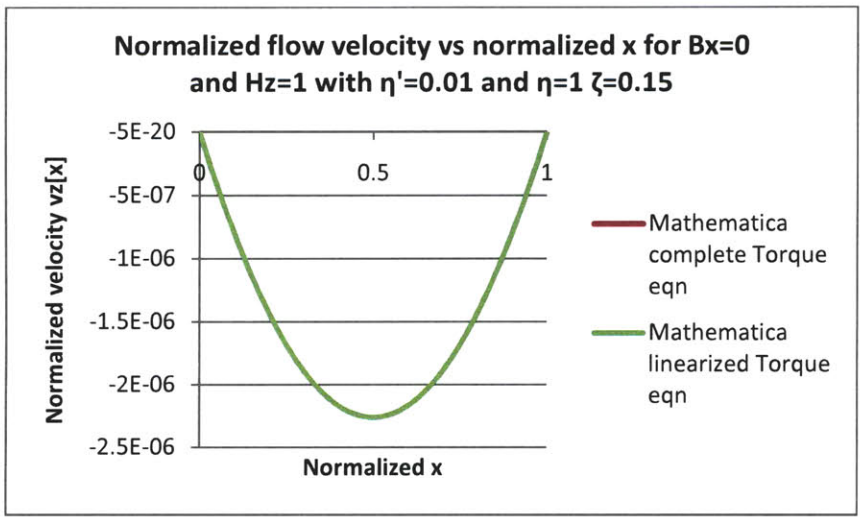

Figure 3-41. Normalized flow velocity $\tilde{v}_z(\tilde{x})$ for an imposed normalized magnetic field with $\tilde{B}_x = 0, \tilde{H}_z = 1$ with $\chi_0 = 1, \tilde{\eta} = 1, \tilde{\zeta} = 0.15, \frac{\partial \tilde{p}'}{\partial \tilde{z}} = 0.00001, \tilde{\Omega} = 1, \tilde{\eta}' = 0.01$. The results obtained with the complete torque equation and the linearized torque equation are in good agreement with their curves overlapping each other.

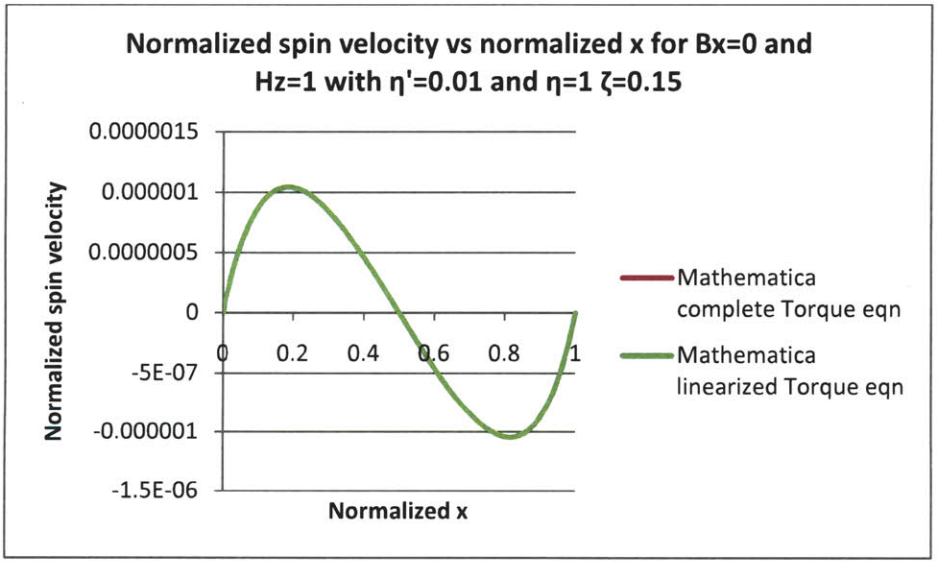

Figure 3-42. Normalized spin velocity $\tilde{\omega}_y(\tilde{x})$ for an imposed normalized magnetic field with $\tilde{B}_x = 0, \tilde{H}_z = 1$ with $\chi_0 = 1, \tilde{\eta} = 1, \tilde{\zeta} = 0.15, \frac{\partial \tilde{p}'}{\partial \tilde{z}} = 0.00001, \tilde{\Omega} = 1, \tilde{\eta}' = 0.01$. The results obtained with the complete torque equation and the linearized torque equation are in good agreement with their curves overlapping each other.

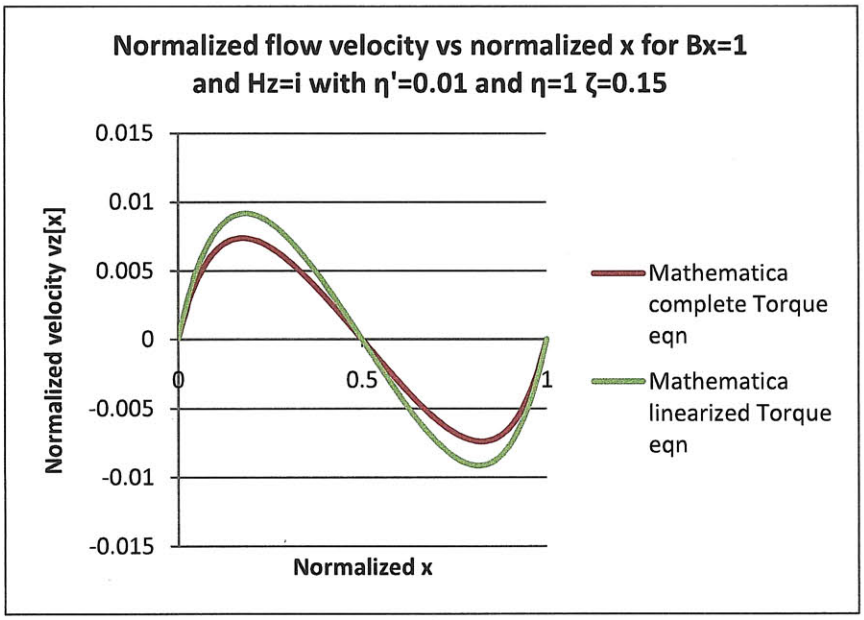

Figure 3-43. Normalized flow velocity $\tilde{v}_z(\tilde{x})$ for an imposed normalized rotating magnetic field with $\tilde{B}_x = 1, \tilde{H}_z = i$ with $\chi_0 = 1, \tilde{\eta} = 1, \tilde{\zeta} = 0.15, \frac{\partial \tilde{p}'}{\partial \tilde{z}} = 0.00001, \tilde{\Omega} = 1, \tilde{\eta}' = 0.01$. The results obtained show differences obtained between the complete torque equation and the linearized torque equation.

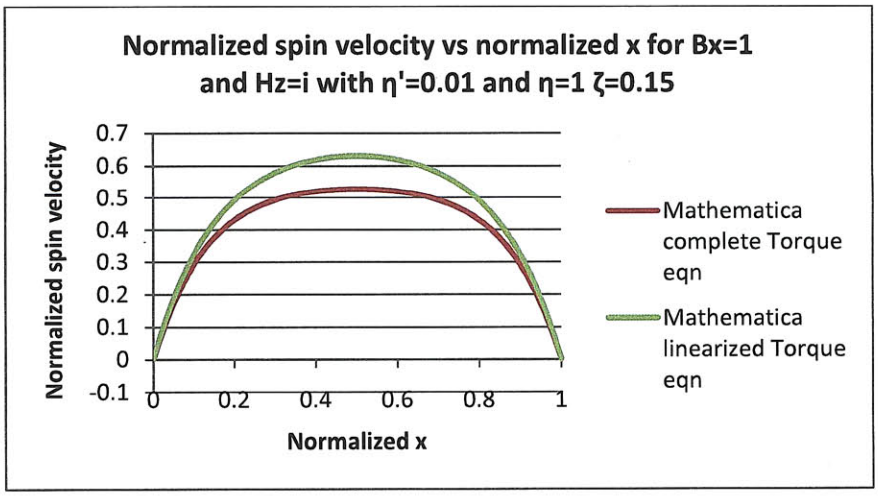

Figure 3-44. Normalized spin velocity $\tilde{\omega}_y(\tilde{x})$ for an imposed normalized rotating magnetic field with $\tilde{B}_x = 1, \tilde{H}_z = i$ with $\chi_0 = 1, \tilde{\eta} = 1, \tilde{\zeta} = 0.15, \frac{\partial \tilde{p}'}{\partial \tilde{z}} = 0.00001, \tilde{\Omega} = 1, \tilde{\eta}' = 0.01$. The results obtained show differences obtained between the complete torque equation and the linearized torque equation.

3.3. Conclusions

This chapter extends the planar Couette flow analytical results of [7] to include perpendicular applied magnetic flux densities B_x at AC frequencies and also analytically derives the effective magnetoviscosity for tangentially applied AC magnetic fields H_z.

This chapter replicates the planar Poiseuille flow results of Zahn [1] and Pioch [2-4] using Mathematica® and COMSOL Multiphysics® with good agreement between the results of the two software packages. The results of Zahn [1] and Pioch [2-4] use non-physical values of vortex viscosity and this chapter extends their analysis to include physical values of vortex viscosity $\zeta = \frac{3}{2}\eta\phi_{vol}$ for dilute suspensions.

[1] M. Zahn and D. R. Greer, "Ferrohydrodynamic pumping in spatially uniform sinusoidally time-varying magnetic fields," *Journal of Magnetism and Magnetic Materials,* vol. 149, pp. 165-173, 1995.

[2] L. L. V. Pioch, "Ferrofluid flow & spin profiles for positive and negative effective viscosities," M. Eng., Dept. of Electrical Engineering and Computer Science, Massachusetts Institute of Technology, 1997.

[3] M. Zahn and L. Pioch, "Ferrofluid flows in AC and traveling wave magnetic fields with effective positive, zero or negative dynamic viscosity," *J. Magn. Magn. Mater.,* vol. 201, p. 144, 1999.

[4] M. Zahn and L. L. Pioch, "Magnetizable fluid behaviour with effective positive, zero or negative dynamic viscosity," *Indian Journal of Engineering & Materials Sciences,* vol. 5, pp. 400-410, 1998.

[5] R. E. Rosensweig, *Ferrohydrodynamics*: Dover Publications, 1997.

[6] M. I. Shliomis, "Effective viscosity of magnetic suspensions," *Soviet Physics JETP,* vol. 34, pp. 1291-1294, 1972.

[7] X. He, "Ferrohydrodynamic flows in uniform and non-uniform rotating magnetic fields," Ph.D thesis, Dept of Electrical Engineering and Computer Science, Massachusetts Institute of Technology, Cambridge, MA, 2006.

Chapter 4. Ferrofluid Flows in Cylindrical Geometry

4.1. Introduction

The classic spin-up experiment involves placing a ferrofluid filled cylinder in a uniform rotating magnetic field and observing the velocity distribution. The opacity of the ferrofluid led many researchers to observe the velocity distribution using streak path techniques with tracer particles only on the surface of the fluid [1-3]. However this led to observations of flow that were counter-rotating to the rotational direction of the magnetic field [4]. This counter-rotating phenomena was explained to be a result of asymmetric tangential stresses on the boundary of the magnetic fluid [5, 6]. It was believed that the flow in the bulk of the fluid would be an entrainment of this surface flow until a new technique, pulsed ultrasound velocimetry, showed that the volume flow below the interface was co-rotating to the rotational direction of the magnetic field [7-9].

Pulsed ultrasound velocimetry is a technique that allows for the measurement of bulk velocity flow measurements of opaque fluids [10-13]. If asymmetric tangential stresses on the boundary of the magnetic fluid entrained the fluid layers below, then by placing a cover and removing the free surface at the top of the cylinder the fluid would conceivably not have any motion [2, 14-17]. Experiments were done with and without the cover on top of the surface and co-rotating motion was observed in the bulk of the fluid in both cases while counter-rotating motion, with a concave shaped meniscus, was observed near the surface [7-9]. The governing mechanism for the flow in this case was believed to be because of spin-diffusion theory.

This chapter will outline this experiment and will go over the spin-diffusion model and simulations that were used to explain and reproduce this phenomena. This chapter will also critique erroneous reasons for flow reversal that were obtained by Finlayson in his COMSOL simulations [18] as well as, incorrect conclusions reached by Elborai in his PhD thesis [8]. This chapter will also correct the value of η' quoted by Chaves [9] for the fluid EMG900_2.

4.2. Experimental Setup

4.2.1. Ultrasound Measurement of Bulk Flows in a Ferrofluid Filled Cylinder with no Free Surface

The bulk flow experiments [7-9, 19] conducted with ultrasound pulsed velocimetry used a three phase two-pole induction motor Y connected stator winding to generate the uniform rotating magnetic field. The rotating field was generated by using balanced three-phase currents each with 120° phase difference, in time and space, from each other. This was done by exciting two phases with ±60° phase difference and grounding the remaining phase allowing the neutral point voltage to float [7-9, 19].

The cylindrical vessel, with interior radius R, was made of polycarbonate with notches made around the container at specific angles between the probe and the radius to the cylinder center. A special cover was used to suppress the asymmetric surface tangential stresses generated by a free surface. The setup is illustrated in Figure 4-1.

The Signal Processing DOP2000 ultrasound velocimeter was used along with Griltex-P1 latex tracer particles produced by EMS CHEMIE at a concentration of 0.01g/ml in experiments

by He, Elborai and Chaves [7-9, 19]. These copolyamide particles are neutrally buoyant in ferrofluid with a density of $1.1 g/ml^3$ and a diameter of 50μm. The ultrasound probes send pulses that get reflected off these tracer particles added to the ferrofluid. The velocity is determined by measuring the Doppler frequency shift in the received pulses while the time of flight gives the distance away the moving particle is from the probe. The velocimeter only measures the component of the velocity parallel to the axis of the transducer. By combining the readings of multiple probes at various angles the rotational velocity profile $v_\phi(r)$ can be determined. The velocity measured at a point in the fluid can be expressed in cylindrical coordinates with no dependence in the ϕ direction as

$$\mathbf{v}(r,z) = v_r(r,z)\mathbf{i}_\mathbf{r} + v_\phi(r,z)\mathbf{i}_\phi + v_z(r,z)\mathbf{i}_\mathbf{z} \tag{4.1}$$

If the probe is placed at an angle α as shown in Figure 4-2, the radius r at a point on the ultrasound path is given by the expression

$$r = \sqrt{\left(x^2 + (R\sin\alpha)^2\right)} \tag{4.2}$$

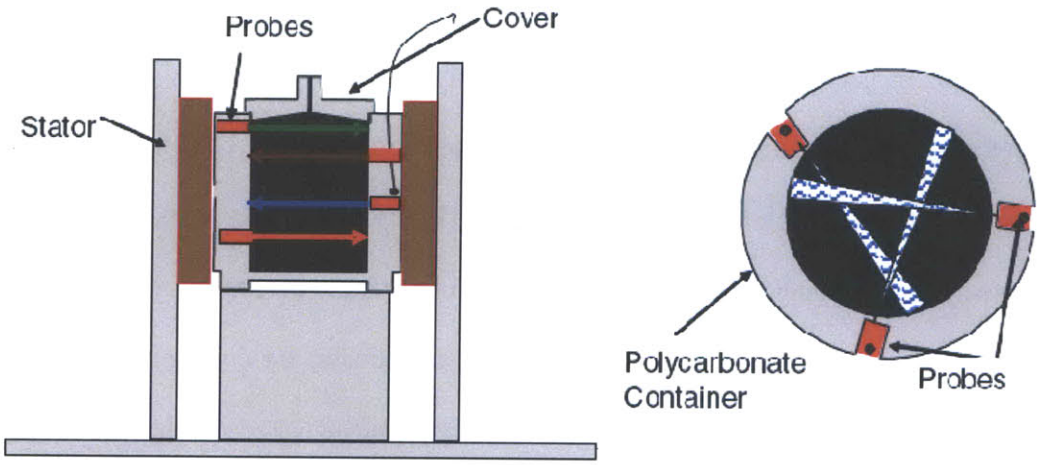

Figure 4-1. Experimental setup illustrating measurement of bulk ferrofluid flow profiles in cylindrical geometry. Left: Ultrasound transducers placed at various heights in the container surrounded by the stator. Right: Top view of probes placed at different incident angles [19].

Resolving the unit vectors $\mathbf{i}_r = \cos\phi\mathbf{i}_x + \sin\phi\mathbf{i}_y$ and $\mathbf{i}_\phi = -\sin\phi\mathbf{i}_x + \cos\phi\mathbf{i}_y$ into Cartesian coordinates and using (4.2) gives

$$\mathbf{v}(r,z) = v_r(r,z)\left(\frac{x}{r}\mathbf{i}_x + \frac{R\sin\alpha}{r}\mathbf{i}_y\right) + v_\phi(r,z)\left(-\frac{R\sin\alpha}{r}\mathbf{i}_x + \frac{x}{r}\mathbf{i}_y\right) + v_z(r,z)\mathbf{i}_z \tag{4.3}$$

where $\cos\phi = \frac{x}{r}$ and $\sin\phi = \frac{R\sin\alpha}{r}$. The ultrasound transducer in Figure 4-2 only measures the velocity v_m in the x-direction given by

$$v_m(x) = \mathbf{v}(r,z)\bullet\mathbf{i}_x = v_r(r)\frac{x}{\sqrt{x^2 + (R\sin\alpha)^2}} - v_\phi(r)\frac{R\sin\alpha}{\sqrt{x^2 + (R\sin\alpha)^2}} \tag{4.4}$$

Rewriting this to solve for v_ϕ gives

$$v_\phi(r) = v_r(r)\frac{x}{R\sin\alpha} - v_m(x)\frac{\sqrt{x^2 + (R\sin\alpha)^2}}{R\sin\alpha} \tag{4.5}$$

requiring that in addition to the measurement $v_m(x)$, a measurement of the radial component of the velocity $v_r(r)$ is needed. This is typically done with the ultrasound probe axis directed along a radial line to the cylinder center.

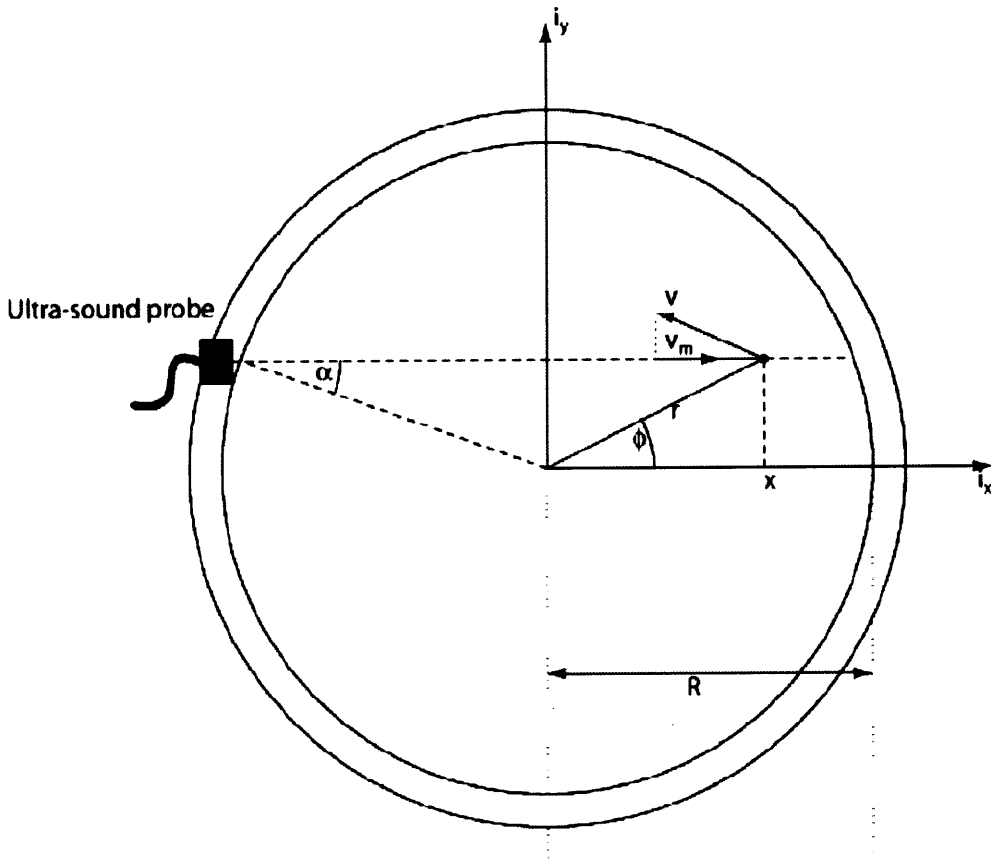

Figure 4-2. Spin-up flow measurement geometry. Ultrasound transducer positioned at angle α with respect to the radial direction. Probe measures x component of velocity vector $v_m(x)$ [7, 8].

4.3. Experimental Results and Conclusions

Chaves conducts several experiments using two fluids EMG705_0 (water based) and EMG900_2 (kerosene based) [9]. Their physical characteristics are tabulated in Table 4-1.

Ferrofluid	η (N s m^{-2})	ρ (kg/m^3)	$\mu_0 M_s$ (mT)	χ	Volume Fraction
EMG705_0	0.0025	1220	21.9	4.99	0.039
EMG900_2	0.0045	1030	23.9	1.19	0.043

Table 4-1. Physical and magnetic properties at room temperature for a subset of fluids used by Chaves [9].

The rotating field generates a well defined circular flow, as seen in Figure 4-3, with negligible circulation in the axial direction in Figure 4-4. Having a consistently shaped velocity profile allows for investigating the effect of various parameters on the magnitude of the rotational velocity of the fluid v_ϕ.

Velocity profiles for the two different liquids (EMG705_0 and EMG900_2) are plotted as a function of frequency (Figure 4-5), magnetic flux density (Figure 4-6) and position along the height of the cylinder (Figure 4-3). It is evident that increasing the frequency, keeping the strength of the field constant, increases the magnitude of the rotational velocity while maintaining the same velocity profile shape. The same direct relationship is true between magnetic flux density and magnitude of rotational velocity.

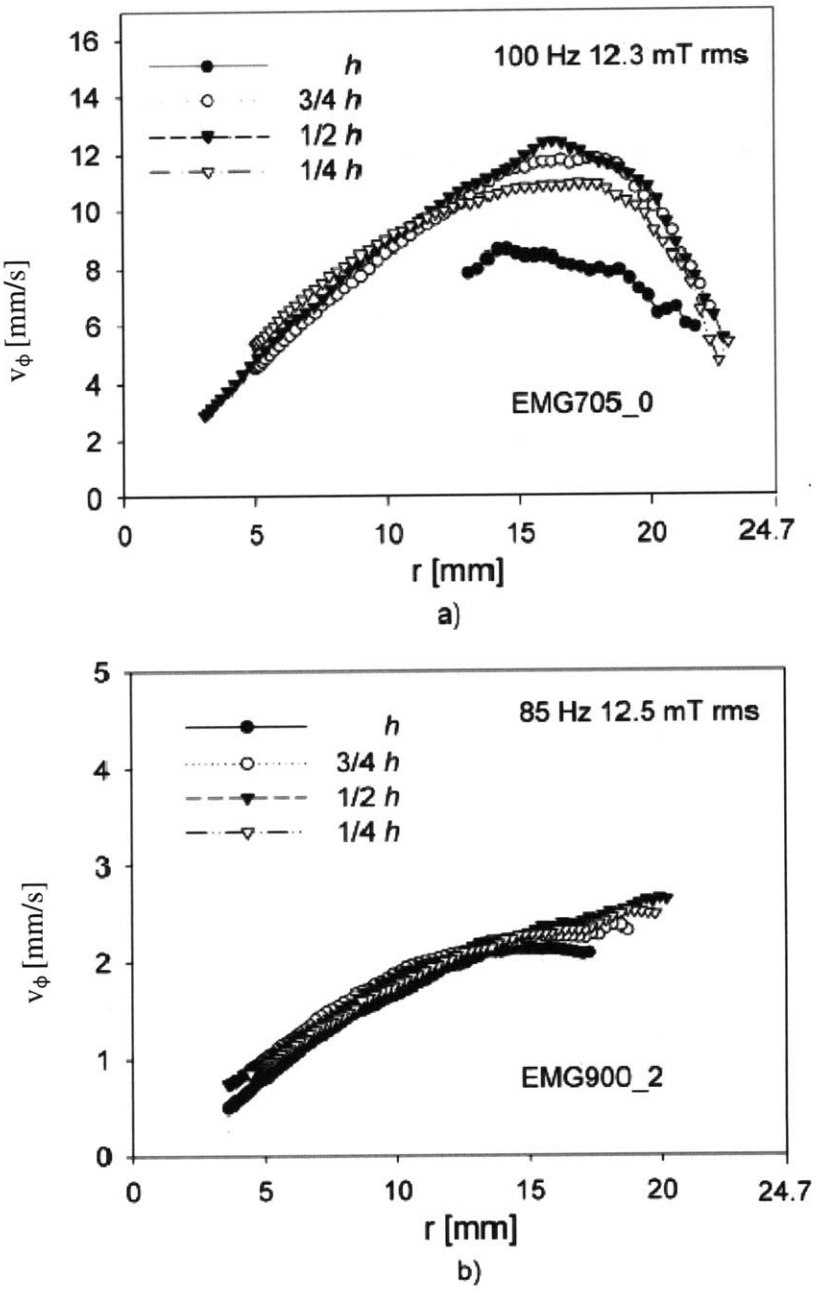

Figure 4-3. Velocity flow profiles for a) EMG705_0 and b) EMG900_2 ferrofluids at various heights along the ferrofluid cylinder with a cover at the top. Plot shows that the ϕ directed velocity profile does not significantly change with height. Plots taken from [9].

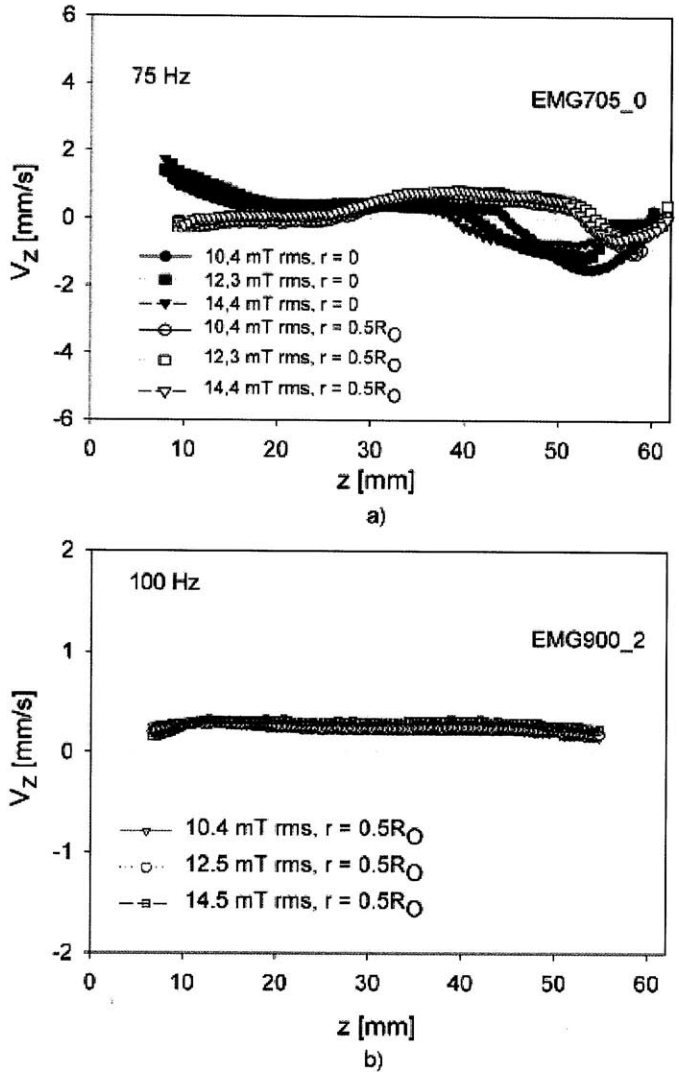

Figure 4-4. Velocity in the axial direction for a) EMG705_0 and b) EMG900_2 ferrofluids. Velocity profiles are for axial lines $r = 0$ (center of cylinder) and $r = 0.5R_0$ where R_0=24.7mm is the radius of the cylindrical vessel used. The z-directed flows are small ($\approx$ 2mm/s) suggesting flow is mainly in the ϕ direction of the rotating field. Plots taken from [9].

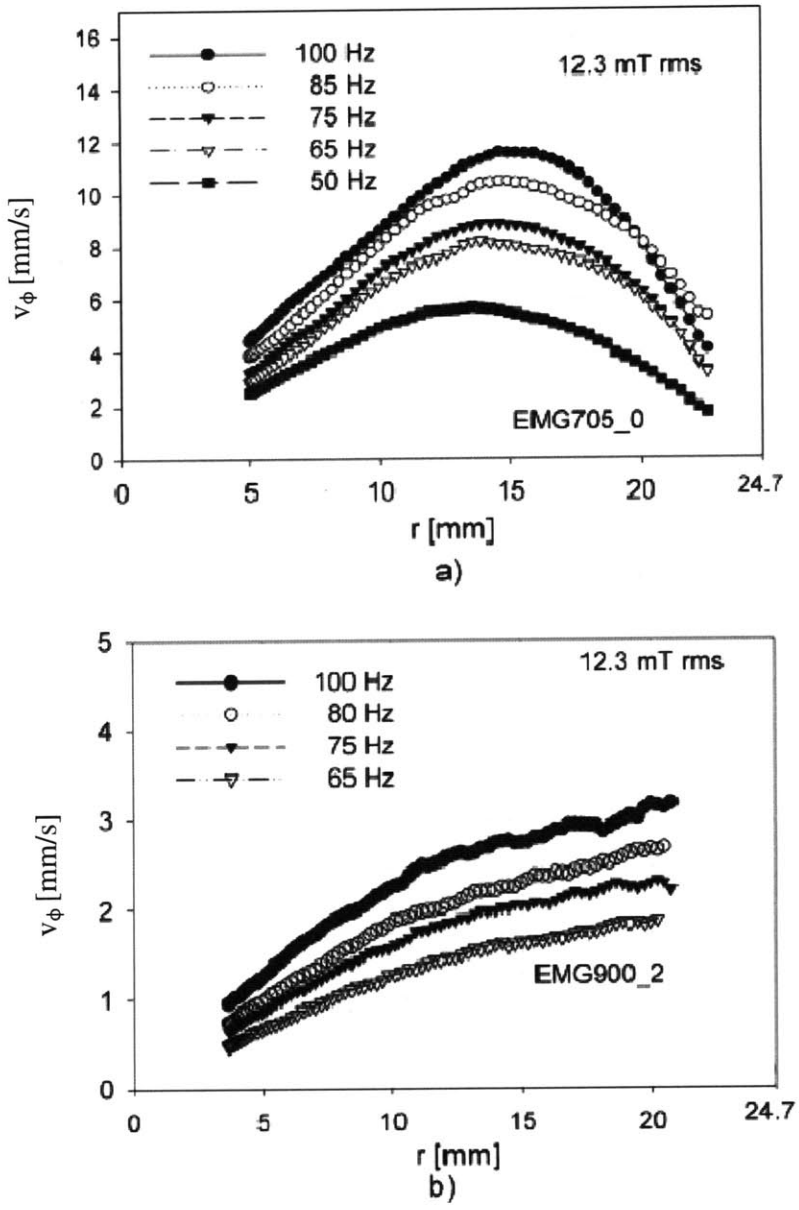

Figure 4-5. Velocity flow profiles for a) EMG705_0 and b) EMG900_2 ferrofluids as a function of frequency at constant rotating flux density of 12.3 mT RMS. Plot shows that increasing frequency proportionally increases the peak magnitude of the rotational velocity. Plots taken from [9].

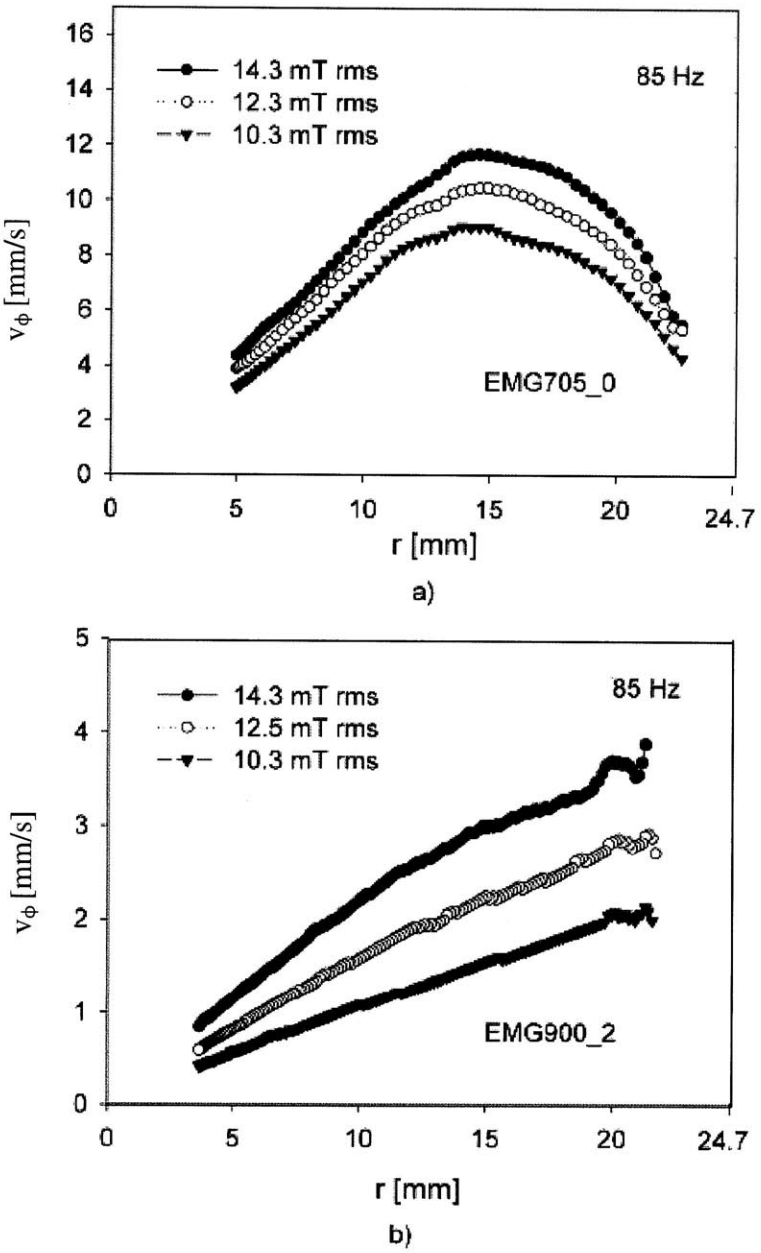

Figure 4-6. Velocity flow profiles for a) EMG705_0 and b) EMG900_2 ferrofluids as a function of strength of applied rotating magnetic flux density at 85 Hz. Plot shows that increasing the strength of the rotating magnetic field increases the magnitude of the rotational velocity. Plots taken from [9].

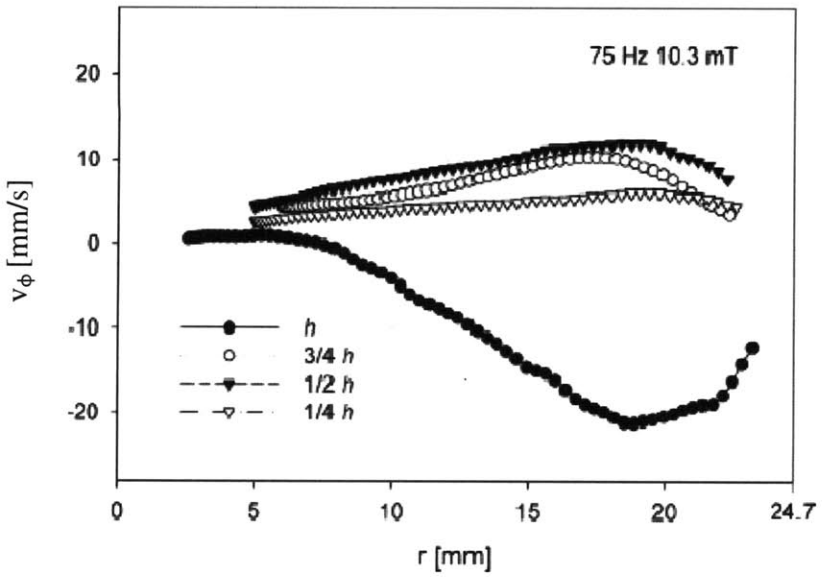

Figure 4-7. Velocity flow profiles for EMG705_0 at different heights in the cylindrical container without a cover. The negative velocity at the surface of the ferrofluid indicates counter-rotating flow opposite to that of the positive co-rotating velocity in the bulk. Plots taken from [9].

Figure 4-7 illustrates that the bulk flow and the flow at the free surface of the ferrofluid are governed by two different mechanisms and can result in opposite flow directions. The flow in the bulk of the fluid is always seen to be co-rotating with the direction of the rotating field. The flow at the surface is caused by asymmetrical tangential stresses that are a function of the meniscus formed with the edges of the container. In Figure 4-7, the ferrofluid 'wets' the surface creating a concave surface shape resulting in counter-rotational flow [6].

Elborai, in his thesis, investigates changing the meniscus shape in two configurations A and B as shown in Figure 4-8 [8]. Configuration B aligns the surface of the ferrofluid with the bottom rim of the iron stack of the stator winding and configuration A aligns the surface with the top rim. In configuration B, the ferrofluid interface is pulled up towards the stronger magnetic field strength resulting in a convex shaped meniscus while in A the stronger field pulls the

interface into a concave shaped meniscus. In both cases the ultrasound probe is placed at the top of the cylinder to measure flows at the ferrofluid-air boundary. The results plotted in Figure 4-9 clearly show that bulk flow and surface flow are in opposite directions and are governed by two different mechanisms. At a free surface the flow is determined by the shape of the meniscus resulting in a co-rotating or counter-rotating flow with a convex or concave shaped meniscus respectively. Elborai goes further to incrementally add ferrofluid to the cylinder of configuration A progressively increasing the height of the ferrofluid. Figure 4-9 shows that initially the ultrasound probe close to the surface of the ferrofluid measures a counter-rotating flow but as more ferrofluid was added the probe being no longer near the surface measures the bulk co-rotating flow.

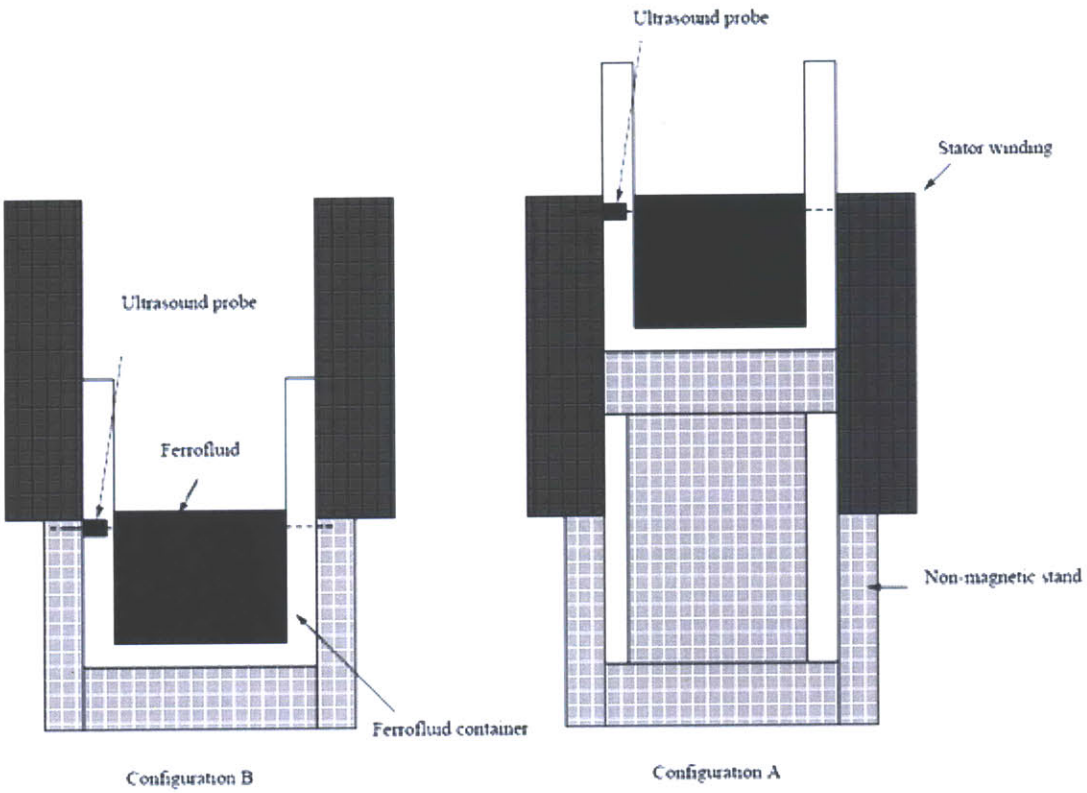

Figure 4-8. Elborai's experimental configuration to change the shape of the meniscus formed at the ferrofluid free surface [8]. Configuration A pulls the meniscus of the ferrofluid downwards into a concave shaped meniscus resulting in counter-rotating flow at the free surface. The meniscus is pulled up into a convex shape by the stator in configuration B resulting in co-rotating flow at the free surface. Figure taken from [8].

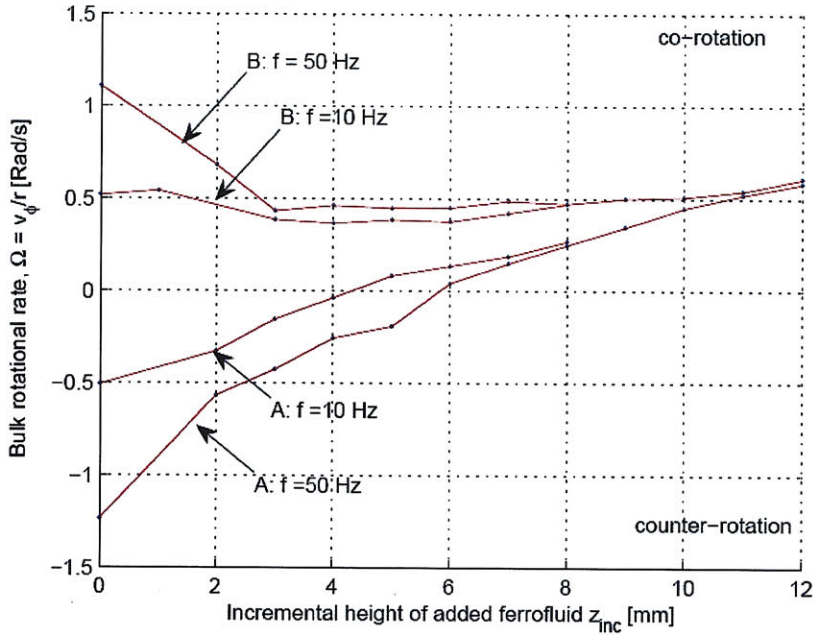

Figure 4-9. Elborai's measured change of rotational rate of MSGW11 ferrofluid as the height of the ferrofluid is increased in increments of 1mm. Experiments were done at two rotating frequencies of 10 and 50Hz. Concave shaped meniscus (A) results in counter-rotating flow while convex shaped meniscus (B) results in co-rotating flow consistent with asymmetric tangential stresses at the ferrofluid-air boundary [6, 8]. As more ferrofluid was added in configuration A, the probe is no longer close to the surface of the ferrofluid and the motion co-rotates similar to that in the bulk of the fluid. Plot taken from [8].

4.3.1. Assumptions and Subtleties of Prior Work

A fundamental assumption made by Elborai, He and Chaves [7-9, 19] was that the demagnetizing effects, due to the shape of the cylinder, did not contribute to the flow. This would be true if the cylinder was infinitely long. For practical purposes a fully filled cylinder of ferrofluid with a height that is significantly greater than its diameter would be a good approximation. However, the ratio of the maximum height of the ferrofluid in the cylinder with respect to the cylinder's diameter used by these authors brings into question their assumption of ignoring demagnetizing effects. The results of Chaves [9, 19], He [7] and Elborai [8] are similar but based on Table 4-2, Chaves's experimental results would appear to be the most accurate by being the set of data that has the least effect due to demagnetizing factors associated with the shape of the cylinder. All further experimental data used in this thesis, for a cylindrical geometry, will be based on Chaves's results.

Author	**Inner diameter of vessel (m)**	**Maximum height of ferrofluid in vessel (m)**	**Ratio of height/diameter**
Elborai [8]	0.0574	0.0500	0.871
He [7]	0.0919	0.0600	0.653
Chaves [9, 19]	0.0494	0.0635	1.285

Table 4-2. Table of ferrofluid cylindrical dimensions used in prior experiments illustrating the invalidity of assuming negligible demagnetizing effects.

A subtlety in all these author's works is the strength of the magnetic flux density used. For all their results the magnetic flux density quoted is the strength of the flux produced by the stator *in the absence* of the ferrofluid. It is not evident that the authors correct for the actual field inside the ferrofluid especially when determining values of spin viscosity η'. This brings into doubt the accuracy of η' that they derive from their experimental results.

4.4. Numerical Simulation of Ferrofluid Spin-up Flow in Cylindrical Geometry

There are different theories for bulk ferrofluid spin-up flow in rotating fields. Shliomis states that the imposed rotating magnetic field is non-uniform itself due to the demagnetizing effects associated with a finite height cylinder [20], while another theory considers inhomogeneous heating of the fluid due to the dissipated energy of the rotating field to create a spatial variation in susceptibility driving the rotational flow [2, 20-22]. Taking the case where the cylinder's height is significantly greater than its diameter, resulting in negligible field non-uniformity in most of the fluid, and assuming that the strength of the magnetic field is weak enough to assume negligible heating effects of the fluid, the only theory that would explain rotational motion in experiments by Chaves, Elborai and He is the spin-diffusion theory [7-9, 19]. This section will explore this limiting case where spin-diffusion is the governing cause of the rotational flow.

4.4.1. Theoretical Model of Experiment

4.4.1.1. Governing Equations

The governing equations outlined here were explained in detail in Chapter 2. There are four governing equations for ferrofluid spin-up flow that need to be solved simultaneously. The two Maxwell's equations applicable to ferrofluid flow are outlined below and can be combined into one equation for magnetic scalar potential.

1) Maxwell's Equations: Ampere's Law

$$\nabla \times \mathbf{H} = \mathbf{J} \tag{4.6}$$

2) Maxwell's Equations: Gauss's Law for Magnetic Flux Density

$$\nabla \cdot \mathbf{B} = 0 \tag{4.7}$$

Since the ferrofluid is a current free region, (4.6) can be rewritten such that $\mathbf{H}$ is the gradient of a magnetic scalar potential ψ as given in (4.8) below.

$$\nabla \times \mathbf{H} = 0 \Rightarrow \mathbf{H} = -\nabla \psi \tag{4.8}$$

(4.7) can be rewritten to include the relation between magnetic flux density and fluid magnetization $\mathbf{M}$.

$$\begin{aligned} &\mathbf{B} = \mu_0(\mathbf{H} + \mathbf{M}) \\ &\nabla \cdot \mathbf{B} = 0 \Rightarrow \mu_0 \nabla \cdot (\mathbf{H} + \mathbf{M}) = 0 \\ &\nabla \cdot \mathbf{H} = -\nabla \cdot \mathbf{M} \end{aligned} \tag{4.9}$$

Substituting (4.8) into (4.9) gives a Poisson's relation between fluid magnetization and magnetic scalar potential.

1) Poisson's Equation

$$\nabla^2\psi = \nabla\bullet\mathbf{M} \tag{4.10}$$

The three other equations that are coupled together are the fluid mechanics equations and the magnetic relaxation equation outlined below.

2) Conservation of Linear Momentum

$$\rho\left[\frac{\partial\mathbf{v}}{\partial t}+(\mathbf{v}\bullet\nabla)\mathbf{v}\right]=-\nabla p'+2\zeta\nabla\times\boldsymbol{\omega}+(\zeta+\eta)\nabla^2\mathbf{v}+\mu_0(\mathbf{M}\bullet\nabla)\mathbf{H} \tag{4.11}$$

3) Conservation of Angular Momentum

$$I\left[\frac{\partial\boldsymbol{\omega}}{\partial t}+(\mathbf{v}\bullet\nabla)\boldsymbol{\omega}\right]=\mu_0\mathbf{M}\times\mathbf{H}+2\zeta(\nabla\times\mathbf{v}-2\boldsymbol{\omega})+\eta'\nabla^2\boldsymbol{\omega} \tag{4.12}$$

4) Magnetic Relaxation Equation

$$\frac{\partial\mathbf{M}}{\partial t}+(\mathbf{v}\bullet\nabla)\mathbf{M}=\boldsymbol{\omega}\times\mathbf{M}-\frac{1}{\tau_{eff}}(\mathbf{M}-\mathbf{M}_{eq}) \tag{4.13}$$

4.4.1.2. Model Assumptions

The applied field is assumed to not be strong enough to magnetically saturate the fluid. The equilibrium magnetization $\mathbf{M}_{eq}$ of the fluid is assumed to be in the linear regime of the Langevin equation as a function of the magnetic field inside the ferrofluid given by

$$\mathbf{M}_{eq}=\chi\mathbf{H}_{fluid} \tag{4.14}$$

To not consider the effect of the non-uniformity of the field on ferrofluid spin-up, an infinitely long cylinder will be modeled since it has no demagnetizing effect in the axial direction and equal demagnetizing factors of ½ in the transverse directions resulting in a uniform field inside the ferrofluid filled cylinder.

The flow is also assumed to be viscous dominated allowing for the inertial terms to be dropped. The left hand side of the linear momentum equation in (4.11) can be set to 0 and the equation reduced to

$$0 = -\nabla p' + 2\zeta \nabla \times \boldsymbol{\omega} + (\zeta + \eta)\nabla^2 \mathbf{v} + \mu_0 (\mathbf{M} \bullet \nabla)\mathbf{H} \tag{4.15}$$

The same can be done for the left hand side of the angular momentum equation in (4.12) and the remaining equation is given as

$$0 = \mu_0 \mathbf{M} \times \mathbf{H} + 2\zeta (\nabla \times \mathbf{v} - 2\boldsymbol{\omega}) + \eta' \nabla^2 \boldsymbol{\omega} \tag{4.16}$$

If the magnetic field is applied in the transverse x-y plane, the spin-velocity $\boldsymbol{\omega}$ is assumed to only be in the z-direction ω_z. This is because in an infinitely long cylinder case, the driving force is created only by the transverse magnetic field which creates a torque only in the z-direction. The spatially varying demagnetizing field of a finite height cylinder would create an internal magnetic field that had components in the transverse (x-y) plane as well as the axial plane (z). In that case, there would be a torque and spin-velocity in all three directions (x, y and z).

4.4.2. Model Setup and Boundary Conditions

4.4.2.1. Modeling the Rotating Magnetic field

There are two ways to model the magnetic field, one is by using a current source boundary condition while the other is by using a scalar potential boundary condition. Both methods will be explored and be shown to be identical. For both cases, the following boundary conditions always apply

$$\mathbf{n}\cdot\|\mathbf{B}\| = 0, \mathbf{n}\times\|\mathbf{H}\| = 0 \quad r = R_0$$

where $\| \ \|$ represents the jump in the value across the boundary $r=R_0$.

1) Surface Current Boundary Condition

The actual experimental setup is similar to Figure 4-10 and involves placing a cylinder of ferrofluid inside a stator winding (itself surrounded by a material with assumed infinite magnetic permeability) of radius R_0 with an air region in between. The resulting magnetic field in the air region is a uniform field imposed by the current source and a dipole field created by the ferrofluid.

The source of the magnetic field is a 3 phase 2 pole stator winding with each phase having 120^0 phase difference from each other. This requires a surface current boundary condition driving the three phase coils in the axial (z) direction of the cylinder which can be described by (4.17) where Ω is the rotational frequency and ϕ the angle from the x axis.

$$\begin{aligned}\mathbf{K}(\phi,t) &= K_0\left[\cos\Omega t\cos\phi+\cos(\Omega t-\frac{2\pi}{3})\cos(\phi-\frac{2\pi}{3})+\cos(\Omega t+\frac{2\pi}{3})\cos(\phi+\frac{2\pi}{3})\right]\mathbf{i}_z \\ \mathbf{K}(\phi,t) &= \frac{3}{2}K_0\cos(\Omega t-\phi)\mathbf{i}_z\end{aligned} \tag{4.17}$$

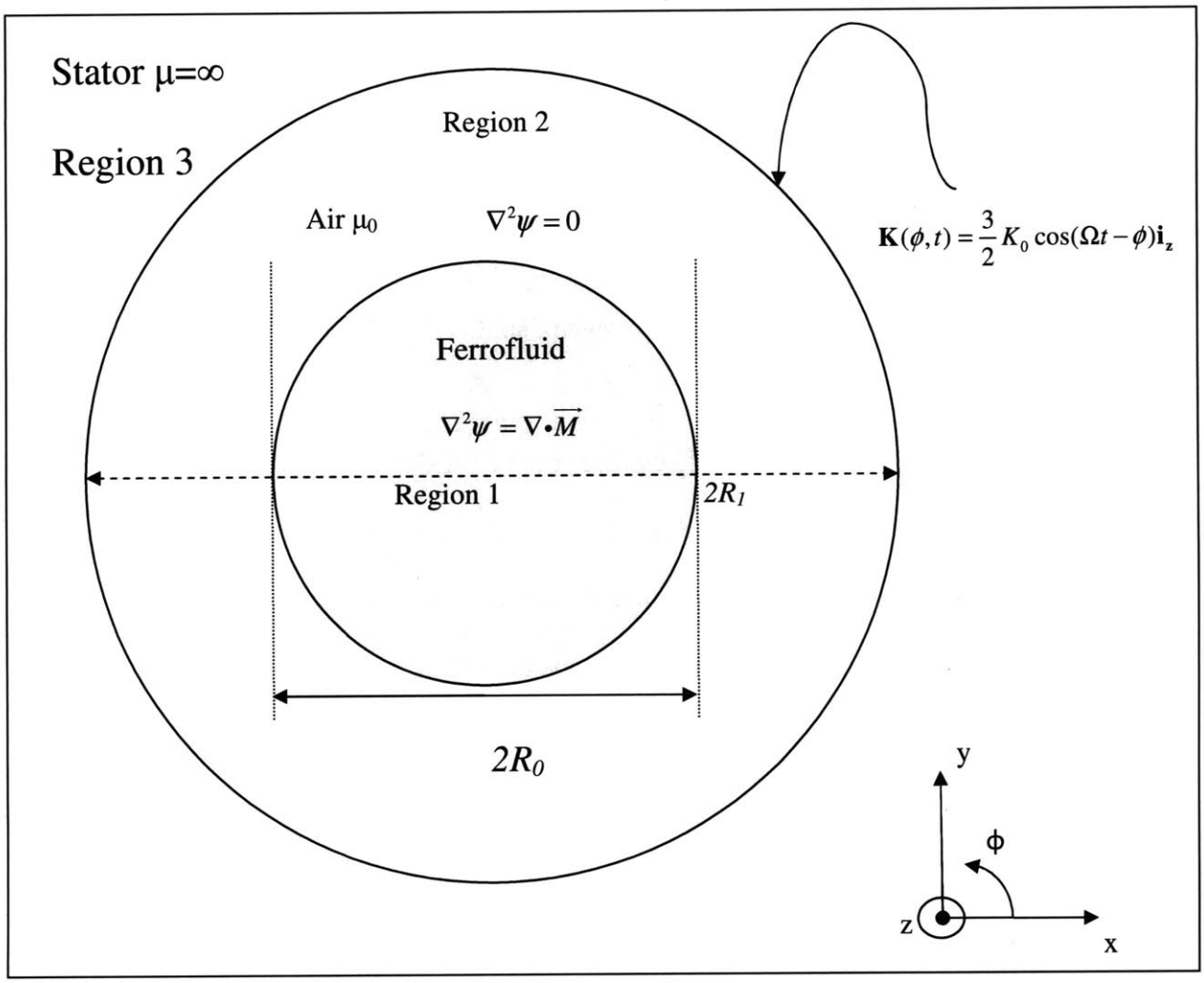

Figure 4-10. . Two dimensional representation of actual spin-up flow experiment. Shaded region represents the infinitely long cylinder of ferrofluid of radius R_0. The unshaded air region separates the ferrofluid from the outer stator winding that has a current boundary condition imposed at $r=R_1$ surrounded by a $\mu = \infty$ region.

2) Scalar Potential Boundary Condition

Although setting up the model using the current boundary condition can be accomplished in COMSOL Multiphysics, it can be difficult to solve. A simpler method of setting up the magnetic field using the magnetic scalar potential can be used. The fact that the only region of interest is the region of ferrofluid and it is only affected by the uniform field imposed allows for this setup to be simplified to a one region problem, similar to Figure 4-11, to aid the numerical simulation process.

It is known that an infinitely long cylinder can be considered a special case of an ellipsoid of revolution with demagnetizing factors of ½ in the transverse (x,y) direction and zero demagnetizing factor in the axial (z) direction. Therefore in the presence of an externally applied uniform magnetic field ($\mathbf{H}_{xext}, \mathbf{H}_{yext}$) the field inside the infinitely long ferrofluid ($\mathbf{H}_{xfluid}, \mathbf{H}_{yfluid}$) cylinder can be given by the following relation.

$$\begin{aligned} \mathbf{H}_{xfluid} &= \mathbf{H}_{xext} - \frac{1}{2}\mathbf{M}_x \\ \mathbf{H}_{yfluid} &= \mathbf{H}_{yext} - \frac{1}{2}\mathbf{M}_y \end{aligned} \tag{4.18}$$

Eqs (4.18) and (4.14) are substituted into $\mathbf{M}_{eq}$ of (4.13) and the only driving force will be due to the uniform external rotating magnetic field ($\mathbf{H}_{xext}, \mathbf{H}_{yext}$). To describe the uniform rotating field in Cartesian coordinates the external fields ($\mathbf{H}_{xext}, \mathbf{H}_{yext}$) are sinusoidal functions of time with rotational frequency Ω and 90^{o} out of phase with each other. Eq (4.19) generates a counter-clockwise uniform rotating magnetic field of magnitude H_0.

$$\begin{aligned} \mathbf{H}_{xext} &= H_0 \cos(\Omega t)\mathbf{i}_x \\ \mathbf{H}_{yext} &= H_0 \sin(\Omega t)\mathbf{i}_y \end{aligned} \tag{4.19}$$

H_0 is related to the surface current as follows

$$H_0 = \frac{3}{2} K_0 \tag{4.20}$$

Since

$$\mathbf{H} = -\nabla \psi \tag{4.21}$$

$\psi(r = R_0)$ can be determined to be the following boundary condition for a counter-clockwise rotating magnetic field.

$$\psi = H_0(x\cos(\Omega t) + y\sin(\Omega t)) \tag{4.22}$$

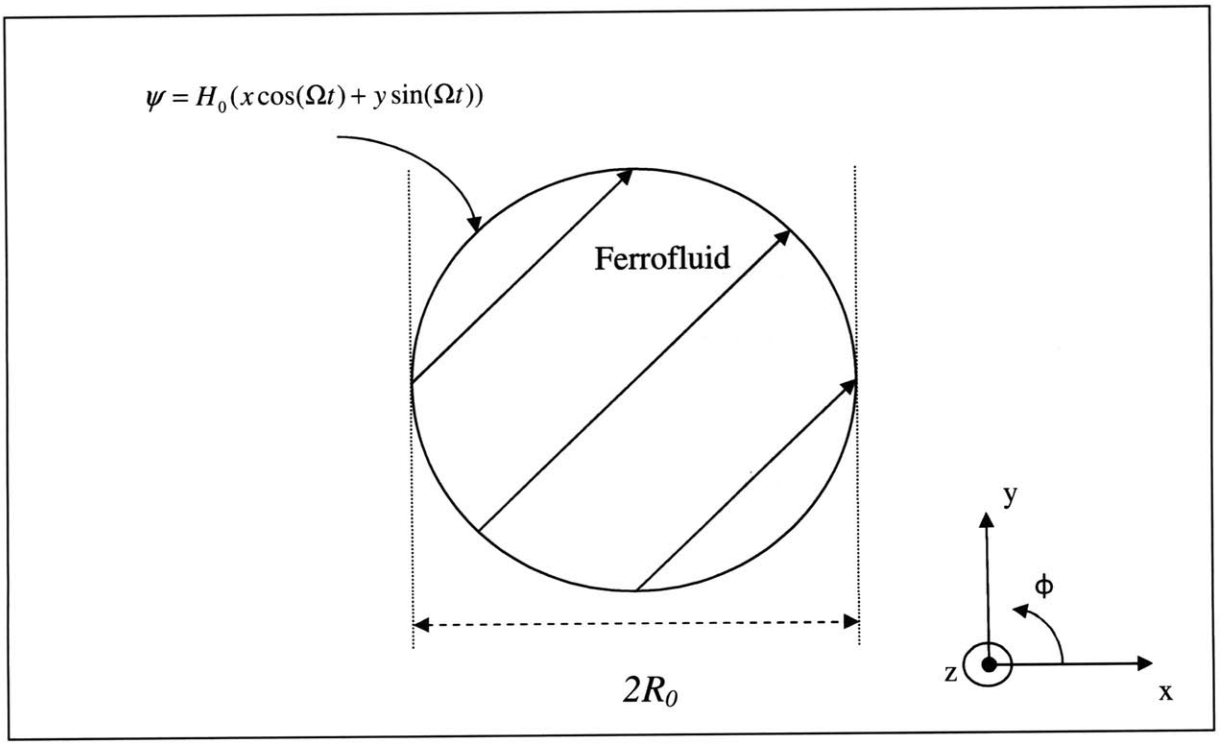

Figure 4-11. One region model setup with shaded circle representing ferrofluid with linear magnetization and boundary condition on magnetic scalar potential. The scalar potential generates a magnetic field rotating in the ϕ direction at frequency Ω. This magnetic field represents the external magnetic field and has to be corrected for demagnetizing effects before being used in the magnetic relaxation equation. The arrows inside the stator show the uniformly distributed rotating magnetic field created inside the ferrofluid at a particular instant in time.

4.4.2.2. Fluid Boundary Conditions

The linear momentum equation in (4.15) requires two vector boundary conditions. For a rigid and stationary boundary the no slip and no-penetration boundary conditions are as follows

$$\mathbf{n}\cdot\|\mathbf{v}\|=0,\mathbf{n}\times\|\mathbf{v}\|=0 \quad r=R_0 \tag{4.23}$$

where $\|\vec{v}\|$ represents the jump in velocity of the fluid across the boundary $r=R_0$. The boundary condition on $\mathbf{v}(r=R_0)$ for this model is

$$\mathbf{v}(r=R_0)=0 \tag{4.24}$$

The conservation of angular momentum in (4.16) requires two vector boundary conditions if $\eta'\neq 0$.The appropriate boundary conditions for the spin-velocity $\boldsymbol{\omega}$ is still a subject of debate and depends on the assumptions for the particle/wall interactions. Two possibilities for this boundary condition are considered.

1. The "spin-no-slip" boundary condition which assumes that the particle/wall interactions are strong enough that there is no relative spin between the particle and surface.

$$\mathbf{n}\cdot\|\boldsymbol{\omega}\|=0,\mathbf{n}\times\|\boldsymbol{\omega}\|=0 \quad r=R_0 \tag{4.25}$$

2. The "spin-vorticity" boundary condition that assumes that antisymmetric stresses vanish at the wall and that the ferrofluid nanoparticles roll along the particle wall interface.

$$\left\|\boldsymbol{\omega}-\frac{1}{2}\nabla\times\mathbf{v}\right\|=0 \quad r=R_0 \tag{4.26}$$

Finlayson, in his paper [18], does COMSOL simulations using the "spin-vorticity" boundary condition which results in flow reversal for all magnetic field strengths which is not

observed experimentally. This result confirms that the "spin-vorticity" boundary condition is not a valid boundary condition to use for modeling ferrofluid flows.

The boundary conditions used for this analysis are the "spin-no-slip" boundary condition at the wall boundary.

$$\omega(r = R_0) = 0 \tag{4.27}$$

Neglecting the effect of "spin-diffusion" by setting $\eta' = 0$, the angular momentum equation in (4.16) reduces from a second order to a zeroth order equation. Therefore there is no boundary condition on the spin-velocity ω implying zero or negligible particle/wall interactions.

4.4.3. COMSOL Simulations

The goal of this section is to reproduce the experimental results of EMG900_2 in Figure 4-6b, using spin-diffusion theory, with COMSOL Multiphysics. The reason why the plot with EMG900_2 will be replicated is to verify Chaves's value for spin-viscosity η' that he determines experimentally to be 6×10^{-10} kg m s^{-1} [9]. This value will be shown to be slightly erroneous due to the fact that the value of the magnetic field used in his paper refers to the magnetic field in the absence of the ferrofluid. It is not clear whether he corrects this value to include the demagnetizing effects for an infinitely long cylinder that this model assumes as seen in (4.18). However, Chaves does allow for order of magnitude errors in his estimated values of ζ and τ_{eff} giving a range of estimated values for spin-viscosity η' from 10^{-8}-10^{-12} kg m s^{-1}.

Equations (4.10)-(4.13) were made non-dimensional with respect to reference parameters such as the radius of the vessel R_0, frequency of the applied rotating field Ω and a reference magnetic field intensity H_0.

$$R_e[\frac{d\bar{\mathbf{v}}}{dt}+(\bar{\mathbf{v}}\bullet\bar{\nabla})\bar{\mathbf{v}}]=-\bar{\nabla}\bar{p}'+2\bar{\zeta}\bar{\nabla}\times\bar{\boldsymbol{\omega}}+(\bar{\zeta}+\bar{\eta})\bar{\nabla}^2\bar{\mathbf{v}}+\left(\bar{\mathbf{M}}\bullet\bar{\nabla}\right)\bar{\mathbf{H}} \tag{4.28}$$

$$R_w[\frac{d\bar{\boldsymbol{\omega}}}{dt}+(\bar{\mathbf{v}}\bullet\bar{\nabla})\bar{\boldsymbol{\omega}}]=\bar{\mathbf{M}}\times\bar{\mathbf{H}}+2\bar{\zeta}(\bar{\nabla}\times\bar{\mathbf{v}}-2\bar{\boldsymbol{\omega}})+\bar{\eta}'\bar{\nabla}^2\bar{\boldsymbol{\omega}} \tag{4.29}$$

$$\frac{d\bar{\mathbf{M}}}{dt}+(\bar{\mathbf{v}}\bullet\bar{\nabla})\bar{\mathbf{M}}=\bar{\boldsymbol{\omega}}\times\bar{\mathbf{M}}-\frac{1}{\Omega\tau_{eff}}(\bar{\mathbf{M}}-\bar{\mathbf{M}}_{eq}) \tag{4.30}$$

$$\nabla^2\bar{\psi}=\nabla\bullet\bar{\mathbf{M}} \tag{4.31}$$

where

$$\bar{\nabla}=\nabla R_0,\ \bar{\mathbf{v}}=\frac{\mathbf{v}}{R_0\Omega},\ \bar{\mathbf{M}}=\frac{\mathbf{M}}{H_0},\ \bar{\mathbf{H}}=\frac{\mathbf{H}}{H_0},\ \bar{t}=t\Omega,\ \bar{p}=\frac{p}{\mu_0H_0^2},\ \bar{\boldsymbol{\omega}}=\frac{\boldsymbol{\omega}}{\Omega},\ \bar{\psi}=\frac{\psi}{H_0R_0}$$
$$\bar{\zeta}=\frac{\zeta\Omega}{\mu_0H_0^2},\ \bar{\eta}=\frac{\eta\Omega}{\mu_0H_0^2},\ R_e=\frac{\rho R_0^2\Omega^2}{\mu_0H_0^2},\ R_w=\frac{I\Omega^2}{\mu_0H_0^2},\ \bar{\eta}'=\frac{\eta'\Omega}{\mu_0H_0^2R_0^2}$$

Equations (4.28)-(4.31) were put into COMSOL in non-dimensional form, setting internal constants such as μ_0=1, and in all cases the transient form of the equations were used. A fluid mechanics module was used to represent the augmented Navier-Stokes equation for (4.28). Two transient convection and diffusion modules were used to represent the magnetic relaxation equation (with zero diffusion) in x and y coordinates for (4.30). A diffusion equation was used for the angular momentum equation in (4.29) with η' the coefficient for the spin diffusion term. A general PDE module was used to represent Poisson's equation in (4.31). The time-dependent terms in the PDE module set of the linear and angular momentum equations were all set to 0.

Table 4-3 lists the necessary constant parameters and the values that Chaves uses for his experiment in Figure 4-6b. In this experiment the variable that Chaves varies is the strength of the magnetic field. This in turn affects certain normalized parameters due to their dependence on the reference magnetic field H_0 and are tabulated in Table 4-4.

Parameter	Value
τ_{eff} (s)	$1x10^{-6}$
ρ (kg/m^3)	1030
η (Ns /m^2)	0.0045
$\mu_0 M_s$ (mT)	23.9
ζ (Ns/m^2)	0.0003
Frequency (Hz)	85
Radius of cylindrical vessel (m)	0.0247
Radius of stator (m)	0.0318
Volume Fraction (%)	4.3
χ	1.19
Ω (rad/s)	534.071
η' (kg m/s)	$6x10^{-10}$

Table 4-3. Table of physical and experimental parameters used by Chaves to generate experimental plot of Figure 4-6b using EMG900_2

Normalized Variable	B_0=143G H_0=11379.6 A/m	B_0= 125G H_0=9947.2 A/m	B_0=103G H_0=8196.5 A/m
$\overline{\eta'} = \frac{\eta'\Omega}{\mu_0 H_0^2 R_0^2}$	$1.61x10^{-6}$	$2.11x10^{-6}$	$3.11x10^{-6}$
$\overline{\zeta} = \frac{\zeta\Omega}{\mu_0 H_0^2}$	0.00048	0.00062	0.00092
$\overline{\eta} = \frac{\eta\Omega}{\mu_0 H_0^2}$	0.0074	0.0097	0.014
$R_e = \frac{\rho R_0^2 \Omega^2}{\mu_0 H_0^2}$	1101.5	1441.5	2123.1

Table 4-4. Table of normalized parameters that depend on the strength of the RMS magnetic field used by Chaves [9].

Two different COMSOL simulations, as described in 4.4.2.1, were done using the normalized equations in Eqs (4.28)-(4.31) and using the normalized parameters for the 143G case in Table 4-4. The first type of simulation was done imposing the surface current boundary condition with a region of air separating the stator from the two dimensional infinitely long cylinder. The second simulation was done using the scalar potential boundary condition method

in only the region of interest - the cylinder of ferrofluid. Both will be shown to be identical with the scalar potential method being easier to implement in COMSOL Multiphysics. Summary of the setup of the COMSOL models used is documented in Appendix B.

4.4.3.1. Simulations Using Surface Current Boundary Condition

The model setup was similar to Figure 4-10 with a normalized radius R_0 of 1 for the cylindrical vessel and a stator normalized radius R_1 of 10 in COMSOL . In the actual experiment a line dipole field would be generated by the ferrofluid in the surrounding free space region. This dipole field could affect the stator winding current if sufficiently close by. From the dimensions of the experiment the stator was not that much larger than the actual cylindrical vessel of ferrofluid, therefore the current in the windings may have been perturbed.

When specifying boundary conditions in a numerical package such as COMSOL Multiphysics the boundary conditions specified are implied to be fixed. To simulate the case where the normalized radius of the stator would have been 1.29 and imposing a fixed surface current boundary condition would be erroneous since the current is actually affected by the dipole field and this effect was not measured by Chaves. The best method to simulate this experiment is to take the value of magnetic field measured in the absence of the ferrofluid and assume that this is an imposed rotating field sufficiently far away such that the current was not perturbed by the dipole field. The normalized boundary condition was imposed at the normalized radius of 5 and was

$$\overline{\mathbf{K}}(\phi,t)=\frac{3}{2}K_0\cos(\bar{t}-\phi)\bar{i}_z \tag{4.32}$$

with K_0 equaling ⅔ such that the magnitude of the current density equals the normalized value of magnetic field $\overline{\mathbf{H}} = 1$.

Figure 4-12 is a COMSOL plot of the velocity field within the ferrofluid cylinder, while Figure 4-13 is a streamline plot of the magnetic field distribution in and around the cylinder of ferrofluid. Figure 4-14 gives the distribution of the magnetic field inside and outside the ferrofluid cylinder as a function of normalized radius. There is a jump in magnetic field at the air-ferrofluid wall corresponding to the additional dipole field created, that decays as the cube of the distance away from the wall, while sufficiently far from the wall the magnetic field is only due to the imposed stator current. The magnetic field and magnetization are mostly uniform inside the cylinder except for a small region at the wall as seen in Figure 4-15 and Figure 4-16. The reason for this is the non-linear effects of the velocity and spin-velocity on the magnetization near the wall. The non-linear effects, however, are very small.

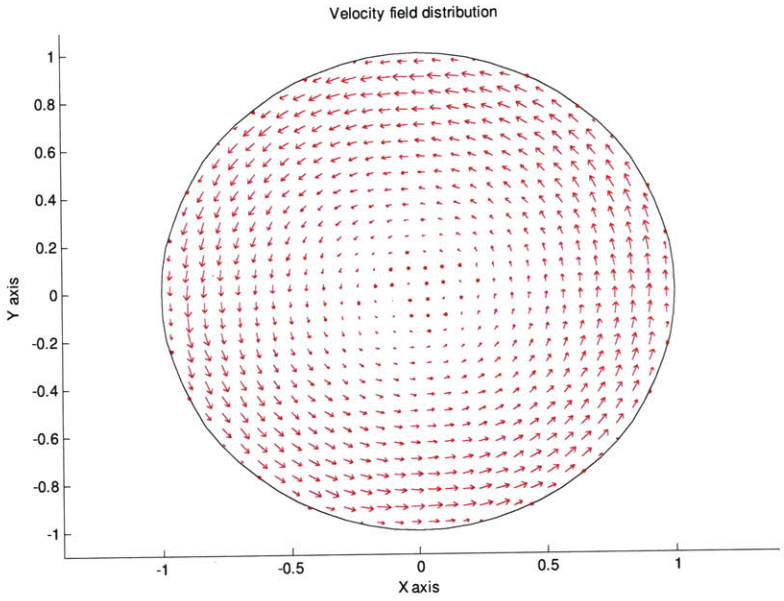

Figure 4-12. Plot of counter-clockwise rotating steady flow of ferrofluid in cylinder surrounded by a stator driven by a surface current boundary condition at $\bar{r}=1$ that generates a counter-clockwise rotating magnetic field. Flow profile is similar to that of rigid-body motion.

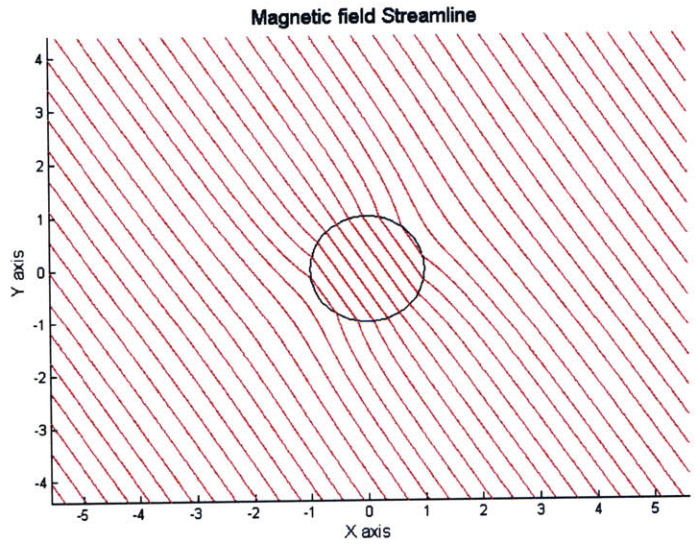

Figure 4-13. COMSOL Streamline plot of magnetic field distribution inside and outside the ferrofluid filled sphere showing a uniform distribution of field inside the cylinder. The field distribution outside the cylinder is the sum of the uniform imposed field and a dipole field created by the ferrofluid.

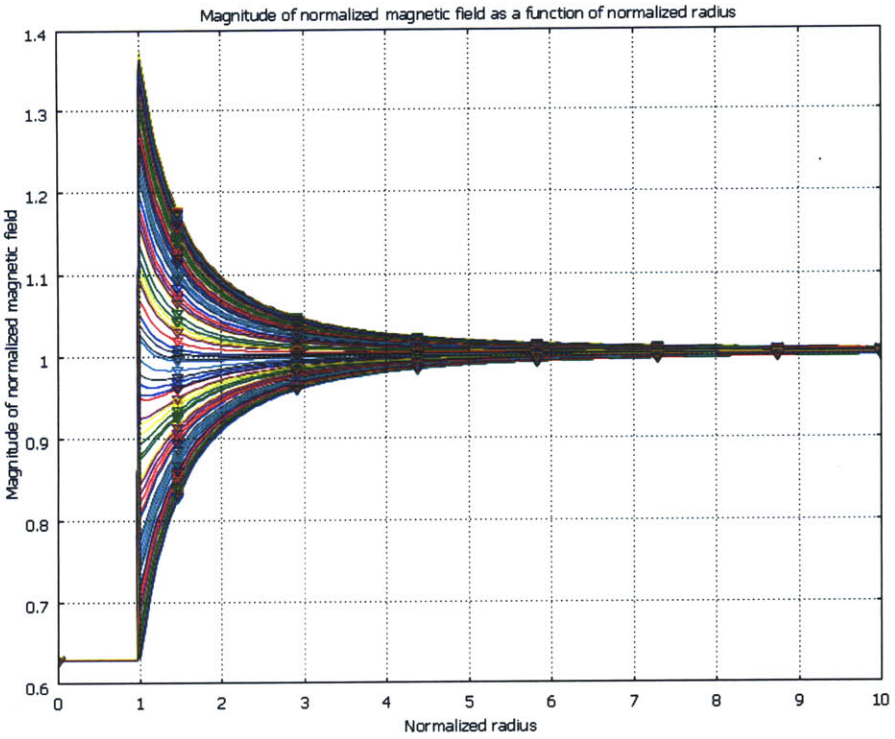

Figure 4-14. Magnitude of normalized magnetic field distribution as a function of normalized radius inside and outside the cylinder of ferrofluid. The different colors represent the magnetic fields at various times. It is evident that the field inside the cylinder is uniform and outside the cylinder it is a uniform and a line dipole field, that decays as the cube of the distance, generated outside. The stator is excited at a normalized radius ($R_1=10$) sufficiently far away from the ferrofluid with $\overline{\mathbf{H}}=1$. Magnitude of the normalized magnetic field inside the ferrofluid is approximately 0.629.

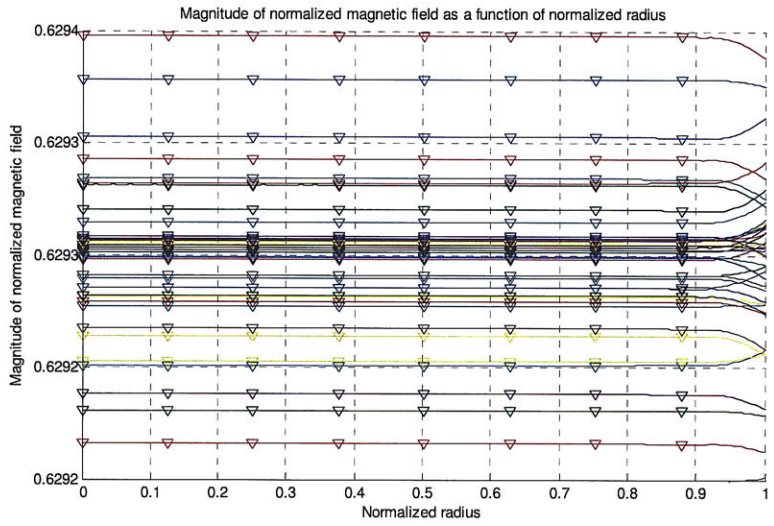

Figure 4-15. Plot of magnitude of normalized magnetic field as a function of normalized radius within the ferrofluid cylinder. Magnetic field is uniform in majority of the fluid except for some variation at the boundary $\bar{r}=1$ due to the velocity and spin velocity affecting the magnetization there. The difference between the magnetic field at the wall and in the rest of the fluid is very small ($\approx 1\text{x}10^{-4}$)

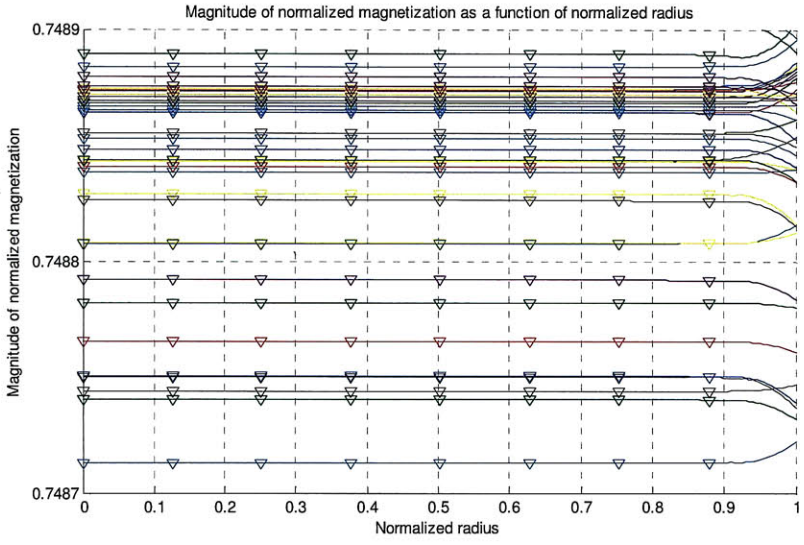

Figure 4-16. Plot of normalized magnitude of magnetization as a function of normalized radius showing that the magnetization at the wall boundary $\bar{r}=1$ deviates from the magnetization in the bulk since there is the greatest change in velocity and spin-velocity near the wall. The non-linearity of the magnetization is very small since the magnitude at the wall changes by $\approx 1\text{x}10^{-4}$ compared to the magnetization in the bulk of the fluid.

4.4.3.2. Simulations Using Magnetic Scalar Potential Boundary Condition

The model was setup similar to Figure 4-11 with a normalized radius R_0 of 1 for the cylindrical vessel. Since the model involved normalized variables the boundary condition imposed in (4.22) has to be normalized and is given by

$$\overline{\psi} = \bar{x}\cos(\bar{t}) + \bar{y}\sin(\bar{t}) \tag{4.33}$$

representing a counter-clockwise rotating magnetic field where

$$\bar{x} = \frac{x}{R_0}, \bar{y} = \frac{y}{R_0} \tag{4.34}$$

The flow pattern obtained is identical to that of Figure 4-12 and is shown in Figure 4-17 along with streamlines of the uniform magnetic field distribution inside the ferrofluid cylinder. The magnetic field distribution within the ferrofluid, in Figure 4-18, can be seen to be mostly uniform in the bulk with some variation at the wall where velocity and spin-velocity affect the magnetization significantly as seen in Figure 4-19.

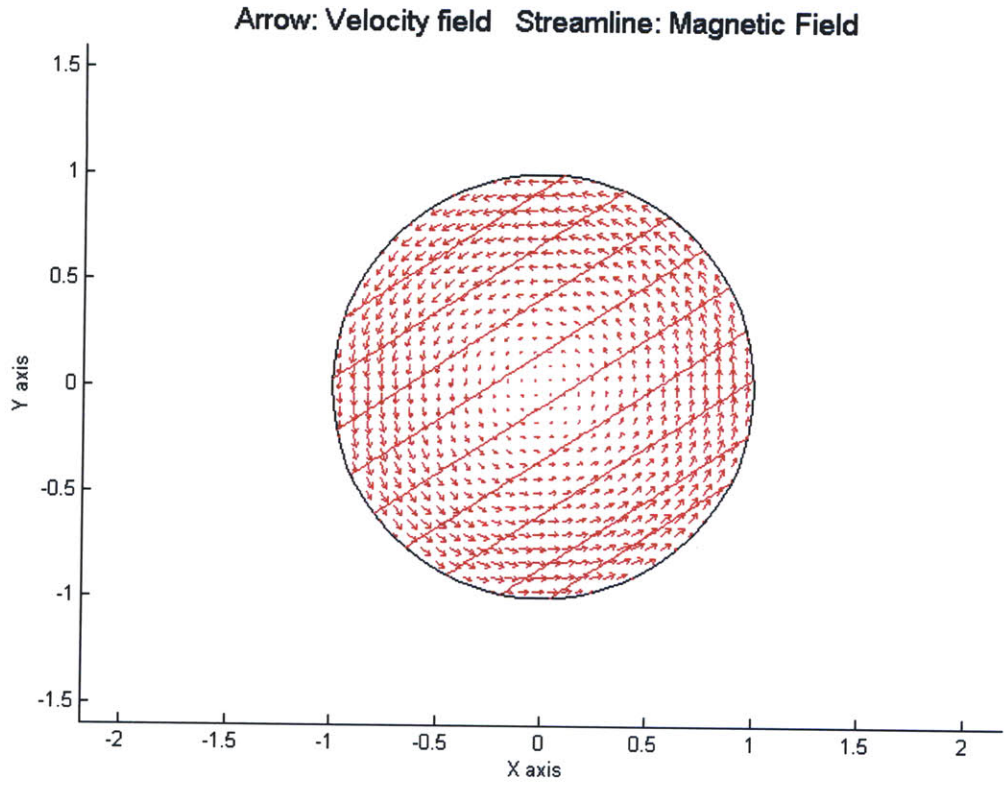

Figure 4-17. Velocity flow profile and magnetic field distribution using scalar potential boundary condition method for a counter-clockwise rotating field. Flow velocity is depicted by arrows counter-rotating while streamlines depict the uniform rotating magnetic field distribution in the region of ferrofluid.

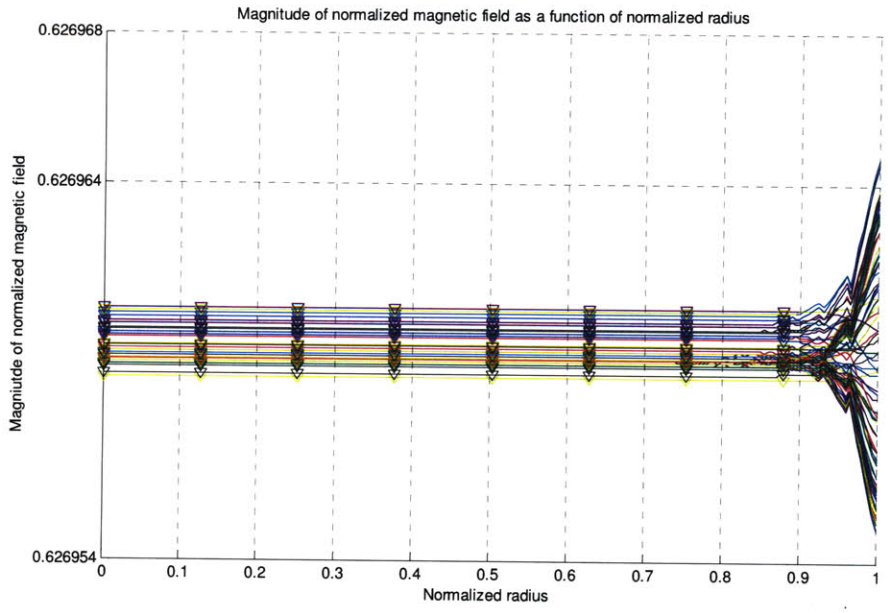

Figure 4-18. Plot of magnitude of normalized magnetic field as a function of normalized radius. The field is shown to be uniform and approximately equal to 0.627.

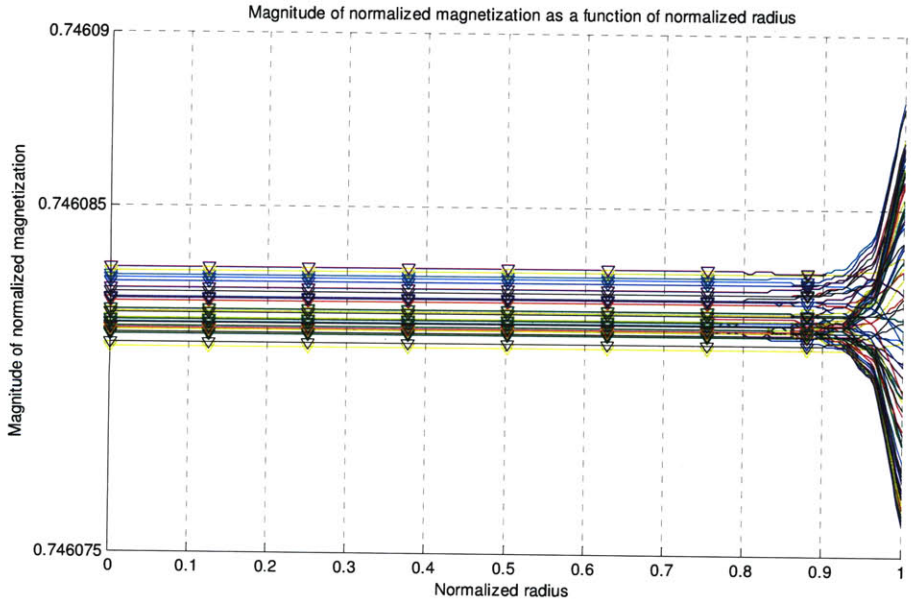

Figure 4-19. Plot of magnitude of normalized magnetization as a function of normalized radius within the ferrofluid cylinder. The different colored lines correspond to different times. The magnetization can be seen to be uniform and approximately equal to 0.746.

4.4.3.3. Comparison of Both Methods

Figure 4-20 compares the velocity profile obtained as a function of normalized radius using both the scalar potential and surface current boundary condition. They can be seen to be almost identical with minor differences due to the more difficult meshing required for the surface current method. The velocity profile is linear in the bulk of the fluid resembling rigid-body rotation except for a small boundary layer at the wall where no-slip boundary conditions of zero velocity has to be satisfied.

Figure 4-21 compares the spin-velocity as a function of normalized radius and is identical for both implementations . The spin velocity is uniform throughout the bulk of the fluid but at the small boundary layer near the wall the spin-velocity has to satisfy the boundary condition of zero spin-velocity.

The plots of velocity and spin-velocity profiles given in Figure 4-20 and Figure 4-21 along with the approximately identical plots obtained for magnetic field (Figure 4-18 and Figure 4-15) and magnetization (Figure 4-19 and Figure 4-16) for the two different methods prove that they are identical. The scalar potential method is easier to mesh and implement and will be used for all other simulations in this thesis.

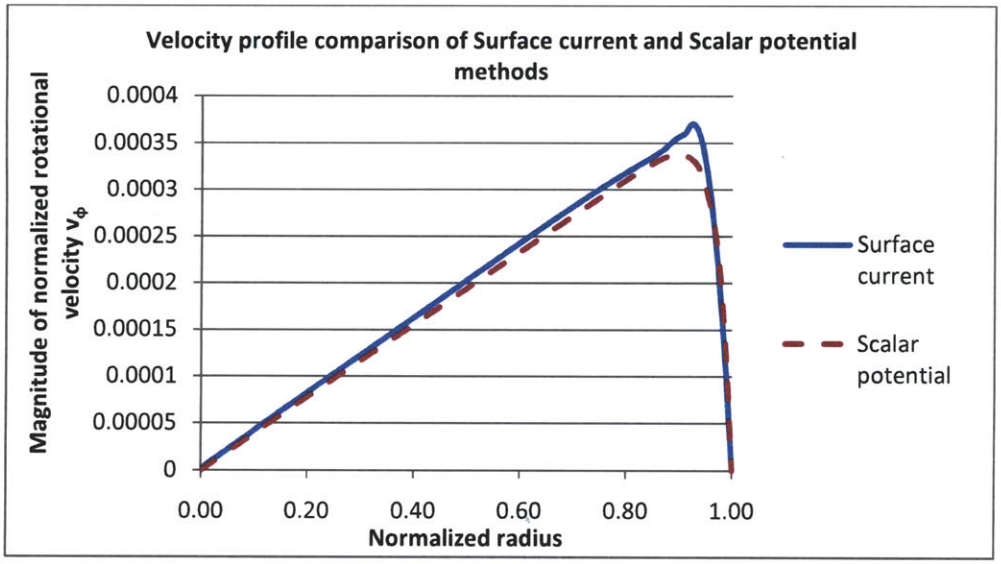

Figure 4-20. Plot of rotational velocity as a function of normalized radius comparing the two different implementations on source boundary conditions - Surface current and scalar potential. Velocity profiles can be seen to be almost identical in both implementations and linear with radius throughout the bulk of the fluid except at the $\bar{r}=1$ boundary where a no-slip boundary condition, $\bar{\mathbf{v}}(\bar{r}=1)=0$, has to be satisfied.

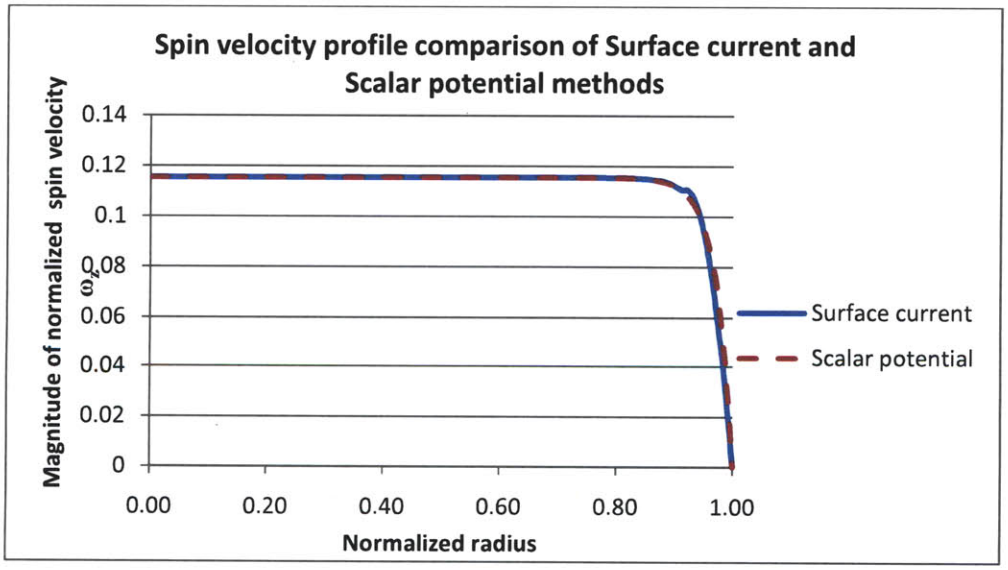

Figure 4-21. Plots of spin-velocity as a function of normalized radius for both model implementations. Spin velocity is shown to be identical and constant within most of the fluid region and going to zero on the $\bar{r}=1$ boundary to satisfy the $\overline{\omega_z}(\bar{r}=1)=0$ boundary condition.

4.4.3.4. Comparison with Analytic Solutions Using a Linear Magnetic Material

If the ferrofluid region in Figure 4-10 is replaced by a linear magnetic material $\mu_1 = \mu_0(1+\chi)$, Poisson's equation can be replaced with Laplace's equation in magnetic scalar potential.

$$\begin{aligned} \nabla^2\psi &= \nabla\bullet\mathbf{M} \\ (1+\chi)\nabla^2\psi &= 0 \\ \nabla^2\psi &= 0 \end{aligned} \tag{4.35}$$

Solutions to Laplace's equation in the individual regions are given as

$$\psi = \begin{cases} r\left(A\cos(\Omega t-\phi)+B\sin(\Omega t-\phi)\right) & 0<r<R_0 \\ r^{-1}\left(C\cos(\Omega t-\phi)+D\sin(\Omega t-\phi)\right)+r\left(E\cos(\Omega t-\phi)+F\sin(\Omega t-\phi)\right) & R_0<r<R_1 \\ r^{-1}\left(G\cos(\Omega t-\phi)+L\sin(\Omega t-\phi)\right) & r>R_1 \end{cases} \tag{4.36}$$

Since $\mu=\infty$ for $r>R_1$,

$$\mathbf{H}(r>R_1)=0 \Rightarrow G=L=0 \tag{4.37}$$

The surface current boundary condition at $r=R_1$ implies

$$\left(H_{\phi 3}-H_{\phi 2}\right)\Big|_{r=R_1} = \frac{3}{2}K_0\cos(\Omega t-\phi) \tag{4.38}$$

$$0+\frac{1}{R_1^{\,2}}\left(\left(C+ER_1^{\,2}\right)\sin(\Omega t-\phi)-\left(D+FR_1^{\,2}\right)\cos(\Omega t-\phi)\right)=\frac{3}{2}K_0\cos(\Omega t-\phi) \tag{4.39}$$

implies that

$$\begin{aligned} C &= -ER_1^2 \\ D+FR_1^2 &= -\frac{3}{2}K_0R_1^{\,2} \end{aligned} \tag{4.40}$$

At $r=R_0$, the tangential magnetic field is continuous resulting in

$$\left(H_{\phi 2}-H_{\phi 1}\right)\Big|_{r=R_0}=0 \tag{4.41}$$

$$\frac{1}{R_0^{\,2}}\left(\left(C+ER_0^2\right)\sin(\Omega t-\phi)+\left(D+FR_0^2\right)\cos(\Omega t-\phi)\right)=\left(A\sin(\Omega t-\phi)+B\cos(\Omega t-\phi)\right) \tag{4.42}$$

resulting in

$$\begin{aligned} A&=\frac{C+ER_0^2}{R_0}\\ B&=\frac{D+FR_0^2}{R_0}\end{aligned} \tag{4.43}$$

The jump in the normal magnetic flux density is also continuous as given in

$$\left(\mu_0 H_{r2}-\mu_1 H_{r1}\right)\Big|_{r=R_0}=0 \tag{4.44}$$

$$\frac{\mu_0}{R_0^{\,2}}\left(C\cos(\Omega t-\phi)-D\sin(\Omega t-\phi)\right)+\mu_0\left(-E\cos(\Omega t-\phi)+F\sin(\Omega t-\phi)\right)=\mu_1\left(-A\cos(\Omega t-\phi)+B\sin(\Omega t-\phi)\right) \tag{4.45}$$

requiring the relationships

$$\begin{aligned} \frac{\mu_0}{R_0^2}\left(C-ER_0^2\right)+\mu_1 A&=0\\ \mu_1 B+\frac{\mu_0}{R_0^2}\left(D-FR_0^2\right)&=0\end{aligned} \tag{4.46}$$

Using (4.40), (4.43) and (4.46) results in

$$A=C=E=0 \tag{4.47}$$

$$B=-\frac{3K_0\mu_0 R_1^2}{\mu_0\left(R_0^2+R_1^2\right)+\mu_1\left(R_1^2-R_0^2\right)} \tag{4.48}$$

$$D=\frac{3K_0 R_1^2(\mu_1-\mu_0)}{2\left(\left(\mu_0-\mu_1\right)R_0^2+R_1^2\left(\mu_1+\mu_0\right)\right)} \tag{4.49}$$

$$F = -\frac{3K_0 R_1^2(\mu_1 + \mu_0)}{2\left(R_1^2(\mu_0 + \mu_1) + R_0^2(\mu_0 - \mu_1)\right)} \tag{4.50}$$

The magnetic field distribution is then given as

$$\mathbf{H} = \begin{cases} B\left(\cos(\Omega t - \phi)\mathbf{i}_\phi - \sin(\Omega t - \phi)\mathbf{i}_r\right) & 0 < r < R_0 \\ \sin(\Omega t - \phi)\left(\frac{D}{r^2} - F\right)\mathbf{i}_r + \cos(\Omega t - \phi)\left(\frac{D}{r^2} + F\right)\mathbf{i}_\phi & R_0 < r < R_1 \\ 0 & r > R_1 \end{cases} \tag{4.51}$$

The field inside the linear magnetic material is uniform and has a magnitude of B. Substituting values used in the simulation of 4.4.3.1 where $R_1=10$, $R_0=1$, $\mu_0=1$ (due to normalization), $\chi=1.19$ and $K_0=2/3$ (since $\overline{\mathbf{H}}=1$) results in a value of

$$B = 0.629307 \tag{4.52}$$

which is approximately equal to the magnitude of the magnetic field strength obtained in Figure 4-15. This confirms that the ferrofluid's magnetization is mostly linear except at the boundary where spin-velocity and velocity effects make it non-linear. The magnitude of the magnetization $\mathbf{M}$ can be calculated to be

$$|\mathbf{M}| = |\chi\mathbf{H}| = 1.19 \times 0.629307 = 0.74888 \tag{4.53}$$

which is approximately equal to the value achieved from simulation in Figure 4-16.

To verify (4.52) for an infinitely long cylinder which has demagnetization coefficients of 1/2, the internal magnetic field within the cylinder can be given as

$$\mathbf{H}_{internal} = \mathbf{H}_{external} - \frac{1}{2}\mathbf{M} \rightarrow \mathbf{M} = \chi\mathbf{H} \rightarrow \mathbf{H}_{internal} = \frac{\mathbf{H}_{external}}{1 + \frac{1}{2}\chi} \tag{4.54}$$

with $\mathbf{H}_{external} = 1$ and $\chi = 1.19$ resulting in $\mathbf{H}_{internal} \approx 0.627$ which is in good agreement with (4.52). The reason for the slight disagreement is because the applied uniform field comes from a source at $R_1=10$ rather than from infinity.

4.4.3.5. COMSOL Simulations of Flows With $\eta'=0$

The conservation of angular momentum equation given in (4.12) has the spin-viscosity term which is the essential component to 'spin-diffusion' theory. Some authors do not include it in their analyses, by setting it to zero, because they believe that η' values are so small that its effect is negligible [2, 5, 20, 23, 24].

By setting the term to zero, the conservation of angular momentum equation reduces to a zeroth order equation in space requiring no boundary condition on spin-velocity $\boldsymbol{\omega}$ at the wall.

$$\cancel{I[\frac{\partial \boldsymbol{\omega}}{\partial t}+(\mathbf{v}\bullet\nabla)\boldsymbol{\omega}]} = \mu_0\mathbf{M}\times\mathbf{H}+2\zeta\left(\nabla\times\mathbf{v}-2\boldsymbol{\omega}\right) \tag{4.55}$$

In the case of the rotating field in the cylinder, the velocity is in the ϕ direction and there is no variation in the $\vec{i}_\phi$ direction resulting in no spatial variation for the spin-velocity ω_z. Having no spatial variation in spin-velocity means that the only driving terms for the linear momentum equation are the viscous and pressure forces.

$$\cancel{\rho[\frac{\partial \mathbf{v}}{\partial t}+(\mathbf{v}\bullet\nabla)\mathbf{v}]} = -\nabla p'+\cancel{2\zeta\nabla\times\boldsymbol{\omega}}+(\zeta+\eta)\nabla^2\mathbf{v}+\cancel{\mu_0(\mathbf{M}\bullet\nabla)\mathbf{H}} \tag{4.56}$$

In an infinitely tall cylinder the magnetic field distribution is uniform inside leading to no Kelvin force density inside the ferrofluid to drive the flow. Therefore, with no driving forces for the flow the state for the ferrofluid is one without motion.

$$\mathbf{F} = \mu_0\left(\mathbf{M}\bullet\nabla\right)\mathbf{H} = 0 \tag{4.57}$$

Simulations of an infinitely tall cylinder of ferrofluid subjected to a uniform rotating field with $\eta'=0$ were done using the parameters for the 143G case of Chaves's EMG900_2 ferrofluid as given in Table 4-3 and Table 4-4. The velocity profile can be seen in Figure 4-22 below and

can be seen to be very small $\approx 10^{-13}$ normalized magnitude. These results are also confirmed by Finlayson in his simulations [18].

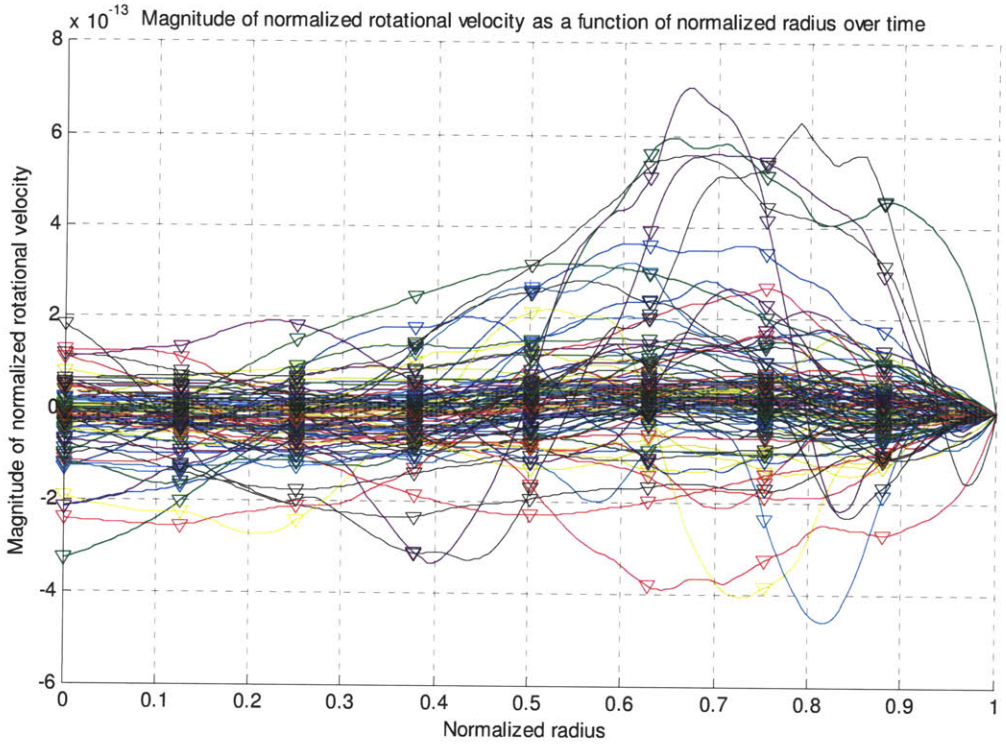

Figure 4-22. Plot of normalized rotational velocity as a function of normalized radius. The different colored lines represent different profiles in time. The magnitude of the velocity is extremely small $\approx 10^{-13}$ normalized magnitude.

4.4.4. Errors in Other Author's Analyses

4.4.4.1. Chaves's Results [9]

Chaves, in his paper, determines the value of η' to be $6x10^{-10}$ kg m s^{-1} but admits for order of magnitude errors in his estimated values of ζ and τ_{eff} giving a range for the spin viscosity of 10^{-8}- 10^{-12} kg m s^{-1}. Using the normalization scheme outlined in 4.4.3 and the normalized parameters in Table 4-4, for the different magnetic field strengths used, COMSOL simulations were done to replicate Figure 4-6b.

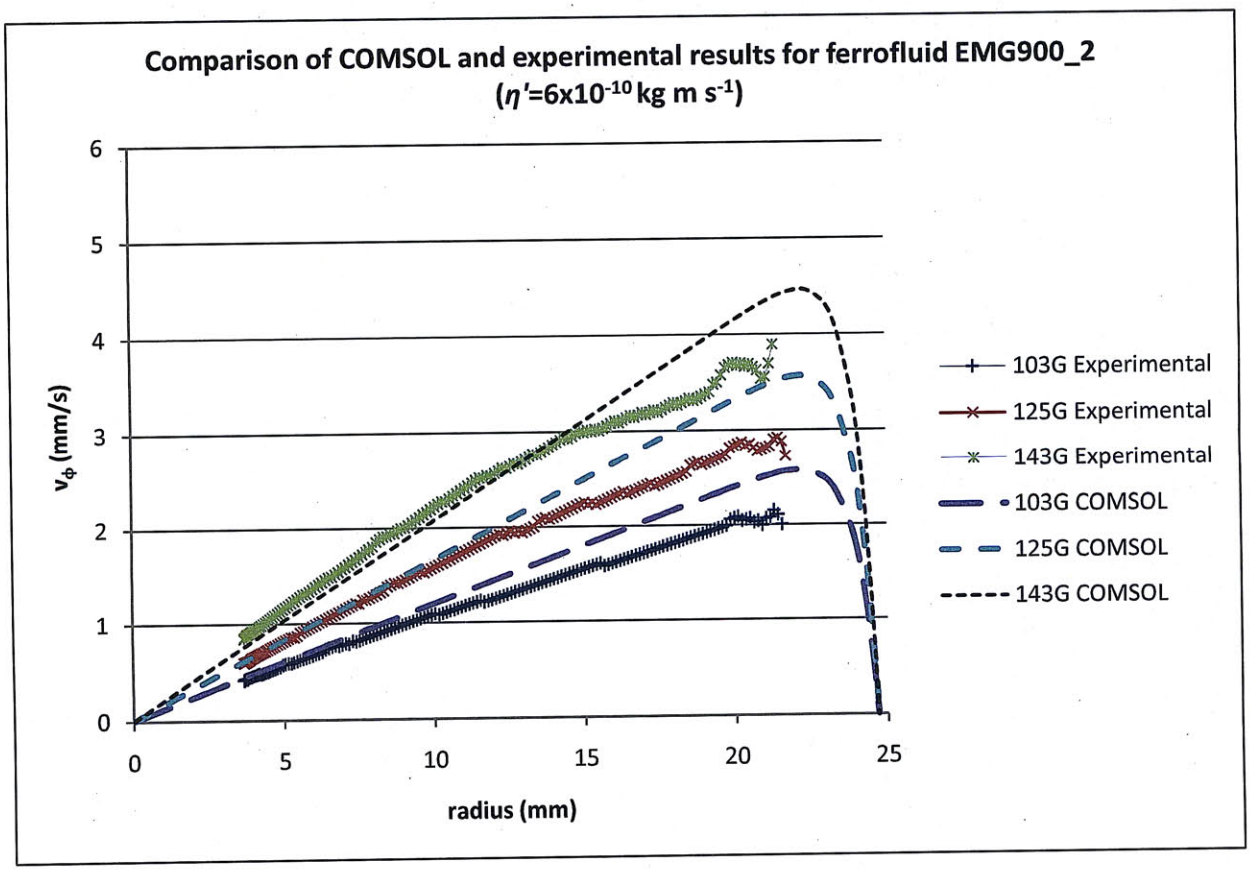

Figure 4-23. Experimental data of Figure 4-6 and COMSOL simulations using parameters from Chaves's paper with $\eta'=6x10^{-10}$ kg m s^{-1}.

Figure 4-23 shows that the COMSOL simulations do not match the experimental results obtained by Chaves. This is because Chaves in his determination of η' used the values of magnetic field which were obtained in the absence of ferrofluid. He did not correct for the value of the magnetic field inside the fluid, given by the relation in (4.18), for an infinitely long cylinder resulting in a higher value for η' than actually needed to replicate the data [25].

The value for η' can be tweaked with the COMSOL model to match the experimental results. Simulations with a value of η'=4.84x10^{-10} kg m s^{-1}was shown to match the experimental results very well as shown in Figure 4-24.

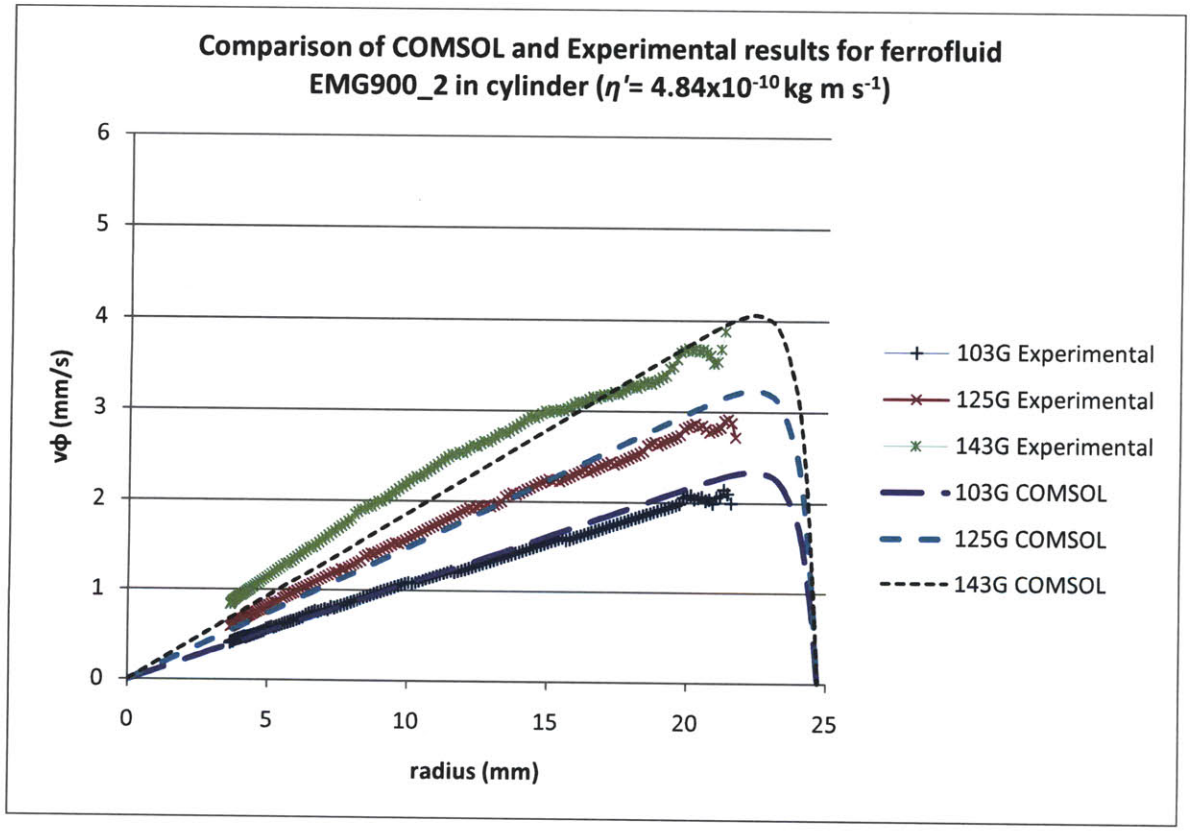

Figure 4-24. Plot of velocity profile as a function of radius for Chaves's experiment showing that a value of η'=4.84x10^{-10} kg m s^{-1}closely matches the experimental results instead of Chaves's quoted value of 6x10^{-10}

4.4.4.2. Elborai's PhD Thesis [8]

Elborai on page 191 of his thesis [8] outlines his normalization scheme for the governing fluid mechanics equations. It appears that Elborai did not normalize the governing equation but instead normalized each term in the set of equations. This leads to some terms in his equations scaled by a constant unitless term. His normalized equations for conservation of linear and angular momentum are given below.

$$\mathrm{R}_e[\frac{\partial \bar{\mathbf{v}}}{\partial \bar{t}}+(\bar{\mathbf{v}}\bullet\bar{\nabla})\bar{\mathbf{v}}]=-\bar{\nabla}\bar{p}'+2\frac{\zeta}{\eta}\bar{\nabla}\times\bar{\boldsymbol{\omega}}+(1+\frac{\zeta}{\eta})\bar{\nabla}^2\bar{\mathbf{v}}+\bar{\mathbf{F}} \tag{4.58}$$

$$\mathrm{R}_e(\frac{I}{\rho R_0^2})[\frac{\partial \bar{\boldsymbol{\omega}}}{\partial \bar{t}}+(\bar{\mathbf{v}}\bullet\bar{\nabla})\bar{\boldsymbol{\omega}}]=\bar{\mathbf{T}}+2\frac{\zeta}{\eta}(\bar{\nabla}\times\bar{\mathbf{v}}-2\bar{\boldsymbol{\omega}})+\frac{\eta'}{R_0^2\eta}\bar{\nabla}^2\bar{\boldsymbol{\omega}}+\frac{\lambda'+\eta'}{R_0^2\eta}\bar{\nabla}(\bar{\nabla}\bullet\bar{\boldsymbol{\omega}}) \tag{4.59}$$

where his normalized variables are given as follows

$$\bar{\nabla}=\nabla R_0,\bar{\mathbf{v}}=\frac{\mathbf{v}}{R_0\Omega},\bar{\mathbf{M}}=\frac{\mathbf{M}}{H_0},\bar{\mathbf{H}}=\frac{\mathbf{H}}{H_0},\bar{t}=t\Omega,\bar{p}=\frac{p}{\mu_0 H_0^2},\bar{\boldsymbol{\omega}}=\frac{\boldsymbol{\omega}}{\Omega},$$
$$R_e=\frac{\rho R_0^2\Omega}{\eta},\bar{\mathbf{F}}=\frac{R_0\mathbf{F}}{\mu_0 H_0^2},\bar{\mathbf{T}}=\frac{\mathbf{T}}{\mu_0 H_0^2}$$

Dimensionalizing his conservation of linear momentum equation with his normalization scheme is shown below.

$$\frac{\rho\Omega R_0^2}{\eta}[\frac{1}{\Omega^2 R_0}\frac{\partial \vec{v}}{\partial t}+\frac{R_0}{\Omega^2 R_0^2}(\mathbf{v}\bullet\nabla)\mathbf{v}]=-\frac{R_0}{\mu_0 H_0^2}\nabla p'+2\frac{\zeta}{\eta}\frac{R_0}{\Omega}\nabla\times\boldsymbol{\omega}+(1+\frac{\zeta}{\eta})\frac{R_0^2}{\Omega R_0}\nabla^2\mathbf{v}+\frac{R_0\mathbf{F}}{\mu_0 H_0^2}$$
$$\frac{\rho R_0}{\eta\Omega}[\frac{\partial \mathbf{v}}{\partial t}+(\mathbf{v}\bullet\nabla)\mathbf{v}]=-\frac{R_0}{\mu_0 H_0^2}\nabla p'+2\frac{\zeta}{\eta}\frac{R_0}{\Omega}\nabla\times\boldsymbol{\omega}+(1+\frac{\zeta}{\eta})\frac{R_0}{\Omega}\nabla^2\mathbf{v}+\frac{R_0\mathbf{F}}{\mu_0 H_0^2}$$
$$\rho[\frac{\partial \mathbf{v}}{\partial t}+(\mathbf{v}\bullet\nabla)\mathbf{v}]=-\frac{\eta\Omega}{\mu_0 H_0^2}\nabla p'+2\zeta\nabla\times\boldsymbol{\omega}+(\eta+\zeta)\nabla^2\mathbf{v}+\frac{\eta\Omega\mathbf{F}}{\mu_0 H_0^2}$$

The result is that the force and pressure terms are scaled by a $\frac{\eta\Omega}{\mu_0 H_0^2}$ term which is unitless but is not necessarily equal to 1. Similarly dimensionalizing his equation for conservation of angular momentum is shown below with the same $\frac{\eta\Omega}{\mu_0 H_0^2}$ term scaling the torque vector.

$$\frac{\rho\Omega R_0^2}{\eta}\left(\frac{I}{\rho R_0^2}\right)\left[\frac{1}{\Omega^2}\frac{\partial\boldsymbol{\omega}}{\partial t}+\frac{R_0}{\Omega^2 R_0}(\mathbf{v}\bullet\nabla)\boldsymbol{\omega}\right]=\frac{\mathbf{T}}{\mu_0 H_0^2}+2\frac{\zeta}{\eta}\left(\frac{R_0}{\Omega R_0}\nabla\times\mathbf{v}-\frac{2}{\Omega}\boldsymbol{\omega}\right)+\frac{\eta'}{R_0^2\eta}\frac{R_0^2}{\Omega}\nabla^2\boldsymbol{\omega}+\frac{\lambda'+\eta'}{R_0^2\eta}\frac{R_0^2}{\Omega}\nabla(\nabla\bullet\boldsymbol{\omega})$$

$$\frac{1}{\eta\Omega}(I)\left[\frac{\partial\boldsymbol{\omega}}{\partial t}+(\mathbf{v}\bullet\nabla)\boldsymbol{\omega}\right]=\frac{\mathbf{T}}{\mu_0 H_0^2}+2\frac{\zeta}{\eta}\left(\frac{1}{\Omega}\nabla\times\mathbf{v}-\frac{2}{\Omega}\boldsymbol{\omega}\right)+\frac{\eta'}{\eta}\frac{1}{\Omega}\nabla^2\boldsymbol{\omega}+\frac{\lambda'+\eta'}{\eta}\frac{1}{\Omega}\nabla(\nabla\bullet\boldsymbol{\omega})$$

$$I\left[\frac{\partial\boldsymbol{\omega}}{\partial t}+(\mathbf{v}\bullet\nabla)\boldsymbol{\omega}\right]=\frac{\mathbf{T}\eta\Omega}{\mu_0 H_0^2}+2\zeta(\nabla\times\mathbf{v}-2\boldsymbol{\omega})+\eta'\nabla^2\boldsymbol{\omega}+(\lambda'+\eta')\nabla(\nabla\bullet\boldsymbol{\omega})$$

This poses as a serious error in his thesis especially if he used the normalized equations for his COMSOL simulations.

Another serious error in Elborai's thesis are his results for simulations with $\eta'=0$. In his thesis, Figures 8-1 (pg 198), 8-2 (pg 198) and 8-3 (pg 201) all show non-zero velocity profiles for a zero spin-viscosity and in the case of an infinitely long cylinder. This is an incorrect result as explained in 4.4.3.4 and is also inconsistent with a similar simulation done by Finlayson [18] with $\eta'=0$. The reason why Elborai might have gotten a non-zero flow was he might have forgotten to remove the "spin-no-slip" boundary condition $\boldsymbol{\omega}(r=R_0)=0$ when he set $\eta'=0$ resulting in Eq. (4.56) having a non-zero curl of spin velocity $\boldsymbol{\omega}$ resulting in non-zero flow. Elborai's figure 8-1 is shown on the next page.

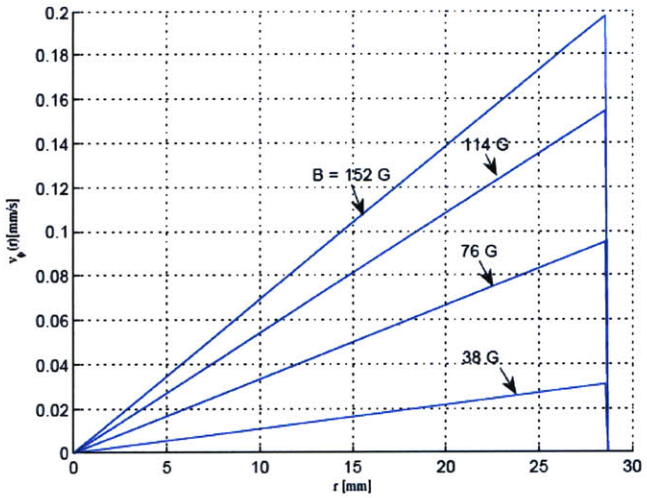

Figure 8-1: Velocity flow profiles obtained by numerically solving the spin-up model without a spin diffusion term (*i.e.*, with spin viscosity $\eta' = 0$). The simulation was run for the parameters of MSG W11 listed in Table 8.1 with $\tau = 1 \times 10^{-5}$ s and $f = 200$ Hz. Note that $\Omega_e = 2\pi f$.

Figure 4-25. Elborai's erroneous plot (Figure 8-1) of velocity profiles with $\eta'=0$ for an infinitely long cylinder in a uniform rotating magnetic field. His plots show non-zero flow when there should be no flow because there is no spatial variation in spin velocity $\boldsymbol{\omega}$. Plot taken from [8].

4.4.4.3. Finlayson's Paper [18]

Finlayson sets up his COMSOL simulations similar to that done using the scalar potential boundary condition method in Figure 4-11 except that Finlayson does not correct for the demagnetizing field associated with an infinitely long cylinder given in (4.18) resulting in an error with his numerical result.

One of Finlayson's conclusions from his simulations was that he observed flow reversal at high magnetic fields. Finlayson associates this result with those obtained by authors who were investigating flows at the free surface and had observed flow reversal [1, 3, 4, 19]. However, the mechanism for this flow reversal had nothing to do with high magnetic fields but rather

depended on the shape of the meniscus formed at the free surface as explained by Rosensweig [6]. Finlayson confuses his result using spin-diffusion theory with the mechanism of tangential stresses at the free surface which are two differing mechanisms even though he does mention it at the end of the first paragraph on page 2 of his paper. Also, this logic of flow reversal at high magnetic fields is not completely correct since the magnetization of the ferrofluid would saturate. It is not clear if he accounts for this since he does not explain the expression he uses for the equilibrium magnetization $\mathbf{M}_{eq}$ which could be the complete Langevin equation or the linear relation given in (4.14).

4.5. Conclusions

This chapter summarizes the assumptions, setup and results of the previously measured bulk flow experiments of spin-up flows in uniform rotating fields by various authors [7-9] . It also outlines the setup for the COMSOL simulations, using spin-diffusion theory, $\eta' \neq 0$, with boundary condition $\omega(r = R_{wall}) = 0$, to explain the experimental results obtained but that neglect the demagnetizing effects associated with the shape of the ferrofluid cylinder. The experimentally fit values of spin viscosity derived by these authors [7-9] do result in COMSOL simulations that are in good agreement with the experimental results but these values of spin viscosity are many orders of magnitude greater than that derived theoretically as seen in Chapter 6. The explanation for this discrepancy is also explained in Chapter 6.

This chapter also explores the case neglecting the effect of spin diffusion ($\eta' = 0$) resulting in negligible flows when an infinitely long ferrofluid filled cylinder is subjected to a uniform rotating magnetic field. Corrections to other author's works are also made in this chapter.

Bibliography

[1] R. Moskowitz and R. E. Rosensweig, "Nonmechanical torque-driven flow of a ferromagnetic fluid by an electromagnetic field," *Appl. Phys. Lett., 11: 301-3 (Nov. 15, 1967).* 1967.

[2] A. Pshenichnikov, *et al.*, "On the rotational effect in nonuniform magnetic fluids," *Magnetohydrodynamics,* vol. 36, pp. 275-281, 2000.

[3] I. Y. Kagan, *et al.*, "Flow of a dielectric ferromagnetic suspension in a rotating magnetic field," *Magnetohydrodynamics,* vol. 9, pp. 258-261, 1973.

[4] R. Brown and T. S. Horsnell, "The Wrong Way Round," *Electrical Review,* vol. 183, 1969.

[5] A. Pshenichnikov and A. Lebedev, "Tangential stresses on the magnetic fluid boundary and rotational effect," *Magnetohydrodynamics,* vol. 36, pp. 254-263, 2000.

[6] R.E.Rosensweig, *et al.*, "Magnetic Fluid Motion in Rotating Field," *Journal of Magnetism and Magnetic Materials,* vol. 85, pp. 171-180, 1990.

[7] X. He, "Ferrohydrodynamic flows in uniform and non-uniform rotating magnetic fields," Ph.D thesis, Dept of Electrical Engineering and Computer Science, Massachusetts Institute of Technology, Cambridge, MA, 2006.

[8] S. Elborai, "Ferrofluid surface and volume flows in uniform rotating magnetic fields," Ph.D thesis, Dept of Electrical Engineering and Computer Science, Massachusetts Institute of Technology, Cambridge, MA, 2006.

[9] A. Chaves, *et al.*, "Spin-up flow of ferrofluids: Asymptotic theory and experimental measurements," vol. 20, p. 053102, 2008.

[10] D. Brito, *et al.*, "Turbulent viscosity measurements relevant to planetary core-mantle dynamics," *Physics of The Earth and Planetary Interiors,* vol. 141, pp. 3-8, 2004.

[11] D. Brito, *et al.*, "Ultrasonic Doppler velocimetry in liquid gallium," *Experiments in Fluids,* vol. 31, pp. 653-663, 2001.

[12] T. Sawada, *et al.*, "Kinematic characteristics of magnetic fluid sloshing in a rectangular container subject to non-uniform magnetic fields," *Experiments in Fluids,* vol. 26, pp. 215-221, 1999.

[13] H. Kikura, *et al.*, "Velocity profile measurement of the Taylor vortex flow of a magnetic fluid using the ultrasonic Doppler method," *Experiments in Fluids,* vol. 26, pp. 208-214, 1999.

[14] A.O.Cebers, *Magn. Gidrodinamkia,* p. 79, 1975.

[15] E.Ya.Blums, *et al.*, *Magnetic fluids*. Berlin: Walter de Gruyter, 1997.

[16] A.N.Vislovich, *Pis'ma Zh. Tekhn. Fiz.,* vol. 1, p. 744, 1975.

[17] V.G.Bashtovoi, *et al.*, *An Introduction to the Thermomechanics of Magnetic Fluids*, 1985.

[18] B. Finlayson, "Modeling a Ferrofluid in a Rotating Magnetic Field," presented at the COMSOL Users' Conference, Boston, 2007.

[19] A. Chaves, *et al.*, "Bulk Flow in Ferrofluids in a Uniform Rotating Magnetic Field," *Physical Review Letters,* vol. 96, pp. 194501-4, 2006.

[20] M. I. Shliomis, *et al.*, "Ferrohydrodynamics: An essay on the progress of ideas," *Chem. Eng. Comm.,* vol. 67, pp. 275 - 290, 1988.

[21] A. V. Lebedev and A. F. Pschenichnikov, "Rotational effect: The influence of free or solid moving boundaries," *Journal of Magnetism and Magnetic Materials,* vol. 122, pp. 227-230, 1993.

[22] A. V. Lebedev and A. F. Pshenichnikov, "Motion of a magnetic fluid in a rotating magnetic field," *Magnetohydrodynamics,* vol. 27, pp. 4-8, 1991.

[23] O. A. Glazov, "Motion of a ferrosuspension in rotating magnetic fields," *Magnetohydrodynamics,* vol. 11, pp. 140-145, 1975.

[24] O. A. Glazov, "Role of higher harmonics in ferrosuspension motion in a rotating magnetic field," *Magnetohydrodynamics,* vol. 11, pp. 434-438, 1975.

[25] A. Chaves and S. Khushrushahi, ed, 2009.

Chapter 5. Experimental Setup of Ferrofluid Spin-up Flows in Spherical Geometry

5.1. Introduction

Spin-diffusion theory, applied to finite height cylindrical vessels in the previous chapter, was shown to reproduce circular co-rotating bulk flows in uniform rotating magnetic fields. The assumption made was that the cylinder had to be significantly taller than its diameter such that non-uniform demagnetizing fields due to the cylindrical shape did not significantly contribute to generating the flow. However, most experiments actually conducted using a three phase two pole stator winding or current driven pairs of coils that limit the height of the imposed magnetic field in the ferrofluid filled cylinder such that these demagnetization effects cannot be disregarded [1-4]. Shliomis believes that the rotating fluid motion is generated as a result of the non-uniform field created due to the non-uniform demagnetizing fields associated with a finite length ferrofluid filled cylinder [5].

To compare whether spin-diffusion or non-uniform fields, due to demagnetizing effects, generate the spin-up flow, an experiment where the non-uniform demagnetizing field effects are insignificant was conducted. An infinitely long cylinder is only useful from a theoretical standpoint since the uniform field demagnetizing factors are equal (to 1/2) in the transverse direction and zero in the axial direction allowing for the creation of a uniform field. A uniform field can also be created if the magnetic material is in the shape of a sphere allowing for equal demagnetizing factors (of 1/3) in all directions. An experiment subjecting a ferrofluid filled

sphere to a uniform rotating magnetic field was performed to determine if non-uniform demagnetizing fields were the primary cause for the spin-up flow.

This chapter will describe the setup of the experiment to subject a ferrofluid filled sphere to a uniform rotating magnetic field, generated inside of two spherical coils in quadrature in time and space called a "fluxball machine", with bulk flows being measured using ultrasound velocimetry. Two 10 cm diameter hollow polypropylene spheres were each filled with a different ferrofluids, EMG705 and MSGW11, with their magnetic and fluid properties given in section 2.2. Each ferrofluid filled sphere was mounted in a special polycarbonate holder, that keeps the sphere fixed and holds the ultrasound probes needed to measure the bulk velocity flows, and tested one at a time in the uniform magnetic field apparatus. A list of the materials used and the design of certain parts are documented in Appendix C.

5.2. Experimental Setup

5.2.1. Probe Holder

The probe holder was made of 0.5 inch thick polycarbonate and was designed in SolidWorks®. Polycarbonate was chosen since it is nonmagnetic, nonconducting, resistant to solvents and high temperature (melting point of ≈115°C) and is easy to machine. These properties made it an excellent choice to be used as a probe holder.

The probe holder had to hold the 10 cm diameter sphere of ferrofluid and had to be machined very carefully to get the correct curvature of the ball. To accomplish this, the probe holder was precisely cut using a computer controlled OMAX waterjet cutter. The individual parts

of the probe holder were then held together with polycarbonate screws (Appendix C). Figure 5-1 illustrates a graphic of the probe holder with the sphere of ferrofluid.

In addition to holding the sphere of ferrofluid fixed and exactly in the center of the fluxball machine, the probe holder had to also hold the individual ultrasound probes at precise angles with respect to the radius. The setup is similar to that explained in section 4.2 except with notches placed underneath, along the equator and along one side of the sphere. A graphic of the various probe angles from the top and side view of the probe holder can be seen in Figure 5-2 and Figure 5-3.

Special individual holders that snugly fit the ultrasound probes were cut out with the waterjet, glued on to notches in the probe holder and drilled through with an 8.3 mm drill bit to allow for the probe to touch the sphere. The exact dimensions of the individual parts for the probe holder are documented in Appendix C. The standard dimensions of the ultrasound probe are given in Table 5-1.

Ultrasound Probe	Characteristics
Diameter	8 mm
Length	10 mm & 30 mm
Case material	Epoxy
Output wire	Radial
Other specification	Non-magnetic

Table 5-1. Ultrasound probe specifications used in this thesis.

Additional notches were also made on the probe holder to allow for the placement of GMW three axis sensors to measure the magnetic field strengths at three positions on the circumference of the sphere. The GMW sensor datasheets are in Appendix C.

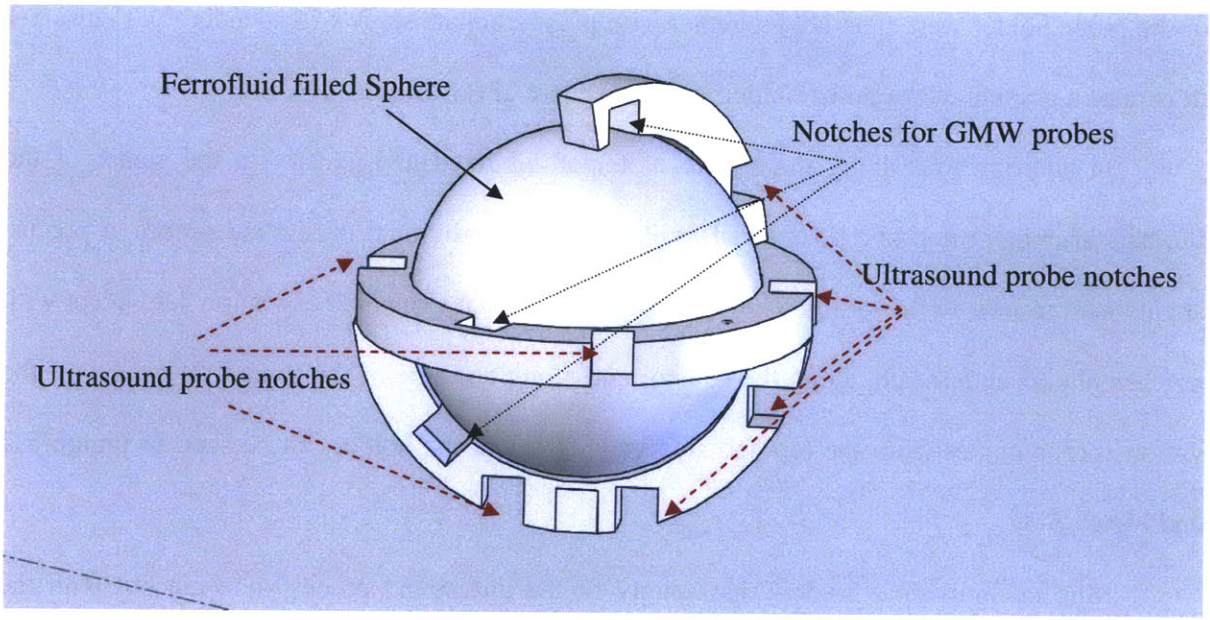

Figure 5-1. SolidWorks design of assembled probe holder (ultrasound probe holders not shown) holding the sphere of ferrofluid. The positions of the notches are shown allowing for the ultrasound beam to be directed at specific angles with respect to the radial direction. Notches for the GMW magnetic field probes can also be seen.

The support rod fits into the support notch in Figure 5-3 and holds the probe holder and sphere of ferrofluid upright and fixed. It is made from low friction material like Teflon because it is needed to slide in and out of the fluxball access holes which can be seen in Figure 5-20.

Figure 5-5 and Figure 5-6 show the top and side views of the actual constructed probe holder containing the sphere of ferrofluid. The notches for the ultrasound probe holder and the GMW magnetic field sensors can be clearly seen.

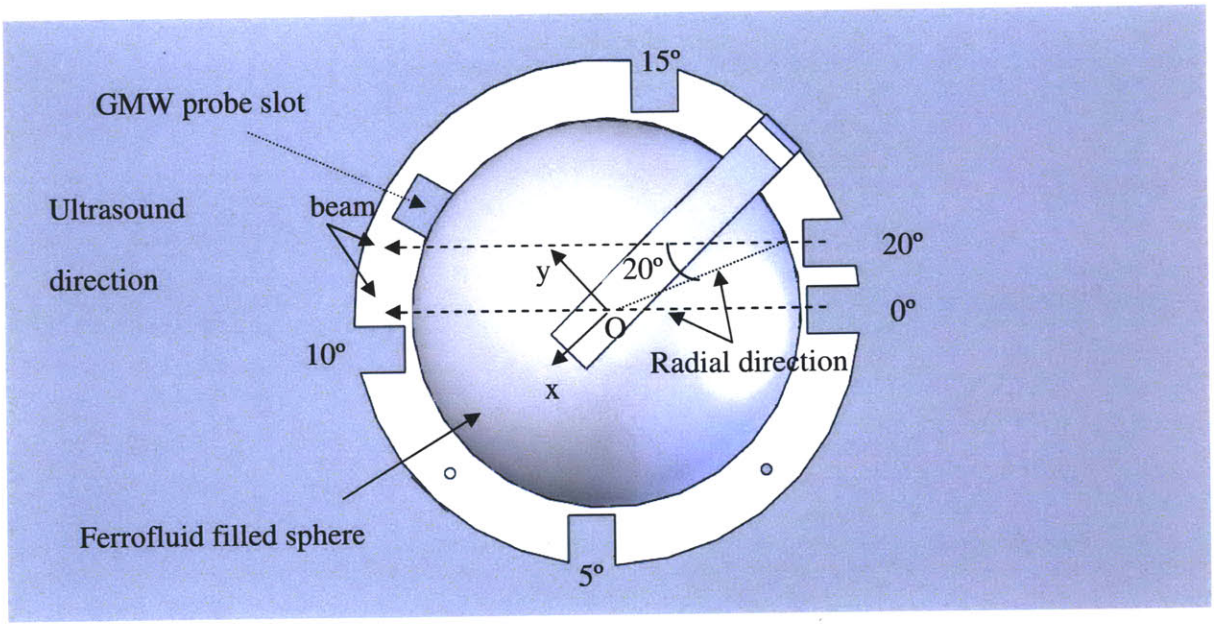

Figure 5-2. Top view of probe holder showing various probe angles, with respect to the radial direction, measured along the equator of the sphere. The probe positioned at 20° to the radial direction is clearly drawn out. Image obtained from SolidWorks design of probe holder.

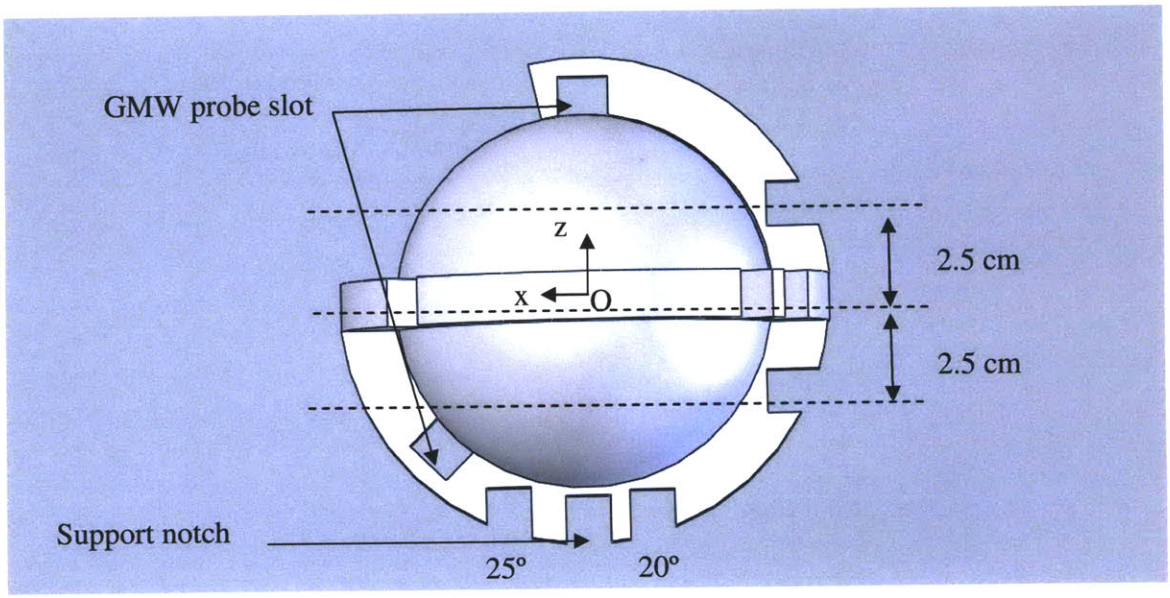

Figure 5-3. Side view of probe holder. Probes are placed at two different heights and also some underneath the sphere of ferrofluid. The angles the probe makes with respect to the radial direction is also noted. The support notch in the center helps to hold the probe holder and sphere of ferrofluid fixed in the fluxball machine. Image obtained from SolidWorks design of probe holder.

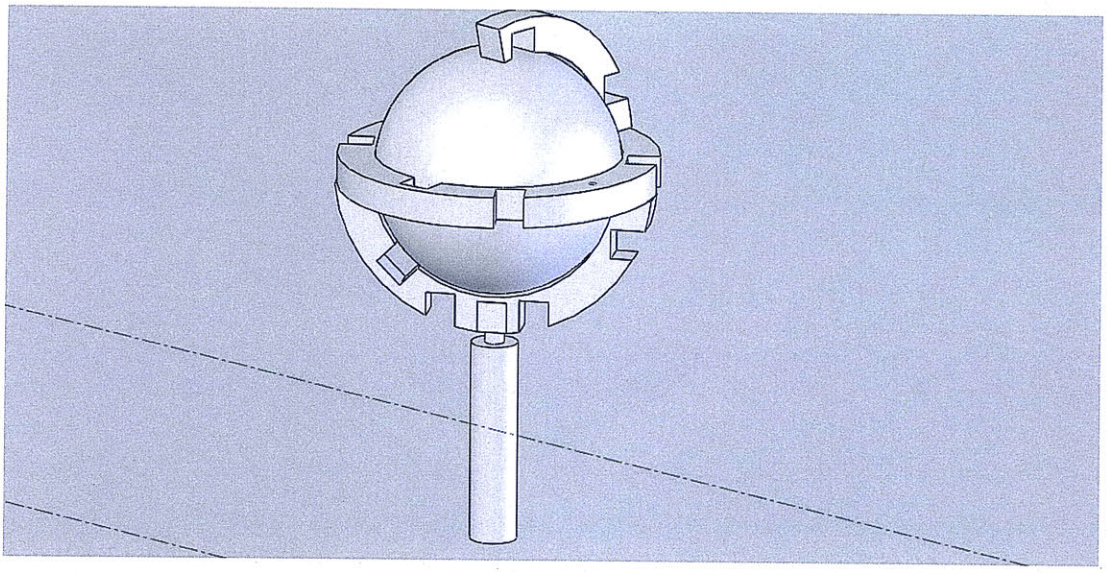

Figure 5-4. SolidWorks Graphic of probe holder with sphere of ferrofluid and support rod needed to keep it firmly in place.

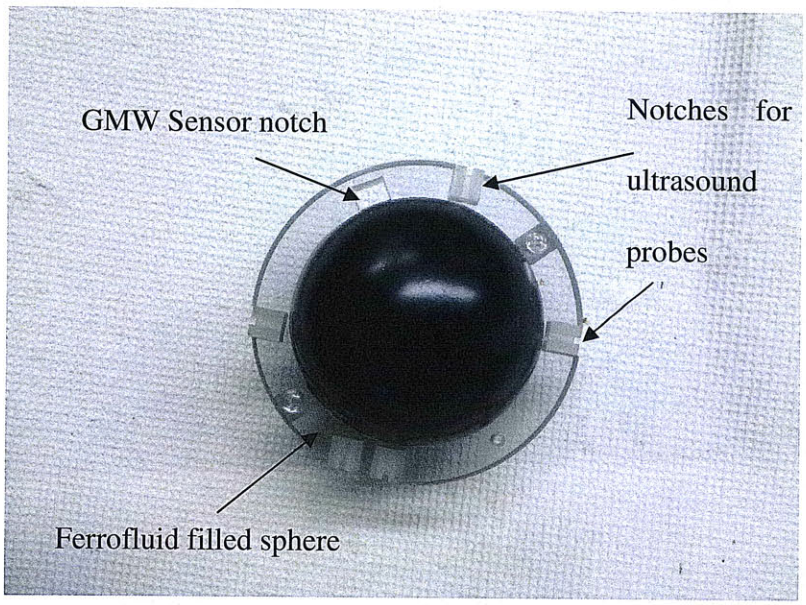

Figure 5-5. Top of assembled probe holder containing sphere of ferrofluid. Notches for the ultrasound probes and the GMW field sensor can be seen.

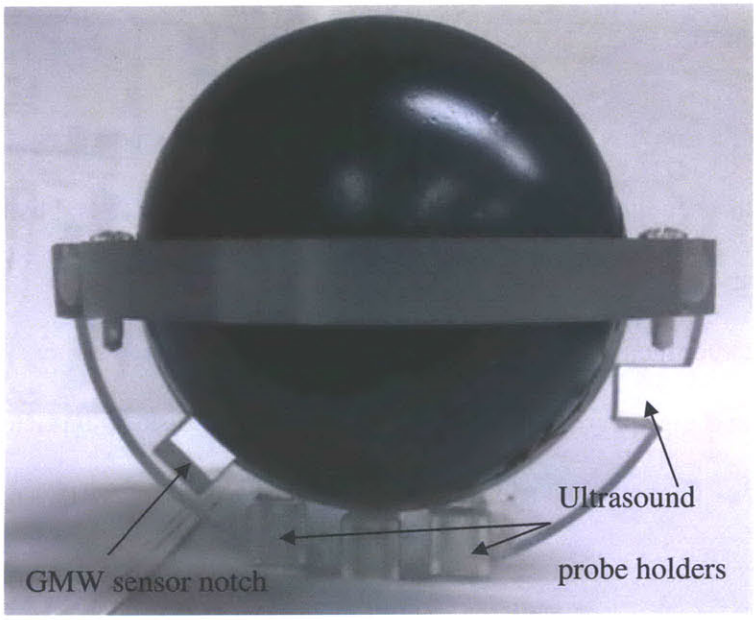

Figure 5-6. Side view of assembled probe holder containing sphere of ferrofluid. Notches for the underball ultrasound probe sensors and GMW field sensors can be seen.

5.2.2. Testing the Probe Holder

Before conducting any experiments with ferrofluid it was necessary to test whether the probe holder would accurately measure a flow that could be easily established experimentally and with simulations.

A simple experiment was conducted using a 10 cm diameter sphere that had the top ¼ surface sawed off and the sphere filled with transformer oil. A disk of diameter 81 mm was then positioned on top of the free surface and was rotated at a constant RPM entraining the fluid layers below.

The setup of the experiment is given in Figure 5-7. The velocity profiles were measured using Signal Processing's DOP2000 velocimeter similar to the process outlined in section 4.2.1. To allow for the measurement of the velocity profiles, Griltex-P1 was added to the transformer oil. Plots of the area under the ultrasound echo curves (Appendix D) were made at various concentrations of Griltex-P1 mixed with the transformer oil. The optimum concentration of Griltex-P1 was found to be 0.008g/ml. The probes were placed at different positions in the probe holder measuring different velocity profiles inside the sphere. The same flow was set up and simulated in COMSOL Multiphysics and the model file is detailed in Appendix D.

The transformer oil used was Shell DIALA A with its physical properties listed below. The viscosity of the oil was measured at 23°C with TA instrument's AR-G2 rheometer while the speed of sound was measured using Signal Processing's DOP2000 velocimeter.

	Viscosity η (Pa s)	Density ρ (kg/m^3)	Speed of sound (m/s)
Shell DIALA (Measured at 23°C)	0.0155	900	1421

Table 5-2. Table of physical properties of Shell DIALA A transformer oil. Viscosity and speed of sound are measured values with value for density taken from the datasheet.

The Brookfield DV-I+ viscometer was used as a motor drive by fitting the LV-1 spindle into a specially made acrylic disk that was the same diameter of the free surface at the top of the ¾ sphere. The dimensions of the disk are documented in Appendix C.

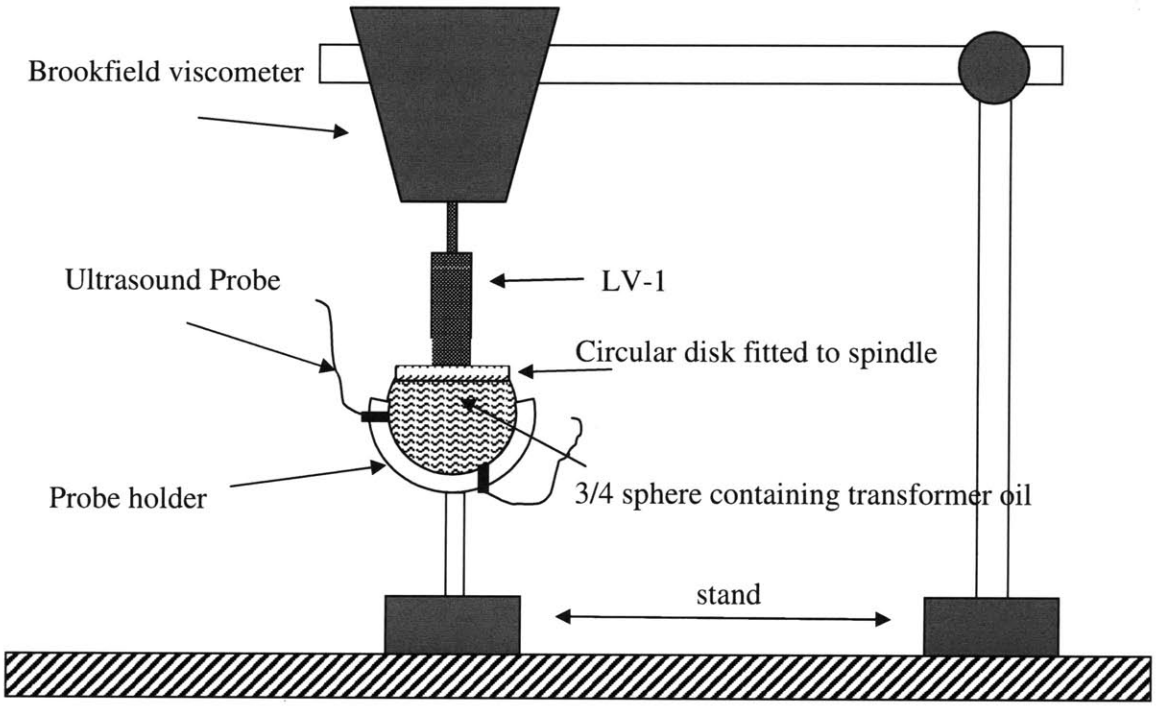

Figure 5-7. Experimental apparatus of flow driven by rotating circular disk entraining flow inside sphere of transformer oil. The flow is measured with ultrasound probes at various positions on the circumference of the sphere.

Figure 5-8 is a picture of the experimental setup with the sphere empty and the ultrasound probes positioned on the equator of the sphere. Figure 5-9 is a picture of the experimental setup with the circular disk attached to the LV-1 placed on the free transformer oil surface of the filled sphere. One probe is placed along the radial direction and the other 20° to the radial direction along the equator. These two probes allow for a calculation of the rotational velocity v_ϕ and the results, seen in Figure 5-10, are in good agreement with the COMSOL simulations.

The ultrasound probe can only measure the velocity in the direction of the ultrasound beam. As a result, Figure 5-11 is a plot of the z-directed velocity as a function of position z (where $z=0$ is the equatorial plane of the sphere) measured by the probe placed underneath the sphere at 25° to the radial direction. The position of the probe can be clearly seen in Figure 5-3. The results are in close agreement with the COMSOL simulations for the same probe position.

Figure 5-12 compares the experimental and COMSOL results for a probe measuring the x-directed velocity as a function of x where $x=z=0$ is the center point of the sphere. The probe is placed at $(y=0,z=-2.5cm)$ in the holder shown in Figure 5-3. The experimental results are in approximate agreement with the results obtained using COMSOL.

The results obtained in this experiment confirms that the probe holder was designed and built to measure flow profiles in the sphere accurately. The probe holder was used for all experiments in this thesis with a Griltex-P1 concentration of 0.008g/ml mixed with the sample fluid.

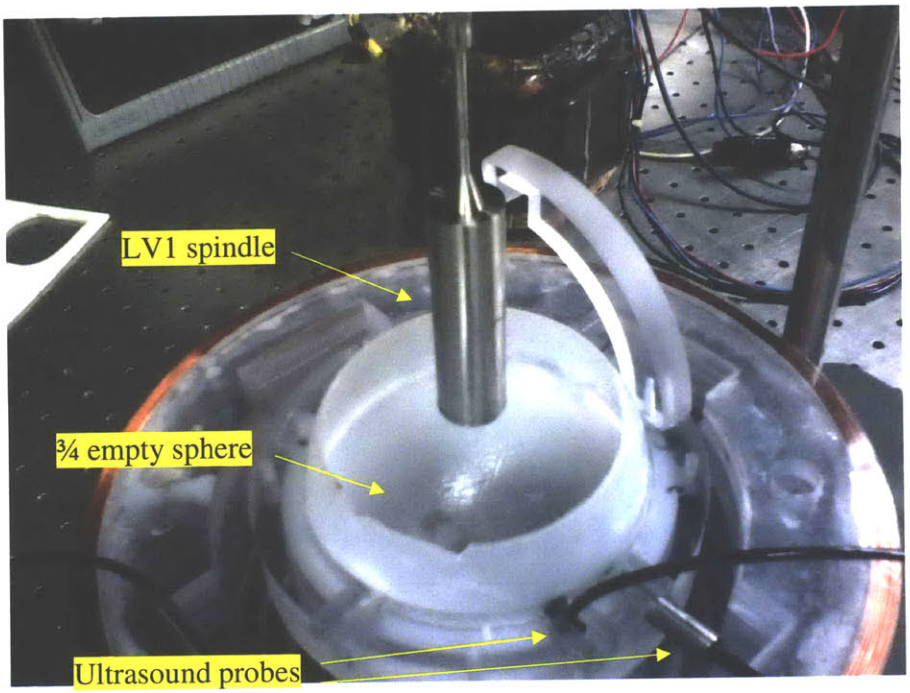

Figure 5-8. Picture of experimental setup showing LV1 spindle (without disk) positioned above 3/4 empty sphere with ultrasound probes positioned on the circumference

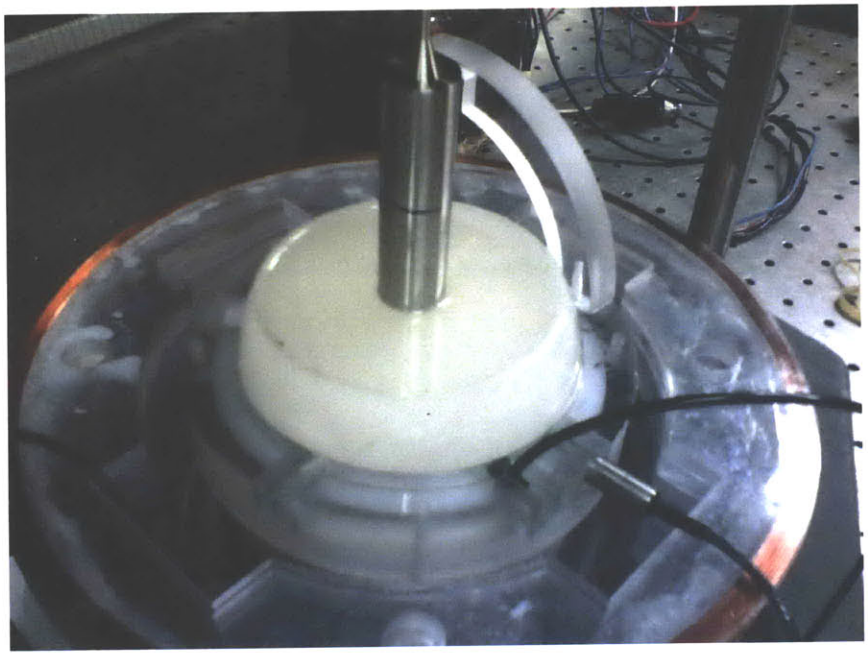

Figure 5-9. Sphere filled with Shell DIALA transformer fluid with disk fitted on LV-1 spindle placed on top of the ¾ sphere.

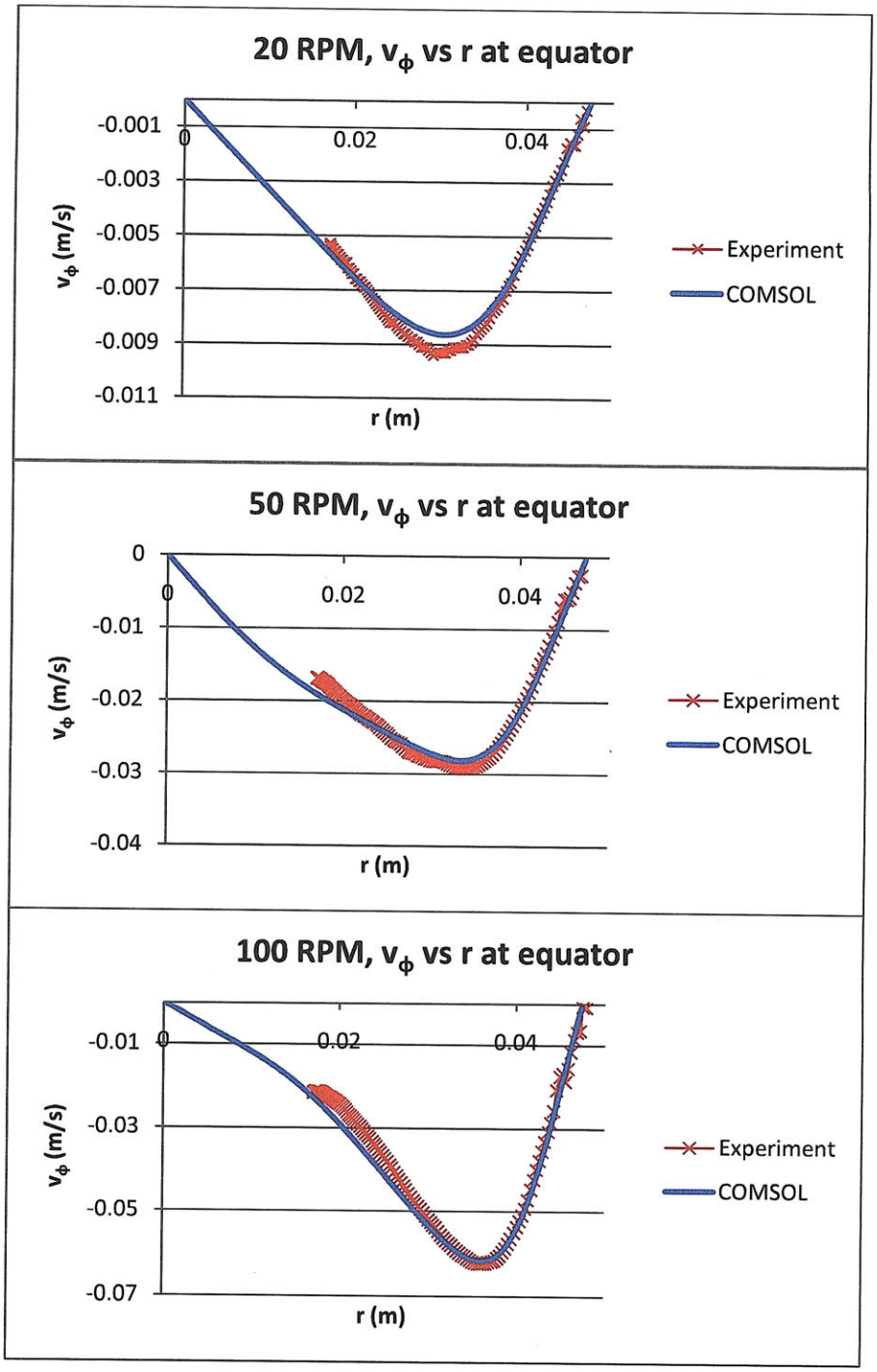

Figure 5-10. Rotational velocity v_ϕ as a function of radius measured at the equator of the ¾ sphere of radius 5cm at three different rotational rates 20, 50 and 100 RPM. Experimental results match those obtained using COMSOL simulations.

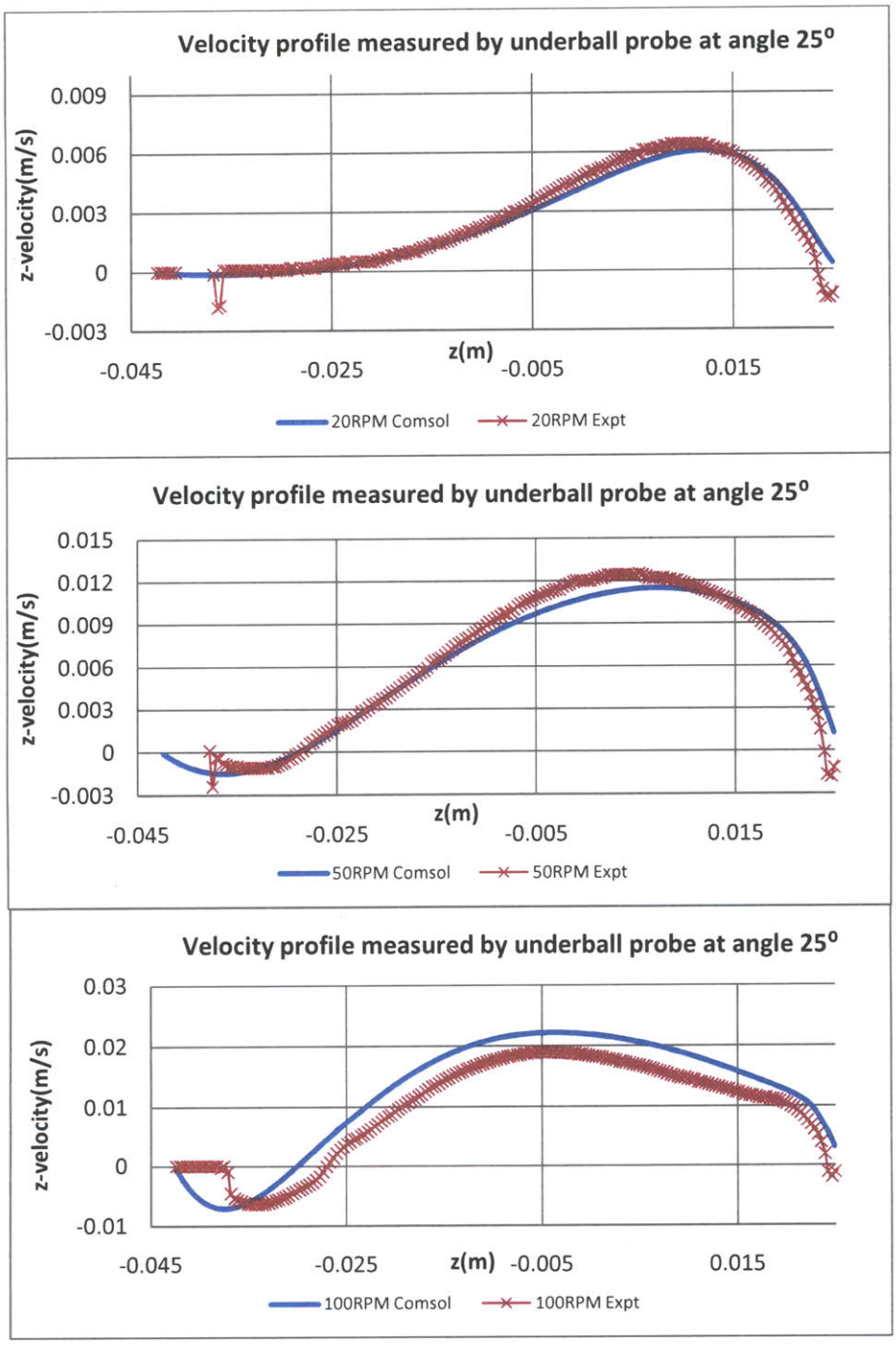

Figure 5-11. Velocity profile measured by probe placed underneath the sphere at 25° to the radial direction as seen in Figure 5-3. The velocity is a function of z position where z=0 is at the equator level of the sphere. Three different experimental rotational rates (20, 50 and 100 RPM) are compared to COMSOL simulations.

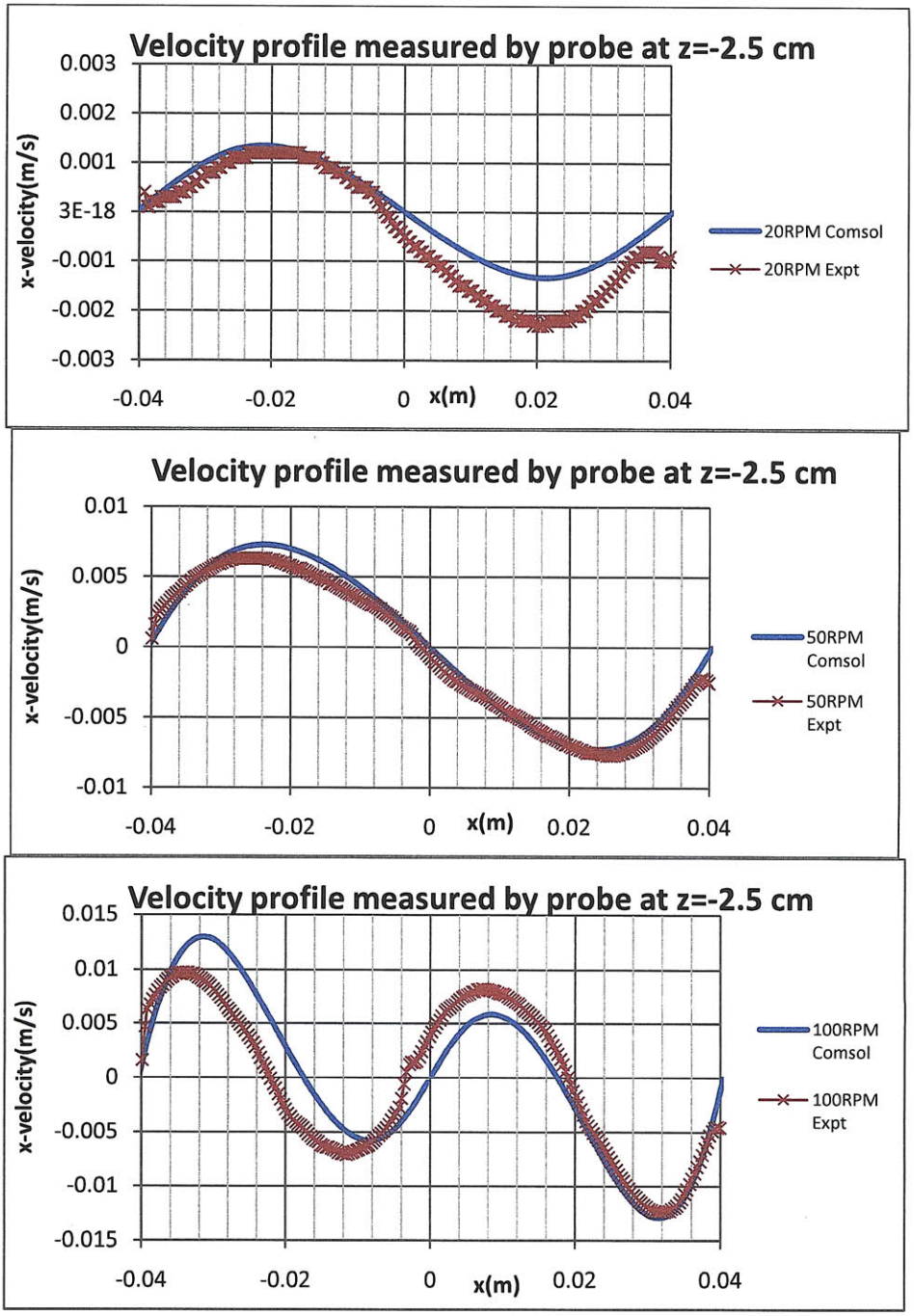

Figure 5-12. Velocity profiles measured from probe placed at z= -2.5 cm as seen in Figure 5-3. The probe measures x-directed velocity as a function of x where x=z=0 is the center position of the sphere. Experimental and simulation profiles are seen for three different rotational rates 20, 50 and 100 RPM.

5.2.3. Fluxball

If a spherical coil is wound of thin wire such that the vertical turns density is uniformly distributed with respect to the z axis as in Figure 5-13, the magnetic field intensity produced inside it will be uniform. In [6], [7] and the rest of this thesis such a spherical coil is commonly referred to as a *fluxball.*

Assuming that the fluxball is made up of N turns of wire, the turn density in $\mathbf{z}$ is $\frac{N}{2R}$ and the number of turns at $r=R$ in an increment of length in the z direction would then be given as $\frac{N}{2R}dz$. Because $z = R\cos\theta, dz = -\sin\theta R d\theta$, the number of turns per unit length $Rd\theta$ along the surface of the sphere can then be determined to be $\frac{N}{2R}\sin\theta$. Multiplying this with the current I in each turn of wire gives the surface current density.

$$\mathbf{K} = \mathbf{i}_\phi \frac{NI}{2R}\frac{(-dz)}{Rd\theta} = \mathbf{i}_\phi \frac{NI}{2R}\sin\theta \tag{5.1}$$

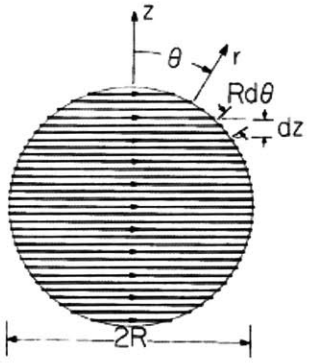

Figure 5-13. Mathematical description of a fluxball of radius R with uniformly distributed windings in z of N total turns each carrying current I resulting in a surface current sheet flowing azimuthally in the ϕ direction but varying sinusoidally with respect to the zenith angle θ [6, 7]. Image taken from [6].

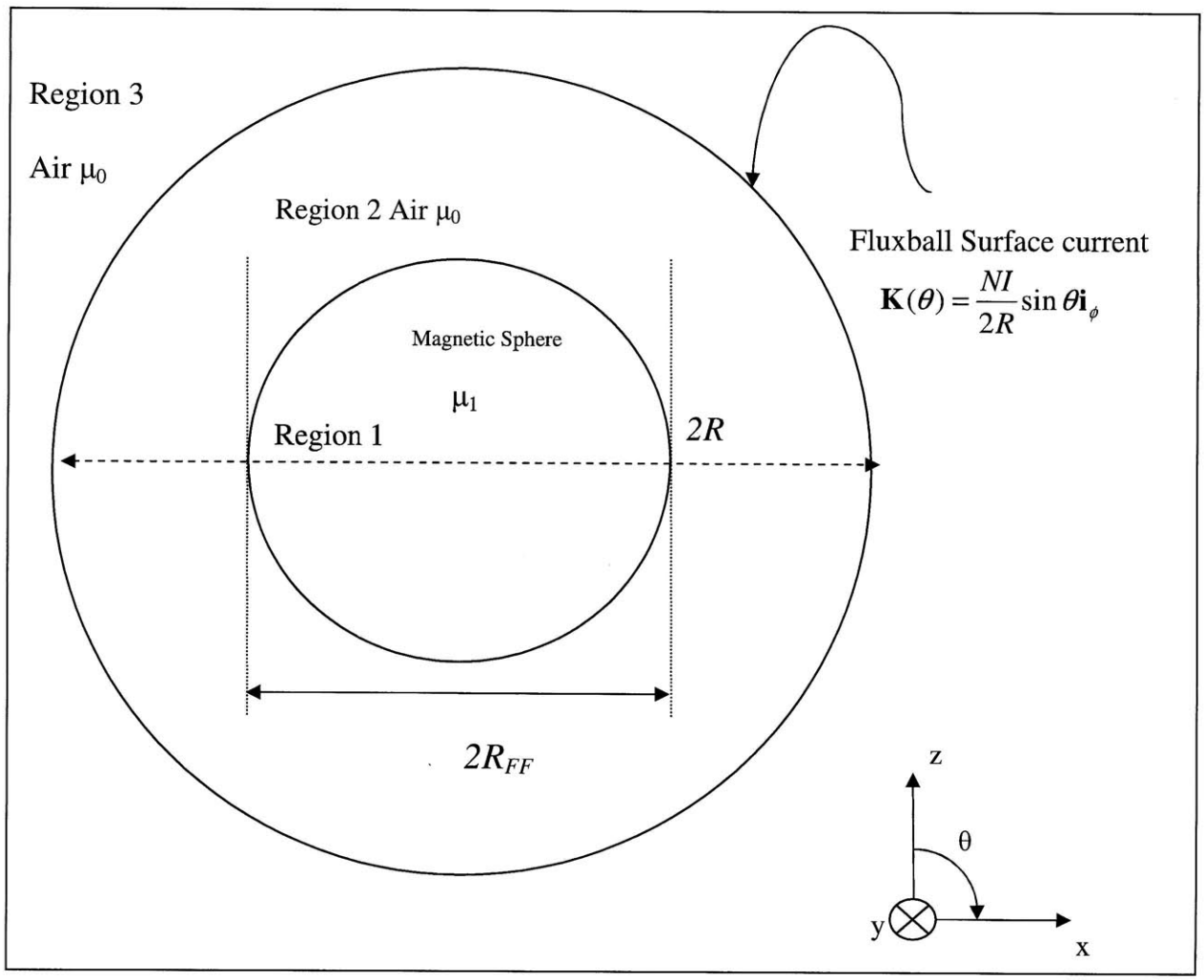

Figure 5-14. Cross-sectional view of fluxball with sphere of linearly magnetic material inside. Sphere and fluxball are both surrounded by a region of air.

If a sphere, containing linear magnetic material with magnetic permeability given as

$$\mu_1 = \mu_0(1+\chi) \tag{5.2}$$

where χ is the magnetic susceptibility, is placed inside this fluxball such that there are three regions of interest as depicted in Figure 5-14. The field distribution in all three regions can be solved using the magnetic scalar potential ψ since $\nabla\times\mathbf{H}=0$ so that

$$\mathbf{H} = -\nabla\psi \tag{5.3}$$

Magnetic flux density can be given as $\mathbf{B}=\mu_0(\mathbf{H}+\mathbf{M})$. Applying Gauss's Law of magnetism ($\nabla\bullet\mathbf{B}=0$) everywhere results in Laplace's equation in magnetic scalar potential ($\nabla^2\psi=0$) in all three regions. The solution to Laplace's equation in spherical coordinates for the three different regions are

$$\psi = \begin{cases} Ar\cos\theta & 0<r<R_{FF} \\ Br\cos\theta+\dfrac{C}{r^2}\cos\theta & R_{FF}<r<R \\ \dfrac{D}{r^2}\cos\theta & r>R \end{cases} \tag{5.4}$$

The magnetic field in each region is

$$\mathbf{H} = -\nabla\psi = \begin{cases} -A\cos\theta\mathbf{i}_r + A\sin\theta\mathbf{i}_\phi & 0<r<R_{FF} \\ \left(-B\cos\theta+\dfrac{2C\cos\theta}{r^3}\right)\mathbf{i}_r + \dfrac{\left(C+Br^3\right)\sin\theta}{r^3}\mathbf{i}_\phi & R_{FF}<r<R \\ \dfrac{2D\cos\theta}{r^3}\mathbf{i}_r + \dfrac{D\sin\theta}{r^3}\mathbf{i}_\phi & r>R \end{cases} \tag{5.5}$$

Boundary conditions at $r=R_{FF}$ require that

$$\begin{aligned} H_{\theta 2} - H_{\theta 1} &= 0 \\ \mu_0 H_{r2} - \mu_1 H_{r1} &= 0 \end{aligned} \tag{5.6}$$

which gives

$$A\mu_1\cos(\theta)+\mu_0(-B\cos(\theta)+\frac{2C\cos(\theta)}{R_{FF}{}^3})=0$$
$$-A\sin(\theta)+\frac{(C+BR_{FF}^3)\sin(\theta)}{R_{FF}^3}=0 \tag{5.7}$$

resulting in

$$A=\frac{3B\mu_0}{2\mu_0+\mu_1}, C=\frac{(B\mu_0-B\mu_1)R_1{}^3}{2\mu_0+\mu_1} \tag{5.8}$$

Boundary conditions at $r=R_1$ require that

$$H_{\theta 3}-H_{\theta 2}=\frac{NI\sin(\theta)}{2R}$$
$$\mu_0 H_{r3}-\mu_0 H_{r2}=0 \tag{5.9}$$

which gives

$$\frac{2D\mu_0\cos(\theta)}{R^3}-\mu_0(-B\cos(\theta)+\frac{2C\cos(\theta)}{R^3})=0$$
$$\frac{D\sin(\theta)}{R^3}-\frac{(C+BR^3)\sin(\theta)}{R^3}=\frac{NI\sin(\theta)}{2R} \tag{5.10}$$

resulting in

$$B=-\frac{NI}{3R}\Rightarrow C=\frac{-(\mu_0-\mu_1)NIR_{FF}^3}{3(2\mu_0+\mu_1)R}$$
$$D=C-\frac{BR^3}{2}=\frac{-(\mu_0-\mu_1)NIR_{FF}^3}{3(2\mu_0+\mu_1)R}+\frac{NIR^2}{6} \tag{5.11}$$

Solving for A gives

$$A=\frac{-NI\mu_0}{(2\mu_0+\mu_1)R}\Rightarrow A=\frac{-NI}{(3+\chi)R} \tag{5.12}$$

and substituting in (5.5) gives

$$\mathbf{H}=\begin{cases} \dfrac{NI}{(3+\chi)R}\cos\theta\mathbf{i}_r - \dfrac{NI}{(3+\chi)R}\sin\theta\mathbf{i}_\phi & 0<r<R_{FF} \\ \left(\dfrac{NI}{3R}\cos(\theta)+\dfrac{2NIR_{FF}^3\chi\cos(\theta)}{3Rr^3(3+\chi)}\right)\mathbf{i}_r + \dfrac{NI(R_{FF}^3\chi-(3+\chi)r^3)\sin(\theta)}{3r^3R(3+\chi)}\mathbf{i}_\phi & R_{FF}<r<R \\ \dfrac{NI\left(2R_{FF}^3\chi+R^3(3+\chi)\right)\cos(\theta)}{3r^3R(3+\chi)}\mathbf{i}_r + \dfrac{NI\left(2R_{FF}^3\chi+R^3(3+\chi)\right)\sin(\theta)}{6r^3R(3+\chi)}\mathbf{i}_\phi & r>R \end{cases} \quad (5.13)$$

where the field inside the magnetic sphere is uniform and can be rewritten as

$$\mathbf{H}=\mathbf{i}_r\left(\frac{NI}{(3+\chi)R}\cos(\theta)\right)-\mathbf{i}_\phi\left(\frac{NI}{(3+\chi)R}\sin(\theta)\right)=\frac{NI}{(3+\chi)R}\mathbf{i}_z \quad (5.14)$$

The field outside the magnetic sphere is the sum of the dipole field, generated by the magnetic sphere, and a uniform field while the field outside the fluxball is purely a dipole field. In the case that the ferrofluid filled sphere is empty ($\chi=0$) (5.13) reduces to (5.15) where the internal uniform field and dipole field outside the fluxball is clearly shown in Figure 5-15.

$$\mathbf{H}=\begin{cases} \dfrac{NI}{3R}\mathbf{i}_z & r<R \\ \dfrac{NI}{6R}\left(\dfrac{R}{r}\right)^3\left(\mathbf{i}_r 2\cos\theta+\mathbf{i}_\phi\sin\theta\right) & r>R \end{cases} \quad (5.15)$$

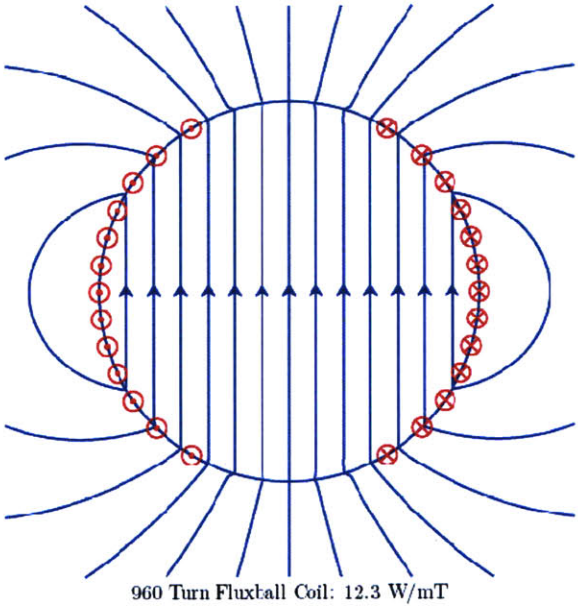

Figure 5-15. Magnetic field lines produced by a fluxball of 960 turns. It produces a 25 mT uniform magnetic field in a spherical region of diameter 8 cm. The power consumed per mT of field density produced is also listed [7]. Image taken from [7].

5.2.4. Lawler's Fluxball Machine [7]

To generate a uniform rotating magnetic field, two concentric orthogonally oriented fluxballs have to be excited with alternating currents that are out of phase by 90° as shown in Figure 5-16. This configuration will be known as a *fluxball machine* for the rest of this thesis.

Lawler, in his thesis [7], built a fluxball machine by stacking and bonding polycarbonate discs and flanges of different radii to support the windings. Pictures of the fluxball machine can be seen in Figure 5-17 through Figure 5-19. A picture showing the winding support structure for the inner fluxball can be seen in Figure 5-20 with the complete fluxball machine, containing a ferrofluid filled sphere of diameter 10 cm inside the test chamber, shown in Figure 5-21.

Table 1-1 outlines Lawler's specifications for the fluxball machine he built. He quotes that the fluxball machine would have an interior **B** field of 5.4 mT/A for each fluxball. This will be shown to be slightly inaccurate in section 5.2.7. The measured dimensions of the built inner fluxball are given in Appendix C.

Characteristic	Inner Fluxball	Outer Fluxball
Interior **B** field	5.4 mT/A	5.4 mT/A
Winding Axis Radius, $r(\theta=0^o)$	10.36 cm	15.04 cm
Quadrature Axis Radius, $r(\theta=90^o)$	11.02 cm	16.75 cm
Peak Current	5 A	5 A
Continuous Current	2 A	2 A
Total Turns	1280	1920
Length of Winding	700 m	1568 m
Total Slots	32	48
Slot Height	5.9 mm	5.9 mm
Flange Height	0.50 mm	0.50 mm

Table 5-3. Magnetic, geometric and electrical specifications for Lawler's fluxball machine [7]. Interior **B** field is slightly erroneous.

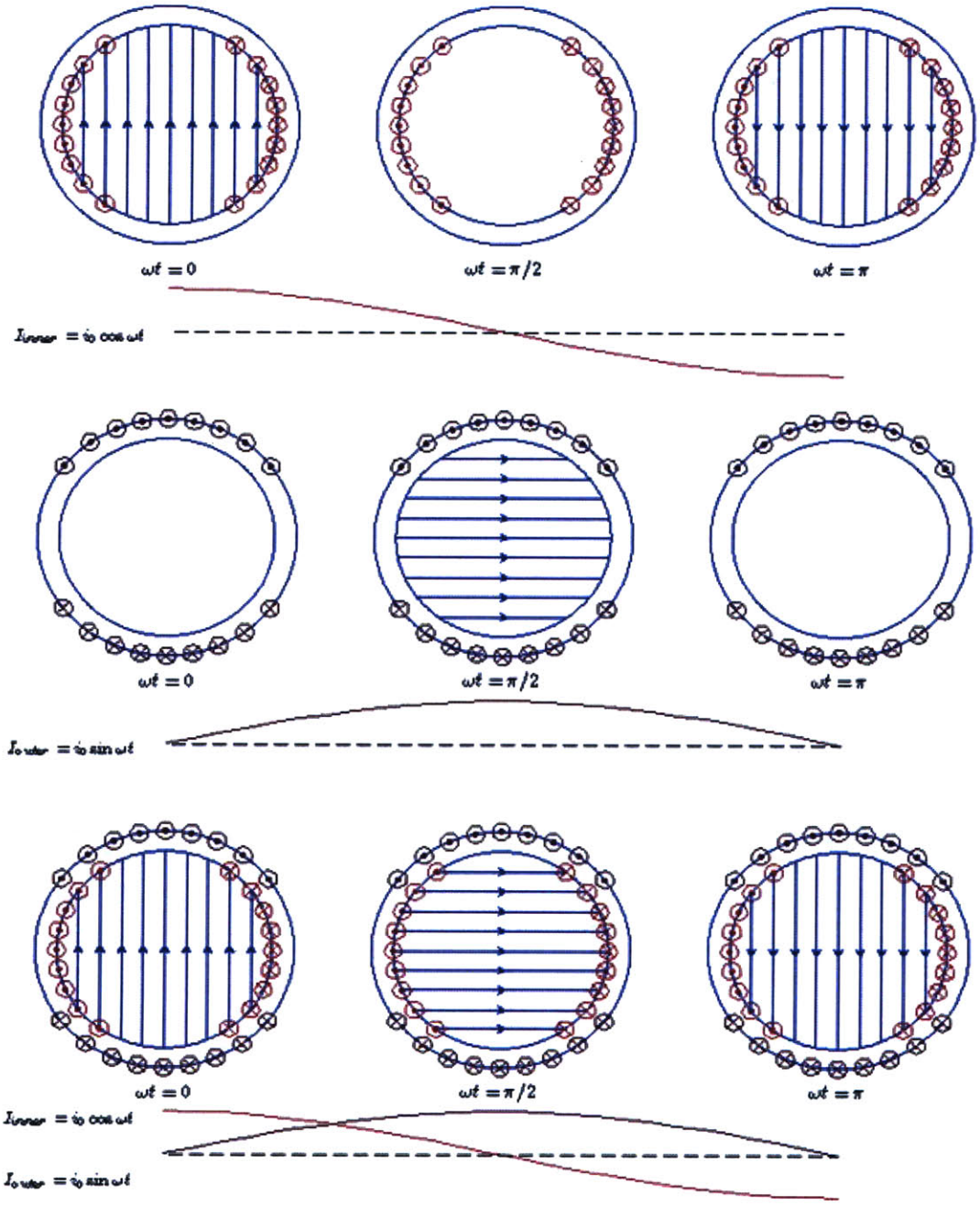

Figure 5-16. The rotating uniform magnetic field is produced by driving the two orthogonal coils with sinusoidal currents that are out of phase by 90° in time . The inner coil (top row) generates the vertical uniform magnetic field while the outer coil (middle row) generates the horizontal magnetic field. Combining them together gives the rotating uniform magnetic field as seen in the last row. Image taken from [7].

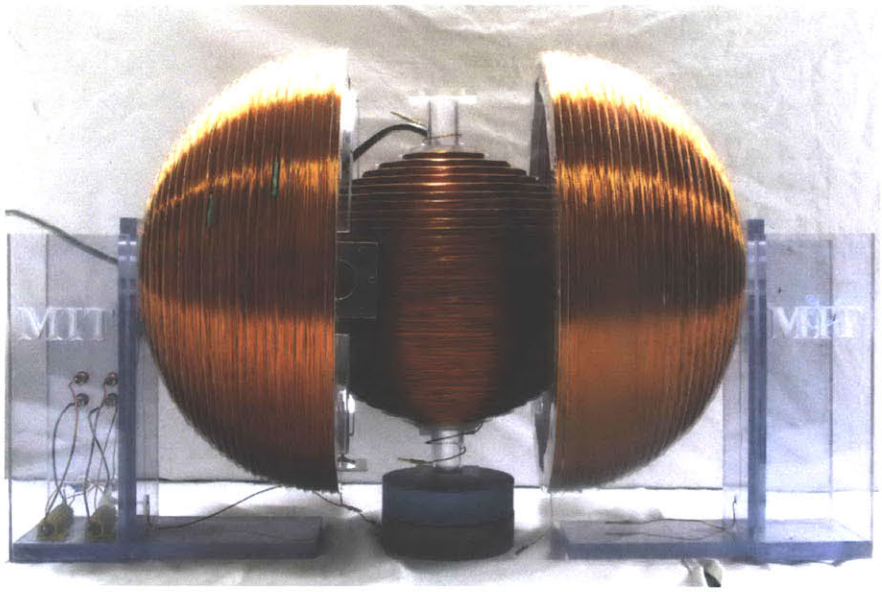

Figure 5-17. Lawler's fluxball [7] machine that was used in this thesis. The outer windings have a radius of 16 cm while the inner winding has a radius of 11 cm. The two windings create uniform rotating magnetic fields in a spherical volume of 15 cm diameter inside the inner fluxball. Image taken from [7].

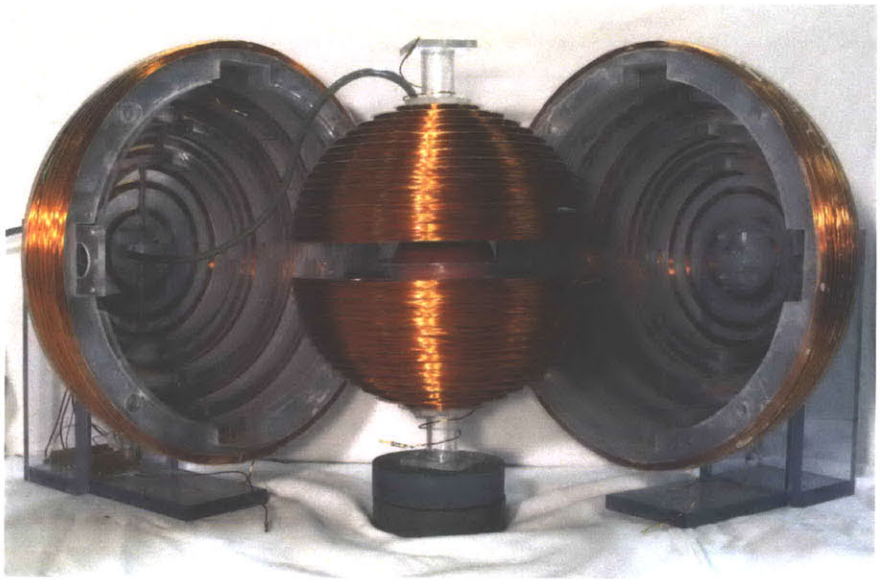

Figure 5-18. An exposed view of the insides of the outer windings. The inner fluxball winding is orthogonal to the outer winding and fits inside the outer winding generating a uniform rotating magnetic field in the region inside the inner fluxball when excited by two phase AC signals. The inner fluxball is slightly separated showing the region inside. Access holes were also made to allow for probes and cables to be inserted inside the inner fluxball. Image taken from [7].

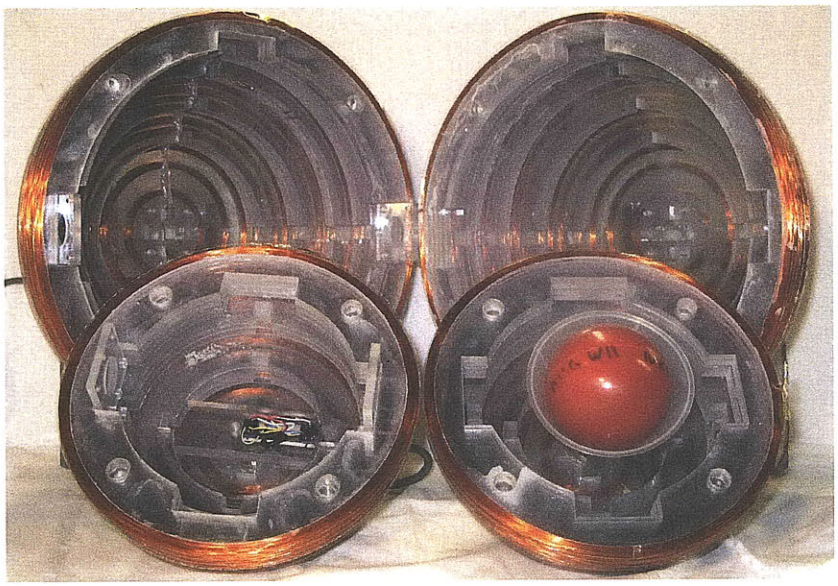

Figure 5-19. Insides of the inner and outer windings are shown. It can be seen that the inner winding has enough space to fit a ferrofluid filled sphere of diameter 10 cm. Image taken from [7].

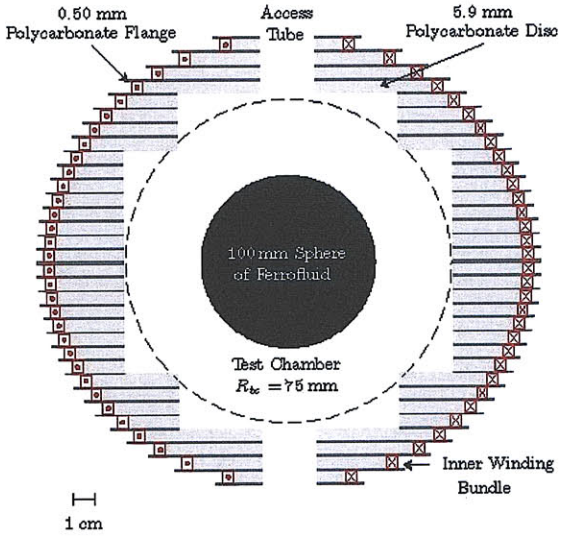

Figure 5-20. Cross-sectional plot of inner fluxball showing the test chamber and the fluxball winding support structures. The access tube at the top and bottom of the inner fluxball can also be seen and is further illustrated with the cable entering the test chamber in Figure 5-18. The ferrofluid filled sphere of diameter 10 cm fits inside the test chamber. Image taken and modified from [7].

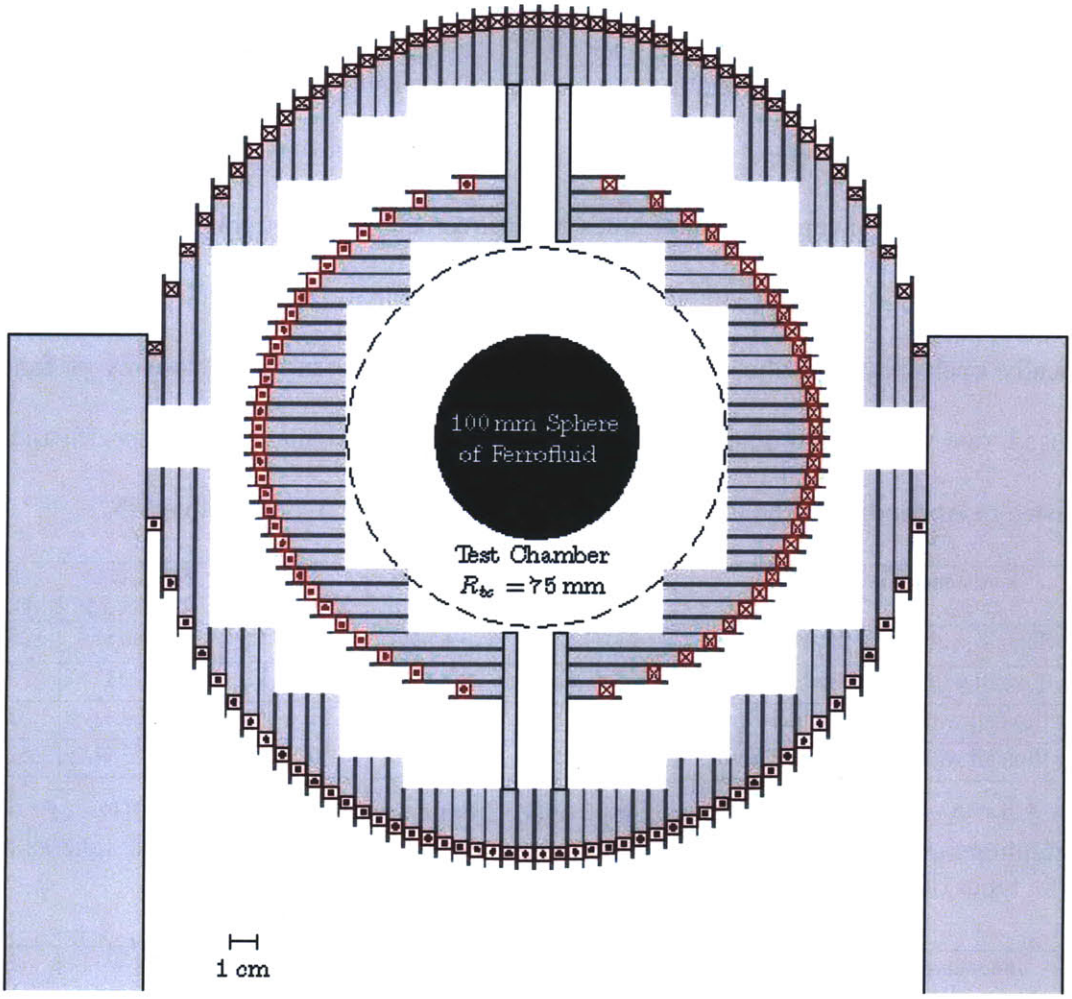

Figure 5-21. Cross-sectional diagram of the complete design for the fluxball machine. The inner fluxball can be seen to fit inside the outer fluxball and that their windings are orthogonal to each other. A uniform rotating magnetic field is created inside the test chamber which will be occupied by a 10 cm diameter sphere of ferrofluid. Image taken and modified from [7].

5.2.5. Lumped Parameter Model of Fluxball Machine

The individual fluxballs of the fluxball machine can be modeled as a series R-L circuit. Measurements of the resistance and inductance were made using the Hewlett-Packard 4192A LF Impedance Analyzer for each fluxball winding with and without spheres of ferrofluid. The measurements are an average of the values taken over a range of frequencies below the self resonant frequency of the individual windings with combinations of electrically shorting and electrically open circuiting the individual fluxballs. Two different sized spheres of ferrofluid were used, one with 10 cm diameter and the other with 7 cm diameter, with specifications for both listed in Appendix C. The measurements are listed in Table 5-4 and Table 5-5.

Resistance for Setup	No Sample	MSG W11 (D=10 cm)	EFH1 (D=10 cm)	MSG W11 (D=7 cm)	EFH1 (D=7 cm)
Inner fluxball with Outer fluxball Open	23.81 Ω	23.85 Ω	23.76 Ω	23.80 Ω	23.80 Ω
Inner fluxball with Outer fluxball Short	23.77 Ω	23.84 Ω	23.76 Ω	23.79 Ω	23.80 Ω
Outer fluxball with Inner fluxball Open	52.70 Ω	52.77 Ω	52.69 Ω	52.64 Ω	52.67 Ω
Outer fluxball with Inner fluxball Short	52.70 Ω	52.76 Ω	52.70 Ω	52.63 Ω	52.66 Ω

Table 5-4. Averaged resistance values over frequency range 10Hz-100Hz of various configurations of the inner and outer fluxball with and without differently sized spheres of two different types of ferrofluid, MSGW11 and EFH1.

Inductances for Setup	No Sample	MSGW11 (D=10 cm)	EFH1 (D=10 cm)	MSG W11 (D=7 cm)	EFH1 (D=7 cm)
Inner fluxball with Outer fluxball Open	0.172 H	0.177 H	0.183 H	0.173 H	0.176 H
Inner fluxball with Outer fluxball Short	0.172 H	0.177 H	0.183 H	0.173 H	0.176 H
Outer fluxball with Inner fluxball Open	0.565 H	0.570 H	0.577 H	0.566 H	0.569 H
Outer fluxball with Inner fluxball Short	0.565 H	0.570 H	0.577 H	0.566 H	0.569 H

Table 5-5. Averaged inductance values over frequency range 10Hz-10kHz of various configurations of the inner and outer fluxball with and without differently sized spheres of two different types of ferrofluid, MSGW11 and EFH1.

5.2.6. Controlling the Fluxball Machine

The purpose of the fluxball machine is to generate a uniform rotating magnetic field at any frequency specified and in any rotational direction. To ensure that the desired magnetic field strength is reached either a current source in series with the fluxball can be used, or a voltage source with the voltage set at a specific level to generate the desired current magnitude. Lawler, in his thesis [7], used the LVC 5050 power amplifier as a voltage source to generate the desired current in the fluxball machine. The same LVC 5050 power amplifiers were used for this thesis and its datasheets are given in Appendix C.

To control this voltage source Lawler used a LabVIEW program that implemented a hard coded PID control system that was simple enough to obtain data for his thesis. However, the previous section showed that the lumped model for the fluxball windings changes with the inclusion of different sized spheres and different types of ferrofluid used. In addition, the R-L model for the fluxball has an impedance that is frequency dependent given by

$$Z_{fluxball} = (R_{fluxball} + R_{fluid}) + j\omega(L_{fluxball} + L_{fluid}) \tag{5.16}$$

A more versatile program was developed with NI LabVIEW 8.2 to dynamically control the voltage and phase applied to the individual fluxballs. The LabVIEW program directly controls the NI PCI-6036E DAQ card which allows for simultaneous measurement of 16 analog inputs and the generation of two analog outputs, one for each fluxball winding, via an NI BNC 2120 connector block. The two output channels are amplified, with a voltage gain of 20, by the LVC 5050 amplifier and fed to the individual fluxball windings. The individual fluxball windings are placed in series with two 1Ω 50W resistors that minimally affect the circuit characteristics but the voltage drop across them represents the current flowing through the

windings. These current measurements along with their phase difference are fed back into the inputs of the DAQ card. The LabVIEW program with the help of the NI LabVIEW 8.2 PID Control Toolkit then adjusts the output channel voltages from the DAQ card to obtain the specified current value through the fluxball windings and ensures that the phase difference between spherical coils is ±90°. The setup for controlling the fluxball machine is drawn out with a circuit diagram shown in Figure 5-23 and datasheets for the parts used are given in Appendix C.

A screen shot of the LabVIEW user interface is shown in Figure 5-22. A detailed description of its functionality and the underlying code is given in Appendix J. The LabVIEW interface allows for the control of the two fluxball windings as well as a third coil. For the purposes of this chapter the controls highlighted in Figure 5-22 are sufficient to control and maintain the phase, magnitude and frequency of the current in the individual fluxball windings.

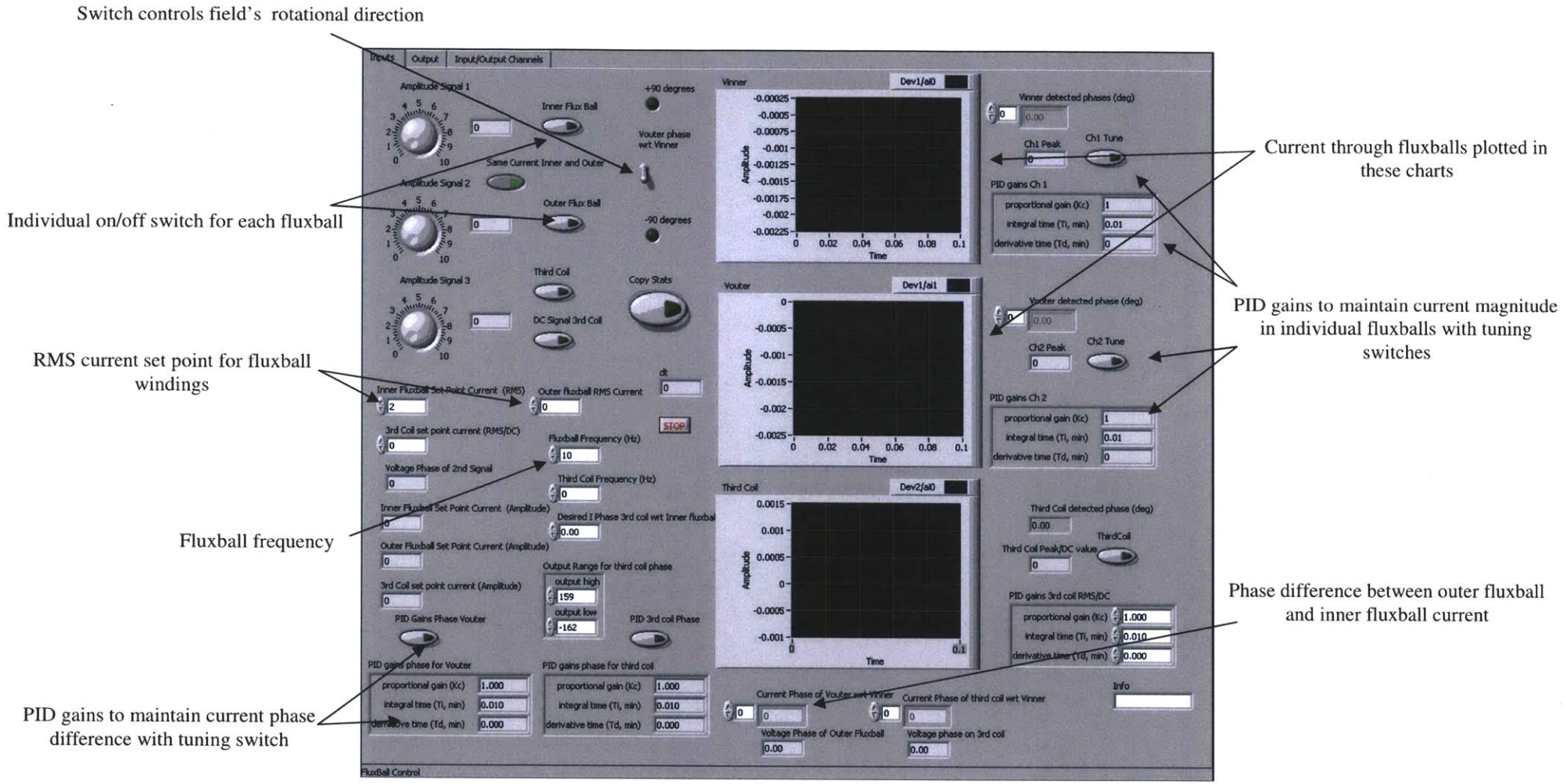

Figure 5-22. Front control panel of program in NI LabVIEW 8.2 showing all the controls needed to maintain the magnitude, phase and frequency of the current in the individual fluxball windings.

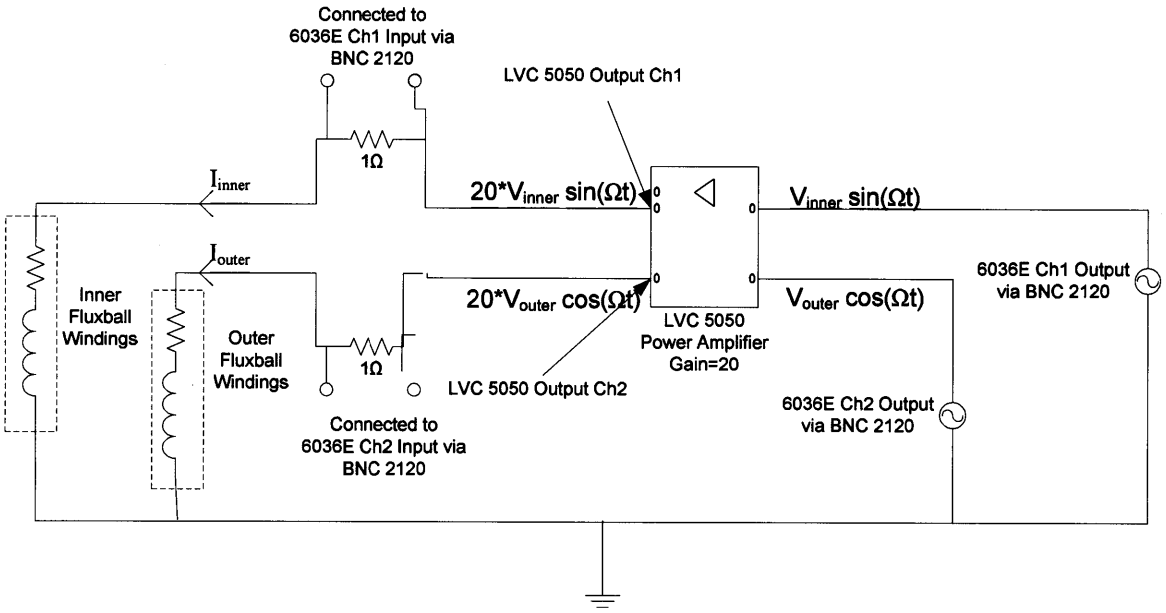

Figure 5-23. Circuit diagram for controlling the fluxball machine. The LabVIEW program is interfaced to the 6036E DAQ card and the two output channels are amplified by the LVC 5050 and fed to the individual fluxball windings. The voltage across the 1Ω resistors represents the currents in the fluxball windings and the magnitude and phases are fed back to the LabVIEW program. A PID control program adjusts the input to the amplifier so that the resulting current can eventually reach the desired set value.

5.2.7. Testing and Characterizing the Fluxball Machine

To test the fluxball machine, three GMW Hall effect three axis magnetic sensors were fitted into the GMW probe slots seen in Figure 5-2 and Figure 5-3 to measure the magnetic field on the circumference of the 10 cm diameter sphere, without ferrofluid, made by the fluxball machine. The specifications for these sensors are included in Appendix C and a picture of one of the sensors is given in Figure 5-24 below.

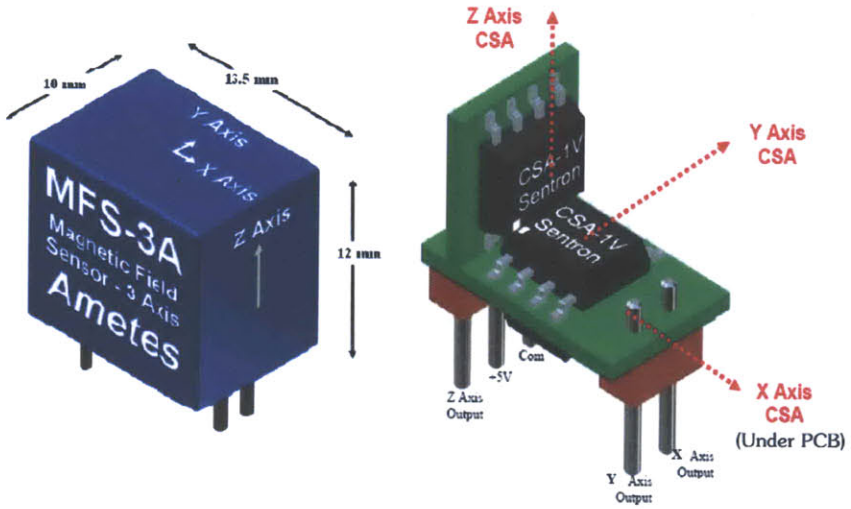

Figure 5-24. GMW three axis magnetic field sensor.

The three sensors labeled GMW Sensors 1-3 were oriented in each slot as shown in Figure 5-25 and Figure 5-26. They were supplied with a constant 5.0 V DC from a supply voltage and voltage signals were read from the pins of the sensors, using a shielded 20 conductor data cable listed in Appendix C, via the input terminals of the BNC 2120 interfaced with the LabVIEW program. The LabVIEW interface panel can be seen in Figure 5-27 and can monitor two sensors at a time. This is because the BNC 2120 has eight BNC inputs, two of which are used to monitor the current through the fluxball leaving 6 terminals to monitor the x, y and z axis

readings of the two sensors. The third sensor values are measured by swapping out the connecting terminals of one of the already measured two sensors.

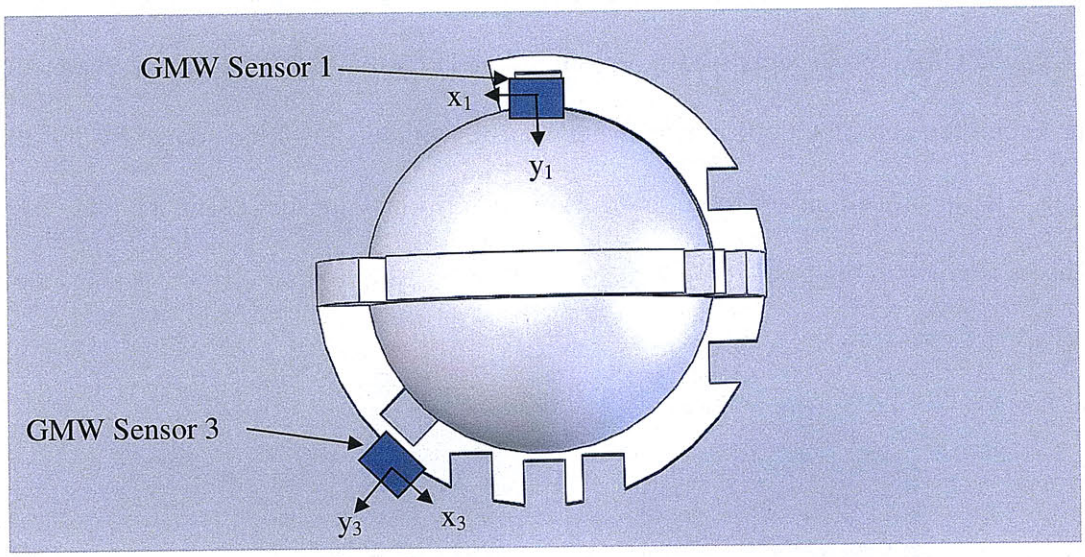

Figure 5-25. Side view of probe holder with empty sphere, showing GMW sensors 1& 3 in dark blue. The individual sensor's axes are oriented as shown and denoted as x_1, y_1 for sensor 1 and x_3, y_3 for sensor 3. Image obtained from SolidWorks design of probe holder.

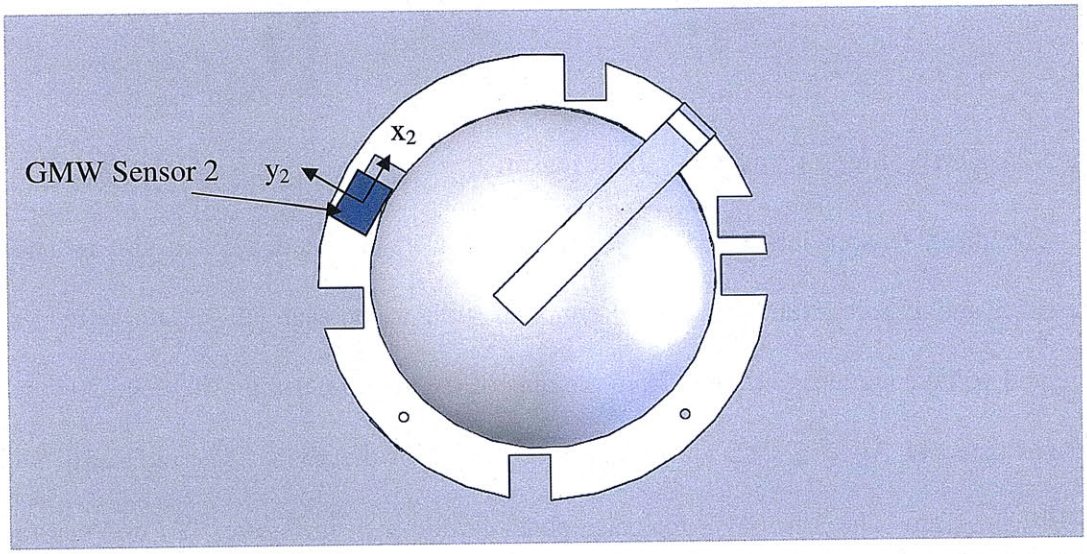

Figure 5-26. Top view of probe holder with empty sphere, showing GMW sensor 2 (dark blue) fitted in slot and sensor's x and y axis (denoted as x_2 and y_2) aligned as shown. Image obtained from SolidWorks design of probe holder.

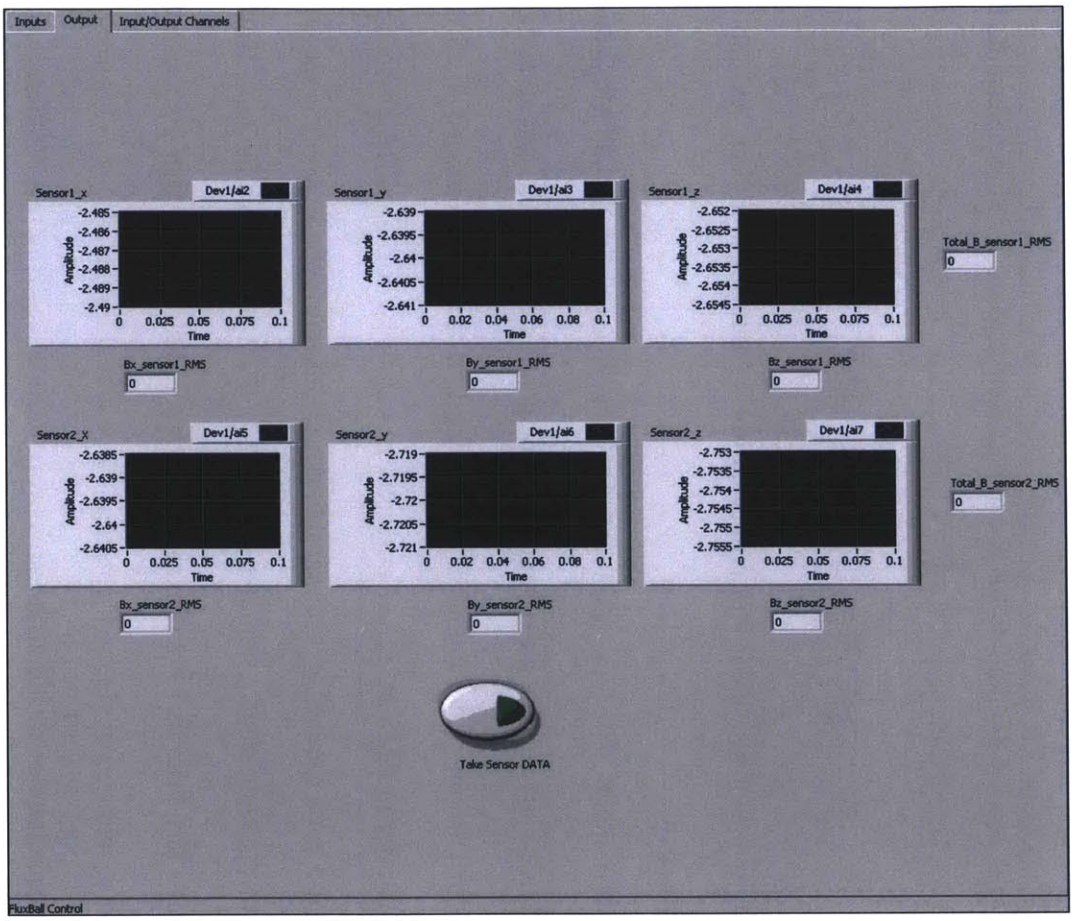

ure 5-27. Panel monitoring x, y and z magnetic field components measured by GMW sensors in LabVIEW program controlling se, magnitude and frequency of the current in the two fluxball windings. Only two sensors can be monitored at a time due to a l nputs on the BNC 2120/6036E DAQ card. The graphs display the voltage waveforms along individual axes of the sensor wl) calculating the RMS flux density magnitude. Clicking on the *Take Sensor DATA* button copies all the data to a text file for p cessing.

Since each sensor measures the magnetic field along the individual axes that its internal current sensors are aligned to, the magnitude of the magnetic field outside the 10 cm diameter sphere picked up by the three individual sensors is given by

$$|\mathbf{B}|_{rms} = \sqrt{B_{xrms}^2 + B_{yrms}^2 + B_{zrms}^2} \tag{5.17}$$

Values of the turn ratio N and the average radius R can be substituted in (5.15) to determine the theoretical flux density for the individual fluxballs

$$|\mathbf{B}| = |\mu_0 \mathbf{H}| = \frac{\mu_0 N}{3R} I = K_w I, \quad K_w = \frac{\mu_0 N}{3R} \tag{5.18}$$

where K_w is known as the winding factor and represents the relationship between the applied current and the magnetic field.

The fluxballs were individually energized at different current magnitudes and frequencies without any ferrofluid filled sphere. The magnitude of the magnetic fields were recorded at these frequencies and fluxball currents and compared to theoretical values as determined in (5.18). Table 5-6 is a list of measured RMS values of magnetic flux density, for the different sensors, when energizing only the inner fluxball at different frequencies and currents. It also lists the error associated with each measurement as compared to the theoretical values for the flux density using the inner fluxball's turn ratio of 1392 turns and an average radius of 10.7 cm. A maximum error of $\approx$ 10% difference with respect to the theoretical value is highlighted. Table 5-7 is a list of measured flux density magnitudes of the different sensors when energizing the 2069 turn outer fluxball of 15.9 cm average radius. A maximum error of 12% difference with respect to the theoretical value is also highlighted. The differing radii of the two exciting coils are counterbalanced by the increase in number of turns for the outer coil such that

$$\frac{N_{inner}}{R_{inner}} \approx \frac{N_{outer}}{R_{outer}} \approx 115 \text{ turns/cm} \tag{5.19}$$

The winding factors for the different fluxballs are determined for each sensor and then averaged. Those sensor averaged winding factors are then averaged for every frequency and current combination to give an average winding factor of 5.09 mT/A (RMS) and 5.03 mT/A (RMS) for the inner and outer fluxballs respectively. This value is approximately equal to the value that Lawler predicted (≈ 5.05 mT/A (RMS) pg 82 of [7]) it to be but Lawler measured values were significantly higher, 5.4 mT/A (RMS). This discrepancy could be because Lawler did his measurements when the fluxball was placed on a steel optical table. Lawler himself, recognizes this discrepancy in his conclusions and calculates that the reflected fields from the steel table could increase the magnetic field by 5% which almost exactly explains his measurements (105% of 5.05mT/A = 5.303 mT/A) and confirms his theoretical results with those in Table 5-6 and Table 5-7. The experiments that were conducted in this thesis were all done with the fluxball machine on a wooden table.

Table 5-8 compares the values of the measured magnetic flux density, for the individual sensors, obtained by energizing the individual fluxballs. It shows that the inner and outer fluxballs generate the same magnetic field when energized with the same current with a maximum error of ≈ 9%. Table 5-9 compares the magnitude of magnetic flux density obtained by the different sensors giving the error in the spatial distribution of the magnetic field, when energizing the individual fluxballs one at a time, due to the construction process of the fluxball machine. A maximum spatial error in magnetic flux of 7% and 10% for the inner fluxball and outer fluxball respectively, was obtained confirming that the fields generated by the individual fluxballs are mostly uniform in the test chamber.

f (Hz)	RMS $I_{innefluxball}$ (A)	B_{mag} (mT) Sensor 1	B_{mag} (mT) Sensor 2	B_{mag} (mT) Sensor 3	$B_{theoretical}$ (mT)	Sensor 1 Error (%)	Sensor 2 Error (%)	Sensor 3 Error (%)	K_w (mT/A) Sensor 1	K_w (mT/A) Sensor 2	K_w (mT/A) Sensor 3	Avg K_w (mT/A)
1	0.354	1.850	1.812	1.724	1.927	3.978	5.950	10.517	5.252	5.125	4.876	5.085
1	0.707	3.731	3.716	3.495	3.853	3.173	3.562	9.298	5.284	5.255	4.943	5.160
1	1.414	7.007	6.938	7.087	7.707	9.077	9.972	8.039	4.955	4.906	5.011	4.957
10	0.354	1.850	1.813	1.756	1.927	3.978	5.898	8.857	5.235	5.128	4.967	5.110
10	0.707	3.727	3.711	3.551	3.853	3.277	3.692	7.844	5.278	5.248	5.022	5.183
10	1.414	7.011	6.937	7.199	7.707	9.025	9.985	6.586	4.958	4.905	5.090	4.985
50	0.354	1.843	1.808	1.747	1.927	4.341	6.158	9.324	5.233	5.114	4.941	5.096
50	0.707	3.723	3.705	3.556	3.853	3.381	3.848	7.715	5.269	5.240	5.029	5.179
50	1.414	7.024	6.931	7.204	7.707	8.857	10.063	6.521	4.967	4.901	5.094	4.987
100	0.354	1.843	1.809	1.742	1.927	4.341	6.106	9.583	5.204	5.117	4.927	5.083
100	0.707	3.724	3.705	3.541	3.853	3.355	3.848	8.104	5.262	5.240	5.008	5.170
									Average	winding	factor	5.09

Table 5-6. Table of measured RMS magnitude of magnetic flux density of the three GMW sensors positioned in the slots of the probe holder for only energizing the inner fluxball. The percentage error compared to the theoretical value of the flux density is also calculated. The winding factors are also calculated for the different frequencies, sensors and fluxball current and averaged. Highlighted values indicate greatest error obtained from measurements.

f (Hz)	RMS $I_{outerfluxball}$ (A)	B_{mag} (mT) Sensor 1	B_{mag} (mT) Sensor 2	B_{mag} (mT) Sensor 3	$B_{theoretical}$ (mT)	Sensor 1 Error (%)	Sensor 2 Error (%)	Sensor 3 Error (%)	K_w (mT/A) Sensor 1	K_w (mT/A) Sensor 2	K_w (mT/A) Sensor 3	Avg K_w (mT/A)
1	0.354	1.845	1.682	1.763	1.927	4.261	12.719	8.516	5.190	4.757	4.987	4.978
1	0.707	3.709	3.407	3.573	3.854	3.768	11.603	7.297	5.245	4.818	5.053	5.0388
1	1.414	7.097	6.636	7.256	7.708	7.932	13.913	5.870	5.020	4.692	5.131	4.9476
10	0.354	1.847	1.731	1.784	1.927	4.157	10.176	7.426	5.213	4.896	5.046	5.0516
10	0.707	3.708	3.496	3.607	3.854	3.794	9.294	6.414	5.240	4.944	5.101	5.0949
10	1.414	7.086	6.787	7.324	7.708	8.075	11.954	4.987	5.010	4.799	5.179	4.9959
50	0.354	1.838	1.726	1.775	1.927	4.624	10.436	7.893	5.210	4.882	5.020	5.0374
50	0.707	3.699	3.467	3.592	3.854	4.027	10.047	6.804	5.226	4.903	5.080	5.0695
100	0.354	1.83	1.735	1.772	1.927	5.039	9.969	8.049	5.165	4.907	5.012	5.028
									Average	winding	factor	5.03

Table 5-7. Table of measured RMS magnitude of magnetic flux density of the three GMW sensors positioned in the probe holder slots only when energizing the outer fluxball. The table also lists the measurement error compared to the theoretical value as well as the average winding factors. Highlighted values indicate greatest error obtained from measurements.

f (Hz)	RMS I (A) through individual fluxball	Sensor 1 Error (%)	Sensor 1 Error (%)	Sensor 1 Error (%)
1	0.354	0.271	7.729	2.212
1	0.707	0.593	9.070	2.183
1	1.414	1.268	4.551	2.329
10	0.354	0.162	4.737	1.570
10	0.707	0.512	6.150	1.553
10	1.414	1.058	2.210	1.707
50	0.354	0.272	4.751	1.577
50	0.707	0.649	6.865	1.002
100	0.354	0.710	4.265	1.693

Table 5-8. Table of errors between the values of measured magnitude of flux density by the different sensors obtained by energizing the inner and outer fluxballs individually. There is a maximum of $\approx$ 9% difference between the magnitude of the magnetic flux generated by the inner and outer fluxballs.

Inner Fluxball					
f (Hz)	RMS $I_{innerfluxball}$ (A)	Sensor 2 Error (%) wrt Sensor 1	Sensor 3 Error (%) wrt Sensor 1	Sensor 1 Error (%) wrt Sensor 2	Sensor 3 Error (%) wrt Sensor 2
1	0.354	2.054	7.162	2.097	4.857
1	0.707	0.402	6.451	0.404	5.947
1	1.414	0.985	1.142	0.995	2.148
10	0.354	2.000	5.132	2.041	3.144
10	0.707	0.429	4.850	0.431	4.312
10	1.414	1.055	2.667	1.067	3.777
50	0.354	1.899	5.568	1.936	3.374
50	0.707	0.483	4.563	0.486	4.022
50	1.414	1.324	2.548	1.342	3.939
100	0.354	1.845	5.326	1.879	3.704
100	0.707	0.510	4.837	0.513	4.426

Outer Fluxball					
f (Hz)	RMS $I_{outerfluxball}$ (A)	Sensor 2 Error (%) wrt Sensor 1	Sensor 3 Error (%) wrt Sensor 1	Sensor 1 Error (%) wrt Sensor 2	Sensor 3 Error (%) wrt Sensor 2
1	0.354	8.835	3.924	9.691	4.816
1	0.707	8.142	3.667	8.864	4.872
1	1.414	6.496	2.212	6.947	9.343
10	0.354	6.280	3.201	6.701	3.062
10	0.707	5.717	2.645	6.064	3.175
10	1.414	4.220	3.373	4.405	7.912
50	0.354	6.094	3.637	6.489	2.839
50	0.707	6.272	2.788	6.692	3.605
100	0.354	5.191	2.957	5.476	2.133

Table 5-9. Table compares the values measured by the sensors with respect to each other to determine the maximum spatial error in magnetic field for both fluxballs when the individual fluxballs are energized. A maximum of ≈ 7% for the inner fluxball and ≈ 10% spatial error for the outer fluxball is highlighted.

5.2.8. Resonant Operation of Fluxball Machine

Table 5-10 compares the electrical properties of the two pole stator winding machine, used by He [3] and Elborai [4] in their experiments with a rotating uniform magnetic field, with those of the two fluxball windings. To provide the same amount of current as the two pole stator winding machine, a larger voltage is required because of the greater impedance that scales with frequency, due to the higher inductance of the individual windings. The winding factor of the combined fluxball machine used in this thesis is taken to be the average of the winding factors of the inner and outer fluxball and is equal to 50.6 G/A (RMS).

Setup	Winding Resistance (Ω)	Winding Inductance (H)	Winding Factor K_w (Gauss/A RMS)
2 pole stator winding [3, 4]	3.1	0.008	38
Inner Fluxball	23.8	0.172	50.9
Outer Fluxball	52.7	0.565	50.3

Table 5-10. Table documenting winding resistance, inductance and winding factor for the inner and outer fluxballs along with the 2 pole stator winding used by He [3] and Elborai [4] in their experiments of generating a rotating field.

The LVC 5050 amplifier used by He [3] and Elborai [4] is the same amplifier used in this thesis and has a maximum RMS voltage output of 106 V (Appendix C) with three possible gains of 20, 70 and 130. The NI PCI 6036E DAQ card has a maximum peak output of 10 V. To operate the fluxball machine at a particular frequency, the DAQ card should not exceed 10 V peak and the output of the amplifier should not exceed an RMS value of 106 V.

Table 5-12 for He's [3] and Elborai's [4] stator winding is a list of impedances calculated at various different frequencies along with the calculated voltage output by the LVC 5050 amplifier and the DAQ card, at various gain settings, for a desired magnetic field strength. It also lists which cases meet these specifications and which do not. Elborai's [4] and He's [3] two pole

stator machine's low impedance allows for all but one case to be satisfied without any modifications to the setup.

Table 5-13 and Table 5-14 list the same output voltages by the LVC 5050 amplifier and 6036E DAQ card necessary for the frequencies and magnetic field strengths for each individual fluxball winding. The outer fluxball actually limits the cases further since to generate a rotating magnetic field both the inner and outer fluxballs have to be energized leaving only three possible frequency/current combinations. Of these three cases two occur at a frequency of 1 Hz, which might not be enough to create the torque needed since the magnetization of the fluid and magnetic field will be mostly collinear, while the one case of 20 Hz is insufficient to do a thorough investigation.

The main problem is the high impedance values at the high frequencies resulting in large voltages needed to generate the currents specified. A good solution is by inserting a series capacitor with the windings to cancel the impedance due to the inductance of the windings at the resonant frequency of the resulting RLC circuit as shown in Figure 5-28.

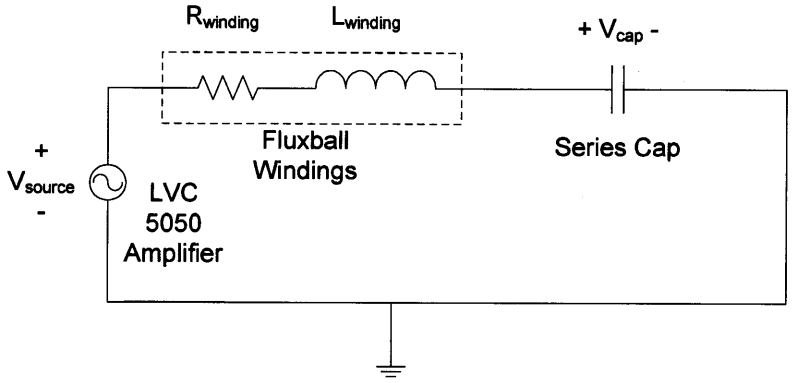

Figure 5-28. Circuit diagram of LVC 5050 amplifier in series with fluxball windings and series capacitor for resonant operation of fluxball.

The voltage drop across the capacitor at resonance can be given as

$$|V_{cap}| = \frac{1}{\Omega C_{cap} R_{winding}} |V_{source}| \tag{5.20}$$

where Ω is the frequency of the sinusoidal signal applied to the fluxball and $R_{winding}$ the resistance of the winding which is the impedance of the RLC circuit at the resonant frequency. The factor $\frac{1}{\Omega C_{cap} R_{winding}}$ given in (5.20) is usually very large for most standard capacitors. This means that any series capacitor chosen to operate at a resonant frequency must have a large enough dielectric breakdown voltage to withstand the high voltages calculated by (5.20).

Two high frequencies (47 Hz and 95 Hz) were chosen for resonant operation and capacitance and voltage drops across the series capacitors were calculated for both fluxball windings as tabulated in Table 5-15 and Table 5-16. It can be seen that at a resonant frequency of 47 Hz the inner fluxball has to have a series capacitance of 66.7 μF rated to withstand an RMS voltage of 102 V, while the outer fluxball needs a series capacitance of 20 μF rated at 334 V RMS. At a resonant frequency of 95 Hz, the inner fluxball has to have a series capacitance of 16.3 μF capable of withstanding 205 V RMS, while the outer fluxball needs a capacitance of 5 μF rated at 675 V RMS. Panasonic AC film capacitors were used because they have high voltage ratings, are compact and can easily be mounted in an enclosure. The datasheet for the enclosure and these capacitors are in Appendix C.

For the 66.7 μF capacitor, four 15 μF capacitors (Digikey #P9413-ND), each rated at 250 V RMS, were put in parallel with a single 6 μF capacitor (Digikey #P9661-ND) rated at 440 V RMS. These five capacitors were mounted with screws in a single enclosure (Digikey #707K-ND) with terminals mounted on the outside. The 20 μF capacitor was assembled with placing four 5 μF capacitors (Digikey #P9660-ND), each rated at 440 V RMS, in parallel with each other

and mounted in a single enclosure. The 16 μF capacitor was made by placing a 10 μF capacitor (Digikey #9411-ND), rated at 250 V RMS, in parallel with a 6 μF capacitor (Digikey #9661-ND) rated at 440 V RMS. For the 5 μF capacitor, which had to withstand an RMS voltage of 675 V, three 15 μF capacitors (Digikey #9413-ND) were placed in series adding up their individual rated voltage of 250 V RMS to a total of 750 V RMS. Both the 16 μF and the 5 μF capacitors were mounted into a single enclosure with two separate output terminals. The enclosures containing the capacitors can be seen in Figure 5-29 with their internal wiring displayed in Figure 5-30.

The individual capacitor boxes were assembled and their capacitances measured. They were also connected in series with the individual fluxball windings and the impedance values of the resulting RLC circuit were also measured at the individual resonant frequencies. These results are tabulated in Table 5-11. It can be seen that at resonance the impedance of the individual windings are mostly real allowing for lower voltages to generate the desired magnetic flux density in the fluxball.

Capacitance Desired (μF)	Measured Capacitance (μF)	Measured Impedance of capacitor in series with fluxball windings (Ω)
20	20.32	Z_{inner}=25.25+0.65j (@47 Hz)
66	68.00	Z_{outer}=54.5-0.8j (@47 Hz)
16	16.23	Z_{inner}=25.28-1.5j (@95 Hz)
5	5.10	Z_{outer}=55+6.91j (@95 Hz)

Table 5-11. Measured values of capacitance and impedance of the RLC circuit at the specified resonant frequency.

f (Hz)	RMS I (A)	B_{mag} (Gauss RMS)	Impedance Z (Ω)	LVC 5050 RMS current (A)	LVC 5050 GAIN=20 6036E Peak Output (V)	LVC 5050 GAIN=70 6036E Peak Output (V)	LVC 5050 GAIN=130 6036E Peak Output (V)	Possible?
1	1.000	38.000	3.100	3.100	0.219	0.063	0.034	YES
1	2.000	76.000	3.100	6.201	0.438	0.125	0.067	YES
1	5.000	190.000	3.100	15.502	1.096	0.313	0.169	YES
20	1.000	38.000	3.259	3.259	0.230	0.066	0.035	YES
20	2.000	76.000	3.259	6.518	0.461	0.132	0.071	YES
20	5.000	190.000	3.259	16.295	1.152	0.329	0.177	YES
50	1.000	38.000	3.991	3.991	0.282	0.081	0.043	YES
50	2.000	76.000	3.991	7.982	0.564	0.161	0.087	YES
50	5.000	190.000	3.991	19.954	1.411	0.403	0.217	YES
100	1.000	38.000	5.906	5.906	0.418	0.119	0.064	YES
100	2.000	76.000	5.906	11.811	0.835	0.239	0.128	YES
100	5.000	190.000	5.906	29.528	2.088	0.597	0.321	YES
1000	1.000	38.000	50.361	50.361	3.561	1.017	0.548	YES
1000	2.000	76.000	50.361	100.722	7.122	2.035	1.096	YES
1000	5.000	190.000	52.400	262.000	18.526	5.293	2.850	NO

Table 5-12. He's [3] and Elborai's [4] 2 pole stator with impedance and magnetic flux density values calculated at different frequencies along with output voltage values of amplifier and 6036E DAQ card. Only one situation does not meet the specifications of current setup and is highlighted in yellow.

f (Hz)	RMS I (A)	B_{mag} (Gauss RMS)	Impedance Z (Ω)	LVC 5050 RMS current (A)	LVC 5050 GAIN=20 6036E Peak Output (V)	LVC 5050 GAIN=70 6036E Peak Output (V)	LVC 5050 GAIN=130 6036E Peak Output (V)	Possible?
1	1	50.9	23.825	23.825	1.685	0.481	0.259	YES
1	2	101.8	23.825	47.649	3.369	0.963	0.518	YES
1	5	254.5	23.825	119.123	8.423	2.407	1.296	NO
1	8	407.2	23.825	190.596	13.477	3.851	2.073	NO
20	1	50.9	32.150	32.150	2.273	0.650	0.350	YES
20	2	101.8	32.150	64.300	4.547	1.299	0.699	YES
20	5	254.5	32.150	160.749	11.367	3.248	1.749	NO
20	8	407.2	32.150	257.199	18.187	5.196	2.798	NO
50	1	50.9	59.045	59.045	4.175	1.193	0.642	YES
50	2	101.8	59.045	118.089	8.350	2.386	1.285	NO
50	5	254.5	59.045	295.223	20.875	5.964	3.212	NO
50	8	407.2	59.045	472.357	33.401	9.543	5.139	NO
100	1	50.9	110.660	110.660	7.825	2.236	1.204	NO
100	2	101.8	110.660	221.321	15.650	4.471	2.408	NO
100	5	254.5	110.660	553.302	39.124	11.178	6.019	NO
100	8	407.2	110.660	885.284	62.599	17.885	9.631	NO
1000	1	50.9	1080.970	1080.970	76.436	21.839	11.759	NO
1000	2	101.8	1080.970	2161.940	152.872	43.678	23.519	NO
1000	5	254.5	1080.970	5404.850	382.181	109.194	58.797	NO

Table 5-13. Lawler's [7] inner fluxball with impedance and magnetic flux density values calculated at different frequencies along with output voltage values of amplifier and 6036E DAQ card. There are only five possible situations to energize the inner fluxball with the current setup to work without any modifications.

f (Hz)	RMS I (A)	Bmag (Gauss RMS)	Impedance Z (Ω)	LVC 5050 RMS current (A)	LVC 5050 GAIN=20 6036E Peak Output (V)	LVC 5050 GAIN=70 6036E Peak Output (V)	LVC 5050 GAIN=130 6036E Peak Output (V)	Possible?
1	1	50.3	52.819	52.819	3.735	1.067	0.575	YES
1	2	100.6	52.819	105.639	7.470	2.134	1.149	YES
1	5	251.5	52.819	264.097	18.674	5.336	2.873	NO
1	8	402.4	52.819	422.555	29.879	8.537	4.597	NO
20	1	50.3	88.421	88.421	6.252	1.786	0.962	YES
20	2	100.6	88.421	176.842	12.505	3.573	1.924	NO
20	5	251.5	88.421	442.105	31.262	8.932	4.809	NO
20	8	402.4	88.421	707.369	50.019	14.291	7.695	NO
50	1	50.3	185.158	185.158	13.093	3.741	2.014	NO
50	2	100.6	185.158	370.316	26.185	7.482	4.029	NO
50	5	251.5	185.158	925.791	65.463	18.704	10.071	NO
50	8	402.4	185.158	1481.265	104.741	29.926	16.114	NO
100	1	50.3	358.890	358.890	25.377	7.251	3.904	NO
100	2	100.6	358.890	717.781	50.755	14.501	7.808	NO
100	5	251.5	358.890	1794.452	126.887	36.253	19.521	NO
100	8	402.4	358.890	2871.123	203.019	58.005	31.234	NO
1000	1	50.3	3550.391	3550.391	251.051	71.729	38.623	NO
1000	2	100.6	3550.391	7100.782	502.101	143.457	77.246	NO
1000	5	251.5	3550.391	17751.954	1255.253	358.644	193.116	NO

Table 5-14. Lawler's [7] outer fluxball with impedance and magnetic flux density values calculated at different frequencies along with output voltage values of amplifier and 6036E DAQ card. There are only three possible situations to energize both fluxballs with the current setup to work without any modifications.

f (Hz)	RMS I (A)	Bmag (Gauss RMS)	Impedance Z (Ω)	LVC 5050 RMS current (A)	LVC 5050 GAIN=20 6036E Peak Output (V)	Series Capacitance (μF)	Vcap RMS (V)
47	1.00	50.90	23.8	23.8	1.68	66.67	50.79
47	2.00	101.80	23.8	47.6	3.37	66.67	101.59
95	1.00	50.90	23.8	23.8	1.68	16.32	102.67
95	2.00	101.80	23.8	47.6	3.37	16.32	205.33

Table 5-15. Table of capacitance and voltage values calculated for capacitors in series with the inner fluxball windings under resonant operation at two frequencies 47 Hz and 95 Hz.

f (Hz)	RMS I (A)	Bmag (Gauss RMS)	Impedance Z (Ω)	LVC 5050 RMS current (A)	LVC 5050 GAIN=20 6036E Peak Output (V)	Series Capacitance (μF)	Vcap RMS (V)
47	1.00	50.30	52.7	52.7	3.73	20.3	166.85
47	2.00	100.60	52.7	105.4	7.45	20.3	333.7
95	1.00	50.30	52.7	52.7	3.73	4.97	337.25
95	2.00	100.60	52.7	105.4	7.45	4.97	674.50

Table 5-16. Table of capacitance and voltage values calculated for capacitors in series with the outer fluxball windings under resonant operation at two frequencies 47 Hz and 95 Hz.

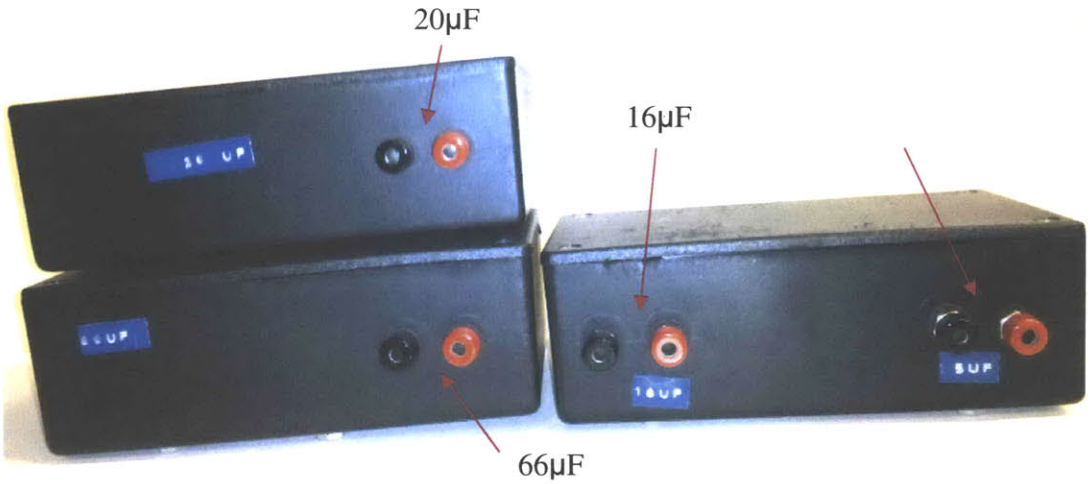

Figure 5-29. Assembled capacitor boxes used for resonant operation of fluxball at 47 Hz and 95 Hz. The 20 μF and the 66 μF capacitors are housed in separate enclosures, while the 16 μF and 5 μF are housed in one enclosure.

Figure 5-30. Capacitor banks with their enclosure lids removed showing their wiring connections. Enclosure at top of the figure is for the 16 μF and 5 μF both together. The 16 μF is made by placing a 10 μF capacitor in parallel with a 6μF capacitor while the 5 μF capacitor is made by three 15 μF capacitors in series. The enclosure at the bottom left with four 15 μF capacitors in parallel with a 6 μF capacitor, is the 66 μF while the bottom right, with 5 μF four in parallel, is for the 20 μF capacitor. The banana plug connection terminals (in red and black) can also be seen.

Bibliography

[1] A. Chaves, *et al.*, "Bulk Flow in Ferrofluids in a Uniform Rotating Magnetic Field," *Physical Review Letters,* vol. 96, pp. 194501-4, 2006.

[2] A. Chaves, *et al.*, "Spin-up flow of ferrofluids: Asymptotic theory and experimental measurements," vol. 20, p. 053102, 2008.

[3] X. He, "Ferrohydrodynamic flows in uniform and non-uniform rotating magnetic fields," Ph.D thesis, Dept of Electrical Engineering and Computer Science, Massachusetts Institute of Technology, Cambridge, MA, 2006.

[4] S. Elborai, "Ferrofluid surface and volume flows in uniform rotating magnetic fields," Ph.D thesis, Dept of Electrical Engineering and Computer Science, Massachusetts Institute of Technology, Cambridge, MA, 2006.

[5] M. I. Shliomis, *et al.*, "Ferrohydrodynamics: An essay on the progress of ideas," *Chem. Eng. Comm.,* vol. 67, pp. 275 - 290, 1988.

[6] H. A. Haus and J. R. Melcher, *Electromagnetic Fields and Energy*. Englewood Cliffs, NJ: Prentice Hall, 1989.

[7] C. Lawler, "A two-phase spherical electric machine for generating rotating uniform magnetic fields," Masters of Science, Dept. of Mechanical Engineering & Dept. of Electrical Engineering and Computer Science, Massachusetts Institute of Technology, Cambridge, MA, 2007.

Chapter 6. Ferrofluid Flows in Spherical Geometry

This chapter will describe the results of the experiments conducted using a ferrofluid filled sphere inside of two spherical coils in quadrature in time and space to generate the uniform magnetic field with bulk flows being measured using ultrasound velocimetry. None or negligible flow was measured concluding that the spin-diffusion effect is not the governing mechanism for the flow.

Researchers that used the spin-diffusion model and were able to simulate their experimental flows [1, 2] using values of spin-viscosity η' ($\approx 10^{-10}$ kg m s^{-1}) that were more than ten orders of magnitude greater than the η' values derived by Rosensweig, Finlayson and Schumacher ($\approx 10^{-20}$ kg m s^{-1}) [3, 4], using an extension of kinetic molecular theory of viscosity in a dilute gas from [5]. This suggests that values experimentally determined for spin-viscosity η' [1, 2, 6] are overstated, to compensate for the actual demagnetizing effects in the cylinder.

Experiments of flow generated in a 2/3 filled sphere further confirm that the non-uniform field, due to demagnetizing effects associated with the shape of the ferrofluid volume, drive the flow. By slightly modifying the fluxball machine, experiments were also performed using a cylindrical geometry under a uniform rotating field generated by the fluxball machine resulting in non-zero flow. Experiments were also conducted where the imposed uniform rotating magnetic field was made non-uniform by using a solenoidal coil and a permanent magnet. Significant measureable flow was obtained in both cases suggesting that both a non-uniform field and a non-uniform distribution of magnetization, similar to Pshenichnikov's conclusions [7], drive the flow.

6.1. Experimental Results From Applying a Uniform Rotating Magnetic Field

Experiments were conducted using the setup described in Chapter 5 with two different Ferrotec® ferrofluids, oil-based EFH1 and water-based MSGW11. The individual ferrofluids were mixed with Griltex-P1 of concentration 0.008g/ml and before any experiment the spheres of ferrofluid were vigorously shaken using an orbital shaker for 30 minutes. The magnetic field strengths used by the fluxball machine were 50.6 and 101.2 RMS Gauss fields corresponding to 1A and 2A RMS current through each spherical winding of the fluxball machine. Figure 6-1 is a picture of the complete experimental setup used for the experiments in this thesis.

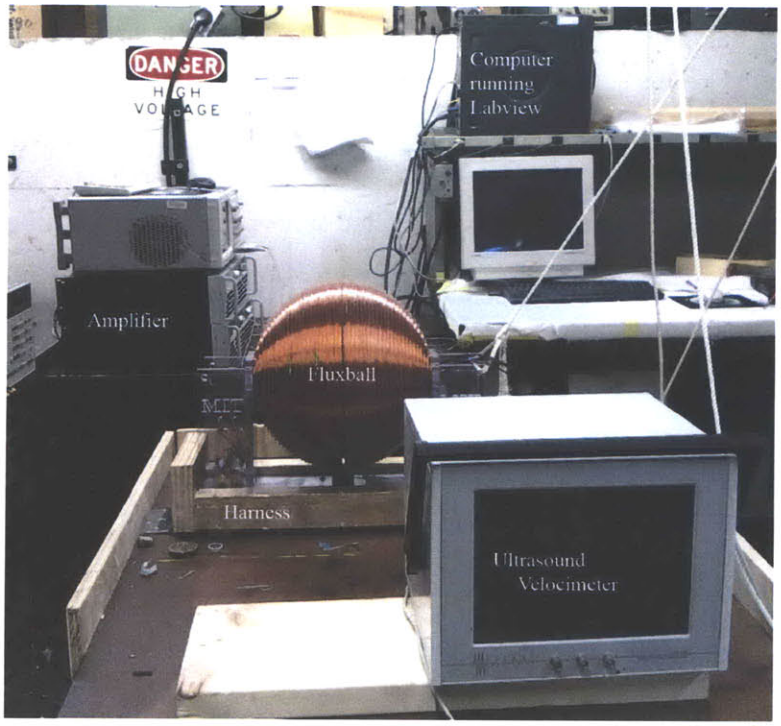

Figure 6-1. Picture of complete experimental setup used in this thesis.

Four ultrasound probes were placed such that they measured velocity profiles along 4 different lines in the x-z plane along the center (y=0) of the ferrofluid filled sphere, as illustrated in Figure 6-2. The four probes, denoted as Channels 1-4, were multiplexed internal to the DOP2000 and they measure the velocity and distance away the moving tracer particles are from the probe. A negative velocity measured by the DOP2000 denotes a particle moving towards the probe, while a positive velocity is for a particle moving away from the probe. Since the beams of the four probes intersect in the y=0 (center of sphere) plane, four velocity vectors can be determined at the four points indicated in Figure 6-2. A current phase difference of +90° between the outer and inner fluxball creates a clockwise rotating uniform magnetic field also illustrated in Figure 6-2. The settings of the DOP2000 ultrasound velocimeter used to obtain all the data in this thesis are given in Table 6-1. The experimental results were conducted allowing sufficient time for the fluxball and the ferrofluid filled sphere to cool to room temperature of ≈25°C to minimize temperature effects on the magnetic susceptibility of the ferrofluid.

Velocimeter Settings	**Value**
Channels	1-4 Multiplexed
PRF	100-200 Hz
Emitting frequency	4 MHz
Power level	High
Burst length	8 cycles
Resolution	0.56mm
Sensitivity	Very High
Time Gain Control (TGC)	Slope, 31dB-61dB
Starting depth	9 mm
Number of gates	180-230
Number of profiles	32
Emission/profile	128

Table 6-1. DOP2000 velocimeter settings used to obtain measurements in this thesis.

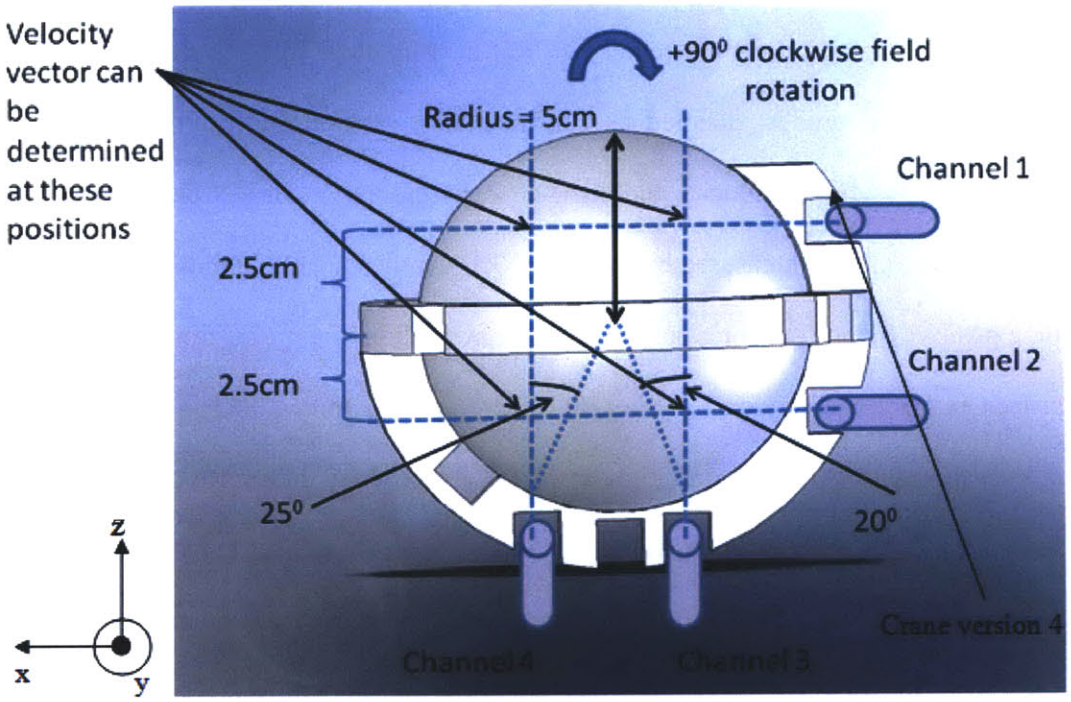

Figure 6-2. Figure depicting positions of the four ultrasound probes (labeled as Channels 1-4), in x-z plane at y=0 (center of the sphere), positioned to measure flows in a ferrofluid filled sphere. A current phase difference of +90° between the outer and inner fluxballs creates a clockwise rotating magnetic field. Image obtained from SolidWorks design of probe holder.

A series of experiments were done investigating different parameters. These different degrees of freedom are tabulated in Table 6-2. Figure 6-5 to Figure 6-8 are plots of a sphere filled with EFH1 ferrofluid subjected to 50.6 G and 101.2 G RMS field in two rotating directions. The profiles are with respect to distance from the probe, with the channel number denoted as a subscript, along the x or z direction as depicted in Figure 6-2. The velocity profiles are truncated to not include the velocity right near the probe surface (distance = 0) because of the saturation of the ultrasound transducer by the echoes near the sphere wall. The profiles are also truncated right where the ultrasound beam hits the inside wall of the sphere at the other end (distance = 10 cm along the sphere's diameter) because of the multiple reflections of echoes

occurring between the different layers of the sphere wall creating a lot of noise. Figure 6-3 is a plot of the raw data obtained by the ultrasound probe 4 using EFH1 at 47 Hz. It clearly shows that there is a lot of noise at the probe surface and at the distance where the ultrasound beam reflects off the inside wall of the sphere. Figure 6-4 is a truncated plot that illustrates the flows in the bulk of the fluid filled sphere.

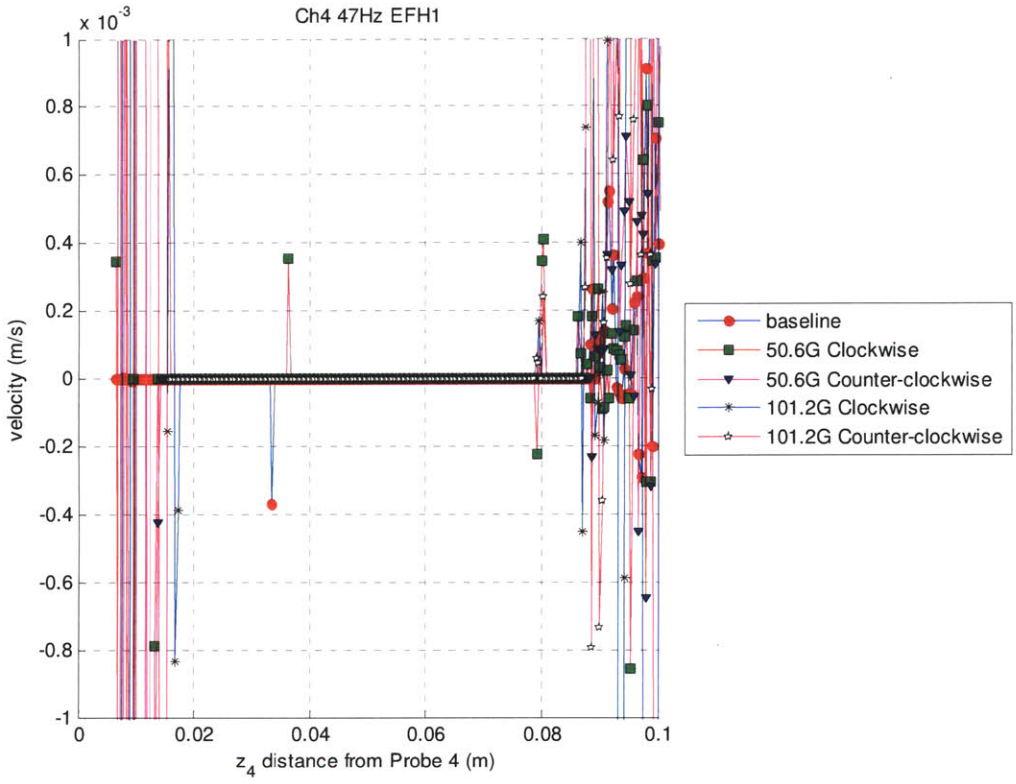

Figure 6-3. Velocity profile at 47 Hz for EFH1 clearly showing saturation of ultrasound probe 4 right near the probe surface (z distance from probe 4 = 0) and multiple reflections at probe wall (z distance from probe 4 =10cm).

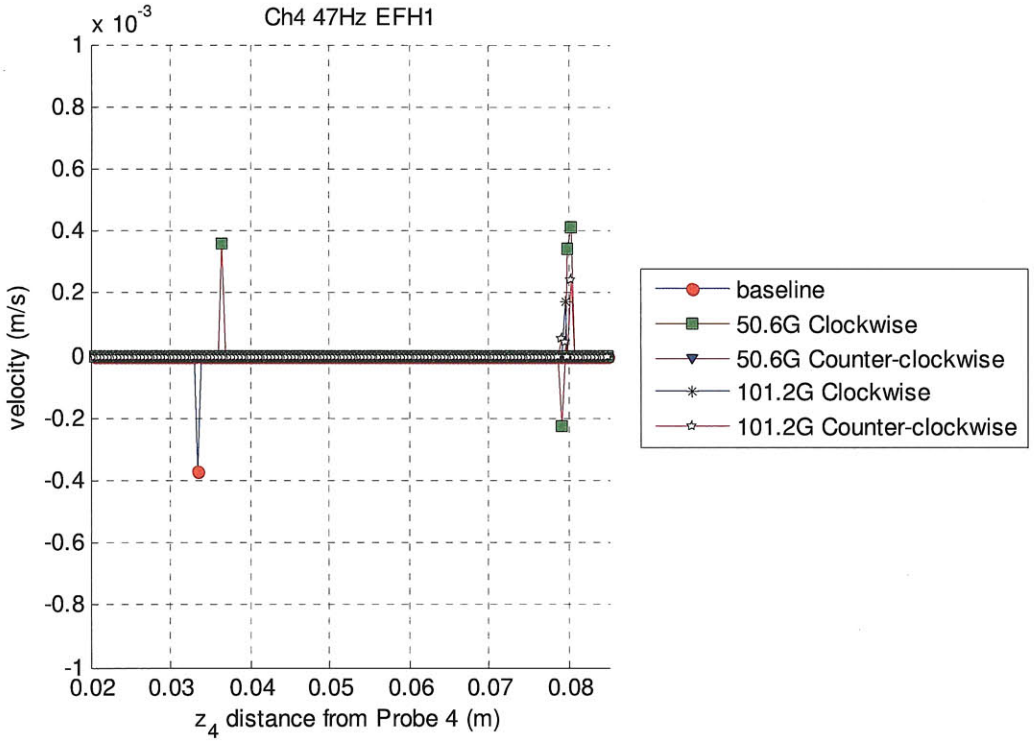

Figure 6-4. Same velocity profile as Figure 6-3 but truncated to remove most of the noise due to saturation of the transducer at zero z-distance from probe 4 and multiple reflections at z-distance from probe 4 of 10 cm.

The baseline case is the velocity profile when no field is applied and under the rotating field there is very little deviation from the baseline. This implies that there is none or negligible flow (<1mm/s) under a uniform rotating field. Any slight deviations from the baseline could be because of instrument noise or due to the maximum 10% spatial non-uniformity of the field in the test chamber of the fluxball machine as explained in section 5.2.7. The negligible flow obtained for EFH1 also occurred at different frequencies and these results are documented in Appendix E.

Parameters investigated	
Fluids used	MSGW11 and EFH1
Frequencies used	15 Hz, 47 Hz and 95 Hz
Magnitude of rotating flux density	50.6 G, 101.2 G
Rotational direction (Phase difference between outer and inner fluxball)	Clockwise (+90°) and counter-clockwise (-90°)

Table 6-2. Table of parameters investigated in experiment subjecting a sphere of ferrofluid to a uniform rotating magnetic field.

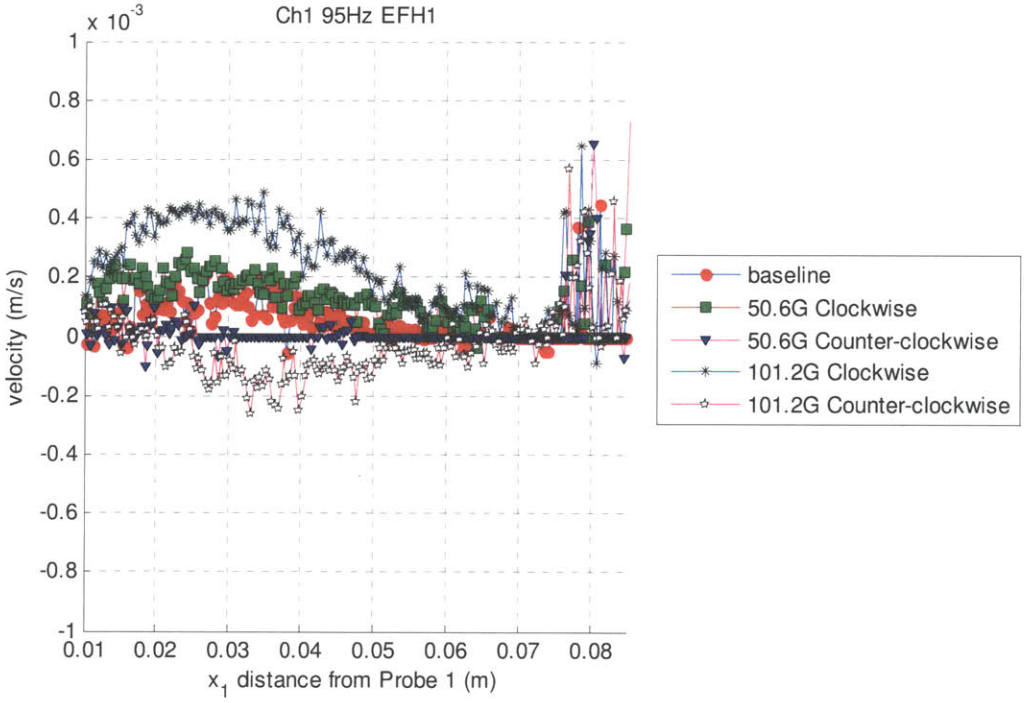

Figure 6-5. Velocity profile as a function of distance away from channel 1 probe at 95 Hz using EFH1. Two field strengths and two rotating directions are investigated. Any flow measured is not significantly more than the baseline and the flow is very small <1mm/s. The slight deviation for the 101.2 G clockwise field could be because of the maximum spatial error of 10% in magnetic field strength in the test chamber of the fluxball machine as described in section 5.2.7 or just noise.

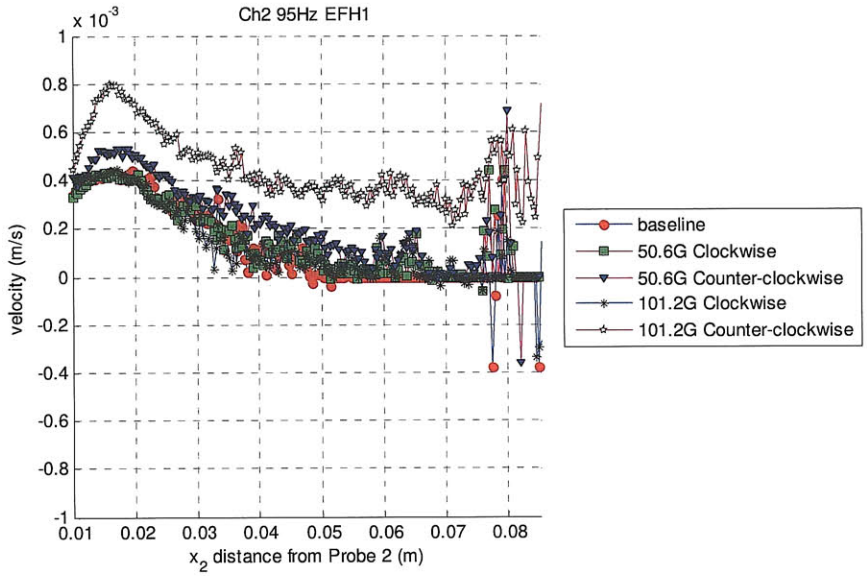

Figure 6-6. Velocity profile as a function of distance away from channel 2 probe at 95 Hz using EFH1. Any flow measured is not significantly more than the baseline and the overall flow is very small <1mm/s The slight deviation for the 101.2 G counter-clockwise field could be because of the maximum spatial error of 10% in magnetic field strength in the test chamber of the fluxball machine as described in section 5.2.7 or just instrument noise.

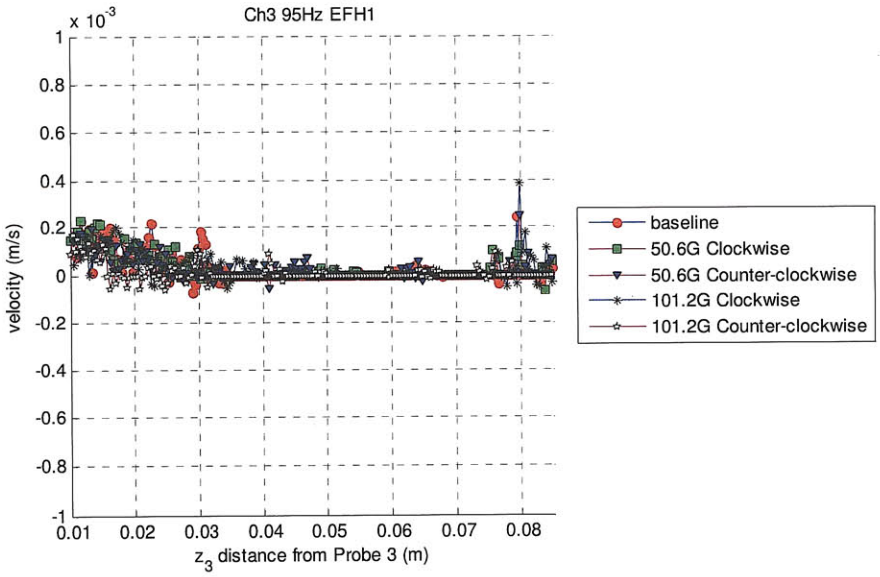

Figure 6-7. Velocity profile as a function of distance away from channel 3 probe at 95 Hz using EFH1. Two field strengths and two rotating directions are investigated. Any flow measured is not significantly more than the baseline and is very small <1mm/s.

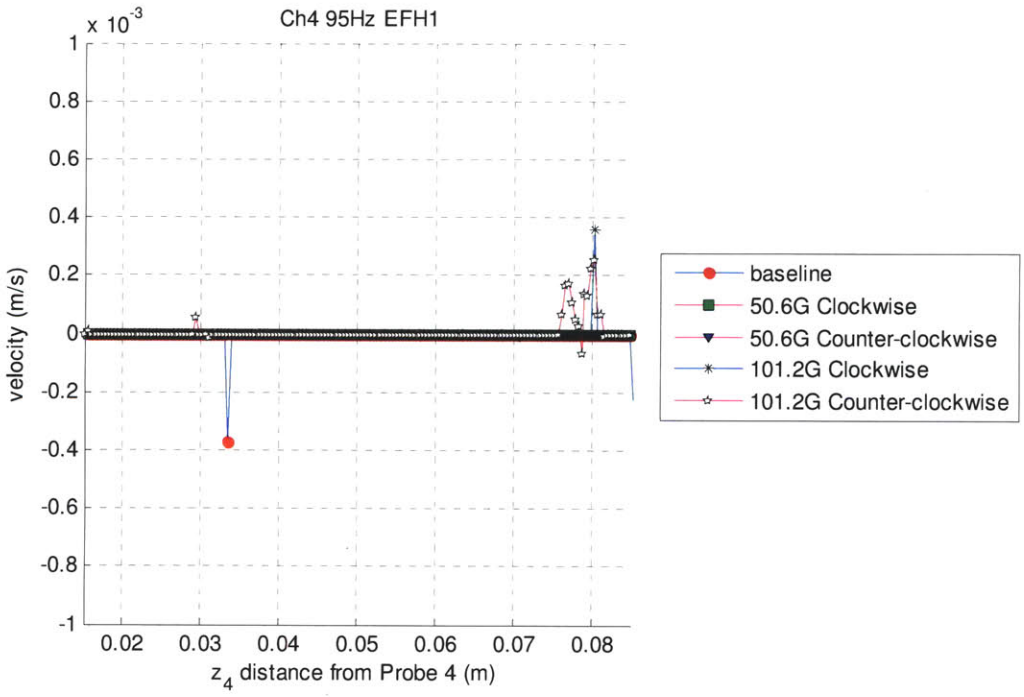

Figure 6-8. Velocity profile as a function of distance away from channel 4 probe at 95 Hz using EFH1. Two field strengths and two rotating directions are investigated. No flow is measured above baseline.

Figure 6-10 through Figure 6-13 are the velocity profiles for a sphere of MSGW11 ferrofluid under the influence of two different rotating directions at a low frequency of 15 Hz. Negligible flow compared to the baseline case, which is the flow measured with no field, confirms the same result as obtained with EFH1 under the influence of a uniform rotating field. Appendix E has plots of a sphere of MSGW11 at other frequencies, 47 Hz and 95 Hz, and they all have none or negligible flow with respect to the baseline case.

To ensure that the experimental setup was working properly, a one inch magnetic stir bar (VWR #58948-138) was inserted into two other spheres of the same ferrofluids and placed in the fluxball machine. The magnitude of the magnetic flux density of the stir bar was measured to be 90 G using the Ametes GMW three axis hall effect sensors. The stir bar and the GMW sensors

are documented in Appendix C. The stir bar would settle at the bottom of the sphere of ferrofluid and the applied rotating field was perpendicular to the magnetic poles of the stir bar. As a result, the stir bar could be heard bouncing around the sphere and erratic non-zero flows were measured. An example of one such flow is given in Figure 6-9 where a velocity profile measured by probe 3 of a sphere of MSGW11 containing a stir bar was excited with a 101.2 G uniform magnetic field rotating in the clockwise direction at frequency 47 Hz. The results confirm that the setup was operating properly and the negligible flow (without the stir bar) is a real result.

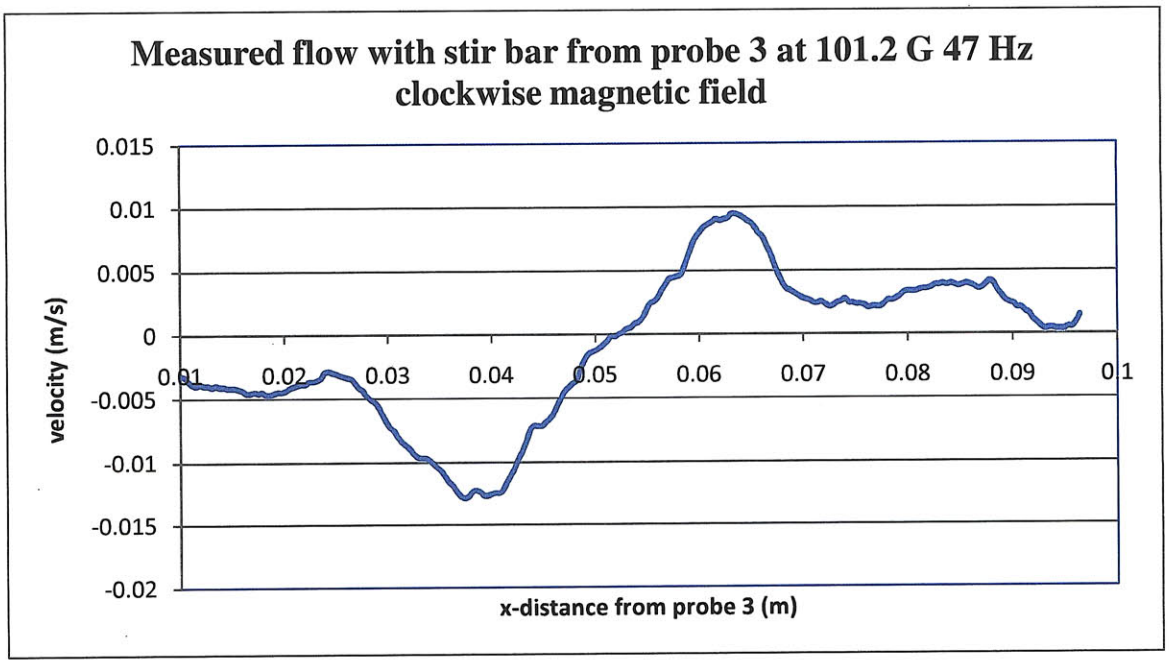

Figure 6-9. Velocity profile as a function of x distance from probe 3 when a magnetic stir bar is added to a sphere of MSGW11 excited at 101.2 G 47 Hz uniform rotating field.

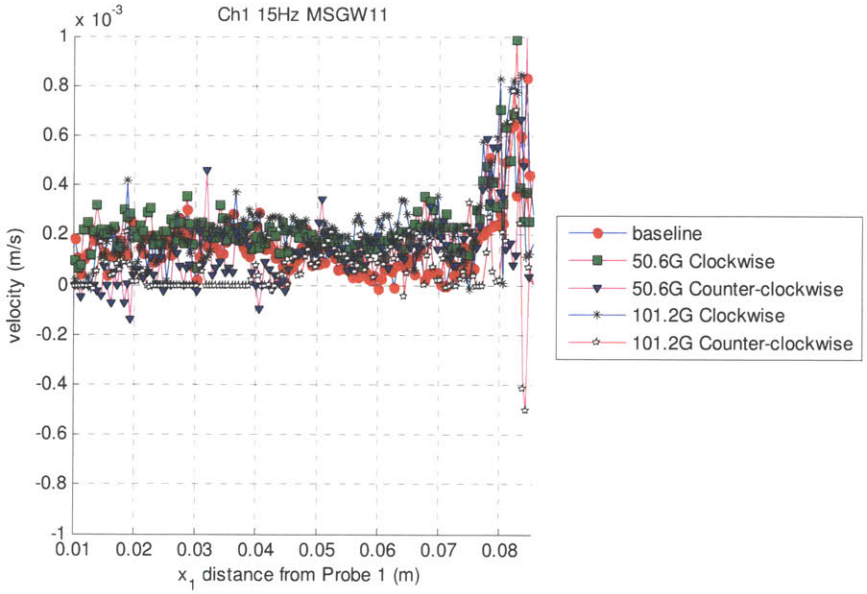

Figure 6-10. Velocity profile as a function of distance away from channel 1 probe at 15 Hz using MSGW11. Two field strengths and two rotating directions are investigated. Negligible flow compared to the baseline is measured.

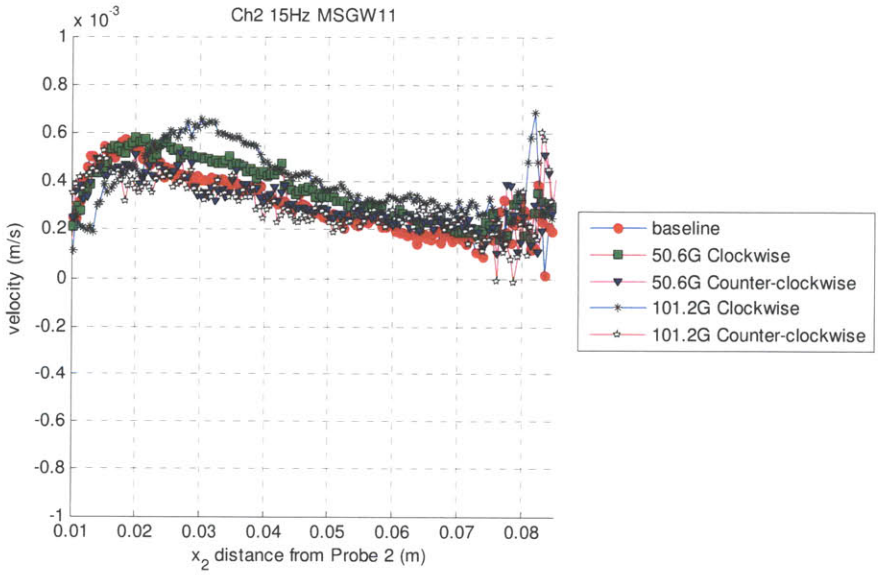

Figure 6-11. Velocity profile as a function of distance away from channel 2 probe at 15 Hz using MSGW11. Two field strengths and two rotating directions are investigated. Negligible flow compared to the baseline is measured.

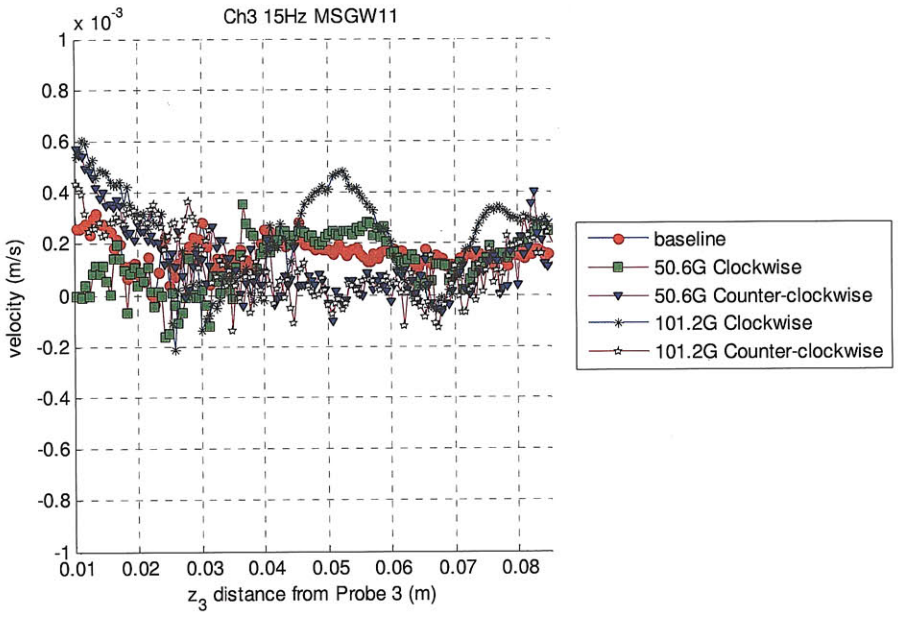

Figure 6-12. Velocity profile as a function of distance away from channel 3 probe at 15 Hz using MSGW11. Two field strengths and two rotating directions are investigated. Negligible flow compared to the baseline is measured.

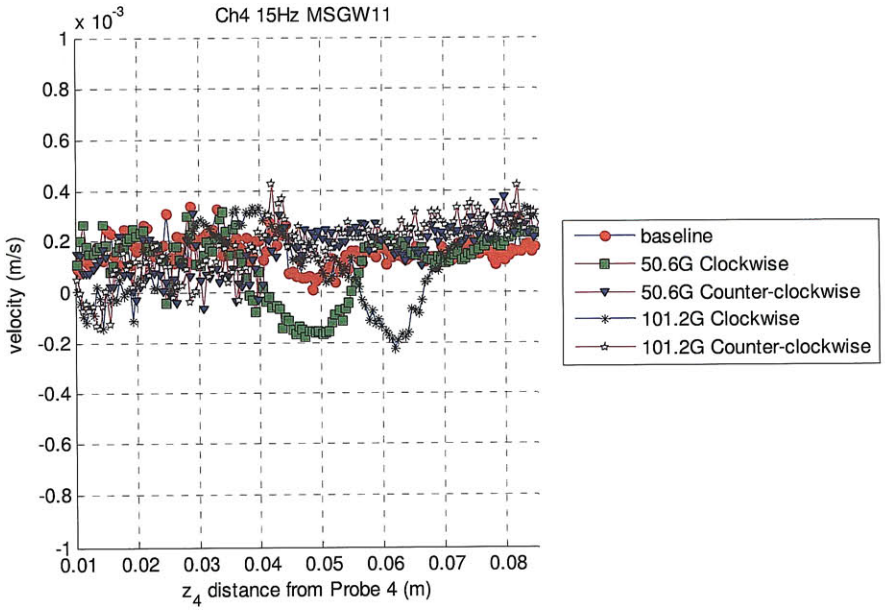

Figure 6-13. Velocity profile as a function of distance away from channel 4 probe at 15 Hz using MSGW11. Two field strengths and two rotating directions are investigated. Negligible flow compared to the baseline is measured.

6.2. Numerical Simulation of Ferrofluid Spin-up Flow in Spherical Geometry in a Uniform Rotating Magnetic Field

To understand the results obtained in the previous section, the experiment was numerically simulated in three dimensions using COMSOL Multiphysics. Two simulations were carried out, one with spin-diffusion theory ($\eta' \neq 0$) and the other without ($\eta' = 0$) for two ferrofluids, Chaves's EMG900_2 [6] and Elborai and He's MSGW11 [1, 2] . Elborai and He's MSGW11 [1, 2] is the same MSGW11 used in Figure 6-10 through Figure 6-13.

6.2.1. Governing Equations

The governing equations used are identical to that used in section 4.4.1.1, and are listed below.

5) Poisson's Equation

$$\nabla^2 \psi = \nabla \cdot \mathbf{M} \tag{6.1}$$

6) Conservation of Linear Momentum

$$\rho\left[\frac{\partial \mathbf{v}}{\partial t} + (\mathbf{v}\cdot\nabla)\mathbf{v}\right] = -\nabla p' + 2\zeta\nabla\times\boldsymbol{\omega} + (\zeta+\eta)\nabla^2\mathbf{v} + \mu_0(\mathbf{M}\cdot\nabla)\mathbf{H} \tag{6.2}$$

7) Conservation of Angular Momentum

$$I\left[\frac{\partial \boldsymbol{\omega}}{\partial t} + (\mathbf{v}\cdot\nabla)\boldsymbol{\omega}\right] = \mu_0\mathbf{M}\times\mathbf{H} + 2\zeta(\nabla\times\mathbf{v} - 2\boldsymbol{\omega}) + \eta'\nabla^2\boldsymbol{\omega} \tag{6.3}$$

8) Magnetic Relaxation Equation

$$\frac{\partial \mathbf{M}}{\partial t} + (\mathbf{v}\cdot\nabla)\mathbf{M} = \boldsymbol{\omega}\times\mathbf{M} - \frac{1}{\tau_{eff}}(\mathbf{M} - \mathbf{M}_{eq}) \tag{6.4}$$

6.2.2. Model Assumptions

The applied field is assumed to not be strong enough to magnetically saturate the fluid. The equilibrium magnetization $\mathbf{M}_{eq}$ of the fluid is assumed to be in the linear regime of the Langevin equation as a function of the magnetic field inside the ferrofluid given by

$$\mathbf{M}_{eq} = \chi \mathbf{H}_{fluid} \tag{6.5}$$

The flow is also assumed to be viscous dominated allowing for the inertial terms to be dropped. The left hand side of the linear and angular momentum equations in (6.2) and (6.3) can be set to 0 and the equations reduced to

$$0 = -\nabla p' + 2\zeta \nabla \times \boldsymbol{\omega} + (\zeta + \eta)\nabla^2 \mathbf{v} + \mu_0 (\mathbf{M} \cdot \nabla)\mathbf{H} \tag{6.6}$$

and,

$$0 = \mu_0 \mathbf{M} \times \mathbf{H} + 2\zeta (\nabla \times \mathbf{v} - 2\boldsymbol{\omega}) + \eta' \nabla^2 \boldsymbol{\omega} \tag{6.7}$$

6.2.3. Model Setup and Boundary Conditions

6.2.3.1. Modeling the Rotating Magnetic Field

Although the model can be setup in COMSOL using current boundary conditions on the fluxballs, similar to Figure 5-14, it can be difficult to solve. A simpler method of setting up the magnetic field is by using the magnetic scalar potential boundary condition similar to that described in section 4.4.2.1. The only region of interest is the region of ferrofluid and it is only affected by the uniform field imposed. This simplifies the problem into a one region problem similar to Figure 6-14, to aid the numerical simulation process.

It is known that a sphere has demagnetizing factors of 1/3 in all directions. Therefore in the presence of an externally applied uniform magnetic field ($\mathbf{H}_{xext}, \mathbf{H}_{yext}, \mathbf{H}_{zext}$) the field inside the sphere of ferrofluid ($\mathbf{H}_{xfluid}, \mathbf{H}_{yfluid}, \mathbf{H}_{zfluid}$) can be given by the following relation.

$$\begin{aligned} \mathbf{H}_{xfluid} &= \mathbf{H}_{xext} - \frac{1}{3}\mathbf{M}_x \\ \mathbf{H}_{yfluid} &= \mathbf{H}_{yext} - \frac{1}{3}\mathbf{M}_y \\ \mathbf{H}_{zfluid} &= \mathbf{H}_{zext} - \frac{1}{3}\mathbf{M}_z \end{aligned} \tag{6.8}$$

Eqs (6.8) are substituted into $\mathbf{M}_{eq}$ of (6.4) and the only driving force will be due to the uniform external rotating magnetic field ($\mathbf{H}_{xext}, \mathbf{H}_{yext}$). To describe the uniform rotating field in Cartesian coordinates the external fields ($\mathbf{H}_{xext}, \mathbf{H}_{yext}$) are sinusoidal functions of time with rotational frequency Ω and 90° out of phase with each other. Eq (6.9) generates a counter-clockwise uniform rotating magnetic field of magnitude H_0.

$$\mathbf{H}_{xext} = H_0 \cos(\Omega t)\mathbf{i}_x$$
$$\mathbf{H}_{yext} = H_0 \sin(\Omega t)\mathbf{i}_y \tag{6.9}$$

Since

$$\mathbf{H} = -\nabla \psi \tag{6.10}$$

$\psi(r = R_0)$ can be determined to be the following boundary condition for a counter-rotating magnetic field.

$$\psi(r = R_0) = H_0(x\cos(\Omega t) + y\sin(\Omega t)) \tag{6.11}$$

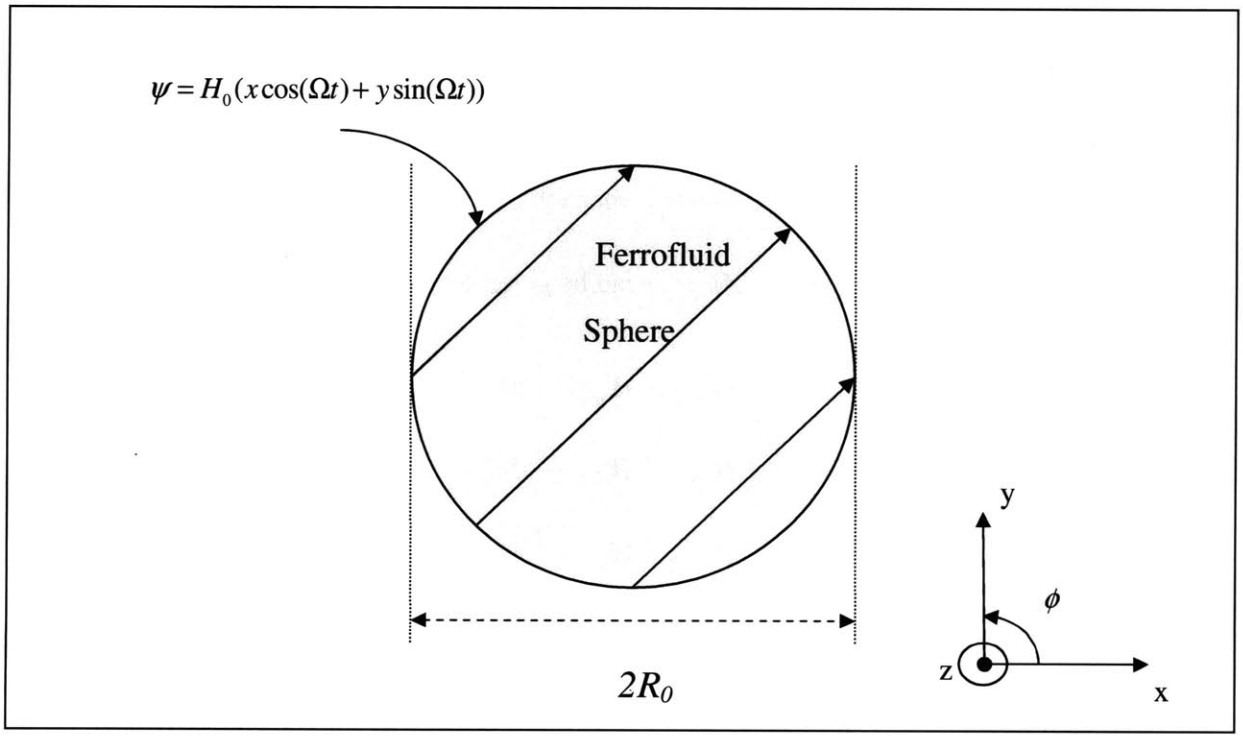

Figure 6-14. One region model setup with shaded circle representing ferrofluid and boundary condition on magnetic scalar potential. The scalar potential generates a magnetic field rotating in the ϕ direction at frequency Ω. This magnetic field represents the external magnetic field and has to be corrected for demagnetizing effects before being used in the magnetic relaxation equation. The arrows inside the stator show the uniformly distributed rotating magnetic field created inside the ferrofluid at a particular instant in time.

6.2.3.2. Fluid Boundary Conditions

The linear momentum equation in (6.6) requires two vector boundary conditions. For a rigid and stationary boundary the no slip and no-penetration boundary conditions are as follows

$$\mathbf{n}\cdot\|\mathbf{v}\| = 0, \mathbf{n}\times\|\mathbf{v}\| = 0 \quad r = R_0 \tag{6.12}$$

where $\|\vec{v}\|$ represents the jump in velocity of the fluid across the boundary $r=R_0$. The boundary condition at $\mathbf{v}(r = R_0)$ is

$$\mathbf{v}(r = R_0) = 0 \tag{6.13}$$

The conservation of angular momentum in (6.7) also requires an initial condition as well as two vector boundary conditions if $\eta' \neq 0$. The "spin-no-slip" boundary condition as described in section 4.4.2.2, which assumes that the particle/wall interactions are strong enough that there is no relative spin between the particle and surface, is applied and given as

$$\boldsymbol{\omega}(r = R_0) = 0 \tag{6.14}$$

Neglecting the effect of "spin-diffusion" by setting $\eta' = 0$, the angular momentum equation in (6.7) reduces from a second order to a zeroth order equation. Therefore there is no boundary condition on the spin-velocity $\boldsymbol{\omega}$ implying zero or negligible particle/wall interactions.

6.2.4. COMSOL Simulations with Spin-Diffusion ($\eta' \neq 0$)

The goal of this section is to simulate the spin-up flow experiment when a sphere of ferrofluid is subjected to a uniform rotating magnetic field and compare the results with those obtained experimentally in the previous section. Elborai [1] and He [2] both use the same MSGW11 fluid that was used to obtain Figure 6-10 through Figure 6-13. In their theses, they determine values for η' and τ that can be used in the COMSOL simulations. The simulations would help gain insight whether or not a flow should have been measured in the spherical case. In addition, Chaves's EMG900_2 fluid used in [6] will also be simulated in the spherical geometry since values of τ and η' are also determined in his paper.

Equations (6.1)-(6.4) were first non-dimensionalized with respect to reference parameters such as the radius of the sphere R_0, rotational frequency Ω and strength of rotating field H_0.

$$\mathrm{R}_e[\frac{d\bar{\mathbf{v}}}{d\bar{t}}+(\bar{\mathbf{v}}\bullet\bar{\nabla})\bar{\mathbf{v}}]=-\bar{\nabla}\bar{p}'+2\bar{\zeta}\bar{\nabla}\times\bar{\boldsymbol{\omega}}+(\bar{\zeta}+\bar{\eta})\bar{\nabla}^2\bar{\mathbf{v}}+\left(\bar{\mathbf{M}}\bullet\bar{\nabla}\right)\bar{\mathbf{H}} \tag{6.15}$$

$$R_w[\frac{d\bar{\boldsymbol{\omega}}}{d\bar{t}}+(\bar{\mathbf{v}}\bullet\bar{\nabla})\bar{\boldsymbol{\omega}}]=\bar{\mathbf{M}}\times\bar{\mathbf{H}}+2\bar{\zeta}(\bar{\nabla}\times\bar{\mathbf{v}}-2\bar{\boldsymbol{\omega}})+\bar{\eta}'\bar{\nabla}^2\bar{\boldsymbol{\omega}} \tag{6.16}$$

$$\frac{d\bar{\mathbf{M}}}{d\bar{t}}+(\bar{\mathbf{v}}\bullet\bar{\nabla})\bar{\mathbf{M}}=\bar{\boldsymbol{\omega}}\times\bar{\mathbf{M}}-\frac{1}{\Omega\tau_{eff}}(\bar{\mathbf{M}}-\bar{\mathbf{M}}_{eq}) \tag{6.17}$$

$$\nabla^2\bar{\psi}=\nabla\bullet\bar{\mathbf{M}} \tag{6.18}$$

where

$$\bar{\nabla}=\nabla R_0,\ \bar{\mathbf{v}}=\frac{\mathbf{v}}{R_0\Omega},\ \bar{\mathbf{M}}=\frac{\mathbf{M}}{H_0},\ \bar{\mathbf{H}}=\frac{\mathbf{H}}{H_0},\ \bar{t}=t\Omega,\ \bar{p}=\frac{p}{\mu_0 H_0^2},\ \bar{\boldsymbol{\omega}}=\frac{\boldsymbol{\omega}}{\Omega},\ \bar{\psi}=\frac{\psi}{H_0R_0}$$

$$\bar{\zeta}=\frac{\zeta\Omega}{\mu_0H_0^2},\ \bar{\eta}=\frac{\eta\Omega}{\mu_0H_0^2},\ R_e=\frac{\rho R_0^2\Omega^2}{\mu_0H_0^2},\ R_w=\frac{I\Omega^2}{\mu_0H_0^2},\ \bar{\eta}'=\frac{\eta'\Omega}{\mu_0H_0^2R_0^2}$$

These equations (6.15)-(6.18) were put into COMSOL in non-dimensional form and in all cases the transient form of the equations were used. A fluid mechanics module was used to represent the augmented Navier-Stokes equation (6.15). Three transient convection and diffusion modules were used to represent the magnetic relaxation equation in x, y and z coordinates (6.17). A diffusion equation was used for the angular momentum equation (6.16) with η' the coefficient for the spin diffusion term and a general PDE module was used to represent Poisson's equation in (6.18). The time-dependent terms in the PDE module set of the linear and angular momentum equations were all set to 0. The general PDE module could potentially be replaced by the AC-DC *Magnetostatics, No Currents* module, both giving the same results.

The results from the previous section are that negligible flow was obtained with MSGW11 at all field strengths and frequencies. The values of η' and τ_{eff} were independently determined by Elborai [1] and He [2]. These are tabulated in Table 6-3.

MSGW11	**τ_{eff}(s)**	**η' (kg m/s)**
Elborai [1]	$1.2\text{x}10^{-5}\pm1.18\text{x}10^{-5}$	$3.15\text{x}10^{-9}\pm1.13\text{x}10^{-9}$
He [2]	$1.57\text{x}10^{-5}\pm1.43\text{x}10^{-5}$	$6.4\text{x}10^{-9}\pm5.4\text{x}10^{-9}$

Table 6-3. Table of η' and τ_{eff} determined by Elborai [1] and He [2] in their theses.

For the COMSOL simulation, an average of the values of η' and τ_{eff} determined by Elborai [1] and He [2] was used resulting in $\tau_{eff} = 1.39\text{x}10^{-5}$ s and $\eta' = 4.78\text{x}10^{-9}$ kg m/s. The parameters for MSGW11 and EMG900_2 are tabulated in Table 6-4. The non-dimensional parameters used in (6.15)-(6.18) were then determined for a RMS rotating flux density of 100 G at 95 Hz and tabulated in Table 6-5. The model files are documented in Appendix F.

The results of the simulation give rotational flow in the spherical case as seen in Figure 6-15 and Figure 6-16. The flow is in the same plane and direction as the rotating field and the magnitude of the dimensional rotational velocity as a function of radius for the two different

fluids in a 10 cm diameter sphere subjected to a rotating field are plotted in Figure 6-17. The magnitude of the velocity obtained is significant and should be easily measured with the DOP2000 velocimeter.

Parameter	EMG900_2 Value	MSGW11 value
τ_{eff} (s)	$1x10^{-6}$	$1.39x10^{-5}$
ρ (kg/m^3)	1030	1200
η (Ns /m^2)	0.0045	0.00202
$\mu_0 M_s$ (mT)	23.9	15.4
ζ (Ns/m^2)	0.0003	0.000083
Frequency (Hz)	95	95
Radius of spherical vessel R_0 (m)	0.05	0.05
Volume Fraction (%)	4.3	2.75
χ	1.19	0.56
η' (kg m/s)	$6x10^{-10}$	$4.78x10^{-9}$

Table 6-4. Table of parameters for EMG900_2 and MSGW11 ferrofluids used in COMSOL simulations.

Normalized Variable	EMG900_2	MSGW11
$\overline{\eta'} = \frac{\eta'\Omega}{\mu_0 H_0^2 R_0^2}$	$9x10^{-7}$	$7.17x10^{-6}$
$\overline{\zeta} = \frac{\zeta\Omega}{\mu_0 H_0^2}$	0.001089	0.000313
$\overline{\eta} = \frac{\eta\Omega}{\mu_0 H_0^2}$	0.0169	0.00758

Table 6-5. Table of normalized parameters that depend on the strength of the RMS magnetic field (B_0=*100 G*, H_0=*7957.75 A/m*) used and the radius of the sphere R_0=*5 cm*.

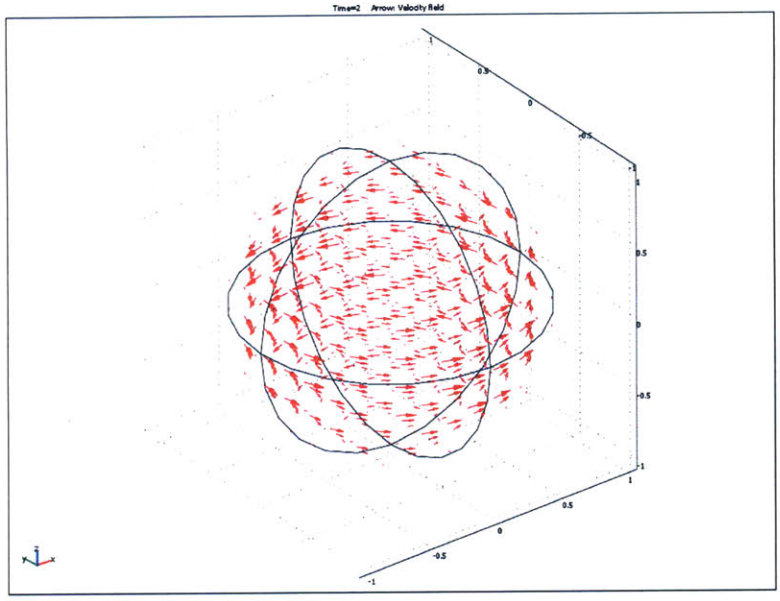

Figure 6-15. Velocity field generated with non-zero spin-viscosity for both MSGW11 and EMG900_2 in sphere. Velocity flow co-rotates in the same direction as the rotating field.

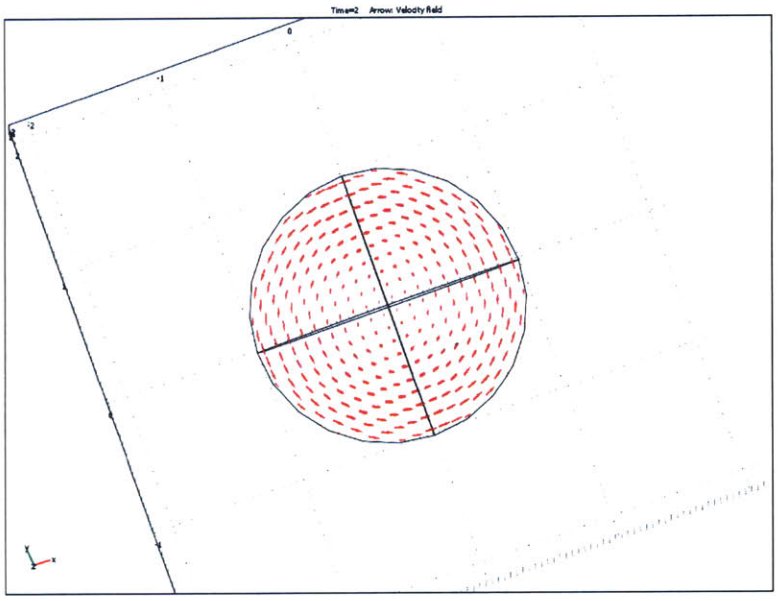

Figure 6-16. Velocity field observed from top of sphere perpendicular to plane of counter-clockwise rotating magnetic field.

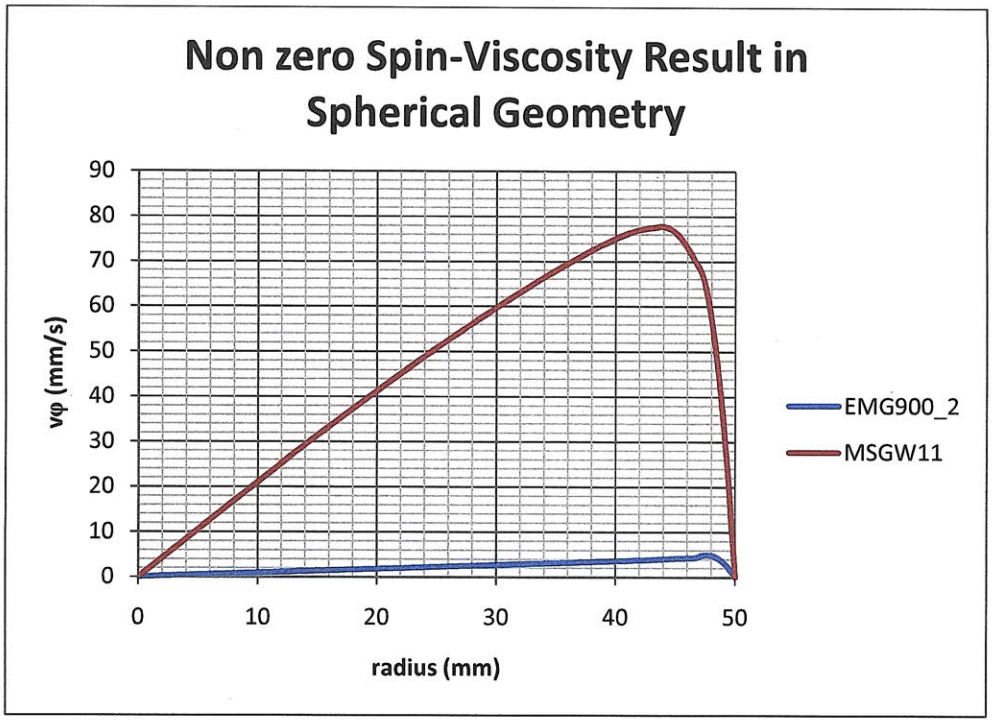

Figure 6-17. Dimensional rotational velocity for 10 cm diameter sphere of ferrofluid with non-zero spin-viscosity in a uniform rotating magnetic field calculated using COMSOL Multiphysics 3.5a. The results of MSGW11 and Chaves's EMG900_2 [6] both have velocity magnitudes that can be measured using the DOP2000.

The normalized magnetic field as a function of radius for both EMG900_2 and MSGW11 are plotted in Figure 6-18 and Figure 6-19. The distribution of magnetic field has slight variations at the wall boundary due to the velocity no-slip boundary condition affecting the magnetization. The magnetization for the EMG900_2 and MSGW11 are plotted in Figure 6-20 and Figure 6-21 respectively.

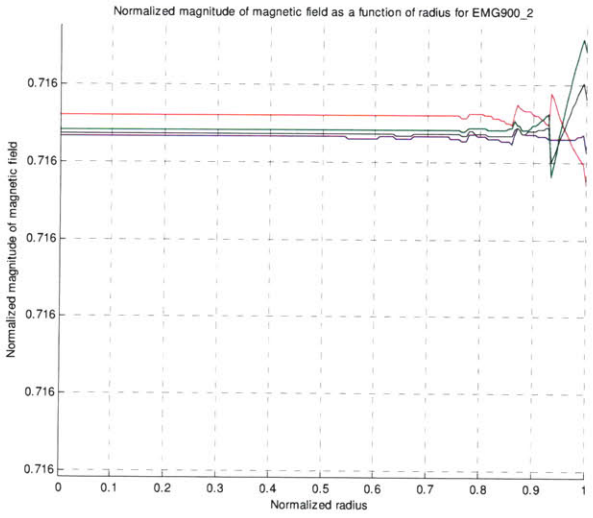

Figure 6-18. Normalized magnitude of magnetic field as a function of radius for EMG900_2 calculated using COMSOL Multiphysics 3.5a. The field is mostly uniform of magnitude 0.716 with slight variation at the wall boundary due to the no-slip velocity boundary condition affecting the magnetization there. The different colored lines correspond to different times in the simulation.

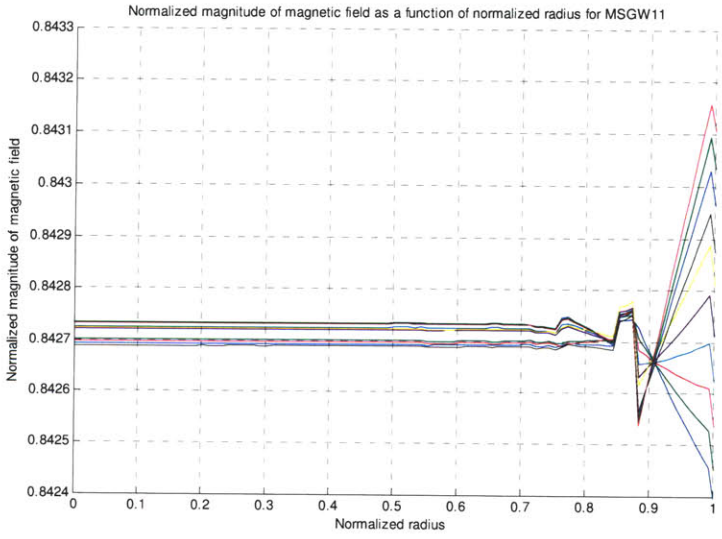

Figure 6-19. Normalized magnitude of magnetic field as a function of normalized radius for MSGW11 calculated using COMSOL Multiphysics 3.5a. Magnetic field is distributed uniformly, of magnitude 0.8427, throughout the fluid with slight variation near the wall boundary due to no-slip velocity boundary condition affecting the magnetization. The different colored lines correspond to different times in the simulation.

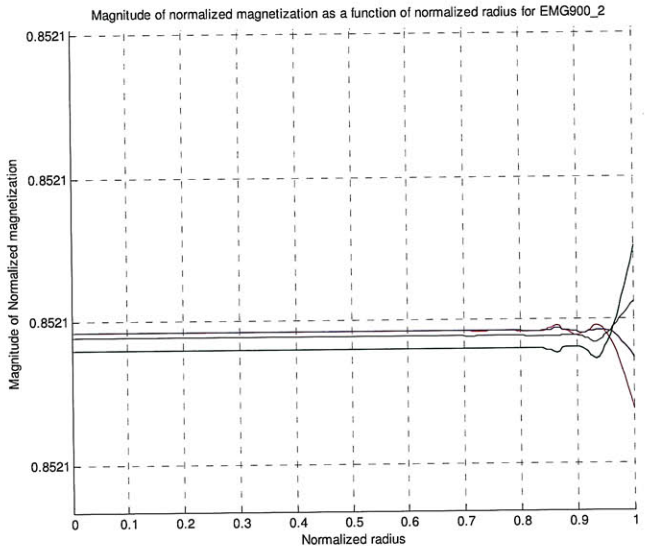

Figure 6-20. Normalized magnitude of magnetization as function of normalized radius for EMG900_2 using COMSOL Multiphysics 3.5a. The different colored lines correspond to different times in the simulation. The magnetization is uniform with magnitude 0.8521 with slight variations near the wall due to the velocity no-slip boundary condition.

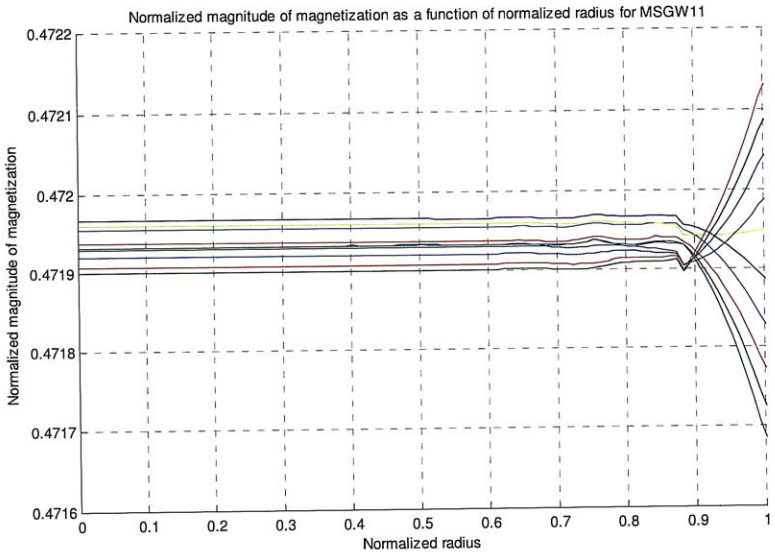

Figure 6-21. Normalized magnitude of magnetization as a function of normalized radius for MSGW11 using COMSOL Multiphysics 3.5a. The different colored lines correspond to different times in the simulations. The magnetization is mostly affected near the wall due to the velocity no-slip boundary condition there and is of magnitude 0.472.

6.2.5. Comparison with Analytic Solutions Using a Linear Magnetic Material

Since the magnetic field is mainly uniform within the ferrofluid as seen in Figure 6-18 and Figure 6-19, the magnetic material can be considered to be almost linear. In section 5.2.3, the magnetic field distribution inside a sphere of linear magnetic material placed inside a fluxball is calculated. To generate a rotating magnetic field, a fluxball machine comprised of two orthogonal fluxballs is used resulting in an equation for the magnetic field inside the linear magnetic material given by

$$|H| = \frac{NI}{(3+\chi)R} \tag{6.19}$$

If $\chi = 0$, with a normalized magnetic field magnitude of 1

$$\frac{NI}{R} = 3 \tag{6.20}$$

Substituting a $\chi = 1.19$ for EMG900_2 gives a normalized magnetic field magnitude of 0.716 similar to that obtained in Figure 6-18. The magnetization can also be calculated using $|\mathbf{M}| = \chi|\mathbf{H}|$ resulting in a normalized value of 0.852 equal to that in Figure 6-20.

Similarly for MSGW11 with a $\chi = 0.56$ results in a normalized magnetic field magnitude of 0.843 and a normalized magnetization of 0.472 as confirmed in Figure 6-19 and Figure 6-21.

6.2.6. Theoretical Determination of Spin-Viscosity η' [3, 4]

Bird, Stewart and Lightfoot [5] derive the dynamic viscosity of a low density gas from a molecular kinetic theory of gases. This theory can be extended to derive a theoretical value for spin-viscosity η' by considering the flux density of internal angular momentum ω, instead of linear momentum as is done in [5], and is given as

$$\text{Angular momentum flux density} = \eta' \nabla \omega \tag{6.21}$$

where the spin-viscosity coefficient η' is the analog to dynamic viscosity η used in [5].

A shear flow in the x-y plane shown in Figure 6-22 has a gradient of x-velocity in the y direction resulting in transfer of linear momentum in the x-direction to the y-direction. The particle's spin direction is in the z-direction which is also transferred in the y-direction. A plot of the distribution of the z-directed spin ω_z as a function of y is given in Figure 6-23.

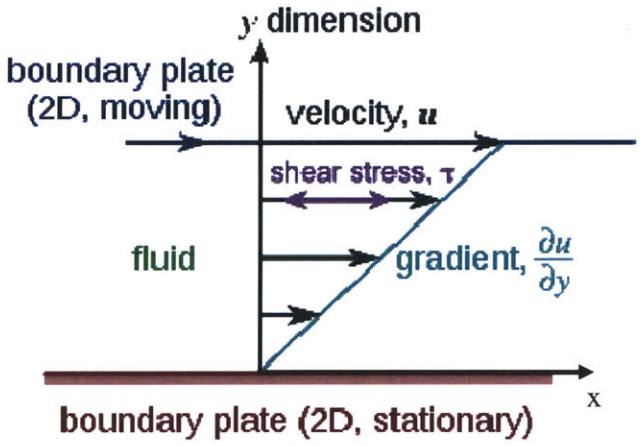

Figure 6-22. Laminar shear flow between two plates resulting in Couette flow http://en.wikipedia.org/wiki/File:Laminar_shear.svg.

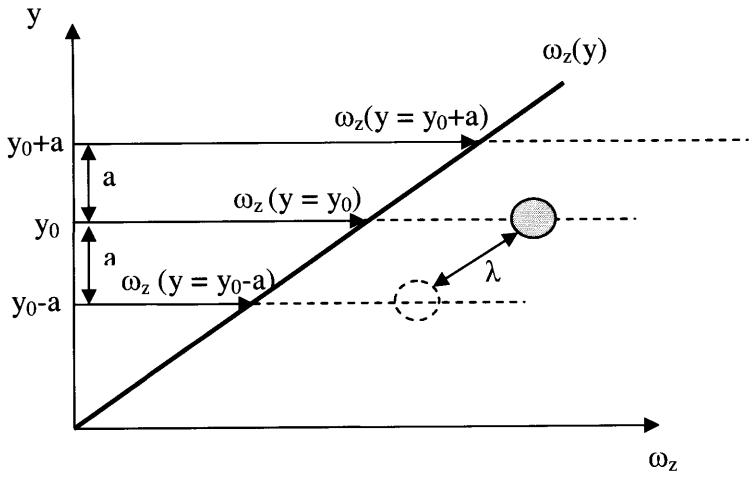

Figure 6-23. Molecular transport of spin velocity ω_z from the plane ($y = y_0-a$) to the plane at y_0. λ is the mean free path of the particle.

The frequency of molecular bombardment per unit area on one side of the plane (y-a) is

$$Z = \frac{1}{4} nu \tag{6.22}$$

where n is the number of molecules per unit volume and u is the magnitude of the average particle velocity given as

$$u = \sqrt{\frac{8kT}{\pi m}} \tag{6.23}$$

where k is the Boltzmann constant, m the mass of the particle and T the average temperature of the fluid. The flux per unit area of internal angular momentum across the planes ($y = y_0+a$) and ($y = y_0-a$) can be given as

$$\text{Angular momentum flux density} = ZmI\omega_z\big|_{y0-a} - ZmI\omega_z\big|_{y0+a} \tag{6.24}$$

where I is the moment of inertia per unit mass. On average a particle reaching a plane would have experienced their last collision at a distance a from the plane given by

$$a = \frac{2}{3}\lambda \tag{6.25}$$

where λ is the mean free path given by

$$\lambda = \frac{1}{\sqrt{2}\pi(2R_2)^2 n} \tag{6.26}$$

with $2R_2$ representing the collision diameter of the particle. Assuming that all particles have spin velocities representative of the region in which they last collided, the spin profile $\omega_z(y)$ is essentially linear over many mean free paths and is given by

$$\begin{aligned} \omega_z\big|_{y0-a} &= \omega_z\big|_{y0} - \frac{2}{3}\lambda \frac{d\omega_z}{dy}\bigg|_{y0} \\ \omega_z\big|_{y0+a} &= \omega_z\big|_{y0} + \frac{2}{3}\lambda \frac{d\omega_z}{dy}\bigg|_{y0} \end{aligned} \tag{6.27}$$

Substituting these equations into (6.24) results in

$$\text{Angular flux density} = -\frac{4}{3} ZmI\lambda \frac{d\omega_z}{dy}\bigg|_{y0} \tag{6.28}$$

where the coefficient to $\frac{d\omega_z}{dy}$ is the spin viscosity term η' as given in (6.21).

$$\eta' = \frac{4}{3} ZmI\lambda \tag{6.29}$$

The ferrofluid nanoparticles have a core radius of R_1 and are coated with a surfactant layer of radius R_2 resulting in a two layered sphere with different mass densities in each layer as seen in Figure 6-24.

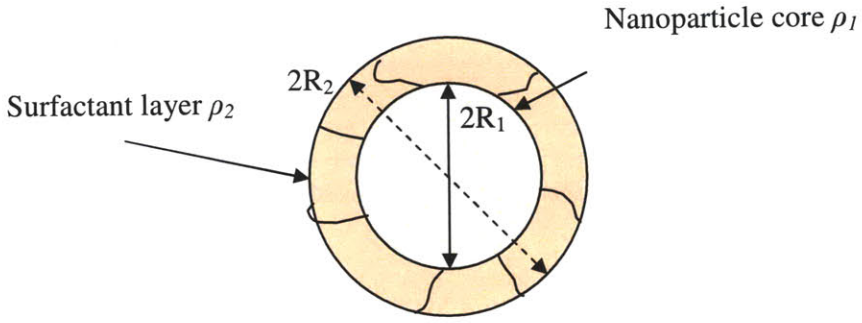

Figure 6-24. Two layered sphere representing nanoparticle of radius R_2 with a core of radius R_1. The core has a mass density of ρ_1 while the surfactant layer has a mass density ρ_2.

The moment of inertia per unit mass I is given as

$$I = \frac{8}{m15}\pi\left[\rho_1 R_1^5 + \rho_2\left(R_2^5 - R_1^5\right)\right] \tag{6.30}$$

Substituting (6.30) into (6.29) results in an estimate for η' as

$$\eta' = \frac{16}{45}\sqrt{\frac{kT}{m}}\frac{1}{\pi^{3/2}\left(2R_2\right)^2}\pi\left[\rho_1 R_1^5 + \rho_2\left(R_2^5 - R_1^5\right)\right] \tag{6.31}$$

where the mass of the two layered nanoparticle is given as

$$m = \frac{4}{3}\pi\left[\left(\rho_1 - \rho_2\right)R_1^3 + \rho_2 R_2^3\right] \tag{6.32}$$

with ρ_1, R_1 the mass density and radius of the core and ρ_2, R_2 the mass density and radius of the particle including the surfactant layer.

Schumacher, in his paper [3] states that "The spin viscosity is estimated using kinetic molecular theory of an ideal gas and multiplied by 1000 to get an estimate for our liquid since

liquid viscosities are typically 100-1000 times larger than gas viscosities". Schumacher [3] calculates that for a particular ferrofluid, with characteristics listed in Table 6-6, a value of $\eta'=6.4x10^{-20}$ is theoretically obtained.

Parameter	Schumacher's Ferrofluid [3]
ρ (kg/m^3)	1187.4
η (Ns /m^2)	0.00385
ζ (Ns/m^2)	0.00193
η' (kg m/s)	6.4x10^{-20}

Table 6-6. List of physical parameters and values used by Schumacher in his theoretical determination of η' [3].

The fluids used in this thesis, EFH1 and MSGW11, and even Chaves's EMG900_2 have parameters with values of the same order of magnitude as those listed in Table 6-6. The theoretical value for η' for these fluids should also be on the order of $\eta' \approx 10^{-20}$ which is many orders of magnitude smaller than the values experimentally determined by He [2], Elborai [1] and Chaves [6].

6.2.7. Rosensweig's Alternate Method of Determining Spin-Viscosity

Rosensweig also theoretically derives an expression for η' using the kinetic theory of dilute gases [4], similar to Schumacher in [3]. In addition to that, Rosensweig also derives an expression for η', in his book [8], using the viscosity of the fluid itself η given by

$$\eta' \sim \eta l^2 \tag{6.33}$$

where l is the characteristic diffusion length and has the same order of magnitude as the average distance between the solid particles defined by the approximate dilute-limit relationship

$$\frac{l}{d} = \left(\frac{\pi}{6\phi_{vol}} \right)^{1/3} \tag{6.34}$$

where d is the particle diameter and ϕ_{vol} is the volume fraction of magnetic nanoparticles in the ferrofluid.

He [2], using values determined for MSGW11 in his thesis (d=5.5-12.4nm, η =0.00202 Ns/m^2, ϕ_{vol} =2.75%), derives a value of η' for MSGW11 to be $\eta' = 0.436 - 2.214 \times 10^{-16}$ [kg m/s] which is also several order of magnitudes smaller than the value determined from his experiments $\eta' \approx$ (1-11.8)x10^{-9} [kg m/s].

6.2.8. COMSOL Simulations with No Spin-Diffusion ($\eta'=0$)

The theoretical η' term is calculated to be extremely small, which is why several authors do not include it in their analysis by setting it to 0 [7, 9-12]. The results obtained are similar to those obtained in the cylindrical geometry and documented in section 4.4.3.5. The model file is documented in Appendix F.

By setting the term to zero, the conservation of angular momentum equation reduces to a zeroth order equation in space requiring no boundary condition on spin-velocity $\boldsymbol{\omega}$ at the wall.

$$I[\frac{\partial \boldsymbol{\omega}}{\partial t}+(\mathbf{v}\bullet\nabla)\boldsymbol{\omega}] = \mu_0\mathbf{M}\times\mathbf{H}+2\zeta(\nabla\times\mathbf{v}-2\boldsymbol{\omega})+\eta'\nabla^2\boldsymbol{\omega} \tag{6.35}$$

The constant demagnetizing factors of 1/3 in all directions for the spherical case results in a magnetization that would only be in the same plane as the rotating magnetic field. Any other ferrofluid container shape would result in a spatially varying demagnetizing field that would result in a spatially varying magnetization. Since the magnetization and applied magnetic field do not vary spatially, there would be no spatial variation in spin-velocity and the magnetic force term would also be zero for a cylinder with non-moving walls.

$$\rho[\frac{\partial \mathbf{v}}{\partial t}+(\mathbf{v}\bullet\nabla)\mathbf{v}] = -\nabla p'+2\zeta\nabla\times\boldsymbol{\omega}+(\zeta+\eta)\nabla^2\mathbf{v}+\mu_0(\mathbf{M}\bullet\nabla)\mathbf{H} \tag{6.36}$$

$$\mathbf{F} = \mu_0(\mathbf{M}\bullet\nabla)\mathbf{H} = 0 \tag{6.37}$$

Simulations of a sphere of ferrofluid subjected to a uniform rotating field with $\eta'=0$ were done using the parameters for both Chaves's EMG900_2 [6] ferrofluid and MSGW11 as given in Table 6-4 and Table 6-5. The velocity profiles for EMG900_2 and MSGW11 are negligible ($\approx 10^{-14}$ normalized velocity magnitude) as seen in Figure 6-25 and Figure 6-26 respectively.

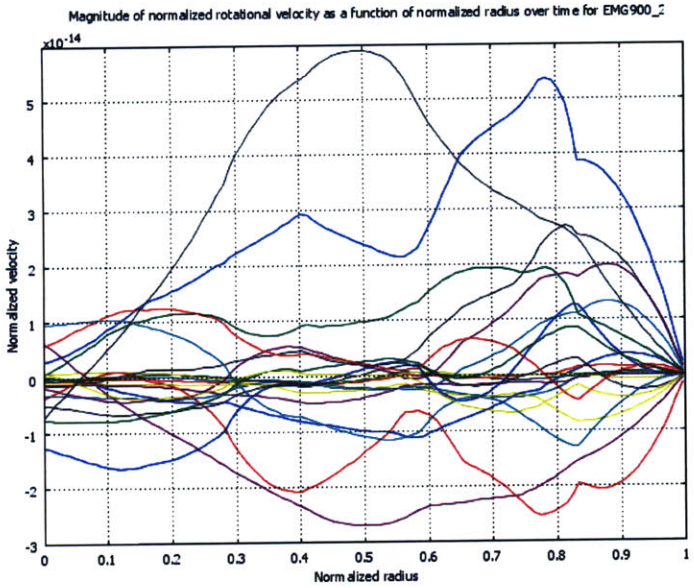

Figure 6-25. Plot of normalized rotational velocity v_ϕ as a function of normalized radius for EMG900_2 calculated using COMSOL Multiphysics 3.5a. The different colored lines represent different profiles in time. The magnitude of the velocity is extremely small $\approx 10^{-14}$ normalized magnitude and is in the noise.

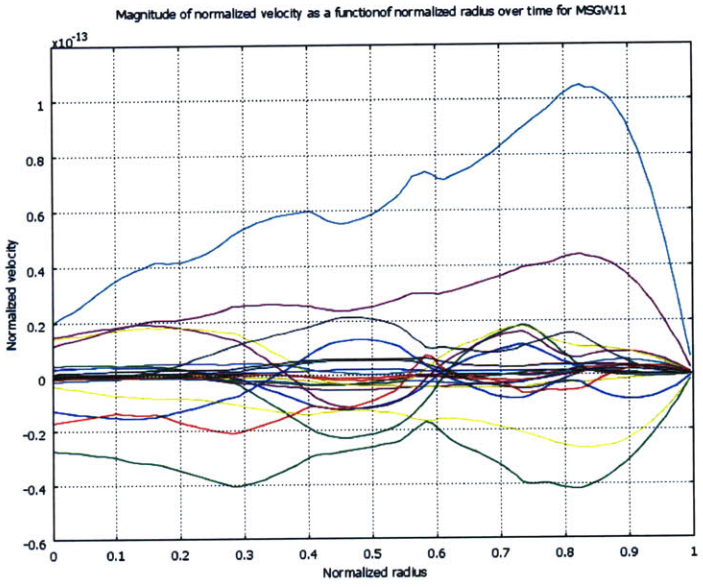

Figure 6-26. . Plot of normalized rotational velocity as a function of normalized radius for MSGW11 calculated using COMSOL Multiphysics 3.5a. The different colored lines represent different profiles in time. The magnitude of the velocity is extremely small $\approx 10^{-13}$ normalized magnitude and is in the noise.

6.3. Conclusions of Spin-up Experiment with Uniform Rotating Magnetic Field

The experiment of applying a uniform rotating magnetic field to a sphere of ferrofluid gave negligible flow as described in section 6.1. This result could not have been possible using the η' values determined experimentally by Chaves [6], He [2] and Elborai [1]. These values were also many orders of magnitude greater than the theoretical derivation of η'.

The negligible flow obtained in the spherical geometry and the non-zero flow in the cylindrical geometry with a stationary lid confirms that flow is generated due to the non-uniform field created by the demagnetizing effects of the shape of the ferrofluid container as stated by Shliomis [12]. The negligible flow in the spherical case could not have been possible using the η' values determined experimentally by Chaves [6], He [2] and Elborai [1]. This also means that the experimentally determined η' values compensates for the demagnetizing effects due to the cylindrical shape of the container and explains why fitted η' values to meeasurements were many orders of magnitude greater than the theoretical derivation of η'.

All these facts along with the negligible flow obtained with $\eta'=0$ (section 6.2.8) conclude that the effects of spin-diffusion are truly negligible. Pshenichnikov [7] takes Shliomis's [12] argument further by stating that the flow is fundamentally created by a spatial non-uniformity in magnetic susceptibility brought about either by a strong bias field or by spatial non-uniform heating of the fluid due to the dissipation energy of the rotating field. To fully investigate this hypothesis, the sphere of ferrofluid is subjected to a non-uniform rotating field and this experiment is detailed in the next section.

6.4. Experimental Setup of Applying a Non-Uniform Rotating Magnetic Field to a Sphere of Ferrofluid

A non-uniform rotating magnetic field is created by superimposing the uniform rotating magnetic field, generated by the fluxball, with the magnetic field imposed by a permanent magnet or a solenoidal coil placed at a particular point on the ferrofluid filled sphere. The field will be mainly non-uniform in the region near the solenoidal coil or permanent magnet and uniform elsewhere.

In the case of the fluxball machine, there was very little room inside the test chamber of the inner fluxball leaving only the option of placing the coil/magnets on top of the sphere of ferrofluid. To allow for this, the *crane* part had to be redesigned to remove the slot for the GMW probe and leave only the slot for the ultrasound probe at z=+2.5 cm as seen in Figure 6-2. The new crane part (named *Crane version 4*) can be seen in Figure 6-2, Figure 6-27 and Figure 6-28 and its dimensions are given in Appendix C.

The experimental results were conducted allowing sufficient time for the fluxball and the ferrofluid filled sphere to cool to room temperature of ≈25°C to minimize temperature effects on the magnetic susceptibility of the ferrofluid.

6.4.1. Design and Construction of the Third Solenoidal Coil

The third solenoidal coil will be referred to as the third coil for the rest of this thesis. The design requirements for the third coil are as follows:

1. The coil has to be able to fit inside the small region above the sphere of ferrofluid and the inside wall of the inner fluxball.
2. It has to have low resistance to prevent significant heating of the ferrofluid filled sphere that would drive convection currents.
3. It has to have high inductance to generate a strong enough magnetic field to make the total field significantly non-uniform in the region near the ferrofluid filled sphere.

To meet these criteria, the third coil was made using 0.5 inch wide insulated copper foil (Alpha-Core Laminax B-series #B0500x0625). The copper foil was of 5 mil thickness with a 0.625 inch wide polyester backing of 1.2 mil thickness and is described in Appendix C. The copper foil automatically limited the coil's height to 0.625 inches and the third coil was made by winding 150 turns of this foil. The resulting dimensions of this solenoidal coil, documented in Appendix C, was small enough to fit inside the small region above the sphere of ferrofluid as seen in the outline diagram of Figure 6-27 and the profile picture of Figure 6-28.

Figure 6-29 and Figure 6-30 are pictures of the actual third coil designed and built. Figure 6-29 also shows that the third coil had its leads coated with Kapton insulating tape to prevent short circuiting of the leads in case the high currents melt the wire insulation. Figure 6-30 illustrates that the windings and the structural integrity of the coil were also held together with the help of cable ties.

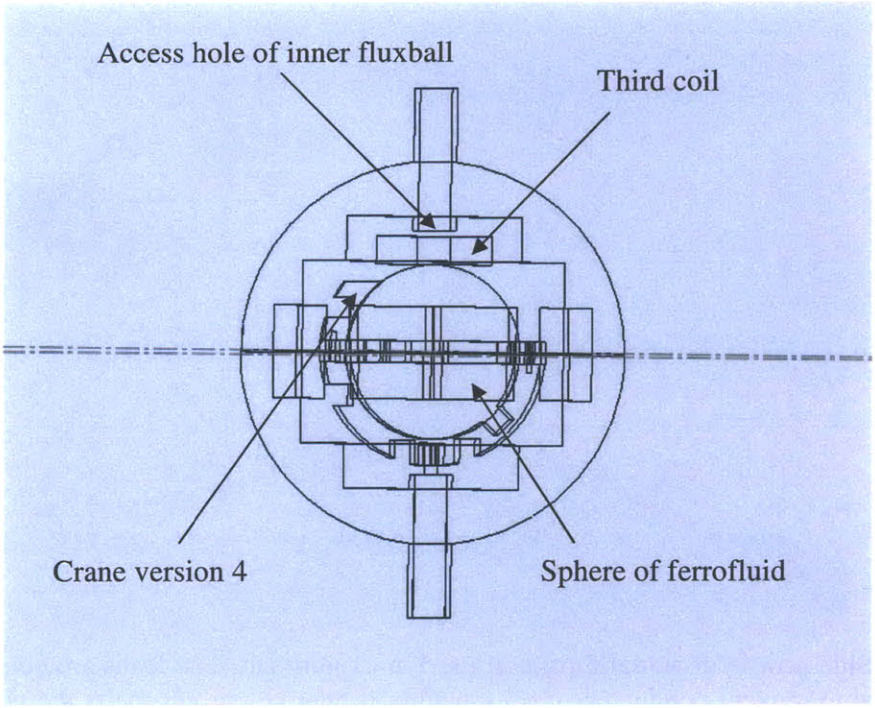

Figure 6-27. Wire diagram showing position of third coil placed on top of ferrofluid sphere with very little room left between access hole of inner fluxball and third coil.

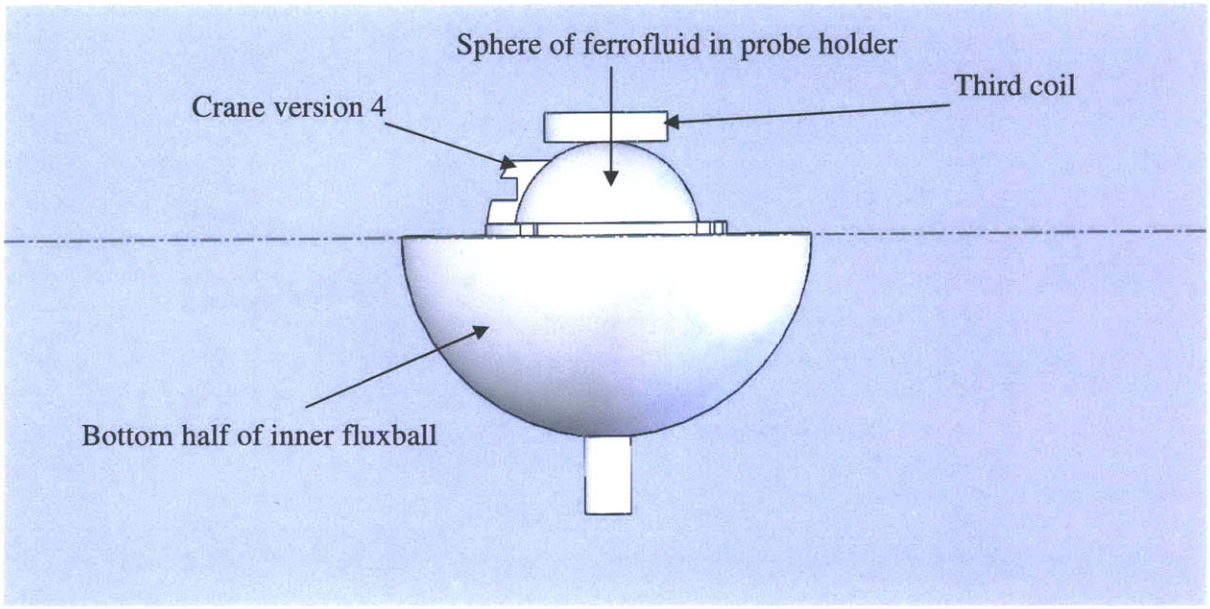

Figure 6-28. Side profile of half of inner fluxball with third coil placed on top of sphere of ferrofluid. The modified crane version 4 is also shown.

Figure 6-29. Side profile of actual third coil used in experiment. The leads are coated in Kapton insulation tape to prevent conductors from touching if enough current melts the wire insulation. The coil also has a tube fitted to its inner annulus to fit inside the inner fluxball's access hole.

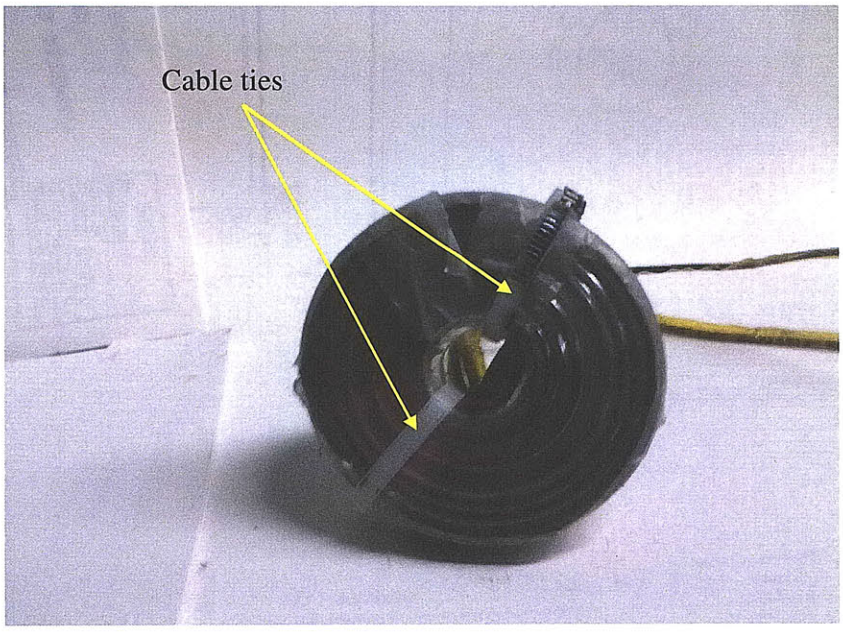

Figure 6-30. Picture showing the underneath of the third coil used in experiment. The windings are held together using cable ties.

6.4.2. Lumped Parameter Model of Third Coil

The third coil can be modeled as an R-L circuit. Measurements of the resistance and inductance of the third coil was made using the Hewlett-Packard 4192A LF Impedance Analyzer. The properties for the third coil are tabulated in Table 6-7 with values of resistance and inductance taken at two frequencies 100 Hz and 1 kHz.

	At 100 Hz	At 1000 Hz
Resistance	0.26 Ω	0.394 Ω
Inductance	0.7 mH	0.688 mH
Self Resonant Frequency	1.98 MHz	

Table 6-7. Table of measured resistance and inductance values for the R-L model of the third coil at two frequencies, 100 Hz and 1 kHz.

6.4.3. Normal Operation of the Third Coil

The purpose of the third coil is to generate a magnetic field at DC as well as at any AC frequency specified. To generate the desired current through the third coil, it would have to be connected to a voltage source which in this case would be the output of the LVC 5050 power amplifier with inputs from a NI PCI-6035E DAQ card. The NI LabVIEW 8.2 program used in section 5.2.6 was used to control the NI PCI-6035E DAQ card which generates an output voltage of 0-10V that is amplified, with a voltage gain of 20, by the LVC 5050 power amplifier and fed to the third coil in series with a 1Ω 200W resistor.

The voltage drop across this resistor represents the current flowing through the third coil and this measurement is fed back to an input of the DAQ card. The LabVIEW program uses the NI LabVIEW 8.2 PID Control Toolkit to then adjust the output channel voltage from the DAQ card to obtain the desired current through the third coil. This measurement also allows for the control of the phase difference between the third coil current and the inner fluxball current

during AC operation of the third coil. Since the third coil will be used in conjunction with the fluxball machine, both the NI PCI-6036E and PCI-6035E DAQ cards have to be used in conjunction with two LVC 5050 power amplifiers and two BNC 2120 connector blocks. The different amplifiers, DAQ cards and connector blocks are numbered and laid out in the circuit diagram for the whole setup as shown in Figure 6-31 and the datasheet for the parts are given in Appendix C.

A screen shot of the LabVIEW user interface (identical to Figure 5-22) is shown in Figure 6-32. The controls highlighted in Figure 6-32 are sufficient to control and maintain the magnitude, frequency (including DC operation) and phase difference between the third coil and inner fluxball currents. The phase difference between the third coil and the inner fluxball is controlled by adjusting the phase of the signal exciting the third coil using the NI LabVIEW 8.2 PID Control Toolkit taking care of the mutual inductance effects between the fluxball and the third coil. The controls for the individual fluxball windings were highlighted in Figure 5-22. A detailed description of the LabVIEW program's functionality and code are given in Appendix J.

The 1Ω 200W resistor was made by placing two 50W 1Ω resistors in series with each other which were themselves placed in parallel with another two 50W 1Ω series resistors. The combined resistance of this arrangement is 1Ω but the power rating is 200W. The resistors were mounted in a metal enclosure (Digikey #HM947-ND) that had heat sinks (Digikey #ATS1145-ND) placed to dissipate the heat generated as seen in Figure 6-34. The inside of the resistor box with the four resistors are shown in Figure 6-35.

The third coil was inserted by fitting the tube (seen in Figure 6-29) into the access hole of the upper half of the inner fluxball. This positions the third coil along the axial line of the inner

fluxball and provides consistency for the numerous experiments conducted. A picture of the third coil inserted into the upper half of the inner fluxball is shown in Figure 6-33.

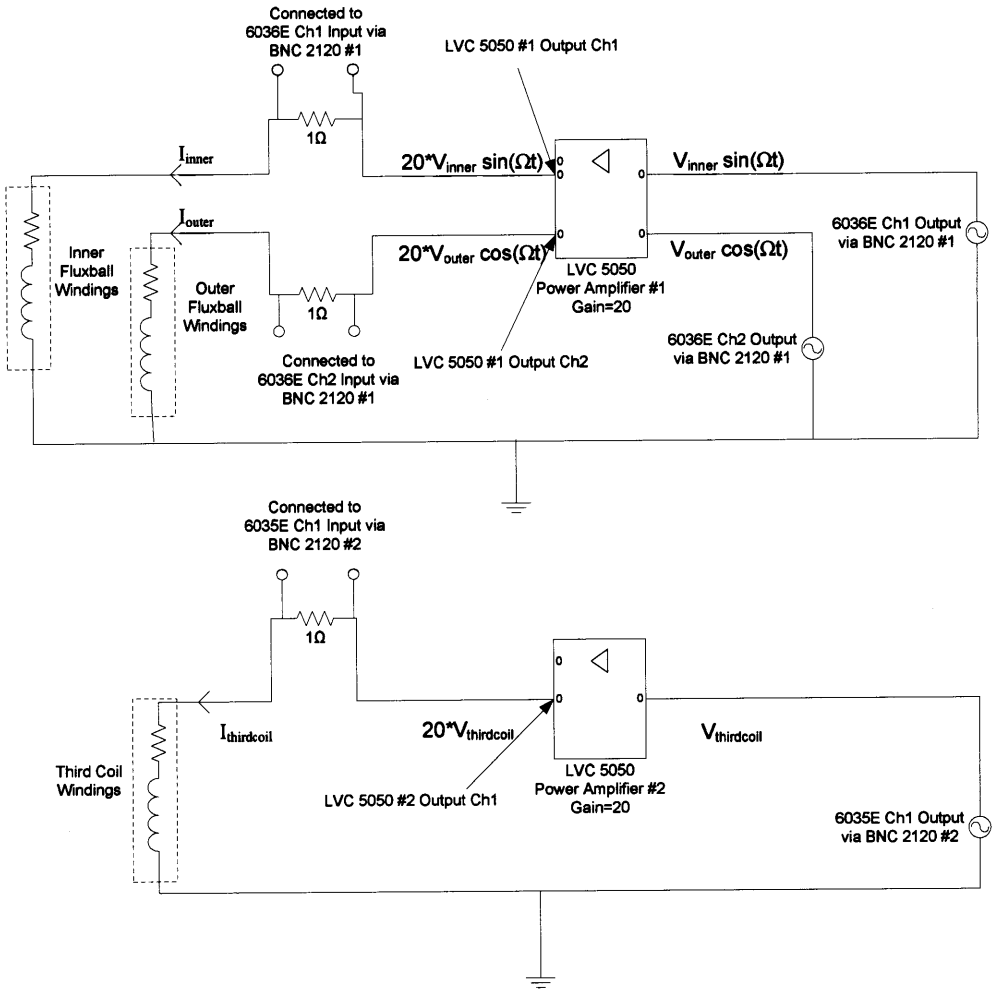

Figure 6-31. Circuit diagram outlining whole setup of controlling fluxball machine as well as third coil. Two LVC 5050 amplifiers, two DAQ cards and two BNC 2120 connector blocks have to be used.

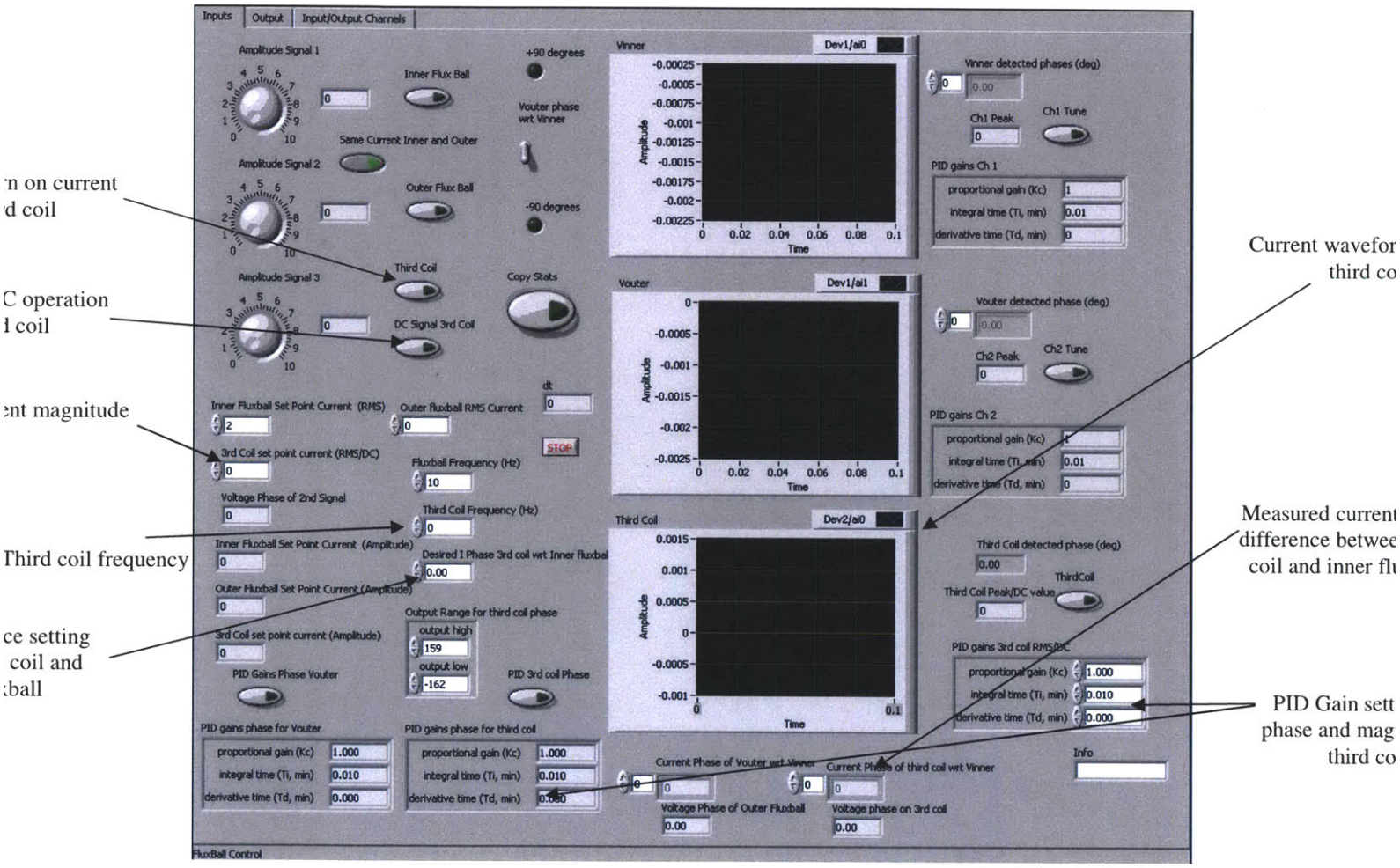

re 6-32. Front control panel of program in NI LabVIEW 8.2 showing all the controls needed to control third coil including setti
nitude, frequency and phase difference between third coil and inner fluxball. It also has a control to drive a DC current through t

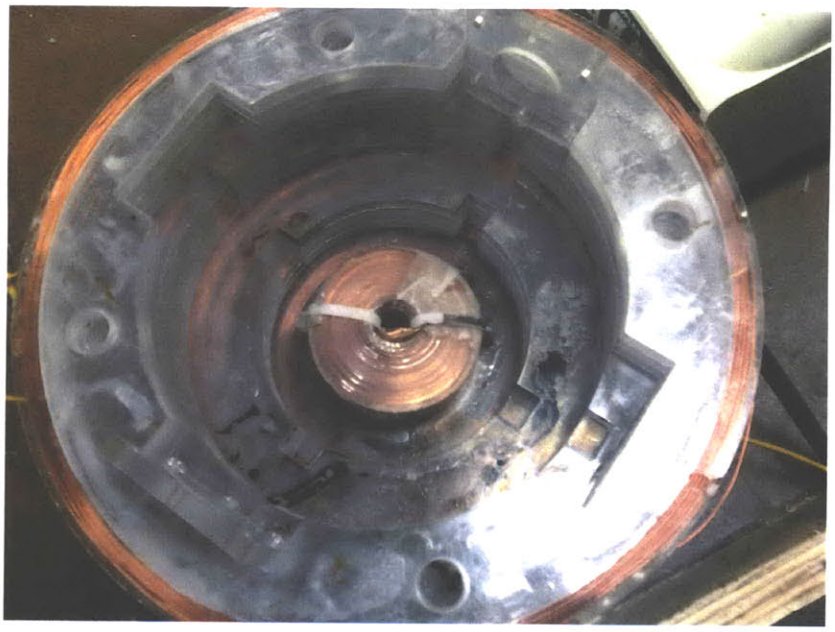

Figure 6-33. Tube inserted in the annulus of third coil (see Figure 6-29) fits inside the inner diameter of the inner fluxball's access tube. This allows for the third coil to be properly aligned along the axis of the fluxball for the numerous experiments conducted.

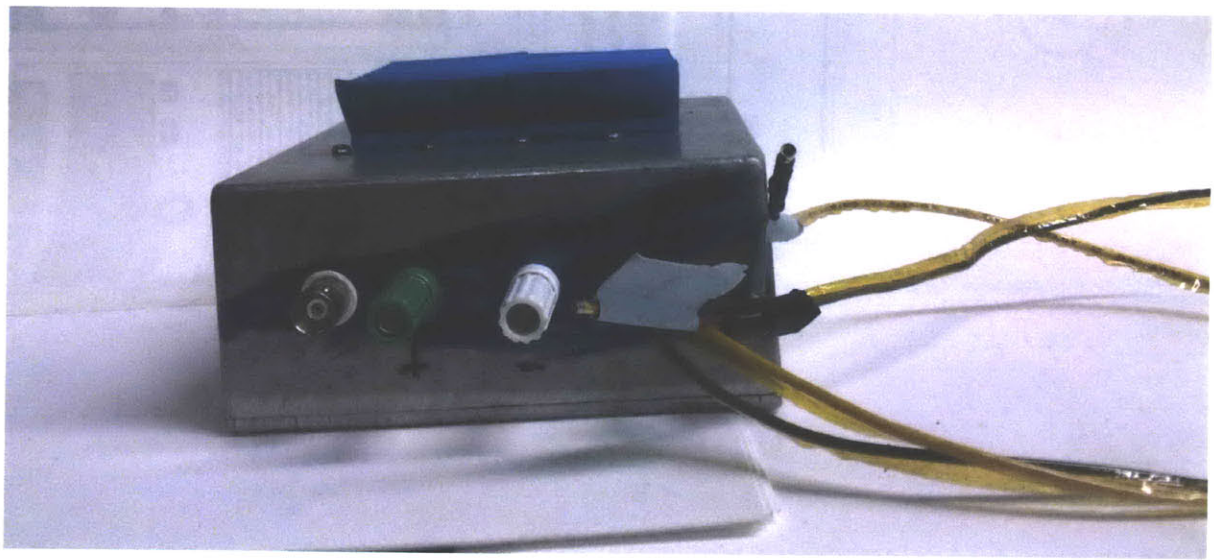

Figure 6-34. 1Ω 200W resistor in enclosure with heat sinks mounted. BNC connector used to connect the resistor in series with the LVC-5050 amplifier. The leads coated in Kapton tape connect the resistor to the third coil. The banana plug leads allow for the voltage measurement across the 1Ω resistor.

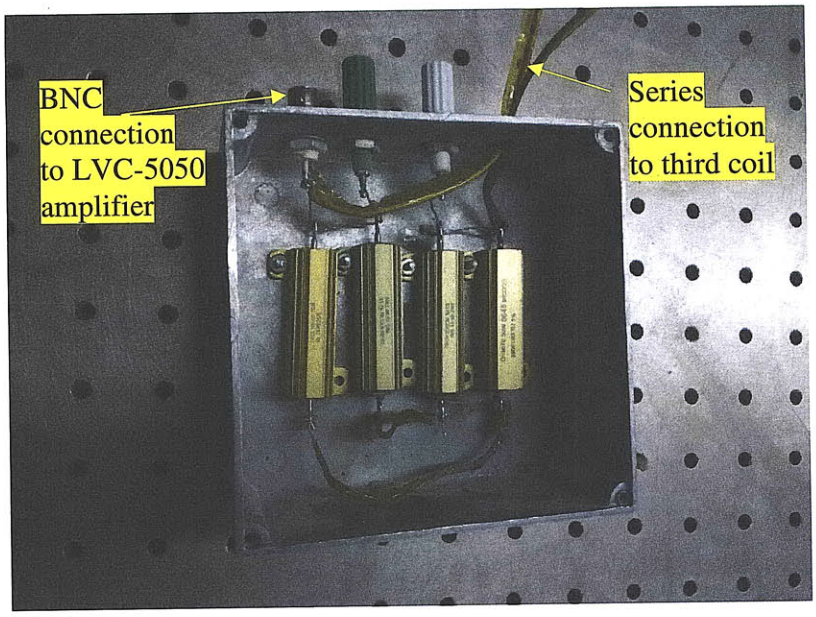

Figure 6-35. 1Ω 200W resistor made by using four 1Ω 50W resistors and mounted in the metal enclosure shown above. Two series 1Ω resistors are placed in parallel with another two series 1Ω resistors. The leads to the coil are coated with Kapton tape with banana plug leads connected to measure the voltage drop across the 1Ω combined resistor.

6.4.4. Magnetic Characteristics of Third Coil

The magnetic field in non-magnetic media in the axial direction (z-direction) of a single circular hoop in the z=0 plane, of radius a about the origin, carrying a constant current I is given by (6.38) [13] where z is the position along the axial direction.

$$B_z = \frac{\mu_0 I a^2}{2\left(z^2 + a^2\right)^{3/2}} \tag{6.38}$$

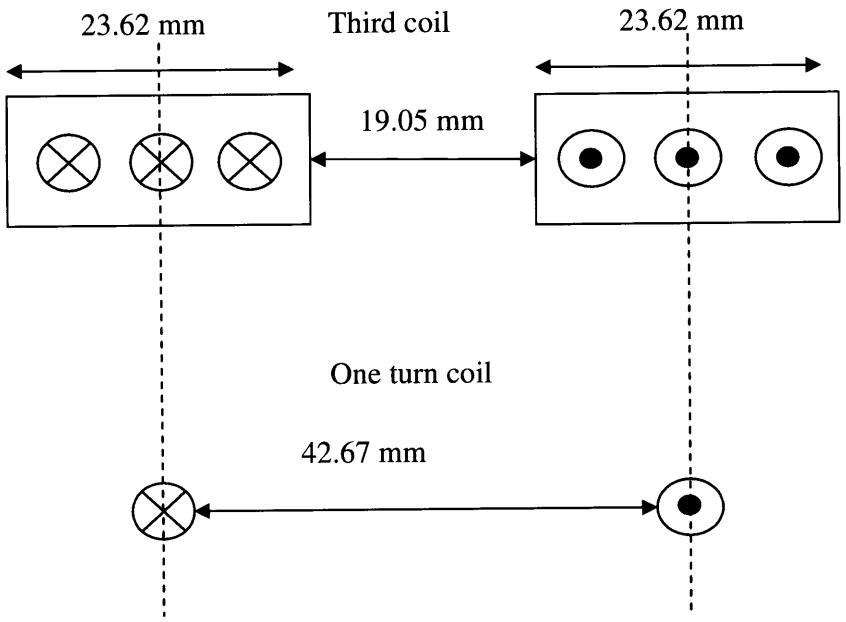

Figure 6-36. Cross-sectional diagram representing dimensions of third coil windings and one turn coil equivalent with radius $a \approx 21.34$ *mm*.

To compare the theoretical axial magnetic field obtained using (6.38) with measured data, the value of a has to be determined. By taking the mean location of the third coil windings as seen in Figure 6-36, the single turn equivalent current loop has an approximate radius $a \approx 21.34$ *mm*.

Measurements of axial magnetic flux density (B_z) as a function of axial distance (z) were made using 1A DC and 1A RMS for different frequencies and plotted in Figure 6-37.

To determine the winding factor K_w for the third coil, several measurements of magnetic flux density as a function of current, at the center of the annulus of the third coil $z=0$, were made for different frequencies including DC. These winding factors were averaged over the several frequency measurements and then averaged over the different current amplitudes to give an overall winding factor of 42.4 Gauss/A. These results are tabulated in Table 6-8.

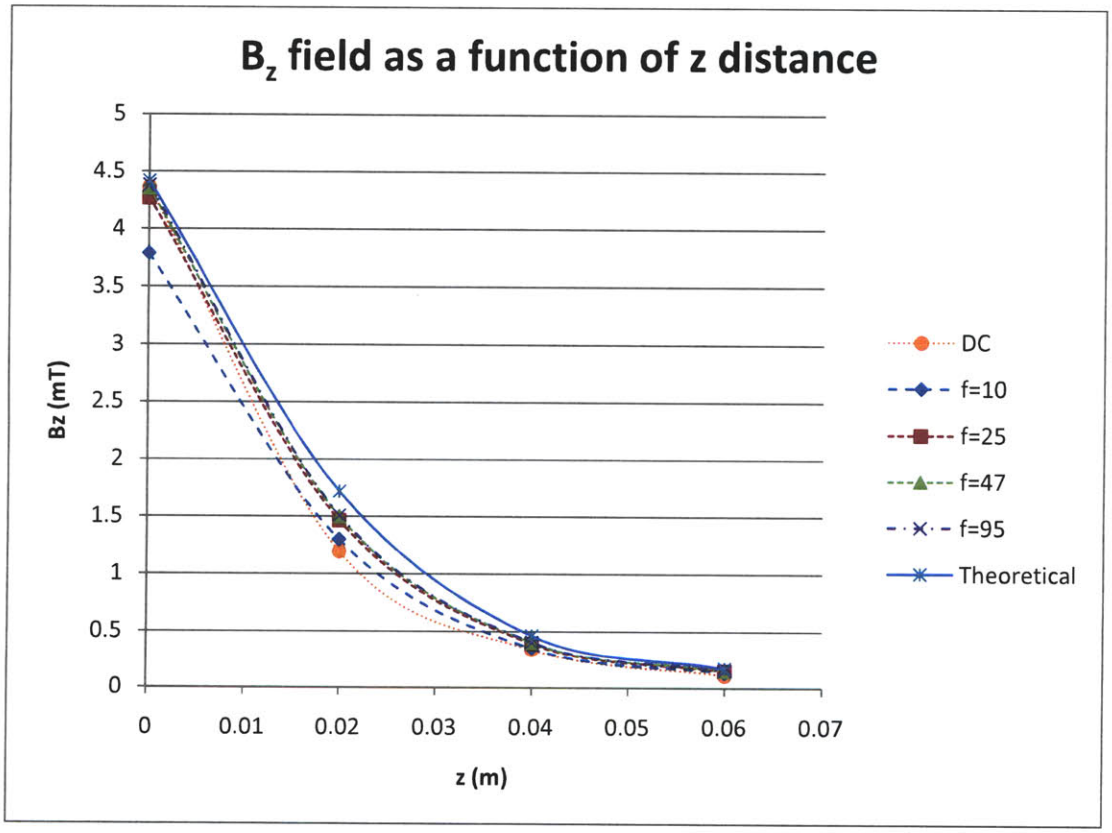

Figure 6-37. Measurement of axial magnetic flux density B_z of third coil as a function of axial distance z at different frequencies and DC. Measured results are very similar to the plot of a theoretical one turn model of third coil with radius $a=21.34mm$.

I(A) RMS/DC	B_z(mT) at DC	B_z(mT) at f = 10 Hz (RMS)	B_z(mT) at f = 25 Hz (RMS	B_z(mT) at f = 47 Hz (RMS)	B_z(mT) at f = 95 Hz (RMS)	Frequency Averaged K_w=B_z/I (mT/A)
1	4.36	3.79	4.27	4.35	4.38	4.23
2	8.74	7.64	8.55	8.75	8.79	4.25
3	13.12	11.53	12.8	13.13	13.22	4.25
					Overall Average K_w	**4.24**

Table 6-8. Table of measured axial flux densities at *r=z=0* (origin of axial direction) at different frequencies and DC. The average winding factor is calculated over the frequency range and an overall average winding factor is calculated for three different current measurements.

For an N turn coil the theoretical magnetic field at z=0 can be calculated by setting z=0 and multiplying Eq (6.38) by N, resulting in a theoretical value of K_w, given in (6.39), in good agreement with experiment results

$$K_w = \frac{N\mu_0}{2a} = 4.42 \text{ mT/A (RMS)} \tag{6.39}$$

6.4.5. Using Permanent Magnets

Neodymium permanent magnets of diameter 1 inch could also be placed on top of the ferrofluid filled sphere instead of the third coil. Five magnets were purchased from K&J Magnetics Inc. with different surface field strengths as tabulated in Table 6-9. The surface field strength was also measured using the F.W. Bell three axis probe and Teslameter. The specifications for the magnets and the Teslameter are documented in Appendix C.

A special holder, as seen in Figure 6-38, was made to fit inside the inner diameter of the inner fluxball access hole and hold the magnet. This would help keep the position of the magnet consistent between experiments. The magnet holder fitted in the access hole, to align it with the axial line of the inner fluxball, can be seen in Figure 6-39.

K&J Magnetics #	Quoted Surface Field Strength (Gauss)	Measured Surface Field Strength (Gauss)	Height (inches)
DX02	1601	1088	1/8
DX04	2952	2580	1/4
DX04B-N52	3309	2910	1/4
DX08	4667	3900	1/2
DX08B-N52	5233	4400	1/2

Table 6-9. Table detailing height and surface field strength of 1 inch diameter neodymium permanent magnets.

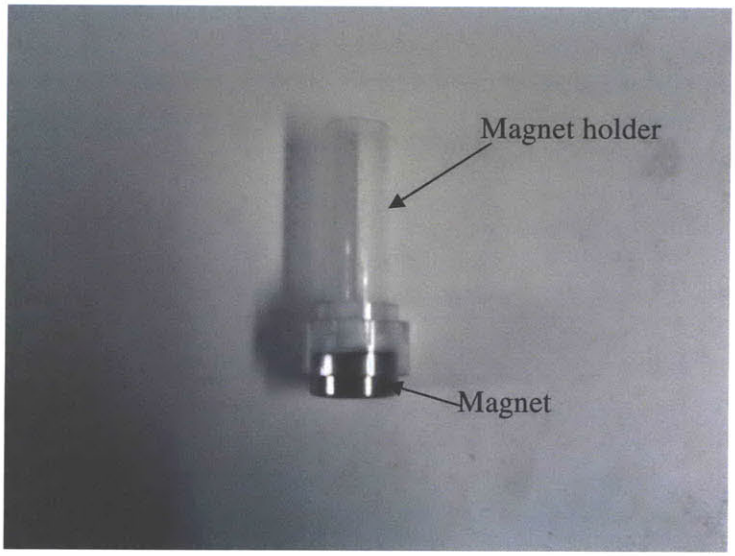

Figure 6-38. Magnet holder to fit inside inner fluxball's access hole.

Figure 6-39. Magnet in holder fitted inside upper half of inner fluxball's access hole.

6.5. Experimental Results With a Non-Uniform Field Imposed

6.5.1. Parameters Investigated in Experiments Using The Third Coil

The experiments conducted with the third coil generated a non-uniform field that resulted in significant flow that was measured with the ultrasound velocimeter. The parameters varied for the experiments conducted are tabulated in Table 6-10. The fluxball field strength of 50.6 G and 101.2 G RMS correspond to 1A and 2A RMS current in the fluxball windings respectively. The third coil is excited using AC frequencies as well as DC. The AC frequencies used are exactly the same as the rotational frequency of the rotating field, in effect, if the rotating field is rotating at 95Hz, the third coil would also be excited at 95Hz. The phase of the third coil under AC operation was also adjusted relative to the phase of the signal exciting the inner fluxball using the LabVIEW program in Figure 6-32. The third coil flux density of 169.6 G and 296.G RMS corresponds to an AC third coil current of 4A and 7A RMS respectively. The ±339.2 G DC corresponds to a DC third coil current of ±8A for the third coil. The experimental results of all cases conducted with the third coil are documented in Appendix G.

Parameters Varied	Values
Rotating field direction	Clockwise and Counter-clockwise
Fluxball rotating field strength (RMS)	50.6G, 101.2G
Rotating Field Frequencies	15Hz, 47Hz, 95Hz
Fluids	EFH1, MSGW11
Third Coil Frequencies	15Hz, 47Hz, 95Hz, DC
Phase of third coil with respect to phase of inner fluxball	0°,+60°,-60°,+120°,-120°,180°
Field strength of third coil (RMS)	169.6G (AC), 296.8G (AC), ±339.2G (DC)

Table 6-10. Table of parameters varied in experiments conducted with magnetic field generated by third coil and fluxball machine.

6.5.2. Parameters Investigated in Experiments Using Permanent Magnets

The experiments conducted with the permanent magnets also generated a non-uniform field that resulted in significant flow that was measured with the ultrasound velocimeter. The parameters varied for the experiments conducted are tabulated in Table 6-11. The fluxball field strength of 50.6 G and 101.2 G RMS correspond to 1A and 2A RMS current in the fluxball windings respectively. The experimental results of all the cases conducted with permanent magnets are documented in Appendix H.

Parameters Varied	Values
Rotating field direction	Clockwise and Counter-clockwise
Fluxball rotating field strength (RMS)	50.6G, 101.2G
Rotating Field Frequencies	15Hz, 47Hz, 95Hz
Fluids	EFH1, MSGW11
Pole of Magnet facing sphere of ferrofluid	North, South
Surface field strength of magnet	1601G, 2952G, 3309G, 4667G, 5223G

Table 6-11. Table of parameters varied in experiments conducted with field generated by permanent magnets and fluxball machine.

6.5.3. Effect of Rotational Direction of Magnetic Field

In general, the ferrofluid flows reverse direction when the rotating field direction is changed from counter-clockwise to clockwise directions. This occurs in experiments involving the third coil as well as the permanent magnets. The flow generated as a result of the non-uniform fields is very complicated and irregular with the creation of several vortices. As a result the flow does not necessarily change symmetrically when the field direction is reversed.

Figure 6-40 and Figure 6-41 are velocity profiles measured by the channel 2 probe with a 50.6 G clockwise and counter-clockwise rotating magnetic field respectively for EFH1 at 95Hz with permanent magnets having their south poles facing the ferrofluid filled sphere. It can be clearly seen that the flow profile reverses as a result of reversal of the rotating field directions. A plot of the velocity vectors determined at the four points in Figure 6-2 are plotted in Figure 6-42 and Figure 6-43 for a clockwise and counter-clockwise rotating field respectively, of rotating field strength 101.2 G at 95Hz using the oil-based EFH1.

The reversal in flow direction is also observed when using the third coil and MSGW11. Figure 6-44 and Figure 6-45 are plots of velocity flow profiles measured by the channel 1 probe for clockwise and counter-clockwise rotating 95 Hz fields respectively for MSGW11 using a third coil which is entirely in phase with the inner fluxball current. The velocity vectors at the four points in Figure 6-2 can also be constructed with data measured by the four probes and is illustrated in Figure 6-46 and Figure 6-47 for clockwise and counter-clockwise rotating field respectively with velocity vectors reversing direction, although not symmetrically, as a result of reversal of field direction.

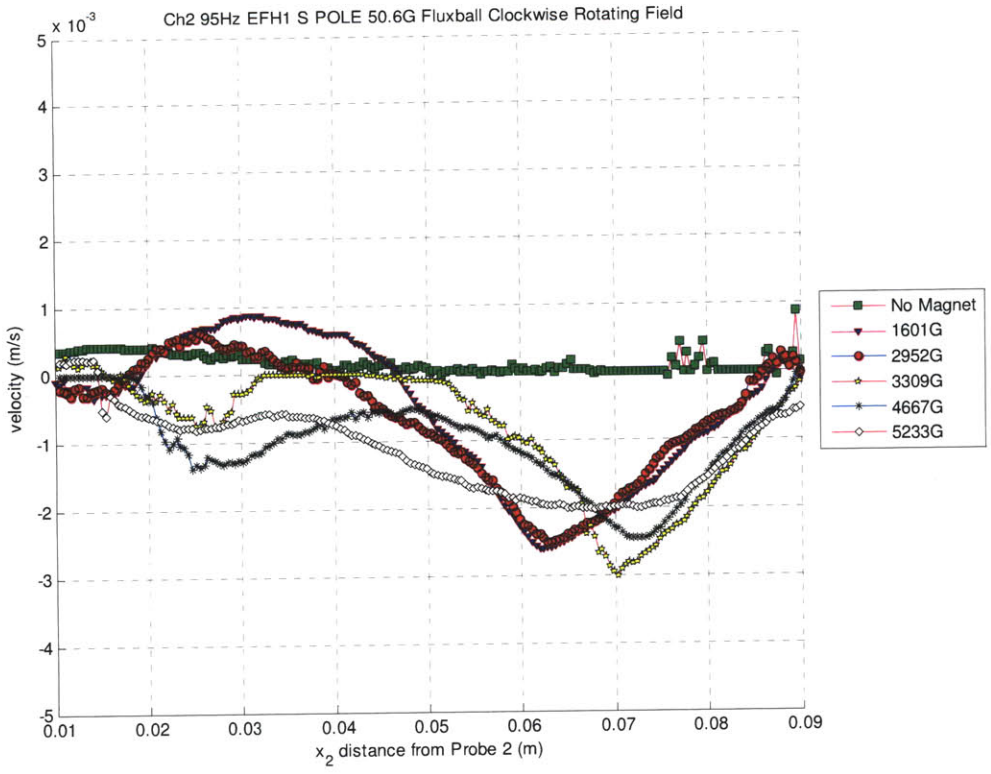

Figure 6-40. Channel 2 velocity profile as a function of distance from Probe 2 for EFH1 at 95 Hz and 50.6 G clockwise rotating magnetic field under the influence of permanent magnets with south poles facing the top of the sphere of ferrofluid.

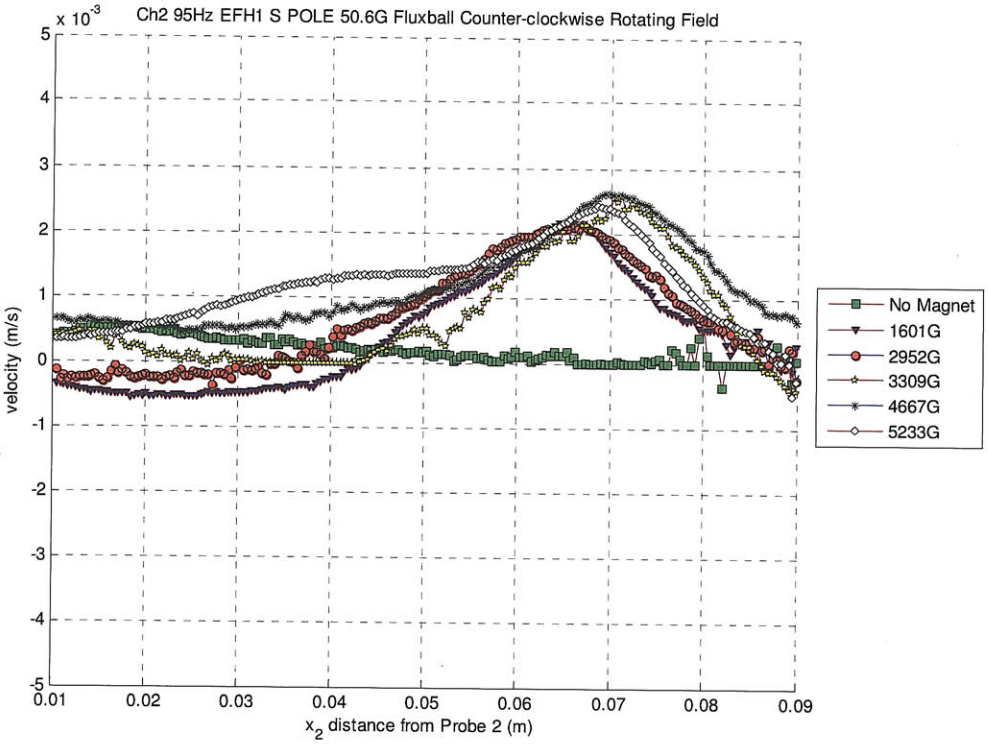

Figure 6-41. Channel 2 velocity profile as a function of distance from Probe 2 for EFH1 at 95Hz and 50.6 G counter-clockwise rotating magnetic field under the influence of permanent magnets with south poles facing the top of the sphere of ferrofluid.

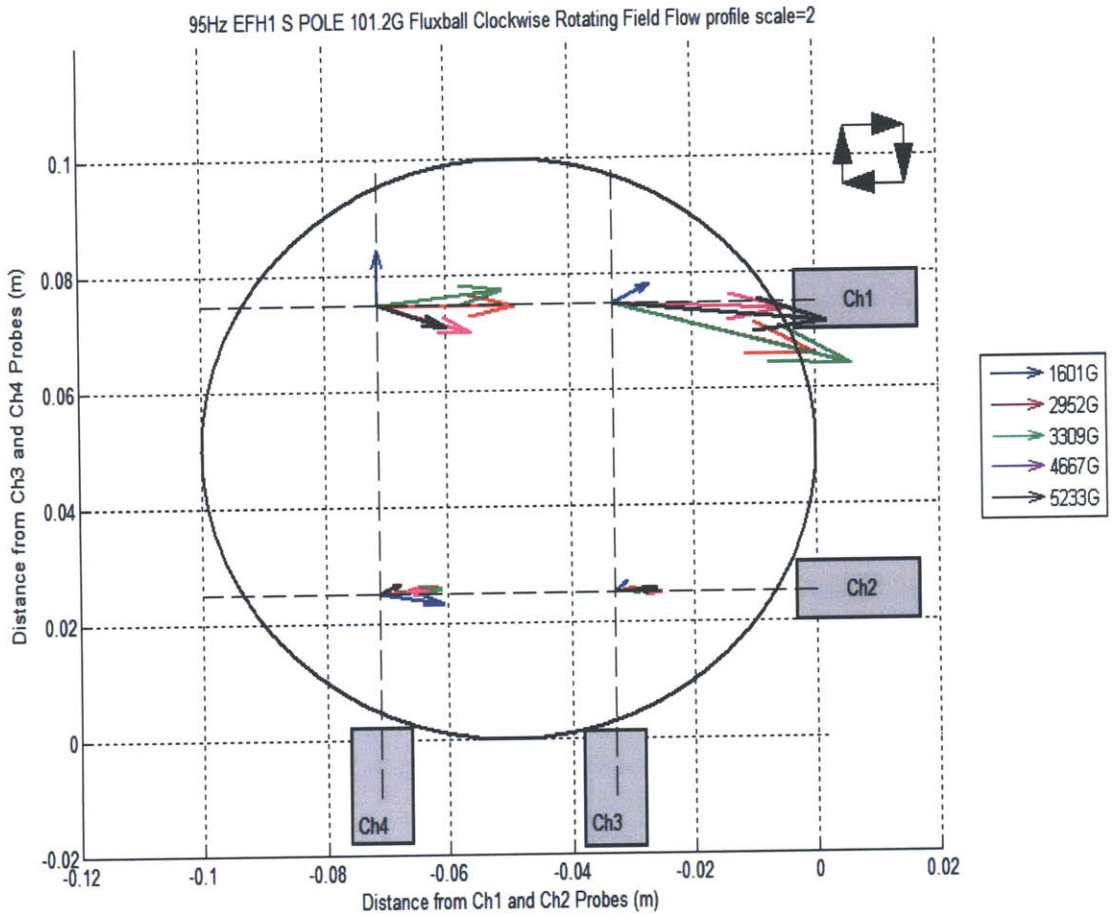

Figure 6-42. Velocity vectors plotted at the points where the four probe beams intersect for EFH1 at a 101.2 G 95 Hz clockwise rotating field with magnets having their south poles facing the top of the ferrofluid filled sphere. The flow pattern follows the clockwise rotating field direction with greater magnitude flow occurring at the top of the sphere. The little flow at the two measurement points near the bottom of the sphere also seems to flow towards the right implying vortices must be forming in the region between the top two points and the bottom two points. The arrows are scaled by a factor of 2 to better see them.

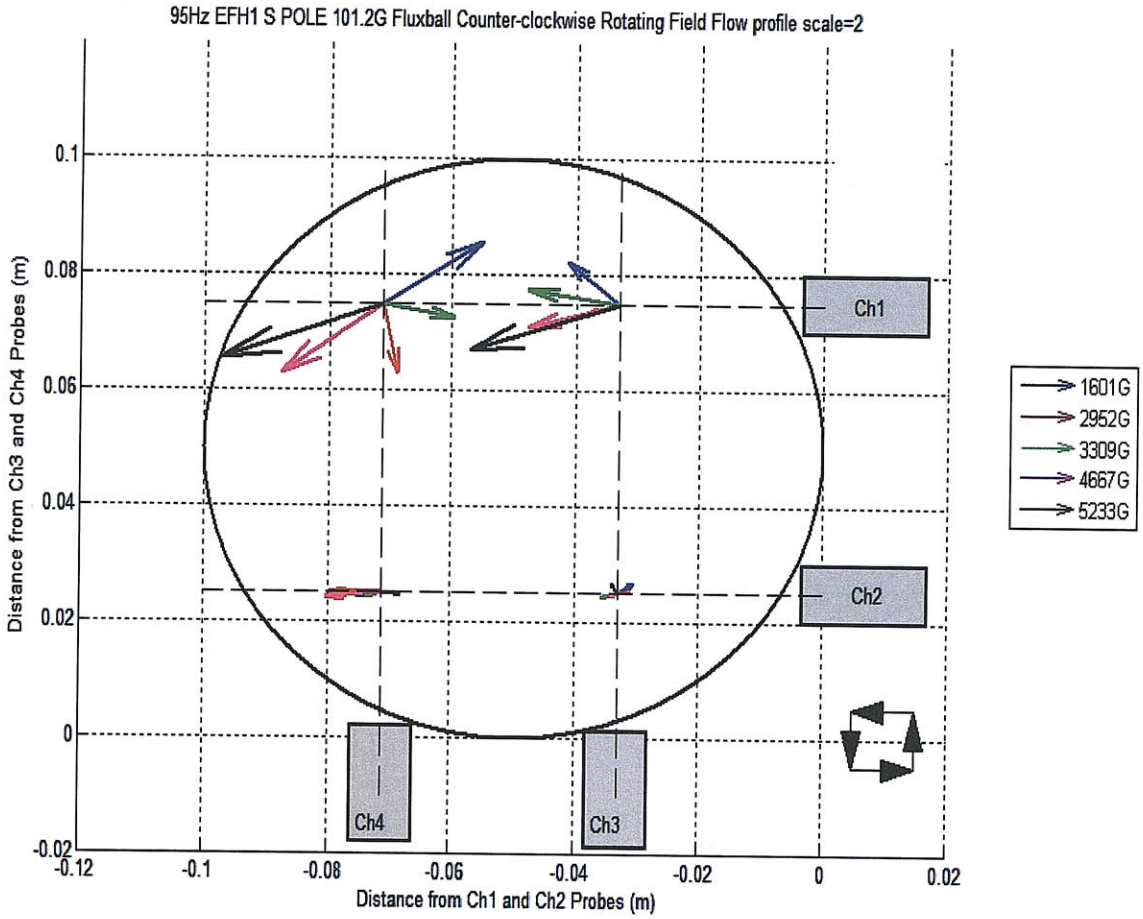

Figure 6-43. Velocity vectors plotted at the points where the four probe beams intersect for EFH1 at a 101.2 G 95 Hz counter-clockwise rotating field with magnets having their south poles facing the top of the ferrofluid filled sphere. The flow pattern generally reverses direction with the counter-clockwise rotating field with greater flow occurring near the region of non-uniform field at the top of the ferrofluid filled sphere near the magnets. The arrows are scaled by a factor of 2 to better see them.

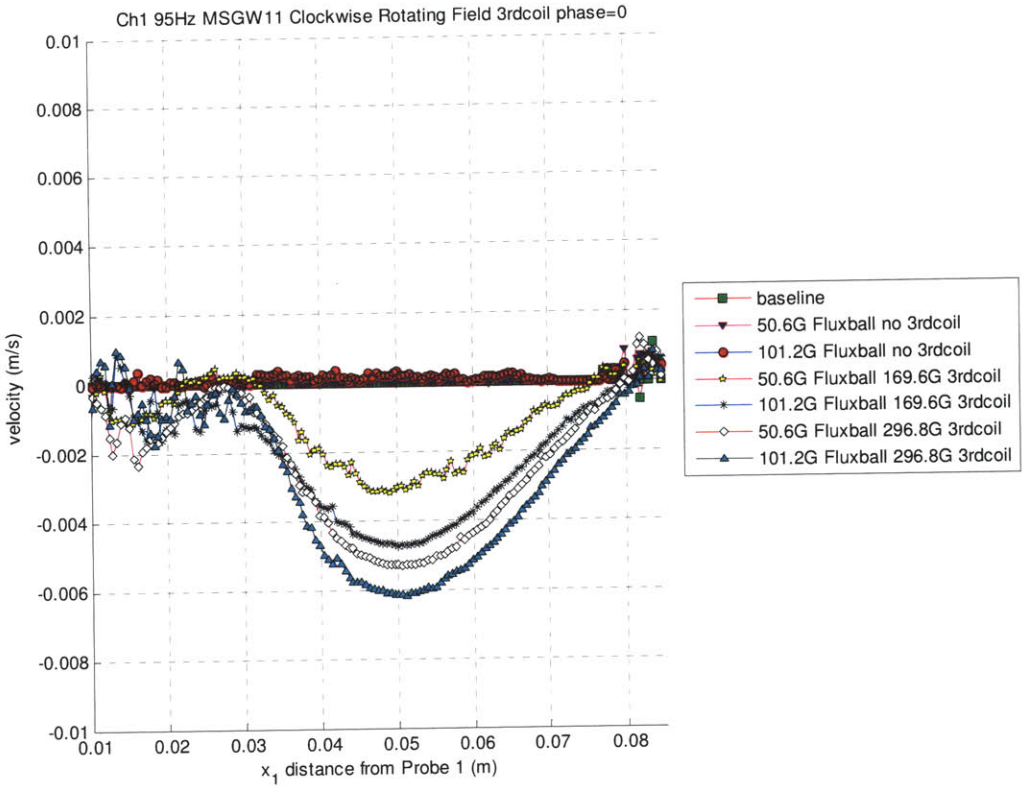

Figure 6-44. MSGW11 velocity flow profile measured by channel 1 probe for 95 Hz clockwise rotating field with the phase of the third coil with respect to the inner fluxball equal to 0. Baseline refers to the flow measured by the velocimeter without any field applied.

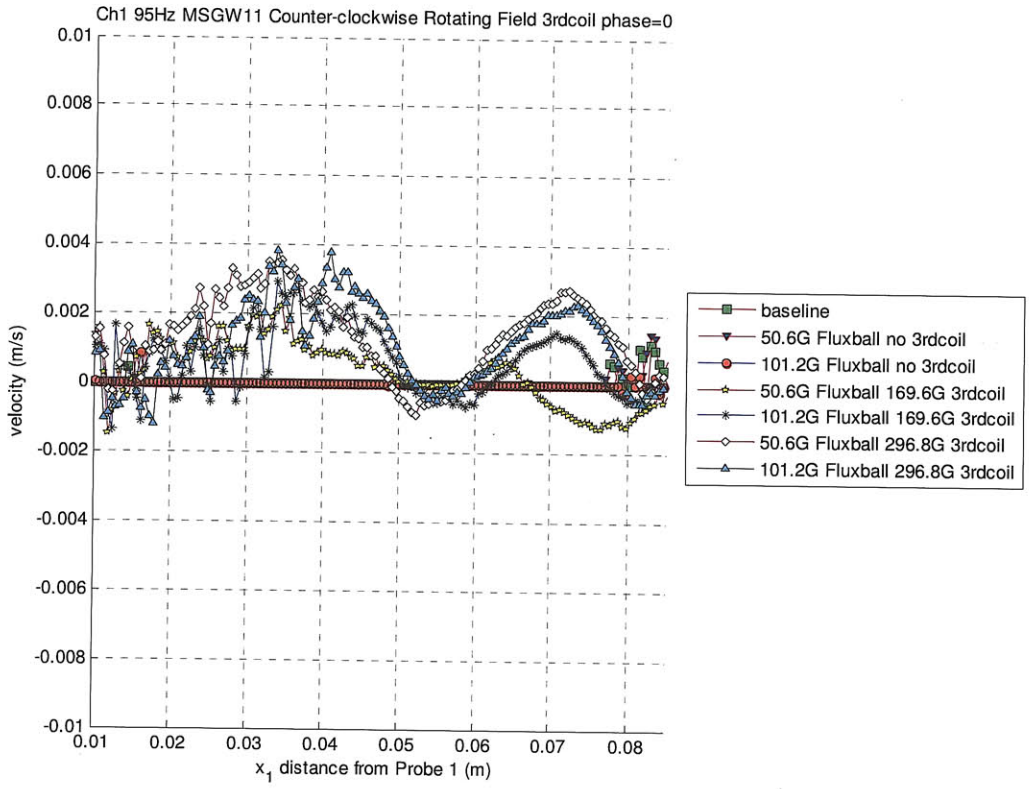

Figure 6-45. MSGW11 velocity flow profile measured by channel 1 probe for 95 Hz counter-clockwise rotating field with the phase of the third coil with respect to the inner fluxball equal to 0. Baseline refers to the flow measured by the velocimeter without any field applied. Flow reverses direction but is not symmetric due to complicated flow patterns. The velocity goes to 0 at around 0.055m implying the presence of two vortices formed.

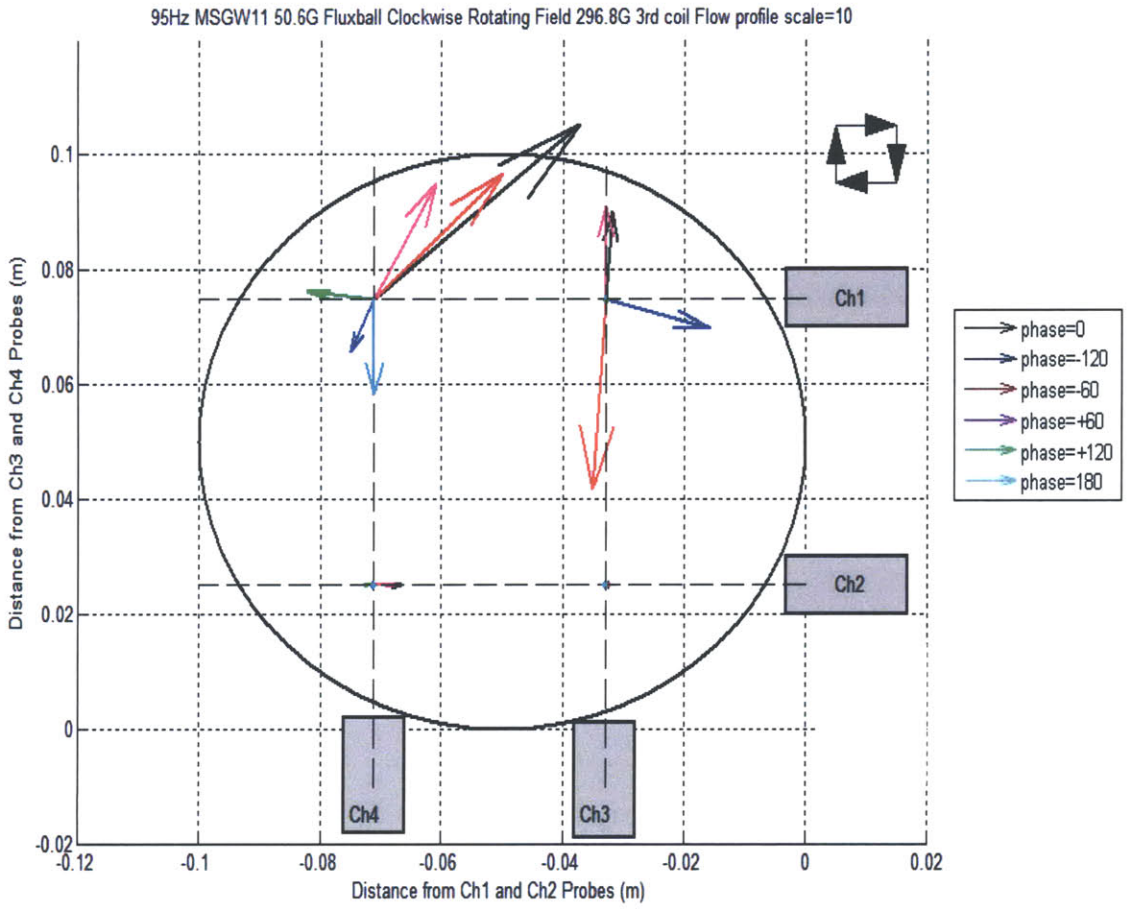

Figure 6-46. MSGW11 velocity flow vectors at four points as determined by the intersection of the four probe beams for a 50.6 G clockwise rotating field with 296.8 G non-uniform field imposed by the third coil. The individual velocity vectors correspond to the phase of the third coil with respect to the inner fluxball current. The arrows are scaled by a factor of 10 to better see them.

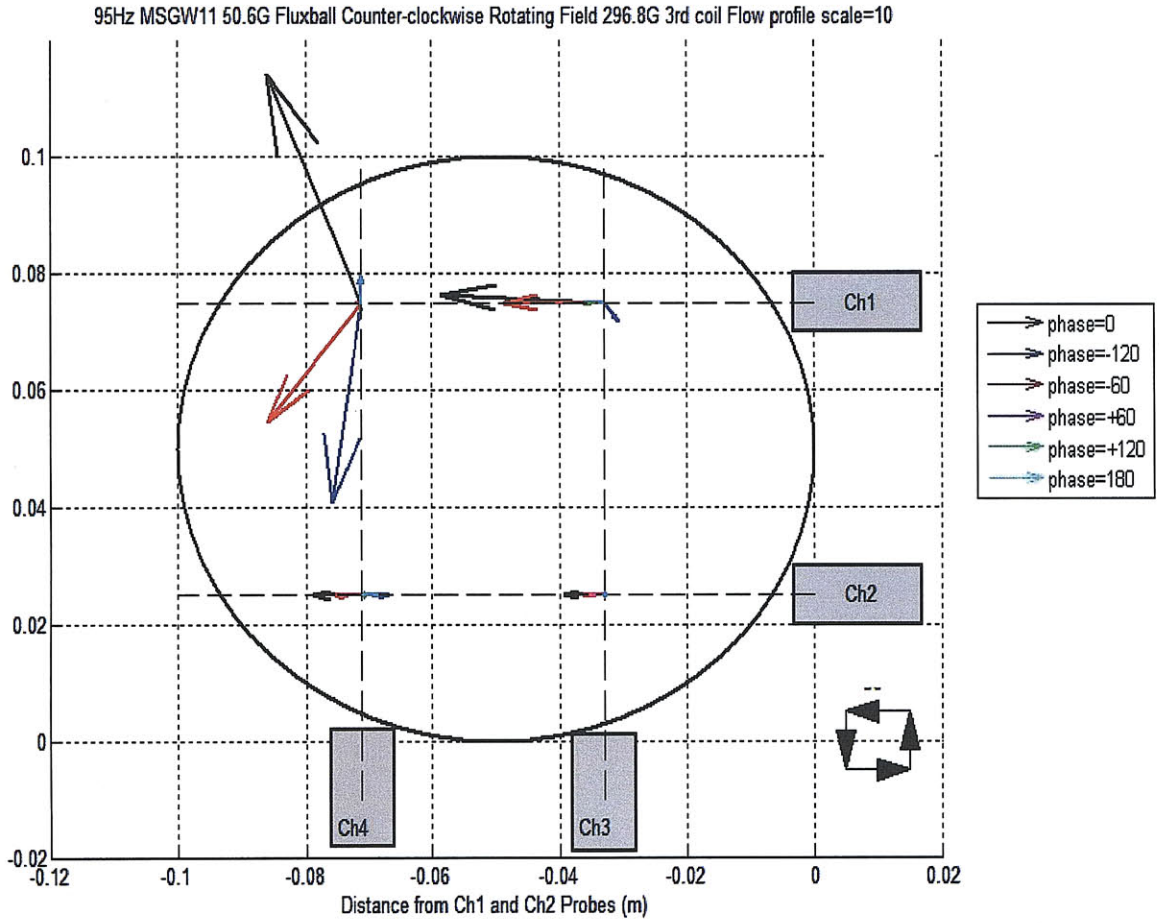

Figure 6-47. MSGW11 velocity flow vectors at four points as determined by the intersection of the four probe beams for a 50.6 G counter-clockwise rotating field with 296.8 G non-uniform field imposed by the third coil. The individual velocity vectors correspond to the phase of the third coil with respect to the inner fluxball current. The flow vectors reverse direction compared to the clockwise rotating field in Figure 6-46. The arrows are scaled by a factor of 10 to better see them.

6.5.4. Effect of Permanent Magnets on Fluid Flow

In the cylindrical case described in Chapter 4, the flow was completely in the v_ϕ direction allowing for a simple determination of field strength on the magnitude of the flow velocity. In the spherical case with a non-uniform field imposed by the magnets, the flow has vortices that are generated making the flow field irregular. In addition, the four probes only measure velocity profiles in the direction of the four ultrasonic beams and do not completely give the entire flow field inside the sphere of ferrofluid. As a result, the effect of the surface strength of the permanent magnets on the flow magnitude is difficult to determine.

Figure 6-48 seems to suggest that the velocity magnitude of the flow profile has a direct correlation with the surface strength of the magnets. But Figure 6-49 which is the flow profile measured by the channel 4 probe with the same driving conditions as Figure 6-48 does not show this behavior since the magnitude of the velocity appears to be the same, further bolstering the fact that the flow is irregular caused by the spatially non-uniform field. Figure 6-50 further illustrates an inverse dependence of magnet strength on the magnitude of velocity proving that the four probes give a limited view on the complicated flow profile generated and the exact dependence of the flow magnitude on the strength of the magnet is difficult to determine. However, one safe conclusion that can be determined is the presence of a stronger magnet definitely increases the likelihood of there being a measureable flow generated.

The strength of the magnet does consistently result in a shift in the position of a vortex formed near the position of the magnet at the top of the ferrofluid filled sphere. A vortex is when the velocity profile goes through zero with opposite polarity of velocity on either side of zero. Figure 6-51 has velocity profiles that reverse direction indicating that vortices are being formed.

The position of these vortices are dependent on the strength of the magnet used, a stronger magnet pushes the profile closer to probe 4 and away from the magnet at z_4=0.1m. This behavior is consistently observable at different frequencies, rotating field direction and even by changing the pole facing the ferrofluid sphere from south to north as seen in Figure 6-52. This shift in the flow profile towards the probe also occurs with MSGW11 as seen in Figure 6-53.

The polarity of the pole facing the ferrofluid filled sphere can affect whether the dominant flow is generated nearer to the magnet or further away from it. Figure 6-53 illustrates that with the north pole facing the MSGW11 filled sphere the flow is more dominant away from the magnet. Figure 6-54 is the velocity vector plot for an MSGW11 filled sphere with the south pole of the magnets facing the sphere. The flow is more dominant nearer to the magnet at the top of the sphere. Figure 6-55 on the other hand, is the velocity vector plot for the same driving conditions as Figure 6-54 except with the north pole of the permanent magnets facing the sphere. The flow in this case is more dominant at the bottom of the sphere with still significant flows at the top. Changing the polarity of the magnet with EFH1 from south to north as seen in Figure 6-56 and Figure 6-57 do illustrate that flows generated with the north pole facing the sphere does tend to increase the flow at the bottom of the ferrofluid sphere. However, this effect seems to be greater in MSGW11 than in EFH1.

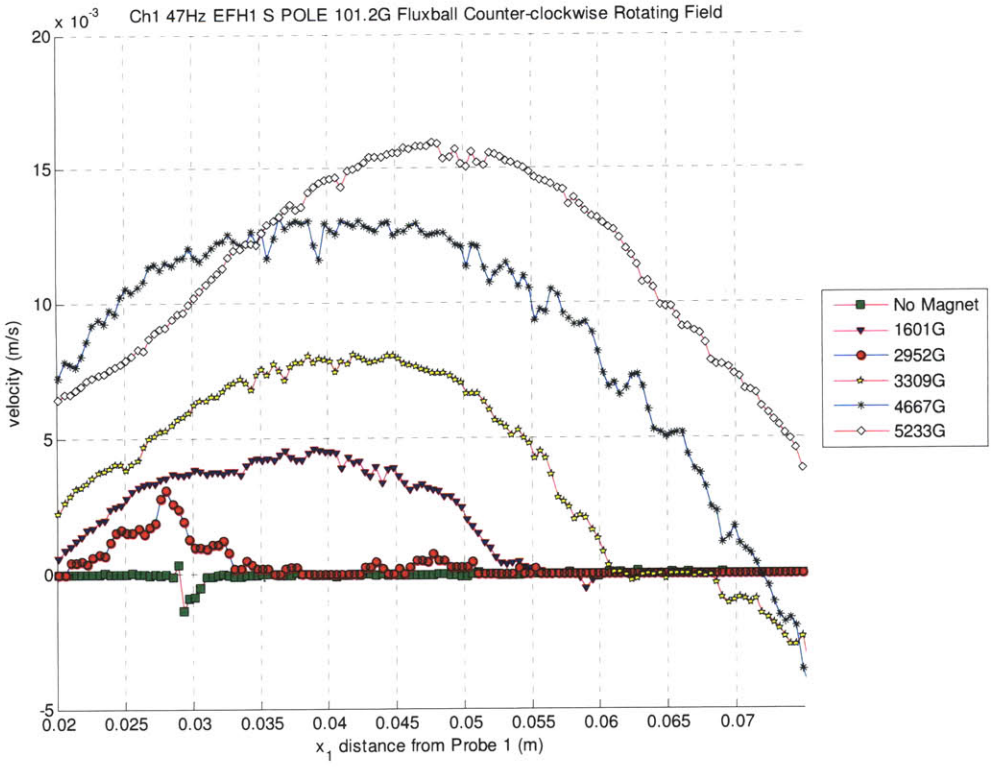

Figure 6-48. Flow profile measured by channel 1 probe for 101.2 G counter-clockwise rotating field at 47 Hz for EFH1 with magnets having their south poles facing the top of the ferrofluid filled sphere. Strength of the magnets seems to directly affect magnitude of flow velocity except for 1601 G and 2952 G permanent magnets.

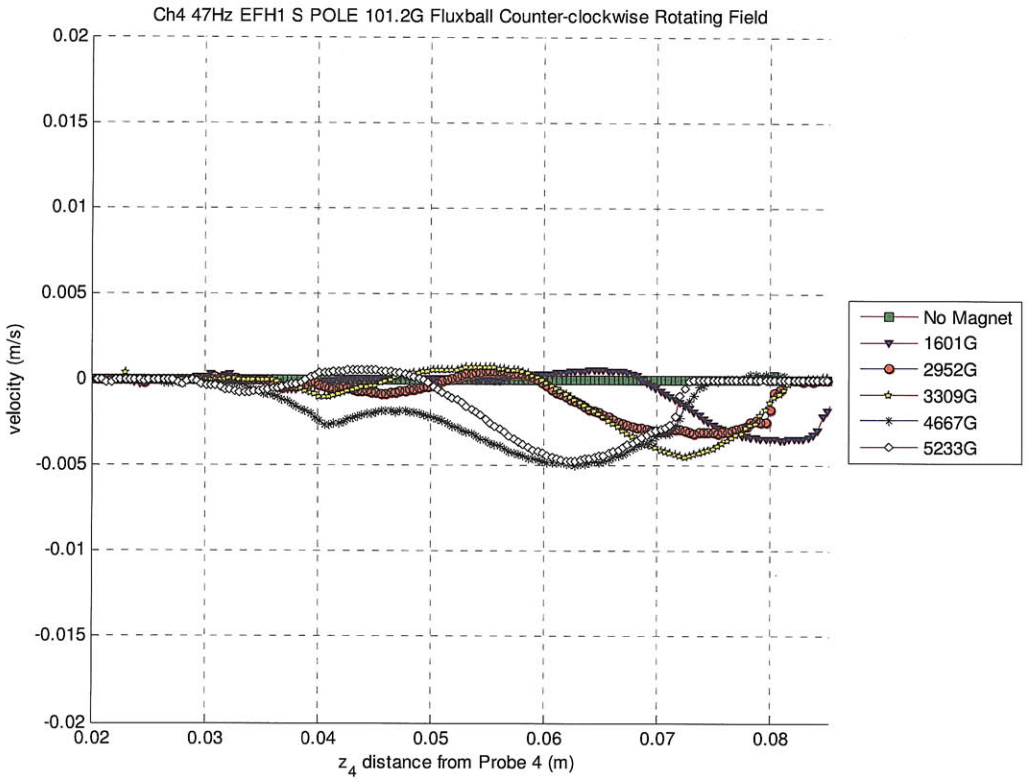

Figure 6-49. Flow field as measured by channel 4 probe for same driving conditions as Figure 6-48 does not show as large an increase in velocity magnitude but does show a reversal of flow direction.

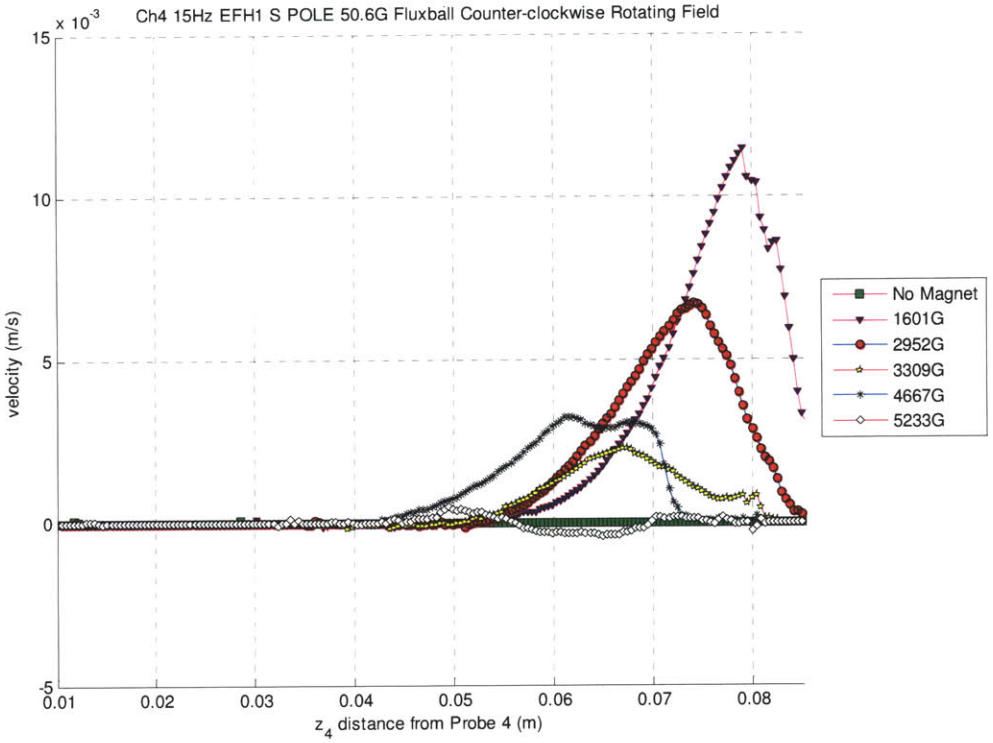

Figure 6-50. Flow profile measured by channel 4 probe in a 50.6 G counter-clockwise rotating field at 15 Hz for EFH1 ferrofluid with magnets having their south poles facing the top of the ferrofluid filled sphere. The magnitude of velocity has an inverse relation with the strength of the magnets used unlike seen in Figure 6-48.

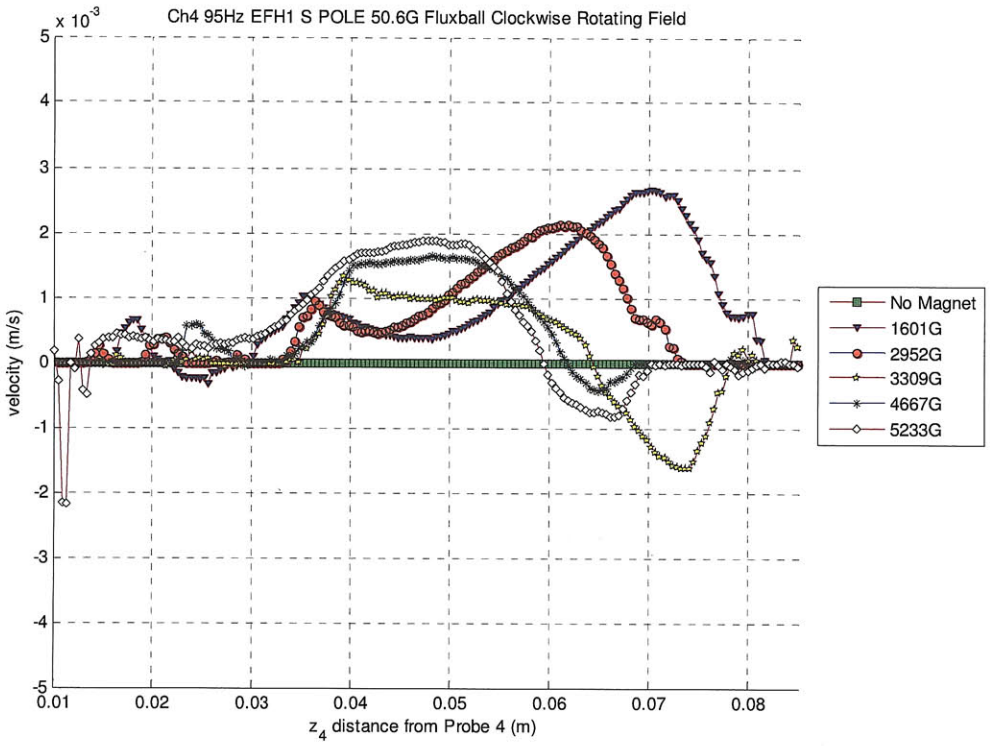

Figure 6-51. Flow measured by channel 4 probe with 50.6 G clockwise rotating magnetic field at 95 Hz with magnets having their south poles facing the top of the EFH1 filled sphere. The velocity profile indicates that there is a vortex formed since the flow direction reverses. As the magnet strength increases there is a shift of the vortex formed away from the magnet at 0.1m from probe 4.

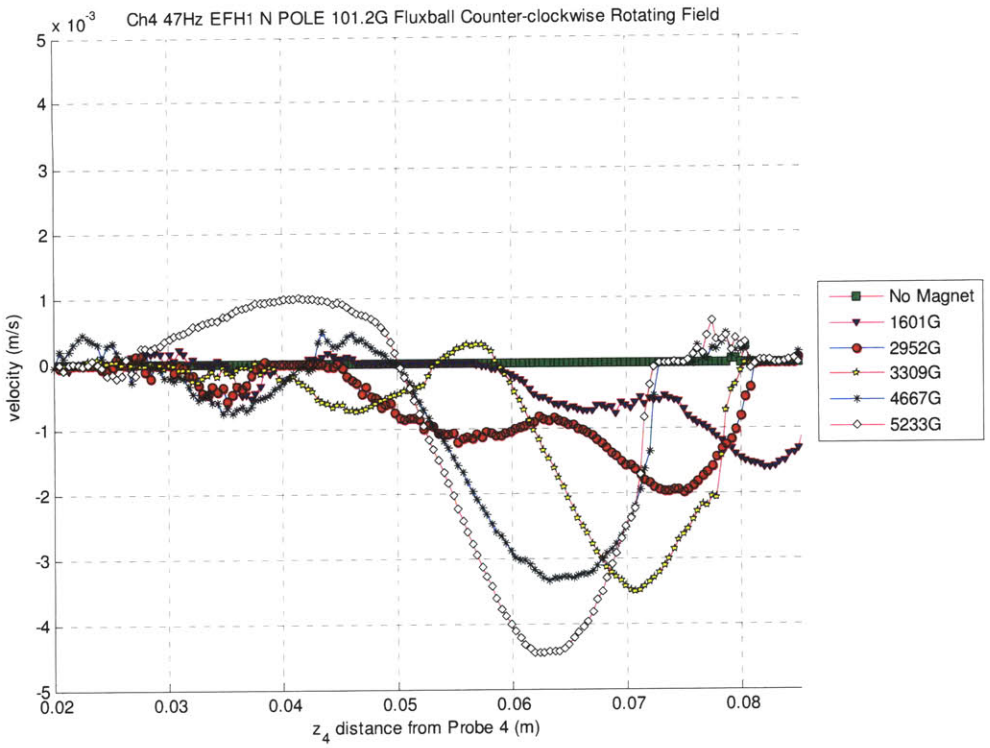

Figure 6-52. Flow measured by channel 4 probe with 101.2 G counter-clockwise rotating magnetic field at 47Hz with magnets having their north poles facing the top of the EFH1 filled sphere. The velocity profile indicates that there is a vortex formed since the flow direction reverses. As the magnet strength increases there is a shift of the vortex formed away from the magnet at 0.1m from probe 4. A vortex is formed when velocity goes through zero with opposite polarity of velocity direction on either side of zero.

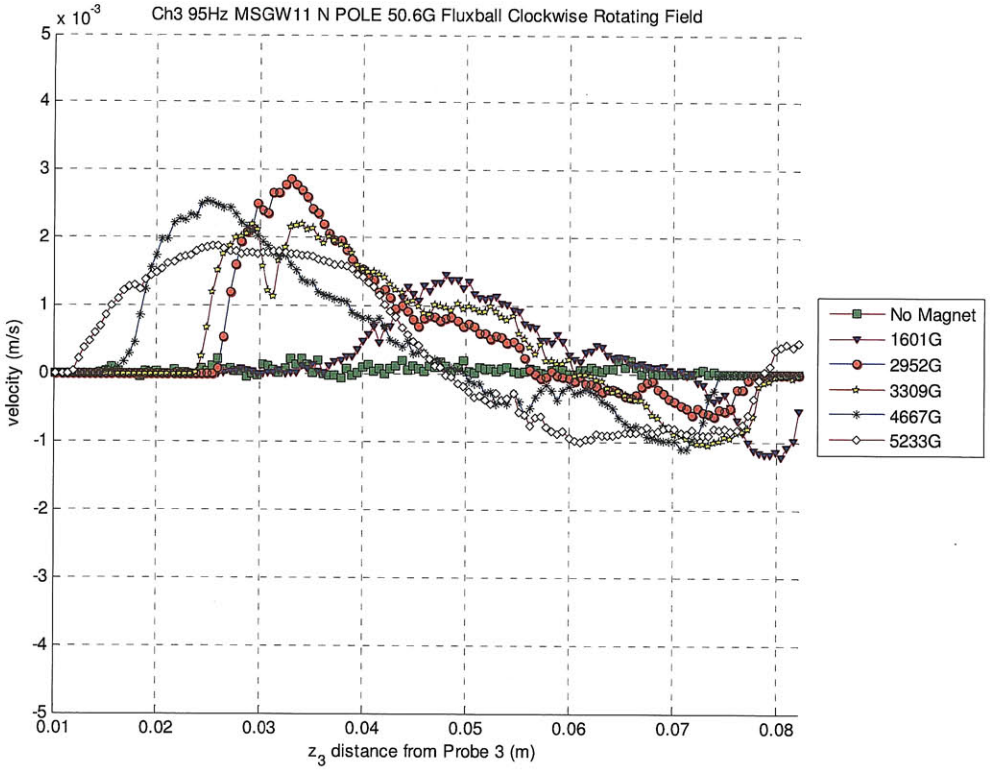

Figure 6-53. Flow measured by channel 3 probe with 50.6 G clockwise rotating magnetic field at 95 Hz with magnets having their north poles facing the top of the MSGW11 filled sphere. The velocity profile here also indicates there is a shift of the vortex away from the magnet at 0.1m from probe 4 but the velocity magnitude is larger away from the magnet.

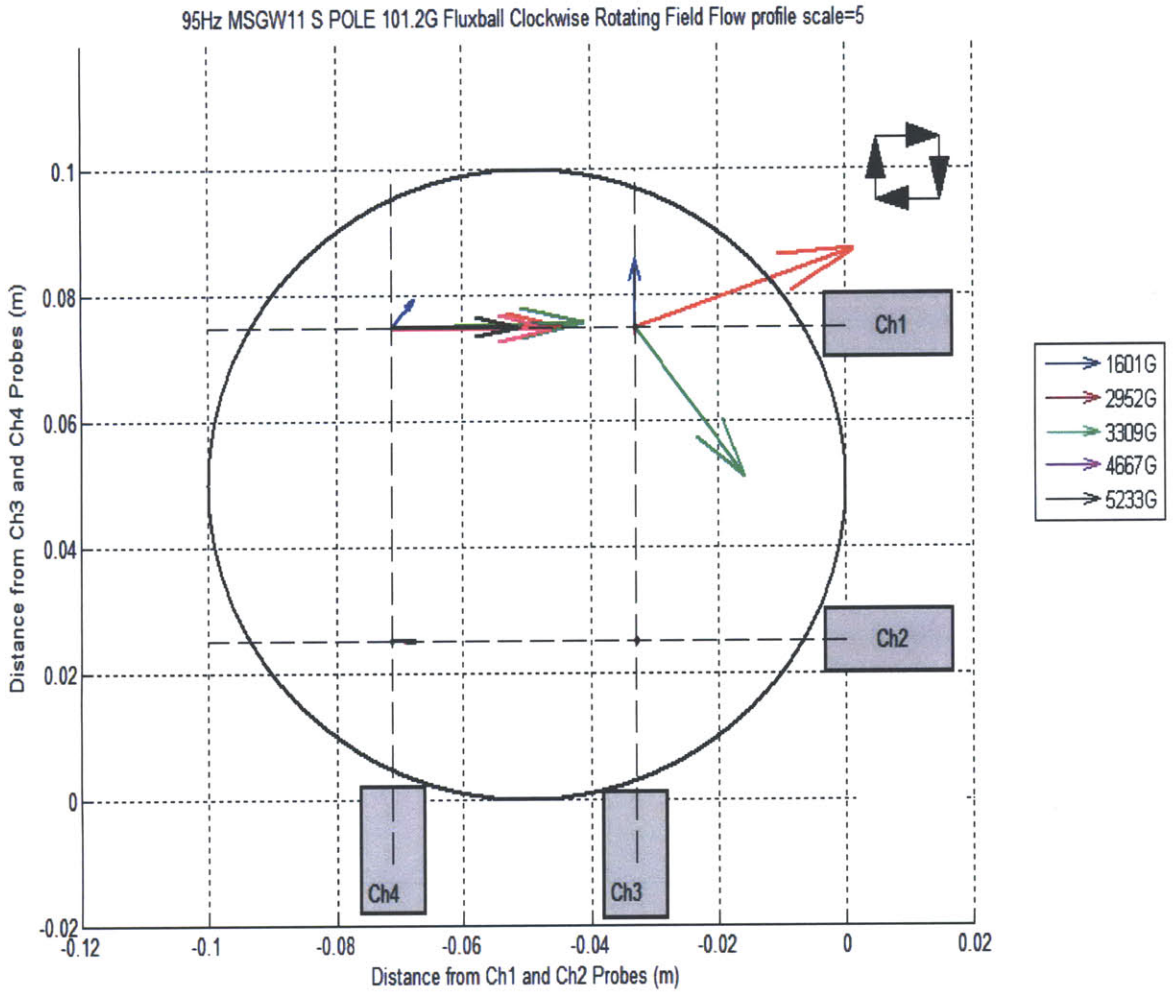

Figure 6-54. MSGW11 velocity flow vectors at four points as determined by the intersection of the four probe beams for a 101.2 G clockwise rotating field with the south pole of the magnets facing the top of the ferrofluid filled sphere. The flow is more dominant near the magnet at the top of the sphere.

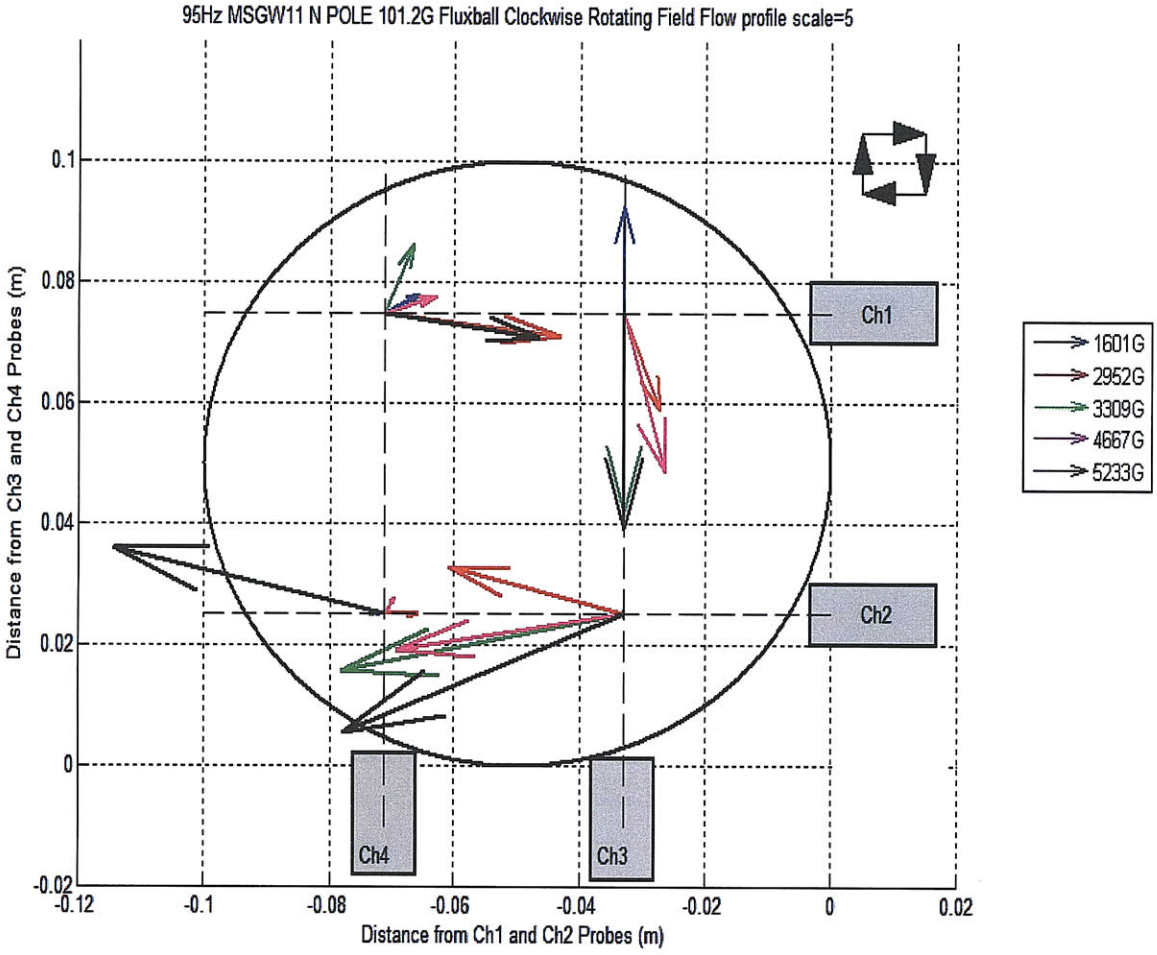

Figure 6-55. MSGW11 velocity flow vectors at four points as determined by the intersection of the four probe beams for a 101.2 G clockwise rotating field with the north pole of the magnets facing the top of the ferrofluid filled sphere. The flow is more dominant away from the magnet at the bottom of the sphere with significant flow still generated near the magnet at the top of the sphere.

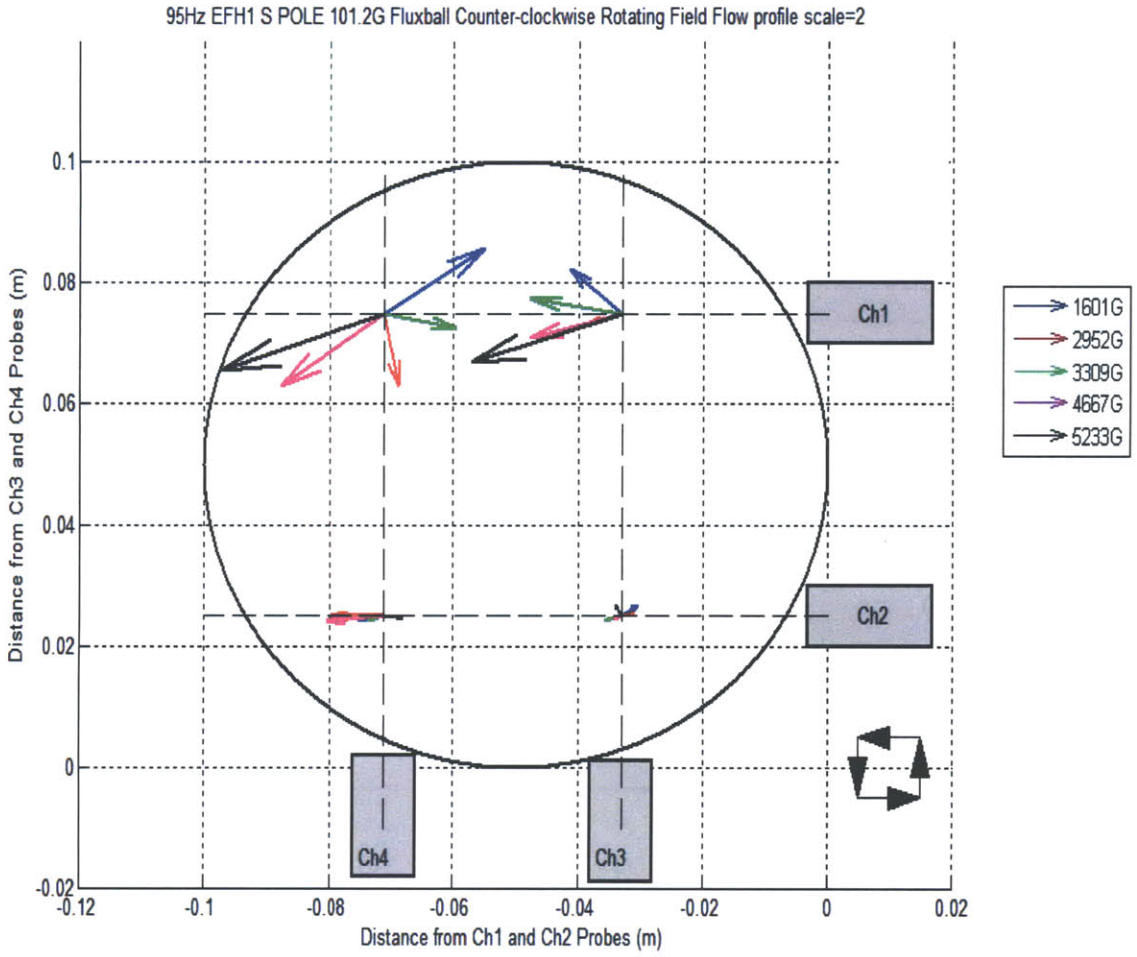

Figure 6-56. EFH1 velocity flow vectors at four points as determined by the intersection of the four probe beams for a 101.2 G counter-clockwise rotating field with the south pole of the magnets facing the top of the ferrofluid filled sphere. The flow profile seems to be more dominant at the top of the sphere near the position of the magnet.

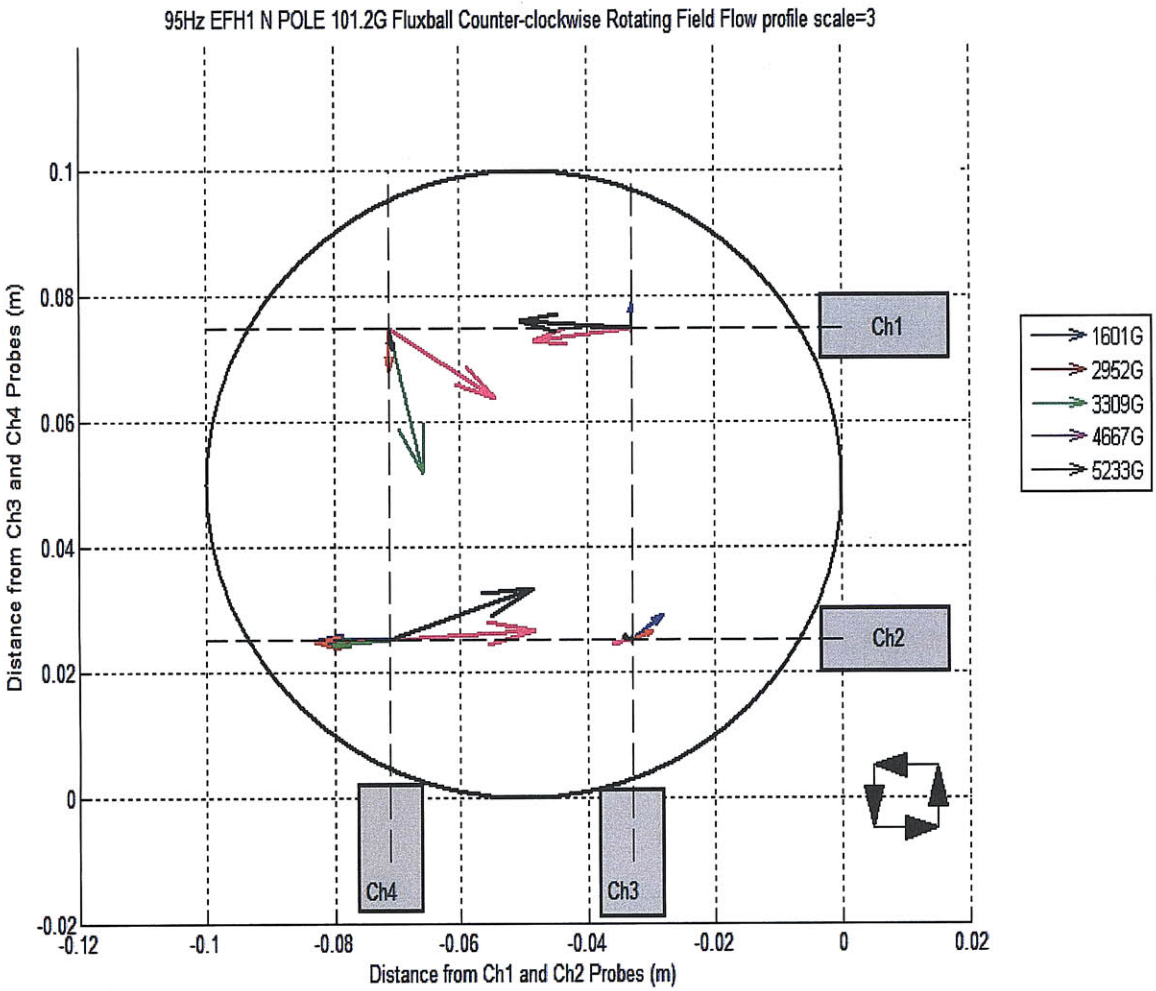

Figure 6-57. EFH1 velocity flow vectors at four points as determined by the intersection of the four probe beams for a 101.2 G counter-clockwise rotating field with the north pole of the magnets facing the ferrofluid filled sphere. The flow profile at the bottom of the sphere is just as significant as the flow at the top near the magnet.

6.5.5. Effect of Strength of Rotating Field On Flow Generated by Permanent Magnets

The strength of the rotating field has a direct effect on the magnitude of the flow generated by the non-uniform field of the permanent magnets. Figure 6-58 is a velocity profile plot measured by channel 4 probe for both EFH1 and MSGW11 at all rotating frequencies with a non-uniform field generated by a 5233 G magnet and a counter-clockwise rotating field of strength 50.6 G. The flow obtained is not significant. Figure 6-59, on the other hand, is the velocity profile obtained for the same case as Figure 6-58 except with a rotating field strength of 101.2 G. The velocity profiles obtained are more significant confirming that the rotating field strength does affect the magnitude of the flow in the case of a non-uniform field generated by permanent magnets.

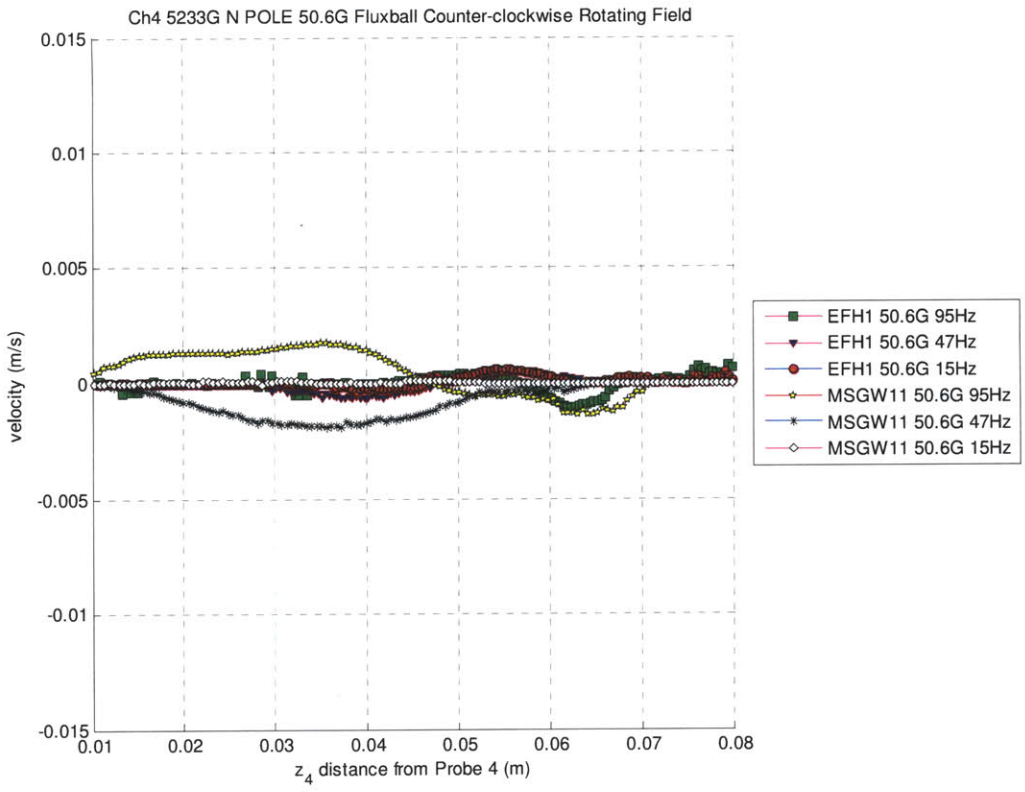

Figure 6-58. Velocity profiles measured by channel 4 probe at all rotating frequencies for both EFH1 and MSGW11 with the strongest magnet of strength 5233 G and a rotating field strength of 50.6 G rotating in the counter-clockwise direction.

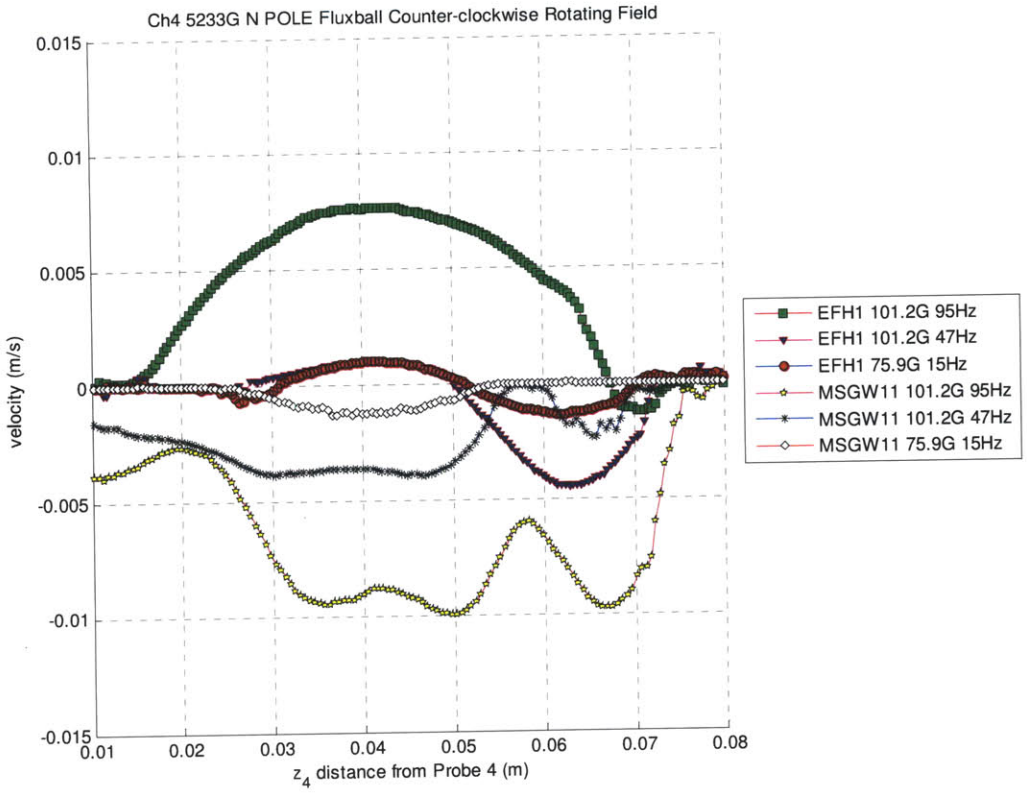

Figure 6-59. Velocity profiles measured by channel 4 probe at all rotating frequencies for both EFH1 and MSGW11 with the strongest magnet of strength 5233 G and a rotating field strength of 101.2 G and 75.9 G rotating in the counter-clockwise direction. The magnitude of flow generated is greater than that obtained in Figure 6-58.

6.5.6. Effect of Strength of Rotating Field and Strength of Non-Uniform AC Field on Flow Generated by Third Coil

The magnitude of the flow generated by the rotating field and the non-uniform field of the third coil is dependent on the strength of the non-uniform field generated by the third coil with a phase difference of 0 with respect to the inner fluxball field. In addition, the strength of the rotating field generated by the fluxball also has a direct dependence on the magnitude of flow. All of these behaviors can be clearly illustrated in the channel 3 measured EFH1 velocity profile for a counter-clockwise rotating and third coil oscillating field of frequency 95 Hz as seen in Figure 6-60.

This result is also obtained for all frequencies, rotational directions and for both EFH1 and MSGW11 as confirmed by the channel 4 measured MSGW11 velocity profile for a clockwise rotating field and third coil oscillating field of frequency 47 Hz in Figure 6-61.

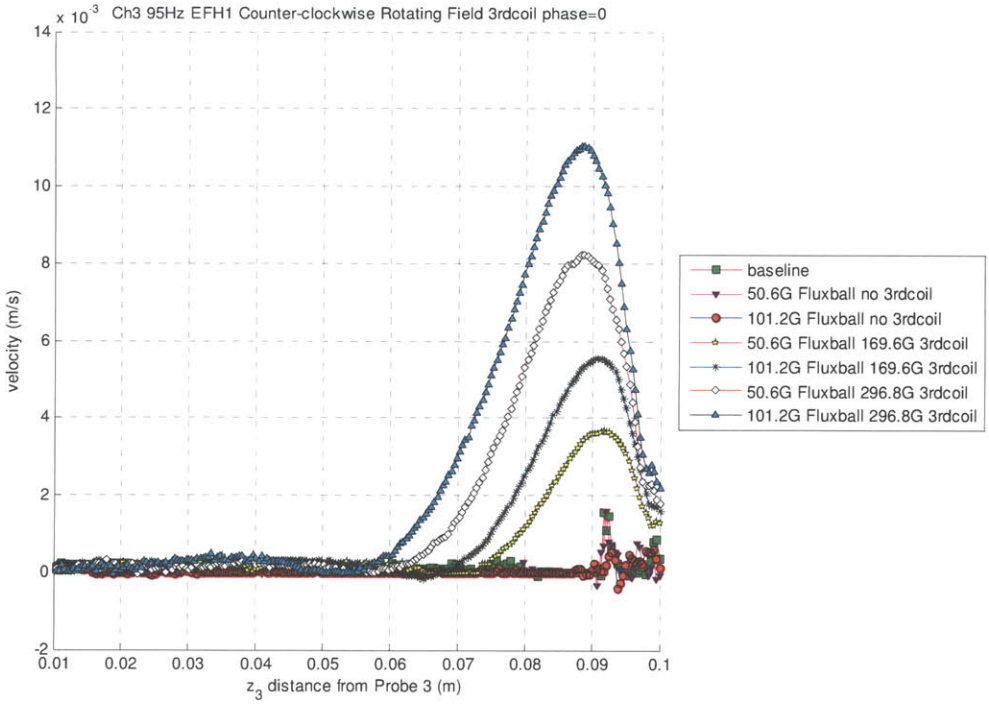

Figure 6-60. EFH1 velocity flow profile measured by channel 3 probe for a counter-clockwise rotating field and third coil oscillating field at 95 Hz. Baseline refers to the flow measured by the velocimeter in the absence of any field. The phase of the third coil with respect to the inner fluxball field is zero. There is a direct dependence of the fluxball rotating field strength and the strength of the non-uniform field imposed on the magnitude of the flow profile.

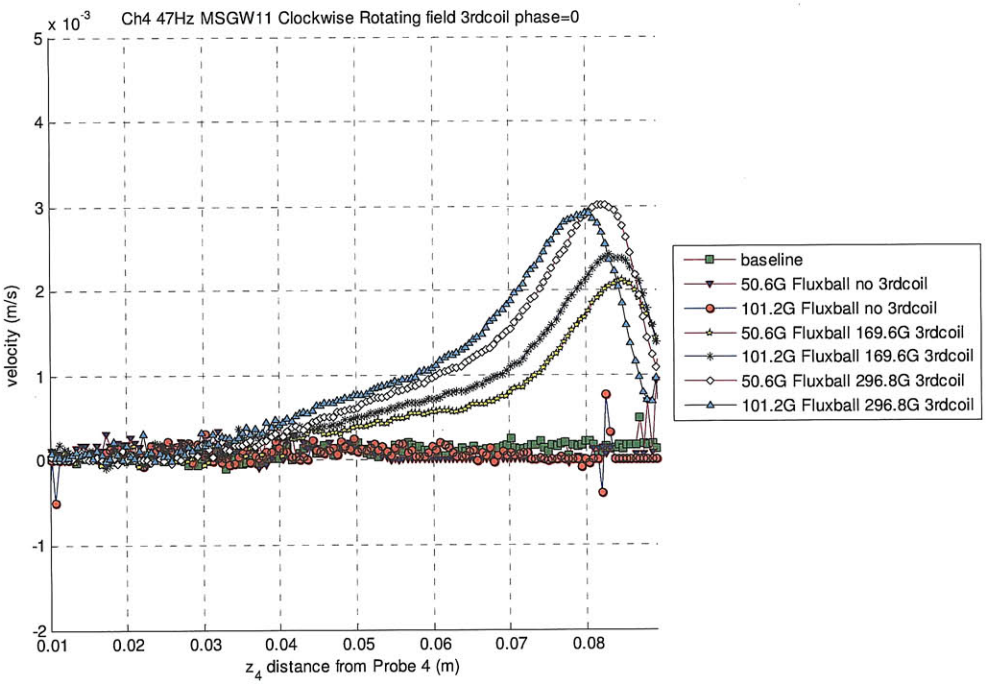

Figure 6-61. MSGW11 velocity profile as measured by channel 4 probe for a 47 Hz clockwise rotating field with a third coil oscillating field frequency of the same value. The strength of the rotating field as well as the non-uniform field generated by the third coil has a direct effect on the magnitude of the flow profile generated.

6.5.7. Effect of Strength of Rotating Field and DC Field on Flow Generated by Third Coil

The experiments conducted by imposing a non-uniform DC field generated by the third coil driven by a DC current instead of AC, all result in significant flow. The polarity of the DC field does not have any effect on the flow, instead the strength of the rotating field has a direct effect on the flow profile creating vortices in many cases, such as the channel 1 velocity profile of MSGW11 under the influence of a 95Hz rotating and DC non-uniform field in Figure 6-62. This behavior is consistent with different field rotational frequencies and with EFH1 as illustrated by the channel 4 velocity profile of a 47Hz counter-clockwise rotating field with an imposed DC non-uniform field in Figure 6-63.

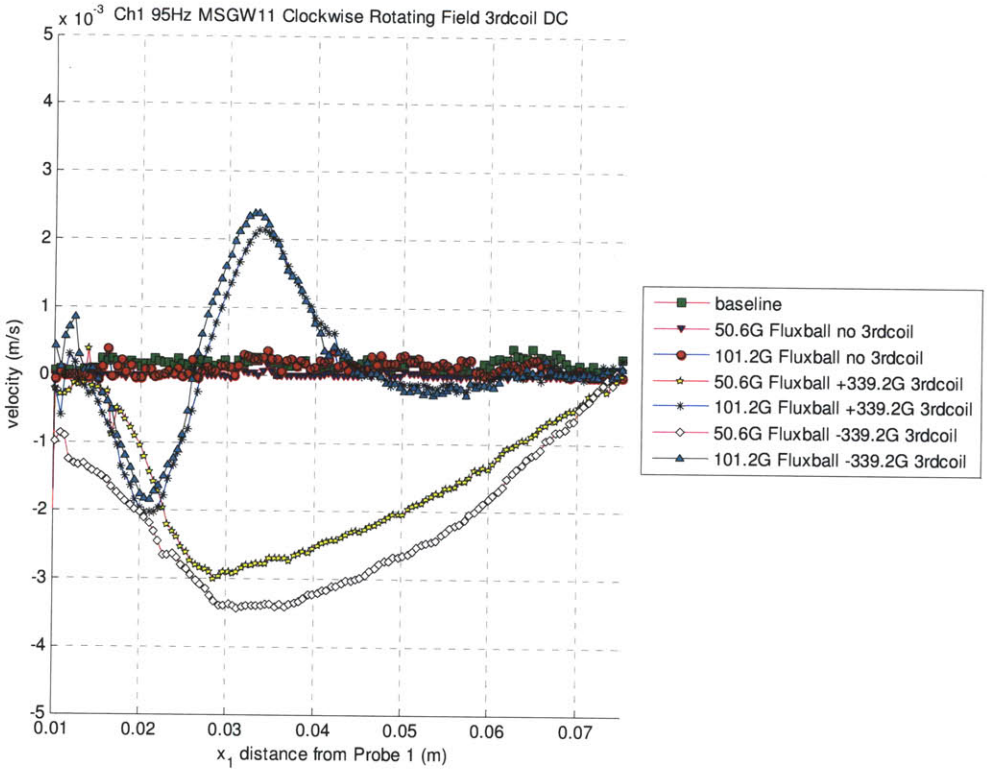

Figure 6-62. MSGW11 velocity profile measured by channel 1 probe for a 95 Hz clockwise rotating field with a non-uniform DC field imposed by the third coil. The flow profile is affected by the strength of the rotating field and not by the polarity of the DC field imposed by the third coil.

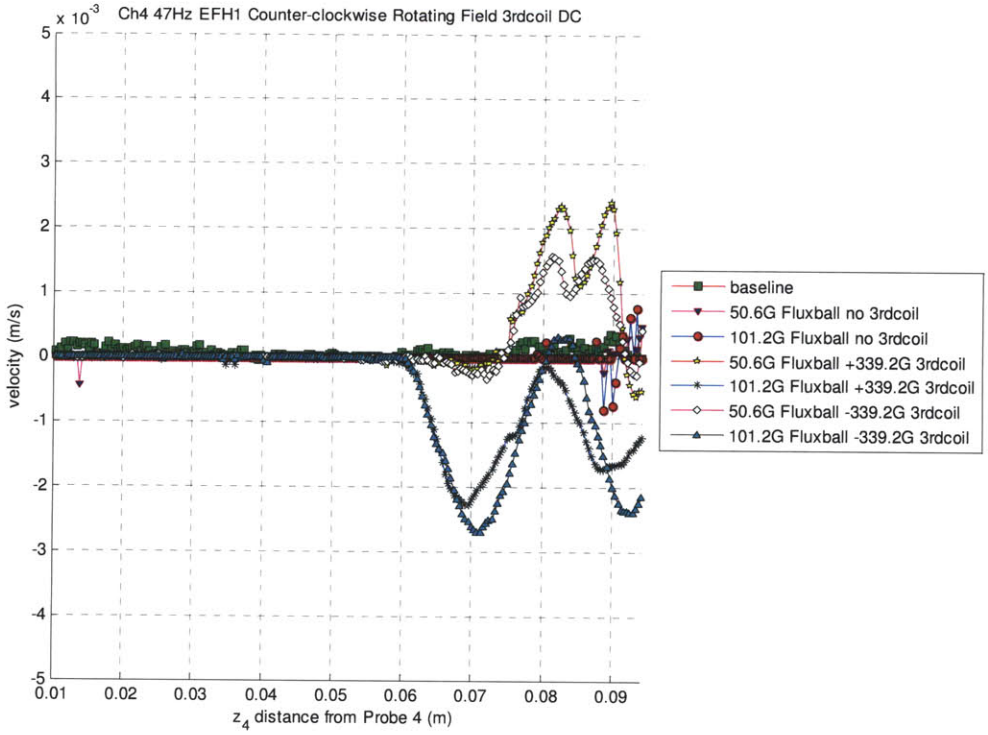

Figure 6-63. EFH1 velocity flow profile generated by a 47 Hz counter-clockwise rotating field with a DC field imposed by the third coil.

6.5.8. Effect of Rotational Frequency and Magnetic Properties of Ferrofluid on Flow

Due to the irregular complicated flow obtained by the non-uniform field imposed it is difficult to determine the dependence of frequency on the magnitude of flow. Figure 6-64 suggests that there is a direct dependence of frequency on the magnitude of the flow generated and type of fluid used (EFH1 having a higher magnetic susceptibility and magnetic saturation than MSGW11). However, Figure 6-65 illustrates that the flow profile behavior is different when measured by different probes and no direct frequency dependence or magnetic fluid dependence on the magnitude of flow can be determined due to the irregularities of the flow profile generated.

In general, the complicated flow that results makes it difficult to draw conclusions about the frequency and magnetic properties dependence on the magnitude of the flow. However all the results do support a safe conclusion that increasing the frequency does increase the chances of measuring non-zero velocity profiles (also bolstered by Figure 6-59) and that there is more likelihood of flow with the more magnetically responsive EFH1 than MSGW11.

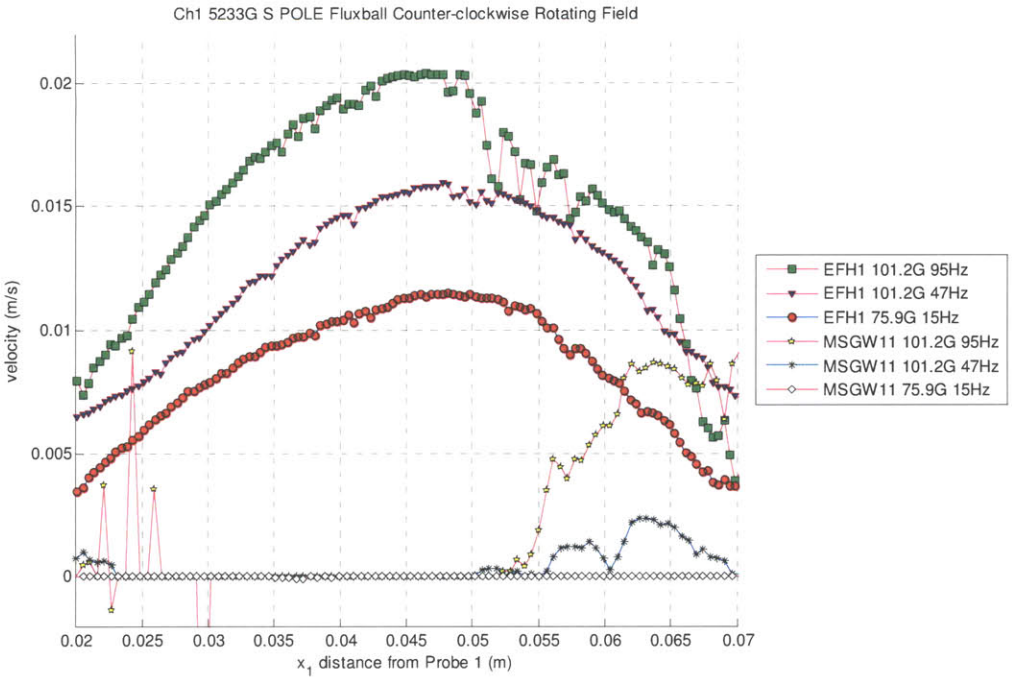

Figure 6-64. Velocity profiles measured by channel 1 probe for both MSGW11 and EFH1, and all three counter-clockwise rotational frequencies (15 Hz, 47 Hz, and 95 Hz) with a non-uniform field imposed by a south pole facing permanent magnet of surface field strength 5233 G on top of the ferrofluid filled sphere. EFH1 is in general more responsive than MSGW11.

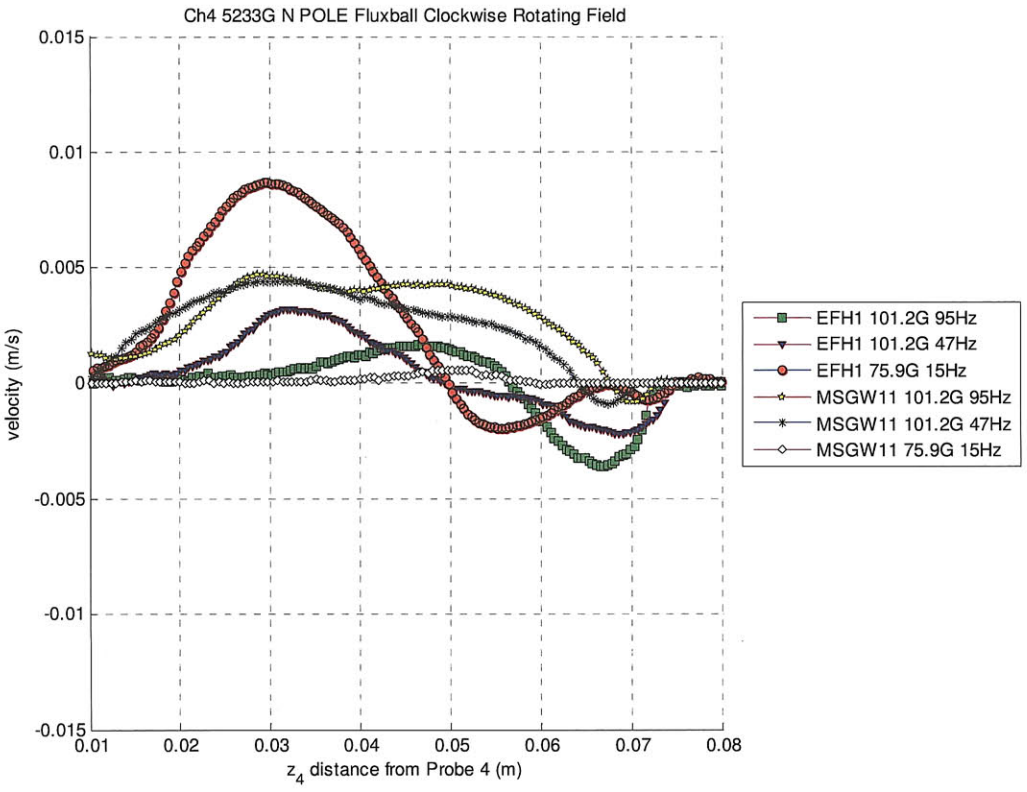

Figure 6-65. Velocity profile measured by channel 4 probe for MSGW11 and EFH1 at all investigated rotational frequencies (15 Hz, 47 Hz and 95 Hz) for a clockwise rotating field and a north pole facing permanent magnet of surface field strength 5233 G on top of the ferrofluid filled sphere.

6.6. Experiments of Non-Zero Flow Driven By Non-Uniform Fields Due to Demagnetizing Effects

6.6.1. Using a 2/3 Full Ferrofluid Filled Sphere

The 10 cm diameter hollow sphere can hold a maximum of ≈ 524 ml of ferrofluid. For this experiment two spheres were filled to 2/3 its maximum volume (≈ 350 ml) with EFH1 and MSGW11 respectively as seen in Figure 6-66. The four ultrasound probes are placed at the positions shown in Figure 6-68 and Figure 6-69 to measure the velocity profiles in those directions.

Figure 6-66. Picture of MSGW11 2/3 full sphere of diameter 10 cm. The ferrofluid can be seen to only occupy 2/3 of the volume of the sphere.

Non-zero flows were measured in the bulk of the ferrofluid 2/3 filled sphere under the influence of a rotating uniform magnetic field. Figure 6-70 to Figure 6-73 are the individual ultrasound probe's measured velocity flow profiles for a 2/3 filled sphere of EFH1 with a 101.2

G RMS uniform rotating magnetic field. Figure 6-74 is a calculated rotational velocity flow profile as a function of radius, at the equator of the sphere approximately 2 cm below the free surface, using the measurements of channel 1 and channel 3 and the equations outlined in section 4.2.1.

The bulk flows measured are a result of the non-uniform field due to the demagnetizing fields associated with the 2/3 full sphere. It is not immediately clear whether surface driven flows would result since the free ferrofluid surface is not in the plane of the rotating field but perpendicular to it as seen in Figure 6-67.

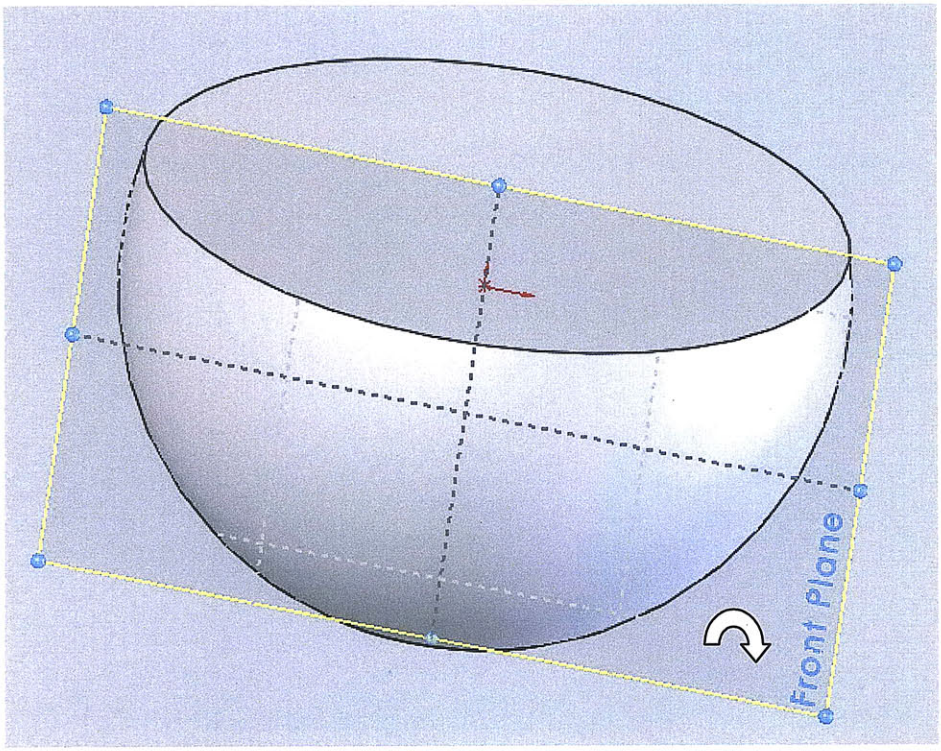

Figure 6-67. 2/3 full sphere with rotating field rotating in the Front Plane indicated.

Figure 6-75 to Figure 6-78 are the individual ultrasound probe's measured velocity flow profiles for a 2/3 filled sphere of EFH1 with a 50.6 G RMS uniform rotating magnetic field. Figure 6-79 is a calculated rotational velocity flow profile as a function of radius, at the equator

of the sphere approximately 2 cm below the free surface, using the measurements of channel 1 and channel 3 and the equations outlined in section 4.2.1.

Experiments were also conducted with a 2/3 full MSGW11 filled sphere of diameter 10 cm, however, no measureable flow was observed. This is because not only is the MSGW11 magnetically less responsive than EFH1, having a lower magnetic susceptibility and magnetic saturation, but the applied magnetic field of the fluxball machine could not be driven higher than 101.2 G RMS to drive the flow.

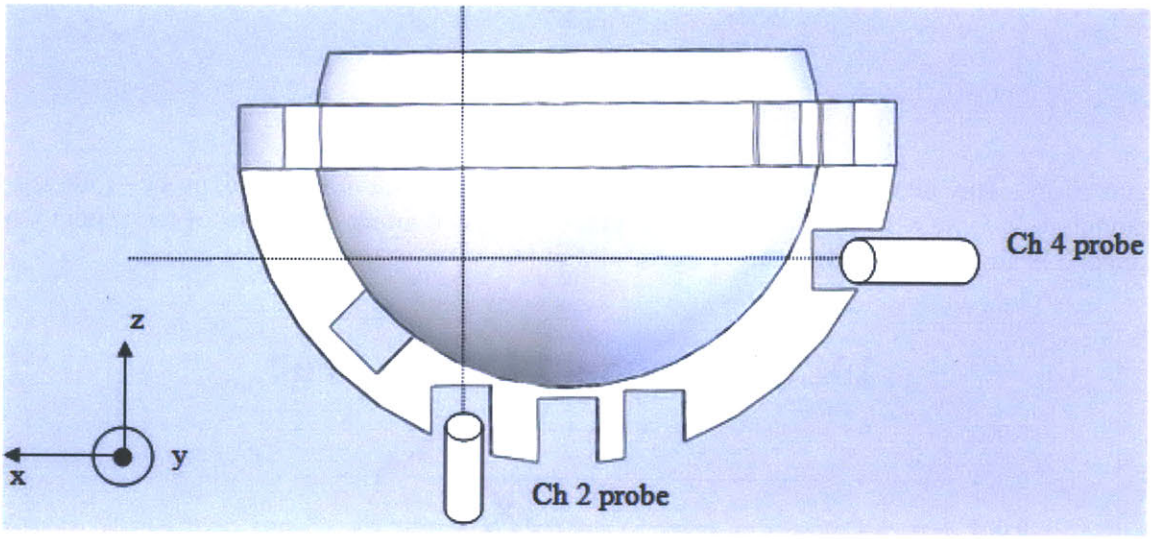

Figure 6-68. Profile view depicting positions of two of the four ultrasound probes (labeled as Channels 2 & 4), in x-z plane. Channel 2 probe placed underneath the sphere while channel 4 is the probe placed 2.5 cm below the equator of the sphere. The sphere shown here has its top portion removed to illustrate how the actual ferrofluid volume looks. The actual sphere was intact and just filled 2/3 full.

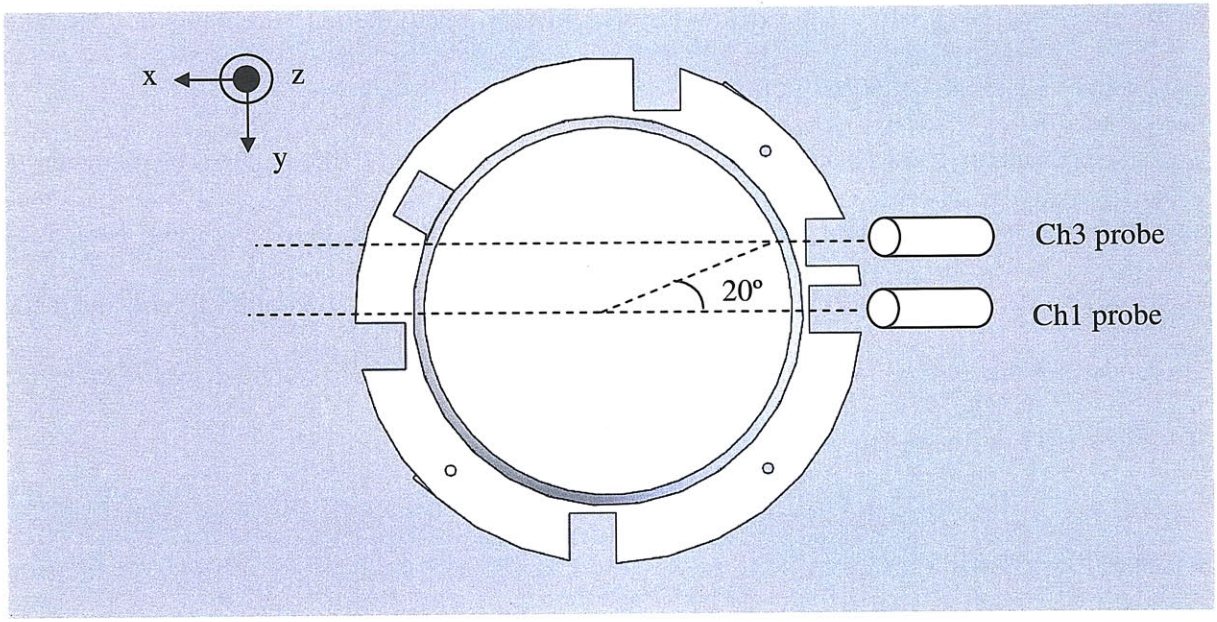

Figure 6-69. Top view depicting positions of two of the four ultrasound probes (labeled as Channels 1 & 3), in x-y plane. Channel 1 is probe is aligned along the radius of the sphere while channel 3 is aligned 20° to the radial direction.

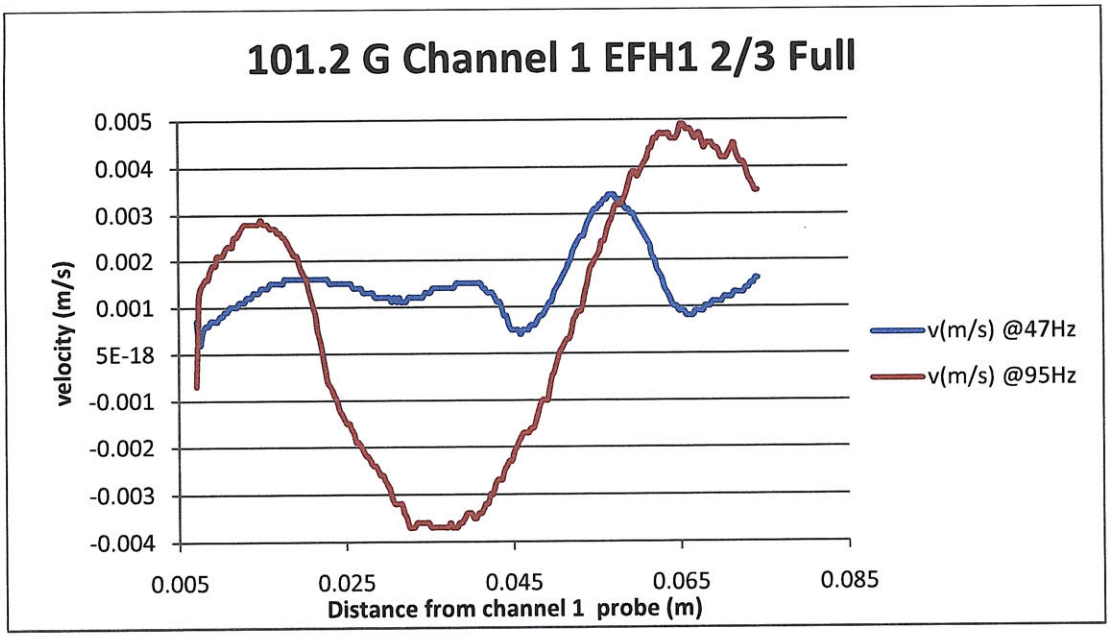

Figure 6-70. EFH1 velocity profile measured by channel 1 probe for 2/3 full sphere at 47 Hz and 95 Hz 101.2 G RMS uniform rotating field.

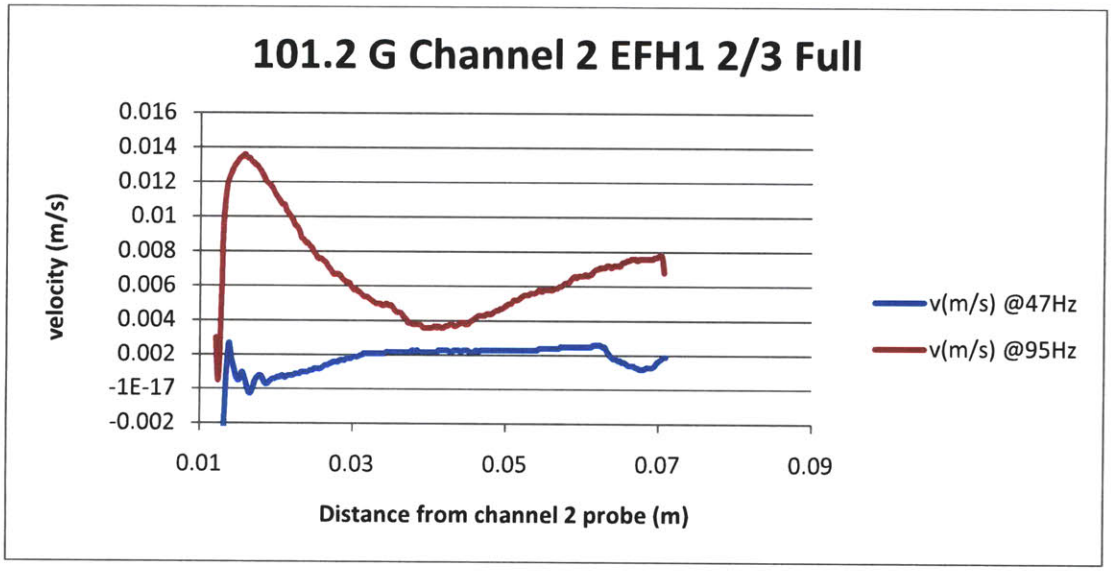

Figure 6-71. EFH1 velocity profile measured by channel 2 probe for 2/3 full sphere at 47 Hz and 95 Hz 101.2 G RMS uniform rotating field.

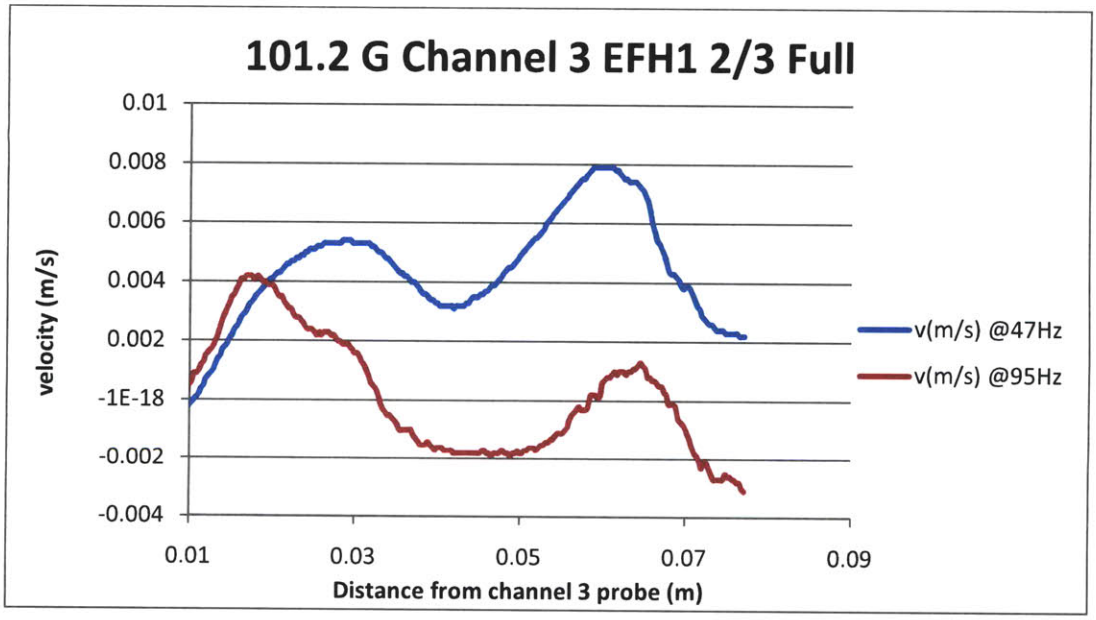

Figure 6-72. EFH1 velocity profile measured by channel 3 probe for 2/3 full sphere at 47 Hz and 95 Hz 101.2 G RMS uniform rotating field.

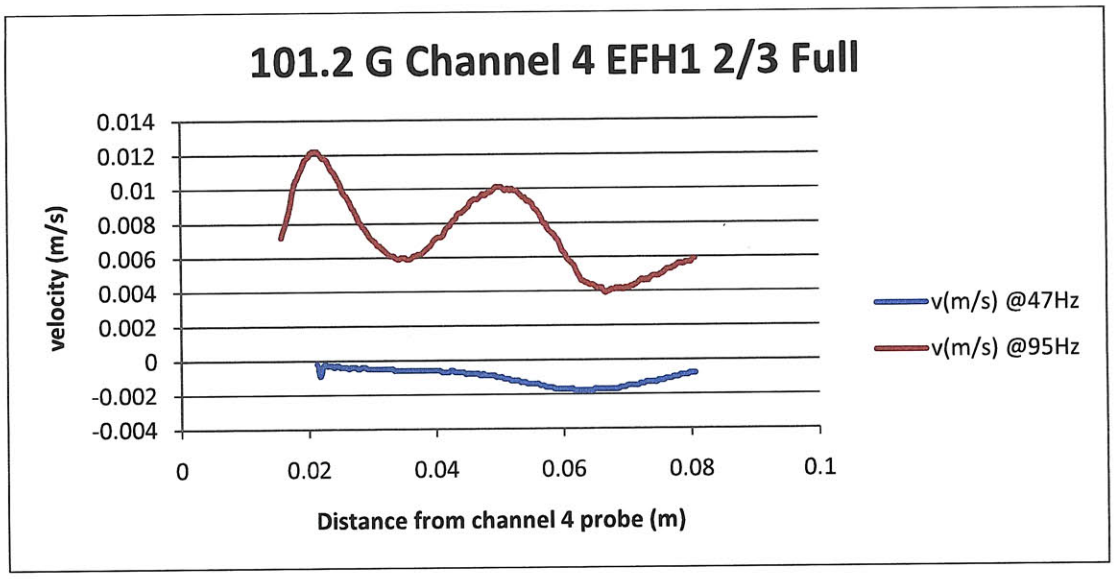

Figure 6-73. EFH1 velocity profile measured by channel 4 probe for 2/3 full sphere at 47 Hz and 95 Hz 101.2 G RMS uniform rotating field.

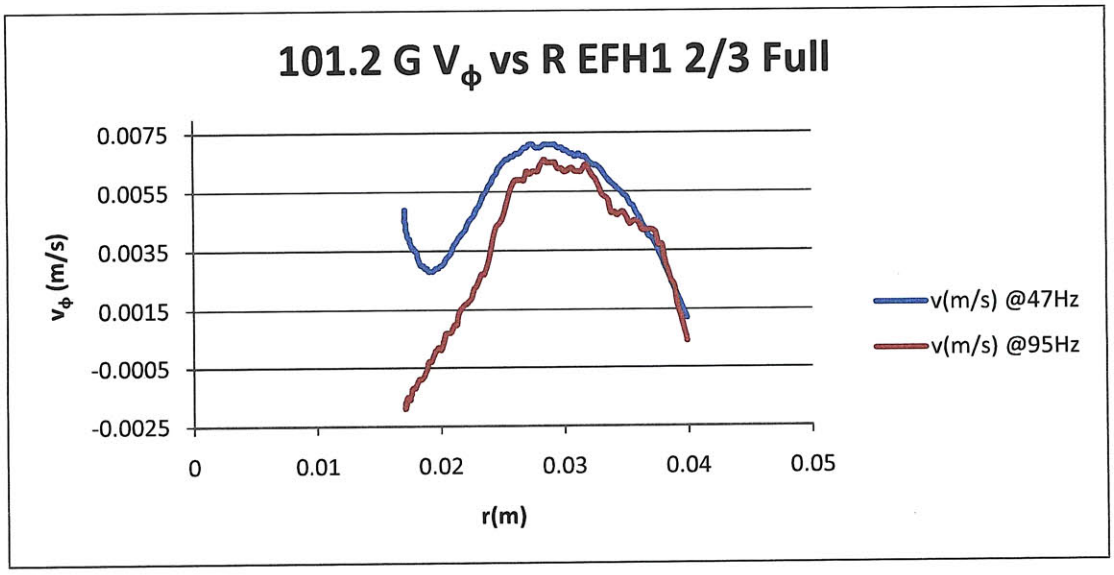

Figure 6-74. Rotational velocity v_φ as a function of radius for 2/3 filled sphere of EFH1, under a 101.2 G RMS uniform rotating magnetic field, measured at the equator of the sphere approximately 2 cm below the free surface.

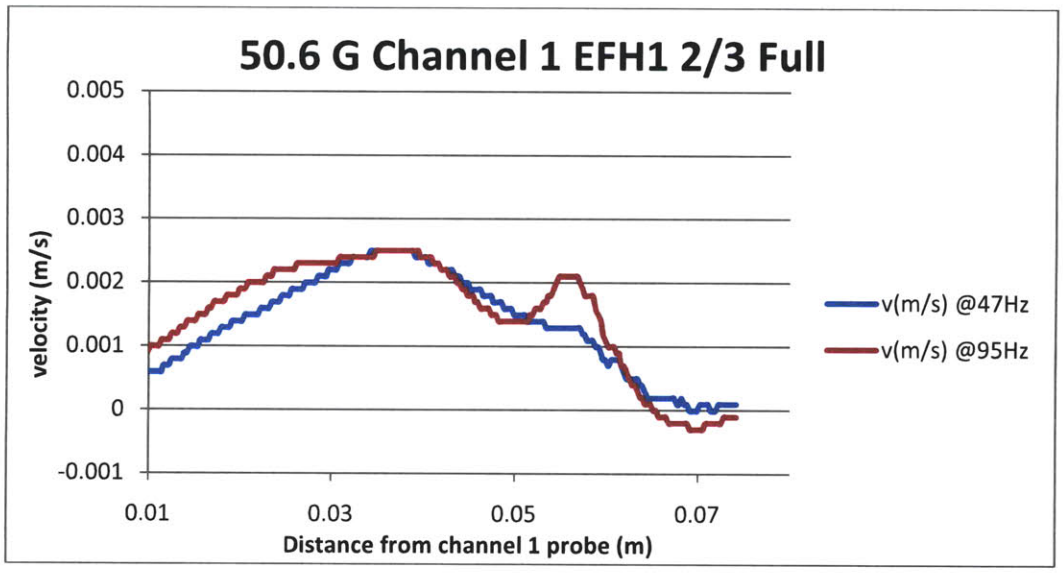

Figure 6-75. EFH1 velocity profile measured by channel 1 probe for 2/3 full sphere at 47 Hz and 95 Hz 50.6 G RMS uniform rotating field.

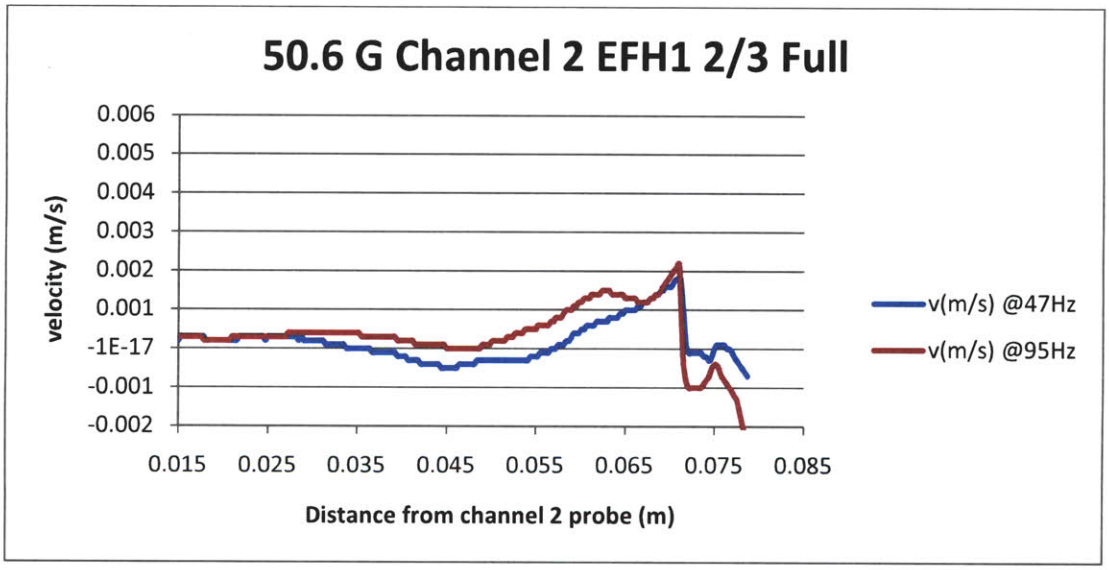

Figure 6-76. EFH1 velocity profile measured by channel 2 probe for 2/3 full sphere at 47 Hz and 95 Hz 50.6 G RMS uniform rotating field.

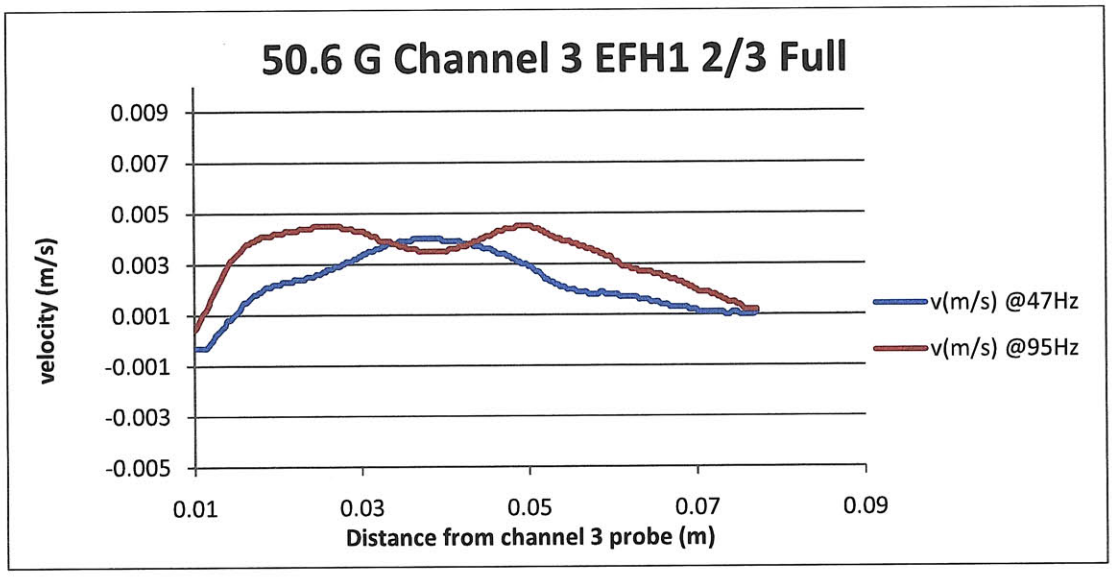

Figure 6-77. EFH1 velocity profile measured by channel 3 probe for 2/3 full sphere at 47 Hz and 95 Hz 50.6 G RMS uniform rotating field.

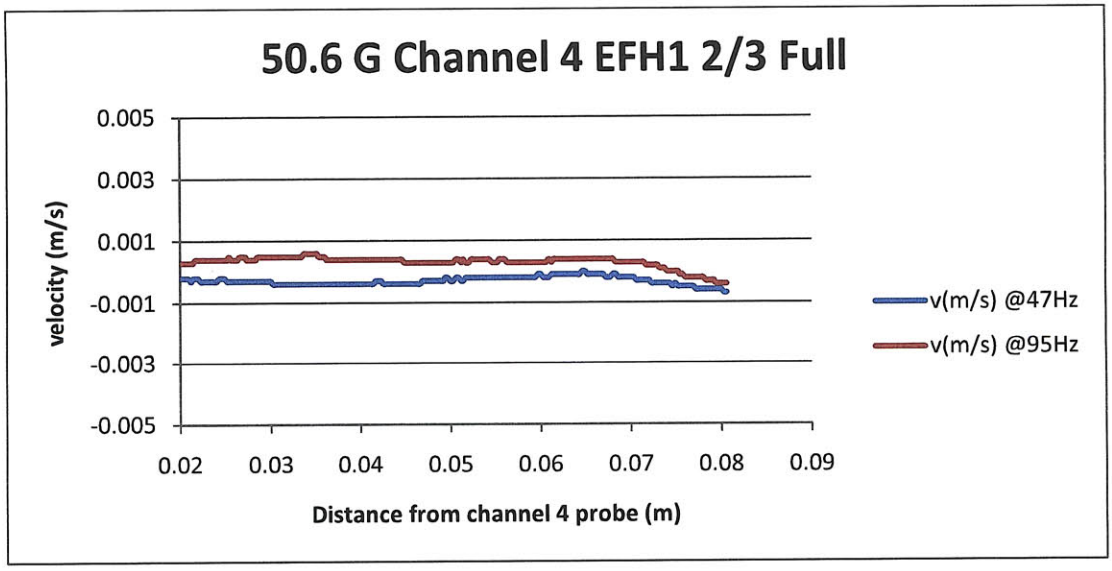

Figure 6-78. EFH1 velocity profile measured by channel 4 probe for 2/3 full sphere at 47 Hz and 95 Hz 50.6 G RMS uniform rotating field.

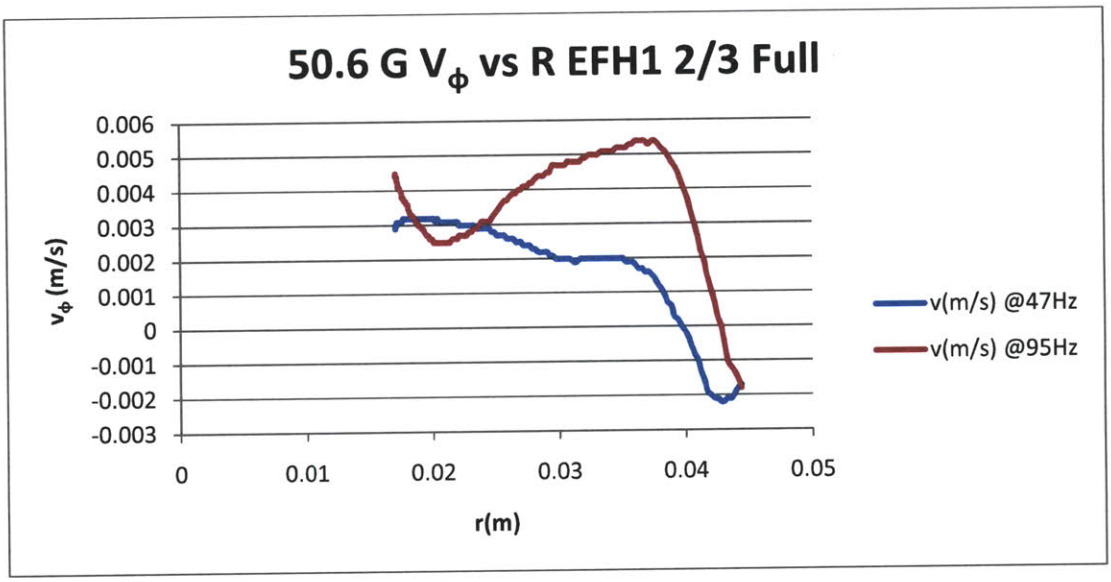

Figure 6-79. Rotational velocity v_φ as a function of radius for 2/3 filled sphere of EFH1, under a 50.6 G RMS uniform rotating field, measured at the equator of the sphere approximately 2 cm below the free surface.

6.6.2. Using a Finite Height Cylinder

He's polycarbonate cylinder, used in his thesis [2], of 91.9 mm diameter and height 60 mm was used to conduct this experiment. A top view picture of the cylinder, as seen in Figure 6-80, shows the grooves on the sides of the cylinder allowing for the placement of the ultrasound probes. A side view of the cylinder, as seen in Figure 6-81, shows support posts that were fitted on its sides to allow for fitting inside the inner fluxball. The cylinder had its lid fitted to prevent the ferrofluid from spilling but it was too difficult to fill the cylinder all the way to ensure no free surface. The cylinder filled with ferrofluid was then placed inside the inner fluxball as shown in Figure 6-82.

The inner fluxball was designed to be fitted inside the outer fluxball vertically, as seen at the left of Figure 6-83. This generates a rotating field in the x-y plane as shown. To carry out the classical cylindrical experiment, the rotating field should be in the plane of the ferrofluid cylinder. This was achieved by placing the cylinder fitted inside the inner fluxball as shown in Figure 6-82 and placing the entire inner fluxball inside the outer fluxball oriented 90° to its designed configuration.

The ultrasound probes were placed one along the radial (α=0°) groove and one along the (α=10°) groove at a height approximately half way from the surface of the ferrofluid towards the bottom of the cylinder, to ensure bulk flow measurements. The results plotted in Figure 6-84 for EFH1 illustrate that non-zero velocities were obtained in a uniform rotating field, generated by the fluxball machine, for two rotational frequencies 10Hz and 95Hz. The flow was measured by ultrasound probes positioned half way from the ferrofluid free surface and the bottom of the cylinder to ensure measurement of bulk flows.

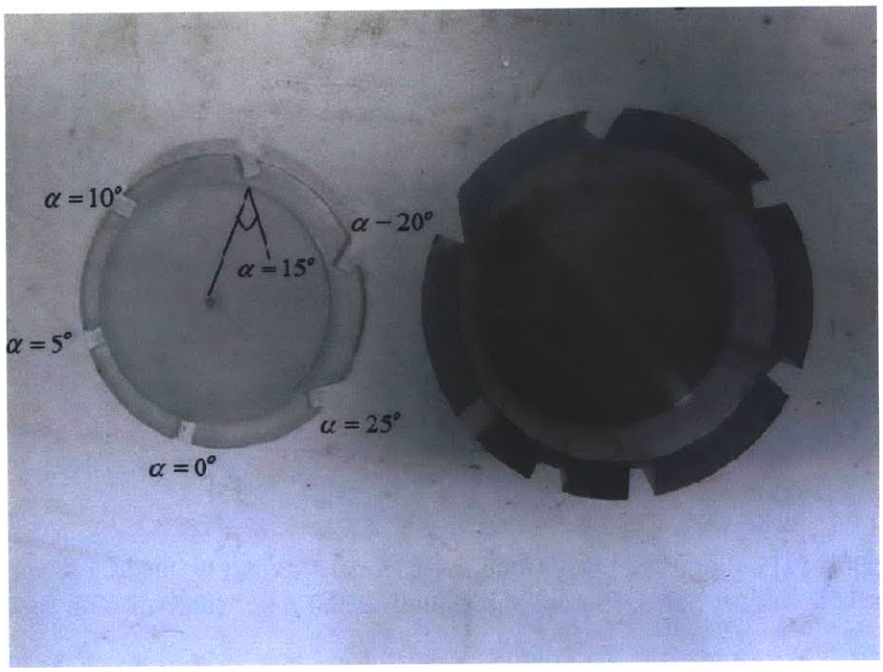

Figure 6-80. Top view of He's [2] cylindrical polycarbonate cylinder with lid. The grooves on the side of the cylinder allow for the placement of ultrasound probes that are at angles (α) with respect to the radial direction as illustrated in Figure 4-2. This image was taken from He's thesis [2].

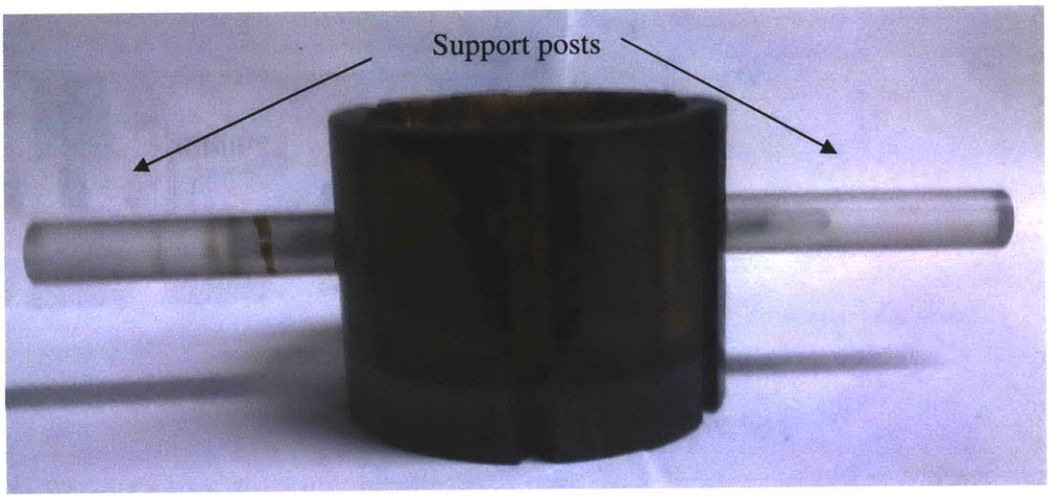

Figure 6-81. Side profile of He's [2] cylinder. Support posts were added to the sides of the cylinder to allow for fitting into the access hole of the inner fluxball.

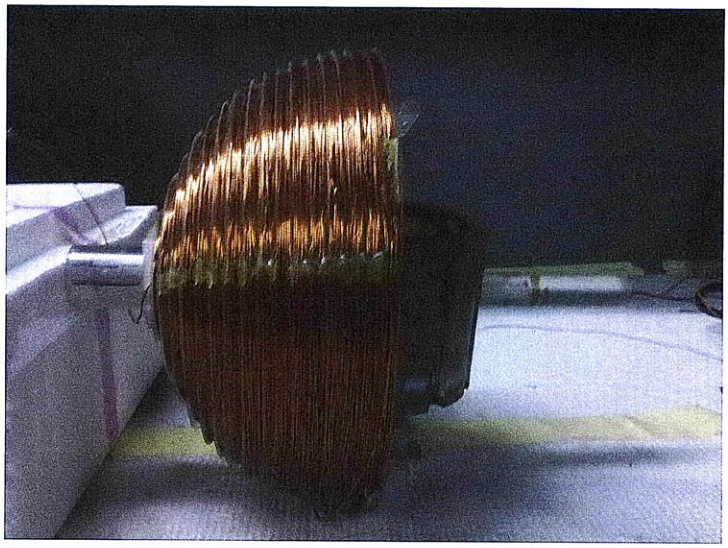

Figure 6-82. He's [2] cylinder securely fitted inside inner fluxball by placing support posts inside the inner fluxball's access holes. Picture shows half of the inner fluxball with the cylinder fitted inside it.

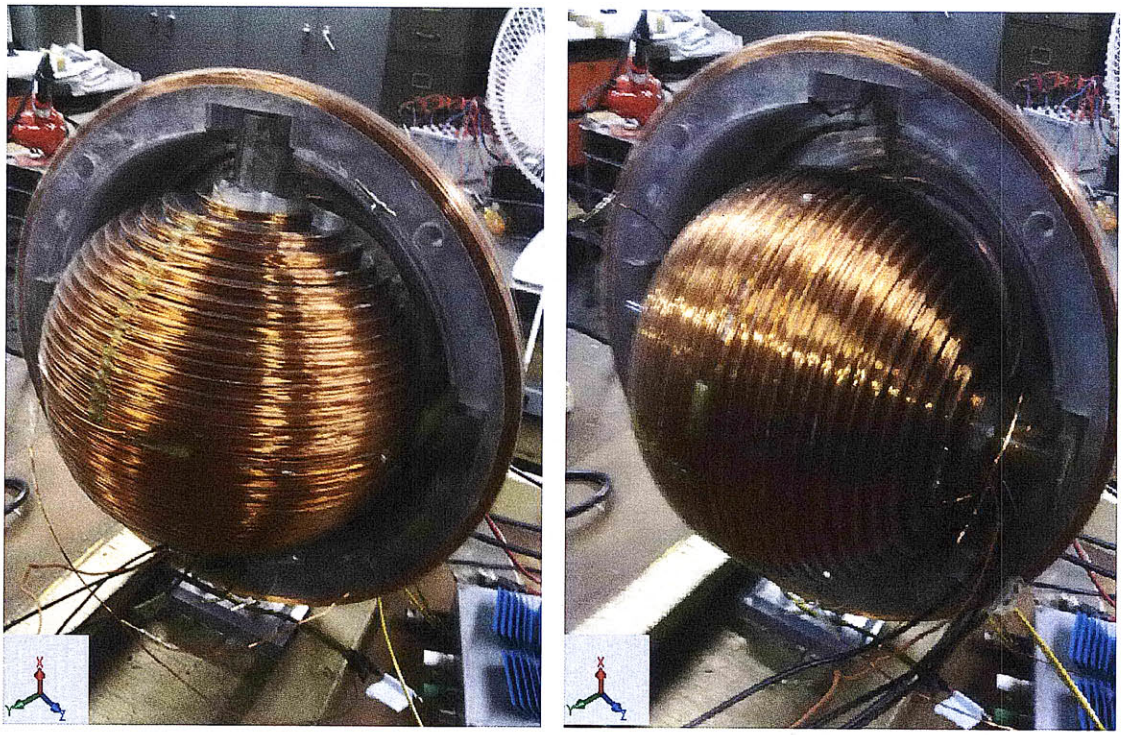

Figure 6-83. Inner fluxball configurations. Left: Inner fluxball designed to be placed vertically generating a rotating magnetic field in the x-y plane. Right: Inner fluxball rotated 90° from designed configuration and generates rotating magnetic field in y-z plane.

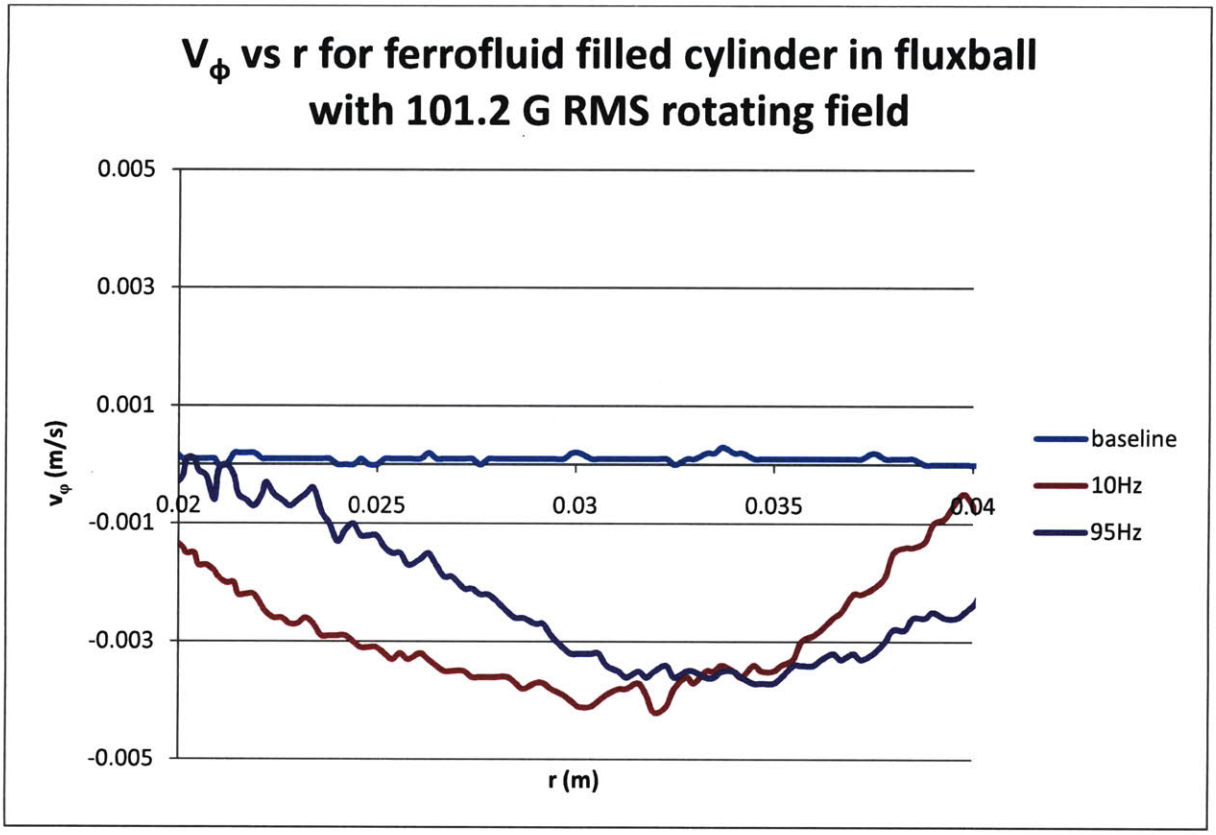

Figure 6-84. EFH1 rotational velocity v_φ as a function of radius for a rotating field strength of 101.2 G RMS for two rotational frequencies 10 Hz and 95 Hz. The flow is measured in the bulk of the fluid half way from the ferrofluid free surface towards the bottom of the cylinder. Baseline represents the measured velocity with no magnetic field applied.

6.7. Conclusions

In this chapter, COMSOL simulations using spin-diffusion theory ($\eta' \neq 0$) with $\omega(r = R_{wall}) = 0$ boundary condition predict non-zero measureable flow for a ferrofluid filled sphere subjected to a uniform rotating magnetic field. COMSOL simulations that neglect the effect of spin-diffusion ($\eta' = 0$) give negligible flow which is in agreement to the results of experiments performed subjecting the spherical geometry to a uniform rotating magnetic field. Measured flows were obtained in geometries where demagnetizing effects associated with the shape were significant (2/3 full sphere and cylinder). These experiments confirm that not only are spin-diffusion effects negligible but that the demagnetizing effects associated with the shape of the container results in a non-uniform field inside the ferrofluid volume driving the flow.

These results also for the first time explain why the experimentally fit values of spin viscosity used by several authors [1, 2, 6], to explain their experimental results obtained in cylindrical geometry (Chapter 4), are many orders of magnitude greater than the theoretical values of spin viscosity derived here in this chapter. The reason for this discrepancy is due to the fact that these experimentally fit spin viscosity values encompass the demagnetizing effects associated with the shape of the cylindrical container resulting in larger values than theory and as a result have mistakenly attributed the effect of spin-diffusion theory to being a possible explanation for the driving force behind spin-up flow.

To further bolster the theory that non-uniform magnetic properties drive the flow, this chapter describes results of experiments where the fully filled ferrofluid sphere is subjected to a non-uniform field imposed by permanent magnets or a third solenoidal coil in addition to the

rotating uniform magnetic field. In both these cases complicated and significant measureable flows were obtained.

Bibliography

[1] S. Elborai, "Ferrofluid surface and volume flows in uniform rotating magnetic fields," Ph.D thesis, Dept of Electrical Engineering and Computer Science, Massachusetts Institute of Technology, Cambridge, MA, 2006.

[2] X. He, "Ferrohydrodynamic flows in uniform and non-uniform rotating magnetic fields," Ph.D thesis, Dept of Electrical Engineering and Computer Science, Massachusetts Institute of Technology, Cambridge, MA, 2006.

[3] K. R. Schumacher, *et al.*, "Experiment and simulation of laminar and turbulent ferrofluid pipe flow in an oscillating magnetic field," *Physical Review E,* vol. 67, p. 026308, 2003.

[4] B. Finlayson and R. E. Rosensweig, M. Zahn, Ed., ed, 2002.

[5] R. B. Bird, *et al.*, *Transport Phenomena*, Second ed.: John Wiley & Sons, Inc, 2002.

[6] A. Chaves, *et al.*, "Spin-up flow of ferrofluids: Asymptotic theory and experimental measurements," vol. 20, p. 053102, 2008.

[7] A. Pshenichnikov, *et al.*, "On the rotational effect in nonuniform magnetic fluids," *Magnetohydrodynamics,* vol. 36, pp. 275-281, 2000.

[8] R. E. Rosensweig, *Ferrohydrodynamics*: Dover Publications, 1997.

[9] O. A. Glazov, "Motion of a ferrosuspension in rotating magnetic fields," *Magnetohydrodynamics,* vol. 11, pp. 140-145, 1975.

[10] O. A. Glazov, "Role of higher harmonics in ferrosuspension motion in a rotating magnetic field," *Magnetohydrodynamics,* vol. 11, pp. 434-438, 1975.

[11] A. Pshenichnikov and A. Lebedev, "Tangential stresses on the magnetic fluid boundary and rotational effect," *Magnetohydrodynamics,* vol. 36, pp. 254-263, 2000.

[12] M. I. Shliomis, *et al.*, "Ferrohydrodynamics: An essay on the progress of ideas," *Chem. Eng. Comm.,* vol. 67, pp. 275 - 290, 1988.

[13] M. Zahn, *Electromagnetic Field Theory: A Problem Solving Approach*: Krieger Publishing Company, 2003.

Chapter 7. COMSOL Simulations of Ferrofluid Flows With Zero Spin-Viscosity (η'=0) in Cylindrical Geometry With Non-Uniform Magnetic Fields

This chapter will describe COMSOL simulations of flows in an infinitely long ferrofluid filled cylinder, assuming zero spin-viscosity, subjected to a uniform rotating field and a non-uniform magnetic field imposed by an infinitely long permanent magnet. The results of this chapter demonstrate that the flows obtained are complicated and irregular and that they have similar characteristics obtained from the spherical geometry experiments of Chapter 6, even though the geometries are not identical.

7.1. Setup of Simulations

7.1.1. Model Geometry

The model is setup as shown in Figure 7-1 with two concentric cylinders, the inner one representing the ferrofluid cylinder while the outer one represents a stator winding. The stator winding with a surface current boundary condition generates the uniform rotating field, while the permanent magnet, magnetized in the y direction, is placed at a distance R_3 above the ferrofluid filled cylinder making the field non-uniform. The strength of the magnet is α times greater than the strength of the rotating field. Air fills the gap between the outer stator winding and the ferrofluid cylinder.

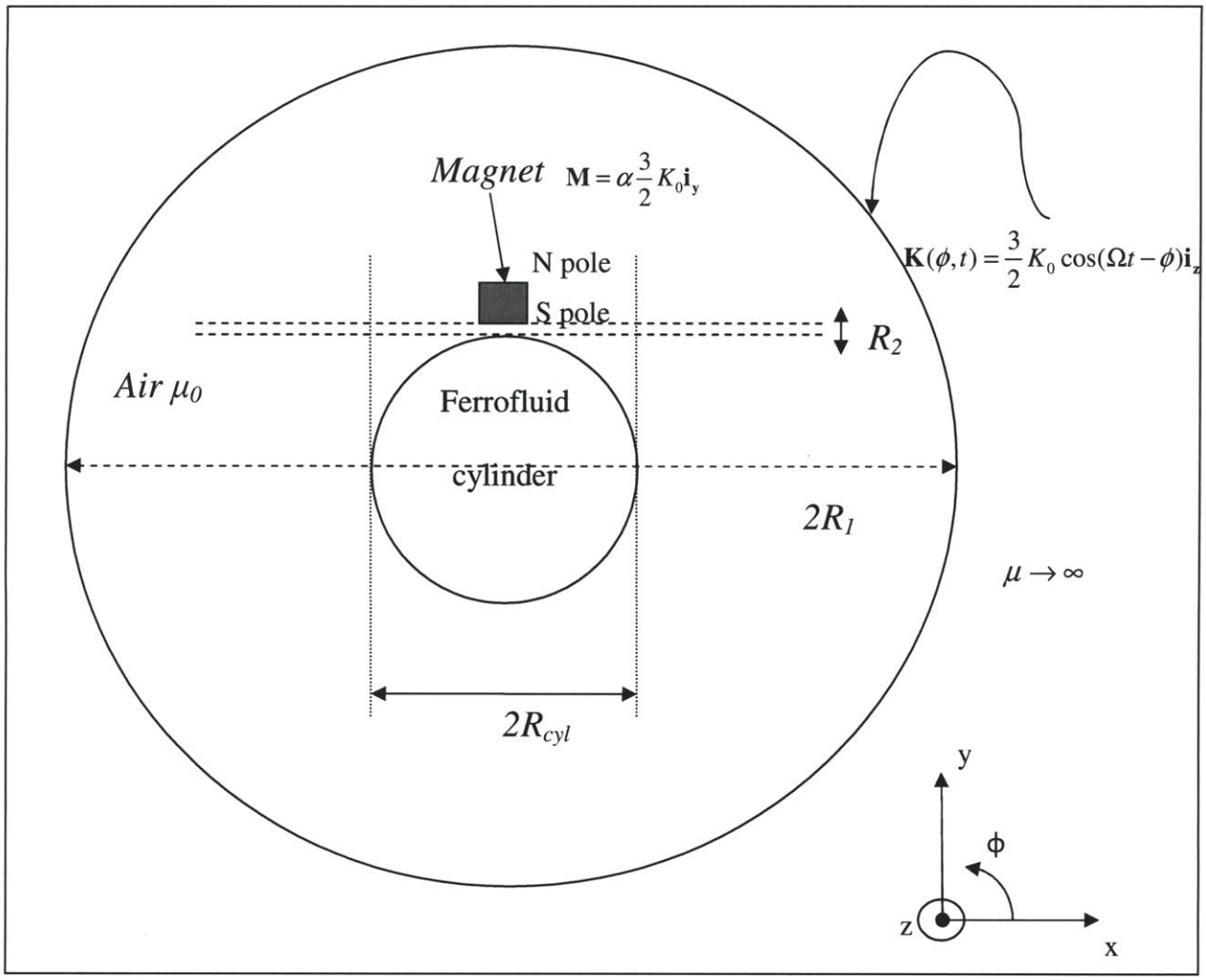

Figure 7-1. Model setup for simulating flows in ferrofluid under the influence of the non-uniform field of the permanent magnet, as well as, the uniform rotating magnet field imposed by current boundary condition far away. The magnet placed at a distance R_2 from the cylinder is magnetized in the y direction and is α times the strength of the rotating field. The south pole of the magnet faces the cylinder as shown.

7.1.2. Governing Equations

Ampere's Law with zero volume current and Gauss's Law for magnetic flux density can be combined to give the first relation between magnetic flux density and ferrofluid magnetization. This relation in (7.1) is derived in Eq. (4.9) and although it could be further reduced to Poisson's equations in terms of a magnetic scalar potential as used in Chapters 4 and 6, the magnetic scalar potential is not used in these models. The reason for this is explained in section 7.1.5.

1) Maxwell's equation

$$\nabla \bullet \mathbf{H} = -\nabla \bullet \mathbf{M} \tag{7.1}$$

The three other equations that are coupled together are the fluid mechanics linear and angular momentum equations and the magnetization relaxation equation outlined below. The spin-viscosity term η' is set to 0 in the conservation of angular momentum equation since results in Chapter 6 suggest its role is insignificant.

2) Conservation of Linear Momentum

$$\rho\left[\frac{\partial \mathbf{v}}{\partial t} + (\mathbf{v} \bullet \nabla)\mathbf{v}\right] = -\nabla p' + 2\zeta \nabla \times \boldsymbol{\omega} + (\zeta + \eta)\nabla^2 \mathbf{v} + \mu_0 (\mathbf{M} \bullet \nabla)\mathbf{H} \tag{7.2}$$

3) Conservation of Angular Momentum

$$I\left[\frac{\partial \boldsymbol{\omega}}{\partial t} + (\mathbf{v} \bullet \nabla)\boldsymbol{\omega}\right] = \mu_0 \mathbf{M} \times \mathbf{H} + 2\zeta(\nabla \times \mathbf{v} - 2\boldsymbol{\omega}) + \cancel{\eta' \nabla^2 \boldsymbol{\omega}} \tag{7.3}$$

4) Magnetization Relaxation Equation

$$\frac{\partial \mathbf{M}}{\partial t} + (\mathbf{v} \bullet \nabla)\mathbf{M} = \boldsymbol{\omega} \times \mathbf{M} - \frac{1}{\tau_{eff}}(\mathbf{M} - \mathbf{M}_{eq}) \tag{7.4}$$

7.1.3. Boundary Conditions

The rotating magnetic field is generated by using a z-directed surface current boundary condition identical to Eq. (4.17). The fluid boundary conditions are no slip on the boundary as given by

$$\mathbf{v}(r = R_{cyl}) = 0 \tag{7.5}$$

Since $\eta' = 0$, there are no boundary conditions on spin velocity ω.

7.1.4. Assumptions

The equilibrium magnetization $\mathbf{M}_{eq}$ of the fluid is not assumed to be in the linear regime of the Langevin equation unlike the previous COMSOL simulations done in Chapters 4 and 6. The equilibrium magnetization is described by the complete Langevin equation as given in Eq (2.17) and is used in these simulations because of the magnetic saturation of the fluid near the permanent magnet.

The flow is also assumed to be viscous dominated allowing for the inertial terms to be dropped. The left hand side of the linear and angular momentum equations in (7.2) and (7.3) are set to 0 and the equations reduce to

$$0 = -\nabla p' + 2\zeta\nabla\times\boldsymbol{\omega} + (\zeta+\eta)\nabla^2\mathbf{v} + \mu_0(\mathbf{M}\cdot\nabla)\mathbf{H} \tag{7.6}$$

$$0 = \mu_0\mathbf{M}\times\mathbf{H} + 2\zeta(\nabla\times\mathbf{v} - 2\boldsymbol{\omega}) + \cancel{\eta'\nabla^2\boldsymbol{\omega}} \tag{7.7}$$

7.1.5. COMSOL Simulations

The COMSOL simulations were done by using non-dimensional forms of equations (7.1) -(7.4) with respect to reference parameters such as radius of the vessel R_0, frequency of the

applied rotating field Ω and a reference magnetic field intensity H_0. For all the simulations used in this chapter, these reference values are given in Table 7-1.

Parameters	Value
Radius of cylindrical vessel R_0 (m)	0.05
Rotational frequency (Hz)	95
Rotational frequency Ω (rad/s)	596.9
Rotational field flux density RMS B_0 (Gauss)	100
Rotational field intensity RMS H_0 (A/m)	7957.75

Table 7-1. Reference values used for normalizing equations for simulations in this section.

The non-dimensional equations are given as

$$\mathrm{R}_e[\frac{d\bar{\mathbf{v}}}{dt}+(\bar{\mathbf{v}}\bullet\bar{\nabla})\bar{\mathbf{v}}]=-\bar{\nabla}\bar{p}'+2\bar{\zeta}\bar{\nabla}\times\bar{\boldsymbol{\omega}}+(\bar{\zeta}+\bar{\eta})\bar{\nabla}^2\bar{\mathbf{v}}+\left(\bar{\mathbf{M}}\bullet\bar{\nabla}\right)\bar{\mathbf{H}} \tag{7.8}$$

$$R_w[\frac{d\bar{\boldsymbol{\omega}}}{dt}+(\bar{\mathbf{v}}\bullet\bar{\nabla})\bar{\boldsymbol{\omega}}]=\bar{\mathbf{M}}\times\bar{\mathbf{H}}+2\bar{\zeta}(\bar{\nabla}\times\bar{\mathbf{v}}-2\bar{\boldsymbol{\omega}}) \tag{7.9}$$

$$\frac{d\bar{\mathbf{M}}}{dt}+(\bar{\mathbf{v}}\bullet\bar{\nabla})\bar{\mathbf{M}}=\bar{\boldsymbol{\omega}}\times\bar{\mathbf{M}}-\frac{1}{\Omega\tau_{eff}}(\bar{\mathbf{M}}-\bar{\mathbf{M}}_{eq}) \tag{7.10}$$

$$\nabla\bullet\bar{\mathbf{H}}=-\nabla\bullet\bar{\mathbf{M}} \tag{7.11}$$

where

$$\bar{\nabla}=\nabla R_0,\ \bar{\mathbf{v}}=\frac{\mathbf{v}}{R_0\Omega},\ \bar{\mathbf{M}}=\frac{\mathbf{M}}{H_0},\ \bar{\mathbf{H}}=\frac{\mathbf{H}}{H_0},\ \bar{t}=t\Omega,\ \bar{p}=\frac{p}{\mu_0H_0^2},\ \bar{\boldsymbol{\omega}}=\frac{\boldsymbol{\omega}}{\Omega},\ \bar{\zeta}=\frac{\zeta\Omega}{\mu_0H_0^2},$$
$$\bar{\eta}=\frac{\eta\Omega}{\mu_0H_0^2},\ R_e=\frac{\rho R_0^2\Omega^2}{\mu_0H_0^2},\ R_w=\frac{I\Omega^2}{\mu_0H_0^2}$$

For all cases the transient form of these equations were entered into COMSOL. A fluid mechanics module was used to represent the augmented Navier-Stokes equation in (7.8), but with setting the density ρ term to 0 to get rid of the inertial terms on the left hand side of (7.8). A diffusion equation was used for the conservation of angular momentum equation, having no convective derivative automatically gets rid of the left hand side of (7.8), with η' representing

the diffusion constant and set to 0. Two transient convection and diffusion modules were used to represent the magnetic relaxation equation (with zero diffusion) in x and y coordinates for (7.10). A *Perpendicular, Induction Currents* module automatically implements (7.11) using a magnetic vector potential **A** where

$$\mathbf{B} = \nabla \times \mathbf{A} \tag{7.12}$$

It is because this module allows for the z-directed surface current boundary condition and the specification of the y-directed magnetization of the permanent magnet that there is no need to work with the magnetic scalar potential method. The magnetic scalar potential method would require using a general PDE module and then handling the permanent magnet's magnetization separately.

The COMSOL model was setup such that R_{cyl} = 1, R_1 = 10 and R_2 = 0.2 normalized distances. The normalized boundary condition was imposed at R_1 and was

$$\overline{\mathbf{K}}(\phi, t) = \frac{3}{2} K_0 \cos(\bar{t} - \phi)\vec{i}_z \tag{7.13}$$

with K_0 equaling ⅔ such that the magnitude of the current density equals the normalized value of magnetic field $\overline{\mathbf{H}} = 1$. The magnetization of the magnet would then be a factor α times the strength of the normalized rotating magnetic field, $\overline{\mathbf{M}} = \alpha\overline{\mathbf{H}}$, where case studies would take α values of 2, 10, 20 and 40. These would correspond to permanent magnets having surface magnetic field strengths of 200 G, 1000 G, 2000 G and 4000 G. For the results in this section the magnet is aligned such that its south pole faces the cylinder of ferrofluid as shown in Figure 7-1.

Both fluids EFH1 and MSGW11 were simulated by normalizing their physical characteristics with respect to values in Table 7-1. These values are tabulated in Table 7-2. The model files for all the cases are documented in Appendix I.

Normalized Variable	EFH1	MSGW11
$\bar{\zeta} = \frac{\zeta\Omega}{\mu_0 H_0^2}$	0.00308	0.000313
$\bar{\eta} = \frac{\eta\Omega}{\mu_0 H_0^2}$	0.0273	0.00758

Table 7-2. Table of normalized parameters that are normalized with respect to reference RMS magnetic field strength (B_0=*100 G*, H_0=*7957.75 A/m*) and frequency Ω=*596.9 rad/s* and reference radius of the cylinder R_0=*5 cm*.

7.2. Simulation Results

7.2.1. Magnetic Field Distribution With No Magnet

In the presence of just a rotating magnetic field, the cylinder of ferrofluid creates its own dipole field that rotates. The sum of the dipole field of the cylinder and the external rotating field creates two regions of strong magnetic field intensity and two regions of weak magnetic field intensity due to addition and cancellation of the uniform field with the dipole field as seen in Figure 7-2. Figure 7-3 is a series of plots of magnetization and magnetic field as a function of time for a rotating field of frequency Ω. The surface plot clearly shows regions of strong and weak magnetic field created as a result of addition and cancellation of the ferrofluid dipole field with the external uniform rotating field with the magnetization (white arrows) following the rotating magnetic field direction. The magnitude of the velocity that results is negligible as was described in section 4.4.3.5.

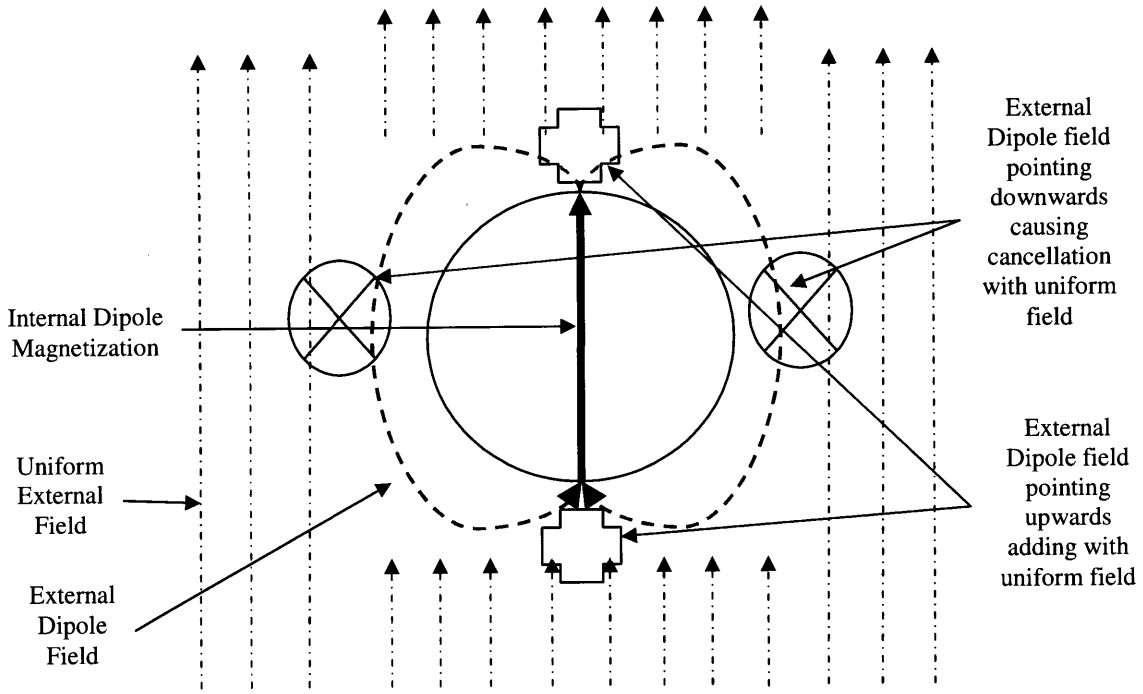

Figure 7-2. Ferrofluid cylinder magnetized vertically creating dipole field that cancels with uniform externally applied field at points marked by crosses, and adds at points marked by grey plus signs.

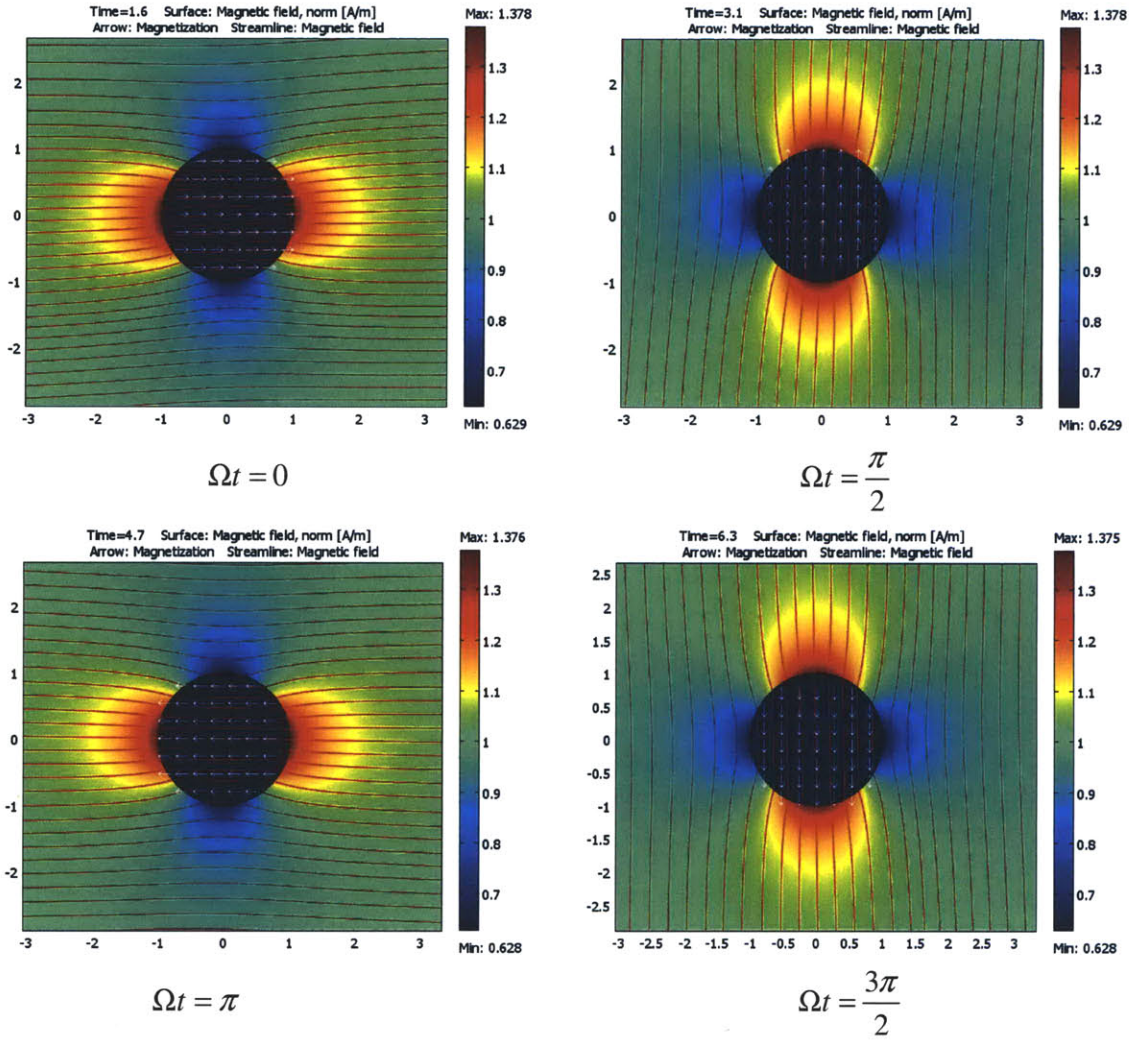

$\Omega t = 0$ $\quad \Omega t = \frac{\pi}{2}$

$\Omega t = \pi$ $\quad \Omega t = \frac{3\pi}{2}$

Figure 7-3. Plots of total magnetic field and magnetization for one period of rotation, at rotational frequency Ω, for a ferrofluid cylinder subjected to a uniform counter-clockwise rotating magnetic field. The magnetization is plotted as white arrows, the streamline plot represents the total magnetic field while the surface plot represents the magnitude of the total magnetic field. The dipole field of the ferrofluid cylinder in addition to the uniform field creates rotating regions of strong (red) and weak (blue) magnetic field outside the ferrofluid cylinder.

7.2.2. Magnetic Field Distribution

The total magnetic field as a result of the uniform rotating magnetic field and the permanent magnet has a similar distribution as Figure 7-2, with cancellation and addition of the magnetic field resulting in regions of strong and weak magnetic field that rotate with the rotating field. This is illustrated in Figure 7-4.

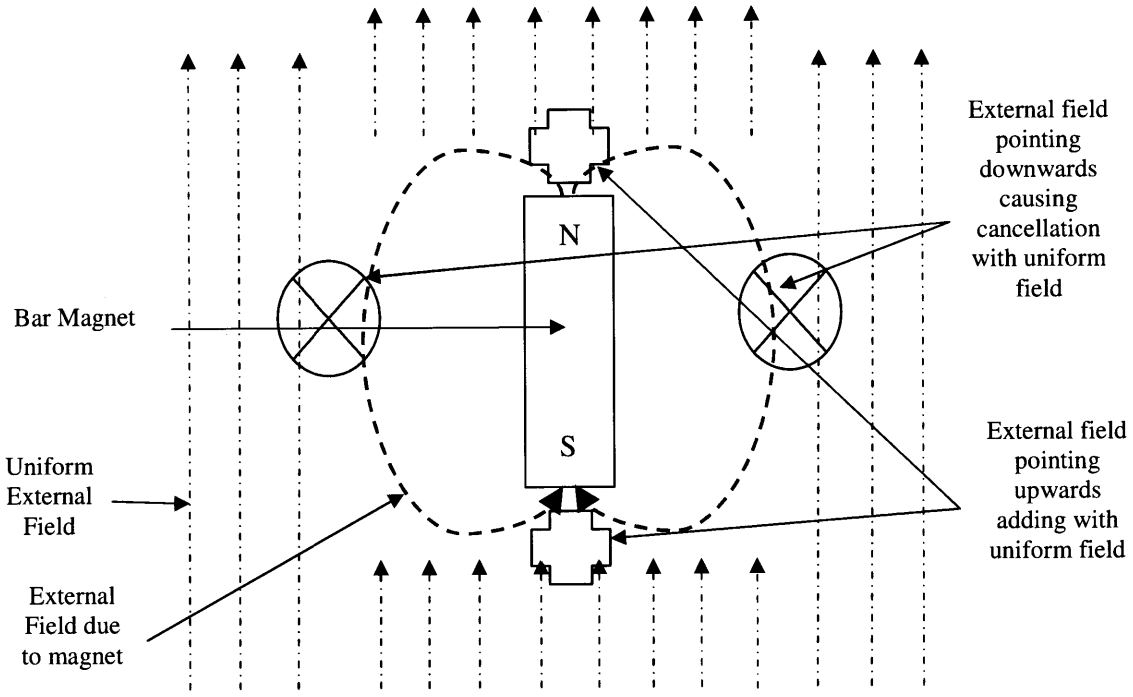

Figure 7-4. Field due to permanent magnet that cancels with uniform externally applied field at points marked by crosses, and adds at points marked by grey plus signs.

In addition, the rotating dipole field of the ferrofluid cylinder also adds to the distribution of the total magnetic field of the permanent magnet and the uniform rotating field. It is difficult to see these effects when plotting magnitude of the magnetic field that is scaled to include the strength of the permanent magnet's field. This is because the permanent magnets used have strengths that are several times the strength of the rotating field as seen in Figure 7-5 which is a magnetic field plot at $\Omega t = \frac{3\pi}{2}$ with a permanent magnet that is 40 times stronger than the strength of the rotating field. Figure 7-6 is the same plot of Figure 7-5 except scaled to see the effect of the uniform rotating field, the dipole field due to the ferrofluid cylinder and the field due to the permanent magnet. The white region represents the magnetic field magnitude that is beyond the values represented by the scale. For all the plots in this chapter, the white regions represents values that are beyond the scale maximum.

Figure 7-7 is a plot of the total magnetic field inside and outside the ferrofluid cylinder scaled to see the total effect of the ferrofluid cylinder's dipole field, the uniform rotating magnetic field and the field due to the permanent magnet. It clearly shows that the field due to the permanent magnet and the uniform rotating magnetic field results in regions of strong and weak magnetic field that rotate with the rotating field inside and outside the ferrofluid cylinder. The region of strong field can be seen inside the ferrofluid cylinder at $\Omega t = \frac{\pi}{2}$ while the region of weak field inside the ferrofluid can be seen at $\Omega t = \frac{3\pi}{2}$. The dipole field due to the ferrofluid filled cylinder can also be seen to be perturbed by the field due to the magnet.

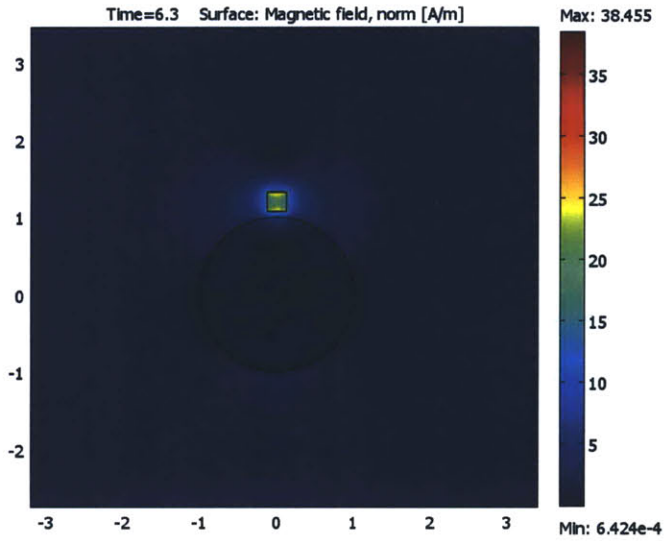

Figure 7-5. Total field distribution of rotating uniform magnetic field and field due to permanent magnet. The permanent magnet is 40 times the strength of the uniform rotating field and the scale reflects this but makes it difficult to see the effect of the ferrofluid cylinder's dipole field interacting with the field due to the permanent magnet and the effect of the field due to the permanent magnet and the uniform rotating field.

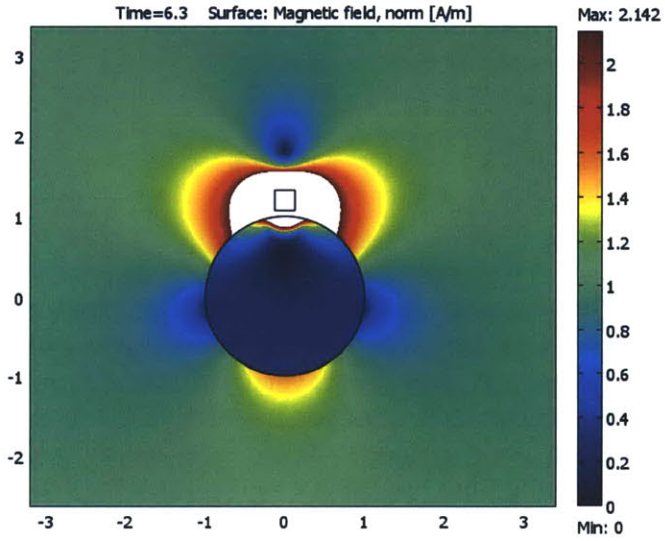

Figure 7-6. Same plot as Figure 7-5 except total field distribution, of rotating uniform magnetic field and field due to permanent magnet, is scaled to see the effects of ferrofluid cylinder's dipole field, the field due to the permanent magnet and the uniform rotating field. The white region represents the region of magnetic field that is beyond the values represented by the color scale.

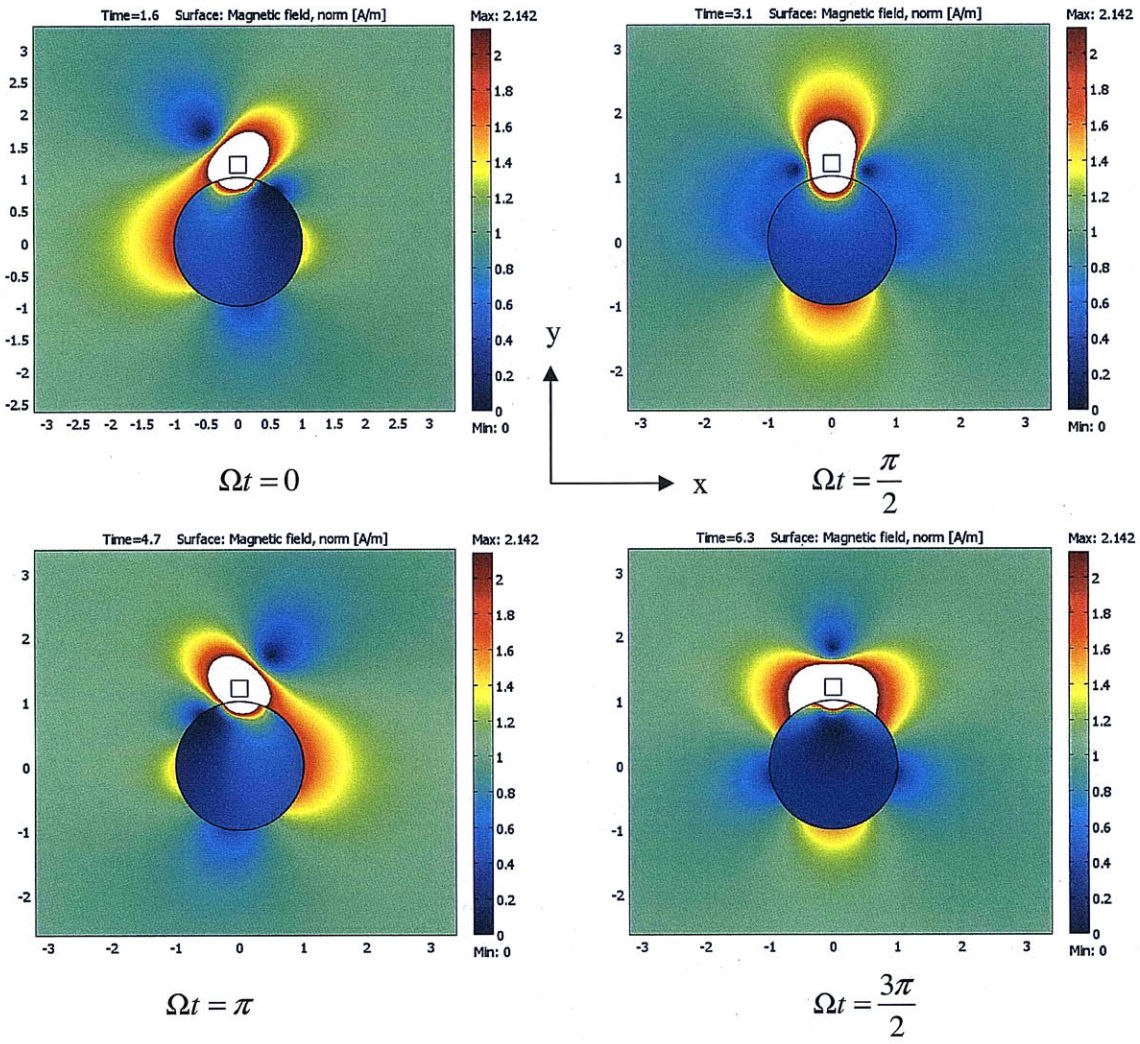

Figure 7-7. Total magnetic distribution with a magnet that is 40 times stronger than the strength of the rotating magnetic field placed on top of the EFH1 filled cylinder. The white region represents magnetic field strengths that are beyond the scale shown. The plots show the evolution in time of the total magnetic field inside and outside the ferrofluid cylinder due to the uniform rotating field, the ferrofluid cylinder's dipole field and the field due to the permanent magnet. The magnetization of the fluid follows the same direction as the white arrows in Figure 7-3 for the same time.

7.2.3. Distribution of Magnetization

The previous section elaborated on the total magnetic field due to the uniform rotating field and the field due to the permanent magnet, creating regions of cancellation (weak field) and addition (strong field) that rotate. The distribution of the ferrofluid's magnetization clearly shows the effect of these rotating regions of strong and weak field as seen in Figure 7-8. The blue circle representing weak magnetization, that can be seen at $\Omega t = \frac{3\pi}{2}$, is the magnetization due to the almost complete cancellation of the magnetic field due to the permanent magnet and the rotating field at a certain distance from the top of the cylinder. The red region of strong magnetization at the top of the cylinder at $\Omega t = \frac{\pi}{2}$ is due to the strong region of the magnetic field that saturates the fluid EFH1 with a normalized value of $\overline{\mathbf{M}} = 4.2$ using reference values defined in section 7.1.5 and EFH1 saturation magnetization value from Table 2-3.

The position of the blue region of magnetization is determined by the strength of the permanent magnet with respect to the rotating field. The stronger the permanent magnet the further away the region of weak field is from the top of the cylinder. This is illustrated in Figure 7-9 for permanent magnets that are 10 and 40 times stronger than the strength of the rotating field.

These results confirm that it is not only the non-uniform field that is responsible for the non-zero velocity profiles that result, but also due to the non-uniform distribution of the magnetization of the ferrofluid.

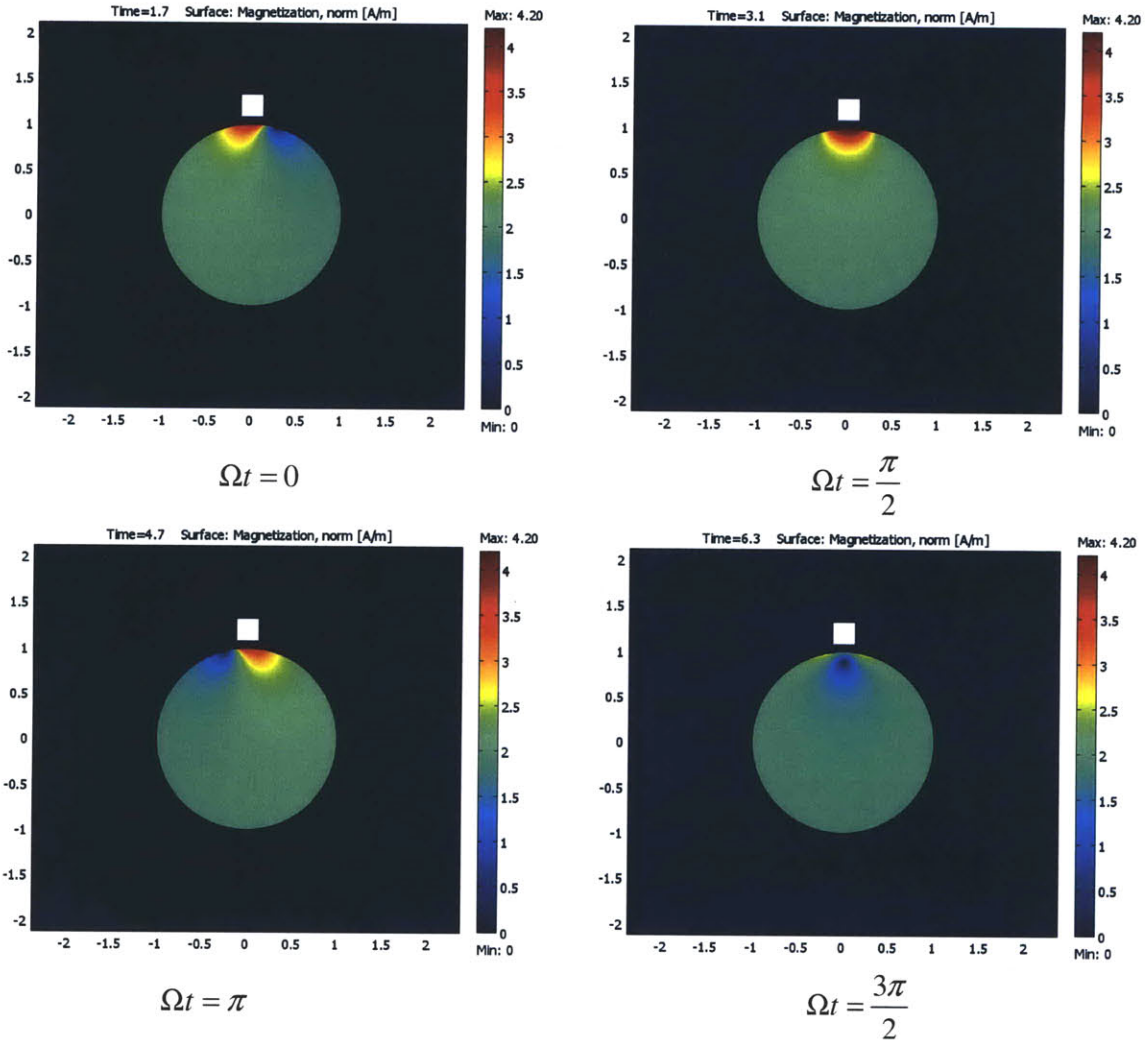

Figure 7-8. Distribution of magnetization in the EFH1 filled cylinder as a function of time in a non-uniform field generated by a uniform rotating field and the field of a permanent magnet that is 10 times stronger than the strength of the rotating field. The blue circle which represents a weak field, due to near complete cancellation of the rotating magnetic field and the field due to the permanent magnet, can be clearly seen to rotate in an arc near the top of the sphere. The red region represents the strong field that saturates the EFH1 with a normalized saturation magnetization of $\overline{\mathbf{M}} = 4.2$. Non-uniform distribution of the magnetization also contributes to the generation of non-zero velocity flows.

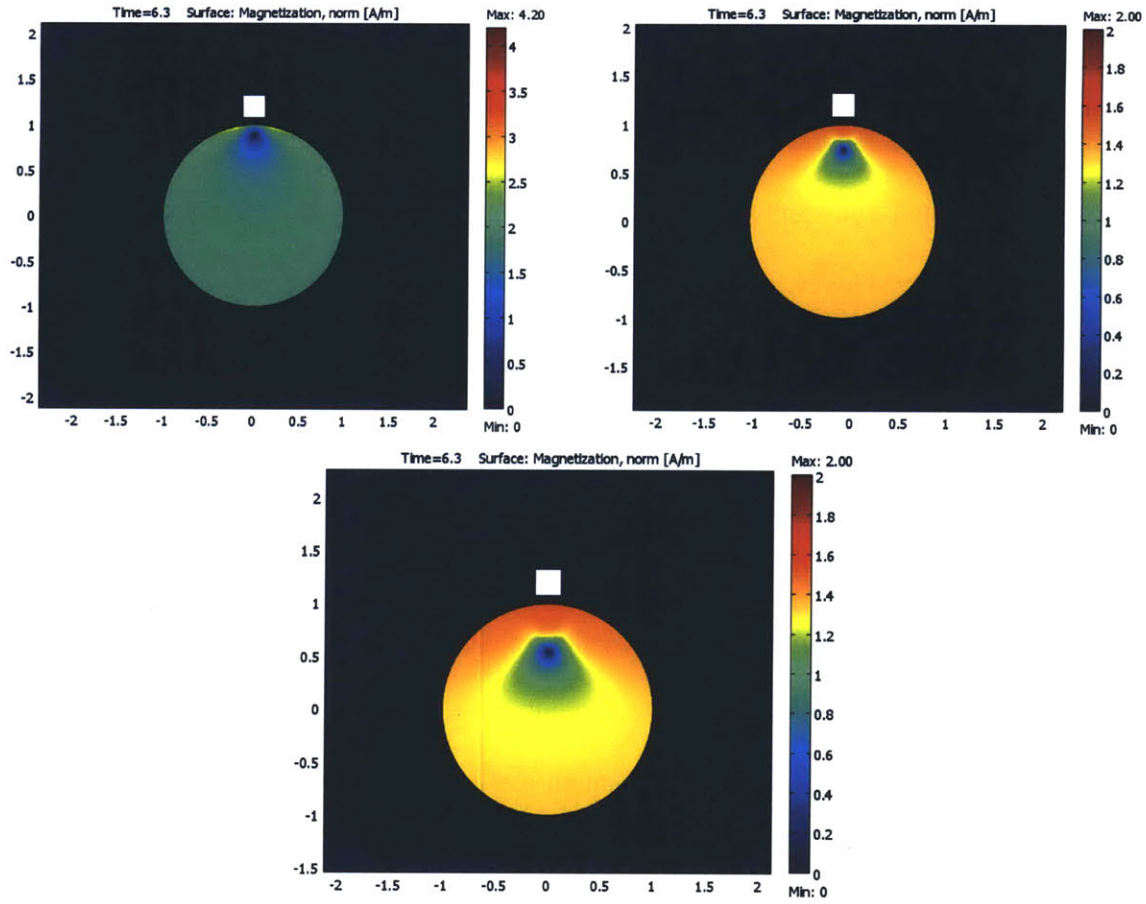

Figure 7-9. Position of region of weak field is dependent on the strength of the permanent magnet, a stronger magnet creates a blue region further away from the top of the cylinder than a weaker magnet. Top Left: For a permanent magnet that is 10 times stronger than the strength of the rotating field, position of the center of the blue circle is at 0.885. Top Right: For a permanent magnet that is 10 times stronger than the strength of the rotating field, position of the center of the blue circle is at 0.739. Bottom: For a permanent magnet that is 40 times stronger than the strength of the rotating field, position of the center of the blue circle is at 0.536.

7.2.4. Distribution of Spin Velocity ω and Torque

Figure 7-10 and Figure 7-11 are plots of torque and spin velocity ω as a function of time for a MSGW11 filled cylinder with a permanent magnet that is 20 times stronger than the strength of the counter-clockwise rotating field. From both of these plots, it can be seen that torque and spin velocity reversal occurs above the region where the total magnetic field inside the fluid is at a minimum (blue region), in this case 0.739.

The reason for this reversal is due to the fact that the magnetic field direction with respect to the ferrofluid magnetization vector changes abruptly as seen by the two points A and B in Figure 7-12. At point A, the magnetization vector with respect to the magnetic field can be seen to create a torque in the +z direction, while at point B the magnetic field lags the magnetization vector because of the distribution of the magnetic field creating a torque in the -z direction as seen in Figure 7-13.

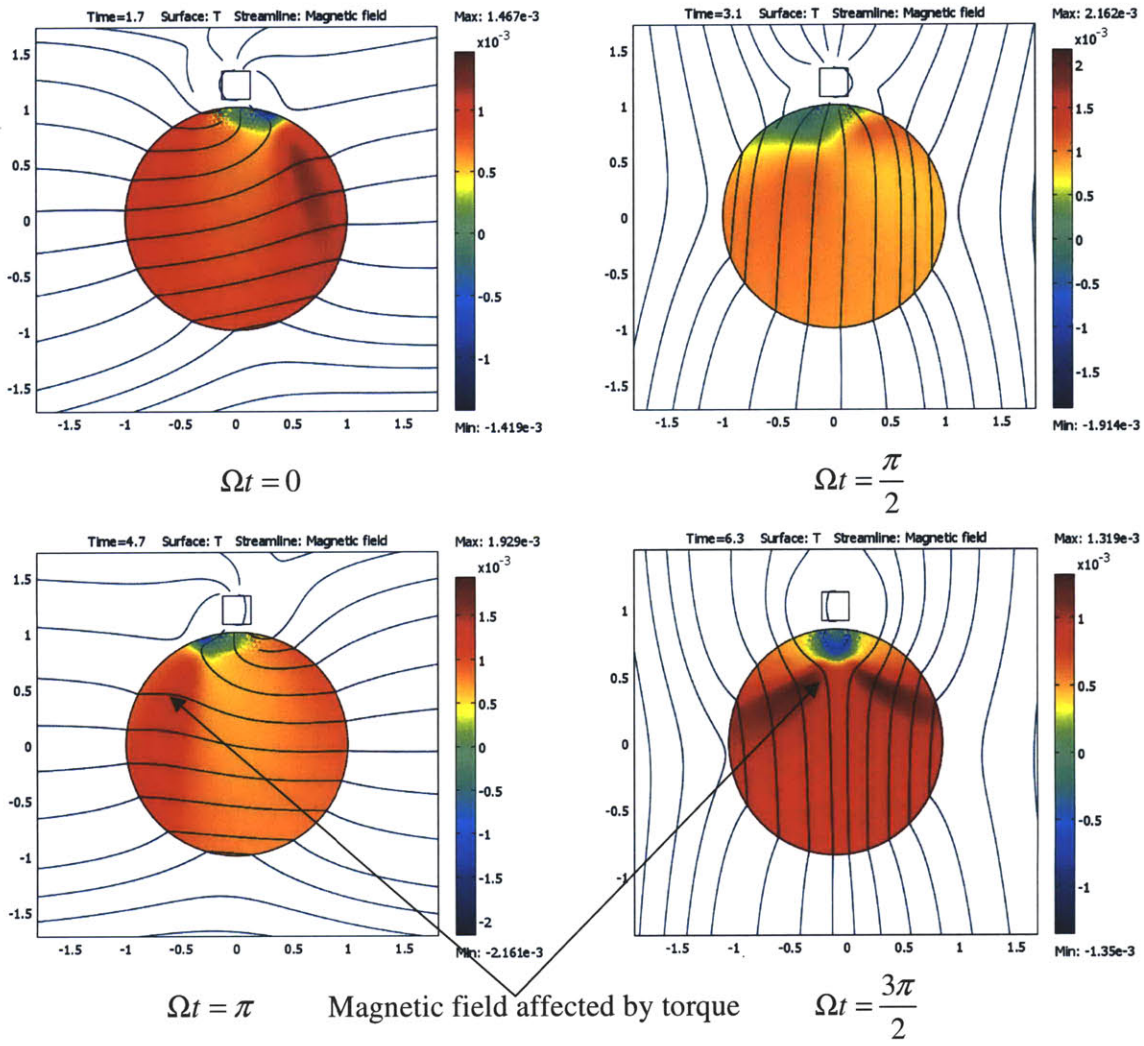

Figure 7-10. Distribution of torque (surface plot) and streamlines of magnetic field as a function of time for MSGW11 filled cylinder with a permanent magnet 20 times stronger than the strength of the counter-clockwise rotating field. Torque distribution can clearly be seen to have regions of torque reversal as seen at $\Omega t = \frac{3\pi}{4}$. The shape of the streamlines of magnetic field inside the cylinder are affected by the torque as shown with arrows.

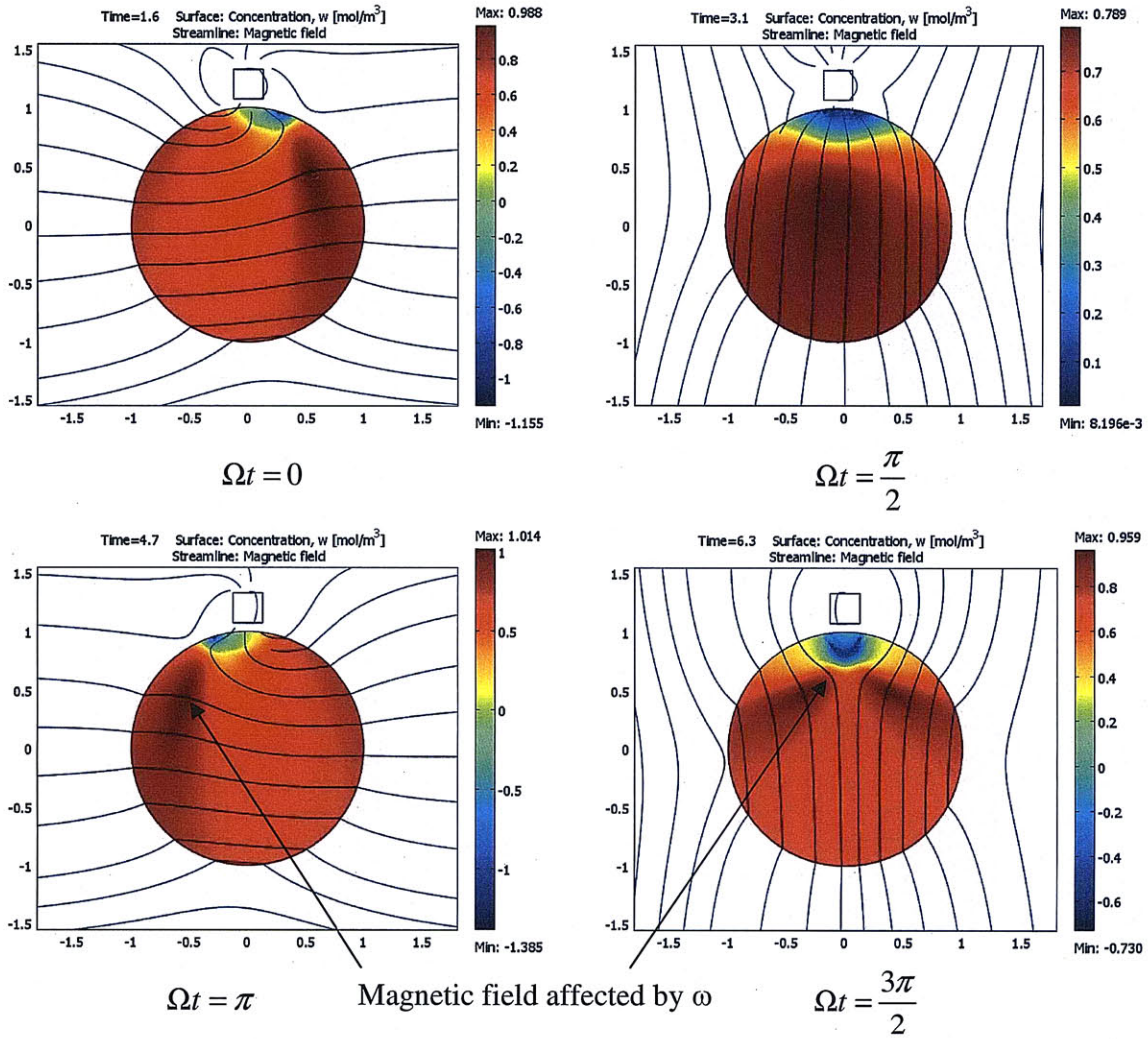

Figure 7-11. Distribution of magnitude of spin velocity ω (surface plot) and streamlines of magnetic field as a function of time for MSGW11 filled cylinder with a permanent magnet 20 times stronger than the strength of the counter-clockwise rotating field. Spin-velocity can clearly be seen to reverse directions as seen at $\Omega t = \frac{3\pi}{2}$. The shape of the streamlines of magnetic field inside the cylinder are affected by the spin-velocity as seen by arrows shown.

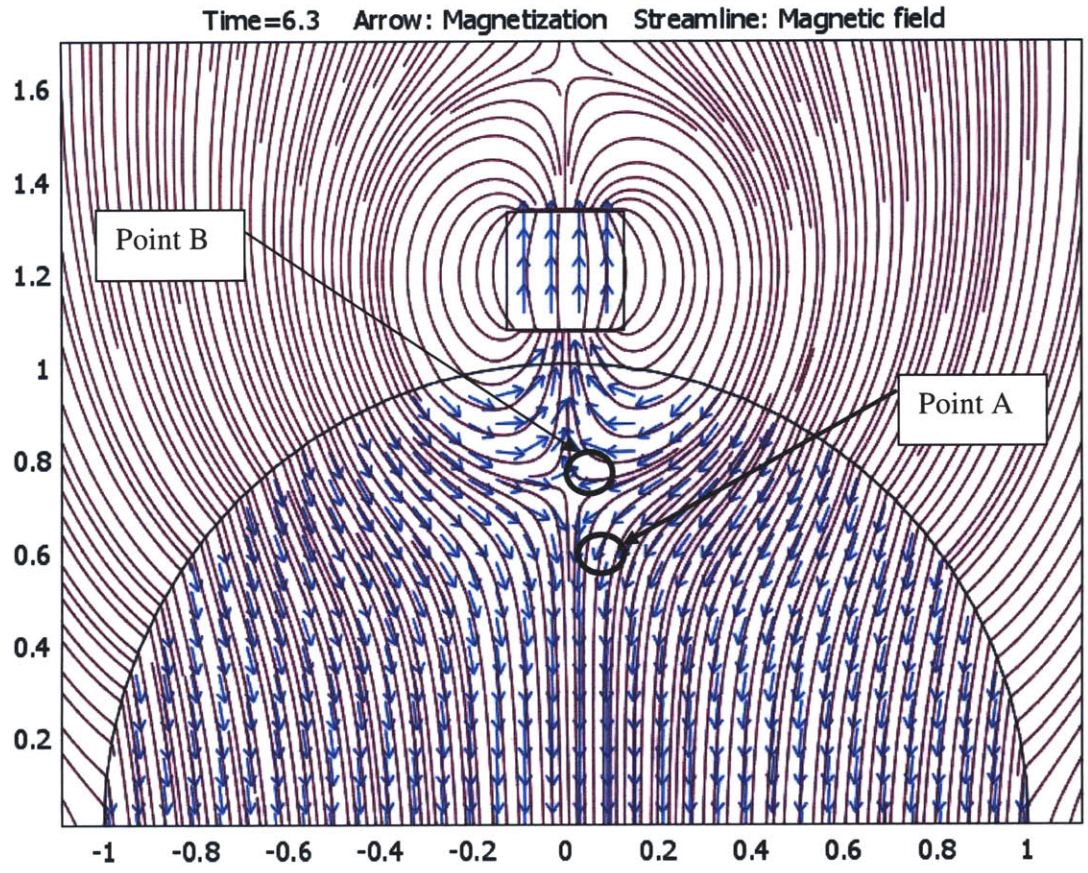

Figure 7-12. Zoomed section near magnet showing magnetic streamlines and magnetization arrows at $\Omega t = \frac{3\pi}{2}$ for MSGW11 filled cylinder with permanent magnet 20 times stronger than the counter-clockwise rotating field. Torque reversal occurs because the field lines of the magnet turn more abruptly upwards at point B than the magnetization vectors causing torque reversal compared to point A.

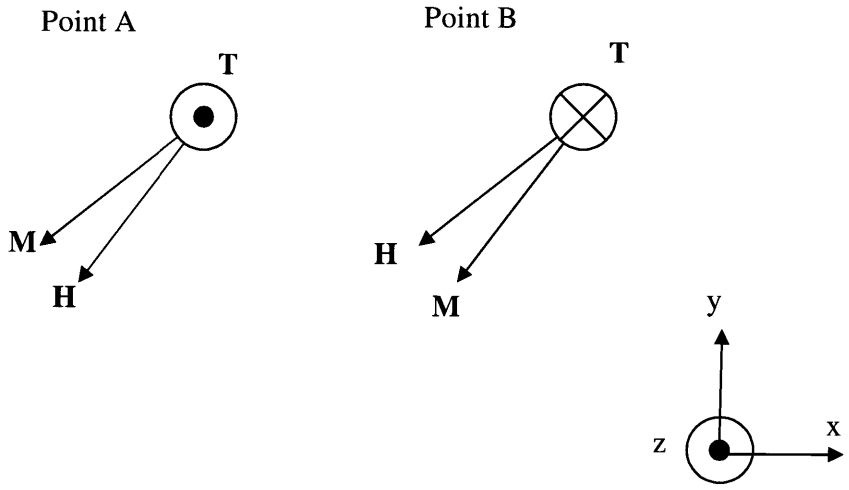

Figure 7-13. Magnetization and magnetic field vectors at two points in Figure 7-12 justifying torque and spin reversal seen in Figure 7-10 and Figure 7-11.

7.2.5. Distribution of velocity

Figure 7-14 and Figure 7-15 show the velocity field distributions represented by vectors and streamlines for an MSGW11 filled ferrofluid cylinder with a permanent magnet that is 20 times stronger than the strength of the rotating field. The flow profile can be seen to be complicated and irregular with the formation of vortices as seen at $\Omega t = \frac{3\pi}{4}, \frac{3\pi}{2}, \frac{7\pi}{4}$. To understand this, Eq (7.7) can be solved for the curl of spin velocity ω as given below

$$\begin{aligned} 0 &= \mu_0 \mathbf{M} \times \mathbf{H} + 2\zeta(\nabla \times \mathbf{v} - 2\boldsymbol{\omega}) \\ 0 &= \mu_0 \nabla \times (\mathbf{M} \times \mathbf{H}) + 2\zeta(-\nabla^2 \mathbf{v} - 2\nabla \times \boldsymbol{\omega}) \\ \nabla \times \boldsymbol{\omega} &= \frac{1}{4\zeta}(\mu_0 \nabla \times (\mathbf{M} \times \mathbf{H}) - 2\zeta \nabla^2 \mathbf{v}) \end{aligned} \tag{7.14}$$

and substituting (7.14) in the linear momentum equation of (7.6) gives

$$\begin{aligned} 0 &= -\nabla p' + \frac{1}{2}(\mu_0 \nabla \times (\mathbf{M} \times \mathbf{H}) - 2\zeta \nabla^2 \mathbf{v}) + (\zeta + \eta)\nabla^2 \mathbf{v} + \mu_0 (\mathbf{M} \cdot \nabla)\mathbf{H} \\ 0 &= -\nabla p' + \eta \nabla^2 \mathbf{v} + \mu_0 (\mathbf{M} \cdot \nabla)\mathbf{H} + \frac{1}{2}(\mu_0 \nabla \times (\mathbf{M} \times \mathbf{H})) \\ 0 &= -\nabla p' + \eta \nabla^2 \mathbf{v} + \mathbf{F} + \frac{1}{2}(\nabla \times \mathbf{T}) \end{aligned} \tag{7.15}$$

where **F** and **T** are defined in section 2.1.2.

Eq (7.15) is the effective linear momentum equation when $\eta' = 0$ that describes the behavior seen in Figure 7-14 and Figure 7-15. The curl of the torque density and the force density term both contribute to creating the vortices and the irregular flow seen. The regions of weak and strong magnetic fields cause the gradient of the force density term to change direction

and is partly responsible for the flow reversal seen at $\Omega t = \frac{3\pi}{2}$ with respect to the velocity vectors at $\Omega t = \frac{\pi}{2}$. Expanding Eq (7.15) using the identity

$$\nabla\times(\mathbf{M}\times\mathbf{H}) = \mathbf{M}(\nabla\bullet\mathbf{H}) - \mathbf{H}(\nabla\bullet\mathbf{M}) + (\mathbf{H}\bullet\nabla)\mathbf{M} - (\mathbf{M}\bullet\nabla)\mathbf{H} \tag{7.16}$$

and the relation in (7.1) gives

$$-\nabla p + \eta\nabla^2\mathbf{v} + \frac{\mu_0}{2}(\mathbf{M}\bullet\nabla\mathbf{H}) + \frac{1}{2}\mathbf{B}(\nabla\bullet\mathbf{H}) + \frac{\mu_0}{2}\mathbf{H}\bullet\nabla\mathbf{M} = 0 \tag{7.17}$$

With the aid of the known vector identity

$$(\mathbf{H}\bullet\nabla)\mathbf{M} + (\mathbf{M}\bullet\nabla)\mathbf{H} = \nabla(\mathbf{H}\bullet\mathbf{M}) - \mathbf{H}\times(\nabla\times\mathbf{M}) - \mathbf{M}\times(\nabla\times\mathbf{H}) \tag{7.18}$$

and the fact that $\nabla\times\mathbf{H} = 0$ results in the expression

$$-\nabla\left\{p + \frac{\mu_0\mathbf{H}\bullet\mathbf{M}}{2}\right\} + \eta\nabla^2\mathbf{v} + \frac{1}{2}\mathbf{B}(\nabla\bullet\mathbf{H}) + \frac{\mu_0}{2}\mathbf{H}\times(\nabla\times\mathbf{M}) = 0 \tag{7.19}$$

The extra pressure term is proportional to the projection of the magnetization on the magnetic field and the pressure distribution is illustrated in Figure 7-16. Figure 7-17 is a plot of the magnitude and direction of the velocity field as a function of time illustrating that the normalized magnitude of velocity is of the order $1\text{x}10^{-3}$-$1\text{x}10^{-2}$. Dimensionalizing this velocity with respect to the reference values given in Table 7-1, gives a velocity of ≈3-30mm/s which is on the same order of measured velocity profiles in the experiment conducted with the spherical geometry.

7.2.6. Effect of Reversing Rotational Field Direction

Reversing the rotational direction of the uniform magnetic field reverses the velocity flow direction to match the reversed direction. Figure 7-18 and Figure 7-19 are plots of counter-clockwise and clockwise rotating magnetic fields that result in flows that follow the field direction. The plots are for EFH1 with a permanent magnet that is 20 times stronger than the strength of the rotating field. This result is similar to the result obtained experimentally with the spherical geometry as explained in section 6.5.3.

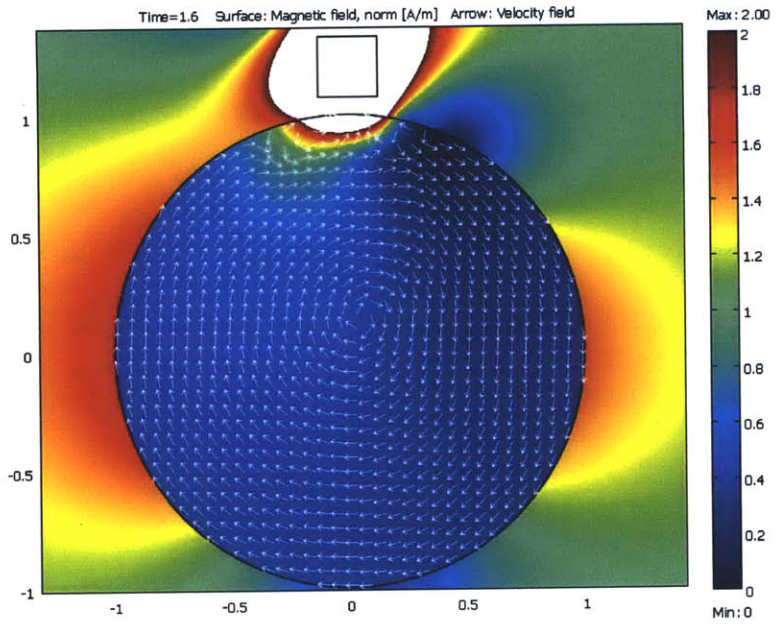

$\Omega t = 0$

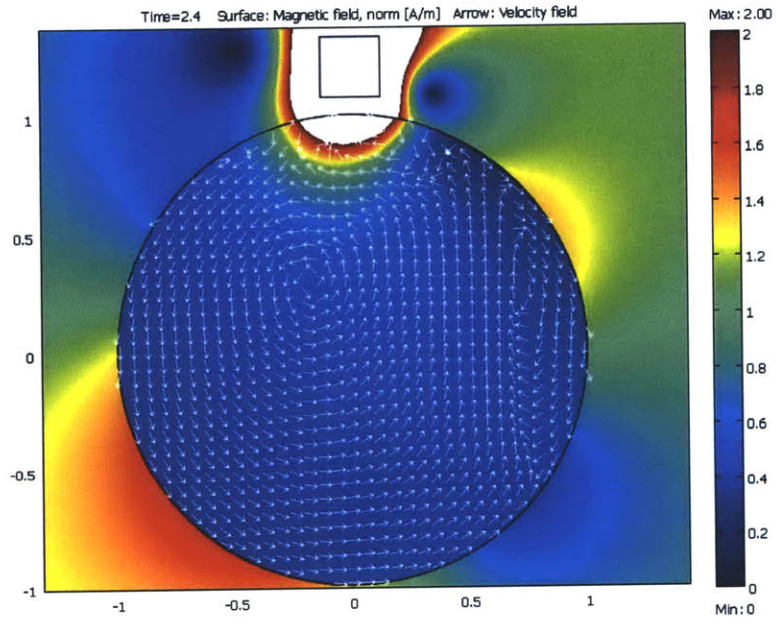

$\Omega t = \frac{\pi}{4}$

(a)

Figure 7-14. Distribution of velocity field, with formation of vortices, for MSGW11 filled cylinder with permanent magnet 20 times stronger than uniform counter-clockwise rotating field as a function of time over one period of rotation (a)-(d).

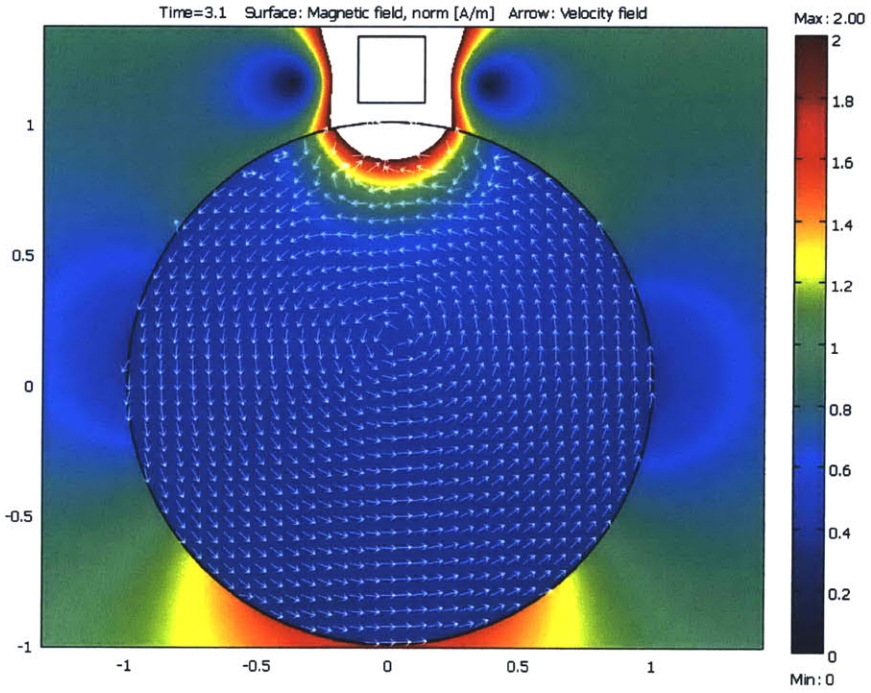

$$\Omega t = \frac{\pi}{2}$$

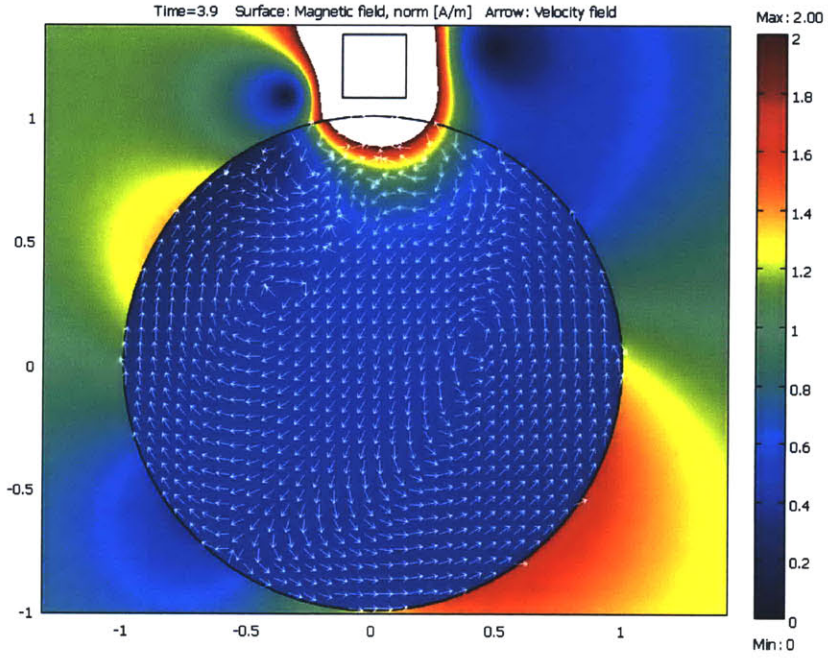

$$\Omega t = \frac{3\pi}{4}$$

(b)

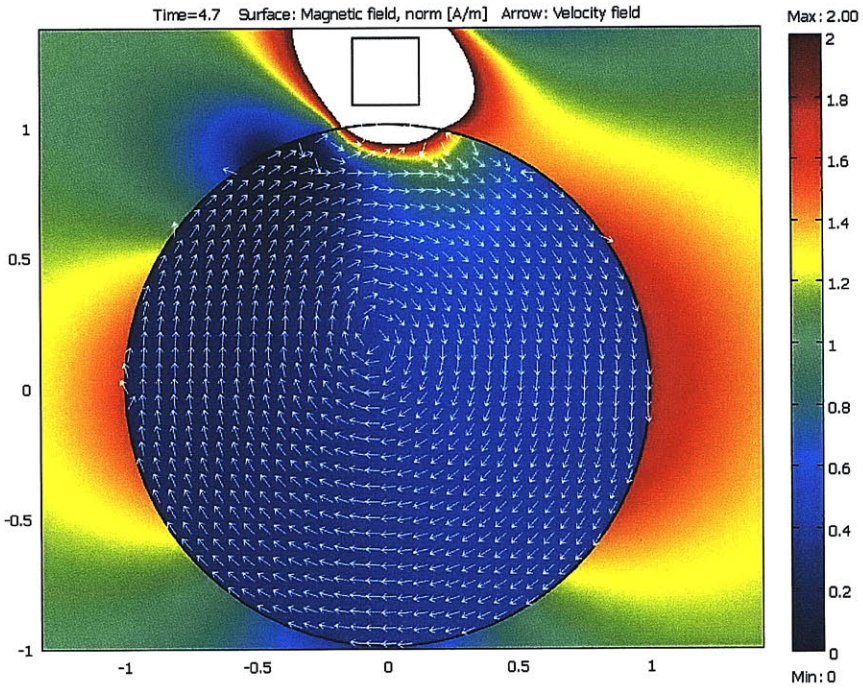

$\Omega t = \pi$

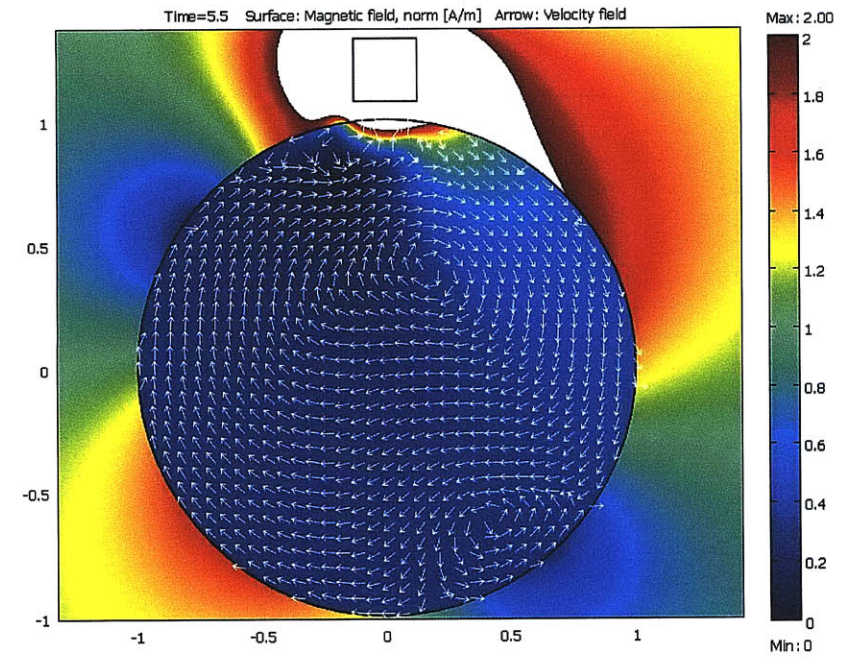

$\Omega t = \frac{5\pi}{4}$

(c)

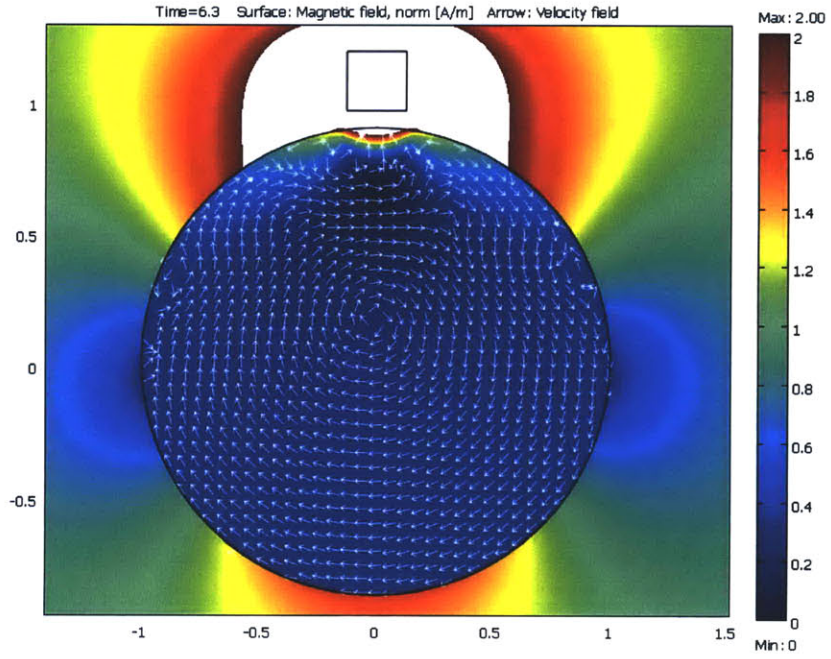

$$\Omega t = \frac{3\pi}{2}$$

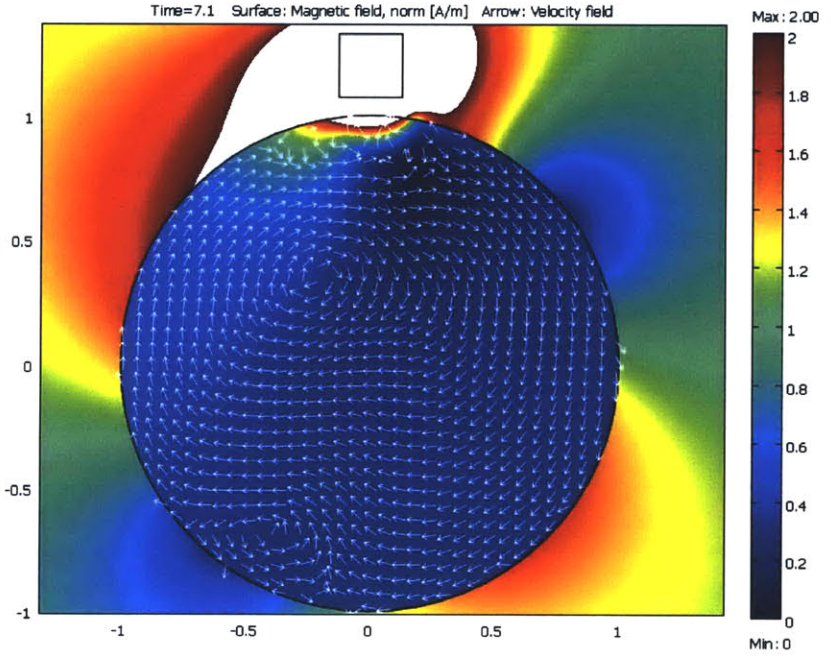

$$\Omega t = \frac{7\pi}{4}$$

(d)

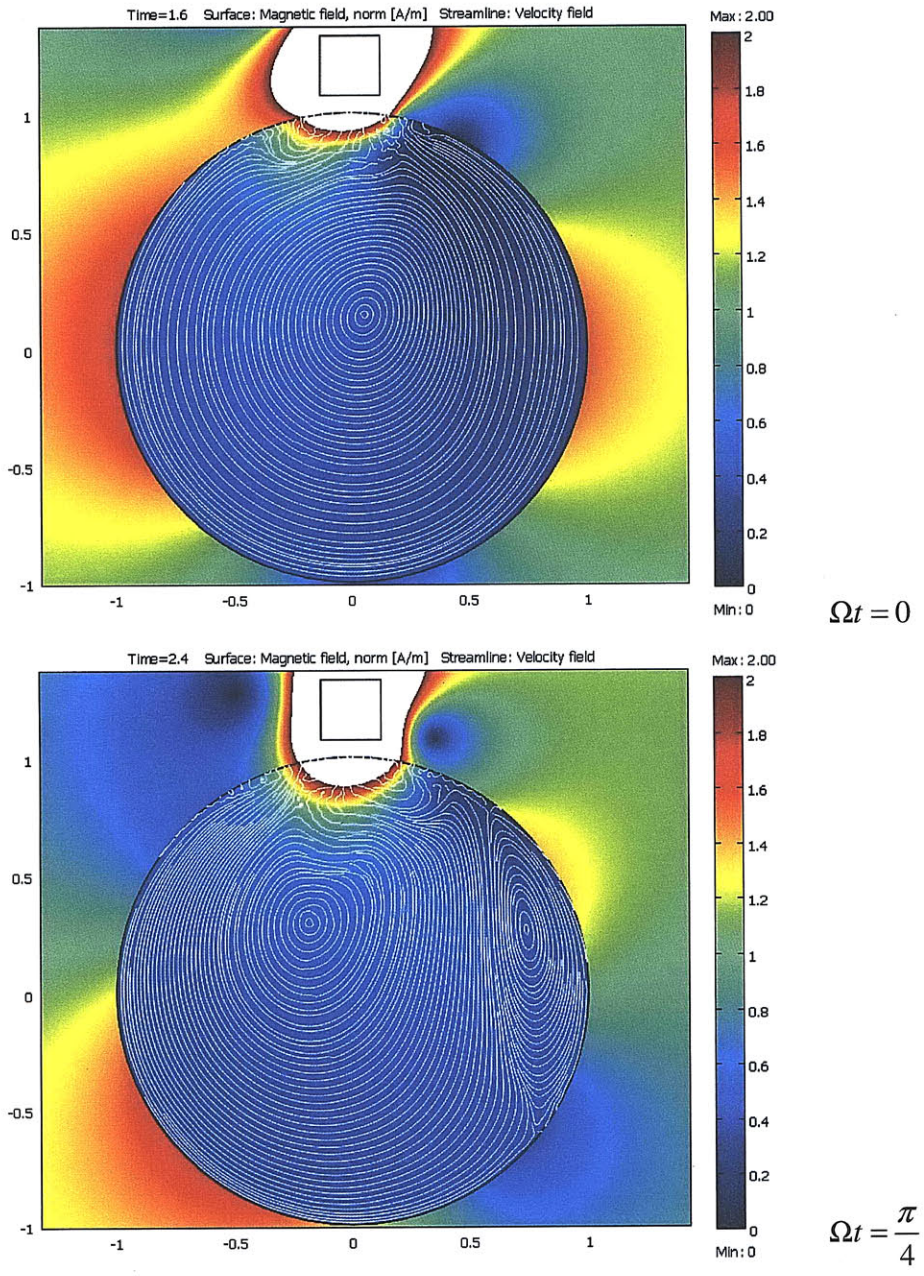

(a)

Figure 7-15. Distribution of velocity streamlines, illustrating vortices formed, for MSGW11 filled cylinder with permanent magnet 20 times stronger than uniform counter-clockwise rotating field as a function of time over one period of rotation (a)-(d).

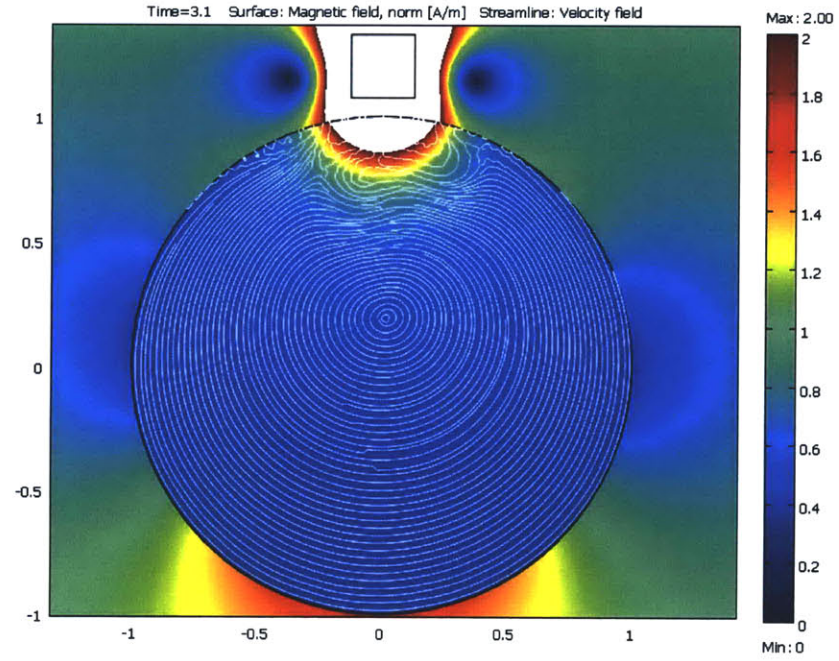

$$\Omega t = \frac{\pi}{2}$$

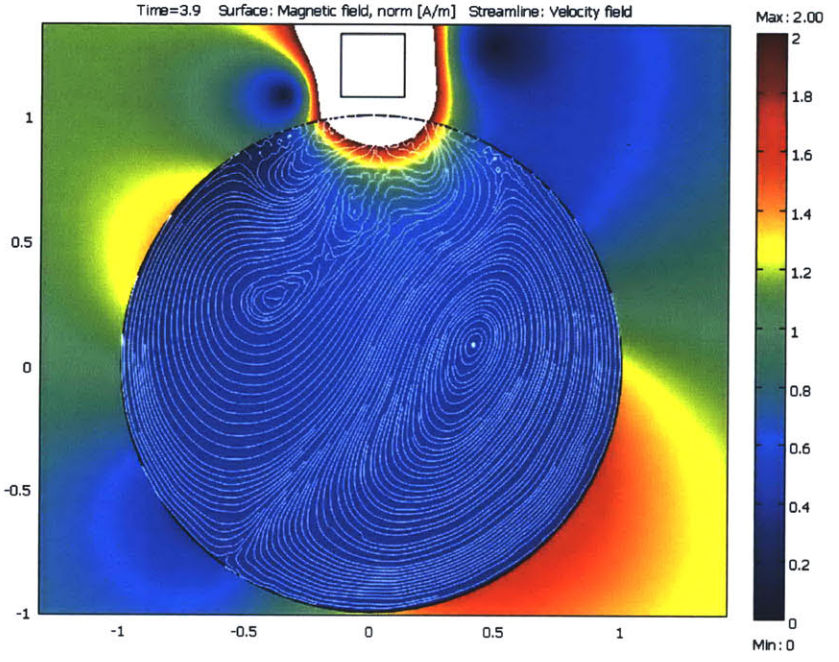

$$\Omega t = \frac{3\pi}{4}$$

(b)

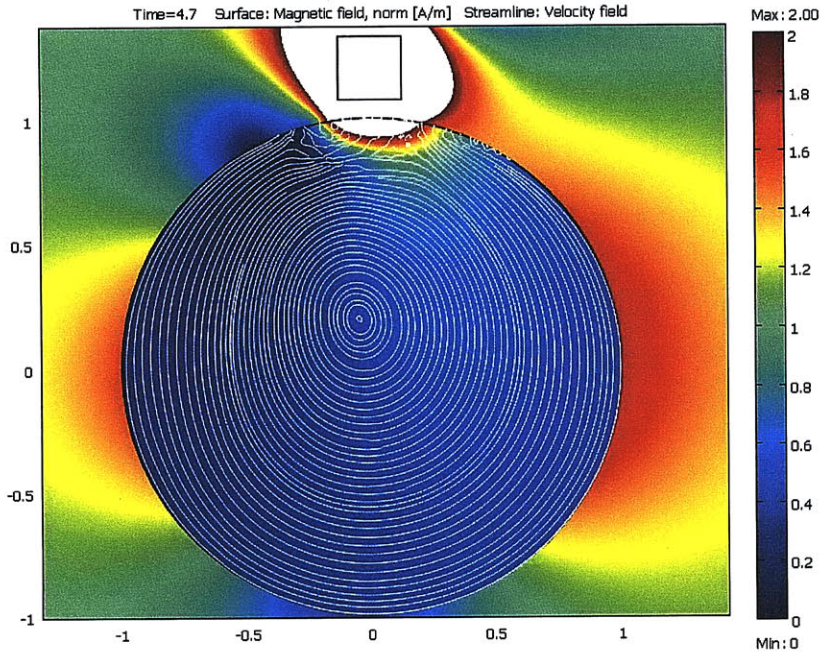

$\Omega t = \pi$

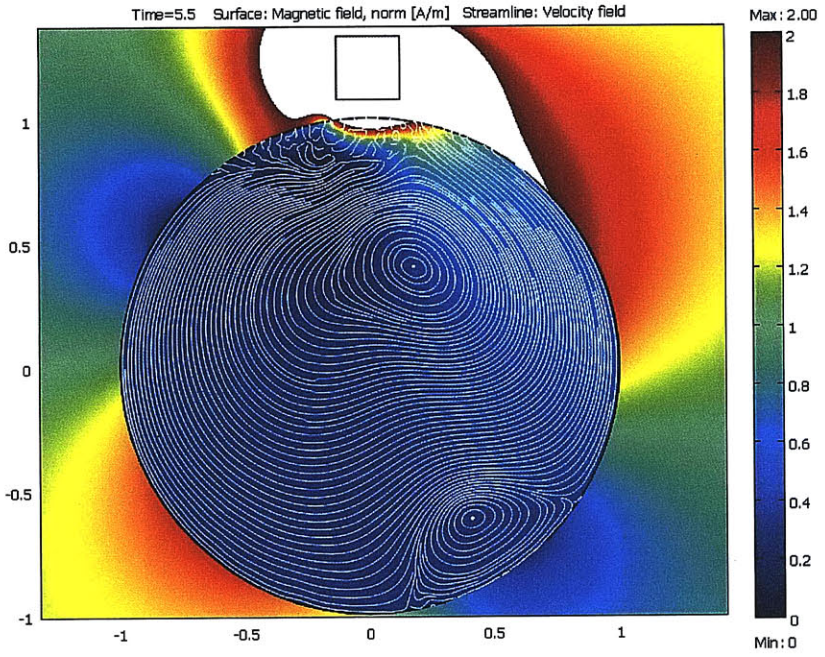

$\Omega t = \frac{5\pi}{4}$

(c)

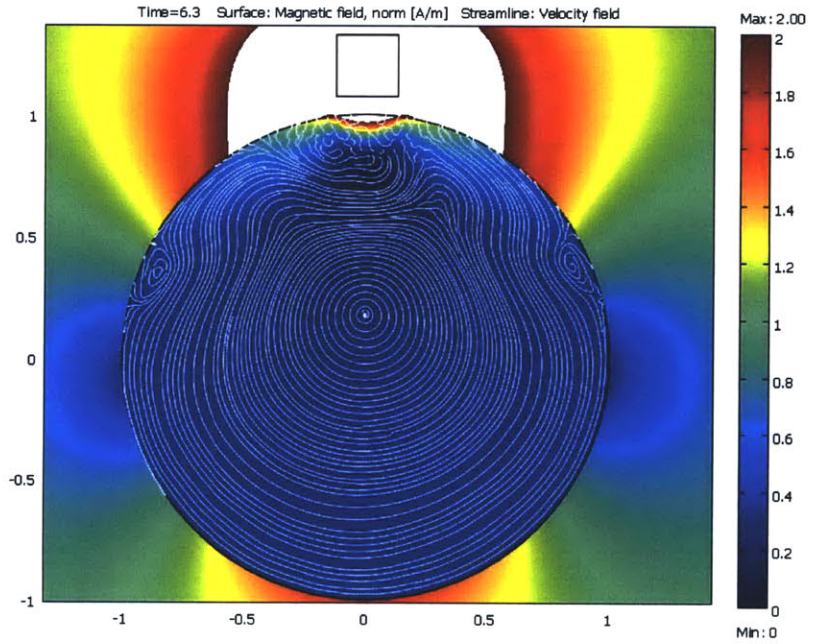

$$\Omega t = \frac{3\pi}{2}$$

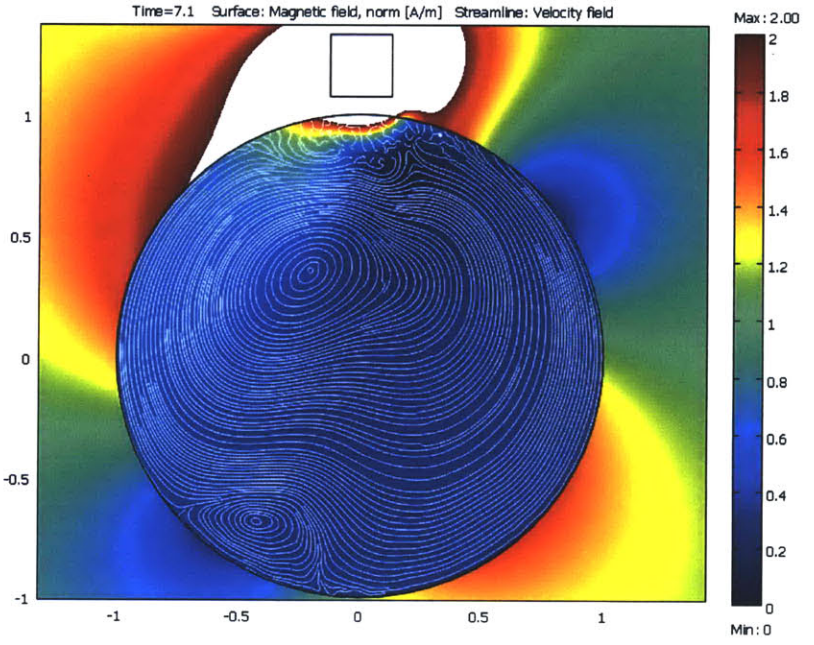

$$\Omega t = \frac{7\pi}{4}$$

(d)

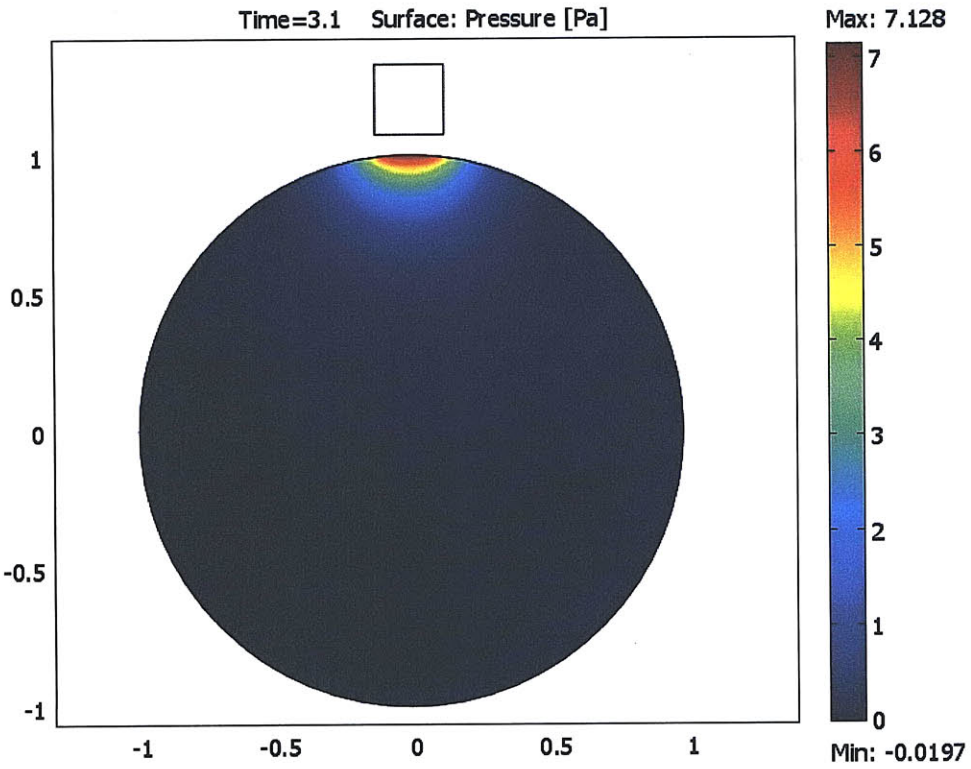

Figure 7-16. Distribution of modified pressure term in (7.19), in the MSGW11 ferrofluid filled sphere with a permanent magnet that is 20 times stronger than the field of the counter-clockwise rotating field. The pressure is strongest near the magnet.

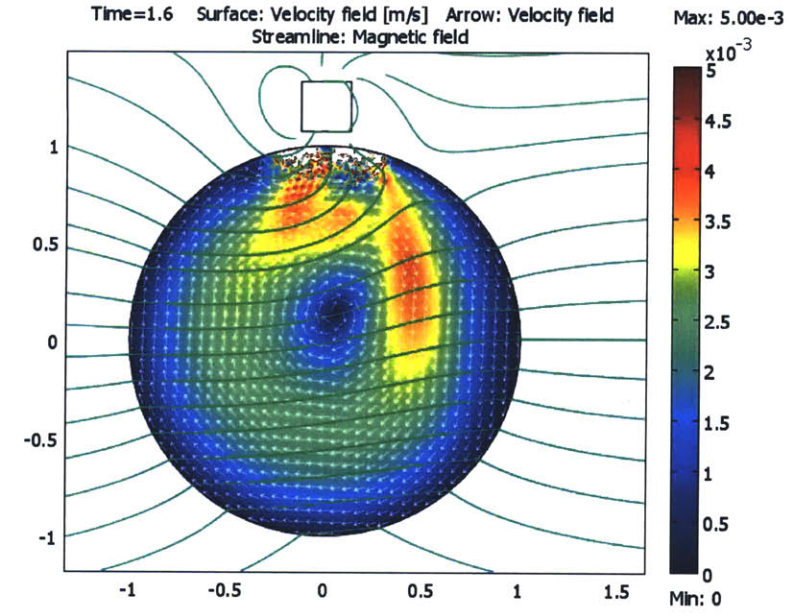

$\Omega t = 0$

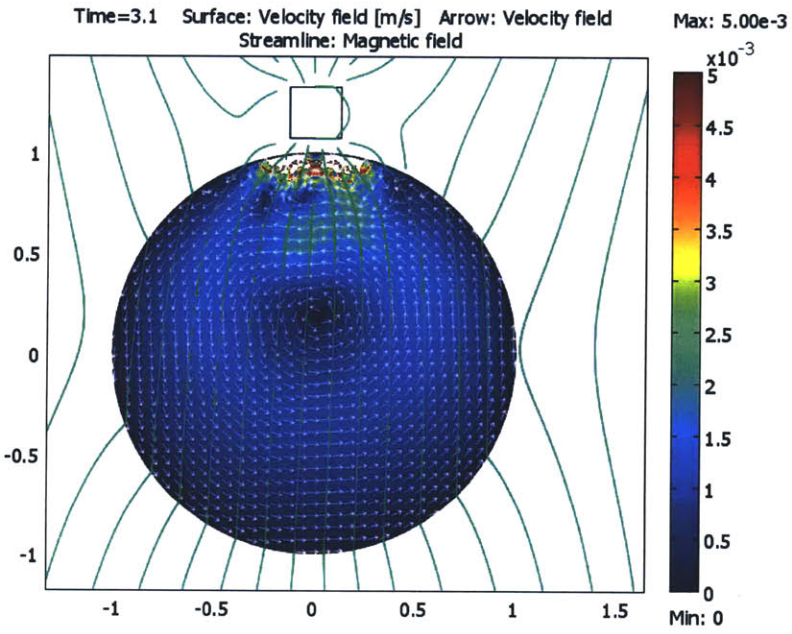

$\Omega t = \frac{\pi}{2}$

(a)

Figure 7-17. Magnitude and direction of velocity field with magnetic field streamlines for MSGW11 filled cylinder with permanent magnet 20 times stronger than uniform rotating field as a function of time over one period of rotation (a)-(b). Dimensional magnitude of velocity is calculated to be on the order of 3-30 mm/s according to these simulations which corroborates experimental results from Chapter 6.

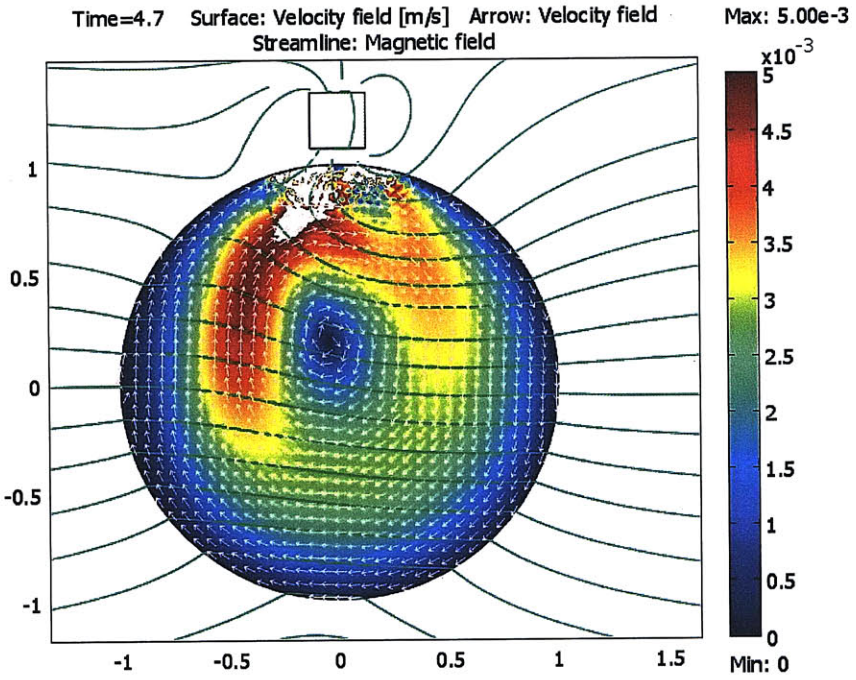

$\Omega t = \pi$

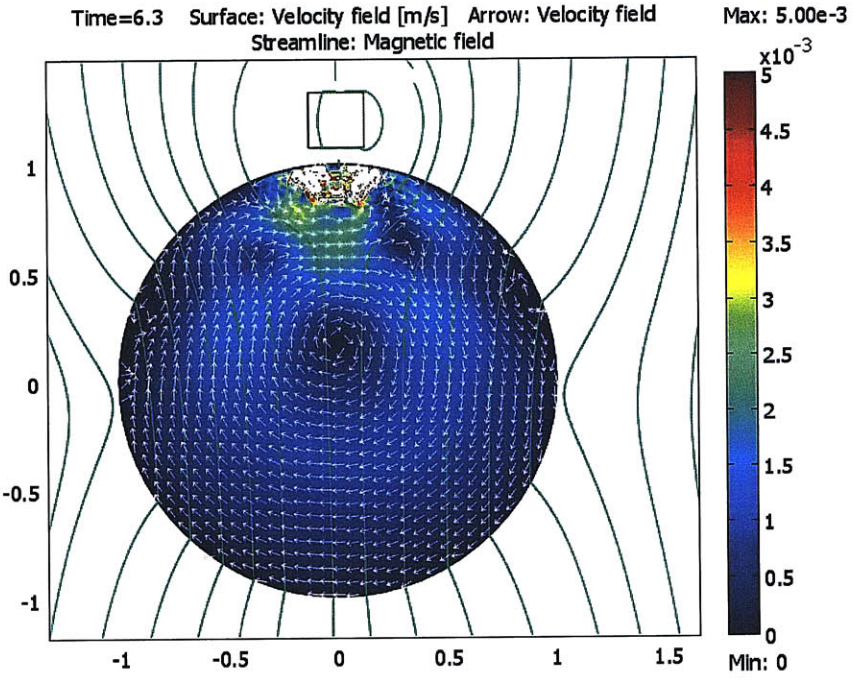

$\Omega t = \frac{3\pi}{2}$

(b)

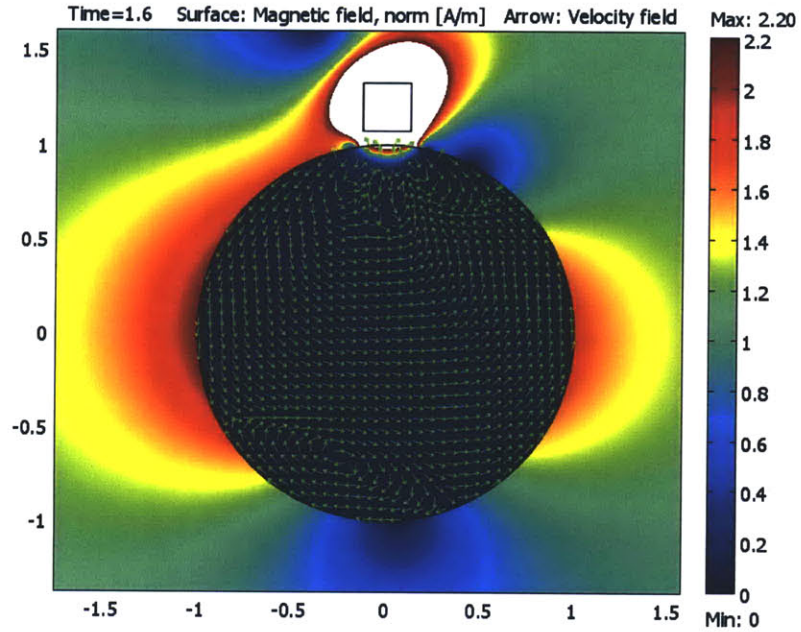

$\Omega t = 0$

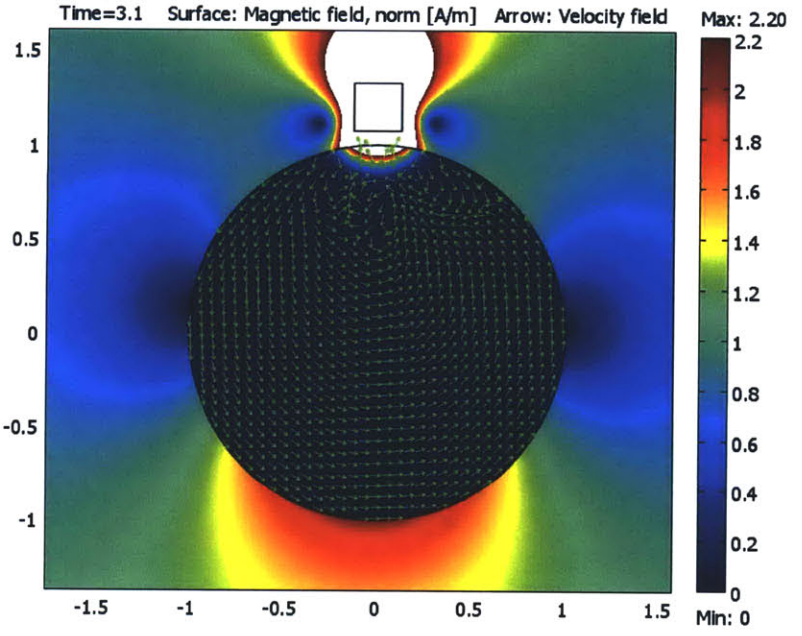

$\Omega t = \frac{\pi}{2}$

(a)

Figure 7-18. Distribution of velocity field for EFH1 filled cylinder with permanent magnet 20 times stronger than uniform rotating field as a function of time over one period of rotation (a)-(b). The rotating field is rotating in the counter-clockwise direction with the velocity over most of the period in the same direction as the rotating field except at $\Omega t = \pi$.

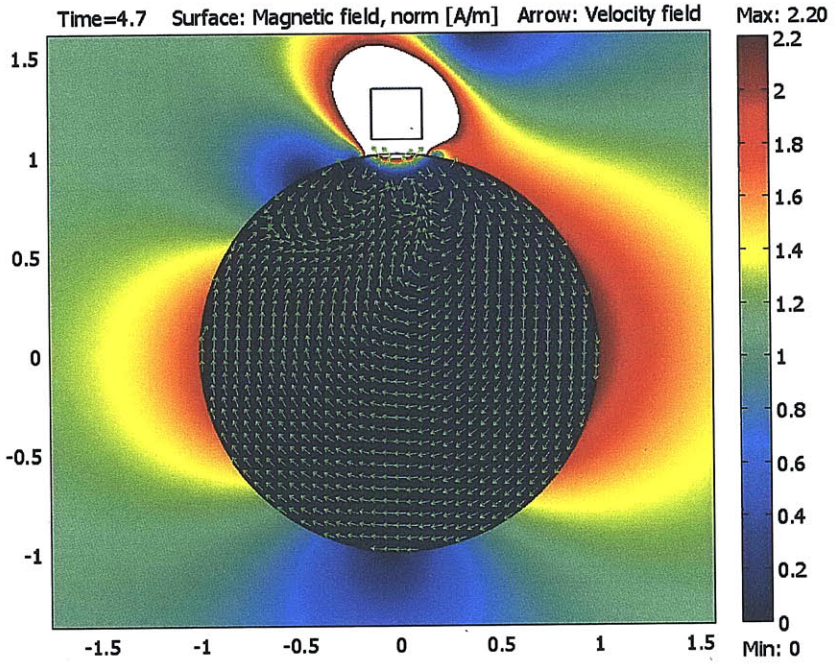

$\Omega t = \pi$

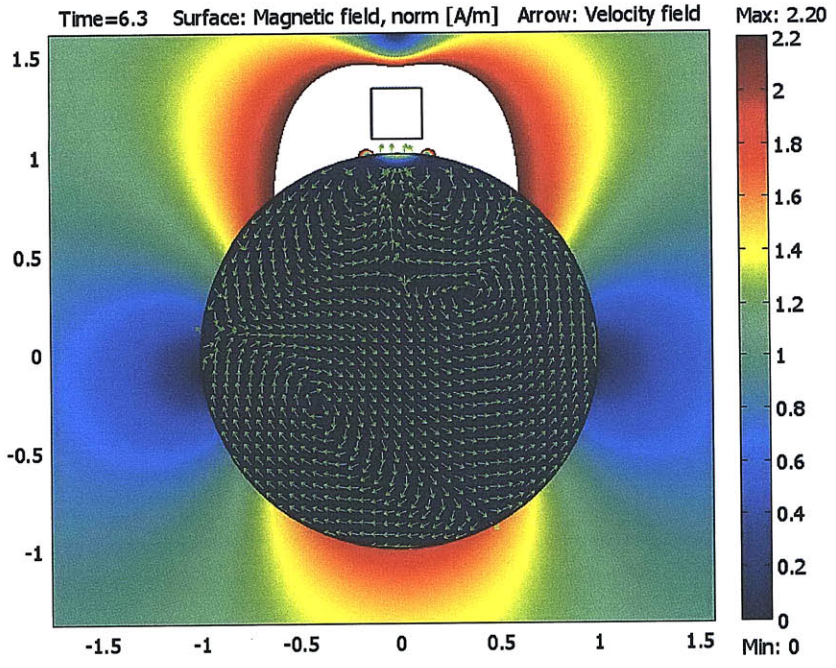

$\Omega t = \frac{3\pi}{2}$

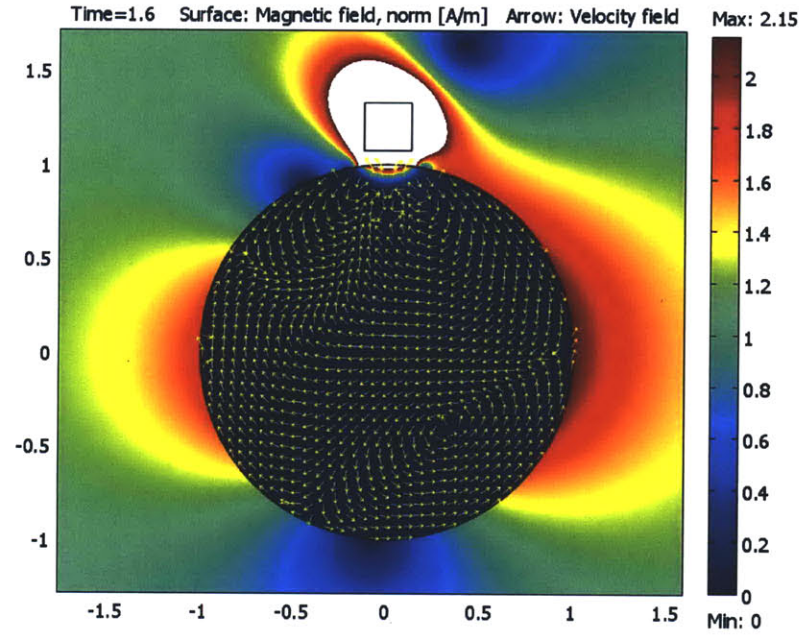

$\Omega t = 0$

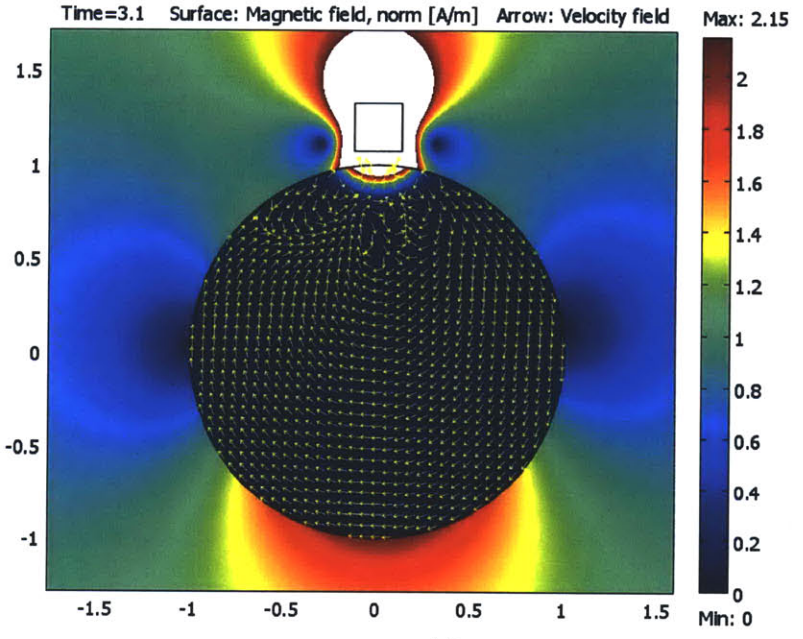

$\Omega t = \frac{\pi}{2}$

(a)

Figure 7-19. Distribution of velocity field for EFH1 filled cylinder with permanent magnet 20 times stronger than uniform rotating field as a function of time over one period of rotation (a)-(b). The rotating field is rotating in the clockwise direction with the velocity flow over most of the period in the same direction except at $\Omega t = \pi$.

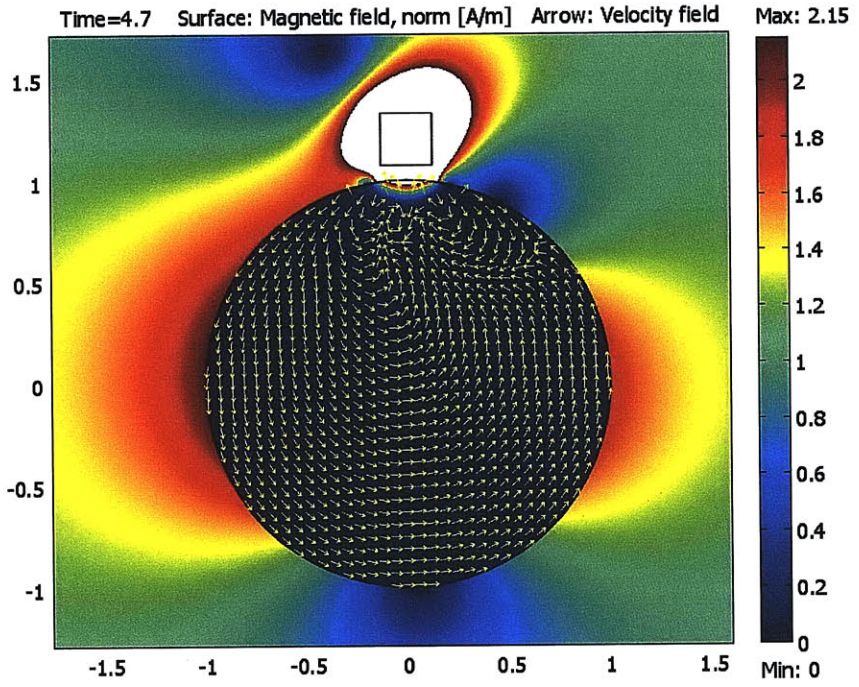

$\Omega t = \pi$

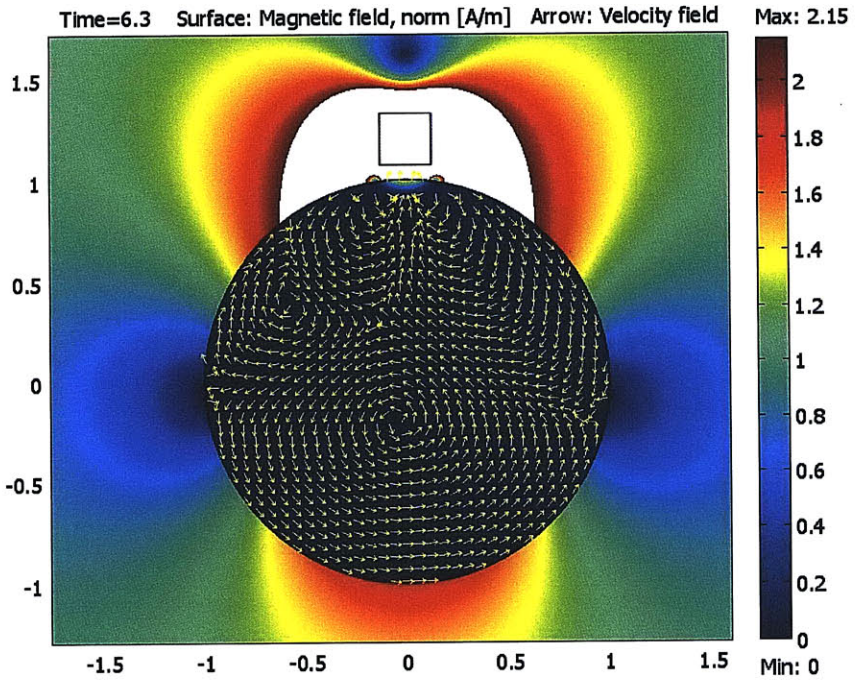

$\Omega t = \frac{3\pi}{2}$

(b)

7.2.7. Non-Uniform Distribution of Spin

Zaitsev and Shliomis [1], in their paper, accounted for the flow in the cylindrical geometry due to the non-uniform distribution of spin velocity $\boldsymbol{\omega}$ brought about by the 'spin-no-slip' boundary condition given by $\boldsymbol{\omega}(r = R_{wall}) = 0$. This required $\eta' \neq 0$ in the conservation of angular momentum equation. The experiments and simulations in Chapter 6 show that the effect of spin-viscosity η' is negligible and flow is a result of the spatially non-uniform field and the non-uniform distribution of the magnetic properties of the ferrofluid.

The results shown in Figure 7-20 illustrate that the non-uniform field and the non-uniform distribution of the magnetization of the ferrofluid creates a non-uniform distribution of spin velocity $\boldsymbol{\omega}$ which is a result and not a starting point for the case of the non-zero flow as stated by Zaitsev and Shliomis [1]. In addition to the magnitude of spin velocity, the results in Figure 7-20 plot the spatial gradient of the spin velocity ω and can be seen to form streamlines of constant values emanating from velocity vortices that also have the maximum value of spin velocity ω as seen at $\Omega t = \frac{\pi}{2}$. At $\Omega t = \frac{3\pi}{2}$, two regions of positive spin velocity coexist with a region of negative spin velocity with the velocity directions reversing direction in each of these regions corresponding to the reversal of spin velocity and torque.

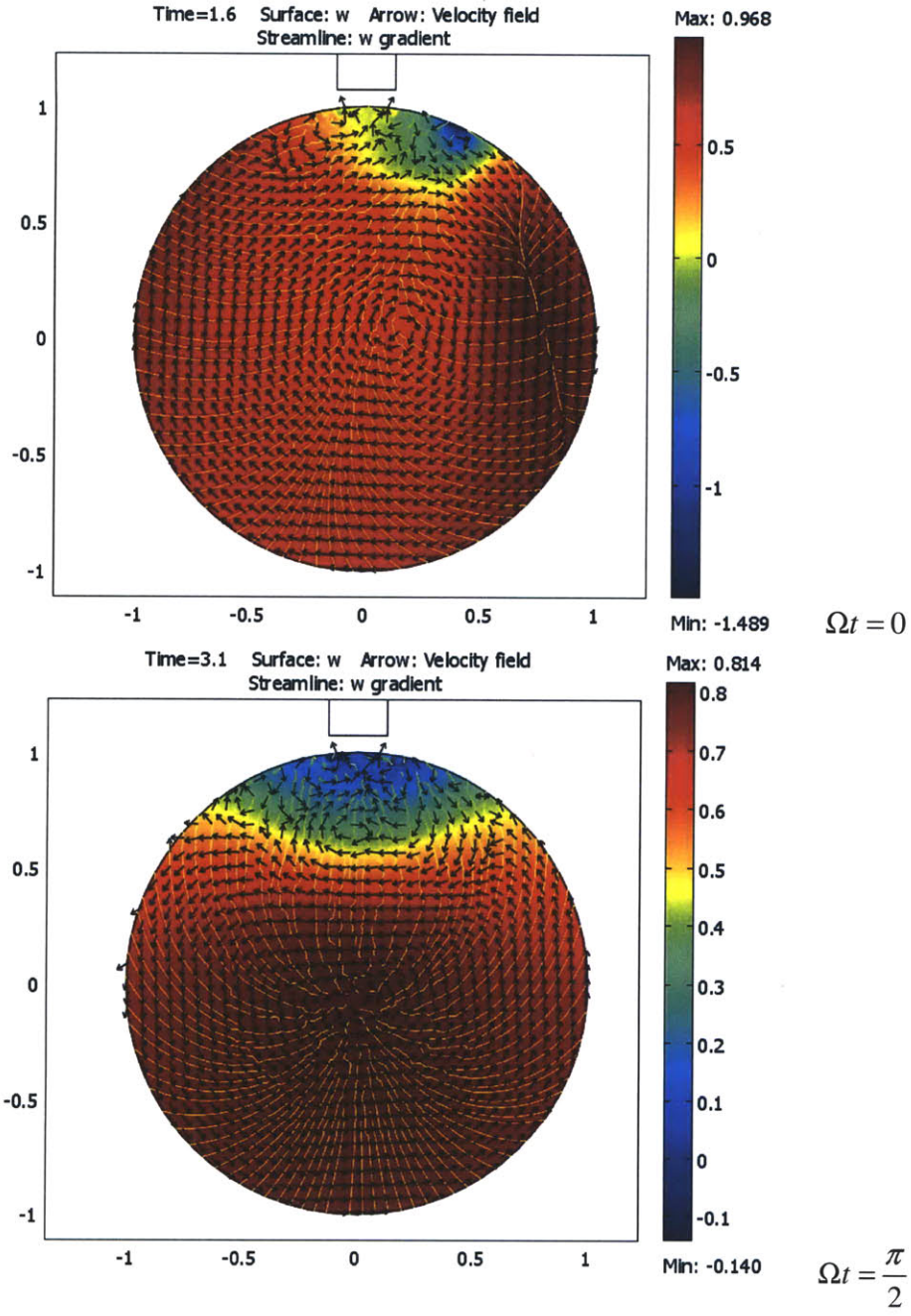

(a)

Figure 7-20. Distribution of magnitude (surface plot) and gradient streamlines of spin velocity **ω** with velocity field across one period of rotating field with permanent magnet 40 times the strength of the counter-clockwise rotating field. Non-uniform distribution of spin velocity and non-zero velocity is a result of the non-uniform field and not the other way round.

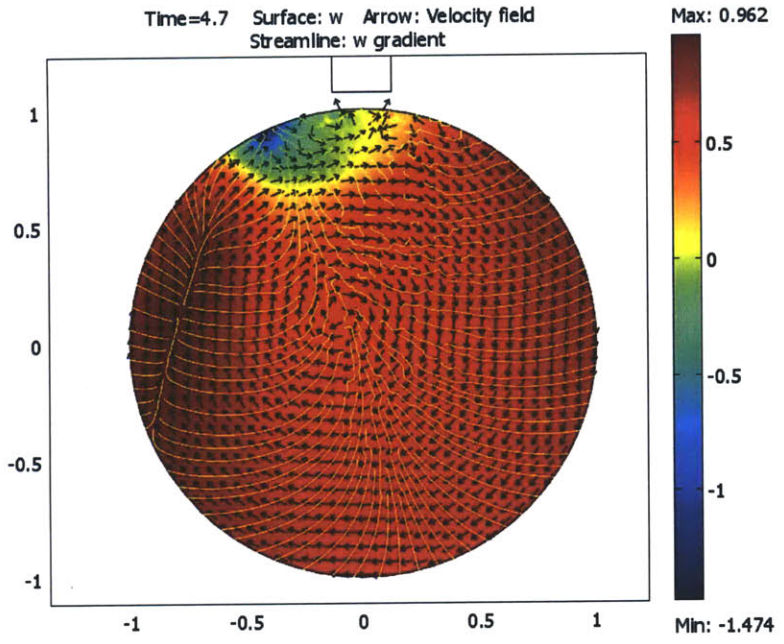

$\Omega t = \pi$

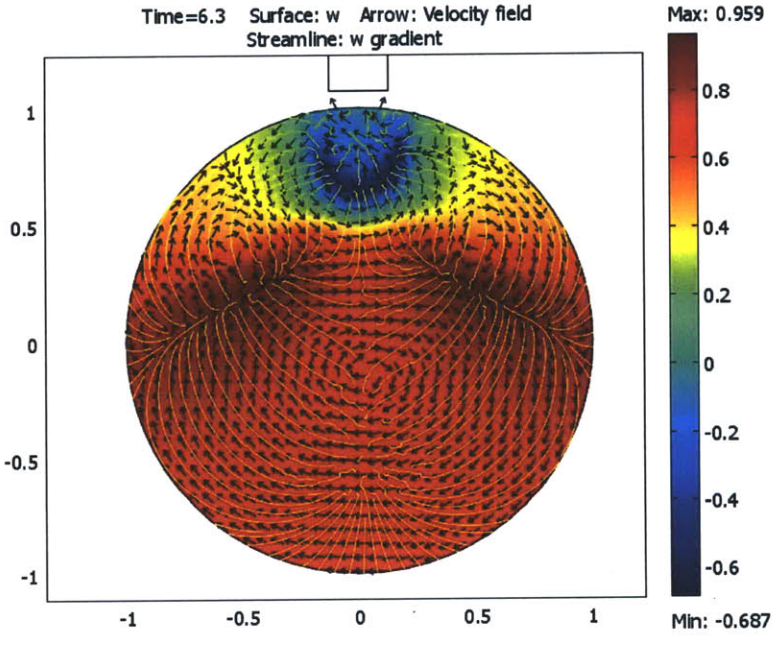

$\Omega t = \frac{3\pi}{2}$

(b)

7.3. Conclusions

This chapter explored, through COMSOL simulations neglecting spin-diffusion ($\eta' = 0$), subjecting an infinitely long cylinder to an external uniform rotating magnetic field with an imposed non-uniform field from an infinitely long permanent magnet placed on the side of the ferrofluid filled cylinder. The results of complicated significant flows were obtained similar to those of the experiments in Chapter 6, which involved using a spherical geometry subjected to a uniform rotating field with a non-uniform field imposed by a solenoidal coil or permanent magnet placed on top of the ferrofluid filled sphere. As a result this chapter confirms the results that a non-uniform field and non-uniform magnetic properties in a ferrofluid result in flow without spin-diffusion effects.

This chapter also illustrates that the non-uniform field and non-uniform magnetic properties in a ferrofluid results in a non-uniform distribution of spin velocity which is the starting assumption for Zaitsev and Shliomis's [1] spin-diffusion theory requiring that $\eta' \neq 0$. A non-uniform distribution of spin velocity is a result and not the cause for flow which is driven by the non-uniform field and non-uniform magnetic properties of the ferrofluid volume.

Bibliography

[1] V. M. Zaitsev and M. I. Shliomis, "Entrainment of ferromagnetic suspension by a rotating field," *Journal of Applied Mechanics and Technical Physics,* vol. 10, pp. 696-700, 1969.

Chapter 8. Thesis Summary and Suggestions for Future Work

This thesis investigated the effect of uniform rotating magnetic fields on ferrofluid spin-up flow by conducting experiments subjecting a ferrofluid filled sphere, with uniform demagnetizing factors in all three Cartesian directions, to a uniform external rotating magnetic field generated by two orthogonally placed spherical coil 'fluxballs' excited by two sinusoidal signals out of phase by 90° in time. The constant demagnetizing factors of a sphere ensured that the field inside the ferrofluid volume would be uniform and negligible measureable flow was obtained using ultrasound velocimetry. Negligible flow was obtained with COMSOL Multiphysics in a spherical geometry using zero spin-viscosity ($\eta'=0$) while simulations of spin-diffusion theory, with non-zero spin-viscosity ($\eta'\neq 0$) and $\omega=0$ boundary condition, predicted flow that should have been measureable by ultrasound velocimetry. Ultrasound velocimetry results from geometries where the demagnetizing effects associated with the shape of the container result in a non-uniform magnetic field within the ferrofluid volume, such as a 2/3 full sphere and a ferrofluid filled cylinder of finite height both subjected to a uniform rotating magnetic field, result in measureable flow (Chapter 6).

These results confirm that spin-diffusion theory is not the governing mechanism for spin-up flow as was previously believed by several authors [1-3]. The demagnetizing effects associated with the shape of the container results in a non-uniform field distribution in the ferrofluid volume, which have been ignored by these authors [1-3], and is the real mechanism driving the flow. As a result, the values of spin viscosity experimentally derived by these authors

[1-3] includes these demagnetizing effects and is the reason why the experimentally fit values of spin viscosity are many orders of magnitude greater than that derived theoretically.

The governing mechanism where non-uniform magnetic properties of the fluid drive the flow is further bolstered by ultrasound measurements of strong flows obtained when the ferrofluid filled sphere was subjected to a non-uniform field imposed by a solenoidal coil or a permanent magnet, in addition to the uniform rotating magnetic field. The results obtained had similar characteristics to COMSOL simulations of an infinitely long cylinder, with zero spin-viscosity ($\eta'=0$) subjected to a non-uniform field of an infinitely long permanent magnet and a uniform rotating field, even though the geometries were different.

In conclusion, this thesis proves that spin-diffusion theory is not the governing mechanism for ferrofluid spin-up flow in a uniform rotating magnetic field. The governing mechanism for the flow is due to non-uniform magnetic properties within the ferrofluid volume either imposed by an external source (magnet/coil) or created due to the demagnetizing effects associated with the shape of the container.

By determining the governing mechanism for spin up flow, this thesis helps understand the mechanism necessary for generating any flows in ferrofluids subjected to magnetic fields and is of value in applications involving ferrofluid pumping in particular MEMS devices.

8.1. Key Contributions

Different models for ferrofluid spin-up flow are studied, through COMSOL Multiphysics numerical simulations in cylindrical and spherical geometries and experiments using rotating magnetic fields with a coil or permanent magnet to create non-uniform magnetic fields. The following points summarize the key contributions to ferrofluid spin-up flow research made in this thesis:

1. Experiments in Chapter 6 of a ferrofluid filled sphere in a uniform rotating field give no measureable flow with an ultrasound velocimeter confirming that the shape of the ferrofluid container is responsible for non-uniform fields within the ferrofluid, due to demagnetizing effects, which drive the flow. This is further corroborated by experiments done in a 2/3 full sphere of ferrofluid and a finite height cylinder subjected to a uniform rotating field resulting in strong flows with velocity of the order of 1-30 mm/s. These experiments confirm that a non-uniform field due to the demagnetizing effects associated with the shape of the ferrofluid volume are the driving mechanisms for spin-up flow.
2. Experimental results (Chapter 6) of non-zero irregular flows obtained in the spherical geometry due to non-uniform fields imposed by a permanent magnet and a solenoidal coil in addition to a uniform rotating magnetic field, also demonstrate that non-uniform magnetic fields and non-uniform distribution of magnetic properties are responsible for driving the flow.
3. Zaitsev and Shliomis [4] in their paper, stated that a non-uniform distribution of spin velocity (non-zero spin-viscosity $\eta' \neq 0$) imposed by a spin velocity boundary condition $\omega=0$, would result in macroscopic rigid body motion in a cylindrical geometry. The experiments

(Chapter 6) and simulations (Chapter 7) done in this thesis, confirm that non-uniform magnetic fields and non-uniform distribution of magnetic properties drive the flow and a non-uniform distribution of spin is a result and not the cause of the macroscopic flow.

4. COMSOL simulation results of non-zero irregular and complicated two dimensional flows in a cylindrical geometry of infinite height due to non-uniform fields imposed by an infinitely long magnet in a uniform rotating field confirm similar experimental observations obtained in the spherical case even though the geometries are different (Chapter 7).
5. Pshenichnikov, in his paper [5], applies a permanent magnet induced bias field perpendicular to the plane of a uniform rotating field to a cuvette containing ferrofluid. In this thesis the simulations (Chapter 7) were conducted with the field of an infinitely long permanent magnet in the same plane as the rotating field. Although the plane of the magnetic field of the permanent magnet, with respect to the plane of the rotating field, is different from the simulations (Chapter 7) done in this thesis and Pshenichnikov's implementation, the results obtained have similar characteristics of flow reversal/vortex formation (as seen in Figure 8-1). Pshenichnikov's results could be attributed to the total magnetic field of the magnet and the uniform rotating field creating regions of strong and weak fields creating vortices/flow reversal. Pshenichnikov's results also confirm the conclusion from this thesis that non-uniform magnetic properties are the governing mechanism driving spin-up flow.

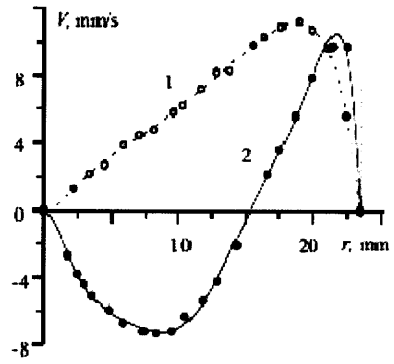

Figure 8-1. Velocity profile for the circular cuvette in the absence of the bias field (curve 1) and with it (curve 2), taken from Pshenichnikov [5].

6. Simulations of velocity profiles with non-zero spin-viscosity ($\eta' \neq 0$) give non-zero flow that have been previously measured by other researchers [1-3] in cylindrical geometry and should be measureable in the spherical geometry. Simulations of velocity profiles with zero spin-viscosity ($\eta' = 0$) give negligible flow in both cylindrical and spherical cases. The experiment of subjecting a ferrofluid filled sphere to a uniform rotating magnetic field gave negligible flow (Chapter 6) confirming that only non-uniform distribution of magnetic properties either imposed by a coil/magnet or due to demagnetizing effects associated with the shape of the container drives the flow.
7. As a result of experiments and simulations (Chapter 4 and Chapter 6) with and without spin viscosity η', spin-diffusion is shown to have a negligible effect on ferrofluid spin-up flow. The value of spin-viscosity is either zero with no boundary condition on spin velocity $\boldsymbol{\omega}$ or an alternative explanation is that the value of spin-viscosity is negligibly small as derived by Schumacher [6] using a modification of the dynamic viscosity derivation of an ideal gas

using molecular kinetic theory [7]. The boundary condition on spin velocity $\boldsymbol{\omega}$ used in this thesis

$$\left\| \boldsymbol{\omega} - \gamma \frac{1}{2} \nabla \times \mathbf{v} \right\| = 0 \tag{8.1}$$

where γ is the spin boundary condition selector that has a value between 0 and 1 and $\|\boldsymbol{\omega}\|$ represents the jump in spin velocity $\boldsymbol{\omega}$ across the fixed boundary. A value of $\gamma = 0$ representing the 'spin-no-slip' ($\boldsymbol{\omega} = 0$) boundary condition would still give measureable flow in the fluid volume while a value of $\gamma = 1$ representing the 'spin-vorticity' ($\boldsymbol{\omega} = \frac{1}{2} \nabla \times \mathbf{v}$) boundary condition results in flow that is in the opposite direction of the rotating magnetic field [8]. A value of γ between 0 and 1 could potentially result in none or negligible flow. Regardless of what the boundary condition on spin velocity is, the experiments of a ferrofluid filled sphere in a uniform rotating field gave negligible flow while experiments where demagnetizing effects are significant (2/3 full sphere and ferrofluid filled finite height cylinder in Chapter 6) result in significant flow justifying the significance of non-uniform magnetic properties within the ferrofluid volume driving the flow.

8. The theoretical value of spin-viscosity (η') derived using a modification of molecular kinetic theory of dilute gases is many orders of magnitude smaller than that obtained experimentally by several researchers by fitting numerical solutions of the governing equations to measurements. The spin-viscosity values experimentally determined by several researchers [1-3] is thus, mathematically overstated to account for the demagnetizing effects associated with the shape of the cylinder, but not considered in their theoretical modeling, and is not the mechanism driving the flow.

8.2. Suggestions for Future Work

In closing, the following directions for future work are suggested to build and extend upon the results presented in this thesis:

1. To confirm negligible flow in an infinitely tall cylinder, a special toroidal structure can be built as shown in Figure 8-2. The vessel can be built in slices that are held together with o-rings to prevent leaks. Helmholtz coils can be used to generate the uniform rotating magnetic field in the ferrofluid volume of each slice. The cross-section of the slices can be seen in the bottom right corner of Figure 8-2. A permanent magnet can be fitted inside the slot at the top of every slice to create a non-uniform field replicating experimentally the simulations in Chapter 7. The slices will have to be made fairly thin to ensure the spatial variation of the magnetic field does not change too much as a function of the ϕ direction.

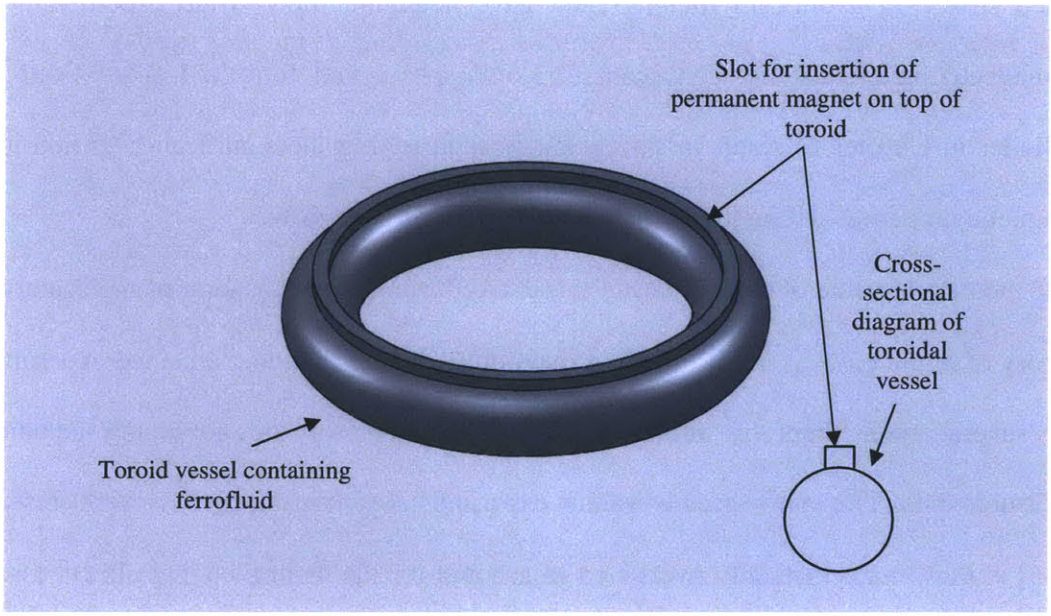

Figure 8-2. Infinitely long cylinder modified to be shaped as a toroid with slot on top for placement of permanent magnet. Cross-sectional diagram of toroidal vessel can also be seen.

2. Simulating the ferrofluid spin-up flows in a 3D finite height cylinder using an improved COMSOL to investigate demagnetizing fields driving ferrofluid rotational flows. The present limitation is the setup of the mesh in 3D and the processing and memory capability of the computer used.
3. The magnetic field from the third coil/magnet is spatially non-uniform and its effect resulted in complicated flows with vortices that were difficult to analytically investigate. Applying a non-uniform field that can be distributed spatially, in a manner such that its effects on ferrofluid flows can be analytically calculated, would be beneficial in understanding the effect of the torque and force densities in generating vortices.
4. Simulating the experiment of a ferrofluid sphere in a non-uniform field as described in Chapter 6 using COMSOL. The reason why it could not be completed in this thesis was because it required a better computer than a dual quad-core computer with more than 100GB of RAM to handle a very fine mesh in three dimensional geometry. A cluster of computers running COMSOL would be ideal.
5. Developing a molecular kinetic theory of viscosity for liquids would aid in determining a more precise analytical determination of spin-viscosity η'.

Bibliography

[1] S. Elborai, "Ferrofluid surface and volume flows in uniform rotating magnetic fields," Ph.D thesis, Dept of Electrical Engineering and Computer Science, Massachusetts Institute of Technology, Cambridge, MA, 2006.

[2] A. Chaves, *et al.*, "Spin-up flow of ferrofluids: Asymptotic theory and experimental measurements," vol. 20, p. 053102, 2008.

[3] X. He, "Ferrohydrodynamic flows in uniform and non-uniform rotating magnetic fields," Ph.D thesis, Dept of Electrical Engineering and Computer Science, Massachusetts Institute of Technology, Cambridge, MA, 2006.

[4] V. M. Zaitsev and M. I. Shliomis, "Entrainment of ferromagnetic suspension by a rotating field," *Journal of Applied Mechanics and Technical Physics,* vol. 10, pp. 696-700, 1969.

[5] A. Pshenichnikov, *et al.*, "On the rotational effect in nonuniform magnetic fluids," *Magnetohydrodynamics,* vol. 36, pp. 275-281, 2000.

[6] K. R. Schumacher, *et al.*, "Experiment and simulation of laminar and turbulent ferrofluid pipe flow in an oscillating magnetic field," *Physical Review E,* vol. 67, p. 026308, 2003.

[7] R. B. Bird, *et al.*, *Transport Phenomena*, Second ed.: John Wiley & Sons, Inc, 2002.

[8] B. Finlayson, "Modeling a Ferrofluid in a Rotating Magnetic Field," presented at the COMSOL Users' Conference, Boston, 2007.

Appendix A : Ferrofluid Flows in Planar Geometry

Supplementary Code

A1. Mathematica Code for Planar Couette Flow With $\tilde{H}_z = 1, \tilde{B}_x = 0$ (Section 3.2.2)

```
In[185]:= << "VectorAnalysis`"
ClearAll[v, B, M, H, eqn, x, y, z, eqn11, eqn12, f, TL, eqnT2, Bx, Hz, Mnorm];SetCoordinates[Cartesian[x, y, z]];

CleanSlate[]
ω = {ωx[x], ωy[x], ωz[x]};v = {0, 0, vz[x]};B = {Bx, By[x], Bz[x]} e^(Ωit);M = {Mx[x], My[x], Mz[x]} e^(Ωit);H = {Hx[x], Hy, Hz} e^(Ωit);
TL = 2 π / Ω;

$Assumptions = Bz[x] ∈ Reals && ωy[x] ∈ Reals && Hz ∈ Reals && Bx ∈ Reals && Ω ∈ Reals && μ0 ∈ Reals && χ0 ∈ Reals &&
   τ ∈ Reals && t ∈ Reals && vz[x] ∈ Reals && Hx[x] ∈ Reals && H ∈ Reals && B ∈ Reals && v ∈ Reals && ω ∈ Reals &&
   Conjugate[ωy[x]] ∈ Reals && Conjugate[ωy[x]]^2 ∈ Reals && Conjugate[Bx] ∈ Reals && Conjugate[Ω] ∈ Reals && Conjugate[Hz] ∈ Reals && p ∈ Reals && vz''[x] ∈ Reals && ξ ∈ Reals &&
   χ0^2 ∈ Reals && ωx[x] ∈ Reals && ωz[x] ∈ Reals && By[x] ∈ Reals && My[x] ∈ Reals && Hy ∈ Reals && Conjugate[ωx[x]] ∈ Reals &&
   Conjugate[ωz[x]] ∈ Reals && Conjugate[My[x]] ∈ Reals && Conjugate[Hy] ∈ Reals && Conjugate[Mx[x]] ∈ Reals && Conjugate[Mz[x]] ∈ Reals && 1/μ0 ∈ Reals && H0 ∈ Reals;



Print["Torque Expression"]
T = μ0 M×Bgrad2[v_, M_] := {∂t M[1] + v[1] ∂x M[1] - (ω×M)[1] + (M[1] - χ0 H[1])/τ, ∂t M[2] + v[2] ∂y M[2] - (ω×M)[2] + (M[2] - χ0 H[2])/τ,
  ∂t M[3] + v[3] ∂z M[3] - (ω×M)[3] + (M[3] - χ0 H[3])/τ}
eqn = grad2[v, M] /. Hz[x] → Bx/μ0 - Mx[x];


eqn8 = eqn[1] == 0eqn7 = eqn[2] == 0
eqn9 = eqn[3] == 0

eqn11 = FullSimplify[Solve[{eqn7, eqn8, eqn9}, Mx[x], {Mz[x], My[x]}]]M = M /. %;eqn12 =
 FullSimplify[Solve[{eqn7, eqn8, eqn9}, My[x], {Mx[x], Mz[x]}]]M = M /. %;
eqn13 = FullSimplify[Solve[{eqn7, eqn8, eqn9}, Mz[x], {Mx[x], My[x]}]]M = M /. %;M = Flatten[M]
```

In[210]:= (* Substituting Zahn's average Torque Density and moving on *)

```
Mxnorm[x] = (χ0 (H̄x (-i + Ω̄)^2 - (H̄x ω̄x[x]^2 + (1 + i Ω̄) (H̄z ω̄y[x] - H̄y ω̄z[x]) + ω̄x[x] (H̄y ω̄y[x] + H̄z ω̄z[x])))) /
   ((χ0 ((-i + Ω̄)^2 - (ω̄x[x])^2) + (1 + i Ω̄) ((-i + Ω̄)^2 - ((ω̄x[x])^2 + (ω̄y[x])^2 + (ω̄z[x])^2))));

Mynorm[x] =
  (χ0 (H̄y (-i + Ω̄)^2 + χ0 (H̄y (-1 - i Ω̄) + H̄z ω̄x[x]) + ω̄x[x] (H̄z + i H̄z Ω̄ - H̄x ω̄y[x]) - (H̄y (ω̄y[x])^2 + (H̄x + i H̄x Ω̄ + H̄z ω̄y[x]) ω̄z[x]))) /
   ((χ0 ((-i + Ω̄)^2 - (ω̄x[x])^2) + (1 + i Ω̄) ((-i + Ω̄)^2 - ((ω̄x[x])^2 + (ω̄y[x])^2 + (ω̄z[x])^2))));

Mznorm[x] =
  (χ0 (H̄z (-i + Ω̄)^2 + χ0 (H̄z (-1 - i Ω̄) - H̄y ω̄x[x]) + (-i (-i + Ω̄) (H̄y ω̄x[x] - H̄x ω̄y[x]) - (H̄x ω̄x[x] + H̄y ω̄y[x]) ω̄z[x] - H̄z (ω̄z[x])^2))) /
   ((χ0 ((-i + Ω̄)^2 - (ω̄x[x])^2) + (1 + i Ω̄) ((-i + Ω̄)^2 - ((ω̄x[x])^2 + (ω̄y[x])^2 + (ω̄z[x])^2))));

Mnorm = Simplify[{Mxnorm[x], Mynorm[x], Mznorm[x]} /. {H̄x → 0, ω̄x[x] → 0, ω̄z[x] → 0, H̄y → 0}]
```

In[214]:= (* Calculating normalized average Torque densities in each direction *)

```
avgTx = 0.5 * Re[My[x] * Conjugate[Hz] - Conjugate[Hy] * Mz[x]] /. {My[x] -> Mnorm[[2]], Mz[x] -> Mnorm[[3]]};
avgTx = FullSimplify[ComplexExpand[%]];
avgTy = -1/2 * Re[Mx[x] * Hz + Mz[x] * Conjugate[Mx[x]]] /. {Mx[x] → Mnorm[[1]], Mz[x] → Mnorm[[3]]};
avgTy = FullSimplify[ComplexExpand[%]];
avgTz = FullSimplify[0.5 * Re[Mx[x] * Conjugate[Hy] - Conjugate[Hx[x]] * My[x]]] /.
   {Mx[x] → Mnorm[[1]], My[x] -> Mnorm[[2]]};

avgTx = avgTx /. {H̄x → 0, ω̄x[x] → 0, ω̄z[x] → 0, H̄y → 0}
avgTy = avgTy /. {H̄x → 0, ω̄x[x] → 0, ω̄z[x] → 0, H̄y → 0}
avgTz = avgTz /. {H̄x → 0, ω̄x[x] → 0, ω̄z[x] → 0, H̄y → 0}



(* Unnormalizing Ty and since this is DC average power will give half the power if it were DC,
so it should be doubled *)

avgTx = FullSimplify[1 * μ0 * avgTx /. {ω̄y[x] -> ωy[x] * τ, ω̄x[x] -> ωx[x] * τ, Ω̄ -> Ω * τ}];
avgTy = FullSimplify[1 * μ0 * avgTy /. {ω̄y[x] -> ωy[x] * τ, ω̄x[x] -> ωx[x] * τ, Ω̄ -> Ω * τ}]
(*
avgTx=FullSimplify[2*μ0 *avgTx]
avgTy=FullSimplify[2*μ0 *avgTy]
*)
```

In[320]:=
```
eqntosolve = 2 ωy[x] + V/d - avgTy/(2 ξ) == 0

eqntosolve = V/d + 2 ωy[x] + (μ0 τ Hz^2 χ0 ωy[x] (-τ^2 Ω^2 + (1 + χ0)^2 + τ^2 ωy[x]^2)) / (4 ξ (τ^4 Ω^4 + τ^2 Ω^2 (2 + χ0 (2 + χ0) - 2 τ^2 ωy[x]^2) + (1 + χ0 + τ^2 ωy[x]^2)^2)) == 0

eqntosolve = r + (P ωy[x] (-Ω̄^2 + (1 + χ0)^2 + ωy[x]^2)) / (2 Vnew (Ω̄^4 + Ω̄^2 (2 + χ0 (2 + χ0) - 2 ωy[x]^2) + (1 + χ0 + ωy[x]^2)^2)) == 0 /. {ωy[x] → (r - 1/2) Vnew}

eqntosolve = r 2 Vnew (Ω̄^4 + Ω̄^2 (2 + χ0 (2 + χ0) - 2 ωy[x]^2) + (1 + χ0 + ωy[x]^2)^2) + P ωy[x] (-Ω̄^2 + (1 + χ0)^2 + ωy[x]^2) == 0 /.
  {ωy[x] → (r - 1/2) Vnew}
Flatten[Solve[eqntosolve, P]]
eqpl = P /. %;
eqplot = eqpl /. {χ0 → 1.55`, r → 0.5` r}

eqplotDC = eqpl/1 /. {χ0 → 1.55`, r → 0.5` r}

Plot[Evaluate[Table[eqplotDC /. {Ω̄ → 0}, {Vnew, 0, 12, 4}]], {r, 0, 1}, AxesLabel → {2 r, PHDC},
 PlotRange → {{0, 1}, {0, 20}}, MaxRecursion → 15, GridLines → Automatic, PlotStyle → {Red, Green, Blue, Black}]
Plot[Evaluate[Table[eqplot /. {Ω̄ → 0.2}, {Vnew, 0, 12, 4}]], {r, 0, 1}, AxesLabel → {2 r, PH},
 PlotRange → {{0, 1}, {0, 20}}, MaxRecursion → 15, GridLines → Automatic, PlotStyle → {Red, Green, Blue, Black}]
Plot[Evaluate[Table[eqplot /. {Ω̄ → 0.4}, {Vnew, 0, 12, 4}]], {r, 0, 1}, AxesLabel → {2 r, PH},
 PlotRange → {{0, 1}, {0, 20}}, MaxRecursion → 15, GridLines → Automatic, PlotStyle → {Red, Green, Blue, Black}]
Plot[Evaluate[Table[eqplot /. {Ω̄ → 1}, {Vnew, 0, 12, 4}]], {r, 0, 1}, AxesLabel → {2 r, PH}, PlotRange → {{0, 1}, {0, 20}},
 MaxRecursion → 15, GridLines → Automatic, PlotStyle → {Red, Green, Blue, Black}]
Plot[Evaluate[Table[eqplot /. {Ω̄→0.8}, {Vnew, 0, 12, 4}]], {r, 0, 1}, AxesLabel→{2r, PH}, PlotRange→{{0,1}, {0,50}},
  MaxRecursion→15, GridLines→Automatic, PlotStyle→{Red, Green, Blue, Black}]
Plot[Evaluate[Table[eqplot /. {Ω̄→1.0}, {Vnew, 0, 12, 4}]], {r, 0, 1}, AxesLabel→{2r, PH}, PlotRange→{{0,1}, {0,50}},
  MaxRecursion→15, GridLines→Automatic, PlotStyle→{Red, Green, Blue, Black}]


Plot[Evaluate[Table[eqplot /. {Ω̄→0}, {Vnew, 4, 12, 4}]], {r, 0, 1}, MaxRecursion→15, GridLines→Automatic, Frame→True,
  PlotRange→{{0,1}, {0,20}}]
Plot[Evaluate[Table[eqplot /. {Ω̄→0.2}, {Vnew, 4, 12, 4}]], {r, 0, 1}, MaxRecursion→15, GridLines→Automatic,
  Frame→True, PlotRange→{{0,1}, {0,20}}]
Plot[Evaluate[Table[eqplot /. {Ω̄→0.4}, {Vnew, 4, 12, 4}]], {r, 0, 1}, MaxRecursion→15, GridLines→Automatic,
  Frame→True, PlotRange→{{0,1}, {0,20}}]
Plot[Evaluate[Table[eqplot /. {Ω̄→0.6}, {Vnew, 4, 12, 4}]], {r, 0, 1}, MaxRecursion→15, GridLines→Automatic,
  Frame→True, PlotRange→{{0,1}, {0,20}}]
Plot[Evaluate[Table[eqplot /. {Ω̄→0.8}, {Vnew, 4, 12, 4}]], {r, 0, 1}, MaxRecursion→15, GridLines→Automatic,
  Frame→True, PlotRange→{{0,1}, {0,20}}]
Plot[Evaluate[Table[eqplot /. {Ω̄→1}, {Vnew, 4, 12, 4}]], {r, 0, 1}, MaxRecursion→15, GridLines→Automatic, Frame→True,
  PlotRange→{{0,1}, {0,20}}]
```

A2. Mathematica Code for Planar Couette Flow With $\tilde{H}_z = 0, \tilde{B}_x = 1$ (Section 3.2.3)

```
<< "VectorAnalysis`"
ClearAll[v, B, M, H, eqn, x, y, z, eqn11, eqn12, f, TL, eqnT2, Bx, Hz, Mnorm]; SetCoordinates[Cartesian[x, y, z]];

CleanSlate[]
ω = {ωx[x], ωy[x], ωz[x]}; v = {0, 0, vz[x]}; B = {Bx, By[x], Bz[x]} e^(Ω i t); M = {Mx[x], My[x], Mz[x]} e^(Ω i t); H = {Hx[x], Hy, Hz} e^(Ω i t);
TL = 2 π / Ω;

$Assumptions = Bz[x] ∈ Reals && ωy[x] ∈ Reals && Hz ∈ Reals && Bx ∈ Reals && Ω ∈ Reals && μ0 ∈ Reals && χ0 ∈ Reals && τ ∈ Reals && t ∈ Reals && vz[x] ∈ Reals && Hx[x] ∈ Reals &&
   H ∈ Reals && B ∈ Reals && v ∈ Reals && ω ∈ Reals && Conjugate[ωy[x]] ∈ Reals && Conjugate[ωy[x]]^2 ∈ Reals && Conjugate[Bx] ∈ Reals && Conjugate[Ω] ∈ Reals && Conjugate[Hz] ∈ Reals && p ∈ Reals && vz''[x] ∈ Reals && ξ ∈ Reals &&
   χ0^2 ∈ Reals && ωx[x] ∈ Reals && ωz[x] ∈ Reals && By[x] ∈ Reals && My[x] ∈ Reals && Hy ∈ Reals && Conjugate[ωx[x]] ∈ Reals && Conjugate[ωz[x]] ∈ Reals && Conjugate[My[x]] ∈ Reals && Conjugate[Hy] ∈ Reals &&
   Conjugate[Mx[x]] ∈ Reals && Conjugate[Mz[x]] ∈ Reals && 1/μ0 ∈ Reals && H0 ∈ Reals;
Null
Null

Print["Torque Expression"]
T = μ0 M × H grad2[v_, M_] := {∂t M[1] + v[1] ∂x M[1] - (ω × M)[1] + (M[1] - χ0 H[1])/τ, ∂t M[2] + v[2] ∂y M[2] - (ω × M)[2] + (M[2] - χ0 H[2])/τ, ∂t M[3] + v[3] ∂x M[3] - (ω × M)[3] + (M[3] - χ0 H[3])/τ}
eqn = grad2[v, M] /. Hx[x] → Bx/μ0 - Mx[x];
Null

eqn8 = eqn[1] == 0 eqn7 = eqn[2] == 0
eqn9 = eqn[3] == 0

eqn11 = FullSimplify[Solve[{eqn7, eqn8, eqn9}, Mx[x], {Mx[x], My[x]}]] M = M /. %; eqn12 = FullSimplify[Solve[{eqn7, eqn8, eqn9}, My[x], {Mx[x], Mz[x]}]] M = M /. %;
eqn13 = FullSimplify[Solve[{eqn7, eqn8, eqn9}, Mz[x], {Mx[x], My[x]}]] M = M /. %; M = Flatten[M]

(* Substituting Zahn's average Torque Density and moving on *)

Mxnorm[x] = (χ0 (Conjugate[Bx] (-i + Ω̄)^2 - (Conjugate[Bx] Conjugate[ωx[x]]^2 + (1 + i Ω̄) (Conjugate[Hz] Conjugate[ωy[x]] - Conjugate[Hy] Conjugate[ωz[x]]) + Conjugate[ωx[x]] (Conjugate[Hy] Conjugate[ωy[x]] + Conjugate[Hz] Conjugate[ωz[x]])))) /
    ((χ0 ((-i + Ω̄)^2 - (Conjugate[ωx[x]])^2) + (1 + i Ω̄) ((-i + Ω̄)^2 - ((Conjugate[ωx[x]])^2 + (Conjugate[ωy[x]])^2 + (Conjugate[ωz[x]])^2)))) /. {Conjugate[Hz] → 0, Conjugate[Hy] → 0, Conjugate[ωx[x]] → 0, Conjugate[ωz[x]] → 0};

Mynorm[x] = (χ0 (Conjugate[Hy] (-i + Ω̄)^2 + χ0 (Conjugate[Hy] (-1 - i Ω̄) + Conjugate[Hz] Conjugate[ωx[x]]) + Conjugate[ωx[x]] (Conjugate[Hz] + i Conjugate[Hz] Ω̄ - Conjugate[Bx] Conjugate[ωy[x]]) - (Conjugate[Hy] (Conjugate[ωy[x]])^2 + (Conjugate[Bx] + i Conjugate[Bx] Ω̄ + Conjugate[Hz] Conjugate[ωy[x]]) Conjugate[ωz[x]]))) /
    ((χ0 ((-i + Ω̄)^2 - (Conjugate[ωx[x]])^2) + (1 + i Ω̄) ((-i + Ω̄)^2 - ((Conjugate[ωx[x]])^2 + (Conjugate[ωy[x]])^2 + (Conjugate[ωz[x]])^2)))) /. {Conjugate[Hz] → 0, Conjugate[Hy] → 0, Conjugate[ωx[x]] → 0, Conjugate[ωz[x]] → 0};

Mznorm[x] = (χ0 (Conjugate[Hz] (-i + Ω̄)^2 + χ0 (Conjugate[Hz] (-1 - i Ω̄) - Conjugate[Hy] Conjugate[ωx[x]]) + (-i (-i + Ω̄) (Conjugate[Hy] Conjugate[ωx[x]] - Conjugate[Bx] Conjugate[ωy[x]]) - (Conjugate[Bx] Conjugate[ωx[x]] + Conjugate[Hy] Conjugate[ωy[x]]) Conjugate[ωz[x]] - Conjugate[Hz] (Conjugate[ωz[x]])^2))) /
    ((χ0 ((-i + Ω̄)^2 - (Conjugate[ωx[x]])^2) + (1 + i Ω̄) ((-i + Ω̄)^2 - ((Conjugate[ωx[x]])^2 + (Conjugate[ωy[x]])^2 + (Conjugate[ωz[x]])^2)))) /. {Conjugate[Hz] → 0, Conjugate[Hy] → 0, Conjugate[ωx[x]] → 0, Conjugate[ωz[x]] → 0};

Mnorm = FullSimplify[{Mxnorm[x], Mynorm[x], Mznorm[x]}]
```

```
Mnorm
(* Calculating normalized average Torque densities in each direction *)

avgTx = 0.5 * Re[My[x]bar * Conjugate[Hz]bar - Conjugate[Hy]bar * Mz[x]bar] /. {My[x]bar -> Mnorm[[2]], Mz[x]bar -> Mnorm[[3]]};
avgTx = FullSimplify[ComplexExpand[%]];
avgTy = 1/2 * Re[Mz[x]bar * Bx - Mz[x]bar * Conjugate[Mx[x]bar]] /. {Mx[x]bar -> Mnorm[[1]], Mz[x]bar -> Mnorm[[3]]};
avgTy = FullSimplify[ComplexExpand[%]];
avgTz = FullSimplify[0.5 * Re[Mx[x]bar * Conjugate[Hy]bar - Conjugate[Hx[x]bar] * My[x]bar]] /. {Mx[x]bar -> Mnorm[[1]], My[x]bar -> Mnorm[[2]]};

avgTx = avgTx /. {Hz -> 0, Hy -> 0, ωx[x]bar -> 0, ωz[x]bar -> 0};
avgTy = avgTy /. {Hz -> 0, Hy -> 0, ωx[x]bar -> 0, ωz[x]bar -> 0}
avgTz = avgTz /. {Hz -> 0, Hy -> 0, ωx[x]bar -> 0, ωz[x]bar -> 0};

(* Unnormalizing Ty  *)

avgTx = FullSimplify[1 * μ0 * avgTx /. {ωy[x]bar -> ωy[x] * τ, ωx[x]bar -> ωx[x] * τ, Ω -> Ω * τ, Hx -> Bx/μ0}];
avgTy = FullSimplify[1 * μ0 * avgTy /. {ωy[x]bar -> ωy[x] * τ, ωx[x]bar -> ωx[x] * τ, Ω -> Ω * τ, Hx -> Bx/μ0}]
eqntosolve = 2 ωy[x] + V/d - avgTy/(2 ξ) == 0

eqntosolve = V/d + 2 ωy[x] + Bx^2 τ χ0 ωy[x] (1 - τ^2 Ω^2 + τ^2 ωy[x]^2) / (4 μ0 ξ (τ^4 Ω^4 + τ^2 Ω^2 (2 + χ0 (2 + χ0) - 2 τ^2 ωy[x]^2) + (1 + χ0 + τ^2 ωy[x]^2)^2)) == 0

eqntosolve = r + ωy[x]bar P (1 - Ω^2 + ωy[x]bar^2) / (Vnew (Ω^4 + Ω^2 (2 + χ0 (2 + χ0) - 2 ωy[x]bar^2) + (1 + χ0 + ωy[x]bar^2)^2)) == 0 /. {ωy[x]bar -> (r - 1/2) Vnew}
FullSimplify[%]

eqntosolve = Simplify[r Vnew (Ω^4 + Ω^2 (2 + χ0 (2 + χ0) - 2 ωy[x]bar^2) + (1 + χ0 + ωy[x]bar^2)^2) + P ωy[x]bar (1 - Ω^2 + ωy[x]bar^2) == 0 /. {ωy[x]bar -> (r - 1/2) Vnew}]

Flatten[Solve[eqntosolve, P]]
eqpl = P /. %;

eqplotDC = eqpl/2.55^-2 /. {χ0 -> 1.55`, r -> 0.5` r}
eqplot = 2 * eqpl/2.55^-2 /. {χ0 -> 1.55`, r -> 0.5` r}

Plot[Evaluate[Table[eqplotDC /. {Ω -> 0}, {Vnew, 0, 36, 12}]], {r, 0, 1}, AxesLabel -> {2 r, PB}, PlotRange -> {{0, 1}, {0, 20}}, MaxRecursion -> 15, GridLines -> Automatic,
 PlotStyle -> {Red, Green, Blue, Black}]
Plot[Evaluate[Table[eqplot /. {Ω -> 0.2}, {Vnew, 0, 36, 12}]], {r, 0, 1}, AxesLabel -> {2 r, PB}, PlotRange -> {{0, 1}, {0, 50}}, MaxRecursion -> 15, GridLines -> Automatic,
 PlotStyle -> {Red, Green, Blue, Black}]
Plot[Evaluate[Table[eqplot /. {Ω -> 0.4}, {Vnew, 0, 36, 12}]], {r, 0, 1}, AxesLabel -> {2 r, PB}, PlotRange -> {{0, 1}, {0, 50}}, MaxRecursion -> 15, GridLines -> Automatic,
 PlotStyle -> {Red, Green, Blue, Black}]
Plot[Evaluate[Table[eqplot /. {Ω -> 0.6}, {Vnew, 0, 36, 12}]], {r, 0, 1}, AxesLabel -> {2 r, PB}, PlotRange -> {{0, 1}, {0, 50}}, MaxRecursion -> 15, GridLines -> Automatic,
 PlotStyle -> {Red, Green, Blue, Black}]
Plot[Evaluate[Table[eqplot /. {Ω -> 0.8}, {Vnew, 0, 36, 12}]], {r, 0, 1}, AxesLabel -> {2 r, PB}, PlotRange -> {{0, 1}, {0, 50}}, MaxRecursion -> 15, GridLines -> Automatic,
 PlotStyle -> {Red, Green, Blue, Black}]
Plot[Evaluate[Table[eqplot /. {Ω -> 1.0}, {Vnew, 0, 36, 12}]], {r, 0, 1}, AxesLabel -> {2 r, PB}, PlotRange -> {{0, 1}, {0, 50}}, MaxRecursion -> 15, GridLines -> Automatic,
 PlotStyle -> {Red, Green, Blue, Black}]
(*
Plot[Evaluate[Table[eqplot /.{Ω→0.2 },{Vnew,12.36,12}]],{r,0,1},MaxRecursion→15,GridLines→Automatic,Frame→True,PlotRange→{{0,1},{0,50}}]
 Plot[Evaluate[Table[eqplot /.{Ω→0.4 },{Vnew,12.36,12}]],{r,0,1},MaxRecursion→15,GridLines→Automatic,Frame→True,PlotRange→{{0,1},{0,50}}]
 Plot[Evaluate[Table[eqplot /.{Ω→0.6 },{Vnew,12.36,12}]],{r,0,1},MaxRecursion→15,GridLines→Automatic,Frame→True,PlotRange→{{0,1},{0,50}}]
 Plot[Evaluate[Table[eqplot /.{Ω→0.8 },{Vnew,12.36,12}]],{r,0,1},MaxRecursion→15,GridLines→Automatic,Frame→True,PlotRange→{{0,1},{0,50}}]
 Plot[Evaluate[Table[eqplot /.{Ω→1},{Vnew,12.36,12}]],{r,0,1},MaxRecursion→15,GridLines→Automatic,Frame→True,PlotRange→{{0,1},{0,50}}]
```

A3. Mathematica Code for Replicating Zahn and Pioch's Results (Section 3.2.4)

$\eta'=0$ case with Complete Torque Equation

```
(*Trying to develop the case in ZahnGreer Fig 5 plots with etaprime zero with complete Torque equation*)

ClearAll[Bx, Hz, vz, ω, A, B]
i = Ik;

Mx = (χ * (ω[x] * Hz + (Ik * Ω + 1) * Bx)) / (ω[x]^2 + (i * Ω + 1) * (i * Ω + 1 + χ));
Mz = (χ * ((i * Ω + 1 + χ) * Hz - Bx * ω[x])) / (ω[x]^2 + (i * Ω + 1) * (i * Ω + 1 + χ));
T = 1/2 * Re[Mz * Conjugate[Bx] - Conjugate[Mx] * (Hz + Mz)];


(* DIMENSIONLESS FLOW AND SPIN VELOCITY EQUATIONS *)

linearegn = 1/2 * (ξ + η) * D[vz[x], {x, 2}] + ξ * D[ω[x], x] - D[p[z], z] == 0
spineqn = η' * D[ω[x], {x, 2}] - ξ * (D[vz[x], x] + 2 * ω[x]) + Torque == 0

T = Simplify[T /. {Mx -> Mx /. {Bx → 10, Hz → 1i, χ → 1, Ω → 1}, Mz -> Mz /. {Bx → 10, Hz → 1i, χ → 1, Ω → 1}, Bx → 10, Hz → 1i, χ → 1, Ω → 1}, ω[x] ∈ Reals];


(* Doing case in Fig 5a ZahnGreer with etaprime=0 *)
eqn1 = linearegn /. {η → 1, ξ → 1, D[p[z], z] → 0.00001};
eqn2 = spineqn /. {Torque → T, ξ → 1, η → 1, η' → 0};
eqn2 = eqn2
eqn3 = D[eqn2, x]
Solve[eqn3, vz''[x]]
eqn4 = eqn1 /. %

xend = 1;
Al = -1; Au = 1; Ainc = (Au - Al) / 200 // N;


Eqnstosolve = {eqn2, eqn4, vz[0] == 0}

fpend[A_] := vz[xend] /. NDSolve[{Eqnstosolve, ω[0] == A}, {vz, ω}, {x, 0, xend}]
fpend@[0.011]

Table[{A, fpend[A]}, {A, Al, Au, Ainc}]
fpA = Interpolation[%]
fpA[A]
rooteqn = FindRoot[fpA[A] == 0, {A, {Al, Au}}]

A = A /. rooteqn;


A = A[[1]]


fpend[A]


eqnresult = NDSolve[{Eqnstosolve, ω[0] == A}, {vz, ω}, {x, 0, xend}]
vz[x] = vz[x] /. eqnresult
ω[x] = ω[x] /. eqnresult
Plot[Evaluate[vz[x]], {x, 0, xend}]
Plot[Evaluate[ω[x]], {x, 0, xend}]
Exceldatavz = Table[Evaluate[vz[x]], {x, 0, xend, 0.01}]
Exceldataωz = Table[Evaluate[ω[x]], {x, 0, xend, 0.01}]
Export["f:\desktop\vzxdata.xls", Exceldatavz, "XLS"]
Export["f:\desktop\wxdata.xls", Exceldataωz, "XLS"]
```

η'=0 case with Linearized Torque Equation

```
(*Trying to develop the case in ZahnGreer Fig 5 plots with etaprime zero with Linearized Torque equation*)

ClearAll[Bx, Hz, vz, ω, A, B]
i = ⅈ;

Mx = (χ * (ω[x] * Hz + (ⅈ * Ω + 1) * Bx)) / (ω[x]^2 + (i * Ω + 1) * (i * Ω + 1 + χ));
Mz = (χ * ((i * Ω + 1 + χ) * Hz - Bx * ω[x])) / (ω[x]^2 + (i * Ω + 1) * (i * Ω + 1 + χ));
T = 1/2 * Re[Hz * Conjugate[Bx] - Conjugate[Mx] * (Hz + Mz)];


(* DIMENSIONLESS FLOW AND SPIN VELOCITY EQUATIONS *)

linearеqn = 1/2 * (ξ + η) * D[vz[x], {x, 2}] + ξ * D[ω[x], x] - D[p[z], z] == 0
spineqn = η' * D[ω[x], {x, 2}] - ξ * (D[vz[x], x] + 2 * ω[x]) + Torque == 0


T0 = (-χ * Re[(χ * Ω^2 + ⅈ * Ω * (Ω^2 + 1 + χ)) * (Hz * Conjugate[Bx])]) / ((Ω^2 + 1 + χ)^2 + (χ * Ω)^2)
α = χ * (Abs[Bx]^2 * (Ω^2 - 1) + (Abs[Hz]^2) * (Ω^2 - (1 + χ)^2)) / (2 * ((Ω^2 + 1 + χ)^2 + (χ * Ω)^2))

Tlinear = Simplify[T0 + α * ω[x] /. {Mx -> Mx /. {Bx → 10, Hz → i, χ → 1, Ω → 1}, Mz -> Mz /. {Bx → 10, Hz → i, χ → 1, Ω → 1}, Bx → 10, Hz → i, χ → 1, Ω → 1}, ω[x] ∈ Reals]

(* Doing case in Fig 5a ZahnGreer with etaprime=0 *)
eqn1 = linearеqn /. {η → 1, ξ → 1, D[p[z], z] → 0.00001};
eqn2 = spineqn /. {Torque → Tlinear, ξ → 1, η → 1, η' → 0};
eqn2 = eqn2
eqn3 = D[eqn2, x]
Solve[eqn3, vz''[x]]
eqn4 = eqn1 /. %

xend = 1;
Al = -1; Au = 1; Ainc = (Au - Al) / 200 // N;


Eqnstosolve = {eqn2, eqn4, vz[0] == 0}

fpend[A_] := vz[xend] /. NDSolve[{Eqnstosolve, ω[0] == A}, {vz, ω}, {x, 0, xend}]
fpend@[0.011]

Table[{A, fpend[A]}, {A, Al, Au, Ainc}]
fpA = Interpolation[%]
fpA[A]
rooteqn = FindRoot[fpA[A] == 0, {A, {Al, Au}}]

A = A /. rooteqn;


A = A[[1]]


fpend[A]


eqnresult = NDSolve[{Eqnstosolve, ω[0] == A}, {vz, ω}, {x, 0, xend}]
vz[x] = vz[x] /. eqnresult
ω[x] = ω[x] /. eqnresult
Plot[Evaluate[vz[x]], {x, 0, xend}]
Plot[Evaluate[ω[x]], {x, 0, xend}]
Exceldatavz = Table[Evaluate[vz[x]], {x, 0, xend, 0.01}]
Exceldatawz = Table[Evaluate[ω[x]], {x, 0, xend, 0.01}]
Export["f:\desktop\vzxdata.xls", Exceldatavz, "XLS"]
Export["f:\desktop\wxdata.xls", Exceldatawz, "XLS"]
```

η'=0.01 with rotating field imposed (Bx=0.1B0,Hz=0.1iH0) with η=ξ=1 with Linearized Torque Equation

```
(*Trying to develop the case in ZahnGreer Fig 5 plots with etaprime nonzero and linearized Torque equation with Bx and Hz fields *)
ClearAll[Bx, Hz, vz, ω, λ, B]
i = Ä;

Mx = (χ * (ω[x] * Hz + (λ * Ω + 1) * Bx)) / (ω[x]^2 + (i * Ω + 1) * (i * Ω + 1 + χ));
Mz = (χ * ((i * Ω + 1 + χ) * Hz - Bx * ω[x])) / (ω[x]^2 + (i * Ω + 1) * (i * Ω + 1 + χ));
T = 1/2 * Re[Mz * Conjugate[Bx] - Conjugate[Mx] * (Hz * Ma)];
(* DIMENSIONLESS FLOW AND SPIN VELOCITY EQUATIONS *)
limearegn = 1/2 * (ξ + η) * D[vz[x], {x, 2}] + ξ * D[ω[x], x] - D[p[z], z] == 0;
spinegn = η' * D[ω[x], {x, 2}] - ξ * (D[vz[x], x] + 2 * ω[x]) + Torque == 0;
T = Simplify[T /. (Hz -> Mx /. {Bx → 0.1, Hz → 0.1 * i, χ → 1, Ω → 1}), Mz -> Mx /. {Bx → 0.1 * i, Hz → 0.1 * i, χ → 1, Ω → 1}, Bx → 0.1, Hz → 0.1 * i, χ → 1, Ω → 1}, ω[x] ∈ Reals];
T0 = (-χ * Re[(χ * Ω^2 + λ * Ω * (Ω^2 + 1 + χ)) * (Hz * Conjugate[Bx])]) / ((Ω^2 + 1 + χ)^2 + (χ * Ω)^2)
α = χ * (Re[Bx]^2 * (Ω^2 - 1) + (Re[Hz]^2) * (Ω^2 - (1 + χ)^2)) / (2 * ((Ω^2 + 1 + χ)^2 + (χ * Ω)^2))
(* Bx→0.1ReB0 and Hz→H0  Rotating magnetic field *)

Tlinear = Simplify[T0 + α * ω[x] /. (Hz -> Mx /. {Bx → 0.1, Hz → 0.1 * i, χ → 1, Ω → 1}), Mz -> Mx /. {Bx → 0.1, Hz → 0.1 * i, χ → 1, Ω → 1}, Bx → 0.1, Hz → 0.1 * i, χ → 1, Ω → 1},
  ω[x] ∈ Reals]
eqn1 = limearegn /. {η → 1, ξ → 1, D[p[z], z] → 0.00001}
eqn2 = spinegn /. {Torque → Tlinear, ξ → 1, η → 1, η' → 0.01};
eqn2 = eqn2
xend = 1;
Al = -1; Au = 1; Ainc = (Au - Al) / 100 // N;
Bl = -1; Bu = 2; Binc = (Bu - Bl) / 100 // N;
boundaryConditions = {vz[0] == 0, vz'[0] == A, ω[0] == 0, ω'[0] == B}
Eqnstosolve = {eqn1, eqn2}
fpend[A_, B_] := vz[xend] /. NDSolve[{Eqnstosolve, vz[0] == 0, vz'[0] == A, ω[0] == 0, ω'[0] == B}, {vz, ω}, {x, 0, xend}, MaxSteps → 10000]
fpendω[A_, B_] := ω[xend] /. NDSolve[{Eqnstosolve, vz[0] == 0, vz'[0] == A, ω[0] == 0, ω'[0] == B}, {vz, ω}, {x, 0, xend}, MaxSteps → 10000]
fpend[1, 1]
data = Table[{fpend[A, B], {A, Al, Au, Ainc}, {B, Bl, Bu, Binc}}];
dataω = Table[{fpendω[A, B], {A, Al, Au, Ainc}, {B, Bl, Bu, Binc}}];
fpA = ListInterpolation[data, {{Al, Au}, {Bl, Bu}}]
fpB = ListInterpolation[datavz, {{Al, Au}, {Bl, Bu}}]
fpA[A, B]
fpB[A, B]
fpA[1, 0.7]
fpB[1, 0.7]
rooteqn = FindRoot[{fpB[A, B] == 0, fpA[A, B] == 0}, {{A, {Al, Au}}, {B, {Bl, Bu}}}]
A = A /. rooteqn
B = B /. rooteqn
A = A[[1]]
B = B[[1]]
Al = A - 5 * Ainc
Au = A + 5 * Ainc
Bl = B - 5 * Binc
Bu = B + 5 * Binc
Clear[A, B]
data = Table[fpend[A, B], {A, Al, Au, Ainc}, {B, Bl, Bu, Binc}];
datavz = Table[fpendω[A, B], {A, Al, Au, Ainc}, {B, Bl, Bu, Binc}];
fpA = ListInterpolation[data, {{Al, Au}, {Bl, Bu}}]
fpB = ListInterpolation[datavz, {{Al, Au}, {Bl, Bu}}]
fpA[A, B]
fpB[A, B]
rooteqn = FindRoot[{fpB[A, B] == 0, fpA[A, B] == 0}, {{A, {Al, Au}}, {B, {Bl, Bu}}}]
A = A /. rooteqn
B = B /. rooteqn
A = A[[1]]
B = B[[1]]
Al = A - 1 * Ainc
Au = A + 1 * Ainc
Bl = B - 1 * Binc
Bu = B + 1 * Binc
Clear[A, B]
data = Table[fpend[A, B], {A, Al, Au, Ainc}, {B, Bl, Bu, Binc}];
datavz = Table[fpendω[A, B], {A, Al, Au, Ainc}, {B, Bl, Bu, Binc}];
fpA = ListInterpolation[data, {{Al, Au}, {Bl, Bu}}]
fpB = ListInterpolation[datavz, {{Al, Au}, {Bl, Bu}}]
fpA[A, B]
fpB[A, B]
rooteqn = FindRoot[{fpB[A, B] == 0, fpA[A, B] == 0}, {{A, {Al, Au}}, {B, {Bl, Bu}}}]
A = A /. rooteqn
B = B /. rooteqn
A = A[[1]]
B = B[[1]]
Al = A - 1 * Ainc
Au = A + 1 * Ainc
Bl = B - 1 * Binc
Bu = B + 1 * Binc
Clear[A, B]
data = Table[fpend[A, B], {A, Al, Au, Ainc}, {B, Bl, Bu, Binc}];
datavz = Table[fpendω[A, B], {A, Al, Au, Ainc}, {B, Bl, Bu, Binc}];
fpA = ListInterpolation[data, {{Al, Au}, {Bl, Bu}}]
fpB = ListInterpolation[datavz, {{Al, Au}, {Bl, Bu}}]
fpA[A, B]
fpB[A, B]
rooteqn = FindRoot[{fpB[A, B] == 0, fpA[A, B] == 0}, {{A, {Al, Au}}, {B, {Bl, Bu}}}]
A = A /. rooteqn
B = B /. rooteqn
A = A[[1]]
B = B[[1]]
fpend[A, B]
fpendω[A, B]
eqnresult = NDSolve[{Eqnstosolve, vz[0] == 0, vz'[0] == A, ω[0] == 0, ω'[0] == B}, {vz, ω}, {x, 0, xend}]
vz[x] = vz[x] /. eqnresult
ω[x] = ω[x] /. eqnresult
Evaluate[vz[1]]
Evaluate[ω[1]]
Plot[Evaluate[vz[x]], {x, 0, xend}]
Plot[Evaluate[ω[x]], {x, 0, xend}]
Exceldatavz = Table[Evaluate[vz[x]], {x, 0, xend, 0.01}]
Exceldataωz = Table[Evaluate[ω[x]], {x, 0, xend, 0.01}]
Export["f:\desktop\vzndata.xls", Exceldatavz, "XLS"]
Export["f:\desktop\wnata.xls", Exceldataωz, "XLS"]
```

η'=0 case with Complete Torque Equation- Lorettas cases Bx=1, Hy=0, η=ξ=0.0592, Ω=5 (Table 3.1 pg 43 of Lorettas thesis)

```
(*Trying to develop the case in ZahnGreer Fig 5 plots with etaprime zero with complete Torque equation*)

ClearAll[Bx, Hz, vz, ω, A, B]
i = ĩ;

Hx = (χ * (ω[x] * Hz + (ĩ * Ω + 1) * Bx)) / (ω[x]^2 + (i * Ω + 1) * (i * Ω + 1 + χ));
Hz = (χ * ((i * Ω + 1 + χ) * Hz - Bx * ω[x])) / (ω[x]^2 + (i * Ω + 1) * (i * Ω + 1 + χ));
T = 1/2 * Re[Hz * Conjugate[Bx] - Conjugate[Hx] * (Hz + Hz)];


(* DIMENSIONLESS FLOW AND SPIN VELOCITY EQUATIONS *)

linearеqn = 1/2 * (ξ + η) * D[vz[x], {x, 2}] + ξ * D[ω[x], x] - D[p[z], z] == 0
spineqn = η' * D[ω[x], {x, 2}] - ξ * (D[vz[x], x] + 2 * ω[x]) + Torque == 0

T = Simplify[T /. {Hx -> Hx /. {Bx → 1, Hz → 0, χ → 1, Ω → 5}, Hz -> Hz /. {Bx → 1, Hz → 0, χ → 1, Ω → 5}, Bx → 1, Hz → 0, χ → 1, Ω → 5}, ω[x] ∈ Reals];


(* Doing case in Fig 5a ZahnGreer with etaprime=0 *)
eqn1 = linearеqn /. {η → 0.0592, ξ → 0.0592, D[p[z], z] → 1};
eqn2 = spineqn /. {Torque → T, ξ → 0.0592, η → 0.0592, η' → 0};
eqn2 = eqn2
eqn3 = D[eqn2, x]
Flatten[Solve[eqn3, vz''[x]]]
eqn4 = eqn1 /. %

xend = 1;
A1 = -15; Au = 15; Ainc = (Au - A1) / 100 // N;


Eqnstosolve = {eqn2, eqn4, vz[0] == 0}

fpend[A_] := vz[xend] /. NDSolve[{Eqnstosolve, ω[0] == A}, {vz, ω}, {x, 0, xend}]
fpend@@[0.011]

Table[{A, fpend[A]}, {A, A1, Au, Ainc}]
fpA = Interpolation[%]
fpA[A]
rooteqn = FindRoot[fpA[A] == 0, {A, {A1, Au}}]

A = A /. rooteqn;


A = A[[1]]


fpend[A]


eqnresult = NDSolve[{Eqnstosolve, ω[0] == A}, {vz, ω}, {x, 0, xend}]
vz[x] = vz[x] /. eqnresult
ω[x] = ω[x] /. eqnresult
Plot[Evaluate[vz[x]], {x, 0, xend}]
Plot[Evaluate[ω[x]], {x, 0, xend}]
Exceldatavz = Table[Evaluate[vz[x]], {x, 0, xend, 0.01}]
Exceldatawz = Table[Evaluate[ω[x]], {x, 0, xend, 0.01}]
Export["f:\desktop\vzxdata.xls", Exceldatavz, "XLS"]
Export["f:\desktop\wxdata.xls", Exceldatawz, "XLS"]
```

η'=0.01 with rotating field imposed (Bx=B0,Hz=iH0) with η=1 ξ=0.15 with Complete Torque Equation

```
(*Trying to develop the case in ZahnGreer Fig 5 plots with etaprime nonzero and complete Torque equation with Bx and Hz fields imposed*)
ClearAll[Bx, Hz, vz, ω, A, B]
i = Î;
Mx = (χ * (ω[x] * Hz + (A * Ω + 1) * Bx)) / (ω[x]^2 + (i * Ω + 1) * (i * Ω + 1 + χ));
Mz = (χ * ((i * Ω + 1 + χ) * Hz - Bx * ω[x])) / (ω[x]^2 + (i * Ω + 1) * (i * Ω + 1 + χ));
T = 1/2 * Re[Mz * Conjugate[Bx] - Conjugate[Mx] * (Hz + Mz)];
(* DIMENSIONLESS FLOW AND SPIN VELOCITY EQUATIONS *)
linearegn = 1/2 * (ξ + η) * D[vz[x], {x, 2}] + ξ * D[ω[x], x] - D[p[z], z] == 0;
spinegn = η' * D[ω[x], {x, 2}] - ξ * (D[vz[x], x] + 2 * ω[x]) + Torque == 0;
(* Bx=0.1mu0H0 and Hz=H0  Rotating magnetic field *)
T = Simplify[T /. {Mx -> Mx /. {Bx → 1, Hz → i, χ → 1, Ω → 1}, Mz -> Mz /. {Bx → 1, Hz → i, χ → 1, Ω → 1}, Bx → 1, Hz → i, χ → 1, Ω → 1}, ω[x] ∈ Reals];
(* Doing case in Fig 5a ZahnGreer with etaprime=0.01  *)
eqn1 = linearegn /. {η → 1, ξ → 0.15, D[p[z], z] → 0.00001}
eqn2 = spinegn /. {Torque → T, ξ → 0.15, η → 1, η' → 0.01};
eqn2 = eqn2
xend = 1;
A1 = 0.11; Au = 0.12; Ainc = (Au - A1) / 100 // N;
B1 = 4; Bu = 4.1; Binc = (Bu - B1) / 100 // N;
boundaryConditions = {vz[0] == 0, vz'[0] == A, ω[0] == 0, ω'[0] == B}
Eqnstosolve = {eqn1, eqn2}
fpend[A_, B_] := vz[xend] /. NDSolve[{Eqnstosolve, vz[0] == 0, vz'[0] == A, ω[0] == 0, ω'[0] == B}, {vz, ω}, {x, 0, xend}, MaxSteps → 10000]
fpendω[A_, B_] := ω[xend] /. NDSolve[{Eqnstosolve, vz[0] == 0, vz'[0] == A, ω[0] == 0, ω'[0] == B}, {vz, ω}, {x, 0, xend}, MaxSteps → 10000]
fpend[1, 1]
data = Table[{fpend[A, B], {A, A1, Au, Ainc}, {B, B1, Bu, Binc}}];
dataω = Table[{fpendω[A, B], {A, A1, Au, Ainc}, {B, B1, Bu, Binc}}];
fpA = ListInterpolation[data, {{A1, Au}, {B1, Bu}}]
fpB = ListInterpolation[dataω, {{A1, Au}, {B1, Bu}}]
fpA[A, B]
fpB[A, B]
fpA[1, 0.7]
fpB[1, 0.7]
rooteqn = FindRoot[{fpB[A, B] == 0, fpA[A, B] == 0}, {{A, {A1, Au}}, {B, {B1, Bu}}}]
A = A /. rooteqn
B = B /. rooteqn
A = A[[1]]
B = B[[1]]
A1 = A - 10 * Ainc
Au = A + 10 * Ainc
B1 = B - 10 * Binc
Bu = B + 10 * Binc
Clear[A, B]
data = Table[{fpend[A, B], {A, A1, Au, Ainc}, {B, B1, Bu, Binc}}];
dataω = Table[{fpendω[A, B], {A, A1, Au, Ainc}, {B, B1, Bu, Binc}}];
fpA = ListInterpolation[data, {{A1, Au}, {B1, Bu}}]
fpB = ListInterpolation[dataω, {{A1, Au}, {B1, Bu}}]
fpA[A, B]
fpB[A, B]
rooteqn = FindRoot[{fpB[A, B] == 0, fpA[A, B] == 0}, {{A, {A1, Au}}, {B, {B1, Bu}}}]
A = A /. rooteqn
B = B /. rooteqn
A = A[[1]]
B = B[[1]]
A1 = A - 5 * Ainc
Au = A + 5 * Ainc
B1 = B - 5 * Binc
Bu = B + 5 * Binc
Clear[A, B]
data = Table[{fpend[A, B], {A, A1, Au, Ainc}, {B, B1, Bu, Binc}}];
dataω = Table[{fpendω[A, B], {A, A1, Au, Ainc}, {B, B1, Bu, Binc}}];
fpA = ListInterpolation[data, {{A1, Au}, {B1, Bu}}]
fpB = ListInterpolation[dataω, {{A1, Au}, {B1, Bu}}]
fpA[A, B]
fpB[A, B]
rooteqn = FindRoot[{fpB[A, B] == 0, fpA[A, B] == 0}, {{A, {A1, Au}}, {B, {B1, Bu}}}]
A = A /. rooteqn
B = B /. rooteqn
A = A[[1]]
B = B[[1]]
A1 = A - 1 * Ainc
Au = A + 1 * Ainc
B1 = B - 1 * Binc
Bu = B + 1 * Binc
Clear[A, B]
data = Table[{fpend[A, B], {A, A1, Au, Ainc}, {B, B1, Bu, Binc}}];
dataω = Table[{fpendω[A, B], {A, A1, Au, Ainc}, {B, B1, Bu, Binc}}];
fpA = ListInterpolation[data, {{A1, Au}, {B1, Bu}}]
fpB = ListInterpolation[dataω, {{A1, Au}, {B1, Bu}}]
fpA[A, B]
fpB[A, B]
rooteqn = FindRoot[{fpB[A, B] == 0, fpA[A, B] == 0}, {{A, {A1, Au}}, {B, {B1, Bu}}}]
A = A /. rooteqn
B = B /. rooteqn
A = A[[1]]
B = B[[1]]
fpend[A, B]
fpendω[A, B]
eqnresult = NDSolve[{Eqnstosolve, vz[0] == 0, vz'[0] == A, ω[0] == 0, ω'[0] == B}, {vz, ω}, {x, 0, xend}]
vz[x] = vz[x] /. eqnresult
ω[x] = ω[x] /. eqnresult
Evaluate[vz[1]]
Evaluate[ω[1]]
Plot[Evaluate[vz[x]], {x, 0, xend}]
Plot[Evaluate[ω[x]], {x, 0, xend}]
Exceldatavz = Table[Evaluate[vz[x]], {x, 0, xend, 0.01}]
Exceldataωz = Table[Evaluate[ω[x]], {x, 0, xend, 0.01}]
Export["f:\desktop\vzxdata.xls", Exceldatavz, "XLS"]
Export["f:\desktop\wxdata.xls", Exceldataωz, "XLS"]
```

A4. COMSOL Simulations of Planar Poiseuille Flow With Non-Zero Spin-viscosity ($\eta' \neq 0$) (Section 3.2.4)

Zahn Greer Analysis with Poisseuille flow imposed and H field only

1. Table of Contents

2. Model Properties

Property	Value
Model name	Zahn Greer Analysis with Poisseuille flow imposed and H field only
Author	Shahriar Khushrushahi
Company	MIT
Department	EECS
Reference	
URL	http://lees.mit.edu/lees/old_files/full/faculty/Zahn/Publications/Ferrohydordynamics/Zahn-Greer-Ferrohydrodynamicspumping1995JMMMv149p165.pdf
Saved date	May 10, 2010 3:39:50 PM
Creation date	Jun 3, 2008 3:14:47 PM
COMSOL version	COMSOL 3.5.0.603

File name: C:\Users\Shahriar\Documents\My Dropbox\Research Files\Software Data Files\Comsol Files\Working_ZahnGreeranalysis\ZahnGreer_Pouisseilleflow_etaprime0point01.mph

Application modes and modules used in this model:

- Geom1 (2D)
  - Perpendicular Induction Currents, Vector Potential (AC/DC Module)
  - Incompressible Navier-Stokes
  - PDE, General Form

2.1. Model description

Zahn Greer Analysis with Poisseuille Flow imposed. This analysis is a steady state analysis with etaprime=0.01 and values for viscosity taken as 1

3. Constants

Name	Expression	Value	Description
Omega	1		Real Angular frequency
f	1		Real Frequency
Hmax	0.1i		Normalized H
Bmax	0.1		Normalized B
zeta	1		normalized vortex viscosity
eta	1		normalized viscosity
etaprime	0.01		normalized spin viscosity
Xi	1		susceptibility
Tau	1		Ferrofluid time constant
mu0	1		Magnetic permeability of free space
rho	1		density of MSGW11
pmax	-1e-4		
vfrac	0.1		

4. Global Expressions

Name	Expression	Unit	Description
T	0.5*real(Mx_emqa*conj(Bmax)-mu0*conj(My_emqa)*(Hmax+Mx_emqa))		

5. Geometry

Number of geometries: 1

5.1. Geom1

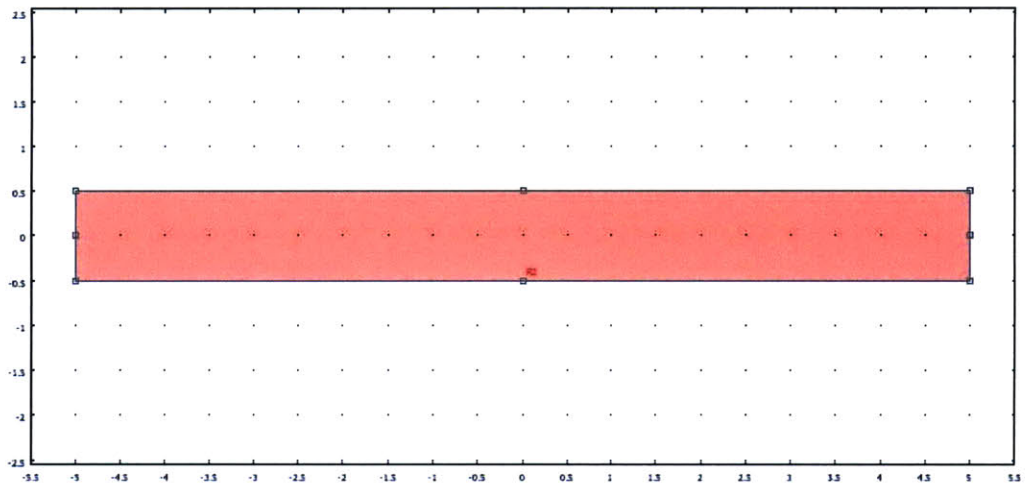

5.1.1. Point mode

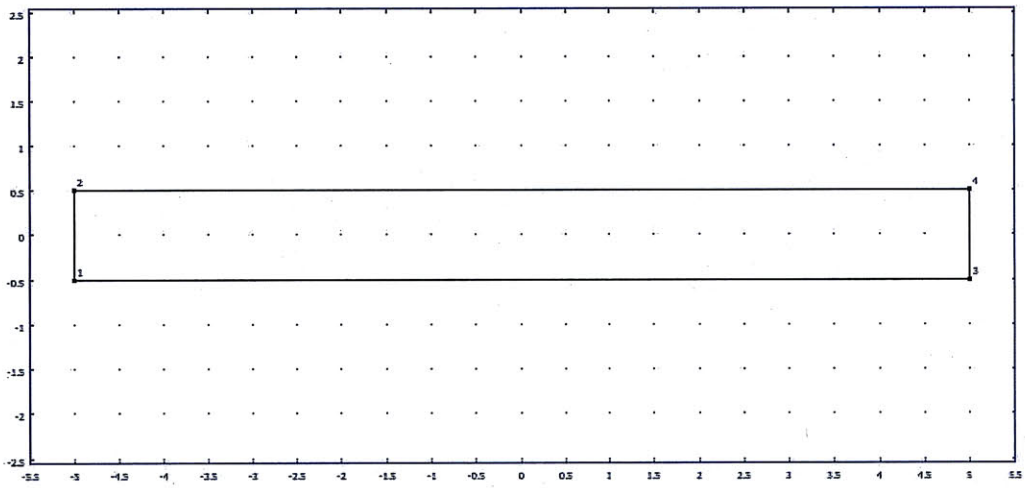

5.1.2. Boundary mode

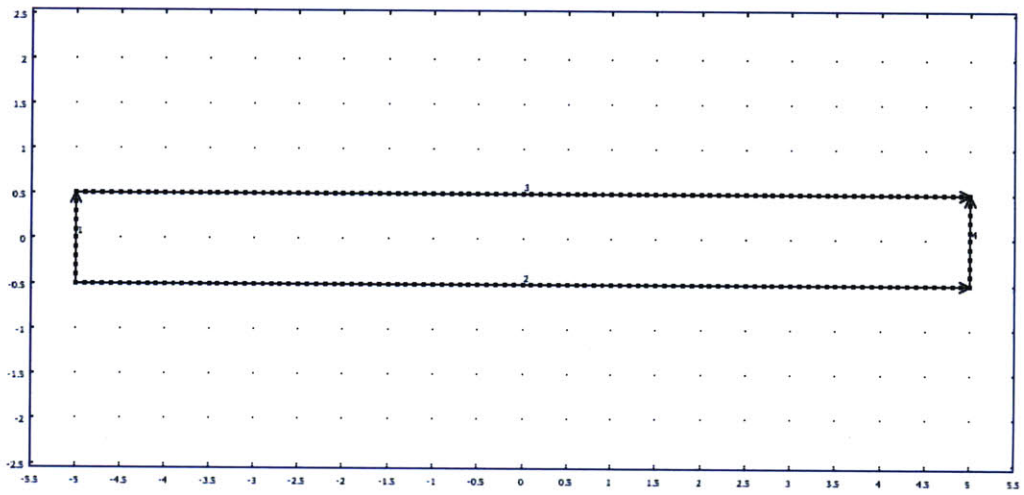

5.1.3. Subdomain mode

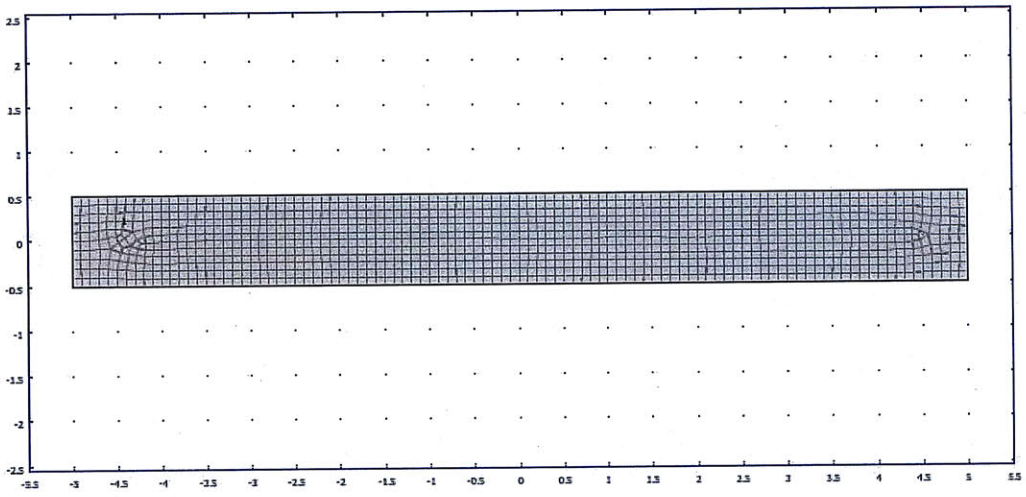

6. Geom1

Space dimensions: 2D

Independent variables: x, y, z

6.1. Mesh

6.1.1. Mesh Statistics

Number of degrees of freedom	21089
Number of mesh points	1293
Number of elements	1182
Triangular	0
Quadrilateral	1182
Number of boundary elements	220
Number of vertex elements	4
Minimum element quality	0.84
Element area ratio	0.318

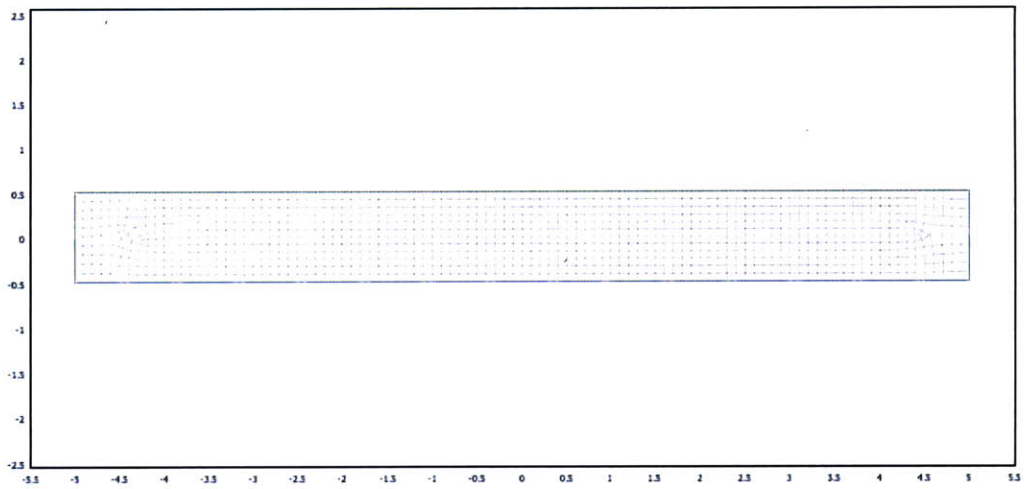

6.2. Application Mode: Perpendicular Induction Currents, Vector Potential (emqa)

Application mode type: Perpendicular Induction Currents, Vector Potential (AC/DC Module)

Application mode name: emqa

6.2.1. Scalar Variables

Name	Variable	Value	Unit	Description
epsilon0	epsilon0_emqa	8.854187817e-12	F/m	Permittivity of vacuum
mu0	mu0_emqa	1	H/m	Permeability of vacuum

6.2.2. Application Mode Properties

Property	Value
Default element type	Lagrange - Quadratic
Analysis type	Transient
Bias application mode	None
Solve for	Total potential
Background field	Magnetic vector potential
Frame	Frame (ref)
Weak constraints	Off

Constraint type	Ideal

6.2.3. Variables

Dependent variables: Az, redAz

Shape functions: shlag(2,'Az')

Interior boundaries active

6.2.4. Boundary Settings

Boundary		1, 4	2	3
Type		Magnetic field	Magnetic field	Magnetic field
Magnetic field (H0)	A/m	{Hmax*flc2hs(t-1,0.05); ((Bmax/mu0)-My_emqa)*flc2hs(t-1,0.01)}	{Hmax*flc2hs(t-1,0.05); ((Bmax/mu0)-My_emqa)*flc2hs(t-1,0.01)}	{Hmax*flc2hs(t-1,0.05); ((Bmax/mu0)-My_emqa)*flc2hs(t-1,0.01)}
Surface current density (Js0z)	A/m	0	Hmax	-Hmax

6.2.5. Subdomain Settings

Subdomain		1
Relative permeability (mur)	1	{(1+(Xi*((j*Omega*Tau+1+Xi)*Hmax-(Bmax*Tau*w/mu0))/((Tau*w)^2+(j*Omega*Tau+1)*(j*Omega*Tau+1+Xi))))/mu0_emqa,0;0,(1+(Xi*((w*Tau)*Hmax+(j*Omega*Tau+1)*(Bmax/mu0))/((w*Tau)^2+(j*Omega*Tau+1)*(j*Omega*Tau+1+Xi))))/mu0_emqa}
magconstrel		B = μ_0H + μ_0M
Magnetization (M)	A/m	{Xi*((j*Omega*Tau+1+Xi)*Hmax-(Bmax*Tau*w/mu0))/((Tau*w)^2+(j*Omega*Tau+1)*(j*Omega*Tau+1+Xi));Xi*((w*Tau)*Hmax+(j*Omega*Tau+1)*(Bmax/mu0))/((w*Tau)^2+(j*Omega*Tau+1)*(j*Omega*Tau+1+Xi))}

6.3. Application Mode: Incompressible Navier-Stokes (ns)

Application mode type: Incompressible Navier-Stokes

Application mode name: ns

6.3.1. Scalar Variables

Name	Variable	Value	Unit	Description
visc_vel_fact	visc_vel_fact_ns	10	1	Viscous velocity factor

6.3.2. Application Mode Properties

Property	Value
Default element type	Lagrange - P_2 P_1
Analysis type	Stationary
Corner smoothing	Off
Frame	Frame (ref)

Weak constraints	Off
Constraint type	Ideal

6.3.3. Variables

Dependent variables: u, v, p, nxw, nyw

Shape functions: shlag(2,'u'), shlag(2,'v'), shlag(1,'p')

Interior boundaries not active

6.3.4. Boundary Settings

Boundary		1	2	3
Type		Inlet	Wall	Wall
intype		**Pressure, no viscous stress**	Velocity	Velocity
outtype		Pressure, no viscous stress	Pressure, no viscous stress	Pressure, no viscous stress
stresstype		**Normal stress, normal flow**	General stress	General stress
velType		**u0**	U0in	U0in
x-velocity (u0)	m/s	**1**	0	0
Pressure (p0)	Pa	**pmax**	0	0
Normal stress (f0)	N/m^2	**pmax**	0	0
Velocity of the tangentially moving wall (uvw)	m/s	0	0	**Umax**
#-velocity of moving wall (uwall)	m/s	0	0	**Umax**

Boundary		4
Type		Outlet
intype		Velocity
outtype		**Normal stress**
stresstype		General stress
velType		U0in
x-velocity (u0)	m/s	0
Pressure (p0)	Pa	0
Normal stress (f0)	N/m^2	0
Velocity of the tangentially moving wall (uvw)	m/s	0
#-velocity of moving wall (uwall)	m/s	0

6.3.5. Subdomain Settings

Subdomain		1
Integration order (gporder)		**4 4 2**
Constraint order (cporder)		**2 2 1**
Density (rho)	kg/m^3	**0**
Dynamic viscosity (eta)	Pa·s	**0.5*(zeta+eta)**
Volume force, x dir. (F_x)	N/m^3	**zeta*wy**

cdon		0

6.4. Application Mode: PDE, General Form (g)

Application mode type: PDE, General Form

Application mode name: g

6.4.1. Application Mode Properties

Property	Value
Default element type	Lagrange - Quadratic
Wave extension	Off
Frame	Frame (ref)
Weak constraints	Off

6.4.2. Variables

Dependent variables: w, w_t

Shape functions: shlag(2,'w')

Interior boundaries not active

6.4.3. Boundary Settings

Boundary		1-4
Type		Dirichlet boundary condition

6.4.4. Subdomain Settings

Subdomain		1
Damping/Mass coefficient (da)		**0**
Source term (f)		**etaprime*wyy-1*zeta*(uy+2*w)+T**
Conservative flux source term (ga)		**{{0;0}}**

7. Solver Settings

Solve using a script: off

Analysis type	Transient
Auto select solver	On
Solver	Time dependent
Solution form	Automatic
Symmetric	auto
Adaptive mesh refinement	Off
Optimization/Sensitivity	Off
Plot while solving	Off

7.1. Direct (UMFPACK)

Solver type: Linear system solver

Parameter	Value
Pivot threshold	0.1
Memory allocation factor	0.7

7.2. Time Stepping

Parameter	Value
Times	range(0,0.1,10)
Relative tolerance	0.01
Absolute tolerance	0.0010
Times to store in output	Specified times
Time steps taken by solver	Free
Maximum BDF order	5
Singular mass matrix	Maybe
Consistent initialization of DAE systems	Backward Euler
Error estimation strategy	Include algebraic
Allow complex numbers	Off

7.3. Advanced

Parameter	Value
Constraint handling method	Elimination
Null-space function	Automatic
Automatic assembly block size	On
Assembly block size	5000
Use Hermitian transpose of constraint matrix and in symmetry detection	Off
Use complex functions with real input	Off
Stop if error due to undefined operation	On
Store solution on file	Off
Type of scaling	Automatic
Manual scaling	
Row equilibration	On
Manual control of reassembly	Off
Load constant	On
Constraint constant	On
Mass constant	On
Damping (mass) constant	On
Jacobian constant	On
Constraint Jacobian constant	On

8. Postprocessing

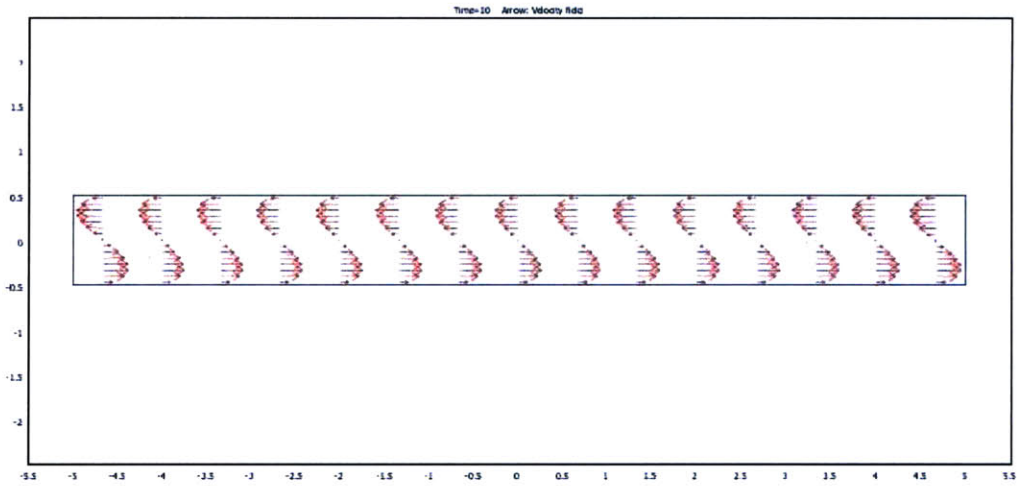

9. Variables

9.1. Boundary

Name	Description	Unit	Expression
dVolbnd_emqa	Area integration contribution	1	1
murbnd_emqa	Relative permeability	1	murbndxx_emqa
Jsz_emqa	Surface current density	A/m	unx * (Hy_emqa_down-Hy_emqa_up)-uny * (Hx_emqa_down-Hx_emqa_up)
unTx_emqa	Maxwell surface stress tensor, x component	Pa	-0.5 * (Bx_emqa_up * Hx_emqa_up+By_emqa_up * Hy_emqa_up) * dnx+(dnx * Hx_emqa_up+dny * Hy_emqa_up) * Bx_emqa_up
dnTx_emqa	Maxwell surface stress tensor, x component	Pa	-0.5 * (Bx_emqa_down * Hx_emqa_down+By_emqa_down * Hy_emqa_down) * unx+(unx * Hx_emqa_down+uny * Hy_emqa_down) * Bx_emqa_down
unTy_emqa	Maxwell surface stress tensor, y component	Pa	-0.5 * (Bx_emqa_up * Hx_emqa_up+By_emqa_up * Hy_emqa_up) * dny+(dnx * Hx_emqa_up+dny * Hy_emqa_up) * By_emqa_up
dnTy_emqa	Maxwell surface stress tensor, y component	Pa	-0.5 * (Bx_emqa_down * Hx_emqa_down+By_emqa_down * Hy_emqa_down) * uny+(unx * Hx_emqa_down+uny * Hy_emqa_down) * By_emqa_down

Qs_emqa	Surface resistive heating	W/m^2	Jsz_emqa * Ez_emqa
nPo_emqa	Power outflow	W/m^2	nx_emqa * Pox_emqa+ny_emqa * Poy_emqa
FsLtzx_emqa	Lorentz surface force contribution, x component	Pa	-Jsz_emqa * By_emqa
FsLtzy_emqa	Lorentz surface force contribution, y component	Pa	Jsz_emqa * Bx_emqa
normFsLtz_emqa	Lorentz surface force contribution, cycle average, norm	Pa	sqrt(abs(FsLtzx_emqa)^2+abs(FsLtzy_emqa)^2)
K_x_ns	Viscous force per area, x component	Pa	eta_ns * (2 * nx_ns * ux+ny_ns * (uy+vx))
T_x_ns	Total force per area, x component	Pa	-nx_ns * p+2 * nx_ns * eta_ns * ux+ny_ns * eta_ns * (uy+vx)
K_y_ns	Viscous force per area, y component	Pa	eta_ns * (nx_ns * (vx+uy)+2 * ny_ns * vy)
T_y_ns	Total force per area, y component	Pa	-ny_ns * p+nx_ns * eta_ns * (vx+uy)+2 * ny_ns * eta_ns * vy

9.2. Subdomain

Name	Description	Unit	Expression
dr_guess_emqa	Width in radial direction default guess	m	0
R0_guess_emqa	Inner radius default guess	m	0
Sx_emqa	Infinite element x coordinate	m	x
S0x_guess_emqa	Inner x coordinate default guess	m	0
Sdx_guess_emqa	Width in x direction default guess	m	0
Sy_emqa	Infinite element y coordinate	m	y
S0y_guess_emqa	Inner y coordinate default guess	m	0
Sdy_guess_emqa	Width in y direction default guess	m	0
curlAx_emqa	Curl of magnetic potential, x component	T	Azy
curlAy_emqa	Curl of magnetic potential, y component	T	-Azx
dVol_emqa	Volume integration contribution	1	detJ_emqa
Bx_emqa	Magnetic flux density, x component	T	curlAx_emqa

By_emqa	Magnetic flux density, y component	T	curlAy_emqa
Hx_emqa	Magnetic field, x component	A/m	Bx_emqa/mu0_emqa-Mx_emqa
Hy_emqa	Magnetic field, y component	A/m	By_emqa/mu0_emqa-My_emqa
mu_emqa	Permeability	H/m	mu0_emqa * mur_emqa
muxx_emqa	Permeability, xx component	H/m	mu0_emqa * murxx_emqa
muxy_emqa	Permeability, xy component	H/m	mu0_emqa * murxy_emqa
muyx_emqa	Permeability, yx component	H/m	mu0_emqa * muryx_emqa
muyy_emqa	Permeability, yy component	H/m	mu0_emqa * muryy_emqa
Jpz_emqa	Potential current density, z component	A/m^2	sigma_emqa * deltaV_emqa/L_emqa
Ez_emqa	Electric field, z component	V/m	-d(Az,t)
Jz_emqa	Total current density, z component	A/m^2	Jpz_emqa+Jiz_emqa+Jez_emqa
Pox_emqa	Power flow, x component	W/m^2	-Ez_emqa * Hy_emqa
Poy_emqa	Power flow, y component	W/m^2	Ez_emqa * Hx_emqa
normE_emqa	Electric field, norm	V/m	abs(Ez_emqa)
Jiz_emqa	Induced current density, z component	A/m^2	sigma_emqa * Ez_emqa
Q_emqa	Resistive heating	W/m^3	Jz_emqa * (Ez_emqa+deltaV_emqa/L_emqa)
W_emqa	Total energy density	J/m^3	Wm_emqa
dW_emqa	Integrand for total energy	J/m^3	dVol_emqa * W_emqa
Wm_emqa	Magnetic energy density	J/m^3	0.5 * (Hx_emqa * Bx_emqa+Hy_emqa * By_emqa+Mx_emqa * Bx_emqa+My_emqa * By_emqa)
FLtzx_emqa	Lorentz force contribution, x component	N/m^3	-Jz_emqa * By_emqa
FLtzy_emqa	Lorentz force contribution, y component	N/m^3	Jz_emqa * Bx_emqa
normFLtz_emqa	Lorentz force contribution, norm	N/m^3	sqrt(abs(FLtzx_emqa)^2+abs(FLtzy_emqa)^2)
normM_emqa	Magnetization, norm	A/m	sqrt(abs(Mx_emqa)^2+abs(My_emqa)^2)
normBr_emqa	Remanent flux density, norm	T	sqrt(abs(Brx_emqa)^2+abs(Bry_emqa)^2)
normH_emqa	Magnetic field, norm	A/m	sqrt(abs(Hx_emqa)^2+abs(Hy_emqa)^2)
normB_emqa	Magnetic flux density, norm	T	sqrt(abs(Bx_emqa)^2+abs(By_emqa)^2)

normJ_emqa	Total current density, norm	A/m^2	abs(Jz_emqa)
Evz_emqa	Lorentz electric field, z component	V/m	d(x,t) * By_emqa-d(y,t) * Bx_emqa
normEv_emqa	Lorentz electric field, norm	V/m	abs(Evz_emqa)
normPo_emqa	Power flow, time average, norm	W/m^2	sqrt(abs(Pox_emqa)^2+abs(Poy_emqa)^2)
U_ns	Velocity field	m/s	sqrt(u^2+v^2)
V_ns	Vorticity	1/s	vx-uy
divU_ns	Divergence of velocity field	1/s	ux+vy
cellRe_ns	Cell Reynolds number	1	rho_ns * U_ns * h/eta_ns
res_u_ns	Equation residual for u	N/m^3	rho_ns * (u * ux+v * uy)+px-F_x_ns-eta_ns * (2 * uxx+uyy+vxy)
res_v_ns	Equation residual for v	N/m^3	rho_ns * (u * vx+v * vy)+py-F_y_ns-eta_ns * (vxx+uyx+2 * vyy)
beta_x_ns	Convective field, x component	kg/(m^2*s)	rho_ns * u
beta_y_ns	Convective field, y component	kg/(m^2*s)	rho_ns * v
Dm_ns	Mean diffusion coefficient	Pa*s	eta_ns
da_ns	Total time scale factor	kg/m^3	rho_ns
taum_ns	GLS time-scale	m^3*s/kg	nojac(1/max(2 * rho_ns * sqrt(emetric(u,v)),48 * eta_ns/h^2))
tauc_ns	GLS time-scale	m^2/s	0.5 * nojac(if(u^2+v^2
res_p_ns	Equation residual for p	kg/(m^3*s)	rho_ns * divU_ns
abswx_g	|grad(w)|		sqrt(wx^2+wy^2)
absga5x_g	|ga5x|		sqrt(ga5x^2+ga5y^2)

A5. COMSOL Simulations of Planar Poiseuille Flow With Zero Spin-viscosity ($\eta'=0$) (Section 3.2.4)

Zahn Greer Analysis with Poisseuille flow imposed and H field only

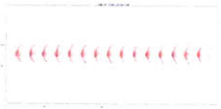

1. Table of Contents

2. Model Properties

Property	Value
Model name	Zahn Greer Analysis with Poisseuille flow imposed and H field only
Author	Shahriar Khushrushahi
Company	MIT
Department	EECS
Reference	
URL	http://lees.mit.edu/lees/old_files/full/faculty/Zahn/Publications/Ferrohydordynamics/Zahn-Greer-Ferrohydrodynamicspumping1995JMMMv149p165.pdf
Saved date	May 7, 2010 11:32:36 AM
Creation date	Jun 3, 2008 3:14:47 PM
COMSOL version	COMSOL 3.5.0.603

File name: C:\Users\Shahriar\Documents\My Dropbox\Research Files\Software Data Files\Comsol Files\Working_ZahnGreeranalysis\ZahnGreer_Pouisseilleflow_etaprime0.mph

Application modes and modules used in this model:

- Geom1 (2D)
  - Perpendicular Induction Currents, Vector Potential (AC/DC Module)
  - Incompressible Navier-Stokes
  - PDE, General Form

2.1. Model description

Zahn Greer Analysis with Poisseuille Flow imposed. This analysis is a steady state analysis with etaprime=0

3. Constants

Name	Expression	Value	Description
Omega	1.3		Real Angular frequency
f	1		Real Frequency
Hmax	0		Normalized H
Bmax	1		Normalized B
zeta	0.1125		normalized vortex viscosity
eta	zeta		normalized viscosity
etaprime	0		normalized spin viscosity
Xi	1		susceptibility
Tau	1		Ferrofluid time constant
mu0	1		Magnetic permeability of free space
rho	1		density of MSGW11
pmax	-1		

4. Global Expressions

Name	Expression	Unit	Description
T	0.5*real(Mx_emqa*conj(Bmax)-mu0*conj(My_emqa)*(Hmax+Mx_emqa))		

5. Geometry

Number of geometries: 1

5.1. Geom1

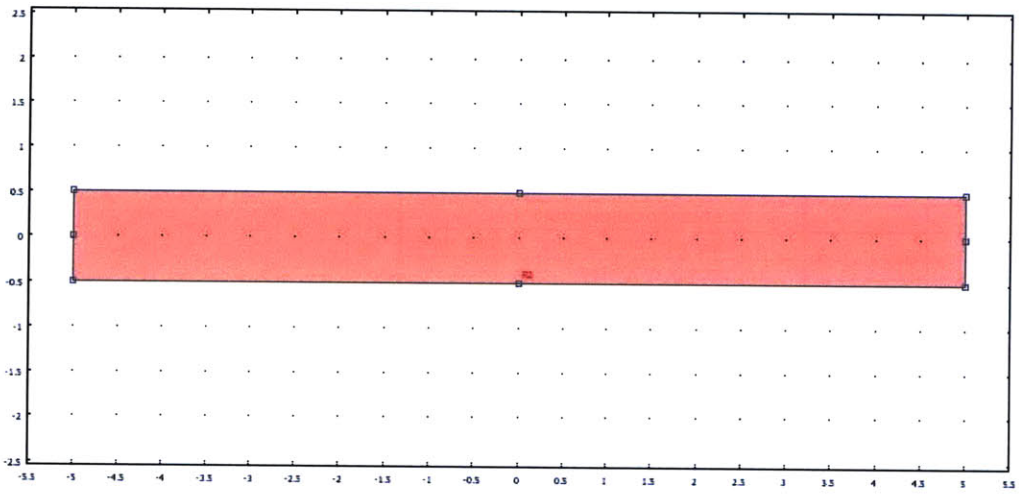

5.1.1. Point mode

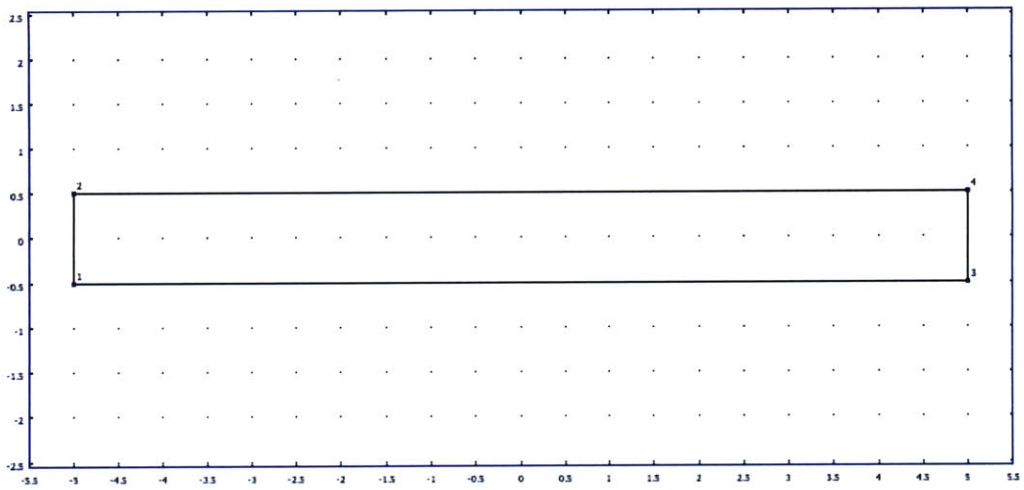

5.1.2. Boundary mode

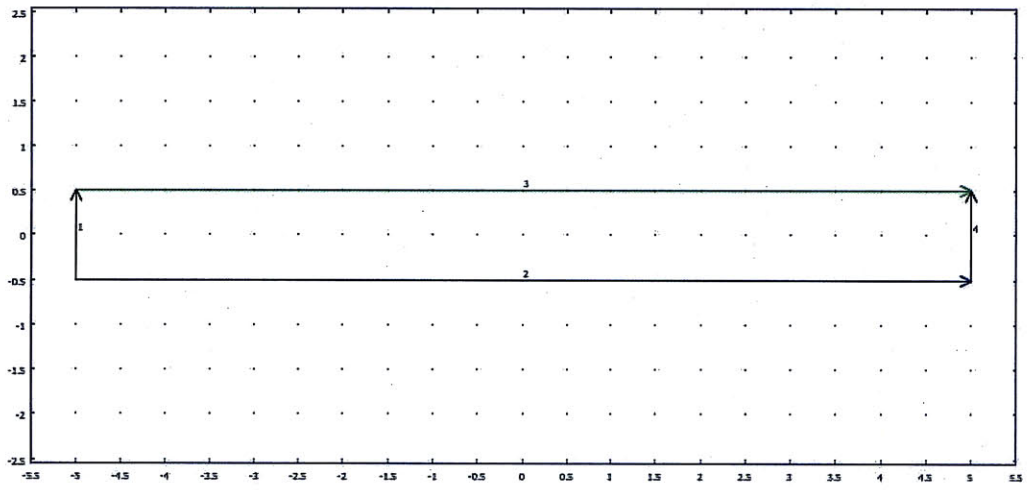

5.1.3. Subdomain mode

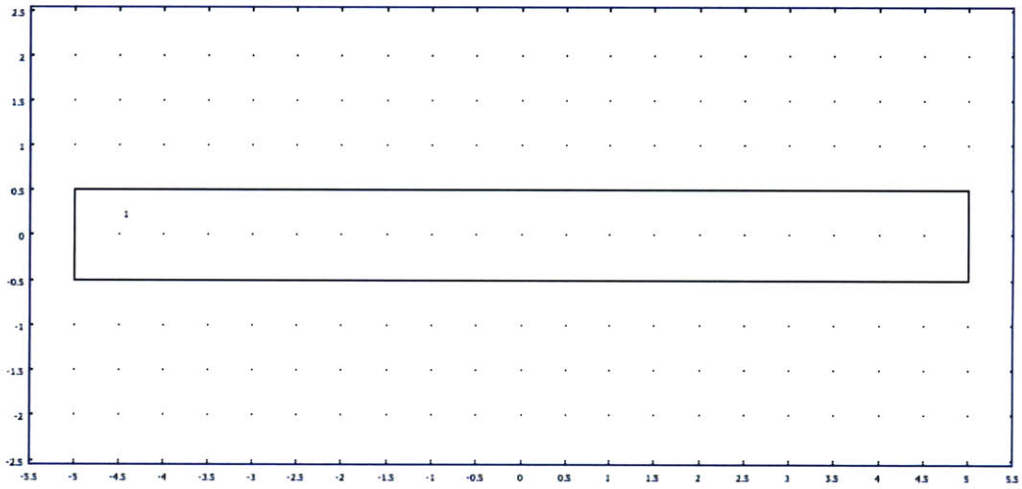

6. Geom1

Space dimensions: 2D

Independent variables: x, y, z

6.1. Mesh

6.1.1. Mesh Statistics

Number of degrees of freedom	762
Number of mesh points	54
Number of elements	70
Triangular	70
Quadrilateral	0
Number of boundary elements	36
Number of vertex elements	4
Minimum element quality	0.9
Element area ratio	0.328

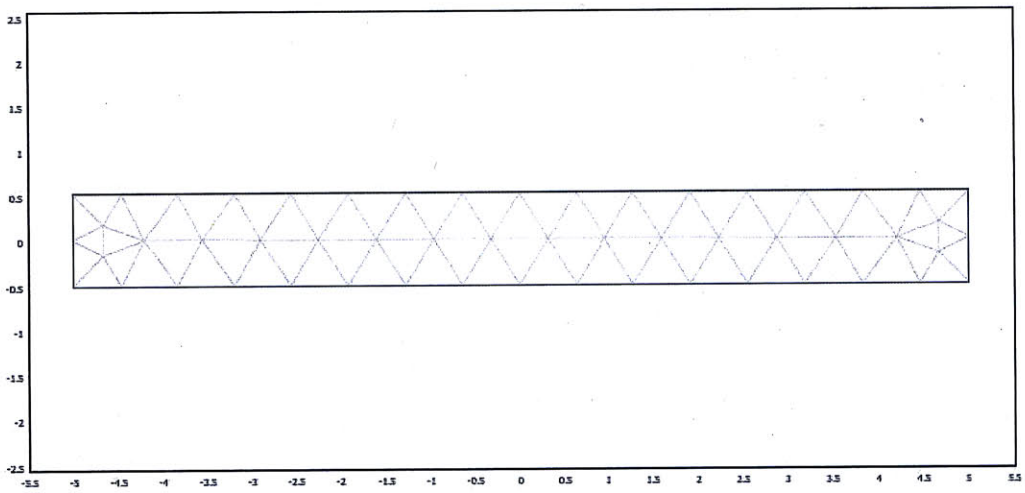

6.2. Application Mode: Perpendicular Induction Currents, Vector Potential (emqa)

Application mode type: Perpendicular Induction Currents, Vector Potential (AC/DC Module)

Application mode name: emqa

6.2.1. Scalar Variables

Name	Variable	Value	Unit	Description
epsilon0	epsilon0_emqa	8.854187817e-12	F/m	Permittivity of vacuum
mu0	mu0_emqa	1	H/m	Permeability of vacuum

6.2.2. Application Mode Properties

Property	Value
Default element type	Lagrange - Quadratic
Analysis type	Transient
Bias application mode	None
Solve for	Total potential
Background field	Magnetic vector potential
Frame	Frame (ref)
Weak constraints	Off

Constraint type	Ideal

6.2.3. Variables

Dependent variables: Az, redAz

Shape functions: shlag(2,'Az')

Interior boundaries active

6.2.4. Boundary Settings

Boundary		1, 4	2	3
Type		Magnetic field	Magnetic field	Magnetic field
Magnetic field (H0)	A/m	{Hmax*flc2hs(t-1,0.05); ((Bmax/mu0)-My_emqa)*flc2hs(t-1,0.05)}	{Hmax*flc2hs(t-1,0.05); ((Bmax/mu0)-My_emqa)*flc2hs(t-1,0.05)}	{Hmax*flc2hs(t-1,0.05); ((Bmax/mu0)-My_emqa) 1,0.05)}
Surface current density (Js0z)	A/m	0	Hmax	-Hmax

6.2.5. Subdomain Settings

Subdomain		1
Relative permeability (mur)	1	{(1+(Xi*((j*Omega*Tau+1+Xi)*Hmax-(Bmax*Tau*w/mu0))/((Tau*w)^2+(j*Omega*Tau+1)*(j*Omega*Tau+1+Xi))))/mu0_emqa,0;0,(1+(Xi*((w*Tau)*Hmax+(j*Omega*Tau+1)*(Bmax/mu0))/((w*Tau)^2+(j*Omega*Tau+1)*(j*Omega*Tau+1+Xi))))/mu0_emqa}
magconstrel		B = μ_0H + μ_0M
Magnetization (M)	A/m	{Xi*((j*Omega*Tau+1+Xi)*Hmax-(Bmax*Tau*w/mu0))/((Tau*w)^2+(j*Omega*Tau+1)*(j*Omega*Tau+1+Xi));Xi*((w*Tau)*Hmax+(j*Omega*Tau+1)*(Bmax/mu0))/((w*Tau)^2+(j*Omega*Tau+1)*(j*Omega*Tau+1+Xi))}

6.3. Application Mode: Incompressible Navier-Stokes (ns)

Application mode type: Incompressible Navier-Stokes

Application mode name: ns

6.3.1. Scalar Variables

Name	Variable	Value	Unit	Description
visc_vel_fact	visc_vel_fact_ns	10	1	Viscous velocity factor

6.3.2. Application Mode Properties

Property	Value
Default element type	Lagrange - P_2 P_1
Analysis type	Stationary
Corner smoothing	Off
Frame	Frame (ref)

Weak constraints	Off
Constraint type	Ideal

6.3.3. Variables

Dependent variables: u, v, p, nxw, nyw

Shape functions: shlag(2,'u'), shlag(2,'v'), shlag(1,'p')

Interior boundaries not active

6.3.4. Boundary Settings

Boundary		1	2	3
Type		Inlet	Wall	Wall
intype		**Pressure, no viscous stress**	Velocity	Velocity
outtype		Pressure, no viscous stress	Pressure, no viscous stress	Pressure, no viscous stress
stresstype		**Normal stress, normal flow**	General stress	General stress
velType		**u0**	U0in	U0in
x-velocity (u0)	m/s	**1**	0	0
Pressure (p0)	Pa	**pmax**	0	0
Normal stress (f0)	N/m^2	**pmax**	0	0
Velocity of the tangentially moving wall (uvw)	m/s	0	0	**Umax**
#-velocity of moving wall (uwall)	m/s	0	0	**Umax**

Boundary		4
Type		Outlet
intype		Velocity
outtype		**Normal stress**
stresstype		General stress
velType		U0in
x-velocity (u0)	m/s	0
Pressure (p0)	Pa	0
Normal stress (f0)	N/m^2	0
Velocity of the tangentially moving wall (uvw)	m/s	0
#-velocity of moving wall (uwall)	m/s	0

6.3.5. Subdomain Settings

Subdomain		1
Integration order (gporder)		**4 4 2**
Constraint order (cporder)		**2 2 1**
Density (rho)	kg/m^3	**0**
Dynamic viscosity (eta)	Pa·s	**0.5*(zeta+eta)**
Volume force, x dir. (F_x)	N/m^3	**zeta*wy**

cdon		0

6.4. Application Mode: PDE, General Form (g)

Application mode type: PDE, General Form

Application mode name: g

6.4.1. Application Mode Properties

Property	Value
Default element type	Lagrange - Quadratic
Wave extension	Off
Frame	Frame (ref)
Weak constraints	Off

6.4.2. Variables

Dependent variables: w, w_t

Shape functions: shlag(2,'w')

Interior boundaries not active

6.4.3. Boundary Settings

Boundary	1-4
Type	Neumann boundary condition

6.4.4. Subdomain Settings

Subdomain	1
Damping/Mass coefficient (da)	0
Source term (f)	etaprime*wyy-1*zeta*(uy+2*w)+T
Conservative flux source term (ga)	{{0;0}}

7. Solver Settings

Solve using a script: off

Analysis type	Transient
Auto select solver	On
Solver	Time dependent
Solution form	Automatic
Symmetric	auto
Adaptive mesh refinement	Off
Optimization/Sensitivity	Off
Plot while solving	Off

7.1. Direct (UMFPACK)

Solver type: Linear system solver

Parameter	Value
Pivot threshold	0.1
Memory allocation factor	0.7

7.2. Time Stepping

Parameter	Value
Times	range(0,0.1,10)
Relative tolerance	0.01
Absolute tolerance	0.0010
Times to store in output	Specified times
Time steps taken by solver	Free
Maximum BDF order	5
Singular mass matrix	Maybe
Consistent initialization of DAE systems	Backward Euler
Error estimation strategy	Include algebraic
Allow complex numbers	On

7.3. Advanced

Parameter	Value
Constraint handling method	Elimination
Null-space function	Automatic
Automatic assembly block size	On
Assembly block size	5000
Use Hermitian transpose of constraint matrix and in symmetry detection	Off
Use complex functions with real input	Off
Stop if error due to undefined operation	On
Store solution on file	Off
Type of scaling	Automatic
Manual scaling	
Row equilibration	On
Manual control of reassembly	Off
Load constant	On
Constraint constant	On
Mass constant	On
Damping (mass) constant	On
Jacobian constant	On
Constraint Jacobian constant	On

8. Postprocessing

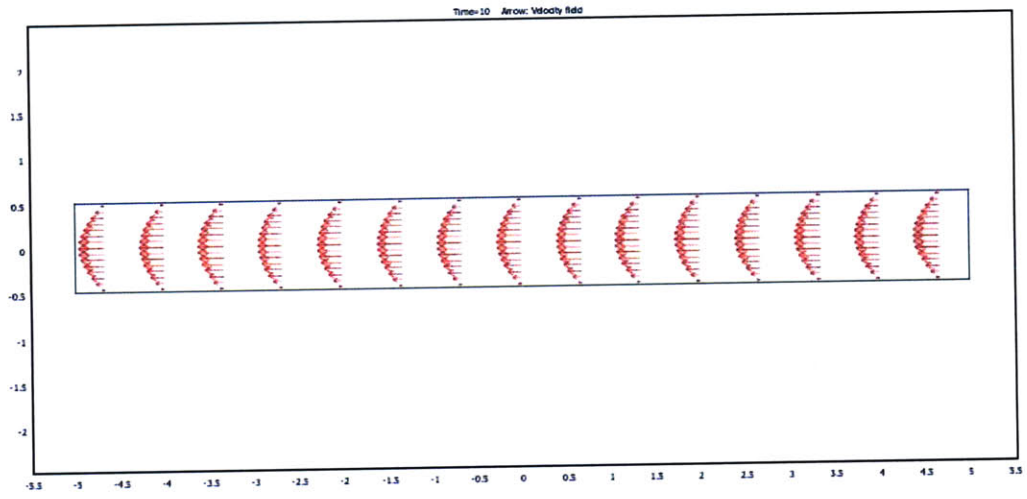

9. Variables

9.1. Boundary

Name	Description	Unit	Expression
dVolbnd_emqa	Area integration contribution	1	1
murbnd_emqa	Relative permeability	1	murbndxx_emqa
Jsz_emqa	Surface current density	A/m	unx * (Hy_emqa_down-Hy_emqa_up)-uny * (Hx_emqa_down-Hx_emqa_up)
unTx_emqa	Maxwell surface stress tensor, x component	Pa	-0.5 * (Bx_emqa_up * Hx_emqa_up+By_emqa_up * Hy_emqa_up) * dnx+(dnx * Hx_emqa_up+dny * Hy_emqa_up) * Bx_emqa_up
dnTx_emqa	Maxwell surface stress tensor, x component	Pa	-0.5 * (Bx_emqa_down * Hx_emqa_down+By_emqa_down * Hy_emqa_down) * unx+(unx * Hx_emqa_down+uny * Hy_emqa_down) * Bx_emqa_down
unTy_emqa	Maxwell surface stress tensor, y component	Pa	-0.5 * (Bx_emqa_up * Hx_emqa_up+By_emqa_up * Hy_emqa_up) * dny+(dnx * Hx_emqa_up+dny * Hy_emqa_up) * By_emqa_up
dnTy_emqa	Maxwell surface stress tensor, y component	Pa	-0.5 * (Bx_emqa_down * Hx_emqa_down+By_emqa_down * Hy_emqa_down) * uny+(unx * Hx_emqa_down+uny * Hy_emqa_down) * By_emqa_down

Qs_emqa	Surface resistive heating	W/m^2	Jsz_emqa * Ez_emqa
nPo_emqa	Power outflow	W/m^2	nx_emqa * Pox_emqa+ny_emqa * Poy_emqa
FsLtzx_emqa	Lorentz surface force contribution, x component	Pa	-Jsz_emqa * By_emqa
FsLtzy_emqa	Lorentz surface force contribution, y component	Pa	Jsz_emqa * Bx_emqa
normFsLtz_emqa	Lorentz surface force contribution, cycle average, norm	Pa	sqrt(abs(FsLtzx_emqa)^2+abs(FsLtzy_emqa)^2)
K_x_ns	Viscous force per area, x component	Pa	eta_ns * (2 * nx_ns * ux+ny_ns * (uy+vx))
T_x_ns	Total force per area, x component	Pa	-nx_ns * p+2 * nx_ns * eta_ns * ux+ny_ns * eta_ns * (uy+vx)
K_y_ns	Viscous force per area, y component	Pa	eta_ns * (nx_ns * (vx+uy)+2 * ny_ns * vy)
T_y_ns	Total force per area, y component	Pa	-ny_ns * p+nx_ns * eta_ns * (vx+uy)+2 * ny_ns * eta_ns * vy

9.2. Subdomain

Name	Description	Unit	Expression
dr_guess_emqa	Width in radial direction default guess	m	0
R0_guess_emqa	Inner radius default guess	m	0
Sx_emqa	Infinite element x coordinate	m	x
S0x_guess_emqa	Inner x coordinate default guess	m	0
Sdx_guess_emqa	Width in x direction default guess	m	0
Sy_emqa	Infinite element y coordinate	m	y
S0y_guess_emqa	Inner y coordinate default guess	m	0
Sdy_guess_emqa	Width in y direction default guess	m	0
curlAx_emqa	Curl of magnetic potential, x component	T	Azy
curlAy_emqa	Curl of magnetic potential, y component	T	-Azx
dVol_emqa	Volume integration contribution	1	detJ_emqa
Bx_emqa	Magnetic flux density, x component	T	curlAx_emqa

By_emqa	Magnetic flux density, y component	T	curlAy_emqa
Hx_emqa	Magnetic field, x component	A/m	Bx_emqa/mu0_emqa-Mx_emqa
Hy_emqa	Magnetic field, y component	A/m	By_emqa/mu0_emqa-My_emqa
mu_emqa	Permeability	H/m	mu0_emqa * mur_emqa
muxx_emqa	Permeability, xx component	H/m	mu0_emqa * murxx_emqa
muxy_emqa	Permeability, xy component	H/m	mu0_emqa * murxy_emqa
muyx_emqa	Permeability, yx component	H/m	mu0_emqa * muryx_emqa
muyy_emqa	Permeability, yy component	H/m	mu0_emqa * muryy_emqa
Jpz_emqa	Potential current density, z component	A/m^2	sigma_emqa * deltaV_emqa/L_emqa
Ez_emqa	Electric field, z component	V/m	-d(Az,t)
Jz_emqa	Total current density, z component	A/m^2	Jpz_emqa+Jiz_emqa+Jez_emqa
Pox_emqa	Power flow, x component	W/m^2	-Ez_emqa * Hy_emqa
Poy_emqa	Power flow, y component	W/m^2	Ez_emqa * Hx_emqa
normE_emqa	Electric field, norm	V/m	abs(Ez_emqa)
Jiz_emqa	Induced current density, z component	A/m^2	sigma_emqa * Ez_emqa
Q_emqa	Resistive heating	W/m^3	Jz_emqa * (Ez_emqa+deltaV_emqa/L_emqa)
W_emqa	Total energy density	J/m^3	Wm_emqa
dW_emqa	Integrand for total energy	J/m^3	dVol_emqa * W_emqa
Wm_emqa	Magnetic energy density	J/m^3	0.5 * (Hx_emqa * Bx_emqa+Hy_emqa * By_emqa+Mx_emqa * Bx_emqa+My_emqa * By_emqa)
FLtzx_emqa	Lorentz force contribution, x component	N/m^3	-Jz_emqa * By_emqa
FLtzy_emqa	Lorentz force contribution, y component	N/m^3	Jz_emqa * Bx_emqa
normFLtz_emqa	Lorentz force contribution, norm	N/m^3	sqrt(abs(FLtzx_emqa)^2+abs(FLtzy_emqa)^2)
normM_emqa	Magnetization, norm	A/m	sqrt(abs(Mx_emqa)^2+abs(My_emqa)^2)
normBr_emqa	Remanent flux density, norm	T	sqrt(abs(Brx_emqa)^2+abs(Bry_emqa)^2)
normH_emqa	Magnetic field, norm	A/m	sqrt(abs(Hx_emqa)^2+abs(Hy_emqa)^2)
normB_emqa	Magnetic flux density, norm	T	sqrt(abs(Bx_emqa)^2+abs(By_emqa)^2)

normJ_emqa	Total current density, norm	A/m^2	abs(Jz_emqa)
Evz_emqa	Lorentz electric field, z component	V/m	d(x,t) * By_emqa-d(y,t) * Bx_emqa
normEv_emqa	Lorentz electric field, norm	V/m	abs(Evz_emqa)
normPo_emqa	Power flow, time average, norm	W/m^2	sqrt(abs(Pox_emqa)^2+abs(Poy_emqa)^2)
U_ns	Velocity field	m/s	sqrt(u^2+v^2)
V_ns	Vorticity	1/s	vx-uy
divU_ns	Divergence of velocity field	1/s	ux+vy
cellRe_ns	Cell Reynolds number	1	rho_ns * U_ns * h/eta_ns
res_u_ns	Equation residual for u	N/m^3	rho_ns * (u * ux+v * uy)+px-F_x_ns-eta_ns * (2 * uxx+uyy+vxy)
res_v_ns	Equation residual for v	N/m^3	rho_ns * (u * vx+v * vy)+py-F_y_ns-eta_ns * (vxx+uyx+2 * vyy)
beta_x_ns	Convective field, x component	kg/(m^2*s)	rho_ns * u
beta_y_ns	Convective field, y component	kg/(m^2*s)	rho_ns * v
Dm_ns	Mean diffusion coefficient	Pa*s	eta_ns
da_ns	Total time scale factor	kg/m^3	rho_ns
taum_ns	GLS time-scale	m^3*s/kg	nojac(1/max(2 * rho_ns * sqrt(emetric(u,v)),48 * eta_ns/h^2))
tauc_ns	GLS time-scale	m^2/s	0.5 * nojac(if(u^2+v^2
res_p_ns	Equation residual for p	kg/(m^3*s)	rho_ns * divU_ns
abswx_g	|grad(w)|		sqrt(wx^2+wy^2)
absga5x_g	|ga5x|		sqrt(ga5x^2+ga5y^2)

Appendix B : COMSOL Simulation of Ferrofluid Flows in Cylindrical Geometry

B1. COMSOL Simulation Using Surface Current Boundary Condition Method (Chaves 143G case, $\eta'=6x10^{-10}$) (Section 4.4.3.1)

COMSOL Model Report

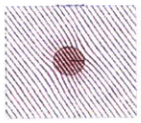

1. Table of Contents

2. Model Properties

Property	Value
Model name	
Author	
Company	
Department	
Reference	
URL	
Saved date	Feb 16, 2010 1:00:57 AM
Creation date	Sep 19, 2008 9:32:16 PM
COMSOL version	COMSOL 3.5.0.603

File name: D:\Documents and Settings\Administrator\Desktop\Comsol_Testbed\GoodFiles\Good2DCylinderfiles\2Dcase_cylinder_surfacecurrent_forceincluded_etaprimenon0_Chaves_airgap_R10.mph

Application modes and modules used in this model:

- Geom1 (2D)
  - Incompressible Navier-Stokes
  - Diffusion
  - Convection and Diffusion
  - Convection and Diffusion
  - Perpendicular Induction Currents, Vector Potential (AC/DC Module)
  - PDE, General Form

- PDE, General Form

2.1. Model description

Rotation of Ferrofluid in a rotating magnetic field in an infinitely long cylinder

Using Parameters from Chaves Paper of 2008 on spinup Flow

Using parameters for EMG900_2 trying to get plot similar to Fig 4b

Using my normalization scheme outlined in VeryifyingShihabsmethod_081205.doc

Excited with surface current on boundary Includes force terms

Etaprime non0 case

3. Constants

Name	Expression	Value	Description
Xi	1.19		
omega	2*pi*f		
zeta	0.00048		
eta	0.0074		
etaprime	1.61e-6		
f	85		
tau	1e-6		
omegatau	omega*tau		
R0	0.027		
l	2/3		

4. Global Expressions

Name	Expression	Unit	Description
FMx	M_x*(Azyx-M_xx)+M_y*(Azyy-M_xy)		\
FMy	M_x*(-Azxx-M_yx)+M_y*(-Azxy-M_yy)		
T	M_x*Hy-M_y*Hx	A*mol/m^4	
M_eqx	Xi*Hx	A/m	
M_eqy	Xi*Hy	A/m	
Hx	Hx_emqa	A/m	
Hy	Hy_emqa	A/m	
phi	atan2(y,x)	rad	

5. Geometry

Number of geometries: 1

5.1. Geom1

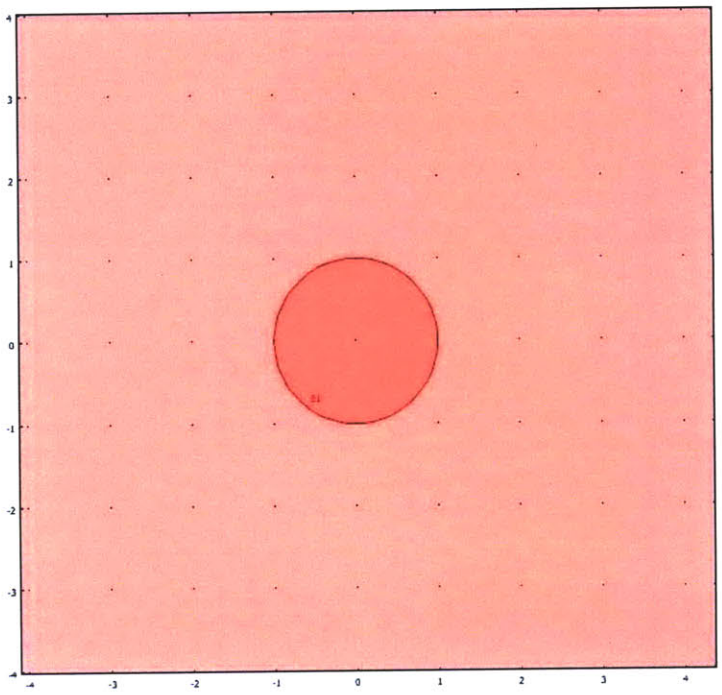

5.1.1. Point mode

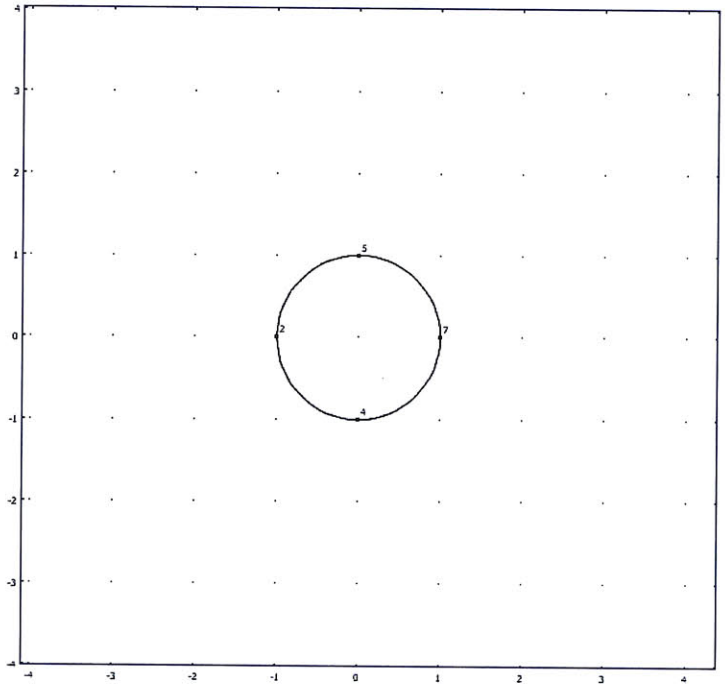

5.1.2. Boundary mode

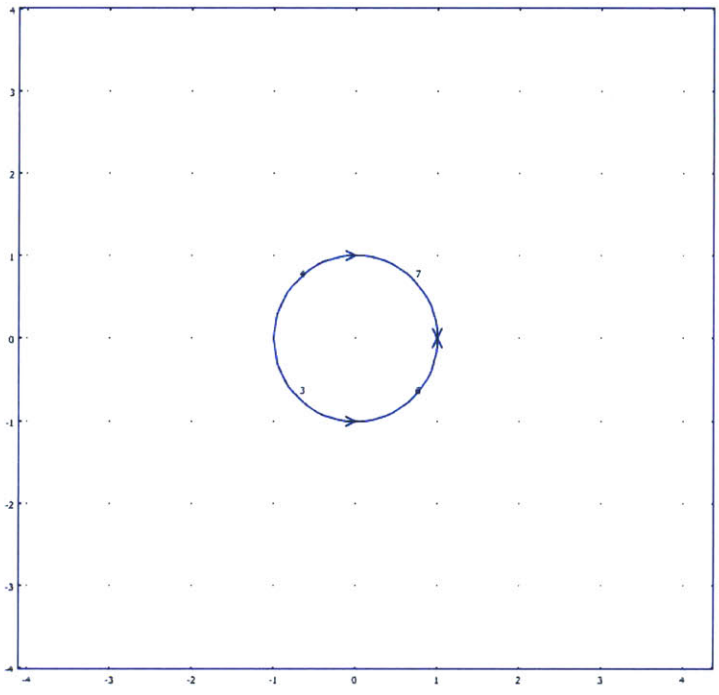

5.1.3. Subdomain mode

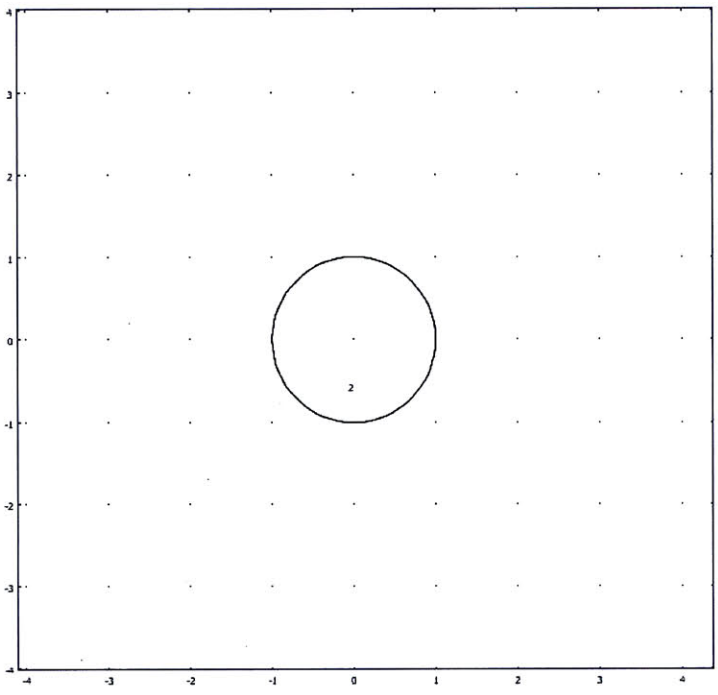

6. Geom 1

Space dimensions: 2D

Independent variables: x, y, z

6.1. Mesh

6.1.1. Mesh Statistics

Number of degrees of freedom	199667
Number of mesh points	5593
Number of elements	11024
Triangular	11024
Quadrilateral	0
Number of boundary elements	188
Number of vertex elements	8
Minimum element quality	0.342
Element area ratio	0.003

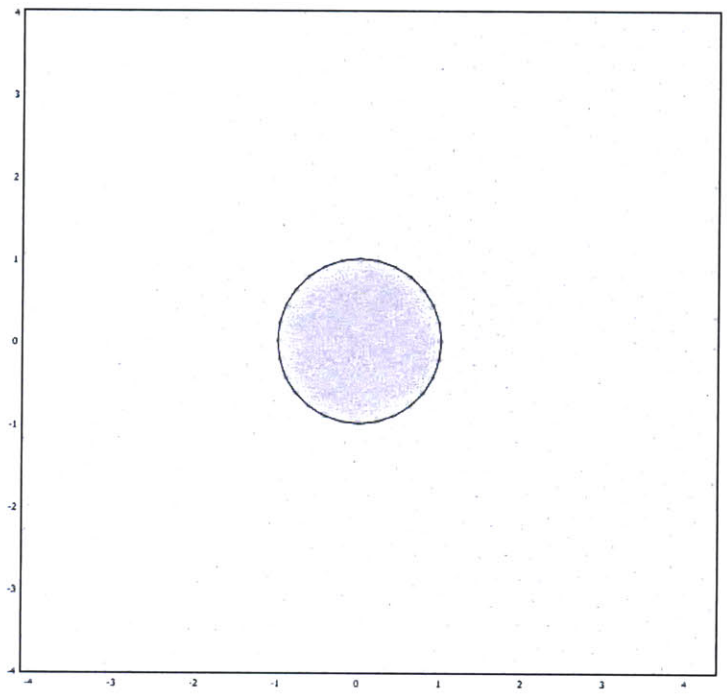

6.2. Application Mode: Incompressible Navier-Stokes (ns)

Application mode type: Incompressible Navier-Stokes

Application mode name: ns

6.2.1. Scalar Variables

Name	Variable	Value	Unit	Description
visc_vel_fact	visc_vel_fact_ns	10	1	Viscous velocity factor

6.2.2. Application Mode Properties

Property	Value
Default element type	Lagrange - P_2 P_1
Analysis type	Transient
Corner smoothing	Off
Frame	Frame (ref)
Weak constraints	Off
Constraint type	Ideal

6.2.3. Variables

Dependent variables: u, v, p, nxw, nyw

Shape functions: shlag(2,'u'), shlag(2,'v'), shlag(1,'p')

Interior boundaries not active

6.2.4. Point Settings

Point	1, 3-8	2
pnton	0	1

6.2.5. Boundary Settings

Boundary	3-4, 6-7
Type	Wall

6.2.6. Subdomain Settings

Subdomain		2
Integration order (gporder)		**4 4 2**
Constraint order (cporder)		**2 2 1**
Density (rho)	kg/m^3	**0**
Dynamic viscosity (eta)	Pa·s	**eta+zeta**
Volume force, x dir. (F_x)	N/m^3	**2*zeta*wy+FMx**
Volume force, y dir. (F_y)	N/m^3	**-2*zeta*wx+FMy**
cdon		**0**

6.3. Application Mode: Diffusion (di)

Application mode type: Diffusion

Application mode name: di

6.3.1. Application Mode Properties

Property	Value
Default element type	Lagrange - Quadratic
Analysis type	Stationary
Frame	Frame (ref)
Weak constraints	Off
Constraint type	Ideal

6.3.2. Variables

Dependent variables: w

Shape functions: shlag(2,'w')

Interior boundaries not active

6.3.3. Boundary Settings

Boundary	3-4, 6-7
Type	Concentration

6.3.4. Subdomain Settings

Subdomain		2
Diffusion coefficient (D)	m^2/s	**etaprime**
Reaction rate (R)	$mol/(m^3 \cdot s)$	**T+2*zeta*(vx-uy-2*w)**

6.4. Application Mode: Convection and Diffusion (cd3)

Application mode type: Convection and Diffusion

Application mode name: cd3

6.4.1. Application Mode Properties

Property	Value
Default element type	Lagrange - Quadratic
Analysis type	Transient
Equation form	Non-conservative
Frame	Frame (ref)
Weak constraints	Off
Constraint type	Ideal

6.4.2. Variables

Dependent variables: M_x

Shape functions: shlag(2,'M_x')

Interior boundaries not active

6.4.3. Boundary Settings

Boundary	3-4, 6-7
Type	Insulation/Symmetry

6.4.4. Subdomain Settings

Subdomain		2
Diffusion coefficient (D)	m^2/s	**0**
Reaction rate (R)	$mol/(m^3 \cdot s)$	**-w*M_y-((M_x-M_eqx)/omegatau)**
x-velocity (u)	m/s	**u**
y-velocity (v)	m/s	**v**

6.5. Application Mode: Convection and Diffusion (cd)

Application mode type: Convection and Diffusion

Application mode name: cd

6.5.1. Application Mode Properties

Property	Value
Default element type	Lagrange - Quadratic
Analysis type	Transient
Equation form	Non-conservative
Frame	Frame (ref)
Weak constraints	Off
Constraint type	Ideal

6.5.2. Variables

Dependent variables: M_y

Shape functions: shlag(2,'M_y')

Interior boundaries not active

6.5.3. Boundary Settings

Boundary	3-4, 6-7
Type	Insulation/Symmetry

6.5.4. Subdomain Settings

Subdomain		2
Diffusion coefficient (D)	m^2/s	**0**
Reaction rate (R)	$mol/(m^3 \cdot s)$	**w*M_x-((M_y-M_eqy)/omegatau)**
x-velocity (u)	m/s	**u**
y-velocity (v)	m/s	**v**

6.6. Application Mode: Perpendicular Induction Currents, Vector Potential (emqa)

Application mode type: Perpendicular Induction Currents, Vector Potential (AC/DC Module)

Application mode name: emqa

6.6.1. Scalar Variables

Name	Variable	Value	Unit	Description
epsilon0	epsilon0_emqa	8.854187817e-12	F/m	Permittivity of vacuum
mu0	mu0_emqa	1	H/m	Permeability of vacuum

6.6.2. Application Mode Properties

Property	Value
Default element type	Lagrange - Quintic
Analysis type	Transient
Bias application mode	None
Solve for	Total potential
Background field	Magnetic vector potential

Frame	Frame (ref)
Weak constraints	Off
Constraint type	Ideal

6.6.3. Variables

Dependent variables: Az, redAz

Shape functions: shlag(5,'Az')

Interior boundaries not active

6.6.4. Boundary Settings

Boundary		1-2, 5, 8
Type		Surface current
Surface current density (Js0z)	A/m	**I*(3/2)*cos(t-phi)*flc2hs(t-1,0.05)**

6.6.5. Subdomain Settings

Subdomain		1	2
magconstrel		**B = $\mu_0\mu_r$H**	**B = μ_0H + μ_0M**
Magnetization (M)	A/m	{0;0}	**{M_x;M_y}**

6.7. Application Mode: PDE, General Form (g)

Application mode type: PDE, General Form

Application mode name: g

6.7.1. Application Mode Properties

Property	Value
Default element type	Lagrange - Quadratic
Wave extension	Off
Frame	Frame (ref)
Weak constraints	Off

6.7.2. Variables

Dependent variables: avgv, avgv_t

Shape functions: shlag(2,'avgv')

Interior boundaries not active

6.7.3. Boundary Settings

Boundary	3-4, 6-7
Type	Dirichlet boundary condition

6.7.4. Subdomain Settings

Subdomain	2
Source term (f)	v
Conservative flux source term (ga)	{{0;0}}

6.8. Application Mode: PDE, General Form (g2)

Application mode type: PDE, General Form

Application mode name: g2

6.8.1. Application Mode Properties

Property	Value
Default element type	Lagrange - Quadratic
Wave extension	Off
Frame	Frame (ref)
Weak constraints	Off

6.8.2. Variables

Dependent variables: u2, u2_t

Shape functions: shlag(2,'u2')

Interior boundaries not active

6.8.3. Boundary Settings

Boundary	3-4, 6-7
Type	Neumann boundary condition

6.8.4. Subdomain Settings

Subdomain	2
Source term (f)	w
Conservative flux source term (ga)	{{0;0}}

7. Solver Settings

Solve using a script: off

Analysis type	Transient
Auto select solver	On
Solver	Time dependent
Solution form	Automatic
Symmetric	auto
Adaptive mesh refinement	Off
Optimization/Sensitivity	Off
Plot while solving	Off

7.1. Direct (UMFPACK)

Solver type: Linear system solver

Parameter	Value
Pivot threshold	0.1
Memory allocation factor	0.7

7.2. Time Stepping

Parameter	Value
Times	range(0,0.1,10)
Relative tolerance	0.01
Absolute tolerance	0.0010
Times to store in output	Specified times
Time steps taken by solver	Free
Maximum BDF order	5
Singular mass matrix	Maybe
Consistent initialization of DAE systems	Backward Euler
Error estimation strategy	Include algebraic
Allow complex numbers	Off

7.3. Advanced

Parameter	Value
Constraint handling method	Elimination
Null-space function	Automatic
Automatic assembly block size	On
Assembly block size	5000
Use Hermitian transpose of constraint matrix and in symmetry detection	Off
Use complex functions with real input	Off
Stop if error due to undefined operation	On
Store solution on file	Off
Type of scaling	Automatic
Manual scaling	
Row equilibration	On
Manual control of reassembly	Off
Load constant	On
Constraint constant	On
Mass constant	On
Damping (mass) constant	On
Jacobian constant	On
Constraint Jacobian constant	On

8. Postprocessing

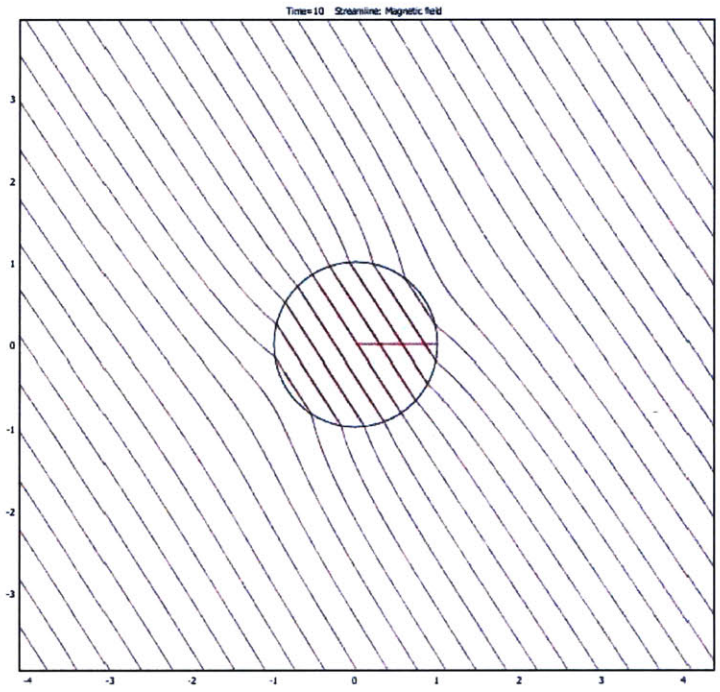

9. Variables

9.1. Boundary

9.1.1. Boundary 1-2, 5, 8

Name	Description	Unit	Expression
K_x_ns	Viscous force per area, x component	Pa	
T_x_ns	Total force per area, x component	Pa	
K_y_ns	Viscous force per area, y component	Pa	
T_y_ns	Total force per area, y component	Pa	
ndflux_w_di	Normal diffusive flux, w	mol/(m^2*s)	
ndflux_M_x_cd3	Normal diffusive flux, M_x	mol/(m^2*s)	

ncflux_M_x_cd3	Normal convective flux, M_x	mol/(m^2*s)	
ntflux_M_x_cd3	Normal total flux, M_x	mol/(m^2*s)	
ndflux_M_y_cd	Normal diffusive flux, M_y	mol/(m^2*s)	
ncflux_M_y_cd	Normal convective flux, M_y	mol/(m^2*s)	
ntflux_M_y_cd	Normal total flux, M_y	mol/(m^2*s)	
dVolbnd_emqa	Area integration contribution	1	1
murbnd_emqa	Relative permeability	1	murbndxx_emqa
Jsz_emqa	Surface current density	A/m	unx * (Hy_emqa_down-Hy_emqa_up)-uny * (Hx_emqa_down-Hx_emqa_up)
unTx_emqa	Maxwell surface stress tensor, x component	Pa	-0.5 * (Bx_emqa_up * Hx_emqa_up+By_emqa_up * Hy_emqa_up) * dnx+(dnx * Hx_emqa_up+dny * Hy_emqa_up) * Bx_emqa_up
dnTx_emqa	Maxwell surface stress tensor, x component	Pa	-0.5 * (Bx_emqa_down * Hx_emqa_down+By_emqa_down * Hy_emqa_down) * unx+(unx * Hx_emqa_down+uny * Hy_emqa_down) * Bx_emqa_down
unTy_emqa	Maxwell surface stress tensor, y component	Pa	-0.5 * (Bx_emqa_up * Hx_emqa_up+By_emqa_up * Hy_emqa_up) * dny+(dnx * Hx_emqa_up+dny * Hy_emqa_up) * By_emqa_up
dnTy_emqa	Maxwell surface stress tensor, y component	Pa	-0.5 * (Bx_emqa_down * Hx_emqa_down+By_emqa_down * Hy_emqa_down) * uny+(unx * Hx_emqa_down+uny * Hy_emqa_down) * By_emqa_down
Qs_emqa	Surface resistive heating	W/m^2	Jsz_emqa * Ez_emqa
nPo_emqa	Power outflow	W/m^2	nx_emqa * Pox_emqa+ny_emqa * Poy_emqa
FsLtzx_emqa	Lorentz surface force contribution, x component	Pa	-Jsz_emqa * By_emqa
FsLtzy_emqa	Lorentz surface force contribution, y component	Pa	Jsz_emqa * Bx_emqa
normFsLtz_emqa	Lorentz surface force contribution, cycle average, norm	Pa	sqrt(abs(FsLtzx_emqa)^2+abs(FsLtzy_emqa)^2)

9.1.2. Boundary 3-4, 6-7

Name	Description	Unit	Expression

K_x_ns	Viscous force per area, x component	Pa	eta_ns * (2 * nx_ns * ux+ny_ns * (uy+vx))
T_x_ns	Total force per area, x component	Pa	-nx_ns * p+2 * nx_ns * eta_ns * ux+ny_ns * eta_ns * (uy+vx)
K_y_ns	Viscous force per area, y component	Pa	eta_ns * (nx_ns * (vx+uy)+2 * ny_ns * vy)
T_y_ns	Total force per area, y component	Pa	-ny_ns * p+nx_ns * eta_ns * (vx+uy)+2 * ny_ns * eta_ns * vy
ndflux_w_di	Normal diffusive flux, w	mol/(m^2*s)	nx_di * dflux_w_x_di+ny_di * dflux_w_y_di
ndflux_M_x_cd3	Normal diffusive flux, M_x	mol/(m^2*s)	nx_cd3 * dflux_M_x_x_cd3+ny_cd3 * dflux_M_x_y_cd3
ncflux_M_x_cd3	Normal convective flux, M_x	mol/(m^2*s)	nx_cd3 * cflux_M_x_x_cd3+ny_cd3 * cflux_M_x_y_cd3
ntflux_M_x_cd3	Normal total flux, M_x	mol/(m^2*s)	nx_cd3 * tflux_M_x_x_cd3+ny_cd3 * tflux_M_x_y_cd3
ndflux_M_y_cd	Normal diffusive flux, M_y	mol/(m^2*s)	nx_cd * dflux_M_y_x_cd+ny_cd * dflux_M_y_y_cd
ncflux_M_y_cd	Normal convective flux, M_y	mol/(m^2*s)	nx_cd * cflux_M_y_x_cd+ny_cd * cflux_M_y_y_cd
ntflux_M_y_cd	Normal total flux, M_y	mol/(m^2*s)	nx_cd * tflux_M_y_x_cd+ny_cd * tflux_M_y_y_cd
dVolbnd_emqa	Area integration contribution	1	1
murbnd_emqa	Relative permeability	1	murbndxx_emqa
Jsz_emqa	Surface current density	A/m	unx * (Hy_emqa_down-Hy_emqa_up)-uny * (Hx_emqa_down-Hx_emqa_up)
unTx_emqa	Maxwell surface stress tensor, x component	Pa	-0.5 * (Bx_emqa_up * Hx_emqa_up+By_emqa_up * Hy_emqa_up) * dnx+(dnx * Hx_emqa_up+dny * Hy_emqa_up) * Bx_emqa_up
dnTx_emqa	Maxwell surface stress tensor, x component	Pa	-0.5 * (Bx_emqa_down * Hx_emqa_down+By_emqa_down * Hy_emqa_down) * unx+(unx * Hx_emqa_down+uny * Hy_emqa_down) * Bx_emqa_down
unTy_emqa	Maxwell surface stress tensor, y component	Pa	-0.5 * (Bx_emqa_up * Hx_emqa_up+By_emqa_up * Hy_emqa_up) * dny+(dnx * Hx_emqa_up+dny * Hy_emqa_up) * By_emqa_up
dnTy_emqa	Maxwell surface stress tensor, y component	Pa	-0.5 * (Bx_emqa_down * Hx_emqa_down+By_emqa_down * Hy_emqa_down) * uny+(unx * Hx_emqa_down+uny * Hy_emqa_down) * By_emqa_down
Qs_emqa	Surface resistive heating	W/m^2	Jsz_emqa * Ez_emqa
nPo_emqa	Power outflow	W/m^2	nx_emqa * Pox_emqa+ny_emqa * Poy_emqa
FsLtzx_emqa	Lorentz surface force contribution, x	Pa	-Jsz_emqa * By_emqa

	component		
FsLtzy_emqa	Lorentz surface force contribution, y component	Pa	Jsz_emqa * Bx_emqa
normFsLtz_emqa	Lorentz surface force contribution, cycle average, norm	Pa	sqrt(abs(FsLtzx_emqa)^2+abs(FsLtzy_emqa)^2)

9.2. Subdomain

9.2.1. Subdomain 1

Name	Description	Unit	Expression
U_ns	Velocity field	m/s	
V_ns	Vorticity	1/s	
divU_ns	Divergence of velocity field	1/s	
cellRe_ns	Cell Reynolds number	1	
res_u_ns	Equation residual for u	N/m^3	
res_v_ns	Equation residual for v	N/m^3	
beta_x_ns	Convective field, x component	kg/(m^2*s)	
beta_y_ns	Convective field, y component	kg/(m^2*s)	
Dm_ns	Mean diffusion coefficient	Pa*s	
da_ns	Total time scale factor	kg/m^3	
taum_ns	GLS time-scale	m^3*s/kg	
tauc_ns	GLS time-scale	m^2/s	
res_p_ns	Equation residual for p	kg/(m^3*s)	
grad_w_x_di	Concentration gradient, w, x component	mol/m^4	
dflux_w_x_di	Diffusive flux, w, x component	mol/(m^2*s)	
grad_w_y_di	Concentration gradient, w, y component	mol/m^4	
dflux_w_y_di	Diffusive flux, w, y component	mol/(m^2*s)	
grad_w_di	Concentration gradient, w	mol/m^4	
dflux_w_di	Diffusive flux, w	mol/(m^2*s)	
grad_M_x_x_cd3	Concentration gradient, M_x, x component	mol/m^4	
dflux_M_x_x_cd3	Diffusive flux, M_x, x component	mol/(m^2*s)	
cflux_M_x_x_cd3	Convective flux, M_x, x component	mol/(m^2*s)	
tflux_M_x_x_cd3	Total flux, M_x, x component	mol/(m^2*s)	
grad_M_x_y_cd3	Concentration gradient, M_x, y component	mol/m^4	

dflux_M_x_y_cd3	Diffusive flux, M_x, y component	mol/(m^2*s)	
cflux_M_x_y_cd3	Convective flux, M_x, y component	mol/(m^2*s)	
tflux_M_x_y_cd3	Total flux, M_x, y component	mol/(m^2*s)	
beta_M_x_x_cd3	Convective field, M_x, x component	m/s	
beta_M_x_y_cd3	Convective field, M_x, y component	m/s	
grad_M_x_cd3	Concentration gradient, M_x	mol/m^4	
dflux_M_x_cd3	Diffusive flux, M_x	mol/(m^2*s)	
cflux_M_x_cd3	Convective flux, M_x	mol/(m^2*s)	
tflux_M_x_cd3	Total flux, M_x	mol/(m^2*s)	
cellPe_M_x_cd3	Cell Peclet number, M_x	1	
Dm_M_x_cd3	Mean diffusion coefficient, M_x	m^2/s	
res_M_x_cd3	Equation residual for M_x	mol/(m^3*s)	
res_sc_M_x_cd3	Shock capturing residual for M_x	mol/(m^3*s)	
da_M_x_cd3	Total time scale factor, M_x	1	
grad_M_y_x_cd	Concentration gradient, M_y, x component	mol/m^4	
dflux_M_y_x_cd	Diffusive flux, M_y, x component	mol/(m^2*s)	
cflux_M_y_x_cd	Convective flux, M_y, x component	mol/(m^2*s)	
tflux_M_y_x_cd	Total flux, M_y, x component	mol/(m^2*s)	
grad_M_y_y_cd	Concentration gradient, M_y, y component	mol/m^4	
dflux_M_y_y_cd	Diffusive flux, M_y, y component	mol/(m^2*s)	
cflux_M_y_y_cd	Convective flux, M_y, y component	mol/(m^2*s)	
tflux_M_y_y_cd	Total flux, M_y, y component	mol/(m^2*s)	
beta_M_y_x_cd	Convective field, M_y, x component	m/s	
beta_M_y_y_cd	Convective field, M_y, y component	m/s	
grad_M_y_cd	Concentration gradient, M_y	mol/m^4	
dflux_M_y_cd	Diffusive flux, M_y	mol/(m^2*s)	
cflux_M_y_cd	Convective flux, M_y	mol/(m^2*s)	
tflux_M_y_cd	Total flux, M_y	mol/(m^2*s)	
cellPe_M_y_cd	Cell Peclet number, M_y	1	
Dm_M_y_cd	Mean diffusion coefficient, M_y	m^2/s	
res_M_y_cd	Equation residual for M_y	mol/(m^3*s)	

res_sc_M_y_cd	Shock capturing residual for M_y	mol/(m^3*s)	
da_M_y_cd	Total time scale factor, M_y	1	
dr_guess_emqa	Width in radial direction default guess	m	0
R0_guess_emqa	Inner radius default guess	m	0
Sx_emqa	Infinite element x coordinate	m	x
S0x_guess_emqa	Inner x coordinate default guess	m	0
Sdx_guess_emqa	Width in x direction default guess	m	0
Sy_emqa	Infinite element y coordinate	m	y
S0y_guess_emqa	Inner y coordinate default guess	m	0
Sdy_guess_emqa	Width in y direction default guess	m	0
curlAx_emqa	Curl of magnetic potential, x component	T	Azy
curlAy_emqa	Curl of magnetic potential, y component	T	-Azx
dVol_emqa	Volume integration contribution	1	detJ_emqa
Bx_emqa	Magnetic flux density, x component	T	curlAx_emqa
By_emqa	Magnetic flux density, y component	T	curlAy_emqa
Hx_emqa	Magnetic field, x component	A/m	Bx_emqa/(mur_emqa * mu0_emqa)
Hy_emqa	Magnetic field, y component	A/m	By_emqa/(mur_emqa * mu0_emqa)
mu_emqa	Permeability	H/m	mu0_emqa * mur_emqa
muxx_emqa	Permeability, xx component	H/m	mu0_emqa * murxx_emqa
muxy_emqa	Permeability, xy component	H/m	mu0_emqa * murxy_emqa
muyx_emqa	Permeability, yx component	H/m	mu0_emqa * muryx_emqa
muyy_emqa	Permeability, yy component	H/m	mu0_emqa * muryy_emqa
Jpz_emqa	Potential current density, z component	A/m^2	sigma_emqa * deltaV_emqa/L_emqa
Ez_emqa	Electric field, z component	V/m	-d(Az,t)
Jz_emqa	Total current density, z component	A/m^2	Jpz_emqa+Jiz_emqa+Jez_emqa
Pox_emqa	Power flow, x component	W/m^2	-Ez_emqa * Hy_emqa
Poy_emqa	Power flow, y component	W/m^2	Ez_emqa * Hx_emqa
normE_emqa	Electric field, norm	V/m	abs(Ez_emqa)

Jiz_emqa	Induced current density, z component	A/m^2	sigma_emqa * Ez_emqa
Q_emqa	Resistive heating	W/m^3	Jz_emqa * (Ez_emqa+deltaV_emqa/L_emqa)
W_emqa	Total energy density	J/m^3	Wm_emqa
dW_emqa	Integrand for total energy	J/m^3	dVol_emqa * W_emqa
Wm_emqa	Magnetic energy density	J/m^3	0.5 * (Hx_emqa * Bx_emqa+Hy_emqa * By_emqa)
FLtzx_emqa	Lorentz force contribution, x component	N/m^3	-Jz_emqa * By_emqa
FLtzy_emqa	Lorentz force contribution, y component	N/m^3	Jz_emqa * Bx_emqa
normFLtz_emqa	Lorentz force contribution, norm	N/m^3	sqrt(abs(FLtzx_emqa)^2+abs(FLtzy_emqa)^2)
normM_emqa	Magnetization, norm	A/m	sqrt(abs(Mx_emqa)^2+abs(My_emqa)^2)
normBr_emqa	Remanent flux density, norm	T	sqrt(abs(Brx_emqa)^2+abs(Bry_emqa)^2)
normH_emqa	Magnetic field, norm	A/m	sqrt(abs(Hx_emqa)^2+abs(Hy_emqa)^2)
normB_emqa	Magnetic flux density, norm	T	sqrt(abs(Bx_emqa)^2+abs(By_emqa)^2)
normJ_emqa	Total current density, norm	A/m^2	abs(Jz_emqa)
Evz_emqa	Lorentz electric field, z component	V/m	d(x,t) * By_emqa-d(y,t) * Bx_emqa
normEv_emqa	Lorentz electric field, norm	V/m	abs(Evz_emqa)
normPo_emqa	Power flow, time average, norm	W/m^2	sqrt(abs(Pox_emqa)^2+abs(Poy_emqa)^2)
absavgvx_g	|grad(avgv)|		
absga8x_g	|ga8x|		
absu2x_g2	|grad(u2)|		
absga9x_g2	|ga9x|		

9.2.2. Subdomain 2

Name	Description	Unit	Expression
U_ns	Velocity field	m/s	sqrt(u^2+v^2)
V_ns	Vorticity	1/s	vx-uy
divU_ns	Divergence of velocity field	1/s	ux+vy
cellRe_ns	Cell Reynolds number	1	rho_ns * U_ns * h/eta_ns
res_u_ns	Equation residual for u	N/m^3	rho_ns * (ut+u * ux+v * uy)+px-F_x_ns-eta_ns * (2 * uxx+uyy+vxy)
res_v_ns	Equation residual for v	N/m^3	rho_ns * (vt+u * vx+v * vy)+py-F_y_ns-eta_ns * (vxx+uyx+2 * vyy)
beta_x_ns	Convective field, x component	kg/(m^2*s)	rho_ns * u
beta_y_ns	Convective field, y	kg/(m^2*s)	rho_ns * v

	component		
Dm_ns	Mean diffusion coefficient	Pa*s	eta_ns
da_ns	Total time scale factor	kg/m^3	rho_ns
taum_ns	GLS time-scale	m^3*s/kg	nojac(1/max(2 * rho_ns * sqrt(emetric(u,v)),48 * eta_ns/h^2))
tauc_ns	GLS time-scale	m^2/s	0.5 * nojac(if(u^2+v^2
res_p_ns	Equation residual for p	kg/(m^3*s)	rho_ns * divU_ns
grad_w_x_di	Concentration gradient, w, x component	mol/m^4	wx
dflux_w_x_di	Diffusive flux, w, x component	mol/(m^2*s)	-Dxx_w_di * wx-Dxy_w_di * wy
grad_w_y_di	Concentration gradient, w, y component	mol/m^4	wy
dflux_w_y_di	Diffusive flux, w, y component	mol/(m^2*s)	-Dyx_w_di * wx-Dyy_w_di * wy
grad_w_di	Concentration gradient, w	mol/m^4	sqrt(grad_w_x_di^2+grad_w_y_di^2)
dflux_w_di	Diffusive flux, w	mol/(m^2*s)	sqrt(dflux_w_x_di^2+dflux_w_y_di^2)
grad_M_x_x_cd3	Concentration gradient, M_x, x component	mol/m^4	M_xx
dflux_M_x_x_cd3	Diffusive flux, M_x, x component	mol/(m^2*s)	-Dxx_M_x_cd3 * M_xx-Dxy_M_x_cd3 * M_xy
cflux_M_x_x_cd3	Convective flux, M_x, x component	mol/(m^2*s)	M_x * u_M_x_cd3
tflux_M_x_x_cd3	Total flux, M_x, x component	mol/(m^2*s)	dflux_M_x_x_cd3+cflux_M_x_x_cd3
grad_M_x_y_cd3	Concentration gradient, M_x, y component	mol/m^4	M_xy
dflux_M_x_y_cd3	Diffusive flux, M_x, y component	mol/(m^2*s)	-Dyx_M_x_cd3 * M_xx-Dyy_M_x_cd3 * M_xy
cflux_M_x_y_cd3	Convective flux, M_x, y component	mol/(m^2*s)	M_x * v_M_x_cd3
tflux_M_x_y_cd3	Total flux, M_x, y component	mol/(m^2*s)	dflux_M_x_y_cd3+cflux_M_x_y_cd3
beta_M_x_x_cd3	Convective field, M_x, x	m/s	u_M_x_cd3

	component		
beta_M_x_y_cd3	Convective field, M_x, y component	m/s	v_M_x_cd3
grad_M_x_cd3	Concentration gradient, M_x	mol/m^4	sqrt(grad_M_x_x_cd3^2+grad_M_x_y_cd3^2)
dflux_M_x_cd3	Diffusive flux, M_x	mol/(m^2*s)	sqrt(dflux_M_x_x_cd3^2+dflux_M_x_y_cd3^2)
cflux_M_x_cd3	Convective flux, M_x	mol/(m^2*s)	sqrt(cflux_M_x_x_cd3^2+cflux_M_x_y_cd3^2)
tflux_M_x_cd3	Total flux, M_x	mol/(m^2*s)	sqrt(tflux_M_x_x_cd3^2+tflux_M_x_y_cd3^2)
cellPe_M_x_cd3	Cell Peclet number, M_x	1	h * sqrt(beta_M_x_x_cd3^2+beta_M_x_y_cd3^2)/Dm_M_x_cd3
Dm_M_x_cd3	Mean diffusion coefficient, M_x	m^2/s	(Dxx_M_x_cd3 * u_M_x_cd3^2+Dxy_M_x_cd3 * u_M_x_cd3 * v_M_x_cd3+Dyx_M_x_cd3 * v_M_x_cd3 * u_M_x_cd3+Dyy_M_x_cd3 * v_M_x_cd3^2)/(u_M_x_cd3^2+v_M_x_cd3^2+eps)
res_M_x_cd3	Equation residual for M_x	mol/(m^3*s)	-Dxx_M_x_cd3 * M_xxx-Dxy_M_x_cd3 * M_xxy+M_xx * u_M_x_cd3-Dyx_M_x_cd3 * M_xyx-Dyy_M_x_cd3 * M_xyy+M_xy * v_M_x_cd3-R_M_x_cd3
res_sc_M_x_cd3	Shock capturing residual for M_x	mol/(m^3*s)	M_xx * u_M_x_cd3+M_xy * v_M_x_cd3-R_M_x_cd3
da_M_x_cd3	Total time scale factor, M_x	1	Dts_M_x_cd3
grad_M_y_x_cd	Concentration gradient, M_y, x component	mol/m^4	M_yx
dflux_M_y_x_cd	Diffusive flux, M_y, x component	mol/(m^2*s)	-Dxx_M_y_cd * M_yx-Dxy_M_y_cd * M_yy
cflux_M_y_x_cd	Convective flux, M_y, x component	mol/(m^2*s)	M_y * u_M_y_cd
tflux_M_y_x_cd	Total flux, M_y, x component	mol/(m^2*s)	dflux_M_y_x_cd+cflux_M_y_x_cd
grad_M_y_y_cd	Concentration gradient, M_y, y component	mol/m^4	M_yy
dflux_M_y_y_cd	Diffusive flux, M_y, y component	mol/(m^2*s)	-Dyx_M_y_cd * M_yx-Dyy_M_y_cd * M_yy
cflux_M_y_y_cd	Convective flux, M_y, y component	mol/(m^2*s)	M_y * v_M_y_cd
tflux_M_y_y_cd	Total flux, M_y, y component	mol/(m^2*s)	dflux_M_y_y_cd+cflux_M_y_y_cd
beta_M_y_x_cd	Convective field, M_y, x component	m/s	u_M_y_cd

beta_M_y_y_cd	Convective field, M_y, y component	m/s	v_M_y_cd
grad_M_y_cd	Concentration gradient, M_y	mol/m^4	sqrt(grad_M_y_x_cd^2+grad_M_y_y_cd^2)
dflux_M_y_cd	Diffusive flux, M_y	mol/(m^2*s)	sqrt(dflux_M_y_x_cd^2+dflux_M_y_y_cd^2)
cflux_M_y_cd	Convective flux, M_y	mol/(m^2*s)	sqrt(cflux_M_y_x_cd^2+cflux_M_y_y_cd^2)
tflux_M_y_cd	Total flux, M_y	mol/(m^2*s)	sqrt(tflux_M_y_x_cd^2+tflux_M_y_y_cd^2)
cellPe_M_y_cd	Cell Peclet number, M_y	1	h * sqrt(beta_M_y_x_cd^2+beta_M_y_y_cd^2)/Dm_M_y_cd
Dm_M_y_cd	Mean diffusion coefficient, M_y	m^2/s	(Dxx_M_y_cd * u_M_y_cd^2+Dxy_M_y_cd * u_M_y_cd * v_M_y_cd+Dyx_M_y_cd * v_M_y_cd * u_M_y_cd+Dyy_M_y_cd * v_M_y_cd^2)/(u_M_y_cd^2+v_M_y_cd^2+eps)
res_M_y_cd	Equation residual for M_y	mol/(m^3*s)	-Dxx_M_y_cd * M_yxx-Dxy_M_y_cd * M_yxy+M_yx * u_M_y_cd-Dyx_M_y_cd * M_yyx-Dyy_M_y_cd * M_yyy+M_yy * v_M_y_cd-R_M_y_cd
res_sc_M_y_cd	Shock capturing residual for M_y	mol/(m^3*s)	M_yx * u_M_y_cd+M_yy * v_M_y_cd-R_M_y_cd
da_M_y_cd	Total time scale factor, M_y	1	Dts_M_y_cd
dr_guess_emqa	Width in radial direction default guess	m	0
R0_guess_emqa	Inner radius default guess	m	0
Sx_emqa	Infinite element x coordinate	m	x
S0x_guess_emqa	Inner x coordinate default guess	m	0
Sdx_guess_emqa	Width in x direction default guess	m	0
Sy_emqa	Infinite element y coordinate	m	y
S0y_guess_emqa	Inner y coordinate default guess	m	0
Sdy_guess_emqa	Width in y direction default guess	m	0
curlAx_emqa	Curl of magnetic potential, x component	T	Azy

curlAy_emqa	Curl of magnetic potential, y component	T	-Azx
dVol_emqa	Volume integration contribution	1	detJ_emqa
Bx_emqa	Magnetic flux density, x component	T	curlAx_emqa
By_emqa	Magnetic flux density, y component	T	curlAy_emqa
Hx_emqa	Magnetic field, x component	A/m	Bx_emqa/mu0_emqa-Mx_emqa
Hy_emqa	Magnetic field, y component	A/m	By_emqa/mu0_emqa-My_emqa
mu_emqa	Permeability	H/m	mu0_emqa * mur_emqa
muxx_emqa	Permeability, xx component	H/m	mu0_emqa * murxx_emqa
muxy_emqa	Permeability, xy component	H/m	mu0_emqa * murxy_emqa
muyx_emqa	Permeability, yx component	H/m	mu0_emqa * muryx_emqa
muyy_emqa	Permeability, yy component	H/m	mu0_emqa * muryy_emqa
Jpz_emqa	Potential current density, z component	A/m^2	sigma_emqa * deltaV_emqa/L_emqa
Ez_emqa	Electric field, z component	V/m	-d(Az,t)
Jz_emqa	Total current density, z component	A/m^2	Jpz_emqa+Jiz_emqa+Jez_emqa
Pox_emqa	Power flow, x component	W/m^2	-Ez_emqa * Hy_emqa
Poy_emqa	Power flow, y component	W/m^2	Ez_emqa * Hx_emqa
normE_emqa	Electric field, norm	V/m	abs(Ez_emqa)
Jiz_emqa	Induced current density, z component	A/m^2	sigma_emqa * Ez_emqa
Q_emqa	Resistive heating	W/m^3	Jz_emqa * (Ez_emqa+deltaV_emqa/L_emqa)
W_emqa	Total energy density	J/m^3	Wm_emqa
dW_emqa	Integrand for total energy	Pa	dVol_emqa * W_emqa
Wm_emqa	Magnetic energy density	J/m^3	0.5 * (Hx_emqa * Bx_emqa+Hy_emqa * By_emqa+Mx_emqa * Bx_emqa+My_emqa * By_emqa)

FLtzx_emqa	Lorentz force contribution, x component	N/m^3	-Jz_emqa * By_emqa
FLtzy_emqa	Lorentz force contribution, y component	N/m^3	Jz_emqa * Bx_emqa
normFLtz_emqa	Lorentz force contribution, norm	N/m^3	sqrt(abs(FLtzx_emqa)^2+abs(FLtzy_emqa)^2)
normM_emqa	Magnetization, norm	A/m	sqrt(abs(Mx_emqa)^2+abs(My_emqa)^2)
normBr_emqa	Remanent flux density, norm	T	sqrt(abs(Brx_emqa)^2+abs(Bry_emqa)^2)
normH_emqa	Magnetic field, norm	A/m	sqrt(abs(Hx_emqa)^2+abs(Hy_emqa)^2)
normB_emqa	Magnetic flux density, norm	T	sqrt(abs(Bx_emqa)^2+abs(By_emqa)^2)
normJ_emqa	Total current density, norm	A/m^2	abs(Jz_emqa)
Evz_emqa	Lorentz electric field, z component	V/m	d(x,t) * By_emqa-d(y,t) * Bx_emqa
normEv_emqa	Lorentz electric field, norm	V/m	abs(Evz_emqa)
normPo_emqa	Power flow, time average, norm	W/m^2	sqrt(abs(Pox_emqa)^2+abs(Poy_emqa)^2)
absavgvx_g	|grad(avgv)|		sqrt(avgvx^2+avgvy^2)
absga8x_g	|ga8x|		sqrt(ga8x^2+ga8y^2)
absu2x_g2	|grad(u2)|		sqrt(u2x^2+u2y^2)
absga9x_g2	|ga9x|		sqrt(ga9x^2+ga9y^2)

B2. COMSOL Simulation Using Scalar Potential Boundary Condition Method (Chaves 143G case, $\eta'=6x10^{-10}$) (Section 4.4.3.2)

2D case cylinder with Chaves's parameters

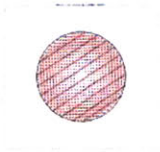

1. Table of Contents

2. Model Properties

Property	Value
Model name	2D case cylinder with Chaves's parameters
Author	Shahriar Khushrushahi
Company	MIT
Department	EECS
Reference	
URL	
Saved date	Feb 16, 2010 1:21:37 PM
Creation date	Sep 19, 2008 9:32:16 PM
COMSOL version	COMSOL 3.5.0.603

File name: D:\Documents and Settings\Administrator\Desktop\Comsol_Testbed\GoodFiles\Good2DCylinderfiles\2Dcylinder_finlaysonsmethod_etaprime6em10_demagfields_Chaves_143G.mph

Application modes and modules used in this model:

- Geom1 (2D)
  - Incompressible Navier-Stokes
  - Diffusion
  - Convection and Diffusion
  - Convection and Diffusion
  - PDE, General Form
  - PDE, General Form

2.1. Model description

Rotation of Ferrofluid in a rotating magnetic field in an infinitely long cylinder

Using Parameters from Chaves Paper of 2008 on spinup Flow

Using parameters for EMG900_2 trying to get plot similar to Fig 5b

The values used in this model correspond to normalizing to 14.3mT values from his paper. The normalized values can be calculated from Calculating_Different_Parameters.xls under EMG900

Using my normalization scheme outlined in VeryifyingShihabsmethod_081205.doc

This method uses scalar potential similar to Finlaysons Comsol paper

Etaprime non0 case

Etaprime of 6e-10 quoted in Chaves's paper is used

3. Constants

Name	Expression	Value	Description
Xi	1.19		
omega	2*pi*f		
zeta	0.00048		
eta	0.0074		
etaprime	1.61e-6		
f	85		
tau	1e-6		
omegatau	omega*tau		
R0	0.027		
I	2/3		
H0	1		

4. Global Expressions

Name	Expression	Unit	Description
FMx	M_x*(-psixx)+M_y*(-psixy)		\
FMy	M_x*(-psiyx)+M_y*(-psiyy)		
T	M_x*Hy-M_y*Hx		
M_eqx	(Xi*Hx)		
M_eqy	(Xi*Hy)		
Hx	-psix-M_x/2		
Hy	-psiy-M_y/2		
phi	atan2(y,x)	rad	

5. Geometry

Number of geometries: 1

5.1. Geom1

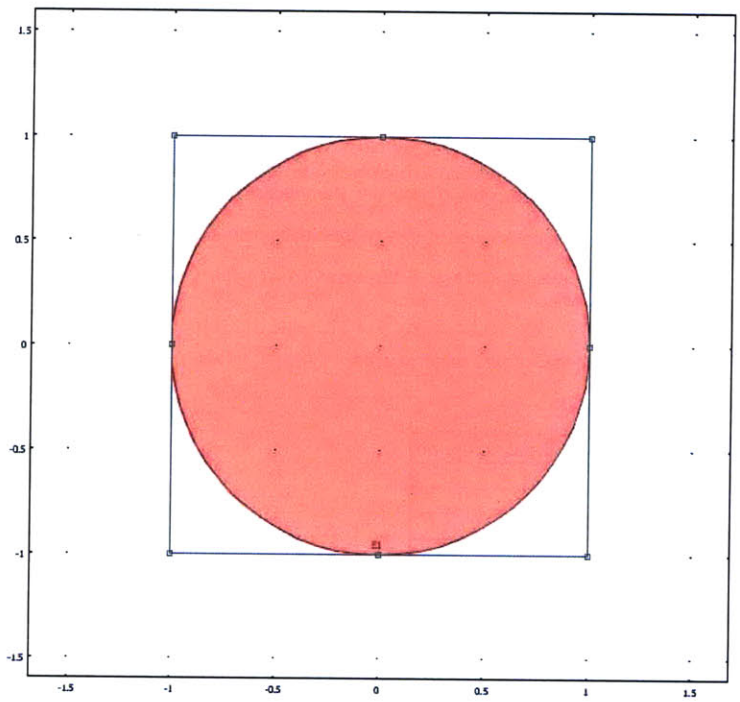

5.1.1. Point mode

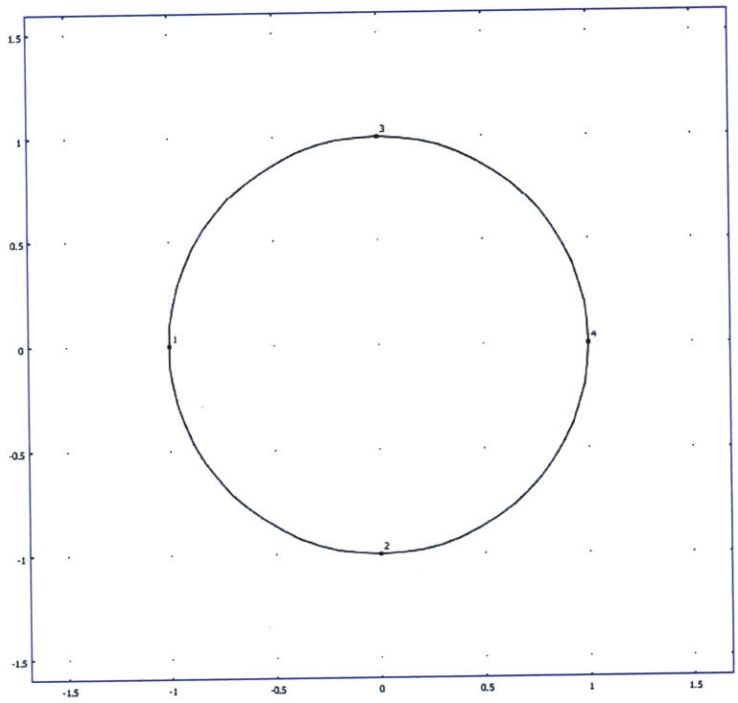

5.1.2. Boundary mode

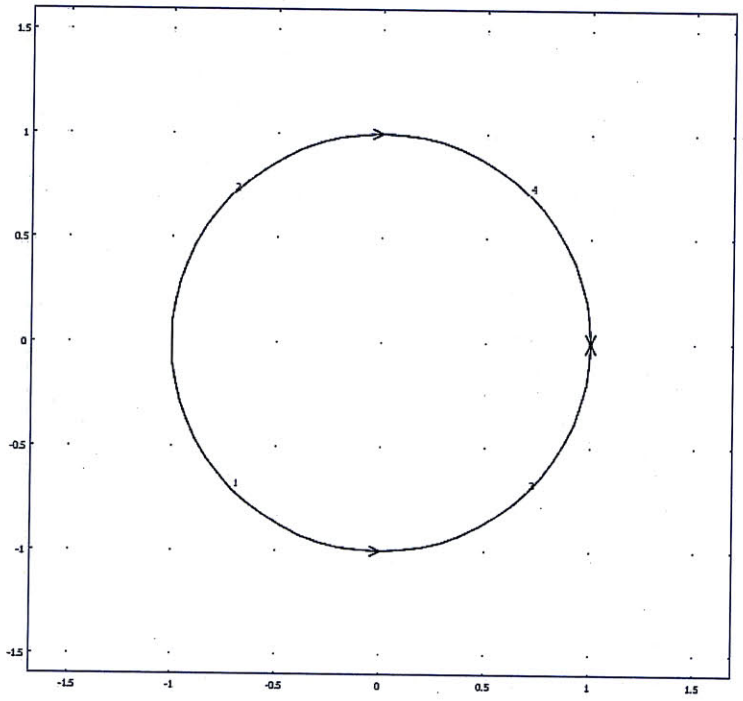

5.1.3. Subdomain mode

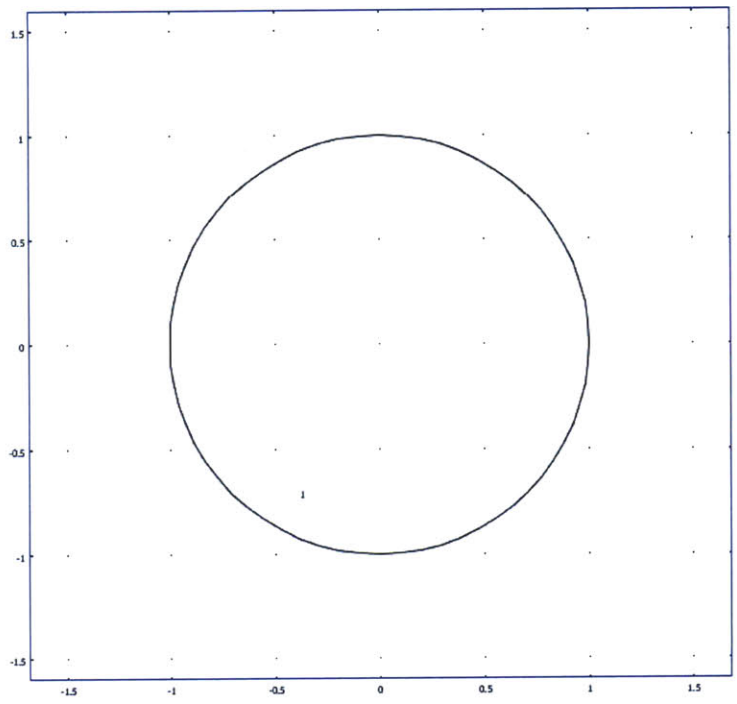

6. Geom1

Space dimensions: 2D

Independent variables: x, y, z

6.1. Mesh

6.1.1. Mesh Statistics

Number of degrees of freedom	66110
Number of mesh points	2319
Number of elements	4476
Triangular	4476
Quadrilateral	0
Number of boundary elements	160
Number of vertex elements	4
Minimum element quality	0.901
Element area ratio	0.254

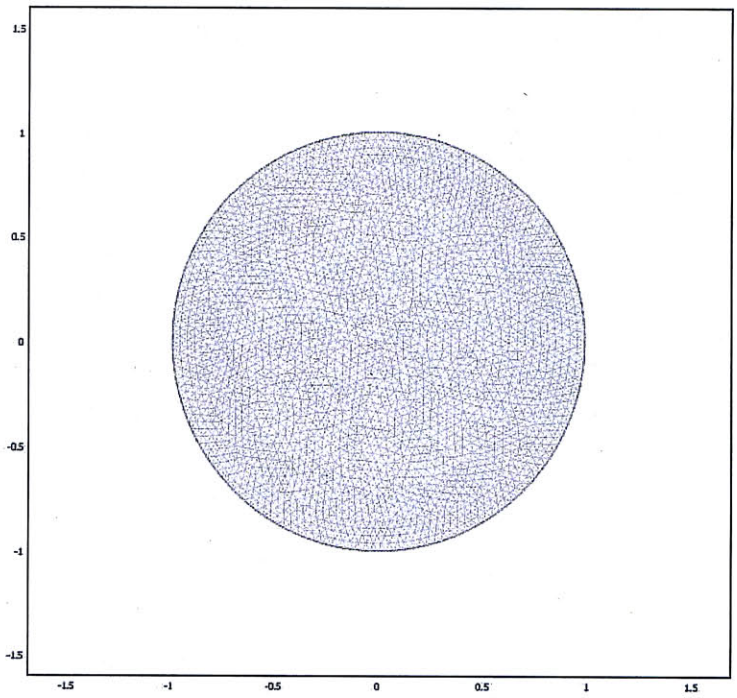

6.2. Application Mode: Incompressible Navier-Stokes (ns)

Application mode type: Incompressible Navier-Stokes

Application mode name: ns

6.2.1. Scalar Variables

Name	Variable	Value	Unit	Description
visc_vel_fact	visc_vel_fact_ns	10	1	Viscous velocity factor

6.2.2. Application Mode Properties

Property	Value
Default element type	Lagrange - P_2 P_1
Analysis type	Transient
Corner smoothing	Off
Frame	Frame (ref)
Weak constraints	Off
Constraint type	Ideal

6.2.3. Variables

Dependent variables: u, v, p, nxw, nyw

Shape functions: shlag(2,'u'), shlag(2,'V'), shlag(1,'p')

Interior boundaries not active

6.2.4. Point Settings

Point	2-4	1
pnton	0	1

6.2.5. Boundary Settings

Boundary	1-4
Type	Wall

6.2.6. Subdomain Settings

Subdomain		1
Integration order (gporder)		**4 4 2**
Constraint order (cporder)		**2 2 1**
Density (rho)	kg/m^3	**0**
Dynamic viscosity (eta)	Pa·s	**eta+zeta**
Volume force, x dir. (F_x)	N/m^3	**2*zeta*wy+FMx**
Volume force, y dir. (F_y)	N/m^3	**-2*zeta*wx+FMy**
cdon		**0**

6.3. Application Mode: Diffusion (di)

Application mode type: Diffusion

Application mode name: di

6.3.1. Application Mode Properties

Property	Value
Default element type	Lagrange - Quadratic
Analysis type	Stationary
Frame	Frame (ref)
Weak constraints	Off
Constraint type	Ideal

6.3.2. Variables

Dependent variables: w

Shape functions: shlag(2,'w')

Interior boundaries not active

6.3.3. Boundary Settings

Boundary	1-4
Type	Concentration

6.3.4. Subdomain Settings

Subdomain		1
Diffusion coefficient (D)	m^2/s	**etaprime**
Reaction rate (R)	$mol/(m^3 \cdot s)$	**T+2*zeta*(vx-uy-2*w)**

6.4. Application Mode: Convection and Diffusion (cd3)

Application mode type: Convection and Diffusion

Application mode name: cd3

6.4.1. Application Mode Properties

Property	Value
Default element type	Lagrange - Quadratic
Analysis type	Transient
Equation form	Non-conservative
Frame	Frame (ref)
Weak constraints	Off
Constraint type	Ideal

6.4.2. Variables

Dependent variables: M_x

Shape functions: shlag(2,'M_x')

Interior boundaries not active

6.4.3. Boundary Settings

Boundary	1-4
Type	Insulation/Symmetry

6.4.4. Subdomain Settings

Subdomain		1
Diffusion coefficient (D)	m^2/s	**0**
Reaction rate (R)	$mol/(m^3 \cdot s)$	**-w*M_y-((M_x-M_eqx)/omegatau)**
x-velocity (u)	m/s	**u**
y-velocity (v)	m/s	**v**

6.5. Application Mode: Convection and Diffusion (cd)

Application mode type: Convection and Diffusion

Application mode name: cd

6.5.1. Application Mode Properties

Property	Value
Default element type	Lagrange - Quadratic
Analysis type	Transient
Equation form	Non-conservative
Frame	Frame (ref)
Weak constraints	Off
Constraint type	Ideal

6.5.2. Variables

Dependent variables: M_y

Shape functions: shlag(2,'M_y')

Interior boundaries not active

6.5.3. Boundary Settings

Boundary	1-4
Type	Insulation/Symmetry

6.5.4. Subdomain Settings

Subdomain		1
Diffusion coefficient (D)	m^2/s	**0**
Reaction rate (R)	$mol/(m^3 \cdot s)$	**w*M_x-((M_y-M_eqy)/omegatau)**
x-velocity (u)	m/s	**u**
y-velocity (v)	m/s	**v**

6.6. Application Mode: PDE, General Form (g)

Application mode type: PDE, General Form

Application mode name: g

6.6.1. Application Mode Properties

Property	Value
Default element type	Lagrange - Quadratic
Wave extension	Off
Frame	Frame (ref)
Weak constraints	Off

6.6.2. Variables

Dependent variables: psi, psi_t

Shape functions: shlag(2,'psi')

Interior boundaries not active

6.6.3. Boundary Settings

Boundary	1-4
Type	Dirichlet boundary condition
(r)	-psi+H0*(x*cos(t)+y*sin(t))

6.6.4. Subdomain Settings

Subdomain	1
Damping/Mass coefficient (da)	0
Source term (f)	-M_xx-M_yy

6.7. Application Mode: PDE, General Form (g2)

Application mode type: PDE, General Form

Application mode name: g2

6.7.1. Application Mode Properties

Property	Value
Default element type	Lagrange - Quadratic
Wave extension	Off
Frame	Frame (ref)
Weak constraints	Off

6.7.2. Variables

Dependent variables: u2, u2_t

Shape functions: shlag(2,'u2')

Interior boundaries not active

6.7.3. Boundary Settings

Boundary	1-4
Type	Dirichlet boundary condition

6.7.4. Subdomain Settings

Subdomain	1
Source term (f)	v
Conservative flux source term (ga)	{{0;0}}

7. Solver Settings

Solve using a script: off

Analysis type	Transient
Auto select solver	On
Solver	Time dependent
Solution form	Automatic
Symmetric	auto
Adaptive mesh refinement	Off
Optimization/Sensitivity	Off
Plot while solving	Off

7.1. Direct (UMFPACK)

Solver type: Linear system solver

Parameter	Value
Pivot threshold	0.1
Memory allocation factor	0.7

7.2. Time Stepping

Parameter	Value
Times	range(0,0.1,10)
Relative tolerance	0.0001
Absolute tolerance	0.000010
Times to store in output	Specified times
Time steps taken by solver	Free
Maximum BDF order	5
Singular mass matrix	Maybe
Consistent initialization of DAE systems	Backward Euler
Error estimation strategy	Include algebraic
Allow complex numbers	Off

7.3. Advanced

Parameter	Value
Constraint handling method	Elimination
Null-space function	Automatic
Automatic assembly block size	On
Assembly block size	5000
Use Hermitian transpose of constraint matrix and in symmetry detection	Off
Use complex functions with real input	Off
Stop if error due to undefined operation	On
Store solution on file	Off
Type of scaling	Automatic
Manual scaling	
Row equilibration	On
Manual control of reassembly	Off
Load constant	On
Constraint constant	On

Mass constant	On
Damping (mass) constant	On
Jacobian constant	On
Constraint Jacobian constant	On

8. Postprocessing

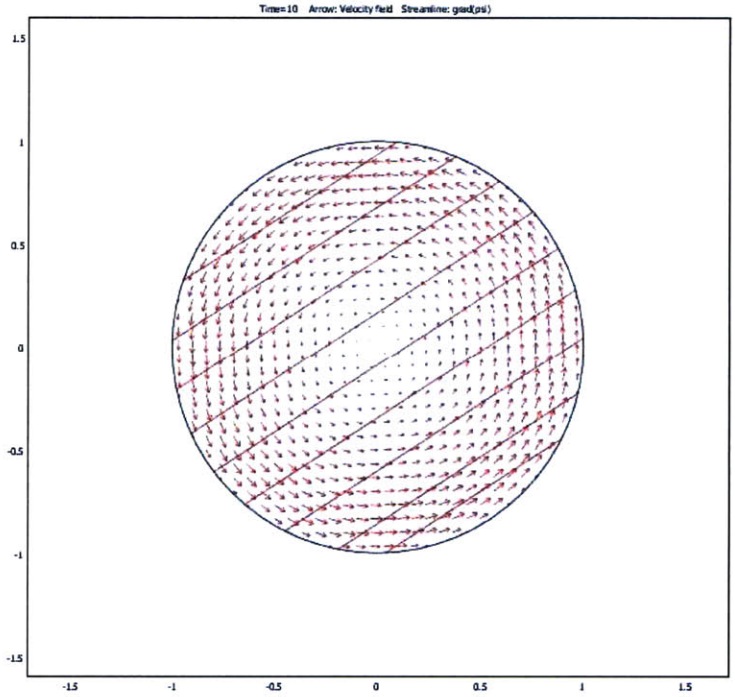

9. Variables

9.1. Boundary

Name	Description	Unit	Expression
K_x_ns	Viscous force per area, x component	Pa	eta_ns * (2 * nx_ns * ux+ny_ns * (uy+vx))
T_x_ns	Total force per area, x component	Pa	-nx_ns * p+2 * nx_ns * eta_ns * ux+ny_ns * eta_ns * (uy+vx)
K_y_ns	Viscous force per area, y component	Pa	eta_ns * (nx_ns * (vx+uy)+2 * ny_ns * vy)
T_y_ns	Total force per area, y component	Pa	-ny_ns * p+nx_ns * eta_ns * (vx+uy)+2 * ny_ns * eta_ns * vy
ndflux_w_di	Normal diffusive flux, w	mol/(m^2*s)	nx_di * dflux_w_x_di+ny_di * dflux_w_y_di

ndflux_M_x_cd3	Normal diffusive flux, M_x	mol/(m^2*s)	nx_cd3 * dflux_M_x_x_cd3+ny_cd3 * dflux_M_x_y_cd3
ncflux_M_x_cd3	Normal convective flux, M_x	mol/(m^2*s)	nx_cd3 * cflux_M_x_x_cd3+ny_cd3 * cflux_M_x_y_cd3
ntflux_M_x_cd3	Normal total flux, M_x	mol/(m^2*s)	nx_cd3 * tflux_M_x_x_cd3+ny_cd3 * tflux_M_x_y_cd3
ndflux_M_y_cd	Normal diffusive flux, M_y	mol/(m^2*s)	nx_cd * dflux_M_y_x_cd+ny_cd * dflux_M_y_y_cd
ncflux_M_y_cd	Normal convective flux, M_y	mol/(m^2*s)	nx_cd * cflux_M_y_x_cd+ny_cd * cflux_M_y_y_cd
ntflux_M_y_cd	Normal total flux, M_y	mol/(m^2*s)	nx_cd * tflux_M_y_x_cd+ny_cd * tflux_M_y_y_cd

9.2. Subdomain

Name	Description	Unit	Expression
U_ns	Velocity field	m/s	sqrt(u^2+v^2)
V_ns	Vorticity	1/s	vx-uy
divU_ns	Divergence of velocity field	1/s	ux+vy
cellRe_ns	Cell Reynolds number	1	rho_ns * U_ns * h/eta_ns
res_u_ns	Equation residual for u	N/m^3	rho_ns * (ut+u * ux+v * uy)+px-F_x_ns-eta_ns * (2 * uxx+uyy+vxy)
res_v_ns	Equation residual for v	N/m^3	rho_ns * (vt+u * vx+v * vy)+py-F_y_ns-eta_ns * (vxx+uyx+2 * vyy)
beta_x_ns	Convective field, x component	kg/(m^2*s)	rho_ns * u
beta_y_ns	Convective field, y component	kg/(m^2*s)	rho_ns * v
Dm_ns	Mean diffusion coefficient	Pa*s	eta_ns
da_ns	Total time scale factor	kg/m^3	rho_ns
taum_ns	GLS time-scale	m^3*s/kg	nojac(1/max(2 * rho_ns * sqrt(emetric(u,v)),48 * eta_ns/h^2))
tauc_ns	GLS time-scale	m^2/s	0.5 * nojac(if(u^2+v^2
res_p_ns	Equation residual for p	kg/(m^3*s)	rho_ns * divU_ns
grad_w_x_di	Concentration gradient, w, x component	mol/m^4	wx
dflux_w_x_di	Diffusive flux, w, x component	mol/(m^2*s)	-Dxx_w_di * wx-Dxy_w_di * wy
grad_w_y_di	Concentration gradient, w, y component	mol/m^4	wy

dflux_w_y_di	Diffusive flux, w, y component	mol/(m^2*s)	-Dyx_w_di * wx-Dyy_w_di * wy
grad_w_di	Concentration gradient, w	mol/m^4	sqrt(grad_w_x_di^2+grad_w_y_di^2)
dflux_w_di	Diffusive flux, w	mol/(m^2*s)	sqrt(dflux_w_x_di^2+dflux_w_y_di^2)
grad_M_x_x_cd3	Concentration gradient, M_x, x component	mol/m^4	M_xx
dflux_M_x_x_cd3	Diffusive flux, M_x, x component	mol/(m^2*s)	-Dxx_M_x_cd3 * M_xx-Dxy_M_x_cd3 * M_xy
cflux_M_x_x_cd3	Convective flux, M_x, x component	mol/(m^2*s)	M_x * u_M_x_cd3
tflux_M_x_x_cd3	Total flux, M_x, x component	mol/(m^2*s)	dflux_M_x_x_cd3+cflux_M_x_x_cd3
grad_M_x_y_cd3	Concentration gradient, M_x, y component	mol/m^4	M_xy
dflux_M_x_y_cd3	Diffusive flux, M_x, y component	mol/(m^2*s)	-Dyx_M_x_cd3 * M_xx-Dyy_M_x_cd3 * M_xy
cflux_M_x_y_cd3	Convective flux, M_x, y component	mol/(m^2*s)	M_x * v_M_x_cd3
tflux_M_x_y_cd3	Total flux, M_x, y component	mol/(m^2*s)	dflux_M_x_y_cd3+cflux_M_x_y_cd3
beta_M_x_x_cd3	Convective field, M_x, x component	m/s	u_M_x_cd3
beta_M_x_y_cd3	Convective field, M_x, y component	m/s	v_M_x_cd3
grad_M_x_cd3	Concentration gradient, M_x	mol/m^4	sqrt(grad_M_x_x_cd3^2+grad_M_x_y_cd3^2)
dflux_M_x_cd3	Diffusive flux, M_x	mol/(m^2*s)	sqrt(dflux_M_x_x_cd3^2+dflux_M_x_y_cd3^2)
cflux_M_x_cd3	Convective flux, M_x	mol/(m^2*s)	sqrt(cflux_M_x_x_cd3^2+cflux_M_x_y_cd3^2)
tflux_M_x_cd3	Total flux, M_x	mol/(m^2*s)	sqrt(tflux_M_x_x_cd3^2+tflux_M_x_y_cd3^2)
cellPe_M_x_cd3	Cell Peclet number, M_x	1	h * sqrt(beta_M_x_x_cd3^2+beta_M_x_y_cd3^2)/Dm_M_x_cd3
Dm_M_x_cd3	Mean diffusion coefficient, M_x	m^2/s	(Dxx_M_x_cd3 * u_M_x_cd3^2+Dxy_M_x_cd3 * u_M_x_cd3 * v_M_x_cd3+Dyx_M_x_cd3 * v_M_x_cd3 * u_M_x_cd3+Dyy_M_x_cd3 * v_M_x_cd3^2)/(u_M_x_cd3^2+v_M_x_cd3^2+eps)

res_M_x_cd3	Equation residual for M_x	mol/(m^3*s)	-Dxx_M_x_cd3 * M_xxx-Dxy_M_x_cd3 * M_xxy+M_xx * u_M_x_cd3-Dyx_M_x_cd3 * M_xyx-Dyy_M_x_cd3 * M_xyy+M_xy * v_M_x_cd3-R_M_x_cd3
res_sc_M_x_cd3	Shock capturing residual for M_x	mol/(m^3*s)	M_xx * u_M_x_cd3+M_xy * v_M_x_cd3-R_M_x_cd3
da_M_x_cd3	Total time scale factor, M_x	1	Dts_M_x_cd3
grad_M_y_x_cd	Concentration gradient, M_y, x component	mol/m^4	M_yx
dflux_M_y_x_cd	Diffusive flux, M_y, x component	mol/(m^2*s)	-Dxx_M_y_cd * M_yx-Dxy_M_y_cd * M_yy
cflux_M_y_x_cd	Convective flux, M_y, x component	mol/(m^2*s)	M_y * u_M_y_cd
tflux_M_y_x_cd	Total flux, M_y, x component	mol/(m^2*s)	dflux_M_y_x_cd+cflux_M_y_x_cd
grad_M_y_y_cd	Concentration gradient, M_y, y component	mol/m^4	M_yy
dflux_M_y_y_cd	Diffusive flux, M_y, y component	mol/(m^2*s)	-Dyx_M_y_cd * M_yx-Dyy_M_y_cd * M_yy
cflux_M_y_y_cd	Convective flux, M_y, y component	mol/(m^2*s)	M_y * v_M_y_cd
tflux_M_y_y_cd	Total flux, M_y, y component	mol/(m^2*s)	dflux_M_y_y_cd+cflux_M_y_y_cd
beta_M_y_x_cd	Convective field, M_y, x component	m/s	u_M_y_cd
beta_M_y_y_cd	Convective field, M_y, y component	m/s	v_M_y_cd
grad_M_y_cd	Concentration gradient, M_y	mol/m^4	sqrt(grad_M_y_x_cd^2+grad_M_y_y_cd^2)
dflux_M_y_cd	Diffusive flux, M_y	mol/(m^2*s)	sqrt(dflux_M_y_x_cd^2+dflux_M_y_y_cd^2)
cflux_M_y_cd	Convective flux, M_y	mol/(m^2*s)	sqrt(cflux_M_y_x_cd^2+cflux_M_y_y_cd^2)
tflux_M_y_cd	Total flux, M_y	mol/(m^2*s)	sqrt(tflux_M_y_x_cd^2+tflux_M_y_y_cd^2)
cellPe_M_y_cd	Cell Peclet number, M_y	1	h * sqrt(beta_M_y_x_cd^2+beta_M_y_y_cd^2)/Dm_M_y_cd

Dm_M_y_cd	Mean diffusion coefficient, M_y	m^2/s	(Dxx_M_y_cd * u_M_y_cd^2+Dxy_M_y_cd * u_M_y_cd * v_M_y_cd+Dyx_M_y_cd * v_M_y_cd * u_M_y_cd+Dyy_M_y_cd * v_M_y_cd^2)/(u_M_y_cd^2+v_M_y_cd^2+eps)
res_M_y_cd	Equation residual for M_y	mol/(m^3*s)	-Dxx_M_y_cd * M_yxx-Dxy_M_y_cd * M_yxy+M_yx * u_M_y_cd-Dyx_M_y_cd * M_yyx-Dyy_M_y_cd * M_yyy+M_yy * v_M_y_cd-R_M_y_cd
res_sc_M_y_cd	Shock capturing residual for M_y	mol/(m^3*s)	M_yx * u_M_y_cd+M_yy * v_M_y_cd-R_M_y_cd
da_M_y_cd	Total time scale factor, M_y	1	Dts_M_y_cd
abspsix_g	|grad(psi)|		sqrt(psix^2+psiy^2)
absga7x_g	|ga7x|		sqrt(ga7x^2+ga7y^2)
absu2x_g2	|grad(u2)|		sqrt(u2x^2+u2y^2)
absga8x_g2	|ga8x|		sqrt(ga8x^2+ga8y^2)

B3. COMSOL Simulation of Chaves 125G Case, $\eta'=6x10^{-10}$ (Section 4.4.4.1)

2D case cylinder with Chaves's parameters

1. Table of Contents

2. Model Properties

Property	Value
Model name	2D case cylinder with Chaves's parameters
Author	Shahriar Khushrushahi
Company	MIT
Department	EECS
Reference	
URL	
Saved date	Feb 16, 2010 1:20:31 PM
Creation date	Sep 19, 2008 9:32:16 PM
COMSOL version	COMSOL 3.5.0.603

File name: D:\Documents and Settings\Administrator\Desktop\Comsol_Testbed\GoodFiles\Good2DCylinderfiles\2Dcylinder_finlaysonsmethod_etaprime6em10_demagfields_Chaves_125G.mph

Application modes and modules used in this model:

- Geom1 (2D)
  - Incompressible Navier-Stokes
  - Diffusion
  - Convection and Diffusion
  - Convection and Diffusion
  - PDE, General Form
  - PDE, General Form

2.1. Model description

Rotation of Ferrofluid in a rotating magnetic field in an infinitely long cylinder

Using Parameters from Chaves Paper of 2008 on spinup Flow

Using parameters for EMG900_2 trying to get plot similar to Fig 5b

The values used in this model correspond to normalizing to 12.5mT values from his paper. The normalized values can be calculated from Calculating_Different_Parameters.xls under EMG900

Using my normalization scheme outlined in VeryifyingShihabsmethod_081205.doc

This method uses scalar potential similar to Finlaysons Comsol paper

Etaprime of 6e-10 quoted by Chaves in his paper is used

3. Constants

Name	Expression	Value	Description
Xi	1.19		
omega	2*pi*f		
zeta	0.00062		
eta	0.0097		
etaprime	2.11e-6		
f	85		
tau	1e-6		
omegatau	omega*tau		
R0	0.027		
I	2/3		
H0	1		

4. Global Expressions

Name	Expression	Unit	Description
FMx	M_x*(-psixx)+M_y*(-psixy)		\
FMy	M_x*(-psiyx)+M_y*(-psiyy)		
T	M_x*Hy-M_y*Hx		
M_eqx	(Xi*Hx)		
M_eqy	(Xi*Hy)		
Hx	-psix-M_x/2		
Hy	-psiy-M_y/2		
phi	atan2(y,x)	rad	

5. Geometry

Number of geometries: 1

5.1. Geom1

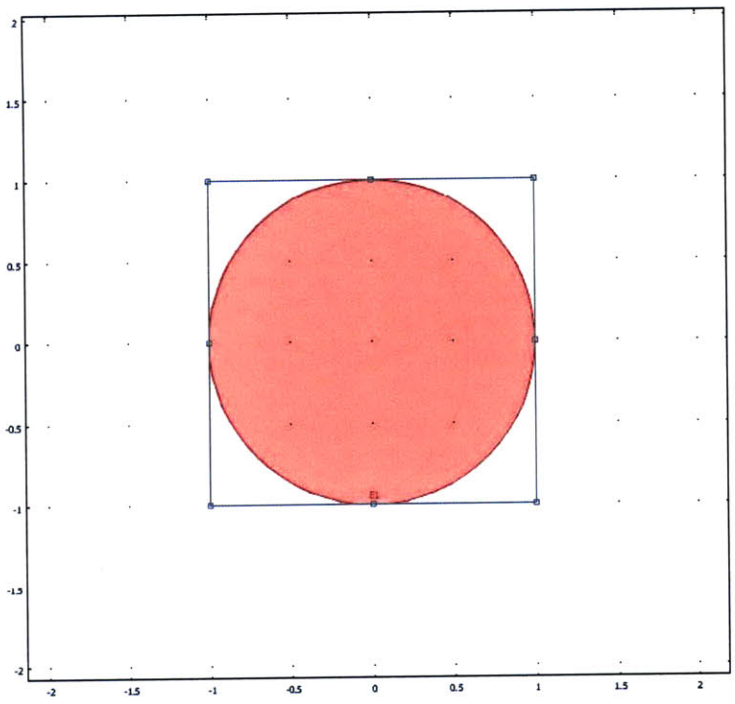

5.1.1. Point mode

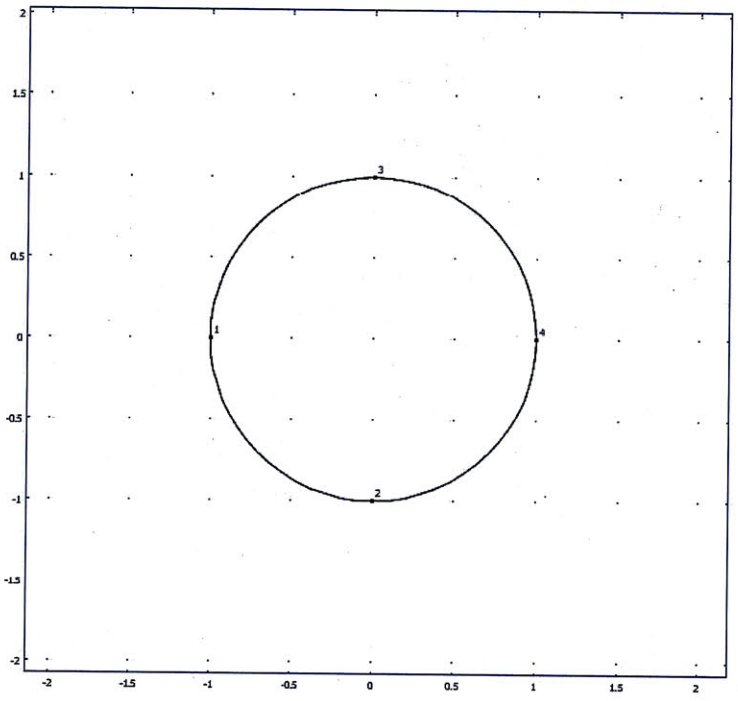

5.1.2. Boundary mode

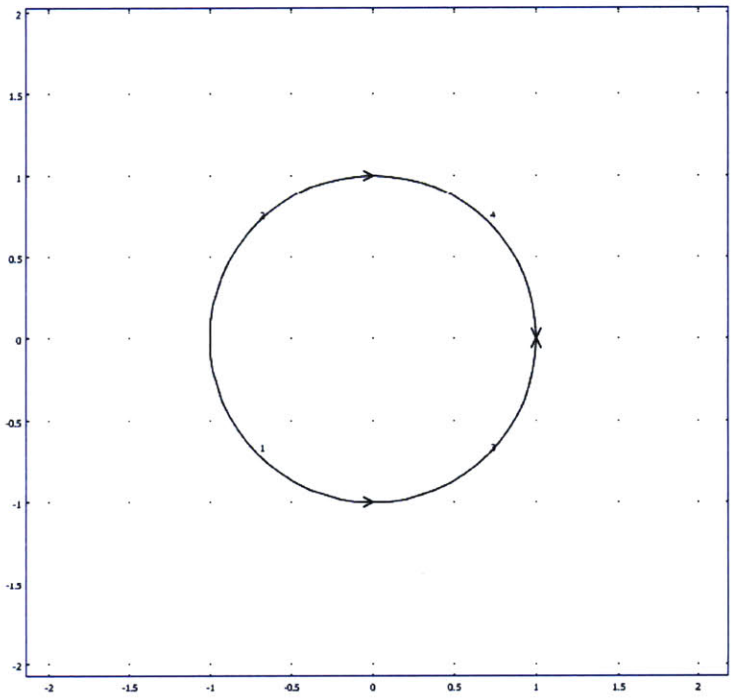

5.1.3. Subdomain mode

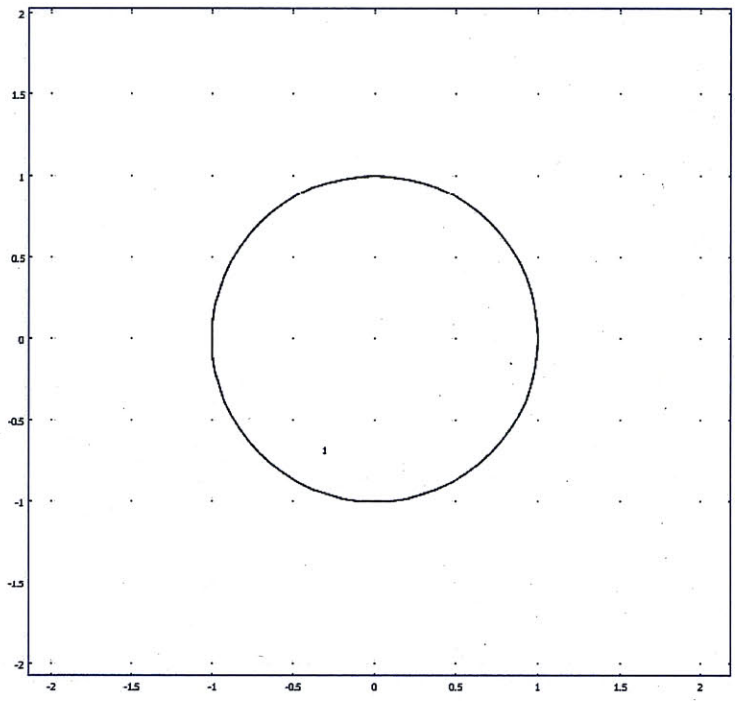

6. Geom1

Space dimensions: 2D

Independent variables: x, y, z

6.1. Mesh

6.1.1. Mesh Statistics

Number of degrees of freedom	66110
Number of mesh points	2319
Number of elements	4476
Triangular	4476
Quadrilateral	0
Number of boundary elements	160
Number of vertex elements	4
Minimum element quality	0.901
Element area ratio	0.254

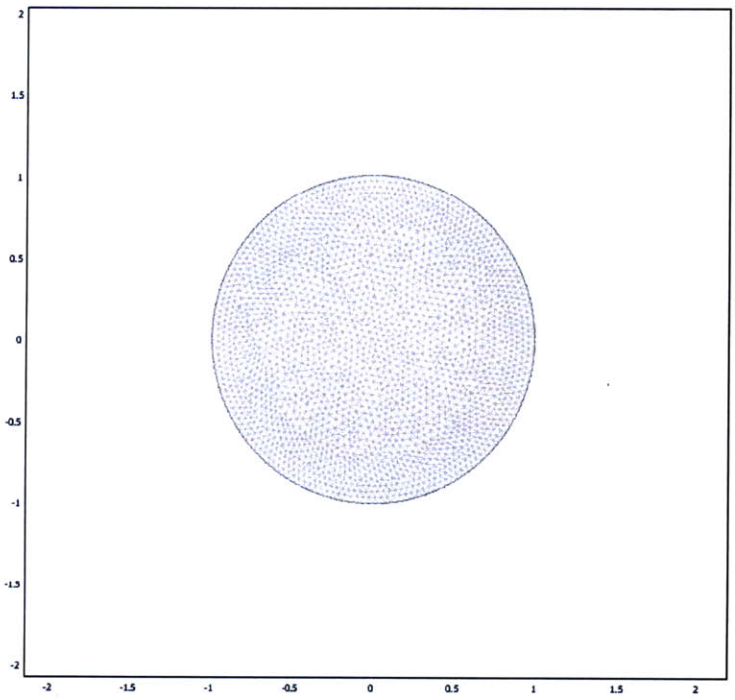

6.2. Application Mode: Incompressible Navier-Stokes (ns)

Application mode type: Incompressible Navier-Stokes

Application mode name: ns

6.2.1. Scalar Variables

Name	Variable	Value	Unit	Description
visc_vel_fact	visc_vel_fact_ns	10	1	Viscous velocity factor

6.2.2. Application Mode Properties

Property	Value
Default element type	Lagrange - P_2 P_1
Analysis type	Transient
Corner smoothing	Off
Frame	Frame (ref)
Weak constraints	Off
Constraint type	Ideal

6.2.3. Variables

Dependent variables: u, v, p, nxw, nyw

Shape functions: shlag(2,'u'), shlag(2,'v'), shlag(1,'p')

Interior boundaries not active

6.2.4. Point Settings

Point	2-4	1
pnton	0	1

6.2.5. Boundary Settings

Boundary	1-4
Type	Wall

6.2.6. Subdomain Settings

Subdomain		1
Integration order (gporder)		**4 4 2**
Constraint order (cporder)		**2 2 1**
Density (rho)	kg/m^3	**0**
Dynamic viscosity (eta)	Pa·s	**eta+zeta**
Volume force, x dir. (F_x)	N/m^3	**2*zeta*wy+FMx**
Volume force, y dir. (F_y)	N/m^3	**-2*zeta*wx+FMy**
cdon		**0**

6.3. Application Mode: Diffusion (di)

Application mode type: Diffusion

Application mode name: di

6.3.1. Application Mode Properties

Property	Value
Default element type	Lagrange - Quadratic
Analysis type	Stationary
Frame	Frame (ref)
Weak constraints	Off
Constraint type	Ideal

6.3.2. Variables

Dependent variables: w

Shape functions: shlag(2,'w')

Interior boundaries not active

6.3.3. Boundary Settings

Boundary	1-4
Type	Concentration

6.3.4. Subdomain Settings

Subdomain		1
Diffusion coefficient (D)	m^2/s	**etaprime**
Reaction rate (R)	$mol/(m^3 \cdot s)$	**T+2*zeta*(vx-uy-2*w)**

6.4. Application Mode: Convection and Diffusion (cd3)

Application mode type: Convection and Diffusion

Application mode name: cd3

6.4.1. Application Mode Properties

Property	Value
Default element type	Lagrange - Quadratic
Analysis type	Transient
Equation form	Non-conservative
Frame	Frame (ref)
Weak constraints	Off
Constraint type	Ideal

6.4.2. Variables

Dependent variables: M_x

Shape functions: shlag(2,'M_x')

Interior boundaries not active

6.4.3. Boundary Settings

Boundary	1-4
Type	Insulation/Symmetry

6.4.4. Subdomain Settings

Subdomain		1
Diffusion coefficient (D)	m^2/s	**0**
Reaction rate (R)	$mol/(m^3 \cdot s)$	**-w*M_y-((M_x-M_eqx)/omegatau)**
x-velocity (u)	m/s	**u**
y-velocity (v)	m/s	**v**

6.5. Application Mode: Convection and Diffusion (cd)

Application mode type: Convection and Diffusion

Application mode name: cd

6.5.1. Application Mode Properties

Property	Value
Default element type	Lagrange - Quadratic
Analysis type	Transient
Equation form	Non-conservative
Frame	Frame (ref)
Weak constraints	Off
Constraint type	Ideal

6.5.2. Variables

Dependent variables: M_y

Shape functions: shlag(2,'M_y')

Interior boundaries not active

6.5.3. Boundary Settings

Boundary	1-4
Type	Insulation/Symmetry

6.5.4. Subdomain Settings

Subdomain		1
Diffusion coefficient (D)	m^2/s	**0**
Reaction rate (R)	$mol/(m^3 \cdot s)$	**w*M_x-((M_y-M_eqy)/omegatau)**
x-velocity (u)	m/s	**u**
y-velocity (v)	m/s	**v**

6.6. Application Mode: PDE, General Form (g)

Application mode type: PDE, General Form

Application mode name: g

6.6.1. Application Mode Properties

Property	Value
Default element type	Lagrange - Quadratic
Wave extension	Off
Frame	Frame (ref)
Weak constraints	Off

6.6.2. Variables

Dependent variables: psi, psi_t

Shape functions: shlag(2,'psi')

Interior boundaries not active

6.6.3. Boundary Settings

Boundary	1-4
Type	Dirichlet boundary condition
(r)	-psi+H0*(x*cos(t)+y*sin(t))

6.6.4. Subdomain Settings

Subdomain	1
Damping/Mass coefficient (da)	0
Source term (f)	-M_xx-M_yy

6.7. Application Mode: PDE, General Form (g2)

Application mode type: PDE, General Form

Application mode name: g2

6.7.1. Application Mode Properties

Property	Value
Default element type	Lagrange - Quadratic
Wave extension	Off
Frame	Frame (ref)
Weak constraints	Off

6.7.2. Variables

Dependent variables: u2, u2_t

Shape functions: shlag(2,'u2')

Interior boundaries not active

6.7.3. Boundary Settings

Boundary	1-4
Type	Dirichlet boundary condition

6.7.4. Subdomain Settings

Subdomain	1
Source term (f)	v
Conservative flux source term (ga)	{{0;0}}

7. Solver Settings

Solve using a script: off

Analysis type	Transient
Auto select solver	On
Solver	Time dependent
Solution form	Automatic
Symmetric	auto
Adaptive mesh refinement	Off
Optimization/Sensitivity	Off
Plot while solving	Off

7.1. Direct (UMFPACK)

Solver type: Linear system solver

Parameter	Value
Pivot threshold	0.1
Memory allocation factor	0.7

7.2. Time Stepping

Parameter	Value
Times	range(0,0.1,10)
Relative tolerance	0.0001
Absolute tolerance	0.000010
Times to store in output	Specified times
Time steps taken by solver	Free
Maximum BDF order	5
Singular mass matrix	Maybe
Consistent initialization of DAE systems	Backward Euler
Error estimation strategy	Include algebraic
Allow complex numbers	Off

7.3. Advanced

Parameter	Value
Constraint handling method	Elimination
Null-space function	Automatic
Automatic assembly block size	On
Assembly block size	5000
Use Hermitian transpose of constraint matrix and in symmetry detection	Off
Use complex functions with real input	Off
Stop if error due to undefined operation	On
Store solution on file	Off
Type of scaling	Automatic
Manual scaling	
Row equilibration	On
Manual control of reassembly	Off
Load constant	On
Constraint constant	On

Mass constant	On
Damping (mass) constant	On
Jacobian constant	On
Constraint Jacobian constant	On

8. Postprocessing

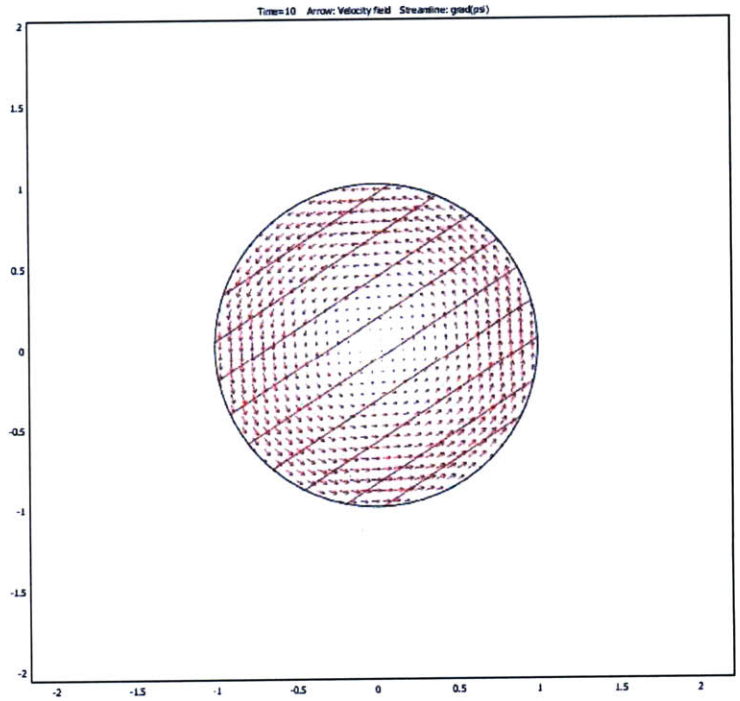

9. Variables

9.1. Boundary

Name	Description	Unit	Expression
K_x_ns	Viscous force per area, x component	Pa	eta_ns * (2 * nx_ns * ux+ny_ns * (uy+vx))
T_x_ns	Total force per area, x component	Pa	-nx_ns * p+2 * nx_ns * eta_ns * ux+ny_ns * eta_ns * (uy+vx)
K_y_ns	Viscous force per area, y component	Pa	eta_ns * (nx_ns * (vx+uy)+2 * ny_ns * vy)
T_y_ns	Total force per area, y component	Pa	-ny_ns * p+nx_ns * eta_ns * (vx+uy)+2 * ny_ns * eta_ns * vy
ndflux_w_di	Normal diffusive flux, w	mol/(m^2*s)	nx_di * dflux_w_x_di+ny_di * dflux_w_y_di

ndflux_M_x_cd3	Normal diffusive flux, M_x	mol/(m^2*s)	nx_cd3 * dflux_M_x_x_cd3+ny_cd3 * dflux_M_x_y_cd3
ncflux_M_x_cd3	Normal convective flux, M_x	mol/(m^2*s)	nx_cd3 * cflux_M_x_x_cd3+ny_cd3 * cflux_M_x_y_cd3
ntflux_M_x_cd3	Normal total flux, M_x	mol/(m^2*s)	nx_cd3 * tflux_M_x_x_cd3+ny_cd3 * tflux_M_x_y_cd3
ndflux_M_y_cd	Normal diffusive flux, M_y	mol/(m^2*s)	nx_cd * dflux_M_y_x_cd+ny_cd * dflux_M_y_y_cd
ncflux_M_y_cd	Normal convective flux, M_y	mol/(m^2*s)	nx_cd * cflux_M_y_x_cd+ny_cd * cflux_M_y_y_cd
ntflux_M_y_cd	Normal total flux, M_y	mol/(m^2*s)	nx_cd * tflux_M_y_x_cd+ny_cd * tflux_M_y_y_cd

9.2. Subdomain

Name	Description	Unit	Expression
U_ns	Velocity field	m/s	sqrt(u^2+v^2)
V_ns	Vorticity	1/s	vx-uy
divU_ns	Divergence of velocity field	1/s	ux+vy
cellRe_ns	Cell Reynolds number	1	rho_ns * U_ns * h/eta_ns
res_u_ns	Equation residual for u	N/m^3	rho_ns * (ut+u * ux+v * uy)+px-F_x_ns-eta_ns * (2 * uxx+uyy+vxy)
res_v_ns	Equation residual for v	N/m^3	rho_ns * (vt+u * vx+v * vy)+py-F_y_ns-eta_ns * (vxx+uyx+2 * vyy)
beta_x_ns	Convective field, x component	kg/(m^2*s)	rho_ns * u
beta_y_ns	Convective field, y component	kg/(m^2*s)	rho_ns * v
Dm_ns	Mean diffusion coefficient	Pa*s	eta_ns
da_ns	Total time scale factor	kg/m^3	rho_ns
taum_ns	GLS time-scale	m^3*s/kg	nojac(1/max(2 * rho_ns * sqrt(emetric(u,v)),48 * eta_ns/h^2))
tauc_ns	GLS time-scale	m^2/s	0.5 * nojac(if(u^2+v^2
res_p_ns	Equation residual for p	kg/(m^3*s)	rho_ns * divU_ns
grad_w_x_di	Concentration gradient, w, x component	mol/m^4	wx
dflux_w_x_di	Diffusive flux, w, x component	mol/(m^2*s)	-Dxx_w_di * wx-Dxy_w_di * wy
grad_w_y_di	Concentration gradient, w, y component	mol/m^4	wy

dflux_w_y_di	Diffusive flux, w, y component	mol/(m^2*s)	-Dyx_w_di * wx-Dyy_w_di * wy
grad_w_di	Concentration gradient, w	mol/m^4	sqrt(grad_w_x_di^2+grad_w_y_di^2)
dflux_w_di	Diffusive flux, w	mol/(m^2*s)	sqrt(dflux_w_x_di^2+dflux_w_y_di^2)
grad_M_x_x_cd3	Concentration gradient, M_x, x component	mol/m^4	M_xx
dflux_M_x_x_cd3	Diffusive flux, M_x, x component	mol/(m^2*s)	-Dxx_M_x_cd3 * M_xx-Dxy_M_x_cd3 * M_xy
cflux_M_x_x_cd3	Convective flux, M_x, x component	mol/(m^2*s)	M_x * u_M_x_cd3
tflux_M_x_x_cd3	Total flux, M_x, x component	mol/(m^2*s)	dflux_M_x_x_cd3+cflux_M_x_x_cd3
grad_M_x_y_cd3	Concentration gradient, M_x, y component	mol/m^4	M_xy
dflux_M_x_y_cd3	Diffusive flux, M_x, y component	mol/(m^2*s)	-Dyx_M_x_cd3 * M_xx-Dyy_M_x_cd3 * M_xy
cflux_M_x_y_cd3	Convective flux, M_x, y component	mol/(m^2*s)	M_x * v_M_x_cd3
tflux_M_x_y_cd3	Total flux, M_x, y component	mol/(m^2*s)	dflux_M_x_y_cd3+cflux_M_x_y_cd3
beta_M_x_x_cd3	Convective field, M_x, x component	m/s	u_M_x_cd3
beta_M_x_y_cd3	Convective field, M_x, y component	m/s	v_M_x_cd3
grad_M_x_cd3	Concentration gradient, M_x	mol/m^4	sqrt(grad_M_x_x_cd3^2+grad_M_x_y_cd3^2)
dflux_M_x_cd3	Diffusive flux, M_x	mol/(m^2*s)	sqrt(dflux_M_x_x_cd3^2+dflux_M_x_y_cd3^2)
cflux_M_x_cd3	Convective flux, M_x	mol/(m^2*s)	sqrt(cflux_M_x_x_cd3^2+cflux_M_x_y_cd3^2)
tflux_M_x_cd3	Total flux, M_x	mol/(m^2*s)	sqrt(tflux_M_x_x_cd3^2+tflux_M_x_y_cd3^2)
cellPe_M_x_cd3	Cell Peclet number, M_x	1	h * sqrt(beta_M_x_x_cd3^2+beta_M_x_y_cd3^2)/Dm_M_x_cd3
Dm_M_x_cd3	Mean diffusion coefficient, M_x	m^2/s	(Dxx_M_x_cd3 * u_M_x_cd3^2+Dxy_M_x_cd3 * u_M_x_cd3 * v_M_x_cd3+Dyx_M_x_cd3 * v_M_x_cd3 * u_M_x_cd3+Dyy_M_x_cd3 * v_M_x_cd3^2)/(u_M_x_cd3^2+v_M_x_cd3^2+eps)

res_M_x_cd3	Equation residual for M_x	mol/(m^3*s)	-Dxx_M_x_cd3 * M_xxx-Dxy_M_x_cd3 * M_xxy+M_xx * u_M_x_cd3-Dyx_M_x_cd3 * M_xyx-Dyy_M_x_cd3 * M_xyy+M_xy * v_M_x_cd3-R_M_x_cd3
res_sc_M_x_cd3	Shock capturing residual for M_x	mol/(m^3*s)	M_xx * u_M_x_cd3+M_xy * v_M_x_cd3-R_M_x_cd3
da_M_x_cd3	Total time scale factor, M_x	1	Dts_M_x_cd3
grad_M_y_x_cd	Concentration gradient, M_y, x component	mol/m^4	M_yx
dflux_M_y_x_cd	Diffusive flux, M_y, x component	mol/(m^2*s)	-Dxx_M_y_cd * M_yx-Dxy_M_y_cd * M_yy
cflux_M_y_x_cd	Convective flux, M_y, x component	mol/(m^2*s)	M_y * u_M_y_cd
tflux_M_y_x_cd	Total flux, M_y, x component	mol/(m^2*s)	dflux_M_y_x_cd+cflux_M_y_x_cd
grad_M_y_y_cd	Concentration gradient, M_y, y component	mol/m^4	M_yy
dflux_M_y_y_cd	Diffusive flux, M_y, y component	mol/(m^2*s)	-Dyx_M_y_cd * M_yx-Dyy_M_y_cd * M_yy
cflux_M_y_y_cd	Convective flux, M_y, y component	mol/(m^2*s)	M_y * v_M_y_cd
tflux_M_y_y_cd	Total flux, M_y, y component	mol/(m^2*s)	dflux_M_y_y_cd+cflux_M_y_y_cd
beta_M_y_x_cd	Convective field, M_y, x component	m/s	u_M_y_cd
beta_M_y_y_cd	Convective field, M_y, y component	m/s	v_M_y_cd
grad_M_y_cd	Concentration gradient, M_y	mol/m^4	sqrt(grad_M_y_x_cd^2+grad_M_y_y_cd^2)
dflux_M_y_cd	Diffusive flux, M_y	mol/(m^2*s)	sqrt(dflux_M_y_x_cd^2+dflux_M_y_y_cd^2)
cflux_M_y_cd	Convective flux, M_y	mol/(m^2*s)	sqrt(cflux_M_y_x_cd^2+cflux_M_y_y_cd^2)
tflux_M_y_cd	Total flux, M_y	mol/(m^2*s)	sqrt(tflux_M_y_x_cd^2+tflux_M_y_y_cd^2)
cellPe_M_y_cd	Cell Peclet number, M_y	1	h * sqrt(beta_M_y_x_cd^2+beta_M_y_y_cd^2)/Dm_M_y_cd

Dm_M_y_cd	Mean diffusion coefficient, M_y	m^2/s	(Dxx_M_y_cd * u_M_y_cd^2+Dxy_M_y_cd * u_M_y_cd * v_M_y_cd+Dyx_M_y_cd * v_M_y_cd * u_M_y_cd+Dyy_M_y_cd * v_M_y_cd^2)/(u_M_y_cd^2+v_M_y_cd^2+eps)
res_M_y_cd	Equation residual for M_y	mol/(m^3*s)	-Dxx_M_y_cd * M_yxx-Dxy_M_y_cd * M_yxy+M_yx * u_M_y_cd-Dyx_M_y_cd * M_yyx-Dyy_M_y_cd * M_yyy+M_yy * v_M_y_cd-R_M_y_cd
res_sc_M_y_cd	Shock capturing residual for M_y	mol/(m^3*s)	M_yx * u_M_y_cd+M_yy * v_M_y_cd-R_M_y_cd
da_M_y_cd	Total time scale factor, M_y	1	Dts_M_y_cd
abspsix_g	|grad(psi)|		sqrt(psix^2+psiy^2)
absga7x_g	|ga7x|		sqrt(ga7x^2+ga7y^2)
absu2x_g2	|grad(u2)|		sqrt(u2x^2+u2y^2)
absga8x_g2	|ga8x|		sqrt(ga8x^2+ga8y^2)

B4. COMSOL Simulation of Chaves 143G Case With Adjusted $\eta'=4.84x10^{-10}$ (Section 4.4.4.1)

2D case cylinder with Chaves's parameters

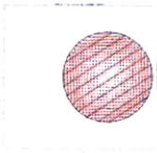

1. Table of Contents

2. Model Properties

Property	Value
Model name	2D case cylinder with Chaves's parameters
Author	Shahriar Khushrushahi
Company	MIT
Department	EECS
Reference	
URL	
Saved date	Mar 9, 2010 1:48:42 PM
Creation date	Sep 19, 2008 9:32:16 PM
COMSOL version	COMSOL 3.5.0.603

File name: D:\Documents and Settings\Administrator\Desktop\Comsol_Testbed\GoodFiles\Good2DCylinderfiles\2Dcylinder_finlaysonsmethod_etaprimefinding_demagfields_Chaves_143G.mph

Application modes and modules used in this model:

- Geom1 (2D)
  - Incompressible Navier-Stokes
  - Diffusion
  - Convection and Diffusion
  - Convection and Diffusion
  - PDE, General Form
  - PDE, General Form

2.1. Model description

Rotation of Ferrofluid in a rotating magnetic field in an infinitely long cylinder

Using Parameters from Chaves Paper of 2008 on spinup Flow

Using parameters for EMG900_2 trying to get plot similar to Fig 5b

The values used in this model correspond to normalizing to 14.3mT values from his paper. The normalized values can be calculated from Calculating_Different_Parameters.xls under EMG900

Using my normalization scheme outlined in VeryifyingShihabsmethod_081205.doc

This method uses scalar potential similar to Finlaysons Comsol paper

Etaprime non0 case

Etaprime of 4.84e-10 for a better fit is used

3. Constants

Name	Expression	Value	Description
Xi	1.19		
omega	2*pi*f		
zeta	0.00048		
eta	0.0074		
etaprime	1.3e-6		
f	85		
tau	1e-6		
omegatau	omega*tau		
R0	0.027		
I	2/3		
H0	1		

4. Global Expressions

Name	Expression	Unit	Description
FMx	M_x*(-psixx)+M_y*(-psixy)		\
FMy	M_x*(-psiyx)+M_y*(-psiyy)		
T	M_x*Hy-M_y*Hx		
M_eqx	(Xi*Hx)		
M_eqy	(Xi*Hy)		
Hx	-psix-M_x/2		
Hy	-psiy-M_y/2		
phi	atan2(y,x)	rad	

5. Geometry

Number of geometries: 1

5.1. Geom1

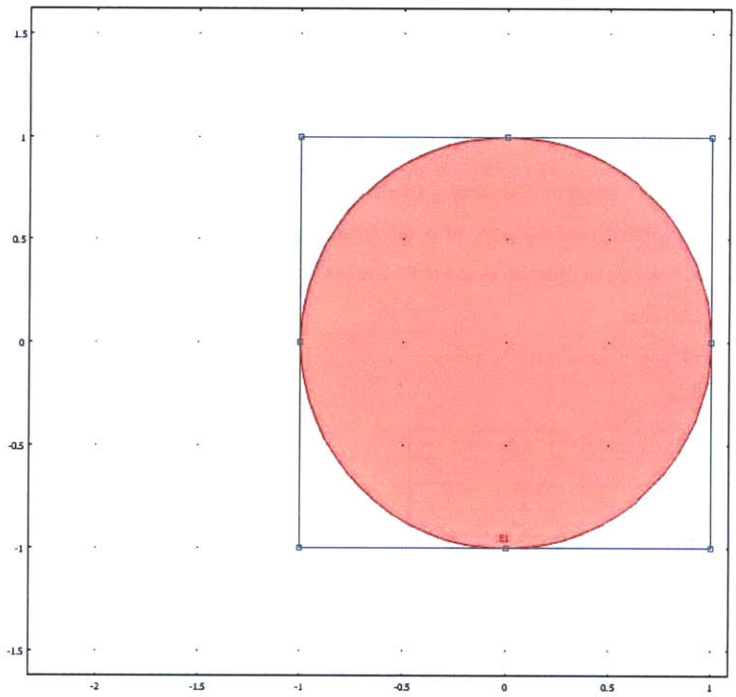

5.1.1. Point mode

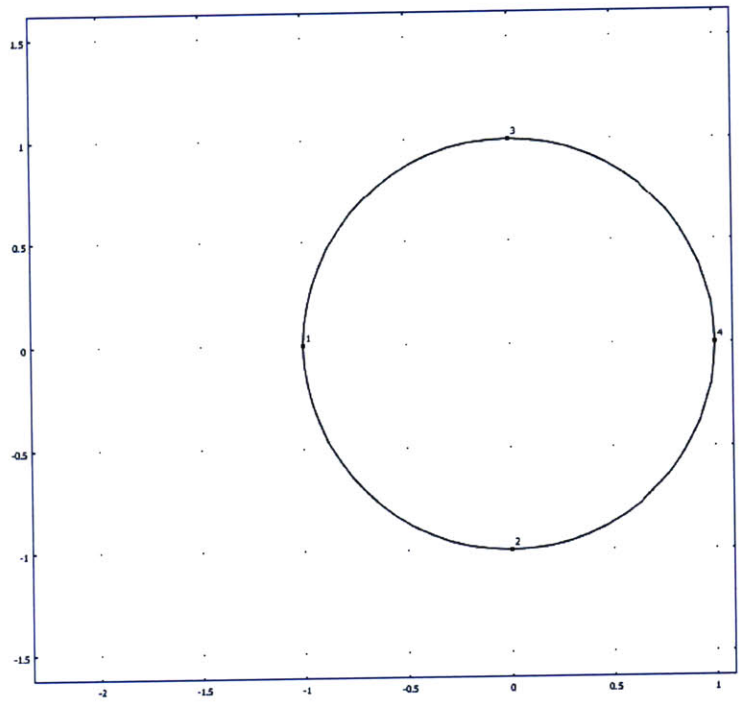

5.1.2. Boundary mode

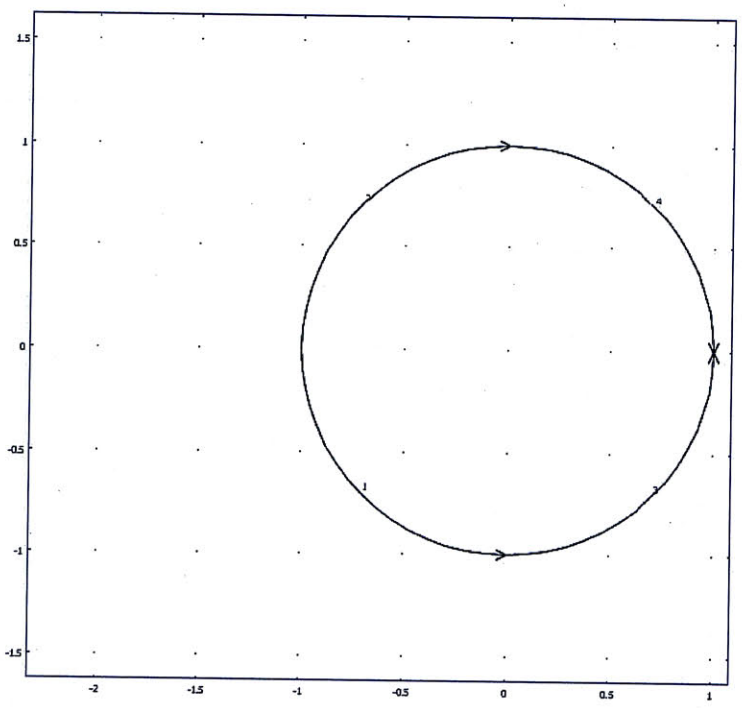

5.1.3. Subdomain mode

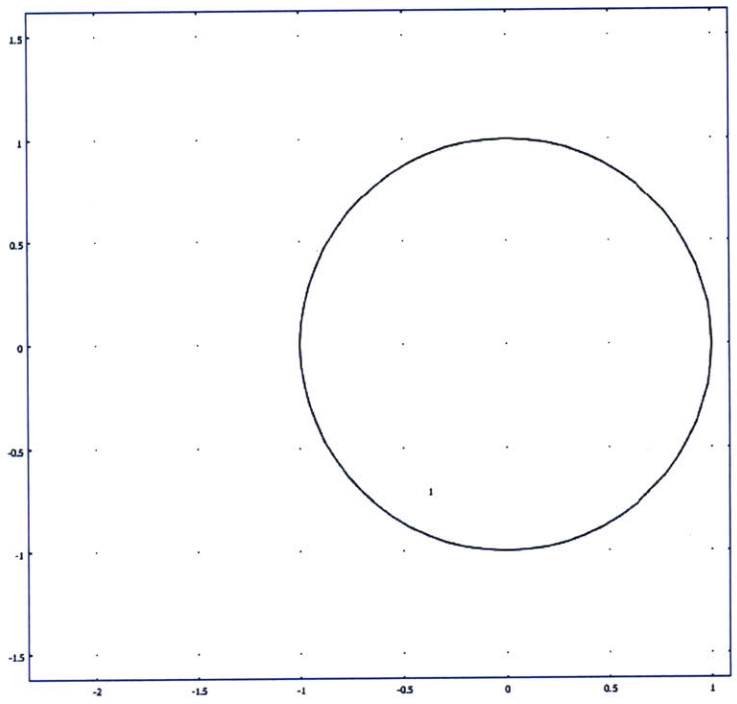

6. Geom1

Space dimensions: 2D

Independent variables: x, y, z

6.1. Mesh

6.1.1. Mesh Statistics

Number of degrees of freedom	66110
Number of mesh points	2319
Number of elements	4476
Triangular	4476
Quadrilateral	0
Number of boundary elements	160
Number of vertex elements	4
Minimum element quality	0.901
Element area ratio	0.254

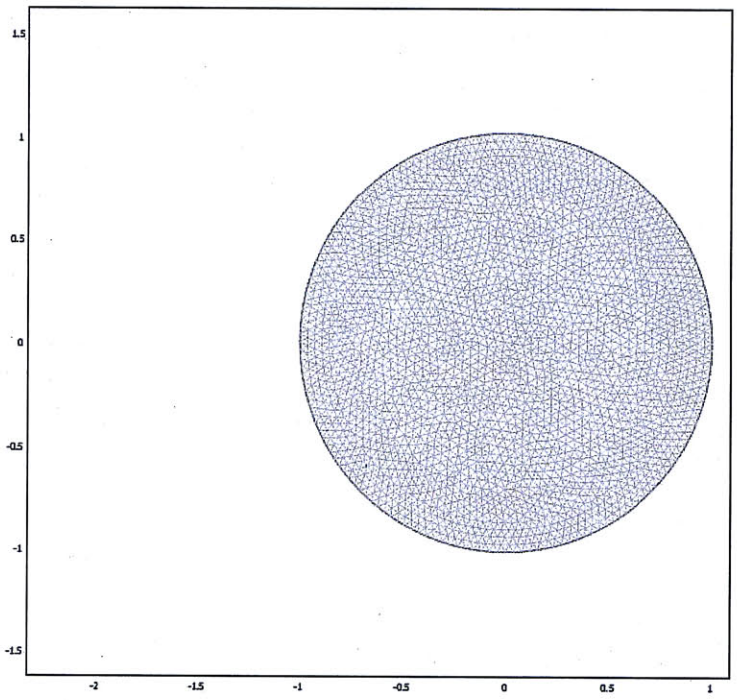

6.2. Application Mode: Incompressible Navier-Stokes (ns)

Application mode type: Incompressible Navier-Stokes

Application mode name: ns

6.2.1. Scalar Variables

Name	Variable	Value	Unit	Description
visc_vel_fact	visc_vel_fact_ns	10	1	Viscous velocity factor

6.2.2. Application Mode Properties

Property	Value
Default element type	Lagrange - P_2 P_1
Analysis type	Transient
Corner smoothing	Off
Frame	Frame (ref)
Weak constraints	Off
Constraint type	Ideal

6.2.3. Variables

Dependent variables: u, v, p, nxw, nyw

Shape functions: shlag(2,'u'), shlag(2,'v'), shlag(1,'p')

Interior boundaries not active

6.2.4. Point Settings

Point	2-4	1
pnton	0	1

6.2.5. Boundary Settings

Boundary	1-4
Type	Wall

6.2.6. Subdomain Settings

Subdomain		1
Integration order (gporder)		**4 4 2**
Constraint order (cporder)		**2 2 1**
Density (rho)	kg/m^3	**0**
Dynamic viscosity (eta)	Pa·s	**eta+zeta**
Volume force, x dir. (F_x)	N/m^3	**2*zeta*wy+FMx**
Volume force, y dir. (F_y)	N/m^3	**-2*zeta*wx+FMy**
cdon		**0**

6.3. Application Mode: Diffusion (di)

Application mode type: Diffusion

Application mode name: di

6.3.1. Application Mode Properties

Property	Value
Default element type	Lagrange - Quadratic
Analysis type	Stationary
Frame	Frame (ref)
Weak constraints	Off
Constraint type	Ideal

6.3.2. Variables

Dependent variables: w

Shape functions: shlag(2,'w')

Interior boundaries not active

6.3.3. Boundary Settings

Boundary	1-4
Type	Concentration

6.3.4. Subdomain Settings

Subdomain		1
Diffusion coefficient (D)	m^2/s	**etaprime**
Reaction rate (R)	$mol/(m^3 \cdot s)$	**T+2*zeta*(vx-uy-2*w)**

6.4. Application Mode: Convection and Diffusion (cd3)

Application mode type: Convection and Diffusion

Application mode name: cd3

6.4.1. Application Mode Properties

Property	Value
Default element type	Lagrange - Quadratic
Analysis type	Transient
Equation form	Non-conservative
Frame	Frame (ref)
Weak constraints	Off
Constraint type	Ideal

6.4.2. Variables

Dependent variables: M_x

Shape functions: shlag(2,'M_x')

Interior boundaries not active

6.4.3. Boundary Settings

Boundary	1-4
Type	Insulation/Symmetry

6.4.4. Subdomain Settings

Subdomain		1
Diffusion coefficient (D)	m^2/s	**0**
Reaction rate (R)	$mol/(m^3 \cdot s)$	**-w*M_y-((M_x-M_eqx)/omegatau)**
x-velocity (u)	m/s	**u**
y-velocity (v)	m/s	**v**

6.5. Application Mode: Convection and Diffusion (cd)

Application mode type: Convection and Diffusion

Application mode name: cd

6.5.1. Application Mode Properties

Property	Value
Default element type	Lagrange - Quadratic
Analysis type	Transient
Equation form	Non-conservative
Frame	Frame (ref)
Weak constraints	Off
Constraint type	Ideal

6.5.2. Variables

Dependent variables: M_y

Shape functions: shlag(2,'M_y')

Interior boundaries not active

6.5.3. Boundary Settings

Boundary	1-4
Type	Insulation/Symmetry

6.5.4. Subdomain Settings

Subdomain		1
Diffusion coefficient (D)	m^2/s	**0**
Reaction rate (R)	$mol/(m^3 \cdot s)$	**w*M_x-((M_y-M_eqy)/omegatau)**
x-velocity (u)	m/s	**u**
y-velocity (v)	m/s	**v**

6.6. Application Mode: PDE, General Form (g)

Application mode type: PDE, General Form

Application mode name: g

6.6.1. Application Mode Properties

Property	Value
Default element type	Lagrange - Quadratic
Wave extension	Off
Frame	Frame (ref)
Weak constraints	Off

6.6.2. Variables

Dependent variables: psi, psi_t

Shape functions: shlag(2,'psi')

Interior boundaries not active

6.6.3. Boundary Settings

Boundary	1-4
Type	Dirichlet boundary condition
(r)	-psi+H0*(x*cos(t)+y*sin(t))

6.6.4. Subdomain Settings

Subdomain	1
Damping/Mass coefficient (da)	0
Source term (f)	-M_xx-M_yy

6.7. Application Mode: PDE, General Form (g2)

Application mode type: PDE, General Form

Application mode name: g2

6.7.1. Application Mode Properties

Property	Value
Default element type	Lagrange - Quadratic
Wave extension	Off
Frame	Frame (ref)
Weak constraints	Off

6.7.2. Variables

Dependent variables: u2, u2_t

Shape functions: shlag(2,'u2')

Interior boundaries not active

6.7.3. Boundary Settings

Boundary	1-4
Type	Dirichlet boundary condition

6.7.4. Subdomain Settings

Subdomain	1
Source term (f)	v
Conservative flux source term (ga)	{{0;0}}

7. Solver Settings

Solve using a script: off

Analysis type	Transient
Auto select solver	On
Solver	Time dependent
Solution form	Automatic
Symmetric	auto
Adaptive mesh refinement	Off
Optimization/Sensitivity	Off
Plot while solving	Off

7.1. Direct (UMFPACK)

Solver type: Linear system solver

Parameter	Value
Pivot threshold	0.1
Memory allocation factor	0.7

7.2. Time Stepping

Parameter	Value
Times	range(0,0.1,10)
Relative tolerance	0.0001
Absolute tolerance	0.000010
Times to store in output	Specified times
Time steps taken by solver	Free
Maximum BDF order	5
Singular mass matrix	Maybe
Consistent initialization of DAE systems	Backward Euler
Error estimation strategy	Include algebraic
Allow complex numbers	Off

7.3. Advanced

Parameter	Value
Constraint handling method	Elimination
Null-space function	Automatic
Automatic assembly block size	On
Assembly block size	5000
Use Hermitian transpose of constraint matrix and in symmetry detection	Off
Use complex functions with real input	Off
Stop if error due to undefined operation	On
Store solution on file	Off
Type of scaling	Automatic
Manual scaling	
Row equilibration	On
Manual control of reassembly	Off
Load constant	On
Constraint constant	On

Mass constant	On
Damping (mass) constant	On
Jacobian constant	On
Constraint Jacobian constant	On

8. Postprocessing

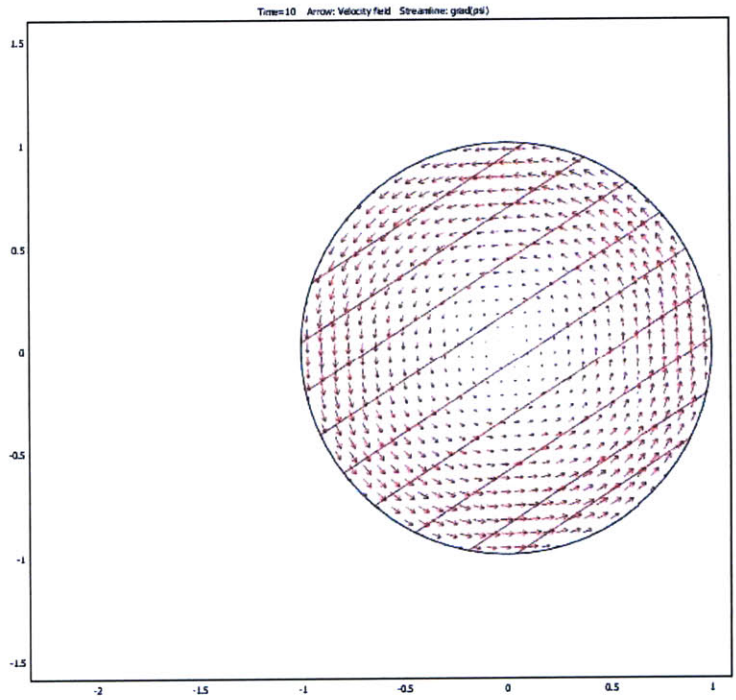

9. Variables

9.1. Boundary

Name	Description	Unit	Expression
K_x_ns	Viscous force per area, x component	Pa	eta_ns * (2 * nx_ns * ux+ny_ns * (uy+vx))
T_x_ns	Total force per area, x component	Pa	-nx_ns * p+2 * nx_ns * eta_ns * ux+ny_ns * eta_ns * (uy+vx)
K_y_ns	Viscous force per area, y component	Pa	eta_ns * (nx_ns * (vx+uy)+2 * ny_ns * vy)
T_y_ns	Total force per area, y component	Pa	-ny_ns * p+nx_ns * eta_ns * (vx+uy)+2 * ny_ns * eta_ns * vy
ndflux_w_di	Normal diffusive flux, w	mol/(m^2*s)	nx_di * dflux_w_x_di+ny_di * dflux_w_y_di

ndflux_M_x_cd3	Normal diffusive flux, M_x	mol/(m^2*s)	nx_cd3 * dflux_M_x_x_cd3+ny_cd3 * dflux_M_x_y_cd3
ncflux_M_x_cd3	Normal convective flux, M_x	mol/(m^2*s)	nx_cd3 * cflux_M_x_x_cd3+ny_cd3 * cflux_M_x_y_cd3
ntflux_M_x_cd3	Normal total flux, M_x	mol/(m^2*s)	nx_cd3 * tflux_M_x_x_cd3+ny_cd3 * tflux_M_x_y_cd3
ndflux_M_y_cd	Normal diffusive flux, M_y	mol/(m^2*s)	nx_cd * dflux_M_y_x_cd+ny_cd * dflux_M_y_y_cd
ncflux_M_y_cd	Normal convective flux, M_y	mol/(m^2*s)	nx_cd * cflux_M_y_x_cd+ny_cd * cflux_M_y_y_cd
ntflux_M_y_cd	Normal total flux, M_y	mol/(m^2*s)	nx_cd * tflux_M_y_x_cd+ny_cd * tflux_M_y_y_cd

9.2. Subdomain

Name	Description	Unit	Expression
U_ns	Velocity field	m/s	sqrt(u^2+v^2)
V_ns	Vorticity	1/s	vx-uy
divU_ns	Divergence of velocity field	1/s	ux+vy
cellRe_ns	Cell Reynolds number	1	rho_ns * U_ns * h/eta_ns
res_u_ns	Equation residual for u	N/m^3	rho_ns * (ut+u * ux+v * uy)+px-F_x_ns-eta_ns * (2 * uxx+uyy+vxy)
res_v_ns	Equation residual for v	N/m^3	rho_ns * (vt+u * vx+v * vy)+py-F_y_ns-eta_ns * (vxx+uyx+2 * vyy)
beta_x_ns	Convective field, x component	kg/(m^2*s)	rho_ns * u
beta_y_ns	Convective field, y component	kg/(m^2*s)	rho_ns * v
Dm_ns	Mean diffusion coefficient	Pa*s	eta_ns
da_ns	Total time scale factor	kg/m^3	rho_ns
taum_ns	GLS time-scale	m^3*s/kg	nojac(1/max(2 * rho_ns * sqrt(emetric(u,v)),48 * eta_ns/h^2))
tauc_ns	GLS time-scale	m^2/s	0.5 * nojac(if(u^2+v^2
res_p_ns	Equation residual for p	kg/(m^3*s)	rho_ns * divU_ns
grad_w_x_di	Concentration gradient, w, x component	mol/m^4	wx
dflux_w_x_di	Diffusive flux, w, x component	mol/(m^2*s)	-Dxx_w_di * wx-Dxy_w_di * wy
grad_w_y_di	Concentration gradient, w, y component	mol/m^4	wy

dflux_w_y_di	Diffusive flux, w, y component	mol/(m^2*s)	-Dyx_w_di * wx-Dyy_w_di * wy
grad_w_di	Concentration gradient, w	mol/m^4	sqrt(grad_w_x_di^2+grad_w_y_di^2)
dflux_w_di	Diffusive flux, w	mol/(m^2*s)	sqrt(dflux_w_x_di^2+dflux_w_y_di^2)
grad_M_x_x_cd3	Concentration gradient, M_x, x component	mol/m^4	M_xx
dflux_M_x_x_cd3	Diffusive flux, M_x, x component	mol/(m^2*s)	-Dxx_M_x_cd3 * M_xx-Dxy_M_x_cd3 * M_xy
cflux_M_x_x_cd3	Convective flux, M_x, x component	mol/(m^2*s)	M_x * u_M_x_cd3
tflux_M_x_x_cd3	Total flux, M_x, x component	mol/(m^2*s)	dflux_M_x_x_cd3+cflux_M_x_x_cd3
grad_M_x_y_cd3	Concentration gradient, M_x, y component	mol/m^4	M_xy
dflux_M_x_y_cd3	Diffusive flux, M_x, y component	mol/(m^2*s)	-Dyx_M_x_cd3 * M_xx-Dyy_M_x_cd3 * M_xy
cflux_M_x_y_cd3	Convective flux, M_x, y component	mol/(m^2*s)	M_x * v_M_x_cd3
tflux_M_x_y_cd3	Total flux, M_x, y component	mol/(m^2*s)	dflux_M_x_y_cd3+cflux_M_x_y_cd3
beta_M_x_x_cd3	Convective field, M_x, x component	m/s	u_M_x_cd3
beta_M_x_y_cd3	Convective field, M_x, y component	m/s	v_M_x_cd3
grad_M_x_cd3	Concentration gradient, M_x	mol/m^4	sqrt(grad_M_x_x_cd3^2+grad_M_x_y_cd3^2)
dflux_M_x_cd3	Diffusive flux, M_x	mol/(m^2*s)	sqrt(dflux_M_x_x_cd3^2+dflux_M_x_y_cd3^2)
cflux_M_x_cd3	Convective flux, M_x	mol/(m^2*s)	sqrt(cflux_M_x_x_cd3^2+cflux_M_x_y_cd3^2)
tflux_M_x_cd3	Total flux, M_x	mol/(m^2*s)	sqrt(tflux_M_x_x_cd3^2+tflux_M_x_y_cd3^2)
cellPe_M_x_cd3	Cell Peclet number, M_x	1	h * sqrt(beta_M_x_x_cd3^2+beta_M_x_y_cd3^2)/Dm_M_x_cd3
Dm_M_x_cd3	Mean diffusion coefficient, M_x	m^2/s	(Dxx_M_x_cd3 * u_M_x_cd3^2+Dxy_M_x_cd3 * u_M_x_cd3 * v_M_x_cd3+Dyx_M_x_cd3 * v_M_x_cd3 * u_M_x_cd3+Dyy_M_x_cd3 * v_M_x_cd3^2)/(u_M_x_cd3^2+v_M_x_cd3^2+eps)

res_M_x_cd3	Equation residual for M_x	mol/(m^3*s)	-Dxx_M_x_cd3 * M_xxx-Dxy_M_x_cd3 * M_xxy+M_xx * u_M_x_cd3-Dyx_M_x_cd3 * M_xyx-Dyy_M_x_cd3 * M_xyy+M_xy * v_M_x_cd3-R_M_x_cd3
res_sc_M_x_cd3	Shock capturing residual for M_x	mol/(m^3*s)	M_xx * u_M_x_cd3+M_xy * v_M_x_cd3-R_M_x_cd3
da_M_x_cd3	Total time scale factor, M_x	1	Dts_M_x_cd3
grad_M_y_x_cd	Concentration gradient, M_y, x component	mol/m^4	M_yx
dflux_M_y_x_cd	Diffusive flux, M_y, x component	mol/(m^2*s)	-Dxx_M_y_cd * M_yx-Dxy_M_y_cd * M_yy
cflux_M_y_x_cd	Convective flux, M_y, x component	mol/(m^2*s)	M_y * u_M_y_cd
tflux_M_y_x_cd	Total flux, M_y, x component	mol/(m^2*s)	dflux_M_y_x_cd+cflux_M_y_x_cd
grad_M_y_y_cd	Concentration gradient, M_y, y component	mol/m^4	M_yy
dflux_M_y_y_cd	Diffusive flux, M_y, y component	mol/(m^2*s)	-Dyx_M_y_cd * M_yx-Dyy_M_y_cd * M_yy
cflux_M_y_y_cd	Convective flux, M_y, y component	mol/(m^2*s)	M_y * v_M_y_cd
tflux_M_y_y_cd	Total flux, M_y, y component	mol/(m^2*s)	dflux_M_y_y_cd+cflux_M_y_y_cd
beta_M_y_x_cd	Convective field, M_y, x component	m/s	u_M_y_cd
beta_M_y_y_cd	Convective field, M_y, y component	m/s	v_M_y_cd
grad_M_y_cd	Concentration gradient, M_y	mol/m^4	sqrt(grad_M_y_x_cd^2+grad_M_y_y_cd^2)
dflux_M_y_cd	Diffusive flux, M_y	mol/(m^2*s)	sqrt(dflux_M_y_x_cd^2+dflux_M_y_y_cd^2)
cflux_M_y_cd	Convective flux, M_y	mol/(m^2*s)	sqrt(cflux_M_y_x_cd^2+cflux_M_y_y_cd^2)
tflux_M_y_cd	Total flux, M_y	mol/(m^2*s)	sqrt(tflux_M_y_x_cd^2+tflux_M_y_y_cd^2)
cellPe_M_y_cd	Cell Peclet number, M_y	1	h * sqrt(beta_M_y_x_cd^2+beta_M_y_y_cd^2)/Dm_M_y_cd

Dm_M_y_cd	Mean diffusion coefficient, M_y	m^2/s	(Dxx_M_y_cd * u_M_y_cd^2+Dxy_M_y_cd * u_M_y_cd * v_M_y_cd+Dyx_M_y_cd * v_M_y_cd * u_M_y_cd+Dyy_M_y_cd * v_M_y_cd^2)/(u_M_y_cd^2+v_M_y_cd^2+eps)
res_M_y_cd	Equation residual for M_y	mol/(m^3*s)	-Dxx_M_y_cd * M_yxx-Dxy_M_y_cd * M_yxy+M_yx * u_M_y_cd-Dyx_M_y_cd * M_yyx-Dyy_M_y_cd * M_yyy+M_yy * v_M_y_cd-R_M_y_cd
res_sc_M_y_cd	Shock capturing residual for M_y	mol/(m^3*s)	M_yx * u_M_y_cd+M_yy * v_M_y_cd-R_M_y_cd
da_M_y_cd	Total time scale factor, M_y	1	Dts_M_y_cd
abspsix_g	|grad(psi)|		sqrt(psix^2+psiy^2)
absga7x_g	|ga7x|		sqrt(ga7x^2+ga7y^2)
absu2x_g2	|grad(u2)|		sqrt(u2x^2+u2y^2)
absga8x_g2	|ga8x|		sqrt(ga8x^2+ga8y^2)

B5. COMSOL Simulation of Chaves 143G case With η'=0 (Section 4.4.3.5)

2D case cylinder with Chaves's parameters

1. Table of Contents

2. Model Properties

Property	Value
Model name	2D case cylinder with Chaves's parameters
Author	Shahriar Khushrushahi
Company	MIT
Department	EECS
Reference	
URL	
Saved date	Feb 17, 2010 5:31:41 PM
Creation date	Sep 19, 2008 9:32:16 PM
COMSOL version	COMSOL 3.5.0.603

File name: D:\Documents and Settings\Administrator\Desktop\Comsol_Testbed\GoodFiles\Good2DCylinderfiles\2Dcylinder_finlaysonsmethod_etaprime0_demagfields_Chaves_143G.mph

Application modes and modules used in this model:

- Geom1 (2D)
  - Incompressible Navier-Stokes
  - Diffusion
  - Convection and Diffusion
  - Convection and Diffusion
  - PDE, General Form
  - PDE, General Form

2.1. Model description

Rotation of Ferrofluid in a rotating magnetic field in an infinitely long cylinder

Using Parameters from Chaves Paper of 2008 on spinup Flow

Using parameters for EMG900_2

The values used in this model correspond to normalizing to 14.3mT values from his paper. The normalized values can be calculated from Calculating_Different_Parameters.xls under EMG900

Using my normalization scheme outlined in VeryifyingShihabsmethod_081205.doc

This method uses scalar potential similar to Finlaysons Comsol paper

Etaprime 0 case

3. Constants

Name	Expression	Value	Description
Xi	1.19		
omega	2*pi*f		
zeta	0.00048		
eta	0.0074		
etaprime	0		
f	85		
tau	1e-6		
omegatau	omega*tau		
R0	0.027		
I	2/3		
H0	1		

4. Global Expressions

Name	Expression	Unit	Description
FMx	M_x*(-psixx)+M_y*(-psixy)		\
FMy	M_x*(-psiyx)+M_y*(-psiyy)		
T	M_x*Hy-M_y*Hx		
M_eqx	(Xi*Hx)		
M_eqy	(Xi*Hy)		
Hx	-psix-M_x/2		
Hy	-psiy-M_y/2		
phi	atan2(y,x)	rad	

5. Geometry

Number of geometries: 1

5.1. Geom1

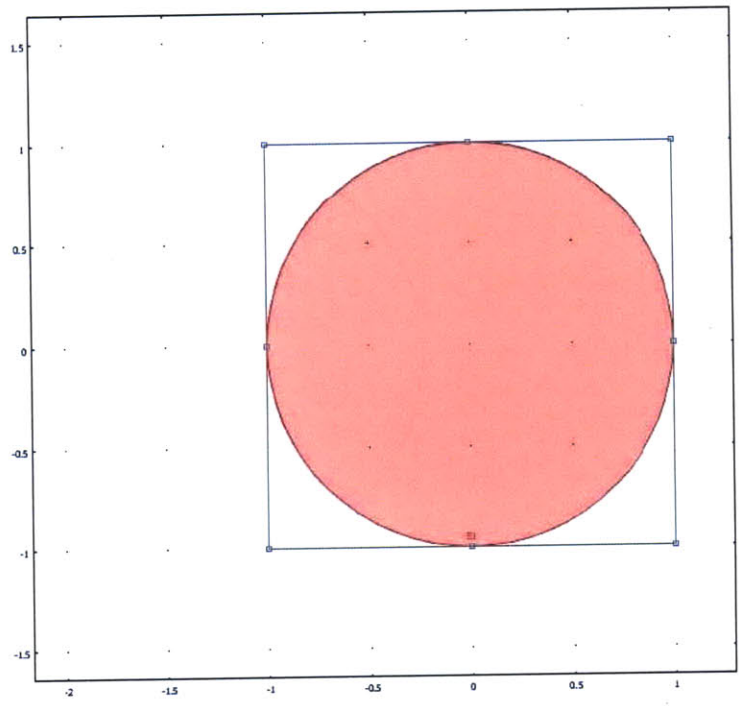

5.1.1. Point mode

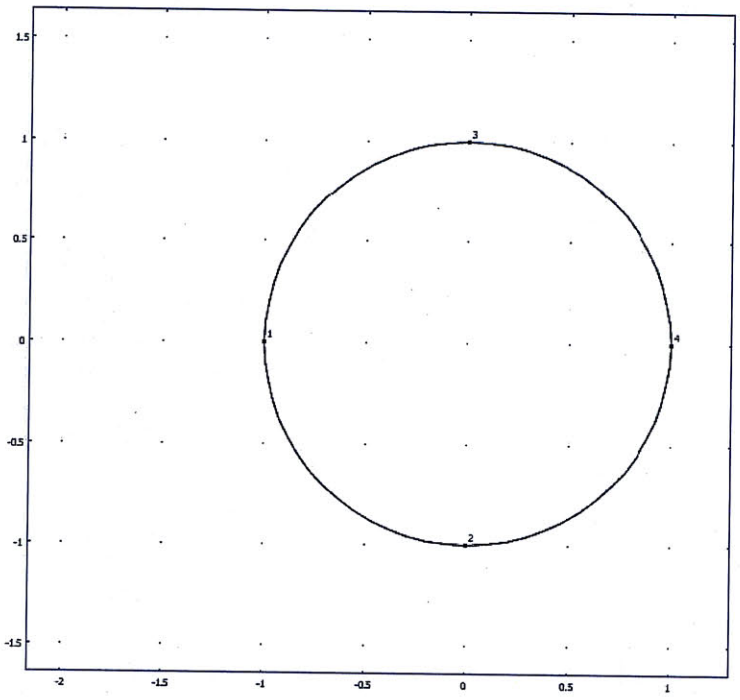

5.1.2. Boundary mode

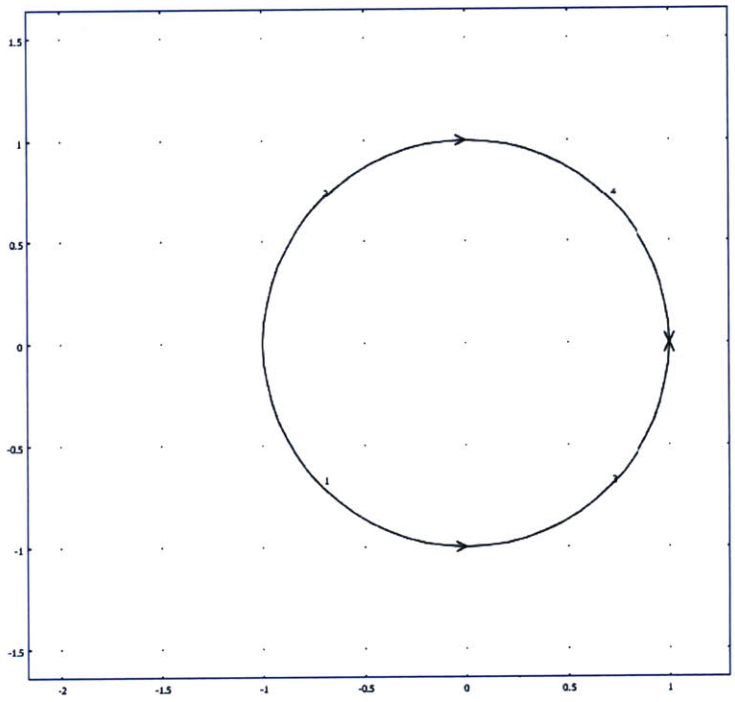

5.1.3. Subdomain mode

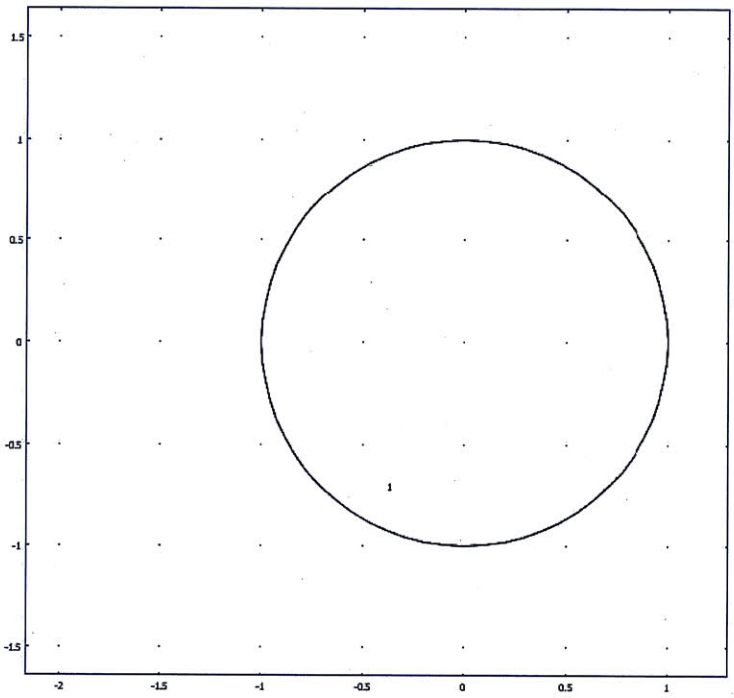

6. Geom1

Space dimensions: 2D

Independent variables: x, y, z

6.1. Mesh

6.1.1. Mesh Statistics

Number of degrees of freedom	66110
Number of mesh points	2319
Number of elements	4476
Triangular	4476
Quadrilateral	0
Number of boundary elements	160
Number of vertex elements	4
Minimum element quality	0.901
Element area ratio	0.254

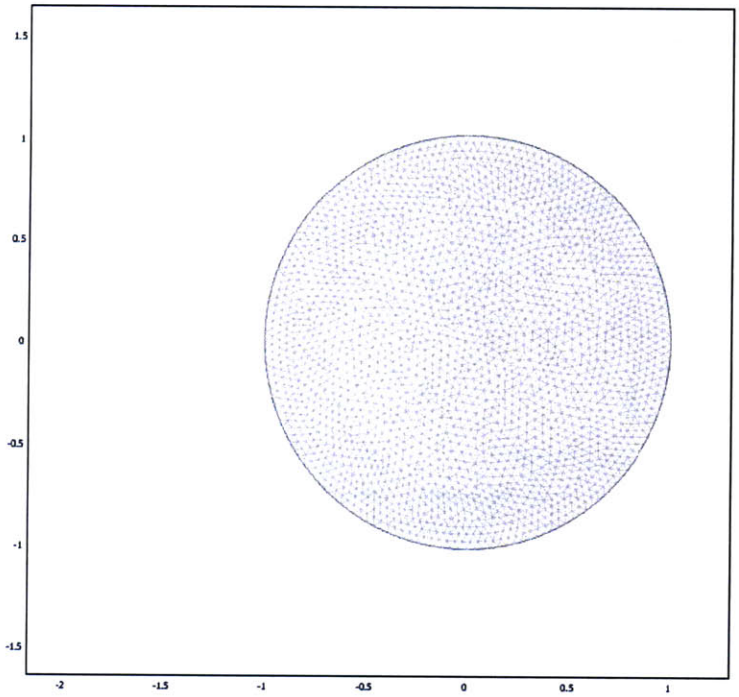

6.2. Application Mode: Incompressible Navier-Stokes (ns)

Application mode type: Incompressible Navier-Stokes

Application mode name: ns

6.2.1. Scalar Variables

Name	Variable	Value	Unit	Description
visc_vel_fact	visc_vel_fact_ns	10	1	Viscous velocity factor

6.2.2. Application Mode Properties

Property	Value
Default element type	Lagrange - P_2 P_1
Analysis type	Transient
Corner smoothing	Off
Frame	Frame (ref)
Weak constraints	Off
Constraint type	Ideal

6.2.3. Variables

Dependent variables: u, v, p, nxw, nyw

Shape functions: shlag(2,'u'), shlag(2,'v'), shlag(1,'p')

Interior boundaries not active

6.2.4. Point Settings

Point	2-4	1
pnton	0	1

6.2.5. Boundary Settings

Boundary	1-4
Type	Wall

6.2.6. Subdomain Settings

Subdomain		1
Integration order (gporder)		**4 4 2**
Constraint order (cporder)		**2 2 1**
Density (rho)	kg/m^3	**0**
Dynamic viscosity (eta)	Pa·s	**eta+zeta**
Volume force, x dir. (F_x)	N/m^3	**2*zeta*wy+FMx**
Volume force, y dir. (F_y)	N/m^3	**-2*zeta*wx+FMy**
cdon		**0**

6.3. Application Mode: Diffusion (di)

Application mode type: Diffusion

Application mode name: di

6.3.1. Application Mode Properties

Property	Value
Default element type	Lagrange - Quadratic
Analysis type	Stationary
Frame	Frame (ref)
Weak constraints	Off
Constraint type	Ideal

6.3.2. Variables

Dependent variables: w

Shape functions: shlag(2,'w')

Interior boundaries not active

6.3.3. Boundary Settings

Boundary	1-4
Type	Insulation/Symmetry

6.3.4. Subdomain Settings

Subdomain		1
Diffusion coefficient (D)	m^2/s	**etaprime**
Reaction rate (R)	$mol/(m^3 \cdot s)$	**T+2*zeta*(vx-uy-2*w)**

6.4. Application Mode: Convection and Diffusion (cd3)

Application mode type: Convection and Diffusion

Application mode name: cd3

6.4.1. Application Mode Properties

Property	Value
Default element type	Lagrange - Quadratic
Analysis type	Transient
Equation form	Non-conservative
Frame	Frame (ref)
Weak constraints	Off
Constraint type	Ideal

6.4.2. Variables

Dependent variables: M_x

Shape functions: shlag(2,'M_x')

Interior boundaries not active

6.4.3. Boundary Settings

Boundary	1-4
Type	Insulation/Symmetry

6.4.4. Subdomain Settings

Subdomain		1
Diffusion coefficient (D)	m^2/s	**0**
Reaction rate (R)	$mol/(m^3 \cdot s)$	**-w*M_y-((M_x-M_eqx)/omegatau)**
x-velocity (u)	m/s	**u**
y-velocity (v)	m/s	**v**

6.5. Application Mode: Convection and Diffusion (cd)

Application mode type: Convection and Diffusion

Application mode name: cd

6.5.1. Application Mode Properties

Property	Value
Default element type	Lagrange - Quadratic
Analysis type	Transient
Equation form	Non-conservative
Frame	Frame (ref)
Weak constraints	Off
Constraint type	Ideal

6.5.2. Variables

Dependent variables: M_y

Shape functions: shlag(2,'M_y')

Interior boundaries not active

6.5.3. Boundary Settings

Boundary	1-4
Type	Insulation/Symmetry

6.5.4. Subdomain Settings

Subdomain		1
Diffusion coefficient (D)	m^2/s	**0**
Reaction rate (R)	$mol/(m^3 \cdot s)$	**w*M_x-((M_y-M_eqy)/omegatau)**
x-velocity (u)	m/s	**u**
y-velocity (v)	m/s	**v**

6.6. Application Mode: PDE, General Form (g)

Application mode type: PDE, General Form

Application mode name: g

6.6.1. Application Mode Properties

Property	Value
Default element type	Lagrange - Quadratic
Wave extension	Off
Frame	Frame (ref)
Weak constraints	Off

6.6.2. Variables

Dependent variables: psi, psi_t

Shape functions: shlag(2,'psi')

Interior boundaries not active

6.6.3. Boundary Settings

Boundary	1-4
Type	Dirichlet boundary condition
(r)	-psi+H0*(x*cos(t)+y*sin(t))

6.6.4. Subdomain Settings

Subdomain	1
Damping/Mass coefficient (da)	0
Source term (f)	-M_xx-M_yy

6.7. Application Mode: PDE, General Form (g2)

Application mode type: PDE, General Form

Application mode name: g2

6.7.1. Application Mode Properties

Property	Value
Default element type	Lagrange - Quadratic
Wave extension	Off
Frame	Frame (ref)
Weak constraints	Off

6.7.2. Variables

Dependent variables: u2, u2_t

Shape functions: shlag(2,'u2')

Interior boundaries not active

6.7.3. Boundary Settings

Boundary	1-4
Type	Dirichlet boundary condition

6.7.4. Subdomain Settings

Subdomain	1
Source term (f)	v
Conservative flux source term (ga)	{{0;0}}

7. Solver Settings

Solve using a script: off

Analysis type	Transient
Auto select solver	On
Solver	Time dependent
Solution form	Automatic
Symmetric	auto
Adaptive mesh refinement	Off
Optimization/Sensitivity	Off
Plot while solving	Off

7.1. Direct (UMFPACK)

Solver type: Linear system solver

Parameter	Value
Pivot threshold	0.1
Memory allocation factor	0.7

7.2. Time Stepping

Parameter	Value
Times	range(0,0.1,10)
Relative tolerance	0.0001
Absolute tolerance	0.000010
Times to store in output	Specified times
Time steps taken by solver	Free
Maximum BDF order	5
Singular mass matrix	Maybe
Consistent initialization of DAE systems	Backward Euler
Error estimation strategy	Include algebraic
Allow complex numbers	Off

7.3. Advanced

Parameter	Value
Constraint handling method	Elimination
Null-space function	Automatic
Automatic assembly block size	On
Assembly block size	5000
Use Hermitian transpose of constraint matrix and in symmetry detection	Off
Use complex functions with real input	Off
Stop if error due to undefined operation	On
Store solution on file	Off
Type of scaling	Automatic
Manual scaling	
Row equilibration	On
Manual control of reassembly	Off
Load constant	On
Constraint constant	On

Mass constant	On
Damping (mass) constant	On
Jacobian constant	On
Constraint Jacobian constant	On

8. Postprocessing

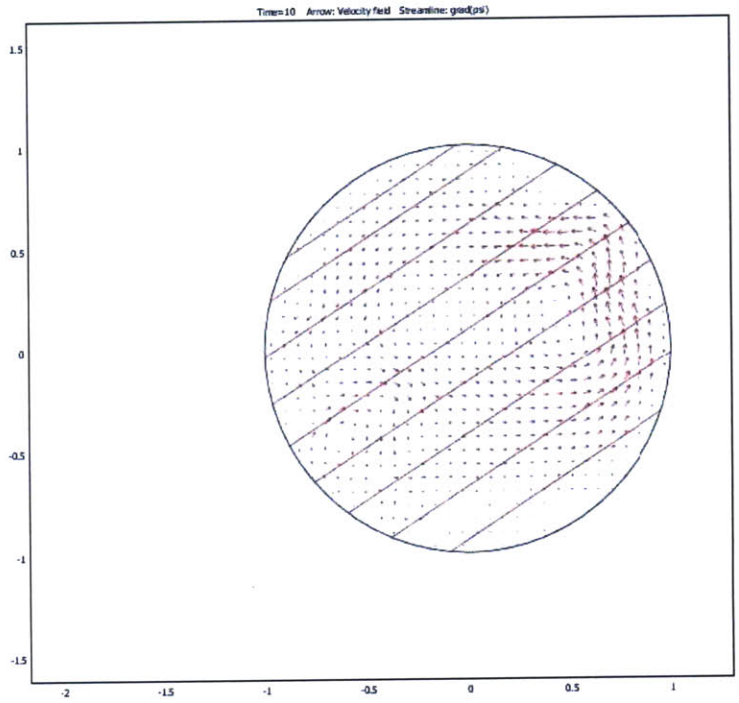

9. Variables

9.1. Boundary

Name	Description	Unit	Expression
K_x_ns	Viscous force per area, x component	Pa	eta_ns * (2 * nx_ns * ux+ny_ns * (uy+vx))
T_x_ns	Total force per area, x component	Pa	-nx_ns * p+2 * nx_ns * eta_ns * ux+ny_ns * eta_ns * (uy+vx)
K_y_ns	Viscous force per area, y component	Pa	eta_ns * (nx_ns * (vx+uy)+2 * ny_ns * vy)
T_y_ns	Total force per area, y component	Pa	-ny_ns * p+nx_ns * eta_ns * (vx+uy)+2 * ny_ns * eta_ns * vy
ndflux_w_di	Normal diffusive flux, w	mol/(m^2*s)	nx_di * dflux_w_x_di+ny_di * dflux_w_y_di

ndflux_M_x_cd3	Normal diffusive flux, M_x	mol/(m^2*s)	nx_cd3 * dflux_M_x_x_cd3+ny_cd3 * dflux_M_x_y_cd3
ncflux_M_x_cd3	Normal convective flux, M_x	mol/(m^2*s)	nx_cd3 * cflux_M_x_x_cd3+ny_cd3 * cflux_M_x_y_cd3
ntflux_M_x_cd3	Normal total flux, M_x	mol/(m^2*s)	nx_cd3 * tflux_M_x_x_cd3+ny_cd3 * tflux_M_x_y_cd3
ndflux_M_y_cd	Normal diffusive flux, M_y	mol/(m^2*s)	nx_cd * dflux_M_y_x_cd+ny_cd * dflux_M_y_y_cd
ncflux_M_y_cd	Normal convective flux, M_y	mol/(m^2*s)	nx_cd * cflux_M_y_x_cd+ny_cd * cflux_M_y_y_cd
ntflux_M_y_cd	Normal total flux, M_y	mol/(m^2*s)	nx_cd * tflux_M_y_x_cd+ny_cd * tflux_M_y_y_cd

9.2. Subdomain

Name	Description	Unit	Expression
U_ns	Velocity field	m/s	sqrt(u^2+v^2)
V_ns	Vorticity	1/s	vx-uy
divU_ns	Divergence of velocity field	1/s	ux+vy
cellRe_ns	Cell Reynolds number	1	rho_ns * U_ns * h/eta_ns
res_u_ns	Equation residual for u	N/m^3	rho_ns * (ut+u * ux+v * uy)+px-F_x_ns-eta_ns * (2 * uxx+uyy+vxy)
res_v_ns	Equation residual for v	N/m^3	rho_ns * (vt+u * vx+v * vy)+py-F_y_ns-eta_ns * (vxx+uyx+2 * vyy)
beta_x_ns	Convective field, x component	kg/(m^2*s)	rho_ns * u
beta_y_ns	Convective field, y component	kg/(m^2*s)	rho_ns * v
Dm_ns	Mean diffusion coefficient	Pa*s	eta_ns
da_ns	Total time scale factor	kg/m^3	rho_ns
taum_ns	GLS time-scale	m^3*s/kg	nojac(1/max(2 * rho_ns * sqrt(emetric(u,v)),48 * eta_ns/h^2))
tauc_ns	GLS time-scale	m^2/s	0.5 * nojac(if(u^2+v^2
res_p_ns	Equation residual for p	kg/(m^3*s)	rho_ns * divU_ns
grad_w_x_di	Concentration gradient, w, x component	mol/m^4	wx
dflux_w_x_di	Diffusive flux, w, x component	mol/(m^2*s)	-Dxx_w_di * wx-Dxy_w_di * wy
grad_w_y_di	Concentration gradient, w, y component	mol/m^4	wy

dflux_w_y_di	Diffusive flux, w, y component	mol/(m^2*s)	-Dyx_w_di * wx-Dyy_w_di * wy
grad_w_di	Concentration gradient, w	mol/m^4	sqrt(grad_w_x_di^2+grad_w_y_di^2)
dflux_w_di	Diffusive flux, w	mol/(m^2*s)	sqrt(dflux_w_x_di^2+dflux_w_y_di^2)
grad_M_x_x_cd3	Concentration gradient, M_x, x component	mol/m^4	M_xx
dflux_M_x_x_cd3	Diffusive flux, M_x, x component	mol/(m^2*s)	-Dxx_M_x_cd3 * M_xx-Dxy_M_x_cd3 * M_xy
cflux_M_x_x_cd3	Convective flux, M_x, x component	mol/(m^2*s)	M_x * u_M_x_cd3
tflux_M_x_x_cd3	Total flux, M_x, x component	mol/(m^2*s)	dflux_M_x_x_cd3+cflux_M_x_x_cd3
grad_M_x_y_cd3	Concentration gradient, M_x, y component	mol/m^4	M_xy
dflux_M_x_y_cd3	Diffusive flux, M_x, y component	mol/(m^2*s)	-Dyx_M_x_cd3 * M_xx-Dyy_M_x_cd3 * M_xy
cflux_M_x_y_cd3	Convective flux, M_x, y component	mol/(m^2*s)	M_x * v_M_x_cd3
tflux_M_x_y_cd3	Total flux, M_x, y component	mol/(m^2*s)	dflux_M_x_y_cd3+cflux_M_x_y_cd3
beta_M_x_x_cd3	Convective field, M_x, x component	m/s	u_M_x_cd3
beta_M_x_y_cd3	Convective field, M_x, y component	m/s	v_M_x_cd3
grad_M_x_cd3	Concentration gradient, M_x	mol/m^4	sqrt(grad_M_x_x_cd3^2+grad_M_x_y_cd3^2)
dflux_M_x_cd3	Diffusive flux, M_x	mol/(m^2*s)	sqrt(dflux_M_x_x_cd3^2+dflux_M_x_y_cd3^2)
cflux_M_x_cd3	Convective flux, M_x	mol/(m^2*s)	sqrt(cflux_M_x_x_cd3^2+cflux_M_x_y_cd3^2)
tflux_M_x_cd3	Total flux, M_x	mol/(m^2*s)	sqrt(tflux_M_x_x_cd3^2+tflux_M_x_y_cd3^2)
cellPe_M_x_cd3	Cell Peclet number, M_x	1	h * sqrt(beta_M_x_x_cd3^2+beta_M_x_y_cd3^2)/Dm_M_x_cd3
Dm_M_x_cd3	Mean diffusion coefficient, M_x	m^2/s	(Dxx_M_x_cd3 * u_M_x_cd3^2+Dxy_M_x_cd3 * u_M_x_cd3 * v_M_x_cd3+Dyx_M_x_cd3 * v_M_x_cd3 * u_M_x_cd3+Dyy_M_x_cd3 * v_M_x_cd3^2)/(u_M_x_cd3^2+v_M_x_cd3^2+eps)

res_M_x_cd3	Equation residual for M_x	mol/(m^3*s)	-Dxx_M_x_cd3 * M_xxx-Dxy_M_x_cd3 * M_xxy+M_xx * u_M_x_cd3-Dyx_M_x_cd3 * M_xyx-Dyy_M_x_cd3 * M_xyy+M_xy * v_M_x_cd3-R_M_x_cd3
res_sc_M_x_cd3	Shock capturing residual for M_x	mol/(m^3*s)	M_xx * u_M_x_cd3+M_xy * v_M_x_cd3-R_M_x_cd3
da_M_x_cd3	Total time scale factor, M_x	1	Dts_M_x_cd3
grad_M_y_x_cd	Concentration gradient, M_y, x component	mol/m^4	M_yx
dflux_M_y_x_cd	Diffusive flux, M_y, x component	mol/(m^2*s)	-Dxx_M_y_cd * M_yx-Dxy_M_y_cd * M_yy
cflux_M_y_x_cd	Convective flux, M_y, x component	mol/(m^2*s)	M_y * u_M_y_cd
tflux_M_y_x_cd	Total flux, M_y, x component	mol/(m^2*s)	dflux_M_y_x_cd+cflux_M_y_x_cd
grad_M_y_y_cd	Concentration gradient, M_y, y component	mol/m^4	M_yy
dflux_M_y_y_cd	Diffusive flux, M_y, y component	mol/(m^2*s)	-Dyx_M_y_cd * M_yx-Dyy_M_y_cd * M_yy
cflux_M_y_y_cd	Convective flux, M_y, y component	mol/(m^2*s)	M_y * v_M_y_cd
tflux_M_y_y_cd	Total flux, M_y, y component	mol/(m^2*s)	dflux_M_y_y_cd+cflux_M_y_y_cd
beta_M_y_x_cd	Convective field, M_y, x component	m/s	u_M_y_cd
beta_M_y_y_cd	Convective field, M_y, y component	m/s	v_M_y_cd
grad_M_y_cd	Concentration gradient, M_y	mol/m^4	sqrt(grad_M_y_x_cd^2+grad_M_y_y_cd^2)
dflux_M_y_cd	Diffusive flux, M_y	mol/(m^2*s)	sqrt(dflux_M_y_x_cd^2+dflux_M_y_y_cd^2)
cflux_M_y_cd	Convective flux, M_y	mol/(m^2*s)	sqrt(cflux_M_y_x_cd^2+cflux_M_y_y_cd^2)
tflux_M_y_cd	Total flux, M_y	mol/(m^2*s)	sqrt(tflux_M_y_x_cd^2+tflux_M_y_y_cd^2)
cellPe_M_y_cd	Cell Peclet number, M_y	1	h * sqrt(beta_M_y_x_cd^2+beta_M_y_y_cd^2)/Dm_M_y_cd

Dm_M_y_cd	Mean diffusion coefficient, M_y	m^2/s	(Dxx_M_y_cd * u_M_y_cd^2+Dxy_M_y_cd * u_M_y_cd * v_M_y_cd+Dyx_M_y_cd * v_M_y_cd * u_M_y_cd+Dyy_M_y_cd * v_M_y_cd^2)/(u_M_y_cd^2+v_M_y_cd^2+eps)
res_M_y_cd	Equation residual for M_y	mol/(m^3*s)	-Dxx_M_y_cd * M_yxx-Dxy_M_y_cd * M_yxy+M_yx * u_M_y_cd-Dyx_M_y_cd * M_yyx-Dyy_M_y_cd * M_yyy+M_yy * v_M_y_cd-R_M_y_cd
res_sc_M_y_cd	Shock capturing residual for M_y	mol/(m^3*s)	M_yx * u_M_y_cd+M_yy * v_M_y_cd-R_M_y_cd
da_M_y_cd	Total time scale factor, M_y	1	Dts_M_y_cd
abspsix_g	|grad(psi)|		sqrt(psix^2+psiy^2)
absga7x_g	|ga7x|		sqrt(ga7x^2+ga7y^2)
absu2x_g2	|grad(u2)|		sqrt(u2x^2+u2y^2)
absga8x_g2	|ga8x|		sqrt(ga8x^2+ga8y^2)

Appendix C : Specifications (refer to Chapters 4-6)

C1. 10 cm Diameter Sphere to Contain Ferrofluid

Part Number: 3748K18 — $4.26 per Pack of 1

Material	Polypropylene
Polypropylene Material	Easy-to-Machine Chemical-Resistant Polypropylene
Backing	Plain Back
Finish	Smooth
Shape	Balls
Ball Type	Hollow
Diameter	3.937"
Diameter Tolerance	±.05"
Translucent	Translucent White
Operating Temperature Range	Up to +220° F
Softening Point	Not Rated
Tensile Strength	Poor
Impact Strength	Poor
Tolerance	Standard
Grade	Not Rated
Hardness	Not Rated
Sphericity	Not Rated
Quantity	1
Specifications Met	Not Rated

C2. 7 cm Diameter Sphere to Contain Ferrofluid

Part Number: 3748K35 — $15.09 per Pack of 10

Material	Polypropylene
Polypropylene Material	Easy-to-Machine Chemical-Resistant Polypropylene
Backing	Plain Back
Finish	Smooth
Shape	Balls
Ball Type	Hollow
Diameter	2.756"
Diameter Tolerance	±.02"
Translucent	Translucent White
Operating Temperature Range	Up to +220° F
Softening Point	Not Rated
Tensile Strength	Poor
Impact Strength	Poor
Tolerance	Standard
Grade	Not Rated
Hardness	Not Rated
Sphericity	Not Rated
Quantity	10
Specifications Met	Not Rated

C3. Teflon Support Rod Stock

Part Number: 8546K15 — $8.16 per Ft.

Material	Fluoropolymers
Fluoropolymer Material	Virgin Electrical Grade Teflon® PTFE
Backing	Plain Back
Finish	Smooth
Shape	Rods and Discs
Rods and Discs Type	Rod
Length	Cut-to-Length
Available Lengths	Sold in 1' increments
Maximum Continuous Length	6'
Diameter	3/4"
Diameter Tolerance	+.005"
Opaque	White
Operating Temperature Range	-350° to +500° F
Softening Point	Not Rated
Performance Characteristic	Electrical Insulator, Weather Resistant, Very Low Friction
Tensile Strength	Poor
Impact Strength	Good
Tolerance	Standard
Hardness	Shore D55
Specifications Met	3A Sanitary Standards (3A) Compliant, Aerospace Material Specifications (AMS), American Society for Testing and Materials (ASTM), Food and Drug Administration (FDA) Compliant, Underwriters Laboratories (UL)
AMS Specification	AMS 3651

C4. Screws to Attach Parts of Probe Holder Together

Part Number: 93140A246 — $4.70 per Pack of 10

Head Style	Pan
Pan Head Style	Pan
Material Type	Plastic
Finish	Plain
Plastic Type	Polycarbonate
Self Locking Element	None
Drive Style	Phillips
System of Measurement	Inch
Inch Thread Size	1/4"-20
Thread Length	Fully Threaded
Length	1"
Decimal Size	.250"
Head Diameter	.492"
Head Height	.175"
Drive	#3
Rockwell Hardness	Not Rated
Minimum Tensile Strength	Not Rated
Operating Temperature	-40° to +212° F
Color	Clear
Specifications Met	Not Rated
Screw Quantity	Individual Screw

C5. Stock Material Used to Make Probe Holder

Part Number: 8707K65 — $360.19 Each

Material	Polycarbonate
Polycarbonate Material	Abrasion-Resistant Polycarbonate
Backing	Plain Back
Finish	Smooth
Shape	Sheets, Bars, Strips, and Cubes
Sheets, Bars, Strips, and Cubes Type	Square Sheet
Thickness	1/2"
Thickness Tolerance	±.025"
Length	48"
Length Tolerance	+1/4"
Width	48"
Width Tolerance	+1/4"
Clear	Clear with No Tint
Operating Temperature Range	-40° to +200° F
Softening Point	+295°F
Performance Characteristic	High Impact Strength, Weather Resistant
Tensile Strength	Good
Impact Strength	Excellent
Tolerance	Standard
Hardness	Not Rated
Specifications Met	Not Rated
Note	Clear hard-coat finish is on both sides.

C6. Plastic Cement

Weld-On Cements for Plastics

Fusing two plastic surfaces together, these adhesives make extra-strong bonds. Application temperature range is 70° to 80° F. Operating temperature range varies with materials being joined. These products are compliant under all state VOC rules in effect on October 1, 2009, except in the Los Angeles area (unless noted).

Weld-On 3 bonds acrylic, butyrate, PETG, polycarbonate, and polystyrene to themselves. Dries clear. **Weld-On 4052** bonds ABS, acrylic, PVC, CPVC, polystyrene, and vinyl to themselves and each other. Dries clear. **Weld-On 4707** bonds ABS to itself. Dries white. **Weld-On 4807** is high strength for joining various types of polystyrene. Dries white.

Weld-On No.	Size	Begins to Harden	Reaches Full Strength		Each
3	1-pt. Can	30-45 sec.	24-48 hrs.	7528A13†	$12.77
4052	1-pt. Can	15 min.	7 days	7352A11	18.00
4052	1-gal. Can	15 min.	7 days	7352A12	90.21
4707	1-pt. Can	10 min.	24-72 hrs.	7352A17†	13.96
4707	1-gal. Can	10 min.	24-72 hrs.	7352A19†	65.30
4807	1-pt. Can	10-15 min.	24-72 hrs.	7352A24	13.47
4807	1-gal. Can	10-15 min.	24-72 hrs.	7352A26	63.91

† This product is compliant under all state VOC rules in effect on October 1, 2009.

C7. GMW Three Axis Magnetic Field Sensor

Ametes *Magnetic Field Sensor • 3 Axis, MFS-3A*

The high magnetic field sensitivity, accurate calibration, high stability and high signal output of the Sentron CSA-1V Hall effect IC enable it to be conveniently used to monitor the extended fields from magnetic items and electric equipment. As a demonstration of the CSA-1V capability, three CSA-1V with sensitive axes mutually perpendicular, are combined in a compact module as the MFS-3A. Three output voltages $V_X = S*B_X$, $V_Y = S*B_Y$ and $V_Z = S*B_Z$ are generated proportional to the magnetic flux density components B_X, B_Y and B_Z with the sensitivity S = 280mV/mT over the field range of ±7.3mT. This enables calculation of the total magnetic flux density, $B = (B_X^2 + B_Y^2 + B_Z^2)^{1/2} = (V_X^2 + V_Y^2 + V_Z^2)^{1/2}/S$.

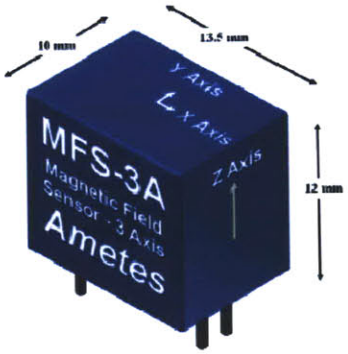

Specifications

* Measures B_X, B_Y, B_Z
* Suitable for environmental magnetic fields
* Field range: ±7.3mT (+/-73G)
* Resolution: ±10μT (+/-0.1G)
* Three linear analog outputs V_X, V_Y, V_Z of 0.5V to 4.5V
* Sensitivity: S = 280mV/mT
* Accuracy: ±3%
* Angular alignment: ±3deg
* Frequency response dc to 100kHz (-3dB)
* Small size: 10 x 13.5 x 12mm (0.39 x 0.53 x 0.47inch)
* Low weight: 2.5g (0.1oz)
* Low power: 36mA max at 5V

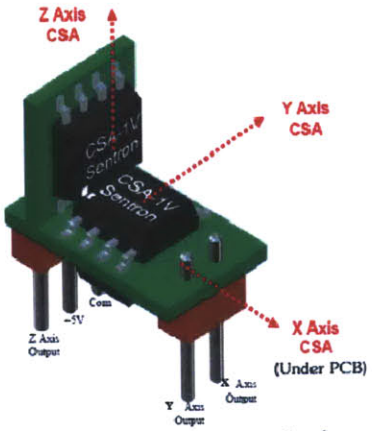

Applications:

* Quality assurance of magnetized materials and items such as sealing strips and permanent magnets by fast and complete characterization of the external magnetic field.
* Detection/separation of magnetic and non-magnetic materials by monitoring the modification of the local or imposed field caused by magnetic item/items.
* Non-contact, non-invasive and continuous "Condition Monitoring" of electrical motors, generators, transformers or inductors by comparing the amplitudes of selected external or "leakage" field spectral components with initial or reference values. Quality assurance of electrical components by leakage field measurement.
* Independent monitoring of the ON/OFF status of large magnets with extended fringing fields. The MFS-3A output can be used to operate warning indicators and/or interlocks. Resolution of ±10μT readily allows measurement of the 500μT (5G) safety level applicable to Magnetic Resonance Imagers (MRI).
* Wearable, battery operated "Personal Magnetic Field Detector" to immediately generate a warning to the wearer that they have entered a region of increased magnitude magnetic field.
* Magnetic field detection and warning or interlock to be incorporated in magnetically sensitive equipment such as time standards or patient support equipment that may be used in the fringe field of an MRI or other large magnet.

Revision 07 May 2007 MFS-3A

Europe - **Senis GmbH: Technoparkstrasse 1, 8005 Zurich, Switzerland. www.senis.ch. +41 (79) 366-8756**
The Americas - GMW Associates: 955 Industrial Road, San Carlos, CA 94070, USA. www.gmw.com. +1 (650) 802-8292

GMW

Sentron CSA-1V
Revised Jan 2005

CSA-1V

Current Sensor

Features:

- Sensitive to a magnetic field parallel to the chip surface
- Very high sensitivity
- Linear output voltage proportional to a magnetic field
- Wide-band: DC to 100kHz
- Very low offset and offset-drift
- Very low noise
- Isolated from current conductor
- Surface mount SOIC-8 package

Applications:

- AC and/or DC current measurement
- Wide-Band Magnetic Field Measurement
- Battery Chargers
- AC-DC Converters
- Motor Control

General Description

The CSA-1V is a single-axis integrated magnetic field sensor based on the Hall effect. The circuit is fabricated using a conventional CMOS technology with an additional ferromagnetic layer. The ferromagnetic layer is used as a magnetic flux concentrator providing a high magnetic gain. Therefore, the circuit features very high magnetic sensitivity, low offset, and low noise.
The CSA-1V is packaged in a standard SOIC-8 full plastic package. This package provides:

- highest isolation for applications with the current conductor on the PCB (up to 600V)
- highest sensitivity for applications with the current lead above the chip.

Package: SOIC-8

Pin Out:

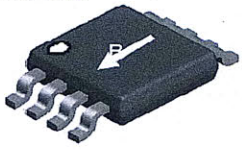

1 A_OUT, analog sensor output
2 V_{DD} pos. supply voltage
3 Not connected
4 PV, programming voltage [1)]
5 GND, supply common
6 PD, programming data [1)]
7 PC, programming clock [1)]
8 CO_OUT, common output

Note 1: Used for factory programming

Manufactured by: Sentron AG (A Melexis Company) • Baarerstrasse 73 • 6300 Zug • Switzerland • Tel: +41 (41) 711 2170 • Fax: +41 (41) 711 2188 www.sentron.ch • sales@sentron.ch •

GMW Associates. 955 Industrial Rd, San Carlos, CA 94070
www.gmw.com. Tel: (650) 802-8292. Fax: (650) 802-8298. Email sales@gmw.com

GMW

Sentron CSA-1V
Revised Jan 2005

Absolute Maximum Ratings

Symbol	Parameter	Min.	Typ.	Max.	Unit	Remarks
V_{SUP}	Supply Voltage	0		6	V	
T	Ambient Temperature	-40		+150	°C	

Recommended Operating Conditions

Symbol	Parameter	Min.	Typ.	Max.	Unit	Remarks
V_{SUP}	Supply Voltage	4.5	5	5.5	V	
I_{OUT}	Output Current	-1		1	mA	
C_L	Load Capacitance			1000	pF	

Electrical Characteristics

At T=-40°C to 150°C, V_{SUP}=4.5V to 5.5V if not otherwise specified.

Symbol	Parameter	Min.	Typ.	Max.	Unit	Test Conditions
I_{SUP}	Supply Current		11	16	mA	
V_{Common}	Common (reference) Output Voltage[2)]	$V_{SUP}/2$ -20mV	$V_{SUP}/2$	$V_{SUP}/2$ +20mV		I_{OUT}=0mA
BW	Bandwidth: DC to		100		kHz	
t_R	Response Time			6	µs	

Note 2: Ratiometric (proportional to V_{SUP})

Characteristics of the Linear Magnetic Field Sensor [3,4)]

With V_{SUP}= 5V and in the temperature range -40°C to 150°C, if not otherwise specified.

Symbol	Parameter	Min.	Typ.	Max.	Unit	Test Conditions
S	Magnetic Sensitivity[3)]	270	280[6)]	290	V/T	B = B_L
ΔS/SΔT	Magn. Sensitivity Temperature Drift	- 0.02		0.02	%/°C	I_{OUT}=0mA T=-20°C to 125°C
Voff	Offset Voltage[3)]	-15	0	15	mV	B=0T, Iout=0mA, T=20°C
Boff	Equivalent Magnetic Offset[3)]	-50	0	50	µT	B=0T, I_{OUT}=0mA T=-20°C to 80°C
ΔVoff/ΔT	Offset Temperature Drift	-0.2	0	0.2	mV/°C	B=0T, I_{OUT}=0mA, T=-20°C to 125°C
B_{FS}	Full Scale Magnetic Field Range[5)]	-7.5		7.5	mT	
B_L	Linear Magnetic Field Range	-5		5	mT	
NL	Non Linearity		0.1	0.2	%	B = B_L
			0.5	1		B = B_{FS}
ΔBnoise	Input referred magnetic noise spectrum density (RMS)			125	nT/√Hz	f=10Hz to 10kHz

Note 3: Ratiometric (proportional to V_{SUP})
Note 4: When the analog output pin A_OUT is used in differential mode (ie Vout = A_OUT – CO_OUT)
Note 5: Device saturates for B>B_{FS} but is not damaged
Note 6: Specification correction: Was 300+/- 10 V/T. Now 280+/- 10 V/T. All parts manufactured to date, have been calibrated to 280+/- V/T

Manufactured by: Sentron AG (A Melexis Company) • Baarerstrasse 73 • 6300 Zug • Switzerland • Tel: +41 (41) 711 2170 • Fax: +41 (41) 711 2188 www.sentron.ch • sales@sentron.ch •

Block Diagram

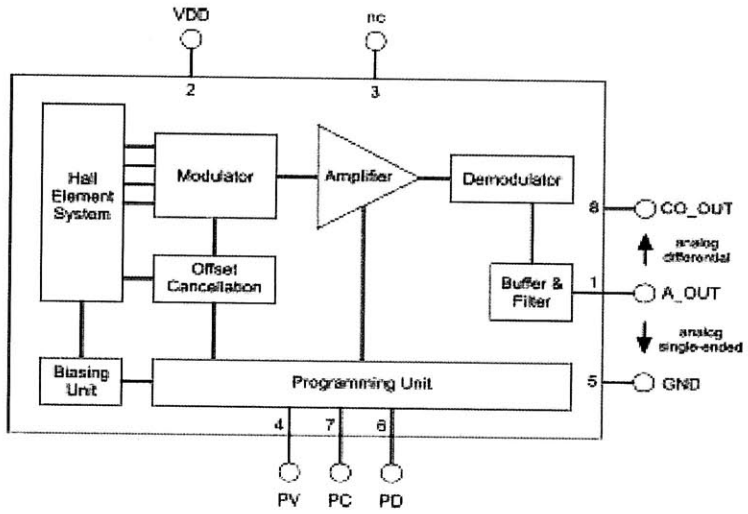

Fig. 1 Block diagram of CSA-1V

IMPORTANT For reliable operation within the specifications the sensor must be connected as follows:

Connect Pin 6 (PD) to Pin 5 (GND)
Connect Pin 7 (PC) to Pin 2 (Vdd)
Connect Pin 4 (PV) to Pin 2 (Vdd)
Put a 100nF capacitor close to the chip between Pin 2 (Vdd) and Pin 5 (GND)

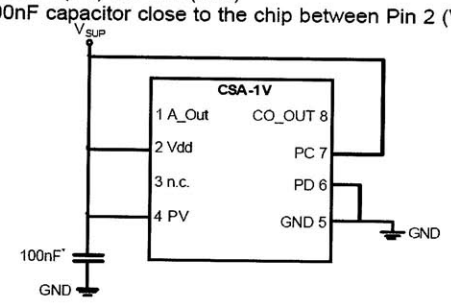

* If the supply voltage is disturbed by EMI it can be useful to place a second capacitor (100pF, ceramic) parallel to the 100nF capacitor.

Fig. 2 Connection diagram of CSA-1V

Package Information SOIC-8

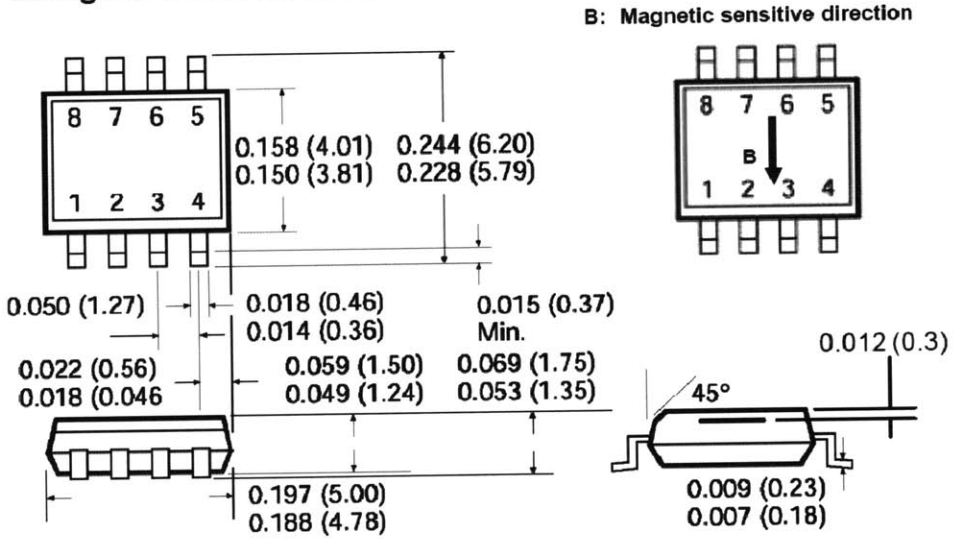

Fig. 3 Package information and magnetic sensitive direction

Ordering Information

Order part number: **CSA-1V-SO**

Parts are supplied on tape and reels.

Quantiites below 2600 pcs are available in cut reels to the quantiity ordered
Quantities above 2600 pcs are available in complete 13", 2600 pc reels

Manufactured by: Sentron AG (A Melexis Company) • Baarerstrasse 73 • 6300 Zug • Switzerland • Tel: +41 (41) 711 2170 • Fax: +41 (41) 711 2188 www.sentron.ch • sales@sentron.ch •

GMW Associates. 955 Industrial Rd, San Carlos, CA 94070
www.gmw.com. Tel: (650) 802-8292. Fax: (650) 802-8298. Email sales@gmw.com

C8. Probe Holder Construction Drawings

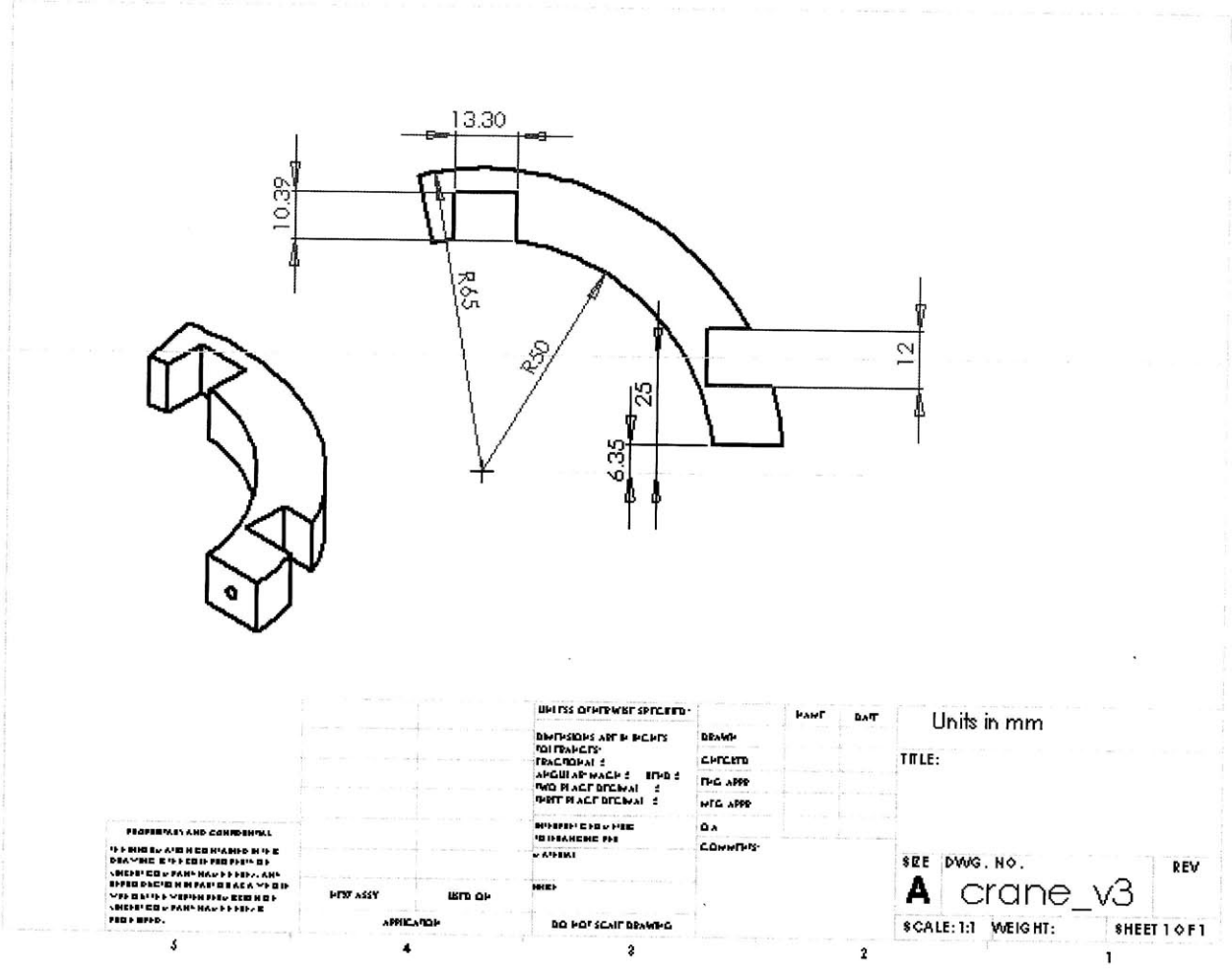

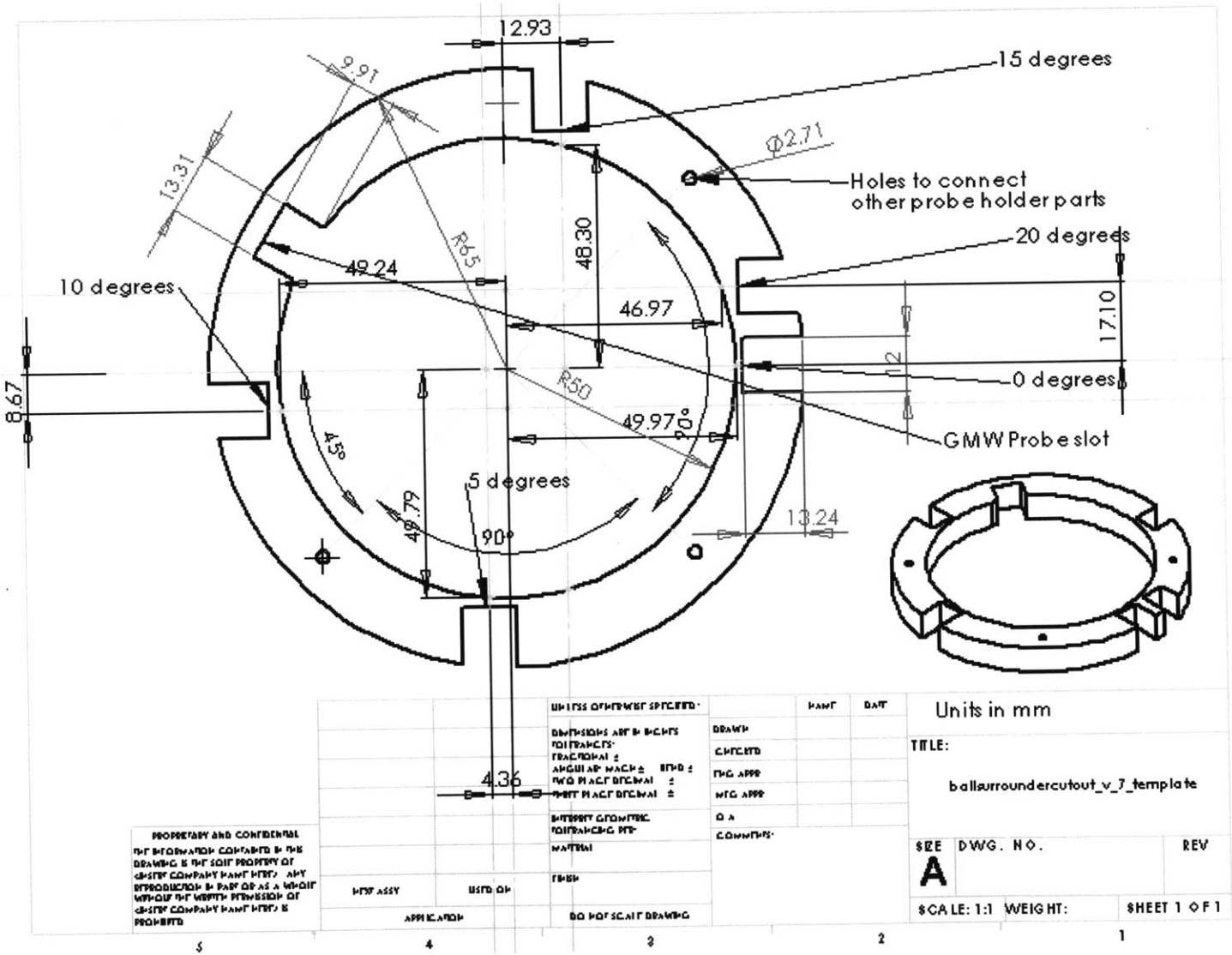
12.93
9.91
13.31
15 degrees
Ø2.71
Holes to connect
other probe holder parts
20 degrees
48.30
49.24
R65
10 degrees
46.97
17.10
2
0 degrees
8.67
R50
49.97
20°
GMW Probe slot
45°
5 degrees
48.79
90°
13.24
4.36
Units in mm
TITLE:
ballsurroundercutout_v_7_template
SIZE
A
DWG. NO.
REV
SCALE: 1:1
WEIGHT:
SHEET 1 OF 1
PROPRIETARY AND CONFIDENTIAL
DRAWN
CHECKED
ENG APPR
MFG APPR
Q A
COMMENTS:
MATERIAL
FINISH
NEXT ASSY
USED ON
APPLICATION
DO NOT SCALE DRAWING

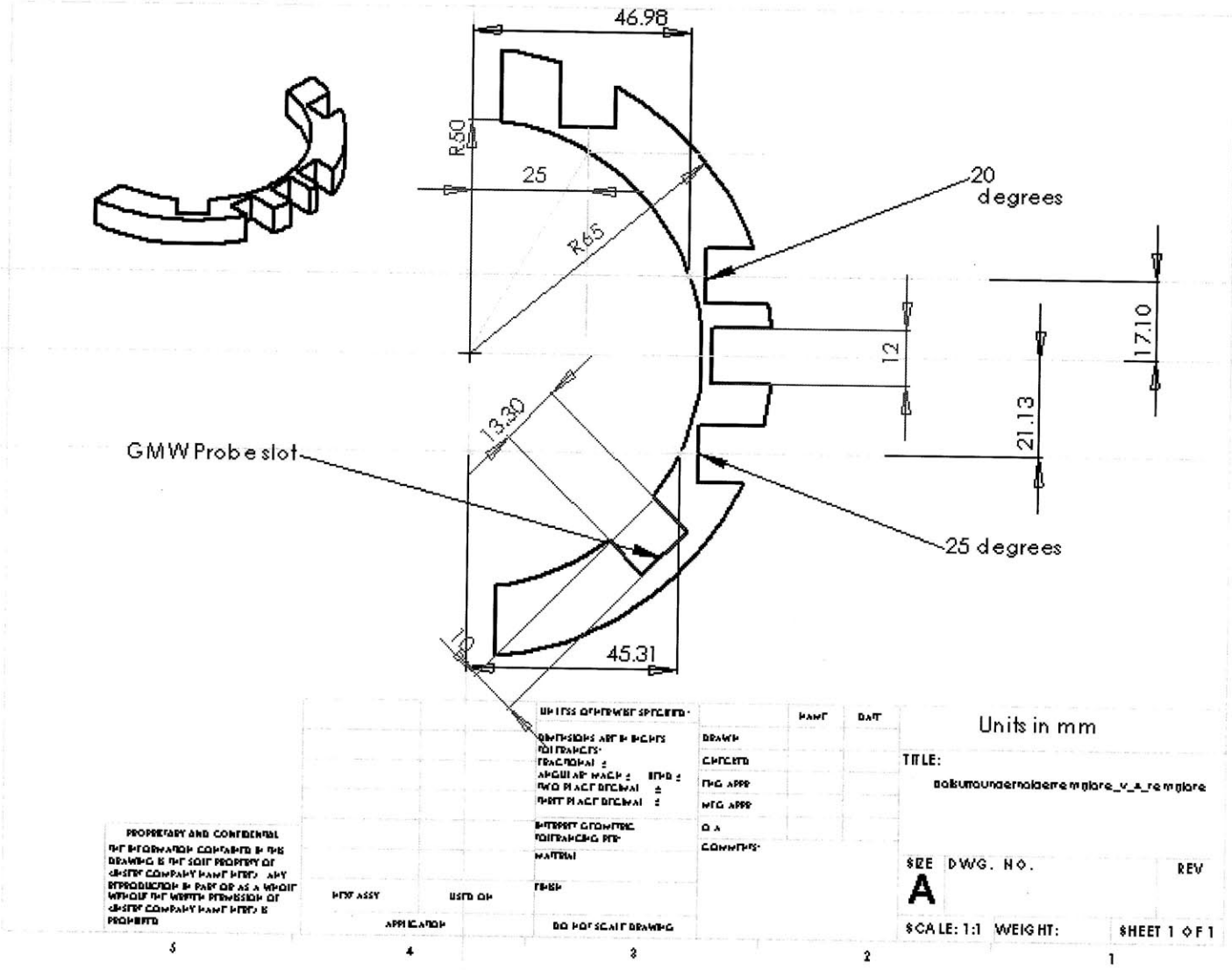
46.98
R.50
25
R65
20
degrees
12
17.10
21.13
13.30
GMW Probe slot
25 degrees
45.31
Units in mm
TITLE:
SIZE
A
DWG. NO.
REV
SCALE: 1:1
WEIGHT:
SHEET 1 OF 1

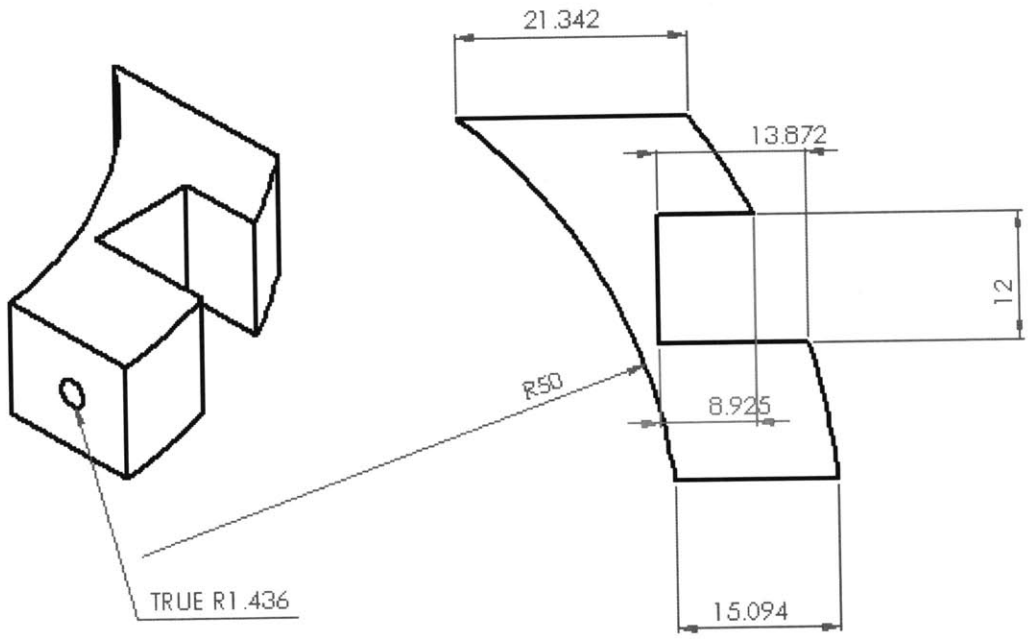

		UNLESS OTHERWISE SPECIFIED:		NAME	DATE
		DIMENSIONS ARE IN INCHES TOLERANCES: FRACTIONAL ± ANGULAR: MACH ± BEND ± TWO PLACE DECIMAL ± THREE PLACE DECIMAL ±	DRAWN		
			CHECKED		
			ENG APPR.		
			MFG APPR.		
		INTERPRET GEOMETRIC TOLERANCING PER:	Q.A.		
		MATERIAL	COMMENTS:		
		FINISH			
NEXT ASSY	USED ON				
APPLICATION		DO NOT SCALE DRAWING			

PROPRIETARY AND CONFIDENTIAL

THE INFORMATION CONTAINED IN THIS DRAWING IS THE SOLE PROPERTY OF <INSERT COMPANY NAME HERE>. ANY REPRODUCTION IN PART OR AS A WHOLE WITHOUT THE WRITTEN PERMISSION OF <INSERT COMPANY NAME HERE> IS PROHIBITED

Units in mm

TITLE:

crane_v4_for3rdcoilcase

SIZE	DWG. NO.	REV
A		
SCALE: 5:1	WEIGHT:	SHEET 1 OF 1

5 4 3 2 1

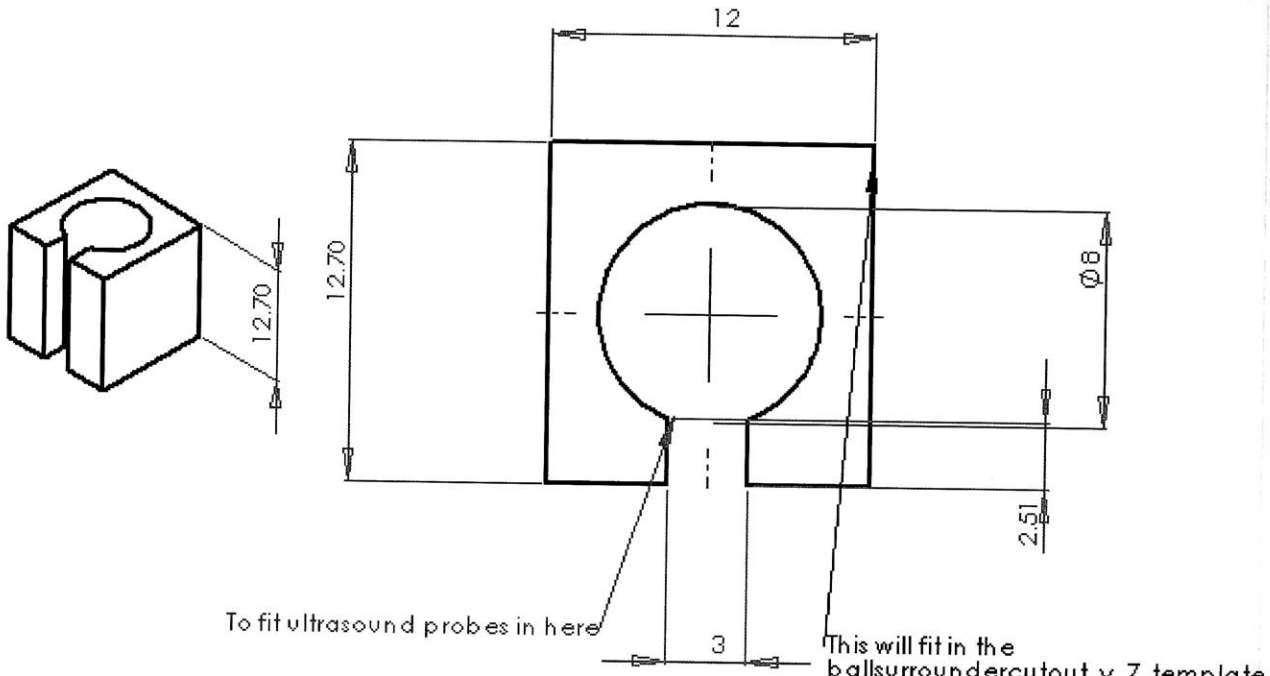

			UNLESS OTHERWISE SPECIFIED:		NAME	DATE	Units in mm
			DIMENSIONS ARE IN INCHES TOLERANCES: FRACTIONAL ± ANGULAR: MACH ± BEND ± TWO PLACE DECIMAL ± THREE PLACE DECIMAL ±	DRAWN			TITLE: probeholder
				CHECKED			
				ENG APPR.			
				MFG APPR.			
			INTERPRET GEOMETRIC TOLERANCING PER:	Q.A.			
			MATERIAL	COMMENTS:			SIZE A DWG. NO. REV
PROPRIETARY AND CONFIDENTIAL THE INFORMATION CONTAINED IN THIS DRAWING IS THE SOLE PROPERTY OF <INSERT COMPANY NAME HERE>. ANY REPRODUCTION IN PART OR AS A WHOLE WITHOUT THE WRITTEN PERMISSION OF <INSERT COMPANY NAME HERE> IS PROHIBITED.			FINISH				SCALE: 2:1 WEIGHT: SHEET 1 OF 1
	NEXT ASSY	USED ON					
	APPLICATION		DO NOT SCALE DRAWING				
5	4		3	2			1

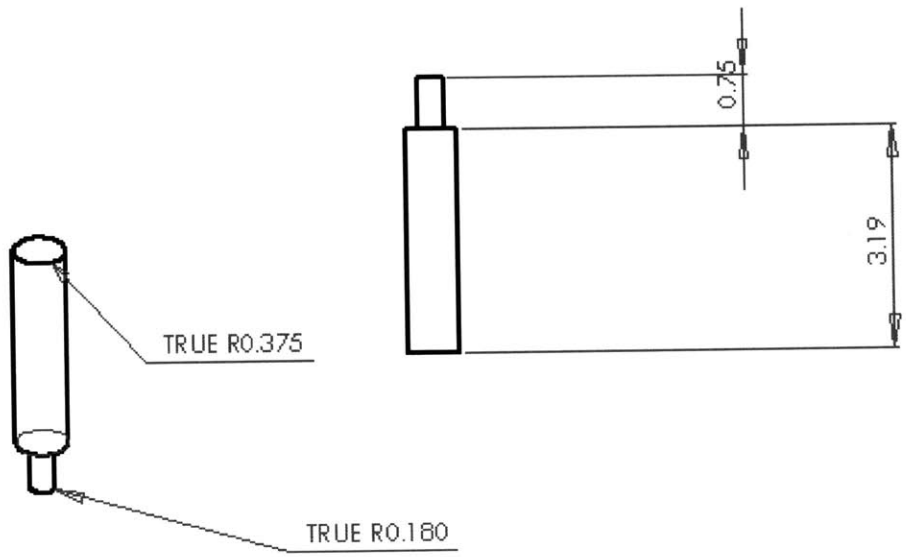

		UNLESS OTHERWISE SPECIFIED:		NAME	DATE
		DIMENSIONS ARE IN INCHES TOLERANCES: FRACTIONAL ± ANGULAR: MACH ± BEND ± TWO PLACE DECIMAL ± THREE PLACE DECIMAL ±	DRAWN		
			CHECKED		
			ENG APPR.		
			MFG APPR.		
		INTERPRET GEOMETRIC TOLERANCING PER:	Q.A.		
		MATERIAL	COMMENTS: Units in inches		
		FINISH			
NEXT ASSY	USED ON				
APPLICATION		DO NOT SCALE DRAWING			

PROPRIETARY AND CONFIDENTIAL

THE INFORMATION CONTAINED IN THIS DRAWING IS THE SOLE PROPERTY OF <INSERT COMPANY NAME HERE>. ANY REPRODUCTION IN PART OR AS A WHOLE WITHOUT THE WRITTEN PERMISSION OF <INSERT COMPANY NAME HERE> IS PROHIBITED

Units in inches

TITLE:

SIZE	DWG. NO.	REV
A	ballholder	
SCALE: 1:2	WEIGHT:	SHEET 1 OF 1

5 4 3 2 1

C9. Brookfield LV1 Spindle Disk Attachment

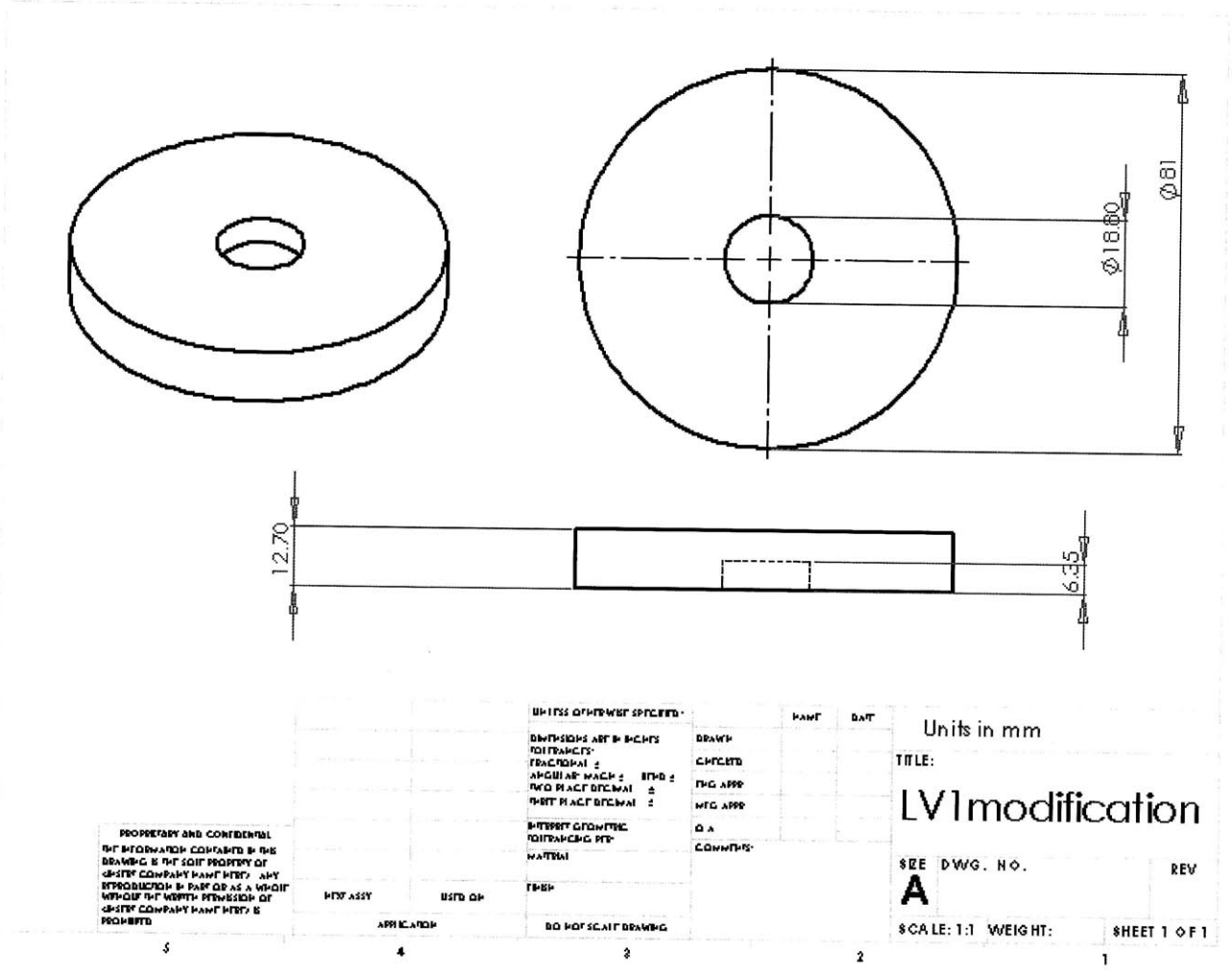

C10. Dimensions of Inner Fluxball

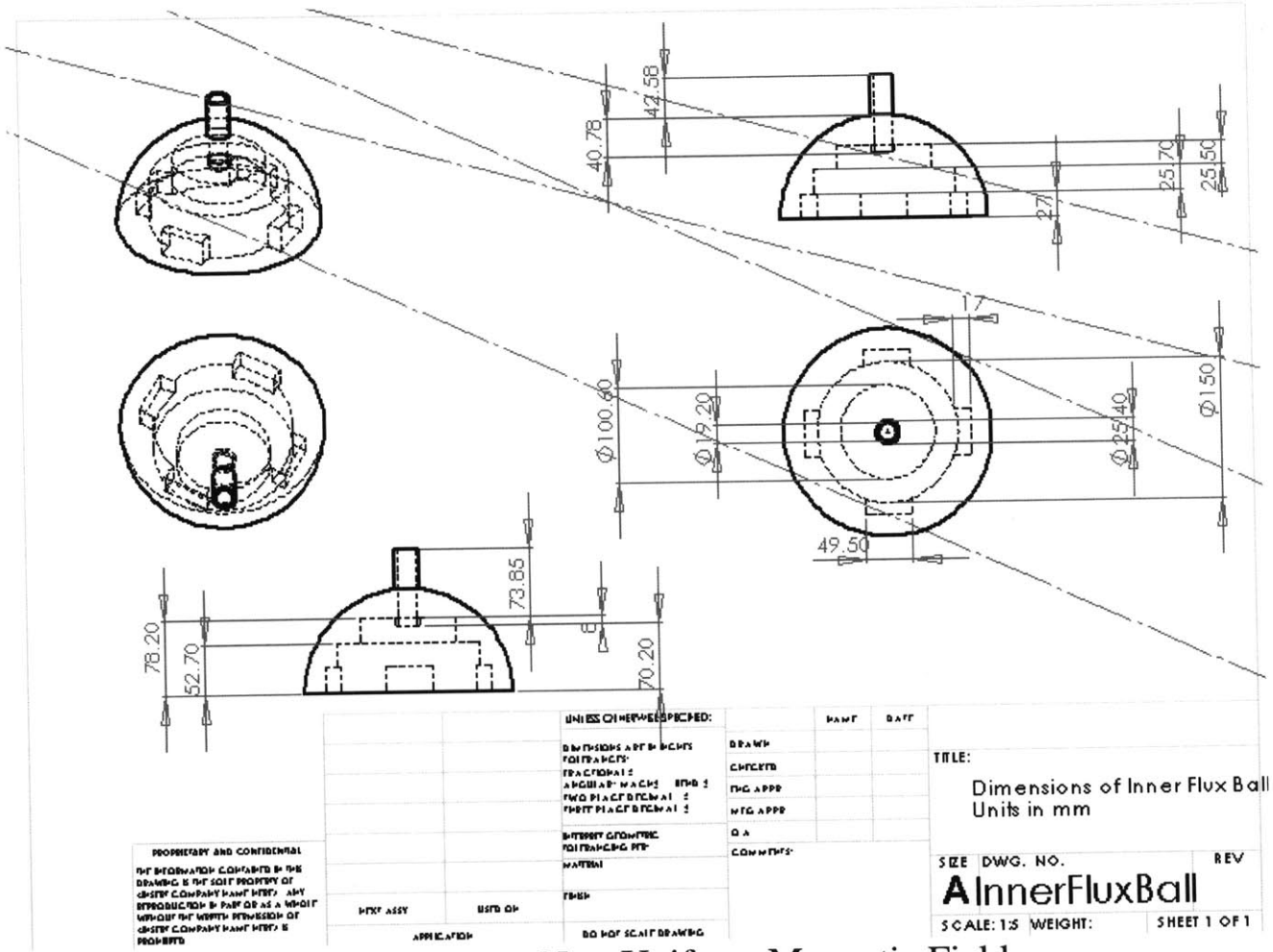

C11. Third Solenoidal Coil Used to Create Non-Uniform Magnetic Field

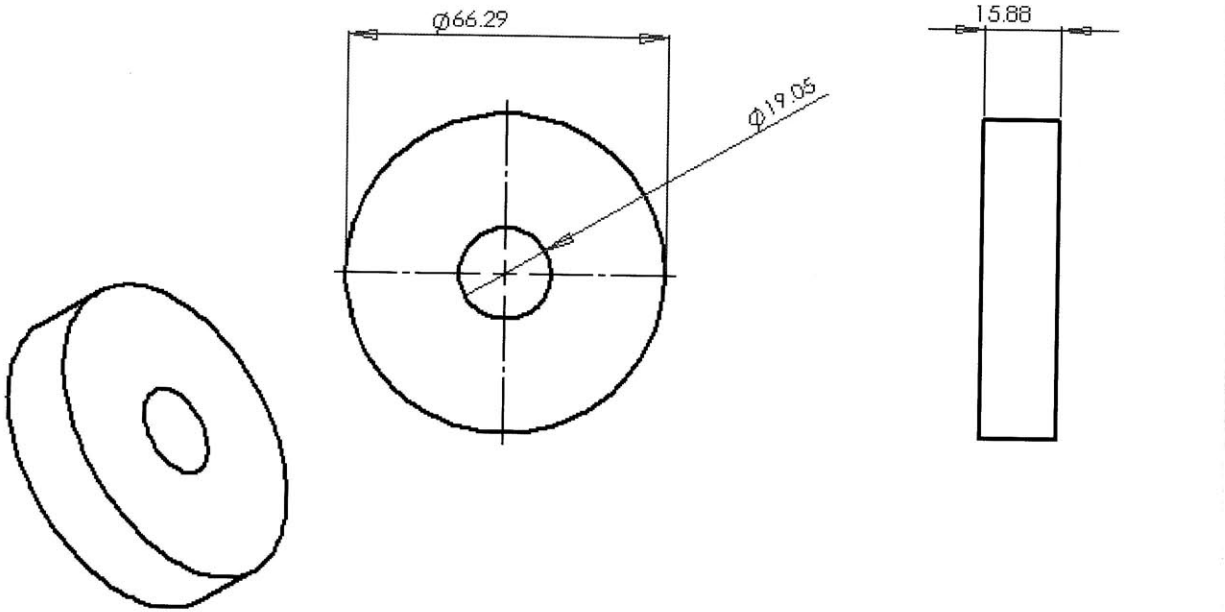

Units in mm

TITLE:

SIZE A

DWG. NO. 3rdcoil_2

REV

SCALE: 1:1 WEIGHT:

SHEET 1 OF 1

C12. LVC 5050 Power Amplifier

There are two amplifiers in the LEES HVRL laboratory. Although they look identical, one is actually an older model where the front panel controls have been disabled. The only voltage controls are the on/off switch and the rear gain selector.

APPLICATION

AE Techron, Inc. **LVC 5050**

The **LVC 5050** is a general purpose, high voltage, medium continuous current, linear power amplifier. It works best when driving loads of 2 - 16 ohms. The **LVC 5050** works well with either pulsed or continuous test signals or environments that have both conditions. The **LVC 5050** has two (2) separate channels that can be operated independently or combined for greater maximum voltage or current. In ***Bridge-mono mode*** the available output voltage doubles. In ***Parallel-mono mode*** the amplifier operates with twice the available output current

FEATURES

- Bi Level ™ Power Supply, amplifier optimizes itself for either, high pulse voltage or low voltage high current, dynamically. The **LVC 5050** produces less heat, higher long term power, with no added distortion.
- Output of 20.0 amperes rms, or 106 volts rms, per channel depending on load.
- Frequency bandwidth of DC to 20 kHz at full power.
- Option of controlled voltage, or controlled current operation, modes changed via a jumper
- User-adjustable voltage or current limiting
- Remote switching to standby mode by contact closure
- External monitoring of voltage and current output
- Equipped with circuitry to protect the amplifier from input overloads, improper output connection (including shorts and improper loads), excessive temperature, voltage or current.
- Shipped ready to operate using single-phase, 120-volt AC mains. Also available in 100, 200, 208, 230 and 240 VAC versions.
- Installs easily into a standard 19 inch rack, or stands alone for bench top operations

INDICATORS AND CONTROLS

- Front panel LEDs indicate signal presence and output overload
- A pushbutton power "On/Off" located on the front panel
- Two gain controls on the front panel for controlled voltage applications
- A back panel slide switch to lift signal ground from chassis ground
- A back panel slide switch to choose between 2 channel, bridge mono and parallel mono operation

Call us or visit our website! When your project or product requires a low noise, low distortion, high power amplifier solution, contact ***AE Techron Inc.*** We are happy to help.

PERFORMANCE (One hour continuous ratings)

Frequency response
+/- 0.1 dB from 20 Hz to 20 kHz at 1 watt

Phase response
+/- 10 Degrees (10 Hz to 20 kHz at 1 watt

Signal-to-noise ratio
At 26 dB gain, better than 105 dB (A-weighted) below full output

THD
Less than 0.05% from 20 Hz to 1 kHz increasing linearly to 0.1% at 20 kHz at full output

I.M. Distortion
<0.05% from 410 milliwatts to full output at 26 dB gain with and 8 ohm load

Slew rate
> 31V per microsecond

Load Impedance
Rated for 16,8,4 and 2 ohm use. Safe with all load types even reactive ones.

Input Impedance
Greater than 10K ohms, balanced, and 5K ohms unbalanced.

Output impedance
Less than 10 milliohms in series with less than 2 microhenries

OUTPUT POWER LVC 5050

Single Channel

	40 mSec			1 Hour Continuous		
Ohms	Watts	Volts	Amps	Watts	Volts	Amps
2	2505	71	35	800	40	20
4	1940	88	22	576	48	12
8	1270	101	12	1205	98.2	12
16	702	106	7	702	106	7

Bridged Mono

	40 mSec			1 Hour Continuous		
Ohms	Watts	Volts	Amps	Watts	Volts	Amps
4	5320	146	36			
8	3003	155	19	3003	155	19
16	2036	180	11	2036	180	11

Parallel Mono

	40 mSec			1 Hour Continuous		
Ohms	Watts	Volts	Amps	Watts	Volts	Amps
1	5320	73	73			
2	4045	90	45			
4	2670	103	26	2416	98.3	25
8	1378	105	13	1324	102.9	13

PHYSICAL CHARACTERISTICS

Chassis: The Amplifier is designed for stand alone, or rack mounted, operation. The Chassis is black steel with a silver finished aluminum front panel. The unit occupies three EIA 19-inch-wide units.

Weight: 77 lbs. (35.2 kg), Shipping 88 lbs. (40.2 kgs)

AC Power: Single phase, 120 volts, 60 Hz, 30 amperes ac service. (Note: 100, 120, 200, 208, 230 or 240 volt, 50-60 Hz models are available Call for specifications.) US models come with 3 blade NEMA TT30P plug.

Cooling: Forced air cooling from the front, through removable filters, to the back.

Dimensions: 19 in. x 16 in. x 5.25 in (48.3 cm x 40.3.0 cm x 13.3 cm)

SUPPORT

When you purchase an ***AE Techron*** amplifier, a full complement of technical and factory support personnel join your team. ***AE Techron Inc.*** provides:

- Applications engineering for your technical questions and customized product needs.
- A one year limited warranty to protect your equipment investment.
- A fully equipped service center to keep your amplifier operating at original performance requirements.

AE Techron Inc.
2507 Warren Street
Elkhart, IN 46516 USA
Phone: 574-295-9495
Fax: 574-295-9496
E-mail: Sales@aetechron.com
Web: www.aetechron.com

C13. National Instruments PCI-6036E DAQ card

Technical Sales
United States
(866) 531-6285
info@ni.com

NI PCI-6036E

200 kS/s, 16-Bit, 16-Analog-Input Multifunction DAQ

- FREE award-winning global services and support at ni.com/support
- Consider NI M Series for 16-bit resolution, 1.25 MS/s, and similar costs with the PCI-6251.
- LabVIEW, LabWindows/CVI, and Measurement Studio for Visual Basic and Visual Studio .NET integration
- Two 16-bit analog outputs; eight digital I/O lines; two 24-bit counters
- NIST-traceable calibration certificate and more than 70 signal conditioning options
- Included NI-DAQmx driver software and additional measurement services

Overview

National Instruments recommends M Series DAQ and NI-DAQmx driver software for new applications. Increase accuracy and perform 16-bit measurements at 1.25 MS/s with the PCI-6251.

Add sensor and high-voltage measurement capability to your E Series device with National Instruments SCC or SCXI signal conditioning. The National Instruments PCI-6036E is a low-cost DAQ board that uses E Series technology to deliver reliable, 16-bit acquisition for a wide range of applications. The NI PCI-6036E has sixteen 16-bit analog inputs and two 16-bit analog outputs. In addition, it has eight digital I/O lines and two 24-bit, 20 MHz counter/timers. Depending on your hard drive, the PCI-6036E can stream to disk at rates up to 200 kS/s.

Using NI hardware and driver software options, you have flexible OS, application development environment, and application software choices. Complete your DAQ system with NI signal conditioning to measure virtually any type of sensor and voltage.

Specifications

Specifications Documents

- Detailed Specifications
- Data Sheet

Specifications Summary

Specifications Summary

General

Product Name	PCI-6036E
Product Family	Multifunction Data Acquisition
Form Factor	PCI

Operating System/Target	Windows , Real-Time , Linux , Mac OS
LabVIEW RT Support	Yes
DAQ Product Family	E Series
RoHS Compliant	No
Analog Input	
Channels	16 , 8
Single-Ended Channels	16
Differential Channels	8
Resolution	16 bits
Sample Rate	200 kS/s
Max Voltage	10 V
Maximum Voltage Range	10 V , -10 V
Maximum Voltage Range Accuracy	7.56 mV
Minimum Voltage Range	50 mV , -50 mV
Minimum Voltage Range Accuracy	0.061 mV
Number of Ranges	4
Simultaneous Sampling	No
On-Board Memory	512 samples
Analog Output	
Channels	2
Resolution	16 bits
Max Voltage	10 V
Maximum Voltage Range	10 V , -10 V
Maximum Voltage Range Accuracy	2.417 mV
Minimum Voltage Range	10 V , -10 V
Minimum Voltage Range Accuracy	2.417 mV
Update Rate	10 kS/s
Current Drive Single	5 mA
Digital I/O	
Bidirectional Channels	8
Input-Only Channels	0

Output-Only Channels	0
Number of Channels	8 , 0 , 0
Timing	Software
Logic Levels	TTL
Input Current Flow	Sinking , Sourcing
Output Current Flow	Sinking , Sourcing
Programmable Input Filters	No
Supports Programmable Power-Up States?	No
Current Drive Single	24 mA
Current Drive All	192 mA
Watchdog Timer	No
Supports Handshaking I/O?	No
Supports Pattern I/O?	No
Maximum Input Range	5 V , 0 V
Maximum Output Range	5 V , 0 V
Counter/Timers	
Counters	2
Number of DMA Channels	1
Buffered Operations	Yes
Debouncing/Glitch Removal	No
GPS Synchronization	No
Maximum Range	5 V , 0 V
Max Source Frequency	20 MHz
Minimum Input Pulse Width	10 ns
Pulse Generation	Yes
Resolution	24 bits
Timebase Stability	100 ppm
Logic Levels	TTL
Physical Specifications	
Length	17.5 cm
Width	10.6 cm

C14. National Instruments PCI-6035E DAQ card

Technical Sales
United States
(866) 531-6285
info@ni.com

NI PCI-6035E

200 kS/s, 16-Bit, 16-Analog-Input Multifunction DAQ

- Two 12-bit analog outputs; 8 digital I/O lines; two 24-bit counters
- Consider NI M Series for 16-bit resolution, 1.25 MS/s, and similar costs with the PCI-6251.
- Included NI-DAQmx driver software and additional measurement services
- LabVIEW, LabWindows/CVI, and Measurement Studio for Visual Basic and Visual Studio .NET integration
- NIST-traceable calibration certificate and more than 70 signal conditioning options
- FREE award-winning global services and support at ni.com/support

Overview

National Instruments recommends M Series DAQ and NI-DAQmx driver software for new applications. Increase accuracy and perform 16-bit measurements at 1.25 MS/s with the PCI-6251.

The National Instruments PCI-6035E low-cost data acquisition board uses E Series technologies to deliver reliable measurements in a wide range of applications. You get up to 200 kS/s sampling and 16-bit resolution with 16 single-ended or eight differential analog inputs. The NI PCI-6035E also features two 12-bit analog outputs. Depending on your hard drive, the PCI-6035E can stream to disk at rates up to 200 kS/s.

Complete your DAQ system with NI signal conditioning to measure virtually any type of sensor and voltage.

Specifications

Specifications Documents

- Detailed Specifications
- Data Sheet

Specifications Summary

Specifications Summary

General

Product Name	PCI-6035E
Product Family	Multifunction Data Acquisition
Form Factor	PCI

Operating System/Target	Windows , Real-Time , Linux , Mac OS
LabVIEW RT Support	Yes
DAQ Product Family	E Series
RoHS Compliant	No
Analog Input	
Channels	16 , 8
Single-Ended Channels	16
Differential Channels	8
Resolution	16 bits
Sample Rate	200 kS/s
Max Voltage	10 V
Maximum Voltage Range	-10 V , 10 V
Maximum Voltage Range Accuracy	7.56 mV
Minimum Voltage Range	-50 mV , 50 mV
Minimum Voltage Range Accuracy	0.061 mV
Number of Ranges	4
Simultaneous Sampling	No
On-Board Memory	512 samples
Analog Output	
Channels	2
Resolution	12 bits
Max Voltage	10 V
Maximum Voltage Range	-10 V , 10 V
Maximum Voltage Range Accuracy	8.127 mV
Minimum Voltage Range	-10 V , 10 V
Minimum Voltage Range Accuracy	8.127 mV
Update Rate	10 kS/s
Current Drive Single	5 mA
Digital I/O	
Bidirectional Channels	8
Input-Only Channels	0

Output-Only Channels	0
Number of Channels	8 , 0 , 0
Timing	Software
Logic Levels	TTL
Input Current Flow	Sinking , Sourcing
Output Current Flow	Sinking , Sourcing
Programmable Input Filters	No
Supports Programmable Power-Up States?	No
Current Drive Single	24 mA
Current Drive All	192 mA
Watchdog Timer	No
Supports Handshaking I/O?	No
Supports Pattern I/O?	No
Maximum Input Range	0 V , 5 V
Maximum Output Range	0 V , 5 V
Counter/Timers	
Counters	2
Number of DMA Channels	1
Buffered Operations	Yes
Debouncing/Glitch Removal	No
GPS Synchronization	No
Maximum Range	0 V , 5 V
Max Source Frequency	20 MHz
Minimum Input Pulse Width	10 ns
Pulse Generation	Yes
Resolution	24 bits
Timebase Stability	100 ppm
Logic Levels	TTL
Physical Specifications	
Length	17.5 cm
Width	10.6 cm

C15. National Instruments BNC 2120

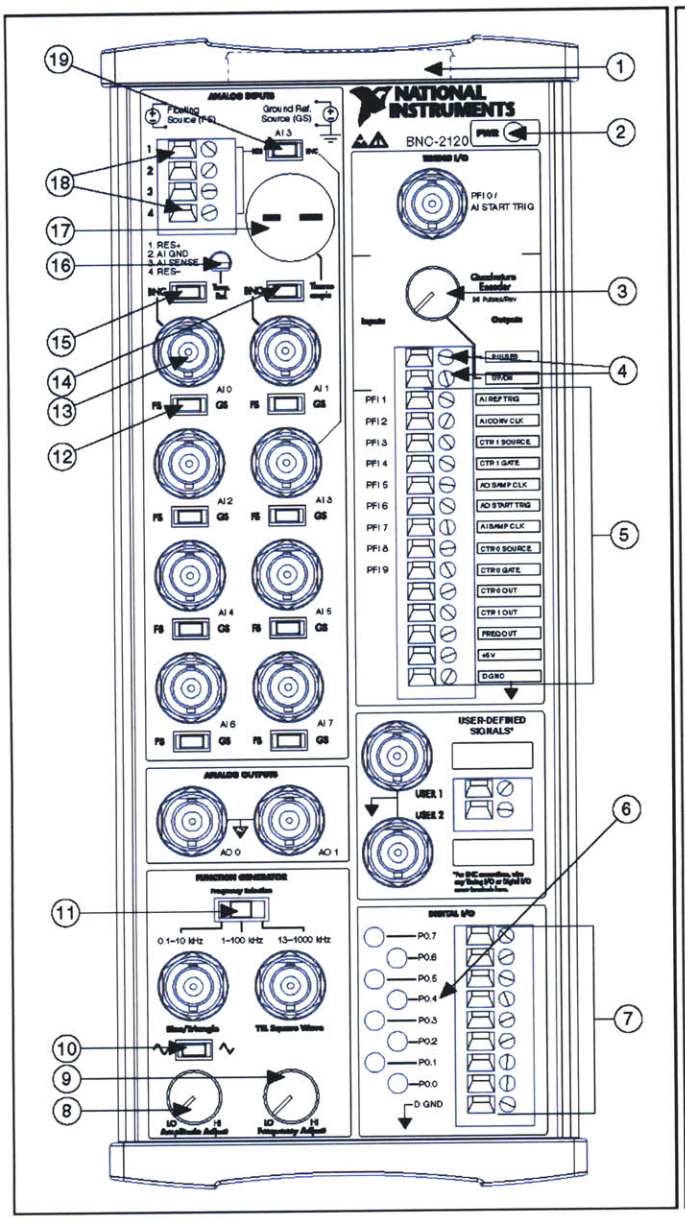

1 68-Position I/O Connector
2 Power Indicator LED
3 Quadrature Encoder Knob
4 Quadrature Encoder Output Screw Terminals
5 TIO Screw Terminals
6 DIO LED State Indicators
7 DIO Screw Terminals
8 Function Generator Amplitude Adjust Knob
9 Function Generator Frequency Adjust Knob
10 Sine/Triangle Waveform Selection Switch
11 Frequency Range Selection Switch
12 Floating Source (FS)/ Ground-Referenced Source (GS) Switch
13 BNC Connector
14 BNC/Thermocouple Selection Switch
15 BNC/Temperature Reference Selection Switch
16 Temperature Reference
17 Thermocouple Input Connector
18 Resistor Measurement Screw Terminals
19 Resistor/BNC Selection Switch

Figure 1. BNC-2120 Front Panel

C16. 50W,1Ω Power Resistor

RH Series Aluminum Housed Wirewound Resistors

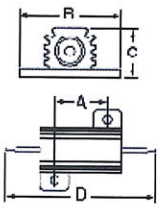

Specifications:
• Terminals: Copper clad steel core • Terminal finish: Tin/Lead 60/40 Sn/Pb with nickel underplate Lead-free Ni/Pd/Au • Operating Temperature Range: -55°C ~ 250°C

Features:
• Molded construction for total environmental protection • Complete welded construction • Meets applicable requirements of MIL-PRF-18546 • Mounts on chassis to utilize heat-sink effect • Excellent stability in operation (<1% change in resistance)

Series	Dimensions (mm) A	B	C	D	Temperature Coefficient (ppm/°C)	Short Time Overload
RH005	11.28	16.41	9.13	28.58	.10Ω ~ .00Ω / ±100	5X Rated Power for 5 Seconds
	11.28	16.41	9.13	28.58	1.0Ω ~ 8.0Ω / ±50	
	11.28	16.41	9.13	28.58	10Ω ~ 1.0KΩ / ±20	
RH010	14.27	20.32	9.91	34.93	.20Ω / ±100	
	14.27	20.32	9.91	34.93	1.0Ω ~ 2.0Ω / ±50	
	14.27	20.32	9.91	34.93	10Ω ~ 25KΩ / ±20	
RH025	18.26	27.43	13.87	49.28	.10Ω / ±100	
	18.26	27.43	13.87	49.28	1.0Ω ~ 8.0Ω / ±50	
	18.26	27.43	13.87	49.28	12Ω ~ 8KΩ / ±20	
RH050	39.67	28.96	15.49	70.64	.15Ω ~ .50 / ±100	
	39.67	28.96	15.49	70.64	1.0Ω ~ 8.0Ω / ±50	
	39.67	28.96	15.49	70.64	10Ω ~ 2.5KΩ / ±20	

Resistance Values RH005, 1%, RHA

.10◆	10	100	2.0K	.20	25◆	75◆	332◆	10K◆
.50◆	12	150◆	10K	1.0◆	33◆	100◆	1.0K◆	25K◆
1.0◆	25	300◆	15K◆	2.0◆	35◆	300◆	2.0K	
5.0◆	30◆	330◆		10◆	50◆	330	2.5K	

Resistance Values RH010, 1%, RHB

.10◆	15	100◆	1.0K◆	.15	.50◆	2.5◆	8.0◆	20	200◆	2.5K◆
1.0◆	20◆	200◆	8.0K◆	.20	1.0	3.3◆	10◆	30	300◆	
3.0◆	25◆	300		.25	1.5◆	5.0◆	12◆	40◆	500◆	
12	40	500◆		.30	2.0◆	6.0	16	100◆	10K	

Resistance Values RH025, 1%, RHC

Resistance Values RH050, 1% RHD

Description	Power Rating (W)	Value Range (Ω)	Digi-Key Part No.◊	Price Each 1	10	50
RH00E, 1%, RHA	5 (7.5)‡	10 ~ 25, 100, 2.0K	RHA-[Value]-ND	3.59	322	3.01
RH00E, 1%, RHA	5 (7.5)‡	10K	RHA-10K-ND	3.55	320	2.99
RH02E, 1%, RHC	25	40, 300	RHC-[Value]-ND	4.15	374	3.49
RH05C, 1%, RHD	50	.15 ~ .50	RHD-[Value]-ND	9.78	880	8.22
RH05C, 1%, RHD	50	1.0, 15-30 1.0K	RHD-[Value]-ND	5.10	459	4.29
RoHS Compliant						
RH00E, 1%, RHA	5 (7.5)‡	.10 ~ .50	RHA-(Value)-ND	3.46	311	2.90
RH00E, 1%, RHA	5 (7.5)‡	1.0 ~ 300	RHA-(Value)-ND	3.25	293	2.73
RH00E, 1%, RHA	5 (7.5)‡	2.0K ~ 10K	RHA-(Value)-ND	3.23	291	2.71
RH00E, 1%, RHA	5 (7.5)‡	15K	RHA-15K-ND	3.38	304	2.84
RH01C, 1%, RHB	10 (12.5)‡	.20	RHB-.20-ND	6.40	576	5.36
RH01C, 1%, RHB	10 (12.5)‡	1.0 ~ 1.0K	RHB-(Value)-ND	2.28	205	1.92
RH01C, 1%, RHB	10 (12.5)‡	2.0K ~ 10K	RHB-(Value)-ND	2.38	214	2.00
RH01C, 1%, RHB	10 (12.5)‡	25K	RHB-25K-ND	3.26	295	2.76
RH02E, 1%, RHC	25	.10	RHC-.10-ND	7.23	651	6.07
RH02E, 1%, RHC	25	1.0 ~ 1.0K	RHC-(Value)-ND	3.78	340	3.18
RH02E, 1%, RHC	25	8.0K	RHC-8.0K-ND	3.03	273	2.55
RH05C, 1%, RHD	50	.15 ~ .50	RHD-(Value)-ND	8.88	799	7.46
RH05C, 1%, RHD	50	1.0 ~ 1.0K	RHD-(Value)-ND	4.63	417	3.89
RH05C, 1%, RHD	50	2.5K	RHD-2.5K-ND	3.90	354	3.30

◊ For complete part number, substitute value from Resistance Value Chart for (Value). ◆ *RoHS Compliant Only*
‡ Power rating indicates wattage printed on parts, new construction allows these resistors to be rated at higher wattage (listed in parentheses) but will only be printed with the higher wattage on customer request.

C17. GMW Sensor cable

Part Number: 7673K43

1-99 Ft. $4.87 pe
100 or more $4.07 pe

Type	Multiconductor Cable and Cord
Multiconductor Cable and Cord Type	Flexible Cable
Flexible Multiconductor Cable Type	Continuous-Flex
Continuous-Flex Multiconductor Cable Type	Standard
Volts	300 VAC
Amps	4
Grounding Wire	Has a green/yellow ground wire. Total number of conductors includes the ground wire.
Gauge (AWG)	20
Number of Conductors	12
Outside Diameter	.48"
Length	Cut-to-length (per foot)
Maximum Continuous Length	100'
Shielded	Shielded
Conductor Type	Stranded
Conductor Material	Copper
Conductor Insulation Material	PVC
Jacket Material	PVC
Jacket Color	Green
Insulation Cord Color(s)	Black
Temperature Range	+23° to +158° F (-5° to +70° C)
Specifications Met	Canadian Standards Association (CSA), Conformite Europeene (CE) Approved, Underwriters Laboratories (UL)
CSA Specification	CSA Certified, FT1 Vertical Flame Test
UL Specification	UL Recognized

MIT 2

C18. Enclosure for Series Capacitors for Resonant Operation of fluxball

Instrument Boxes

RoHS COMPLIANT

Economical cases molded of high impact material. Mating cover has interlocking flange on lid, countersunk holes for flush mounting. Internal grooved guides to hold PC boards and circuit cards from .062 to .093 thick. Ideal for prototype or production usage. • Low cost • Sturdy construction

Cases supplied with cover and mounting screws

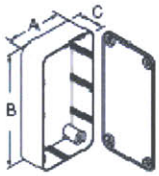

Dimensions Inches (mm)			Color/ Material	Digi-Key Part No.	Price Each		
A	B	C			1	10	100
3.75 (95.25)	6.25 (158.75)	2.00 (50.80)	Black ABS	707K-ND	14.04	13.04	12.02

C19. Panasonic AC Film Capacitors for Resonant Operation of Fluxball

Panasonic **AC Film Capacitors**

Stack Type: Panasonic's "stack type" construction offers significant reduction in case size (compared to oil-filled can type) with a built-in mounting foot.

Features: • Compact size compared to oil-filled type capacitors • 0.187 inch (4.75mm) terminals standard (0.250 inch [6.35mm] available) • 180, 200, 230 are standard voltages • U.L. 810 (File # E76560) and C.S.A listed (CSA-C22.2 No. 0-M91 File # LR99617) • JIS standard is available. (JIS C 4908) • Primary applications: refrigerator., motor run., lighting, etc. • Flame retardant plastic case is rated 94V-0

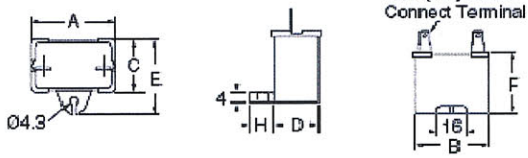

Voltage VAC	Cap. µF	Dimensions (mm) A	B	C	D	E	F	H	Digi-Key Part No.	Pricing 1	10	100	500	Panasonic Part No.
Wound Type - Q Case														
250	10	49.7	48.3	24.0	22.5	34.5	34.5	11.5	P9411-ND◆	6.75	54.00	459.00	2025.00	JS251106-BA
	12	50.0	48.5	26.7	25.3	37.5	36.0	11.5	P9412-ND◆	7.68	61.40	521.90	2302.50	JS251126-BA
	15	50.0	48.5	30.5	28.8	41.0	36.0	11.5	P9413-ND	9.08	72.60	617.10	2722.50	JS251156-BA
440	4	49.7	48.3	24.0	22.5	34.5	34.5	11.5	P9659-ND◆	7.85	62.80	533.80	2355.00	DS441405-BA
	5	50.0	48.5	26.7	25.3	37.5	36.0	11.5	P9660-ND◆	8.38	67.00	569.50	2512.50	DS441505-BA
	6	50.0	48.5	30.5	28.8	41.0	41.5	11.5	P9661-ND◆	9.58	76.60	651.10	2872.50	DS441605-BA

C20. Stir Bar

VWR® Spinbar® Stir Bars, Octagon

Supplier: VWR International

Teflon® resin-coated, octagon-shaped stirring bars have a molded-on pivot ring.

L x Dia., mm (in.)	VWR Catalog#	Unit	Price
12.7 x 3 ($^1/_2$ x $^1/_8$)*	58948-091	Case of 50	$311.15
		Each	$9.31
12.7 x 7.9 ($^1/_2$ x $^5/_{16}$)	58948-116	Case of 50	$299.69
		Each	$8.99
12.7 x 9.5 ($^1/_2$ x $^3/_8$)	58947-120	Each	$8.85
15.9 x 7.9 ($^5/_8$ x $^5/_{16}$)	58948-218	Each	$4.17
15.9 x 9.5 ($^5/_8$ x $^3/_8$)	58947-122	Each	$5.50
22.2 x 7.9 ($^7/_8$ x $^5/_{16}$)	58947-106	Each	$4.52
22.2 x 9.5 ($^7/_8$ x $^3/_8$)	58947-124	Each	$5.65
25.4 x 7.9 (1 x $^5/_{16}$)	*58948-138*	Each	$8.54

C21. Alpha-Core Laminax Copper Foil Used for Third Coil

B-Series

The metal foil is bonded to the insulator. Dimensions and the width of margins may be varied as required. Film backed foil is used as a winding conductor in transformers and coils, replacing interleaved winding of two individual materials. It is also used as electrostatic and grounding shields in many types of equipment.

Backet Conductor

B 0.500" Wide Copper Foil **$24.04 (CT Sales Tax)** 1 100 ft roll

Weight: 0.32 lbs

B0500x0625

To Customize call 800-836-5920 0.005" thick (+$25.93)

0.0014"-0.010" thick Foil insulated with 0.625" wide Polyester, Nomex® or Kapton® Film Polyester 1.2 mil

C22. Permanent Magnets by K&J Magnetics, Inc

Home » NEODYMIUM DISC MAGNETS » DX02 Checkout

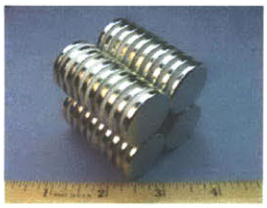

Description | Technical | Downloads

- Dimensions: 1" dia. x 1/8" thick
- Tolerances: ±0.004" x ±0.004"
- Material: NdFeB, Grade N42
- Plating/Coating: Ni-Cu-Ni (Nickel)
- Magnetization Direction: Axial (Poles on Flat Ends)
- Weight: 0.426 oz. (12.1 g)
- Pull Force, Case 1: 12.60 lbs
- Pull Force, Case 2: 57.00 lbs
- Surface Field: 1601 Gauss
- Max Operating Temp: 176°F (80°C)
- Brmax: 13,200 Gauss
- BHmax: 42 MGOe

Here is a strong NdFeB disc in the very popular 1" diameter size. The nice thin shape allows the DX02 to be used inconspicuously for a wide array of applications.

This size is also available in grade N52 as part number DX02-N52 and in grade N52 with Gold plating as part number DX02G-N52.

DX02: 1 for $2.00

Quantity: 1

Add to cart

Home » NEODYMIUM DISC MAGNETS » DX04 Checkout

Description | Technical | Downloads

- Dimensions: 1" dia. x 1/4" thick
- Tolerances: ±0.004" x ±0.004"
- Material: NdFeB, Grade N42
- Plating/Coating: Ni-Cu-Ni (Nickel)
- Magnetization Direction: Axial (Poles on Flat Ends)
- Weight: 0.851 oz. (24.1 g)
- Pull Force, Case 1: 27.20 lbs
- Pull Force, Case 2: 59.00 lbs
- Surface Field: 2952 Gauss
- Max Operating Temp: 176°F (80°C)
- Brmax: 13,200 Gauss
- BHmax: 42 MGOe

These sturdy, NdFeB magnet discs are incredibly strong and must be handled with caution. They are grade N42 and triple plated (like all of our nickel plated magnets) with nickel-copper-nickel plating. Each of these discs has a pull force of over 25 lbs.

This size is also available in grade N52 with Black Nickel plating as part number DX04B-N52.

DX04: 1 for $4.00

Quantity: 1

Add to cart

Home » NEODYMIUM DISC MAGNETS » DX04B-N52

Checkout

Description | Technical | Downloads

- Dimensions: 1" dia. x 1/4" thick
- Tolerances: ±0.004" x ±0.004"
- Material: NdFeB, Grade N52
- Plating/Coating: Ni-Cu-Black Ni (Black Nickel)
- Magnetization Direction: Axial (Poles on Flat Ends)
- Weight: 0.851 oz. (24.1 g)
- Pull Force, Case 1: 33.68 lbs
- Pull Force, Case 2: 73.05 lbs
- Surface Field: 3309 Gauss
- Max Operating Temp: 176°F (80°C)
- Brmax: 14,800 Gauss
- BHmax: 52 MGOe

This is a very strong and sturdy neodymium disc magnet. With N52 strength, these magnets should not be taken lightly. They must be handled with care because they can quite easily give a nasty pinch if you get beween two of them. They are triple plated in black nickel which gives the discs an attractive, shiny black appearance. The DX04B is one of our best magician's magnets because of it's compact size and high strength-to-size ratio.

This size is also available in grade N42 with standard Nickel plating as part number DX04.

DX04B-N52: 1 for $5.45

Quantity: 1

Add to cart

Home » NEODYMIUM DISC MAGNETS » DX08

Checkout

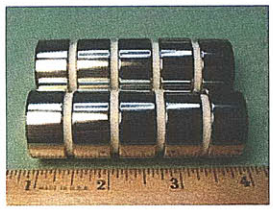

Description | Technical | Downloads

- Dimensions: 1" dia. x 1/2" thick
- Tolerances: ±0.004" x ±0.004"
- Material: NdFeB, Grade N42
- Plating/Coating: Ni-Cu-Ni (Nickel)
- Magnetization Direction: Axial (Poles on Flat Ends)
- Weight: 1.70 oz. (48.3 g)
- Pull Force, Case 1: 44.00 lbs
- Pull Force, Case 2: 60.80 lbs
- Surface Field: 4667 Gauss
- Max Operating Temp: 176°F (80°C)
- Brmax: 13,200 Gauss
- BHmax: 42 MGOe

These strong discs are very powerful and will pinch and do harm if they are not handled properly. One magnet is capable of holding over 40 lbs of steel!

This size is also available in grade N50 with Black Nickel plating as part number DX08B-N52.

DX08: 1 for $7.00

Quantity: 1

Add to cart

Home » NEODYMIUM DISC MAGNETS » DX08B-N52

Checkout

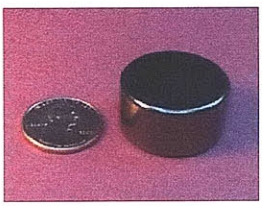

Description | Technical | Downloads

- Dimensions: 1" dia. x 1/2" thick
- Tolerances: ±0.004" x ±0.004"
- Material: NdFeB, Grade N52
- Plating/Coating: Ni-Cu-Black Ni (Black Nickel)
- Magnetization Direction: Axial (Poles on Flat Ends)
- Weight: 1.70 oz. (48.3 g)
- Pull Force, Case 1: 54.48 lbs
- Pull Force, Case 2: 75.28 lbs
- Surface Field: 5233 Gauss
- Max Operating Temp: 176°F (80°C)
- Brmax: 14,800 Gauss
- BHmax: 52 MGOe

The DX08B is the same size as our popular DX08, but is grade N52. There is a very noticeable difference in strength between the N52 and N42 versions of this magnet. The DX08B-N52 will pinch even harder than the standard DX08. If you need a very powerful magnet, this is the one for you. Unbelieveably strong!!

This size is also available in grade N42 with standard Nickel plating as part number DX08.

DX08B-N52: 1 for $11.35

Quantity: 1

Add to cart

C23. F.W. Bell Three Probe and 7030 Teslameter

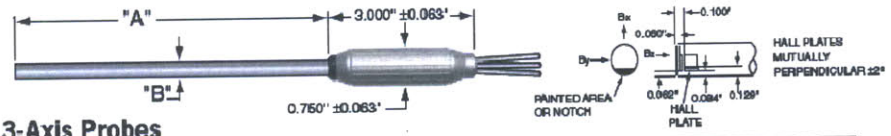

Standard 3-Axis Probes

Model	A	B	C	D	E	F	G	Stem Material	Linearity % of Reading	Frequency Range	Sensitivity	Nominal Active Area	Oper. Temp. Range	Temp. Stability (Max) Zero (G/°C)	Temp. Stability (Max) Calibrate (%/°C)
ZOA73-3208-05 ZOA73-3208-05-T ZOA73-3208-15 ZOA73-3208-15-T ZOA73-3208-30 ZOA73-3208-30-T	8.0" ±0.125"	0.312" ±0.005"	N/A	N/A	N/A	N/A	N/A	Alum.	0.25% to 10kG	DC to 400Hz	1X	0.060" Dia.	0°C to +75°C	±0.100	– 0.040

Description

The Model 7030 three-channel GAUSS/TESLA METER from F.W. Bell leads the way for Advanced Hall Effect Magnetic measuring technology. The easy-to-use front panel programming feature incorporates the latest in user control operations. The 7030 is capable of simultaneously measuring and displaying *seven different parameters per channel* – flux density, frequency, temperature, min, max, peak and valley. With the 7030's vector summation feature, that makes a total of 27 different parameters.

This high accuracy instrument is fully equipped to meet most magnetic measuring applications. Bell's exclusive dynamic probe correcting software increases the 7030 measurement capabilities to make it *the most versatile magnetic measuring tool in the world.*

Key features include high-resolution, high-accuracy and high-speed with a large graphic electroluminescent display. The 7030 features 50 kHz frequency response, temperature and frequency measurements, Auto Zero, Auto Range, Hold functions for Peak, Valley, Min and Max, corrected and uncorrected outputs for each channel and Vector Summation and angle. The Model 7030 provides the user with gauss, tesla, Oe, A/m, IEEE-488 and RS-232 communications ports and Classifier output.

The 7030 operates with Bell's fifth generation Hall Effect probes. These probes provide temperature compensation and measurement readings (0°C to +75°C) while monitoring the magnetic field. The easy-to-read 1/4 VGA display is easily viewable in most light conditions and can be customized to meet a user's specific needs. Applications range from basic magnetic measuring to sensitive complicated three-axis vector summing requirements. All instruments are fully CE compliant.

Features

- Bright 1/4-VGA Readout
- Large electroluminescent graphic display
- Over 100 standard probes available
- Automatic probe coefficient correction
- Displays in Gauss, Tesla, Amp/meter or Oe
- Relative Mode
- Fully menu-driven for easy operation
- Auto Zero and Auto Calibration
- IEEE-488 and RS-232 interface
- CE Compliant
- Manufactured to ISO 9000 standards
- Comprehensive Technical Support

SPECIFICATION

Ranges	300mG (30µT)* 3kG(300mT) 3G (300µT)* 30kG (3T) 30G (3mT) 300kG(30T)† 300G (30mT) * Low field probe † High field probe
Resolution	1 µG (0.1nT) to 1G (0.1mT) (Depending on probe selection)
Accuracy (Displayed Reading)	
dc basic	±0.05% of reading
ac basic	±2% of reading
Frequency Range	
dc mode	dc to 250Hz
ac mode	20Hz to 50kHz
Accuracy (Corrected Analog Output)	
dc basic	±0.1% of range
ac basic	±2% of range
Frequency Range	dc to 500Hz
Frequency Range (Uncorrected Analog Output)	
dc mode	dc to 100Hz
ac mode	20Hz to 50kHz
Analog Output	
Output Voltage	±3V F.S. or ±10V F.S. or adjustable from 0.1 - 9.9V
Source Impedance	<100 ohms
Connector	Standard BNC
Additional Influences	
Temperature Coefficient	±(0.02% of reading ±1 count)/ °C
Temperature Range	
Operating	0°C to +50°C
Storage	-20°C to +60°C
Front Panel Display	1/4 VGA, 320 x 240 pixels Electroluminescent graphic display with 4 shades of amber 4.7" (119 mm) W x 3.5" (89mm) H
Communication Ports	
RS-232	Standard 9-pin "D" connector
Baud Rate	300,600,1200,2400,4800,9600,19200,38400 bits/sec
IEEE-488	Standard 24-pin GPIB connector
Protocol	IEEE-1987.2 and SCPI-1999
Power	Volts: 100/120 or 220/240 Frequency: 50-60 Hz or 50-60 Hz Current: 1.0 A (max) or 0.5 A (max)
Size	
Width	16.3" (414 mm)
Height	5.2" (132mm)
Depth	13.5" (343mm)
Weight	
Net	19.6 lbs. (8.9 kg)
Shipping	25.8 lbs. (11.6 kg)

Due to continuous process improvement, specifications subject to change without notice.

Hall Effect GAUSSMETERS

F.W. BELL®

SYPRIS TEST & MEASUREMENT

C24. Aluminum Enclosure

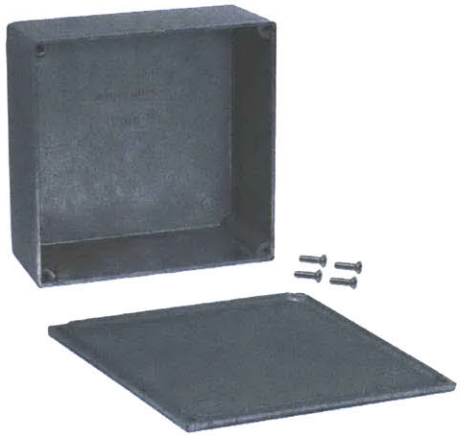

Fig. 3 – Diecast Aluminum Enclosures - 1590 Series

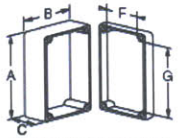

Lid adds 4mm to height of box (except for 1500Z series).
For dimensions A, B, and C, see charts below.

Lid Height for 1590 Heavy Duty Watertight Diecast Aluminum Alloy Enclosure	
Part No.	Dimensions - Inch (mm)
1590Z100	0.5 (13)
1590Z110	0.5 (13)
1590Z120	0.6 (15)
1590Z130	0.5 (13)
1590Z150	0.8 (20)
1590Z160	0.8 (20)

Part No.	Dimensions - Inch (mm) F	G
1590A	0.9 (23)	3.0 (76)
1590B	1.7 (43)	3.8 (97)
1590BB	3.1 (77)	4.0 (102)
1590C	3.1 (77)	4.1 (104)
1590D	4.1 (104)	6.9 (173)
1590DD	4.1 (104)	6.9 (173)
1590E	4.1 (104)	6.9 (173)
1590F	6.8 (173)	6.9 (173)
1590H	0.9 (23)	1.4 (36)
1590J	3.1 (79)	5.1 (130)

Part No.	Dimensions - Inch (mm) F	G
1590K	4.3 (109)	4.3 (109)
1590LB	1.4 (36)	1.4 (36)
1590P1	2.9 (74)	5.4 (137)
1590S	2.6 (66)	3.7 (94)
1590T	2.5 (64)	4.1 (104)
1590U	4.1 (104)	4.1 (104)
1590V	4.1 (104)	4.1 (104)
1590G	1.3 (33)	3.3 (84)
1590N1	1.9 (49)	4.1(104)
1590R1	4.0 (102)	6.9 (175)

1590 Series: Drilled and tapped with lid and 6-32 x 1/2" (12.7mm) countersunk Phillips screws. Choice of standard, flanged or watertight lid. Interlocking flanged lid provides complete RF shielding. Watertight lid has a factory poured silicone rubber gasket around the perimeter to provide protection against dust and water.

1590Z Series: Watertight, heavy duty - thick wall. Two piece "tongue and groove" construction with a neoprene gasket provides protection against dust and water. Four recessed stainless steel machine screws and individual neoprene "O" rings secure lid. Optional M4 x 6mm copper grounding screws with designated enclosures. Designed to meet IP65.

Fig. 3 - 1590 Diecast Aluminum Alloy Enclosures

Un-painted	1.97 (50)	1.97 (50)	0.93 (21)†	HM949-ND	7.14	5.95	5.49	1590LLB
	2.0 (51)	2.0 (51)	1.1 (29)	HM157-ND	7.59	6.32	5.93	1590LB
	2.1 (53)	1.5 (38)	1.1 (29)	HM365-ND	6.52	5.43	5.02	1590H
	3.6 (91)	1.5 (38)	1.1 (29)	HM150-ND	7.36	6.14	5.67	1590A
	3.62 (92)	3.52 (92)	1.5 (38)†	HM955-ND	10.20	8.50	7.85	1590Y
	3.9 (99)	2.0 (51)	0.8 (20)	HM941-ND	7.99	6.57	6.07	1590S
	4.4 (112)	3.2 (81)	1.6 (41)	HM159-ND	11.10	9.26	8.54	1590S
	4.4 (112)	2.3 (59)	1.1 (29)	HM151-ND	9.40	7.01	6.47	1590B
	4.7 (119)	3.7 (94)	1.2 (30)	HM152-ND	10.94	9.12	8.42	1590BB
	4.7 (119)	3.7 (94)	2.1 (53)	HM153-ND	12.30	10.25	9.47	1590C
	4.7 (120)	4.7 (120)	1.1 (29)†	HM949-ND	12.75	10.63	9.11	1590Q
	4.7 (119)	4.7 (119)	2.2 (56)	HM160-ND	16.80	14.00	12.93	1590U
	4.7 (119)	4.7 (119)	3.5 (89)	HM161-ND	23.12	19.27	17.79	1590V
	4.7 (119)	3.1 (79)	2.2 (56)	HM159-ND	11.44	9.54	8.80	1590T
	4.8 (122)	2.6 (66)	1.4 (36)	HM942-ND	11.46	9.56	8.82	1590N1
	4.9 (124)	4.9 (124)	3.0 (76)	HM367-ND	21.02	17.52	16.16	1590K
	4.92 (125)	4.92 (125)	2.1 (53)†	HM947-ND	19.38	16.15	13.84	1590KK
	5.7 (145)	3.7 (94)	1.8 (45)	HM365-ND	12.92	10.77	9.94	1590J
	6.0 (152)	3.2 (81)	1.8 (45)	HM349-ND	15.02	12.52	11.56	1590P1
	7.4 (188)	4.7 (119)	2.1 (53)	HM154-ND	20.14	16.79	15.49	1590D
	7.4 (188)	4.7 (119)	3.1 (79)	HM155-ND	21.53	17.96	16.57	1590E
	7.4 (188)	7.4 (188)	2.5 (64)	HM156-ND	28.94	24.12	22.27	1590F
	7.4 (188)	4.7 (119)	1.3 (33)	HM347-ND	17.70	14.76	13.92	1590DD
	7.6 (193)	4.4 (112)	2.2 (56)	HM943-ND	24.10	20.09	18.54	1590R1

C25. Heat Sinks

BGA Cooling Solutions

maxiFLOW™ Heat Sink Using Thermal Tape

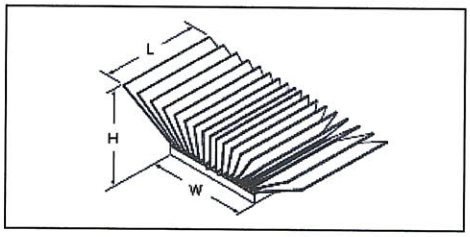

Dimensions (mm)			Thermal Resist. @ 200 LFM (°in/sec.)			Price Each		
L	W	H	Unducted Flow	Ducted Flow	Digi-Key Part No.	1	10	100
31	31	7.5	6.9	5.3	ATS1105-ND	9.03	5.79	4.92
32.5	32.5	7.5	5.9	4.2	ATS1106-ND	9.13	5.95	4.99
33	33	7.5	5.9	4.2	ATS1107-ND	7.92	5.97	4.99
35	35	7.5	5.3	3.4	ATS1108-ND	7.97	5.91	4.92
37.5	37.5	7.5	4.9	3.3	ATS1109-ND	7.94	5.96	4.97
40	40	7.5	4.5	3.2	ATS1110-ND	9.02	6.02	5.01
42.5	42.5	7.5	4.3	3.0	ATS1111-ND	9.11	6.09	5.07
45	45	7.5	4.0	2.6	ATS1112-ND	9.19	6.14	5.12
15	15	12.5	11.7	9.4	ATS1113-ND	9.35	6.27	5.22
17	17	12.5	11.1	9.0	ATS1114-ND	9.45	6.34	5.29
19	19	12.5	10.2	9.4	ATS1115-ND	9.52	6.39	5.33
21	21	12.5	7.2	5.7	ATS1116-ND	9.62	6.47	5.39
23	23	12.5	6.7	5.4	ATS1117-ND	9.71	6.54	5.45
25	25	12.5	5.2	4.0	ATS1118-ND	9.78	6.59	5.49
27	27	12.5	4.9	3.9	ATS1119-ND	9.99	6.66	5.55
29	29	12.5	4.5	3.7	ATS1120-ND	9.99	6.74	5.61
30	30	12.5	4.4	3.6	ATS1121-ND	9.07	6.91	5.67
31	31	12.5	4.3	3.5	ATS1122-ND	9.14	6.96	5.72
32.5	32.5	12.5	3.5	2.9	ATS1123-ND	9.24	6.93	5.79
33	33	12.5	3.5	2.7	ATS1124-ND	9.29	6.97	5.91
35	35	12.5	3.0	2.2	ATS1125-ND	9.34	7.01	5.94
37.5	37.5	12.5	2.6	2.1	ATS1126-ND	9.43	7.09	5.90
40	40	12.5	2.6	2.0	ATS1127-ND	9.53	7.15	5.96
42.5	42.5	12.5	2.4	2.0	ATS1128-ND	9.62	7.02	6.02
45	45	12.5	2.1	1.6	ATS1129-ND	9.72	7.09	6.09
15	15	17.5	9.7	7.1	ATS1130-ND	9.92	7.16	6.14
17	17	17.5	9.3	6.9	ATS1131-ND	9.91	7.23	6.20
19	19	17.5	7.7	6.4	ATS1132-ND	10.01	7.30	6.26
21	21	17.5	5.4	4.3	ATS1133-ND	9.71	7.39	6.33
23	23	17.5	5.1	4.1	ATS1134-ND	9.80	7.46	6.39
25	25	17.5	3.9	3.0	ATS1135-ND	9.99	7.53	6.45
27	27	17.5	3.7	2.9	ATS1136-ND	10.01	7.62	6.53
29	29	17.5	3.5	2.9	ATS1137-ND	10.10	7.69	6.59
30	30	17.5	3.4	2.7	ATS1138-ND	10.19	7.76	6.65
31	31	17.5	3.3	2.7	ATS1139-ND	10.30	7.84	6.72
32.5	32.5	17.5	2.7	2.1	ATS1140-ND	10.40	7.91	6.79
33	33	17.5	2.7	2.1	ATS1141-ND	10.44	7.95	6.91
35	35	17.5	2.3	1.7	ATS1142-ND	10.51	9.00	6.96
37.5	37.5	17.5	2.1	1.6	ATS1143-ND	10.60	9.07	6.92
40	40	17.5	2.0	1.6	ATS1144-ND	10.72	9.16	6.99
42.5	42.5	17.5	1.9	1.5	ATS1145-ND	10.93	8.25	7.07
45	45	17.5	1.6	1.3	ATS1146-ND	10.93	9.32	7.13

C26. Kapton Tape

High Temperature Tape					
High Temperature Kapton Tape, 2.7-mil, Amber KAPTON Polyimide Film, Silicone Adhesive	1/2" x 36 yds.	3M541312-ND	26.60	—	5413 1/2"
High Temperature Kapton Tape, 2.7-mil, Amber KAPTON Polyimide Film, Silicone Adhesive	3/4" x 36 yds.	3M541334-ND	39.90	—	5413 3/4"
Wave Solder Tape, Low Static, 2.7-mil, Amber Polyimide Film, Silicone Adhesive	1/2" x 36 yds.	3M591912-ND	28.65	—	5419 1/2"
Wave Solder Tape, Low Static, 2.7-mil, Amber Polyimide Film, Silicone Adhesive	3/4" x 36 yds.	3M591934-ND	40.93	—	5419 3/4"
Wave Solder Tape, Water-Soluble, PVA Film Backing, Water-soluble Synthetic Adhesive	1/2" x 36 yds.	3M541412-ND	27.07	—	5414 1/2"
Wave Solder Tape, Water-Soluble, PVA Film Backing, Water-soluble Synthetic Adhesive	3/4" x 36 yds.	3M541434-ND	46.85	—	5414 3/4"

Appendix D : Testing the Probe holder

D1. Determining GrilTex-P1 Concentration (Section 5.2.2)

The area under the echo graph obtained for various concentrations of the experiment outlined in *Testing the probe holder* section was plotted for the various probes used. The area

under the echo curve can be seen to be dependent on concentration for very low concentrations and is then fairly constant with concentration with a consistent greatest area obtained for a Griltex-P1 concentration of 0.008g/ml. The graphs below are plots of the area under the curves for the various probes used at three different rotational rates.

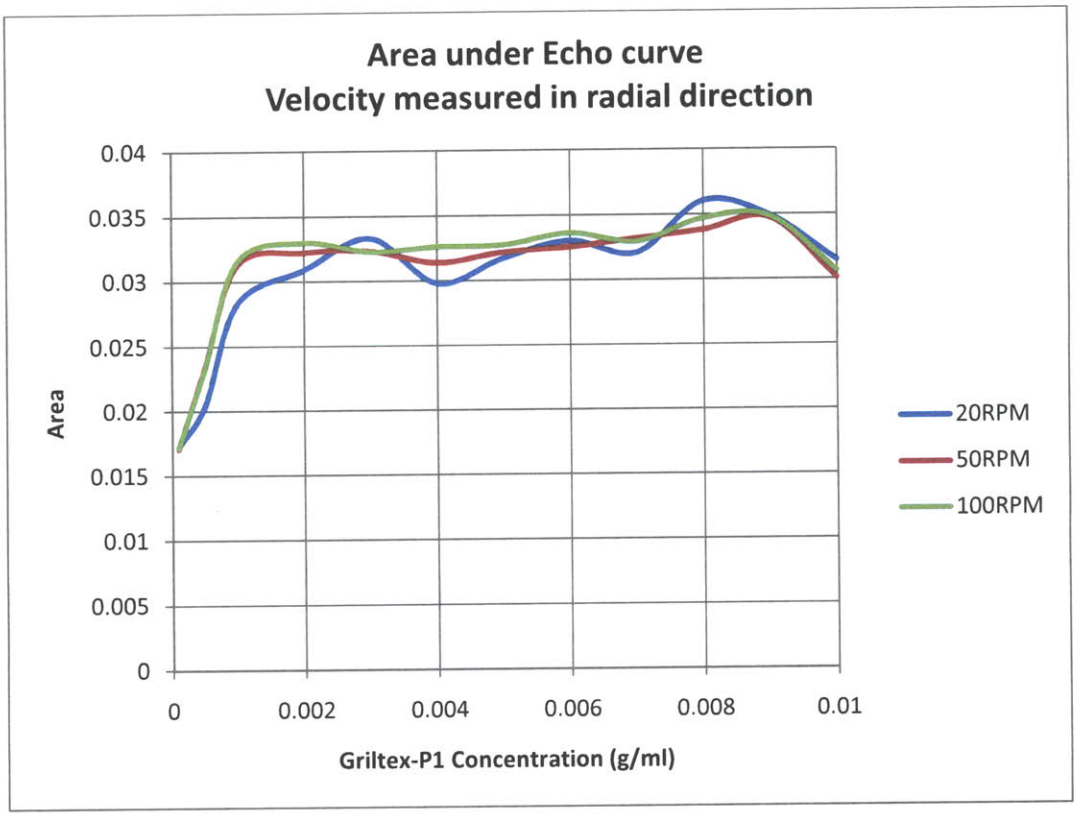

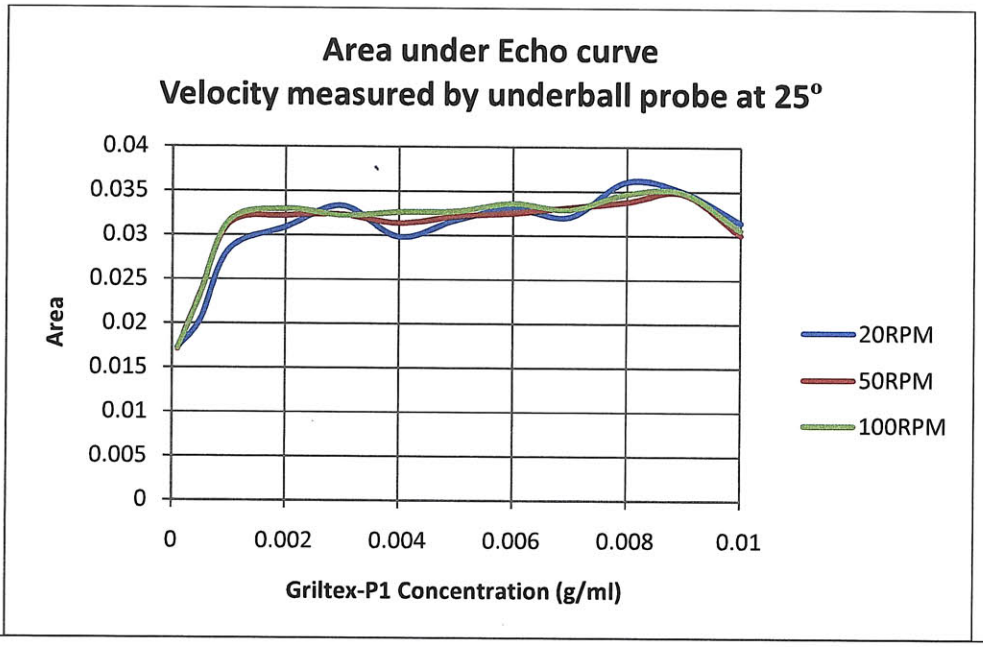
Area under Echo curve
Velocity measured by underball probe at 25°
Area
0.04
0.035
0.03
0.025
0.02
0.015
0.01
0.005
0
0
0.002
0.004
0.006
0.008
0.01
Griltex-P1 Concentration (g/ml)
20RPM
50RPM
100RPM

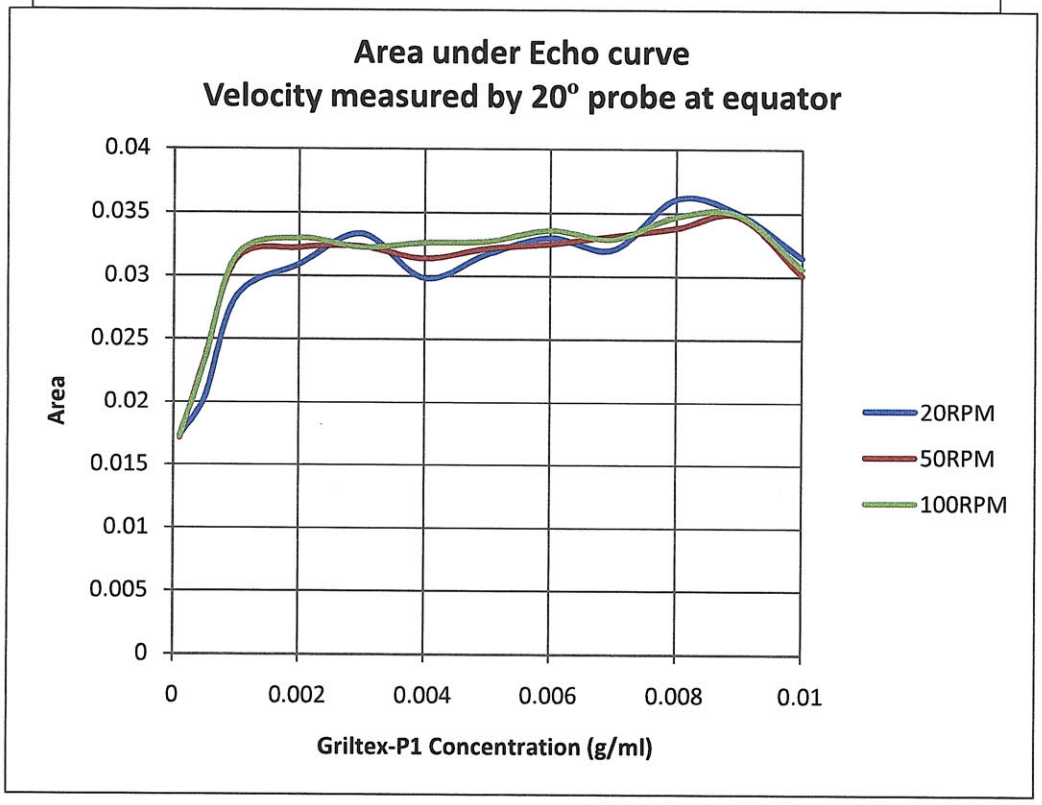
Area under Echo curve
Velocity measured by 20° probe at equator
Area
0.04
0.035
0.03
0.025
0.02
0.015
0.01
0.005
0
0
0.002
0.004
0.006
0.008
0.01
Griltex-P1 Concentration (g/ml)
20RPM
50RPM
100RPM

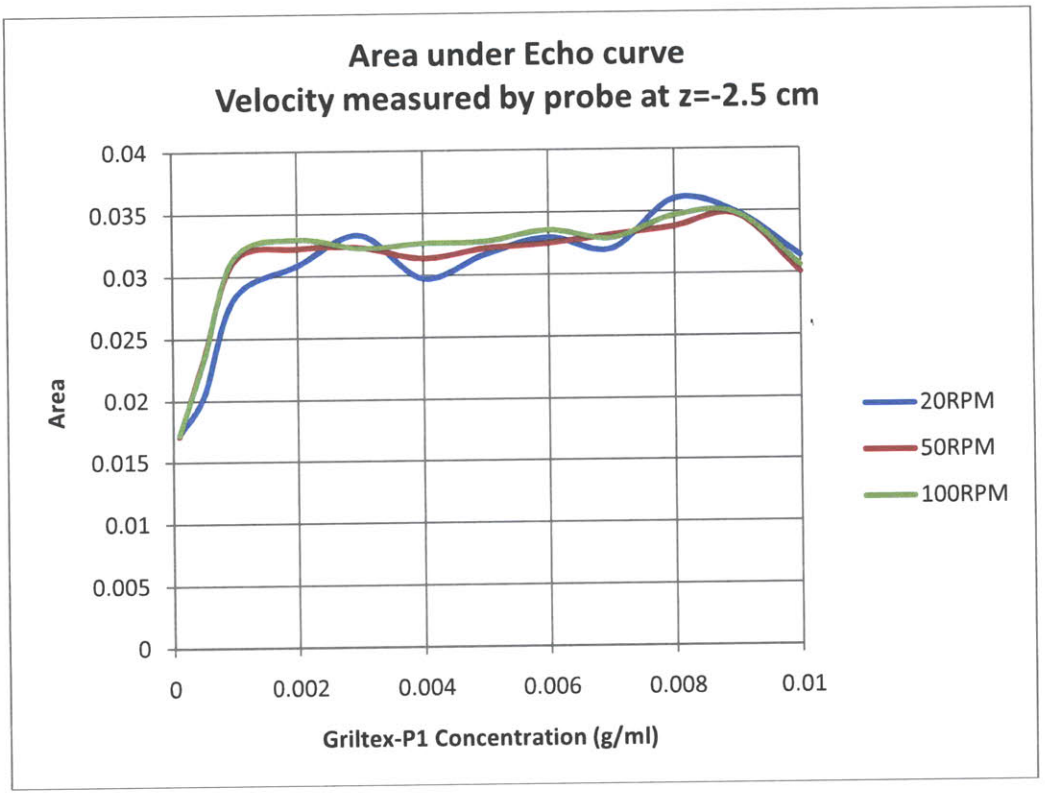
Area under Echo curve
Velocity measured by probe at z=-2.5 cm
Area
0.04
0.035
0.03
0.025
0.02
0.015
0.01
0.005
0
0
0.002
0.004
0.006
0.008
0.01
Griltex-P1 Concentration (g/ml)
20RPM
50RPM
100RPM

D2. COMSOL Model File for Shell DIALA A Transformer Oil Experiment (Section 5.2.2)

COMSOL Model Report

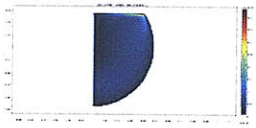

1. Table of Contents

2. Model Properties

Property	Value
Model name	
Author	
Company	
Department	
Reference	
URL	
Saved date	Apr 30, 2008 12:45:26 PM
Creation date	Mar 18, 2008 7:40:16 PM
COMSOL version	COMSOL 3.5.0.603

File name: C:\Users\Shahriar\Documents\My Dropbox\Research Files\Software Data Files\Comsol Files\Working_Rotatingcylinderinsphere\2Dsawedoffspheretoprotating_v_4_SHELLDIALAoil.mph

Application modes and modules used in this model:

- Geom1 (Axial symmetry (2D))
  - Swirl Flow (Chemical Engineering Module)
- Geom2 (3D)

D3.

3. Geometry

Number of geometries: 2

3.1. Geom1

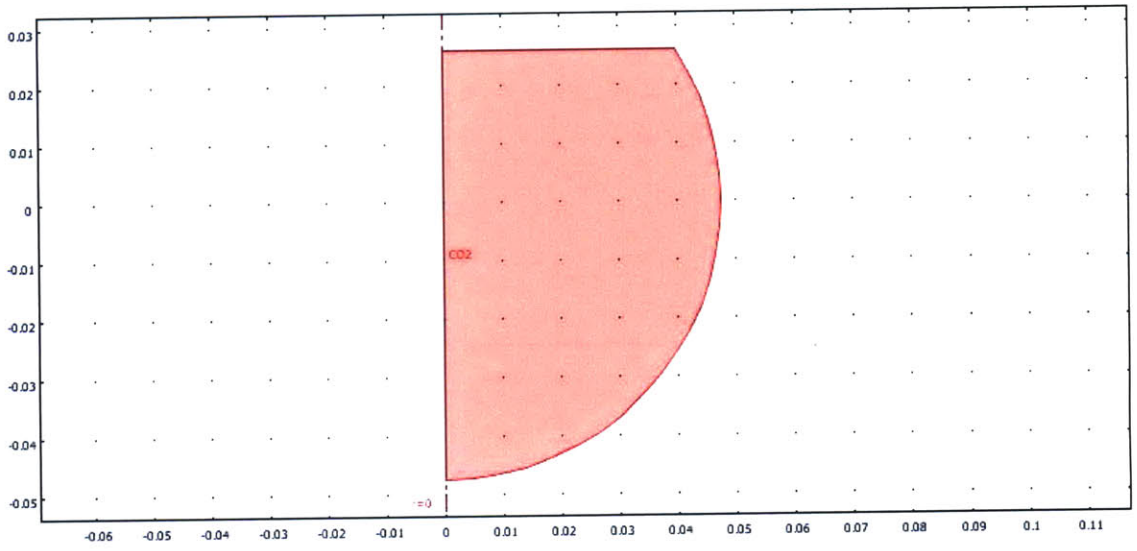

3.1.1. Point mode

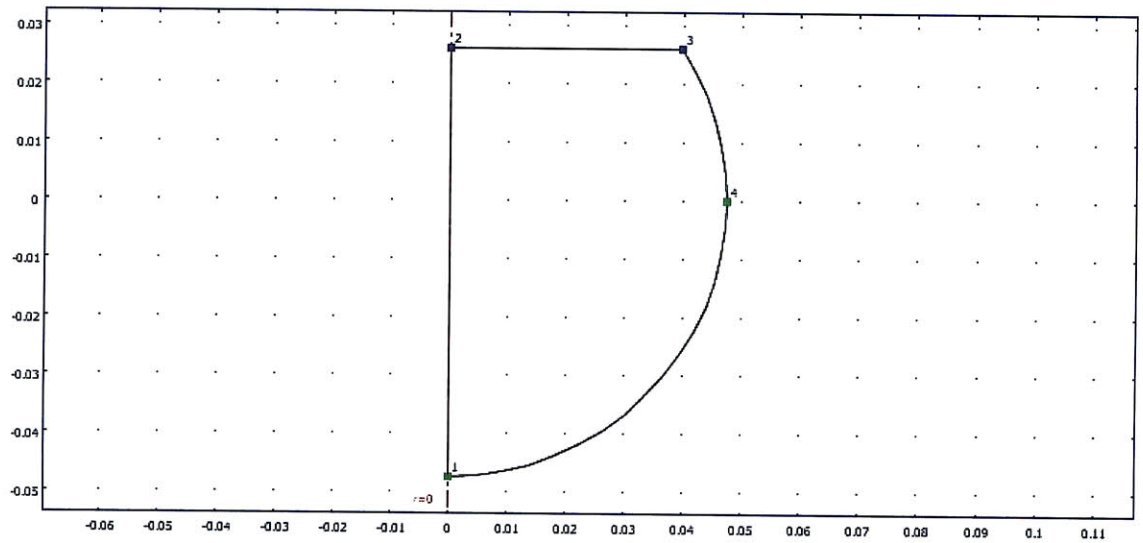

3.1.2. Boundary mode

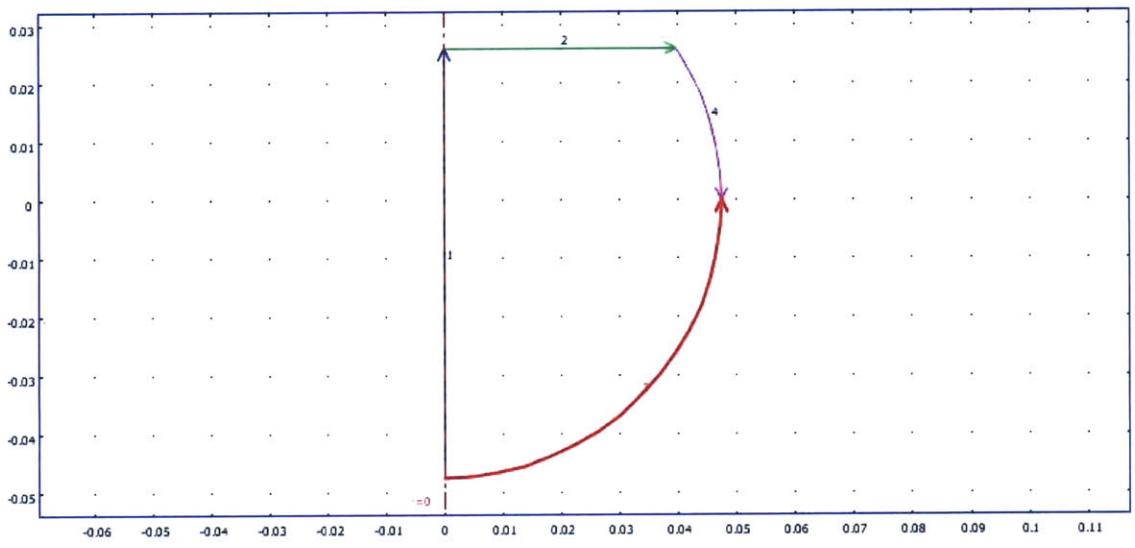

3.1.3. Subdomain mode

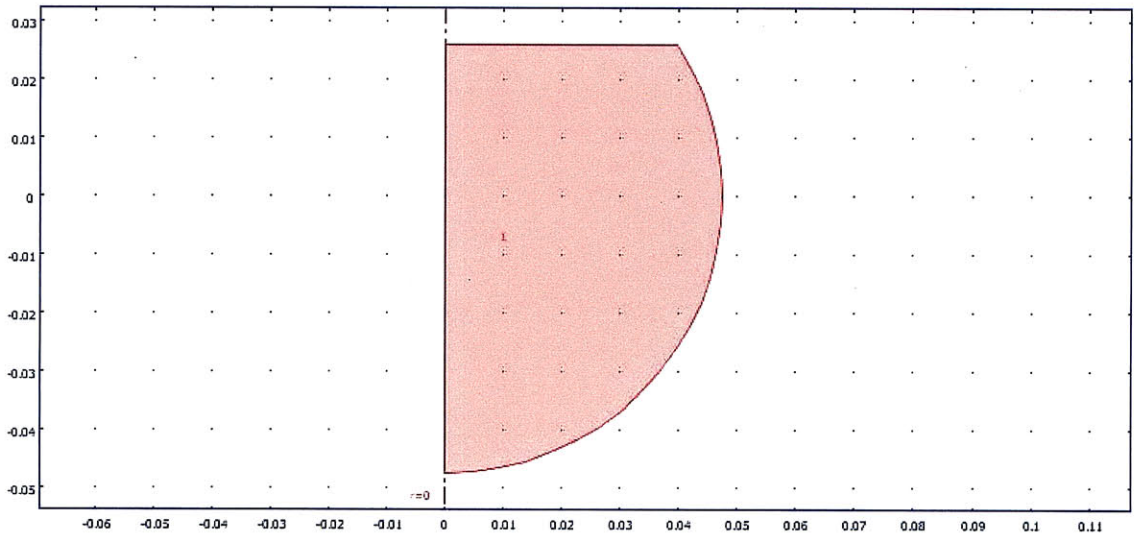
0.03
0.02
0.01
0
-0.01
-0.02
-0.03
-0.04
-0.05
r=0
-0.06
-0.05
-0.04
-0.03
-0.02
-0.01
0
0.01
0.02
0.03
0.04
0.05
0.06
0.07
0.08
0.09
0.1
0.11

3.2. Geom2

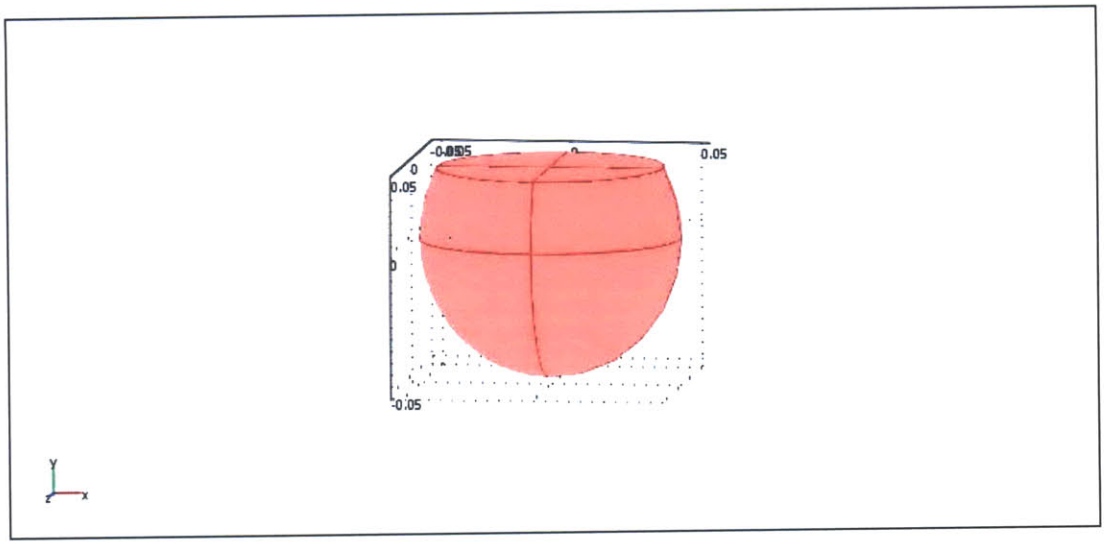

3.2.1. Point mode

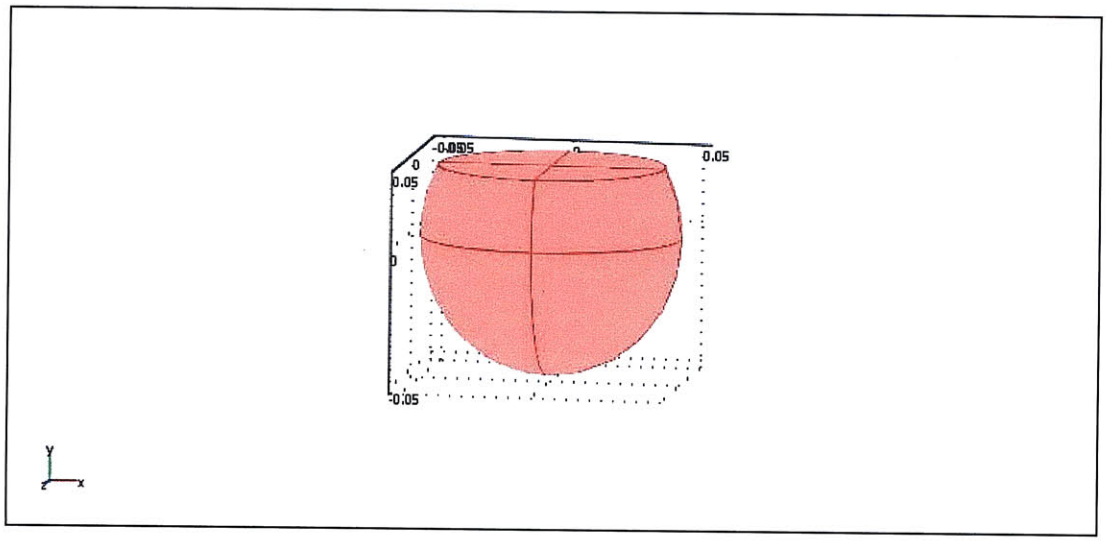

3.2.2. Edge mode

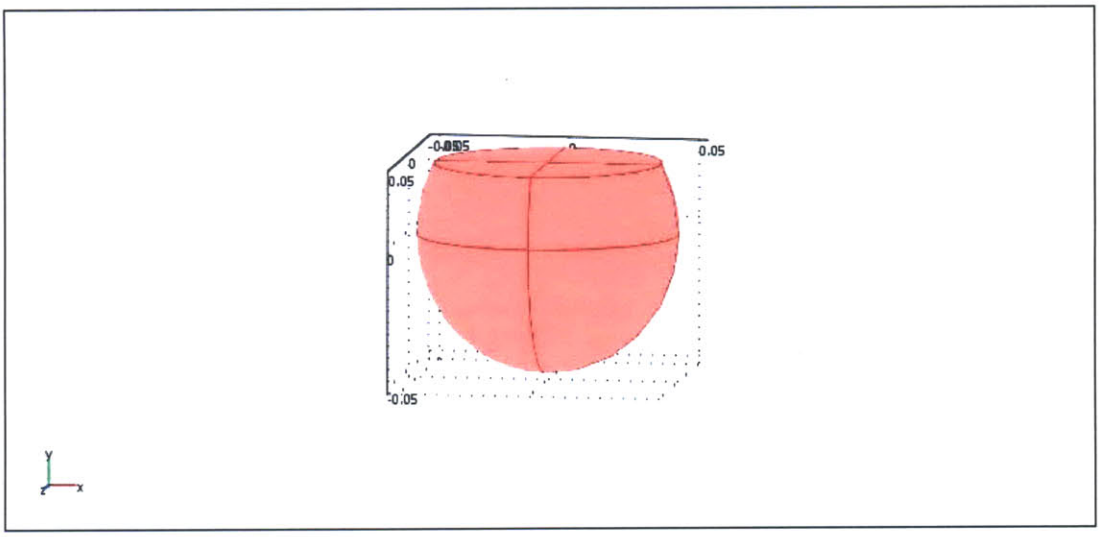

3.2.3. Boundary mode

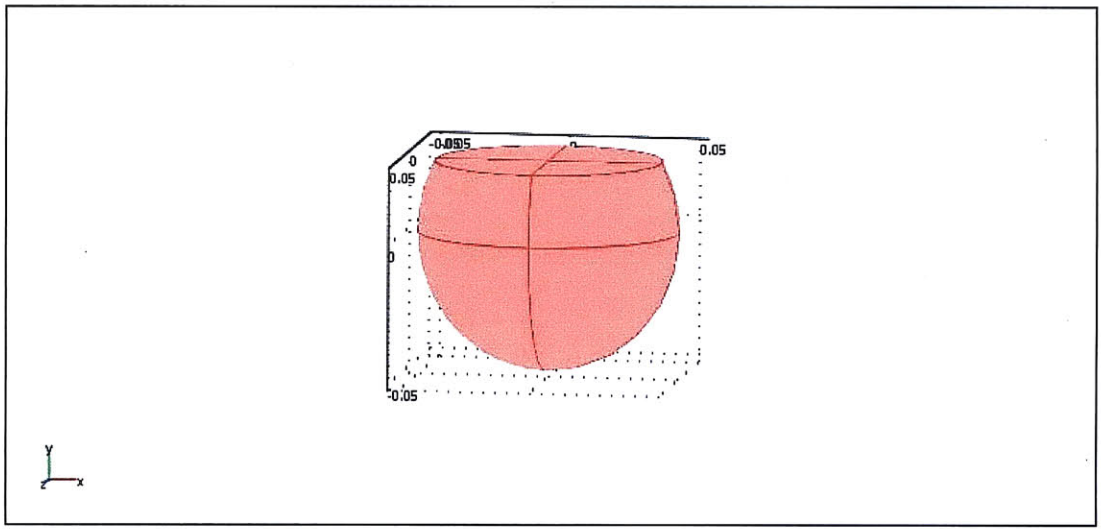

3.2.4. Subdomain mode

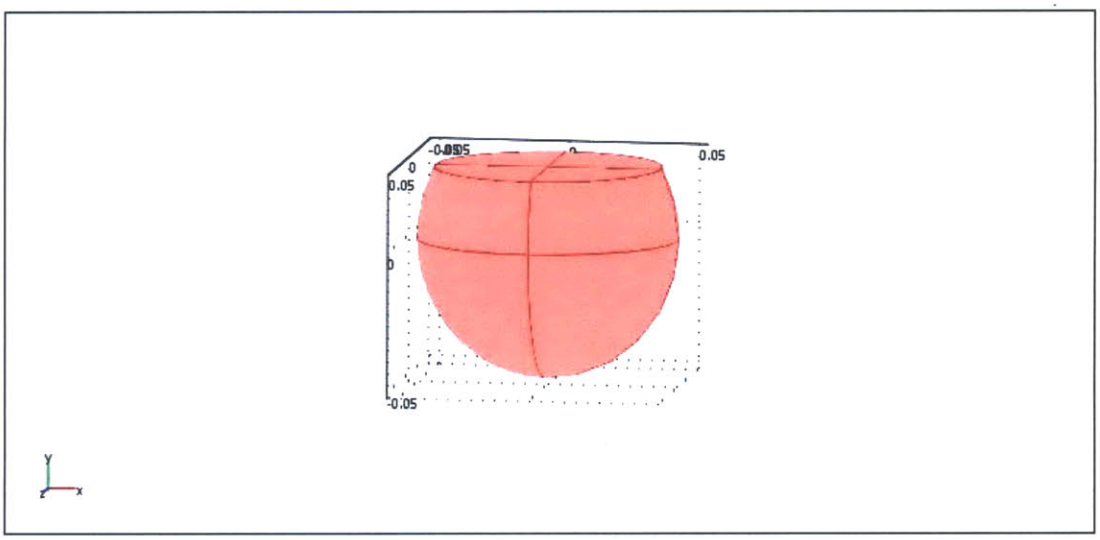

4. Geom1

Space dimensions: Axial symmetry (2D)

Independent variables: r, phi, z

4.1. Mesh

4.1.1. Mesh Statistics

Number of degrees of freedom	13657
Number of mesh points	1072
Number of elements	2052
Triangular	2052
Quadrilateral	0
Number of boundary elements	90
Number of vertex elements	4

Minimum element quality	0.685
Element area ratio	0.13

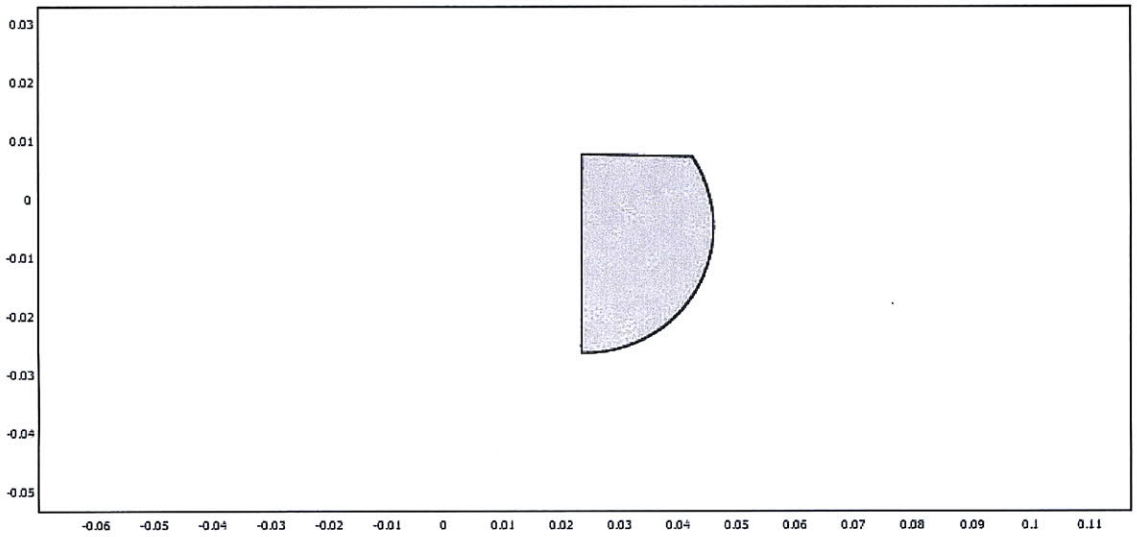

4.2. Application Mode: Swirl Flow (chns)

Application mode type: Swirl Flow (Chemical Engineering Module)

Application mode name: chns

4.2.1. Scalar Variables

Name	Variable	Value	Unit	Description
visc_vel_fact	visc_vel_fact_chns	10	1	Viscous velocity factor

4.2.2. Application Mode Properties

Property	Value

Default element type	Lagrange - P_2 P_1
Analysis type	Stationary
Corner smoothing	Off
Weakly compressible flow	Off
Turbulence model	None
Realizability	Off
Non-Newtonian flow	Off
Brinkman on by default	Off
Two-phase flow	Single-phase flow
Swirl velocity	On
Frame	Frame (ref)
Weak constraints	Off
Constraint type	Ideal

4.2.3. Variables

Dependent variables: u, v, w, p, logk, logd, logw, phi, psi, nrw, nzw

Shape functions: shlag(2,'u'), shlag(2,'v'), shlag(2,'w'), shlag(1,'p')

Interior boundaries not active

4.2.4. Point Settings

Point		1, 4	2-3
pnton		0	**1**

4.2.5. Boundary Settings

Boundary		1	2	3-4
Type		Symmetry boundary	Inlet	Wall
velType		U0in	**u0**	U0in
symtype		**Axial symmetry**	Symmetry	Symmetry
φ-velocity (w0)	m/s	0	**-(2*pi*RPM/60)*r**	0

4.2.6. Subdomain Settings

Subdomain		1
Integration order (gporder)		**4 4 4 2**
Constraint order (cporder)		**2 2 2 1**
Density (rho)	kg/m^3	**900**
Dynamic viscosity (eta)	Pa s	**0.01545**
cdon		**0**
Surface tension coefficient (sigma)	N/m	**0**
Parameter controlling interface thickness (epsilon)	m	**hmax_chns**

5. Geom2

Space dimensions: 3D

Independent variables: x, y, z

5.1. Scalar Expressions

Name	Expression	Unit	Description
u_3D	u_2D*sin(atan2(x,z))+w_2D*cos(atan2(x,z))		u-component 3D
v_3D	v_2D		v-component 3D
w_3D	u_2D*cos(atan2(x,z))-w_2D*sin(atan2(x,z))		w-component 3D
Velocity_3D	sqrt(u_3D^2+v_3D^2+w_3D^2)		Magnitude of 3D Velocity

5.2. Mesh

5.2.1. Mesh Statistics

Number of degrees of freedom	13657
Number of mesh points	1586
Number of elements	7685
Tetrahedral	7685
Prism	0
Hexahedral	0
Number of boundary elements	1106
Triangular	1106
Quadrilateral	0
Number of edge elements	128
Number of vertex elements	10
Minimum element quality	0.361
Element volume ratio	0.115

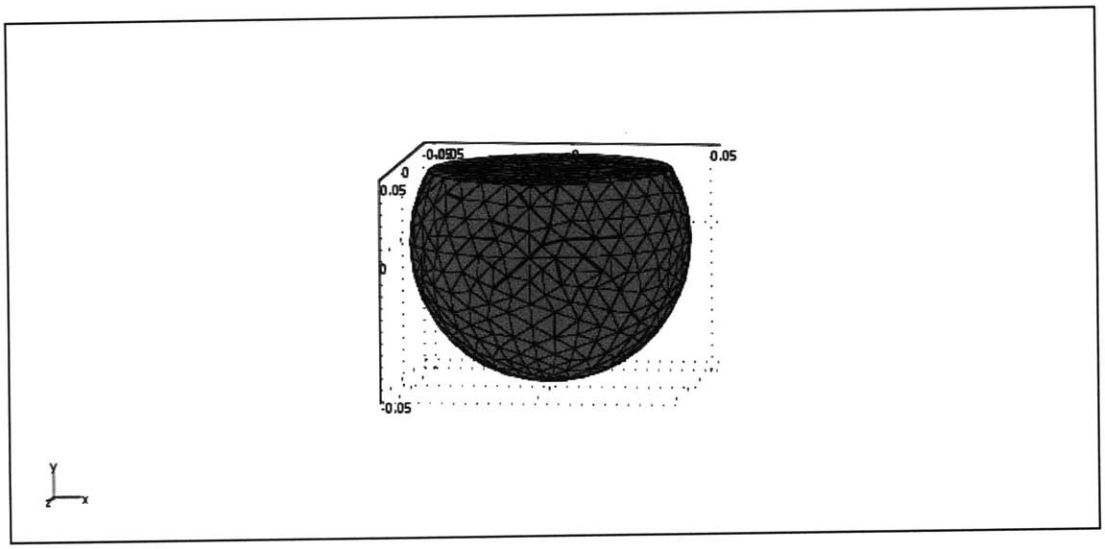

6. Extrusion Coupling Variables

6.1. Geom1

6.1.1. Source Subdomain: 1

Name	Value
Expression	v
Transformation type	General
Source transformation	r, z,
Destination Subdomain	1 (Geom2)
Destination transformation	sqrt(x^2+y^2), y,
Name	v_2D

6.1.2. Source Subdomain: 1

Name	Value

Expression	u
Transformation type	General
Source transformation	r, z,
Destination Subdomain	1 (Geom2)
Destination transformation	sqrt(x^2+y^2), y,
Name	u_2D

6.1.3. Source Subdomain: 1

Name	Value
Expression	w
Transformation type	General
Source transformation	r, z,
Destination Subdomain	1 (Geom2)
Destination transformation	sqrt(x^2+z^2), y,
Name	w_2D

7. Solver Settings

Solve using a script: off

Analysis type	Stationary
Auto select solver	On
Solver	Parametric
Solution form	Automatic
Symmetric	auto
Adaptive mesh refinement	Off
Optimization/Sensitivity	Off
Plot while solving	Off

7.1. Direct (PARDISO)

Solver type: Linear system solver

Parameter	Value
Preordering algorithm	Nested dissection
Row preordering	On
Bunch-Kaufmann	Off
Pivoting perturbation	1.0E-8
Relative tolerance	1.0E-6
Factor in error estimate	400.0
Check tolerances	On

7.2. Stationary

Parameter	Value
Linearity	Automatic
Relative tolerance	1.0E-6
Maximum number of iterations	250
Manual tuning of damping parameters	Off
Highly nonlinear problem	On
Initial damping factor	1.0
Minimum damping factor	1.0E-4
Restriction for step size update	10.0

7.3. Parametric

Parameter	Value
Parameter name	RPM
Parameter values	1 20 50 100
Predictor	Linear
Manual tuning of parameter step size	Off
Initial step size	0.0
Minimum step size	0.0
Maximum step size	0.0

7.4. Advanced

Parameter	Value
Constraint handling method	Elimination
Null-space function	Automatic
Automatic assembly block size	On
Assembly block size	1000
Use Hermitian transpose of constraint matrix and in symmetry detection	Off
Use complex functions with real input	Off
Stop if error due to undefined operation	On
Store solution on file	Off
Type of scaling	None
Manual scaling	
Row equilibration	On
Manual control of reassembly	Off
Load constant	On
Constraint constant	On
Mass constant	On
Damping (mass) constant	On
Jacobian constant	On
Constraint Jacobian constant	On

8. Postprocessing

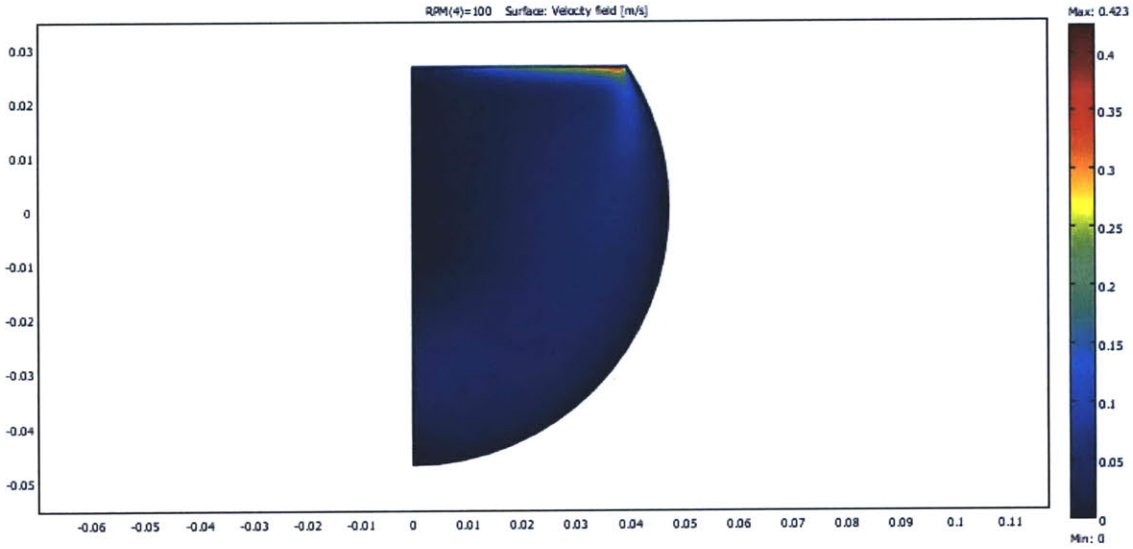
RPM(4)=100 Surface: Velocity field [m/s]
Max: 0.423
0.4
0.35
0.3
0.25
0.2
0.15
0.1
0.05
0
Min: 0
0.03
0.02
0.01
0
-0.01
-0.02
-0.03
-0.04
-0.05
-0.06 -0.05 -0.04 -0.03 -0.02 -0.01 0 0.01 0.02 0.03 0.04 0.05 0.06 0.07 0.08 0.09 0.1 0.11

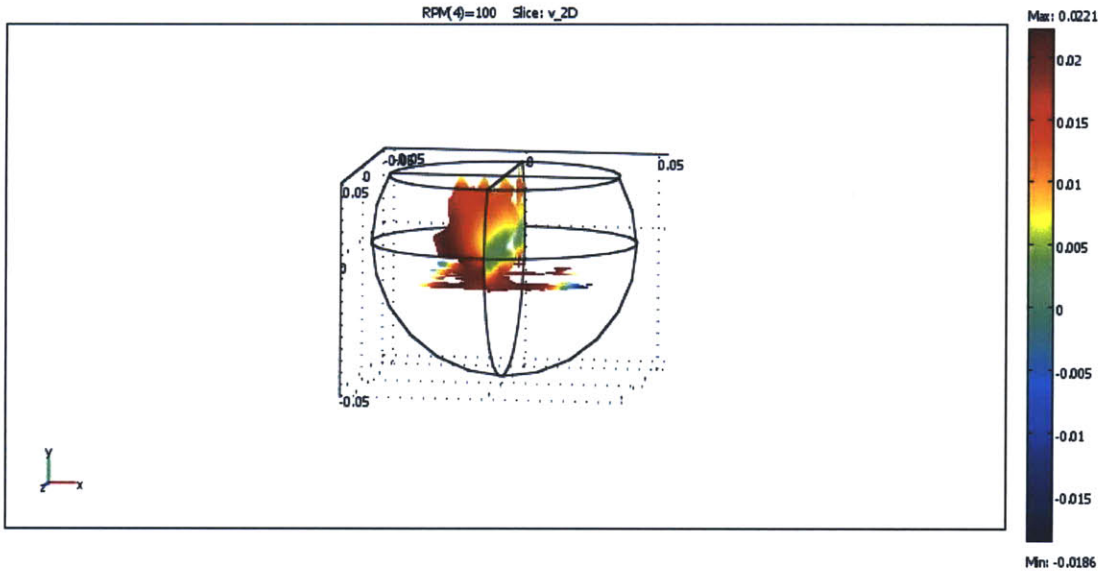

9. Variables

9.1. Boundary

Name	Description	Unit	Expression
K_r_chns	Viscous force per area, r component	Pa	eta_chns * (2 * nr_chns * ur+nz_chns * (uz+vr))
T_r_chns	Total force per area, r component	Pa	-nr_chns * p+2 * nr_chns * eta_chns * ur+nz_chns * eta_chns * (uz+vr)
K_z_chns	Viscous force per area, z component	Pa	eta_chns * (nr_chns * (vr+uz)+2 * nz_chns * vz)
T_z_chns	Total force per area, z component	Pa	-nz_chns * p+nr_chns * eta_chns * (vr+uz)+2 * nz_chns * eta_chns * vz
K_phi_chns	Viscous force per area, phi component	Pa	eta_chns * (nr_chns * wr+nz_chns * wz-nr_chns * w/r)
T_phi_chns	Total force per area, phi component	Pa	eta_chns * (nr_chns * wr+nz_chns * wz-nr_chns * w/r)

9.2. Subdomain

Name	Description	Unit	Expression

U_chns	Velocity field	m/s	sqrt(u^2+v^2+w^2)
Vr_chns	Vorticity, r component	1/s	-wz
Vz_chns	Vorticity, z component	1/s	wr+w/r
Vphi_chns	Vorticity, phi component	1/s	uz-vr
V_chns	Vorticity	1/s	sqrt(Vr_chns^2+Vz_chns^2+Vphi_chns^2)
divU_chns	Divergence of velocity field	1/s	ur+vz+u/r
cellRe_chns	Cell Reynolds number	1	rho_chns * U_chns * h/eta_chns
res_u_chns	Equation residual for u	Pa	r * (rho_chns * (u * ur+v * uz)+pr-F_r_chns)-rho_chns * w^2+2 * eta_chns * (u/r-ur)-eta_chns * r * (2 * urr+uzz+vrz)
res_v_chns	Equation residual for v	Pa	r * (rho_chns * (u * vr+v * vz)+pz-F_z_chns)-eta_chns * (r * (vrr +uzr)+2 * r * vzz+uz+vr)
res_w_chns	Equation residual for w	Pa	r * (rho_chns * (u * wr+v * wz)-F_phi_chns)+rho_chns * u * w-eta_chns * (wr-w/r)-eta_chns * r * wrr-r * eta_chns * wzz
beta_r_chns	Convective field, r component	Pa*s	r * rho_chns * u
beta_z_chns	Convective field, z component	Pa*s	r * rho_chns * v
Dm_chns	Mean diffusion coefficient	kg/s	r * eta_chns
da_chns	Total time scale factor	kg/m^2	r * rho_chns
taum_chns	GLS time-scale	m^3*s/kg	nojac(1/max(2 * rho_chns * sqrt(emetric(u,v)),48 * eta_chns/ h^2))
tauc_chns	GLS time-scale	m^2/s	0.5 * nojac(if(u^2+v^2
res_p_chns	Equation residual for p	kg/(m^2*s)	rho_chns * r * divU_chns

Appendix E : Results of Uniform Rotating Magnetic Field Applied to Sphere of Ferrofluid (Section 6.1)

E1. EFH1 at 47 Hz

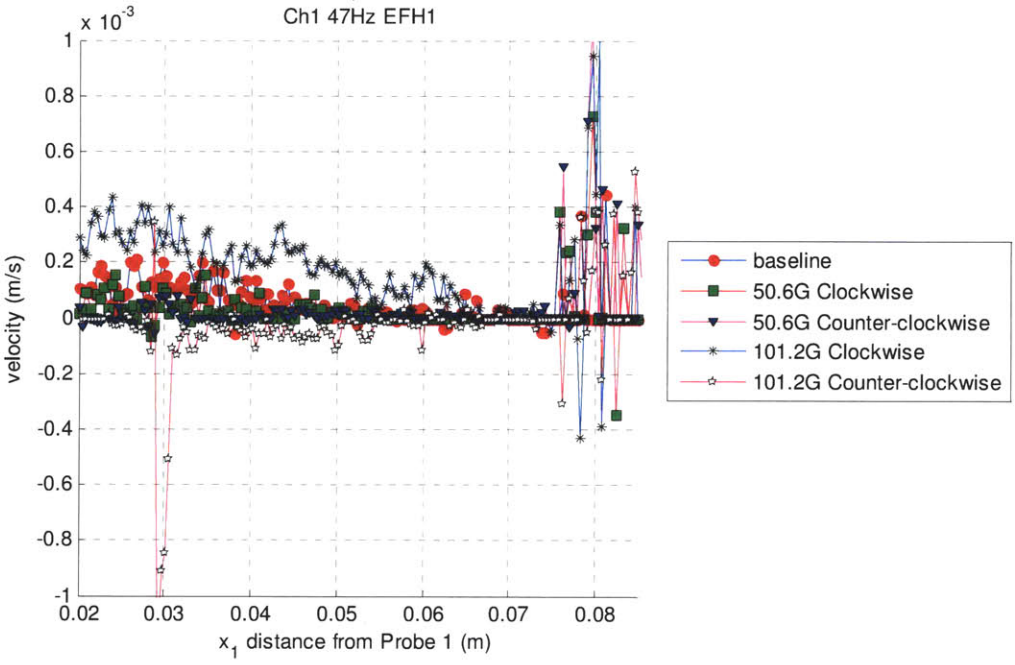

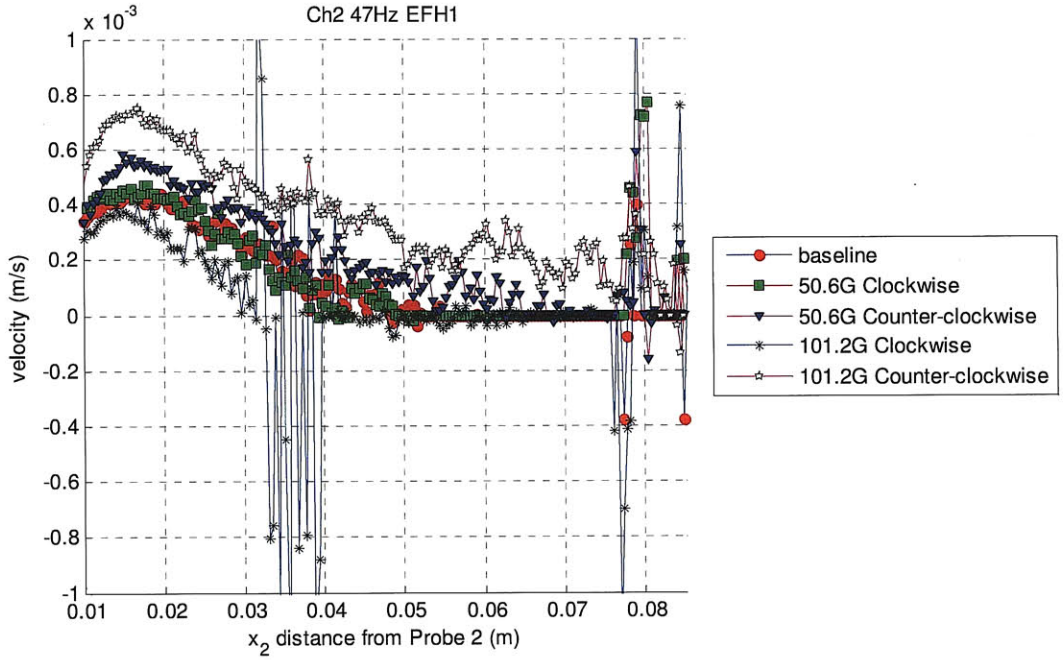
Ch2 47Hz EFH1
x 10^-3
velocity (m/s)
x2 distance from Probe 2 (m)
baseline
50.6G Clockwise
50.6G Counter-clockwise
101.2G Clockwise
101.2G Counter-clockwise

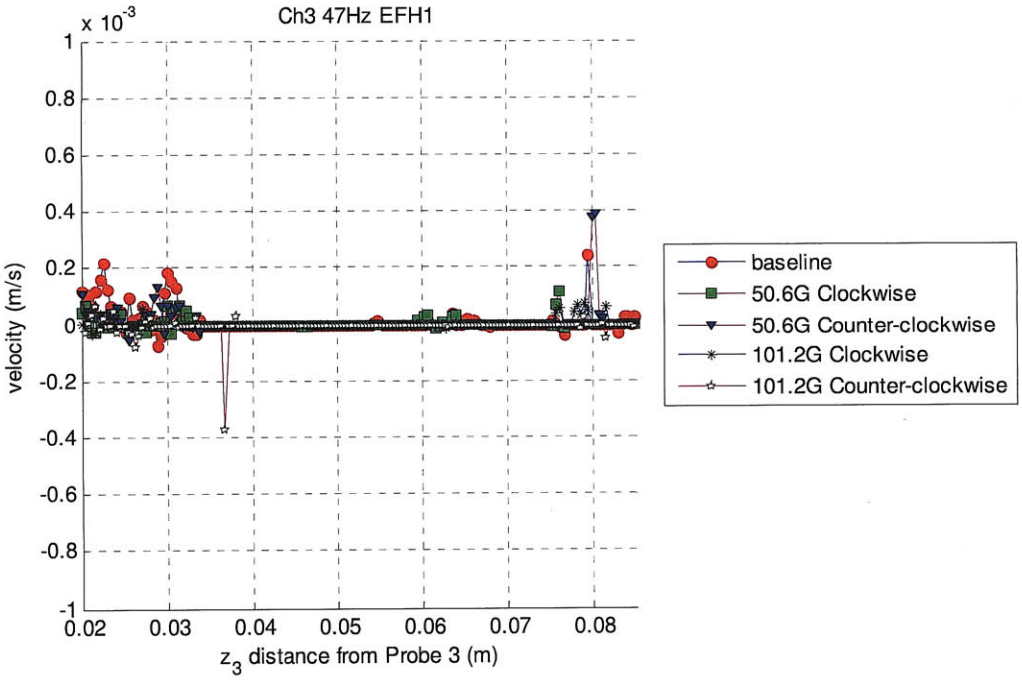
Ch3 47Hz EFH1
x 10^-3
velocity (m/s)
z3 distance from Probe 3 (m)
baseline
50.6G Clockwise
50.6G Counter-clockwise
101.2G Clockwise
101.2G Counter-clockwise

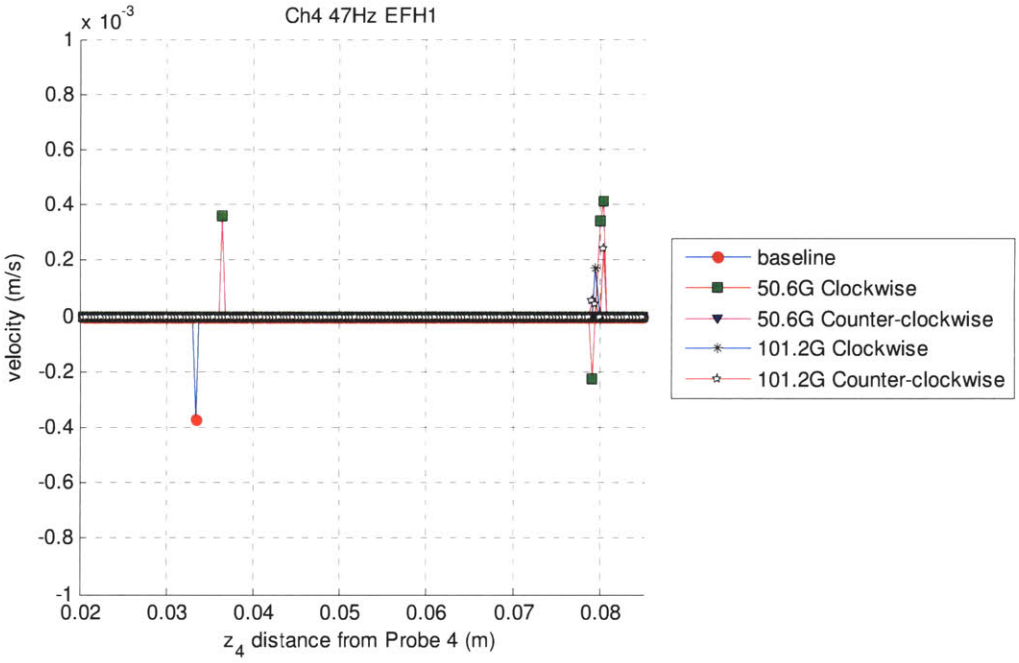

E2. EFH1 at 15 Hz

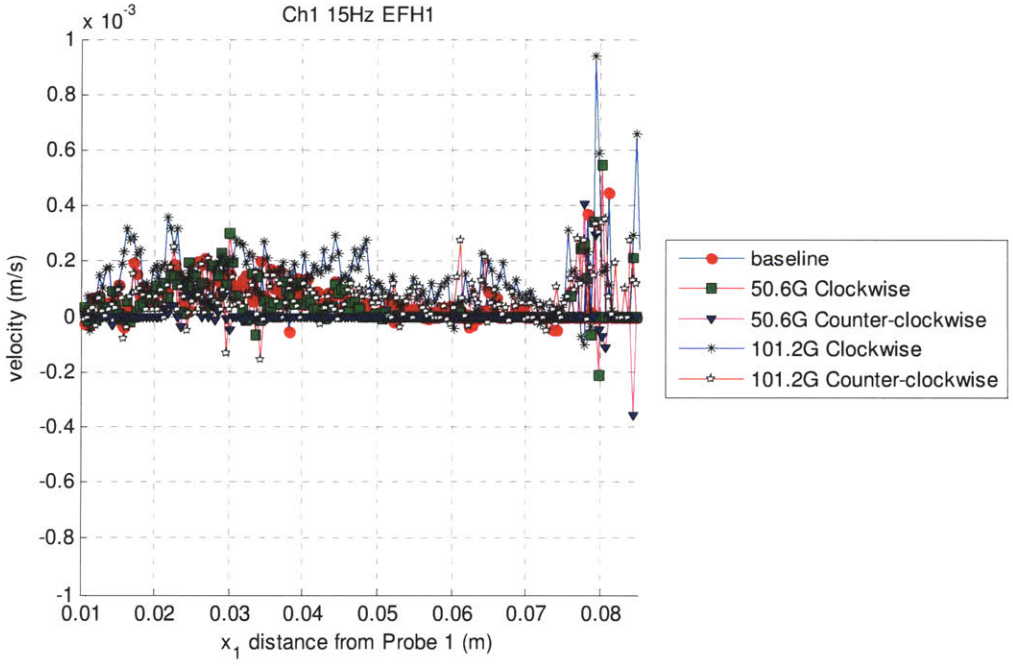

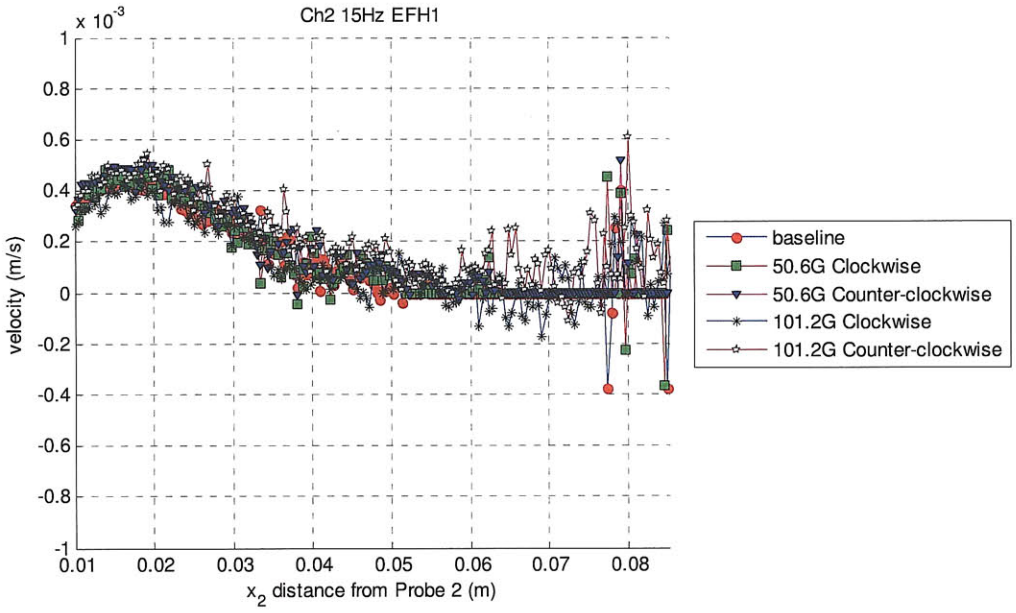
Ch2 15Hz EFH1
x 10^-3
velocity (m/s)
x2 distance from Probe 2 (m)
baseline
50.6G Clockwise
50.6G Counter-clockwise
101.2G Clockwise
101.2G Counter-clockwise

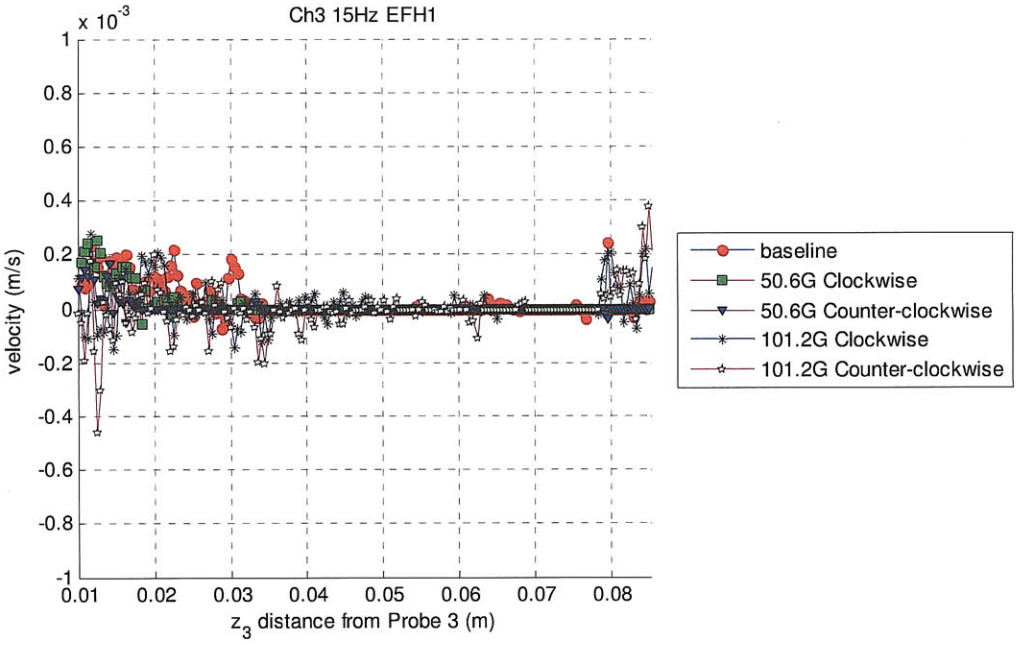
Ch3 15Hz EFH1
x 10^-3
velocity (m/s)
z3 distance from Probe 3 (m)
baseline
50.6G Clockwise
50.6G Counter-clockwise
101.2G Clockwise
101.2G Counter-clockwise

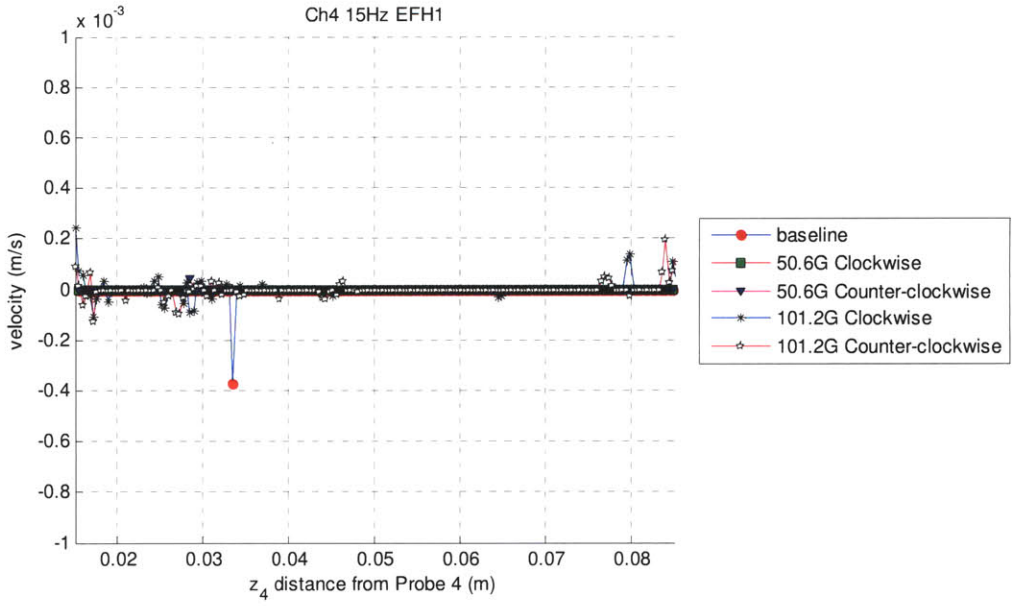

E3. MSGW11 at 95 Hz

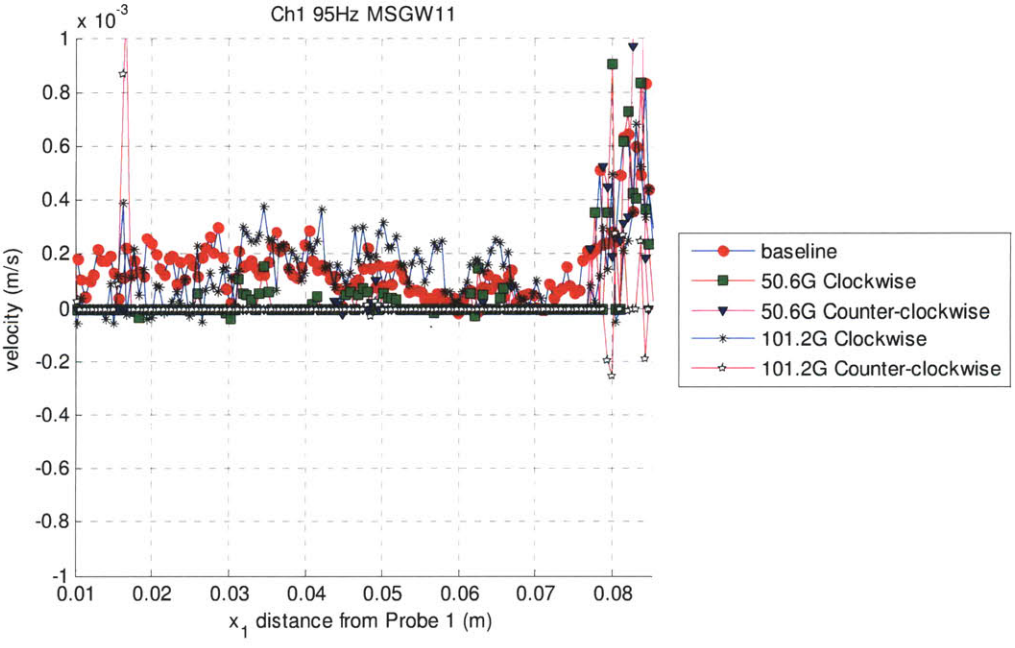

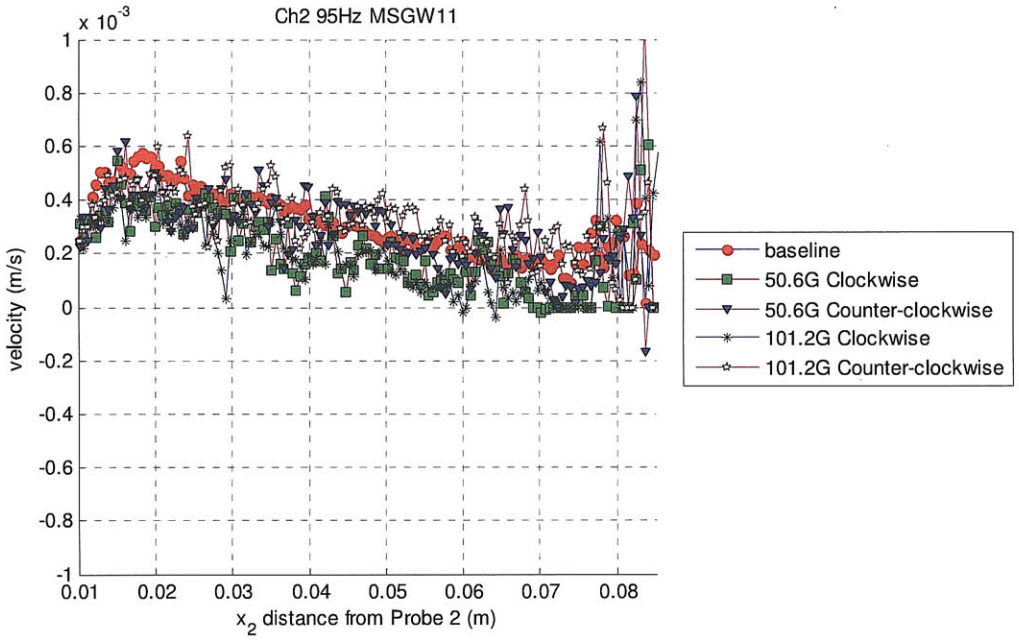
Ch2 95Hz MSGW11
x 10^-3
velocity (m/s)
x2 distance from Probe 2 (m)
baseline
50.6G Clockwise
50.6G Counter-clockwise
101.2G Clockwise
101.2G Counter-clockwise

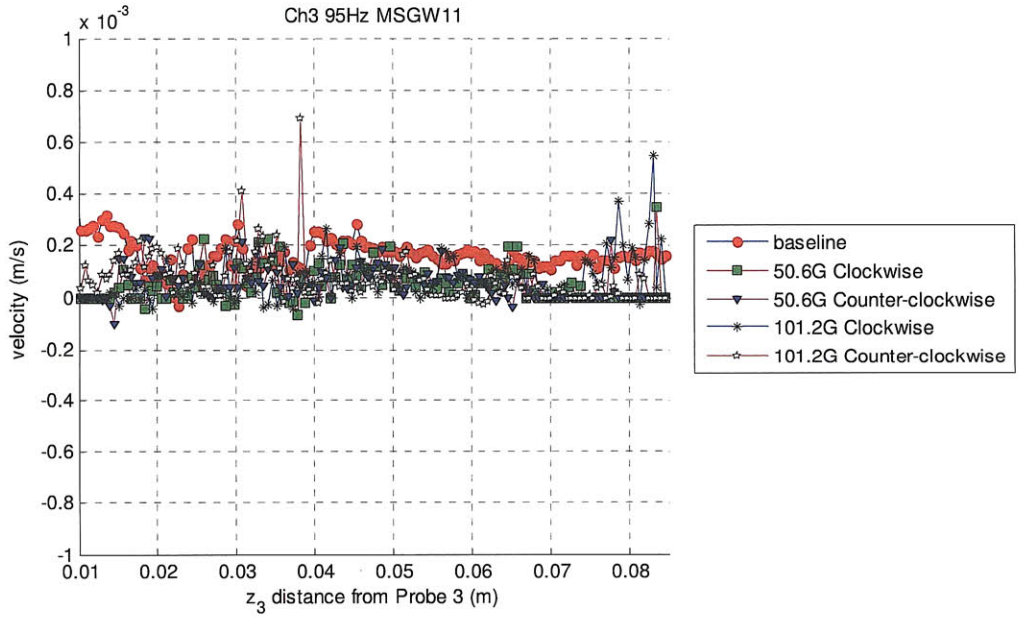
Ch3 95Hz MSGW11
x 10^-3
velocity (m/s)
z3 distance from Probe 3 (m)
baseline
50.6G Clockwise
50.6G Counter-clockwise
101.2G Clockwise
101.2G Counter-clockwise

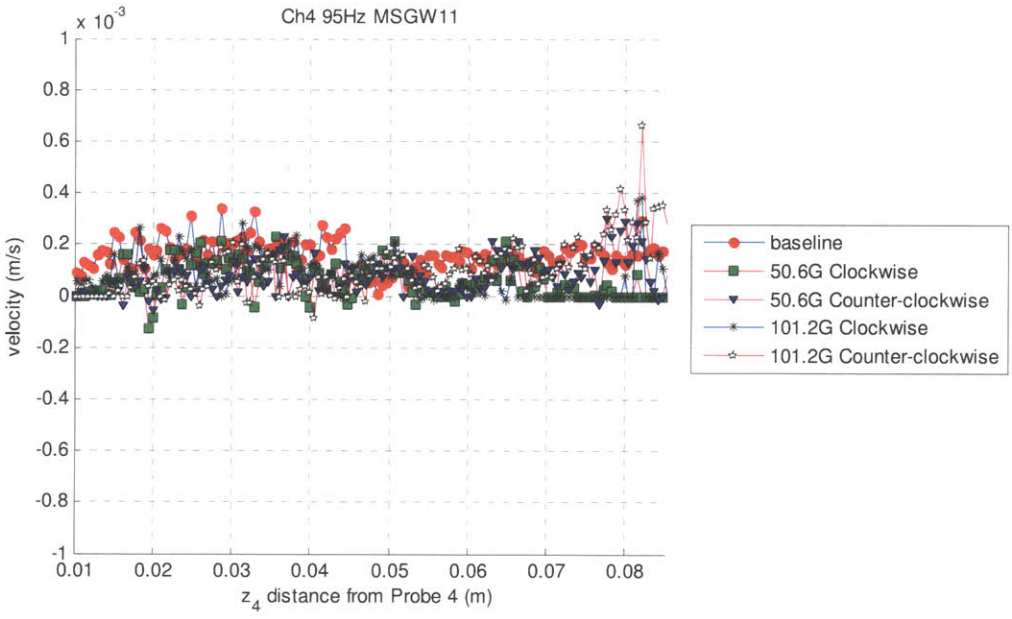

E4. MSGW11 at 47 Hz

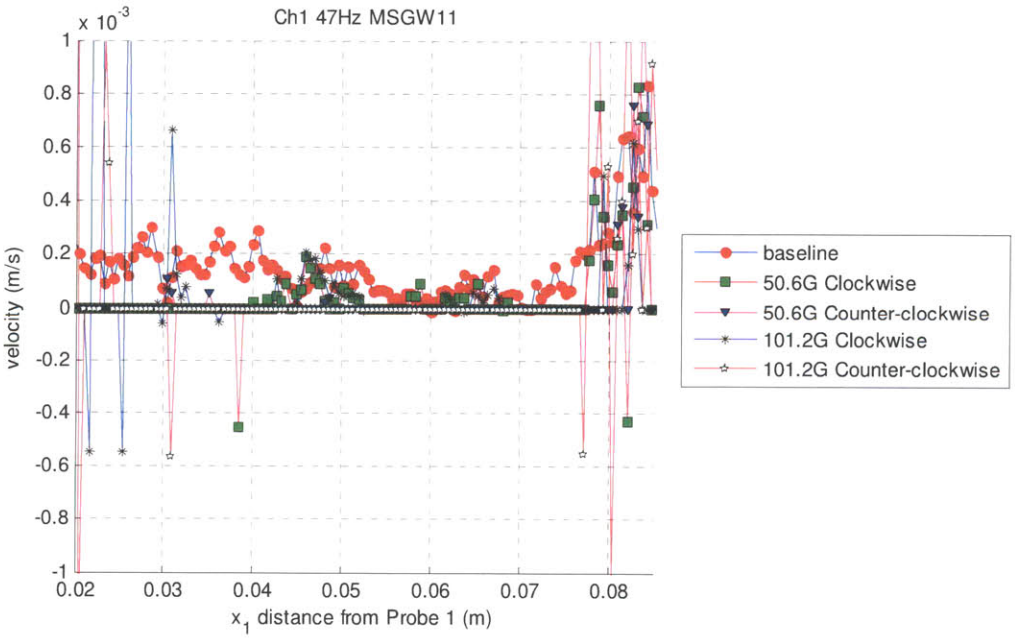

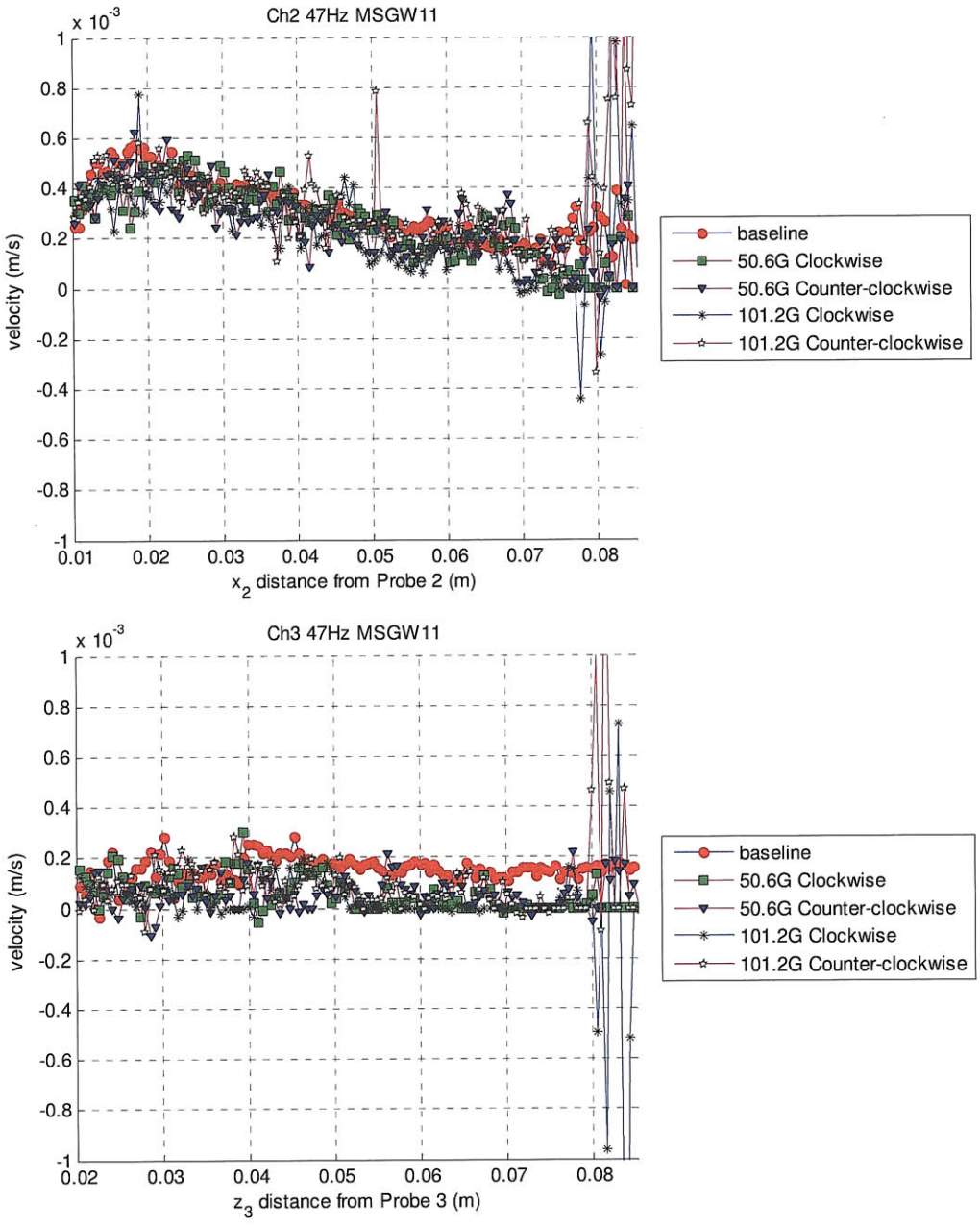
Ch2 47Hz MSGW11
x 10^-3
velocity (m/s)
x2 distance from Probe 2 (m)
baseline
50.6G Clockwise
50.6G Counter-clockwise
101.2G Clockwise
101.2G Counter-clockwise
Ch3 47Hz MSGW11
x 10^-3
velocity (m/s)
z3 distance from Probe 3 (m)
baseline
50.6G Clockwise
50.6G Counter-clockwise
101.2G Clockwise
101.2G Counter-clockwise

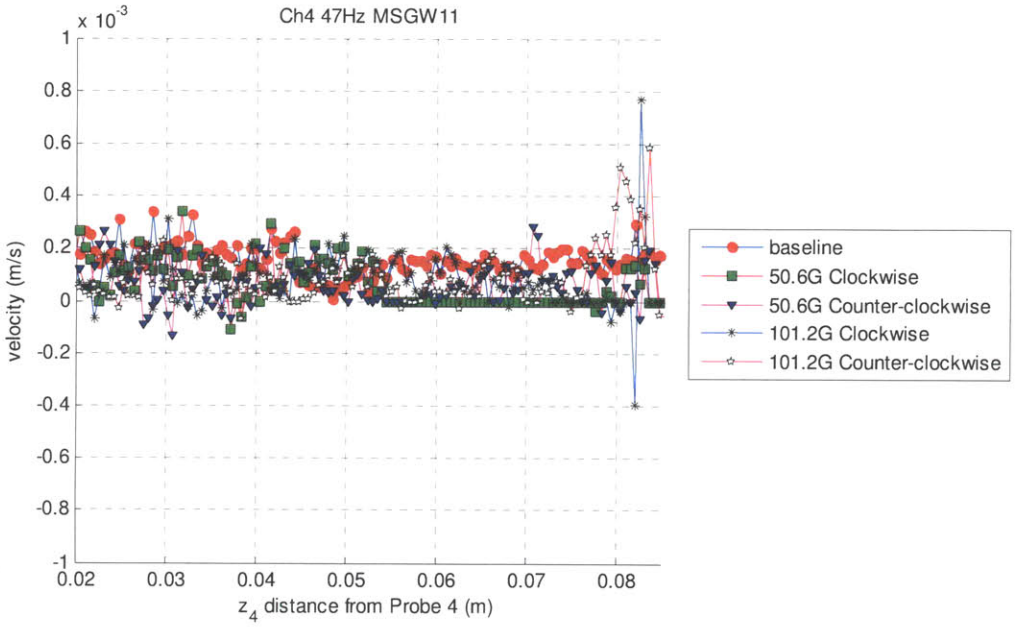
Ch4 47Hz MSGW11
x 10^-3
1
0.8
0.6
0.4
0.2
0
-0.2
-0.4
-0.6
-0.8
-1
velocity (m/s)
0.02
0.03
0.04
0.05
0.06
0.07
0.08
z4 distance from Probe 4 (m)
baseline
50.6G Clockwise
50.6G Counter-clockwise
101.2G Clockwise
101.2G Counter-clockwise

Appendix F : COMSOL Simulations of Spherical Geometry in Uniform Rotating Magnetic Fields

F1. MSGW11 Filled Sphere with 100G Rotating Field with ($\eta' \neq 0$) (Section 6.2.4)

Ferrofluid in 3D Cylinder with rotating H field

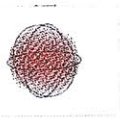

1. Table of Contents

2. Model Properties

Property	Value
Model name	Ferrofluid in 3D Cylinder with rotating H field
Author	Shahriar
Company	MIT
Department	EECS
Reference	
URL	
Saved date	Mar 26, 2010 6:31:35 PM
Creation date	Oct 6, 2008 11:21:14 PM
COMSOL version	COMSOL 3.5.0.608

File name: F:\Research Files\Software Data Files\Comsol Files\Good3DSpherefiles\3Dcase_sphere_MSGW11_scalarpotentialmethod_fluxball_100G.mph

Application modes and modules used in this model:

- Geom1 (3D)
  - Incompressible Navier-Stokes
  - Diffusion
  - Convection and Diffusion
  - Convection and Diffusion
  - Convection and Diffusion
  - PDE, General Form
  - PDE, General Form

2.1. Model description

Model is with a rotating magnetic field in a cylinder with ferrofluid with boundary condition of omega=0. If this boundary condition is removed there is no flow.

Parameters picked are similar to those from Chaves's papers normalized. Look at Calculation_normalized_velocity_alexchaves.xls

3. Constants

Name	Expression	Value	Description
Xi	0.56	0.56	
omega	2*pi*f	596.902604	
f	95	95	
zeta	0.0003125	3.125e-4	
eta	7.58e-3	0.00758	
etaprime	7.17e-6	7.17e-6	
H0	1	1	
Tau	1.39e-5	1.39e-5	
omegatau	omega*Tau	0.008297	
R0	0.05	0.05	

4. Global Expressions

Name	Expression	Unit	Description
FMx	M_x*(d(Hx,x))+M_y*(d(Hx,y))+M_z*(d(Hx,z))		
FMy	M_x*(d(Hy,x))+M_y*(d(Hy,y))+M_z*(d(Hy,z))		
FMz	M_x*(d(Hz,x))+M_y*(d(Hz,y))+M_z*(d(Hz,z))		
T	M_x*Hy-M_y*Hx		
M_eqx	Xi*Hx		
M_eqy	Xi*Hy		
M_eqz	Xi*Hz		
Hx	-psix-M_x/3		
Hy	-psiy-M_y/3		
Hz	-psiz-M_z/3		
potential	H0*(x*cos(t)+y*sin(t))		

5. Geometry

Number of geometries: 1

5.1. Geom1

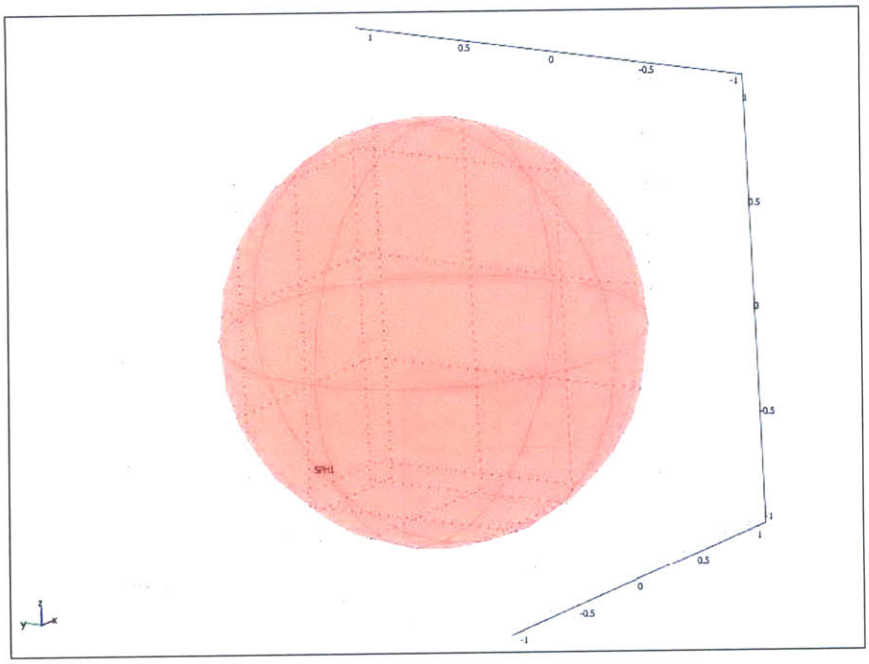

5.1.1. Point mode

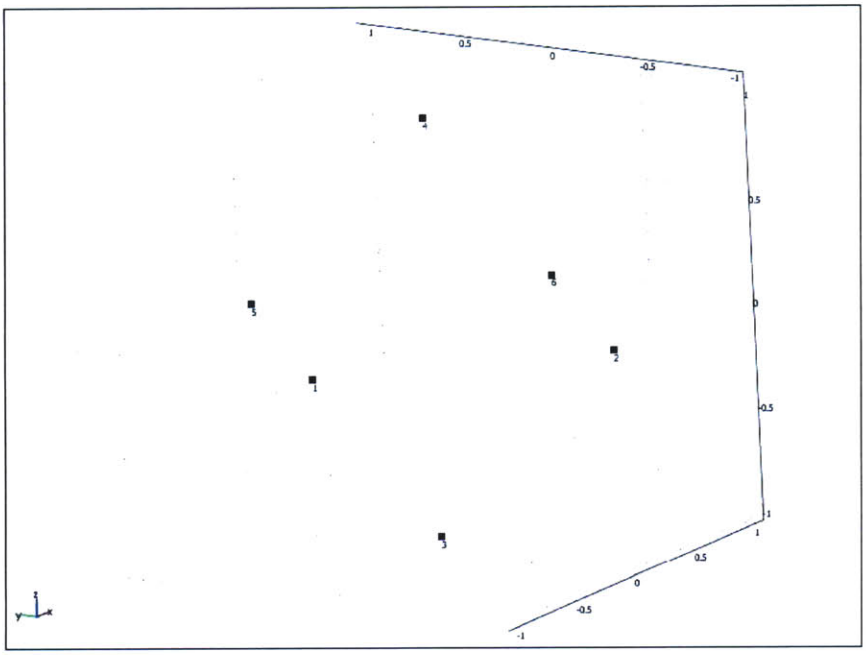

5.1.2. Edge mode

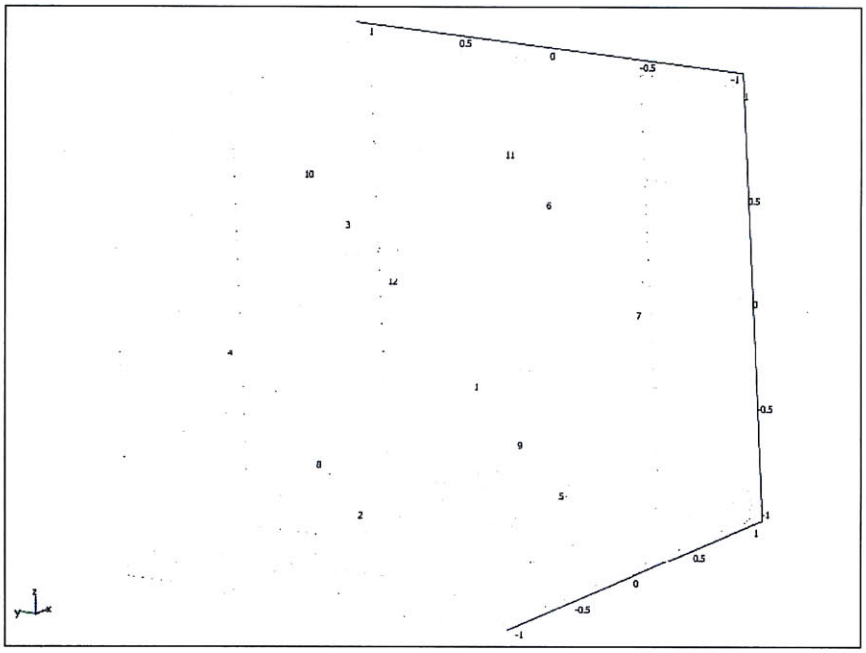

5.1.3. Boundary mode

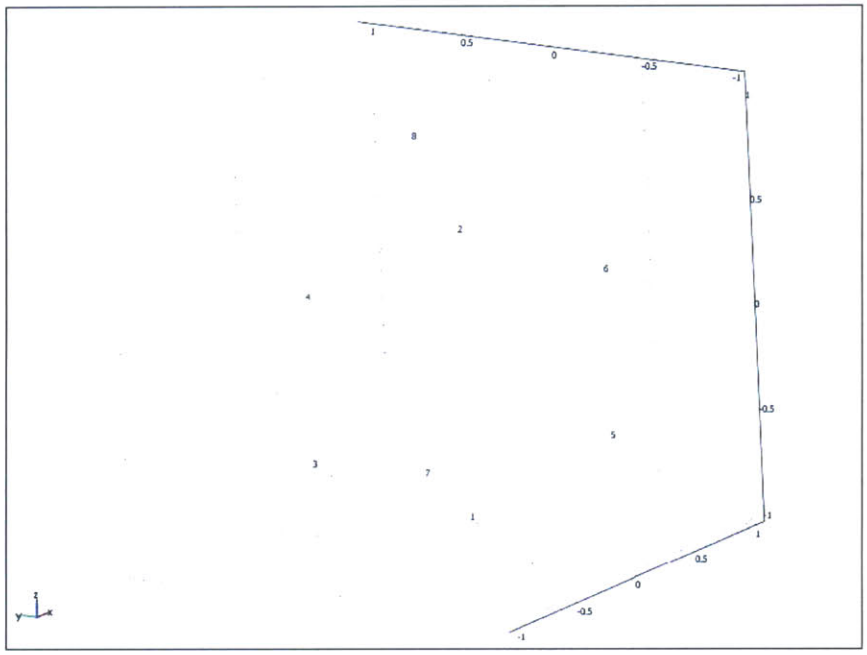

5.1.4. Subdomain mode

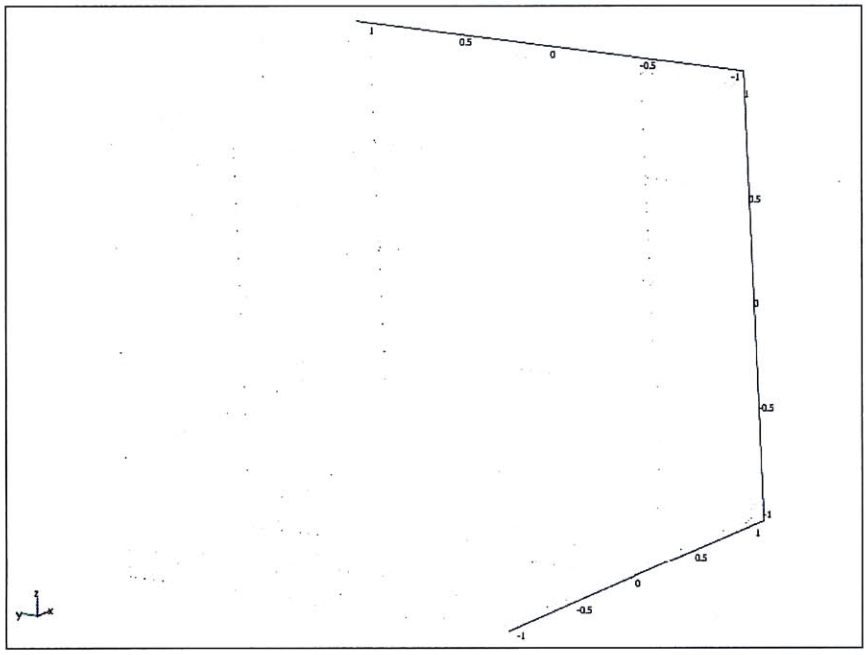

6. Geom1

Space dimensions: 3D

Independent variables: x, y, z

6.1. Scalar Expressions

Name	Expression	Unit	Description
r	sqrt(x^2+y^2+z^2)	m	
phi	atan2(y,x)	rad	
theta	atan2(x,z)	rad	

6.2. Mesh

6.2.1. Mesh Statistics

Number of degrees of freedom	704248
Number of mesh points	10168
Number of elements	54859
Tetrahedral	54859
Prism	0
Hexahedral	0
Number of boundary elements	3852
Triangular	3852
Quadrilateral	0
Number of edge elements	180
Number of vertex elements	6
Minimum element quality	0.355
Element volume ratio	0.058

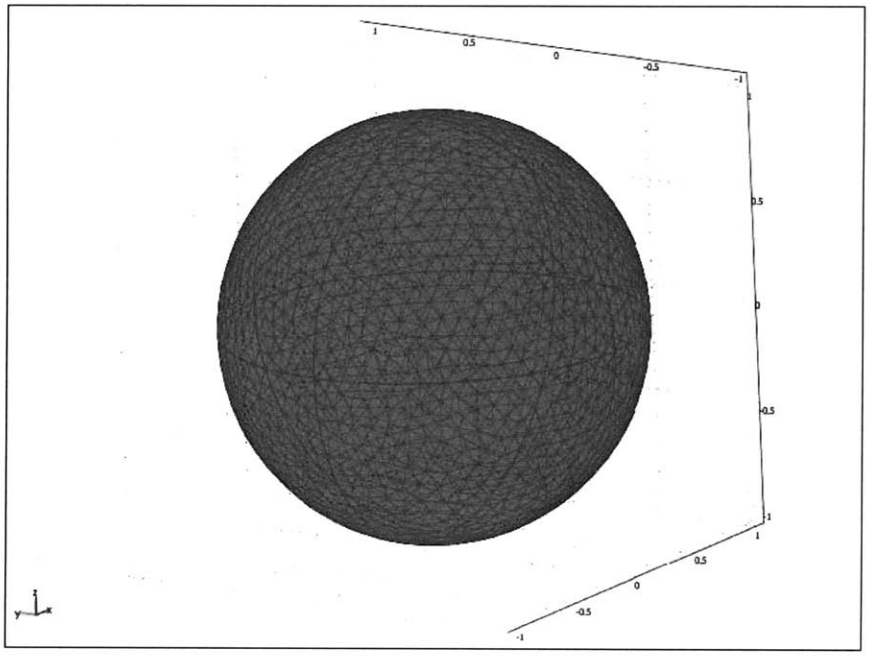

6.3. Application Mode: Incompressible Navier-Stokes (ns)

Application mode type: Incompressible Navier-Stokes

Application mode name: ns

6.3.1. Scalar Variables

Name	Variable	Value	Unit	Description
visc_vel_fact	visc_vel_fact_ns	10	1	Viscous velocity factor

6.3.2. Application Mode Properties

Property	Value
Default element type	Lagrange - P_2 P_1
Analysis type	Stationary
Corner smoothing	Off
Frame	Frame (ref)
Weak constraints	Off
Constraint type	Ideal

6.3.3. Variables

Dependent variables: u, v, w, p, nxw, nyw, nzw

Shape functions: shlag(2,'u'), shlag(2,'v'), shlag(2,'w'), shlag(1,'p')

Interior boundaries not active

6.3.4. Point Settings

Point	1-4, 6	5
pnton	0	1

6.3.5. Boundary Settings

Boundary	1-8
Type	Wall

6.3.6. Subdomain Settings

Subdomain		1
Integration order (gporder)		4 4 4 2
Constraint order (cporder)		2 2 2 1
Density (rho)	kg/m^3	0
Dynamic viscosity (eta)	Pa·s	eta+zeta
Volume force, x dir. (F_x)	N/m^3	2*zeta*sy+FMx
Volume force, y dir. (F_y)	N/m^3	-2*zeta*sx+FMy
Volume force, z dir. (F_z)	N/m^3	FMz
cdon		0

6.4. Application Mode: Diffusion (di)

Application mode type: Diffusion

Application mode name: di

6.4.1. Application Mode Properties

Property	Value
Default element type	Lagrange - Quadratic
Analysis type	Stationary
Frame	Frame (ref)
Weak constraints	Off
Constraint type	Ideal

6.4.2. Variables

Dependent variables: s

Shape functions: shlag(2,'s')

Interior boundaries not active

6.4.3. Boundary Settings

Boundary	1-8
Type	Concentration

6.4.4. Subdomain Settings

Subdomain		1
Diffusion coefficient (D)	m^2/s	etaprime
Reaction rate (R)	$mol/(m^3 \cdot s)$	T+2*zeta*(vx-uy-2*s)

6.5. Application Mode: Convection and Diffusion (cd)

Application mode type: Convection and Diffusion

Application mode name: cd

6.5.1. Application Mode Properties

Property	Value
Default element type	Lagrange - Quadratic
Analysis type	Transient
Equation form	Non-conservative
Frame	Frame (ref)
Weak constraints	Off
Constraint type	Ideal

6.5.2. Variables

Dependent variables: M_x

Shape functions: shlag(2,'M_x')

Interior boundaries not active

6.5.3. Boundary Settings

Boundary	1-8
Type	Insulation/Symmetry

6.5.4. Subdomain Settings

Subdomain		1
Diffusion coefficient (D)	m^2/s	0
Reaction rate (R)	$mol/(m^3 \cdot s)$	-s*M_y-((M_x-M_eqx)/(omegatau))
x-velocity (u)	m/s	u
y-velocity (v)	m/s	v
z-velocity (w)	m/s	w

6.6. Application Mode: Convection and Diffusion (cd2)

Application mode type: Convection and Diffusion

Application mode name: cd2

6.6.1. Application Mode Properties

Property	Value
Default element type	Lagrange - Quadratic
Analysis type	Transient
Equation form	Non-conservative
Frame	Frame (ref)
Weak constraints	Off
Constraint type	Ideal

6.6.2. Variables

Dependent variables: M_y

Shape functions: shlag(2,'M_y')

Interior boundaries not active

6.6.3. Boundary Settings

Boundary	1-8
Type	Insulation/Symmetry

6.6.4. Subdomain Settings

Subdomain		1
Diffusion coefficient (D)	m^2/s	0
Reaction rate (R)	$mol/(m^3 \cdot s)$	s*M_x-((M_y-M_eqy)/omegatau)
x-velocity (u)	m/s	u
y-velocity (v)	m/s	v
z-velocity (w)	m/s	w

6.7. Application Mode: Convection and Diffusion (cd3)

Application mode type: Convection and Diffusion

Application mode name: cd3

6.7.1. Application Mode Properties

Property	Value
Default element type	Lagrange - Quadratic
Analysis type	Transient
Equation form	Non-conservative
Frame	Frame (ref)
Weak constraints	Off
Constraint type	Ideal

6.7.2. Variables

Dependent variables: M_z

Shape functions: shlag(2,'M_z')

Interior boundaries not active

6.7.3. Boundary Settings

Boundary	1-8
Type	Insulation/Symmetry

6.7.4. Subdomain Settings

Subdomain		1
Diffusion coefficient (D)	m^2/s	0
Reaction rate (R)	$mol/(m^3 \cdot s)$	-((M_z-M_eqz)/omegatau)
x-velocity (u)	m/s	u
y-velocity (v)	m/s	v
z-velocity (w)	m/s	w

6.8. Application Mode: PDE, General Form (g2)

Application mode type: PDE, General Form

Application mode name: g2

6.8.1. Application Mode Properties

Property	Value
Default element type	Lagrange - Quadratic
Wave extension	Off
Frame	Frame (ref)
Weak constraints	Off

6.8.2. Variables

Dependent variables: avgv, avgv_t

Shape functions: shlag(2,'avgv')

Interior boundaries not active

6.8.3. Boundary Settings

Boundary	1-8
Type	Dirichlet boundary condition

6.8.4. Subdomain Settings

Subdomain	1
Source term (f)	v
Conservative flux source term (ga)	{{0;0;0}}

6.9. Application Mode: PDE, General Form (g)

Application mode type: PDE, General Form

Application mode name: g

6.9.1. Application Mode Properties

Property	Value
Default element type	Lagrange - Quadratic
Wave extension	Off
Frame	Frame (ref)
Weak constraints	Off

6.9.2. Variables

Dependent variables: psi, psi_t

Shape functions: shlag(2,'psi')

Interior boundaries not active

6.9.3. Boundary Settings

Boundary	1-8
Type	Dirichlet boundary condition
(r)	-psi+potential

6.9.4. Subdomain Settings

Subdomain	1
Damping/Mass coefficient (da)	0
Source term (f)	-d(M_x,x)-d(M_y,y)-d(M_z,z)

7. Solver Settings

Solve using a script: off

Analysis type	Stationary
Auto select solver	On
Solver	Time dependent
Solution form	Automatic
Symmetric	auto
Adaptive mesh refinement	Off
Optimization/Sensitivity	Off
Plot while solving	Off

7.1. Direct (PARDISO)

Solver type: Linear system solver

Parameter	Value
Preordering algorithm	Nested dissection
Row preordering	On
Bunch-Kaufmann	Off
Pivoting perturbation	1.0E-8
Relative tolerance	1.0E-6
Factor in error estimate	400.0
Check tolerances	Off

7.2. Time Stepping

Parameter	Value
Times	range(0,0.1,2)
Relative tolerance	0.001
Absolute tolerance	0.00010
Times to store in output	Specified times
Time steps taken by solver	Free
Maximum BDF order	5
Singular mass matrix	Maybe
Consistent initialization of DAE systems	Backward Euler
Error estimation strategy	Exclude algebraic
Allow complex numbers	Off

7.3. Advanced

Parameter	Value
Constraint handling method	Elimination
Null-space function	Automatic
Automatic assembly block size	On
Assembly block size	5000
Use Hermitian transpose of constraint matrix and in symmetry detection	Off
Use complex functions with real input	Off
Stop if error due to undefined operation	On
Store solution on file	Off
Type of scaling	Automatic
Manual scaling	
Row equilibration	On
Manual control of reassembly	Off
Load constant	On
Constraint constant	On
Mass constant	On

Damping (mass) constant	On
Jacobian constant	On
Constraint Jacobian constant	On

8. Postprocessing

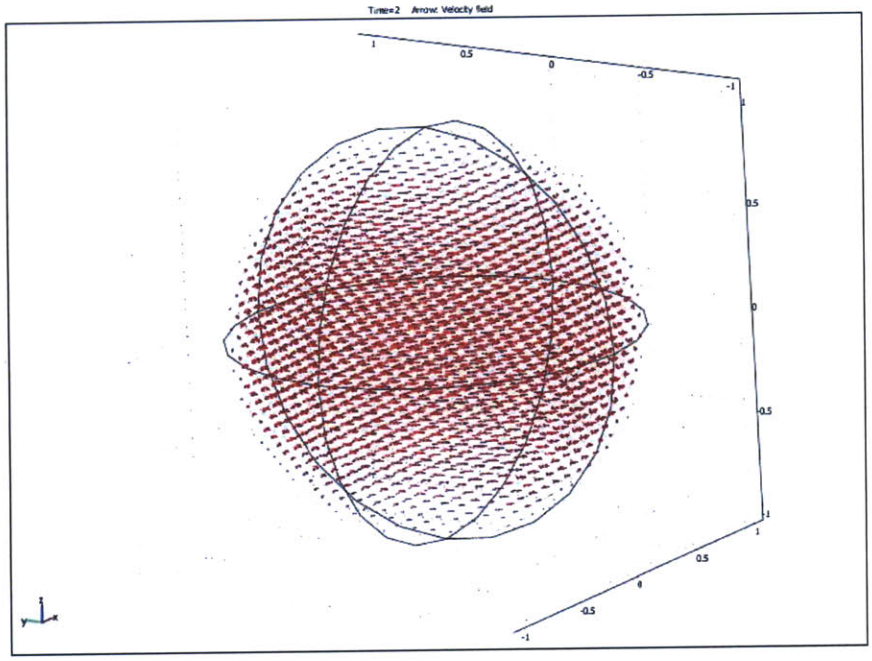

9. Variables

9.1. Boundary

Name	Description	Unit	Expression
K_x_ns	Viscous force per area, x component	Pa	eta_ns * (2 * nx_ns * ux+ny_ns * (uy+vx)+nz_ns * (uz+wx))
T_x_ns	Total force per area, x component	Pa	-nx_ns * p+2 * nx_ns * eta_ns * ux+ny_ns * eta_ns * (uy+vx)+nz_ns * eta_ns * (uz+wx)
K_y_ns	Viscous force per area, y component	Pa	eta_ns * (nx_ns * (vx+uy)+2 * ny_ns * vy+nz_ns * (vz+wy))
T_y_ns	Total force per area, y component	Pa	-ny_ns * p+nx_ns * eta_ns * (vx+uy)+2 * ny_ns * eta_ns * vy+nz_ns * eta_ns * (vz+wy)
K_z_ns	Viscous force per area, z component	Pa	eta_ns * (nx_ns * (wx+uz)+ny_ns * (wy+vz)+2 * nz_ns * wz)
T_z_ns	Total force per area, z component	Pa	-nz_ns * p+nx_ns * eta_ns * (wx+uz)+ny_ns * eta_ns * (wy+vz)+2 * nz_ns * eta_ns * wz
ndflux_s_di	Normal diffusive flux, s	mol/(m^2*s)	nx_di * dflux_s_x_di+ny_di * dflux_s_y_di+nz_di * dflux_s_z_di
ndflux_M_x_cd	Normal diffusive flux, M_x	mol/(m^2*s)	nx_cd * dflux_M_x_x_cd+ny_cd * dflux_M_x_y_cd+nz_cd * dflux_M_x_z_cd
ncflux_M_x_cd	Normal convective flux, M_x	mol/(m^2*s)	nx_cd * cflux_M_x_x_cd+ny_cd * cflux_M_x_y_cd+nz_cd * cflux_M_x_z_cd
ntflux_M_x_cd	Normal total flux, M_x	mol/(m^2*s)	nx_cd * tflux_M_x_x_cd+ny_cd * tflux_M_x_y_cd+nz_cd * tflux_M_x_z_cd

ndflux_M_y_cd2	Normal diffusive flux, M_y	mol/(m^2*s)	nx_cd2 * dflux_M_y_x_cd2+ny_cd2 * dflux_M_y_y_cd2+nz_cd2 * dflux_M_y_z_cd2
ncflux_M_y_cd2	Normal convective flux, M_y	mol/(m^2*s)	nx_cd2 * cflux_M_y_x_cd2+ny_cd2 * cflux_M_y_y_cd2+nz_cd2 * cflux_M_y_z_cd2
ntflux_M_y_cd2	Normal total flux, M_y	mol/(m^2*s)	nx_cd2 * tflux_M_y_x_cd2+ny_cd2 * tflux_M_y_y_cd2+nz_cd2 * tflux_M_y_z_cd2
ndflux_M_z_cd3	Normal diffusive flux, M_z	mol/(m^2*s)	nx_cd3 * dflux_M_z_x_cd3+ny_cd3 * dflux_M_z_y_cd3+nz_cd3 * dflux_M_z_z_cd3
ncflux_M_z_cd3	Normal convective flux, M_z	mol/(m^2*s)	nx_cd3 * cflux_M_z_x_cd3+ny_cd3 * cflux_M_z_y_cd3+nz_cd3 * cflux_M_z_z_cd3
ntflux_M_z_cd3	Normal total flux, M_z	mol/(m^2*s)	nx_cd3 * tflux_M_z_x_cd3+ny_cd3 * tflux_M_z_y_cd3+nz_cd3 * tflux_M_z_z_cd3

9.2. Subdomain

Name	Description	Unit	Expression
U_ns	Velocity field	m/s	sqrt(u^2+v^2+w^2)
Vx_ns	Vorticity, x component	1/s	wy-vz
Vy_ns	Vorticity, y component	1/s	uz-wx
Vz_ns	Vorticity, z component	1/s	vx-uy
V_ns	Vorticity	1/s	sqrt(Vx_ns^2+Vy_ns^2+Vz_ns^2)
divU_ns	Divergence of velocity field	1/s	ux+vy+wz
cellRe_ns	Cell Reynolds number	1	rho_ns * U_ns * h/eta_ns
res_u_ns	Equation residual for u	N/m^3	rho_ns * (u * ux+v * uy+w * uz)+px-F_x_ns+if(gmg_level>0,0,-eta_ns * (2 * uxx+uyy+vxy+uzz+wxz))
res_v_ns	Equation residual for v	N/m^3	rho_ns * (u * vx+v * vy+w * vz)+py-F_y_ns+if(gmg_level>0,0,-eta_ns * (vxx+uyx+2 * vyy+vzz+wyz))
res_w_ns	Equation residual for w	N/m^3	rho_ns * (u * wx+v * wy+w * wz)+pz-F_z_ns+if(gmg_level>0,0,-eta_ns * (wxx+uzx+wyy+vzy+2 * wzz))
beta_x_ns	Convective field, x component	kg/(m^2*s)	rho_ns * u
beta_y_ns	Convective field, y component	kg/(m^2*s)	rho_ns * v
beta_z_ns	Convective field, z component	kg/(m^2*s)	rho_ns * w
Dm_ns	Mean diffusion coefficient	Pa*s	eta_ns
da_ns	Total time scale factor	kg/m^3	rho_ns
taum_ns	GLS time-scale	m^3*s/kg	nojac(1/max(2 * rho_ns * sqrt(emetric(u,v,w)),48 * eta_ns/h^2))
tauc_ns	GLS time-scale	m^2/s	0.5 * nojac(if(u^2+v^2+w^2
res_p_ns	Equation residual for p	kg/(m^3*s)	rho_ns * divU_ns
grad_s_x_di	Concentration gradient, s, x component	mol/m^4	sx
dflux_s_x_di	Diffusive flux, s, x component	mol/(m^2*s)	-Dxx_s_di * sx-Dxy_s_di * sy-Dxz_s_di * sz

grad_s_y_di	Concentration gradient, s, y component	mol/m^4	sy
dflux_s_y_di	Diffusive flux, s, y component	mol/(m^2*s)	-Dyx_s_di * sx-Dyy_s_di * sy-Dyz_s_di * sz
grad_s_z_di	Concentration gradient, s, z component	mol/m^4	sz
dflux_s_z_di	Diffusive flux, s, z component	mol/(m^2*s)	-Dzx_s_di * sx-Dzy_s_di * sy-Dzz_s_di * sz
grad_s_di	Concentration gradient, s	mol/m^4	sqrt(grad_s_x_di^2+grad_s_y_di^2+grad_s_z_di^2)
dflux_s_di	Diffusive flux, s	mol/(m^2*s)	sqrt(dflux_s_x_di^2+dflux_s_y_di^2+dflux_s_z_di^2)
grad_M_x_x_cd	Concentration gradient, M_x, x component	mol/m^4	M_xx
dflux_M_x_x_cd	Diffusive flux, M_x, x component	mol/(m^2*s)	-Dxx_M_x_cd * M_xx-Dxy_M_x_cd * M_xy-Dxz_M_x_cd * M_xz
cflux_M_x_x_cd	Convective flux, M_x, x component	mol/(m^2*s)	M_x * u_M_x_cd
tflux_M_x_x_cd	Total flux, M_x, x component	mol/(m^2*s)	dflux_M_x_x_cd+cflux_M_x_x_cd
grad_M_x_y_cd	Concentration gradient, M_x, y component	mol/m^4	M_xy
dflux_M_x_y_cd	Diffusive flux, M_x, y component	mol/(m^2*s)	-Dyx_M_x_cd * M_xx-Dyy_M_x_cd * M_xy-Dyz_M_x_cd * M_xz
cflux_M_x_y_cd	Convective flux, M_x, y component	mol/(m^2*s)	M_x * v_M_x_cd
tflux_M_x_y_cd	Total flux, M_x, y component	mol/(m^2*s)	dflux_M_x_y_cd+cflux_M_x_y_cd
grad_M_x_z_cd	Concentration gradient, M_x, z component	mol/m^4	M_xz
dflux_M_x_z_cd	Diffusive flux, M_x, z component	mol/(m^2*s)	-Dzx_M_x_cd * M_xx-Dzy_M_x_cd * M_xy-Dzz_M_x_cd * M_xz
cflux_M_x_z_cd	Convective flux, M_x, z component	mol/(m^2*s)	M_x * w_M_x_cd
tflux_M_x_z_cd	Total flux, M_x, z component	mol/(m^2*s)	dflux_M_x_z_cd+cflux_M_x_z_cd
beta_M_x_x_cd	Convective field, M_x, x component	m/s	u_M_x_cd
beta_M_x_y_cd	Convective field, M_x, y component	m/s	v_M_x_cd

beta_M_x_z_cd	Convective field, M_x, z component	m/s	w_M_x_cd
grad_M_x_cd	Concentration gradient, M_x	mol/m^4	sqrt(grad_M_x_x_cd^2+grad_M_x_y_cd^2+grad_M_x_z_cd^2)
dflux_M_x_cd	Diffusive flux, M_x	mol/(m^2*s)	sqrt(dflux_M_x_x_cd^2+dflux_M_x_y_cd^2+dflux_M_x_z_cd^2)
cflux_M_x_cd	Convective flux, M_x	mol/(m^2*s)	sqrt(cflux_M_x_x_cd^2+cflux_M_x_y_cd^2+cflux_M_x_z_cd^2)
tflux_M_x_cd	Total flux, M_x	mol/(m^2*s)	sqrt(tflux_M_x_x_cd^2+tflux_M_x_y_cd^2+tflux_M_x_z_cd^2)
cellPe_M_x_cd	Cell Peclet number, M_x	1	h * sqrt(beta_M_x_x_cd^2+beta_M_x_y_cd^2+beta_M_x_z_cd^2)/Dm_M_x_cd
Dm_M_x_cd	Mean diffusion coefficient, M_x	m^2/s	(Dxx_M_x_cd * u_M_x_cd^2+Dxy_M_x_cd * u_M_x_cd * v_M_x_cd+Dxz_M_x_cd * u_M_x_cd * w_M_x_cd+Dyx_M_x_cd * v_M_x_cd * u_M_x_cd+Dyy_M_x_cd * v_M_x_cd^2+Dyz_M_x_cd * v_M_x_cd * w_M_x_cd+Dzx_M_x_cd * w_M_x_cd * u_M_x_cd+Dzy_M_x_cd * w_M_x_cd * v_M_x_cd+Dzz_M_x_cd * w_M_x_cd^2)/(u_M_x_cd^2+v_M_x_cd^2+w_M_x_cd^2+eps)
res_M_x_cd	Equation residual for M_x	mol/(m^3*s)	-Dxx_M_x_cd * M_xxx-Dxy_M_x_cd * M_xxy-Dxz_M_x_cd * M_xxz+M_xx * u_M_x_cd-Dyx_M_x_cd * M_xyx-Dyy_M_x_cd * M_xyy-Dyz_M_x_cd * M_xyz+M_xy * v_M_x_cd-Dzx_M_x_cd * M_xzx-Dzy_M_x_cd * M_xzy-Dzz_M_x_cd * M_xzz+M_xz * w_M_x_cd-R_M_x_cd
res_sc_M_x_cd	Shock capturing residual for M_x	mol/(m^3*s)	M_xx * u_M_x_cd+M_xy * v_M_x_cd+M_xz * w_M_x_cd-R_M_x_cd
da_M_x_cd	Total time scale factor, M_x	1	Dts_M_x_cd
grad_M_y_x_cd2	Concentration gradient, M_y, x component	mol/m^4	M_yx
dflux_M_y_x_cd2	Diffusive flux, M_y, x component	mol/(m^2*s)	-Dxx_M_y_cd2 * M_yx-Dxy_M_y_cd2 * M_yy-Dxz_M_y_cd2 * M_yz
cflux_M_y_x_cd2	Convective flux, M_y, x component	mol/(m^2*s)	M_y * u_M_y_cd2
tflux_M_y_x_cd2	Total flux, M_y, x component	mol/(m^2*s)	dflux_M_y_x_cd2+cflux_M_y_x_cd2
grad_M_y_y_cd2	Concentration gradient, M_y, y component	mol/m^4	M_yy
dflux_M_y_y_cd2	Diffusive flux, M_y, y component	mol/(m^2*s)	-Dyx_M_y_cd2 * M_yx-Dyy_M_y_cd2 * M_yy-Dyz_M_y_cd2 * M_yz
cflux_M_y_y_cd2	Convective flux, M_y, y component	mol/(m^2*s)	M_y * v_M_y_cd2
tflux_M_y_y_cd2	Total flux, M_y, y component	mol/(m^2*s)	dflux_M_y_y_cd2+cflux_M_y_y_cd2
grad_M_y_z_cd2	Concentration gradient, M_y, z component	mol/m^4	M_yz
dflux_M_y_z_cd2	Diffusive flux, M_y, z	mol/(m^2*s)	-Dzx_M_y_cd2 * M_yx-Dzy_M_y_cd2 * M_yy-Dzz_M_y_cd2 * M_yz

	component		
cflux_M_y_z_cd2	Convective flux, M_y, z component	mol/(m^2*s)	M_y * w_M_y_cd2
tflux_M_y_z_cd2	Total flux, M_y, z component	mol/(m^2*s)	dflux_M_y_z_cd2+cflux_M_y_z_cd2
beta_M_y_x_cd2	Convective field, M_y, x component	m/s	u_M_y_cd2
beta_M_y_y_cd2	Convective field, M_y, y component	m/s	v_M_y_cd2
beta_M_y_z_cd2	Convective field, M_y, z component	m/s	w_M_y_cd2
grad_M_y_cd2	Concentration gradient, M_y	mol/m^4	sqrt(grad_M_y_x_cd2^2+grad_M_y_y_cd2^2+grad_M_y_z_cd2^2)
dflux_M_y_cd2	Diffusive flux, M_y	mol/(m^2*s)	sqrt(dflux_M_y_x_cd2^2+dflux_M_y_y_cd2^2+dflux_M_y_z_cd2^2)
cflux_M_y_cd2	Convective flux, M_y	mol/(m^2*s)	sqrt(cflux_M_y_x_cd2^2+cflux_M_y_y_cd2^2+cflux_M_y_z_cd2^2)
tflux_M_y_cd2	Total flux, M_y	mol/(m^2*s)	sqrt(tflux_M_y_x_cd2^2+tflux_M_y_y_cd2^2+tflux_M_y_z_cd2^2)
cellPe_M_y_cd2	Cell Peclet number, M_y	1	h * sqrt(beta_M_y_x_cd2^2+beta_M_y_y_cd2^2+beta_M_y_z_cd2^2)/Dm_M_y_cd2
Dm_M_y_cd2	Mean diffusion coefficient, M_y	m^2/s	(Dxx_M_y_cd2 * u_M_y_cd2^2+Dxy_M_y_cd2 * u_M_y_cd2 * v_M_y_cd2+Dxz_M_y_cd2 * u_M_y_cd2 * w_M_y_cd2+Dyx_M_y_cd2 * v_M_y_cd2 * u_M_y_cd2+Dyy_M_y_cd2 * v_M_y_cd2^2+Dyz_M_y_cd2 * v_M_y_cd2 * w_M_y_cd2+Dzx_M_y_cd2 * w_M_y_cd2 * u_M_y_cd2+Dzy_M_y_cd2 * w_M_y_cd2 * v_M_y_cd2+Dzz_M_y_cd2 * w_M_y_cd2^2)/(u_M_y_cd2^2+v_M_y_cd2^2+w_M_y_cd2^2+eps)
res_M_y_cd2	Equation residual for M_y	mol/(m^3*s)	-Dxx_M_y_cd2 * M_yxx-Dxy_M_y_cd2 * M_yxy-Dxz_M_y_cd2 * M_yxz+M_yx * u_M_y_cd2-Dyx_M_y_cd2 * M_yyx-Dyy_M_y_cd2 * M_yyy-Dyz_M_y_cd2 * M_yyz+M_yy * v_M_y_cd2-Dzx_M_y_cd2 * M_yzx-Dzy_M_y_cd2 * M_yzy-Dzz_M_y_cd2 * M_yzz+M_yz * w_M_y_cd2-R_M_y_cd2
res_sc_M_y_cd2	Shock capturing residual for M_y	mol/(m^3*s)	M_yx * u_M_y_cd2+M_yy * v_M_y_cd2+M_yz * w_M_y_cd2-R_M_y_cd2
da_M_y_cd2	Total time scale factor, M_y	1	Dts_M_y_cd2
grad_M_z_x_cd3	Concentration gradient, M_z, x component	mol/m^4	M_zx
dflux_M_z_x_cd3	Diffusive flux, M_z, x component	mol/(m^2*s)	-Dxx_M_z_cd3 * M_zx-Dxy_M_z_cd3 * M_zy-Dxz_M_z_cd3 * M_zz
cflux_M_z_x_cd3	Convective flux, M_z, x component	mol/(m^2*s)	M_z * u_M_z_cd3
tflux_M_z_x_cd3	Total flux, M_z, x component	mol/(m^2*s)	dflux_M_z_x_cd3+cflux_M_z_x_cd3
grad_M_z_y_cd3	Concentration gradient, M_z, y component	mol/m^4	M_zy
dflux_M_z_y_cd3	Diffusive flux, M_z, y	mol/(m^2*s)	-Dyx_M_z_cd3 * M_zx-Dyy_M_z_cd3 * M_zy-Dyz_M_z_cd3 * M_zz

	component		
cflux_M_z_y_cd3	Convective flux, M_z, y component	mol/(m^2*s)	M_z * v_M_z_cd3
tflux_M_z_y_cd3	Total flux, M_z, y component	mol/(m^2*s)	dflux_M_z_y_cd3+cflux_M_z_y_cd3
grad_M_z_z_cd3	Concentration gradient, M_z, z component	mol/m^4	M_zz
dflux_M_z_z_cd3	Diffusive flux, M_z, z component	mol/(m^2*s)	-Dzx_M_z_cd3 * M_zx-Dzy_M_z_cd3 * M_zy-Dzz_M_z_cd3 * M_zz
cflux_M_z_z_cd3	Convective flux, M_z, z component	mol/(m^2*s)	M_z * w_M_z_cd3
tflux_M_z_z_cd3	Total flux, M_z, z component	mol/(m^2*s)	dflux_M_z_z_cd3+cflux_M_z_z_cd3
beta_M_z_x_cd3	Convective field, M_z, x component	m/s	u_M_z_cd3
beta_M_z_y_cd3	Convective field, M_z, y component	m/s	v_M_z_cd3
beta_M_z_z_cd3	Convective field, M_z, z component	m/s	w_M_z_cd3
grad_M_z_cd3	Concentration gradient, M_z	mol/m^4	sqrt(grad_M_z_x_cd3^2+grad_M_z_y_cd3^2+grad_M_z_z_cd3^2)
dflux_M_z_cd3	Diffusive flux, M_z	mol/(m^2*s)	sqrt(dflux_M_z_x_cd3^2+dflux_M_z_y_cd3^2+dflux_M_z_z_cd3^2)
cflux_M_z_cd3	Convective flux, M_z	mol/(m^2*s)	sqrt(cflux_M_z_x_cd3^2+cflux_M_z_y_cd3^2+cflux_M_z_z_cd3^2)
tflux_M_z_cd3	Total flux, M_z	mol/(m^2*s)	sqrt(tflux_M_z_x_cd3^2+tflux_M_z_y_cd3^2+tflux_M_z_z_cd3^2)
cellPe_M_z_cd3	Cell Peclet number, M_z	1	h * sqrt(beta_M_z_x_cd3^2+beta_M_z_y_cd3^2+beta_M_z_z_cd3^2)/Dm_M_z_cd3
Dm_M_z_cd3	Mean diffusion coefficient, M_z	m^2/s	(Dxx_M_z_cd3 * u_M_z_cd3^2+Dxy_M_z_cd3 * u_M_z_cd3 * v_M_z_cd3+Dxz_M_z_cd3 * u_M_z_cd3 * w_M_z_cd3+Dyx_M_z_cd3 * v_M_z_cd3 * u_M_z_cd3+Dyy_M_z_cd3 * v_M_z_cd3^2+Dyz_M_z_cd3 * v_M_z_cd3 * w_M_z_cd3+Dzx_M_z_cd3 * w_M_z_cd3 * u_M_z_cd3+Dzy_M_z_cd3 * w_M_z_cd3 * v_M_z_cd3+Dzz_M_z_cd3 * w_M_z_cd3^2)/(u_M_z_cd3^2+v_M_z_cd3^2+w_M_z_cd3^2+eps)
res_M_z_cd3	Equation residual for M_z	mol/(m^3*s)	-Dxx_M_z_cd3 * M_zxx-Dxy_M_z_cd3 * M_zxy-Dxz_M_z_cd3 * M_zxz+M_zx * u_M_z_cd3-Dyx_M_z_cd3 * M_zyx-Dyy_M_z_cd3 * M_zyy-Dyz_M_z_cd3 * M_zyz+M_zy * v_M_z_cd3-Dzx_M_z_cd3 * M_zzx-Dzy_M_z_cd3 * M_zzy-Dzz_M_z_cd3 * M_zzz+M_zz * w_M_z_cd3-R_M_z_cd3
res_sc_M_z_cd3	Shock capturing residual for M_z	mol/(m^3*s)	M_zx * u_M_z_cd3+M_zy * v_M_z_cd3+M_zz * w_M_z_cd3-R_M_z_cd3
da_M_z_cd3	Total time scale factor, M_z	1	Dts_M_z_cd3
absavgvx_g2	|grad(avgv)|		sqrt(avgvx^2+avgvy^2+avgvz^2)
absga9x_g2	|ga9x|		sqrt(ga9x^2+ga9y^2+ga9z^2)
abspsix_g	|grad(psi)|		sqrt(psix^2+psiy^2+psiz^2)
absga10x_g	|ga10x|		sqrt(ga10x^2+ga10y^2+ga10z^2)

F2. MSGW11 Filled Sphere with 100G Rotating Field with ($\eta'=0$) (Section 6.2.8)

Ferrofluid in 3D Cylinder with rotating H field

1. Table of Contents

2. Model Properties

Property	Value
Model name	Ferrofluid in 3D Cylinder with rotating H field
Author	Shahriar
Company	MIT
Department	EECS
Reference	
URL	
Saved date	May 12, 2010 9:40:54 PM
Creation date	Oct 6, 2008 11:21:14 PM
COMSOL version	COMSOL 3.5.0.608

File name: F:\Research Files\Software Data Files\Comsol Files\Good3DSpherefiles \3Dcase_sphere_MSGW11_scalarpotentialmethod_etaprime0_fluxball_100G.mph

Application modes and modules used in this model:

- Geom1 (3D)
  - Incompressible Navier-Stokes
  - Diffusion
  - Convection and Diffusion
  - Convection and Diffusion
  - Convection and Diffusion
  - PDE, General Form
  - PDE, General Form

2.1. Model description

Model is with a rotating magnetic field in a cylinder with ferrofluid with no boundary condition since etaprime=0 there is no flow as a result

Parameters picked are similar to those from Chaves's papers normalized. Look at Calculation_normalized_velocity_alexchaves.xls

3. Constants

Name	Expression	Value	Description
Xi	0.56	0.56	
omega	2*pi*f	596.902604	
f	95	95	
zeta	0.0003125	3.125e-4	
eta	7.58e-3	0.00758	
etaprime	0	0	
H0	1	1	
Tau	1.39e-5	1.39e-5	
omegatau	omega*Tau	0.008297	
R0	0.05	0.05	

4. Global Expressions

Name	Expression	Unit	Description
FMx	M_x*(d(Hx,x))+M_y*(d(Hx,y))+M_z*(d(Hx,z))		
FMy	M_x*(d(Hy,x))+M_y*(d(Hy,y))+M_z*(d(Hy,z))		
FMz	M_x*(d(Hz,x))+M_y*(d(Hz,y))+M_z*(d(Hz,z))		
T	M_x*Hy-M_y*Hx		
M_eqx	Xi*Hx		
M_eqy	Xi*Hy		
M_eqz	Xi*Hz		
Hx	-psix-M_x/3		
Hy	-psiy-M_y/3		
Hz	-psiz-M_z/3		
potential	H0*(x*cos(t)+y*sin(t))		

5. Geometry

Number of geometries: 1

5.1. Geom1

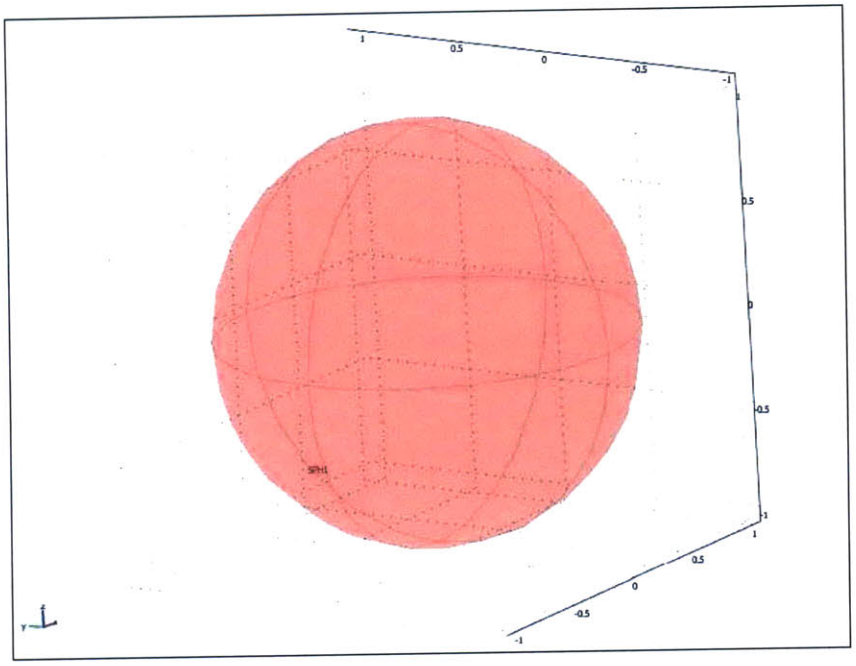

5.1.1. Point mode

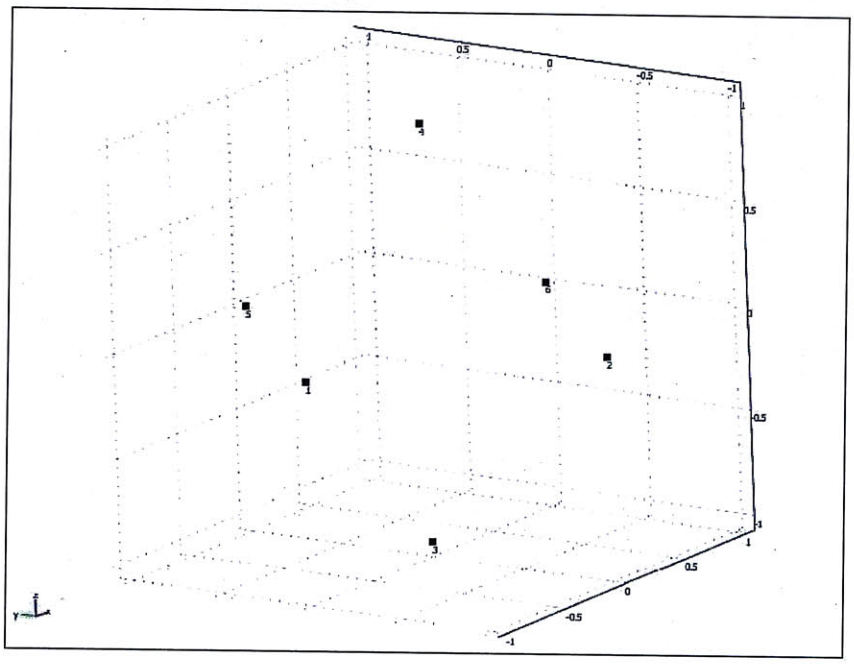

5.1.2. Edge mode

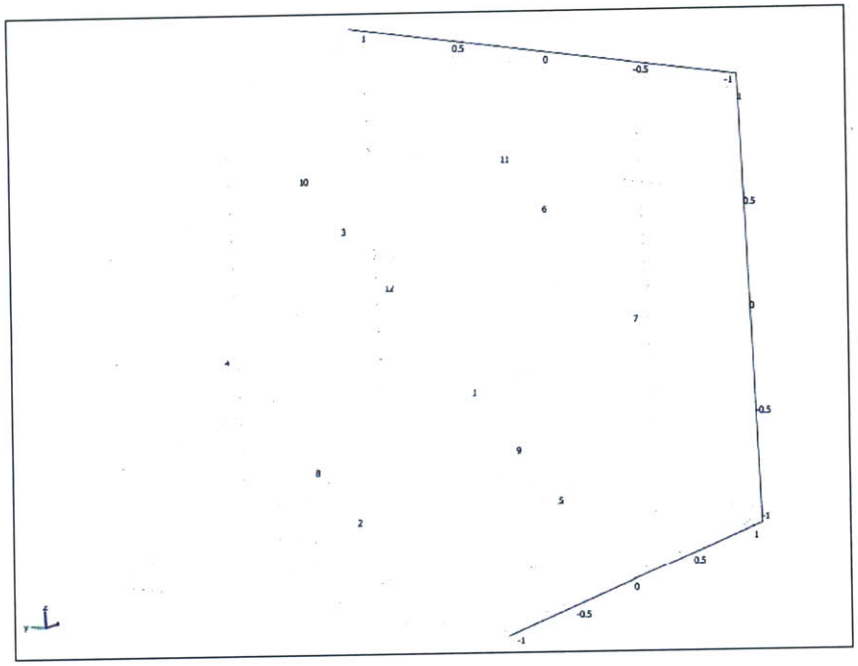

5.1.3. Boundary mode

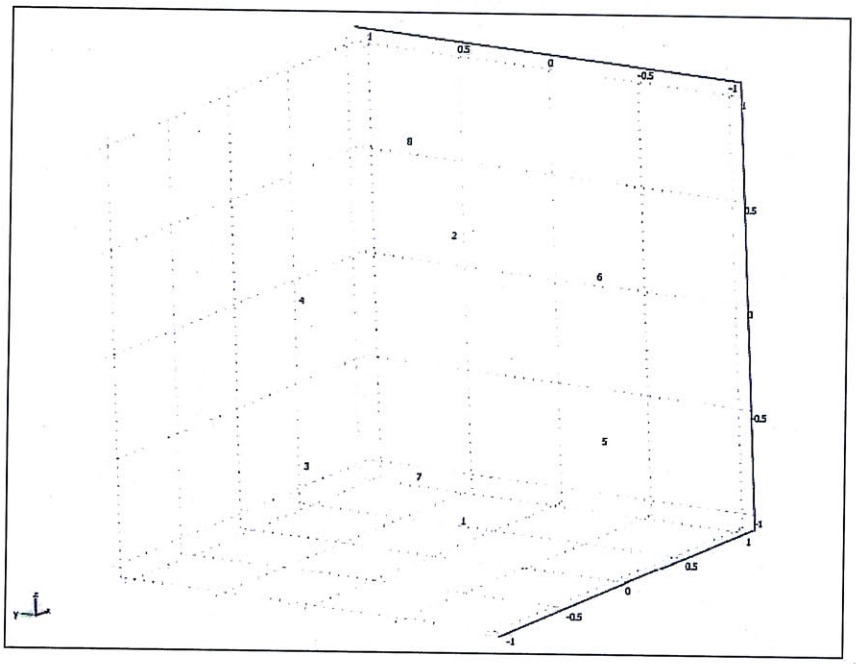

5.1.4. Subdomain mode

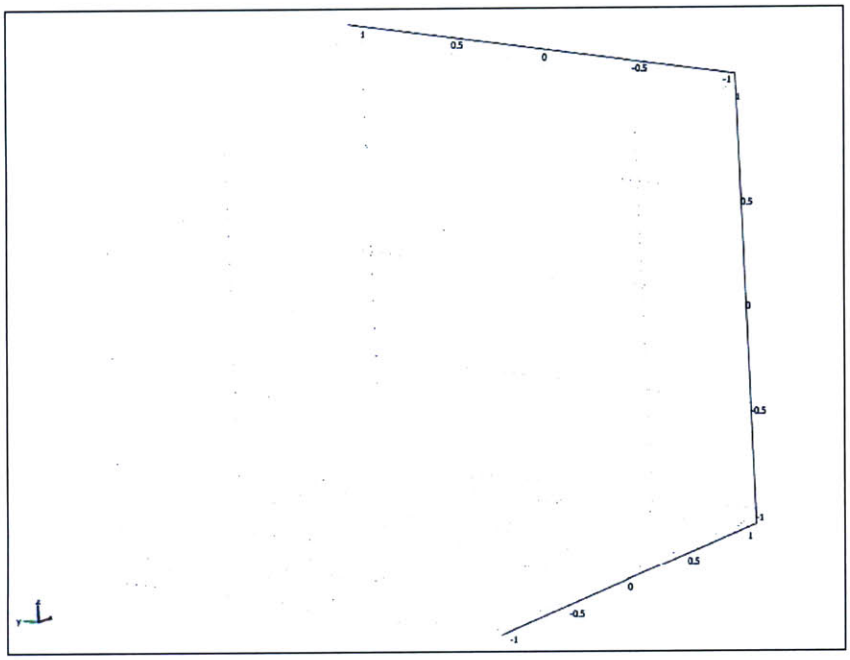

6. Geom1

Space dimensions: 3D

Independent variables: x, y, z

6.1. Scalar Expressions

Name	Expression	Unit	Description
r	sqrt(x^2+y^2+z^2)	m	
phi	atan2(y,x)	rad	
theta	atan2(x,z)	rad	

6.2. Mesh

6.2.1. Mesh Statistics

Number of degrees of freedom	123448
Number of mesh points	1867
Number of elements	9156
Tetrahedral	9156
Prism	0
Hexahedral	0
Number of boundary elements	1240
Triangular	1240
Quadrilateral	0
Number of edge elements	96
Number of vertex elements	6
Minimum element quality	0.36
Element volume ratio	0.079

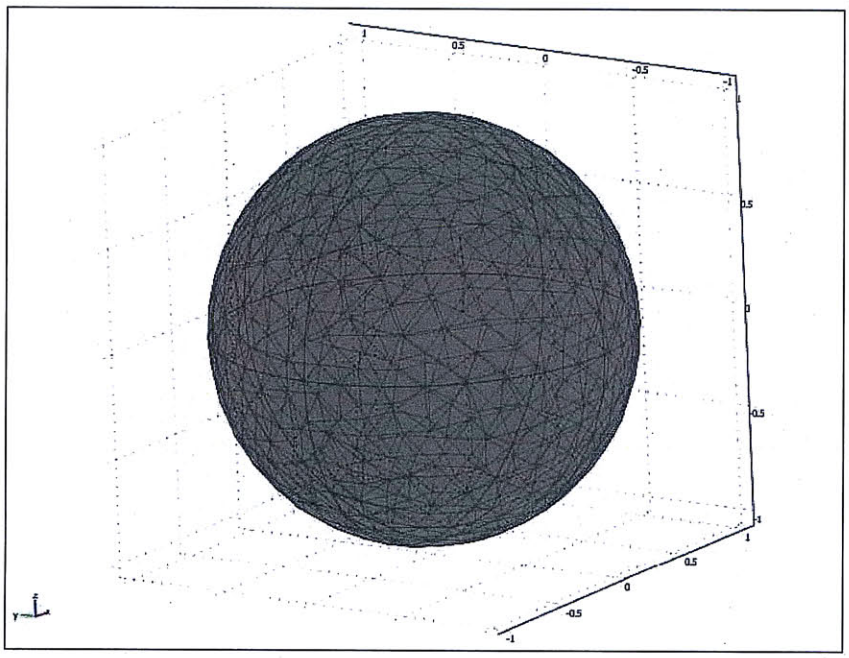

6.3. Application Mode: Incompressible Navier-Stokes (ns)

Application mode type: Incompressible Navier-Stokes

Application mode name: ns

6.3.1. Scalar Variables

Name	Variable	Value	Unit	Description
visc_vel_fact	visc_vel_fact_ns	10	1	Viscous velocity factor

6.3.2. Application Mode Properties

Property	Value
Default element type	Lagrange - P_2 P_1
Analysis type	Stationary
Corner smoothing	Off
Frame	Frame (ref)
Weak constraints	Off
Constraint type	Ideal

6.3.3. Variables

Dependent variables: u, v, w, p, nxw, nyw, nzw

Shape functions: shlag(2,'u'), shlag(2,'v'), shlag(2,'w'), shlag(1,'p')

Interior boundaries not active

6.3.4. Point Settings

Point	1-4, 6	5
pnton	0	1

6.3.5. Boundary Settings

Boundary	1-8
Type	Wall

6.3.6. Subdomain Settings

Subdomain		1
Integration order (gporder)		4 4 4 2
Constraint order (cporder)		2 2 2 1
Density (rho)	kg/m^3	0
Dynamic viscosity (eta)	Pa·s	eta+zeta
Volume force, x dir. (F_x)	N/m^3	2*zeta*sy+FMx
Volume force, y dir. (F_y)	N/m^3	-2*zeta*sx+FMy
Volume force, z dir. (F_z)	N/m^3	FMz
cdon		0

6.4. Application Mode: Diffusion (di)

Application mode type: Diffusion

Application mode name: di

6.4.1. Application Mode Properties

Property	Value
Default element type	Lagrange - Quadratic
Analysis type	Stationary
Frame	Frame (ref)
Weak constraints	Off
Constraint type	Ideal

6.4.2. Variables

Dependent variables: s

Shape functions: shlag(2,'s')

Interior boundaries not active

6.4.3. Boundary Settings

Boundary	1-8
Type	Insulation/Symmetry

6.4.4. Subdomain Settings

Subdomain		1
Diffusion coefficient (D)	m^2/s	etaprime
Reaction rate (R)	$mol/(m^3 \cdot s)$	T+2*zeta*(vx-uy-2*s)

6.5. Application Mode: Convection and Diffusion (cd)

Application mode type: Convection and Diffusion

Application mode name: cd

6.5.1. Application Mode Properties

Property	Value
Default element type	Lagrange - Quadratic
Analysis type	Transient
Equation form	Non-conservative
Frame	Frame (ref)
Weak constraints	Off
Constraint type	Ideal

6.5.2. Variables

Dependent variables: M_x

Shape functions: shlag(2,'M_x')

Interior boundaries not active

6.5.3. Boundary Settings

Boundary	1-8
Type	Insulation/Symmetry

6.5.4. Subdomain Settings

Subdomain		1
Diffusion coefficient (D)	m^2/s	**0**
Reaction rate (R)	$mol/(m^3 \cdot s)$	**-s*M_y-((M_x-M_eqx)/(omegatau))**
x-velocity (u)	m/s	**u**
y-velocity (v)	m/s	**v**
z-velocity (w)	m/s	**w**

6.6. Application Mode: Convection and Diffusion (cd2)

Application mode type: Convection and Diffusion

Application mode name: cd2

6.6.1. Application Mode Properties

Property	Value
Default element type	Lagrange - Quadratic
Analysis type	Transient
Equation form	Non-conservative
Frame	Frame (ref)
Weak constraints	Off
Constraint type	Ideal

6.6.2. Variables

Dependent variables: M_y

Shape functions: shlag(2,'M_y')

Interior boundaries not active

6.6.3. Boundary Settings

Boundary	1-8
Type	Insulation/Symmetry

6.6.4. Subdomain Settings

Subdomain		1
Diffusion coefficient (D)	m^2/s	0
Reaction rate (R)	$mol/(m^3 \cdot s)$	s*M_x-((M_y-M_eqy)/omegatau)
x-velocity (u)	m/s	u
y-velocity (v)	m/s	v
z-velocity (w)	m/s	w

6.7. Application Mode: Convection and Diffusion (cd3)

Application mode type: Convection and Diffusion

Application mode name: cd3

6.7.1. Application Mode Properties

Property	Value
Default element type	Lagrange - Quadratic
Analysis type	Transient
Equation form	Non-conservative
Frame	Frame (ref)
Weak constraints	Off
Constraint type	Ideal

6.7.2. Variables

Dependent variables: M_z

Shape functions: shlag(2,'M_z')

Interior boundaries not active

6.7.3. Boundary Settings

Boundary	1-8
Type	Insulation/Symmetry

6.7.4. Subdomain Settings

Subdomain		1
Diffusion coefficient (D)	m^2/s	0
Reaction rate (R)	$mol/(m^3 \cdot s)$	-((M_z-M_eqz)/omegatau)
x-velocity (u)	m/s	u
y-velocity (v)	m/s	v
z-velocity (w)	m/s	w

6.8. Application Mode: PDE, General Form (g2)

Application mode type: PDE, General Form

Application mode name: g2

6.8.1. Application Mode Properties

Property	Value
Default element type	Lagrange - Quadratic
Wave extension	Off
Frame	Frame (ref)
Weak constraints	Off

6.8.2. Variables

Dependent variables: avgv, avgv_t

Shape functions: shlag(2,'avgv')

Interior boundaries not active

6.8.3. Boundary Settings

Boundary	1-8
Type	Dirichlet boundary condition

6.8.4. Subdomain Settings

Subdomain	1
Source term (f)	v
Conservative flux source term (ga)	{{0;0;0}}

6.9. Application Mode: PDE, General Form (g)

Application mode type: PDE, General Form

Application mode name: g

6.9.1. Application Mode Properties

Property	Value
Default element type	Lagrange - Quadratic
Wave extension	Off
Frame	Frame (ref)
Weak constraints	Off

6.9.2. Variables

Dependent variables: psi, psi_t

Shape functions: shlag(2,'psi')

Interior boundaries not active

6.9.3. Boundary Settings

Boundary	1-8
Type	Dirichlet boundary condition
(r)	-psi+potential

6.9.4. Subdomain Settings

Subdomain	1
Damping/Mass coefficient (da)	0
Source term (f)	-d(M_x,x)-d(M_y,y)-d(M_z,z)

7. Solver Settings

Solve using a script: off

Analysis type	Stationary
Auto select solver	On
Solver	Time dependent
Solution form	Automatic
Symmetric	auto
Adaptive mesh refinement	Off
Optimization/Sensitivity	Off
Plot while solving	Off

7.1. Direct (PARDISO)

Solver type: Linear system solver

Parameter	Value
Preordering algorithm	Nested dissection
Row preordering	On
Bunch-Kaufmann	Off
Pivoting perturbation	1.0E-8
Relative tolerance	1.0E-6
Factor in error estimate	400.0
Check tolerances	Off

7.2. Time Stepping

Parameter	Value
Times	range(0,0.1,2)
Relative tolerance	0.001
Absolute tolerance	0.00010
Times to store in output	Specified times
Time steps taken by solver	Free
Maximum BDF order	5
Singular mass matrix	Maybe
Consistent initialization of DAE systems	Backward Euler
Error estimation strategy	Exclude algebraic
Allow complex numbers	Off

7.3. Advanced

Parameter	Value
Constraint handling method	Elimination
Null-space function	Automatic
Automatic assembly block size	On
Assembly block size	5000
Use Hermitian transpose of constraint matrix and in symmetry detection	Off
Use complex functions with real input	Off
Stop if error due to undefined operation	On
Store solution on file	Off
Type of scaling	Automatic
Manual scaling	
Row equilibration	On
Manual control of reassembly	Off
Load constant	On
Constraint constant	On
Mass constant	On

Damping (mass) constant	On
Jacobian constant	On
Constraint Jacobian constant	On

8. Postprocessing

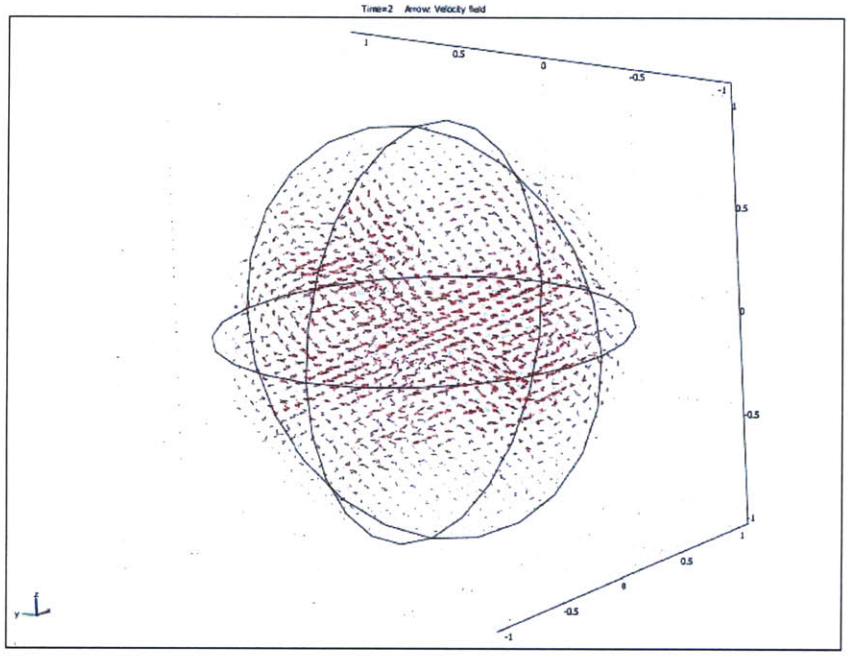

9. Variables

9.1. Boundary

Name	Description	Unit	Expression
K_x_ns	Viscous force per area, x component	Pa	eta_ns * (2 * nx_ns * ux+ny_ns * (uy+vx)+nz_ns * (uz+wx))
T_x_ns	Total force per area, x component	Pa	-nx_ns * p+2 * nx_ns * eta_ns * ux+ny_ns * eta_ns * (uy+vx)+nz_ns * eta_ns * (uz+wx)
K_y_ns	Viscous force per area, y component	Pa	eta_ns * (nx_ns * (vx+uy)+2 * ny_ns * vy+nz_ns * (vz+wy))
T_y_ns	Total force per area, y component	Pa	-ny_ns * p+nx_ns * eta_ns * (vx+uy)+2 * ny_ns * eta_ns * vy+nz_ns * eta_ns * (vz+wy)
K_z_ns	Viscous force per area, z component	Pa	eta_ns * (nx_ns * (wx+uz)+ny_ns * (wy+vz)+2 * nz_ns * wz)
T_z_ns	Total force per area, z component	Pa	-nz_ns * p+nx_ns * eta_ns * (wx+uz)+ny_ns * eta_ns * (wy+vz)+2 * nz_ns * eta_ns * wz
ndflux_s_di	Normal diffusive flux, s	mol/(m^2*s)	nx_di * dflux_s_x_di+ny_di * dflux_s_y_di+nz_di * dflux_s_z_di
ndflux_M_x_cd	Normal diffusive flux, M_x	mol/(m^2*s)	nx_cd * dflux_M_x_x_cd+ny_cd * dflux_M_x_y_cd+nz_cd * dflux_M_x_z_cd
ncflux_M_x_cd	Normal convective flux, M_x	mol/(m^2*s)	nx_cd * cflux_M_x_x_cd+ny_cd * cflux_M_x_y_cd+nz_cd * cflux_M_x_z_cd
ntflux_M_x_cd	Normal total flux, M_x	mol/(m^2*s)	nx_cd * tflux_M_x_x_cd+ny_cd * tflux_M_x_y_cd+nz_cd * tflux_M_x_z_cd

ndflux_M_y_cd2	Normal diffusive flux, M_y	mol/(m^2*s)	nx_cd2 * dflux_M_y_x_cd2+ny_cd2 * dflux_M_y_y_cd2+nz_cd2 * dflux_M_y_z_cd2
ncflux_M_y_cd2	Normal convective flux, M_y	mol/(m^2*s)	nx_cd2 * cflux_M_y_x_cd2+ny_cd2 * cflux_M_y_y_cd2+nz_cd2 * cflux_M_y_z_cd2
ntflux_M_y_cd2	Normal total flux, M_y	mol/(m^2*s)	nx_cd2 * tflux_M_y_x_cd2+ny_cd2 * tflux_M_y_y_cd2+nz_cd2 * tflux_M_y_z_cd2
ndflux_M_z_cd3	Normal diffusive flux, M_z	mol/(m^2*s)	nx_cd3 * dflux_M_z_x_cd3+ny_cd3 * dflux_M_z_y_cd3+nz_cd3 * dflux_M_z_z_cd3
ncflux_M_z_cd3	Normal convective flux, M_z	mol/(m^2*s)	nx_cd3 * cflux_M_z_x_cd3+ny_cd3 * cflux_M_z_y_cd3+nz_cd3 * cflux_M_z_z_cd3
ntflux_M_z_cd3	Normal total flux, M_z	mol/(m^2*s)	nx_cd3 * tflux_M_z_x_cd3+ny_cd3 * tflux_M_z_y_cd3+nz_cd3 * tflux_M_z_z_cd3

9.2. Subdomain

Name	Description	Unit	Expression
U_ns	Velocity field	m/s	sqrt(u^2+v^2+w^2)
Vx_ns	Vorticity, x component	1/s	wy-vz
Vy_ns	Vorticity, y component	1/s	uz-wx
Vz_ns	Vorticity, z component	1/s	vx-uy
V_ns	Vorticity	1/s	sqrt(Vx_ns^2+Vy_ns^2+Vz_ns^2)
divU_ns	Divergence of velocity field	1/s	ux+vy+wz
cellRe_ns	Cell Reynolds number	1	rho_ns * U_ns * h/eta_ns
res_u_ns	Equation residual for u	N/m^3	rho_ns * (u * ux+v * uy+w * uz)+px-F_x_ns+if(gmg_level>0,0,-eta_ns * (2 * uxx+uyy+vxy+uzz+wxz))
res_v_ns	Equation residual for v	N/m^3	rho_ns * (u * vx+v * vy+w * vz)+py-F_y_ns+if(gmg_level>0,0,-eta_ns * (vxx+uyx+2 * vyy+vzz+wyz))
res_w_ns	Equation residual for w	N/m^3	rho_ns * (u * wx+v * wy+w * wz)+pz-F_z_ns+if(gmg_level>0,0,-eta_ns * (wxx+uzx+wyy+vzy+2 * wzz))
beta_x_ns	Convective field, x component	kg/(m^2*s)	rho_ns * u
beta_y_ns	Convective field, y component	kg/(m^2*s)	rho_ns * v
beta_z_ns	Convective field, z component	kg/(m^2*s)	rho_ns * w
Dm_ns	Mean diffusion coefficient	Pa*s	eta_ns
da_ns	Total time scale factor	kg/m^3	rho_ns
taum_ns	GLS time-scale	m^3*s/kg	nojac(1/max(2 * rho_ns * sqrt(emetric(u,v,w)),48 * eta_ns/h^2))
tauc_ns	GLS time-scale	m^2/s	0.5 * nojac(if(u^2+v^2+w^2
res_p_ns	Equation residual for p	kg/(m^3*s)	rho_ns * divU_ns
grad_s_x_di	Concentration gradient, s, x component	mol/m^4	sx
dflux_s_x_di	Diffusive flux, s, x component	mol/(m^2*s)	-Dxx_s_di * sx-Dxy_s_di * sy-Dxz_s_di * sz

grad_s_y_di	Concentration gradient, s, y component	mol/m^4	sy
dflux_s_y_di	Diffusive flux, s, y component	mol/(m^2*s)	-Dyx_s_di * sx-Dyy_s_di * sy-Dyz_s_di * sz
grad_s_z_di	Concentration gradient, s, z component	mol/m^4	sz
dflux_s_z_di	Diffusive flux, s, z component	mol/(m^2*s)	-Dzx_s_di * sx-Dzy_s_di * sy-Dzz_s_di * sz
grad_s_di	Concentration gradient, s	mol/m^4	sqrt(grad_s_x_di^2+grad_s_y_di^2+grad_s_z_di^2)
dflux_s_di	Diffusive flux, s	mol/(m^2*s)	sqrt(dflux_s_x_di^2+dflux_s_y_di^2+dflux_s_z_di^2)
grad_M_x_x_cd	Concentration gradient, M_x, x component	mol/m^4	M_xx
dflux_M_x_x_cd	Diffusive flux, M_x, x component	mol/(m^2*s)	-Dxx_M_x_cd * M_xx-Dxy_M_x_cd * M_xy-Dxz_M_x_cd * M_xz
cflux_M_x_x_cd	Convective flux, M_x, x component	mol/(m^2*s)	M_x * u_M_x_cd
tflux_M_x_x_cd	Total flux, M_x, x component	mol/(m^2*s)	dflux_M_x_x_cd+cflux_M_x_x_cd
grad_M_x_y_cd	Concentration gradient, M_x, y component	mol/m^4	M_xy
dflux_M_x_y_cd	Diffusive flux, M_x, y component	mol/(m^2*s)	-Dyx_M_x_cd * M_xx-Dyy_M_x_cd * M_xy-Dyz_M_x_cd * M_xz
cflux_M_x_y_cd	Convective flux, M_x, y component	mol/(m^2*s)	M_x * v_M_x_cd
tflux_M_x_y_cd	Total flux, M_x, y component	mol/(m^2*s)	dflux_M_x_y_cd+cflux_M_x_y_cd
grad_M_x_z_cd	Concentration gradient, M_x, z component	mol/m^4	M_xz
dflux_M_x_z_cd	Diffusive flux, M_x, z component	mol/(m^2*s)	-Dzx_M_x_cd * M_xx-Dzy_M_x_cd * M_xy-Dzz_M_x_cd * M_xz
cflux_M_x_z_cd	Convective flux, M_x, z component	mol/(m^2*s)	M_x * w_M_x_cd
tflux_M_x_z_cd	Total flux, M_x, z component	mol/(m^2*s)	dflux_M_x_z_cd+cflux_M_x_z_cd
beta_M_x_x_cd	Convective field, M_x, x component	m/s	u_M_x_cd
beta_M_x_y_cd	Convective field, M_x, y component	m/s	v_M_x_cd

beta_M_x_z_cd	Convective field, M_x, z component	m/s	w_M_x_cd
grad_M_x_cd	Concentration gradient, M_x	mol/m^4	sqrt(grad_M_x_x_cd^2+grad_M_x_y_cd^2+grad_M_x_z_cd^2)
dflux_M_x_cd	Diffusive flux, M_x	mol/(m^2*s)	sqrt(dflux_M_x_x_cd^2+dflux_M_x_y_cd^2+dflux_M_x_z_cd^2)
cflux_M_x_cd	Convective flux, M_x	mol/(m^2*s)	sqrt(cflux_M_x_x_cd^2+cflux_M_x_y_cd^2+cflux_M_x_z_cd^2)
tflux_M_x_cd	Total flux, M_x	mol/(m^2*s)	sqrt(tflux_M_x_x_cd^2+tflux_M_x_y_cd^2+tflux_M_x_z_cd^2)
cellPe_M_x_cd	Cell Peclet number, M_x	1	h * sqrt(beta_M_x_x_cd^2+beta_M_x_y_cd^2+beta_M_x_z_cd^2)/Dm_M_x_cd
Dm_M_x_cd	Mean diffusion coefficient, M_x	m^2/s	(Dxx_M_x_cd * u_M_x_cd^2+Dxy_M_x_cd * u_M_x_cd * v_M_x_cd+Dxz_M_x_cd * u_M_x_cd * w_M_x_cd+Dyx_M_x_cd * v_M_x_cd * u_M_x_cd+Dyy_M_x_cd * v_M_x_cd^2+Dyz_M_x_cd * v_M_x_cd * w_M_x_cd+Dzx_M_x_cd * w_M_x_cd * u_M_x_cd+Dzy_M_x_cd * w_M_x_cd * v_M_x_cd+Dzz_M_x_cd * w_M_x_cd^2)/(u_M_x_cd^2+v_M_x_cd^2+w_M_x_cd^2+eps)
res_M_x_cd	Equation residual for M_x	mol/(m^3*s)	-Dxx_M_x_cd * M_xxx-Dxy_M_x_cd * M_xxy-Dxz_M_x_cd * M_xxz+M_xx * u_M_x_cd-Dyx_M_x_cd * M_xyx-Dyy_M_x_cd * M_xyy-Dyz_M_x_cd * M_xyz+M_xy * v_M_x_cd-Dzx_M_x_cd * M_xzx-Dzy_M_x_cd * M_xzy-Dzz_M_x_cd * M_xzz+M_xz * w_M_x_cd-R_M_x_cd
res_sc_M_x_cd	Shock capturing residual for M_x	mol/(m^3*s)	M_xx * u_M_x_cd+M_xy * v_M_x_cd+M_xz * w_M_x_cd-R_M_x_cd
da_M_x_cd	Total time scale factor, M_x	1	Dts_M_x_cd
grad_M_y_x_cd2	Concentration gradient, M_y, x component	mol/m^4	M_yx
dflux_M_y_x_cd2	Diffusive flux, M_y, x component	mol/(m^2*s)	-Dxx_M_y_cd2 * M_yx-Dxy_M_y_cd2 * M_yy-Dxz_M_y_cd2 * M_yz
cflux_M_y_x_cd2	Convective flux, M_y, x component	mol/(m^2*s)	M_y * u_M_y_cd2
tflux_M_y_x_cd2	Total flux, M_y, x component	mol/(m^2*s)	dflux_M_y_x_cd2+cflux_M_y_x_cd2
grad_M_y_y_cd2	Concentration gradient, M_y, y component	mol/m^4	M_yy
dflux_M_y_y_cd2	Diffusive flux, M_y, y component	mol/(m^2*s)	-Dyx_M_y_cd2 * M_yx-Dyy_M_y_cd2 * M_yy-Dyz_M_y_cd2 * M_yz
cflux_M_y_y_cd2	Convective flux, M_y, y component	mol/(m^2*s)	M_y * v_M_y_cd2
tflux_M_y_y_cd2	Total flux, M_y, y component	mol/(m^2*s)	dflux_M_y_y_cd2+cflux_M_y_y_cd2
grad_M_y_z_cd2	Concentration gradient, M_y, z component	mol/m^4	M_yz
dflux_M_y_z_cd2	Diffusive flux, M_y, z	mol/(m^2*s)	-Dzx_M_y_cd2 * M_yx-Dzy_M_y_cd2 * M_yy-Dzz_M_y_cd2 * M_yz

	component		
cflux_M_y_z_cd2	Convective flux, M_y, z component	mol/(m^2*s)	M_y * w_M_y_cd2
tflux_M_y_z_cd2	Total flux, M_y, z component	mol/(m^2*s)	dflux_M_y_z_cd2+cflux_M_y_z_cd2
beta_M_y_x_cd2	Convective field, M_y, x component	m/s	u_M_y_cd2
beta_M_y_y_cd2	Convective field, M_y, y component	m/s	v_M_y_cd2
beta_M_y_z_cd2	Convective field, M_y, z component	m/s	w_M_y_cd2
grad_M_y_cd2	Concentration gradient, M_y	mol/m^4	sqrt(grad_M_y_x_cd2^2+grad_M_y_y_cd2^2+grad_M_y_z_cd2^2)
dflux_M_y_cd2	Diffusive flux, M_y	mol/(m^2*s)	sqrt(dflux_M_y_x_cd2^2+dflux_M_y_y_cd2^2+dflux_M_y_z_cd2^2)
cflux_M_y_cd2	Convective flux, M_y	mol/(m^2*s)	sqrt(cflux_M_y_x_cd2^2+cflux_M_y_y_cd2^2+cflux_M_y_z_cd2^2)
tflux_M_y_cd2	Total flux, M_y	mol/(m^2*s)	sqrt(tflux_M_y_x_cd2^2+tflux_M_y_y_cd2^2+tflux_M_y_z_cd2^2)
cellPe_M_y_cd2	Cell Peclet number, M_y	1	h * sqrt(beta_M_y_x_cd2^2+beta_M_y_y_cd2^2+beta_M_y_z_cd2^2)/Dm_M_y_cd2
Dm_M_y_cd2	Mean diffusion coefficient, M_y	m^2/s	(Dxx_M_y_cd2 * u_M_y_cd2^2+Dxy_M_y_cd2 * u_M_y_cd2 * v_M_y_cd2+Dxz_M_y_cd2 * u_M_y_cd2 * w_M_y_cd2+Dyx_M_y_cd2 * v_M_y_cd2 * u_M_y_cd2+Dyy_M_y_cd2 * v_M_y_cd2^2+Dyz_M_y_cd2 * v_M_y_cd2 * w_M_y_cd2+Dzx_M_y_cd2 * w_M_y_cd2 * u_M_y_cd2+Dzy_M_y_cd2 * w_M_y_cd2 * v_M_y_cd2+Dzz_M_y_cd2 * w_M_y_cd2^2)/(u_M_y_cd2^2+v_M_y_cd2^2+w_M_y_cd2^2+eps)
res_M_y_cd2	Equation residual for M_y	mol/(m^3*s)	-Dxx_M_y_cd2 * M_yxx-Dxy_M_y_cd2 * M_yxy-Dxz_M_y_cd2 * M_yxz+M_yx * u_M_y_cd2-Dyx_M_y_cd2 * M_yyx-Dyy_M_y_cd2 * M_yyy-Dyz_M_y_cd2 * M_yyz+M_yy * v_M_y_cd2-Dzx_M_y_cd2 * M_yzx-Dzy_M_y_cd2 * M_yzy-Dzz_M_y_cd2 * M_yzz+M_yz * w_M_y_cd2-R_M_y_cd2
res_sc_M_y_cd2	Shock capturing residual for M_y	mol/(m^3*s)	M_yx * u_M_y_cd2+M_yy * v_M_y_cd2+M_yz * w_M_y_cd2-R_M_y_cd2
da_M_y_cd2	Total time scale factor, M_y	1	Dts_M_y_cd2
grad_M_z_x_cd3	Concentration gradient, M_z, x component	mol/m^4	M_zx
dflux_M_z_x_cd3	Diffusive flux, M_z, x component	mol/(m^2*s)	-Dxx_M_z_cd3 * M_zx-Dxy_M_z_cd3 * M_zy-Dxz_M_z_cd3 * M_zz
cflux_M_z_x_cd3	Convective flux, M_z, x component	mol/(m^2*s)	M_z * u_M_z_cd3
tflux_M_z_x_cd3	Total flux, M_z, x component	mol/(m^2*s)	dflux_M_z_x_cd3+cflux_M_z_x_cd3
grad_M_z_y_cd3	Concentration gradient, M_z, y component	mol/m^4	M_zy
dflux_M_z_y_cd3	Diffusive flux, M_z, y	mol/(m^2*s)	-Dyx_M_z_cd3 * M_zx-Dyy_M_z_cd3 * M_zy-Dyz_M_z_cd3 * M_zz

	component		
cflux_M_z_y_cd3	Convective flux, M_z, y component	mol/(m^2*s)	M_z * v_M_z_cd3
tflux_M_z_y_cd3	Total flux, M_z, y component	mol/(m^2*s)	dflux_M_z_y_cd3+cflux_M_z_y_cd3
grad_M_z_z_cd3	Concentration gradient, M_z, z component	mol/m^4	M_zz
dflux_M_z_z_cd3	Diffusive flux, M_z, z component	mol/(m^2*s)	-Dzx_M_z_cd3 * M_zx-Dzy_M_z_cd3 * M_zy-Dzz_M_z_cd3 * M_zz
cflux_M_z_z_cd3	Convective flux, M_z, z component	mol/(m^2*s)	M_z * w_M_z_cd3
tflux_M_z_z_cd3	Total flux, M_z, z component	mol/(m^2*s)	dflux_M_z_z_cd3+cflux_M_z_z_cd3
beta_M_z_x_cd3	Convective field, M_z, x component	m/s	u_M_z_cd3
beta_M_z_y_cd3	Convective field, M_z, y component	m/s	v_M_z_cd3
beta_M_z_z_cd3	Convective field, M_z, z component	m/s	w_M_z_cd3
grad_M_z_cd3	Concentration gradient, M_z	mol/m^4	sqrt(grad_M_z_x_cd3^2+grad_M_z_y_cd3^2+grad_M_z_z_cd3^2)
dflux_M_z_cd3	Diffusive flux, M_z	mol/(m^2*s)	sqrt(dflux_M_z_x_cd3^2+dflux_M_z_y_cd3^2+dflux_M_z_z_cd3^2)
cflux_M_z_cd3	Convective flux, M_z	mol/(m^2*s)	sqrt(cflux_M_z_x_cd3^2+cflux_M_z_y_cd3^2+cflux_M_z_z_cd3^2)
tflux_M_z_cd3	Total flux, M_z	mol/(m^2*s)	sqrt(tflux_M_z_x_cd3^2+tflux_M_z_y_cd3^2+tflux_M_z_z_cd3^2)
cellPe_M_z_cd3	Cell Peclet number, M_z	1	h * sqrt(beta_M_z_x_cd3^2+beta_M_z_y_cd3^2+beta_M_z_z_cd3^2)/Dm_M_z_cd3
Dm_M_z_cd3	Mean diffusion coefficient, M_z	m^2/s	(Dxx_M_z_cd3 * u_M_z_cd3^2+Dxy_M_z_cd3 * v_M_z_cd3+Dxz_M_z_cd3 * u_M_z_cd3 * w_M_z_cd3+Dyx_M_z_cd3 * v_M_z_cd3 * u_M_z_cd3+Dyy_M_z_cd3 * v_M_z_cd3^2+Dyz_M_z_cd3 * v_M_z_cd3 * w_M_z_cd3+Dzx_M_z_cd3 * w_M_z_cd3 * u_M_z_cd3+Dzy_M_z_cd3 * w_M_z_cd3 * v_M_z_cd3+Dzz_M_z_cd3 * w_M_z_cd3^2)/(u_M_z_cd3^2+v_M_z_cd3^2+w_M_z_cd3^2+eps)
res_M_z_cd3	Equation residual for M_z	mol/(m^3*s)	-Dxx_M_z_cd3 * M_zxx-Dxy_M_z_cd3 * M_zxy-Dxz_M_z_cd3 * M_zxz+M_zx * u_M_z_cd3-Dyx_M_z_cd3 * M_zyx-Dyy_M_z_cd3 * M_zyy-Dyz_M_z_cd3 * M_zyz+M_zy * v_M_z_cd3-Dzx_M_z_cd3 * M_zzx-Dzy_M_z_cd3 * M_zzy-Dzz_M_z_cd3 * M_zzz+M_zz * w_M_z_cd3-R_M_z_cd3
res_sc_M_z_cd3	Shock capturing residual for M_z	mol/(m^3*s)	M_zx * u_M_z_cd3+M_zy * v_M_z_cd3+M_zz * w_M_z_cd3-R_M_z_cd3
da_M_z_cd3	Total time scale factor, M_z	1	Dts_M_z_cd3
absavgvx_g2	|grad(avgv)|		sqrt(avgvx^2+avgvy^2+avgvz^2)
absga9x_g2	|ga9x|		sqrt(ga9x^2+ga9y^2+ga9z^2)
abspsix_g	|grad(psi)|		sqrt(psix^2+psiy^2+psiz^2)
absga10x_g	|ga10x|		sqrt(ga10x^2+ga10y^2+ga10z^2)

F3. EMG900_2 Model files

These files are identical to those for the MSGW11 cases in this Appendix except with different normalized variables used as described in Table 6-5.

Appendix G : Experimental Results with Non-Uniform Fields Generated Using Third Coil (Section 6.4)

G1. EFH1 Filled Sphere with Third Coil Oscillating at Same Frequency as Rotating Field at 95Hz

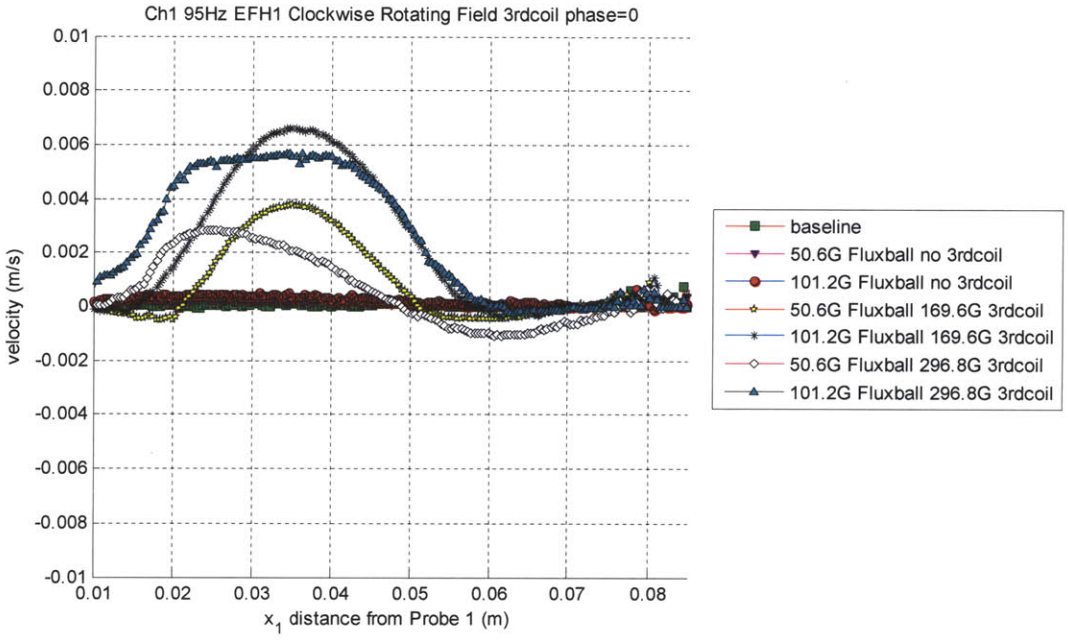

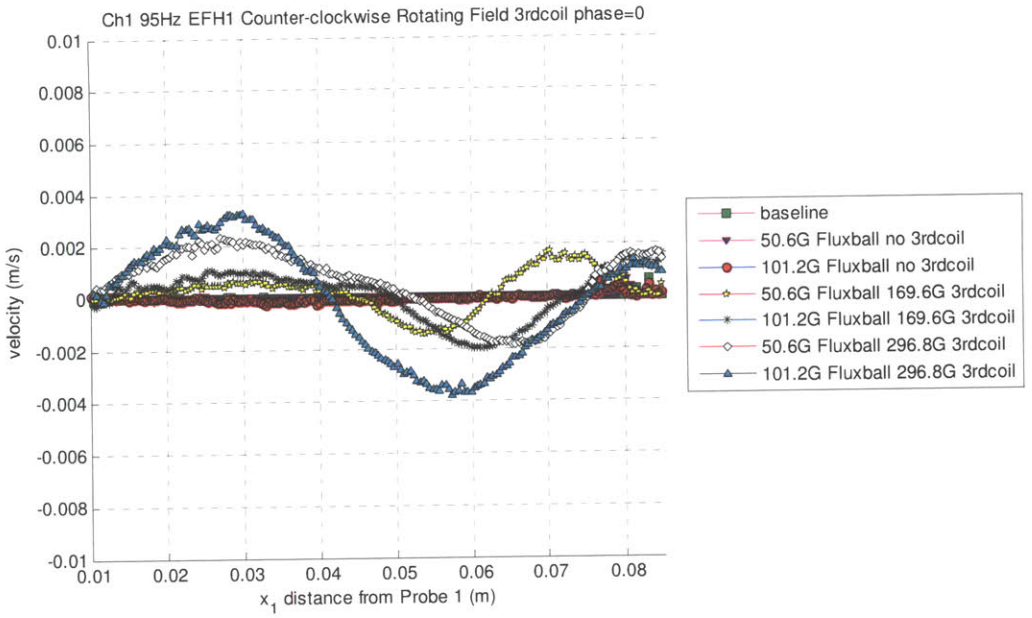
Ch1 95Hz EFH1 Counter-clockwise Rotating Field 3rdcoil phase=0
velocity (m/s)
0.01
0.008
0.006
0.004
0.002
0
-0.002
-0.004
-0.006
-0.008
-0.01
0.01
0.02
0.03
0.04
0.05
0.06
0.07
0.08
x1 distance from Probe 1 (m)
baseline
50.6G Fluxball no 3rdcoil
101.2G Fluxball no 3rdcoil
50.6G Fluxball 169.6G 3rdcoil
101.2G Fluxball 169.6G 3rdcoil
50.6G Fluxball 296.8G 3rdcoil
101.2G Fluxball 296.8G 3rdcoil

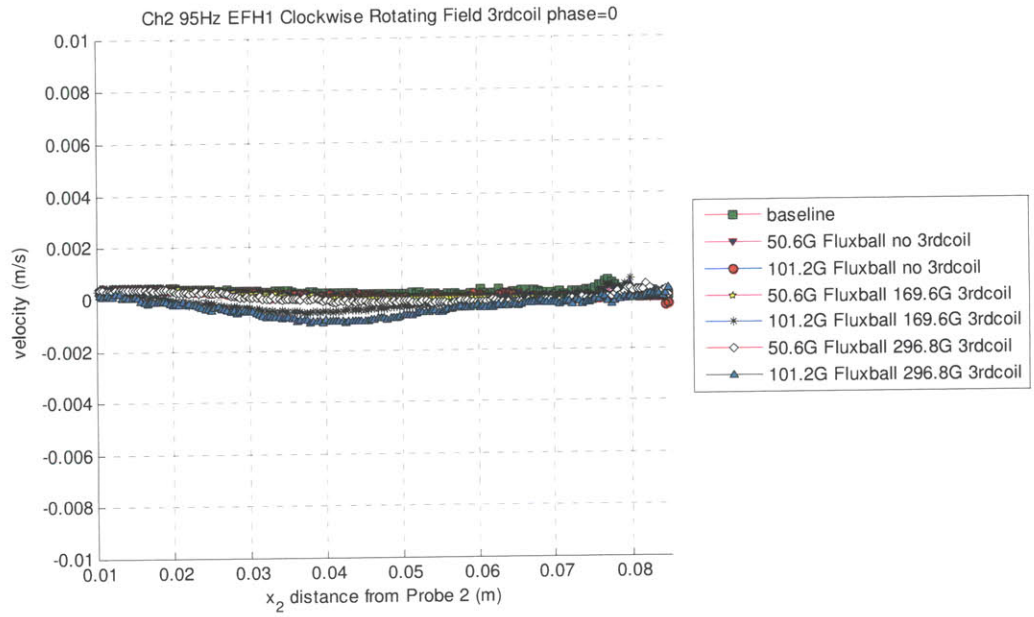
Ch2 95Hz EFH1 Clockwise Rotating Field 3rdcoil phase=0
velocity (m/s)
0.01
0.008
0.006
0.004
0.002
0
-0.002
-0.004
-0.006
-0.008
-0.01
0.01
0.02
0.03
0.04
0.05
0.06
0.07
0.08
x2 distance from Probe 2 (m)
baseline
50.6G Fluxball no 3rdcoil
101.2G Fluxball no 3rdcoil
50.6G Fluxball 169.6G 3rdcoil
101.2G Fluxball 169.6G 3rdcoil
50.6G Fluxball 296.8G 3rdcoil
101.2G Fluxball 296.8G 3rdcoil

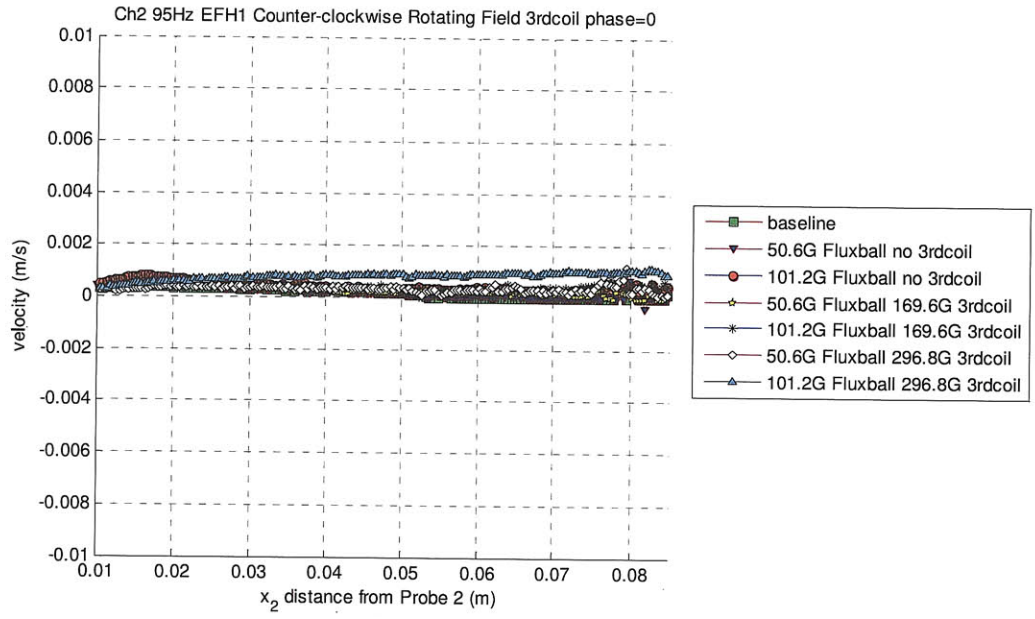
Ch2 95Hz EFH1 Counter-clockwise Rotating Field 3rdcoil phase=0
velocity (m/s)
0.01
0.008
0.006
0.004
0.002
0
-0.002
-0.004
-0.006
-0.008
-0.01
0.01 0.02 0.03 0.04 0.05 0.06 0.07 0.08
x2 distance from Probe 2 (m)
baseline
50.6G Fluxball no 3rdcoil
101.2G Fluxball no 3rdcoil
50.6G Fluxball 169.6G 3rdcoil
101.2G Fluxball 169.6G 3rdcoil
50.6G Fluxball 296.8G 3rdcoil
101.2G Fluxball 296.8G 3rdcoil

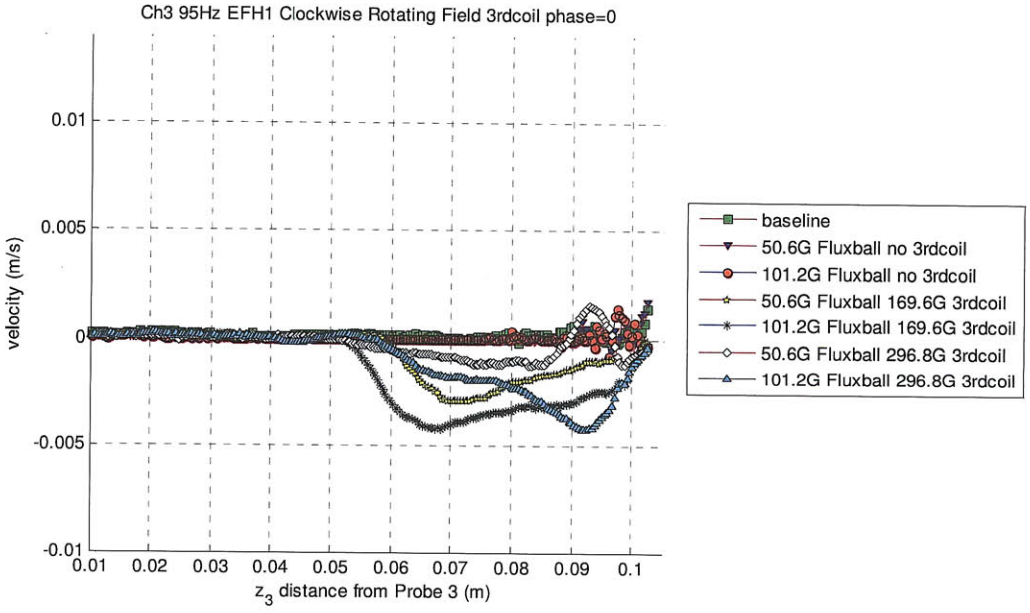
Ch3 95Hz EFH1 Clockwise Rotating Field 3rdcoil phase=0
velocity (m/s)
0.01
0.005
0
-0.005
-0.01
0.01 0.02 0.03 0.04 0.05 0.06 0.07 0.08 0.09 0.1
z3 distance from Probe 3 (m)
baseline
50.6G Fluxball no 3rdcoil
101.2G Fluxball no 3rdcoil
50.6G Fluxball 169.6G 3rdcoil
101.2G Fluxball 169.6G 3rdcoil
50.6G Fluxball 296.8G 3rdcoil
101.2G Fluxball 296.8G 3rdcoil

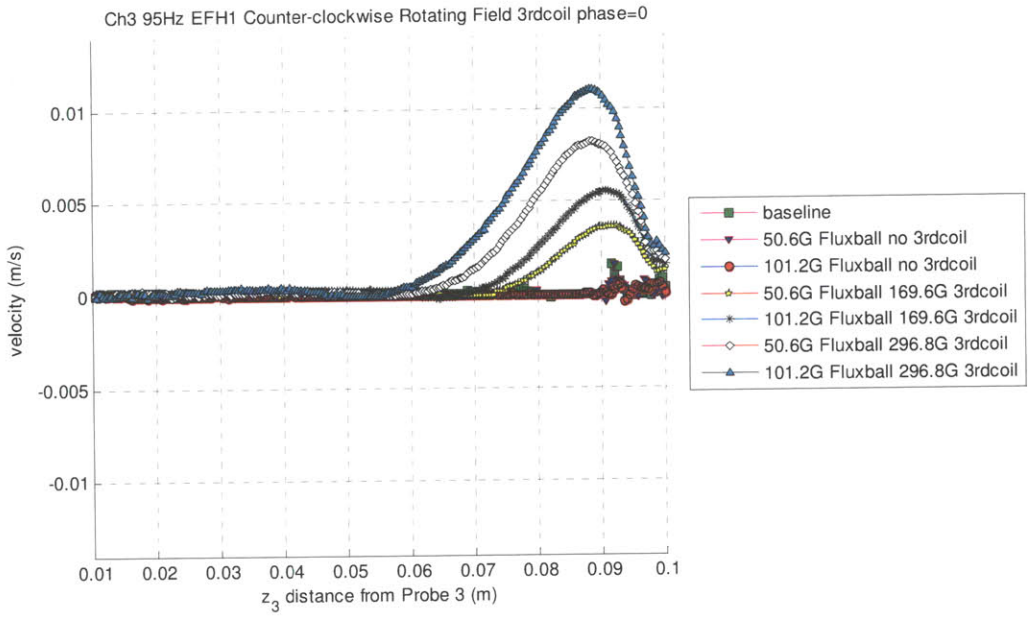
Ch3 95Hz EFH1 Counter-clockwise Rotating Field 3rdcoil phase=0
velocity (m/s)
0.01
0.005
0
-0.005
-0.01
0.01 0.02 0.03 0.04 0.05 0.06 0.07 0.08 0.09 0.1
z3 distance from Probe 3 (m)
baseline
50.6G Fluxball no 3rdcoil
101.2G Fluxball no 3rdcoil
50.6G Fluxball 169.6G 3rdcoil
101.2G Fluxball 169.6G 3rdcoil
50.6G Fluxball 296.8G 3rdcoil
101.2G Fluxball 296.8G 3rdcoil

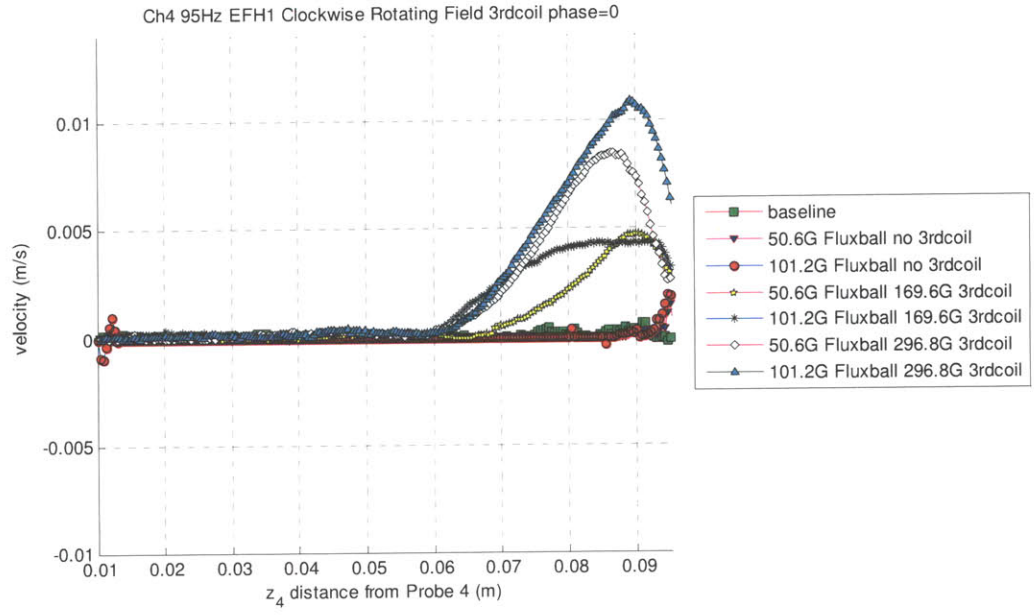
Ch4 95Hz EFH1 Clockwise Rotating Field 3rdcoil phase=0
velocity (m/s)
0.01
0.005
0
-0.005
-0.01
0.01 0.02 0.03 0.04 0.05 0.06 0.07 0.08 0.09
z4 distance from Probe 4 (m)
baseline
50.6G Fluxball no 3rdcoil
101.2G Fluxball no 3rdcoil
50.6G Fluxball 169.6G 3rdcoil
101.2G Fluxball 169.6G 3rdcoil
50.6G Fluxball 296.8G 3rdcoil
101.2G Fluxball 296.8G 3rdcoil

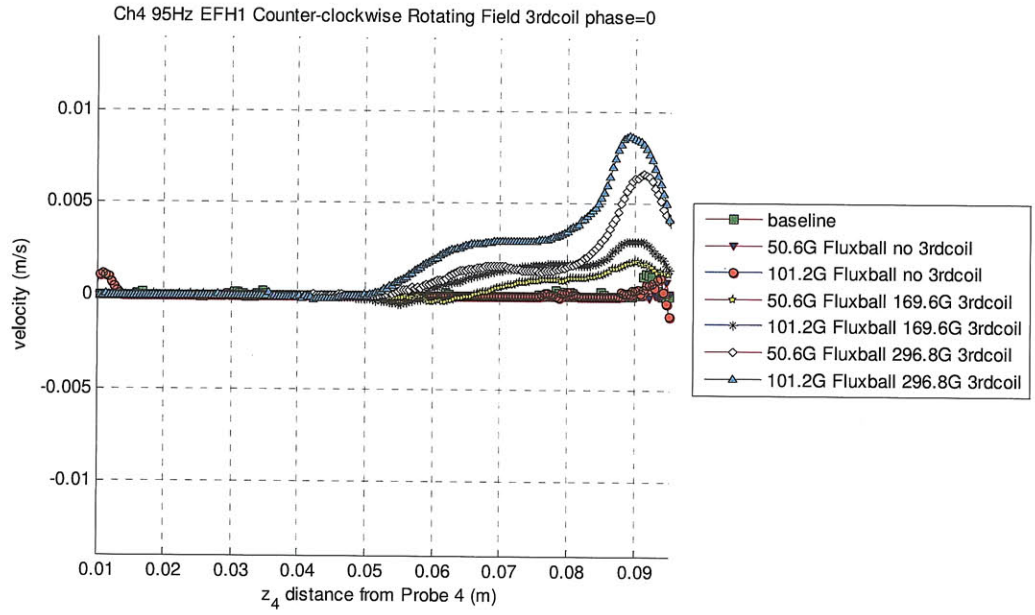
Ch4 95Hz EFH1 Counter-clockwise Rotating Field 3rdcoil phase=0
velocity (m/s)
0.01
0.005
0
-0.005
-0.01
0.01 0.02 0.03 0.04 0.05 0.06 0.07 0.08 0.09
z4 distance from Probe 4 (m)
baseline
50.6G Fluxball no 3rdcoil
101.2G Fluxball no 3rdcoil
50.6G Fluxball 169.6G 3rdcoil
101.2G Fluxball 169.6G 3rdcoil
50.6G Fluxball 296.8G 3rdcoil
101.2G Fluxball 296.8G 3rdcoil

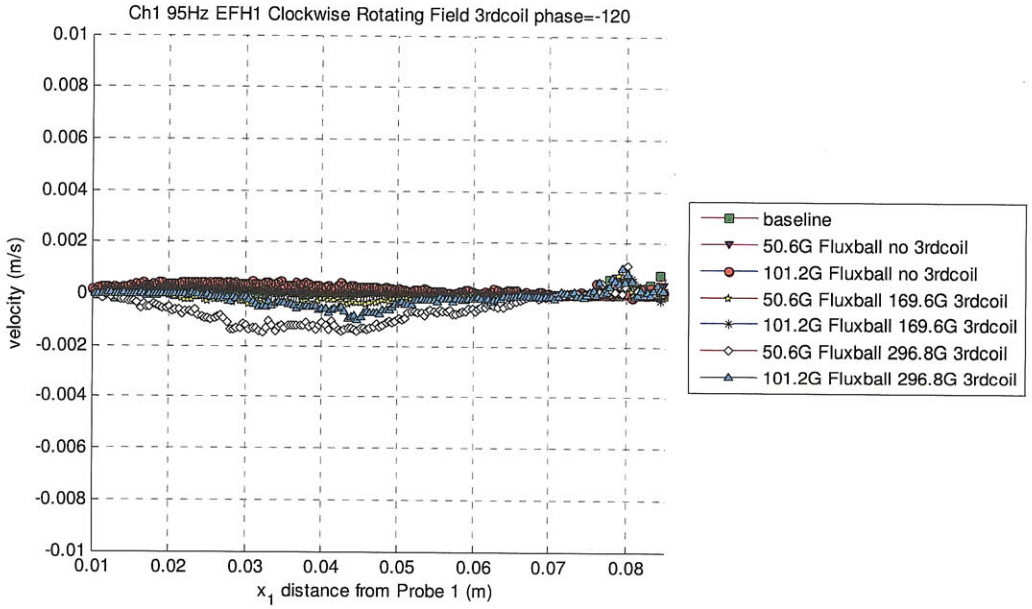
Ch1 95Hz EFH1 Clockwise Rotating Field 3rdcoil phase=-120
velocity (m/s)
0.01
0.008
0.006
0.004
0.002
0
-0.002
-0.004
-0.006
-0.008
-0.01
0.01 0.02 0.03 0.04 0.05 0.06 0.07 0.08
x1 distance from Probe 1 (m)
baseline
50.6G Fluxball no 3rdcoil
101.2G Fluxball no 3rdcoil
50.6G Fluxball 169.6G 3rdcoil
101.2G Fluxball 169.6G 3rdcoil
50.6G Fluxball 296.8G 3rdcoil
101.2G Fluxball 296.8G 3rdcoil

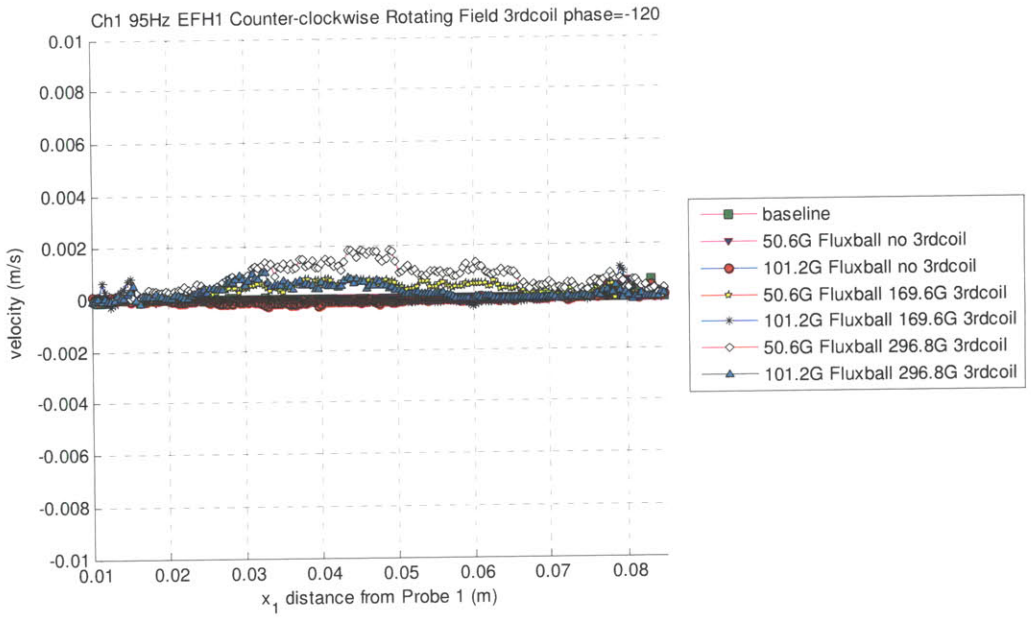
Ch1 95Hz EFH1 Counter-clockwise Rotating Field 3rdcoil phase=-120
velocity (m/s)
0.01
0.008
0.006
0.004
0.002
0
-0.002
-0.004
-0.006
-0.008
-0.01
0.01
0.02
0.03
0.04
0.05
0.06
0.07
0.08
x1 distance from Probe 1 (m)
baseline
50.6G Fluxball no 3rdcoil
101.2G Fluxball no 3rdcoil
50.6G Fluxball 169.6G 3rdcoil
101.2G Fluxball 169.6G 3rdcoil
50.6G Fluxball 296.8G 3rdcoil
101.2G Fluxball 296.8G 3rdcoil

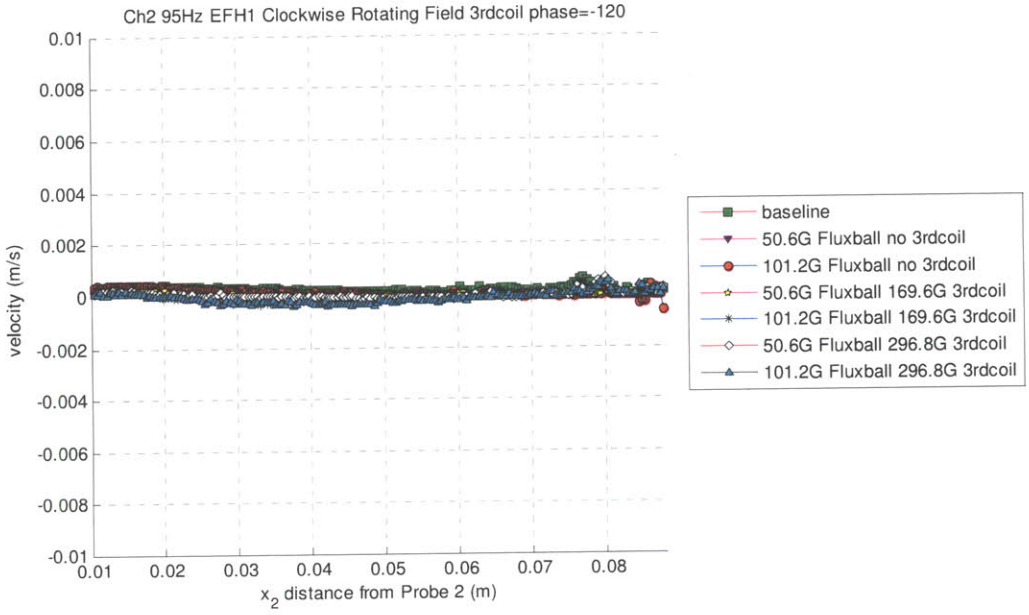
Ch2 95Hz EFH1 Clockwise Rotating Field 3rdcoil phase=-120
velocity (m/s)
0.01
0.008
0.006
0.004
0.002
0
-0.002
-0.004
-0.006
-0.008
-0.01
0.01
0.02
0.03
0.04
0.05
0.06
0.07
0.08
x2 distance from Probe 2 (m)
baseline
50.6G Fluxball no 3rdcoil
101.2G Fluxball no 3rdcoil
50.6G Fluxball 169.6G 3rdcoil
101.2G Fluxball 169.6G 3rdcoil
50.6G Fluxball 296.8G 3rdcoil
101.2G Fluxball 296.8G 3rdcoil

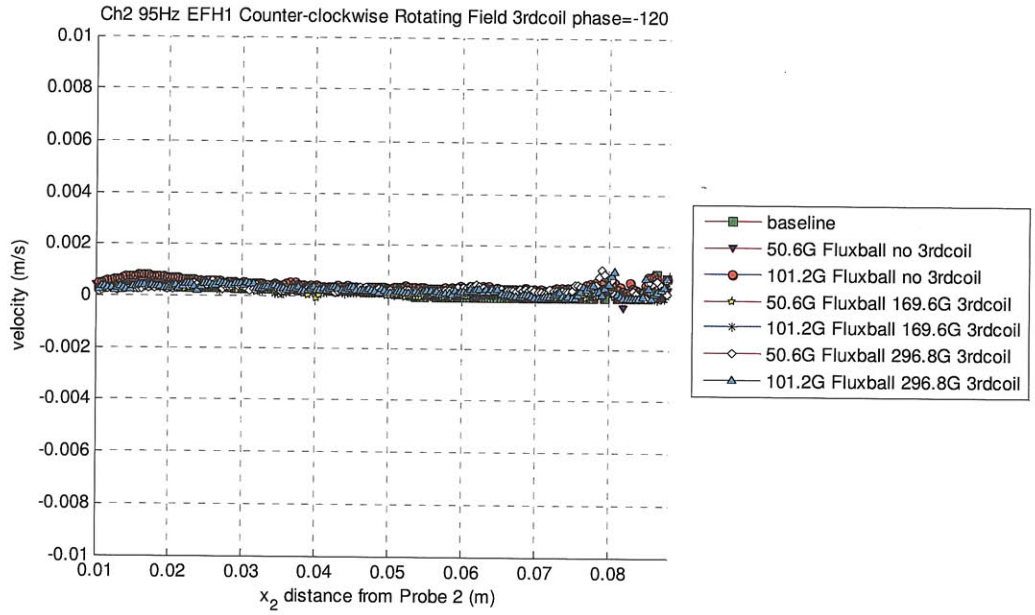
Ch2 95Hz EFH1 Counter-clockwise Rotating Field 3rdcoil phase=-120
velocity (m/s)
0.01
0.008
0.006
0.004
0.002
0
-0.002
-0.004
-0.006
-0.008
-0.01
0.01 0.02 0.03 0.04 0.05 0.06 0.07 0.08
x2 distance from Probe 2 (m)
baseline
50.6G Fluxball no 3rdcoil
101.2G Fluxball no 3rdcoil
50.6G Fluxball 169.6G 3rdcoil
101.2G Fluxball 169.6G 3rdcoil
50.6G Fluxball 296.8G 3rdcoil
101.2G Fluxball 296.8G 3rdcoil

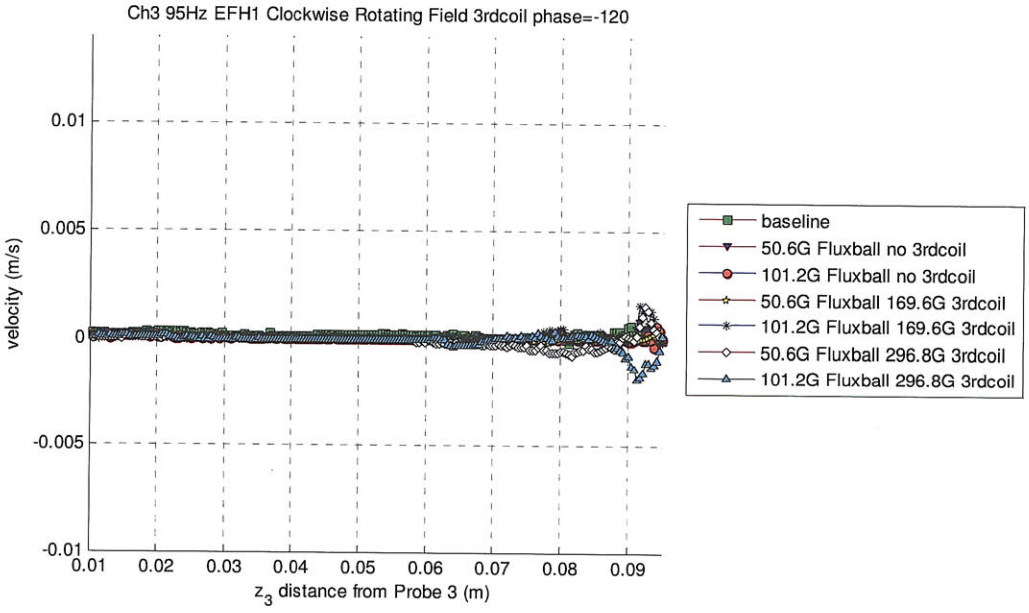
Ch3 95Hz EFH1 Clockwise Rotating Field 3rdcoil phase=-120
velocity (m/s)
0.01
0.005
0
-0.005
-0.01
0.01 0.02 0.03 0.04 0.05 0.06 0.07 0.08 0.09
z3 distance from Probe 3 (m)
baseline
50.6G Fluxball no 3rdcoil
101.2G Fluxball no 3rdcoil
50.6G Fluxball 169.6G 3rdcoil
101.2G Fluxball 169.6G 3rdcoil
50.6G Fluxball 296.8G 3rdcoil
101.2G Fluxball 296.8G 3rdcoil

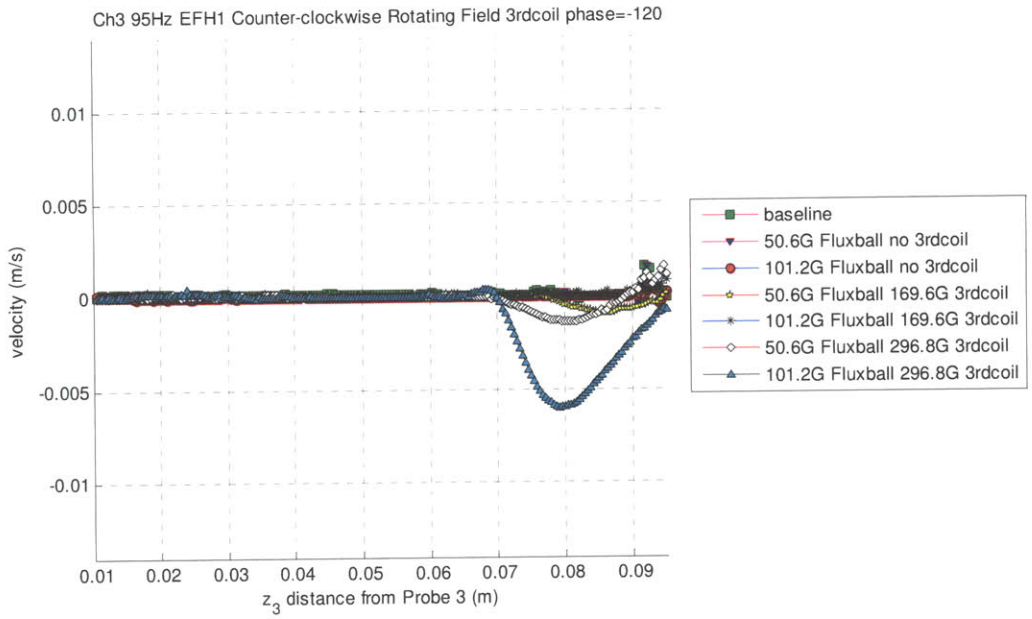
Ch3 95Hz EFH1 Counter-clockwise Rotating Field 3rdcoil phase=-120
velocity (m/s)
0.01
0.005
0
-0.005
-0.01
0.01 0.02 0.03 0.04 0.05 0.06 0.07 0.08 0.09
z3 distance from Probe 3 (m)
baseline
50.6G Fluxball no 3rdcoil
101.2G Fluxball no 3rdcoil
50.6G Fluxball 169.6G 3rdcoil
101.2G Fluxball 169.6G 3rdcoil
50.6G Fluxball 296.8G 3rdcoil
101.2G Fluxball 296.8G 3rdcoil

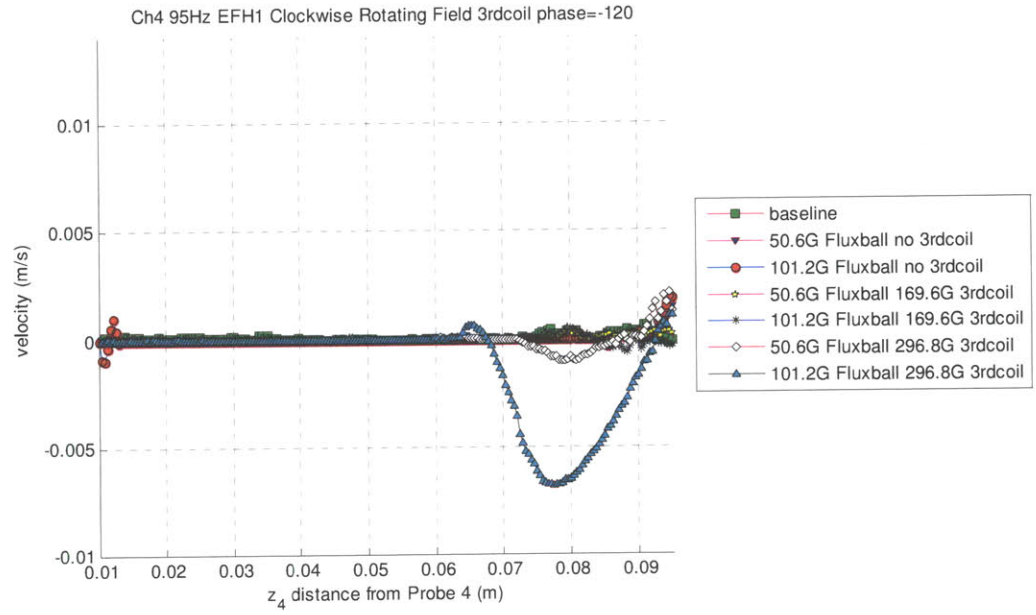
Ch4 95Hz EFH1 Clockwise Rotating Field 3rdcoil phase=-120
velocity (m/s)
0.01
0.005
0
-0.005
-0.01
0.01 0.02 0.03 0.04 0.05 0.06 0.07 0.08 0.09
z4 distance from Probe 4 (m)
baseline
50.6G Fluxball no 3rdcoil
101.2G Fluxball no 3rdcoil
50.6G Fluxball 169.6G 3rdcoil
101.2G Fluxball 169.6G 3rdcoil
50.6G Fluxball 296.8G 3rdcoil
101.2G Fluxball 296.8G 3rdcoil

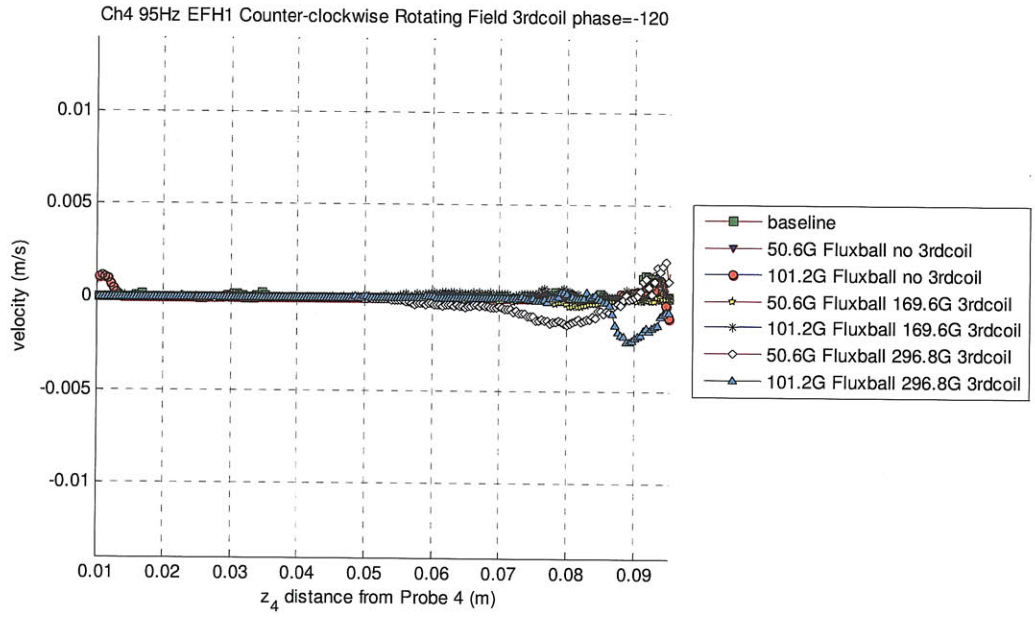
Ch4 95Hz EFH1 Counter-clockwise Rotating Field 3rdcoil phase=-120
velocity (m/s)
0.01
0.005
0
-0.005
-0.01
0.01 0.02 0.03 0.04 0.05 0.06 0.07 0.08 0.09
z4 distance from Probe 4 (m)
baseline
50.6G Fluxball no 3rdcoil
101.2G Fluxball no 3rdcoil
50.6G Fluxball 169.6G 3rdcoil
101.2G Fluxball 169.6G 3rdcoil
50.6G Fluxball 296.8G 3rdcoil
101.2G Fluxball 296.8G 3rdcoil

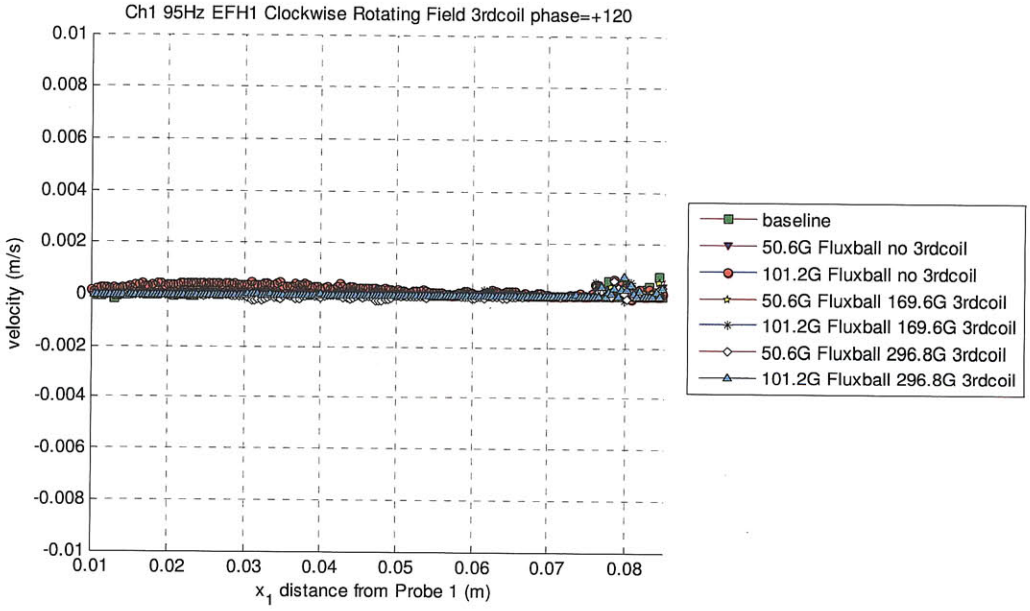
Ch1 95Hz EFH1 Clockwise Rotating Field 3rdcoil phase=+120
velocity (m/s)
0.01
0.008
0.006
0.004
0.002
0
-0.002
-0.004
-0.006
-0.008
-0.01
0.01 0.02 0.03 0.04 0.05 0.06 0.07 0.08
x1 distance from Probe 1 (m)
baseline
50.6G Fluxball no 3rdcoil
101.2G Fluxball no 3rdcoil
50.6G Fluxball 169.6G 3rdcoil
101.2G Fluxball 169.6G 3rdcoil
50.6G Fluxball 296.8G 3rdcoil
101.2G Fluxball 296.8G 3rdcoil

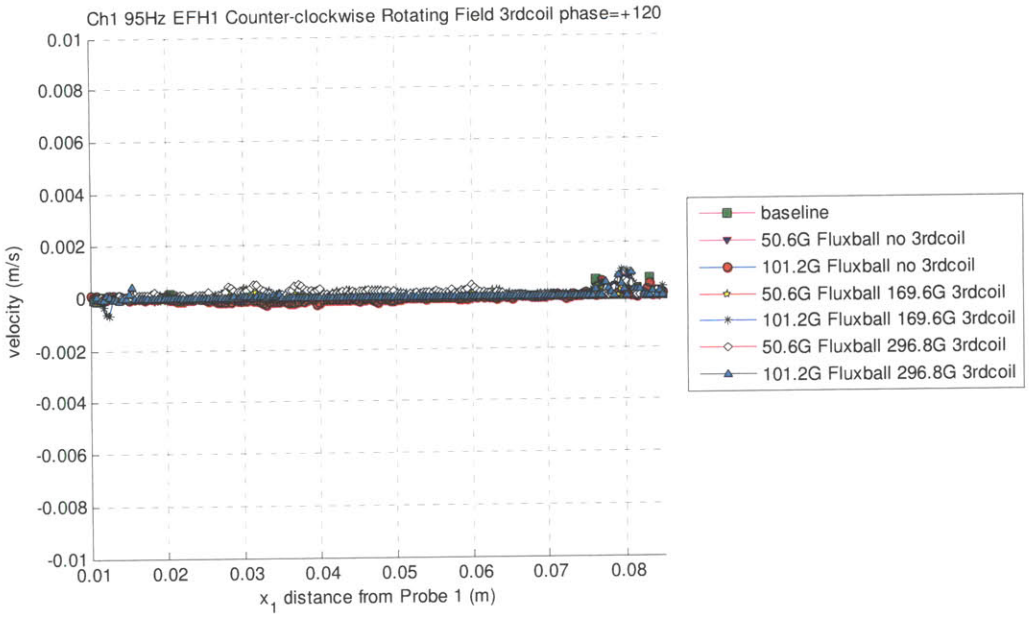
Ch1 95Hz EFH1 Counter-clockwise Rotating Field 3rdcoil phase=+120
velocity (m/s)
0.01
0.008
0.006
0.004
0.002
0
-0.002
-0.004
-0.006
-0.008
-0.01
0.01
0.02
0.03
0.04
0.05
0.06
0.07
0.08
x1 distance from Probe 1 (m)
baseline
50.6G Fluxball no 3rdcoil
101.2G Fluxball no 3rdcoil
50.6G Fluxball 169.6G 3rdcoil
101.2G Fluxball 169.6G 3rdcoil
50.6G Fluxball 296.8G 3rdcoil
101.2G Fluxball 296.8G 3rdcoil

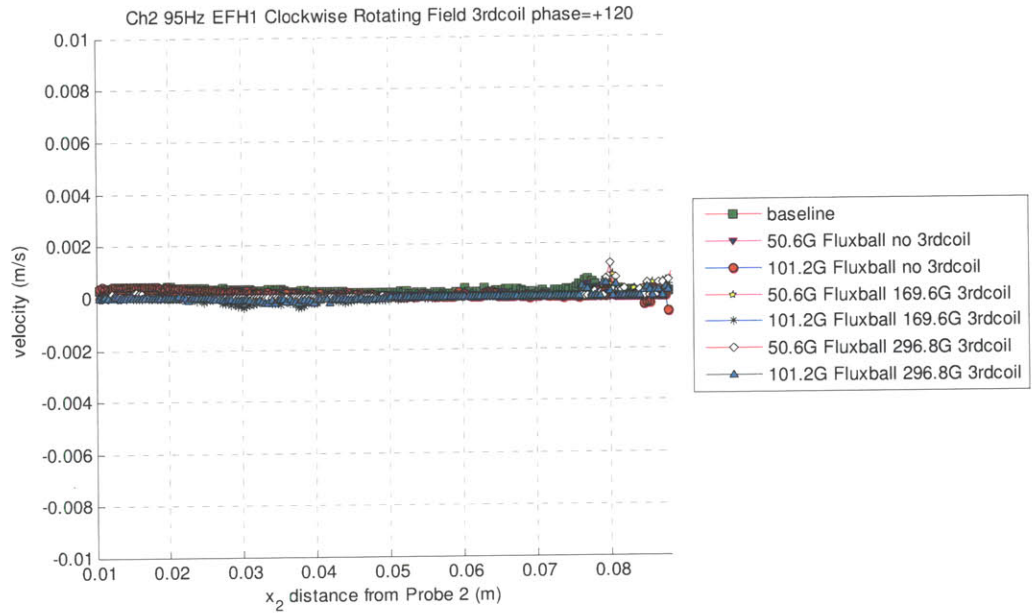
Ch2 95Hz EFH1 Clockwise Rotating Field 3rdcoil phase=+120
velocity (m/s)
0.01
0.008
0.006
0.004
0.002
0
-0.002
-0.004
-0.006
-0.008
-0.01
0.01
0.02
0.03
0.04
0.05
0.06
0.07
0.08
x2 distance from Probe 2 (m)
baseline
50.6G Fluxball no 3rdcoil
101.2G Fluxball no 3rdcoil
50.6G Fluxball 169.6G 3rdcoil
101.2G Fluxball 169.6G 3rdcoil
50.6G Fluxball 296.8G 3rdcoil
101.2G Fluxball 296.8G 3rdcoil

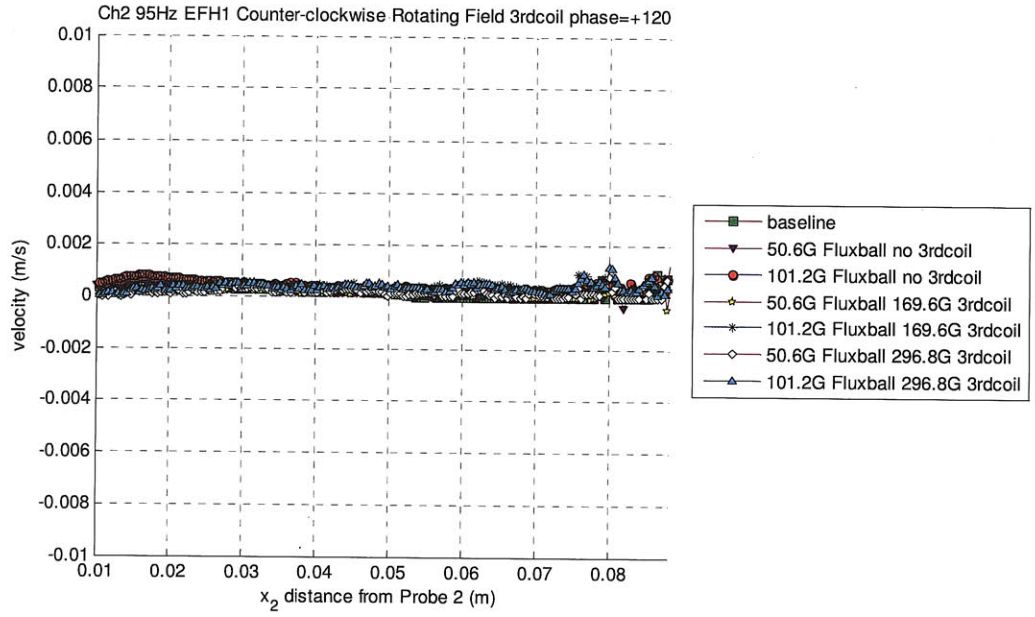
Ch2 95Hz EFH1 Counter-clockwise Rotating Field 3rdcoil phase=+120
velocity (m/s)
0.01
0.008
0.006
0.004
0.002
0
-0.002
-0.004
-0.006
-0.008
-0.01
0.01 0.02 0.03 0.04 0.05 0.06 0.07 0.08
x2 distance from Probe 2 (m)
baseline
50.6G Fluxball no 3rdcoil
101.2G Fluxball no 3rdcoil
50.6G Fluxball 169.6G 3rdcoil
101.2G Fluxball 169.6G 3rdcoil
50.6G Fluxball 296.8G 3rdcoil
101.2G Fluxball 296.8G 3rdcoil

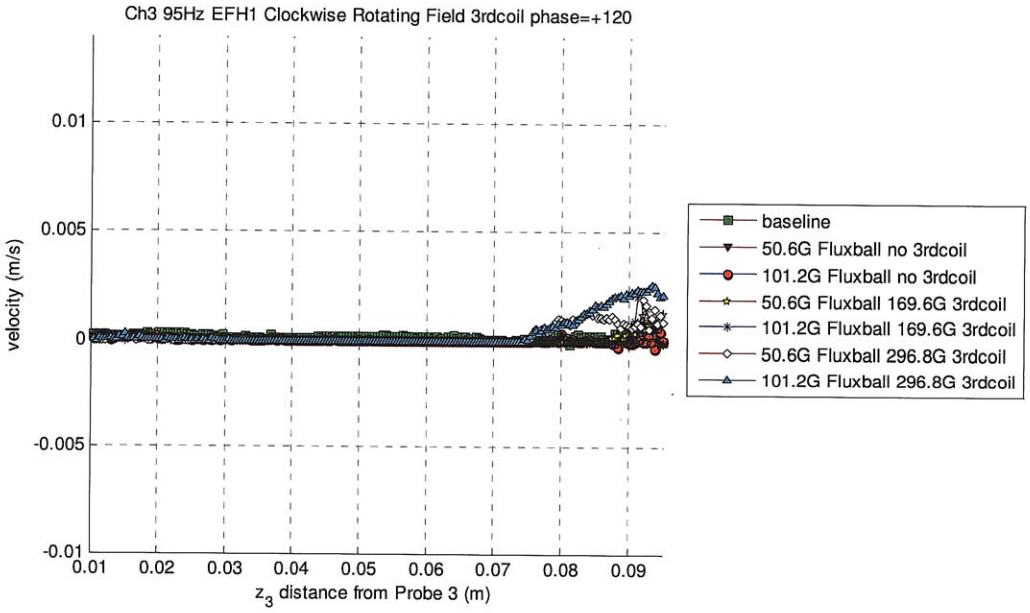
Ch3 95Hz EFH1 Clockwise Rotating Field 3rdcoil phase=+120
velocity (m/s)
0.01
0.005
0
-0.005
-0.01
0.01 0.02 0.03 0.04 0.05 0.06 0.07 0.08 0.09
z3 distance from Probe 3 (m)
baseline
50.6G Fluxball no 3rdcoil
101.2G Fluxball no 3rdcoil
50.6G Fluxball 169.6G 3rdcoil
101.2G Fluxball 169.6G 3rdcoil
50.6G Fluxball 296.8G 3rdcoil
101.2G Fluxball 296.8G 3rdcoil

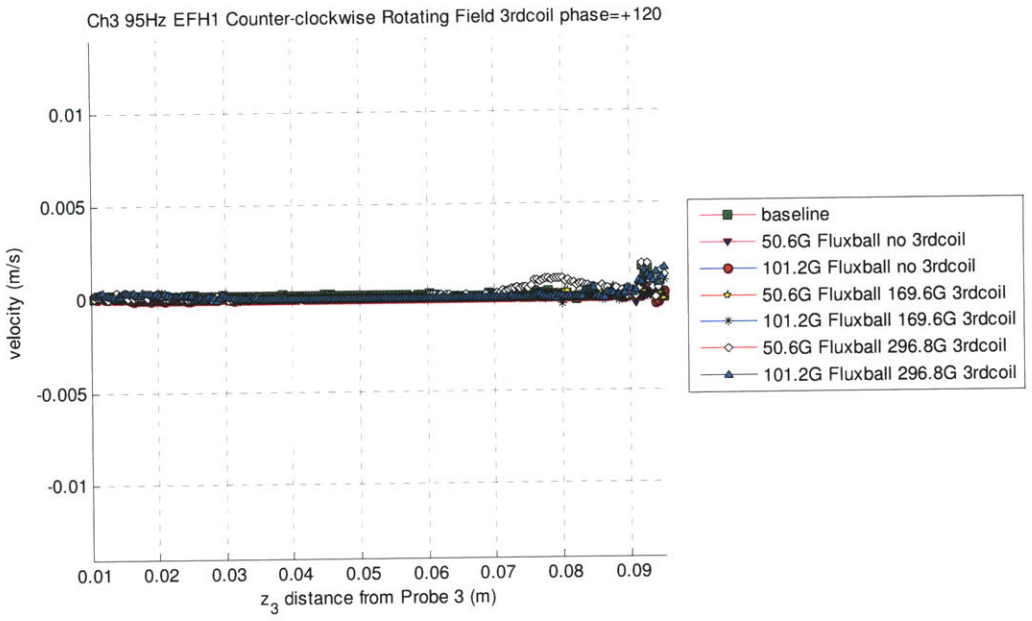
Ch3 95Hz EFH1 Counter-clockwise Rotating Field 3rdcoil phase=+120
velocity (m/s)
0.01
0.005
0
-0.005
-0.01
0.01 0.02 0.03 0.04 0.05 0.06 0.07 0.08 0.09
z3 distance from Probe 3 (m)
baseline
50.6G Fluxball no 3rdcoil
101.2G Fluxball no 3rdcoil
50.6G Fluxball 169.6G 3rdcoil
101.2G Fluxball 169.6G 3rdcoil
50.6G Fluxball 296.8G 3rdcoil
101.2G Fluxball 296.8G 3rdcoil

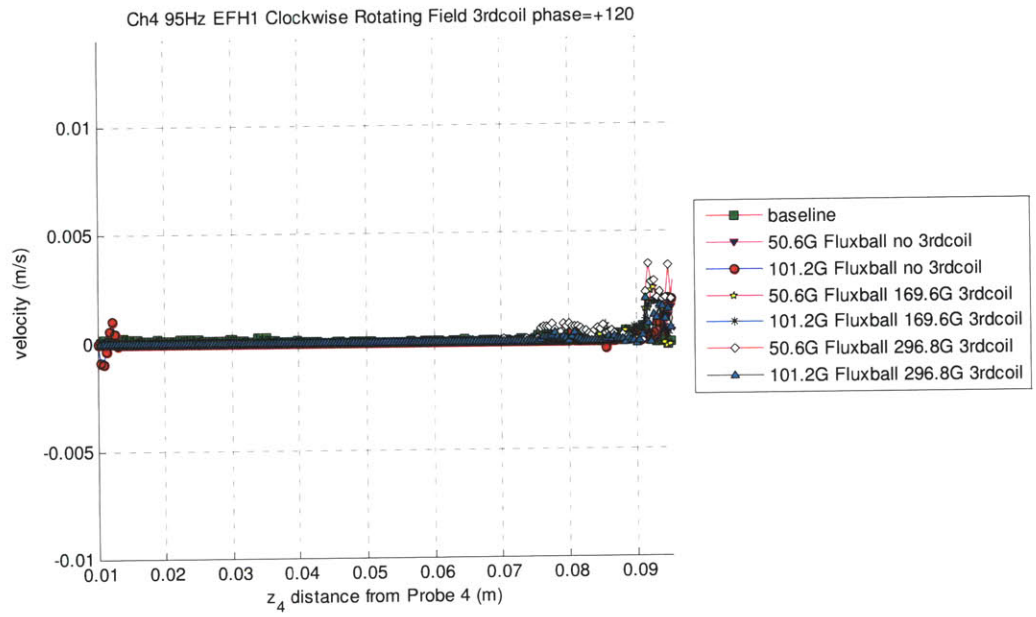
Ch4 95Hz EFH1 Clockwise Rotating Field 3rdcoil phase=+120
velocity (m/s)
0.01
0.005
0
-0.005
-0.01
0.01 0.02 0.03 0.04 0.05 0.06 0.07 0.08 0.09
z4 distance from Probe 4 (m)
baseline
50.6G Fluxball no 3rdcoil
101.2G Fluxball no 3rdcoil
50.6G Fluxball 169.6G 3rdcoil
101.2G Fluxball 169.6G 3rdcoil
50.6G Fluxball 296.8G 3rdcoil
101.2G Fluxball 296.8G 3rdcoil

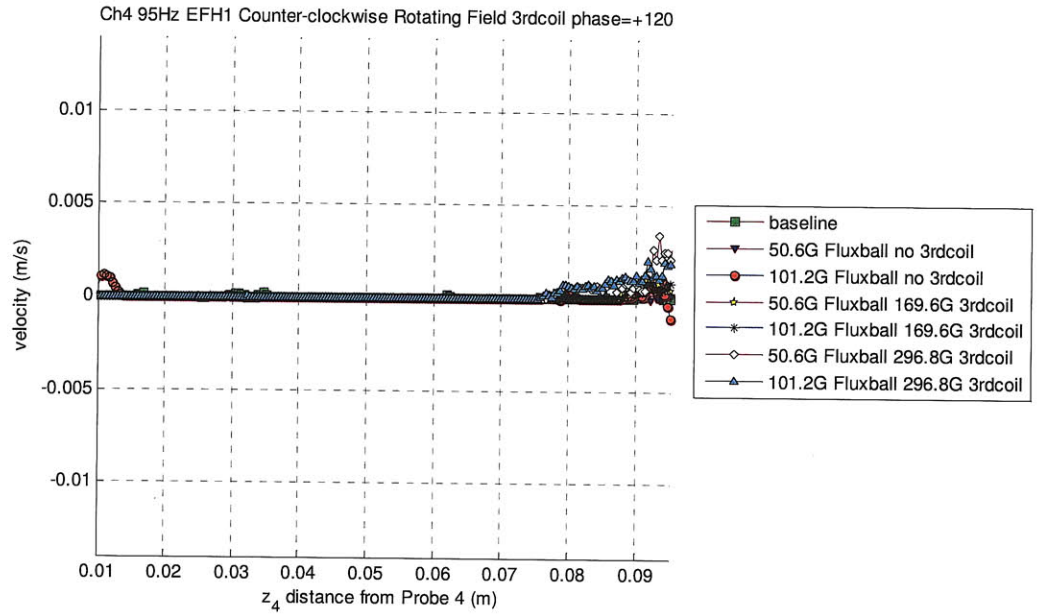
Ch4 95Hz EFH1 Counter-clockwise Rotating Field 3rdcoil phase=+120
velocity (m/s)
0.01
0.005
0
-0.005
-0.01
0.01 0.02 0.03 0.04 0.05 0.06 0.07 0.08 0.09
z4 distance from Probe 4 (m)
baseline
50.6G Fluxball no 3rdcoil
101.2G Fluxball no 3rdcoil
50.6G Fluxball 169.6G 3rdcoil
101.2G Fluxball 169.6G 3rdcoil
50.6G Fluxball 296.8G 3rdcoil
101.2G Fluxball 296.8G 3rdcoil

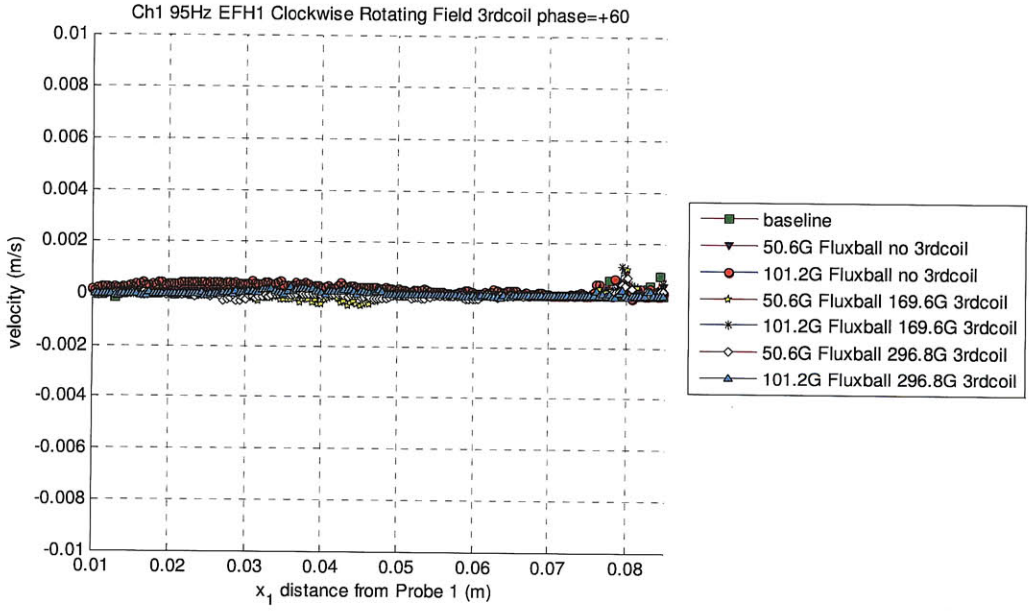
Ch1 95Hz EFH1 Clockwise Rotating Field 3rdcoil phase=+60
velocity (m/s)
0.01
0.008
0.006
0.004
0.002
0
-0.002
-0.004
-0.006
-0.008
-0.01
0.01 0.02 0.03 0.04 0.05 0.06 0.07 0.08
x1 distance from Probe 1 (m)
baseline
50.6G Fluxball no 3rdcoil
101.2G Fluxball no 3rdcoil
50.6G Fluxball 169.6G 3rdcoil
101.2G Fluxball 169.6G 3rdcoil
50.6G Fluxball 296.8G 3rdcoil
101.2G Fluxball 296.8G 3rdcoil

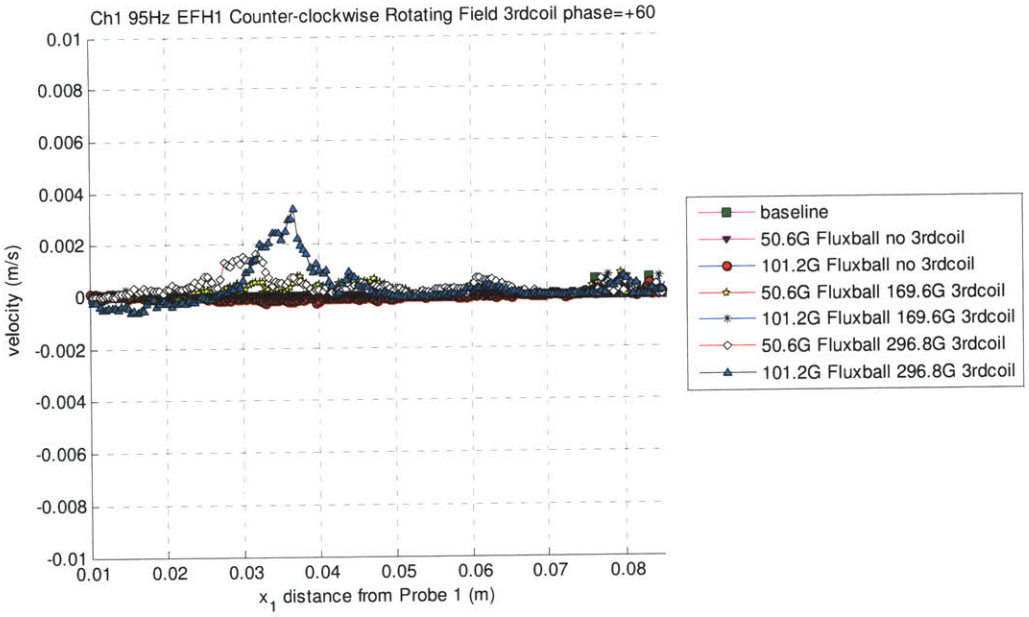
Ch1 95Hz EFH1 Counter-clockwise Rotating Field 3rdcoil phase=+60
velocity (m/s)
0.01
0.008
0.006
0.004
0.002
0
-0.002
-0.004
-0.006
-0.008
-0.01
0.01
0.02
0.03
0.04
0.05
0.06
0.07
0.08
x1 distance from Probe 1 (m)
baseline
50.6G Fluxball no 3rdcoil
101.2G Fluxball no 3rdcoil
50.6G Fluxball 169.6G 3rdcoil
101.2G Fluxball 169.6G 3rdcoil
50.6G Fluxball 296.8G 3rdcoil
101.2G Fluxball 296.8G 3rdcoil

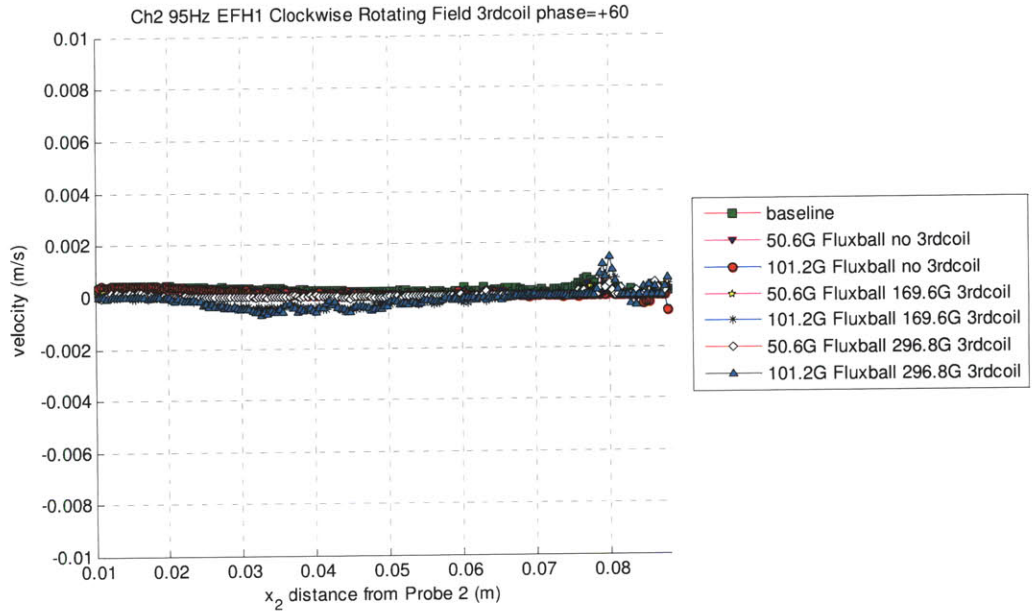
Ch2 95Hz EFH1 Clockwise Rotating Field 3rdcoil phase=+60
velocity (m/s)
0.01
0.008
0.006
0.004
0.002
0
-0.002
-0.004
-0.006
-0.008
-0.01
0.01
0.02
0.03
0.04
0.05
0.06
0.07
0.08
x2 distance from Probe 2 (m)
baseline
50.6G Fluxball no 3rdcoil
101.2G Fluxball no 3rdcoil
50.6G Fluxball 169.6G 3rdcoil
101.2G Fluxball 169.6G 3rdcoil
50.6G Fluxball 296.8G 3rdcoil
101.2G Fluxball 296.8G 3rdcoil

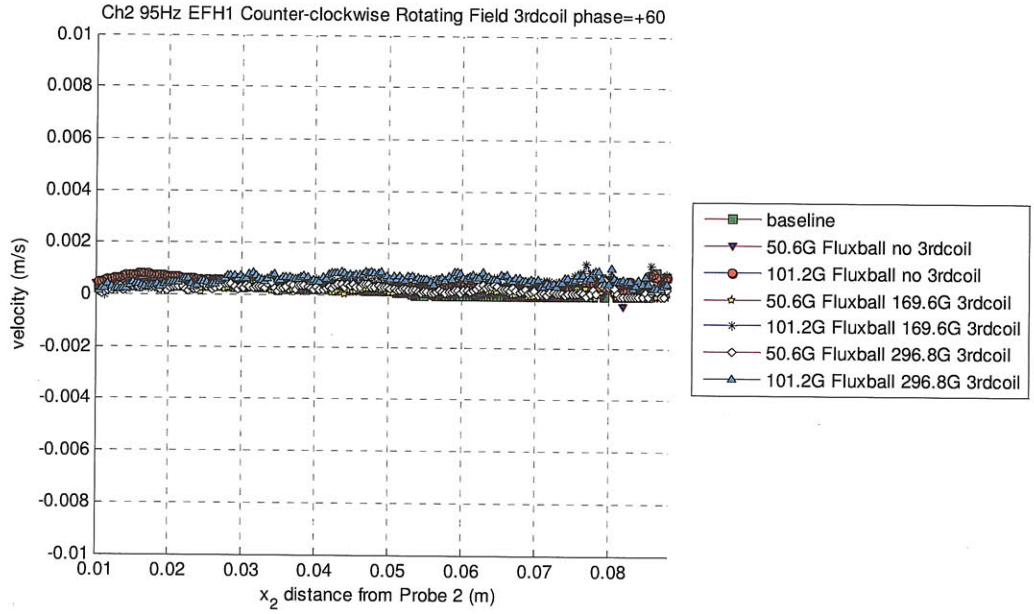
Ch2 95Hz EFH1 Counter-clockwise Rotating Field 3rdcoil phase=+60
velocity (m/s)
0.01
0.008
0.006
0.004
0.002
0
-0.002
-0.004
-0.006
-0.008
-0.01
0.01 0.02 0.03 0.04 0.05 0.06 0.07 0.08
x2 distance from Probe 2 (m)
baseline
50.6G Fluxball no 3rdcoil
101.2G Fluxball no 3rdcoil
50.6G Fluxball 169.6G 3rdcoil
101.2G Fluxball 169.6G 3rdcoil
50.6G Fluxball 296.8G 3rdcoil
101.2G Fluxball 296.8G 3rdcoil

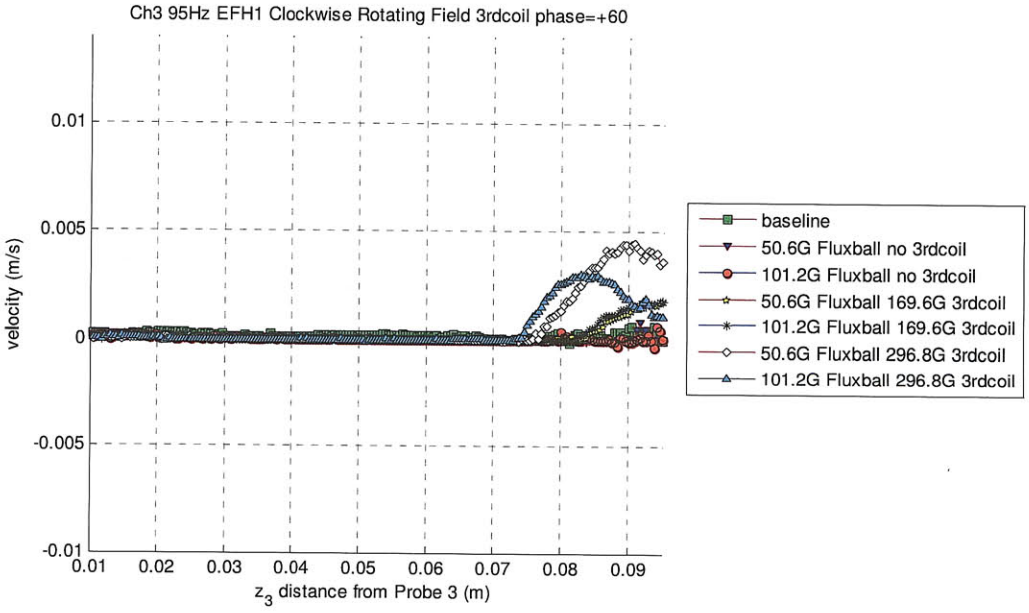
Ch3 95Hz EFH1 Clockwise Rotating Field 3rdcoil phase=+60
velocity (m/s)
0.01
0.005
0
-0.005
-0.01
0.01 0.02 0.03 0.04 0.05 0.06 0.07 0.08 0.09
z3 distance from Probe 3 (m)
baseline
50.6G Fluxball no 3rdcoil
101.2G Fluxball no 3rdcoil
50.6G Fluxball 169.6G 3rdcoil
101.2G Fluxball 169.6G 3rdcoil
50.6G Fluxball 296.8G 3rdcoil
101.2G Fluxball 296.8G 3rdcoil

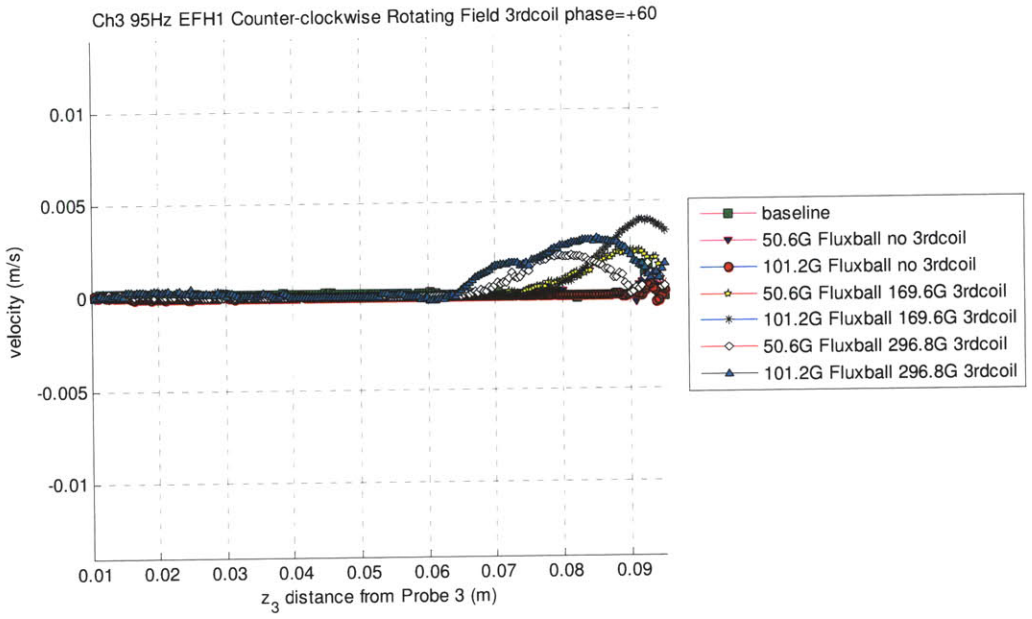
Ch3 95Hz EFH1 Counter-clockwise Rotating Field 3rdcoil phase=+60
velocity (m/s)
0.01
0.005
0
-0.005
-0.01
0.01 0.02 0.03 0.04 0.05 0.06 0.07 0.08 0.09
z3 distance from Probe 3 (m)
baseline
50.6G Fluxball no 3rdcoil
101.2G Fluxball no 3rdcoil
50.6G Fluxball 169.6G 3rdcoil
101.2G Fluxball 169.6G 3rdcoil
50.6G Fluxball 296.8G 3rdcoil
101.2G Fluxball 296.8G 3rdcoil

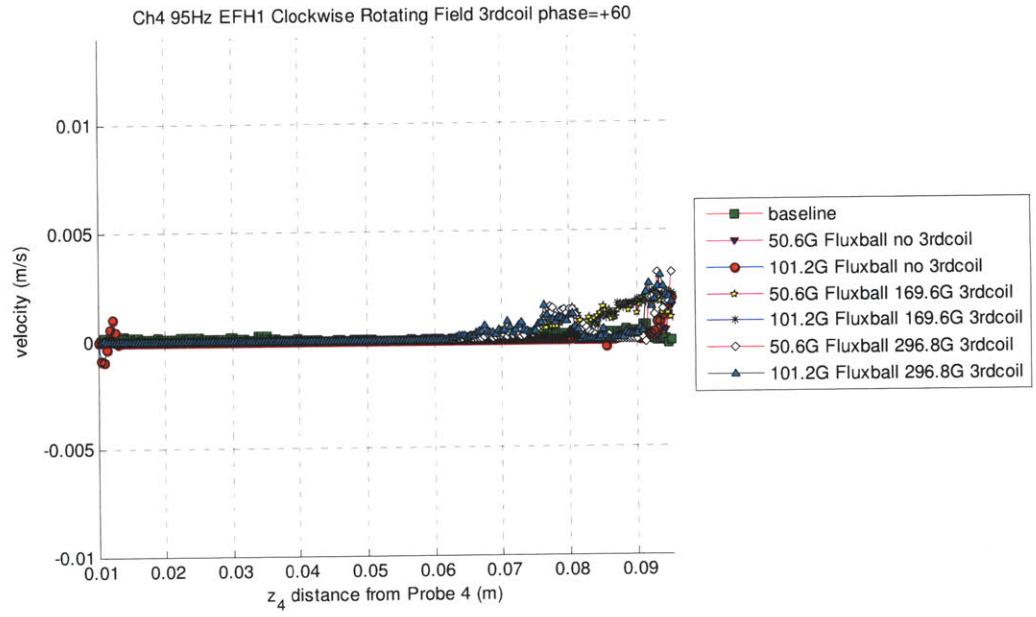
Ch4 95Hz EFH1 Clockwise Rotating Field 3rdcoil phase=+60
velocity (m/s)
0.01
0.005
0
-0.005
-0.01
0.01 0.02 0.03 0.04 0.05 0.06 0.07 0.08 0.09
z4 distance from Probe 4 (m)
baseline
50.6G Fluxball no 3rdcoil
101.2G Fluxball no 3rdcoil
50.6G Fluxball 169.6G 3rdcoil
101.2G Fluxball 169.6G 3rdcoil
50.6G Fluxball 296.8G 3rdcoil
101.2G Fluxball 296.8G 3rdcoil

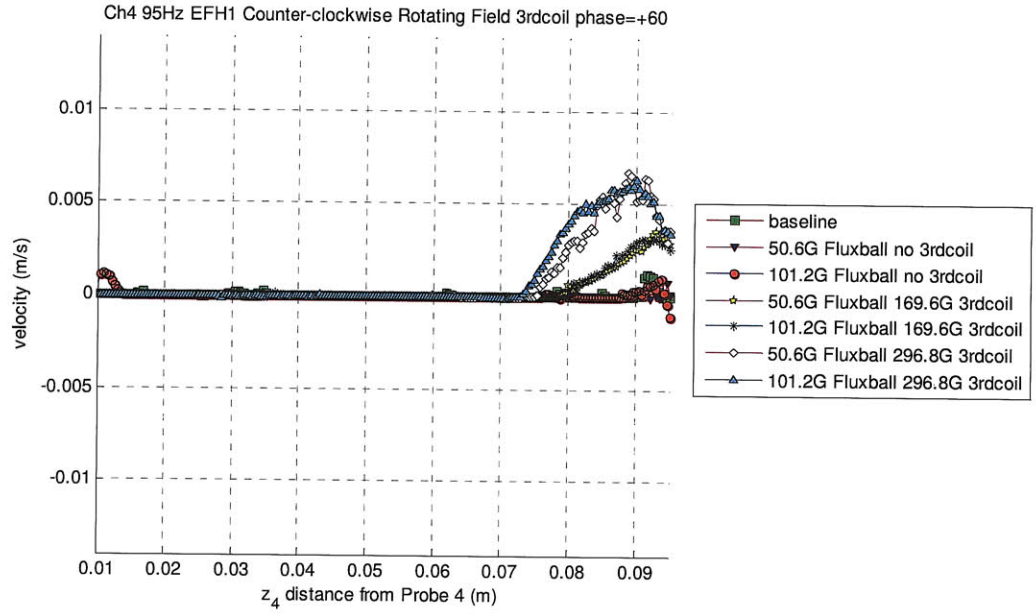
Ch4 95Hz EFH1 Counter-clockwise Rotating Field 3rdcoil phase=+60
velocity (m/s)
0.01
0.005
0
-0.005
-0.01
0.01 0.02 0.03 0.04 0.05 0.06 0.07 0.08 0.09
z4 distance from Probe 4 (m)
baseline
50.6G Fluxball no 3rdcoil
101.2G Fluxball no 3rdcoil
50.6G Fluxball 169.6G 3rdcoil
101.2G Fluxball 169.6G 3rdcoil
50.6G Fluxball 296.8G 3rdcoil
101.2G Fluxball 296.8G 3rdcoil

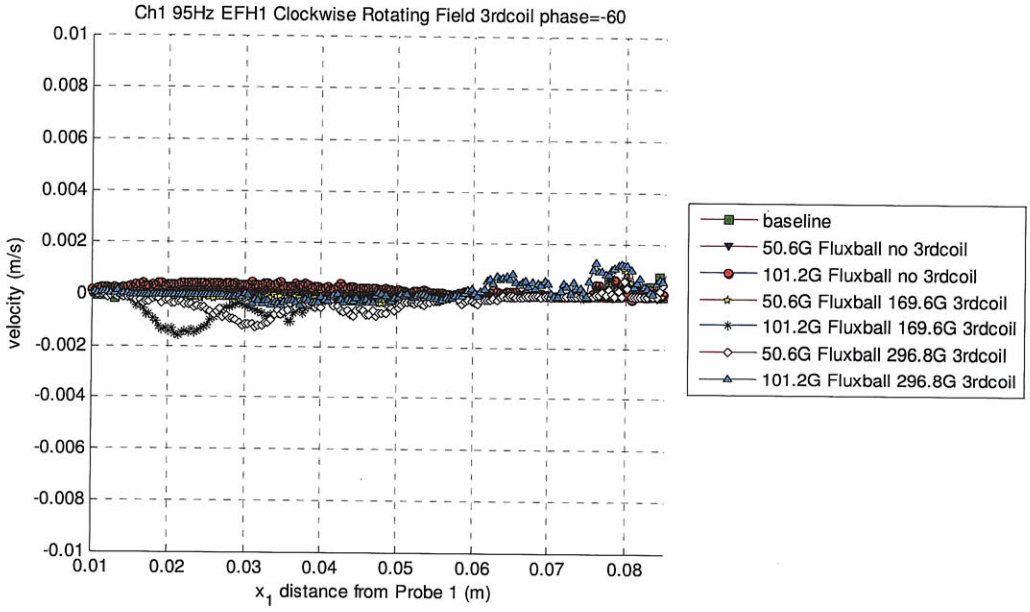
Ch1 95Hz EFH1 Clockwise Rotating Field 3rdcoil phase=-60
velocity (m/s)
0.01
0.008
0.006
0.004
0.002
0
-0.002
-0.004
-0.006
-0.008
-0.01
0.01 0.02 0.03 0.04 0.05 0.06 0.07 0.08
x1 distance from Probe 1 (m)
baseline
50.6G Fluxball no 3rdcoil
101.2G Fluxball no 3rdcoil
50.6G Fluxball 169.6G 3rdcoil
101.2G Fluxball 169.6G 3rdcoil
50.6G Fluxball 296.8G 3rdcoil
101.2G Fluxball 296.8G 3rdcoil

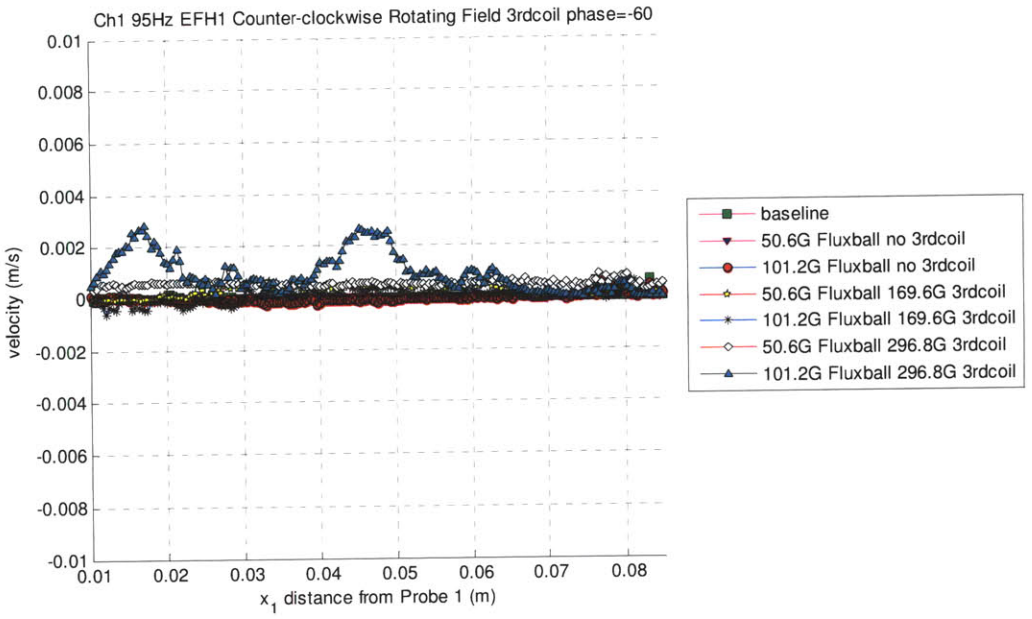
Ch1 95Hz EFH1 Counter-clockwise Rotating Field 3rdcoil phase=-60
velocity (m/s)
0.01
0.008
0.006
0.004
0.002
0
-0.002
-0.004
-0.006
-0.008
-0.01
0.01
0.02
0.03
0.04
0.05
0.06
0.07
0.08
x1 distance from Probe 1 (m)
baseline
50.6G Fluxball no 3rdcoil
101.2G Fluxball no 3rdcoil
50.6G Fluxball 169.6G 3rdcoil
101.2G Fluxball 169.6G 3rdcoil
50.6G Fluxball 296.8G 3rdcoil
101.2G Fluxball 296.8G 3rdcoil

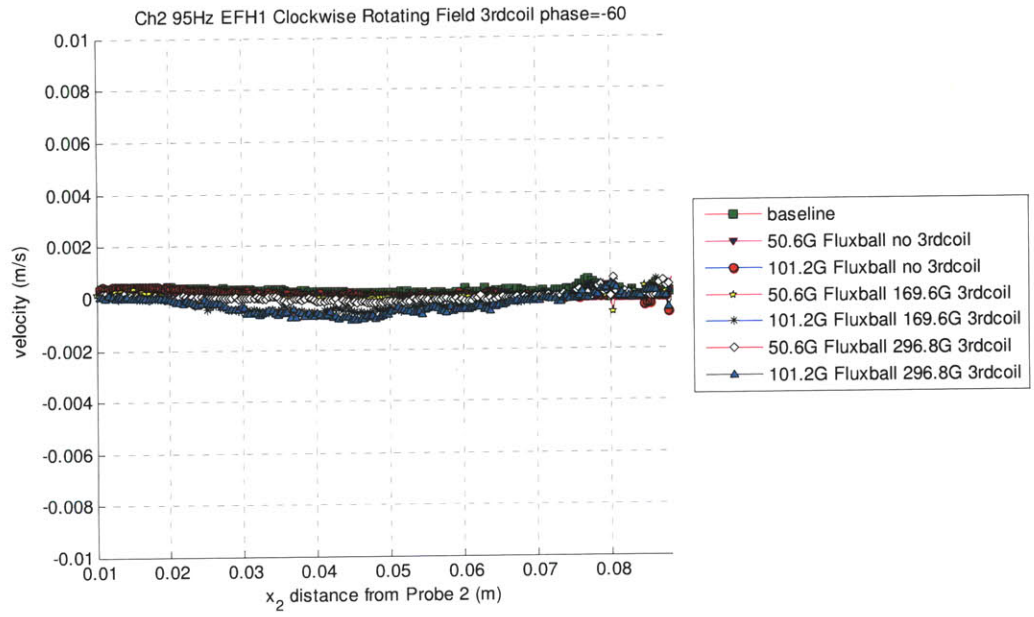
Ch2 95Hz EFH1 Clockwise Rotating Field 3rdcoil phase=-60
velocity (m/s)
0.01
0.008
0.006
0.004
0.002
0
-0.002
-0.004
-0.006
-0.008
-0.01
0.01
0.02
0.03
0.04
0.05
0.06
0.07
0.08
x2 distance from Probe 2 (m)
baseline
50.6G Fluxball no 3rdcoil
101.2G Fluxball no 3rdcoil
50.6G Fluxball 169.6G 3rdcoil
101.2G Fluxball 169.6G 3rdcoil
50.6G Fluxball 296.8G 3rdcoil
101.2G Fluxball 296.8G 3rdcoil

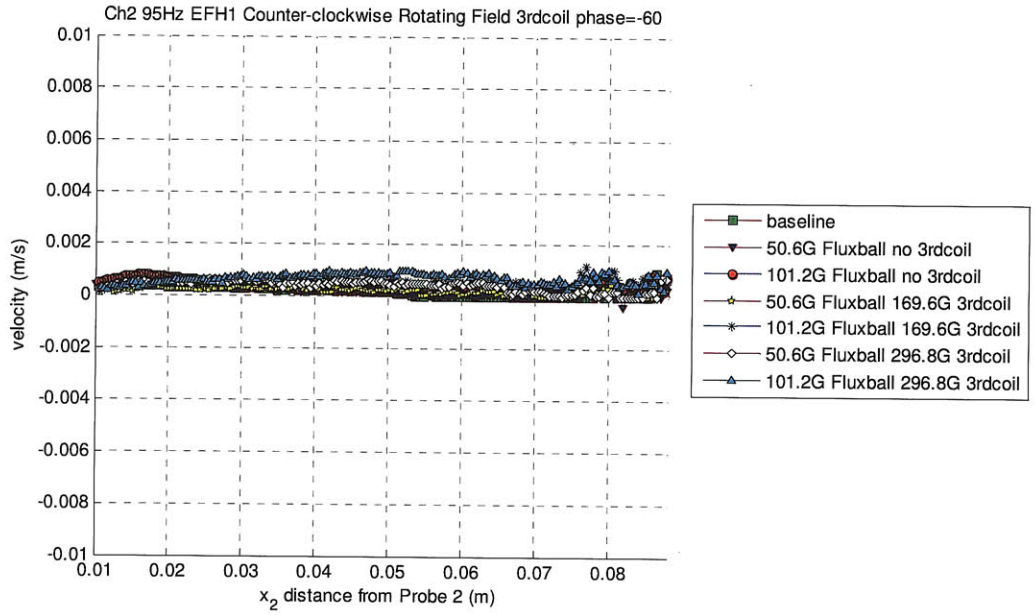
Ch2 95Hz EFH1 Counter-clockwise Rotating Field 3rdcoil phase=-60
velocity (m/s)
0.01
0.008
0.006
0.004
0.002
0
-0.002
-0.004
-0.006
-0.008
-0.01
0.01 0.02 0.03 0.04 0.05 0.06 0.07 0.08
x2 distance from Probe 2 (m)
baseline
50.6G Fluxball no 3rdcoil
101.2G Fluxball no 3rdcoil
50.6G Fluxball 169.6G 3rdcoil
101.2G Fluxball 169.6G 3rdcoil
50.6G Fluxball 296.8G 3rdcoil
101.2G Fluxball 296.8G 3rdcoil

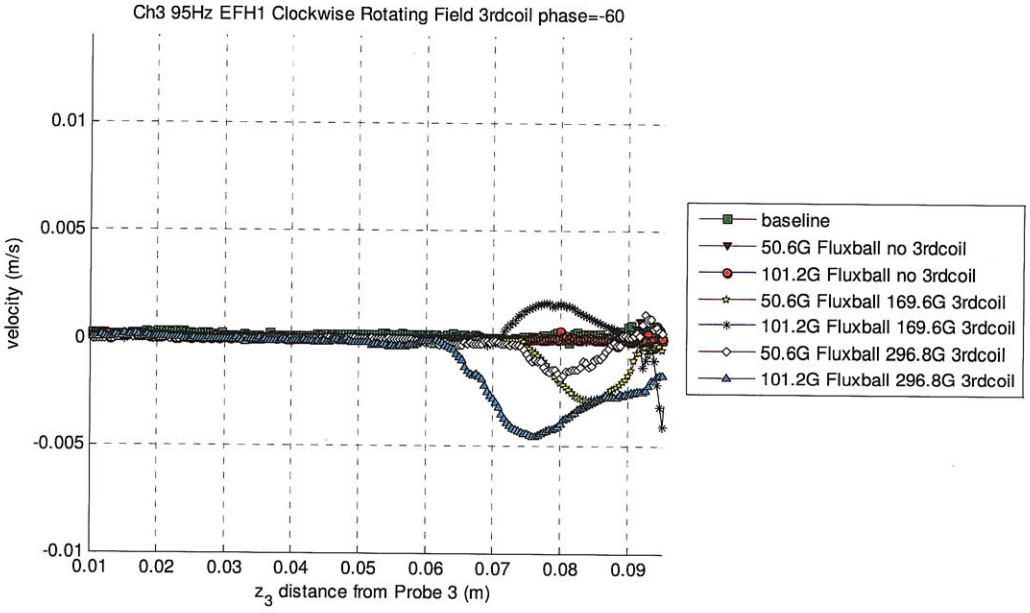
Ch3 95Hz EFH1 Clockwise Rotating Field 3rdcoil phase=-60
velocity (m/s)
0.01
0.005
0
-0.005
-0.01
0.01 0.02 0.03 0.04 0.05 0.06 0.07 0.08 0.09
z3 distance from Probe 3 (m)
baseline
50.6G Fluxball no 3rdcoil
101.2G Fluxball no 3rdcoil
50.6G Fluxball 169.6G 3rdcoil
101.2G Fluxball 169.6G 3rdcoil
50.6G Fluxball 296.8G 3rdcoil
101.2G Fluxball 296.8G 3rdcoil

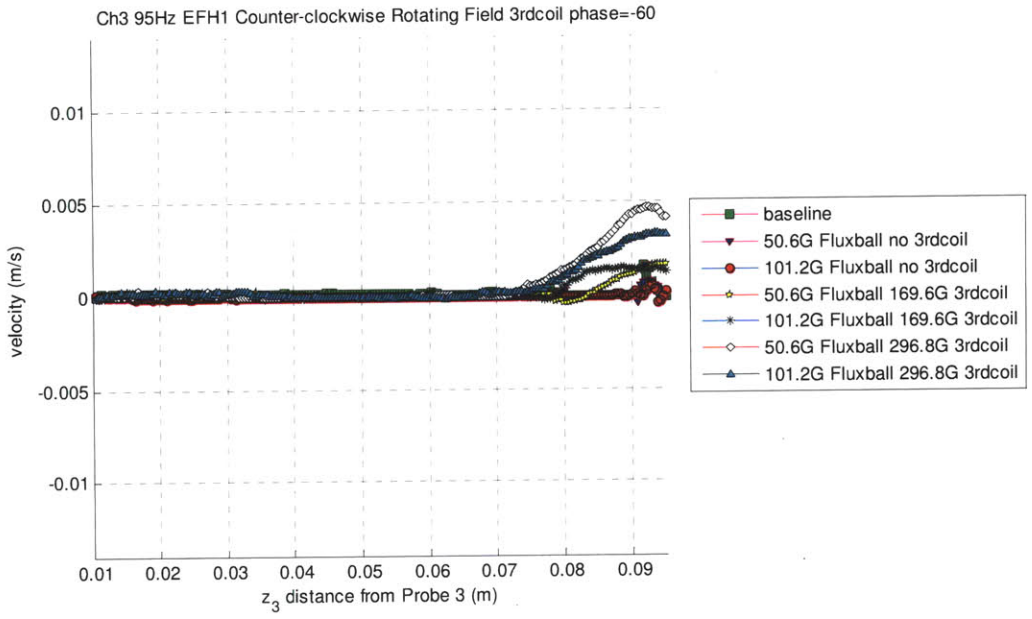
Ch3 95Hz EFH1 Counter-clockwise Rotating Field 3rdcoil phase=-60
velocity (m/s)
0.01
0.005
0
-0.005
-0.01
0.01 0.02 0.03 0.04 0.05 0.06 0.07 0.08 0.09
z3 distance from Probe 3 (m)
baseline
50.6G Fluxball no 3rdcoil
101.2G Fluxball no 3rdcoil
50.6G Fluxball 169.6G 3rdcoil
101.2G Fluxball 169.6G 3rdcoil
50.6G Fluxball 296.8G 3rdcoil
101.2G Fluxball 296.8G 3rdcoil

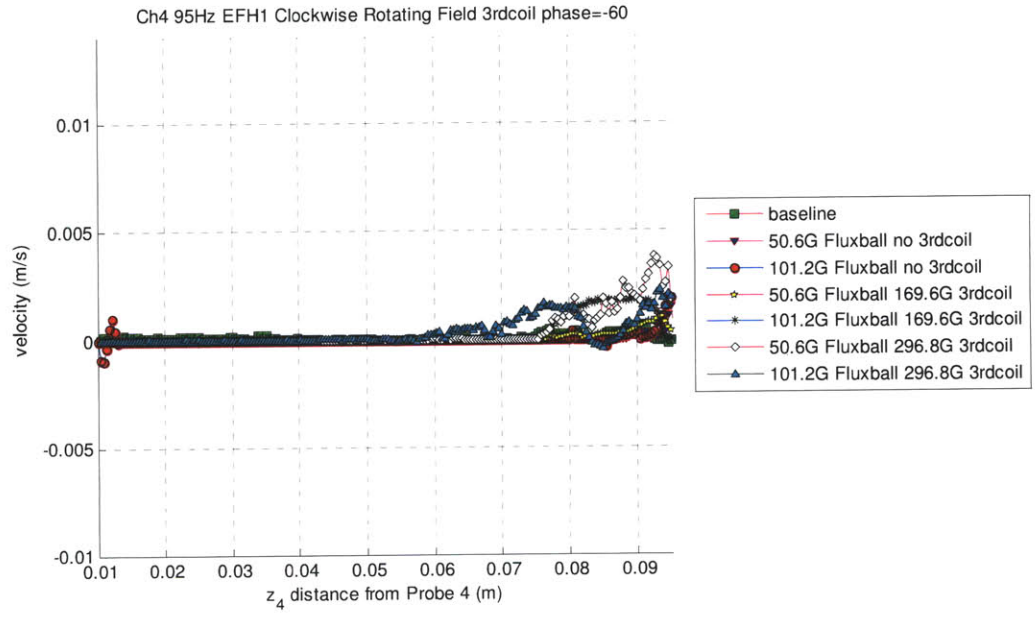
Ch4 95Hz EFH1 Clockwise Rotating Field 3rdcoil phase=-60
velocity (m/s)
0.01
0.005
0
-0.005
-0.01
0.01 0.02 0.03 0.04 0.05 0.06 0.07 0.08 0.09
z4 distance from Probe 4 (m)
baseline
50.6G Fluxball no 3rdcoil
101.2G Fluxball no 3rdcoil
50.6G Fluxball 169.6G 3rdcoil
101.2G Fluxball 169.6G 3rdcoil
50.6G Fluxball 296.8G 3rdcoil
101.2G Fluxball 296.8G 3rdcoil

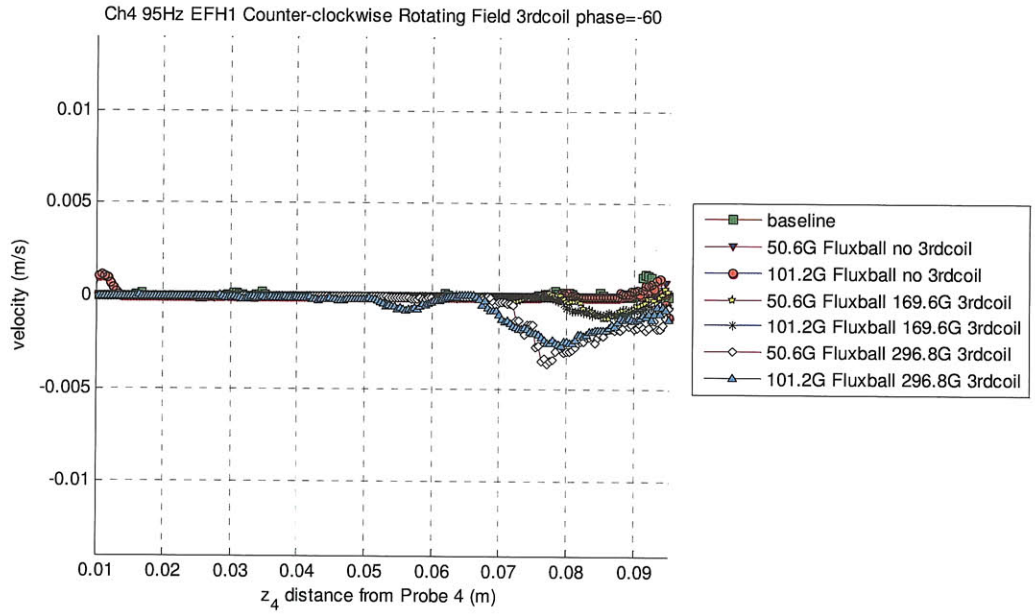
Ch4 95Hz EFH1 Counter-clockwise Rotating Field 3rdcoil phase=-60
velocity (m/s)
0.01
0.005
0
-0.005
-0.01
0.01 0.02 0.03 0.04 0.05 0.06 0.07 0.08 0.09
z4 distance from Probe 4 (m)
baseline
50.6G Fluxball no 3rdcoil
101.2G Fluxball no 3rdcoil
50.6G Fluxball 169.6G 3rdcoil
101.2G Fluxball 169.6G 3rdcoil
50.6G Fluxball 296.8G 3rdcoil
101.2G Fluxball 296.8G 3rdcoil

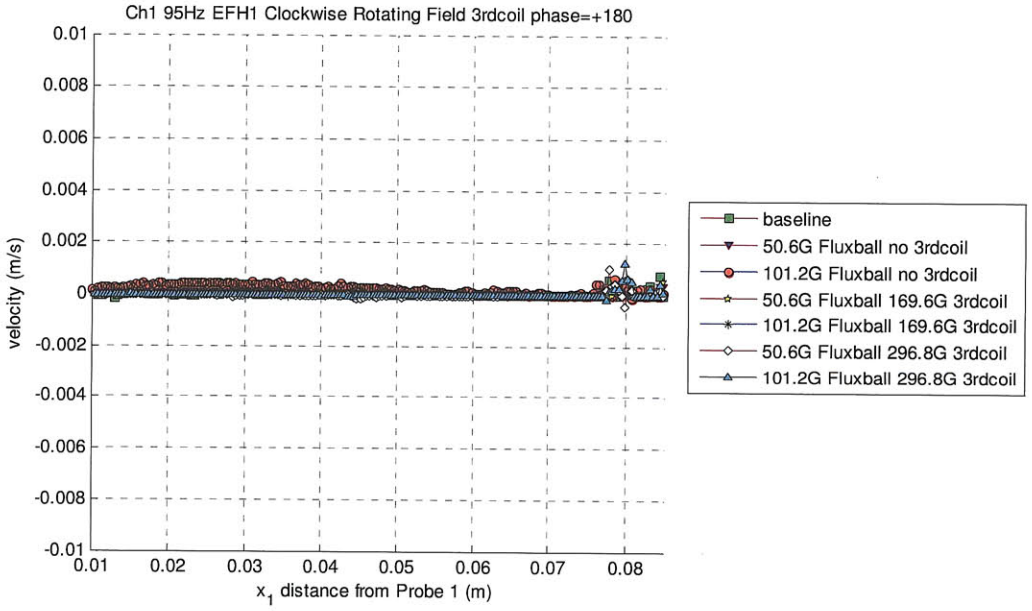
Ch1 95Hz EFH1 Clockwise Rotating Field 3rdcoil phase=+180
velocity (m/s)
0.01
0.008
0.006
0.004
0.002
0
-0.002
-0.004
-0.006
-0.008
-0.01
0.01 0.02 0.03 0.04 0.05 0.06 0.07 0.08
x1 distance from Probe 1 (m)
baseline
50.6G Fluxball no 3rdcoil
101.2G Fluxball no 3rdcoil
50.6G Fluxball 169.6G 3rdcoil
101.2G Fluxball 169.6G 3rdcoil
50.6G Fluxball 296.8G 3rdcoil
101.2G Fluxball 296.8G 3rdcoil

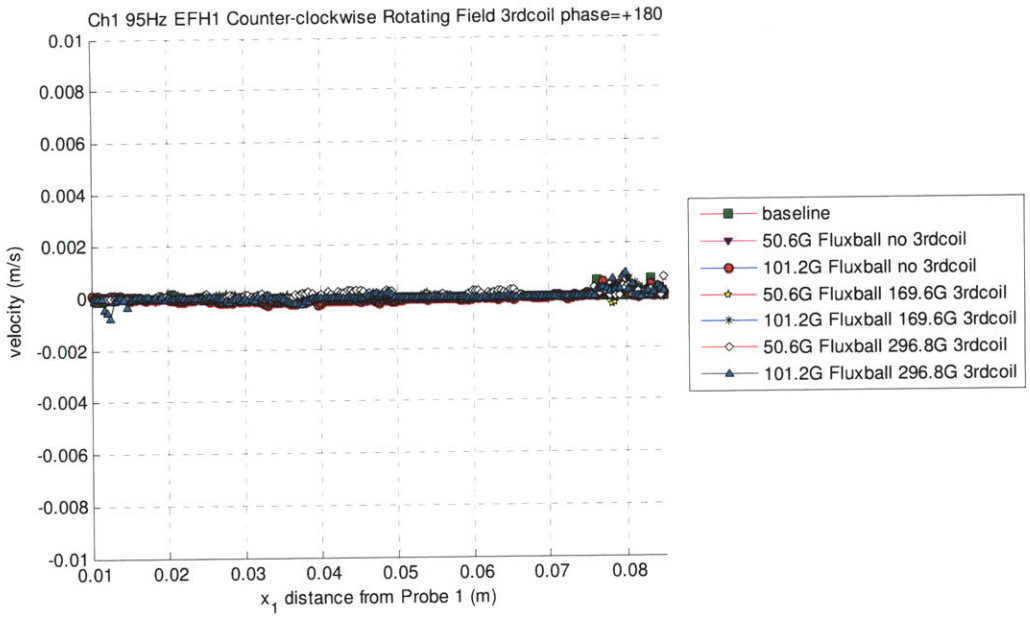
Ch1 95Hz EFH1 Counter-clockwise Rotating Field 3rdcoil phase=+180
velocity (m/s)
0.01
0.008
0.006
0.004
0.002
0
-0.002
-0.004
-0.006
-0.008
-0.01
0.01
0.02
0.03
0.04
0.05
0.06
0.07
0.08
x1 distance from Probe 1 (m)
baseline
50.6G Fluxball no 3rdcoil
101.2G Fluxball no 3rdcoil
50.6G Fluxball 169.6G 3rdcoil
101.2G Fluxball 169.6G 3rdcoil
50.6G Fluxball 296.8G 3rdcoil
101.2G Fluxball 296.8G 3rdcoil

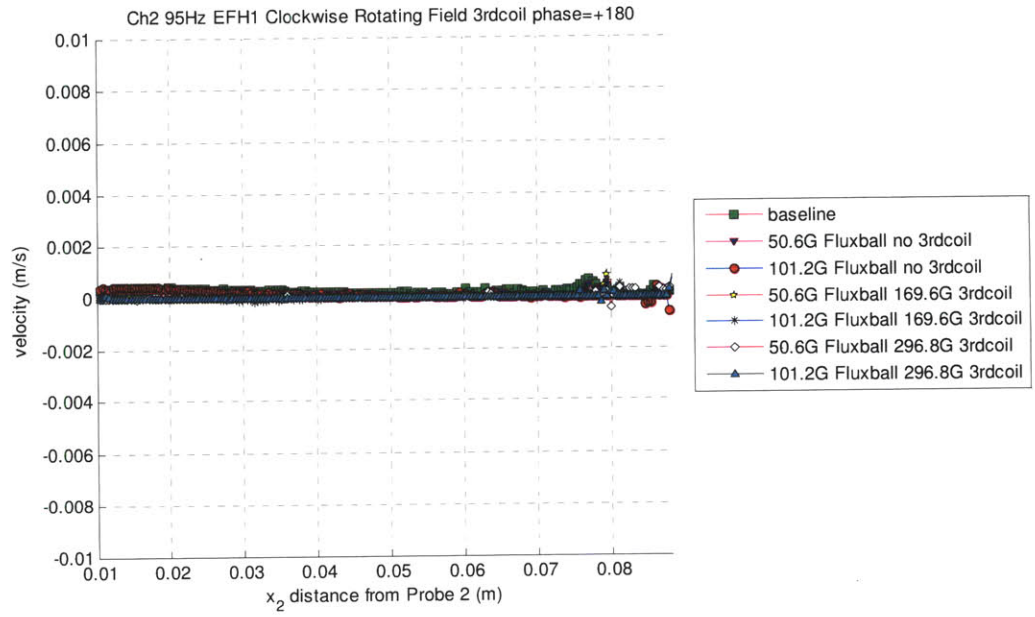
Ch2 95Hz EFH1 Clockwise Rotating Field 3rdcoil phase=+180
velocity (m/s)
0.01
0.008
0.006
0.004
0.002
0
-0.002
-0.004
-0.006
-0.008
-0.01
0.01
0.02
0.03
0.04
0.05
0.06
0.07
0.08
x2 distance from Probe 2 (m)
baseline
50.6G Fluxball no 3rdcoil
101.2G Fluxball no 3rdcoil
50.6G Fluxball 169.6G 3rdcoil
101.2G Fluxball 169.6G 3rdcoil
50.6G Fluxball 296.8G 3rdcoil
101.2G Fluxball 296.8G 3rdcoil

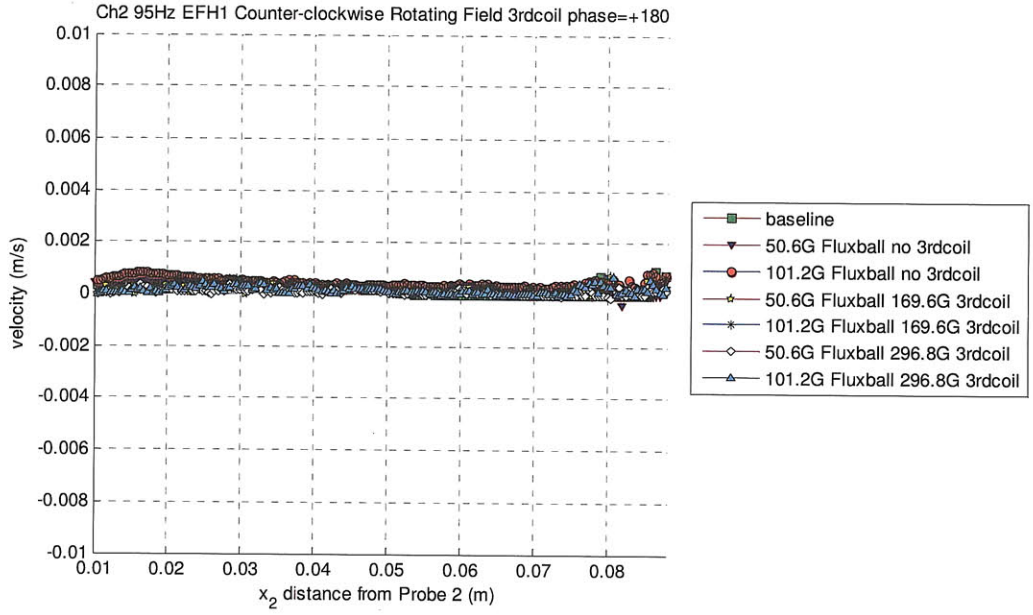
Ch2 95Hz EFH1 Counter-clockwise Rotating Field 3rdcoil phase=+180
velocity (m/s)
0.01
0.008
0.006
0.004
0.002
0
-0.002
-0.004
-0.006
-0.008
-0.01
0.01 0.02 0.03 0.04 0.05 0.06 0.07 0.08
x2 distance from Probe 2 (m)
baseline
50.6G Fluxball no 3rdcoil
101.2G Fluxball no 3rdcoil
50.6G Fluxball 169.6G 3rdcoil
101.2G Fluxball 169.6G 3rdcoil
50.6G Fluxball 296.8G 3rdcoil
101.2G Fluxball 296.8G 3rdcoil

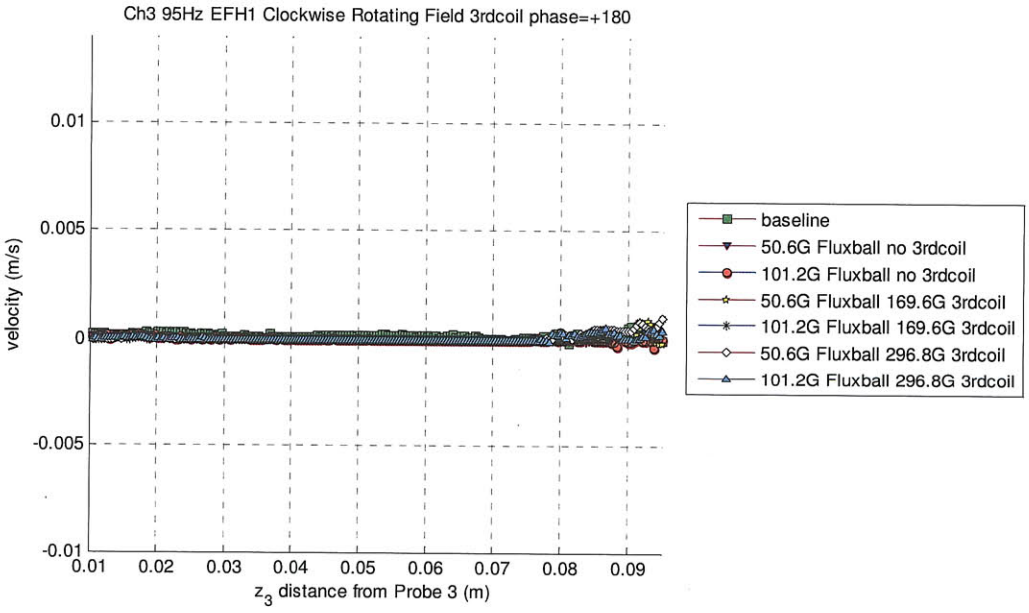
Ch3 95Hz EFH1 Clockwise Rotating Field 3rdcoil phase=+180
velocity (m/s)
0.01
0.005
0
-0.005
-0.01
0.01 0.02 0.03 0.04 0.05 0.06 0.07 0.08 0.09
z3 distance from Probe 3 (m)
baseline
50.6G Fluxball no 3rdcoil
101.2G Fluxball no 3rdcoil
50.6G Fluxball 169.6G 3rdcoil
101.2G Fluxball 169.6G 3rdcoil
50.6G Fluxball 296.8G 3rdcoil
101.2G Fluxball 296.8G 3rdcoil

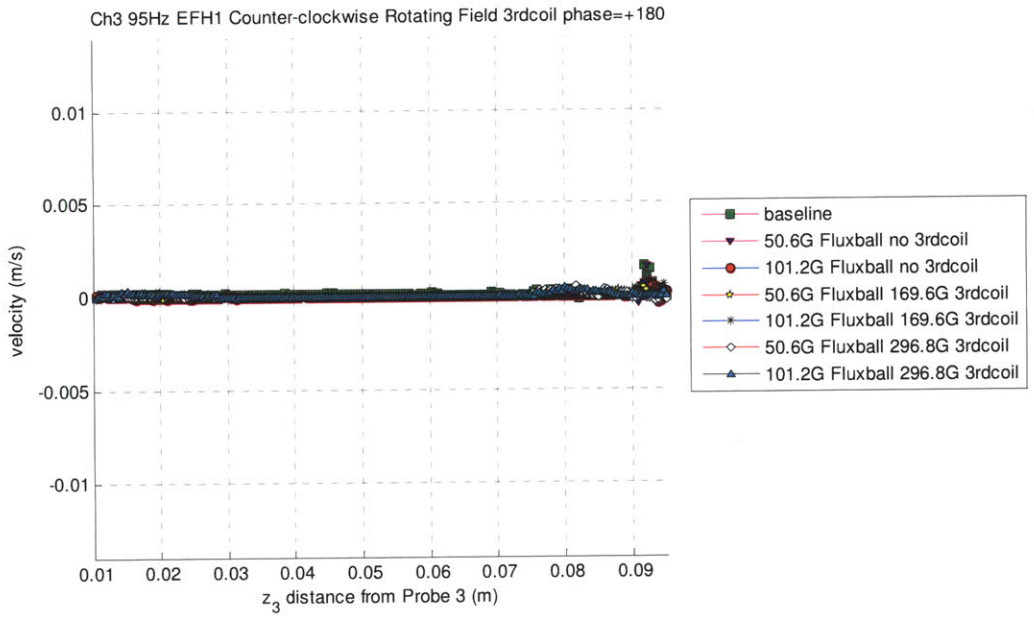
Ch3 95Hz EFH1 Counter-clockwise Rotating Field 3rdcoil phase=+180
velocity (m/s)
0.01
0.005
0
-0.005
-0.01
0.01 0.02 0.03 0.04 0.05 0.06 0.07 0.08 0.09
z_3 distance from Probe 3 (m)
baseline
50.6G Fluxball no 3rdcoil
101.2G Fluxball no 3rdcoil
50.6G Fluxball 169.6G 3rdcoil
101.2G Fluxball 169.6G 3rdcoil
50.6G Fluxball 296.8G 3rdcoil
101.2G Fluxball 296.8G 3rdcoil

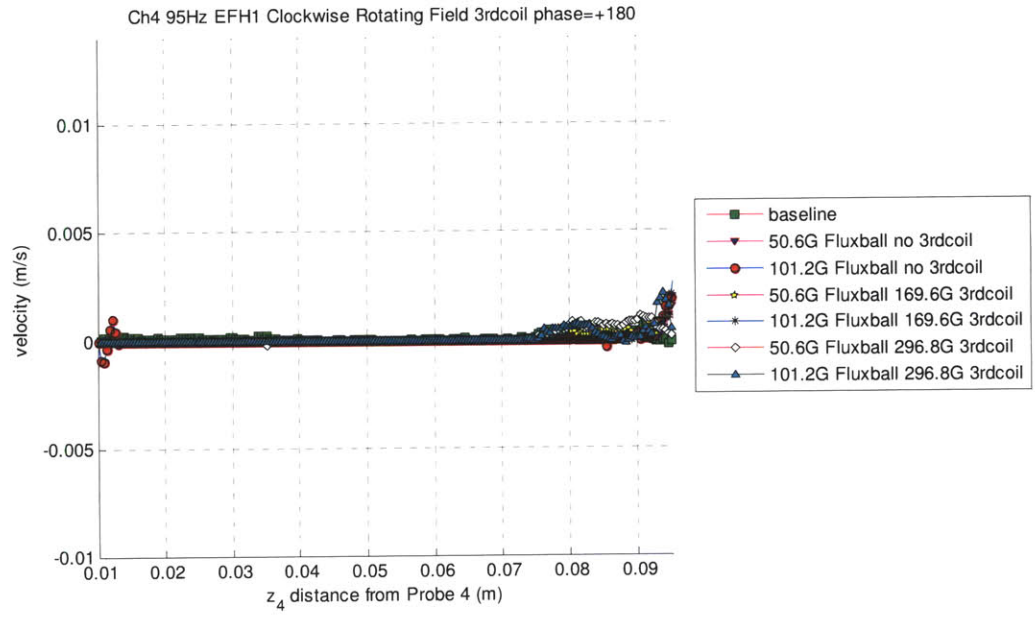
Ch4 95Hz EFH1 Clockwise Rotating Field 3rdcoil phase=+180
velocity (m/s)
0.01
0.005
0
-0.005
-0.01
0.01 0.02 0.03 0.04 0.05 0.06 0.07 0.08 0.09
z_4 distance from Probe 4 (m)
baseline
50.6G Fluxball no 3rdcoil
101.2G Fluxball no 3rdcoil
50.6G Fluxball 169.6G 3rdcoil
101.2G Fluxball 169.6G 3rdcoil
50.6G Fluxball 296.8G 3rdcoil
101.2G Fluxball 296.8G 3rdcoil

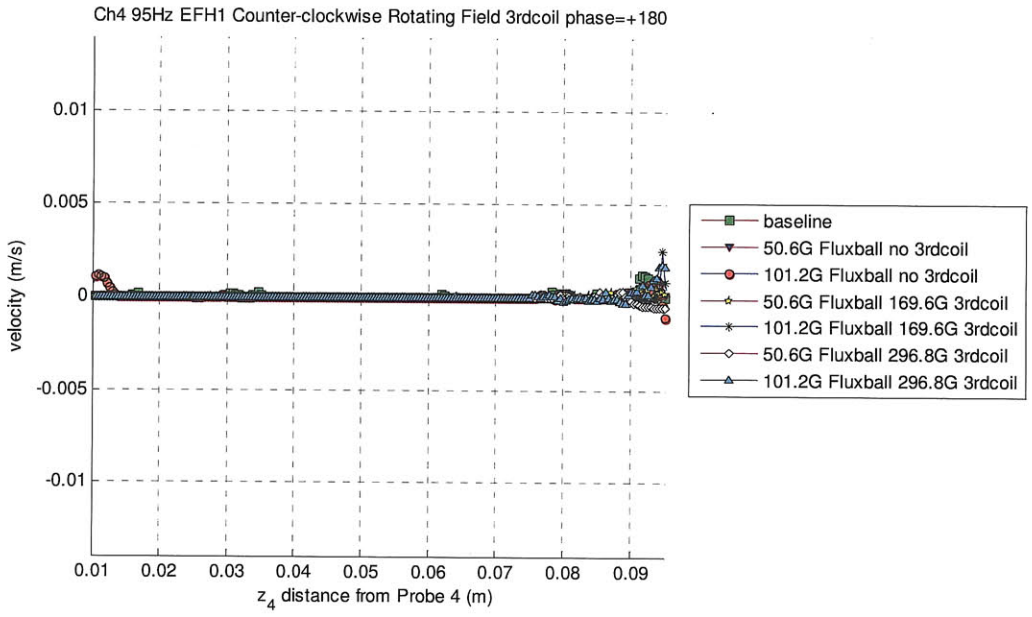
Ch4 95Hz EFH1 Counter-clockwise Rotating Field 3rdcoil phase=+180
velocity (m/s)
0.01
0.005
0
-0.005
-0.01
0.01 0.02 0.03 0.04 0.05 0.06 0.07 0.08 0.09
z4 distance from Probe 4 (m)
baseline
50.6G Fluxball no 3rdcoil
101.2G Fluxball no 3rdcoil
50.6G Fluxball 169.6G 3rdcoil
101.2G Fluxball 169.6G 3rdcoil
50.6G Fluxball 296.8G 3rdcoil
101.2G Fluxball 296.8G 3rdcoil

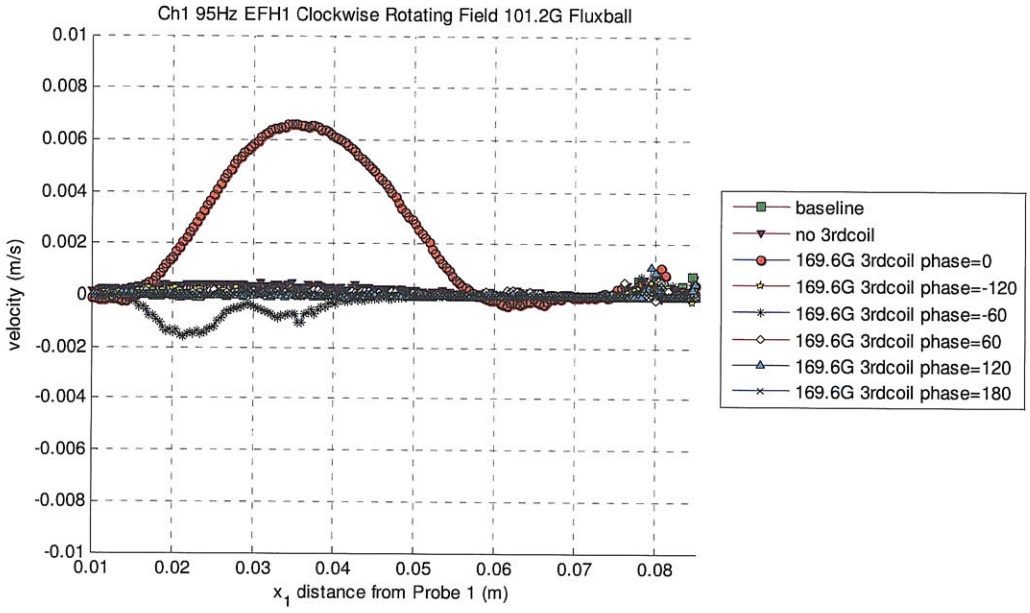
Ch1 95Hz EFH1 Clockwise Rotating Field 101.2G Fluxball
velocity (m/s)
0.01
0.008
0.006
0.004
0.002
0
-0.002
-0.004
-0.006
-0.008
-0.01
0.01 0.02 0.03 0.04 0.05 0.06 0.07 0.08
x1 distance from Probe 1 (m)
baseline
no 3rdcoil
169.6G 3rdcoil phase=0
169.6G 3rdcoil phase=-120
169.6G 3rdcoil phase=-60
169.6G 3rdcoil phase=60
169.6G 3rdcoil phase=120
169.6G 3rdcoil phase=180

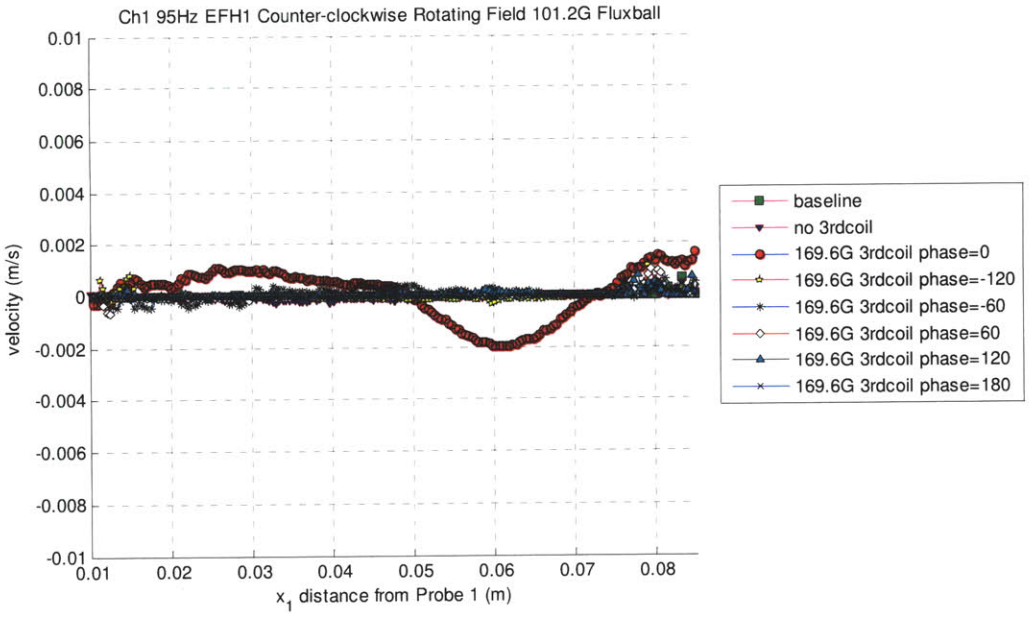
Ch1 95Hz EFH1 Counter-clockwise Rotating Field 101.2G Fluxball
velocity (m/s)
0.01
0.008
0.006
0.004
0.002
0
-0.002
-0.004
-0.006
-0.008
-0.01
0.01
0.02
0.03
0.04
0.05
0.06
0.07
0.08
x1 distance from Probe 1 (m)
baseline
no 3rdcoil
169.6G 3rdcoil phase=0
169.6G 3rdcoil phase=-120
169.6G 3rdcoil phase=-60
169.6G 3rdcoil phase=60
169.6G 3rdcoil phase=120
169.6G 3rdcoil phase=180

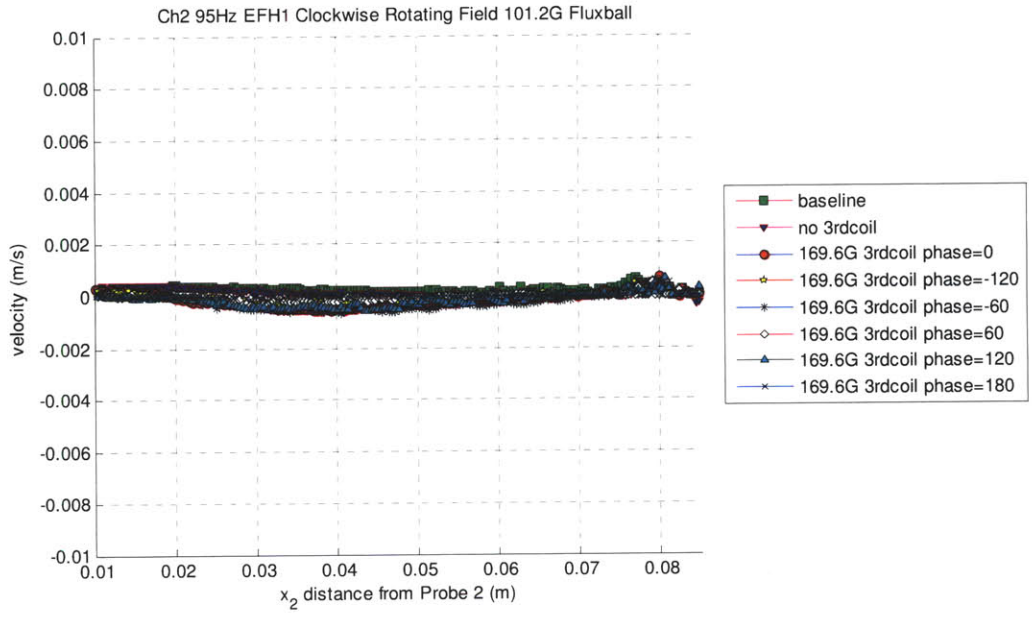
Ch2 95Hz EFH1 Clockwise Rotating Field 101.2G Fluxball
velocity (m/s)
0.01
0.008
0.006
0.004
0.002
0
-0.002
-0.004
-0.006
-0.008
-0.01
0.01
0.02
0.03
0.04
0.05
0.06
0.07
0.08
x2 distance from Probe 2 (m)
baseline
no 3rdcoil
169.6G 3rdcoil phase=0
169.6G 3rdcoil phase=-120
169.6G 3rdcoil phase=-60
169.6G 3rdcoil phase=60
169.6G 3rdcoil phase=120
169.6G 3rdcoil phase=180

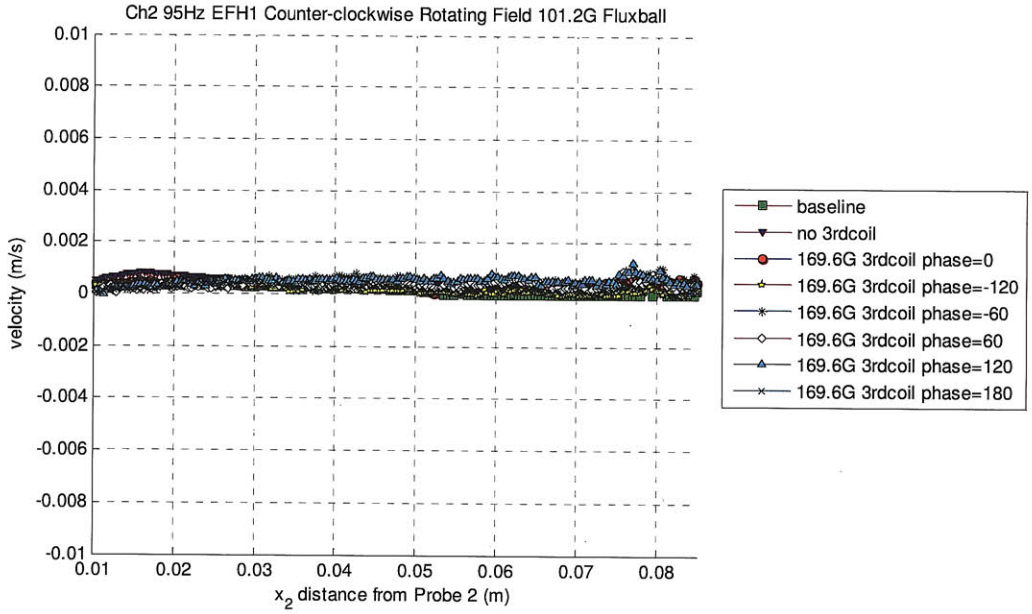
Ch2 95Hz EFH1 Counter-clockwise Rotating Field 101.2G Fluxball
velocity (m/s)
0.01
0.008
0.006
0.004
0.002
0
-0.002
-0.004
-0.006
-0.008
-0.01
0.01
0.02
0.03
0.04
0.05
0.06
0.07
0.08
x2 distance from Probe 2 (m)
baseline
no 3rdcoil
169.6G 3rdcoil phase=0
169.6G 3rdcoil phase=-120
169.6G 3rdcoil phase=-60
169.6G 3rdcoil phase=60
169.6G 3rdcoil phase=120
169.6G 3rdcoil phase=180

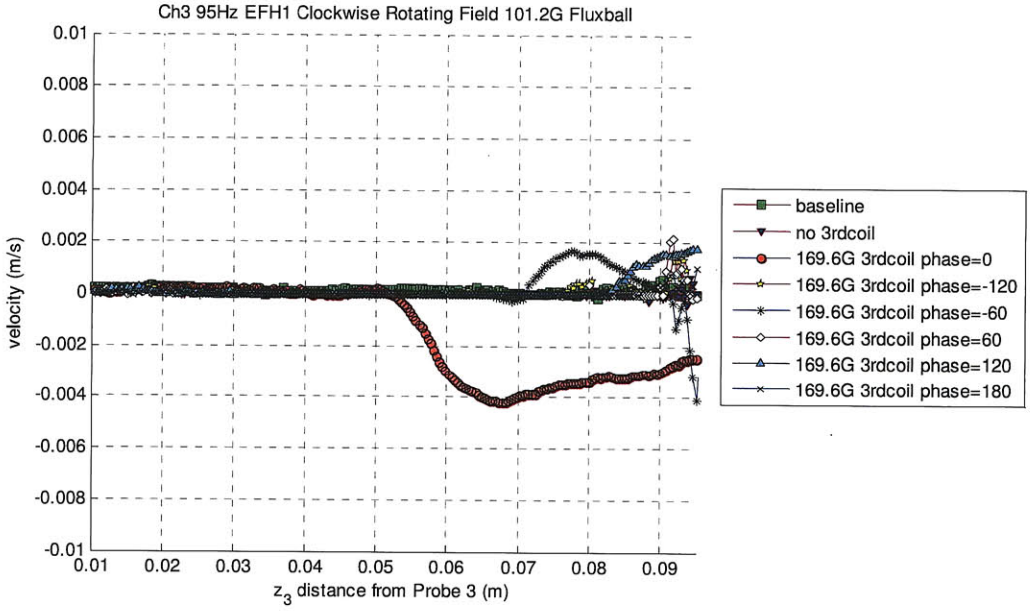
Ch3 95Hz EFH1 Clockwise Rotating Field 101.2G Fluxball
velocity (m/s)
0.01
0.008
0.006
0.004
0.002
0
-0.002
-0.004
-0.006
-0.008
-0.01
0.01
0.02
0.03
0.04
0.05
0.06
0.07
0.08
0.09
z3 distance from Probe 3 (m)
baseline
no 3rdcoil
169.6G 3rdcoil phase=0
169.6G 3rdcoil phase=-120
169.6G 3rdcoil phase=-60
169.6G 3rdcoil phase=60
169.6G 3rdcoil phase=120
169.6G 3rdcoil phase=180

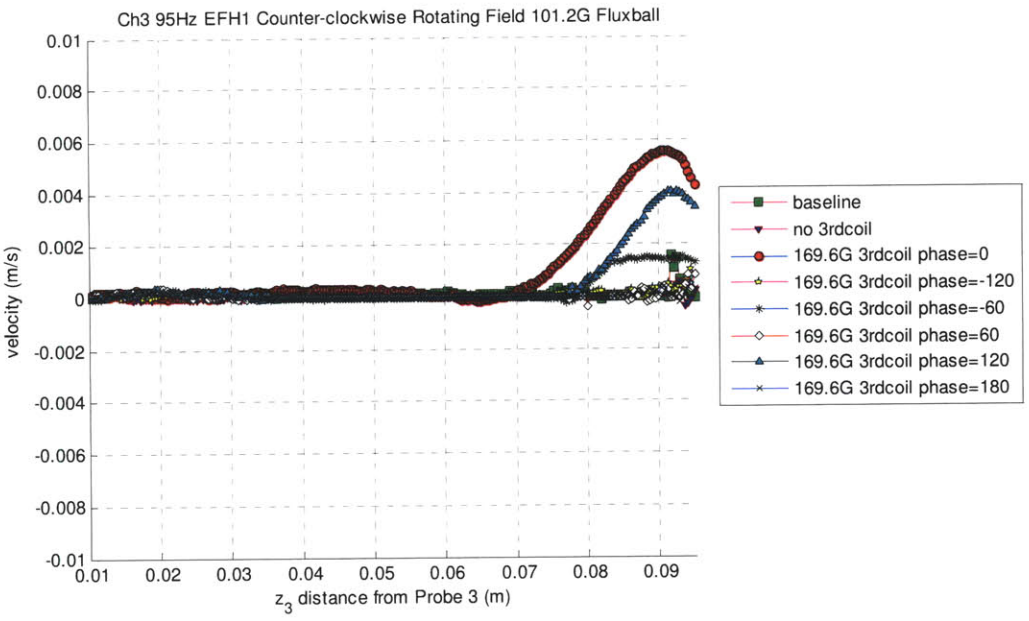
Ch3 95Hz EFH1 Counter-clockwise Rotating Field 101.2G Fluxball
velocity (m/s)
0.01
0.008
0.006
0.004
0.002
0
-0.002
-0.004
-0.006
-0.008
-0.01
0.01 0.02 0.03 0.04 0.05 0.06 0.07 0.08 0.09
z3 distance from Probe 3 (m)
baseline
no 3rdcoil
169.6G 3rdcoil phase=0
169.6G 3rdcoil phase=-120
169.6G 3rdcoil phase=-60
169.6G 3rdcoil phase=60
169.6G 3rdcoil phase=120
169.6G 3rdcoil phase=180

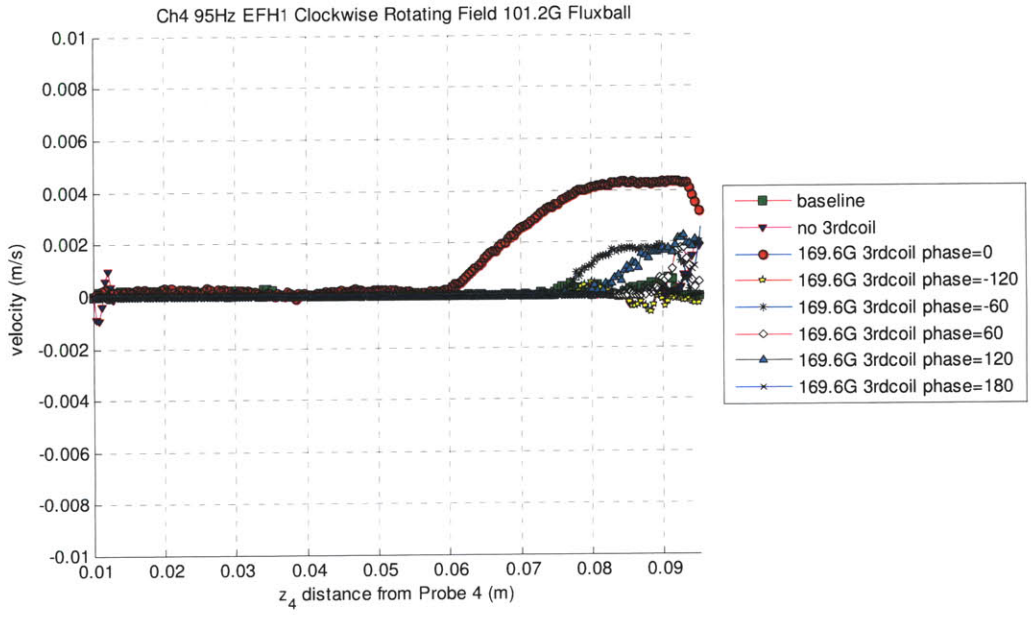
Ch4 95Hz EFH1 Clockwise Rotating Field 101.2G Fluxball
velocity (m/s)
0.01
0.008
0.006
0.004
0.002
0
-0.002
-0.004
-0.006
-0.008
-0.01
0.01 0.02 0.03 0.04 0.05 0.06 0.07 0.08 0.09
z4 distance from Probe 4 (m)
baseline
no 3rdcoil
169.6G 3rdcoil phase=0
169.6G 3rdcoil phase=-120
169.6G 3rdcoil phase=-60
169.6G 3rdcoil phase=60
169.6G 3rdcoil phase=120
169.6G 3rdcoil phase=180

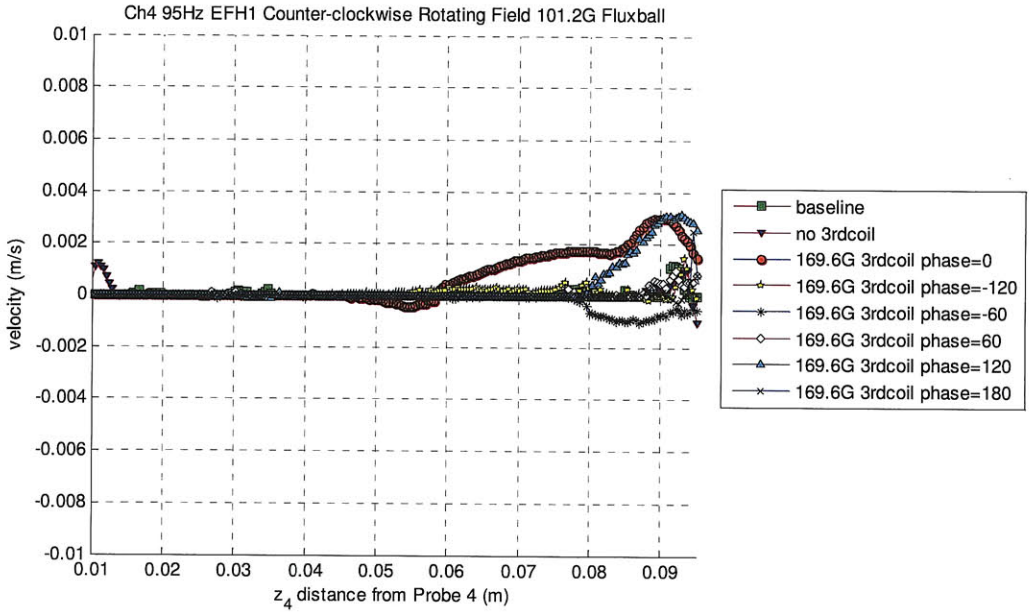
Ch4 95Hz EFH1 Counter-clockwise Rotating Field 101.2G Fluxball
velocity (m/s)
0.01
0.008
0.006
0.004
0.002
0
-0.002
-0.004
-0.006
-0.008
-0.01
0.01 0.02 0.03 0.04 0.05 0.06 0.07 0.08 0.09
z4 distance from Probe 4 (m)
baseline
no 3rdcoil
169.6G 3rdcoil phase=0
169.6G 3rdcoil phase=-120
169.6G 3rdcoil phase=-60
169.6G 3rdcoil phase=60
169.6G 3rdcoil phase=120
169.6G 3rdcoil phase=180

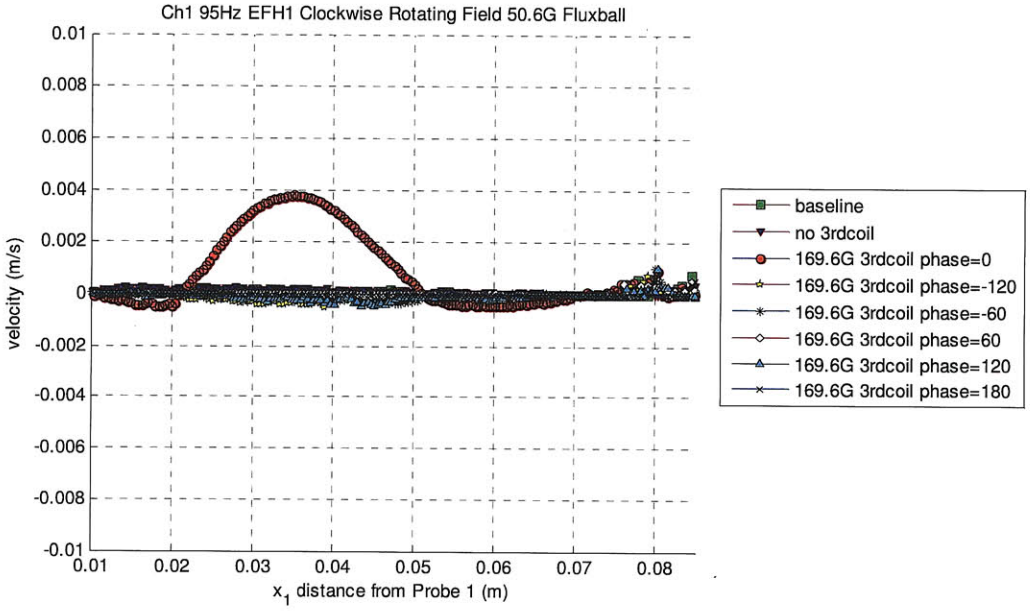
Ch1 95Hz EFH1 Clockwise Rotating Field 50.6G Fluxball
velocity (m/s)
0.01
0.008
0.006
0.004
0.002
0
-0.002
-0.004
-0.006
-0.008
-0.01
0.01 0.02 0.03 0.04 0.05 0.06 0.07 0.08
x1 distance from Probe 1 (m)
baseline
no 3rdcoil
169.6G 3rdcoil phase=0
169.6G 3rdcoil phase=-120
169.6G 3rdcoil phase=-60
169.6G 3rdcoil phase=60
169.6G 3rdcoil phase=120
169.6G 3rdcoil phase=180

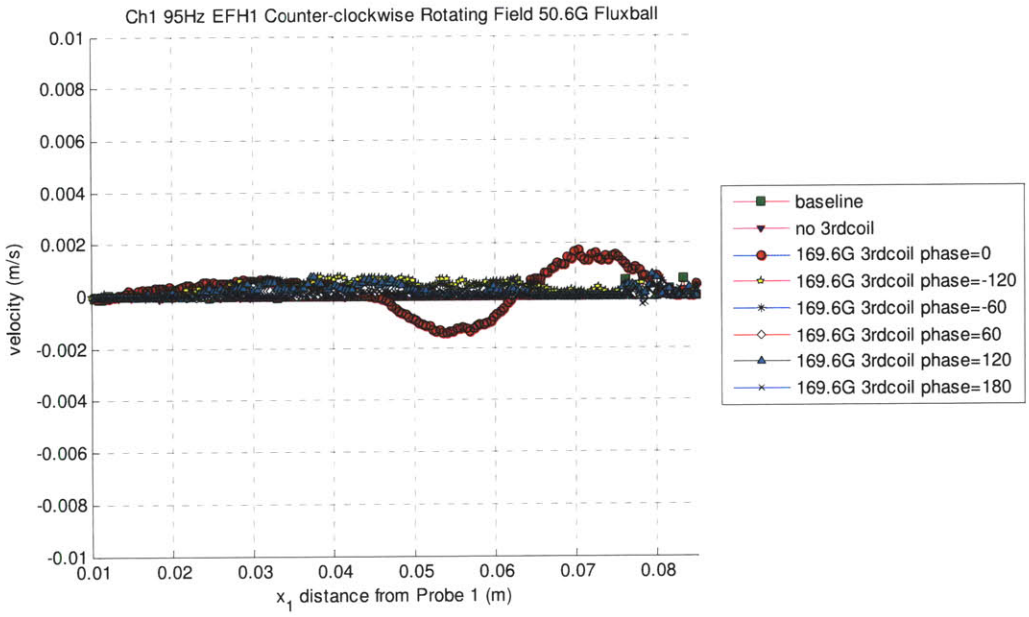
Ch1 95Hz EFH1 Counter-clockwise Rotating Field 50.6G Fluxball
velocity (m/s)
0.01
0.008
0.006
0.004
0.002
0
-0.002
-0.004
-0.006
-0.008
-0.01
0.01
0.02
0.03
0.04
0.05
0.06
0.07
0.08
x1 distance from Probe 1 (m)
baseline
no 3rdcoil
169.6G 3rdcoil phase=0
169.6G 3rdcoil phase=-120
169.6G 3rdcoil phase=-60
169.6G 3rdcoil phase=60
169.6G 3rdcoil phase=120
169.6G 3rdcoil phase=180

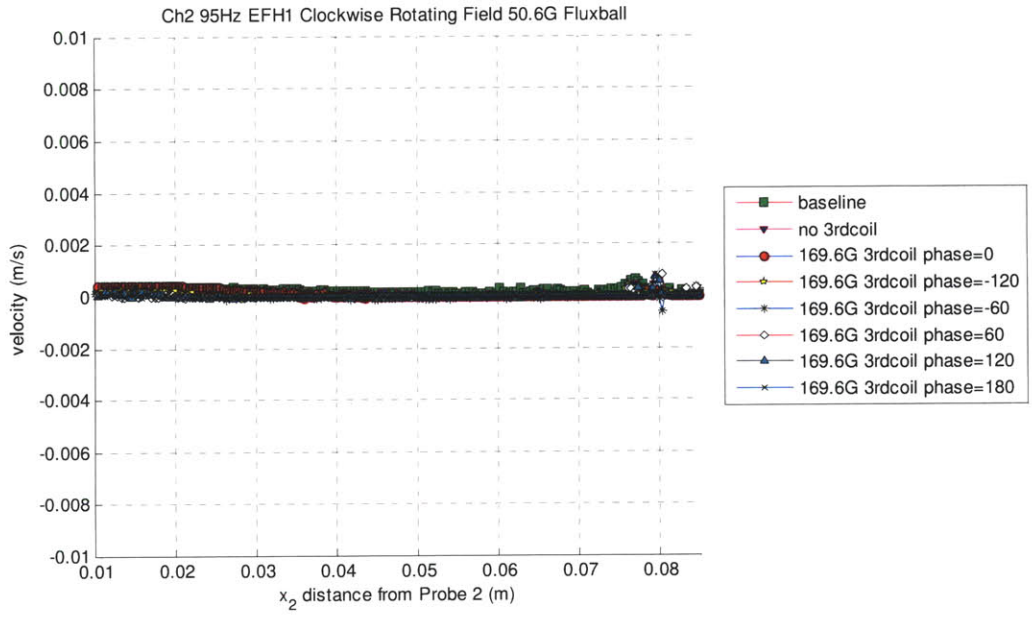
Ch2 95Hz EFH1 Clockwise Rotating Field 50.6G Fluxball
velocity (m/s)
0.01
0.008
0.006
0.004
0.002
0
-0.002
-0.004
-0.006
-0.008
-0.01
0.01
0.02
0.03
0.04
0.05
0.06
0.07
0.08
x2 distance from Probe 2 (m)
baseline
no 3rdcoil
169.6G 3rdcoil phase=0
169.6G 3rdcoil phase=-120
169.6G 3rdcoil phase=-60
169.6G 3rdcoil phase=60
169.6G 3rdcoil phase=120
169.6G 3rdcoil phase=180

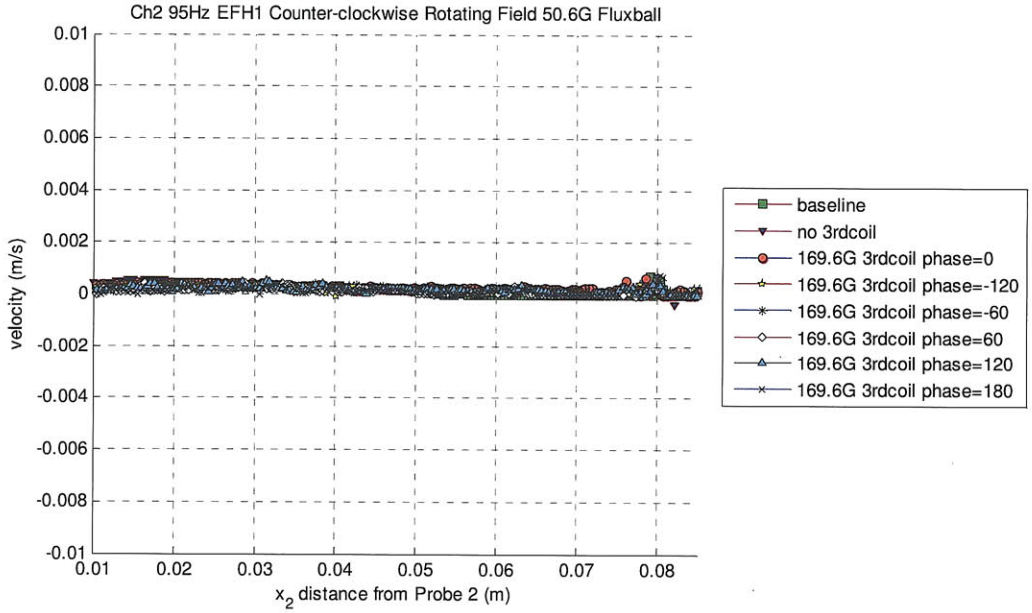
Ch2 95Hz EFH1 Counter-clockwise Rotating Field 50.6G Fluxball
velocity (m/s)
0.01
0.008
0.006
0.004
0.002
0
-0.002
-0.004
-0.006
-0.008
-0.01
0.01 0.02 0.03 0.04 0.05 0.06 0.07 0.08
x2 distance from Probe 2 (m)
baseline
no 3rdcoil
169.6G 3rdcoil phase=0
169.6G 3rdcoil phase=-120
169.6G 3rdcoil phase=-60
169.6G 3rdcoil phase=60
169.6G 3rdcoil phase=120
169.6G 3rdcoil phase=180

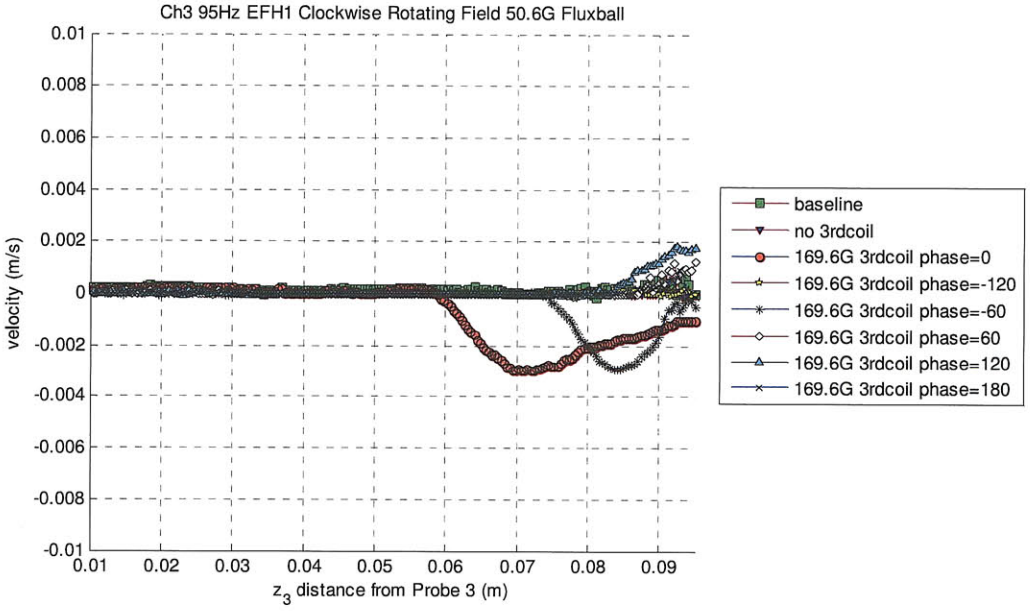
Ch3 95Hz EFH1 Clockwise Rotating Field 50.6G Fluxball
velocity (m/s)
0.01
0.008
0.006
0.004
0.002
0
-0.002
-0.004
-0.006
-0.008
-0.01
0.01 0.02 0.03 0.04 0.05 0.06 0.07 0.08 0.09
z3 distance from Probe 3 (m)
baseline
no 3rdcoil
169.6G 3rdcoil phase=0
169.6G 3rdcoil phase=-120
169.6G 3rdcoil phase=-60
169.6G 3rdcoil phase=60
169.6G 3rdcoil phase=120
169.6G 3rdcoil phase=180

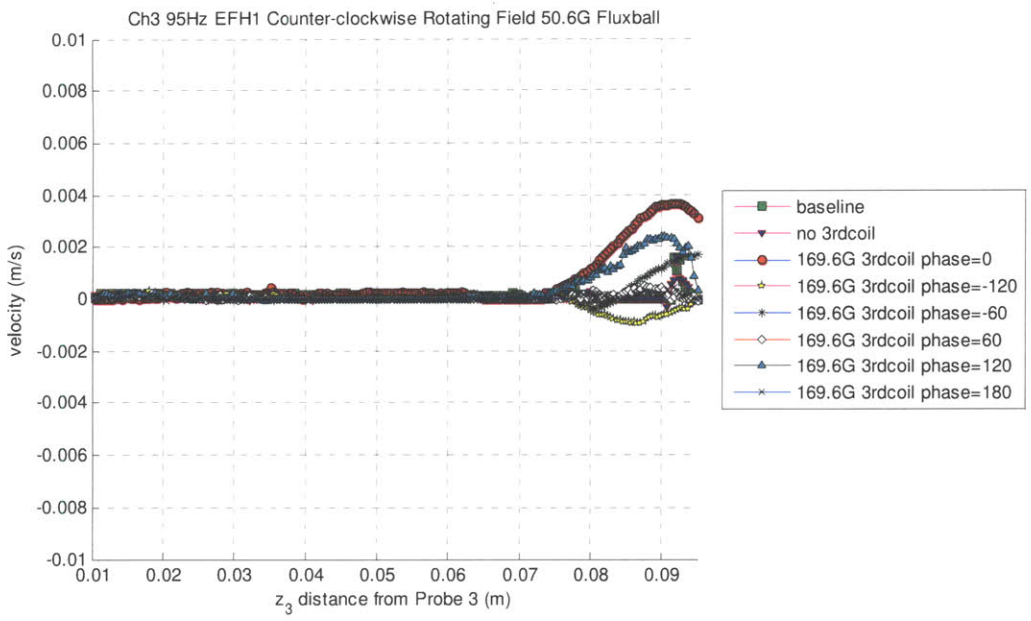
Ch3 95Hz EFH1 Counter-clockwise Rotating Field 50.6G Fluxball
velocity (m/s)
0.01
0.008
0.006
0.004
0.002
0
-0.002
-0.004
-0.006
-0.008
-0.01
0.01 0.02 0.03 0.04 0.05 0.06 0.07 0.08 0.09
z3 distance from Probe 3 (m)
baseline
no 3rdcoil
169.6G 3rdcoil phase=0
169.6G 3rdcoil phase=-120
169.6G 3rdcoil phase=-60
169.6G 3rdcoil phase=60
169.6G 3rdcoil phase=120
169.6G 3rdcoil phase=180

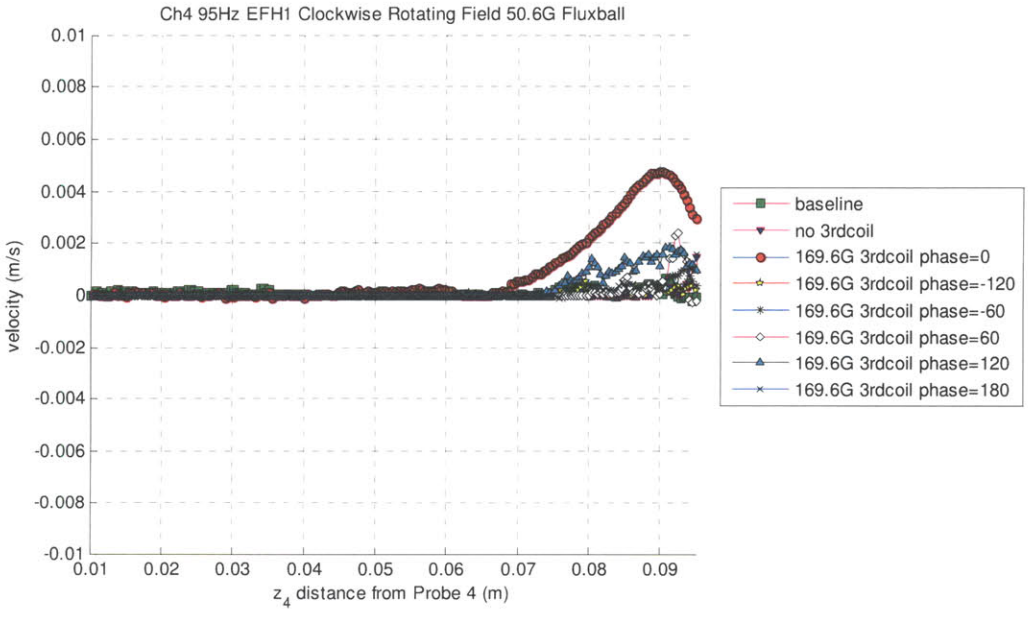
Ch4 95Hz EFH1 Clockwise Rotating Field 50.6G Fluxball
velocity (m/s)
0.01
0.008
0.006
0.004
0.002
0
-0.002
-0.004
-0.006
-0.008
-0.01
0.01 0.02 0.03 0.04 0.05 0.06 0.07 0.08 0.09
z4 distance from Probe 4 (m)
baseline
no 3rdcoil
169.6G 3rdcoil phase=0
169.6G 3rdcoil phase=-120
169.6G 3rdcoil phase=-60
169.6G 3rdcoil phase=60
169.6G 3rdcoil phase=120
169.6G 3rdcoil phase=180

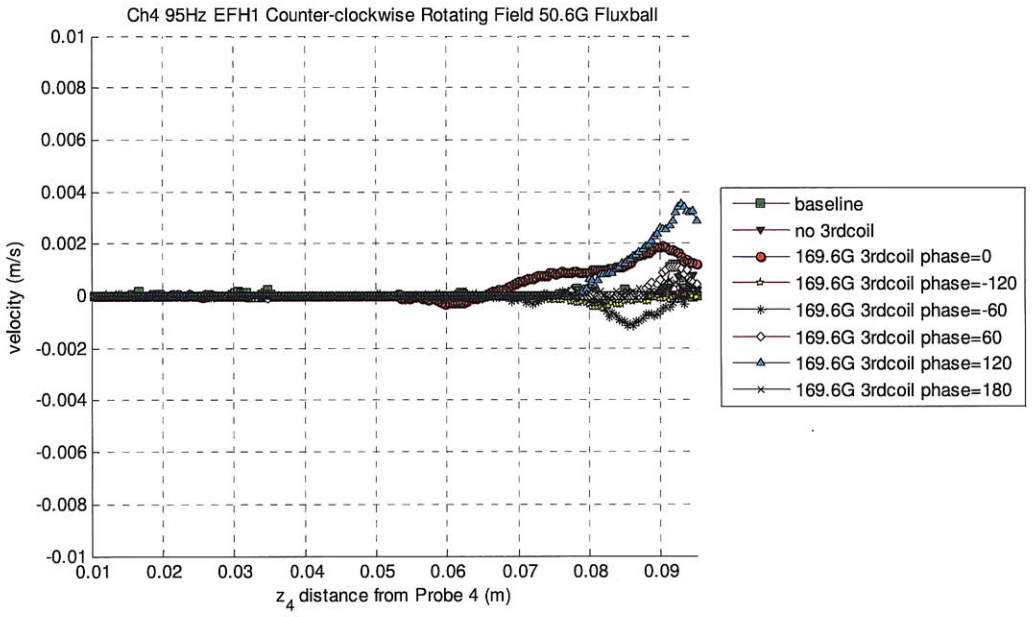
Ch4 95Hz EFH1 Counter-clockwise Rotating Field 50.6G Fluxball
velocity (m/s)
0.01
0.008
0.006
0.004
0.002
0
-0.002
-0.004
-0.006
-0.008
-0.01
0.01 0.02 0.03 0.04 0.05 0.06 0.07 0.08 0.09
z4 distance from Probe 4 (m)
baseline
no 3rdcoil
169.6G 3rdcoil phase=0
169.6G 3rdcoil phase=-120
169.6G 3rdcoil phase=-60
169.6G 3rdcoil phase=60
169.6G 3rdcoil phase=120
169.6G 3rdcoil phase=180

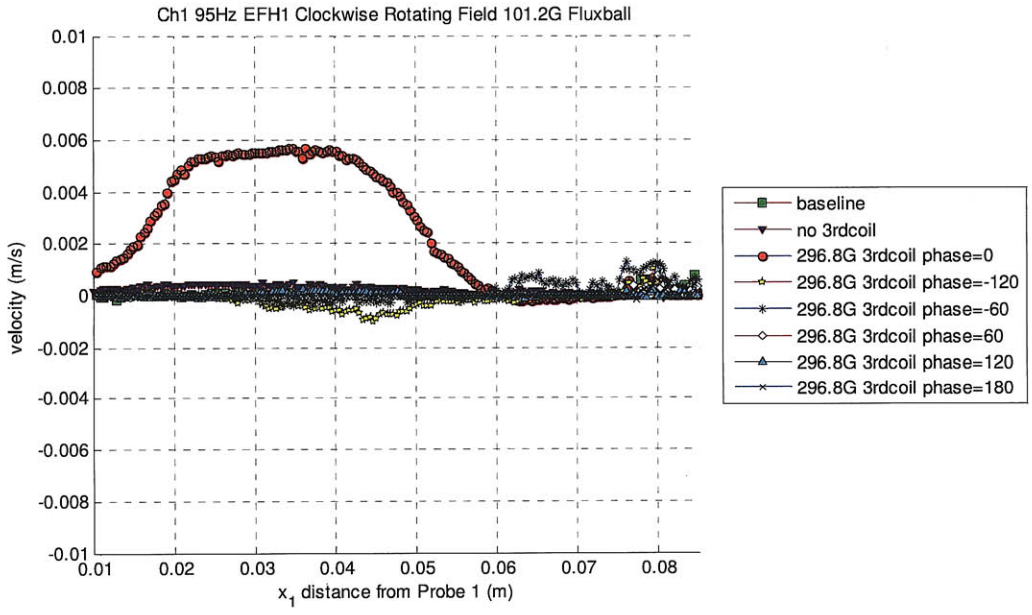
Ch1 95Hz EFH1 Clockwise Rotating Field 101.2G Fluxball
velocity (m/s)
0.01
0.008
0.006
0.004
0.002
0
-0.002
-0.004
-0.006
-0.008
-0.01
0.01 0.02 0.03 0.04 0.05 0.06 0.07 0.08
x1 distance from Probe 1 (m)
baseline
no 3rdcoil
296.8G 3rdcoil phase=0
296.8G 3rdcoil phase=-120
296.8G 3rdcoil phase=-60
296.8G 3rdcoil phase=60
296.8G 3rdcoil phase=120
296.8G 3rdcoil phase=180

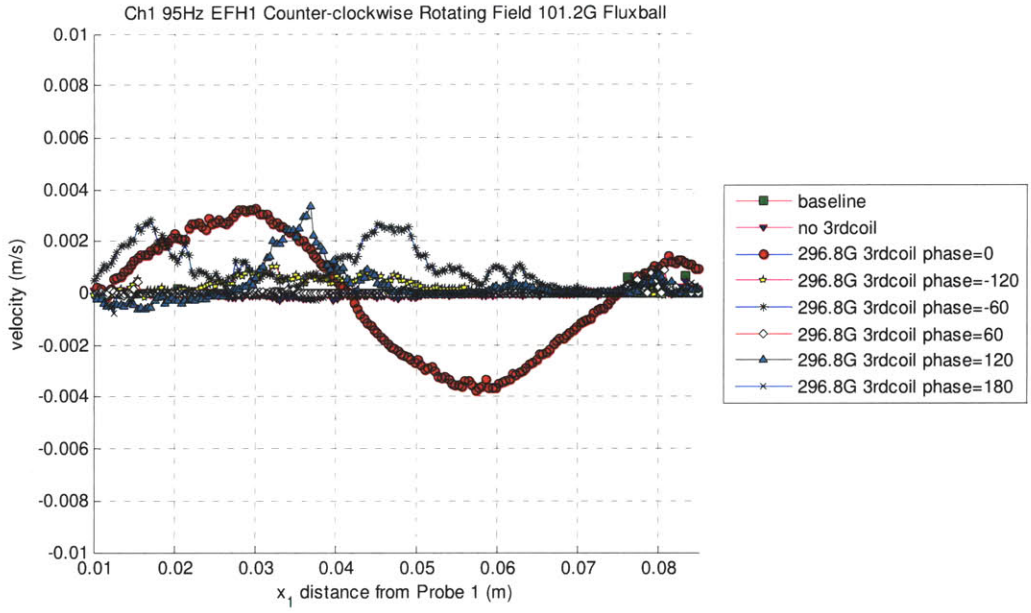
Ch1 95Hz EFH1 Counter-clockwise Rotating Field 101.2G Fluxball
velocity (m/s)
0.01
0.008
0.006
0.004
0.002
0
-0.002
-0.004
-0.006
-0.008
-0.01
0.01
0.02
0.03
0.04
0.05
0.06
0.07
0.08
x1 distance from Probe 1 (m)
baseline
no 3rdcoil
296.8G 3rdcoil phase=0
296.8G 3rdcoil phase=-120
296.8G 3rdcoil phase=-60
296.8G 3rdcoil phase=60
296.8G 3rdcoil phase=120
296.8G 3rdcoil phase=180

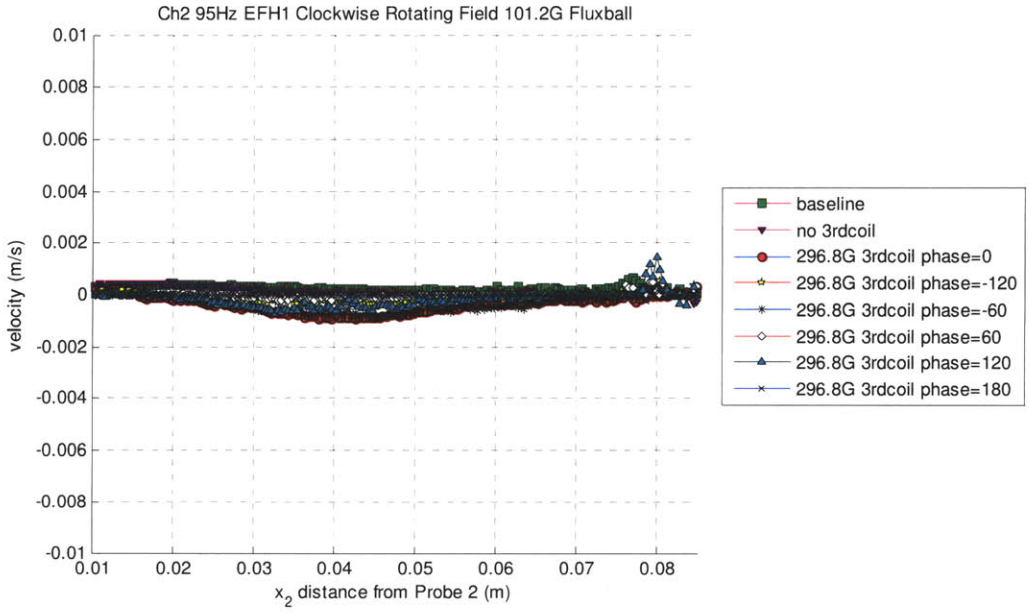
Ch2 95Hz EFH1 Clockwise Rotating Field 101.2G Fluxball
velocity (m/s)
0.01
0.008
0.006
0.004
0.002
0
-0.002
-0.004
-0.006
-0.008
-0.01
0.01
0.02
0.03
0.04
0.05
0.06
0.07
0.08
x2 distance from Probe 2 (m)
baseline
no 3rdcoil
296.8G 3rdcoil phase=0
296.8G 3rdcoil phase=-120
296.8G 3rdcoil phase=-60
296.8G 3rdcoil phase=60
296.8G 3rdcoil phase=120
296.8G 3rdcoil phase=180

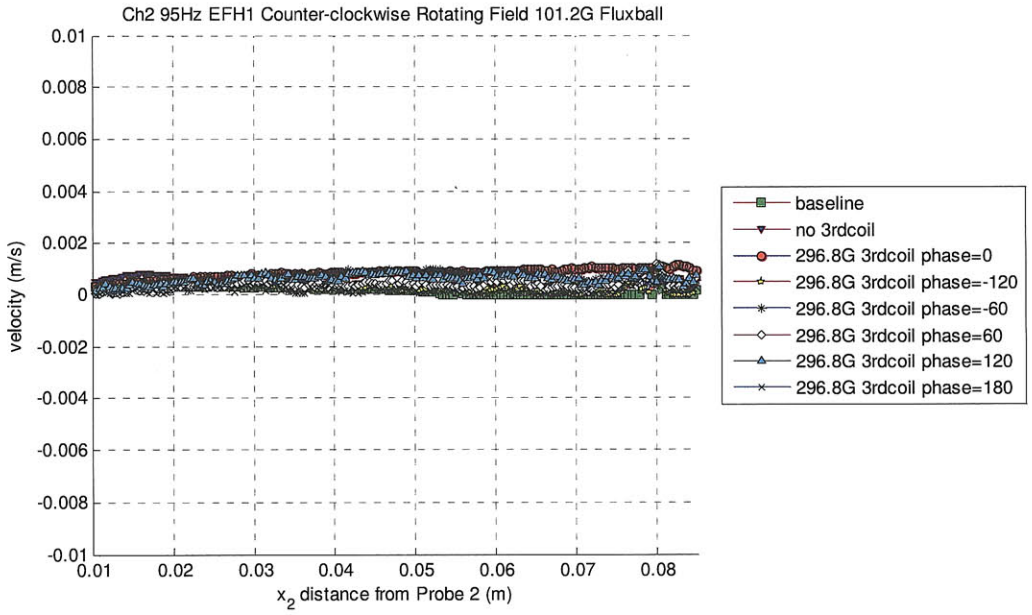
Ch2 95Hz EFH1 Counter-clockwise Rotating Field 101.2G Fluxball
velocity (m/s)
0.01
0.008
0.006
0.004
0.002
0
-0.002
-0.004
-0.006
-0.008
-0.01
0.01
0.02
0.03
0.04
0.05
0.06
0.07
0.08
x2 distance from Probe 2 (m)
baseline
no 3rdcoil
296.8G 3rdcoil phase=0
296.8G 3rdcoil phase=-120
296.8G 3rdcoil phase=-60
296.8G 3rdcoil phase=60
296.8G 3rdcoil phase=120
296.8G 3rdcoil phase=180

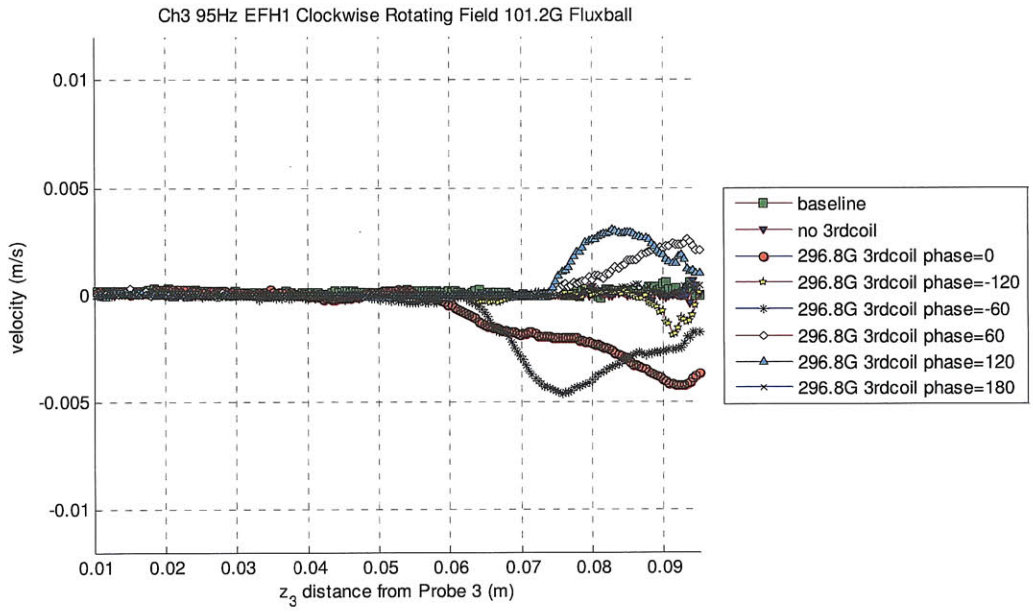
Ch3 95Hz EFH1 Clockwise Rotating Field 101.2G Fluxball
velocity (m/s)
0.01
0.005
0
-0.005
-0.01
0.01
0.02
0.03
0.04
0.05
0.06
0.07
0.08
0.09
z3 distance from Probe 3 (m)
baseline
no 3rdcoil
296.8G 3rdcoil phase=0
296.8G 3rdcoil phase=-120
296.8G 3rdcoil phase=-60
296.8G 3rdcoil phase=60
296.8G 3rdcoil phase=120
296.8G 3rdcoil phase=180

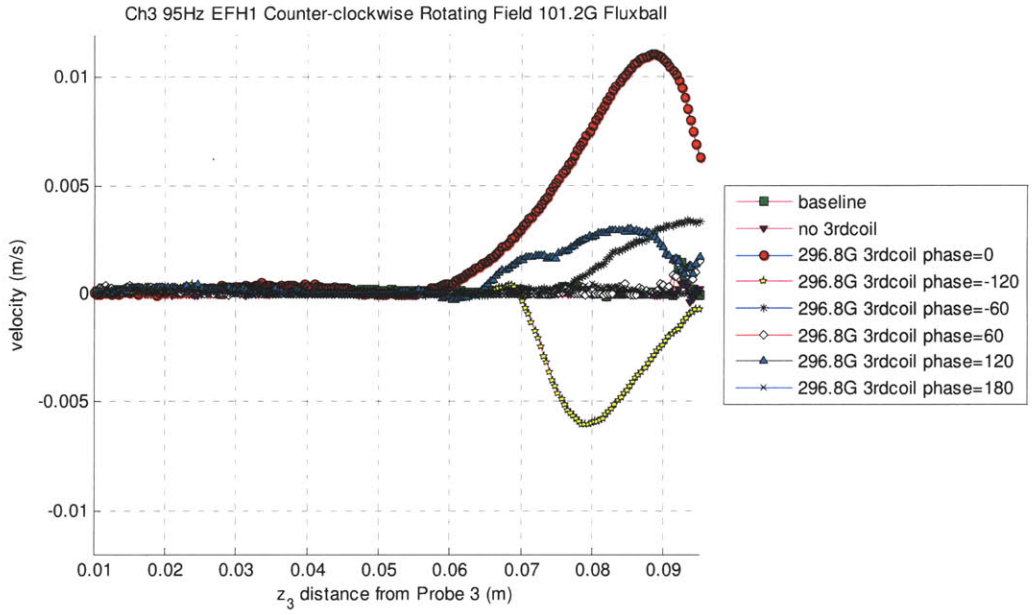
Ch3 95Hz EFH1 Counter-clockwise Rotating Field 101.2G Fluxball
velocity (m/s)
0.01
0.005
0
-0.005
-0.01
0.01
0.02
0.03
0.04
0.05
0.06
0.07
0.08
0.09
z3 distance from Probe 3 (m)
baseline
no 3rdcoil
296.8G 3rdcoil phase=0
296.8G 3rdcoil phase=-120
296.8G 3rdcoil phase=-60
296.8G 3rdcoil phase=60
296.8G 3rdcoil phase=120
296.8G 3rdcoil phase=180

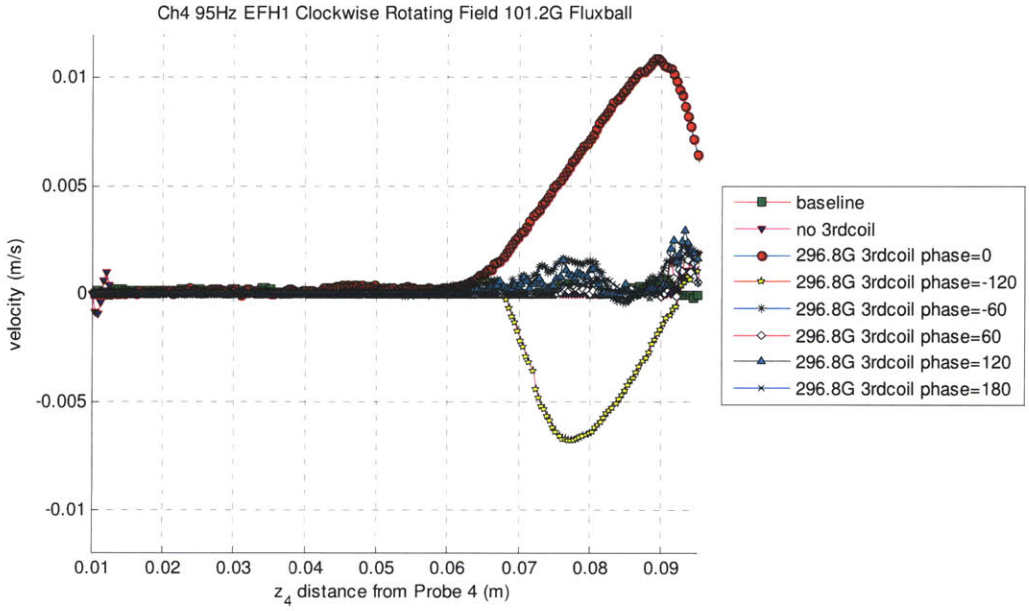
Ch4 95Hz EFH1 Clockwise Rotating Field 101.2G Fluxball
velocity (m/s)
0.01
0.005
0
-0.005
-0.01
0.01
0.02
0.03
0.04
0.05
0.06
0.07
0.08
0.09
z4 distance from Probe 4 (m)
baseline
no 3rdcoil
296.8G 3rdcoil phase=0
296.8G 3rdcoil phase=-120
296.8G 3rdcoil phase=-60
296.8G 3rdcoil phase=60
296.8G 3rdcoil phase=120
296.8G 3rdcoil phase=180

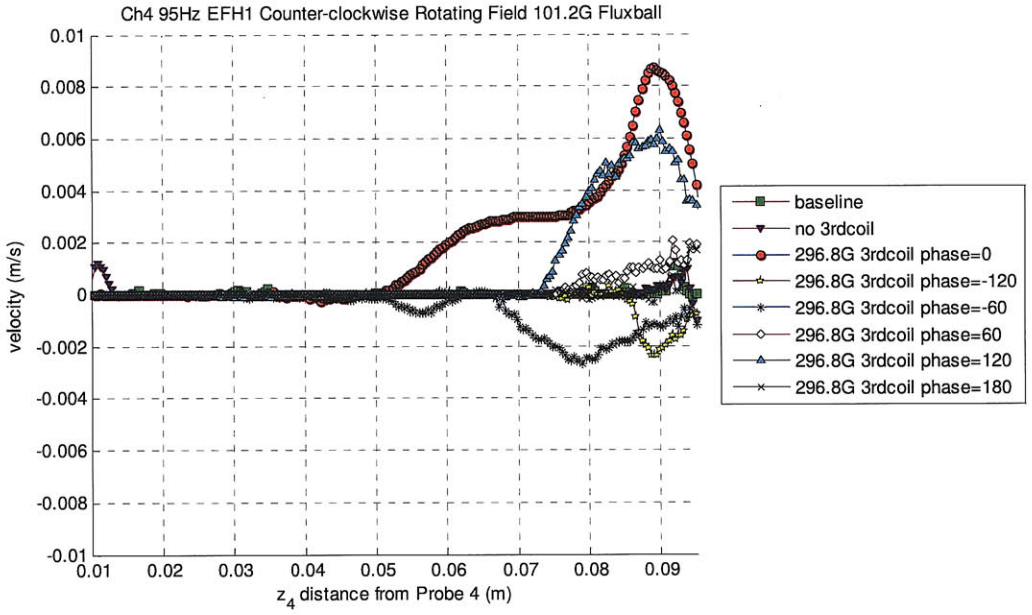
Ch4 95Hz EFH1 Counter-clockwise Rotating Field 101.2G Fluxball
velocity (m/s)
0.01
0.008
0.006
0.004
0.002
0
-0.002
-0.004
-0.006
-0.008
-0.01
0.01 0.02 0.03 0.04 0.05 0.06 0.07 0.08 0.09
z4 distance from Probe 4 (m)
baseline
no 3rdcoil
296.8G 3rdcoil phase=0
296.8G 3rdcoil phase=-120
296.8G 3rdcoil phase=-60
296.8G 3rdcoil phase=60
296.8G 3rdcoil phase=120
296.8G 3rdcoil phase=180

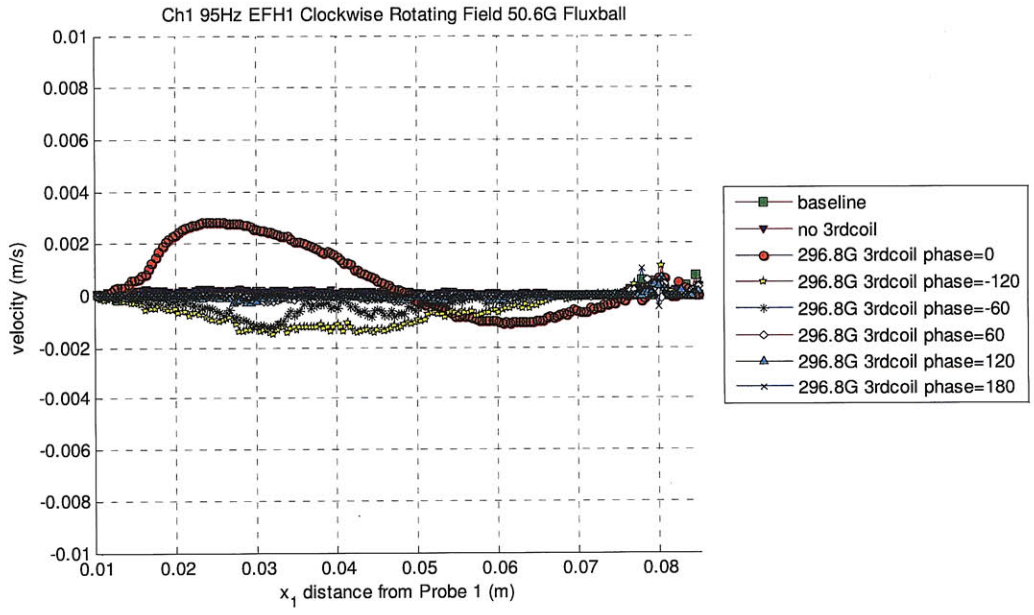
Ch1 95Hz EFH1 Clockwise Rotating Field 50.6G Fluxball
velocity (m/s)
0.01
0.008
0.006
0.004
0.002
0
-0.002
-0.004
-0.006
-0.008
-0.01
0.01 0.02 0.03 0.04 0.05 0.06 0.07 0.08
x1 distance from Probe 1 (m)
baseline
no 3rdcoil
296.8G 3rdcoil phase=0
296.8G 3rdcoil phase=-120
296.8G 3rdcoil phase=-60
296.8G 3rdcoil phase=60
296.8G 3rdcoil phase=120
296.8G 3rdcoil phase=180

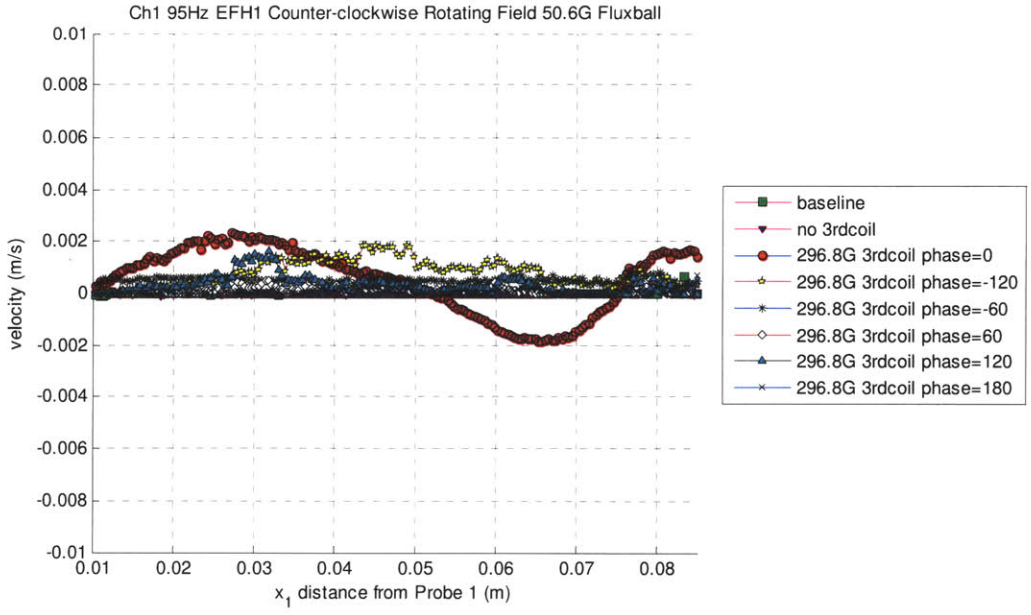
Ch1 95Hz EFH1 Counter-clockwise Rotating Field 50.6G Fluxball
velocity (m/s)
0.01
0.008
0.006
0.004
0.002
0
-0.002
-0.004
-0.006
-0.008
-0.01
0.01
0.02
0.03
0.04
0.05
0.06
0.07
0.08
x1 distance from Probe 1 (m)
baseline
no 3rdcoil
296.8G 3rdcoil phase=0
296.8G 3rdcoil phase=-120
296.8G 3rdcoil phase=-60
296.8G 3rdcoil phase=60
296.8G 3rdcoil phase=120
296.8G 3rdcoil phase=180

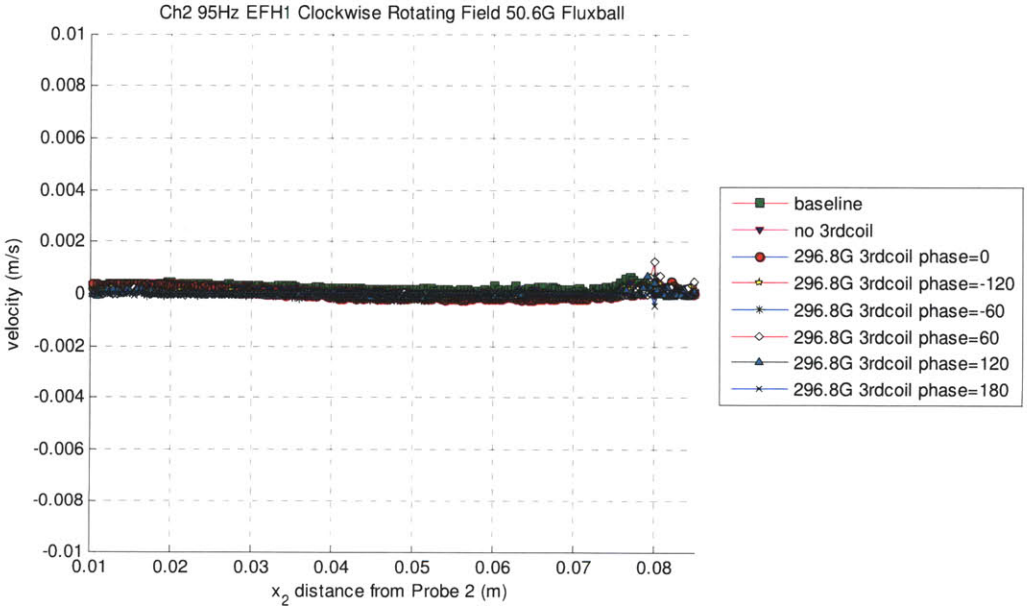
Ch2 95Hz EFH1 Clockwise Rotating Field 50.6G Fluxball
velocity (m/s)
0.01
0.008
0.006
0.004
0.002
0
-0.002
-0.004
-0.006
-0.008
-0.01
0.01
0.02
0.03
0.04
0.05
0.06
0.07
0.08
x2 distance from Probe 2 (m)
baseline
no 3rdcoil
296.8G 3rdcoil phase=0
296.8G 3rdcoil phase=-120
296.8G 3rdcoil phase=-60
296.8G 3rdcoil phase=60
296.8G 3rdcoil phase=120
296.8G 3rdcoil phase=180

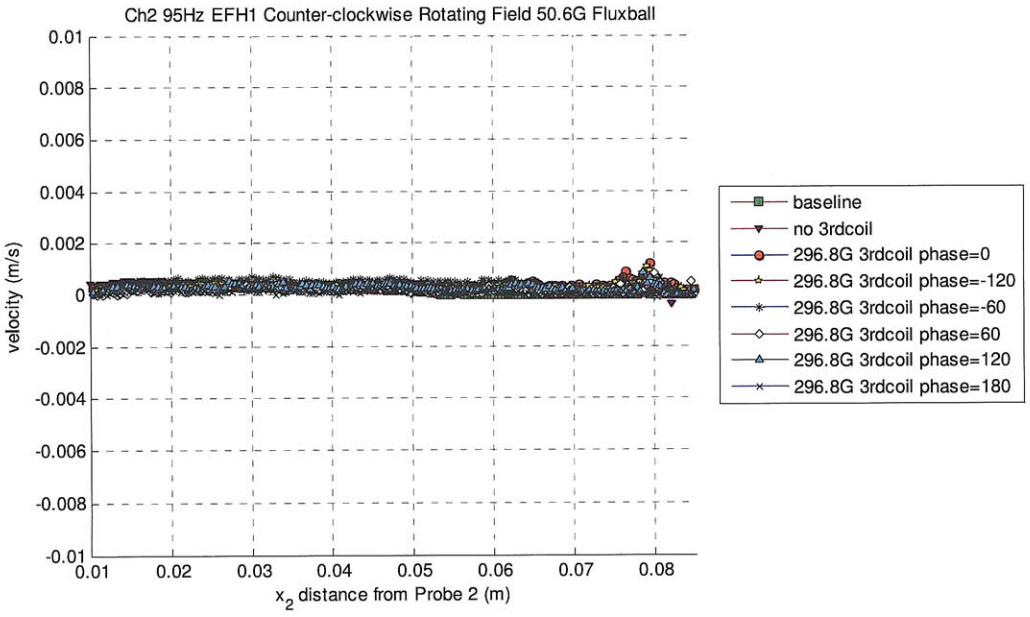
Ch2 95Hz EFH1 Counter-clockwise Rotating Field 50.6G Fluxball
velocity (m/s)
0.01
0.008
0.006
0.004
0.002
0
-0.002
-0.004
-0.006
-0.008
-0.01
0.01
0.02
0.03
0.04
0.05
0.06
0.07
0.08
x2 distance from Probe 2 (m)
baseline
no 3rdcoil
296.8G 3rdcoil phase=0
296.8G 3rdcoil phase=-120
296.8G 3rdcoil phase=-60
296.8G 3rdcoil phase=60
296.8G 3rdcoil phase=120
296.8G 3rdcoil phase=180

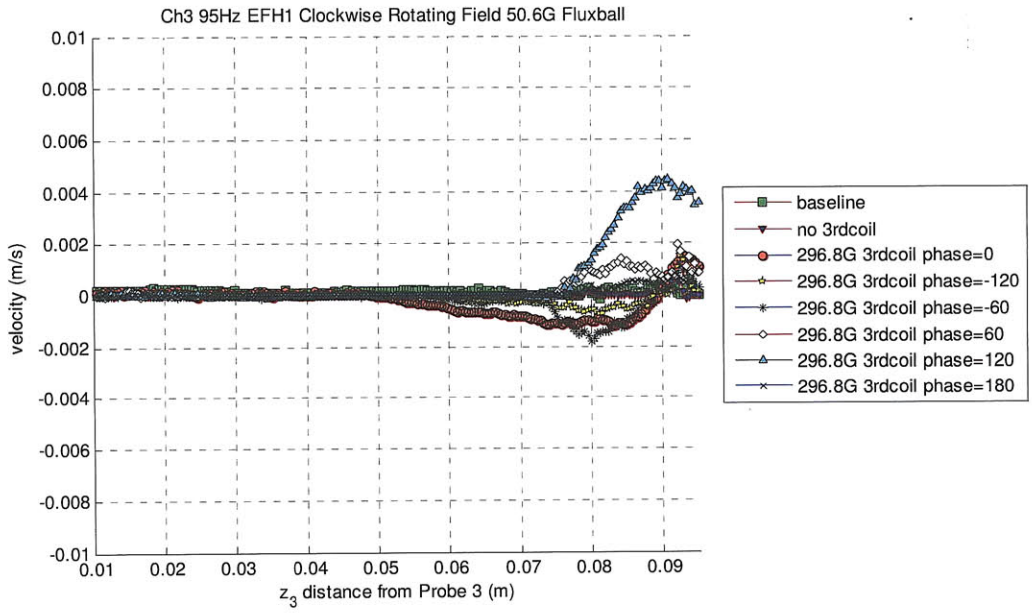
Ch3 95Hz EFH1 Clockwise Rotating Field 50.6G Fluxball
velocity (m/s)
0.01
0.008
0.006
0.004
0.002
0
-0.002
-0.004
-0.006
-0.008
-0.01
0.01
0.02
0.03
0.04
0.05
0.06
0.07
0.08
0.09
z3 distance from Probe 3 (m)
baseline
no 3rdcoil
296.8G 3rdcoil phase=0
296.8G 3rdcoil phase=-120
296.8G 3rdcoil phase=-60
296.8G 3rdcoil phase=60
296.8G 3rdcoil phase=120
296.8G 3rdcoil phase=180

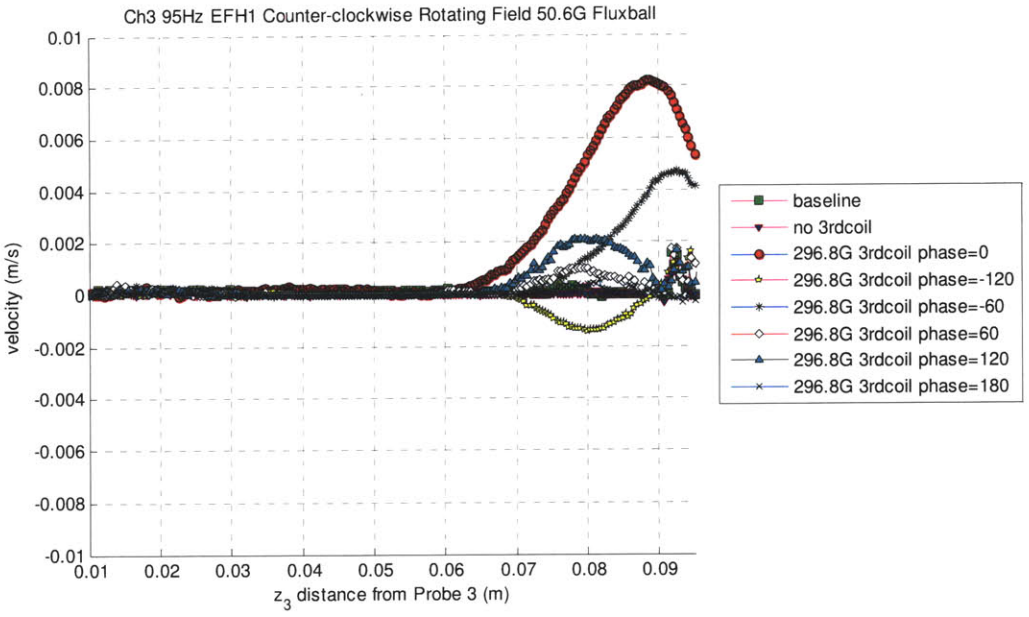
Ch3 95Hz EFH1 Counter-clockwise Rotating Field 50.6G Fluxball
velocity (m/s)
0.01
0.008
0.006
0.004
0.002
0
-0.002
-0.004
-0.006
-0.008
-0.01
0.01 0.02 0.03 0.04 0.05 0.06 0.07 0.08 0.09
z3 distance from Probe 3 (m)
baseline
no 3rdcoil
296.8G 3rdcoil phase=0
296.8G 3rdcoil phase=-120
296.8G 3rdcoil phase=-60
296.8G 3rdcoil phase=60
296.8G 3rdcoil phase=120
296.8G 3rdcoil phase=180

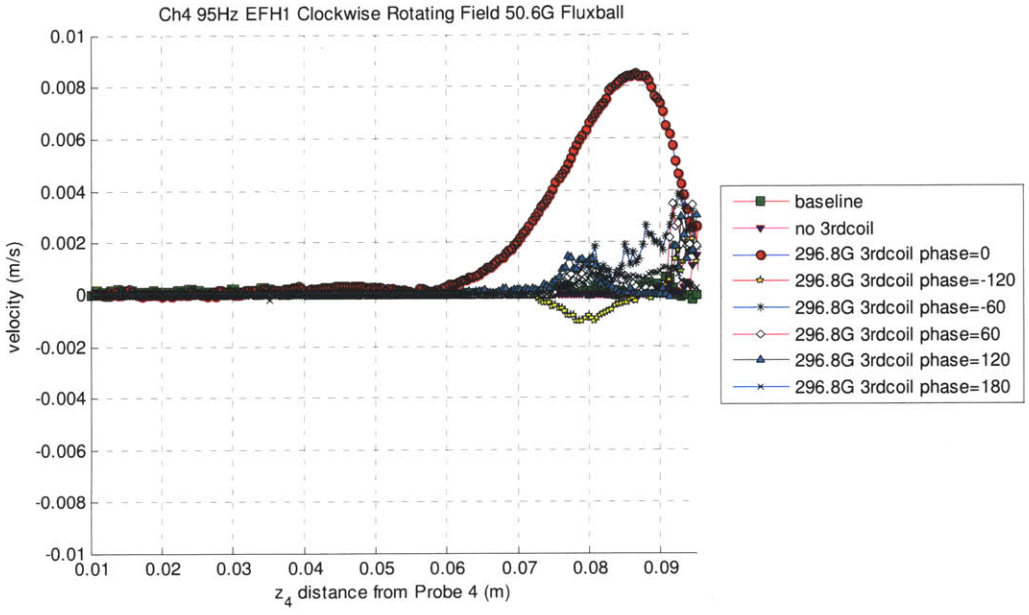
Ch4 95Hz EFH1 Clockwise Rotating Field 50.6G Fluxball
velocity (m/s)
0.01
0.008
0.006
0.004
0.002
0
-0.002
-0.004
-0.006
-0.008
-0.01
0.01 0.02 0.03 0.04 0.05 0.06 0.07 0.08 0.09
z4 distance from Probe 4 (m)
baseline
no 3rdcoil
296.8G 3rdcoil phase=0
296.8G 3rdcoil phase=-120
296.8G 3rdcoil phase=-60
296.8G 3rdcoil phase=60
296.8G 3rdcoil phase=120
296.8G 3rdcoil phase=180

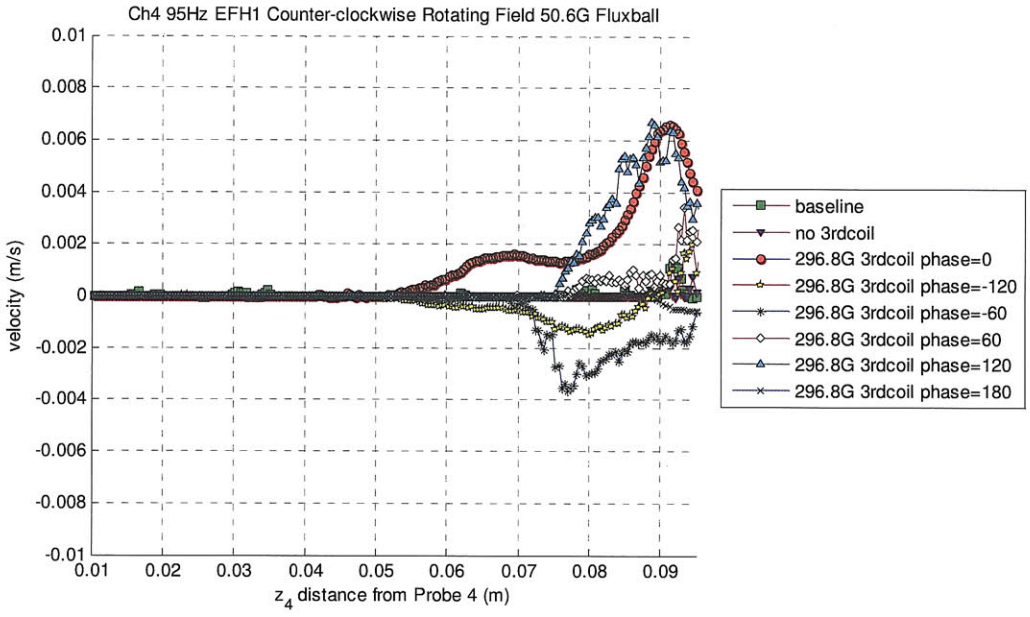
Ch4 95Hz EFH1 Counter-clockwise Rotating Field 50.6G Fluxball
velocity (m/s)
0.01
0.008
0.006
0.004
0.002
0
-0.002
-0.004
-0.006
-0.008
-0.01
0.01 0.02 0.03 0.04 0.05 0.06 0.07 0.08 0.09
z4 distance from Probe 4 (m)
baseline
no 3rdcoil
296.8G 3rdcoil phase=0
296.8G 3rdcoil phase=-120
296.8G 3rdcoil phase=-60
296.8G 3rdcoil phase=60
296.8G 3rdcoil phase=120
296.8G 3rdcoil phase=180

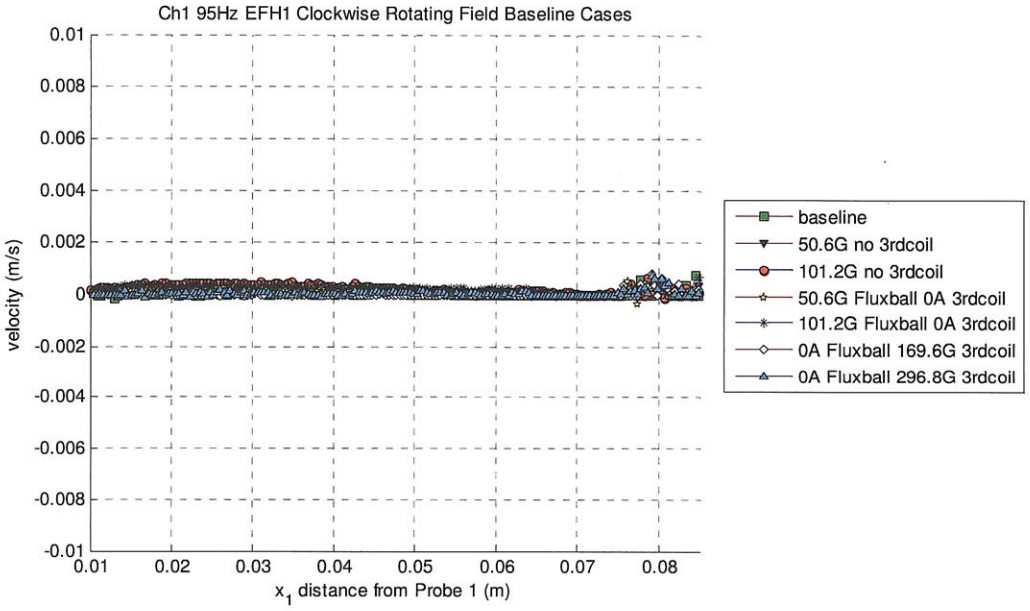
Ch1 95Hz EFH1 Clockwise Rotating Field Baseline Cases
velocity (m/s)
0.01
0.008
0.006
0.004
0.002
0
-0.002
-0.004
-0.006
-0.008
-0.01
0.01 0.02 0.03 0.04 0.05 0.06 0.07 0.08
x1 distance from Probe 1 (m)
baseline
50.6G no 3rdcoil
101.2G no 3rdcoil
50.6G Fluxball 0A 3rdcoil
101.2G Fluxball 0A 3rdcoil
0A Fluxball 169.6G 3rdcoil
0A Fluxball 296.8G 3rdcoil

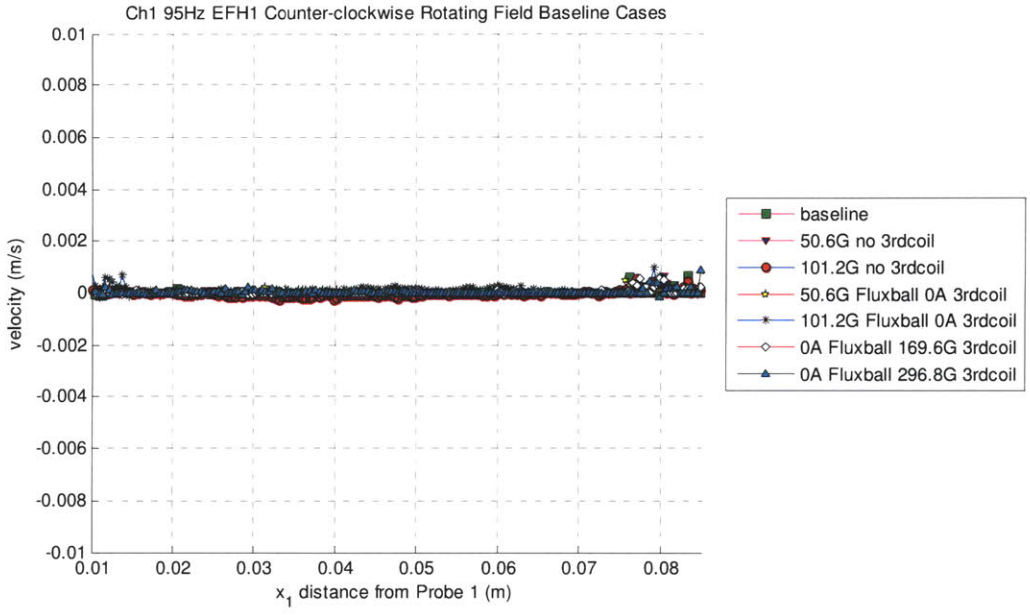
Ch1 95Hz EFH1 Counter-clockwise Rotating Field Baseline Cases
velocity (m/s)
0.01
0.008
0.006
0.004
0.002
0
-0.002
-0.004
-0.006
-0.008
-0.01
0.01
0.02
0.03
0.04
0.05
0.06
0.07
0.08
x1 distance from Probe 1 (m)
baseline
50.6G no 3rdcoil
101.2G no 3rdcoil
50.6G Fluxball 0A 3rdcoil
101.2G Fluxball 0A 3rdcoil
0A Fluxball 169.6G 3rdcoil
0A Fluxball 296.8G 3rdcoil

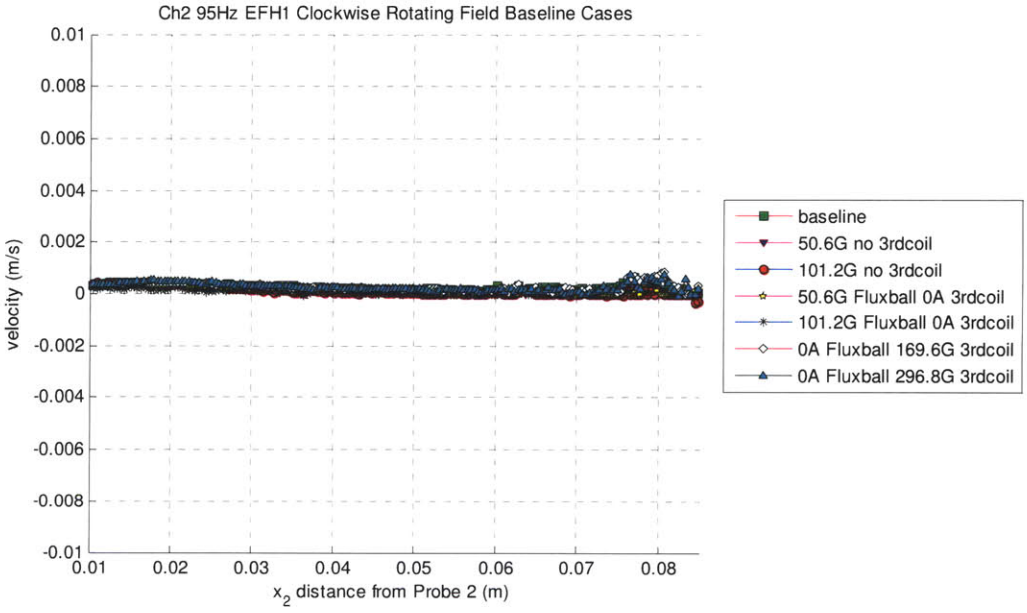
Ch2 95Hz EFH1 Clockwise Rotating Field Baseline Cases
velocity (m/s)
0.01
0.008
0.006
0.004
0.002
0
-0.002
-0.004
-0.006
-0.008
-0.01
0.01
0.02
0.03
0.04
0.05
0.06
0.07
0.08
x2 distance from Probe 2 (m)
baseline
50.6G no 3rdcoil
101.2G no 3rdcoil
50.6G Fluxball 0A 3rdcoil
101.2G Fluxball 0A 3rdcoil
0A Fluxball 169.6G 3rdcoil
0A Fluxball 296.8G 3rdcoil

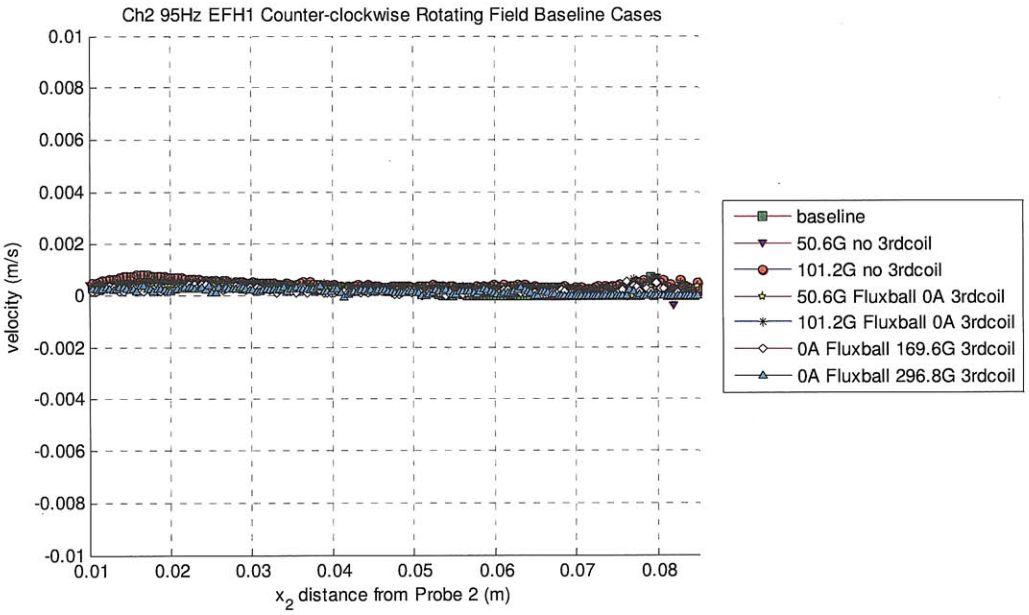
Ch2 95Hz EFH1 Counter-clockwise Rotating Field Baseline Cases
velocity (m/s)
0.01
0.008
0.006
0.004
0.002
0
-0.002
-0.004
-0.006
-0.008
-0.01
0.01
0.02
0.03
0.04
0.05
0.06
0.07
0.08
x2 distance from Probe 2 (m)
baseline
50.6G no 3rdcoil
101.2G no 3rdcoil
50.6G Fluxball 0A 3rdcoil
101.2G Fluxball 0A 3rdcoil
0A Fluxball 169.6G 3rdcoil
0A Fluxball 296.8G 3rdcoil

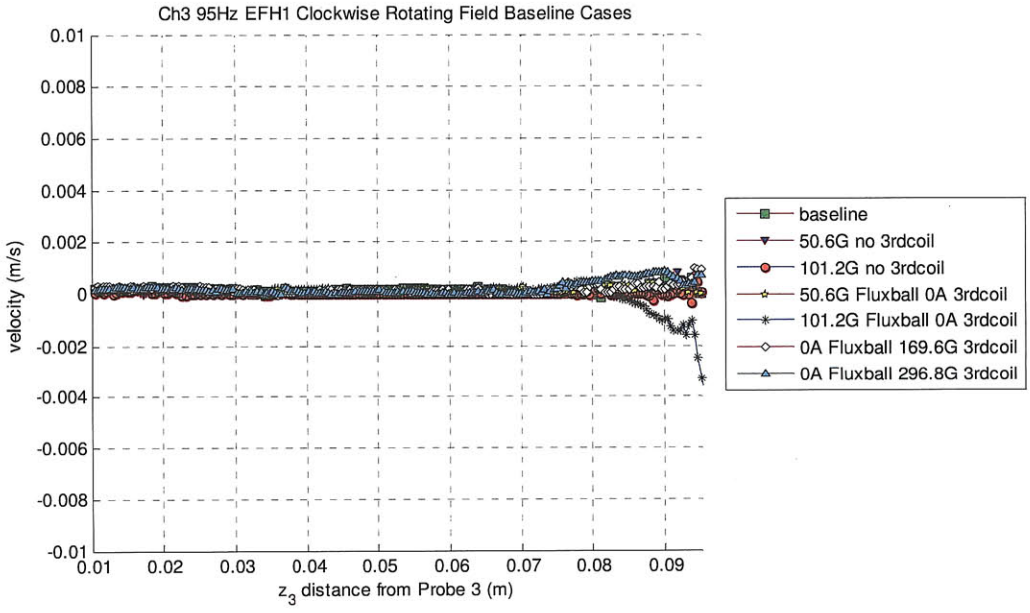
Ch3 95Hz EFH1 Clockwise Rotating Field Baseline Cases
velocity (m/s)
0.01
0.008
0.006
0.004
0.002
0
-0.002
-0.004
-0.006
-0.008
-0.01
0.01
0.02
0.03
0.04
0.05
0.06
0.07
0.08
0.09
z3 distance from Probe 3 (m)
baseline
50.6G no 3rdcoil
101.2G no 3rdcoil
50.6G Fluxball 0A 3rdcoil
101.2G Fluxball 0A 3rdcoil
0A Fluxball 169.6G 3rdcoil
0A Fluxball 296.8G 3rdcoil

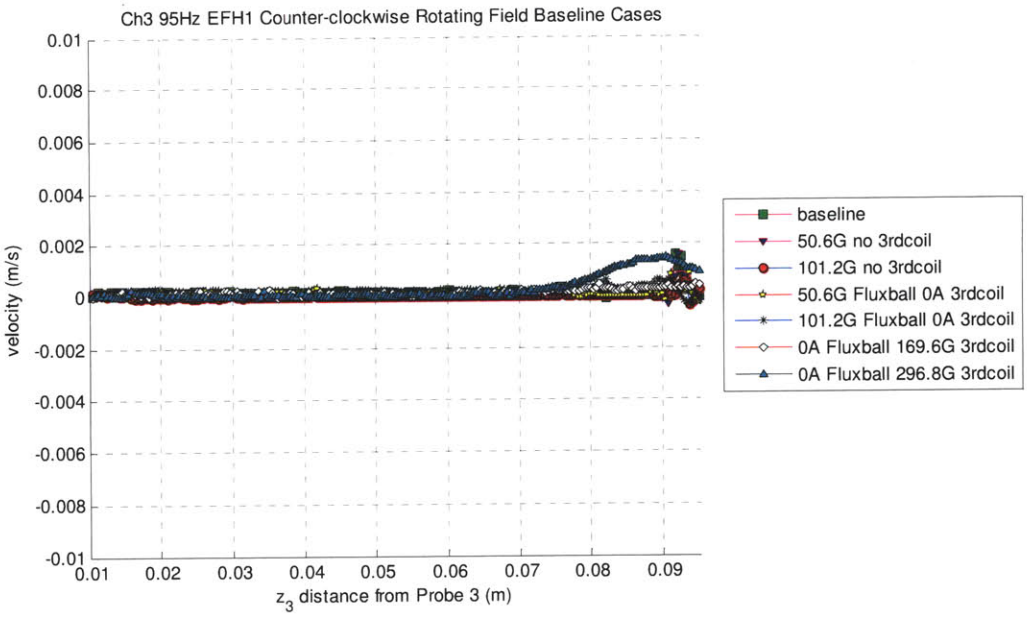
Ch3 95Hz EFH1 Counter-clockwise Rotating Field Baseline Cases
velocity (m/s)
0.01
0.008
0.006
0.004
0.002
0
-0.002
-0.004
-0.006
-0.008
-0.01
0.01 0.02 0.03 0.04 0.05 0.06 0.07 0.08 0.09
z3 distance from Probe 3 (m)
baseline
50.6G no 3rdcoil
101.2G no 3rdcoil
50.6G Fluxball 0A 3rdcoil
101.2G Fluxball 0A 3rdcoil
0A Fluxball 169.6G 3rdcoil
0A Fluxball 296.8G 3rdcoil

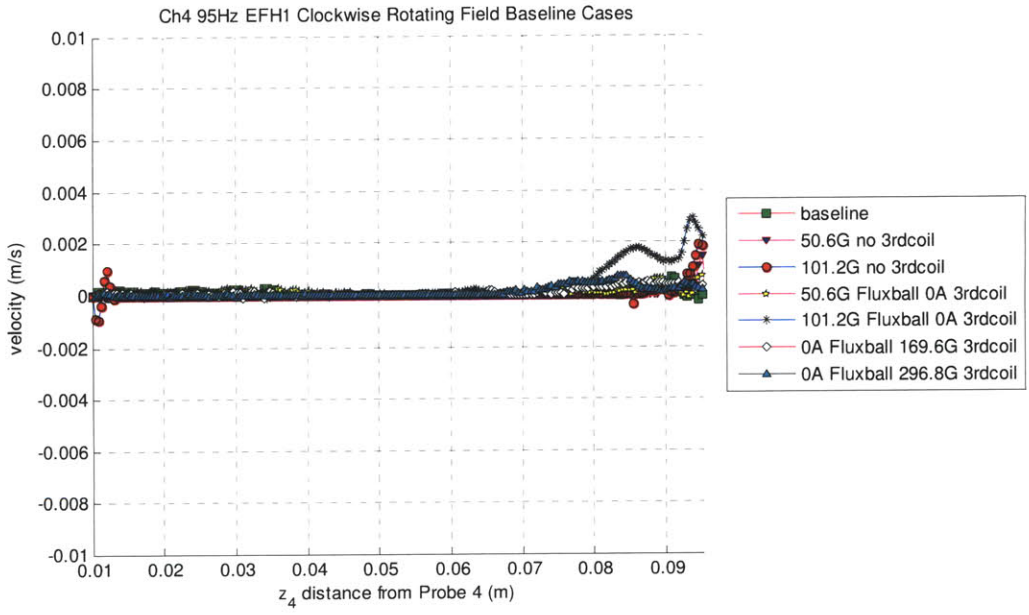
Ch4 95Hz EFH1 Clockwise Rotating Field Baseline Cases
velocity (m/s)
0.01
0.008
0.006
0.004
0.002
0
-0.002
-0.004
-0.006
-0.008
-0.01
0.01 0.02 0.03 0.04 0.05 0.06 0.07 0.08 0.09
z4 distance from Probe 4 (m)
baseline
50.6G no 3rdcoil
101.2G no 3rdcoil
50.6G Fluxball 0A 3rdcoil
101.2G Fluxball 0A 3rdcoil
0A Fluxball 169.6G 3rdcoil
0A Fluxball 296.8G 3rdcoil

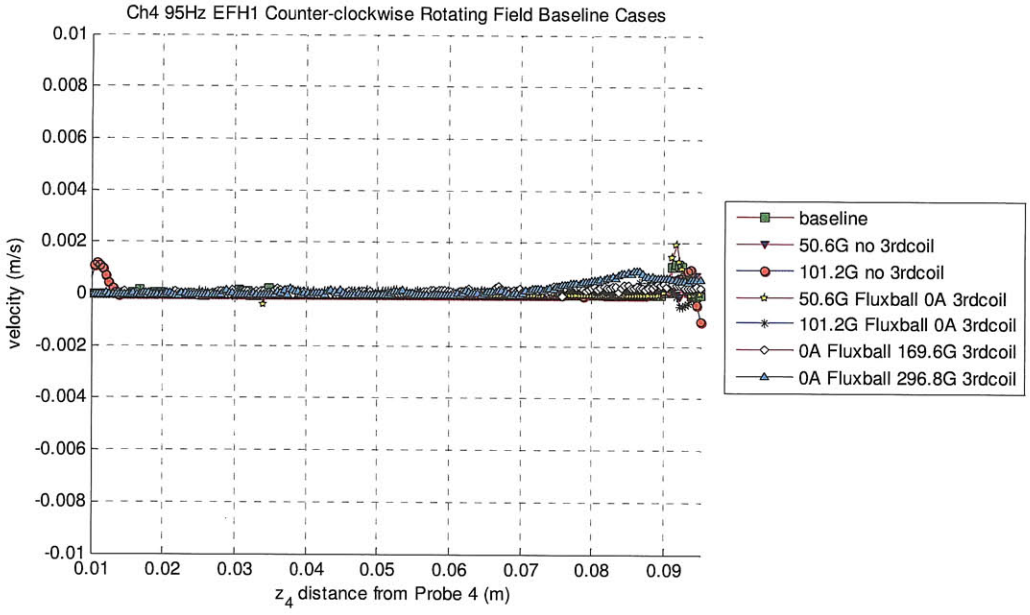
Ch4 95Hz EFH1 Counter-clockwise Rotating Field Baseline Cases
velocity (m/s)
0.01
0.008
0.006
0.004
0.002
0
-0.002
-0.004
-0.006
-0.008
-0.01
0.01 0.02 0.03 0.04 0.05 0.06 0.07 0.08 0.09
z4 distance from Probe 4 (m)
baseline
50.6G no 3rdcoil
101.2G no 3rdcoil
50.6G Fluxball 0A 3rdcoil
101.2G Fluxball 0A 3rdcoil
0A Fluxball 169.6G 3rdcoil
0A Fluxball 296.8G 3rdcoil

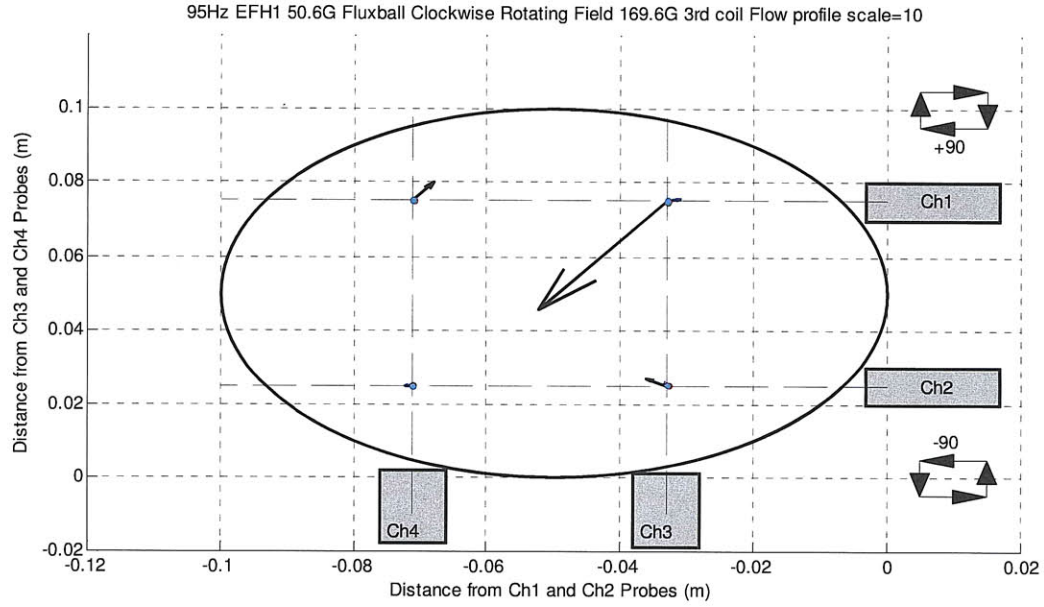
95Hz EFH1 50.6G Fluxball Clockwise Rotating Field 169.6G 3rd coil Flow profile scale=10
Distance from Ch3 and Ch4 Probes (m)
0.1
0.08
0.06
0.04
0.02
0
-0.02
-0.12 -0.1 -0.08 -0.06 -0.04 -0.02 0 0.02
Distance from Ch1 and Ch2 Probes (m)
+90
Ch1
Ch2
-90
Ch4
Ch3

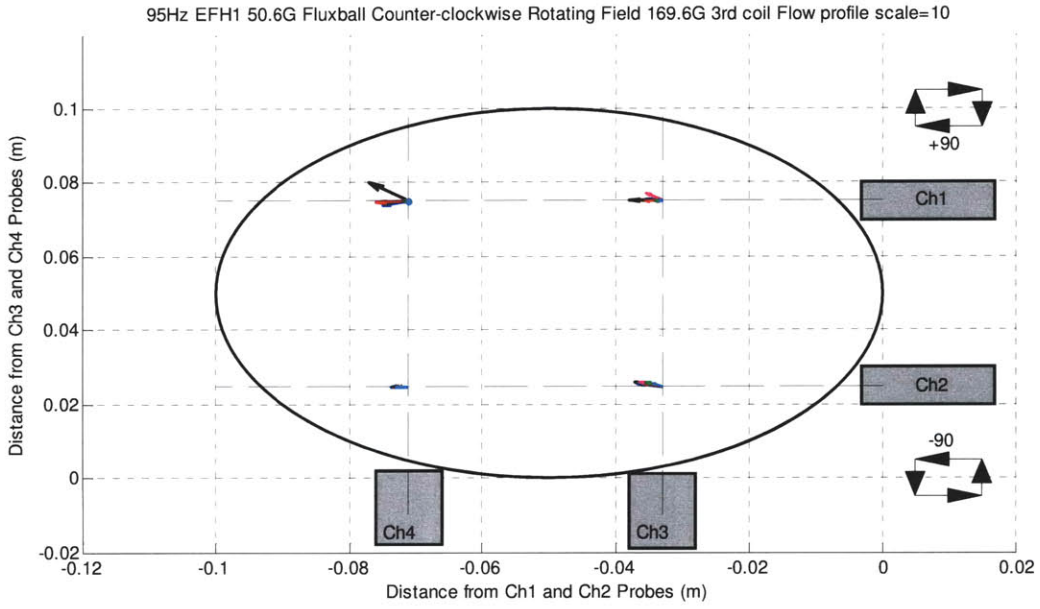
95Hz EFH1 50.6G Fluxball Counter-clockwise Rotating Field 169.6G 3rd coil Flow profile scale=10
Distance from Ch3 and Ch4 Probes (m)
Distance from Ch1 and Ch2 Probes (m)
+90
-90
Ch1
Ch2
Ch3
Ch4
0.1
0.08
0.06
0.04
0.02
0
-0.02
-0.12
-0.1
-0.08
-0.06
-0.04
-0.02
0
0.02

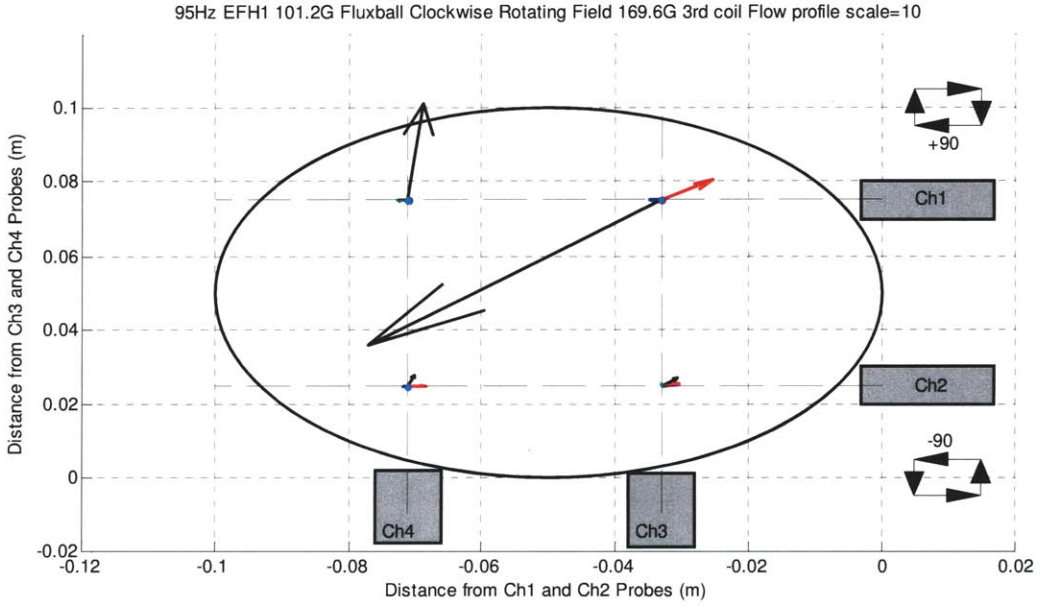
95Hz EFH1 101.2G Fluxball Clockwise Rotating Field 169.6G 3rd coil Flow profile scale=10
Distance from Ch3 and Ch4 Probes (m)
Distance from Ch1 and Ch2 Probes (m)
+90
-90
Ch1
Ch2
Ch3
Ch4
0.1
0.08
0.06
0.04
0.02
0
-0.02
-0.12
-0.1
-0.08
-0.06
-0.04
-0.02
0
0.02

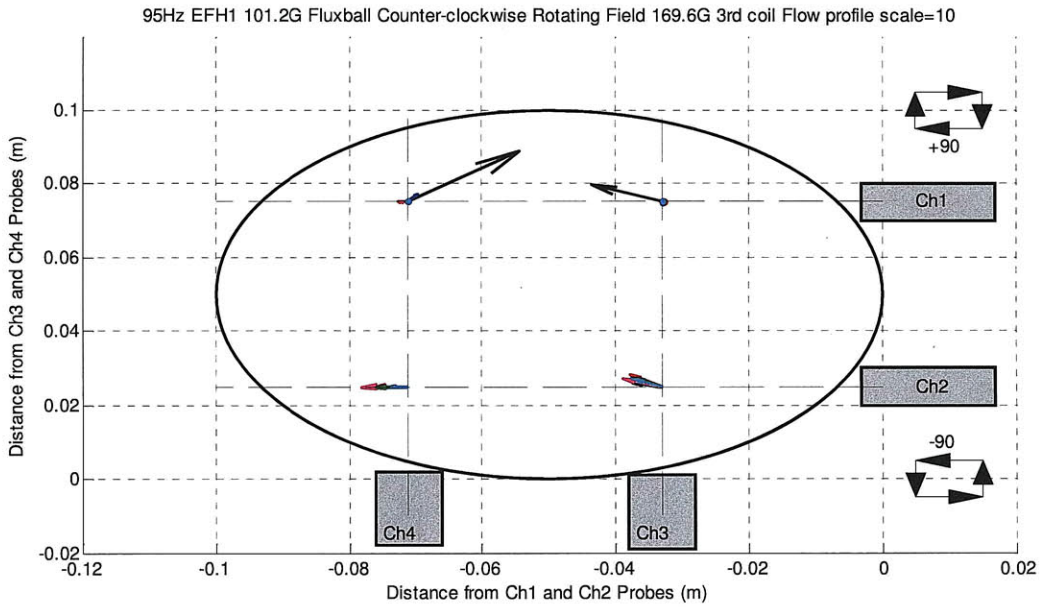
95Hz EFH1 101.2G Fluxball Counter-clockwise Rotating Field 169.6G 3rd coil Flow profile scale=10
Distance from Ch3 and Ch4 Probes (m)
Distance from Ch1 and Ch2 Probes (m)
+90
-90
Ch1
Ch2
Ch3
Ch4
0.1
0.08
0.06
0.04
0.02
0
-0.02
-0.12
-0.1
-0.08
-0.06
-0.04
-0.02
0
0.02

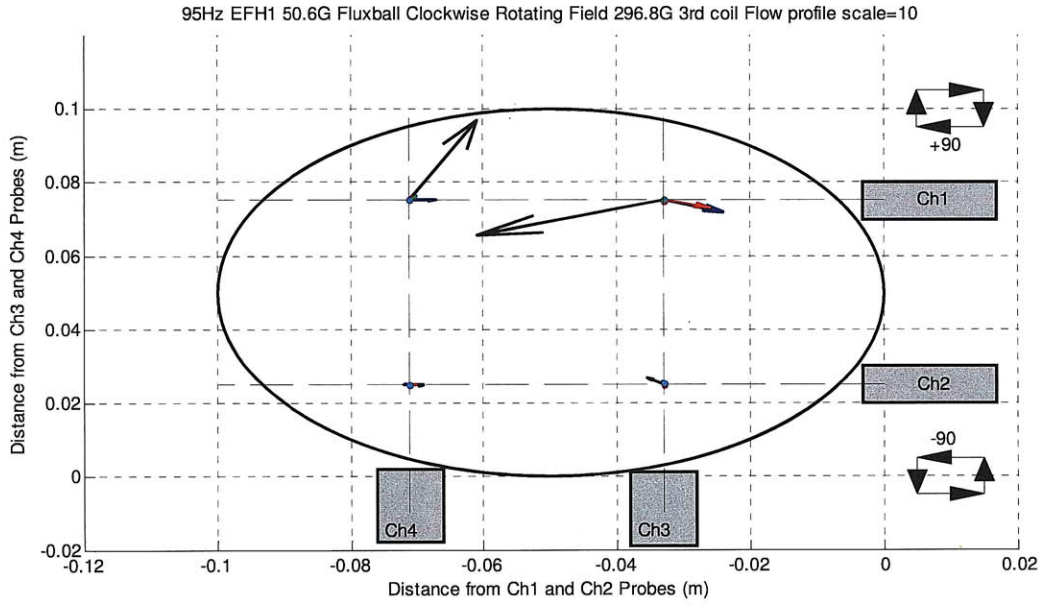
95Hz EFH1 50.6G Fluxball Clockwise Rotating Field 296.8G 3rd coil Flow profile scale=10
Distance from Ch3 and Ch4 Probes (m)
Distance from Ch1 and Ch2 Probes (m)
+90
-90
Ch1
Ch2
Ch3
Ch4
0.1
0.08
0.06
0.04
0.02
0
-0.02
-0.12
-0.1
-0.08
-0.06
-0.04
-0.02
0
0.02

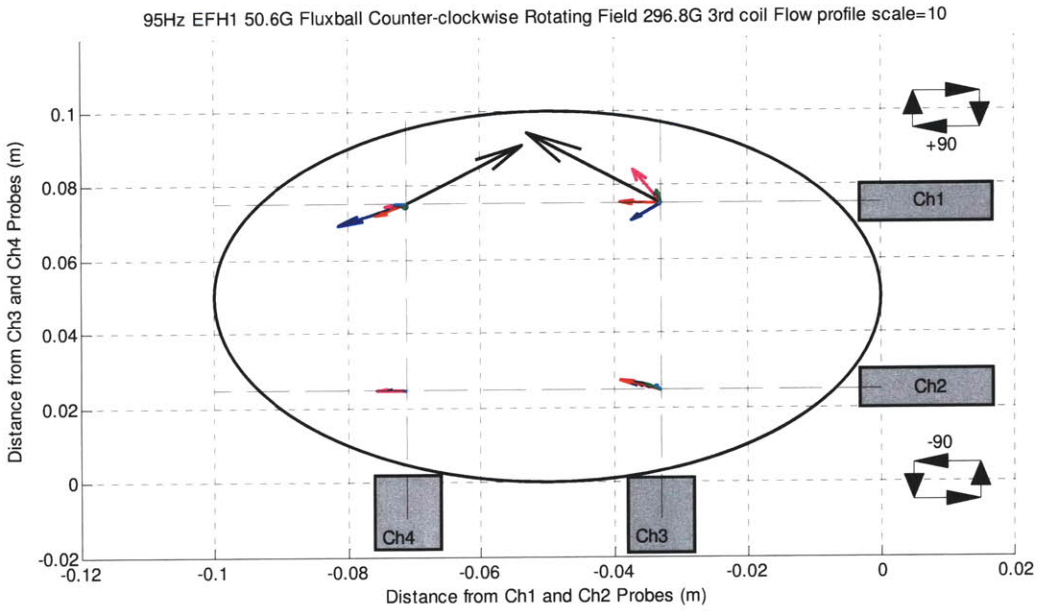
95Hz EFH1 50.6G Fluxball Counter-clockwise Rotating Field 296.8G 3rd coil Flow profile scale=10
Distance from Ch3 and Ch4 Probes (m)
Distance from Ch1 and Ch2 Probes (m)
+90
-90
Ch1
Ch2
Ch3
Ch4
0.1
0.08
0.06
0.04
0.02
0
-0.02
-0.12
-0.1
-0.08
-0.06
-0.04
-0.02
0
0.02

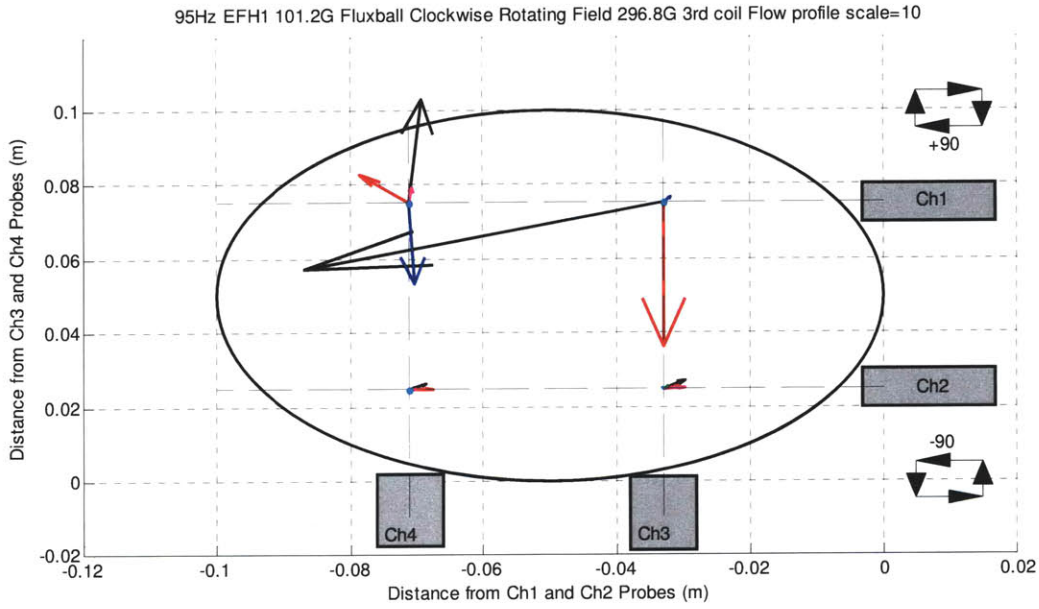
95Hz EFH1 101.2G Fluxball Clockwise Rotating Field 296.8G 3rd coil Flow profile scale=10
Distance from Ch3 and Ch4 Probes (m)
Distance from Ch1 and Ch2 Probes (m)
+90
-90
Ch1
Ch2
Ch3
Ch4
0.1
0.08
0.06
0.04
0.02
0
-0.02
-0.12
-0.1
-0.08
-0.06
-0.04
-0.02
0
0.02

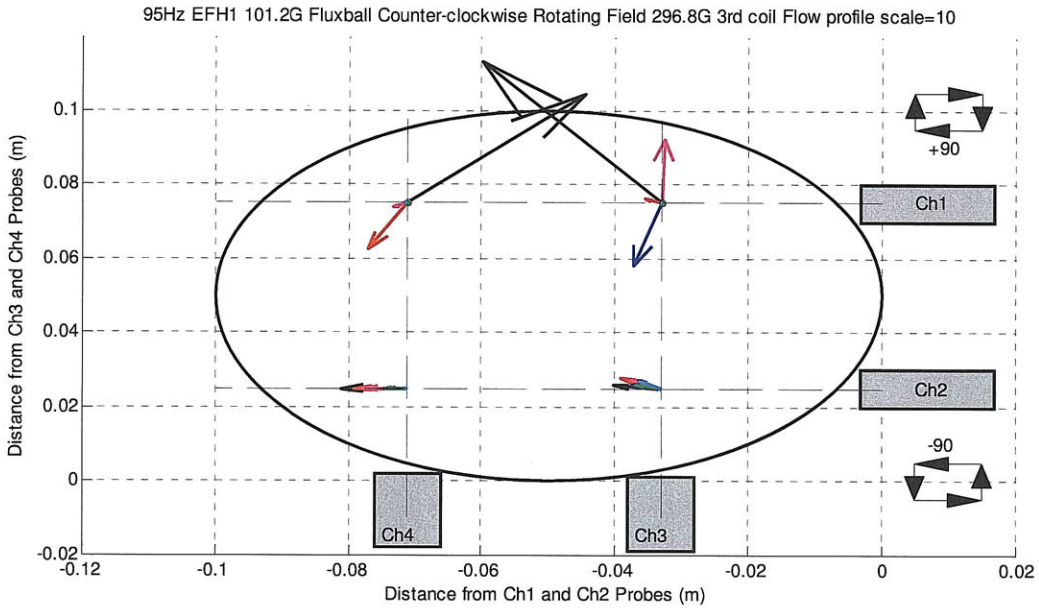
95Hz EFH1 101.2G Fluxball Counter-clockwise Rotating Field 296.8G 3rd coil Flow profile scale=10
Distance from Ch3 and Ch4 Probes (m)
Distance from Ch1 and Ch2 Probes (m)
0.1
0.08
0.06
0.04
0.02
0
-0.02
-0.12
-0.1
-0.08
-0.06
-0.04
-0.02
0
0.02
+90
-90
Ch1
Ch2
Ch3
Ch4

G2. EFH1 Filled Sphere with Third Coil Oscillating at Same Frequency as Rotating Field at 47Hz

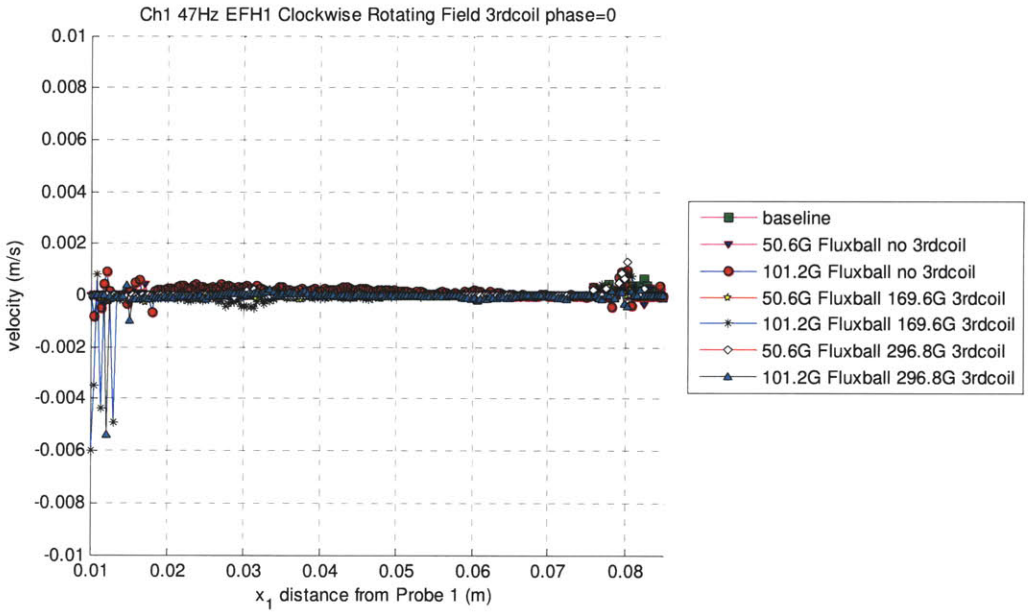

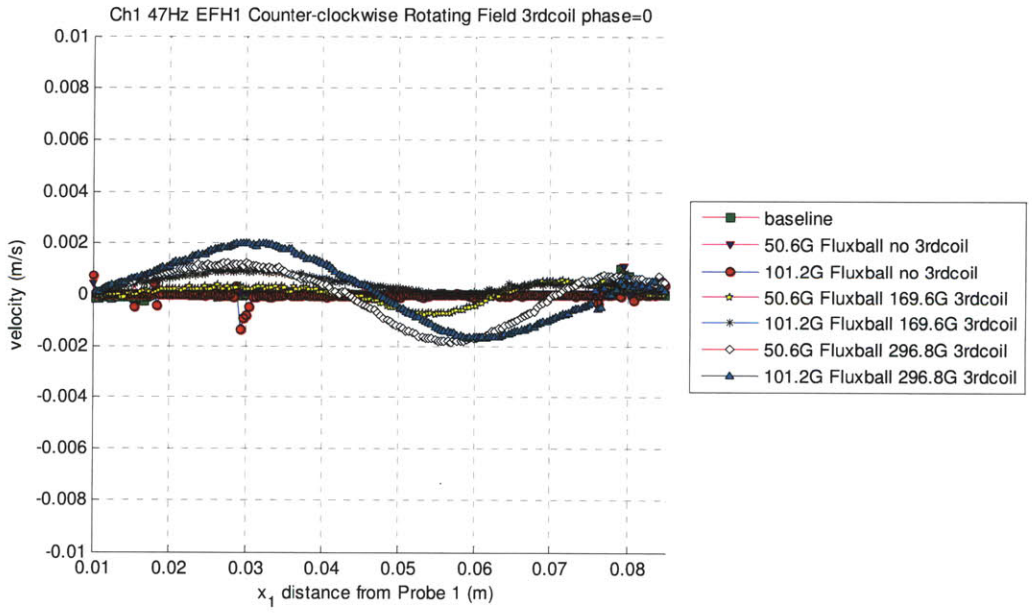

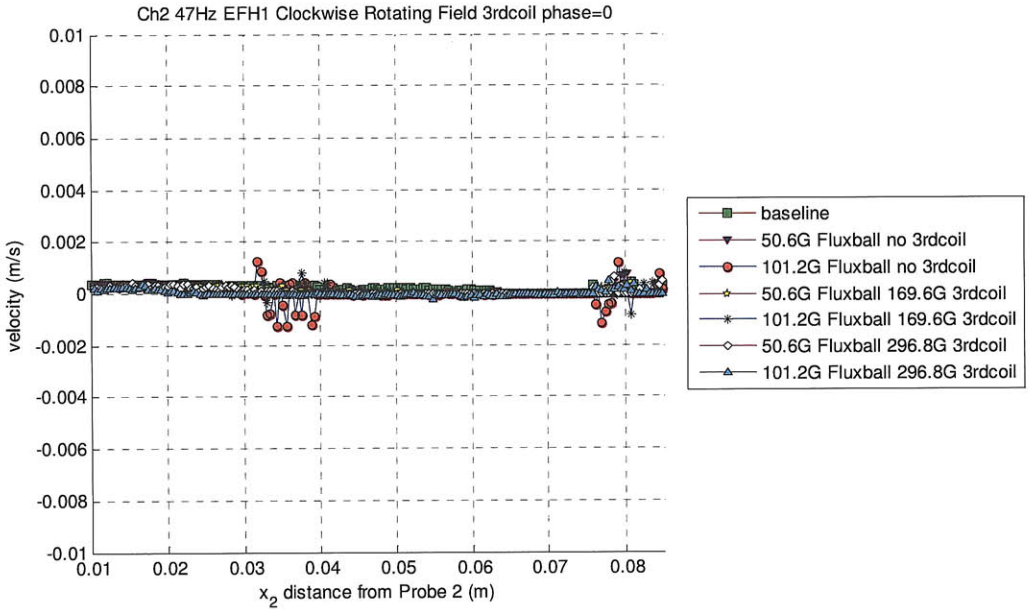
Ch2 47Hz EFH1 Clockwise Rotating Field 3rdcoil phase=0
velocity (m/s)
0.01
0.008
0.006
0.004
0.002
0
-0.002
-0.004
-0.006
-0.008
-0.01
0.01 0.02 0.03 0.04 0.05 0.06 0.07 0.08
x2 distance from Probe 2 (m)
baseline
50.6G Fluxball no 3rdcoil
101.2G Fluxball no 3rdcoil
50.6G Fluxball 169.6G 3rdcoil
101.2G Fluxball 169.6G 3rdcoil
50.6G Fluxball 296.8G 3rdcoil
101.2G Fluxball 296.8G 3rdcoil

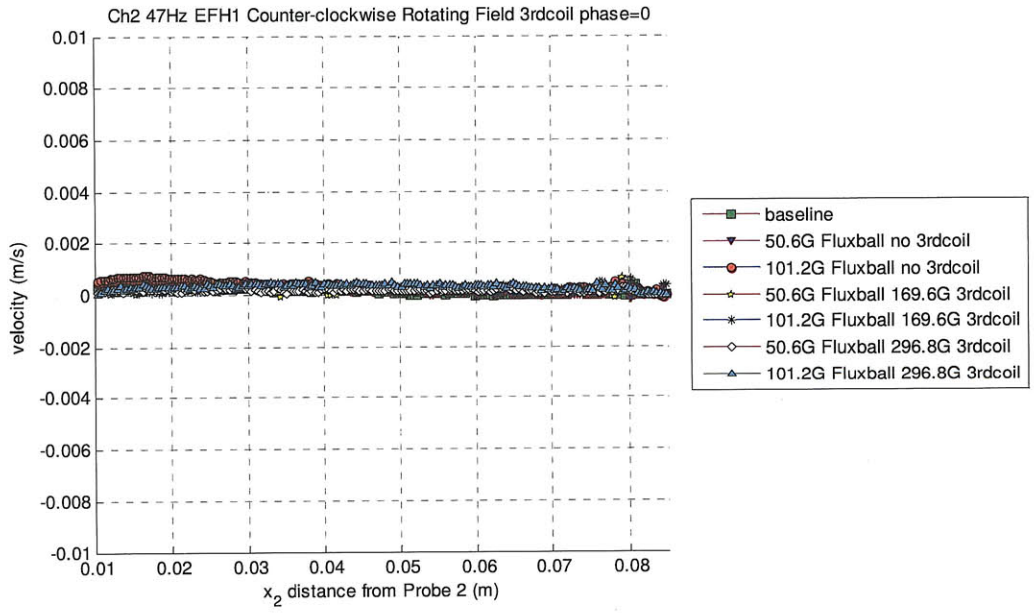
Ch2 47Hz EFH1 Counter-clockwise Rotating Field 3rdcoil phase=0
velocity (m/s)
0.01
0.008
0.006
0.004
0.002
0
-0.002
-0.004
-0.006
-0.008
-0.01
0.01 0.02 0.03 0.04 0.05 0.06 0.07 0.08
x2 distance from Probe 2 (m)
baseline
50.6G Fluxball no 3rdcoil
101.2G Fluxball no 3rdcoil
50.6G Fluxball 169.6G 3rdcoil
101.2G Fluxball 169.6G 3rdcoil
50.6G Fluxball 296.8G 3rdcoil
101.2G Fluxball 296.8G 3rdcoil

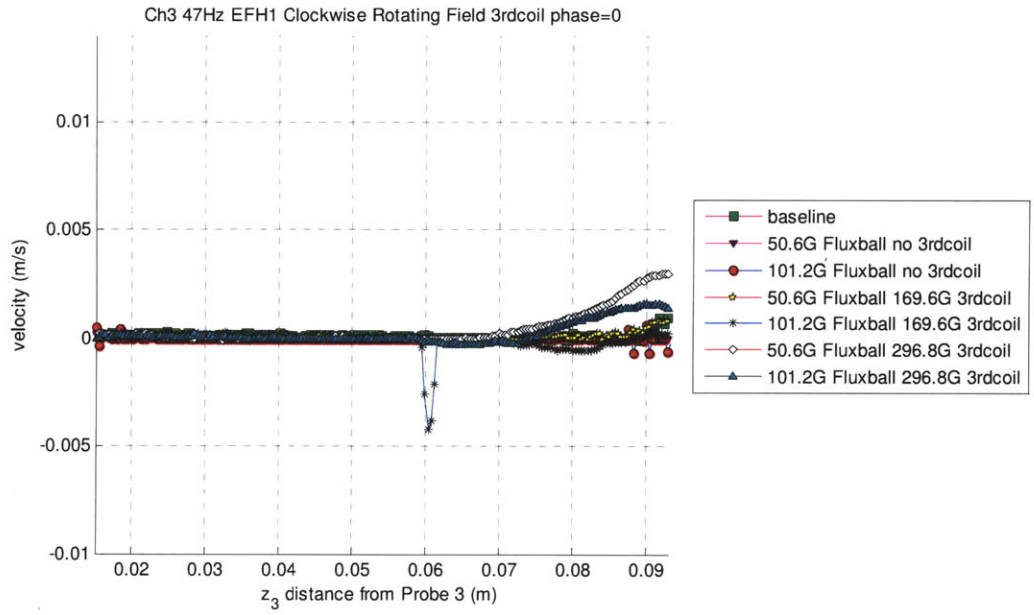
Ch3 47Hz EFH1 Clockwise Rotating Field 3rdcoil phase=0
velocity (m/s)
0.01
0.005
0
-0.005
-0.01
0.02
0.03
0.04
0.05
0.06
0.07
0.08
0.09
z3 distance from Probe 3 (m)
baseline
50.6G Fluxball no 3rdcoil
101.2G Fluxball no 3rdcoil
50.6G Fluxball 169.6G 3rdcoil
101.2G Fluxball 169.6G 3rdcoil
50.6G Fluxball 296.8G 3rdcoil
101.2G Fluxball 296.8G 3rdcoil

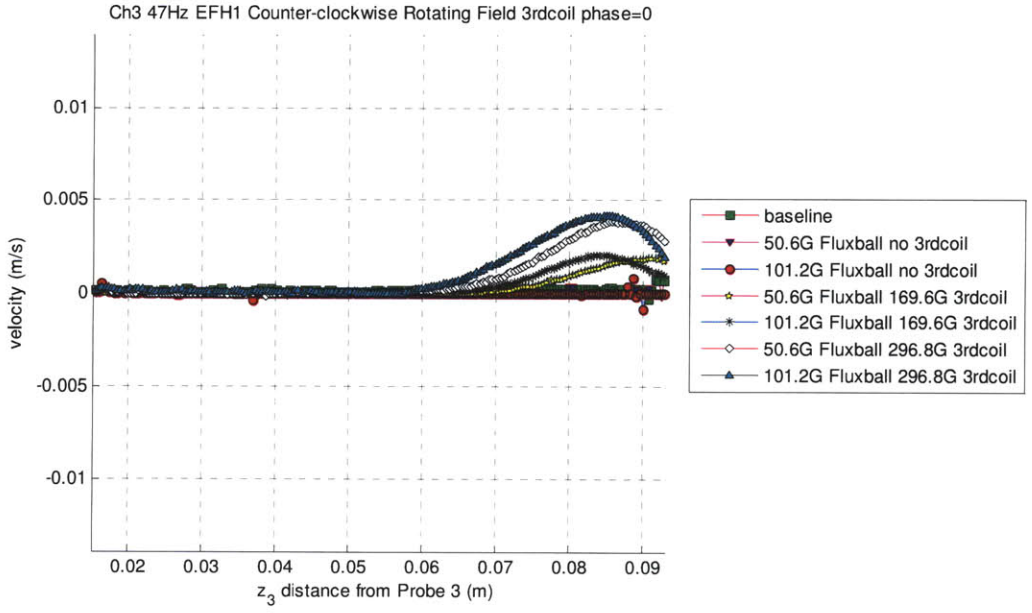
Ch3 47Hz EFH1 Counter-clockwise Rotating Field 3rdcoil phase=0
velocity (m/s)
0.01
0.005
0
-0.005
-0.01
0.02
0.03
0.04
0.05
0.06
0.07
0.08
0.09
z3 distance from Probe 3 (m)
baseline
50.6G Fluxball no 3rdcoil
101.2G Fluxball no 3rdcoil
50.6G Fluxball 169.6G 3rdcoil
101.2G Fluxball 169.6G 3rdcoil
50.6G Fluxball 296.8G 3rdcoil
101.2G Fluxball 296.8G 3rdcoil

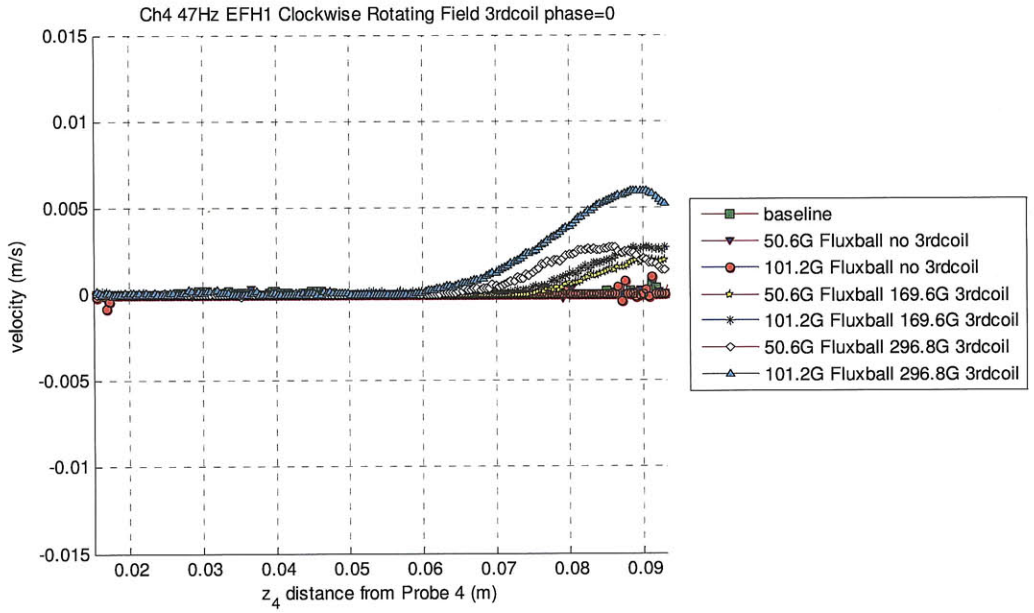
Ch4 47Hz EFH1 Clockwise Rotating Field 3rdcoil phase=0
velocity (m/s)
0.015
0.01
0.005
0
-0.005
-0.01
-0.015
0.02
0.03
0.04
0.05
0.06
0.07
0.08
0.09
z4 distance from Probe 4 (m)
baseline
50.6G Fluxball no 3rdcoil
101.2G Fluxball no 3rdcoil
50.6G Fluxball 169.6G 3rdcoil
101.2G Fluxball 169.6G 3rdcoil
50.6G Fluxball 296.8G 3rdcoil
101.2G Fluxball 296.8G 3rdcoil

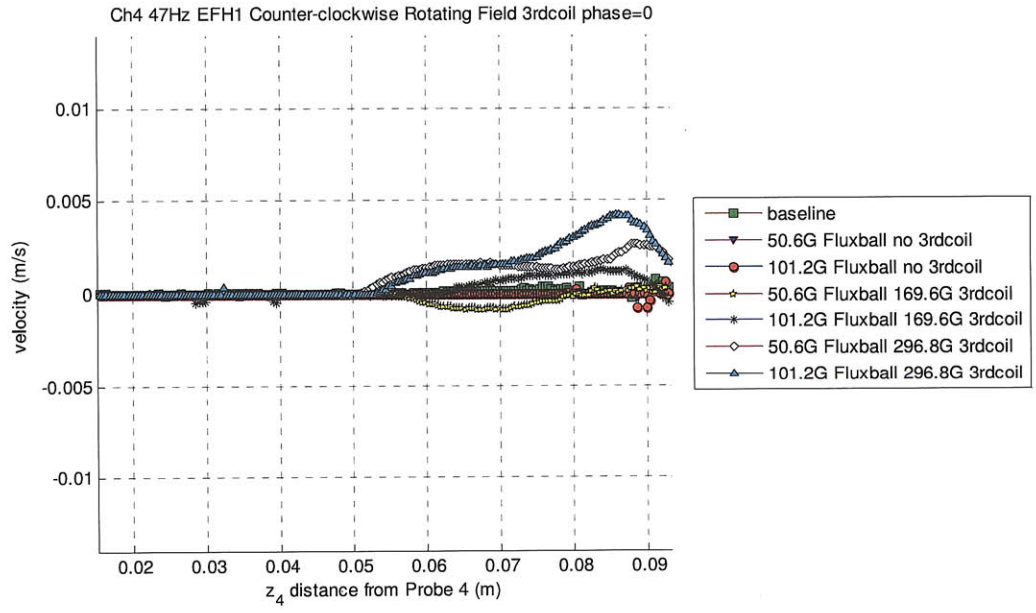
Ch4 47Hz EFH1 Counter-clockwise Rotating Field 3rdcoil phase=0
velocity (m/s)
0.01
0.005
0
-0.005
-0.01
0.02
0.03
0.04
0.05
0.06
0.07
0.08
0.09
z4 distance from Probe 4 (m)
baseline
50.6G Fluxball no 3rdcoil
101.2G Fluxball no 3rdcoil
50.6G Fluxball 169.6G 3rdcoil
101.2G Fluxball 169.6G 3rdcoil
50.6G Fluxball 296.8G 3rdcoil
101.2G Fluxball 296.8G 3rdcoil

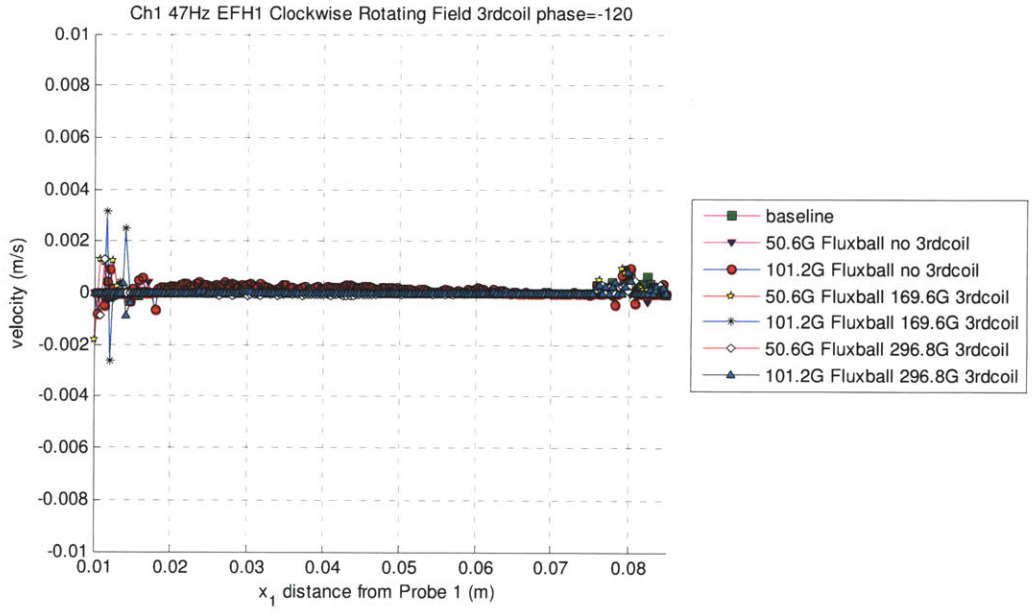
Ch1 47Hz EFH1 Clockwise Rotating Field 3rdcoil phase=-120
velocity (m/s)
x1 distance from Probe 1 (m)
baseline
50.6G Fluxball no 3rdcoil
101.2G Fluxball no 3rdcoil
50.6G Fluxball 169.6G 3rdcoil
101.2G Fluxball 169.6G 3rdcoil
50.6G Fluxball 296.8G 3rdcoil
101.2G Fluxball 296.8G 3rdcoil

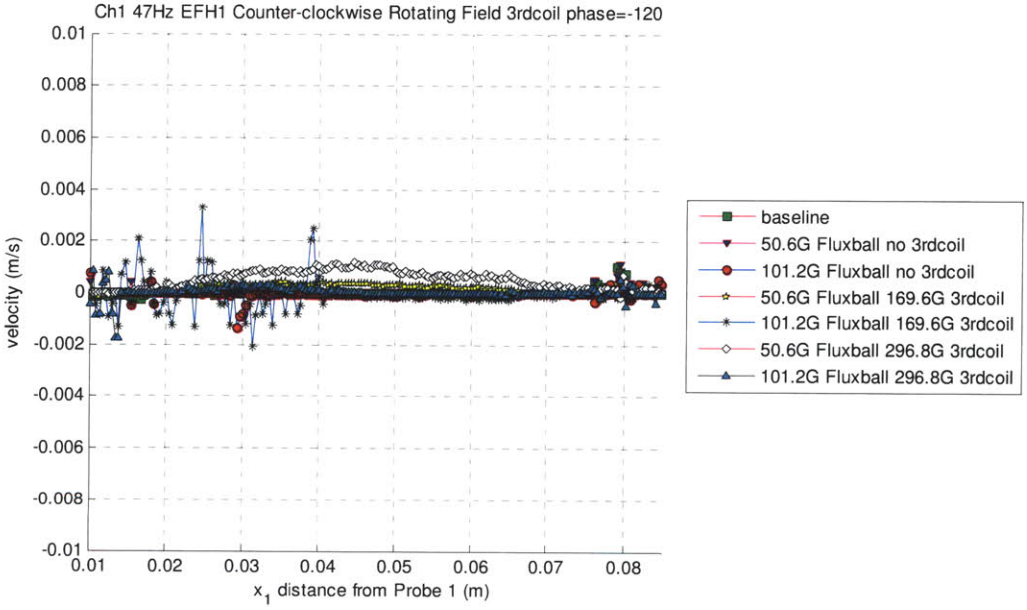
Ch1 47Hz EFH1 Counter-clockwise Rotating Field 3rdcoil phase=-120
velocity (m/s)
x1 distance from Probe 1 (m)
baseline
50.6G Fluxball no 3rdcoil
101.2G Fluxball no 3rdcoil
50.6G Fluxball 169.6G 3rdcoil
101.2G Fluxball 169.6G 3rdcoil
50.6G Fluxball 296.8G 3rdcoil
101.2G Fluxball 296.8G 3rdcoil

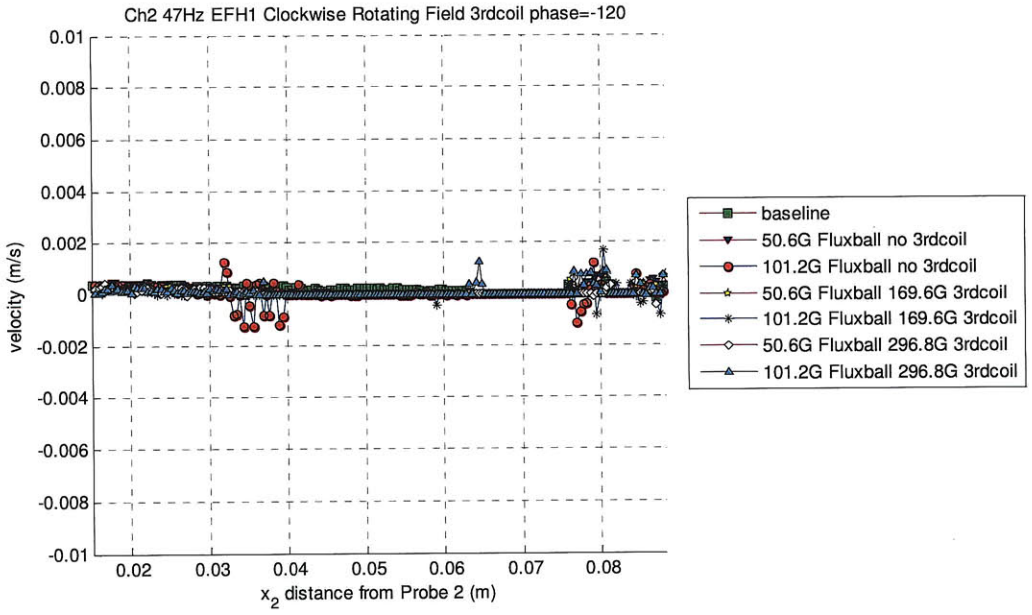
Ch2 47Hz EFH1 Clockwise Rotating Field 3rdcoil phase=-120
velocity (m/s)
0.01
0.008
0.006
0.004
0.002
0
-0.002
-0.004
-0.006
-0.008
-0.01
0.02
0.03
0.04
0.05
0.06
0.07
0.08
x2 distance from Probe 2 (m)
baseline
50.6G Fluxball no 3rdcoil
101.2G Fluxball no 3rdcoil
50.6G Fluxball 169.6G 3rdcoil
101.2G Fluxball 169.6G 3rdcoil
50.6G Fluxball 296.8G 3rdcoil
101.2G Fluxball 296.8G 3rdcoil

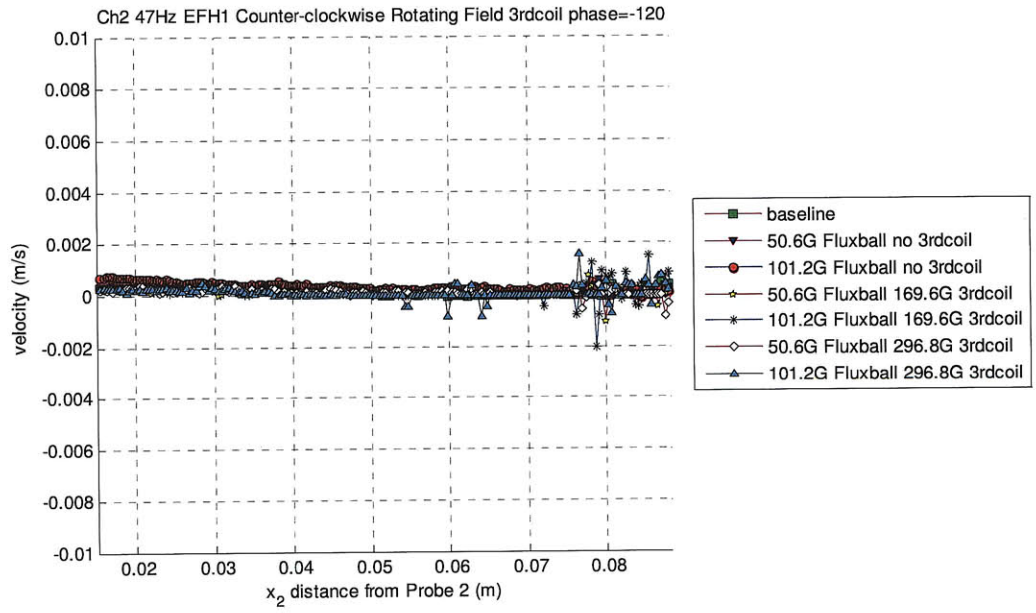
Ch2 47Hz EFH1 Counter-clockwise Rotating Field 3rdcoil phase=-120
velocity (m/s)
0.01
0.008
0.006
0.004
0.002
0
-0.002
-0.004
-0.006
-0.008
-0.01
0.02
0.03
0.04
0.05
0.06
0.07
0.08
x2 distance from Probe 2 (m)
baseline
50.6G Fluxball no 3rdcoil
101.2G Fluxball no 3rdcoil
50.6G Fluxball 169.6G 3rdcoil
101.2G Fluxball 169.6G 3rdcoil
50.6G Fluxball 296.8G 3rdcoil
101.2G Fluxball 296.8G 3rdcoil

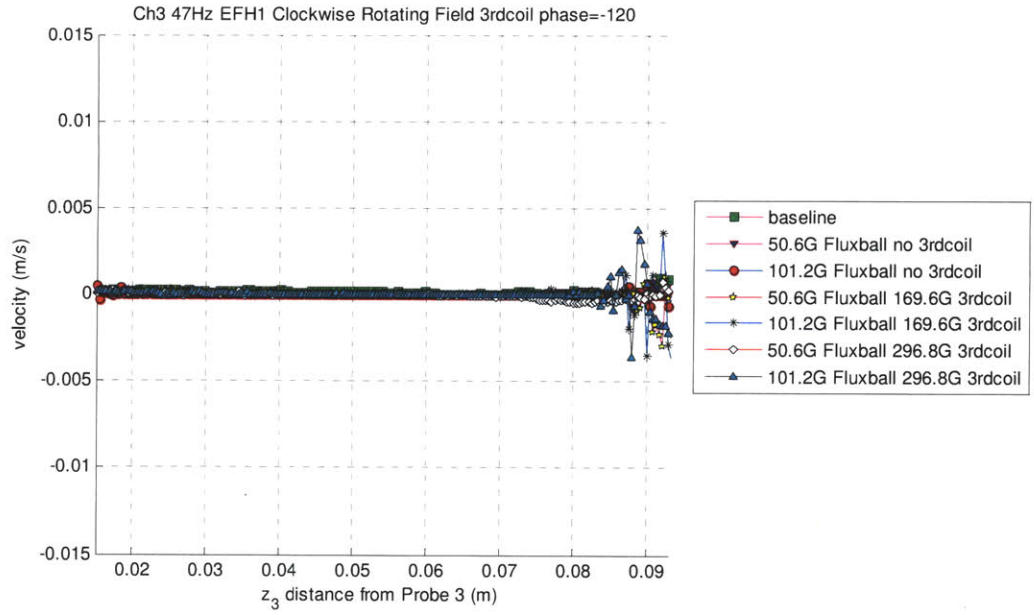
Ch3 47Hz EFH1 Clockwise Rotating Field 3rdcoil phase=-120
velocity (m/s)
0.015
0.01
0.005
0
-0.005
-0.01
-0.015
0.02
0.03
0.04
0.05
0.06
0.07
0.08
0.09
z_3 distance from Probe 3 (m)
baseline
50.6G Fluxball no 3rdcoil
101.2G Fluxball no 3rdcoil
50.6G Fluxball 169.6G 3rdcoil
101.2G Fluxball 169.6G 3rdcoil
50.6G Fluxball 296.8G 3rdcoil
101.2G Fluxball 296.8G 3rdcoil

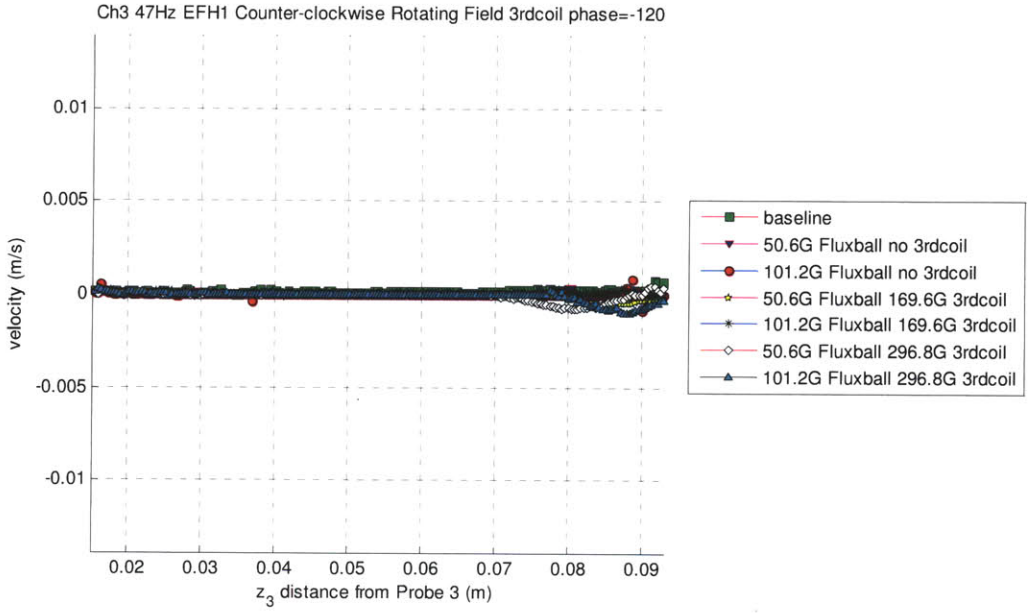
Ch3 47Hz EFH1 Counter-clockwise Rotating Field 3rdcoil phase=-120
velocity (m/s)
0.01
0.005
0
-0.005
-0.01
0.02
0.03
0.04
0.05
0.06
0.07
0.08
0.09
z_3 distance from Probe 3 (m)
baseline
50.6G Fluxball no 3rdcoil
101.2G Fluxball no 3rdcoil
50.6G Fluxball 169.6G 3rdcoil
101.2G Fluxball 169.6G 3rdcoil
50.6G Fluxball 296.8G 3rdcoil
101.2G Fluxball 296.8G 3rdcoil

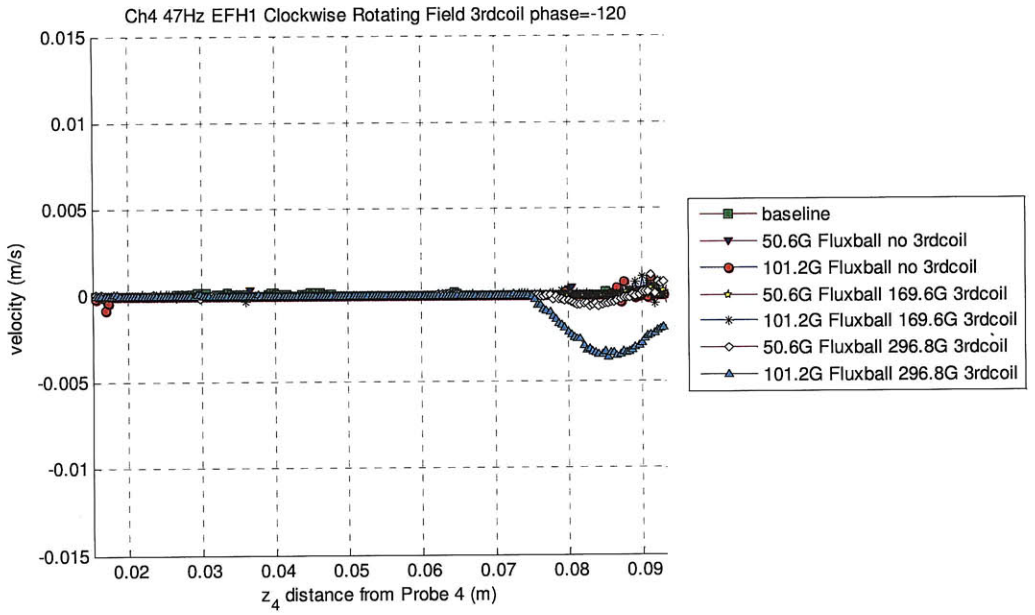
Ch4 47Hz EFH1 Clockwise Rotating Field 3rdcoil phase=-120
0.015
0.01
0.005
0
-0.005
-0.01
-0.015
velocity (m/s)
0.02
0.03
0.04
0.05
0.06
0.07
0.08
0.09
z4 distance from Probe 4 (m)
baseline
50.6G Fluxball no 3rdcoil
101.2G Fluxball no 3rdcoil
50.6G Fluxball 169.6G 3rdcoil
101.2G Fluxball 169.6G 3rdcoil
50.6G Fluxball 296.8G 3rdcoil
101.2G Fluxball 296.8G 3rdcoil

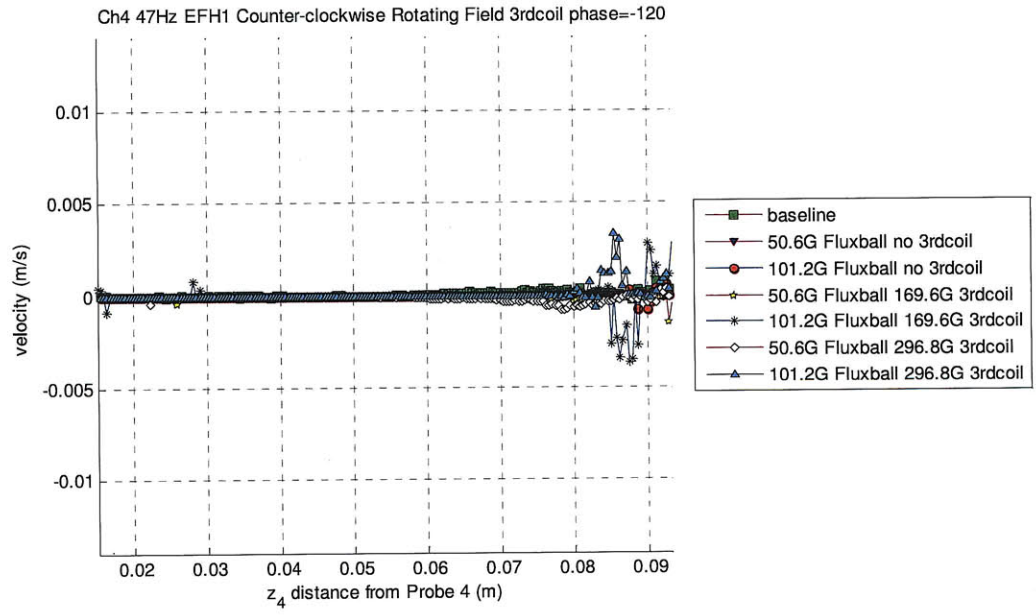
Ch4 47Hz EFH1 Counter-clockwise Rotating Field 3rdcoil phase=-120
0.01
0.005
0
-0.005
-0.01
velocity (m/s)
0.02
0.03
0.04
0.05
0.06
0.07
0.08
0.09
z4 distance from Probe 4 (m)
baseline
50.6G Fluxball no 3rdcoil
101.2G Fluxball no 3rdcoil
50.6G Fluxball 169.6G 3rdcoil
101.2G Fluxball 169.6G 3rdcoil
50.6G Fluxball 296.8G 3rdcoil
101.2G Fluxball 296.8G 3rdcoil

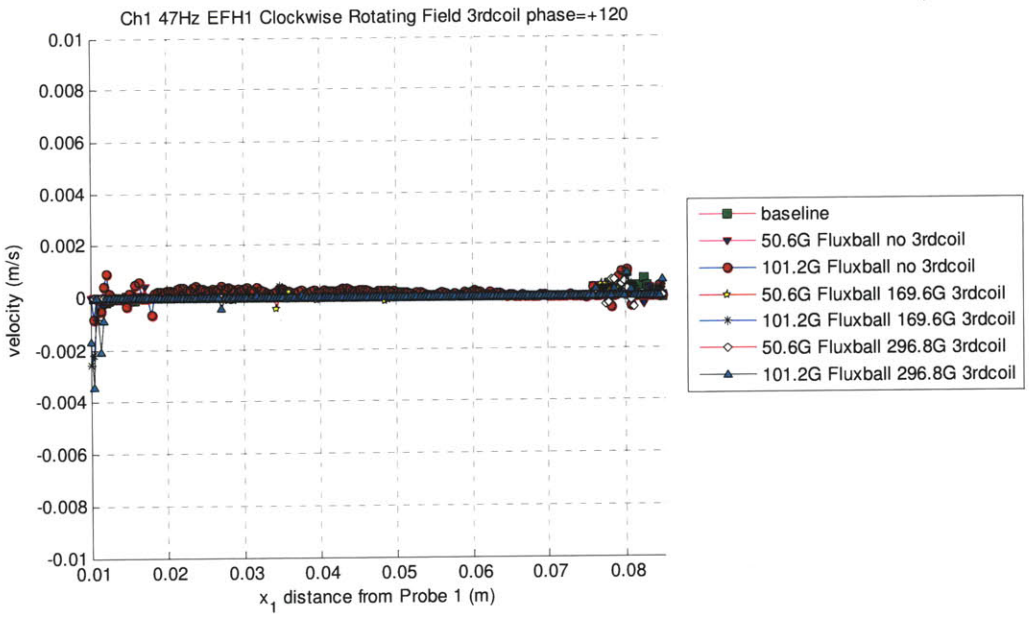
Ch1 47Hz EFH1 Clockwise Rotating Field 3rdcoil phase=+120
velocity (m/s)
0.01
0.008
0.006
0.004
0.002
0
-0.002
-0.004
-0.006
-0.008
-0.01
0.01
0.02
0.03
0.04
0.05
0.06
0.07
0.08
x1 distance from Probe 1 (m)
baseline
50.6G Fluxball no 3rdcoil
101.2G Fluxball no 3rdcoil
50.6G Fluxball 169.6G 3rdcoil
101.2G Fluxball 169.6G 3rdcoil
50.6G Fluxball 296.8G 3rdcoil
101.2G Fluxball 296.8G 3rdcoil

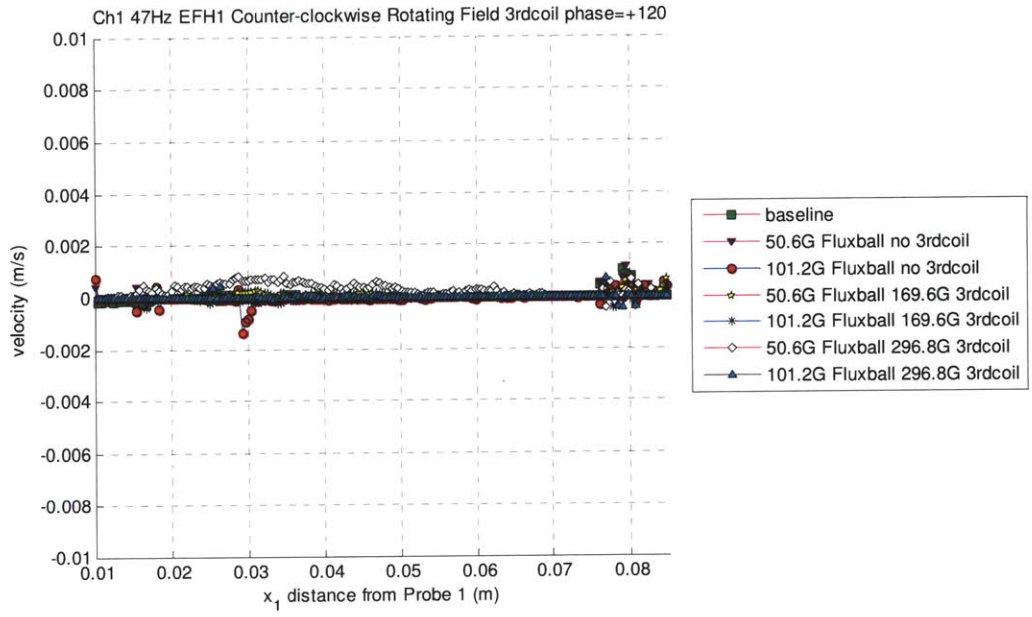
Ch1 47Hz EFH1 Counter-clockwise Rotating Field 3rdcoil phase=+120
velocity (m/s)
0.01
0.008
0.006
0.004
0.002
0
-0.002
-0.004
-0.006
-0.008
-0.01
0.01
0.02
0.03
0.04
0.05
0.06
0.07
0.08
x1 distance from Probe 1 (m)
baseline
50.6G Fluxball no 3rdcoil
101.2G Fluxball no 3rdcoil
50.6G Fluxball 169.6G 3rdcoil
101.2G Fluxball 169.6G 3rdcoil
50.6G Fluxball 296.8G 3rdcoil
101.2G Fluxball 296.8G 3rdcoil

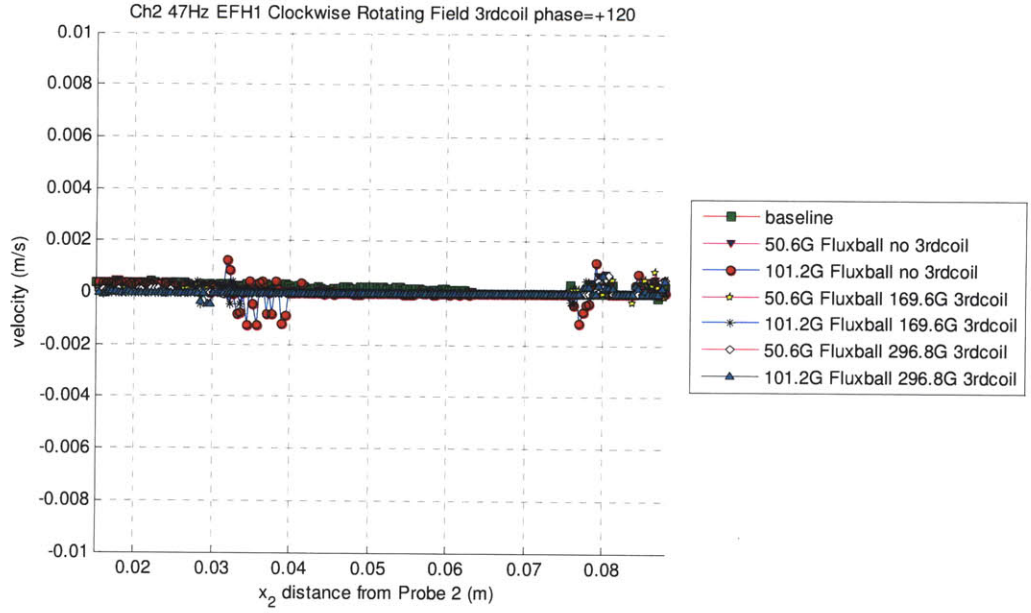
Ch2 47Hz EFH1 Clockwise Rotating Field 3rdcoil phase=+120
velocity (m/s)
0.01
0.008
0.006
0.004
0.002
0
-0.002
-0.004
-0.006
-0.008
-0.01
0.02
0.03
0.04
0.05
0.06
0.07
0.08
x2 distance from Probe 2 (m)
baseline
50.6G Fluxball no 3rdcoil
101.2G Fluxball no 3rdcoil
50.6G Fluxball 169.6G 3rdcoil
101.2G Fluxball 169.6G 3rdcoil
50.6G Fluxball 296.8G 3rdcoil
101.2G Fluxball 296.8G 3rdcoil

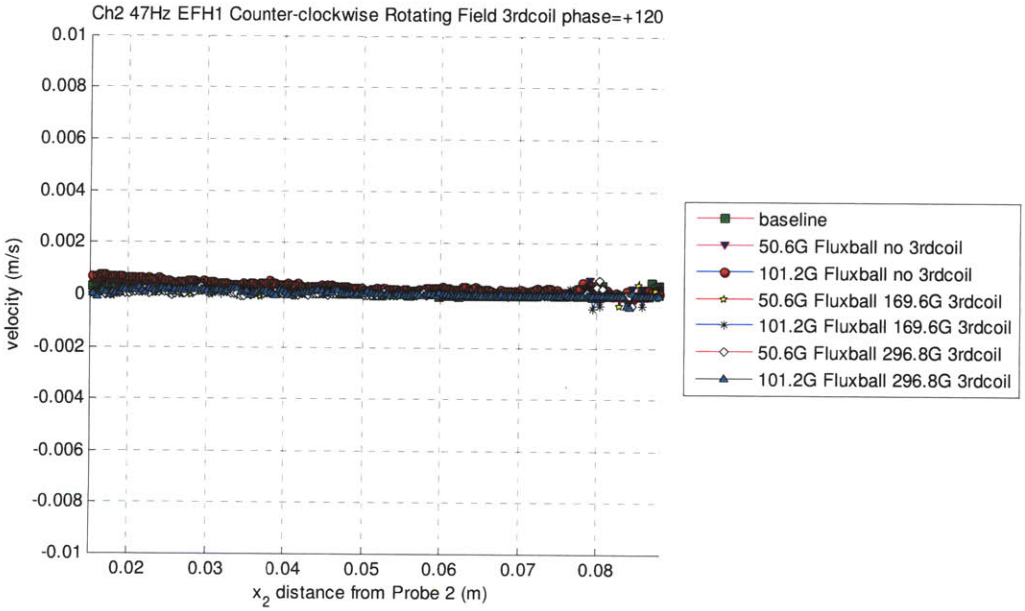
Ch2 47Hz EFH1 Counter-clockwise Rotating Field 3rdcoil phase=+120
velocity (m/s)
0.01
0.008
0.006
0.004
0.002
0
-0.002
-0.004
-0.006
-0.008
-0.01
0.02
0.03
0.04
0.05
0.06
0.07
0.08
x2 distance from Probe 2 (m)
baseline
50.6G Fluxball no 3rdcoil
101.2G Fluxball no 3rdcoil
50.6G Fluxball 169.6G 3rdcoil
101.2G Fluxball 169.6G 3rdcoil
50.6G Fluxball 296.8G 3rdcoil
101.2G Fluxball 296.8G 3rdcoil

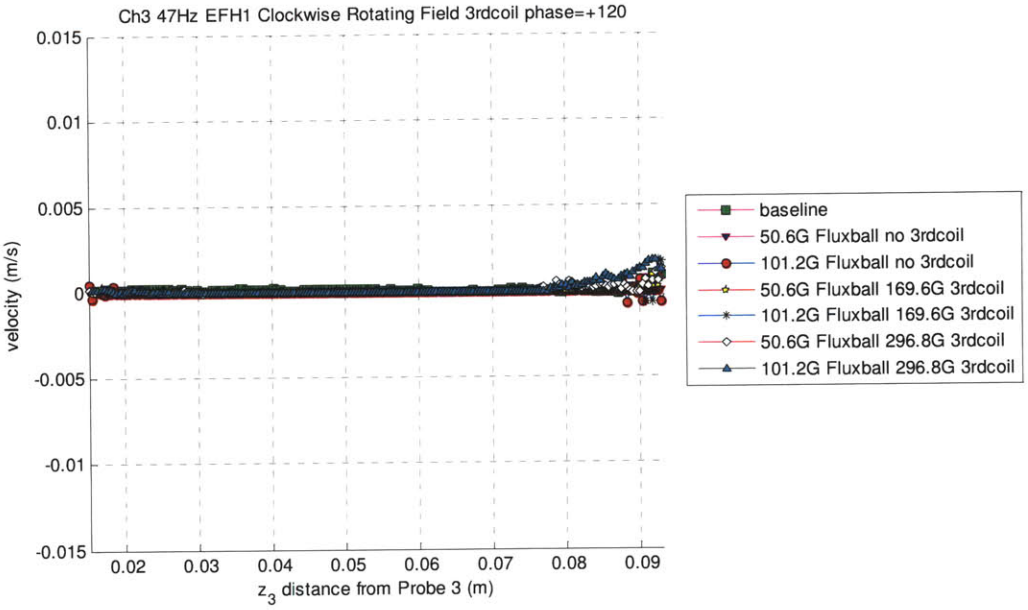
Ch3 47Hz EFH1 Clockwise Rotating Field 3rdcoil phase=+120
velocity (m/s)
0.015
0.01
0.005
0
-0.005
-0.01
-0.015
0.02
0.03
0.04
0.05
0.06
0.07
0.08
0.09
z3 distance from Probe 3 (m)
baseline
50.6G Fluxball no 3rdcoil
101.2G Fluxball no 3rdcoil
50.6G Fluxball 169.6G 3rdcoil
101.2G Fluxball 169.6G 3rdcoil
50.6G Fluxball 296.8G 3rdcoil
101.2G Fluxball 296.8G 3rdcoil

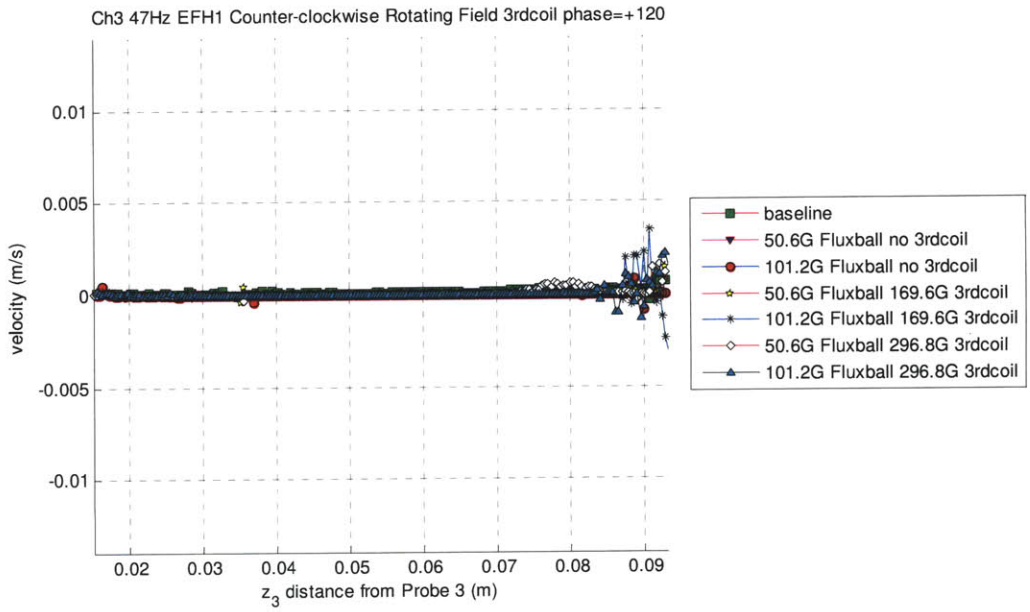
Ch3 47Hz EFH1 Counter-clockwise Rotating Field 3rdcoil phase=+120
velocity (m/s)
0.01
0.005
0
-0.005
-0.01
0.02
0.03
0.04
0.05
0.06
0.07
0.08
0.09
z3 distance from Probe 3 (m)
baseline
50.6G Fluxball no 3rdcoil
101.2G Fluxball no 3rdcoil
50.6G Fluxball 169.6G 3rdcoil
101.2G Fluxball 169.6G 3rdcoil
50.6G Fluxball 296.8G 3rdcoil
101.2G Fluxball 296.8G 3rdcoil

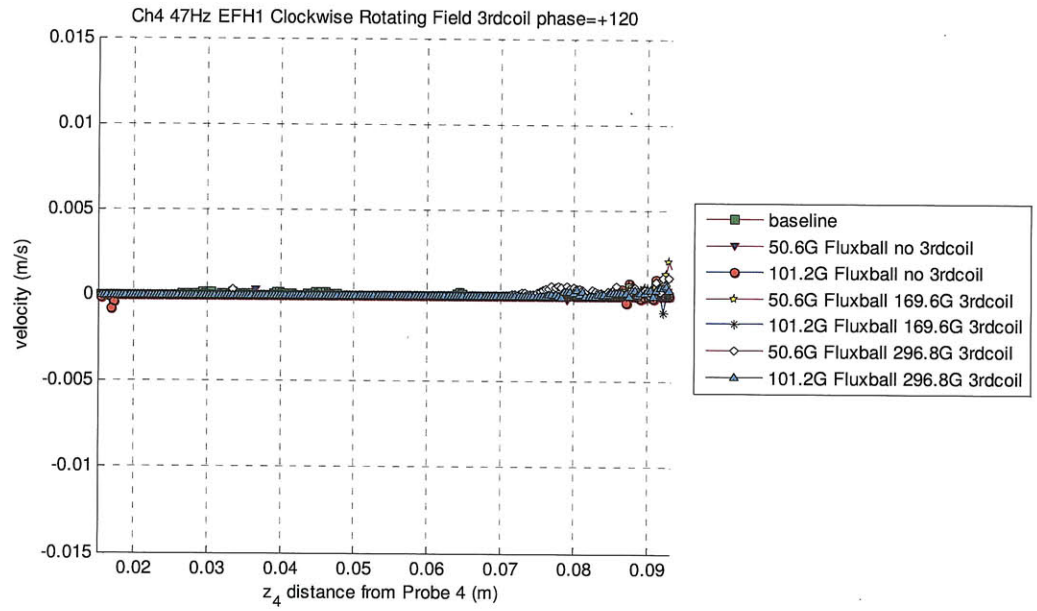
Ch4 47Hz EFH1 Clockwise Rotating Field 3rdcoil phase=+120
velocity (m/s)
0.015
0.01
0.005
0
-0.005
-0.01
-0.015
0.02
0.03
0.04
0.05
0.06
0.07
0.08
0.09
z4 distance from Probe 4 (m)
baseline
50.6G Fluxball no 3rdcoil
101.2G Fluxball no 3rdcoil
50.6G Fluxball 169.6G 3rdcoil
101.2G Fluxball 169.6G 3rdcoil
50.6G Fluxball 296.8G 3rdcoil
101.2G Fluxball 296.8G 3rdcoil

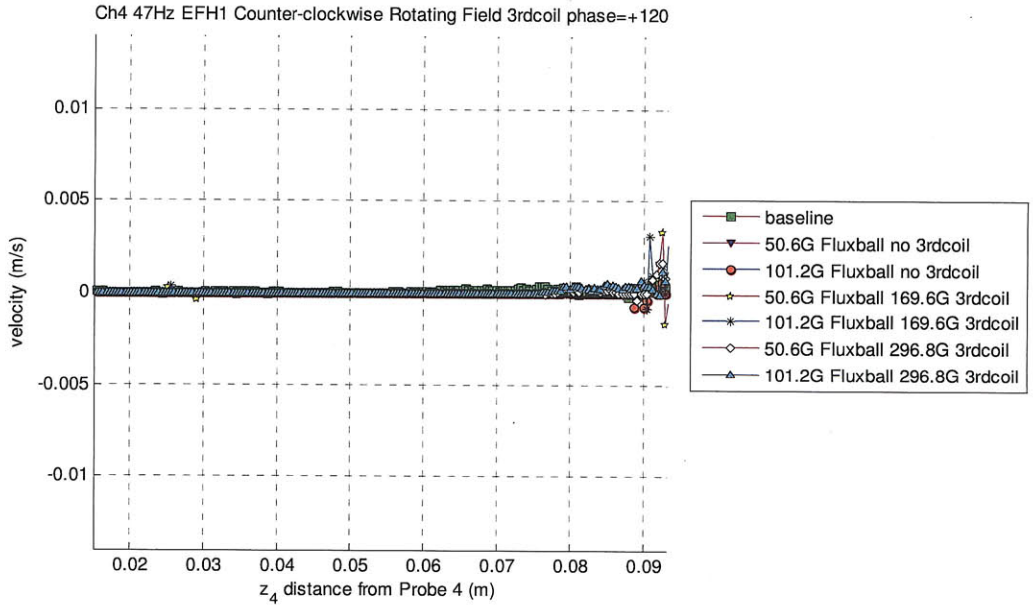
Ch4 47Hz EFH1 Counter-clockwise Rotating Field 3rdcoil phase=+120
velocity (m/s)
0.01
0.005
0
-0.005
-0.01
0.02
0.03
0.04
0.05
0.06
0.07
0.08
0.09
z4 distance from Probe 4 (m)
baseline
50.6G Fluxball no 3rdcoil
101.2G Fluxball no 3rdcoil
50.6G Fluxball 169.6G 3rdcoil
101.2G Fluxball 169.6G 3rdcoil
50.6G Fluxball 296.8G 3rdcoil
101.2G Fluxball 296.8G 3rdcoil

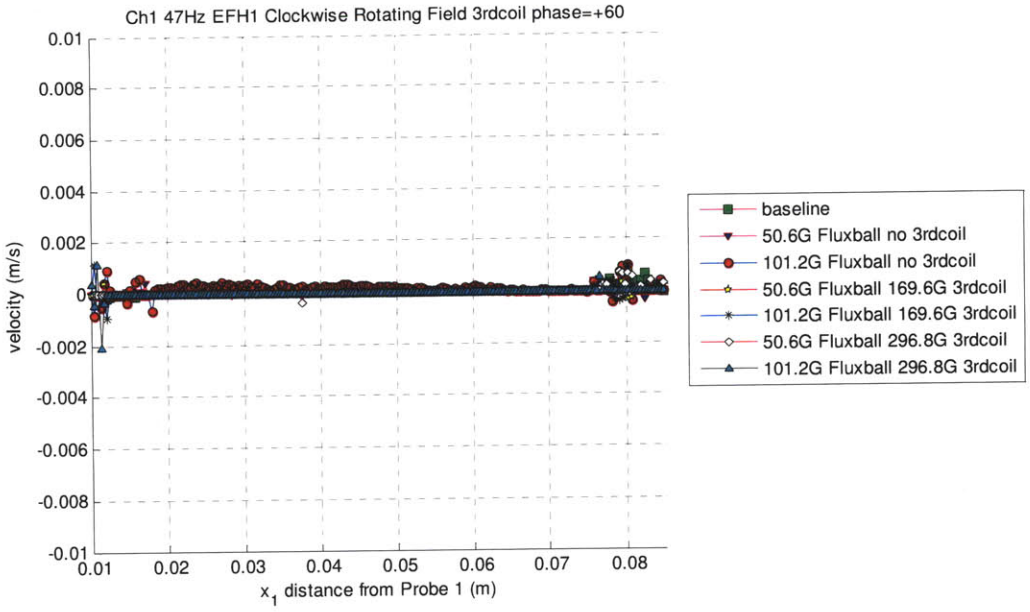
Ch1 47Hz EFH1 Clockwise Rotating Field 3rdcoil phase=+60
velocity (m/s)
x1 distance from Probe 1 (m)
baseline
50.6G Fluxball no 3rdcoil
101.2G Fluxball no 3rdcoil
50.6G Fluxball 169.6G 3rdcoil
101.2G Fluxball 169.6G 3rdcoil
50.6G Fluxball 296.8G 3rdcoil
101.2G Fluxball 296.8G 3rdcoil

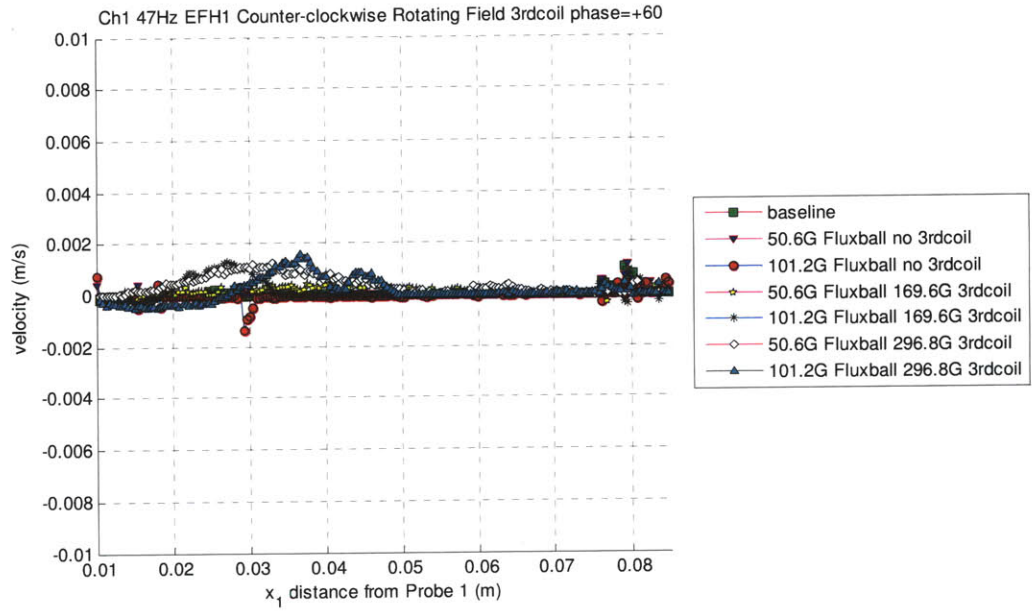
Ch1 47Hz EFH1 Counter-clockwise Rotating Field 3rdcoil phase=+60
velocity (m/s)
x1 distance from Probe 1 (m)
baseline
50.6G Fluxball no 3rdcoil
101.2G Fluxball no 3rdcoil
50.6G Fluxball 169.6G 3rdcoil
101.2G Fluxball 169.6G 3rdcoil
50.6G Fluxball 296.8G 3rdcoil
101.2G Fluxball 296.8G 3rdcoil

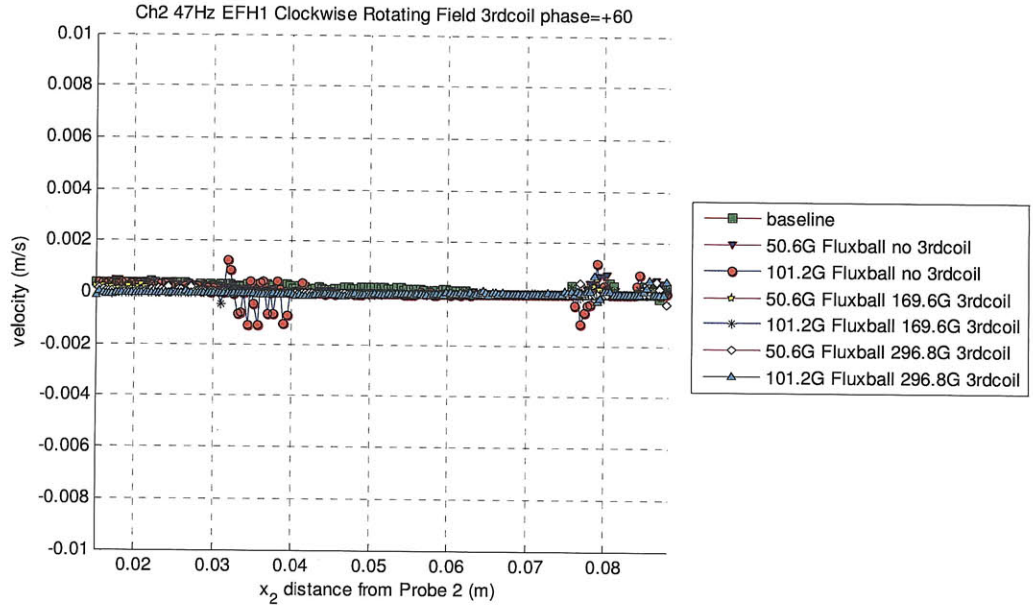
Ch2 47Hz EFH1 Clockwise Rotating Field 3rdcoil phase=+60
velocity (m/s)
0.01
0.008
0.006
0.004
0.002
0
-0.002
-0.004
-0.006
-0.008
-0.01
0.02
0.03
0.04
0.05
0.06
0.07
0.08
x2 distance from Probe 2 (m)
baseline
50.6G Fluxball no 3rdcoil
101.2G Fluxball no 3rdcoil
50.6G Fluxball 169.6G 3rdcoil
101.2G Fluxball 169.6G 3rdcoil
50.6G Fluxball 296.8G 3rdcoil
101.2G Fluxball 296.8G 3rdcoil

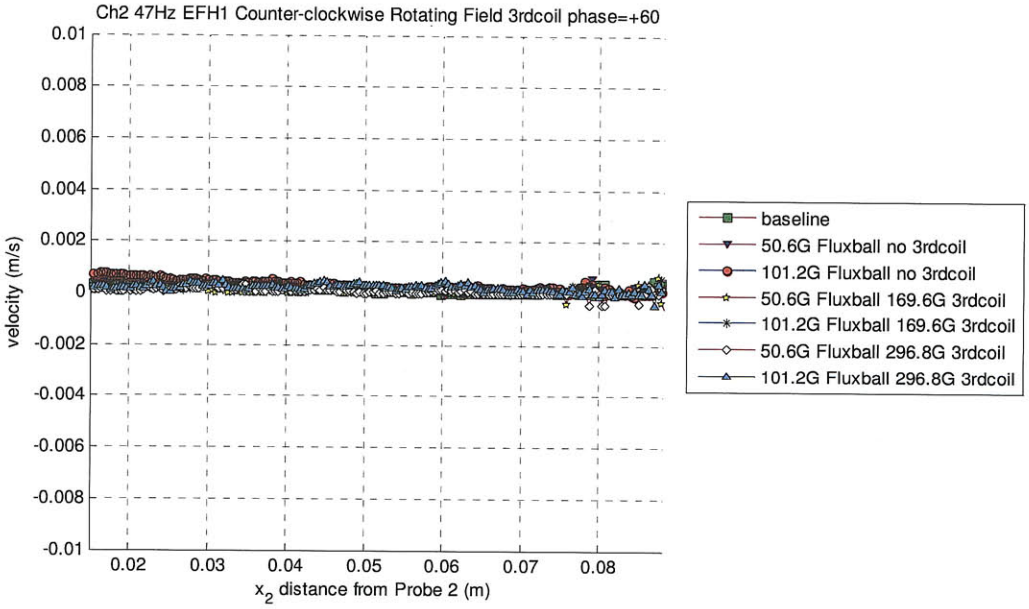
Ch2 47Hz EFH1 Counter-clockwise Rotating Field 3rdcoil phase=+60
velocity (m/s)
0.01
0.008
0.006
0.004
0.002
0
-0.002
-0.004
-0.006
-0.008
-0.01
0.02
0.03
0.04
0.05
0.06
0.07
0.08
x2 distance from Probe 2 (m)
baseline
50.6G Fluxball no 3rdcoil
101.2G Fluxball no 3rdcoil
50.6G Fluxball 169.6G 3rdcoil
101.2G Fluxball 169.6G 3rdcoil
50.6G Fluxball 296.8G 3rdcoil
101.2G Fluxball 296.8G 3rdcoil

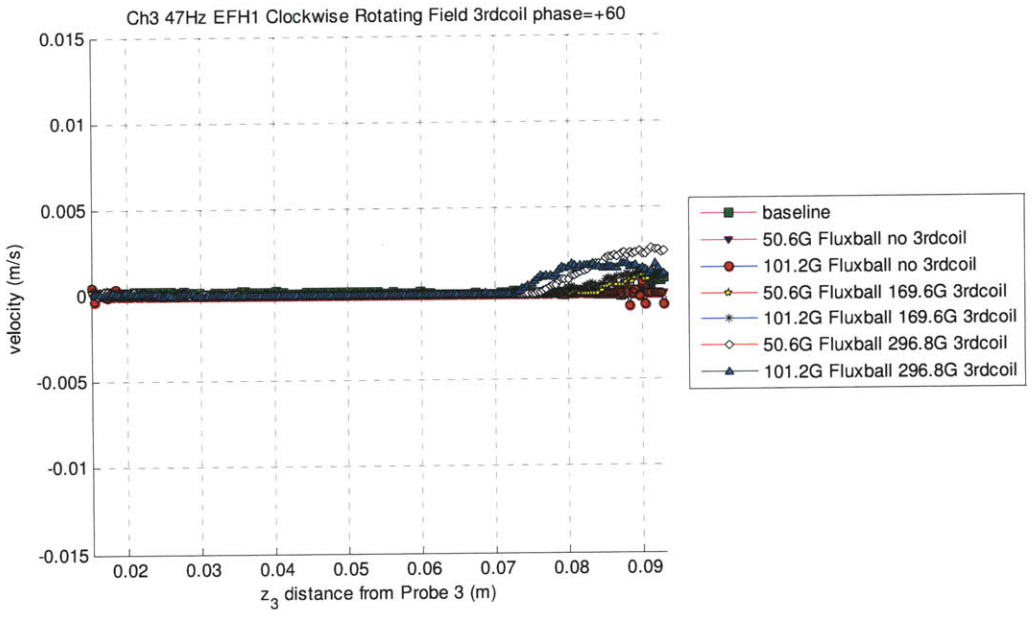
Ch3 47Hz EFH1 Clockwise Rotating Field 3rdcoil phase=+60
velocity (m/s)
0.015
0.01
0.005
0
-0.005
-0.01
-0.015
0.02
0.03
0.04
0.05
0.06
0.07
0.08
0.09
z3 distance from Probe 3 (m)
baseline
50.6G Fluxball no 3rdcoil
101.2G Fluxball no 3rdcoil
50.6G Fluxball 169.6G 3rdcoil
101.2G Fluxball 169.6G 3rdcoil
50.6G Fluxball 296.8G 3rdcoil
101.2G Fluxball 296.8G 3rdcoil

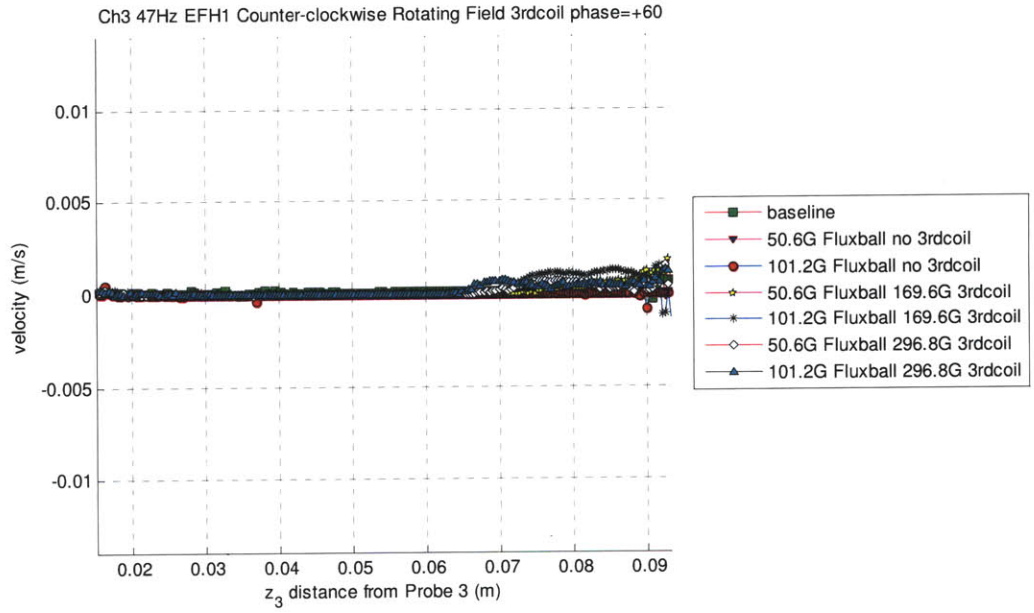
Ch3 47Hz EFH1 Counter-clockwise Rotating Field 3rdcoil phase=+60
velocity (m/s)
0.01
0.005
0
-0.005
-0.01
0.02
0.03
0.04
0.05
0.06
0.07
0.08
0.09
z3 distance from Probe 3 (m)
baseline
50.6G Fluxball no 3rdcoil
101.2G Fluxball no 3rdcoil
50.6G Fluxball 169.6G 3rdcoil
101.2G Fluxball 169.6G 3rdcoil
50.6G Fluxball 296.8G 3rdcoil
101.2G Fluxball 296.8G 3rdcoil

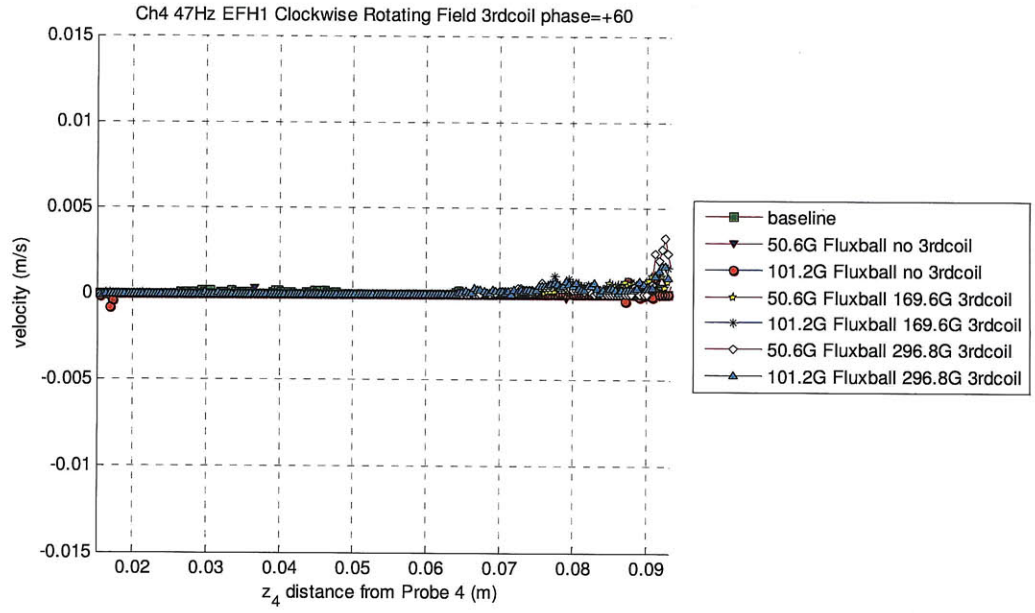
Ch4 47Hz EFH1 Clockwise Rotating Field 3rdcoil phase=+60
velocity (m/s)
0.015
0.01
0.005
0
-0.005
-0.01
-0.015
0.02
0.03
0.04
0.05
0.06
0.07
0.08
0.09
z4 distance from Probe 4 (m)
baseline
50.6G Fluxball no 3rdcoil
101.2G Fluxball no 3rdcoil
50.6G Fluxball 169.6G 3rdcoil
101.2G Fluxball 169.6G 3rdcoil
50.6G Fluxball 296.8G 3rdcoil
101.2G Fluxball 296.8G 3rdcoil

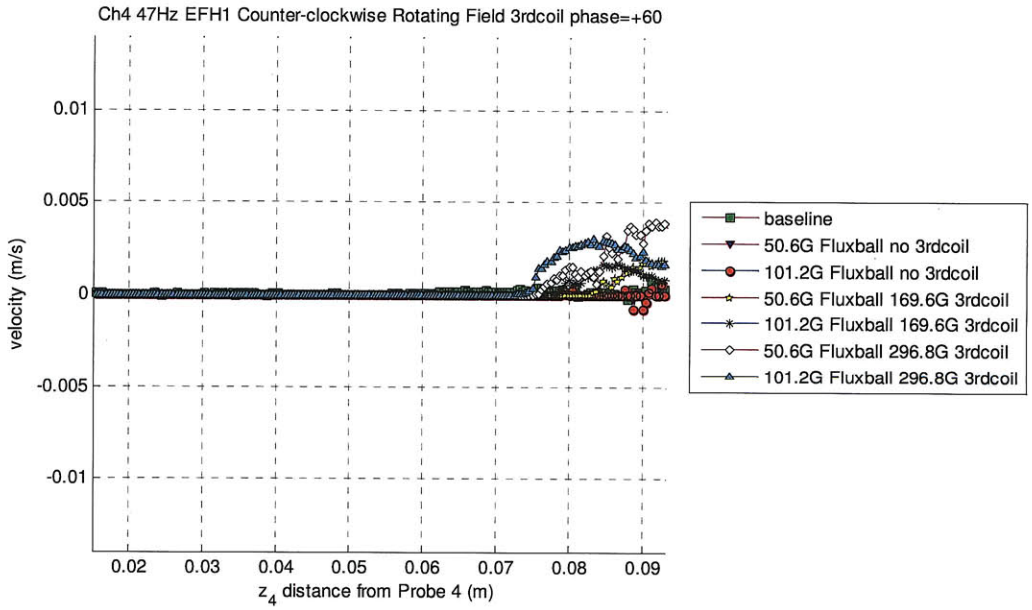
Ch4 47Hz EFH1 Counter-clockwise Rotating Field 3rdcoil phase=+60
velocity (m/s)
0.01
0.005
0
-0.005
-0.01
0.02
0.03
0.04
0.05
0.06
0.07
0.08
0.09
z4 distance from Probe 4 (m)
baseline
50.6G Fluxball no 3rdcoil
101.2G Fluxball no 3rdcoil
50.6G Fluxball 169.6G 3rdcoil
101.2G Fluxball 169.6G 3rdcoil
50.6G Fluxball 296.8G 3rdcoil
101.2G Fluxball 296.8G 3rdcoil

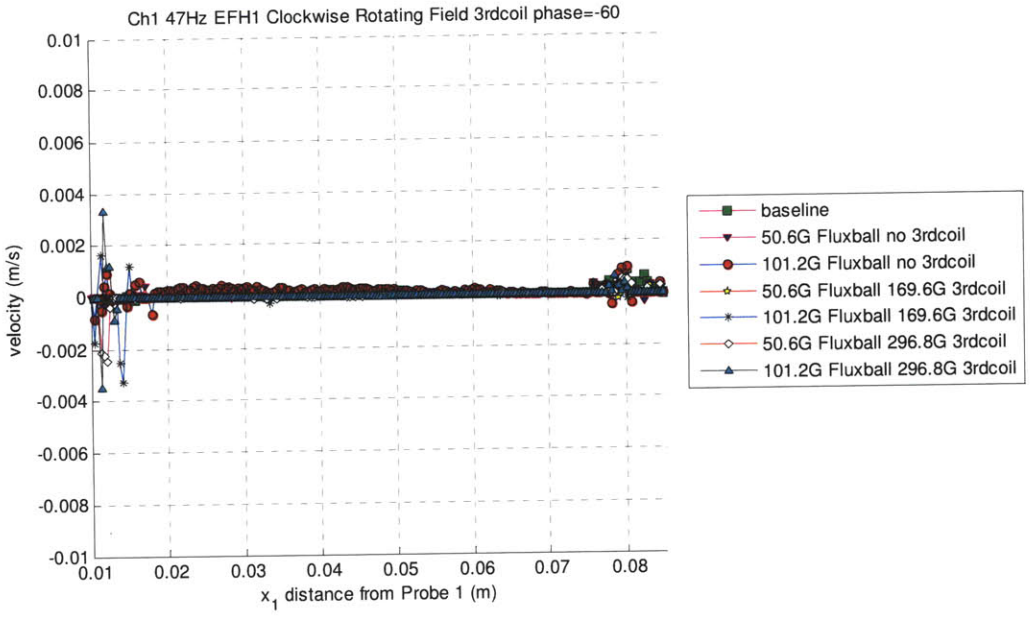
Ch1 47Hz EFH1 Clockwise Rotating Field 3rdcoil phase=-60
velocity (m/s)
0.01
0.008
0.006
0.004
0.002
0
-0.002
-0.004
-0.006
-0.008
-0.01
0.01
0.02
0.03
0.04
0.05
0.06
0.07
0.08
x1 distance from Probe 1 (m)
baseline
50.6G Fluxball no 3rdcoil
101.2G Fluxball no 3rdcoil
50.6G Fluxball 169.6G 3rdcoil
101.2G Fluxball 169.6G 3rdcoil
50.6G Fluxball 296.8G 3rdcoil
101.2G Fluxball 296.8G 3rdcoil

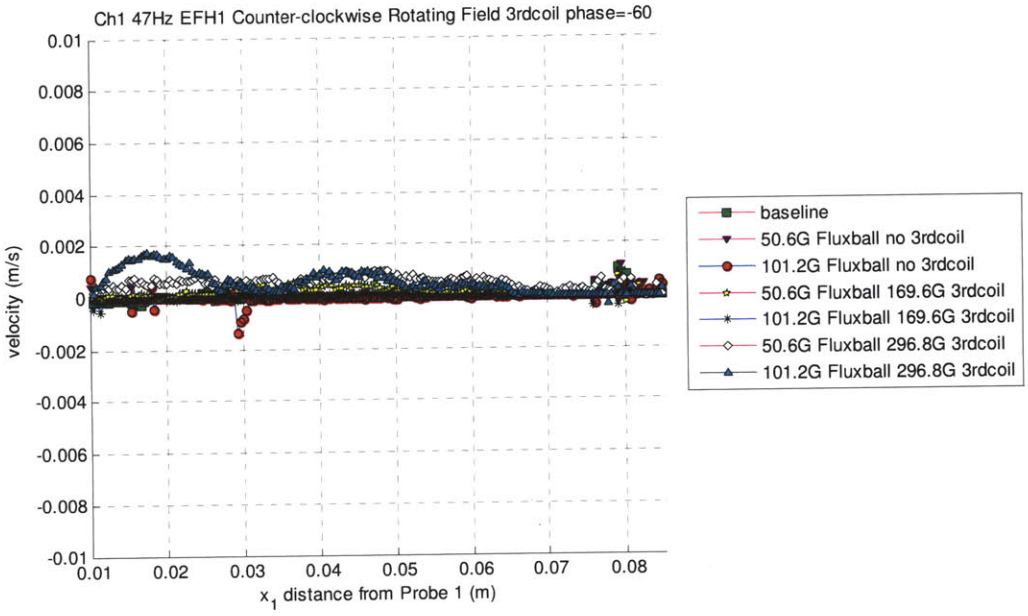
Ch1 47Hz EFH1 Counter-clockwise Rotating Field 3rdcoil phase=-60
velocity (m/s)
0.01
0.008
0.006
0.004
0.002
0
-0.002
-0.004
-0.006
-0.008
-0.01
0.01
0.02
0.03
0.04
0.05
0.06
0.07
0.08
x1 distance from Probe 1 (m)
baseline
50.6G Fluxball no 3rdcoil
101.2G Fluxball no 3rdcoil
50.6G Fluxball 169.6G 3rdcoil
101.2G Fluxball 169.6G 3rdcoil
50.6G Fluxball 296.8G 3rdcoil
101.2G Fluxball 296.8G 3rdcoil

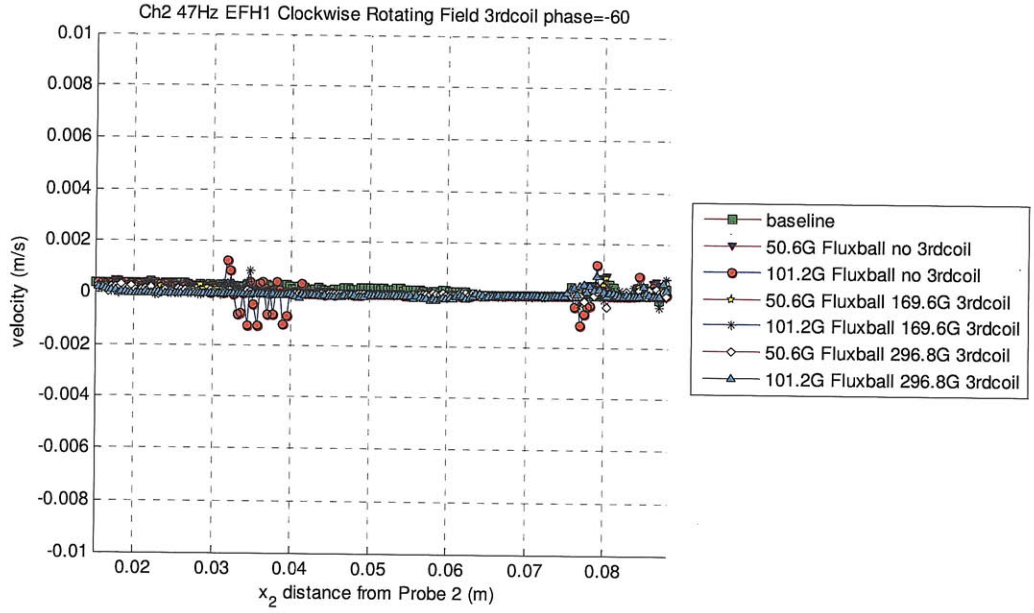
Ch2 47Hz EFH1 Clockwise Rotating Field 3rdcoil phase=-60
velocity (m/s)
0.01
0.008
0.006
0.004
0.002
0
-0.002
-0.004
-0.006
-0.008
-0.01
0.02
0.03
0.04
0.05
0.06
0.07
0.08
x2 distance from Probe 2 (m)
baseline
50.6G Fluxball no 3rdcoil
101.2G Fluxball no 3rdcoil
50.6G Fluxball 169.6G 3rdcoil
101.2G Fluxball 169.6G 3rdcoil
50.6G Fluxball 296.8G 3rdcoil
101.2G Fluxball 296.8G 3rdcoil

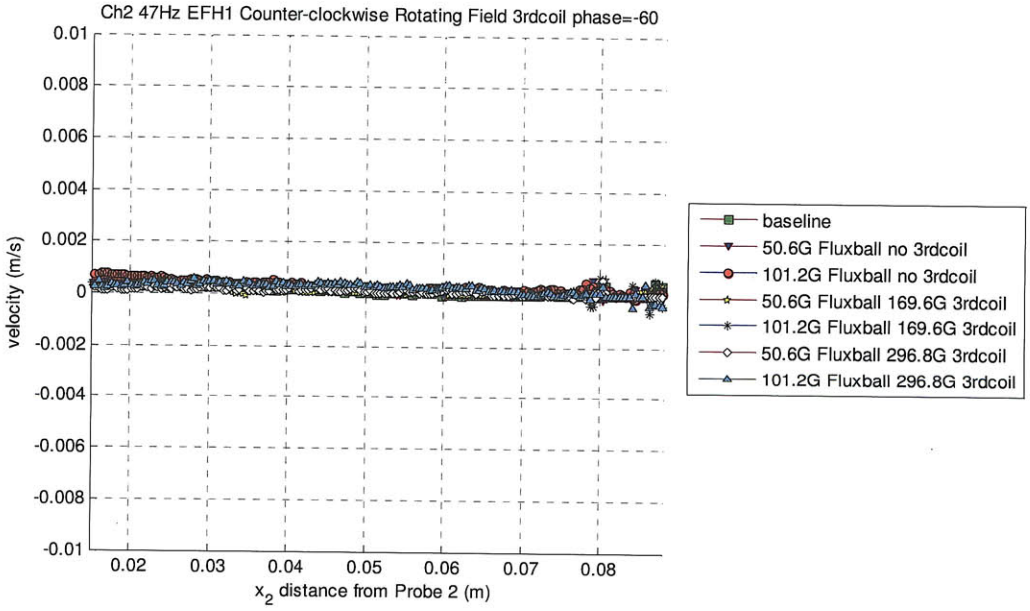
Ch2 47Hz EFH1 Counter-clockwise Rotating Field 3rdcoil phase=-60
velocity (m/s)
0.01
0.008
0.006
0.004
0.002
0
-0.002
-0.004
-0.006
-0.008
-0.01
0.02
0.03
0.04
0.05
0.06
0.07
0.08
x2 distance from Probe 2 (m)
baseline
50.6G Fluxball no 3rdcoil
101.2G Fluxball no 3rdcoil
50.6G Fluxball 169.6G 3rdcoil
101.2G Fluxball 169.6G 3rdcoil
50.6G Fluxball 296.8G 3rdcoil
101.2G Fluxball 296.8G 3rdcoil

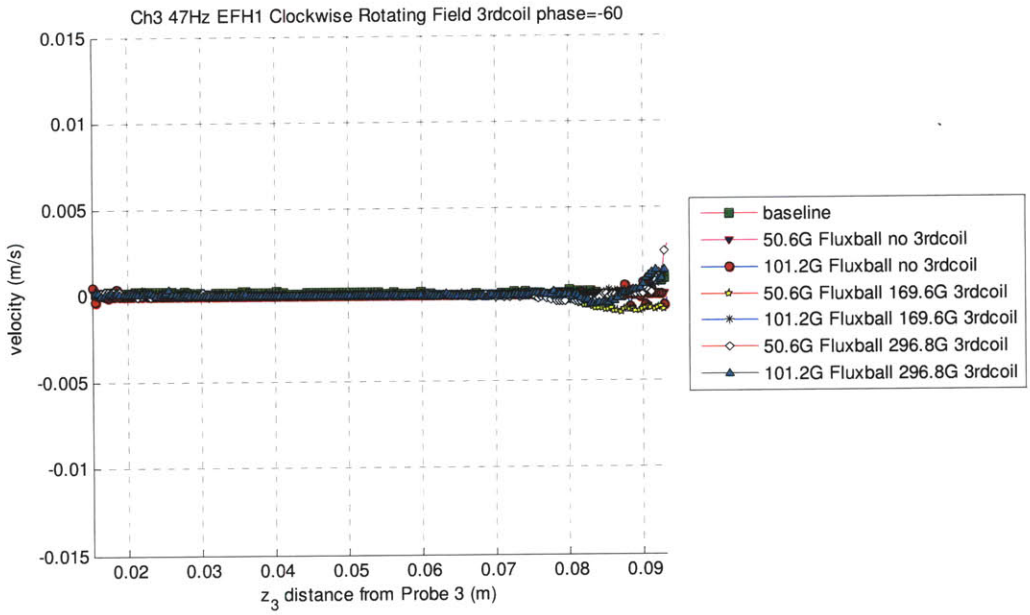
Ch3 47Hz EFH1 Clockwise Rotating Field 3rdcoil phase=-60
velocity (m/s)
0.015
0.01
0.005
0
-0.005
-0.01
-0.015
0.02
0.03
0.04
0.05
0.06
0.07
0.08
0.09
z_3 distance from Probe 3 (m)
baseline
50.6G Fluxball no 3rdcoil
101.2G Fluxball no 3rdcoil
50.6G Fluxball 169.6G 3rdcoil
101.2G Fluxball 169.6G 3rdcoil
50.6G Fluxball 296.8G 3rdcoil
101.2G Fluxball 296.8G 3rdcoil

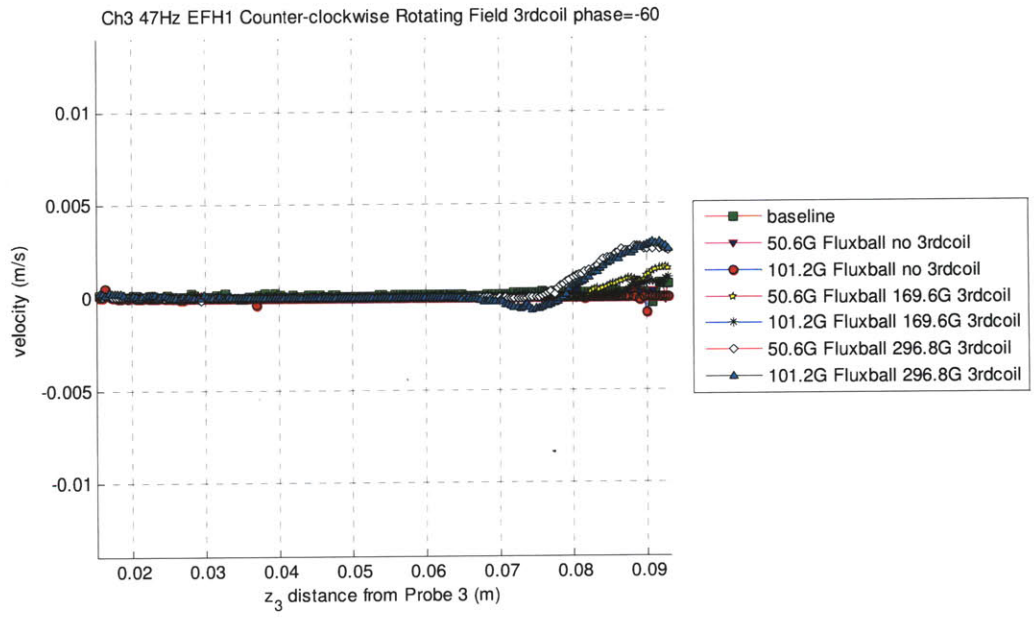
Ch3 47Hz EFH1 Counter-clockwise Rotating Field 3rdcoil phase=-60
velocity (m/s)
0.01
0.005
0
-0.005
-0.01
0.02
0.03
0.04
0.05
0.06
0.07
0.08
0.09
z_3 distance from Probe 3 (m)
baseline
50.6G Fluxball no 3rdcoil
101.2G Fluxball no 3rdcoil
50.6G Fluxball 169.6G 3rdcoil
101.2G Fluxball 169.6G 3rdcoil
50.6G Fluxball 296.8G 3rdcoil
101.2G Fluxball 296.8G 3rdcoil

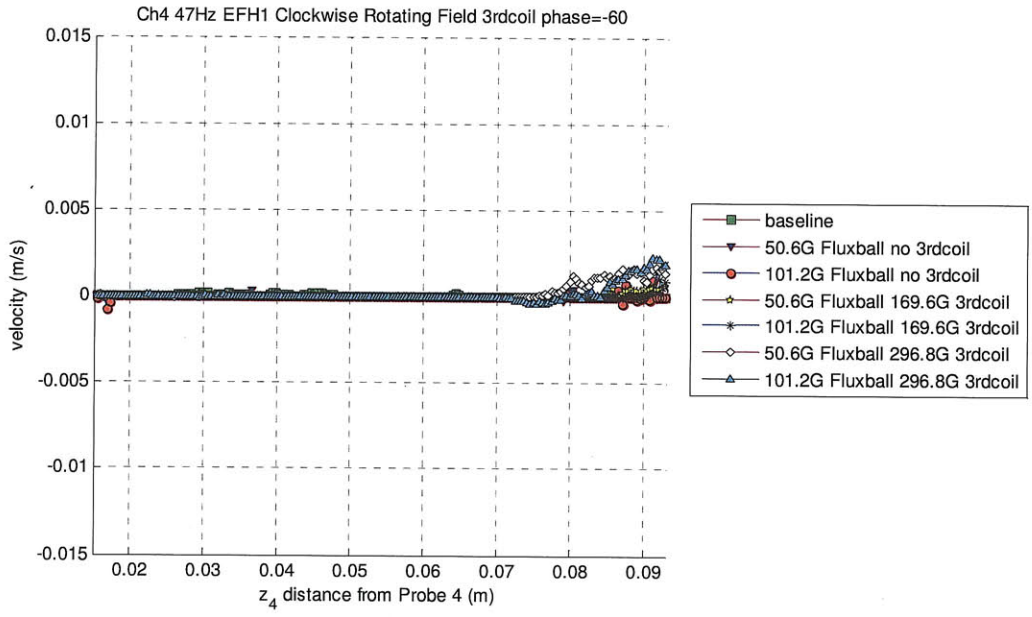
Ch4 47Hz EFH1 Clockwise Rotating Field 3rdcoil phase=-60
velocity (m/s)
0.015
0.01
0.005
0
-0.005
-0.01
-0.015
0.02
0.03
0.04
0.05
0.06
0.07
0.08
0.09
z4 distance from Probe 4 (m)
baseline
50.6G Fluxball no 3rdcoil
101.2G Fluxball no 3rdcoil
50.6G Fluxball 169.6G 3rdcoil
101.2G Fluxball 169.6G 3rdcoil
50.6G Fluxball 296.8G 3rdcoil
101.2G Fluxball 296.8G 3rdcoil

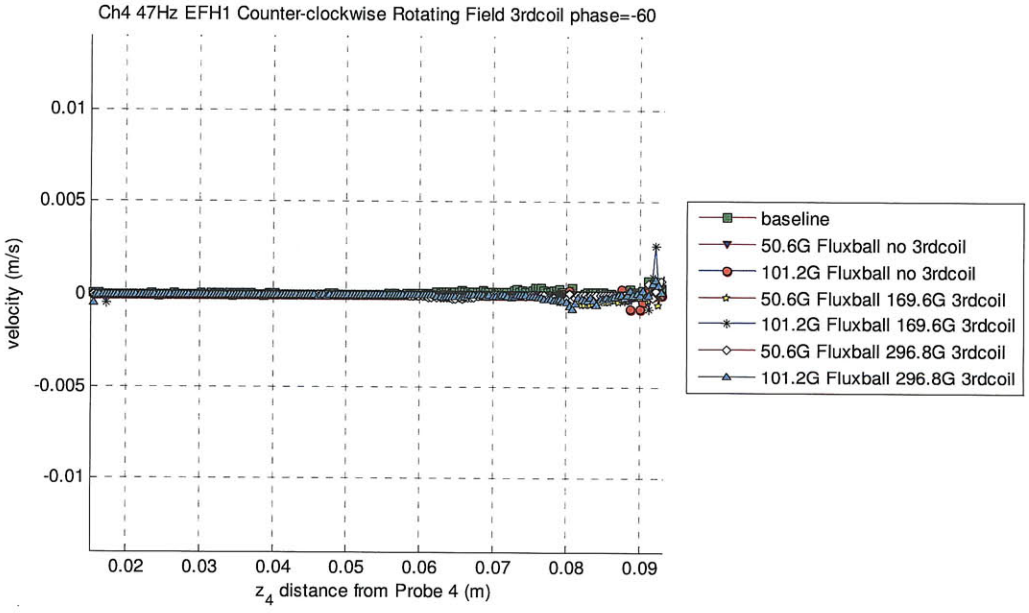
Ch4 47Hz EFH1 Counter-clockwise Rotating Field 3rdcoil phase=-60
velocity (m/s)
0.01
0.005
0
-0.005
-0.01
0.02
0.03
0.04
0.05
0.06
0.07
0.08
0.09
z4 distance from Probe 4 (m)
baseline
50.6G Fluxball no 3rdcoil
101.2G Fluxball no 3rdcoil
50.6G Fluxball 169.6G 3rdcoil
101.2G Fluxball 169.6G 3rdcoil
50.6G Fluxball 296.8G 3rdcoil
101.2G Fluxball 296.8G 3rdcoil

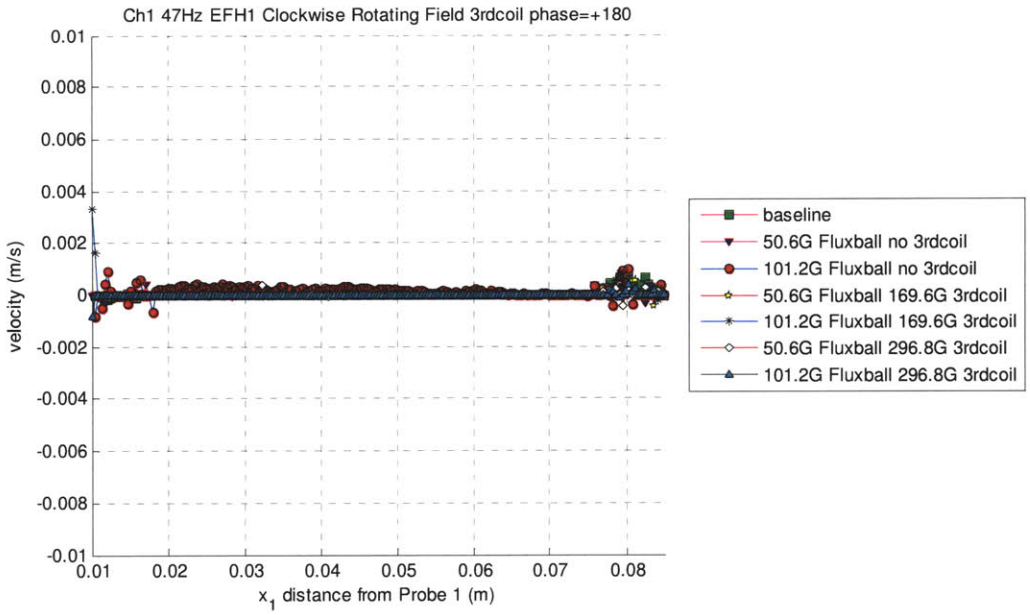
Ch1 47Hz EFH1 Clockwise Rotating Field 3rdcoil phase=+180
velocity (m/s)
x1 distance from Probe 1 (m)
baseline
50.6G Fluxball no 3rdcoil
101.2G Fluxball no 3rdcoil
50.6G Fluxball 169.6G 3rdcoil
101.2G Fluxball 169.6G 3rdcoil
50.6G Fluxball 296.8G 3rdcoil
101.2G Fluxball 296.8G 3rdcoil

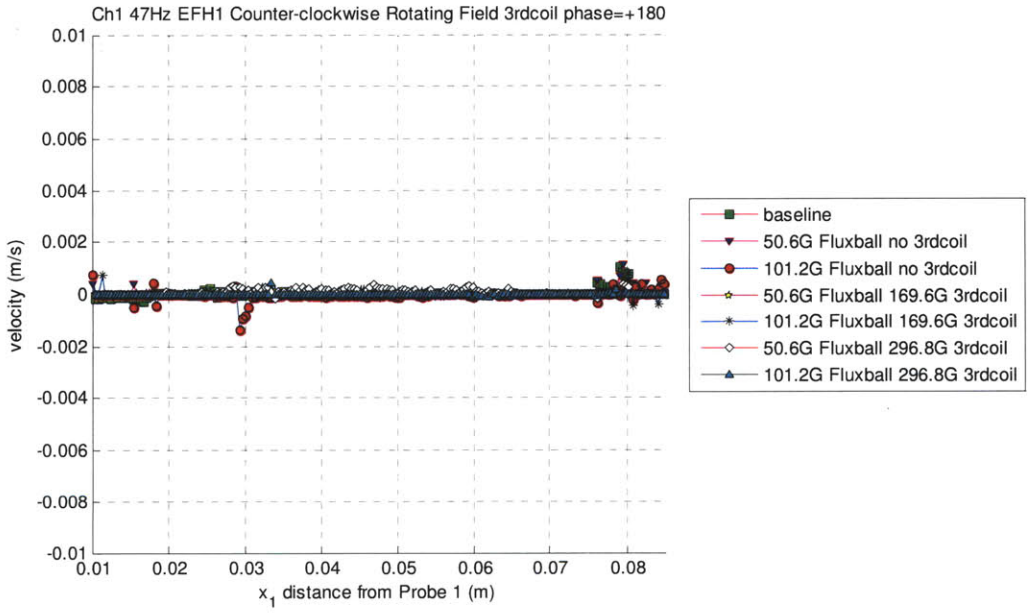
Ch1 47Hz EFH1 Counter-clockwise Rotating Field 3rdcoil phase=+180
velocity (m/s)
x1 distance from Probe 1 (m)
baseline
50.6G Fluxball no 3rdcoil
101.2G Fluxball no 3rdcoil
50.6G Fluxball 169.6G 3rdcoil
101.2G Fluxball 169.6G 3rdcoil
50.6G Fluxball 296.8G 3rdcoil
101.2G Fluxball 296.8G 3rdcoil

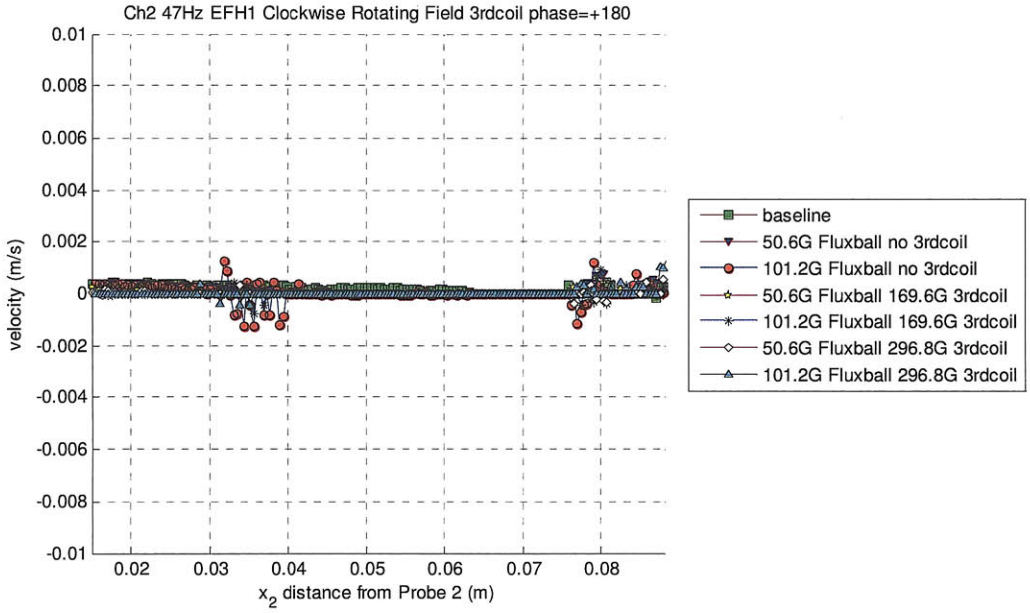
Ch2 47Hz EFH1 Clockwise Rotating Field 3rdcoil phase=+180
velocity (m/s)
0.01
0.008
0.006
0.004
0.002
0
-0.002
-0.004
-0.006
-0.008
-0.01
0.02
0.03
0.04
0.05
0.06
0.07
0.08
x2 distance from Probe 2 (m)
baseline
50.6G Fluxball no 3rdcoil
101.2G Fluxball no 3rdcoil
50.6G Fluxball 169.6G 3rdcoil
101.2G Fluxball 169.6G 3rdcoil
50.6G Fluxball 296.8G 3rdcoil
101.2G Fluxball 296.8G 3rdcoil

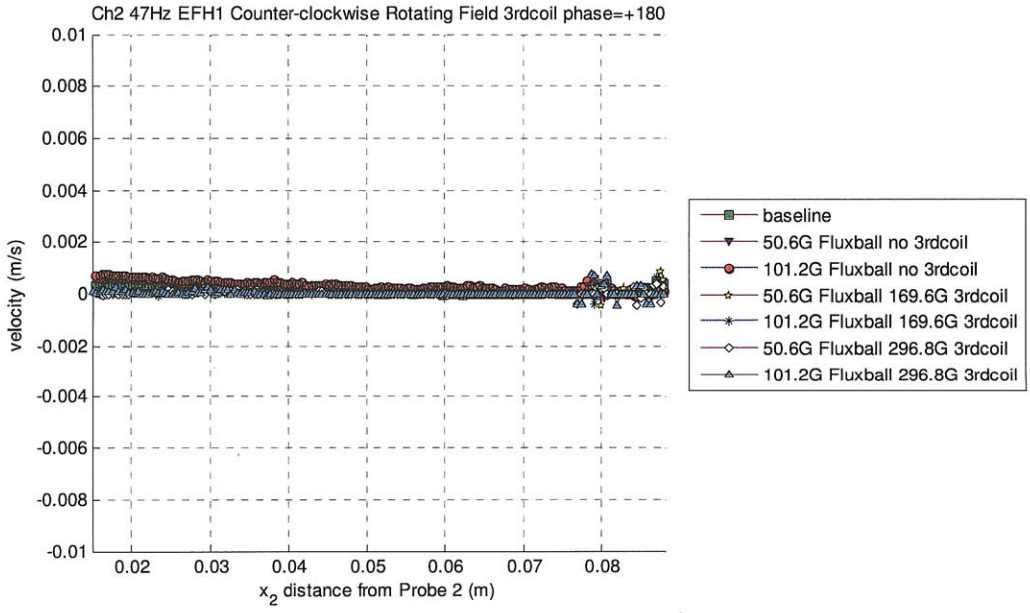
Ch2 47Hz EFH1 Counter-clockwise Rotating Field 3rdcoil phase=+180
velocity (m/s)
0.01
0.008
0.006
0.004
0.002
0
-0.002
-0.004
-0.006
-0.008
-0.01
0.02
0.03
0.04
0.05
0.06
0.07
0.08
x2 distance from Probe 2 (m)
baseline
50.6G Fluxball no 3rdcoil
101.2G Fluxball no 3rdcoil
50.6G Fluxball 169.6G 3rdcoil
101.2G Fluxball 169.6G 3rdcoil
50.6G Fluxball 296.8G 3rdcoil
101.2G Fluxball 296.8G 3rdcoil

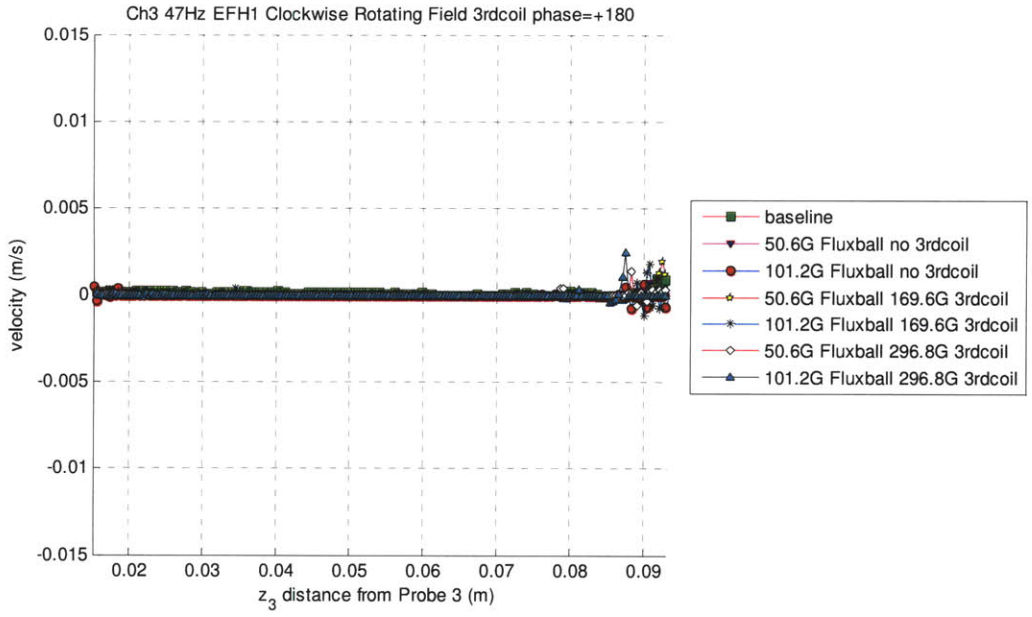
Ch3 47Hz EFH1 Clockwise Rotating Field 3rdcoil phase=+180
velocity (m/s)
0.015
0.01
0.005
0
-0.005
-0.01
-0.015
0.02
0.03
0.04
0.05
0.06
0.07
0.08
0.09
z3 distance from Probe 3 (m)
baseline
50.6G Fluxball no 3rdcoil
101.2G Fluxball no 3rdcoil
50.6G Fluxball 169.6G 3rdcoil
101.2G Fluxball 169.6G 3rdcoil
50.6G Fluxball 296.8G 3rdcoil
101.2G Fluxball 296.8G 3rdcoil

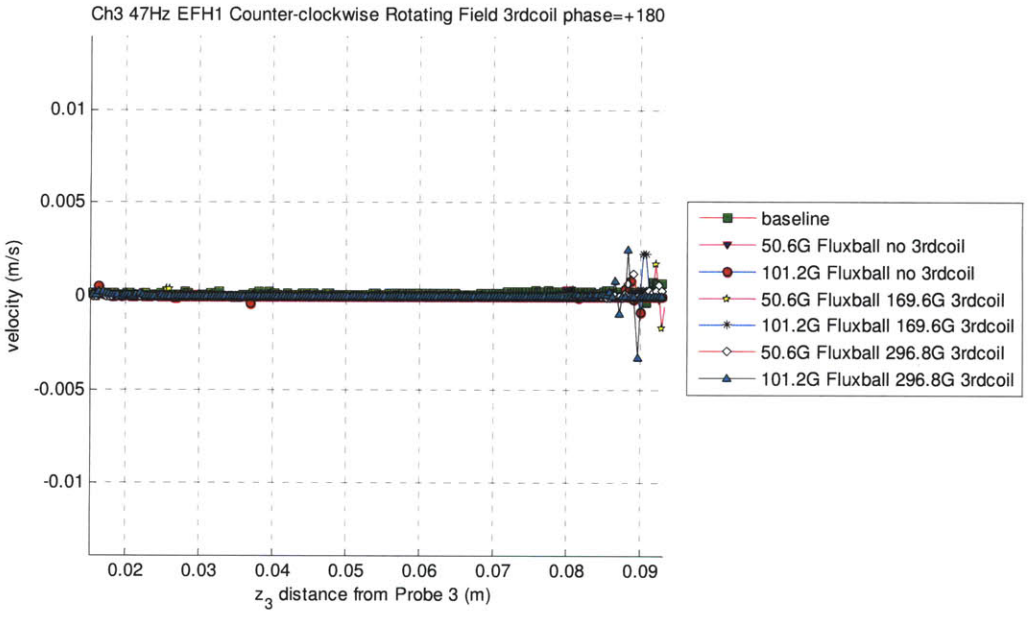
Ch3 47Hz EFH1 Counter-clockwise Rotating Field 3rdcoil phase=+180
velocity (m/s)
0.01
0.005
0
-0.005
-0.01
0.02
0.03
0.04
0.05
0.06
0.07
0.08
0.09
z3 distance from Probe 3 (m)
baseline
50.6G Fluxball no 3rdcoil
101.2G Fluxball no 3rdcoil
50.6G Fluxball 169.6G 3rdcoil
101.2G Fluxball 169.6G 3rdcoil
50.6G Fluxball 296.8G 3rdcoil
101.2G Fluxball 296.8G 3rdcoil

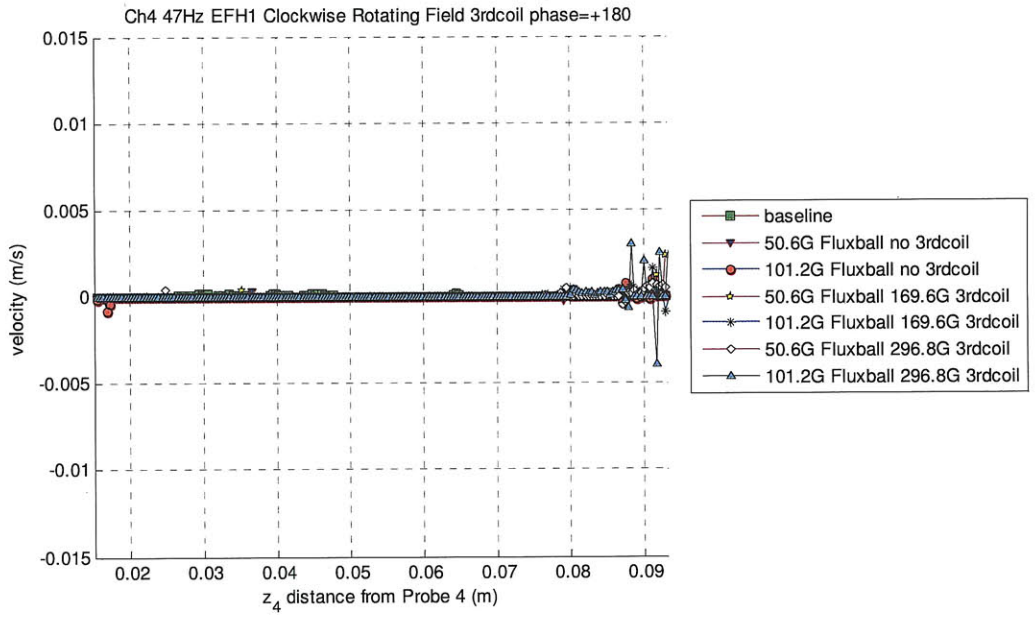
Ch4 47Hz EFH1 Clockwise Rotating Field 3rdcoil phase=+180
0.015
0.01
0.005
0
-0.005
-0.01
-0.015
velocity (m/s)
0.02
0.03
0.04
0.05
0.06
0.07
0.08
0.09
z4 distance from Probe 4 (m)
baseline
50.6G Fluxball no 3rdcoil
101.2G Fluxball no 3rdcoil
50.6G Fluxball 169.6G 3rdcoil
101.2G Fluxball 169.6G 3rdcoil
50.6G Fluxball 296.8G 3rdcoil
101.2G Fluxball 296.8G 3rdcoil

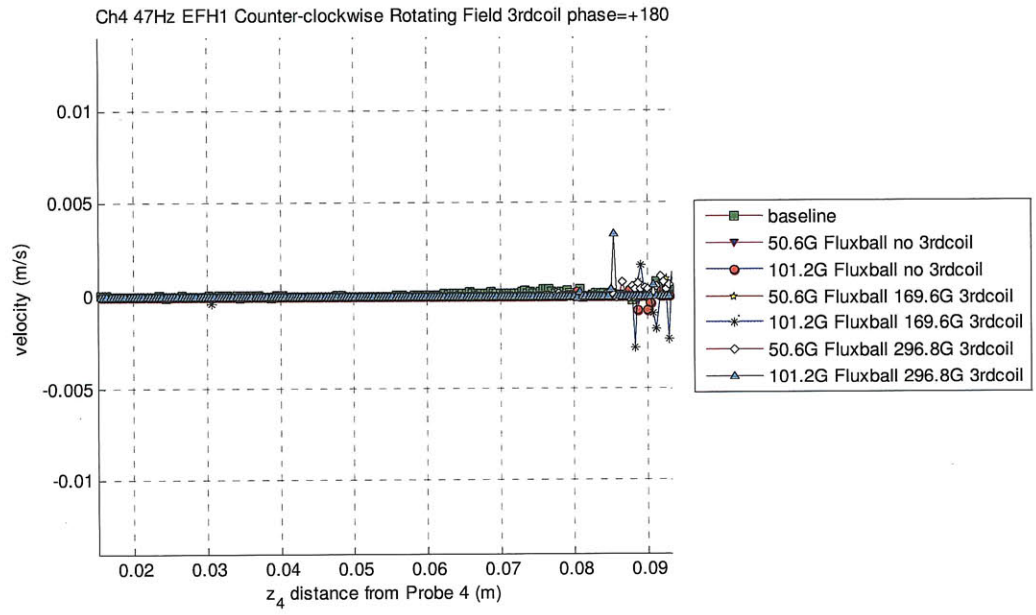
Ch4 47Hz EFH1 Counter-clockwise Rotating Field 3rdcoil phase=+180
0.01
0.005
0
-0.005
-0.01
velocity (m/s)
0.02
0.03
0.04
0.05
0.06
0.07
0.08
0.09
z4 distance from Probe 4 (m)
baseline
50.6G Fluxball no 3rdcoil
101.2G Fluxball no 3rdcoil
50.6G Fluxball 169.6G 3rdcoil
101.2G Fluxball 169.6G 3rdcoil
50.6G Fluxball 296.8G 3rdcoil
101.2G Fluxball 296.8G 3rdcoil

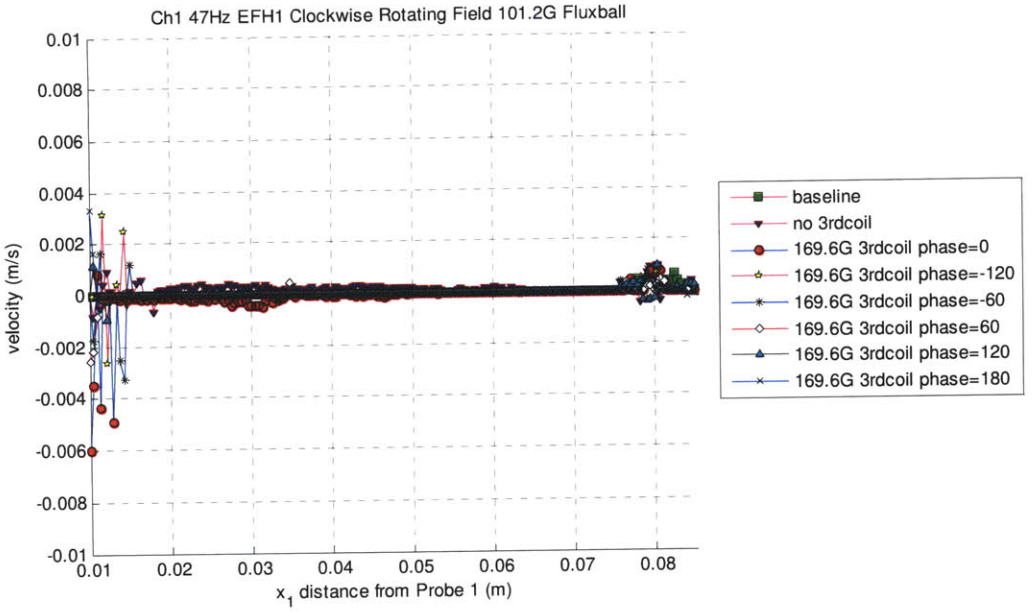
Ch1 47Hz EFH1 Clockwise Rotating Field 101.2G Fluxball
velocity (m/s)
0.01
0.008
0.006
0.004
0.002
0
-0.002
-0.004
-0.006
-0.008
-0.01
0.01
0.02
0.03
0.04
0.05
0.06
0.07
0.08
x1 distance from Probe 1 (m)
baseline
no 3rdcoil
169.6G 3rdcoil phase=0
169.6G 3rdcoil phase=-120
169.6G 3rdcoil phase=-60
169.6G 3rdcoil phase=60
169.6G 3rdcoil phase=120
169.6G 3rdcoil phase=180

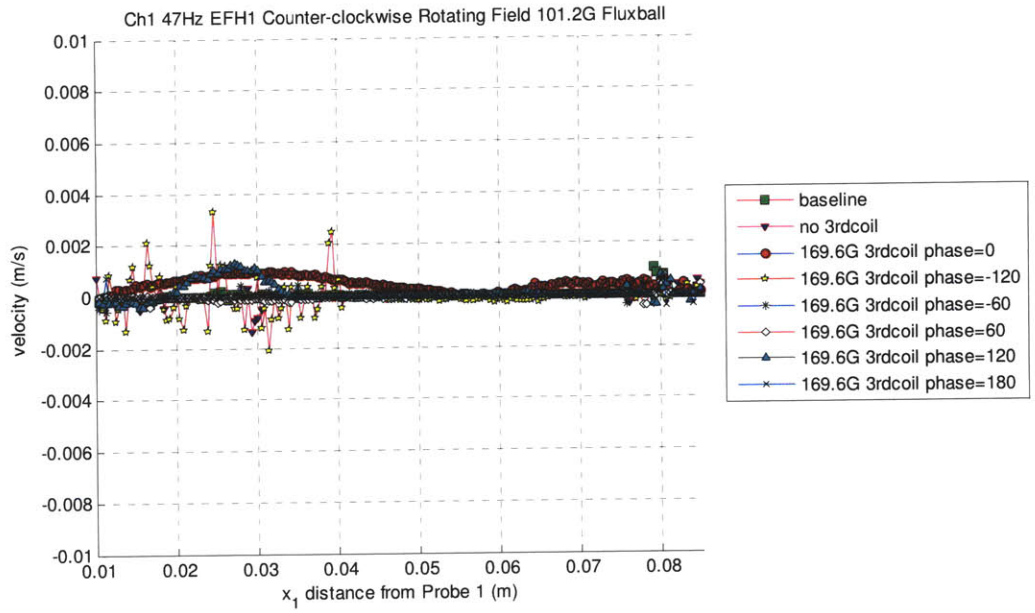
Ch1 47Hz EFH1 Counter-clockwise Rotating Field 101.2G Fluxball
velocity (m/s)
0.01
0.008
0.006
0.004
0.002
0
-0.002
-0.004
-0.006
-0.008
-0.01
0.01
0.02
0.03
0.04
0.05
0.06
0.07
0.08
x1 distance from Probe 1 (m)
baseline
no 3rdcoil
169.6G 3rdcoil phase=0
169.6G 3rdcoil phase=-120
169.6G 3rdcoil phase=-60
169.6G 3rdcoil phase=60
169.6G 3rdcoil phase=120
169.6G 3rdcoil phase=180

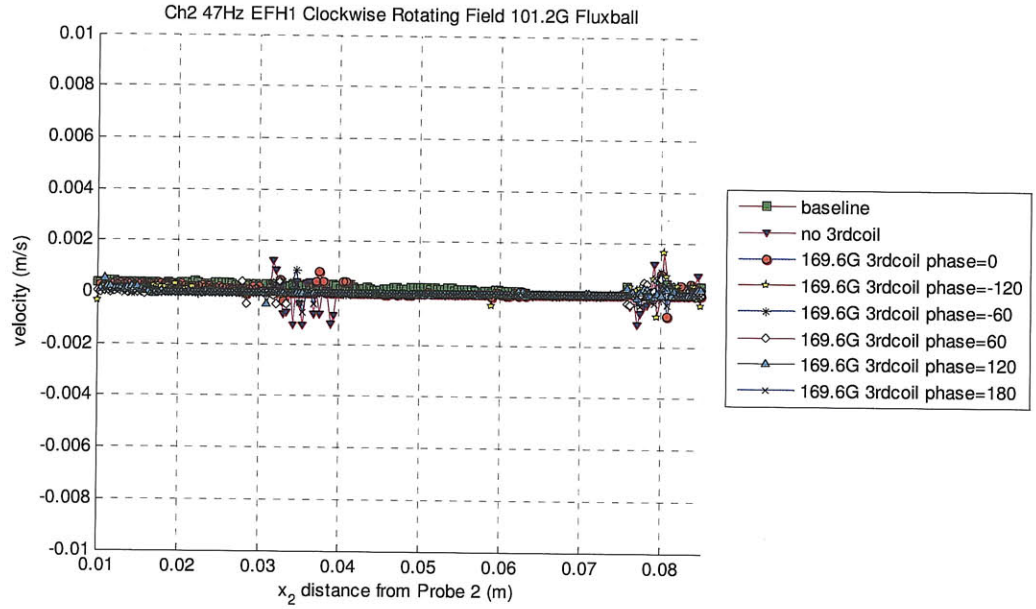
Ch2 47Hz EFH1 Clockwise Rotating Field 101.2G Fluxball
velocity (m/s)
0.01
0.008
0.006
0.004
0.002
0
-0.002
-0.004
-0.006
-0.008
-0.01
0.01
0.02
0.03
0.04
0.05
0.06
0.07
0.08
x2 distance from Probe 2 (m)
baseline
no 3rdcoil
169.6G 3rdcoil phase=0
169.6G 3rdcoil phase=-120
169.6G 3rdcoil phase=-60
169.6G 3rdcoil phase=60
169.6G 3rdcoil phase=120
169.6G 3rdcoil phase=180

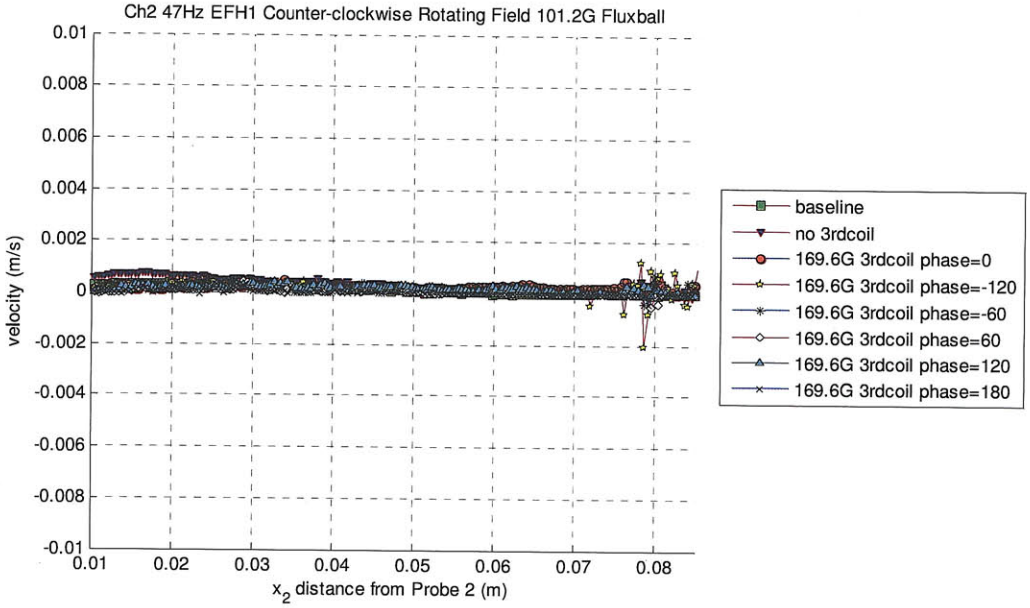
Ch2 47Hz EFH1 Counter-clockwise Rotating Field 101.2G Fluxball
velocity (m/s)
0.01
0.008
0.006
0.004
0.002
0
-0.002
-0.004
-0.006
-0.008
-0.01
0.01
0.02
0.03
0.04
0.05
0.06
0.07
0.08
x2 distance from Probe 2 (m)
baseline
no 3rdcoil
169.6G 3rdcoil phase=0
169.6G 3rdcoil phase=-120
169.6G 3rdcoil phase=-60
169.6G 3rdcoil phase=60
169.6G 3rdcoil phase=120
169.6G 3rdcoil phase=180

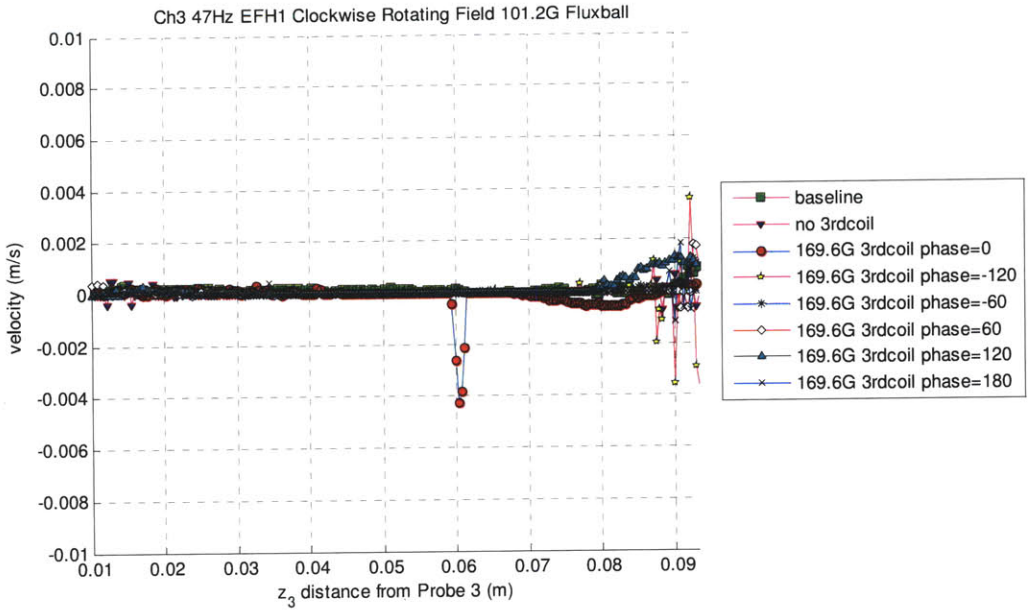
Ch3 47Hz EFH1 Clockwise Rotating Field 101.2G Fluxball
velocity (m/s)
0.01
0.008
0.006
0.004
0.002
0
-0.002
-0.004
-0.006
-0.008
-0.01
0.01 0.02 0.03 0.04 0.05 0.06 0.07 0.08 0.09
z3 distance from Probe 3 (m)
baseline
no 3rdcoil
169.6G 3rdcoil phase=0
169.6G 3rdcoil phase=-120
169.6G 3rdcoil phase=-60
169.6G 3rdcoil phase=60
169.6G 3rdcoil phase=120
169.6G 3rdcoil phase=180

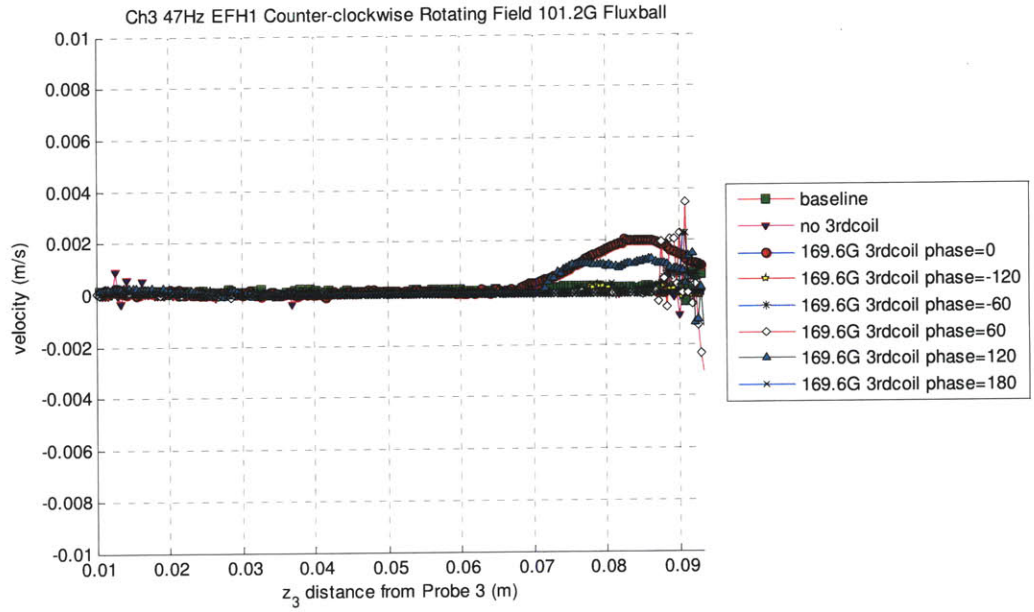
Ch3 47Hz EFH1 Counter-clockwise Rotating Field 101.2G Fluxball
velocity (m/s)
0.01
0.008
0.006
0.004
0.002
0
-0.002
-0.004
-0.006
-0.008
-0.01
0.01 0.02 0.03 0.04 0.05 0.06 0.07 0.08 0.09
z3 distance from Probe 3 (m)
baseline
no 3rdcoil
169.6G 3rdcoil phase=0
169.6G 3rdcoil phase=-120
169.6G 3rdcoil phase=-60
169.6G 3rdcoil phase=60
169.6G 3rdcoil phase=120
169.6G 3rdcoil phase=180

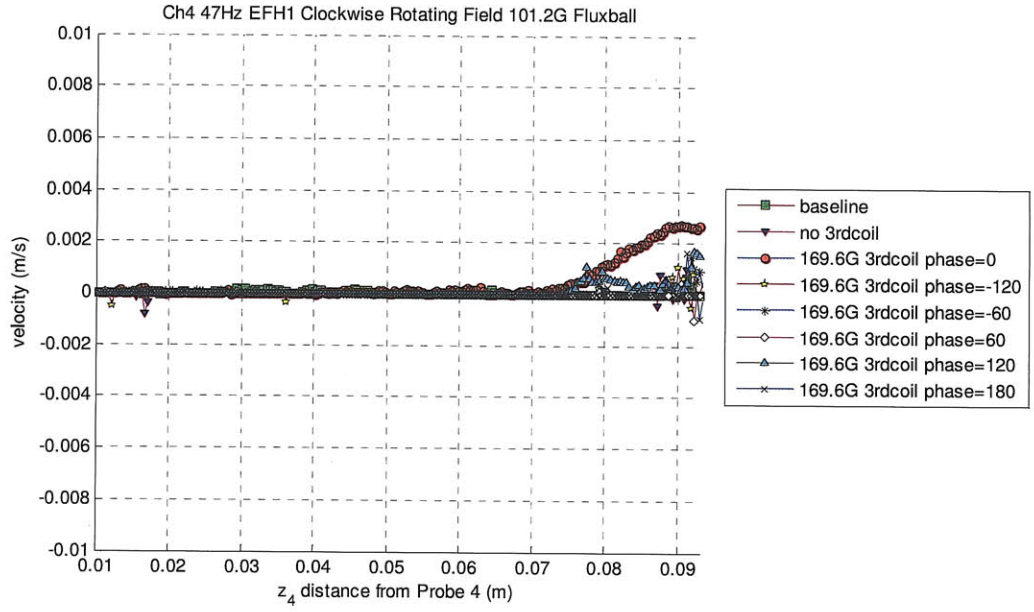
Ch4 47Hz EFH1 Clockwise Rotating Field 101.2G Fluxball
velocity (m/s)
0.01
0.008
0.006
0.004
0.002
0
-0.002
-0.004
-0.006
-0.008
-0.01
0.01 0.02 0.03 0.04 0.05 0.06 0.07 0.08 0.09
z4 distance from Probe 4 (m)
baseline
no 3rdcoil
169.6G 3rdcoil phase=0
169.6G 3rdcoil phase=-120
169.6G 3rdcoil phase=-60
169.6G 3rdcoil phase=60
169.6G 3rdcoil phase=120
169.6G 3rdcoil phase=180

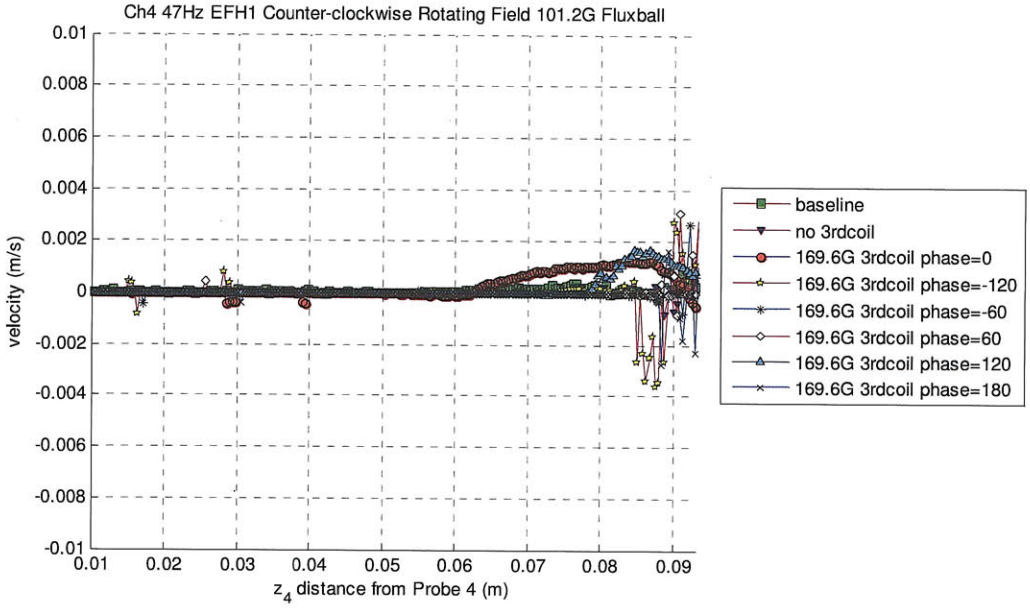
Ch4 47Hz EFH1 Counter-clockwise Rotating Field 101.2G Fluxball
velocity (m/s)
0.01
0.008
0.006
0.004
0.002
0
-0.002
-0.004
-0.006
-0.008
-0.01
0.01 0.02 0.03 0.04 0.05 0.06 0.07 0.08 0.09
z4 distance from Probe 4 (m)
baseline
no 3rdcoil
169.6G 3rdcoil phase=0
169.6G 3rdcoil phase=-120
169.6G 3rdcoil phase=-60
169.6G 3rdcoil phase=60
169.6G 3rdcoil phase=120
169.6G 3rdcoil phase=180

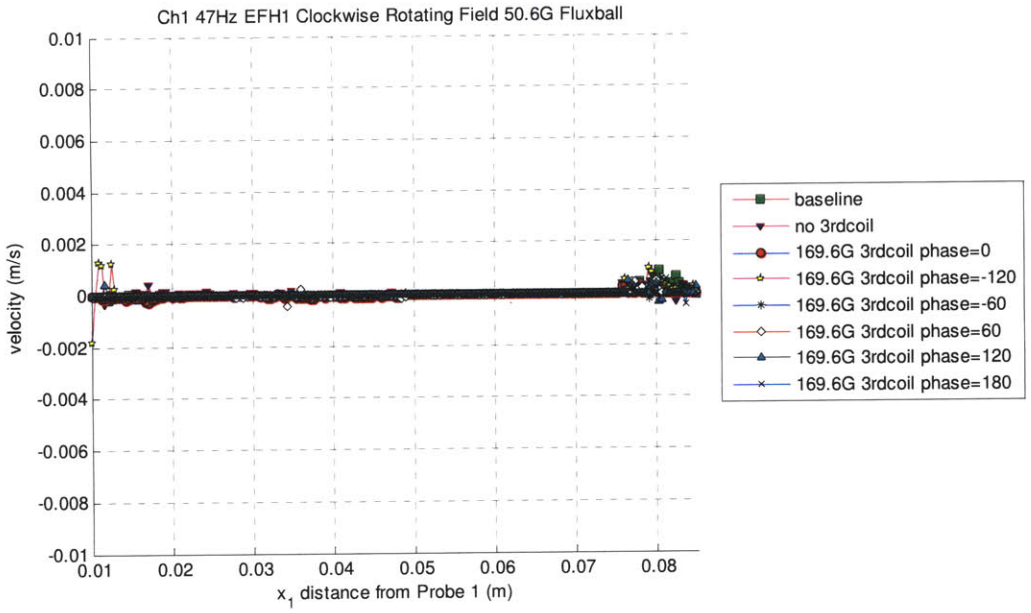
Ch1 47Hz EFH1 Clockwise Rotating Field 50.6G Fluxball
velocity (m/s)
x1 distance from Probe 1 (m)
baseline
no 3rdcoil
169.6G 3rdcoil phase=0
169.6G 3rdcoil phase=-120
169.6G 3rdcoil phase=-60
169.6G 3rdcoil phase=60
169.6G 3rdcoil phase=120
169.6G 3rdcoil phase=180

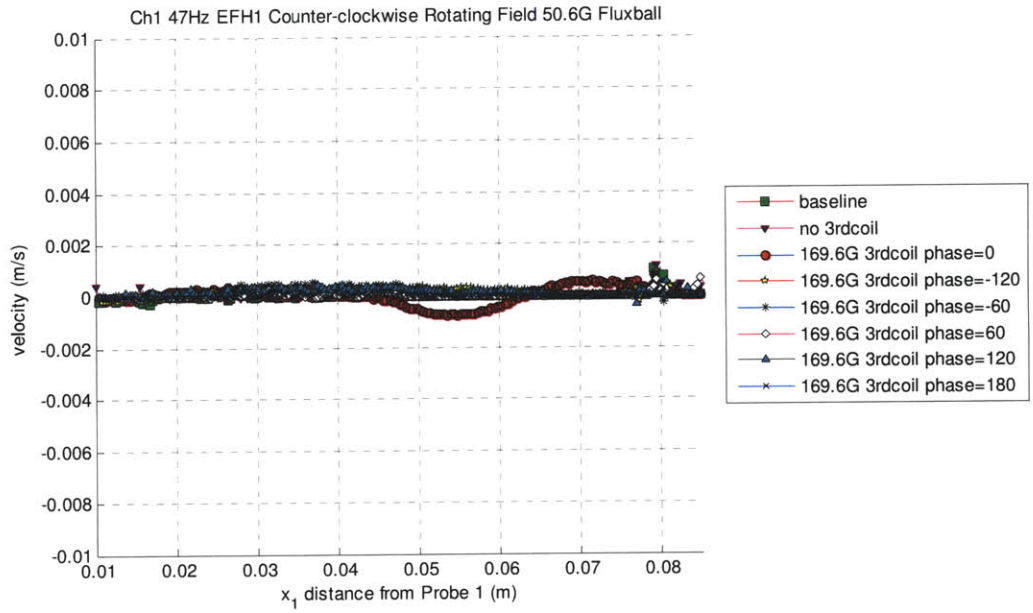
Ch1 47Hz EFH1 Counter-clockwise Rotating Field 50.6G Fluxball
velocity (m/s)
x1 distance from Probe 1 (m)
baseline
no 3rdcoil
169.6G 3rdcoil phase=0
169.6G 3rdcoil phase=-120
169.6G 3rdcoil phase=-60
169.6G 3rdcoil phase=60
169.6G 3rdcoil phase=120
169.6G 3rdcoil phase=180

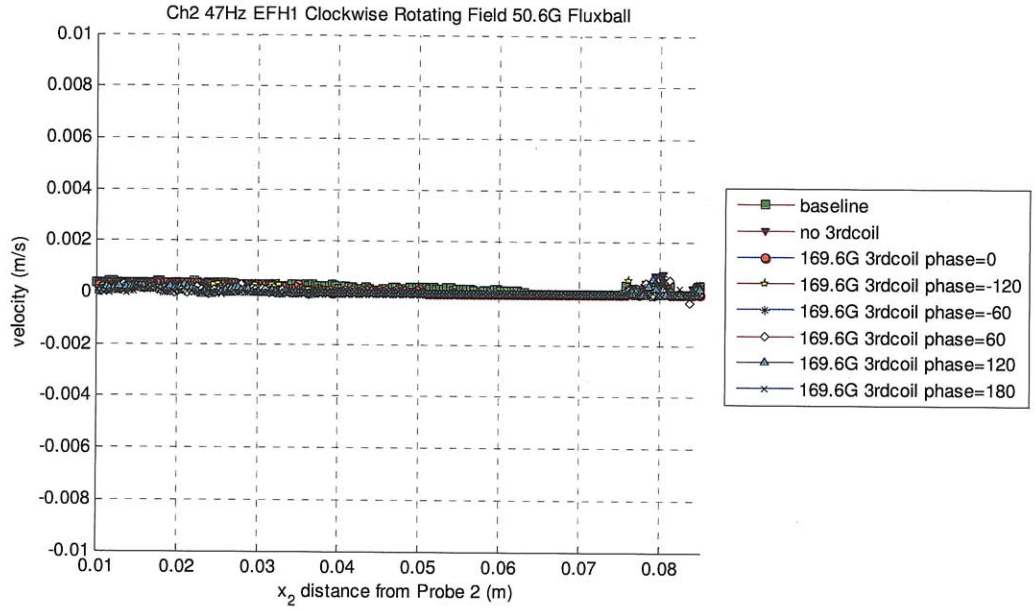
Ch2 47Hz EFH1 Clockwise Rotating Field 50.6G Fluxball
velocity (m/s)
0.01
0.008
0.006
0.004
0.002
0
-0.002
-0.004
-0.006
-0.008
-0.01
0.01
0.02
0.03
0.04
0.05
0.06
0.07
0.08
x2 distance from Probe 2 (m)
baseline
no 3rdcoil
169.6G 3rdcoil phase=0
169.6G 3rdcoil phase=-120
169.6G 3rdcoil phase=-60
169.6G 3rdcoil phase=60
169.6G 3rdcoil phase=120
169.6G 3rdcoil phase=180

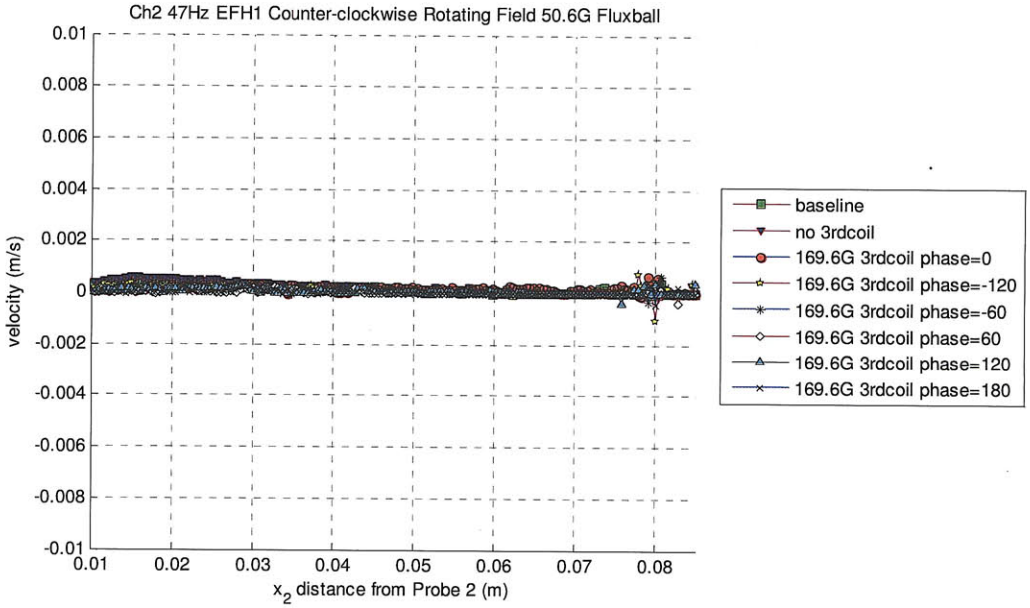
Ch2 47Hz EFH1 Counter-clockwise Rotating Field 50.6G Fluxball
velocity (m/s)
0.01
0.008
0.006
0.004
0.002
0
-0.002
-0.004
-0.006
-0.008
-0.01
0.01
0.02
0.03
0.04
0.05
0.06
0.07
0.08
x2 distance from Probe 2 (m)
baseline
no 3rdcoil
169.6G 3rdcoil phase=0
169.6G 3rdcoil phase=-120
169.6G 3rdcoil phase=-60
169.6G 3rdcoil phase=60
169.6G 3rdcoil phase=120
169.6G 3rdcoil phase=180

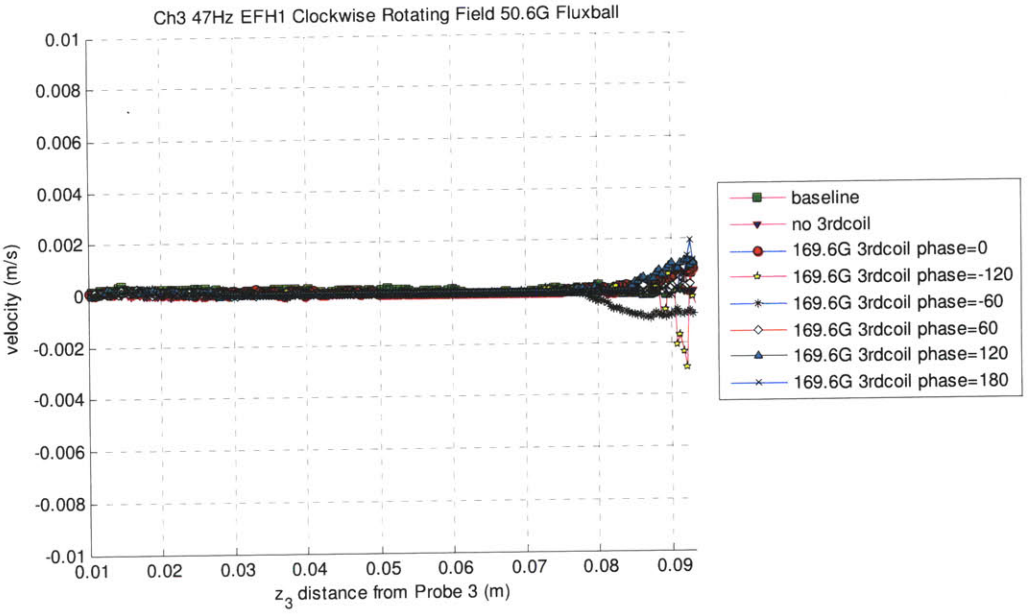
Ch3 47Hz EFH1 Clockwise Rotating Field 50.6G Fluxball
velocity (m/s)
0.01
0.008
0.006
0.004
0.002
0
-0.002
-0.004
-0.006
-0.008
-0.01
0.01 0.02 0.03 0.04 0.05 0.06 0.07 0.08 0.09
z3 distance from Probe 3 (m)
baseline
no 3rdcoil
169.6G 3rdcoil phase=0
169.6G 3rdcoil phase=-120
169.6G 3rdcoil phase=-60
169.6G 3rdcoil phase=60
169.6G 3rdcoil phase=120
169.6G 3rdcoil phase=180

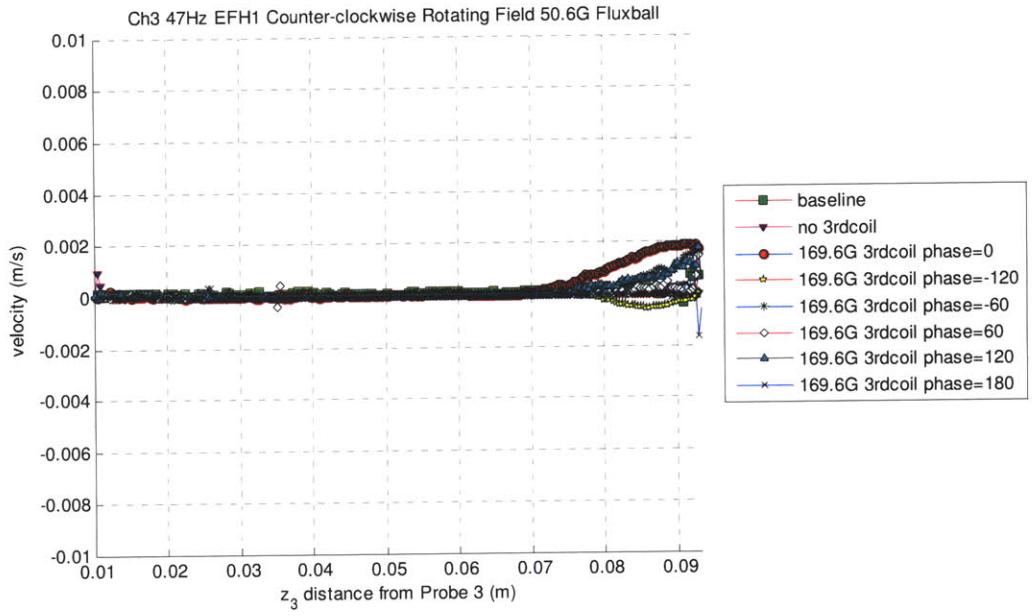
Ch3 47Hz EFH1 Counter-clockwise Rotating Field 50.6G Fluxball
velocity (m/s)
0.01
0.008
0.006
0.004
0.002
0
-0.002
-0.004
-0.006
-0.008
-0.01
0.01 0.02 0.03 0.04 0.05 0.06 0.07 0.08 0.09
z3 distance from Probe 3 (m)
baseline
no 3rdcoil
169.6G 3rdcoil phase=0
169.6G 3rdcoil phase=-120
169.6G 3rdcoil phase=-60
169.6G 3rdcoil phase=60
169.6G 3rdcoil phase=120
169.6G 3rdcoil phase=180

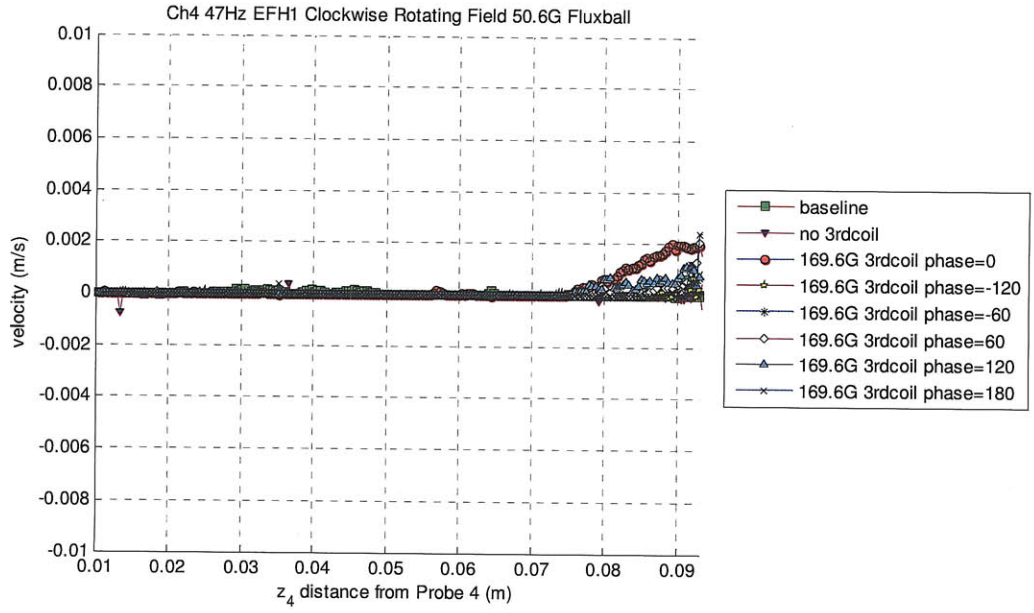
Ch4 47Hz EFH1 Clockwise Rotating Field 50.6G Fluxball
velocity (m/s)
0.01
0.008
0.006
0.004
0.002
0
-0.002
-0.004
-0.006
-0.008
-0.01
0.01 0.02 0.03 0.04 0.05 0.06 0.07 0.08 0.09
z4 distance from Probe 4 (m)
baseline
no 3rdcoil
169.6G 3rdcoil phase=0
169.6G 3rdcoil phase=-120
169.6G 3rdcoil phase=-60
169.6G 3rdcoil phase=60
169.6G 3rdcoil phase=120
169.6G 3rdcoil phase=180

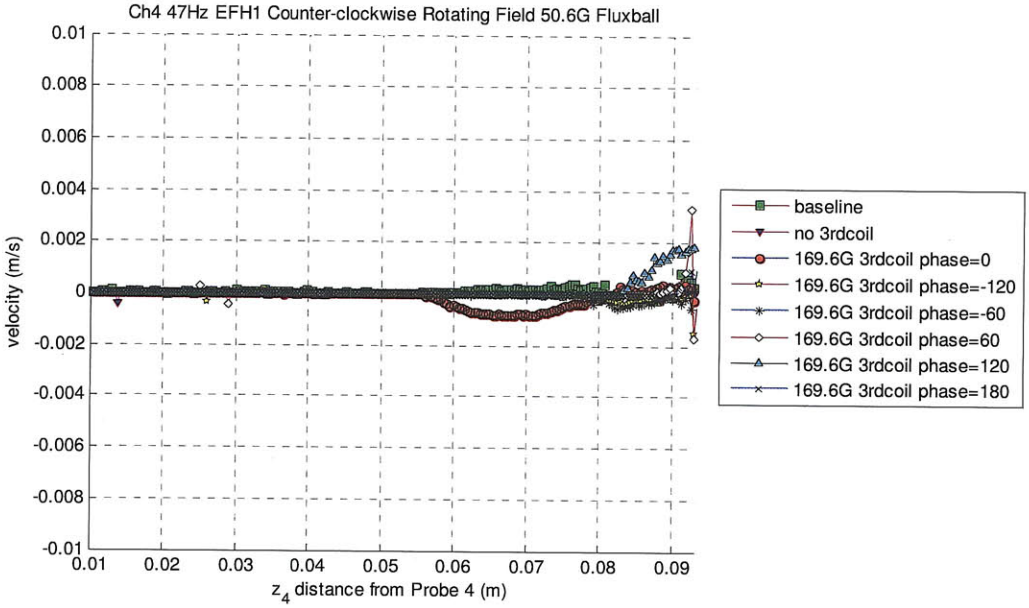
Ch4 47Hz EFH1 Counter-clockwise Rotating Field 50.6G Fluxball
velocity (m/s)
0.01
0.008
0.006
0.004
0.002
0
-0.002
-0.004
-0.006
-0.008
-0.01
0.01 0.02 0.03 0.04 0.05 0.06 0.07 0.08 0.09
z4 distance from Probe 4 (m)
baseline
no 3rdcoil
169.6G 3rdcoil phase=0
169.6G 3rdcoil phase=-120
169.6G 3rdcoil phase=-60
169.6G 3rdcoil phase=60
169.6G 3rdcoil phase=120
169.6G 3rdcoil phase=180

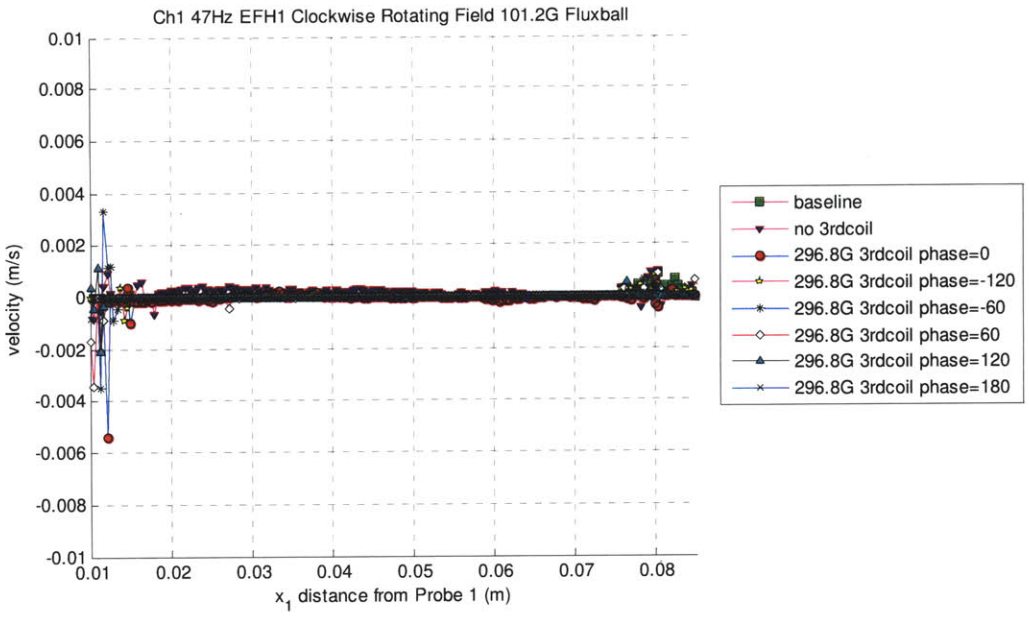
Ch1 47Hz EFH1 Clockwise Rotating Field 101.2G Fluxball
velocity (m/s)
x1 distance from Probe 1 (m)
baseline
no 3rdcoil
296.8G 3rdcoil phase=0
296.8G 3rdcoil phase=-120
296.8G 3rdcoil phase=-60
296.8G 3rdcoil phase=60
296.8G 3rdcoil phase=120
296.8G 3rdcoil phase=180

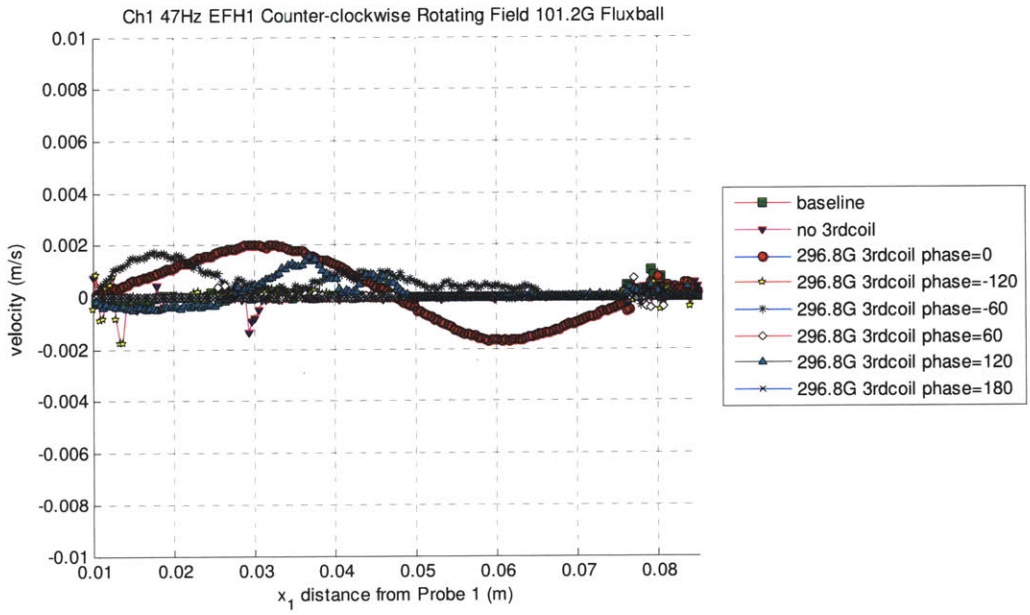
Ch1 47Hz EFH1 Counter-clockwise Rotating Field 101.2G Fluxball
velocity (m/s)
x1 distance from Probe 1 (m)
baseline
no 3rdcoil
296.8G 3rdcoil phase=0
296.8G 3rdcoil phase=-120
296.8G 3rdcoil phase=-60
296.8G 3rdcoil phase=60
296.8G 3rdcoil phase=120
296.8G 3rdcoil phase=180

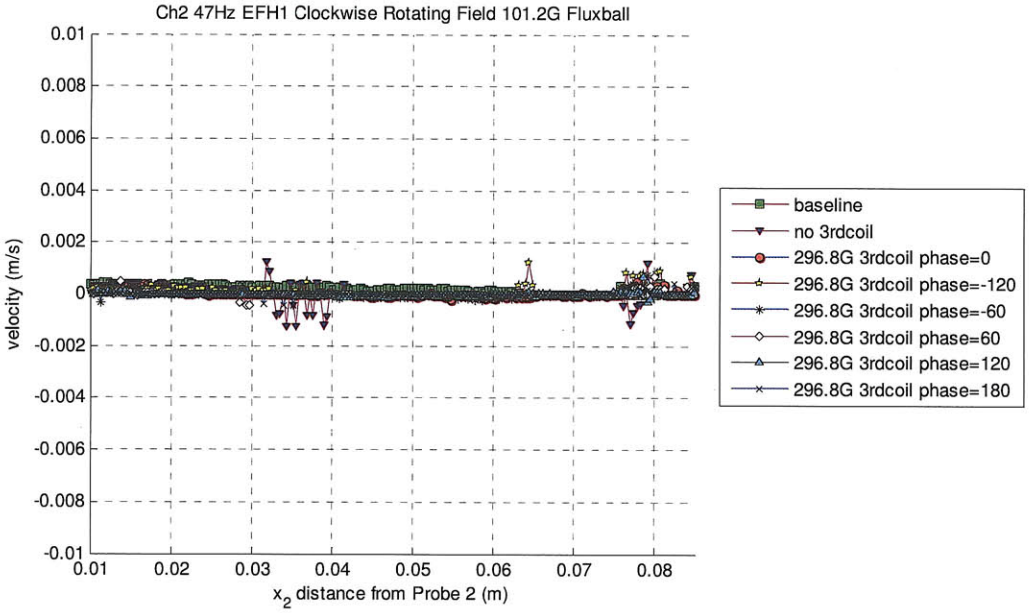
Ch2 47Hz EFH1 Clockwise Rotating Field 101.2G Fluxball
velocity (m/s)
0.01
0.008
0.006
0.004
0.002
0
-0.002
-0.004
-0.006
-0.008
-0.01
0.01
0.02
0.03
0.04
0.05
0.06
0.07
0.08
x2 distance from Probe 2 (m)
baseline
no 3rdcoil
296.8G 3rdcoil phase=0
296.8G 3rdcoil phase=-120
296.8G 3rdcoil phase=-60
296.8G 3rdcoil phase=60
296.8G 3rdcoil phase=120
296.8G 3rdcoil phase=180

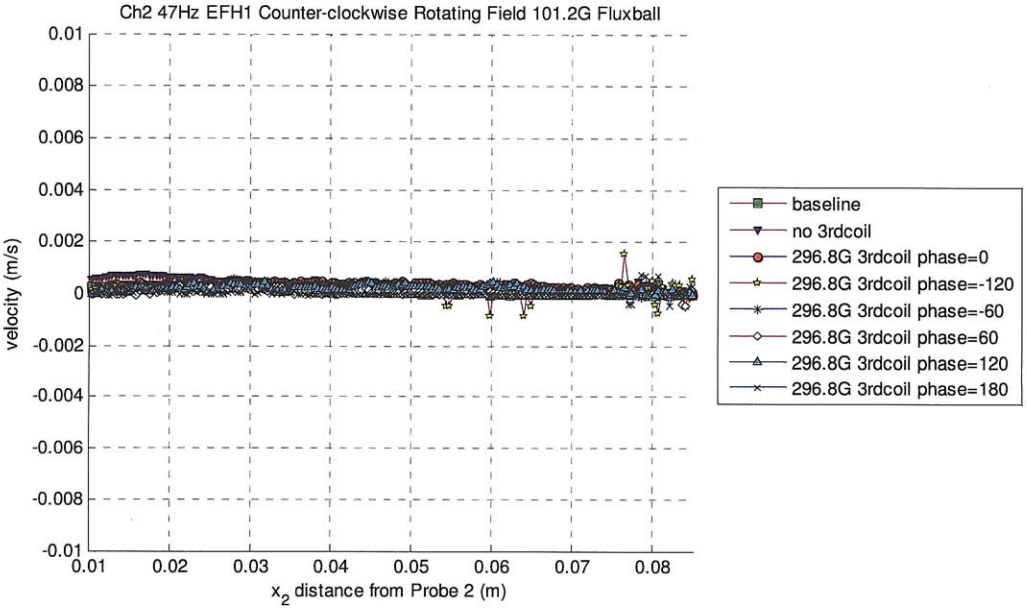
Ch2 47Hz EFH1 Counter-clockwise Rotating Field 101.2G Fluxball
velocity (m/s)
0.01
0.008
0.006
0.004
0.002
0
-0.002
-0.004
-0.006
-0.008
-0.01
0.01
0.02
0.03
0.04
0.05
0.06
0.07
0.08
x2 distance from Probe 2 (m)
baseline
no 3rdcoil
296.8G 3rdcoil phase=0
296.8G 3rdcoil phase=-120
296.8G 3rdcoil phase=-60
296.8G 3rdcoil phase=60
296.8G 3rdcoil phase=120
296.8G 3rdcoil phase=180

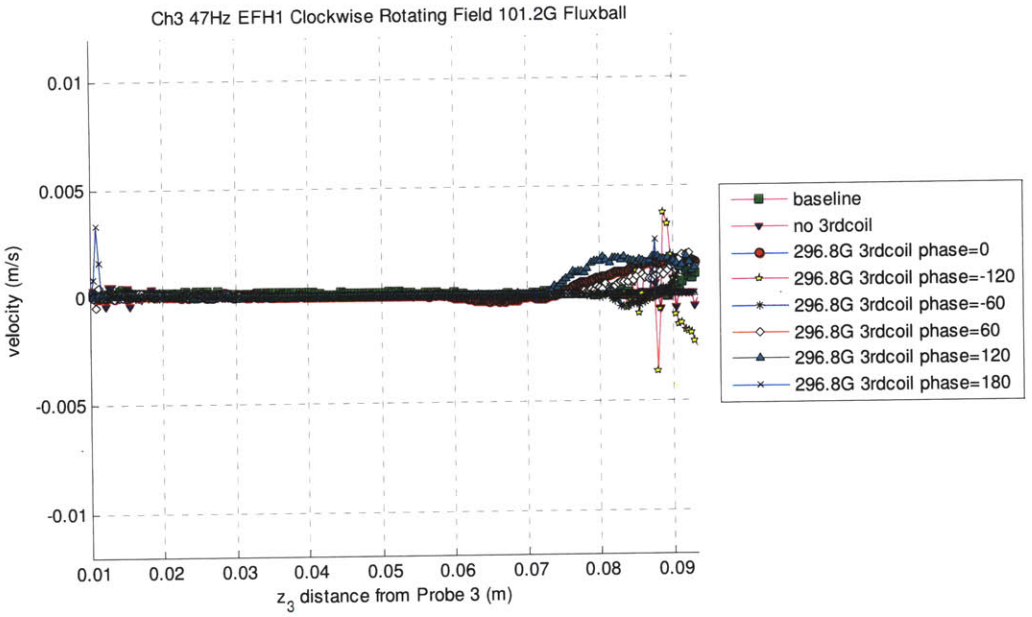
Ch3 47Hz EFH1 Clockwise Rotating Field 101.2G Fluxball
velocity (m/s)
0.01
0.005
0
-0.005
-0.01
0.01
0.02
0.03
0.04
0.05
0.06
0.07
0.08
0.09
z3 distance from Probe 3 (m)
baseline
no 3rdcoil
296.8G 3rdcoil phase=0
296.8G 3rdcoil phase=-120
296.8G 3rdcoil phase=-60
296.8G 3rdcoil phase=60
296.8G 3rdcoil phase=120
296.8G 3rdcoil phase=180

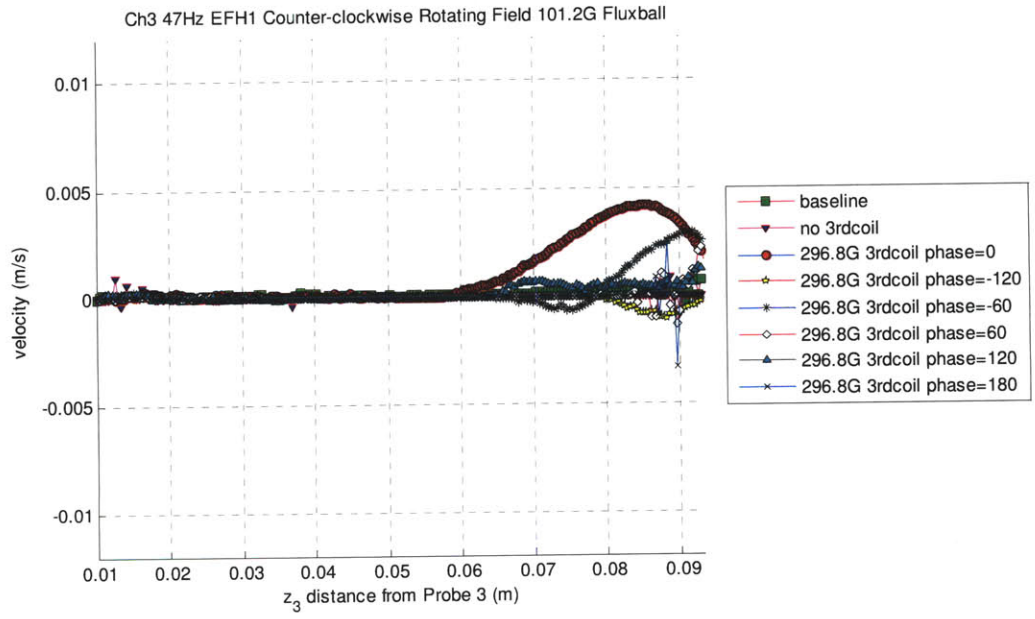
Ch3 47Hz EFH1 Counter-clockwise Rotating Field 101.2G Fluxball
velocity (m/s)
0.01
0.005
0
-0.005
-0.01
0.01
0.02
0.03
0.04
0.05
0.06
0.07
0.08
0.09
z3 distance from Probe 3 (m)
baseline
no 3rdcoil
296.8G 3rdcoil phase=0
296.8G 3rdcoil phase=-120
296.8G 3rdcoil phase=-60
296.8G 3rdcoil phase=60
296.8G 3rdcoil phase=120
296.8G 3rdcoil phase=180

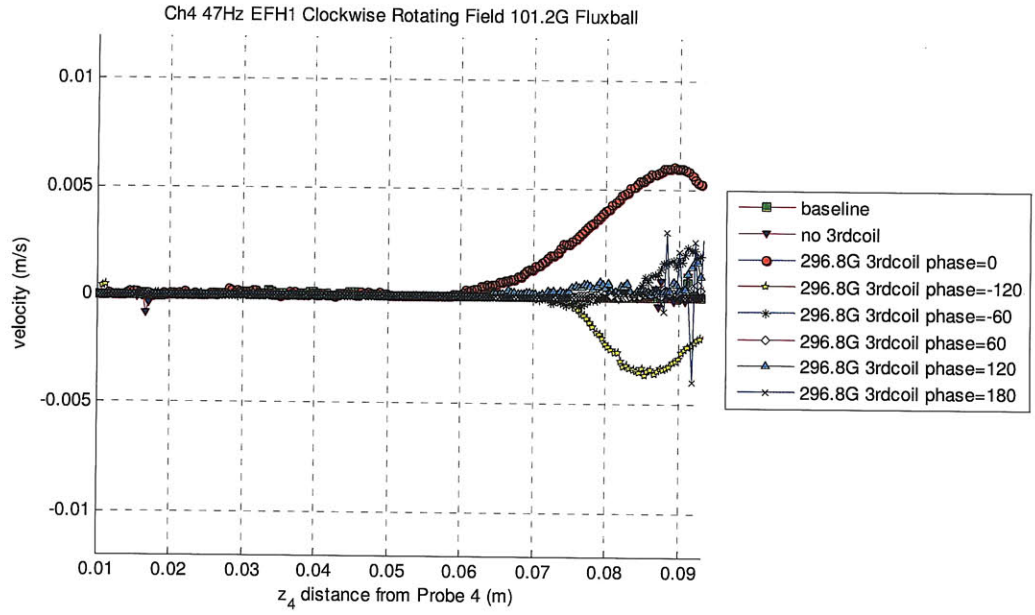
Ch4 47Hz EFH1 Clockwise Rotating Field 101.2G Fluxball
velocity (m/s)
0.01
0.005
0
-0.005
-0.01
0.01 0.02 0.03 0.04 0.05 0.06 0.07 0.08 0.09
z4 distance from Probe 4 (m)
baseline
no 3rdcoil
296.8G 3rdcoil phase=0
296.8G 3rdcoil phase=-120
296.8G 3rdcoil phase=-60
296.8G 3rdcoil phase=60
296.8G 3rdcoil phase=120
296.8G 3rdcoil phase=180

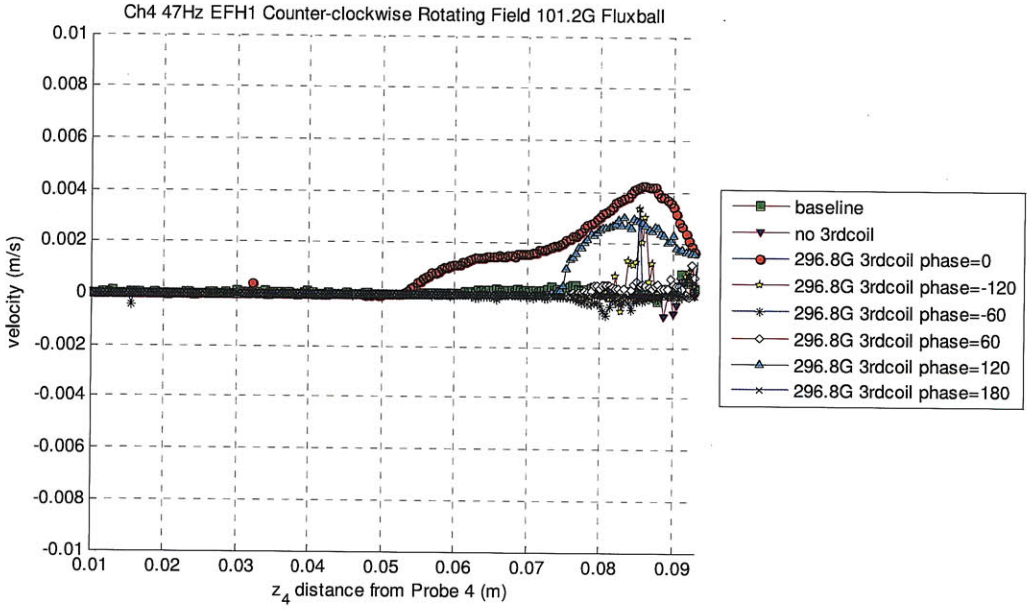
Ch4 47Hz EFH1 Counter-clockwise Rotating Field 101.2G Fluxball
velocity (m/s)
0.01
0.008
0.006
0.004
0.002
0
-0.002
-0.004
-0.006
-0.008
-0.01
0.01 0.02 0.03 0.04 0.05 0.06 0.07 0.08 0.09
z4 distance from Probe 4 (m)
baseline
no 3rdcoil
296.8G 3rdcoil phase=0
296.8G 3rdcoil phase=-120
296.8G 3rdcoil phase=-60
296.8G 3rdcoil phase=60
296.8G 3rdcoil phase=120
296.8G 3rdcoil phase=180

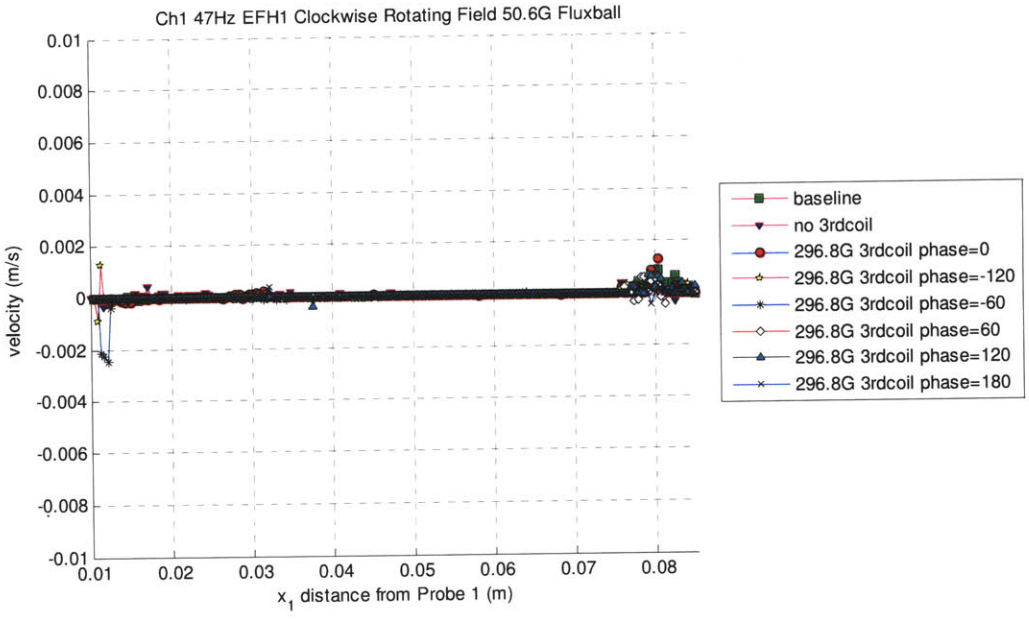
Ch1 47Hz EFH1 Clockwise Rotating Field 50.6G Fluxball
velocity (m/s)
x1 distance from Probe 1 (m)
baseline
no 3rdcoil
296.8G 3rdcoil phase=0
296.8G 3rdcoil phase=-120
296.8G 3rdcoil phase=-60
296.8G 3rdcoil phase=60
296.8G 3rdcoil phase=120
296.8G 3rdcoil phase=180

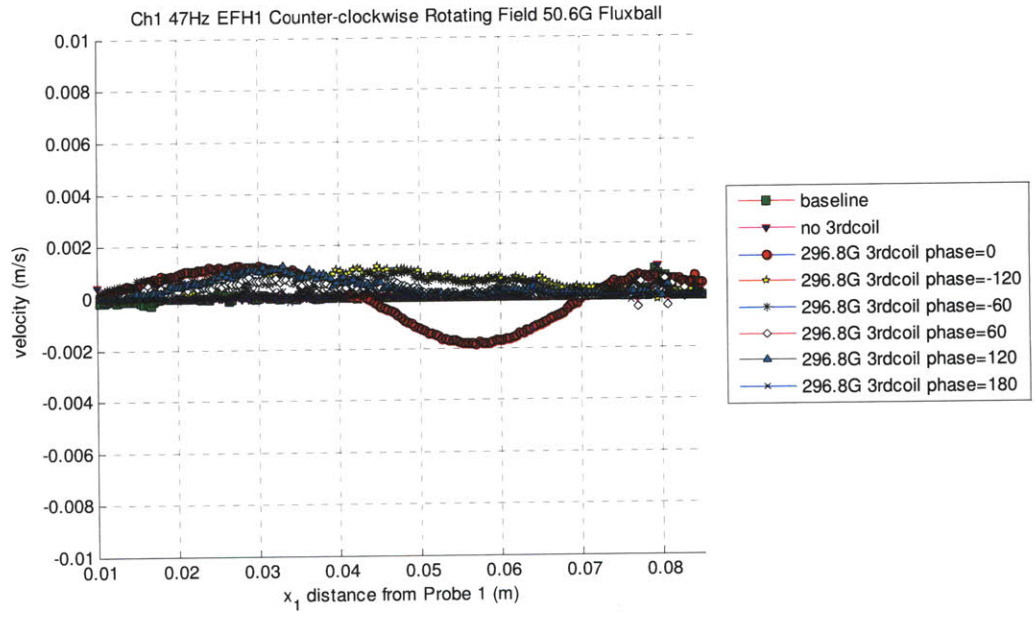
Ch1 47Hz EFH1 Counter-clockwise Rotating Field 50.6G Fluxball
velocity (m/s)
x1 distance from Probe 1 (m)
baseline
no 3rdcoil
296.8G 3rdcoil phase=0
296.8G 3rdcoil phase=-120
296.8G 3rdcoil phase=-60
296.8G 3rdcoil phase=60
296.8G 3rdcoil phase=120
296.8G 3rdcoil phase=180

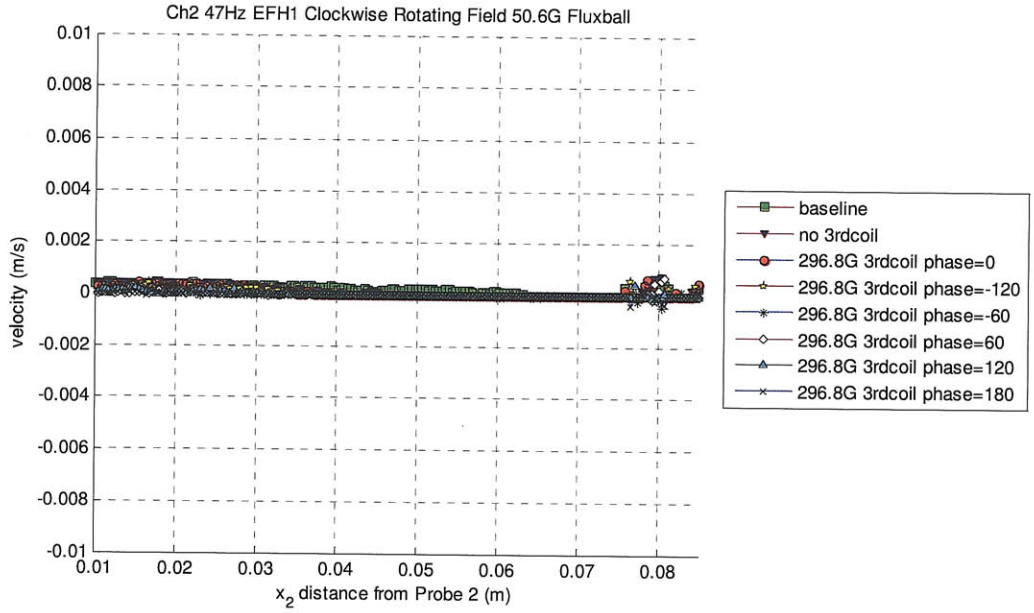
Ch2 47Hz EFH1 Clockwise Rotating Field 50.6G Fluxball
velocity (m/s)
0.01
0.008
0.006
0.004
0.002
0
-0.002
-0.004
-0.006
-0.008
-0.01
0.01
0.02
0.03
0.04
0.05
0.06
0.07
0.08
x2 distance from Probe 2 (m)
baseline
no 3rdcoil
296.8G 3rdcoil phase=0
296.8G 3rdcoil phase=-120
296.8G 3rdcoil phase=-60
296.8G 3rdcoil phase=60
296.8G 3rdcoil phase=120
296.8G 3rdcoil phase=180

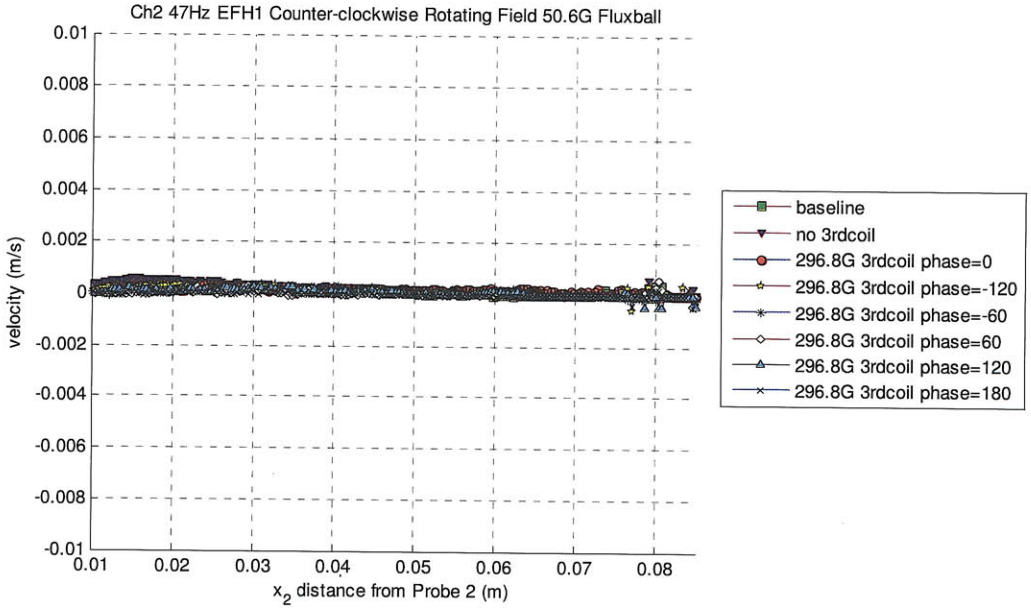
Ch2 47Hz EFH1 Counter-clockwise Rotating Field 50.6G Fluxball
velocity (m/s)
0.01
0.008
0.006
0.004
0.002
0
-0.002
-0.004
-0.006
-0.008
-0.01
0.01
0.02
0.03
0.04
0.05
0.06
0.07
0.08
x2 distance from Probe 2 (m)
baseline
no 3rdcoil
296.8G 3rdcoil phase=0
296.8G 3rdcoil phase=-120
296.8G 3rdcoil phase=-60
296.8G 3rdcoil phase=60
296.8G 3rdcoil phase=120
296.8G 3rdcoil phase=180

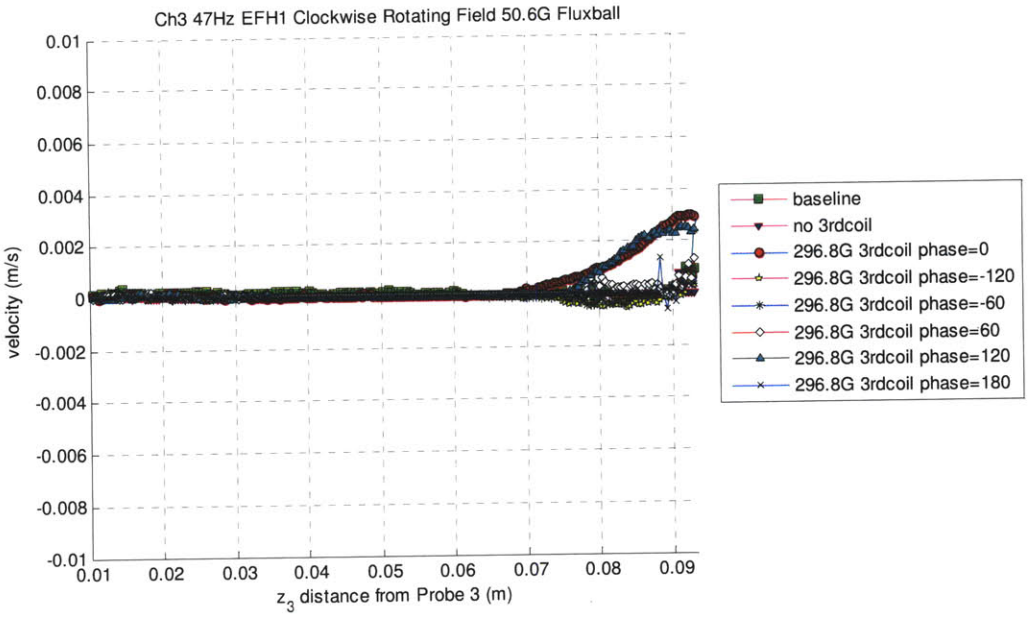
Ch3 47Hz EFH1 Clockwise Rotating Field 50.6G Fluxball
velocity (m/s)
0.01
0.008
0.006
0.004
0.002
0
-0.002
-0.004
-0.006
-0.008
-0.01
0.01 0.02 0.03 0.04 0.05 0.06 0.07 0.08 0.09
z3 distance from Probe 3 (m)
baseline
no 3rdcoil
296.8G 3rdcoil phase=0
296.8G 3rdcoil phase=-120
296.8G 3rdcoil phase=-60
296.8G 3rdcoil phase=60
296.8G 3rdcoil phase=120
296.8G 3rdcoil phase=180

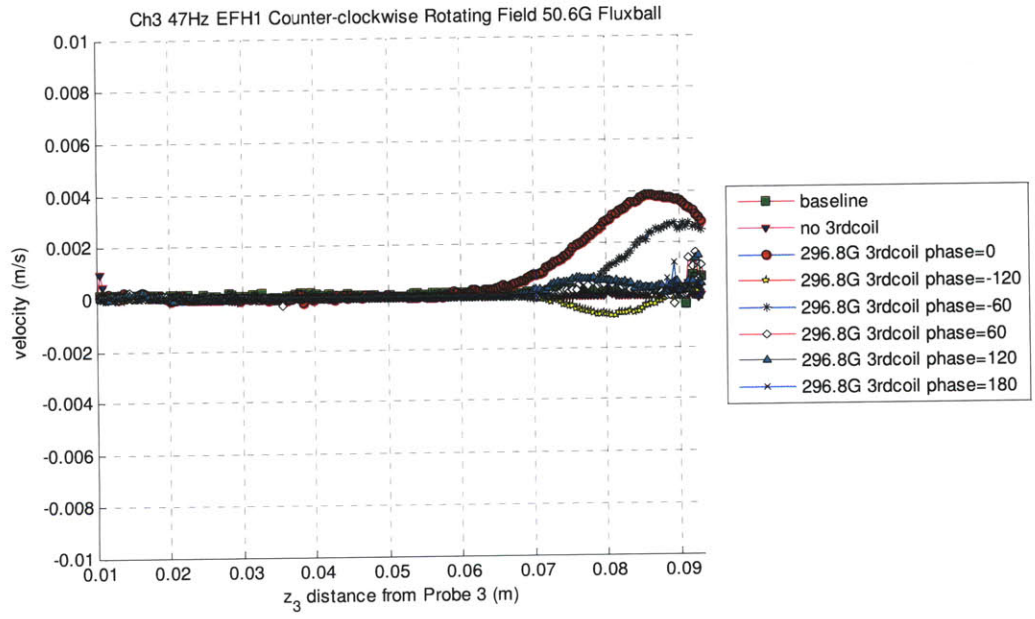
Ch3 47Hz EFH1 Counter-clockwise Rotating Field 50.6G Fluxball
velocity (m/s)
0.01
0.008
0.006
0.004
0.002
0
-0.002
-0.004
-0.006
-0.008
-0.01
0.01 0.02 0.03 0.04 0.05 0.06 0.07 0.08 0.09
z3 distance from Probe 3 (m)
baseline
no 3rdcoil
296.8G 3rdcoil phase=0
296.8G 3rdcoil phase=-120
296.8G 3rdcoil phase=-60
296.8G 3rdcoil phase=60
296.8G 3rdcoil phase=120
296.8G 3rdcoil phase=180

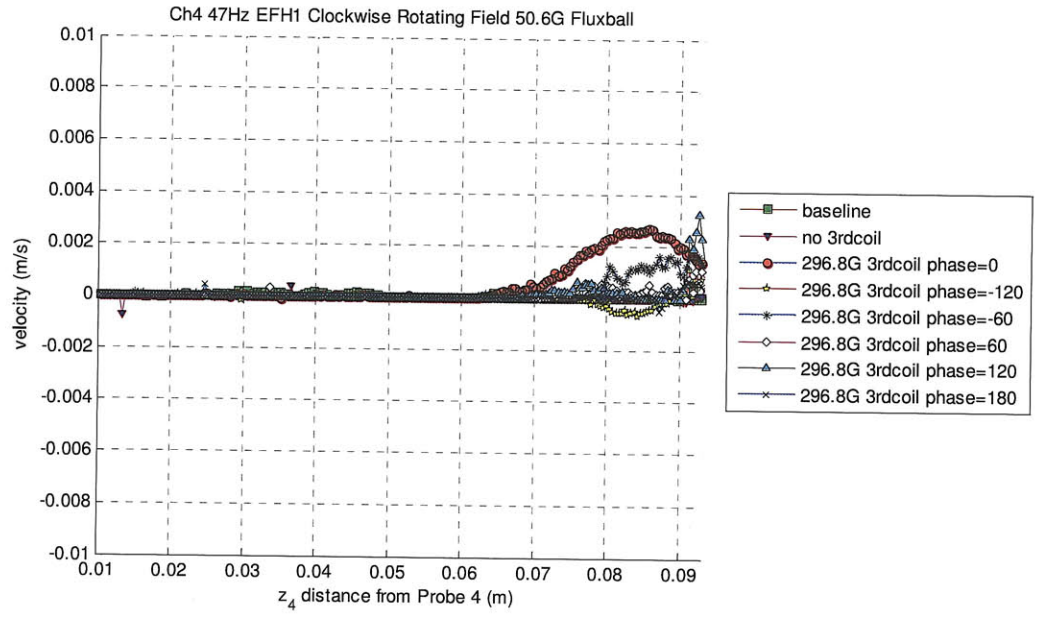
Ch4 47Hz EFH1 Clockwise Rotating Field 50.6G Fluxball
velocity (m/s)
0.01
0.008
0.006
0.004
0.002
0
-0.002
-0.004
-0.006
-0.008
-0.01
0.01 0.02 0.03 0.04 0.05 0.06 0.07 0.08 0.09
z4 distance from Probe 4 (m)
baseline
no 3rdcoil
296.8G 3rdcoil phase=0
296.8G 3rdcoil phase=-120
296.8G 3rdcoil phase=-60
296.8G 3rdcoil phase=60
296.8G 3rdcoil phase=120
296.8G 3rdcoil phase=180

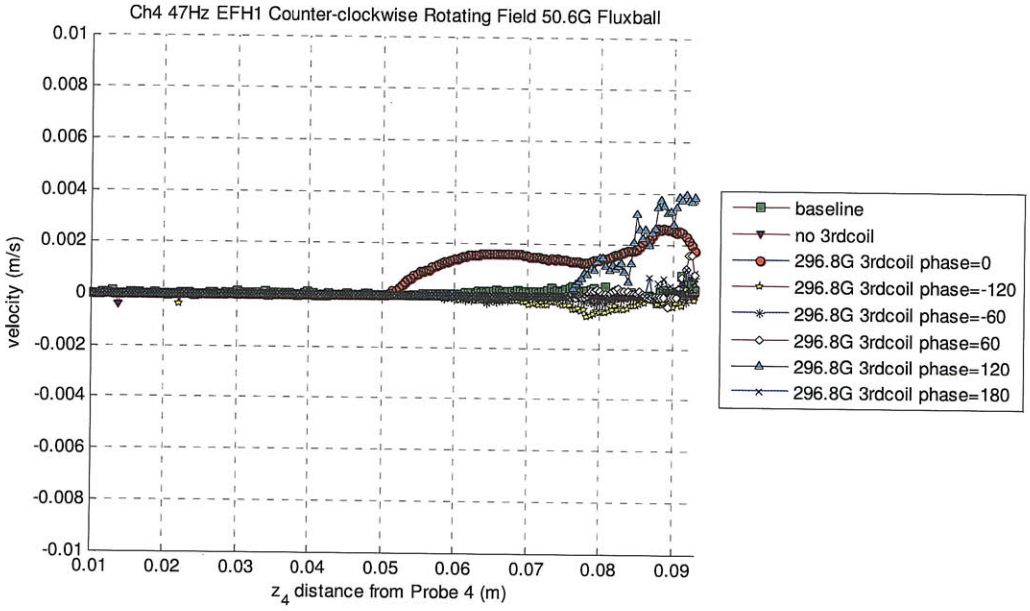
Ch4 47Hz EFH1 Counter-clockwise Rotating Field 50.6G Fluxball
velocity (m/s)
0.01
0.008
0.006
0.004
0.002
0
-0.002
-0.004
-0.006
-0.008
-0.01
0.01 0.02 0.03 0.04 0.05 0.06 0.07 0.08 0.09
z4 distance from Probe 4 (m)
baseline
no 3rdcoil
296.8G 3rdcoil phase=0
296.8G 3rdcoil phase=-120
296.8G 3rdcoil phase=-60
296.8G 3rdcoil phase=60
296.8G 3rdcoil phase=120
296.8G 3rdcoil phase=180

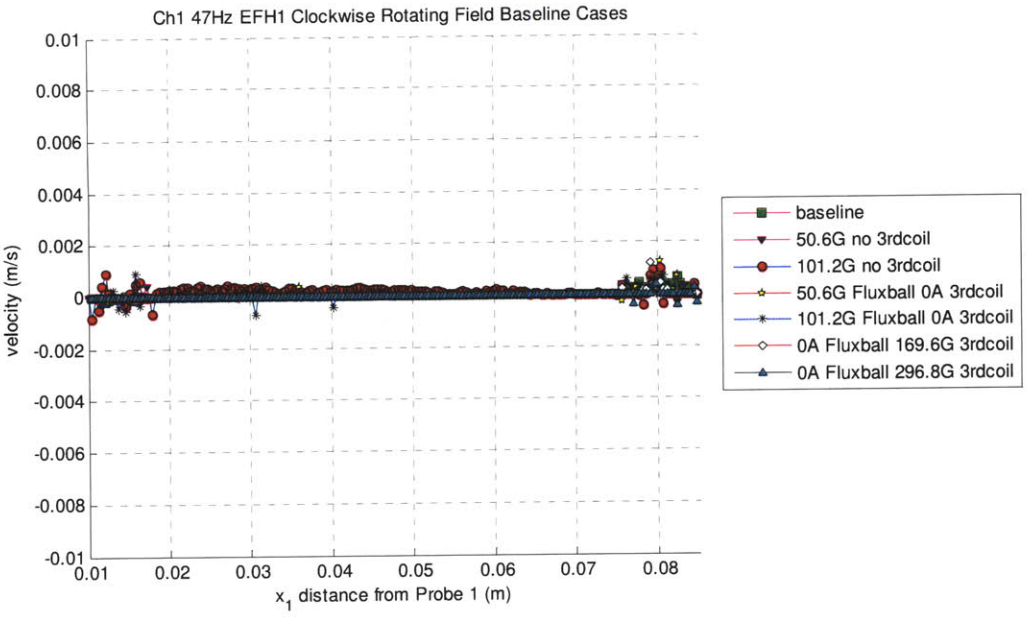
Ch1 47Hz EFH1 Clockwise Rotating Field Baseline Cases
velocity (m/s)
0.01
0.008
0.006
0.004
0.002
0
-0.002
-0.004
-0.006
-0.008
-0.01
0.01
0.02
0.03
0.04
0.05
0.06
0.07
0.08
x1 distance from Probe 1 (m)
baseline
50.6G no 3rdcoil
101.2G no 3rdcoil
50.6G Fluxball 0A 3rdcoil
101.2G Fluxball 0A 3rdcoil
0A Fluxball 169.6G 3rdcoil
0A Fluxball 296.8G 3rdcoil

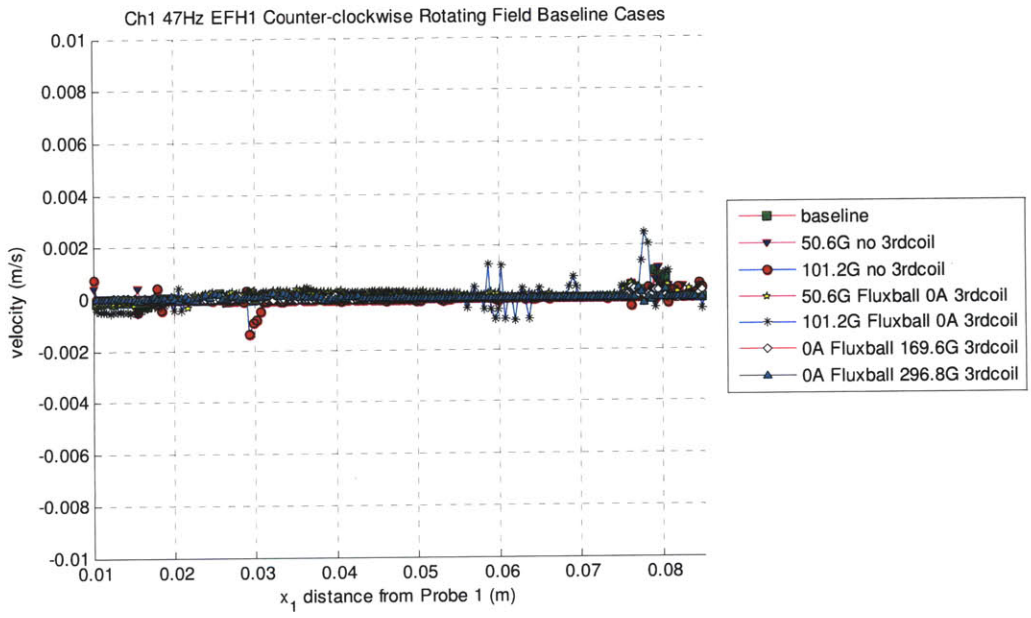
Ch1 47Hz EFH1 Counter-clockwise Rotating Field Baseline Cases
velocity (m/s)
0.01
0.008
0.006
0.004
0.002
0
-0.002
-0.004
-0.006
-0.008
-0.01
0.01
0.02
0.03
0.04
0.05
0.06
0.07
0.08
x1 distance from Probe 1 (m)
baseline
50.6G no 3rdcoil
101.2G no 3rdcoil
50.6G Fluxball 0A 3rdcoil
101.2G Fluxball 0A 3rdcoil
0A Fluxball 169.6G 3rdcoil
0A Fluxball 296.8G 3rdcoil

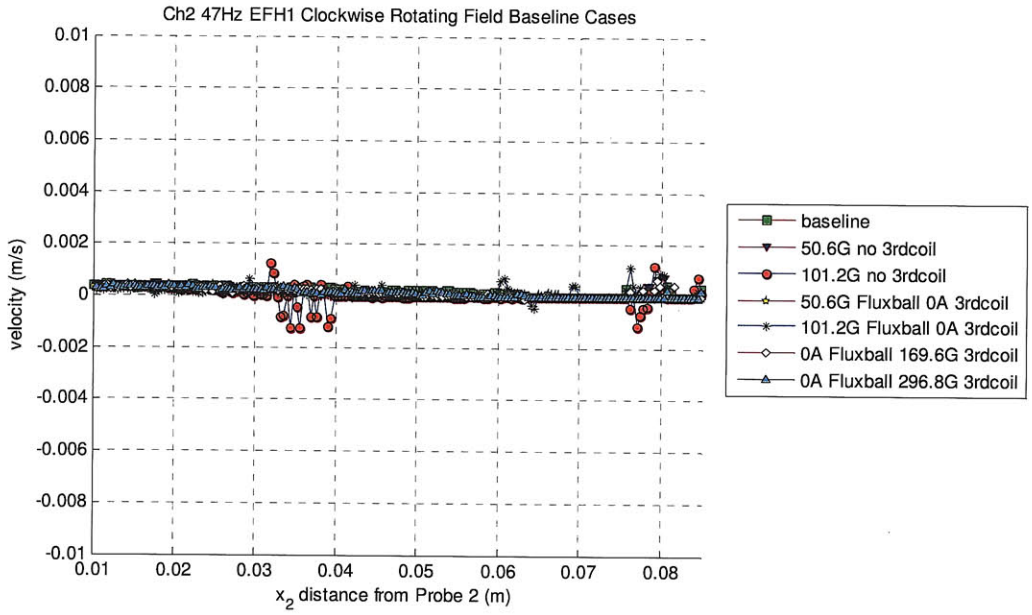
Ch2 47Hz EFH1 Clockwise Rotating Field Baseline Cases
velocity (m/s)
0.01
0.008
0.006
0.004
0.002
0
-0.002
-0.004
-0.006
-0.008
-0.01
0.01
0.02
0.03
0.04
0.05
0.06
0.07
0.08
x2 distance from Probe 2 (m)
baseline
50.6G no 3rdcoil
101.2G no 3rdcoil
50.6G Fluxball 0A 3rdcoil
101.2G Fluxball 0A 3rdcoil
0A Fluxball 169.6G 3rdcoil
0A Fluxball 296.8G 3rdcoil

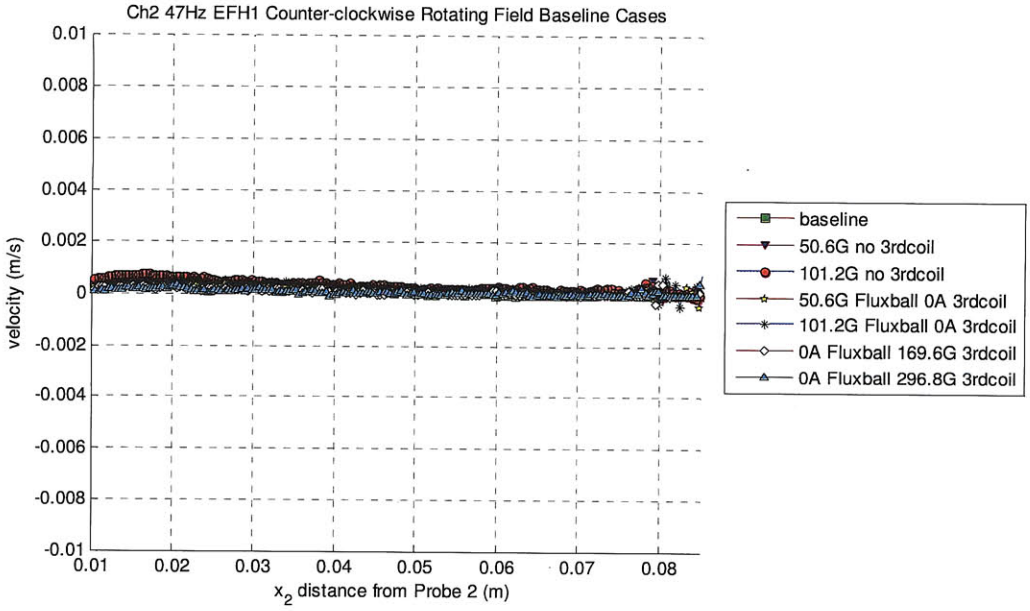
Ch2 47Hz EFH1 Counter-clockwise Rotating Field Baseline Cases
velocity (m/s)
0.01
0.008
0.006
0.004
0.002
0
-0.002
-0.004
-0.006
-0.008
-0.01
0.01
0.02
0.03
0.04
0.05
0.06
0.07
0.08
x2 distance from Probe 2 (m)
baseline
50.6G no 3rdcoil
101.2G no 3rdcoil
50.6G Fluxball 0A 3rdcoil
101.2G Fluxball 0A 3rdcoil
0A Fluxball 169.6G 3rdcoil
0A Fluxball 296.8G 3rdcoil

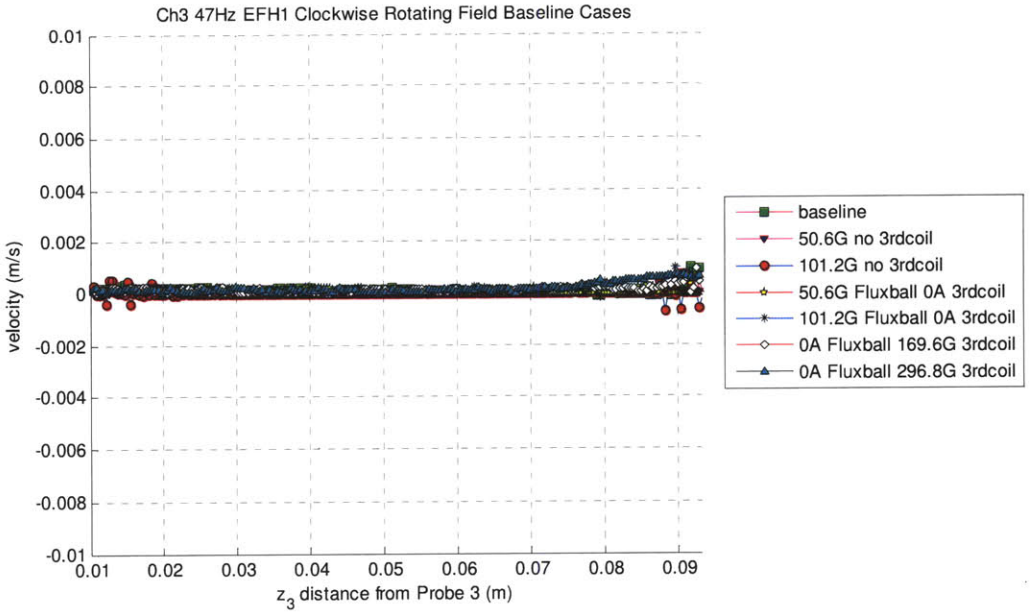
Ch3 47Hz EFH1 Clockwise Rotating Field Baseline Cases
velocity (m/s)
0.01
0.008
0.006
0.004
0.002
0
-0.002
-0.004
-0.006
-0.008
-0.01
0.01 0.02 0.03 0.04 0.05 0.06 0.07 0.08 0.09
z3 distance from Probe 3 (m)
baseline
50.6G no 3rdcoil
101.2G no 3rdcoil
50.6G Fluxball 0A 3rdcoil
101.2G Fluxball 0A 3rdcoil
0A Fluxball 169.6G 3rdcoil
0A Fluxball 296.8G 3rdcoil

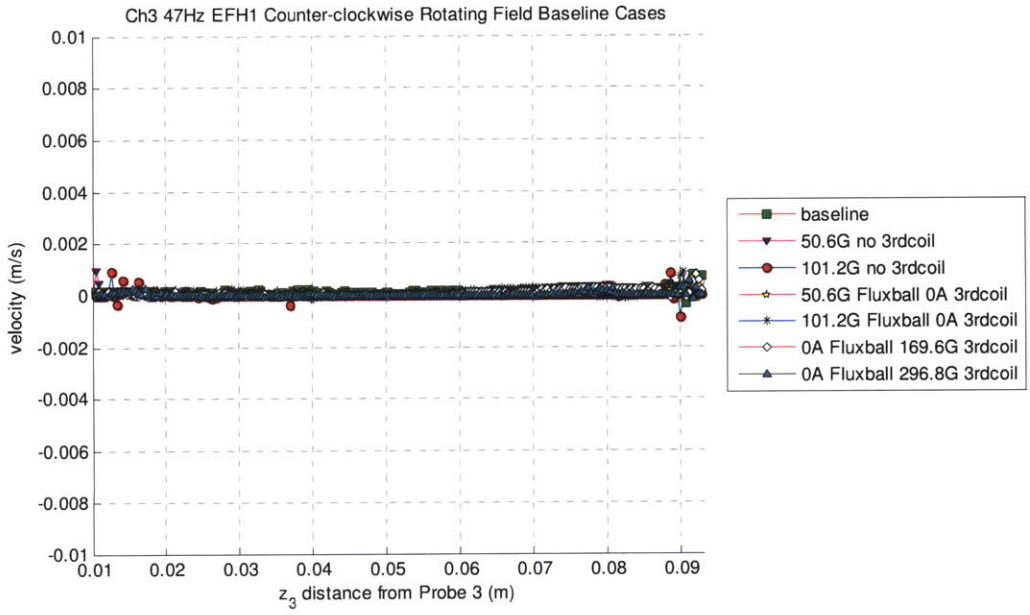
Ch3 47Hz EFH1 Counter-clockwise Rotating Field Baseline Cases
velocity (m/s)
0.01
0.008
0.006
0.004
0.002
0
-0.002
-0.004
-0.006
-0.008
-0.01
0.01 0.02 0.03 0.04 0.05 0.06 0.07 0.08 0.09
z3 distance from Probe 3 (m)
baseline
50.6G no 3rdcoil
101.2G no 3rdcoil
50.6G Fluxball 0A 3rdcoil
101.2G Fluxball 0A 3rdcoil
0A Fluxball 169.6G 3rdcoil
0A Fluxball 296.8G 3rdcoil

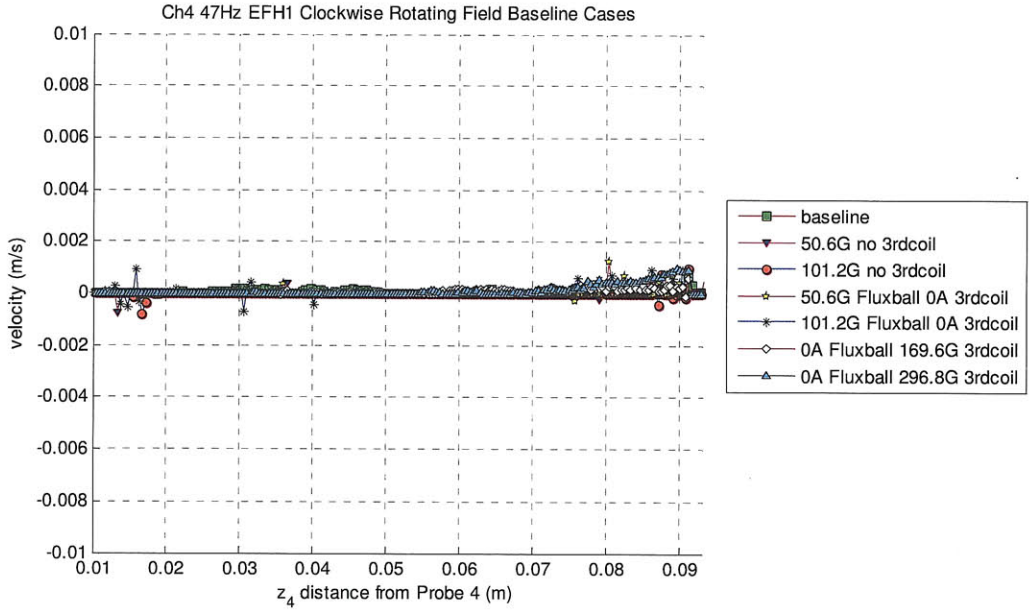
Ch4 47Hz EFH1 Clockwise Rotating Field Baseline Cases
velocity (m/s)
0.01
0.008
0.006
0.004
0.002
0
-0.002
-0.004
-0.006
-0.008
-0.01
0.01
0.02
0.03
0.04
0.05
0.06
0.07
0.08
0.09
z4 distance from Probe 4 (m)
baseline
50.6G no 3rdcoil
101.2G no 3rdcoil
50.6G Fluxball 0A 3rdcoil
101.2G Fluxball 0A 3rdcoil
0A Fluxball 169.6G 3rdcoil
0A Fluxball 296.8G 3rdcoil

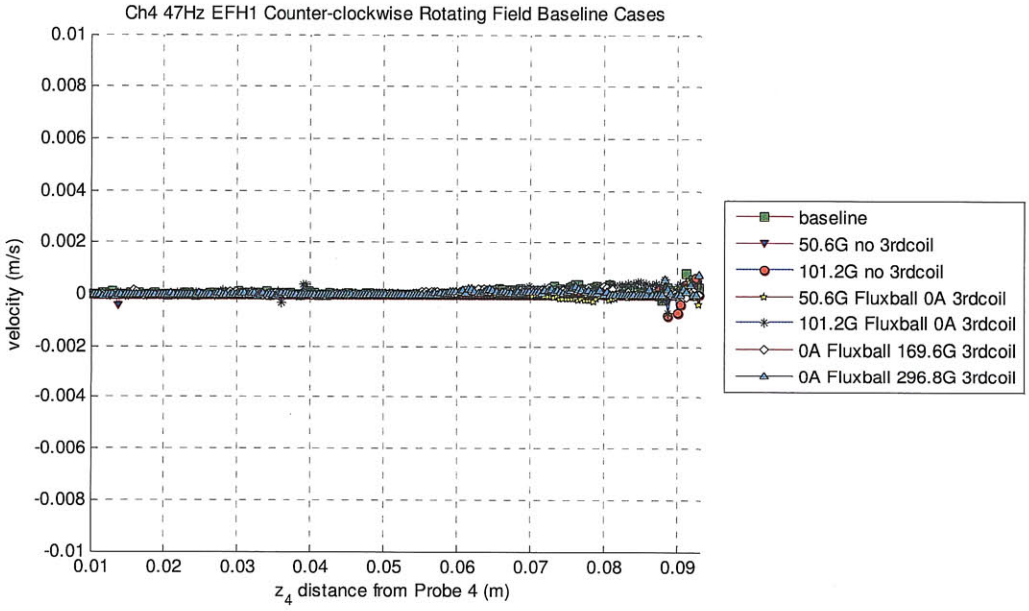
Ch4 47Hz EFH1 Counter-clockwise Rotating Field Baseline Cases
velocity (m/s)
0.01
0.008
0.006
0.004
0.002
0
-0.002
-0.004
-0.006
-0.008
-0.01
0.01
0.02
0.03
0.04
0.05
0.06
0.07
0.08
0.09
z4 distance from Probe 4 (m)
baseline
50.6G no 3rdcoil
101.2G no 3rdcoil
50.6G Fluxball 0A 3rdcoil
101.2G Fluxball 0A 3rdcoil
0A Fluxball 169.6G 3rdcoil
0A Fluxball 296.8G 3rdcoil

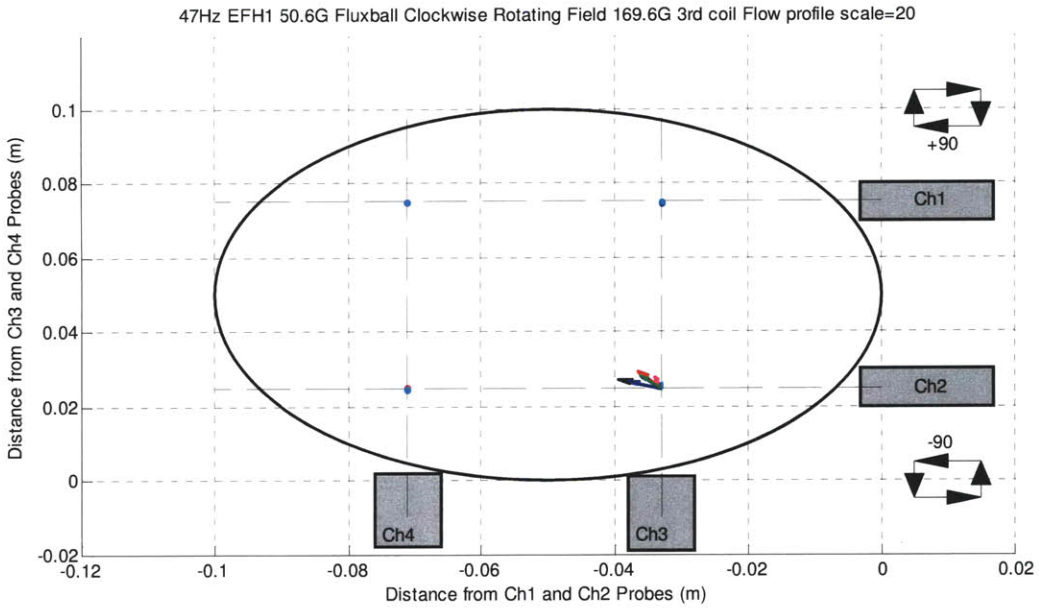
47Hz EFH1 50.6G Fluxball Clockwise Rotating Field 169.6G 3rd coil Flow profile scale=20
Distance from Ch3 and Ch4 Probes (m)
Distance from Ch1 and Ch2 Probes (m)
0.1
0.08
0.06
0.04
0.02
0
-0.02
-0.12
-0.1
-0.08
-0.06
-0.04
-0.02
0
0.02
+90
-90
Ch1
Ch2
Ch3
Ch4

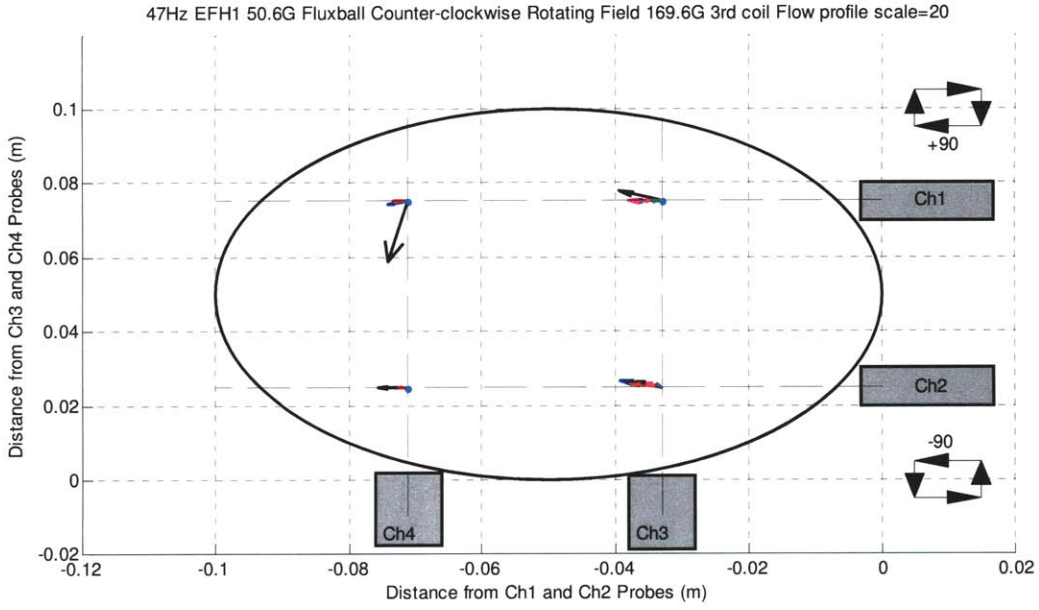
47Hz EFH1 50.6G Fluxball Counter-clockwise Rotating Field 169.6G 3rd coil Flow profile scale=20
Distance from Ch3 and Ch4 Probes (m)
Distance from Ch1 and Ch2 Probes (m)
0.1
0.08
0.06
0.04
0.02
0
-0.02
-0.12
-0.1
-0.08
-0.06
-0.04
-0.02
0
0.02
+90
-90
Ch1
Ch2
Ch3
Ch4

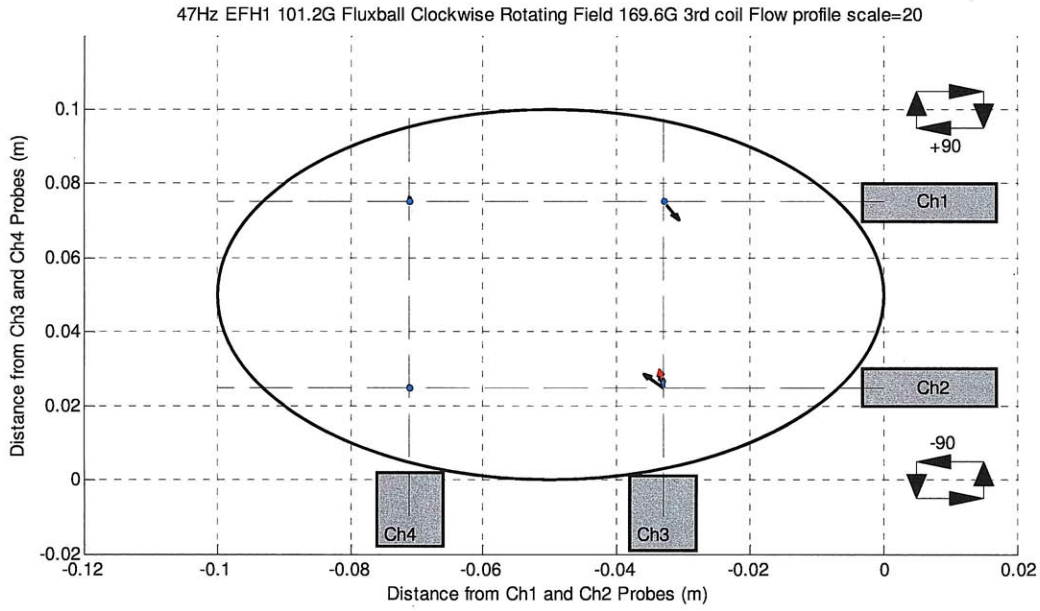
47Hz EFH1 101.2G Fluxball Clockwise Rotating Field 169.6G 3rd coil Flow profile scale=20
Distance from Ch3 and Ch4 Probes (m)
Distance from Ch1 and Ch2 Probes (m)
+90
-90
Ch1
Ch2
Ch3
Ch4
0.1
0.08
0.06
0.04
0.02
0
-0.02
-0.12
-0.1
-0.08
-0.06
-0.04
-0.02
0
0.02

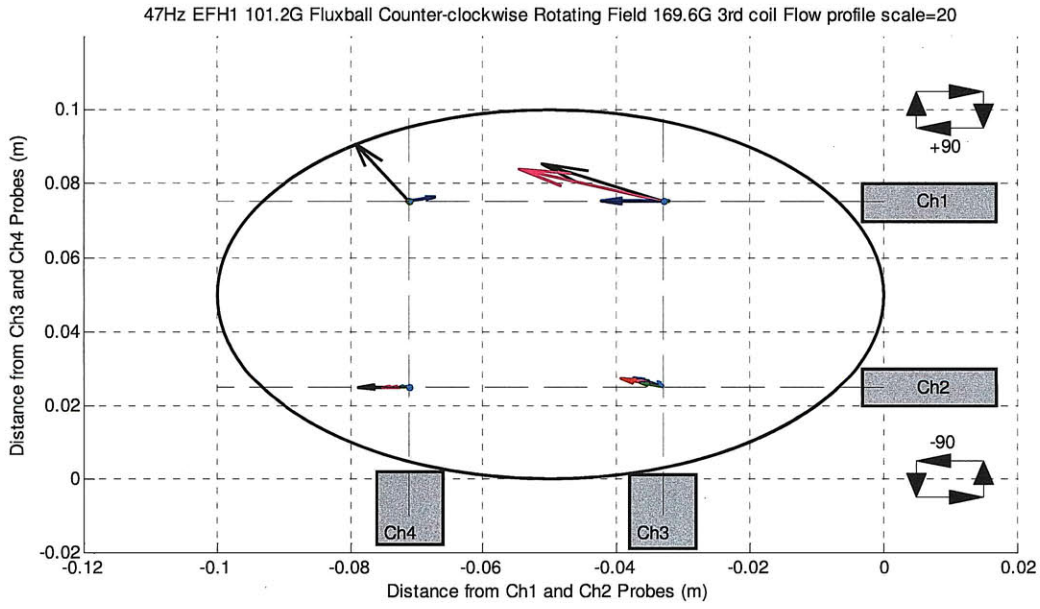
47Hz EFH1 101.2G Fluxball Counter-clockwise Rotating Field 169.6G 3rd coil Flow profile scale=20
Distance from Ch3 and Ch4 Probes (m)
Distance from Ch1 and Ch2 Probes (m)
+90
-90
Ch1
Ch2
Ch3
Ch4
0.1
0.08
0.06
0.04
0.02
0
-0.02
-0.12
-0.1
-0.08
-0.06
-0.04
-0.02
0
0.02

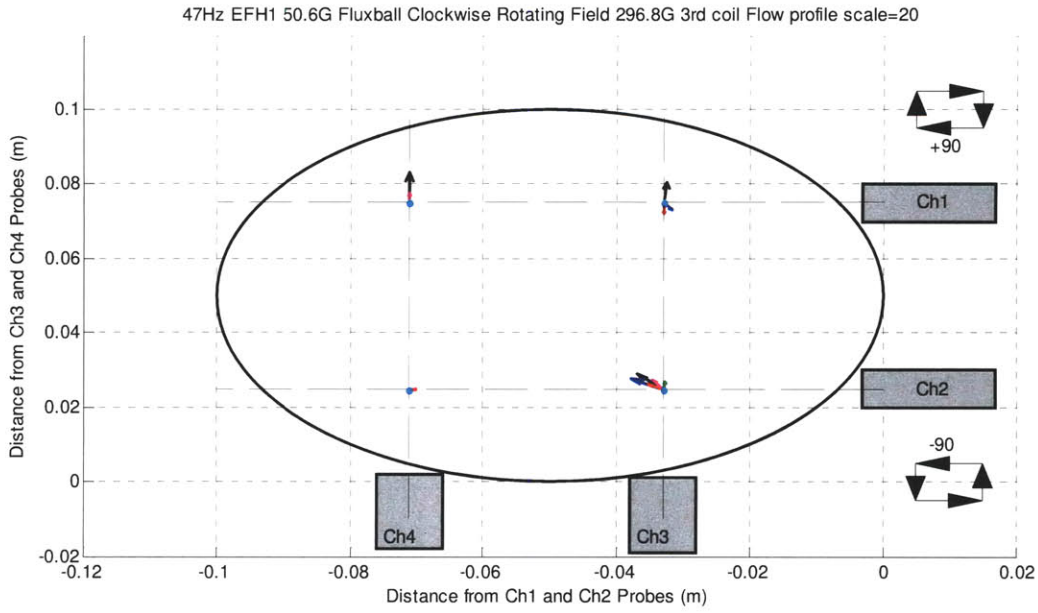
47Hz EFH1 50.6G Fluxball Clockwise Rotating Field 296.8G 3rd coil Flow profile scale=20
Distance from Ch3 and Ch4 Probes (m)
Distance from Ch1 and Ch2 Probes (m)
+90
-90
Ch1
Ch2
Ch3
Ch4
0.1
0.08
0.06
0.04
0.02
0
-0.02
-0.12
-0.1
-0.08
-0.06
-0.04
-0.02
0
0.02

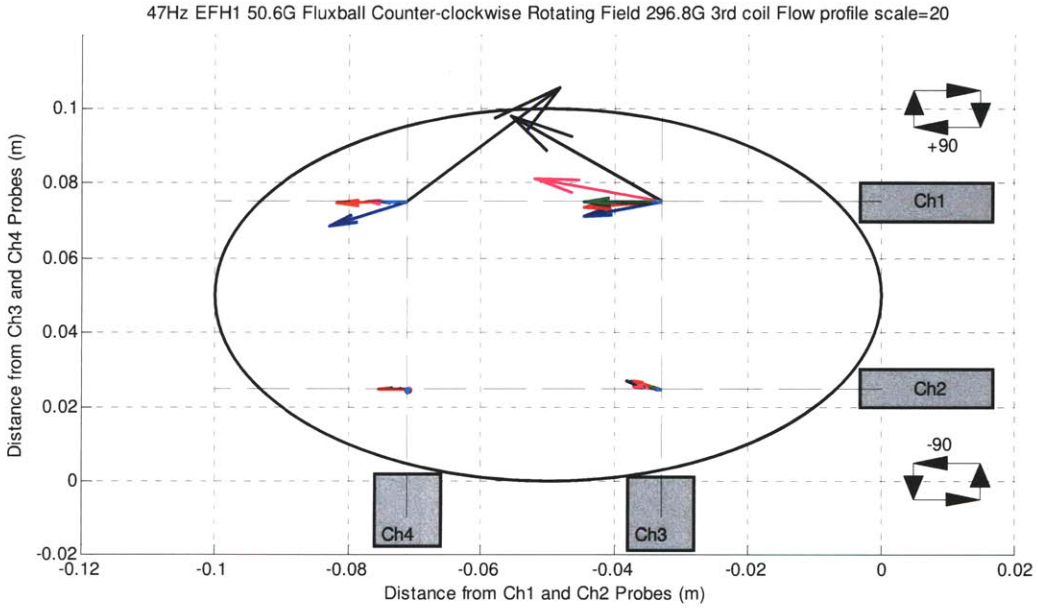
47Hz EFH1 50.6G Fluxball Counter-clockwise Rotating Field 296.8G 3rd coil Flow profile scale=20
Distance from Ch3 and Ch4 Probes (m)
Distance from Ch1 and Ch2 Probes (m)
+90
-90
Ch1
Ch2
Ch3
Ch4
0.1
0.08
0.06
0.04
0.02
0
-0.02
-0.12
-0.1
-0.08
-0.06
-0.04
-0.02
0
0.02

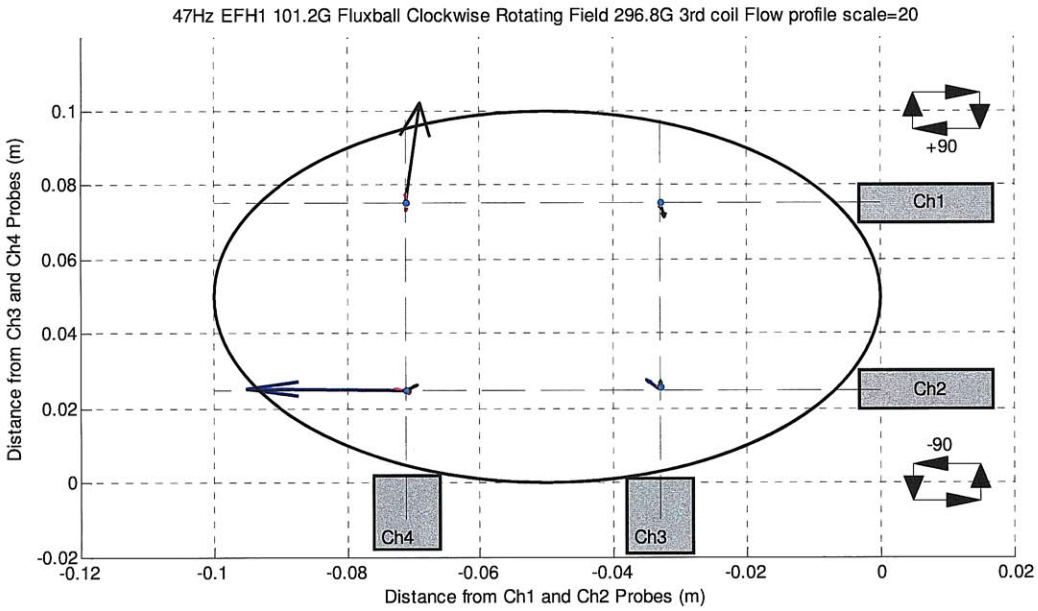
47Hz EFH1 101.2G Fluxball Clockwise Rotating Field 296.8G 3rd coil Flow profile scale=20
Distance from Ch3 and Ch4 Probes (m)
Distance from Ch1 and Ch2 Probes (m)
0.1
0.08
0.06
0.04
0.02
0
-0.02
-0.12
-0.1
-0.08
-0.06
-0.04
-0.02
0
0.02
+90
-90
Ch1
Ch2
Ch3
Ch4

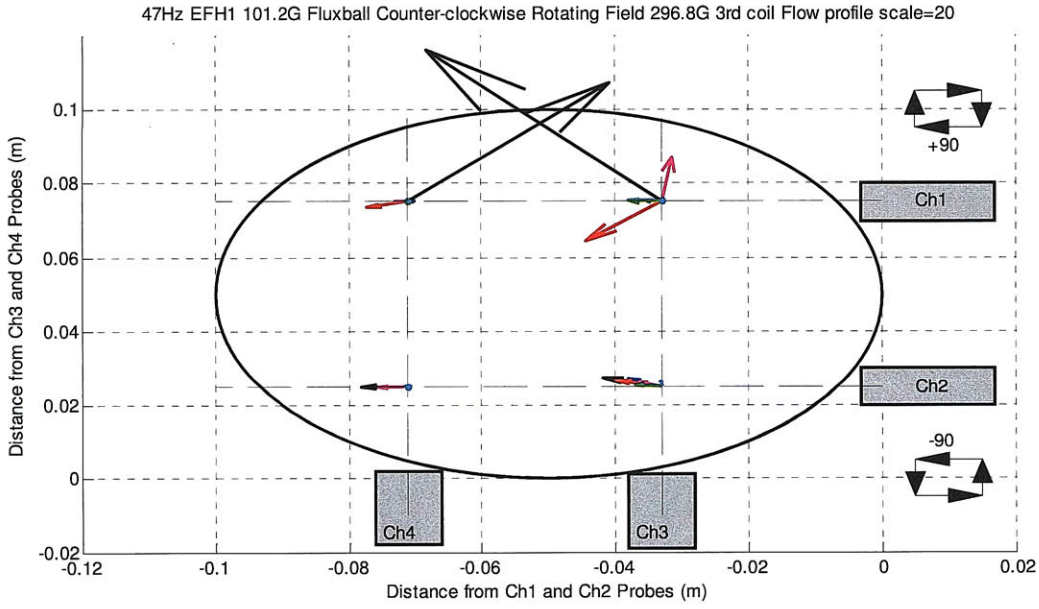
47Hz EFH1 101.2G Fluxball Counter-clockwise Rotating Field 296.8G 3rd coil Flow profile scale=20
Distance from Ch3 and Ch4 Probes (m)
Distance from Ch1 and Ch2 Probes (m)
0.1
0.08
0.06
0.04
0.02
0
-0.02
-0.12
-0.1
-0.08
-0.06
-0.04
-0.02
0
0.02
+90
-90
Ch1
Ch2
Ch3
Ch4

G3. EFH1 Filled Sphere with Third Coil Oscillating at Same Frequency as Rotating Field at 15Hz

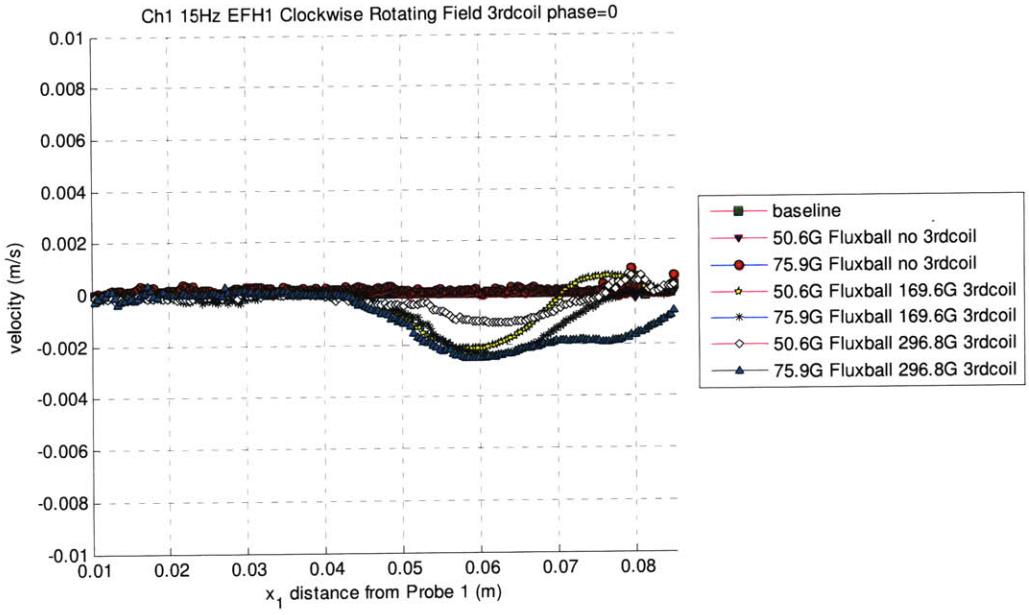

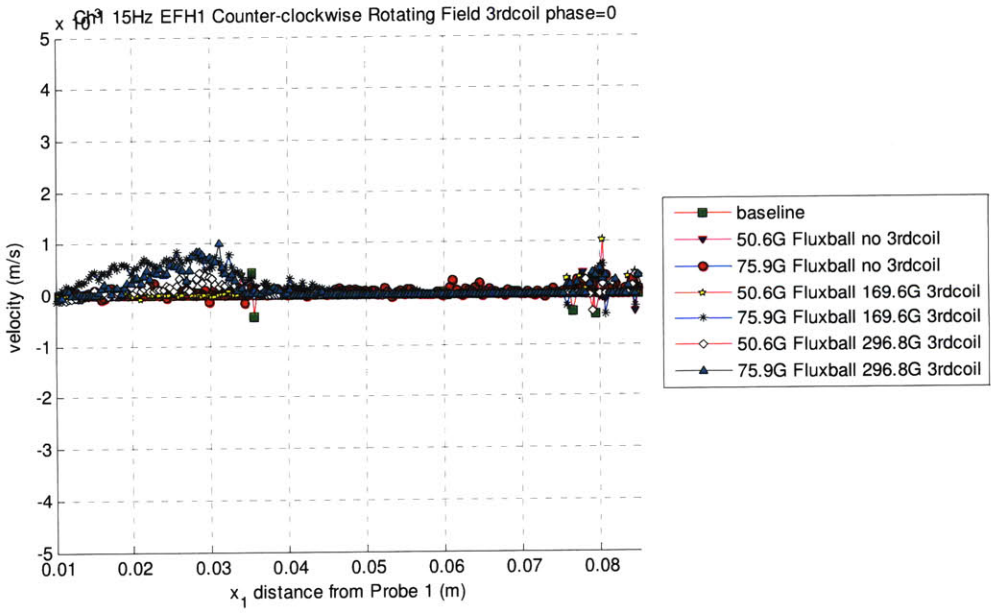

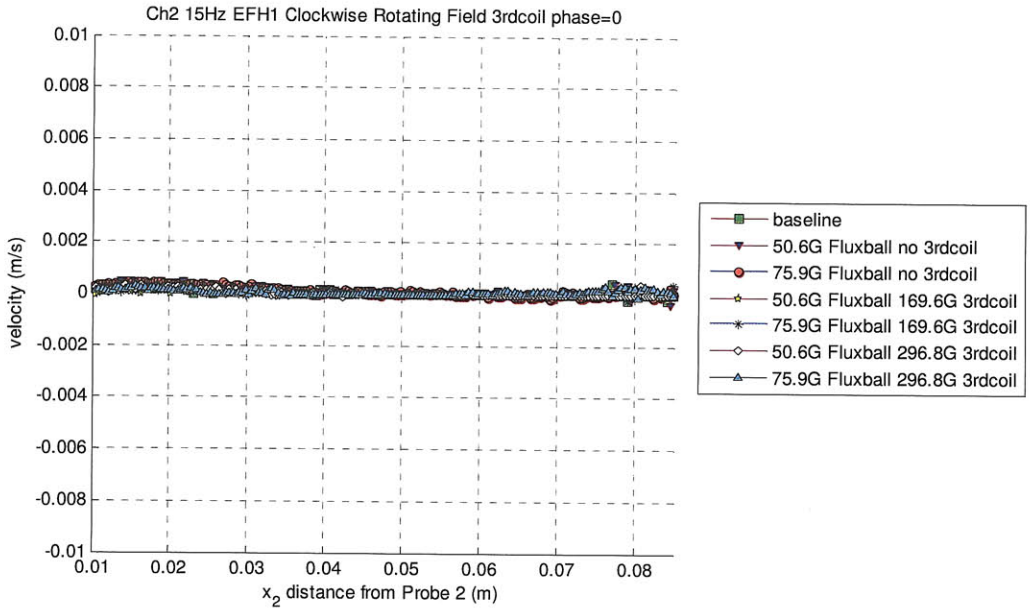
Ch2 15Hz EFH1 Clockwise Rotating Field 3rdcoil phase=0
velocity (m/s)
0.01
0.008
0.006
0.004
0.002
0
-0.002
-0.004
-0.006
-0.008
-0.01
0.01 0.02 0.03 0.04 0.05 0.06 0.07 0.08
x2 distance from Probe 2 (m)
baseline
50.6G Fluxball no 3rdcoil
75.9G Fluxball no 3rdcoil
50.6G Fluxball 169.6G 3rdcoil
75.9G Fluxball 169.6G 3rdcoil
50.6G Fluxball 296.8G 3rdcoil
75.9G Fluxball 296.8G 3rdcoil

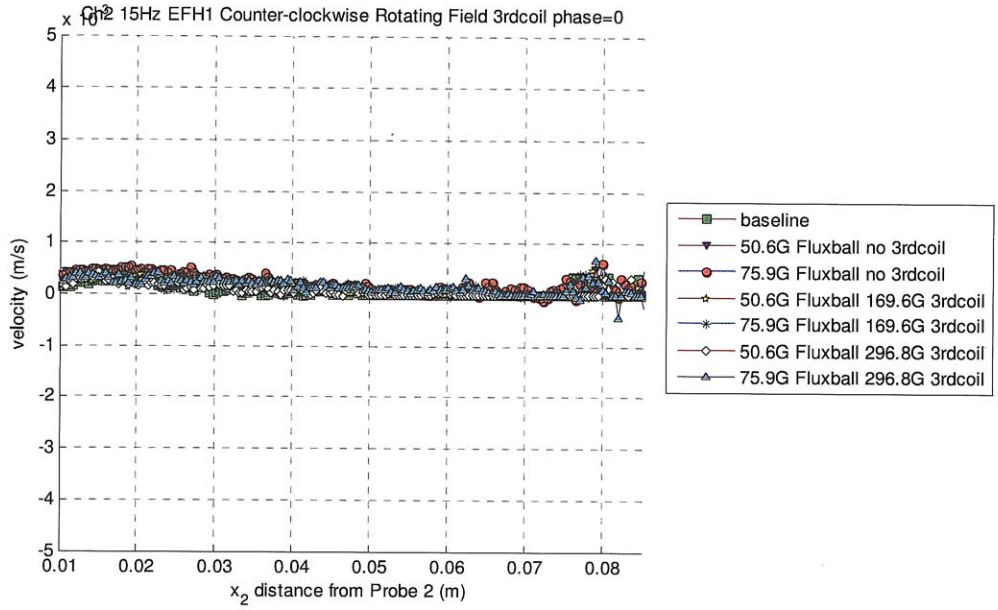
Ch2 15Hz EFH1 Counter-clockwise Rotating Field 3rdcoil phase=0
x 10-2
velocity (m/s)
5
4
3
2
1
0
-1
-2
-3
-4
-5
0.01 0.02 0.03 0.04 0.05 0.06 0.07 0.08
x2 distance from Probe 2 (m)
baseline
50.6G Fluxball no 3rdcoil
75.9G Fluxball no 3rdcoil
50.6G Fluxball 169.6G 3rdcoil
75.9G Fluxball 169.6G 3rdcoil
50.6G Fluxball 296.8G 3rdcoil
75.9G Fluxball 296.8G 3rdcoil

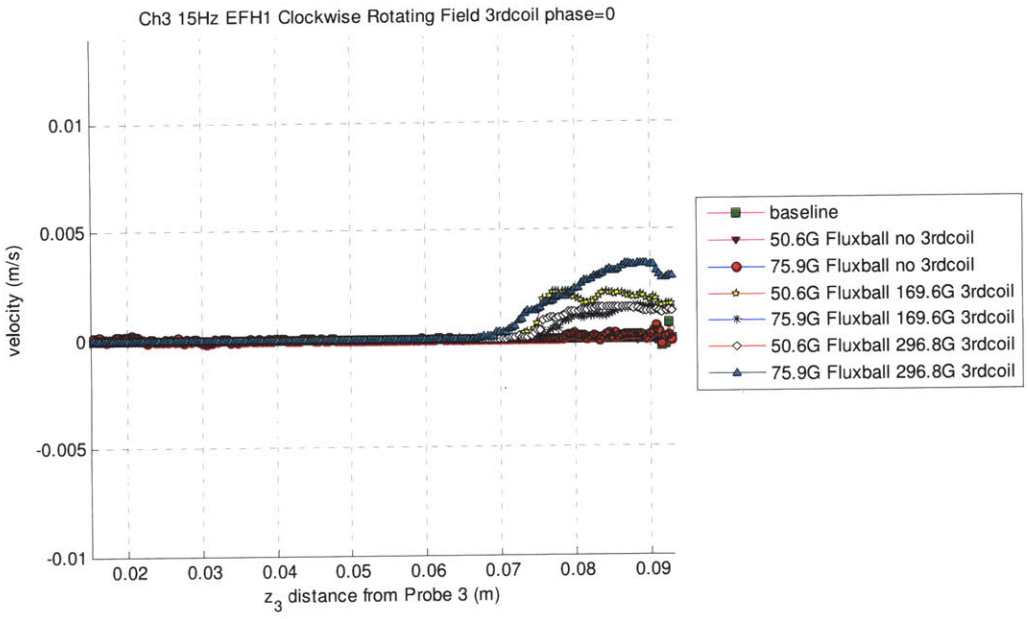
Ch3 15Hz EFH1 Clockwise Rotating Field 3rdcoil phase=0
velocity (m/s)
0.01
0.005
0
-0.005
-0.01
0.02
0.03
0.04
0.05
0.06
0.07
0.08
0.09
z_3 distance from Probe 3 (m)
baseline
50.6G Fluxball no 3rdcoil
75.9G Fluxball no 3rdcoil
50.6G Fluxball 169.6G 3rdcoil
75.9G Fluxball 169.6G 3rdcoil
50.6G Fluxball 296.8G 3rdcoil
75.9G Fluxball 296.8G 3rdcoil

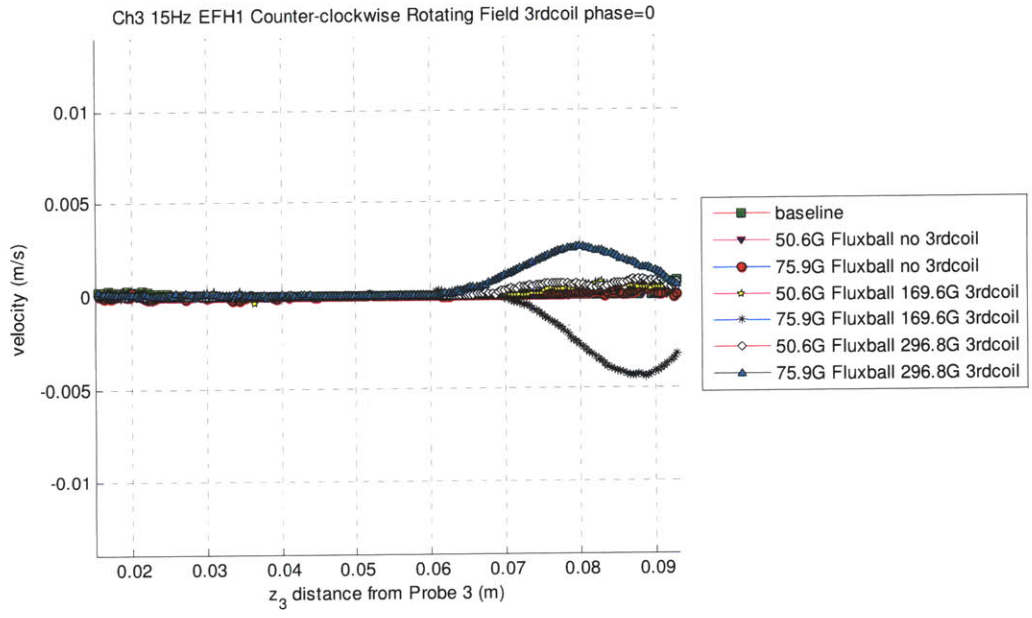
Ch3 15Hz EFH1 Counter-clockwise Rotating Field 3rdcoil phase=0
velocity (m/s)
0.01
0.005
0
-0.005
-0.01
0.02
0.03
0.04
0.05
0.06
0.07
0.08
0.09
z_3 distance from Probe 3 (m)
baseline
50.6G Fluxball no 3rdcoil
75.9G Fluxball no 3rdcoil
50.6G Fluxball 169.6G 3rdcoil
75.9G Fluxball 169.6G 3rdcoil
50.6G Fluxball 296.8G 3rdcoil
75.9G Fluxball 296.8G 3rdcoil

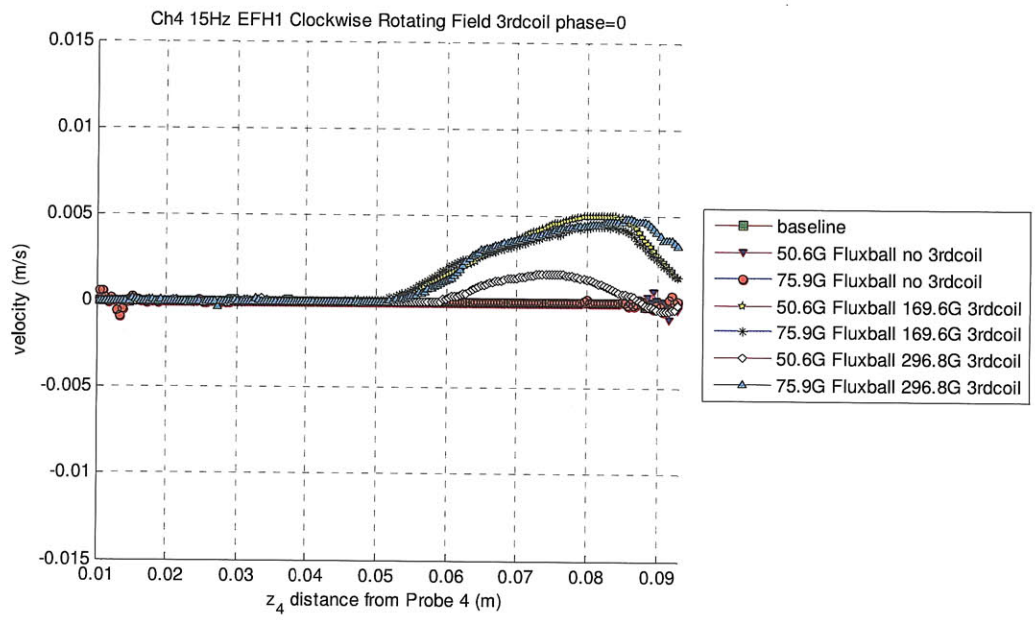
Ch4 15Hz EFH1 Clockwise Rotating Field 3rdcoil phase=0
velocity (m/s)
0.015
0.01
0.005
0
-0.005
-0.01
-0.015
0.01
0.02
0.03
0.04
0.05
0.06
0.07
0.08
0.09
z4 distance from Probe 4 (m)
baseline
50.6G Fluxball no 3rdcoil
75.9G Fluxball no 3rdcoil
50.6G Fluxball 169.6G 3rdcoil
75.9G Fluxball 169.6G 3rdcoil
50.6G Fluxball 296.8G 3rdcoil
75.9G Fluxball 296.8G 3rdcoil

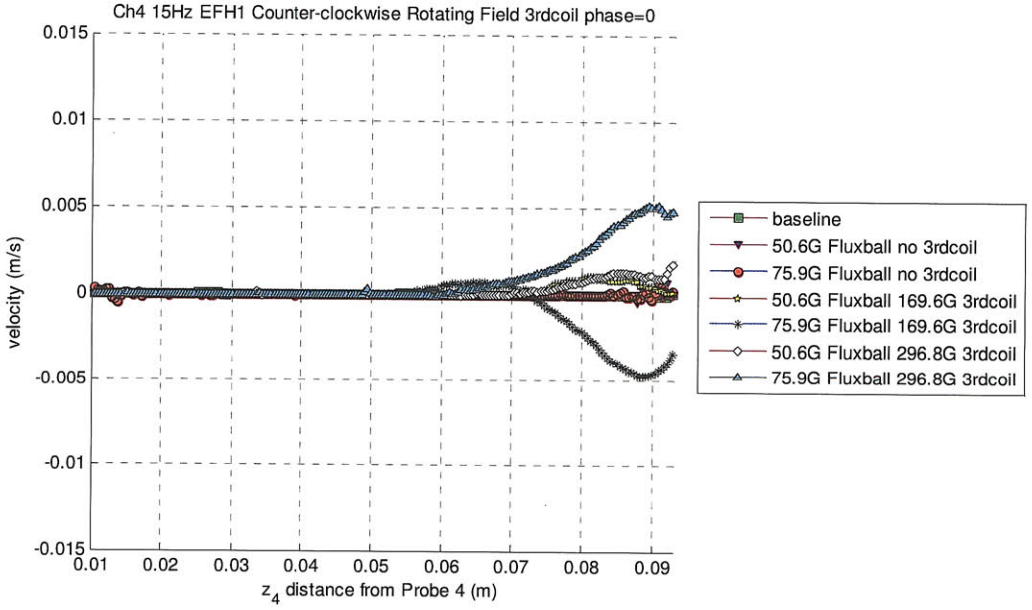
Ch4 15Hz EFH1 Counter-clockwise Rotating Field 3rdcoil phase=0
velocity (m/s)
0.015
0.01
0.005
0
-0.005
-0.01
-0.015
0.01
0.02
0.03
0.04
0.05
0.06
0.07
0.08
0.09
z4 distance from Probe 4 (m)
baseline
50.6G Fluxball no 3rdcoil
75.9G Fluxball no 3rdcoil
50.6G Fluxball 169.6G 3rdcoil
75.9G Fluxball 169.6G 3rdcoil
50.6G Fluxball 296.8G 3rdcoil
75.9G Fluxball 296.8G 3rdcoil

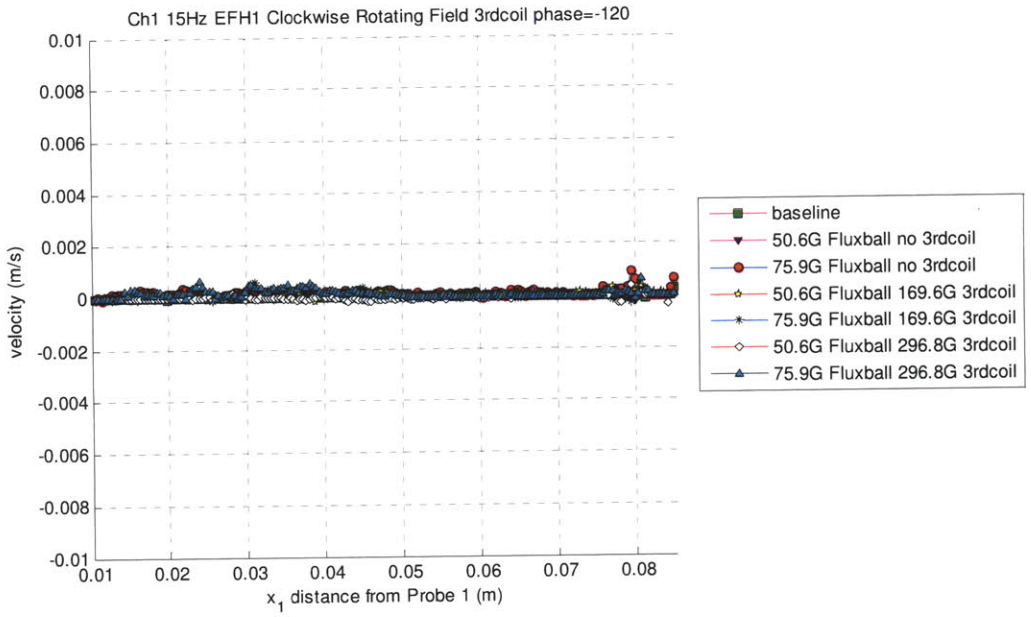
Ch1 15Hz EFH1 Clockwise Rotating Field 3rdcoil phase=-120
velocity (m/s)
x1 distance from Probe 1 (m)
baseline
50.6G Fluxball no 3rdcoil
75.9G Fluxball no 3rdcoil
50.6G Fluxball 169.6G 3rdcoil
75.9G Fluxball 169.6G 3rdcoil
50.6G Fluxball 296.8G 3rdcoil
75.9G Fluxball 296.8G 3rdcoil

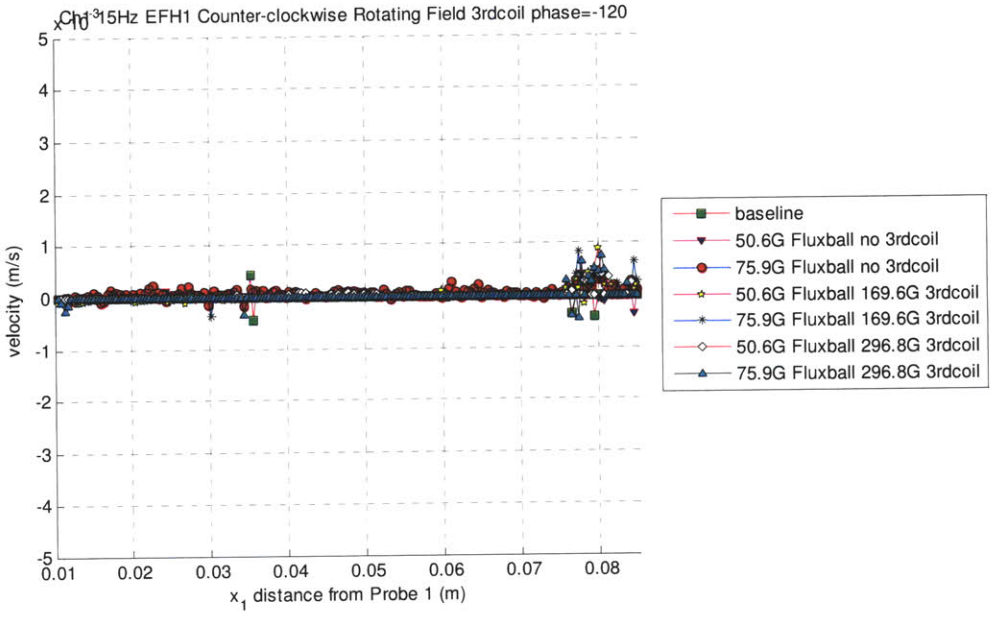
Ch1 15Hz EFH1 Counter-clockwise Rotating Field 3rdcoil phase=-120
x 10^-3
velocity (m/s)
x1 distance from Probe 1 (m)
baseline
50.6G Fluxball no 3rdcoil
75.9G Fluxball no 3rdcoil
50.6G Fluxball 169.6G 3rdcoil
75.9G Fluxball 169.6G 3rdcoil
50.6G Fluxball 296.8G 3rdcoil
75.9G Fluxball 296.8G 3rdcoil

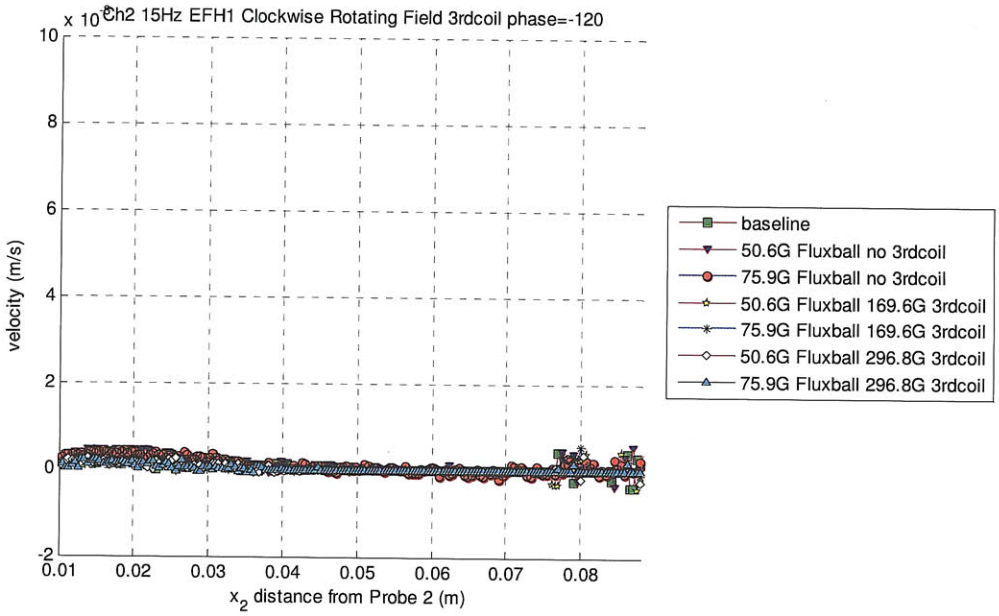
x 10^-5
Ch2 15Hz EFH1 Clockwise Rotating Field 3rdcoil phase=-120
velocity (m/s)
x2 distance from Probe 2 (m)
baseline
50.6G Fluxball no 3rdcoil
75.9G Fluxball no 3rdcoil
50.6G Fluxball 169.6G 3rdcoil
75.9G Fluxball 169.6G 3rdcoil
50.6G Fluxball 296.8G 3rdcoil
75.9G Fluxball 296.8G 3rdcoil

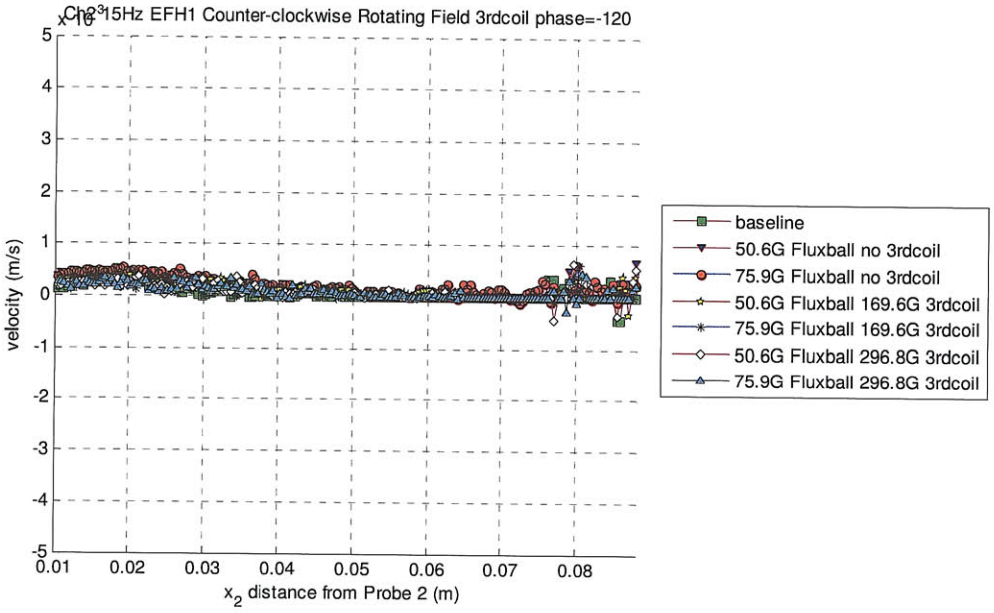
x 10^-6
Ch2 15Hz EFH1 Counter-clockwise Rotating Field 3rdcoil phase=-120
velocity (m/s)
x2 distance from Probe 2 (m)
baseline
50.6G Fluxball no 3rdcoil
75.9G Fluxball no 3rdcoil
50.6G Fluxball 169.6G 3rdcoil
75.9G Fluxball 169.6G 3rdcoil
50.6G Fluxball 296.8G 3rdcoil
75.9G Fluxball 296.8G 3rdcoil

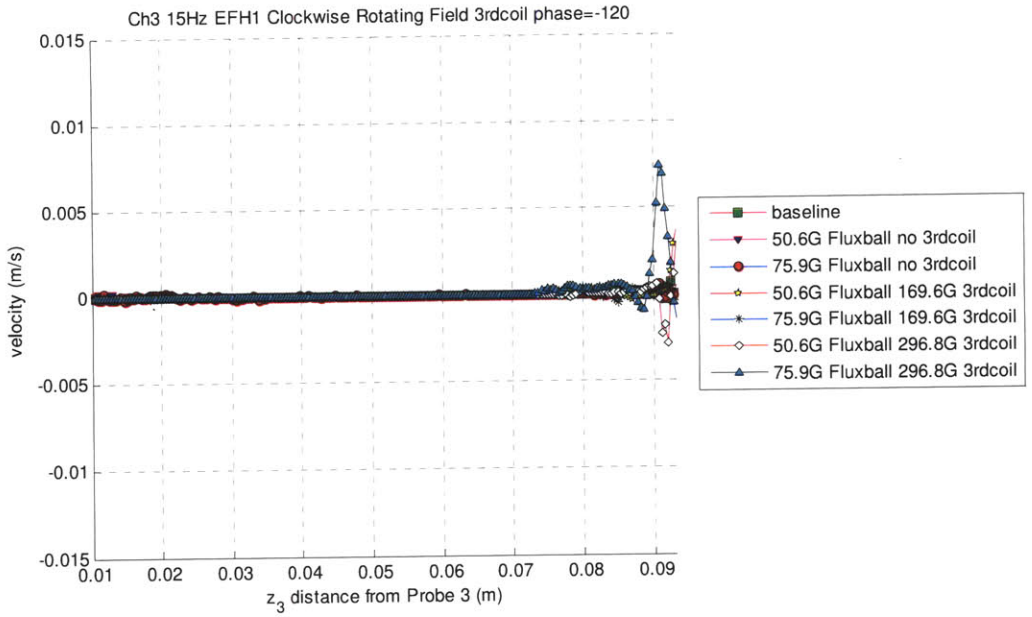
Ch3 15Hz EFH1 Clockwise Rotating Field 3rdcoil phase=-120
velocity (m/s)
0.015
0.01
0.005
0
-0.005
-0.01
-0.015
0.01
0.02
0.03
0.04
0.05
0.06
0.07
0.08
0.09
z3 distance from Probe 3 (m)
baseline
50.6G Fluxball no 3rdcoil
75.9G Fluxball no 3rdcoil
50.6G Fluxball 169.6G 3rdcoil
75.9G Fluxball 169.6G 3rdcoil
50.6G Fluxball 296.8G 3rdcoil
75.9G Fluxball 296.8G 3rdcoil

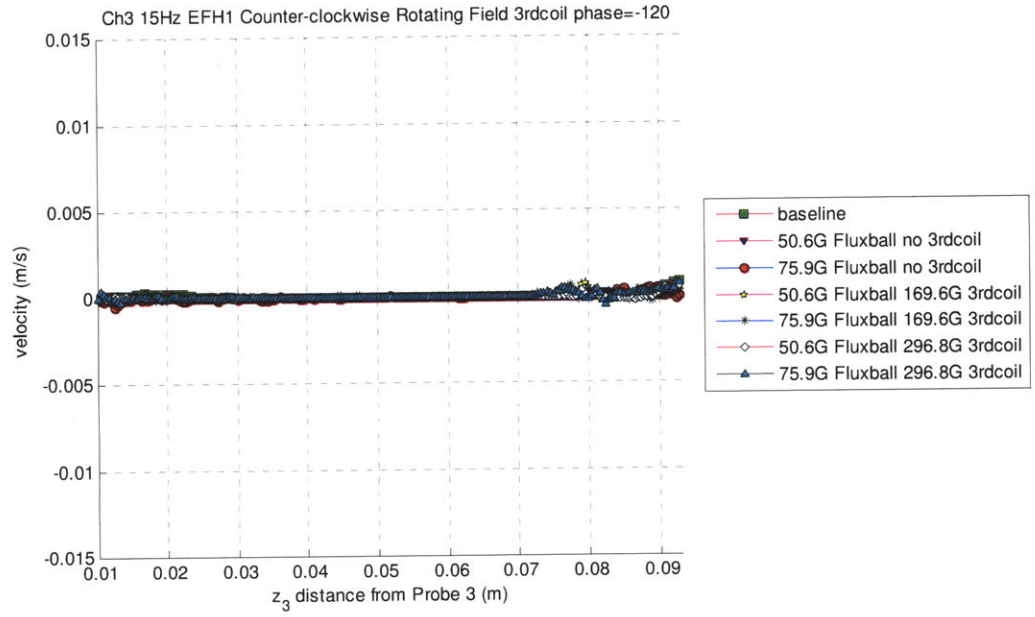
Ch3 15Hz EFH1 Counter-clockwise Rotating Field 3rdcoil phase=-120
velocity (m/s)
0.015
0.01
0.005
0
-0.005
-0.01
-0.015
0.01
0.02
0.03
0.04
0.05
0.06
0.07
0.08
0.09
z3 distance from Probe 3 (m)
baseline
50.6G Fluxball no 3rdcoil
75.9G Fluxball no 3rdcoil
50.6G Fluxball 169.6G 3rdcoil
75.9G Fluxball 169.6G 3rdcoil
50.6G Fluxball 296.8G 3rdcoil
75.9G Fluxball 296.8G 3rdcoil

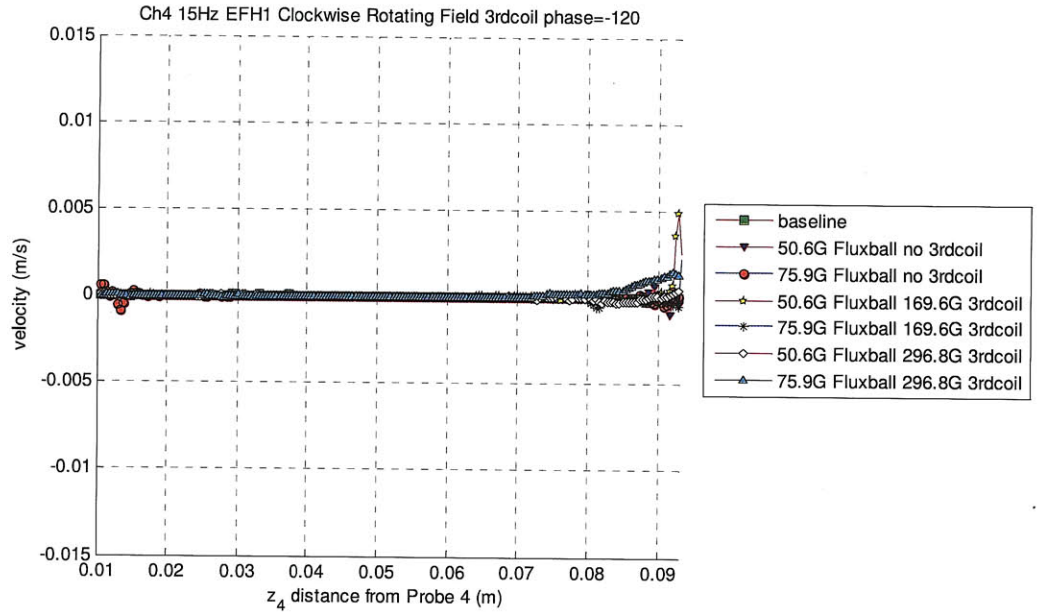
Ch4 15Hz EFH1 Clockwise Rotating Field 3rdcoil phase=-120
velocity (m/s)
0.015
0.01
0.005
0
-0.005
-0.01
-0.015
0.01
0.02
0.03
0.04
0.05
0.06
0.07
0.08
0.09
z4 distance from Probe 4 (m)
baseline
50.6G Fluxball no 3rdcoil
75.9G Fluxball no 3rdcoil
50.6G Fluxball 169.6G 3rdcoil
75.9G Fluxball 169.6G 3rdcoil
50.6G Fluxball 296.8G 3rdcoil
75.9G Fluxball 296.8G 3rdcoil

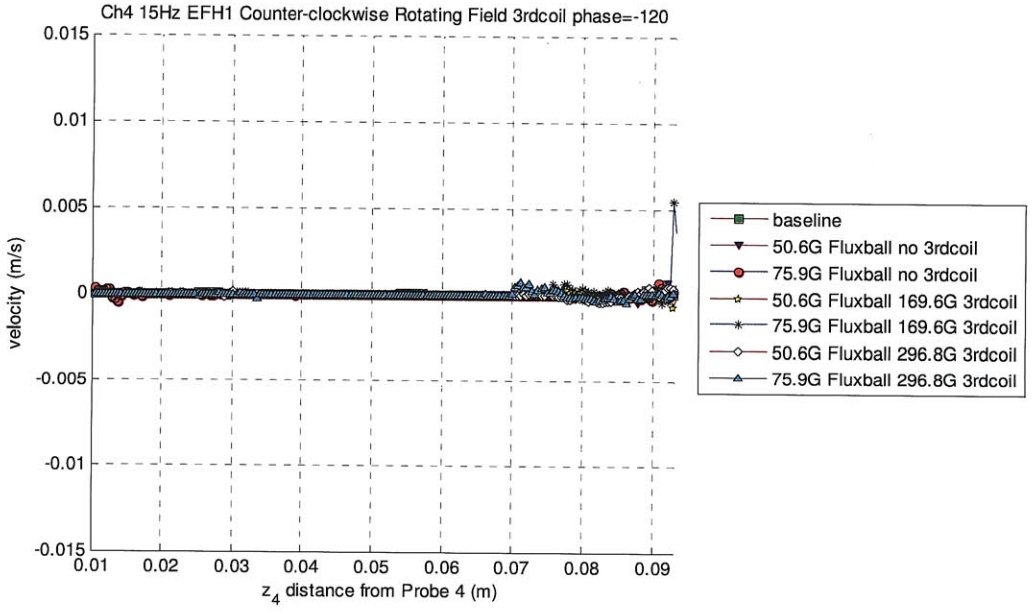
Ch4 15Hz EFH1 Counter-clockwise Rotating Field 3rdcoil phase=-120
velocity (m/s)
0.015
0.01
0.005
0
-0.005
-0.01
-0.015
0.01
0.02
0.03
0.04
0.05
0.06
0.07
0.08
0.09
z4 distance from Probe 4 (m)
baseline
50.6G Fluxball no 3rdcoil
75.9G Fluxball no 3rdcoil
50.6G Fluxball 169.6G 3rdcoil
75.9G Fluxball 169.6G 3rdcoil
50.6G Fluxball 296.8G 3rdcoil
75.9G Fluxball 296.8G 3rdcoil

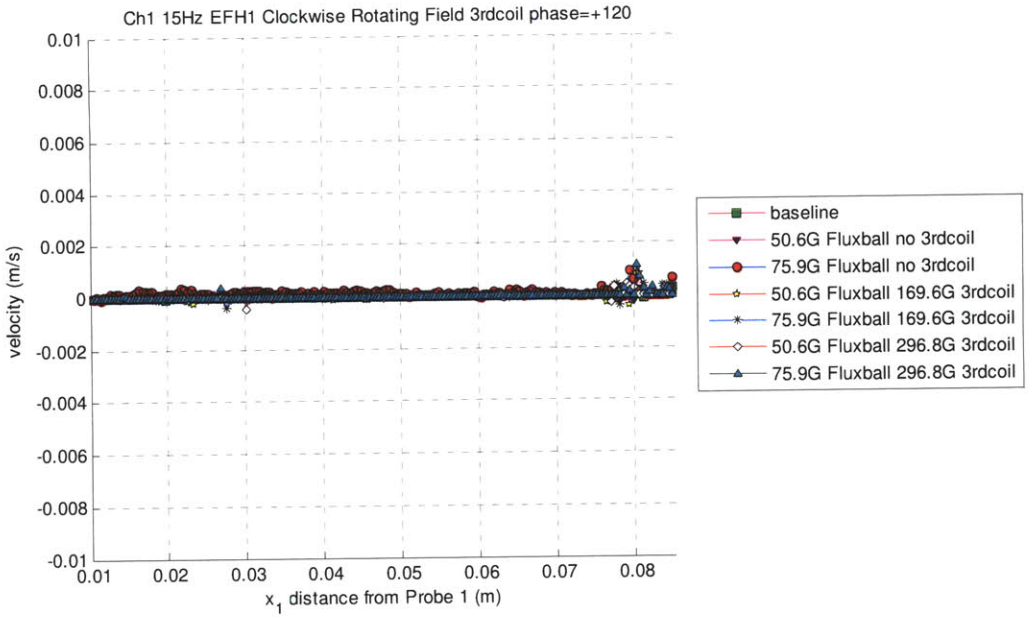
Ch1 15Hz EFH1 Clockwise Rotating Field 3rdcoil phase=+120
velocity (m/s)
0.01
0.008
0.006
0.004
0.002
0
-0.002
-0.004
-0.006
-0.008
-0.01
0.01
0.02
0.03
0.04
0.05
0.06
0.07
0.08
x1 distance from Probe 1 (m)
baseline
50.6G Fluxball no 3rdcoil
75.9G Fluxball no 3rdcoil
50.6G Fluxball 169.6G 3rdcoil
75.9G Fluxball 169.6G 3rdcoil
50.6G Fluxball 296.8G 3rdcoil
75.9G Fluxball 296.8G 3rdcoil

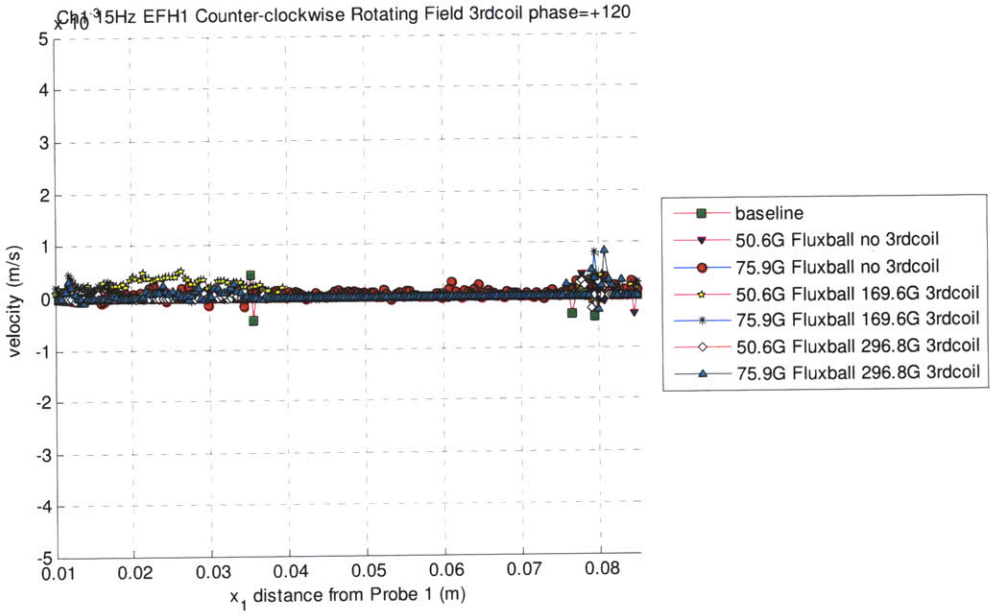
Ch1 15Hz EFH1 Counter-clockwise Rotating Field 3rdcoil phase=+120
x 10
velocity (m/s)
5
4
3
2
1
0
-1
-2
-3
-4
-5
0.01
0.02
0.03
0.04
0.05
0.06
0.07
0.08
x1 distance from Probe 1 (m)
baseline
50.6G Fluxball no 3rdcoil
75.9G Fluxball no 3rdcoil
50.6G Fluxball 169.6G 3rdcoil
75.9G Fluxball 169.6G 3rdcoil
50.6G Fluxball 296.8G 3rdcoil
75.9G Fluxball 296.8G 3rdcoil

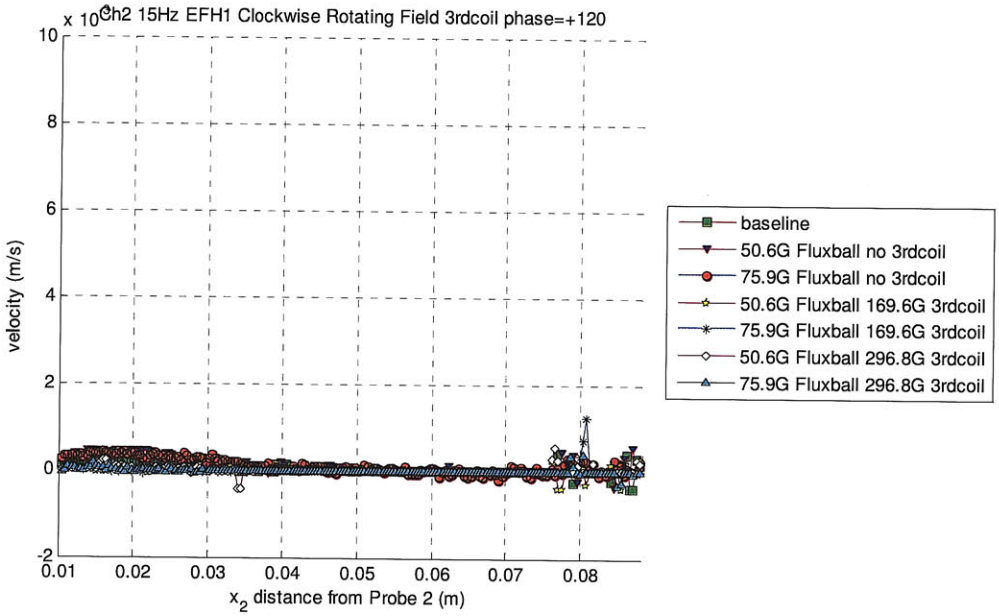
x 10^-3
Ch2 15Hz EFH1 Clockwise Rotating Field 3rdcoil phase=+120
velocity (m/s)
x2 distance from Probe 2 (m)
baseline
50.6G Fluxball no 3rdcoil
75.9G Fluxball no 3rdcoil
50.6G Fluxball 169.6G 3rdcoil
75.9G Fluxball 169.6G 3rdcoil
50.6G Fluxball 296.8G 3rdcoil
75.9G Fluxball 296.8G 3rdcoil

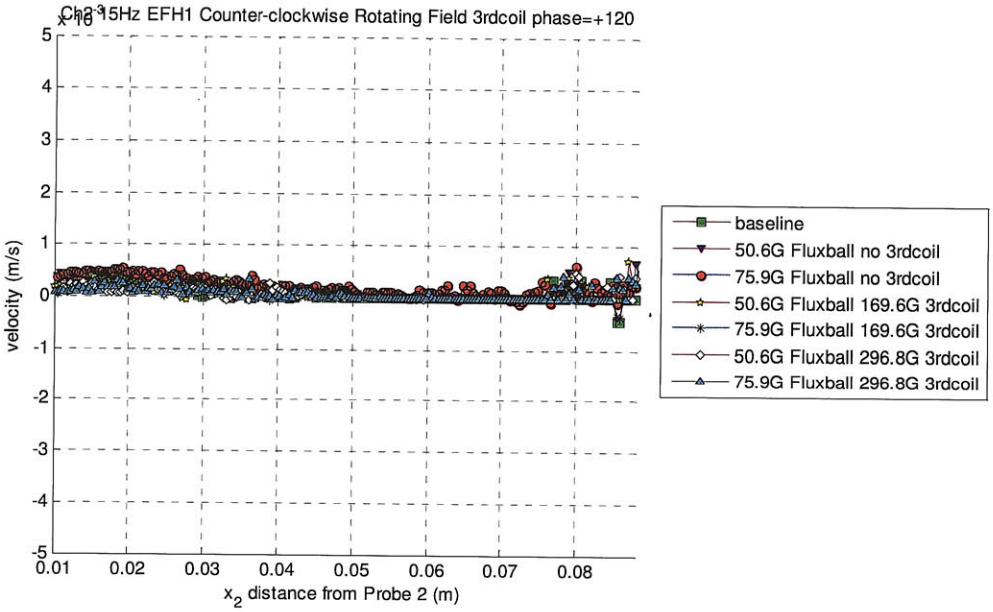
x 10^-3
Ch2 15Hz EFH1 Counter-clockwise Rotating Field 3rdcoil phase=+120
velocity (m/s)
x2 distance from Probe 2 (m)
baseline
50.6G Fluxball no 3rdcoil
75.9G Fluxball no 3rdcoil
50.6G Fluxball 169.6G 3rdcoil
75.9G Fluxball 169.6G 3rdcoil
50.6G Fluxball 296.8G 3rdcoil
75.9G Fluxball 296.8G 3rdcoil

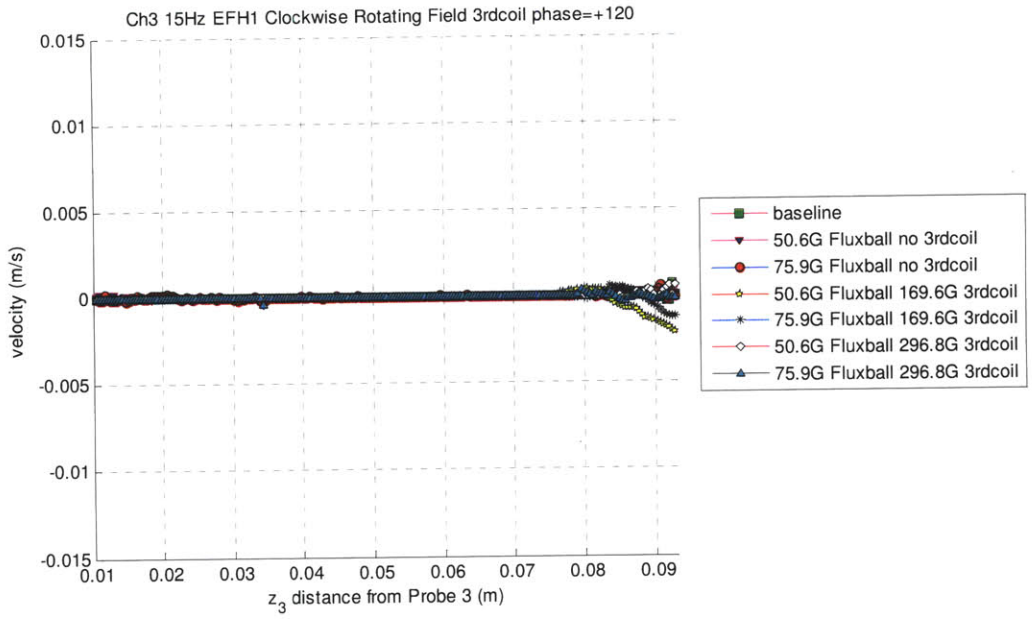
Ch3 15Hz EFH1 Clockwise Rotating Field 3rdcoil phase=+120
velocity (m/s)
0.015
0.01
0.005
0
-0.005
-0.01
-0.015
0.01
0.02
0.03
0.04
0.05
0.06
0.07
0.08
0.09
z3 distance from Probe 3 (m)
baseline
50.6G Fluxball no 3rdcoil
75.9G Fluxball no 3rdcoil
50.6G Fluxball 169.6G 3rdcoil
75.9G Fluxball 169.6G 3rdcoil
50.6G Fluxball 296.8G 3rdcoil
75.9G Fluxball 296.8G 3rdcoil

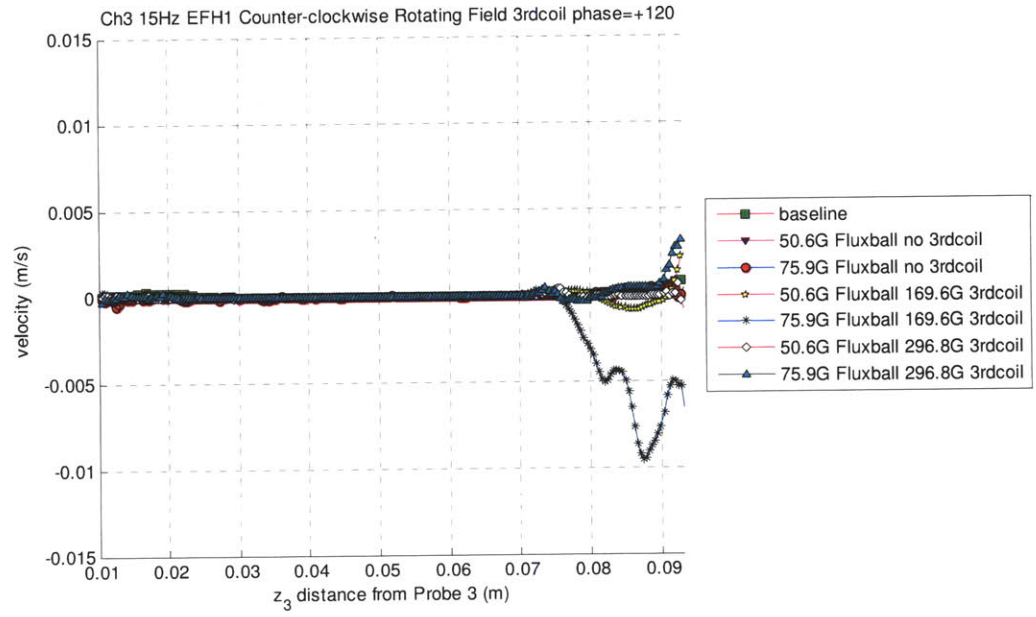
Ch3 15Hz EFH1 Counter-clockwise Rotating Field 3rdcoil phase=+120
velocity (m/s)
0.015
0.01
0.005
0
-0.005
-0.01
-0.015
0.01
0.02
0.03
0.04
0.05
0.06
0.07
0.08
0.09
z3 distance from Probe 3 (m)
baseline
50.6G Fluxball no 3rdcoil
75.9G Fluxball no 3rdcoil
50.6G Fluxball 169.6G 3rdcoil
75.9G Fluxball 169.6G 3rdcoil
50.6G Fluxball 296.8G 3rdcoil
75.9G Fluxball 296.8G 3rdcoil

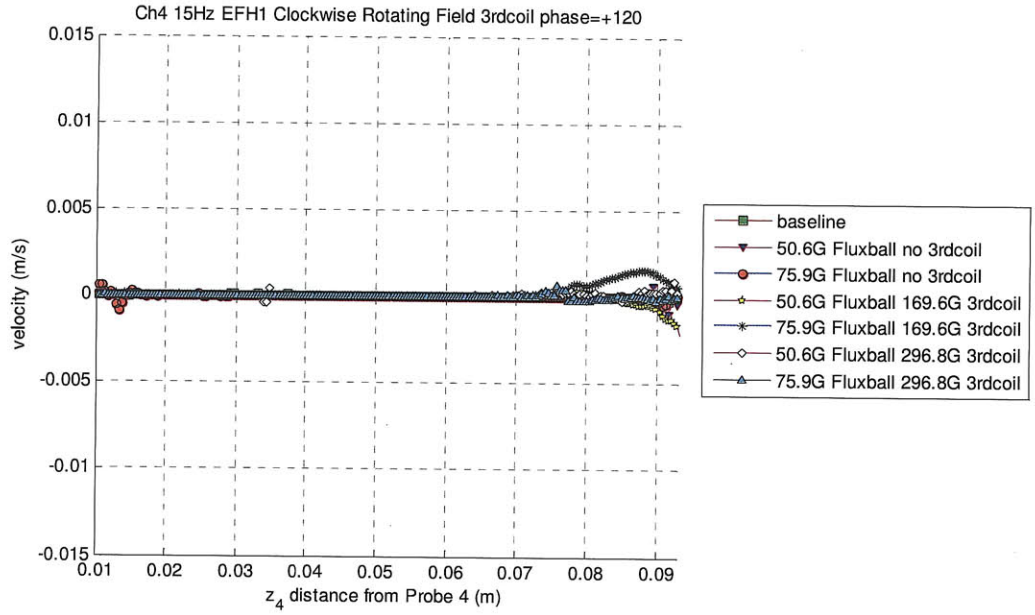
Ch4 15Hz EFH1 Clockwise Rotating Field 3rdcoil phase=+120
velocity (m/s)
0.015
0.01
0.005
0
-0.005
-0.01
-0.015
0.01
0.02
0.03
0.04
0.05
0.06
0.07
0.08
0.09
z4 distance from Probe 4 (m)
baseline
50.6G Fluxball no 3rdcoil
75.9G Fluxball no 3rdcoil
50.6G Fluxball 169.6G 3rdcoil
75.9G Fluxball 169.6G 3rdcoil
50.6G Fluxball 296.8G 3rdcoil
75.9G Fluxball 296.8G 3rdcoil

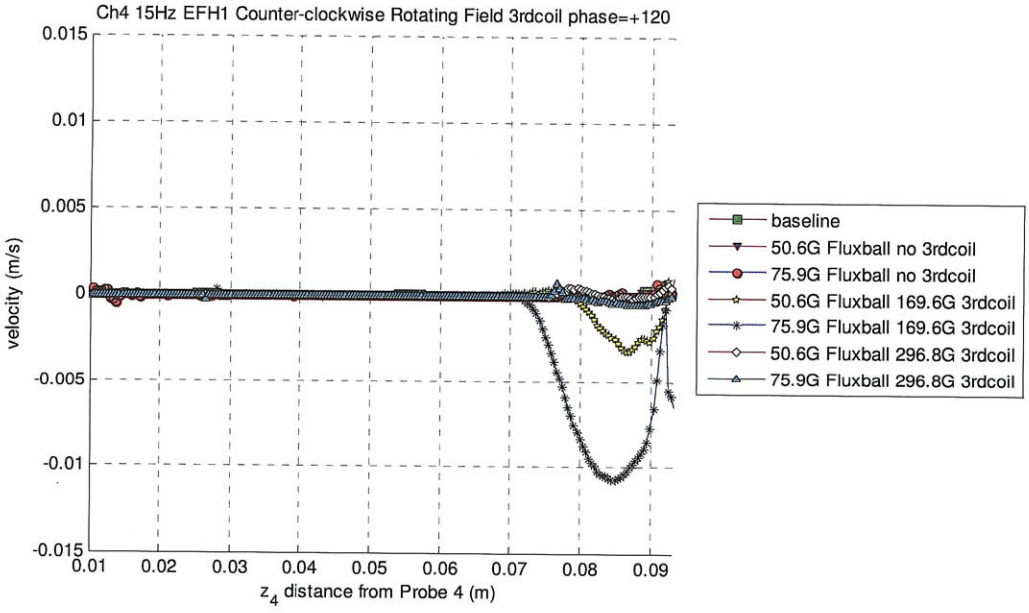
Ch4 15Hz EFH1 Counter-clockwise Rotating Field 3rdcoil phase=+120
velocity (m/s)
0.015
0.01
0.005
0
-0.005
-0.01
-0.015
0.01
0.02
0.03
0.04
0.05
0.06
0.07
0.08
0.09
z4 distance from Probe 4 (m)
baseline
50.6G Fluxball no 3rdcoil
75.9G Fluxball no 3rdcoil
50.6G Fluxball 169.6G 3rdcoil
75.9G Fluxball 169.6G 3rdcoil
50.6G Fluxball 296.8G 3rdcoil
75.9G Fluxball 296.8G 3rdcoil

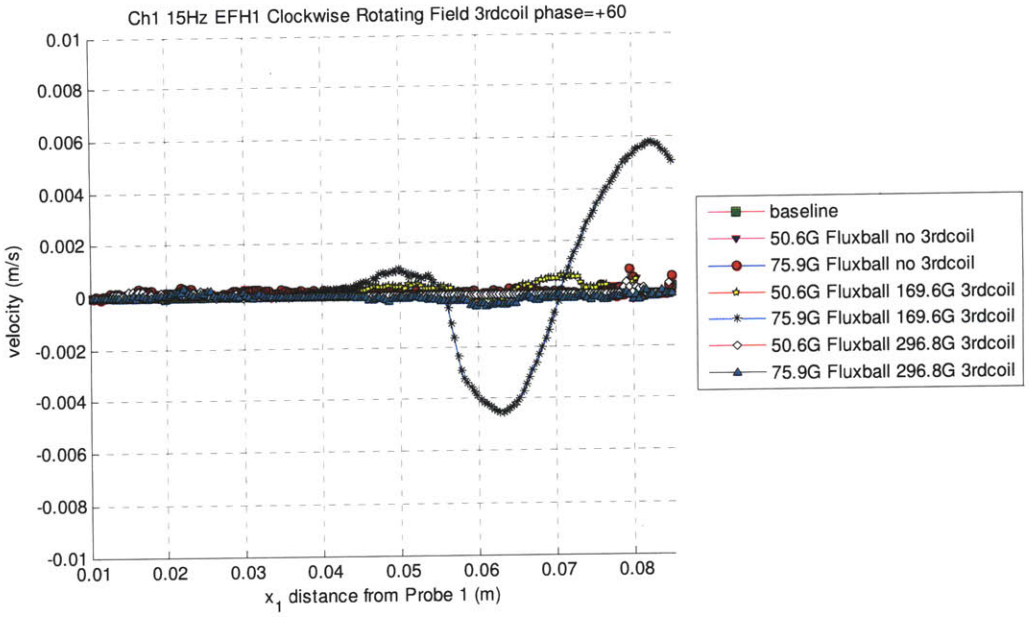
Ch1 15Hz EFH1 Clockwise Rotating Field 3rdcoil phase=+60
velocity (m/s)
0.01
0.008
0.006
0.004
0.002
0
-0.002
-0.004
-0.006
-0.008
-0.01
0.01
0.02
0.03
0.04
0.05
0.06
0.07
0.08
x1 distance from Probe 1 (m)
baseline
50.6G Fluxball no 3rdcoil
75.9G Fluxball no 3rdcoil
50.6G Fluxball 169.6G 3rdcoil
75.9G Fluxball 169.6G 3rdcoil
50.6G Fluxball 296.8G 3rdcoil
75.9G Fluxball 296.8G 3rdcoil

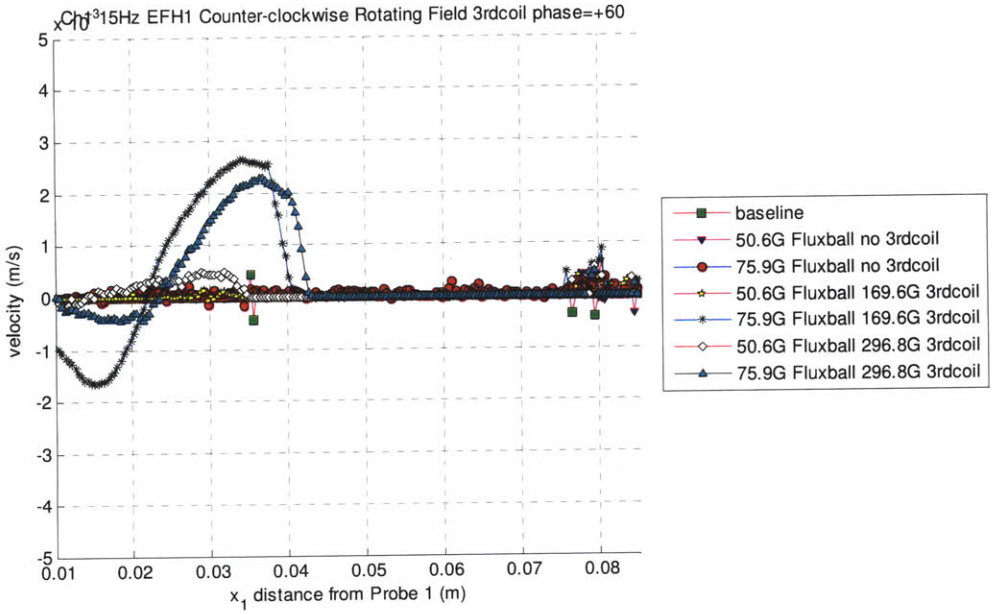
Ch1 15Hz EFH1 Counter-clockwise Rotating Field 3rdcoil phase=+60
x10-3
velocity (m/s)
5
4
3
2
1
0
-1
-2
-3
-4
-5
0.01
0.02
0.03
0.04
0.05
0.06
0.07
0.08
x1 distance from Probe 1 (m)
baseline
50.6G Fluxball no 3rdcoil
75.9G Fluxball no 3rdcoil
50.6G Fluxball 169.6G 3rdcoil
75.9G Fluxball 169.6G 3rdcoil
50.6G Fluxball 296.8G 3rdcoil
75.9G Fluxball 296.8G 3rdcoil

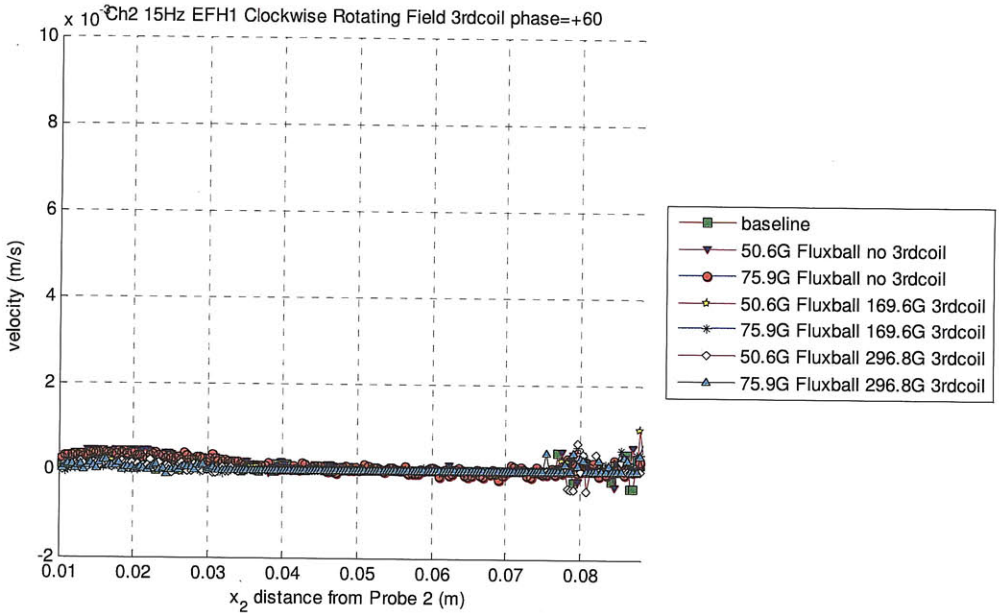
x 10^-3 Ch2 15Hz EFH1 Clockwise Rotating Field 3rdcoil phase=+60
velocity (m/s)
x2 distance from Probe 2 (m)
baseline
50.6G Fluxball no 3rdcoil
75.9G Fluxball no 3rdcoil
50.6G Fluxball 169.6G 3rdcoil
75.9G Fluxball 169.6G 3rdcoil
50.6G Fluxball 296.8G 3rdcoil
75.9G Fluxball 296.8G 3rdcoil

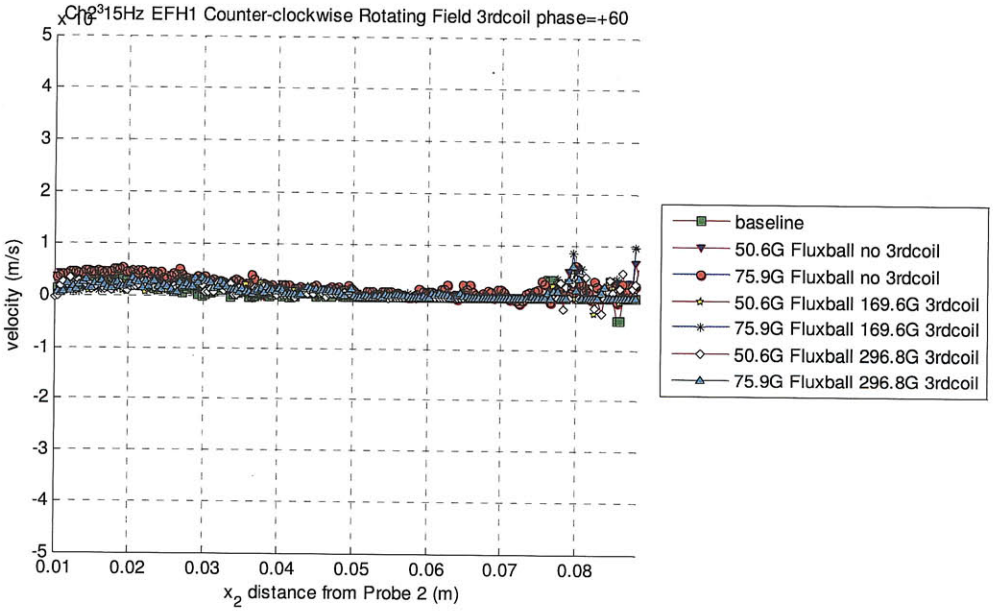
x 10^-3 Ch2 15Hz EFH1 Counter-clockwise Rotating Field 3rdcoil phase=+60
velocity (m/s)
x2 distance from Probe 2 (m)
baseline
50.6G Fluxball no 3rdcoil
75.9G Fluxball no 3rdcoil
50.6G Fluxball 169.6G 3rdcoil
75.9G Fluxball 169.6G 3rdcoil
50.6G Fluxball 296.8G 3rdcoil
75.9G Fluxball 296.8G 3rdcoil

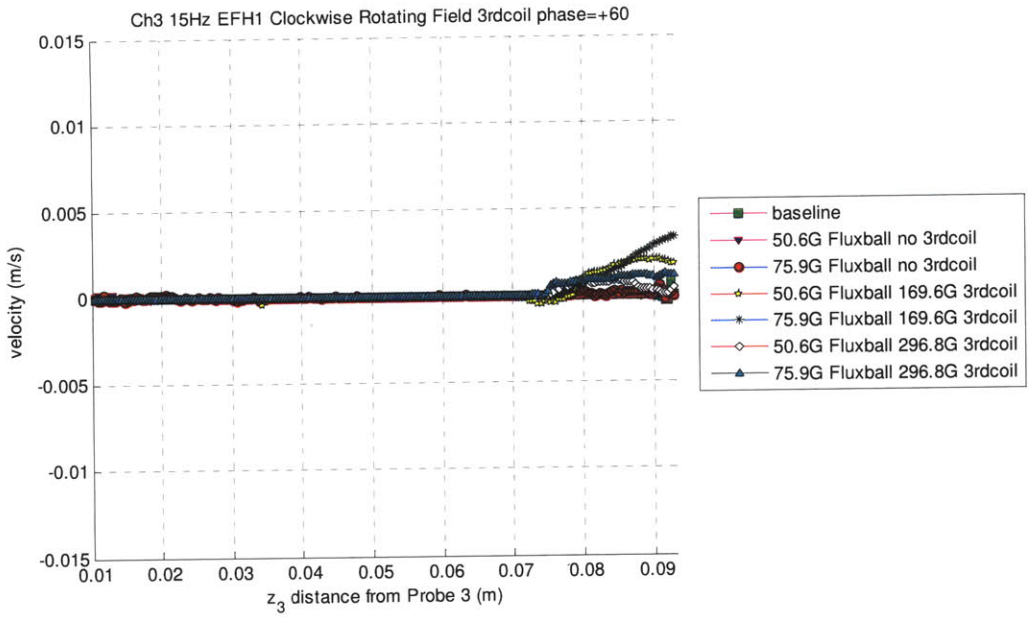
Ch3 15Hz EFH1 Clockwise Rotating Field 3rdcoil phase=+60
velocity (m/s)
0.015
0.01
0.005
0
-0.005
-0.01
-0.015
0.01
0.02
0.03
0.04
0.05
0.06
0.07
0.08
0.09
z3 distance from Probe 3 (m)
baseline
50.6G Fluxball no 3rdcoil
75.9G Fluxball no 3rdcoil
50.6G Fluxball 169.6G 3rdcoil
75.9G Fluxball 169.6G 3rdcoil
50.6G Fluxball 296.8G 3rdcoil
75.9G Fluxball 296.8G 3rdcoil

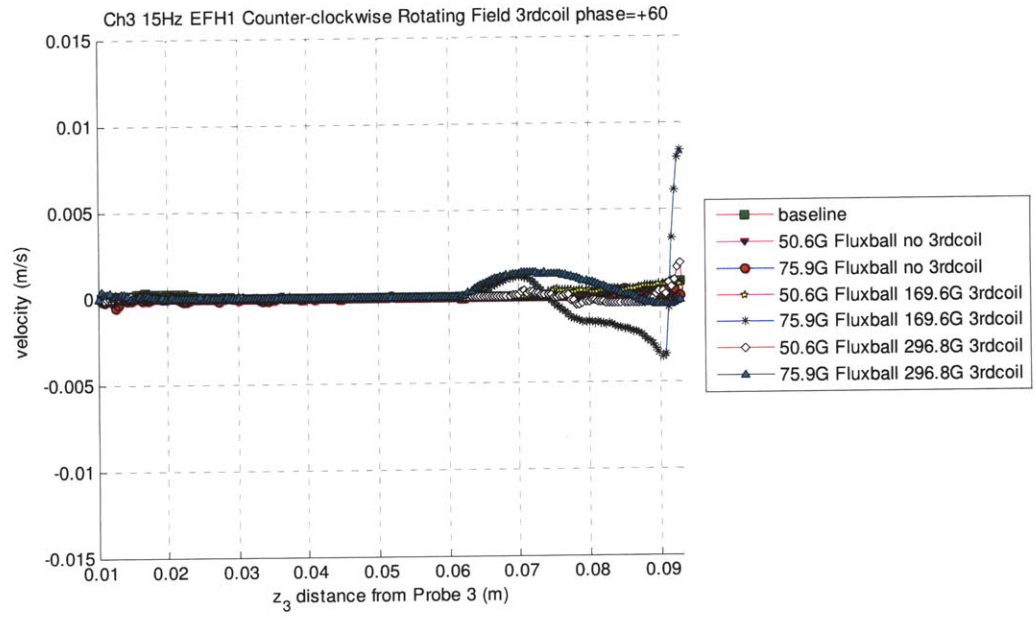
Ch3 15Hz EFH1 Counter-clockwise Rotating Field 3rdcoil phase=+60
velocity (m/s)
0.015
0.01
0.005
0
-0.005
-0.01
-0.015
0.01
0.02
0.03
0.04
0.05
0.06
0.07
0.08
0.09
z3 distance from Probe 3 (m)
baseline
50.6G Fluxball no 3rdcoil
75.9G Fluxball no 3rdcoil
50.6G Fluxball 169.6G 3rdcoil
75.9G Fluxball 169.6G 3rdcoil
50.6G Fluxball 296.8G 3rdcoil
75.9G Fluxball 296.8G 3rdcoil

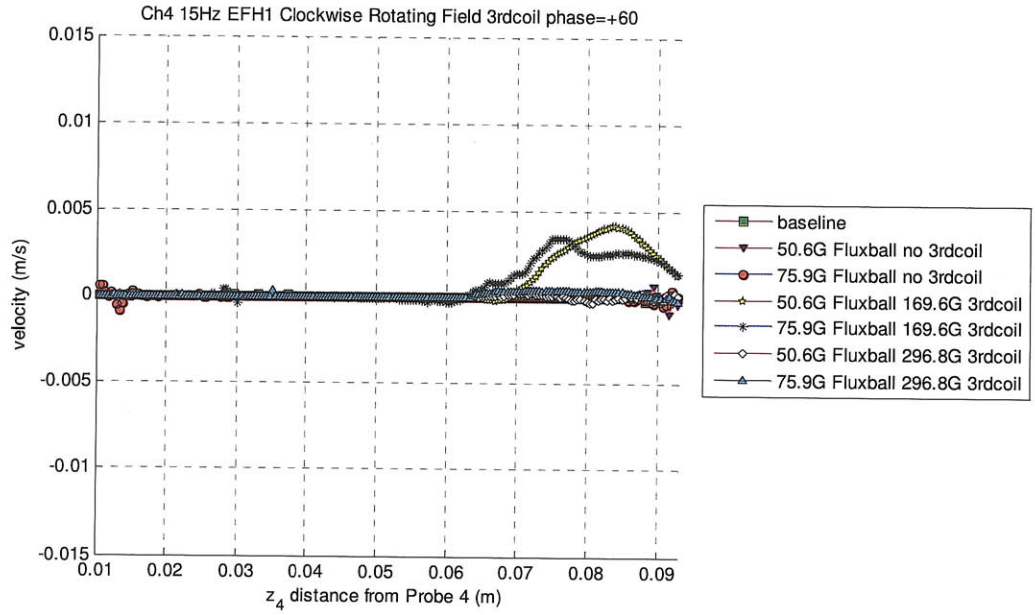
Ch4 15Hz EFH1 Clockwise Rotating Field 3rdcoil phase=+60
velocity (m/s)
0.015
0.01
0.005
0
-0.005
-0.01
-0.015
0.01
0.02
0.03
0.04
0.05
0.06
0.07
0.08
0.09
z4 distance from Probe 4 (m)
baseline
50.6G Fluxball no 3rdcoil
75.9G Fluxball no 3rdcoil
50.6G Fluxball 169.6G 3rdcoil
75.9G Fluxball 169.6G 3rdcoil
50.6G Fluxball 296.8G 3rdcoil
75.9G Fluxball 296.8G 3rdcoil

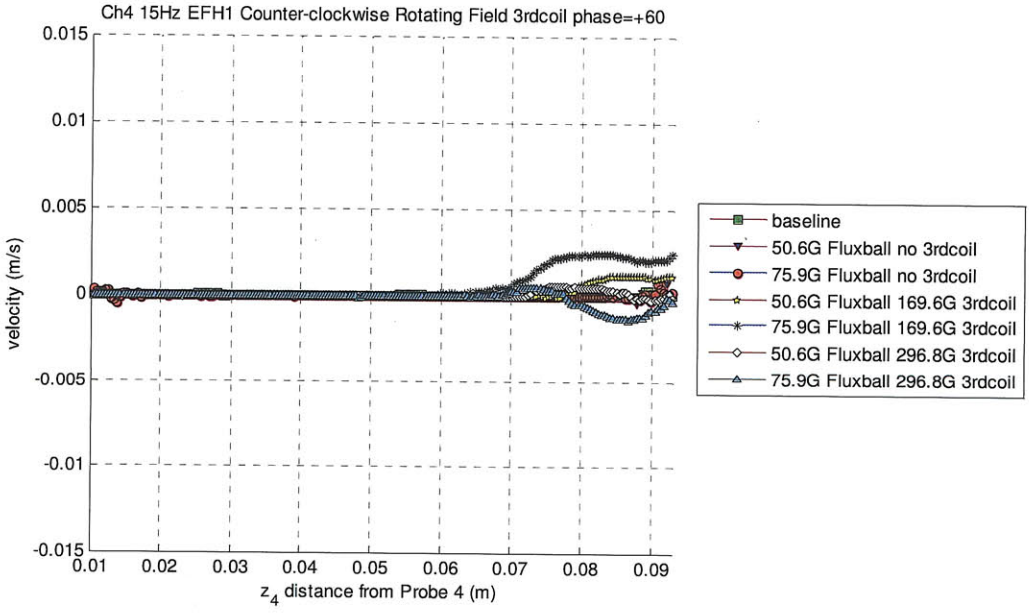
Ch4 15Hz EFH1 Counter-clockwise Rotating Field 3rdcoil phase=+60
velocity (m/s)
0.015
0.01
0.005
0
-0.005
-0.01
-0.015
0.01
0.02
0.03
0.04
0.05
0.06
0.07
0.08
0.09
z4 distance from Probe 4 (m)
baseline
50.6G Fluxball no 3rdcoil
75.9G Fluxball no 3rdcoil
50.6G Fluxball 169.6G 3rdcoil
75.9G Fluxball 169.6G 3rdcoil
50.6G Fluxball 296.8G 3rdcoil
75.9G Fluxball 296.8G 3rdcoil

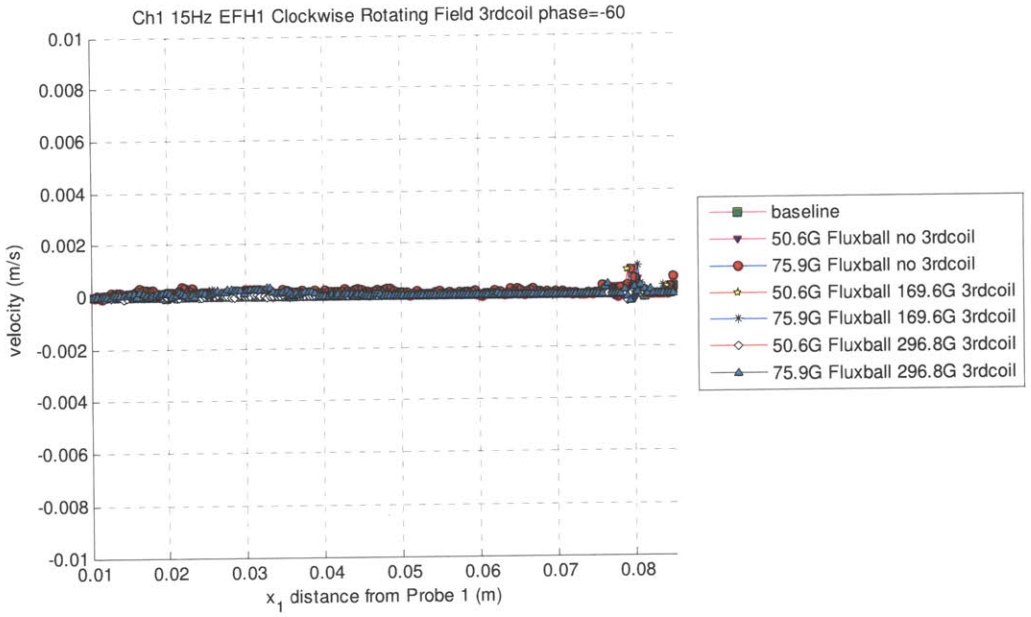
Ch1 15Hz EFH1 Clockwise Rotating Field 3rdcoil phase=-60
velocity (m/s)
0.01
0.008
0.006
0.004
0.002
0
-0.002
-0.004
-0.006
-0.008
-0.01
0.01
0.02
0.03
0.04
0.05
0.06
0.07
0.08
x1 distance from Probe 1 (m)
baseline
50.6G Fluxball no 3rdcoil
75.9G Fluxball no 3rdcoil
50.6G Fluxball 169.6G 3rdcoil
75.9G Fluxball 169.6G 3rdcoil
50.6G Fluxball 296.8G 3rdcoil
75.9G Fluxball 296.8G 3rdcoil

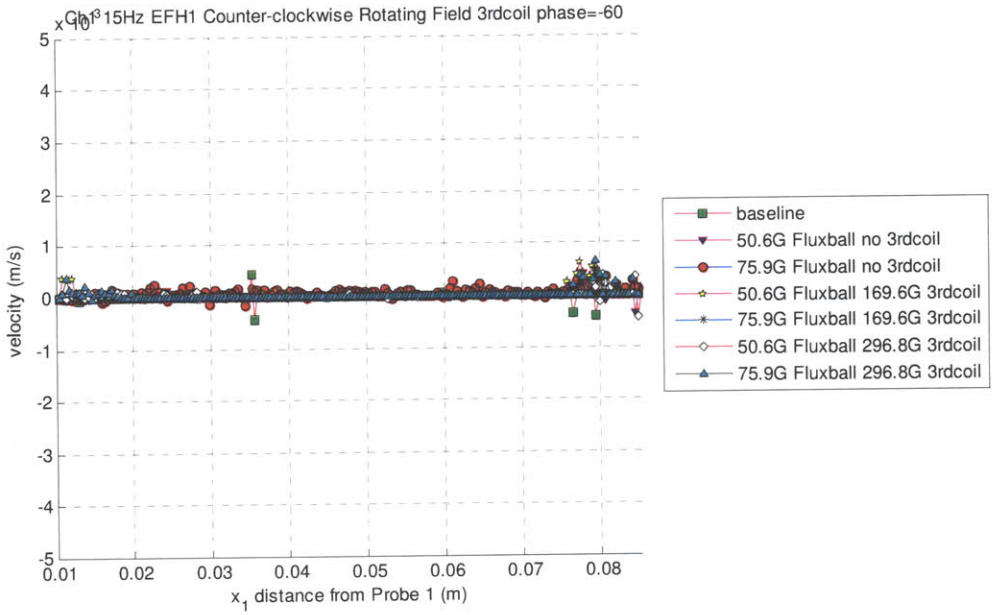
Ch1 15Hz EFH1 Counter-clockwise Rotating Field 3rdcoil phase=-60
x 10^-3
velocity (m/s)
5
4
3
2
1
0
-1
-2
-3
-4
-5
0.01
0.02
0.03
0.04
0.05
0.06
0.07
0.08
x1 distance from Probe 1 (m)
baseline
50.6G Fluxball no 3rdcoil
75.9G Fluxball no 3rdcoil
50.6G Fluxball 169.6G 3rdcoil
75.9G Fluxball 169.6G 3rdcoil
50.6G Fluxball 296.8G 3rdcoil
75.9G Fluxball 296.8G 3rdcoil

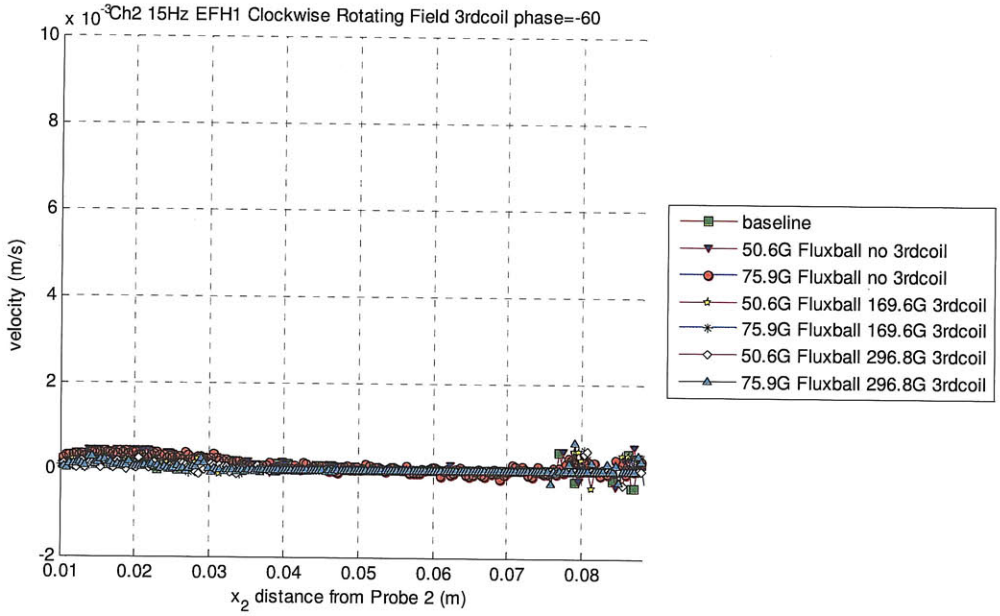
x 10^-3 Ch2 15Hz EFH1 Clockwise Rotating Field 3rdcoil phase=-60
velocity (m/s)
x2 distance from Probe 2 (m)
baseline
50.6G Fluxball no 3rdcoil
75.9G Fluxball no 3rdcoil
50.6G Fluxball 169.6G 3rdcoil
75.9G Fluxball 169.6G 3rdcoil
50.6G Fluxball 296.8G 3rdcoil
75.9G Fluxball 296.8G 3rdcoil

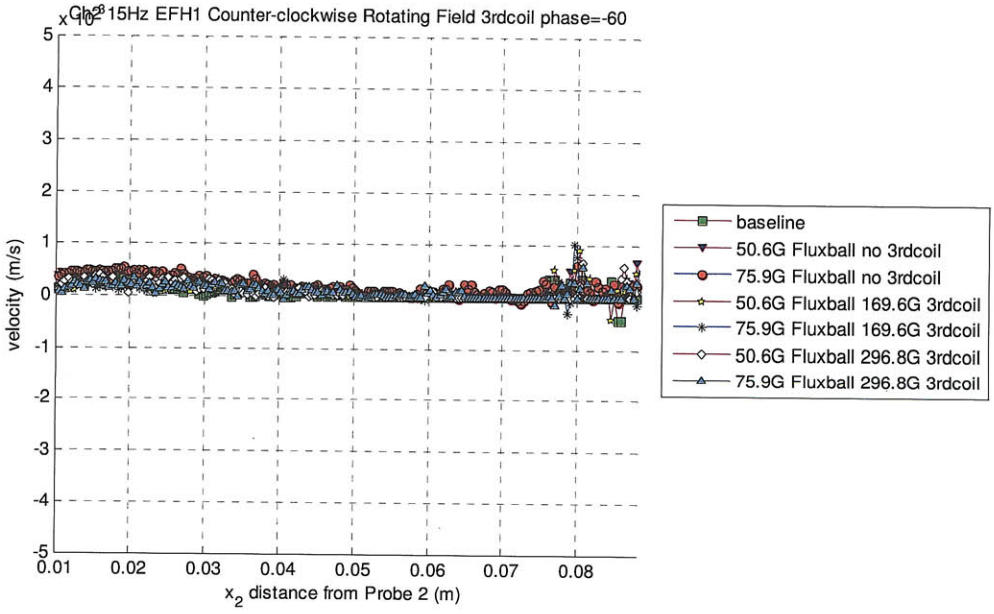
x 10^-3 Ch2 15Hz EFH1 Counter-clockwise Rotating Field 3rdcoil phase=-60
velocity (m/s)
x2 distance from Probe 2 (m)
baseline
50.6G Fluxball no 3rdcoil
75.9G Fluxball no 3rdcoil
50.6G Fluxball 169.6G 3rdcoil
75.9G Fluxball 169.6G 3rdcoil
50.6G Fluxball 296.8G 3rdcoil
75.9G Fluxball 296.8G 3rdcoil

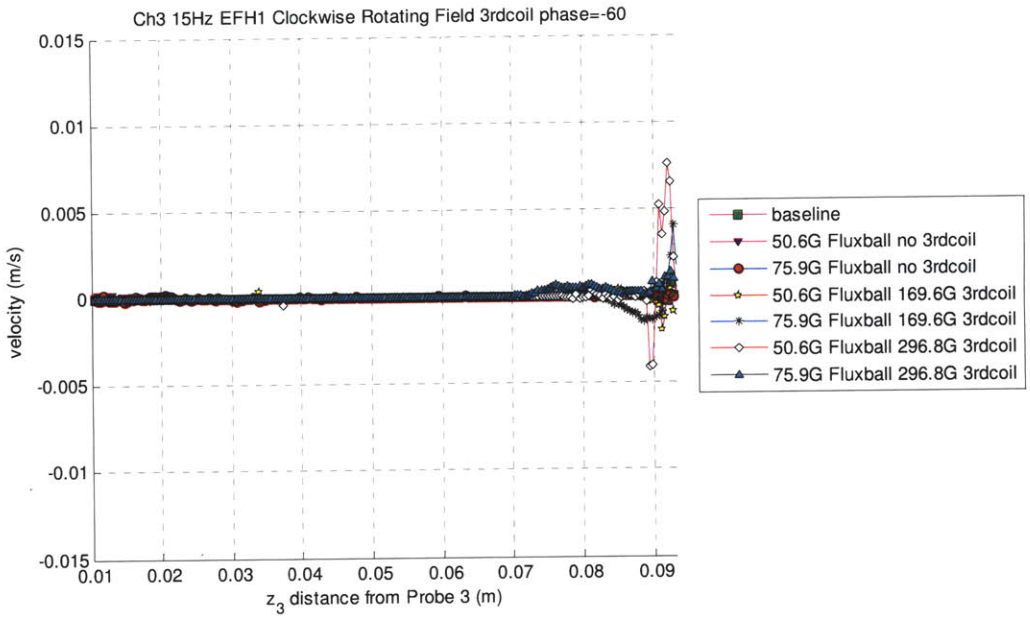
Ch3 15Hz EFH1 Clockwise Rotating Field 3rdcoil phase=-60
velocity (m/s)
0.015
0.01
0.005
0
-0.005
-0.01
-0.015
0.01
0.02
0.03
0.04
0.05
0.06
0.07
0.08
0.09
z_3 distance from Probe 3 (m)
baseline
50.6G Fluxball no 3rdcoil
75.9G Fluxball no 3rdcoil
50.6G Fluxball 169.6G 3rdcoil
75.9G Fluxball 169.6G 3rdcoil
50.6G Fluxball 296.8G 3rdcoil
75.9G Fluxball 296.8G 3rdcoil

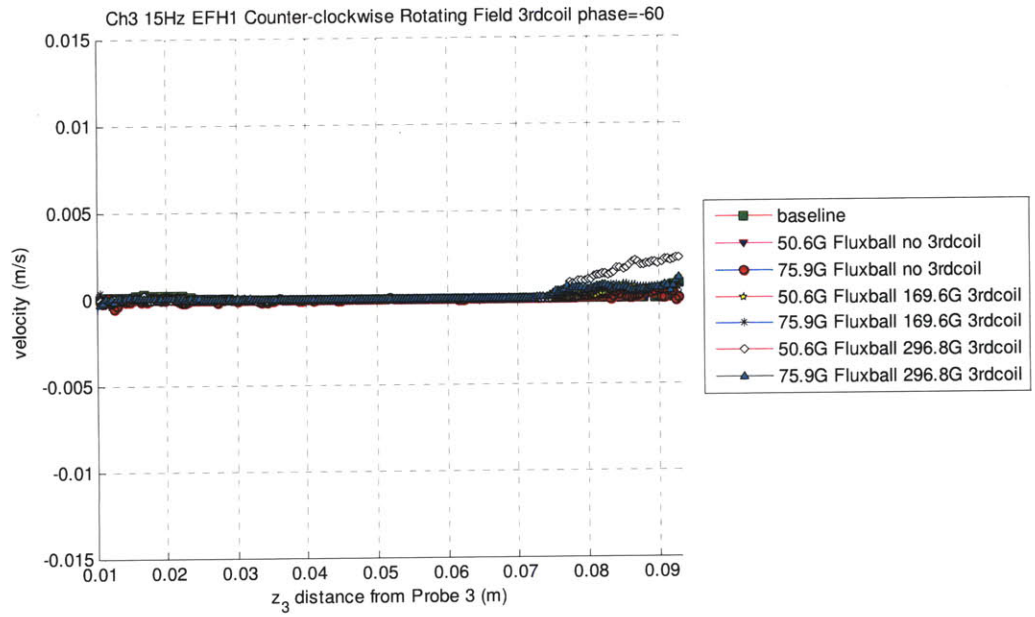
Ch3 15Hz EFH1 Counter-clockwise Rotating Field 3rdcoil phase=-60
velocity (m/s)
0.015
0.01
0.005
0
-0.005
-0.01
-0.015
0.01
0.02
0.03
0.04
0.05
0.06
0.07
0.08
0.09
z_3 distance from Probe 3 (m)
baseline
50.6G Fluxball no 3rdcoil
75.9G Fluxball no 3rdcoil
50.6G Fluxball 169.6G 3rdcoil
75.9G Fluxball 169.6G 3rdcoil
50.6G Fluxball 296.8G 3rdcoil
75.9G Fluxball 296.8G 3rdcoil

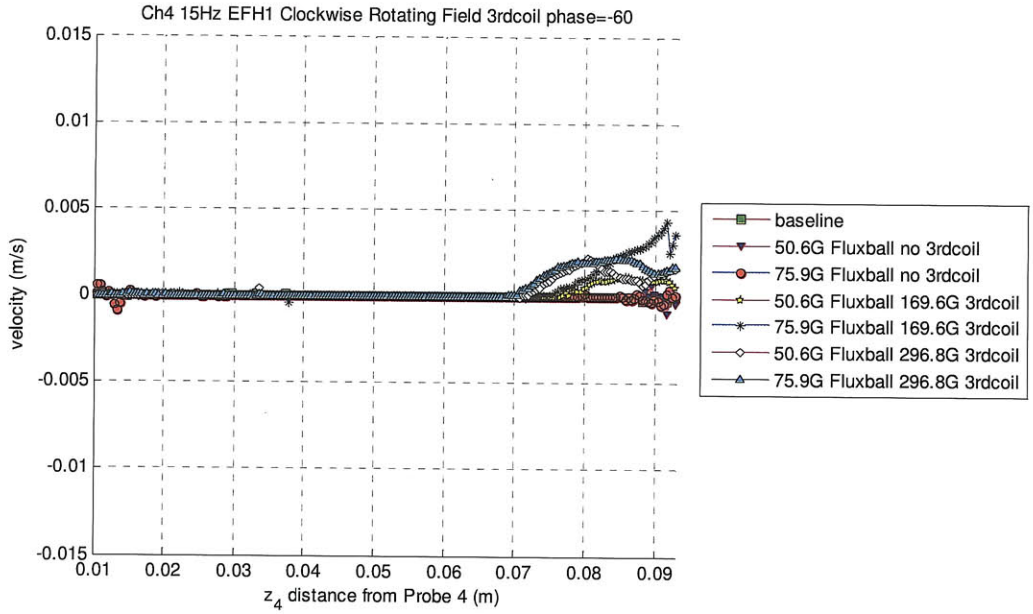
Ch4 15Hz EFH1 Clockwise Rotating Field 3rdcoil phase=-60
velocity (m/s)
0.015
0.01
0.005
0
-0.005
-0.01
-0.015
0.01
0.02
0.03
0.04
0.05
0.06
0.07
0.08
0.09
z4 distance from Probe 4 (m)
baseline
50.6G Fluxball no 3rdcoil
75.9G Fluxball no 3rdcoil
50.6G Fluxball 169.6G 3rdcoil
75.9G Fluxball 169.6G 3rdcoil
50.6G Fluxball 296.8G 3rdcoil
75.9G Fluxball 296.8G 3rdcoil

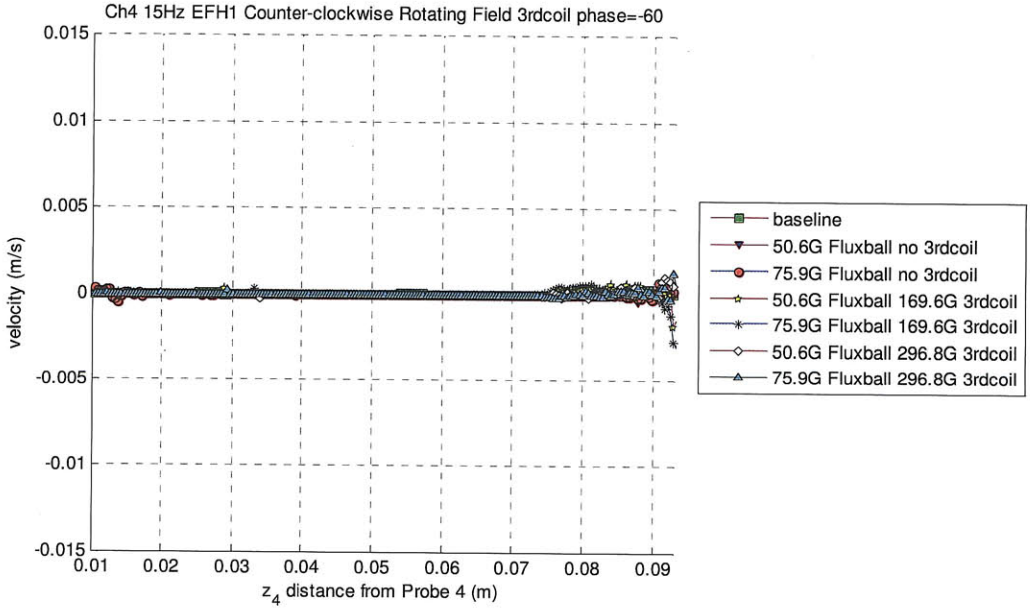
Ch4 15Hz EFH1 Counter-clockwise Rotating Field 3rdcoil phase=-60
velocity (m/s)
0.015
0.01
0.005
0
-0.005
-0.01
-0.015
0.01
0.02
0.03
0.04
0.05
0.06
0.07
0.08
0.09
z4 distance from Probe 4 (m)
baseline
50.6G Fluxball no 3rdcoil
75.9G Fluxball no 3rdcoil
50.6G Fluxball 169.6G 3rdcoil
75.9G Fluxball 169.6G 3rdcoil
50.6G Fluxball 296.8G 3rdcoil
75.9G Fluxball 296.8G 3rdcoil

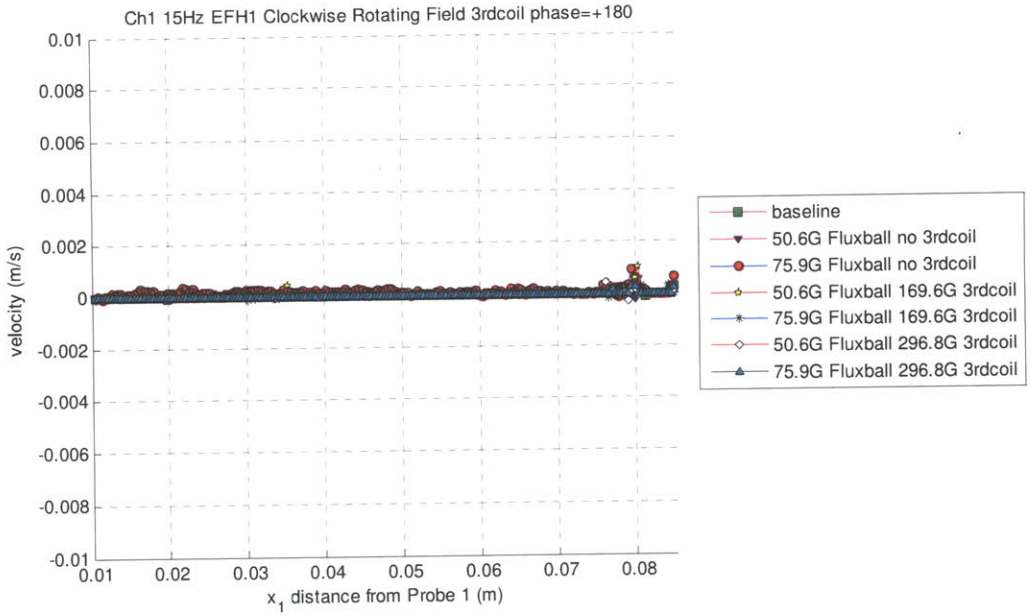
Ch1 15Hz EFH1 Clockwise Rotating Field 3rdcoil phase=+180
velocity (m/s)
0.01
0.008
0.006
0.004
0.002
0
-0.002
-0.004
-0.006
-0.008
-0.01
0.01
0.02
0.03
0.04
0.05
0.06
0.07
0.08
x1 distance from Probe 1 (m)
baseline
50.6G Fluxball no 3rdcoil
75.9G Fluxball no 3rdcoil
50.6G Fluxball 169.6G 3rdcoil
75.9G Fluxball 169.6G 3rdcoil
50.6G Fluxball 296.8G 3rdcoil
75.9G Fluxball 296.8G 3rdcoil

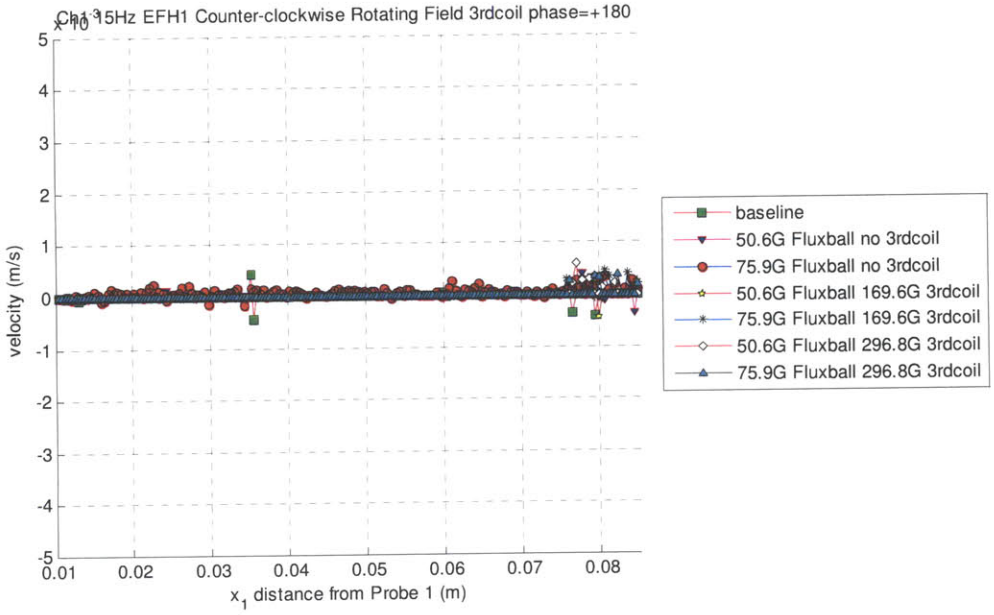
Ch1 15Hz EFH1 Counter-clockwise Rotating Field 3rdcoil phase=+180
x 10-3
velocity (m/s)
5
4
3
2
1
0
-1
-2
-3
-4
-5
0.01
0.02
0.03
0.04
0.05
0.06
0.07
0.08
x1 distance from Probe 1 (m)
baseline
50.6G Fluxball no 3rdcoil
75.9G Fluxball no 3rdcoil
50.6G Fluxball 169.6G 3rdcoil
75.9G Fluxball 169.6G 3rdcoil
50.6G Fluxball 296.8G 3rdcoil
75.9G Fluxball 296.8G 3rdcoil

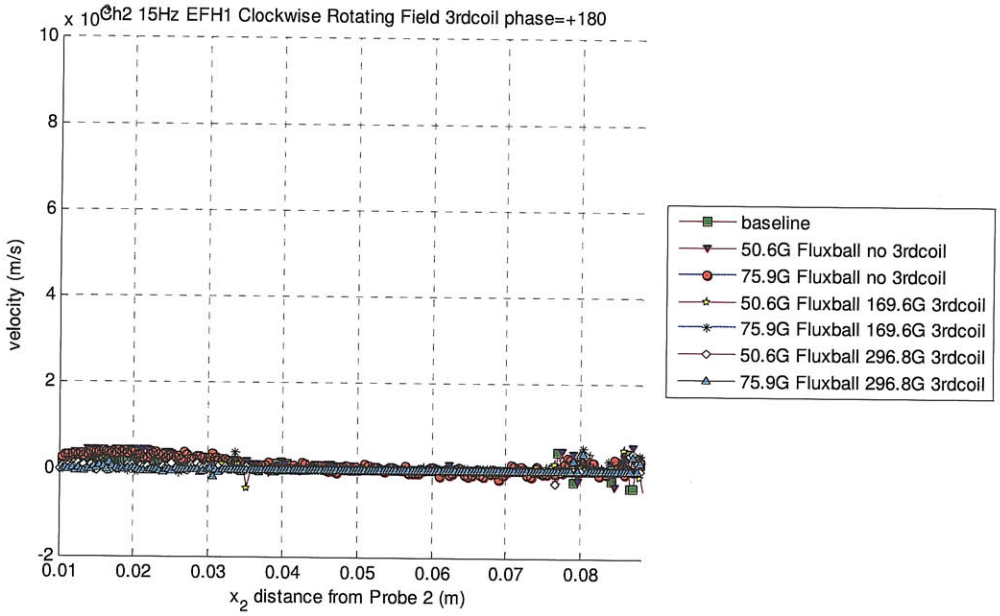
x 10^-3
Ch2 15Hz EFH1 Clockwise Rotating Field 3rdcoil phase=+180
velocity (m/s)
x2 distance from Probe 2 (m)
baseline
50.6G Fluxball no 3rdcoil
75.9G Fluxball no 3rdcoil
50.6G Fluxball 169.6G 3rdcoil
75.9G Fluxball 169.6G 3rdcoil
50.6G Fluxball 296.8G 3rdcoil
75.9G Fluxball 296.8G 3rdcoil

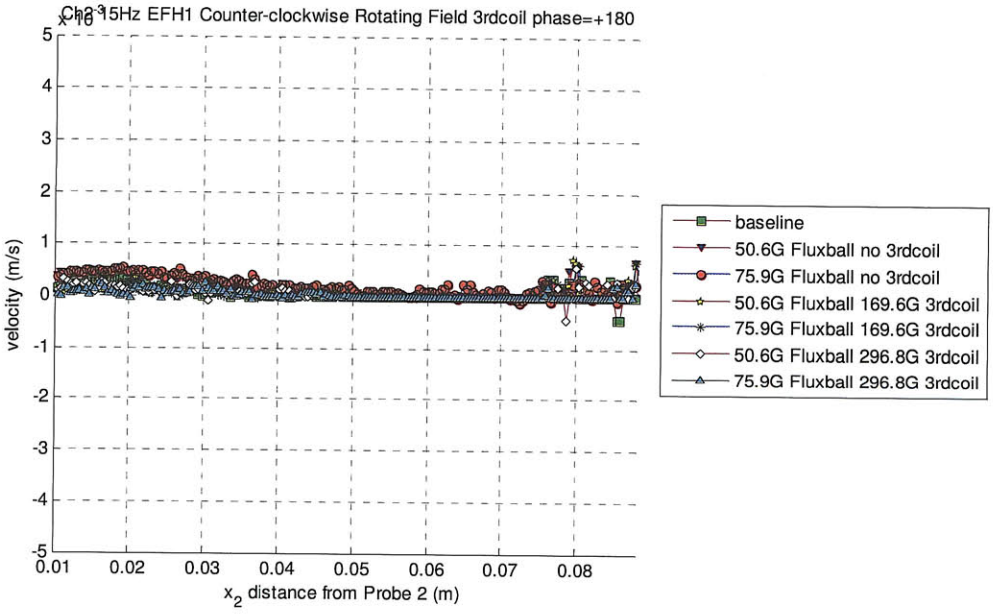
x 10^-3
Ch2 15Hz EFH1 Counter-clockwise Rotating Field 3rdcoil phase=+180
velocity (m/s)
x2 distance from Probe 2 (m)
baseline
50.6G Fluxball no 3rdcoil
75.9G Fluxball no 3rdcoil
50.6G Fluxball 169.6G 3rdcoil
75.9G Fluxball 169.6G 3rdcoil
50.6G Fluxball 296.8G 3rdcoil
75.9G Fluxball 296.8G 3rdcoil

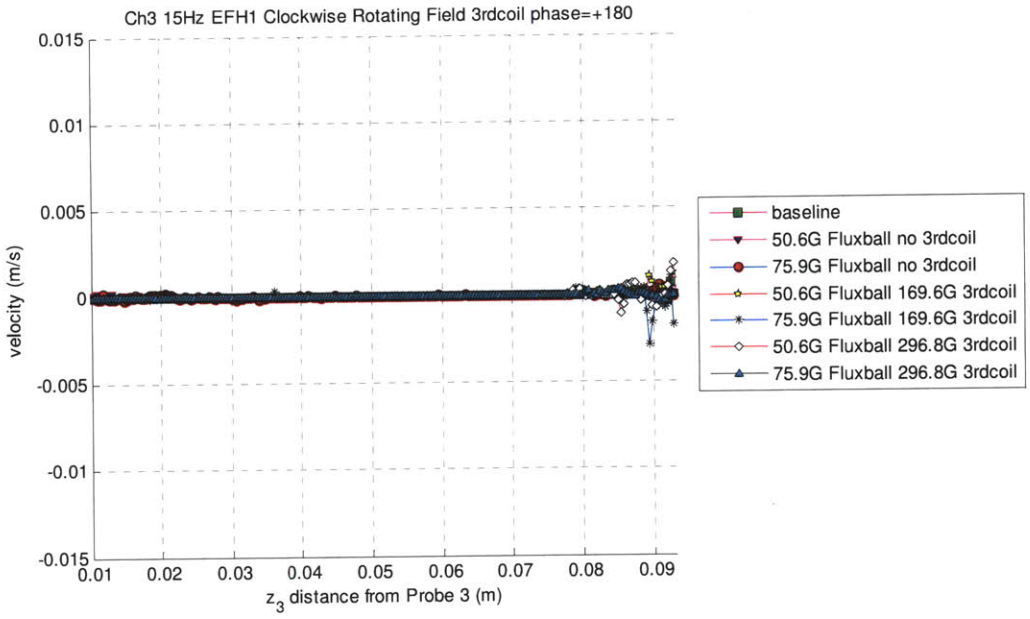
Ch3 15Hz EFH1 Clockwise Rotating Field 3rdcoil phase=+180
velocity (m/s)
0.015
0.01
0.005
0
-0.005
-0.01
-0.015
0.01
0.02
0.03
0.04
0.05
0.06
0.07
0.08
0.09
z_3 distance from Probe 3 (m)
baseline
50.6G Fluxball no 3rdcoil
75.9G Fluxball no 3rdcoil
50.6G Fluxball 169.6G 3rdcoil
75.9G Fluxball 169.6G 3rdcoil
50.6G Fluxball 296.8G 3rdcoil
75.9G Fluxball 296.8G 3rdcoil

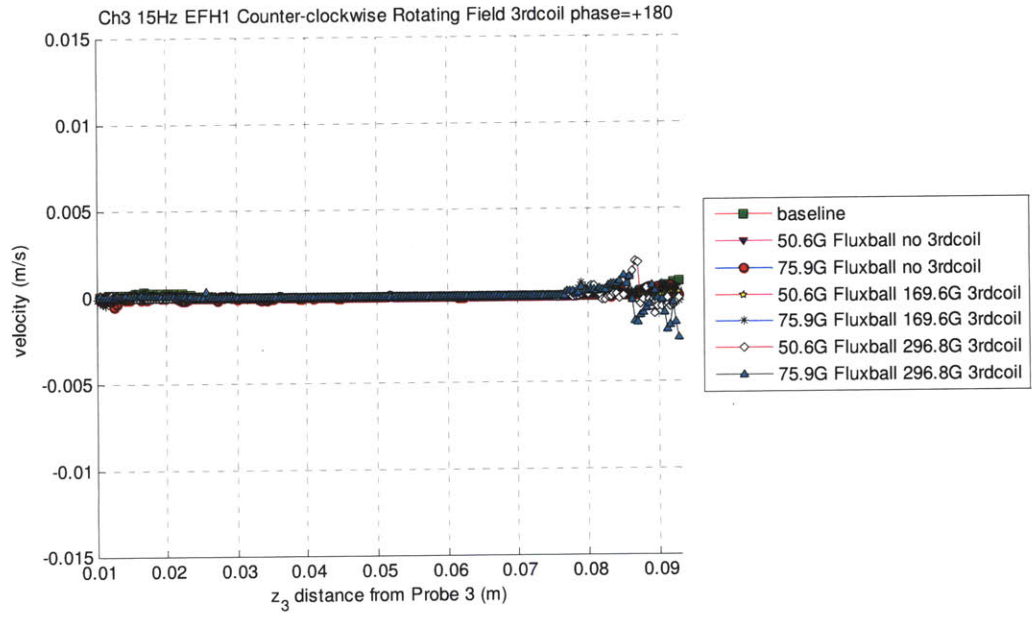
Ch3 15Hz EFH1 Counter-clockwise Rotating Field 3rdcoil phase=+180
velocity (m/s)
0.015
0.01
0.005
0
-0.005
-0.01
-0.015
0.01
0.02
0.03
0.04
0.05
0.06
0.07
0.08
0.09
z_3 distance from Probe 3 (m)
baseline
50.6G Fluxball no 3rdcoil
75.9G Fluxball no 3rdcoil
50.6G Fluxball 169.6G 3rdcoil
75.9G Fluxball 169.6G 3rdcoil
50.6G Fluxball 296.8G 3rdcoil
75.9G Fluxball 296.8G 3rdcoil

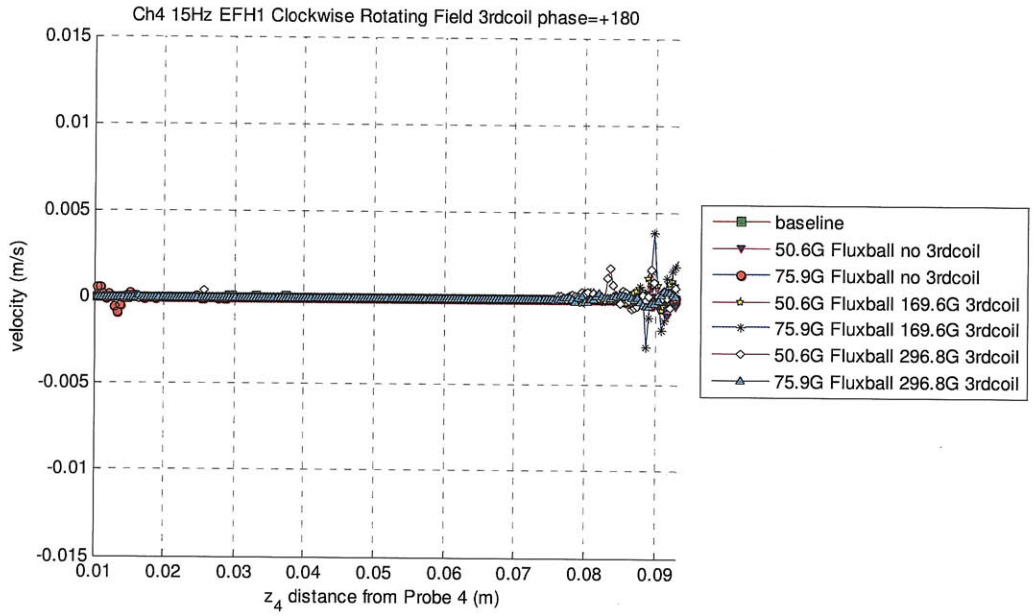
Ch4 15Hz EFH1 Clockwise Rotating Field 3rdcoil phase=+180
velocity (m/s)
0.015
0.01
0.005
0
-0.005
-0.01
-0.015
0.01
0.02
0.03
0.04
0.05
0.06
0.07
0.08
0.09
z4 distance from Probe 4 (m)
baseline
50.6G Fluxball no 3rdcoil
75.9G Fluxball no 3rdcoil
50.6G Fluxball 169.6G 3rdcoil
75.9G Fluxball 169.6G 3rdcoil
50.6G Fluxball 296.8G 3rdcoil
75.9G Fluxball 296.8G 3rdcoil

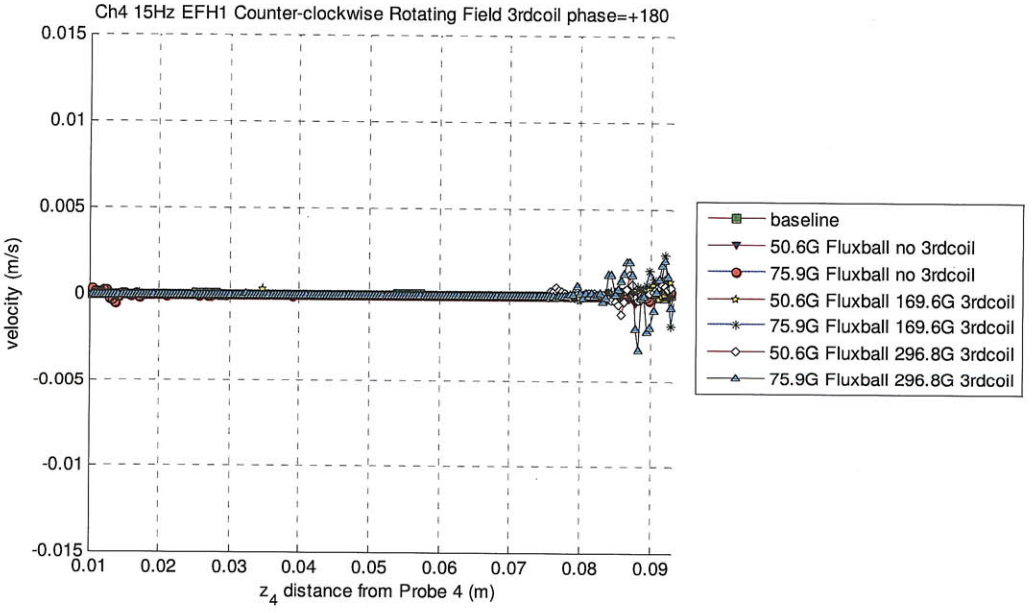
Ch4 15Hz EFH1 Counter-clockwise Rotating Field 3rdcoil phase=+180
velocity (m/s)
0.015
0.01
0.005
0
-0.005
-0.01
-0.015
0.01
0.02
0.03
0.04
0.05
0.06
0.07
0.08
0.09
z4 distance from Probe 4 (m)
baseline
50.6G Fluxball no 3rdcoil
75.9G Fluxball no 3rdcoil
50.6G Fluxball 169.6G 3rdcoil
75.9G Fluxball 169.6G 3rdcoil
50.6G Fluxball 296.8G 3rdcoil
75.9G Fluxball 296.8G 3rdcoil

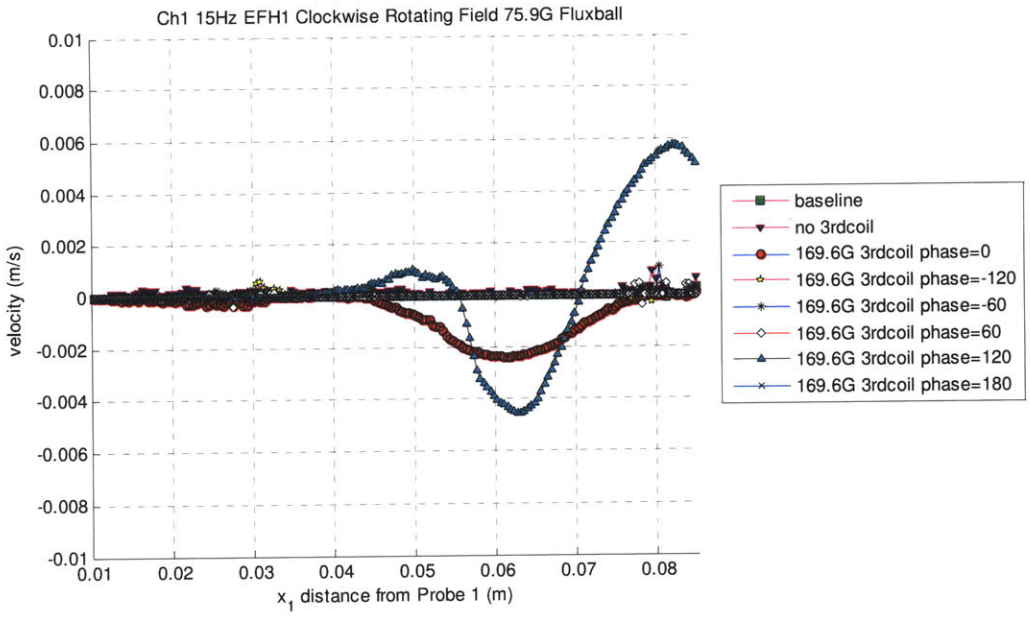
Ch1 15Hz EFH1 Clockwise Rotating Field 75.9G Fluxball
velocity (m/s)
0.01
0.008
0.006
0.004
0.002
0
-0.002
-0.004
-0.006
-0.008
-0.01
0.01
0.02
0.03
0.04
0.05
0.06
0.07
0.08
x1 distance from Probe 1 (m)
baseline
no 3rdcoil
169.6G 3rdcoil phase=0
169.6G 3rdcoil phase=-120
169.6G 3rdcoil phase=-60
169.6G 3rdcoil phase=60
169.6G 3rdcoil phase=120
169.6G 3rdcoil phase=180

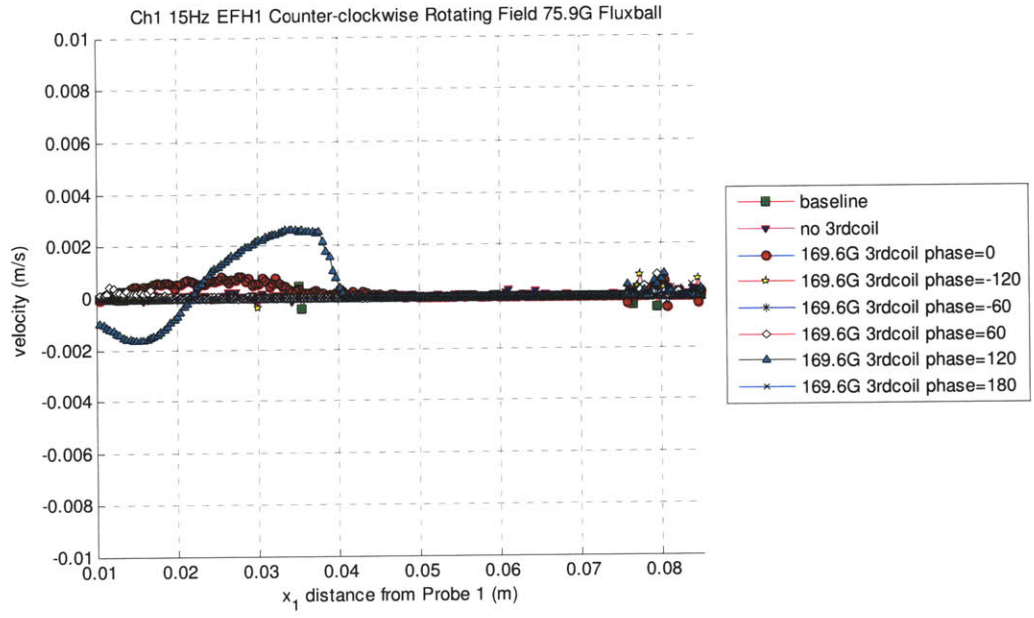
Ch1 15Hz EFH1 Counter-clockwise Rotating Field 75.9G Fluxball
velocity (m/s)
0.01
0.008
0.006
0.004
0.002
0
-0.002
-0.004
-0.006
-0.008
-0.01
0.01
0.02
0.03
0.04
0.05
0.06
0.07
0.08
x1 distance from Probe 1 (m)
baseline
no 3rdcoil
169.6G 3rdcoil phase=0
169.6G 3rdcoil phase=-120
169.6G 3rdcoil phase=-60
169.6G 3rdcoil phase=60
169.6G 3rdcoil phase=120
169.6G 3rdcoil phase=180

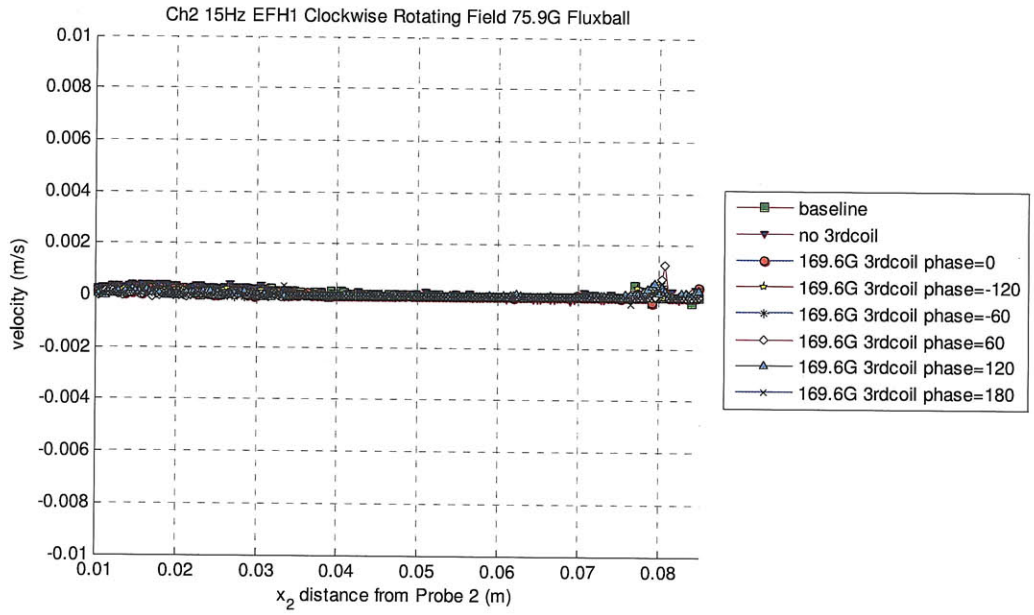
Ch2 15Hz EFH1 Clockwise Rotating Field 75.9G Fluxball
velocity (m/s)
0.01
0.008
0.006
0.004
0.002
0
-0.002
-0.004
-0.006
-0.008
-0.01
0.01
0.02
0.03
0.04
0.05
0.06
0.07
0.08
x2 distance from Probe 2 (m)
baseline
no 3rdcoil
169.6G 3rdcoil phase=0
169.6G 3rdcoil phase=-120
169.6G 3rdcoil phase=-60
169.6G 3rdcoil phase=60
169.6G 3rdcoil phase=120
169.6G 3rdcoil phase=180

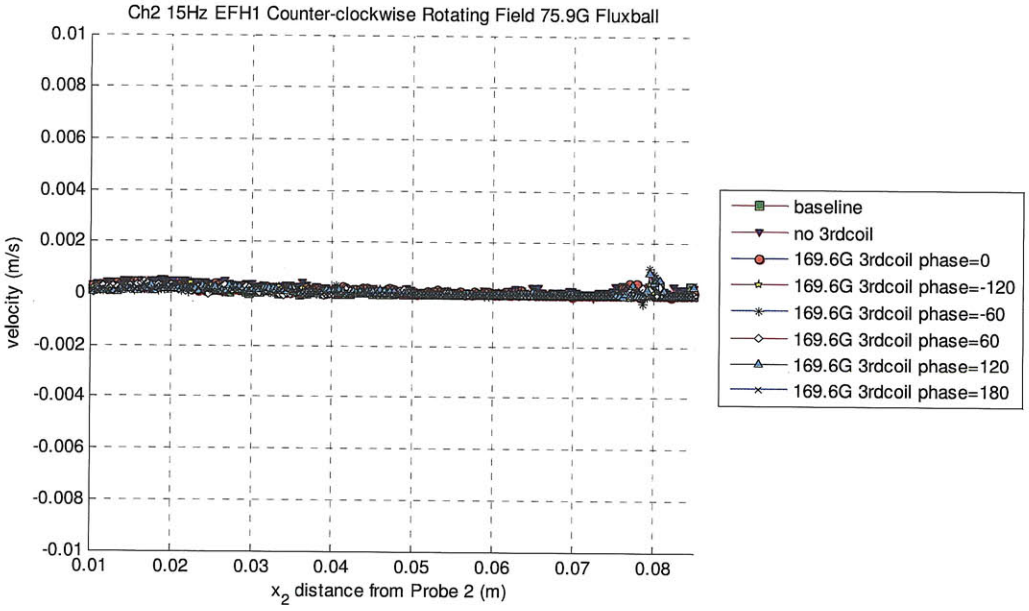
Ch2 15Hz EFH1 Counter-clockwise Rotating Field 75.9G Fluxball
velocity (m/s)
0.01
0.008
0.006
0.004
0.002
0
-0.002
-0.004
-0.006
-0.008
-0.01
0.01
0.02
0.03
0.04
0.05
0.06
0.07
0.08
x2 distance from Probe 2 (m)
baseline
no 3rdcoil
169.6G 3rdcoil phase=0
169.6G 3rdcoil phase=-120
169.6G 3rdcoil phase=-60
169.6G 3rdcoil phase=60
169.6G 3rdcoil phase=120
169.6G 3rdcoil phase=180

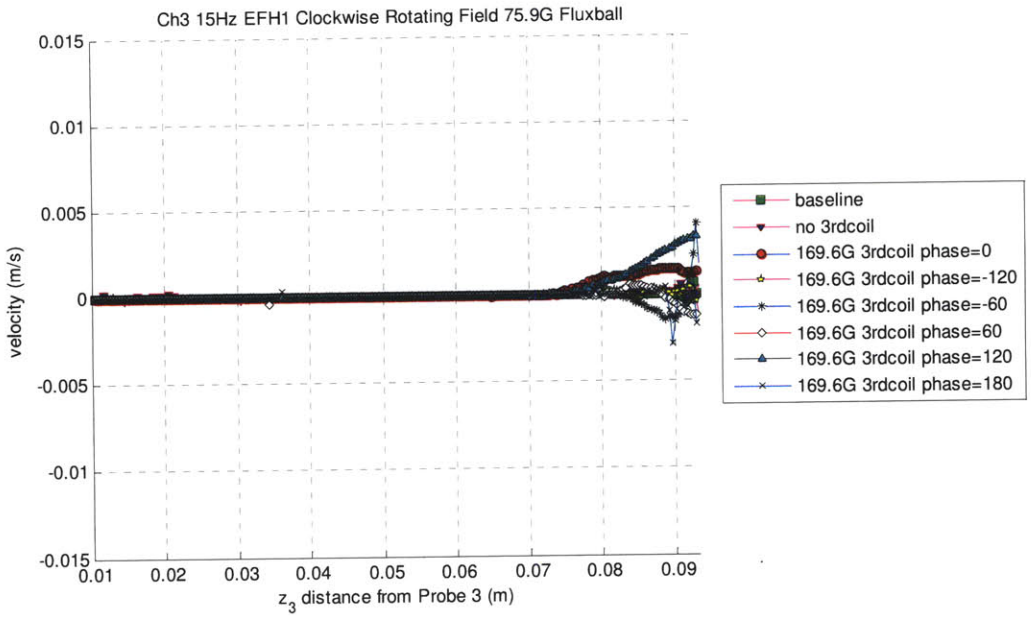
Ch3 15Hz EFH1 Clockwise Rotating Field 75.9G Fluxball
velocity (m/s)
0.015
0.01
0.005
0
-0.005
-0.01
-0.015
0.01
0.02
0.03
0.04
0.05
0.06
0.07
0.08
0.09
z3 distance from Probe 3 (m)
baseline
no 3rdcoil
169.6G 3rdcoil phase=0
169.6G 3rdcoil phase=-120
169.6G 3rdcoil phase=-60
169.6G 3rdcoil phase=60
169.6G 3rdcoil phase=120
169.6G 3rdcoil phase=180

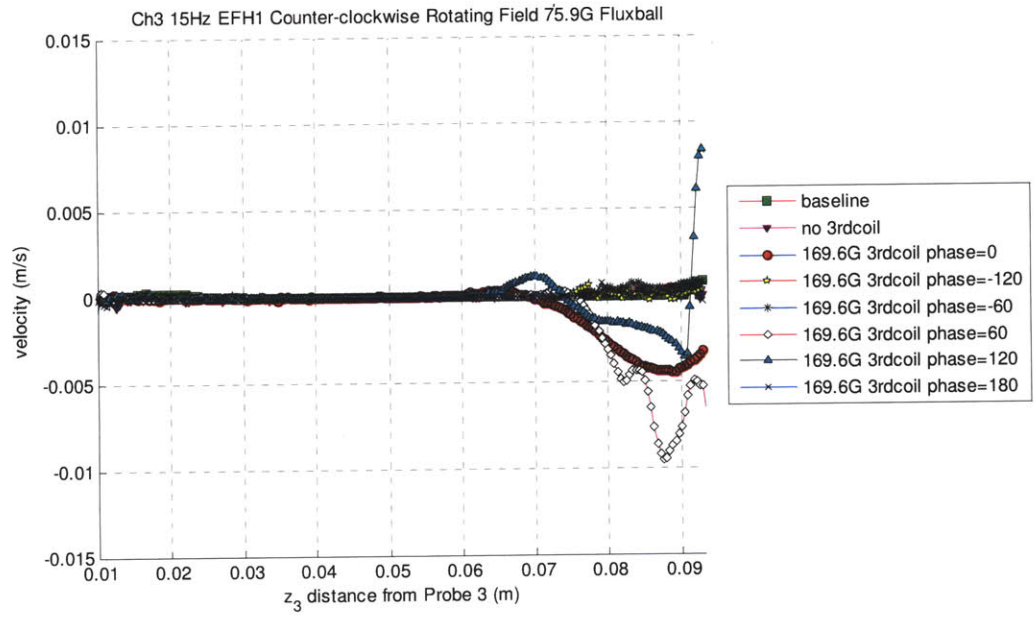
Ch3 15Hz EFH1 Counter-clockwise Rotating Field 75.9G Fluxball
velocity (m/s)
0.015
0.01
0.005
0
-0.005
-0.01
-0.015
0.01
0.02
0.03
0.04
0.05
0.06
0.07
0.08
0.09
z3 distance from Probe 3 (m)
baseline
no 3rdcoil
169.6G 3rdcoil phase=0
169.6G 3rdcoil phase=-120
169.6G 3rdcoil phase=-60
169.6G 3rdcoil phase=60
169.6G 3rdcoil phase=120
169.6G 3rdcoil phase=180

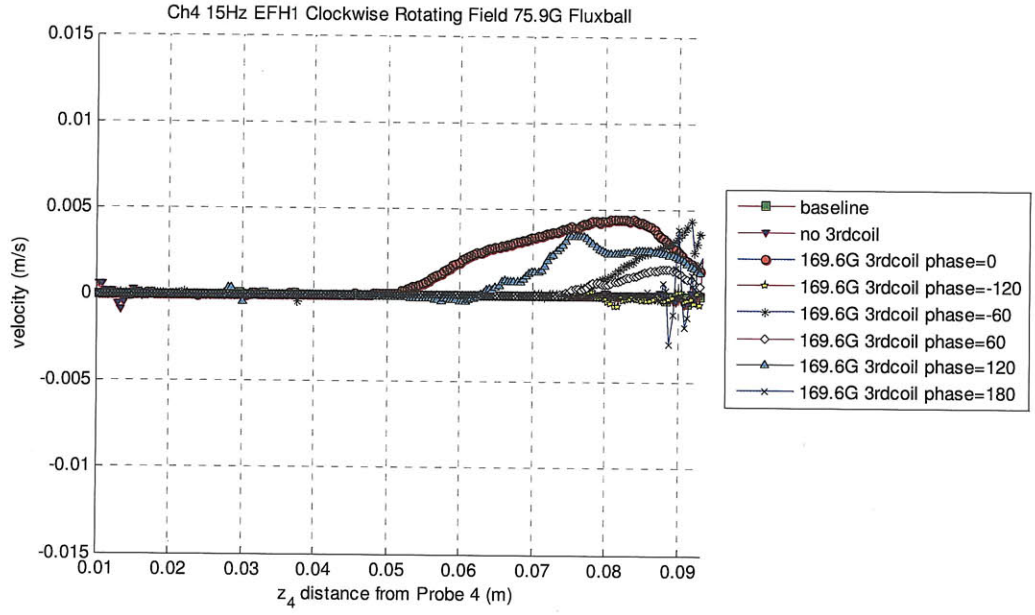
Ch4 15Hz EFH1 Clockwise Rotating Field 75.9G Fluxball
velocity (m/s)
0.015
0.01
0.005
0
-0.005
-0.01
-0.015
0.01
0.02
0.03
0.04
0.05
0.06
0.07
0.08
0.09
z4 distance from Probe 4 (m)
baseline
no 3rdcoil
169.6G 3rdcoil phase=0
169.6G 3rdcoil phase=-120
169.6G 3rdcoil phase=-60
169.6G 3rdcoil phase=60
169.6G 3rdcoil phase=120
169.6G 3rdcoil phase=180

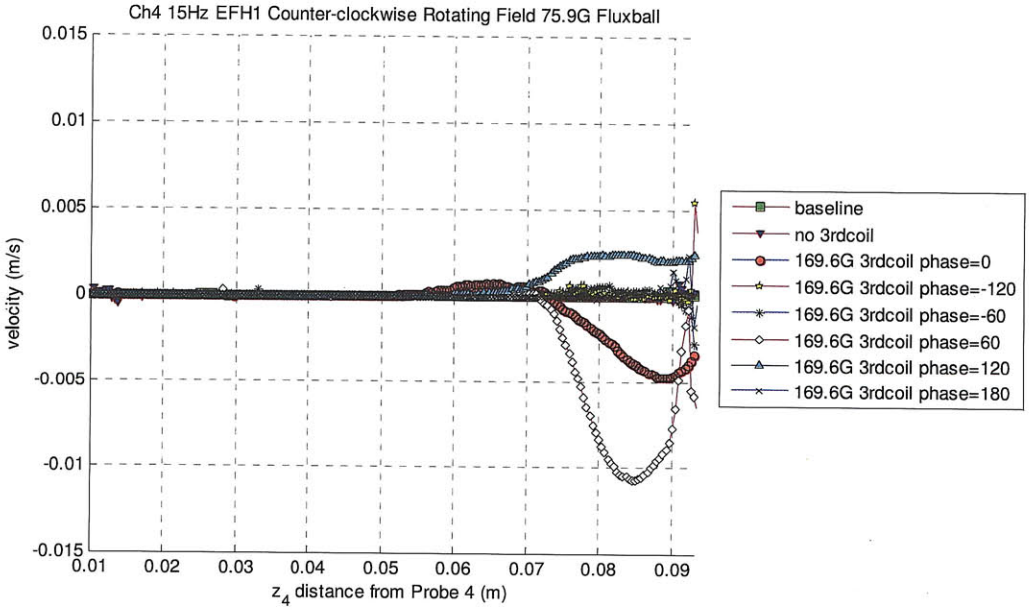
Ch4 15Hz EFH1 Counter-clockwise Rotating Field 75.9G Fluxball
velocity (m/s)
0.015
0.01
0.005
0
-0.005
-0.01
-0.015
0.01
0.02
0.03
0.04
0.05
0.06
0.07
0.08
0.09
z4 distance from Probe 4 (m)
baseline
no 3rdcoil
169.6G 3rdcoil phase=0
169.6G 3rdcoil phase=-120
169.6G 3rdcoil phase=-60
169.6G 3rdcoil phase=60
169.6G 3rdcoil phase=120
169.6G 3rdcoil phase=180

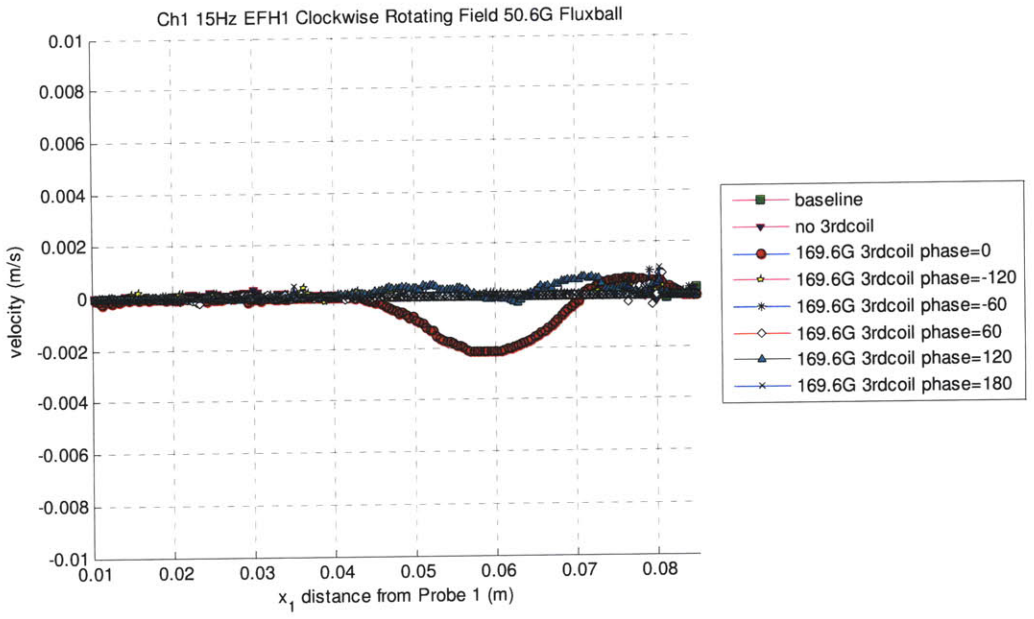
Ch1 15Hz EFH1 Clockwise Rotating Field 50.6G Fluxball
velocity (m/s)
x1 distance from Probe 1 (m)
baseline
no 3rdcoil
169.6G 3rdcoil phase=0
169.6G 3rdcoil phase=-120
169.6G 3rdcoil phase=-60
169.6G 3rdcoil phase=60
169.6G 3rdcoil phase=120
169.6G 3rdcoil phase=180

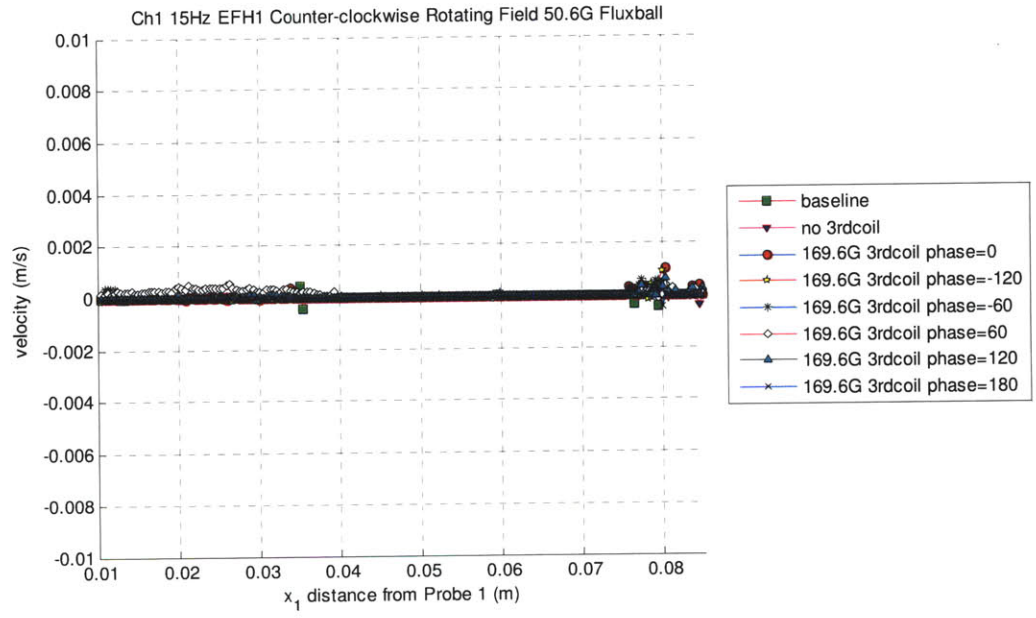
Ch1 15Hz EFH1 Counter-clockwise Rotating Field 50.6G Fluxball
velocity (m/s)
x1 distance from Probe 1 (m)
baseline
no 3rdcoil
169.6G 3rdcoil phase=0
169.6G 3rdcoil phase=-120
169.6G 3rdcoil phase=-60
169.6G 3rdcoil phase=60
169.6G 3rdcoil phase=120
169.6G 3rdcoil phase=180

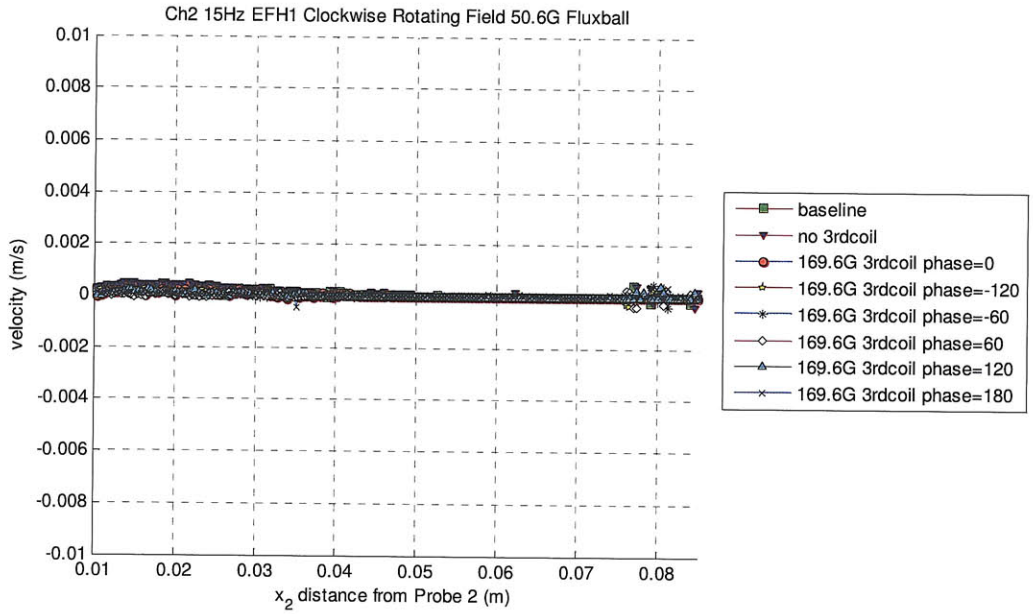
Ch2 15Hz EFH1 Clockwise Rotating Field 50.6G Fluxball
velocity (m/s)
0.01
0.008
0.006
0.004
0.002
0
-0.002
-0.004
-0.006
-0.008
-0.01
0.01
0.02
0.03
0.04
0.05
0.06
0.07
0.08
x2 distance from Probe 2 (m)
baseline
no 3rdcoil
169.6G 3rdcoil phase=0
169.6G 3rdcoil phase=-120
169.6G 3rdcoil phase=-60
169.6G 3rdcoil phase=60
169.6G 3rdcoil phase=120
169.6G 3rdcoil phase=180

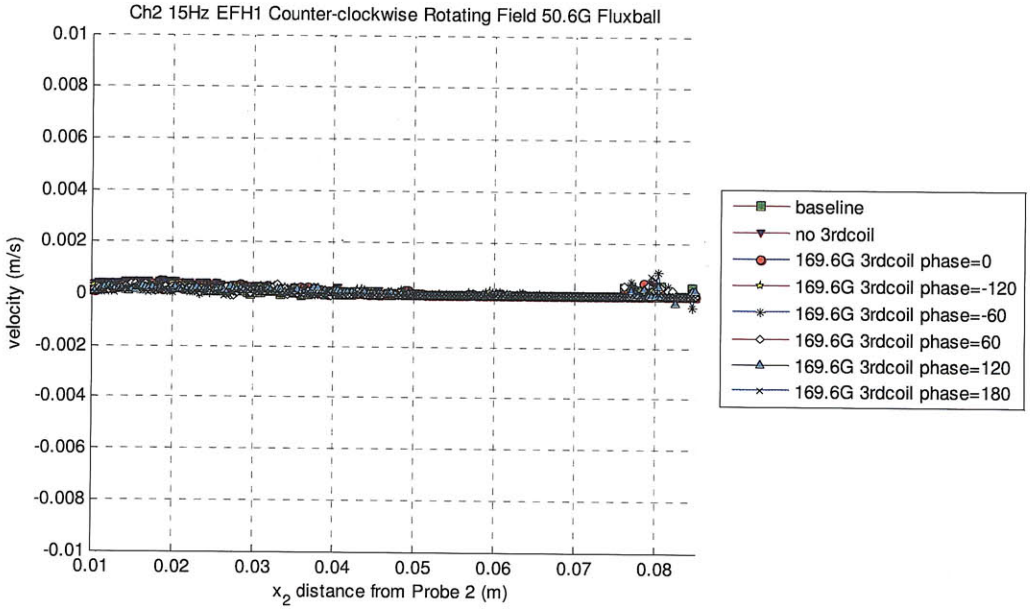
Ch2 15Hz EFH1 Counter-clockwise Rotating Field 50.6G Fluxball
velocity (m/s)
0.01
0.008
0.006
0.004
0.002
0
-0.002
-0.004
-0.006
-0.008
-0.01
0.01
0.02
0.03
0.04
0.05
0.06
0.07
0.08
x2 distance from Probe 2 (m)
baseline
no 3rdcoil
169.6G 3rdcoil phase=0
169.6G 3rdcoil phase=-120
169.6G 3rdcoil phase=-60
169.6G 3rdcoil phase=60
169.6G 3rdcoil phase=120
169.6G 3rdcoil phase=180

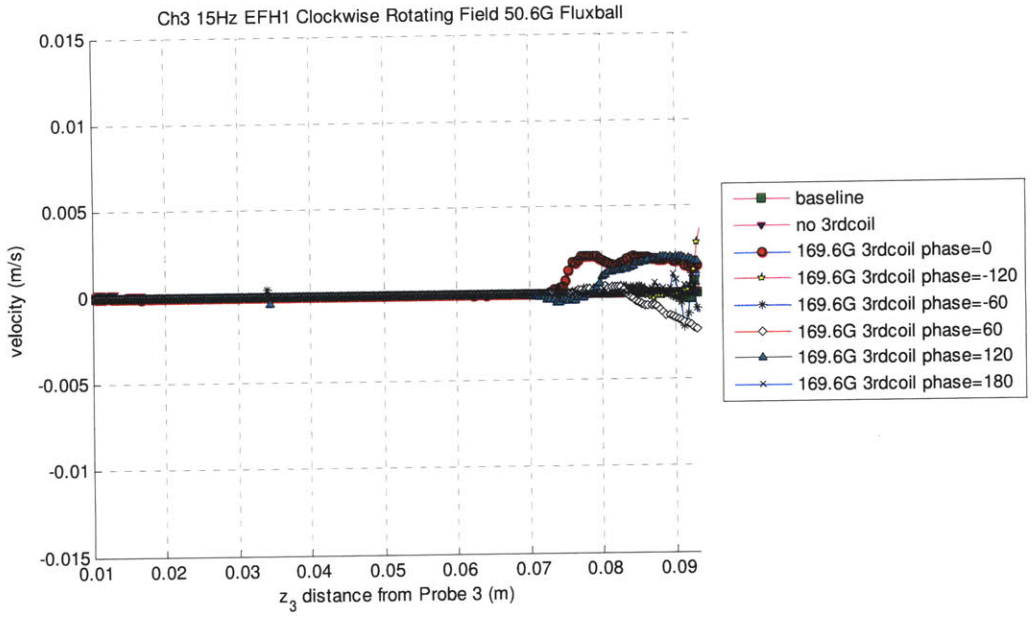
Ch3 15Hz EFH1 Clockwise Rotating Field 50.6G Fluxball
velocity (m/s)
0.015
0.01
0.005
0
-0.005
-0.01
-0.015
0.01
0.02
0.03
0.04
0.05
0.06
0.07
0.08
0.09
z3 distance from Probe 3 (m)
baseline
no 3rdcoil
169.6G 3rdcoil phase=0
169.6G 3rdcoil phase=-120
169.6G 3rdcoil phase=-60
169.6G 3rdcoil phase=60
169.6G 3rdcoil phase=120
169.6G 3rdcoil phase=180

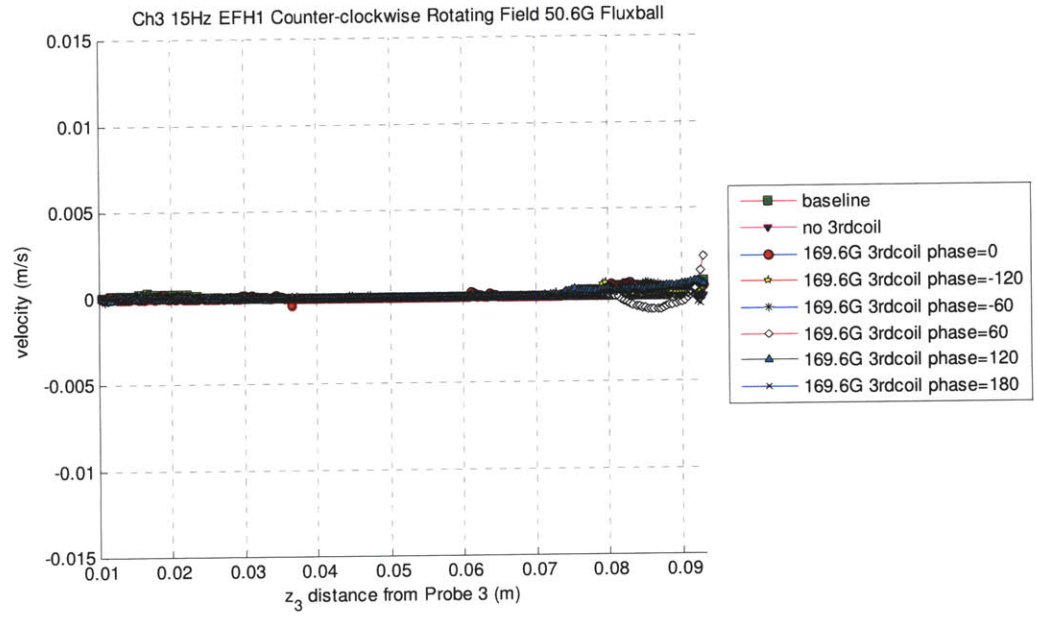
Ch3 15Hz EFH1 Counter-clockwise Rotating Field 50.6G Fluxball
velocity (m/s)
0.015
0.01
0.005
0
-0.005
-0.01
-0.015
0.01
0.02
0.03
0.04
0.05
0.06
0.07
0.08
0.09
z3 distance from Probe 3 (m)
baseline
no 3rdcoil
169.6G 3rdcoil phase=0
169.6G 3rdcoil phase=-120
169.6G 3rdcoil phase=-60
169.6G 3rdcoil phase=60
169.6G 3rdcoil phase=120
169.6G 3rdcoil phase=180

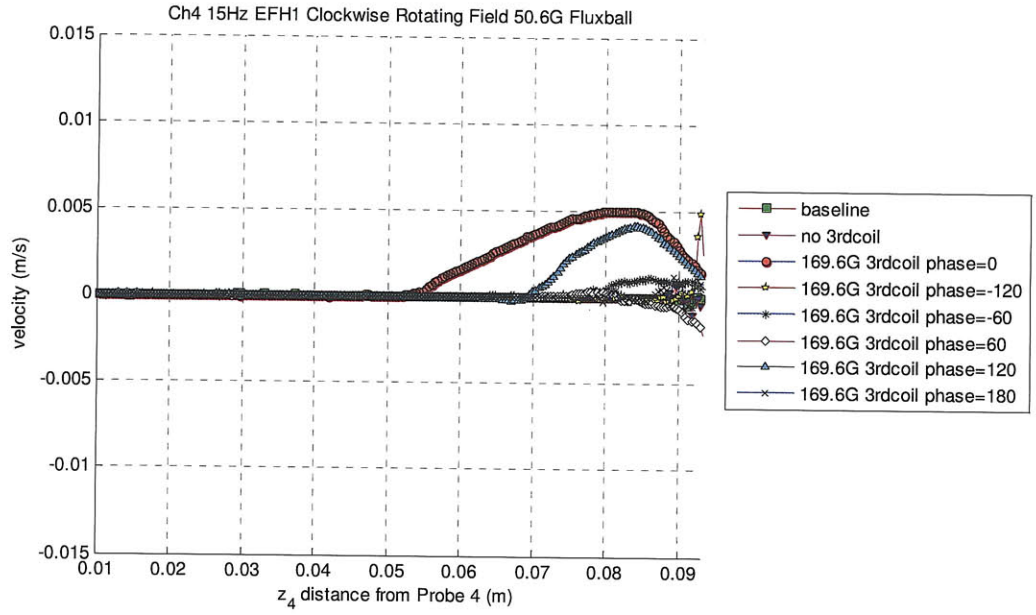
Ch4 15Hz EFH1 Clockwise Rotating Field 50.6G Fluxball
velocity (m/s)
0.015
0.01
0.005
0
-0.005
-0.01
-0.015
0.01
0.02
0.03
0.04
0.05
0.06
0.07
0.08
0.09
z4 distance from Probe 4 (m)
baseline
no 3rdcoil
169.6G 3rdcoil phase=0
169.6G 3rdcoil phase=-120
169.6G 3rdcoil phase=-60
169.6G 3rdcoil phase=60
169.6G 3rdcoil phase=120
169.6G 3rdcoil phase=180

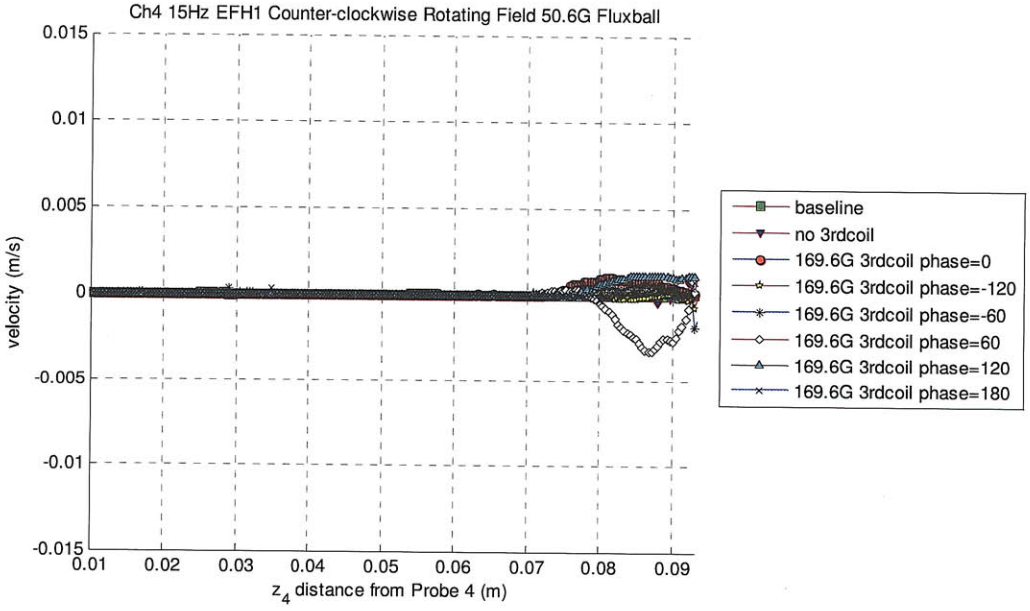
Ch4 15Hz EFH1 Counter-clockwise Rotating Field 50.6G Fluxball
velocity (m/s)
0.015
0.01
0.005
0
-0.005
-0.01
-0.015
0.01
0.02
0.03
0.04
0.05
0.06
0.07
0.08
0.09
z4 distance from Probe 4 (m)
baseline
no 3rdcoil
169.6G 3rdcoil phase=0
169.6G 3rdcoil phase=-120
169.6G 3rdcoil phase=-60
169.6G 3rdcoil phase=60
169.6G 3rdcoil phase=120
169.6G 3rdcoil phase=180

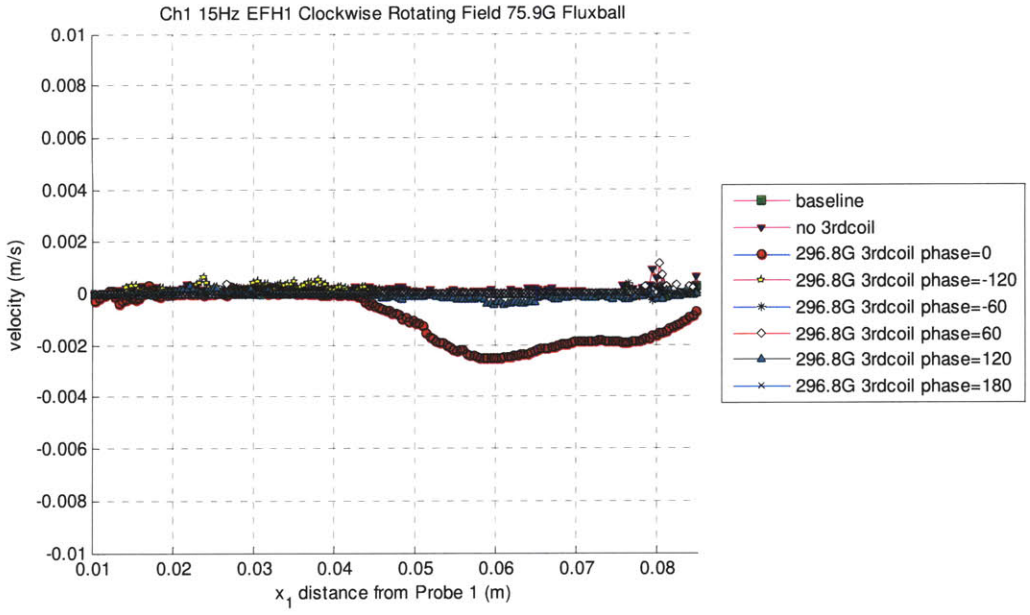
Ch1 15Hz EFH1 Clockwise Rotating Field 75.9G Fluxball
velocity (m/s)
x1 distance from Probe 1 (m)
baseline
no 3rdcoil
296.8G 3rdcoil phase=0
296.8G 3rdcoil phase=-120
296.8G 3rdcoil phase=-60
296.8G 3rdcoil phase=60
296.8G 3rdcoil phase=120
296.8G 3rdcoil phase=180

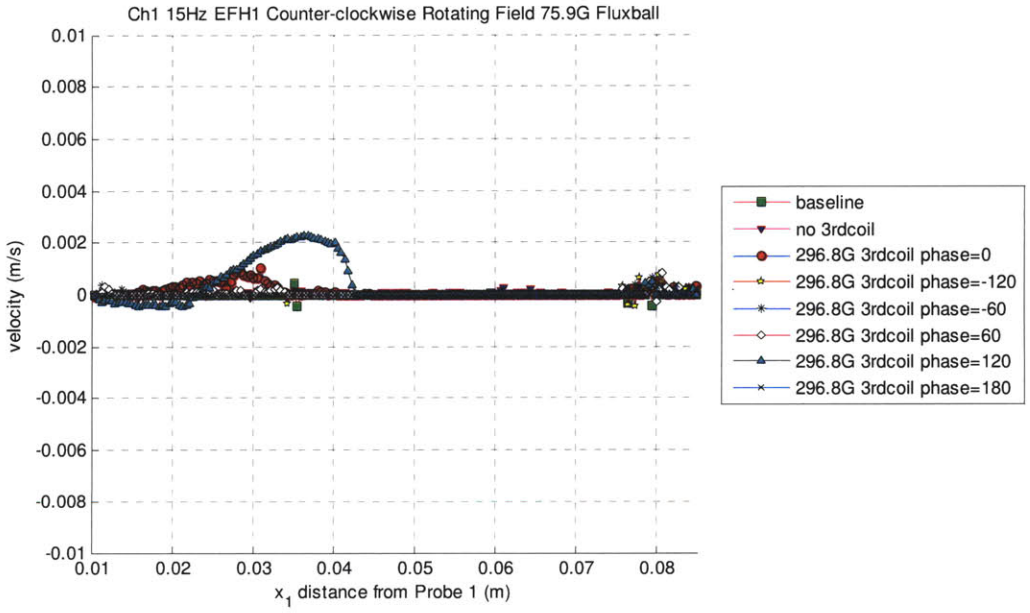
Ch1 15Hz EFH1 Counter-clockwise Rotating Field 75.9G Fluxball
velocity (m/s)
x1 distance from Probe 1 (m)
baseline
no 3rdcoil
296.8G 3rdcoil phase=0
296.8G 3rdcoil phase=-120
296.8G 3rdcoil phase=-60
296.8G 3rdcoil phase=60
296.8G 3rdcoil phase=120
296.8G 3rdcoil phase=180

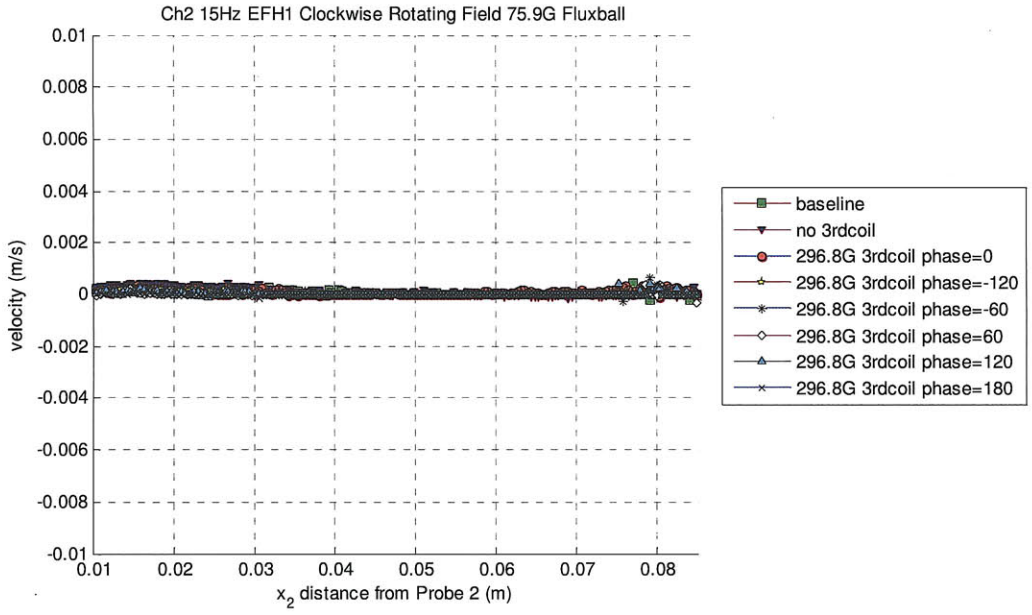
Ch2 15Hz EFH1 Clockwise Rotating Field 75.9G Fluxball
velocity (m/s)
0.01
0.008
0.006
0.004
0.002
0
-0.002
-0.004
-0.006
-0.008
-0.01
0.01
0.02
0.03
0.04
0.05
0.06
0.07
0.08
x2 distance from Probe 2 (m)
baseline
no 3rdcoil
296.8G 3rdcoil phase=0
296.8G 3rdcoil phase=-120
296.8G 3rdcoil phase=-60
296.8G 3rdcoil phase=60
296.8G 3rdcoil phase=120
296.8G 3rdcoil phase=180

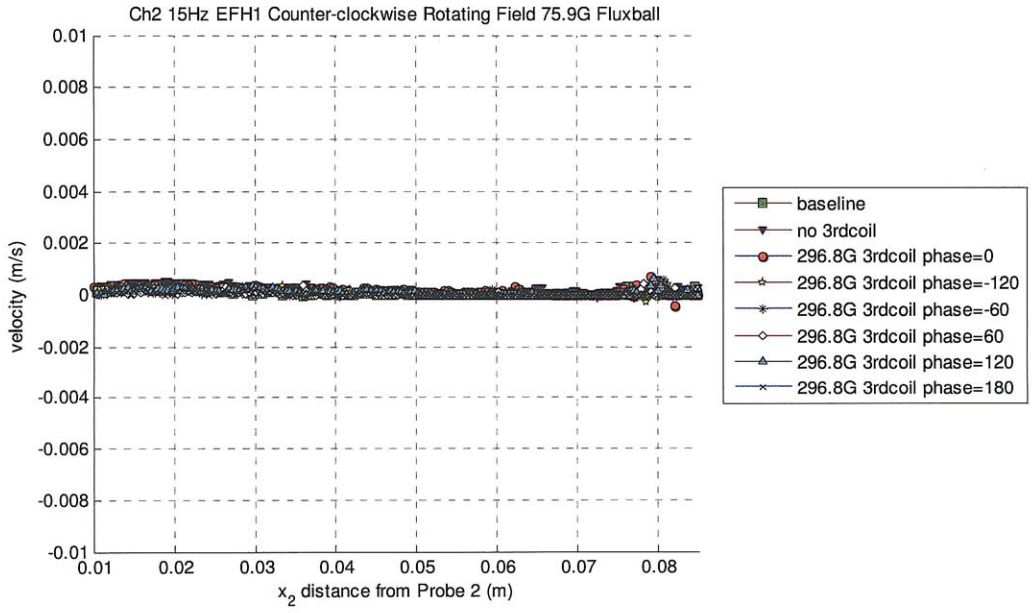
Ch2 15Hz EFH1 Counter-clockwise Rotating Field 75.9G Fluxball
velocity (m/s)
0.01
0.008
0.006
0.004
0.002
0
-0.002
-0.004
-0.006
-0.008
-0.01
0.01
0.02
0.03
0.04
0.05
0.06
0.07
0.08
x2 distance from Probe 2 (m)
baseline
no 3rdcoil
296.8G 3rdcoil phase=0
296.8G 3rdcoil phase=-120
296.8G 3rdcoil phase=-60
296.8G 3rdcoil phase=60
296.8G 3rdcoil phase=120
296.8G 3rdcoil phase=180

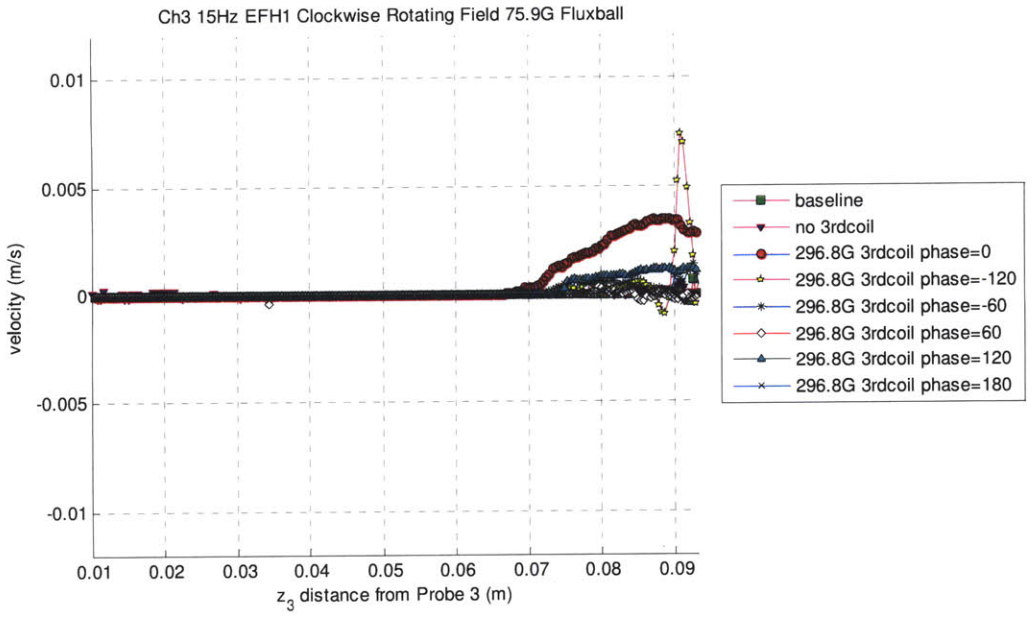
Ch3 15Hz EFH1 Clockwise Rotating Field 75.9G Fluxball
velocity (m/s)
0.01
0.005
0
-0.005
-0.01
0.01 0.02 0.03 0.04 0.05 0.06 0.07 0.08 0.09
z3 distance from Probe 3 (m)
baseline
no 3rdcoil
296.8G 3rdcoil phase=0
296.8G 3rdcoil phase=-120
296.8G 3rdcoil phase=-60
296.8G 3rdcoil phase=60
296.8G 3rdcoil phase=120
296.8G 3rdcoil phase=180

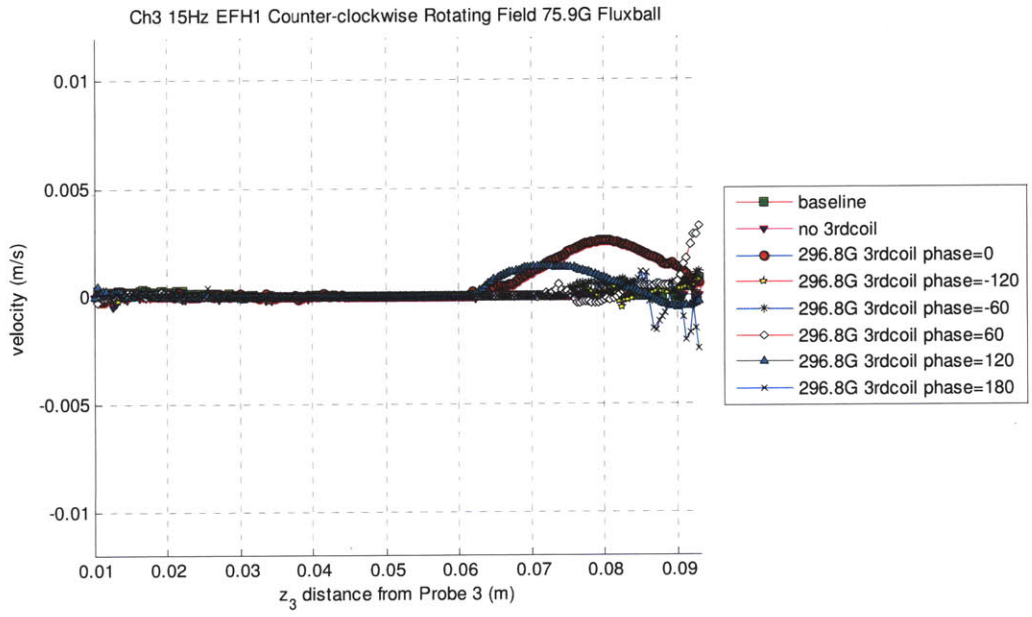
Ch3 15Hz EFH1 Counter-clockwise Rotating Field 75.9G Fluxball
velocity (m/s)
0.01
0.005
0
-0.005
-0.01
0.01 0.02 0.03 0.04 0.05 0.06 0.07 0.08 0.09
z3 distance from Probe 3 (m)
baseline
no 3rdcoil
296.8G 3rdcoil phase=0
296.8G 3rdcoil phase=-120
296.8G 3rdcoil phase=-60
296.8G 3rdcoil phase=60
296.8G 3rdcoil phase=120
296.8G 3rdcoil phase=180

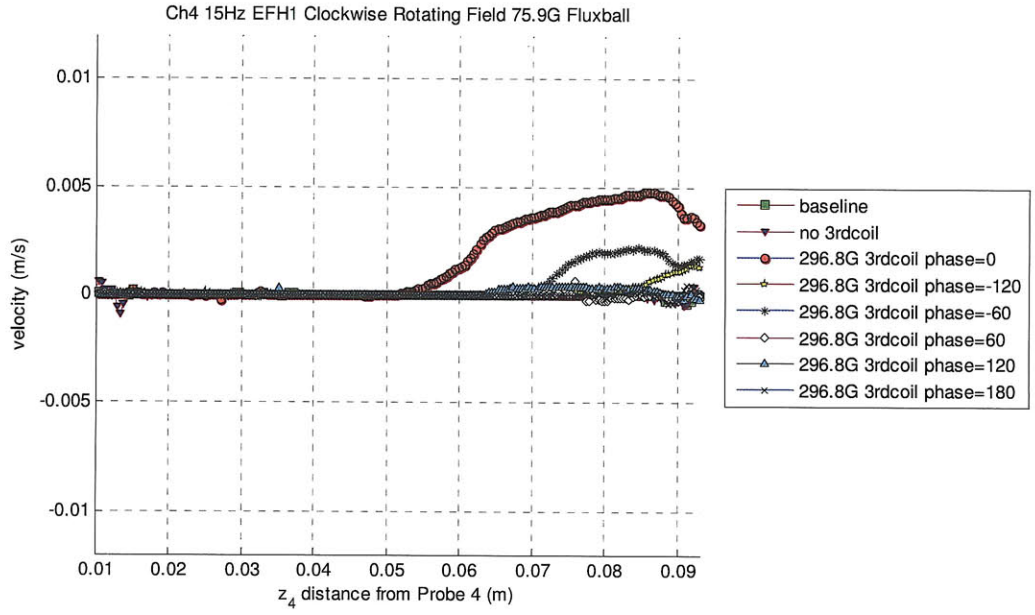
Ch4 15Hz EFH1 Clockwise Rotating Field 75.9G Fluxball
velocity (m/s)
0.01
0.005
0
-0.005
-0.01
0.01
0.02
0.03
0.04
0.05
0.06
0.07
0.08
0.09
z4 distance from Probe 4 (m)
baseline
no 3rdcoil
296.8G 3rdcoil phase=0
296.8G 3rdcoil phase=-120
296.8G 3rdcoil phase=-60
296.8G 3rdcoil phase=60
296.8G 3rdcoil phase=120
296.8G 3rdcoil phase=180

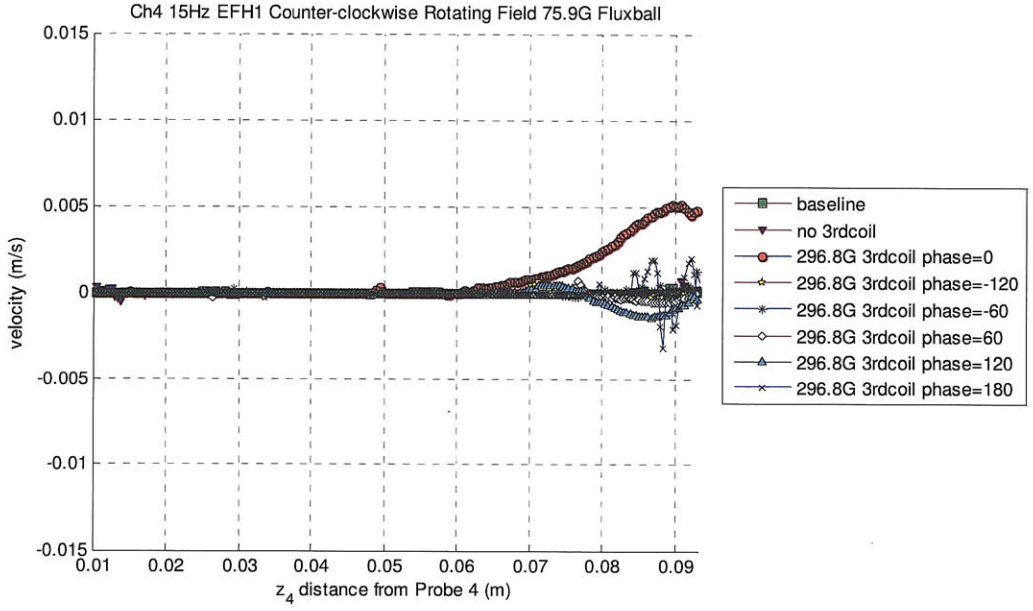
Ch4 15Hz EFH1 Counter-clockwise Rotating Field 75.9G Fluxball
velocity (m/s)
0.015
0.01
0.005
0
-0.005
-0.01
-0.015
0.01
0.02
0.03
0.04
0.05
0.06
0.07
0.08
0.09
z4 distance from Probe 4 (m)
baseline
no 3rdcoil
296.8G 3rdcoil phase=0
296.8G 3rdcoil phase=-120
296.8G 3rdcoil phase=-60
296.8G 3rdcoil phase=60
296.8G 3rdcoil phase=120
296.8G 3rdcoil phase=180

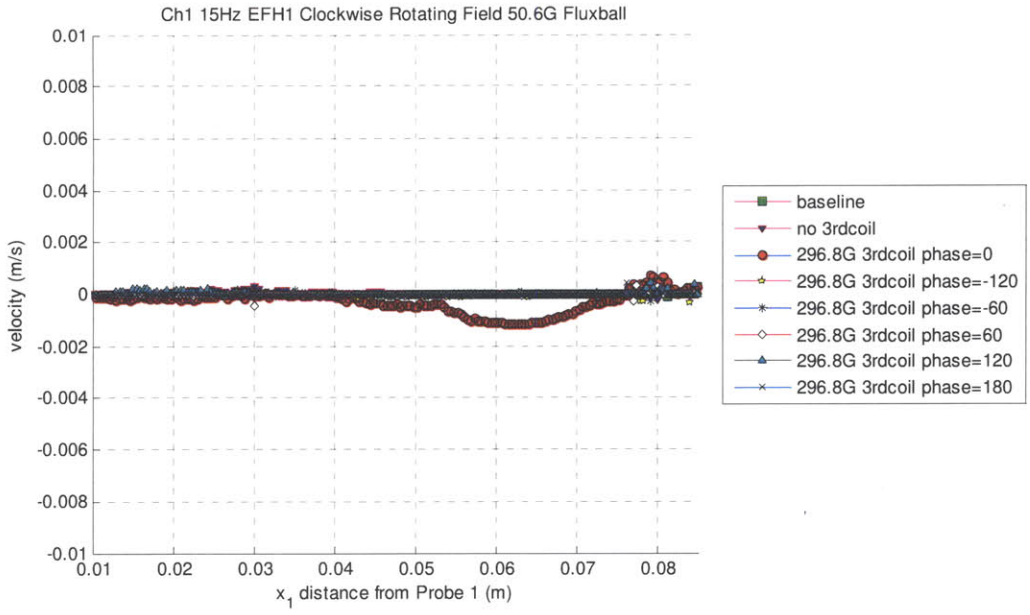
Ch1 15Hz EFH1 Clockwise Rotating Field 50.6G Fluxball
velocity (m/s)
0.01
0.008
0.006
0.004
0.002
0
-0.002
-0.004
-0.006
-0.008
-0.01
0.01
0.02
0.03
0.04
0.05
0.06
0.07
0.08
x1 distance from Probe 1 (m)
baseline
no 3rdcoil
296.8G 3rdcoil phase=0
296.8G 3rdcoil phase=-120
296.8G 3rdcoil phase=-60
296.8G 3rdcoil phase=60
296.8G 3rdcoil phase=120
296.8G 3rdcoil phase=180

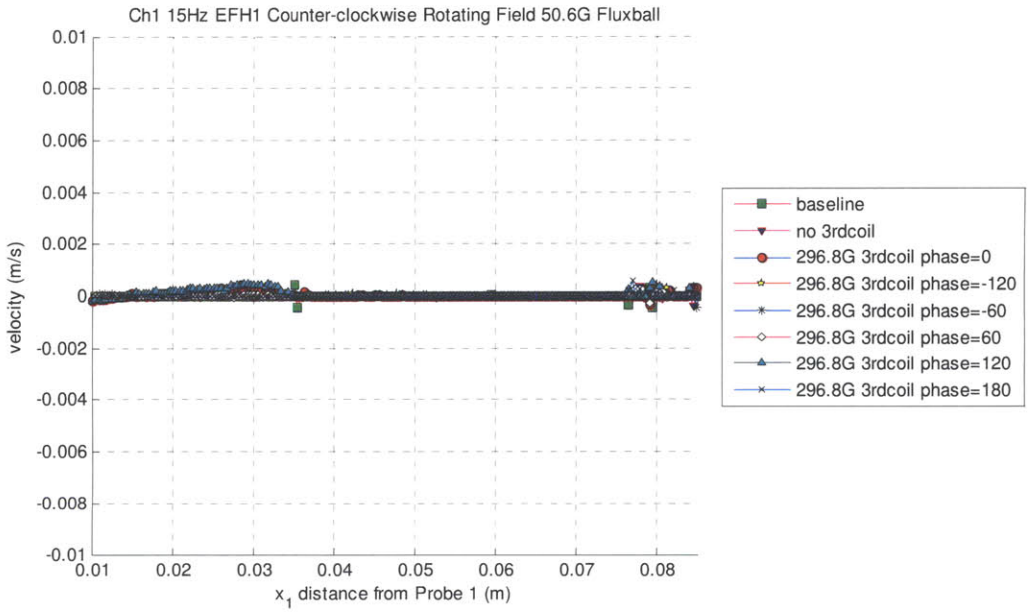
Ch1 15Hz EFH1 Counter-clockwise Rotating Field 50.6G Fluxball
velocity (m/s)
0.01
0.008
0.006
0.004
0.002
0
-0.002
-0.004
-0.006
-0.008
-0.01
0.01
0.02
0.03
0.04
0.05
0.06
0.07
0.08
x1 distance from Probe 1 (m)
baseline
no 3rdcoil
296.8G 3rdcoil phase=0
296.8G 3rdcoil phase=-120
296.8G 3rdcoil phase=-60
296.8G 3rdcoil phase=60
296.8G 3rdcoil phase=120
296.8G 3rdcoil phase=180

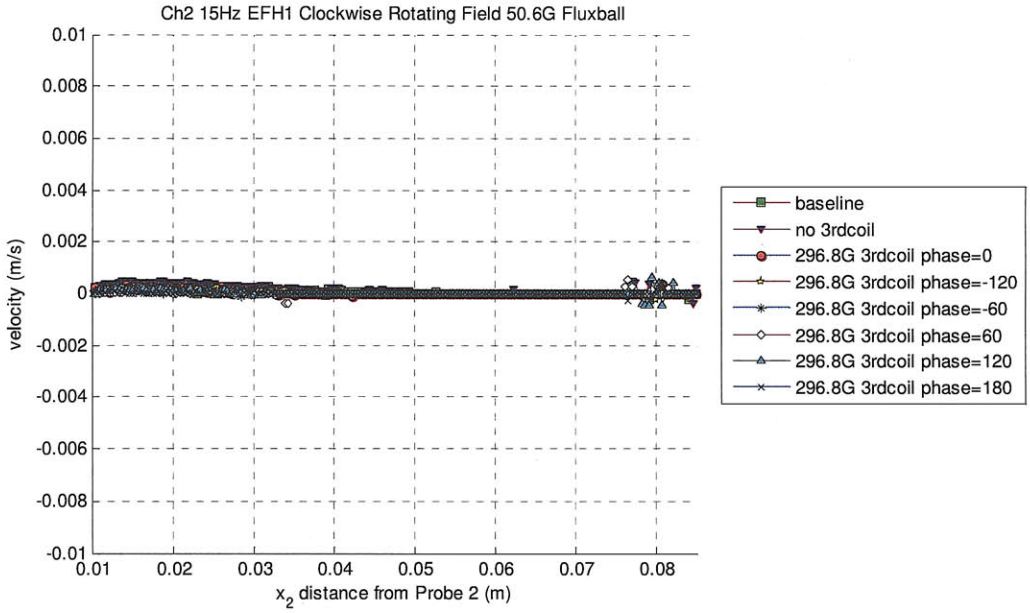
Ch2 15Hz EFH1 Clockwise Rotating Field 50.6G Fluxball
velocity (m/s)
0.01
0.008
0.006
0.004
0.002
0
-0.002
-0.004
-0.006
-0.008
-0.01
0.01
0.02
0.03
0.04
0.05
0.06
0.07
0.08
x2 distance from Probe 2 (m)
baseline
no 3rdcoil
296.8G 3rdcoil phase=0
296.8G 3rdcoil phase=-120
296.8G 3rdcoil phase=-60
296.8G 3rdcoil phase=60
296.8G 3rdcoil phase=120
296.8G 3rdcoil phase=180

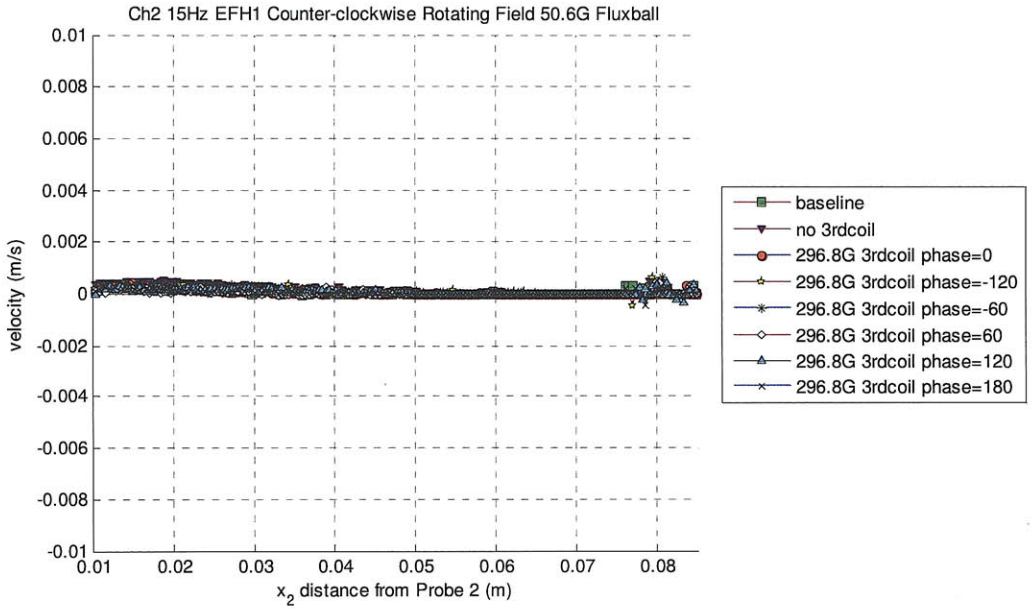
Ch2 15Hz EFH1 Counter-clockwise Rotating Field 50.6G Fluxball
velocity (m/s)
0.01
0.008
0.006
0.004
0.002
0
-0.002
-0.004
-0.006
-0.008
-0.01
0.01
0.02
0.03
0.04
0.05
0.06
0.07
0.08
x2 distance from Probe 2 (m)
baseline
no 3rdcoil
296.8G 3rdcoil phase=0
296.8G 3rdcoil phase=-120
296.8G 3rdcoil phase=-60
296.8G 3rdcoil phase=60
296.8G 3rdcoil phase=120
296.8G 3rdcoil phase=180

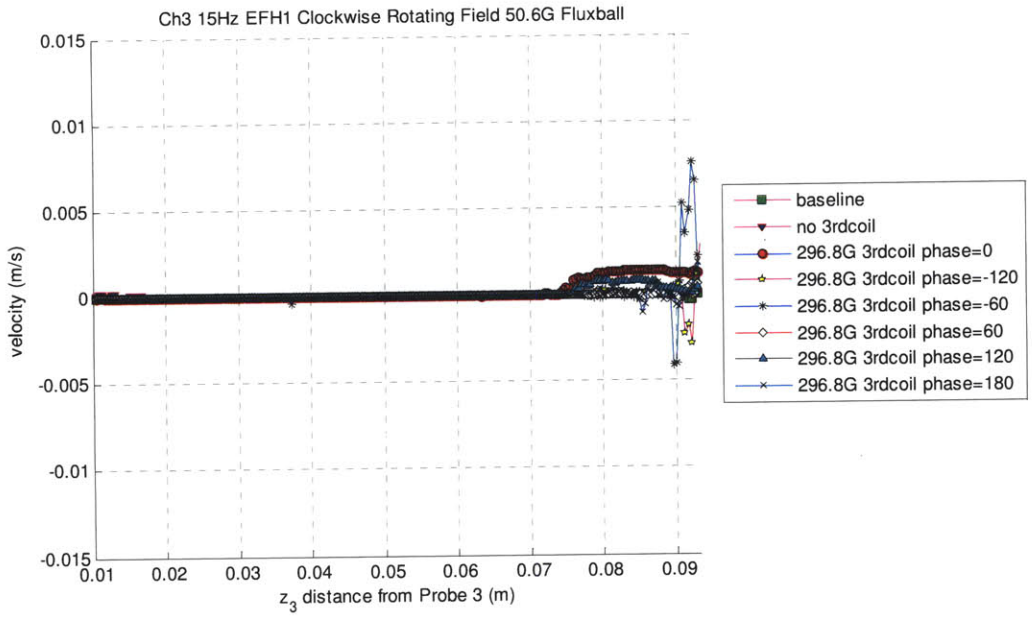
Ch3 15Hz EFH1 Clockwise Rotating Field 50.6G Fluxball
velocity (m/s)
0.015
0.01
0.005
0
-0.005
-0.01
-0.015
0.01
0.02
0.03
0.04
0.05
0.06
0.07
0.08
0.09
z_3 distance from Probe 3 (m)
baseline
no 3rdcoil
296.8G 3rdcoil phase=0
296.8G 3rdcoil phase=-120
296.8G 3rdcoil phase=-60
296.8G 3rdcoil phase=60
296.8G 3rdcoil phase=120
296.8G 3rdcoil phase=180

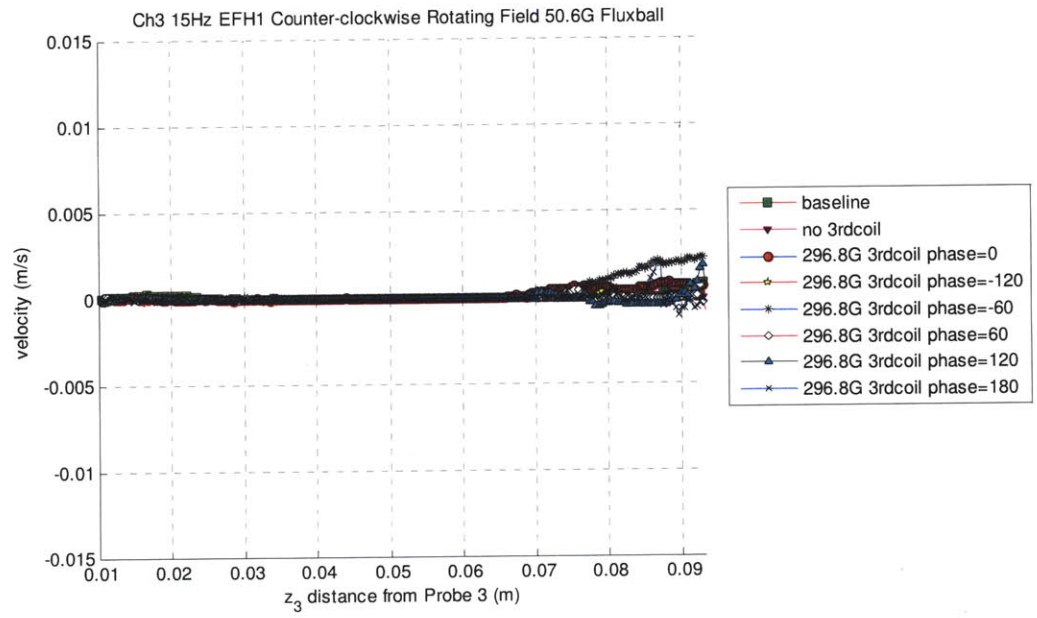
Ch3 15Hz EFH1 Counter-clockwise Rotating Field 50.6G Fluxball
velocity (m/s)
0.015
0.01
0.005
0
-0.005
-0.01
-0.015
0.01
0.02
0.03
0.04
0.05
0.06
0.07
0.08
0.09
z_3 distance from Probe 3 (m)
baseline
no 3rdcoil
296.8G 3rdcoil phase=0
296.8G 3rdcoil phase=-120
296.8G 3rdcoil phase=-60
296.8G 3rdcoil phase=60
296.8G 3rdcoil phase=120
296.8G 3rdcoil phase=180

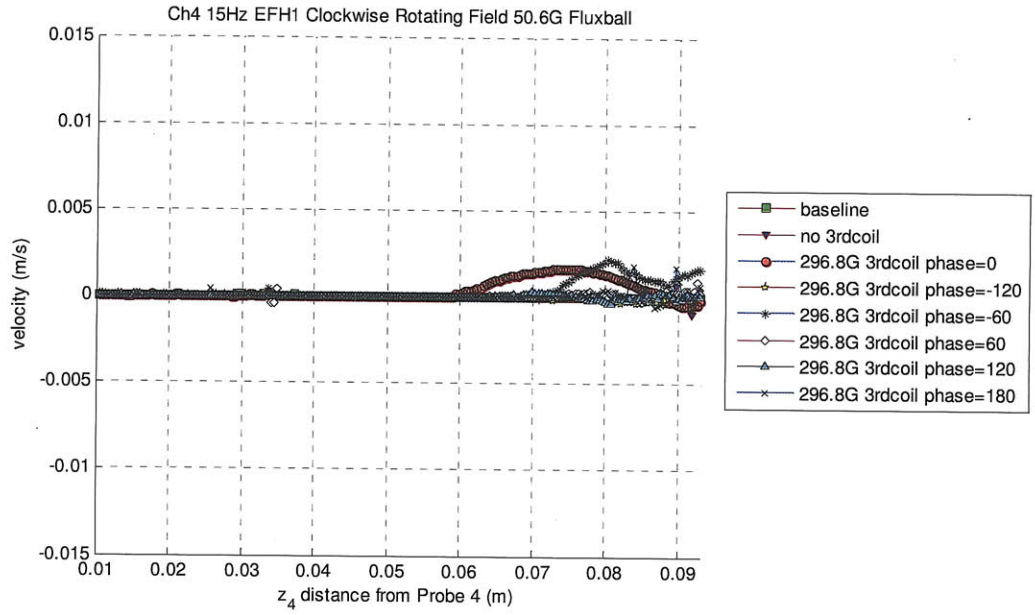
Ch4 15Hz EFH1 Clockwise Rotating Field 50.6G Fluxball
velocity (m/s)
0.015
0.01
0.005
0
-0.005
-0.01
-0.015
0.01
0.02
0.03
0.04
0.05
0.06
0.07
0.08
0.09
z4 distance from Probe 4 (m)
baseline
no 3rdcoil
296.8G 3rdcoil phase=0
296.8G 3rdcoil phase=-120
296.8G 3rdcoil phase=-60
296.8G 3rdcoil phase=60
296.8G 3rdcoil phase=120
296.8G 3rdcoil phase=180

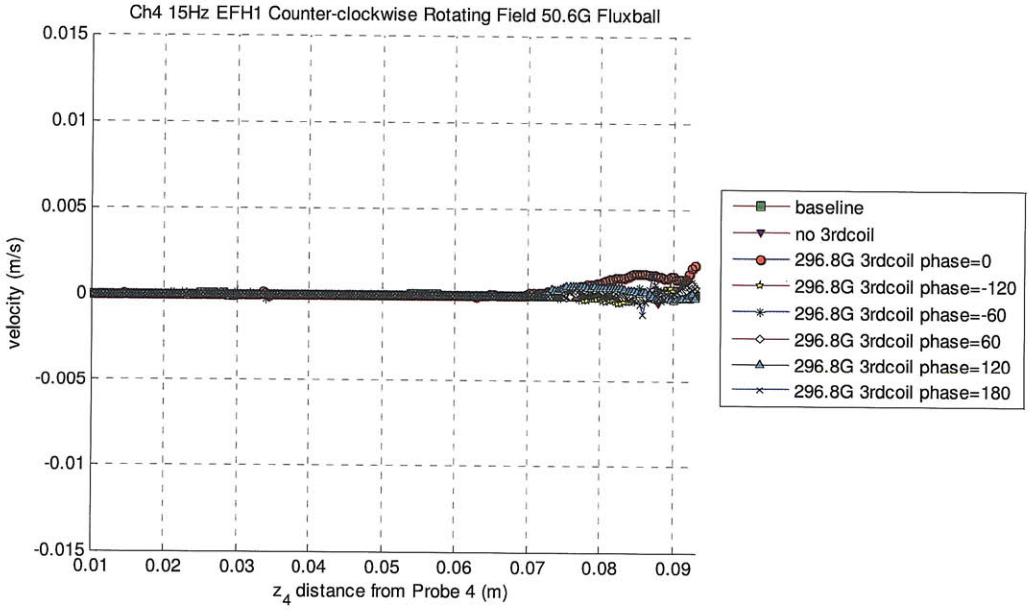
Ch4 15Hz EFH1 Counter-clockwise Rotating Field 50.6G Fluxball
velocity (m/s)
0.015
0.01
0.005
0
-0.005
-0.01
-0.015
0.01
0.02
0.03
0.04
0.05
0.06
0.07
0.08
0.09
z4 distance from Probe 4 (m)
baseline
no 3rdcoil
296.8G 3rdcoil phase=0
296.8G 3rdcoil phase=-120
296.8G 3rdcoil phase=-60
296.8G 3rdcoil phase=60
296.8G 3rdcoil phase=120
296.8G 3rdcoil phase=180

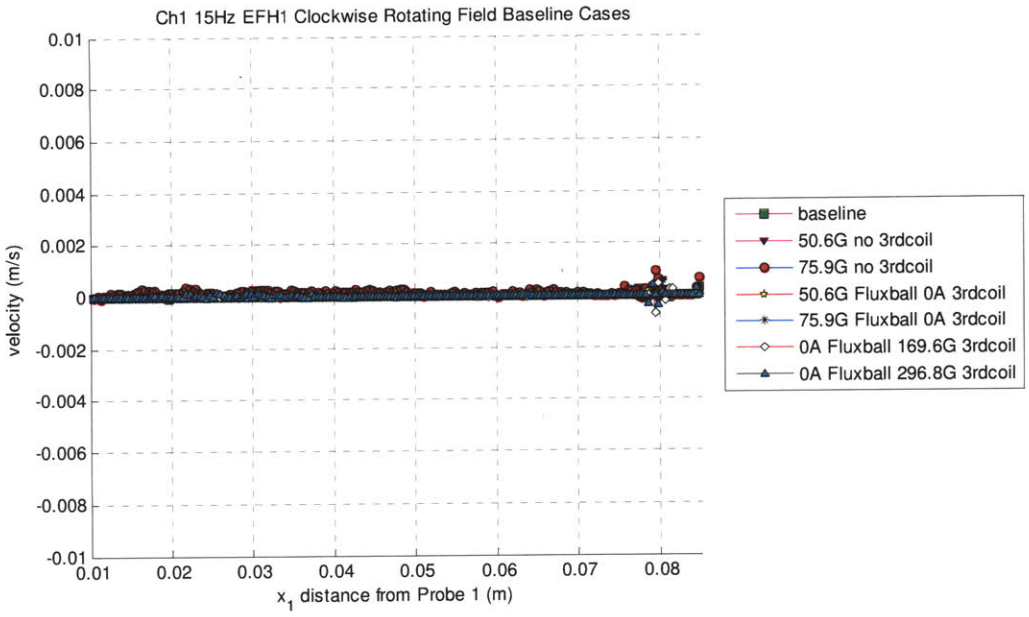
Ch1 15Hz EFH1 Clockwise Rotating Field Baseline Cases
velocity (m/s)
0.01
0.008
0.006
0.004
0.002
0
-0.002
-0.004
-0.006
-0.008
-0.01
0.01
0.02
0.03
0.04
0.05
0.06
0.07
0.08
x1 distance from Probe 1 (m)
baseline
50.6G no 3rdcoil
75.9G no 3rdcoil
50.6G Fluxball 0A 3rdcoil
75.9G Fluxball 0A 3rdcoil
0A Fluxball 169.6G 3rdcoil
0A Fluxball 296.8G 3rdcoil

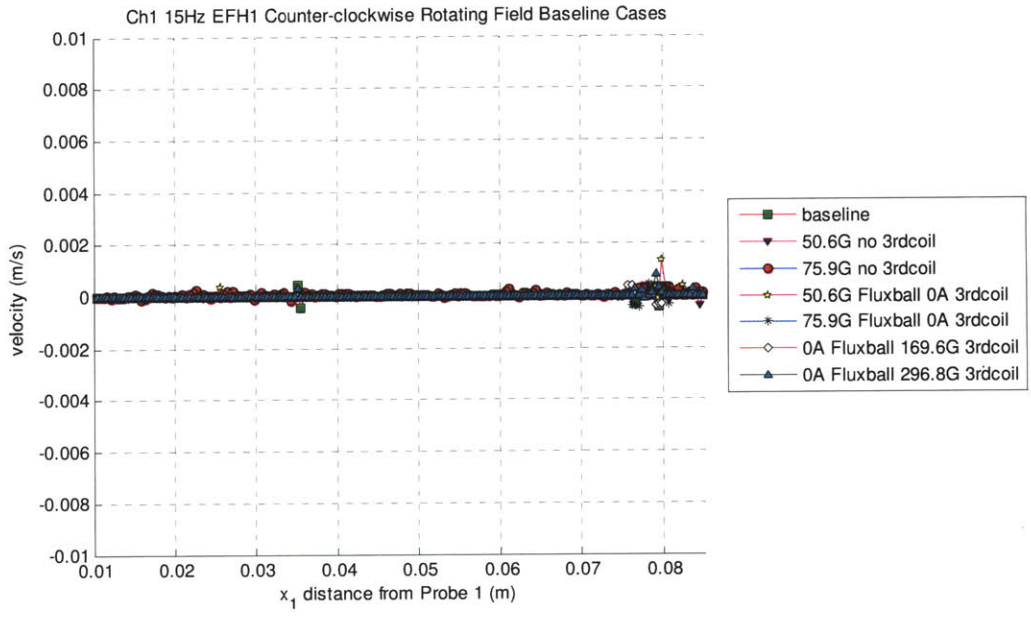
Ch1 15Hz EFH1 Counter-clockwise Rotating Field Baseline Cases
velocity (m/s)
0.01
0.008
0.006
0.004
0.002
0
-0.002
-0.004
-0.006
-0.008
-0.01
0.01
0.02
0.03
0.04
0.05
0.06
0.07
0.08
x1 distance from Probe 1 (m)
baseline
50.6G no 3rdcoil
75.9G no 3rdcoil
50.6G Fluxball 0A 3rdcoil
75.9G Fluxball 0A 3rdcoil
0A Fluxball 169.6G 3rdcoil
0A Fluxball 296.8G 3rdcoil

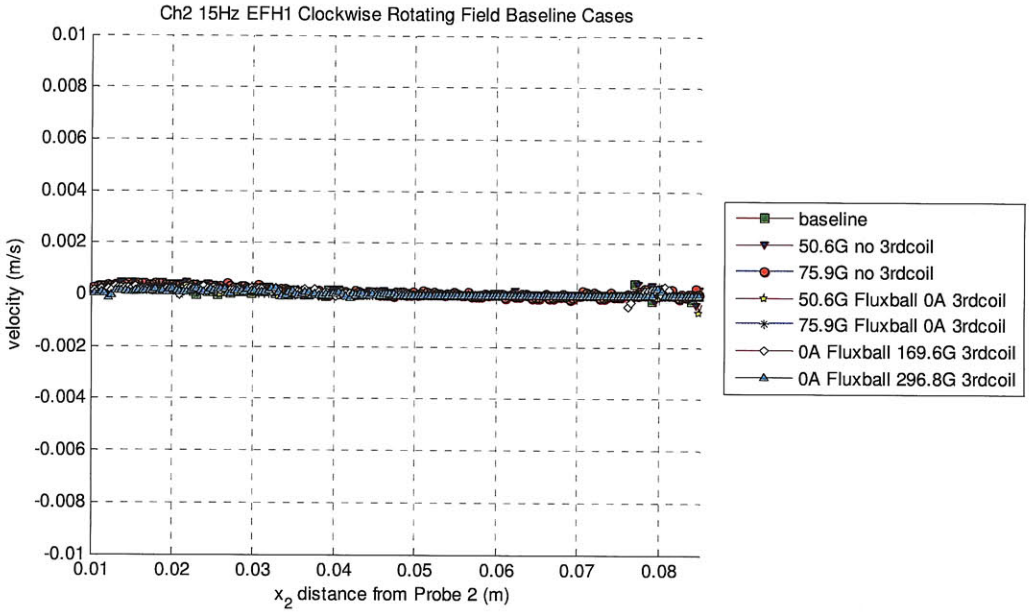
Ch2 15Hz EFH1 Clockwise Rotating Field Baseline Cases
velocity (m/s)
0.01
0.008
0.006
0.004
0.002
0
-0.002
-0.004
-0.006
-0.008
-0.01
0.01
0.02
0.03
0.04
0.05
0.06
0.07
0.08
x2 distance from Probe 2 (m)
baseline
50.6G no 3rdcoil
75.9G no 3rdcoil
50.6G Fluxball 0A 3rdcoil
75.9G Fluxball 0A 3rdcoil
0A Fluxball 169.6G 3rdcoil
0A Fluxball 296.8G 3rdcoil

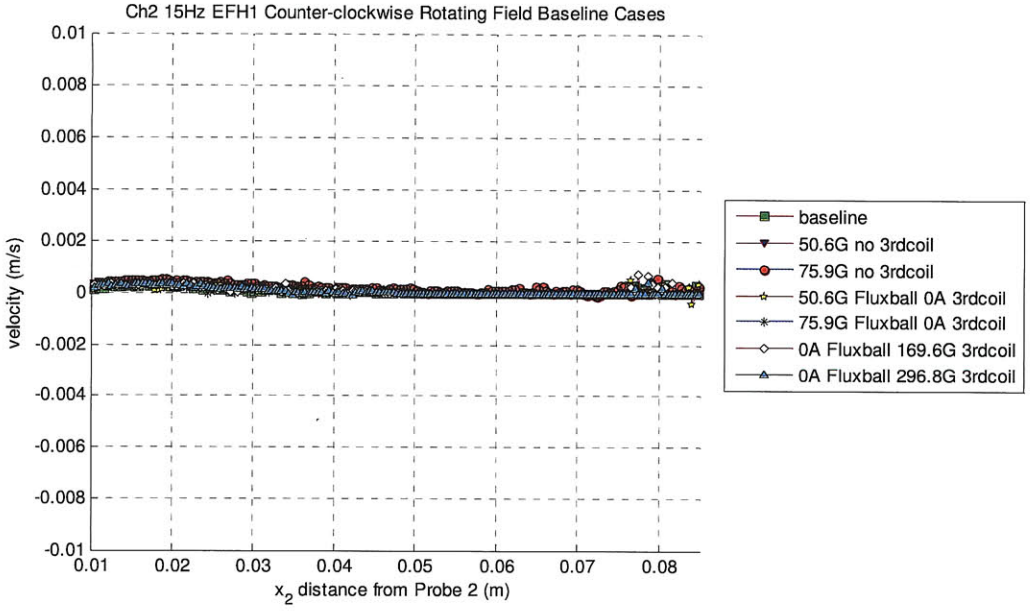
Ch2 15Hz EFH1 Counter-clockwise Rotating Field Baseline Cases
velocity (m/s)
0.01
0.008
0.006
0.004
0.002
0
-0.002
-0.004
-0.006
-0.008
-0.01
0.01
0.02
0.03
0.04
0.05
0.06
0.07
0.08
x2 distance from Probe 2 (m)
baseline
50.6G no 3rdcoil
75.9G no 3rdcoil
50.6G Fluxball 0A 3rdcoil
75.9G Fluxball 0A 3rdcoil
0A Fluxball 169.6G 3rdcoil
0A Fluxball 296.8G 3rdcoil

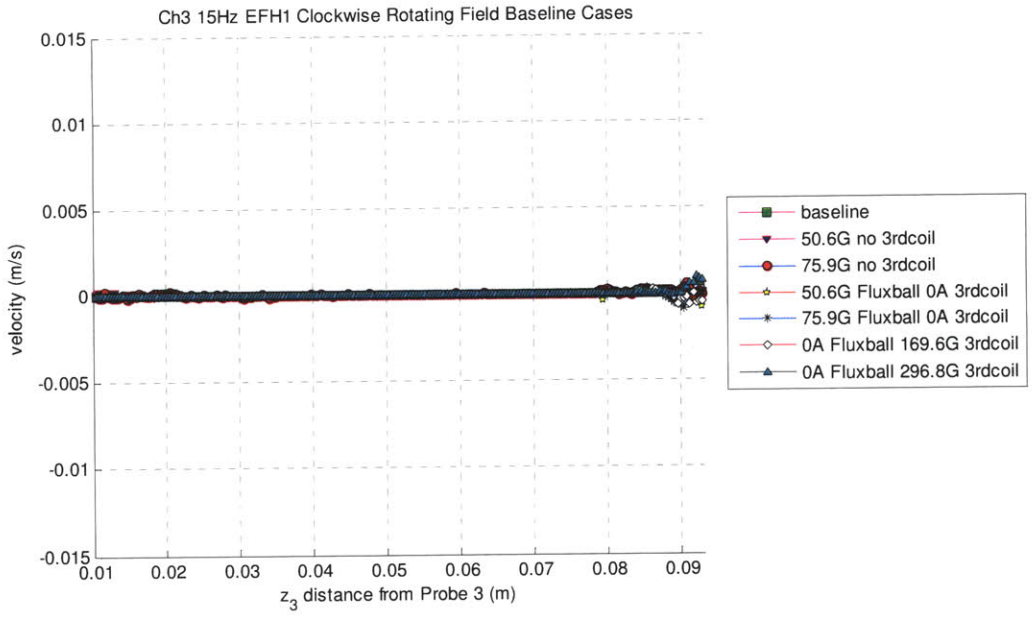
Ch3 15Hz EFH1 Clockwise Rotating Field Baseline Cases
velocity (m/s)
0.015
0.01
0.005
0
-0.005
-0.01
-0.015
0.01
0.02
0.03
0.04
0.05
0.06
0.07
0.08
0.09
z_3 distance from Probe 3 (m)
baseline
50.6G no 3rdcoil
75.9G no 3rdcoil
50.6G Fluxball 0A 3rdcoil
75.9G Fluxball 0A 3rdcoil
0A Fluxball 169.6G 3rdcoil
0A Fluxball 296.8G 3rdcoil

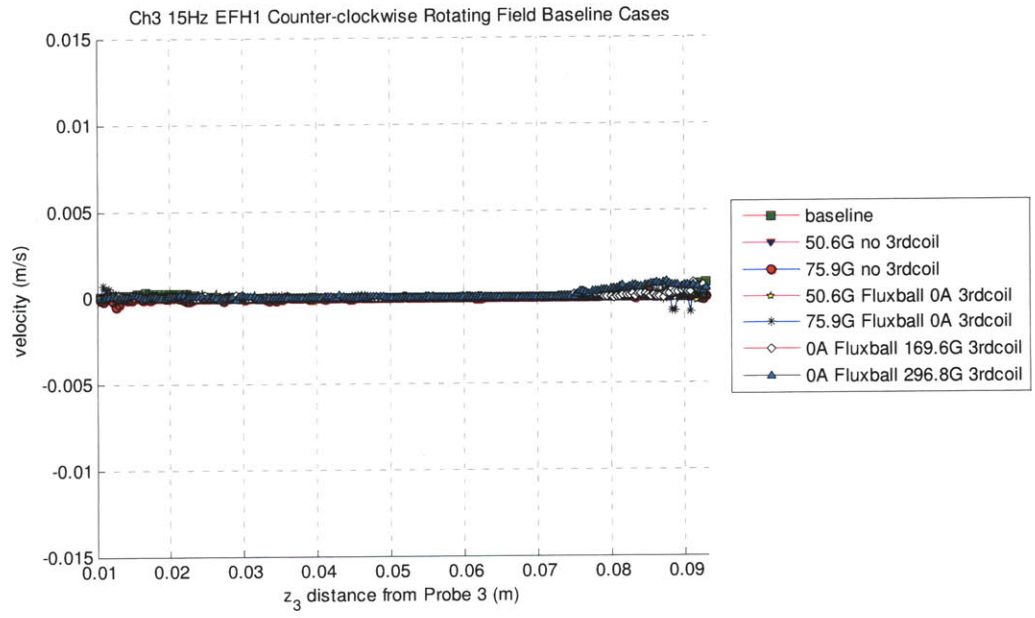
Ch3 15Hz EFH1 Counter-clockwise Rotating Field Baseline Cases
velocity (m/s)
0.015
0.01
0.005
0
-0.005
-0.01
-0.015
0.01
0.02
0.03
0.04
0.05
0.06
0.07
0.08
0.09
z_3 distance from Probe 3 (m)
baseline
50.6G no 3rdcoil
75.9G no 3rdcoil
50.6G Fluxball 0A 3rdcoil
75.9G Fluxball 0A 3rdcoil
0A Fluxball 169.6G 3rdcoil
0A Fluxball 296.8G 3rdcoil

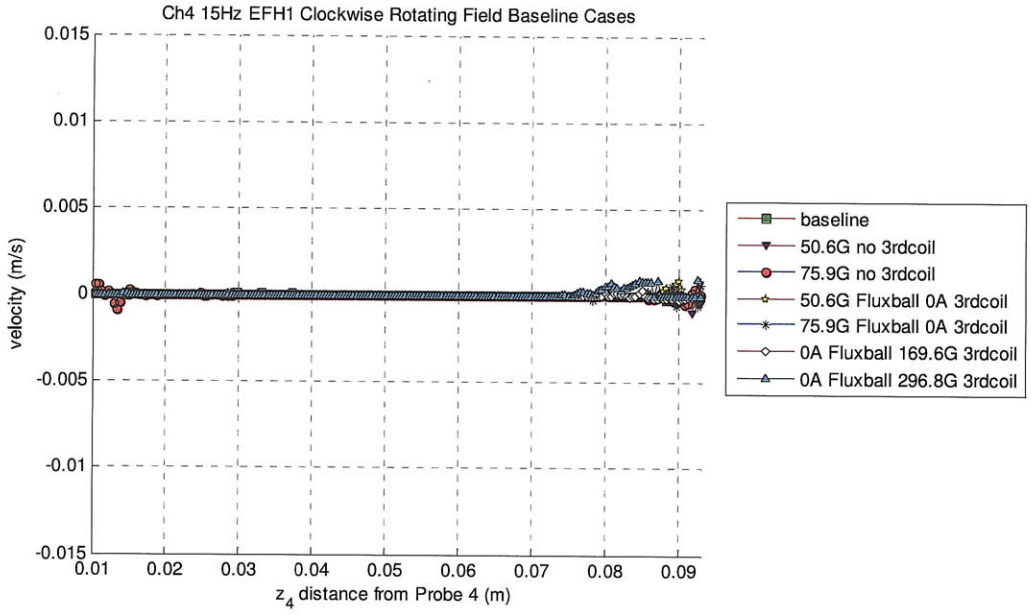
Ch4 15Hz EFH1 Clockwise Rotating Field Baseline Cases
velocity (m/s)
0.015
0.01
0.005
0
-0.005
-0.01
-0.015
0.01
0.02
0.03
0.04
0.05
0.06
0.07
0.08
0.09
z4 distance from Probe 4 (m)
baseline
50.6G no 3rdcoil
75.9G no 3rdcoil
50.6G Fluxball 0A 3rdcoil
75.9G Fluxball 0A 3rdcoil
0A Fluxball 169.6G 3rdcoil
0A Fluxball 296.8G 3rdcoil

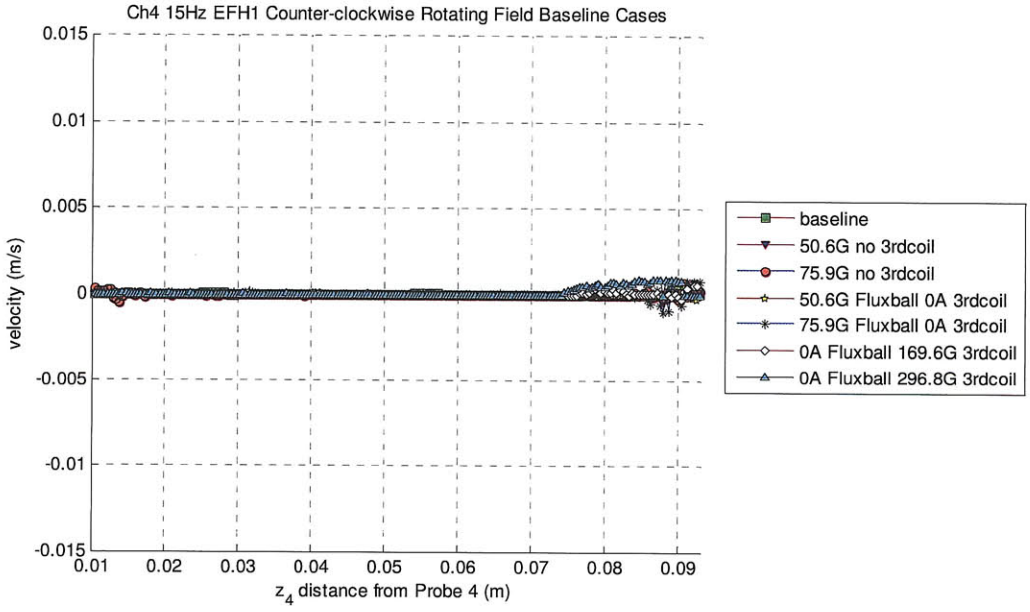
Ch4 15Hz EFH1 Counter-clockwise Rotating Field Baseline Cases
velocity (m/s)
0.015
0.01
0.005
0
-0.005
-0.01
-0.015
0.01
0.02
0.03
0.04
0.05
0.06
0.07
0.08
0.09
z4 distance from Probe 4 (m)
baseline
50.6G no 3rdcoil
75.9G no 3rdcoil
50.6G Fluxball 0A 3rdcoil
75.9G Fluxball 0A 3rdcoil
0A Fluxball 169.6G 3rdcoil
0A Fluxball 296.8G 3rdcoil

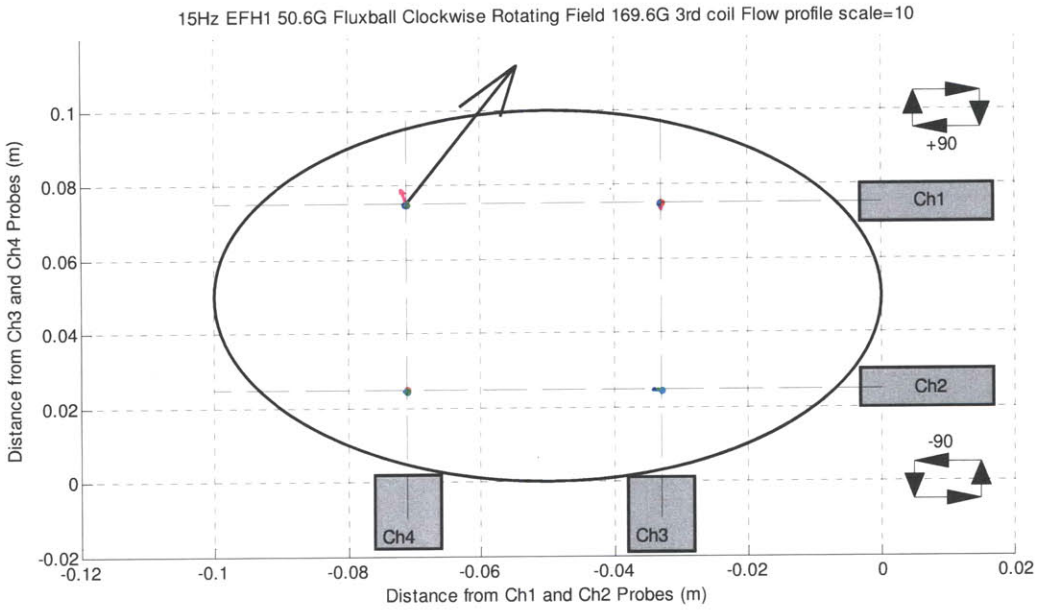
15Hz EFH1 50.6G Fluxball Clockwise Rotating Field 169.6G 3rd coil Flow profile scale=10
Distance from Ch3 and Ch4 Probes (m)
Distance from Ch1 and Ch2 Probes (m)
0.1
0.08
0.06
0.04
0.02
0
-0.02
-0.12
-0.1
-0.08
-0.06
-0.04
-0.02
0
0.02
+90
-90
Ch1
Ch2
Ch3
Ch4

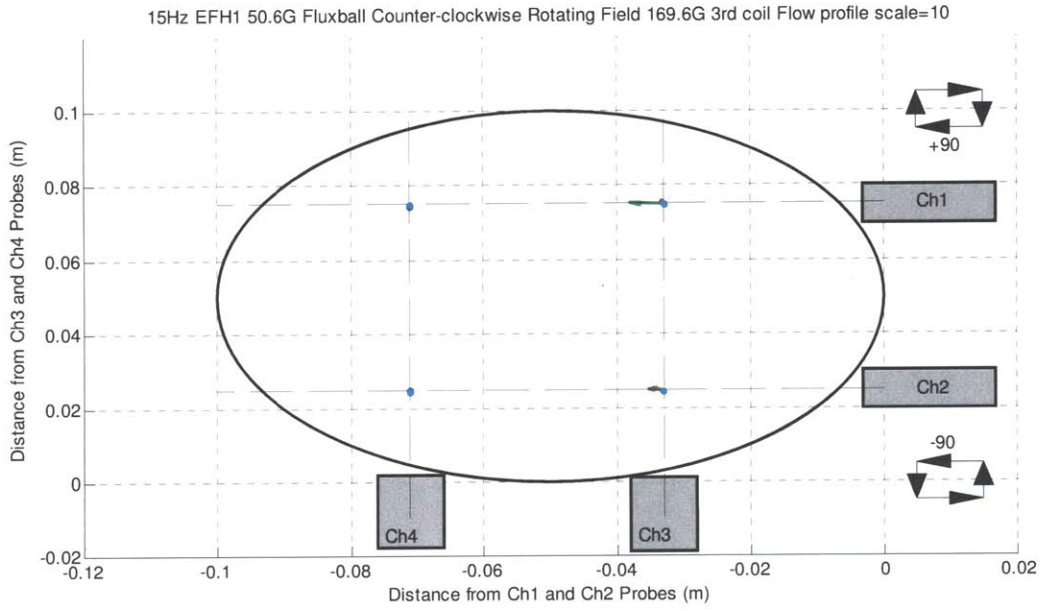
15Hz EFH1 50.6G Fluxball Counter-clockwise Rotating Field 169.6G 3rd coil Flow profile scale=10
Distance from Ch3 and Ch4 Probes (m)
Distance from Ch1 and Ch2 Probes (m)
0.1
0.08
0.06
0.04
0.02
0
-0.02
-0.12
-0.1
-0.08
-0.06
-0.04
-0.02
0
0.02
+90
-90
Ch1
Ch2
Ch3
Ch4

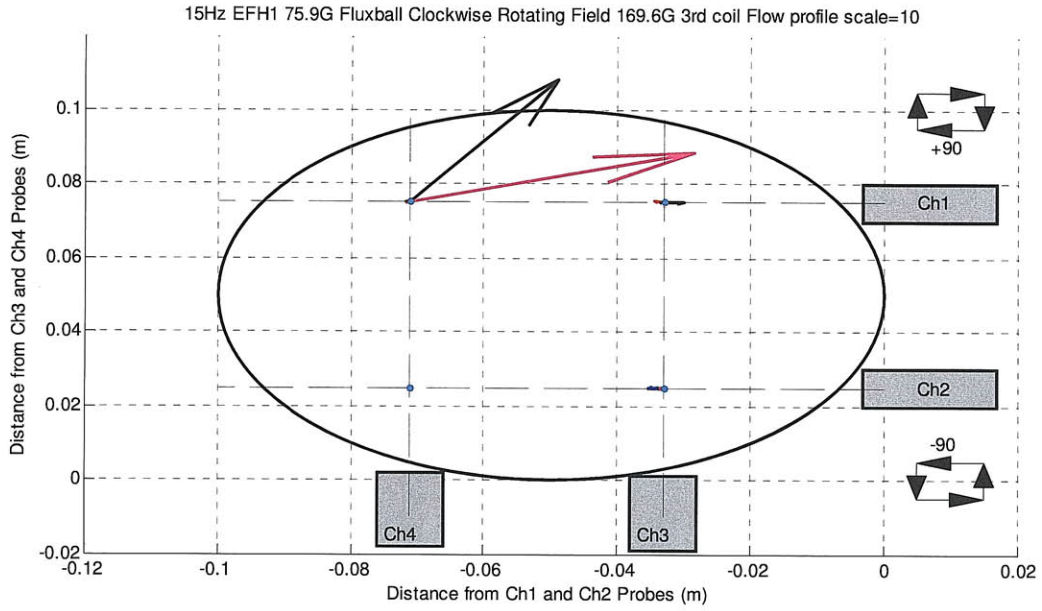
15Hz EFH1 75.9G Fluxball Clockwise Rotating Field 169.6G 3rd coil Flow profile scale=10
Distance from Ch3 and Ch4 Probes (m)
Distance from Ch1 and Ch2 Probes (m)
0.1
0.08
0.06
0.04
0.02
0
-0.02
-0.12
-0.1
-0.08
-0.06
-0.04
-0.02
0
0.02
+90
-90
Ch1
Ch2
Ch3
Ch4

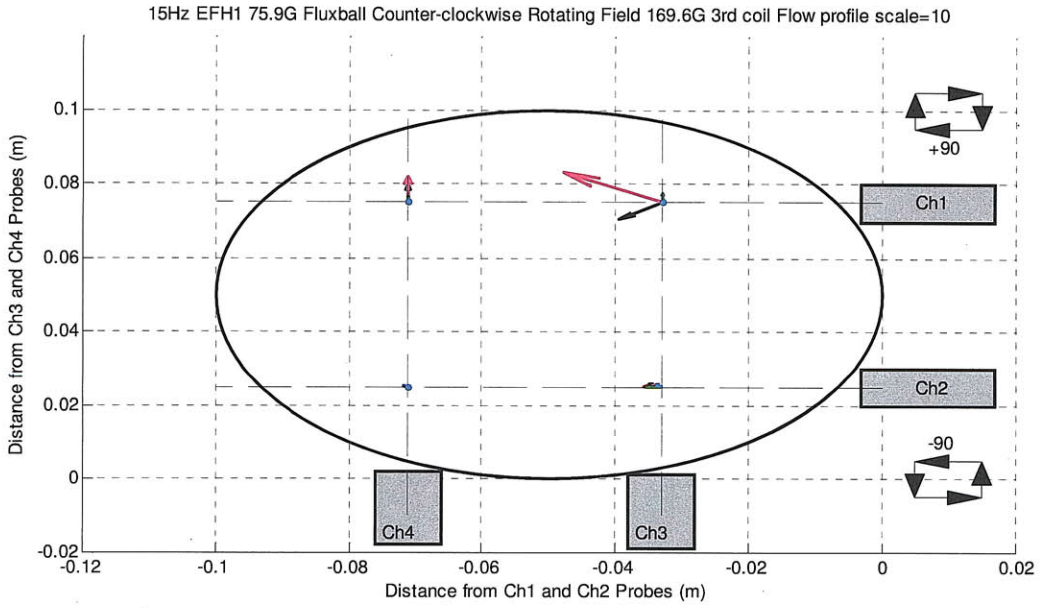
15Hz EFH1 75.9G Fluxball Counter-clockwise Rotating Field 169.6G 3rd coil Flow profile scale=10
Distance from Ch3 and Ch4 Probes (m)
Distance from Ch1 and Ch2 Probes (m)
0.1
0.08
0.06
0.04
0.02
0
-0.02
-0.12
-0.1
-0.08
-0.06
-0.04
-0.02
0
0.02
+90
-90
Ch1
Ch2
Ch3
Ch4

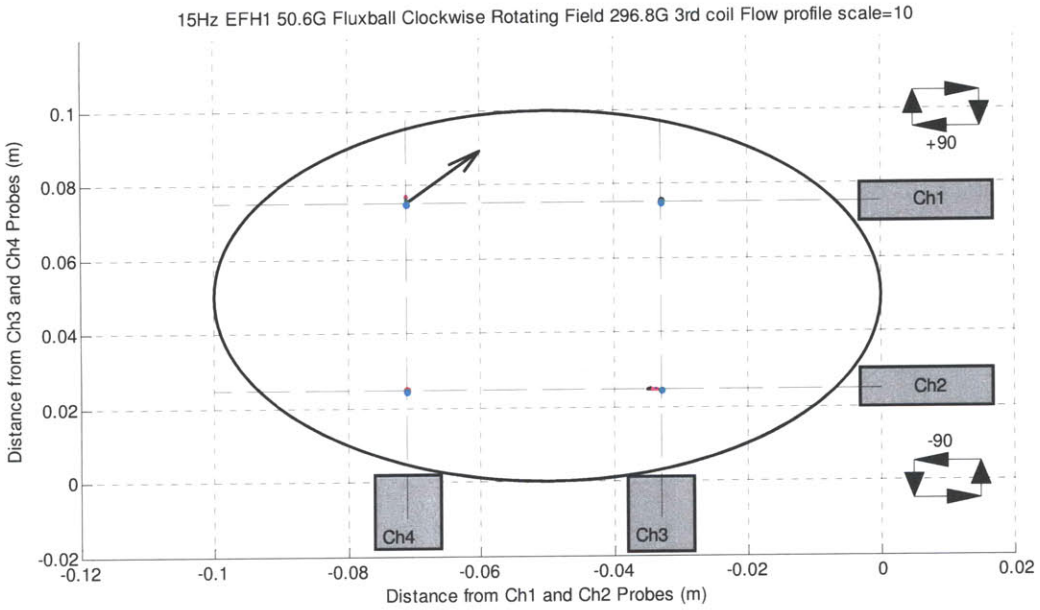
15Hz EFH1 50.6G Fluxball Clockwise Rotating Field 296.8G 3rd coil Flow profile scale=10
Distance from Ch3 and Ch4 Probes (m)
Distance from Ch1 and Ch2 Probes (m)
+90
-90
Ch1
Ch2
Ch3
Ch4
0.1
0.08
0.06
0.04
0.02
0
-0.02
-0.12
-0.1
-0.08
-0.06
-0.04
-0.02
0
0.02

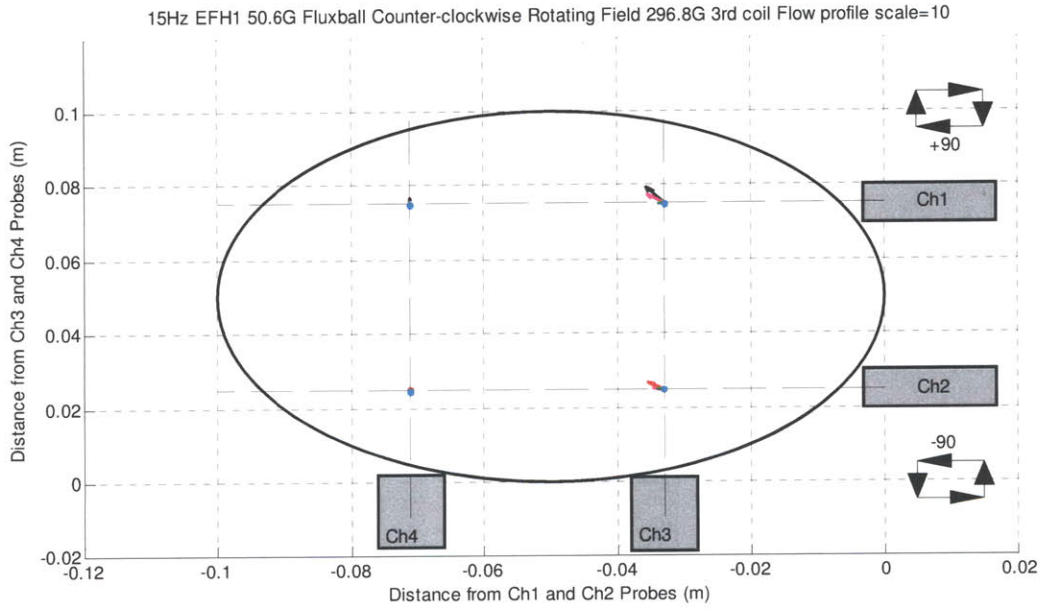
15Hz EFH1 50.6G Fluxball Counter-clockwise Rotating Field 296.8G 3rd coil Flow profile scale=10
Distance from Ch3 and Ch4 Probes (m)
Distance from Ch1 and Ch2 Probes (m)
+90
-90
Ch1
Ch2
Ch3
Ch4
0.1
0.08
0.06
0.04
0.02
0
-0.02
-0.12
-0.1
-0.08
-0.06
-0.04
-0.02
0
0.02

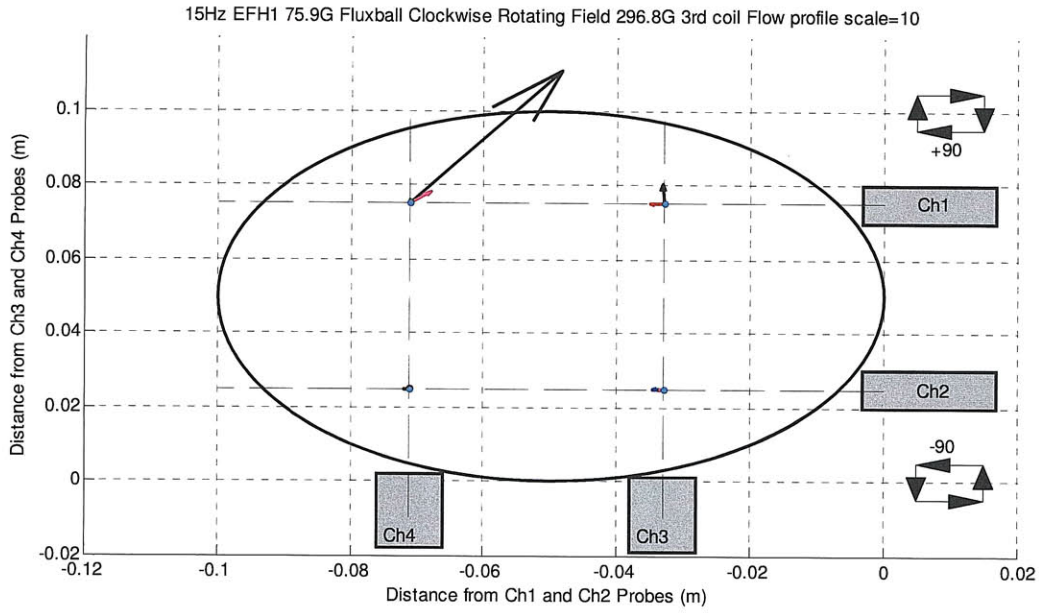
15Hz EFH1 75.9G Fluxball Clockwise Rotating Field 296.8G 3rd coil Flow profile scale=10
Distance from Ch3 and Ch4 Probes (m)
Distance from Ch1 and Ch2 Probes (m)
0.1
0.08
0.06
0.04
0.02
0
-0.02
-0.12
-0.1
-0.08
-0.06
-0.04
-0.02
0
0.02
+90
-90
Ch1
Ch2
Ch3
Ch4

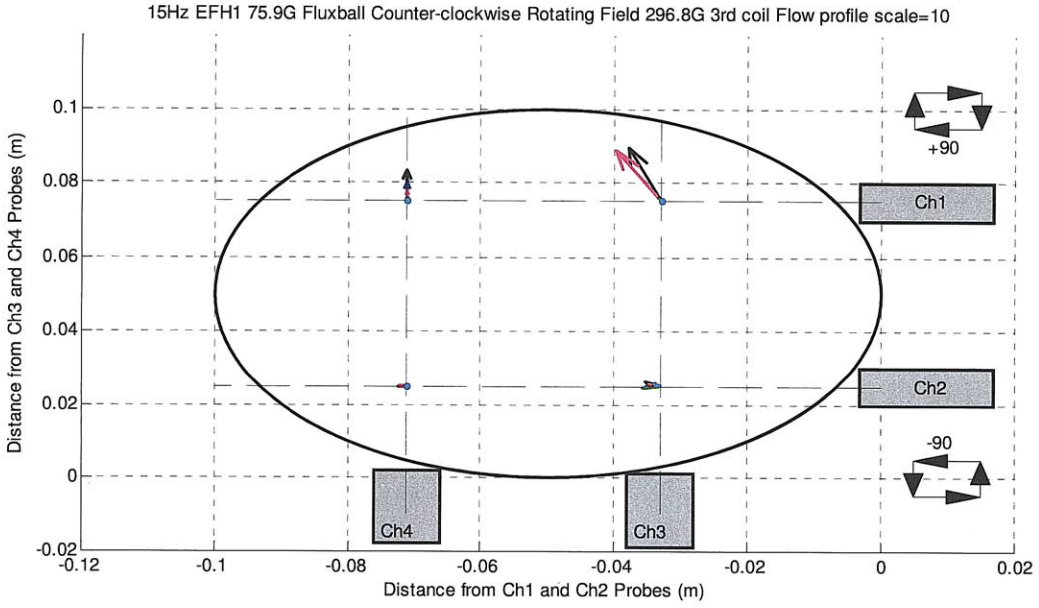
15Hz EFH1 75.9G Fluxball Counter-clockwise Rotating Field 296.8G 3rd coil Flow profile scale=10
Distance from Ch3 and Ch4 Probes (m)
Distance from Ch1 and Ch2 Probes (m)
0.1
0.08
0.06
0.04
0.02
0
-0.02
-0.12
-0.1
-0.08
-0.06
-0.04
-0.02
0
0.02
+90
-90
Ch1
Ch2
Ch3
Ch4

G4. MSGW11 Filled Sphere with Third Coil Oscillating at Same Frequency as Rotating Field at 95Hz

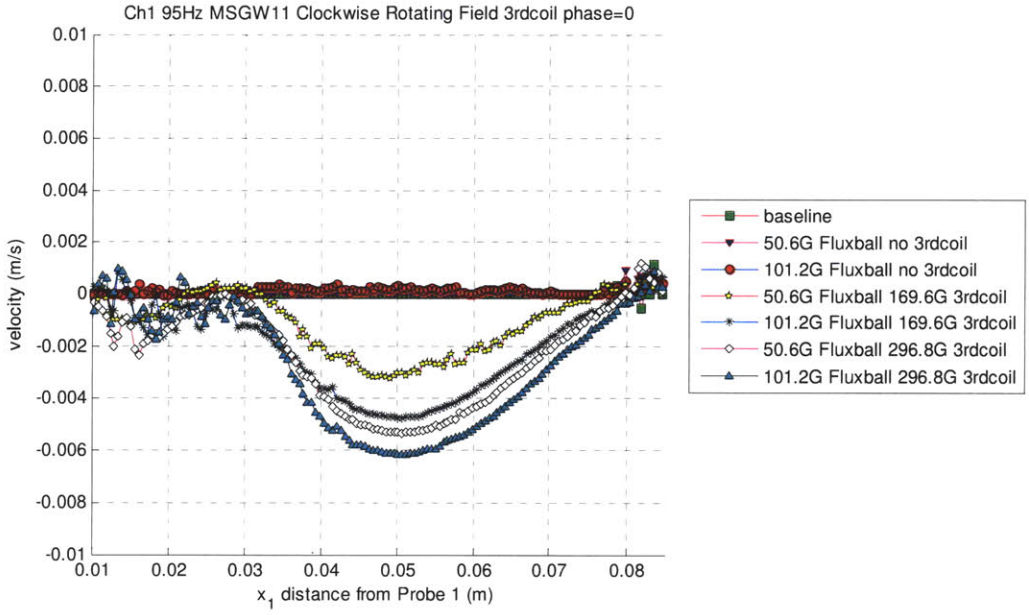

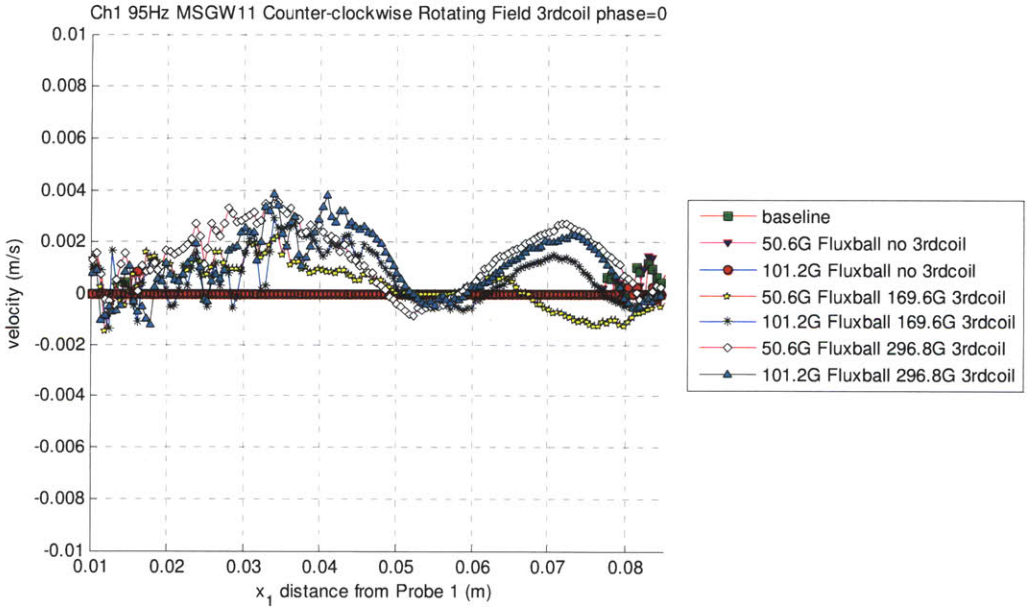

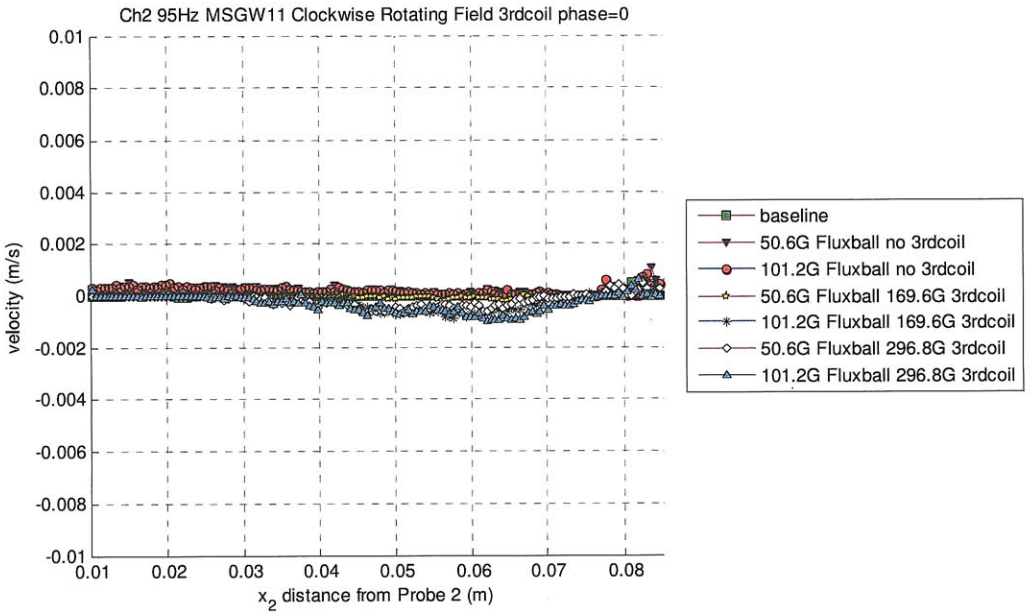
Ch2 95Hz MSGW11 Clockwise Rotating Field 3rdcoil phase=0
velocity (m/s)
0.01
0.008
0.006
0.004
0.002
0
-0.002
-0.004
-0.006
-0.008
-0.01
0.01
0.02
0.03
0.04
0.05
0.06
0.07
0.08
x2 distance from Probe 2 (m)
baseline
50.6G Fluxball no 3rdcoil
101.2G Fluxball no 3rdcoil
50.6G Fluxball 169.6G 3rdcoil
101.2G Fluxball 169.6G 3rdcoil
50.6G Fluxball 296.8G 3rdcoil
101.2G Fluxball 296.8G 3rdcoil

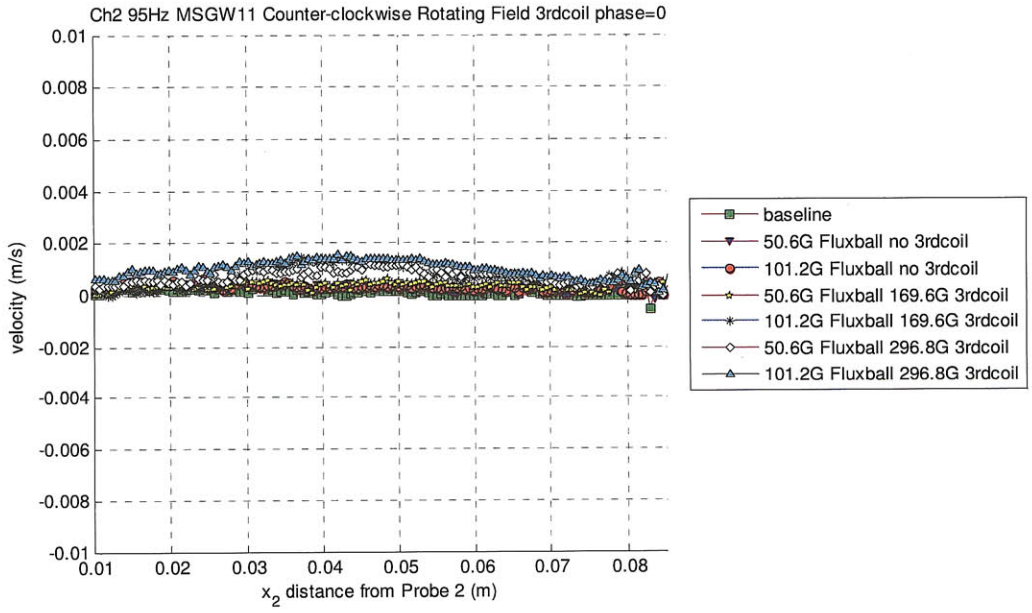
Ch2 95Hz MSGW11 Counter-clockwise Rotating Field 3rdcoil phase=0
velocity (m/s)
0.01
0.008
0.006
0.004
0.002
0
-0.002
-0.004
-0.006
-0.008
-0.01
0.01
0.02
0.03
0.04
0.05
0.06
0.07
0.08
x2 distance from Probe 2 (m)
baseline
50.6G Fluxball no 3rdcoil
101.2G Fluxball no 3rdcoil
50.6G Fluxball 169.6G 3rdcoil
101.2G Fluxball 169.6G 3rdcoil
50.6G Fluxball 296.8G 3rdcoil
101.2G Fluxball 296.8G 3rdcoil

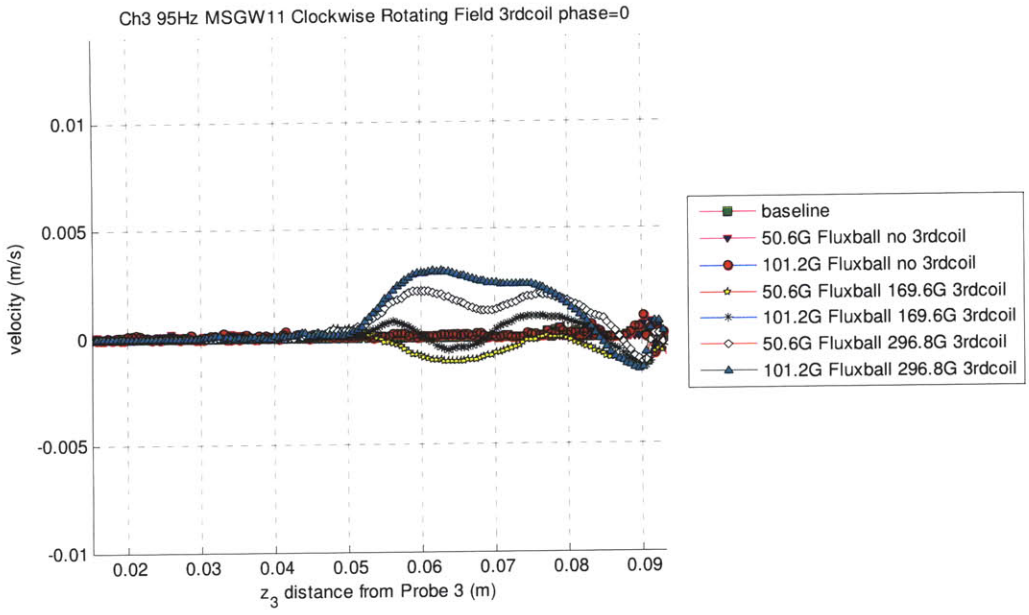
Ch3 95Hz MSGW11 Clockwise Rotating Field 3rdcoil phase=0
velocity (m/s)
0.01
0.005
0
-0.005
-0.01
0.02
0.03
0.04
0.05
0.06
0.07
0.08
0.09
z_3 distance from Probe 3 (m)
baseline
50.6G Fluxball no 3rdcoil
101.2G Fluxball no 3rdcoil
50.6G Fluxball 169.6G 3rdcoil
101.2G Fluxball 169.6G 3rdcoil
50.6G Fluxball 296.8G 3rdcoil
101.2G Fluxball 296.8G 3rdcoil

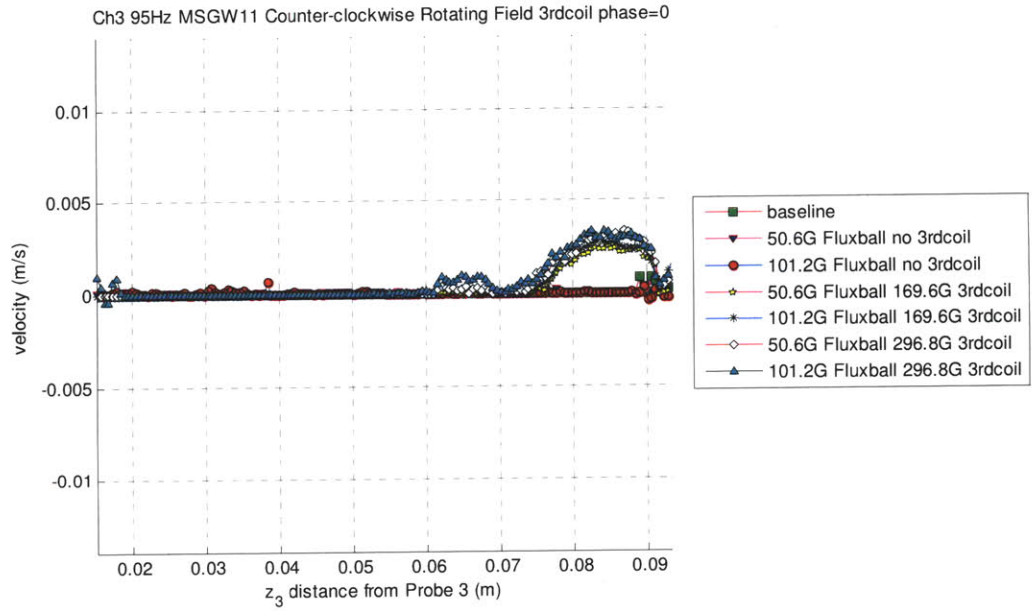
Ch3 95Hz MSGW11 Counter-clockwise Rotating Field 3rdcoil phase=0
velocity (m/s)
0.01
0.005
0
-0.005
-0.01
0.02
0.03
0.04
0.05
0.06
0.07
0.08
0.09
z_3 distance from Probe 3 (m)
baseline
50.6G Fluxball no 3rdcoil
101.2G Fluxball no 3rdcoil
50.6G Fluxball 169.6G 3rdcoil
101.2G Fluxball 169.6G 3rdcoil
50.6G Fluxball 296.8G 3rdcoil
101.2G Fluxball 296.8G 3rdcoil

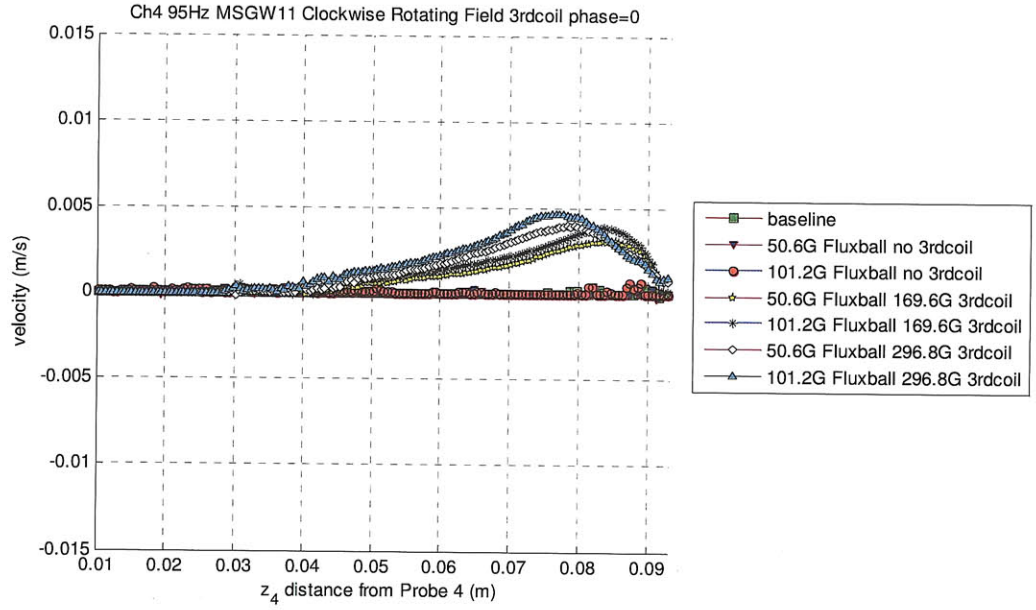
Ch4 95Hz MSGW11 Clockwise Rotating Field 3rdcoil phase=0
velocity (m/s)
0.015
0.01
0.005
0
-0.005
-0.01
-0.015
0.01
0.02
0.03
0.04
0.05
0.06
0.07
0.08
0.09
z4 distance from Probe 4 (m)
baseline
50.6G Fluxball no 3rdcoil
101.2G Fluxball no 3rdcoil
50.6G Fluxball 169.6G 3rdcoil
101.2G Fluxball 169.6G 3rdcoil
50.6G Fluxball 296.8G 3rdcoil
101.2G Fluxball 296.8G 3rdcoil

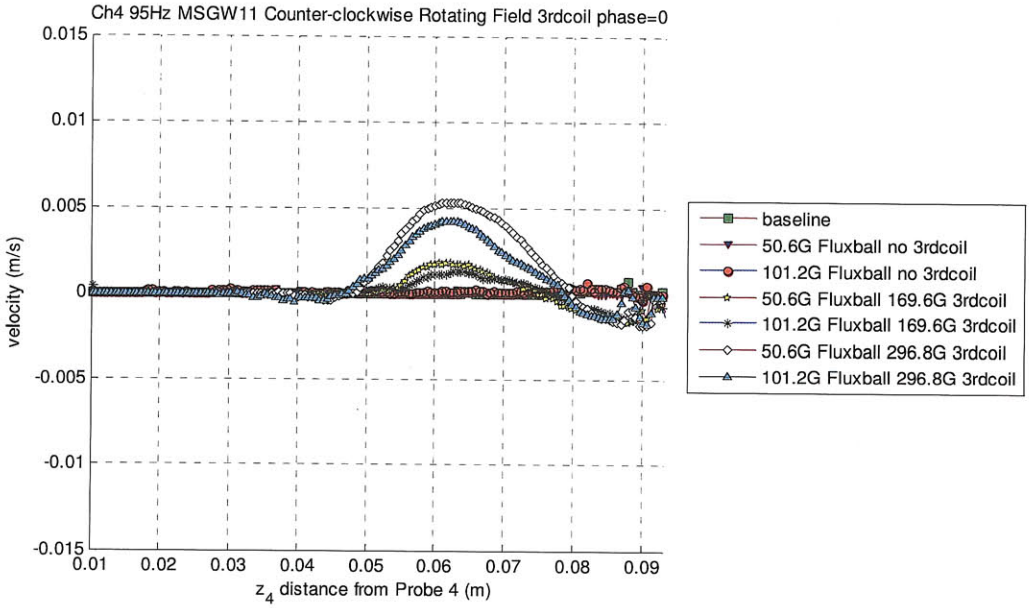
Ch4 95Hz MSGW11 Counter-clockwise Rotating Field 3rdcoil phase=0
velocity (m/s)
0.015
0.01
0.005
0
-0.005
-0.01
-0.015
0.01
0.02
0.03
0.04
0.05
0.06
0.07
0.08
0.09
z4 distance from Probe 4 (m)
baseline
50.6G Fluxball no 3rdcoil
101.2G Fluxball no 3rdcoil
50.6G Fluxball 169.6G 3rdcoil
101.2G Fluxball 169.6G 3rdcoil
50.6G Fluxball 296.8G 3rdcoil
101.2G Fluxball 296.8G 3rdcoil

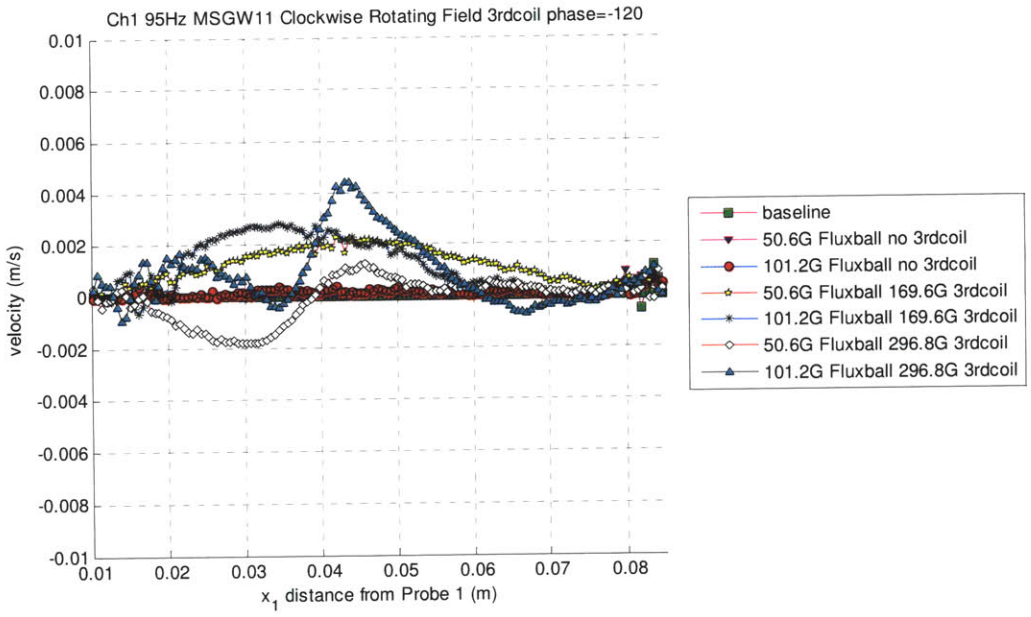
Ch1 95Hz MSGW11 Clockwise Rotating Field 3rdcoil phase=-120
velocity (m/s)
x1 distance from Probe 1 (m)
baseline
50.6G Fluxball no 3rdcoil
101.2G Fluxball no 3rdcoil
50.6G Fluxball 169.6G 3rdcoil
101.2G Fluxball 169.6G 3rdcoil
50.6G Fluxball 296.8G 3rdcoil
101.2G Fluxball 296.8G 3rdcoil

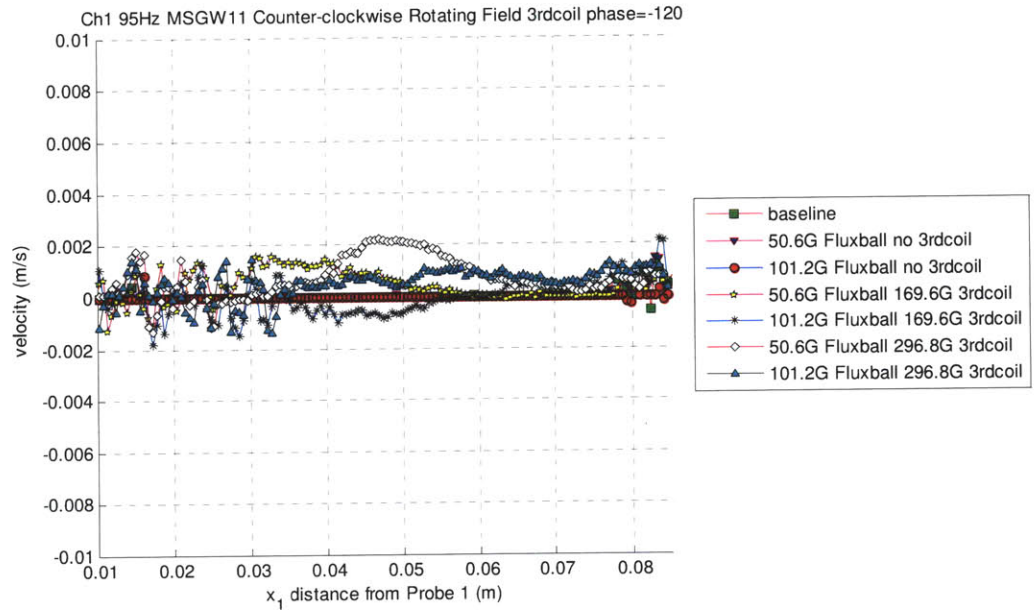
Ch1 95Hz MSGW11 Counter-clockwise Rotating Field 3rdcoil phase=-120
velocity (m/s)
x1 distance from Probe 1 (m)
baseline
50.6G Fluxball no 3rdcoil
101.2G Fluxball no 3rdcoil
50.6G Fluxball 169.6G 3rdcoil
101.2G Fluxball 169.6G 3rdcoil
50.6G Fluxball 296.8G 3rdcoil
101.2G Fluxball 296.8G 3rdcoil

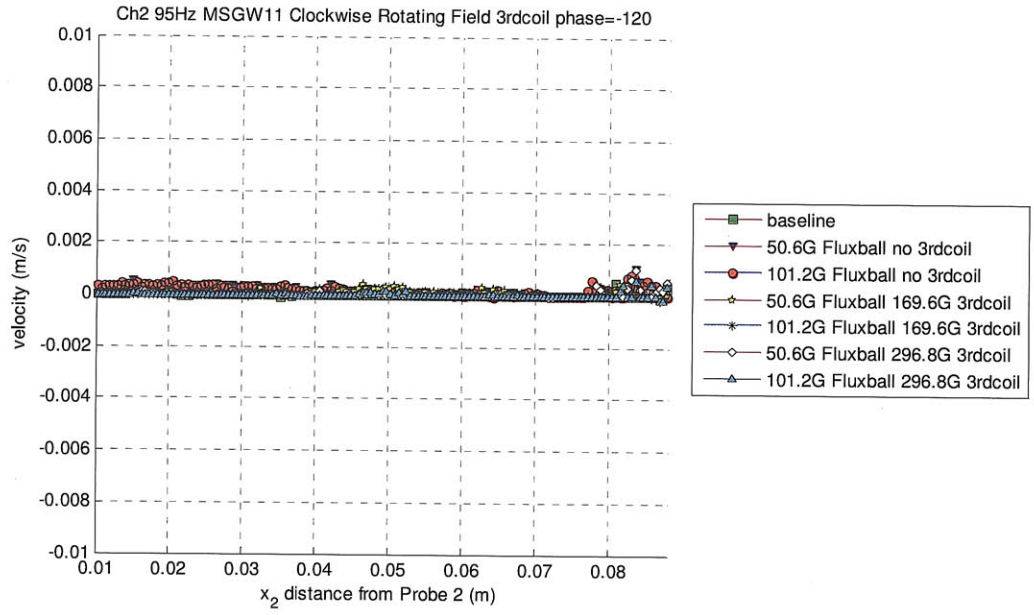
Ch2 95Hz MSGW11 Clockwise Rotating Field 3rdcoil phase=-120
velocity (m/s)
0.01
0.008
0.006
0.004
0.002
0
-0.002
-0.004
-0.006
-0.008
-0.01
0.01 0.02 0.03 0.04 0.05 0.06 0.07 0.08
x2 distance from Probe 2 (m)
baseline
50.6G Fluxball no 3rdcoil
101.2G Fluxball no 3rdcoil
50.6G Fluxball 169.6G 3rdcoil
101.2G Fluxball 169.6G 3rdcoil
50.6G Fluxball 296.8G 3rdcoil
101.2G Fluxball 296.8G 3rdcoil

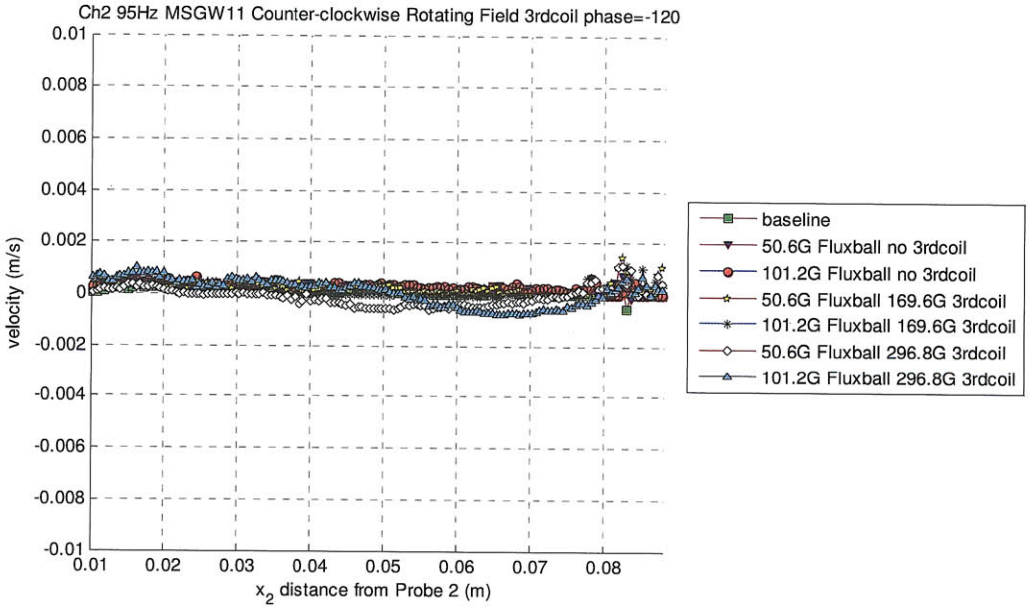
Ch2 95Hz MSGW11 Counter-clockwise Rotating Field 3rdcoil phase=-120
velocity (m/s)
0.01
0.008
0.006
0.004
0.002
0
-0.002
-0.004
-0.006
-0.008
-0.01
0.01 0.02 0.03 0.04 0.05 0.06 0.07 0.08
x2 distance from Probe 2 (m)
baseline
50.6G Fluxball no 3rdcoil
101.2G Fluxball no 3rdcoil
50.6G Fluxball 169.6G 3rdcoil
101.2G Fluxball 169.6G 3rdcoil
50.6G Fluxball 296.8G 3rdcoil
101.2G Fluxball 296.8G 3rdcoil

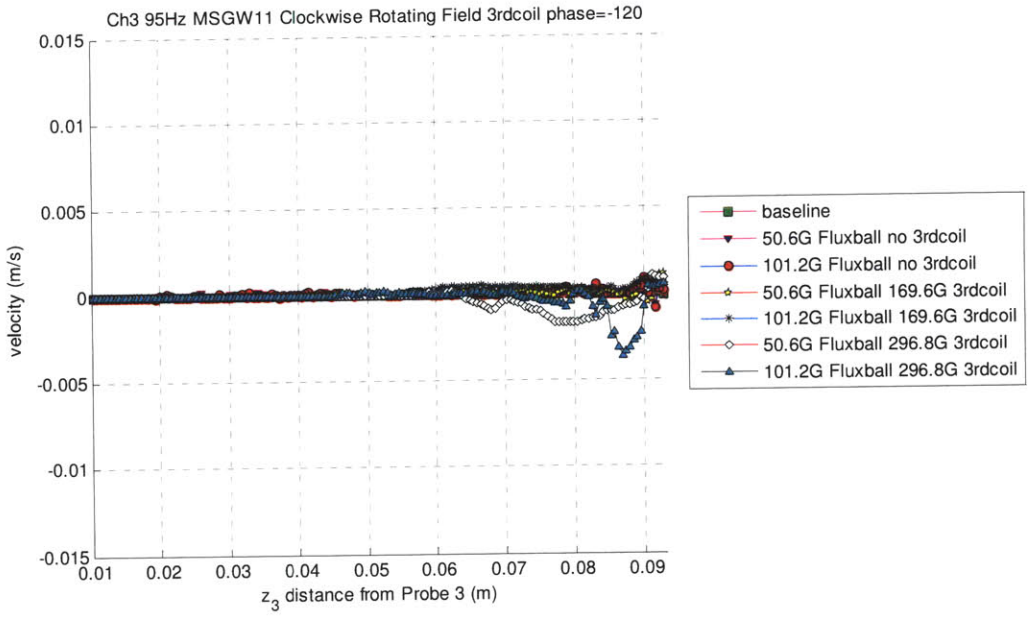
Ch3 95Hz MSGW11 Clockwise Rotating Field 3rdcoil phase=-120
velocity (m/s)
0.015
0.01
0.005
0
-0.005
-0.01
-0.015
0.01
0.02
0.03
0.04
0.05
0.06
0.07
0.08
0.09
z3 distance from Probe 3 (m)
baseline
50.6G Fluxball no 3rdcoil
101.2G Fluxball no 3rdcoil
50.6G Fluxball 169.6G 3rdcoil
101.2G Fluxball 169.6G 3rdcoil
50.6G Fluxball 296.8G 3rdcoil
101.2G Fluxball 296.8G 3rdcoil

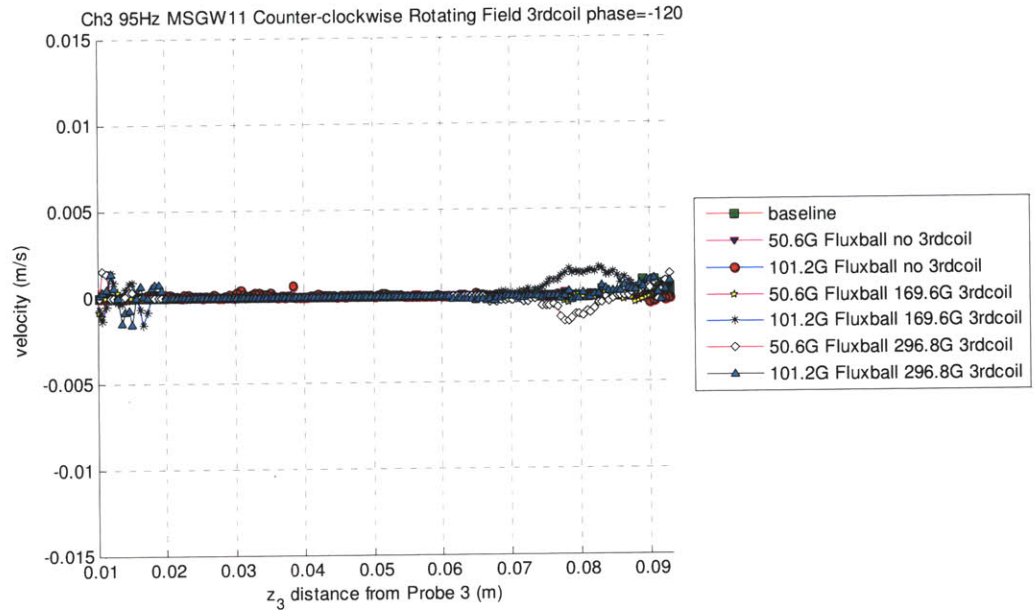
Ch3 95Hz MSGW11 Counter-clockwise Rotating Field 3rdcoil phase=-120
velocity (m/s)
0.015
0.01
0.005
0
-0.005
-0.01
-0.015
0.01
0.02
0.03
0.04
0.05
0.06
0.07
0.08
0.09
z3 distance from Probe 3 (m)
baseline
50.6G Fluxball no 3rdcoil
101.2G Fluxball no 3rdcoil
50.6G Fluxball 169.6G 3rdcoil
101.2G Fluxball 169.6G 3rdcoil
50.6G Fluxball 296.8G 3rdcoil
101.2G Fluxball 296.8G 3rdcoil

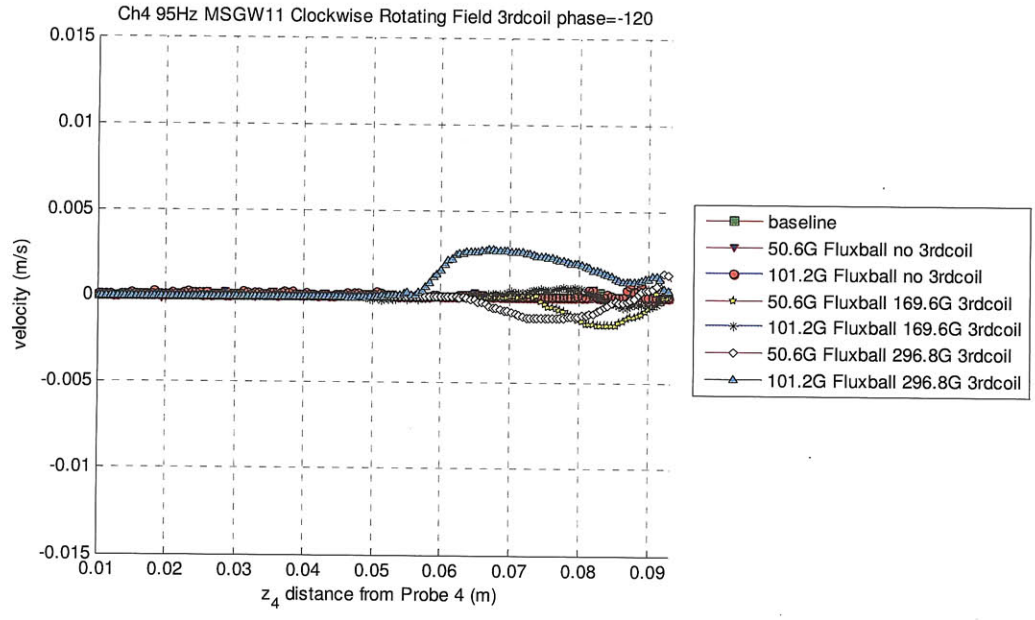
Ch4 95Hz MSGW11 Clockwise Rotating Field 3rdcoil phase=-120
velocity (m/s)
0.015
0.01
0.005
0
-0.005
-0.01
-0.015
0.01
0.02
0.03
0.04
0.05
0.06
0.07
0.08
0.09
z4 distance from Probe 4 (m)
baseline
50.6G Fluxball no 3rdcoil
101.2G Fluxball no 3rdcoil
50.6G Fluxball 169.6G 3rdcoil
101.2G Fluxball 169.6G 3rdcoil
50.6G Fluxball 296.8G 3rdcoil
101.2G Fluxball 296.8G 3rdcoil

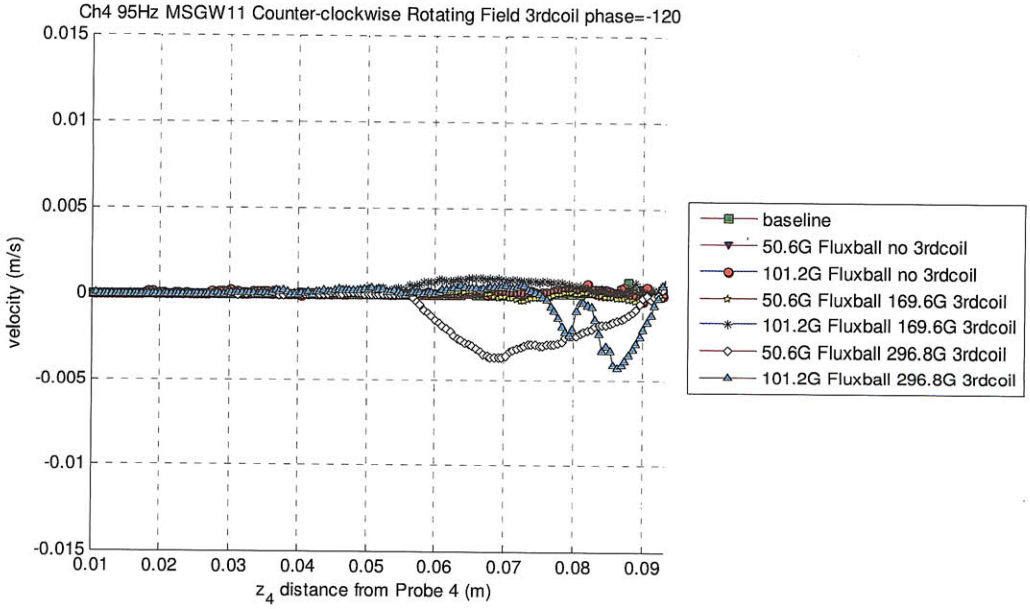
Ch4 95Hz MSGW11 Counter-clockwise Rotating Field 3rdcoil phase=-120
velocity (m/s)
0.015
0.01
0.005
0
-0.005
-0.01
-0.015
0.01
0.02
0.03
0.04
0.05
0.06
0.07
0.08
0.09
z4 distance from Probe 4 (m)
baseline
50.6G Fluxball no 3rdcoil
101.2G Fluxball no 3rdcoil
50.6G Fluxball 169.6G 3rdcoil
101.2G Fluxball 169.6G 3rdcoil
50.6G Fluxball 296.8G 3rdcoil
101.2G Fluxball 296.8G 3rdcoil

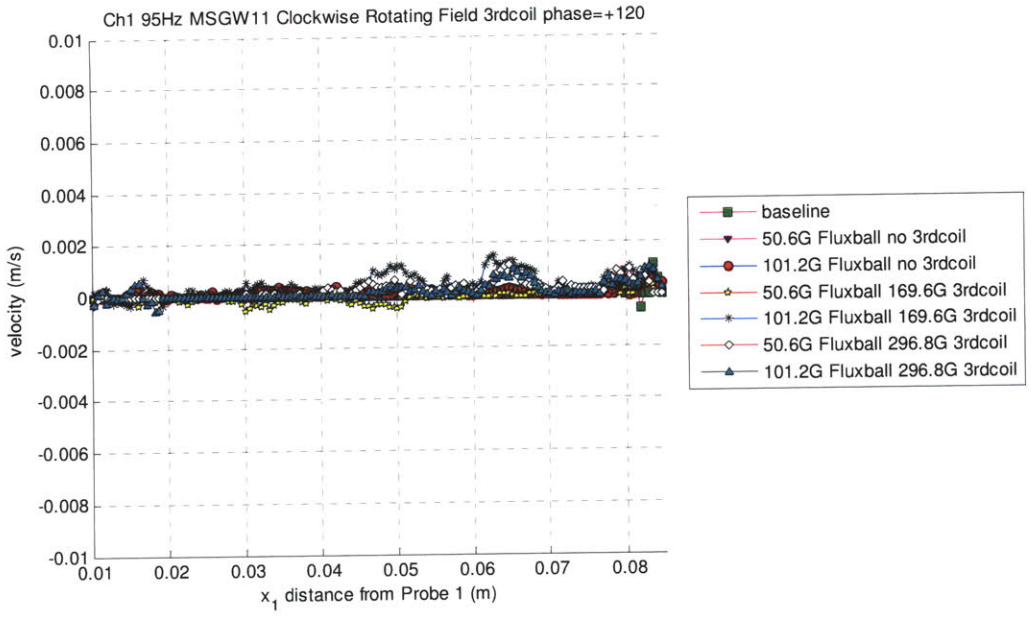
Ch1 95Hz MSGW11 Clockwise Rotating Field 3rdcoil phase=+120
velocity (m/s)
0.01
0.008
0.006
0.004
0.002
0
-0.002
-0.004
-0.006
-0.008
-0.01
0.01
0.02
0.03
0.04
0.05
0.06
0.07
0.08
x1 distance from Probe 1 (m)
baseline
50.6G Fluxball no 3rdcoil
101.2G Fluxball no 3rdcoil
50.6G Fluxball 169.6G 3rdcoil
101.2G Fluxball 169.6G 3rdcoil
50.6G Fluxball 296.8G 3rdcoil
101.2G Fluxball 296.8G 3rdcoil

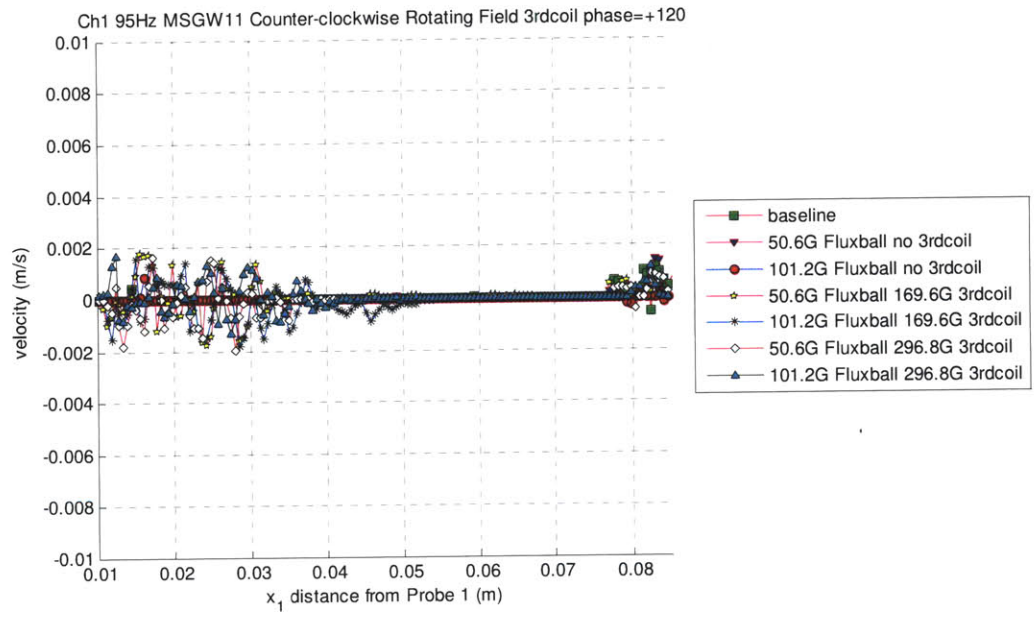
Ch1 95Hz MSGW11 Counter-clockwise Rotating Field 3rdcoil phase=+120
velocity (m/s)
0.01
0.008
0.006
0.004
0.002
0
-0.002
-0.004
-0.006
-0.008
-0.01
0.01
0.02
0.03
0.04
0.05
0.06
0.07
0.08
x1 distance from Probe 1 (m)
baseline
50.6G Fluxball no 3rdcoil
101.2G Fluxball no 3rdcoil
50.6G Fluxball 169.6G 3rdcoil
101.2G Fluxball 169.6G 3rdcoil
50.6G Fluxball 296.8G 3rdcoil
101.2G Fluxball 296.8G 3rdcoil

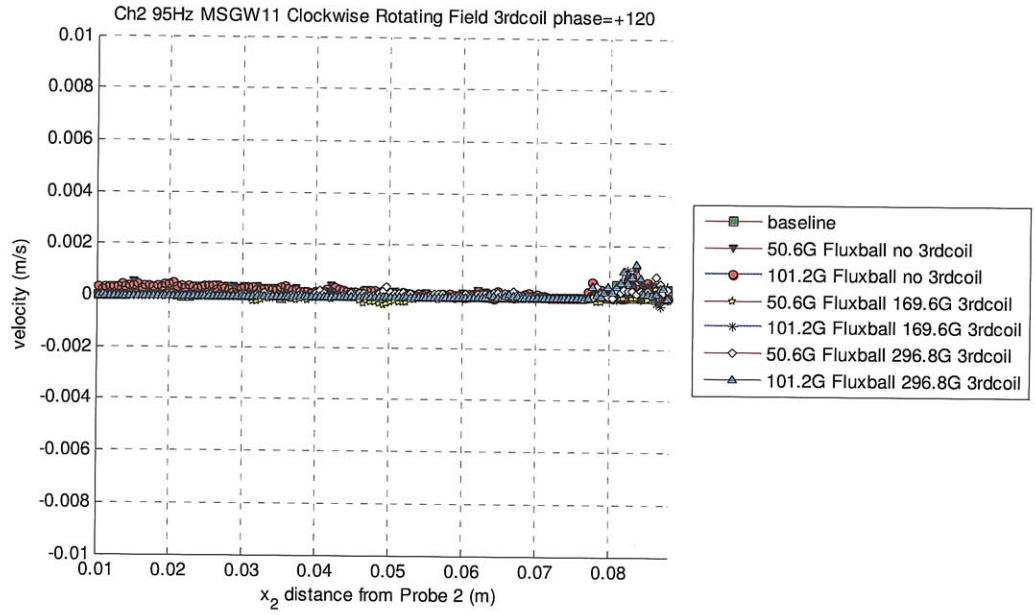
Ch2 95Hz MSGW11 Clockwise Rotating Field 3rdcoil phase=+120
velocity (m/s)
0.01
0.008
0.006
0.004
0.002
0
-0.002
-0.004
-0.006
-0.008
-0.01
0.01 0.02 0.03 0.04 0.05 0.06 0.07 0.08
x2 distance from Probe 2 (m)
baseline
50.6G Fluxball no 3rdcoil
101.2G Fluxball no 3rdcoil
50.6G Fluxball 169.6G 3rdcoil
101.2G Fluxball 169.6G 3rdcoil
50.6G Fluxball 296.8G 3rdcoil
101.2G Fluxball 296.8G 3rdcoil

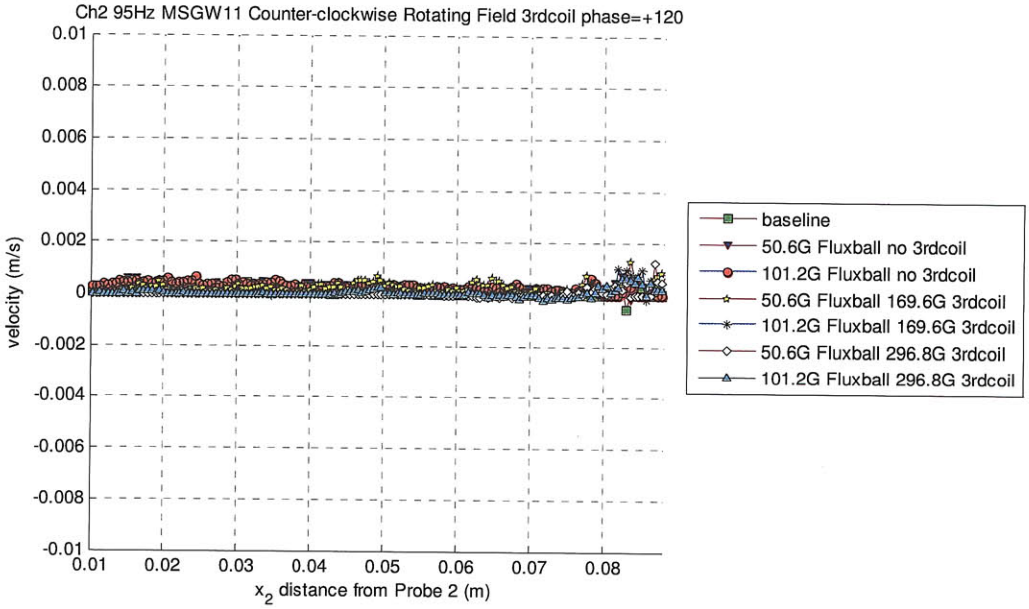
Ch2 95Hz MSGW11 Counter-clockwise Rotating Field 3rdcoil phase=+120
velocity (m/s)
0.01
0.008
0.006
0.004
0.002
0
-0.002
-0.004
-0.006
-0.008
-0.01
0.01 0.02 0.03 0.04 0.05 0.06 0.07 0.08
x2 distance from Probe 2 (m)
baseline
50.6G Fluxball no 3rdcoil
101.2G Fluxball no 3rdcoil
50.6G Fluxball 169.6G 3rdcoil
101.2G Fluxball 169.6G 3rdcoil
50.6G Fluxball 296.8G 3rdcoil
101.2G Fluxball 296.8G 3rdcoil

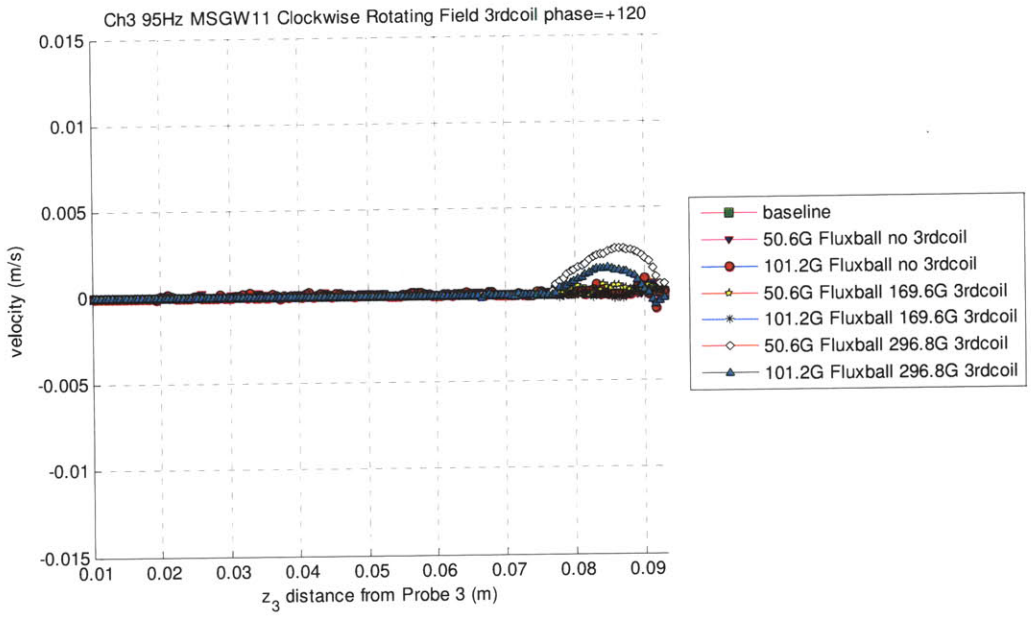
Ch3 95Hz MSGW11 Clockwise Rotating Field 3rdcoil phase=+120
velocity (m/s)
0.015
0.01
0.005
0
-0.005
-0.01
-0.015
0.01
0.02
0.03
0.04
0.05
0.06
0.07
0.08
0.09
z_3 distance from Probe 3 (m)
baseline
50.6G Fluxball no 3rdcoil
101.2G Fluxball no 3rdcoil
50.6G Fluxball 169.6G 3rdcoil
101.2G Fluxball 169.6G 3rdcoil
50.6G Fluxball 296.8G 3rdcoil
101.2G Fluxball 296.8G 3rdcoil

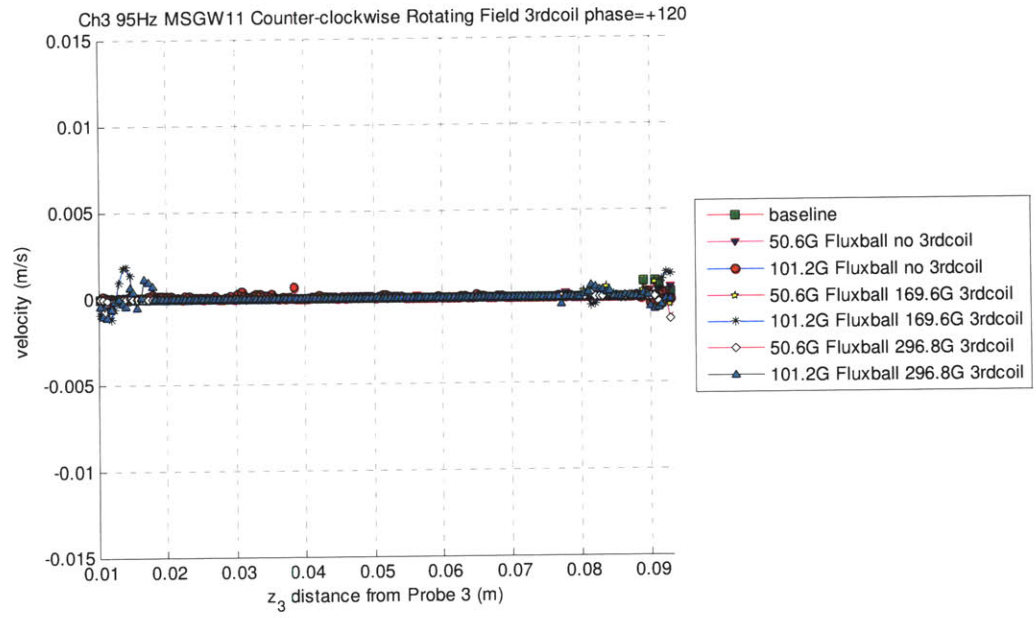
Ch3 95Hz MSGW11 Counter-clockwise Rotating Field 3rdcoil phase=+120
velocity (m/s)
0.015
0.01
0.005
0
-0.005
-0.01
-0.015
0.01
0.02
0.03
0.04
0.05
0.06
0.07
0.08
0.09
z_3 distance from Probe 3 (m)
baseline
50.6G Fluxball no 3rdcoil
101.2G Fluxball no 3rdcoil
50.6G Fluxball 169.6G 3rdcoil
101.2G Fluxball 169.6G 3rdcoil
50.6G Fluxball 296.8G 3rdcoil
101.2G Fluxball 296.8G 3rdcoil

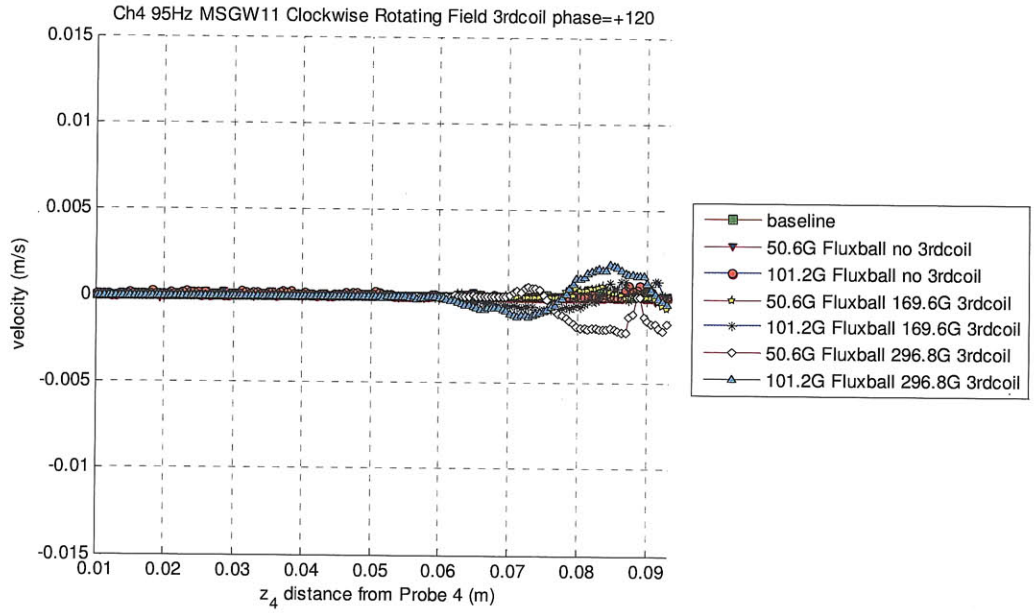
Ch4 95Hz MSGW11 Clockwise Rotating Field 3rdcoil phase=+120
velocity (m/s)
0.015
0.01
0.005
0
-0.005
-0.01
-0.015
0.01
0.02
0.03
0.04
0.05
0.06
0.07
0.08
0.09
z4 distance from Probe 4 (m)
baseline
50.6G Fluxball no 3rdcoil
101.2G Fluxball no 3rdcoil
50.6G Fluxball 169.6G 3rdcoil
101.2G Fluxball 169.6G 3rdcoil
50.6G Fluxball 296.8G 3rdcoil
101.2G Fluxball 296.8G 3rdcoil

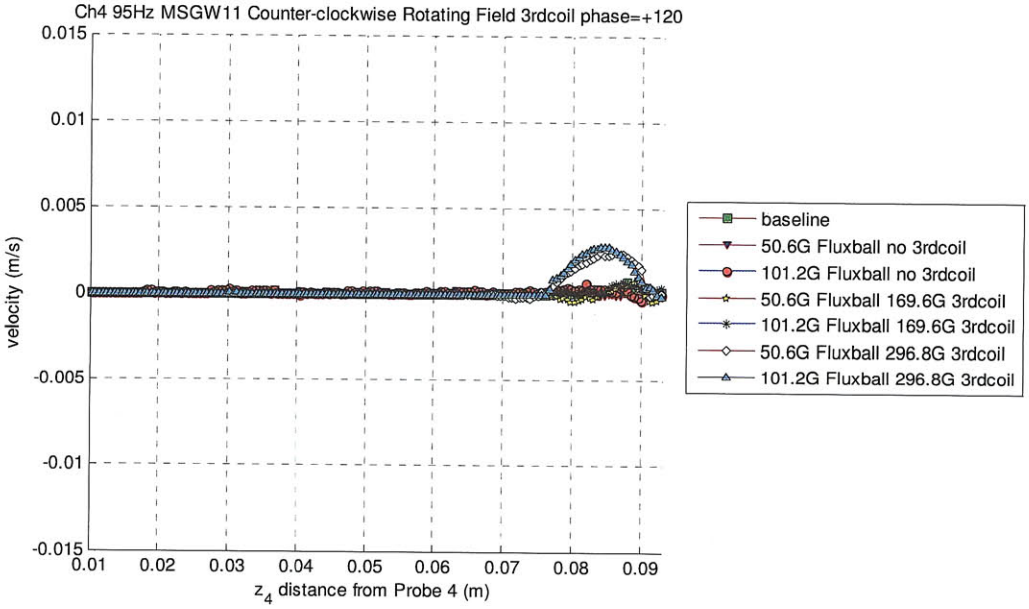
Ch4 95Hz MSGW11 Counter-clockwise Rotating Field 3rdcoil phase=+120
velocity (m/s)
0.015
0.01
0.005
0
-0.005
-0.01
-0.015
0.01
0.02
0.03
0.04
0.05
0.06
0.07
0.08
0.09
z4 distance from Probe 4 (m)
baseline
50.6G Fluxball no 3rdcoil
101.2G Fluxball no 3rdcoil
50.6G Fluxball 169.6G 3rdcoil
101.2G Fluxball 169.6G 3rdcoil
50.6G Fluxball 296.8G 3rdcoil
101.2G Fluxball 296.8G 3rdcoil

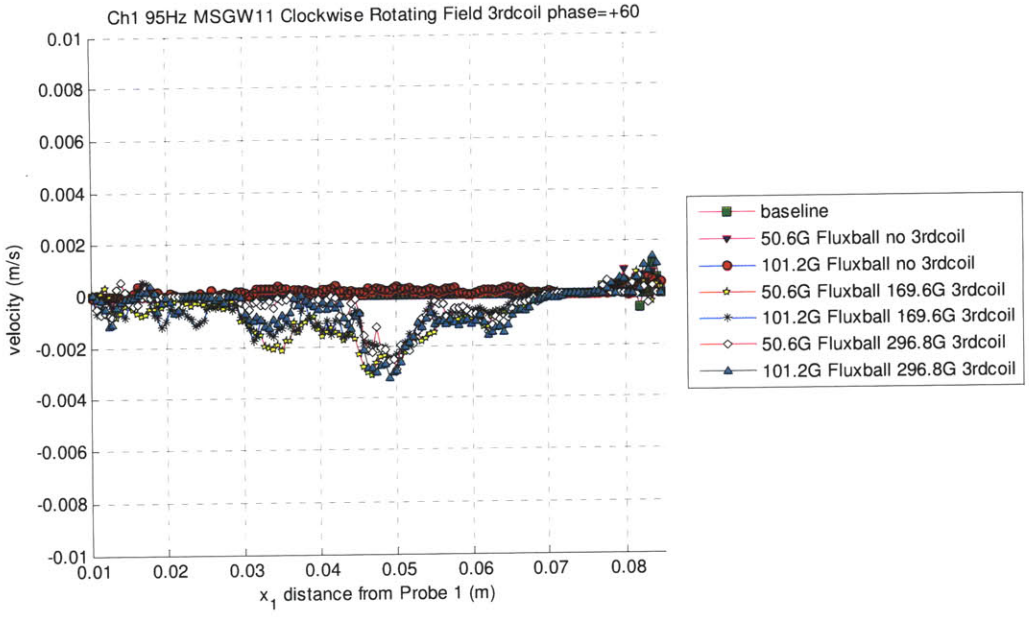
Ch1 95Hz MSGW11 Clockwise Rotating Field 3rdcoil phase=+60
velocity (m/s)
x1 distance from Probe 1 (m)
baseline
50.6G Fluxball no 3rdcoil
101.2G Fluxball no 3rdcoil
50.6G Fluxball 169.6G 3rdcoil
101.2G Fluxball 169.6G 3rdcoil
50.6G Fluxball 296.8G 3rdcoil
101.2G Fluxball 296.8G 3rdcoil

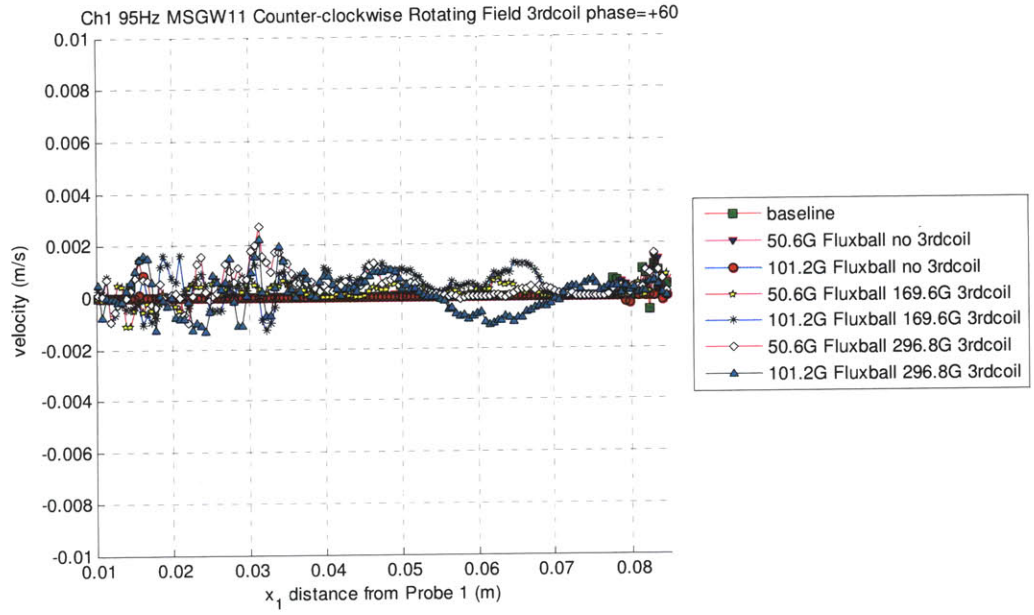
Ch1 95Hz MSGW11 Counter-clockwise Rotating Field 3rdcoil phase=+60
velocity (m/s)
x1 distance from Probe 1 (m)
baseline
50.6G Fluxball no 3rdcoil
101.2G Fluxball no 3rdcoil
50.6G Fluxball 169.6G 3rdcoil
101.2G Fluxball 169.6G 3rdcoil
50.6G Fluxball 296.8G 3rdcoil
101.2G Fluxball 296.8G 3rdcoil

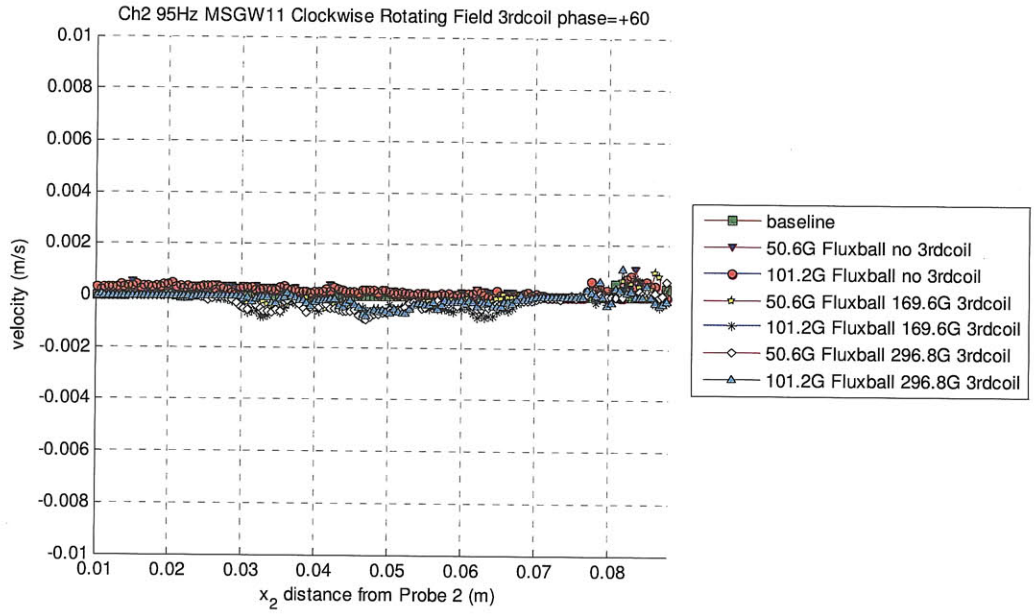
Ch2 95Hz MSGW11 Clockwise Rotating Field 3rdcoil phase=+60
velocity (m/s)
0.01
0.008
0.006
0.004
0.002
0
-0.002
-0.004
-0.006
-0.008
-0.01
0.01
0.02
0.03
0.04
0.05
0.06
0.07
0.08
x2 distance from Probe 2 (m)
baseline
50.6G Fluxball no 3rdcoil
101.2G Fluxball no 3rdcoil
50.6G Fluxball 169.6G 3rdcoil
101.2G Fluxball 169.6G 3rdcoil
50.6G Fluxball 296.8G 3rdcoil
101.2G Fluxball 296.8G 3rdcoil

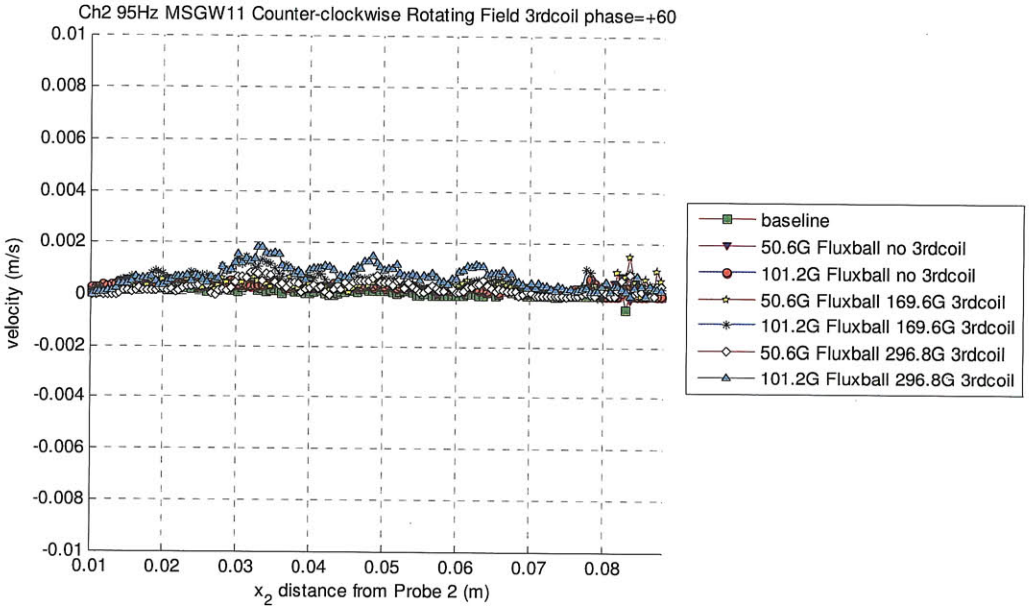
Ch2 95Hz MSGW11 Counter-clockwise Rotating Field 3rdcoil phase=+60
velocity (m/s)
0.01
0.008
0.006
0.004
0.002
0
-0.002
-0.004
-0.006
-0.008
-0.01
0.01
0.02
0.03
0.04
0.05
0.06
0.07
0.08
x2 distance from Probe 2 (m)
baseline
50.6G Fluxball no 3rdcoil
101.2G Fluxball no 3rdcoil
50.6G Fluxball 169.6G 3rdcoil
101.2G Fluxball 169.6G 3rdcoil
50.6G Fluxball 296.8G 3rdcoil
101.2G Fluxball 296.8G 3rdcoil

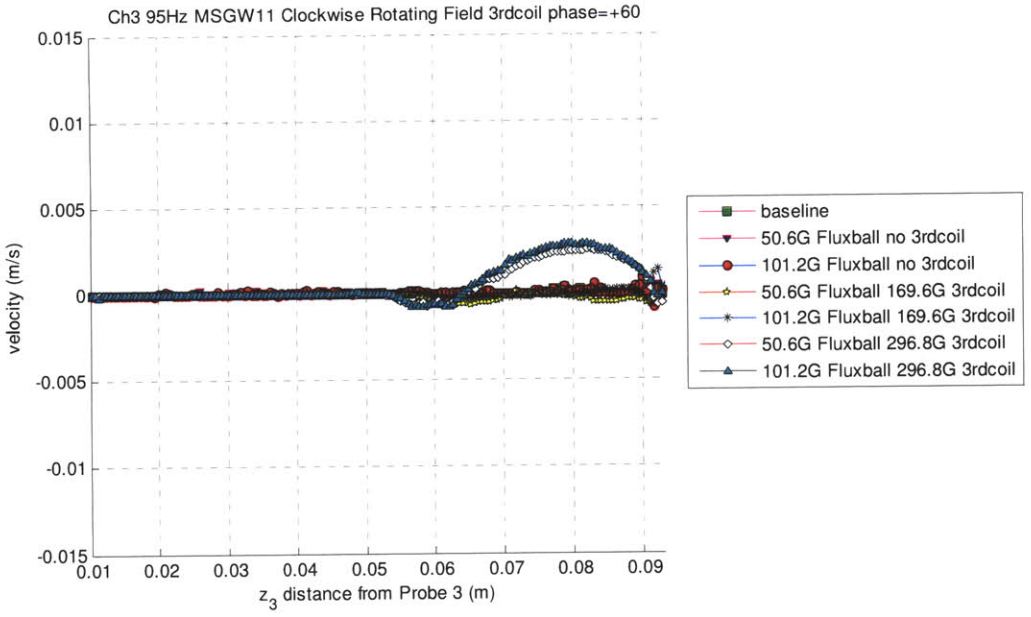
Ch3 95Hz MSGW11 Clockwise Rotating Field 3rdcoil phase=+60
velocity (m/s)
0.015
0.01
0.005
0
-0.005
-0.01
-0.015
0.01
0.02
0.03
0.04
0.05
0.06
0.07
0.08
0.09
z_3 distance from Probe 3 (m)
baseline
50.6G Fluxball no 3rdcoil
101.2G Fluxball no 3rdcoil
50.6G Fluxball 169.6G 3rdcoil
101.2G Fluxball 169.6G 3rdcoil
50.6G Fluxball 296.8G 3rdcoil
101.2G Fluxball 296.8G 3rdcoil

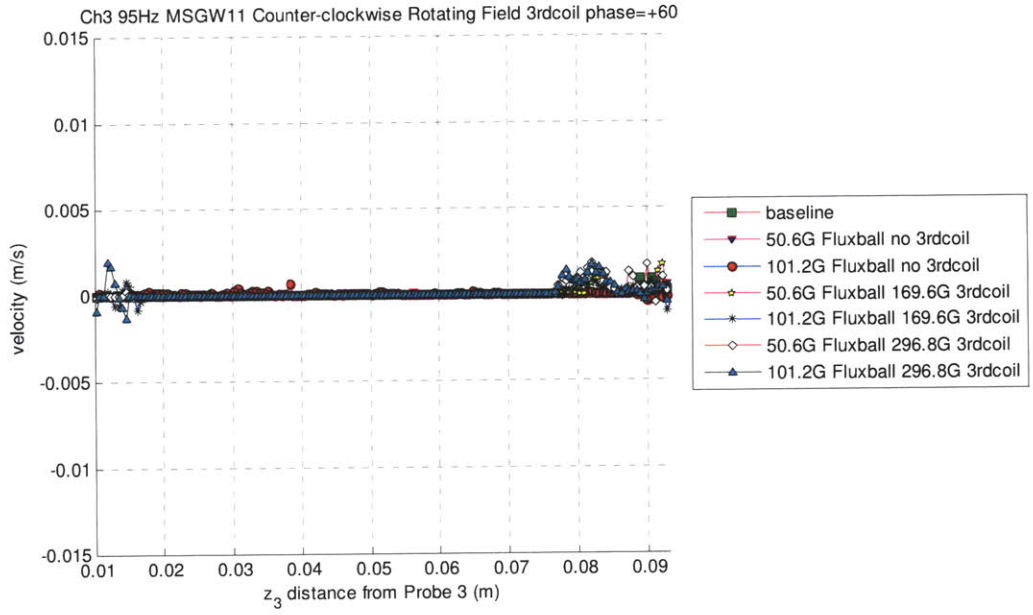
Ch3 95Hz MSGW11 Counter-clockwise Rotating Field 3rdcoil phase=+60
velocity (m/s)
0.015
0.01
0.005
0
-0.005
-0.01
-0.015
0.01
0.02
0.03
0.04
0.05
0.06
0.07
0.08
0.09
z_3 distance from Probe 3 (m)
baseline
50.6G Fluxball no 3rdcoil
101.2G Fluxball no 3rdcoil
50.6G Fluxball 169.6G 3rdcoil
101.2G Fluxball 169.6G 3rdcoil
50.6G Fluxball 296.8G 3rdcoil
101.2G Fluxball 296.8G 3rdcoil

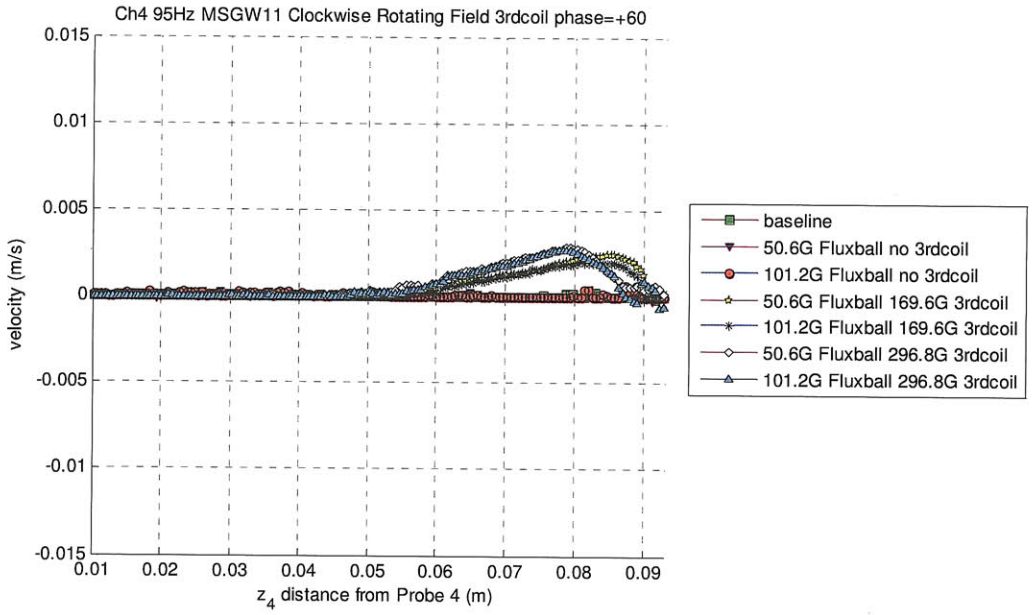
Ch4 95Hz MSGW11 Clockwise Rotating Field 3rdcoil phase=+60
velocity (m/s)
0.015
0.01
0.005
0
-0.005
-0.01
-0.015
0.01
0.02
0.03
0.04
0.05
0.06
0.07
0.08
0.09
z4 distance from Probe 4 (m)
baseline
50.6G Fluxball no 3rdcoil
101.2G Fluxball no 3rdcoil
50.6G Fluxball 169.6G 3rdcoil
101.2G Fluxball 169.6G 3rdcoil
50.6G Fluxball 296.8G 3rdcoil
101.2G Fluxball 296.8G 3rdcoil

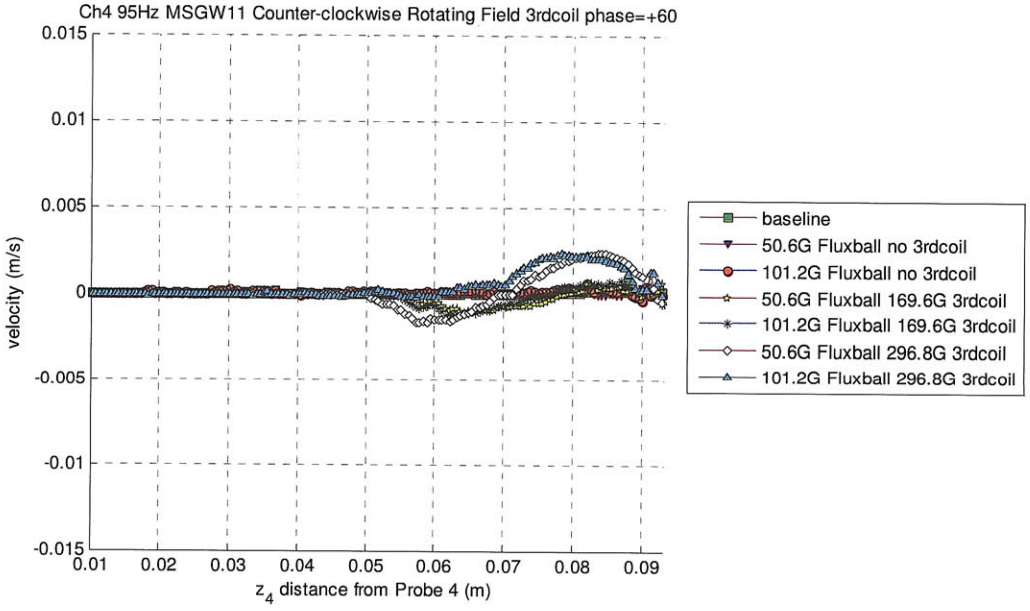
Ch4 95Hz MSGW11 Counter-clockwise Rotating Field 3rdcoil phase=+60
velocity (m/s)
0.015
0.01
0.005
0
-0.005
-0.01
-0.015
0.01
0.02
0.03
0.04
0.05
0.06
0.07
0.08
0.09
z4 distance from Probe 4 (m)
baseline
50.6G Fluxball no 3rdcoil
101.2G Fluxball no 3rdcoil
50.6G Fluxball 169.6G 3rdcoil
101.2G Fluxball 169.6G 3rdcoil
50.6G Fluxball 296.8G 3rdcoil
101.2G Fluxball 296.8G 3rdcoil

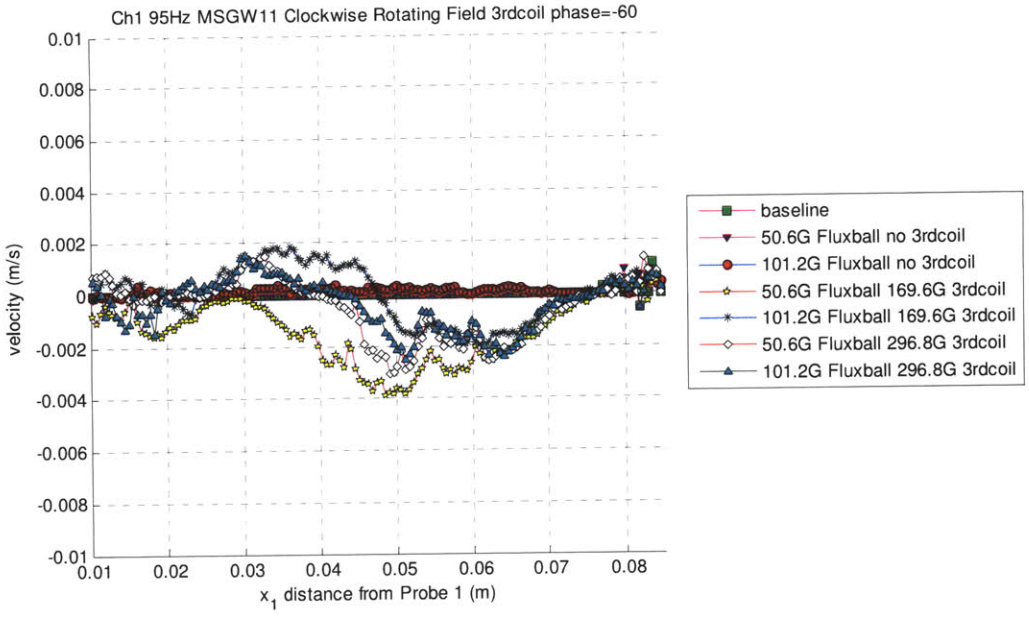
Ch1 95Hz MSGW11 Clockwise Rotating Field 3rdcoil phase=-60
velocity (m/s)
0.01
0.008
0.006
0.004
0.002
0
-0.002
-0.004
-0.006
-0.008
-0.01
0.01
0.02
0.03
0.04
0.05
0.06
0.07
0.08
x1 distance from Probe 1 (m)
baseline
50.6G Fluxball no 3rdcoil
101.2G Fluxball no 3rdcoil
50.6G Fluxball 169.6G 3rdcoil
101.2G Fluxball 169.6G 3rdcoil
50.6G Fluxball 296.8G 3rdcoil
101.2G Fluxball 296.8G 3rdcoil

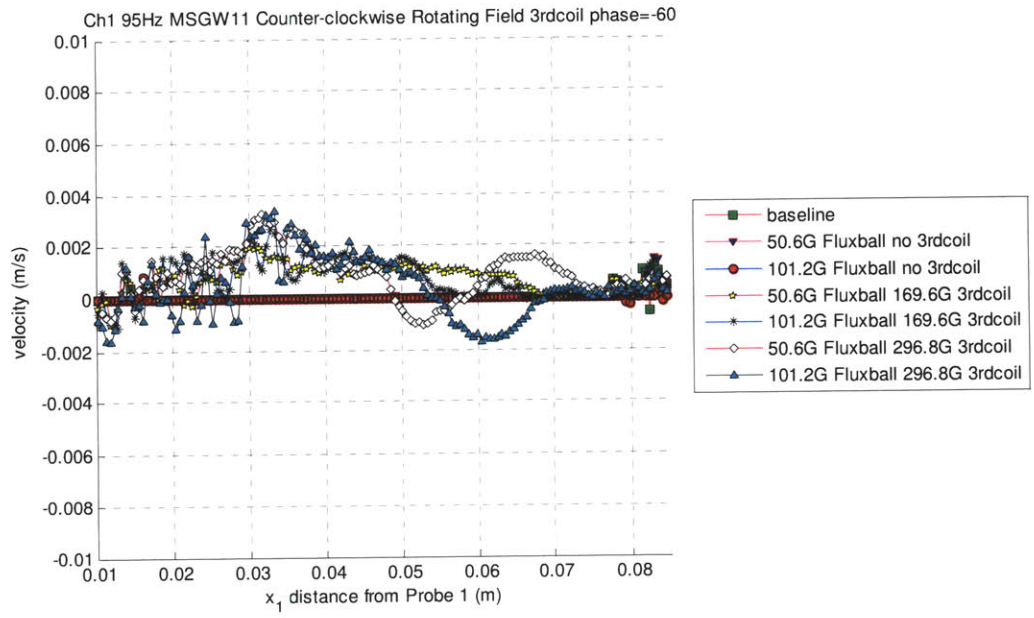
Ch1 95Hz MSGW11 Counter-clockwise Rotating Field 3rdcoil phase=-60
velocity (m/s)
0.01
0.008
0.006
0.004
0.002
0
-0.002
-0.004
-0.006
-0.008
-0.01
0.01
0.02
0.03
0.04
0.05
0.06
0.07
0.08
x1 distance from Probe 1 (m)
baseline
50.6G Fluxball no 3rdcoil
101.2G Fluxball no 3rdcoil
50.6G Fluxball 169.6G 3rdcoil
101.2G Fluxball 169.6G 3rdcoil
50.6G Fluxball 296.8G 3rdcoil
101.2G Fluxball 296.8G 3rdcoil

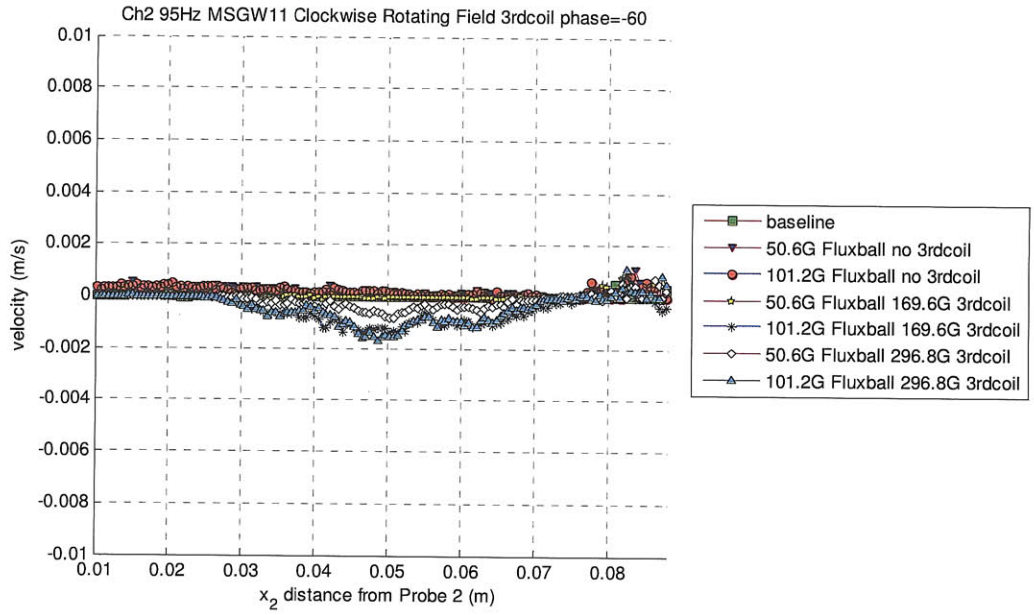
Ch2 95Hz MSGW11 Clockwise Rotating Field 3rdcoil phase=-60
velocity (m/s)
0.01
0.008
0.006
0.004
0.002
0
-0.002
-0.004
-0.006
-0.008
-0.01
0.01 0.02 0.03 0.04 0.05 0.06 0.07 0.08
x2 distance from Probe 2 (m)
baseline
50.6G Fluxball no 3rdcoil
101.2G Fluxball no 3rdcoil
50.6G Fluxball 169.6G 3rdcoil
101.2G Fluxball 169.6G 3rdcoil
50.6G Fluxball 296.8G 3rdcoil
101.2G Fluxball 296.8G 3rdcoil

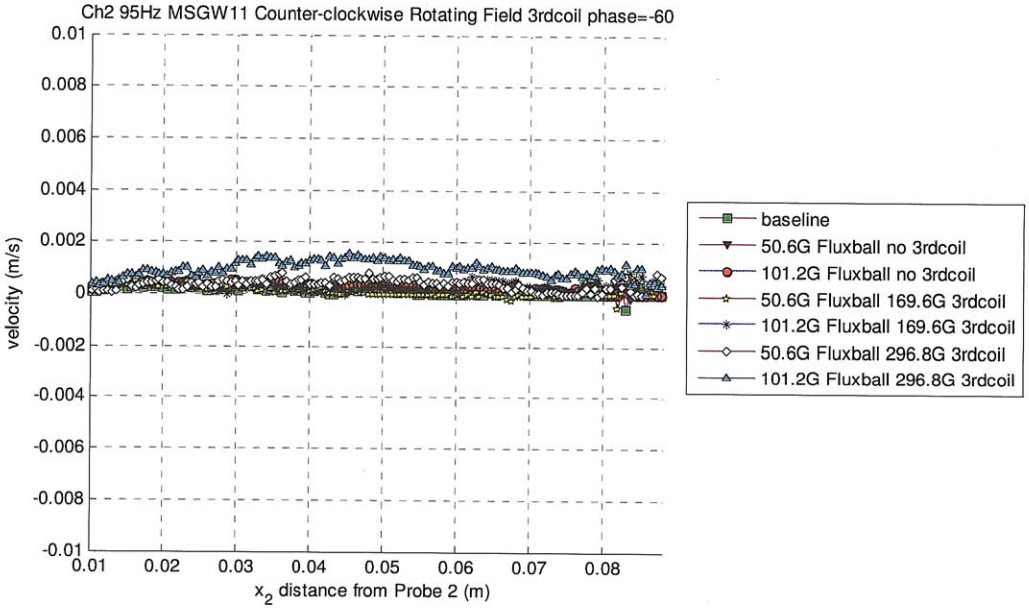
Ch2 95Hz MSGW11 Counter-clockwise Rotating Field 3rdcoil phase=-60
velocity (m/s)
0.01
0.008
0.006
0.004
0.002
0
-0.002
-0.004
-0.006
-0.008
-0.01
0.01 0.02 0.03 0.04 0.05 0.06 0.07 0.08
x2 distance from Probe 2 (m)
baseline
50.6G Fluxball no 3rdcoil
101.2G Fluxball no 3rdcoil
50.6G Fluxball 169.6G 3rdcoil
101.2G Fluxball 169.6G 3rdcoil
50.6G Fluxball 296.8G 3rdcoil
101.2G Fluxball 296.8G 3rdcoil

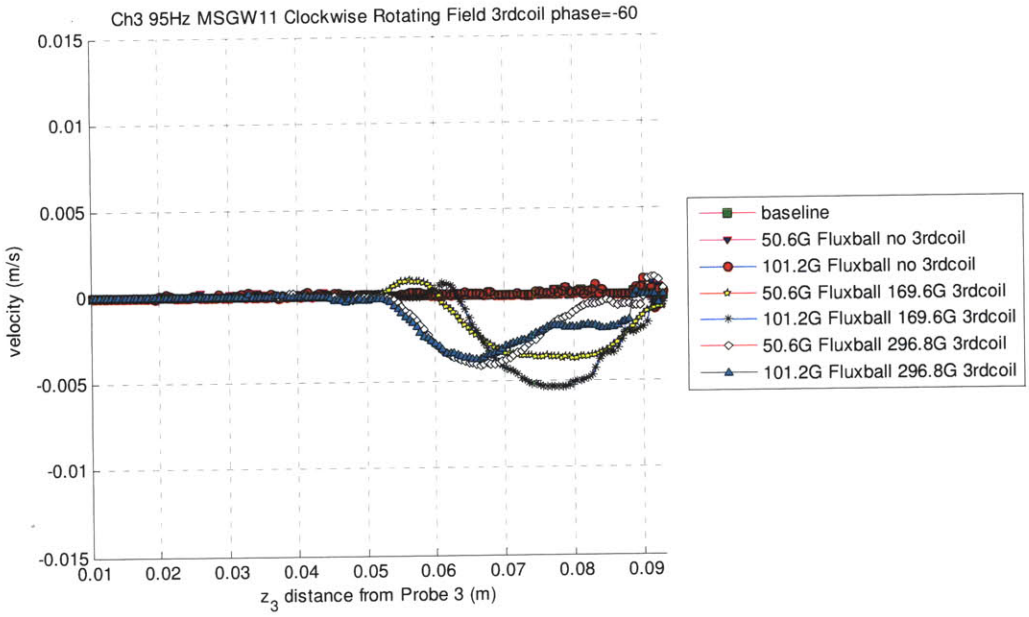
Ch3 95Hz MSGW11 Clockwise Rotating Field 3rdcoil phase=-60
velocity (m/s)
0.015
0.01
0.005
0
-0.005
-0.01
-0.015
0.01
0.02
0.03
0.04
0.05
0.06
0.07
0.08
0.09
z3 distance from Probe 3 (m)
baseline
50.6G Fluxball no 3rdcoil
101.2G Fluxball no 3rdcoil
50.6G Fluxball 169.6G 3rdcoil
101.2G Fluxball 169.6G 3rdcoil
50.6G Fluxball 296.8G 3rdcoil
101.2G Fluxball 296.8G 3rdcoil

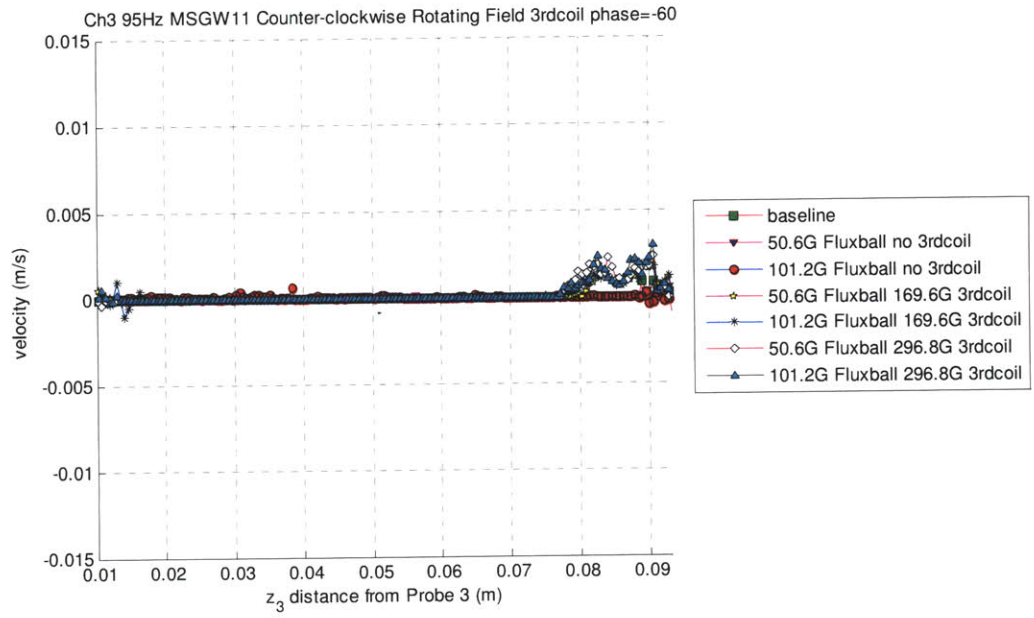
Ch3 95Hz MSGW11 Counter-clockwise Rotating Field 3rdcoil phase=-60
velocity (m/s)
0.015
0.01
0.005
0
-0.005
-0.01
-0.015
0.01
0.02
0.03
0.04
0.05
0.06
0.07
0.08
0.09
z3 distance from Probe 3 (m)
baseline
50.6G Fluxball no 3rdcoil
101.2G Fluxball no 3rdcoil
50.6G Fluxball 169.6G 3rdcoil
101.2G Fluxball 169.6G 3rdcoil
50.6G Fluxball 296.8G 3rdcoil
101.2G Fluxball 296.8G 3rdcoil

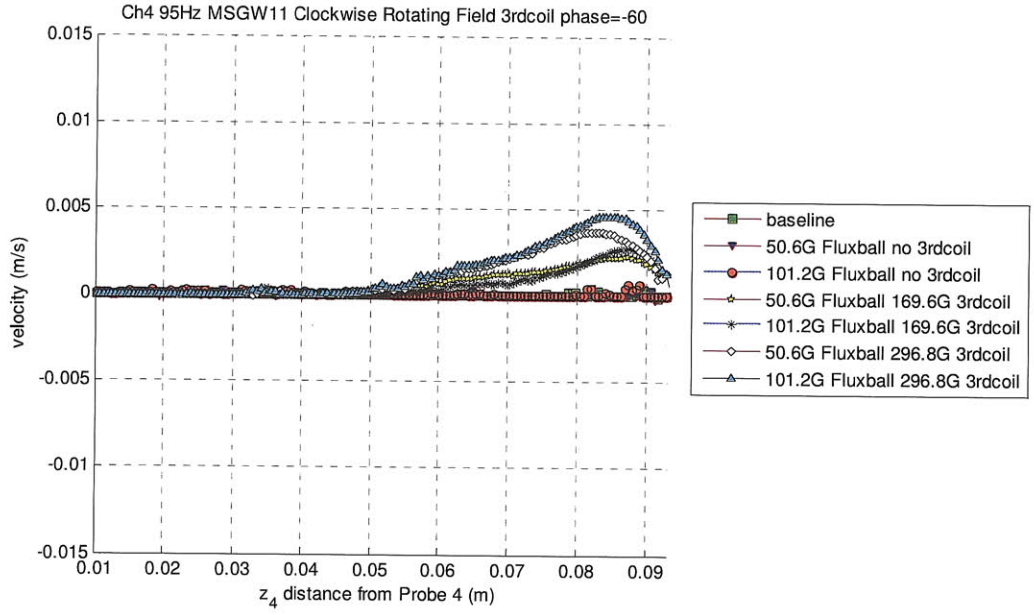
Ch4 95Hz MSGW11 Clockwise Rotating Field 3rdcoil phase=-60
velocity (m/s)
0.015
0.01
0.005
0
-0.005
-0.01
-0.015
0.01
0.02
0.03
0.04
0.05
0.06
0.07
0.08
0.09
z4 distance from Probe 4 (m)
baseline
50.6G Fluxball no 3rdcoil
101.2G Fluxball no 3rdcoil
50.6G Fluxball 169.6G 3rdcoil
101.2G Fluxball 169.6G 3rdcoil
50.6G Fluxball 296.8G 3rdcoil
101.2G Fluxball 296.8G 3rdcoil

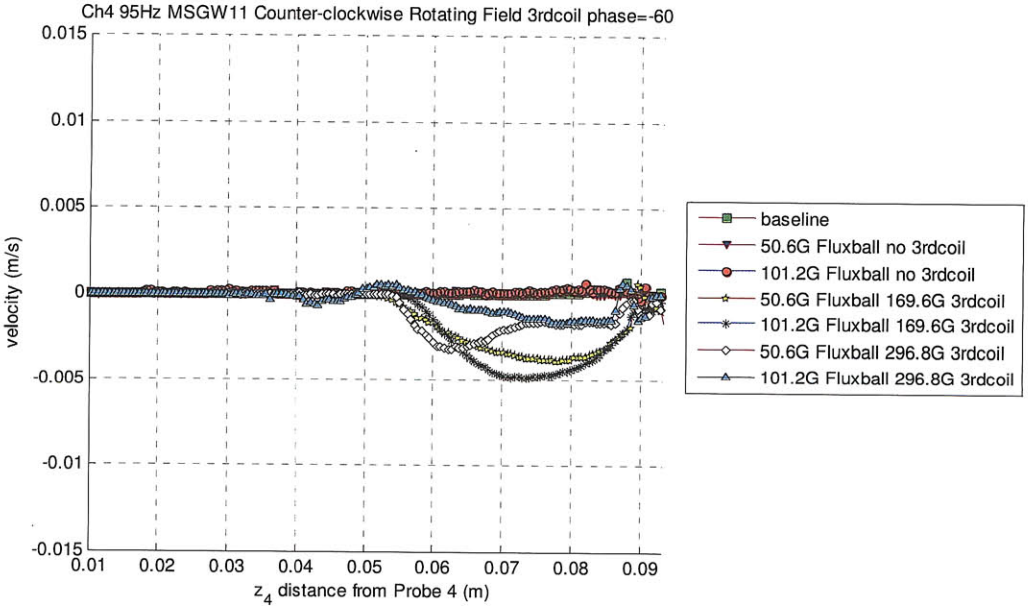
Ch4 95Hz MSGW11 Counter-clockwise Rotating Field 3rdcoil phase=-60
velocity (m/s)
0.015
0.01
0.005
0
-0.005
-0.01
-0.015
0.01
0.02
0.03
0.04
0.05
0.06
0.07
0.08
0.09
z4 distance from Probe 4 (m)
baseline
50.6G Fluxball no 3rdcoil
101.2G Fluxball no 3rdcoil
50.6G Fluxball 169.6G 3rdcoil
101.2G Fluxball 169.6G 3rdcoil
50.6G Fluxball 296.8G 3rdcoil
101.2G Fluxball 296.8G 3rdcoil

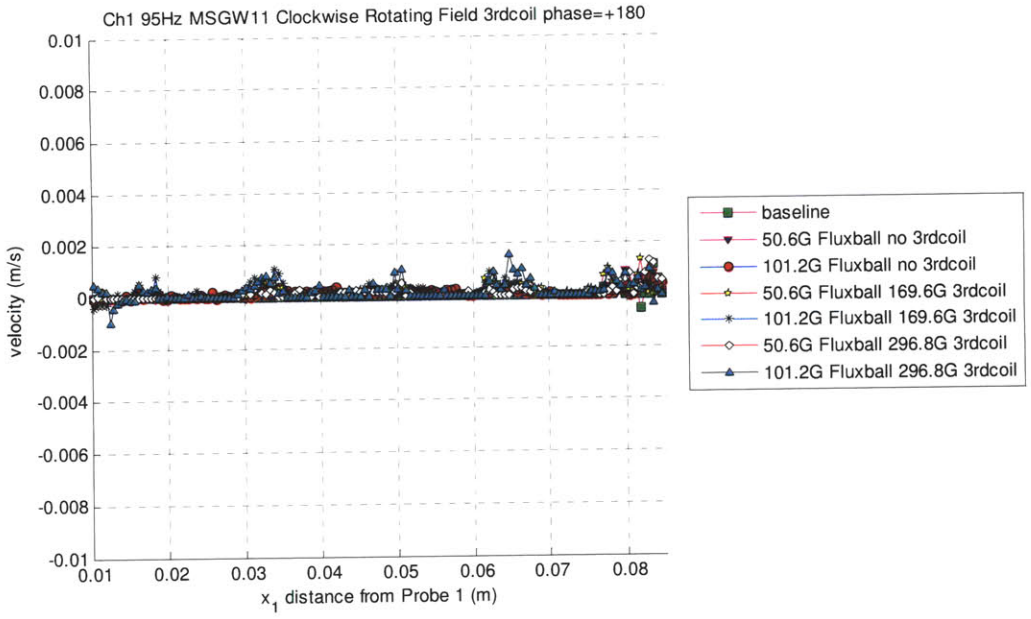
Ch1 95Hz MSGW11 Clockwise Rotating Field 3rdcoil phase=+180
velocity (m/s)
0.01
0.008
0.006
0.004
0.002
0
-0.002
-0.004
-0.006
-0.008
-0.01
0.01
0.02
0.03
0.04
0.05
0.06
0.07
0.08
x1 distance from Probe 1 (m)
baseline
50.6G Fluxball no 3rdcoil
101.2G Fluxball no 3rdcoil
50.6G Fluxball 169.6G 3rdcoil
101.2G Fluxball 169.6G 3rdcoil
50.6G Fluxball 296.8G 3rdcoil
101.2G Fluxball 296.8G 3rdcoil

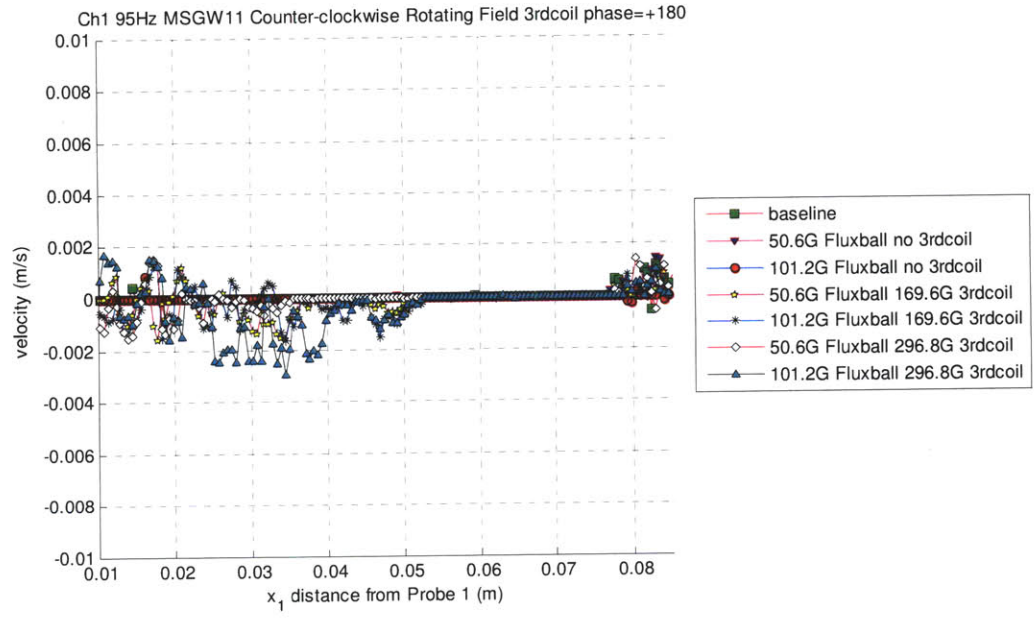
Ch1 95Hz MSGW11 Counter-clockwise Rotating Field 3rdcoil phase=+180
velocity (m/s)
0.01
0.008
0.006
0.004
0.002
0
-0.002
-0.004
-0.006
-0.008
-0.01
0.01
0.02
0.03
0.04
0.05
0.06
0.07
0.08
x1 distance from Probe 1 (m)
baseline
50.6G Fluxball no 3rdcoil
101.2G Fluxball no 3rdcoil
50.6G Fluxball 169.6G 3rdcoil
101.2G Fluxball 169.6G 3rdcoil
50.6G Fluxball 296.8G 3rdcoil
101.2G Fluxball 296.8G 3rdcoil

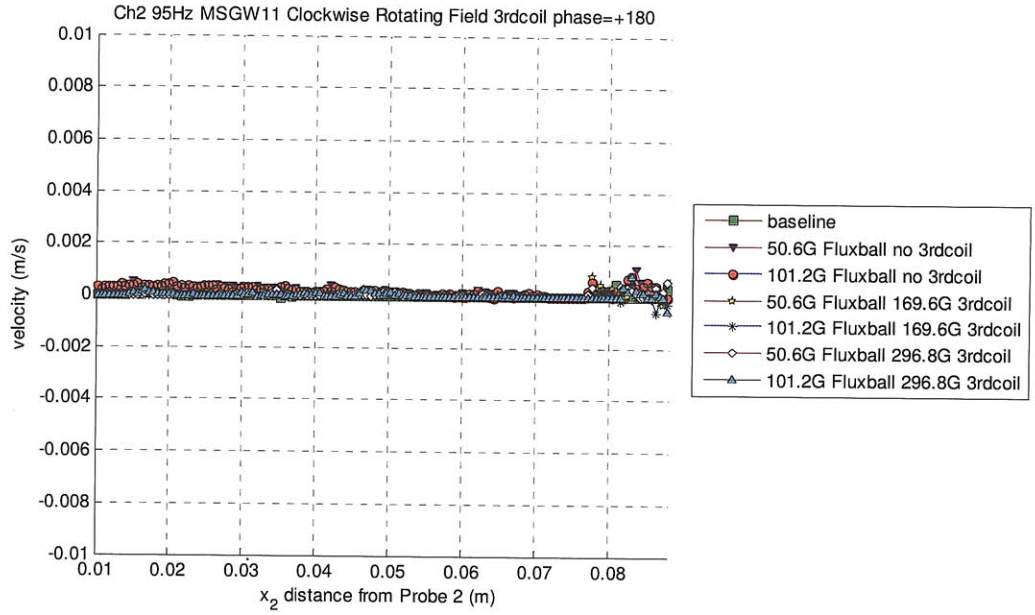
Ch2 95Hz MSGW11 Clockwise Rotating Field 3rdcoil phase=+180
velocity (m/s)
0.01
0.008
0.006
0.004
0.002
0
-0.002
-0.004
-0.006
-0.008
-0.01
0.01
0.02
0.03
0.04
0.05
0.06
0.07
0.08
x2 distance from Probe 2 (m)
baseline
50.6G Fluxball no 3rdcoil
101.2G Fluxball no 3rdcoil
50.6G Fluxball 169.6G 3rdcoil
101.2G Fluxball 169.6G 3rdcoil
50.6G Fluxball 296.8G 3rdcoil
101.2G Fluxball 296.8G 3rdcoil

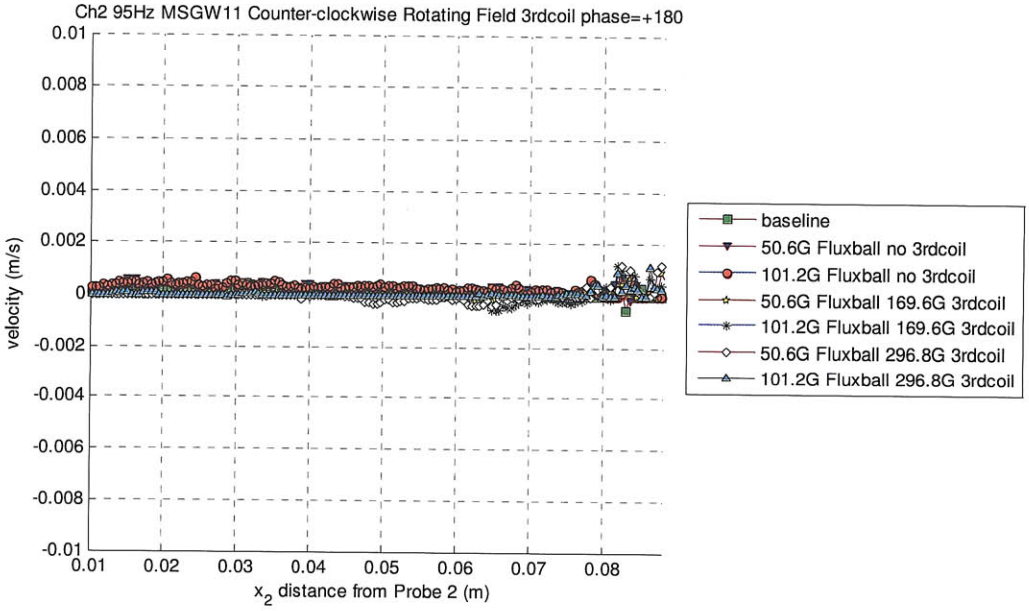
Ch2 95Hz MSGW11 Counter-clockwise Rotating Field 3rdcoil phase=+180
velocity (m/s)
0.01
0.008
0.006
0.004
0.002
0
-0.002
-0.004
-0.006
-0.008
-0.01
0.01
0.02
0.03
0.04
0.05
0.06
0.07
0.08
x2 distance from Probe 2 (m)
baseline
50.6G Fluxball no 3rdcoil
101.2G Fluxball no 3rdcoil
50.6G Fluxball 169.6G 3rdcoil
101.2G Fluxball 169.6G 3rdcoil
50.6G Fluxball 296.8G 3rdcoil
101.2G Fluxball 296.8G 3rdcoil

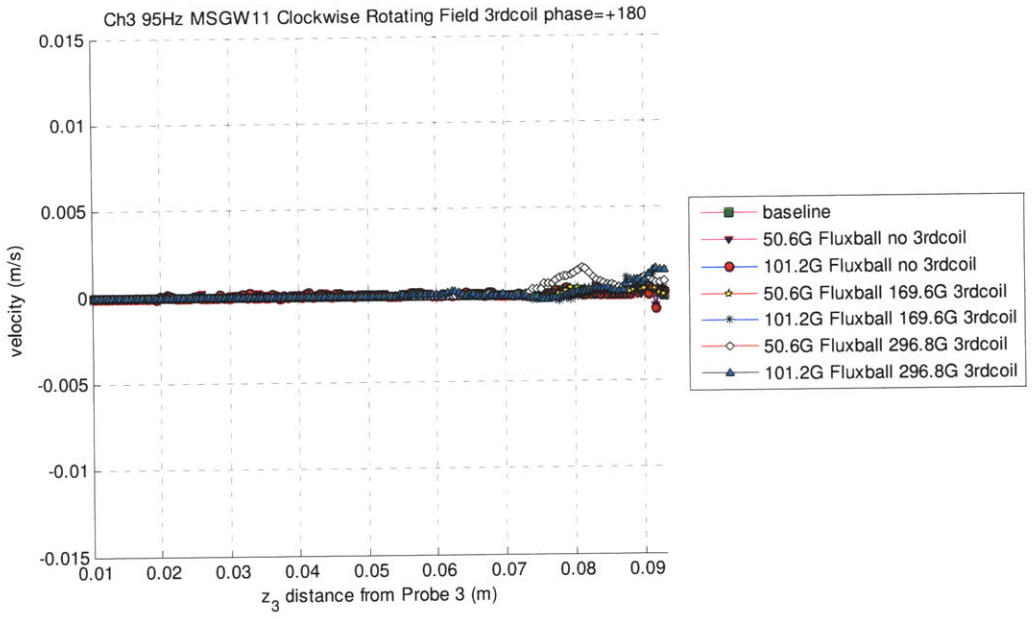
Ch3 95Hz MSGW11 Clockwise Rotating Field 3rdcoil phase=+180
velocity (m/s)
0.015
0.01
0.005
0
-0.005
-0.01
-0.015
0.01
0.02
0.03
0.04
0.05
0.06
0.07
0.08
0.09
z_3 distance from Probe 3 (m)
baseline
50.6G Fluxball no 3rdcoil
101.2G Fluxball no 3rdcoil
50.6G Fluxball 169.6G 3rdcoil
101.2G Fluxball 169.6G 3rdcoil
50.6G Fluxball 296.8G 3rdcoil
101.2G Fluxball 296.8G 3rdcoil

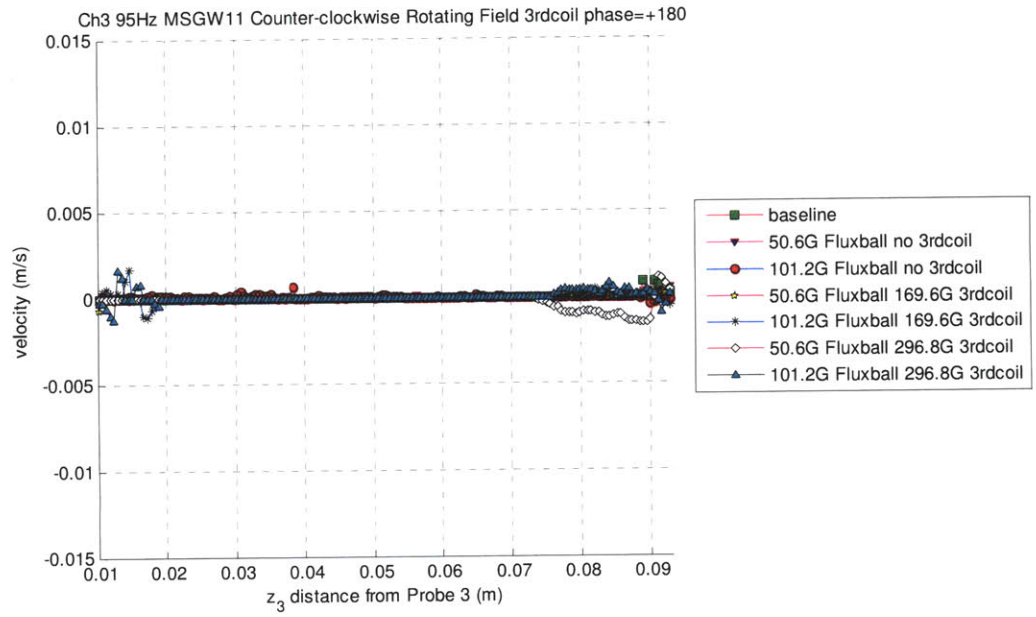
Ch3 95Hz MSGW11 Counter-clockwise Rotating Field 3rdcoil phase=+180
velocity (m/s)
0.015
0.01
0.005
0
-0.005
-0.01
-0.015
0.01
0.02
0.03
0.04
0.05
0.06
0.07
0.08
0.09
z_3 distance from Probe 3 (m)
baseline
50.6G Fluxball no 3rdcoil
101.2G Fluxball no 3rdcoil
50.6G Fluxball 169.6G 3rdcoil
101.2G Fluxball 169.6G 3rdcoil
50.6G Fluxball 296.8G 3rdcoil
101.2G Fluxball 296.8G 3rdcoil

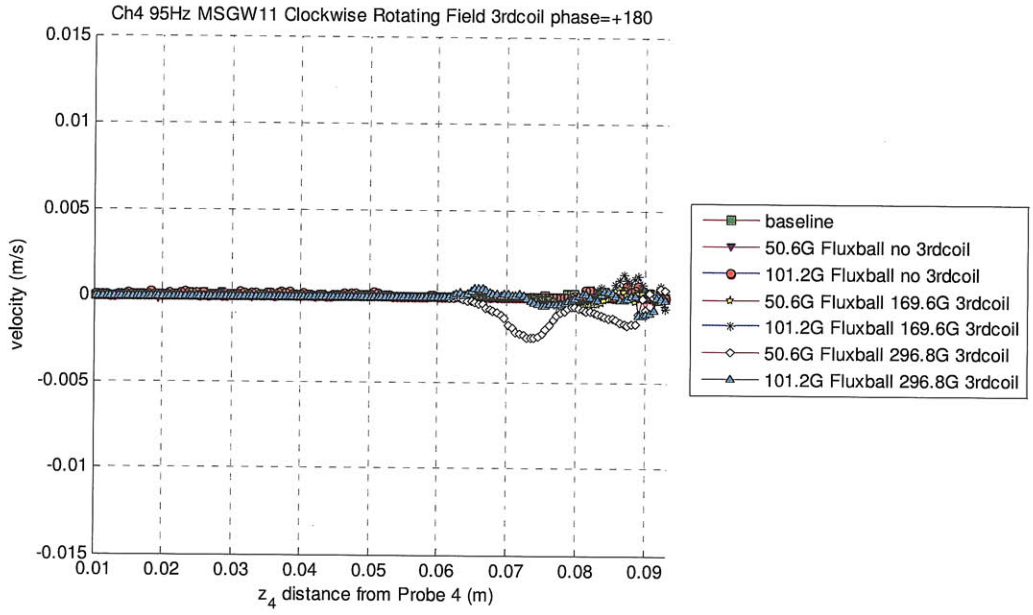
Ch4 95Hz MSGW11 Clockwise Rotating Field 3rdcoil phase=+180
velocity (m/s)
0.015
0.01
0.005
0
-0.005
-0.01
-0.015
0.01
0.02
0.03
0.04
0.05
0.06
0.07
0.08
0.09
z4 distance from Probe 4 (m)
baseline
50.6G Fluxball no 3rdcoil
101.2G Fluxball no 3rdcoil
50.6G Fluxball 169.6G 3rdcoil
101.2G Fluxball 169.6G 3rdcoil
50.6G Fluxball 296.8G 3rdcoil
101.2G Fluxball 296.8G 3rdcoil

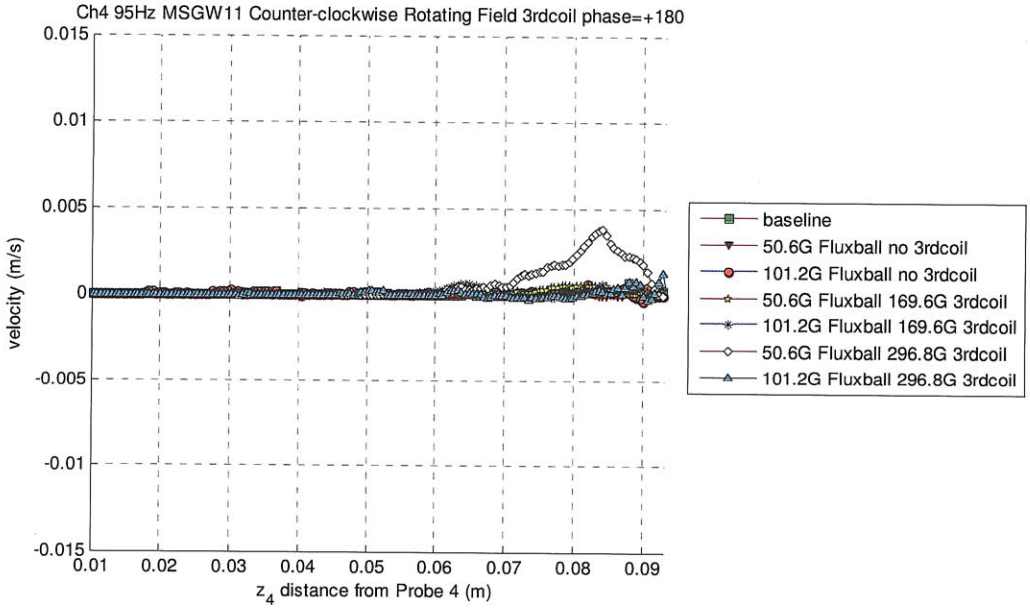
Ch4 95Hz MSGW11 Counter-clockwise Rotating Field 3rdcoil phase=+180
velocity (m/s)
0.015
0.01
0.005
0
-0.005
-0.01
-0.015
0.01
0.02
0.03
0.04
0.05
0.06
0.07
0.08
0.09
z4 distance from Probe 4 (m)
baseline
50.6G Fluxball no 3rdcoil
101.2G Fluxball no 3rdcoil
50.6G Fluxball 169.6G 3rdcoil
101.2G Fluxball 169.6G 3rdcoil
50.6G Fluxball 296.8G 3rdcoil
101.2G Fluxball 296.8G 3rdcoil

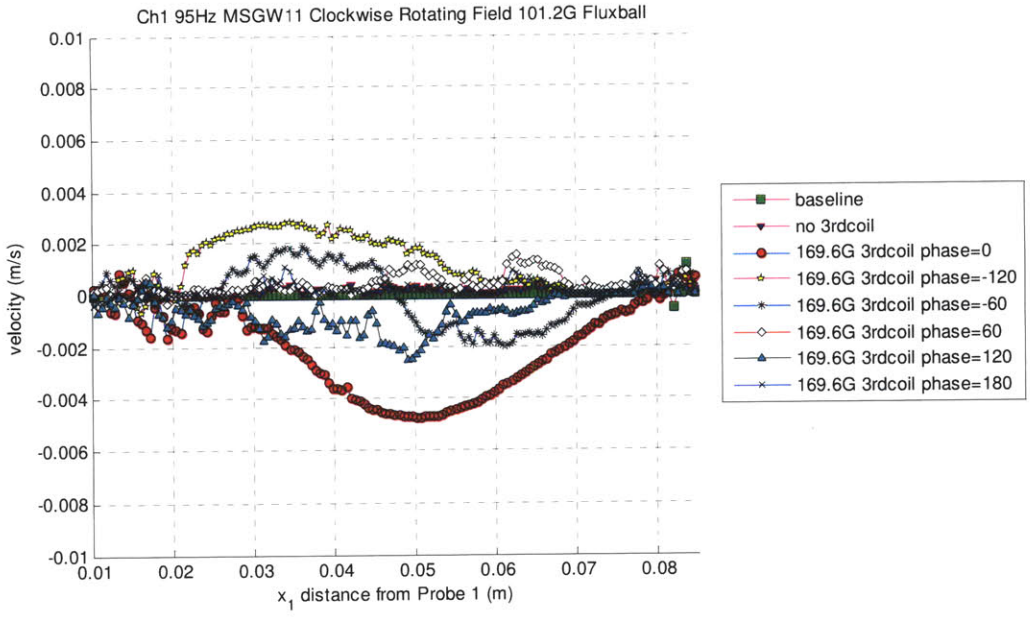
Ch1 95Hz MSGW11 Clockwise Rotating Field 101.2G Fluxball
velocity (m/s)
x1 distance from Probe 1 (m)
baseline
no 3rdcoil
169.6G 3rdcoil phase=0
169.6G 3rdcoil phase=-120
169.6G 3rdcoil phase=-60
169.6G 3rdcoil phase=60
169.6G 3rdcoil phase=120
169.6G 3rdcoil phase=180

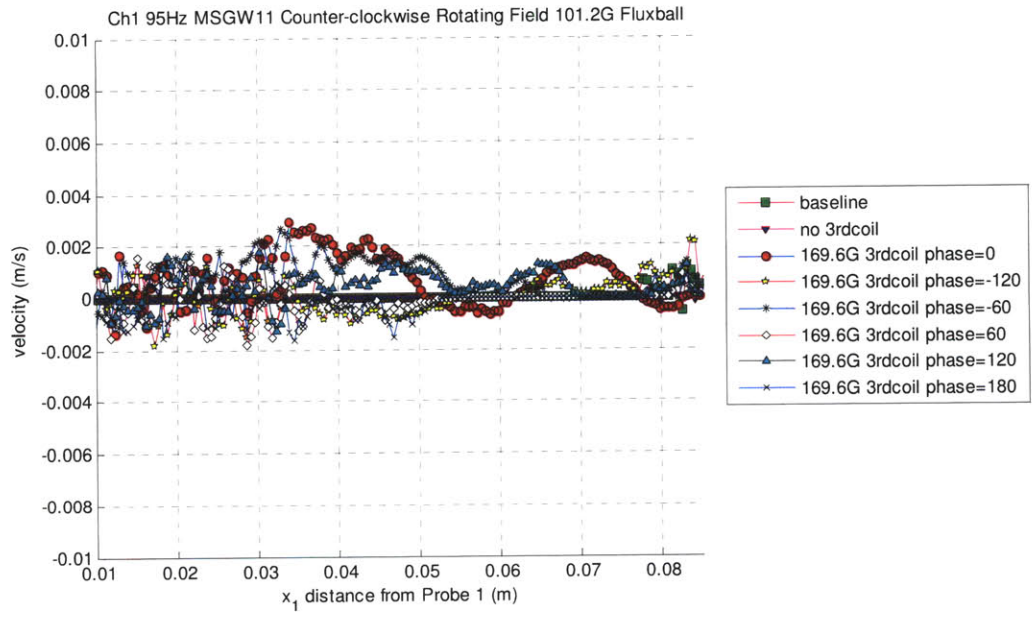
Ch1 95Hz MSGW11 Counter-clockwise Rotating Field 101.2G Fluxball
velocity (m/s)
x1 distance from Probe 1 (m)
baseline
no 3rdcoil
169.6G 3rdcoil phase=0
169.6G 3rdcoil phase=-120
169.6G 3rdcoil phase=-60
169.6G 3rdcoil phase=60
169.6G 3rdcoil phase=120
169.6G 3rdcoil phase=180

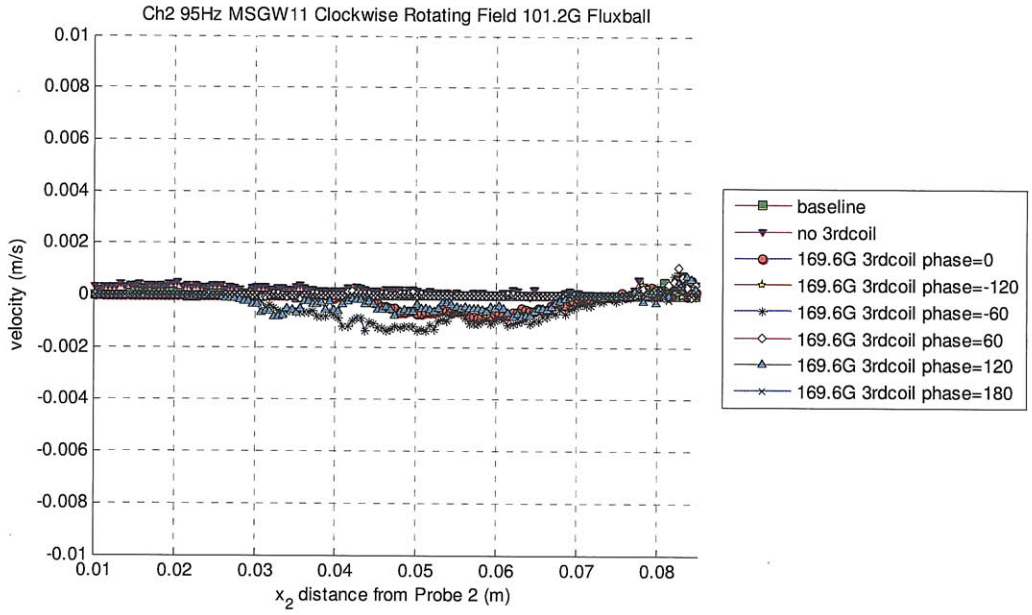
Ch2 95Hz MSGW11 Clockwise Rotating Field 101.2G Fluxball
velocity (m/s)
0.01
0.008
0.006
0.004
0.002
0
-0.002
-0.004
-0.006
-0.008
-0.01
0.01
0.02
0.03
0.04
0.05
0.06
0.07
0.08
x2 distance from Probe 2 (m)
baseline
no 3rdcoil
169.6G 3rdcoil phase=0
169.6G 3rdcoil phase=-120
169.6G 3rdcoil phase=-60
169.6G 3rdcoil phase=60
169.6G 3rdcoil phase=120
169.6G 3rdcoil phase=180

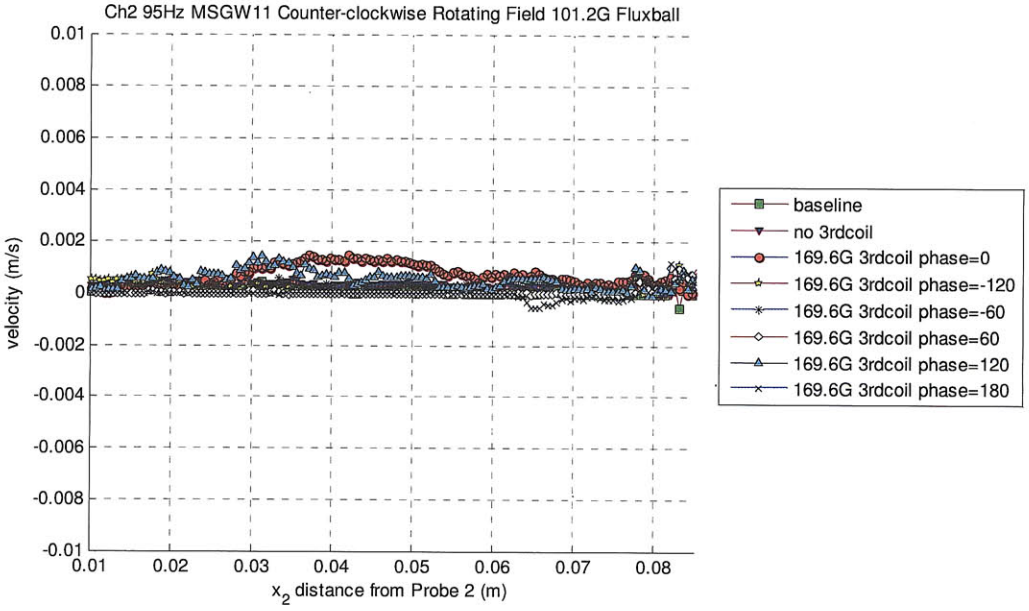
Ch2 95Hz MSGW11 Counter-clockwise Rotating Field 101.2G Fluxball
velocity (m/s)
0.01
0.008
0.006
0.004
0.002
0
-0.002
-0.004
-0.006
-0.008
-0.01
0.01
0.02
0.03
0.04
0.05
0.06
0.07
0.08
x2 distance from Probe 2 (m)
baseline
no 3rdcoil
169.6G 3rdcoil phase=0
169.6G 3rdcoil phase=-120
169.6G 3rdcoil phase=-60
169.6G 3rdcoil phase=60
169.6G 3rdcoil phase=120
169.6G 3rdcoil phase=180

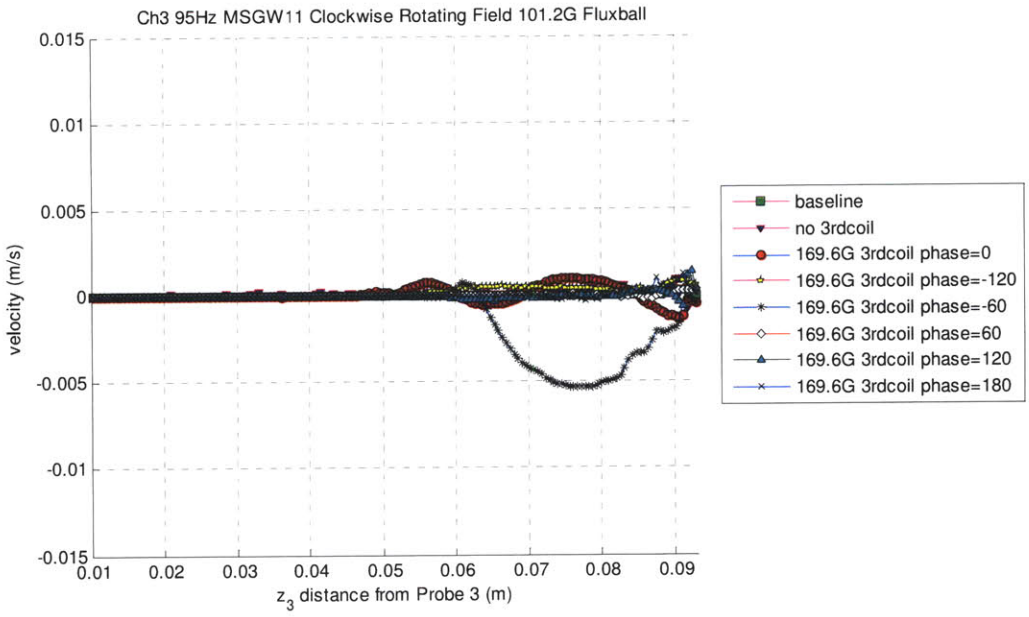
Ch3 95Hz MSGW11 Clockwise Rotating Field 101.2G Fluxball
velocity (m/s)
0.015
0.01
0.005
0
-0.005
-0.01
-0.015
0.01
0.02
0.03
0.04
0.05
0.06
0.07
0.08
0.09
z3 distance from Probe 3 (m)
baseline
no 3rdcoil
169.6G 3rdcoil phase=0
169.6G 3rdcoil phase=-120
169.6G 3rdcoil phase=-60
169.6G 3rdcoil phase=60
169.6G 3rdcoil phase=120
169.6G 3rdcoil phase=180

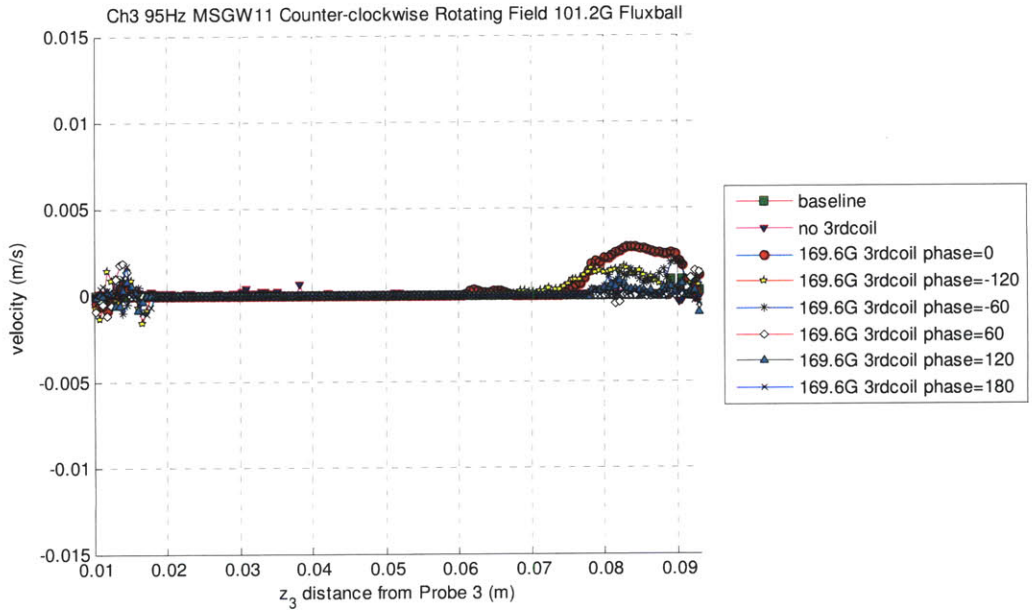
Ch3 95Hz MSGW11 Counter-clockwise Rotating Field 101.2G Fluxball
velocity (m/s)
0.015
0.01
0.005
0
-0.005
-0.01
-0.015
0.01
0.02
0.03
0.04
0.05
0.06
0.07
0.08
0.09
z3 distance from Probe 3 (m)
baseline
no 3rdcoil
169.6G 3rdcoil phase=0
169.6G 3rdcoil phase=-120
169.6G 3rdcoil phase=-60
169.6G 3rdcoil phase=60
169.6G 3rdcoil phase=120
169.6G 3rdcoil phase=180

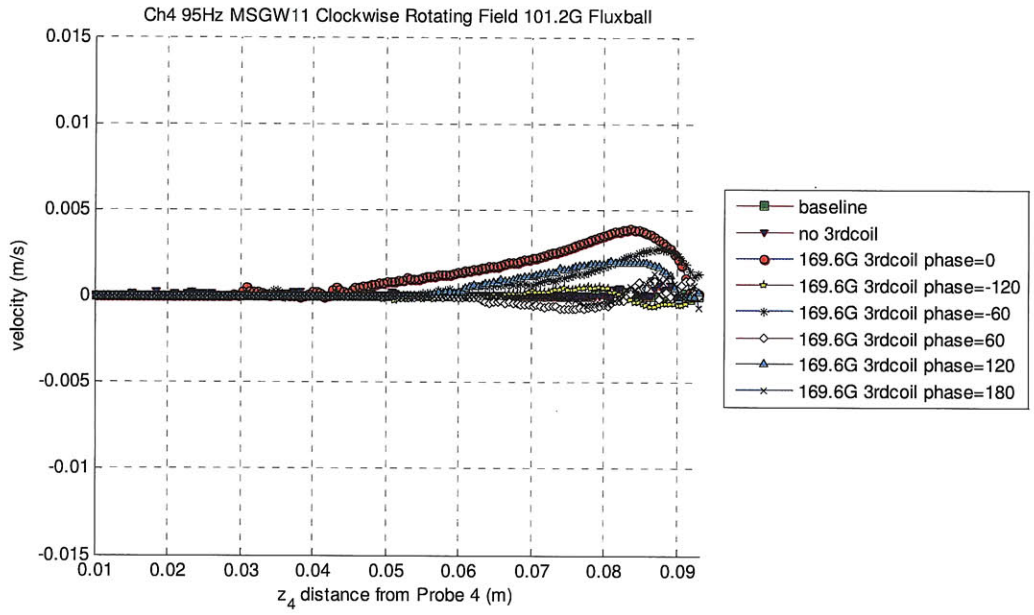
Ch4 95Hz MSGW11 Clockwise Rotating Field 101.2G Fluxball
velocity (m/s)
0.015
0.01
0.005
0
-0.005
-0.01
-0.015
0.01
0.02
0.03
0.04
0.05
0.06
0.07
0.08
0.09
z4 distance from Probe 4 (m)
baseline
no 3rdcoil
169.6G 3rdcoil phase=0
169.6G 3rdcoil phase=-120
169.6G 3rdcoil phase=-60
169.6G 3rdcoil phase=60
169.6G 3rdcoil phase=120
169.6G 3rdcoil phase=180

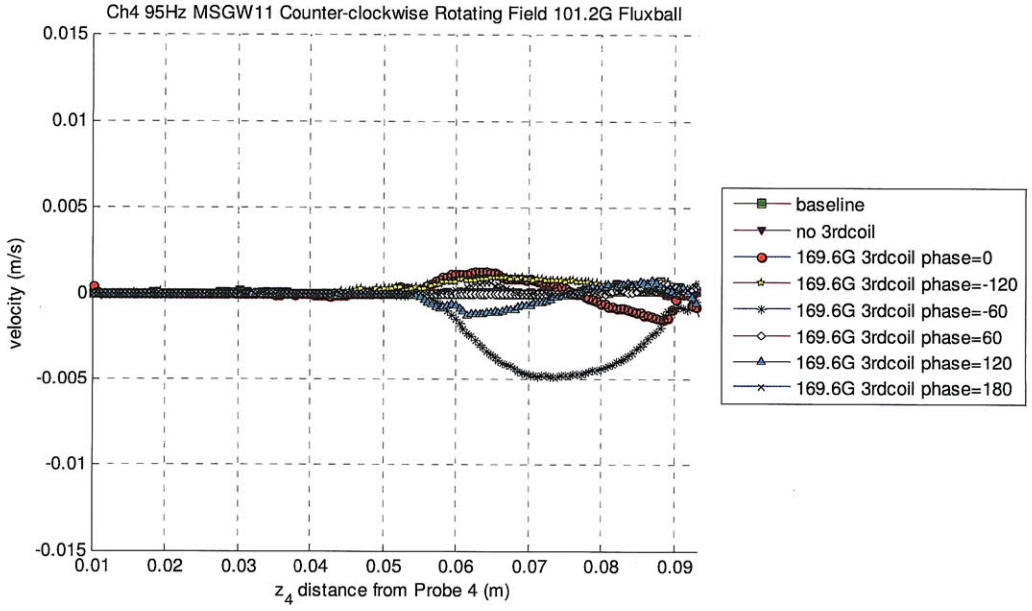
Ch4 95Hz MSGW11 Counter-clockwise Rotating Field 101.2G Fluxball
velocity (m/s)
0.015
0.01
0.005
0
-0.005
-0.01
-0.015
0.01
0.02
0.03
0.04
0.05
0.06
0.07
0.08
0.09
z4 distance from Probe 4 (m)
baseline
no 3rdcoil
169.6G 3rdcoil phase=0
169.6G 3rdcoil phase=-120
169.6G 3rdcoil phase=-60
169.6G 3rdcoil phase=60
169.6G 3rdcoil phase=120
169.6G 3rdcoil phase=180

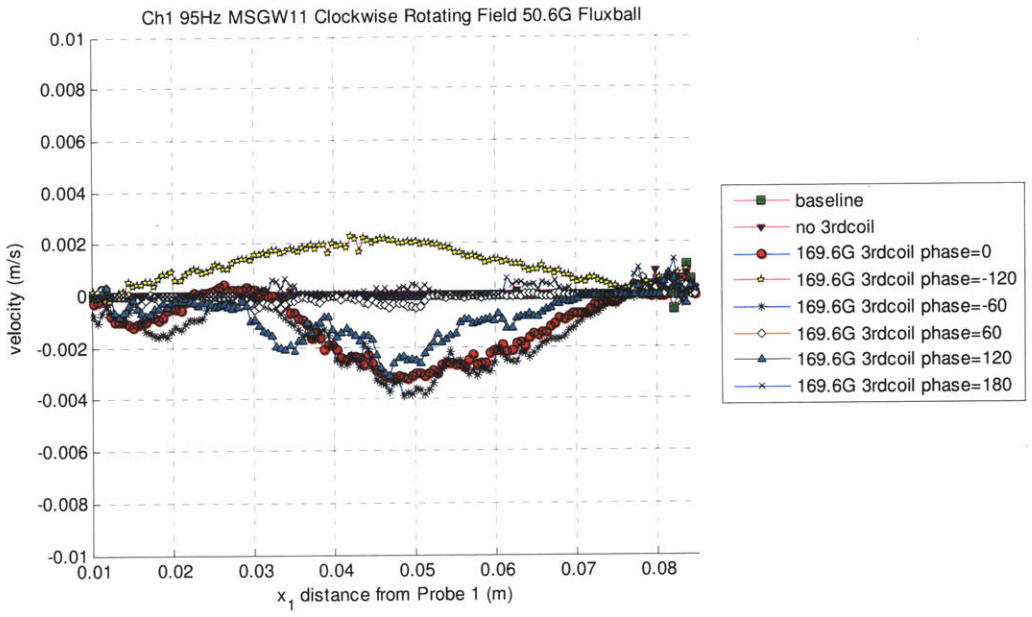
Ch1 95Hz MSGW11 Clockwise Rotating Field 50.6G Fluxball
velocity (m/s)
x1 distance from Probe 1 (m)
baseline
no 3rdcoil
169.6G 3rdcoil phase=0
169.6G 3rdcoil phase=-120
169.6G 3rdcoil phase=-60
169.6G 3rdcoil phase=60
169.6G 3rdcoil phase=120
169.6G 3rdcoil phase=180

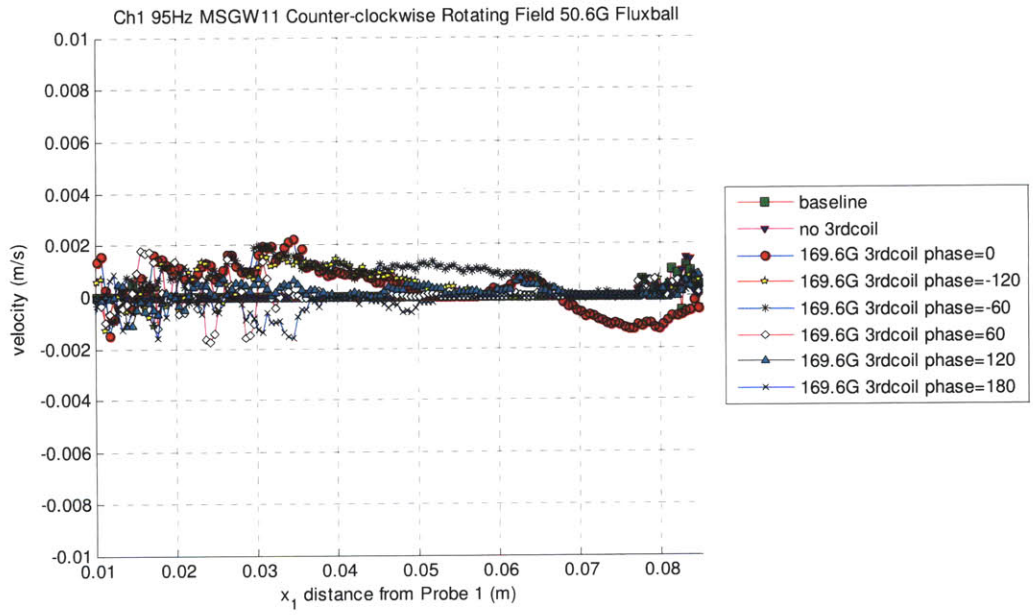
Ch1 95Hz MSGW11 Counter-clockwise Rotating Field 50.6G Fluxball
velocity (m/s)
x1 distance from Probe 1 (m)
baseline
no 3rdcoil
169.6G 3rdcoil phase=0
169.6G 3rdcoil phase=-120
169.6G 3rdcoil phase=-60
169.6G 3rdcoil phase=60
169.6G 3rdcoil phase=120
169.6G 3rdcoil phase=180

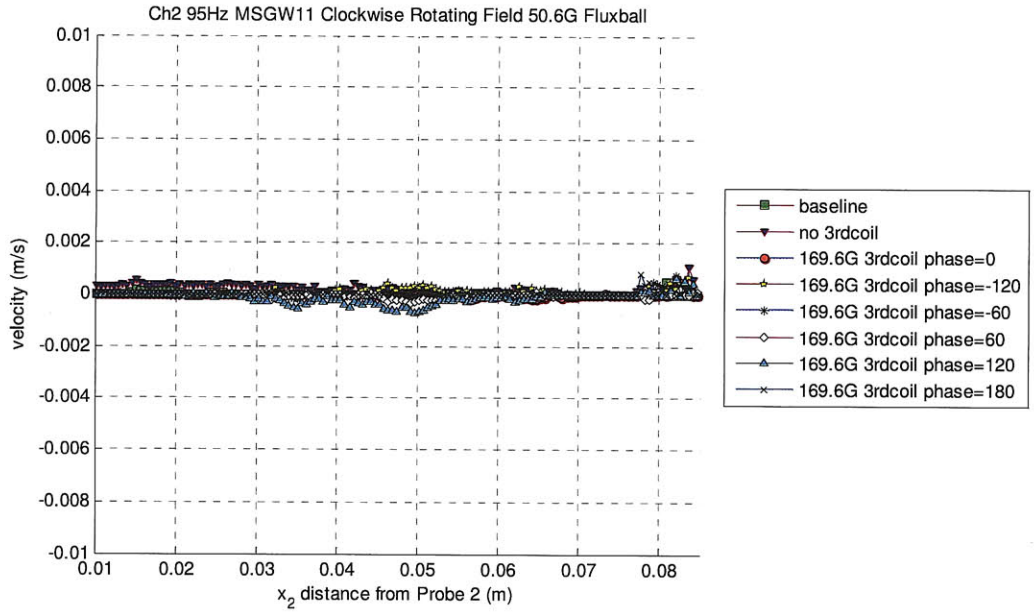
Ch2 95Hz MSGW11 Clockwise Rotating Field 50.6G Fluxball
velocity (m/s)
0.01
0.008
0.006
0.004
0.002
0
-0.002
-0.004
-0.006
-0.008
-0.01
0.01
0.02
0.03
0.04
0.05
0.06
0.07
0.08
x2 distance from Probe 2 (m)
baseline
no 3rdcoil
169.6G 3rdcoil phase=0
169.6G 3rdcoil phase=-120
169.6G 3rdcoil phase=-60
169.6G 3rdcoil phase=60
169.6G 3rdcoil phase=120
169.6G 3rdcoil phase=180

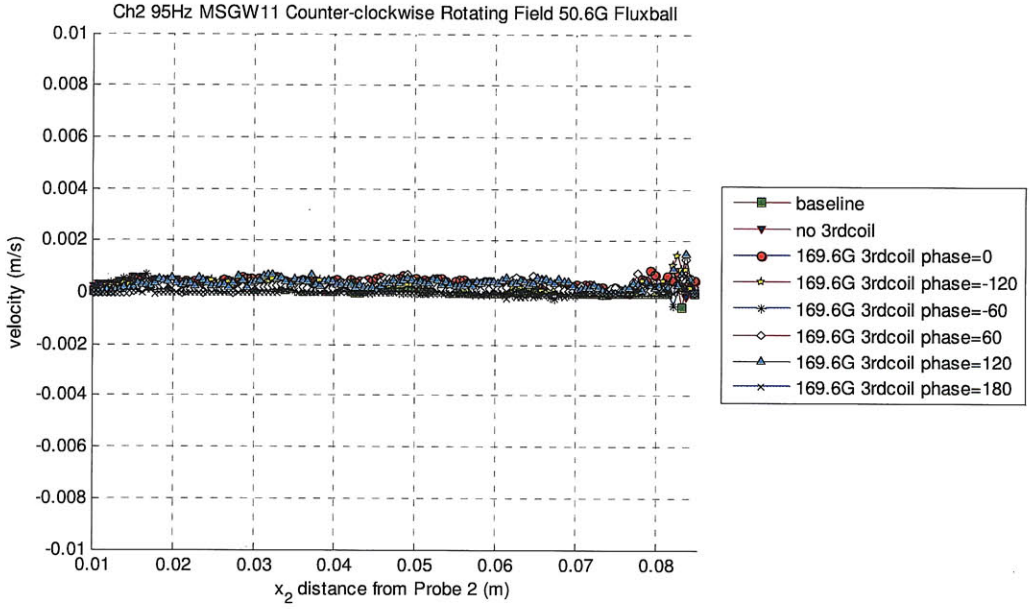
Ch2 95Hz MSGW11 Counter-clockwise Rotating Field 50.6G Fluxball
velocity (m/s)
0.01
0.008
0.006
0.004
0.002
0
-0.002
-0.004
-0.006
-0.008
-0.01
0.01
0.02
0.03
0.04
0.05
0.06
0.07
0.08
x2 distance from Probe 2 (m)
baseline
no 3rdcoil
169.6G 3rdcoil phase=0
169.6G 3rdcoil phase=-120
169.6G 3rdcoil phase=-60
169.6G 3rdcoil phase=60
169.6G 3rdcoil phase=120
169.6G 3rdcoil phase=180

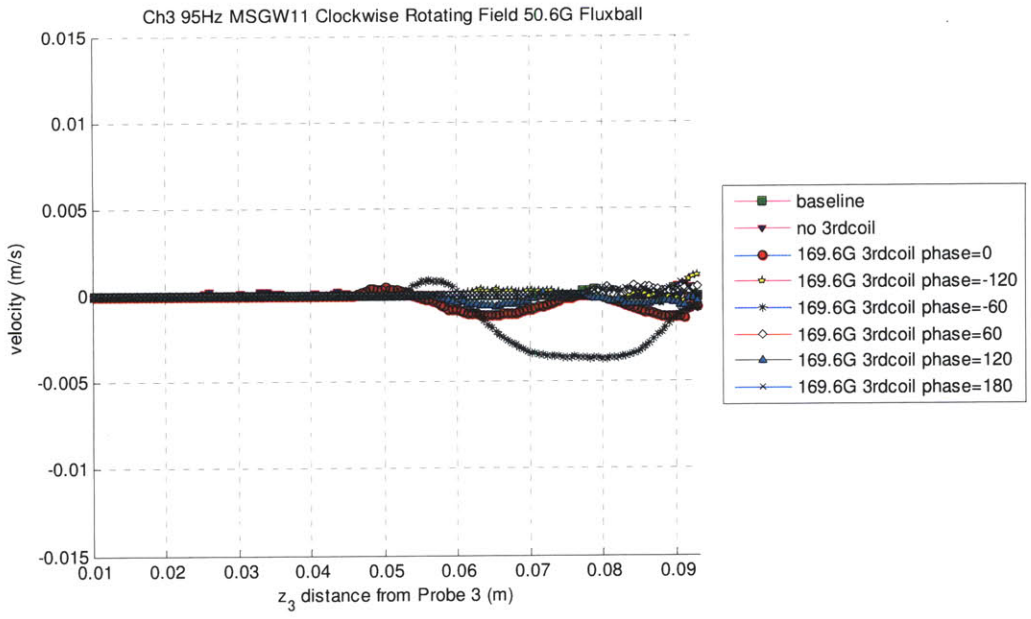
Ch3 95Hz MSGW11 Clockwise Rotating Field 50.6G Fluxball
velocity (m/s)
0.015
0.01
0.005
0
-0.005
-0.01
-0.015
0.01
0.02
0.03
0.04
0.05
0.06
0.07
0.08
0.09
z3 distance from Probe 3 (m)
baseline
no 3rdcoil
169.6G 3rdcoil phase=0
169.6G 3rdcoil phase=-120
169.6G 3rdcoil phase=-60
169.6G 3rdcoil phase=60
169.6G 3rdcoil phase=120
169.6G 3rdcoil phase=180

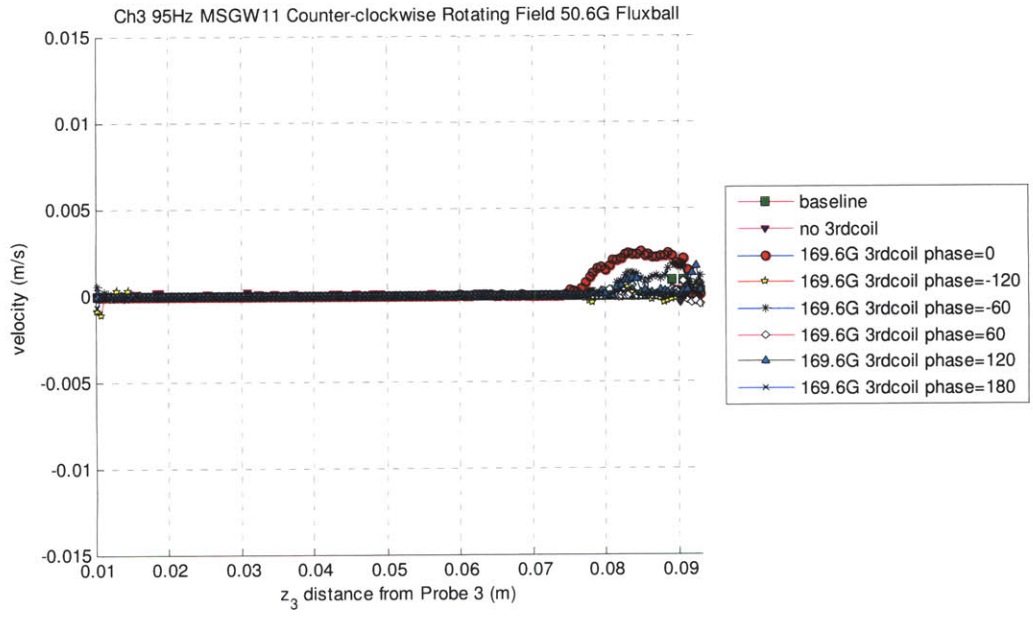
Ch3 95Hz MSGW11 Counter-clockwise Rotating Field 50.6G Fluxball
velocity (m/s)
0.015
0.01
0.005
0
-0.005
-0.01
-0.015
0.01
0.02
0.03
0.04
0.05
0.06
0.07
0.08
0.09
z3 distance from Probe 3 (m)
baseline
no 3rdcoil
169.6G 3rdcoil phase=0
169.6G 3rdcoil phase=-120
169.6G 3rdcoil phase=-60
169.6G 3rdcoil phase=60
169.6G 3rdcoil phase=120
169.6G 3rdcoil phase=180

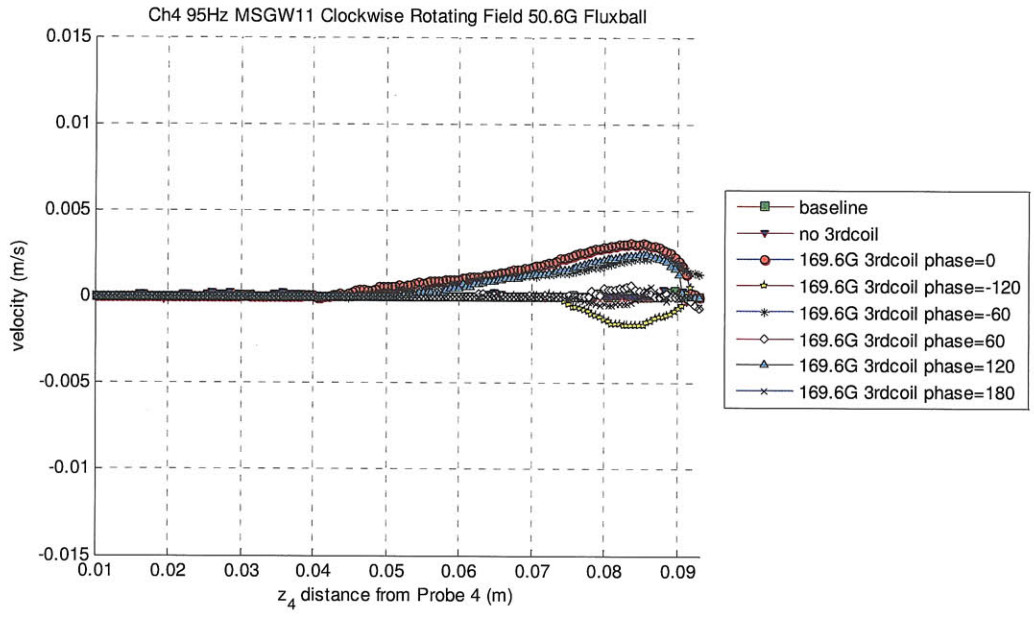
Ch4 95Hz MSGW11 Clockwise Rotating Field 50.6G Fluxball
velocity (m/s)
0.015
0.01
0.005
0
-0.005
-0.01
-0.015
0.01
0.02
0.03
0.04
0.05
0.06
0.07
0.08
0.09
z4 distance from Probe 4 (m)
baseline
no 3rdcoil
169.6G 3rdcoil phase=0
169.6G 3rdcoil phase=-120
169.6G 3rdcoil phase=-60
169.6G 3rdcoil phase=60
169.6G 3rdcoil phase=120
169.6G 3rdcoil phase=180

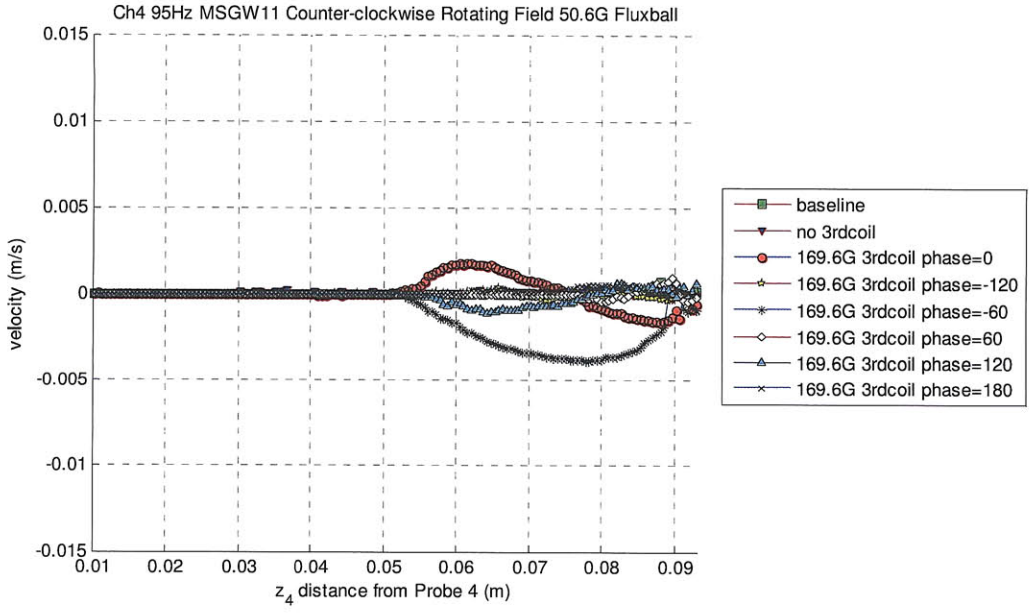
Ch4 95Hz MSGW11 Counter-clockwise Rotating Field 50.6G Fluxball
velocity (m/s)
0.015
0.01
0.005
0
-0.005
-0.01
-0.015
0.01
0.02
0.03
0.04
0.05
0.06
0.07
0.08
0.09
z4 distance from Probe 4 (m)
baseline
no 3rdcoil
169.6G 3rdcoil phase=0
169.6G 3rdcoil phase=-120
169.6G 3rdcoil phase=-60
169.6G 3rdcoil phase=60
169.6G 3rdcoil phase=120
169.6G 3rdcoil phase=180

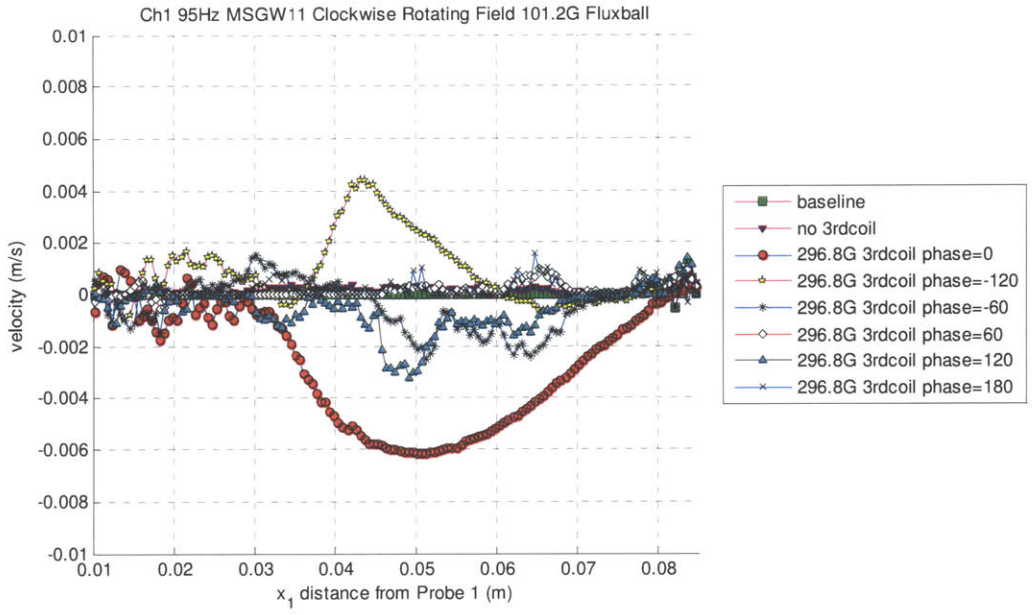
Ch1 95Hz MSGW11 Clockwise Rotating Field 101.2G Fluxball
velocity (m/s)
x1 distance from Probe 1 (m)
baseline
no 3rdcoil
296.8G 3rdcoil phase=0
296.8G 3rdcoil phase=-120
296.8G 3rdcoil phase=-60
296.8G 3rdcoil phase=60
296.8G 3rdcoil phase=120
296.8G 3rdcoil phase=180

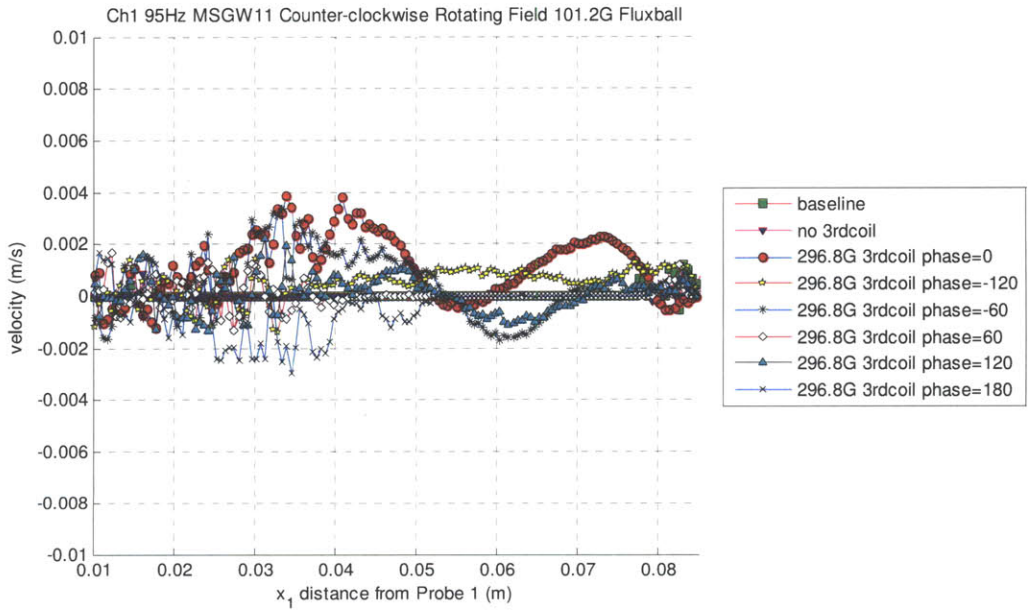
Ch1 95Hz MSGW11 Counter-clockwise Rotating Field 101.2G Fluxball
velocity (m/s)
x1 distance from Probe 1 (m)
baseline
no 3rdcoil
296.8G 3rdcoil phase=0
296.8G 3rdcoil phase=-120
296.8G 3rdcoil phase=-60
296.8G 3rdcoil phase=60
296.8G 3rdcoil phase=120
296.8G 3rdcoil phase=180

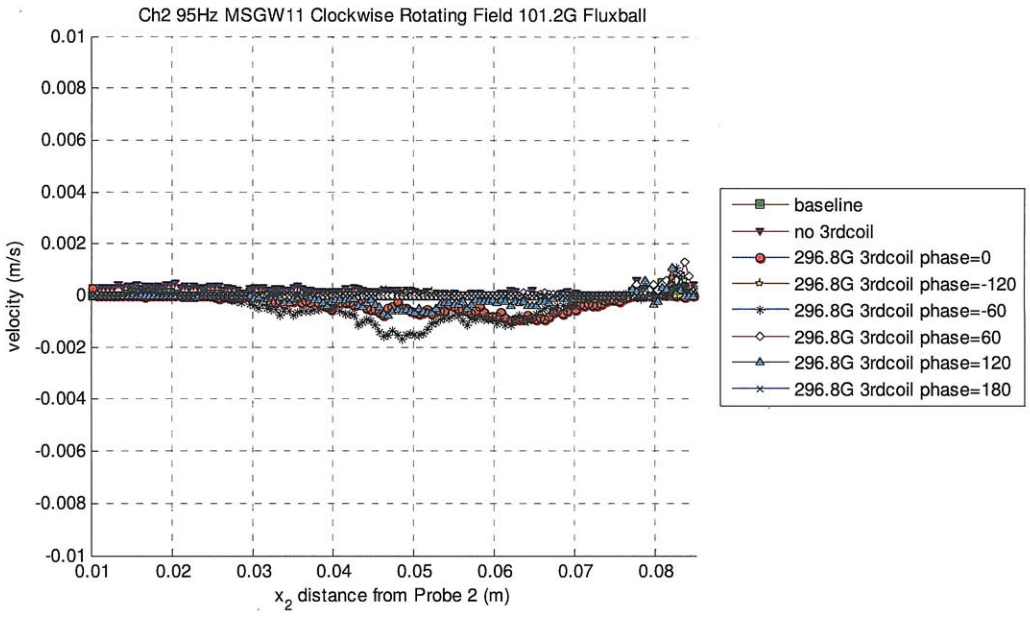
Ch2 95Hz MSGW11 Clockwise Rotating Field 101.2G Fluxball
velocity (m/s)
0.01
0.008
0.006
0.004
0.002
0
-0.002
-0.004
-0.006
-0.008
-0.01
0.01
0.02
0.03
0.04
0.05
0.06
0.07
0.08
x2 distance from Probe 2 (m)
baseline
no 3rdcoil
296.8G 3rdcoil phase=0
296.8G 3rdcoil phase=-120
296.8G 3rdcoil phase=-60
296.8G 3rdcoil phase=60
296.8G 3rdcoil phase=120
296.8G 3rdcoil phase=180

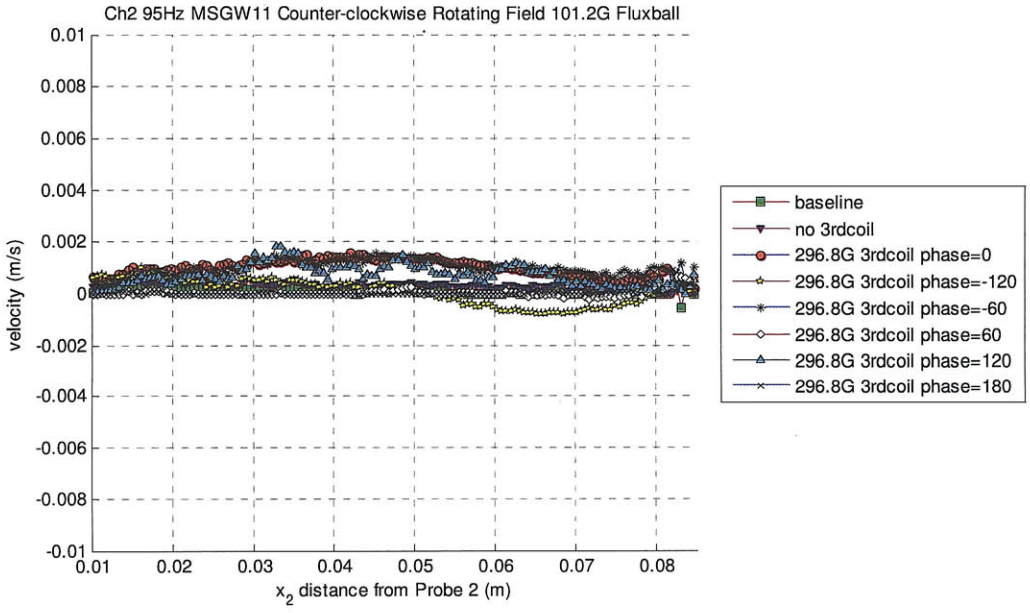
Ch2 95Hz MSGW11 Counter-clockwise Rotating Field 101.2G Fluxball
velocity (m/s)
0.01
0.008
0.006
0.004
0.002
0
-0.002
-0.004
-0.006
-0.008
-0.01
0.01
0.02
0.03
0.04
0.05
0.06
0.07
0.08
x2 distance from Probe 2 (m)
baseline
no 3rdcoil
296.8G 3rdcoil phase=0
296.8G 3rdcoil phase=-120
296.8G 3rdcoil phase=-60
296.8G 3rdcoil phase=60
296.8G 3rdcoil phase=120
296.8G 3rdcoil phase=180

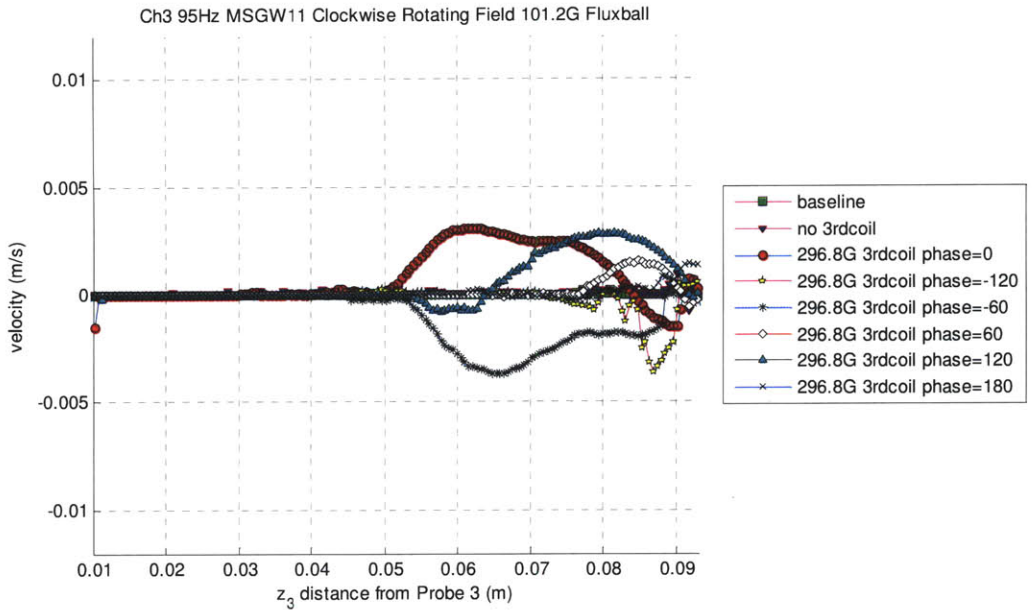
Ch3 95Hz MSGW11 Clockwise Rotating Field 101.2G Fluxball
velocity (m/s)
0.01
0.005
0
-0.005
-0.01
0.01
0.02
0.03
0.04
0.05
0.06
0.07
0.08
0.09
z_3 distance from Probe 3 (m)
baseline
no 3rdcoil
296.8G 3rdcoil phase=0
296.8G 3rdcoil phase=-120
296.8G 3rdcoil phase=-60
296.8G 3rdcoil phase=60
296.8G 3rdcoil phase=120
296.8G 3rdcoil phase=180

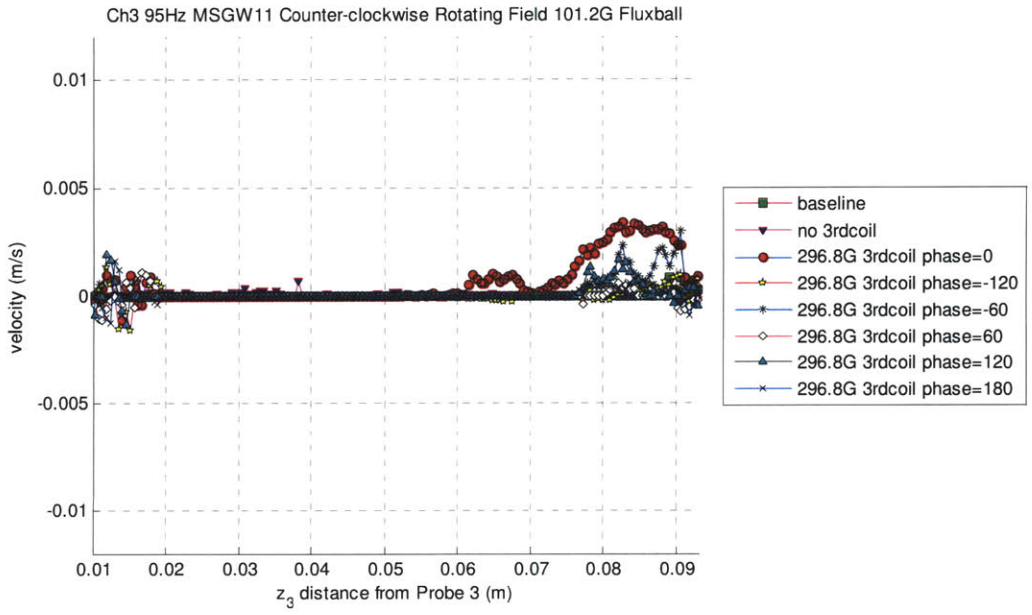
Ch3 95Hz MSGW11 Counter-clockwise Rotating Field 101.2G Fluxball
velocity (m/s)
0.01
0.005
0
-0.005
-0.01
0.01
0.02
0.03
0.04
0.05
0.06
0.07
0.08
0.09
z_3 distance from Probe 3 (m)
baseline
no 3rdcoil
296.8G 3rdcoil phase=0
296.8G 3rdcoil phase=-120
296.8G 3rdcoil phase=-60
296.8G 3rdcoil phase=60
296.8G 3rdcoil phase=120
296.8G 3rdcoil phase=180

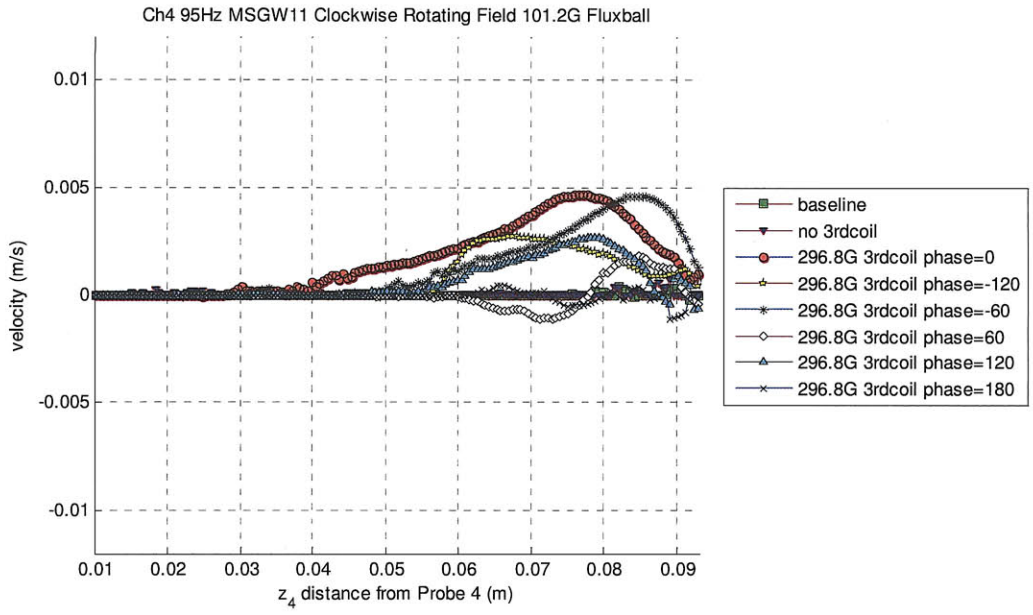
Ch4 95Hz MSGW11 Clockwise Rotating Field 101.2G Fluxball
velocity (m/s)
0.01
0.005
0
-0.005
-0.01
0.01
0.02
0.03
0.04
0.05
0.06
0.07
0.08
0.09
z4 distance from Probe 4 (m)
baseline
no 3rdcoil
296.8G 3rdcoil phase=0
296.8G 3rdcoil phase=-120
296.8G 3rdcoil phase=-60
296.8G 3rdcoil phase=60
296.8G 3rdcoil phase=120
296.8G 3rdcoil phase=180

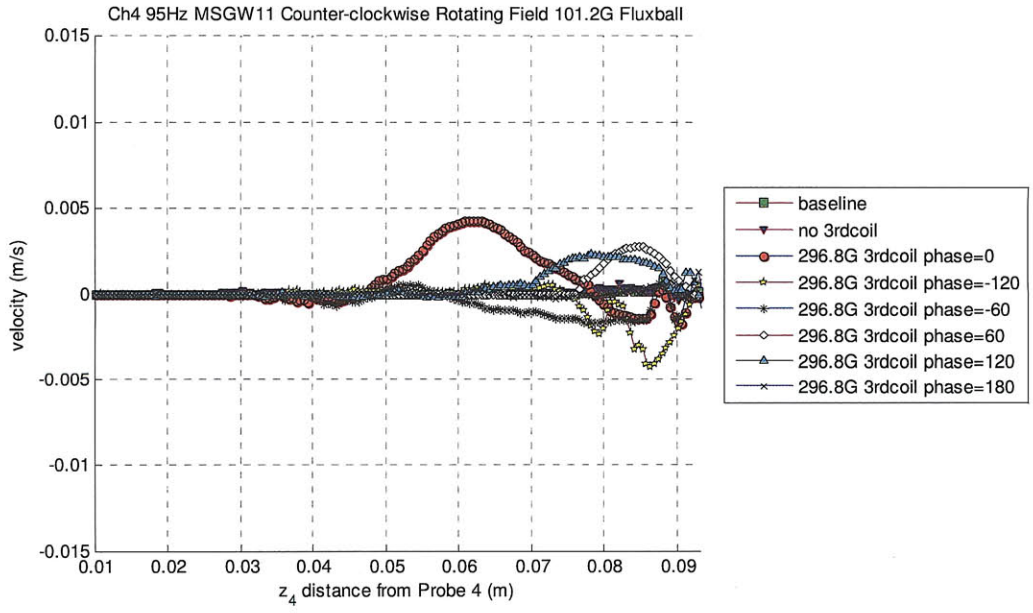
Ch4 95Hz MSGW11 Counter-clockwise Rotating Field 101.2G Fluxball
velocity (m/s)
0.015
0.01
0.005
0
-0.005
-0.01
-0.015
0.01
0.02
0.03
0.04
0.05
0.06
0.07
0.08
0.09
z4 distance from Probe 4 (m)
baseline
no 3rdcoil
296.8G 3rdcoil phase=0
296.8G 3rdcoil phase=-120
296.8G 3rdcoil phase=-60
296.8G 3rdcoil phase=60
296.8G 3rdcoil phase=120
296.8G 3rdcoil phase=180

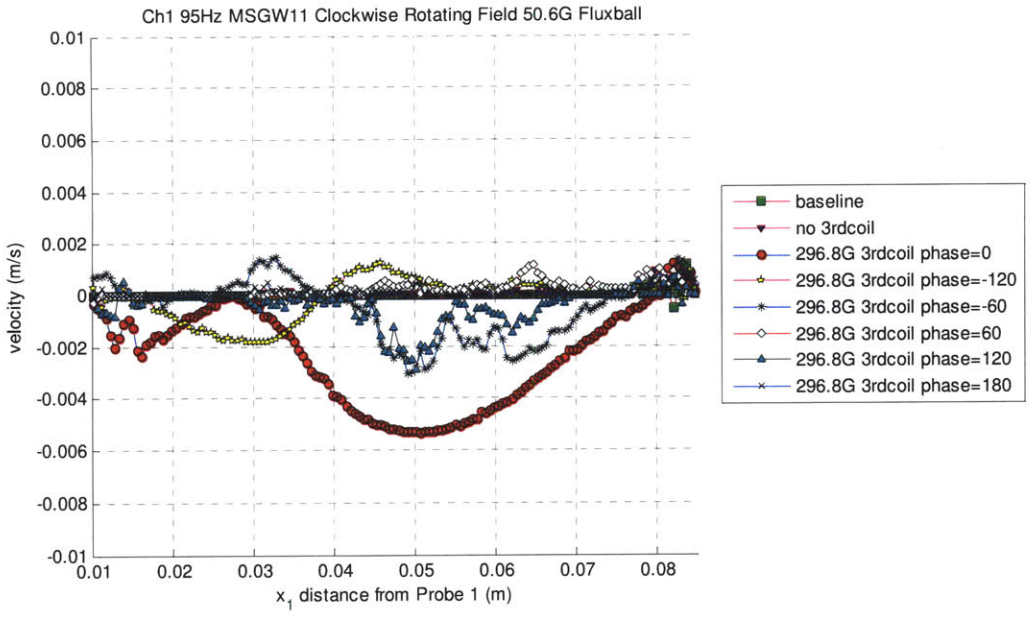
Ch1 95Hz MSGW11 Clockwise Rotating Field 50.6G Fluxball
velocity (m/s)
0.01
0.008
0.006
0.004
0.002
0
-0.002
-0.004
-0.006
-0.008
-0.01
0.01
0.02
0.03
0.04
0.05
0.06
0.07
0.08
x1 distance from Probe 1 (m)
baseline
no 3rdcoil
296.8G 3rdcoil phase=0
296.8G 3rdcoil phase=-120
296.8G 3rdcoil phase=-60
296.8G 3rdcoil phase=60
296.8G 3rdcoil phase=120
296.8G 3rdcoil phase=180

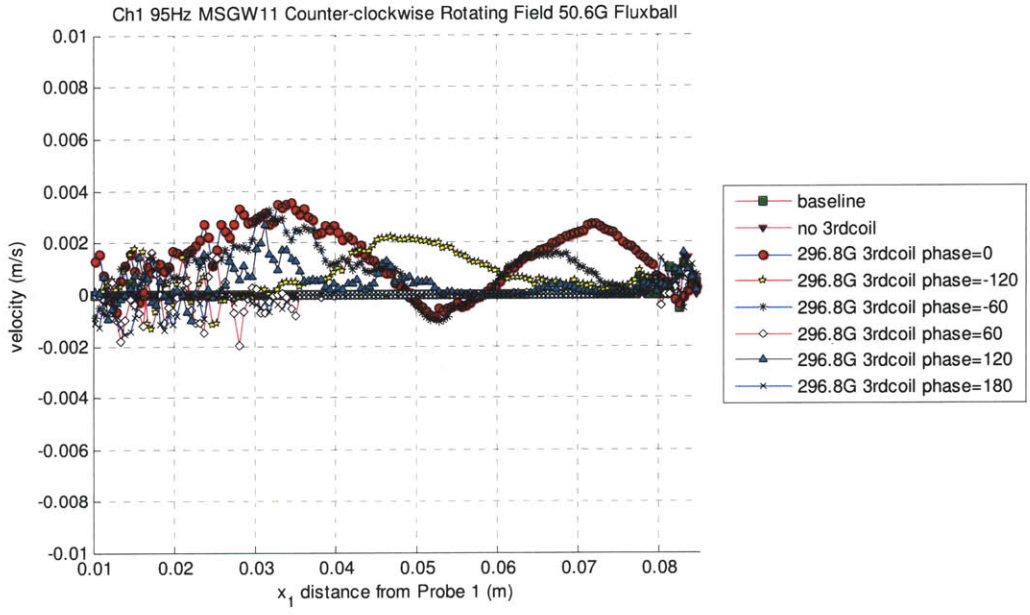
Ch1 95Hz MSGW11 Counter-clockwise Rotating Field 50.6G Fluxball
velocity (m/s)
0.01
0.008
0.006
0.004
0.002
0
-0.002
-0.004
-0.006
-0.008
-0.01
0.01
0.02
0.03
0.04
0.05
0.06
0.07
0.08
x1 distance from Probe 1 (m)
baseline
no 3rdcoil
296.8G 3rdcoil phase=0
296.8G 3rdcoil phase=-120
296.8G 3rdcoil phase=-60
296.8G 3rdcoil phase=60
296.8G 3rdcoil phase=120
296.8G 3rdcoil phase=180

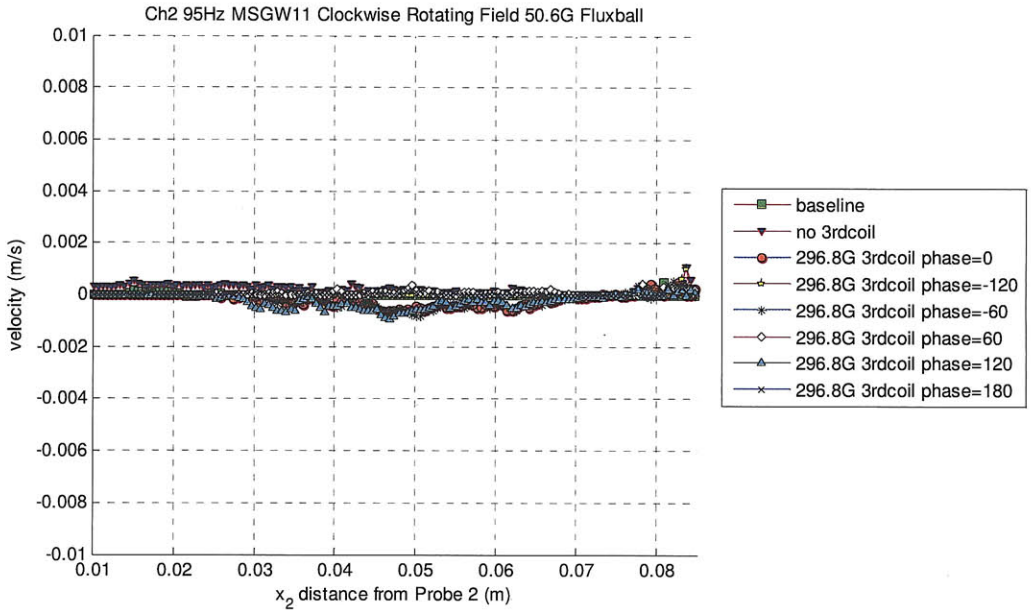
Ch2 95Hz MSGW11 Clockwise Rotating Field 50.6G Fluxball
velocity (m/s)
0.01
0.008
0.006
0.004
0.002
0
-0.002
-0.004
-0.006
-0.008
-0.01
0.01
0.02
0.03
0.04
0.05
0.06
0.07
0.08
x2 distance from Probe 2 (m)
baseline
no 3rdcoil
296.8G 3rdcoil phase=0
296.8G 3rdcoil phase=-120
296.8G 3rdcoil phase=-60
296.8G 3rdcoil phase=60
296.8G 3rdcoil phase=120
296.8G 3rdcoil phase=180

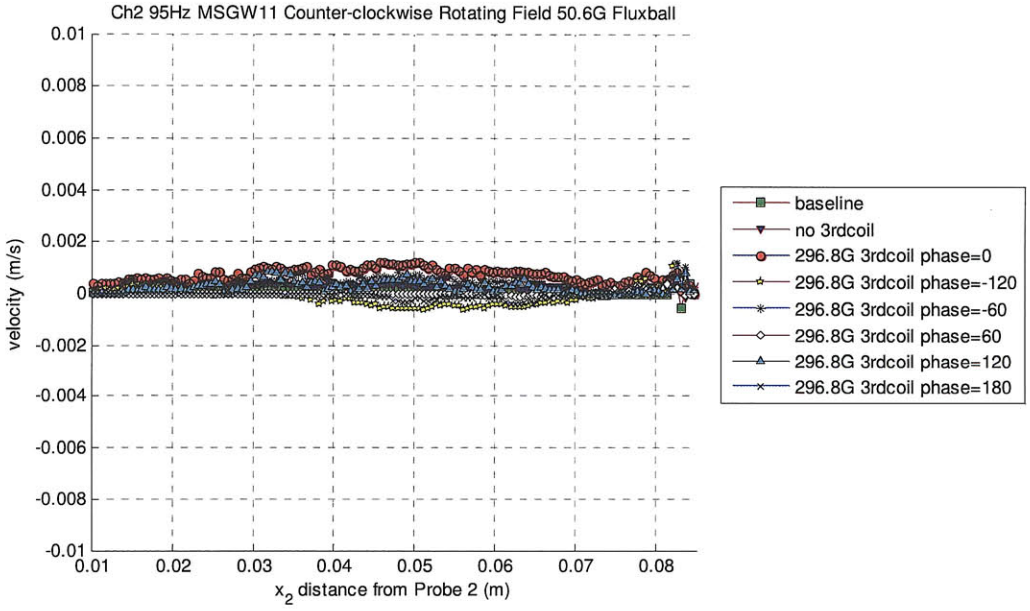
Ch2 95Hz MSGW11 Counter-clockwise Rotating Field 50.6G Fluxball
velocity (m/s)
0.01
0.008
0.006
0.004
0.002
0
-0.002
-0.004
-0.006
-0.008
-0.01
0.01
0.02
0.03
0.04
0.05
0.06
0.07
0.08
x2 distance from Probe 2 (m)
baseline
no 3rdcoil
296.8G 3rdcoil phase=0
296.8G 3rdcoil phase=-120
296.8G 3rdcoil phase=-60
296.8G 3rdcoil phase=60
296.8G 3rdcoil phase=120
296.8G 3rdcoil phase=180

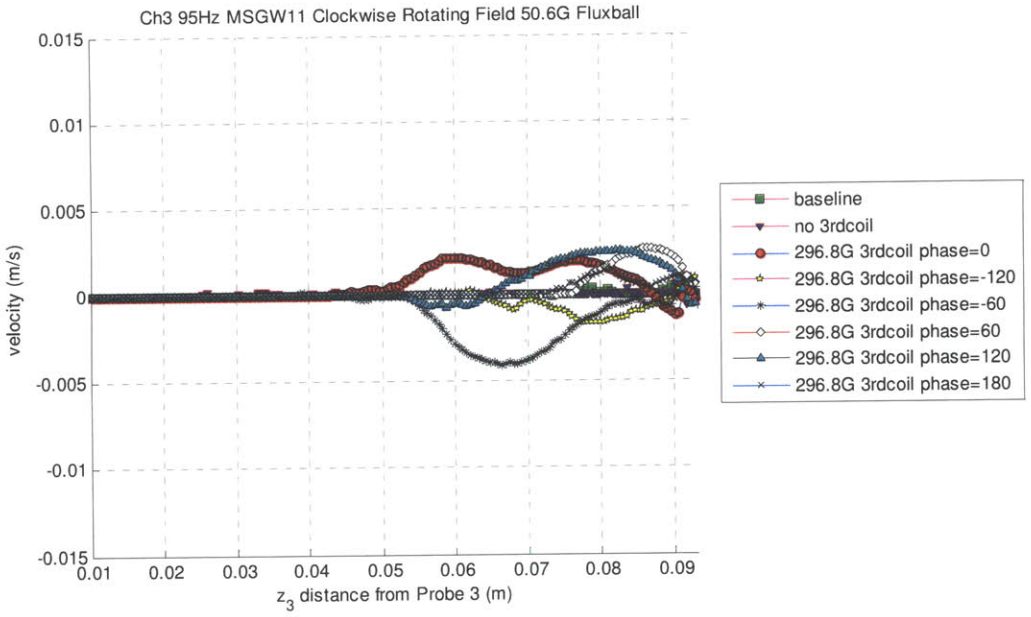
Ch3 95Hz MSGW11 Clockwise Rotating Field 50.6G Fluxball
velocity (m/s)
0.015
0.01
0.005
0
-0.005
-0.01
-0.015
0.01
0.02
0.03
0.04
0.05
0.06
0.07
0.08
0.09
z3 distance from Probe 3 (m)
baseline
no 3rdcoil
296.8G 3rdcoil phase=0
296.8G 3rdcoil phase=-120
296.8G 3rdcoil phase=-60
296.8G 3rdcoil phase=60
296.8G 3rdcoil phase=120
296.8G 3rdcoil phase=180

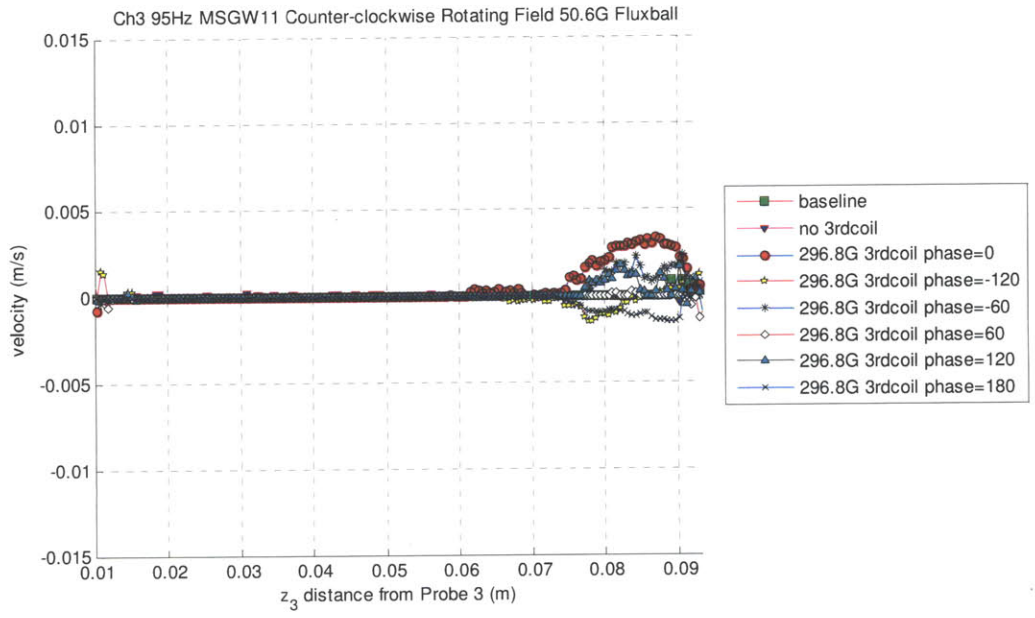
Ch3 95Hz MSGW11 Counter-clockwise Rotating Field 50.6G Fluxball
velocity (m/s)
0.015
0.01
0.005
0
-0.005
-0.01
-0.015
0.01
0.02
0.03
0.04
0.05
0.06
0.07
0.08
0.09
z3 distance from Probe 3 (m)
baseline
no 3rdcoil
296.8G 3rdcoil phase=0
296.8G 3rdcoil phase=-120
296.8G 3rdcoil phase=-60
296.8G 3rdcoil phase=60
296.8G 3rdcoil phase=120
296.8G 3rdcoil phase=180

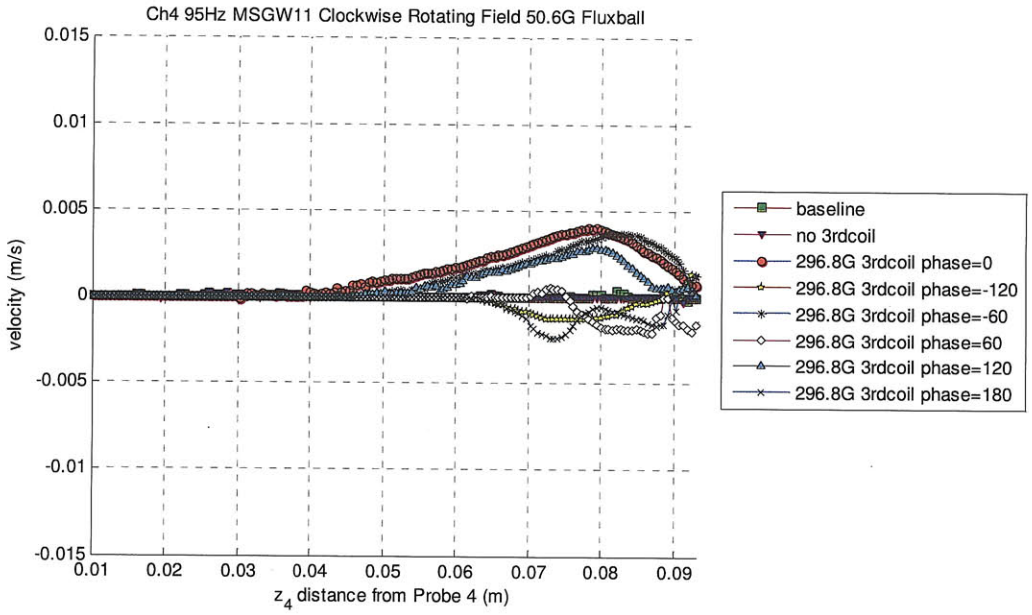
Ch4 95Hz MSGW11 Clockwise Rotating Field 50.6G Fluxball
velocity (m/s)
0.015
0.01
0.005
0
-0.005
-0.01
-0.015
0.01
0.02
0.03
0.04
0.05
0.06
0.07
0.08
0.09
z4 distance from Probe 4 (m)
baseline
no 3rdcoil
296.8G 3rdcoil phase=0
296.8G 3rdcoil phase=-120
296.8G 3rdcoil phase=-60
296.8G 3rdcoil phase=60
296.8G 3rdcoil phase=120
296.8G 3rdcoil phase=180

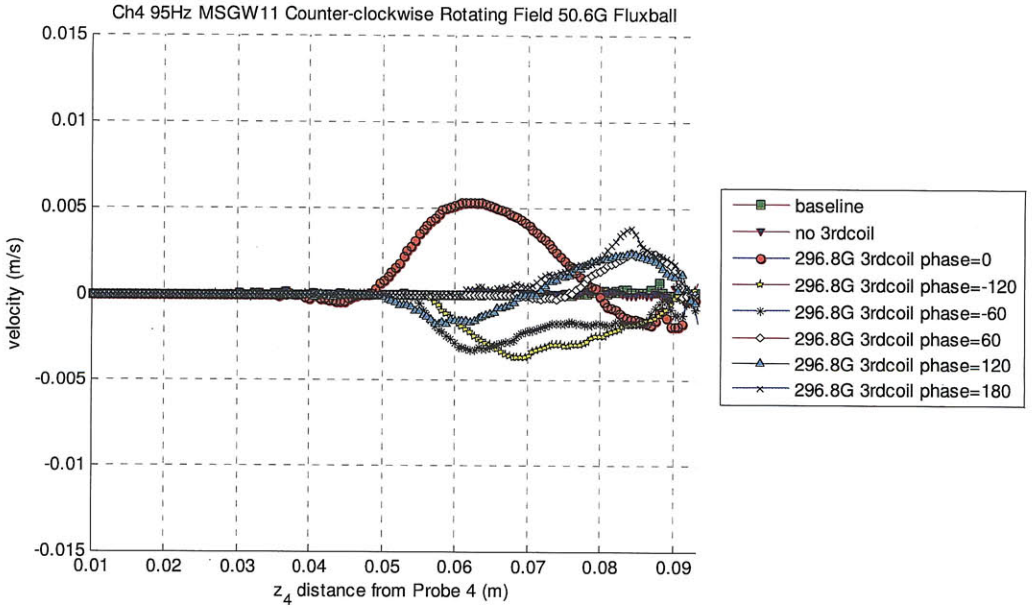
Ch4 95Hz MSGW11 Counter-clockwise Rotating Field 50.6G Fluxball
velocity (m/s)
0.015
0.01
0.005
0
-0.005
-0.01
-0.015
0.01
0.02
0.03
0.04
0.05
0.06
0.07
0.08
0.09
z4 distance from Probe 4 (m)
baseline
no 3rdcoil
296.8G 3rdcoil phase=0
296.8G 3rdcoil phase=-120
296.8G 3rdcoil phase=-60
296.8G 3rdcoil phase=60
296.8G 3rdcoil phase=120
296.8G 3rdcoil phase=180

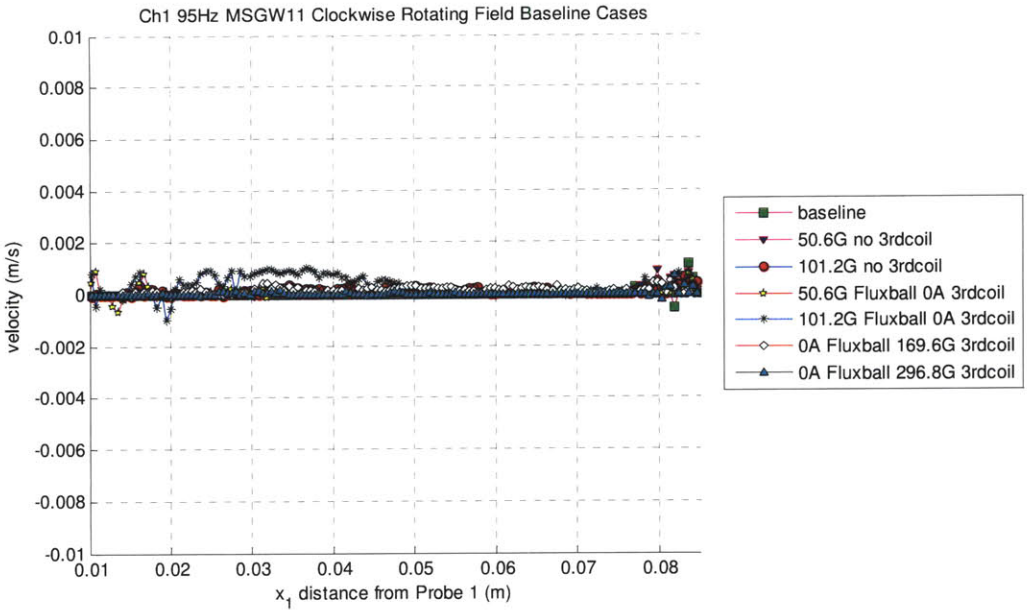
Ch1 95Hz MSGW11 Clockwise Rotating Field Baseline Cases
velocity (m/s)
0.01
0.008
0.006
0.004
0.002
0
-0.002
-0.004
-0.006
-0.008
-0.01
0.01
0.02
0.03
0.04
0.05
0.06
0.07
0.08
x1 distance from Probe 1 (m)
baseline
50.6G no 3rdcoil
101.2G no 3rdcoil
50.6G Fluxball 0A 3rdcoil
101.2G Fluxball 0A 3rdcoil
0A Fluxball 169.6G 3rdcoil
0A Fluxball 296.8G 3rdcoil

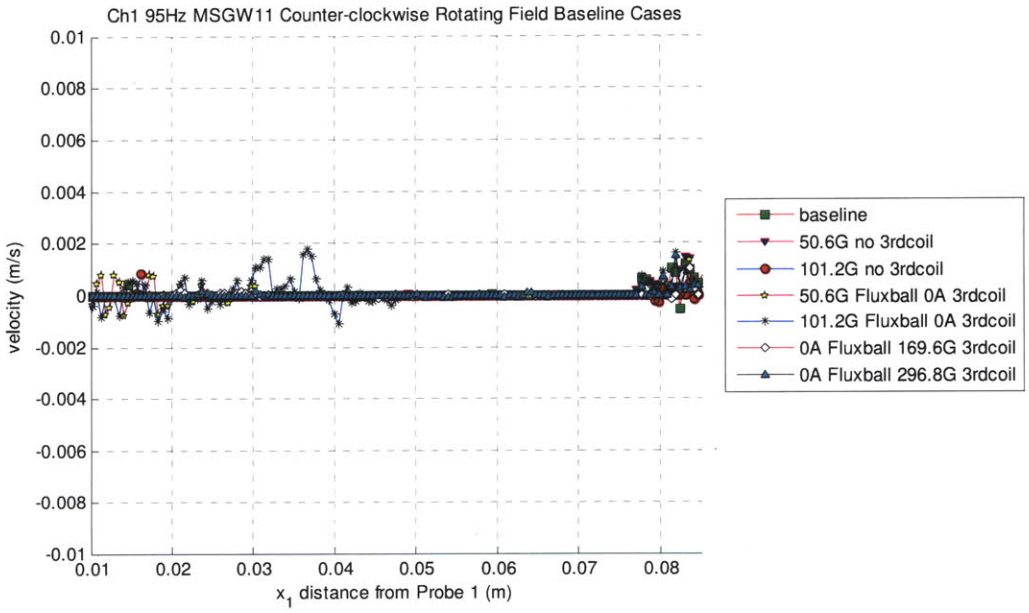
Ch1 95Hz MSGW11 Counter-clockwise Rotating Field Baseline Cases
velocity (m/s)
0.01
0.008
0.006
0.004
0.002
0
-0.002
-0.004
-0.006
-0.008
-0.01
0.01
0.02
0.03
0.04
0.05
0.06
0.07
0.08
x1 distance from Probe 1 (m)
baseline
50.6G no 3rdcoil
101.2G no 3rdcoil
50.6G Fluxball 0A 3rdcoil
101.2G Fluxball 0A 3rdcoil
0A Fluxball 169.6G 3rdcoil
0A Fluxball 296.8G 3rdcoil

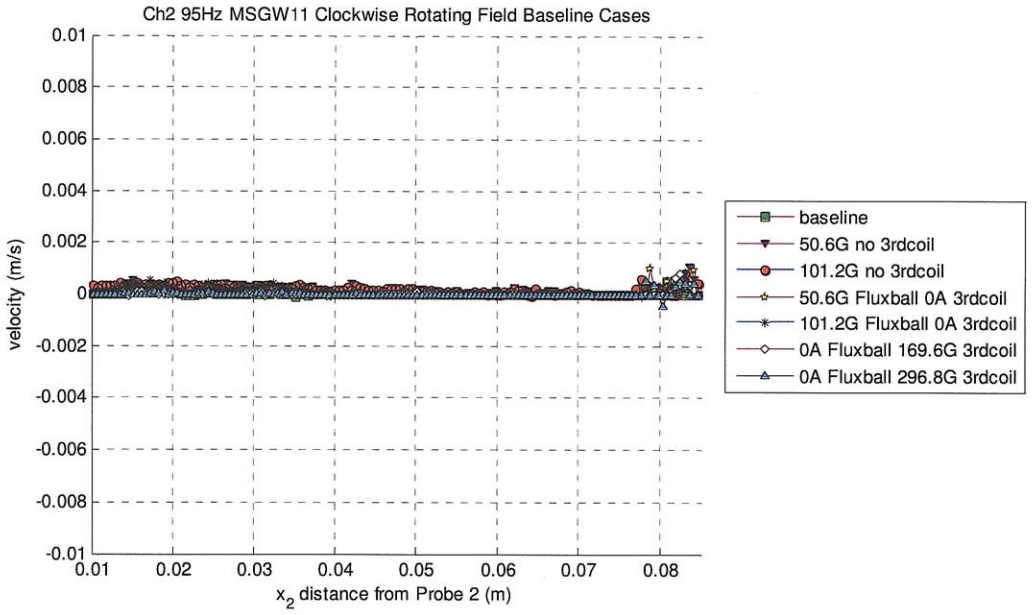
Ch2 95Hz MSGW11 Clockwise Rotating Field Baseline Cases
velocity (m/s)
0.01
0.008
0.006
0.004
0.002
0
-0.002
-0.004
-0.006
-0.008
-0.01
0.01
0.02
0.03
0.04
0.05
0.06
0.07
0.08
x2 distance from Probe 2 (m)
baseline
50.6G no 3rdcoil
101.2G no 3rdcoil
50.6G Fluxball 0A 3rdcoil
101.2G Fluxball 0A 3rdcoil
0A Fluxball 169.6G 3rdcoil
0A Fluxball 296.8G 3rdcoil

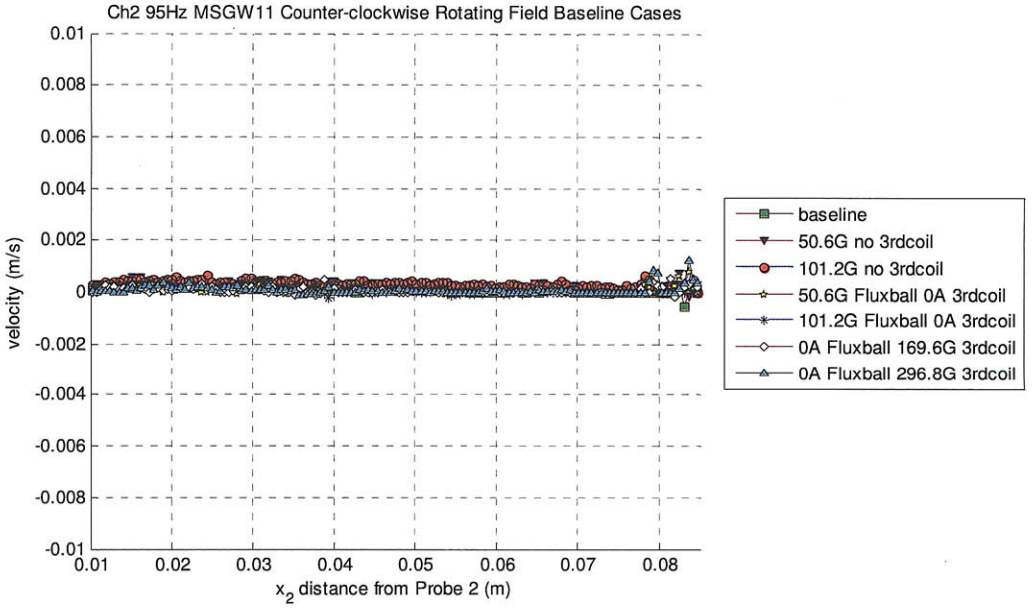
Ch2 95Hz MSGW11 Counter-clockwise Rotating Field Baseline Cases
velocity (m/s)
0.01
0.008
0.006
0.004
0.002
0
-0.002
-0.004
-0.006
-0.008
-0.01
0.01
0.02
0.03
0.04
0.05
0.06
0.07
0.08
x2 distance from Probe 2 (m)
baseline
50.6G no 3rdcoil
101.2G no 3rdcoil
50.6G Fluxball 0A 3rdcoil
101.2G Fluxball 0A 3rdcoil
0A Fluxball 169.6G 3rdcoil
0A Fluxball 296.8G 3rdcoil

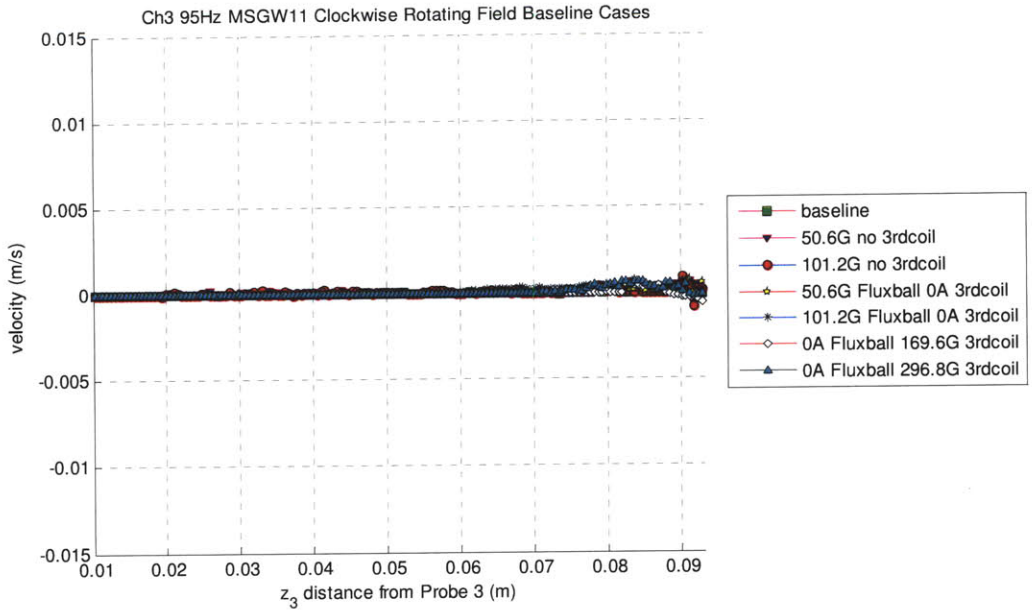
Ch3 95Hz MSGW11 Clockwise Rotating Field Baseline Cases
velocity (m/s)
0.015
0.01
0.005
0
-0.005
-0.01
-0.015
0.01
0.02
0.03
0.04
0.05
0.06
0.07
0.08
0.09
z3 distance from Probe 3 (m)
baseline
50.6G no 3rdcoil
101.2G no 3rdcoil
50.6G Fluxball 0A 3rdcoil
101.2G Fluxball 0A 3rdcoil
0A Fluxball 169.6G 3rdcoil
0A Fluxball 296.8G 3rdcoil

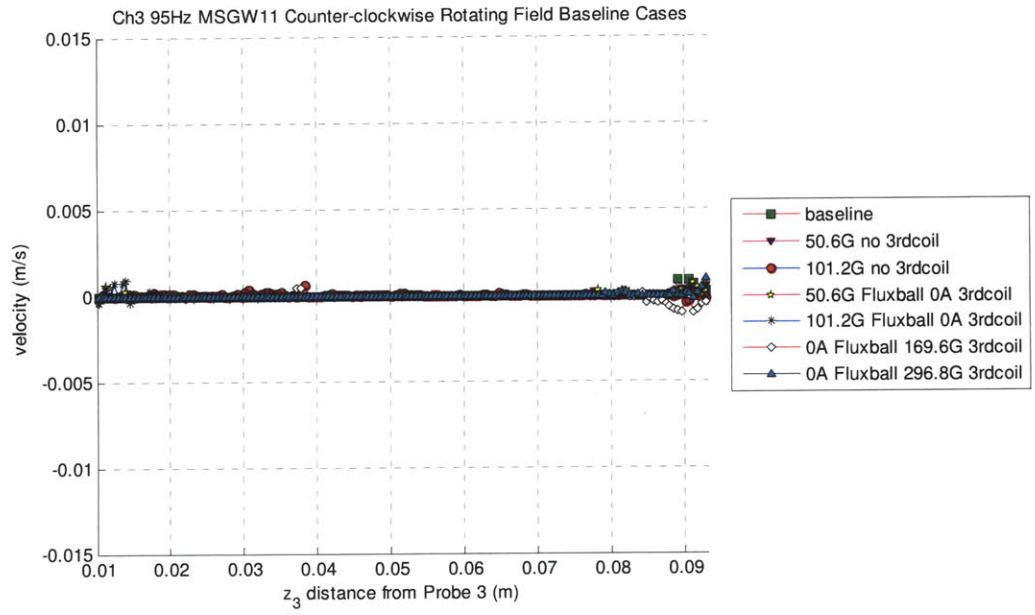
Ch3 95Hz MSGW11 Counter-clockwise Rotating Field Baseline Cases
velocity (m/s)
0.015
0.01
0.005
0
-0.005
-0.01
-0.015
0.01
0.02
0.03
0.04
0.05
0.06
0.07
0.08
0.09
z3 distance from Probe 3 (m)
baseline
50.6G no 3rdcoil
101.2G no 3rdcoil
50.6G Fluxball 0A 3rdcoil
101.2G Fluxball 0A 3rdcoil
0A Fluxball 169.6G 3rdcoil
0A Fluxball 296.8G 3rdcoil

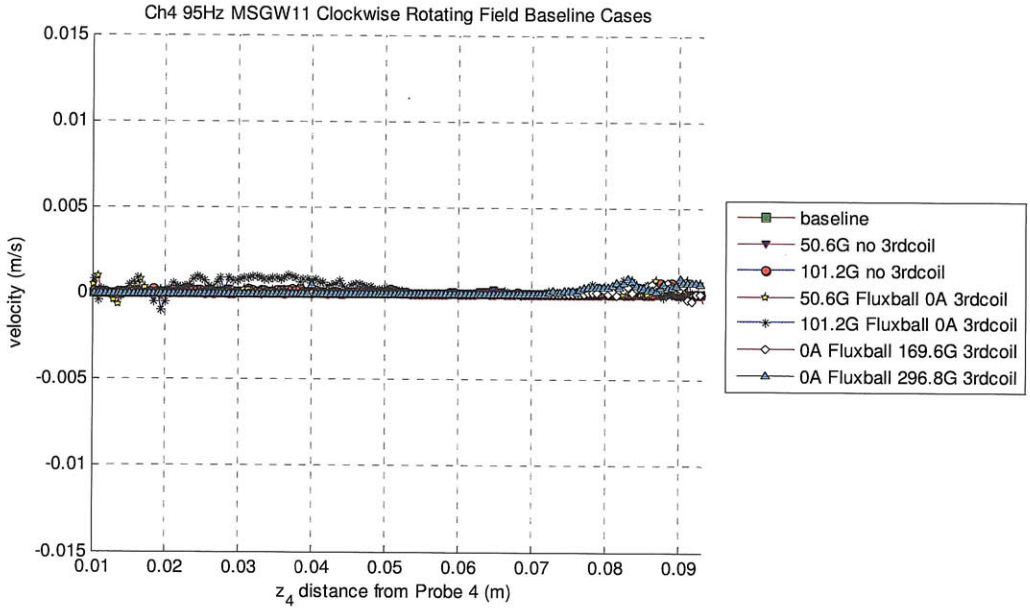
Ch4 95Hz MSGW11 Clockwise Rotating Field Baseline Cases
velocity (m/s)
0.015
0.01
0.005
0
-0.005
-0.01
-0.015
0.01
0.02
0.03
0.04
0.05
0.06
0.07
0.08
0.09
z4 distance from Probe 4 (m)
baseline
50.6G no 3rdcoil
101.2G no 3rdcoil
50.6G Fluxball 0A 3rdcoil
101.2G Fluxball 0A 3rdcoil
0A Fluxball 169.6G 3rdcoil
0A Fluxball 296.8G 3rdcoil

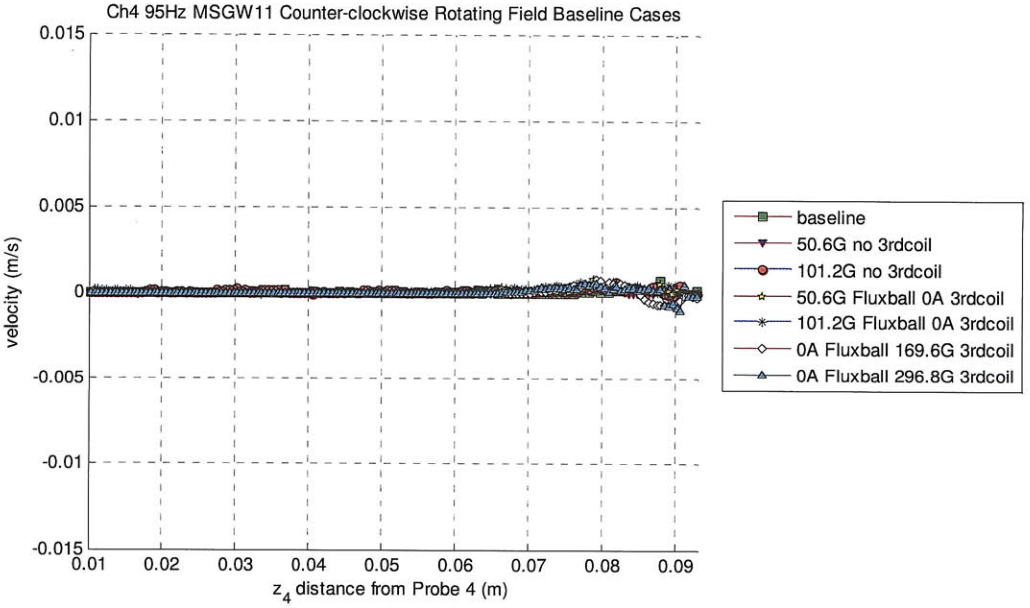
Ch4 95Hz MSGW11 Counter-clockwise Rotating Field Baseline Cases
velocity (m/s)
0.015
0.01
0.005
0
-0.005
-0.01
-0.015
0.01
0.02
0.03
0.04
0.05
0.06
0.07
0.08
0.09
z4 distance from Probe 4 (m)
baseline
50.6G no 3rdcoil
101.2G no 3rdcoil
50.6G Fluxball 0A 3rdcoil
101.2G Fluxball 0A 3rdcoil
0A Fluxball 169.6G 3rdcoil
0A Fluxball 296.8G 3rdcoil

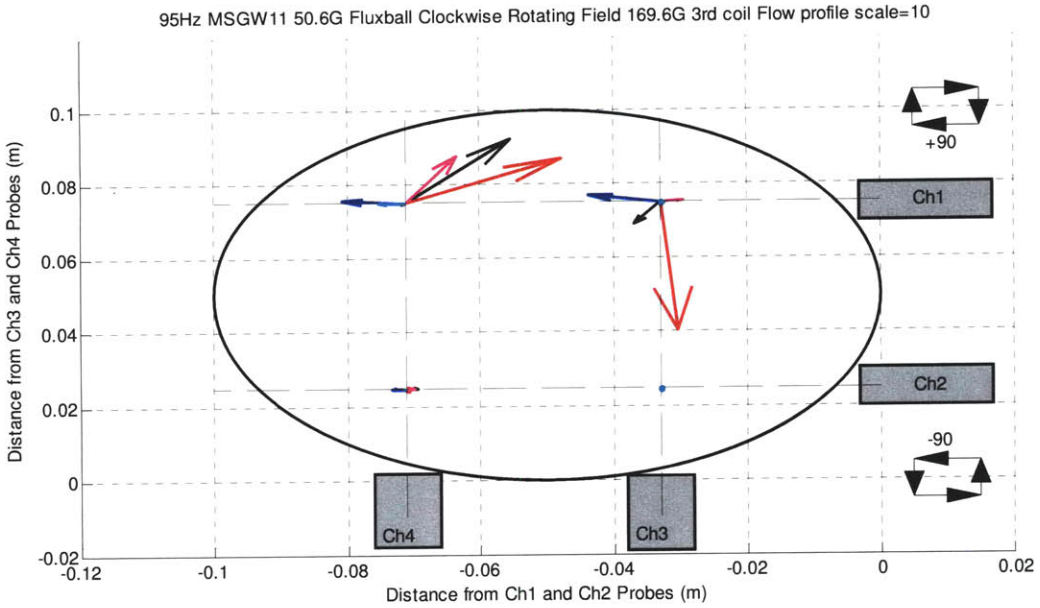
95Hz MSGW11 50.6G Fluxball Clockwise Rotating Field 169.6G 3rd coil Flow profile scale=10
Distance from Ch3 and Ch4 Probes (m)
Distance from Ch1 and Ch2 Probes (m)
0.1
0.08
0.06
0.04
0.02
0
-0.02
-0.12
-0.1
-0.08
-0.06
-0.04
-0.02
0
0.02
+90
-90
Ch1
Ch2
Ch3
Ch4

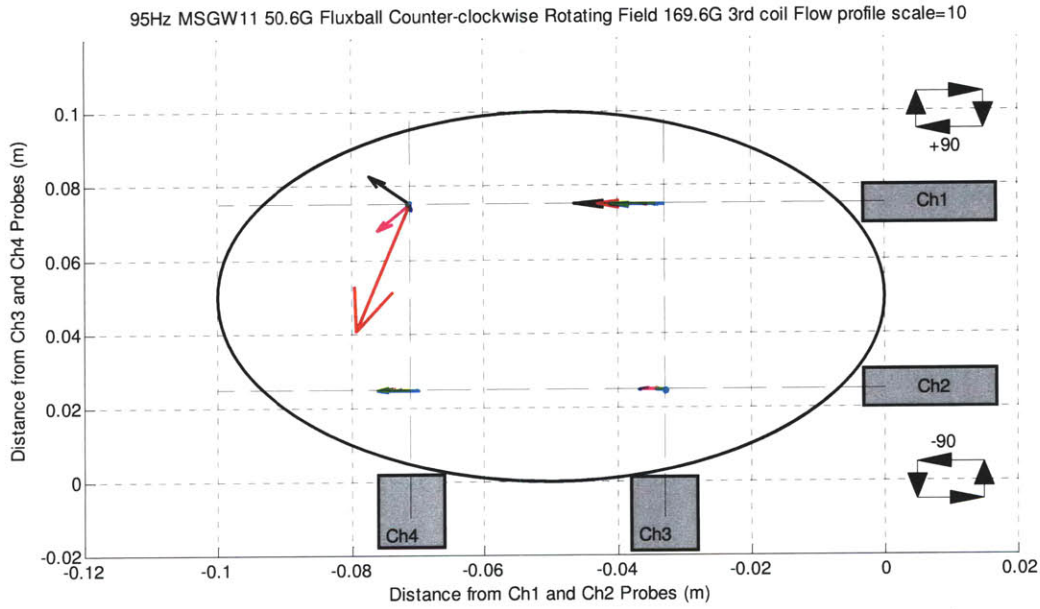
95Hz MSGW11 50.6G Fluxball Counter-clockwise Rotating Field 169.6G 3rd coil Flow profile scale=10
Distance from Ch3 and Ch4 Probes (m)
Distance from Ch1 and Ch2 Probes (m)
0.1
0.08
0.06
0.04
0.02
0
-0.02
-0.12
-0.1
-0.08
-0.06
-0.04
-0.02
0
0.02
+90
-90
Ch1
Ch2
Ch3
Ch4

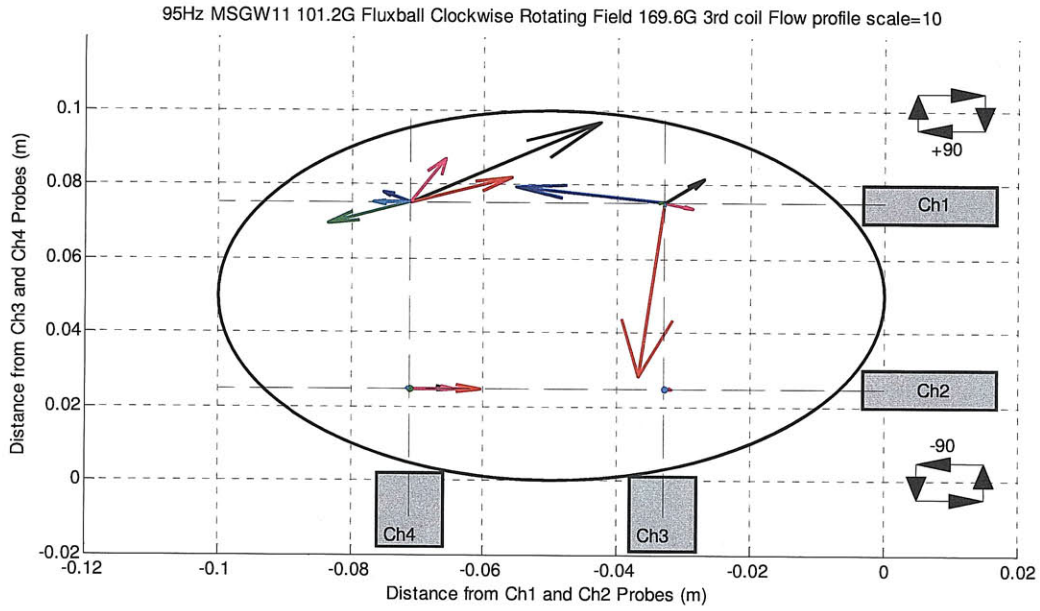
95Hz MSGW11 101.2G Fluxball Clockwise Rotating Field 169.6G 3rd coil Flow profile scale=10
Distance from Ch3 and Ch4 Probes (m)
Distance from Ch1 and Ch2 Probes (m)
0.1
0.08
0.06
0.04
0.02
0
-0.02
-0.12
-0.1
-0.08
-0.06
-0.04
-0.02
0
0.02
+90
-90
Ch1
Ch2
Ch3
Ch4

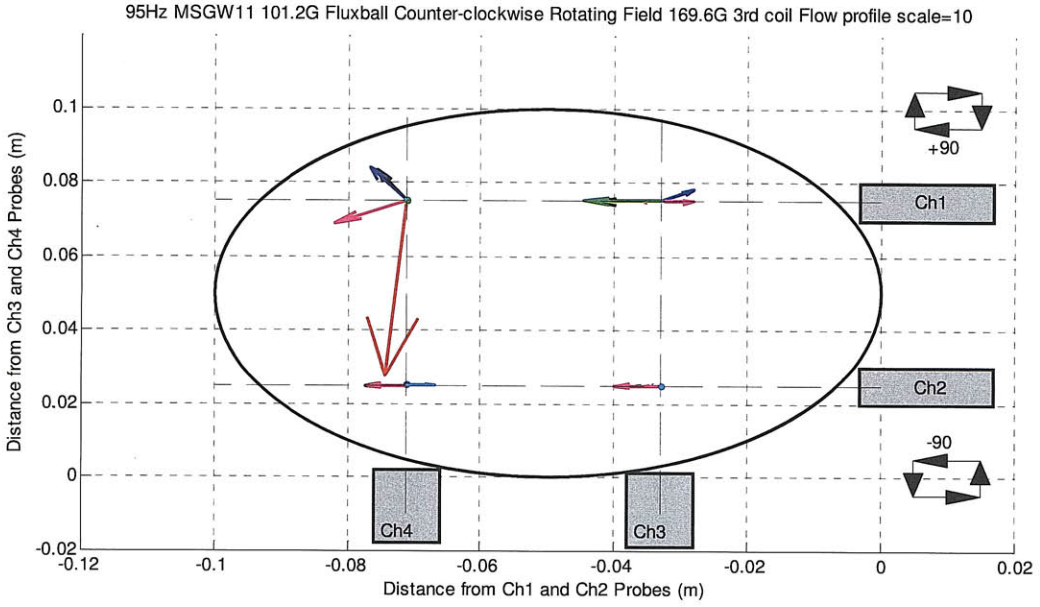
95Hz MSGW11 101.2G Fluxball Counter-clockwise Rotating Field 169.6G 3rd coil Flow profile scale=10
Distance from Ch3 and Ch4 Probes (m)
Distance from Ch1 and Ch2 Probes (m)
0.1
0.08
0.06
0.04
0.02
0
-0.02
-0.12
-0.1
-0.08
-0.06
-0.04
-0.02
0
0.02
+90
-90
Ch1
Ch2
Ch3
Ch4

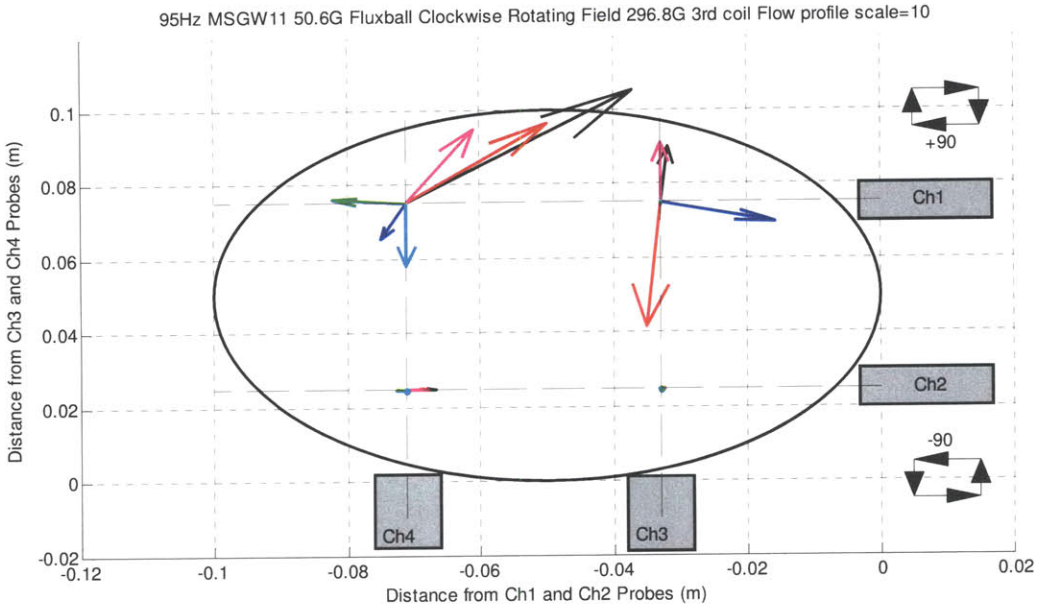
95Hz MSGW11 50.6G Fluxball Clockwise Rotating Field 296.8G 3rd coil Flow profile scale=10
Distance from Ch3 and Ch4 Probes (m)
Distance from Ch1 and Ch2 Probes (m)
0.1
0.08
0.06
0.04
0.02
0
-0.02
-0.12
-0.1
-0.08
-0.06
-0.04
-0.02
0
0.02
+90
-90
Ch1
Ch2
Ch3
Ch4

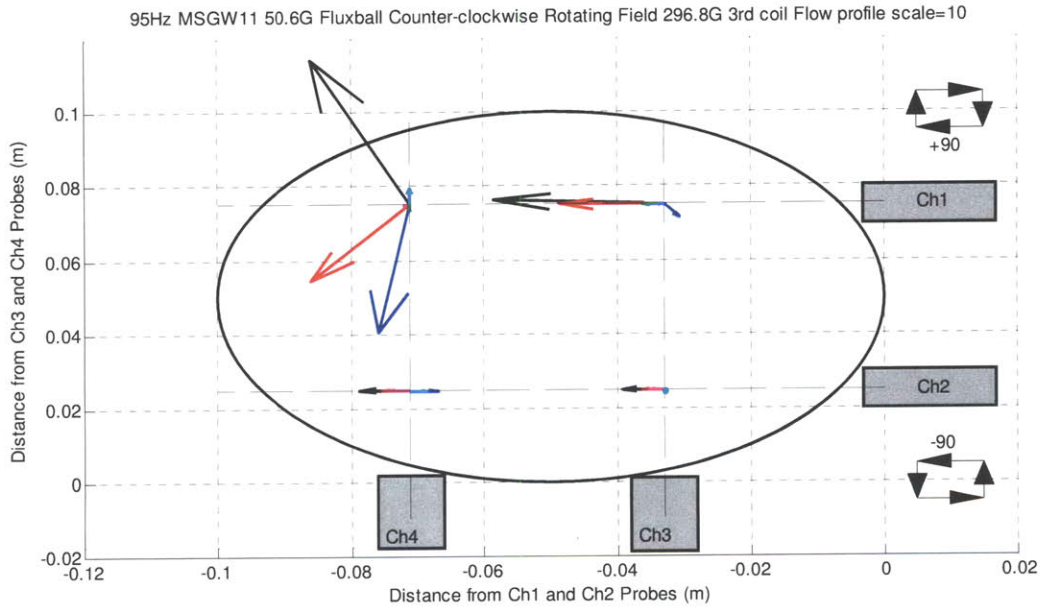
95Hz MSGW11 50.6G Fluxball Counter-clockwise Rotating Field 296.8G 3rd coil Flow profile scale=10
Distance from Ch3 and Ch4 Probes (m)
Distance from Ch1 and Ch2 Probes (m)
0.1
0.08
0.06
0.04
0.02
0
-0.02
-0.12
-0.1
-0.08
-0.06
-0.04
-0.02
0
0.02
+90
-90
Ch1
Ch2
Ch3
Ch4

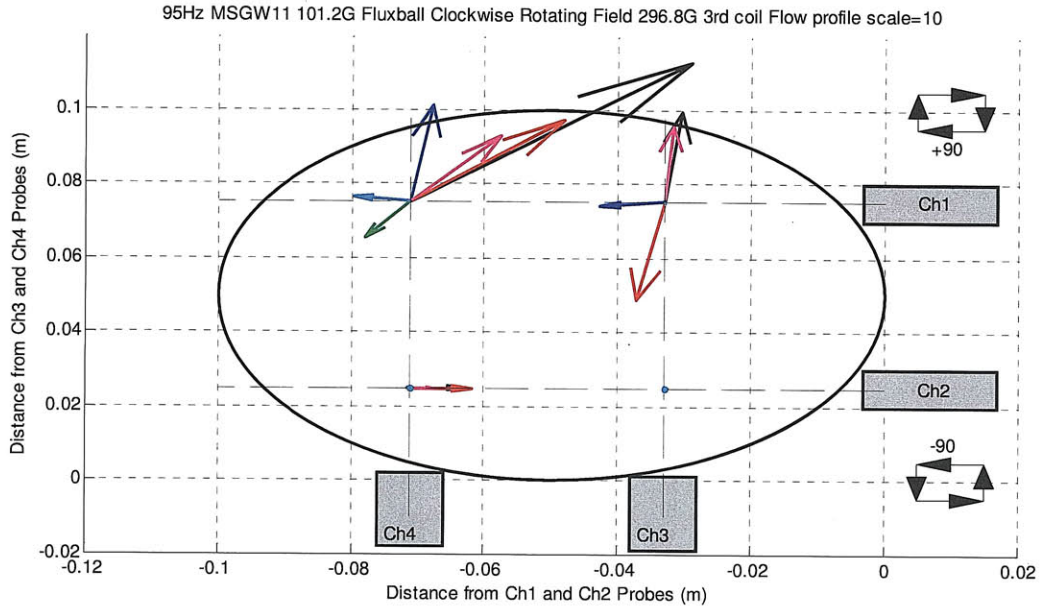
95Hz MSGW11 101.2G Fluxball Clockwise Rotating Field 296.8G 3rd coil Flow profile scale=10
Distance from Ch3 and Ch4 Probes (m)
Distance from Ch1 and Ch2 Probes (m)
+90
-90
Ch1
Ch2
Ch3
Ch4
0.1
0.08
0.06
0.04
0.02
0
-0.02
-0.12
-0.1
-0.08
-0.06
-0.04
-0.02
0
0.02

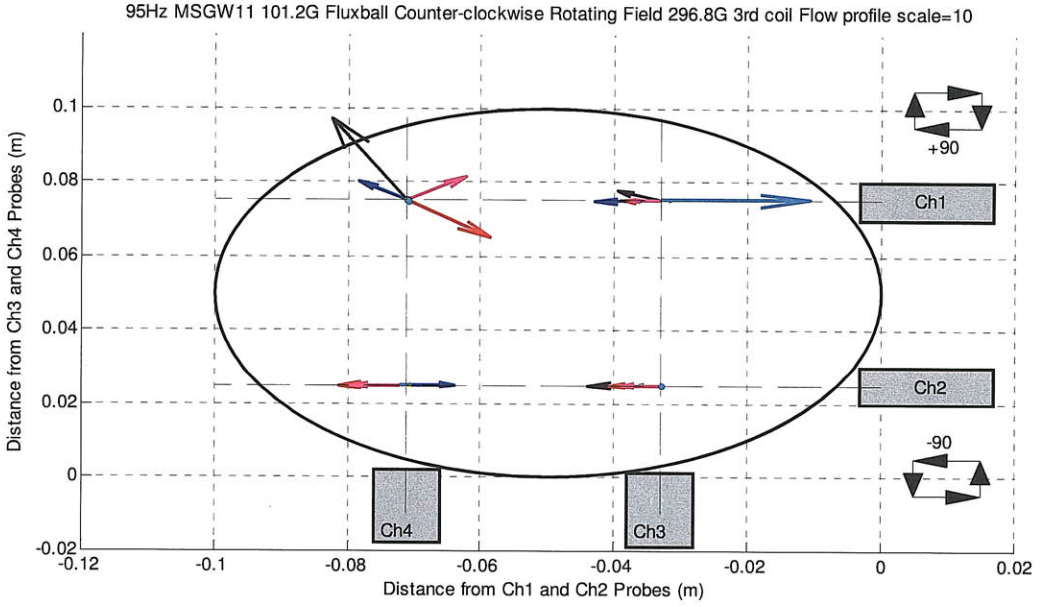
95Hz MSGW11 101.2G Fluxball Counter-clockwise Rotating Field 296.8G 3rd coil Flow profile scale=10
Distance from Ch3 and Ch4 Probes (m)
Distance from Ch1 and Ch2 Probes (m)
+90
-90
Ch1
Ch2
Ch3
Ch4
0.1
0.08
0.06
0.04
0.02
0
-0.02
-0.12
-0.1
-0.08
-0.06
-0.04
-0.02
0
0.02

G5. MSGW11 Filled Sphere with Third Coil Oscillating at Same Frequency as Rotating Field at 47Hz

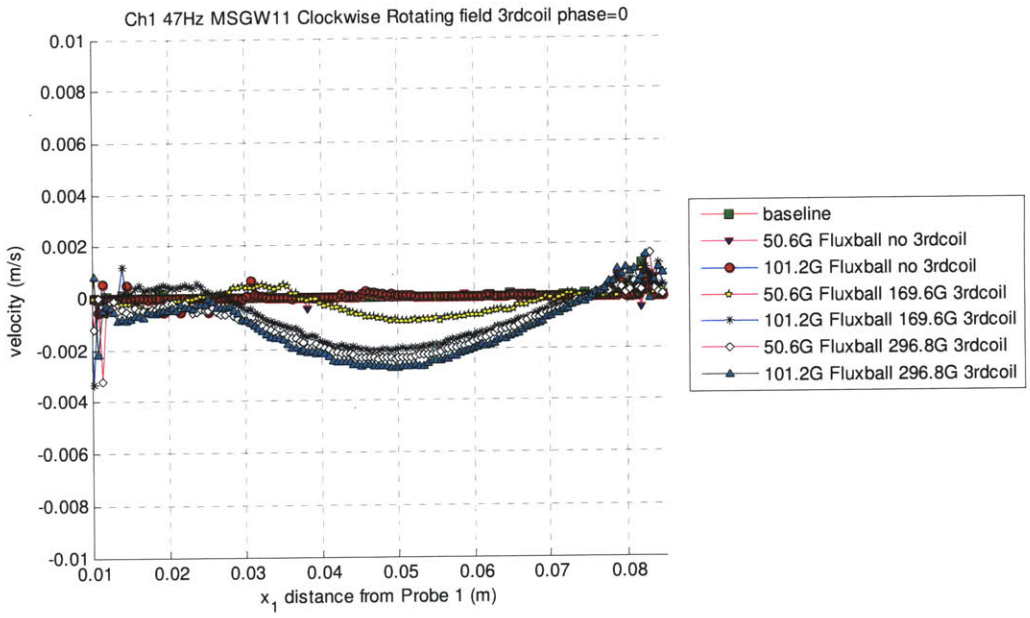

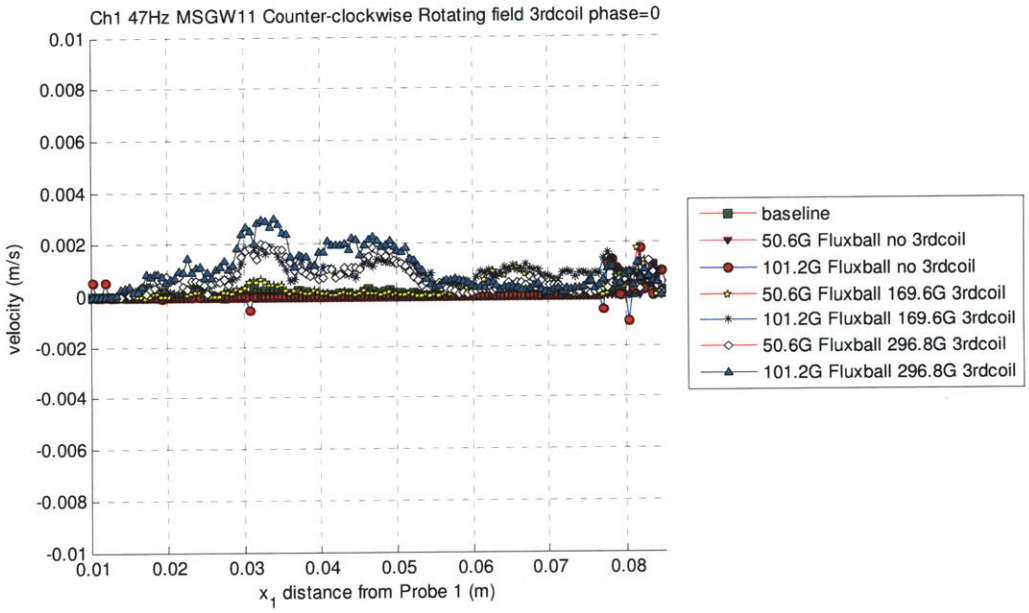

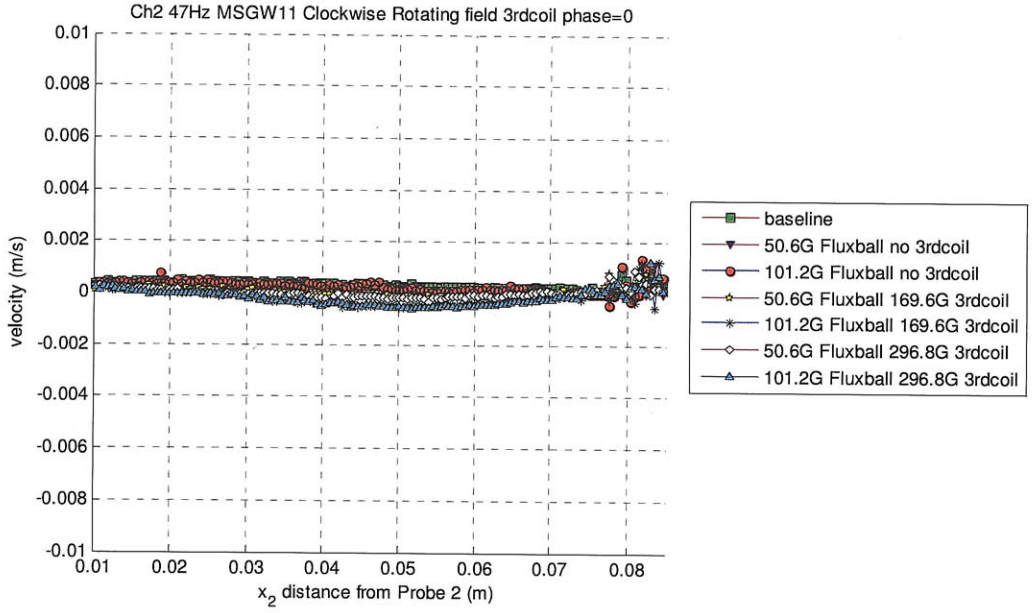
Ch2 47Hz MSGW11 Clockwise Rotating field 3rdcoil phase=0
velocity (m/s)
0.01
0.008
0.006
0.004
0.002
0
-0.002
-0.004
-0.006
-0.008
-0.01
0.01 0.02 0.03 0.04 0.05 0.06 0.07 0.08
x2 distance from Probe 2 (m)
baseline
50.6G Fluxball no 3rdcoil
101.2G Fluxball no 3rdcoil
50.6G Fluxball 169.6G 3rdcoil
101.2G Fluxball 169.6G 3rdcoil
50.6G Fluxball 296.8G 3rdcoil
101.2G Fluxball 296.8G 3rdcoil

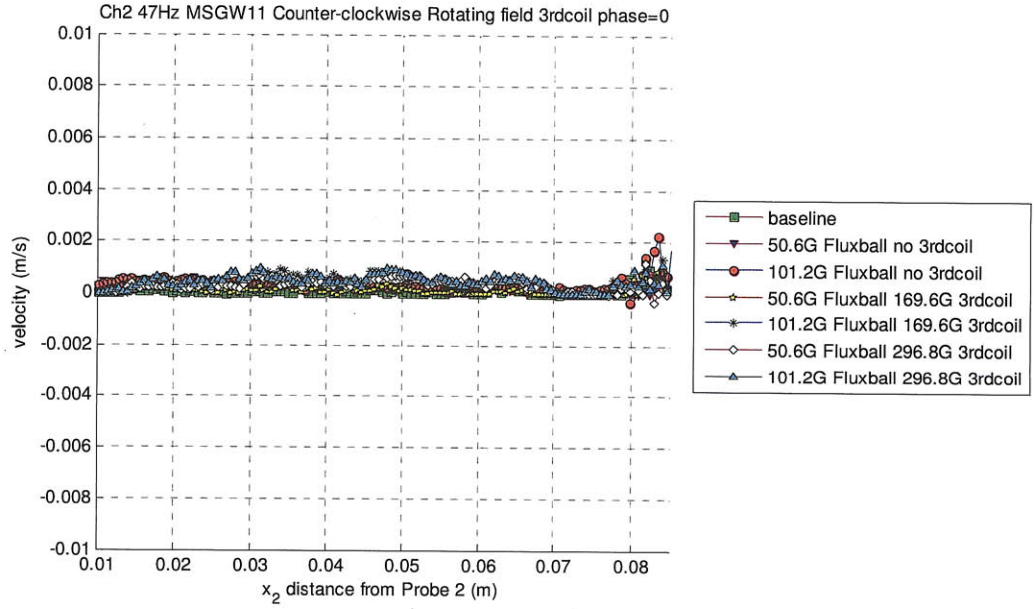
Ch2 47Hz MSGW11 Counter-clockwise Rotating field 3rdcoil phase=0
velocity (m/s)
0.01
0.008
0.006
0.004
0.002
0
-0.002
-0.004
-0.006
-0.008
-0.01
0.01 0.02 0.03 0.04 0.05 0.06 0.07 0.08
x2 distance from Probe 2 (m)
baseline
50.6G Fluxball no 3rdcoil
101.2G Fluxball no 3rdcoil
50.6G Fluxball 169.6G 3rdcoil
101.2G Fluxball 169.6G 3rdcoil
50.6G Fluxball 296.8G 3rdcoil
101.2G Fluxball 296.8G 3rdcoil

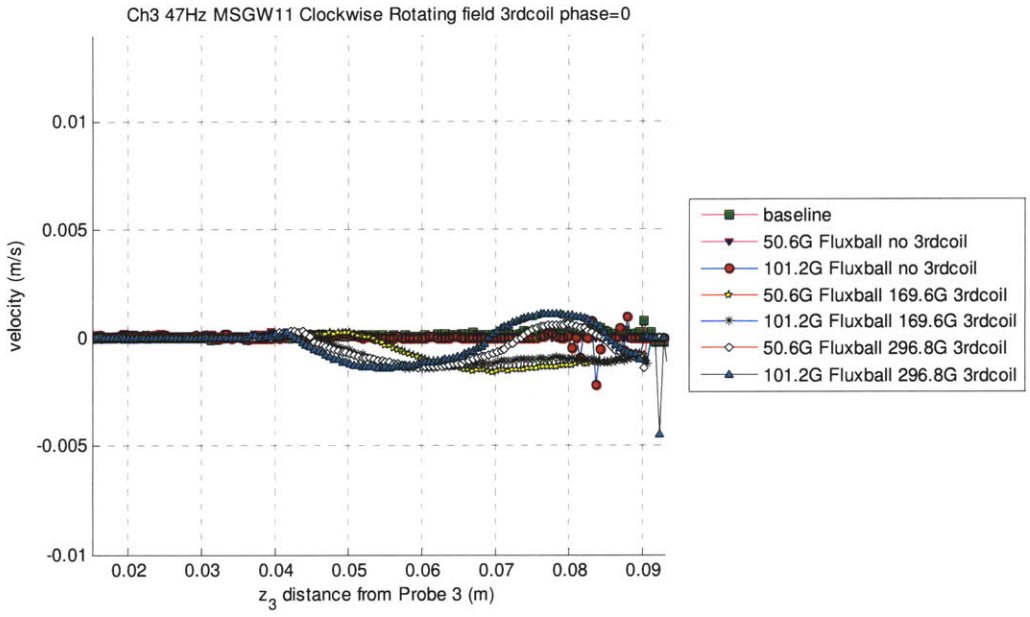
Ch3 47Hz MSGW11 Clockwise Rotating field 3rdcoil phase=0
velocity (m/s)
0.01
0.005
0
-0.005
-0.01
0.02
0.03
0.04
0.05
0.06
0.07
0.08
0.09
z_3 distance from Probe 3 (m)
baseline
50.6G Fluxball no 3rdcoil
101.2G Fluxball no 3rdcoil
50.6G Fluxball 169.6G 3rdcoil
101.2G Fluxball 169.6G 3rdcoil
50.6G Fluxball 296.8G 3rdcoil
101.2G Fluxball 296.8G 3rdcoil

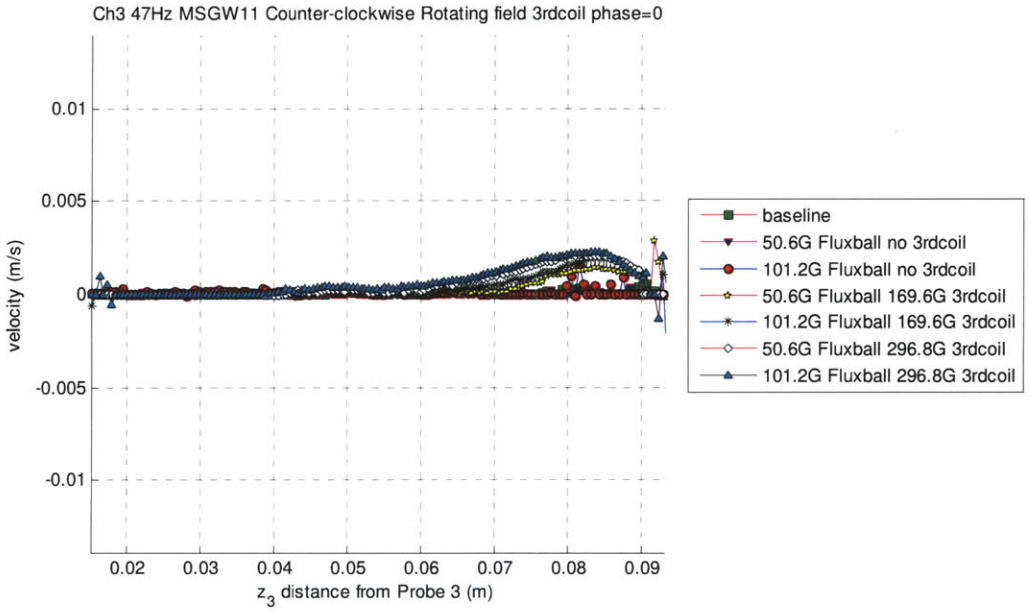
Ch3 47Hz MSGW11 Counter-clockwise Rotating field 3rdcoil phase=0
velocity (m/s)
0.01
0.005
0
-0.005
-0.01
0.02
0.03
0.04
0.05
0.06
0.07
0.08
0.09
z_3 distance from Probe 3 (m)
baseline
50.6G Fluxball no 3rdcoil
101.2G Fluxball no 3rdcoil
50.6G Fluxball 169.6G 3rdcoil
101.2G Fluxball 169.6G 3rdcoil
50.6G Fluxball 296.8G 3rdcoil
101.2G Fluxball 296.8G 3rdcoil

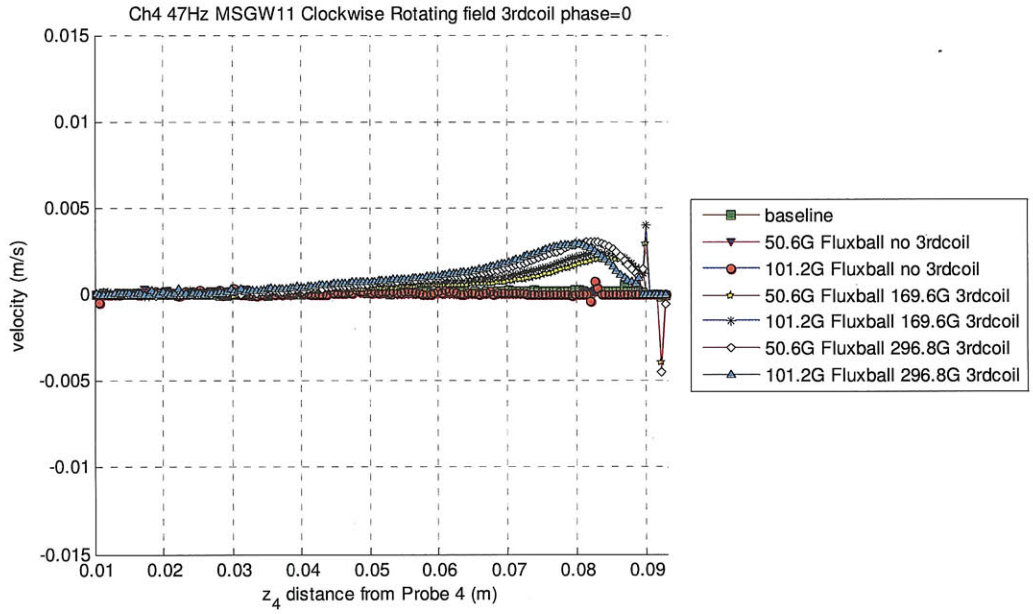
Ch4 47Hz MSGW11 Clockwise Rotating field 3rdcoil phase=0
velocity (m/s)
0.015
0.01
0.005
0
-0.005
-0.01
-0.015
0.01
0.02
0.03
0.04
0.05
0.06
0.07
0.08
0.09
z4 distance from Probe 4 (m)
baseline
50.6G Fluxball no 3rdcoil
101.2G Fluxball no 3rdcoil
50.6G Fluxball 169.6G 3rdcoil
101.2G Fluxball 169.6G 3rdcoil
50.6G Fluxball 296.8G 3rdcoil
101.2G Fluxball 296.8G 3rdcoil

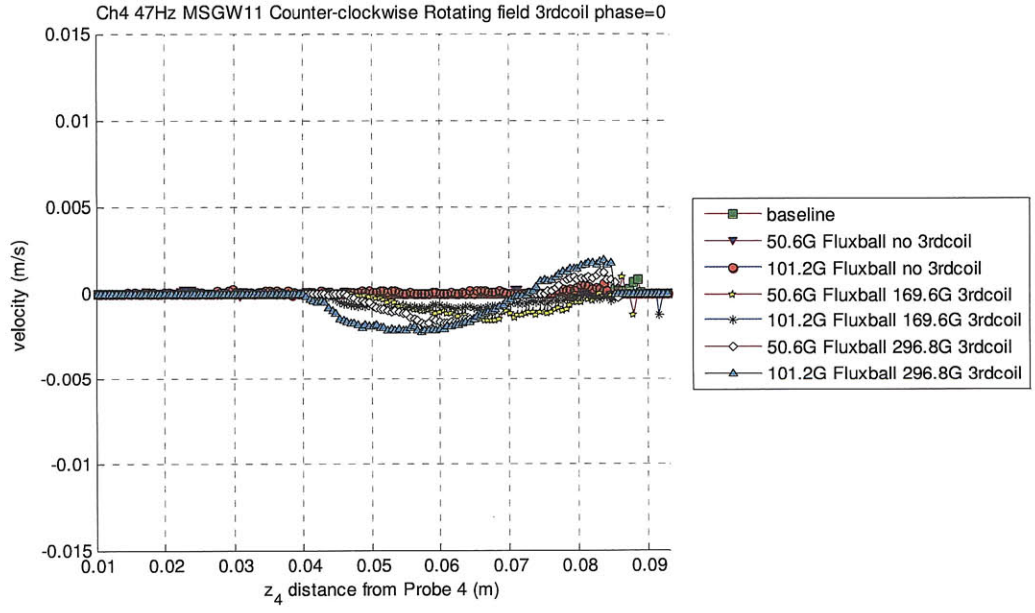
Ch4 47Hz MSGW11 Counter-clockwise Rotating field 3rdcoil phase=0
velocity (m/s)
0.015
0.01
0.005
0
-0.005
-0.01
-0.015
0.01
0.02
0.03
0.04
0.05
0.06
0.07
0.08
0.09
z4 distance from Probe 4 (m)
baseline
50.6G Fluxball no 3rdcoil
101.2G Fluxball no 3rdcoil
50.6G Fluxball 169.6G 3rdcoil
101.2G Fluxball 169.6G 3rdcoil
50.6G Fluxball 296.8G 3rdcoil
101.2G Fluxball 296.8G 3rdcoil

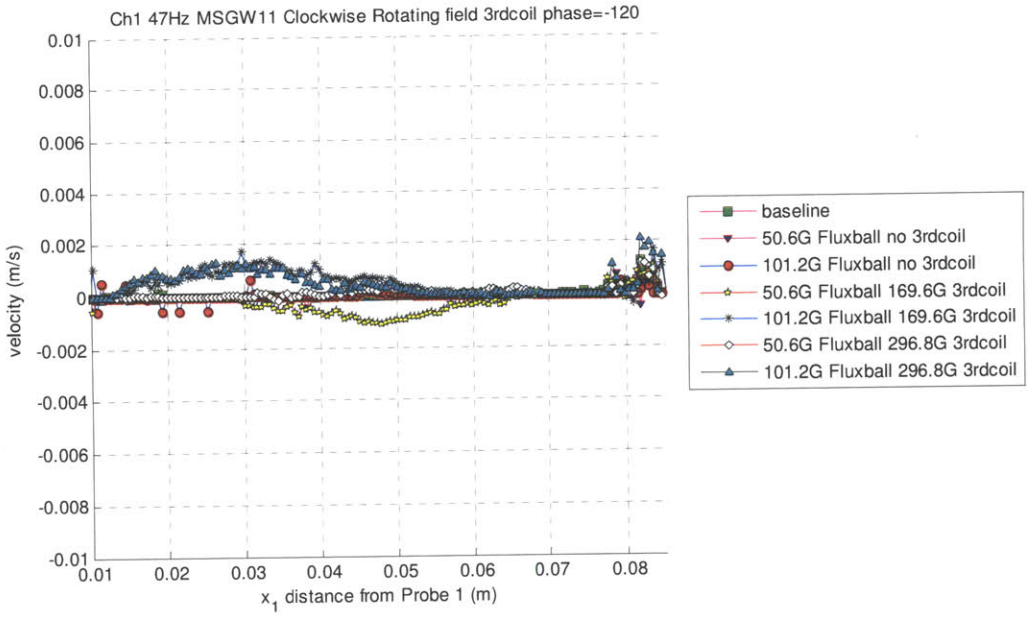
Ch1 47Hz MSGW11 Clockwise Rotating field 3rdcoil phase=-120
velocity (m/s)
0.01
0.008
0.006
0.004
0.002
0
-0.002
-0.004
-0.006
-0.008
-0.01
0.01
0.02
0.03
0.04
0.05
0.06
0.07
0.08
x1 distance from Probe 1 (m)
baseline
50.6G Fluxball no 3rdcoil
101.2G Fluxball no 3rdcoil
50.6G Fluxball 169.6G 3rdcoil
101.2G Fluxball 169.6G 3rdcoil
50.6G Fluxball 296.8G 3rdcoil
101.2G Fluxball 296.8G 3rdcoil

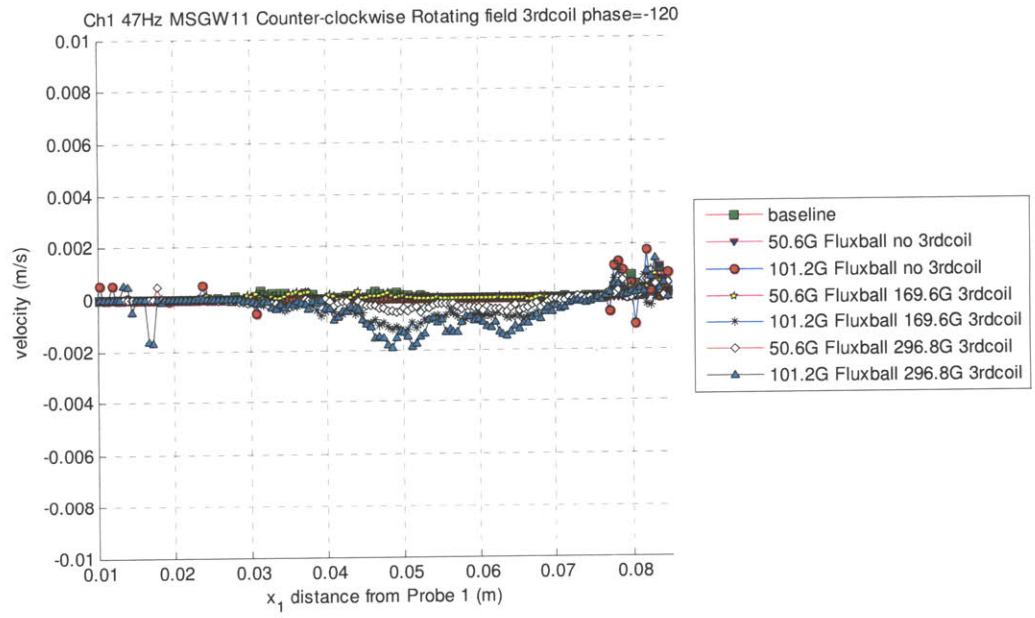
Ch1 47Hz MSGW11 Counter-clockwise Rotating field 3rdcoil phase=-120
velocity (m/s)
0.01
0.008
0.006
0.004
0.002
0
-0.002
-0.004
-0.006
-0.008
-0.01
0.01
0.02
0.03
0.04
0.05
0.06
0.07
0.08
x1 distance from Probe 1 (m)
baseline
50.6G Fluxball no 3rdcoil
101.2G Fluxball no 3rdcoil
50.6G Fluxball 169.6G 3rdcoil
101.2G Fluxball 169.6G 3rdcoil
50.6G Fluxball 296.8G 3rdcoil
101.2G Fluxball 296.8G 3rdcoil

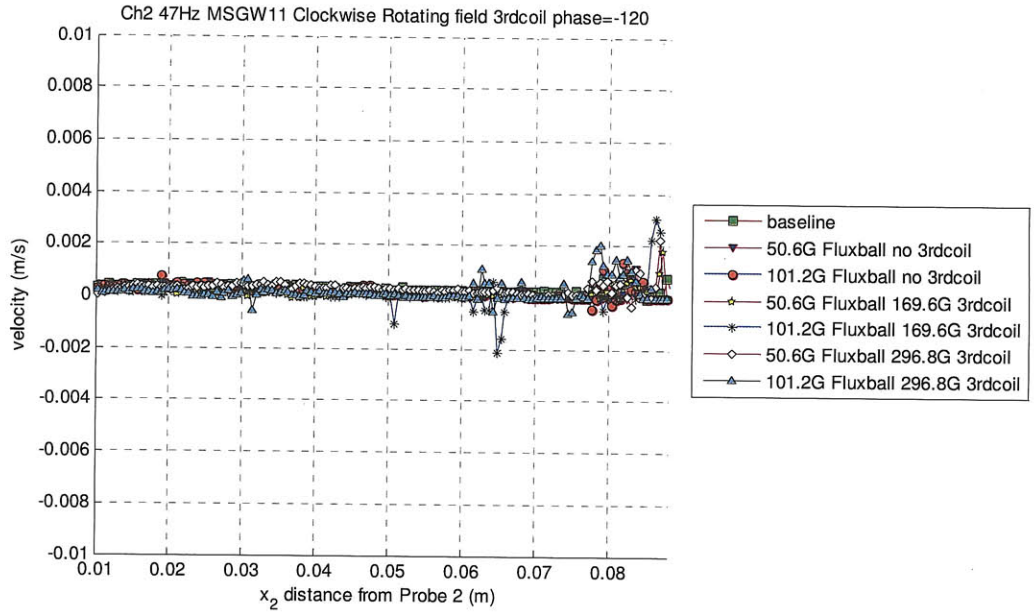
Ch2 47Hz MSGW11 Clockwise Rotating field 3rdcoil phase=-120
velocity (m/s)
0.01
0.008
0.006
0.004
0.002
0
-0.002
-0.004
-0.006
-0.008
-0.01
0.01 0.02 0.03 0.04 0.05 0.06 0.07 0.08
x2 distance from Probe 2 (m)
baseline
50.6G Fluxball no 3rdcoil
101.2G Fluxball no 3rdcoil
50.6G Fluxball 169.6G 3rdcoil
101.2G Fluxball 169.6G 3rdcoil
50.6G Fluxball 296.8G 3rdcoil
101.2G Fluxball 296.8G 3rdcoil

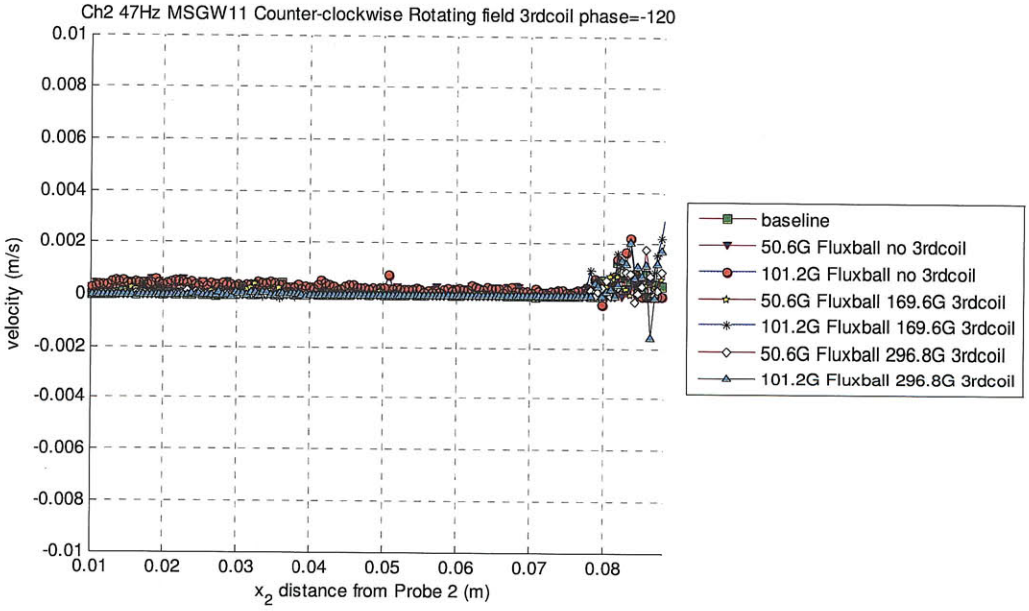
Ch2 47Hz MSGW11 Counter-clockwise Rotating field 3rdcoil phase=-120
velocity (m/s)
0.01
0.008
0.006
0.004
0.002
0
-0.002
-0.004
-0.006
-0.008
-0.01
0.01 0.02 0.03 0.04 0.05 0.06 0.07 0.08
x2 distance from Probe 2 (m)
baseline
50.6G Fluxball no 3rdcoil
101.2G Fluxball no 3rdcoil
50.6G Fluxball 169.6G 3rdcoil
101.2G Fluxball 169.6G 3rdcoil
50.6G Fluxball 296.8G 3rdcoil
101.2G Fluxball 296.8G 3rdcoil

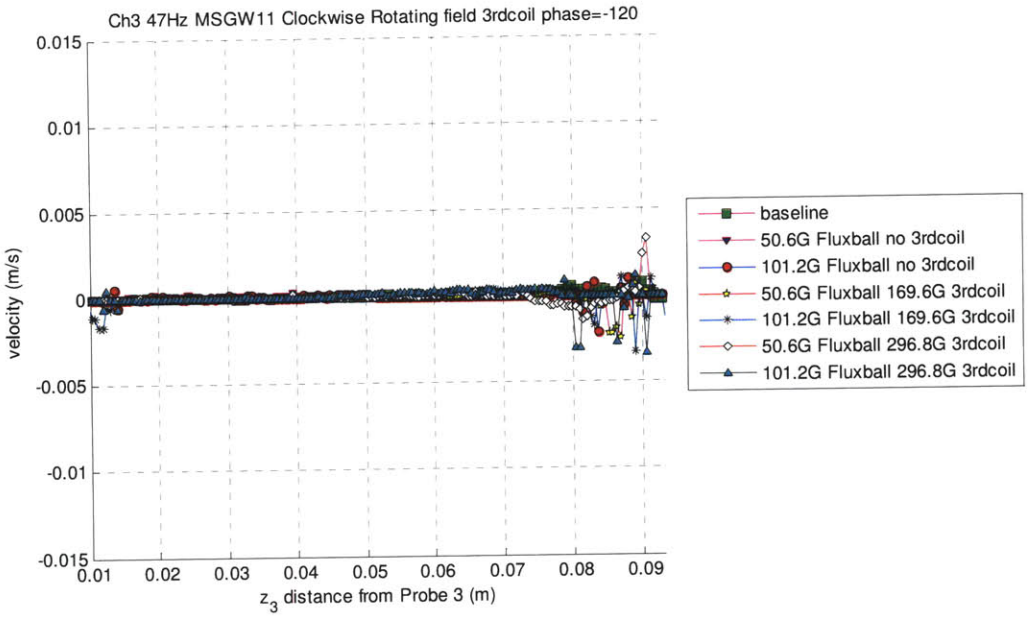
Ch3 47Hz MSGW11 Clockwise Rotating field 3rdcoil phase=-120
velocity (m/s)
0.015
0.01
0.005
0
-0.005
-0.01
-0.015
0.01
0.02
0.03
0.04
0.05
0.06
0.07
0.08
0.09
z3 distance from Probe 3 (m)
baseline
50.6G Fluxball no 3rdcoil
101.2G Fluxball no 3rdcoil
50.6G Fluxball 169.6G 3rdcoil
101.2G Fluxball 169.6G 3rdcoil
50.6G Fluxball 296.8G 3rdcoil
101.2G Fluxball 296.8G 3rdcoil

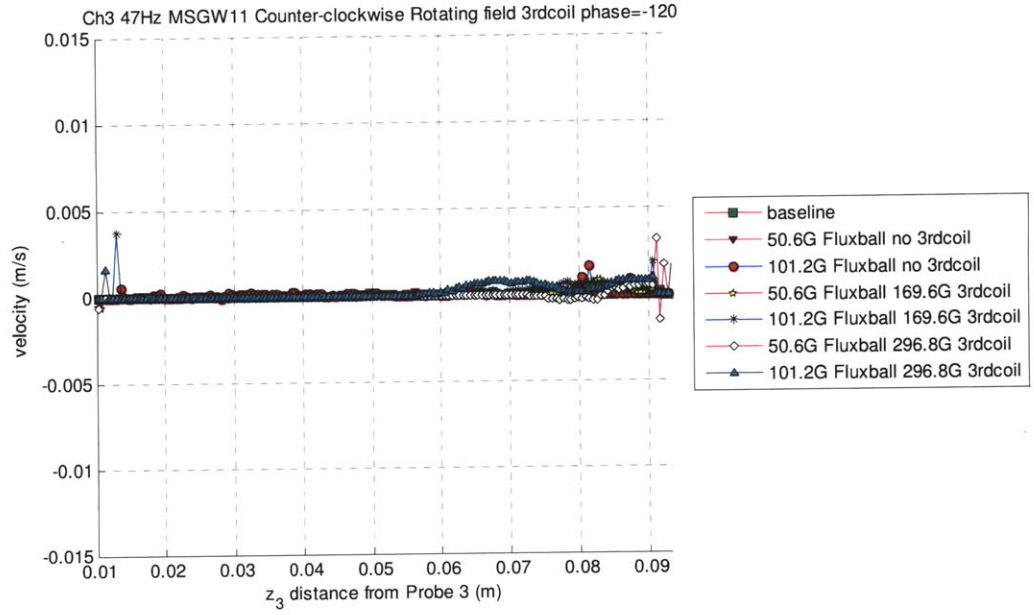
Ch3 47Hz MSGW11 Counter-clockwise Rotating field 3rdcoil phase=-120
velocity (m/s)
0.015
0.01
0.005
0
-0.005
-0.01
-0.015
0.01
0.02
0.03
0.04
0.05
0.06
0.07
0.08
0.09
z3 distance from Probe 3 (m)
baseline
50.6G Fluxball no 3rdcoil
101.2G Fluxball no 3rdcoil
50.6G Fluxball 169.6G 3rdcoil
101.2G Fluxball 169.6G 3rdcoil
50.6G Fluxball 296.8G 3rdcoil
101.2G Fluxball 296.8G 3rdcoil

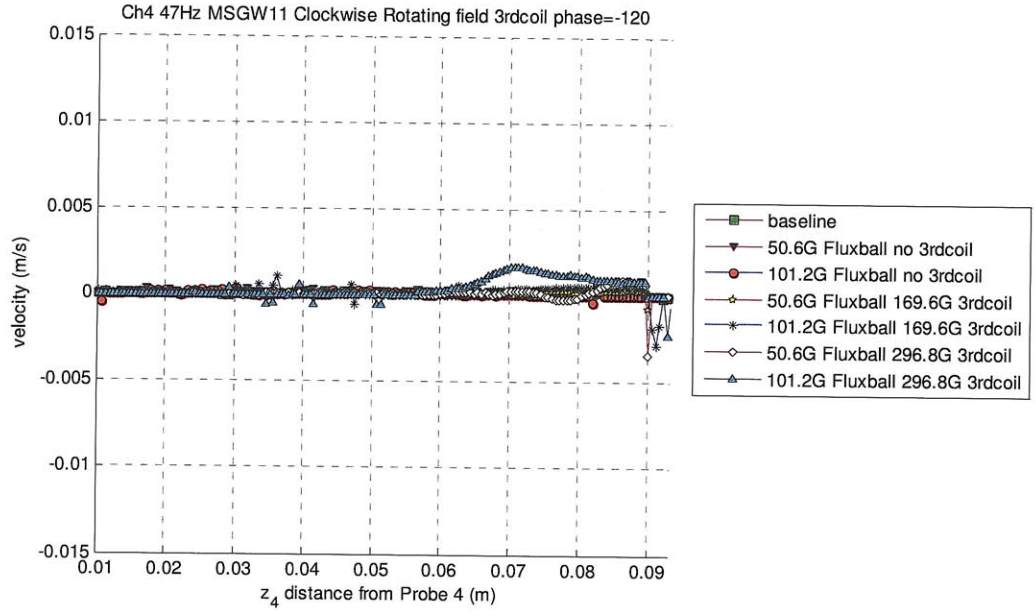
Ch4 47Hz MSGW11 Clockwise Rotating field 3rdcoil phase=-120
velocity (m/s)
0.015
0.01
0.005
0
-0.005
-0.01
-0.015
0.01
0.02
0.03
0.04
0.05
0.06
0.07
0.08
0.09
z4 distance from Probe 4 (m)
baseline
50.6G Fluxball no 3rdcoil
101.2G Fluxball no 3rdcoil
50.6G Fluxball 169.6G 3rdcoil
101.2G Fluxball 169.6G 3rdcoil
50.6G Fluxball 296.8G 3rdcoil
101.2G Fluxball 296.8G 3rdcoil

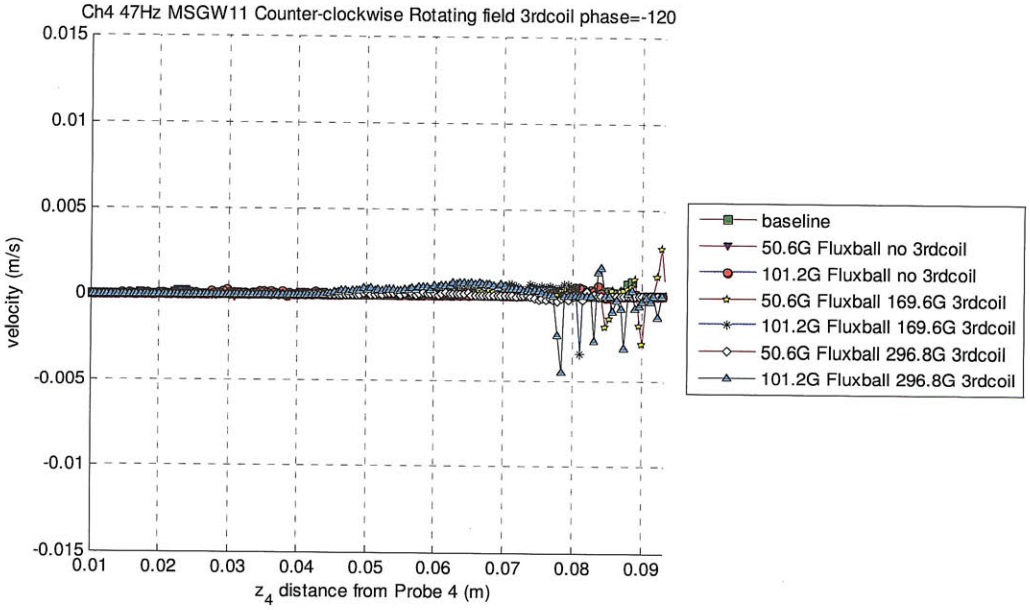
Ch4 47Hz MSGW11 Counter-clockwise Rotating field 3rdcoil phase=-120
velocity (m/s)
0.015
0.01
0.005
0
-0.005
-0.01
-0.015
0.01
0.02
0.03
0.04
0.05
0.06
0.07
0.08
0.09
z4 distance from Probe 4 (m)
baseline
50.6G Fluxball no 3rdcoil
101.2G Fluxball no 3rdcoil
50.6G Fluxball 169.6G 3rdcoil
101.2G Fluxball 169.6G 3rdcoil
50.6G Fluxball 296.8G 3rdcoil
101.2G Fluxball 296.8G 3rdcoil

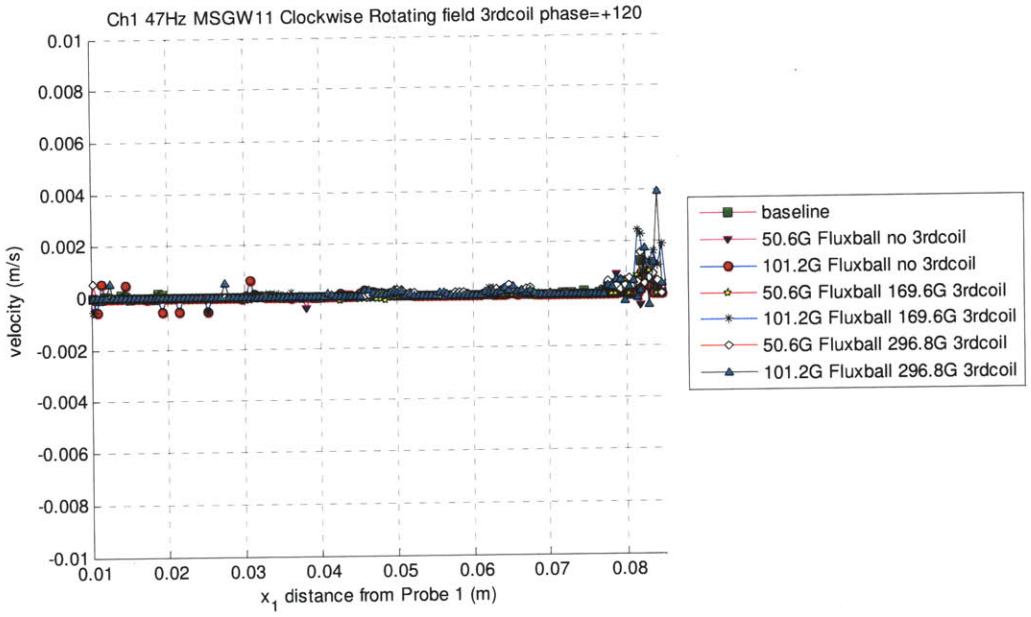
Ch1 47Hz MSGW11 Clockwise Rotating field 3rdcoil phase=+120
velocity (m/s)
0.01
0.008
0.006
0.004
0.002
0
-0.002
-0.004
-0.006
-0.008
-0.01
0.01
0.02
0.03
0.04
0.05
0.06
0.07
0.08
x1 distance from Probe 1 (m)
baseline
50.6G Fluxball no 3rdcoil
101.2G Fluxball no 3rdcoil
50.6G Fluxball 169.6G 3rdcoil
101.2G Fluxball 169.6G 3rdcoil
50.6G Fluxball 296.8G 3rdcoil
101.2G Fluxball 296.8G 3rdcoil

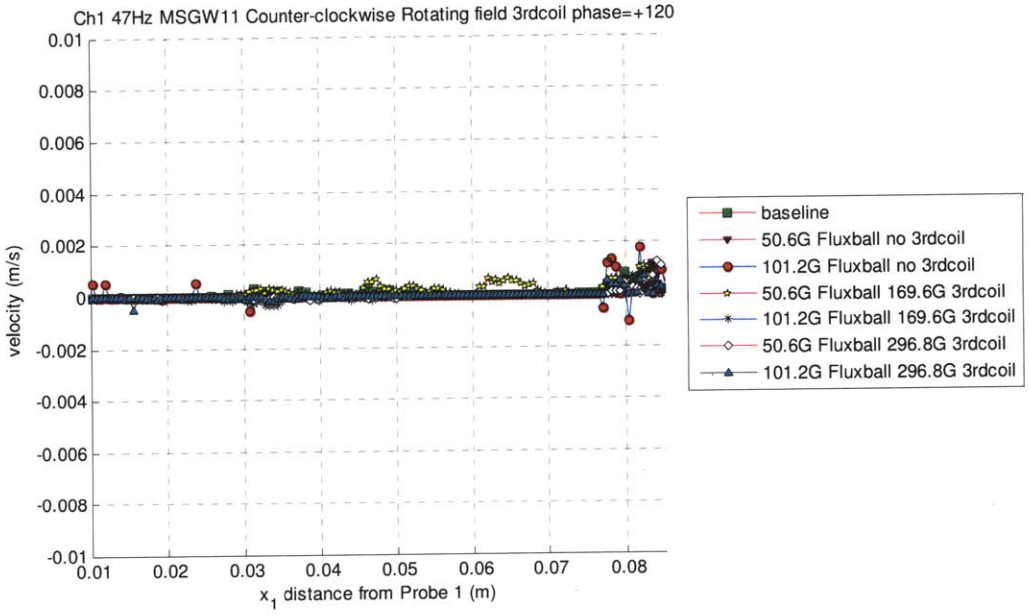
Ch1 47Hz MSGW11 Counter-clockwise Rotating field 3rdcoil phase=+120
velocity (m/s)
0.01
0.008
0.006
0.004
0.002
0
-0.002
-0.004
-0.006
-0.008
-0.01
0.01
0.02
0.03
0.04
0.05
0.06
0.07
0.08
x1 distance from Probe 1 (m)
baseline
50.6G Fluxball no 3rdcoil
101.2G Fluxball no 3rdcoil
50.6G Fluxball 169.6G 3rdcoil
101.2G Fluxball 169.6G 3rdcoil
50.6G Fluxball 296.8G 3rdcoil
101.2G Fluxball 296.8G 3rdcoil

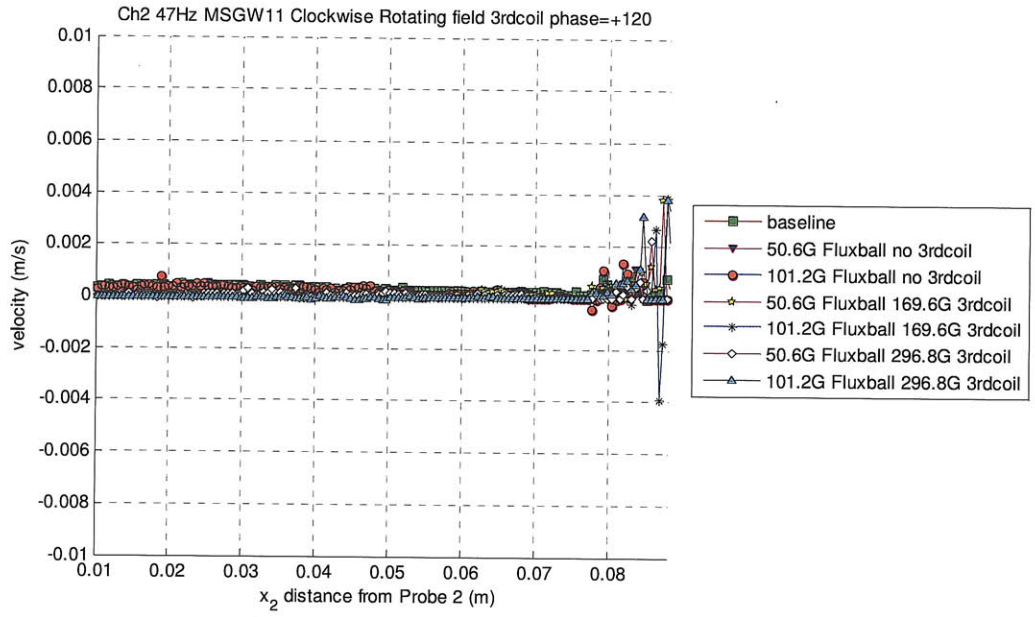
Ch2 47Hz MSGW11 Clockwise Rotating field 3rdcoil phase=+120
velocity (m/s)
0.01
0.008
0.006
0.004
0.002
0
-0.002
-0.004
-0.006
-0.008
-0.01
0.01 0.02 0.03 0.04 0.05 0.06 0.07 0.08
x2 distance from Probe 2 (m)
baseline
50.6G Fluxball no 3rdcoil
101.2G Fluxball no 3rdcoil
50.6G Fluxball 169.6G 3rdcoil
101.2G Fluxball 169.6G 3rdcoil
50.6G Fluxball 296.8G 3rdcoil
101.2G Fluxball 296.8G 3rdcoil

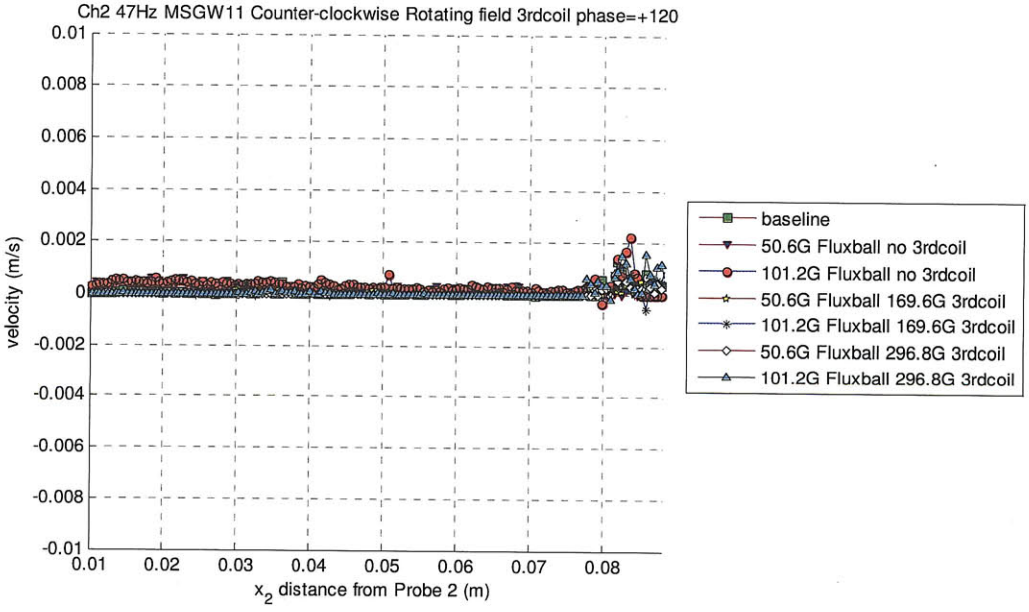
Ch2 47Hz MSGW11 Counter-clockwise Rotating field 3rdcoil phase=+120
velocity (m/s)
0.01
0.008
0.006
0.004
0.002
0
-0.002
-0.004
-0.006
-0.008
-0.01
0.01 0.02 0.03 0.04 0.05 0.06 0.07 0.08
x2 distance from Probe 2 (m)
baseline
50.6G Fluxball no 3rdcoil
101.2G Fluxball no 3rdcoil
50.6G Fluxball 169.6G 3rdcoil
101.2G Fluxball 169.6G 3rdcoil
50.6G Fluxball 296.8G 3rdcoil
101.2G Fluxball 296.8G 3rdcoil

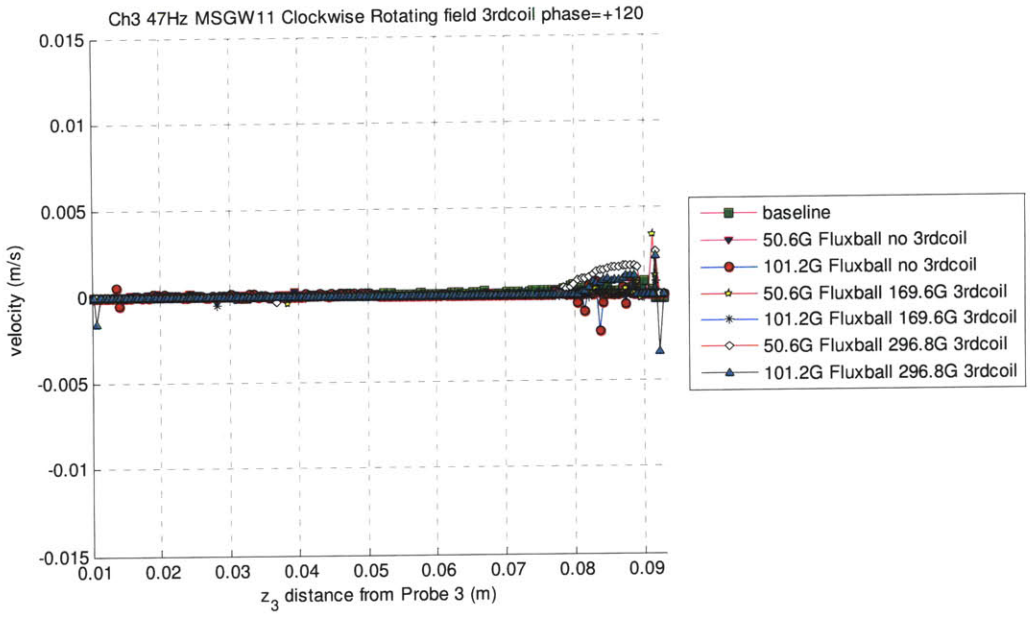
Ch3 47Hz MSGW11 Clockwise Rotating field 3rdcoil phase=+120
velocity (m/s)
0.015
0.01
0.005
0
-0.005
-0.01
-0.015
0.01
0.02
0.03
0.04
0.05
0.06
0.07
0.08
0.09
z_3 distance from Probe 3 (m)
baseline
50.6G Fluxball no 3rdcoil
101.2G Fluxball no 3rdcoil
50.6G Fluxball 169.6G 3rdcoil
101.2G Fluxball 169.6G 3rdcoil
50.6G Fluxball 296.8G 3rdcoil
101.2G Fluxball 296.8G 3rdcoil

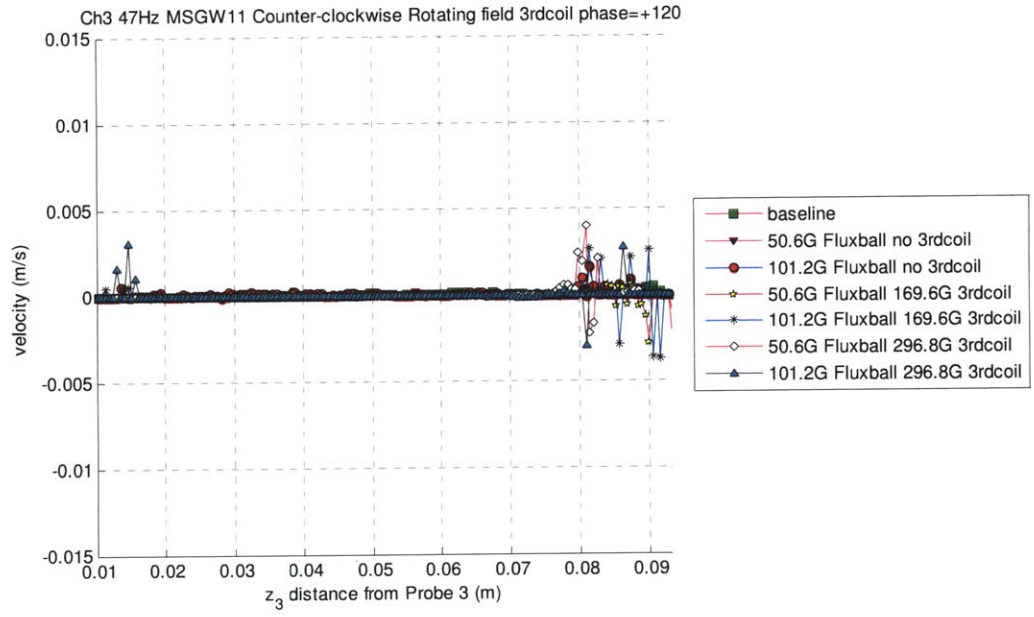
Ch3 47Hz MSGW11 Counter-clockwise Rotating field 3rdcoil phase=+120
velocity (m/s)
0.015
0.01
0.005
0
-0.005
-0.01
-0.015
0.01
0.02
0.03
0.04
0.05
0.06
0.07
0.08
0.09
z_3 distance from Probe 3 (m)
baseline
50.6G Fluxball no 3rdcoil
101.2G Fluxball no 3rdcoil
50.6G Fluxball 169.6G 3rdcoil
101.2G Fluxball 169.6G 3rdcoil
50.6G Fluxball 296.8G 3rdcoil
101.2G Fluxball 296.8G 3rdcoil

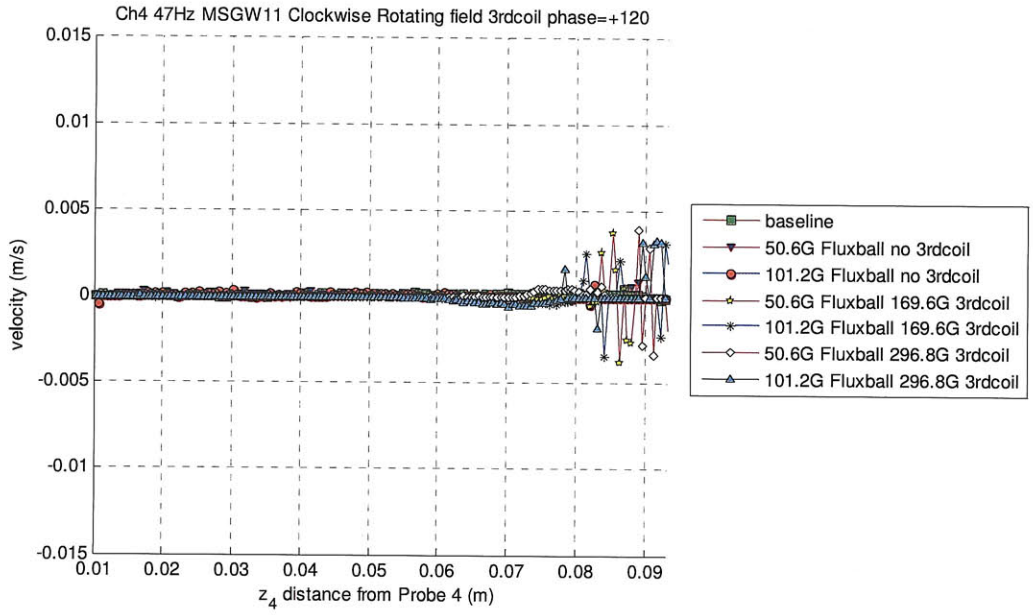
Ch4 47Hz MSGW11 Clockwise Rotating field 3rdcoil phase=+120
velocity (m/s)
0.015
0.01
0.005
0
-0.005
-0.01
-0.015
0.01
0.02
0.03
0.04
0.05
0.06
0.07
0.08
0.09
z4 distance from Probe 4 (m)
baseline
50.6G Fluxball no 3rdcoil
101.2G Fluxball no 3rdcoil
50.6G Fluxball 169.6G 3rdcoil
101.2G Fluxball 169.6G 3rdcoil
50.6G Fluxball 296.8G 3rdcoil
101.2G Fluxball 296.8G 3rdcoil

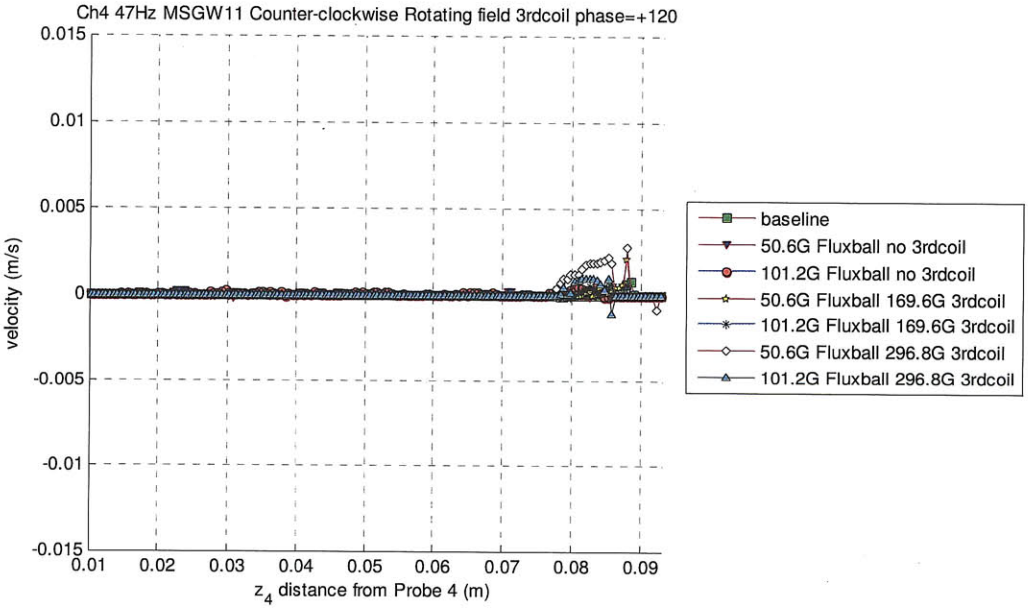
Ch4 47Hz MSGW11 Counter-clockwise Rotating field 3rdcoil phase=+120
velocity (m/s)
0.015
0.01
0.005
0
-0.005
-0.01
-0.015
0.01
0.02
0.03
0.04
0.05
0.06
0.07
0.08
0.09
z4 distance from Probe 4 (m)
baseline
50.6G Fluxball no 3rdcoil
101.2G Fluxball no 3rdcoil
50.6G Fluxball 169.6G 3rdcoil
101.2G Fluxball 169.6G 3rdcoil
50.6G Fluxball 296.8G 3rdcoil
101.2G Fluxball 296.8G 3rdcoil

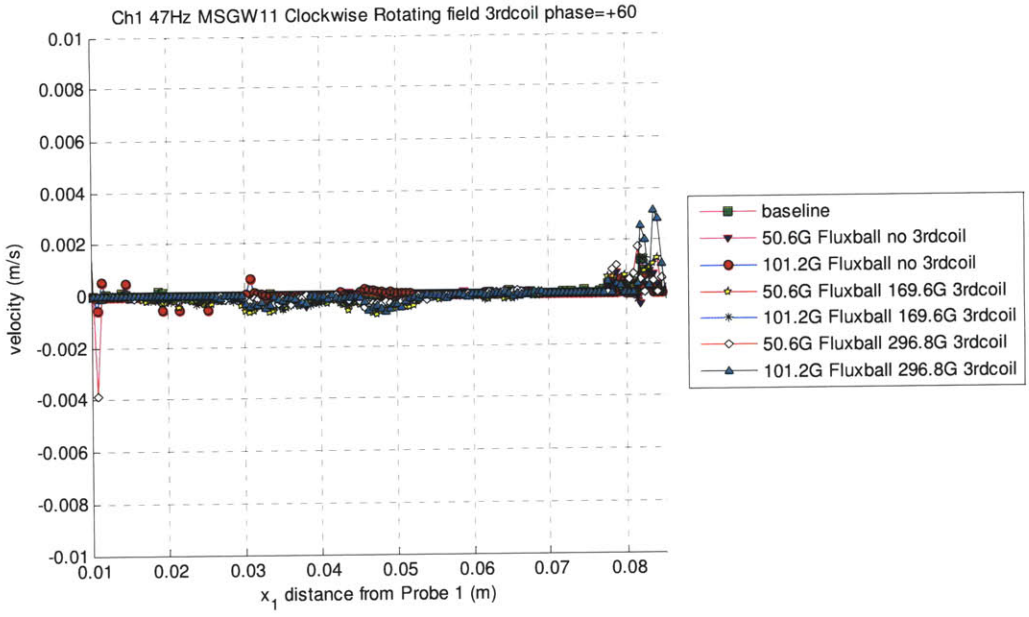
Ch1 47Hz MSGW11 Clockwise Rotating field 3rdcoil phase=+60
velocity (m/s)
0.01
0.008
0.006
0.004
0.002
0
-0.002
-0.004
-0.006
-0.008
-0.01
0.01
0.02
0.03
0.04
0.05
0.06
0.07
0.08
x1 distance from Probe 1 (m)
baseline
50.6G Fluxball no 3rdcoil
101.2G Fluxball no 3rdcoil
50.6G Fluxball 169.6G 3rdcoil
101.2G Fluxball 169.6G 3rdcoil
50.6G Fluxball 296.8G 3rdcoil
101.2G Fluxball 296.8G 3rdcoil

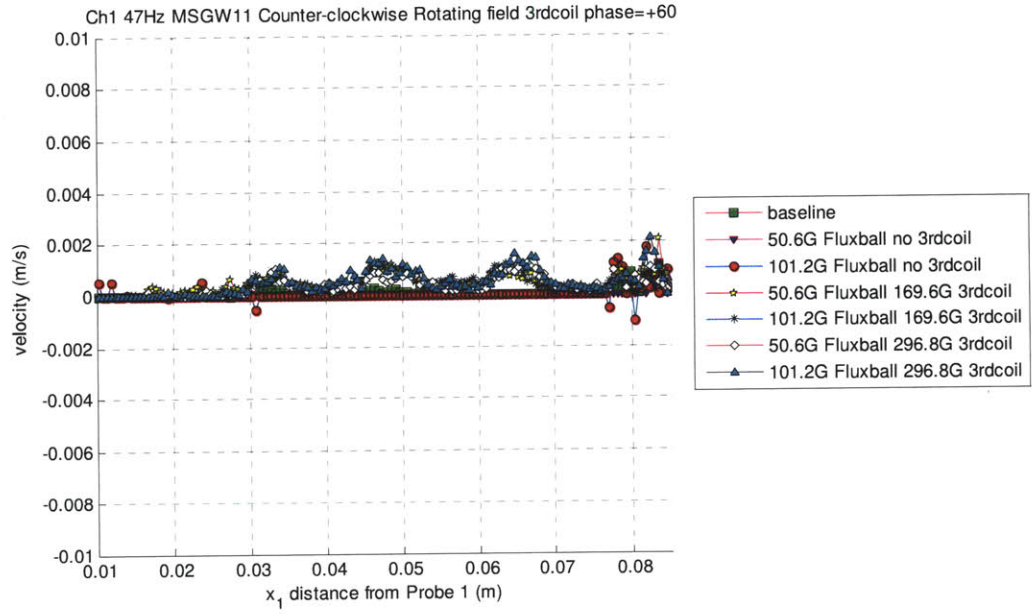
Ch1 47Hz MSGW11 Counter-clockwise Rotating field 3rdcoil phase=+60
velocity (m/s)
0.01
0.008
0.006
0.004
0.002
0
-0.002
-0.004
-0.006
-0.008
-0.01
0.01
0.02
0.03
0.04
0.05
0.06
0.07
0.08
x1 distance from Probe 1 (m)
baseline
50.6G Fluxball no 3rdcoil
101.2G Fluxball no 3rdcoil
50.6G Fluxball 169.6G 3rdcoil
101.2G Fluxball 169.6G 3rdcoil
50.6G Fluxball 296.8G 3rdcoil
101.2G Fluxball 296.8G 3rdcoil

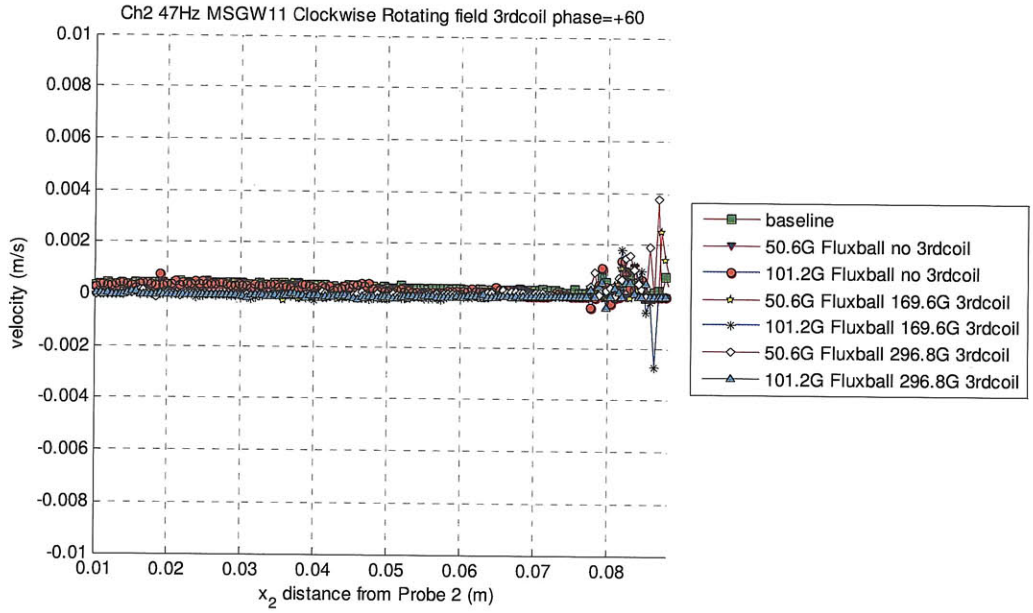
Ch2 47Hz MSGW11 Clockwise Rotating field 3rdcoil phase=+60
velocity (m/s)
0.01
0.008
0.006
0.004
0.002
0
-0.002
-0.004
-0.006
-0.008
-0.01
0.01 0.02 0.03 0.04 0.05 0.06 0.07 0.08
x2 distance from Probe 2 (m)
baseline
50.6G Fluxball no 3rdcoil
101.2G Fluxball no 3rdcoil
50.6G Fluxball 169.6G 3rdcoil
101.2G Fluxball 169.6G 3rdcoil
50.6G Fluxball 296.8G 3rdcoil
101.2G Fluxball 296.8G 3rdcoil

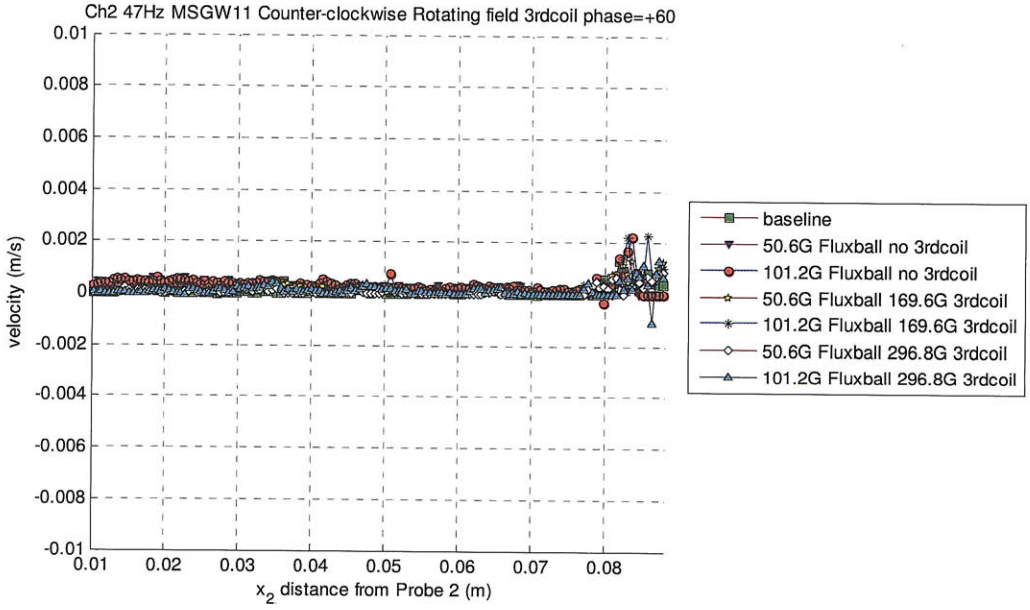
Ch2 47Hz MSGW11 Counter-clockwise Rotating field 3rdcoil phase=+60
velocity (m/s)
0.01
0.008
0.006
0.004
0.002
0
-0.002
-0.004
-0.006
-0.008
-0.01
0.01 0.02 0.03 0.04 0.05 0.06 0.07 0.08
x2 distance from Probe 2 (m)
baseline
50.6G Fluxball no 3rdcoil
101.2G Fluxball no 3rdcoil
50.6G Fluxball 169.6G 3rdcoil
101.2G Fluxball 169.6G 3rdcoil
50.6G Fluxball 296.8G 3rdcoil
101.2G Fluxball 296.8G 3rdcoil

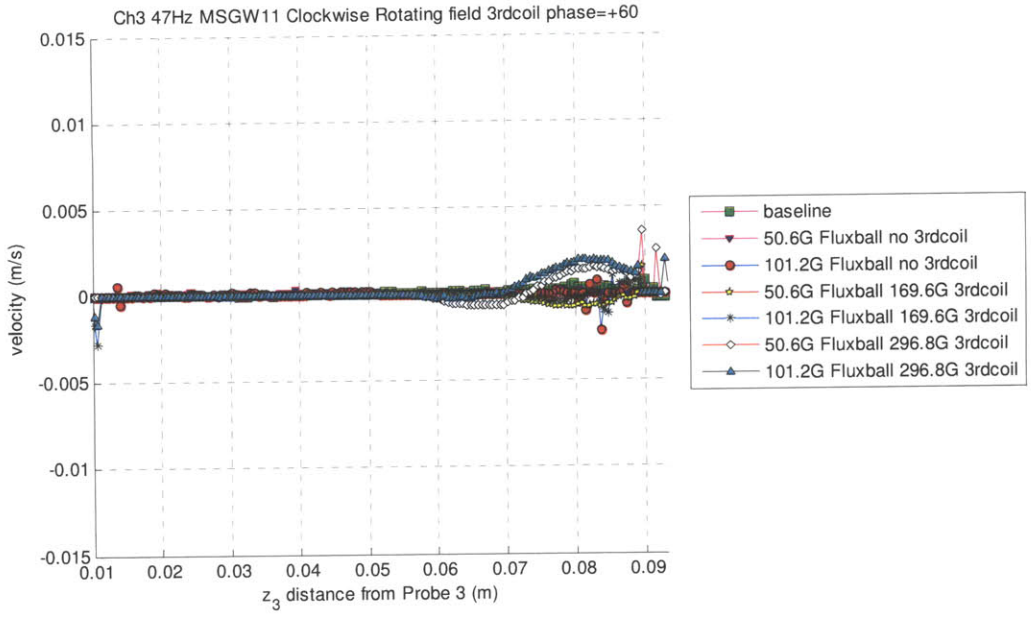
Ch3 47Hz MSGW11 Clockwise Rotating field 3rdcoil phase=+60
velocity (m/s)
0.015
0.01
0.005
0
-0.005
-0.01
-0.015
0.01
0.02
0.03
0.04
0.05
0.06
0.07
0.08
0.09
z3 distance from Probe 3 (m)
baseline
50.6G Fluxball no 3rdcoil
101.2G Fluxball no 3rdcoil
50.6G Fluxball 169.6G 3rdcoil
101.2G Fluxball 169.6G 3rdcoil
50.6G Fluxball 296.8G 3rdcoil
101.2G Fluxball 296.8G 3rdcoil

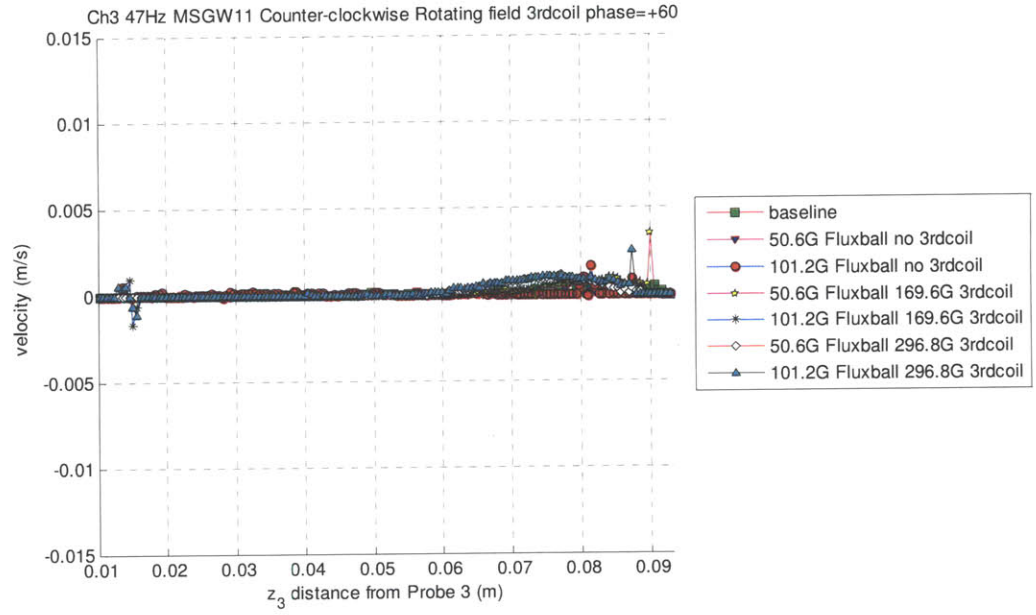
Ch3 47Hz MSGW11 Counter-clockwise Rotating field 3rdcoil phase=+60
velocity (m/s)
0.015
0.01
0.005
0
-0.005
-0.01
-0.015
0.01
0.02
0.03
0.04
0.05
0.06
0.07
0.08
0.09
z3 distance from Probe 3 (m)
baseline
50.6G Fluxball no 3rdcoil
101.2G Fluxball no 3rdcoil
50.6G Fluxball 169.6G 3rdcoil
101.2G Fluxball 169.6G 3rdcoil
50.6G Fluxball 296.8G 3rdcoil
101.2G Fluxball 296.8G 3rdcoil

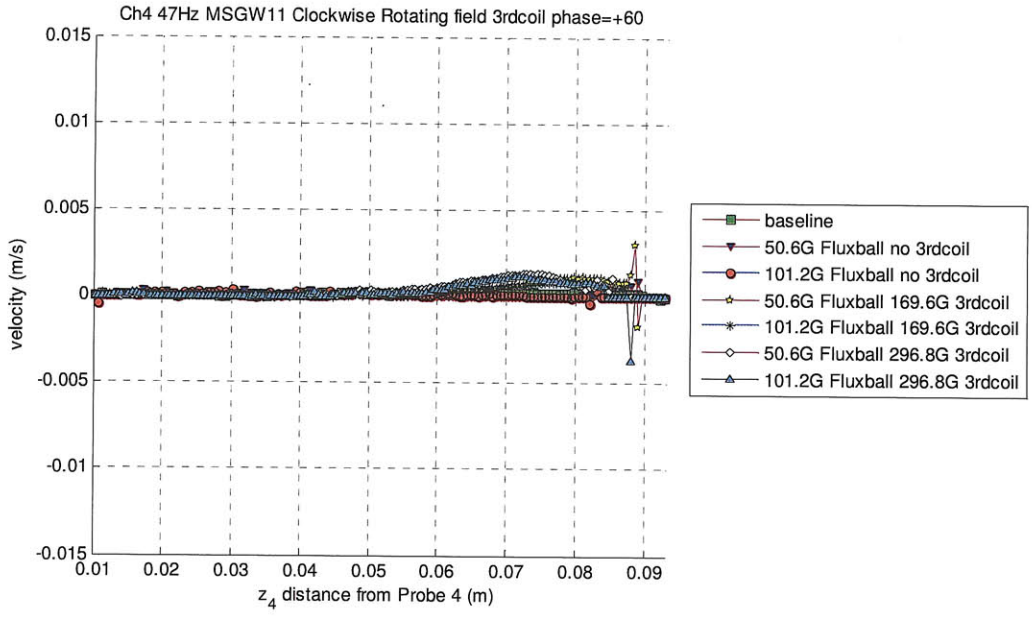
Ch4 47Hz MSGW11 Clockwise Rotating field 3rdcoil phase=+60
velocity (m/s)
0.015
0.01
0.005
0
-0.005
-0.01
-0.015
0.01
0.02
0.03
0.04
0.05
0.06
0.07
0.08
0.09
z4 distance from Probe 4 (m)
baseline
50.6G Fluxball no 3rdcoil
101.2G Fluxball no 3rdcoil
50.6G Fluxball 169.6G 3rdcoil
101.2G Fluxball 169.6G 3rdcoil
50.6G Fluxball 296.8G 3rdcoil
101.2G Fluxball 296.8G 3rdcoil

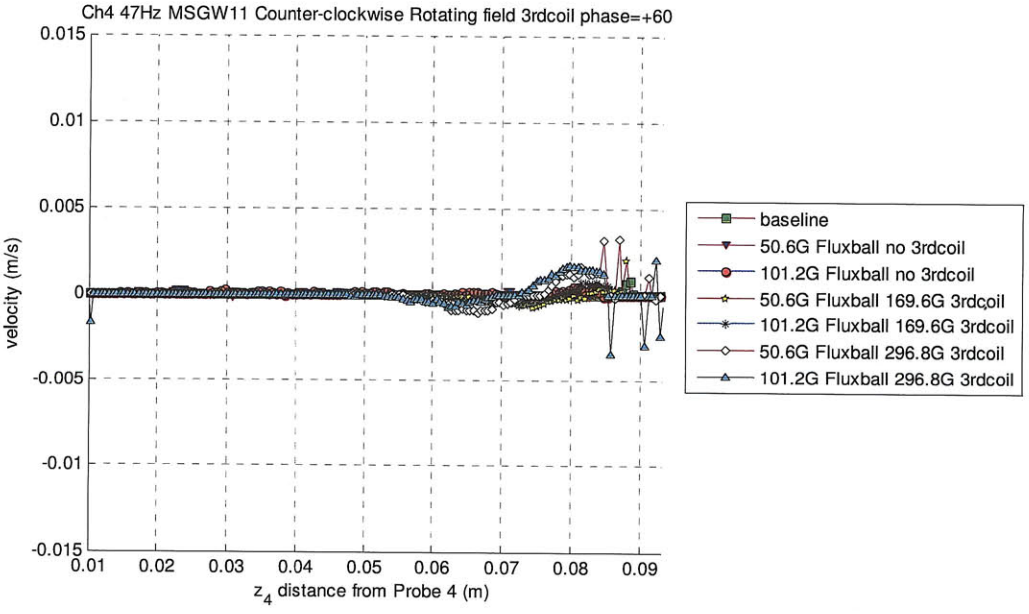
Ch4 47Hz MSGW11 Counter-clockwise Rotating field 3rdcoil phase=+60
velocity (m/s)
0.015
0.01
0.005
0
-0.005
-0.01
-0.015
0.01
0.02
0.03
0.04
0.05
0.06
0.07
0.08
0.09
z4 distance from Probe 4 (m)
baseline
50.6G Fluxball no 3rdcoil
101.2G Fluxball no 3rdcoil
50.6G Fluxball 169.6G 3rdcoil
101.2G Fluxball 169.6G 3rdcoil
50.6G Fluxball 296.8G 3rdcoil
101.2G Fluxball 296.8G 3rdcoil

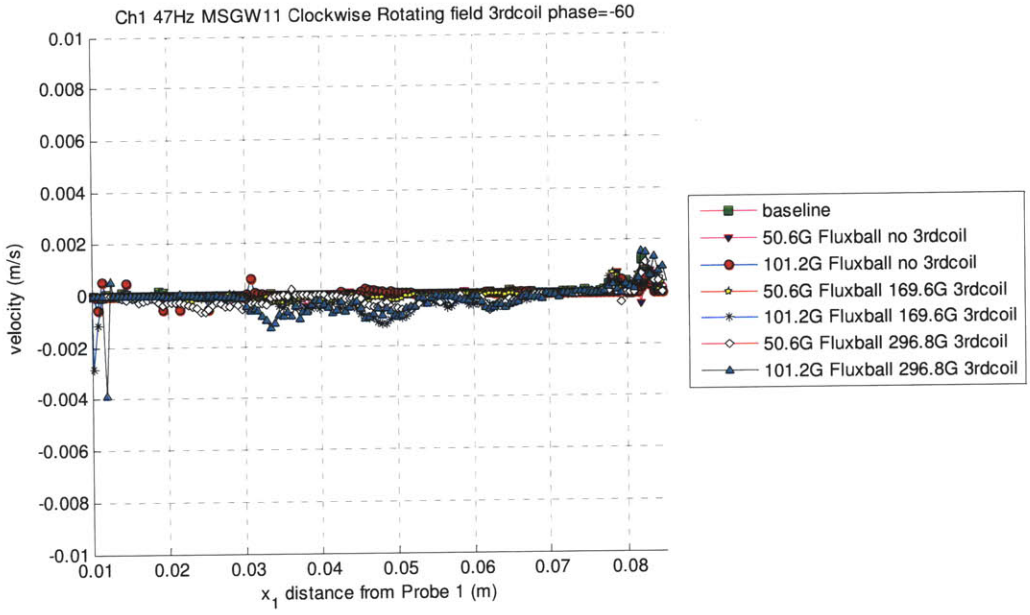
Ch1 47Hz MSGW11 Clockwise Rotating field 3rdcoil phase=-60
velocity (m/s)
0.01
0.008
0.006
0.004
0.002
0
-0.002
-0.004
-0.006
-0.008
-0.01
0.01
0.02
0.03
0.04
0.05
0.06
0.07
0.08
x1 distance from Probe 1 (m)
baseline
50.6G Fluxball no 3rdcoil
101.2G Fluxball no 3rdcoil
50.6G Fluxball 169.6G 3rdcoil
101.2G Fluxball 169.6G 3rdcoil
50.6G Fluxball 296.8G 3rdcoil
101.2G Fluxball 296.8G 3rdcoil

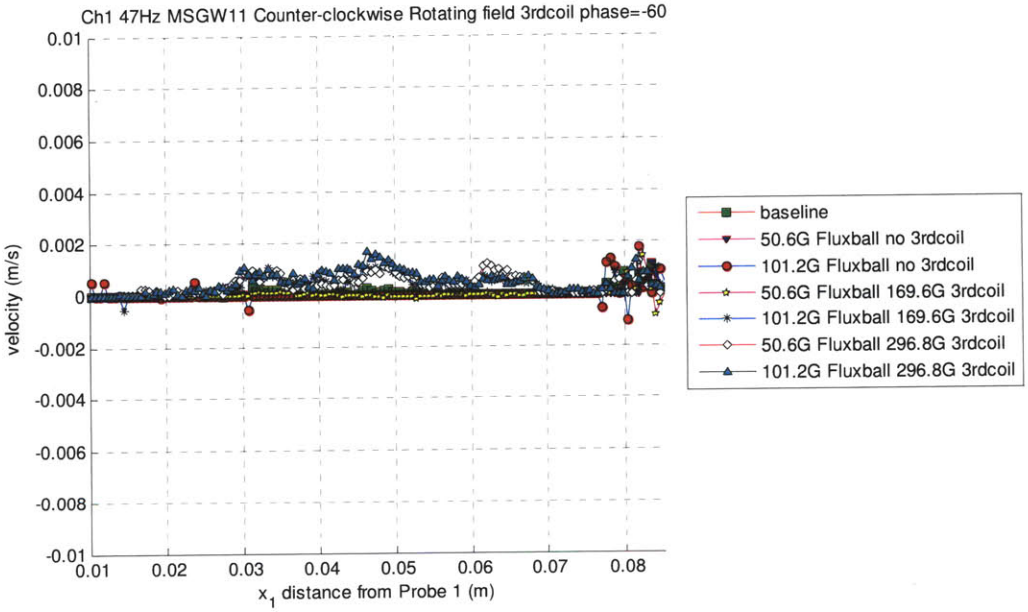
Ch1 47Hz MSGW11 Counter-clockwise Rotating field 3rdcoil phase=-60
velocity (m/s)
0.01
0.008
0.006
0.004
0.002
0
-0.002
-0.004
-0.006
-0.008
-0.01
0.01
0.02
0.03
0.04
0.05
0.06
0.07
0.08
x1 distance from Probe 1 (m)
baseline
50.6G Fluxball no 3rdcoil
101.2G Fluxball no 3rdcoil
50.6G Fluxball 169.6G 3rdcoil
101.2G Fluxball 169.6G 3rdcoil
50.6G Fluxball 296.8G 3rdcoil
101.2G Fluxball 296.8G 3rdcoil

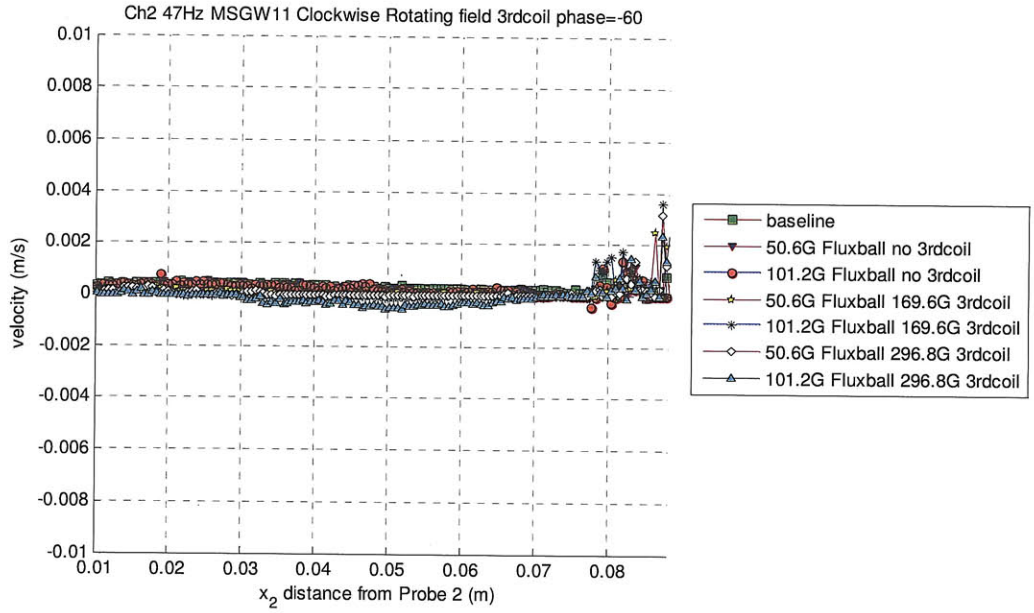
Ch2 47Hz MSGW11 Clockwise Rotating field 3rdcoil phase=-60
velocity (m/s)
0.01
0.008
0.006
0.004
0.002
0
-0.002
-0.004
-0.006
-0.008
-0.01
0.01 0.02 0.03 0.04 0.05 0.06 0.07 0.08
x2 distance from Probe 2 (m)
baseline
50.6G Fluxball no 3rdcoil
101.2G Fluxball no 3rdcoil
50.6G Fluxball 169.6G 3rdcoil
101.2G Fluxball 169.6G 3rdcoil
50.6G Fluxball 296.8G 3rdcoil
101.2G Fluxball 296.8G 3rdcoil

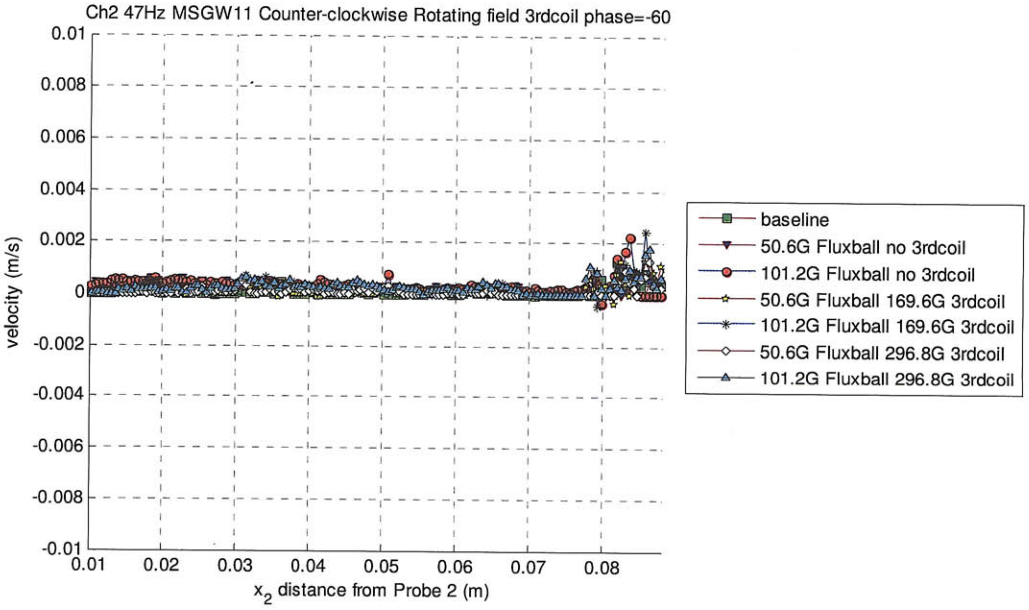
Ch2 47Hz MSGW11 Counter-clockwise Rotating field 3rdcoil phase=-60
velocity (m/s)
0.01
0.008
0.006
0.004
0.002
0
-0.002
-0.004
-0.006
-0.008
-0.01
0.01 0.02 0.03 0.04 0.05 0.06 0.07 0.08
x2 distance from Probe 2 (m)
baseline
50.6G Fluxball no 3rdcoil
101.2G Fluxball no 3rdcoil
50.6G Fluxball 169.6G 3rdcoil
101.2G Fluxball 169.6G 3rdcoil
50.6G Fluxball 296.8G 3rdcoil
101.2G Fluxball 296.8G 3rdcoil

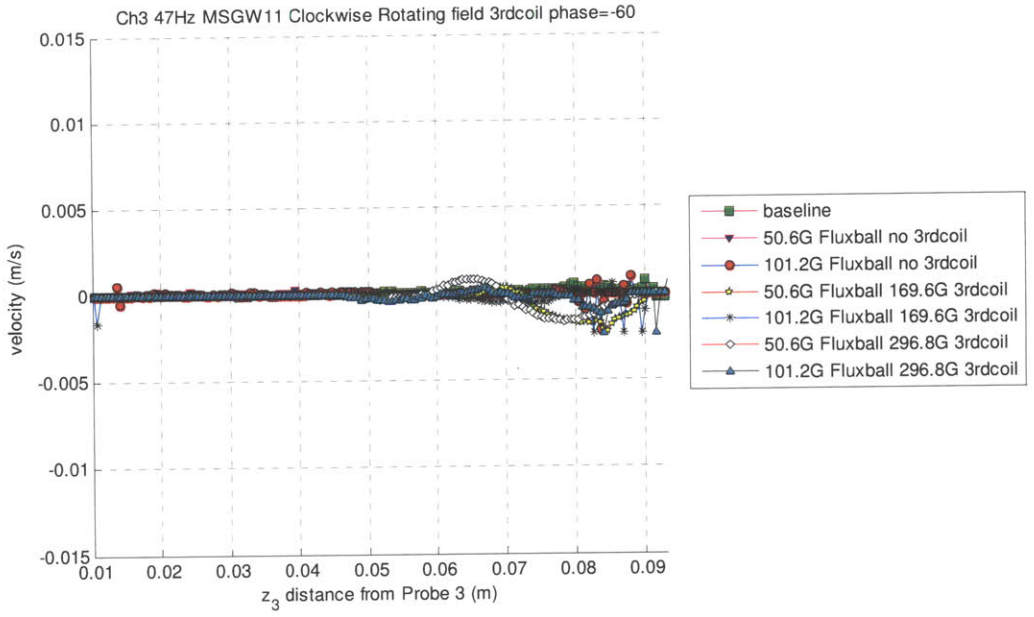
Ch3 47Hz MSGW11 Clockwise Rotating field 3rdcoil phase=-60
velocity (m/s)
0.015
0.01
0.005
0
-0.005
-0.01
-0.015
0.01
0.02
0.03
0.04
0.05
0.06
0.07
0.08
0.09
z_3 distance from Probe 3 (m)
baseline
50.6G Fluxball no 3rdcoil
101.2G Fluxball no 3rdcoil
50.6G Fluxball 169.6G 3rdcoil
101.2G Fluxball 169.6G 3rdcoil
50.6G Fluxball 296.8G 3rdcoil
101.2G Fluxball 296.8G 3rdcoil

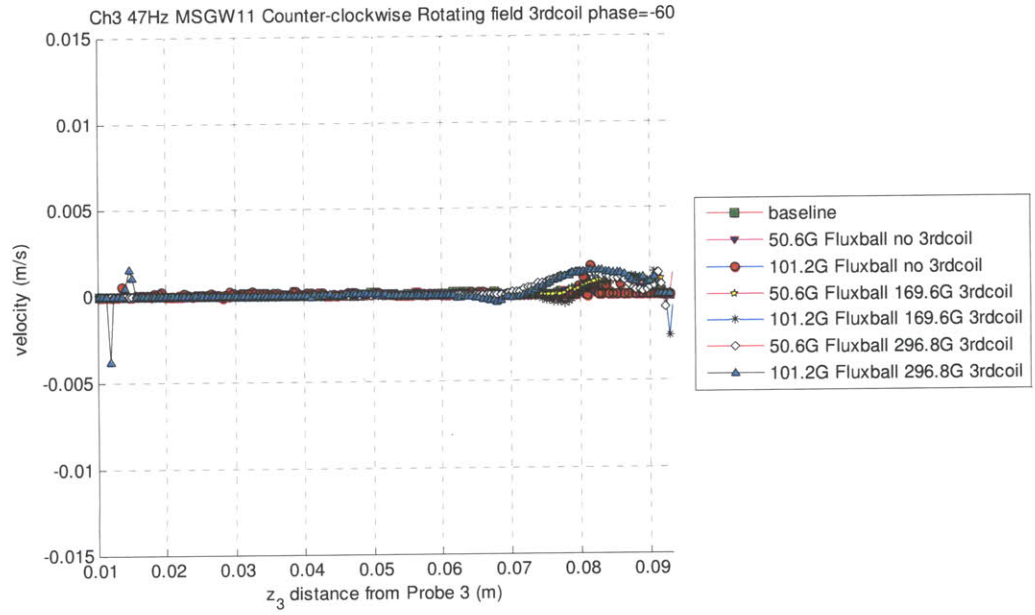
Ch3 47Hz MSGW11 Counter-clockwise Rotating field 3rdcoil phase=-60
velocity (m/s)
0.015
0.01
0.005
0
-0.005
-0.01
-0.015
0.01
0.02
0.03
0.04
0.05
0.06
0.07
0.08
0.09
z_3 distance from Probe 3 (m)
baseline
50.6G Fluxball no 3rdcoil
101.2G Fluxball no 3rdcoil
50.6G Fluxball 169.6G 3rdcoil
101.2G Fluxball 169.6G 3rdcoil
50.6G Fluxball 296.8G 3rdcoil
101.2G Fluxball 296.8G 3rdcoil

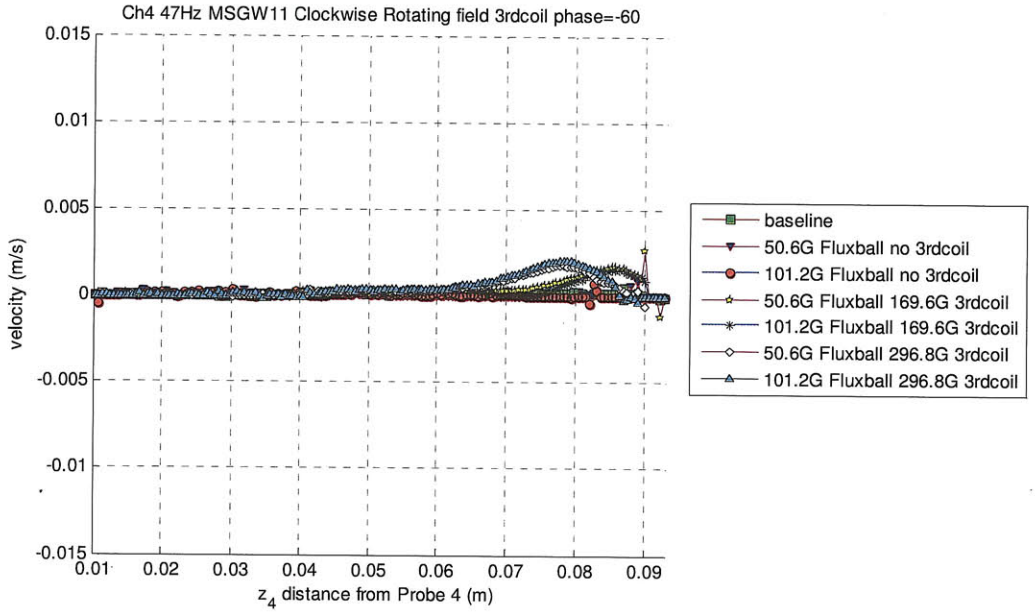
Ch4 47Hz MSGW11 Clockwise Rotating field 3rdcoil phase=-60
velocity (m/s)
0.015
0.01
0.005
0
-0.005
-0.01
-0.015
0.01
0.02
0.03
0.04
0.05
0.06
0.07
0.08
0.09
z4 distance from Probe 4 (m)
baseline
50.6G Fluxball no 3rdcoil
101.2G Fluxball no 3rdcoil
50.6G Fluxball 169.6G 3rdcoil
101.2G Fluxball 169.6G 3rdcoil
50.6G Fluxball 296.8G 3rdcoil
101.2G Fluxball 296.8G 3rdcoil

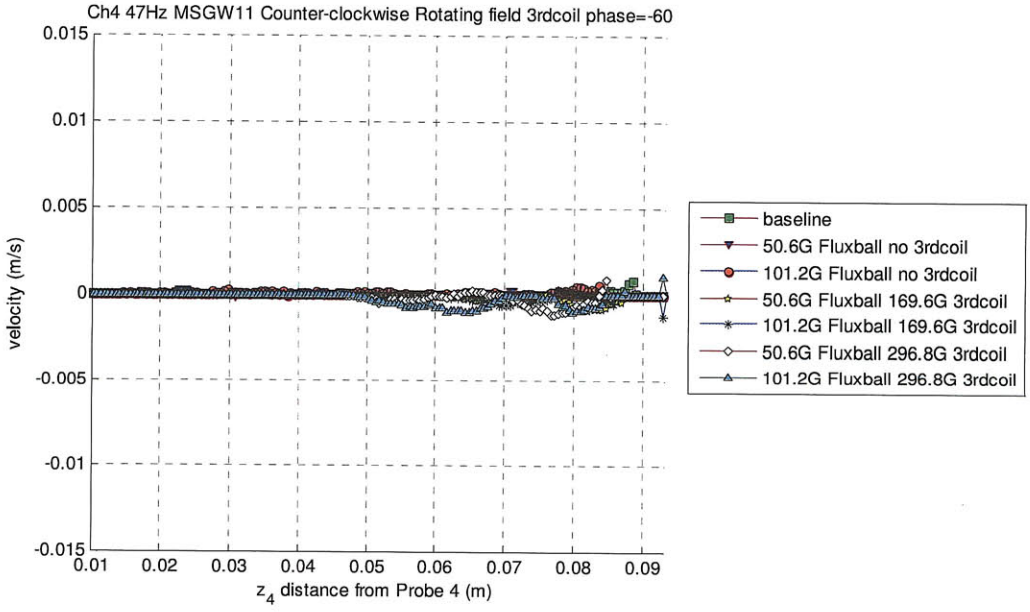
Ch4 47Hz MSGW11 Counter-clockwise Rotating field 3rdcoil phase=-60
velocity (m/s)
0.015
0.01
0.005
0
-0.005
-0.01
-0.015
0.01
0.02
0.03
0.04
0.05
0.06
0.07
0.08
0.09
z4 distance from Probe 4 (m)
baseline
50.6G Fluxball no 3rdcoil
101.2G Fluxball no 3rdcoil
50.6G Fluxball 169.6G 3rdcoil
101.2G Fluxball 169.6G 3rdcoil
50.6G Fluxball 296.8G 3rdcoil
101.2G Fluxball 296.8G 3rdcoil

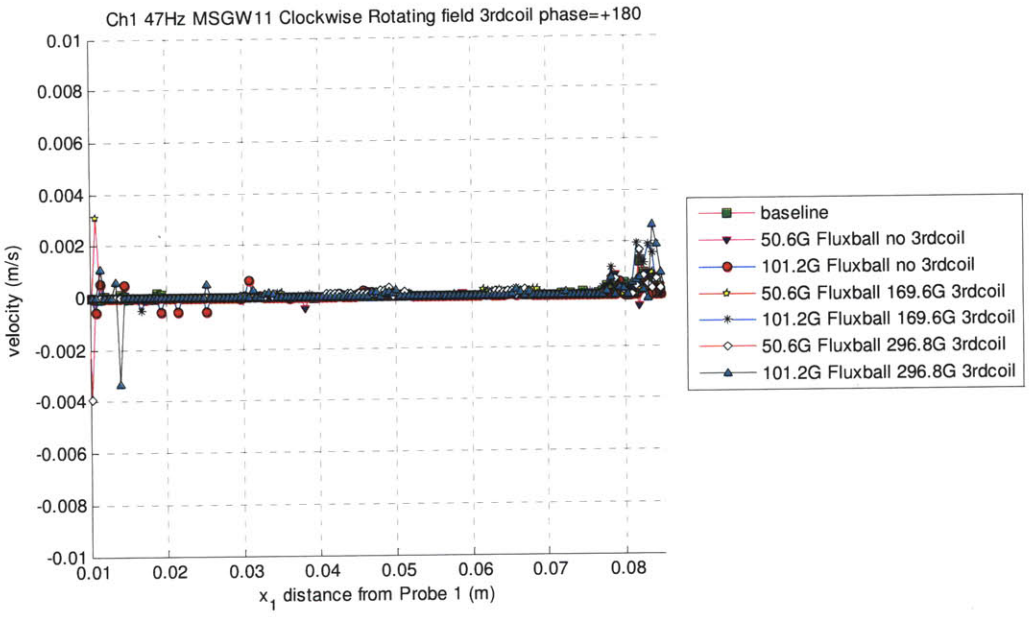
Ch1 47Hz MSGW11 Clockwise Rotating field 3rdcoil phase=+180
velocity (m/s)
0.01
0.008
0.006
0.004
0.002
0
-0.002
-0.004
-0.006
-0.008
-0.01
0.01
0.02
0.03
0.04
0.05
0.06
0.07
0.08
x1 distance from Probe 1 (m)
baseline
50.6G Fluxball no 3rdcoil
101.2G Fluxball no 3rdcoil
50.6G Fluxball 169.6G 3rdcoil
101.2G Fluxball 169.6G 3rdcoil
50.6G Fluxball 296.8G 3rdcoil
101.2G Fluxball 296.8G 3rdcoil

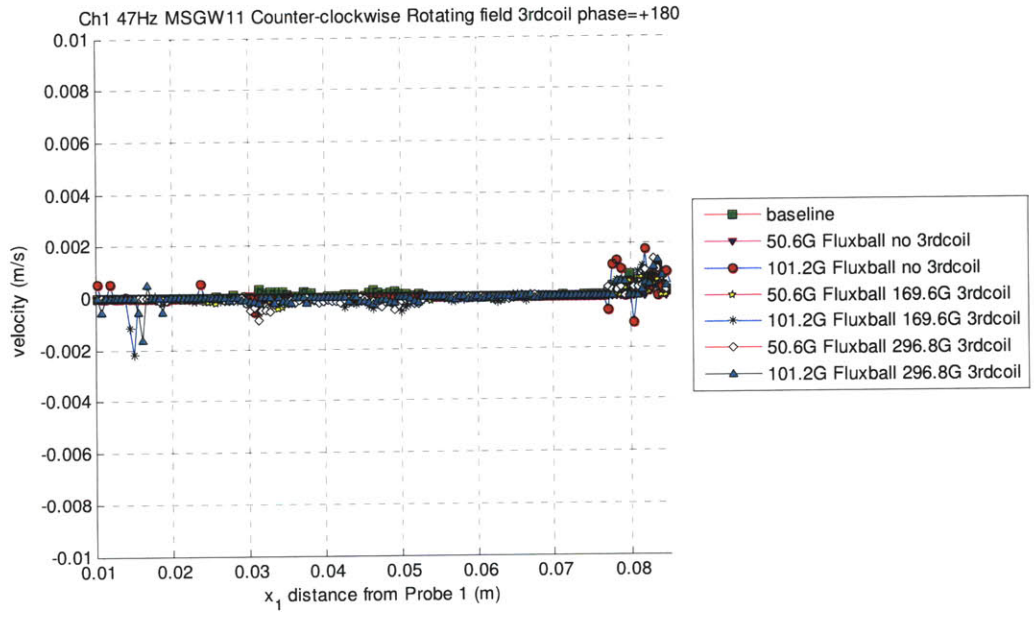
Ch1 47Hz MSGW11 Counter-clockwise Rotating field 3rdcoil phase=+180
velocity (m/s)
0.01
0.008
0.006
0.004
0.002
0
-0.002
-0.004
-0.006
-0.008
-0.01
0.01
0.02
0.03
0.04
0.05
0.06
0.07
0.08
x1 distance from Probe 1 (m)
baseline
50.6G Fluxball no 3rdcoil
101.2G Fluxball no 3rdcoil
50.6G Fluxball 169.6G 3rdcoil
101.2G Fluxball 169.6G 3rdcoil
50.6G Fluxball 296.8G 3rdcoil
101.2G Fluxball 296.8G 3rdcoil

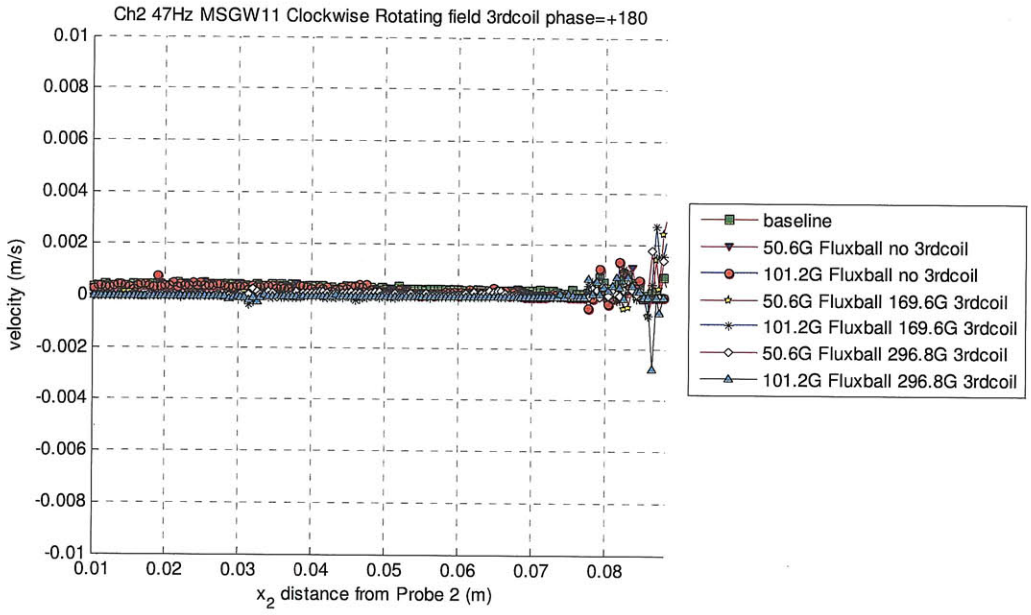
Ch2 47Hz MSGW11 Clockwise Rotating field 3rdcoil phase=+180
velocity (m/s)
0.01
0.008
0.006
0.004
0.002
0
-0.002
-0.004
-0.006
-0.008
-0.01
0.01 0.02 0.03 0.04 0.05 0.06 0.07 0.08
x2 distance from Probe 2 (m)
baseline
50.6G Fluxball no 3rdcoil
101.2G Fluxball no 3rdcoil
50.6G Fluxball 169.6G 3rdcoil
101.2G Fluxball 169.6G 3rdcoil
50.6G Fluxball 296.8G 3rdcoil
101.2G Fluxball 296.8G 3rdcoil

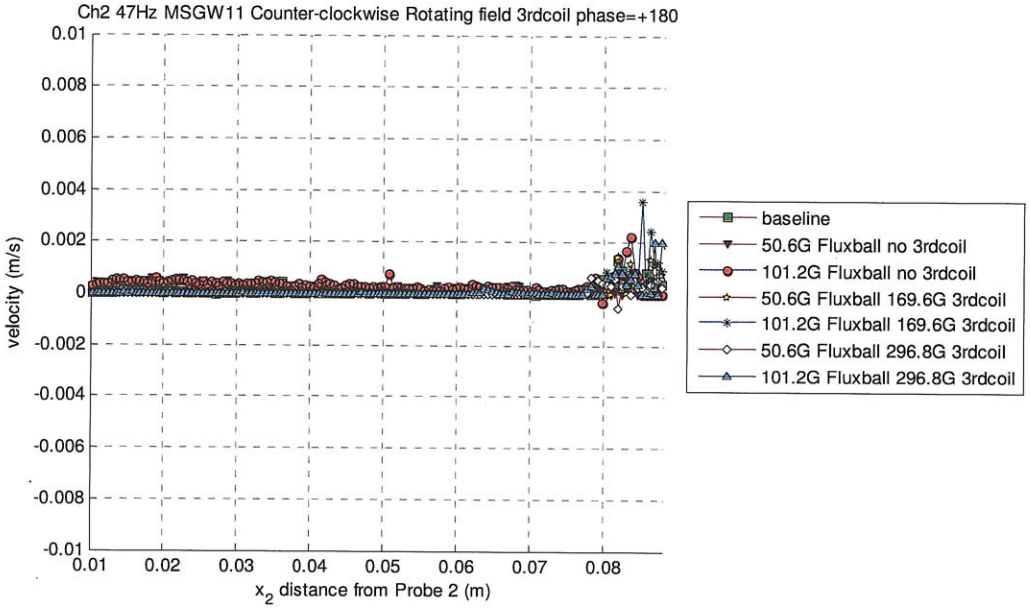
Ch2 47Hz MSGW11 Counter-clockwise Rotating field 3rdcoil phase=+180
velocity (m/s)
0.01
0.008
0.006
0.004
0.002
0
-0.002
-0.004
-0.006
-0.008
-0.01
0.01 0.02 0.03 0.04 0.05 0.06 0.07 0.08
x2 distance from Probe 2 (m)
baseline
50.6G Fluxball no 3rdcoil
101.2G Fluxball no 3rdcoil
50.6G Fluxball 169.6G 3rdcoil
101.2G Fluxball 169.6G 3rdcoil
50.6G Fluxball 296.8G 3rdcoil
101.2G Fluxball 296.8G 3rdcoil

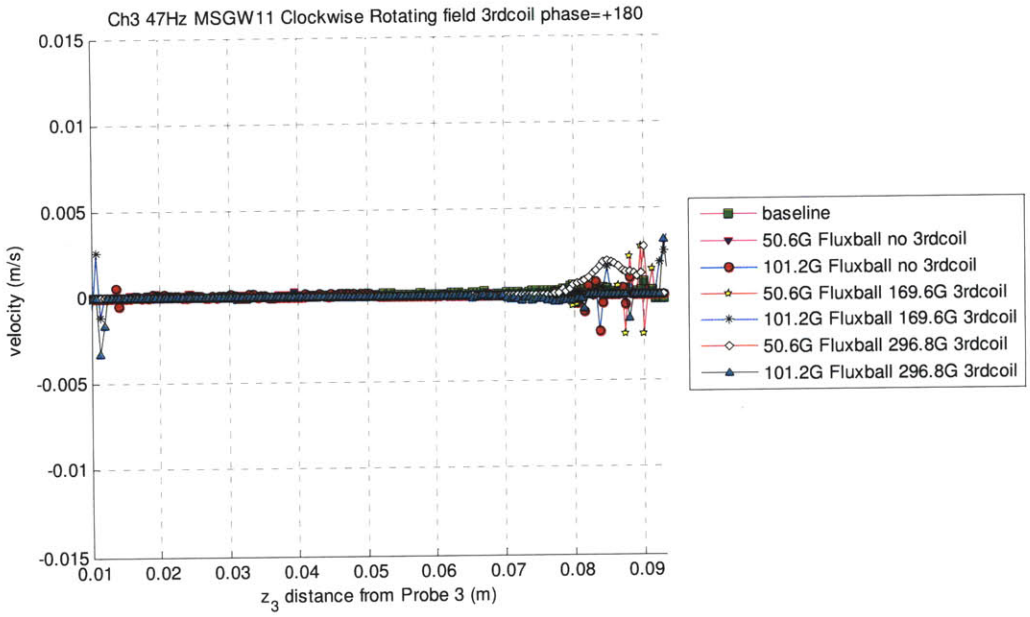
Ch3 47Hz MSGW11 Clockwise Rotating field 3rdcoil phase=+180
velocity (m/s)
0.015
0.01
0.005
0
-0.005
-0.01
-0.015
0.01
0.02
0.03
0.04
0.05
0.06
0.07
0.08
0.09
z_3 distance from Probe 3 (m)
baseline
50.6G Fluxball no 3rdcoil
101.2G Fluxball no 3rdcoil
50.6G Fluxball 169.6G 3rdcoil
101.2G Fluxball 169.6G 3rdcoil
50.6G Fluxball 296.8G 3rdcoil
101.2G Fluxball 296.8G 3rdcoil

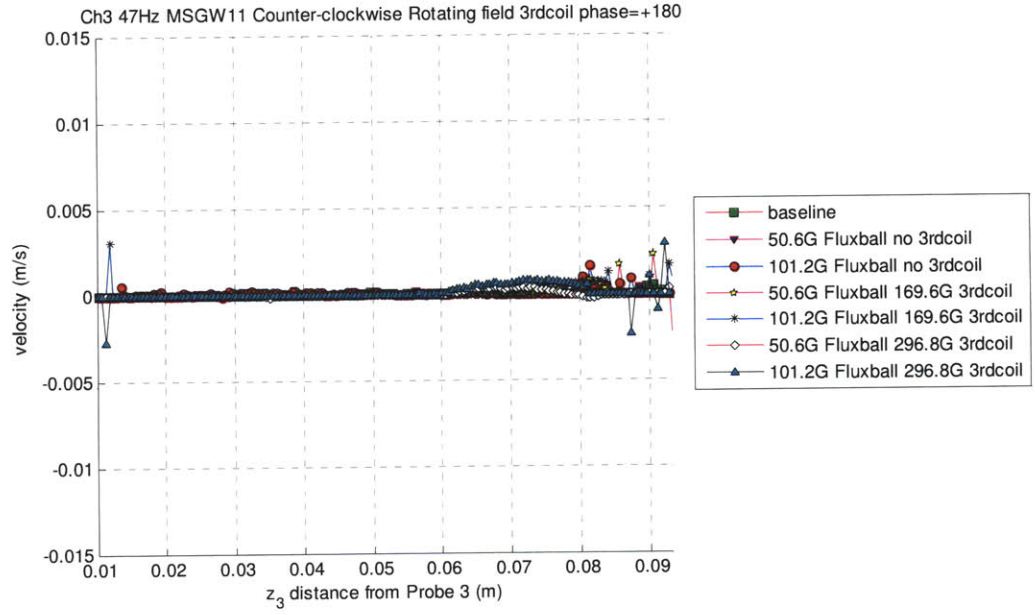
Ch3 47Hz MSGW11 Counter-clockwise Rotating field 3rdcoil phase=+180
velocity (m/s)
0.015
0.01
0.005
0
-0.005
-0.01
-0.015
0.01
0.02
0.03
0.04
0.05
0.06
0.07
0.08
0.09
z_3 distance from Probe 3 (m)
baseline
50.6G Fluxball no 3rdcoil
101.2G Fluxball no 3rdcoil
50.6G Fluxball 169.6G 3rdcoil
101.2G Fluxball 169.6G 3rdcoil
50.6G Fluxball 296.8G 3rdcoil
101.2G Fluxball 296.8G 3rdcoil

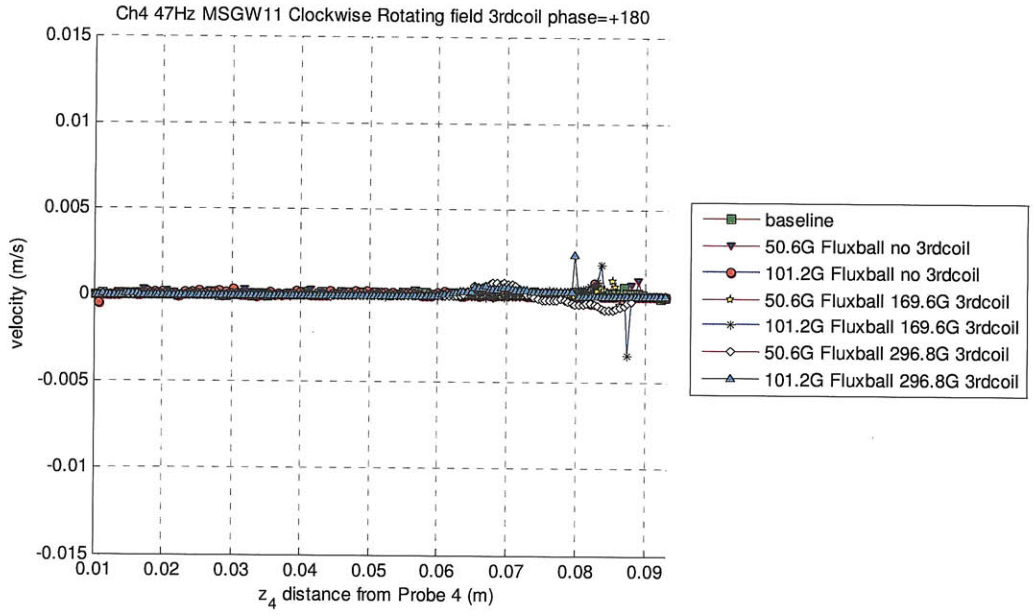
Ch4 47Hz MSGW11 Clockwise Rotating field 3rdcoil phase=+180
velocity (m/s)
0.015
0.01
0.005
0
-0.005
-0.01
-0.015
0.01
0.02
0.03
0.04
0.05
0.06
0.07
0.08
0.09
z4 distance from Probe 4 (m)
baseline
50.6G Fluxball no 3rdcoil
101.2G Fluxball no 3rdcoil
50.6G Fluxball 169.6G 3rdcoil
101.2G Fluxball 169.6G 3rdcoil
50.6G Fluxball 296.8G 3rdcoil
101.2G Fluxball 296.8G 3rdcoil

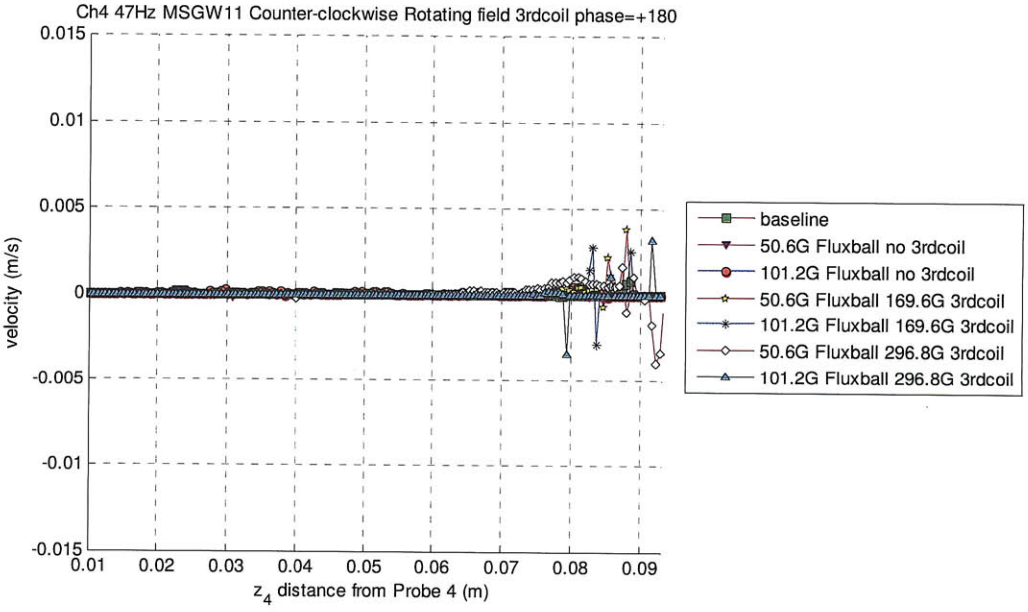
Ch4 47Hz MSGW11 Counter-clockwise Rotating field 3rdcoil phase=+180
velocity (m/s)
0.015
0.01
0.005
0
-0.005
-0.01
-0.015
0.01
0.02
0.03
0.04
0.05
0.06
0.07
0.08
0.09
z4 distance from Probe 4 (m)
baseline
50.6G Fluxball no 3rdcoil
101.2G Fluxball no 3rdcoil
50.6G Fluxball 169.6G 3rdcoil
101.2G Fluxball 169.6G 3rdcoil
50.6G Fluxball 296.8G 3rdcoil
101.2G Fluxball 296.8G 3rdcoil

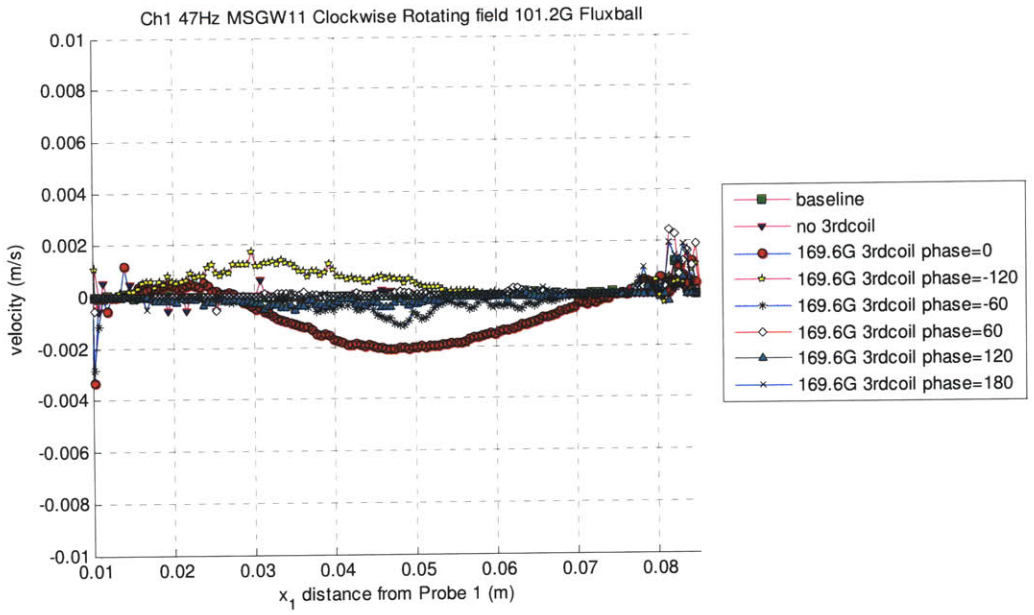
Ch1 47Hz MSGW11 Clockwise Rotating field 101.2G Fluxball
velocity (m/s)
x1 distance from Probe 1 (m)
baseline
no 3rdcoil
169.6G 3rdcoil phase=0
169.6G 3rdcoil phase=-120
169.6G 3rdcoil phase=-60
169.6G 3rdcoil phase=60
169.6G 3rdcoil phase=120
169.6G 3rdcoil phase=180

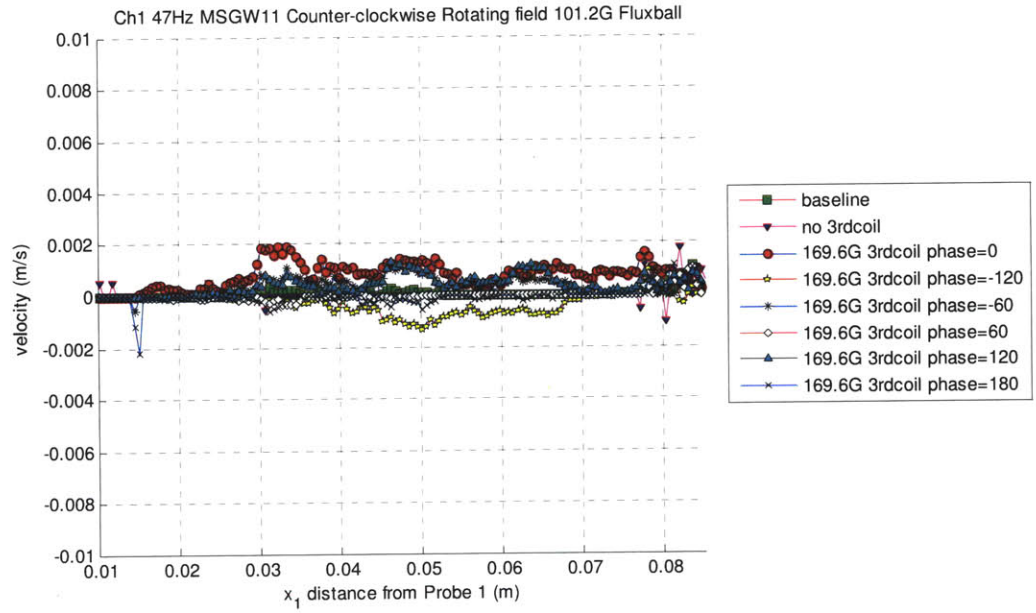
Ch1 47Hz MSGW11 Counter-clockwise Rotating field 101.2G Fluxball
velocity (m/s)
x1 distance from Probe 1 (m)
baseline
no 3rdcoil
169.6G 3rdcoil phase=0
169.6G 3rdcoil phase=-120
169.6G 3rdcoil phase=-60
169.6G 3rdcoil phase=60
169.6G 3rdcoil phase=120
169.6G 3rdcoil phase=180

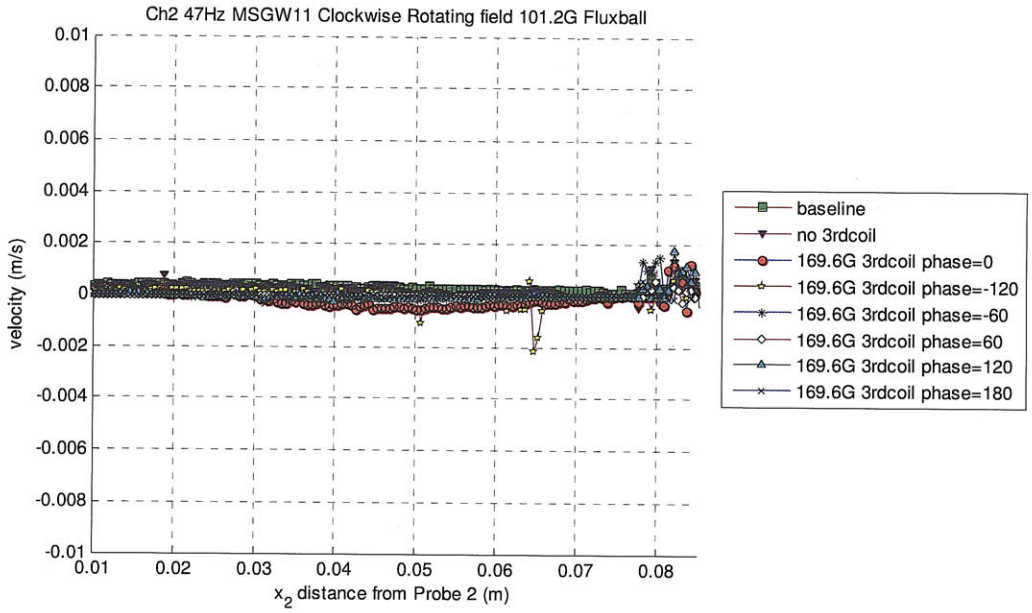
Ch2 47Hz MSGW11 Clockwise Rotating field 101.2G Fluxball
velocity (m/s)
x_2 distance from Probe 2 (m)
baseline
no 3rdcoil
169.6G 3rdcoil phase=0
169.6G 3rdcoil phase=-120
169.6G 3rdcoil phase=-60
169.6G 3rdcoil phase=60
169.6G 3rdcoil phase=120
169.6G 3rdcoil phase=180

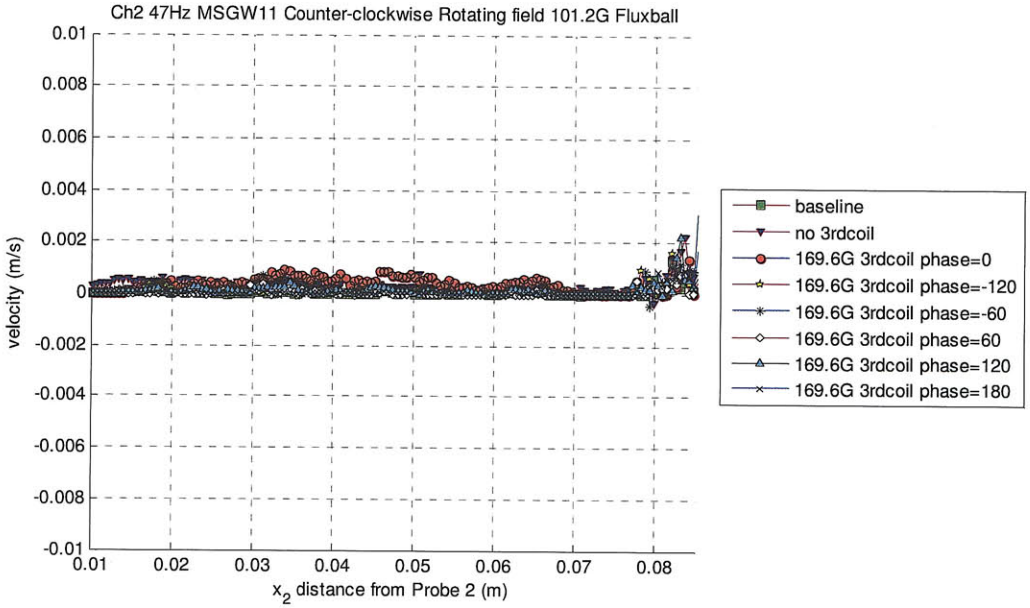
Ch2 47Hz MSGW11 Counter-clockwise Rotating field 101.2G Fluxball
velocity (m/s)
x_2 distance from Probe 2 (m)
baseline
no 3rdcoil
169.6G 3rdcoil phase=0
169.6G 3rdcoil phase=-120
169.6G 3rdcoil phase=-60
169.6G 3rdcoil phase=60
169.6G 3rdcoil phase=120
169.6G 3rdcoil phase=180

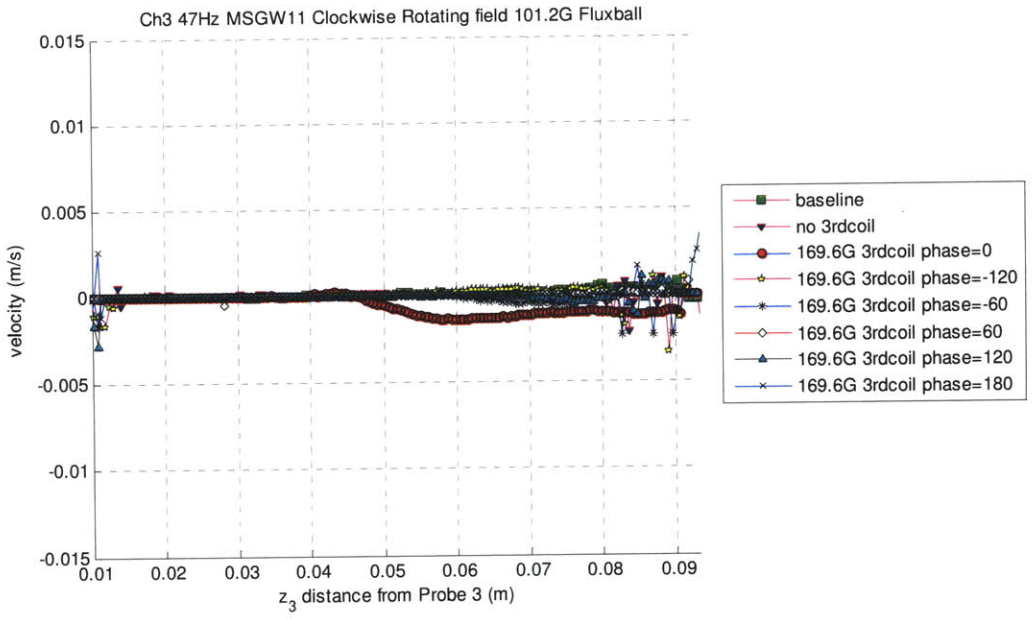
Ch3 47Hz MSGW11 Clockwise Rotating field 101.2G Fluxball
velocity (m/s)
0.015
0.01
0.005
0
-0.005
-0.01
-0.015
0.01
0.02
0.03
0.04
0.05
0.06
0.07
0.08
0.09
z3 distance from Probe 3 (m)
baseline
no 3rdcoil
169.6G 3rdcoil phase=0
169.6G 3rdcoil phase=-120
169.6G 3rdcoil phase=-60
169.6G 3rdcoil phase=60
169.6G 3rdcoil phase=120
169.6G 3rdcoil phase=180

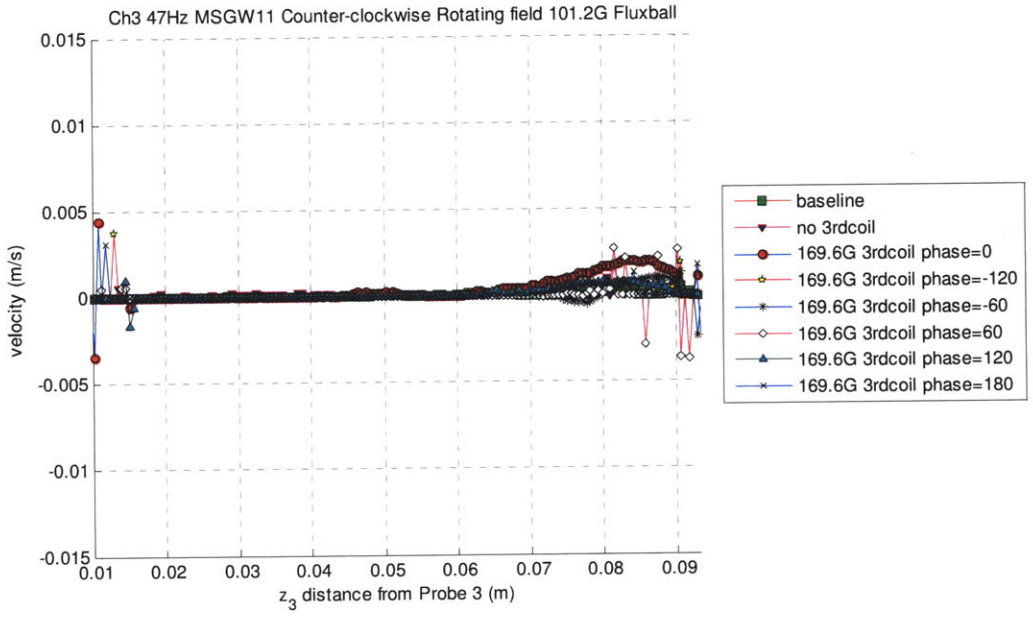
Ch3 47Hz MSGW11 Counter-clockwise Rotating field 101.2G Fluxball
velocity (m/s)
0.015
0.01
0.005
0
-0.005
-0.01
-0.015
0.01
0.02
0.03
0.04
0.05
0.06
0.07
0.08
0.09
z3 distance from Probe 3 (m)
baseline
no 3rdcoil
169.6G 3rdcoil phase=0
169.6G 3rdcoil phase=-120
169.6G 3rdcoil phase=-60
169.6G 3rdcoil phase=60
169.6G 3rdcoil phase=120
169.6G 3rdcoil phase=180

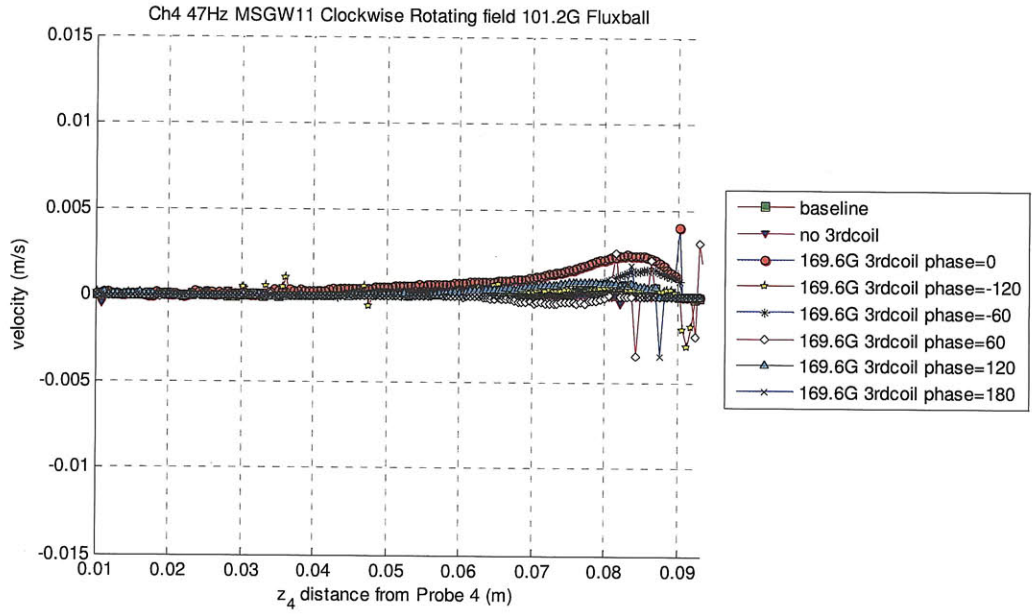
Ch4 47Hz MSGW11 Clockwise Rotating field 101.2G Fluxball
velocity (m/s)
0.015
0.01
0.005
0
-0.005
-0.01
-0.015
0.01
0.02
0.03
0.04
0.05
0.06
0.07
0.08
0.09
z4 distance from Probe 4 (m)
baseline
no 3rdcoil
169.6G 3rdcoil phase=0
169.6G 3rdcoil phase=-120
169.6G 3rdcoil phase=-60
169.6G 3rdcoil phase=60
169.6G 3rdcoil phase=120
169.6G 3rdcoil phase=180

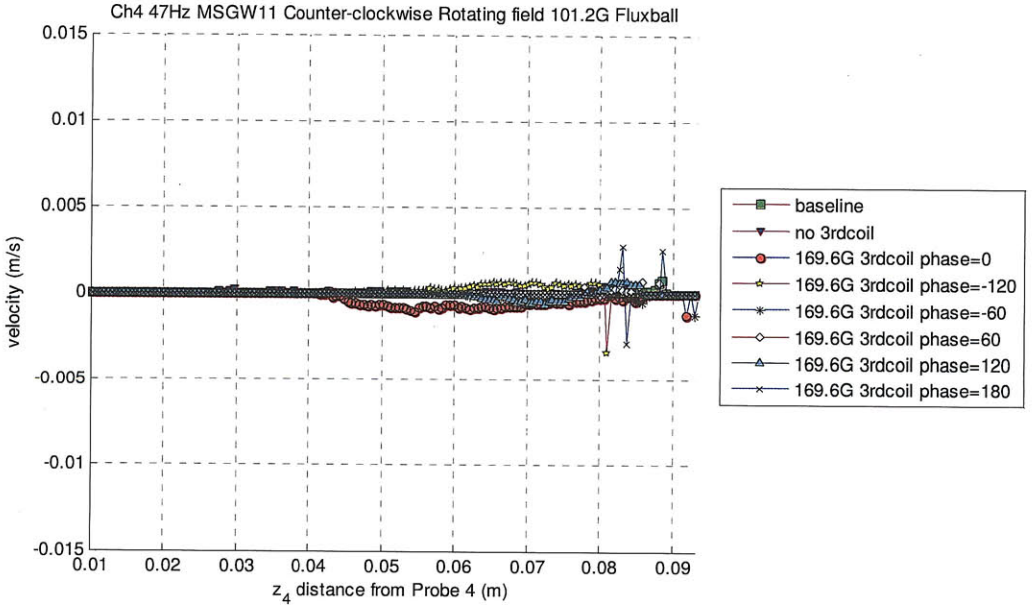
Ch4 47Hz MSGW11 Counter-clockwise Rotating field 101.2G Fluxball
velocity (m/s)
0.015
0.01
0.005
0
-0.005
-0.01
-0.015
0.01
0.02
0.03
0.04
0.05
0.06
0.07
0.08
0.09
z4 distance from Probe 4 (m)
baseline
no 3rdcoil
169.6G 3rdcoil phase=0
169.6G 3rdcoil phase=-120
169.6G 3rdcoil phase=-60
169.6G 3rdcoil phase=60
169.6G 3rdcoil phase=120
169.6G 3rdcoil phase=180

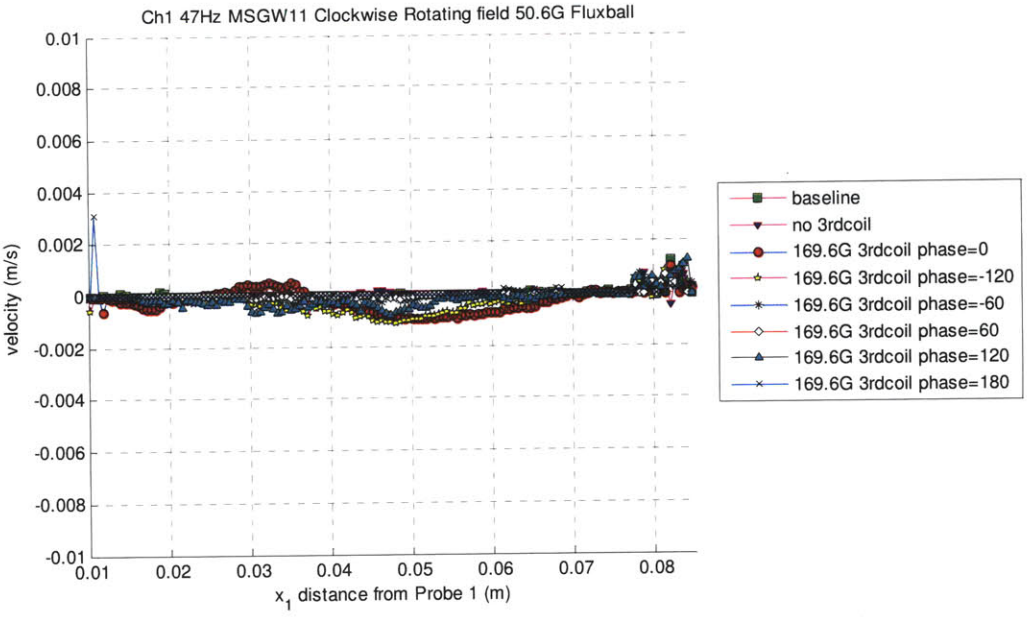
Ch1 47Hz MSGW11 Clockwise Rotating field 50.6G Fluxball
velocity (m/s)
x1 distance from Probe 1 (m)
baseline
no 3rdcoil
169.6G 3rdcoil phase=0
169.6G 3rdcoil phase=-120
169.6G 3rdcoil phase=-60
169.6G 3rdcoil phase=60
169.6G 3rdcoil phase=120
169.6G 3rdcoil phase=180

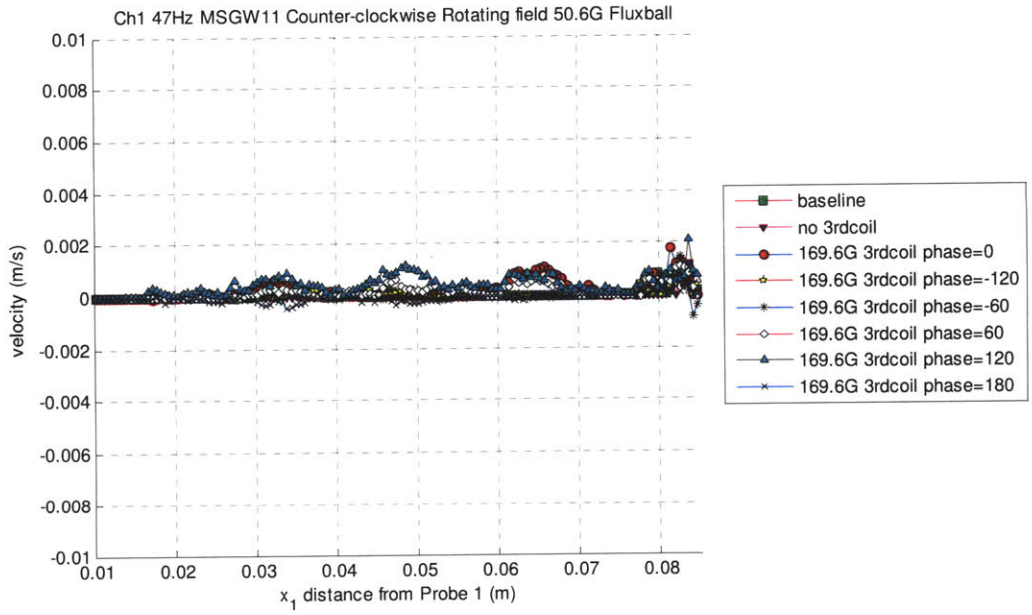
Ch1 47Hz MSGW11 Counter-clockwise Rotating field 50.6G Fluxball
velocity (m/s)
x1 distance from Probe 1 (m)
baseline
no 3rdcoil
169.6G 3rdcoil phase=0
169.6G 3rdcoil phase=-120
169.6G 3rdcoil phase=-60
169.6G 3rdcoil phase=60
169.6G 3rdcoil phase=120
169.6G 3rdcoil phase=180

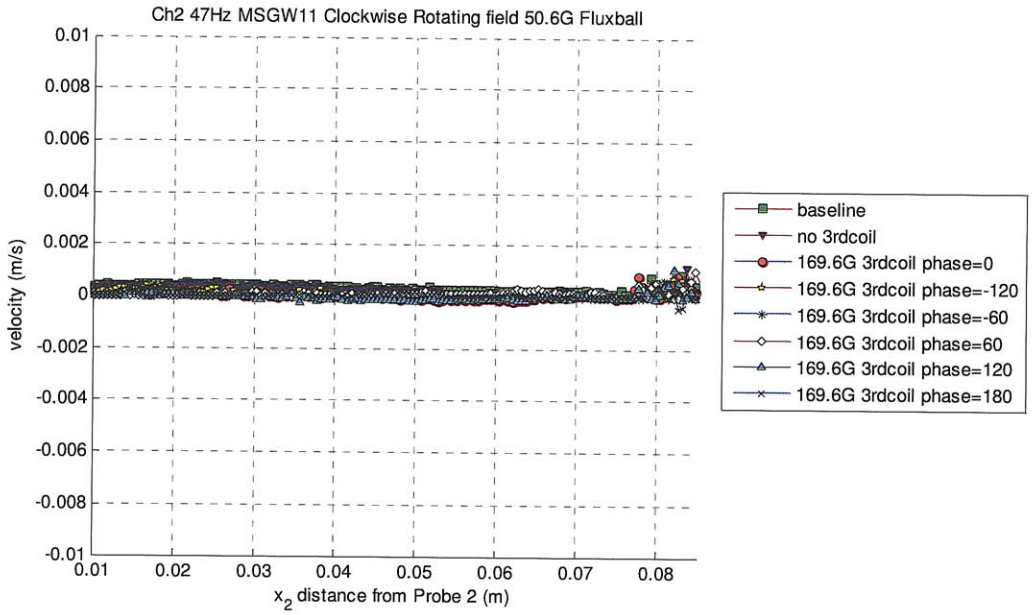
Ch2 47Hz MSGW11 Clockwise Rotating field 50.6G Fluxball
velocity (m/s)
0.01
0.008
0.006
0.004
0.002
0
-0.002
-0.004
-0.006
-0.008
-0.01
0.01
0.02
0.03
0.04
0.05
0.06
0.07
0.08
x2 distance from Probe 2 (m)
baseline
no 3rdcoil
169.6G 3rdcoil phase=0
169.6G 3rdcoil phase=-120
169.6G 3rdcoil phase=-60
169.6G 3rdcoil phase=60
169.6G 3rdcoil phase=120
169.6G 3rdcoil phase=180

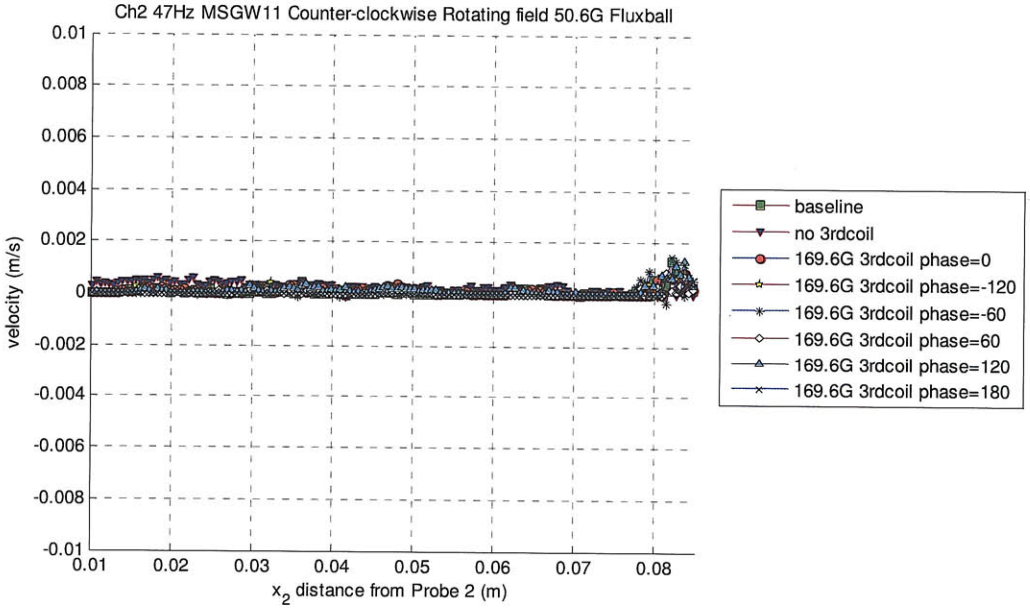
Ch2 47Hz MSGW11 Counter-clockwise Rotating field 50.6G Fluxball
velocity (m/s)
0.01
0.008
0.006
0.004
0.002
0
-0.002
-0.004
-0.006
-0.008
-0.01
0.01
0.02
0.03
0.04
0.05
0.06
0.07
0.08
x2 distance from Probe 2 (m)
baseline
no 3rdcoil
169.6G 3rdcoil phase=0
169.6G 3rdcoil phase=-120
169.6G 3rdcoil phase=-60
169.6G 3rdcoil phase=60
169.6G 3rdcoil phase=120
169.6G 3rdcoil phase=180

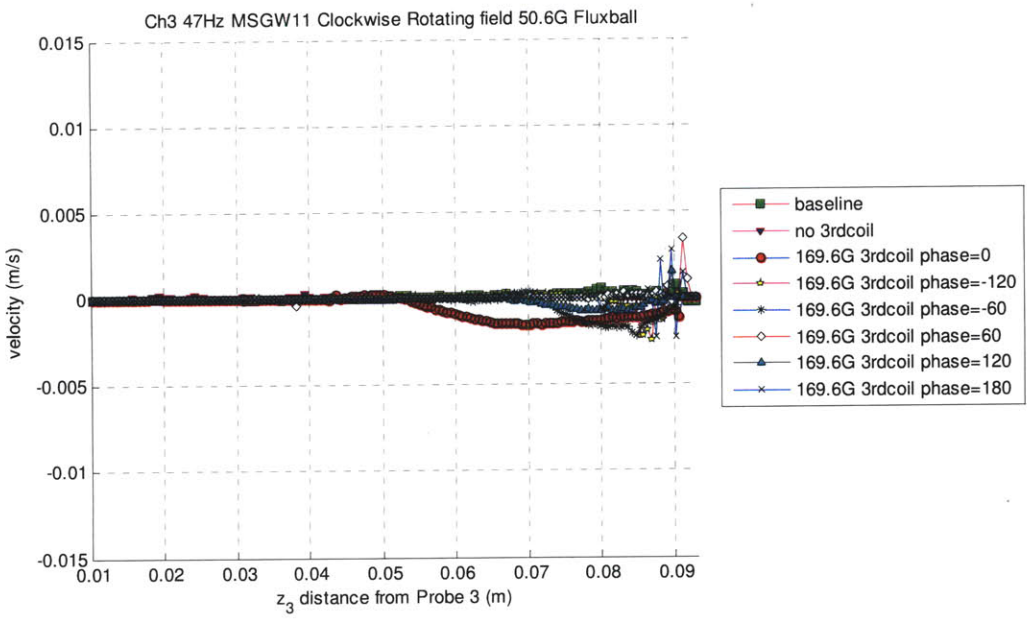
Ch3 47Hz MSGW11 Clockwise Rotating field 50.6G Fluxball
velocity (m/s)
0.015
0.01
0.005
0
-0.005
-0.01
-0.015
0.01
0.02
0.03
0.04
0.05
0.06
0.07
0.08
0.09
z_3 distance from Probe 3 (m)
baseline
no 3rdcoil
169.6G 3rdcoil phase=0
169.6G 3rdcoil phase=-120
169.6G 3rdcoil phase=-60
169.6G 3rdcoil phase=60
169.6G 3rdcoil phase=120
169.6G 3rdcoil phase=180

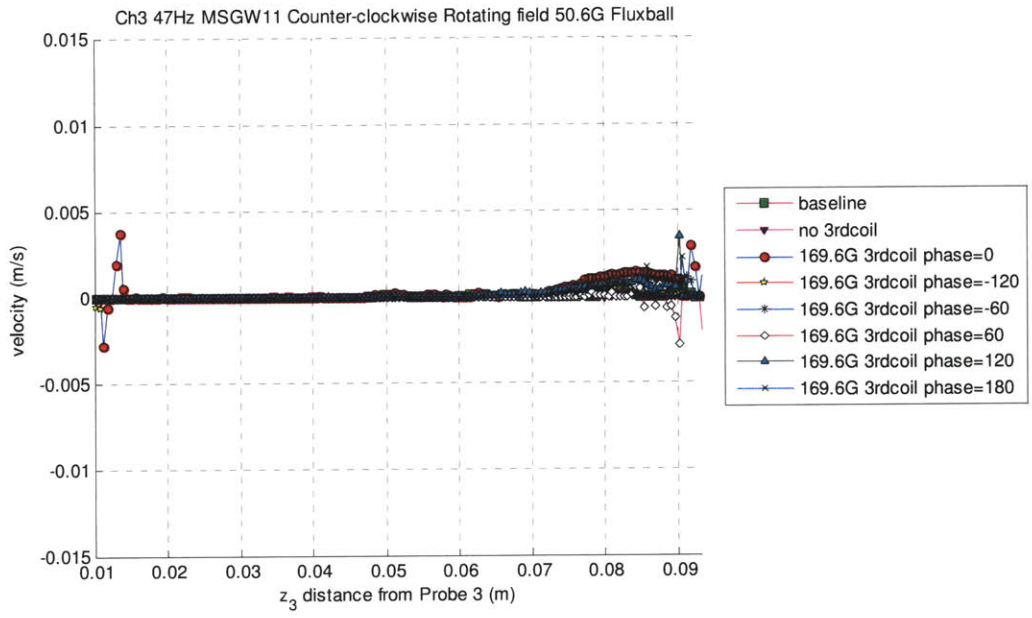
Ch3 47Hz MSGW11 Counter-clockwise Rotating field 50.6G Fluxball
velocity (m/s)
0.015
0.01
0.005
0
-0.005
-0.01
-0.015
0.01
0.02
0.03
0.04
0.05
0.06
0.07
0.08
0.09
z_3 distance from Probe 3 (m)
baseline
no 3rdcoil
169.6G 3rdcoil phase=0
169.6G 3rdcoil phase=-120
169.6G 3rdcoil phase=-60
169.6G 3rdcoil phase=60
169.6G 3rdcoil phase=120
169.6G 3rdcoil phase=180

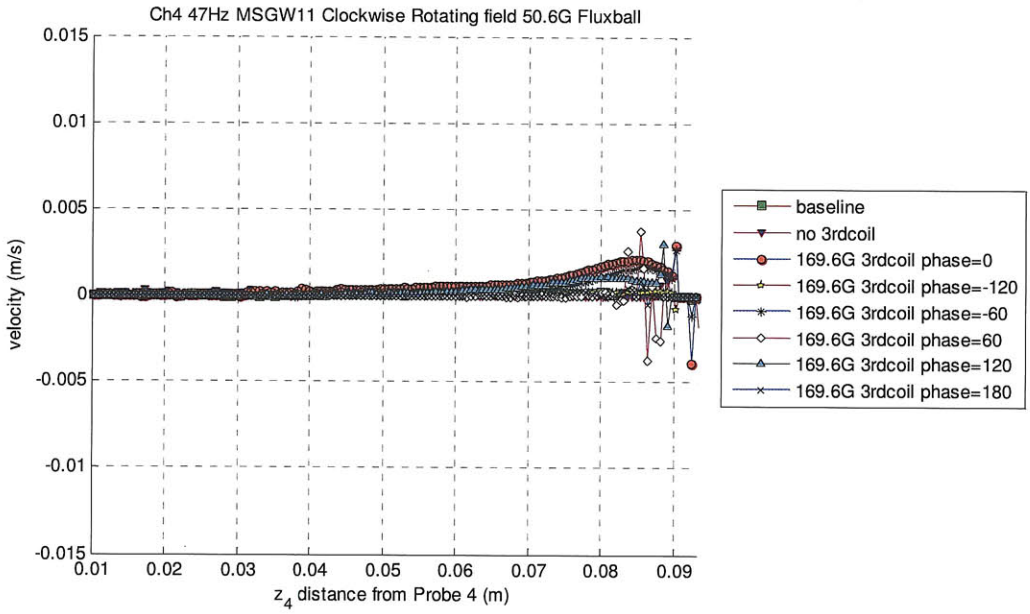
Ch4 47Hz MSGW11 Clockwise Rotating field 50.6G Fluxball
velocity (m/s)
0.015
0.01
0.005
0
-0.005
-0.01
-0.015
0.01
0.02
0.03
0.04
0.05
0.06
0.07
0.08
0.09
z4 distance from Probe 4 (m)
baseline
no 3rdcoil
169.6G 3rdcoil phase=0
169.6G 3rdcoil phase=-120
169.6G 3rdcoil phase=-60
169.6G 3rdcoil phase=60
169.6G 3rdcoil phase=120
169.6G 3rdcoil phase=180

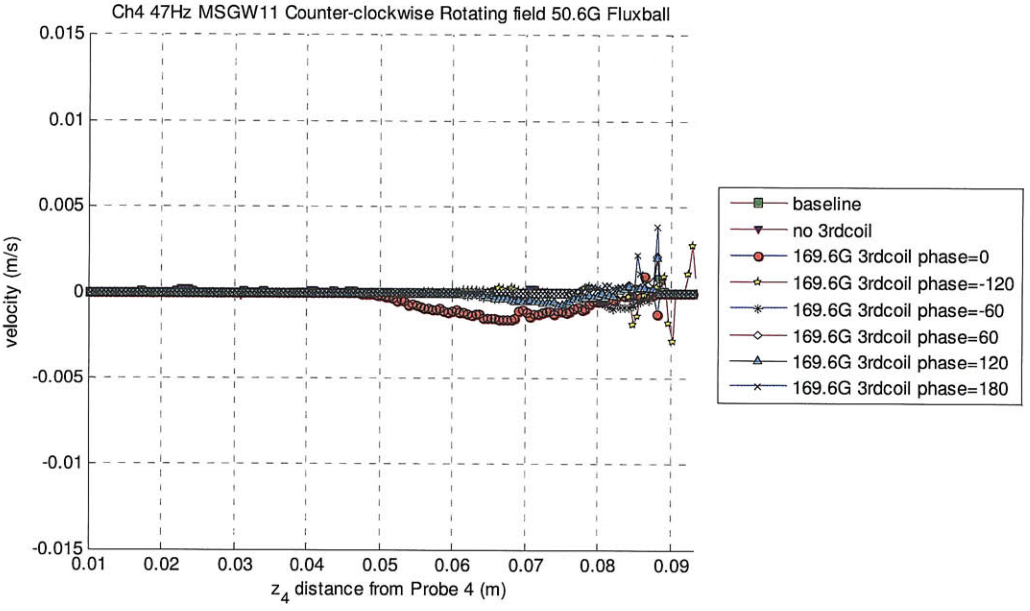
Ch4 47Hz MSGW11 Counter-clockwise Rotating field 50.6G Fluxball
velocity (m/s)
0.015
0.01
0.005
0
-0.005
-0.01
-0.015
0.01
0.02
0.03
0.04
0.05
0.06
0.07
0.08
0.09
z4 distance from Probe 4 (m)
baseline
no 3rdcoil
169.6G 3rdcoil phase=0
169.6G 3rdcoil phase=-120
169.6G 3rdcoil phase=-60
169.6G 3rdcoil phase=60
169.6G 3rdcoil phase=120
169.6G 3rdcoil phase=180

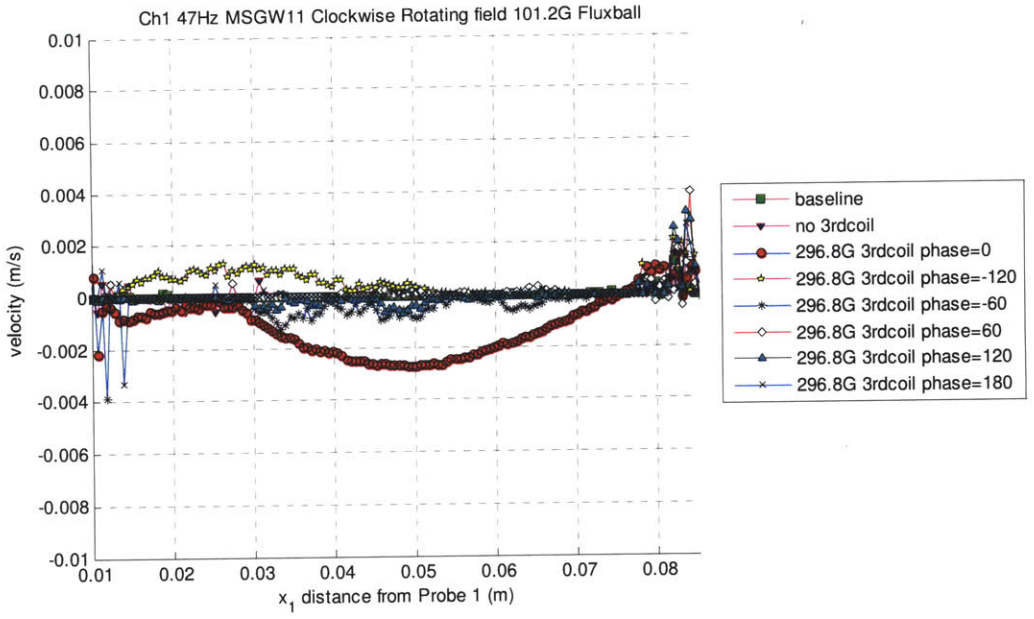
Ch1 47Hz MSGW11 Clockwise Rotating field 101.2G Fluxball
velocity (m/s)
x1 distance from Probe 1 (m)
baseline
no 3rdcoil
296.8G 3rdcoil phase=0
296.8G 3rdcoil phase=-120
296.8G 3rdcoil phase=-60
296.8G 3rdcoil phase=60
296.8G 3rdcoil phase=120
296.8G 3rdcoil phase=180

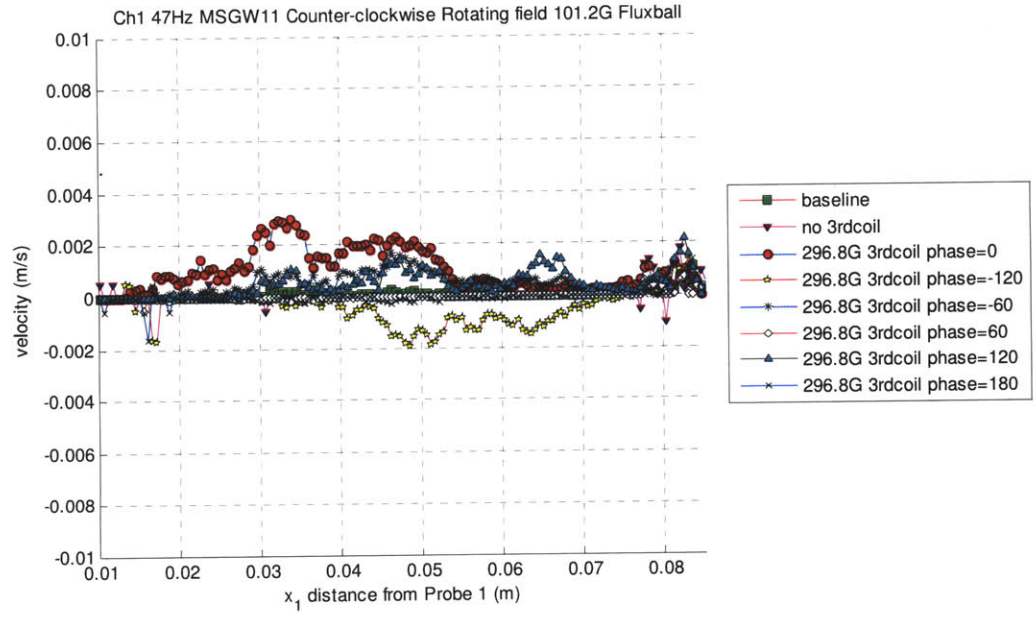
Ch1 47Hz MSGW11 Counter-clockwise Rotating field 101.2G Fluxball
velocity (m/s)
x1 distance from Probe 1 (m)
baseline
no 3rdcoil
296.8G 3rdcoil phase=0
296.8G 3rdcoil phase=-120
296.8G 3rdcoil phase=-60
296.8G 3rdcoil phase=60
296.8G 3rdcoil phase=120
296.8G 3rdcoil phase=180

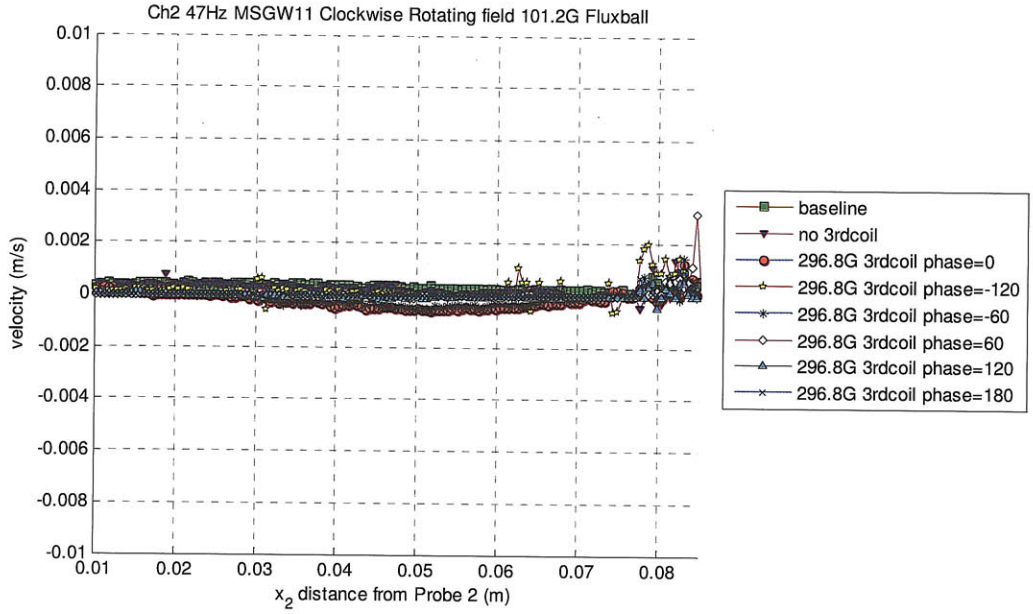
Ch2 47Hz MSGW11 Clockwise Rotating field 101.2G Fluxball
velocity (m/s)
0.01
0.008
0.006
0.004
0.002
0
-0.002
-0.004
-0.006
-0.008
-0.01
0.01
0.02
0.03
0.04
0.05
0.06
0.07
0.08
x2 distance from Probe 2 (m)
baseline
no 3rdcoil
296.8G 3rdcoil phase=0
296.8G 3rdcoil phase=-120
296.8G 3rdcoil phase=-60
296.8G 3rdcoil phase=60
296.8G 3rdcoil phase=120
296.8G 3rdcoil phase=180

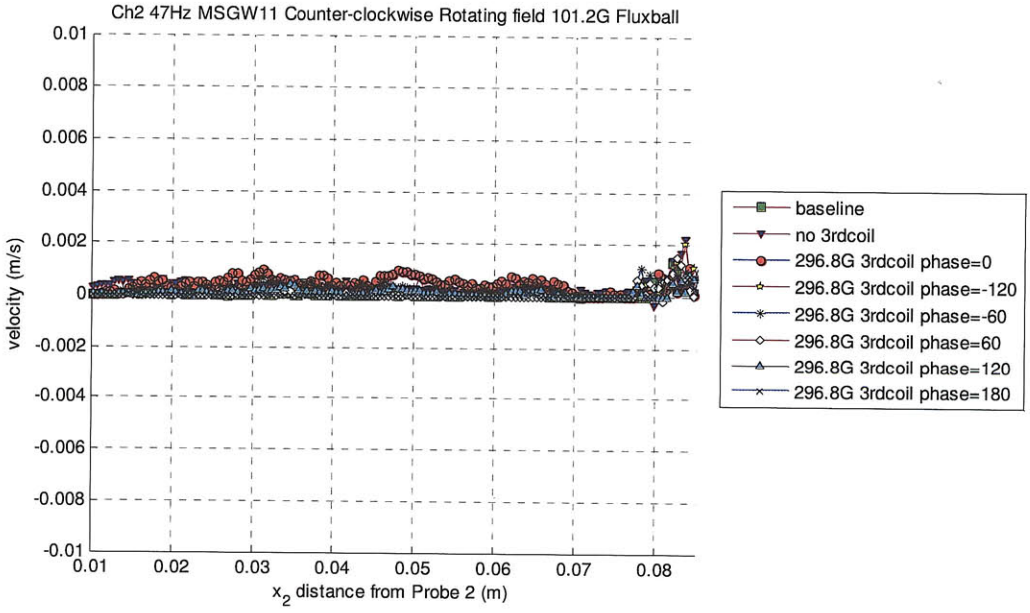
Ch2 47Hz MSGW11 Counter-clockwise Rotating field 101.2G Fluxball
velocity (m/s)
0.01
0.008
0.006
0.004
0.002
0
-0.002
-0.004
-0.006
-0.008
-0.01
0.01
0.02
0.03
0.04
0.05
0.06
0.07
0.08
x2 distance from Probe 2 (m)
baseline
no 3rdcoil
296.8G 3rdcoil phase=0
296.8G 3rdcoil phase=-120
296.8G 3rdcoil phase=-60
296.8G 3rdcoil phase=60
296.8G 3rdcoil phase=120
296.8G 3rdcoil phase=180

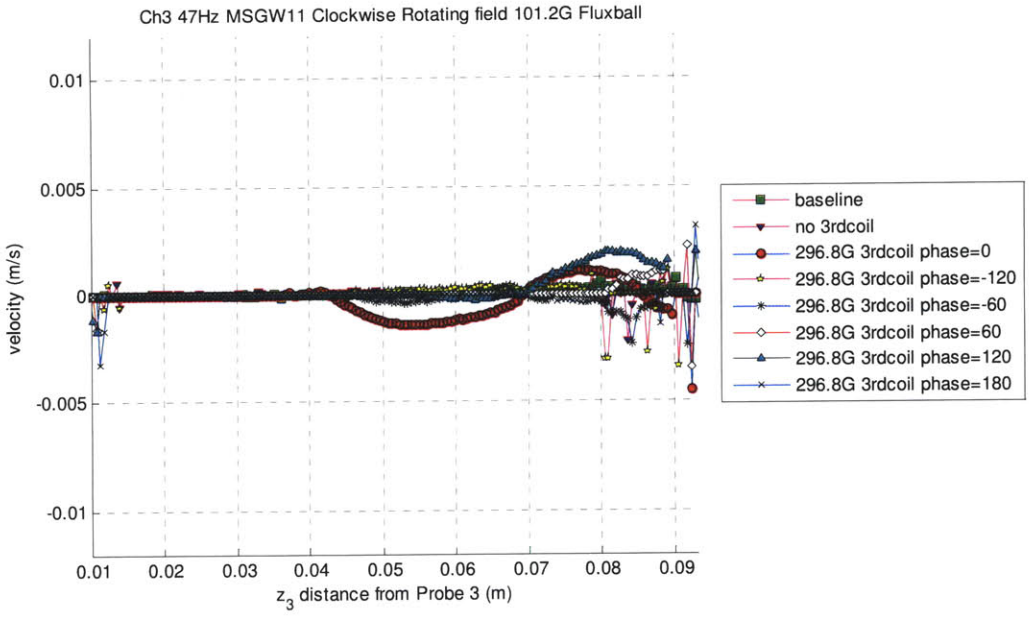
Ch3 47Hz MSGW11 Clockwise Rotating field 101.2G Fluxball
velocity (m/s)
0.01
0.005
0
-0.005
-0.01
0.01
0.02
0.03
0.04
0.05
0.06
0.07
0.08
0.09
z3 distance from Probe 3 (m)
baseline
no 3rdcoil
296.8G 3rdcoil phase=0
296.8G 3rdcoil phase=-120
296.8G 3rdcoil phase=-60
296.8G 3rdcoil phase=60
296.8G 3rdcoil phase=120
296.8G 3rdcoil phase=180

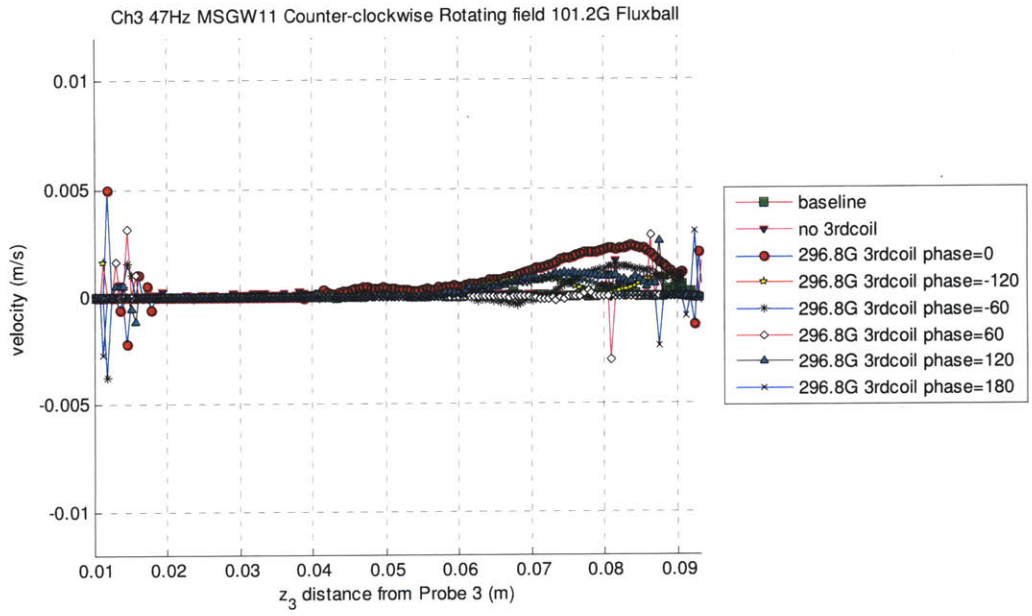
Ch3 47Hz MSGW11 Counter-clockwise Rotating field 101.2G Fluxball
velocity (m/s)
0.01
0.005
0
-0.005
-0.01
0.01
0.02
0.03
0.04
0.05
0.06
0.07
0.08
0.09
z3 distance from Probe 3 (m)
baseline
no 3rdcoil
296.8G 3rdcoil phase=0
296.8G 3rdcoil phase=-120
296.8G 3rdcoil phase=-60
296.8G 3rdcoil phase=60
296.8G 3rdcoil phase=120
296.8G 3rdcoil phase=180

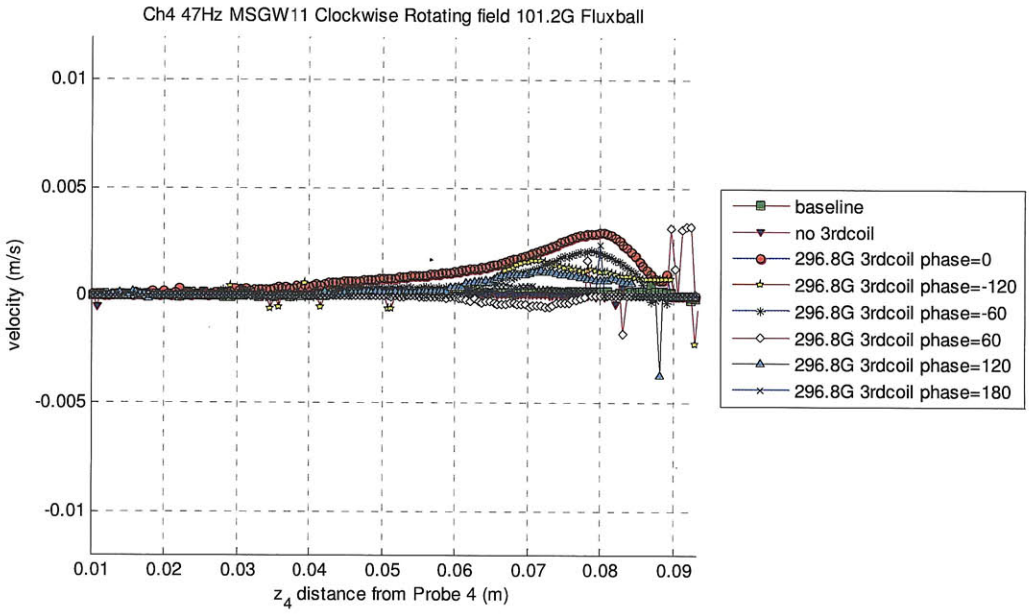
Ch4 47Hz MSGW11 Clockwise Rotating field 101.2G Fluxball
velocity (m/s)
0.01
0.005
0
-0.005
-0.01
0.01 0.02 0.03 0.04 0.05 0.06 0.07 0.08 0.09
z4 distance from Probe 4 (m)
baseline
no 3rdcoil
296.8G 3rdcoil phase=0
296.8G 3rdcoil phase=-120
296.8G 3rdcoil phase=-60
296.8G 3rdcoil phase=60
296.8G 3rdcoil phase=120
296.8G 3rdcoil phase=180

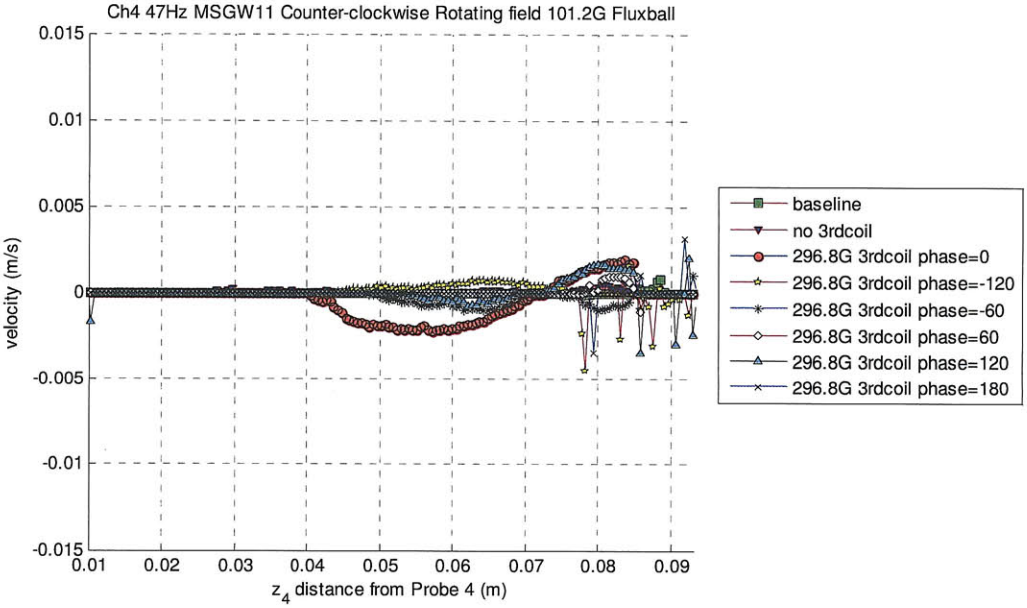
Ch4 47Hz MSGW11 Counter-clockwise Rotating field 101.2G Fluxball
velocity (m/s)
0.015
0.01
0.005
0
-0.005
-0.01
-0.015
0.01 0.02 0.03 0.04 0.05 0.06 0.07 0.08 0.09
z4 distance from Probe 4 (m)
baseline
no 3rdcoil
296.8G 3rdcoil phase=0
296.8G 3rdcoil phase=-120
296.8G 3rdcoil phase=-60
296.8G 3rdcoil phase=60
296.8G 3rdcoil phase=120
296.8G 3rdcoil phase=180

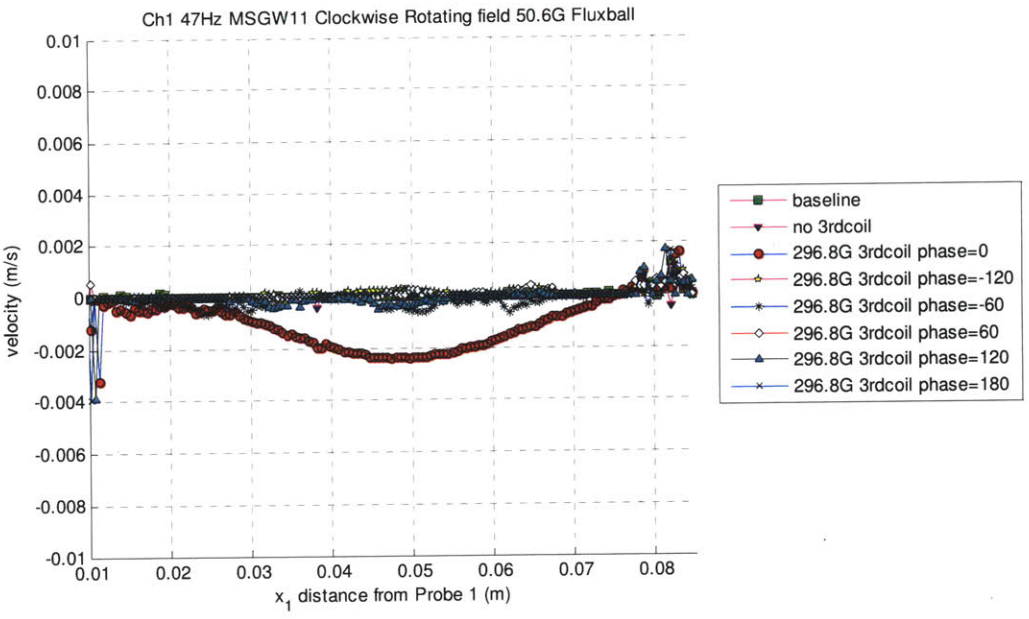
Ch1 47Hz MSGW11 Clockwise Rotating field 50.6G Fluxball
velocity (m/s)
0.01
0.008
0.006
0.004
0.002
0
-0.002
-0.004
-0.006
-0.008
-0.01
0.01
0.02
0.03
0.04
0.05
0.06
0.07
0.08
x1 distance from Probe 1 (m)
baseline
no 3rdcoil
296.8G 3rdcoil phase=0
296.8G 3rdcoil phase=-120
296.8G 3rdcoil phase=-60
296.8G 3rdcoil phase=60
296.8G 3rdcoil phase=120
296.8G 3rdcoil phase=180

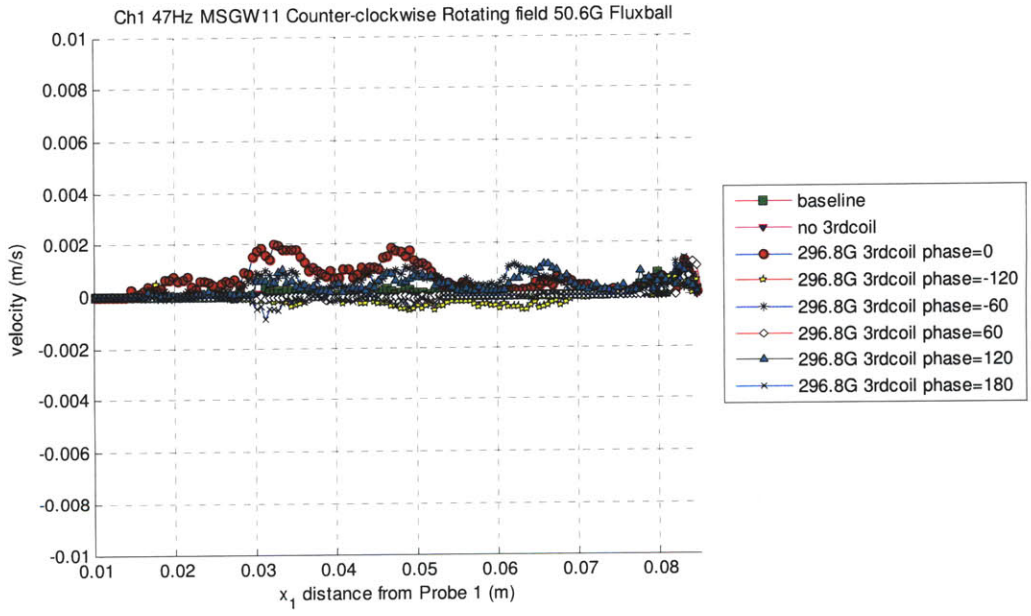
Ch1 47Hz MSGW11 Counter-clockwise Rotating field 50.6G Fluxball
velocity (m/s)
0.01
0.008
0.006
0.004
0.002
0
-0.002
-0.004
-0.006
-0.008
-0.01
0.01
0.02
0.03
0.04
0.05
0.06
0.07
0.08
x1 distance from Probe 1 (m)
baseline
no 3rdcoil
296.8G 3rdcoil phase=0
296.8G 3rdcoil phase=-120
296.8G 3rdcoil phase=-60
296.8G 3rdcoil phase=60
296.8G 3rdcoil phase=120
296.8G 3rdcoil phase=180

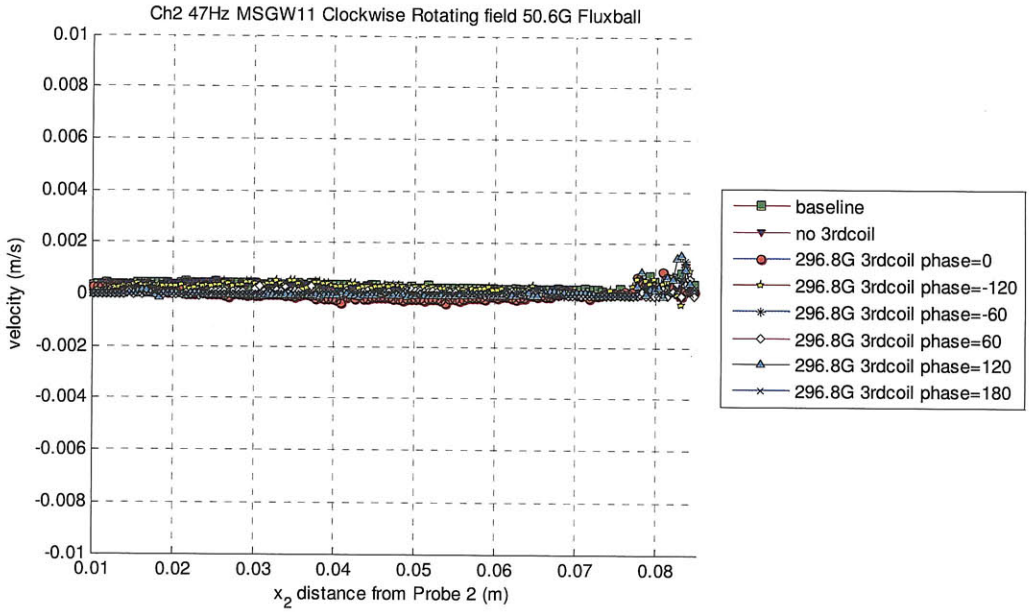
Ch2 47Hz MSGW11 Clockwise Rotating field 50.6G Fluxball
velocity (m/s)
0.01
0.008
0.006
0.004
0.002
0
-0.002
-0.004
-0.006
-0.008
-0.01
0.01
0.02
0.03
0.04
0.05
0.06
0.07
0.08
x2 distance from Probe 2 (m)
baseline
no 3rdcoil
296.8G 3rdcoil phase=0
296.8G 3rdcoil phase=-120
296.8G 3rdcoil phase=-60
296.8G 3rdcoil phase=60
296.8G 3rdcoil phase=120
296.8G 3rdcoil phase=180

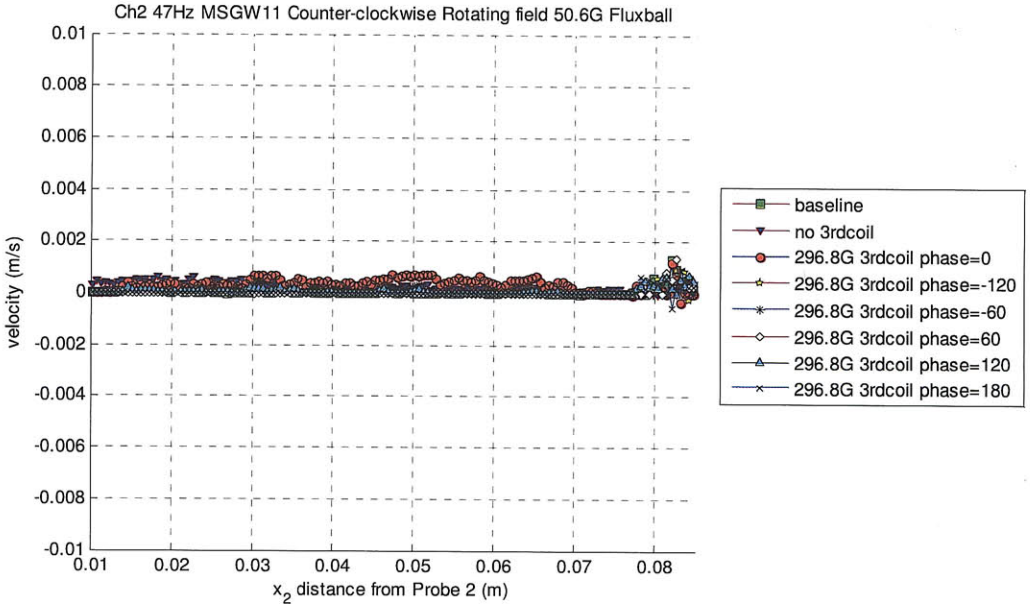
Ch2 47Hz MSGW11 Counter-clockwise Rotating field 50.6G Fluxball
velocity (m/s)
0.01
0.008
0.006
0.004
0.002
0
-0.002
-0.004
-0.006
-0.008
-0.01
0.01
0.02
0.03
0.04
0.05
0.06
0.07
0.08
x2 distance from Probe 2 (m)
baseline
no 3rdcoil
296.8G 3rdcoil phase=0
296.8G 3rdcoil phase=-120
296.8G 3rdcoil phase=-60
296.8G 3rdcoil phase=60
296.8G 3rdcoil phase=120
296.8G 3rdcoil phase=180

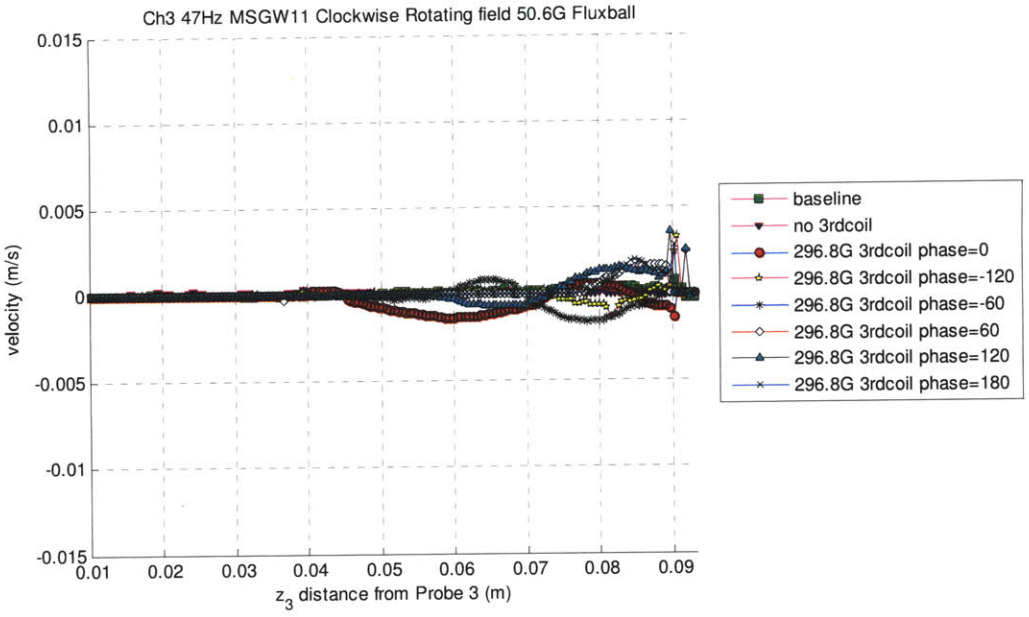
Ch3 47Hz MSGW11 Clockwise Rotating field 50.6G Fluxball
velocity (m/s)
0.015
0.01
0.005
0
-0.005
-0.01
-0.015
0.01
0.02
0.03
0.04
0.05
0.06
0.07
0.08
0.09
z3 distance from Probe 3 (m)
baseline
no 3rdcoil
296.8G 3rdcoil phase=0
296.8G 3rdcoil phase=-120
296.8G 3rdcoil phase=-60
296.8G 3rdcoil phase=60
296.8G 3rdcoil phase=120
296.8G 3rdcoil phase=180

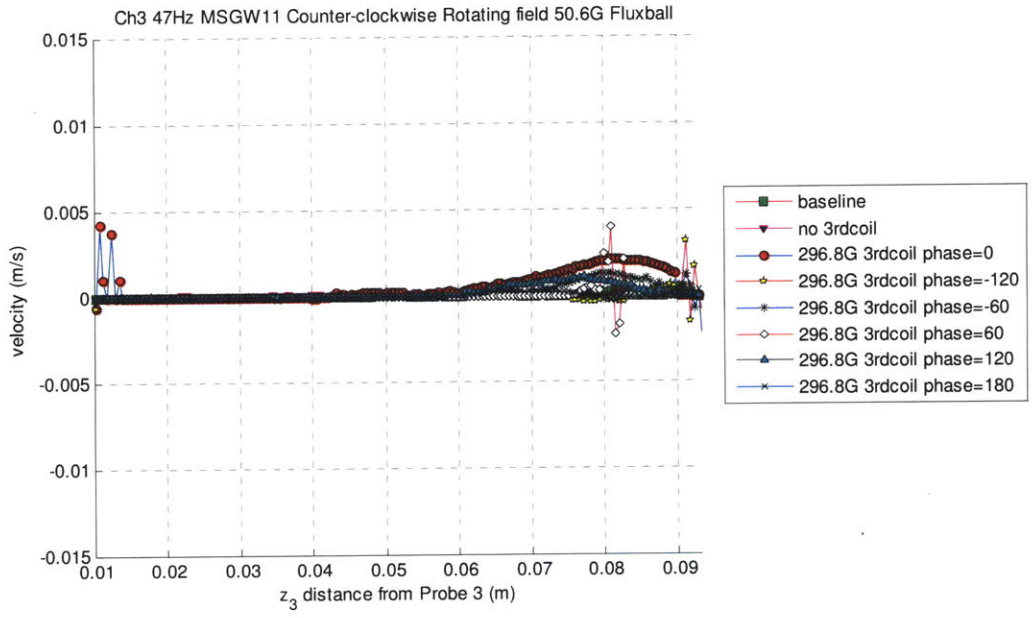
Ch3 47Hz MSGW11 Counter-clockwise Rotating field 50.6G Fluxball
velocity (m/s)
0.015
0.01
0.005
0
-0.005
-0.01
-0.015
0.01
0.02
0.03
0.04
0.05
0.06
0.07
0.08
0.09
z3 distance from Probe 3 (m)
baseline
no 3rdcoil
296.8G 3rdcoil phase=0
296.8G 3rdcoil phase=-120
296.8G 3rdcoil phase=-60
296.8G 3rdcoil phase=60
296.8G 3rdcoil phase=120
296.8G 3rdcoil phase=180

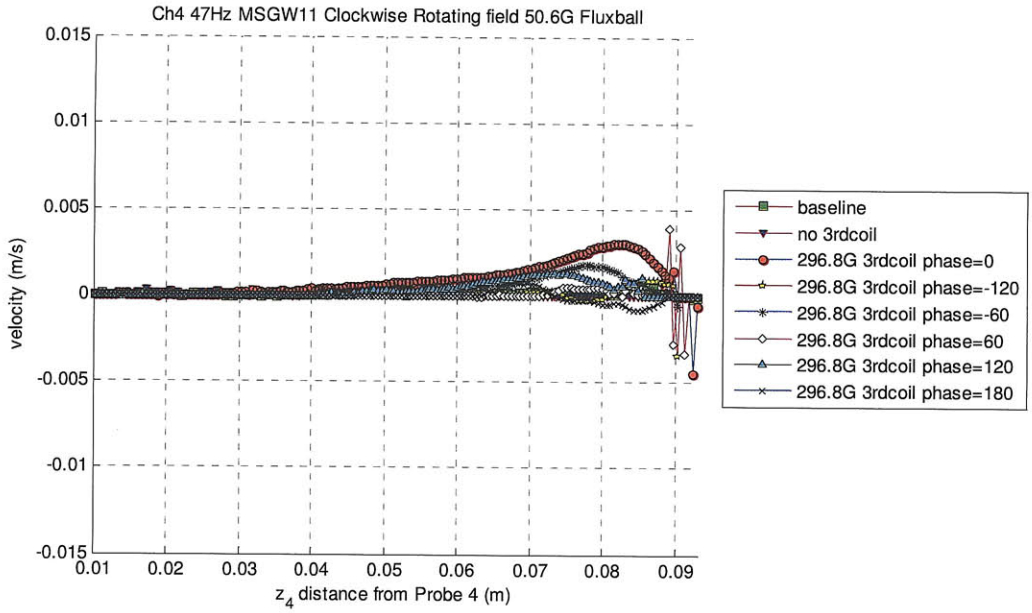
Ch4 47Hz MSGW11 Clockwise Rotating field 50.6G Fluxball
velocity (m/s)
0.015
0.01
0.005
0
-0.005
-0.01
-0.015
0.01
0.02
0.03
0.04
0.05
0.06
0.07
0.08
0.09
z4 distance from Probe 4 (m)
baseline
no 3rdcoil
296.8G 3rdcoil phase=0
296.8G 3rdcoil phase=-120
296.8G 3rdcoil phase=-60
296.8G 3rdcoil phase=60
296.8G 3rdcoil phase=120
296.8G 3rdcoil phase=180

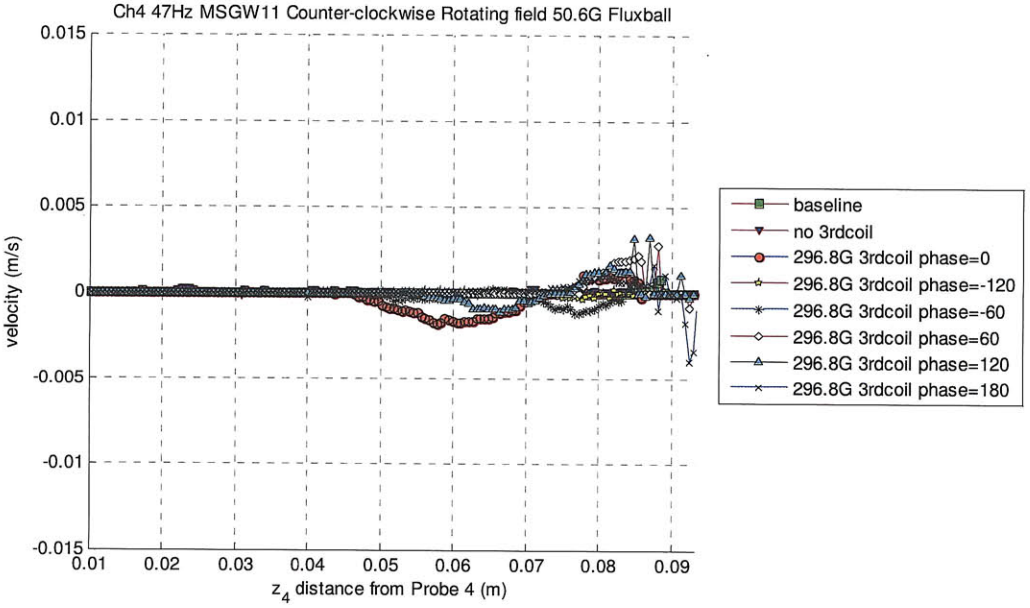
Ch4 47Hz MSGW11 Counter-clockwise Rotating field 50.6G Fluxball
velocity (m/s)
0.015
0.01
0.005
0
-0.005
-0.01
-0.015
0.01
0.02
0.03
0.04
0.05
0.06
0.07
0.08
0.09
z4 distance from Probe 4 (m)
baseline
no 3rdcoil
296.8G 3rdcoil phase=0
296.8G 3rdcoil phase=-120
296.8G 3rdcoil phase=-60
296.8G 3rdcoil phase=60
296.8G 3rdcoil phase=120
296.8G 3rdcoil phase=180

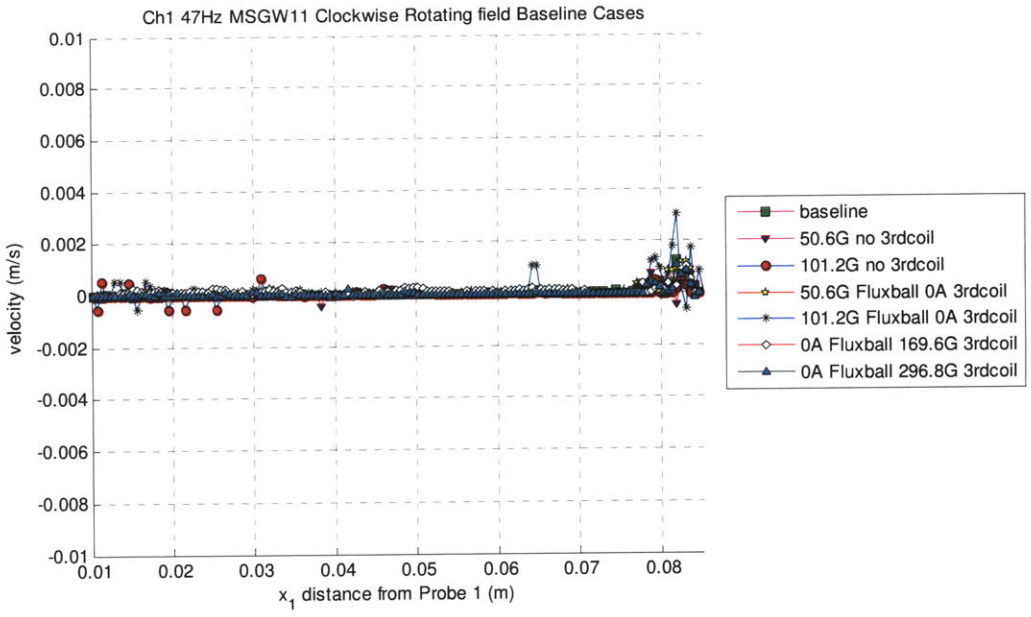
Ch1 47Hz MSGW11 Clockwise Rotating field Baseline Cases
velocity (m/s)
x1 distance from Probe 1 (m)
baseline
50.6G no 3rdcoil
101.2G no 3rdcoil
50.6G Fluxball 0A 3rdcoil
101.2G Fluxball 0A 3rdcoil
0A Fluxball 169.6G 3rdcoil
0A Fluxball 296.8G 3rdcoil

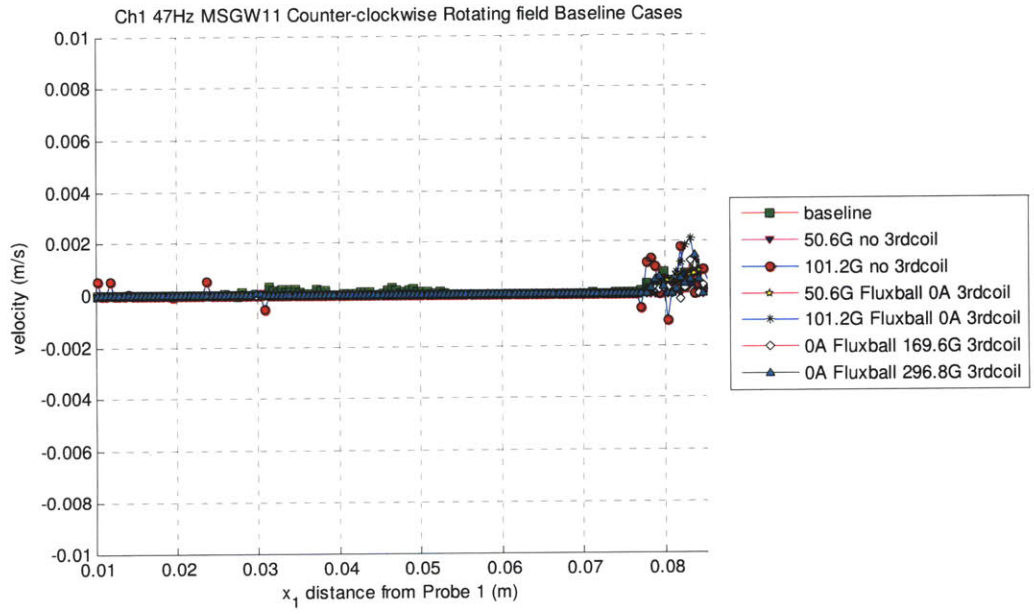
Ch1 47Hz MSGW11 Counter-clockwise Rotating field Baseline Cases
velocity (m/s)
x1 distance from Probe 1 (m)
baseline
50.6G no 3rdcoil
101.2G no 3rdcoil
50.6G Fluxball 0A 3rdcoil
101.2G Fluxball 0A 3rdcoil
0A Fluxball 169.6G 3rdcoil
0A Fluxball 296.8G 3rdcoil

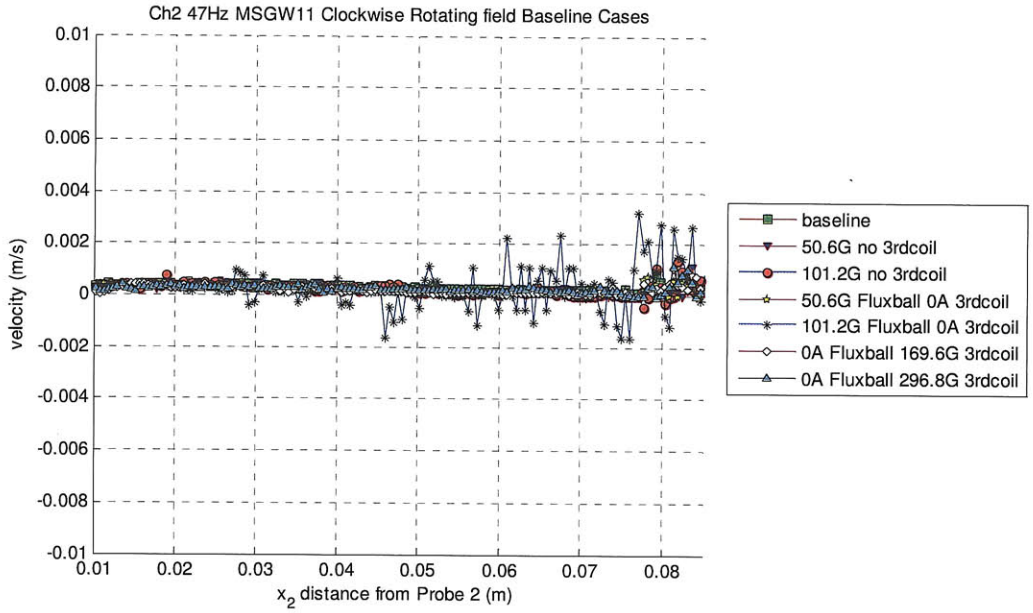
Ch2 47Hz MSGW11 Clockwise Rotating field Baseline Cases
velocity (m/s)
0.01
0.008
0.006
0.004
0.002
0
-0.002
-0.004
-0.006
-0.008
-0.01
0.01
0.02
0.03
0.04
0.05
0.06
0.07
0.08
x2 distance from Probe 2 (m)
baseline
50.6G no 3rdcoil
101.2G no 3rdcoil
50.6G Fluxball 0A 3rdcoil
101.2G Fluxball 0A 3rdcoil
0A Fluxball 169.6G 3rdcoil
0A Fluxball 296.8G 3rdcoil

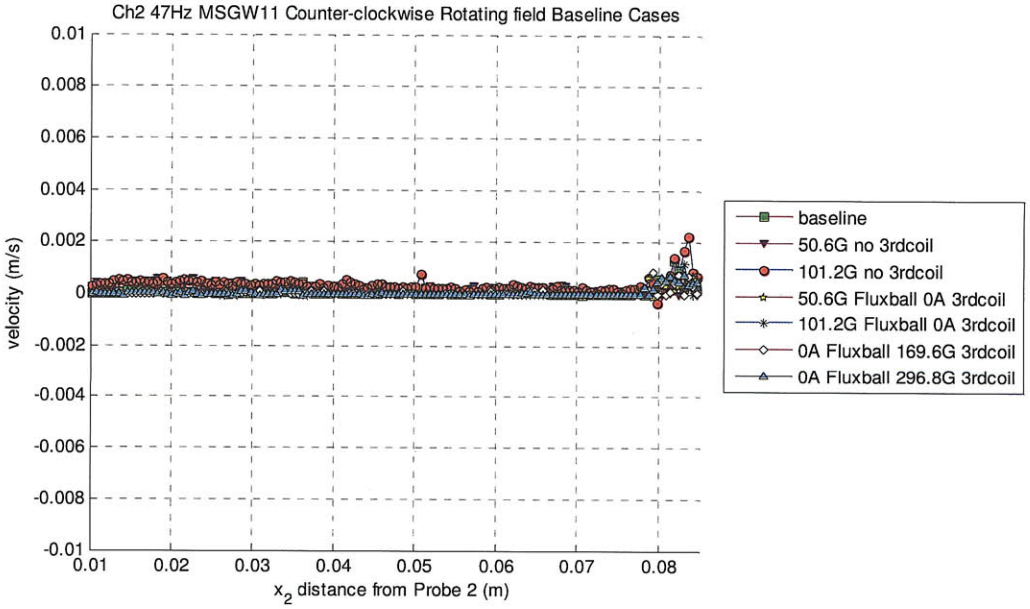
Ch2 47Hz MSGW11 Counter-clockwise Rotating field Baseline Cases
velocity (m/s)
0.01
0.008
0.006
0.004
0.002
0
-0.002
-0.004
-0.006
-0.008
-0.01
0.01
0.02
0.03
0.04
0.05
0.06
0.07
0.08
x2 distance from Probe 2 (m)
baseline
50.6G no 3rdcoil
101.2G no 3rdcoil
50.6G Fluxball 0A 3rdcoil
101.2G Fluxball 0A 3rdcoil
0A Fluxball 169.6G 3rdcoil
0A Fluxball 296.8G 3rdcoil

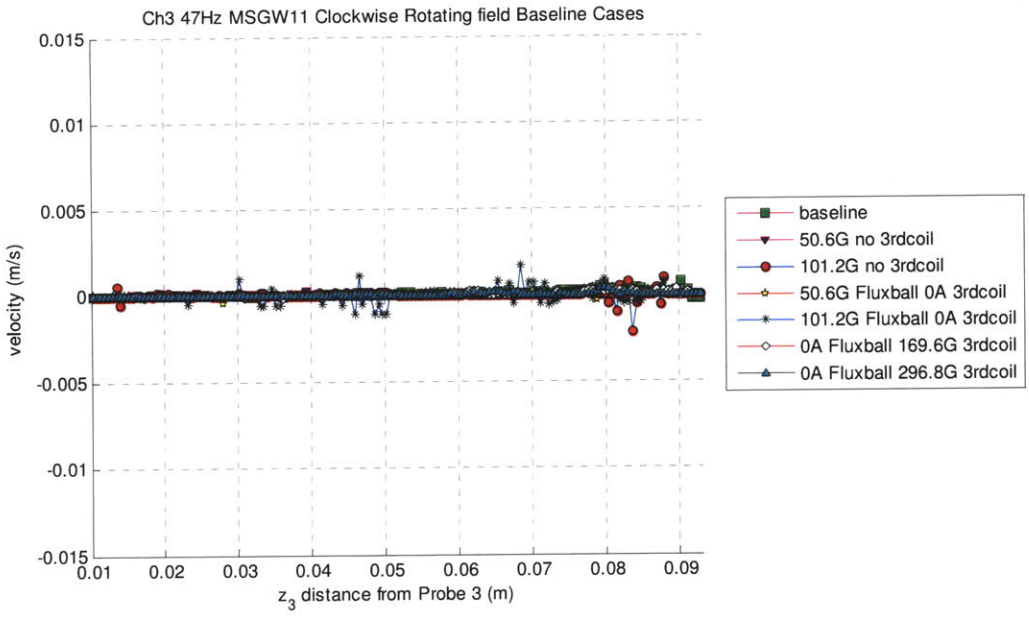
Ch3 47Hz MSGW11 Clockwise Rotating field Baseline Cases
velocity (m/s)
0.015
0.01
0.005
0
-0.005
-0.01
-0.015
0.01
0.02
0.03
0.04
0.05
0.06
0.07
0.08
0.09
z_3 distance from Probe 3 (m)
baseline
50.6G no 3rdcoil
101.2G no 3rdcoil
50.6G Fluxball 0A 3rdcoil
101.2G Fluxball 0A 3rdcoil
0A Fluxball 169.6G 3rdcoil
0A Fluxball 296.8G 3rdcoil

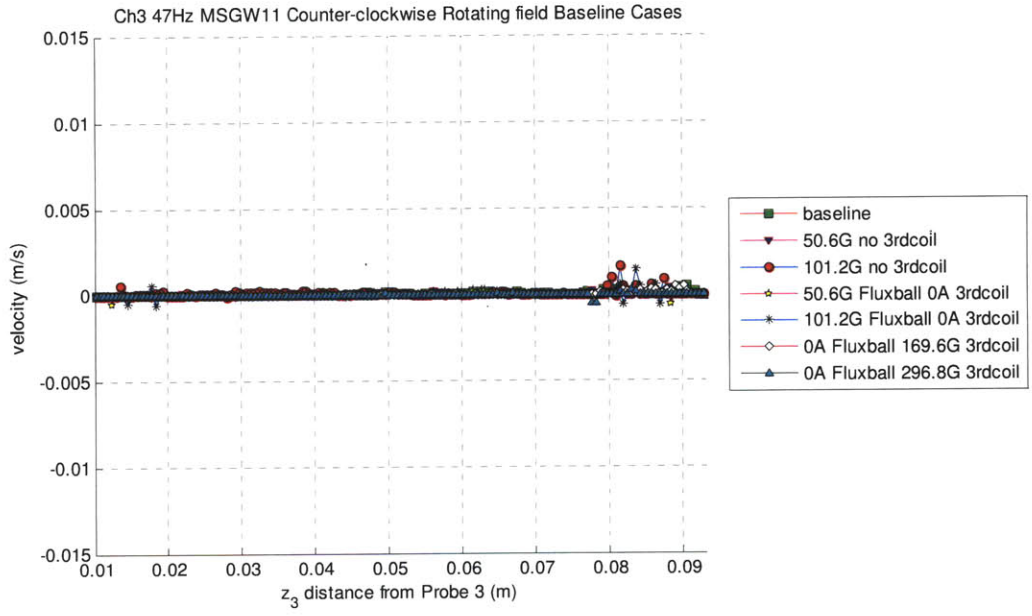
Ch3 47Hz MSGW11 Counter-clockwise Rotating field Baseline Cases
velocity (m/s)
0.015
0.01
0.005
0
-0.005
-0.01
-0.015
0.01
0.02
0.03
0.04
0.05
0.06
0.07
0.08
0.09
z_3 distance from Probe 3 (m)
baseline
50.6G no 3rdcoil
101.2G no 3rdcoil
50.6G Fluxball 0A 3rdcoil
101.2G Fluxball 0A 3rdcoil
0A Fluxball 169.6G 3rdcoil
0A Fluxball 296.8G 3rdcoil

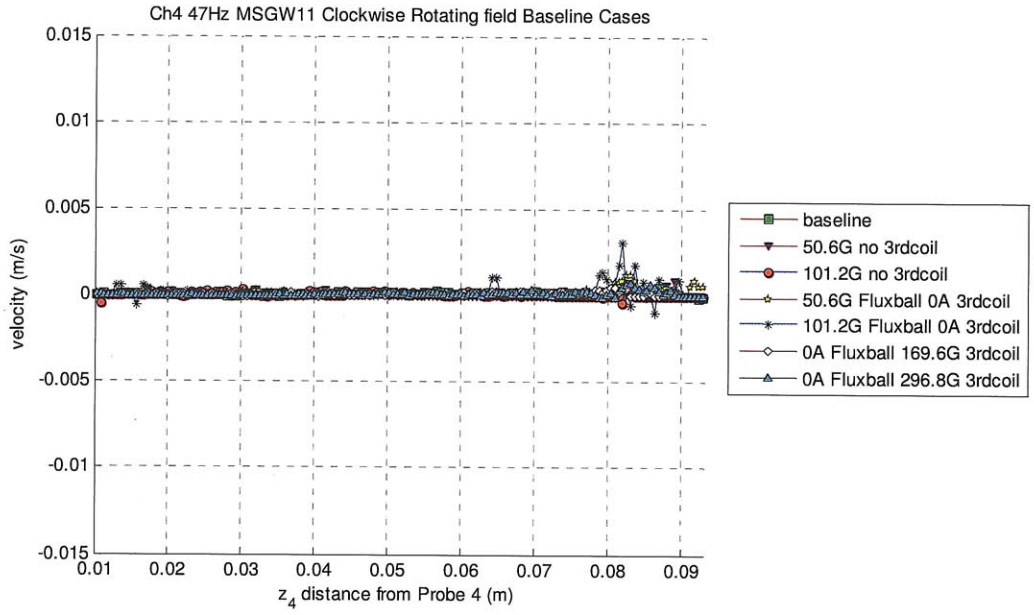
Ch4 47Hz MSGW11 Clockwise Rotating field Baseline Cases
velocity (m/s)
0.015
0.01
0.005
0
-0.005
-0.01
-0.015
0.01
0.02
0.03
0.04
0.05
0.06
0.07
0.08
0.09
z4 distance from Probe 4 (m)
baseline
50.6G no 3rdcoil
101.2G no 3rdcoil
50.6G Fluxball 0A 3rdcoil
101.2G Fluxball 0A 3rdcoil
0A Fluxball 169.6G 3rdcoil
0A Fluxball 296.8G 3rdcoil

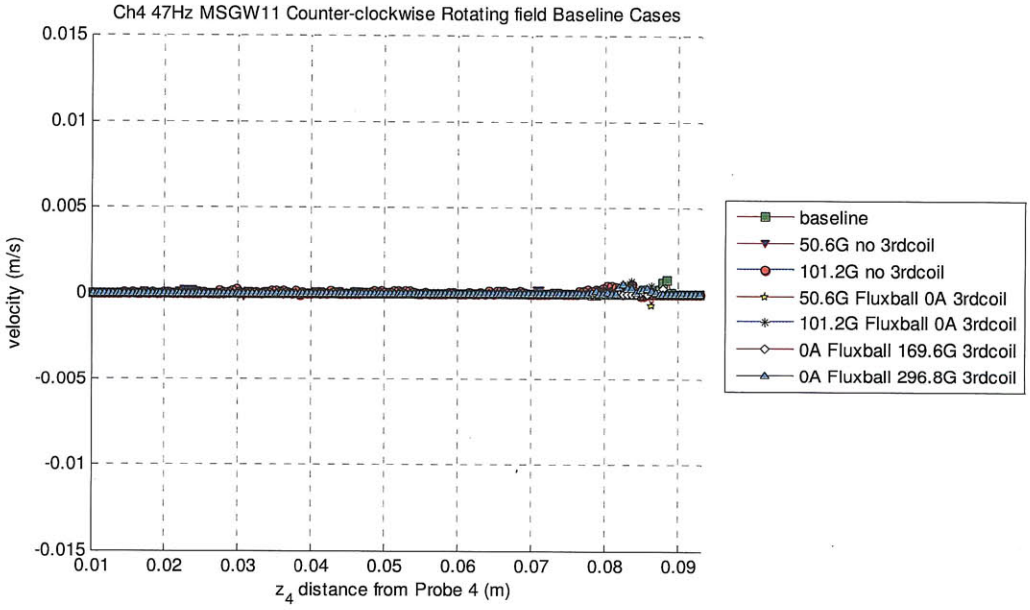
Ch4 47Hz MSGW11 Counter-clockwise Rotating field Baseline Cases
velocity (m/s)
0.015
0.01
0.005
0
-0.005
-0.01
-0.015
0.01
0.02
0.03
0.04
0.05
0.06
0.07
0.08
0.09
z4 distance from Probe 4 (m)
baseline
50.6G no 3rdcoil
101.2G no 3rdcoil
50.6G Fluxball 0A 3rdcoil
101.2G Fluxball 0A 3rdcoil
0A Fluxball 169.6G 3rdcoil
0A Fluxball 296.8G 3rdcoil

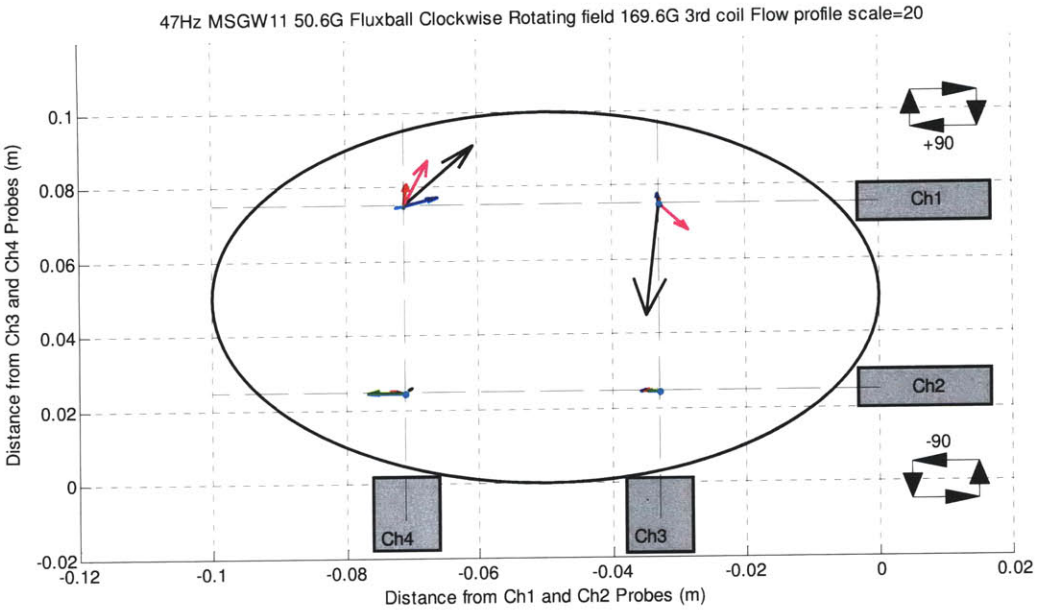
47Hz MSGW11 50.6G Fluxball Clockwise Rotating field 169.6G 3rd coil Flow profile scale=20
Distance from Ch3 and Ch4 Probes (m)
Distance from Ch1 and Ch2 Probes (m)
+90
-90
Ch1
Ch2
Ch3
Ch4
0.1
0.08
0.06
0.04
0.02
0
-0.02
-0.12
-0.1
-0.08
-0.06
-0.04
-0.02
0
0.02

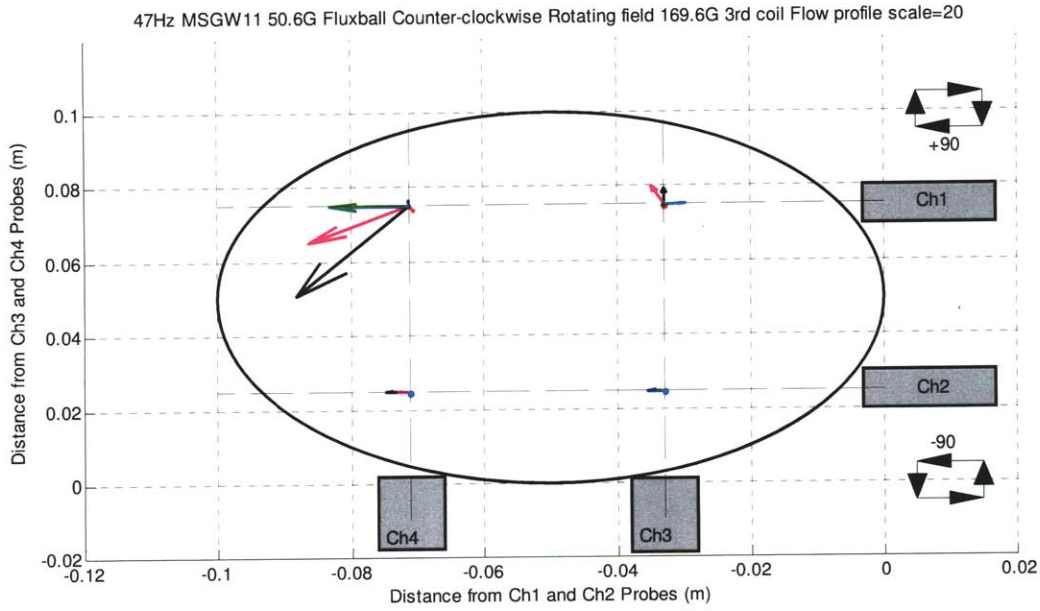
47Hz MSGW11 50.6G Fluxball Counter-clockwise Rotating field 169.6G 3rd coil Flow profile scale=20
Distance from Ch3 and Ch4 Probes (m)
Distance from Ch1 and Ch2 Probes (m)
+90
-90
Ch1
Ch2
Ch3
Ch4
0.1
0.08
0.06
0.04
0.02
0
-0.02
-0.12
-0.1
-0.08
-0.06
-0.04
-0.02
0
0.02

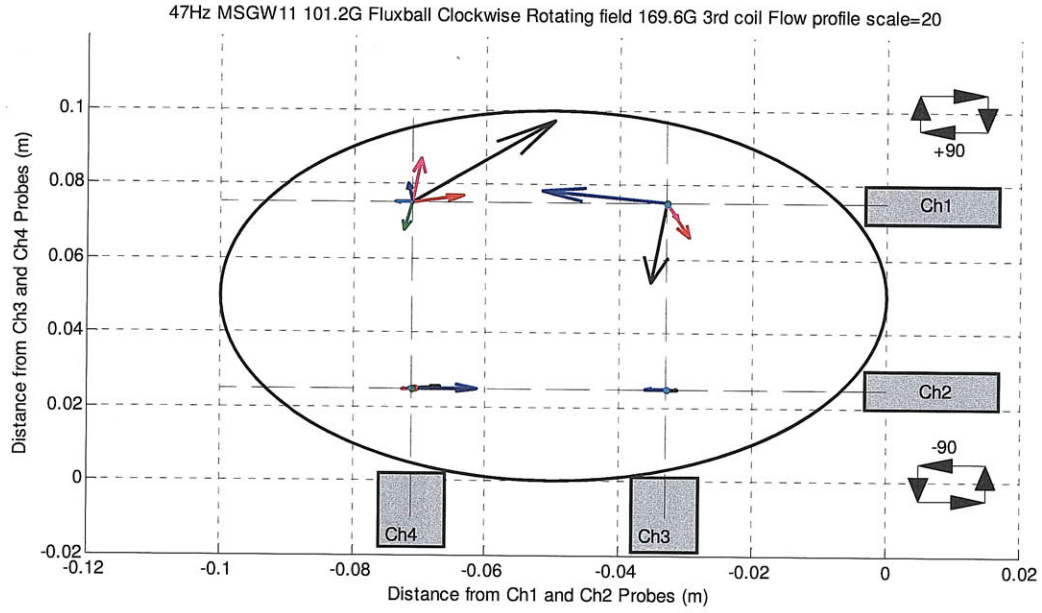
47Hz MSGW11 101.2G Fluxball Clockwise Rotating field 169.6G 3rd coil Flow profile scale=20
Distance from Ch3 and Ch4 Probes (m)
Distance from Ch1 and Ch2 Probes (m)
0.1
0.08
0.06
0.04
0.02
0
-0.02
-0.12
-0.1
-0.08
-0.06
-0.04
-0.02
0
0.02
+90
-90
Ch1
Ch2
Ch3
Ch4

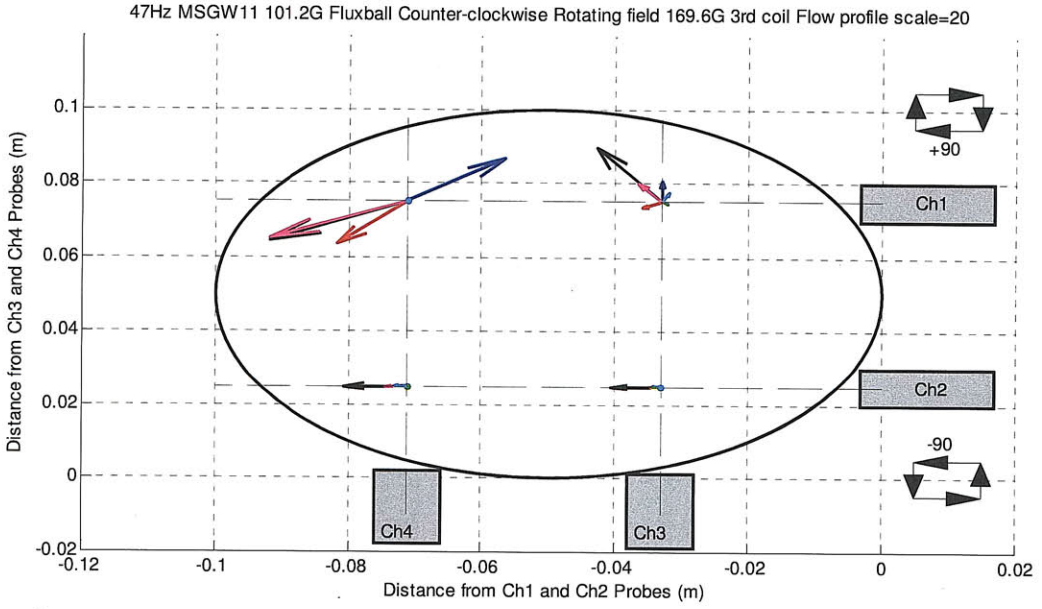
47Hz MSGW11 101.2G Fluxball Counter-clockwise Rotating field 169.6G 3rd coil Flow profile scale=20
Distance from Ch3 and Ch4 Probes (m)
Distance from Ch1 and Ch2 Probes (m)
0.1
0.08
0.06
0.04
0.02
0
-0.02
-0.12
-0.1
-0.08
-0.06
-0.04
-0.02
0
0.02
+90
-90
Ch1
Ch2
Ch3
Ch4

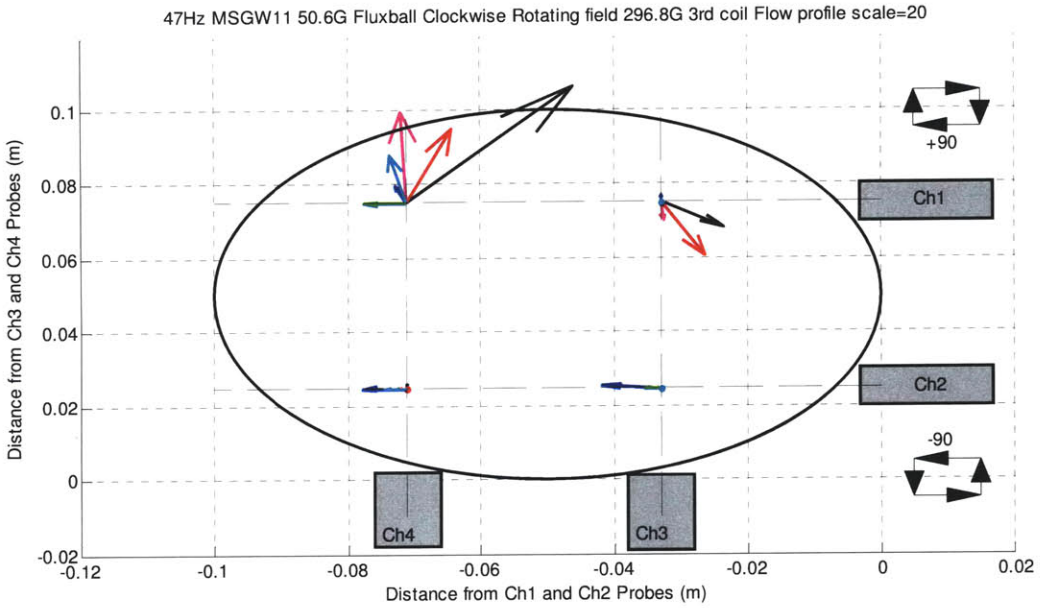
47Hz MSGW11 50.6G Fluxball Clockwise Rotating field 296.8G 3rd coil Flow profile scale=20
Distance from Ch3 and Ch4 Probes (m)
Distance from Ch1 and Ch2 Probes (m)
0.1
0.08
0.06
0.04
0.02
0
-0.02
-0.12
-0.1
-0.08
-0.06
-0.04
-0.02
0
0.02
+90
-90
Ch1
Ch2
Ch3
Ch4

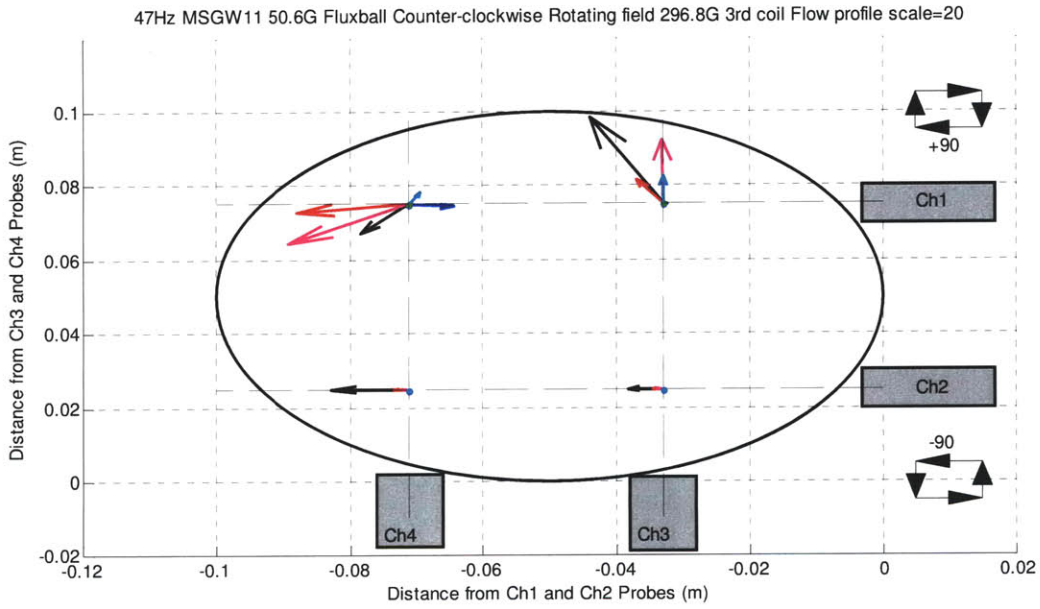
47Hz MSGW11 50.6G Fluxball Counter-clockwise Rotating field 296.8G 3rd coil Flow profile scale=20
Distance from Ch3 and Ch4 Probes (m)
Distance from Ch1 and Ch2 Probes (m)
0.1
0.08
0.06
0.04
0.02
0
-0.02
-0.12
-0.1
-0.08
-0.06
-0.04
-0.02
0
0.02
+90
-90
Ch1
Ch2
Ch3
Ch4

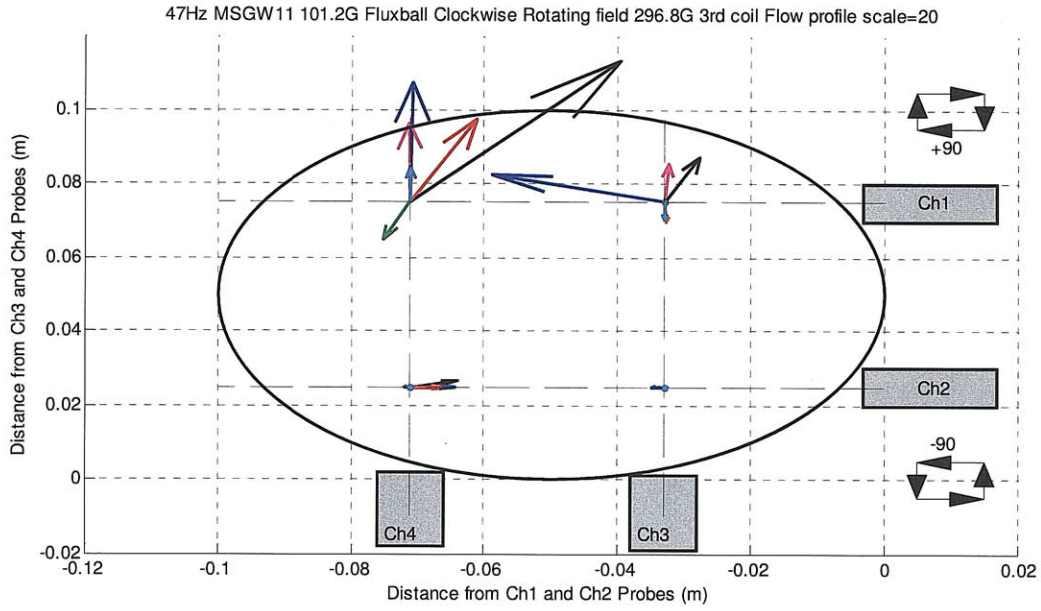
47Hz MSGW11 101.2G Fluxball Clockwise Rotating field 296.8G 3rd coil Flow profile scale=20
Distance from Ch3 and Ch4 Probes (m)
Distance from Ch1 and Ch2 Probes (m)
0.1
0.08
0.06
0.04
0.02
0
-0.02
-0.12
-0.1
-0.08
-0.06
-0.04
-0.02
0
0.02
+90
-90
Ch1
Ch2
Ch3
Ch4

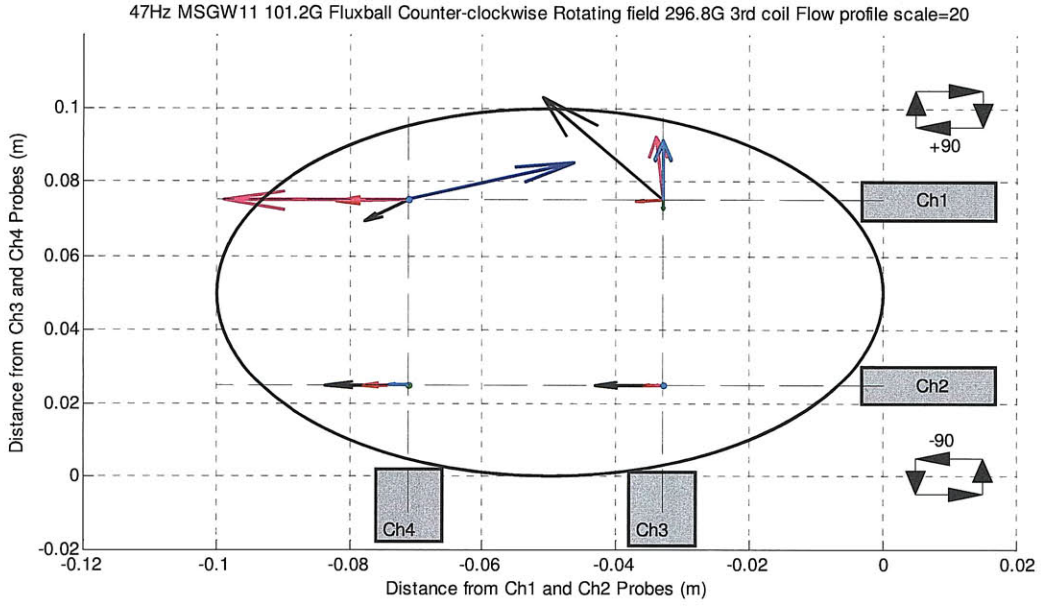
47Hz MSGW11 101.2G Fluxball Counter-clockwise Rotating field 296.8G 3rd coil Flow profile scale=20
Distance from Ch3 and Ch4 Probes (m)
Distance from Ch1 and Ch2 Probes (m)
0.1
0.08
0.06
0.04
0.02
0
-0.02
-0.12
-0.1
-0.08
-0.06
-0.04
-0.02
0
0.02
+90
-90
Ch1
Ch2
Ch3
Ch4

G6. MSGW11 Filled Sphere with Third Coil Oscillating at Same Frequency as Rotating Field at 15Hz

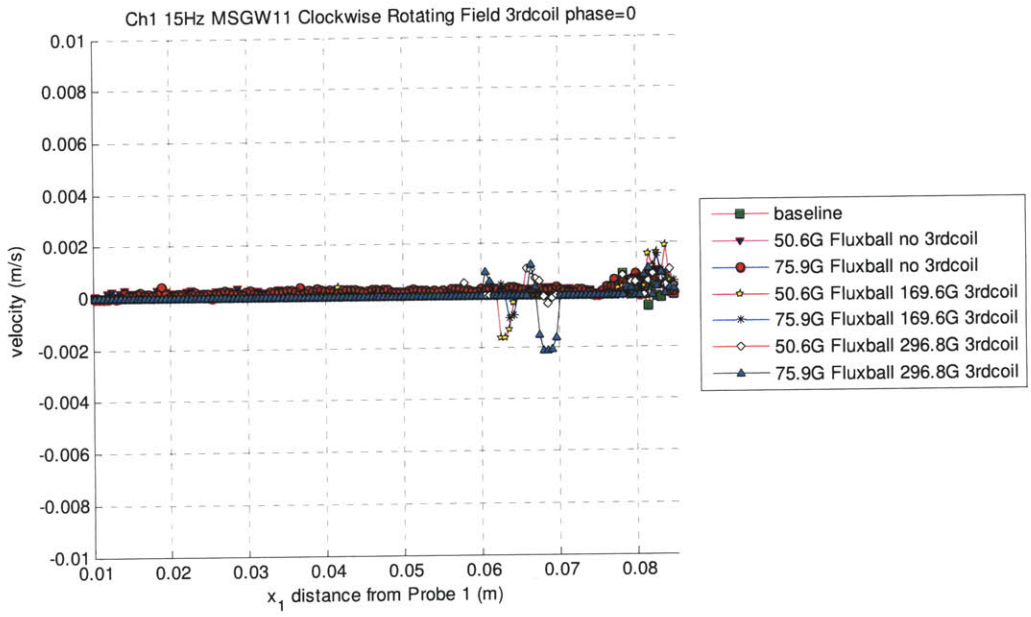

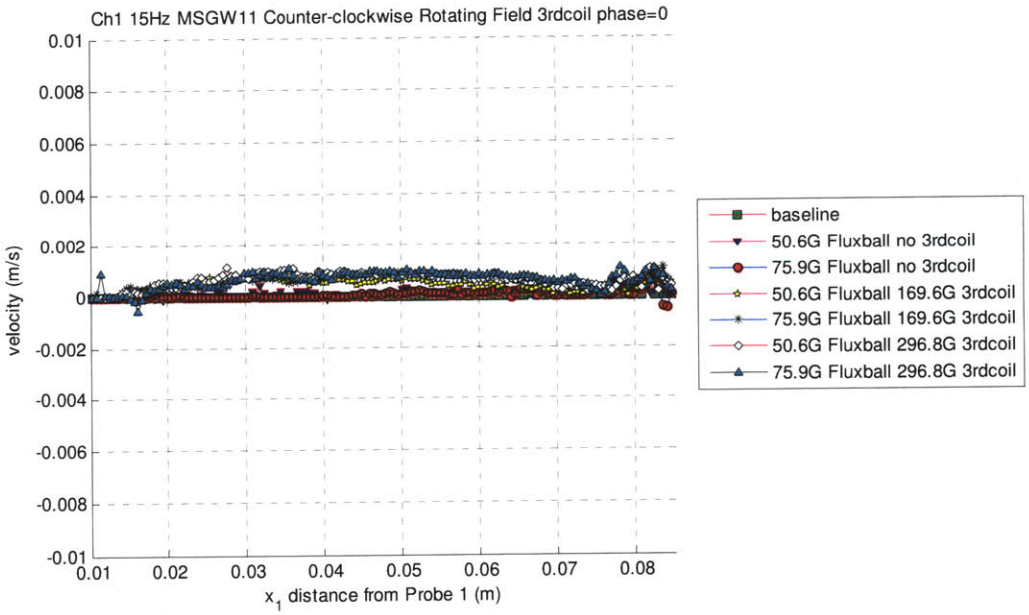

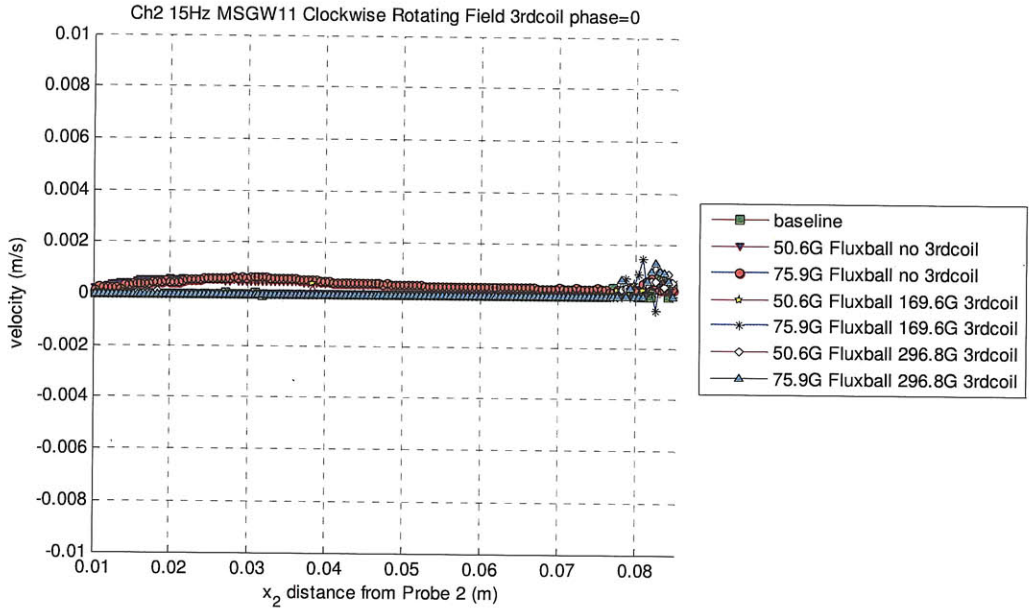
Ch2 15Hz MSGW11 Clockwise Rotating Field 3rdcoil phase=0
velocity (m/s)
0.01
0.008
0.006
0.004
0.002
0
-0.002
-0.004
-0.006
-0.008
-0.01
0.01 0.02 0.03 0.04 0.05 0.06 0.07 0.08
x2 distance from Probe 2 (m)
baseline
50.6G Fluxball no 3rdcoil
75.9G Fluxball no 3rdcoil
50.6G Fluxball 169.6G 3rdcoil
75.9G Fluxball 169.6G 3rdcoil
50.6G Fluxball 296.8G 3rdcoil
75.9G Fluxball 296.8G 3rdcoil

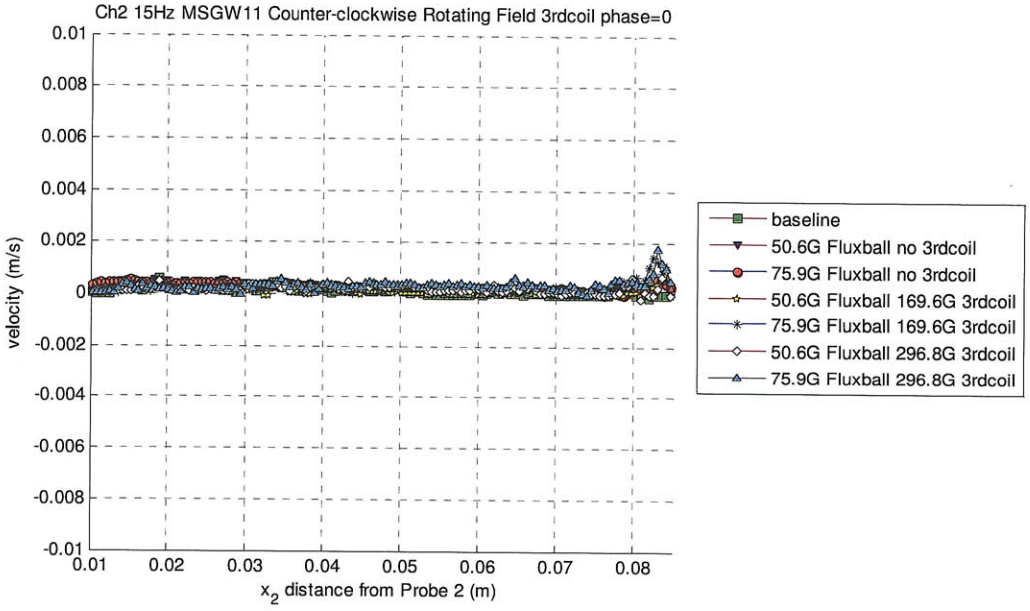
Ch2 15Hz MSGW11 Counter-clockwise Rotating Field 3rdcoil phase=0
velocity (m/s)
0.01
0.008
0.006
0.004
0.002
0
-0.002
-0.004
-0.006
-0.008
-0.01
0.01 0.02 0.03 0.04 0.05 0.06 0.07 0.08
x2 distance from Probe 2 (m)
baseline
50.6G Fluxball no 3rdcoil
75.9G Fluxball no 3rdcoil
50.6G Fluxball 169.6G 3rdcoil
75.9G Fluxball 169.6G 3rdcoil
50.6G Fluxball 296.8G 3rdcoil
75.9G Fluxball 296.8G 3rdcoil

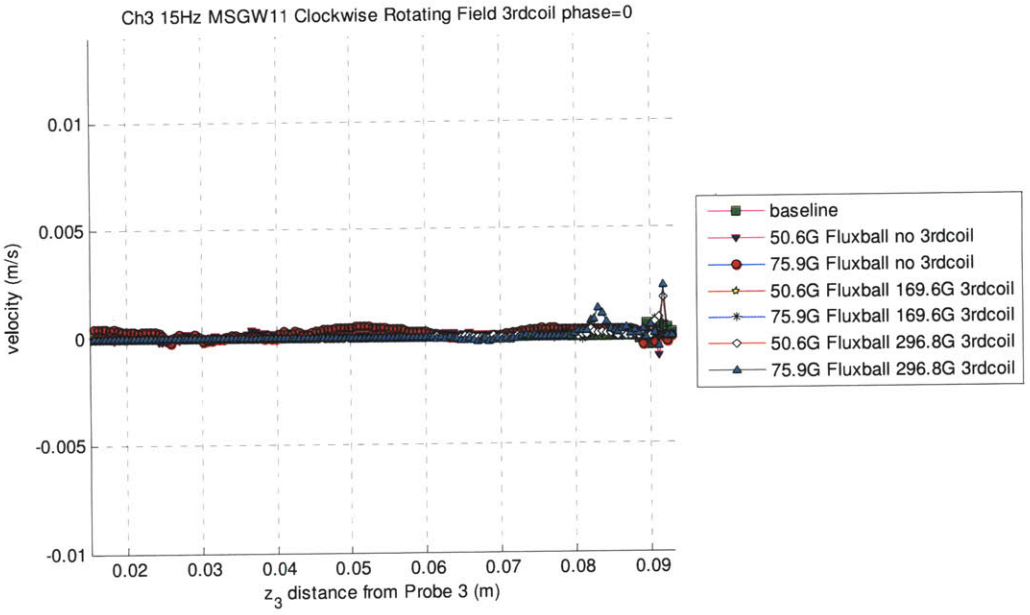
Ch3 15Hz MSGW11 Clockwise Rotating Field 3rdcoil phase=0
velocity (m/s)
0.01
0.005
0
-0.005
-0.01
0.02
0.03
0.04
0.05
0.06
0.07
0.08
0.09
z_3 distance from Probe 3 (m)
baseline
50.6G Fluxball no 3rdcoil
75.9G Fluxball no 3rdcoil
50.6G Fluxball 169.6G 3rdcoil
75.9G Fluxball 169.6G 3rdcoil
50.6G Fluxball 296.8G 3rdcoil
75.9G Fluxball 296.8G 3rdcoil

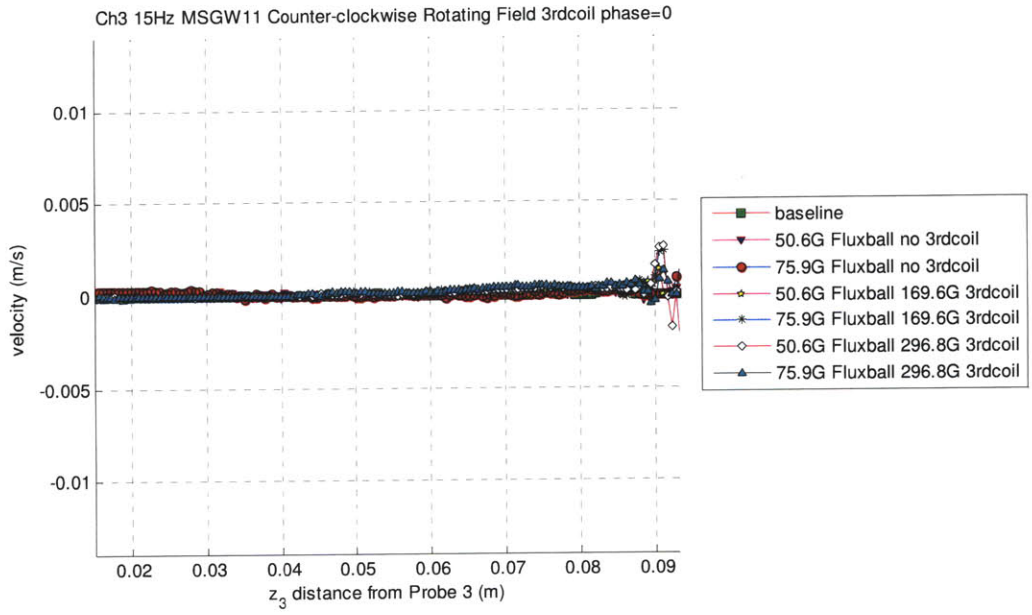
Ch3 15Hz MSGW11 Counter-clockwise Rotating Field 3rdcoil phase=0
velocity (m/s)
0.01
0.005
0
-0.005
-0.01
0.02
0.03
0.04
0.05
0.06
0.07
0.08
0.09
z_3 distance from Probe 3 (m)
baseline
50.6G Fluxball no 3rdcoil
75.9G Fluxball no 3rdcoil
50.6G Fluxball 169.6G 3rdcoil
75.9G Fluxball 169.6G 3rdcoil
50.6G Fluxball 296.8G 3rdcoil
75.9G Fluxball 296.8G 3rdcoil

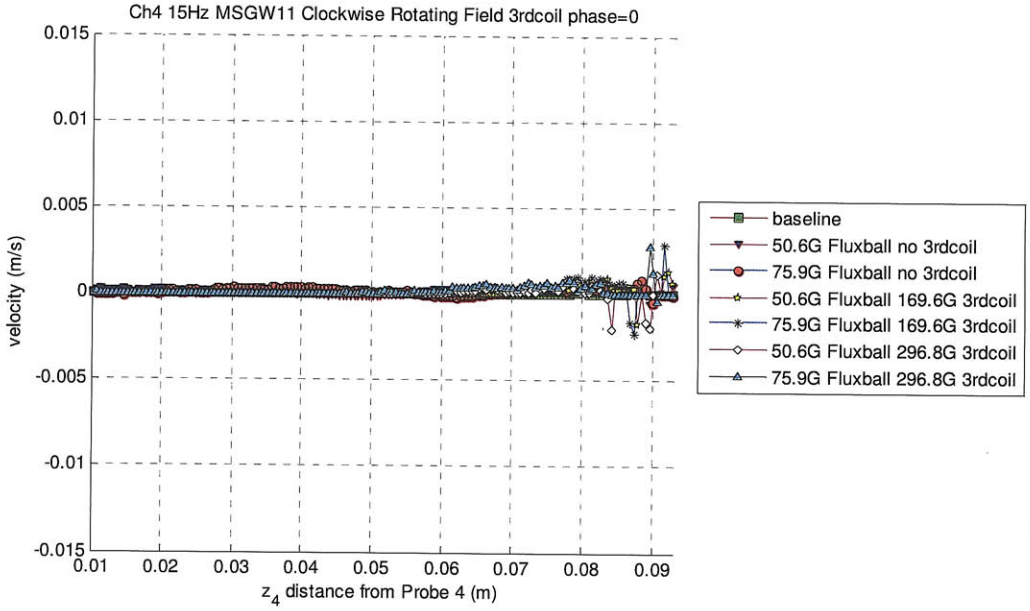
Ch4 15Hz MSGW11 Clockwise Rotating Field 3rdcoil phase=0
velocity (m/s)
0.015
0.01
0.005
0
-0.005
-0.01
-0.015
0.01
0.02
0.03
0.04
0.05
0.06
0.07
0.08
0.09
z4 distance from Probe 4 (m)
baseline
50.6G Fluxball no 3rdcoil
75.9G Fluxball no 3rdcoil
50.6G Fluxball 169.6G 3rdcoil
75.9G Fluxball 169.6G 3rdcoil
50.6G Fluxball 296.8G 3rdcoil
75.9G Fluxball 296.8G 3rdcoil

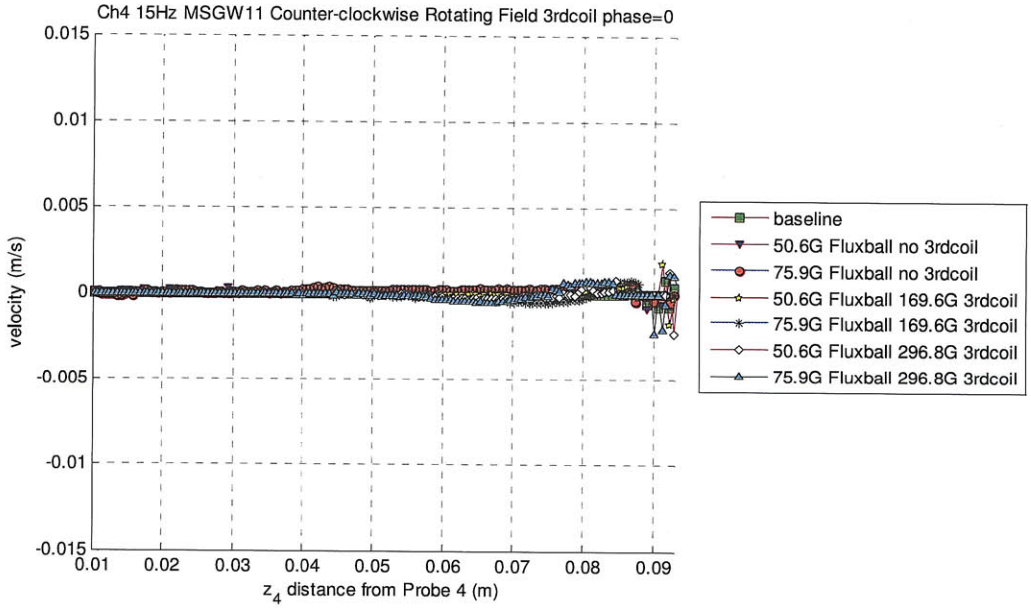
Ch4 15Hz MSGW11 Counter-clockwise Rotating Field 3rdcoil phase=0
velocity (m/s)
0.015
0.01
0.005
0
-0.005
-0.01
-0.015
0.01
0.02
0.03
0.04
0.05
0.06
0.07
0.08
0.09
z4 distance from Probe 4 (m)
baseline
50.6G Fluxball no 3rdcoil
75.9G Fluxball no 3rdcoil
50.6G Fluxball 169.6G 3rdcoil
75.9G Fluxball 169.6G 3rdcoil
50.6G Fluxball 296.8G 3rdcoil
75.9G Fluxball 296.8G 3rdcoil

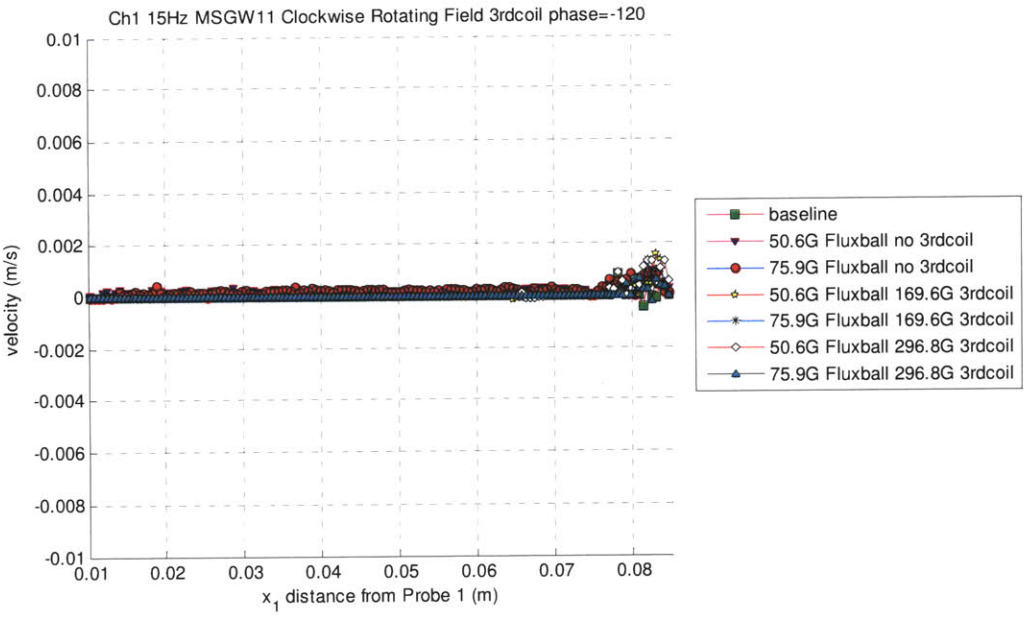
Ch1 15Hz MSGW11 Clockwise Rotating Field 3rdcoil phase=-120
velocity (m/s)
0.01
0.008
0.006
0.004
0.002
0
-0.002
-0.004
-0.006
-0.008
-0.01
0.01
0.02
0.03
0.04
0.05
0.06
0.07
0.08
x1 distance from Probe 1 (m)
baseline
50.6G Fluxball no 3rdcoil
75.9G Fluxball no 3rdcoil
50.6G Fluxball 169.6G 3rdcoil
75.9G Fluxball 169.6G 3rdcoil
50.6G Fluxball 296.8G 3rdcoil
75.9G Fluxball 296.8G 3rdcoil

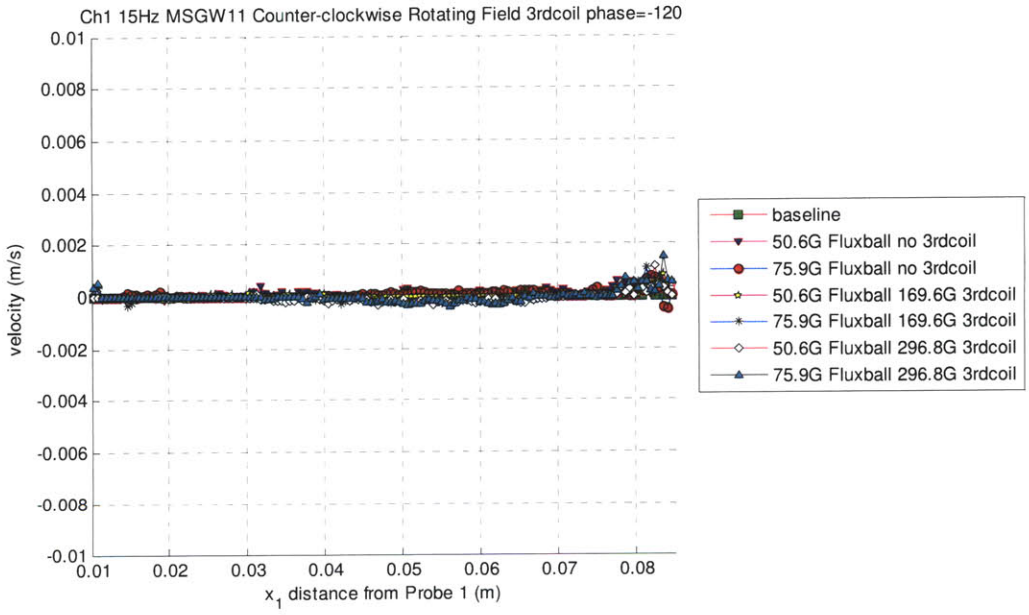
Ch1 15Hz MSGW11 Counter-clockwise Rotating Field 3rdcoil phase=-120
velocity (m/s)
0.01
0.008
0.006
0.004
0.002
0
-0.002
-0.004
-0.006
-0.008
-0.01
0.01
0.02
0.03
0.04
0.05
0.06
0.07
0.08
x1 distance from Probe 1 (m)
baseline
50.6G Fluxball no 3rdcoil
75.9G Fluxball no 3rdcoil
50.6G Fluxball 169.6G 3rdcoil
75.9G Fluxball 169.6G 3rdcoil
50.6G Fluxball 296.8G 3rdcoil
75.9G Fluxball 296.8G 3rdcoil

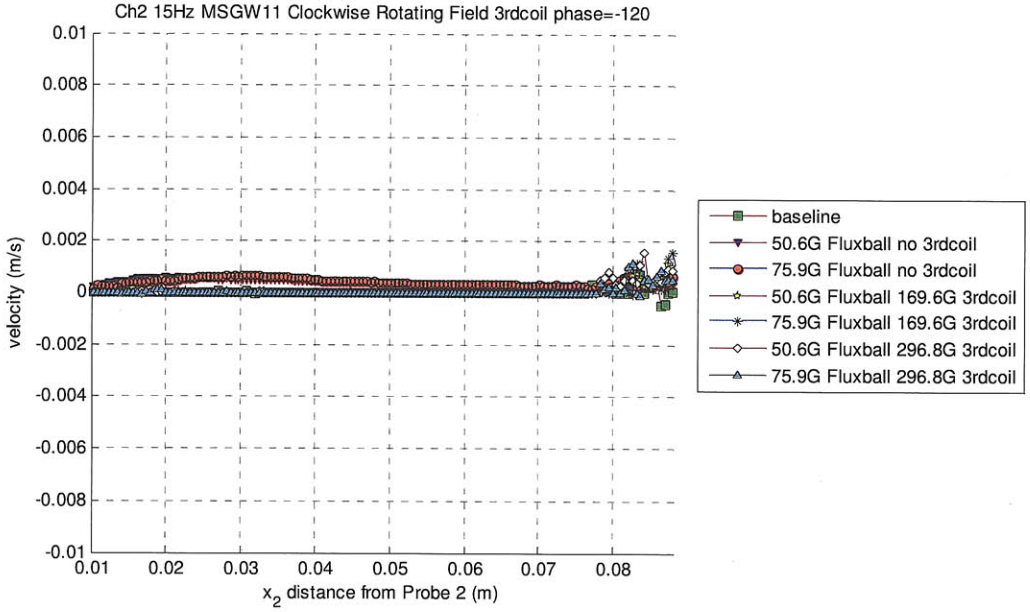
Ch2 15Hz MSGW11 Clockwise Rotating Field 3rdcoil phase=-120
velocity (m/s)
0.01
0.008
0.006
0.004
0.002
0
-0.002
-0.004
-0.006
-0.008
-0.01
0.01
0.02
0.03
0.04
0.05
0.06
0.07
0.08
x2 distance from Probe 2 (m)
baseline
50.6G Fluxball no 3rdcoil
75.9G Fluxball no 3rdcoil
50.6G Fluxball 169.6G 3rdcoil
75.9G Fluxball 169.6G 3rdcoil
50.6G Fluxball 296.8G 3rdcoil
75.9G Fluxball 296.8G 3rdcoil

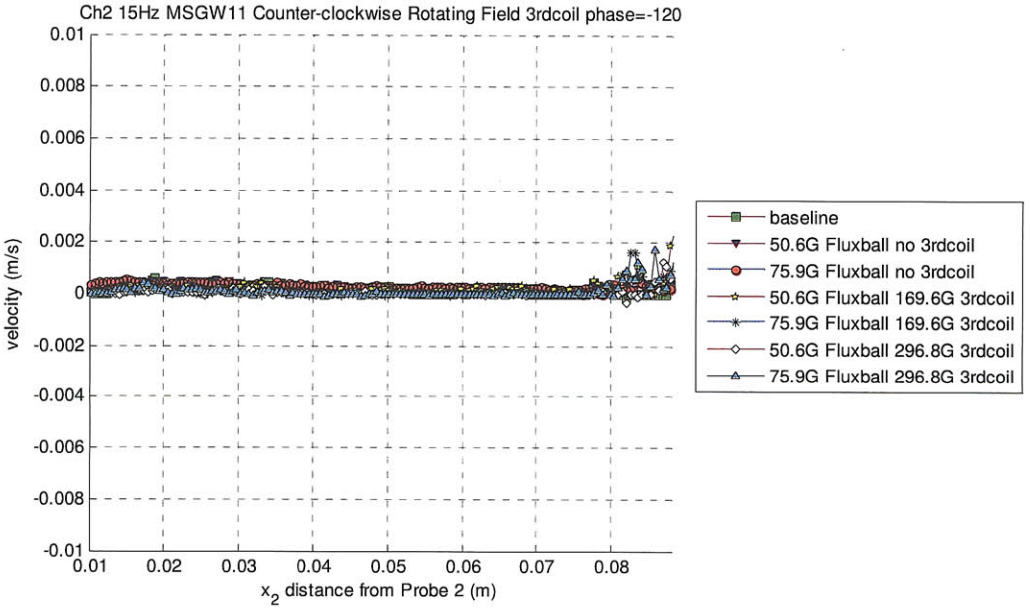
Ch2 15Hz MSGW11 Counter-clockwise Rotating Field 3rdcoil phase=-120
velocity (m/s)
0.01
0.008
0.006
0.004
0.002
0
-0.002
-0.004
-0.006
-0.008
-0.01
0.01
0.02
0.03
0.04
0.05
0.06
0.07
0.08
x2 distance from Probe 2 (m)
baseline
50.6G Fluxball no 3rdcoil
75.9G Fluxball no 3rdcoil
50.6G Fluxball 169.6G 3rdcoil
75.9G Fluxball 169.6G 3rdcoil
50.6G Fluxball 296.8G 3rdcoil
75.9G Fluxball 296.8G 3rdcoil

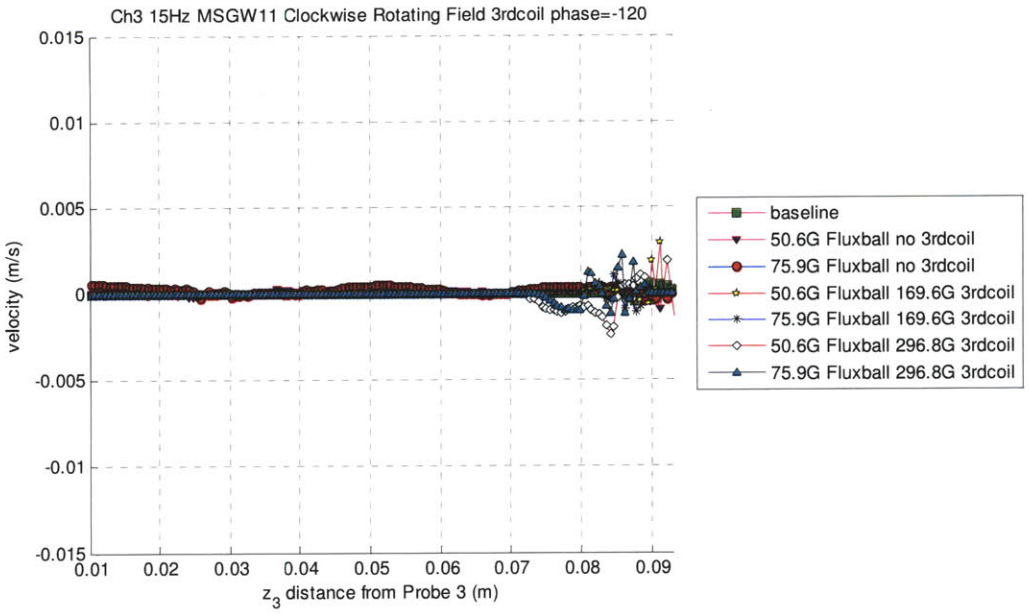
Ch3 15Hz MSGW11 Clockwise Rotating Field 3rdcoil phase=-120
velocity (m/s)
0.015
0.01
0.005
0
-0.005
-0.01
-0.015
0.01
0.02
0.03
0.04
0.05
0.06
0.07
0.08
0.09
z_3 distance from Probe 3 (m)
baseline
50.6G Fluxball no 3rdcoil
75.9G Fluxball no 3rdcoil
50.6G Fluxball 169.6G 3rdcoil
75.9G Fluxball 169.6G 3rdcoil
50.6G Fluxball 296.8G 3rdcoil
75.9G Fluxball 296.8G 3rdcoil

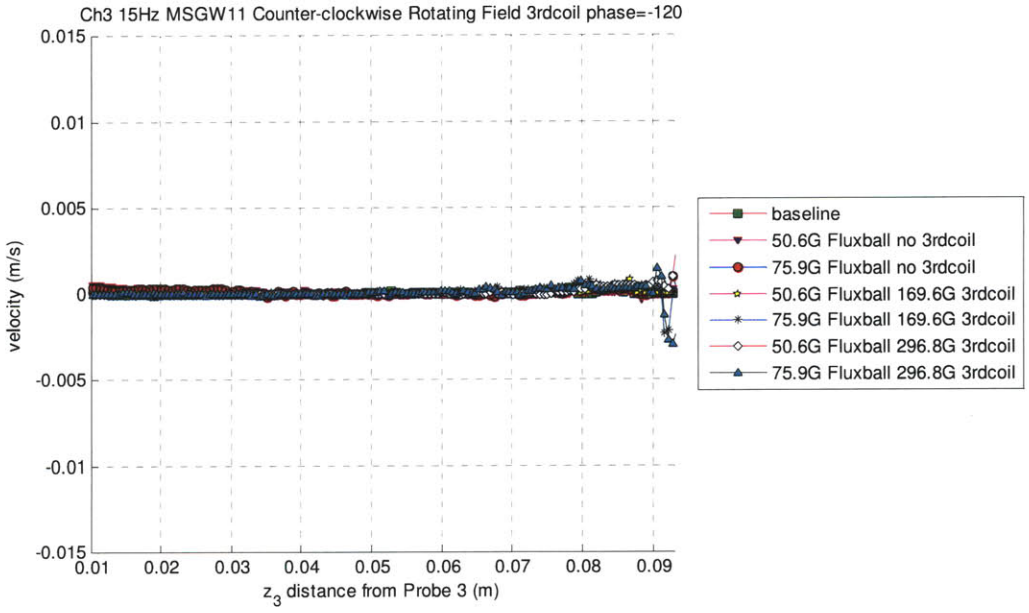
Ch3 15Hz MSGW11 Counter-clockwise Rotating Field 3rdcoil phase=-120
velocity (m/s)
0.015
0.01
0.005
0
-0.005
-0.01
-0.015
0.01
0.02
0.03
0.04
0.05
0.06
0.07
0.08
0.09
z_3 distance from Probe 3 (m)
baseline
50.6G Fluxball no 3rdcoil
75.9G Fluxball no 3rdcoil
50.6G Fluxball 169.6G 3rdcoil
75.9G Fluxball 169.6G 3rdcoil
50.6G Fluxball 296.8G 3rdcoil
75.9G Fluxball 296.8G 3rdcoil

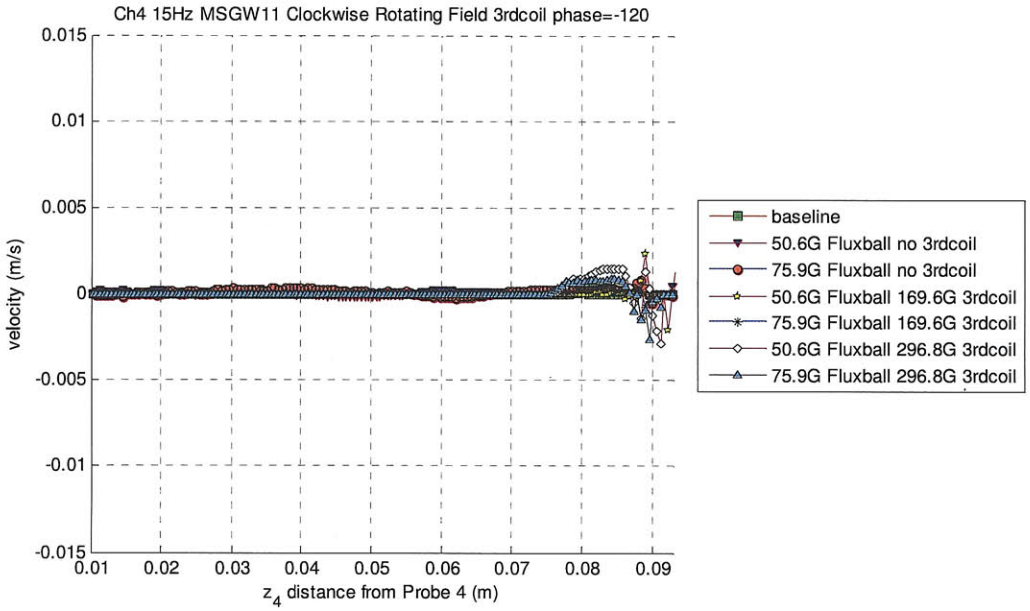
Ch4 15Hz MSGW11 Clockwise Rotating Field 3rdcoil phase=-120
velocity (m/s)
0.015
0.01
0.005
0
-0.005
-0.01
-0.015
0.01
0.02
0.03
0.04
0.05
0.06
0.07
0.08
0.09
z4 distance from Probe 4 (m)
baseline
50.6G Fluxball no 3rdcoil
75.9G Fluxball no 3rdcoil
50.6G Fluxball 169.6G 3rdcoil
75.9G Fluxball 169.6G 3rdcoil
50.6G Fluxball 296.8G 3rdcoil
75.9G Fluxball 296.8G 3rdcoil

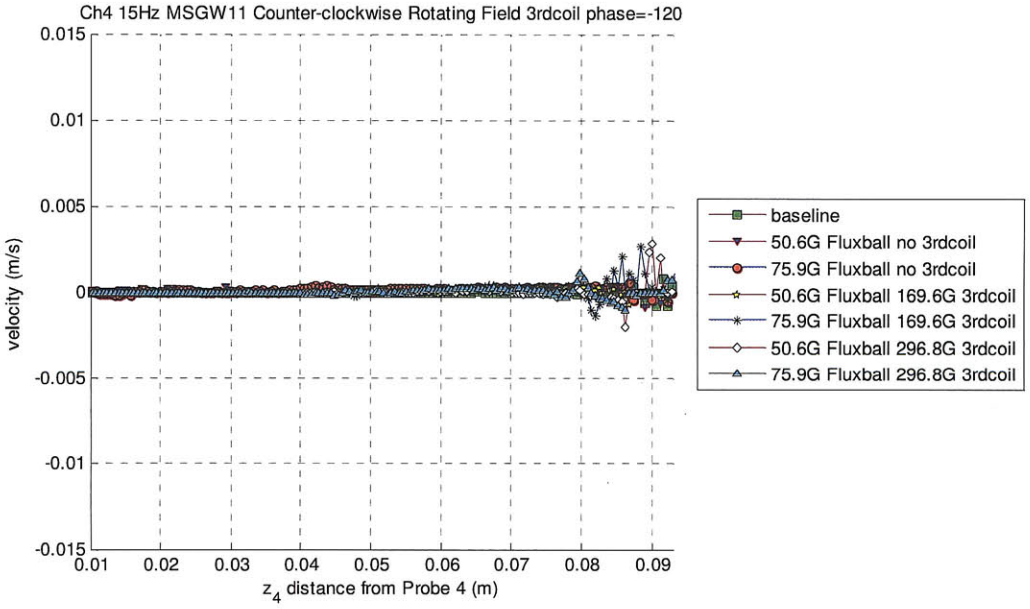
Ch4 15Hz MSGW11 Counter-clockwise Rotating Field 3rdcoil phase=-120
velocity (m/s)
0.015
0.01
0.005
0
-0.005
-0.01
-0.015
0.01
0.02
0.03
0.04
0.05
0.06
0.07
0.08
0.09
z4 distance from Probe 4 (m)
baseline
50.6G Fluxball no 3rdcoil
75.9G Fluxball no 3rdcoil
50.6G Fluxball 169.6G 3rdcoil
75.9G Fluxball 169.6G 3rdcoil
50.6G Fluxball 296.8G 3rdcoil
75.9G Fluxball 296.8G 3rdcoil

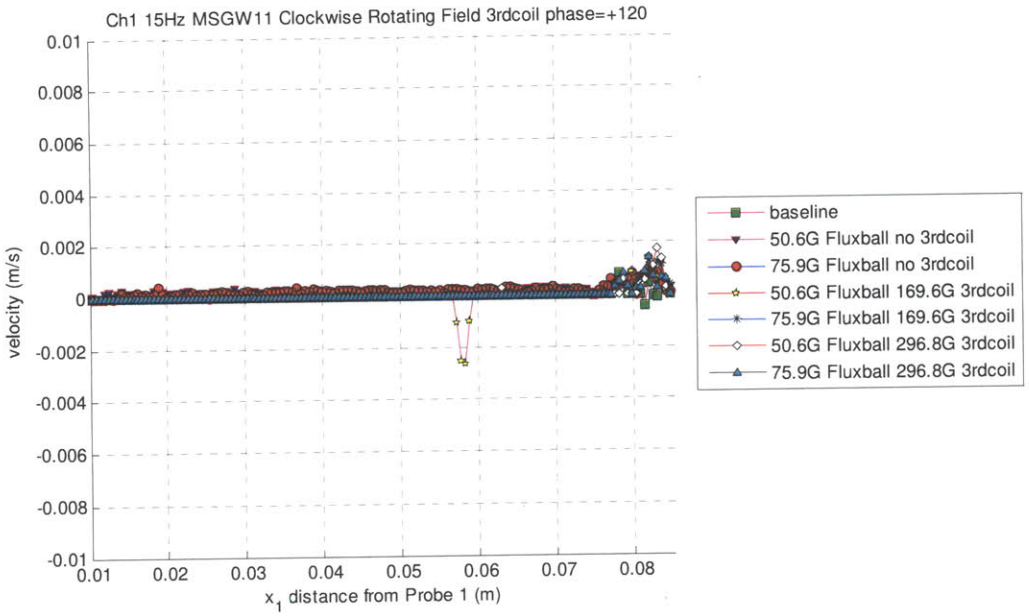
Ch1 15Hz MSGW11 Clockwise Rotating Field 3rdcoil phase=+120
velocity (m/s)
0.01
0.008
0.006
0.004
0.002
0
-0.002
-0.004
-0.006
-0.008
-0.01
0.01
0.02
0.03
0.04
0.05
0.06
0.07
0.08
x1 distance from Probe 1 (m)
baseline
50.6G Fluxball no 3rdcoil
75.9G Fluxball no 3rdcoil
50.6G Fluxball 169.6G 3rdcoil
75.9G Fluxball 169.6G 3rdcoil
50.6G Fluxball 296.8G 3rdcoil
75.9G Fluxball 296.8G 3rdcoil

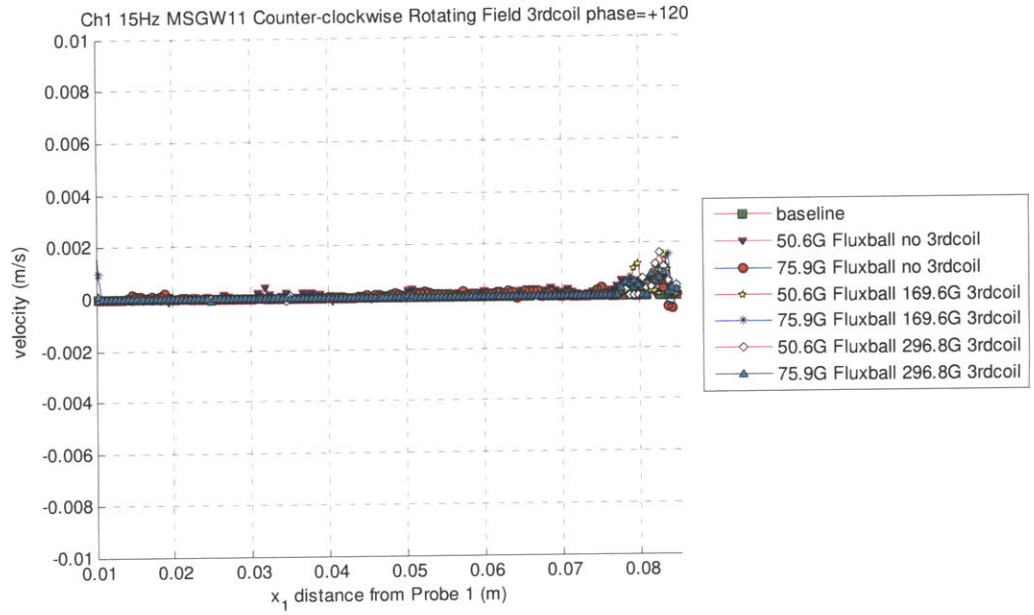
Ch1 15Hz MSGW11 Counter-clockwise Rotating Field 3rdcoil phase=+120
velocity (m/s)
0.01
0.008
0.006
0.004
0.002
0
-0.002
-0.004
-0.006
-0.008
-0.01
0.01
0.02
0.03
0.04
0.05
0.06
0.07
0.08
x1 distance from Probe 1 (m)
baseline
50.6G Fluxball no 3rdcoil
75.9G Fluxball no 3rdcoil
50.6G Fluxball 169.6G 3rdcoil
75.9G Fluxball 169.6G 3rdcoil
50.6G Fluxball 296.8G 3rdcoil
75.9G Fluxball 296.8G 3rdcoil

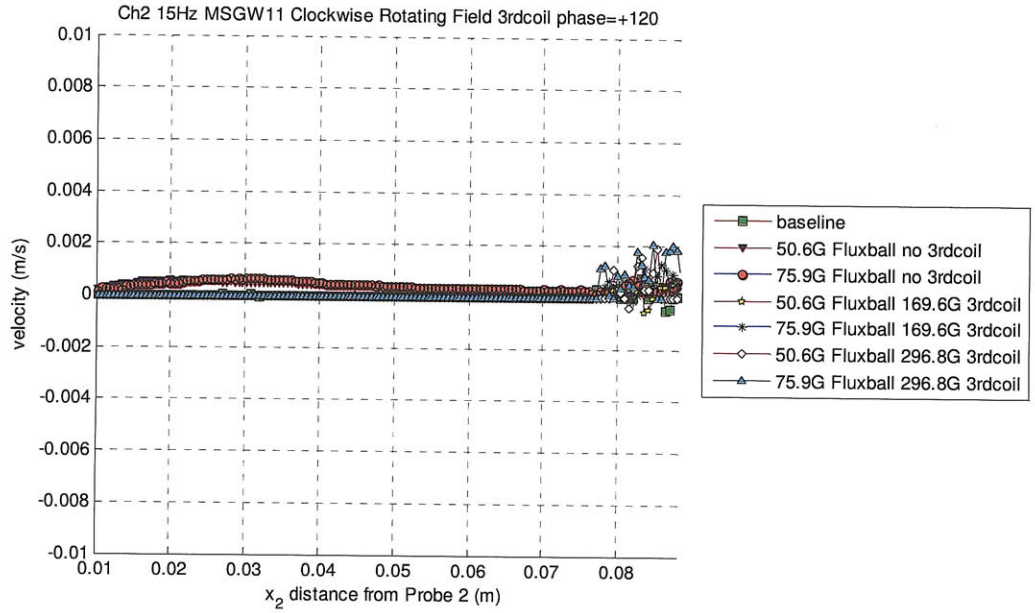
Ch2 15Hz MSGW11 Clockwise Rotating Field 3rdcoil phase=+120
velocity (m/s)
0.01
0.008
0.006
0.004
0.002
0
-0.002
-0.004
-0.006
-0.008
-0.01
0.01
0.02
0.03
0.04
0.05
0.06
0.07
0.08
x2 distance from Probe 2 (m)
baseline
50.6G Fluxball no 3rdcoil
75.9G Fluxball no 3rdcoil
50.6G Fluxball 169.6G 3rdcoil
75.9G Fluxball 169.6G 3rdcoil
50.6G Fluxball 296.8G 3rdcoil
75.9G Fluxball 296.8G 3rdcoil

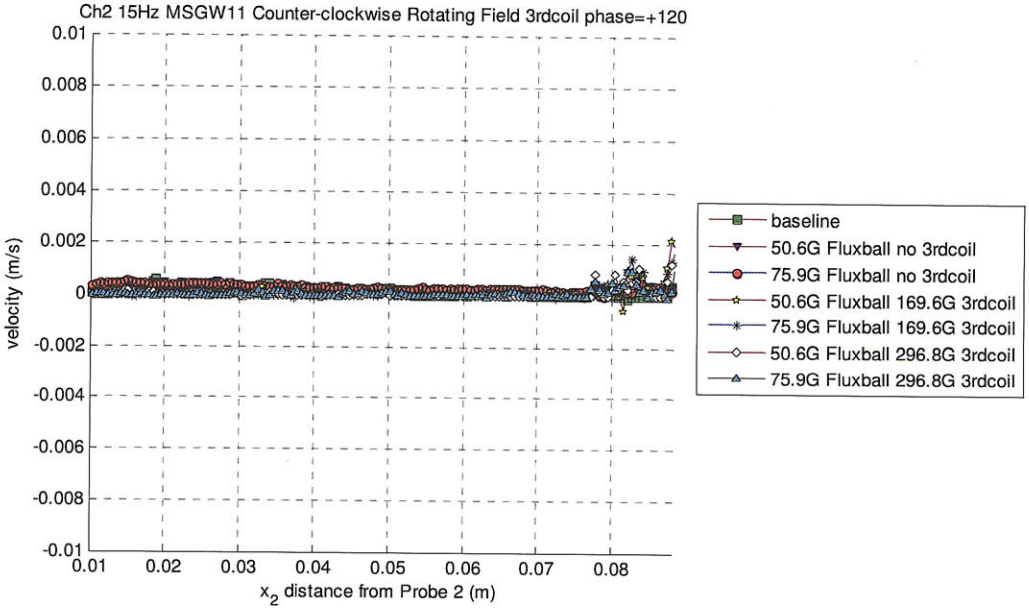
Ch2 15Hz MSGW11 Counter-clockwise Rotating Field 3rdcoil phase=+120
velocity (m/s)
0.01
0.008
0.006
0.004
0.002
0
-0.002
-0.004
-0.006
-0.008
-0.01
0.01
0.02
0.03
0.04
0.05
0.06
0.07
0.08
x2 distance from Probe 2 (m)
baseline
50.6G Fluxball no 3rdcoil
75.9G Fluxball no 3rdcoil
50.6G Fluxball 169.6G 3rdcoil
75.9G Fluxball 169.6G 3rdcoil
50.6G Fluxball 296.8G 3rdcoil
75.9G Fluxball 296.8G 3rdcoil

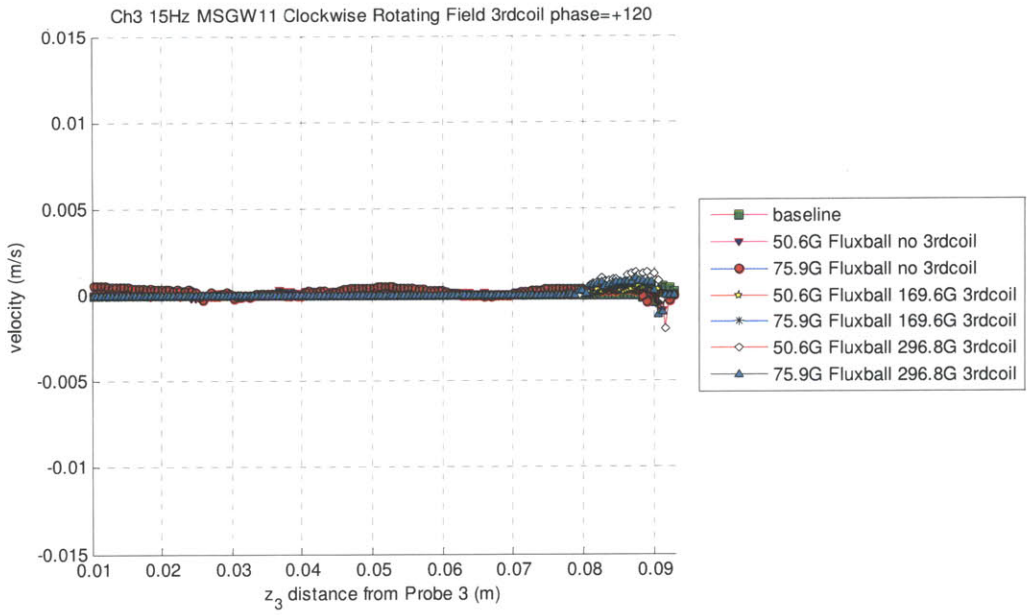
Ch3 15Hz MSGW11 Clockwise Rotating Field 3rdcoil phase=+120
velocity (m/s)
0.015
0.01
0.005
0
-0.005
-0.01
-0.015
0.01
0.02
0.03
0.04
0.05
0.06
0.07
0.08
0.09
z_3 distance from Probe 3 (m)
baseline
50.6G Fluxball no 3rdcoil
75.9G Fluxball no 3rdcoil
50.6G Fluxball 169.6G 3rdcoil
75.9G Fluxball 169.6G 3rdcoil
50.6G Fluxball 296.8G 3rdcoil
75.9G Fluxball 296.8G 3rdcoil

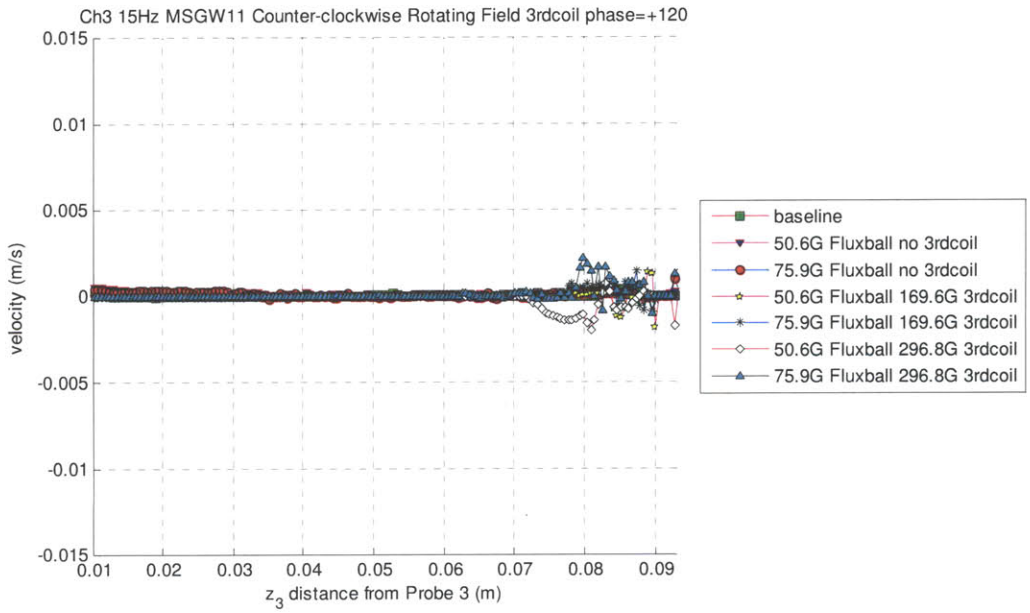
Ch3 15Hz MSGW11 Counter-clockwise Rotating Field 3rdcoil phase=+120
velocity (m/s)
0.015
0.01
0.005
0
-0.005
-0.01
-0.015
0.01
0.02
0.03
0.04
0.05
0.06
0.07
0.08
0.09
z_3 distance from Probe 3 (m)
baseline
50.6G Fluxball no 3rdcoil
75.9G Fluxball no 3rdcoil
50.6G Fluxball 169.6G 3rdcoil
75.9G Fluxball 169.6G 3rdcoil
50.6G Fluxball 296.8G 3rdcoil
75.9G Fluxball 296.8G 3rdcoil

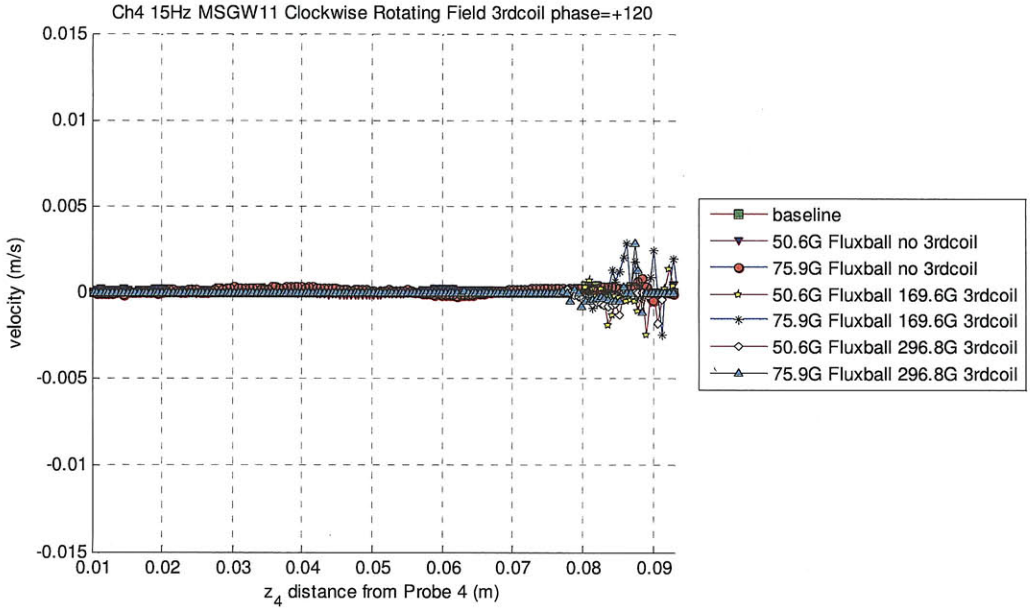
Ch4 15Hz MSGW11 Clockwise Rotating Field 3rdcoil phase=+120
velocity (m/s)
0.015
0.01
0.005
0
-0.005
-0.01
-0.015
0.01
0.02
0.03
0.04
0.05
0.06
0.07
0.08
0.09
z4 distance from Probe 4 (m)
baseline
50.6G Fluxball no 3rdcoil
75.9G Fluxball no 3rdcoil
50.6G Fluxball 169.6G 3rdcoil
75.9G Fluxball 169.6G 3rdcoil
50.6G Fluxball 296.8G 3rdcoil
75.9G Fluxball 296.8G 3rdcoil

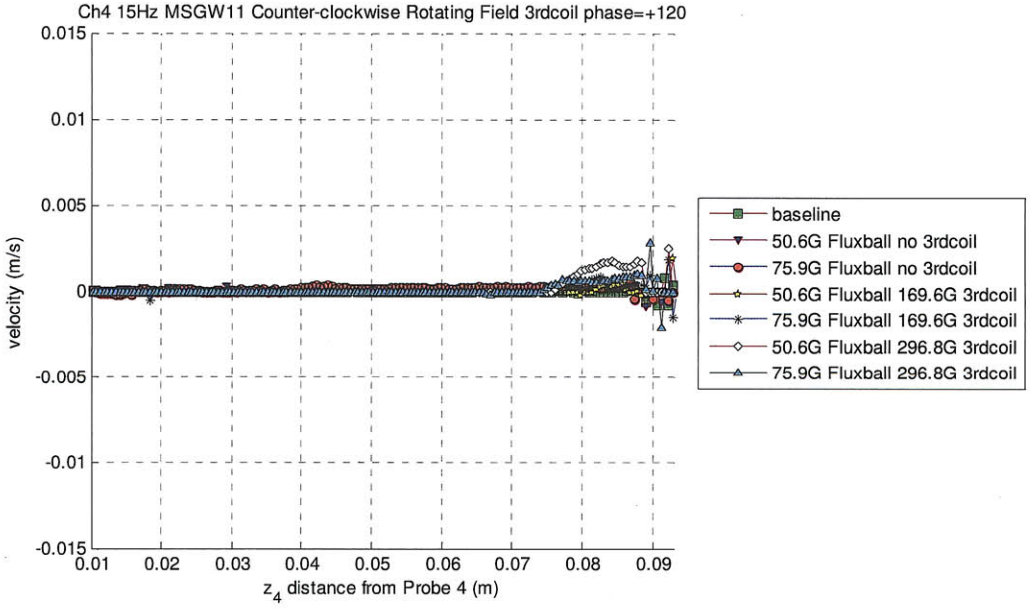
Ch4 15Hz MSGW11 Counter-clockwise Rotating Field 3rdcoil phase=+120
velocity (m/s)
0.015
0.01
0.005
0
-0.005
-0.01
-0.015
0.01
0.02
0.03
0.04
0.05
0.06
0.07
0.08
0.09
z4 distance from Probe 4 (m)
baseline
50.6G Fluxball no 3rdcoil
75.9G Fluxball no 3rdcoil
50.6G Fluxball 169.6G 3rdcoil
75.9G Fluxball 169.6G 3rdcoil
50.6G Fluxball 296.8G 3rdcoil
75.9G Fluxball 296.8G 3rdcoil

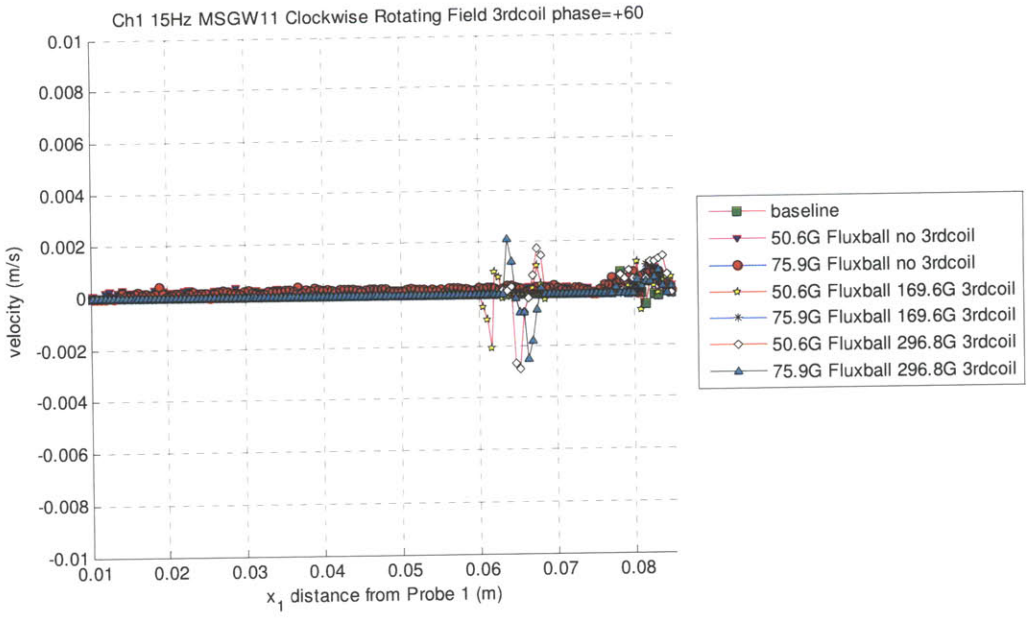
Ch1 15Hz MSGW11 Clockwise Rotating Field 3rdcoil phase=+60
velocity (m/s)
0.01
0.008
0.006
0.004
0.002
0
-0.002
-0.004
-0.006
-0.008
-0.01
0.01
0.02
0.03
0.04
0.05
0.06
0.07
0.08
x1 distance from Probe 1 (m)
baseline
50.6G Fluxball no 3rdcoil
75.9G Fluxball no 3rdcoil
50.6G Fluxball 169.6G 3rdcoil
75.9G Fluxball 169.6G 3rdcoil
50.6G Fluxball 296.8G 3rdcoil
75.9G Fluxball 296.8G 3rdcoil

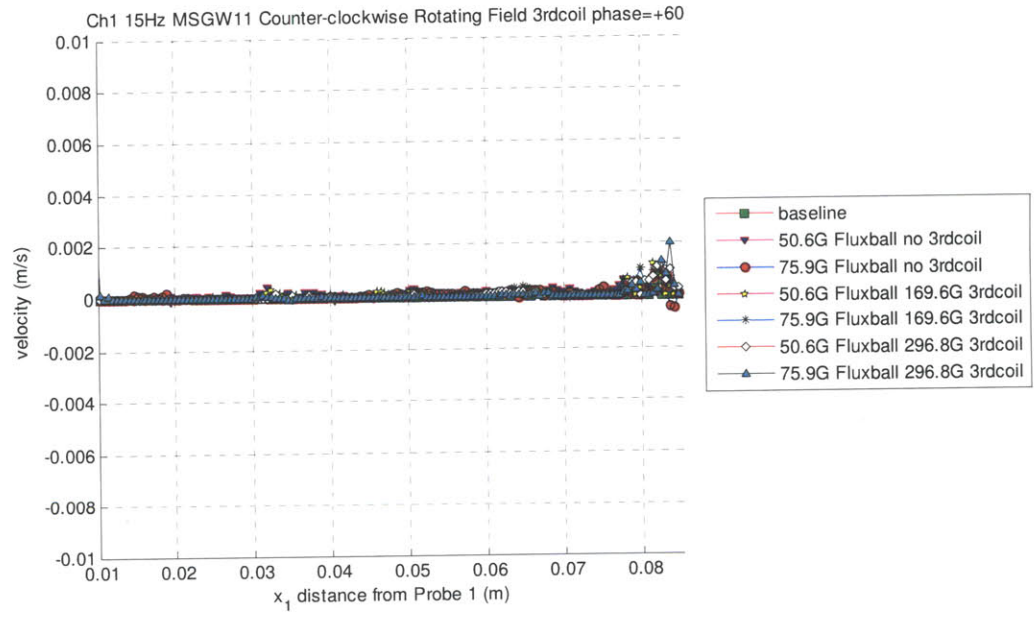
Ch1 15Hz MSGW11 Counter-clockwise Rotating Field 3rdcoil phase=+60
velocity (m/s)
0.01
0.008
0.006
0.004
0.002
0
-0.002
-0.004
-0.006
-0.008
-0.01
0.01
0.02
0.03
0.04
0.05
0.06
0.07
0.08
x1 distance from Probe 1 (m)
baseline
50.6G Fluxball no 3rdcoil
75.9G Fluxball no 3rdcoil
50.6G Fluxball 169.6G 3rdcoil
75.9G Fluxball 169.6G 3rdcoil
50.6G Fluxball 296.8G 3rdcoil
75.9G Fluxball 296.8G 3rdcoil

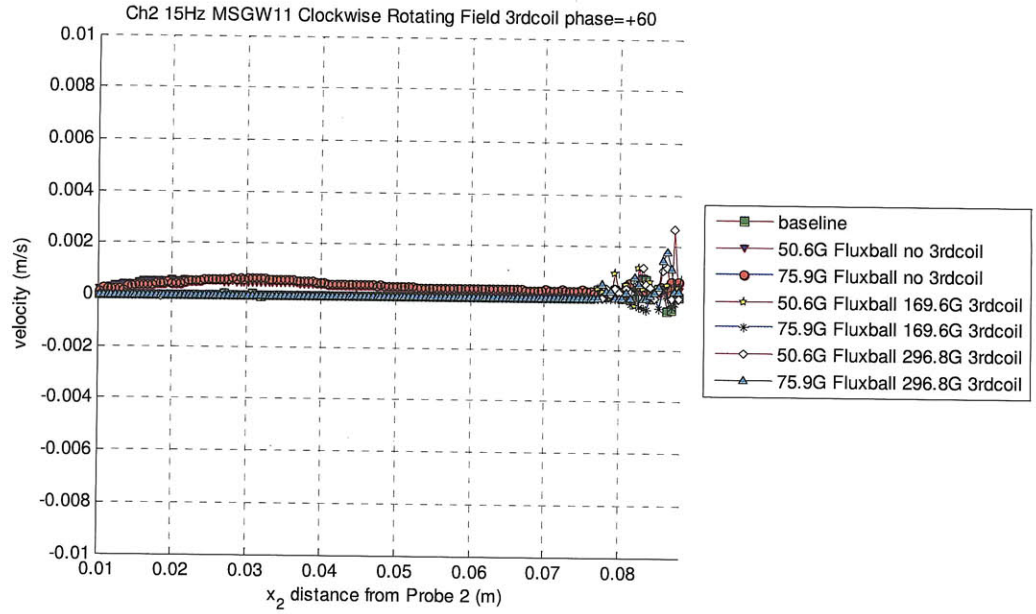
Ch2 15Hz MSGW11 Clockwise Rotating Field 3rdcoil phase=+60
velocity (m/s)
0.01
0.008
0.006
0.004
0.002
0
-0.002
-0.004
-0.006
-0.008
-0.01
0.01 0.02 0.03 0.04 0.05 0.06 0.07 0.08
x2 distance from Probe 2 (m)
baseline
50.6G Fluxball no 3rdcoil
75.9G Fluxball no 3rdcoil
50.6G Fluxball 169.6G 3rdcoil
75.9G Fluxball 169.6G 3rdcoil
50.6G Fluxball 296.8G 3rdcoil
75.9G Fluxball 296.8G 3rdcoil

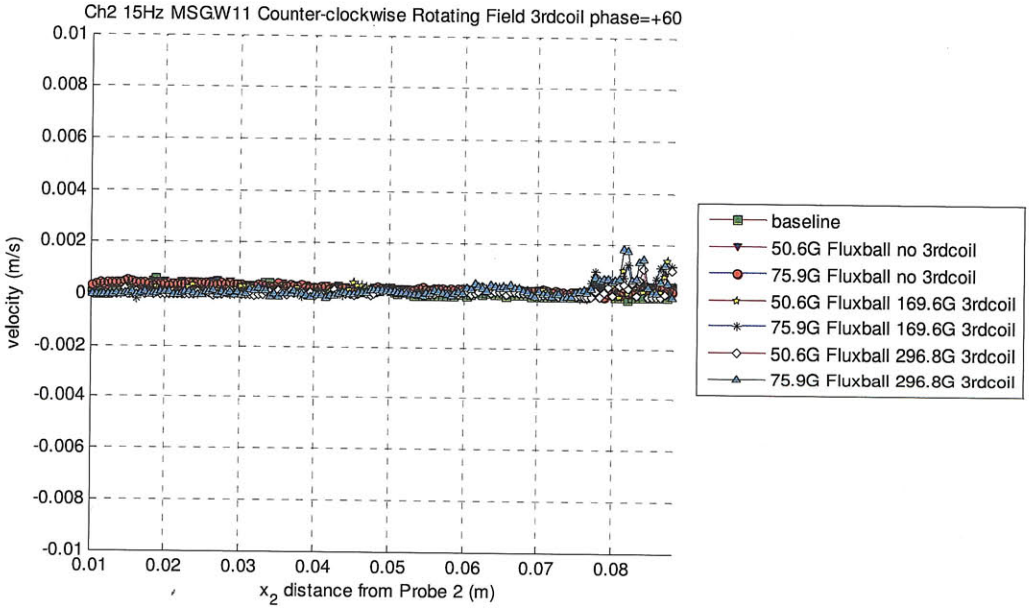
Ch2 15Hz MSGW11 Counter-clockwise Rotating Field 3rdcoil phase=+60
velocity (m/s)
0.01
0.008
0.006
0.004
0.002
0
-0.002
-0.004
-0.006
-0.008
-0.01
0.01 0.02 0.03 0.04 0.05 0.06 0.07 0.08
x2 distance from Probe 2 (m)
baseline
50.6G Fluxball no 3rdcoil
75.9G Fluxball no 3rdcoil
50.6G Fluxball 169.6G 3rdcoil
75.9G Fluxball 169.6G 3rdcoil
50.6G Fluxball 296.8G 3rdcoil
75.9G Fluxball 296.8G 3rdcoil

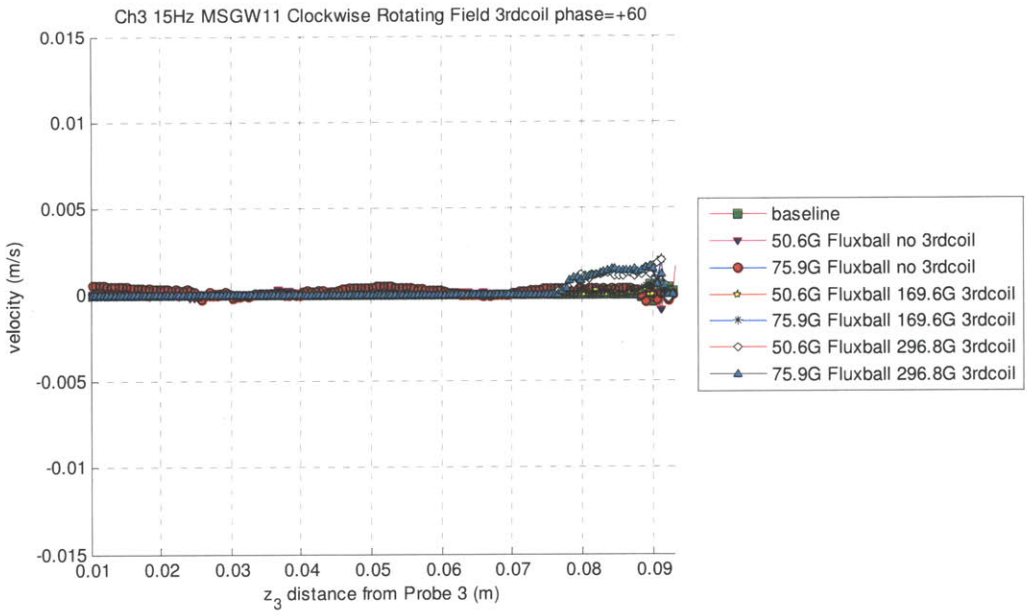
Ch3 15Hz MSGW11 Clockwise Rotating Field 3rdcoil phase=+60
velocity (m/s)
0.015
0.01
0.005
0
-0.005
-0.01
-0.015
0.01
0.02
0.03
0.04
0.05
0.06
0.07
0.08
0.09
z_3 distance from Probe 3 (m)
baseline
50.6G Fluxball no 3rdcoil
75.9G Fluxball no 3rdcoil
50.6G Fluxball 169.6G 3rdcoil
75.9G Fluxball 169.6G 3rdcoil
50.6G Fluxball 296.8G 3rdcoil
75.9G Fluxball 296.8G 3rdcoil

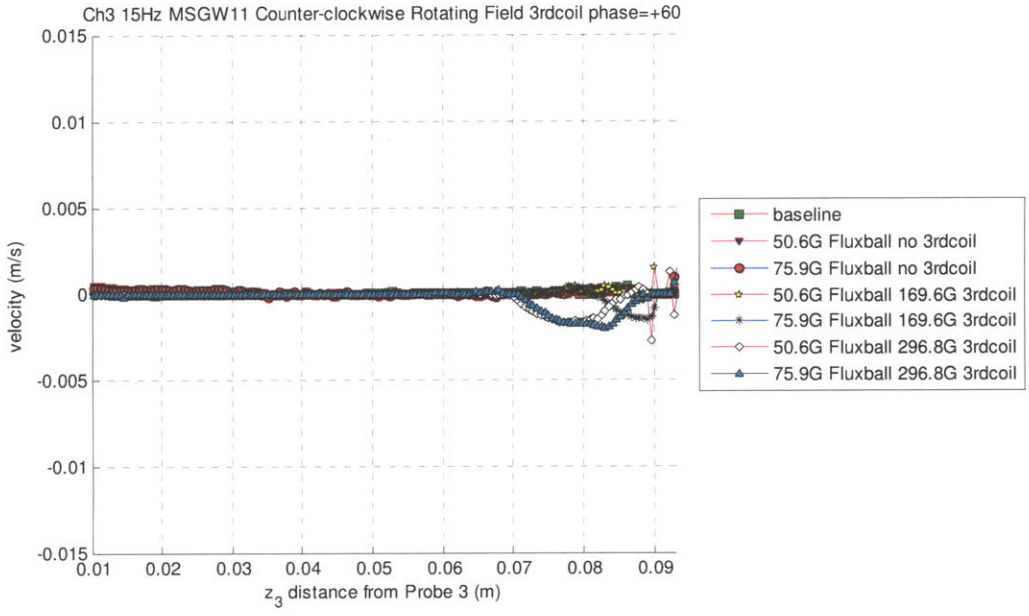
Ch3 15Hz MSGW11 Counter-clockwise Rotating Field 3rdcoil phase=+60
velocity (m/s)
0.015
0.01
0.005
0
-0.005
-0.01
-0.015
0.01
0.02
0.03
0.04
0.05
0.06
0.07
0.08
0.09
z_3 distance from Probe 3 (m)
baseline
50.6G Fluxball no 3rdcoil
75.9G Fluxball no 3rdcoil
50.6G Fluxball 169.6G 3rdcoil
75.9G Fluxball 169.6G 3rdcoil
50.6G Fluxball 296.8G 3rdcoil
75.9G Fluxball 296.8G 3rdcoil

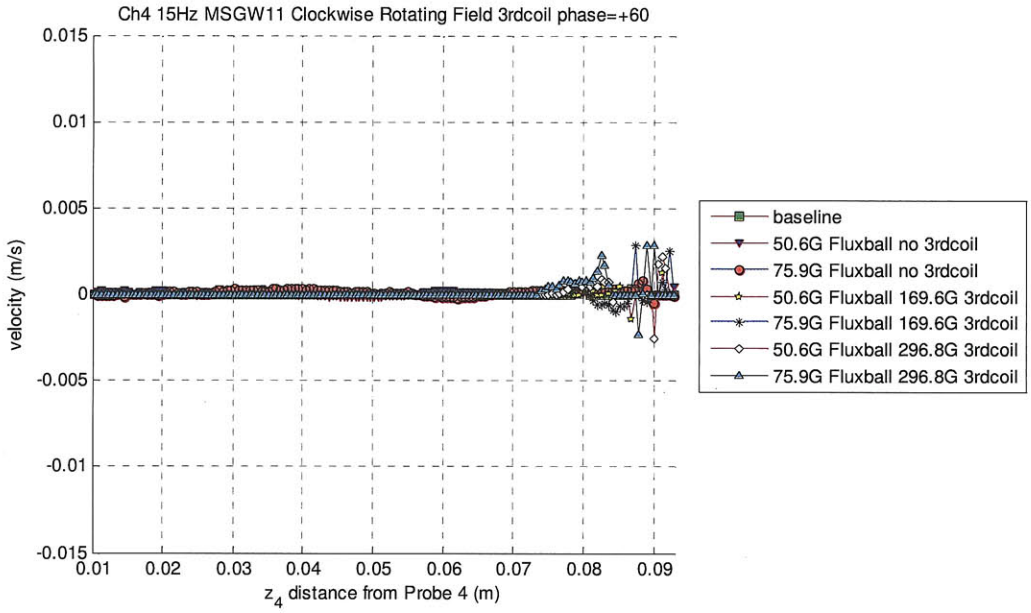
Ch4 15Hz MSGW11 Clockwise Rotating Field 3rdcoil phase=+60
velocity (m/s)
0.015
0.01
0.005
0
-0.005
-0.01
-0.015
0.01
0.02
0.03
0.04
0.05
0.06
0.07
0.08
0.09
z4 distance from Probe 4 (m)
baseline
50.6G Fluxball no 3rdcoil
75.9G Fluxball no 3rdcoil
50.6G Fluxball 169.6G 3rdcoil
75.9G Fluxball 169.6G 3rdcoil
50.6G Fluxball 296.8G 3rdcoil
75.9G Fluxball 296.8G 3rdcoil

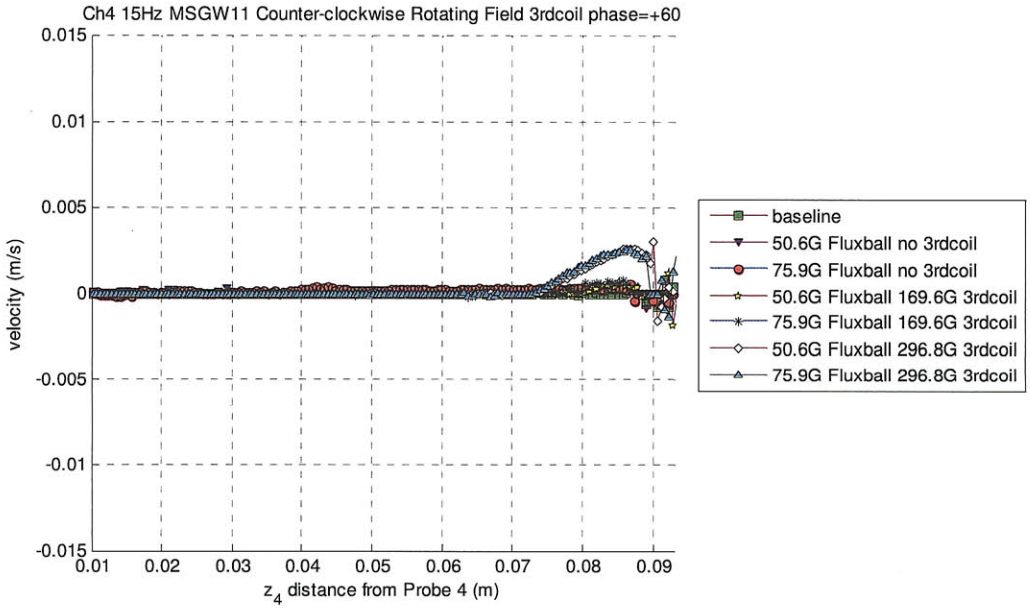
Ch4 15Hz MSGW11 Counter-clockwise Rotating Field 3rdcoil phase=+60
velocity (m/s)
0.015
0.01
0.005
0
-0.005
-0.01
-0.015
0.01
0.02
0.03
0.04
0.05
0.06
0.07
0.08
0.09
z4 distance from Probe 4 (m)
baseline
50.6G Fluxball no 3rdcoil
75.9G Fluxball no 3rdcoil
50.6G Fluxball 169.6G 3rdcoil
75.9G Fluxball 169.6G 3rdcoil
50.6G Fluxball 296.8G 3rdcoil
75.9G Fluxball 296.8G 3rdcoil

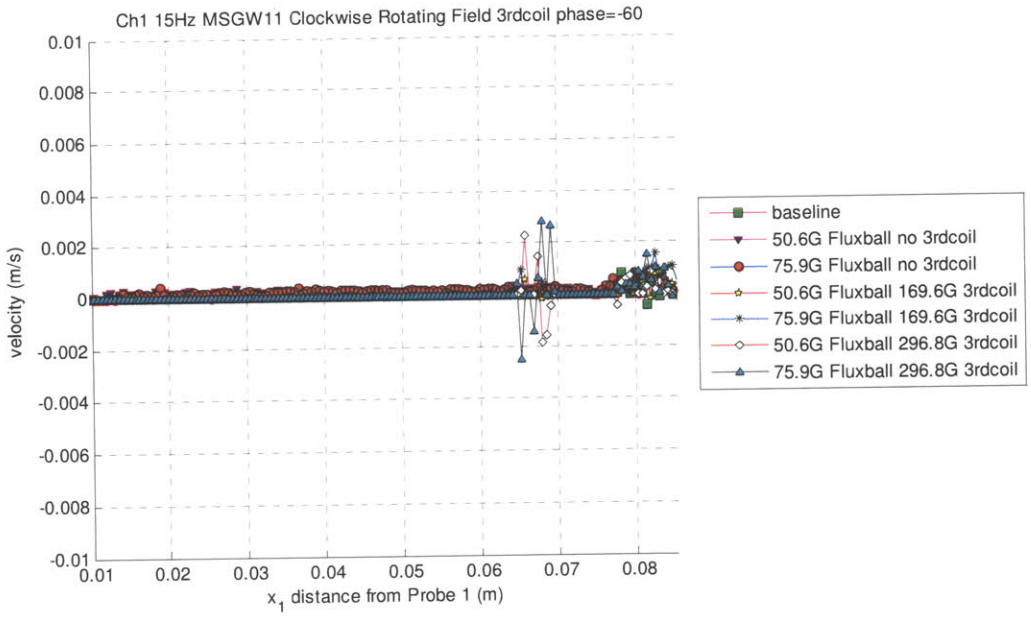
Ch1 15Hz MSGW11 Clockwise Rotating Field 3rdcoil phase=-60
velocity (m/s)
0.01
0.008
0.006
0.004
0.002
0
-0.002
-0.004
-0.006
-0.008
-0.01
0.01
0.02
0.03
0.04
0.05
0.06
0.07
0.08
x1 distance from Probe 1 (m)
baseline
50.6G Fluxball no 3rdcoil
75.9G Fluxball no 3rdcoil
50.6G Fluxball 169.6G 3rdcoil
75.9G Fluxball 169.6G 3rdcoil
50.6G Fluxball 296.8G 3rdcoil
75.9G Fluxball 296.8G 3rdcoil

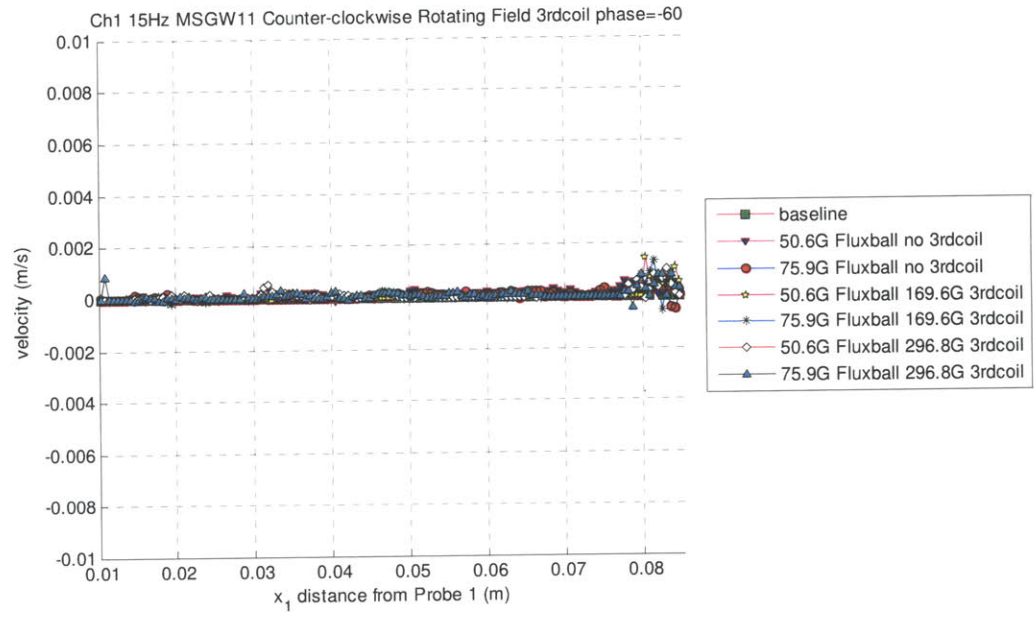
Ch1 15Hz MSGW11 Counter-clockwise Rotating Field 3rdcoil phase=-60
velocity (m/s)
0.01
0.008
0.006
0.004
0.002
0
-0.002
-0.004
-0.006
-0.008
-0.01
0.01
0.02
0.03
0.04
0.05
0.06
0.07
0.08
x1 distance from Probe 1 (m)
baseline
50.6G Fluxball no 3rdcoil
75.9G Fluxball no 3rdcoil
50.6G Fluxball 169.6G 3rdcoil
75.9G Fluxball 169.6G 3rdcoil
50.6G Fluxball 296.8G 3rdcoil
75.9G Fluxball 296.8G 3rdcoil

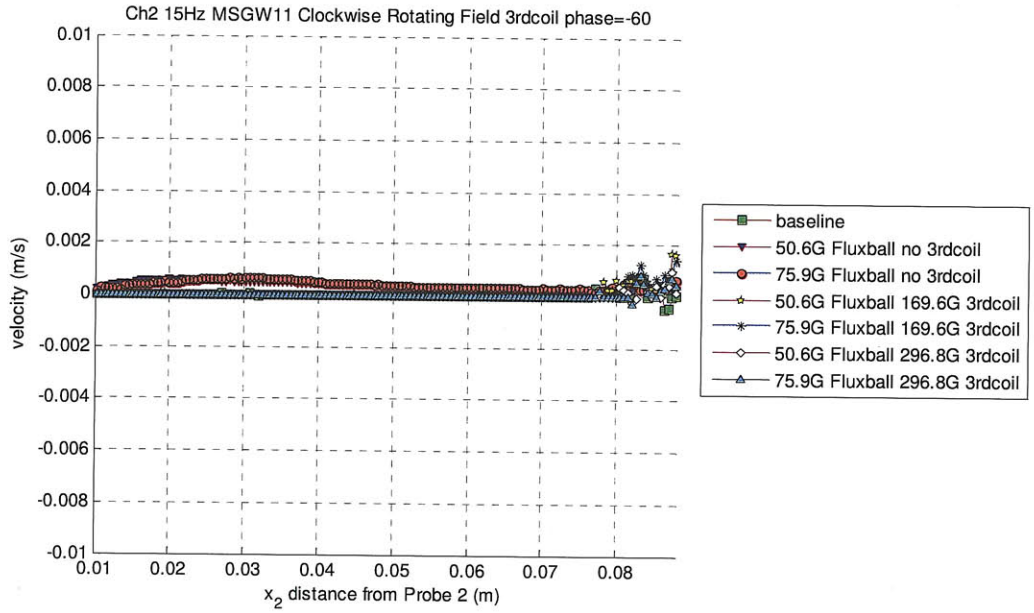
Ch2 15Hz MSGW11 Clockwise Rotating Field 3rdcoil phase=-60
velocity (m/s)
0.01
0.008
0.006
0.004
0.002
0
-0.002
-0.004
-0.006
-0.008
-0.01
0.01
0.02
0.03
0.04
0.05
0.06
0.07
0.08
x2 distance from Probe 2 (m)
baseline
50.6G Fluxball no 3rdcoil
75.9G Fluxball no 3rdcoil
50.6G Fluxball 169.6G 3rdcoil
75.9G Fluxball 169.6G 3rdcoil
50.6G Fluxball 296.8G 3rdcoil
75.9G Fluxball 296.8G 3rdcoil

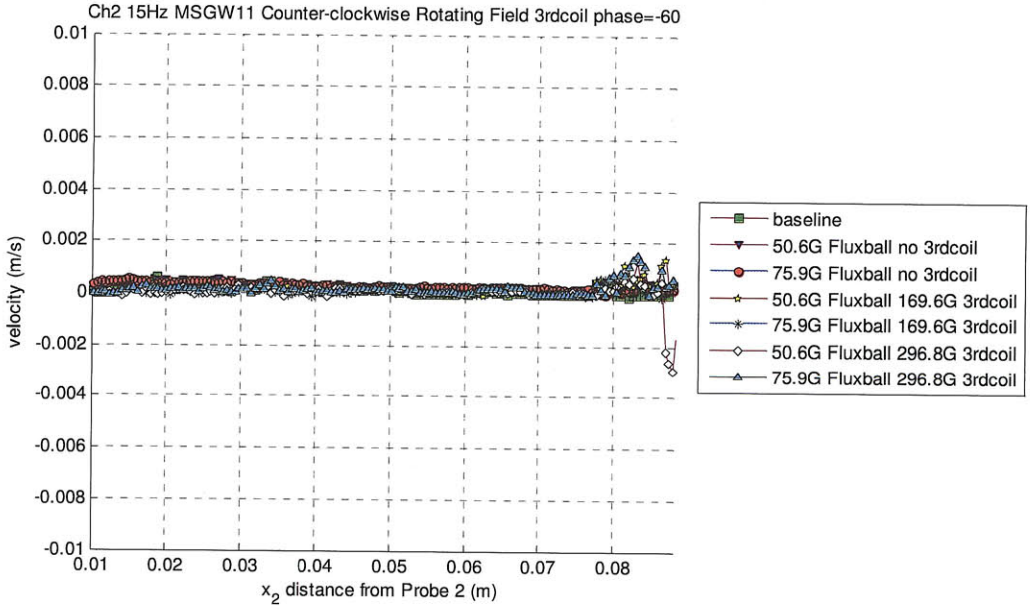
Ch2 15Hz MSGW11 Counter-clockwise Rotating Field 3rdcoil phase=-60
velocity (m/s)
0.01
0.008
0.006
0.004
0.002
0
-0.002
-0.004
-0.006
-0.008
-0.01
0.01
0.02
0.03
0.04
0.05
0.06
0.07
0.08
x2 distance from Probe 2 (m)
baseline
50.6G Fluxball no 3rdcoil
75.9G Fluxball no 3rdcoil
50.6G Fluxball 169.6G 3rdcoil
75.9G Fluxball 169.6G 3rdcoil
50.6G Fluxball 296.8G 3rdcoil
75.9G Fluxball 296.8G 3rdcoil

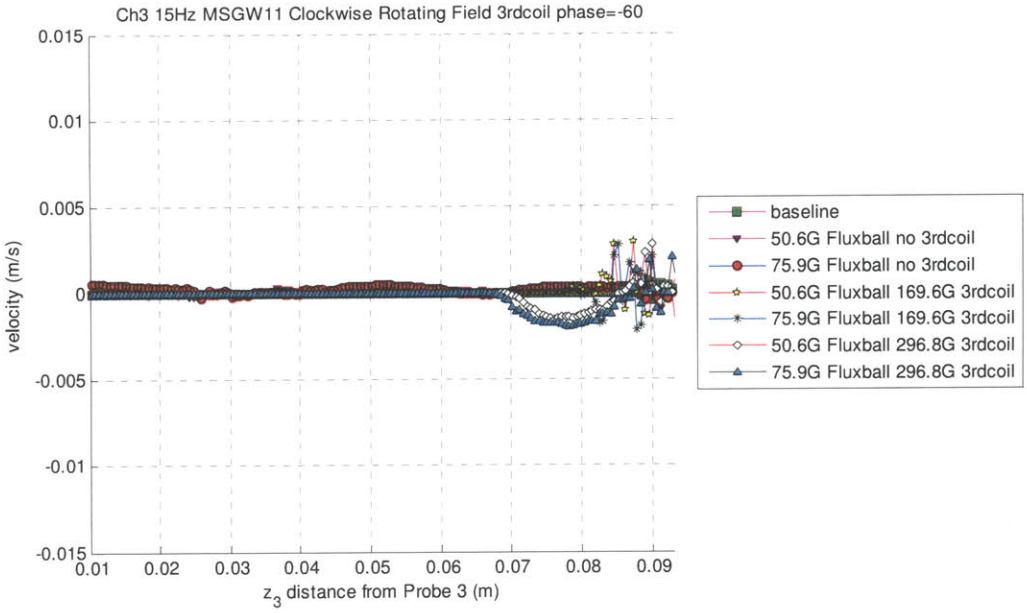
Ch3 15Hz MSGW11 Clockwise Rotating Field 3rdcoil phase=-60
velocity (m/s)
0.015
0.01
0.005
0
-0.005
-0.01
-0.015
0.01
0.02
0.03
0.04
0.05
0.06
0.07
0.08
0.09
z3 distance from Probe 3 (m)
baseline
50.6G Fluxball no 3rdcoil
75.9G Fluxball no 3rdcoil
50.6G Fluxball 169.6G 3rdcoil
75.9G Fluxball 169.6G 3rdcoil
50.6G Fluxball 296.8G 3rdcoil
75.9G Fluxball 296.8G 3rdcoil

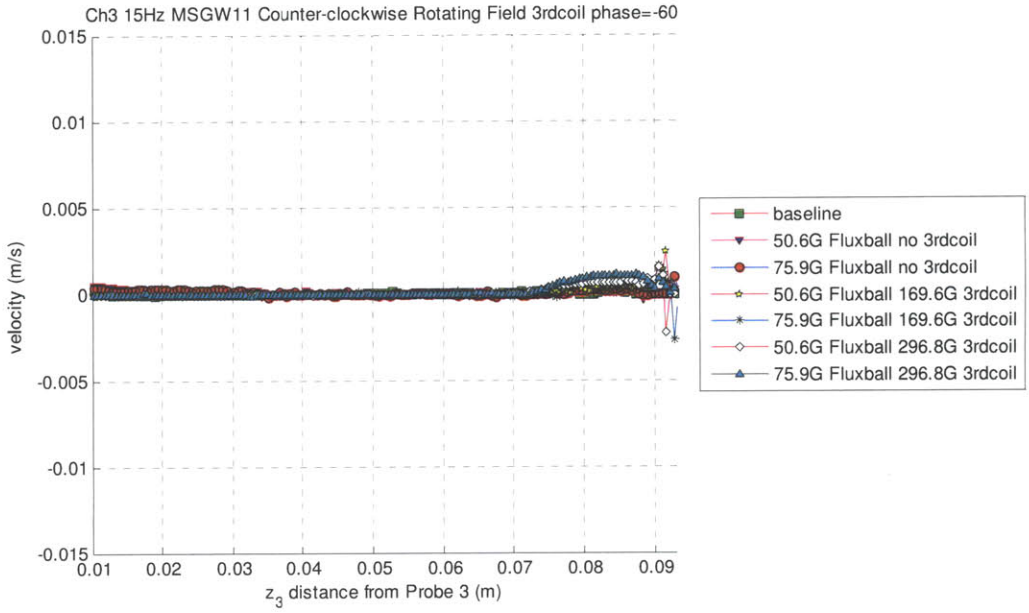
Ch3 15Hz MSGW11 Counter-clockwise Rotating Field 3rdcoil phase=-60
velocity (m/s)
0.015
0.01
0.005
0
-0.005
-0.01
-0.015
0.01
0.02
0.03
0.04
0.05
0.06
0.07
0.08
0.09
z3 distance from Probe 3 (m)
baseline
50.6G Fluxball no 3rdcoil
75.9G Fluxball no 3rdcoil
50.6G Fluxball 169.6G 3rdcoil
75.9G Fluxball 169.6G 3rdcoil
50.6G Fluxball 296.8G 3rdcoil
75.9G Fluxball 296.8G 3rdcoil

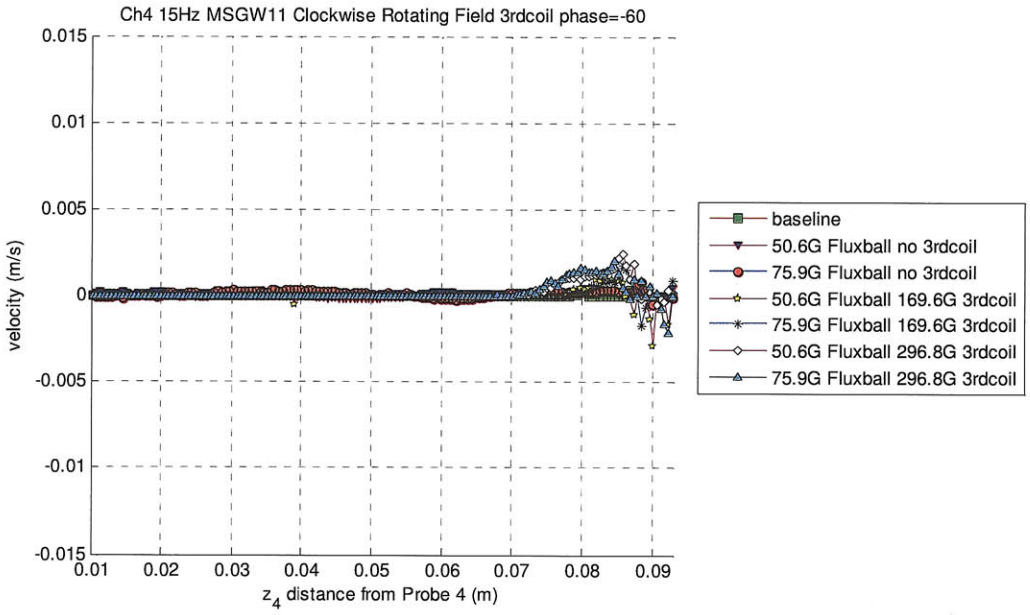
Ch4 15Hz MSGW11 Clockwise Rotating Field 3rdcoil phase=-60
velocity (m/s)
0.015
0.01
0.005
0
-0.005
-0.01
-0.015
0.01
0.02
0.03
0.04
0.05
0.06
0.07
0.08
0.09
z4 distance from Probe 4 (m)
baseline
50.6G Fluxball no 3rdcoil
75.9G Fluxball no 3rdcoil
50.6G Fluxball 169.6G 3rdcoil
75.9G Fluxball 169.6G 3rdcoil
50.6G Fluxball 296.8G 3rdcoil
75.9G Fluxball 296.8G 3rdcoil

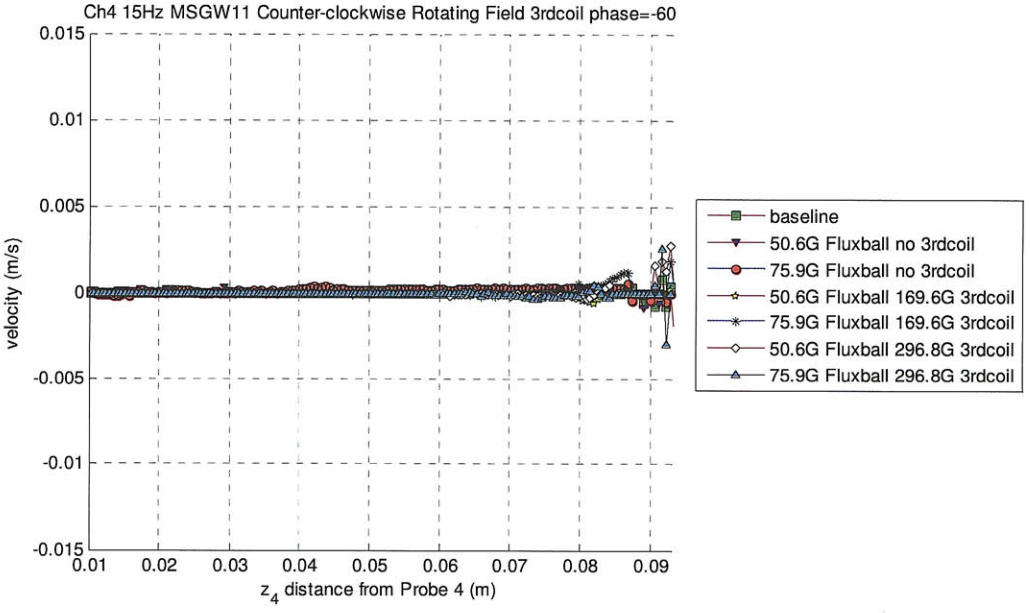
Ch4 15Hz MSGW11 Counter-clockwise Rotating Field 3rdcoil phase=-60
velocity (m/s)
0.015
0.01
0.005
0
-0.005
-0.01
-0.015
0.01
0.02
0.03
0.04
0.05
0.06
0.07
0.08
0.09
z4 distance from Probe 4 (m)
baseline
50.6G Fluxball no 3rdcoil
75.9G Fluxball no 3rdcoil
50.6G Fluxball 169.6G 3rdcoil
75.9G Fluxball 169.6G 3rdcoil
50.6G Fluxball 296.8G 3rdcoil
75.9G Fluxball 296.8G 3rdcoil

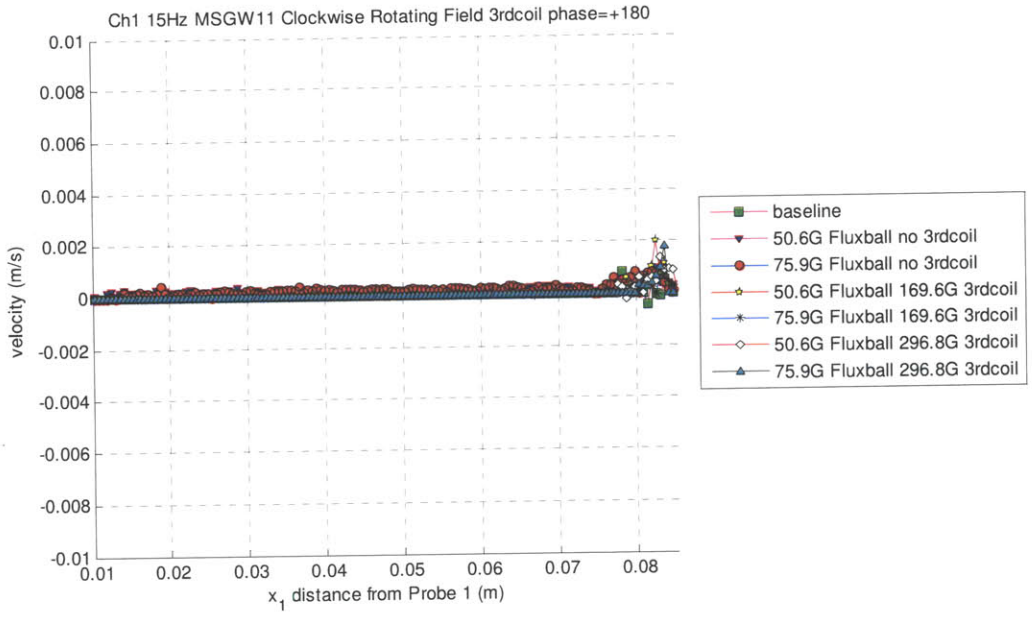
Ch1 15Hz MSGW11 Clockwise Rotating Field 3rdcoil phase=+180
velocity (m/s)
0.01
0.008
0.006
0.004
0.002
0
-0.002
-0.004
-0.006
-0.008
-0.01
0.01
0.02
0.03
0.04
0.05
0.06
0.07
0.08
x1 distance from Probe 1 (m)
baseline
50.6G Fluxball no 3rdcoil
75.9G Fluxball no 3rdcoil
50.6G Fluxball 169.6G 3rdcoil
75.9G Fluxball 169.6G 3rdcoil
50.6G Fluxball 296.8G 3rdcoil
75.9G Fluxball 296.8G 3rdcoil

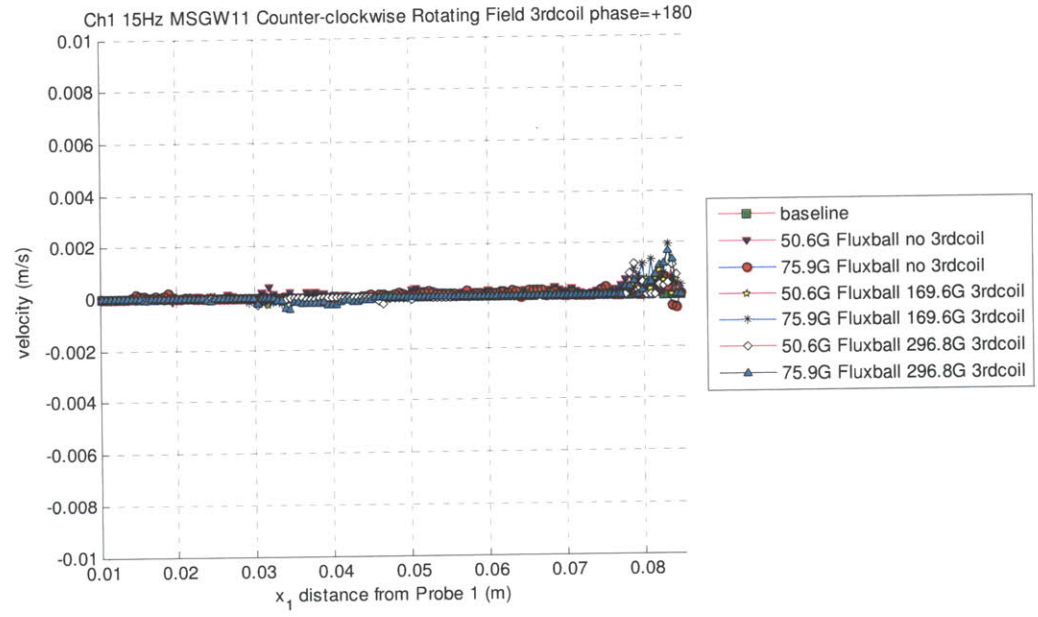
Ch1 15Hz MSGW11 Counter-clockwise Rotating Field 3rdcoil phase=+180
velocity (m/s)
0.01
0.008
0.006
0.004
0.002
0
-0.002
-0.004
-0.006
-0.008
-0.01
0.01
0.02
0.03
0.04
0.05
0.06
0.07
0.08
x1 distance from Probe 1 (m)
baseline
50.6G Fluxball no 3rdcoil
75.9G Fluxball no 3rdcoil
50.6G Fluxball 169.6G 3rdcoil
75.9G Fluxball 169.6G 3rdcoil
50.6G Fluxball 296.8G 3rdcoil
75.9G Fluxball 296.8G 3rdcoil

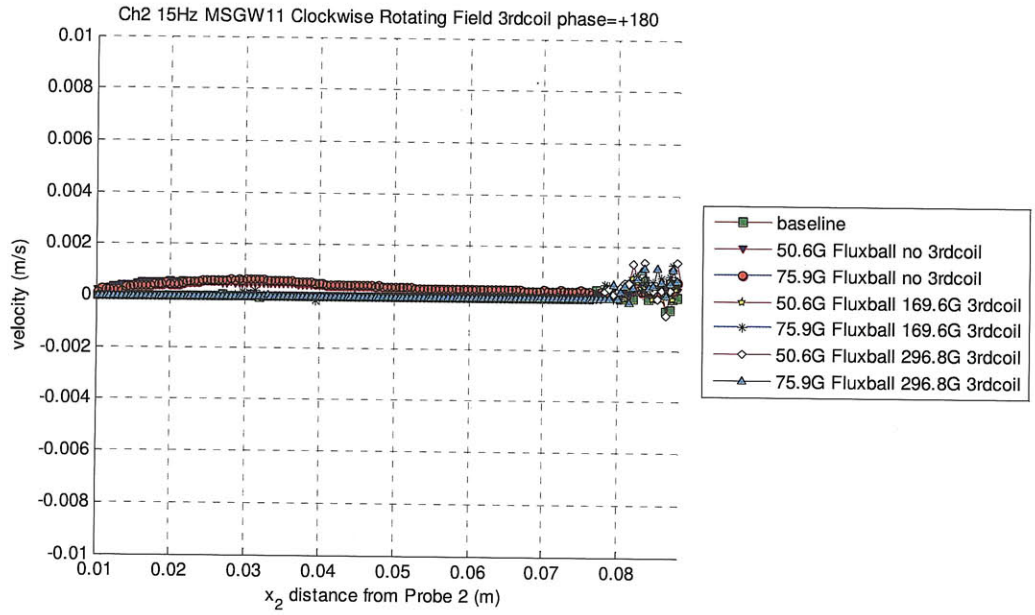
Ch2 15Hz MSGW11 Clockwise Rotating Field 3rdcoil phase=+180
velocity (m/s)
0.01
0.008
0.006
0.004
0.002
0
-0.002
-0.004
-0.006
-0.008
-0.01
0.01
0.02
0.03
0.04
0.05
0.06
0.07
0.08
x2 distance from Probe 2 (m)
baseline
50.6G Fluxball no 3rdcoil
75.9G Fluxball no 3rdcoil
50.6G Fluxball 169.6G 3rdcoil
75.9G Fluxball 169.6G 3rdcoil
50.6G Fluxball 296.8G 3rdcoil
75.9G Fluxball 296.8G 3rdcoil

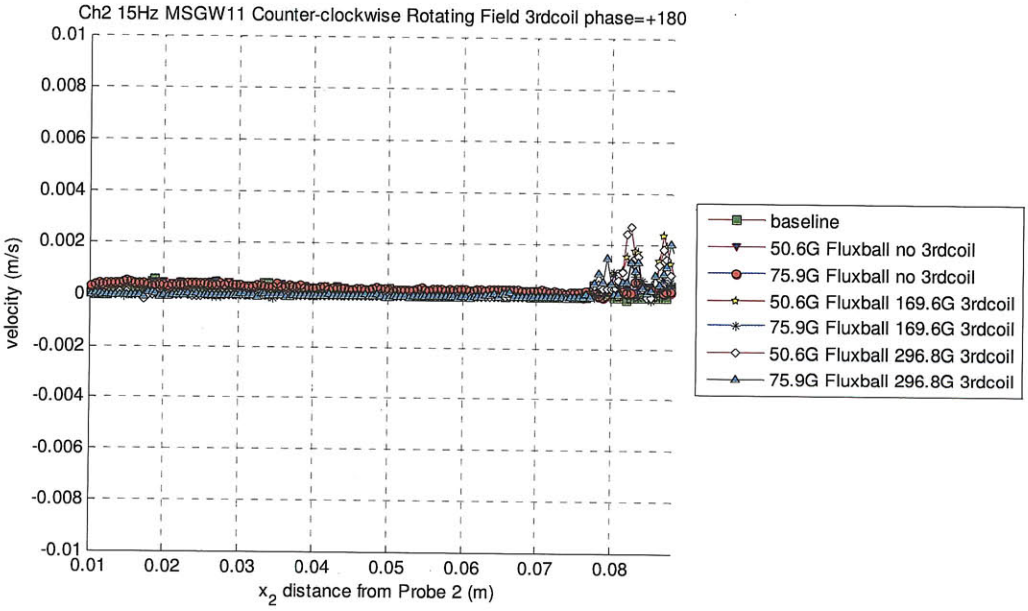
Ch2 15Hz MSGW11 Counter-clockwise Rotating Field 3rdcoil phase=+180
velocity (m/s)
0.01
0.008
0.006
0.004
0.002
0
-0.002
-0.004
-0.006
-0.008
-0.01
0.01
0.02
0.03
0.04
0.05
0.06
0.07
0.08
x2 distance from Probe 2 (m)
baseline
50.6G Fluxball no 3rdcoil
75.9G Fluxball no 3rdcoil
50.6G Fluxball 169.6G 3rdcoil
75.9G Fluxball 169.6G 3rdcoil
50.6G Fluxball 296.8G 3rdcoil
75.9G Fluxball 296.8G 3rdcoil

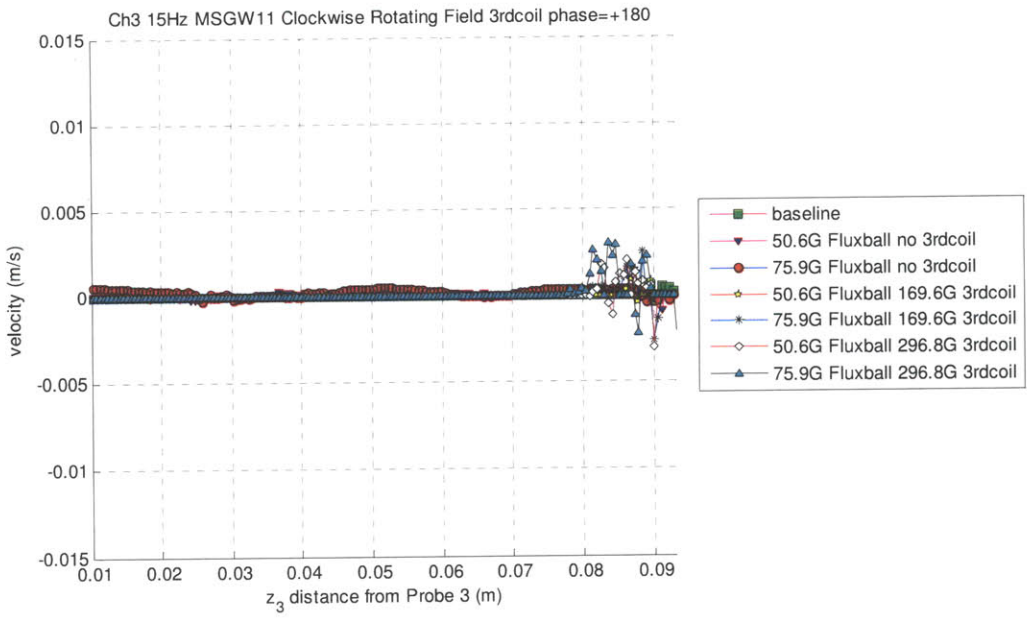
Ch3 15Hz MSGW11 Clockwise Rotating Field 3rdcoil phase=+180
velocity (m/s)
0.015
0.01
0.005
0
-0.005
-0.01
-0.015
0.01
0.02
0.03
0.04
0.05
0.06
0.07
0.08
0.09
z_3 distance from Probe 3 (m)
baseline
50.6G Fluxball no 3rdcoil
75.9G Fluxball no 3rdcoil
50.6G Fluxball 169.6G 3rdcoil
75.9G Fluxball 169.6G 3rdcoil
50.6G Fluxball 296.8G 3rdcoil
75.9G Fluxball 296.8G 3rdcoil

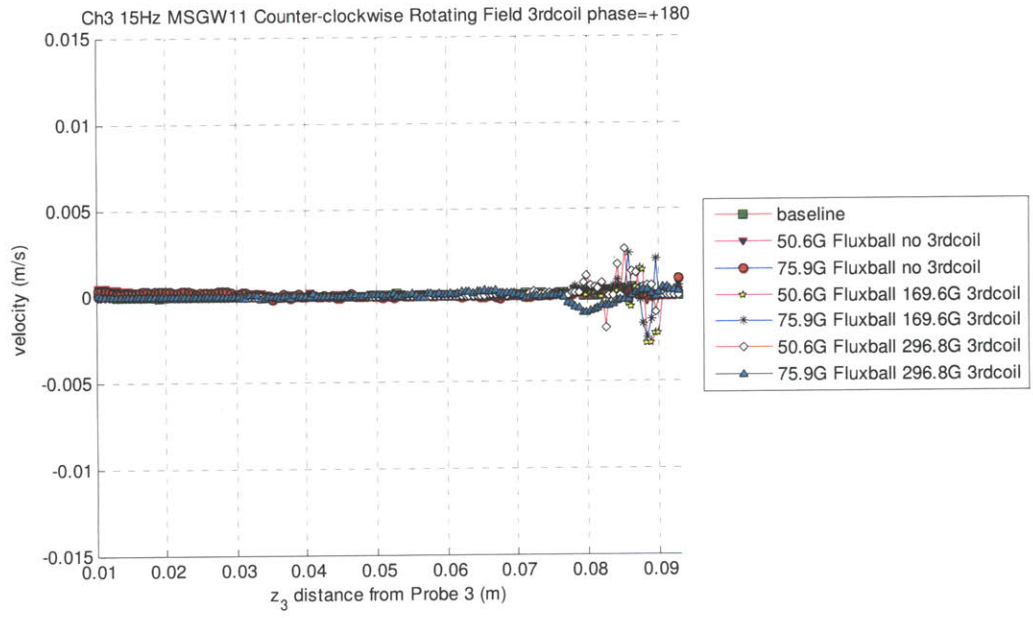
Ch3 15Hz MSGW11 Counter-clockwise Rotating Field 3rdcoil phase=+180
velocity (m/s)
0.015
0.01
0.005
0
-0.005
-0.01
-0.015
0.01
0.02
0.03
0.04
0.05
0.06
0.07
0.08
0.09
z_3 distance from Probe 3 (m)
baseline
50.6G Fluxball no 3rdcoil
75.9G Fluxball no 3rdcoil
50.6G Fluxball 169.6G 3rdcoil
75.9G Fluxball 169.6G 3rdcoil
50.6G Fluxball 296.8G 3rdcoil
75.9G Fluxball 296.8G 3rdcoil

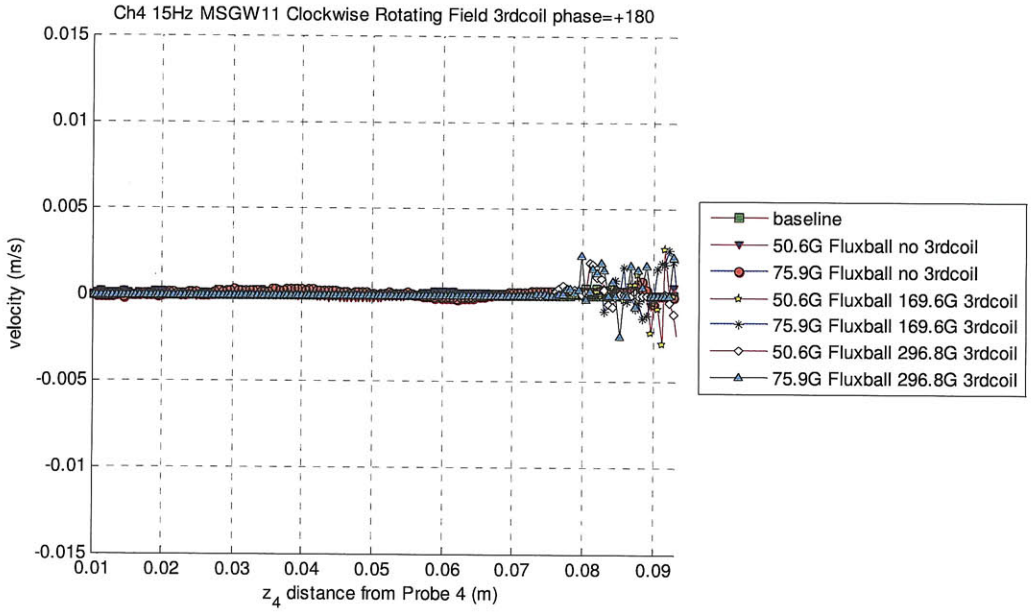
Ch4 15Hz MSGW11 Clockwise Rotating Field 3rdcoil phase=+180
velocity (m/s)
0.015
0.01
0.005
0
-0.005
-0.01
-0.015
0.01
0.02
0.03
0.04
0.05
0.06
0.07
0.08
0.09
z4 distance from Probe 4 (m)
baseline
50.6G Fluxball no 3rdcoil
75.9G Fluxball no 3rdcoil
50.6G Fluxball 169.6G 3rdcoil
75.9G Fluxball 169.6G 3rdcoil
50.6G Fluxball 296.8G 3rdcoil
75.9G Fluxball 296.8G 3rdcoil

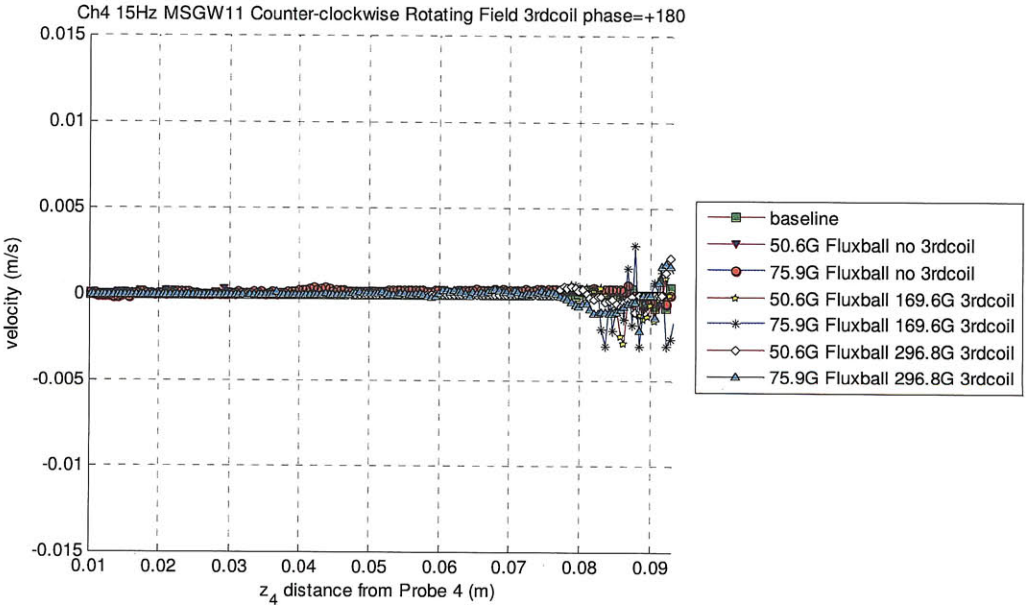
Ch4 15Hz MSGW11 Counter-clockwise Rotating Field 3rdcoil phase=+180
velocity (m/s)
0.015
0.01
0.005
0
-0.005
-0.01
-0.015
0.01
0.02
0.03
0.04
0.05
0.06
0.07
0.08
0.09
z4 distance from Probe 4 (m)
baseline
50.6G Fluxball no 3rdcoil
75.9G Fluxball no 3rdcoil
50.6G Fluxball 169.6G 3rdcoil
75.9G Fluxball 169.6G 3rdcoil
50.6G Fluxball 296.8G 3rdcoil
75.9G Fluxball 296.8G 3rdcoil

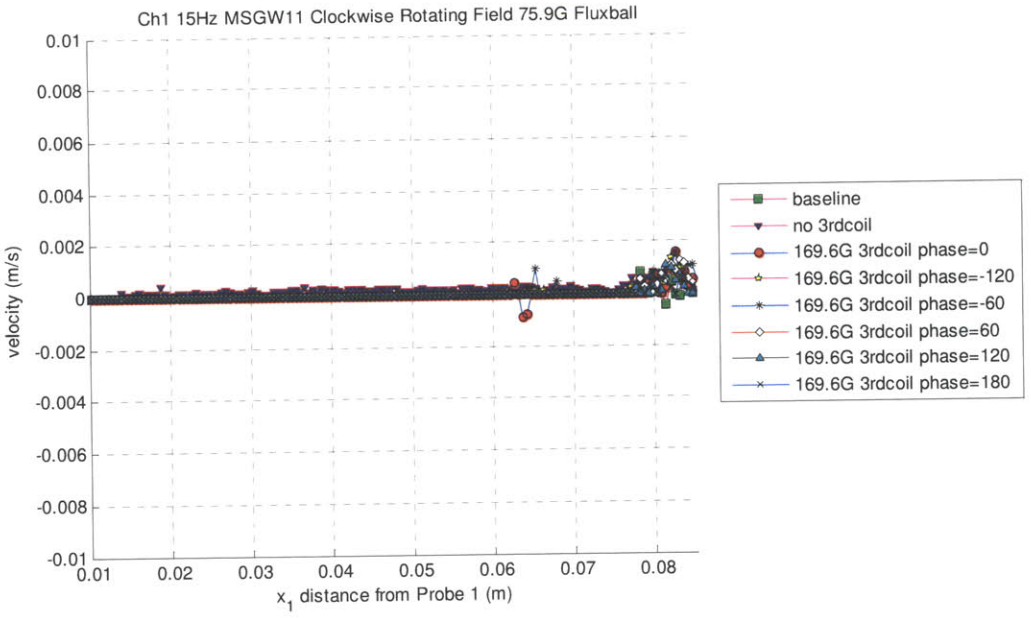
Ch1 15Hz MSGW11 Clockwise Rotating Field 75.9G Fluxball
velocity (m/s)
x1 distance from Probe 1 (m)
baseline
no 3rdcoil
169.6G 3rdcoil phase=0
169.6G 3rdcoil phase=-120
169.6G 3rdcoil phase=-60
169.6G 3rdcoil phase=60
169.6G 3rdcoil phase=120
169.6G 3rdcoil phase=180

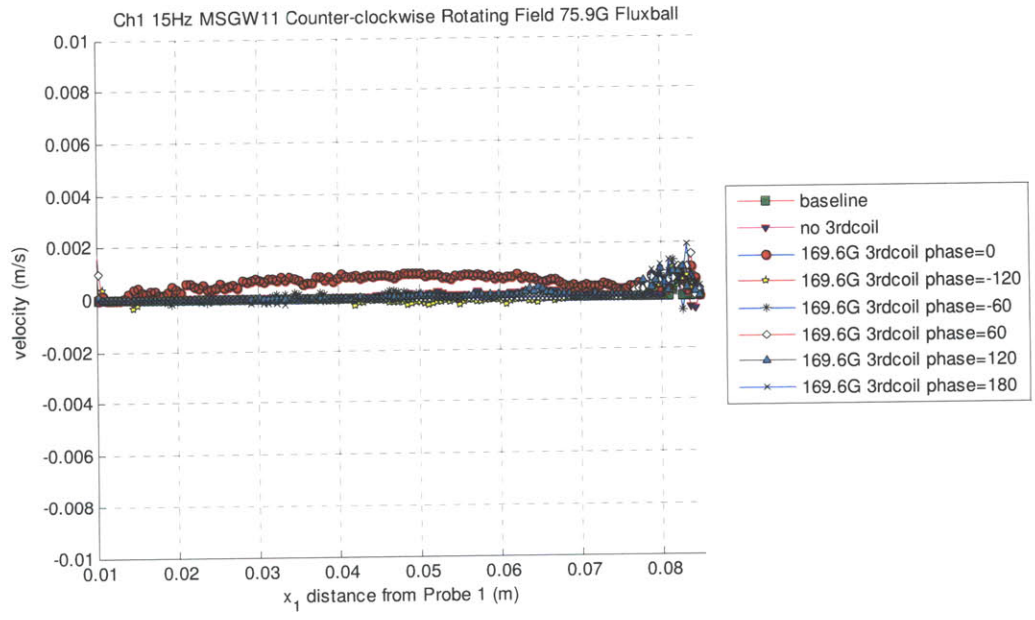
Ch1 15Hz MSGW11 Counter-clockwise Rotating Field 75.9G Fluxball
velocity (m/s)
x1 distance from Probe 1 (m)
baseline
no 3rdcoil
169.6G 3rdcoil phase=0
169.6G 3rdcoil phase=-120
169.6G 3rdcoil phase=-60
169.6G 3rdcoil phase=60
169.6G 3rdcoil phase=120
169.6G 3rdcoil phase=180

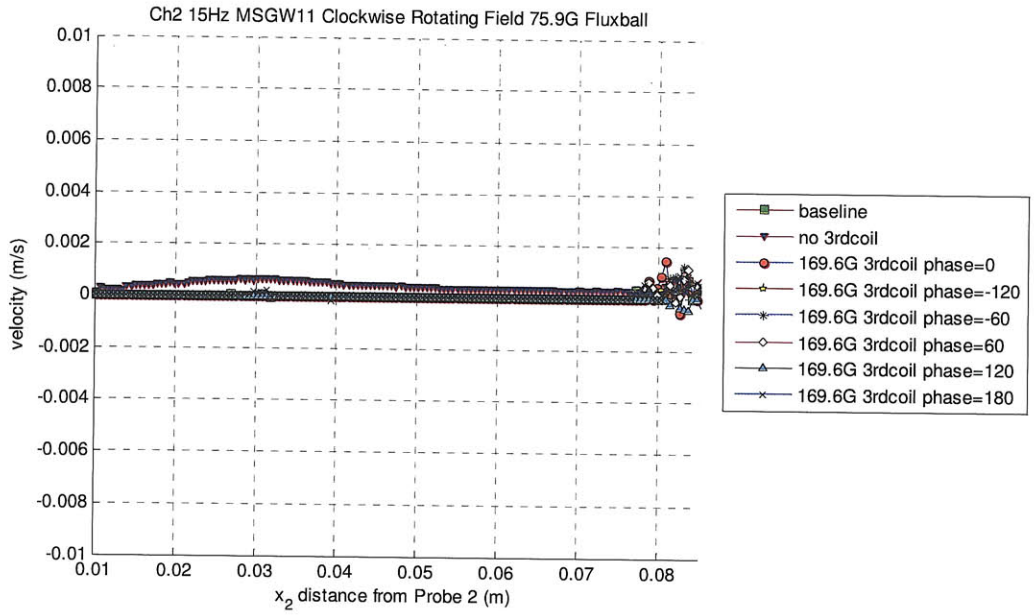
Ch2 15Hz MSGW11 Clockwise Rotating Field 75.9G Fluxball
velocity (m/s)
0.01
0.008
0.006
0.004
0.002
0
-0.002
-0.004
-0.006
-0.008
-0.01
0.01
0.02
0.03
0.04
0.05
0.06
0.07
0.08
x2 distance from Probe 2 (m)
baseline
no 3rdcoil
169.6G 3rdcoil phase=0
169.6G 3rdcoil phase=-120
169.6G 3rdcoil phase=-60
169.6G 3rdcoil phase=60
169.6G 3rdcoil phase=120
169.6G 3rdcoil phase=180

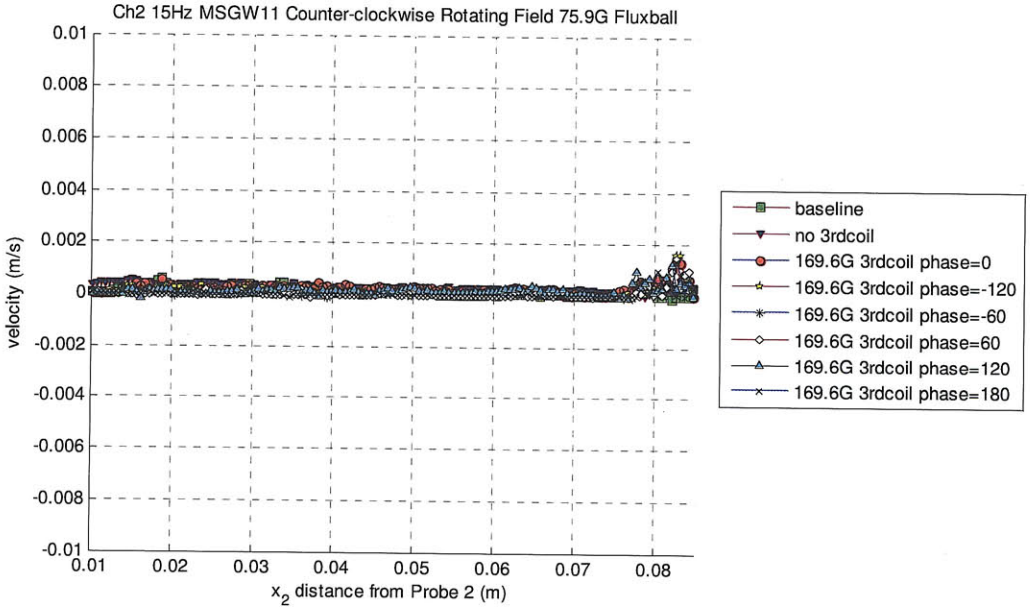
Ch2 15Hz MSGW11 Counter-clockwise Rotating Field 75.9G Fluxball
velocity (m/s)
0.01
0.008
0.006
0.004
0.002
0
-0.002
-0.004
-0.006
-0.008
-0.01
0.01
0.02
0.03
0.04
0.05
0.06
0.07
0.08
x2 distance from Probe 2 (m)
baseline
no 3rdcoil
169.6G 3rdcoil phase=0
169.6G 3rdcoil phase=-120
169.6G 3rdcoil phase=-60
169.6G 3rdcoil phase=60
169.6G 3rdcoil phase=120
169.6G 3rdcoil phase=180

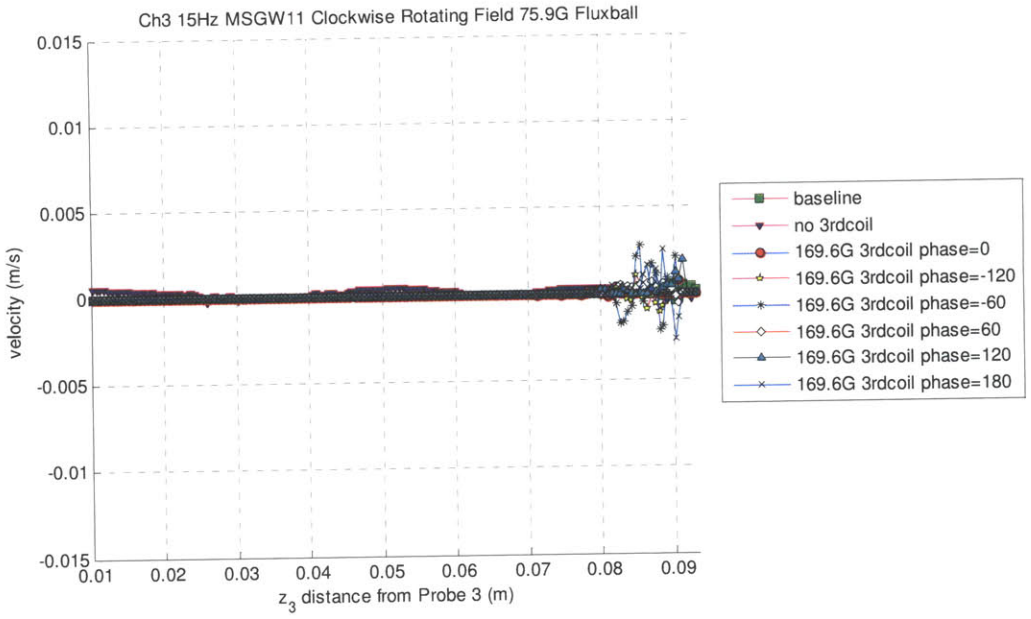
Ch3 15Hz MSGW11 Clockwise Rotating Field 75.9G Fluxball
velocity (m/s)
0.015
0.01
0.005
0
-0.005
-0.01
-0.015
0.01
0.02
0.03
0.04
0.05
0.06
0.07
0.08
0.09
z3 distance from Probe 3 (m)
baseline
no 3rdcoil
169.6G 3rdcoil phase=0
169.6G 3rdcoil phase=-120
169.6G 3rdcoil phase=-60
169.6G 3rdcoil phase=60
169.6G 3rdcoil phase=120
169.6G 3rdcoil phase=180

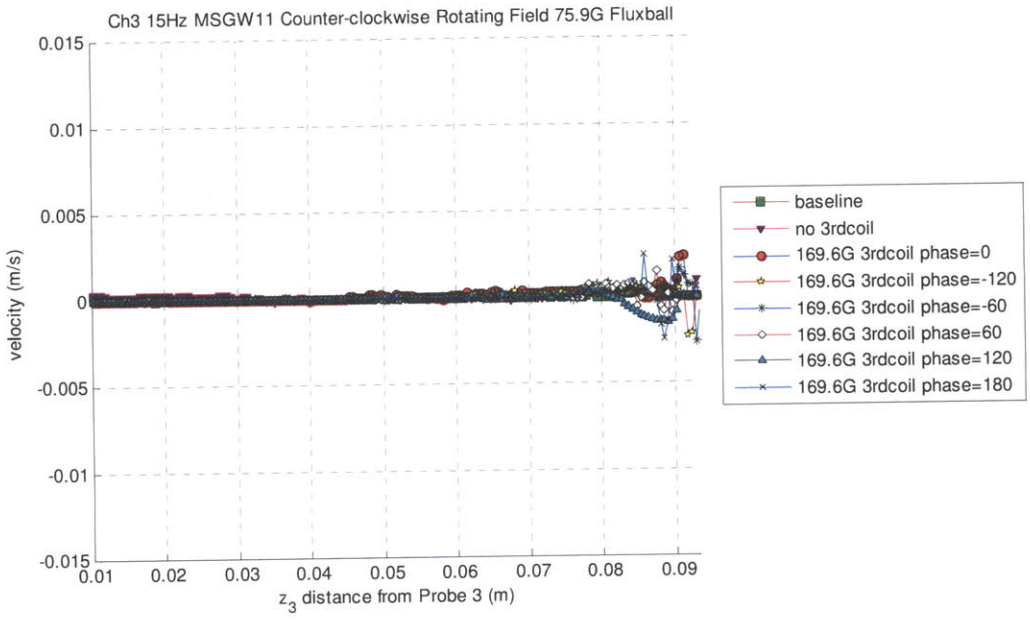
Ch3 15Hz MSGW11 Counter-clockwise Rotating Field 75.9G Fluxball
velocity (m/s)
0.015
0.01
0.005
0
-0.005
-0.01
-0.015
0.01
0.02
0.03
0.04
0.05
0.06
0.07
0.08
0.09
z3 distance from Probe 3 (m)
baseline
no 3rdcoil
169.6G 3rdcoil phase=0
169.6G 3rdcoil phase=-120
169.6G 3rdcoil phase=-60
169.6G 3rdcoil phase=60
169.6G 3rdcoil phase=120
169.6G 3rdcoil phase=180

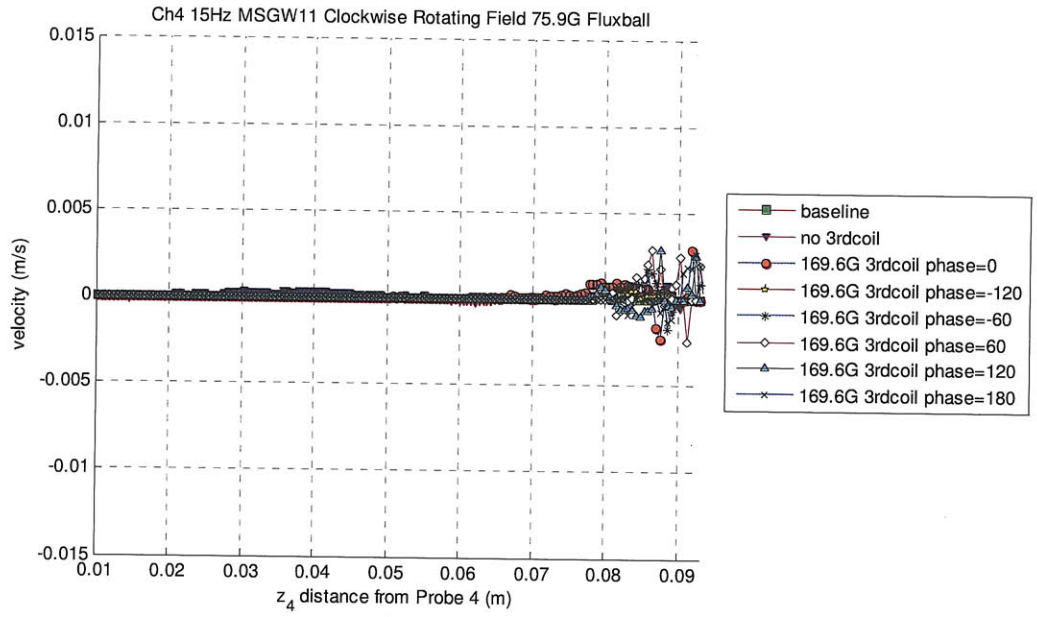
Ch4 15Hz MSGW11 Clockwise Rotating Field 75.9G Fluxball
velocity (m/s)
0.015
0.01
0.005
0
-0.005
-0.01
-0.015
0.01
0.02
0.03
0.04
0.05
0.06
0.07
0.08
0.09
z4 distance from Probe 4 (m)
baseline
no 3rdcoil
169.6G 3rdcoil phase=0
169.6G 3rdcoil phase=-120
169.6G 3rdcoil phase=-60
169.6G 3rdcoil phase=60
169.6G 3rdcoil phase=120
169.6G 3rdcoil phase=180

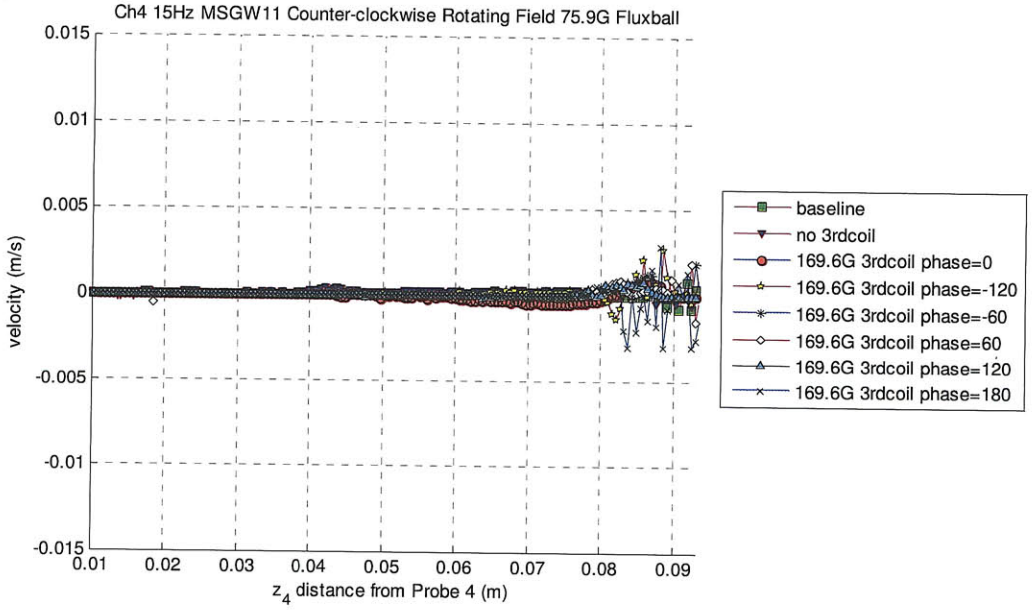
Ch4 15Hz MSGW11 Counter-clockwise Rotating Field 75.9G Fluxball
velocity (m/s)
0.015
0.01
0.005
0
-0.005
-0.01
-0.015
0.01
0.02
0.03
0.04
0.05
0.06
0.07
0.08
0.09
z4 distance from Probe 4 (m)
baseline
no 3rdcoil
169.6G 3rdcoil phase=0
169.6G 3rdcoil phase=-120
169.6G 3rdcoil phase=-60
169.6G 3rdcoil phase=60
169.6G 3rdcoil phase=120
169.6G 3rdcoil phase=180

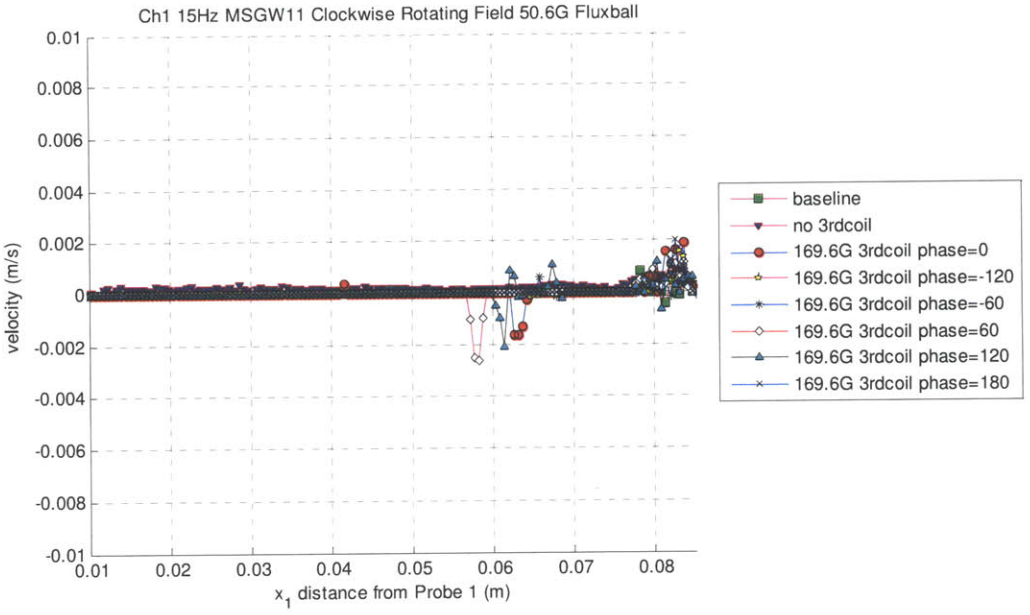
Ch1 15Hz MSGW11 Clockwise Rotating Field 50.6G Fluxball
velocity (m/s)
x1 distance from Probe 1 (m)
baseline
no 3rdcoil
169.6G 3rdcoil phase=0
169.6G 3rdcoil phase=-120
169.6G 3rdcoil phase=-60
169.6G 3rdcoil phase=60
169.6G 3rdcoil phase=120
169.6G 3rdcoil phase=180

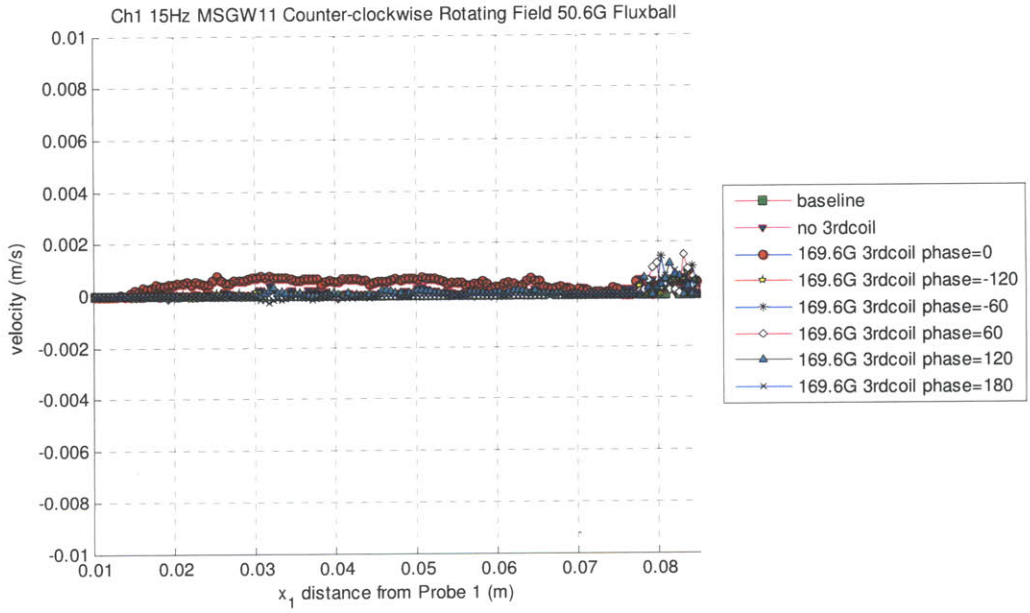
Ch1 15Hz MSGW11 Counter-clockwise Rotating Field 50.6G Fluxball
velocity (m/s)
x1 distance from Probe 1 (m)
baseline
no 3rdcoil
169.6G 3rdcoil phase=0
169.6G 3rdcoil phase=-120
169.6G 3rdcoil phase=-60
169.6G 3rdcoil phase=60
169.6G 3rdcoil phase=120
169.6G 3rdcoil phase=180

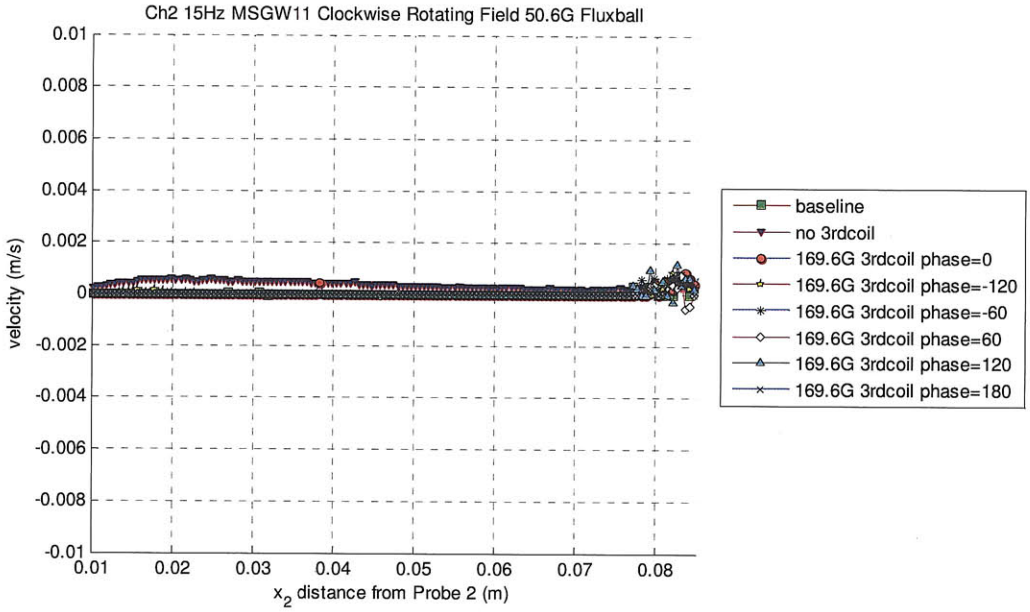
Ch2 15Hz MSGW11 Clockwise Rotating Field 50.6G Fluxball
velocity (m/s)
0.01
0.008
0.006
0.004
0.002
0
-0.002
-0.004
-0.006
-0.008
-0.01
0.01
0.02
0.03
0.04
0.05
0.06
0.07
0.08
x2 distance from Probe 2 (m)
baseline
no 3rdcoil
169.6G 3rdcoil phase=0
169.6G 3rdcoil phase=-120
169.6G 3rdcoil phase=-60
169.6G 3rdcoil phase=60
169.6G 3rdcoil phase=120
169.6G 3rdcoil phase=180

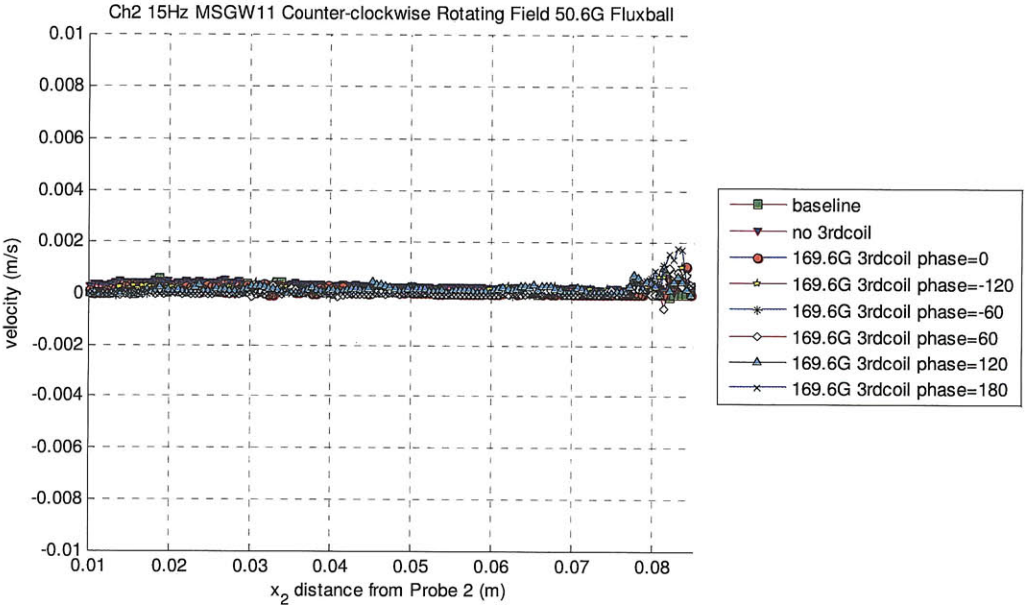
Ch2 15Hz MSGW11 Counter-clockwise Rotating Field 50.6G Fluxball
velocity (m/s)
0.01
0.008
0.006
0.004
0.002
0
-0.002
-0.004
-0.006
-0.008
-0.01
0.01
0.02
0.03
0.04
0.05
0.06
0.07
0.08
x2 distance from Probe 2 (m)
baseline
no 3rdcoil
169.6G 3rdcoil phase=0
169.6G 3rdcoil phase=-120
169.6G 3rdcoil phase=-60
169.6G 3rdcoil phase=60
169.6G 3rdcoil phase=120
169.6G 3rdcoil phase=180

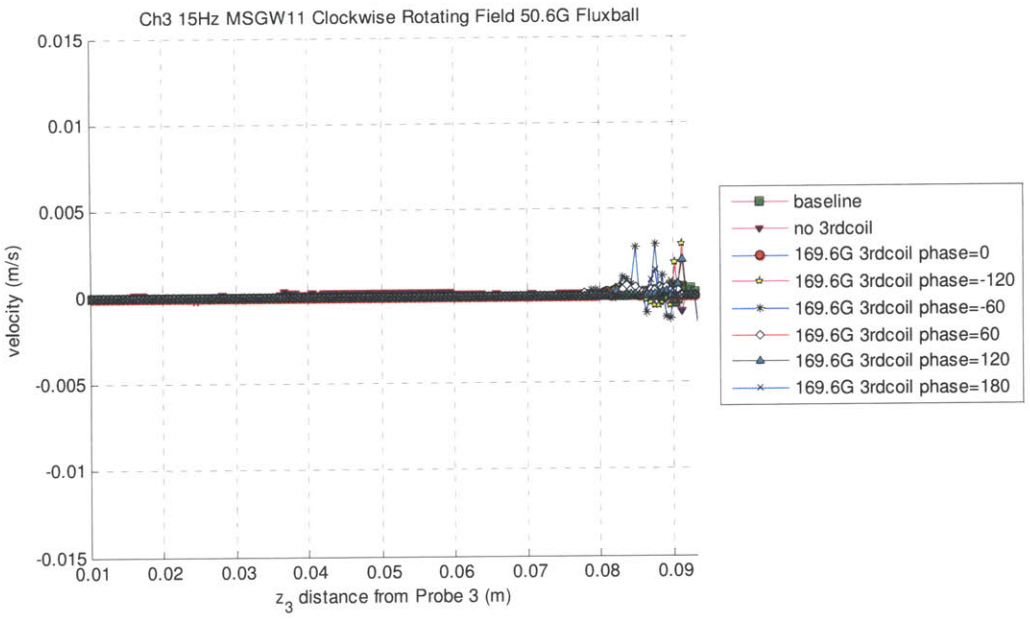
Ch3 15Hz MSGW11 Clockwise Rotating Field 50.6G Fluxball
velocity (m/s)
0.015
0.01
0.005
0
-0.005
-0.01
-0.015
0.01
0.02
0.03
0.04
0.05
0.06
0.07
0.08
0.09
z_3 distance from Probe 3 (m)
baseline
no 3rdcoil
169.6G 3rdcoil phase=0
169.6G 3rdcoil phase=-120
169.6G 3rdcoil phase=-60
169.6G 3rdcoil phase=60
169.6G 3rdcoil phase=120
169.6G 3rdcoil phase=180

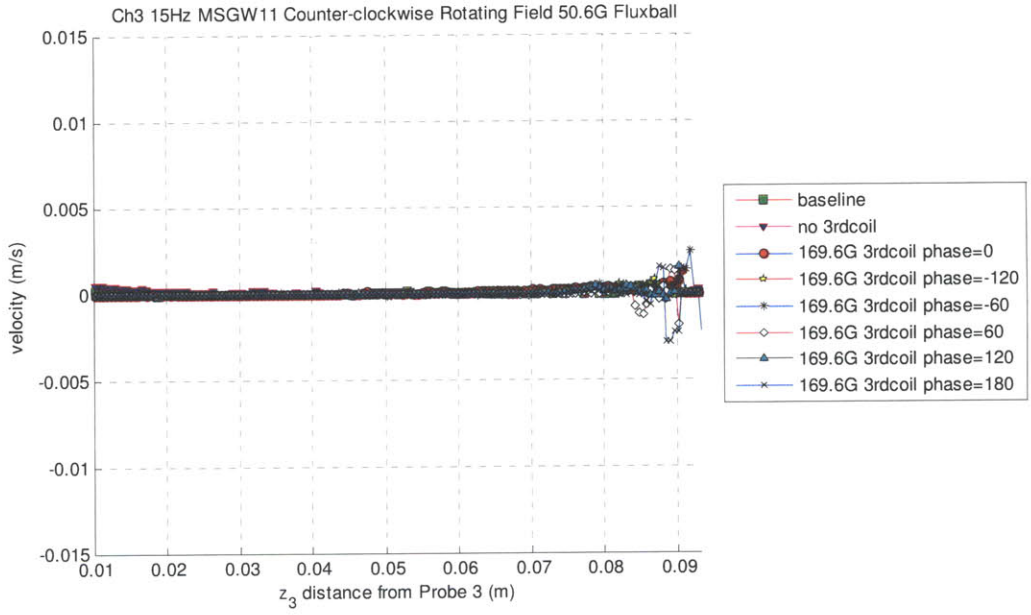
Ch3 15Hz MSGW11 Counter-clockwise Rotating Field 50.6G Fluxball
velocity (m/s)
0.015
0.01
0.005
0
-0.005
-0.01
-0.015
0.01
0.02
0.03
0.04
0.05
0.06
0.07
0.08
0.09
z_3 distance from Probe 3 (m)
baseline
no 3rdcoil
169.6G 3rdcoil phase=0
169.6G 3rdcoil phase=-120
169.6G 3rdcoil phase=-60
169.6G 3rdcoil phase=60
169.6G 3rdcoil phase=120
169.6G 3rdcoil phase=180

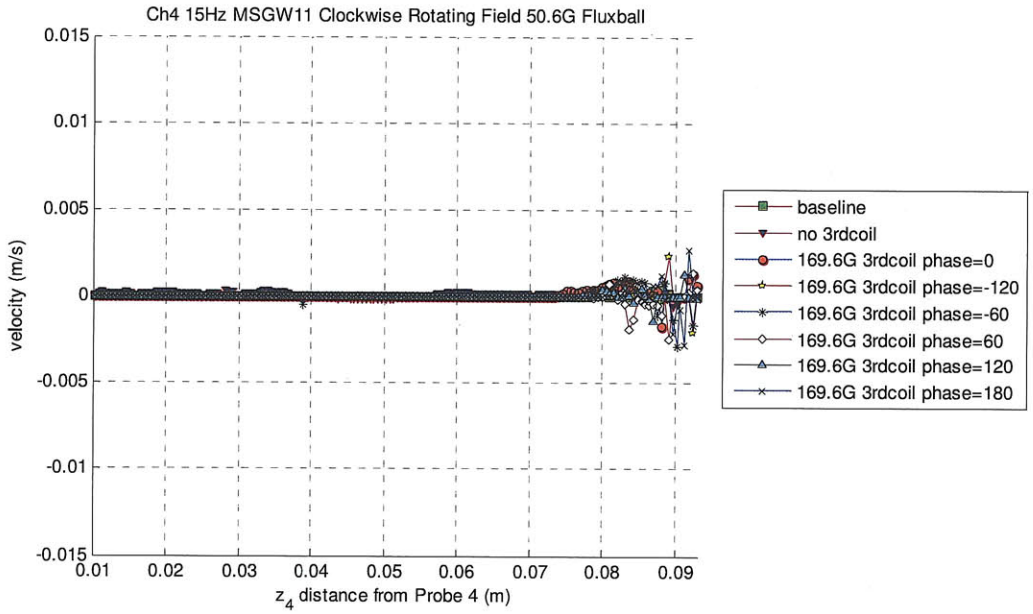
Ch4 15Hz MSGW11 Clockwise Rotating Field 50.6G Fluxball
velocity (m/s)
0.015
0.01
0.005
0
-0.005
-0.01
-0.015
0.01
0.02
0.03
0.04
0.05
0.06
0.07
0.08
0.09
z4 distance from Probe 4 (m)
baseline
no 3rdcoil
169.6G 3rdcoil phase=0
169.6G 3rdcoil phase=-120
169.6G 3rdcoil phase=-60
169.6G 3rdcoil phase=60
169.6G 3rdcoil phase=120
169.6G 3rdcoil phase=180

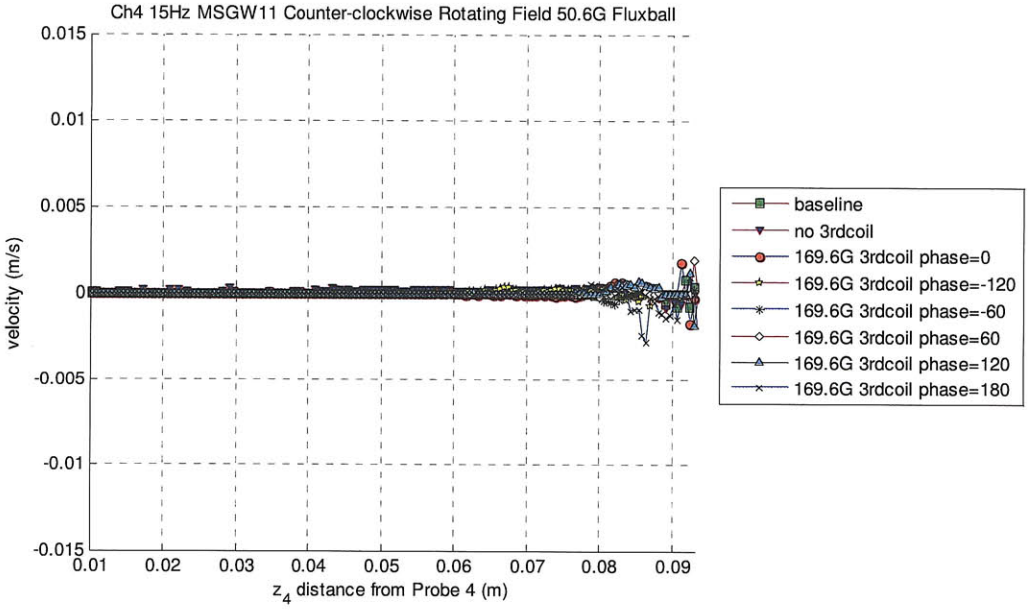
Ch4 15Hz MSGW11 Counter-clockwise Rotating Field 50.6G Fluxball
velocity (m/s)
0.015
0.01
0.005
0
-0.005
-0.01
-0.015
0.01
0.02
0.03
0.04
0.05
0.06
0.07
0.08
0.09
z4 distance from Probe 4 (m)
baseline
no 3rdcoil
169.6G 3rdcoil phase=0
169.6G 3rdcoil phase=-120
169.6G 3rdcoil phase=-60
169.6G 3rdcoil phase=60
169.6G 3rdcoil phase=120
169.6G 3rdcoil phase=180

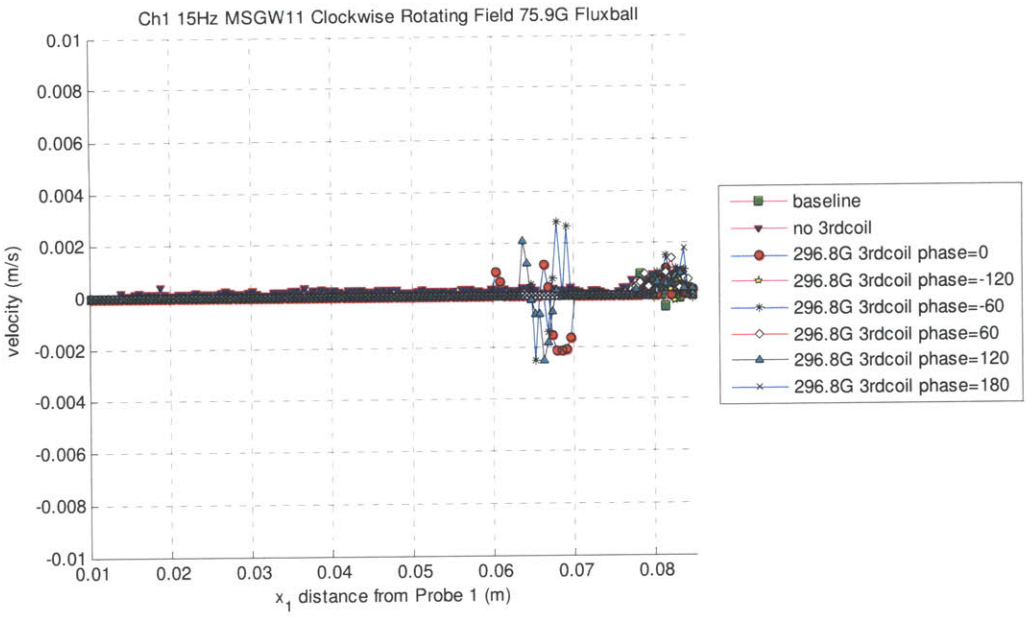
Ch1 15Hz MSGW11 Clockwise Rotating Field 75.9G Fluxball
velocity (m/s)
x1 distance from Probe 1 (m)
baseline
no 3rdcoil
296.8G 3rdcoil phase=0
296.8G 3rdcoil phase=-120
296.8G 3rdcoil phase=-60
296.8G 3rdcoil phase=60
296.8G 3rdcoil phase=120
296.8G 3rdcoil phase=180

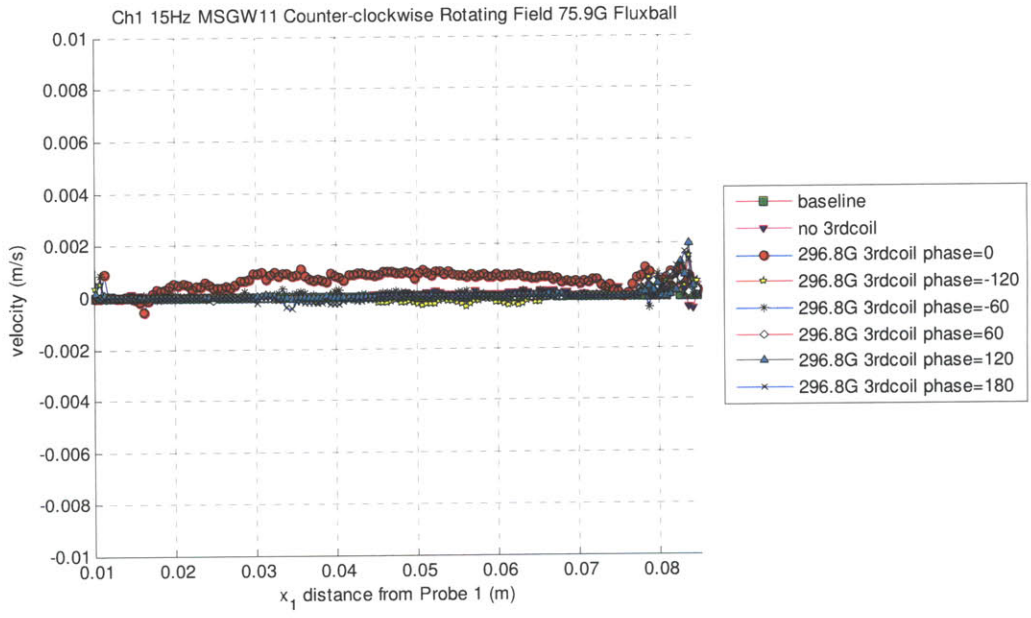
Ch1 15Hz MSGW11 Counter-clockwise Rotating Field 75.9G Fluxball
velocity (m/s)
x1 distance from Probe 1 (m)
baseline
no 3rdcoil
296.8G 3rdcoil phase=0
296.8G 3rdcoil phase=-120
296.8G 3rdcoil phase=-60
296.8G 3rdcoil phase=60
296.8G 3rdcoil phase=120
296.8G 3rdcoil phase=180

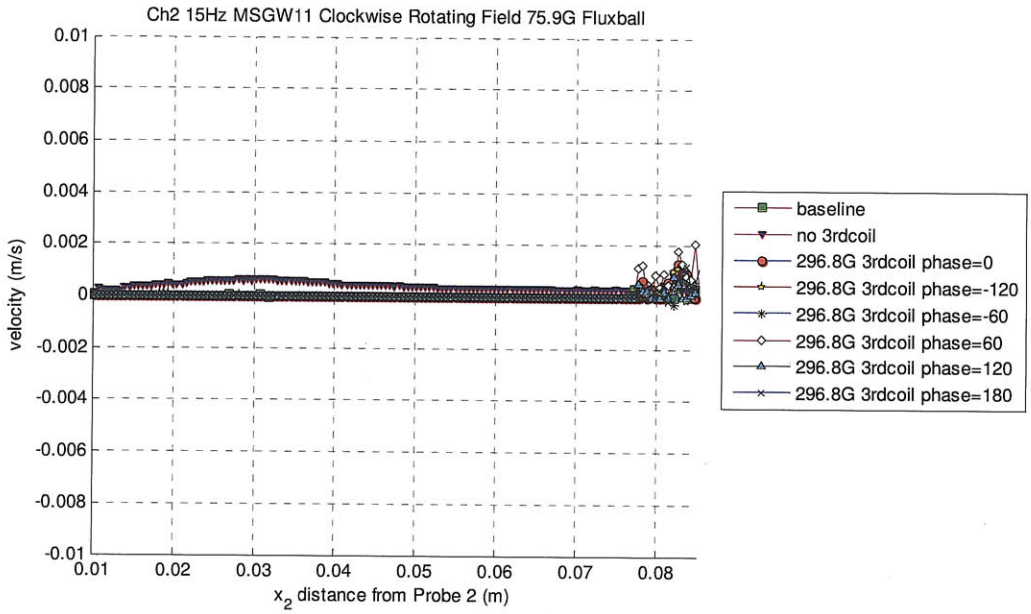
Ch2 15Hz MSGW11 Clockwise Rotating Field 75.9G Fluxball
velocity (m/s)
0.01
0.008
0.006
0.004
0.002
0
-0.002
-0.004
-0.006
-0.008
-0.01
0.01
0.02
0.03
0.04
0.05
0.06
0.07
0.08
x2 distance from Probe 2 (m)
baseline
no 3rdcoil
296.8G 3rdcoil phase=0
296.8G 3rdcoil phase=-120
296.8G 3rdcoil phase=-60
296.8G 3rdcoil phase=60
296.8G 3rdcoil phase=120
296.8G 3rdcoil phase=180

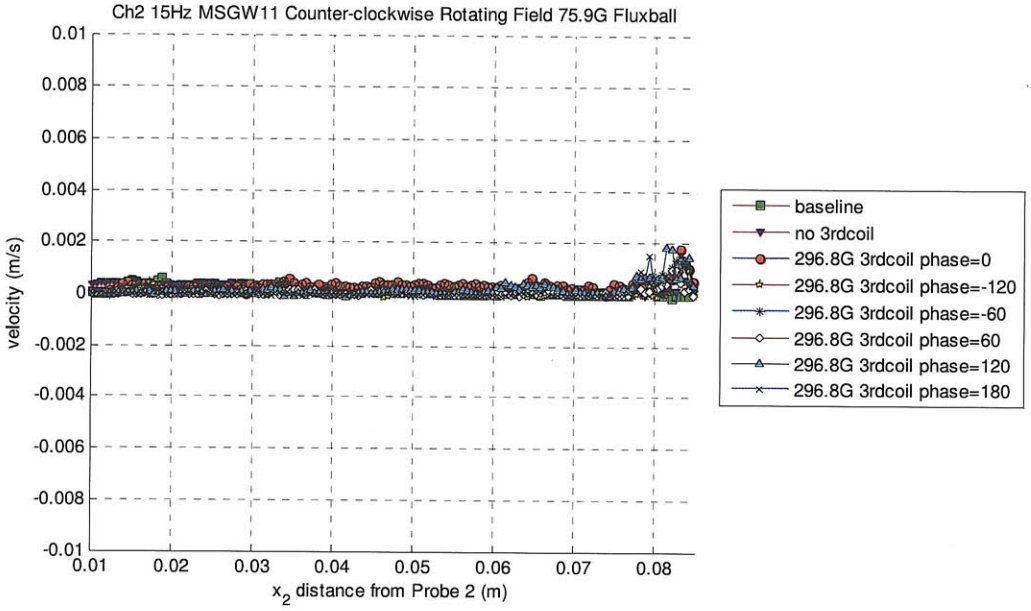
Ch2 15Hz MSGW11 Counter-clockwise Rotating Field 75.9G Fluxball
velocity (m/s)
0.01
0.008
0.006
0.004
0.002
0
-0.002
-0.004
-0.006
-0.008
-0.01
0.01
0.02
0.03
0.04
0.05
0.06
0.07
0.08
x2 distance from Probe 2 (m)
baseline
no 3rdcoil
296.8G 3rdcoil phase=0
296.8G 3rdcoil phase=-120
296.8G 3rdcoil phase=-60
296.8G 3rdcoil phase=60
296.8G 3rdcoil phase=120
296.8G 3rdcoil phase=180

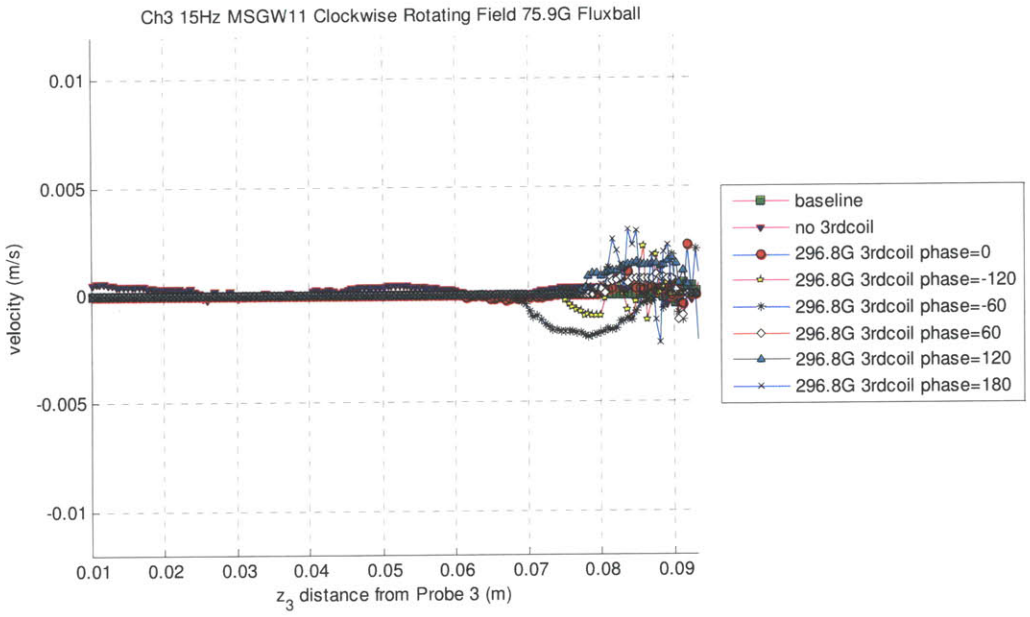
Ch3 15Hz MSGW11 Clockwise Rotating Field 75.9G Fluxball
velocity (m/s)
0.01
0.005
0
-0.005
-0.01
0.01
0.02
0.03
0.04
0.05
0.06
0.07
0.08
0.09
z3 distance from Probe 3 (m)
baseline
no 3rdcoil
296.8G 3rdcoil phase=0
296.8G 3rdcoil phase=-120
296.8G 3rdcoil phase=-60
296.8G 3rdcoil phase=60
296.8G 3rdcoil phase=120
296.8G 3rdcoil phase=180

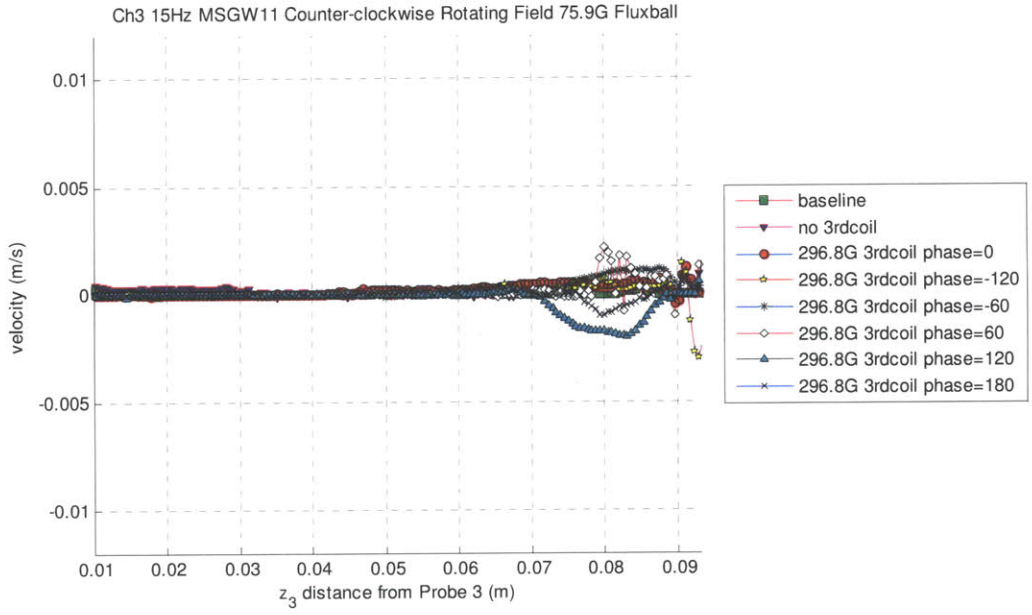
Ch3 15Hz MSGW11 Counter-clockwise Rotating Field 75.9G Fluxball
velocity (m/s)
0.01
0.005
0
-0.005
-0.01
0.01
0.02
0.03
0.04
0.05
0.06
0.07
0.08
0.09
z3 distance from Probe 3 (m)
baseline
no 3rdcoil
296.8G 3rdcoil phase=0
296.8G 3rdcoil phase=-120
296.8G 3rdcoil phase=-60
296.8G 3rdcoil phase=60
296.8G 3rdcoil phase=120
296.8G 3rdcoil phase=180

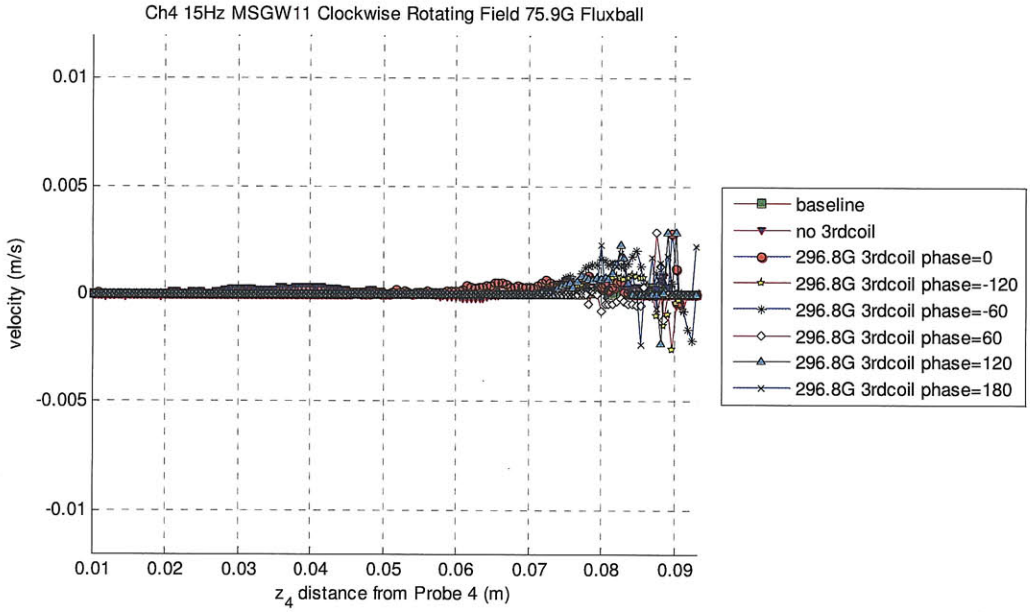
Ch4 15Hz MSGW11 Clockwise Rotating Field 75.9G Fluxball
velocity (m/s)
0.01
0.005
0
-0.005
-0.01
0.01
0.02
0.03
0.04
0.05
0.06
0.07
0.08
0.09
z4 distance from Probe 4 (m)
baseline
no 3rdcoil
296.8G 3rdcoil phase=0
296.8G 3rdcoil phase=-120
296.8G 3rdcoil phase=-60
296.8G 3rdcoil phase=60
296.8G 3rdcoil phase=120
296.8G 3rdcoil phase=180

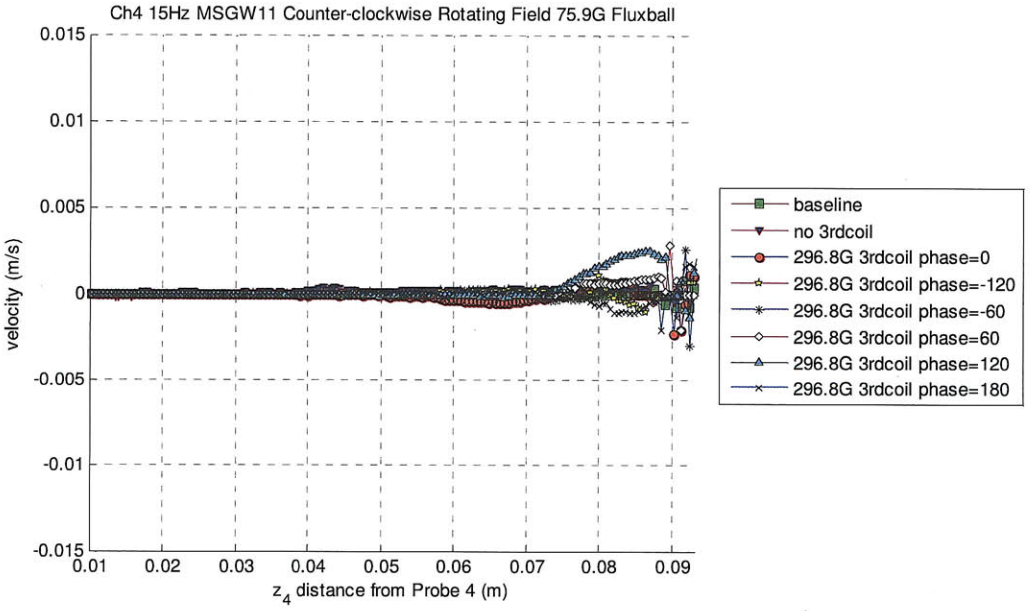
Ch4 15Hz MSGW11 Counter-clockwise Rotating Field 75.9G Fluxball
velocity (m/s)
0.015
0.01
0.005
0
-0.005
-0.01
-0.015
0.01
0.02
0.03
0.04
0.05
0.06
0.07
0.08
0.09
z4 distance from Probe 4 (m)
baseline
no 3rdcoil
296.8G 3rdcoil phase=0
296.8G 3rdcoil phase=-120
296.8G 3rdcoil phase=-60
296.8G 3rdcoil phase=60
296.8G 3rdcoil phase=120
296.8G 3rdcoil phase=180

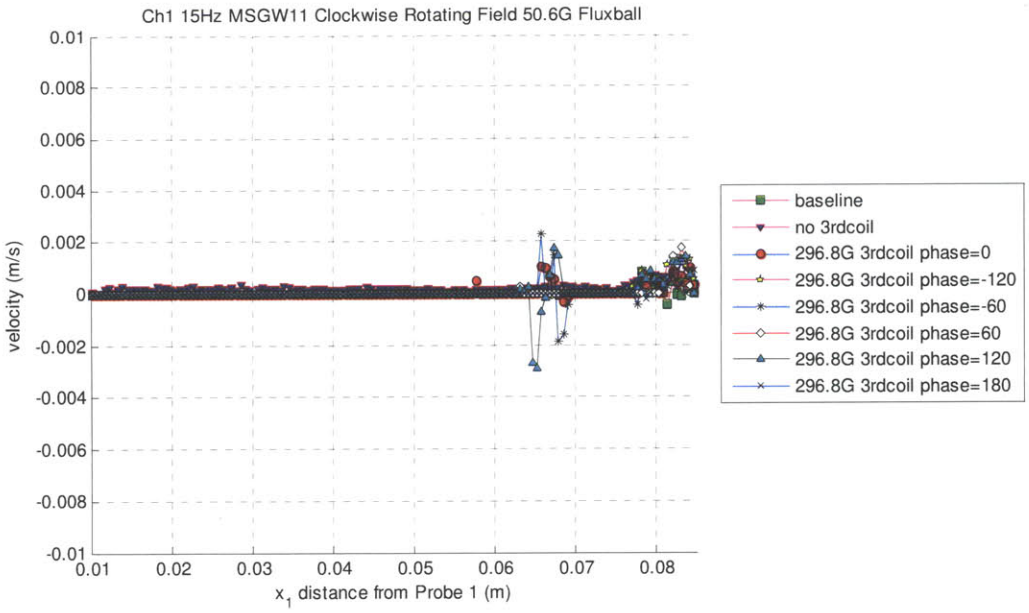
Ch1 15Hz MSGW11 Clockwise Rotating Field 50.6G Fluxball
velocity (m/s)
x1 distance from Probe 1 (m)
baseline
no 3rdcoil
296.8G 3rdcoil phase=0
296.8G 3rdcoil phase=-120
296.8G 3rdcoil phase=-60
296.8G 3rdcoil phase=60
296.8G 3rdcoil phase=120
296.8G 3rdcoil phase=180

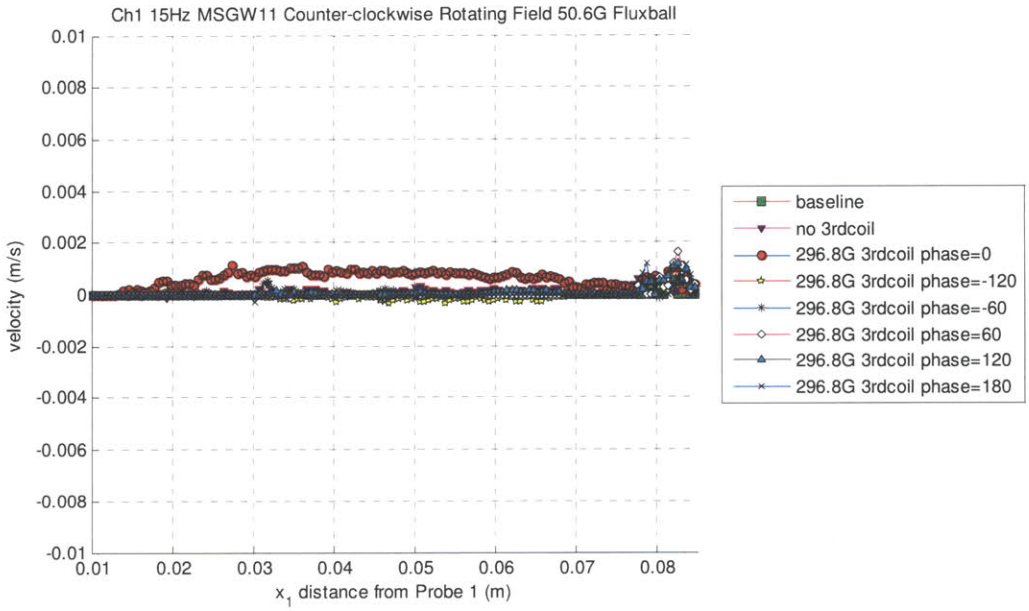
Ch1 15Hz MSGW11 Counter-clockwise Rotating Field 50.6G Fluxball
velocity (m/s)
x1 distance from Probe 1 (m)
baseline
no 3rdcoil
296.8G 3rdcoil phase=0
296.8G 3rdcoil phase=-120
296.8G 3rdcoil phase=-60
296.8G 3rdcoil phase=60
296.8G 3rdcoil phase=120
296.8G 3rdcoil phase=180

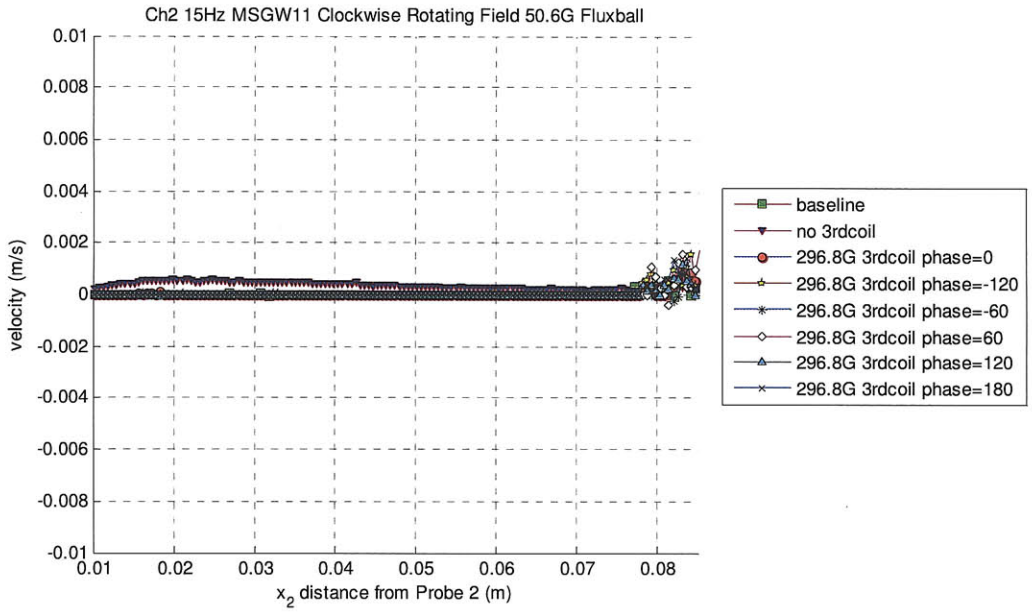
Ch2 15Hz MSGW11 Clockwise Rotating Field 50.6G Fluxball
velocity (m/s)
0.01
0.008
0.006
0.004
0.002
0
-0.002
-0.004
-0.006
-0.008
-0.01
0.01
0.02
0.03
0.04
0.05
0.06
0.07
0.08
x2 distance from Probe 2 (m)
baseline
no 3rdcoil
296.8G 3rdcoil phase=0
296.8G 3rdcoil phase=-120
296.8G 3rdcoil phase=-60
296.8G 3rdcoil phase=60
296.8G 3rdcoil phase=120
296.8G 3rdcoil phase=180

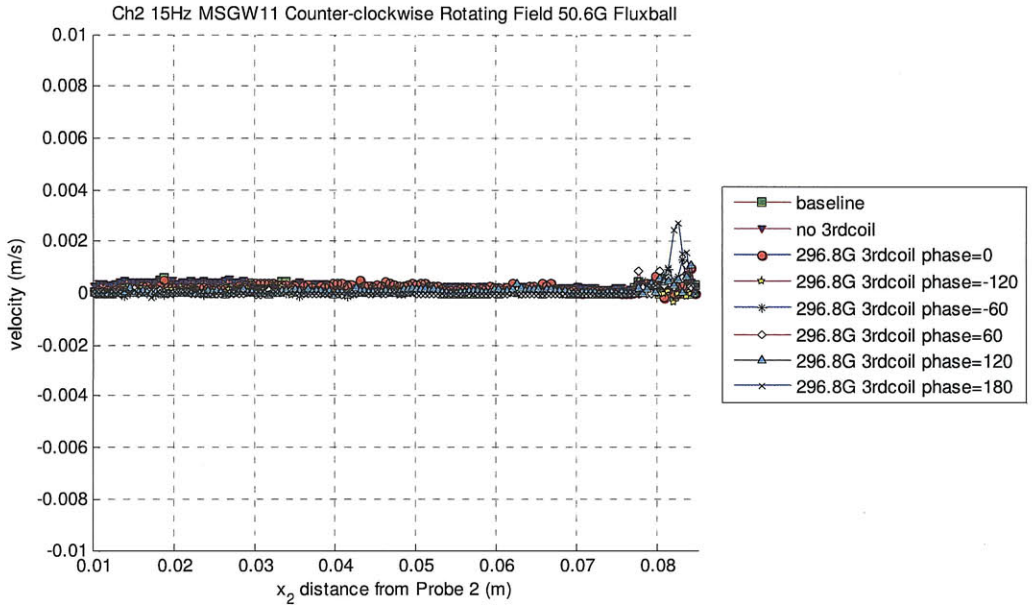
Ch2 15Hz MSGW11 Counter-clockwise Rotating Field 50.6G Fluxball
velocity (m/s)
0.01
0.008
0.006
0.004
0.002
0
-0.002
-0.004
-0.006
-0.008
-0.01
0.01
0.02
0.03
0.04
0.05
0.06
0.07
0.08
x2 distance from Probe 2 (m)
baseline
no 3rdcoil
296.8G 3rdcoil phase=0
296.8G 3rdcoil phase=-120
296.8G 3rdcoil phase=-60
296.8G 3rdcoil phase=60
296.8G 3rdcoil phase=120
296.8G 3rdcoil phase=180

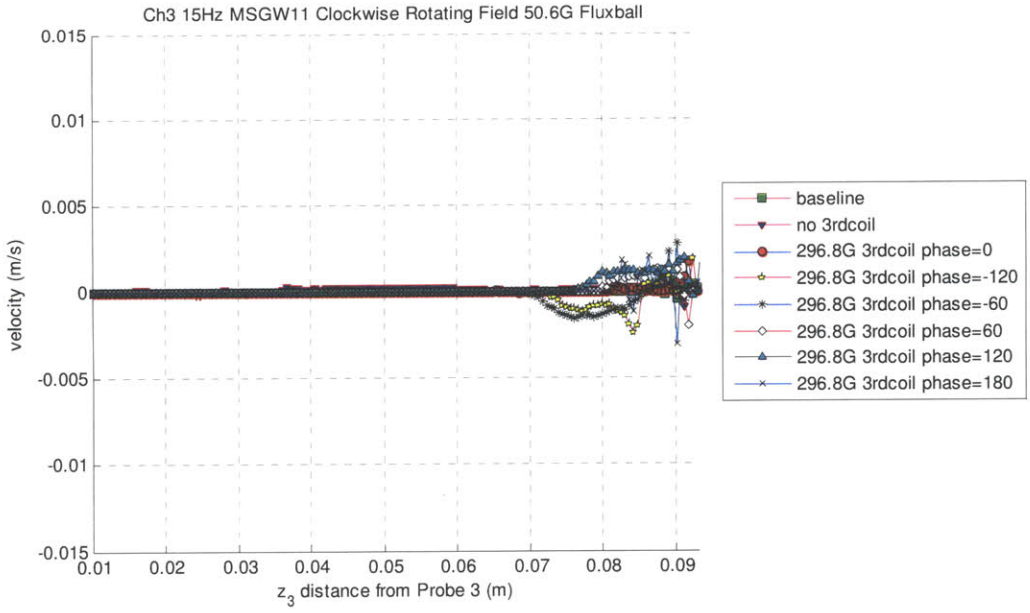
Ch3 15Hz MSGW11 Clockwise Rotating Field 50.6G Fluxball
velocity (m/s)
0.015
0.01
0.005
0
-0.005
-0.01
-0.015
0.01
0.02
0.03
0.04
0.05
0.06
0.07
0.08
0.09
z3 distance from Probe 3 (m)
baseline
no 3rdcoil
296.8G 3rdcoil phase=0
296.8G 3rdcoil phase=-120
296.8G 3rdcoil phase=-60
296.8G 3rdcoil phase=60
296.8G 3rdcoil phase=120
296.8G 3rdcoil phase=180

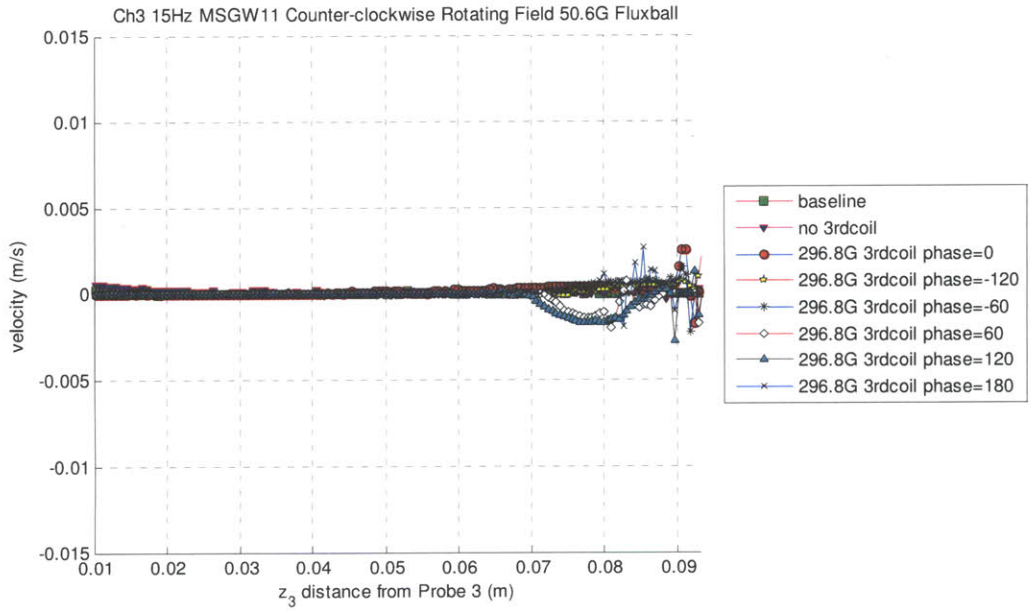
Ch3 15Hz MSGW11 Counter-clockwise Rotating Field 50.6G Fluxball
velocity (m/s)
0.015
0.01
0.005
0
-0.005
-0.01
-0.015
0.01
0.02
0.03
0.04
0.05
0.06
0.07
0.08
0.09
z3 distance from Probe 3 (m)
baseline
no 3rdcoil
296.8G 3rdcoil phase=0
296.8G 3rdcoil phase=-120
296.8G 3rdcoil phase=-60
296.8G 3rdcoil phase=60
296.8G 3rdcoil phase=120
296.8G 3rdcoil phase=180

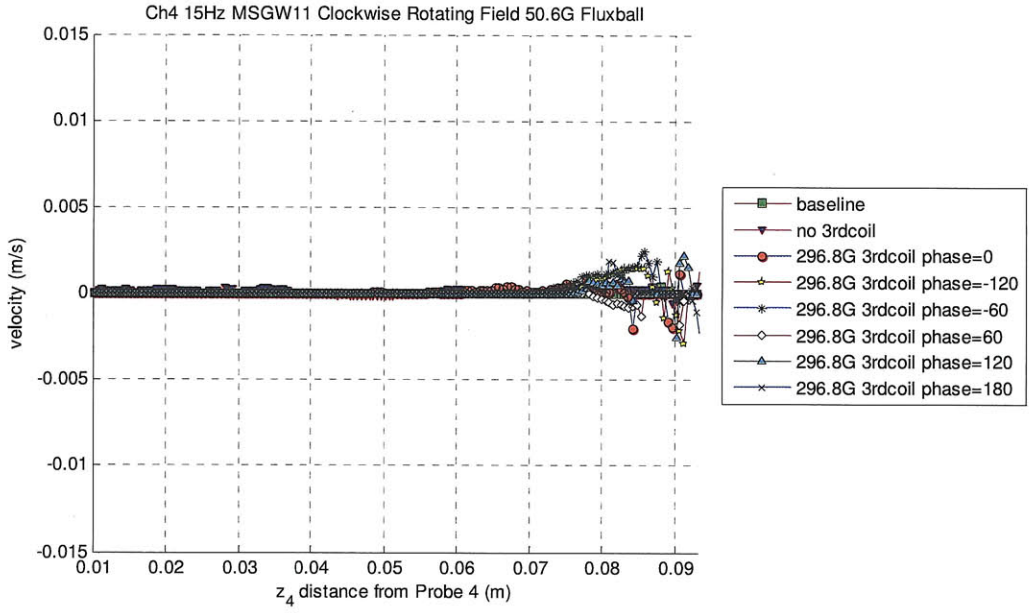
Ch4 15Hz MSGW11 Clockwise Rotating Field 50.6G Fluxball
velocity (m/s)
0.015
0.01
0.005
0
-0.005
-0.01
-0.015
0.01
0.02
0.03
0.04
0.05
0.06
0.07
0.08
0.09
z4 distance from Probe 4 (m)
baseline
no 3rdcoil
296.8G 3rdcoil phase=0
296.8G 3rdcoil phase=-120
296.8G 3rdcoil phase=-60
296.8G 3rdcoil phase=60
296.8G 3rdcoil phase=120
296.8G 3rdcoil phase=180

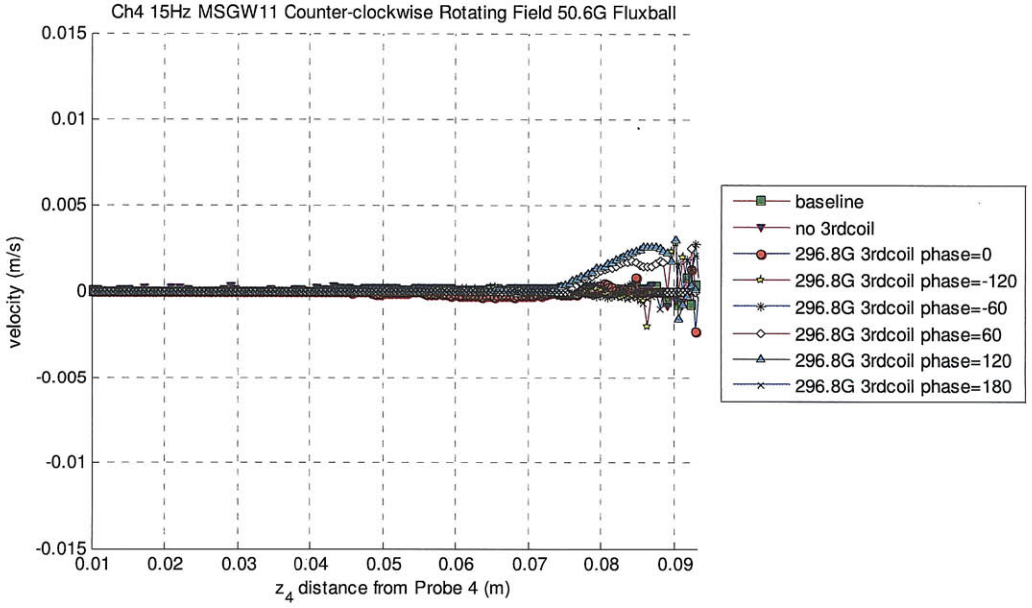
Ch4 15Hz MSGW11 Counter-clockwise Rotating Field 50.6G Fluxball
velocity (m/s)
0.015
0.01
0.005
0
-0.005
-0.01
-0.015
0.01
0.02
0.03
0.04
0.05
0.06
0.07
0.08
0.09
z4 distance from Probe 4 (m)
baseline
no 3rdcoil
296.8G 3rdcoil phase=0
296.8G 3rdcoil phase=-120
296.8G 3rdcoil phase=-60
296.8G 3rdcoil phase=60
296.8G 3rdcoil phase=120
296.8G 3rdcoil phase=180

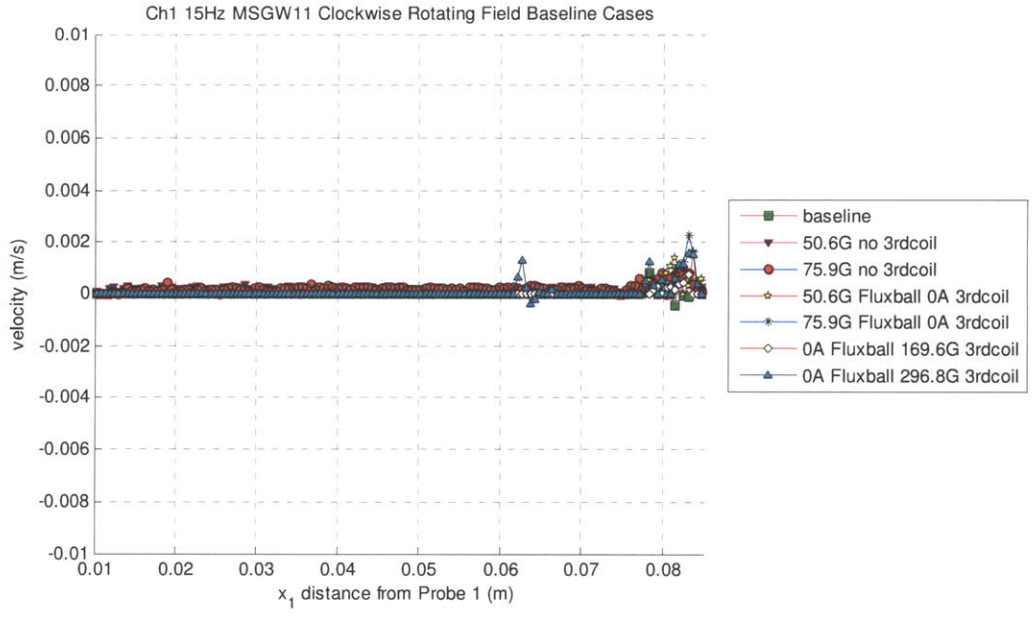
Ch1 15Hz MSGW11 Clockwise Rotating Field Baseline Cases
velocity (m/s)
x1 distance from Probe 1 (m)
baseline
50.6G no 3rdcoil
75.9G no 3rdcoil
50.6G Fluxball 0A 3rdcoil
75.9G Fluxball 0A 3rdcoil
0A Fluxball 169.6G 3rdcoil
0A Fluxball 296.8G 3rdcoil

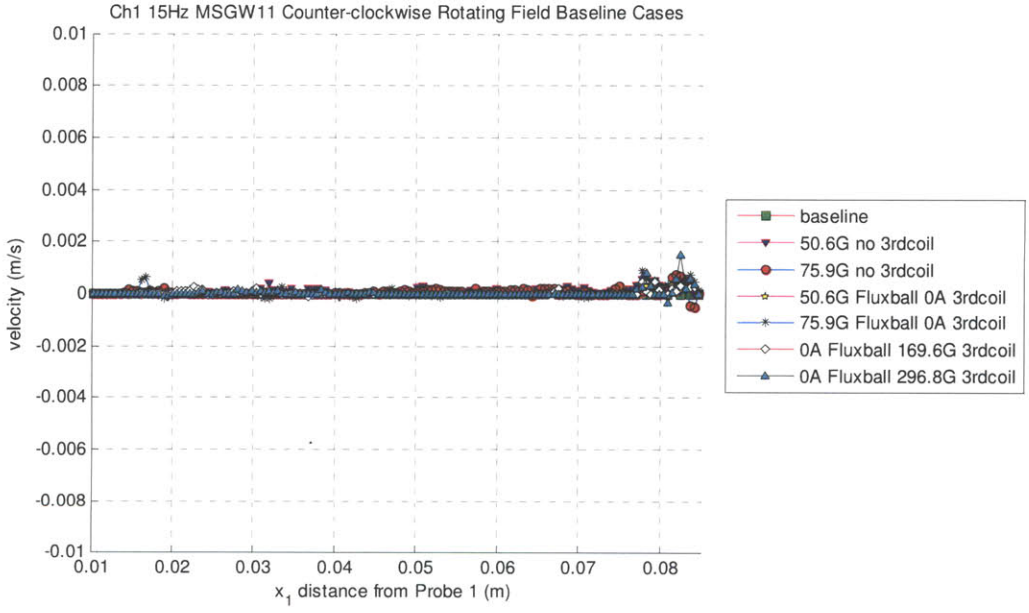
Ch1 15Hz MSGW11 Counter-clockwise Rotating Field Baseline Cases
velocity (m/s)
x1 distance from Probe 1 (m)
baseline
50.6G no 3rdcoil
75.9G no 3rdcoil
50.6G Fluxball 0A 3rdcoil
75.9G Fluxball 0A 3rdcoil
0A Fluxball 169.6G 3rdcoil
0A Fluxball 296.8G 3rdcoil

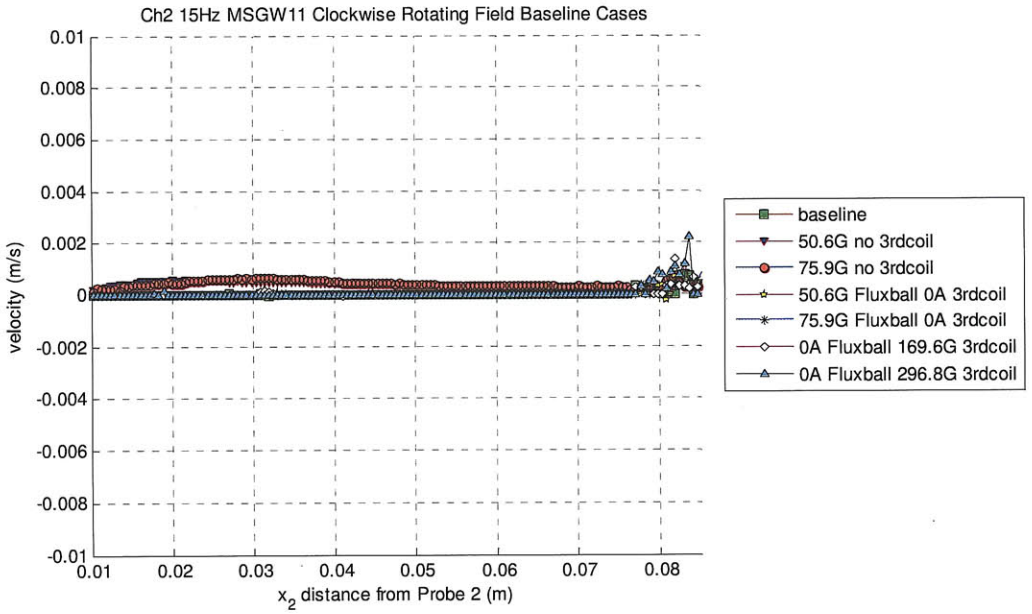
Ch2 15Hz MSGW11 Clockwise Rotating Field Baseline Cases
velocity (m/s)
0.01
0.008
0.006
0.004
0.002
0
-0.002
-0.004
-0.006
-0.008
-0.01
0.01
0.02
0.03
0.04
0.05
0.06
0.07
0.08
x2 distance from Probe 2 (m)
baseline
50.6G no 3rdcoil
75.9G no 3rdcoil
50.6G Fluxball 0A 3rdcoil
75.9G Fluxball 0A 3rdcoil
0A Fluxball 169.6G 3rdcoil
0A Fluxball 296.8G 3rdcoil

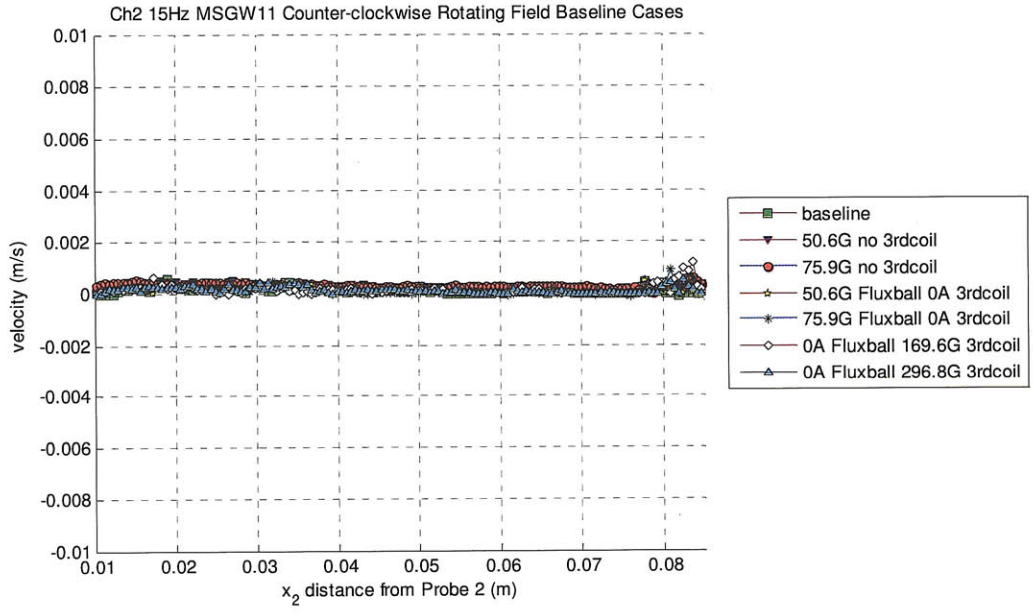
Ch2 15Hz MSGW11 Counter-clockwise Rotating Field Baseline Cases
velocity (m/s)
0.01
0.008
0.006
0.004
0.002
0
-0.002
-0.004
-0.006
-0.008
-0.01
0.01
0.02
0.03
0.04
0.05
0.06
0.07
0.08
x2 distance from Probe 2 (m)
baseline
50.6G no 3rdcoil
75.9G no 3rdcoil
50.6G Fluxball 0A 3rdcoil
75.9G Fluxball 0A 3rdcoil
0A Fluxball 169.6G 3rdcoil
0A Fluxball 296.8G 3rdcoil

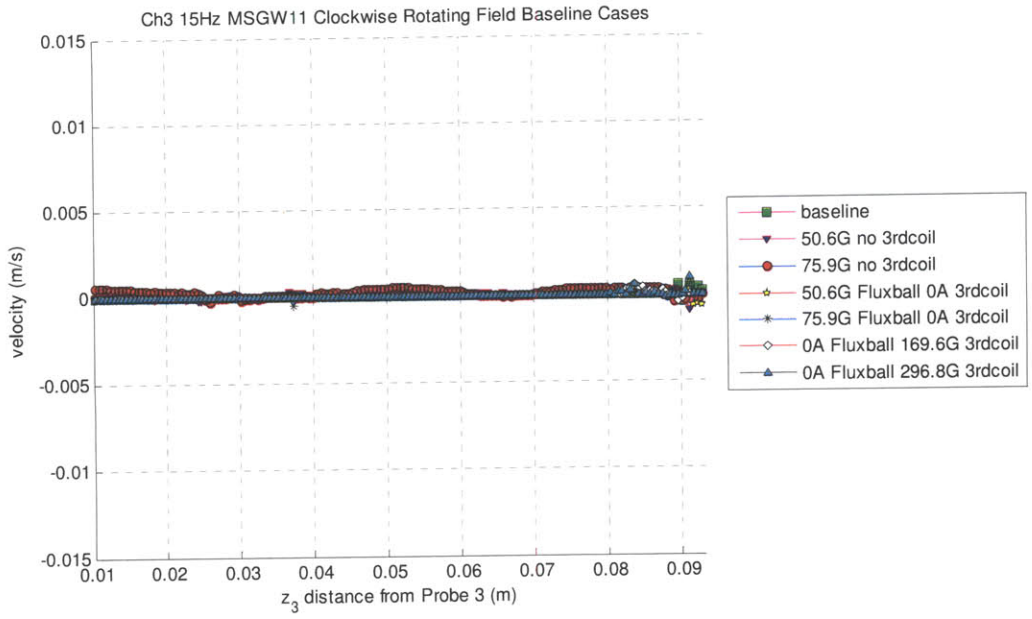
Ch3 15Hz MSGW11 Clockwise Rotating Field Baseline Cases
velocity (m/s)
0.015
0.01
0.005
0
-0.005
-0.01
-0.015
0.01
0.02
0.03
0.04
0.05
0.06
0.07
0.08
0.09
z3 distance from Probe 3 (m)
baseline
50.6G no 3rdcoil
75.9G no 3rdcoil
50.6G Fluxball 0A 3rdcoil
75.9G Fluxball 0A 3rdcoil
0A Fluxball 169.6G 3rdcoil
0A Fluxball 296.8G 3rdcoil

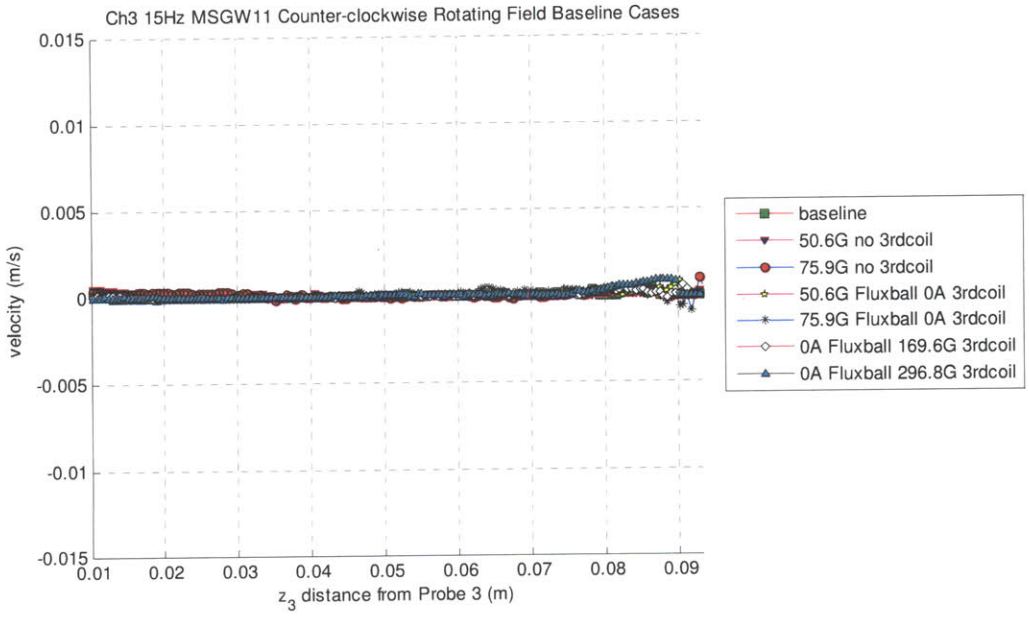
Ch3 15Hz MSGW11 Counter-clockwise Rotating Field Baseline Cases
velocity (m/s)
0.015
0.01
0.005
0
-0.005
-0.01
-0.015
0.01
0.02
0.03
0.04
0.05
0.06
0.07
0.08
0.09
z3 distance from Probe 3 (m)
baseline
50.6G no 3rdcoil
75.9G no 3rdcoil
50.6G Fluxball 0A 3rdcoil
75.9G Fluxball 0A 3rdcoil
0A Fluxball 169.6G 3rdcoil
0A Fluxball 296.8G 3rdcoil

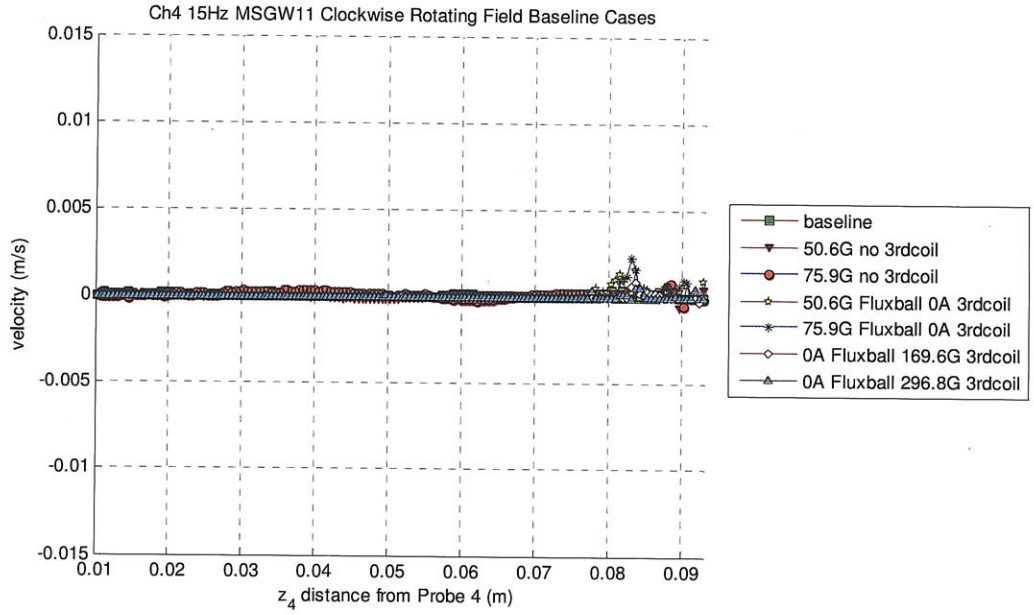
Ch4 15Hz MSGW11 Clockwise Rotating Field Baseline Cases
velocity (m/s)
0.015
0.01
0.005
0
-0.005
-0.01
-0.015
0.01
0.02
0.03
0.04
0.05
0.06
0.07
0.08
0.09
z4 distance from Probe 4 (m)
baseline
50.6G no 3rdcoil
75.9G no 3rdcoil
50.6G Fluxball 0A 3rdcoil
75.9G Fluxball 0A 3rdcoil
0A Fluxball 169.6G 3rdcoil
0A Fluxball 296.8G 3rdcoil

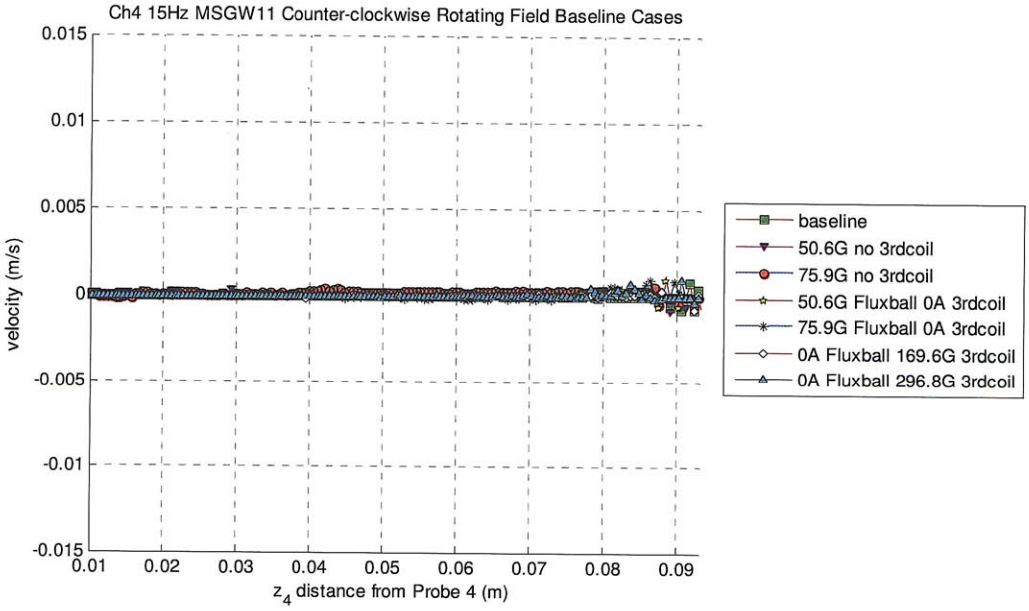
Ch4 15Hz MSGW11 Counter-clockwise Rotating Field Baseline Cases
velocity (m/s)
0.015
0.01
0.005
0
-0.005
-0.01
-0.015
0.01
0.02
0.03
0.04
0.05
0.06
0.07
0.08
0.09
z4 distance from Probe 4 (m)
baseline
50.6G no 3rdcoil
75.9G no 3rdcoil
50.6G Fluxball 0A 3rdcoil
75.9G Fluxball 0A 3rdcoil
0A Fluxball 169.6G 3rdcoil
0A Fluxball 296.8G 3rdcoil

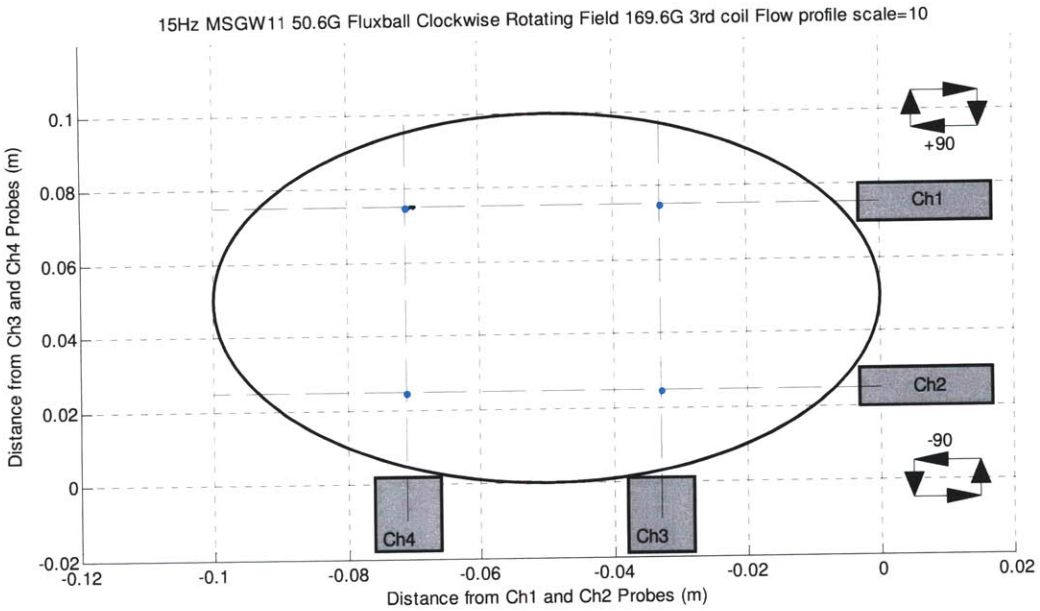
15Hz MSGW11 50.6G Fluxball Clockwise Rotating Field 169.6G 3rd coil Flow profile scale=10
Distance from Ch3 and Ch4 Probes (m)
Distance from Ch1 and Ch2 Probes (m)
0.1
0.08
0.06
0.04
0.02
0
-0.02
-0.12
-0.1
-0.08
-0.06
-0.04
-0.02
0
0.02
+90
-90
Ch1
Ch2
Ch3
Ch4

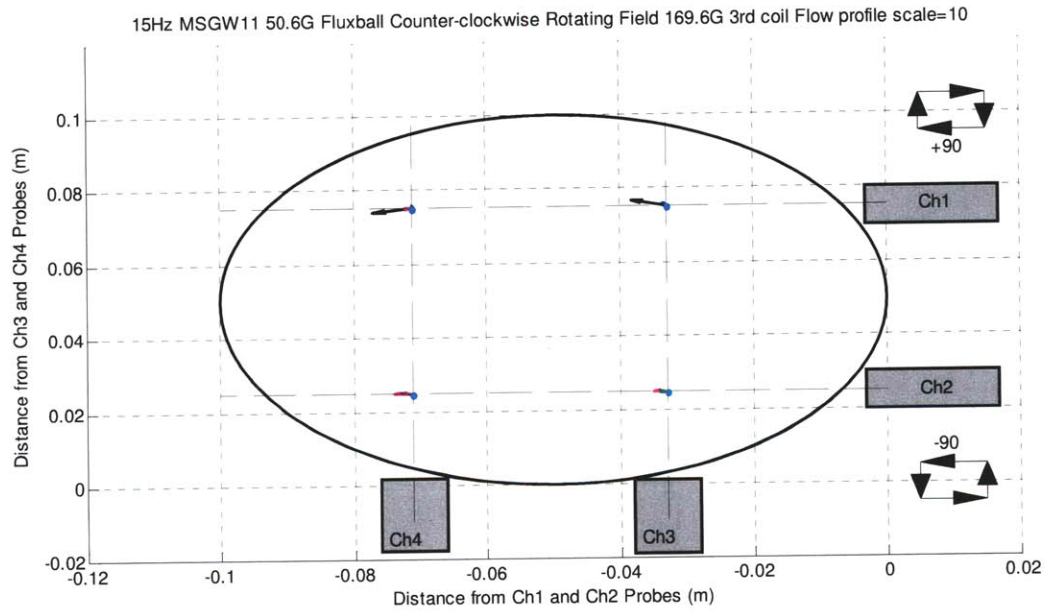
15Hz MSGW11 50.6G Fluxball Counter-clockwise Rotating Field 169.6G 3rd coil Flow profile scale=10
Distance from Ch3 and Ch4 Probes (m)
Distance from Ch1 and Ch2 Probes (m)
0.1
0.08
0.06
0.04
0.02
0
-0.02
-0.12
-0.1
-0.08
-0.06
-0.04
-0.02
0
0.02
+90
-90
Ch1
Ch2
Ch3
Ch4

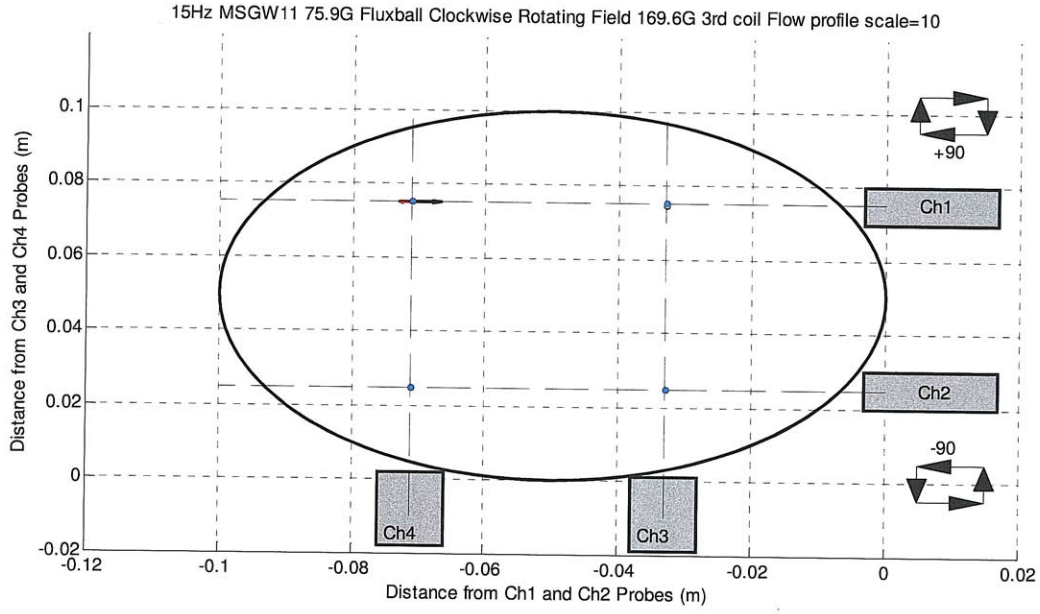
15Hz MSGW11 75.9G Fluxball Clockwise Rotating Field 169.6G 3rd coil Flow profile scale=10
Distance from Ch3 and Ch4 Probes (m)
Distance from Ch1 and Ch2 Probes (m)
0.1
0.08
0.06
0.04
0.02
0
-0.02
-0.12
-0.1
-0.08
-0.06
-0.04
-0.02
0
0.02
+90
-90
Ch1
Ch2
Ch3
Ch4

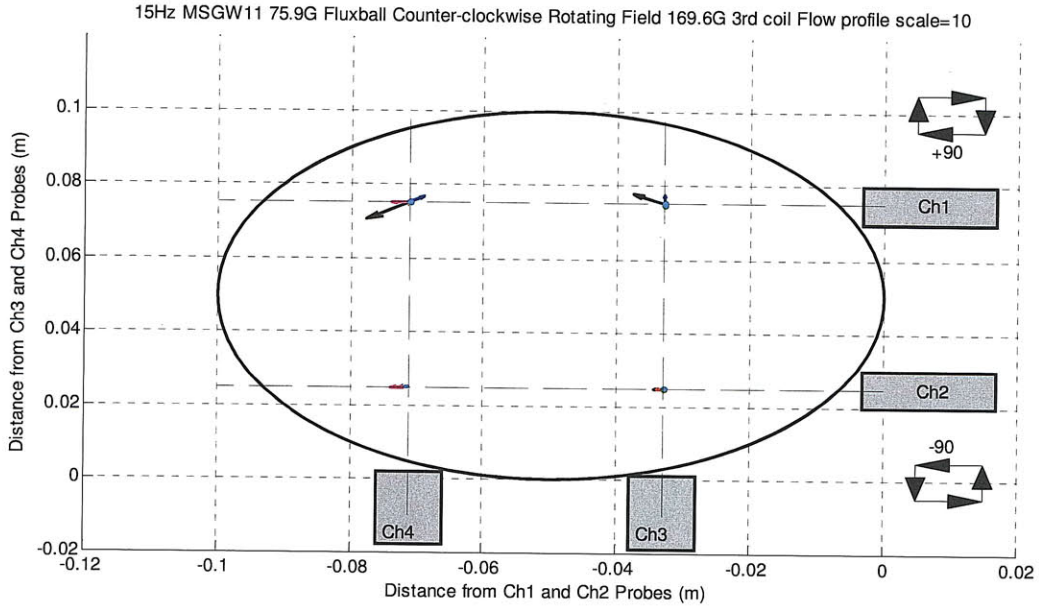
15Hz MSGW11 75.9G Fluxball Counter-clockwise Rotating Field 169.6G 3rd coil Flow profile scale=10
Distance from Ch3 and Ch4 Probes (m)
Distance from Ch1 and Ch2 Probes (m)
0.1
0.08
0.06
0.04
0.02
0
-0.02
-0.12
-0.1
-0.08
-0.06
-0.04
-0.02
0
0.02
+90
-90
Ch1
Ch2
Ch3
Ch4

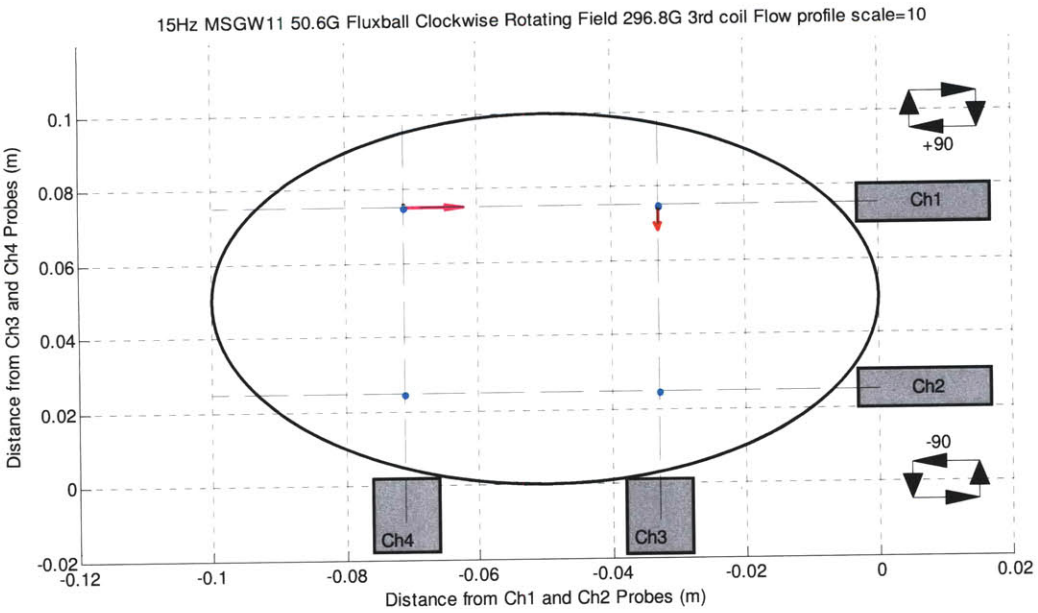
15Hz MSGW11 50.6G Fluxball Clockwise Rotating Field 296.8G 3rd coil Flow profile scale=10
Distance from Ch3 and Ch4 Probes (m)
Distance from Ch1 and Ch2 Probes (m)
0.1
0.08
0.06
0.04
0.02
0
-0.02
-0.12
-0.1
-0.08
-0.06
-0.04
-0.02
0
0.02
+90
-90
Ch1
Ch2
Ch3
Ch4

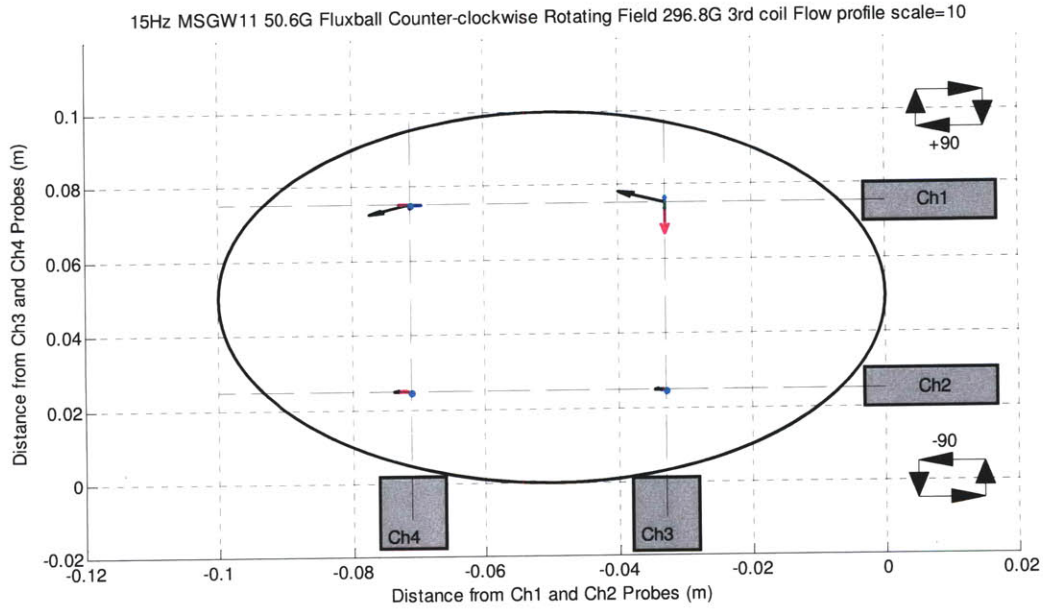
15Hz MSGW11 50.6G Fluxball Counter-clockwise Rotating Field 296.8G 3rd coil Flow profile scale=10
Distance from Ch3 and Ch4 Probes (m)
Distance from Ch1 and Ch2 Probes (m)
0.1
0.08
0.06
0.04
0.02
0
-0.02
-0.12
-0.1
-0.08
-0.06
-0.04
-0.02
0
0.02
+90
-90
Ch1
Ch2
Ch3
Ch4

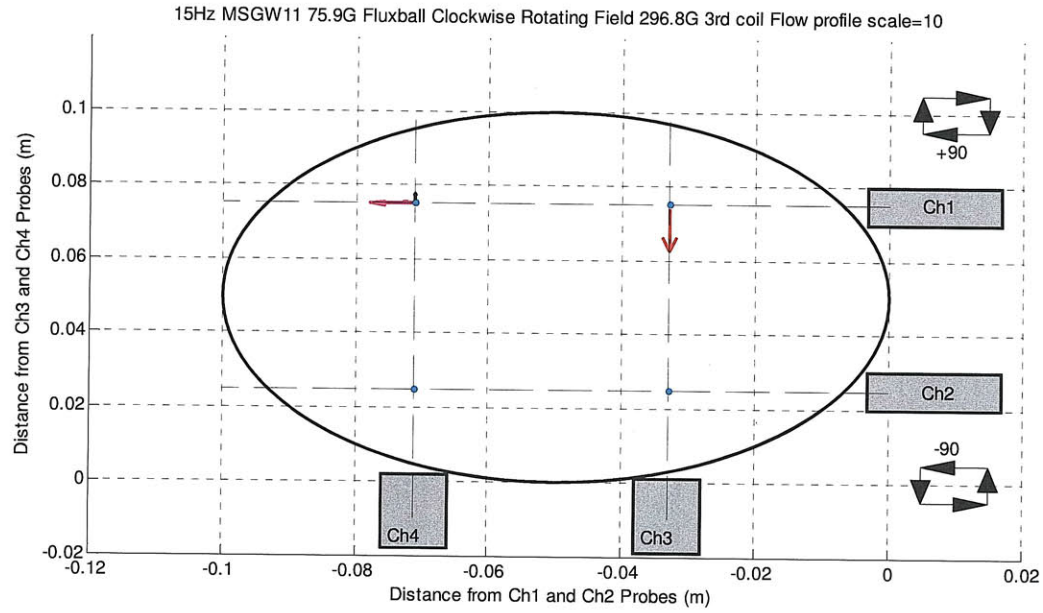
15Hz MSGW11 75.9G Fluxball Clockwise Rotating Field 296.8G 3rd coil Flow profile scale=10
Distance from Ch3 and Ch4 Probes (m)
Distance from Ch1 and Ch2 Probes (m)
0.1
0.08
0.06
0.04
0.02
0
-0.02
-0.12
-0.1
-0.08
-0.06
-0.04
-0.02
0
0.02
+90
-90
Ch1
Ch2
Ch3
Ch4

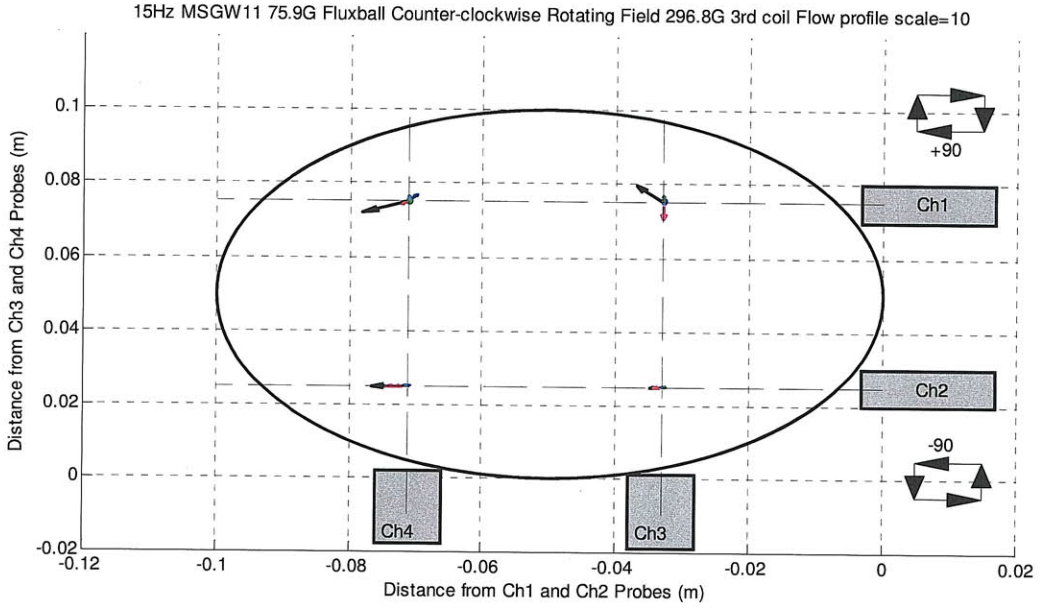
15Hz MSGW11 75.9G Fluxball Counter-clockwise Rotating Field 296.8G 3rd coil Flow profile scale=10
Distance from Ch3 and Ch4 Probes (m)
Distance from Ch1 and Ch2 Probes (m)
0.1
0.08
0.06
0.04
0.02
0
-0.02
-0.12
-0.1
-0.08
-0.06
-0.04
-0.02
0
0.02
+90
-90
Ch1
Ch2
Ch3
Ch4

G7. EFH1 Filled Sphere with Third Coil Imposing DC Field

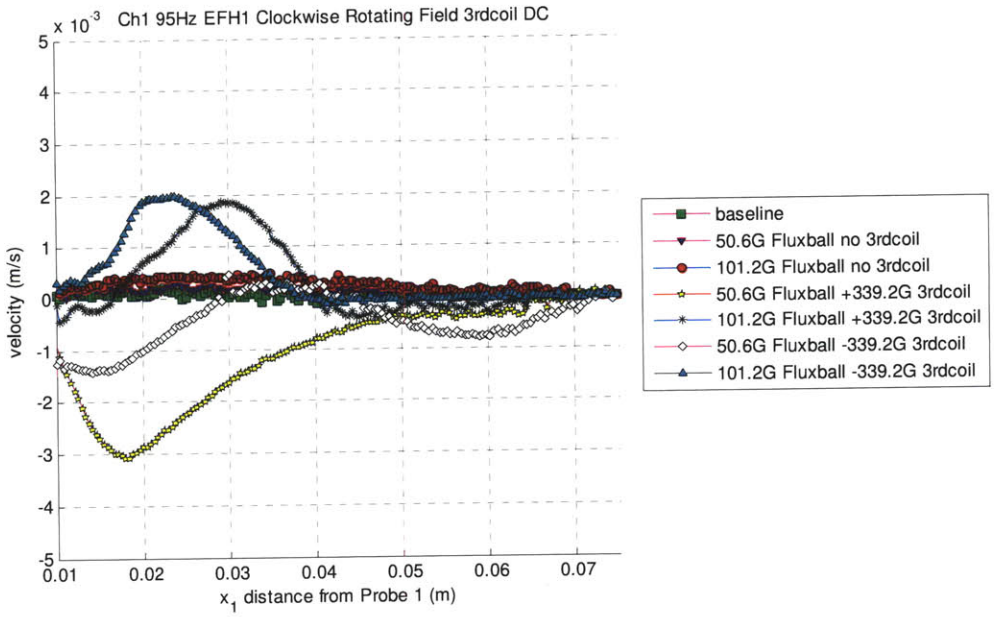

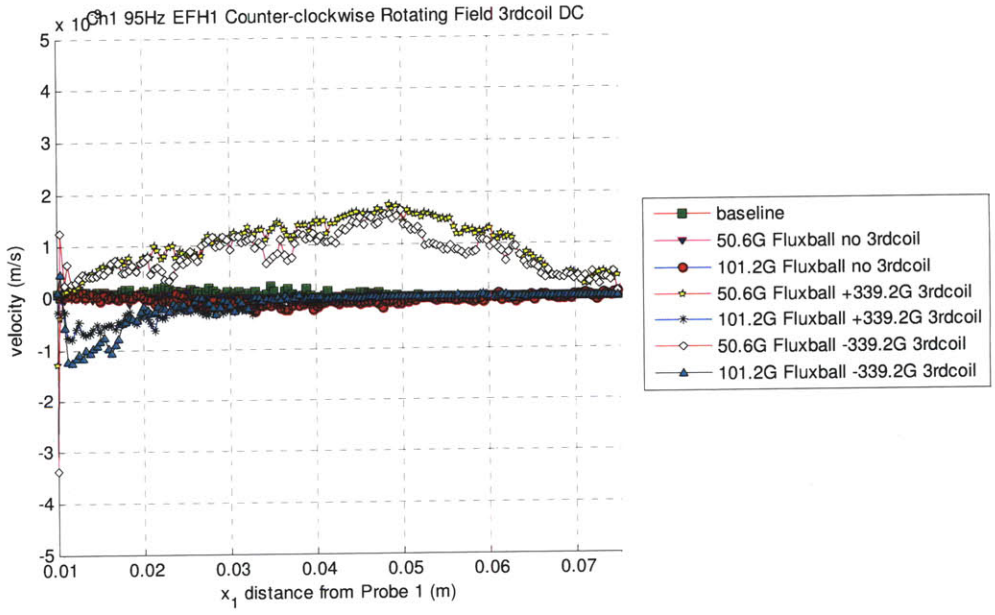

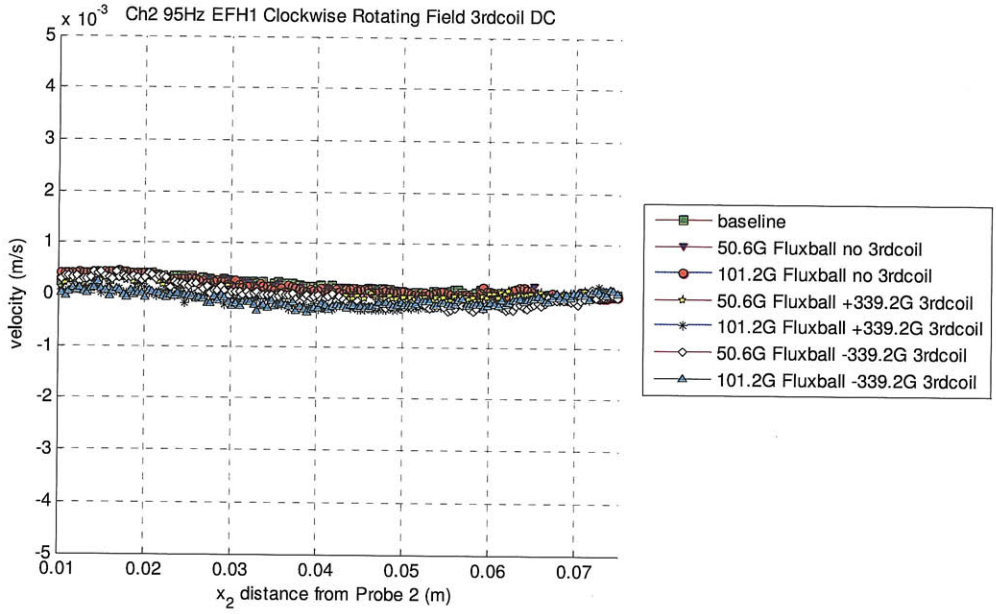
x 10^-3 Ch2 95Hz EFH1 Clockwise Rotating Field 3rdcoil DC
velocity (m/s)
x2 distance from Probe 2 (m)
baseline
50.6G Fluxball no 3rdcoil
101.2G Fluxball no 3rdcoil
50.6G Fluxball +339.2G 3rdcoil
101.2G Fluxball +339.2G 3rdcoil
50.6G Fluxball -339.2G 3rdcoil
101.2G Fluxball -339.2G 3rdcoil

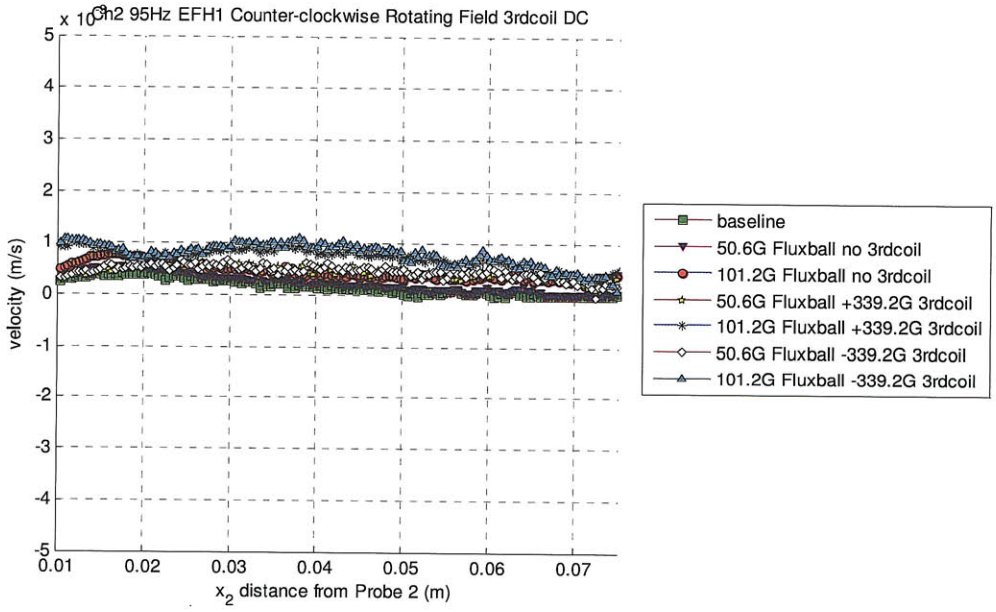
x 10^-3 Ch2 95Hz EFH1 Counter-clockwise Rotating Field 3rdcoil DC
velocity (m/s)
x2 distance from Probe 2 (m)
baseline
50.6G Fluxball no 3rdcoil
101.2G Fluxball no 3rdcoil
50.6G Fluxball +339.2G 3rdcoil
101.2G Fluxball +339.2G 3rdcoil
50.6G Fluxball -339.2G 3rdcoil
101.2G Fluxball -339.2G 3rdcoil

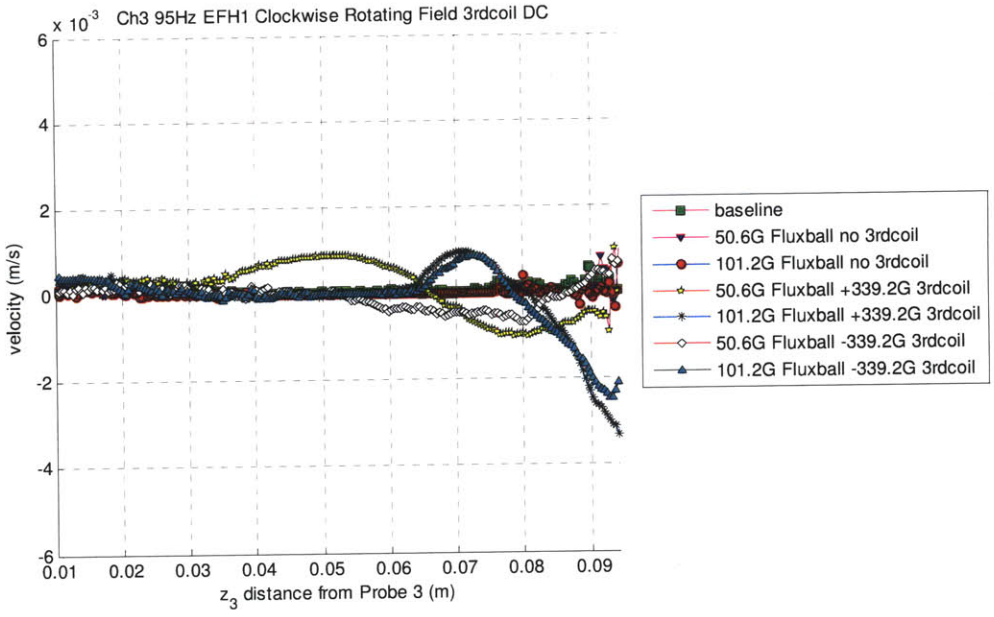
x 10^-3
Ch3 95Hz EFH1 Clockwise Rotating Field 3rdcoil DC
velocity (m/s)
z3 distance from Probe 3 (m)
baseline
50.6G Fluxball no 3rdcoil
101.2G Fluxball no 3rdcoil
50.6G Fluxball +339.2G 3rdcoil
101.2G Fluxball +339.2G 3rdcoil
50.6G Fluxball -339.2G 3rdcoil
101.2G Fluxball -339.2G 3rdcoil

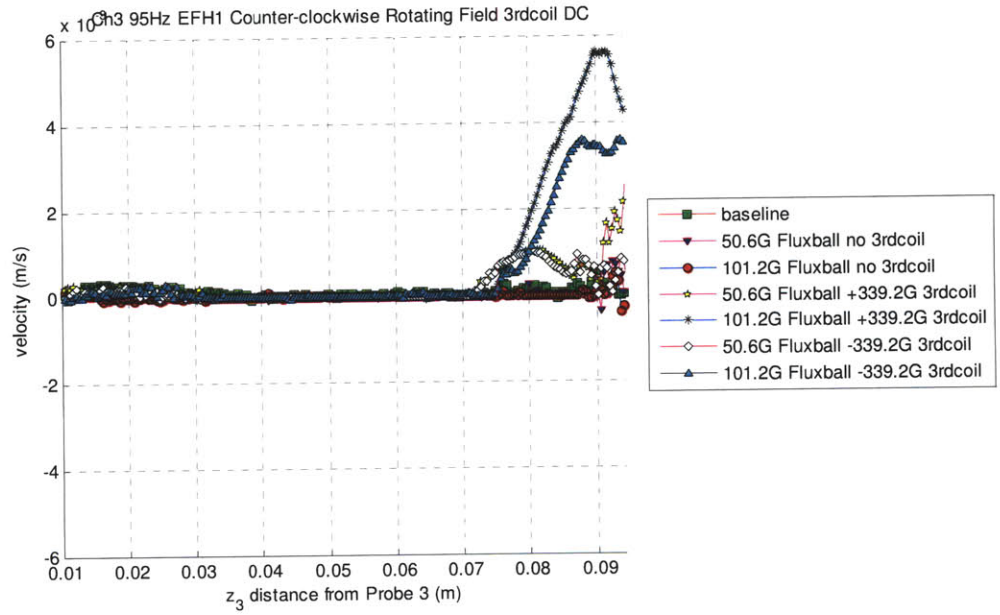
x 10^-3
Ch3 95Hz EFH1 Counter-clockwise Rotating Field 3rdcoil DC
velocity (m/s)
z3 distance from Probe 3 (m)
baseline
50.6G Fluxball no 3rdcoil
101.2G Fluxball no 3rdcoil
50.6G Fluxball +339.2G 3rdcoil
101.2G Fluxball +339.2G 3rdcoil
50.6G Fluxball -339.2G 3rdcoil
101.2G Fluxball -339.2G 3rdcoil

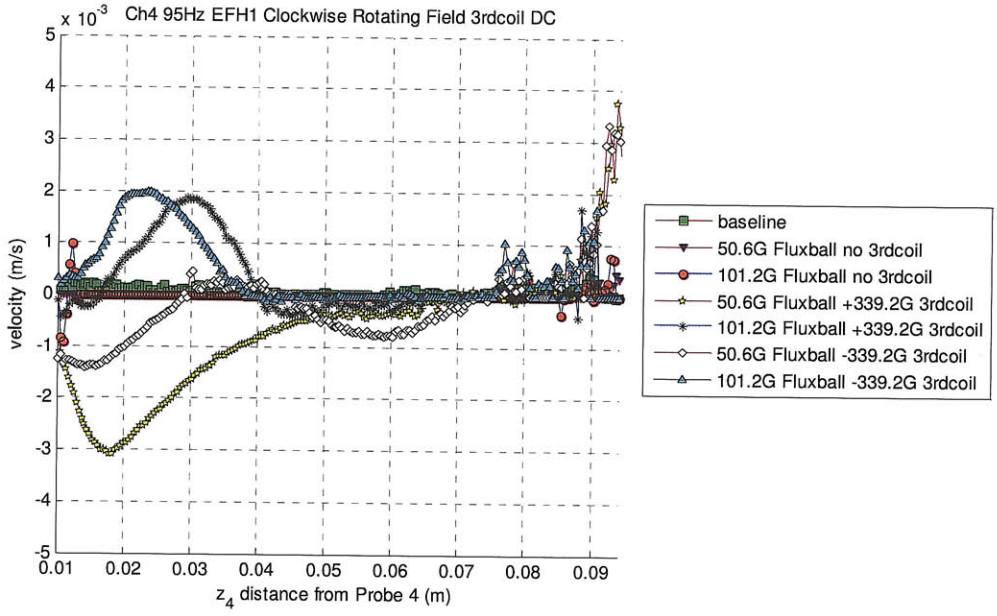
x 10^-3 Ch4 95Hz EFH1 Clockwise Rotating Field 3rdcoil DC
velocity (m/s)
z4 distance from Probe 4 (m)
baseline
50.6G Fluxball no 3rdcoil
101.2G Fluxball no 3rdcoil
50.6G Fluxball +339.2G 3rdcoil
101.2G Fluxball +339.2G 3rdcoil
50.6G Fluxball -339.2G 3rdcoil
101.2G Fluxball -339.2G 3rdcoil

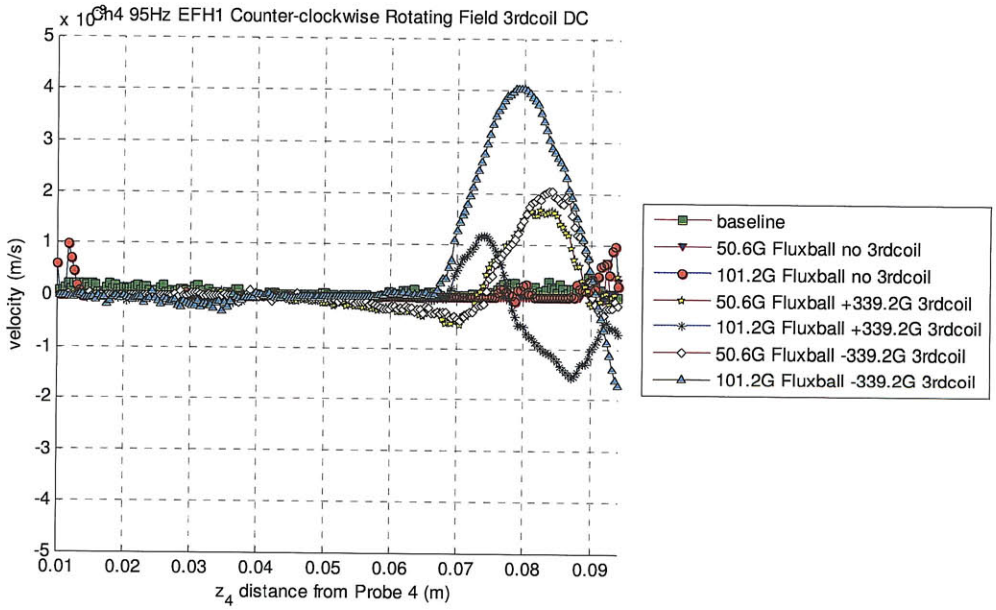
x 10^-3 Ch4 95Hz EFH1 Counter-clockwise Rotating Field 3rdcoil DC
velocity (m/s)
z4 distance from Probe 4 (m)
baseline
50.6G Fluxball no 3rdcoil
101.2G Fluxball no 3rdcoil
50.6G Fluxball +339.2G 3rdcoil
101.2G Fluxball +339.2G 3rdcoil
50.6G Fluxball -339.2G 3rdcoil
101.2G Fluxball -339.2G 3rdcoil

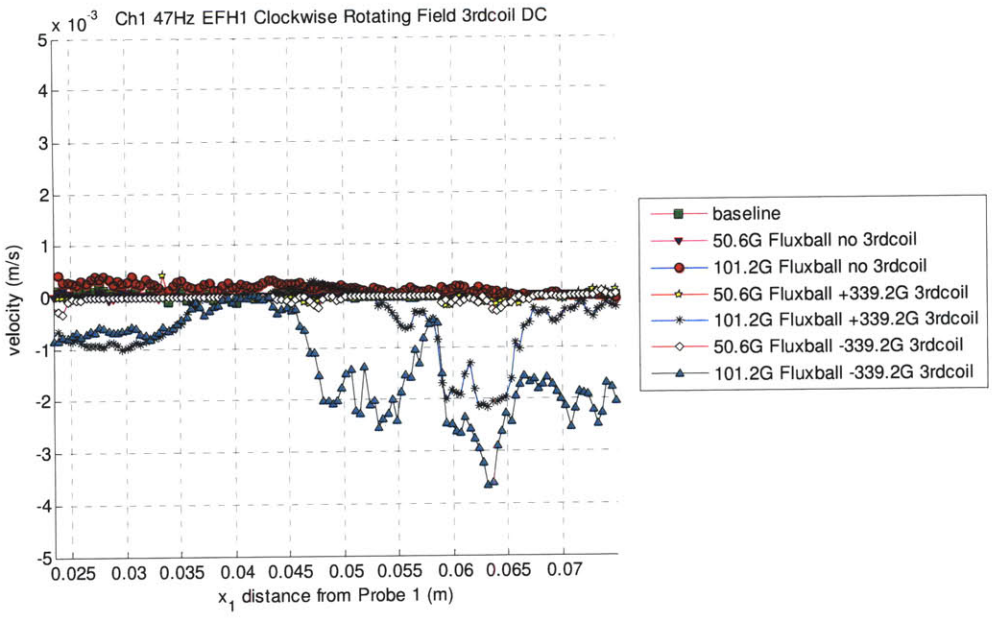
x 10^-3 Ch1 47Hz EFH1 Clockwise Rotating Field 3rdcoil DC
velocity (m/s)
x1 distance from Probe 1 (m)
baseline
50.6G Fluxball no 3rdcoil
101.2G Fluxball no 3rdcoil
50.6G Fluxball +339.2G 3rdcoil
101.2G Fluxball +339.2G 3rdcoil
50.6G Fluxball -339.2G 3rdcoil
101.2G Fluxball -339.2G 3rdcoil

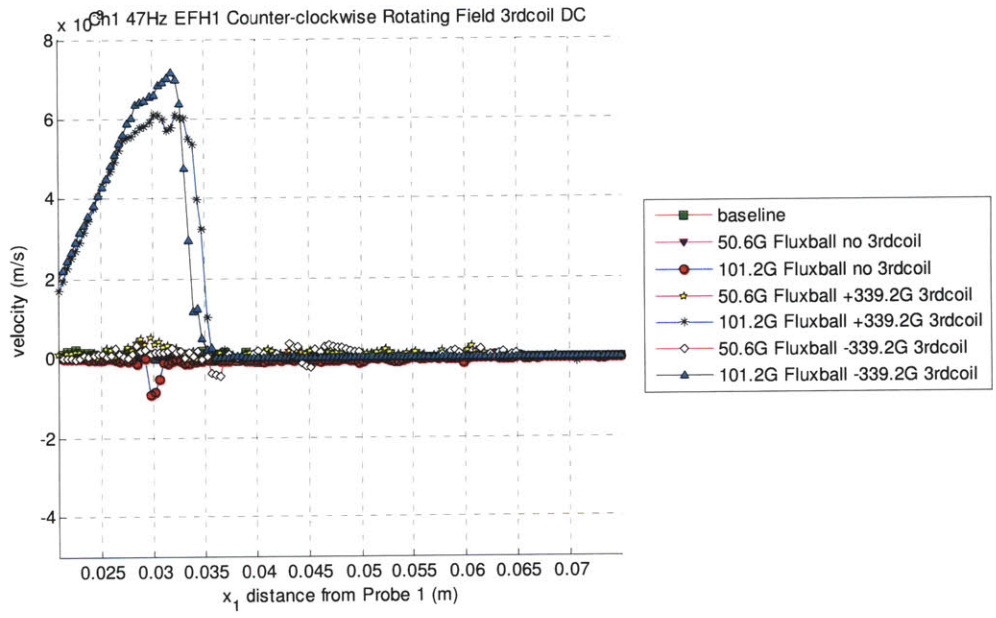
x 10^-3 Ch1 47Hz EFH1 Counter-clockwise Rotating Field 3rdcoil DC
velocity (m/s)
x1 distance from Probe 1 (m)
baseline
50.6G Fluxball no 3rdcoil
101.2G Fluxball no 3rdcoil
50.6G Fluxball +339.2G 3rdcoil
101.2G Fluxball +339.2G 3rdcoil
50.6G Fluxball -339.2G 3rdcoil
101.2G Fluxball -339.2G 3rdcoil

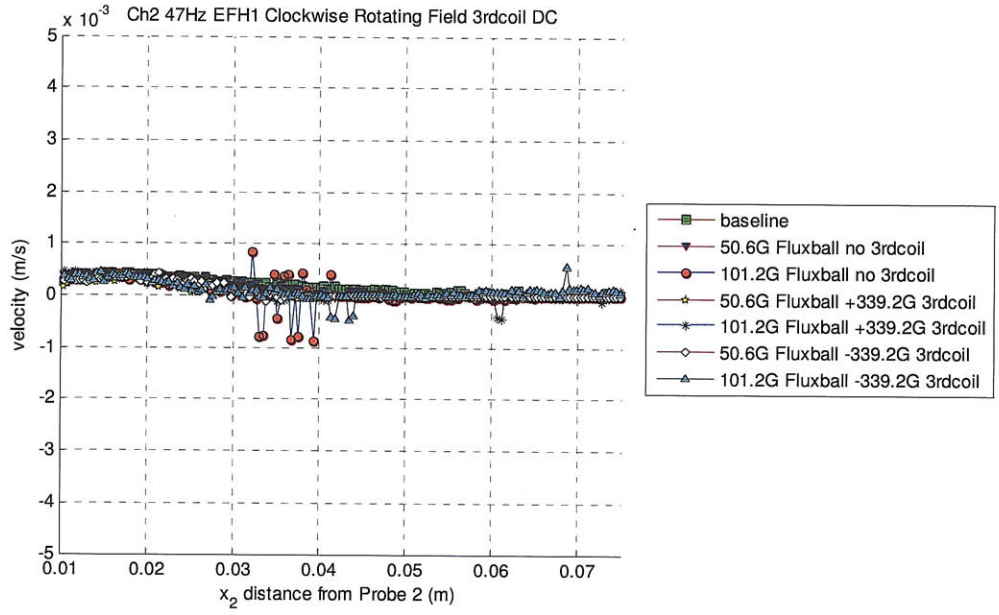
x 10^-3 Ch2 47Hz EFH1 Clockwise Rotating Field 3rdcoil DC
velocity (m/s)
x2 distance from Probe 2 (m)
baseline
50.6G Fluxball no 3rdcoil
101.2G Fluxball no 3rdcoil
50.6G Fluxball +339.2G 3rdcoil
101.2G Fluxball +339.2G 3rdcoil
50.6G Fluxball -339.2G 3rdcoil
101.2G Fluxball -339.2G 3rdcoil

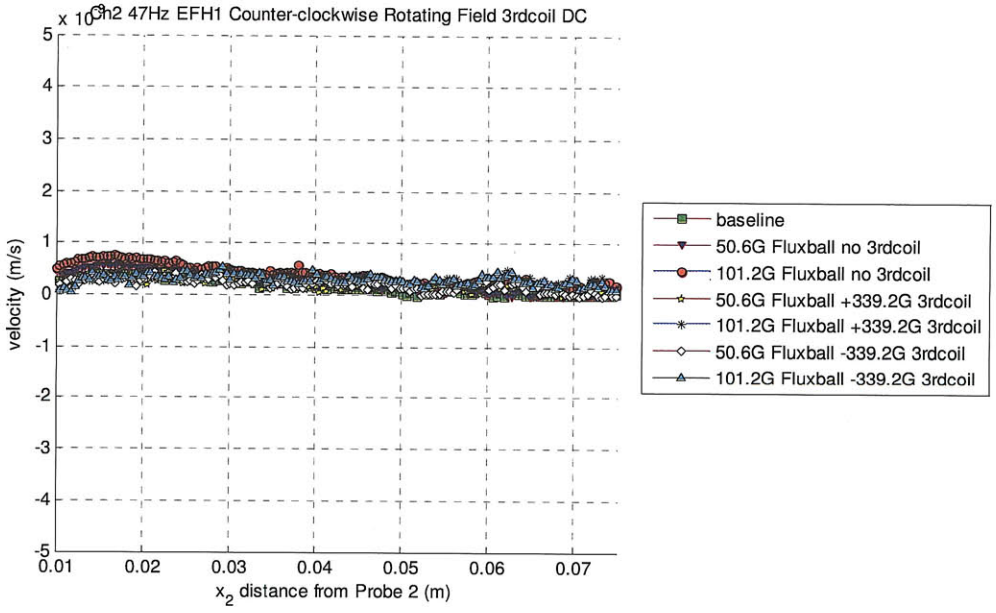
x 10^-3 Ch2 47Hz EFH1 Counter-clockwise Rotating Field 3rdcoil DC
velocity (m/s)
x2 distance from Probe 2 (m)
baseline
50.6G Fluxball no 3rdcoil
101.2G Fluxball no 3rdcoil
50.6G Fluxball +339.2G 3rdcoil
101.2G Fluxball +339.2G 3rdcoil
50.6G Fluxball -339.2G 3rdcoil
101.2G Fluxball -339.2G 3rdcoil

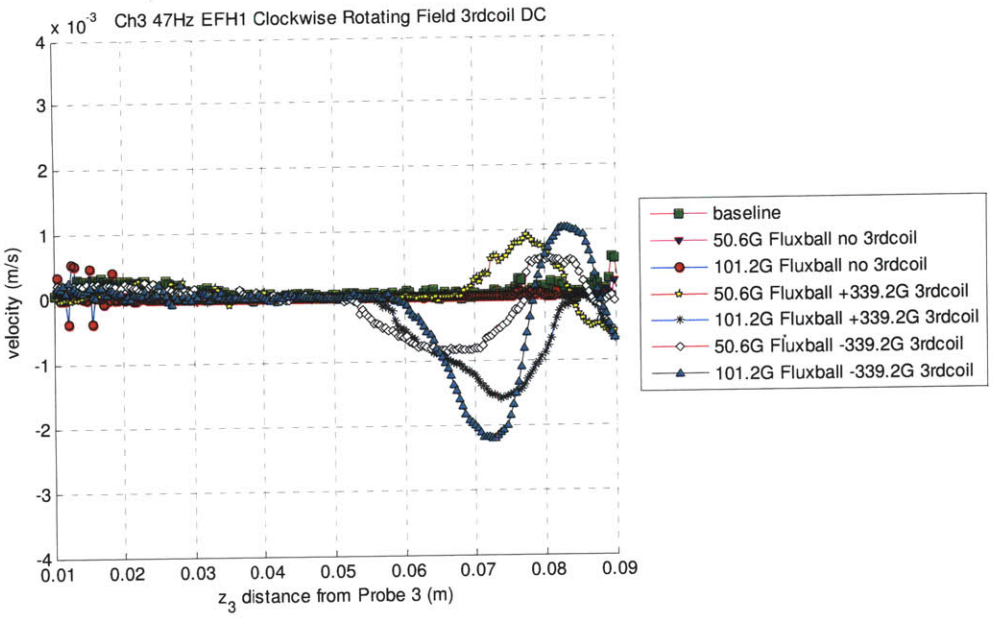
x 10^-3 Ch3 47Hz EFH1 Clockwise Rotating Field 3rdcoil DC
velocity (m/s)
z3 distance from Probe 3 (m)
baseline
50.6G Fluxball no 3rdcoil
101.2G Fluxball no 3rdcoil
50.6G Fluxball +339.2G 3rdcoil
101.2G Fluxball +339.2G 3rdcoil
50.6G Fluxball -339.2G 3rdcoil
101.2G Fluxball -339.2G 3rdcoil

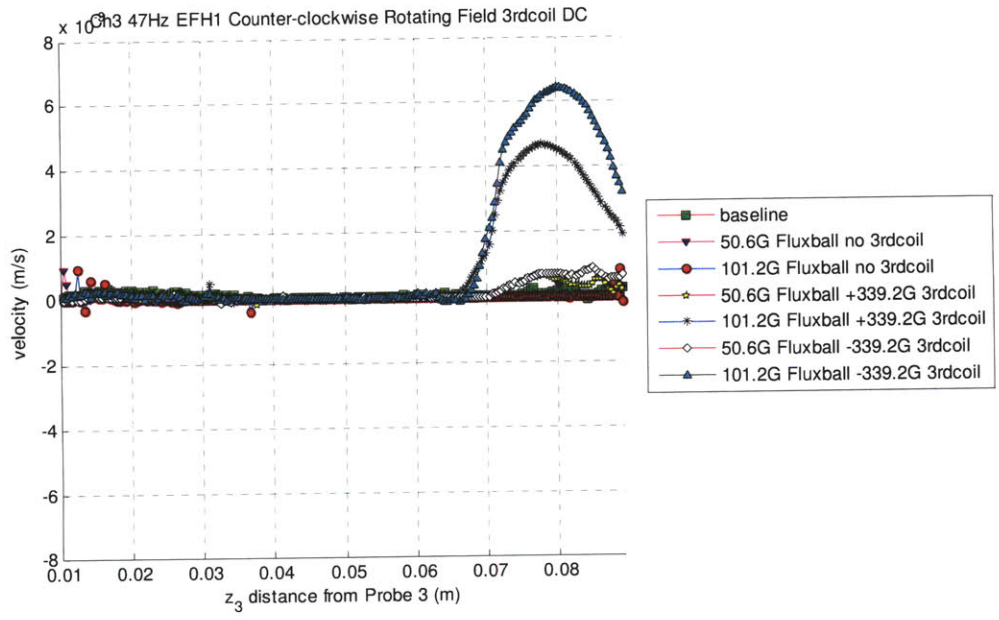
x 10^-3 Ch3 47Hz EFH1 Counter-clockwise Rotating Field 3rdcoil DC
velocity (m/s)
z3 distance from Probe 3 (m)
baseline
50.6G Fluxball no 3rdcoil
101.2G Fluxball no 3rdcoil
50.6G Fluxball +339.2G 3rdcoil
101.2G Fluxball +339.2G 3rdcoil
50.6G Fluxball -339.2G 3rdcoil
101.2G Fluxball -339.2G 3rdcoil

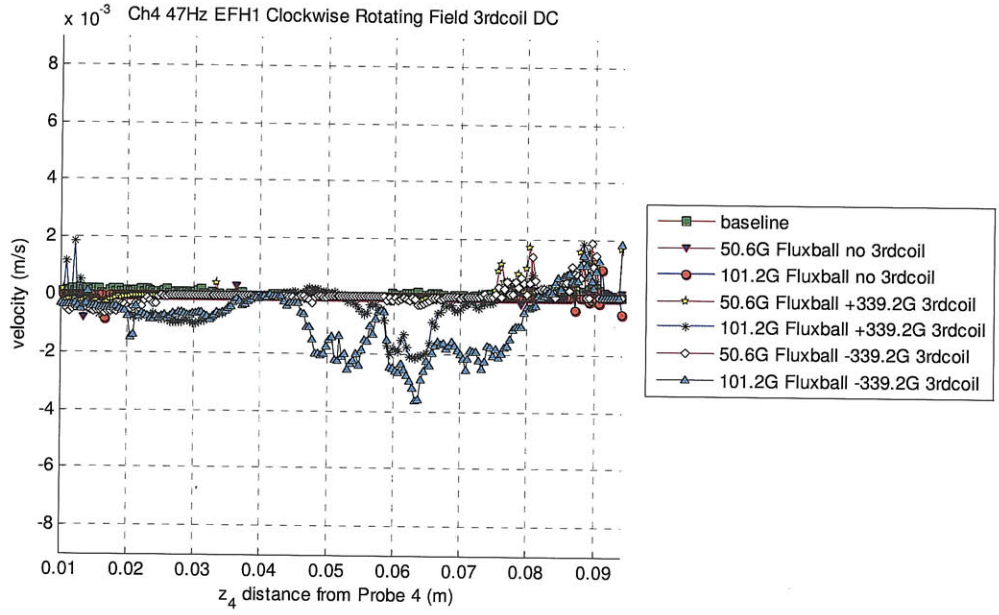
x 10^-3 Ch4 47Hz EFH1 Clockwise Rotating Field 3rdcoil DC
velocity (m/s)
z4 distance from Probe 4 (m)
baseline
50.6G Fluxball no 3rdcoil
101.2G Fluxball no 3rdcoil
50.6G Fluxball +339.2G 3rdcoil
101.2G Fluxball +339.2G 3rdcoil
50.6G Fluxball -339.2G 3rdcoil
101.2G Fluxball -339.2G 3rdcoil

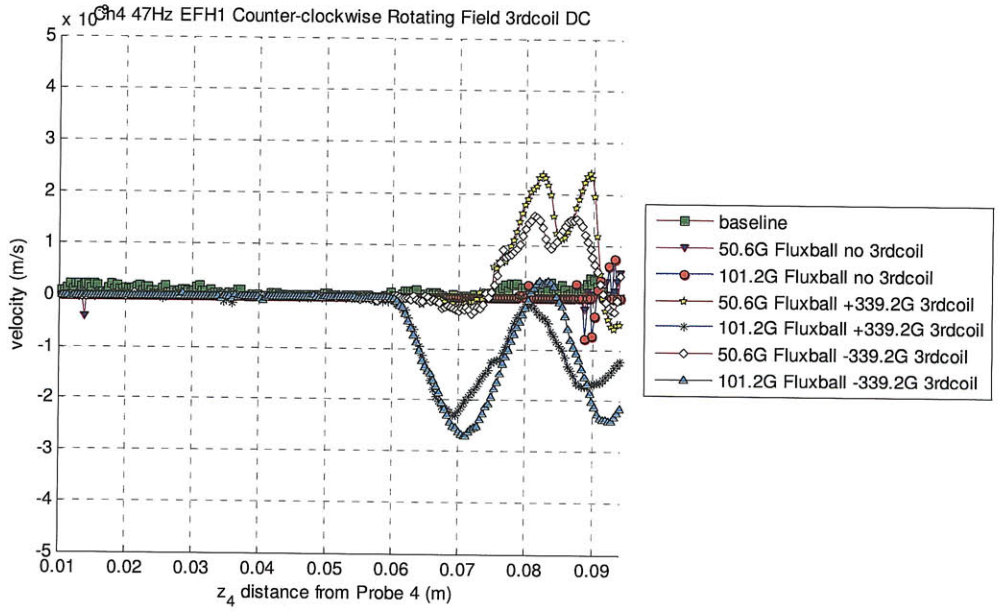
x 10^-3 Ch4 47Hz EFH1 Counter-clockwise Rotating Field 3rdcoil DC
velocity (m/s)
z4 distance from Probe 4 (m)
baseline
50.6G Fluxball no 3rdcoil
101.2G Fluxball no 3rdcoil
50.6G Fluxball +339.2G 3rdcoil
101.2G Fluxball +339.2G 3rdcoil
50.6G Fluxball -339.2G 3rdcoil
101.2G Fluxball -339.2G 3rdcoil

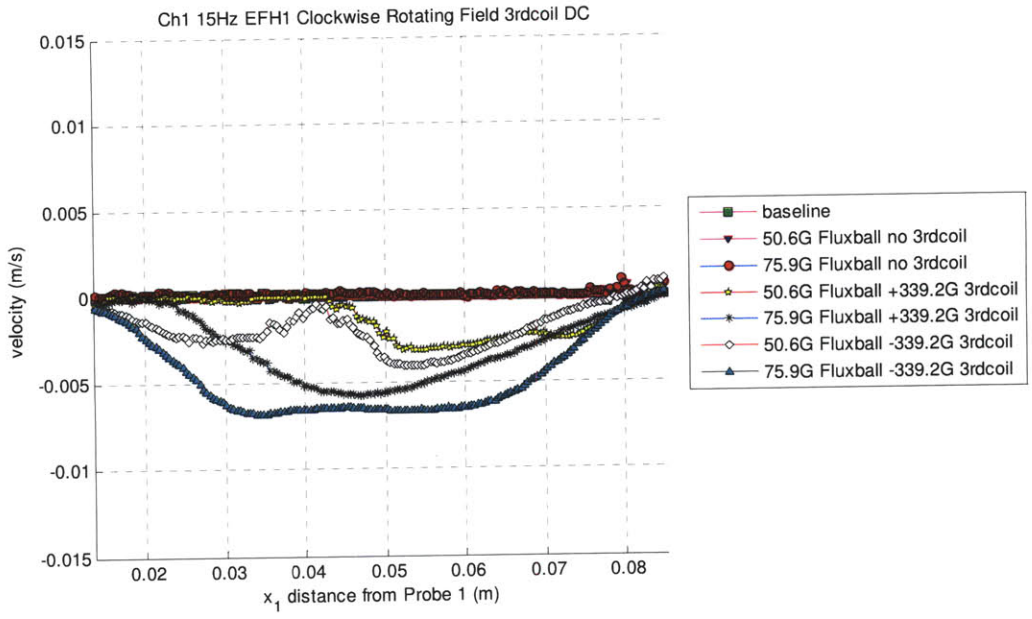
Ch1 15Hz EFH1 Clockwise Rotating Field 3rdcoil DC
velocity (m/s)
0.015
0.01
0.005
0
-0.005
-0.01
-0.015
0.02
0.03
0.04
0.05
0.06
0.07
0.08
x1 distance from Probe 1 (m)
baseline
50.6G Fluxball no 3rdcoil
75.9G Fluxball no 3rdcoil
50.6G Fluxball +339.2G 3rdcoil
75.9G Fluxball +339.2G 3rdcoil
50.6G Fluxball -339.2G 3rdcoil
75.9G Fluxball -339.2G 3rdcoil

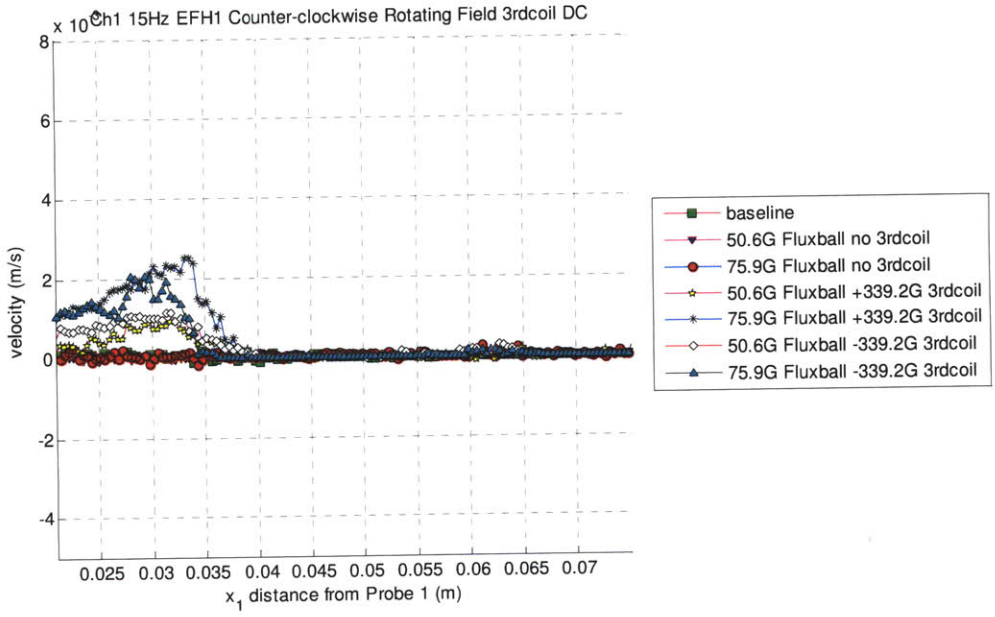
Ch1 15Hz EFH1 Counter-clockwise Rotating Field 3rdcoil DC
x 10
velocity (m/s)
8
6
4
2
0
-2
-4
0.025
0.03
0.035
0.04
0.045
0.05
0.055
0.06
0.065
0.07
x1 distance from Probe 1 (m)
baseline
50.6G Fluxball no 3rdcoil
75.9G Fluxball no 3rdcoil
50.6G Fluxball +339.2G 3rdcoil
75.9G Fluxball +339.2G 3rdcoil
50.6G Fluxball -339.2G 3rdcoil
75.9G Fluxball -339.2G 3rdcoil

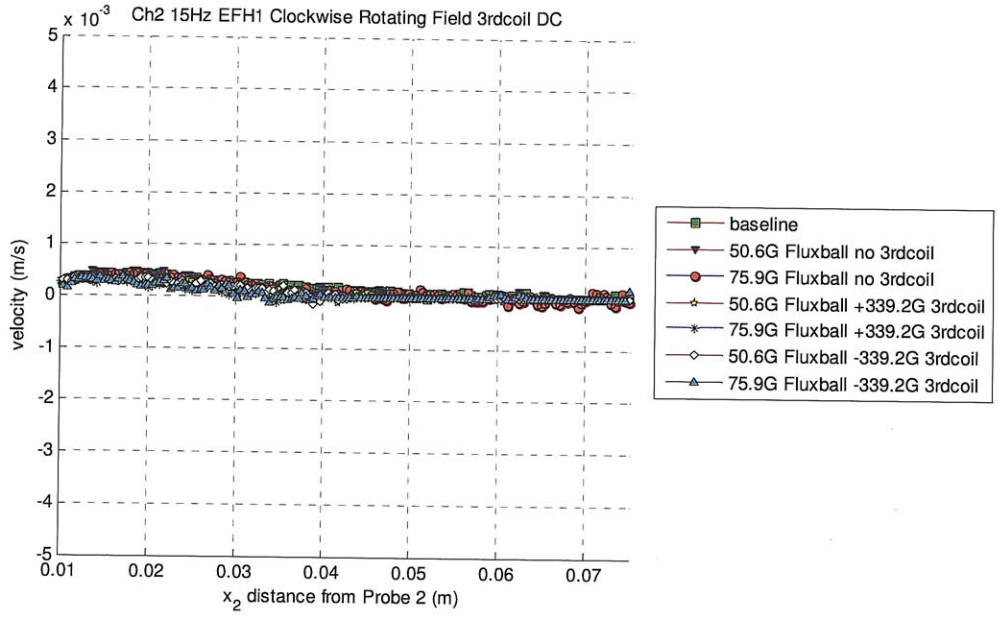
x 10^-3 Ch2 15Hz EFH1 Clockwise Rotating Field 3rdcoil DC
velocity (m/s)
x2 distance from Probe 2 (m)
baseline
50.6G Fluxball no 3rdcoil
75.9G Fluxball no 3rdcoil
50.6G Fluxball +339.2G 3rdcoil
75.9G Fluxball +339.2G 3rdcoil
50.6G Fluxball -339.2G 3rdcoil
75.9G Fluxball -339.2G 3rdcoil

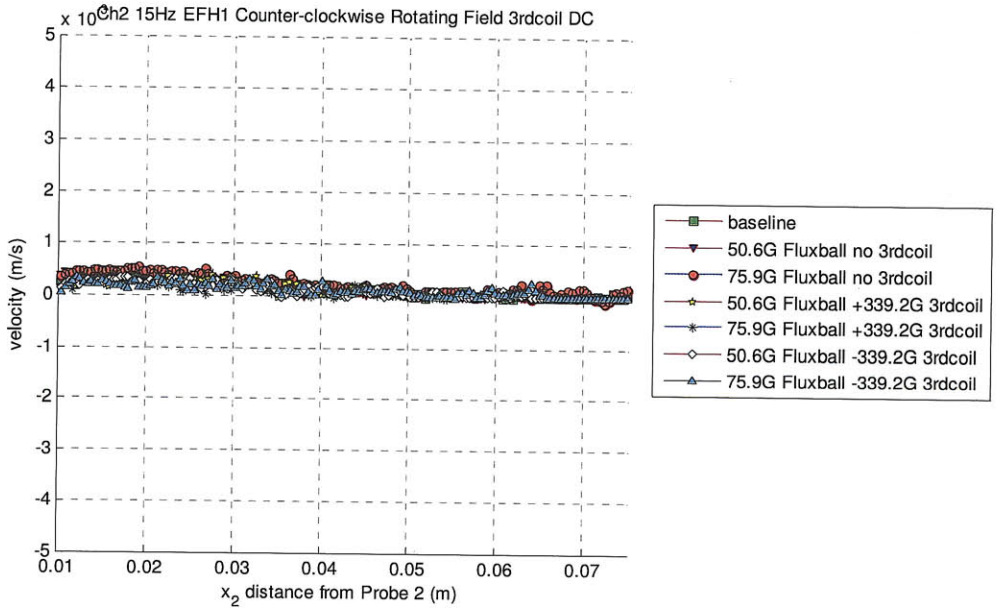
x 10^-3 Ch2 15Hz EFH1 Counter-clockwise Rotating Field 3rdcoil DC
velocity (m/s)
x2 distance from Probe 2 (m)
baseline
50.6G Fluxball no 3rdcoil
75.9G Fluxball no 3rdcoil
50.6G Fluxball +339.2G 3rdcoil
75.9G Fluxball +339.2G 3rdcoil
50.6G Fluxball -339.2G 3rdcoil
75.9G Fluxball -339.2G 3rdcoil

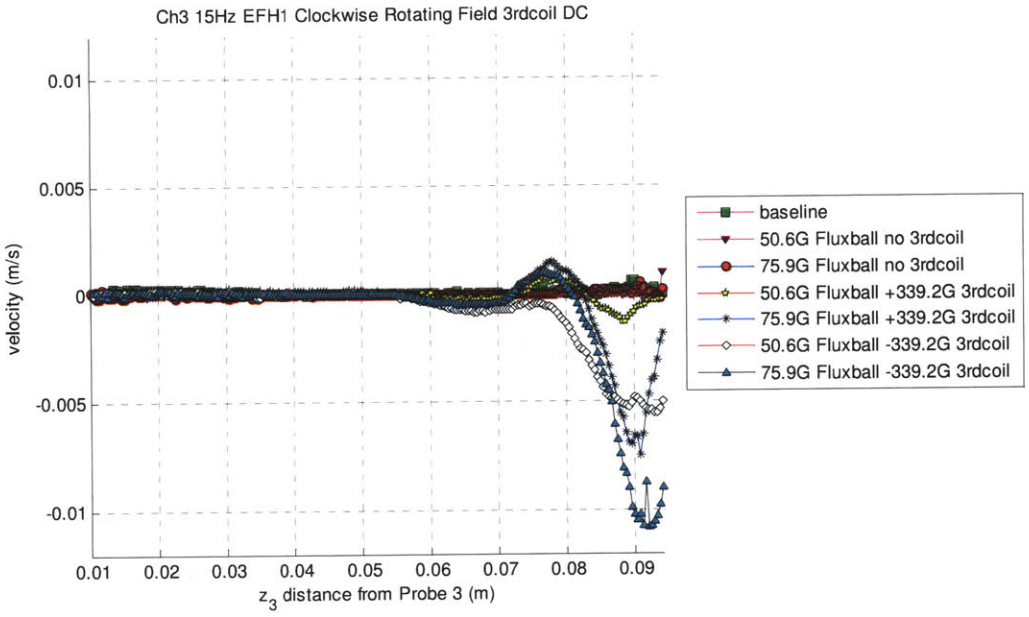
Ch3 15Hz EFH1 Clockwise Rotating Field 3rdcoil DC
velocity (m/s)
0.01
0.005
0
-0.005
-0.01
0.01 0.02 0.03 0.04 0.05 0.06 0.07 0.08 0.09
z3 distance from Probe 3 (m)
baseline
50.6G Fluxball no 3rdcoil
75.9G Fluxball no 3rdcoil
50.6G Fluxball +339.2G 3rdcoil
75.9G Fluxball +339.2G 3rdcoil
50.6G Fluxball -339.2G 3rdcoil
75.9G Fluxball -339.2G 3rdcoil

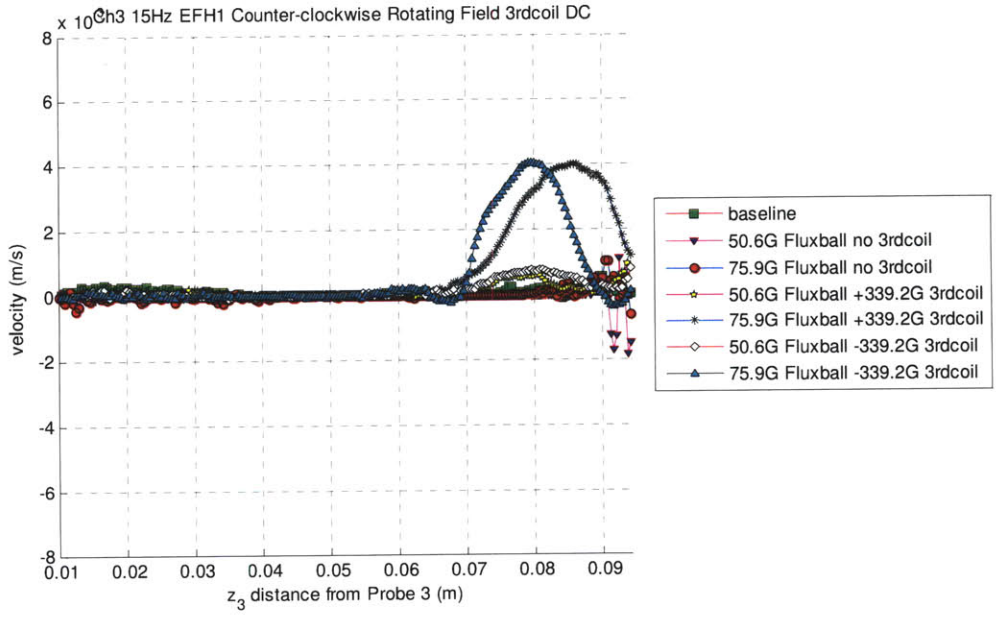
Ch3 15Hz EFH1 Counter-clockwise Rotating Field 3rdcoil DC
x 10
velocity (m/s)
8
6
4
2
0
-2
-4
-6
-8
0.01 0.02 0.03 0.04 0.05 0.06 0.07 0.08 0.09
z3 distance from Probe 3 (m)
baseline
50.6G Fluxball no 3rdcoil
75.9G Fluxball no 3rdcoil
50.6G Fluxball +339.2G 3rdcoil
75.9G Fluxball +339.2G 3rdcoil
50.6G Fluxball -339.2G 3rdcoil
75.9G Fluxball -339.2G 3rdcoil

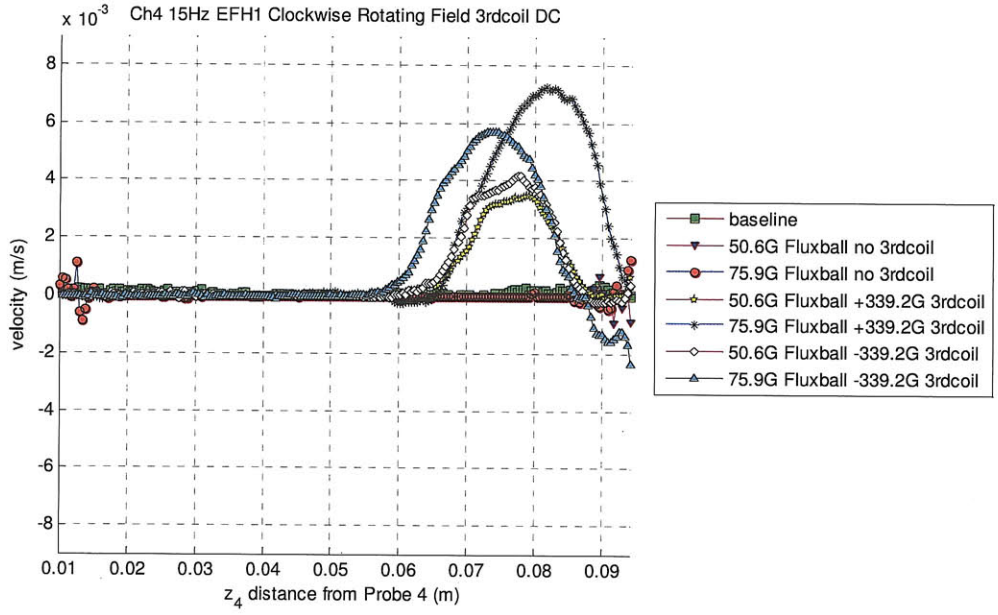
x 10^-3
Ch4 15Hz EFH1 Clockwise Rotating Field 3rdcoil DC
velocity (m/s)
z4 distance from Probe 4 (m)
baseline
50.6G Fluxball no 3rdcoil
75.9G Fluxball no 3rdcoil
50.6G Fluxball +339.2G 3rdcoil
75.9G Fluxball +339.2G 3rdcoil
50.6G Fluxball -339.2G 3rdcoil
75.9G Fluxball -339.2G 3rdcoil

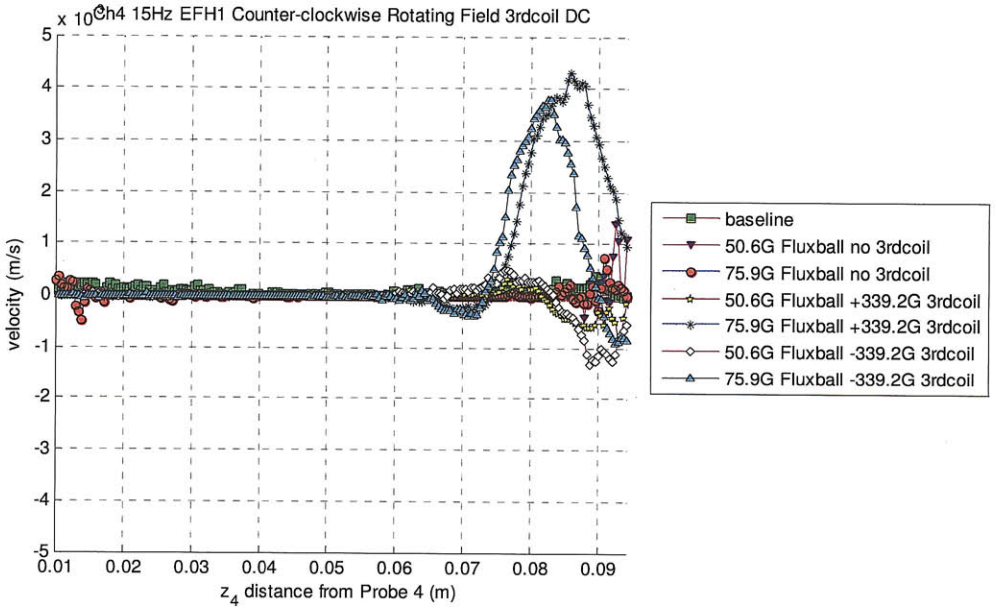
x 10^-3
Ch4 15Hz EFH1 Counter-clockwise Rotating Field 3rdcoil DC
velocity (m/s)
z4 distance from Probe 4 (m)
baseline
50.6G Fluxball no 3rdcoil
75.9G Fluxball no 3rdcoil
50.6G Fluxball +339.2G 3rdcoil
75.9G Fluxball +339.2G 3rdcoil
50.6G Fluxball -339.2G 3rdcoil
75.9G Fluxball -339.2G 3rdcoil

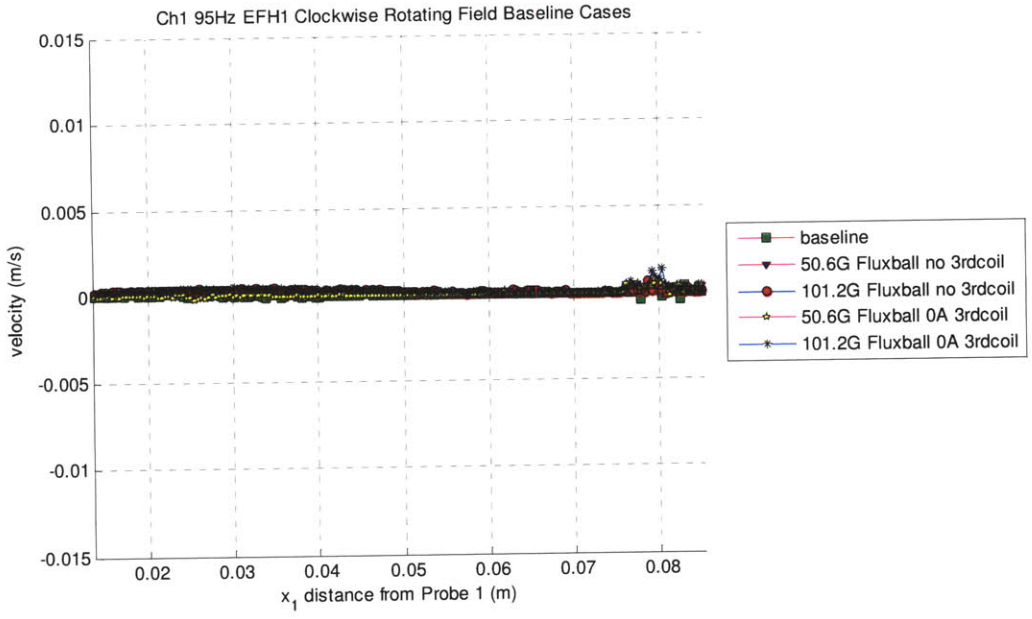
Ch1 95Hz EFH1 Clockwise Rotating Field Baseline Cases
0.015
0.01
0.005
0
-0.005
-0.01
-0.015
velocity (m/s)
0.02
0.03
0.04
0.05
0.06
0.07
0.08
x1 distance from Probe 1 (m)
baseline
50.6G Fluxball no 3rdcoil
101.2G Fluxball no 3rdcoil
50.6G Fluxball 0A 3rdcoil
101.2G Fluxball 0A 3rdcoil

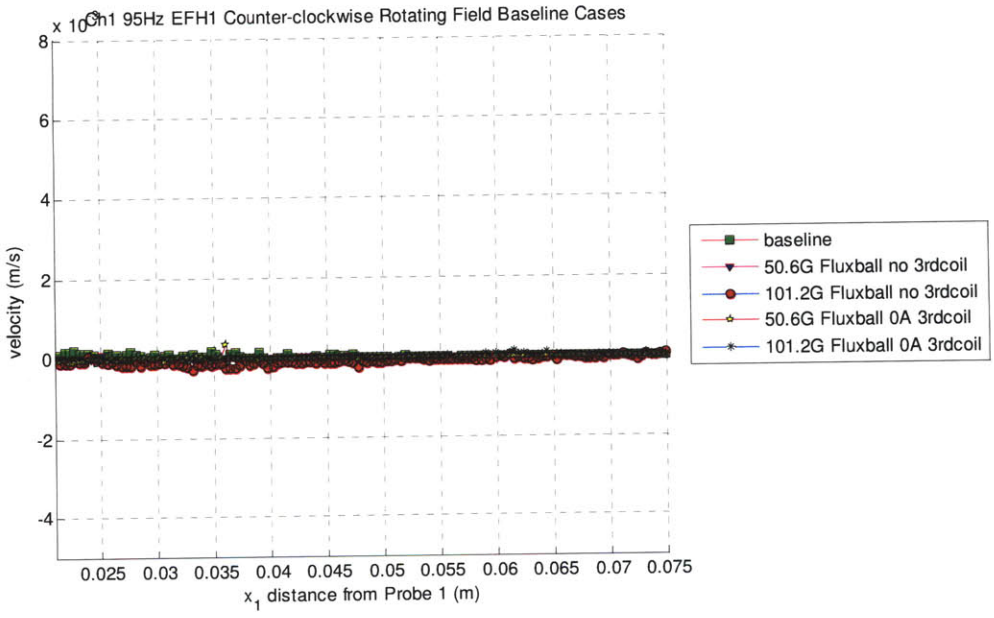
x 10^-3
Ch1 95Hz EFH1 Counter-clockwise Rotating Field Baseline Cases
8
6
4
2
0
-2
-4
velocity (m/s)
0.025
0.03
0.035
0.04
0.045
0.05
0.055
0.06
0.065
0.07
0.075
x1 distance from Probe 1 (m)
baseline
50.6G Fluxball no 3rdcoil
101.2G Fluxball no 3rdcoil
50.6G Fluxball 0A 3rdcoil
101.2G Fluxball 0A 3rdcoil

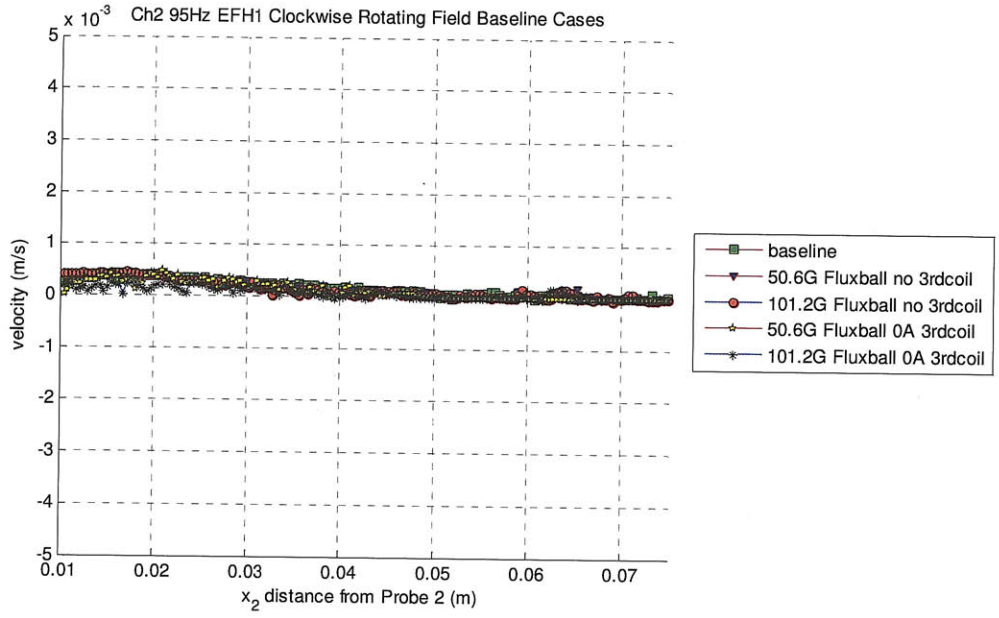
x 10^-3 Ch2 95Hz EFH1 Clockwise Rotating Field Baseline Cases
velocity (m/s)
x2 distance from Probe 2 (m)
baseline
50.6G Fluxball no 3rdcoil
101.2G Fluxball no 3rdcoil
50.6G Fluxball 0A 3rdcoil
101.2G Fluxball 0A 3rdcoil

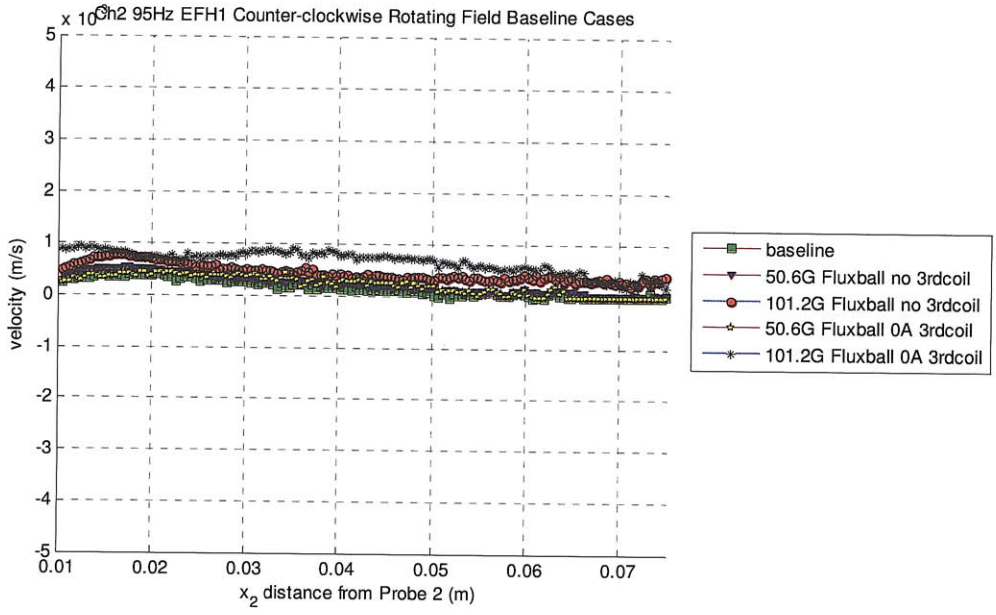
x 10^-3 Ch2 95Hz EFH1 Counter-clockwise Rotating Field Baseline Cases
velocity (m/s)
x2 distance from Probe 2 (m)
baseline
50.6G Fluxball no 3rdcoil
101.2G Fluxball no 3rdcoil
50.6G Fluxball 0A 3rdcoil
101.2G Fluxball 0A 3rdcoil

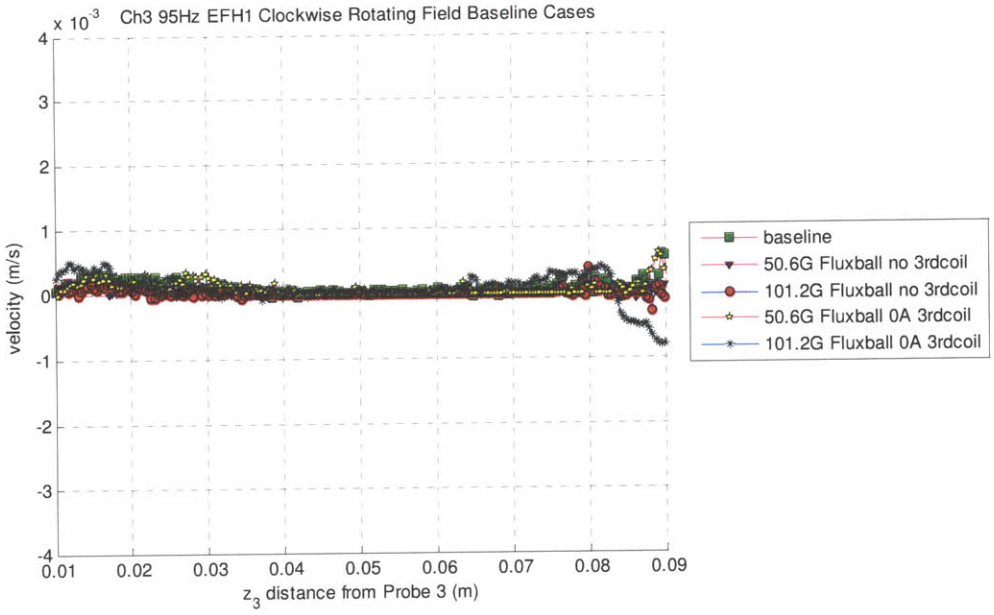
x 10^-3
Ch3 95Hz EFH1 Clockwise Rotating Field Baseline Cases
velocity (m/s)
z3 distance from Probe 3 (m)
baseline
50.6G Fluxball no 3rdcoil
101.2G Fluxball no 3rdcoil
50.6G Fluxball 0A 3rdcoil
101.2G Fluxball 0A 3rdcoil

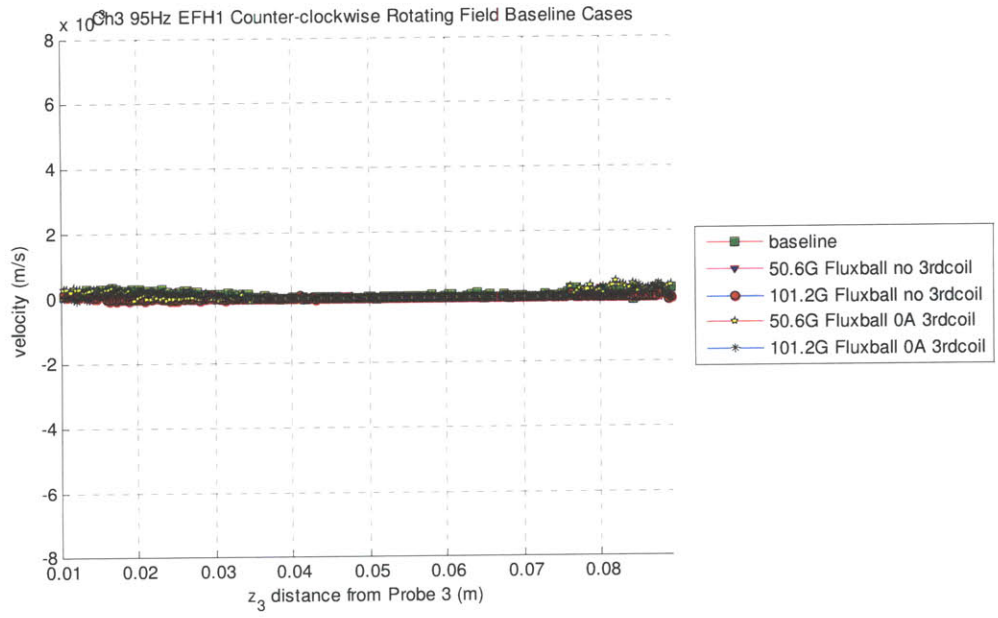
x 10^-3
Ch3 95Hz EFH1 Counter-clockwise Rotating Field Baseline Cases
velocity (m/s)
z3 distance from Probe 3 (m)
baseline
50.6G Fluxball no 3rdcoil
101.2G Fluxball no 3rdcoil
50.6G Fluxball 0A 3rdcoil
101.2G Fluxball 0A 3rdcoil

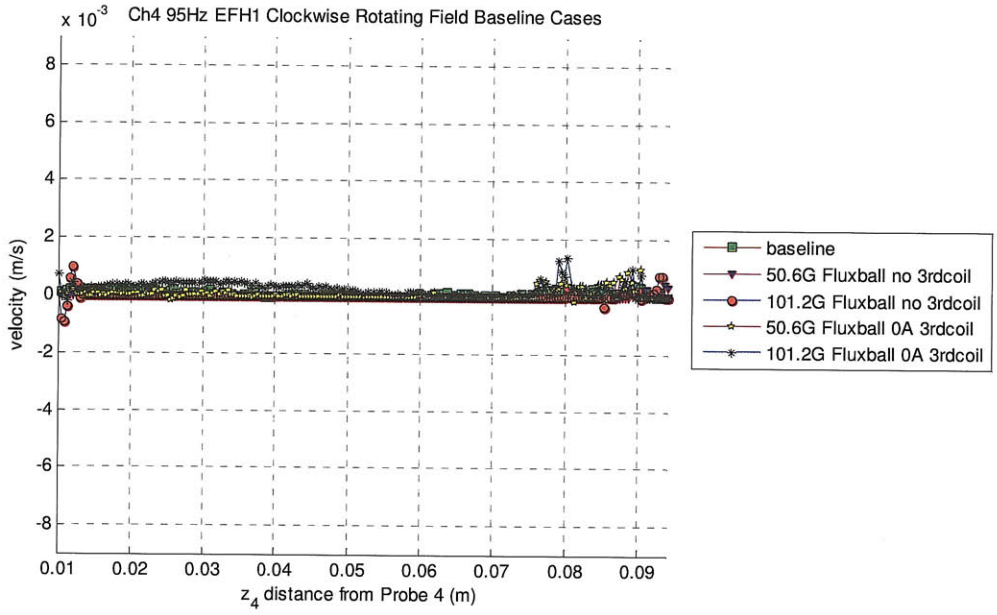
x 10^-3
Ch4 95Hz EFH1 Clockwise Rotating Field Baseline Cases
velocity (m/s)
z4 distance from Probe 4 (m)
baseline
50.6G Fluxball no 3rdcoil
101.2G Fluxball no 3rdcoil
50.6G Fluxball 0A 3rdcoil
101.2G Fluxball 0A 3rdcoil

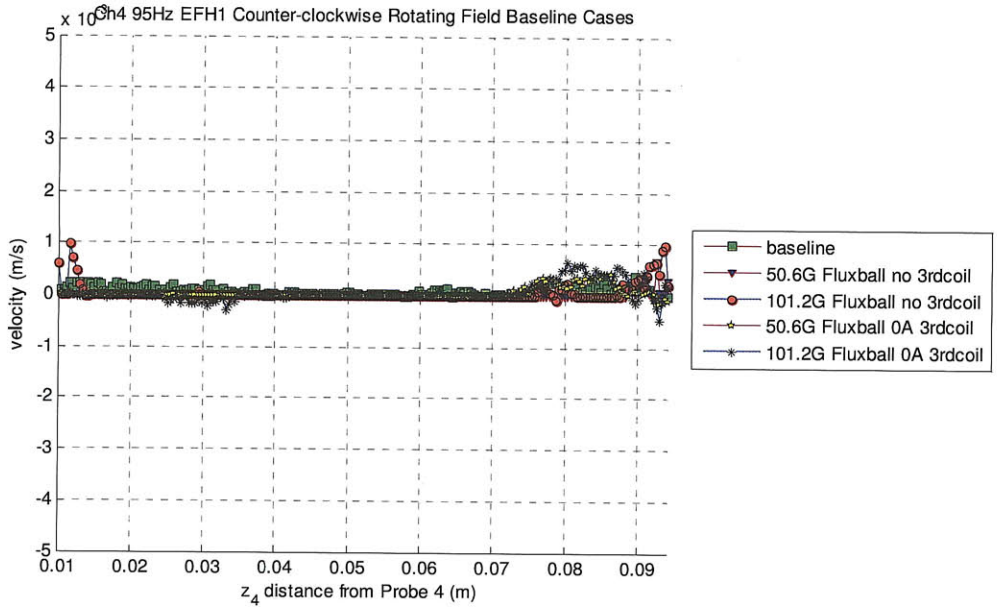
x 10^-3
Ch4 95Hz EFH1 Counter-clockwise Rotating Field Baseline Cases
velocity (m/s)
z4 distance from Probe 4 (m)
baseline
50.6G Fluxball no 3rdcoil
101.2G Fluxball no 3rdcoil
50.6G Fluxball 0A 3rdcoil
101.2G Fluxball 0A 3rdcoil

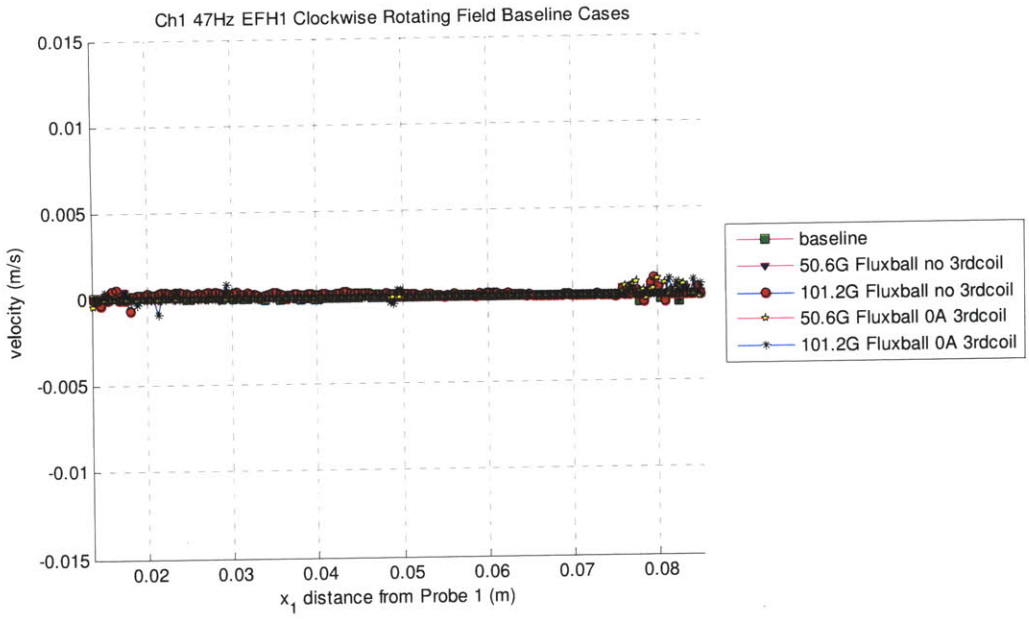
Ch1 47Hz EFH1 Clockwise Rotating Field Baseline Cases
0.015
0.01
0.005
0
-0.005
-0.01
-0.015
velocity (m/s)
0.02
0.03
0.04
0.05
0.06
0.07
0.08
x1 distance from Probe 1 (m)
baseline
50.6G Fluxball no 3rdcoil
101.2G Fluxball no 3rdcoil
50.6G Fluxball 0A 3rdcoil
101.2G Fluxball 0A 3rdcoil

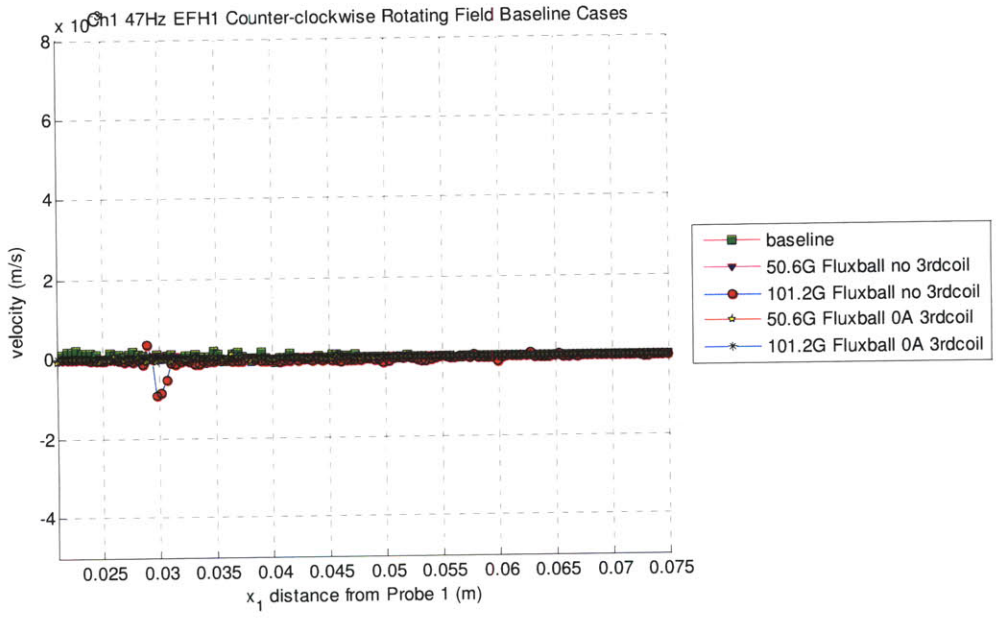
x 10^-3
Ch1 47Hz EFH1 Counter-clockwise Rotating Field Baseline Cases
8
6
4
2
0
-2
-4
velocity (m/s)
0.025
0.03
0.035
0.04
0.045
0.05
0.055
0.06
0.065
0.07
0.075
x1 distance from Probe 1 (m)
baseline
50.6G Fluxball no 3rdcoil
101.2G Fluxball no 3rdcoil
50.6G Fluxball 0A 3rdcoil
101.2G Fluxball 0A 3rdcoil

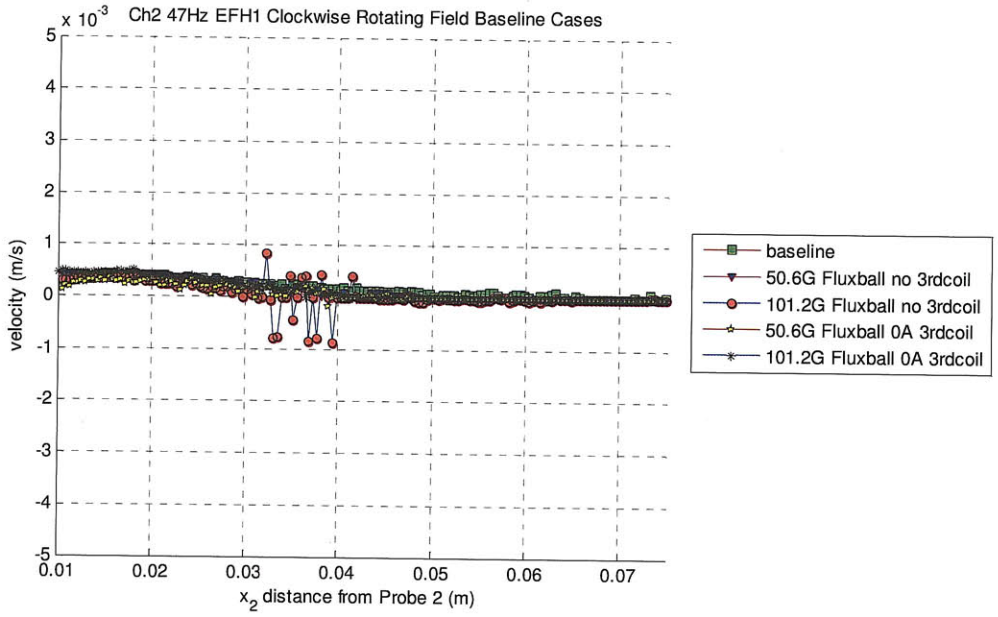
x 10^-3
Ch2 47Hz EFH1 Clockwise Rotating Field Baseline Cases
velocity (m/s)
x2 distance from Probe 2 (m)
baseline
50.6G Fluxball no 3rdcoil
101.2G Fluxball no 3rdcoil
50.6G Fluxball 0A 3rdcoil
101.2G Fluxball 0A 3rdcoil

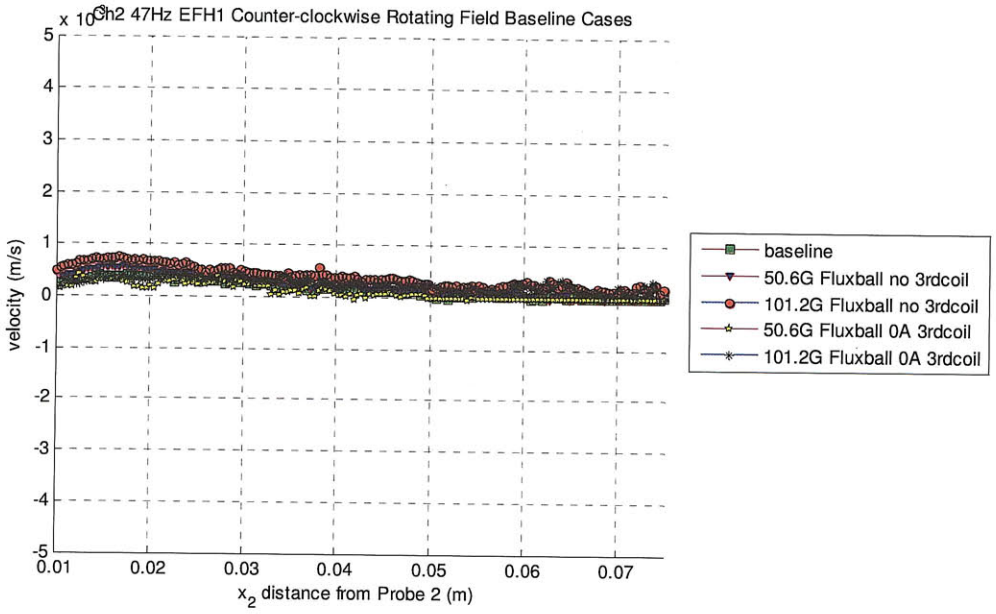
x 10^-3
Ch2 47Hz EFH1 Counter-clockwise Rotating Field Baseline Cases
velocity (m/s)
x2 distance from Probe 2 (m)
baseline
50.6G Fluxball no 3rdcoil
101.2G Fluxball no 3rdcoil
50.6G Fluxball 0A 3rdcoil
101.2G Fluxball 0A 3rdcoil

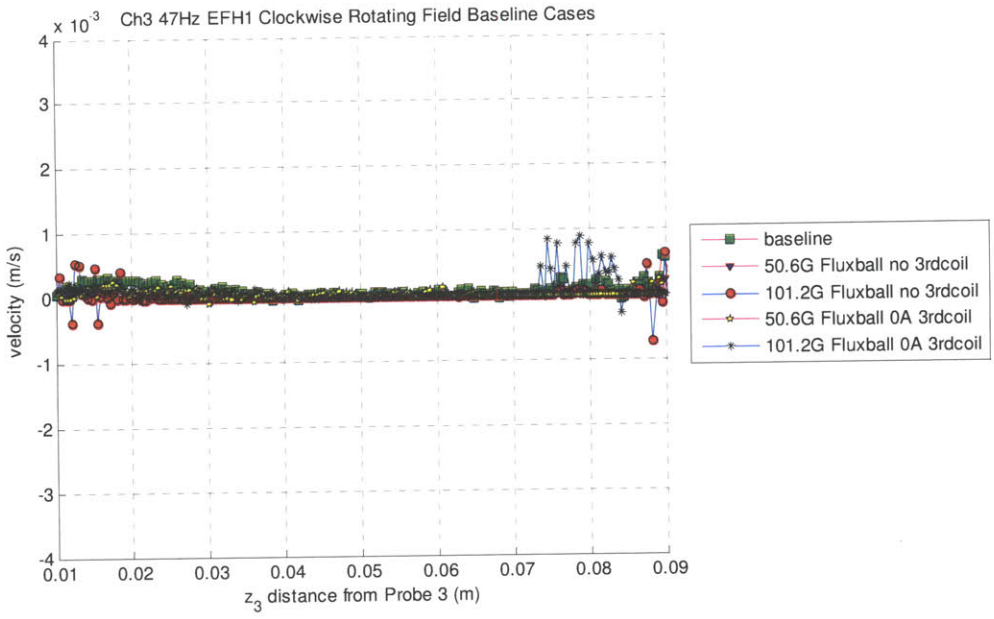
x 10^-3
Ch3 47Hz EFH1 Clockwise Rotating Field Baseline Cases
velocity (m/s)
z3 distance from Probe 3 (m)
baseline
50.6G Fluxball no 3rdcoil
101.2G Fluxball no 3rdcoil
50.6G Fluxball 0A 3rdcoil
101.2G Fluxball 0A 3rdcoil

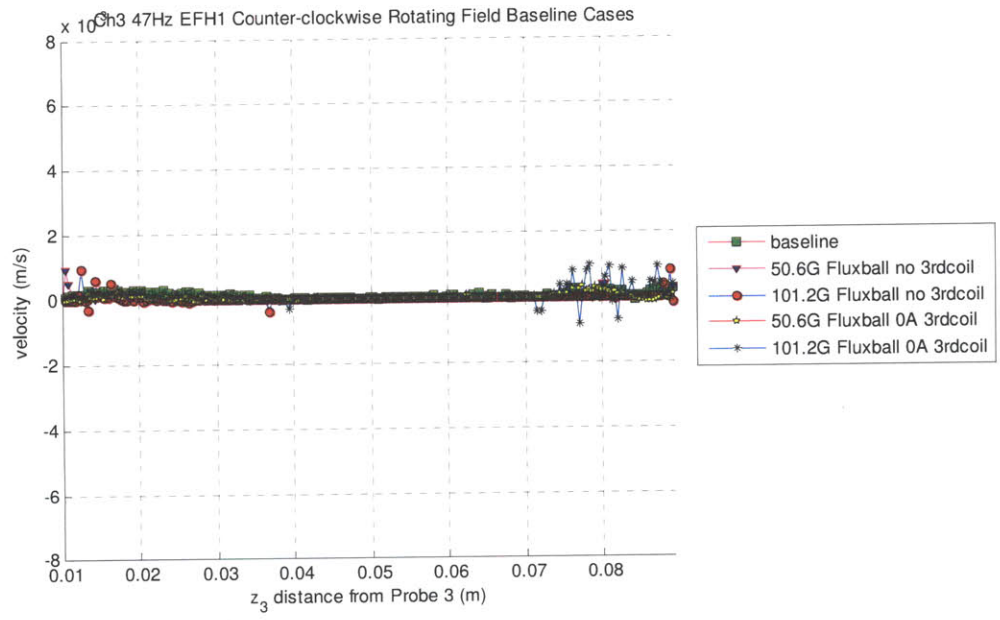
x 10^-3
Ch3 47Hz EFH1 Counter-clockwise Rotating Field Baseline Cases
velocity (m/s)
z3 distance from Probe 3 (m)
baseline
50.6G Fluxball no 3rdcoil
101.2G Fluxball no 3rdcoil
50.6G Fluxball 0A 3rdcoil
101.2G Fluxball 0A 3rdcoil

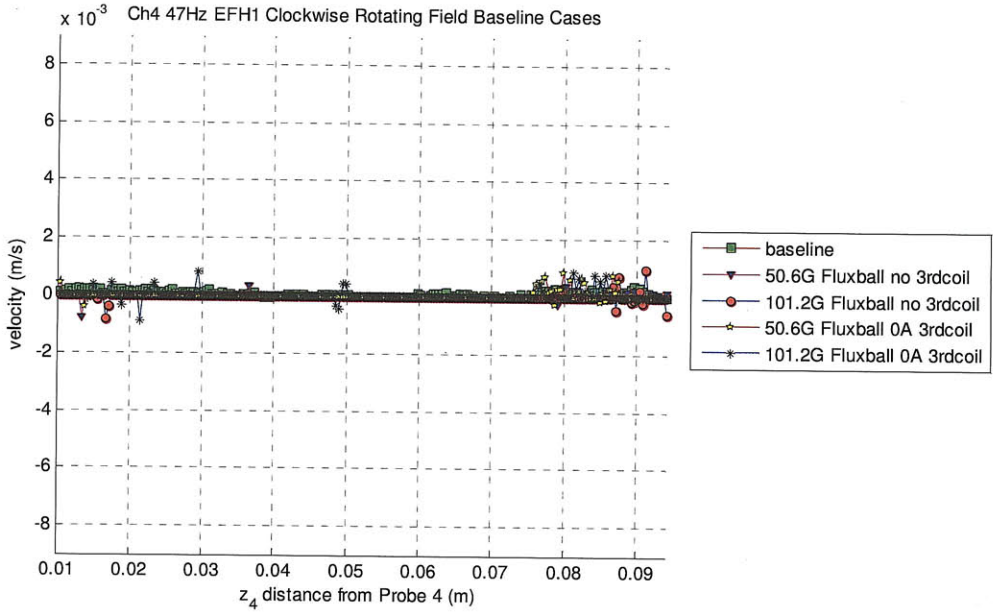
x 10^-3
Ch4 47Hz EFH1 Clockwise Rotating Field Baseline Cases
velocity (m/s)
z4 distance from Probe 4 (m)
baseline
50.6G Fluxball no 3rdcoil
101.2G Fluxball no 3rdcoil
50.6G Fluxball 0A 3rdcoil
101.2G Fluxball 0A 3rdcoil

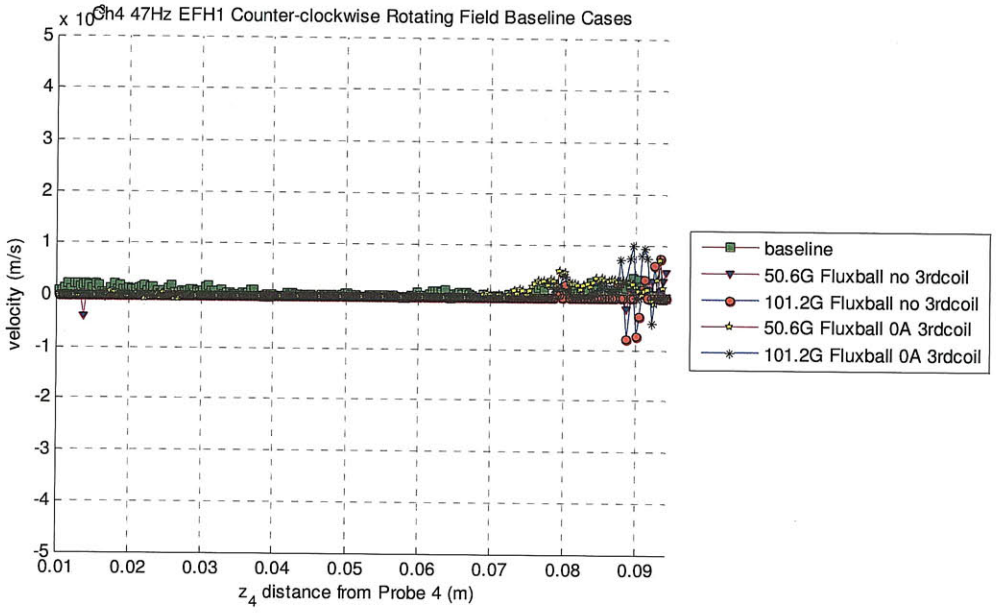
x 10^-3
Ch4 47Hz EFH1 Counter-clockwise Rotating Field Baseline Cases
velocity (m/s)
z4 distance from Probe 4 (m)
baseline
50.6G Fluxball no 3rdcoil
101.2G Fluxball no 3rdcoil
50.6G Fluxball 0A 3rdcoil
101.2G Fluxball 0A 3rdcoil

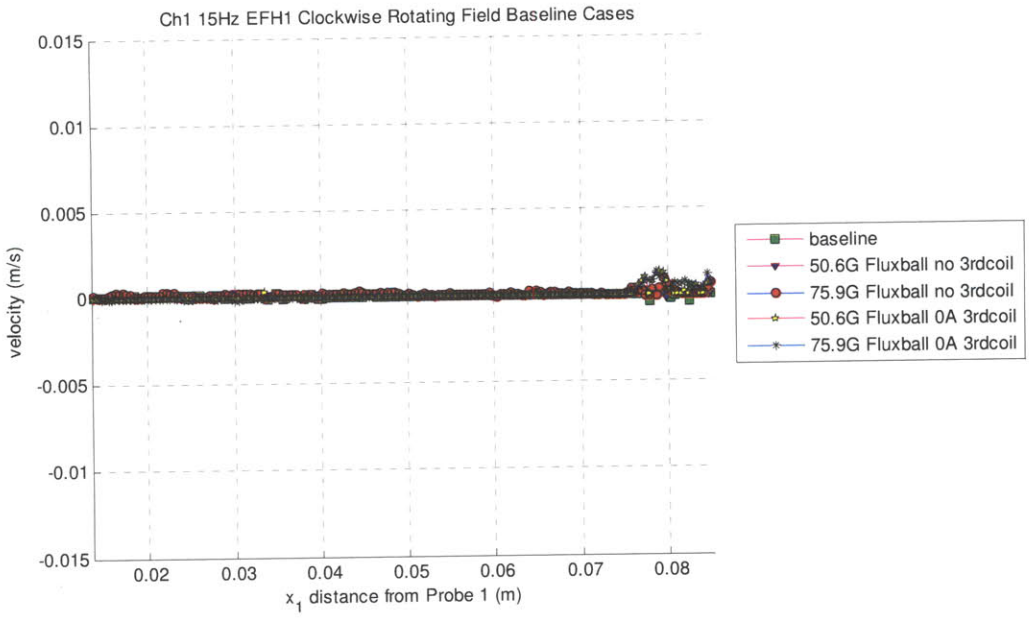
Ch1 15Hz EFH1 Clockwise Rotating Field Baseline Cases
velocity (m/s)
0.015
0.01
0.005
0
-0.005
-0.01
-0.015
0.02
0.03
0.04
0.05
0.06
0.07
0.08
x1 distance from Probe 1 (m)
baseline
50.6G Fluxball no 3rdcoil
75.9G Fluxball no 3rdcoil
50.6G Fluxball 0A 3rdcoil
75.9G Fluxball 0A 3rdcoil

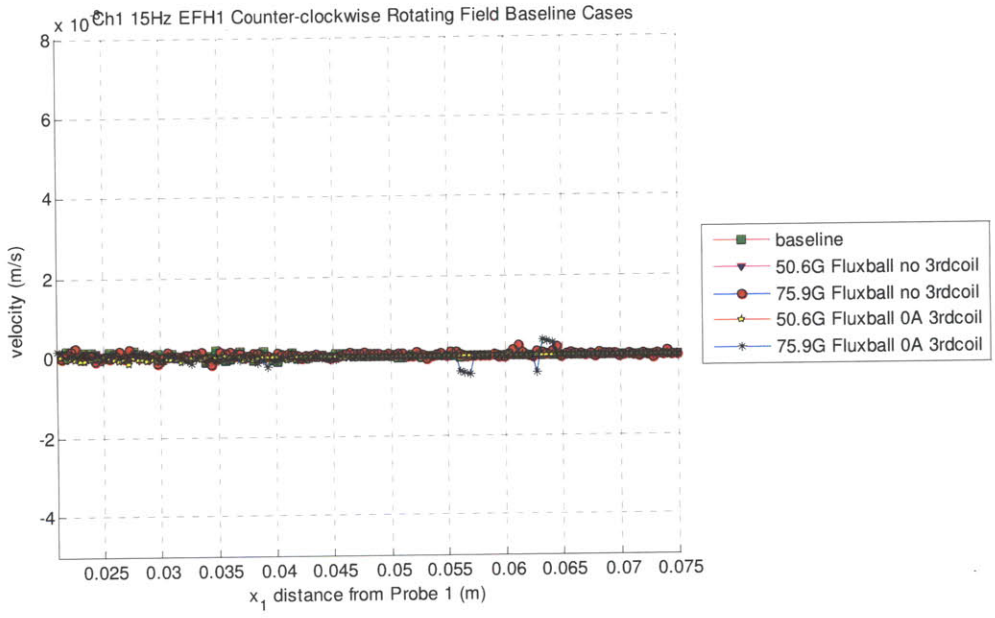
Ch1 15Hz EFH1 Counter-clockwise Rotating Field Baseline Cases
x 10^-3
velocity (m/s)
8
6
4
2
0
-2
-4
0.025
0.03
0.035
0.04
0.045
0.05
0.055
0.06
0.065
0.07
0.075
x1 distance from Probe 1 (m)
baseline
50.6G Fluxball no 3rdcoil
75.9G Fluxball no 3rdcoil
50.6G Fluxball 0A 3rdcoil
75.9G Fluxball 0A 3rdcoil

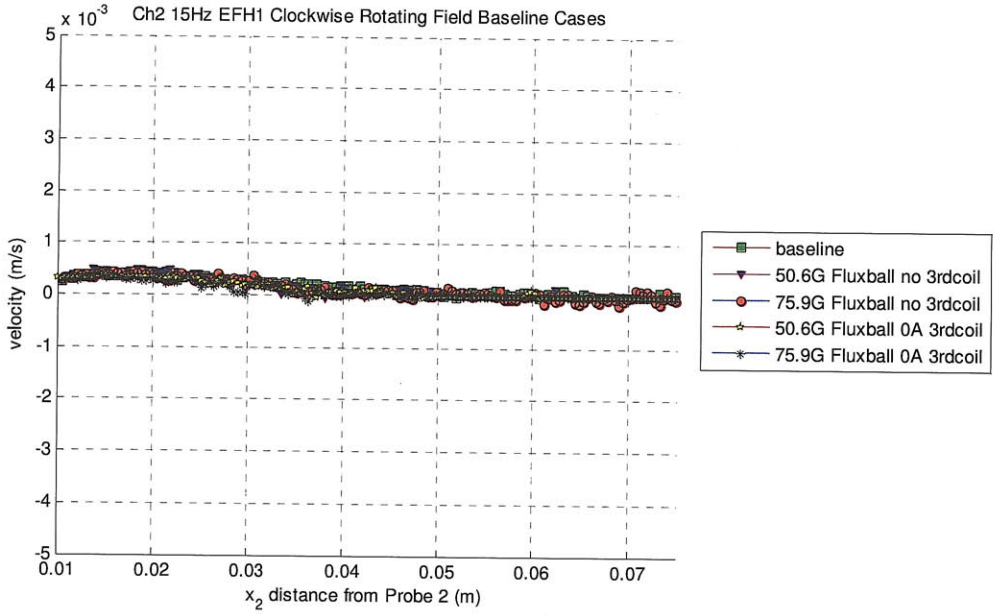
x 10^-3
Ch2 15Hz EFH1 Clockwise Rotating Field Baseline Cases
velocity (m/s)
x2 distance from Probe 2 (m)
baseline
50.6G Fluxball no 3rdcoil
75.9G Fluxball no 3rdcoil
50.6G Fluxball 0A 3rdcoil
75.9G Fluxball 0A 3rdcoil

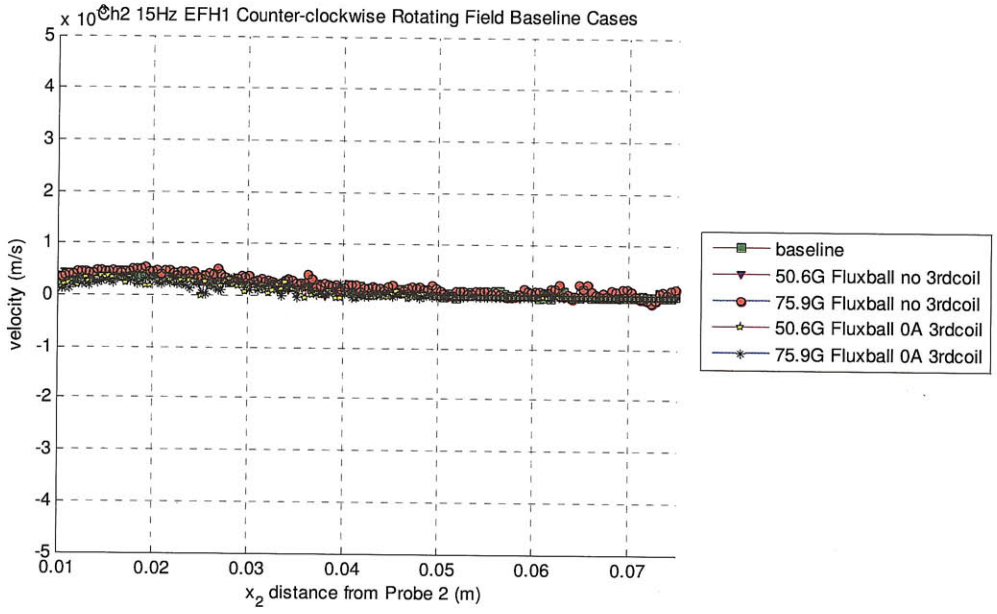
x 10^-3
Ch2 15Hz EFH1 Counter-clockwise Rotating Field Baseline Cases
velocity (m/s)
x2 distance from Probe 2 (m)
baseline
50.6G Fluxball no 3rdcoil
75.9G Fluxball no 3rdcoil
50.6G Fluxball 0A 3rdcoil
75.9G Fluxball 0A 3rdcoil

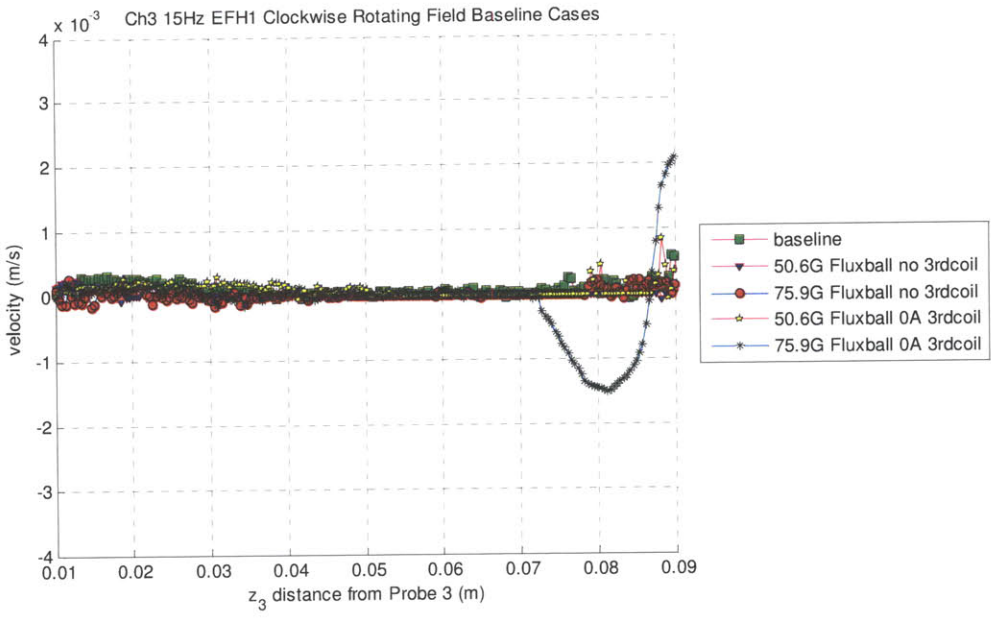
x 10^-3
Ch3 15Hz EFH1 Clockwise Rotating Field Baseline Cases
velocity (m/s)
z3 distance from Probe 3 (m)
baseline
50.6G Fluxball no 3rdcoil
75.9G Fluxball no 3rdcoil
50.6G Fluxball 0A 3rdcoil
75.9G Fluxball 0A 3rdcoil

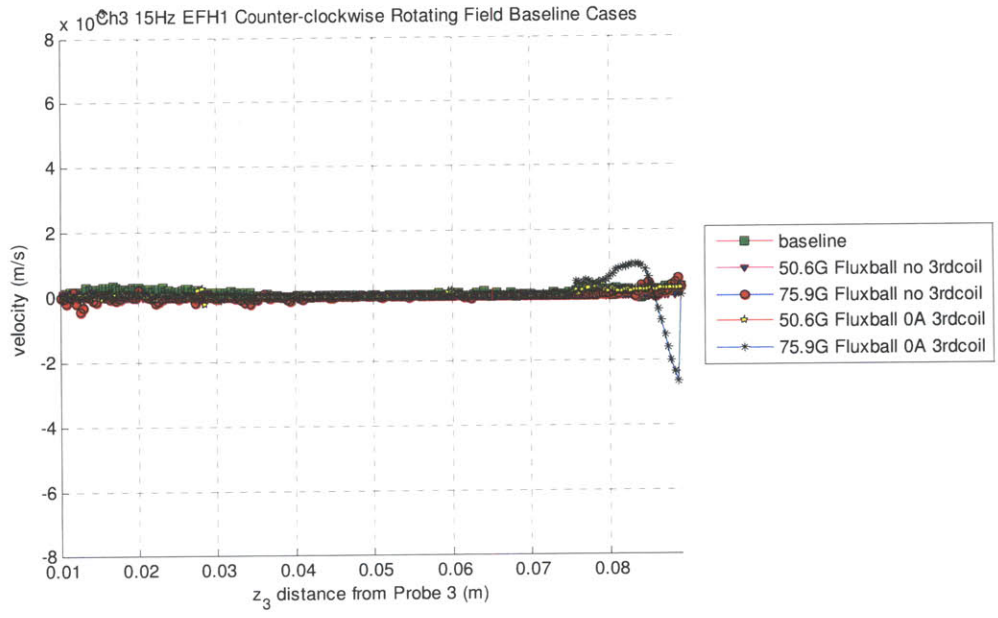
x 10^-3
Ch3 15Hz EFH1 Counter-clockwise Rotating Field Baseline Cases
velocity (m/s)
z3 distance from Probe 3 (m)
baseline
50.6G Fluxball no 3rdcoil
75.9G Fluxball no 3rdcoil
50.6G Fluxball 0A 3rdcoil
75.9G Fluxball 0A 3rdcoil

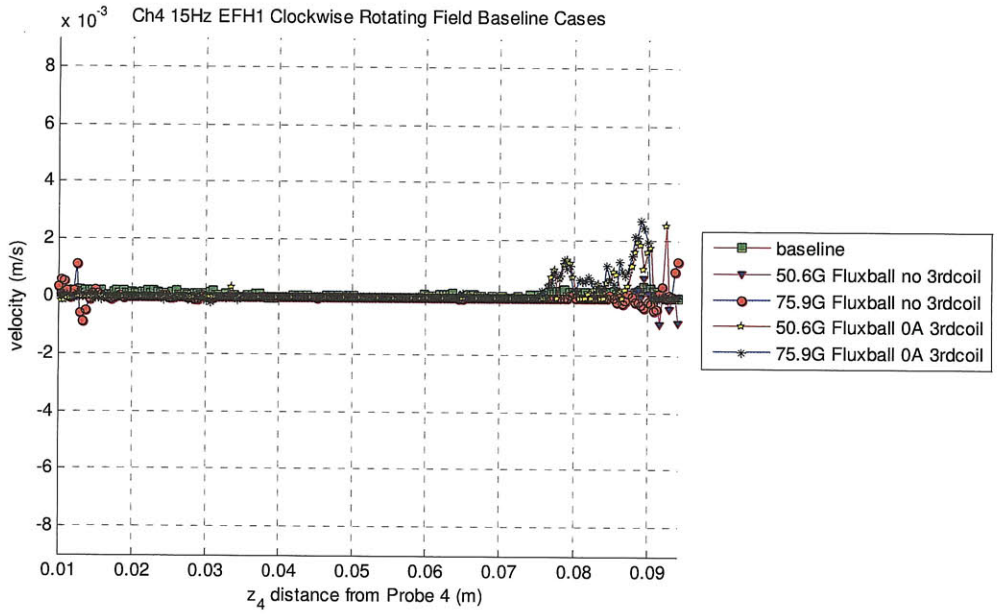
x 10^-3
Ch4 15Hz EFH1 Clockwise Rotating Field Baseline Cases
velocity (m/s)
z4 distance from Probe 4 (m)
baseline
50.6G Fluxball no 3rdcoil
75.9G Fluxball no 3rdcoil
50.6G Fluxball 0A 3rdcoil
75.9G Fluxball 0A 3rdcoil

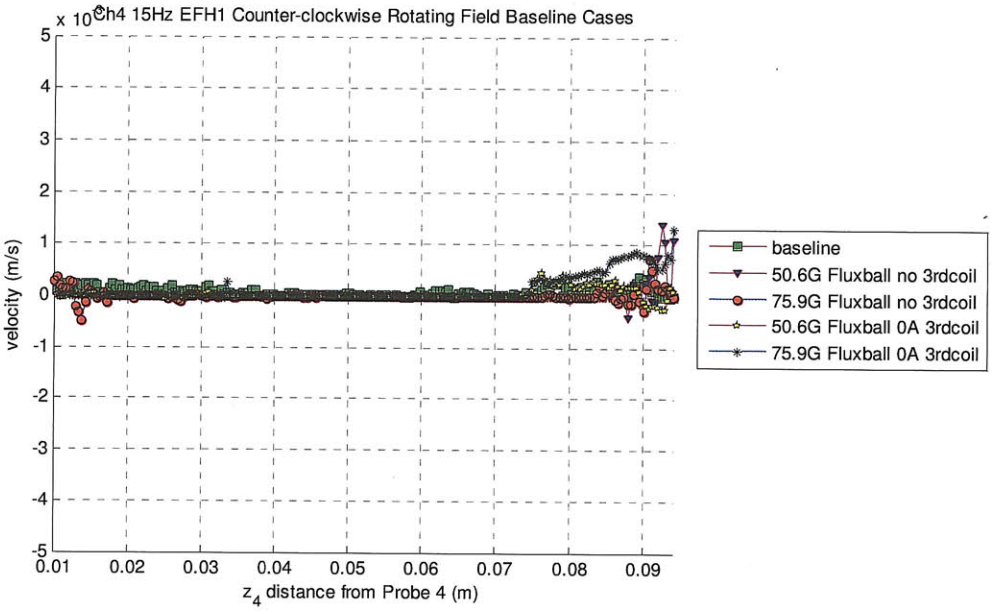
x 10^-3
Ch4 15Hz EFH1 Counter-clockwise Rotating Field Baseline Cases
velocity (m/s)
z4 distance from Probe 4 (m)
baseline
50.6G Fluxball no 3rdcoil
75.9G Fluxball no 3rdcoil
50.6G Fluxball 0A 3rdcoil
75.9G Fluxball 0A 3rdcoil

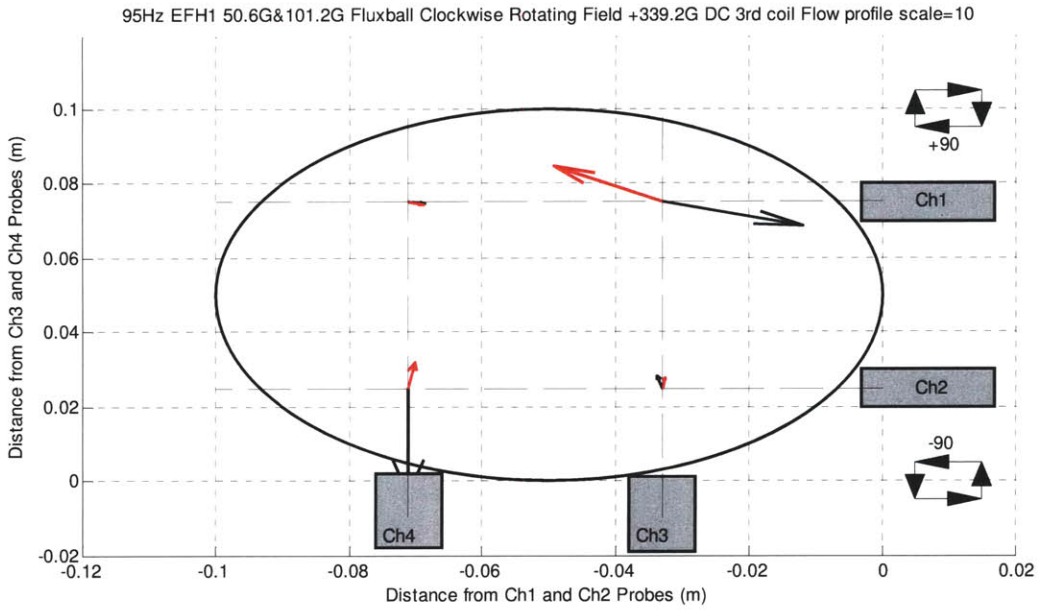
95Hz EFH1 50.6G&101.2G Fluxball Clockwise Rotating Field +339.2G DC 3rd coil Flow profile scale=10
Distance from Ch3 and Ch4 Probes (m)
Distance from Ch1 and Ch2 Probes (m)
+90
-90
Ch1
Ch2
Ch3
Ch4
0.1
0.08
0.06
0.04
0.02
0
-0.02
-0.12
-0.1
-0.08
-0.06
-0.04
-0.02
0
0.02

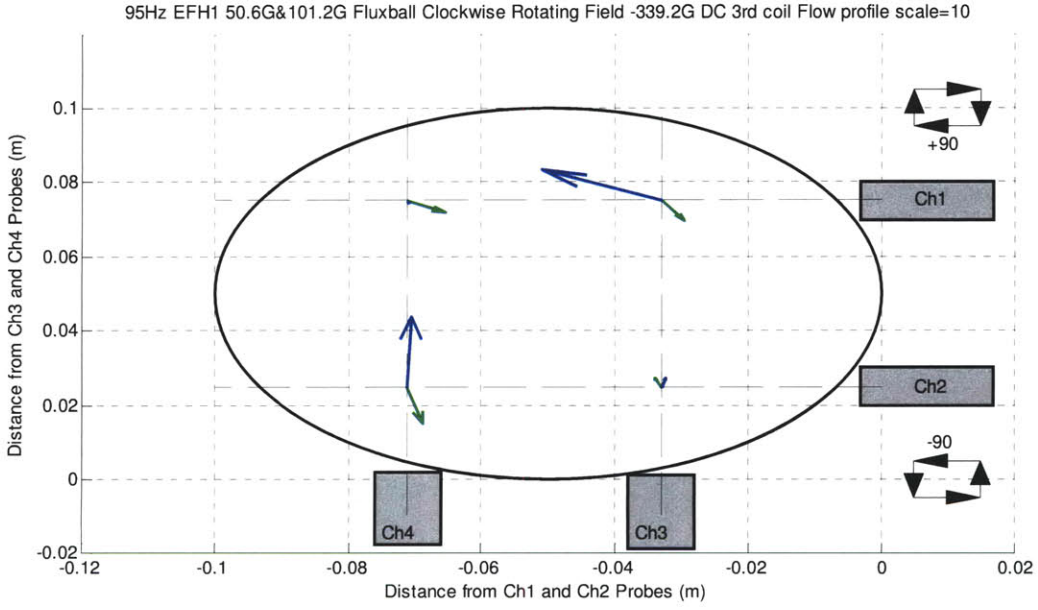
95Hz EFH1 50.6G&101.2G Fluxball Clockwise Rotating Field -339.2G DC 3rd coil Flow profile scale=10
Distance from Ch3 and Ch4 Probes (m)
Distance from Ch1 and Ch2 Probes (m)
+90
-90
Ch1
Ch2
Ch3
Ch4
0.1
0.08
0.06
0.04
0.02
0
-0.02
-0.12
-0.1
-0.08
-0.06
-0.04
-0.02
0
0.02

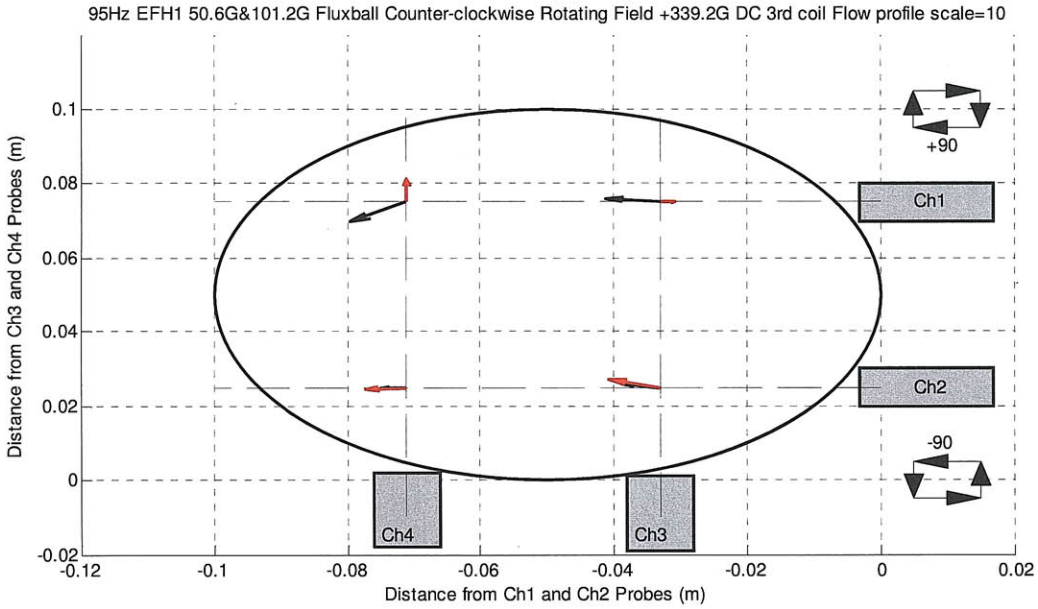
95Hz EFH1 50.6G&101.2G Fluxball Counter-clockwise Rotating Field +339.2G DC 3rd coil Flow profile scale=10
Distance from Ch3 and Ch4 Probes (m)
Distance from Ch1 and Ch2 Probes (m)
+90
-90
Ch1
Ch2
Ch3
Ch4
0.1
0.08
0.06
0.04
0.02
0
-0.02
-0.12
-0.1
-0.08
-0.06
-0.04
-0.02
0
0.02

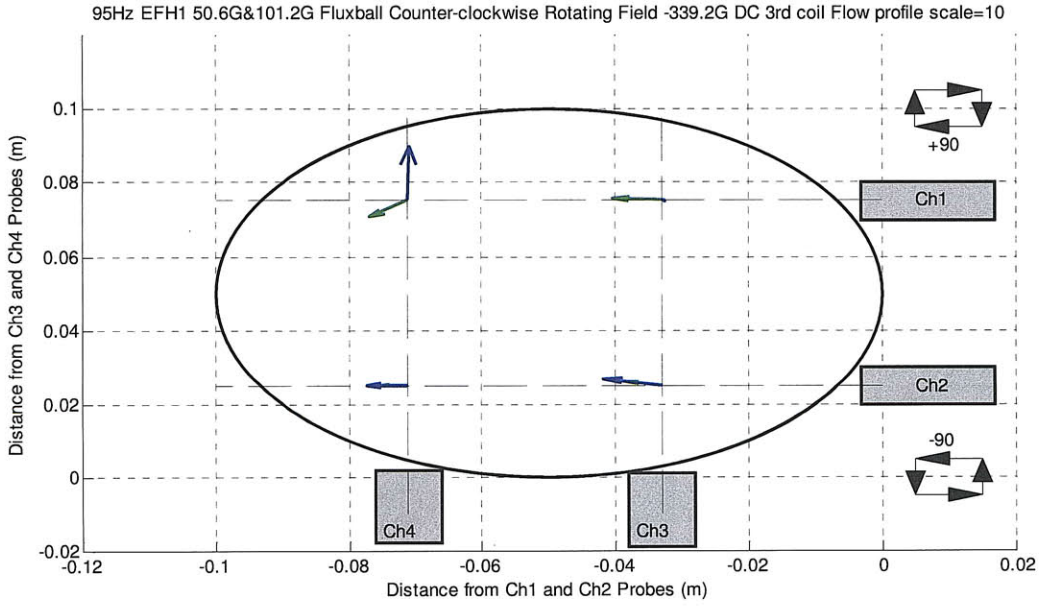
95Hz EFH1 50.6G&101.2G Fluxball Counter-clockwise Rotating Field -339.2G DC 3rd coil Flow profile scale=10
Distance from Ch3 and Ch4 Probes (m)
Distance from Ch1 and Ch2 Probes (m)
+90
-90
Ch1
Ch2
Ch3
Ch4
0.1
0.08
0.06
0.04
0.02
0
-0.02
-0.12
-0.1
-0.08
-0.06
-0.04
-0.02
0
0.02

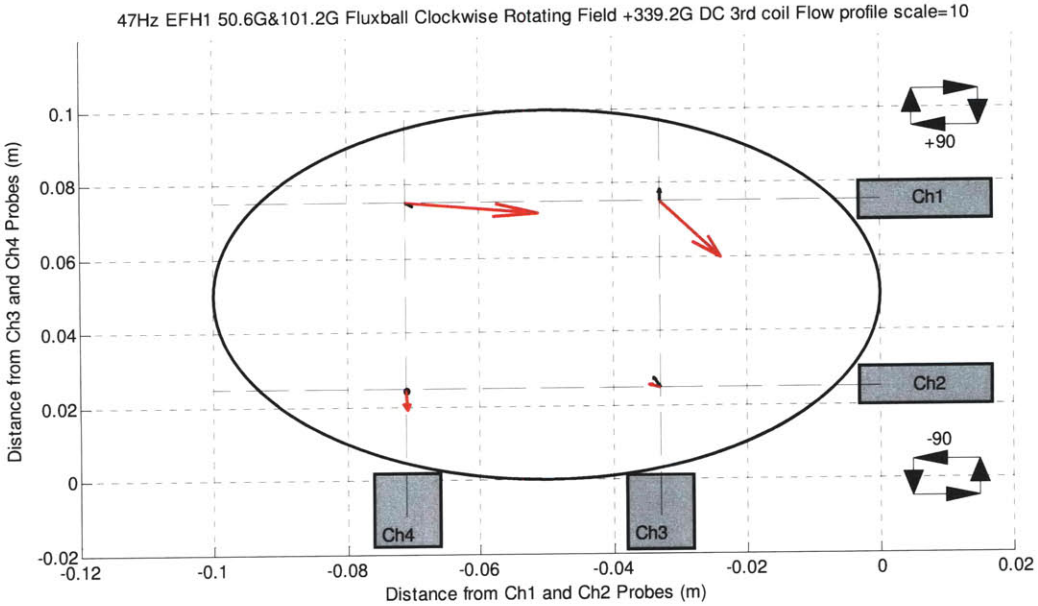
47Hz EFH1 50.6G&101.2G Fluxball Clockwise Rotating Field +339.2G DC 3rd coil Flow profile scale=10
Distance from Ch3 and Ch4 Probes (m)
Distance from Ch1 and Ch2 Probes (m)
+90
-90
Ch1
Ch2
Ch3
Ch4
0.1
0.08
0.06
0.04
0.02
0
-0.02
-0.12
-0.1
-0.08
-0.06
-0.04
-0.02
0
0.02

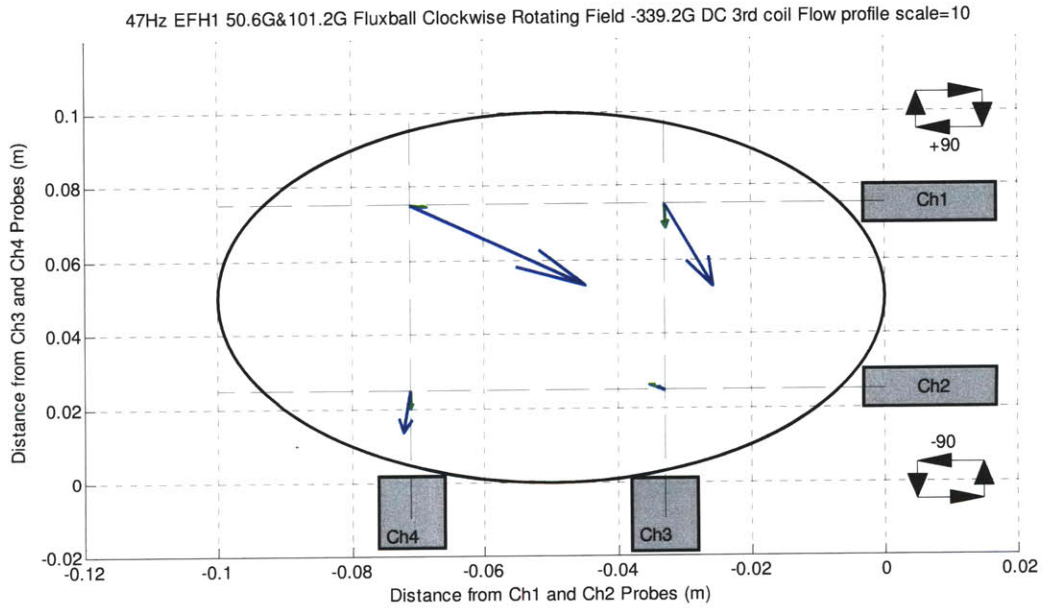
47Hz EFH1 50.6G&101.2G Fluxball Clockwise Rotating Field -339.2G DC 3rd coil Flow profile scale=10
Distance from Ch3 and Ch4 Probes (m)
Distance from Ch1 and Ch2 Probes (m)
+90
-90
Ch1
Ch2
Ch3
Ch4
0.1
0.08
0.06
0.04
0.02
0
-0.02
-0.12
-0.1
-0.08
-0.06
-0.04
-0.02
0
0.02

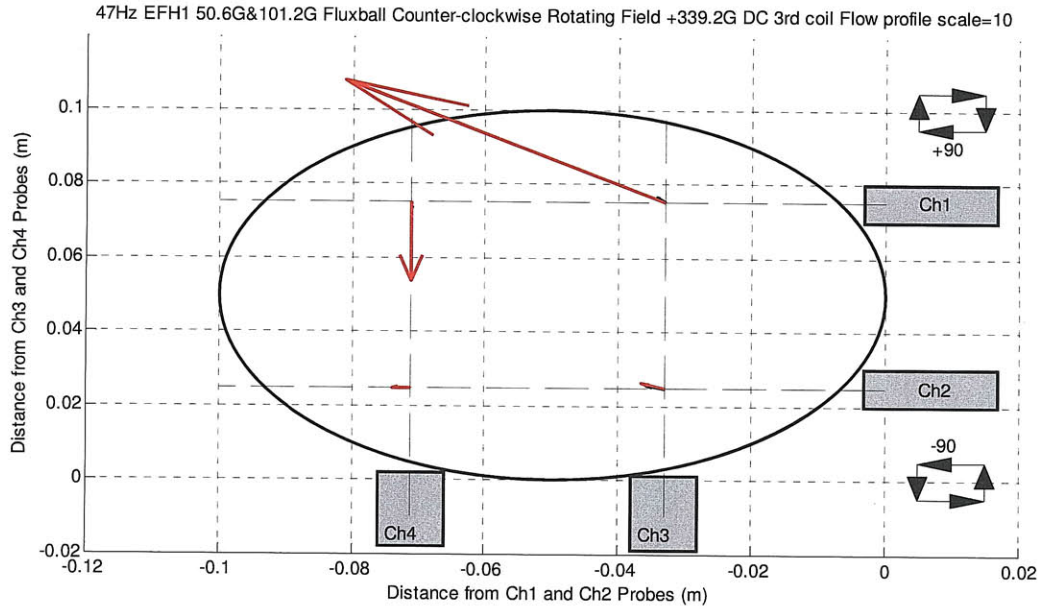
47Hz EFH1 50.6G&101.2G Fluxball Counter-clockwise Rotating Field +339.2G DC 3rd coil Flow profile scale=10
Distance from Ch3 and Ch4 Probes (m)
Distance from Ch1 and Ch2 Probes (m)
0.1
0.08
0.06
0.04
0.02
0
-0.02
-0.12
-0.1
-0.08
-0.06
-0.04
-0.02
0
0.02
+90
-90
Ch1
Ch2
Ch3
Ch4

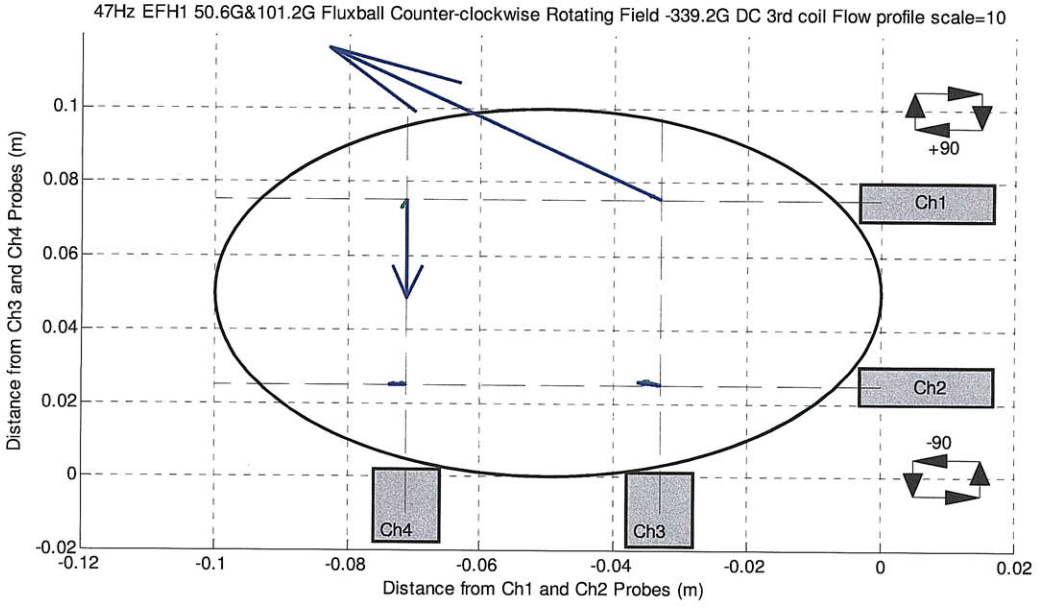
47Hz EFH1 50.6G&101.2G Fluxball Counter-clockwise Rotating Field -339.2G DC 3rd coil Flow profile scale=10
Distance from Ch3 and Ch4 Probes (m)
Distance from Ch1 and Ch2 Probes (m)
0.1
0.08
0.06
0.04
0.02
0
-0.02
-0.12
-0.1
-0.08
-0.06
-0.04
-0.02
0
0.02
+90
-90
Ch1
Ch2
Ch3
Ch4

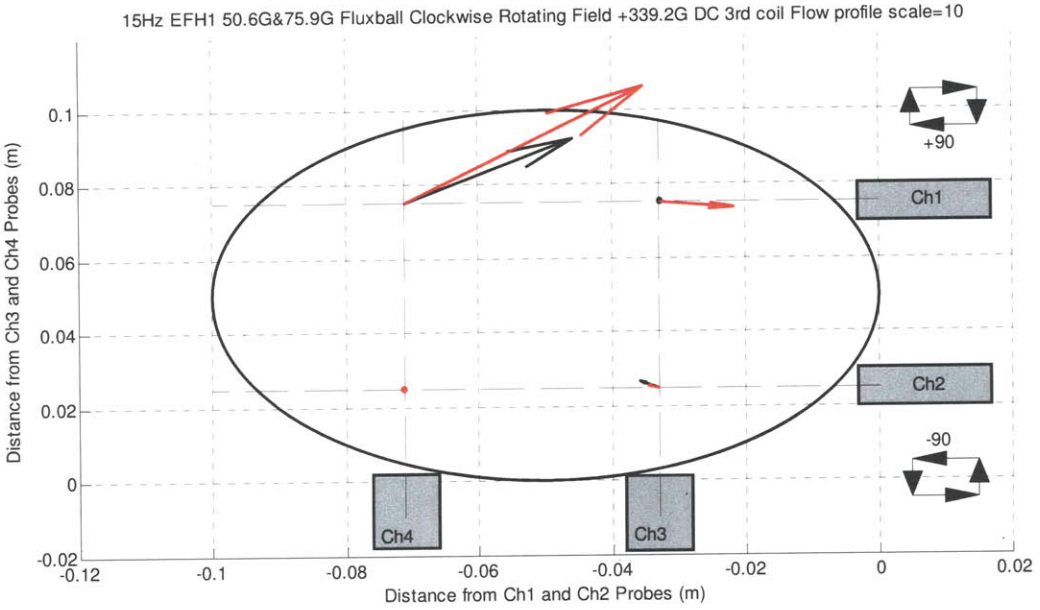
15Hz EFH1 50.6G&75.9G Fluxball Clockwise Rotating Field +339.2G DC 3rd coil Flow profile scale=10
Distance from Ch3 and Ch4 Probes (m)
Distance from Ch1 and Ch2 Probes (m)
0.1
0.08
0.06
0.04
0.02
0
-0.02
-0.12
-0.1
-0.08
-0.06
-0.04
-0.02
0
0.02
+90
-90
Ch1
Ch2
Ch3
Ch4

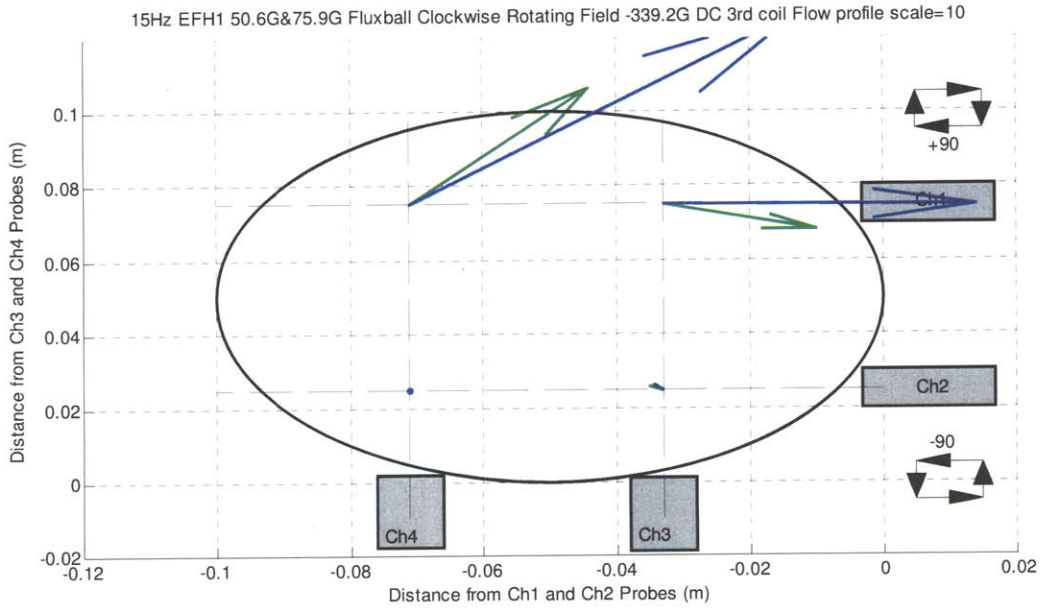
15Hz EFH1 50.6G&75.9G Fluxball Clockwise Rotating Field -339.2G DC 3rd coil Flow profile scale=10
Distance from Ch3 and Ch4 Probes (m)
Distance from Ch1 and Ch2 Probes (m)
0.1
0.08
0.06
0.04
0.02
0
-0.02
-0.12
-0.1
-0.08
-0.06
-0.04
-0.02
0
0.02
+90
-90
Ch1
Ch2
Ch3
Ch4

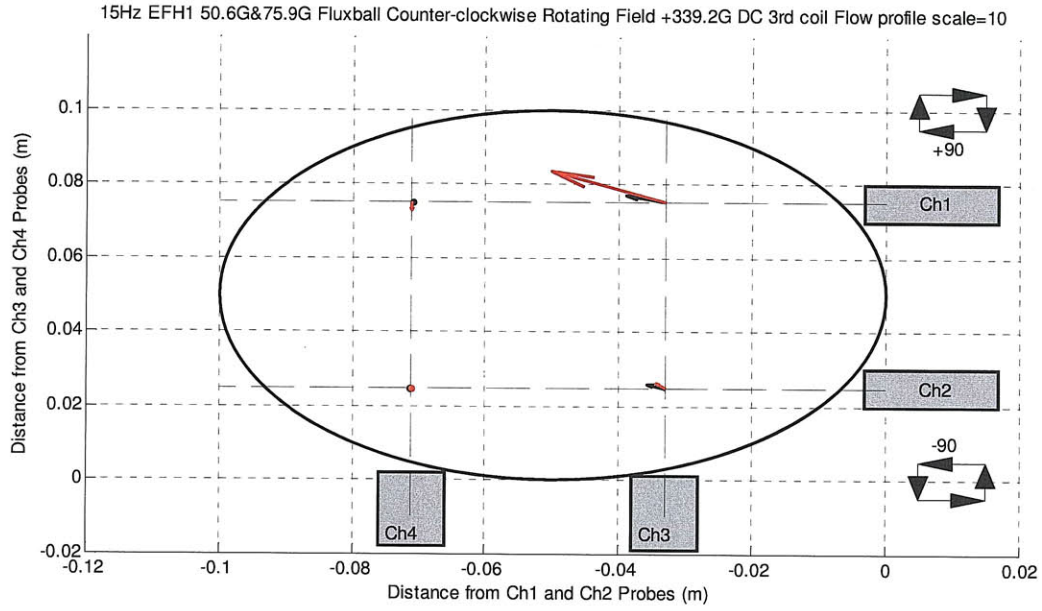
15Hz EFH1 50.6G&75.9G Fluxball Counter-clockwise Rotating Field +339.2G DC 3rd coil Flow profile scale=10
Distance from Ch3 and Ch4 Probes (m)
Distance from Ch1 and Ch2 Probes (m)
+90
-90
Ch1
Ch2
Ch3
Ch4
0.1
0.08
0.06
0.04
0.02
0
-0.02
-0.12
-0.1
-0.08
-0.06
-0.04
-0.02
0
0.02

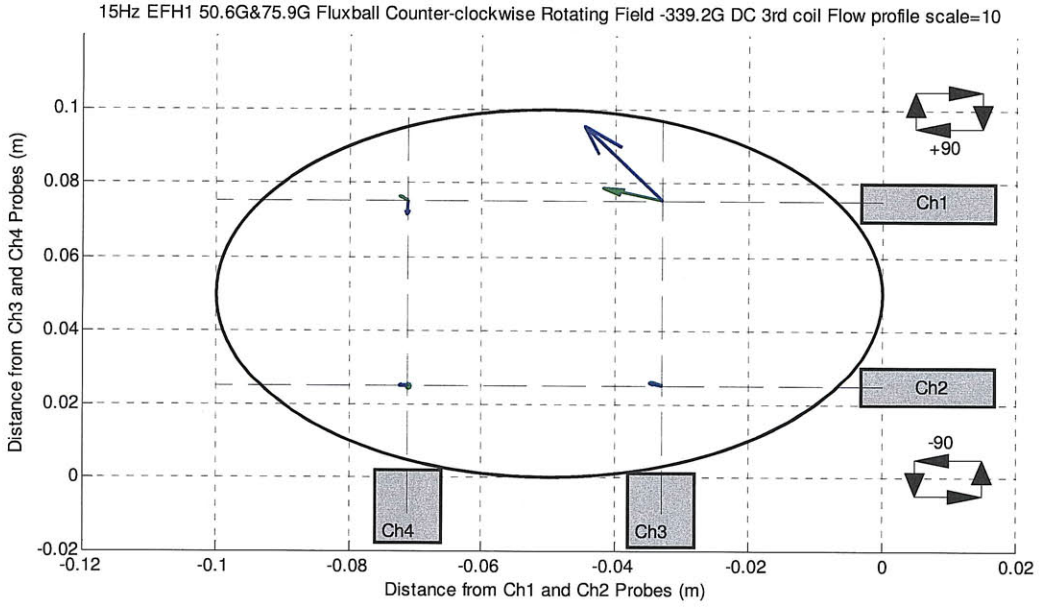
15Hz EFH1 50.6G&75.9G Fluxball Counter-clockwise Rotating Field -339.2G DC 3rd coil Flow profile scale=10
Distance from Ch3 and Ch4 Probes (m)
Distance from Ch1 and Ch2 Probes (m)
+90
-90
Ch1
Ch2
Ch3
Ch4
0.1
0.08
0.06
0.04
0.02
0
-0.02
-0.12
-0.1
-0.08
-0.06
-0.04
-0.02
0
0.02

G8. MSGW11 Filled Sphere with Third Coil Imposing DC Field

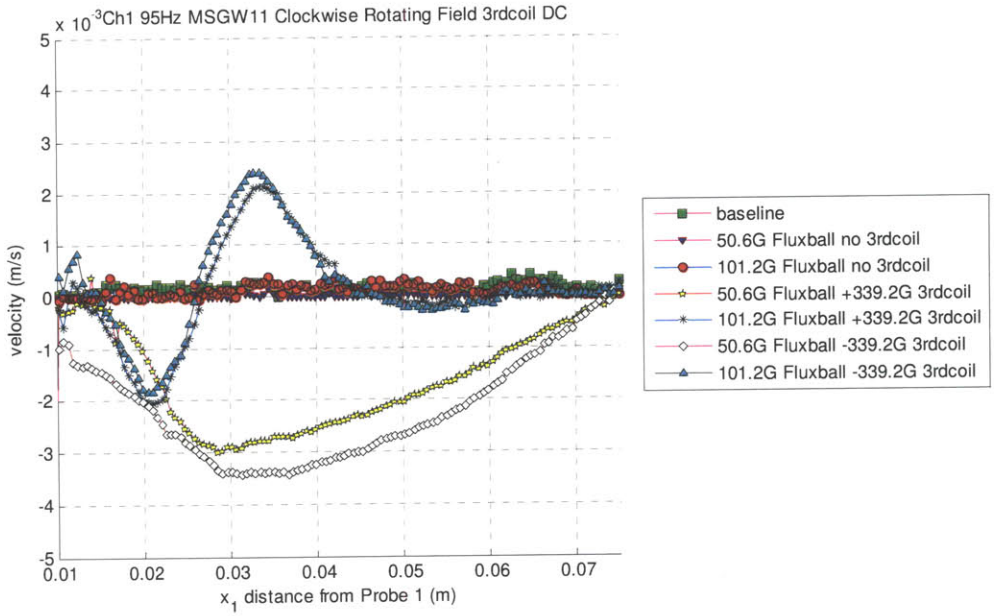

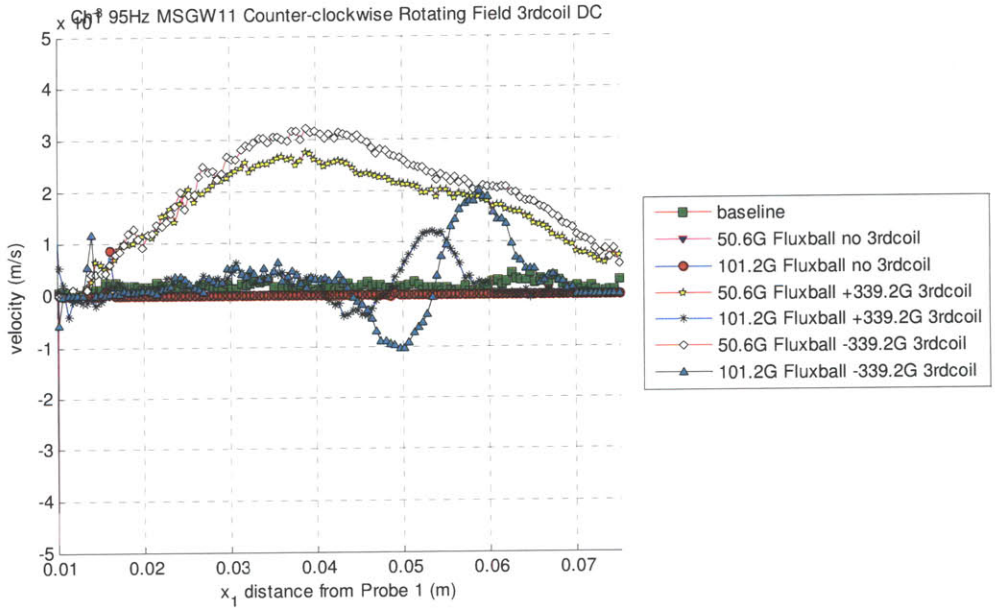

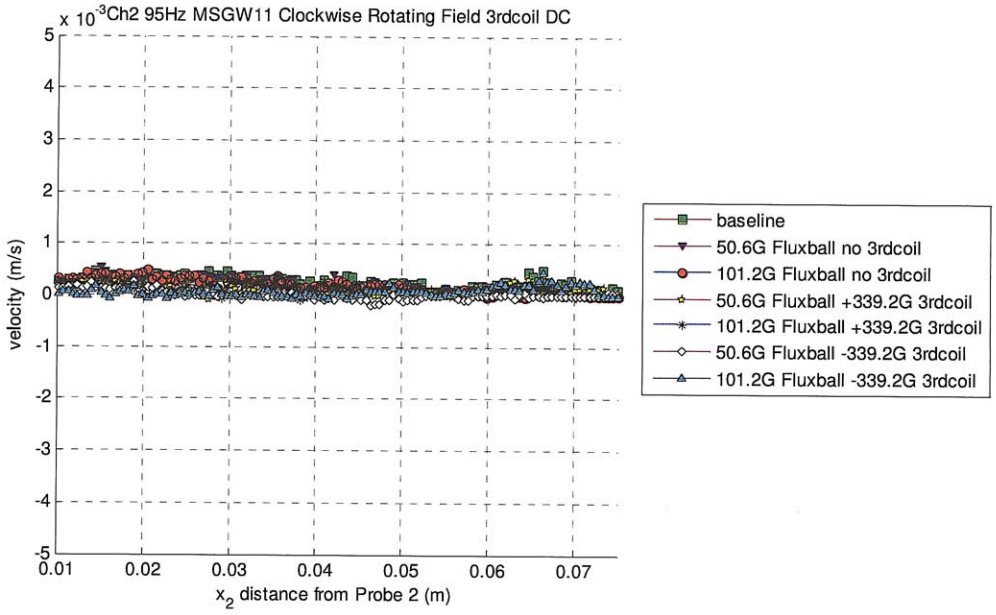
x 10^-3Ch2 95Hz MSGW11 Clockwise Rotating Field 3rdcoil DC
velocity (m/s)
x2 distance from Probe 2 (m)
baseline
50.6G Fluxball no 3rdcoil
101.2G Fluxball no 3rdcoil
50.6G Fluxball +339.2G 3rdcoil
101.2G Fluxball +339.2G 3rdcoil
50.6G Fluxball -339.2G 3rdcoil
101.2G Fluxball -339.2G 3rdcoil

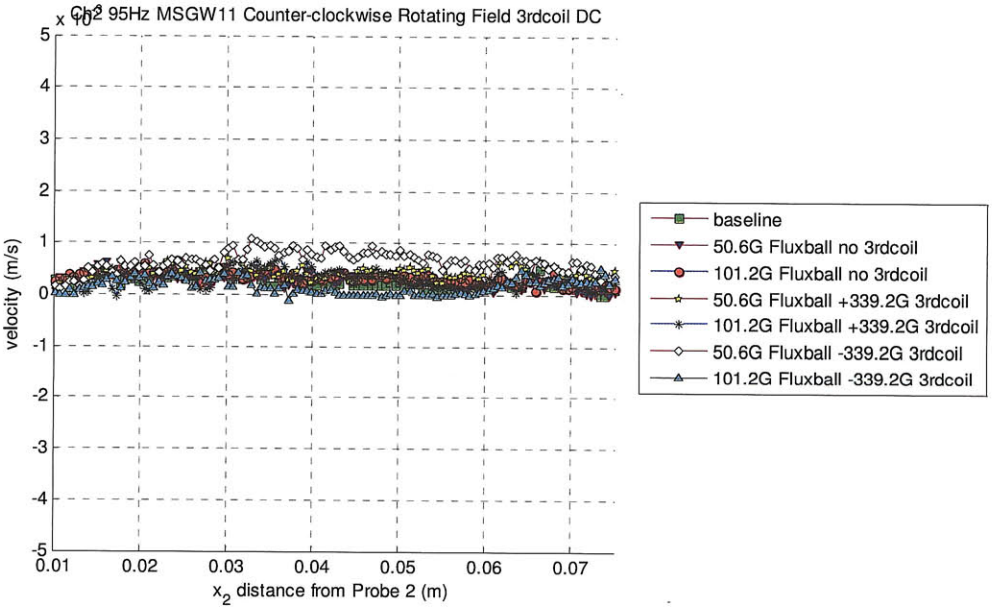
x 10^-3Ch2 95Hz MSGW11 Counter-clockwise Rotating Field 3rdcoil DC
velocity (m/s)
x2 distance from Probe 2 (m)
baseline
50.6G Fluxball no 3rdcoil
101.2G Fluxball no 3rdcoil
50.6G Fluxball +339.2G 3rdcoil
101.2G Fluxball +339.2G 3rdcoil
50.6G Fluxball -339.2G 3rdcoil
101.2G Fluxball -339.2G 3rdcoil

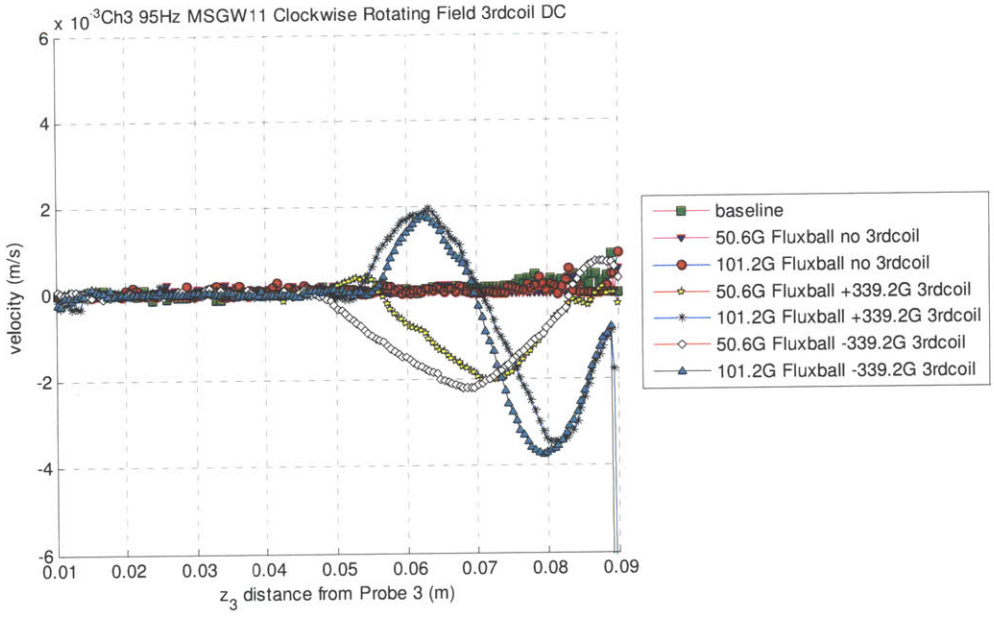
x 10^-3Ch3 95Hz MSGW11 Clockwise Rotating Field 3rdcoil DC
velocity (m/s)
z3 distance from Probe 3 (m)
baseline
50.6G Fluxball no 3rdcoil
101.2G Fluxball no 3rdcoil
50.6G Fluxball +339.2G 3rdcoil
101.2G Fluxball +339.2G 3rdcoil
50.6G Fluxball -339.2G 3rdcoil
101.2G Fluxball -339.2G 3rdcoil

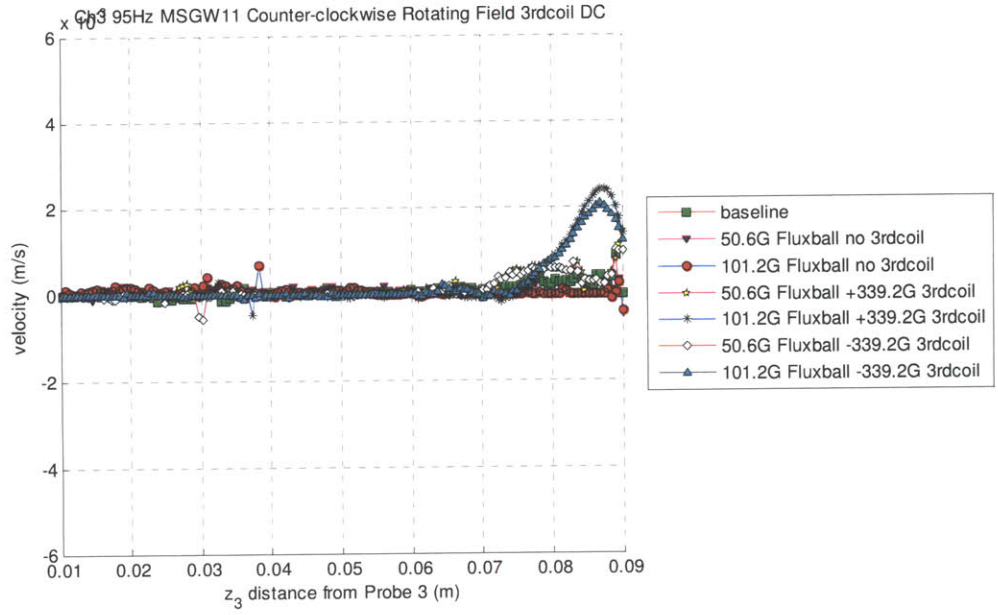
Ch3 95Hz MSGW11 Counter-clockwise Rotating Field 3rdcoil DC
velocity (m/s)
z3 distance from Probe 3 (m)
baseline
50.6G Fluxball no 3rdcoil
101.2G Fluxball no 3rdcoil
50.6G Fluxball +339.2G 3rdcoil
101.2G Fluxball +339.2G 3rdcoil
50.6G Fluxball -339.2G 3rdcoil
101.2G Fluxball -339.2G 3rdcoil

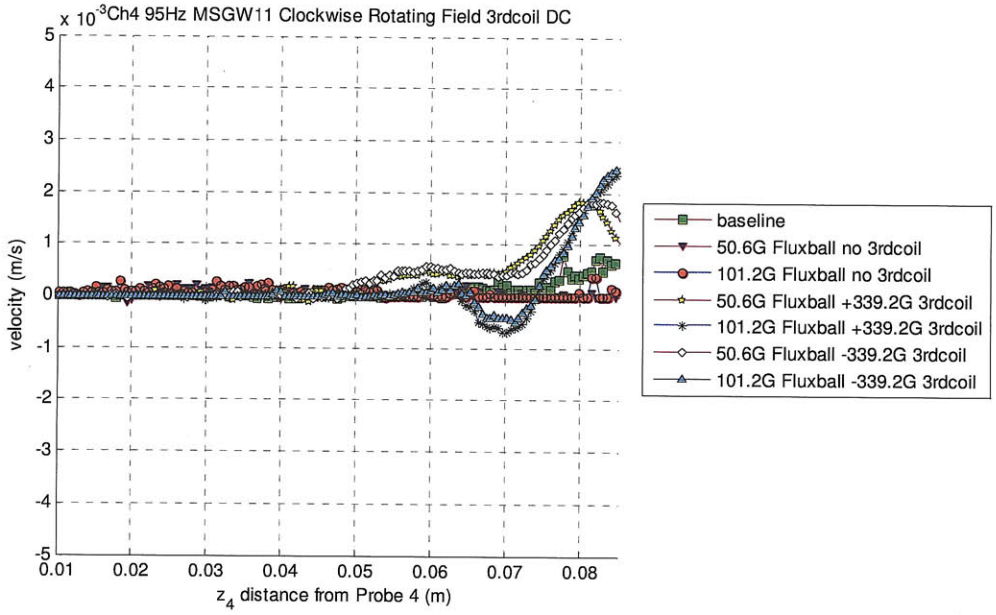
x 10^-3 Ch4 95Hz MSGW11 Clockwise Rotating Field 3rdcoil DC
velocity (m/s)
z4 distance from Probe 4 (m)
baseline
50.6G Fluxball no 3rdcoil
101.2G Fluxball no 3rdcoil
50.6G Fluxball +339.2G 3rdcoil
101.2G Fluxball +339.2G 3rdcoil
50.6G Fluxball -339.2G 3rdcoil
101.2G Fluxball -339.2G 3rdcoil

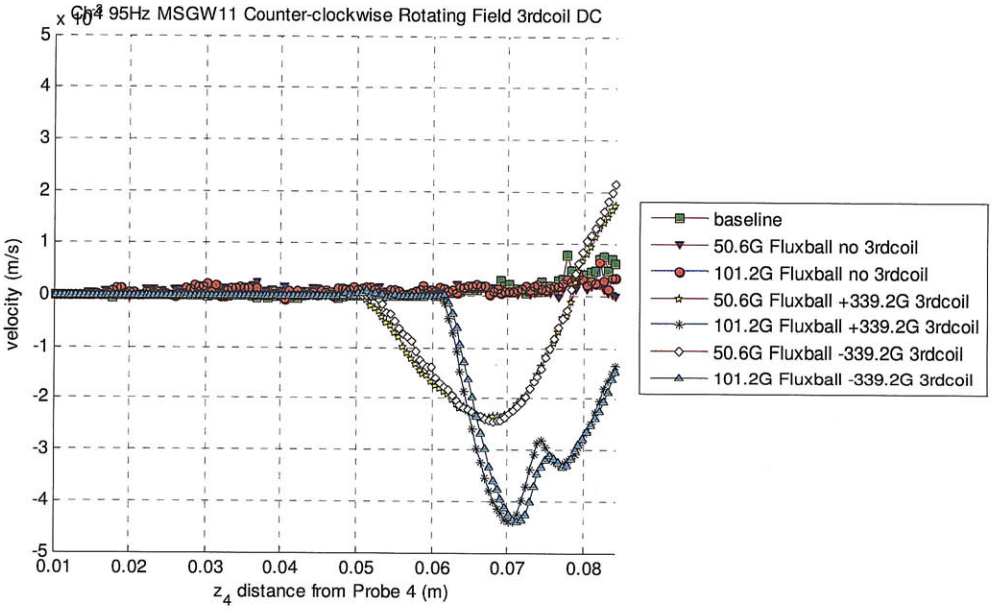
x 10^-3 Ch4 95Hz MSGW11 Counter-clockwise Rotating Field 3rdcoil DC
velocity (m/s)
z4 distance from Probe 4 (m)
baseline
50.6G Fluxball no 3rdcoil
101.2G Fluxball no 3rdcoil
50.6G Fluxball +339.2G 3rdcoil
101.2G Fluxball +339.2G 3rdcoil
50.6G Fluxball -339.2G 3rdcoil
101.2G Fluxball -339.2G 3rdcoil

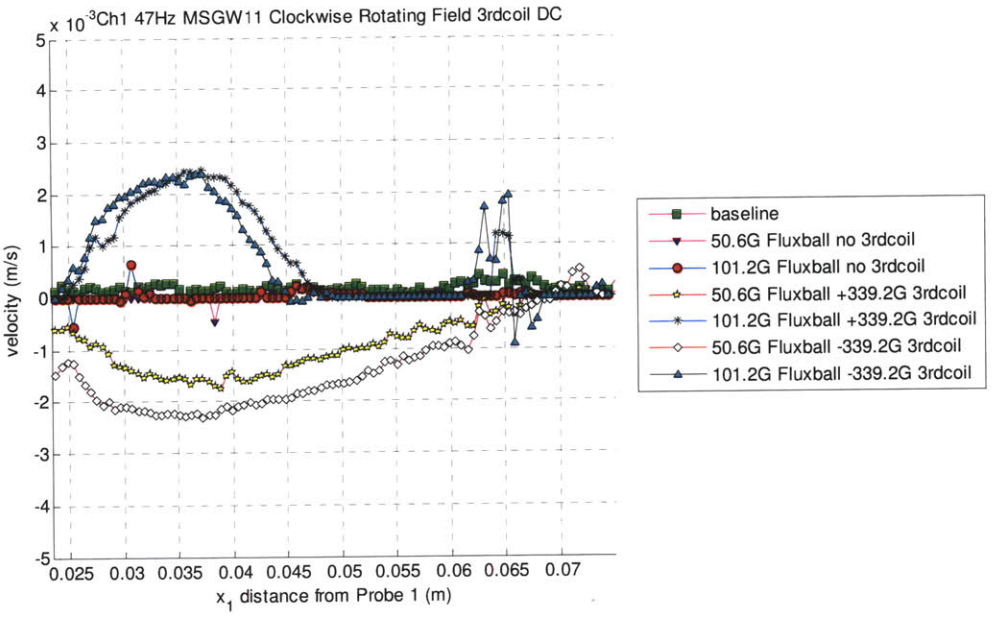
x 10^-3Ch1 47Hz MSGW11 Clockwise Rotating Field 3rdcoil DC
velocity (m/s)
x1 distance from Probe 1 (m)
baseline
50.6G Fluxball no 3rdcoil
101.2G Fluxball no 3rdcoil
50.6G Fluxball +339.2G 3rdcoil
101.2G Fluxball +339.2G 3rdcoil
50.6G Fluxball -339.2G 3rdcoil
101.2G Fluxball -339.2G 3rdcoil

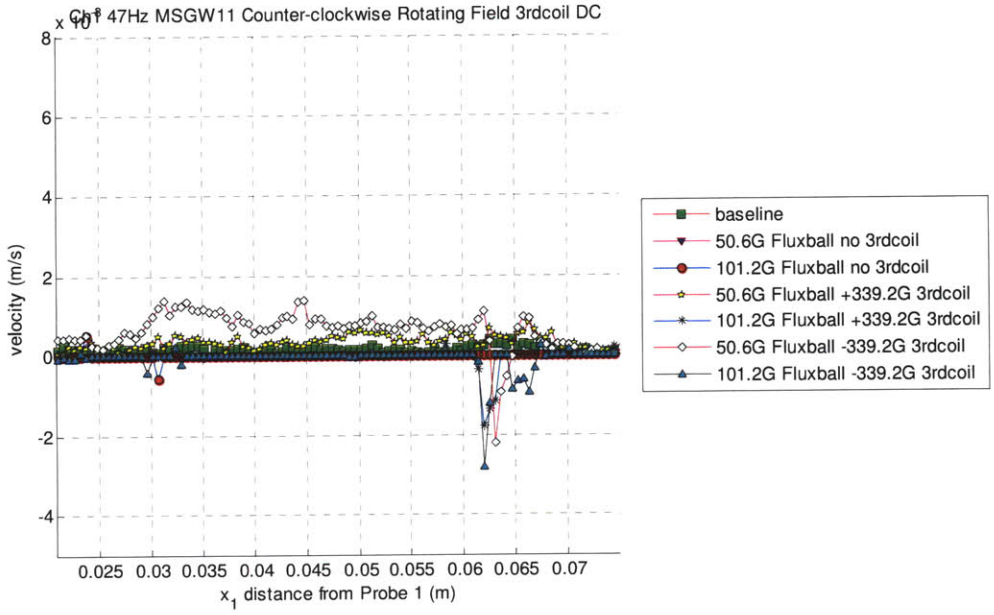
Ch1 47Hz MSGW11 Counter-clockwise Rotating Field 3rdcoil DC
velocity (m/s)
x1 distance from Probe 1 (m)
baseline
50.6G Fluxball no 3rdcoil
101.2G Fluxball no 3rdcoil
50.6G Fluxball +339.2G 3rdcoil
101.2G Fluxball +339.2G 3rdcoil
50.6G Fluxball -339.2G 3rdcoil
101.2G Fluxball -339.2G 3rdcoil

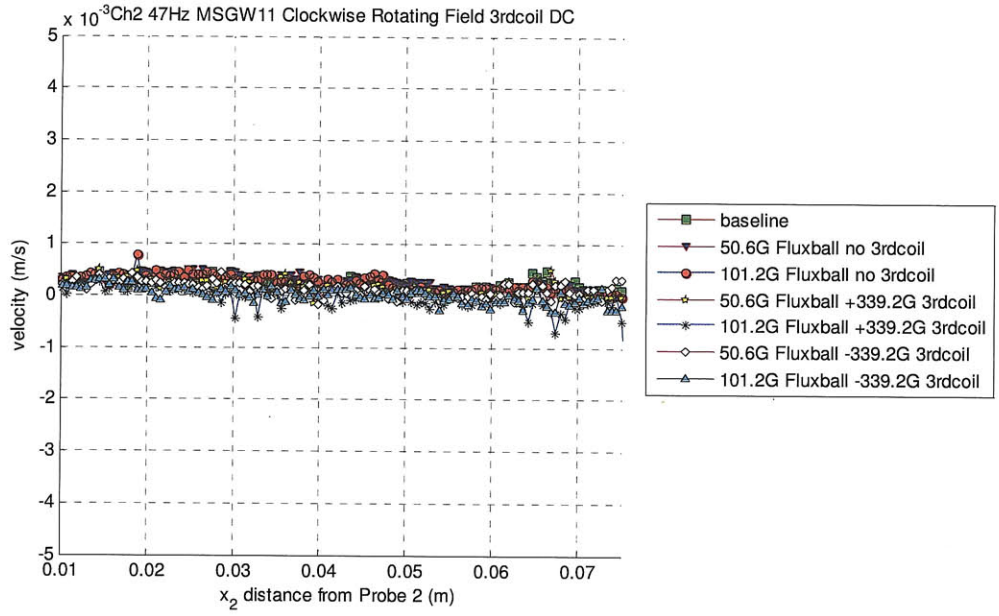
x 10^-3Ch2 47Hz MSGW11 Clockwise Rotating Field 3rdcoil DC
velocity (m/s)
x2 distance from Probe 2 (m)
baseline
50.6G Fluxball no 3rdcoil
101.2G Fluxball no 3rdcoil
50.6G Fluxball +339.2G 3rdcoil
101.2G Fluxball +339.2G 3rdcoil
50.6G Fluxball -339.2G 3rdcoil
101.2G Fluxball -339.2G 3rdcoil

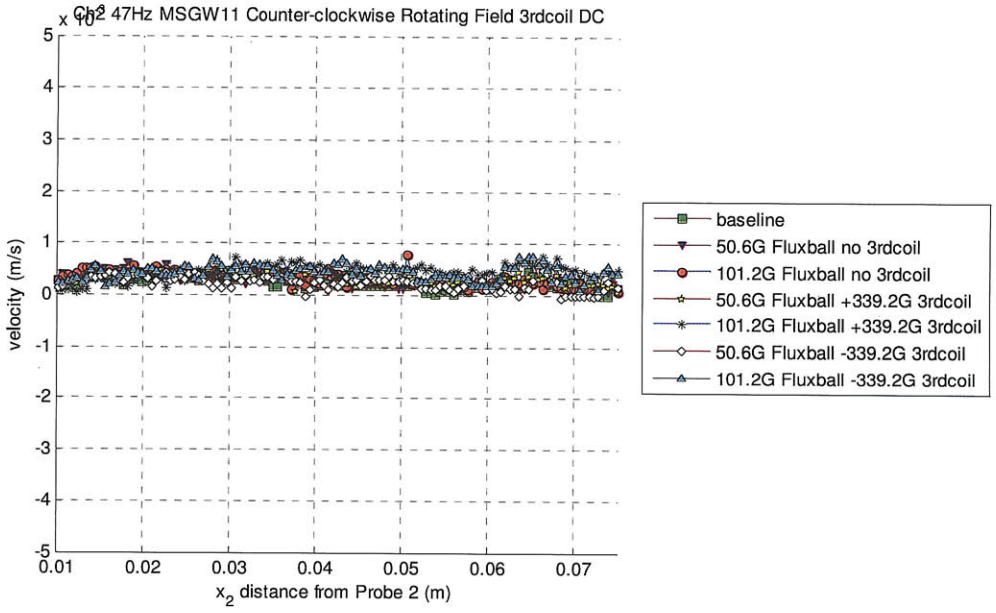
x 10^-3Ch2 47Hz MSGW11 Counter-clockwise Rotating Field 3rdcoil DC
velocity (m/s)
x2 distance from Probe 2 (m)
baseline
50.6G Fluxball no 3rdcoil
101.2G Fluxball no 3rdcoil
50.6G Fluxball +339.2G 3rdcoil
101.2G Fluxball +339.2G 3rdcoil
50.6G Fluxball -339.2G 3rdcoil
101.2G Fluxball -339.2G 3rdcoil

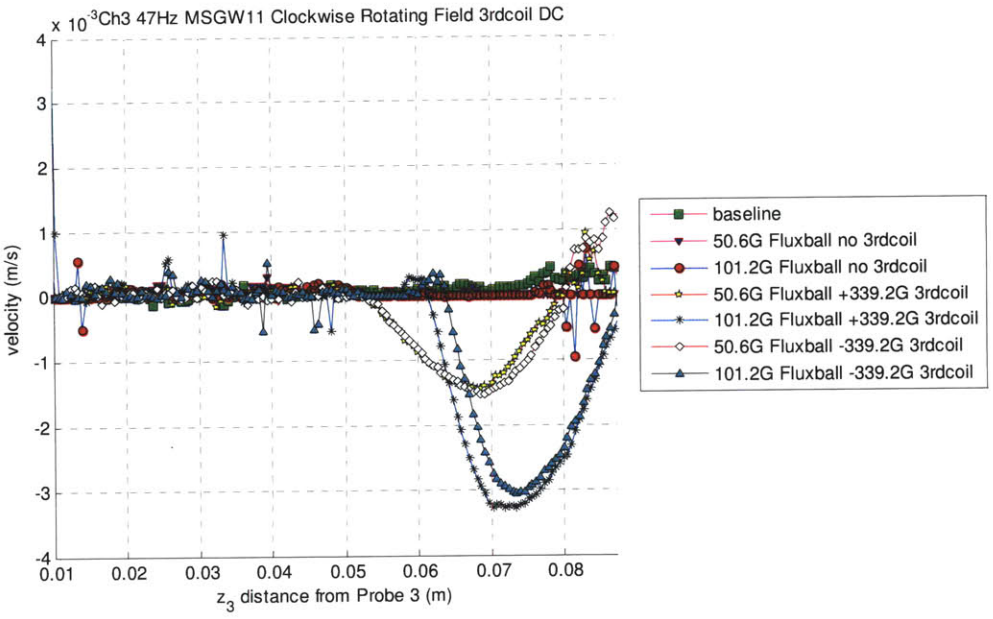
x 10^-3Ch3 47Hz MSGW11 Clockwise Rotating Field 3rdcoil DC
velocity (m/s)
z3 distance from Probe 3 (m)
baseline
50.6G Fluxball no 3rdcoil
101.2G Fluxball no 3rdcoil
50.6G Fluxball +339.2G 3rdcoil
101.2G Fluxball +339.2G 3rdcoil
50.6G Fluxball -339.2G 3rdcoil
101.2G Fluxball -339.2G 3rdcoil

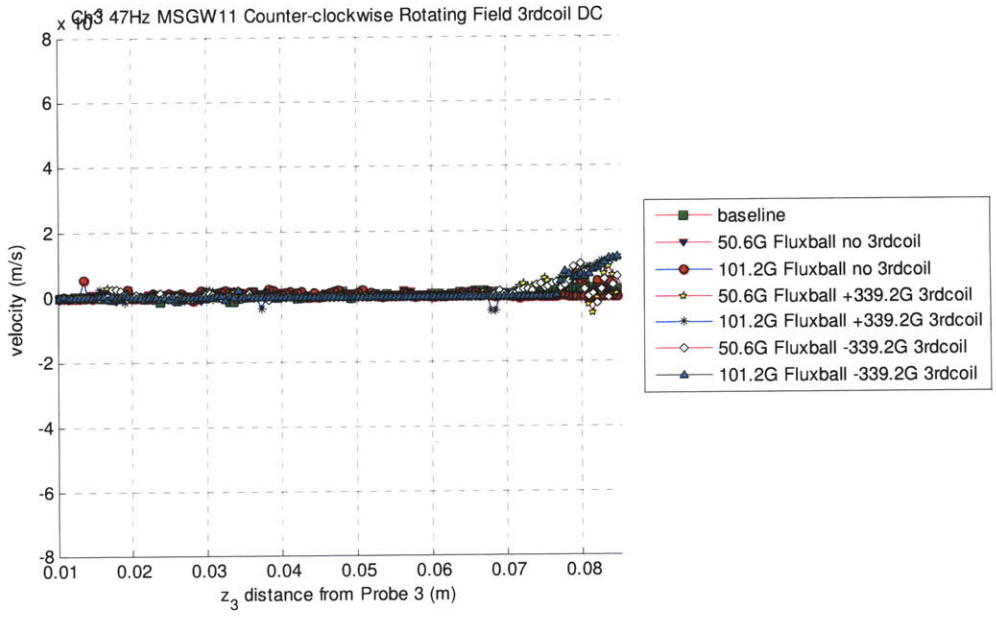
Ch3 47Hz MSGW11 Counter-clockwise Rotating Field 3rdcoil DC
velocity (m/s)
z3 distance from Probe 3 (m)
baseline
50.6G Fluxball no 3rdcoil
101.2G Fluxball no 3rdcoil
50.6G Fluxball +339.2G 3rdcoil
101.2G Fluxball +339.2G 3rdcoil
50.6G Fluxball -339.2G 3rdcoil
101.2G Fluxball -339.2G 3rdcoil

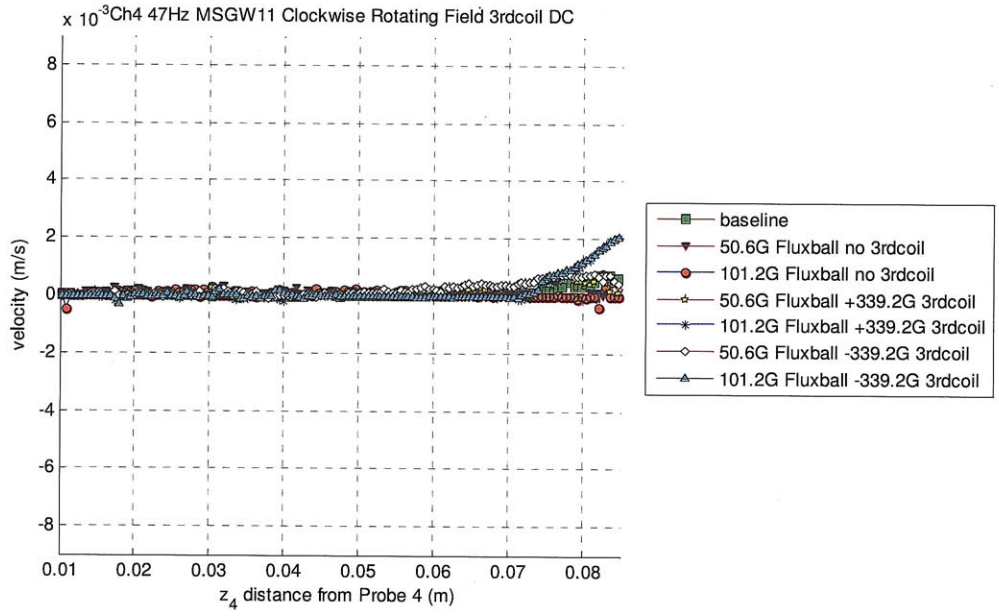
x 10^-3Ch4 47Hz MSGW11 Clockwise Rotating Field 3rdcoil DC
velocity (m/s)
z4 distance from Probe 4 (m)
baseline
50.6G Fluxball no 3rdcoil
101.2G Fluxball no 3rdcoil
50.6G Fluxball +339.2G 3rdcoil
101.2G Fluxball +339.2G 3rdcoil
50.6G Fluxball -339.2G 3rdcoil
101.2G Fluxball -339.2G 3rdcoil

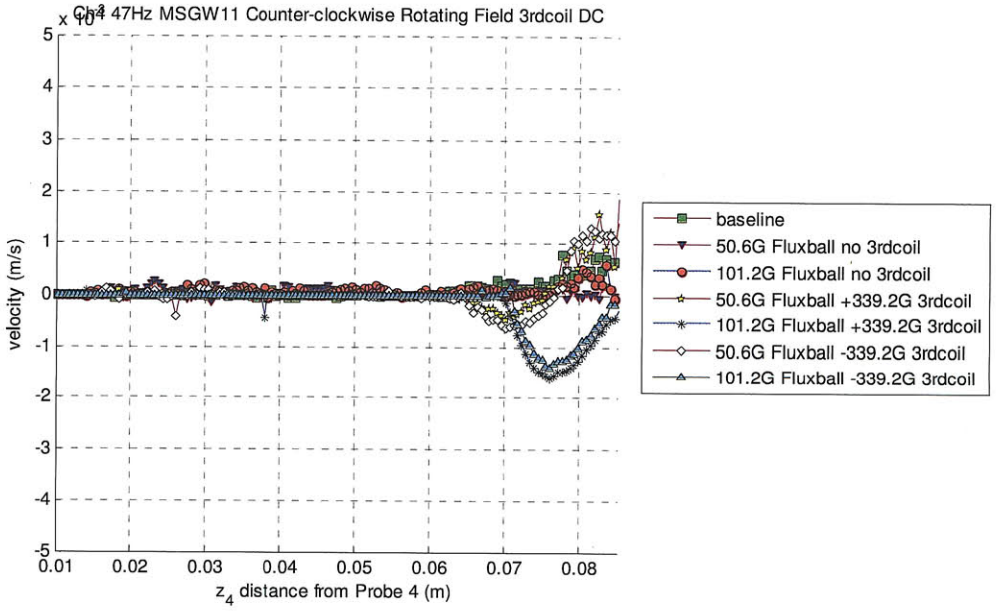
x 10^-3Ch4 47Hz MSGW11 Counter-clockwise Rotating Field 3rdcoil DC
velocity (m/s)
z4 distance from Probe 4 (m)
baseline
50.6G Fluxball no 3rdcoil
101.2G Fluxball no 3rdcoil
50.6G Fluxball +339.2G 3rdcoil
101.2G Fluxball +339.2G 3rdcoil
50.6G Fluxball -339.2G 3rdcoil
101.2G Fluxball -339.2G 3rdcoil

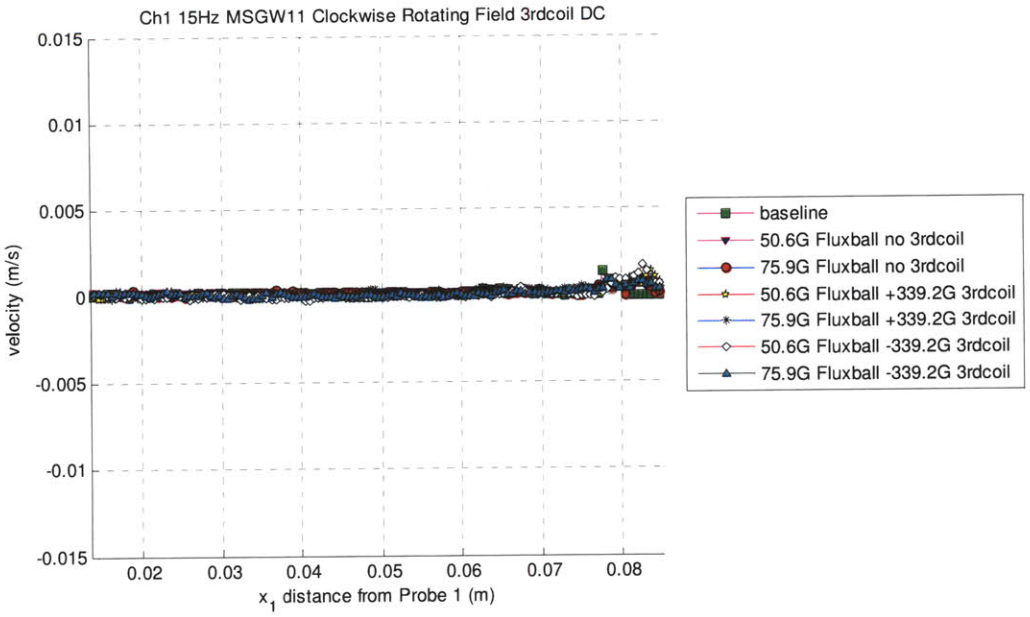
Ch1 15Hz MSGW11 Clockwise Rotating Field 3rdcoil DC
velocity (m/s)
0.015
0.01
0.005
0
-0.005
-0.01
-0.015
0.02
0.03
0.04
0.05
0.06
0.07
0.08
x1 distance from Probe 1 (m)
baseline
50.6G Fluxball no 3rdcoil
75.9G Fluxball no 3rdcoil
50.6G Fluxball +339.2G 3rdcoil
75.9G Fluxball +339.2G 3rdcoil
50.6G Fluxball -339.2G 3rdcoil
75.9G Fluxball -339.2G 3rdcoil

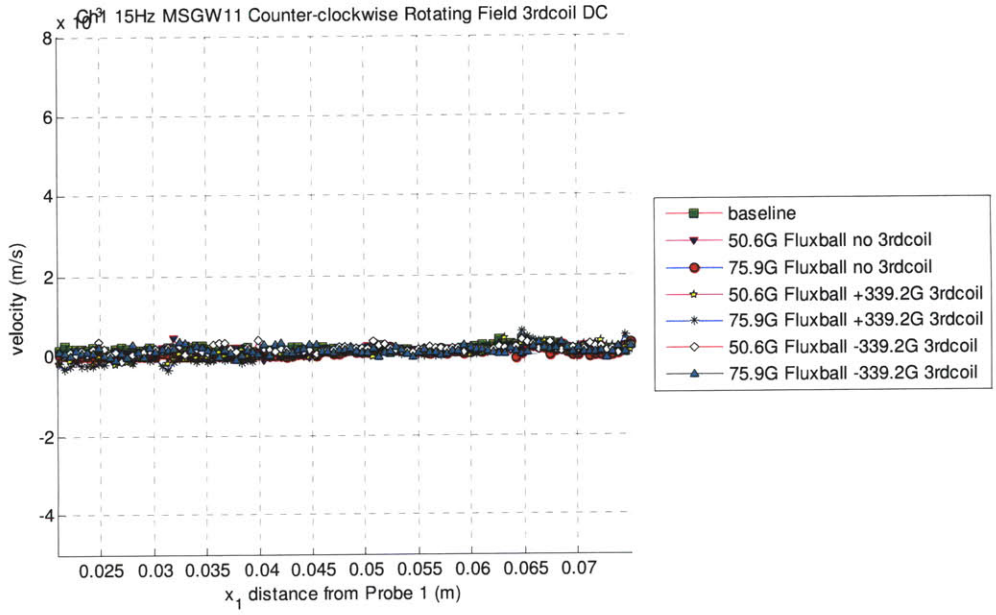
Ch1 15Hz MSGW11 Counter-clockwise Rotating Field 3rdcoil DC
x 10^-3
velocity (m/s)
8
6
4
2
0
-2
-4
0.025
0.03
0.035
0.04
0.045
0.05
0.055
0.06
0.065
0.07
x1 distance from Probe 1 (m)
baseline
50.6G Fluxball no 3rdcoil
75.9G Fluxball no 3rdcoil
50.6G Fluxball +339.2G 3rdcoil
75.9G Fluxball +339.2G 3rdcoil
50.6G Fluxball -339.2G 3rdcoil
75.9G Fluxball -339.2G 3rdcoil

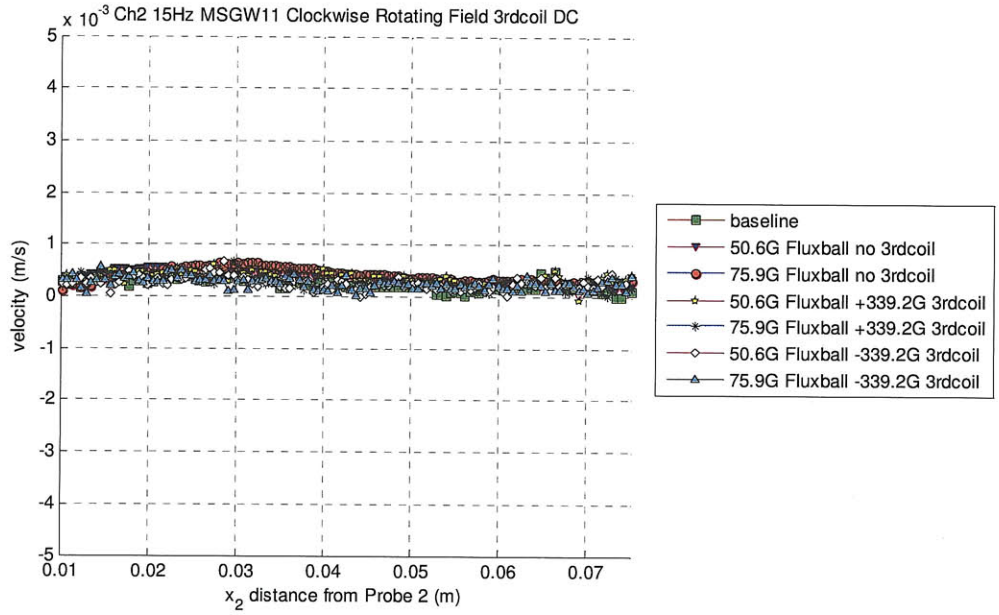
x 10^-3 Ch2 15Hz MSGW11 Clockwise Rotating Field 3rdcoil DC
velocity (m/s)
x2 distance from Probe 2 (m)
baseline
50.6G Fluxball no 3rdcoil
75.9G Fluxball no 3rdcoil
50.6G Fluxball +339.2G 3rdcoil
75.9G Fluxball +339.2G 3rdcoil
50.6G Fluxball -339.2G 3rdcoil
75.9G Fluxball -339.2G 3rdcoil

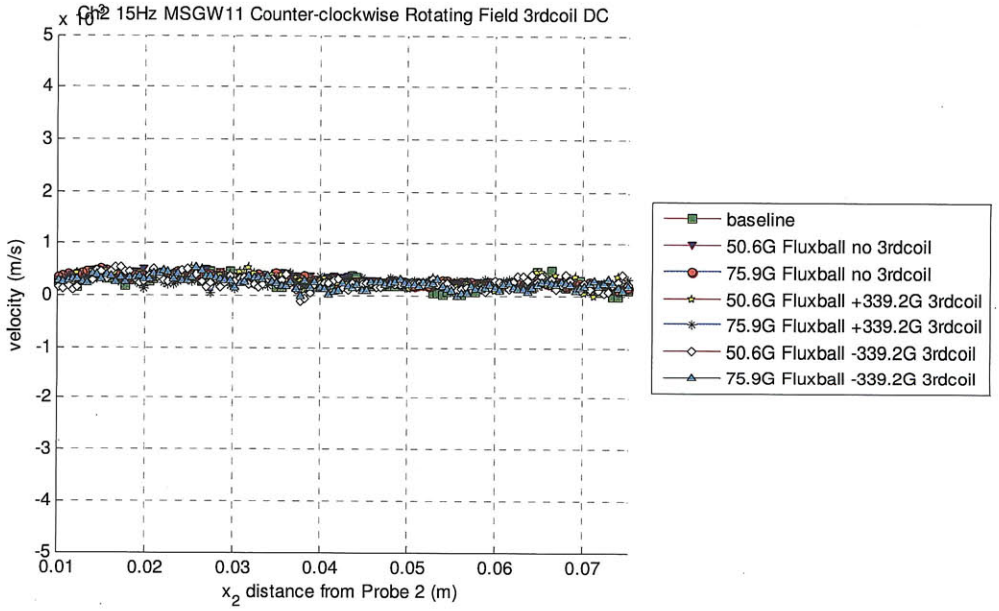
x 10^-3 Ch2 15Hz MSGW11 Counter-clockwise Rotating Field 3rdcoil DC
velocity (m/s)
x2 distance from Probe 2 (m)
baseline
50.6G Fluxball no 3rdcoil
75.9G Fluxball no 3rdcoil
50.6G Fluxball +339.2G 3rdcoil
75.9G Fluxball +339.2G 3rdcoil
50.6G Fluxball -339.2G 3rdcoil
75.9G Fluxball -339.2G 3rdcoil

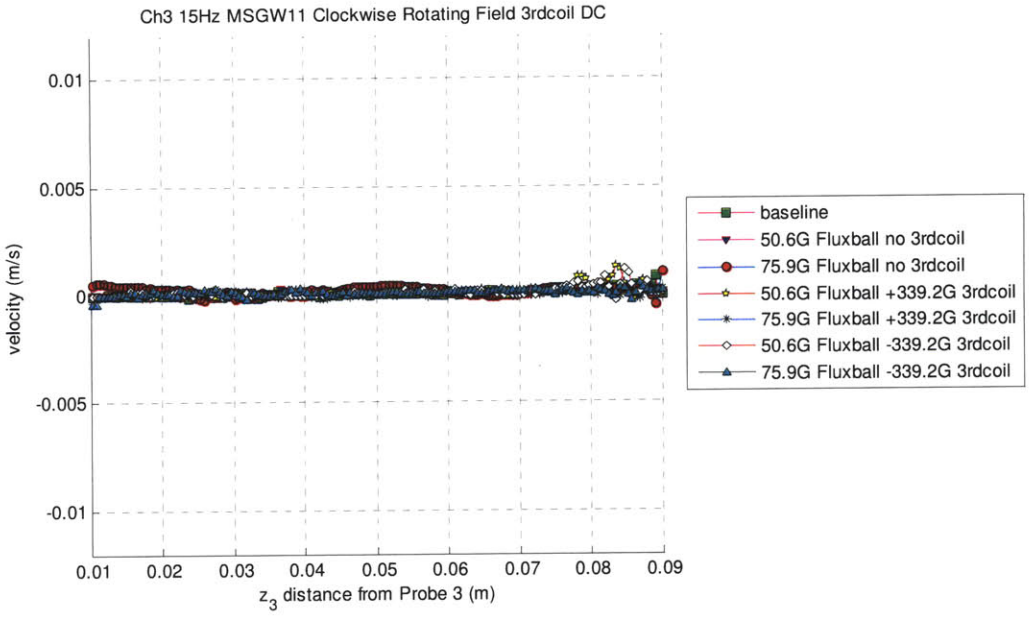
Ch3 15Hz MSGW11 Clockwise Rotating Field 3rdcoil DC
velocity (m/s)
0.01
0.005
0
-0.005
-0.01
0.01
0.02
0.03
0.04
0.05
0.06
0.07
0.08
0.09
z_3 distance from Probe 3 (m)
baseline
50.6G Fluxball no 3rdcoil
75.9G Fluxball no 3rdcoil
50.6G Fluxball +339.2G 3rdcoil
75.9G Fluxball +339.2G 3rdcoil
50.6G Fluxball -339.2G 3rdcoil
75.9G Fluxball -339.2G 3rdcoil

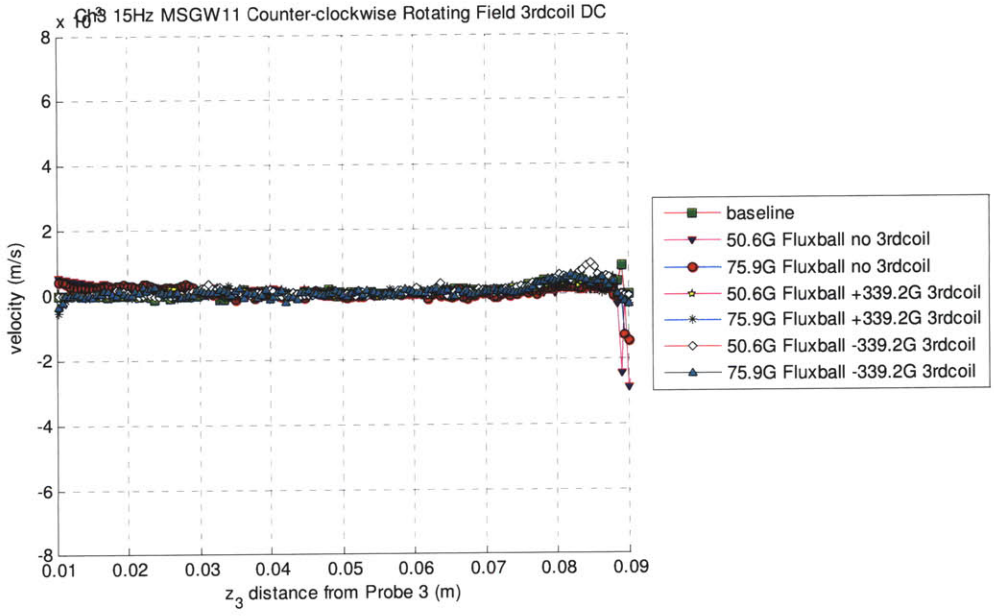
Ch3 15Hz MSGW11 Counter-clockwise Rotating Field 3rdcoil DC
x 10^-3
velocity (m/s)
8
6
4
2
0
-2
-4
-6
-8
0.01
0.02
0.03
0.04
0.05
0.06
0.07
0.08
0.09
z_3 distance from Probe 3 (m)
baseline
50.6G Fluxball no 3rdcoil
75.9G Fluxball no 3rdcoil
50.6G Fluxball +339.2G 3rdcoil
75.9G Fluxball +339.2G 3rdcoil
50.6G Fluxball -339.2G 3rdcoil
75.9G Fluxball -339.2G 3rdcoil

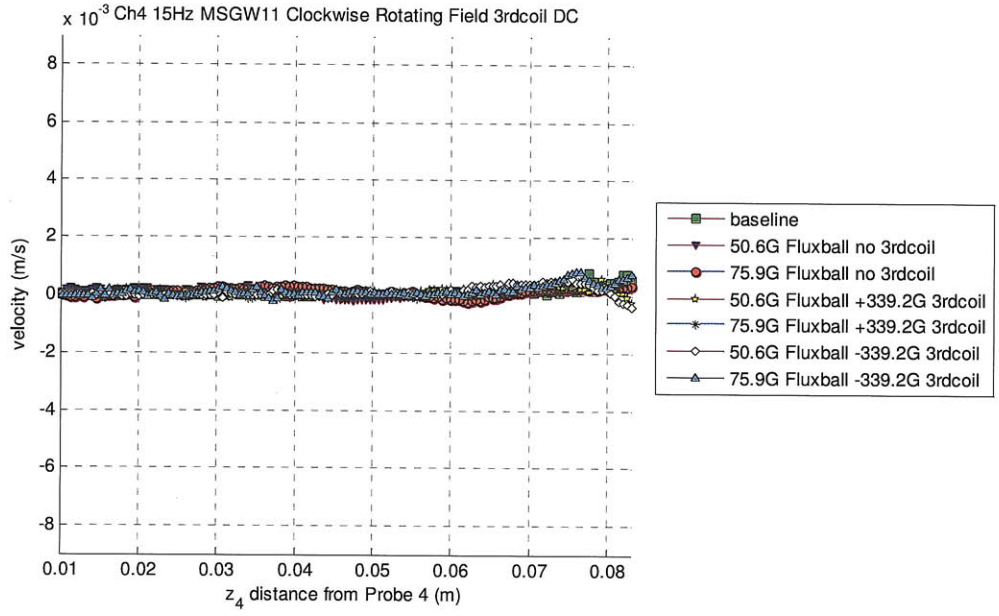
x 10^-3 Ch4 15Hz MSGW11 Clockwise Rotating Field 3rdcoil DC
velocity (m/s)
z4 distance from Probe 4 (m)
baseline
50.6G Fluxball no 3rdcoil
75.9G Fluxball no 3rdcoil
50.6G Fluxball +339.2G 3rdcoil
75.9G Fluxball +339.2G 3rdcoil
50.6G Fluxball -339.2G 3rdcoil
75.9G Fluxball -339.2G 3rdcoil

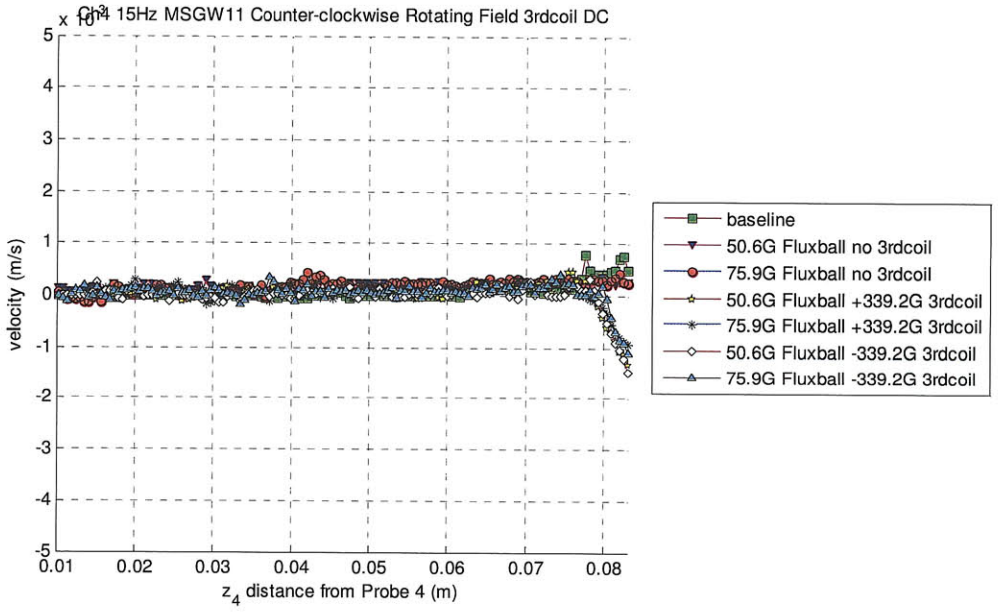
x 10^-3 Ch4 15Hz MSGW11 Counter-clockwise Rotating Field 3rdcoil DC
velocity (m/s)
z4 distance from Probe 4 (m)
baseline
50.6G Fluxball no 3rdcoil
75.9G Fluxball no 3rdcoil
50.6G Fluxball +339.2G 3rdcoil
75.9G Fluxball +339.2G 3rdcoil
50.6G Fluxball -339.2G 3rdcoil
75.9G Fluxball -339.2G 3rdcoil

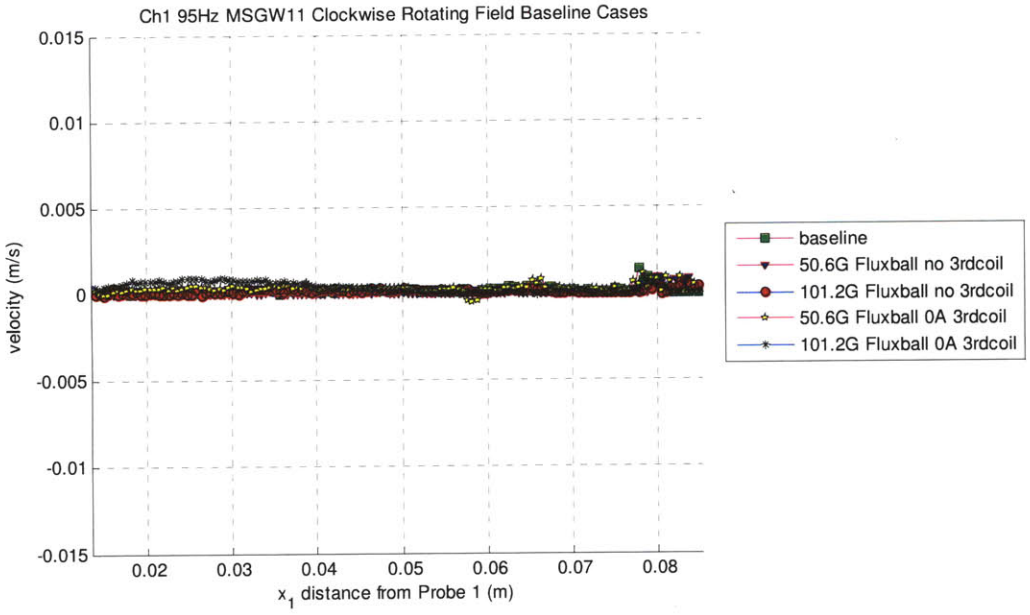
Ch1 95Hz MSGW11 Clockwise Rotating Field Baseline Cases
velocity (m/s)
0.015
0.01
0.005
0
-0.005
-0.01
-0.015
0.02
0.03
0.04
0.05
0.06
0.07
0.08
x1 distance from Probe 1 (m)
baseline
50.6G Fluxball no 3rdcoil
101.2G Fluxball no 3rdcoil
50.6G Fluxball 0A 3rdcoil
101.2G Fluxball 0A 3rdcoil

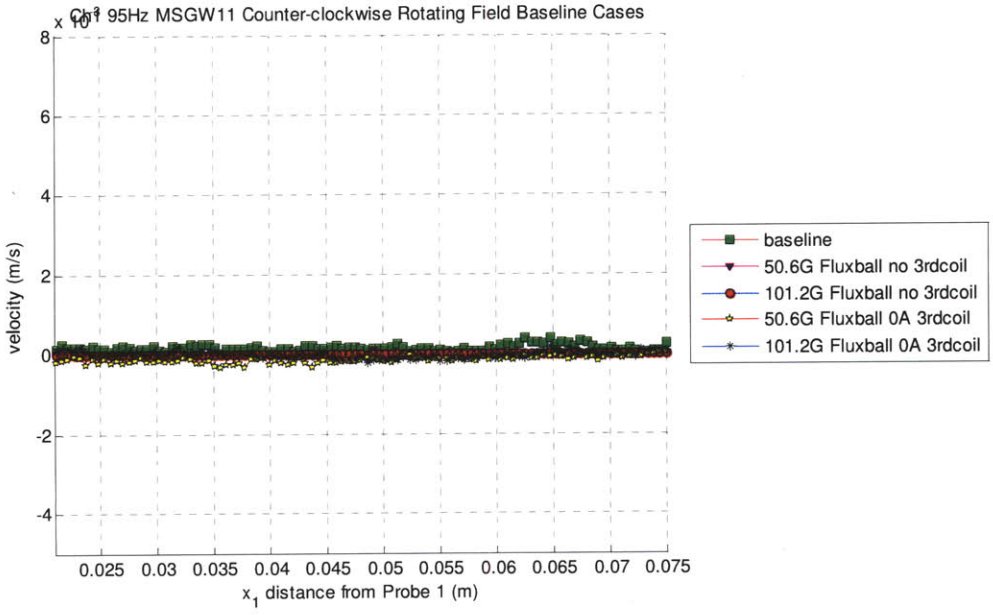
Ch3 95Hz MSGW11 Counter-clockwise Rotating Field Baseline Cases
x 10-4
velocity (m/s)
8
6
4
2
0
-2
-4
0.025
0.03
0.035
0.04
0.045
0.05
0.055
0.06
0.065
0.07
0.075
x1 distance from Probe 1 (m)
baseline
50.6G Fluxball no 3rdcoil
101.2G Fluxball no 3rdcoil
50.6G Fluxball 0A 3rdcoil
101.2G Fluxball 0A 3rdcoil

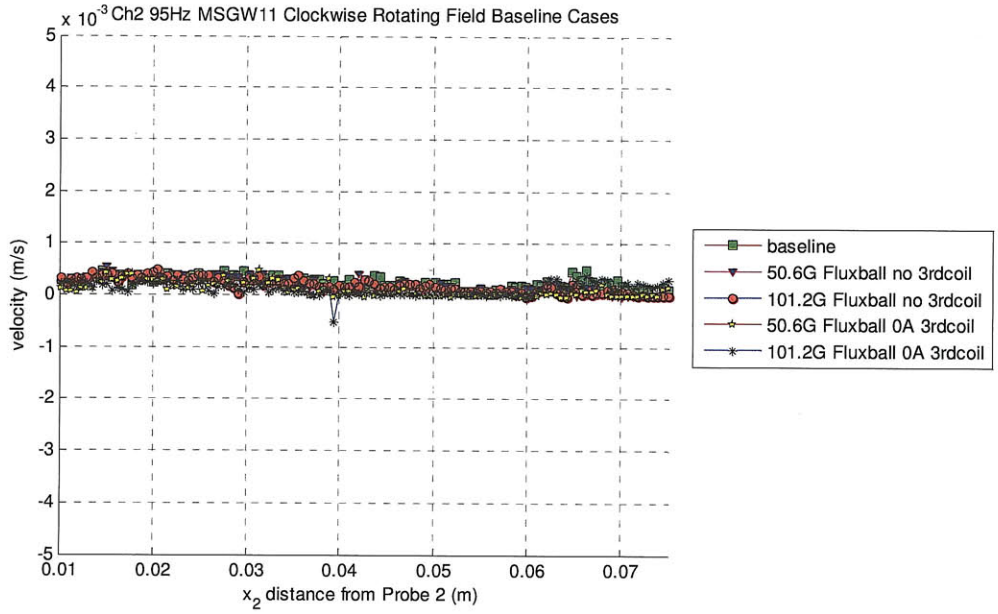
x 10^-3 Ch2 95Hz MSGW11 Clockwise Rotating Field Baseline Cases
velocity (m/s)
x2 distance from Probe 2 (m)
baseline
50.6G Fluxball no 3rdcoil
101.2G Fluxball no 3rdcoil
50.6G Fluxball 0A 3rdcoil
101.2G Fluxball 0A 3rdcoil

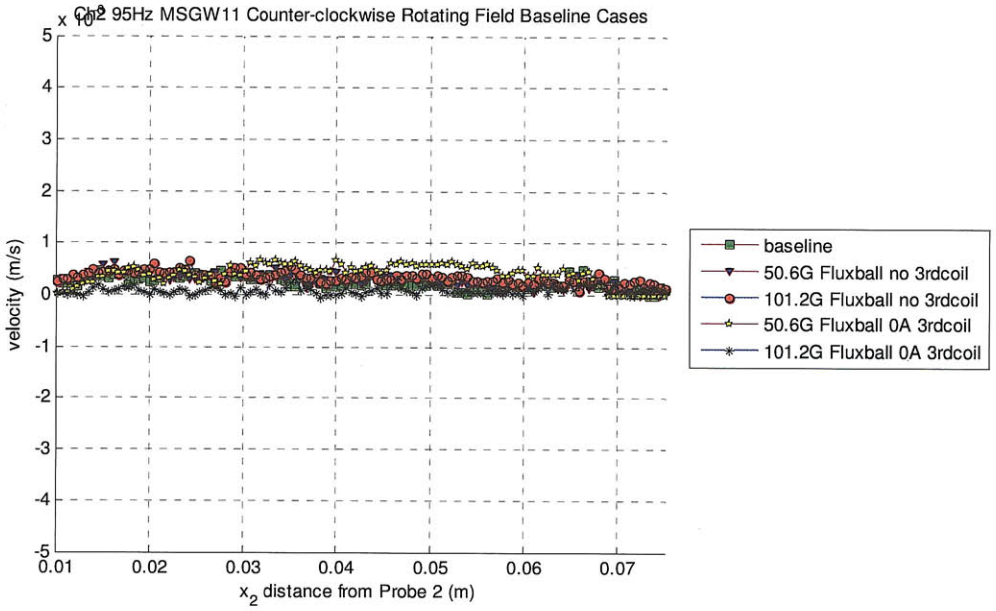
x 10^-3 Ch2 95Hz MSGW11 Counter-clockwise Rotating Field Baseline Cases
velocity (m/s)
x2 distance from Probe 2 (m)
baseline
50.6G Fluxball no 3rdcoil
101.2G Fluxball no 3rdcoil
50.6G Fluxball 0A 3rdcoil
101.2G Fluxball 0A 3rdcoil

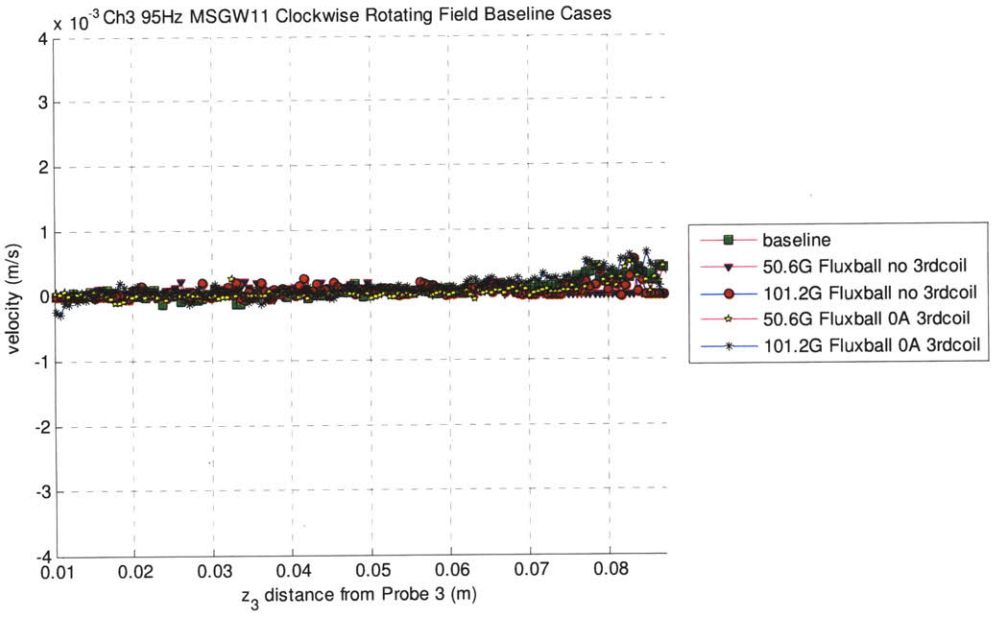
x 10^-3 Ch3 95Hz MSGW11 Clockwise Rotating Field Baseline Cases
velocity (m/s)
z3 distance from Probe 3 (m)
baseline
50.6G Fluxball no 3rdcoil
101.2G Fluxball no 3rdcoil
50.6G Fluxball 0A 3rdcoil
101.2G Fluxball 0A 3rdcoil

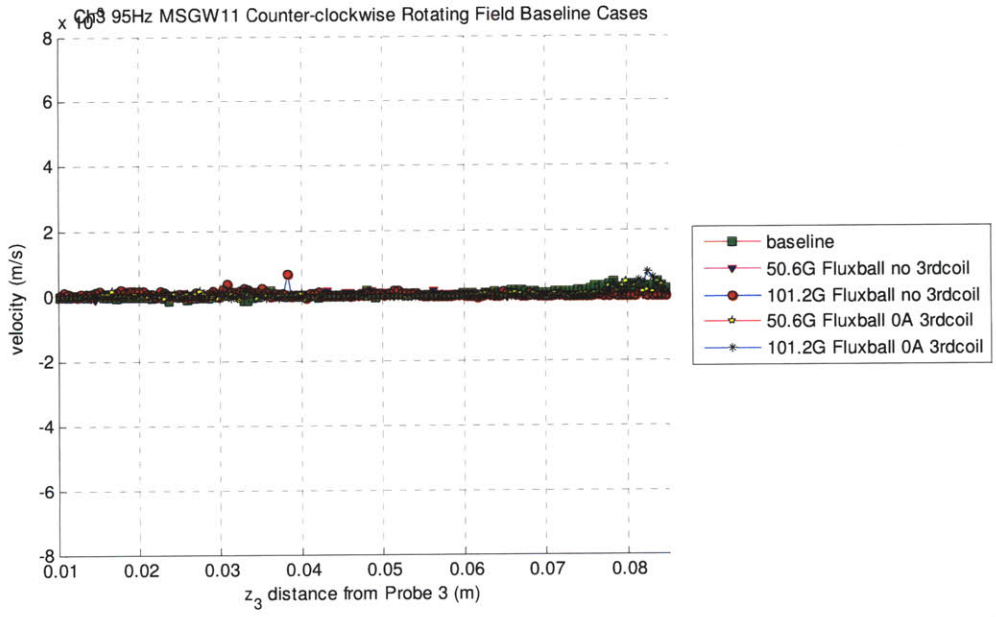
x 10^-3 Ch3 95Hz MSGW11 Counter-clockwise Rotating Field Baseline Cases
velocity (m/s)
z3 distance from Probe 3 (m)
baseline
50.6G Fluxball no 3rdcoil
101.2G Fluxball no 3rdcoil
50.6G Fluxball 0A 3rdcoil
101.2G Fluxball 0A 3rdcoil

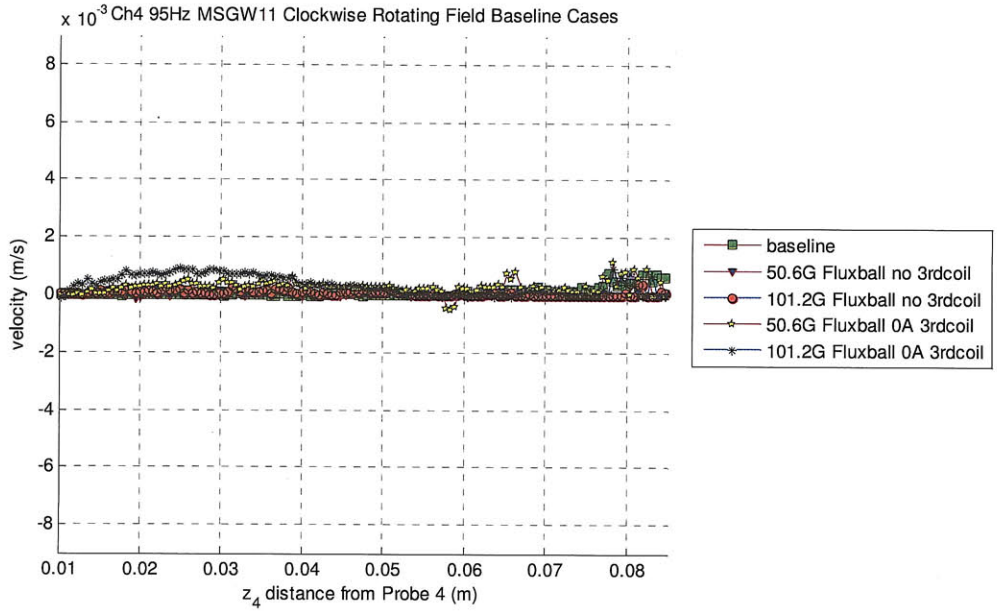
x 10^-3 Ch4 95Hz MSGW11 Clockwise Rotating Field Baseline Cases
velocity (m/s)
z4 distance from Probe 4 (m)
baseline
50.6G Fluxball no 3rdcoil
101.2G Fluxball no 3rdcoil
50.6G Fluxball 0A 3rdcoil
101.2G Fluxball 0A 3rdcoil

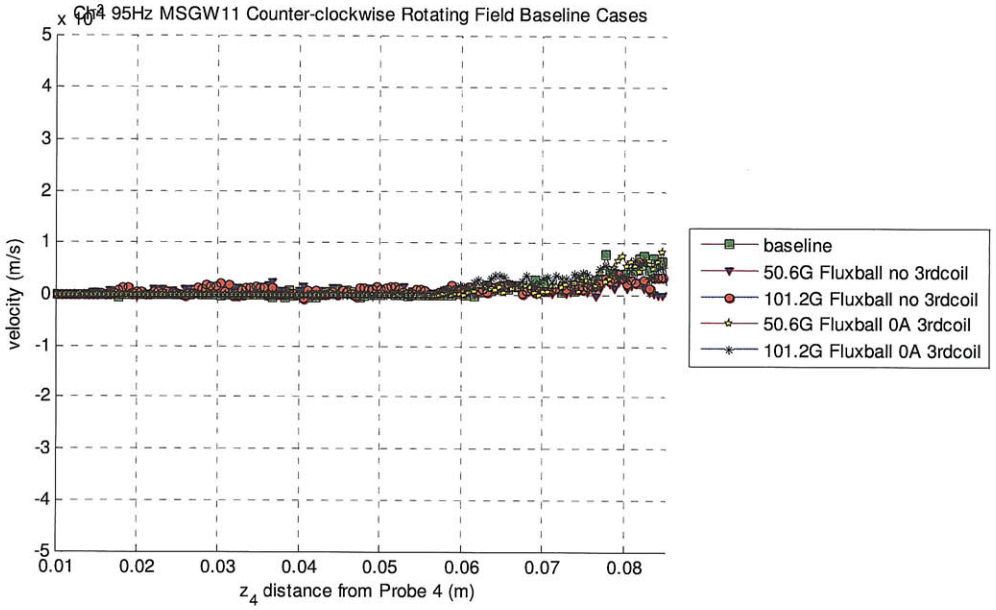
x 10^-3 Ch4 95Hz MSGW11 Counter-clockwise Rotating Field Baseline Cases
velocity (m/s)
z4 distance from Probe 4 (m)
baseline
50.6G Fluxball no 3rdcoil
101.2G Fluxball no 3rdcoil
50.6G Fluxball 0A 3rdcoil
101.2G Fluxball 0A 3rdcoil

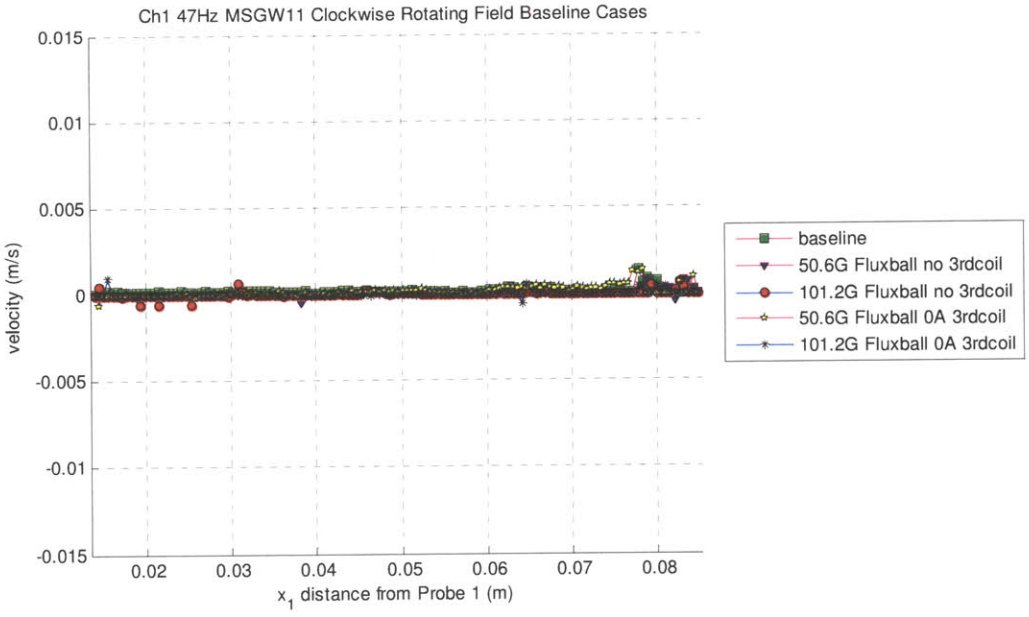
Ch1 47Hz MSGW11 Clockwise Rotating Field Baseline Cases
0.015
0.01
0.005
0
-0.005
-0.01
-0.015
velocity (m/s)
0.02
0.03
0.04
0.05
0.06
0.07
0.08
x1 distance from Probe 1 (m)
baseline
50.6G Fluxball no 3rdcoil
101.2G Fluxball no 3rdcoil
50.6G Fluxball 0A 3rdcoil
101.2G Fluxball 0A 3rdcoil

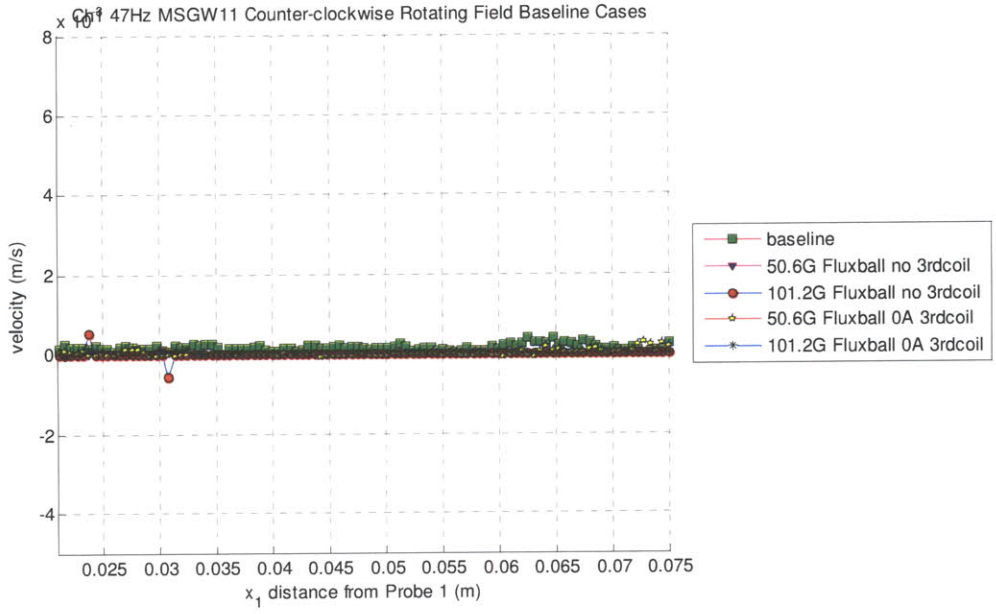
Ch1 47Hz MSGW11 Counter-clockwise Rotating Field Baseline Cases
x 10^-3
8
6
4
2
0
-2
-4
velocity (m/s)
0.025
0.03
0.035
0.04
0.045
0.05
0.055
0.06
0.065
0.07
0.075
x1 distance from Probe 1 (m)
baseline
50.6G Fluxball no 3rdcoil
101.2G Fluxball no 3rdcoil
50.6G Fluxball 0A 3rdcoil
101.2G Fluxball 0A 3rdcoil

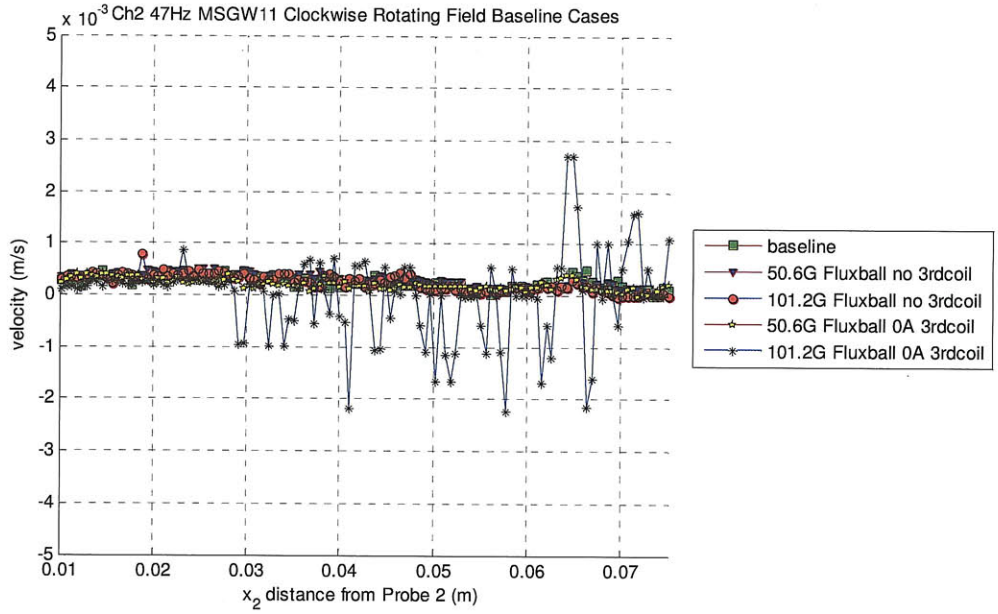
x 10^-3 Ch2 47Hz MSGW11 Clockwise Rotating Field Baseline Cases
velocity (m/s)
x2 distance from Probe 2 (m)
baseline
50.6G Fluxball no 3rdcoil
101.2G Fluxball no 3rdcoil
50.6G Fluxball 0A 3rdcoil
101.2G Fluxball 0A 3rdcoil

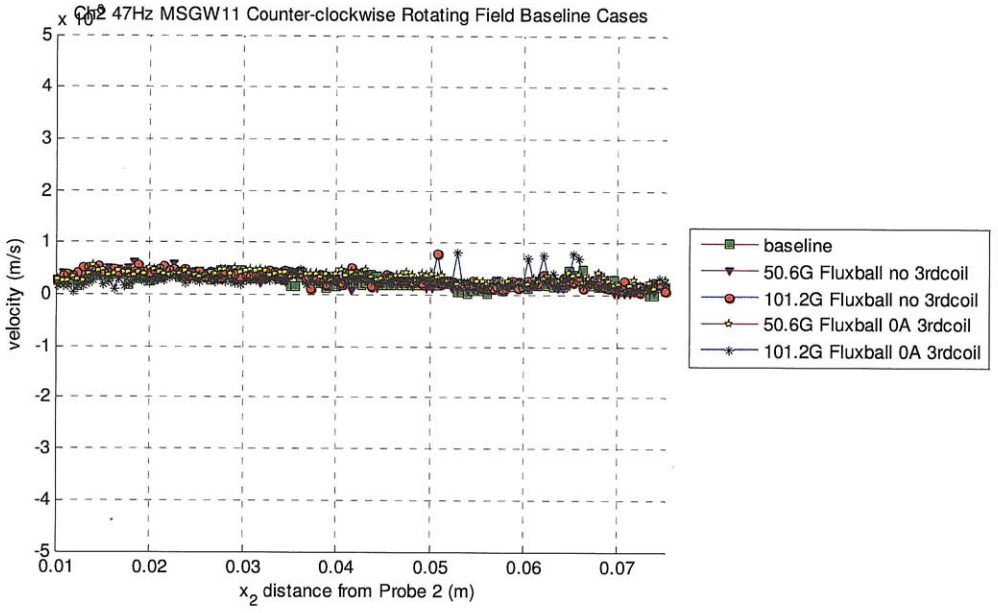
Ch2 47Hz MSGW11 Counter-clockwise Rotating Field Baseline Cases
velocity (m/s)
x2 distance from Probe 2 (m)
baseline
50.6G Fluxball no 3rdcoil
101.2G Fluxball no 3rdcoil
50.6G Fluxball 0A 3rdcoil
101.2G Fluxball 0A 3rdcoil

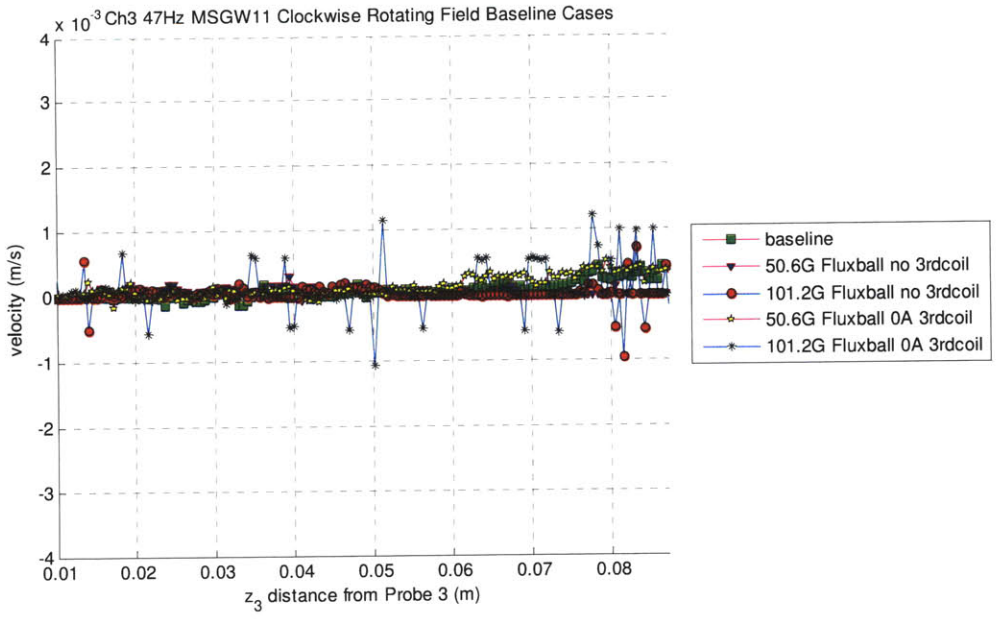
x 10^-3 Ch3 47Hz MSGW11 Clockwise Rotating Field Baseline Cases
velocity (m/s)
z3 distance from Probe 3 (m)
baseline
50.6G Fluxball no 3rdcoil
101.2G Fluxball no 3rdcoil
50.6G Fluxball 0A 3rdcoil
101.2G Fluxball 0A 3rdcoil

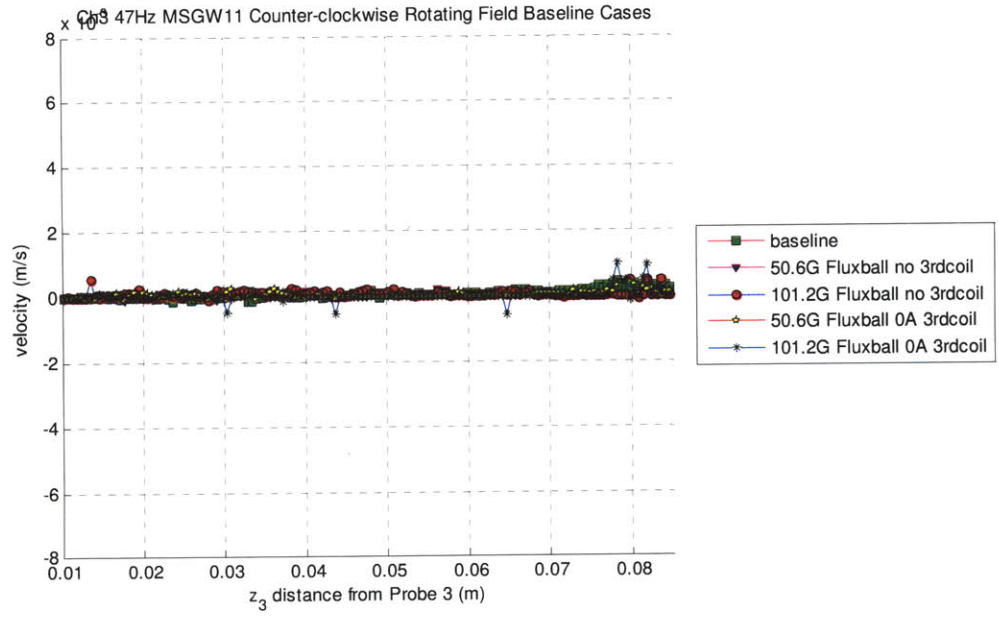
Ch3 47Hz MSGW11 Counter-clockwise Rotating Field Baseline Cases
velocity (m/s)
z3 distance from Probe 3 (m)
baseline
50.6G Fluxball no 3rdcoil
101.2G Fluxball no 3rdcoil
50.6G Fluxball 0A 3rdcoil
101.2G Fluxball 0A 3rdcoil

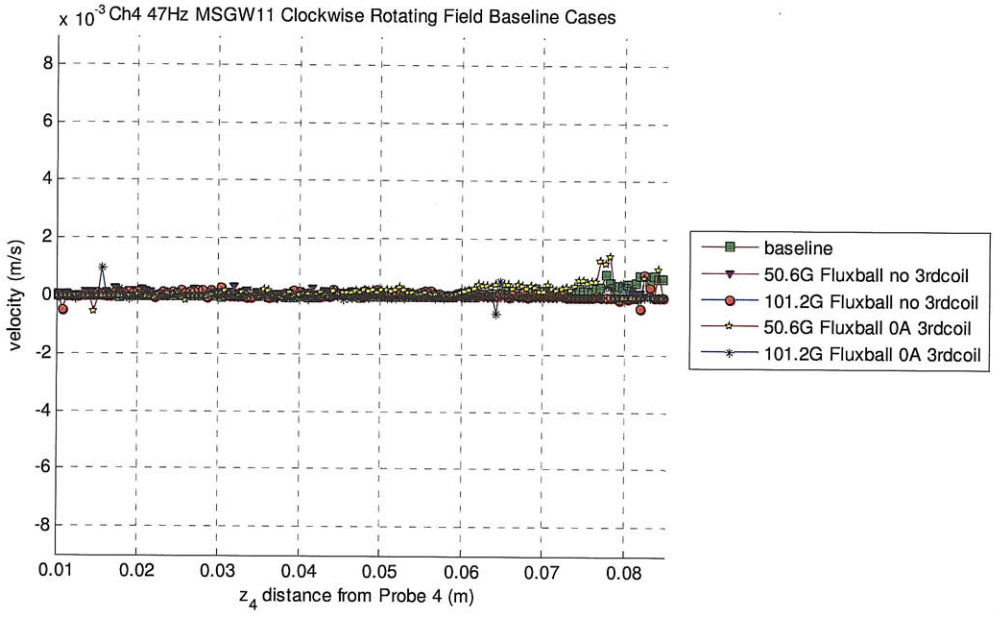
x 10^-3 Ch4 47Hz MSGW11 Clockwise Rotating Field Baseline Cases
velocity (m/s)
z4 distance from Probe 4 (m)
baseline
50.6G Fluxball no 3rdcoil
101.2G Fluxball no 3rdcoil
50.6G Fluxball 0A 3rdcoil
101.2G Fluxball 0A 3rdcoil

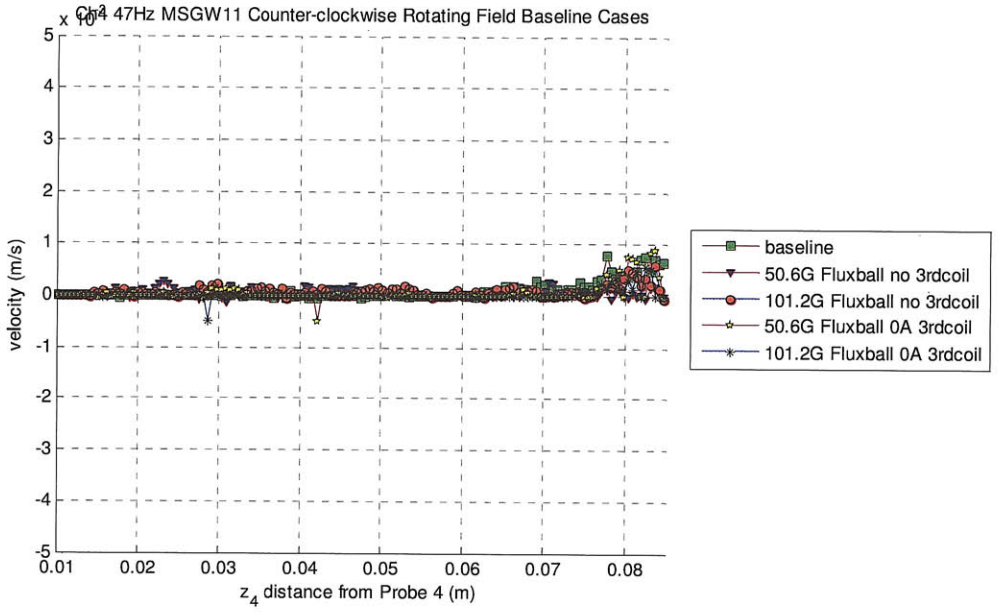
x 10^-4 Ch4 47Hz MSGW11 Counter-clockwise Rotating Field Baseline Cases
velocity (m/s)
z4 distance from Probe 4 (m)
baseline
50.6G Fluxball no 3rdcoil
101.2G Fluxball no 3rdcoil
50.6G Fluxball 0A 3rdcoil
101.2G Fluxball 0A 3rdcoil

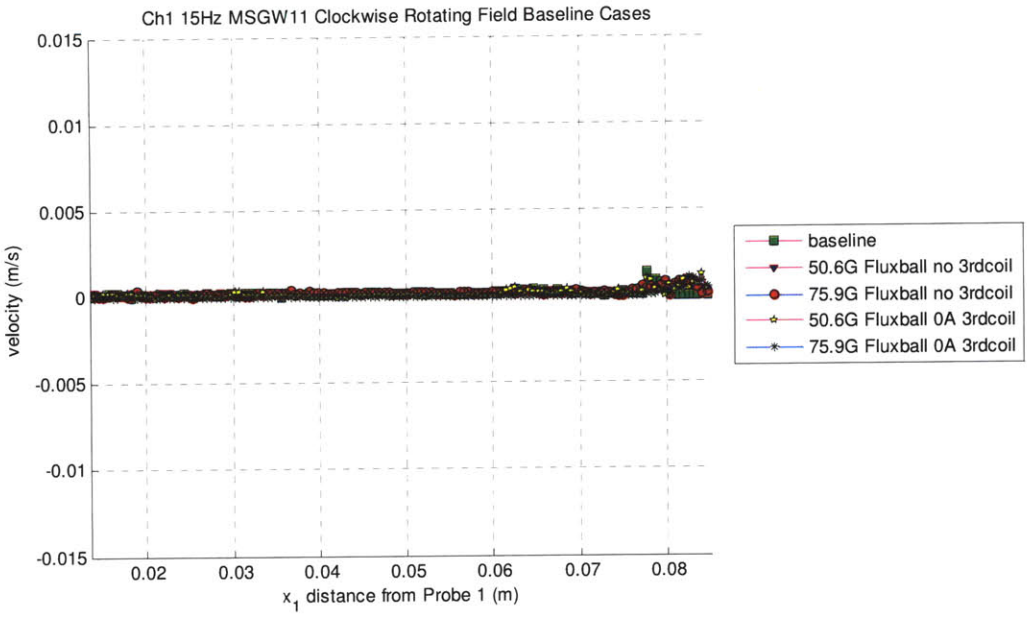
Ch1 15Hz MSGW11 Clockwise Rotating Field Baseline Cases
velocity (m/s)
0.015
0.01
0.005
0
-0.005
-0.01
-0.015
0.02
0.03
0.04
0.05
0.06
0.07
0.08
x1 distance from Probe 1 (m)
baseline
50.6G Fluxball no 3rdcoil
75.9G Fluxball no 3rdcoil
50.6G Fluxball 0A 3rdcoil
75.9G Fluxball 0A 3rdcoil

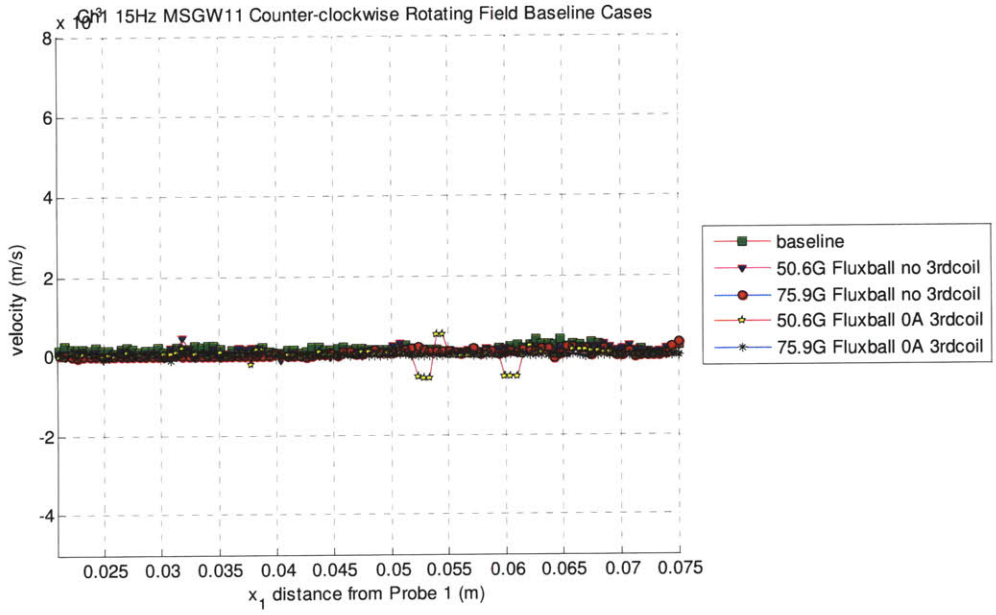
Ch1 15Hz MSGW11 Counter-clockwise Rotating Field Baseline Cases
x 10-3
velocity (m/s)
8
6
4
2
0
-2
-4
0.025
0.03
0.035
0.04
0.045
0.05
0.055
0.06
0.065
0.07
0.075
x1 distance from Probe 1 (m)
baseline
50.6G Fluxball no 3rdcoil
75.9G Fluxball no 3rdcoil
50.6G Fluxball 0A 3rdcoil
75.9G Fluxball 0A 3rdcoil

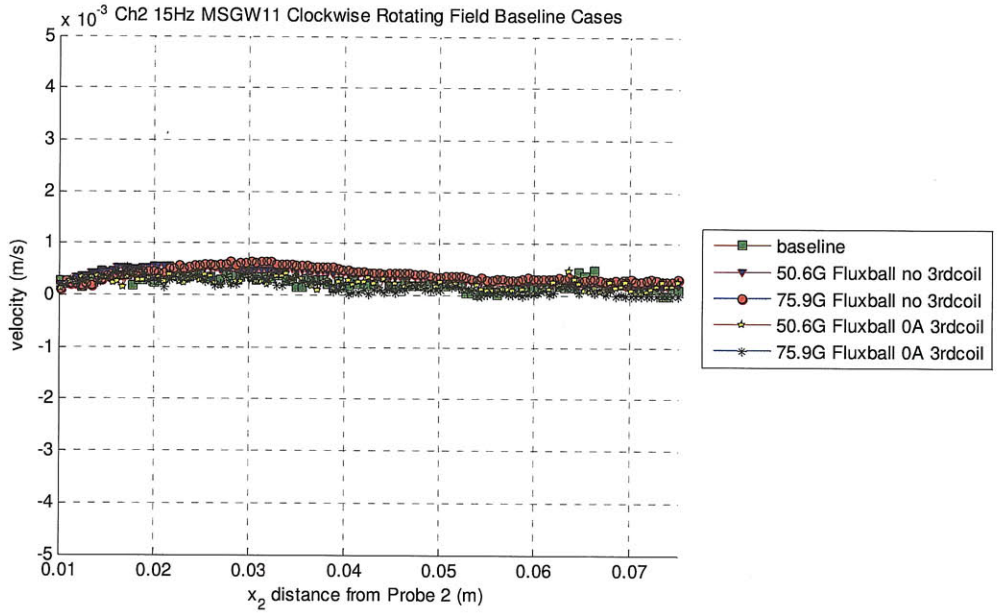
x 10^-3 Ch2 15Hz MSGW11 Clockwise Rotating Field Baseline Cases
velocity (m/s)
x2 distance from Probe 2 (m)
baseline
50.6G Fluxball no 3rdcoil
75.9G Fluxball no 3rdcoil
50.6G Fluxball 0A 3rdcoil
75.9G Fluxball 0A 3rdcoil

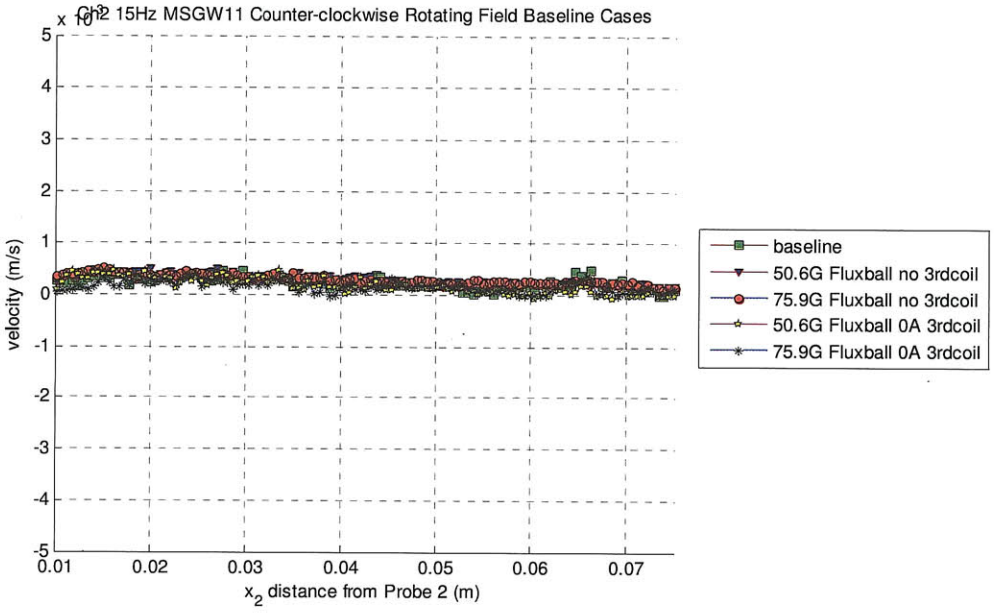
x 10^-3 Ch2 15Hz MSGW11 Counter-clockwise Rotating Field Baseline Cases
velocity (m/s)
x2 distance from Probe 2 (m)
baseline
50.6G Fluxball no 3rdcoil
75.9G Fluxball no 3rdcoil
50.6G Fluxball 0A 3rdcoil
75.9G Fluxball 0A 3rdcoil

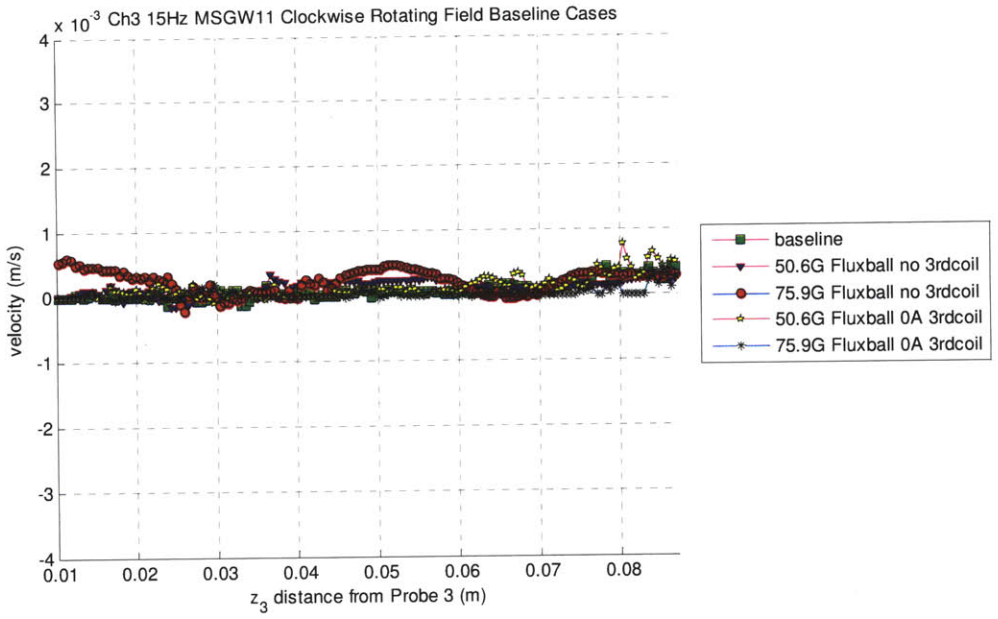
x 10^-3 Ch3 15Hz MSGW11 Clockwise Rotating Field Baseline Cases
velocity (m/s)
z3 distance from Probe 3 (m)
baseline
50.6G Fluxball no 3rdcoil
75.9G Fluxball no 3rdcoil
50.6G Fluxball 0A 3rdcoil
75.9G Fluxball 0A 3rdcoil

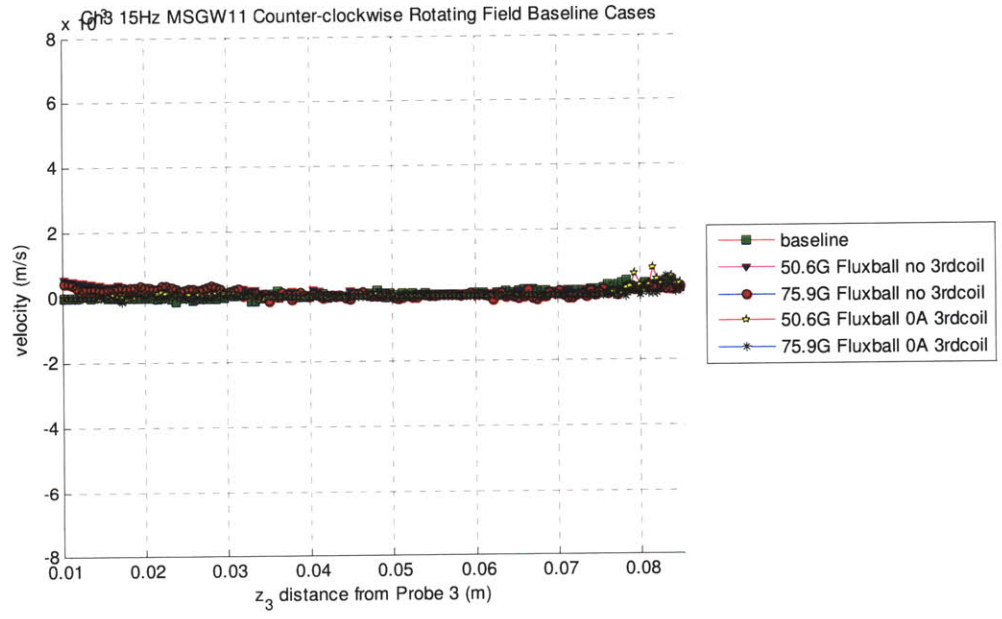
Ch3 15Hz MSGW11 Counter-clockwise Rotating Field Baseline Cases
velocity (m/s)
z3 distance from Probe 3 (m)
baseline
50.6G Fluxball no 3rdcoil
75.9G Fluxball no 3rdcoil
50.6G Fluxball 0A 3rdcoil
75.9G Fluxball 0A 3rdcoil

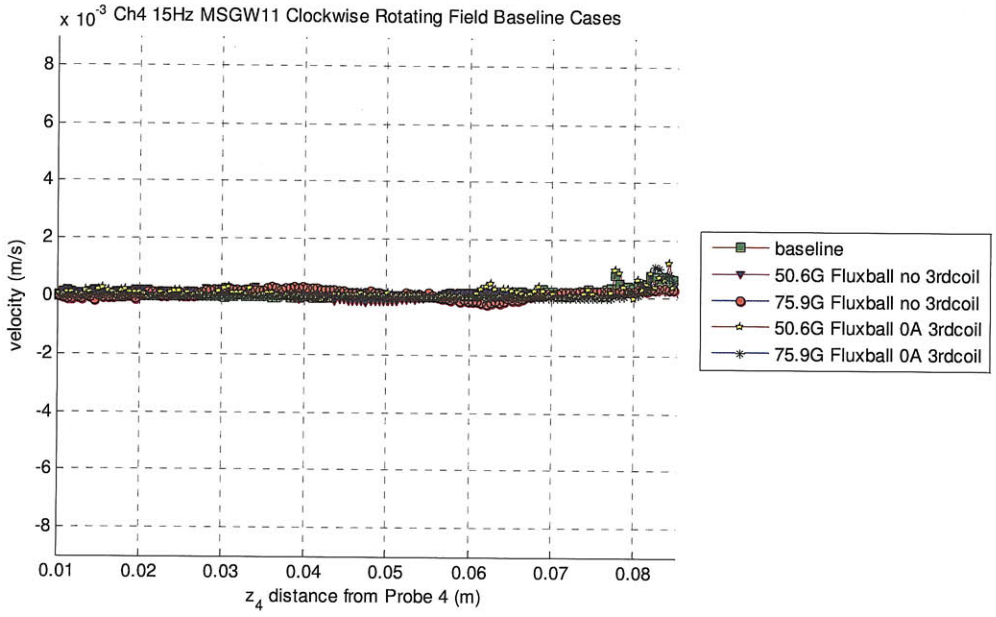
x 10^-3 Ch4 15Hz MSGW11 Clockwise Rotating Field Baseline Cases
velocity (m/s)
z4 distance from Probe 4 (m)
baseline
50.6G Fluxball no 3rdcoil
75.9G Fluxball no 3rdcoil
50.6G Fluxball 0A 3rdcoil
75.9G Fluxball 0A 3rdcoil

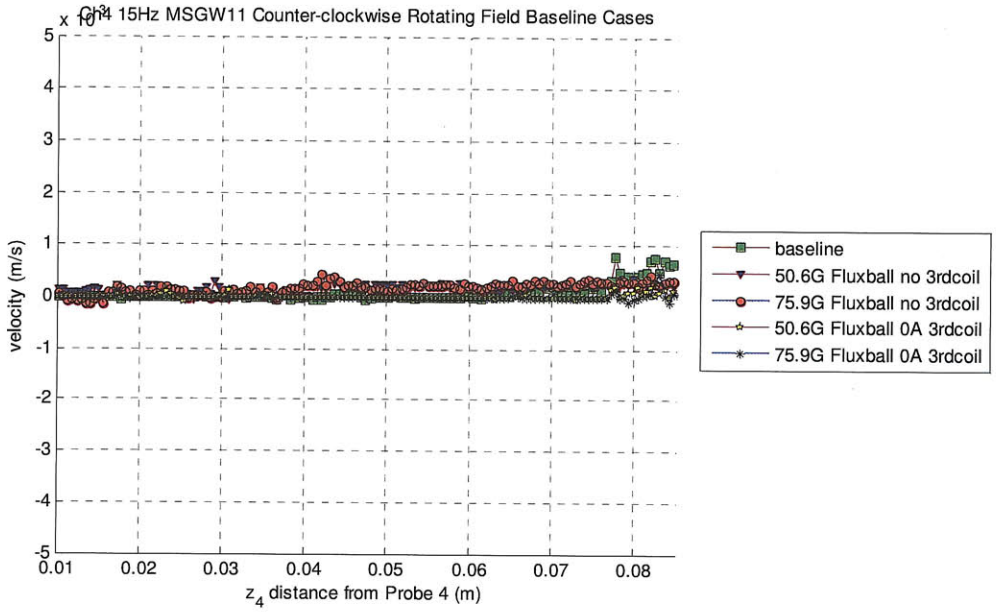
x 10^-3 Ch4 15Hz MSGW11 Counter-clockwise Rotating Field Baseline Cases
velocity (m/s)
z4 distance from Probe 4 (m)
baseline
50.6G Fluxball no 3rdcoil
75.9G Fluxball no 3rdcoil
50.6G Fluxball 0A 3rdcoil
75.9G Fluxball 0A 3rdcoil

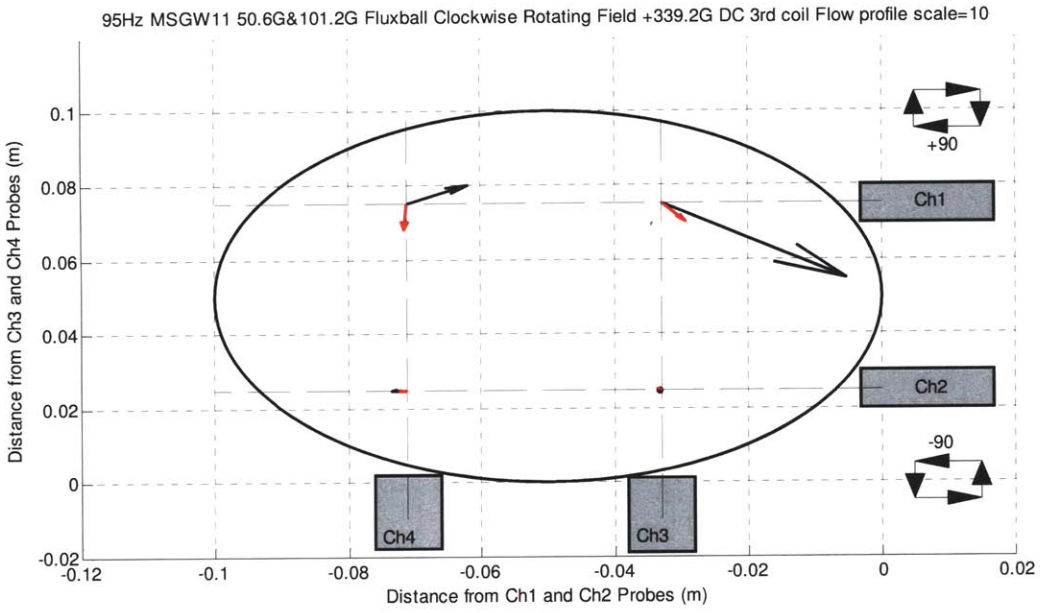
95Hz MSGW11 50.6G&101.2G Fluxball Clockwise Rotating Field +339.2G DC 3rd coil Flow profile scale=10
Distance from Ch3 and Ch4 Probes (m)
Distance from Ch1 and Ch2 Probes (m)
+90
-90
Ch1
Ch2
Ch3
Ch4
0.1
0.08
0.06
0.04
0.02
0
-0.02
-0.12
-0.1
-0.08
-0.06
-0.04
-0.02
0
0.02

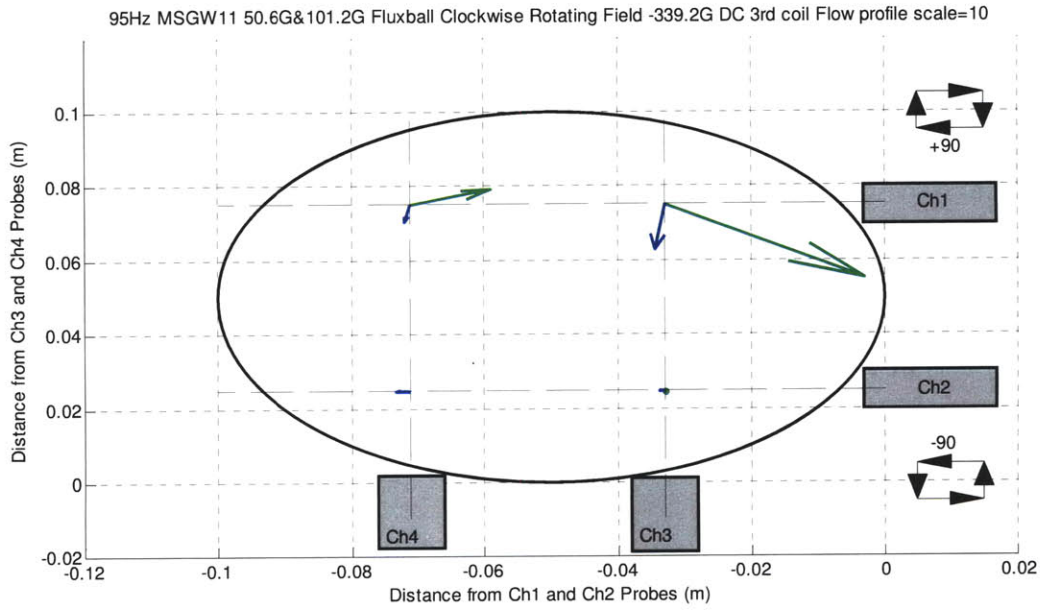
95Hz MSGW11 50.6G&101.2G Fluxball Clockwise Rotating Field -339.2G DC 3rd coil Flow profile scale=10
Distance from Ch3 and Ch4 Probes (m)
Distance from Ch1 and Ch2 Probes (m)
+90
-90
Ch1
Ch2
Ch3
Ch4
0.1
0.08
0.06
0.04
0.02
0
-0.02
-0.12
-0.1
-0.08
-0.06
-0.04
-0.02
0
0.02

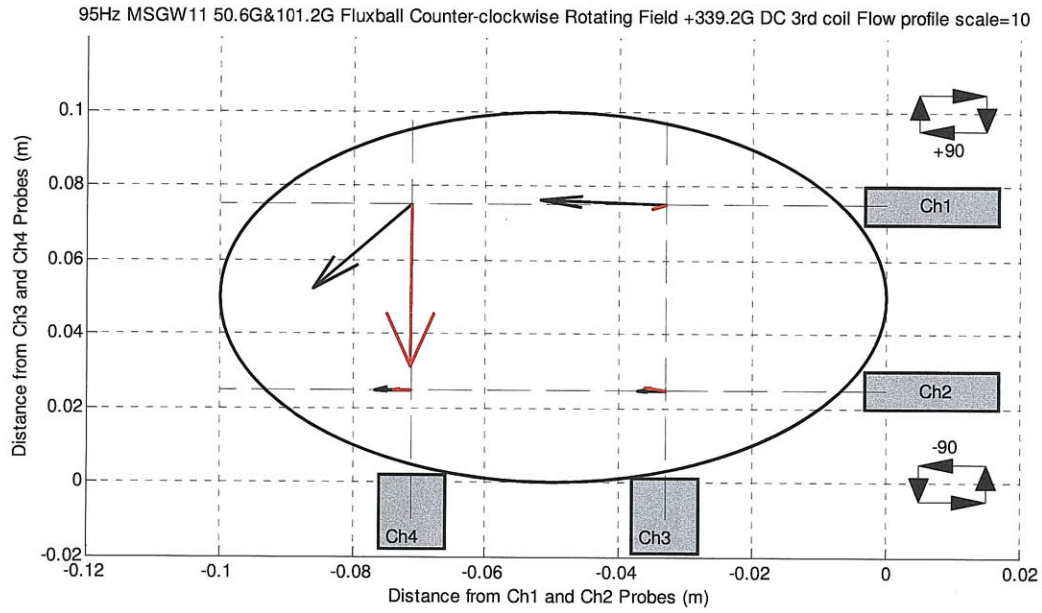
95Hz MSGW11 50.6G&101.2G Fluxball Counter-clockwise Rotating Field +339.2G DC 3rd coil Flow profile scale=10
Distance from Ch3 and Ch4 Probes (m)
Distance from Ch1 and Ch2 Probes (m)
+90
-90
Ch1
Ch2
Ch3
Ch4
0.1
0.08
0.06
0.04
0.02
0
-0.02
-0.12
-0.1
-0.08
-0.06
-0.04
-0.02
0
0.02

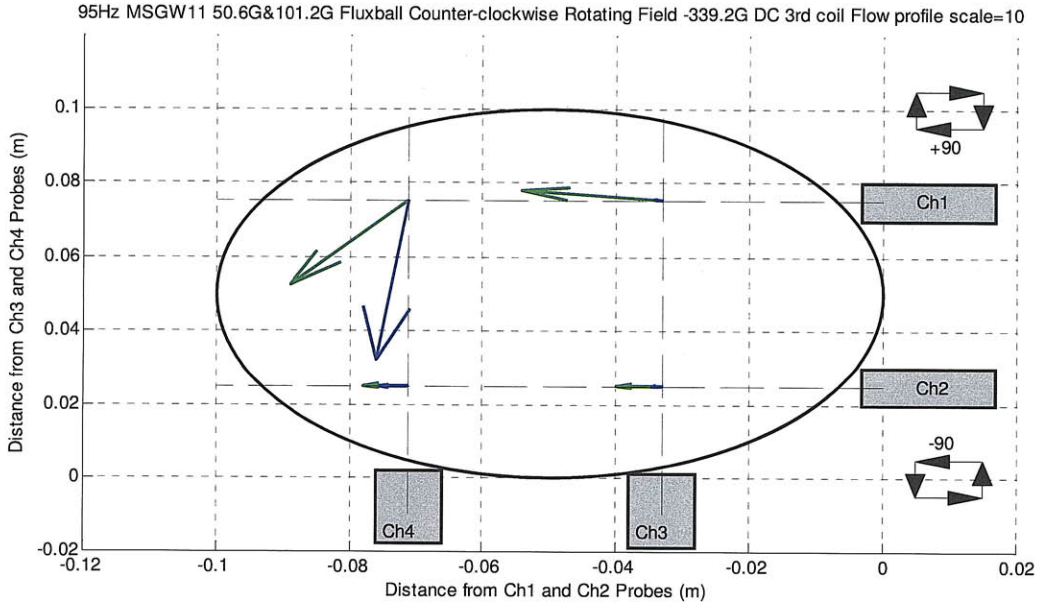
95Hz MSGW11 50.6G&101.2G Fluxball Counter-clockwise Rotating Field -339.2G DC 3rd coil Flow profile scale=10
Distance from Ch3 and Ch4 Probes (m)
Distance from Ch1 and Ch2 Probes (m)
+90
-90
Ch1
Ch2
Ch3
Ch4
0.1
0.08
0.06
0.04
0.02
0
-0.02
-0.12
-0.1
-0.08
-0.06
-0.04
-0.02
0
0.02

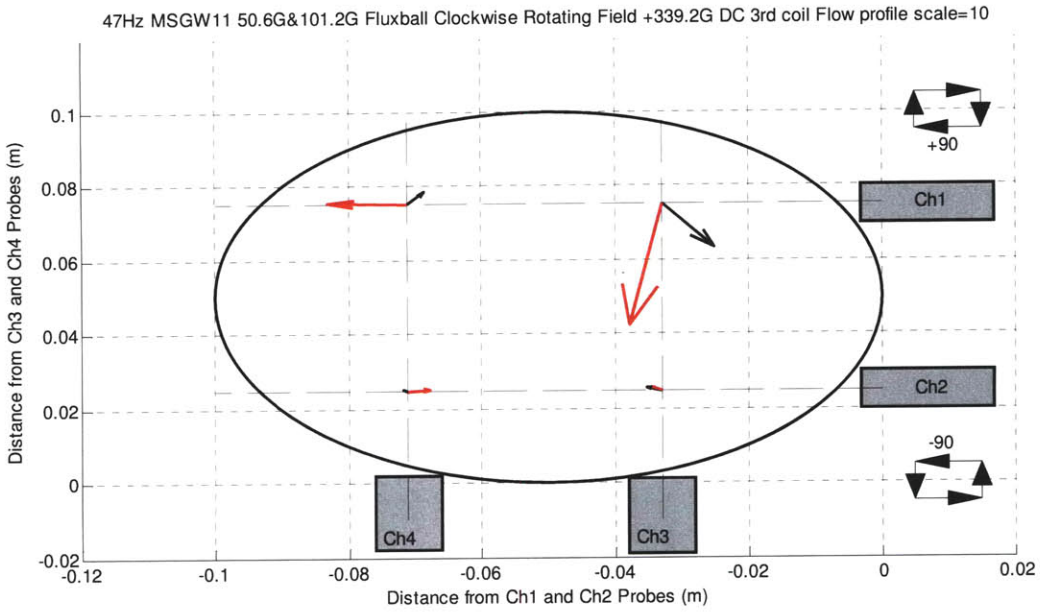
47Hz MSGW11 50.6G&101.2G Fluxball Clockwise Rotating Field +339.2G DC 3rd coil Flow profile scale=10
Distance from Ch3 and Ch4 Probes (m)
Distance from Ch1 and Ch2 Probes (m)
+90
-90
Ch1
Ch2
Ch3
Ch4
0.1
0.08
0.06
0.04
0.02
0
-0.02
-0.12
-0.1
-0.08
-0.06
-0.04
-0.02
0
0.02

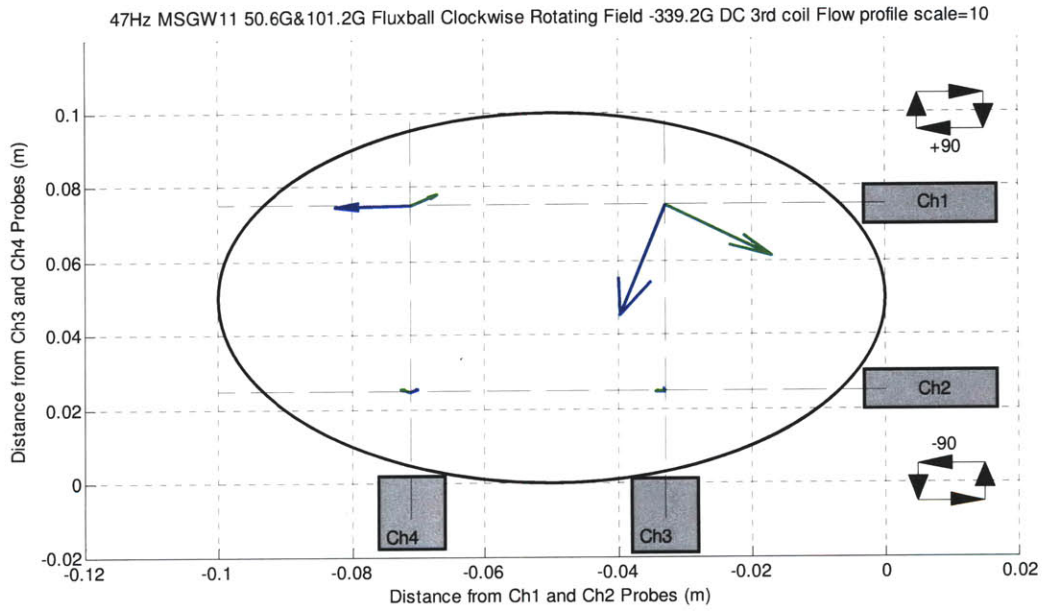
47Hz MSGW11 50.6G&101.2G Fluxball Clockwise Rotating Field -339.2G DC 3rd coil Flow profile scale=10
Distance from Ch3 and Ch4 Probes (m)
Distance from Ch1 and Ch2 Probes (m)
+90
-90
Ch1
Ch2
Ch3
Ch4
0.1
0.08
0.06
0.04
0.02
0
-0.02
-0.12
-0.1
-0.08
-0.06
-0.04
-0.02
0
0.02

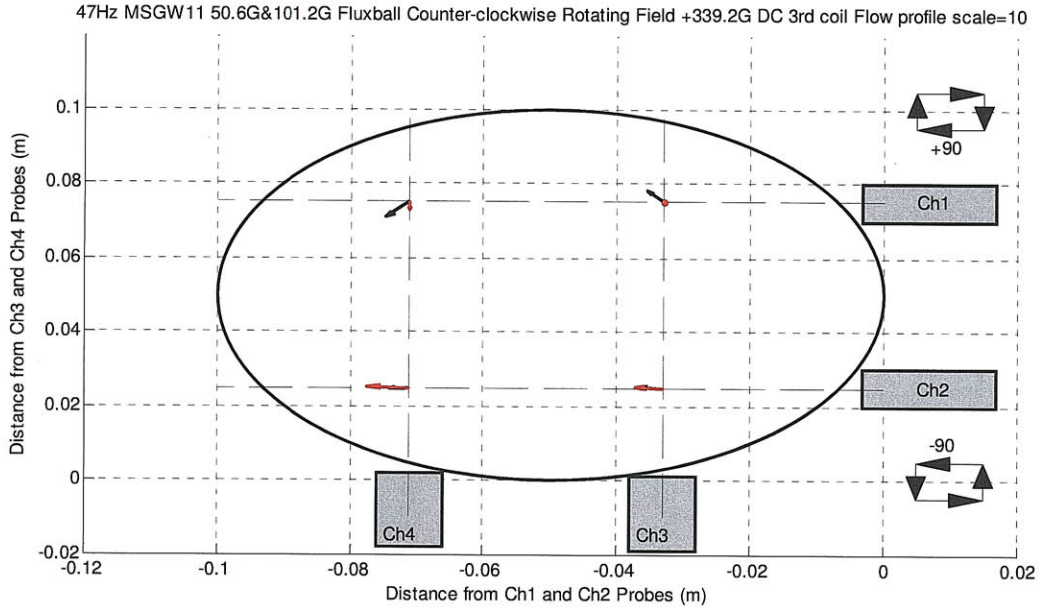
47Hz MSGW11 50.6G&101.2G Fluxball Counter-clockwise Rotating Field +339.2G DC 3rd coil Flow profile scale=10
Distance from Ch3 and Ch4 Probes (m)
Distance from Ch1 and Ch2 Probes (m)
+90
-90
Ch1
Ch2
Ch3
Ch4
0.1
0.08
0.06
0.04
0.02
0
-0.02
-0.12
-0.1
-0.08
-0.06
-0.04
-0.02
0
0.02

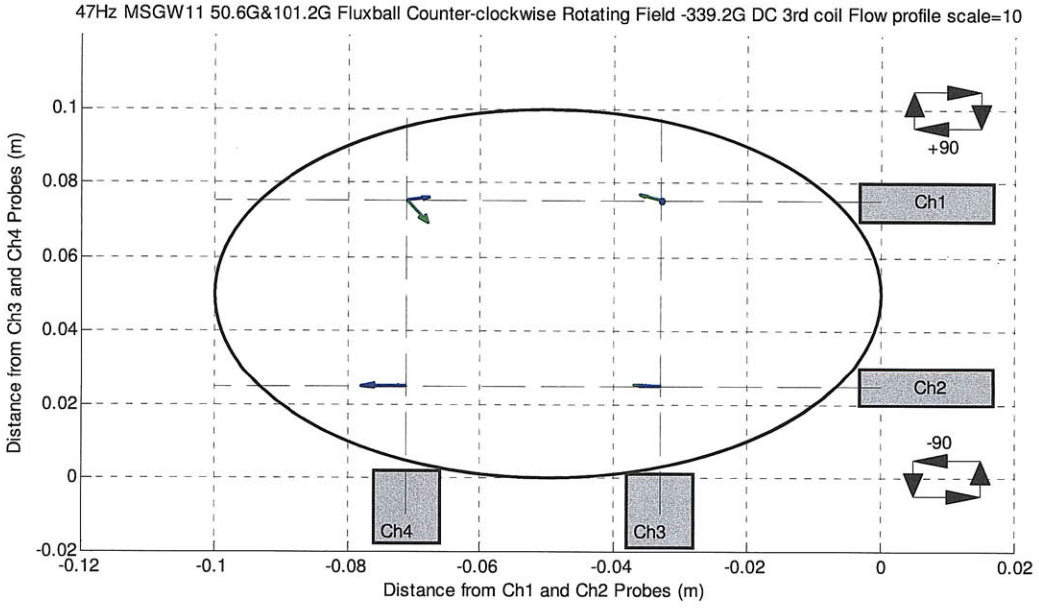
47Hz MSGW11 50.6G&101.2G Fluxball Counter-clockwise Rotating Field -339.2G DC 3rd coil Flow profile scale=10
Distance from Ch3 and Ch4 Probes (m)
Distance from Ch1 and Ch2 Probes (m)
+90
-90
Ch1
Ch2
Ch3
Ch4
0.1
0.08
0.06
0.04
0.02
0
-0.02
-0.12
-0.1
-0.08
-0.06
-0.04
-0.02
0
0.02

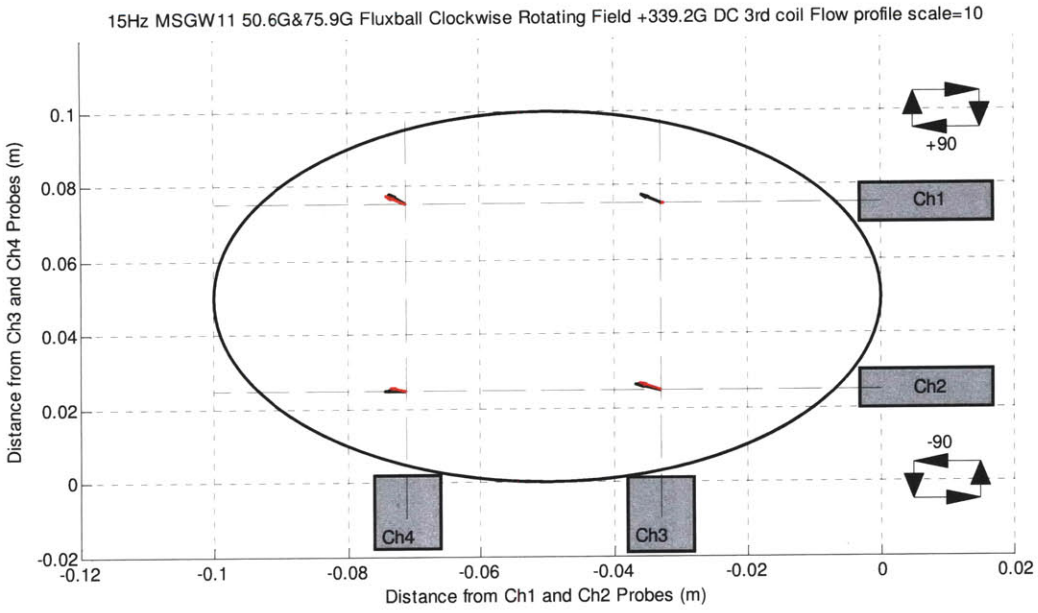
15Hz MSGW11 50.6G&75.9G Fluxball Clockwise Rotating Field +339.2G DC 3rd coil Flow profile scale=10
Distance from Ch3 and Ch4 Probes (m)
Distance from Ch1 and Ch2 Probes (m)
+90
-90
Ch1
Ch2
Ch3
Ch4
0.1
0.08
0.06
0.04
0.02
0
-0.02
-0.12
-0.1
-0.08
-0.06
-0.04
-0.02
0
0.02

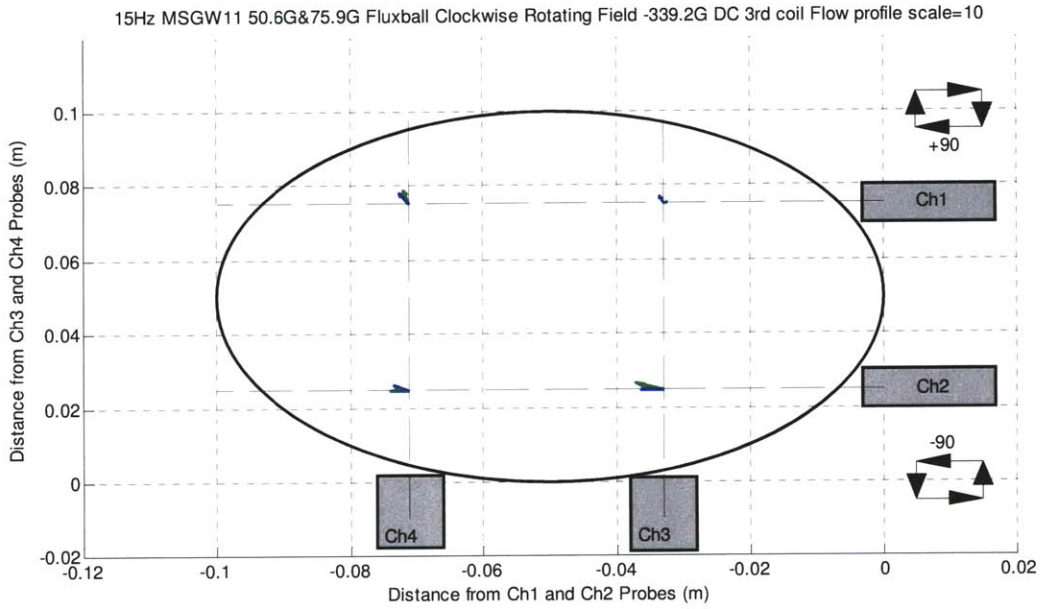
15Hz MSGW11 50.6G&75.9G Fluxball Clockwise Rotating Field -339.2G DC 3rd coil Flow profile scale=10
Distance from Ch3 and Ch4 Probes (m)
Distance from Ch1 and Ch2 Probes (m)
+90
-90
Ch1
Ch2
Ch3
Ch4
0.1
0.08
0.06
0.04
0.02
0
-0.02
-0.12
-0.1
-0.08
-0.06
-0.04
-0.02
0
0.02

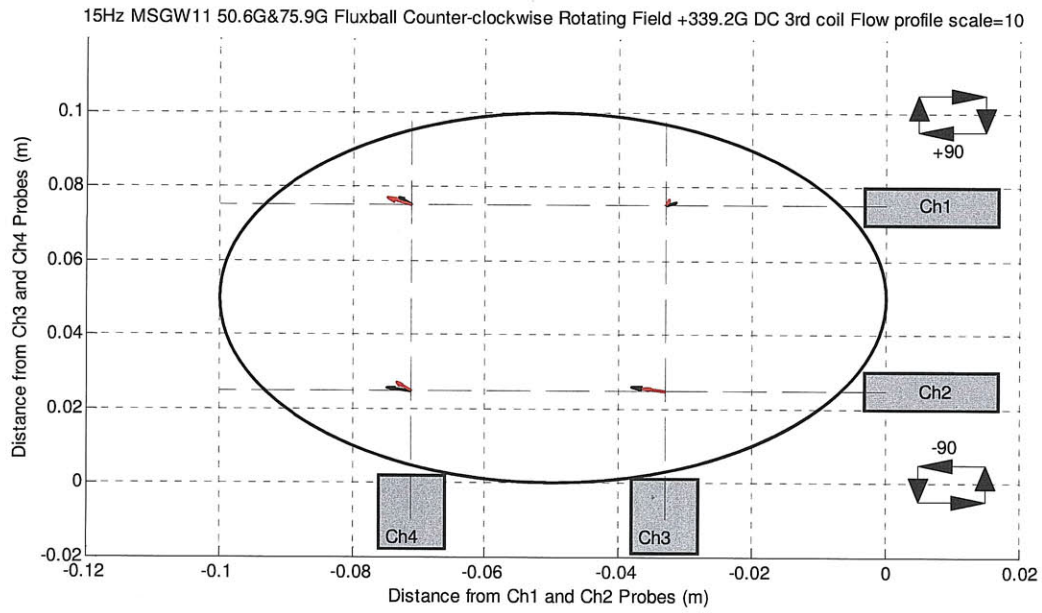
15Hz MSGW11 50.6G&75.9G Fluxball Counter-clockwise Rotating Field +339.2G DC 3rd coil Flow profile scale=10
Distance from Ch3 and Ch4 Probes (m)
Distance from Ch1 and Ch2 Probes (m)
+90
-90
Ch1
Ch2
Ch3
Ch4
0.1
0.08
0.06
0.04
0.02
0
-0.02
-0.12
-0.1
-0.08
-0.06
-0.04
-0.02
0
0.02

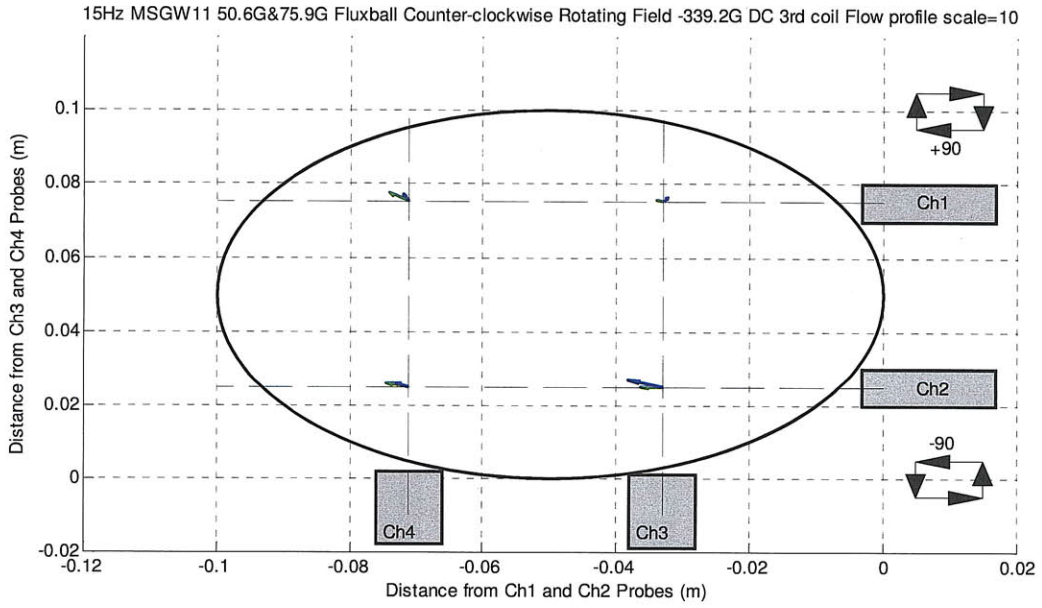
15Hz MSGW11 50.6G&75.9G Fluxball Counter-clockwise Rotating Field -339.2G DC 3rd coil Flow profile scale=10
Distance from Ch3 and Ch4 Probes (m)
Distance from Ch1 and Ch2 Probes (m)
+90
-90
Ch1
Ch2
Ch3
Ch4
0.1
0.08
0.06
0.04
0.02
0
-0.02
-0.12
-0.1
-0.08
-0.06
-0.04
-0.02
0
0.02

G9. Comparison of Different Fluids with Third Coil Oscillating at Different Frequencies with Phase Difference=0 with Respect to Inner Coil

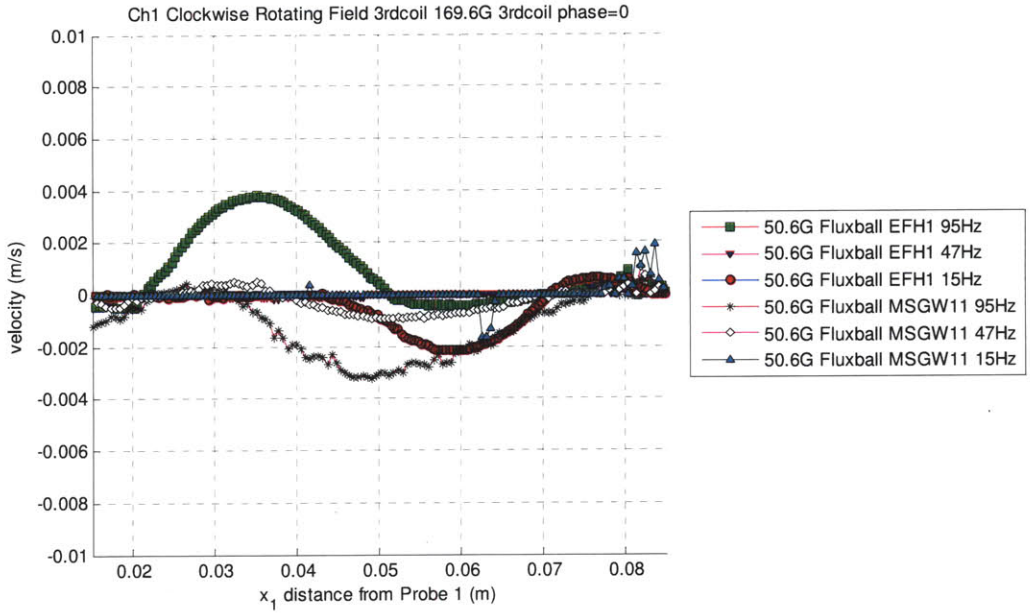

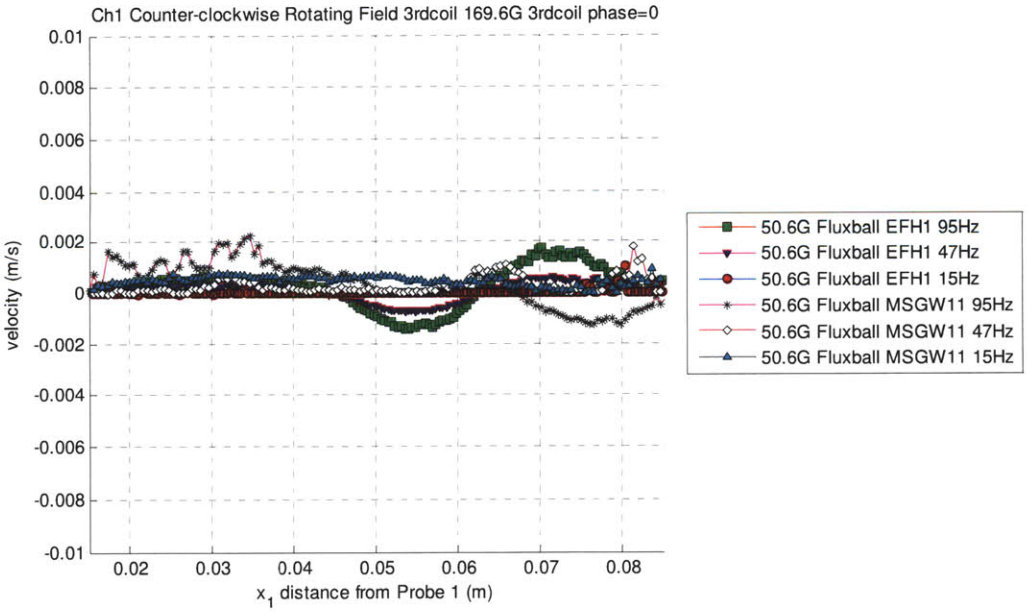

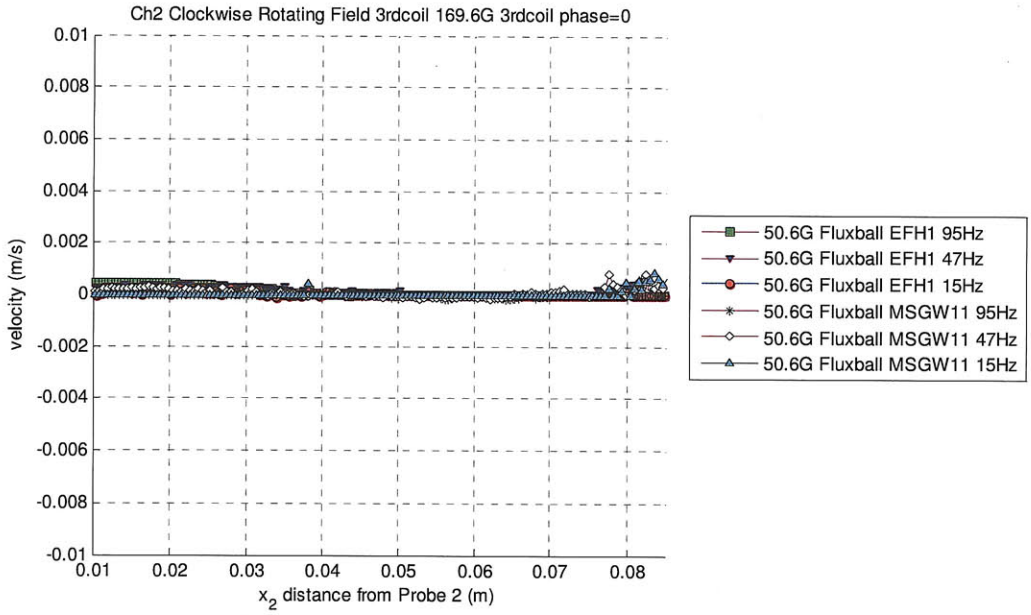
Ch2 Clockwise Rotating Field 3rdcoil 169.6G 3rdcoil phase=0
velocity (m/s)
0.01
0.008
0.006
0.004
0.002
0
-0.002
-0.004
-0.006
-0.008
-0.01
0.01
0.02
0.03
0.04
0.05
0.06
0.07
0.08
x2 distance from Probe 2 (m)
50.6G Fluxball EFH1 95Hz
50.6G Fluxball EFH1 47Hz
50.6G Fluxball EFH1 15Hz
50.6G Fluxball MSGW11 95Hz
50.6G Fluxball MSGW11 47Hz
50.6G Fluxball MSGW11 15Hz

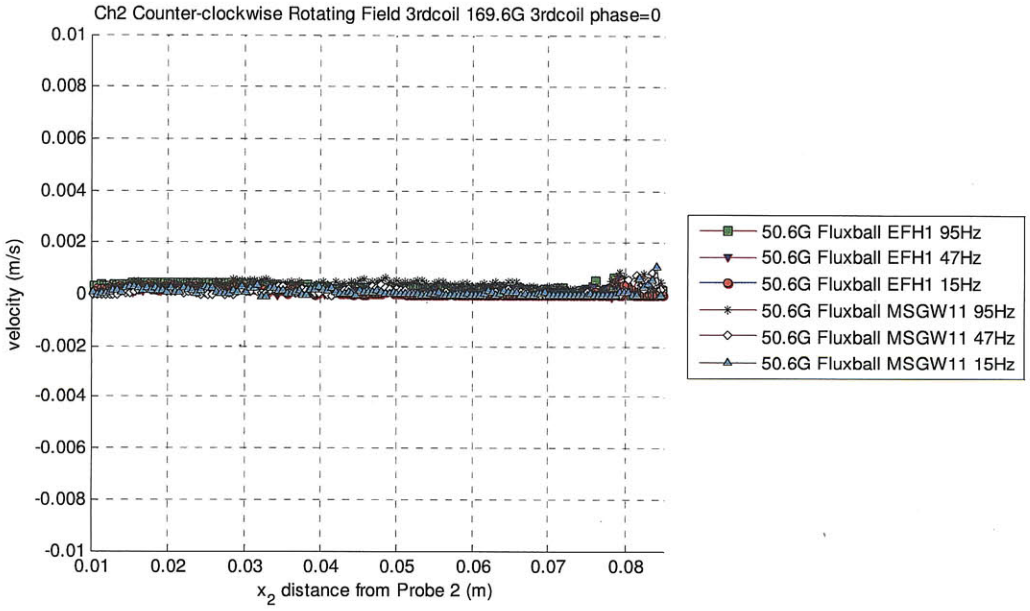
Ch2 Counter-clockwise Rotating Field 3rdcoil 169.6G 3rdcoil phase=0
velocity (m/s)
0.01
0.008
0.006
0.004
0.002
0
-0.002
-0.004
-0.006
-0.008
-0.01
0.01
0.02
0.03
0.04
0.05
0.06
0.07
0.08
x2 distance from Probe 2 (m)
50.6G Fluxball EFH1 95Hz
50.6G Fluxball EFH1 47Hz
50.6G Fluxball EFH1 15Hz
50.6G Fluxball MSGW11 95Hz
50.6G Fluxball MSGW11 47Hz
50.6G Fluxball MSGW11 15Hz

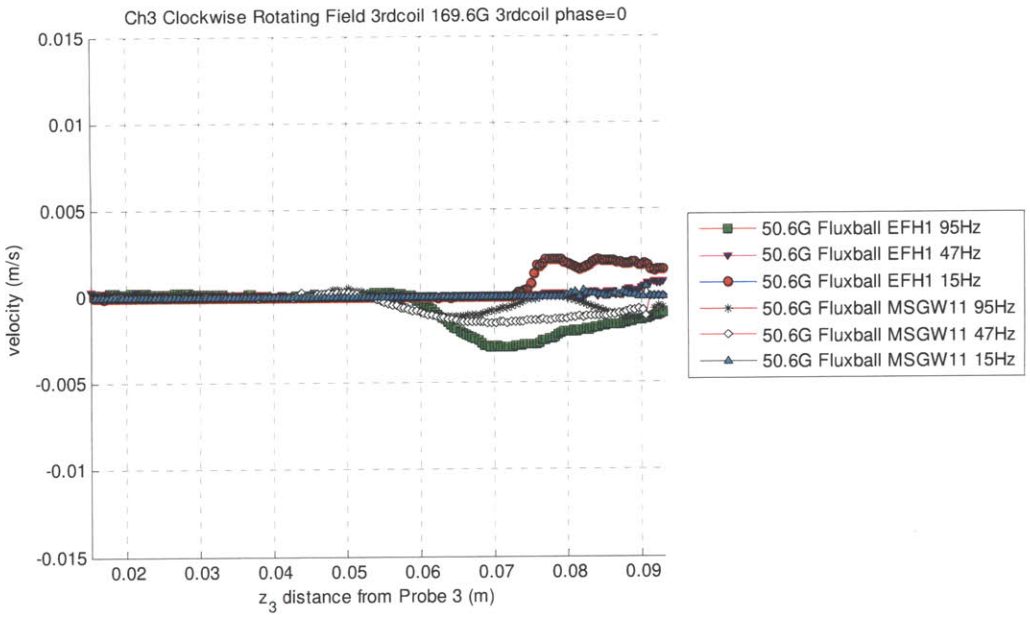
Ch3 Clockwise Rotating Field 3rdcoil 169.6G 3rdcoil phase=0
0.015
0.01
0.005
0
-0.005
-0.01
-0.015
velocity (m/s)
0.02
0.03
0.04
0.05
0.06
0.07
0.08
0.09
z3 distance from Probe 3 (m)
50.6G Fluxball EFH1 95Hz
50.6G Fluxball EFH1 47Hz
50.6G Fluxball EFH1 15Hz
50.6G Fluxball MSGW11 95Hz
50.6G Fluxball MSGW11 47Hz
50.6G Fluxball MSGW11 15Hz

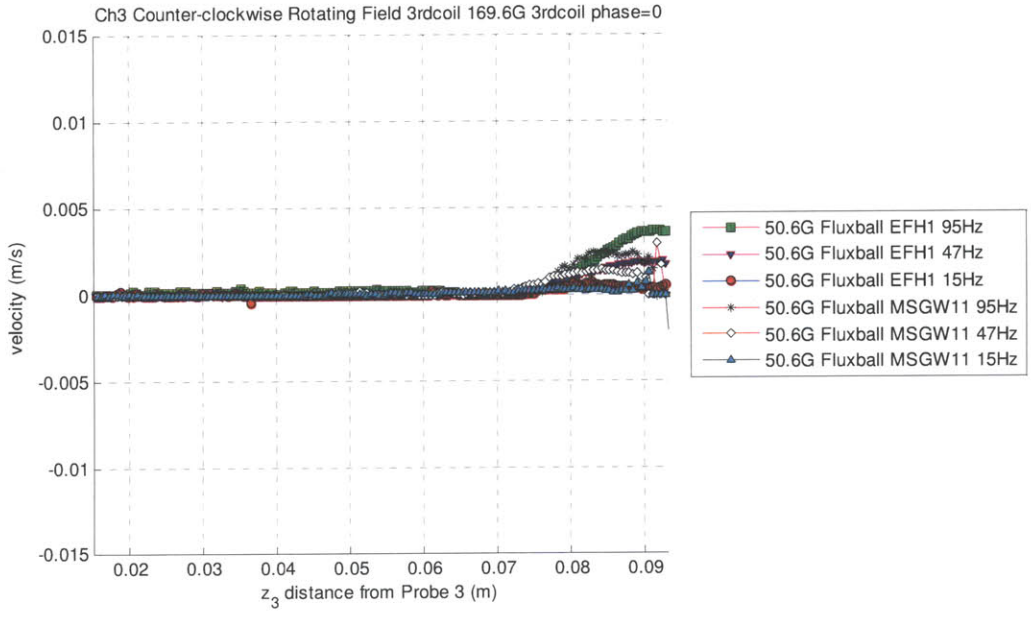
Ch3 Counter-clockwise Rotating Field 3rdcoil 169.6G 3rdcoil phase=0
0.015
0.01
0.005
0
-0.005
-0.01
-0.015
velocity (m/s)
0.02
0.03
0.04
0.05
0.06
0.07
0.08
0.09
z3 distance from Probe 3 (m)
50.6G Fluxball EFH1 95Hz
50.6G Fluxball EFH1 47Hz
50.6G Fluxball EFH1 15Hz
50.6G Fluxball MSGW11 95Hz
50.6G Fluxball MSGW11 47Hz
50.6G Fluxball MSGW11 15Hz

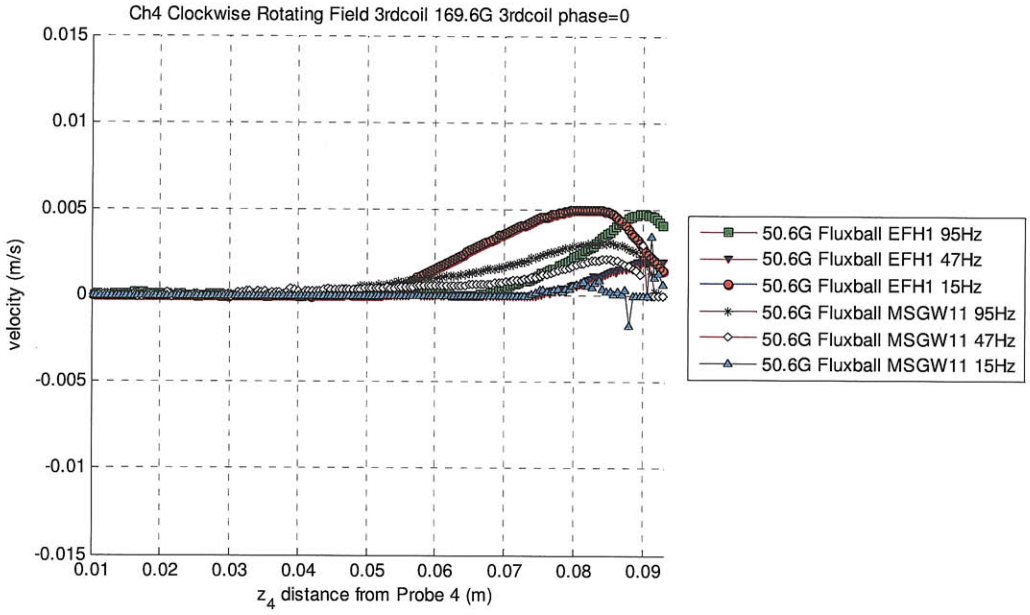
Ch4 Clockwise Rotating Field 3rdcoil 169.6G 3rdcoil phase=0
velocity (m/s)
0.015
0.01
0.005
0
-0.005
-0.01
-0.015
0.01
0.02
0.03
0.04
0.05
0.06
0.07
0.08
0.09
z4 distance from Probe 4 (m)
50.6G Fluxball EFH1 95Hz
50.6G Fluxball EFH1 47Hz
50.6G Fluxball EFH1 15Hz
50.6G Fluxball MSGW11 95Hz
50.6G Fluxball MSGW11 47Hz
50.6G Fluxball MSGW11 15Hz

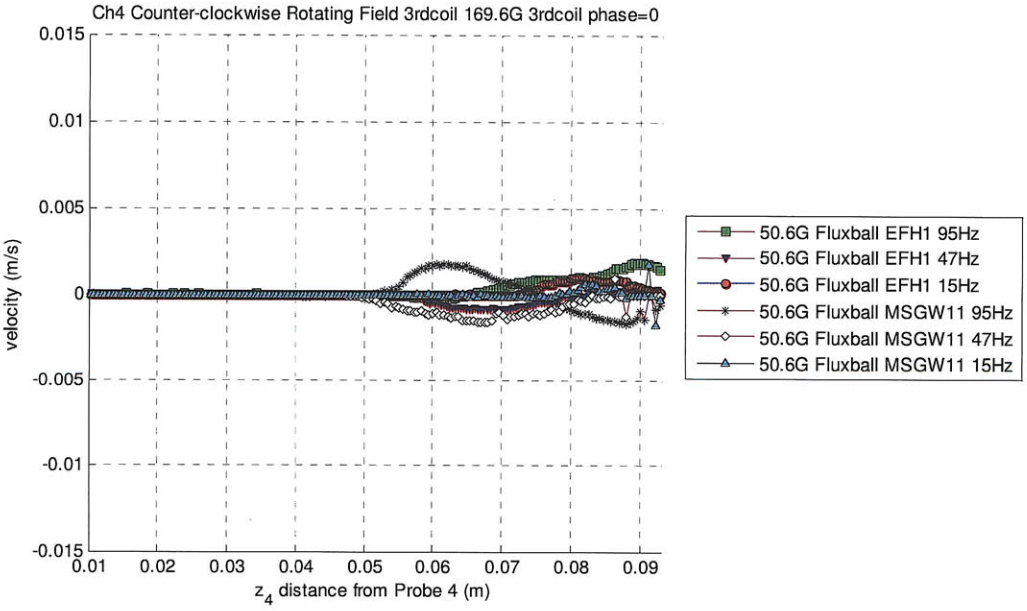
Ch4 Counter-clockwise Rotating Field 3rdcoil 169.6G 3rdcoil phase=0
velocity (m/s)
0.015
0.01
0.005
0
-0.005
-0.01
-0.015
0.01
0.02
0.03
0.04
0.05
0.06
0.07
0.08
0.09
z4 distance from Probe 4 (m)
50.6G Fluxball EFH1 95Hz
50.6G Fluxball EFH1 47Hz
50.6G Fluxball EFH1 15Hz
50.6G Fluxball MSGW11 95Hz
50.6G Fluxball MSGW11 47Hz
50.6G Fluxball MSGW11 15Hz

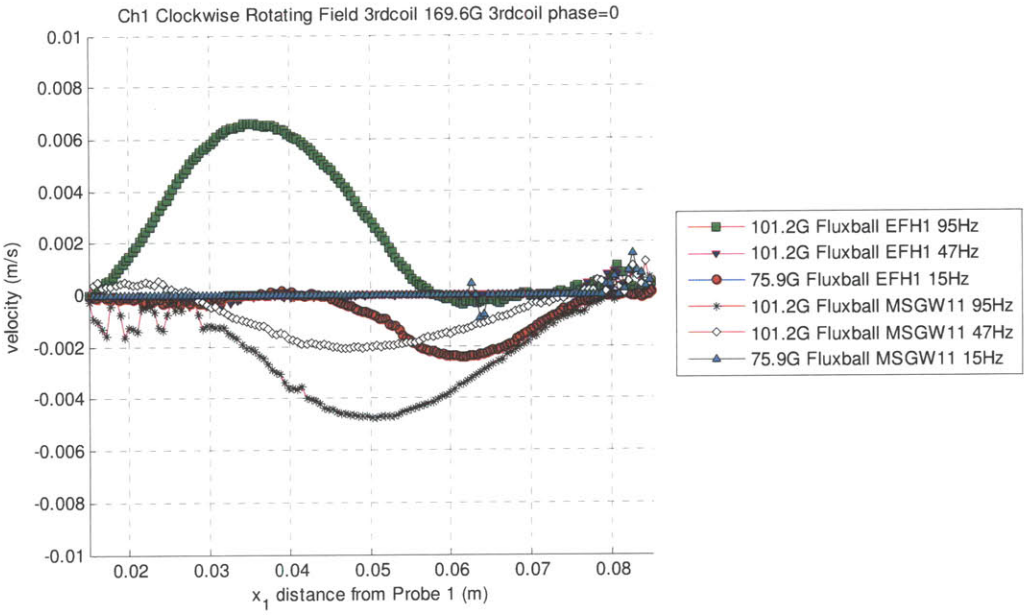
Ch1 Clockwise Rotating Field 3rdcoil 169.6G 3rdcoil phase=0
velocity (m/s)
0.01
0.008
0.006
0.004
0.002
0
-0.002
-0.004
-0.006
-0.008
-0.01
0.02
0.03
0.04
0.05
0.06
0.07
0.08
x1 distance from Probe 1 (m)
101.2G Fluxball EFH1 95Hz
101.2G Fluxball EFH1 47Hz
75.9G Fluxball EFH1 15Hz
101.2G Fluxball MSGW11 95Hz
101.2G Fluxball MSGW11 47Hz
75.9G Fluxball MSGW11 15Hz

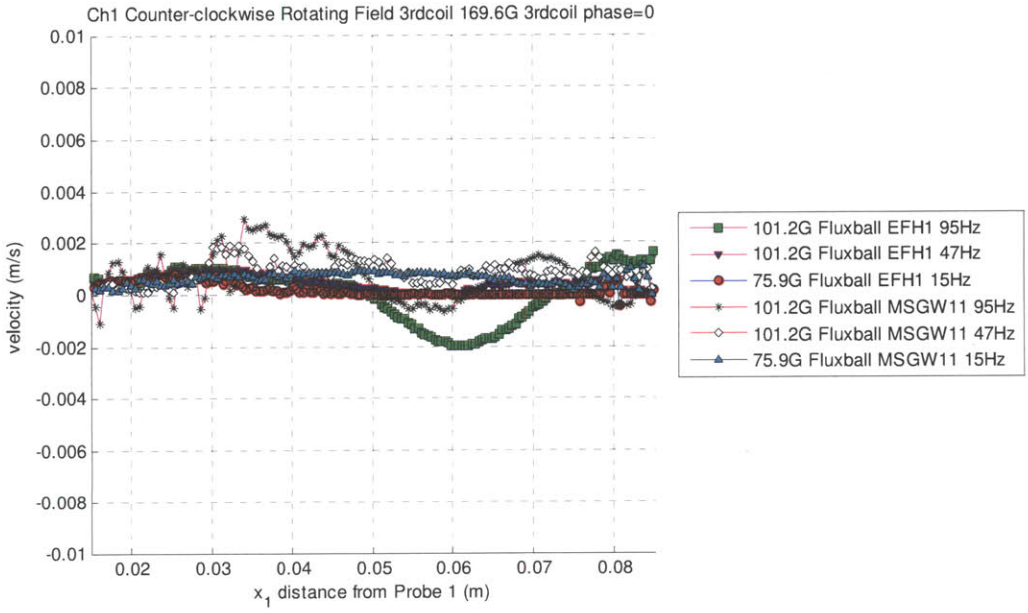
Ch1 Counter-clockwise Rotating Field 3rdcoil 169.6G 3rdcoil phase=0
velocity (m/s)
0.01
0.008
0.006
0.004
0.002
0
-0.002
-0.004
-0.006
-0.008
-0.01
0.02
0.03
0.04
0.05
0.06
0.07
0.08
x1 distance from Probe 1 (m)
101.2G Fluxball EFH1 95Hz
101.2G Fluxball EFH1 47Hz
75.9G Fluxball EFH1 15Hz
101.2G Fluxball MSGW11 95Hz
101.2G Fluxball MSGW11 47Hz
75.9G Fluxball MSGW11 15Hz

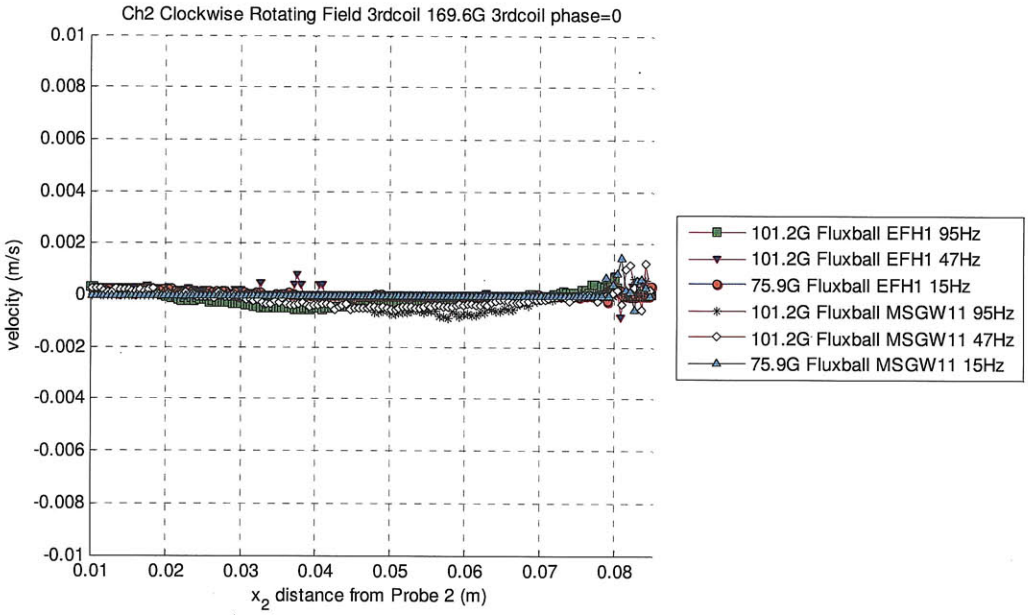
Ch2 Clockwise Rotating Field 3rdcoil 169.6G 3rdcoil phase=0
velocity (m/s)
0.01
0.008
0.006
0.004
0.002
0
-0.002
-0.004
-0.006
-0.008
-0.01
0.01 0.02 0.03 0.04 0.05 0.06 0.07 0.08
x2 distance from Probe 2 (m)
101.2G Fluxball EFH1 95Hz
101.2G Fluxball EFH1 47Hz
75.9G Fluxball EFH1 15Hz
101.2G Fluxball MSGW11 95Hz
101.2G Fluxball MSGW11 47Hz
75.9G Fluxball MSGW11 15Hz

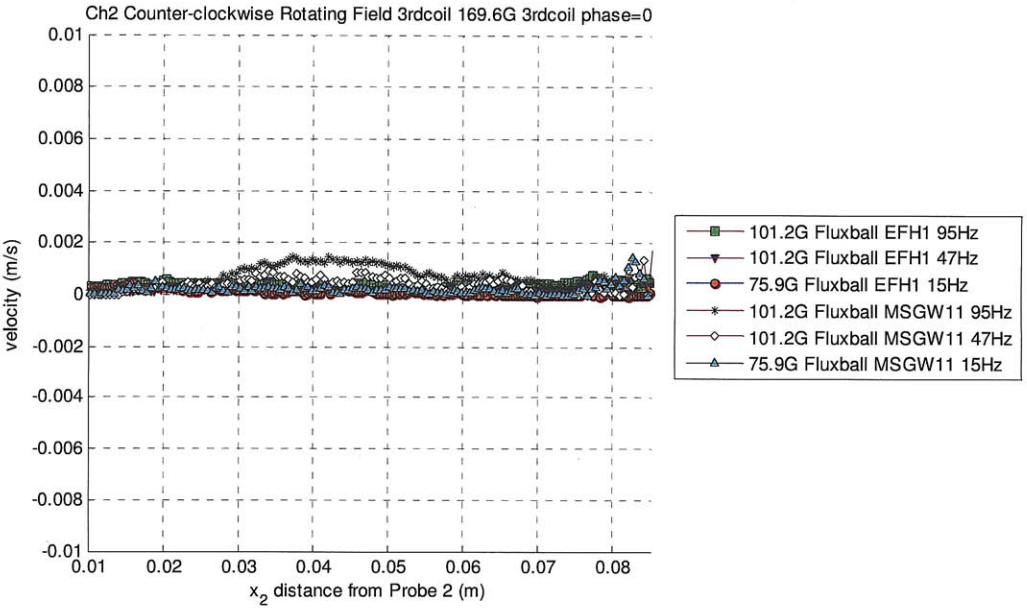
Ch2 Counter-clockwise Rotating Field 3rdcoil 169.6G 3rdcoil phase=0
velocity (m/s)
0.01
0.008
0.006
0.004
0.002
0
-0.002
-0.004
-0.006
-0.008
-0.01
0.01 0.02 0.03 0.04 0.05 0.06 0.07 0.08
x2 distance from Probe 2 (m)
101.2G Fluxball EFH1 95Hz
101.2G Fluxball EFH1 47Hz
75.9G Fluxball EFH1 15Hz
101.2G Fluxball MSGW11 95Hz
101.2G Fluxball MSGW11 47Hz
75.9G Fluxball MSGW11 15Hz

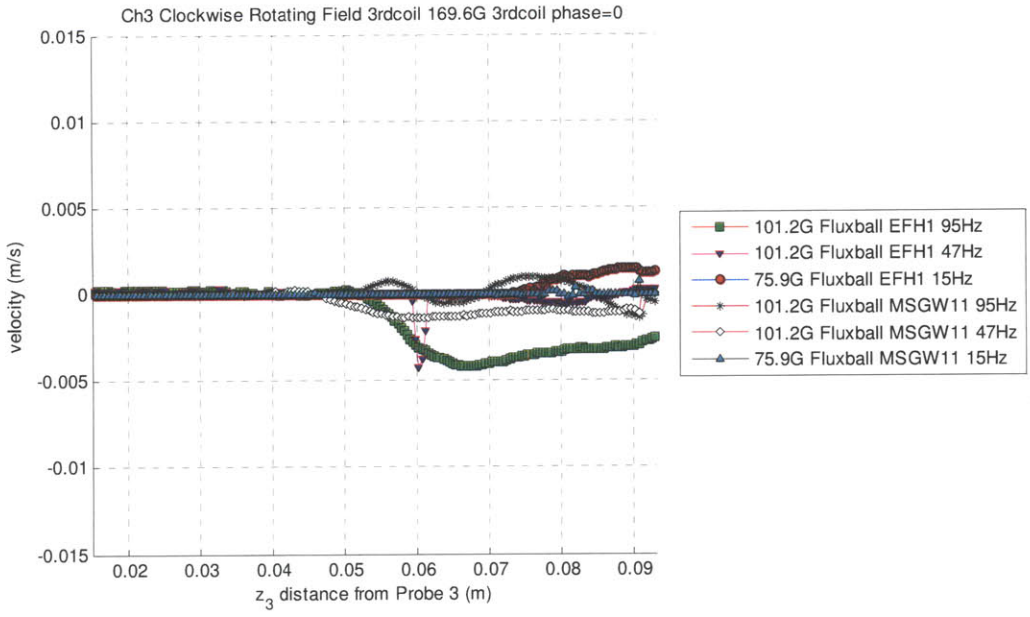
Ch3 Clockwise Rotating Field 3rdcoil 169.6G 3rdcoil phase=0
velocity (m/s)
0.015
0.01
0.005
0
-0.005
-0.01
-0.015
0.02
0.03
0.04
0.05
0.06
0.07
0.08
0.09
z3 distance from Probe 3 (m)
101.2G Fluxball EFH1 95Hz
101.2G Fluxball EFH1 47Hz
75.9G Fluxball EFH1 15Hz
101.2G Fluxball MSGW11 95Hz
101.2G Fluxball MSGW11 47Hz
75.9G Fluxball MSGW11 15Hz

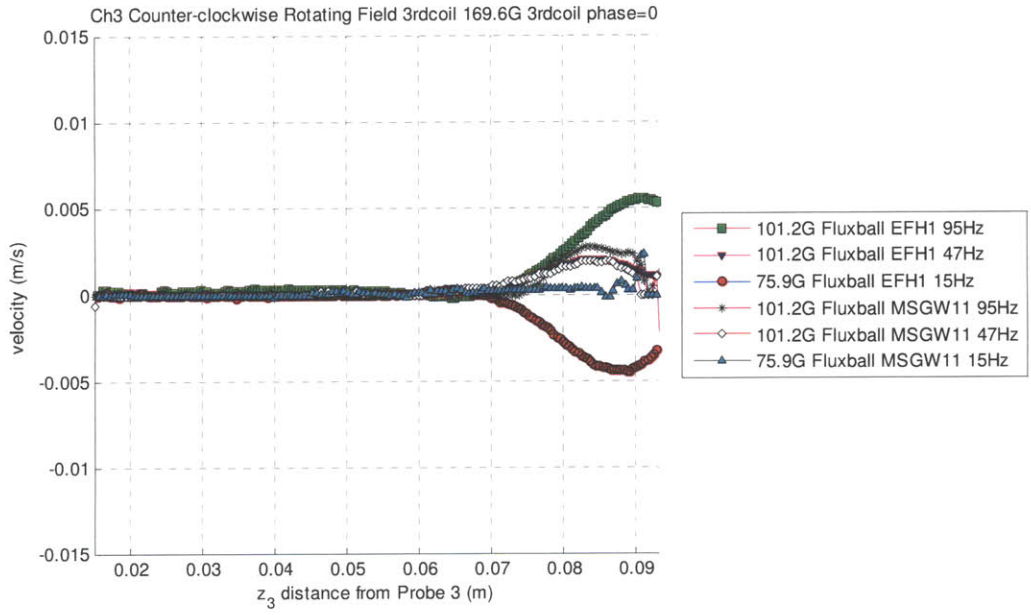
Ch3 Counter-clockwise Rotating Field 3rdcoil 169.6G 3rdcoil phase=0
velocity (m/s)
0.015
0.01
0.005
0
-0.005
-0.01
-0.015
0.02
0.03
0.04
0.05
0.06
0.07
0.08
0.09
z3 distance from Probe 3 (m)
101.2G Fluxball EFH1 95Hz
101.2G Fluxball EFH1 47Hz
75.9G Fluxball EFH1 15Hz
101.2G Fluxball MSGW11 95Hz
101.2G Fluxball MSGW11 47Hz
75.9G Fluxball MSGW11 15Hz

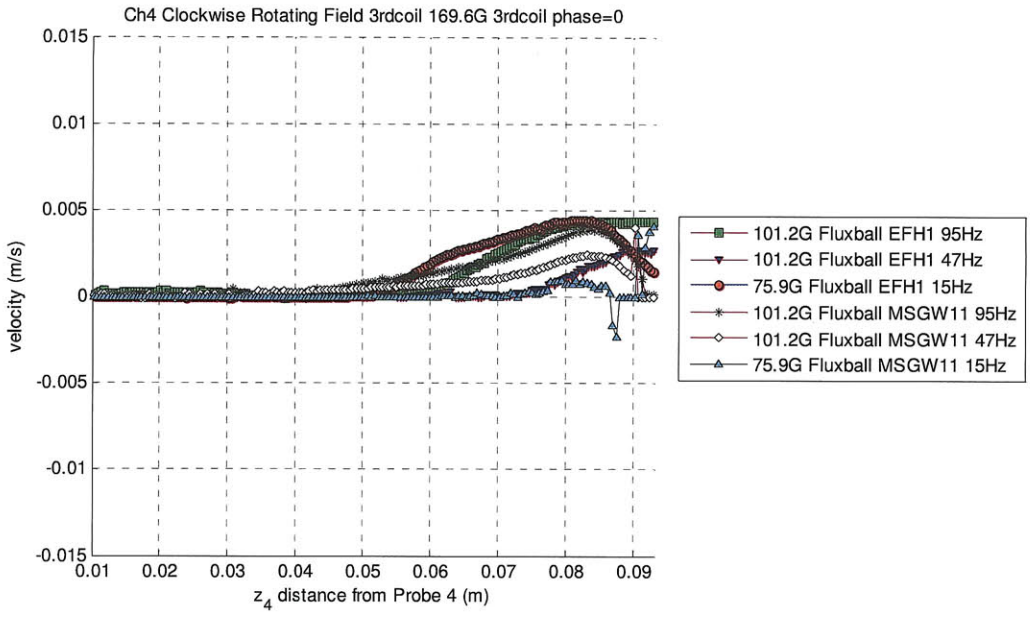
Ch4 Clockwise Rotating Field 3rdcoil 169.6G 3rdcoil phase=0
0.015
0.01
0.005
0
-0.005
-0.01
-0.015
velocity (m/s)
0.01
0.02
0.03
0.04
0.05
0.06
0.07
0.08
0.09
z4 distance from Probe 4 (m)
101.2G Fluxball EFH1 95Hz
101.2G Fluxball EFH1 47Hz
75.9G Fluxball EFH1 15Hz
101.2G Fluxball MSGW11 95Hz
101.2G Fluxball MSGW11 47Hz
75.9G Fluxball MSGW11 15Hz

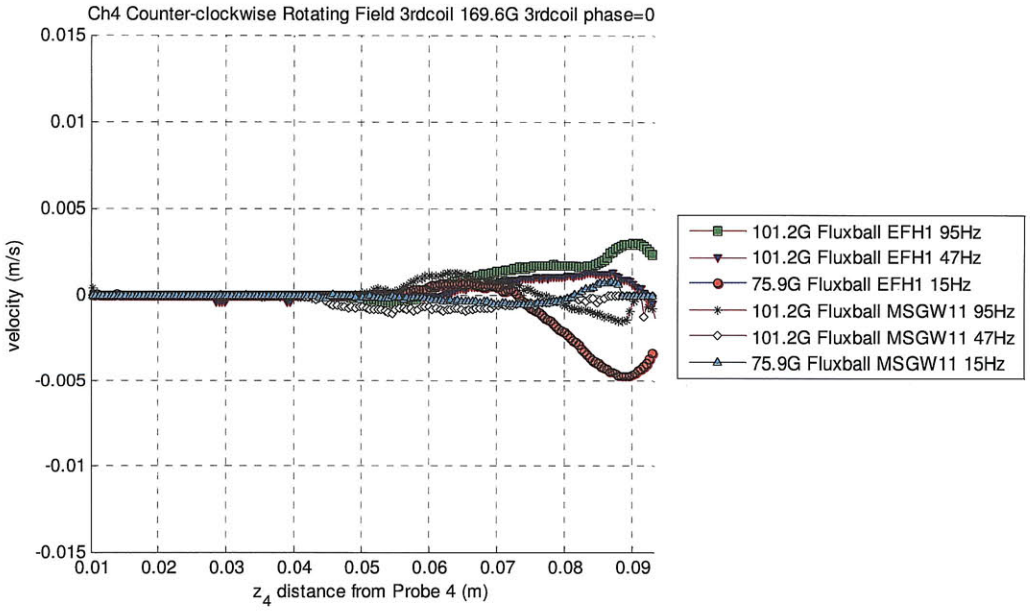
Ch4 Counter-clockwise Rotating Field 3rdcoil 169.6G 3rdcoil phase=0
0.015
0.01
0.005
0
-0.005
-0.01
-0.015
velocity (m/s)
0.01
0.02
0.03
0.04
0.05
0.06
0.07
0.08
0.09
z4 distance from Probe 4 (m)
101.2G Fluxball EFH1 95Hz
101.2G Fluxball EFH1 47Hz
75.9G Fluxball EFH1 15Hz
101.2G Fluxball MSGW11 95Hz
101.2G Fluxball MSGW11 47Hz
75.9G Fluxball MSGW11 15Hz

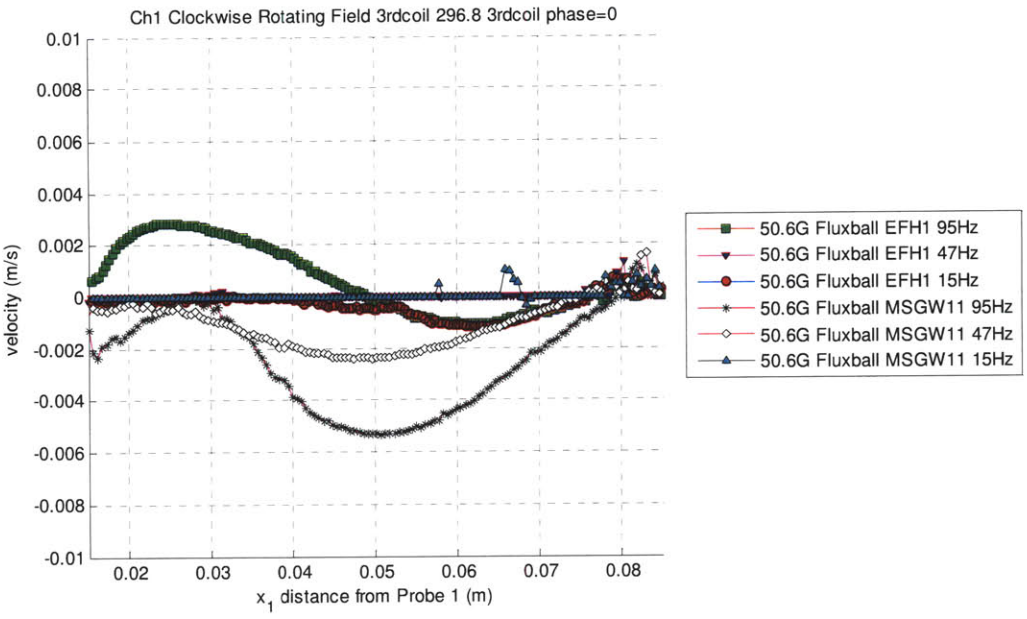
Ch1 Clockwise Rotating Field 3rdcoil 296.8 3rdcoil phase=0
velocity (m/s)
0.01
0.008
0.006
0.004
0.002
0
-0.002
-0.004
-0.006
-0.008
-0.01
0.02
0.03
0.04
0.05
0.06
0.07
0.08
x1 distance from Probe 1 (m)
50.6G Fluxball EFH1 95Hz
50.6G Fluxball EFH1 47Hz
50.6G Fluxball EFH1 15Hz
50.6G Fluxball MSGW11 95Hz
50.6G Fluxball MSGW11 47Hz
50.6G Fluxball MSGW11 15Hz

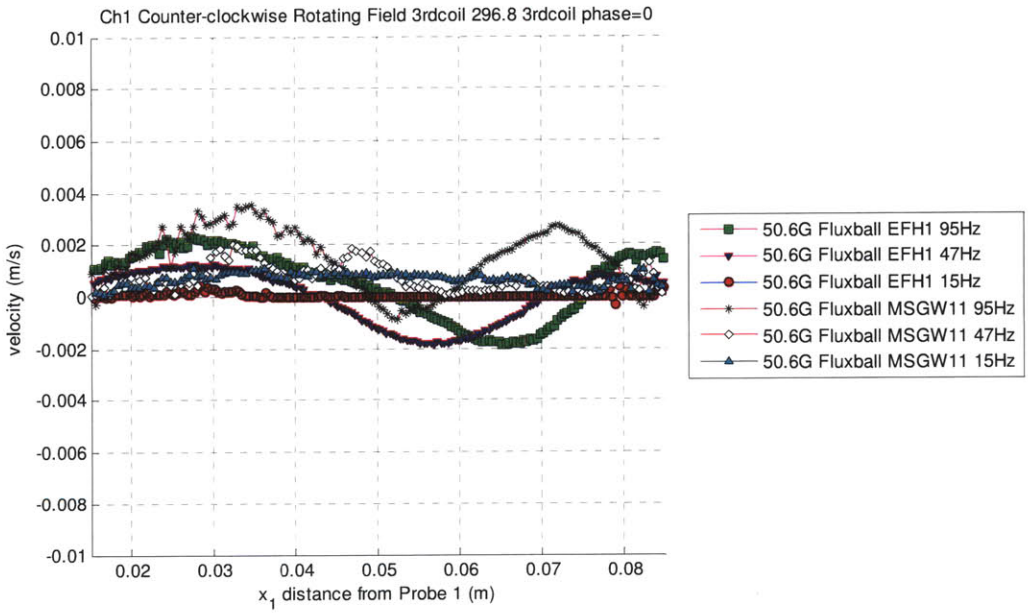
Ch1 Counter-clockwise Rotating Field 3rdcoil 296.8 3rdcoil phase=0
velocity (m/s)
0.01
0.008
0.006
0.004
0.002
0
-0.002
-0.004
-0.006
-0.008
-0.01
0.02
0.03
0.04
0.05
0.06
0.07
0.08
x1 distance from Probe 1 (m)
50.6G Fluxball EFH1 95Hz
50.6G Fluxball EFH1 47Hz
50.6G Fluxball EFH1 15Hz
50.6G Fluxball MSGW11 95Hz
50.6G Fluxball MSGW11 47Hz
50.6G Fluxball MSGW11 15Hz

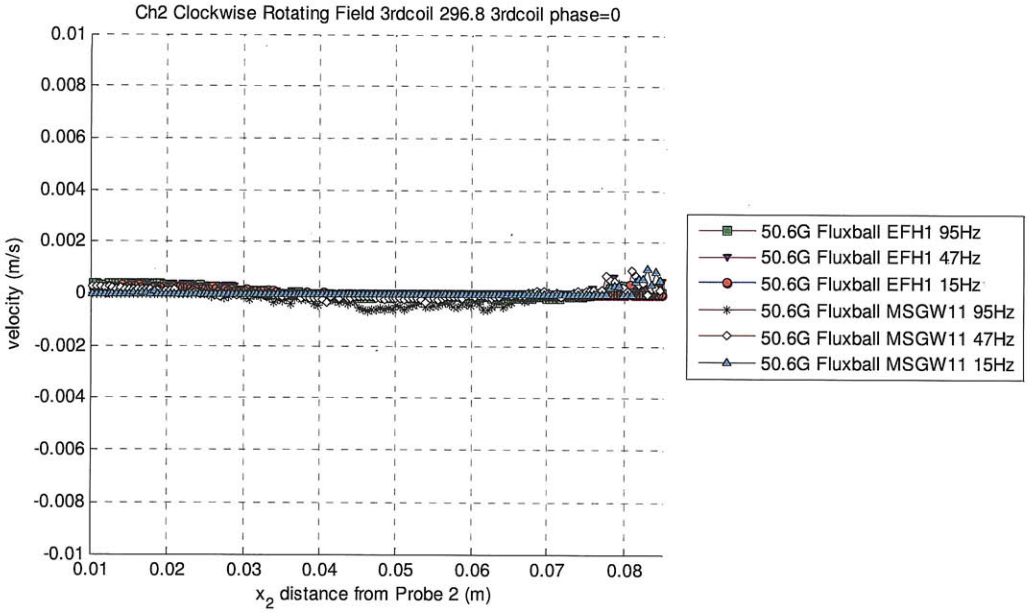
Ch2 Clockwise Rotating Field 3rdcoil 296.8 3rdcoil phase=0
velocity (m/s)
0.01
0.008
0.006
0.004
0.002
0
-0.002
-0.004
-0.006
-0.008
-0.01
0.01
0.02
0.03
0.04
0.05
0.06
0.07
0.08
x2 distance from Probe 2 (m)
50.6G Fluxball EFH1 95Hz
50.6G Fluxball EFH1 47Hz
50.6G Fluxball EFH1 15Hz
50.6G Fluxball MSGW11 95Hz
50.6G Fluxball MSGW11 47Hz
50.6G Fluxball MSGW11 15Hz

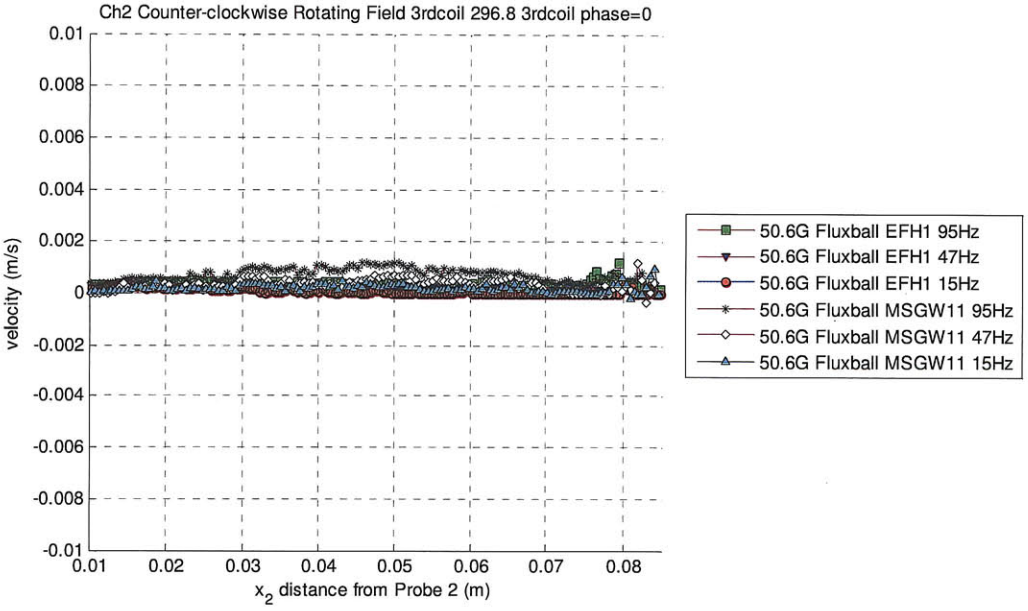
Ch2 Counter-clockwise Rotating Field 3rdcoil 296.8 3rdcoil phase=0
velocity (m/s)
0.01
0.008
0.006
0.004
0.002
0
-0.002
-0.004
-0.006
-0.008
-0.01
0.01
0.02
0.03
0.04
0.05
0.06
0.07
0.08
x2 distance from Probe 2 (m)
50.6G Fluxball EFH1 95Hz
50.6G Fluxball EFH1 47Hz
50.6G Fluxball EFH1 15Hz
50.6G Fluxball MSGW11 95Hz
50.6G Fluxball MSGW11 47Hz
50.6G Fluxball MSGW11 15Hz

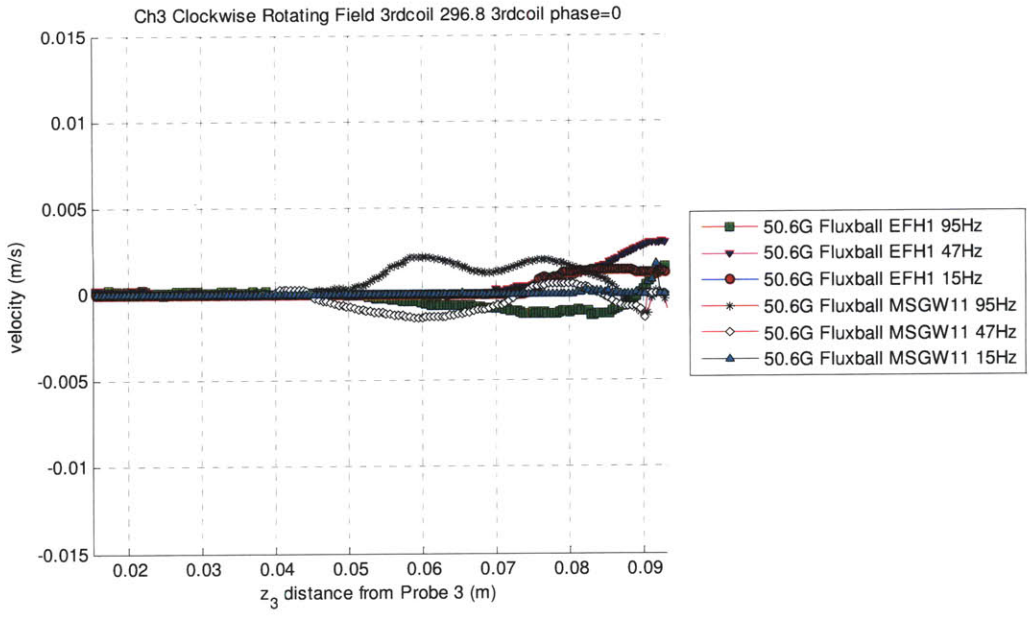
Ch3 Clockwise Rotating Field 3rdcoil 296.8 3rdcoil phase=0
0.015
0.01
0.005
0
-0.005
-0.01
-0.015
velocity (m/s)
0.02
0.03
0.04
0.05
0.06
0.07
0.08
0.09
z3 distance from Probe 3 (m)
50.6G Fluxball EFH1 95Hz
50.6G Fluxball EFH1 47Hz
50.6G Fluxball EFH1 15Hz
50.6G Fluxball MSGW11 95Hz
50.6G Fluxball MSGW11 47Hz
50.6G Fluxball MSGW11 15Hz

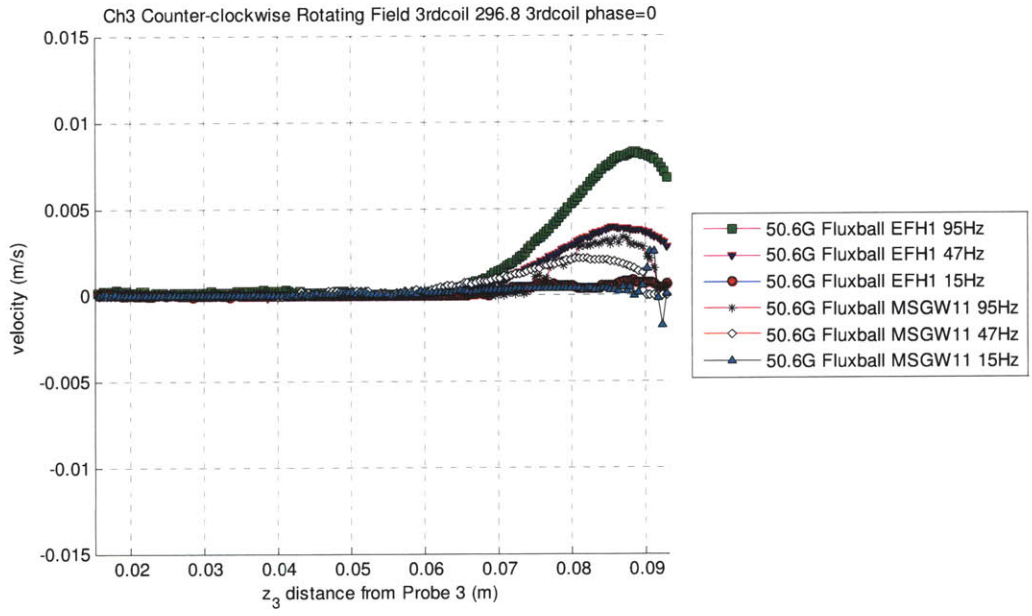
Ch3 Counter-clockwise Rotating Field 3rdcoil 296.8 3rdcoil phase=0
0.015
0.01
0.005
0
-0.005
-0.01
-0.015
velocity (m/s)
0.02
0.03
0.04
0.05
0.06
0.07
0.08
0.09
z3 distance from Probe 3 (m)
50.6G Fluxball EFH1 95Hz
50.6G Fluxball EFH1 47Hz
50.6G Fluxball EFH1 15Hz
50.6G Fluxball MSGW11 95Hz
50.6G Fluxball MSGW11 47Hz
50.6G Fluxball MSGW11 15Hz

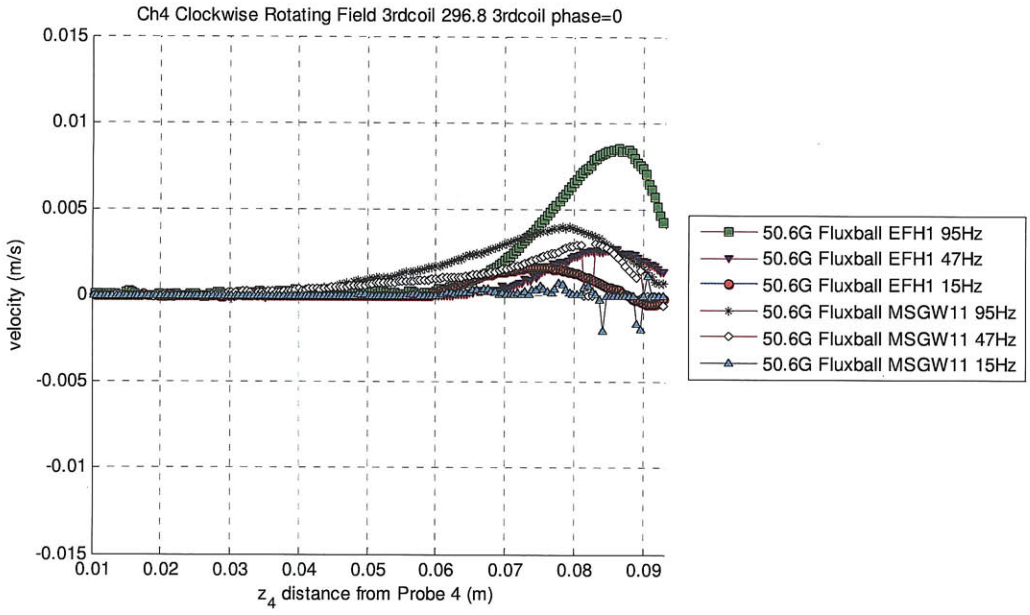
Ch4 Clockwise Rotating Field 3rdcoil 296.8 3rdcoil phase=0
velocity (m/s)
0.015
0.01
0.005
0
-0.005
-0.01
-0.015
0.01 0.02 0.03 0.04 0.05 0.06 0.07 0.08 0.09
z4 distance from Probe 4 (m)
50.6G Fluxball EFH1 95Hz
50.6G Fluxball EFH1 47Hz
50.6G Fluxball EFH1 15Hz
50.6G Fluxball MSGW11 95Hz
50.6G Fluxball MSGW11 47Hz
50.6G Fluxball MSGW11 15Hz

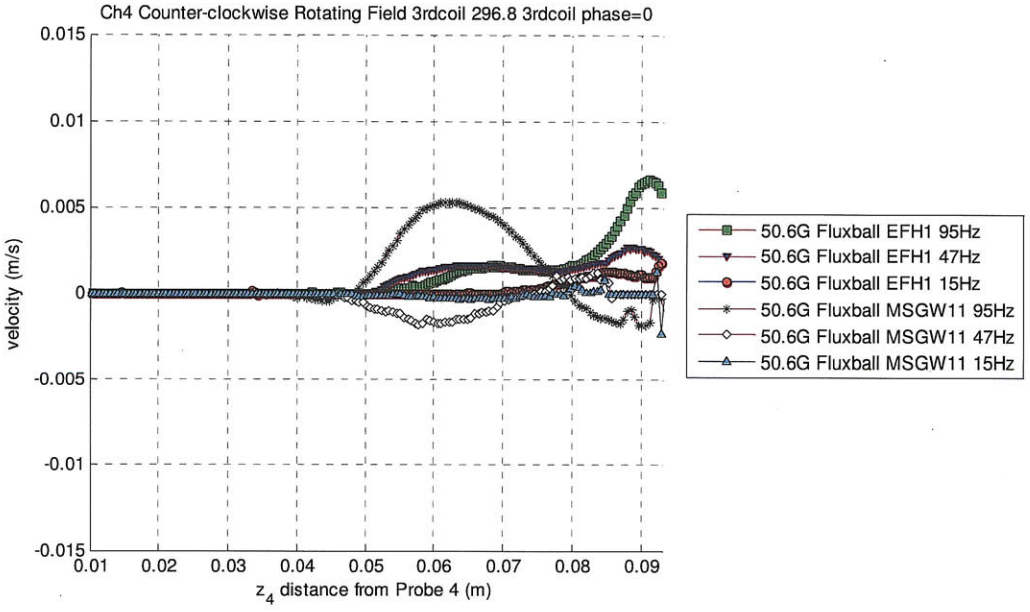
Ch4 Counter-clockwise Rotating Field 3rdcoil 296.8 3rdcoil phase=0
velocity (m/s)
0.015
0.01
0.005
0
-0.005
-0.01
-0.015
0.01 0.02 0.03 0.04 0.05 0.06 0.07 0.08 0.09
z4 distance from Probe 4 (m)
50.6G Fluxball EFH1 95Hz
50.6G Fluxball EFH1 47Hz
50.6G Fluxball EFH1 15Hz
50.6G Fluxball MSGW11 95Hz
50.6G Fluxball MSGW11 47Hz
50.6G Fluxball MSGW11 15Hz

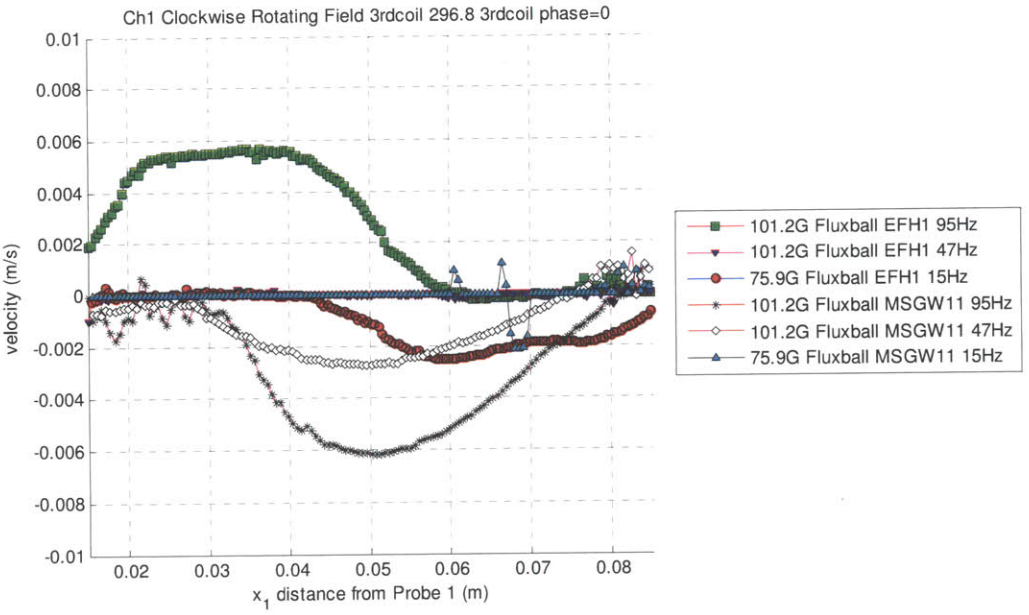
Ch1 Clockwise Rotating Field 3rdcoil 296.8 3rdcoil phase=0
velocity (m/s)
0.01
0.008
0.006
0.004
0.002
0
-0.002
-0.004
-0.006
-0.008
-0.01
0.02
0.03
0.04
0.05
0.06
0.07
0.08
x1 distance from Probe 1 (m)
101.2G Fluxball EFH1 95Hz
101.2G Fluxball EFH1 47Hz
75.9G Fluxball EFH1 15Hz
101.2G Fluxball MSGW11 95Hz
101.2G Fluxball MSGW11 47Hz
75.9G Fluxball MSGW11 15Hz

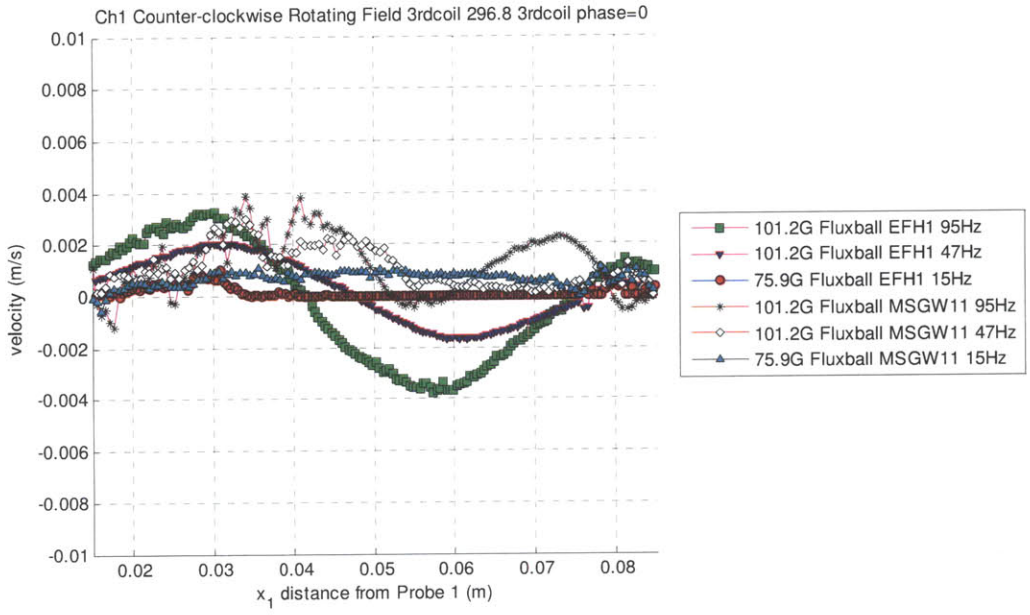
Ch1 Counter-clockwise Rotating Field 3rdcoil 296.8 3rdcoil phase=0
velocity (m/s)
0.01
0.008
0.006
0.004
0.002
0
-0.002
-0.004
-0.006
-0.008
-0.01
0.02
0.03
0.04
0.05
0.06
0.07
0.08
x1 distance from Probe 1 (m)
101.2G Fluxball EFH1 95Hz
101.2G Fluxball EFH1 47Hz
75.9G Fluxball EFH1 15Hz
101.2G Fluxball MSGW11 95Hz
101.2G Fluxball MSGW11 47Hz
75.9G Fluxball MSGW11 15Hz

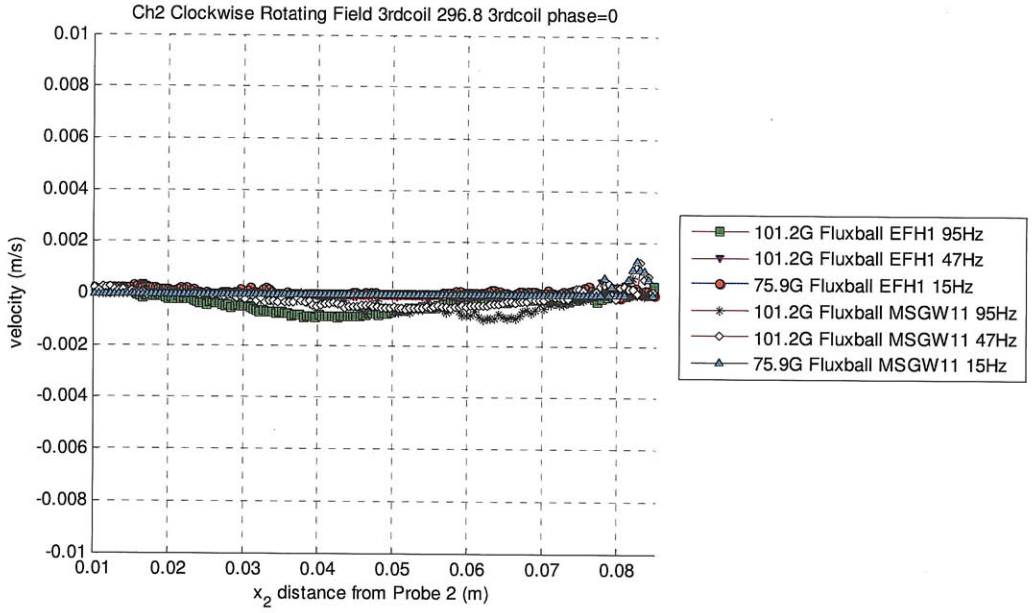
Ch2 Clockwise Rotating Field 3rdcoil 296.8 3rdcoil phase=0
velocity (m/s)
0.01
0.008
0.006
0.004
0.002
0
-0.002
-0.004
-0.006
-0.008
-0.01
0.01 0.02 0.03 0.04 0.05 0.06 0.07 0.08
x2 distance from Probe 2 (m)
101.2G Fluxball EFH1 95Hz
101.2G Fluxball EFH1 47Hz
75.9G Fluxball EFH1 15Hz
101.2G Fluxball MSGW11 95Hz
101.2G Fluxball MSGW11 47Hz
75.9G Fluxball MSGW11 15Hz

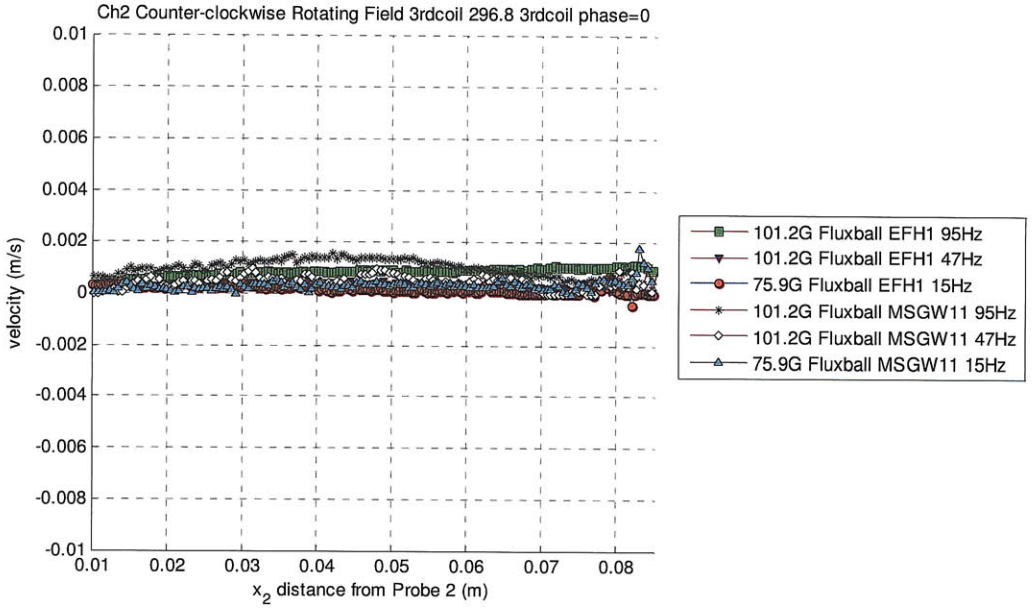
Ch2 Counter-clockwise Rotating Field 3rdcoil 296.8 3rdcoil phase=0
velocity (m/s)
0.01
0.008
0.006
0.004
0.002
0
-0.002
-0.004
-0.006
-0.008
-0.01
0.01 0.02 0.03 0.04 0.05 0.06 0.07 0.08
x2 distance from Probe 2 (m)
101.2G Fluxball EFH1 95Hz
101.2G Fluxball EFH1 47Hz
75.9G Fluxball EFH1 15Hz
101.2G Fluxball MSGW11 95Hz
101.2G Fluxball MSGW11 47Hz
75.9G Fluxball MSGW11 15Hz

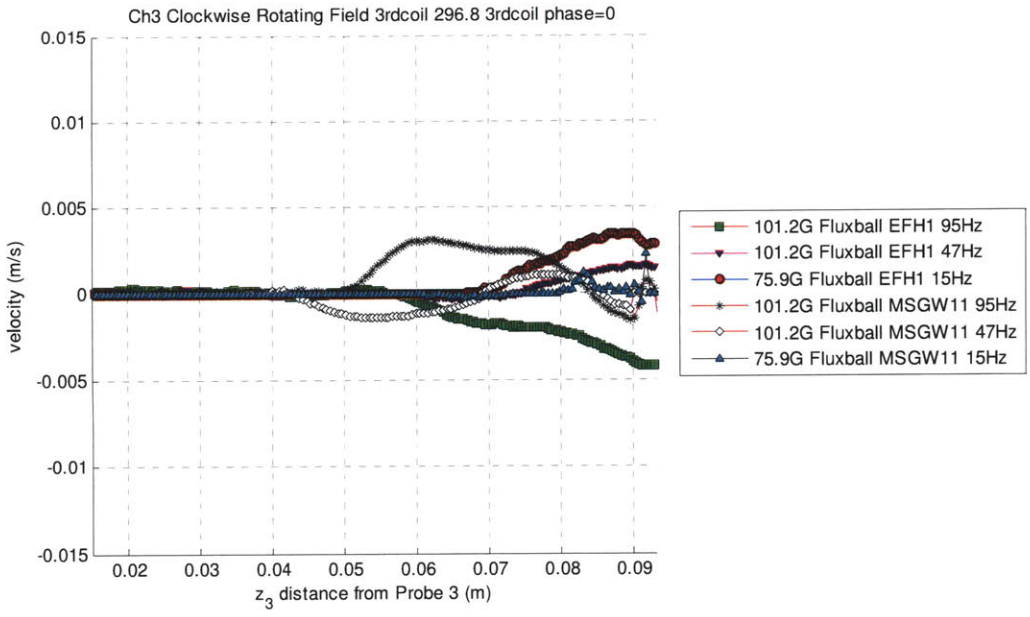
Ch3 Clockwise Rotating Field 3rdcoil 296.8 3rdcoil phase=0
velocity (m/s)
0.015
0.01
0.005
0
-0.005
-0.01
-0.015
0.02
0.03
0.04
0.05
0.06
0.07
0.08
0.09
z_3 distance from Probe 3 (m)
101.2G Fluxball EFH1 95Hz
101.2G Fluxball EFH1 47Hz
75.9G Fluxball EFH1 15Hz
101.2G Fluxball MSGW11 95Hz
101.2G Fluxball MSGW11 47Hz
75.9G Fluxball MSGW11 15Hz

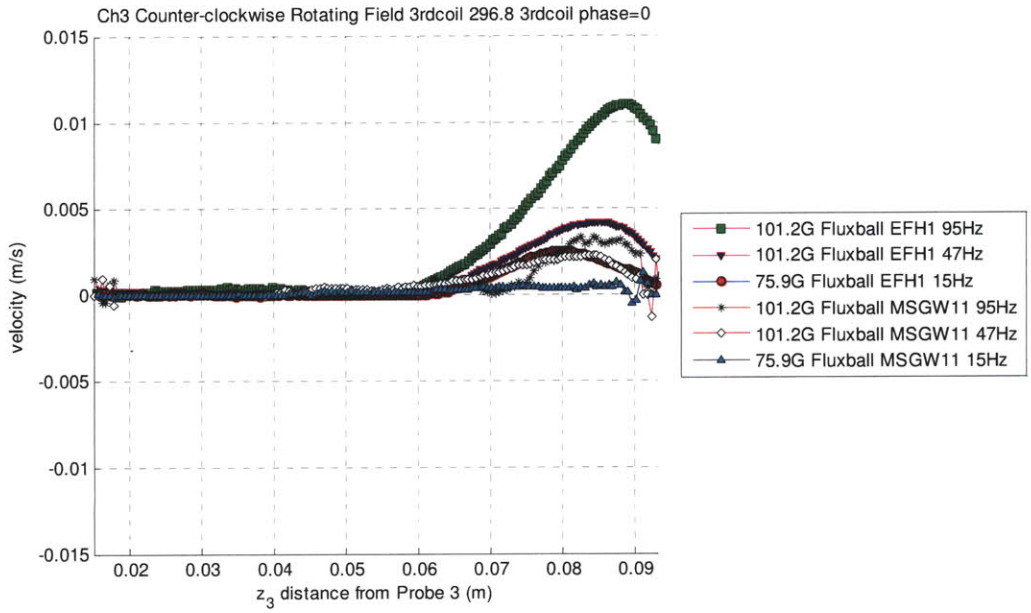
Ch3 Counter-clockwise Rotating Field 3rdcoil 296.8 3rdcoil phase=0
velocity (m/s)
0.015
0.01
0.005
0
-0.005
-0.01
-0.015
0.02
0.03
0.04
0.05
0.06
0.07
0.08
0.09
z_3 distance from Probe 3 (m)
101.2G Fluxball EFH1 95Hz
101.2G Fluxball EFH1 47Hz
75.9G Fluxball EFH1 15Hz
101.2G Fluxball MSGW11 95Hz
101.2G Fluxball MSGW11 47Hz
75.9G Fluxball MSGW11 15Hz

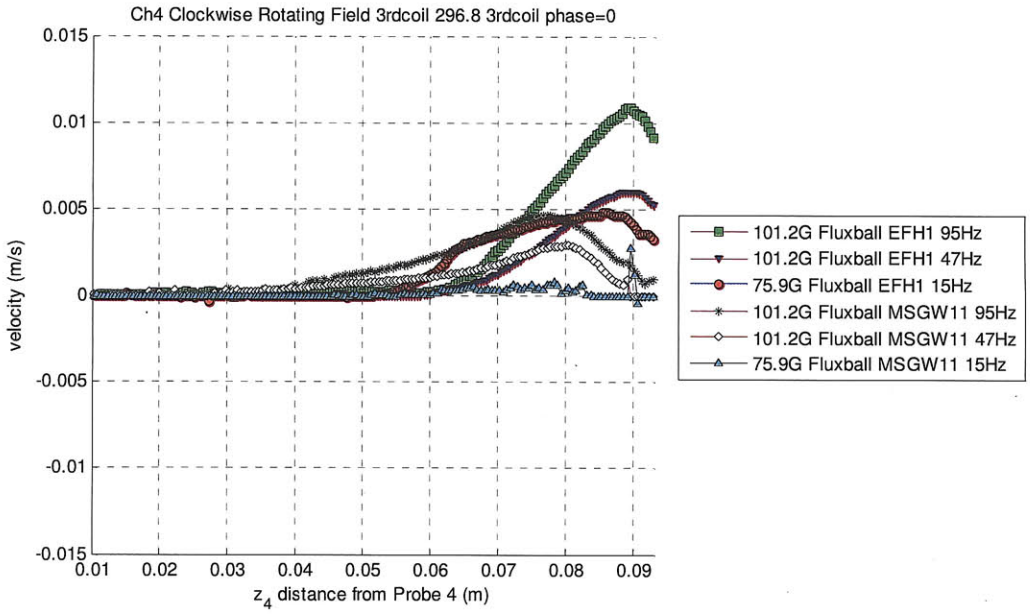
Ch4 Clockwise Rotating Field 3rdcoil 296.8 3rdcoil phase=0
velocity (m/s)
0.015
0.01
0.005
0
-0.005
-0.01
-0.015
0.01 0.02 0.03 0.04 0.05 0.06 0.07 0.08 0.09
z4 distance from Probe 4 (m)
101.2G Fluxball EFH1 95Hz
101.2G Fluxball EFH1 47Hz
75.9G Fluxball EFH1 15Hz
101.2G Fluxball MSGW11 95Hz
101.2G Fluxball MSGW11 47Hz
75.9G Fluxball MSGW11 15Hz

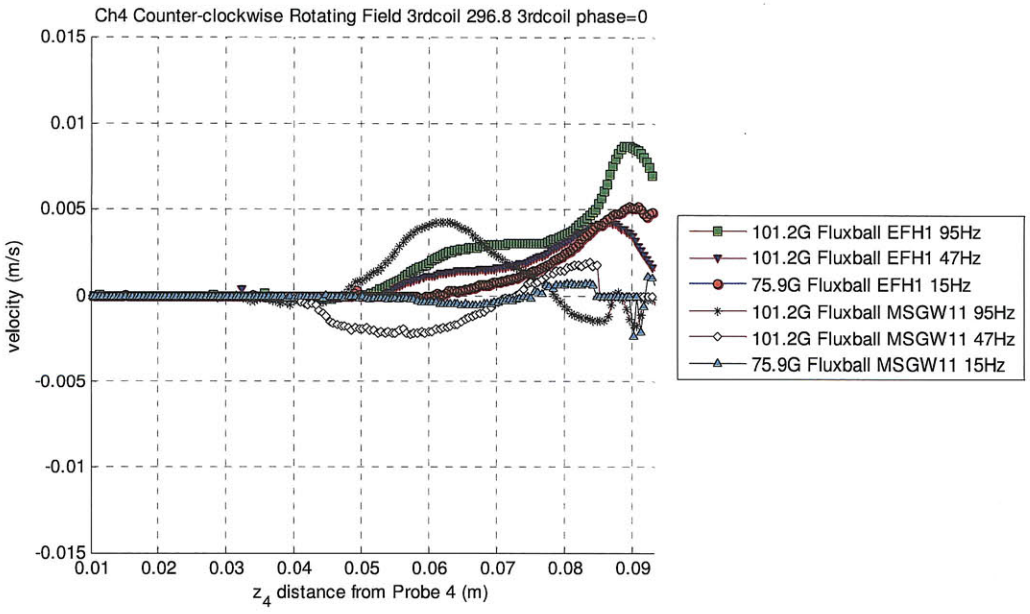
Ch4 Counter-clockwise Rotating Field 3rdcoil 296.8 3rdcoil phase=0
velocity (m/s)
0.015
0.01
0.005
0
-0.005
-0.01
-0.015
0.01 0.02 0.03 0.04 0.05 0.06 0.07 0.08 0.09
z4 distance from Probe 4 (m)
101.2G Fluxball EFH1 95Hz
101.2G Fluxball EFH1 47Hz
75.9G Fluxball EFH1 15Hz
101.2G Fluxball MSGW11 95Hz
101.2G Fluxball MSGW11 47Hz
75.9G Fluxball MSGW11 15Hz

G10. Comparison of Different Fluids with Third Coil Oscillating at Different Frequencies with Phase Difference=60 with Respect to Inner Coil

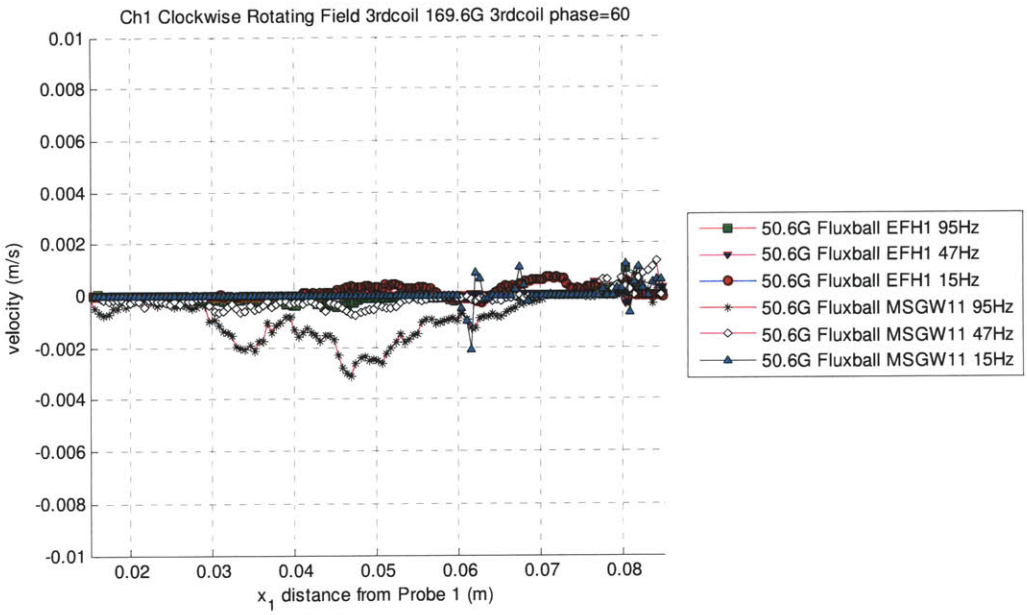

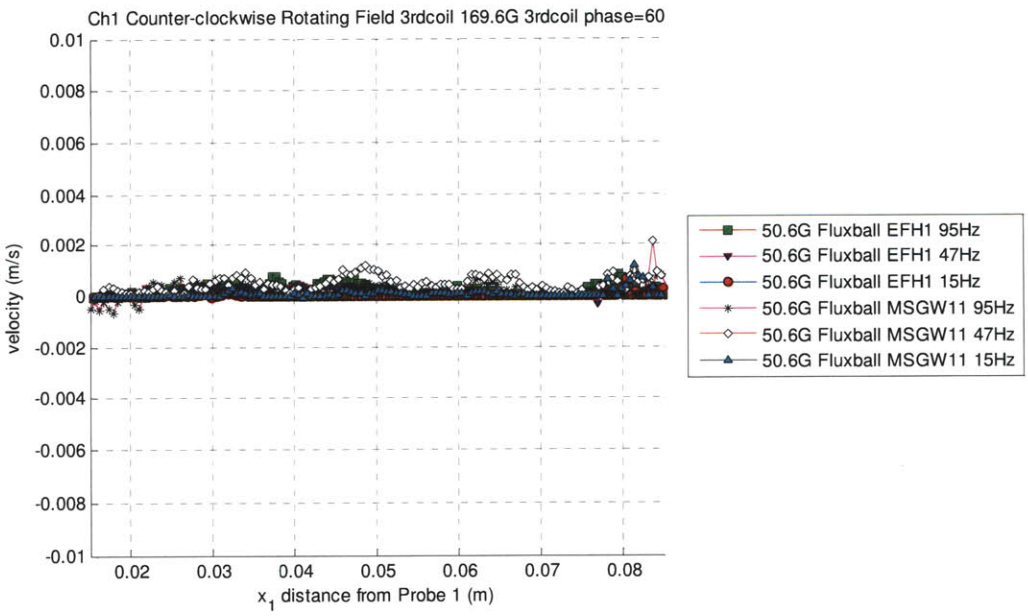

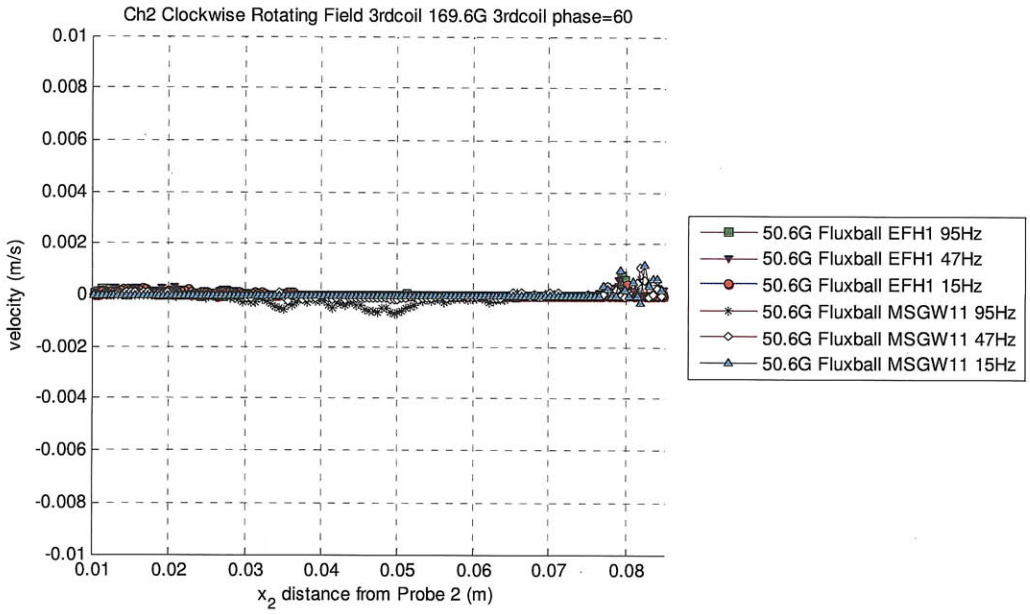
Ch2 Clockwise Rotating Field 3rdcoil 169.6G 3rdcoil phase=60
velocity (m/s)
0.01
0.008
0.006
0.004
0.002
0
-0.002
-0.004
-0.006
-0.008
-0.01
0.01
0.02
0.03
0.04
0.05
0.06
0.07
0.08
x2 distance from Probe 2 (m)
50.6G Fluxball EFH1 95Hz
50.6G Fluxball EFH1 47Hz
50.6G Fluxball EFH1 15Hz
50.6G Fluxball MSGW11 95Hz
50.6G Fluxball MSGW11 47Hz
50.6G Fluxball MSGW11 15Hz

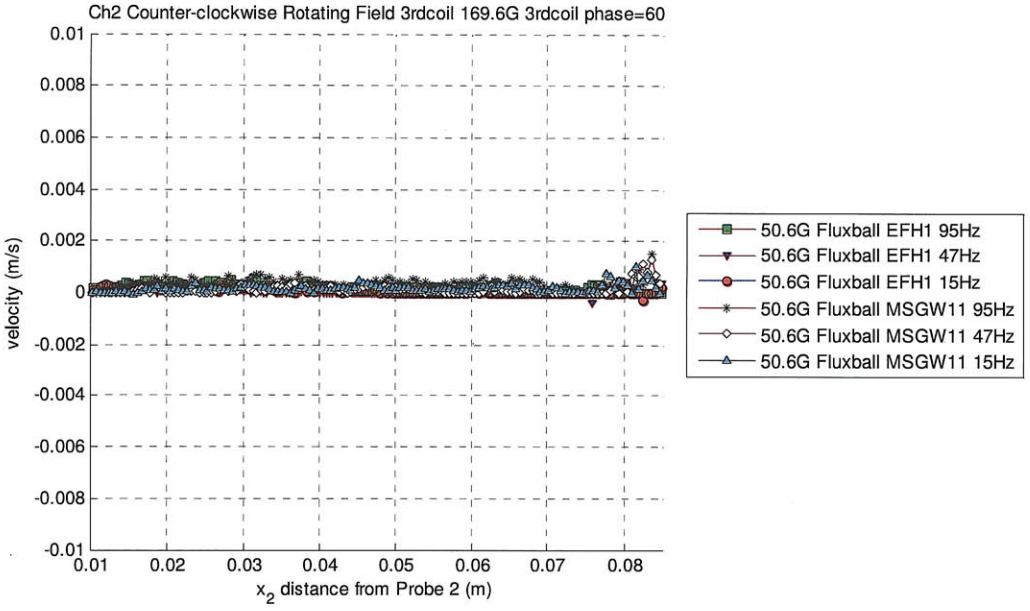
Ch2 Counter-clockwise Rotating Field 3rdcoil 169.6G 3rdcoil phase=60
velocity (m/s)
0.01
0.008
0.006
0.004
0.002
0
-0.002
-0.004
-0.006
-0.008
-0.01
0.01
0.02
0.03
0.04
0.05
0.06
0.07
0.08
x2 distance from Probe 2 (m)
50.6G Fluxball EFH1 95Hz
50.6G Fluxball EFH1 47Hz
50.6G Fluxball EFH1 15Hz
50.6G Fluxball MSGW11 95Hz
50.6G Fluxball MSGW11 47Hz
50.6G Fluxball MSGW11 15Hz

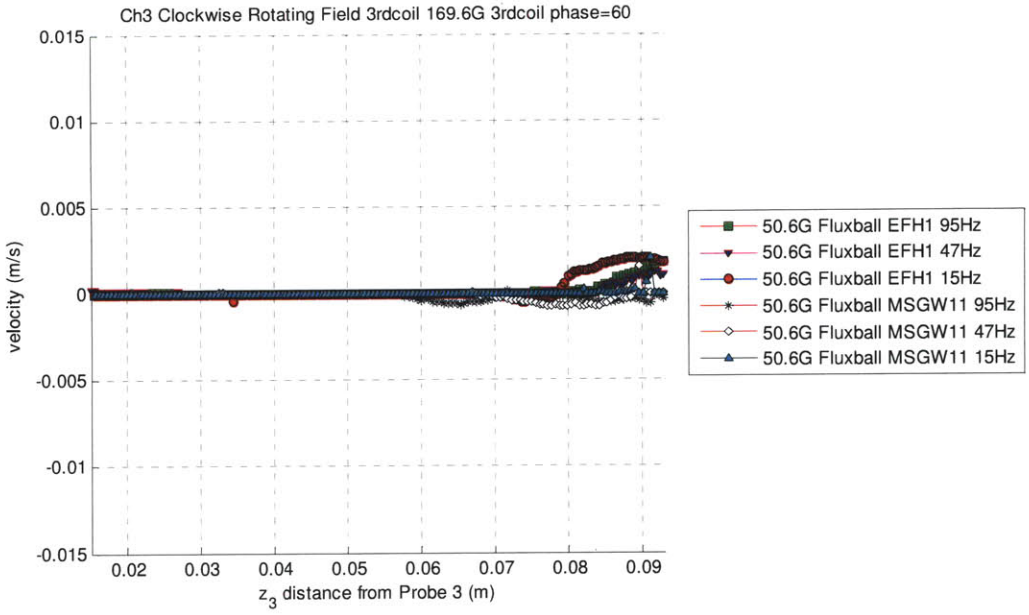
Ch3 Clockwise Rotating Field 3rdcoil 169.6G 3rdcoil phase=60
velocity (m/s)
0.015
0.01
0.005
0
-0.005
-0.01
-0.015
0.02
0.03
0.04
0.05
0.06
0.07
0.08
0.09
z_3 distance from Probe 3 (m)
50.6G Fluxball EFH1 95Hz
50.6G Fluxball EFH1 47Hz
50.6G Fluxball EFH1 15Hz
50.6G Fluxball MSGW11 95Hz
50.6G Fluxball MSGW11 47Hz
50.6G Fluxball MSGW11 15Hz

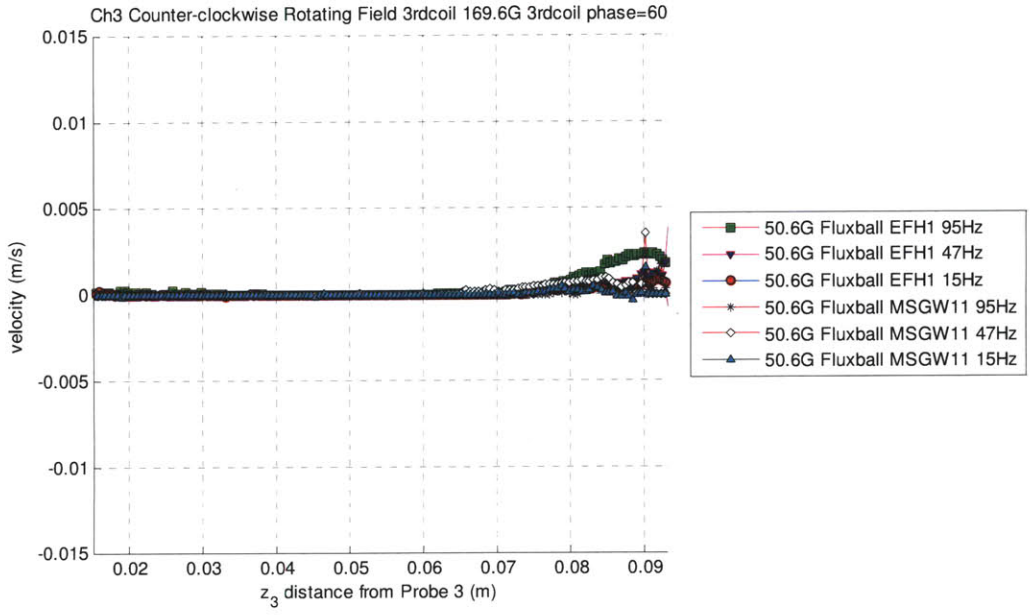
Ch3 Counter-clockwise Rotating Field 3rdcoil 169.6G 3rdcoil phase=60
velocity (m/s)
0.015
0.01
0.005
0
-0.005
-0.01
-0.015
0.02
0.03
0.04
0.05
0.06
0.07
0.08
0.09
z_3 distance from Probe 3 (m)
50.6G Fluxball EFH1 95Hz
50.6G Fluxball EFH1 47Hz
50.6G Fluxball EFH1 15Hz
50.6G Fluxball MSGW11 95Hz
50.6G Fluxball MSGW11 47Hz
50.6G Fluxball MSGW11 15Hz

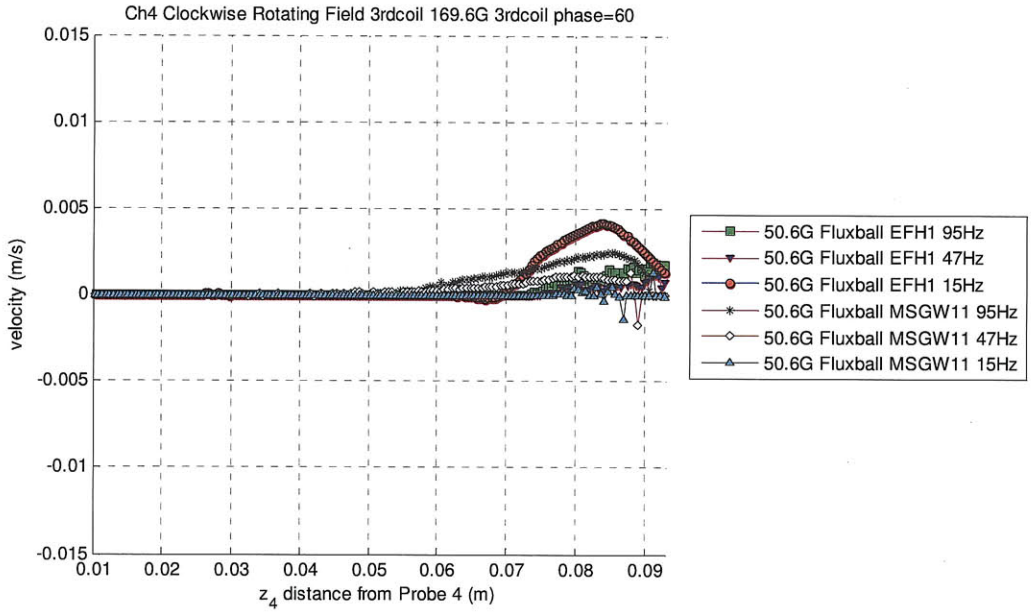
Ch4 Clockwise Rotating Field 3rdcoil 169.6G 3rdcoil phase=60
0.015
0.01
0.005
0
-0.005
-0.01
-0.015
velocity (m/s)
0.01
0.02
0.03
0.04
0.05
0.06
0.07
0.08
0.09
z4 distance from Probe 4 (m)
50.6G Fluxball EFH1 95Hz
50.6G Fluxball EFH1 47Hz
50.6G Fluxball EFH1 15Hz
50.6G Fluxball MSGW11 95Hz
50.6G Fluxball MSGW11 47Hz
50.6G Fluxball MSGW11 15Hz

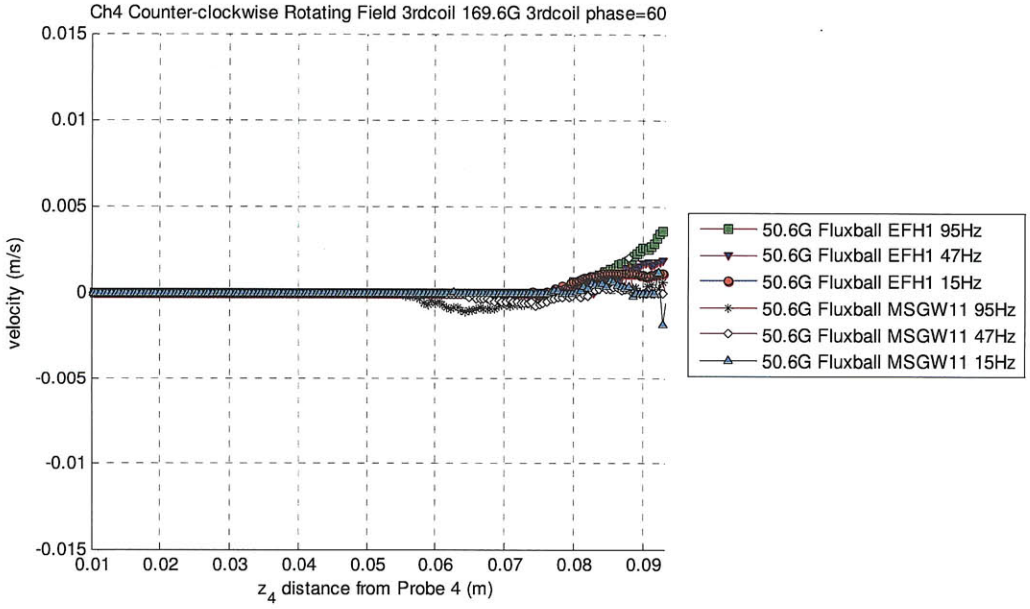
Ch4 Counter-clockwise Rotating Field 3rdcoil 169.6G 3rdcoil phase=60
0.015
0.01
0.005
0
-0.005
-0.01
-0.015
velocity (m/s)
0.01
0.02
0.03
0.04
0.05
0.06
0.07
0.08
0.09
z4 distance from Probe 4 (m)
50.6G Fluxball EFH1 95Hz
50.6G Fluxball EFH1 47Hz
50.6G Fluxball EFH1 15Hz
50.6G Fluxball MSGW11 95Hz
50.6G Fluxball MSGW11 47Hz
50.6G Fluxball MSGW11 15Hz

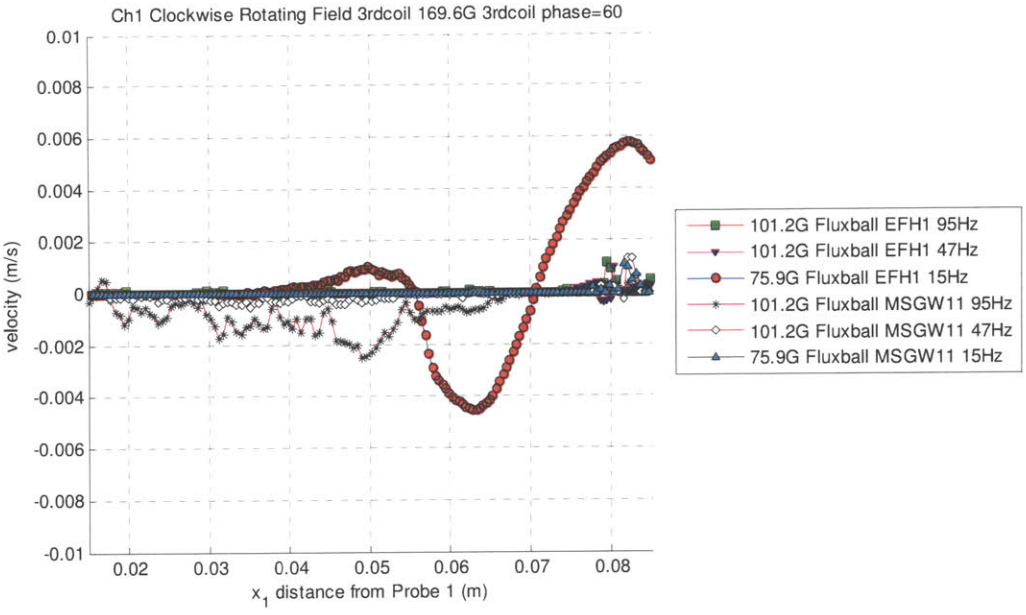
Ch1 Clockwise Rotating Field 3rdcoil 169.6G 3rdcoil phase=60
velocity (m/s)
0.01
0.008
0.006
0.004
0.002
0
-0.002
-0.004
-0.006
-0.008
-0.01
0.02
0.03
0.04
0.05
0.06
0.07
0.08
x1 distance from Probe 1 (m)
101.2G Fluxball EFH1 95Hz
101.2G Fluxball EFH1 47Hz
75.9G Fluxball EFH1 15Hz
101.2G Fluxball MSGW11 95Hz
101.2G Fluxball MSGW11 47Hz
75.9G Fluxball MSGW11 15Hz

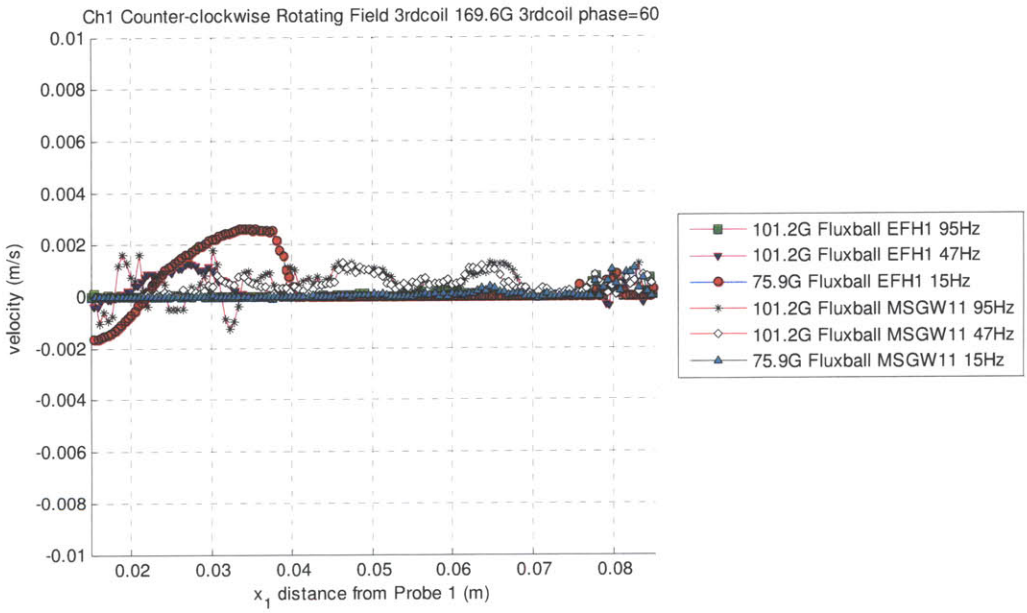
Ch1 Counter-clockwise Rotating Field 3rdcoil 169.6G 3rdcoil phase=60
velocity (m/s)
0.01
0.008
0.006
0.004
0.002
0
-0.002
-0.004
-0.006
-0.008
-0.01
0.02
0.03
0.04
0.05
0.06
0.07
0.08
x1 distance from Probe 1 (m)
101.2G Fluxball EFH1 95Hz
101.2G Fluxball EFH1 47Hz
75.9G Fluxball EFH1 15Hz
101.2G Fluxball MSGW11 95Hz
101.2G Fluxball MSGW11 47Hz
75.9G Fluxball MSGW11 15Hz

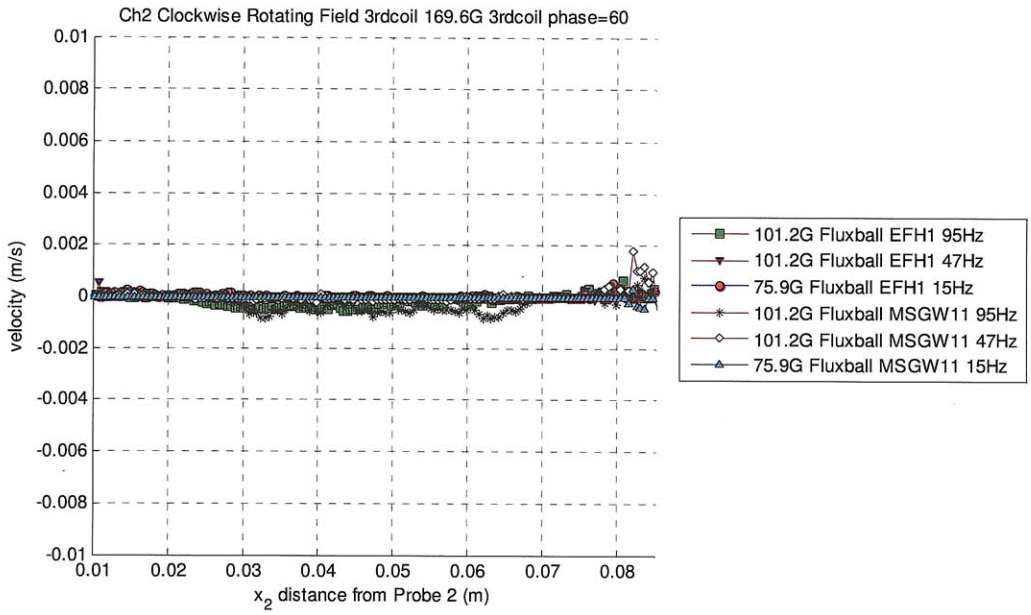
Ch2 Clockwise Rotating Field 3rdcoil 169.6G 3rdcoil phase=60
velocity (m/s)
0.01
0.008
0.006
0.004
0.002
0
-0.002
-0.004
-0.006
-0.008
-0.01
0.01 0.02 0.03 0.04 0.05 0.06 0.07 0.08
x2 distance from Probe 2 (m)
101.2G Fluxball EFH1 95Hz
101.2G Fluxball EFH1 47Hz
75.9G Fluxball EFH1 15Hz
101.2G Fluxball MSGW11 95Hz
101.2G Fluxball MSGW11 47Hz
75.9G Fluxball MSGW11 15Hz

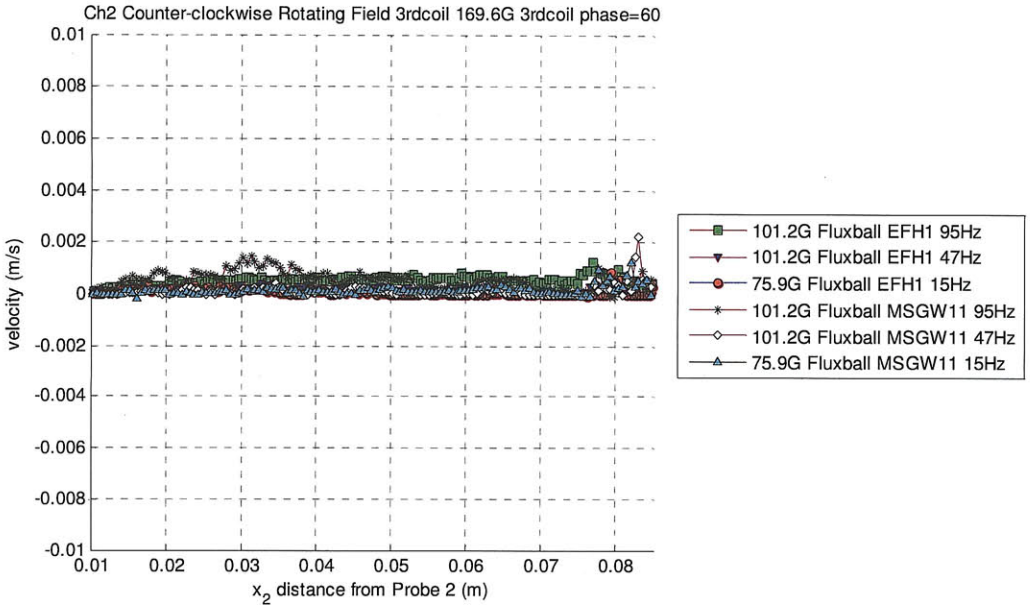
Ch2 Counter-clockwise Rotating Field 3rdcoil 169.6G 3rdcoil phase=60
velocity (m/s)
0.01
0.008
0.006
0.004
0.002
0
-0.002
-0.004
-0.006
-0.008
-0.01
0.01 0.02 0.03 0.04 0.05 0.06 0.07 0.08
x2 distance from Probe 2 (m)
101.2G Fluxball EFH1 95Hz
101.2G Fluxball EFH1 47Hz
75.9G Fluxball EFH1 15Hz
101.2G Fluxball MSGW11 95Hz
101.2G Fluxball MSGW11 47Hz
75.9G Fluxball MSGW11 15Hz

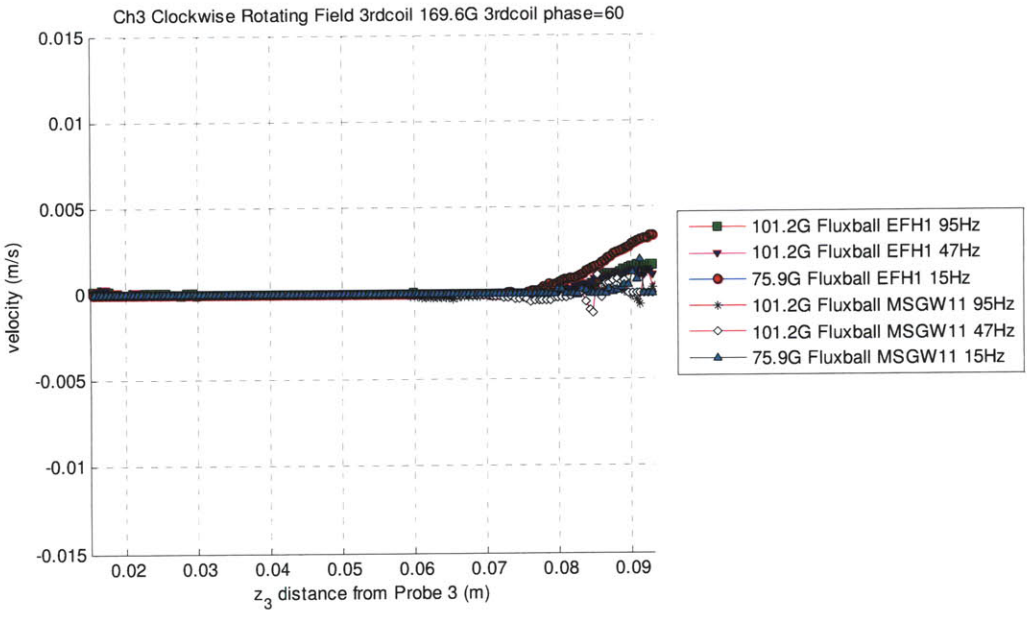
Ch3 Clockwise Rotating Field 3rdcoil 169.6G 3rdcoil phase=60
velocity (m/s)
0.015
0.01
0.005
0
-0.005
-0.01
-0.015
0.02
0.03
0.04
0.05
0.06
0.07
0.08
0.09
z_3 distance from Probe 3 (m)
101.2G Fluxball EFH1 95Hz
101.2G Fluxball EFH1 47Hz
75.9G Fluxball EFH1 15Hz
101.2G Fluxball MSGW11 95Hz
101.2G Fluxball MSGW11 47Hz
75.9G Fluxball MSGW11 15Hz

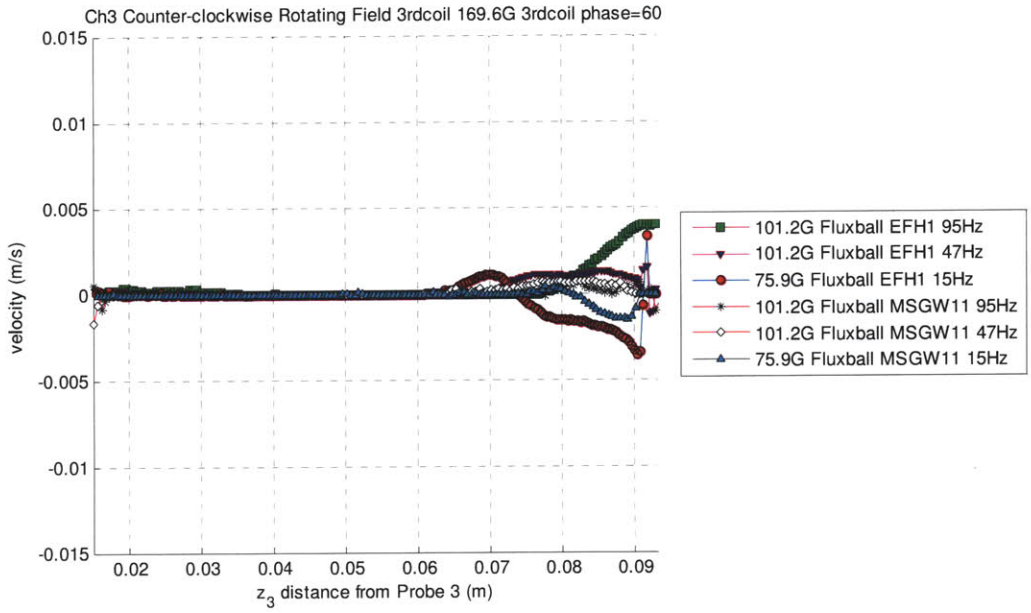
Ch3 Counter-clockwise Rotating Field 3rdcoil 169.6G 3rdcoil phase=60
velocity (m/s)
0.015
0.01
0.005
0
-0.005
-0.01
-0.015
0.02
0.03
0.04
0.05
0.06
0.07
0.08
0.09
z_3 distance from Probe 3 (m)
101.2G Fluxball EFH1 95Hz
101.2G Fluxball EFH1 47Hz
75.9G Fluxball EFH1 15Hz
101.2G Fluxball MSGW11 95Hz
101.2G Fluxball MSGW11 47Hz
75.9G Fluxball MSGW11 15Hz

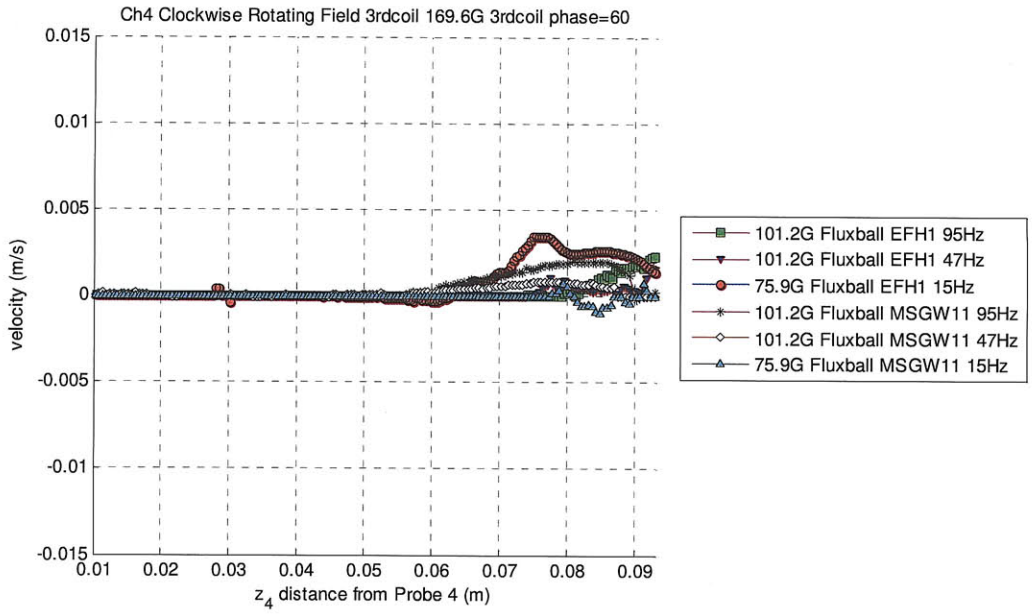
Ch4 Clockwise Rotating Field 3rdcoil 169.6G 3rdcoil phase=60
velocity (m/s)
0.015
0.01
0.005
0
-0.005
-0.01
-0.015
0.01
0.02
0.03
0.04
0.05
0.06
0.07
0.08
0.09
z4 distance from Probe 4 (m)
101.2G Fluxball EFH1 95Hz
101.2G Fluxball EFH1 47Hz
75.9G Fluxball EFH1 15Hz
101.2G Fluxball MSGW11 95Hz
101.2G Fluxball MSGW11 47Hz
75.9G Fluxball MSGW11 15Hz

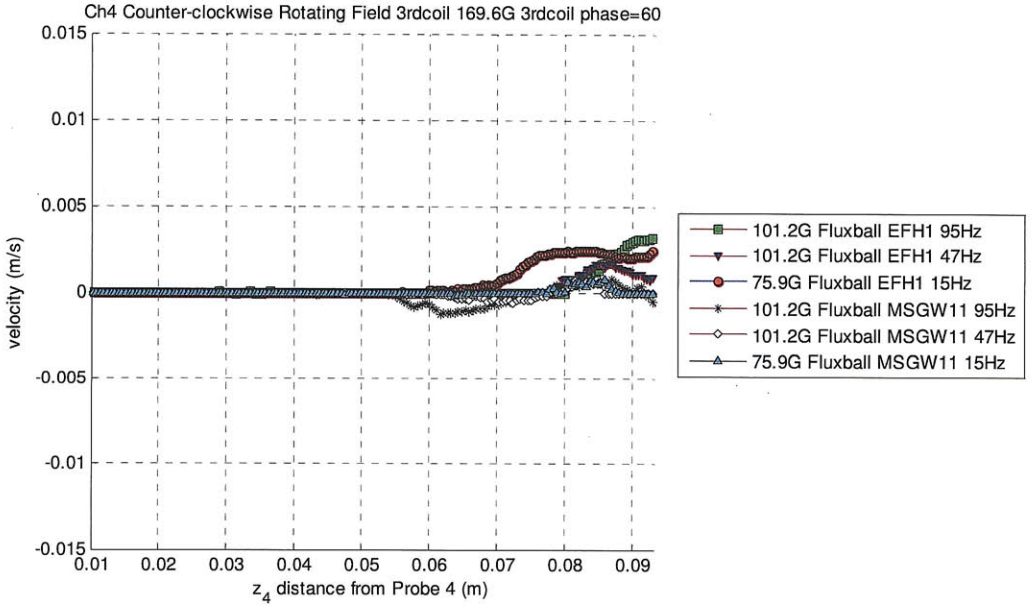
Ch4 Counter-clockwise Rotating Field 3rdcoil 169.6G 3rdcoil phase=60
velocity (m/s)
0.015
0.01
0.005
0
-0.005
-0.01
-0.015
0.01
0.02
0.03
0.04
0.05
0.06
0.07
0.08
0.09
z4 distance from Probe 4 (m)
101.2G Fluxball EFH1 95Hz
101.2G Fluxball EFH1 47Hz
75.9G Fluxball EFH1 15Hz
101.2G Fluxball MSGW11 95Hz
101.2G Fluxball MSGW11 47Hz
75.9G Fluxball MSGW11 15Hz

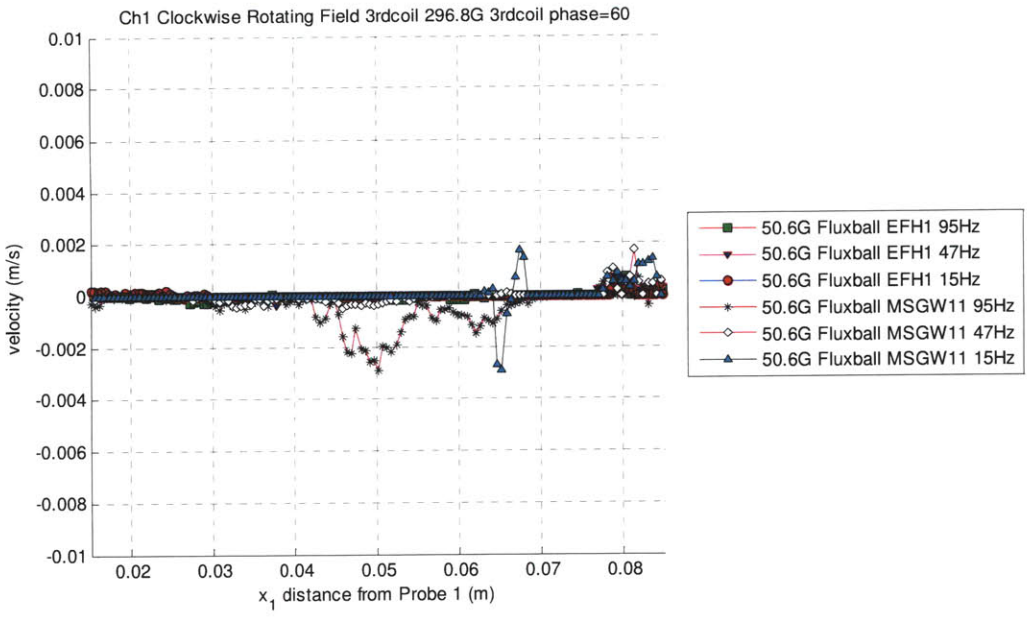
Ch1 Clockwise Rotating Field 3rdcoil 296.8G 3rdcoil phase=60
velocity (m/s)
0.01
0.008
0.006
0.004
0.002
0
-0.002
-0.004
-0.006
-0.008
-0.01
0.02
0.03
0.04
0.05
0.06
0.07
0.08
x1 distance from Probe 1 (m)
50.6G Fluxball EFH1 95Hz
50.6G Fluxball EFH1 47Hz
50.6G Fluxball EFH1 15Hz
50.6G Fluxball MSGW11 95Hz
50.6G Fluxball MSGW11 47Hz
50.6G Fluxball MSGW11 15Hz

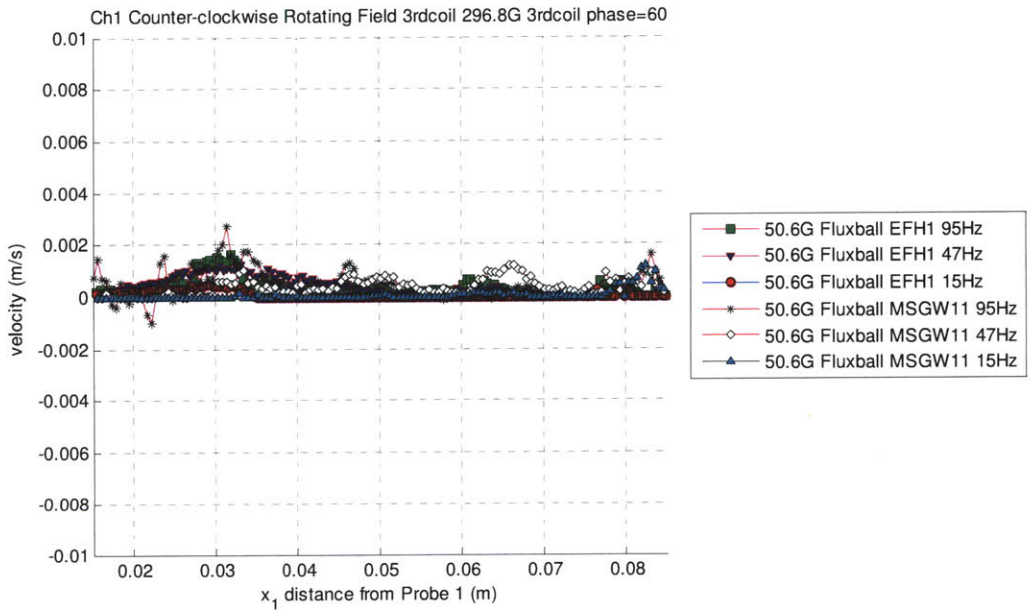
Ch1 Counter-clockwise Rotating Field 3rdcoil 296.8G 3rdcoil phase=60
velocity (m/s)
0.01
0.008
0.006
0.004
0.002
0
-0.002
-0.004
-0.006
-0.008
-0.01
0.02
0.03
0.04
0.05
0.06
0.07
0.08
x1 distance from Probe 1 (m)
50.6G Fluxball EFH1 95Hz
50.6G Fluxball EFH1 47Hz
50.6G Fluxball EFH1 15Hz
50.6G Fluxball MSGW11 95Hz
50.6G Fluxball MSGW11 47Hz
50.6G Fluxball MSGW11 15Hz

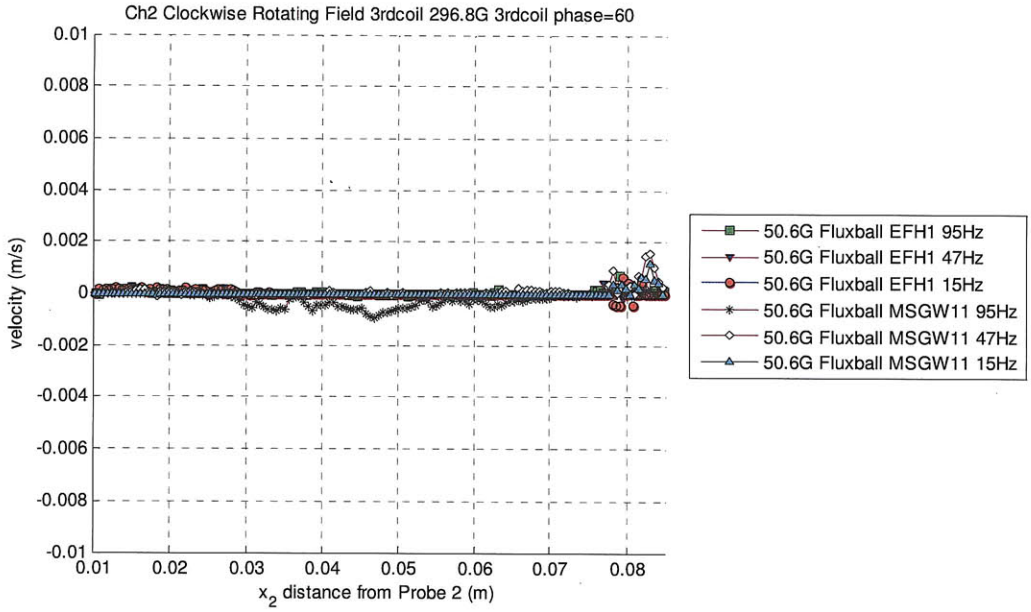
Ch2 Clockwise Rotating Field 3rdcoil 296.8G 3rdcoil phase=60
velocity (m/s)
0.01
0.008
0.006
0.004
0.002
0
-0.002
-0.004
-0.006
-0.008
-0.01
0.01 0.02 0.03 0.04 0.05 0.06 0.07 0.08
x2 distance from Probe 2 (m)
50.6G Fluxball EFH1 95Hz
50.6G Fluxball EFH1 47Hz
50.6G Fluxball EFH1 15Hz
50.6G Fluxball MSGW11 95Hz
50.6G Fluxball MSGW11 47Hz
50.6G Fluxball MSGW11 15Hz

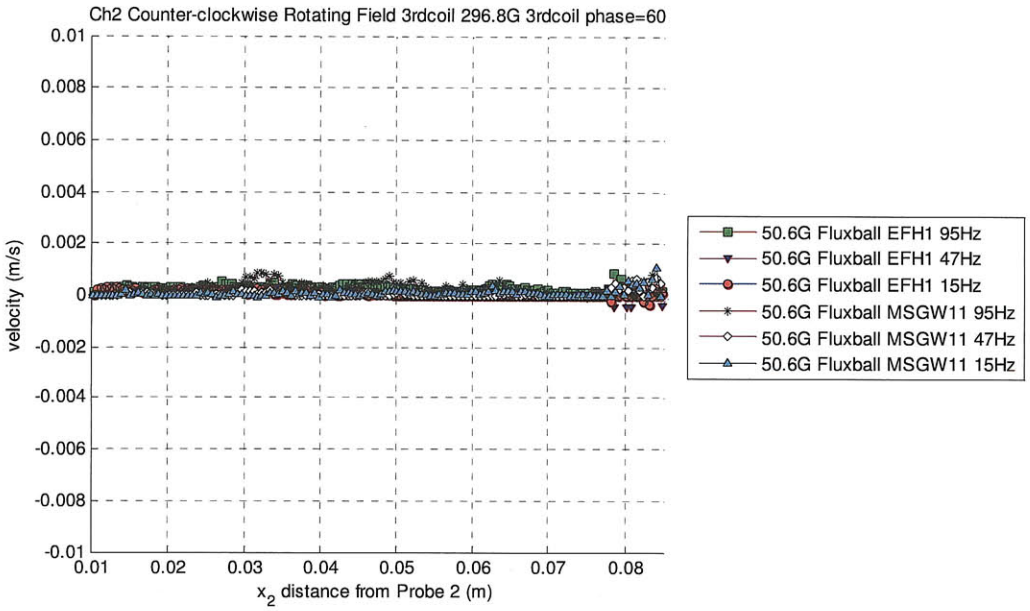
Ch2 Counter-clockwise Rotating Field 3rdcoil 296.8G 3rdcoil phase=60
velocity (m/s)
0.01
0.008
0.006
0.004
0.002
0
-0.002
-0.004
-0.006
-0.008
-0.01
0.01 0.02 0.03 0.04 0.05 0.06 0.07 0.08
x2 distance from Probe 2 (m)
50.6G Fluxball EFH1 95Hz
50.6G Fluxball EFH1 47Hz
50.6G Fluxball EFH1 15Hz
50.6G Fluxball MSGW11 95Hz
50.6G Fluxball MSGW11 47Hz
50.6G Fluxball MSGW11 15Hz

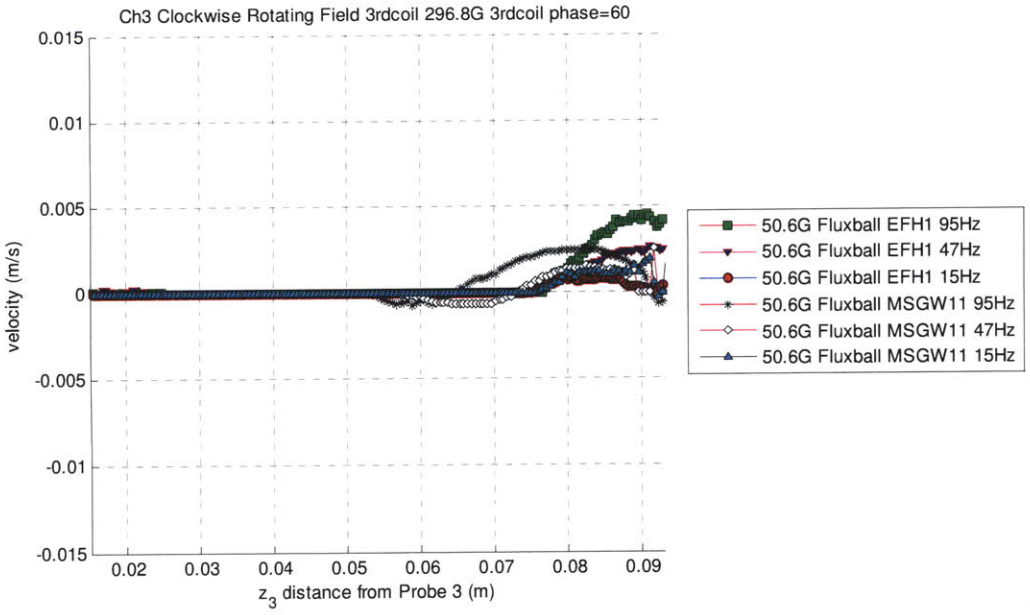
Ch3 Clockwise Rotating Field 3rdcoil 296.8G 3rdcoil phase=60
velocity (m/s)
0.015
0.01
0.005
0
-0.005
-0.01
-0.015
0.02
0.03
0.04
0.05
0.06
0.07
0.08
0.09
z_3 distance from Probe 3 (m)
50.6G Fluxball EFH1 95Hz
50.6G Fluxball EFH1 47Hz
50.6G Fluxball EFH1 15Hz
50.6G Fluxball MSGW11 95Hz
50.6G Fluxball MSGW11 47Hz
50.6G Fluxball MSGW11 15Hz

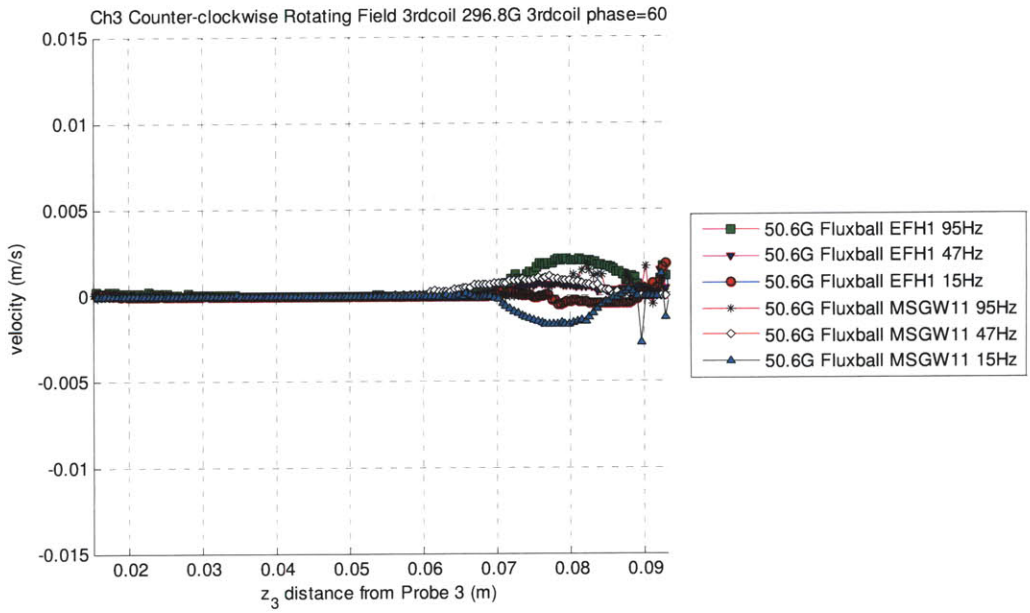
Ch3 Counter-clockwise Rotating Field 3rdcoil 296.8G 3rdcoil phase=60
velocity (m/s)
0.015
0.01
0.005
0
-0.005
-0.01
-0.015
0.02
0.03
0.04
0.05
0.06
0.07
0.08
0.09
z_3 distance from Probe 3 (m)
50.6G Fluxball EFH1 95Hz
50.6G Fluxball EFH1 47Hz
50.6G Fluxball EFH1 15Hz
50.6G Fluxball MSGW11 95Hz
50.6G Fluxball MSGW11 47Hz
50.6G Fluxball MSGW11 15Hz

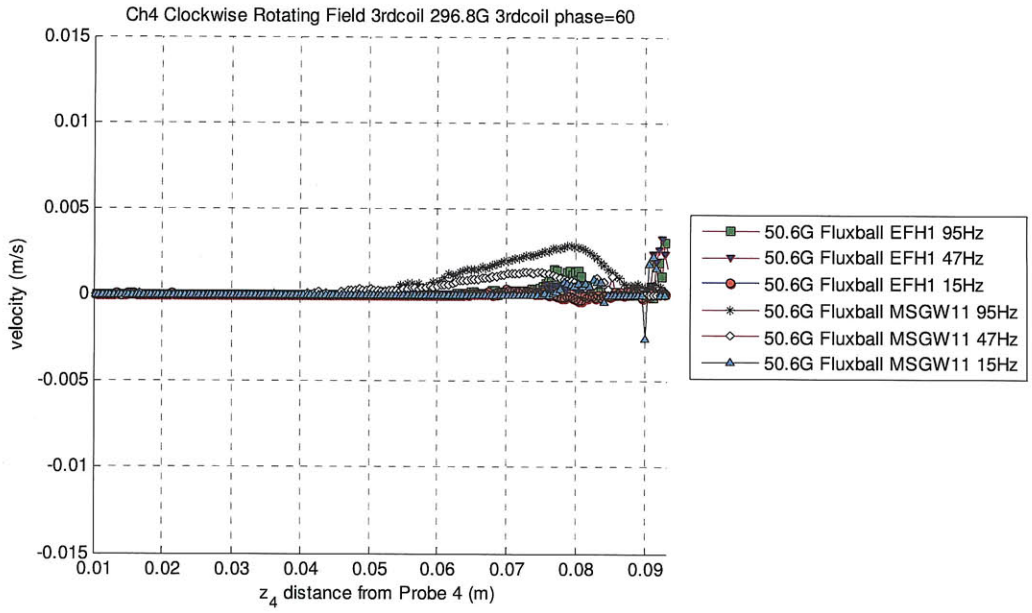
Ch4 Clockwise Rotating Field 3rdcoil 296.8G 3rdcoil phase=60
0.015
0.01
0.005
0
-0.005
-0.01
-0.015
velocity (m/s)
0.01
0.02
0.03
0.04
0.05
0.06
0.07
0.08
0.09
z4 distance from Probe 4 (m)
50.6G Fluxball EFH1 95Hz
50.6G Fluxball EFH1 47Hz
50.6G Fluxball EFH1 15Hz
50.6G Fluxball MSGW11 95Hz
50.6G Fluxball MSGW11 47Hz
50.6G Fluxball MSGW11 15Hz

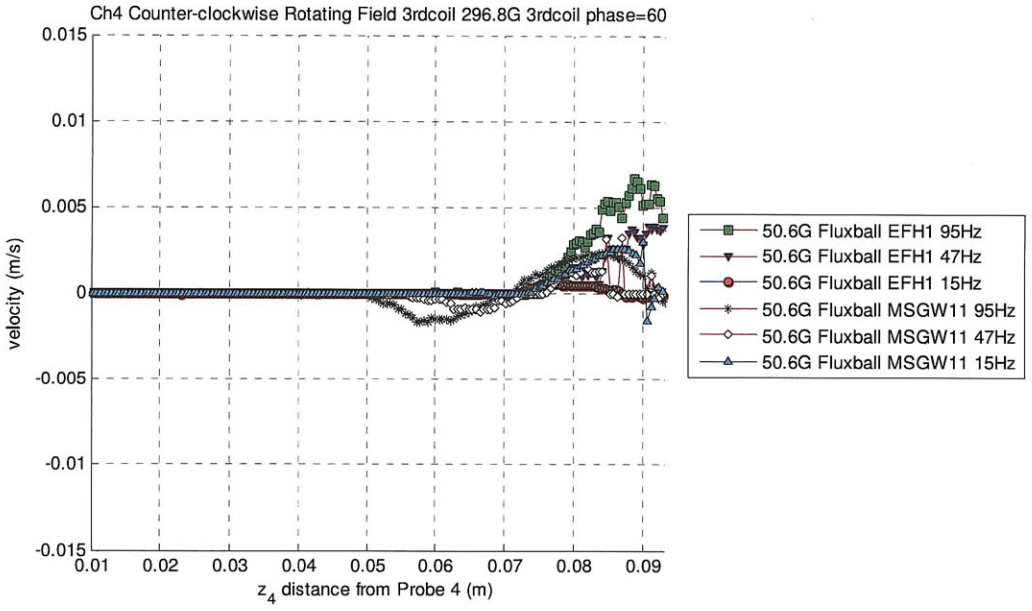
Ch4 Counter-clockwise Rotating Field 3rdcoil 296.8G 3rdcoil phase=60
0.015
0.01
0.005
0
-0.005
-0.01
-0.015
velocity (m/s)
0.01
0.02
0.03
0.04
0.05
0.06
0.07
0.08
0.09
z4 distance from Probe 4 (m)
50.6G Fluxball EFH1 95Hz
50.6G Fluxball EFH1 47Hz
50.6G Fluxball EFH1 15Hz
50.6G Fluxball MSGW11 95Hz
50.6G Fluxball MSGW11 47Hz
50.6G Fluxball MSGW11 15Hz

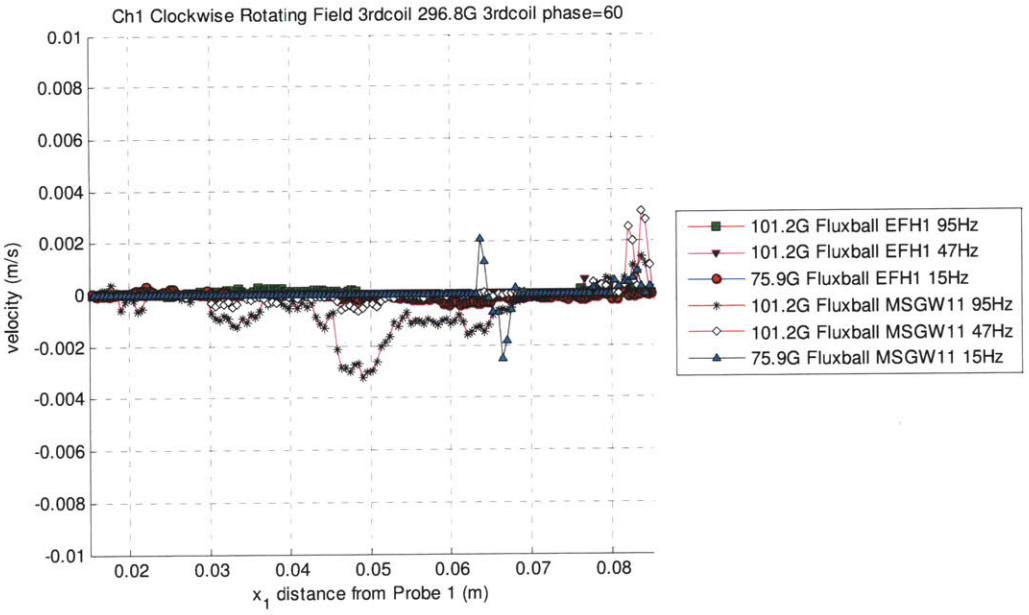
Ch1 Clockwise Rotating Field 3rdcoil 296.8G 3rdcoil phase=60
velocity (m/s)
0.01
0.008
0.006
0.004
0.002
0
-0.002
-0.004
-0.006
-0.008
-0.01
0.02
0.03
0.04
0.05
0.06
0.07
0.08
x1 distance from Probe 1 (m)
101.2G Fluxball EFH1 95Hz
101.2G Fluxball EFH1 47Hz
75.9G Fluxball EFH1 15Hz
101.2G Fluxball MSGW11 95Hz
101.2G Fluxball MSGW11 47Hz
75.9G Fluxball MSGW11 15Hz

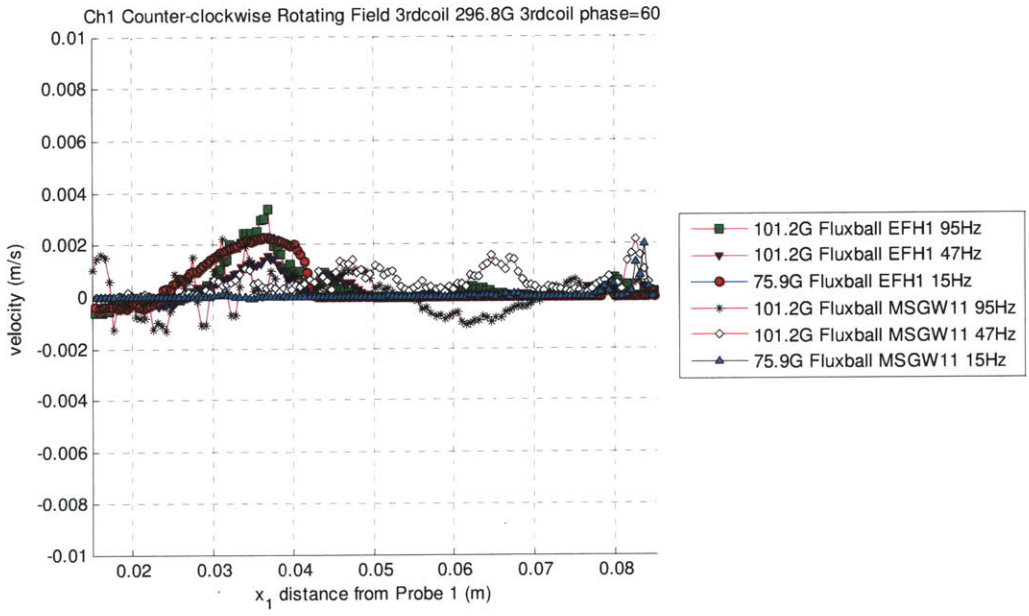
Ch1 Counter-clockwise Rotating Field 3rdcoil 296.8G 3rdcoil phase=60
velocity (m/s)
0.01
0.008
0.006
0.004
0.002
0
-0.002
-0.004
-0.006
-0.008
-0.01
0.02
0.03
0.04
0.05
0.06
0.07
0.08
x1 distance from Probe 1 (m)
101.2G Fluxball EFH1 95Hz
101.2G Fluxball EFH1 47Hz
75.9G Fluxball EFH1 15Hz
101.2G Fluxball MSGW11 95Hz
101.2G Fluxball MSGW11 47Hz
75.9G Fluxball MSGW11 15Hz

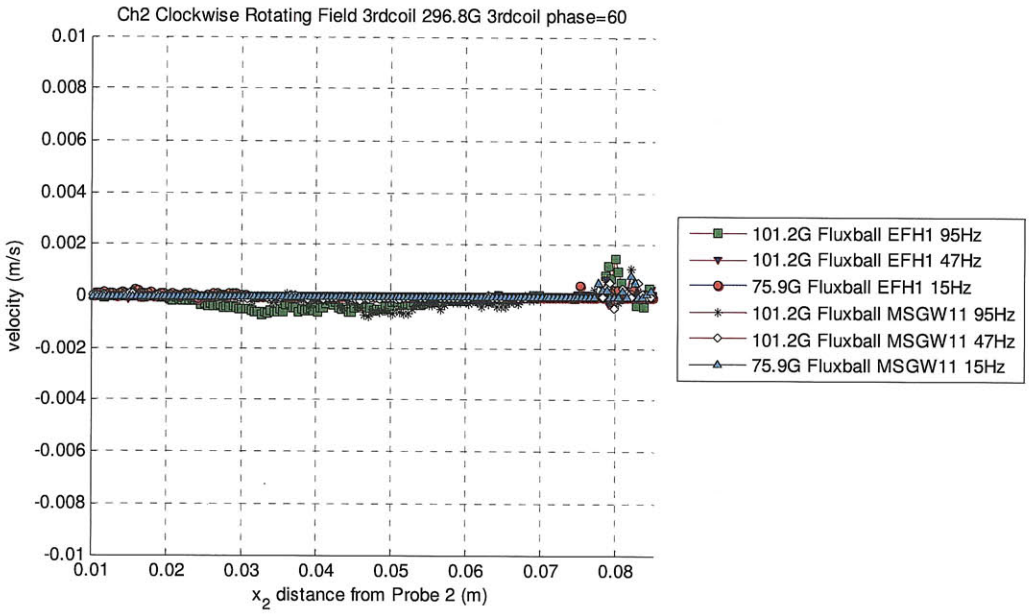
Ch2 Clockwise Rotating Field 3rdcoil 296.8G 3rdcoil phase=60
velocity (m/s)
0.01
0.008
0.006
0.004
0.002
0
-0.002
-0.004
-0.006
-0.008
-0.01
0.01 0.02 0.03 0.04 0.05 0.06 0.07 0.08
x2 distance from Probe 2 (m)
101.2G Fluxball EFH1 95Hz
101.2G Fluxball EFH1 47Hz
75.9G Fluxball EFH1 15Hz
101.2G Fluxball MSGW11 95Hz
101.2G Fluxball MSGW11 47Hz
75.9G Fluxball MSGW11 15Hz

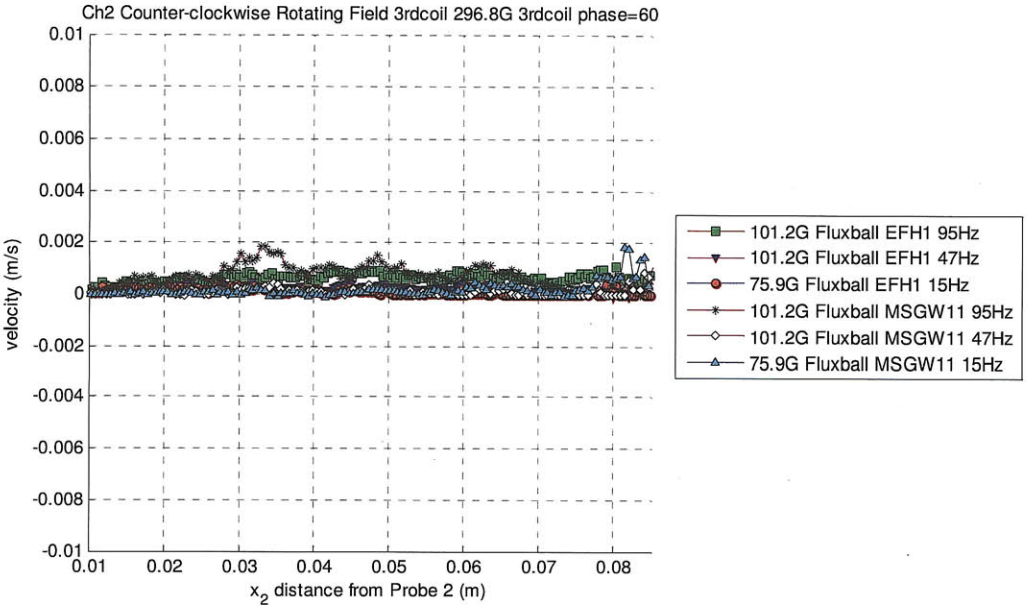
Ch2 Counter-clockwise Rotating Field 3rdcoil 296.8G 3rdcoil phase=60
velocity (m/s)
0.01
0.008
0.006
0.004
0.002
0
-0.002
-0.004
-0.006
-0.008
-0.01
0.01 0.02 0.03 0.04 0.05 0.06 0.07 0.08
x2 distance from Probe 2 (m)
101.2G Fluxball EFH1 95Hz
101.2G Fluxball EFH1 47Hz
75.9G Fluxball EFH1 15Hz
101.2G Fluxball MSGW11 95Hz
101.2G Fluxball MSGW11 47Hz
75.9G Fluxball MSGW11 15Hz

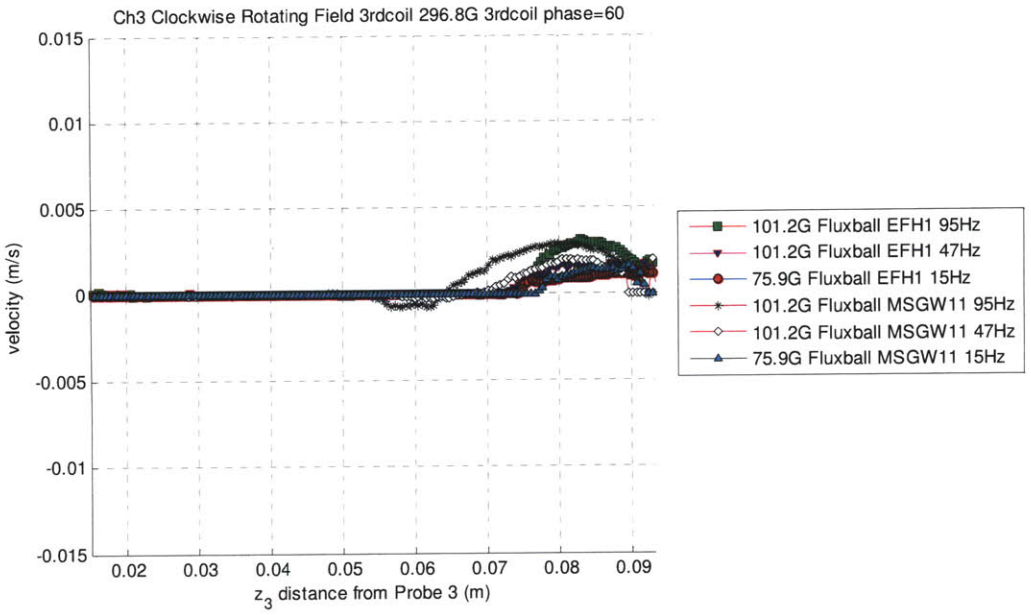
Ch3 Clockwise Rotating Field 3rdcoil 296.8G 3rdcoil phase=60
velocity (m/s)
0.015
0.01
0.005
0
-0.005
-0.01
-0.015
0.02
0.03
0.04
0.05
0.06
0.07
0.08
0.09
z3 distance from Probe 3 (m)
101.2G Fluxball EFH1 95Hz
101.2G Fluxball EFH1 47Hz
75.9G Fluxball EFH1 15Hz
101.2G Fluxball MSGW11 95Hz
101.2G Fluxball MSGW11 47Hz
75.9G Fluxball MSGW11 15Hz

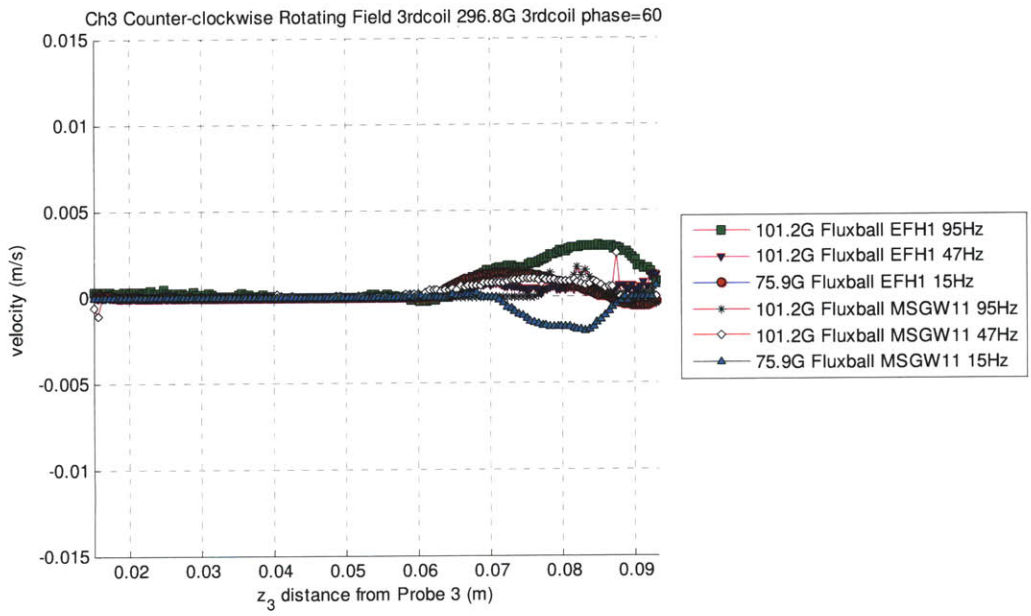
Ch3 Counter-clockwise Rotating Field 3rdcoil 296.8G 3rdcoil phase=60
velocity (m/s)
0.015
0.01
0.005
0
-0.005
-0.01
-0.015
0.02
0.03
0.04
0.05
0.06
0.07
0.08
0.09
z3 distance from Probe 3 (m)
101.2G Fluxball EFH1 95Hz
101.2G Fluxball EFH1 47Hz
75.9G Fluxball EFH1 15Hz
101.2G Fluxball MSGW11 95Hz
101.2G Fluxball MSGW11 47Hz
75.9G Fluxball MSGW11 15Hz

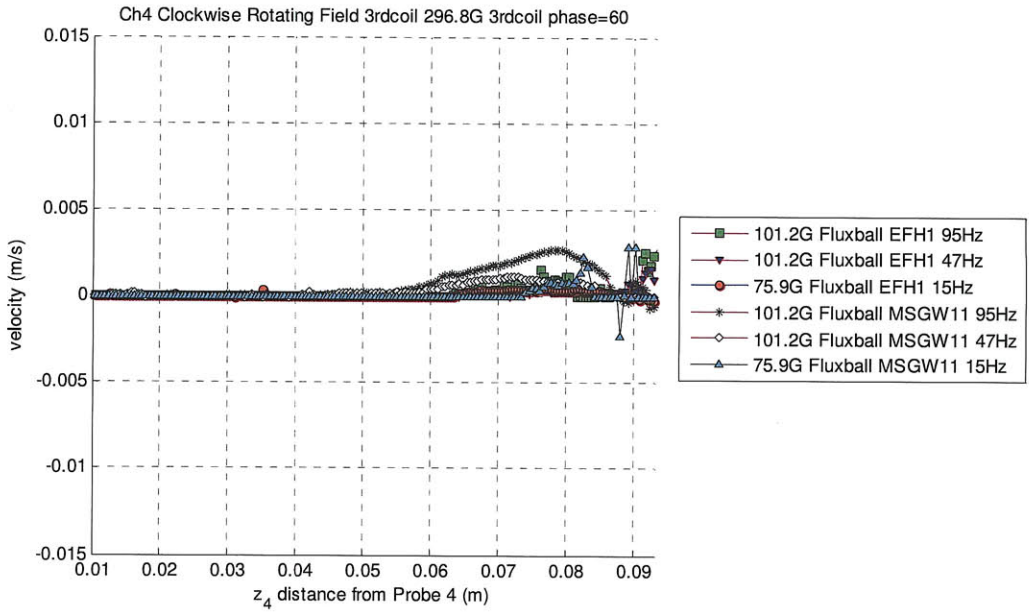
Ch4 Clockwise Rotating Field 3rdcoil 296.8G 3rdcoil phase=60
velocity (m/s)
0.015
0.01
0.005
0
-0.005
-0.01
-0.015
0.01
0.02
0.03
0.04
0.05
0.06
0.07
0.08
0.09
z4 distance from Probe 4 (m)
101.2G Fluxball EFH1 95Hz
101.2G Fluxball EFH1 47Hz
75.9G Fluxball EFH1 15Hz
101.2G Fluxball MSGW11 95Hz
101.2G Fluxball MSGW11 47Hz
75.9G Fluxball MSGW11 15Hz

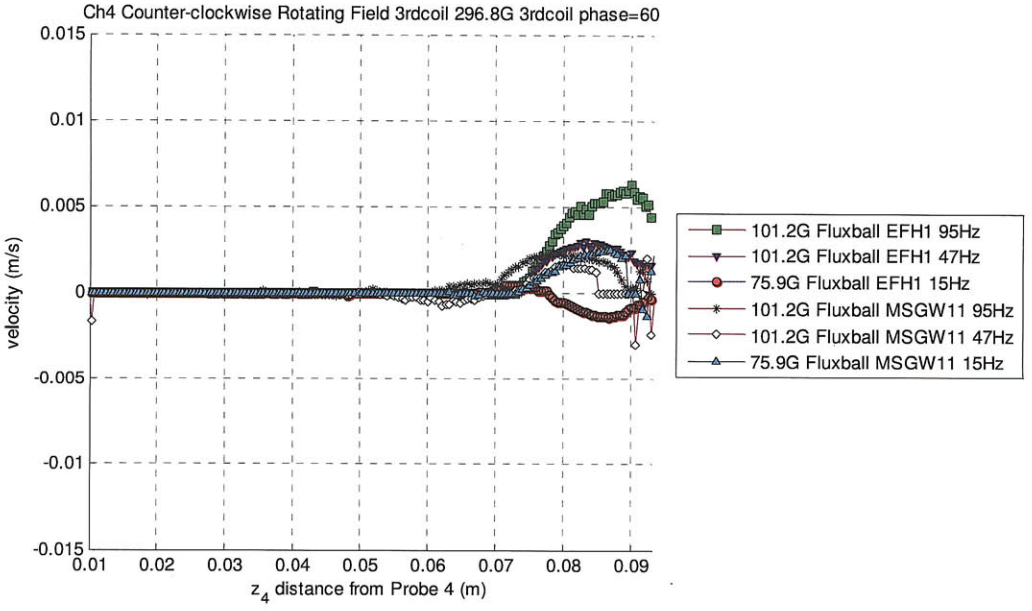
Ch4 Counter-clockwise Rotating Field 3rdcoil 296.8G 3rdcoil phase=60
velocity (m/s)
0.015
0.01
0.005
0
-0.005
-0.01
-0.015
0.01
0.02
0.03
0.04
0.05
0.06
0.07
0.08
0.09
z4 distance from Probe 4 (m)
101.2G Fluxball EFH1 95Hz
101.2G Fluxball EFH1 47Hz
75.9G Fluxball EFH1 15Hz
101.2G Fluxball MSGW11 95Hz
101.2G Fluxball MSGW11 47Hz
75.9G Fluxball MSGW11 15Hz

G11. Comparison of Different Fluids with Third Coil Oscillating at Different Frequencies with Phase Difference=-60 with Respect to Inner Coil

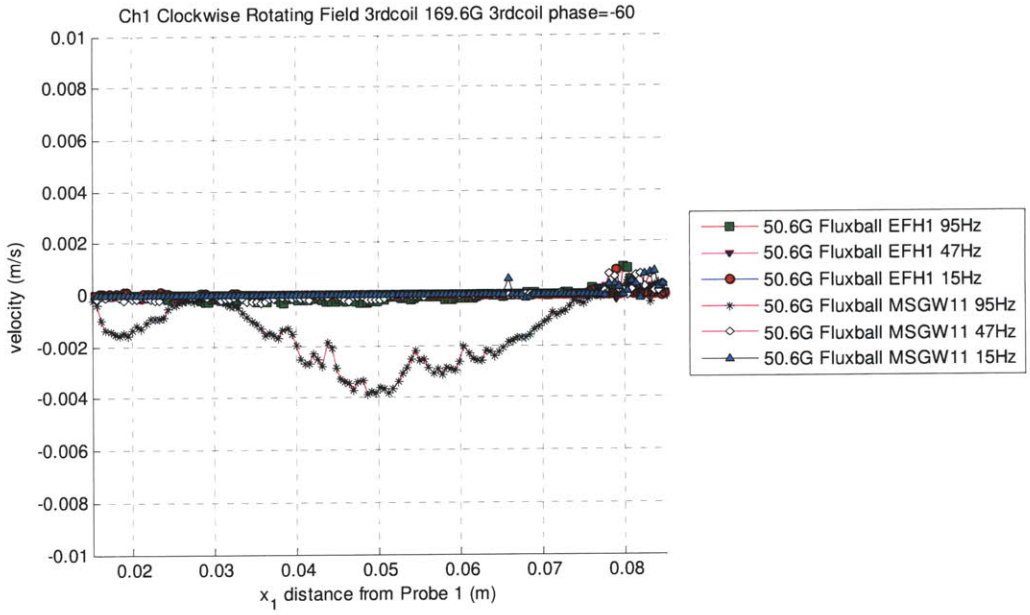

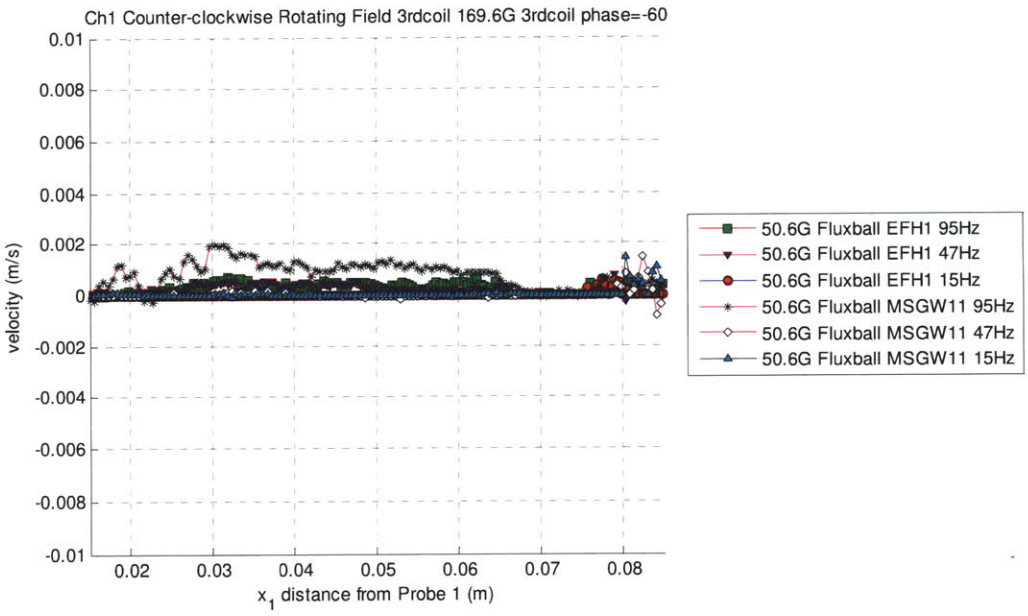

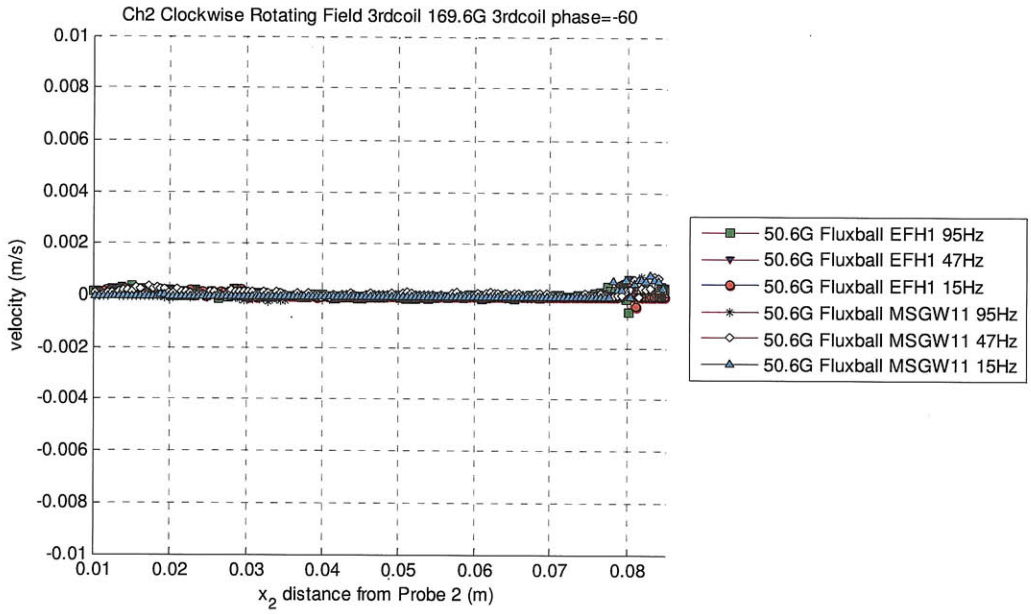
Ch2 Clockwise Rotating Field 3rdcoil 169.6G 3rdcoil phase=-60
velocity (m/s)
0.01
0.008
0.006
0.004
0.002
0
-0.002
-0.004
-0.006
-0.008
-0.01
0.01 0.02 0.03 0.04 0.05 0.06 0.07 0.08
x2 distance from Probe 2 (m)
50.6G Fluxball EFH1 95Hz
50.6G Fluxball EFH1 47Hz
50.6G Fluxball EFH1 15Hz
50.6G Fluxball MSGW11 95Hz
50.6G Fluxball MSGW11 47Hz
50.6G Fluxball MSGW11 15Hz

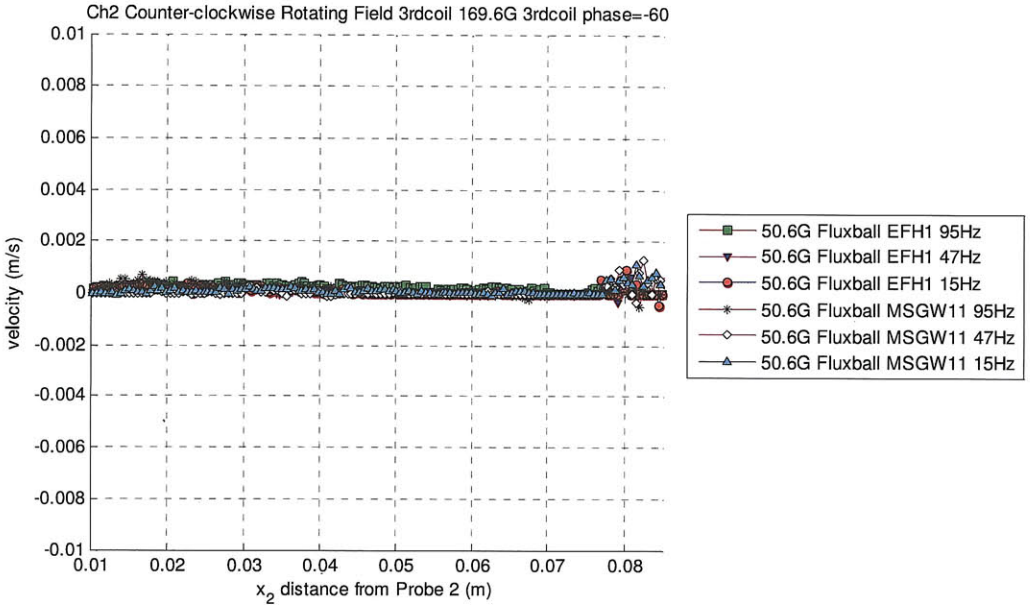
Ch2 Counter-clockwise Rotating Field 3rdcoil 169.6G 3rdcoil phase=-60
velocity (m/s)
0.01
0.008
0.006
0.004
0.002
0
-0.002
-0.004
-0.006
-0.008
-0.01
0.01 0.02 0.03 0.04 0.05 0.06 0.07 0.08
x2 distance from Probe 2 (m)
50.6G Fluxball EFH1 95Hz
50.6G Fluxball EFH1 47Hz
50.6G Fluxball EFH1 15Hz
50.6G Fluxball MSGW11 95Hz
50.6G Fluxball MSGW11 47Hz
50.6G Fluxball MSGW11 15Hz

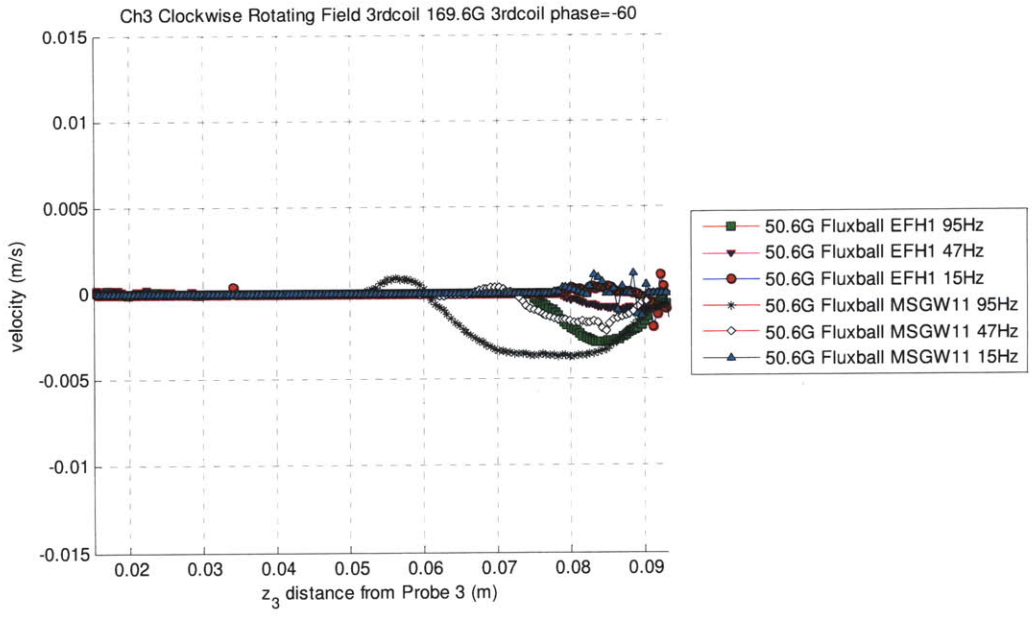
Ch3 Clockwise Rotating Field 3rdcoil 169.6G 3rdcoil phase=-60
velocity (m/s)
0.015
0.01
0.005
0
-0.005
-0.01
-0.015
0.02
0.03
0.04
0.05
0.06
0.07
0.08
0.09
z_3 distance from Probe 3 (m)
50.6G Fluxball EFH1 95Hz
50.6G Fluxball EFH1 47Hz
50.6G Fluxball EFH1 15Hz
50.6G Fluxball MSGW11 95Hz
50.6G Fluxball MSGW11 47Hz
50.6G Fluxball MSGW11 15Hz

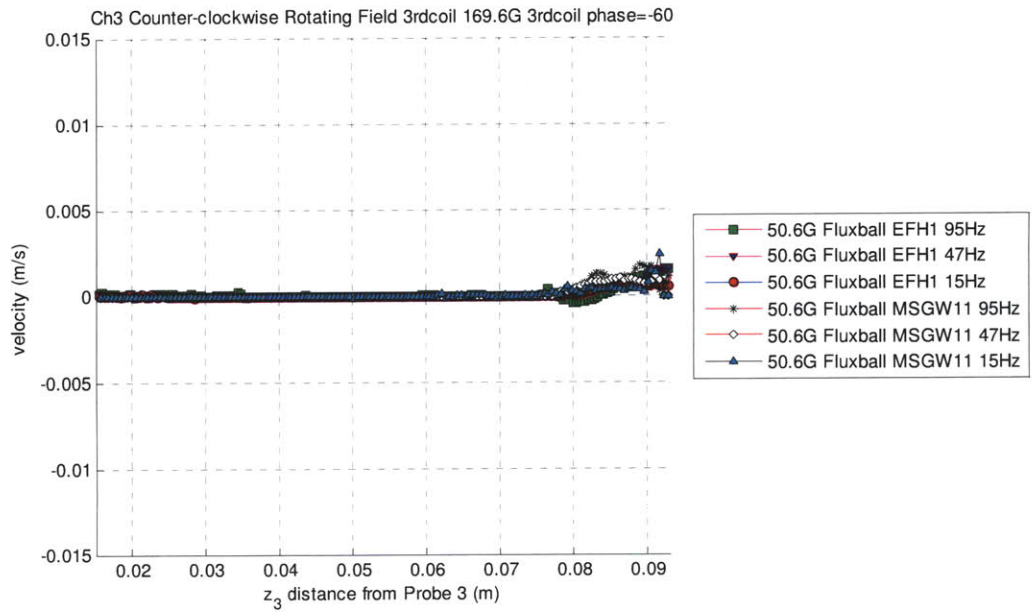
Ch3 Counter-clockwise Rotating Field 3rdcoil 169.6G 3rdcoil phase=-60
velocity (m/s)
0.015
0.01
0.005
0
-0.005
-0.01
-0.015
0.02
0.03
0.04
0.05
0.06
0.07
0.08
0.09
z_3 distance from Probe 3 (m)
50.6G Fluxball EFH1 95Hz
50.6G Fluxball EFH1 47Hz
50.6G Fluxball EFH1 15Hz
50.6G Fluxball MSGW11 95Hz
50.6G Fluxball MSGW11 47Hz
50.6G Fluxball MSGW11 15Hz

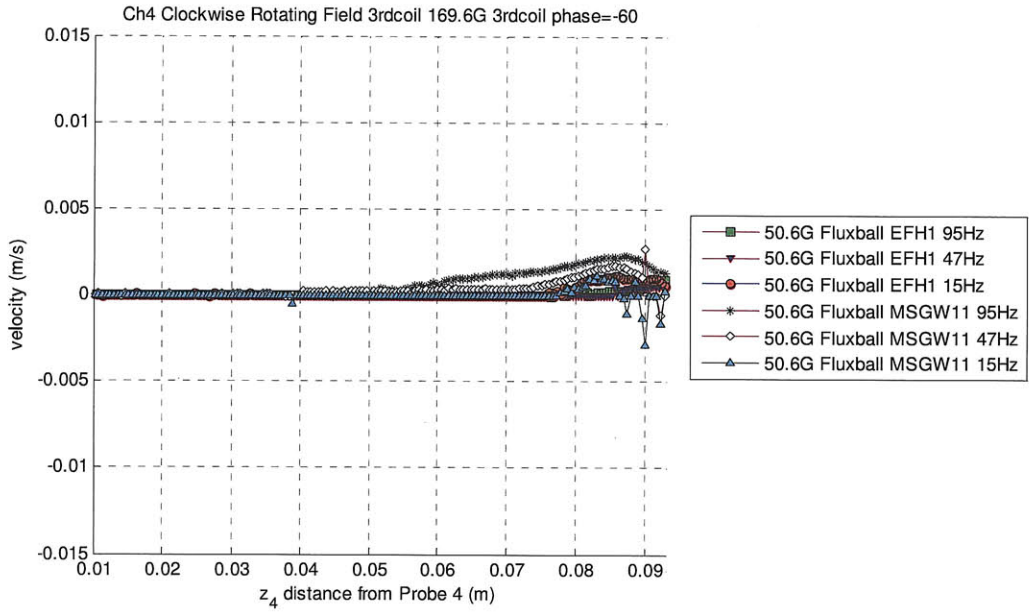
Ch4 Clockwise Rotating Field 3rdcoil 169.6G 3rdcoil phase=-60
0.015
0.01
0.005
0
-0.005
-0.01
-0.015
velocity (m/s)
0.01
0.02
0.03
0.04
0.05
0.06
0.07
0.08
0.09
z4 distance from Probe 4 (m)
50.6G Fluxball EFH1 95Hz
50.6G Fluxball EFH1 47Hz
50.6G Fluxball EFH1 15Hz
50.6G Fluxball MSGW11 95Hz
50.6G Fluxball MSGW11 47Hz
50.6G Fluxball MSGW11 15Hz

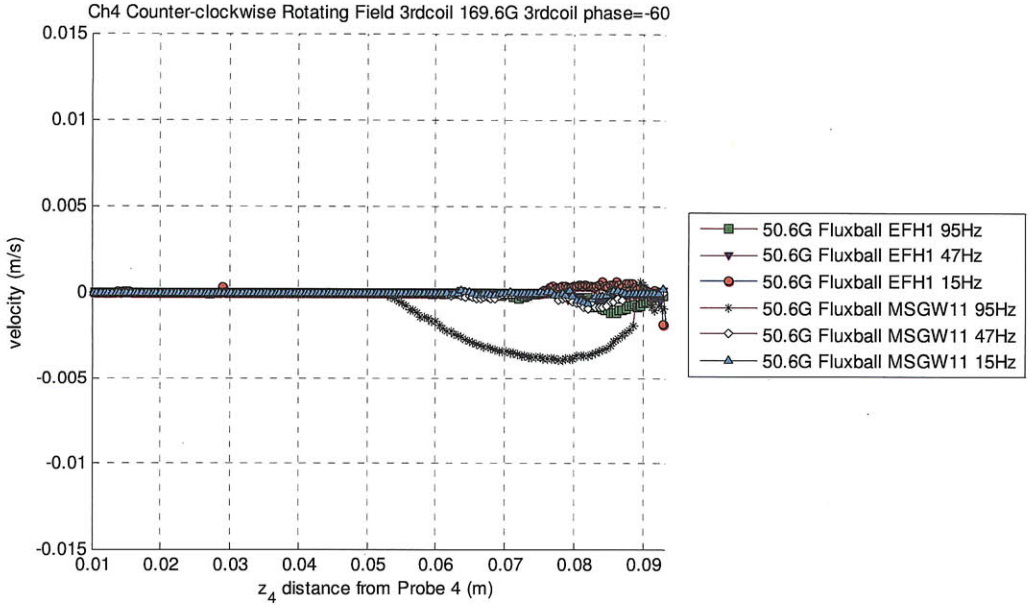
Ch4 Counter-clockwise Rotating Field 3rdcoil 169.6G 3rdcoil phase=-60
0.015
0.01
0.005
0
-0.005
-0.01
-0.015
velocity (m/s)
0.01
0.02
0.03
0.04
0.05
0.06
0.07
0.08
0.09
z4 distance from Probe 4 (m)
50.6G Fluxball EFH1 95Hz
50.6G Fluxball EFH1 47Hz
50.6G Fluxball EFH1 15Hz
50.6G Fluxball MSGW11 95Hz
50.6G Fluxball MSGW11 47Hz
50.6G Fluxball MSGW11 15Hz

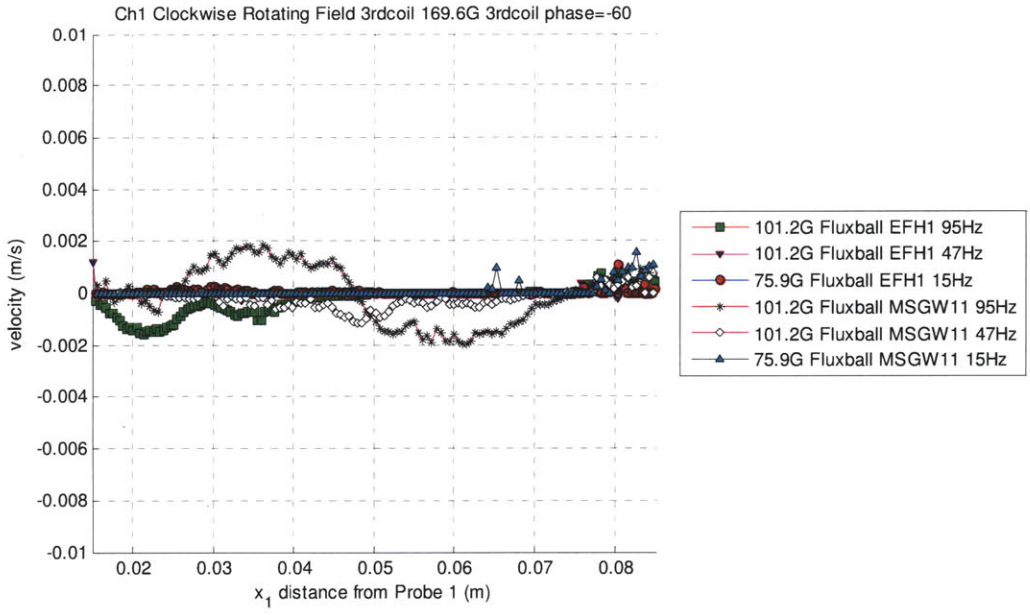
Ch1 Clockwise Rotating Field 3rdcoil 169.6G 3rdcoil phase=-60
velocity (m/s)
0.01
0.008
0.006
0.004
0.002
0
-0.002
-0.004
-0.006
-0.008
-0.01
0.02
0.03
0.04
0.05
0.06
0.07
0.08
x1 distance from Probe 1 (m)
101.2G Fluxball EFH1 95Hz
101.2G Fluxball EFH1 47Hz
75.9G Fluxball EFH1 15Hz
101.2G Fluxball MSGW11 95Hz
101.2G Fluxball MSGW11 47Hz
75.9G Fluxball MSGW11 15Hz

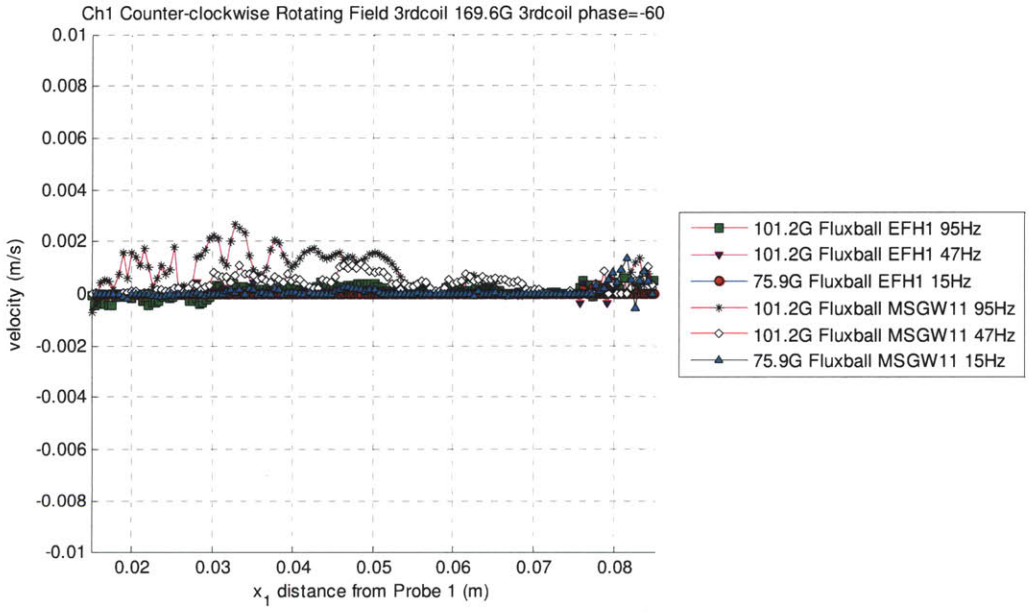
Ch1 Counter-clockwise Rotating Field 3rdcoil 169.6G 3rdcoil phase=-60
velocity (m/s)
0.01
0.008
0.006
0.004
0.002
0
-0.002
-0.004
-0.006
-0.008
-0.01
0.02
0.03
0.04
0.05
0.06
0.07
0.08
x1 distance from Probe 1 (m)
101.2G Fluxball EFH1 95Hz
101.2G Fluxball EFH1 47Hz
75.9G Fluxball EFH1 15Hz
101.2G Fluxball MSGW11 95Hz
101.2G Fluxball MSGW11 47Hz
75.9G Fluxball MSGW11 15Hz

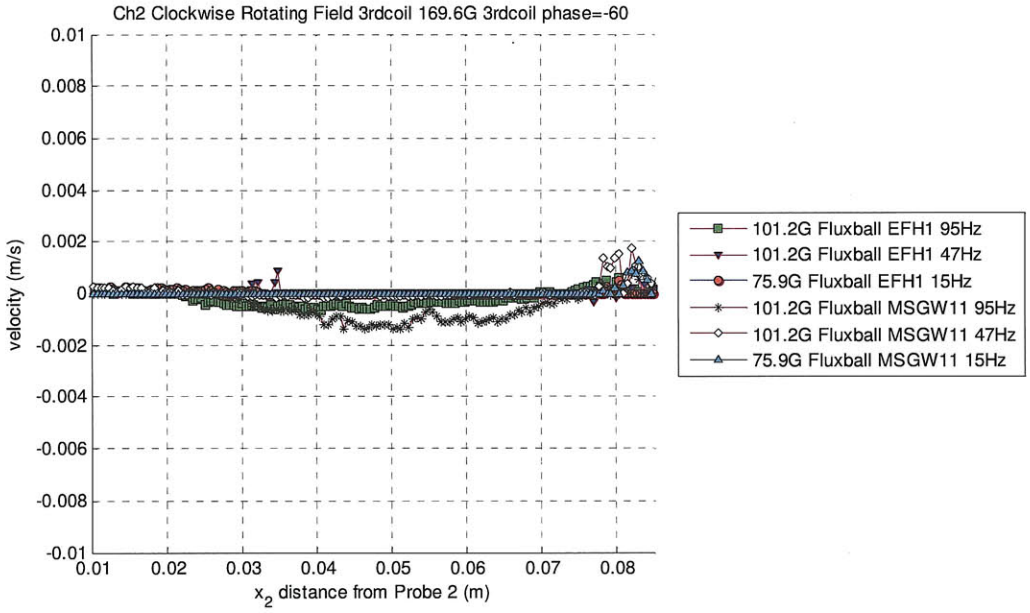
Ch2 Clockwise Rotating Field 3rdcoil 169.6G 3rdcoil phase=-60
velocity (m/s)
0.01
0.008
0.006
0.004
0.002
0
-0.002
-0.004
-0.006
-0.008
-0.01
0.01 0.02 0.03 0.04 0.05 0.06 0.07 0.08
x2 distance from Probe 2 (m)
101.2G Fluxball EFH1 95Hz
101.2G Fluxball EFH1 47Hz
75.9G Fluxball EFH1 15Hz
101.2G Fluxball MSGW11 95Hz
101.2G Fluxball MSGW11 47Hz
75.9G Fluxball MSGW11 15Hz

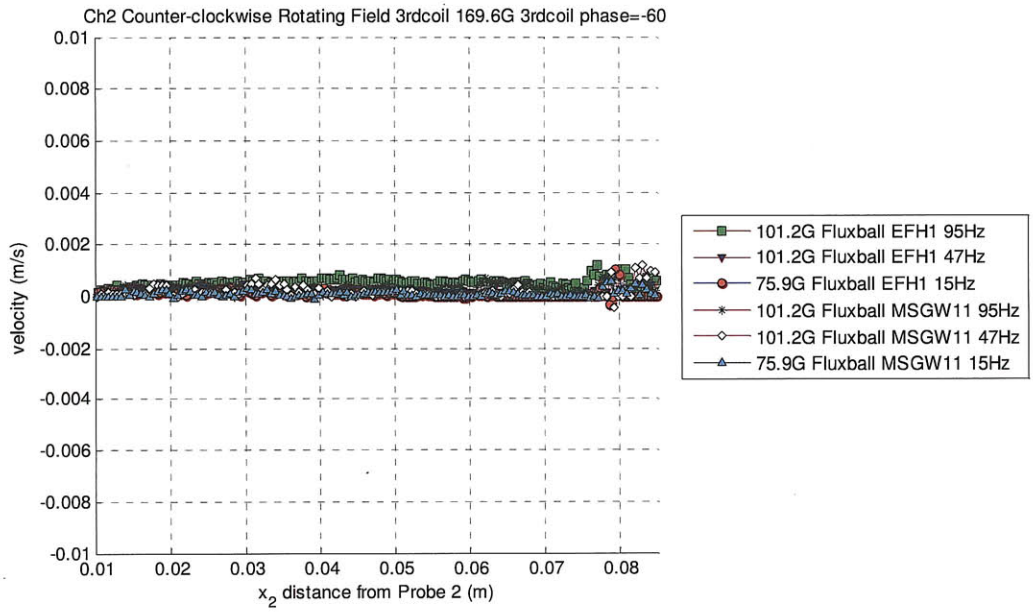
Ch2 Counter-clockwise Rotating Field 3rdcoil 169.6G 3rdcoil phase=-60
velocity (m/s)
0.01
0.008
0.006
0.004
0.002
0
-0.002
-0.004
-0.006
-0.008
-0.01
0.01 0.02 0.03 0.04 0.05 0.06 0.07 0.08
x2 distance from Probe 2 (m)
101.2G Fluxball EFH1 95Hz
101.2G Fluxball EFH1 47Hz
75.9G Fluxball EFH1 15Hz
101.2G Fluxball MSGW11 95Hz
101.2G Fluxball MSGW11 47Hz
75.9G Fluxball MSGW11 15Hz

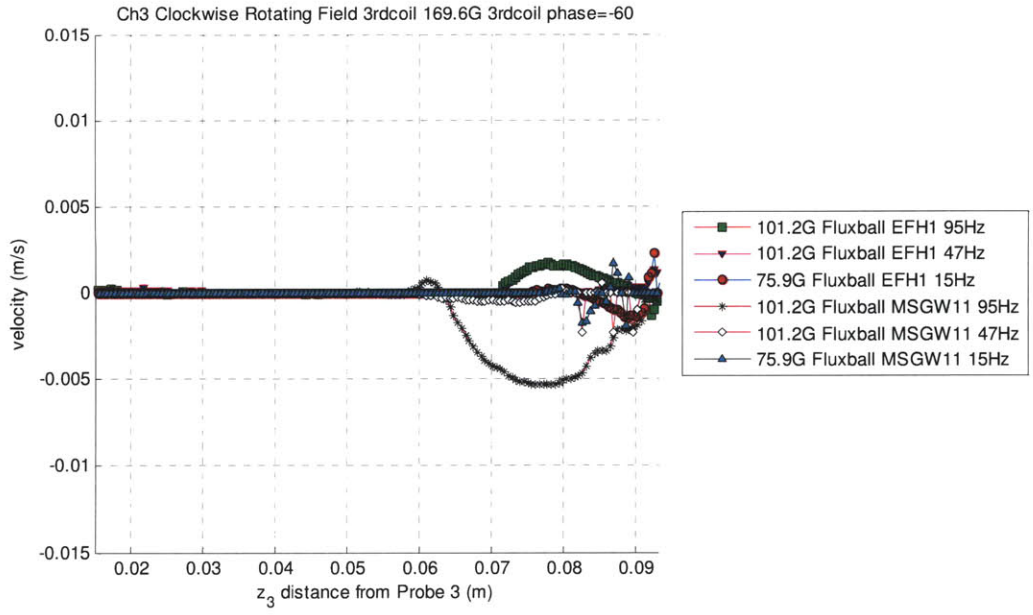
Ch3 Clockwise Rotating Field 3rdcoil 169.6G 3rdcoil phase=-60
velocity (m/s)
0.015
0.01
0.005
0
-0.005
-0.01
-0.015
0.02
0.03
0.04
0.05
0.06
0.07
0.08
0.09
z3 distance from Probe 3 (m)
101.2G Fluxball EFH1 95Hz
101.2G Fluxball EFH1 47Hz
75.9G Fluxball EFH1 15Hz
101.2G Fluxball MSGW11 95Hz
101.2G Fluxball MSGW11 47Hz
75.9G Fluxball MSGW11 15Hz

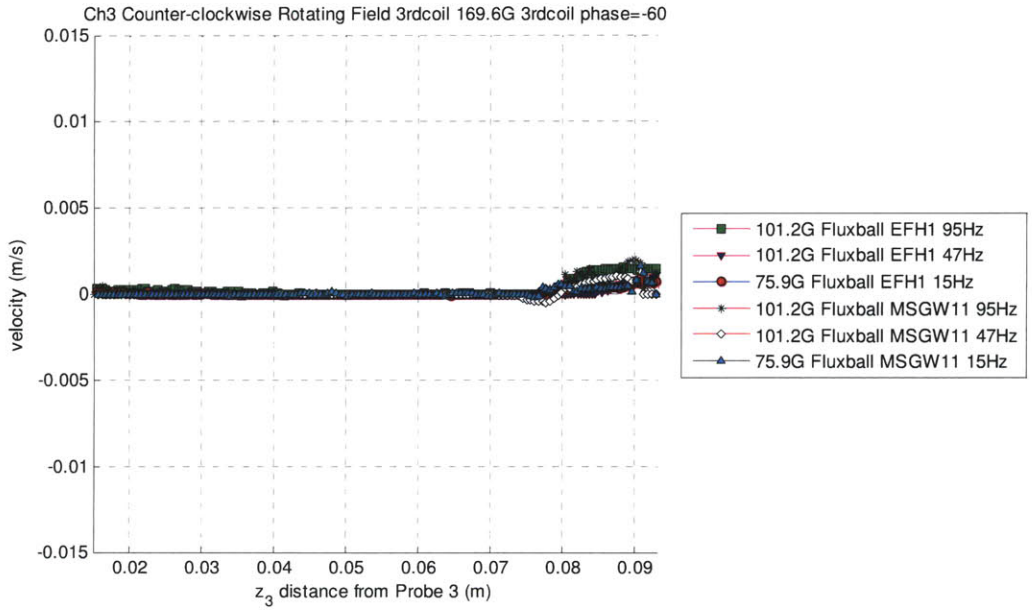
Ch3 Counter-clockwise Rotating Field 3rdcoil 169.6G 3rdcoil phase=-60
velocity (m/s)
0.015
0.01
0.005
0
-0.005
-0.01
-0.015
0.02
0.03
0.04
0.05
0.06
0.07
0.08
0.09
z3 distance from Probe 3 (m)
101.2G Fluxball EFH1 95Hz
101.2G Fluxball EFH1 47Hz
75.9G Fluxball EFH1 15Hz
101.2G Fluxball MSGW11 95Hz
101.2G Fluxball MSGW11 47Hz
75.9G Fluxball MSGW11 15Hz

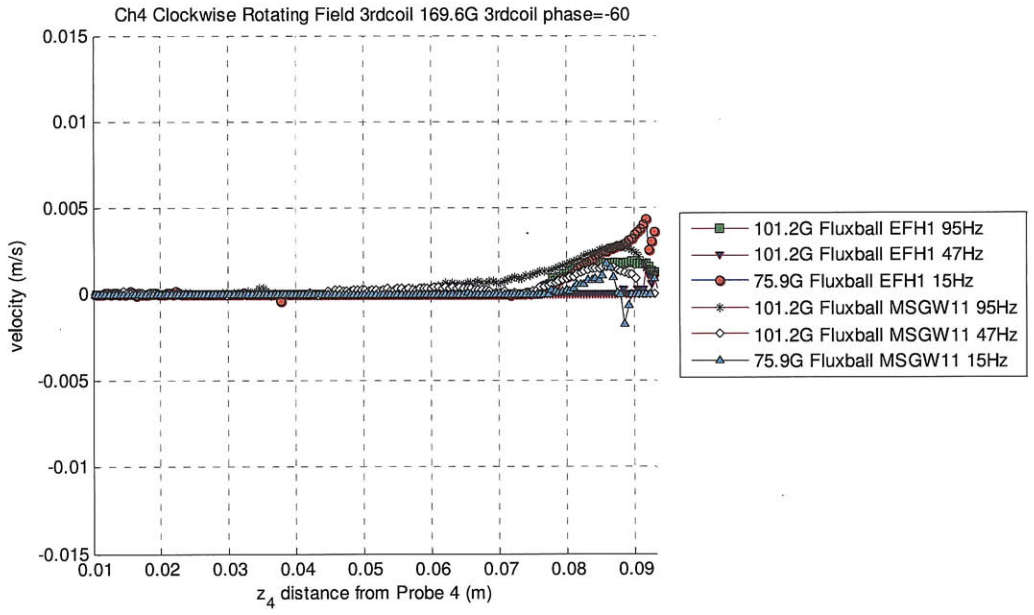
Ch4 Clockwise Rotating Field 3rdcoil 169.6G 3rdcoil phase=-60
velocity (m/s)
0.015
0.01
0.005
0
-0.005
-0.01
-0.015
0.01
0.02
0.03
0.04
0.05
0.06
0.07
0.08
0.09
z4 distance from Probe 4 (m)
101.2G Fluxball EFH1 95Hz
101.2G Fluxball EFH1 47Hz
75.9G Fluxball EFH1 15Hz
101.2G Fluxball MSGW11 95Hz
101.2G Fluxball MSGW11 47Hz
75.9G Fluxball MSGW11 15Hz

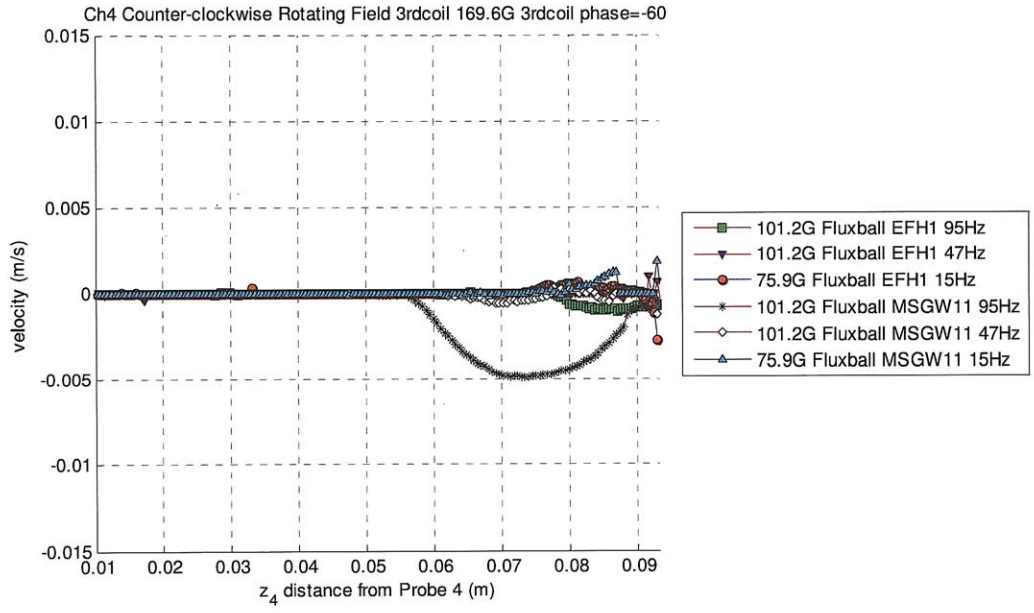
Ch4 Counter-clockwise Rotating Field 3rdcoil 169.6G 3rdcoil phase=-60
velocity (m/s)
0.015
0.01
0.005
0
-0.005
-0.01
-0.015
0.01
0.02
0.03
0.04
0.05
0.06
0.07
0.08
0.09
z4 distance from Probe 4 (m)
101.2G Fluxball EFH1 95Hz
101.2G Fluxball EFH1 47Hz
75.9G Fluxball EFH1 15Hz
101.2G Fluxball MSGW11 95Hz
101.2G Fluxball MSGW11 47Hz
75.9G Fluxball MSGW11 15Hz

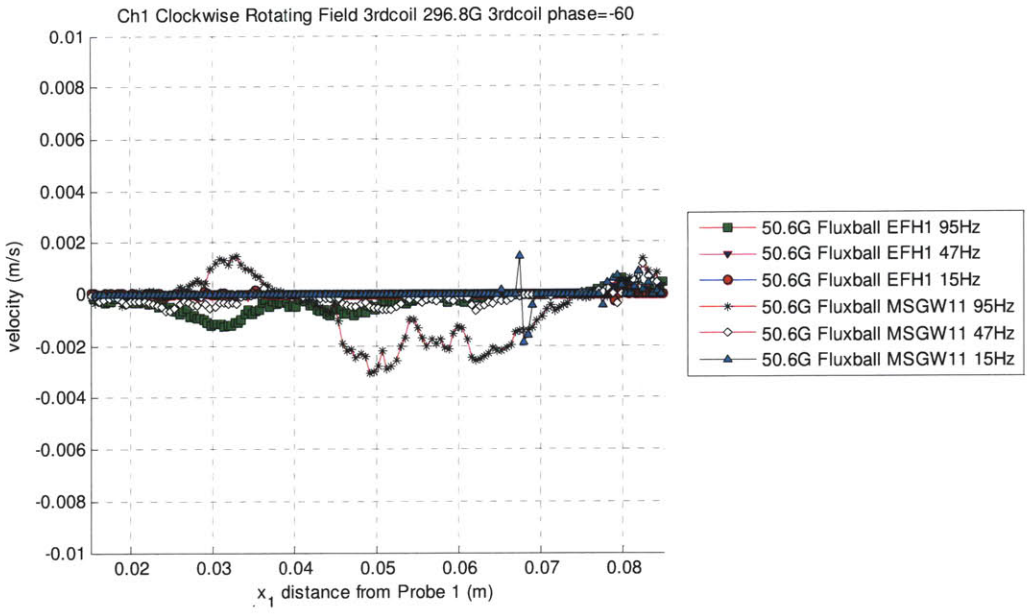
Ch1 Clockwise Rotating Field 3rdcoil 296.8G 3rdcoil phase=-60
velocity (m/s)
0.01
0.008
0.006
0.004
0.002
0
-0.002
-0.004
-0.006
-0.008
-0.01
0.02
0.03
0.04
0.05
0.06
0.07
0.08
x1 distance from Probe 1 (m)
50.6G Fluxball EFH1 95Hz
50.6G Fluxball EFH1 47Hz
50.6G Fluxball EFH1 15Hz
50.6G Fluxball MSGW11 95Hz
50.6G Fluxball MSGW11 47Hz
50.6G Fluxball MSGW11 15Hz

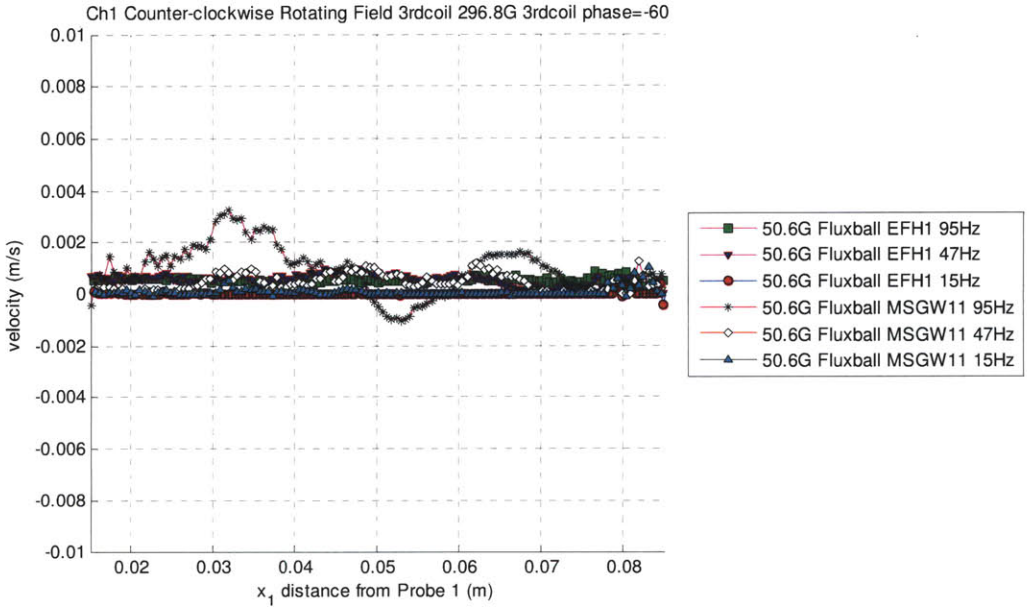
Ch1 Counter-clockwise Rotating Field 3rdcoil 296.8G 3rdcoil phase=-60
velocity (m/s)
0.01
0.008
0.006
0.004
0.002
0
-0.002
-0.004
-0.006
-0.008
-0.01
0.02
0.03
0.04
0.05
0.06
0.07
0.08
x1 distance from Probe 1 (m)
50.6G Fluxball EFH1 95Hz
50.6G Fluxball EFH1 47Hz
50.6G Fluxball EFH1 15Hz
50.6G Fluxball MSGW11 95Hz
50.6G Fluxball MSGW11 47Hz
50.6G Fluxball MSGW11 15Hz

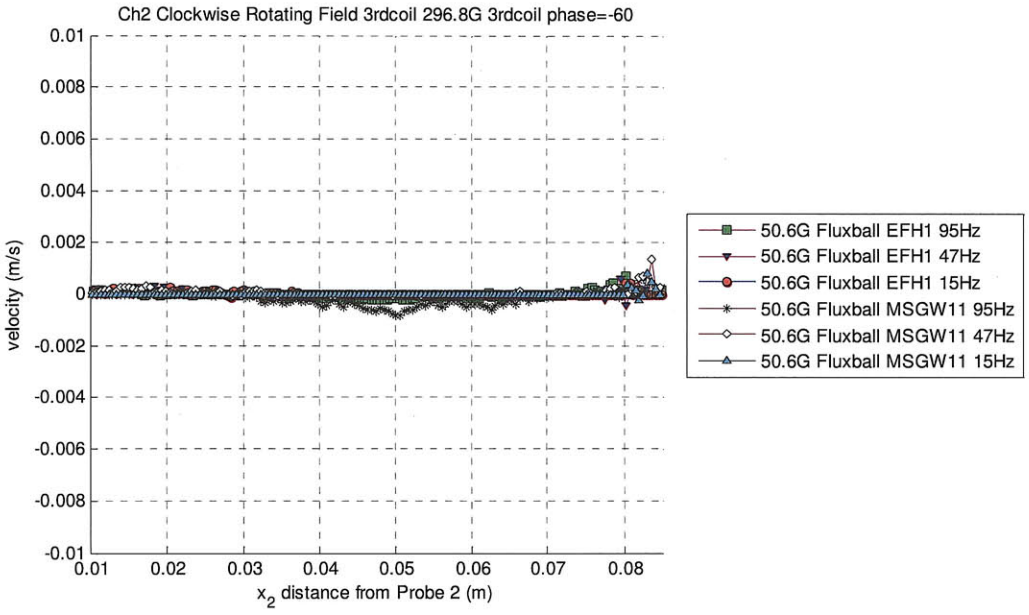
Ch2 Clockwise Rotating Field 3rdcoil 296.8G 3rdcoil phase=-60
velocity (m/s)
0.01
0.008
0.006
0.004
0.002
0
-0.002
-0.004
-0.006
-0.008
-0.01
0.01 0.02 0.03 0.04 0.05 0.06 0.07 0.08
x2 distance from Probe 2 (m)
50.6G Fluxball EFH1 95Hz
50.6G Fluxball EFH1 47Hz
50.6G Fluxball EFH1 15Hz
50.6G Fluxball MSGW11 95Hz
50.6G Fluxball MSGW11 47Hz
50.6G Fluxball MSGW11 15Hz

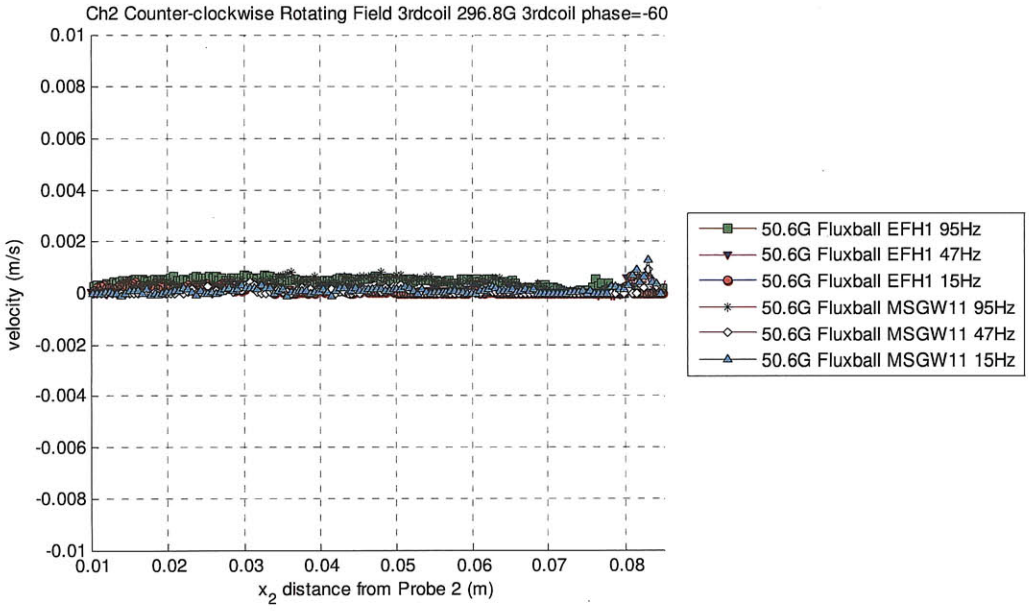
Ch2 Counter-clockwise Rotating Field 3rdcoil 296.8G 3rdcoil phase=-60
velocity (m/s)
0.01
0.008
0.006
0.004
0.002
0
-0.002
-0.004
-0.006
-0.008
-0.01
0.01 0.02 0.03 0.04 0.05 0.06 0.07 0.08
x2 distance from Probe 2 (m)
50.6G Fluxball EFH1 95Hz
50.6G Fluxball EFH1 47Hz
50.6G Fluxball EFH1 15Hz
50.6G Fluxball MSGW11 95Hz
50.6G Fluxball MSGW11 47Hz
50.6G Fluxball MSGW11 15Hz

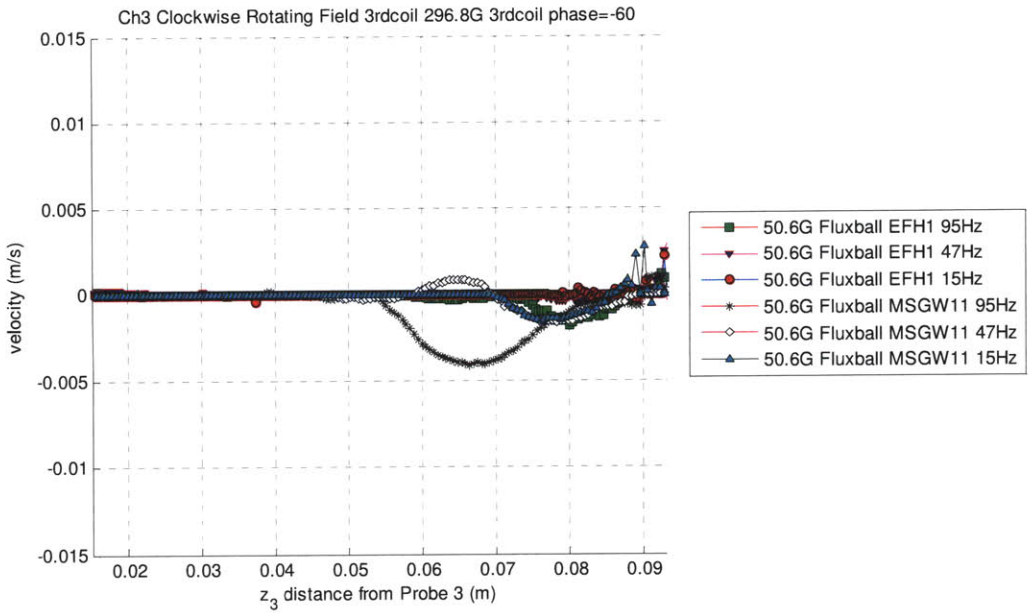
Ch3 Clockwise Rotating Field 3rdcoil 296.8G 3rdcoil phase=-60
velocity (m/s)
0.015
0.01
0.005
0
-0.005
-0.01
-0.015
0.02
0.03
0.04
0.05
0.06
0.07
0.08
0.09
z_3 distance from Probe 3 (m)
50.6G Fluxball EFH1 95Hz
50.6G Fluxball EFH1 47Hz
50.6G Fluxball EFH1 15Hz
50.6G Fluxball MSGW11 95Hz
50.6G Fluxball MSGW11 47Hz
50.6G Fluxball MSGW11 15Hz

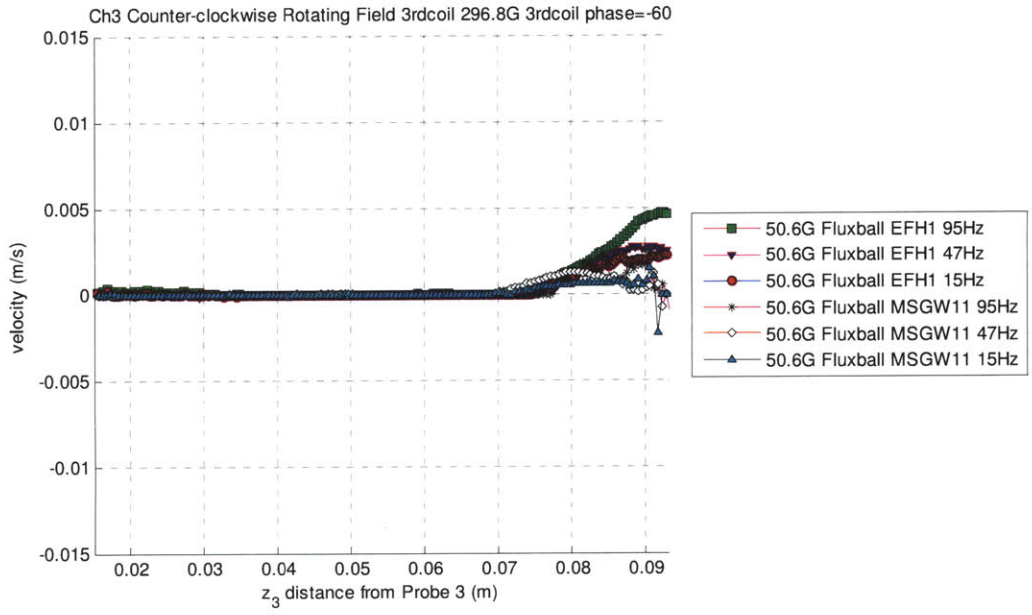
Ch3 Counter-clockwise Rotating Field 3rdcoil 296.8G 3rdcoil phase=-60
velocity (m/s)
0.015
0.01
0.005
0
-0.005
-0.01
-0.015
0.02
0.03
0.04
0.05
0.06
0.07
0.08
0.09
z_3 distance from Probe 3 (m)
50.6G Fluxball EFH1 95Hz
50.6G Fluxball EFH1 47Hz
50.6G Fluxball EFH1 15Hz
50.6G Fluxball MSGW11 95Hz
50.6G Fluxball MSGW11 47Hz
50.6G Fluxball MSGW11 15Hz

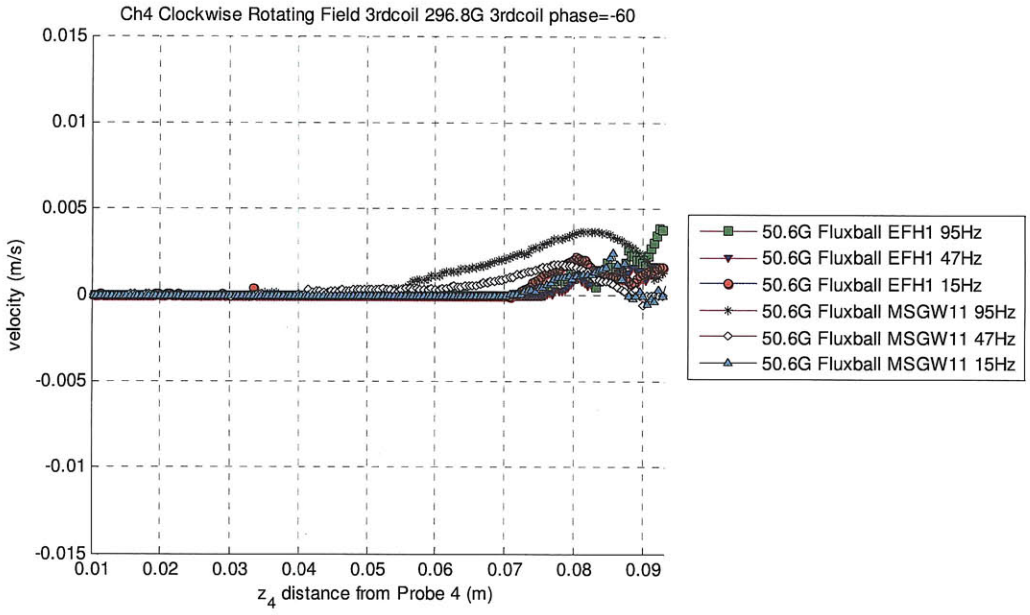
Ch4 Clockwise Rotating Field 3rdcoil 296.8G 3rdcoil phase=-60
velocity (m/s)
0.015
0.01
0.005
0
-0.005
-0.01
-0.015
0.01
0.02
0.03
0.04
0.05
0.06
0.07
0.08
0.09
z4 distance from Probe 4 (m)
50.6G Fluxball EFH1 95Hz
50.6G Fluxball EFH1 47Hz
50.6G Fluxball EFH1 15Hz
50.6G Fluxball MSGW11 95Hz
50.6G Fluxball MSGW11 47Hz
50.6G Fluxball MSGW11 15Hz

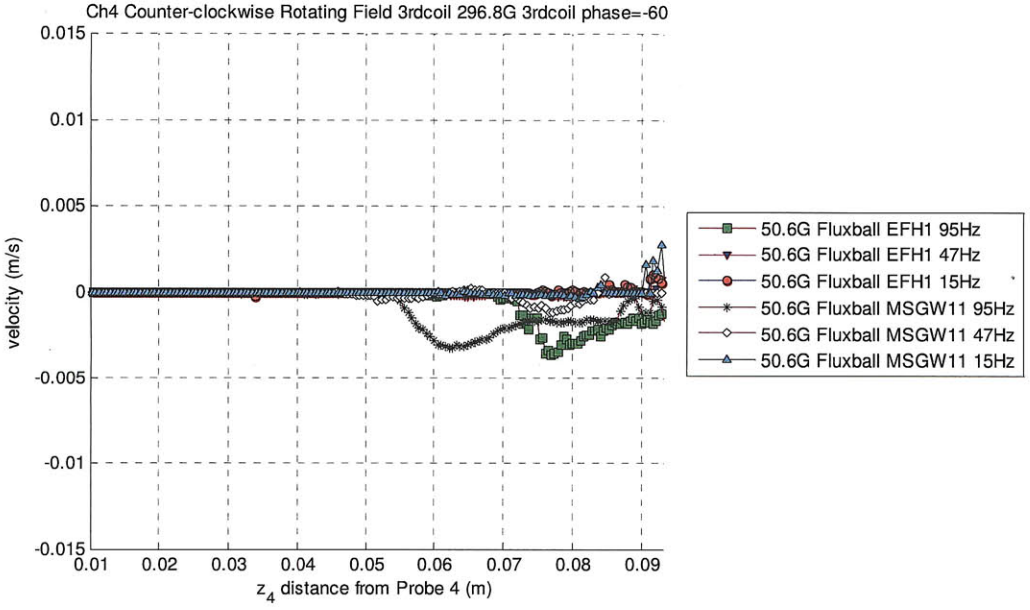
Ch4 Counter-clockwise Rotating Field 3rdcoil 296.8G 3rdcoil phase=-60
velocity (m/s)
0.015
0.01
0.005
0
-0.005
-0.01
-0.015
0.01
0.02
0.03
0.04
0.05
0.06
0.07
0.08
0.09
z4 distance from Probe 4 (m)
50.6G Fluxball EFH1 95Hz
50.6G Fluxball EFH1 47Hz
50.6G Fluxball EFH1 15Hz
50.6G Fluxball MSGW11 95Hz
50.6G Fluxball MSGW11 47Hz
50.6G Fluxball MSGW11 15Hz

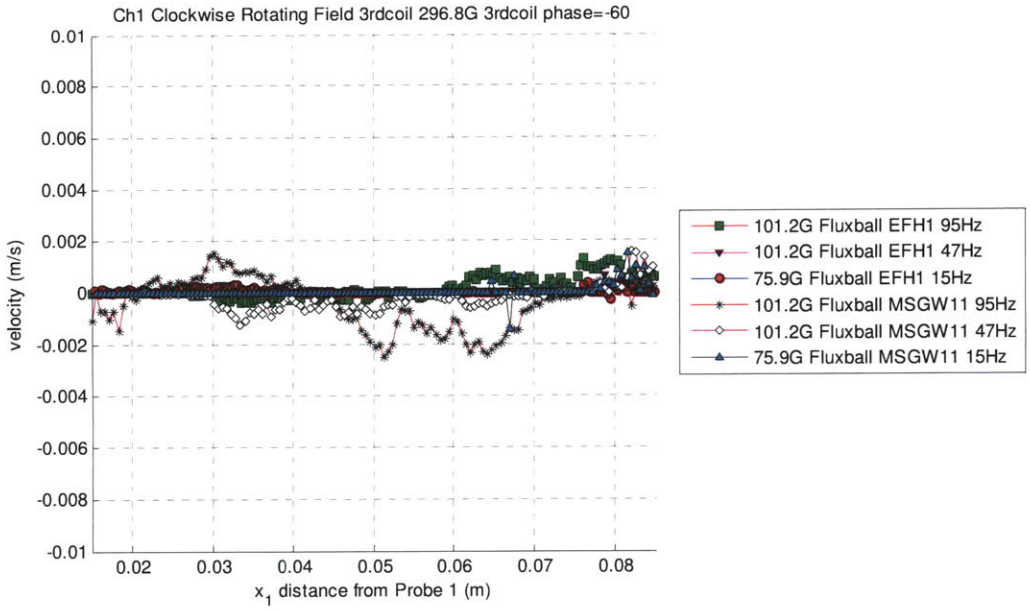
Ch1 Clockwise Rotating Field 3rdcoil 296.8G 3rdcoil phase=-60
velocity (m/s)
0.01
0.008
0.006
0.004
0.002
0
-0.002
-0.004
-0.006
-0.008
-0.01
0.02
0.03
0.04
0.05
0.06
0.07
0.08
x1 distance from Probe 1 (m)
101.2G Fluxball EFH1 95Hz
101.2G Fluxball EFH1 47Hz
75.9G Fluxball EFH1 15Hz
101.2G Fluxball MSGW11 95Hz
101.2G Fluxball MSGW11 47Hz
75.9G Fluxball MSGW11 15Hz

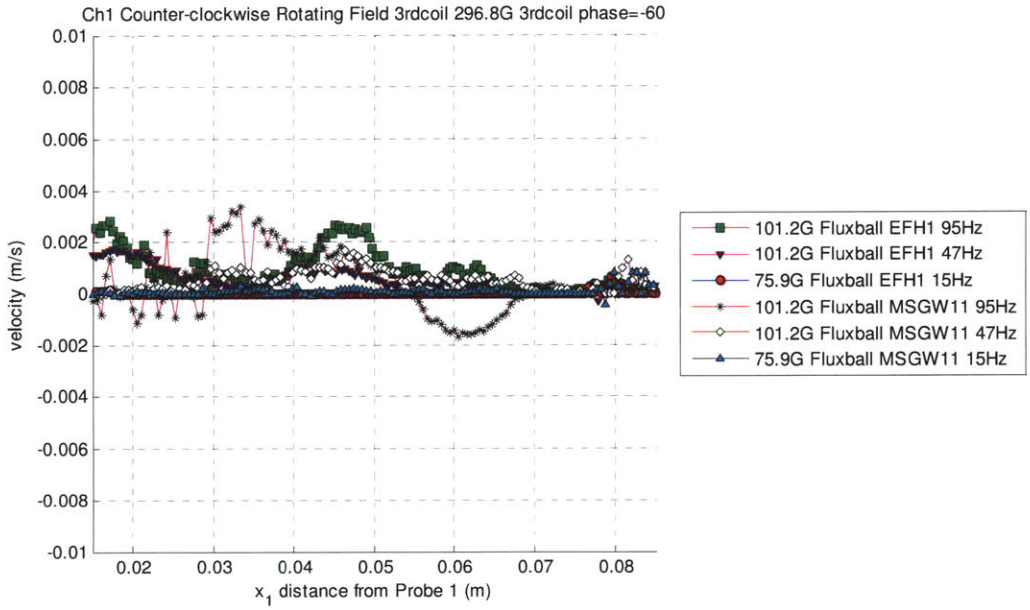
Ch1 Counter-clockwise Rotating Field 3rdcoil 296.8G 3rdcoil phase=-60
velocity (m/s)
0.01
0.008
0.006
0.004
0.002
0
-0.002
-0.004
-0.006
-0.008
-0.01
0.02
0.03
0.04
0.05
0.06
0.07
0.08
x1 distance from Probe 1 (m)
101.2G Fluxball EFH1 95Hz
101.2G Fluxball EFH1 47Hz
75.9G Fluxball EFH1 15Hz
101.2G Fluxball MSGW11 95Hz
101.2G Fluxball MSGW11 47Hz
75.9G Fluxball MSGW11 15Hz

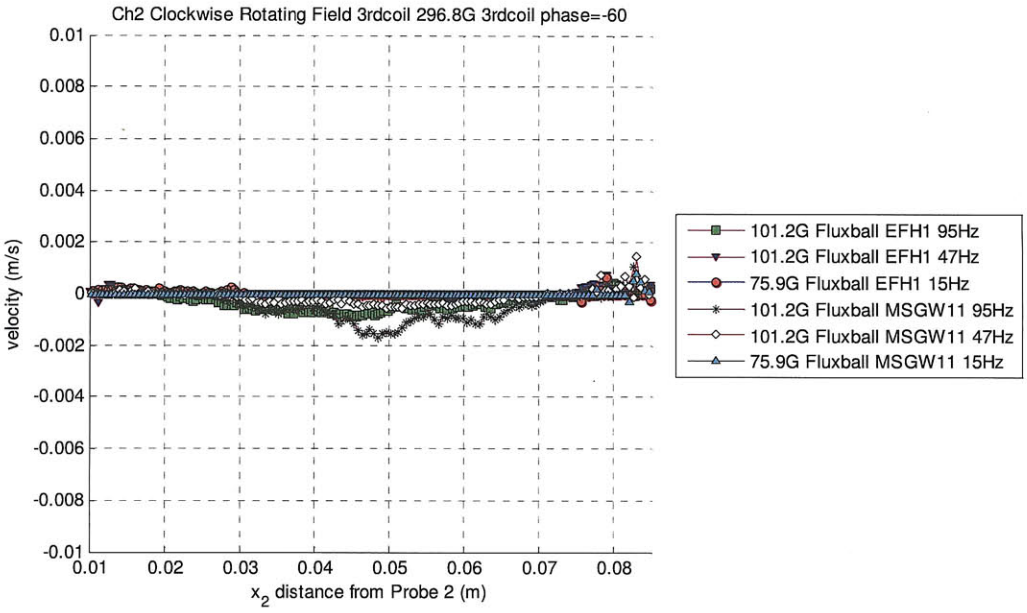
Ch2 Clockwise Rotating Field 3rdcoil 296.8G 3rdcoil phase=-60
velocity (m/s)
0.01
0.008
0.006
0.004
0.002
0
-0.002
-0.004
-0.006
-0.008
-0.01
0.01 0.02 0.03 0.04 0.05 0.06 0.07 0.08
x2 distance from Probe 2 (m)
101.2G Fluxball EFH1 95Hz
101.2G Fluxball EFH1 47Hz
75.9G Fluxball EFH1 15Hz
101.2G Fluxball MSGW11 95Hz
101.2G Fluxball MSGW11 47Hz
75.9G Fluxball MSGW11 15Hz

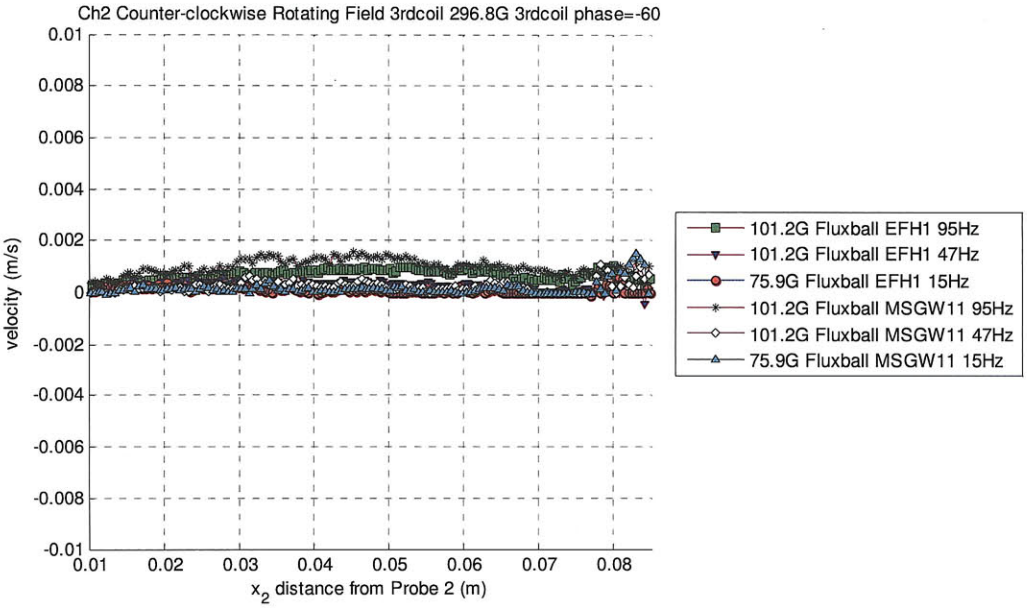
Ch2 Counter-clockwise Rotating Field 3rdcoil 296.8G 3rdcoil phase=-60
velocity (m/s)
0.01
0.008
0.006
0.004
0.002
0
-0.002
-0.004
-0.006
-0.008
-0.01
0.01 0.02 0.03 0.04 0.05 0.06 0.07 0.08
x2 distance from Probe 2 (m)
101.2G Fluxball EFH1 95Hz
101.2G Fluxball EFH1 47Hz
75.9G Fluxball EFH1 15Hz
101.2G Fluxball MSGW11 95Hz
101.2G Fluxball MSGW11 47Hz
75.9G Fluxball MSGW11 15Hz

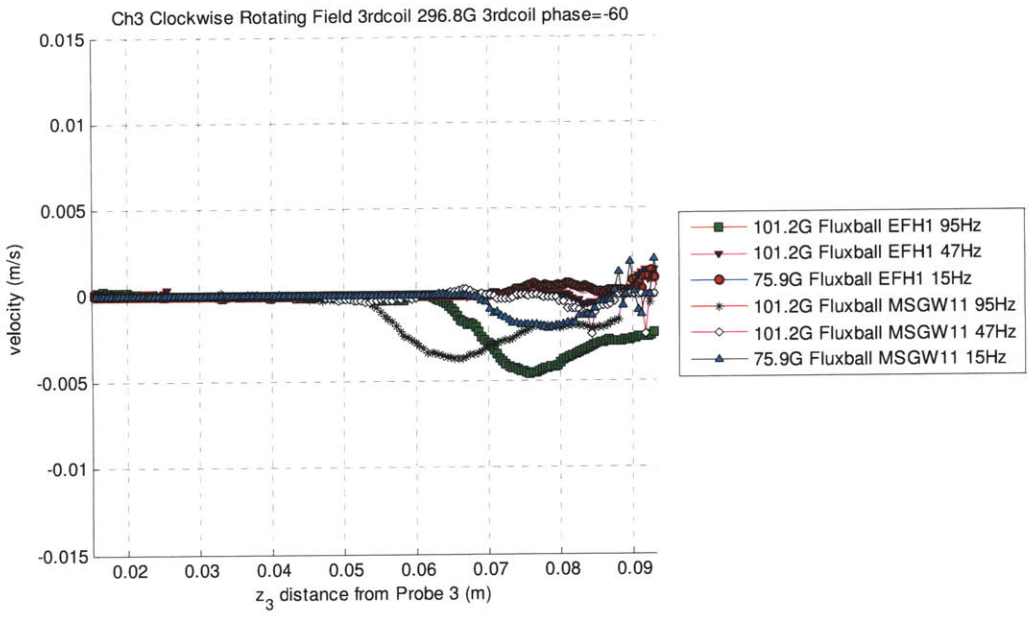
Ch3 Clockwise Rotating Field 3rdcoil 296.8G 3rdcoil phase=-60
velocity (m/s)
0.015
0.01
0.005
0
-0.005
-0.01
-0.015
0.02
0.03
0.04
0.05
0.06
0.07
0.08
0.09
z_3 distance from Probe 3 (m)
101.2G Fluxball EFH1 95Hz
101.2G Fluxball EFH1 47Hz
75.9G Fluxball EFH1 15Hz
101.2G Fluxball MSGW11 95Hz
101.2G Fluxball MSGW11 47Hz
75.9G Fluxball MSGW11 15Hz

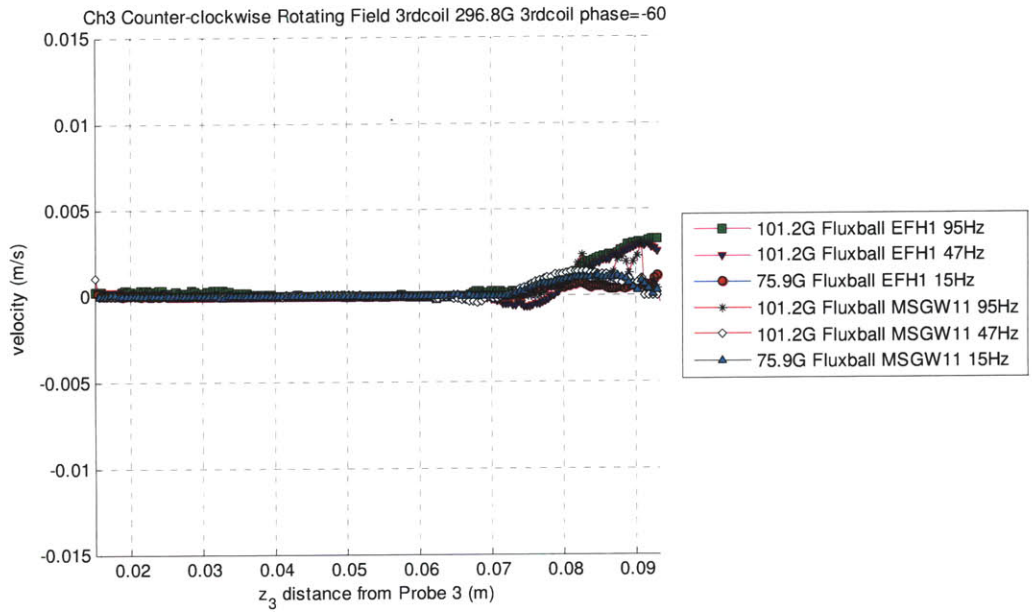
Ch3 Counter-clockwise Rotating Field 3rdcoil 296.8G 3rdcoil phase=-60
velocity (m/s)
0.015
0.01
0.005
0
-0.005
-0.01
-0.015
0.02
0.03
0.04
0.05
0.06
0.07
0.08
0.09
z_3 distance from Probe 3 (m)
101.2G Fluxball EFH1 95Hz
101.2G Fluxball EFH1 47Hz
75.9G Fluxball EFH1 15Hz
101.2G Fluxball MSGW11 95Hz
101.2G Fluxball MSGW11 47Hz
75.9G Fluxball MSGW11 15Hz

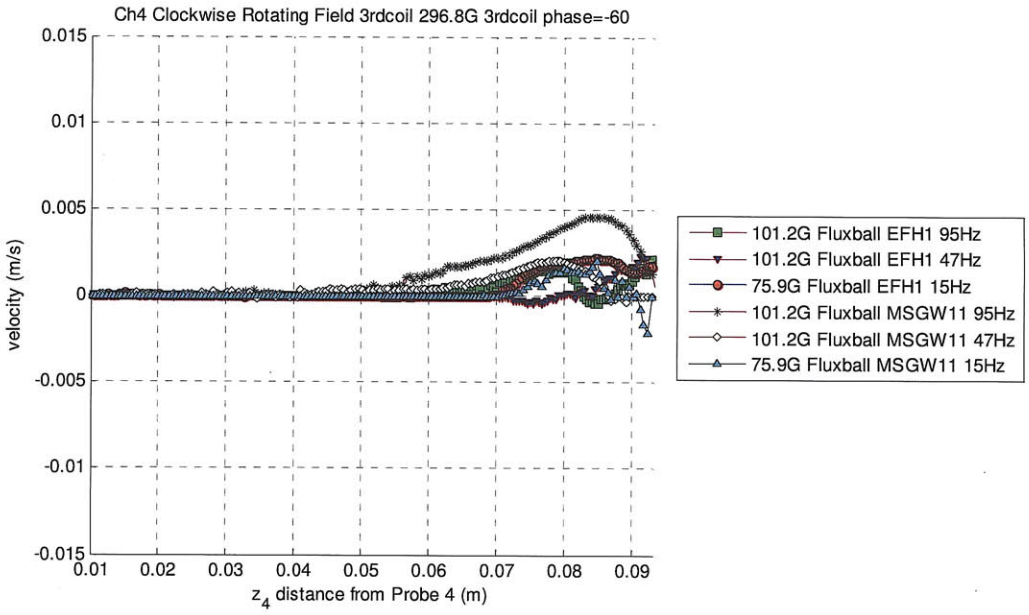
Ch4 Clockwise Rotating Field 3rdcoil 296.8G 3rdcoil phase=-60
velocity (m/s)
0.015
0.01
0.005
0
-0.005
-0.01
-0.015
0.01
0.02
0.03
0.04
0.05
0.06
0.07
0.08
0.09
z4 distance from Probe 4 (m)
101.2G Fluxball EFH1 95Hz
101.2G Fluxball EFH1 47Hz
75.9G Fluxball EFH1 15Hz
101.2G Fluxball MSGW11 95Hz
101.2G Fluxball MSGW11 47Hz
75.9G Fluxball MSGW11 15Hz

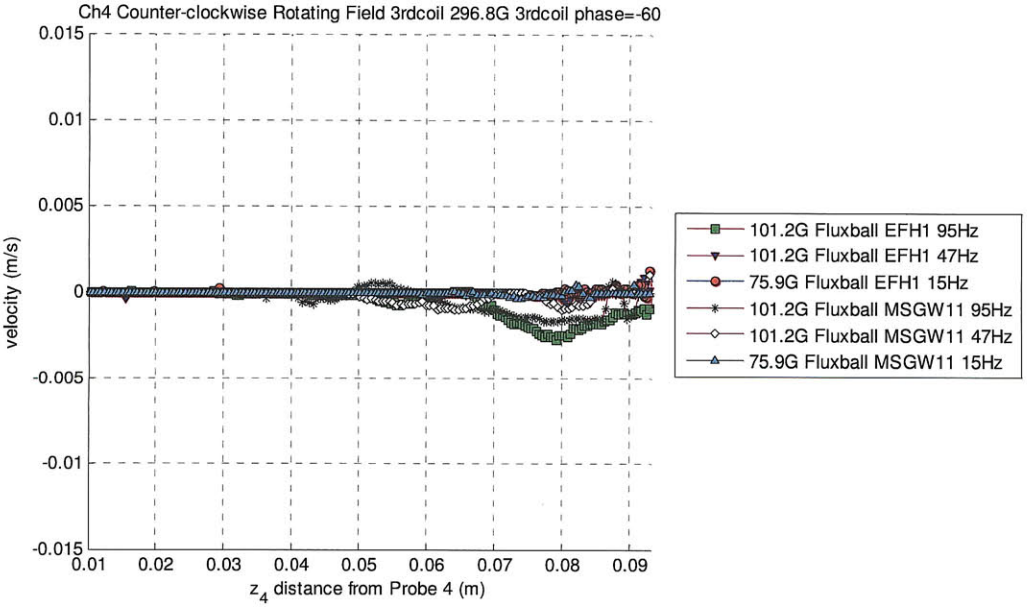
Ch4 Counter-clockwise Rotating Field 3rdcoil 296.8G 3rdcoil phase=-60
velocity (m/s)
0.015
0.01
0.005
0
-0.005
-0.01
-0.015
0.01
0.02
0.03
0.04
0.05
0.06
0.07
0.08
0.09
z4 distance from Probe 4 (m)
101.2G Fluxball EFH1 95Hz
101.2G Fluxball EFH1 47Hz
75.9G Fluxball EFH1 15Hz
101.2G Fluxball MSGW11 95Hz
101.2G Fluxball MSGW11 47Hz
75.9G Fluxball MSGW11 15Hz

G12. Comparison of Different Fluids with Third Coil Oscillating at Different Frequencies with Phase Difference=120 with Respect to Inner Coil

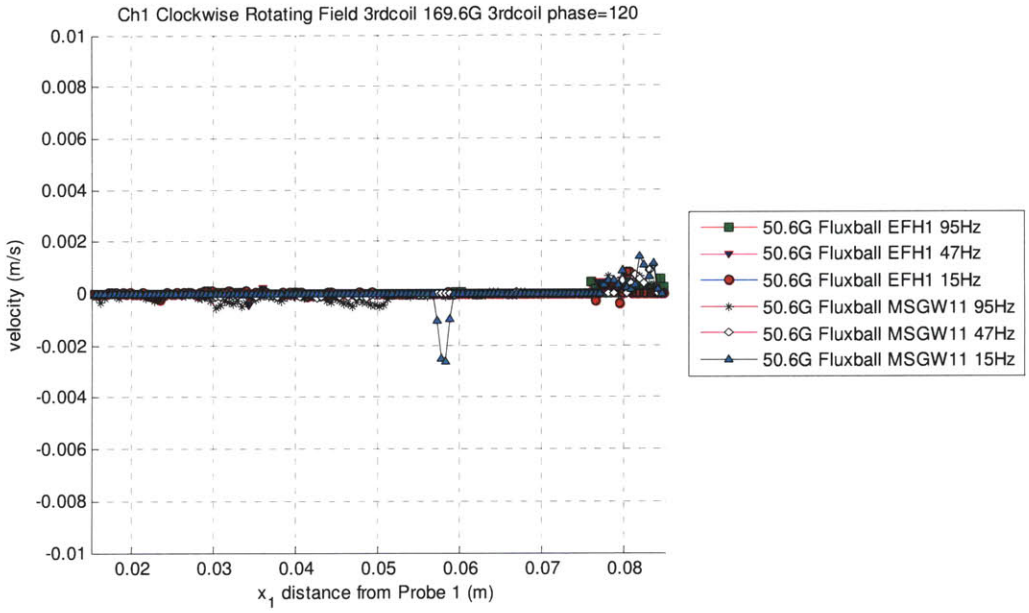

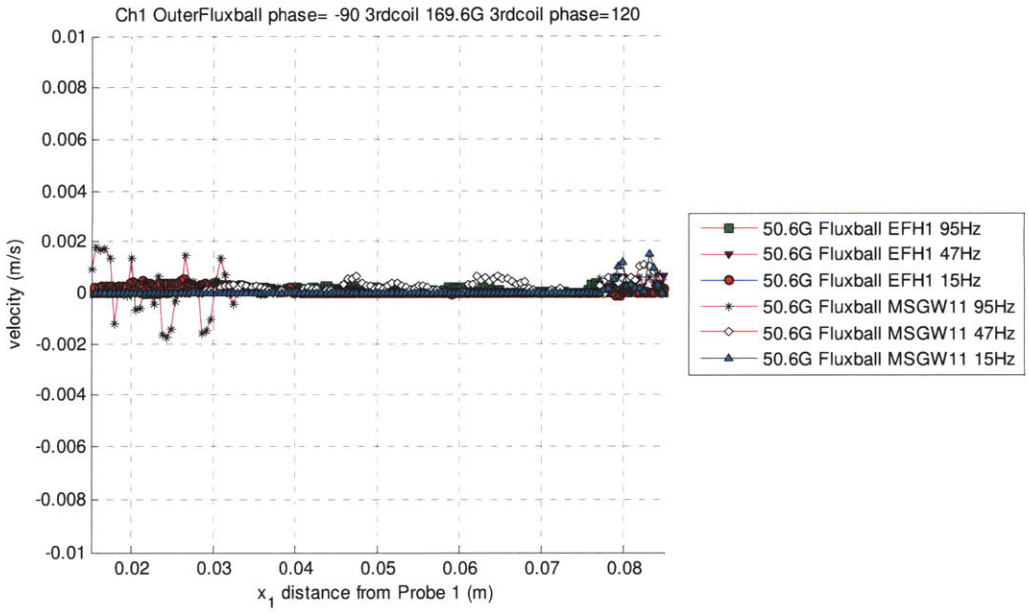

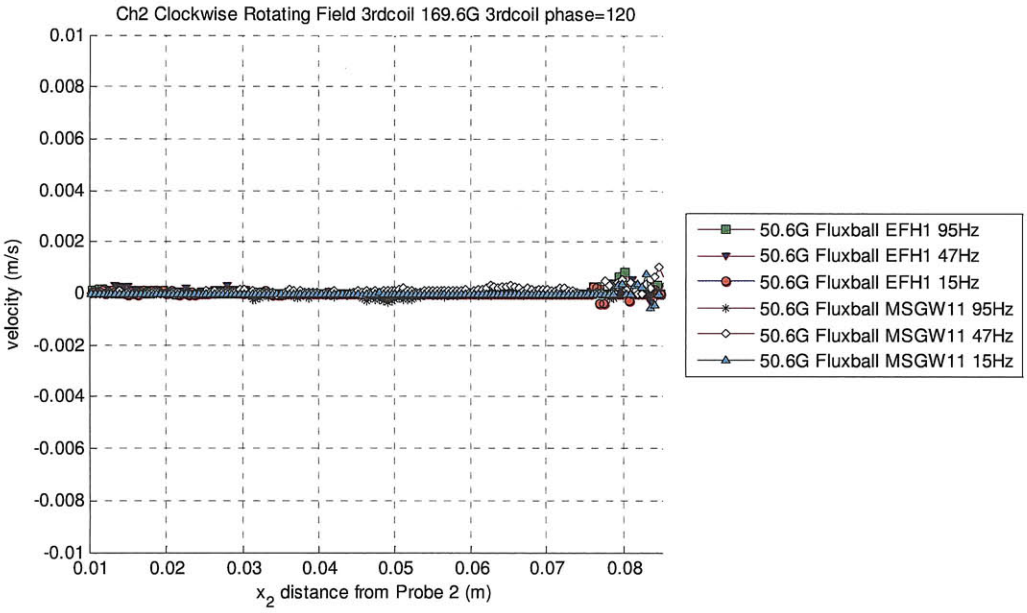
Ch2 Clockwise Rotating Field 3rdcoil 169.6G 3rdcoil phase=120
velocity (m/s)
0.01
0.008
0.006
0.004
0.002
0
-0.002
-0.004
-0.006
-0.008
-0.01
0.01
0.02
0.03
0.04
0.05
0.06
0.07
0.08
x2 distance from Probe 2 (m)
50.6G Fluxball EFH1 95Hz
50.6G Fluxball EFH1 47Hz
50.6G Fluxball EFH1 15Hz
50.6G Fluxball MSGW11 95Hz
50.6G Fluxball MSGW11 47Hz
50.6G Fluxball MSGW11 15Hz

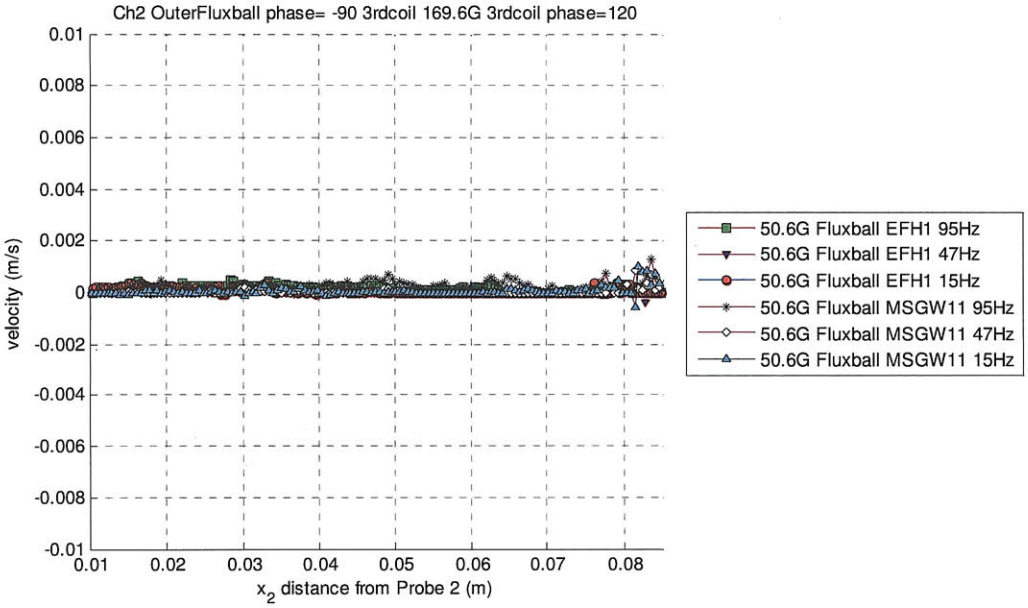
Ch2 OuterFluxball phase= -90 3rdcoil 169.6G 3rdcoil phase=120
velocity (m/s)
0.01
0.008
0.006
0.004
0.002
0
-0.002
-0.004
-0.006
-0.008
-0.01
0.01
0.02
0.03
0.04
0.05
0.06
0.07
0.08
x2 distance from Probe 2 (m)
50.6G Fluxball EFH1 95Hz
50.6G Fluxball EFH1 47Hz
50.6G Fluxball EFH1 15Hz
50.6G Fluxball MSGW11 95Hz
50.6G Fluxball MSGW11 47Hz
50.6G Fluxball MSGW11 15Hz

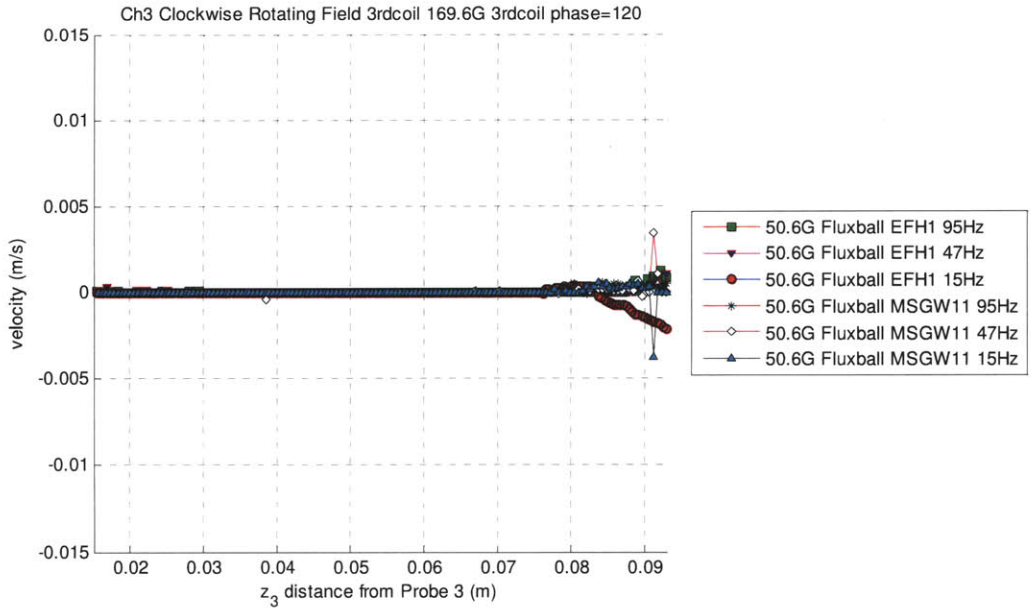
Ch3 Clockwise Rotating Field 3rdcoil 169.6G 3rdcoil phase=120
velocity (m/s)
0.015
0.01
0.005
0
-0.005
-0.01
-0.015
0.02
0.03
0.04
0.05
0.06
0.07
0.08
0.09
z_3 distance from Probe 3 (m)
50.6G Fluxball EFH1 95Hz
50.6G Fluxball EFH1 47Hz
50.6G Fluxball EFH1 15Hz
50.6G Fluxball MSGW11 95Hz
50.6G Fluxball MSGW11 47Hz
50.6G Fluxball MSGW11 15Hz

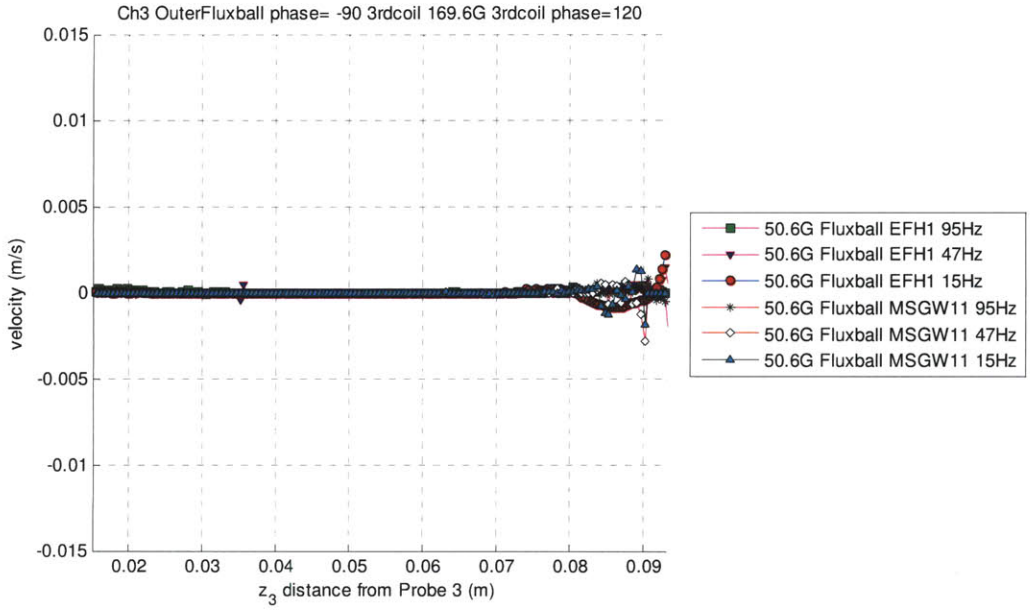
Ch3 OuterFluxball phase= -90 3rdcoil 169.6G 3rdcoil phase=120
velocity (m/s)
0.015
0.01
0.005
0
-0.005
-0.01
-0.015
0.02
0.03
0.04
0.05
0.06
0.07
0.08
0.09
z_3 distance from Probe 3 (m)
50.6G Fluxball EFH1 95Hz
50.6G Fluxball EFH1 47Hz
50.6G Fluxball EFH1 15Hz
50.6G Fluxball MSGW11 95Hz
50.6G Fluxball MSGW11 47Hz
50.6G Fluxball MSGW11 15Hz

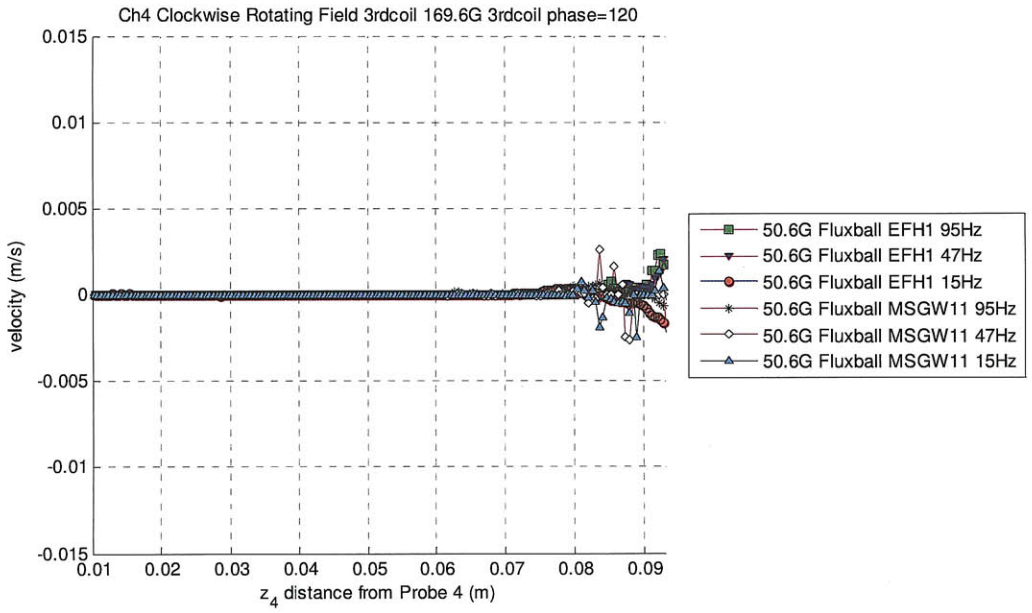
Ch4 Clockwise Rotating Field 3rdcoil 169.6G 3rdcoil phase=120
0.015
0.01
0.005
0
-0.005
-0.01
-0.015
velocity (m/s)
0.01
0.02
0.03
0.04
0.05
0.06
0.07
0.08
0.09
z4 distance from Probe 4 (m)
50.6G Fluxball EFH1 95Hz
50.6G Fluxball EFH1 47Hz
50.6G Fluxball EFH1 15Hz
50.6G Fluxball MSGW11 95Hz
50.6G Fluxball MSGW11 47Hz
50.6G Fluxball MSGW11 15Hz

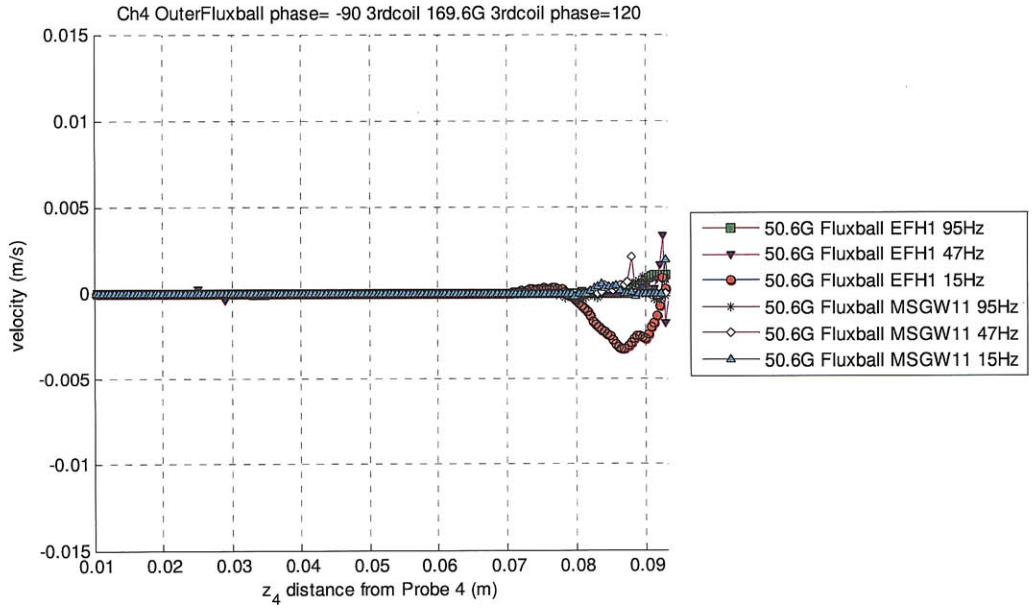
Ch4 OuterFluxball phase= -90 3rdcoil 169.6G 3rdcoil phase=120
0.015
0.01
0.005
0
-0.005
-0.01
-0.015
velocity (m/s)
0.01
0.02
0.03
0.04
0.05
0.06
0.07
0.08
0.09
z4 distance from Probe 4 (m)
50.6G Fluxball EFH1 95Hz
50.6G Fluxball EFH1 47Hz
50.6G Fluxball EFH1 15Hz
50.6G Fluxball MSGW11 95Hz
50.6G Fluxball MSGW11 47Hz
50.6G Fluxball MSGW11 15Hz

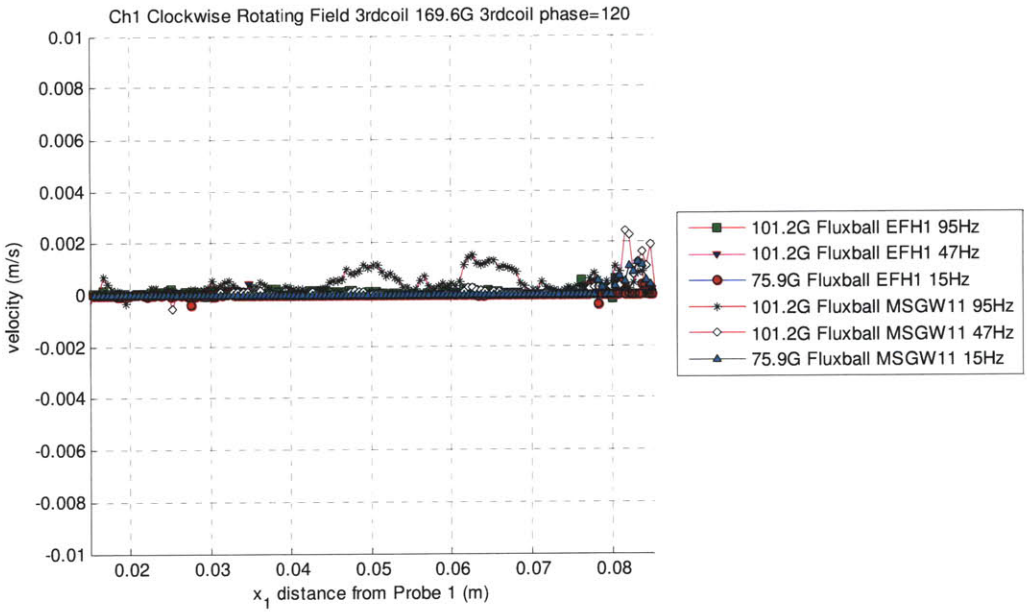
Ch1 Clockwise Rotating Field 3rdcoil 169.6G 3rdcoil phase=120
velocity (m/s)
0.01
0.008
0.006
0.004
0.002
0
-0.002
-0.004
-0.006
-0.008
-0.01
0.02
0.03
0.04
0.05
0.06
0.07
0.08
x1 distance from Probe 1 (m)
101.2G Fluxball EFH1 95Hz
101.2G Fluxball EFH1 47Hz
75.9G Fluxball EFH1 15Hz
101.2G Fluxball MSGW11 95Hz
101.2G Fluxball MSGW11 47Hz
75.9G Fluxball MSGW11 15Hz

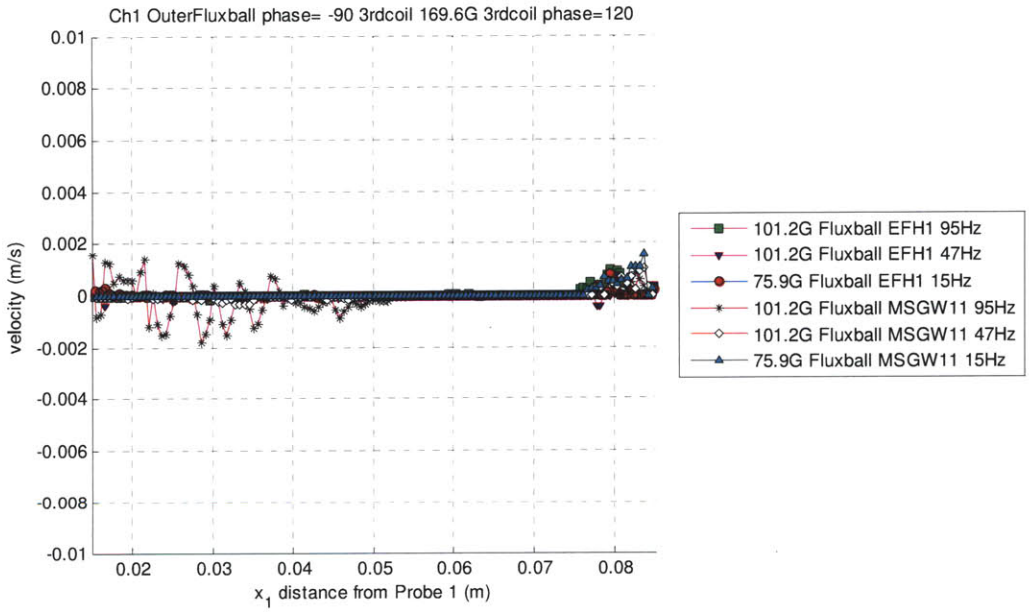
Ch1 OuterFluxball phase= -90 3rdcoil 169.6G 3rdcoil phase=120
velocity (m/s)
0.01
0.008
0.006
0.004
0.002
0
-0.002
-0.004
-0.006
-0.008
-0.01
0.02
0.03
0.04
0.05
0.06
0.07
0.08
x1 distance from Probe 1 (m)
101.2G Fluxball EFH1 95Hz
101.2G Fluxball EFH1 47Hz
75.9G Fluxball EFH1 15Hz
101.2G Fluxball MSGW11 95Hz
101.2G Fluxball MSGW11 47Hz
75.9G Fluxball MSGW11 15Hz

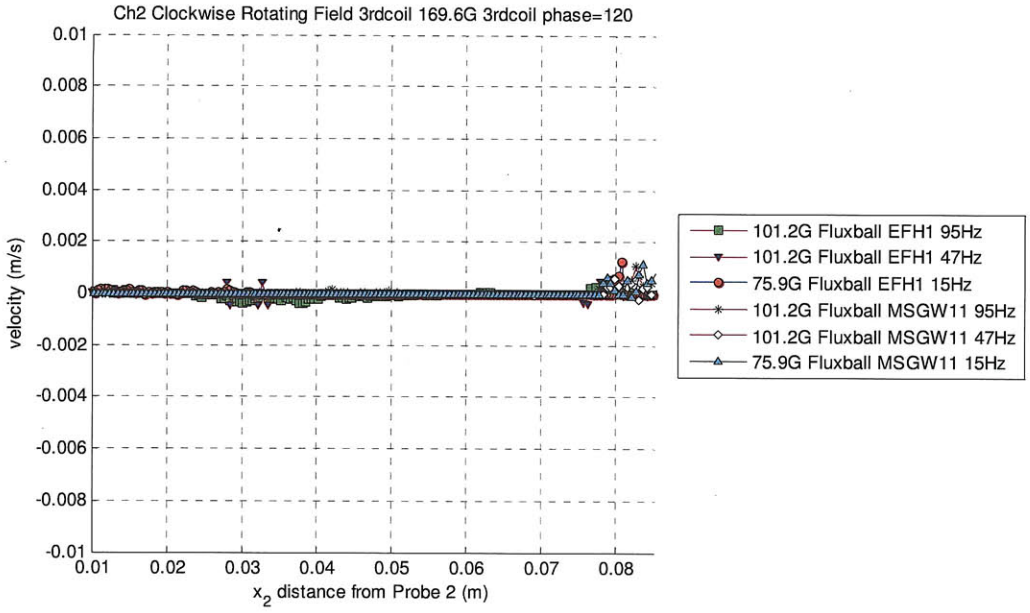
Ch2 Clockwise Rotating Field 3rdcoil 169.6G 3rdcoil phase=120
velocity (m/s)
0.01
0.008
0.006
0.004
0.002
0
-0.002
-0.004
-0.006
-0.008
-0.01
0.01 0.02 0.03 0.04 0.05 0.06 0.07 0.08
x2 distance from Probe 2 (m)
101.2G Fluxball EFH1 95Hz
101.2G Fluxball EFH1 47Hz
75.9G Fluxball EFH1 15Hz
101.2G Fluxball MSGW11 95Hz
101.2G Fluxball MSGW11 47Hz
75.9G Fluxball MSGW11 15Hz

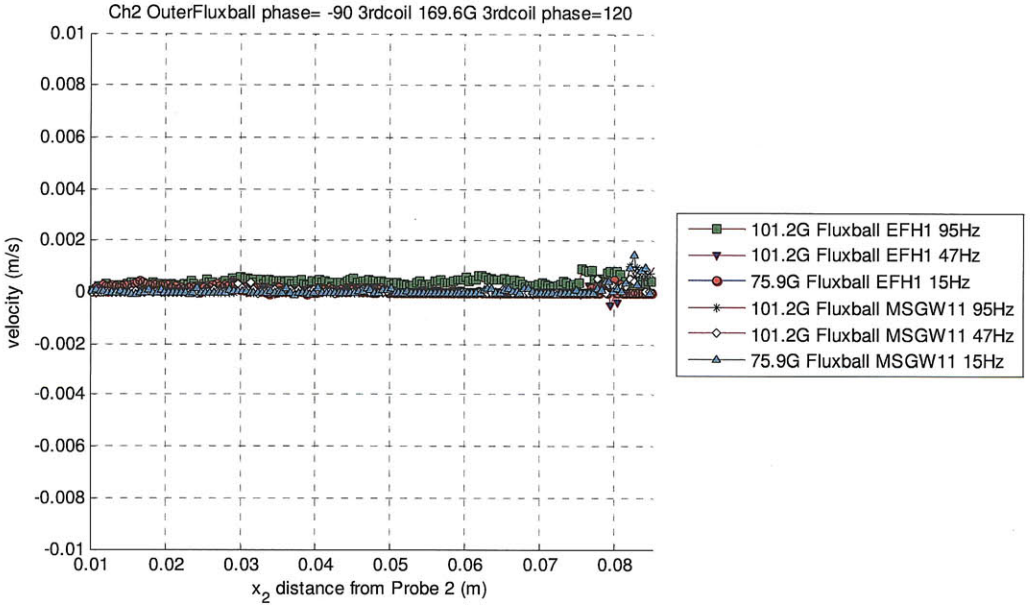
Ch2 OuterFluxball phase= -90 3rdcoil 169.6G 3rdcoil phase=120
velocity (m/s)
0.01
0.008
0.006
0.004
0.002
0
-0.002
-0.004
-0.006
-0.008
-0.01
0.01 0.02 0.03 0.04 0.05 0.06 0.07 0.08
x2 distance from Probe 2 (m)
101.2G Fluxball EFH1 95Hz
101.2G Fluxball EFH1 47Hz
75.9G Fluxball EFH1 15Hz
101.2G Fluxball MSGW11 95Hz
101.2G Fluxball MSGW11 47Hz
75.9G Fluxball MSGW11 15Hz

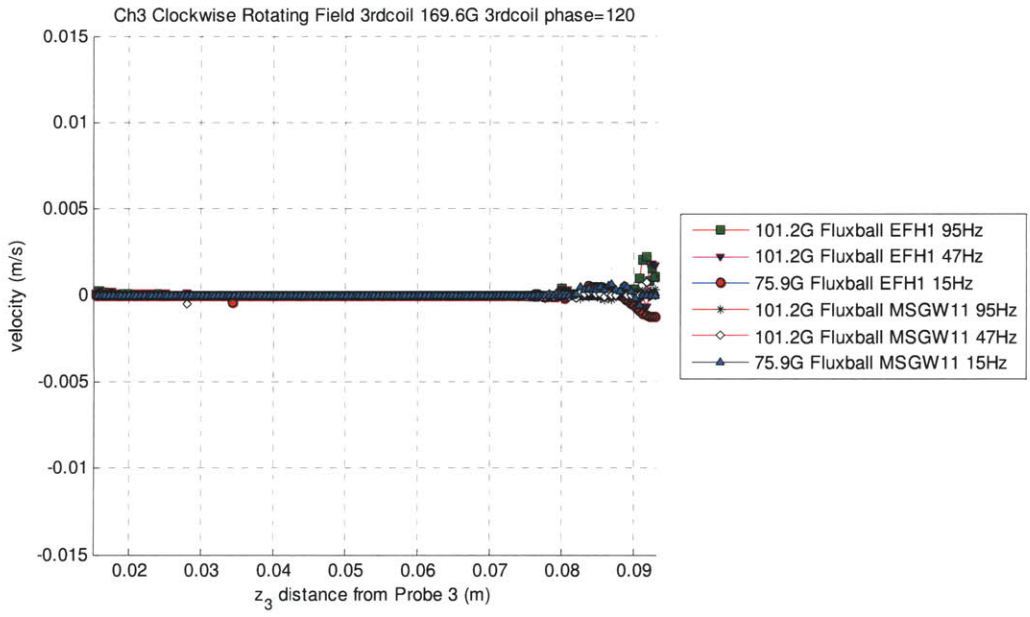
Ch3 Clockwise Rotating Field 3rdcoil 169.6G 3rdcoil phase=120
velocity (m/s)
0.015
0.01
0.005
0
-0.005
-0.01
-0.015
0.02
0.03
0.04
0.05
0.06
0.07
0.08
0.09
z3 distance from Probe 3 (m)
101.2G Fluxball EFH1 95Hz
101.2G Fluxball EFH1 47Hz
75.9G Fluxball EFH1 15Hz
101.2G Fluxball MSGW11 95Hz
101.2G Fluxball MSGW11 47Hz
75.9G Fluxball MSGW11 15Hz

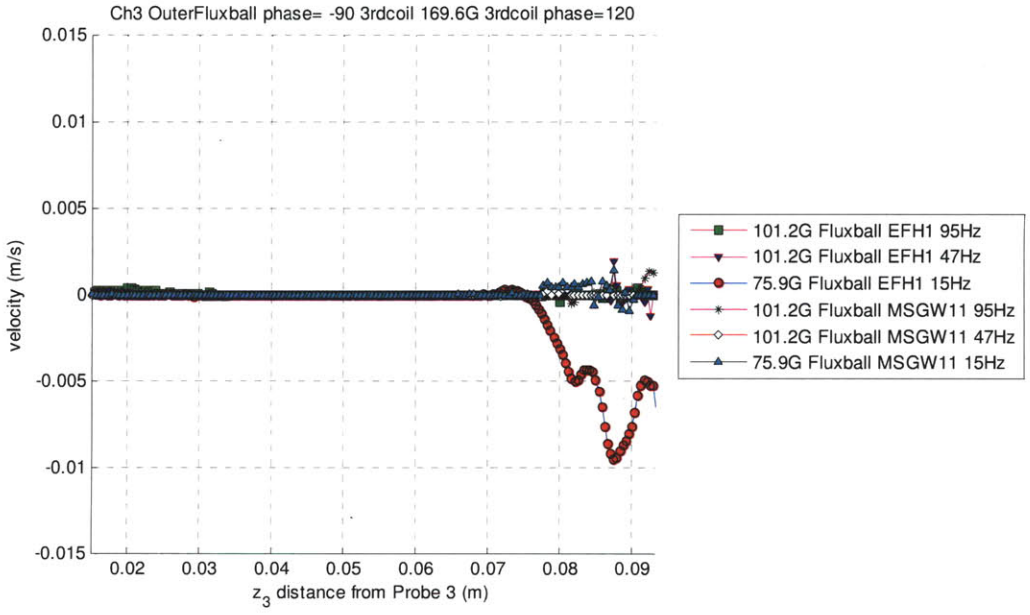
Ch3 OuterFluxball phase= -90 3rdcoil 169.6G 3rdcoil phase=120
velocity (m/s)
0.015
0.01
0.005
0
-0.005
-0.01
-0.015
0.02
0.03
0.04
0.05
0.06
0.07
0.08
0.09
z3 distance from Probe 3 (m)
101.2G Fluxball EFH1 95Hz
101.2G Fluxball EFH1 47Hz
75.9G Fluxball EFH1 15Hz
101.2G Fluxball MSGW11 95Hz
101.2G Fluxball MSGW11 47Hz
75.9G Fluxball MSGW11 15Hz

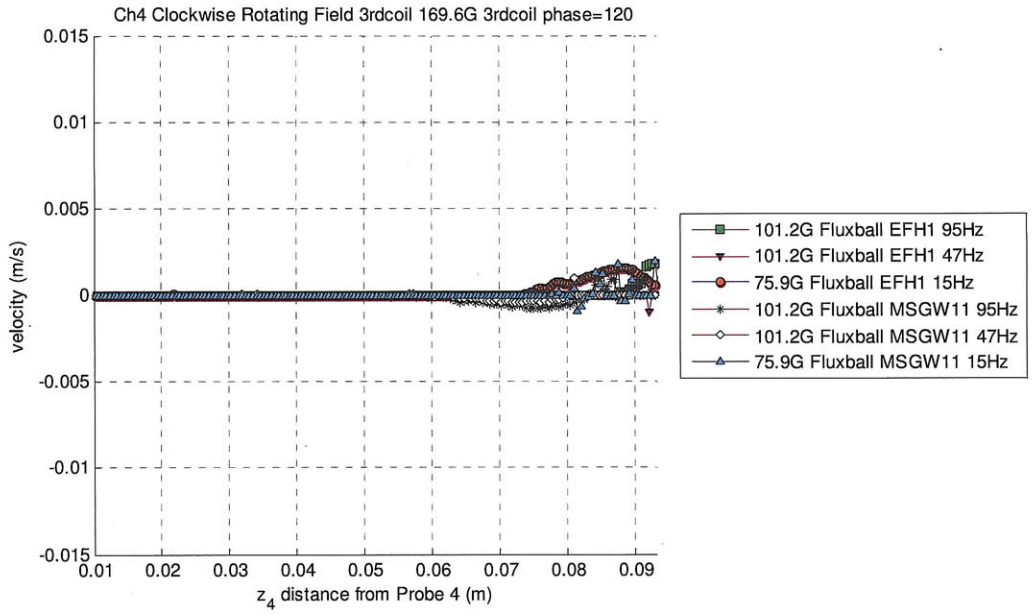
Ch4 Clockwise Rotating Field 3rdcoil 169.6G 3rdcoil phase=120
velocity (m/s)
0.015
0.01
0.005
0
-0.005
-0.01
-0.015
0.01
0.02
0.03
0.04
0.05
0.06
0.07
0.08
0.09
z4 distance from Probe 4 (m)
101.2G Fluxball EFH1 95Hz
101.2G Fluxball EFH1 47Hz
75.9G Fluxball EFH1 15Hz
101.2G Fluxball MSGW11 95Hz
101.2G Fluxball MSGW11 47Hz
75.9G Fluxball MSGW11 15Hz

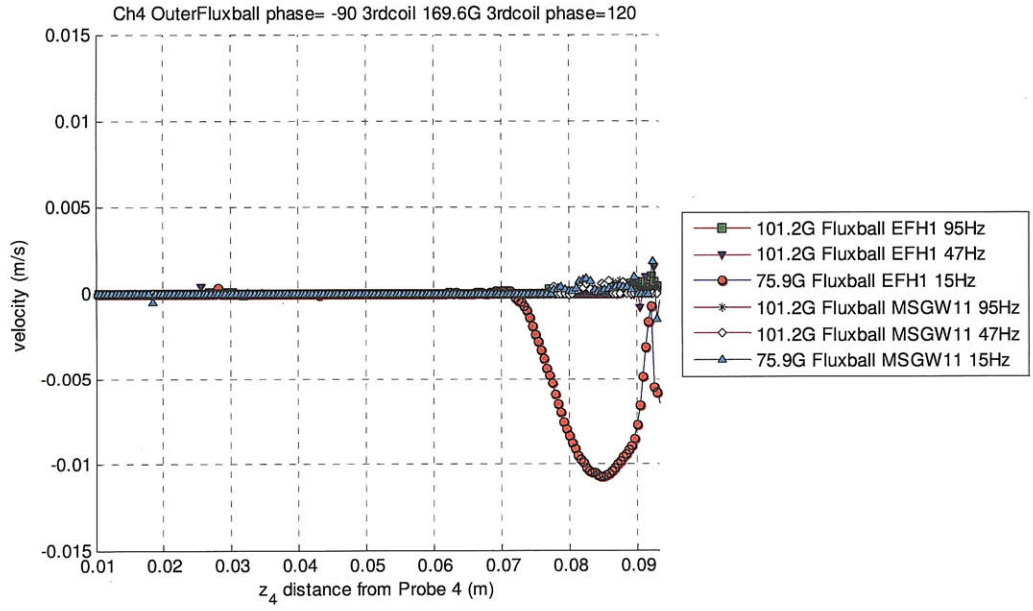
Ch4 OuterFluxball phase= -90 3rdcoil 169.6G 3rdcoil phase=120
velocity (m/s)
0.015
0.01
0.005
0
-0.005
-0.01
-0.015
0.01
0.02
0.03
0.04
0.05
0.06
0.07
0.08
0.09
z4 distance from Probe 4 (m)
101.2G Fluxball EFH1 95Hz
101.2G Fluxball EFH1 47Hz
75.9G Fluxball EFH1 15Hz
101.2G Fluxball MSGW11 95Hz
101.2G Fluxball MSGW11 47Hz
75.9G Fluxball MSGW11 15Hz

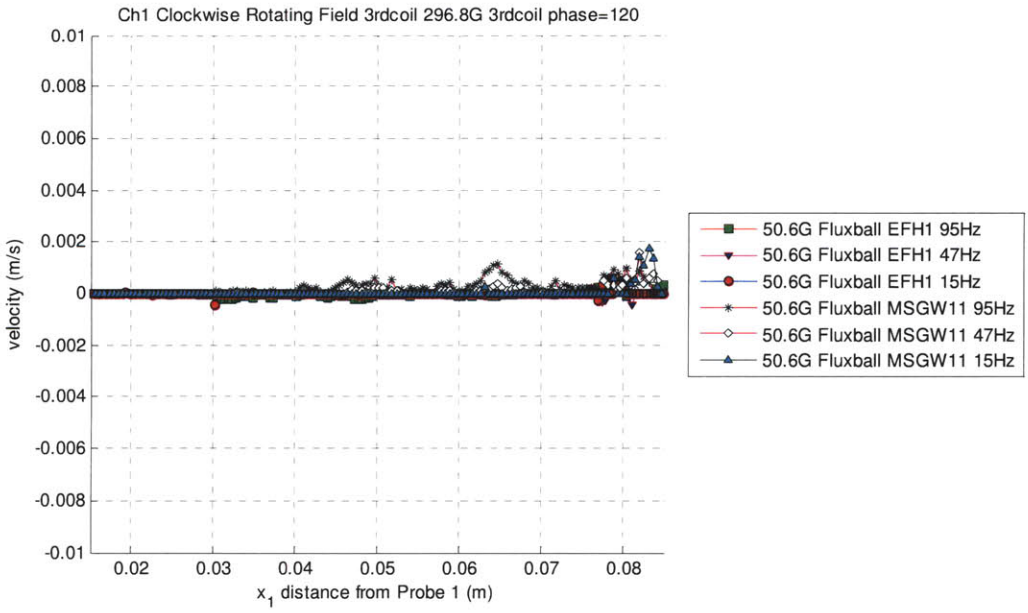
Ch1 Clockwise Rotating Field 3rdcoil 296.8G 3rdcoil phase=120
velocity (m/s)
0.01
0.008
0.006
0.004
0.002
0
-0.002
-0.004
-0.006
-0.008
-0.01
0.02
0.03
0.04
0.05
0.06
0.07
0.08
x1 distance from Probe 1 (m)
50.6G Fluxball EFH1 95Hz
50.6G Fluxball EFH1 47Hz
50.6G Fluxball EFH1 15Hz
50.6G Fluxball MSGW11 95Hz
50.6G Fluxball MSGW11 47Hz
50.6G Fluxball MSGW11 15Hz

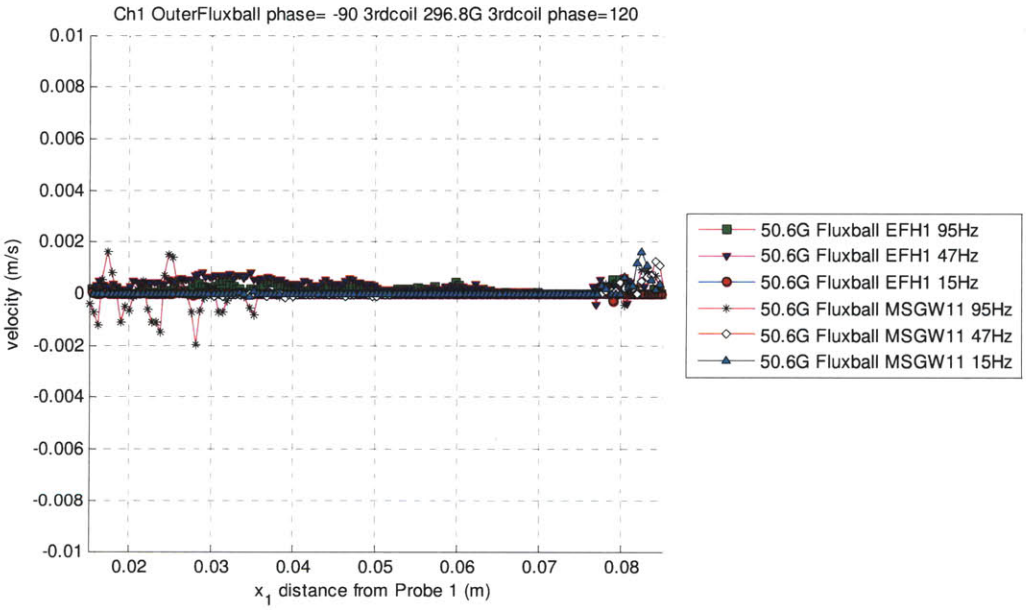
Ch1 OuterFluxball phase= -90 3rdcoil 296.8G 3rdcoil phase=120
velocity (m/s)
0.01
0.008
0.006
0.004
0.002
0
-0.002
-0.004
-0.006
-0.008
-0.01
0.02
0.03
0.04
0.05
0.06
0.07
0.08
x1 distance from Probe 1 (m)
50.6G Fluxball EFH1 95Hz
50.6G Fluxball EFH1 47Hz
50.6G Fluxball EFH1 15Hz
50.6G Fluxball MSGW11 95Hz
50.6G Fluxball MSGW11 47Hz
50.6G Fluxball MSGW11 15Hz

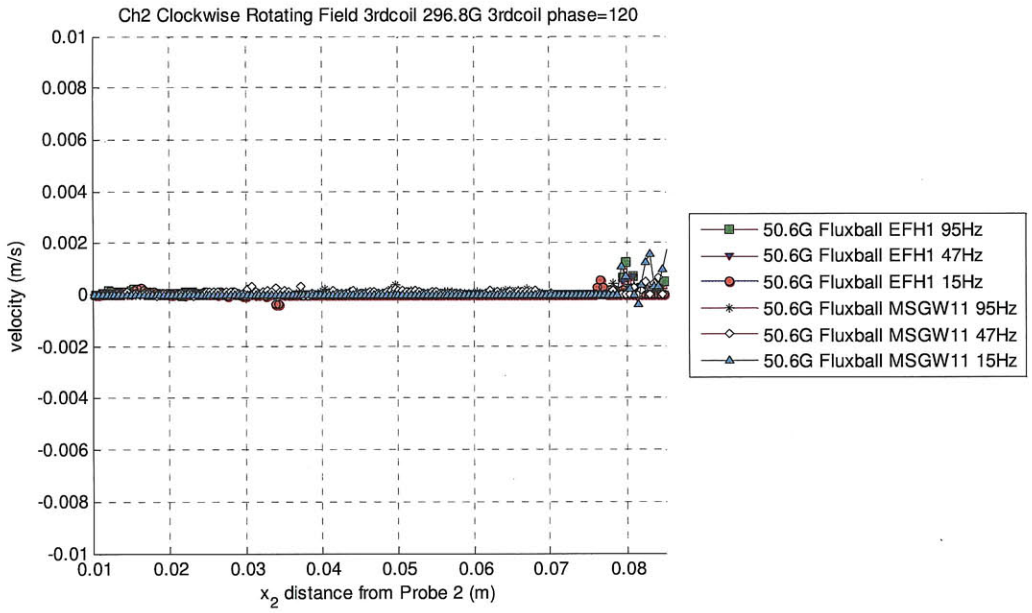
Ch2 Clockwise Rotating Field 3rdcoil 296.8G 3rdcoil phase=120
velocity (m/s)
0.01
0.008
0.006
0.004
0.002
0
-0.002
-0.004
-0.006
-0.008
-0.01
0.01 0.02 0.03 0.04 0.05 0.06 0.07 0.08
x2 distance from Probe 2 (m)
50.6G Fluxball EFH1 95Hz
50.6G Fluxball EFH1 47Hz
50.6G Fluxball EFH1 15Hz
50.6G Fluxball MSGW11 95Hz
50.6G Fluxball MSGW11 47Hz
50.6G Fluxball MSGW11 15Hz

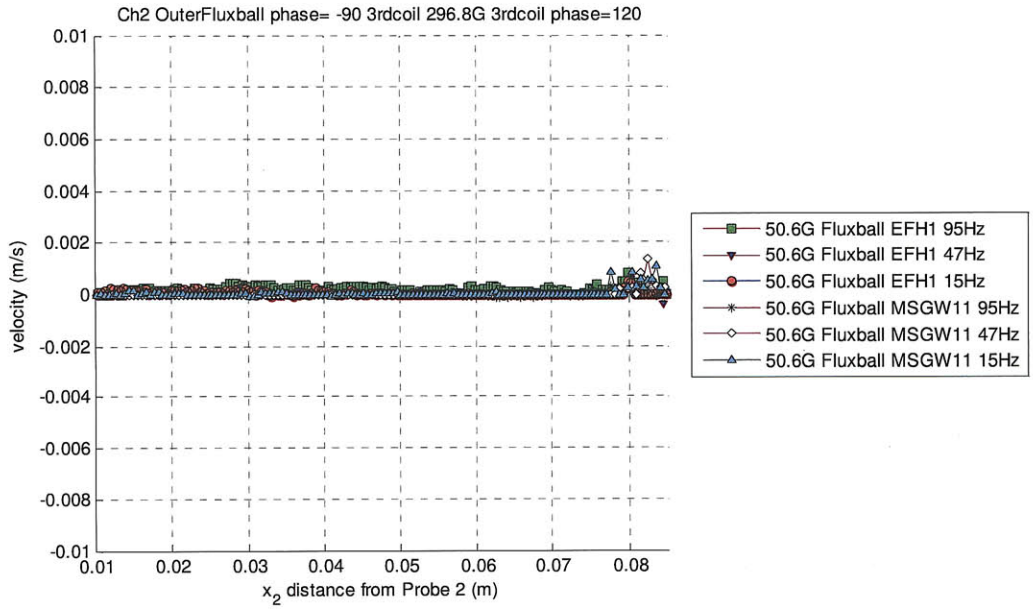
Ch2 OuterFluxball phase= -90 3rdcoil 296.8G 3rdcoil phase=120
velocity (m/s)
0.01
0.008
0.006
0.004
0.002
0
-0.002
-0.004
-0.006
-0.008
-0.01
0.01 0.02 0.03 0.04 0.05 0.06 0.07 0.08
x2 distance from Probe 2 (m)
50.6G Fluxball EFH1 95Hz
50.6G Fluxball EFH1 47Hz
50.6G Fluxball EFH1 15Hz
50.6G Fluxball MSGW11 95Hz
50.6G Fluxball MSGW11 47Hz
50.6G Fluxball MSGW11 15Hz

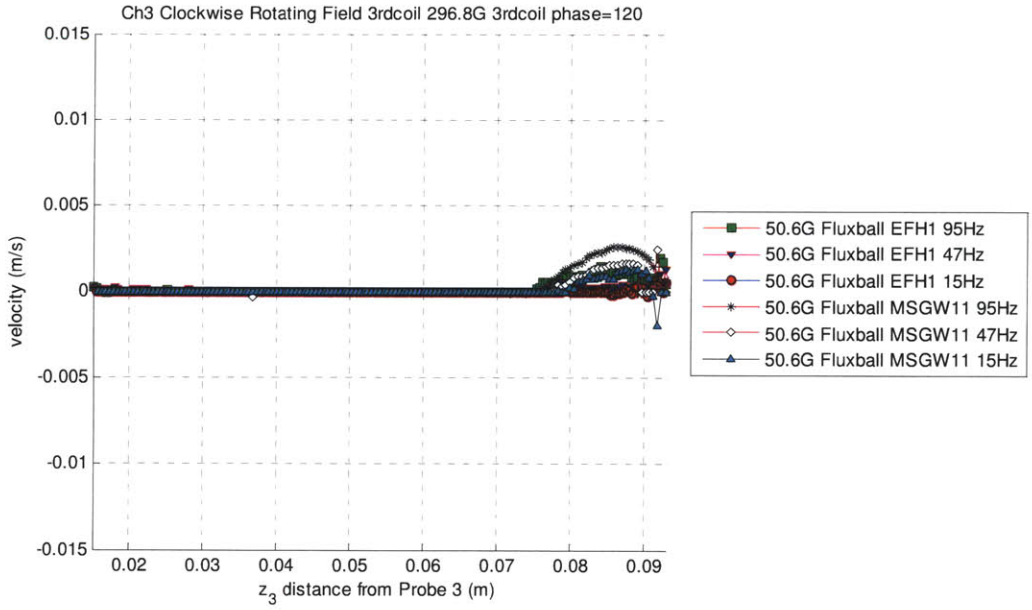
Ch3 Clockwise Rotating Field 3rdcoil 296.8G 3rdcoil phase=120
0.015
0.01
0.005
0
-0.005
-0.01
-0.015
velocity (m/s)
0.02
0.03
0.04
0.05
0.06
0.07
0.08
0.09
z3 distance from Probe 3 (m)
50.6G Fluxball EFH1 95Hz
50.6G Fluxball EFH1 47Hz
50.6G Fluxball EFH1 15Hz
50.6G Fluxball MSGW11 95Hz
50.6G Fluxball MSGW11 47Hz
50.6G Fluxball MSGW11 15Hz

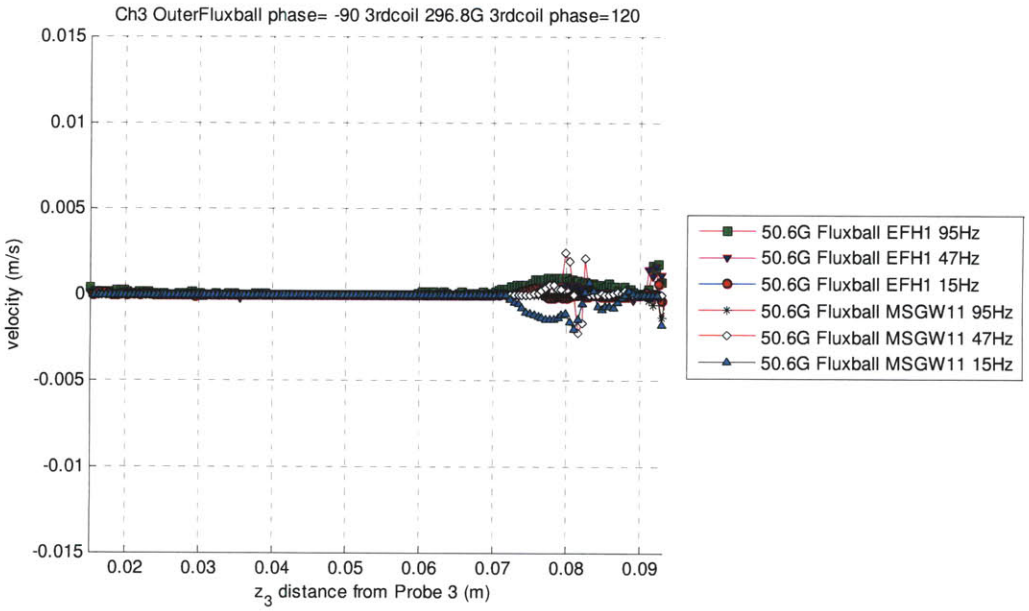
Ch3 OuterFluxball phase= -90 3rdcoil 296.8G 3rdcoil phase=120
0.015
0.01
0.005
0
-0.005
-0.01
-0.015
velocity (m/s)
0.02
0.03
0.04
0.05
0.06
0.07
0.08
0.09
z3 distance from Probe 3 (m)
50.6G Fluxball EFH1 95Hz
50.6G Fluxball EFH1 47Hz
50.6G Fluxball EFH1 15Hz
50.6G Fluxball MSGW11 95Hz
50.6G Fluxball MSGW11 47Hz
50.6G Fluxball MSGW11 15Hz

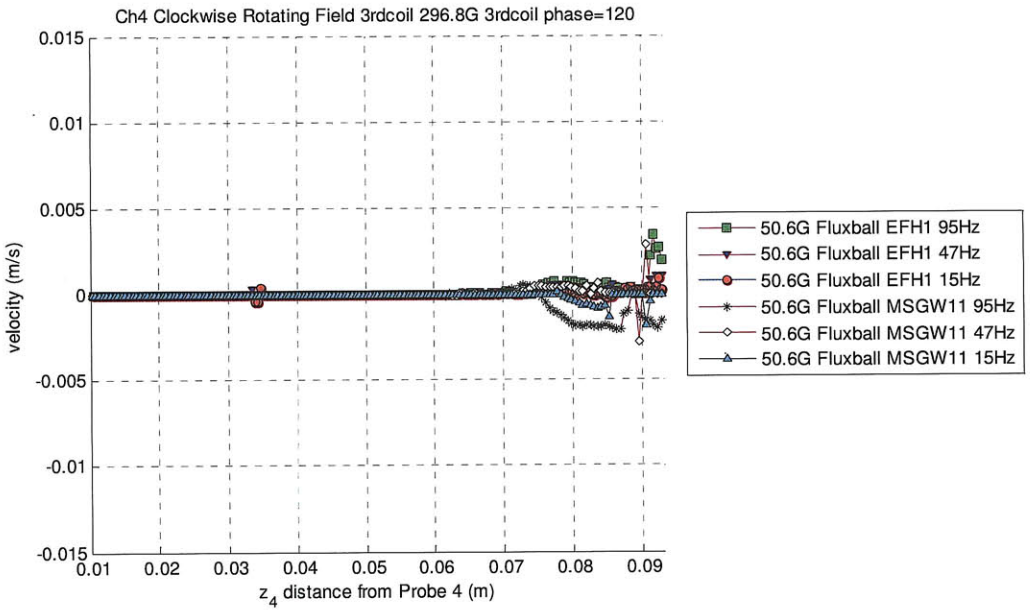
Ch4 Clockwise Rotating Field 3rdcoil 296.8G 3rdcoil phase=120
velocity (m/s)
0.015
0.01
0.005
0
-0.005
-0.01
-0.015
0.01
0.02
0.03
0.04
0.05
0.06
0.07
0.08
0.09
z4 distance from Probe 4 (m)
50.6G Fluxball EFH1 95Hz
50.6G Fluxball EFH1 47Hz
50.6G Fluxball EFH1 15Hz
50.6G Fluxball MSGW11 95Hz
50.6G Fluxball MSGW11 47Hz
50.6G Fluxball MSGW11 15Hz

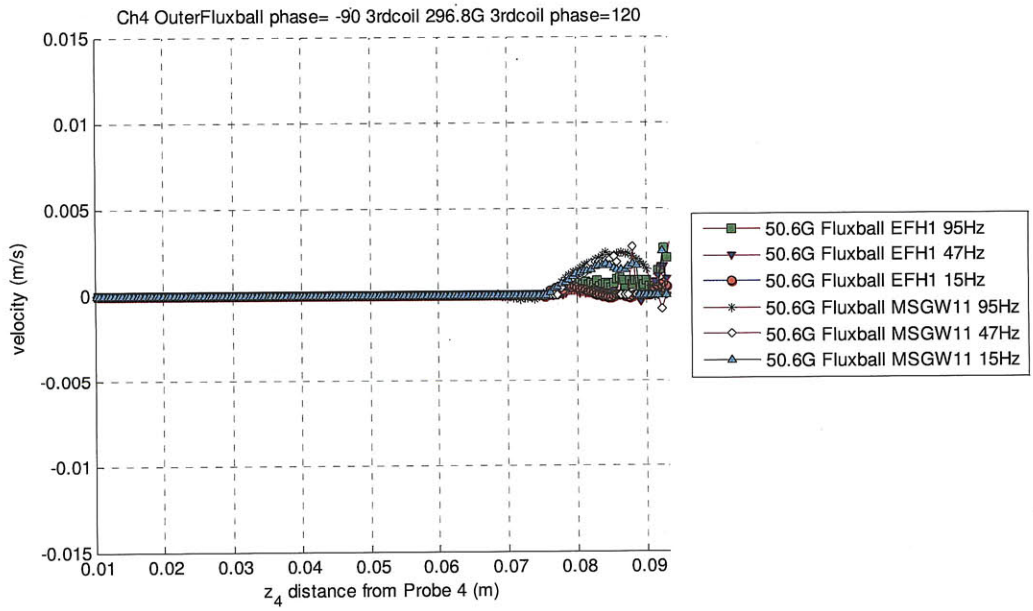
Ch4 OuterFluxball phase= -90 3rdcoil 296.8G 3rdcoil phase=120
velocity (m/s)
0.015
0.01
0.005
0
-0.005
-0.01
-0.015
0.01
0.02
0.03
0.04
0.05
0.06
0.07
0.08
0.09
z4 distance from Probe 4 (m)
50.6G Fluxball EFH1 95Hz
50.6G Fluxball EFH1 47Hz
50.6G Fluxball EFH1 15Hz
50.6G Fluxball MSGW11 95Hz
50.6G Fluxball MSGW11 47Hz
50.6G Fluxball MSGW11 15Hz

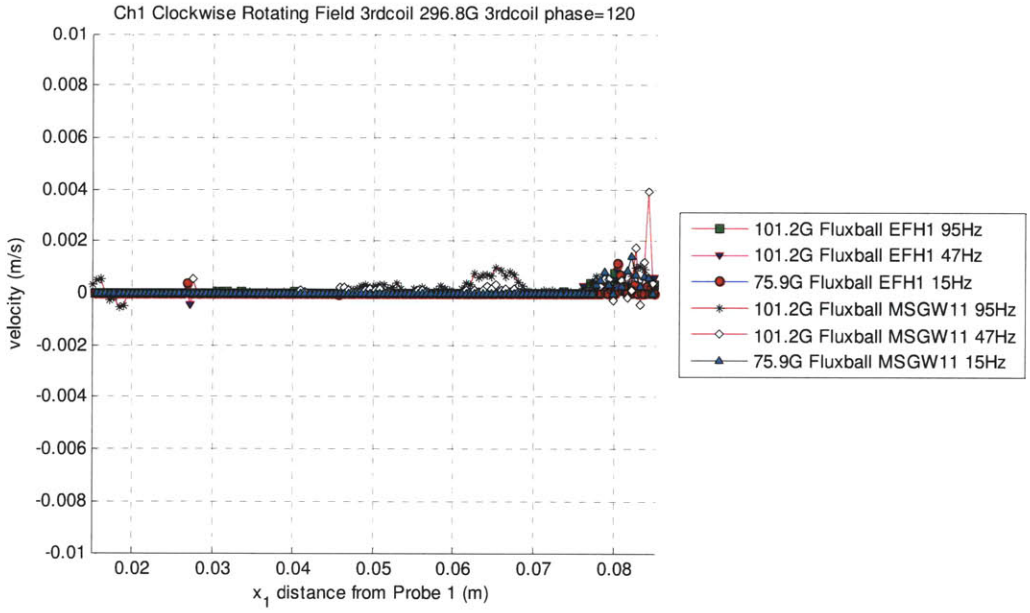
Ch1 Clockwise Rotating Field 3rdcoil 296.8G 3rdcoil phase=120
velocity (m/s)
0.01
0.008
0.006
0.004
0.002
0
-0.002
-0.004
-0.006
-0.008
-0.01
0.02
0.03
0.04
0.05
0.06
0.07
0.08
x1 distance from Probe 1 (m)
101.2G Fluxball EFH1 95Hz
101.2G Fluxball EFH1 47Hz
75.9G Fluxball EFH1 15Hz
101.2G Fluxball MSGW11 95Hz
101.2G Fluxball MSGW11 47Hz
75.9G Fluxball MSGW11 15Hz

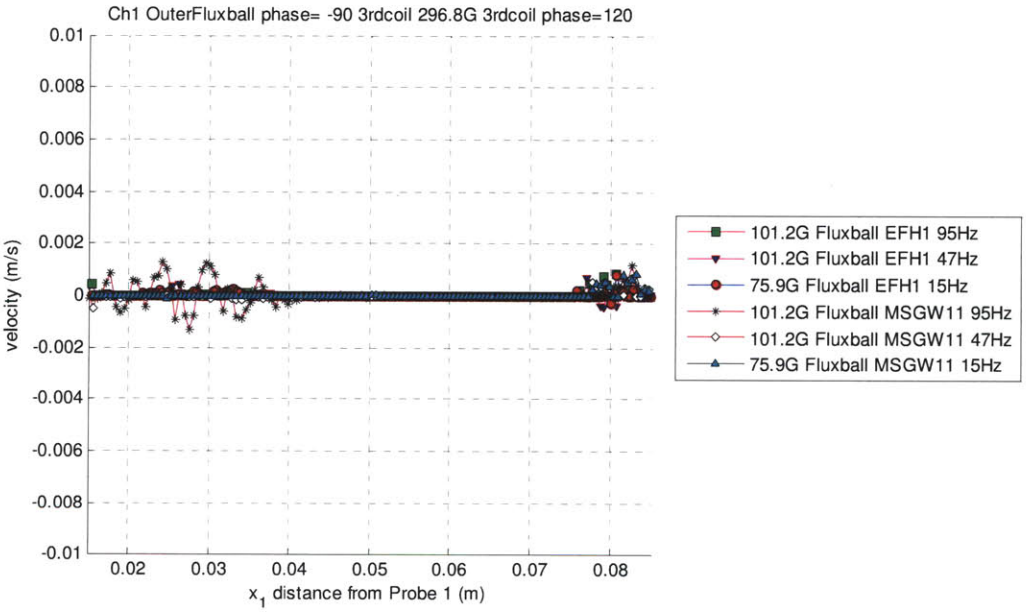
Ch1 OuterFluxball phase= -90 3rdcoil 296.8G 3rdcoil phase=120
velocity (m/s)
0.01
0.008
0.006
0.004
0.002
0
-0.002
-0.004
-0.006
-0.008
-0.01
0.02
0.03
0.04
0.05
0.06
0.07
0.08
x1 distance from Probe 1 (m)
101.2G Fluxball EFH1 95Hz
101.2G Fluxball EFH1 47Hz
75.9G Fluxball EFH1 15Hz
101.2G Fluxball MSGW11 95Hz
101.2G Fluxball MSGW11 47Hz
75.9G Fluxball MSGW11 15Hz

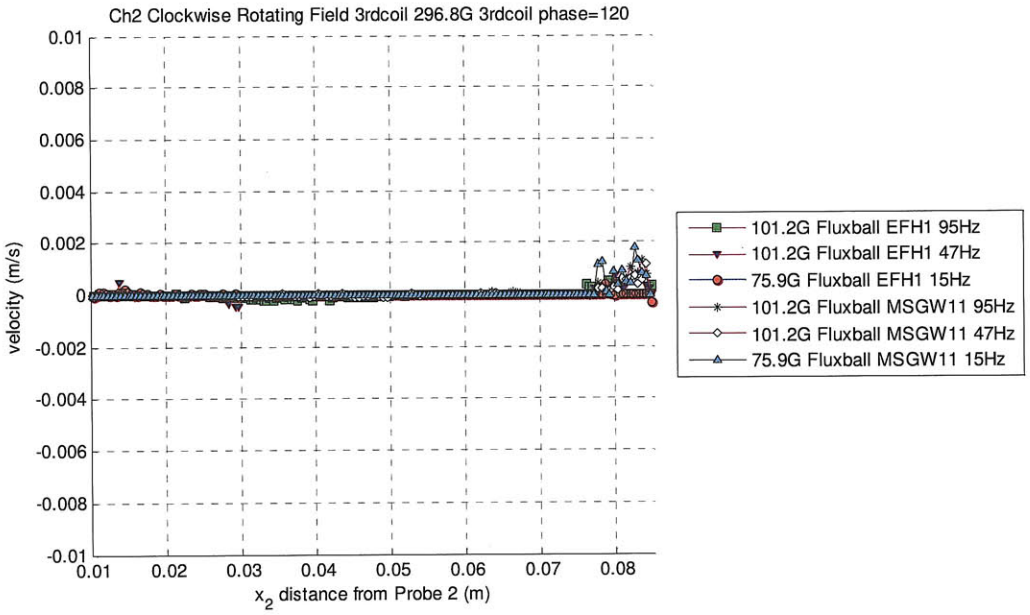
Ch2 Clockwise Rotating Field 3rdcoil 296.8G 3rdcoil phase=120
velocity (m/s)
0.01
0.008
0.006
0.004
0.002
0
-0.002
-0.004
-0.006
-0.008
-0.01
0.01
0.02
0.03
0.04
0.05
0.06
0.07
0.08
x2 distance from Probe 2 (m)
101.2G Fluxball EFH1 95Hz
101.2G Fluxball EFH1 47Hz
75.9G Fluxball EFH1 15Hz
101.2G Fluxball MSGW11 95Hz
101.2G Fluxball MSGW11 47Hz
75.9G Fluxball MSGW11 15Hz

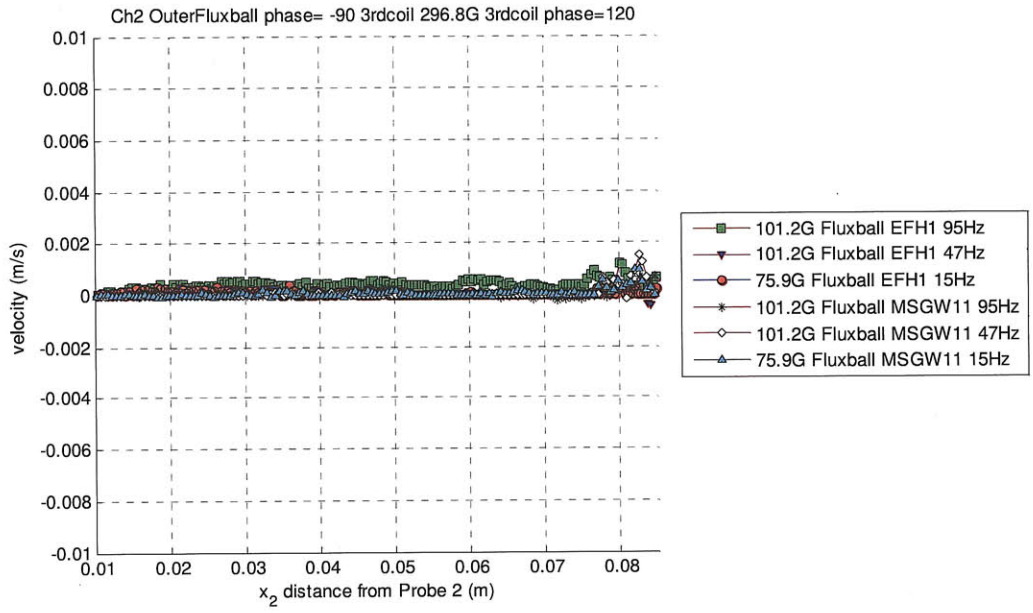
Ch2 OuterFluxball phase= -90 3rdcoil 296.8G 3rdcoil phase=120
velocity (m/s)
0.01
0.008
0.006
0.004
0.002
0
-0.002
-0.004
-0.006
-0.008
-0.01
0.01
0.02
0.03
0.04
0.05
0.06
0.07
0.08
x2 distance from Probe 2 (m)
101.2G Fluxball EFH1 95Hz
101.2G Fluxball EFH1 47Hz
75.9G Fluxball EFH1 15Hz
101.2G Fluxball MSGW11 95Hz
101.2G Fluxball MSGW11 47Hz
75.9G Fluxball MSGW11 15Hz

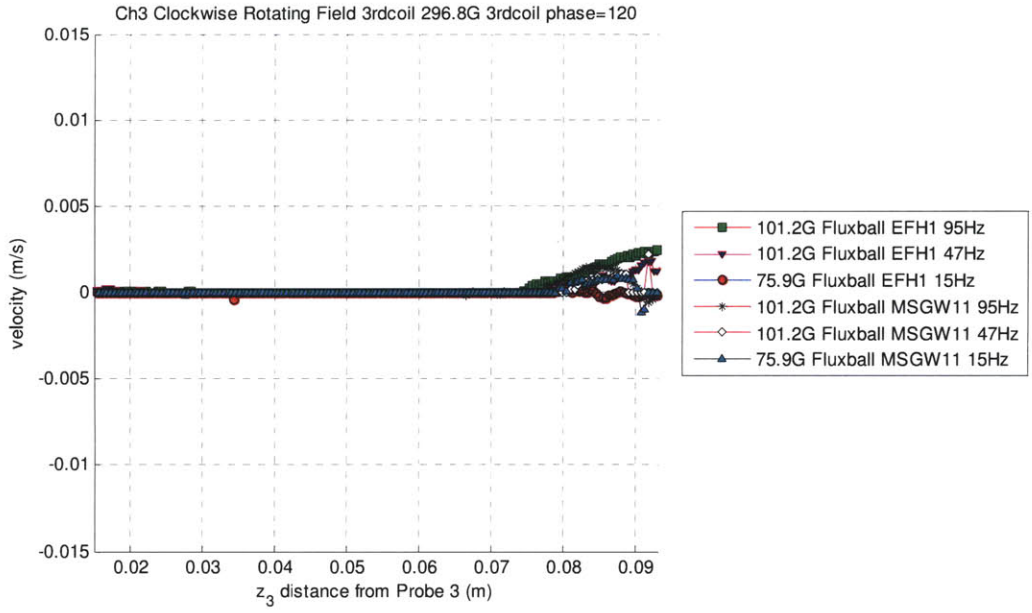
Ch3 Clockwise Rotating Field 3rdcoil 296.8G 3rdcoil phase=120
velocity (m/s)
0.015
0.01
0.005
0
-0.005
-0.01
-0.015
0.02
0.03
0.04
0.05
0.06
0.07
0.08
0.09
z3 distance from Probe 3 (m)
101.2G Fluxball EFH1 95Hz
101.2G Fluxball EFH1 47Hz
75.9G Fluxball EFH1 15Hz
101.2G Fluxball MSGW11 95Hz
101.2G Fluxball MSGW11 47Hz
75.9G Fluxball MSGW11 15Hz

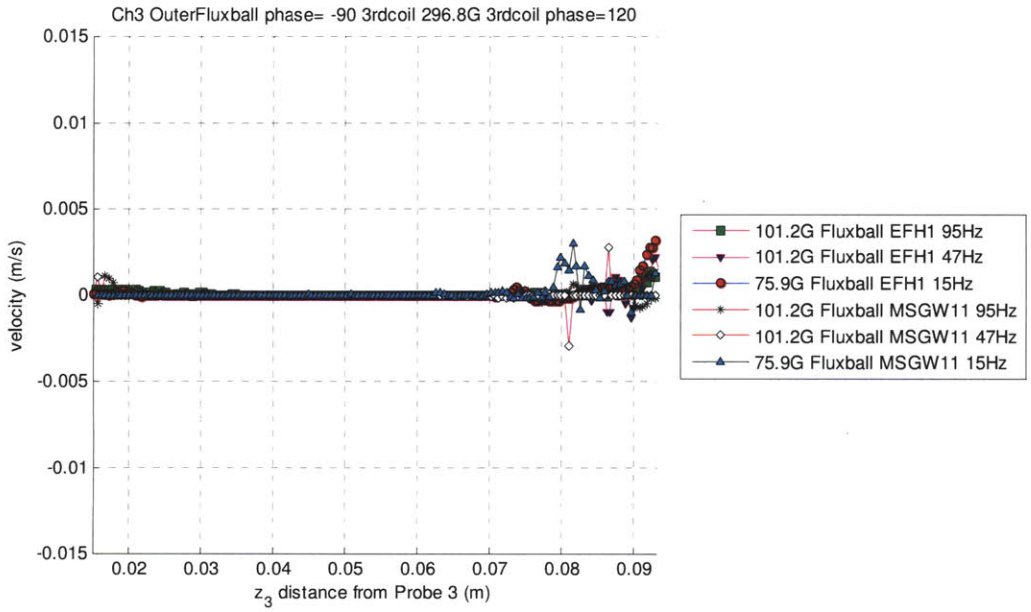
Ch3 OuterFluxball phase= -90 3rdcoil 296.8G 3rdcoil phase=120
velocity (m/s)
0.015
0.01
0.005
0
-0.005
-0.01
-0.015
0.02
0.03
0.04
0.05
0.06
0.07
0.08
0.09
z3 distance from Probe 3 (m)
101.2G Fluxball EFH1 95Hz
101.2G Fluxball EFH1 47Hz
75.9G Fluxball EFH1 15Hz
101.2G Fluxball MSGW11 95Hz
101.2G Fluxball MSGW11 47Hz
75.9G Fluxball MSGW11 15Hz

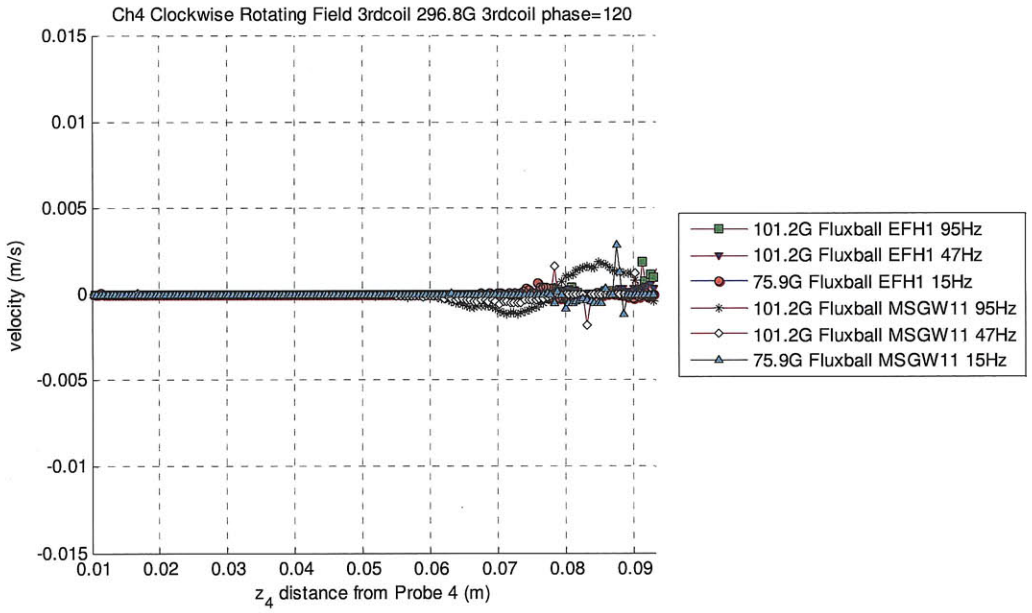
Ch4 Clockwise Rotating Field 3rdcoil 296.8G 3rdcoil phase=120
velocity (m/s)
0.015
0.01
0.005
0
-0.005
-0.01
-0.015
0.01
0.02
0.03
0.04
0.05
0.06
0.07
0.08
0.09
z4 distance from Probe 4 (m)
101.2G Fluxball EFH1 95Hz
101.2G Fluxball EFH1 47Hz
75.9G Fluxball EFH1 15Hz
101.2G Fluxball MSGW11 95Hz
101.2G Fluxball MSGW11 47Hz
75.9G Fluxball MSGW11 15Hz

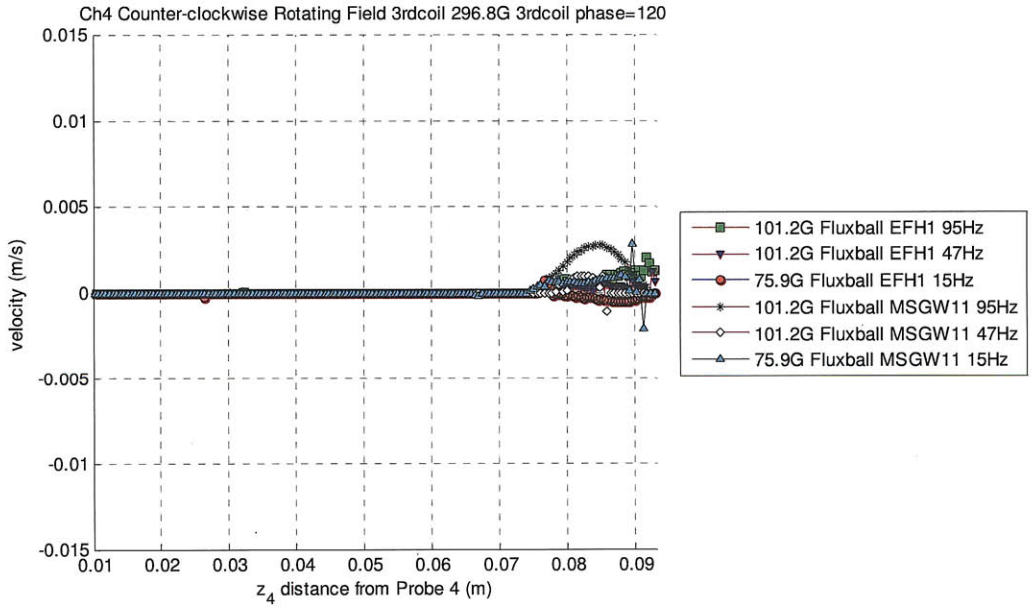
Ch4 Counter-clockwise Rotating Field 3rdcoil 296.8G 3rdcoil phase=120
velocity (m/s)
0.015
0.01
0.005
0
-0.005
-0.01
-0.015
0.01
0.02
0.03
0.04
0.05
0.06
0.07
0.08
0.09
z4 distance from Probe 4 (m)
101.2G Fluxball EFH1 95Hz
101.2G Fluxball EFH1 47Hz
75.9G Fluxball EFH1 15Hz
101.2G Fluxball MSGW11 95Hz
101.2G Fluxball MSGW11 47Hz
75.9G Fluxball MSGW11 15Hz

G13. Comparison of Different Fluids with Third Coil Oscillating at Different Frequencies with Phase Difference=-120 with Respect to Inner Coil

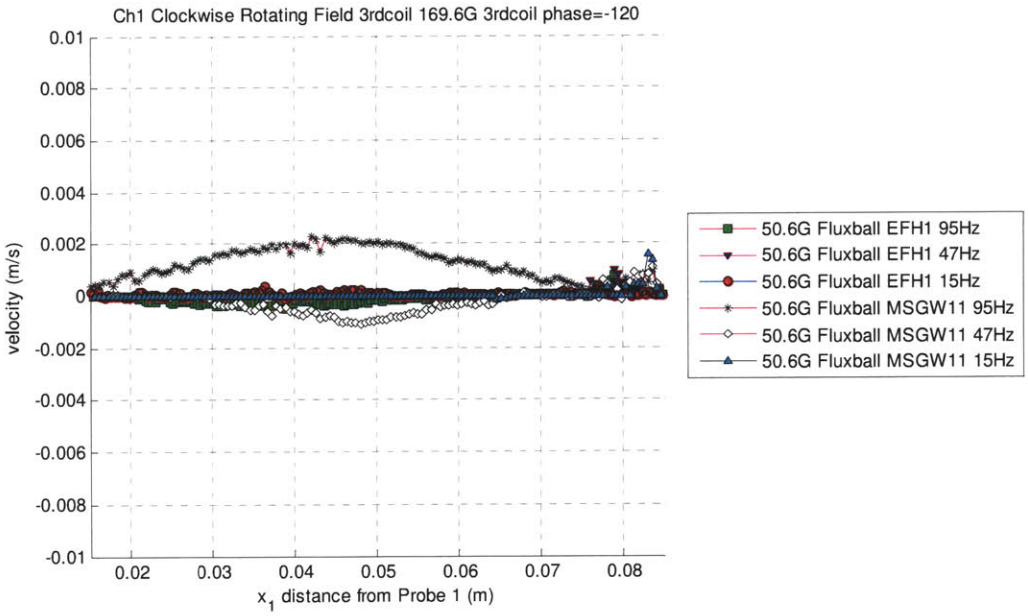

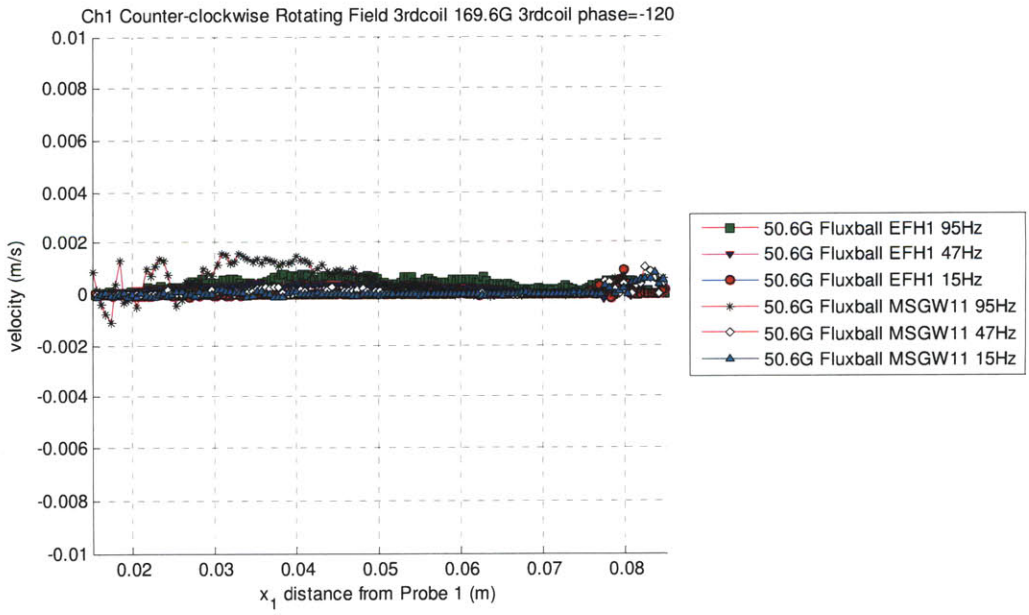

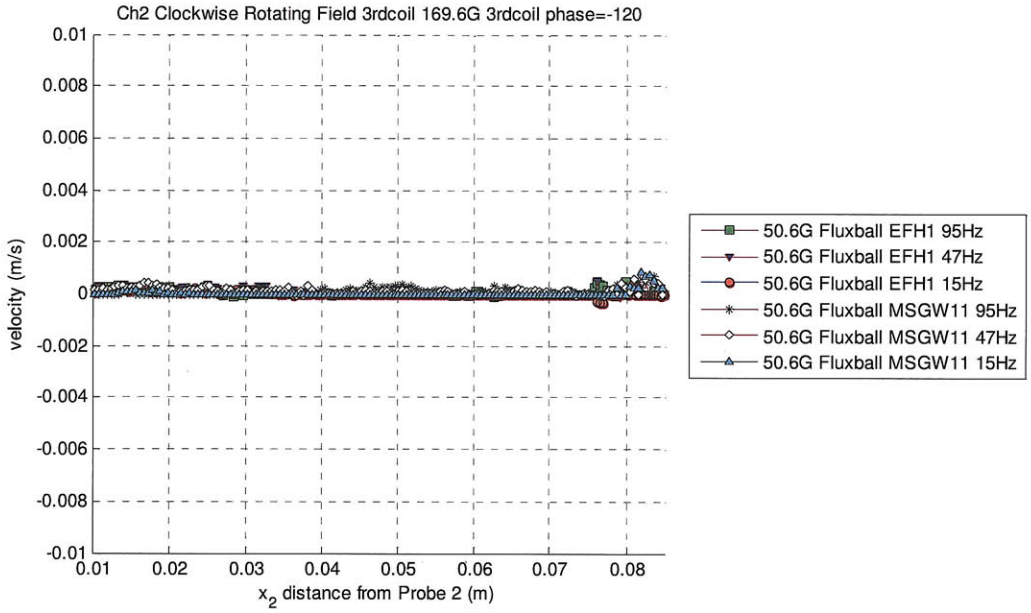
Ch2 Clockwise Rotating Field 3rdcoil 169.6G 3rdcoil phase=-120
velocity (m/s)
0.01
0.008
0.006
0.004
0.002
0
-0.002
-0.004
-0.006
-0.008
-0.01
0.01
0.02
0.03
0.04
0.05
0.06
0.07
0.08
x2 distance from Probe 2 (m)
50.6G Fluxball EFH1 95Hz
50.6G Fluxball EFH1 47Hz
50.6G Fluxball EFH1 15Hz
50.6G Fluxball MSGW11 95Hz
50.6G Fluxball MSGW11 47Hz
50.6G Fluxball MSGW11 15Hz

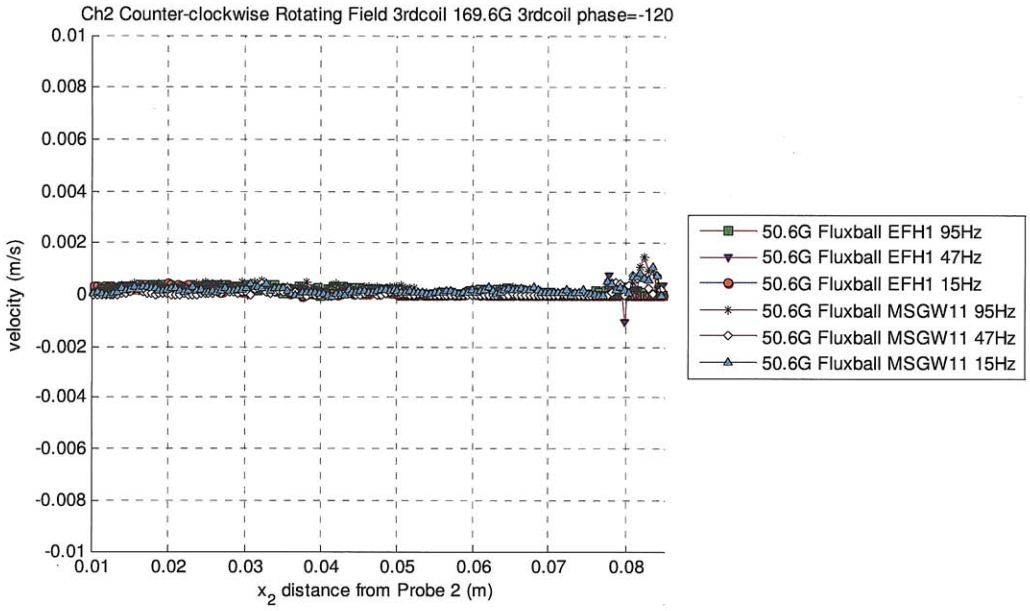
Ch2 Counter-clockwise Rotating Field 3rdcoil 169.6G 3rdcoil phase=-120
velocity (m/s)
0.01
0.008
0.006
0.004
0.002
0
-0.002
-0.004
-0.006
-0.008
-0.01
0.01
0.02
0.03
0.04
0.05
0.06
0.07
0.08
x2 distance from Probe 2 (m)
50.6G Fluxball EFH1 95Hz
50.6G Fluxball EFH1 47Hz
50.6G Fluxball EFH1 15Hz
50.6G Fluxball MSGW11 95Hz
50.6G Fluxball MSGW11 47Hz
50.6G Fluxball MSGW11 15Hz

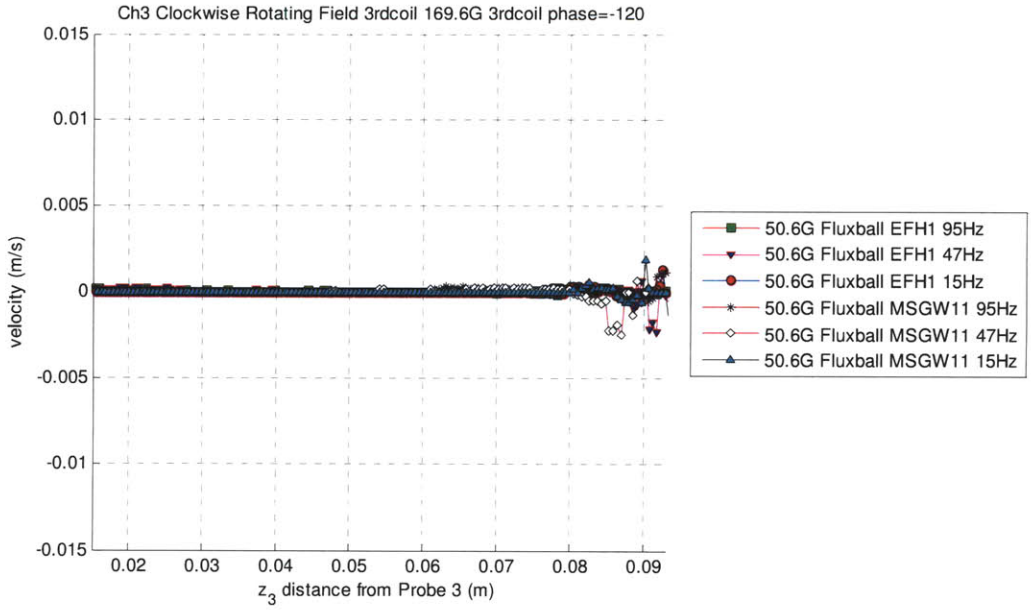
Ch3 Clockwise Rotating Field 3rdcoil 169.6G 3rdcoil phase=-120
velocity (m/s)
0.015
0.01
0.005
0
-0.005
-0.01
-0.015
0.02
0.03
0.04
0.05
0.06
0.07
0.08
0.09
z3 distance from Probe 3 (m)
50.6G Fluxball EFH1 95Hz
50.6G Fluxball EFH1 47Hz
50.6G Fluxball EFH1 15Hz
50.6G Fluxball MSGW11 95Hz
50.6G Fluxball MSGW11 47Hz
50.6G Fluxball MSGW11 15Hz

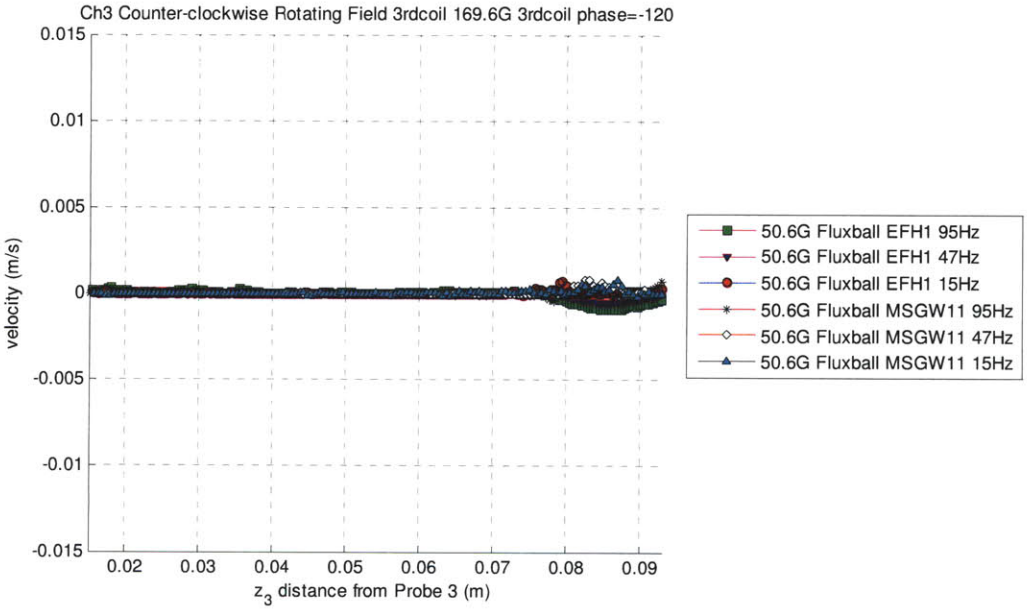
Ch3 Counter-clockwise Rotating Field 3rdcoil 169.6G 3rdcoil phase=-120
velocity (m/s)
0.015
0.01
0.005
0
-0.005
-0.01
-0.015
0.02
0.03
0.04
0.05
0.06
0.07
0.08
0.09
z3 distance from Probe 3 (m)
50.6G Fluxball EFH1 95Hz
50.6G Fluxball EFH1 47Hz
50.6G Fluxball EFH1 15Hz
50.6G Fluxball MSGW11 95Hz
50.6G Fluxball MSGW11 47Hz
50.6G Fluxball MSGW11 15Hz

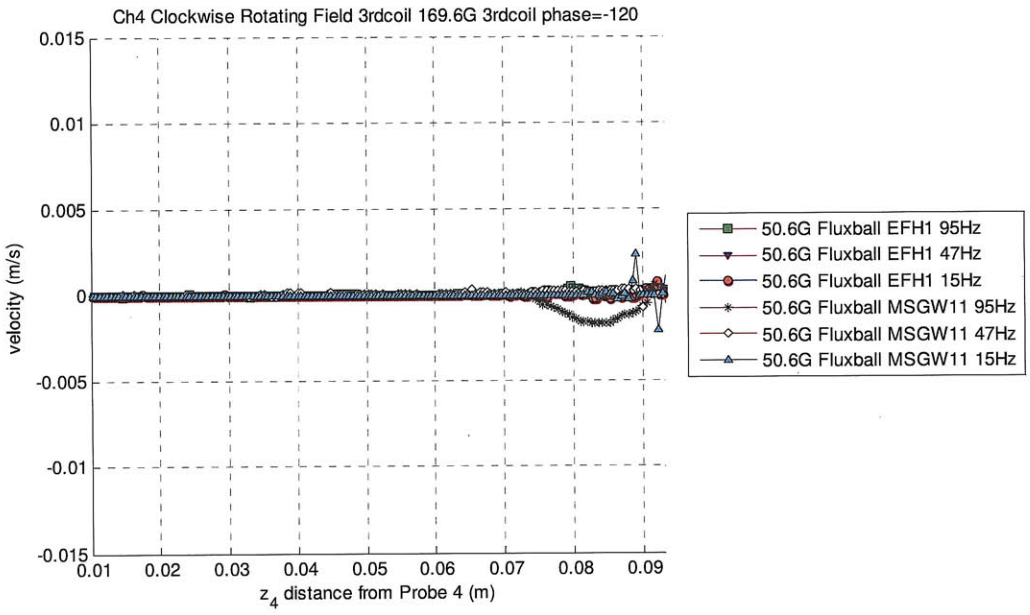
Ch4 Clockwise Rotating Field 3rdcoil 169.6G 3rdcoil phase=-120
velocity (m/s)
0.015
0.01
0.005
0
-0.005
-0.01
-0.015
0.01
0.02
0.03
0.04
0.05
0.06
0.07
0.08
0.09
z4 distance from Probe 4 (m)
50.6G Fluxball EFH1 95Hz
50.6G Fluxball EFH1 47Hz
50.6G Fluxball EFH1 15Hz
50.6G Fluxball MSGW11 95Hz
50.6G Fluxball MSGW11 47Hz
50.6G Fluxball MSGW11 15Hz

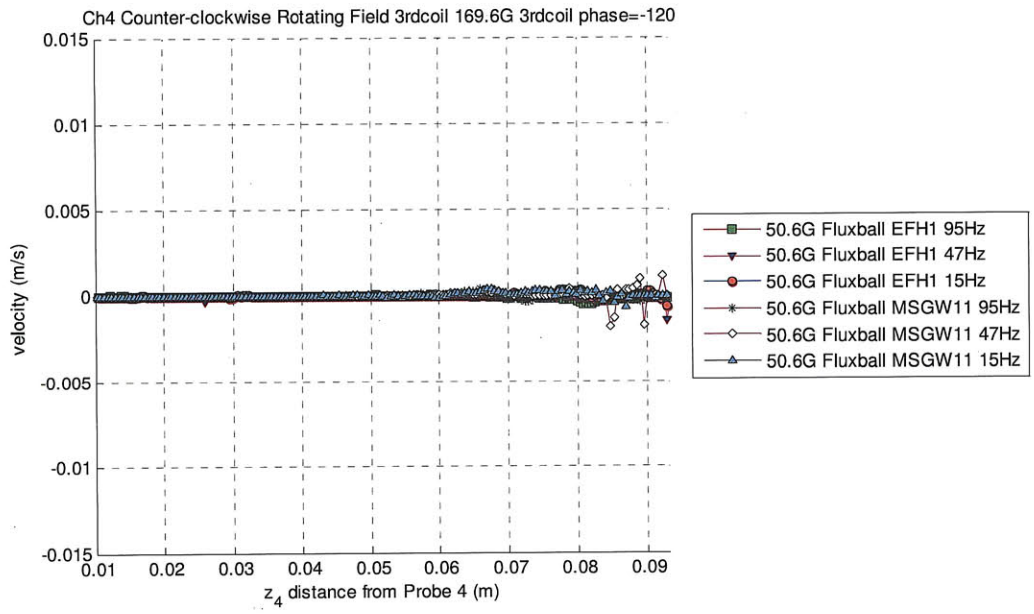
Ch4 Counter-clockwise Rotating Field 3rdcoil 169.6G 3rdcoil phase=-120
velocity (m/s)
0.015
0.01
0.005
0
-0.005
-0.01
-0.015
0.01
0.02
0.03
0.04
0.05
0.06
0.07
0.08
0.09
z4 distance from Probe 4 (m)
50.6G Fluxball EFH1 95Hz
50.6G Fluxball EFH1 47Hz
50.6G Fluxball EFH1 15Hz
50.6G Fluxball MSGW11 95Hz
50.6G Fluxball MSGW11 47Hz
50.6G Fluxball MSGW11 15Hz

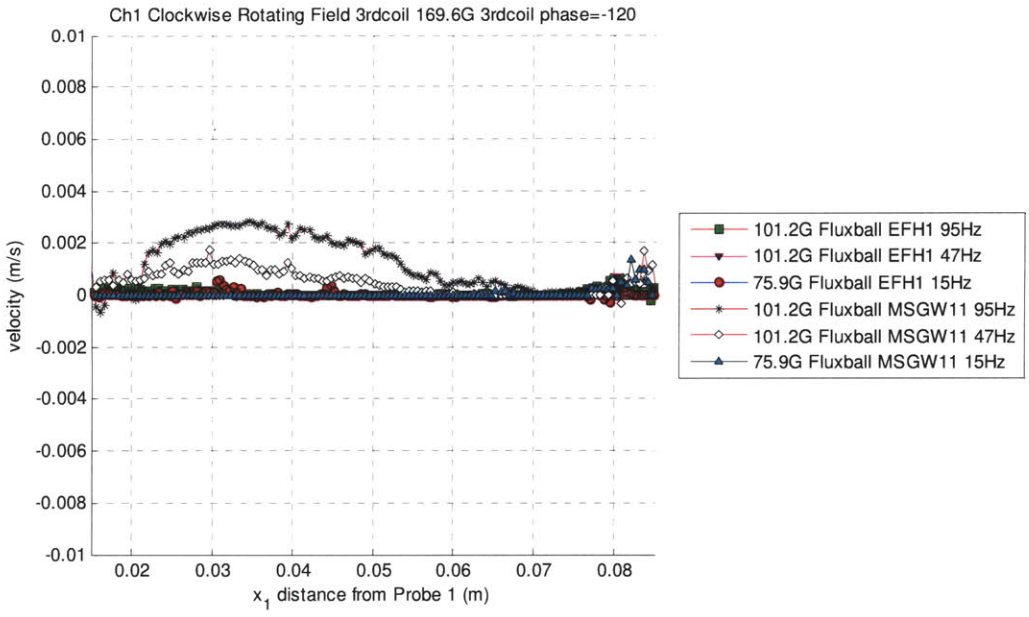
Ch1 Clockwise Rotating Field 3rdcoil 169.6G 3rdcoil phase=-120
velocity (m/s)
0.01
0.008
0.006
0.004
0.002
0
-0.002
-0.004
-0.006
-0.008
-0.01
0.02
0.03
0.04
0.05
0.06
0.07
0.08
x1 distance from Probe 1 (m)
101.2G Fluxball EFH1 95Hz
101.2G Fluxball EFH1 47Hz
75.9G Fluxball EFH1 15Hz
101.2G Fluxball MSGW11 95Hz
101.2G Fluxball MSGW11 47Hz
75.9G Fluxball MSGW11 15Hz

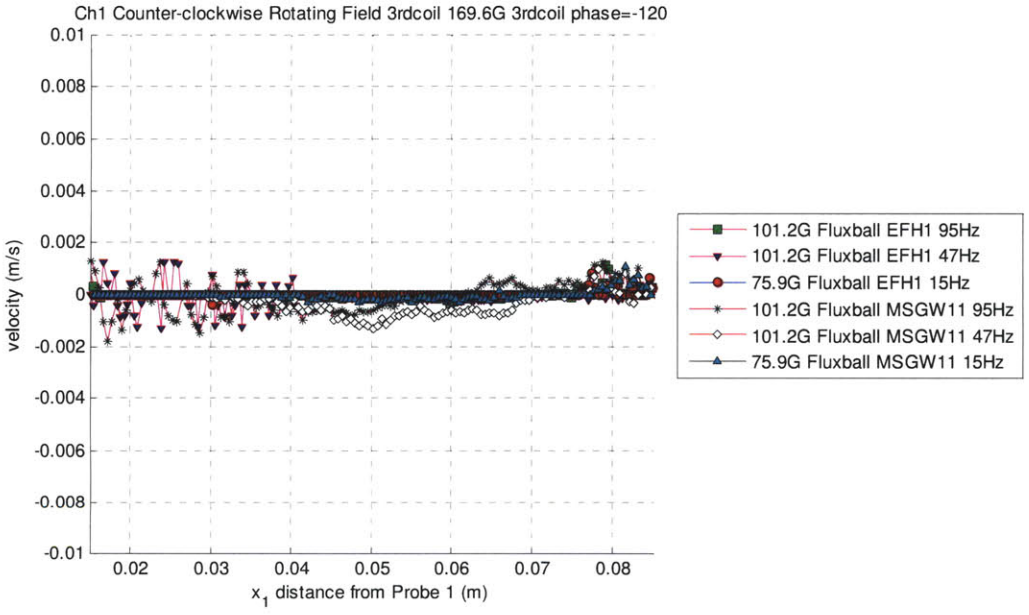
Ch1 Counter-clockwise Rotating Field 3rdcoil 169.6G 3rdcoil phase=-120
velocity (m/s)
0.01
0.008
0.006
0.004
0.002
0
-0.002
-0.004
-0.006
-0.008
-0.01
0.02
0.03
0.04
0.05
0.06
0.07
0.08
x1 distance from Probe 1 (m)
101.2G Fluxball EFH1 95Hz
101.2G Fluxball EFH1 47Hz
75.9G Fluxball EFH1 15Hz
101.2G Fluxball MSGW11 95Hz
101.2G Fluxball MSGW11 47Hz
75.9G Fluxball MSGW11 15Hz

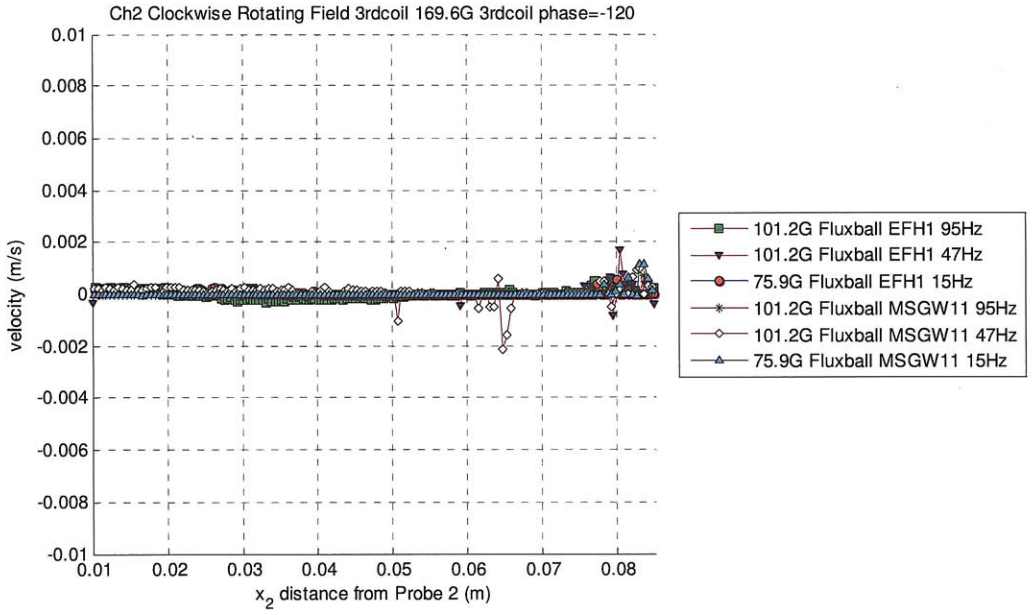
Ch2 Clockwise Rotating Field 3rdcoil 169.6G 3rdcoil phase=-120
velocity (m/s)
0.01
0.008
0.006
0.004
0.002
0
-0.002
-0.004
-0.006
-0.008
-0.01
0.01
0.02
0.03
0.04
0.05
0.06
0.07
0.08
x2 distance from Probe 2 (m)
101.2G Fluxball EFH1 95Hz
101.2G Fluxball EFH1 47Hz
75.9G Fluxball EFH1 15Hz
101.2G Fluxball MSGW11 95Hz
101.2G Fluxball MSGW11 47Hz
75.9G Fluxball MSGW11 15Hz

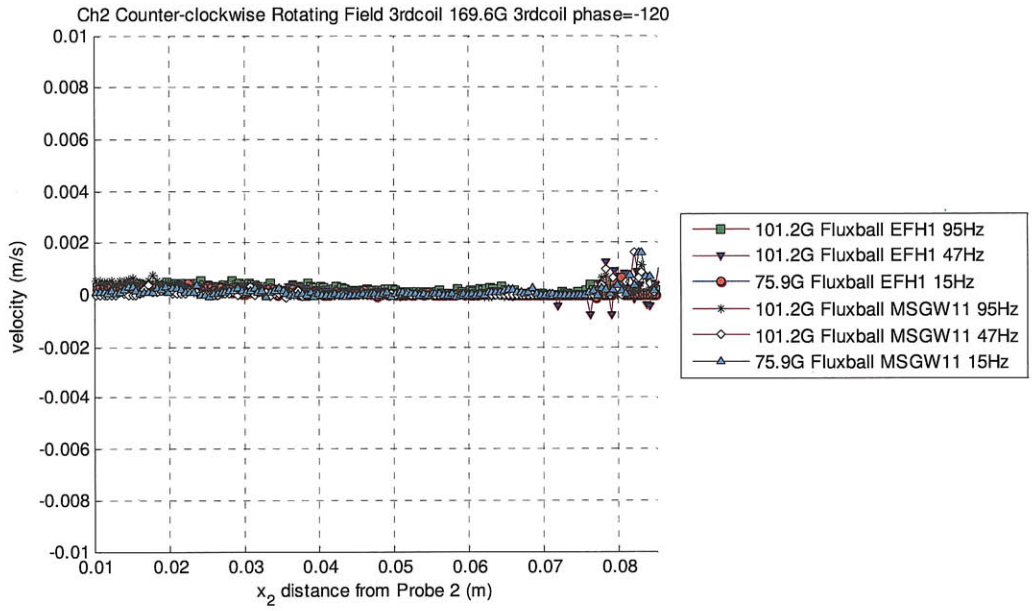
Ch2 Counter-clockwise Rotating Field 3rdcoil 169.6G 3rdcoil phase=-120
velocity (m/s)
0.01
0.008
0.006
0.004
0.002
0
-0.002
-0.004
-0.006
-0.008
-0.01
0.01
0.02
0.03
0.04
0.05
0.06
0.07
0.08
x2 distance from Probe 2 (m)
101.2G Fluxball EFH1 95Hz
101.2G Fluxball EFH1 47Hz
75.9G Fluxball EFH1 15Hz
101.2G Fluxball MSGW11 95Hz
101.2G Fluxball MSGW11 47Hz
75.9G Fluxball MSGW11 15Hz

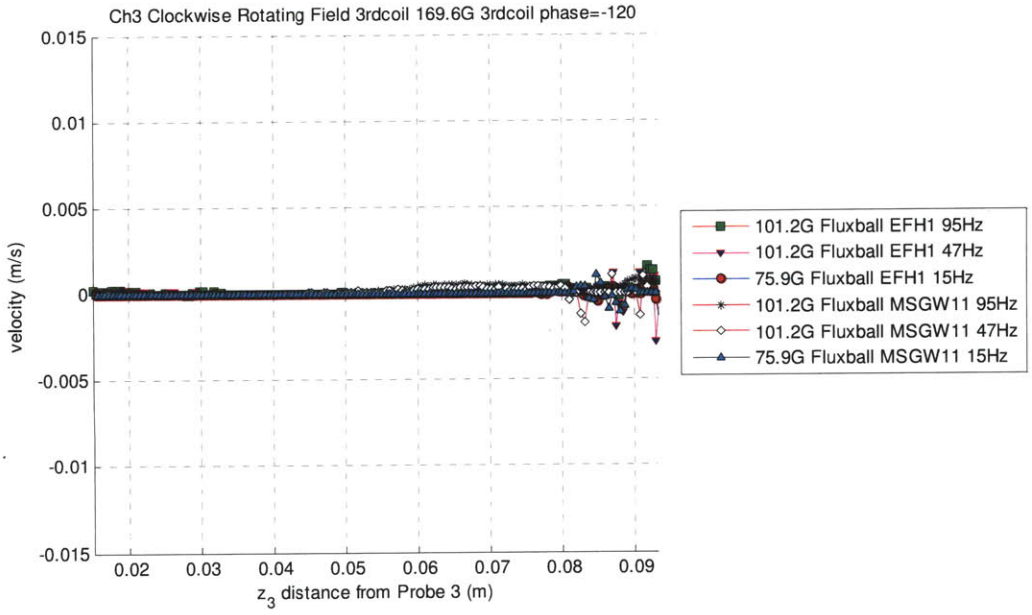
Ch3 Clockwise Rotating Field 3rdcoil 169.6G 3rdcoil phase=-120
velocity (m/s)
0.015
0.01
0.005
0
-0.005
-0.01
-0.015
0.02
0.03
0.04
0.05
0.06
0.07
0.08
0.09
z_3 distance from Probe 3 (m)
101.2G Fluxball EFH1 95Hz
101.2G Fluxball EFH1 47Hz
75.9G Fluxball EFH1 15Hz
101.2G Fluxball MSGW11 95Hz
101.2G Fluxball MSGW11 47Hz
75.9G Fluxball MSGW11 15Hz

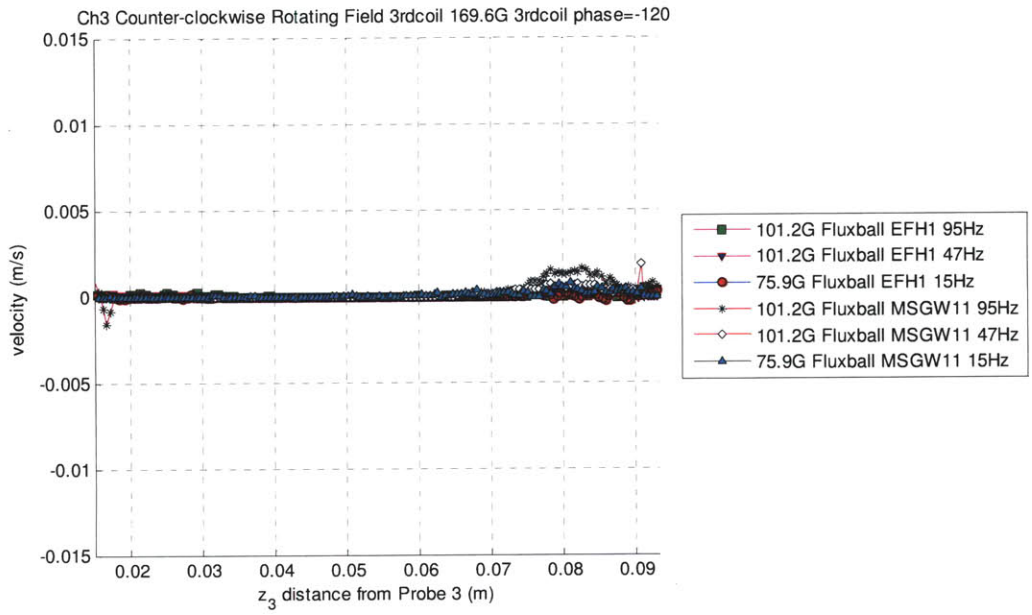
Ch3 Counter-clockwise Rotating Field 3rdcoil 169.6G 3rdcoil phase=-120
velocity (m/s)
0.015
0.01
0.005
0
-0.005
-0.01
-0.015
0.02
0.03
0.04
0.05
0.06
0.07
0.08
0.09
z_3 distance from Probe 3 (m)
101.2G Fluxball EFH1 95Hz
101.2G Fluxball EFH1 47Hz
75.9G Fluxball EFH1 15Hz
101.2G Fluxball MSGW11 95Hz
101.2G Fluxball MSGW11 47Hz
75.9G Fluxball MSGW11 15Hz

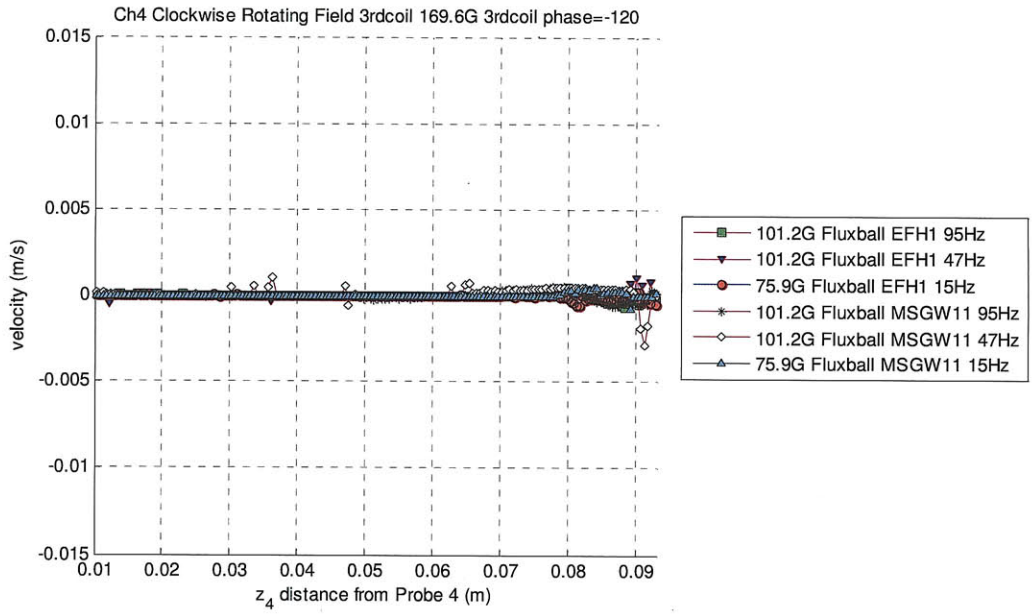
Ch4 Clockwise Rotating Field 3rdcoil 169.6G 3rdcoil phase=-120
velocity (m/s)
0.015
0.01
0.005
0
-0.005
-0.01
-0.015
0.01
0.02
0.03
0.04
0.05
0.06
0.07
0.08
0.09
z4 distance from Probe 4 (m)
101.2G Fluxball EFH1 95Hz
101.2G Fluxball EFH1 47Hz
75.9G Fluxball EFH1 15Hz
101.2G Fluxball MSGW11 95Hz
101.2G Fluxball MSGW11 47Hz
75.9G Fluxball MSGW11 15Hz

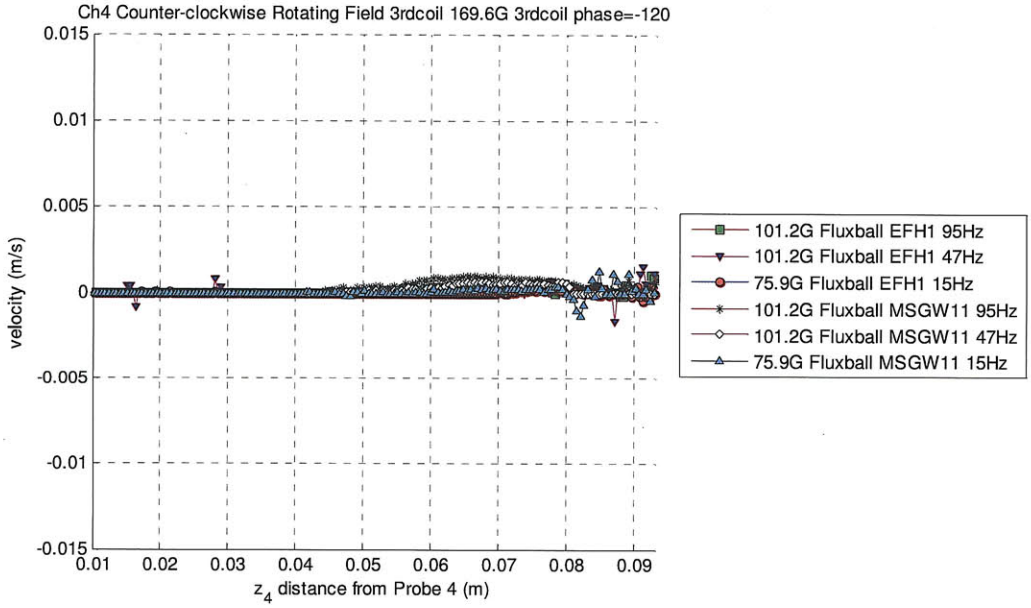
Ch4 Counter-clockwise Rotating Field 3rdcoil 169.6G 3rdcoil phase=-120
velocity (m/s)
0.015
0.01
0.005
0
-0.005
-0.01
-0.015
0.01
0.02
0.03
0.04
0.05
0.06
0.07
0.08
0.09
z4 distance from Probe 4 (m)
101.2G Fluxball EFH1 95Hz
101.2G Fluxball EFH1 47Hz
75.9G Fluxball EFH1 15Hz
101.2G Fluxball MSGW11 95Hz
101.2G Fluxball MSGW11 47Hz
75.9G Fluxball MSGW11 15Hz

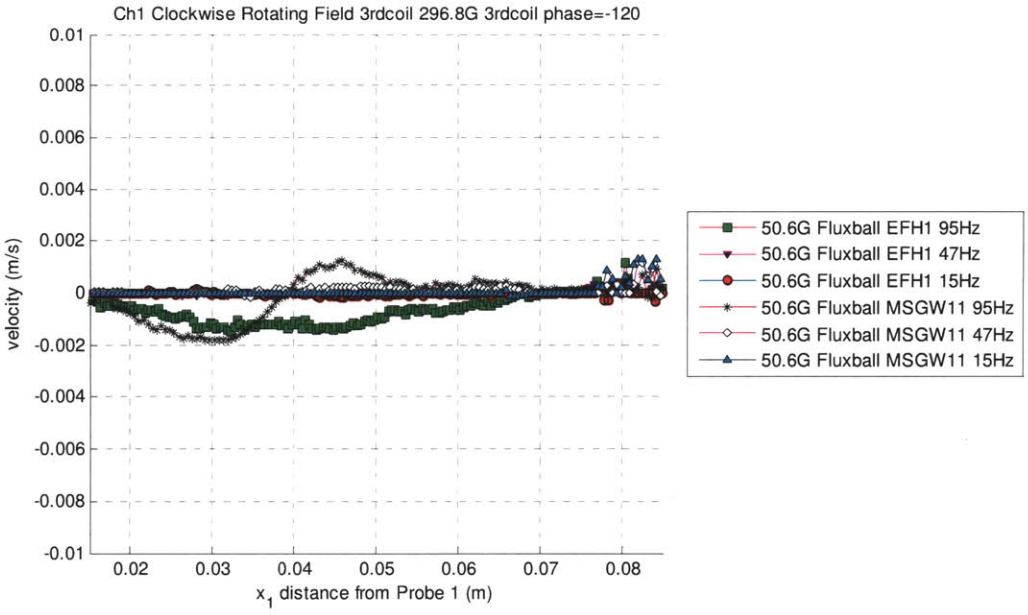
Ch1 Clockwise Rotating Field 3rdcoil 296.8G 3rdcoil phase=-120
velocity (m/s)
0.01
0.008
0.006
0.004
0.002
0
-0.002
-0.004
-0.006
-0.008
-0.01
0.02
0.03
0.04
0.05
0.06
0.07
0.08
x1 distance from Probe 1 (m)
50.6G Fluxball EFH1 95Hz
50.6G Fluxball EFH1 47Hz
50.6G Fluxball EFH1 15Hz
50.6G Fluxball MSGW11 95Hz
50.6G Fluxball MSGW11 47Hz
50.6G Fluxball MSGW11 15Hz

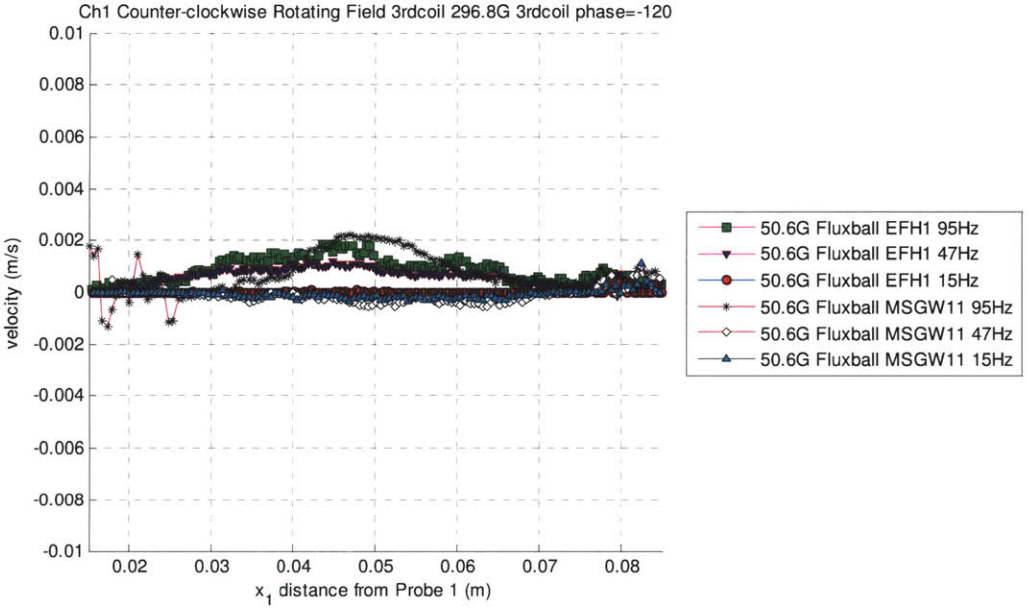
Ch1 Counter-clockwise Rotating Field 3rdcoil 296.8G 3rdcoil phase=-120
velocity (m/s)
0.01
0.008
0.006
0.004
0.002
0
-0.002
-0.004
-0.006
-0.008
-0.01
0.02
0.03
0.04
0.05
0.06
0.07
0.08
x1 distance from Probe 1 (m)
50.6G Fluxball EFH1 95Hz
50.6G Fluxball EFH1 47Hz
50.6G Fluxball EFH1 15Hz
50.6G Fluxball MSGW11 95Hz
50.6G Fluxball MSGW11 47Hz
50.6G Fluxball MSGW11 15Hz

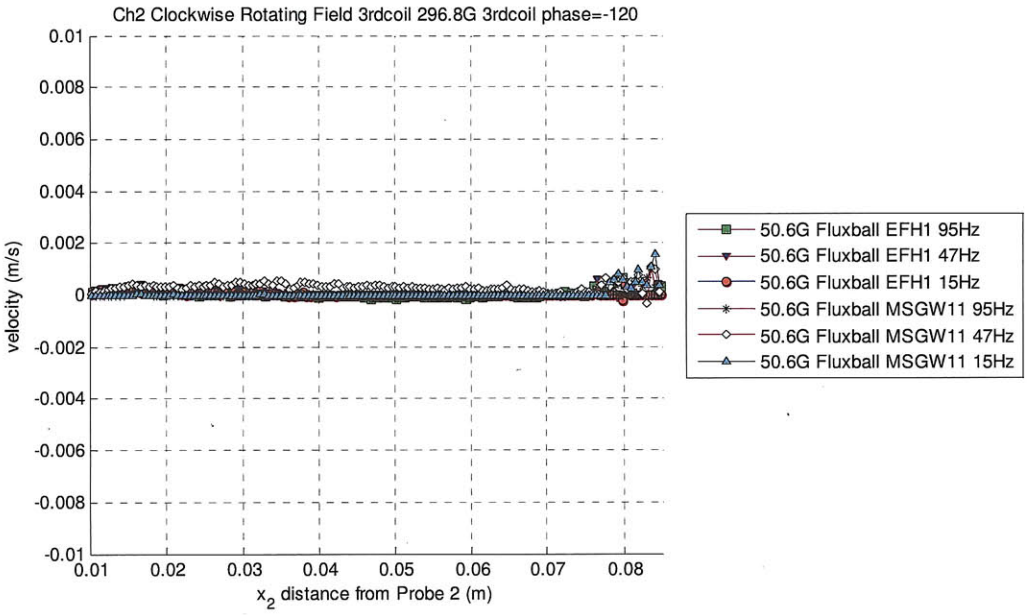
Ch2 Clockwise Rotating Field 3rdcoil 296.8G 3rdcoil phase=-120
velocity (m/s)
0.01
0.008
0.006
0.004
0.002
0
-0.002
-0.004
-0.006
-0.008
-0.01
0.01
0.02
0.03
0.04
0.05
0.06
0.07
0.08
x2 distance from Probe 2 (m)
50.6G Fluxball EFH1 95Hz
50.6G Fluxball EFH1 47Hz
50.6G Fluxball EFH1 15Hz
50.6G Fluxball MSGW11 95Hz
50.6G Fluxball MSGW11 47Hz
50.6G Fluxball MSGW11 15Hz

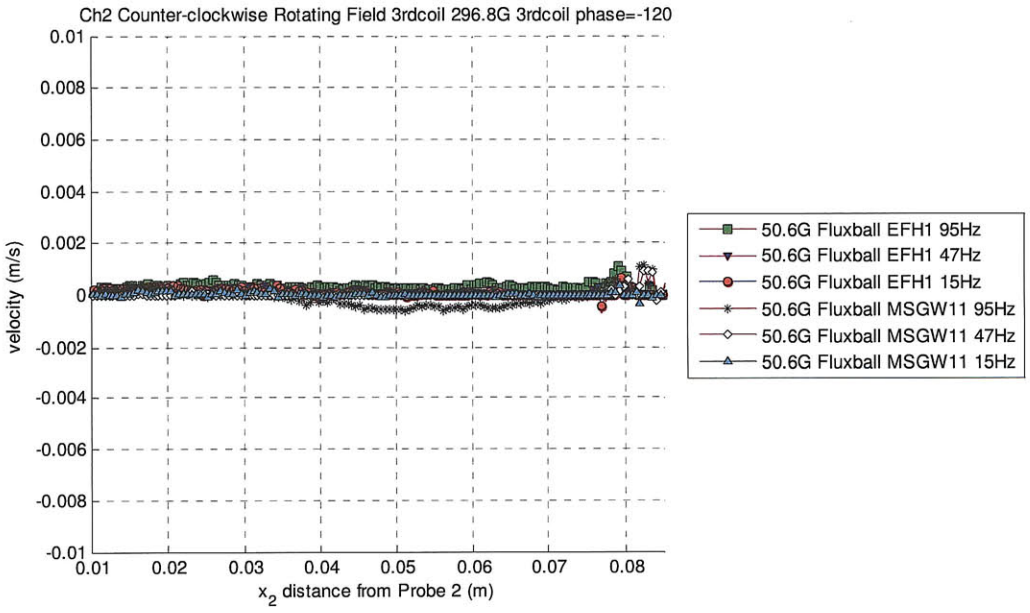
Ch2 Counter-clockwise Rotating Field 3rdcoil 296.8G 3rdcoil phase=-120
velocity (m/s)
0.01
0.008
0.006
0.004
0.002
0
-0.002
-0.004
-0.006
-0.008
-0.01
0.01
0.02
0.03
0.04
0.05
0.06
0.07
0.08
x2 distance from Probe 2 (m)
50.6G Fluxball EFH1 95Hz
50.6G Fluxball EFH1 47Hz
50.6G Fluxball EFH1 15Hz
50.6G Fluxball MSGW11 95Hz
50.6G Fluxball MSGW11 47Hz
50.6G Fluxball MSGW11 15Hz

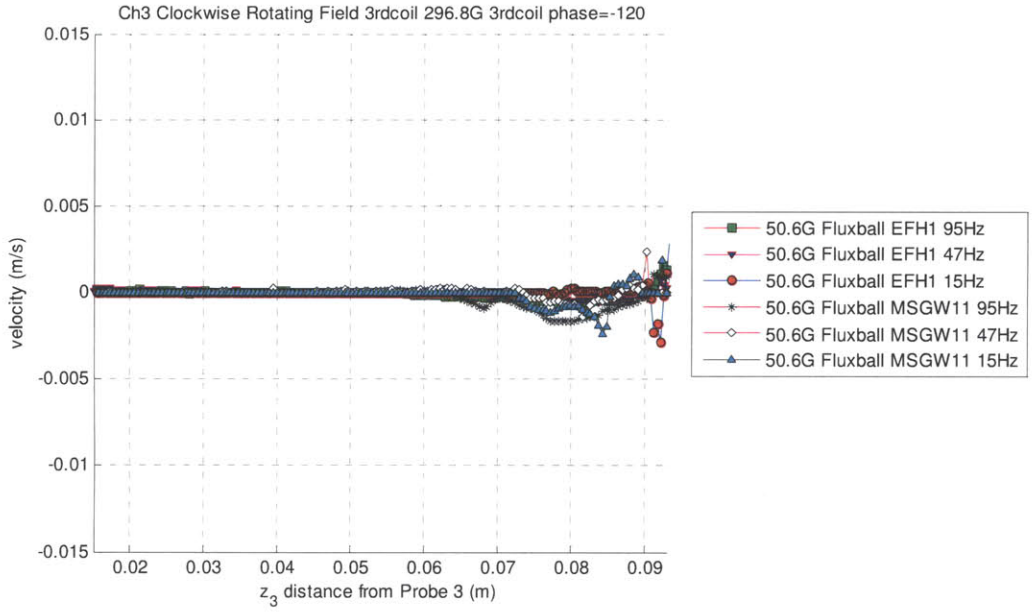
Ch3 Clockwise Rotating Field 3rdcoil 296.8G 3rdcoil phase=-120
velocity (m/s)
0.015
0.01
0.005
0
-0.005
-0.01
-0.015
0.02
0.03
0.04
0.05
0.06
0.07
0.08
0.09
z3 distance from Probe 3 (m)
50.6G Fluxball EFH1 95Hz
50.6G Fluxball EFH1 47Hz
50.6G Fluxball EFH1 15Hz
50.6G Fluxball MSGW11 95Hz
50.6G Fluxball MSGW11 47Hz
50.6G Fluxball MSGW11 15Hz

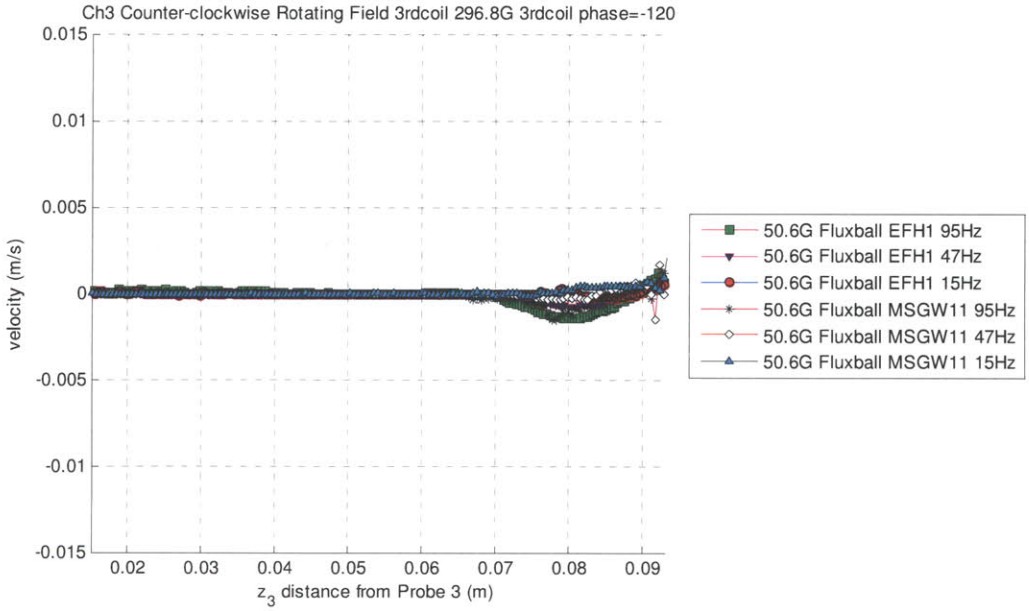
Ch3 Counter-clockwise Rotating Field 3rdcoil 296.8G 3rdcoil phase=-120
velocity (m/s)
0.015
0.01
0.005
0
-0.005
-0.01
-0.015
0.02
0.03
0.04
0.05
0.06
0.07
0.08
0.09
z3 distance from Probe 3 (m)
50.6G Fluxball EFH1 95Hz
50.6G Fluxball EFH1 47Hz
50.6G Fluxball EFH1 15Hz
50.6G Fluxball MSGW11 95Hz
50.6G Fluxball MSGW11 47Hz
50.6G Fluxball MSGW11 15Hz

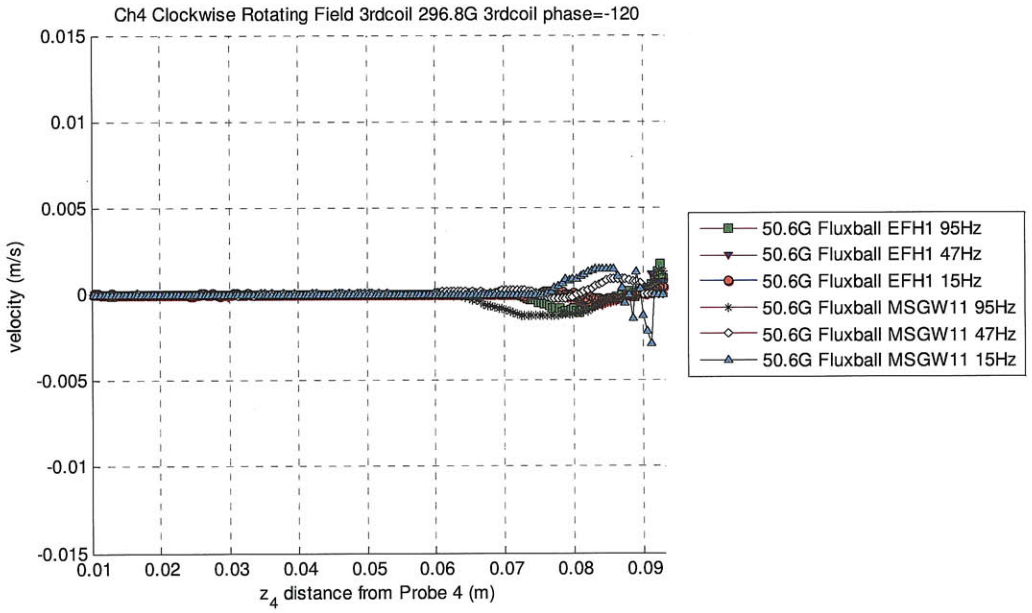
Ch4 Clockwise Rotating Field 3rdcoil 296.8G 3rdcoil phase=-120
0.015
0.01
0.005
0
-0.005
-0.01
-0.015
velocity (m/s)
0.01
0.02
0.03
0.04
0.05
0.06
0.07
0.08
0.09
z4 distance from Probe 4 (m)
50.6G Fluxball EFH1 95Hz
50.6G Fluxball EFH1 47Hz
50.6G Fluxball EFH1 15Hz
50.6G Fluxball MSGW11 95Hz
50.6G Fluxball MSGW11 47Hz
50.6G Fluxball MSGW11 15Hz

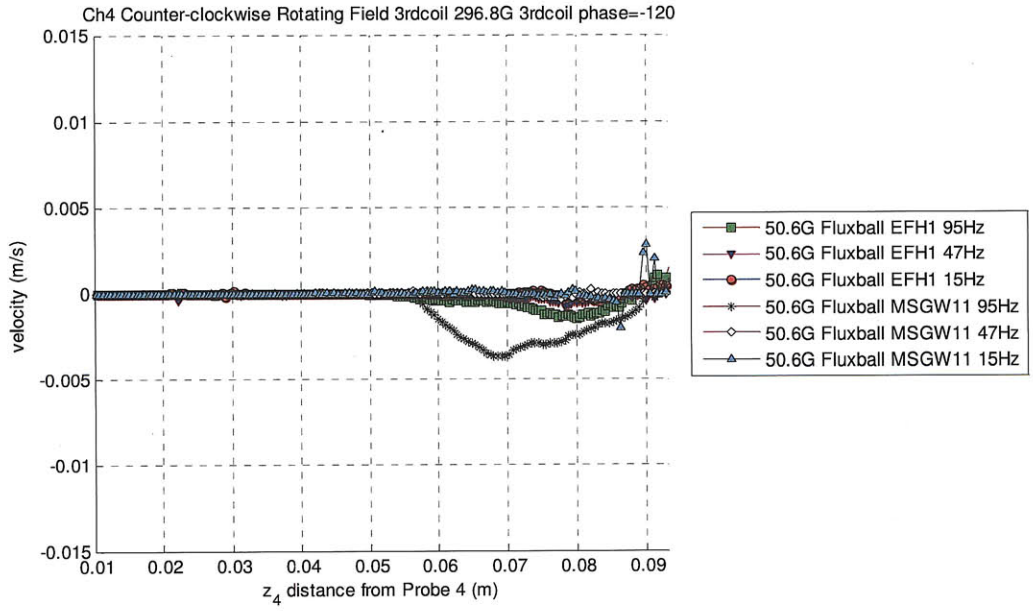
Ch4 Counter-clockwise Rotating Field 3rdcoil 296.8G 3rdcoil phase=-120
0.015
0.01
0.005
0
-0.005
-0.01
-0.015
velocity (m/s)
0.01
0.02
0.03
0.04
0.05
0.06
0.07
0.08
0.09
z4 distance from Probe 4 (m)
50.6G Fluxball EFH1 95Hz
50.6G Fluxball EFH1 47Hz
50.6G Fluxball EFH1 15Hz
50.6G Fluxball MSGW11 95Hz
50.6G Fluxball MSGW11 47Hz
50.6G Fluxball MSGW11 15Hz

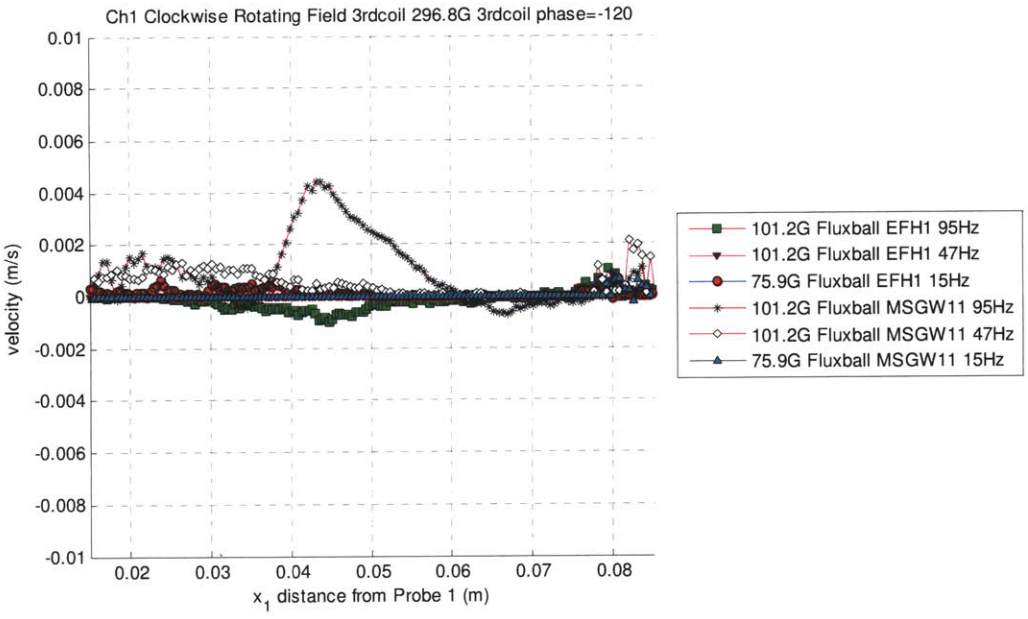
Ch1 Clockwise Rotating Field 3rdcoil 296.8G 3rdcoil phase=-120
velocity (m/s)
0.01
0.008
0.006
0.004
0.002
0
-0.002
-0.004
-0.006
-0.008
-0.01
0.02
0.03
0.04
0.05
0.06
0.07
0.08
x1 distance from Probe 1 (m)
101.2G Fluxball EFH1 95Hz
101.2G Fluxball EFH1 47Hz
75.9G Fluxball EFH1 15Hz
101.2G Fluxball MSGW11 95Hz
101.2G Fluxball MSGW11 47Hz
75.9G Fluxball MSGW11 15Hz

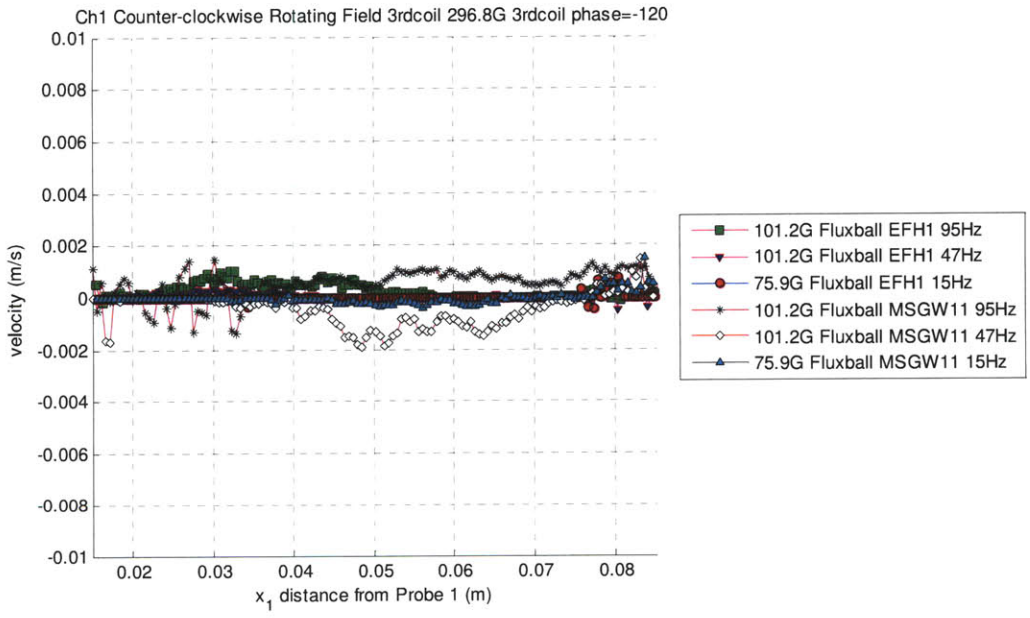
Ch1 Counter-clockwise Rotating Field 3rdcoil 296.8G 3rdcoil phase=-120
velocity (m/s)
0.01
0.008
0.006
0.004
0.002
0
-0.002
-0.004
-0.006
-0.008
-0.01
0.02
0.03
0.04
0.05
0.06
0.07
0.08
x1 distance from Probe 1 (m)
101.2G Fluxball EFH1 95Hz
101.2G Fluxball EFH1 47Hz
75.9G Fluxball EFH1 15Hz
101.2G Fluxball MSGW11 95Hz
101.2G Fluxball MSGW11 47Hz
75.9G Fluxball MSGW11 15Hz

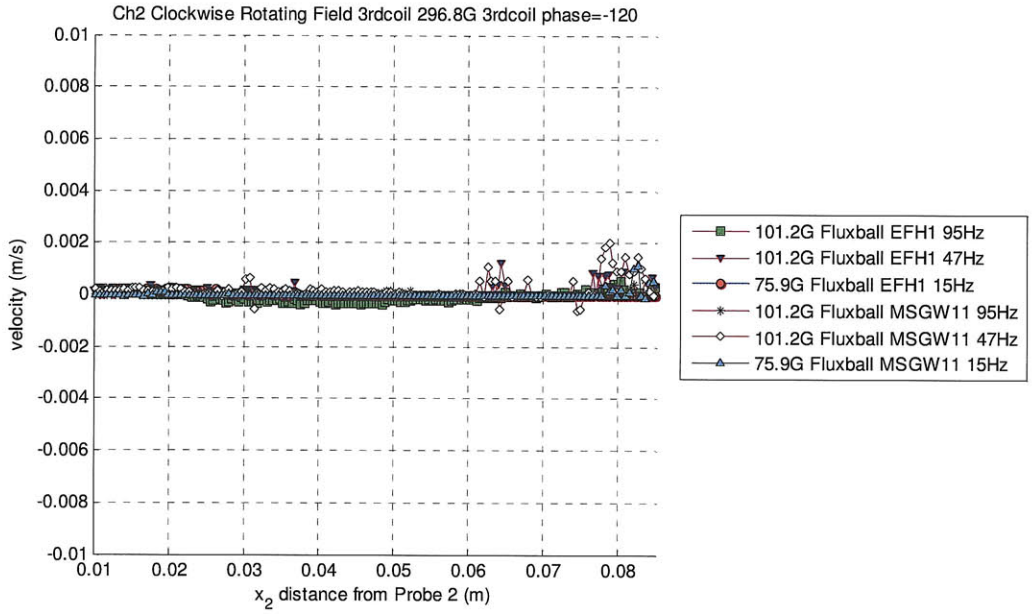
Ch2 Clockwise Rotating Field 3rdcoil 296.8G 3rdcoil phase=-120
velocity (m/s)
0.01
0.008
0.006
0.004
0.002
0
-0.002
-0.004
-0.006
-0.008
-0.01
0.01
0.02
0.03
0.04
0.05
0.06
0.07
0.08
x2 distance from Probe 2 (m)
101.2G Fluxball EFH1 95Hz
101.2G Fluxball EFH1 47Hz
75.9G Fluxball EFH1 15Hz
101.2G Fluxball MSGW11 95Hz
101.2G Fluxball MSGW11 47Hz
75.9G Fluxball MSGW11 15Hz

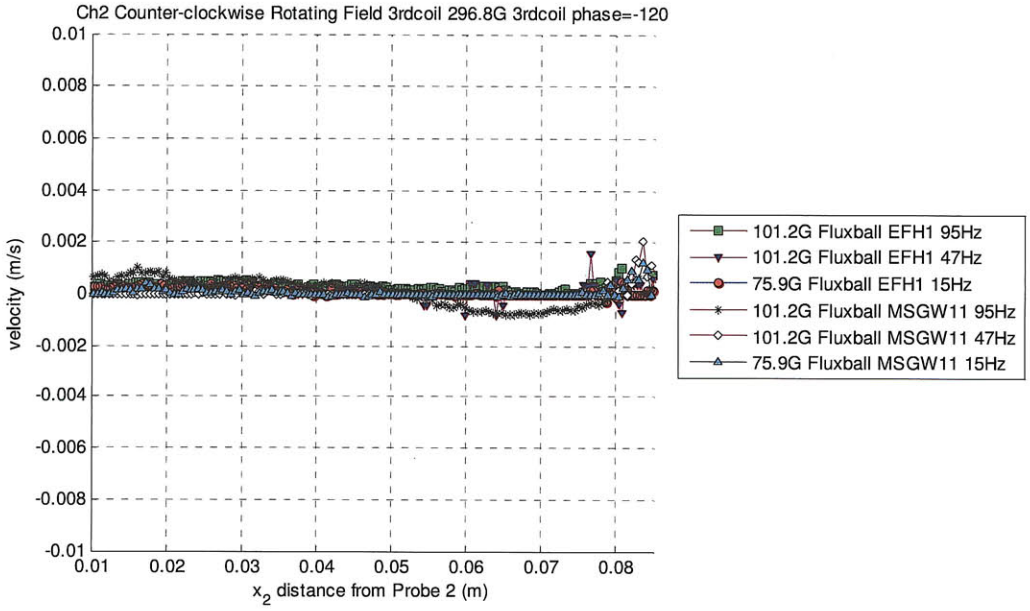
Ch2 Counter-clockwise Rotating Field 3rdcoil 296.8G 3rdcoil phase=-120
velocity (m/s)
0.01
0.008
0.006
0.004
0.002
0
-0.002
-0.004
-0.006
-0.008
-0.01
0.01
0.02
0.03
0.04
0.05
0.06
0.07
0.08
x2 distance from Probe 2 (m)
101.2G Fluxball EFH1 95Hz
101.2G Fluxball EFH1 47Hz
75.9G Fluxball EFH1 15Hz
101.2G Fluxball MSGW11 95Hz
101.2G Fluxball MSGW11 47Hz
75.9G Fluxball MSGW11 15Hz

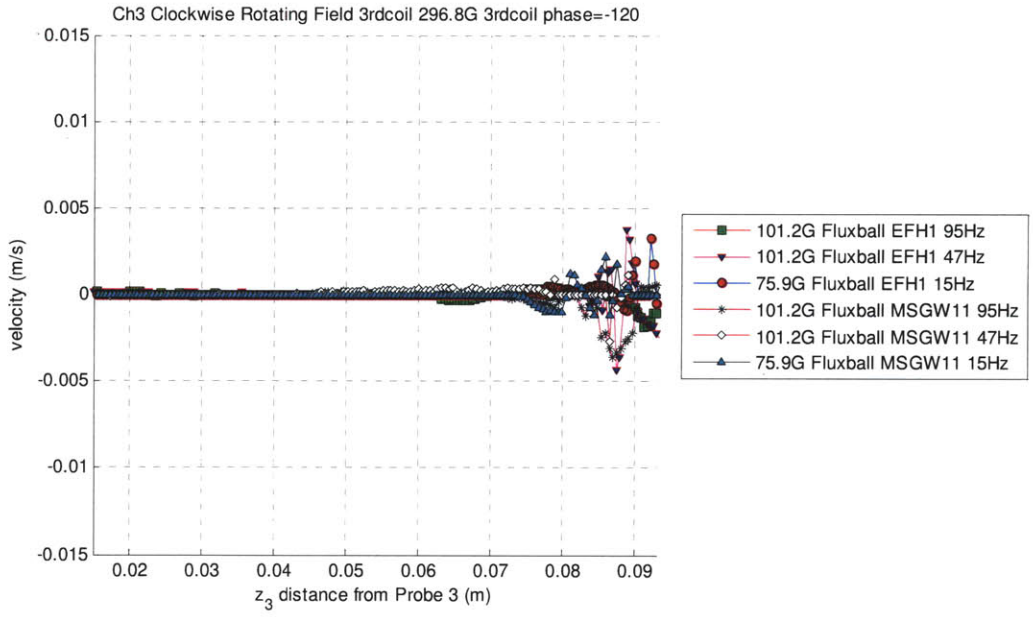
Ch3 Clockwise Rotating Field 3rdcoil 296.8G 3rdcoil phase=-120
velocity (m/s)
0.015
0.01
0.005
0
-0.005
-0.01
-0.015
0.02
0.03
0.04
0.05
0.06
0.07
0.08
0.09
z_3 distance from Probe 3 (m)
101.2G Fluxball EFH1 95Hz
101.2G Fluxball EFH1 47Hz
75.9G Fluxball EFH1 15Hz
101.2G Fluxball MSGW11 95Hz
101.2G Fluxball MSGW11 47Hz
75.9G Fluxball MSGW11 15Hz

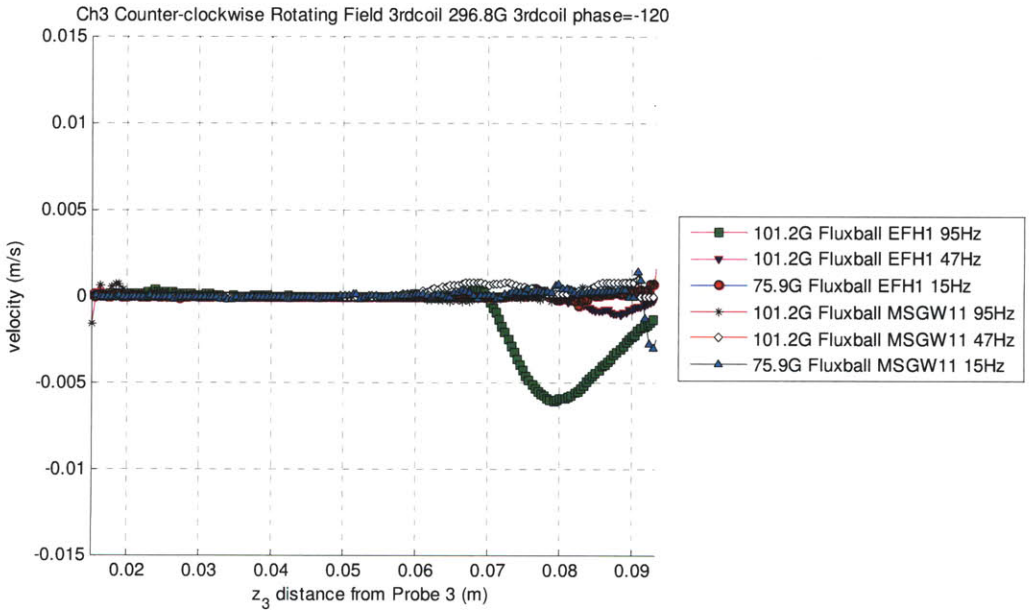
Ch3 Counter-clockwise Rotating Field 3rdcoil 296.8G 3rdcoil phase=-120
velocity (m/s)
0.015
0.01
0.005
0
-0.005
-0.01
-0.015
0.02
0.03
0.04
0.05
0.06
0.07
0.08
0.09
z_3 distance from Probe 3 (m)
101.2G Fluxball EFH1 95Hz
101.2G Fluxball EFH1 47Hz
75.9G Fluxball EFH1 15Hz
101.2G Fluxball MSGW11 95Hz
101.2G Fluxball MSGW11 47Hz
75.9G Fluxball MSGW11 15Hz

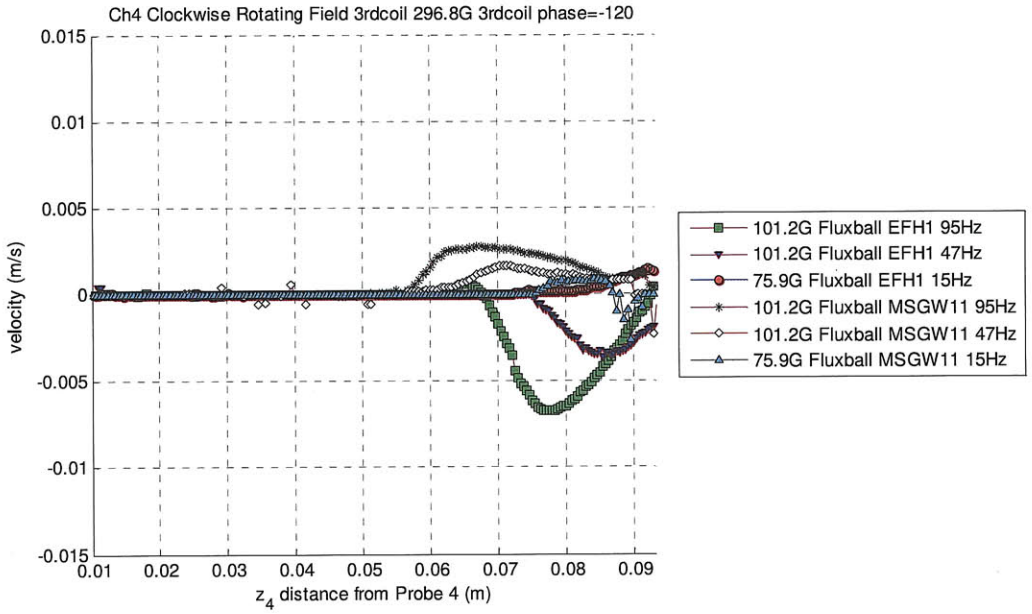
Ch4 Clockwise Rotating Field 3rdcoil 296.8G 3rdcoil phase=-120
velocity (m/s)
0.015
0.01
0.005
0
-0.005
-0.01
-0.015
0.01
0.02
0.03
0.04
0.05
0.06
0.07
0.08
0.09
z4 distance from Probe 4 (m)
101.2G Fluxball EFH1 95Hz
101.2G Fluxball EFH1 47Hz
75.9G Fluxball EFH1 15Hz
101.2G Fluxball MSGW11 95Hz
101.2G Fluxball MSGW11 47Hz
75.9G Fluxball MSGW11 15Hz

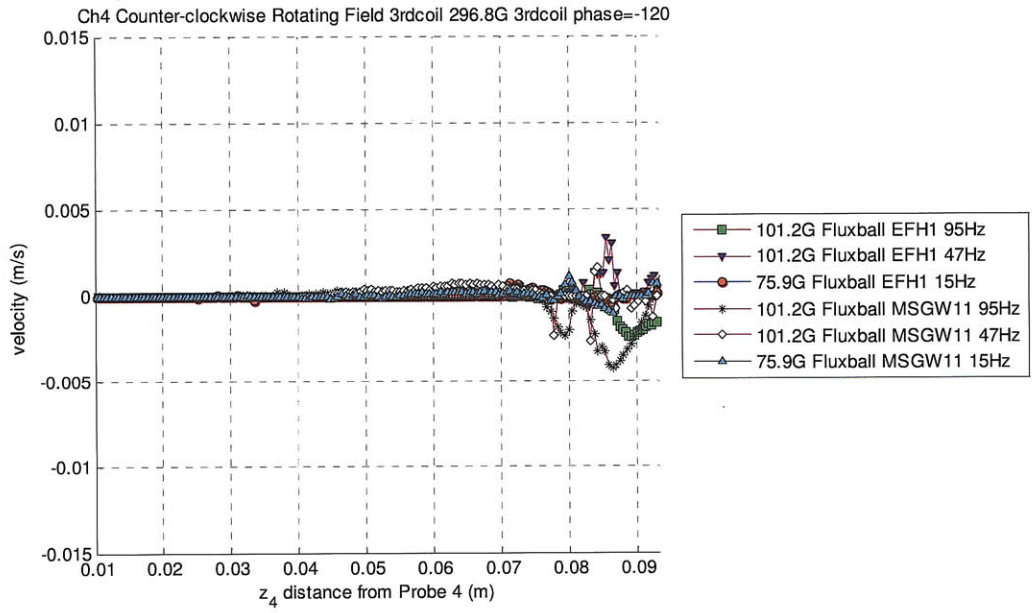
Ch4 Counter-clockwise Rotating Field 3rdcoil 296.8G 3rdcoil phase=-120
velocity (m/s)
0.015
0.01
0.005
0
-0.005
-0.01
-0.015
0.01
0.02
0.03
0.04
0.05
0.06
0.07
0.08
0.09
z4 distance from Probe 4 (m)
101.2G Fluxball EFH1 95Hz
101.2G Fluxball EFH1 47Hz
75.9G Fluxball EFH1 15Hz
101.2G Fluxball MSGW11 95Hz
101.2G Fluxball MSGW11 47Hz
75.9G Fluxball MSGW11 15Hz

G14. Comparison of Different Fluids with Third Coil Oscillating at Different Frequencies with Phase Difference=180 with Respect to Inner Coil

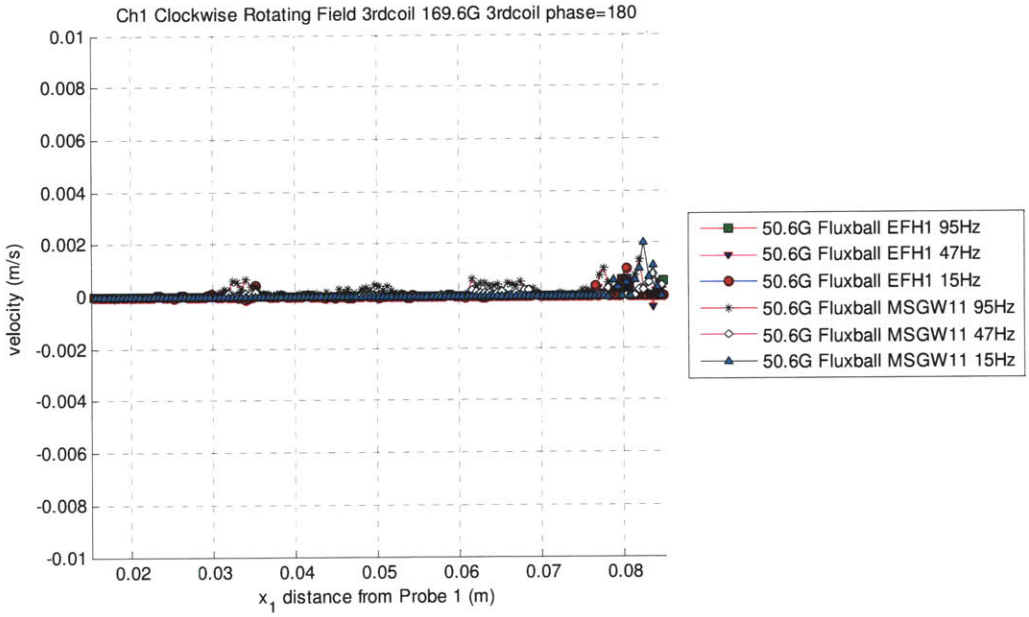

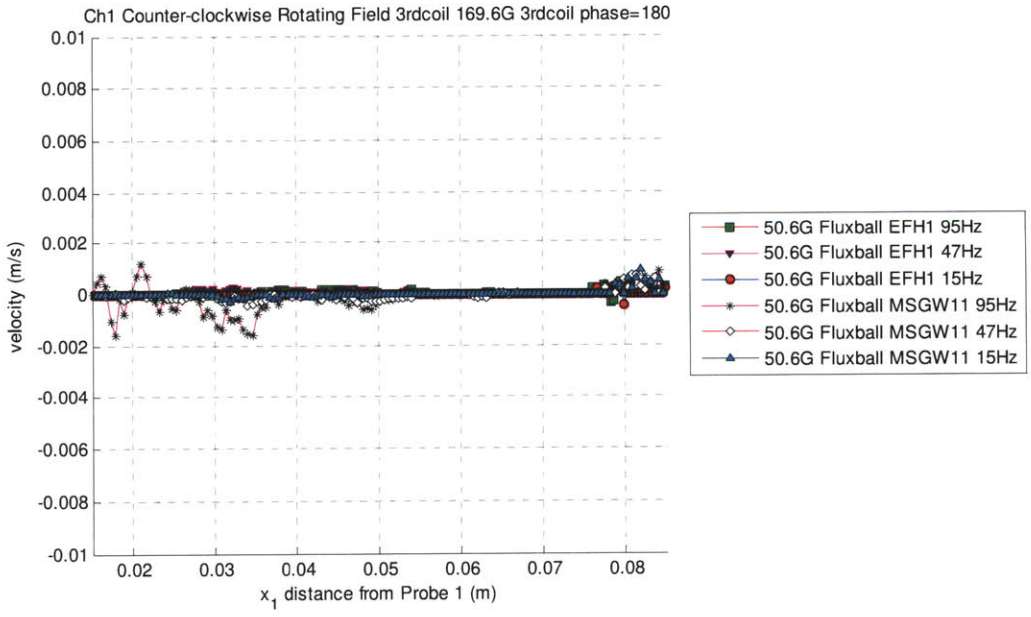

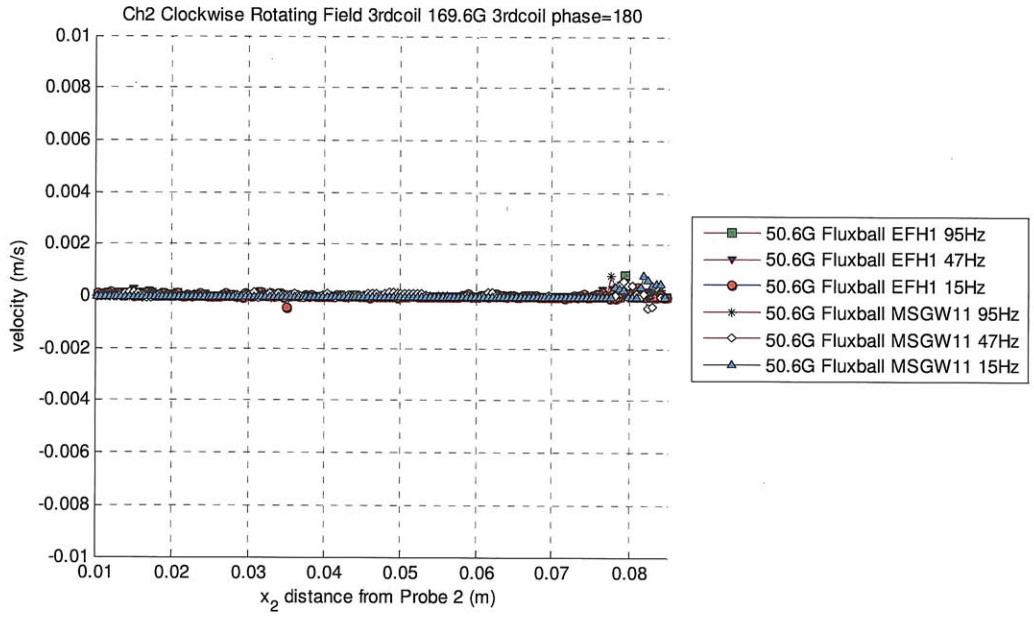
Ch2 Clockwise Rotating Field 3rdcoil 169.6G 3rdcoil phase=180
velocity (m/s)
0.01
0.008
0.006
0.004
0.002
0
-0.002
-0.004
-0.006
-0.008
-0.01
0.01 0.02 0.03 0.04 0.05 0.06 0.07 0.08
x2 distance from Probe 2 (m)
50.6G Fluxball EFH1 95Hz
50.6G Fluxball EFH1 47Hz
50.6G Fluxball EFH1 15Hz
50.6G Fluxball MSGW11 95Hz
50.6G Fluxball MSGW11 47Hz
50.6G Fluxball MSGW11 15Hz

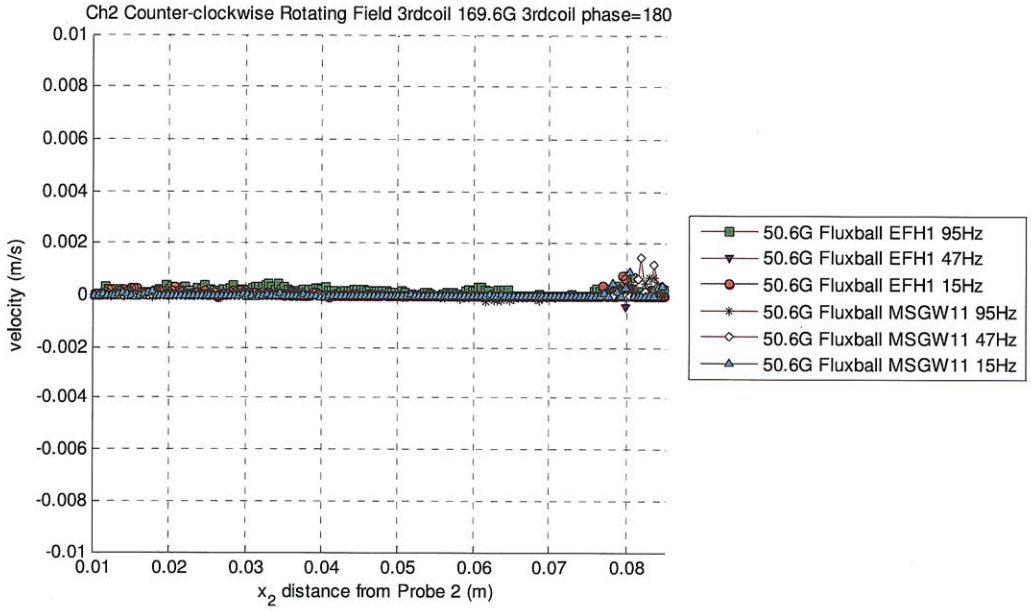
Ch2 Counter-clockwise Rotating Field 3rdcoil 169.6G 3rdcoil phase=180
velocity (m/s)
0.01
0.008
0.006
0.004
0.002
0
-0.002
-0.004
-0.006
-0.008
-0.01
0.01 0.02 0.03 0.04 0.05 0.06 0.07 0.08
x2 distance from Probe 2 (m)
50.6G Fluxball EFH1 95Hz
50.6G Fluxball EFH1 47Hz
50.6G Fluxball EFH1 15Hz
50.6G Fluxball MSGW11 95Hz
50.6G Fluxball MSGW11 47Hz
50.6G Fluxball MSGW11 15Hz

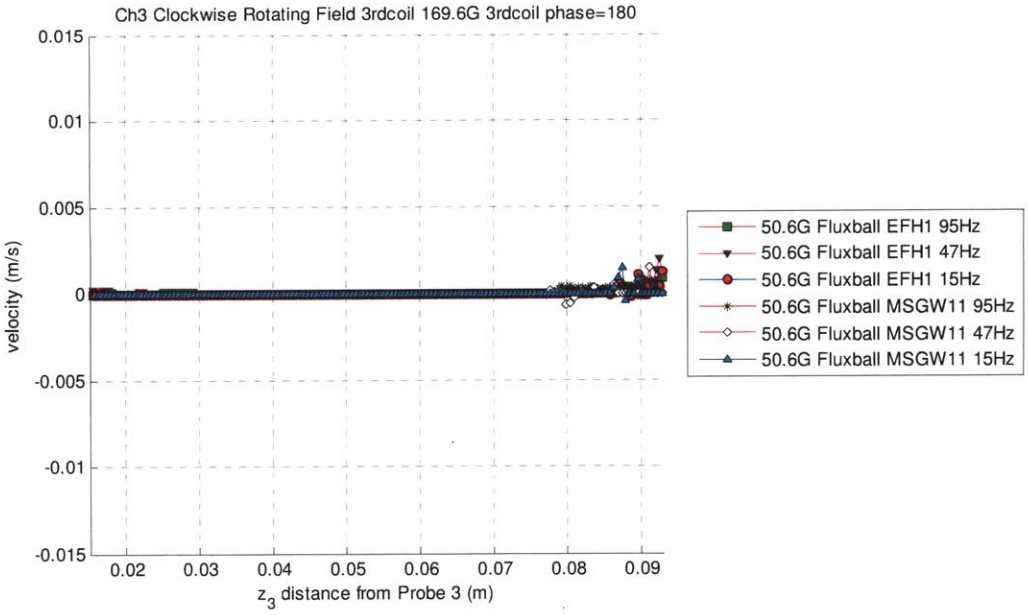
Ch3 Clockwise Rotating Field 3rdcoil 169.6G 3rdcoil phase=180
0.015
0.01
0.005
0
-0.005
-0.01
-0.015
velocity (m/s)
0.02
0.03
0.04
0.05
0.06
0.07
0.08
0.09
z_3 distance from Probe 3 (m)
50.6G Fluxball EFH1 95Hz
50.6G Fluxball EFH1 47Hz
50.6G Fluxball EFH1 15Hz
50.6G Fluxball MSGW11 95Hz
50.6G Fluxball MSGW11 47Hz
50.6G Fluxball MSGW11 15Hz

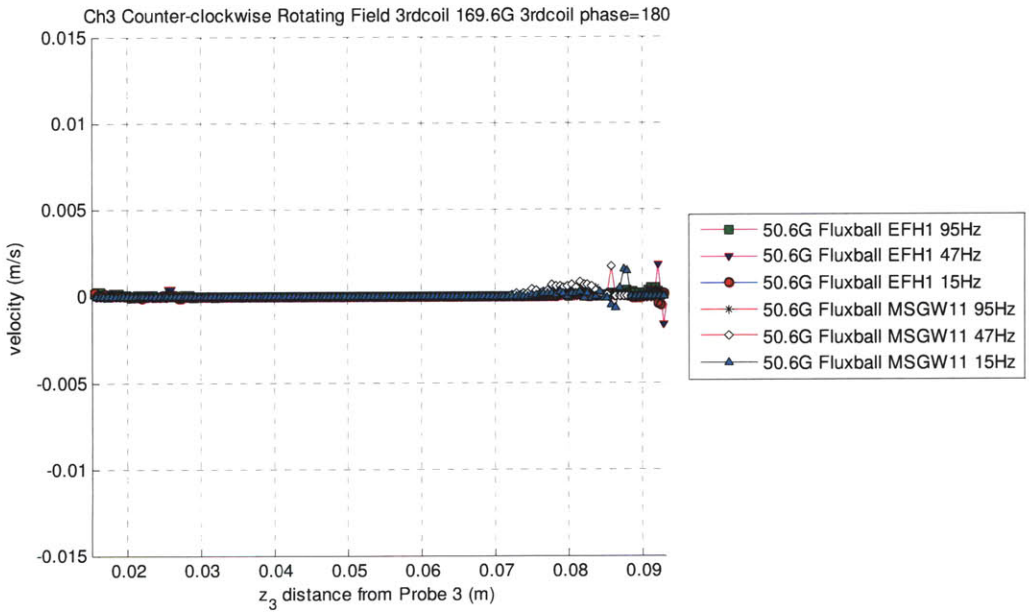
Ch3 Counter-clockwise Rotating Field 3rdcoil 169.6G 3rdcoil phase=180
0.015
0.01
0.005
0
-0.005
-0.01
-0.015
velocity (m/s)
0.02
0.03
0.04
0.05
0.06
0.07
0.08
0.09
z_3 distance from Probe 3 (m)
50.6G Fluxball EFH1 95Hz
50.6G Fluxball EFH1 47Hz
50.6G Fluxball EFH1 15Hz
50.6G Fluxball MSGW11 95Hz
50.6G Fluxball MSGW11 47Hz
50.6G Fluxball MSGW11 15Hz

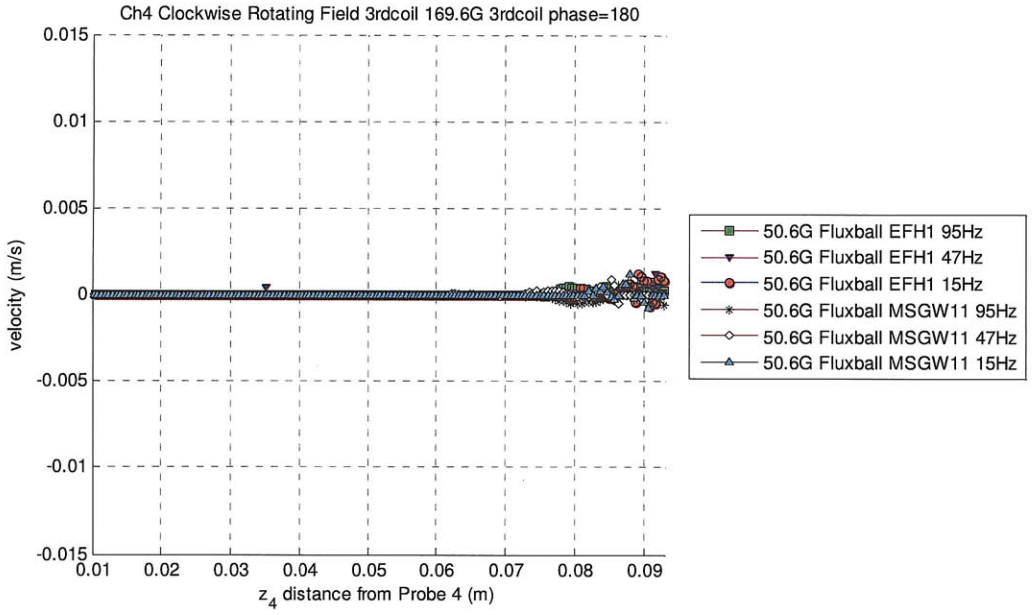
Ch4 Clockwise Rotating Field 3rdcoil 169.6G 3rdcoil phase=180
velocity (m/s)
0.015
0.01
0.005
0
-0.005
-0.01
-0.015
0.01
0.02
0.03
0.04
0.05
0.06
0.07
0.08
0.09
z4 distance from Probe 4 (m)
50.6G Fluxball EFH1 95Hz
50.6G Fluxball EFH1 47Hz
50.6G Fluxball EFH1 15Hz
50.6G Fluxball MSGW11 95Hz
50.6G Fluxball MSGW11 47Hz
50.6G Fluxball MSGW11 15Hz

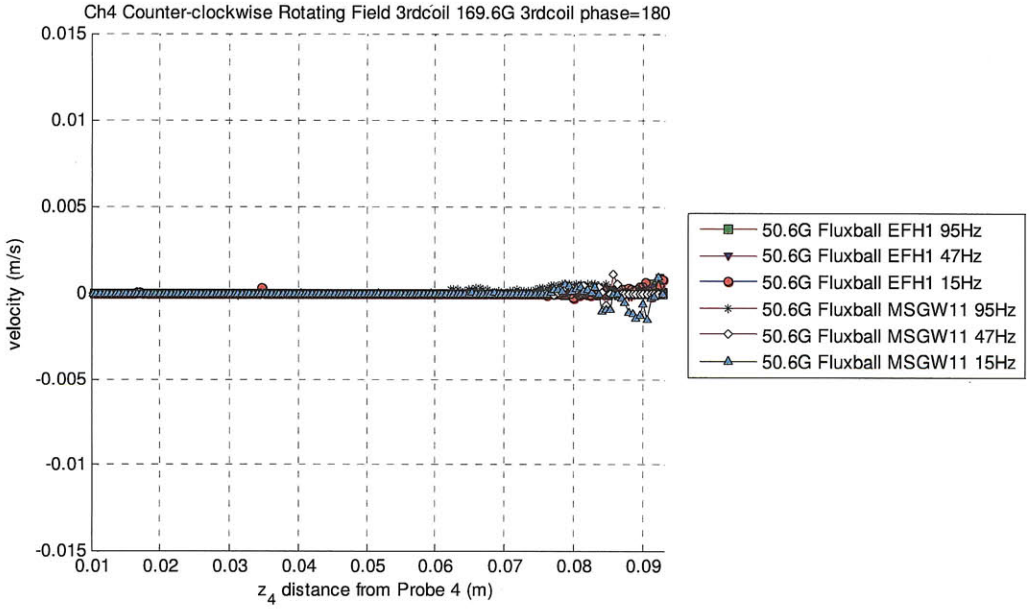
Ch4 Counter-clockwise Rotating Field 3rdcoil 169.6G 3rdcoil phase=180
velocity (m/s)
0.015
0.01
0.005
0
-0.005
-0.01
-0.015
0.01
0.02
0.03
0.04
0.05
0.06
0.07
0.08
0.09
z4 distance from Probe 4 (m)
50.6G Fluxball EFH1 95Hz
50.6G Fluxball EFH1 47Hz
50.6G Fluxball EFH1 15Hz
50.6G Fluxball MSGW11 95Hz
50.6G Fluxball MSGW11 47Hz
50.6G Fluxball MSGW11 15Hz

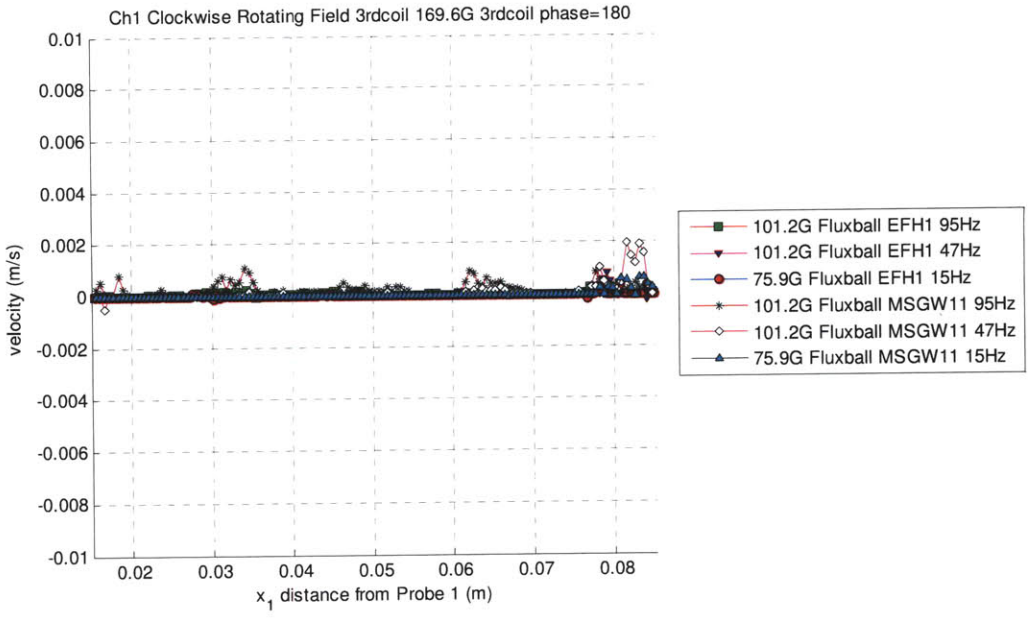
Ch1 Clockwise Rotating Field 3rdcoil 169.6G 3rdcoil phase=180
velocity (m/s)
0.01
0.008
0.006
0.004
0.002
0
-0.002
-0.004
-0.006
-0.008
-0.01
0.02
0.03
0.04
0.05
0.06
0.07
0.08
x1 distance from Probe 1 (m)
101.2G Fluxball EFH1 95Hz
101.2G Fluxball EFH1 47Hz
75.9G Fluxball EFH1 15Hz
101.2G Fluxball MSGW11 95Hz
101.2G Fluxball MSGW11 47Hz
75.9G Fluxball MSGW11 15Hz

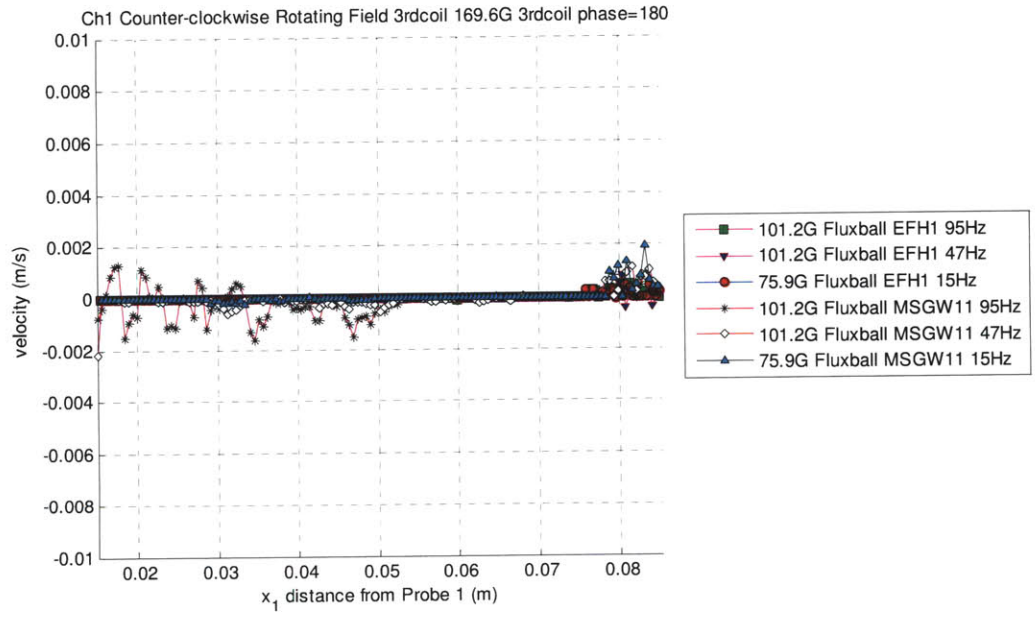
Ch1 Counter-clockwise Rotating Field 3rdcoil 169.6G 3rdcoil phase=180
velocity (m/s)
0.01
0.008
0.006
0.004
0.002
0
-0.002
-0.004
-0.006
-0.008
-0.01
0.02
0.03
0.04
0.05
0.06
0.07
0.08
x1 distance from Probe 1 (m)
101.2G Fluxball EFH1 95Hz
101.2G Fluxball EFH1 47Hz
75.9G Fluxball EFH1 15Hz
101.2G Fluxball MSGW11 95Hz
101.2G Fluxball MSGW11 47Hz
75.9G Fluxball MSGW11 15Hz

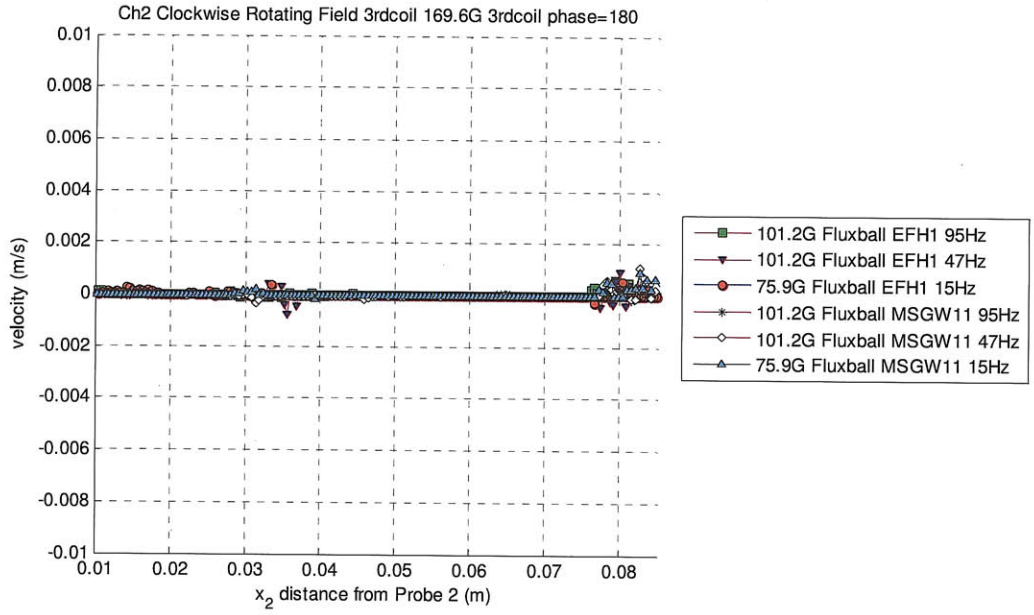
Ch2 Clockwise Rotating Field 3rdcoil 169.6G 3rdcoil phase=180
velocity (m/s)
0.01
0.008
0.006
0.004
0.002
0
-0.002
-0.004
-0.006
-0.008
-0.01
0.01 0.02 0.03 0.04 0.05 0.06 0.07 0.08
x2 distance from Probe 2 (m)
101.2G Fluxball EFH1 95Hz
101.2G Fluxball EFH1 47Hz
75.9G Fluxball EFH1 15Hz
101.2G Fluxball MSGW11 95Hz
101.2G Fluxball MSGW11 47Hz
75.9G Fluxball MSGW11 15Hz

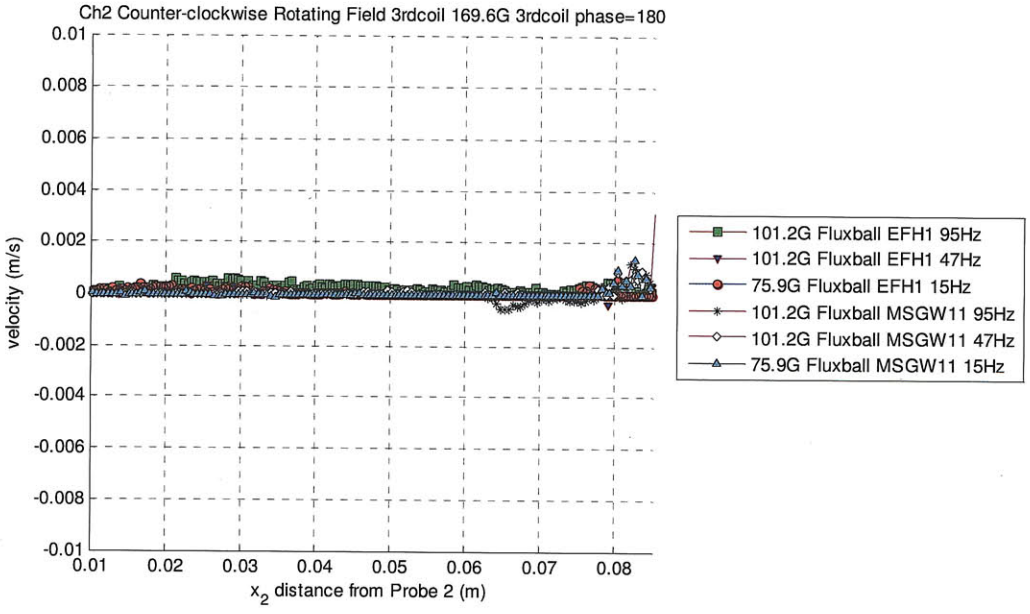
Ch2 Counter-clockwise Rotating Field 3rdcoil 169.6G 3rdcoil phase=180
velocity (m/s)
0.01
0.008
0.006
0.004
0.002
0
-0.002
-0.004
-0.006
-0.008
-0.01
0.01 0.02 0.03 0.04 0.05 0.06 0.07 0.08
x2 distance from Probe 2 (m)
101.2G Fluxball EFH1 95Hz
101.2G Fluxball EFH1 47Hz
75.9G Fluxball EFH1 15Hz
101.2G Fluxball MSGW11 95Hz
101.2G Fluxball MSGW11 47Hz
75.9G Fluxball MSGW11 15Hz

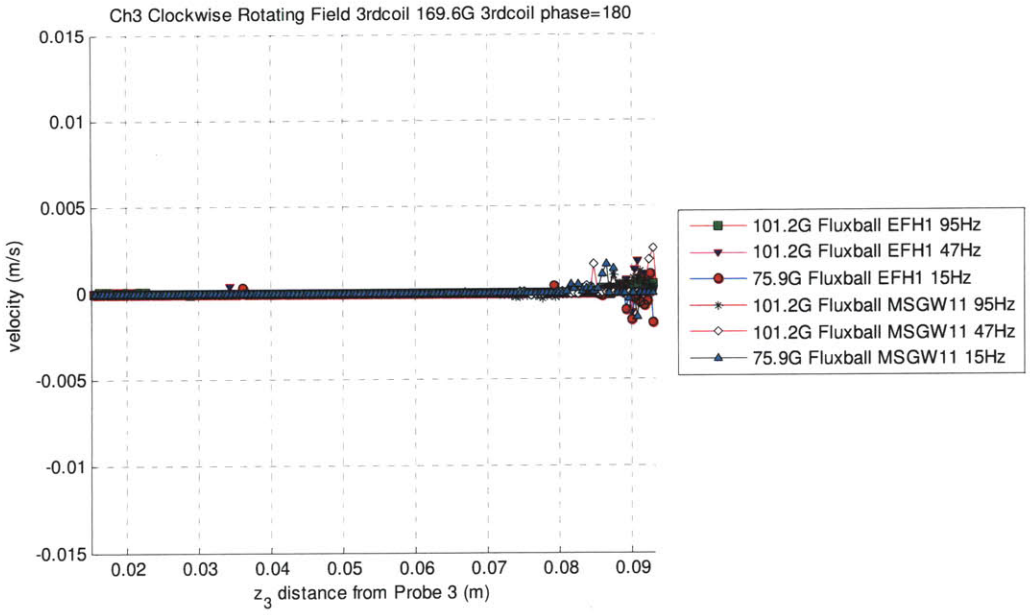
Ch3 Clockwise Rotating Field 3rdcoil 169.6G 3rdcoil phase=180
0.015
0.01
0.005
0
-0.005
-0.01
-0.015
velocity (m/s)
0.02
0.03
0.04
0.05
0.06
0.07
0.08
0.09
z3 distance from Probe 3 (m)
101.2G Fluxball EFH1 95Hz
101.2G Fluxball EFH1 47Hz
75.9G Fluxball EFH1 15Hz
101.2G Fluxball MSGW11 95Hz
101.2G Fluxball MSGW11 47Hz
75.9G Fluxball MSGW11 15Hz

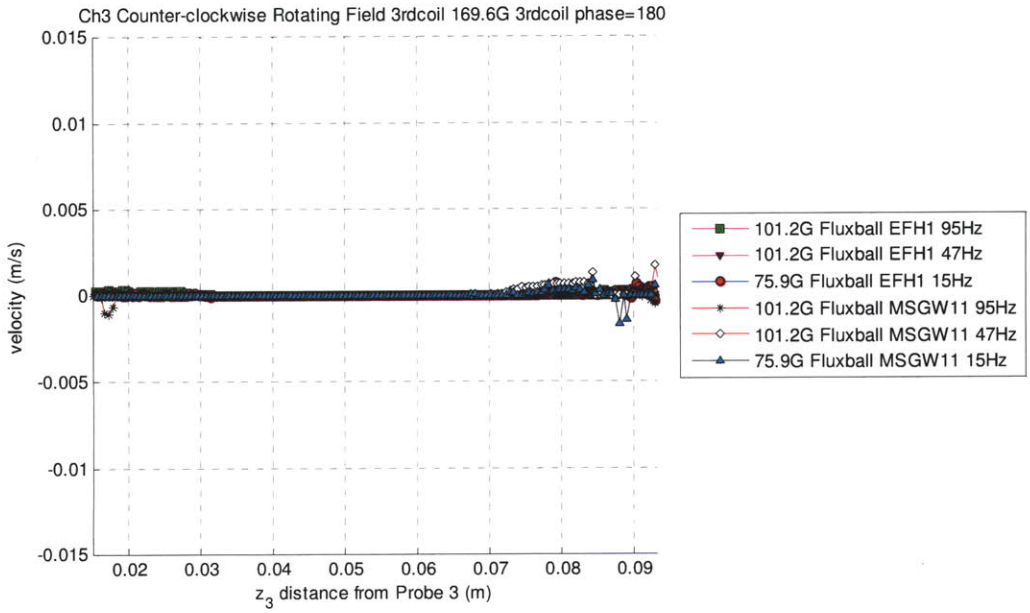
Ch3 Counter-clockwise Rotating Field 3rdcoil 169.6G 3rdcoil phase=180
0.015
0.01
0.005
0
-0.005
-0.01
-0.015
velocity (m/s)
0.02
0.03
0.04
0.05
0.06
0.07
0.08
0.09
z3 distance from Probe 3 (m)
101.2G Fluxball EFH1 95Hz
101.2G Fluxball EFH1 47Hz
75.9G Fluxball EFH1 15Hz
101.2G Fluxball MSGW11 95Hz
101.2G Fluxball MSGW11 47Hz
75.9G Fluxball MSGW11 15Hz

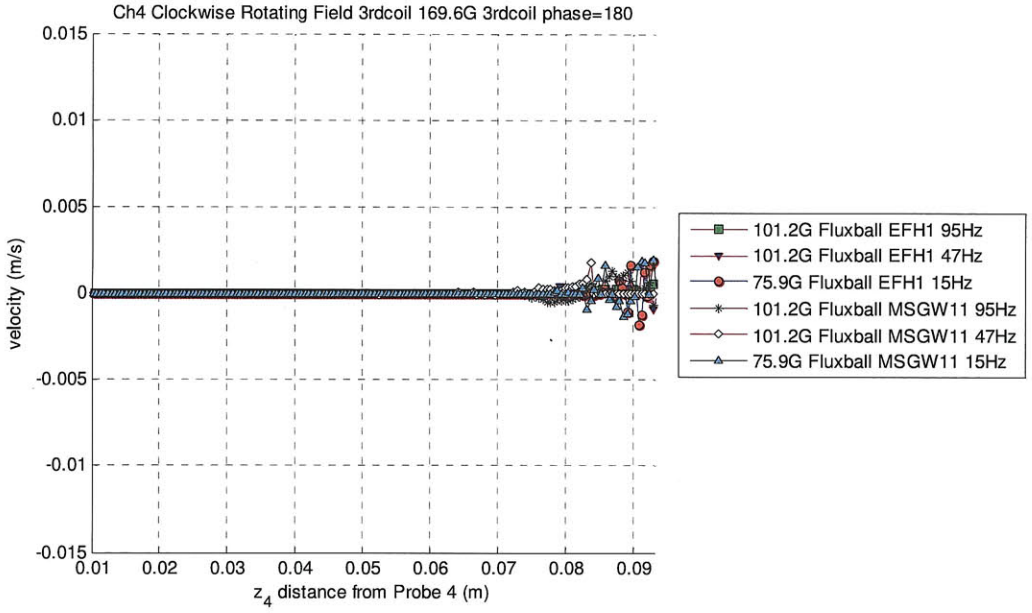
Ch4 Clockwise Rotating Field 3rdcoil 169.6G 3rdcoil phase=180
0.015
0.01
0.005
0
-0.005
-0.01
-0.015
velocity (m/s)
0.01
0.02
0.03
0.04
0.05
0.06
0.07
0.08
0.09
z4 distance from Probe 4 (m)
101.2G Fluxball EFH1 95Hz
101.2G Fluxball EFH1 47Hz
75.9G Fluxball EFH1 15Hz
101.2G Fluxball MSGW11 95Hz
101.2G Fluxball MSGW11 47Hz
75.9G Fluxball MSGW11 15Hz

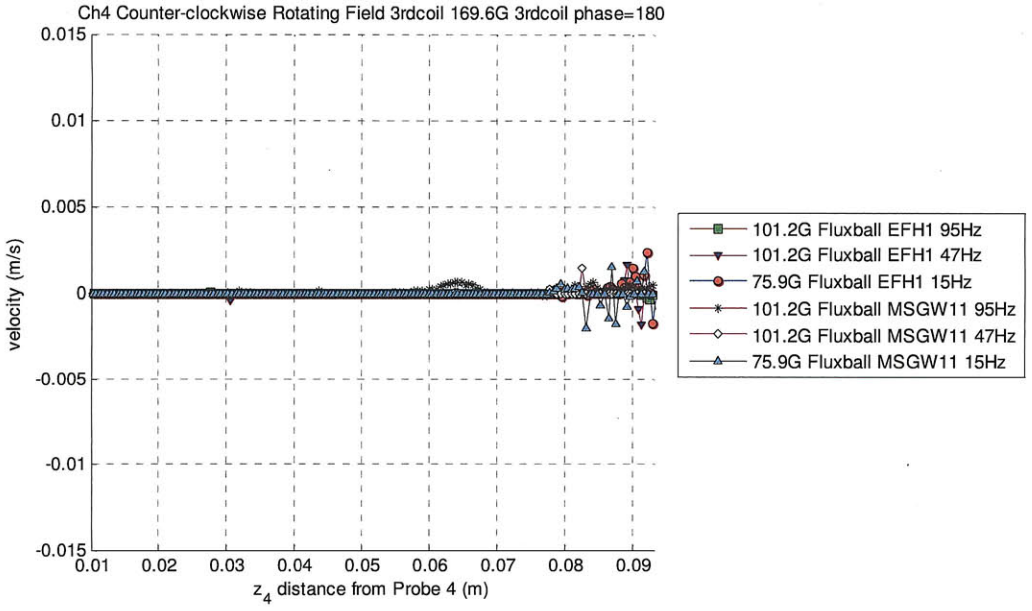
Ch4 Counter-clockwise Rotating Field 3rdcoil 169.6G 3rdcoil phase=180
0.015
0.01
0.005
0
-0.005
-0.01
-0.015
velocity (m/s)
0.01
0.02
0.03
0.04
0.05
0.06
0.07
0.08
0.09
z4 distance from Probe 4 (m)
101.2G Fluxball EFH1 95Hz
101.2G Fluxball EFH1 47Hz
75.9G Fluxball EFH1 15Hz
101.2G Fluxball MSGW11 95Hz
101.2G Fluxball MSGW11 47Hz
75.9G Fluxball MSGW11 15Hz

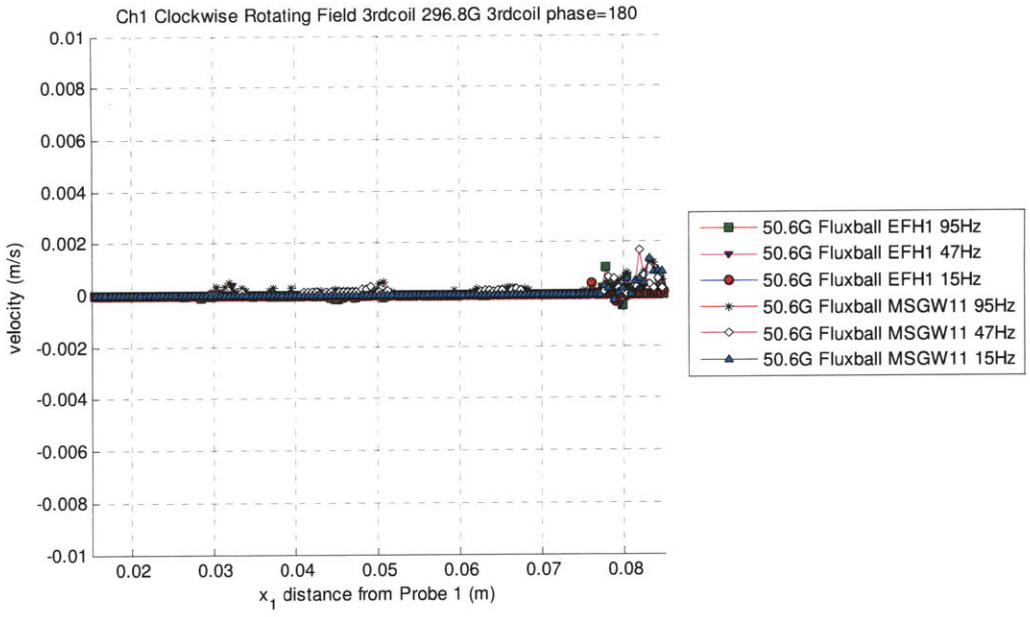
Ch1 Clockwise Rotating Field 3rdcoil 296.8G 3rdcoil phase=180
velocity (m/s)
0.01
0.008
0.006
0.004
0.002
0
-0.002
-0.004
-0.006
-0.008
-0.01
0.02
0.03
0.04
0.05
0.06
0.07
0.08
x1 distance from Probe 1 (m)
50.6G Fluxball EFH1 95Hz
50.6G Fluxball EFH1 47Hz
50.6G Fluxball EFH1 15Hz
50.6G Fluxball MSGW11 95Hz
50.6G Fluxball MSGW11 47Hz
50.6G Fluxball MSGW11 15Hz

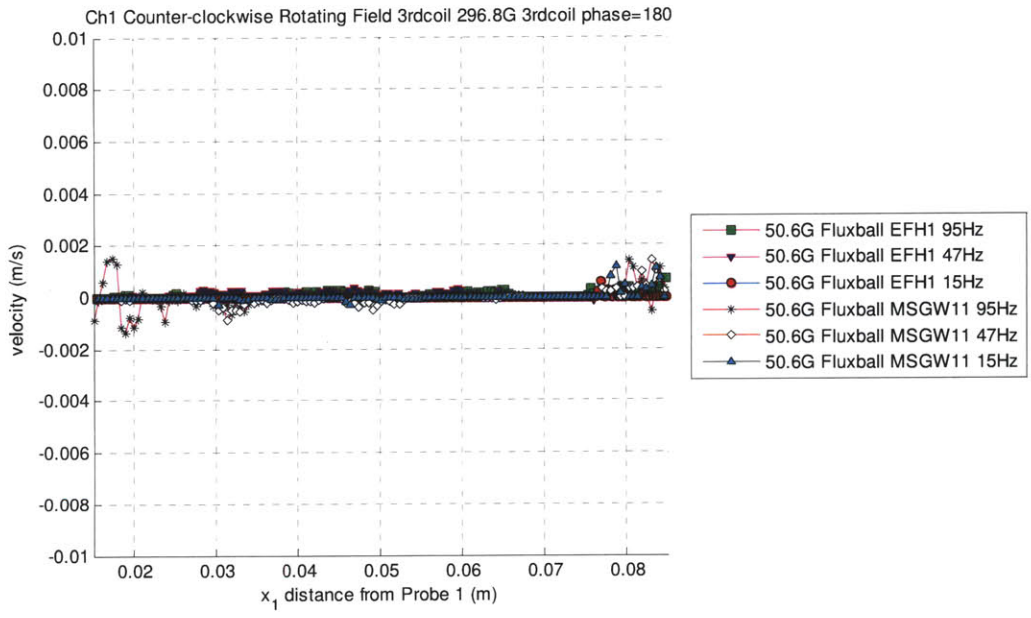
Ch1 Counter-clockwise Rotating Field 3rdcoil 296.8G 3rdcoil phase=180
velocity (m/s)
0.01
0.008
0.006
0.004
0.002
0
-0.002
-0.004
-0.006
-0.008
-0.01
0.02
0.03
0.04
0.05
0.06
0.07
0.08
x1 distance from Probe 1 (m)
50.6G Fluxball EFH1 95Hz
50.6G Fluxball EFH1 47Hz
50.6G Fluxball EFH1 15Hz
50.6G Fluxball MSGW11 95Hz
50.6G Fluxball MSGW11 47Hz
50.6G Fluxball MSGW11 15Hz

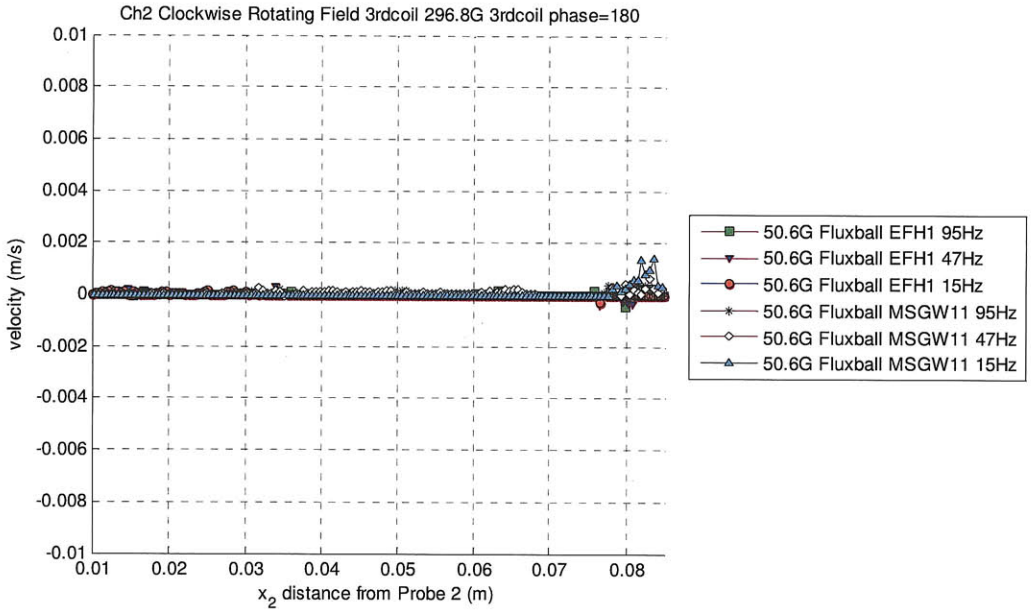
Ch2 Clockwise Rotating Field 3rdcoil 296.8G 3rdcoil phase=180
velocity (m/s)
0.01
0.008
0.006
0.004
0.002
0
-0.002
-0.004
-0.006
-0.008
-0.01
0.01 0.02 0.03 0.04 0.05 0.06 0.07 0.08
x2 distance from Probe 2 (m)
50.6G Fluxball EFH1 95Hz
50.6G Fluxball EFH1 47Hz
50.6G Fluxball EFH1 15Hz
50.6G Fluxball MSGW11 95Hz
50.6G Fluxball MSGW11 47Hz
50.6G Fluxball MSGW11 15Hz

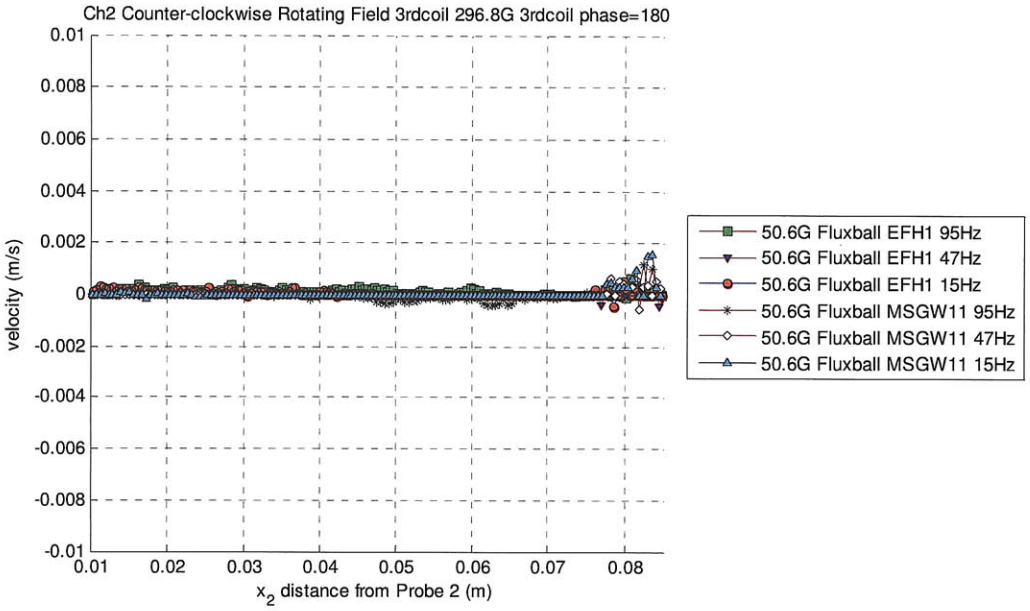
Ch2 Counter-clockwise Rotating Field 3rdcoil 296.8G 3rdcoil phase=180
velocity (m/s)
0.01
0.008
0.006
0.004
0.002
0
-0.002
-0.004
-0.006
-0.008
-0.01
0.01 0.02 0.03 0.04 0.05 0.06 0.07 0.08
x2 distance from Probe 2 (m)
50.6G Fluxball EFH1 95Hz
50.6G Fluxball EFH1 47Hz
50.6G Fluxball EFH1 15Hz
50.6G Fluxball MSGW11 95Hz
50.6G Fluxball MSGW11 47Hz
50.6G Fluxball MSGW11 15Hz

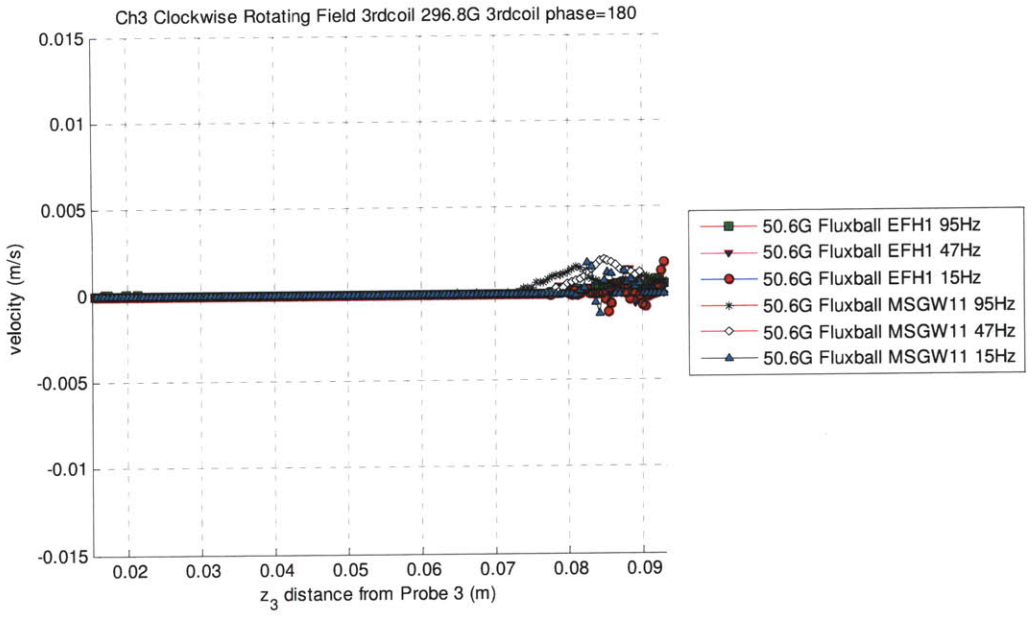
Ch3 Clockwise Rotating Field 3rdcoil 296.8G 3rdcoil phase=180
velocity (m/s)
0.015
0.01
0.005
0
-0.005
-0.01
-0.015
0.02
0.03
0.04
0.05
0.06
0.07
0.08
0.09
z3 distance from Probe 3 (m)
50.6G Fluxball EFH1 95Hz
50.6G Fluxball EFH1 47Hz
50.6G Fluxball EFH1 15Hz
50.6G Fluxball MSGW11 95Hz
50.6G Fluxball MSGW11 47Hz
50.6G Fluxball MSGW11 15Hz

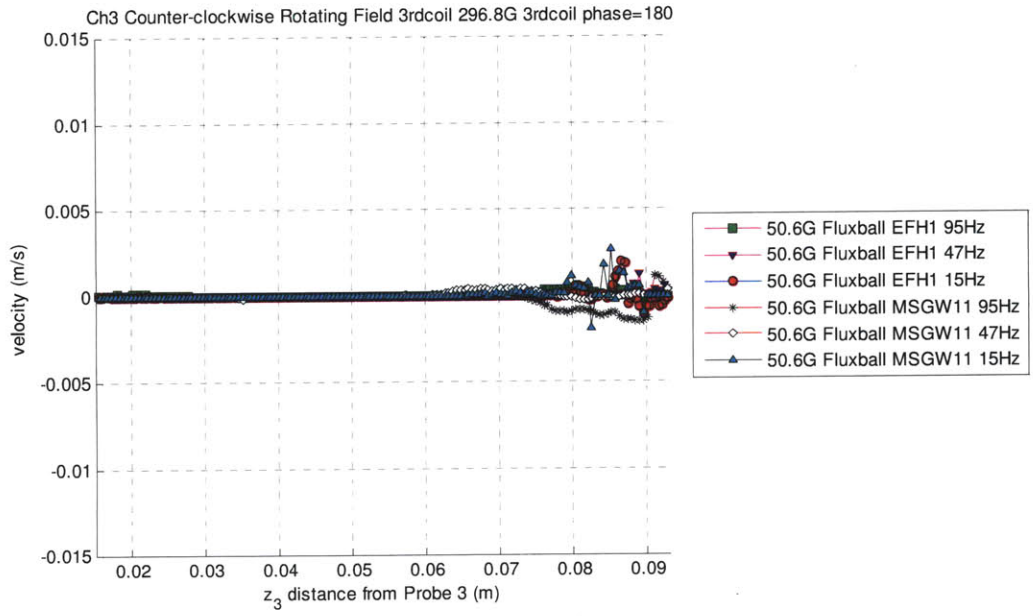
Ch3 Counter-clockwise Rotating Field 3rdcoil 296.8G 3rdcoil phase=180
velocity (m/s)
0.015
0.01
0.005
0
-0.005
-0.01
-0.015
0.02
0.03
0.04
0.05
0.06
0.07
0.08
0.09
z3 distance from Probe 3 (m)
50.6G Fluxball EFH1 95Hz
50.6G Fluxball EFH1 47Hz
50.6G Fluxball EFH1 15Hz
50.6G Fluxball MSGW11 95Hz
50.6G Fluxball MSGW11 47Hz
50.6G Fluxball MSGW11 15Hz

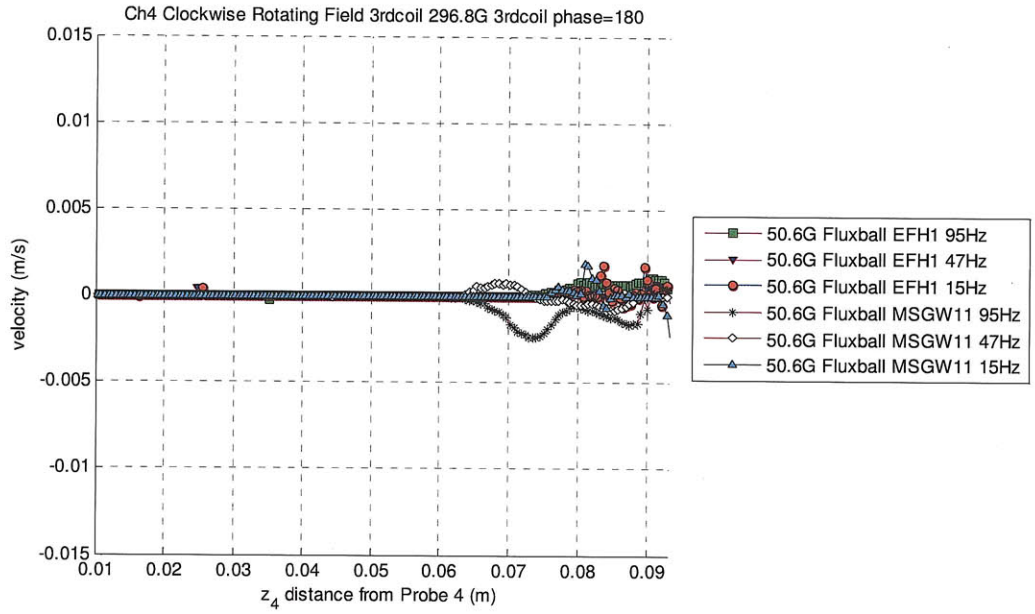
Ch4 Clockwise Rotating Field 3rdcoil 296.8G 3rdcoil phase=180
velocity (m/s)
0.015
0.01
0.005
0
-0.005
-0.01
-0.015
0.01
0.02
0.03
0.04
0.05
0.06
0.07
0.08
0.09
z4 distance from Probe 4 (m)
50.6G Fluxball EFH1 95Hz
50.6G Fluxball EFH1 47Hz
50.6G Fluxball EFH1 15Hz
50.6G Fluxball MSGW11 95Hz
50.6G Fluxball MSGW11 47Hz
50.6G Fluxball MSGW11 15Hz

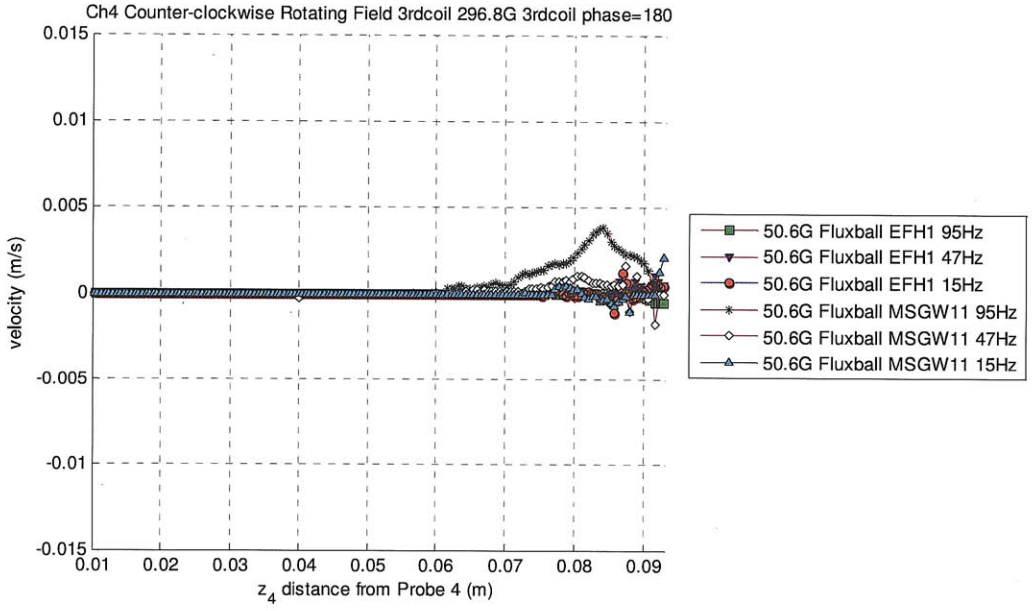
Ch4 Counter-clockwise Rotating Field 3rdcoil 296.8G 3rdcoil phase=180
velocity (m/s)
0.015
0.01
0.005
0
-0.005
-0.01
-0.015
0.01
0.02
0.03
0.04
0.05
0.06
0.07
0.08
0.09
z4 distance from Probe 4 (m)
50.6G Fluxball EFH1 95Hz
50.6G Fluxball EFH1 47Hz
50.6G Fluxball EFH1 15Hz
50.6G Fluxball MSGW11 95Hz
50.6G Fluxball MSGW11 47Hz
50.6G Fluxball MSGW11 15Hz

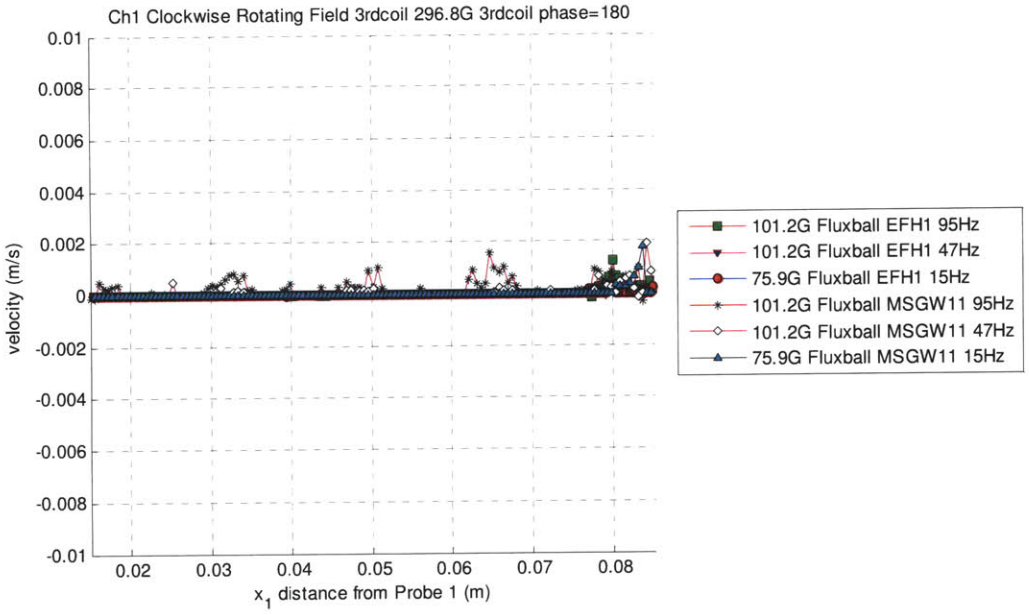
Ch1 Clockwise Rotating Field 3rdcoil 296.8G 3rdcoil phase=180
velocity (m/s)
0.01
0.008
0.006
0.004
0.002
0
-0.002
-0.004
-0.006
-0.008
-0.01
0.02
0.03
0.04
0.05
0.06
0.07
0.08
x1 distance from Probe 1 (m)
101.2G Fluxball EFH1 95Hz
101.2G Fluxball EFH1 47Hz
75.9G Fluxball EFH1 15Hz
101.2G Fluxball MSGW11 95Hz
101.2G Fluxball MSGW11 47Hz
75.9G Fluxball MSGW11 15Hz

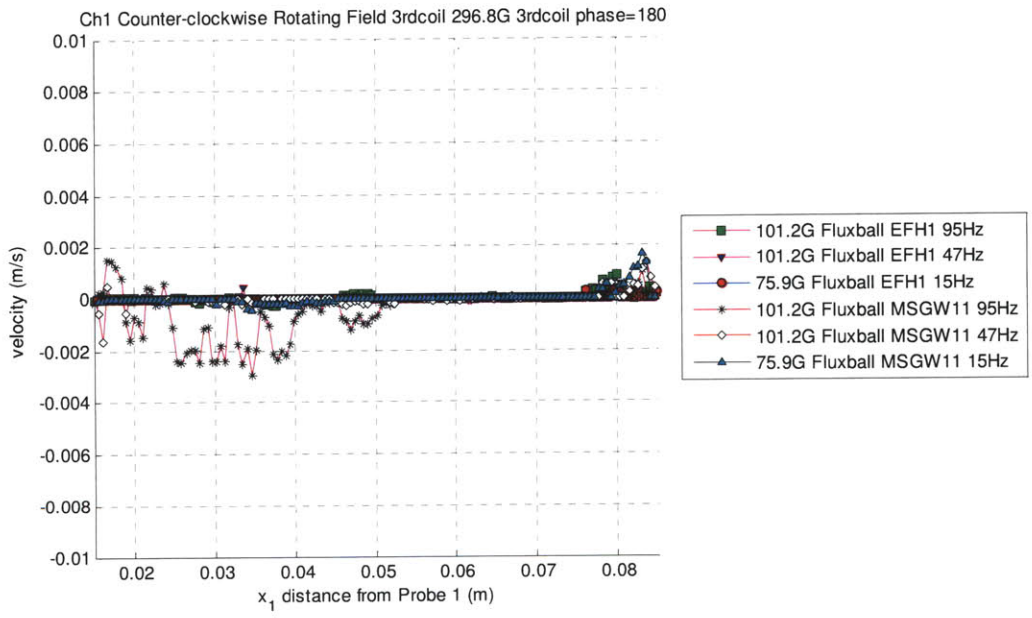
Ch1 Counter-clockwise Rotating Field 3rdcoil 296.8G 3rdcoil phase=180
velocity (m/s)
0.01
0.008
0.006
0.004
0.002
0
-0.002
-0.004
-0.006
-0.008
-0.01
0.02
0.03
0.04
0.05
0.06
0.07
0.08
x1 distance from Probe 1 (m)
101.2G Fluxball EFH1 95Hz
101.2G Fluxball EFH1 47Hz
75.9G Fluxball EFH1 15Hz
101.2G Fluxball MSGW11 95Hz
101.2G Fluxball MSGW11 47Hz
75.9G Fluxball MSGW11 15Hz

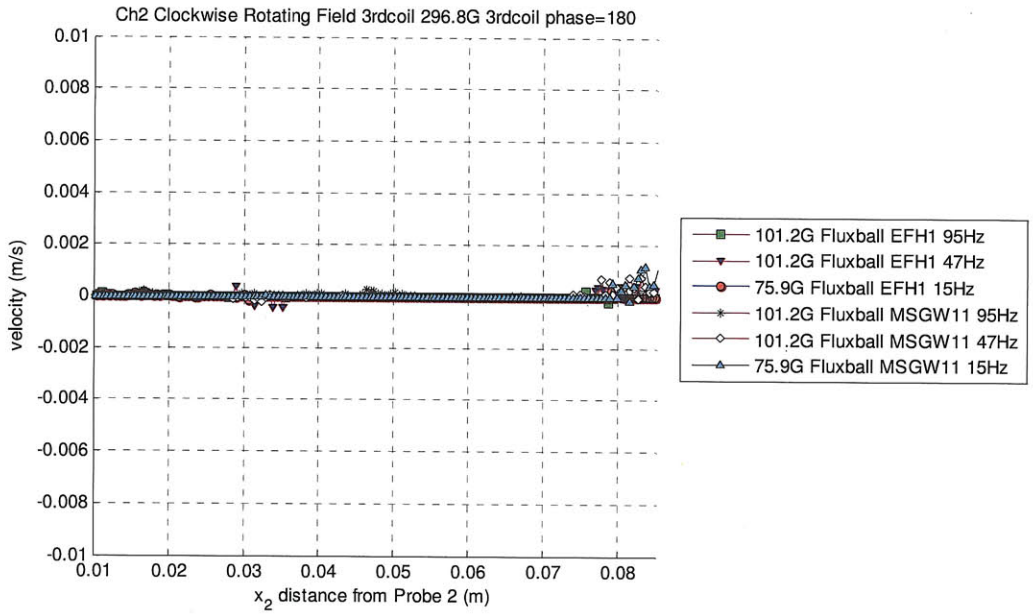
Ch2 Clockwise Rotating Field 3rdcoil 296.8G 3rdcoil phase=180
velocity (m/s)
0.01
0.008
0.006
0.004
0.002
0
-0.002
-0.004
-0.006
-0.008
-0.01
0.01 0.02 0.03 0.04 0.05 0.06 0.07 0.08
x2 distance from Probe 2 (m)
101.2G Fluxball EFH1 95Hz
101.2G Fluxball EFH1 47Hz
75.9G Fluxball EFH1 15Hz
101.2G Fluxball MSGW11 95Hz
101.2G Fluxball MSGW11 47Hz
75.9G Fluxball MSGW11 15Hz

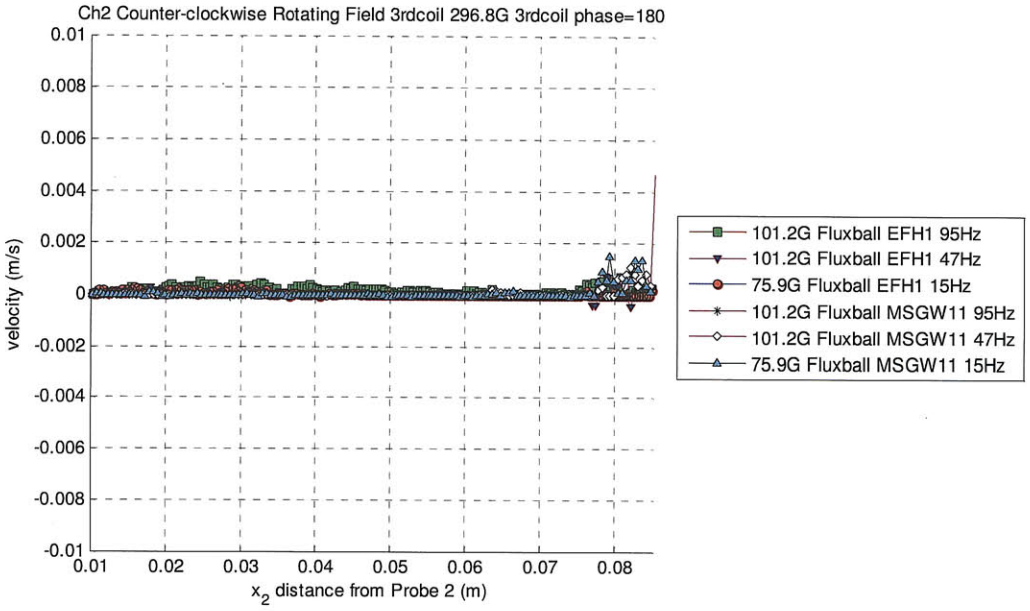
Ch2 Counter-clockwise Rotating Field 3rdcoil 296.8G 3rdcoil phase=180
velocity (m/s)
0.01
0.008
0.006
0.004
0.002
0
-0.002
-0.004
-0.006
-0.008
-0.01
0.01 0.02 0.03 0.04 0.05 0.06 0.07 0.08
x2 distance from Probe 2 (m)
101.2G Fluxball EFH1 95Hz
101.2G Fluxball EFH1 47Hz
75.9G Fluxball EFH1 15Hz
101.2G Fluxball MSGW11 95Hz
101.2G Fluxball MSGW11 47Hz
75.9G Fluxball MSGW11 15Hz

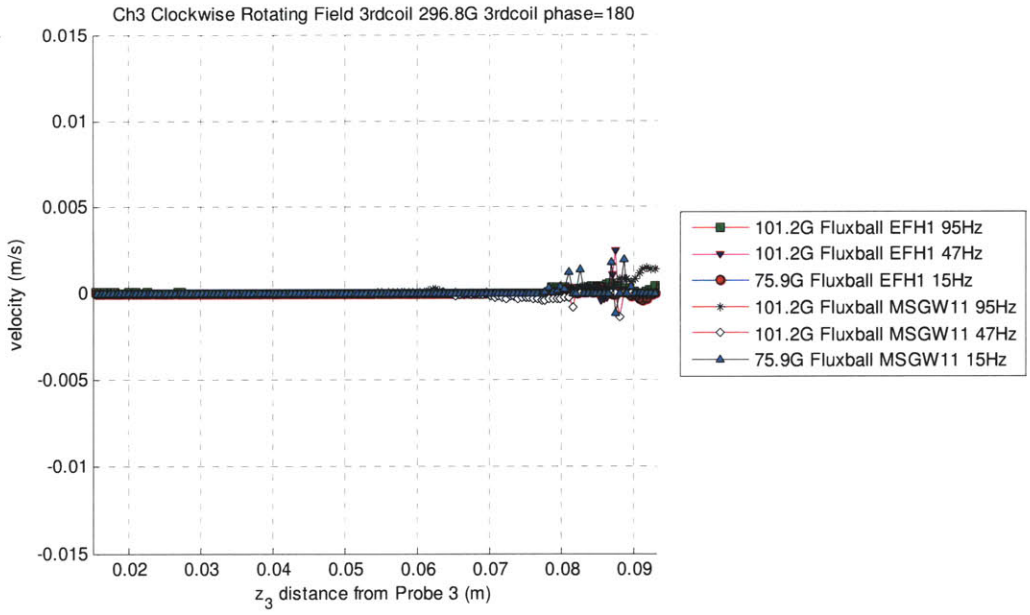
Ch3 Clockwise Rotating Field 3rdcoil 296.8G 3rdcoil phase=180
velocity (m/s)
0.015
0.01
0.005
0
-0.005
-0.01
-0.015
0.02
0.03
0.04
0.05
0.06
0.07
0.08
0.09
z_3 distance from Probe 3 (m)
101.2G Fluxball EFH1 95Hz
101.2G Fluxball EFH1 47Hz
75.9G Fluxball EFH1 15Hz
101.2G Fluxball MSGW11 95Hz
101.2G Fluxball MSGW11 47Hz
75.9G Fluxball MSGW11 15Hz

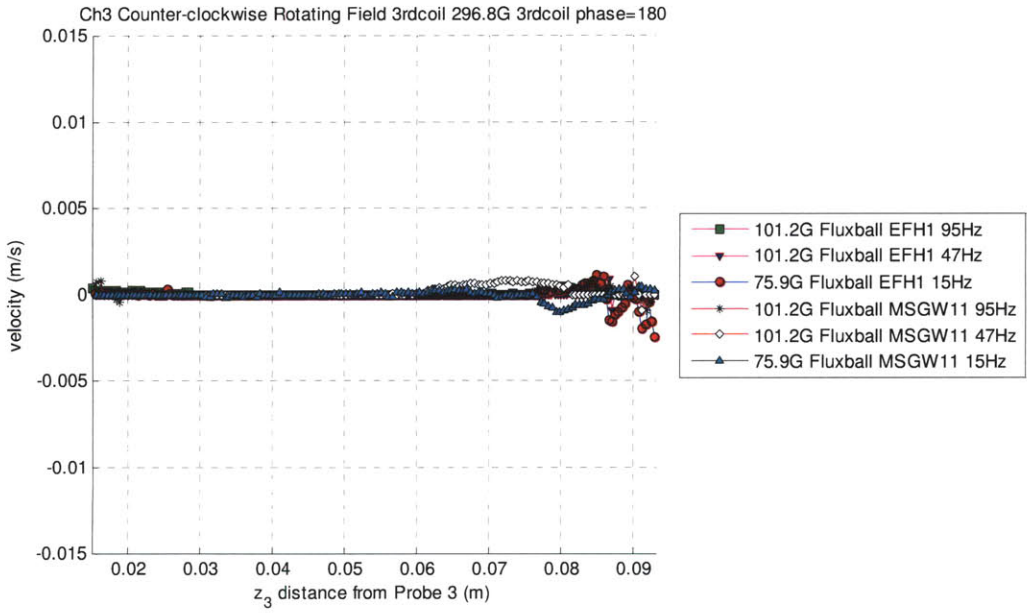
Ch3 Counter-clockwise Rotating Field 3rdcoil 296.8G 3rdcoil phase=180
velocity (m/s)
0.015
0.01
0.005
0
-0.005
-0.01
-0.015
0.02
0.03
0.04
0.05
0.06
0.07
0.08
0.09
z_3 distance from Probe 3 (m)
101.2G Fluxball EFH1 95Hz
101.2G Fluxball EFH1 47Hz
75.9G Fluxball EFH1 15Hz
101.2G Fluxball MSGW11 95Hz
101.2G Fluxball MSGW11 47Hz
75.9G Fluxball MSGW11 15Hz

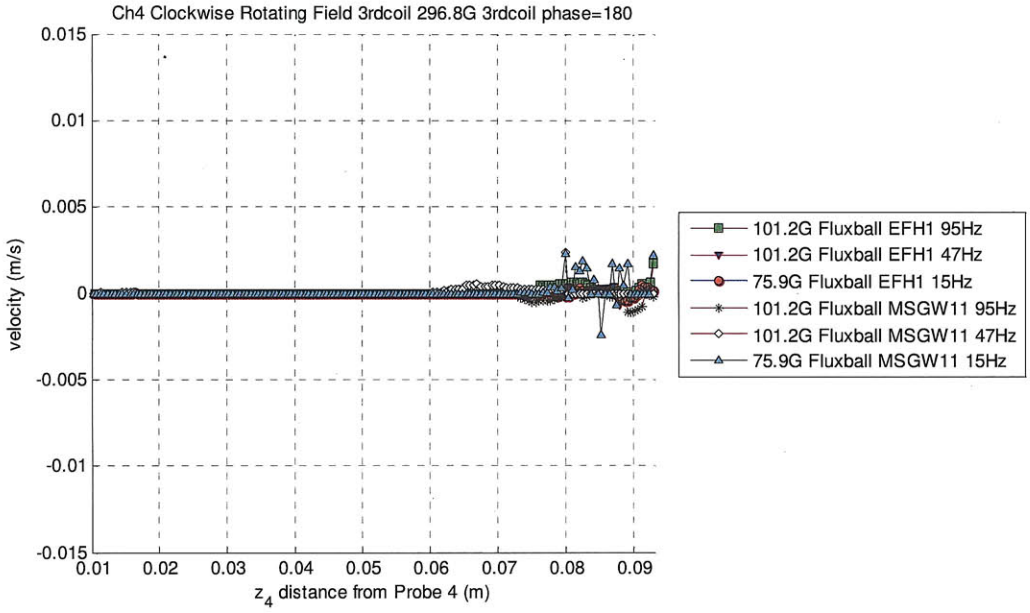
Ch4 Clockwise Rotating Field 3rdcoil 296.8G 3rdcoil phase=180
0.015
0.01
0.005
0
-0.005
-0.01
-0.015
velocity (m/s)
0.01
0.02
0.03
0.04
0.05
0.06
0.07
0.08
0.09
z4 distance from Probe 4 (m)
101.2G Fluxball EFH1 95Hz
101.2G Fluxball EFH1 47Hz
75.9G Fluxball EFH1 15Hz
101.2G Fluxball MSGW11 95Hz
101.2G Fluxball MSGW11 47Hz
75.9G Fluxball MSGW11 15Hz

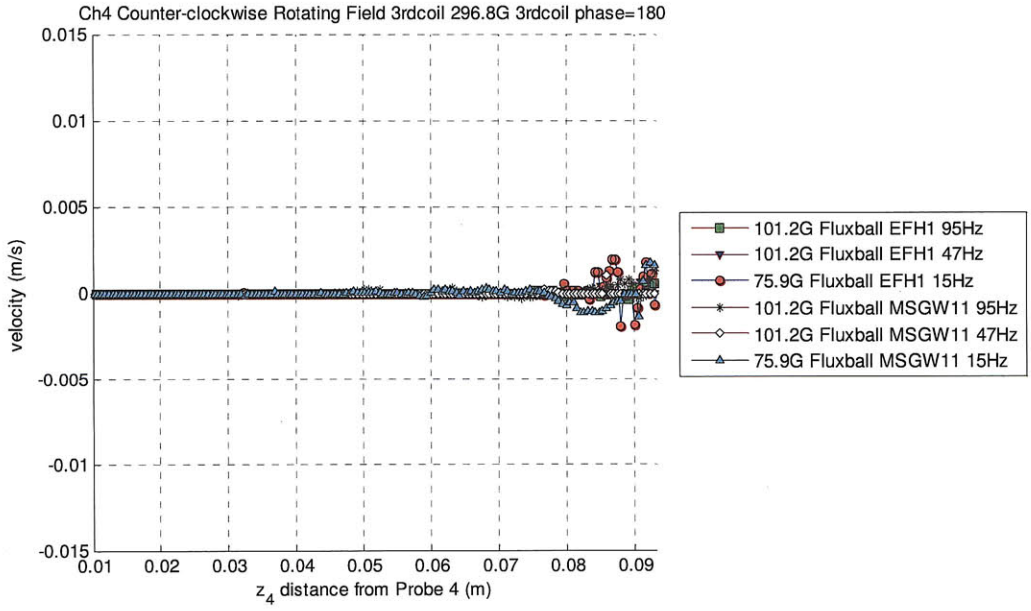
Ch4 Counter-clockwise Rotating Field 3rdcoil 296.8G 3rdcoil phase=180
0.015
0.01
0.005
0
-0.005
-0.01
-0.015
velocity (m/s)
0.01
0.02
0.03
0.04
0.05
0.06
0.07
0.08
0.09
z4 distance from Probe 4 (m)
101.2G Fluxball EFH1 95Hz
101.2G Fluxball EFH1 47Hz
75.9G Fluxball EFH1 15Hz
101.2G Fluxball MSGW11 95Hz
101.2G Fluxball MSGW11 47Hz
75.9G Fluxball MSGW11 15Hz

G15. Comparison of Different Fluids with Third Coil at DC

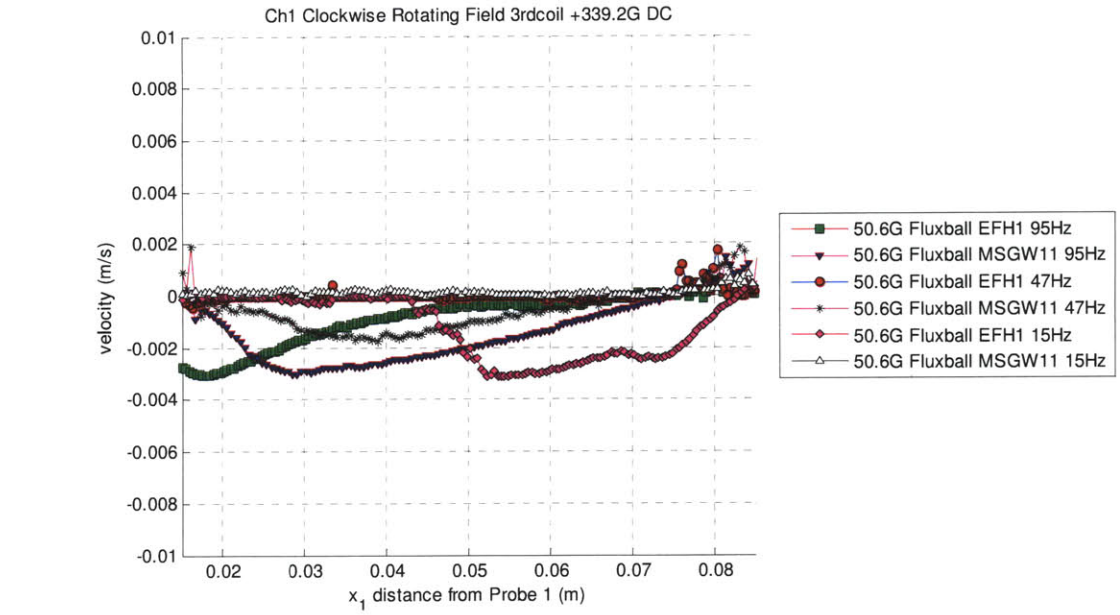

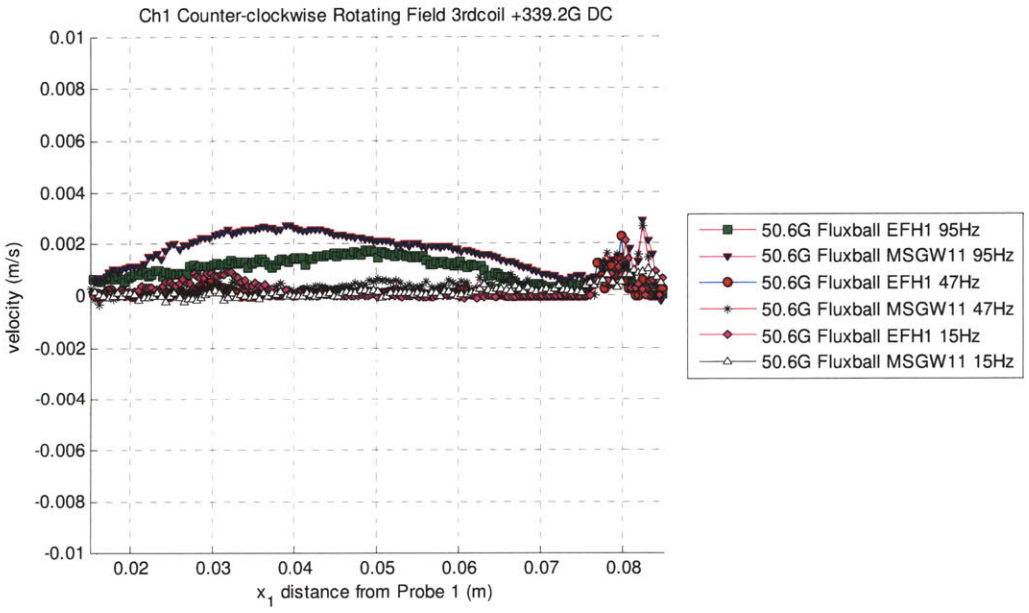

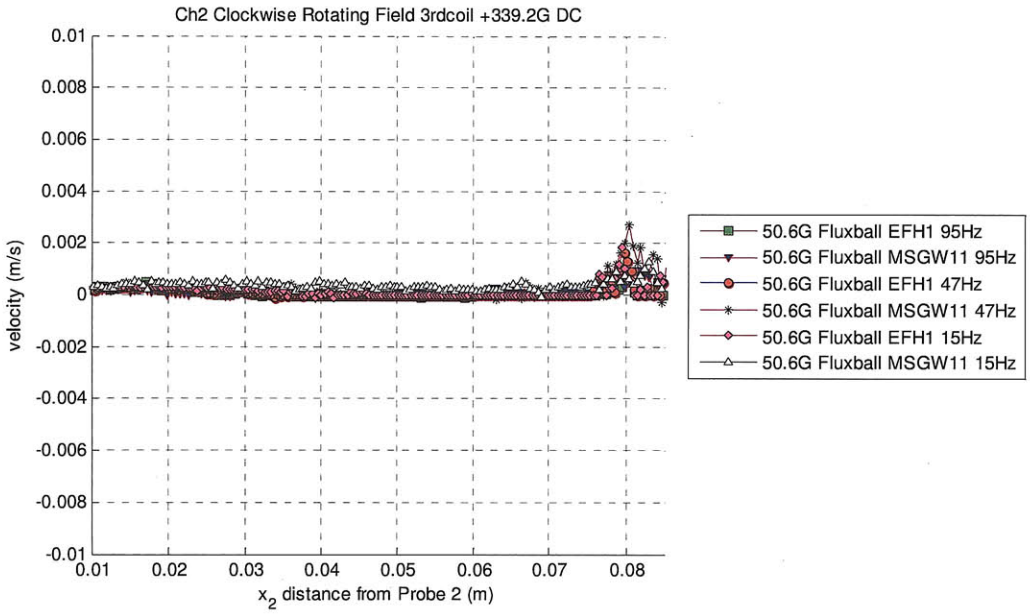
Ch2 Clockwise Rotating Field 3rdcoil +339.2G DC
velocity (m/s)
0.01
0.008
0.006
0.004
0.002
0
-0.002
-0.004
-0.006
-0.008
-0.01
0.01
0.02
0.03
0.04
0.05
0.06
0.07
0.08
x2 distance from Probe 2 (m)
50.6G Fluxball EFH1 95Hz
50.6G Fluxball MSGW11 95Hz
50.6G Fluxball EFH1 47Hz
50.6G Fluxball MSGW11 47Hz
50.6G Fluxball EFH1 15Hz
50.6G Fluxball MSGW11 15Hz

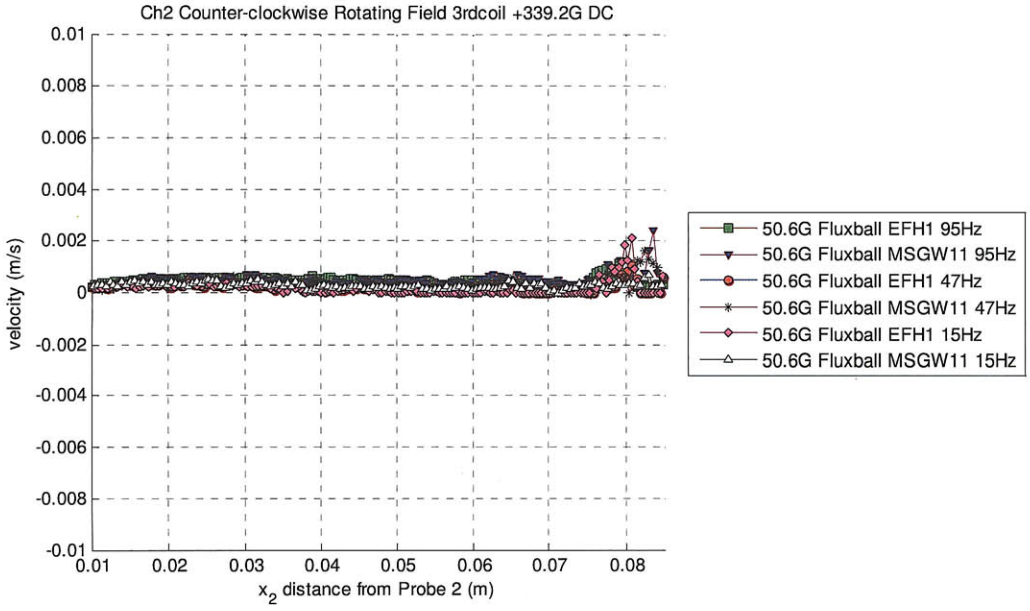
Ch2 Counter-clockwise Rotating Field 3rdcoil +339.2G DC
velocity (m/s)
0.01
0.008
0.006
0.004
0.002
0
-0.002
-0.004
-0.006
-0.008
-0.01
0.01
0.02
0.03
0.04
0.05
0.06
0.07
0.08
x2 distance from Probe 2 (m)
50.6G Fluxball EFH1 95Hz
50.6G Fluxball MSGW11 95Hz
50.6G Fluxball EFH1 47Hz
50.6G Fluxball MSGW11 47Hz
50.6G Fluxball EFH1 15Hz
50.6G Fluxball MSGW11 15Hz

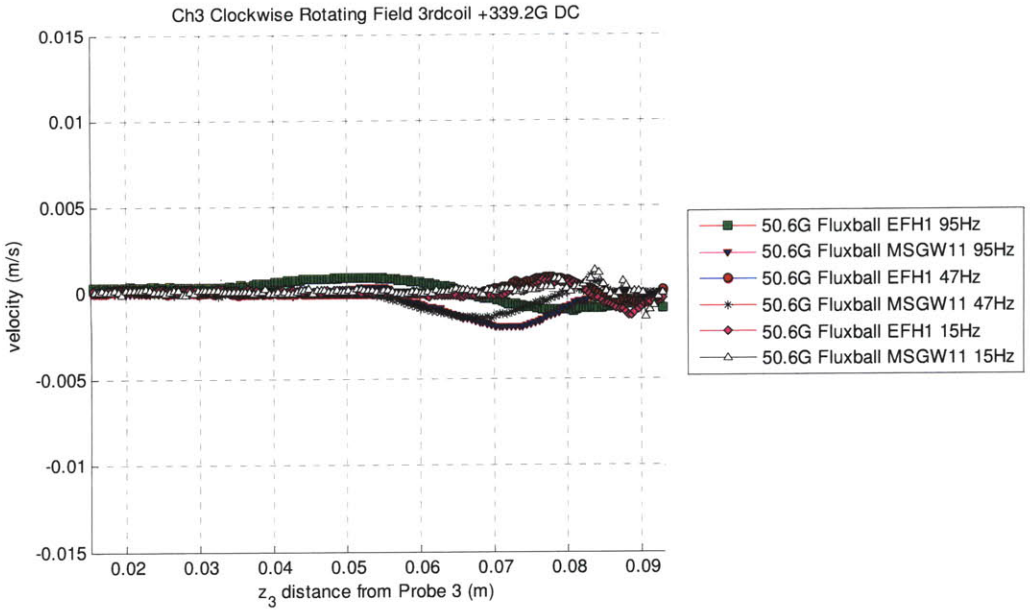
Ch3 Clockwise Rotating Field 3rdcoil +339.2G DC
velocity (m/s)
0.015
0.01
0.005
0
-0.005
-0.01
-0.015
0.02
0.03
0.04
0.05
0.06
0.07
0.08
0.09
z_3 distance from Probe 3 (m)
50.6G Fluxball EFH1 95Hz
50.6G Fluxball MSGW11 95Hz
50.6G Fluxball EFH1 47Hz
50.6G Fluxball MSGW11 47Hz
50.6G Fluxball EFH1 15Hz
50.6G Fluxball MSGW11 15Hz

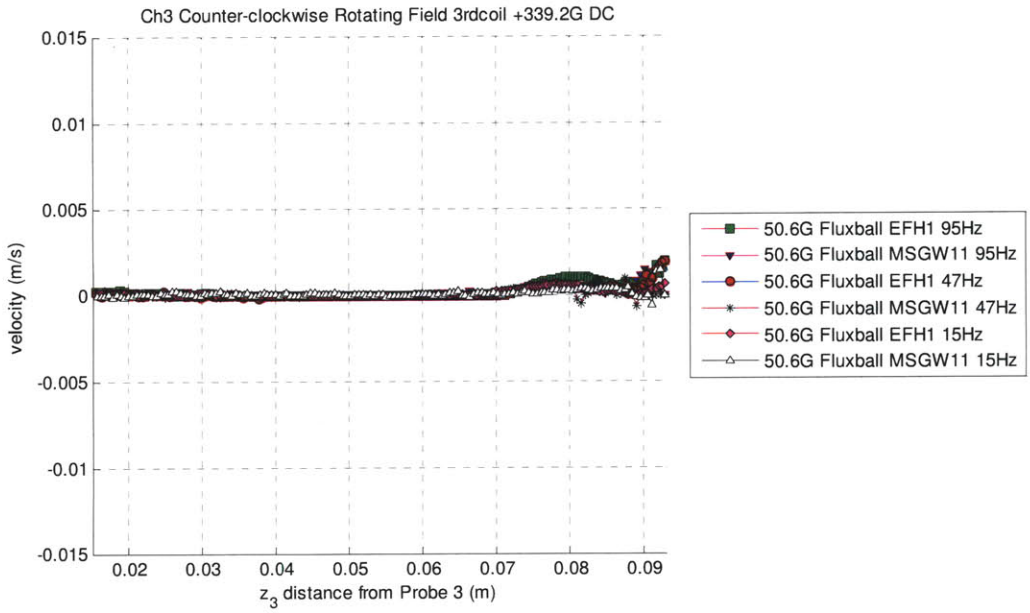
Ch3 Counter-clockwise Rotating Field 3rdcoil +339.2G DC
velocity (m/s)
0.015
0.01
0.005
0
-0.005
-0.01
-0.015
0.02
0.03
0.04
0.05
0.06
0.07
0.08
0.09
z_3 distance from Probe 3 (m)
50.6G Fluxball EFH1 95Hz
50.6G Fluxball MSGW11 95Hz
50.6G Fluxball EFH1 47Hz
50.6G Fluxball MSGW11 47Hz
50.6G Fluxball EFH1 15Hz
50.6G Fluxball MSGW11 15Hz

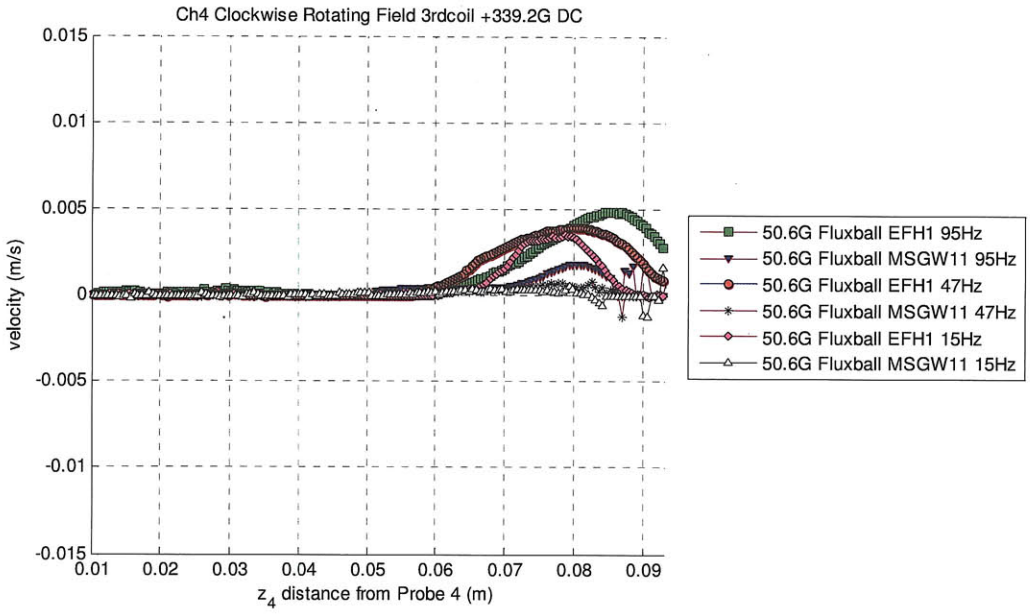
Ch4 Clockwise Rotating Field 3rdcoil +339.2G DC
velocity (m/s)
0.015
0.01
0.005
0
-0.005
-0.01
-0.015
0.01
0.02
0.03
0.04
0.05
0.06
0.07
0.08
0.09
z4 distance from Probe 4 (m)
50.6G Fluxball EFH1 95Hz
50.6G Fluxball MSGW11 95Hz
50.6G Fluxball EFH1 47Hz
50.6G Fluxball MSGW11 47Hz
50.6G Fluxball EFH1 15Hz
50.6G Fluxball MSGW11 15Hz

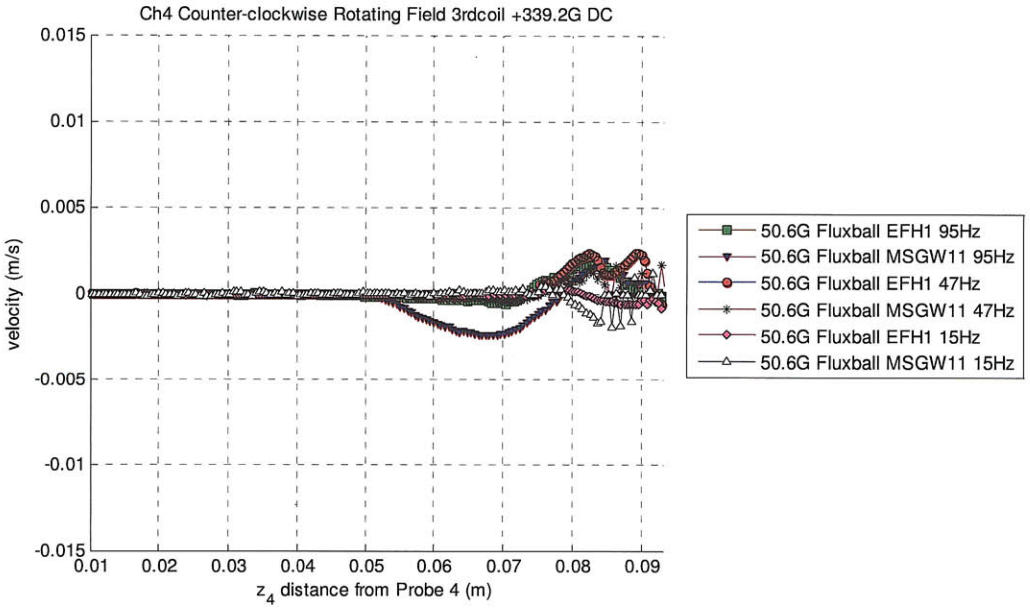
Ch4 Counter-clockwise Rotating Field 3rdcoil +339.2G DC
velocity (m/s)
0.015
0.01
0.005
0
-0.005
-0.01
-0.015
0.01
0.02
0.03
0.04
0.05
0.06
0.07
0.08
0.09
z4 distance from Probe 4 (m)
50.6G Fluxball EFH1 95Hz
50.6G Fluxball MSGW11 95Hz
50.6G Fluxball EFH1 47Hz
50.6G Fluxball MSGW11 47Hz
50.6G Fluxball EFH1 15Hz
50.6G Fluxball MSGW11 15Hz

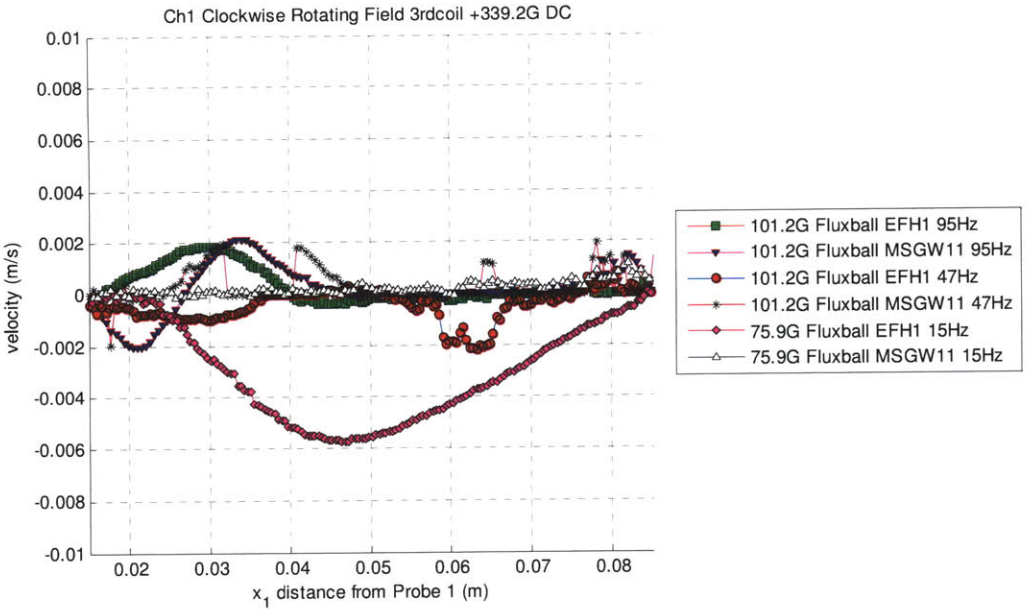
Ch1 Clockwise Rotating Field 3rdcoil +339.2G DC
velocity (m/s)
0.01
0.008
0.006
0.004
0.002
0
-0.002
-0.004
-0.006
-0.008
-0.01
0.02
0.03
0.04
0.05
0.06
0.07
0.08
x1 distance from Probe 1 (m)
101.2G Fluxball EFH1 95Hz
101.2G Fluxball MSGW11 95Hz
101.2G Fluxball EFH1 47Hz
101.2G Fluxball MSGW11 47Hz
75.9G Fluxball EFH1 15Hz
75.9G Fluxball MSGW11 15Hz

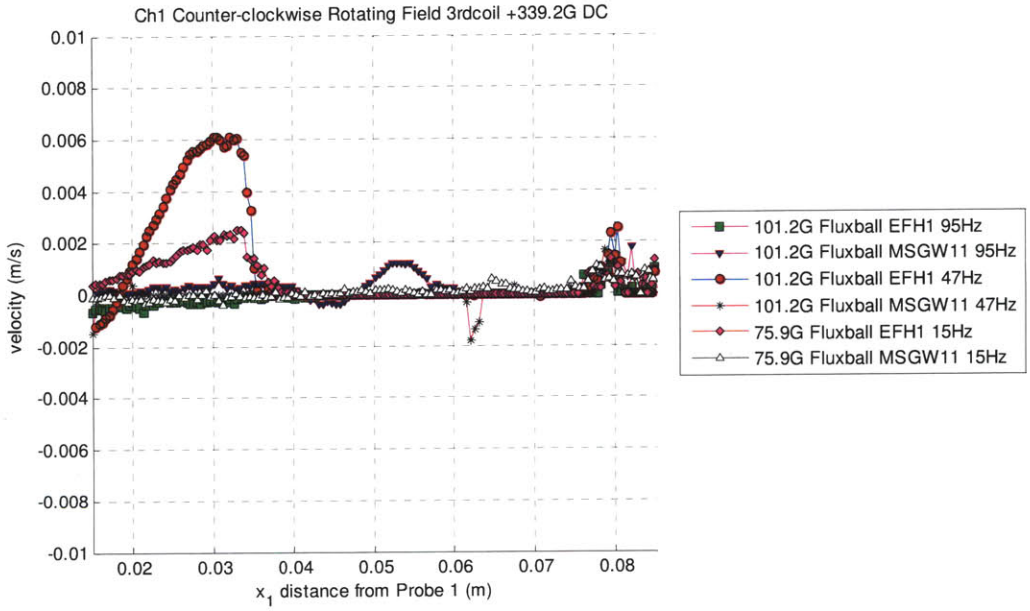
Ch1 Counter-clockwise Rotating Field 3rdcoil +339.2G DC
velocity (m/s)
0.01
0.008
0.006
0.004
0.002
0
-0.002
-0.004
-0.006
-0.008
-0.01
0.02
0.03
0.04
0.05
0.06
0.07
0.08
x1 distance from Probe 1 (m)
101.2G Fluxball EFH1 95Hz
101.2G Fluxball MSGW11 95Hz
101.2G Fluxball EFH1 47Hz
101.2G Fluxball MSGW11 47Hz
75.9G Fluxball EFH1 15Hz
75.9G Fluxball MSGW11 15Hz

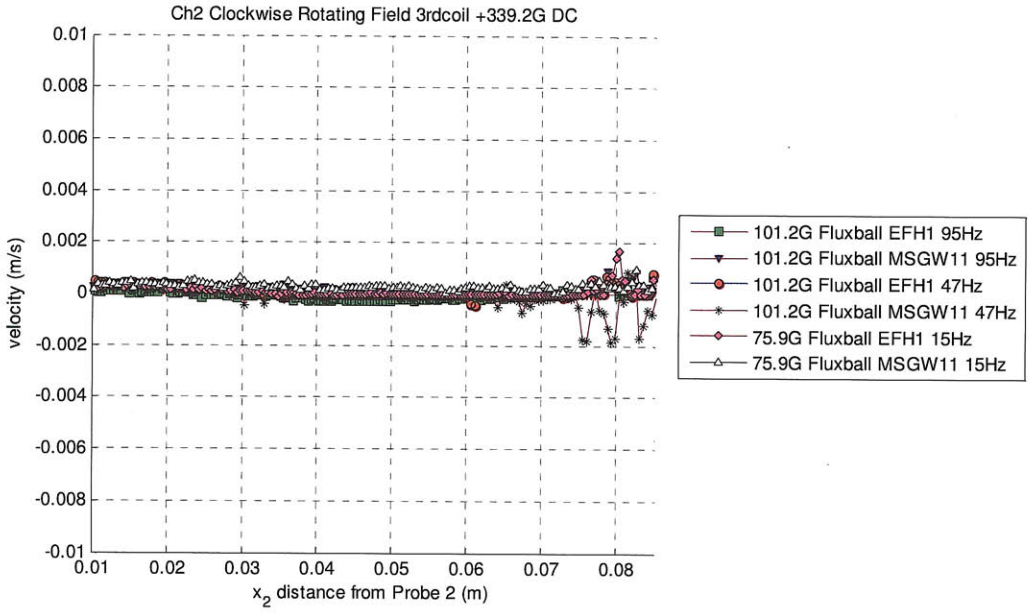
Ch2 Clockwise Rotating Field 3rdcoil +339.2G DC
velocity (m/s)
0.01
0.008
0.006
0.004
0.002
0
-0.002
-0.004
-0.006
-0.008
-0.01
0.01 0.02 0.03 0.04 0.05 0.06 0.07 0.08
x2 distance from Probe 2 (m)
101.2G Fluxball EFH1 95Hz
101.2G Fluxball MSGW11 95Hz
101.2G Fluxball EFH1 47Hz
101.2G Fluxball MSGW11 47Hz
75.9G Fluxball EFH1 15Hz
75.9G Fluxball MSGW11 15Hz

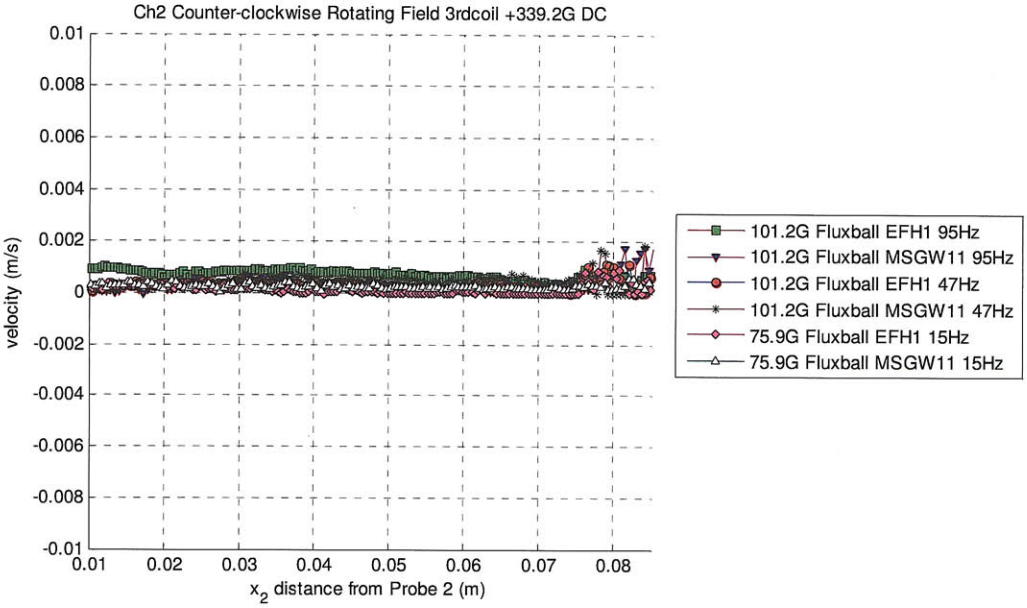
Ch2 Counter-clockwise Rotating Field 3rdcoil +339.2G DC
velocity (m/s)
0.01
0.008
0.006
0.004
0.002
0
-0.002
-0.004
-0.006
-0.008
-0.01
0.01 0.02 0.03 0.04 0.05 0.06 0.07 0.08
x2 distance from Probe 2 (m)
101.2G Fluxball EFH1 95Hz
101.2G Fluxball MSGW11 95Hz
101.2G Fluxball EFH1 47Hz
101.2G Fluxball MSGW11 47Hz
75.9G Fluxball EFH1 15Hz
75.9G Fluxball MSGW11 15Hz

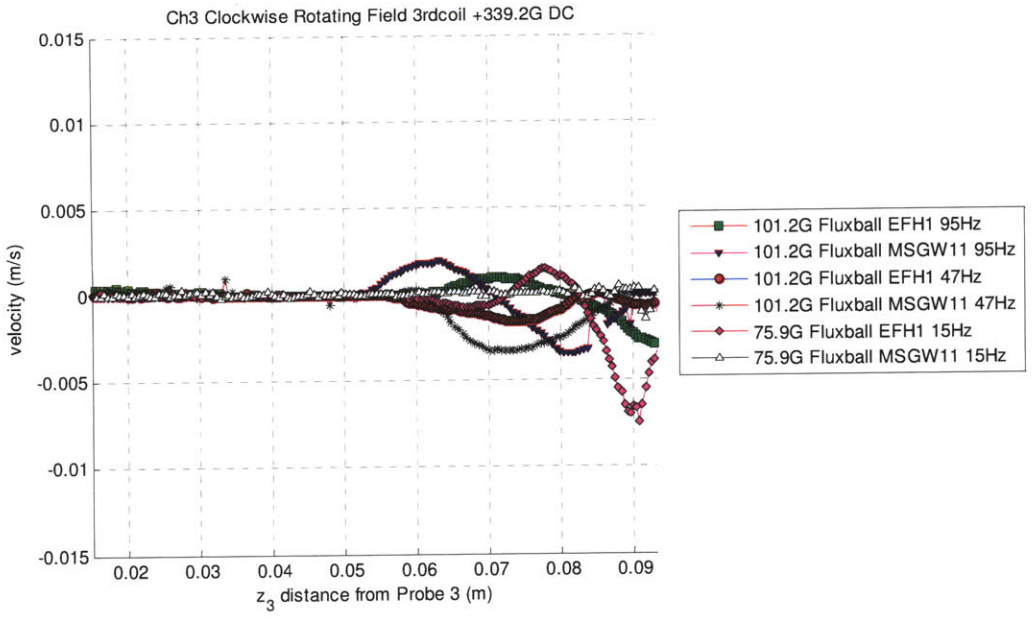
Ch3 Clockwise Rotating Field 3rdcoil +339.2G DC
0.015
0.01
0.005
0
-0.005
-0.01
-0.015
velocity (m/s)
0.02
0.03
0.04
0.05
0.06
0.07
0.08
0.09
z3 distance from Probe 3 (m)
101.2G Fluxball EFH1 95Hz
101.2G Fluxball MSGW11 95Hz
101.2G Fluxball EFH1 47Hz
101.2G Fluxball MSGW11 47Hz
75.9G Fluxball EFH1 15Hz
75.9G Fluxball MSGW11 15Hz

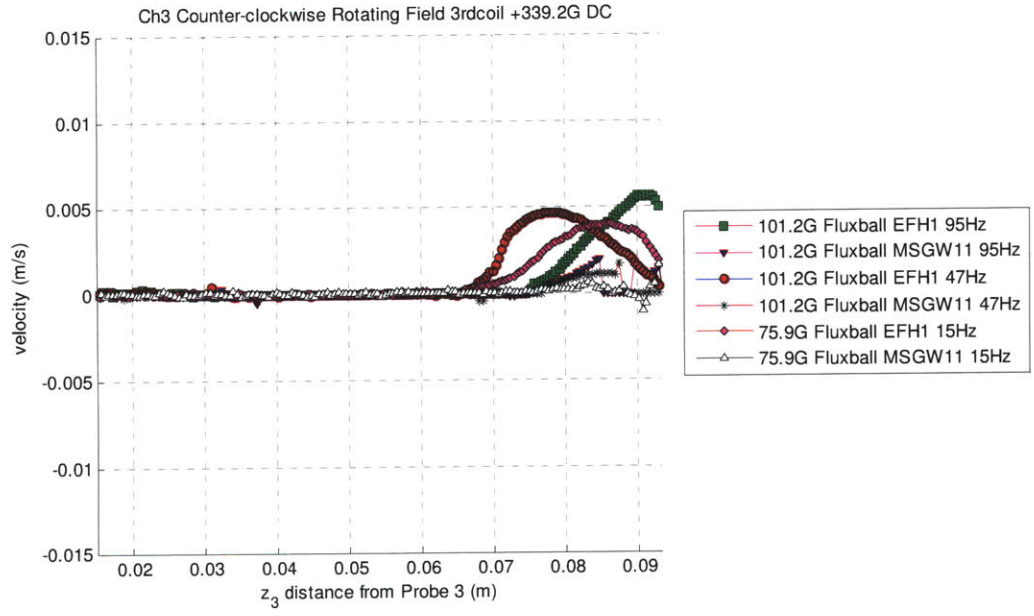
Ch3 Counter-clockwise Rotating Field 3rdcoil +339.2G DC
0.015
0.01
0.005
0
-0.005
-0.01
-0.015
velocity (m/s)
0.02
0.03
0.04
0.05
0.06
0.07
0.08
0.09
z3 distance from Probe 3 (m)
101.2G Fluxball EFH1 95Hz
101.2G Fluxball MSGW11 95Hz
101.2G Fluxball EFH1 47Hz
101.2G Fluxball MSGW11 47Hz
75.9G Fluxball EFH1 15Hz
75.9G Fluxball MSGW11 15Hz

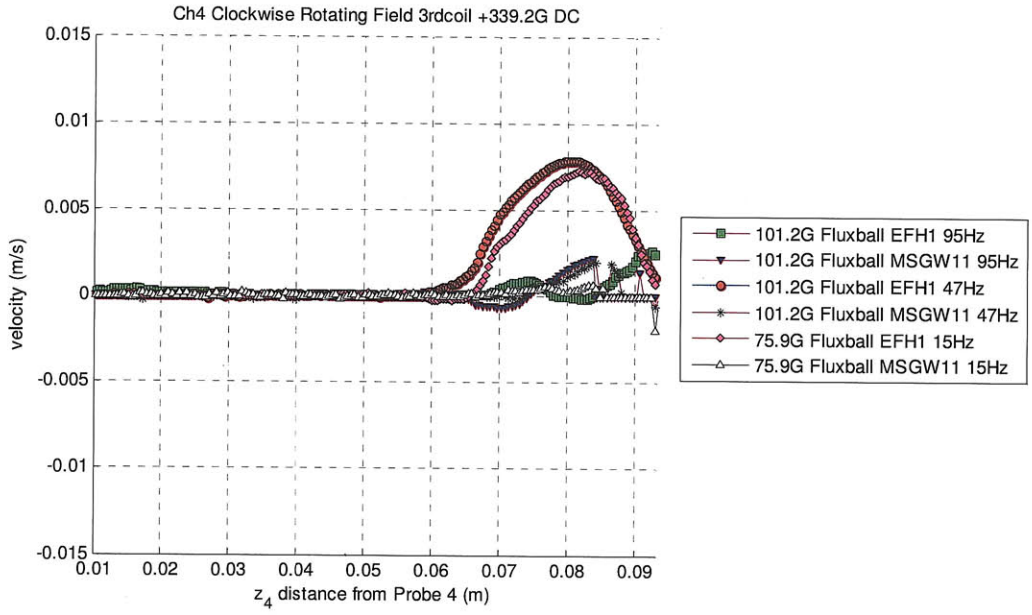
Ch4 Clockwise Rotating Field 3rdcoil +339.2G DC
velocity (m/s)
0.015
0.01
0.005
0
-0.005
-0.01
-0.015
0.01 0.02 0.03 0.04 0.05 0.06 0.07 0.08 0.09
z4 distance from Probe 4 (m)
101.2G Fluxball EFH1 95Hz
101.2G Fluxball MSGW11 95Hz
101.2G Fluxball EFH1 47Hz
101.2G Fluxball MSGW11 47Hz
75.9G Fluxball EFH1 15Hz
75.9G Fluxball MSGW11 15Hz

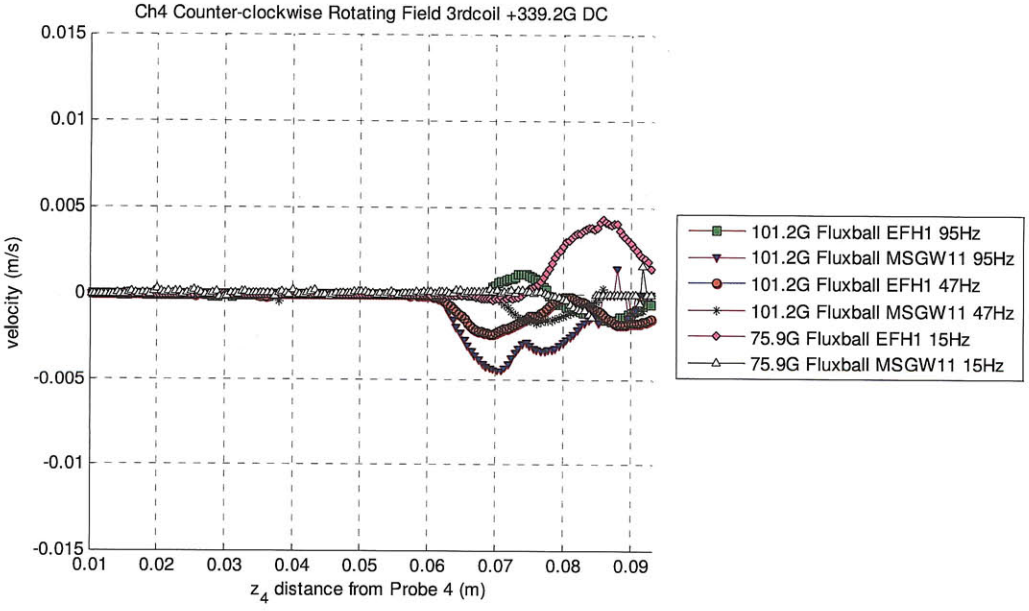
Ch4 Counter-clockwise Rotating Field 3rdcoil +339.2G DC
velocity (m/s)
0.015
0.01
0.005
0
-0.005
-0.01
-0.015
0.01 0.02 0.03 0.04 0.05 0.06 0.07 0.08 0.09
z4 distance from Probe 4 (m)
101.2G Fluxball EFH1 95Hz
101.2G Fluxball MSGW11 95Hz
101.2G Fluxball EFH1 47Hz
101.2G Fluxball MSGW11 47Hz
75.9G Fluxball EFH1 15Hz
75.9G Fluxball MSGW11 15Hz

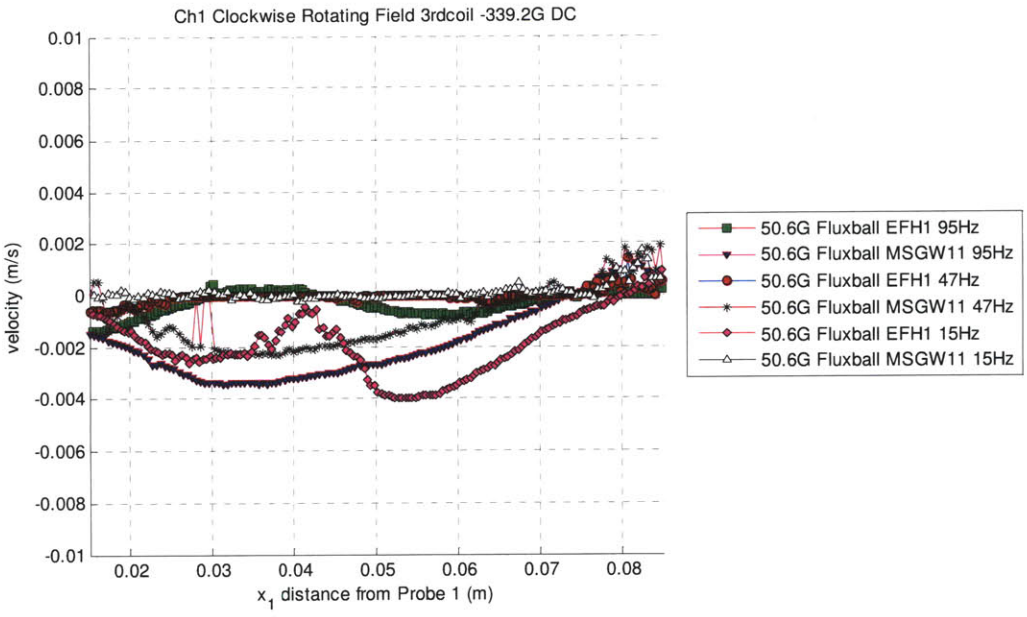
Ch1 Clockwise Rotating Field 3rdcoil -339.2G DC
velocity (m/s)
0.01
0.008
0.006
0.004
0.002
0
-0.002
-0.004
-0.006
-0.008
-0.01
0.02
0.03
0.04
0.05
0.06
0.07
0.08
x1 distance from Probe 1 (m)
50.6G Fluxball EFH1 95Hz
50.6G Fluxball MSGW11 95Hz
50.6G Fluxball EFH1 47Hz
50.6G Fluxball MSGW11 47Hz
50.6G Fluxball EFH1 15Hz
50.6G Fluxball MSGW11 15Hz

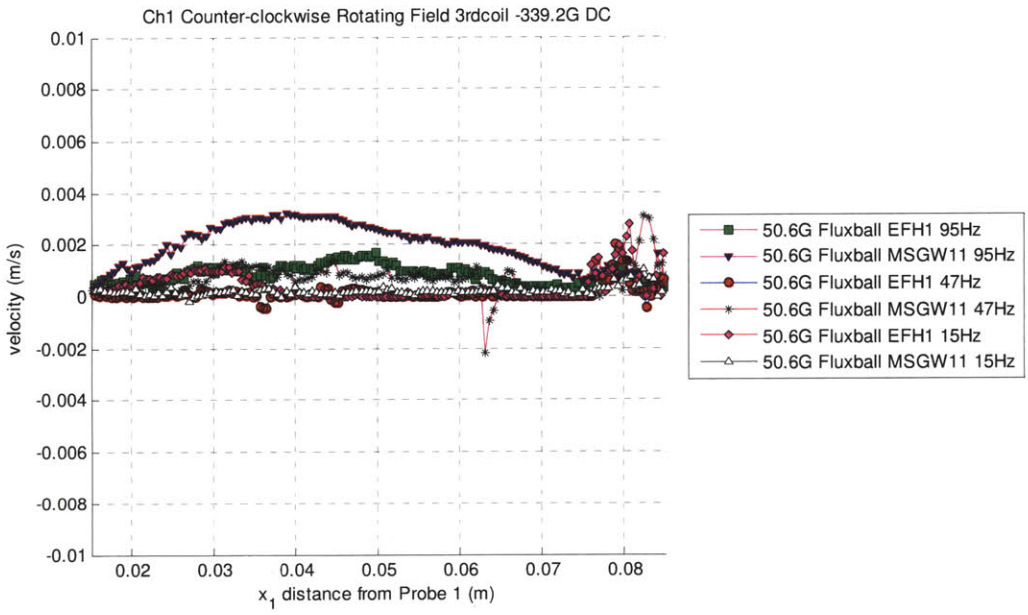
Ch1 Counter-clockwise Rotating Field 3rdcoil -339.2G DC
velocity (m/s)
0.01
0.008
0.006
0.004
0.002
0
-0.002
-0.004
-0.006
-0.008
-0.01
0.02
0.03
0.04
0.05
0.06
0.07
0.08
x1 distance from Probe 1 (m)
50.6G Fluxball EFH1 95Hz
50.6G Fluxball MSGW11 95Hz
50.6G Fluxball EFH1 47Hz
50.6G Fluxball MSGW11 47Hz
50.6G Fluxball EFH1 15Hz
50.6G Fluxball MSGW11 15Hz

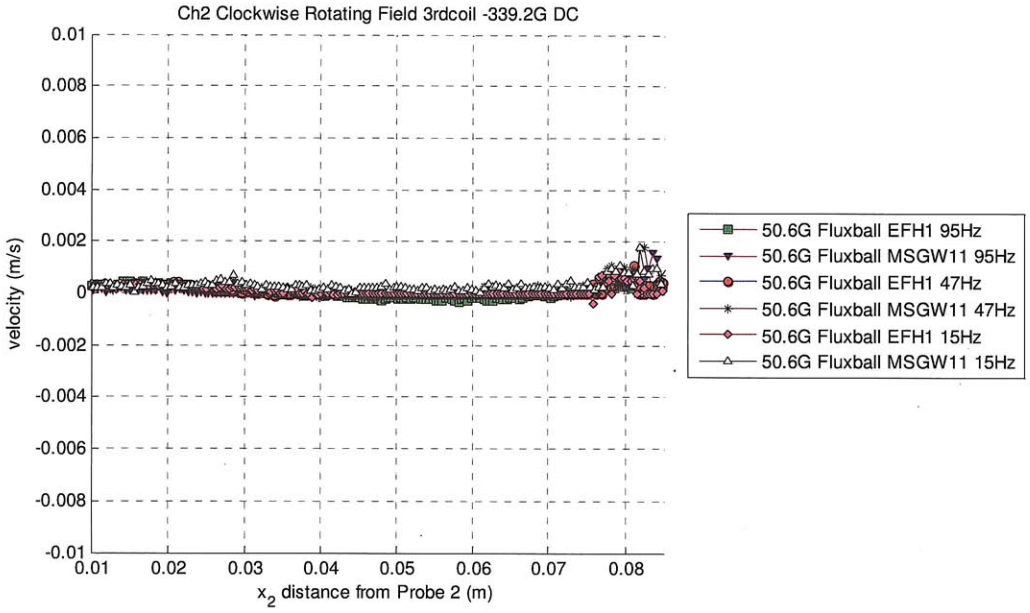
Ch2 Clockwise Rotating Field 3rdcoil -339.2G DC
velocity (m/s)
0.01
0.008
0.006
0.004
0.002
0
-0.002
-0.004
-0.006
-0.008
-0.01
0.01
0.02
0.03
0.04
0.05
0.06
0.07
0.08
x2 distance from Probe 2 (m)
50.6G Fluxball EFH1 95Hz
50.6G Fluxball MSGW11 95Hz
50.6G Fluxball EFH1 47Hz
50.6G Fluxball MSGW11 47Hz
50.6G Fluxball EFH1 15Hz
50.6G Fluxball MSGW11 15Hz

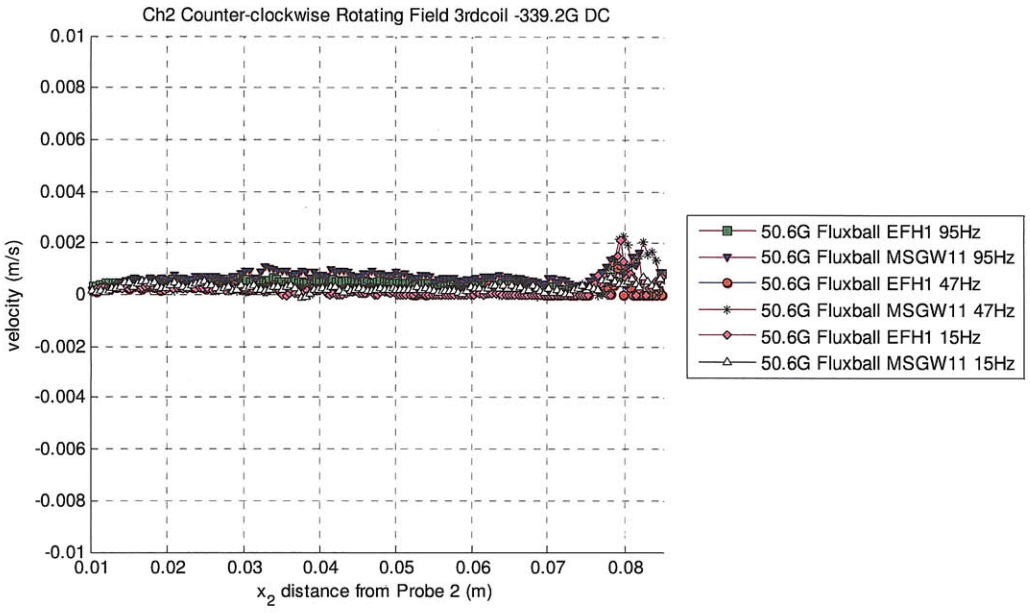
Ch2 Counter-clockwise Rotating Field 3rdcoil -339.2G DC
velocity (m/s)
0.01
0.008
0.006
0.004
0.002
0
-0.002
-0.004
-0.006
-0.008
-0.01
0.01
0.02
0.03
0.04
0.05
0.06
0.07
0.08
x2 distance from Probe 2 (m)
50.6G Fluxball EFH1 95Hz
50.6G Fluxball MSGW11 95Hz
50.6G Fluxball EFH1 47Hz
50.6G Fluxball MSGW11 47Hz
50.6G Fluxball EFH1 15Hz
50.6G Fluxball MSGW11 15Hz

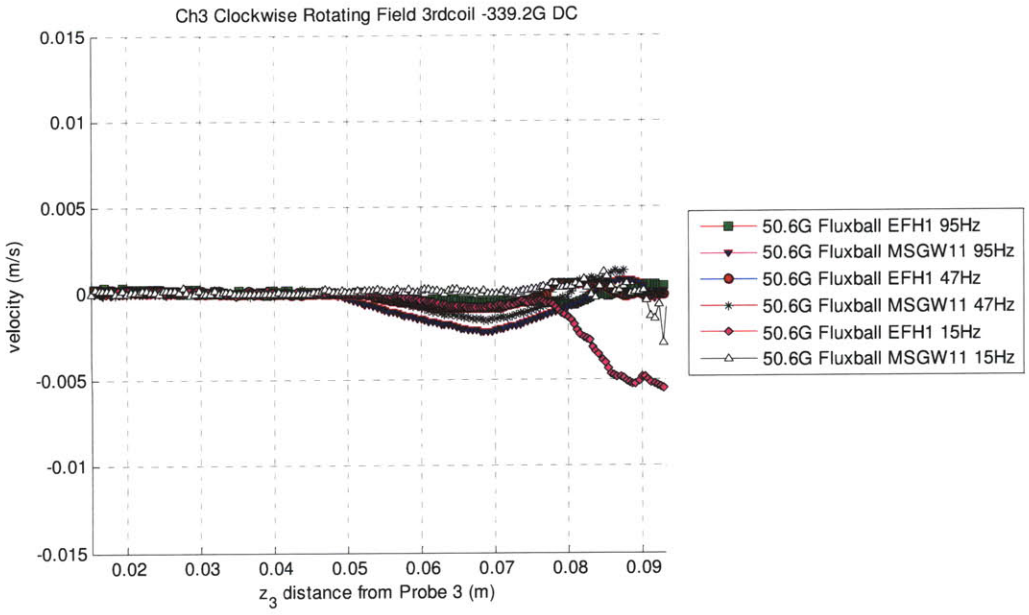
Ch3 Clockwise Rotating Field 3rdcoil -339.2G DC
velocity (m/s)
0.015
0.01
0.005
0
-0.005
-0.01
-0.015
0.02
0.03
0.04
0.05
0.06
0.07
0.08
0.09
z_3 distance from Probe 3 (m)
50.6G Fluxball EFH1 95Hz
50.6G Fluxball MSGW11 95Hz
50.6G Fluxball EFH1 47Hz
50.6G Fluxball MSGW11 47Hz
50.6G Fluxball EFH1 15Hz
50.6G Fluxball MSGW11 15Hz

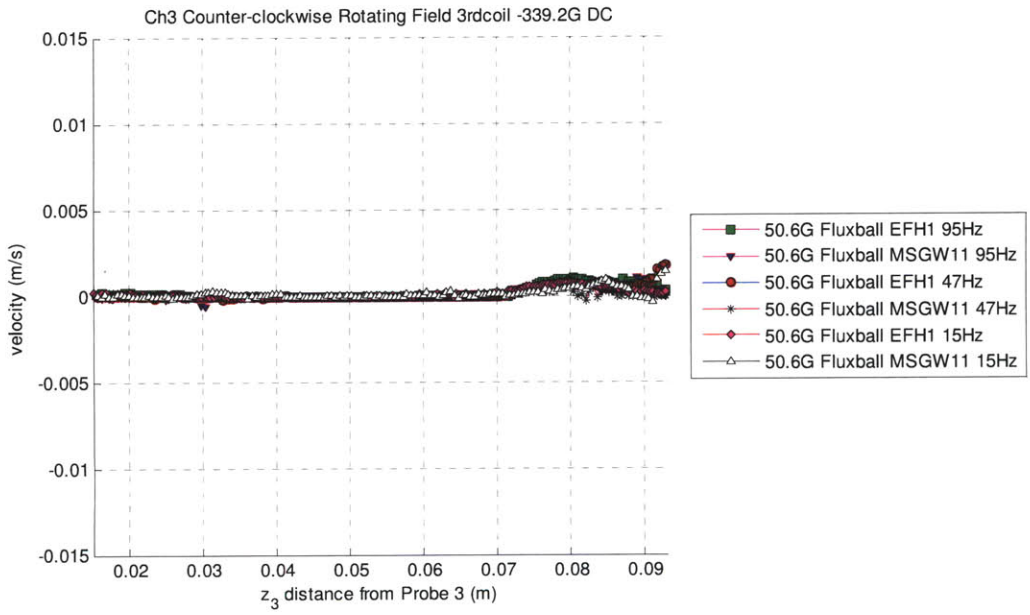
Ch3 Counter-clockwise Rotating Field 3rdcoil -339.2G DC
velocity (m/s)
0.015
0.01
0.005
0
-0.005
-0.01
-0.015
0.02
0.03
0.04
0.05
0.06
0.07
0.08
0.09
z_3 distance from Probe 3 (m)
50.6G Fluxball EFH1 95Hz
50.6G Fluxball MSGW11 95Hz
50.6G Fluxball EFH1 47Hz
50.6G Fluxball MSGW11 47Hz
50.6G Fluxball EFH1 15Hz
50.6G Fluxball MSGW11 15Hz

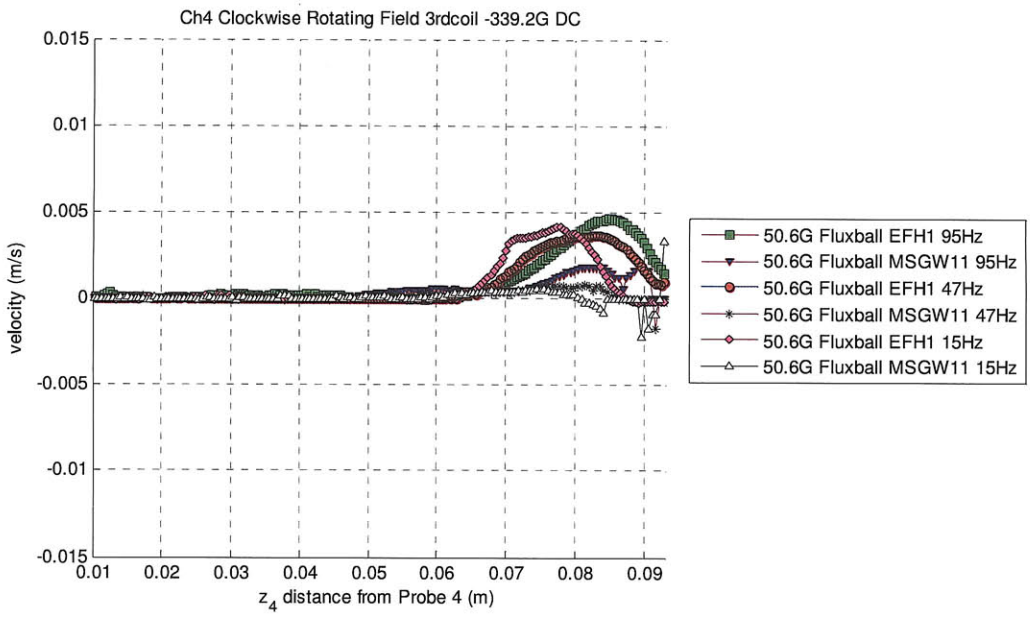
Ch4 Clockwise Rotating Field 3rdcoil -339.2G DC
velocity (m/s)
0.015
0.01
0.005
0
-0.005
-0.01
-0.015
0.01
0.02
0.03
0.04
0.05
0.06
0.07
0.08
0.09
z4 distance from Probe 4 (m)
50.6G Fluxball EFH1 95Hz
50.6G Fluxball MSGW11 95Hz
50.6G Fluxball EFH1 47Hz
50.6G Fluxball MSGW11 47Hz
50.6G Fluxball EFH1 15Hz
50.6G Fluxball MSGW11 15Hz

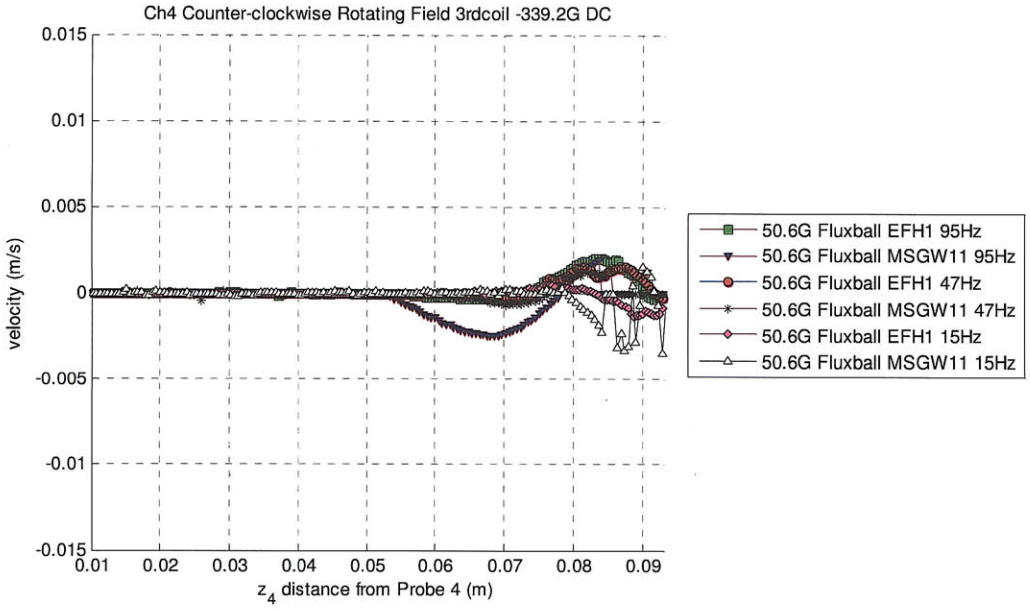
Ch4 Counter-clockwise Rotating Field 3rdcoil -339.2G DC
velocity (m/s)
0.015
0.01
0.005
0
-0.005
-0.01
-0.015
0.01
0.02
0.03
0.04
0.05
0.06
0.07
0.08
0.09
z4 distance from Probe 4 (m)
50.6G Fluxball EFH1 95Hz
50.6G Fluxball MSGW11 95Hz
50.6G Fluxball EFH1 47Hz
50.6G Fluxball MSGW11 47Hz
50.6G Fluxball EFH1 15Hz
50.6G Fluxball MSGW11 15Hz

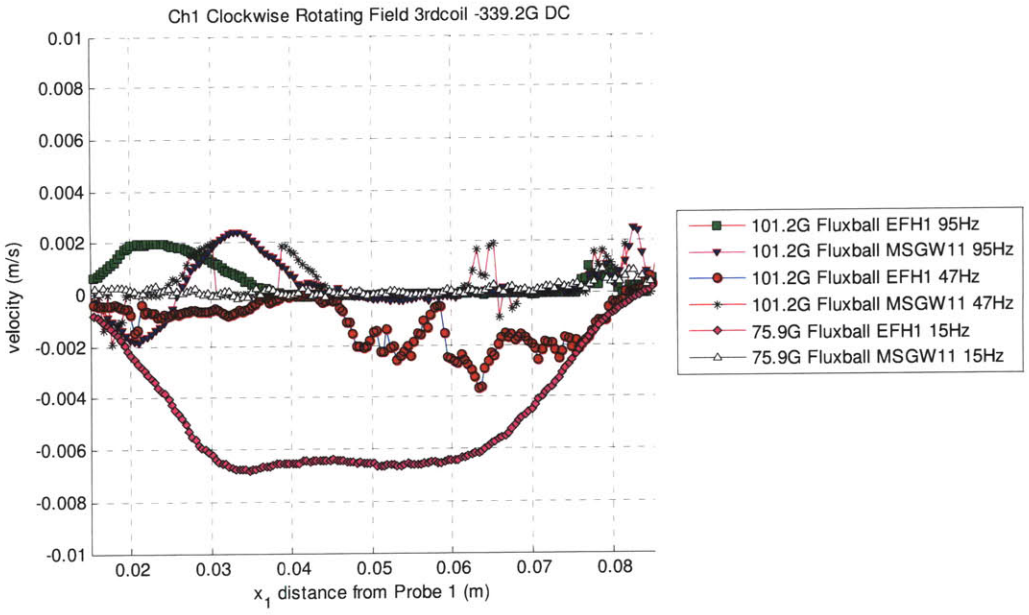
Ch1 Clockwise Rotating Field 3rdcoil -339.2G DC
velocity (m/s)
0.01
0.008
0.006
0.004
0.002
0
-0.002
-0.004
-0.006
-0.008
-0.01
0.02
0.03
0.04
0.05
0.06
0.07
0.08
x1 distance from Probe 1 (m)
101.2G Fluxball EFH1 95Hz
101.2G Fluxball MSGW11 95Hz
101.2G Fluxball EFH1 47Hz
101.2G Fluxball MSGW11 47Hz
75.9G Fluxball EFH1 15Hz
75.9G Fluxball MSGW11 15Hz

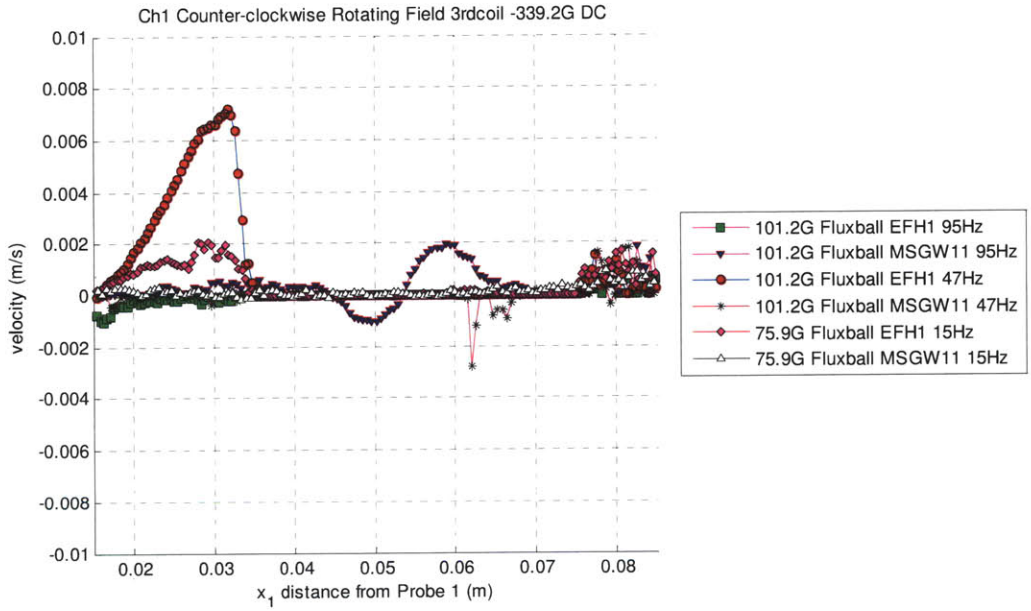
Ch1 Counter-clockwise Rotating Field 3rdcoil -339.2G DC
velocity (m/s)
0.01
0.008
0.006
0.004
0.002
0
-0.002
-0.004
-0.006
-0.008
-0.01
0.02
0.03
0.04
0.05
0.06
0.07
0.08
x1 distance from Probe 1 (m)
101.2G Fluxball EFH1 95Hz
101.2G Fluxball MSGW11 95Hz
101.2G Fluxball EFH1 47Hz
101.2G Fluxball MSGW11 47Hz
75.9G Fluxball EFH1 15Hz
75.9G Fluxball MSGW11 15Hz

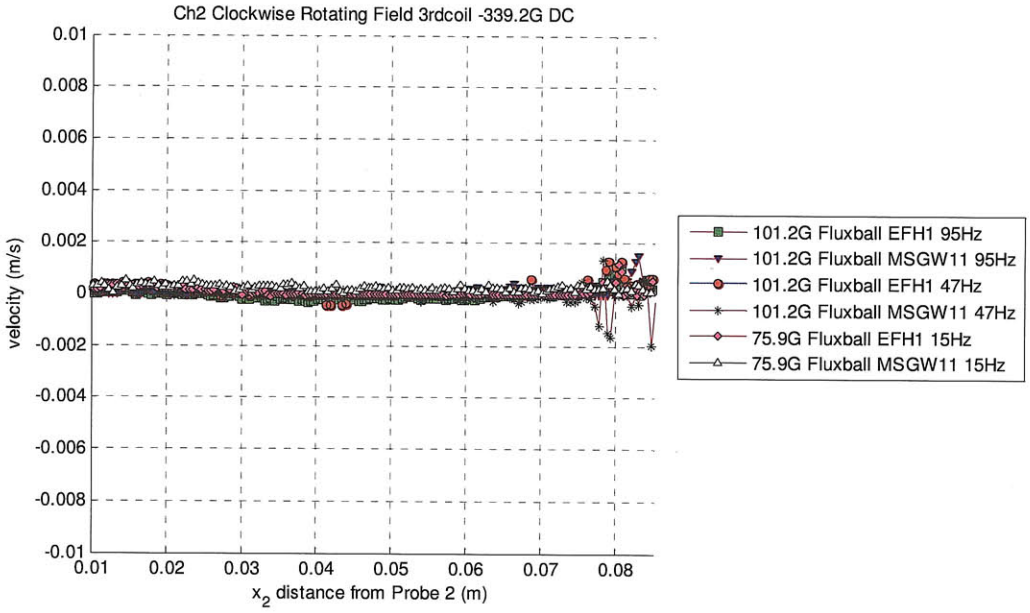
Ch2 Clockwise Rotating Field 3rdcoil -339.2G DC
velocity (m/s)
0.01
0.008
0.006
0.004
0.002
0
-0.002
-0.004
-0.006
-0.008
-0.01
0.01 0.02 0.03 0.04 0.05 0.06 0.07 0.08
x2 distance from Probe 2 (m)
101.2G Fluxball EFH1 95Hz
101.2G Fluxball MSGW11 95Hz
101.2G Fluxball EFH1 47Hz
101.2G Fluxball MSGW11 47Hz
75.9G Fluxball EFH1 15Hz
75.9G Fluxball MSGW11 15Hz

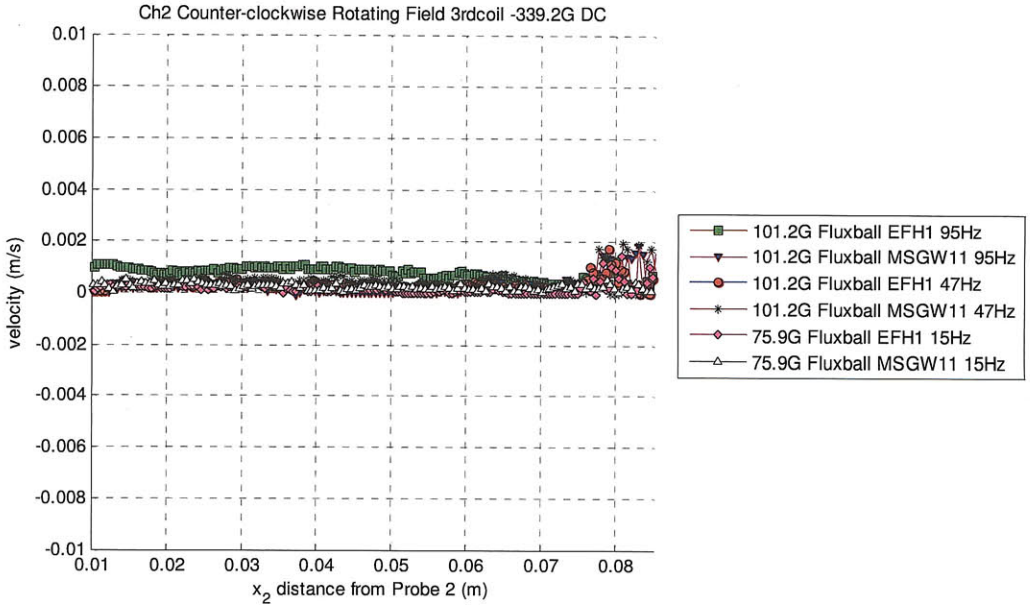
Ch2 Counter-clockwise Rotating Field 3rdcoil -339.2G DC
velocity (m/s)
0.01
0.008
0.006
0.004
0.002
0
-0.002
-0.004
-0.006
-0.008
-0.01
0.01 0.02 0.03 0.04 0.05 0.06 0.07 0.08
x2 distance from Probe 2 (m)
101.2G Fluxball EFH1 95Hz
101.2G Fluxball MSGW11 95Hz
101.2G Fluxball EFH1 47Hz
101.2G Fluxball MSGW11 47Hz
75.9G Fluxball EFH1 15Hz
75.9G Fluxball MSGW11 15Hz

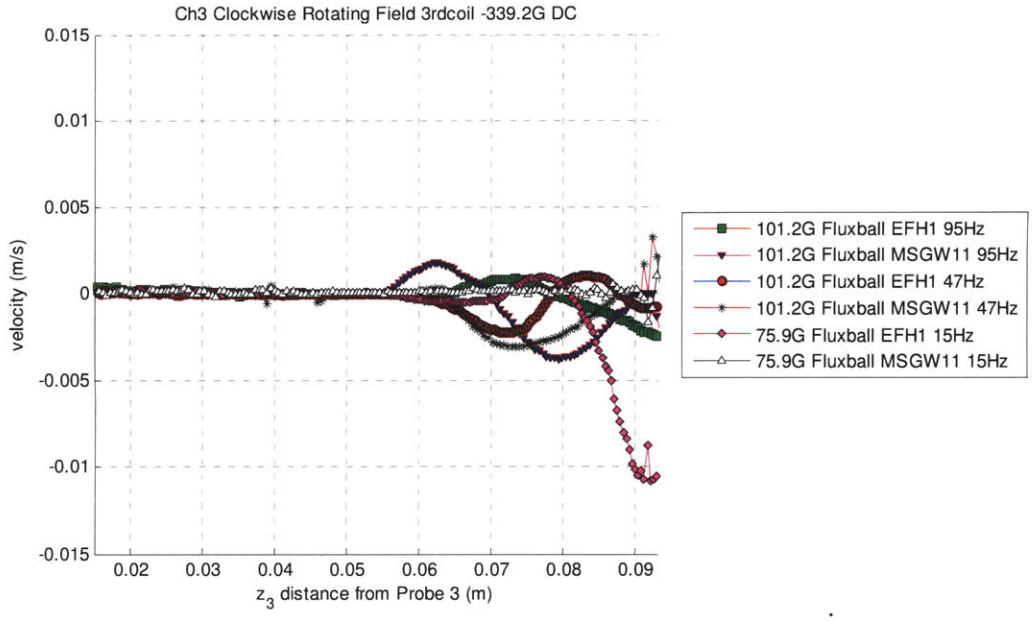
Ch3 Clockwise Rotating Field 3rdcoil -339.2G DC
velocity (m/s)
0.015
0.01
0.005
0
-0.005
-0.01
-0.015
0.02
0.03
0.04
0.05
0.06
0.07
0.08
0.09
z3 distance from Probe 3 (m)
101.2G Fluxball EFH1 95Hz
101.2G Fluxball MSGW11 95Hz
101.2G Fluxball EFH1 47Hz
101.2G Fluxball MSGW11 47Hz
75.9G Fluxball EFH1 15Hz
75.9G Fluxball MSGW11 15Hz

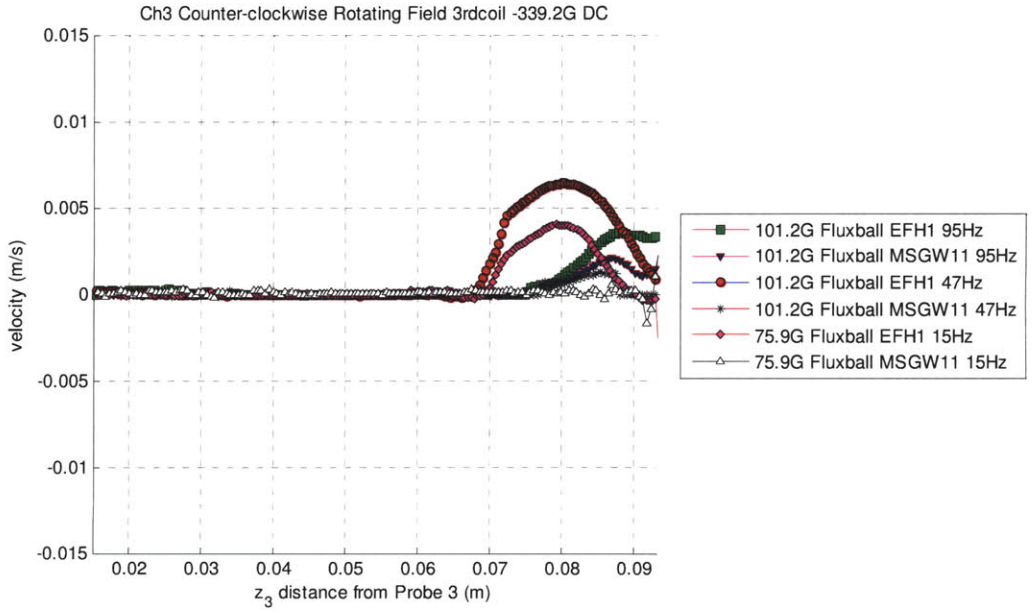
Ch3 Counter-clockwise Rotating Field 3rdcoil -339.2G DC
velocity (m/s)
0.015
0.01
0.005
0
-0.005
-0.01
-0.015
0.02
0.03
0.04
0.05
0.06
0.07
0.08
0.09
z3 distance from Probe 3 (m)
101.2G Fluxball EFH1 95Hz
101.2G Fluxball MSGW11 95Hz
101.2G Fluxball EFH1 47Hz
101.2G Fluxball MSGW11 47Hz
75.9G Fluxball EFH1 15Hz
75.9G Fluxball MSGW11 15Hz

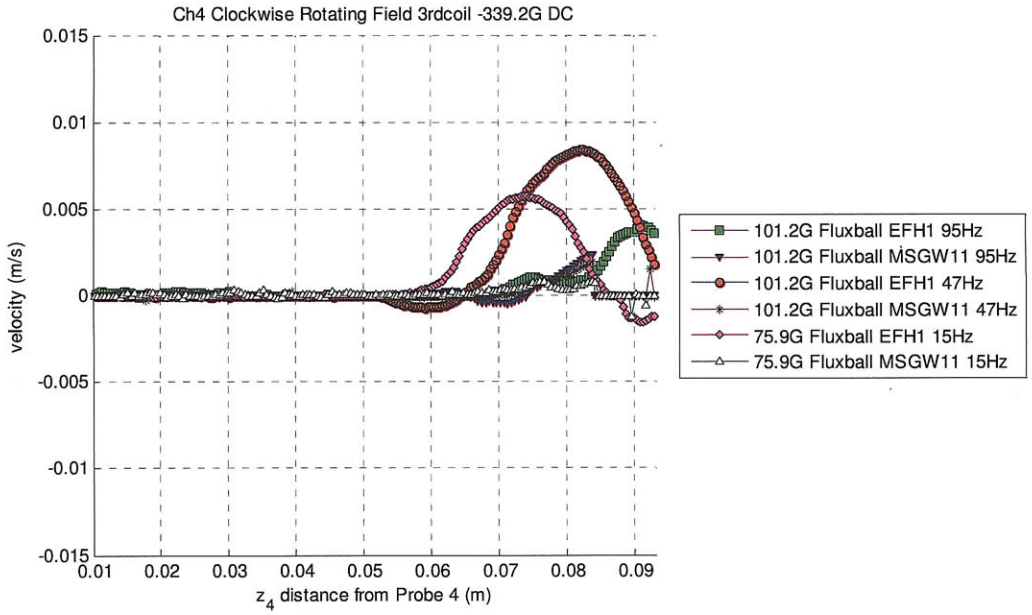
Ch4 Clockwise Rotating Field 3rdcoil -339.2G DC
velocity (m/s)
0.015
0.01
0.005
0
-0.005
-0.01
-0.015
0.01
0.02
0.03
0.04
0.05
0.06
0.07
0.08
0.09
z4 distance from Probe 4 (m)
101.2G Fluxball EFH1 95Hz
101.2G Fluxball MSGW11 95Hz
101.2G Fluxball EFH1 47Hz
101.2G Fluxball MSGW11 47Hz
75.9G Fluxball EFH1 15Hz
75.9G Fluxball MSGW11 15Hz

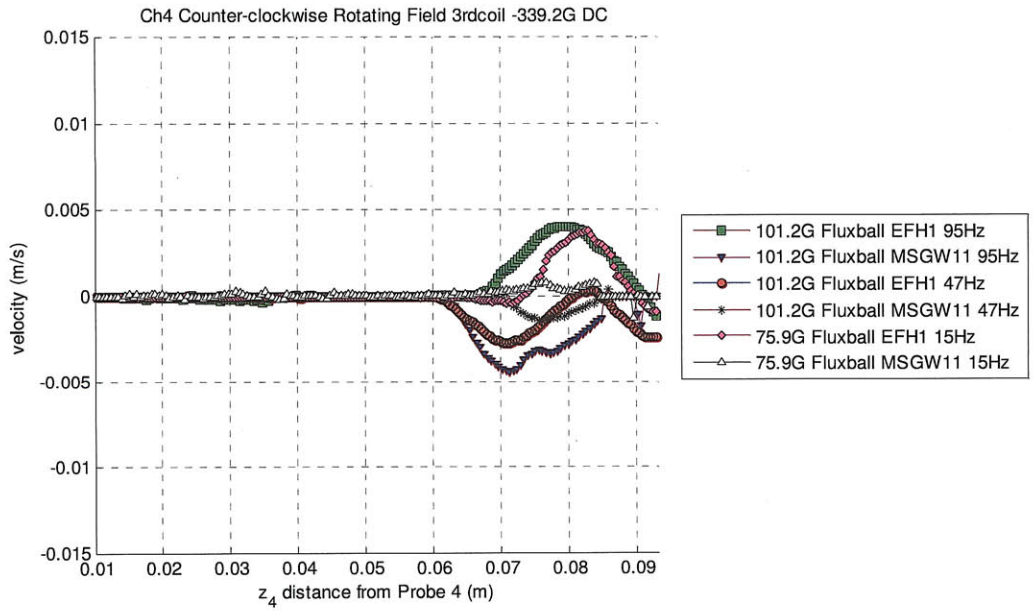
Ch4 Counter-clockwise Rotating Field 3rdcoil -339.2G DC
velocity (m/s)
0.015
0.01
0.005
0
-0.005
-0.01
-0.015
0.01
0.02
0.03
0.04
0.05
0.06
0.07
0.08
0.09
z4 distance from Probe 4 (m)
101.2G Fluxball EFH1 95Hz
101.2G Fluxball MSGW11 95Hz
101.2G Fluxball EFH1 47Hz
101.2G Fluxball MSGW11 47Hz
75.9G Fluxball EFH1 15Hz
75.9G Fluxball MSGW11 15Hz

Appendix H : Experimental Results with Non-Uniform Fields Generated Using Permanent Magnets (Section 6.4)

H1. EFH1 Filled Sphere with South Pole Facing Magnets on Top of Sphere at 95Hz

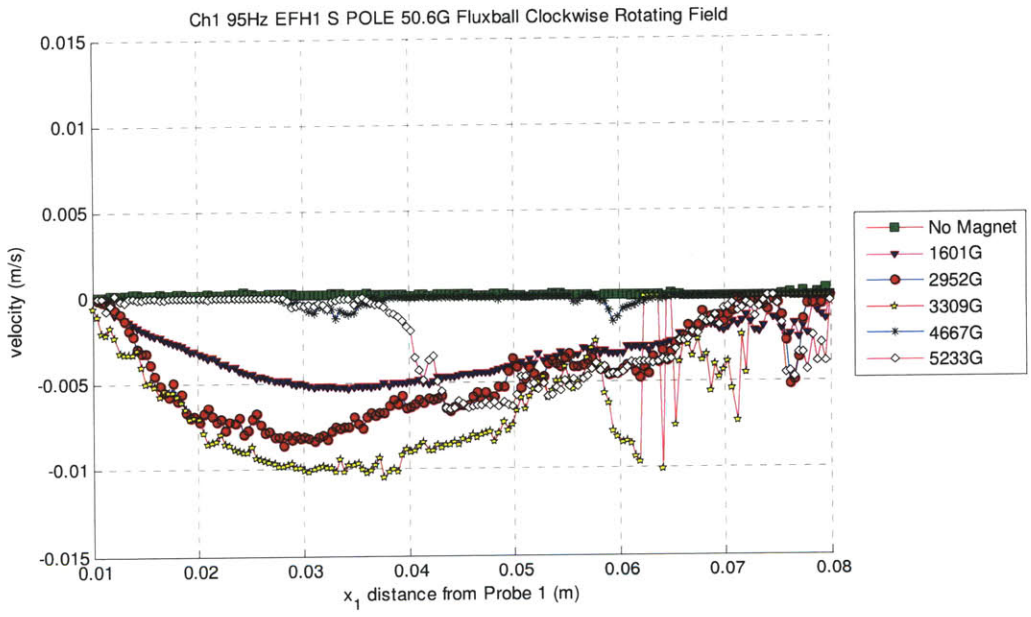

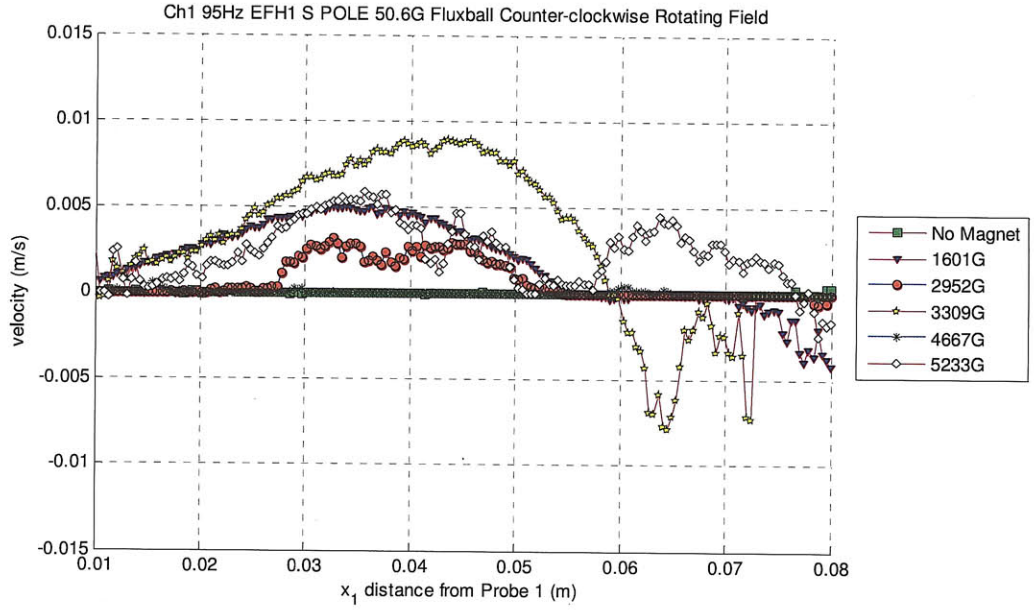
Ch1 95Hz EFH1 S POLE 50.6G Fluxball Counter-clockwise Rotating Field
velocity (m/s)
0.015
0.01
0.005
0
-0.005
-0.01
-0.015
0.01
0.02
0.03
0.04
0.05
0.06
0.07
0.08
x1 distance from Probe 1 (m)
No Magnet
1601G
2952G
3309G
4667G
5233G

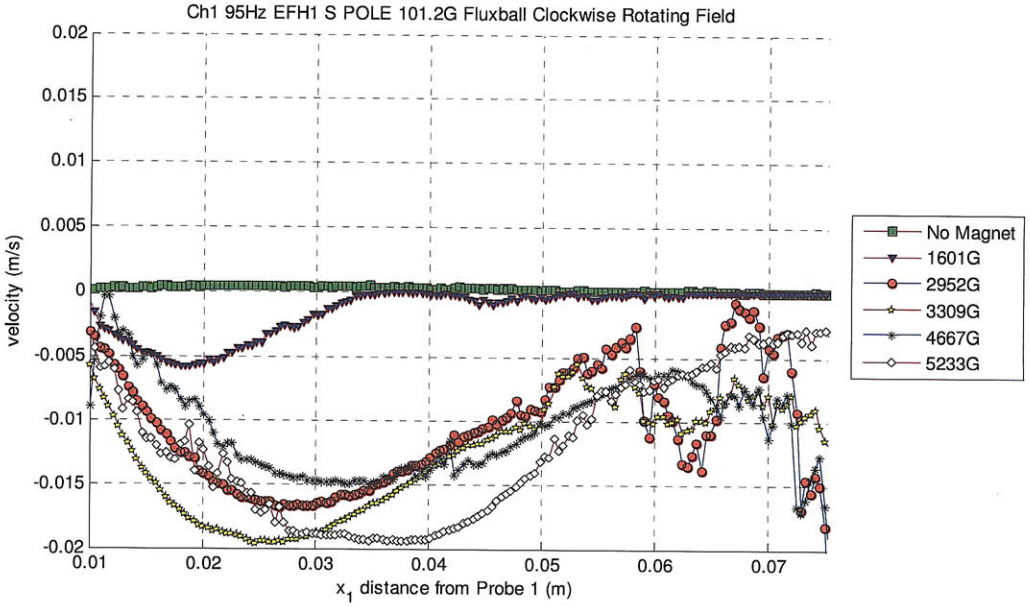
Ch1 95Hz EFH1 S POLE 101.2G Fluxball Clockwise Rotating Field
velocity (m/s)
0.02
0.015
0.01
0.005
0
-0.005
-0.01
-0.015
-0.02
0.01
0.02
0.03
0.04
0.05
0.06
0.07
x1 distance from Probe 1 (m)
No Magnet
1601G
2952G
3309G
4667G
5233G

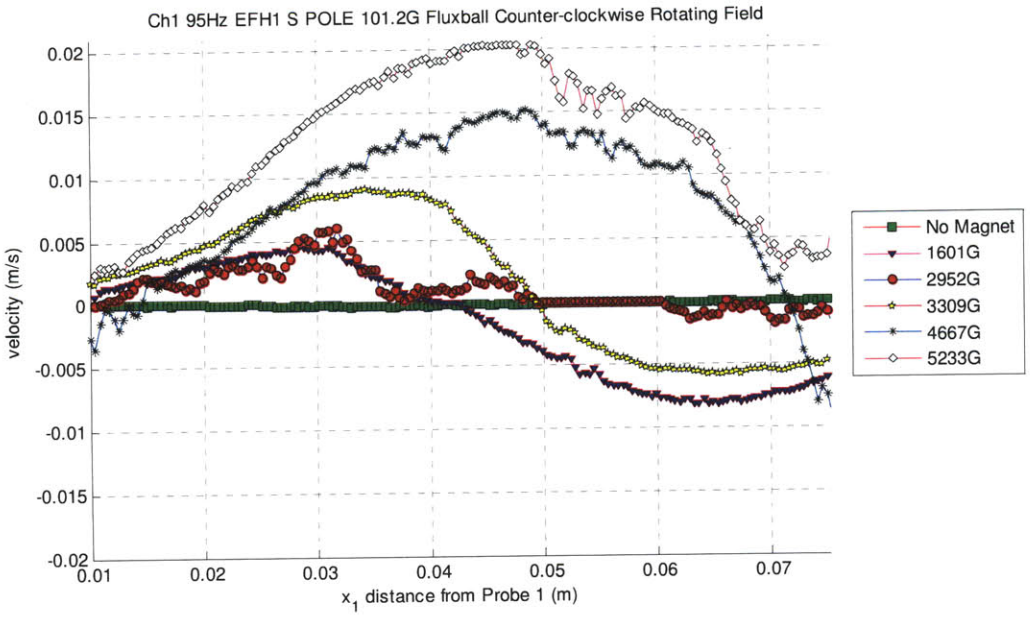
Ch1 95Hz EFH1 S POLE 101.2G Fluxball Counter-clockwise Rotating Field
velocity (m/s)
0.02
0.015
0.01
0.005
0
-0.005
-0.01
-0.015
-0.02
0.01
0.02
0.03
0.04
0.05
0.06
0.07
x1 distance from Probe 1 (m)
No Magnet
1601G
2952G
3309G
4667G
5233G

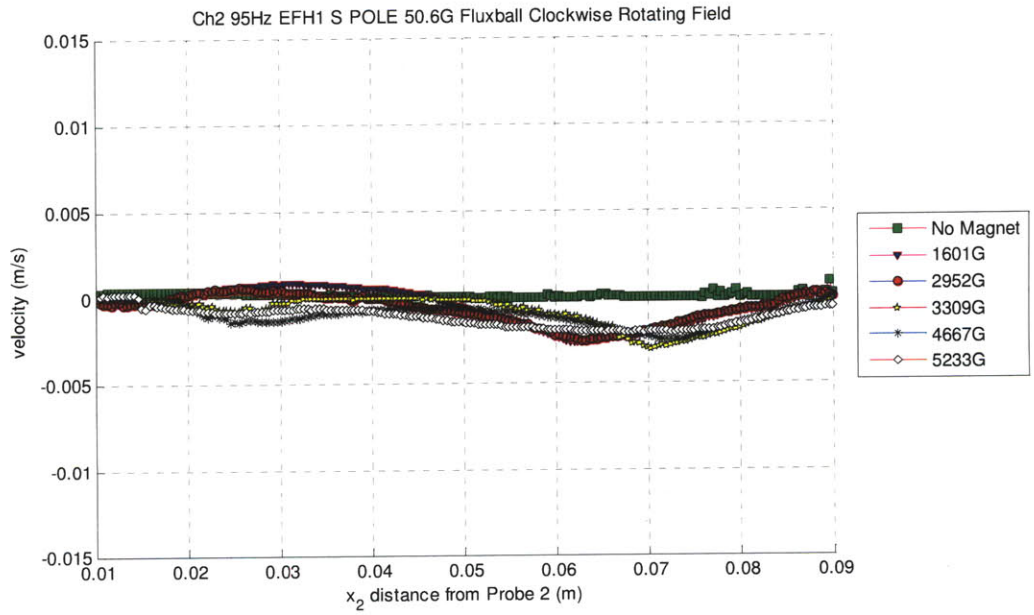
Ch2 95Hz EFH1 S POLE 50.6G Fluxball Clockwise Rotating Field
velocity (m/s)
0.015
0.01
0.005
0
-0.005
-0.01
-0.015
0.01
0.02
0.03
0.04
0.05
0.06
0.07
0.08
0.09
x2 distance from Probe 2 (m)
No Magnet
1601G
2952G
3309G
4667G
5233G

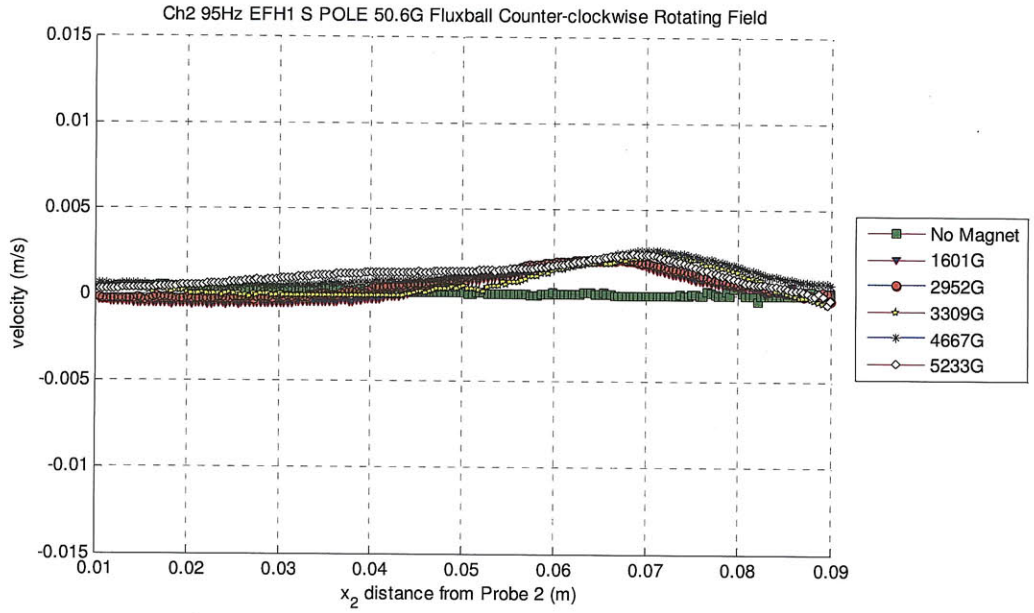
Ch2 95Hz EFH1 S POLE 50.6G Fluxball Counter-clockwise Rotating Field
velocity (m/s)
0.015
0.01
0.005
0
-0.005
-0.01
-0.015
0.01
0.02
0.03
0.04
0.05
0.06
0.07
0.08
0.09
x2 distance from Probe 2 (m)
No Magnet
1601G
2952G
3309G
4667G
5233G

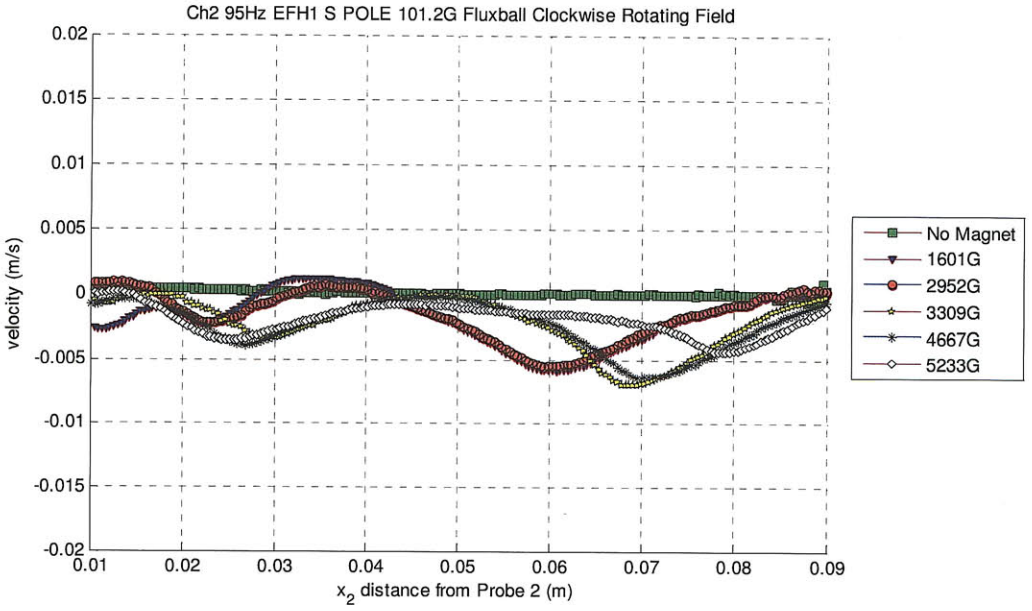
Ch2 95Hz EFH1 S POLE 101.2G Fluxball Clockwise Rotating Field
velocity (m/s)
0.02
0.015
0.01
0.005
0
-0.005
-0.01
-0.015
-0.02
0.01
0.02
0.03
0.04
0.05
0.06
0.07
0.08
0.09
x2 distance from Probe 2 (m)
No Magnet
1601G
2952G
3309G
4667G
5233G

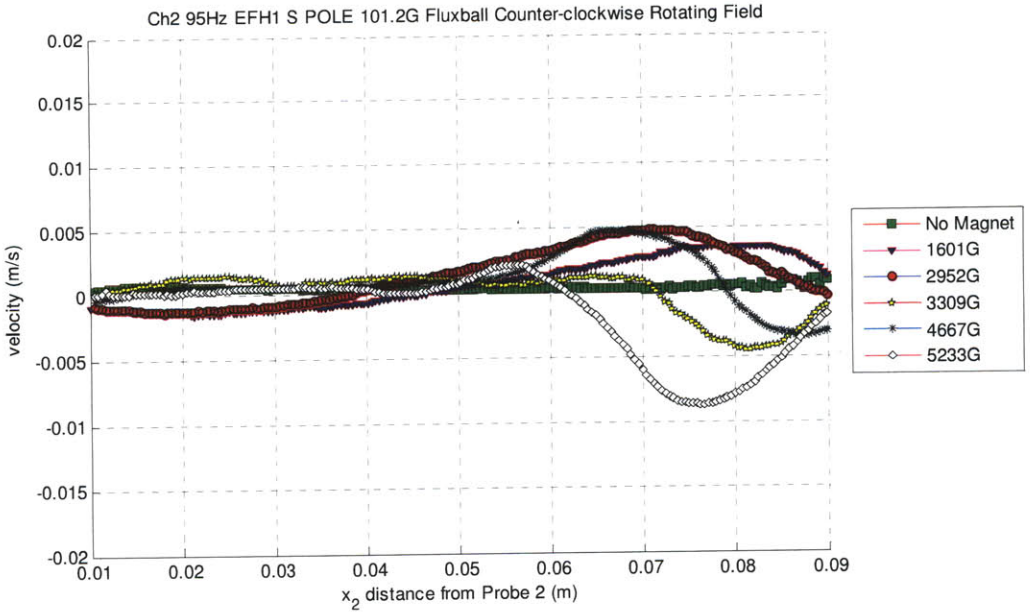
Ch2 95Hz EFH1 S POLE 101.2G Fluxball Counter-clockwise Rotating Field
velocity (m/s)
0.02
0.015
0.01
0.005
0
-0.005
-0.01
-0.015
-0.02
0.01
0.02
0.03
0.04
0.05
0.06
0.07
0.08
0.09
x_2 distance from Probe 2 (m)
No Magnet
1601G
2952G
3309G
4667G
5233G

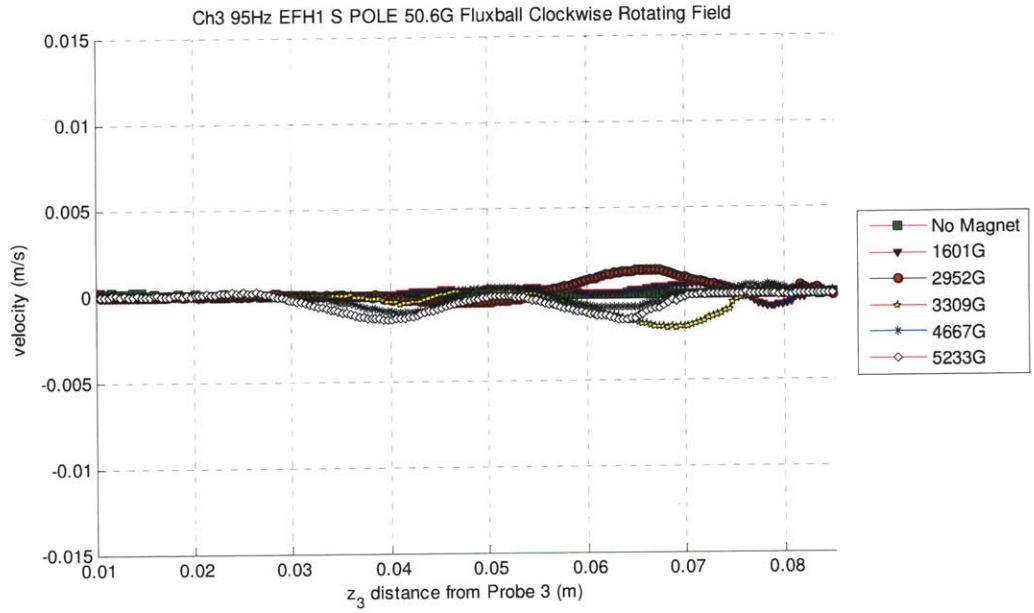
Ch3 95Hz EFH1 S POLE 50.6G Fluxball Clockwise Rotating Field
velocity (m/s)
0.015
0.01
0.005
0
-0.005
-0.01
-0.015
0.01
0.02
0.03
0.04
0.05
0.06
0.07
0.08
z_3 distance from Probe 3 (m)
No Magnet
1601G
2952G
3309G
4667G
5233G

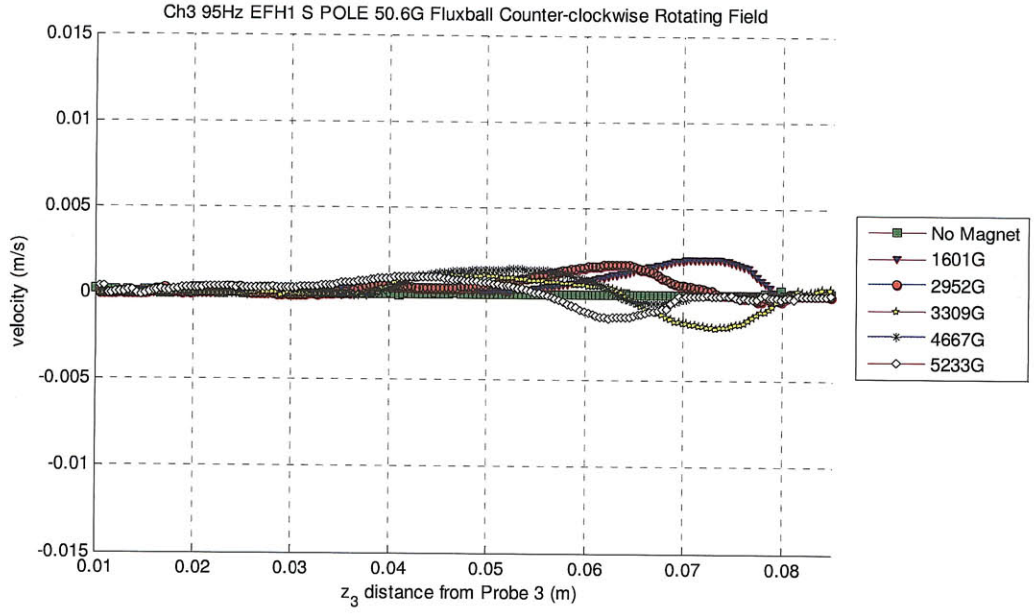
Ch3 95Hz EFH1 S POLE 50.6G Fluxball Counter-clockwise Rotating Field
velocity (m/s)
0.015
0.01
0.005
0
-0.005
-0.01
-0.015
0.01
0.02
0.03
0.04
0.05
0.06
0.07
0.08
z_3 distance from Probe 3 (m)
No Magnet
1601G
2952G
3309G
4667G
5233G

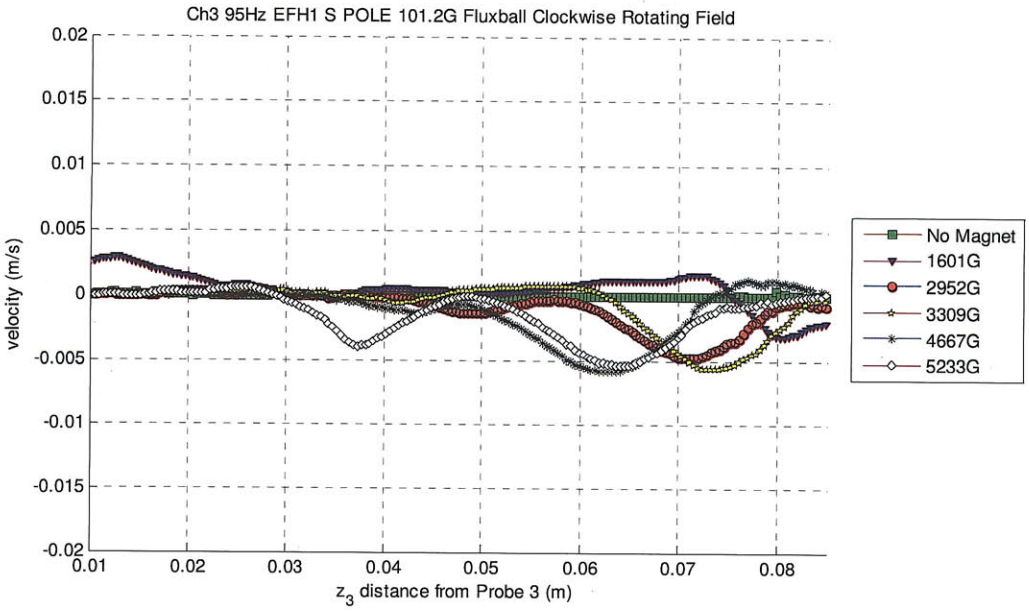
Ch3 95Hz EFH1 S POLE 101.2G Fluxball Clockwise Rotating Field
velocity (m/s)
0.02
0.015
0.01
0.005
0
-0.005
-0.01
-0.015
-0.02
0.01
0.02
0.03
0.04
0.05
0.06
0.07
0.08
z_3 distance from Probe 3 (m)
No Magnet
1601G
2952G
3309G
4667G
5233G

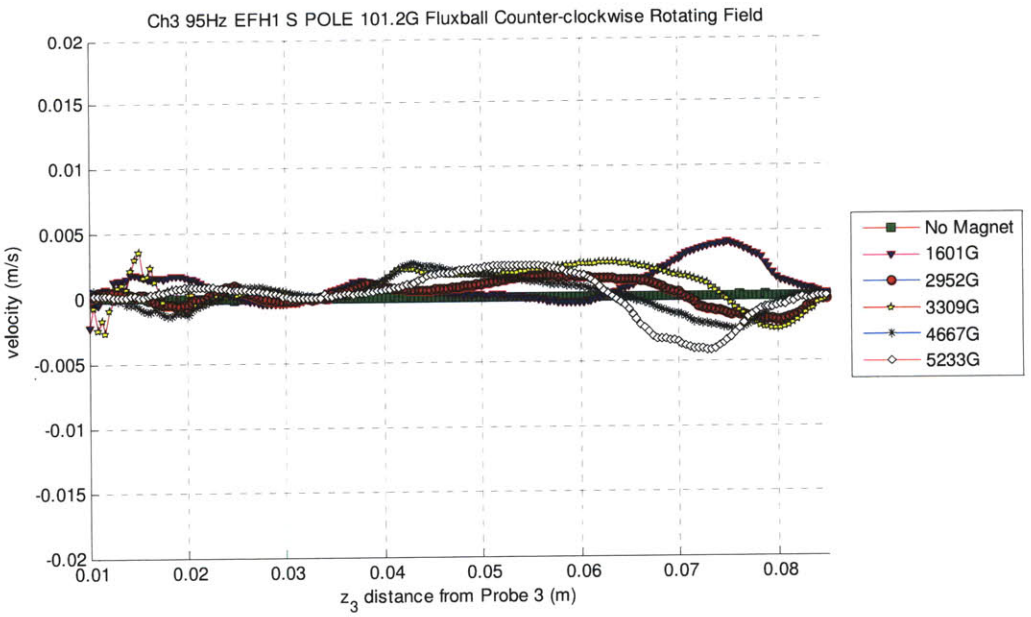
Ch3 95Hz EFH1 S POLE 101.2G Fluxball Counter-clockwise Rotating Field
velocity (m/s)
0.02
0.015
0.01
0.005
0
-0.005
-0.01
-0.015
-0.02
0.01
0.02
0.03
0.04
0.05
0.06
0.07
0.08
z_3 distance from Probe 3 (m)
No Magnet
1601G
2952G
3309G
4667G
5233G

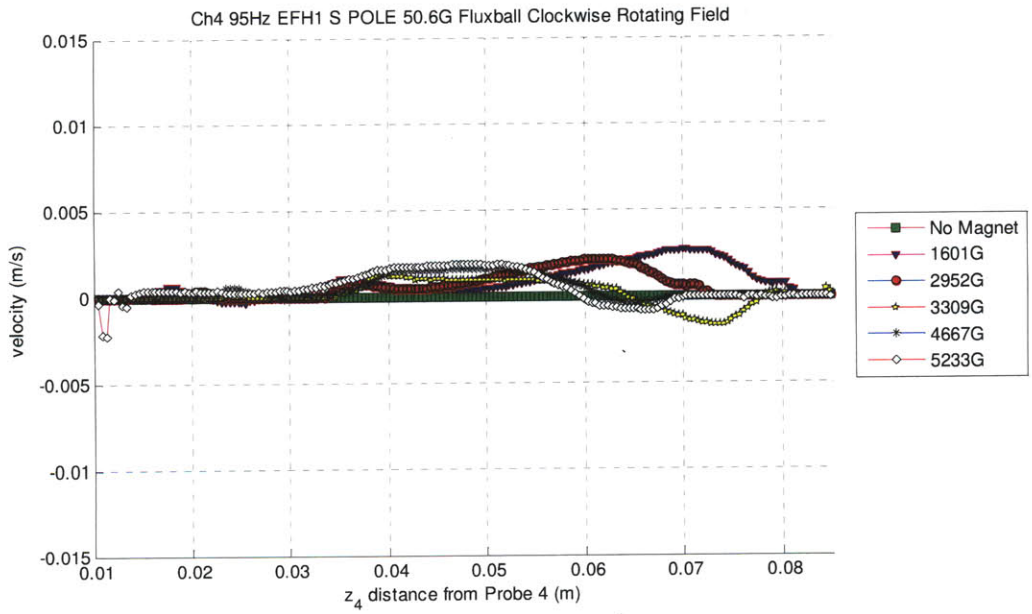
Ch4 95Hz EFH1 S POLE 50.6G Fluxball Clockwise Rotating Field
velocity (m/s)
0.015
0.01
0.005
0
-0.005
-0.01
-0.015
0.01
0.02
0.03
0.04
0.05
0.06
0.07
0.08
z_4 distance from Probe 4 (m)
No Magnet
1601G
2952G
3309G
4667G
5233G

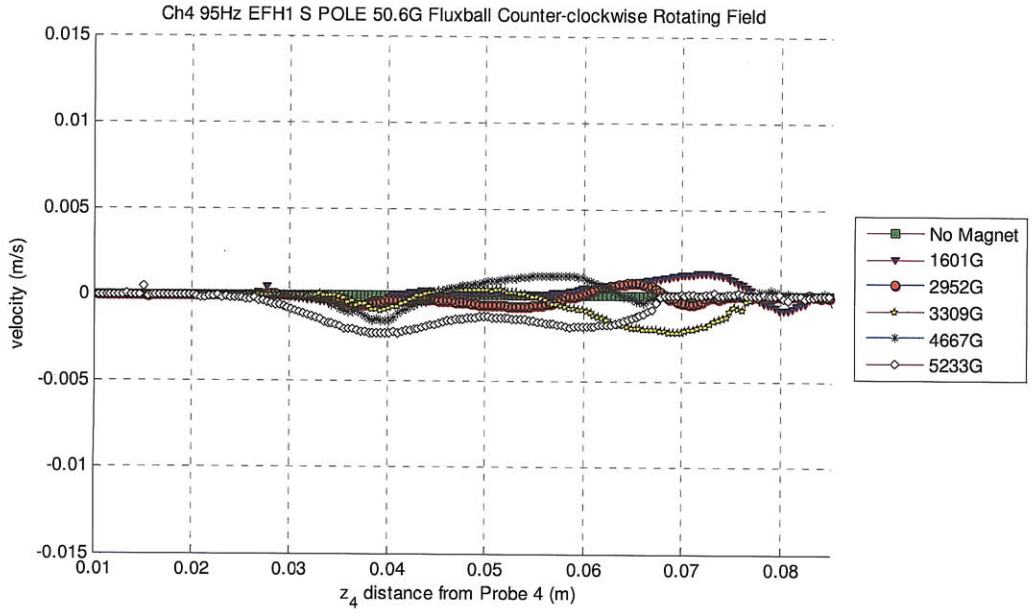
Ch4 95Hz EFH1 S POLE 50.6G Fluxball Counter-clockwise Rotating Field
velocity (m/s)
0.015
0.01
0.005
0
-0.005
-0.01
-0.015
0.01
0.02
0.03
0.04
0.05
0.06
0.07
0.08
z_4 distance from Probe 4 (m)
No Magnet
1601G
2952G
3309G
4667G
5233G

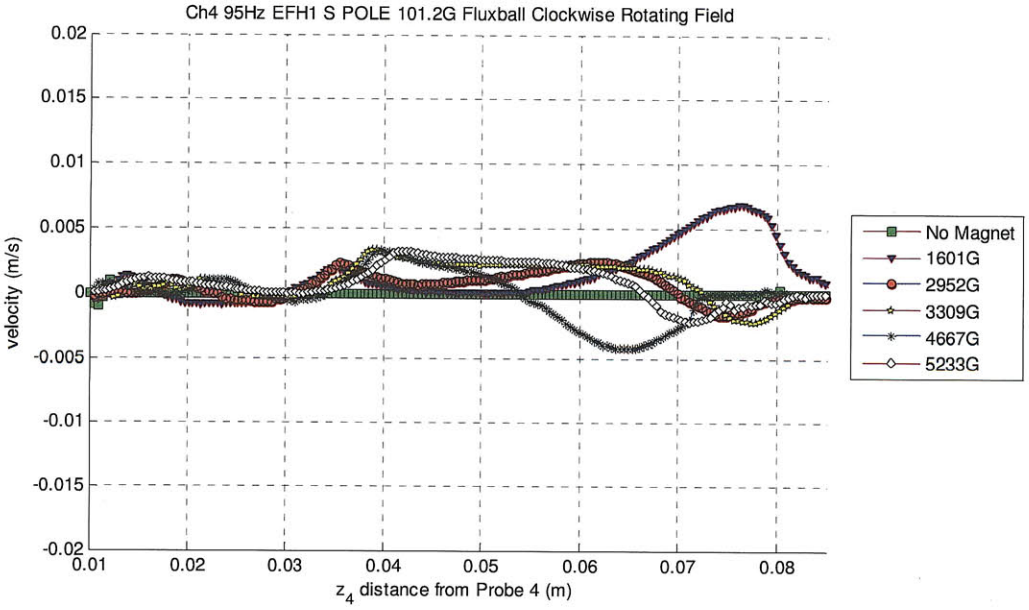
Ch4 95Hz EFH1 S POLE 101.2G Fluxball Clockwise Rotating Field
velocity (m/s)
0.02
0.015
0.01
0.005
0
-0.005
-0.01
-0.015
-0.02
0.01
0.02
0.03
0.04
0.05
0.06
0.07
0.08
z_4 distance from Probe 4 (m)
No Magnet
1601G
2952G
3309G
4667G
5233G

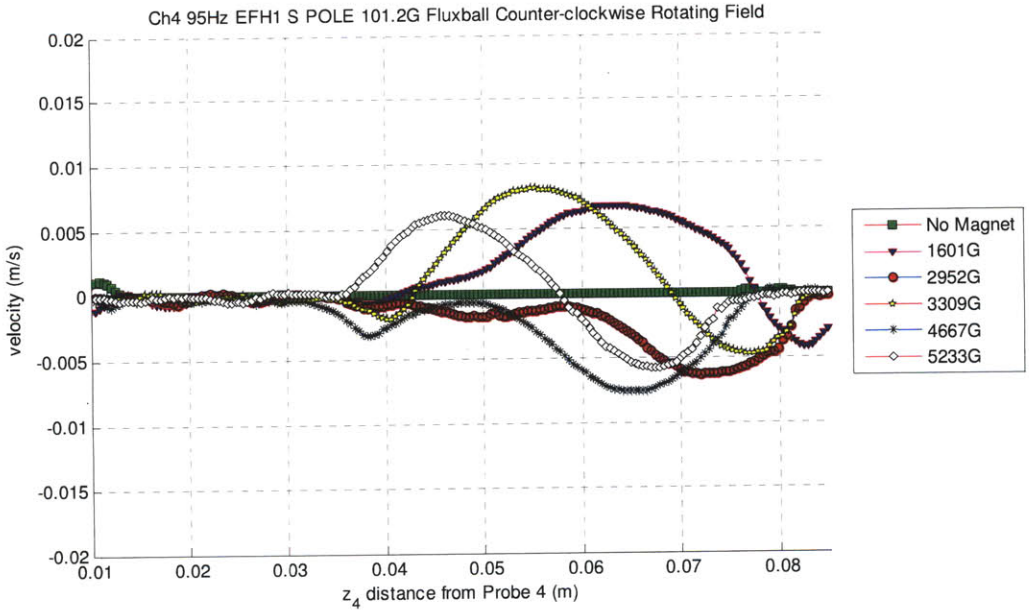
Ch4 95Hz EFH1 S POLE 101.2G Fluxball Counter-clockwise Rotating Field
velocity (m/s)
z_4 distance from Probe 4 (m)
No Magnet
1601G
2952G
3309G
4667G
5233G

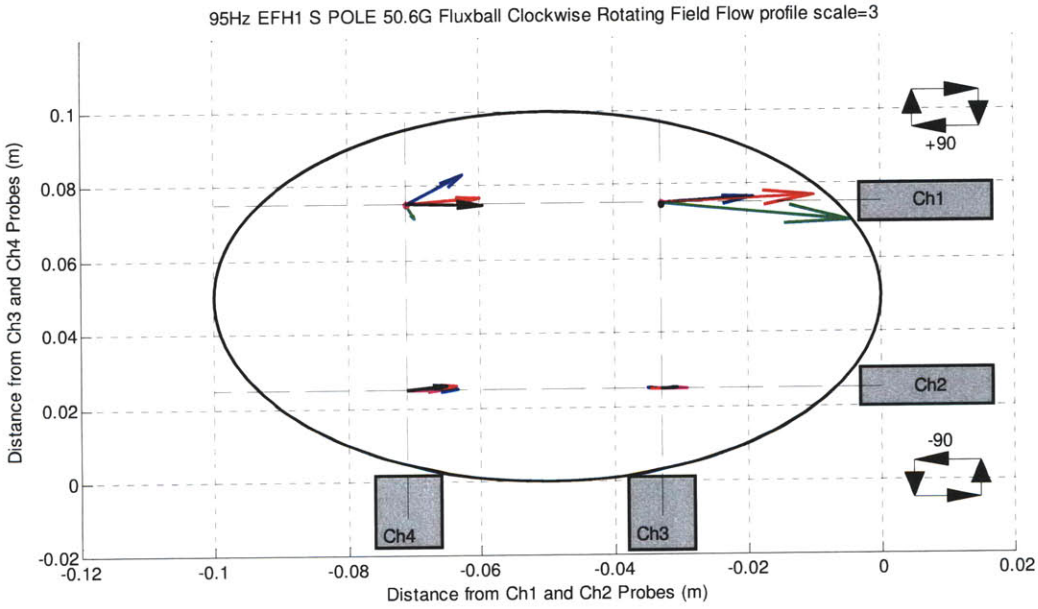
95Hz EFH1 S POLE 50.6G Fluxball Clockwise Rotating Field Flow profile scale=3
Distance from Ch3 and Ch4 Probes (m)
Distance from Ch1 and Ch2 Probes (m)
+90
-90
Ch1
Ch2
Ch3
Ch4

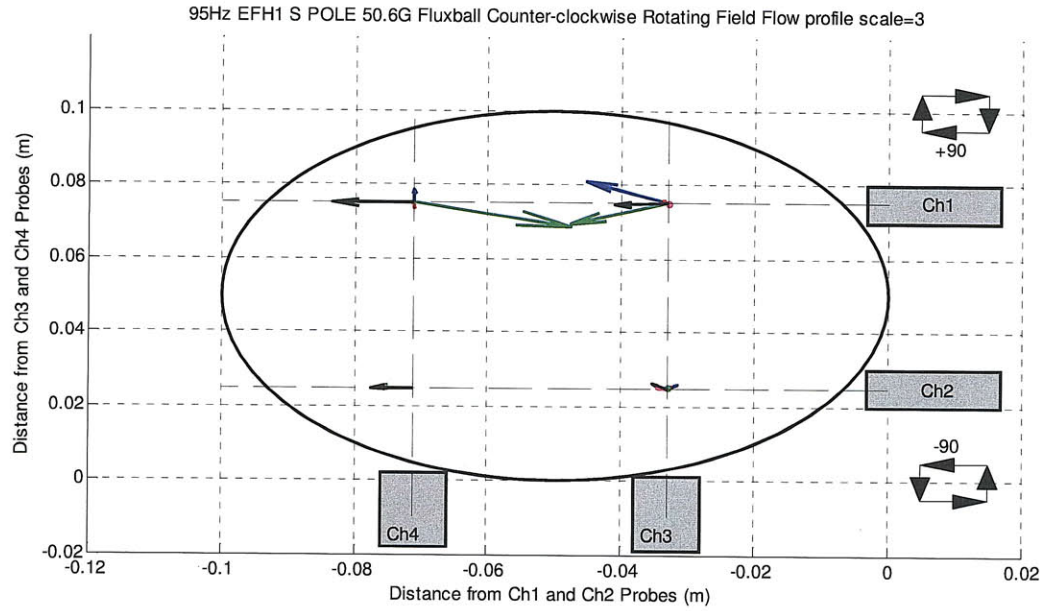
95Hz EFH1 S POLE 50.6G Fluxball Counter-clockwise Rotating Field Flow profile scale=3
Distance from Ch3 and Ch4 Probes (m)
Distance from Ch1 and Ch2 Probes (m)
+90
-90
Ch1
Ch2
Ch3
Ch4
0.1
0.08
0.06
0.04
0.02
0
-0.02
-0.12
-0.1
-0.08
-0.06
-0.04
-0.02
0
0.02

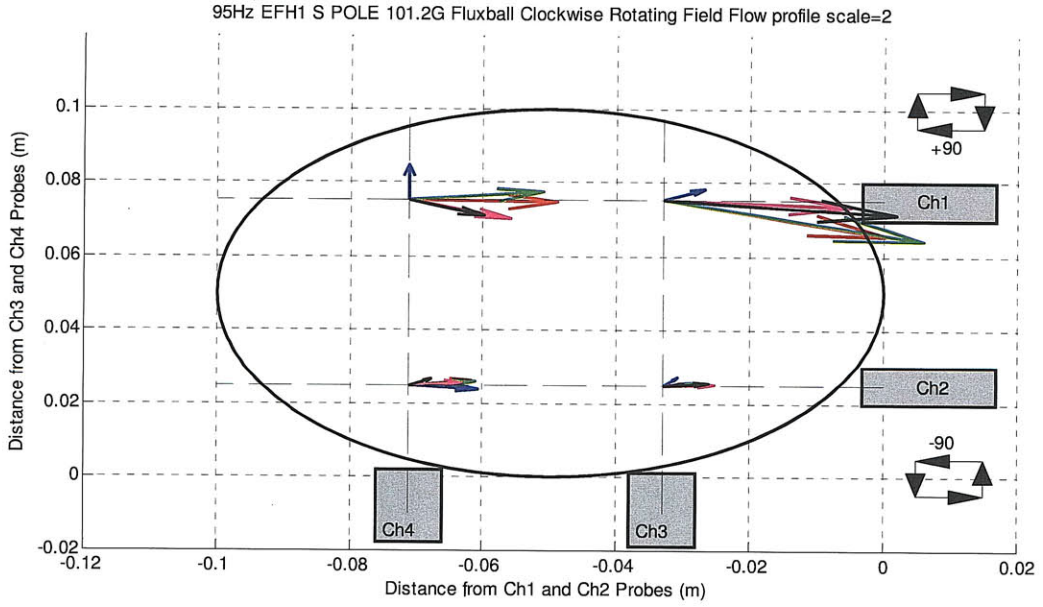
95Hz EFH1 S POLE 101.2G Fluxball Clockwise Rotating Field Flow profile scale=2
Distance from Ch3 and Ch4 Probes (m)
Distance from Ch1 and Ch2 Probes (m)
+90
-90
Ch1
Ch2
Ch3
Ch4
0.1
0.08
0.06
0.04
0.02
0
-0.02
-0.12
-0.1
-0.08
-0.06
-0.04
-0.02
0
0.02

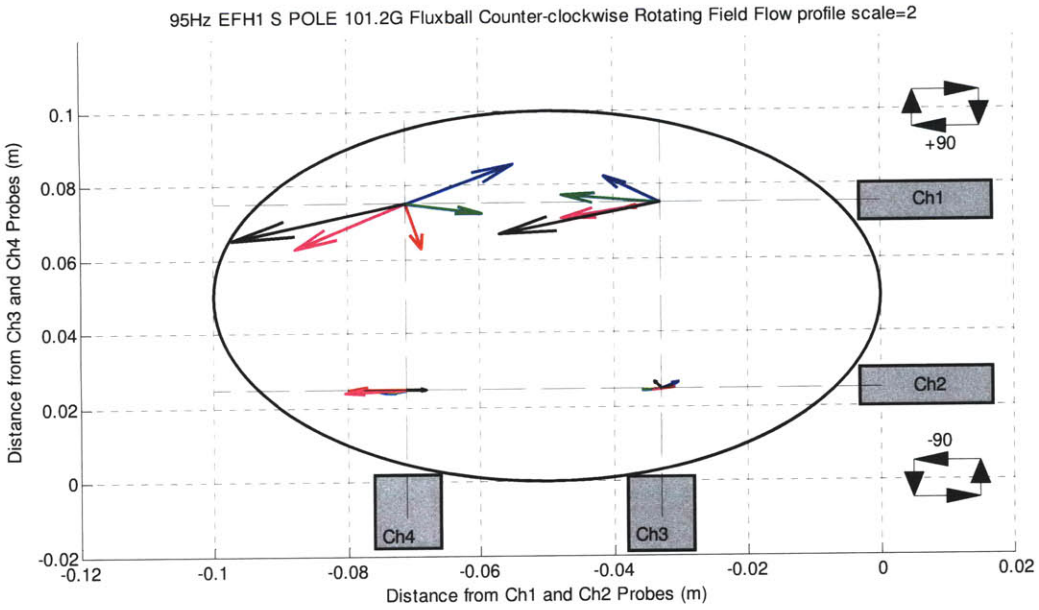
95Hz EFH1 S POLE 101.2G Fluxball Counter-clockwise Rotating Field Flow profile scale=2
Distance from Ch3 and Ch4 Probes (m)
Distance from Ch1 and Ch2 Probes (m)
0.1
0.08
0.06
0.04
0.02
0
-0.02
-0.12
-0.1
-0.08
-0.06
-0.04
-0.02
0
0.02
+90
-90
Ch1
Ch2
Ch3
Ch4

H2. EFH1 Filled Sphere with South Pole Facing Magnets on Top of Sphere at 47Hz

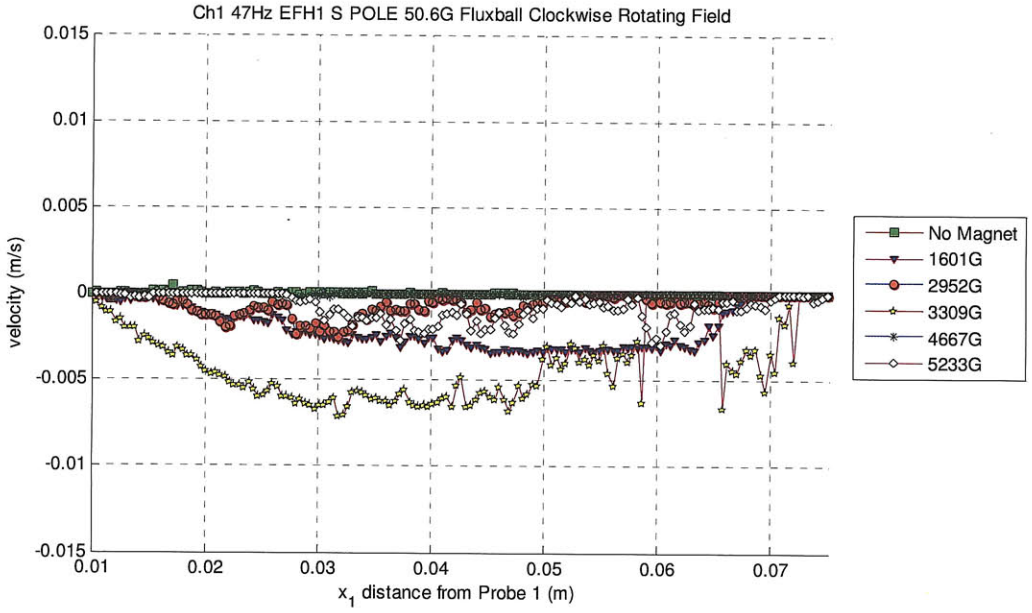

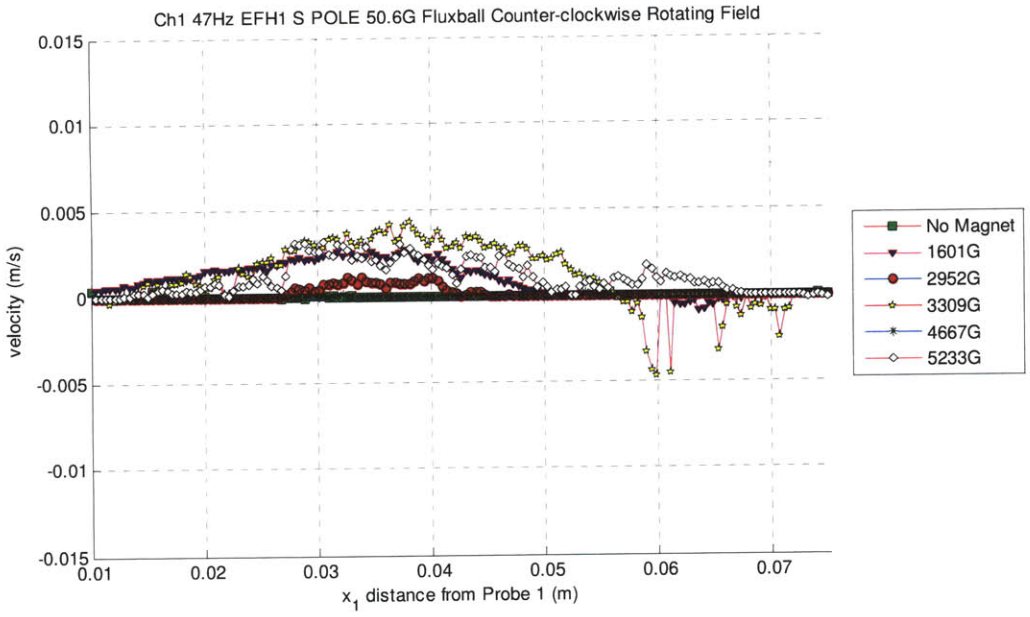
Ch1 47Hz EFH1 S POLE 50.6G Fluxball Counter-clockwise Rotating Field
velocity (m/s)
0.015
0.01
0.005
0
-0.005
-0.01
-0.015
0.01
0.02
0.03
0.04
0.05
0.06
0.07
x1 distance from Probe 1 (m)
No Magnet
1601G
2952G
3309G
4667G
5233G

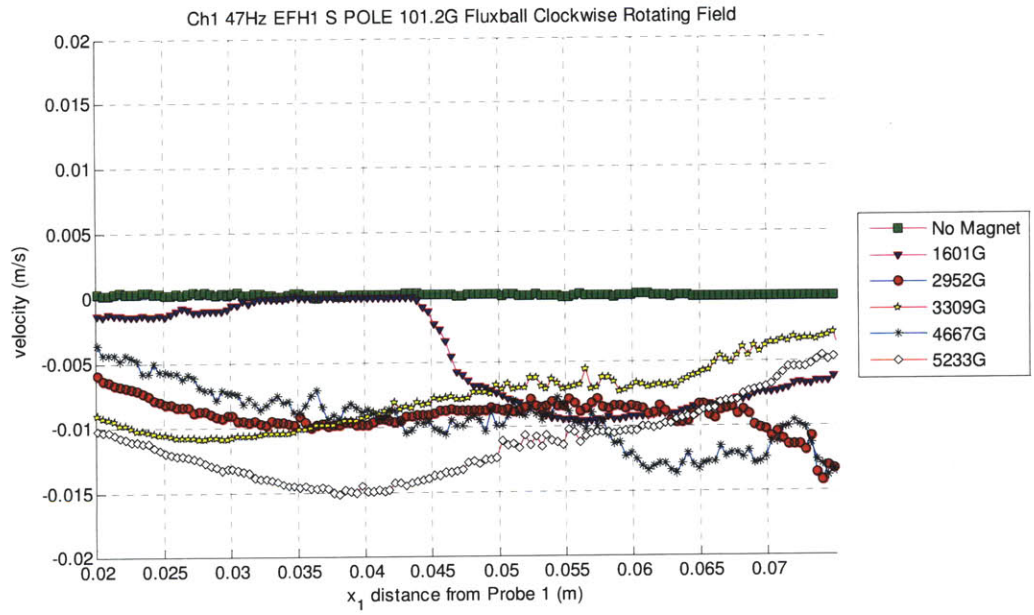
Ch1 47Hz EFH1 S POLE 101.2G Fluxball Clockwise Rotating Field
velocity (m/s)
0.02
0.015
0.01
0.005
0
-0.005
-0.01
-0.015
-0.02
0.02
0.025
0.03
0.035
0.04
0.045
0.05
0.055
0.06
0.065
0.07
x1 distance from Probe 1 (m)
No Magnet
1601G
2952G
3309G
4667G
5233G

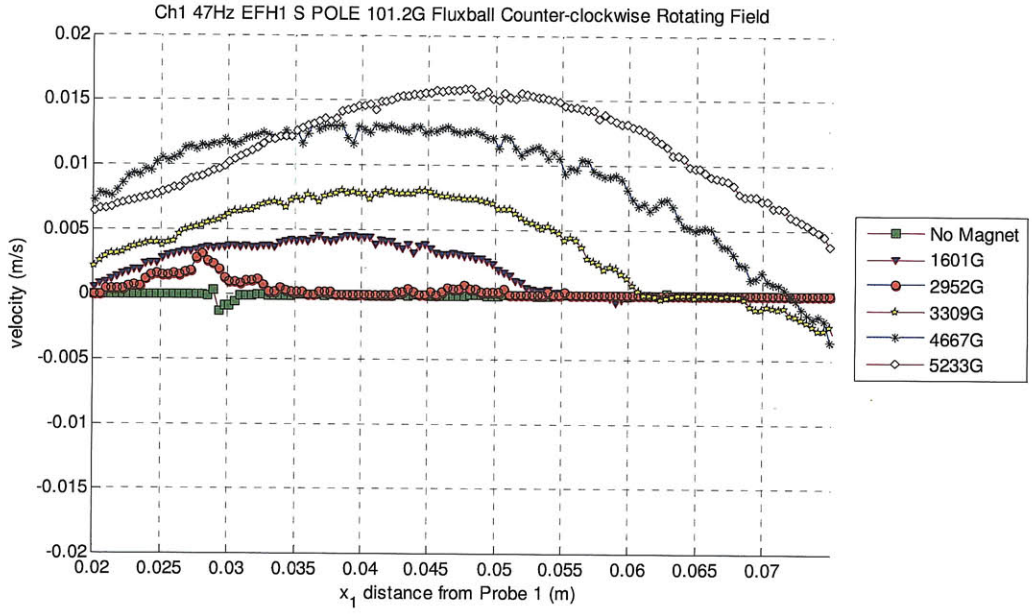
Ch1 47Hz EFH1 S POLE 101.2G Fluxball Counter-clockwise Rotating Field
velocity (m/s)
0.02
0.015
0.01
0.005
0
-0.005
-0.01
-0.015
-0.02
0.02 0.025 0.03 0.035 0.04 0.045 0.05 0.055 0.06 0.065 0.07
x1 distance from Probe 1 (m)
No Magnet
1601G
2952G
3309G
4667G
5233G

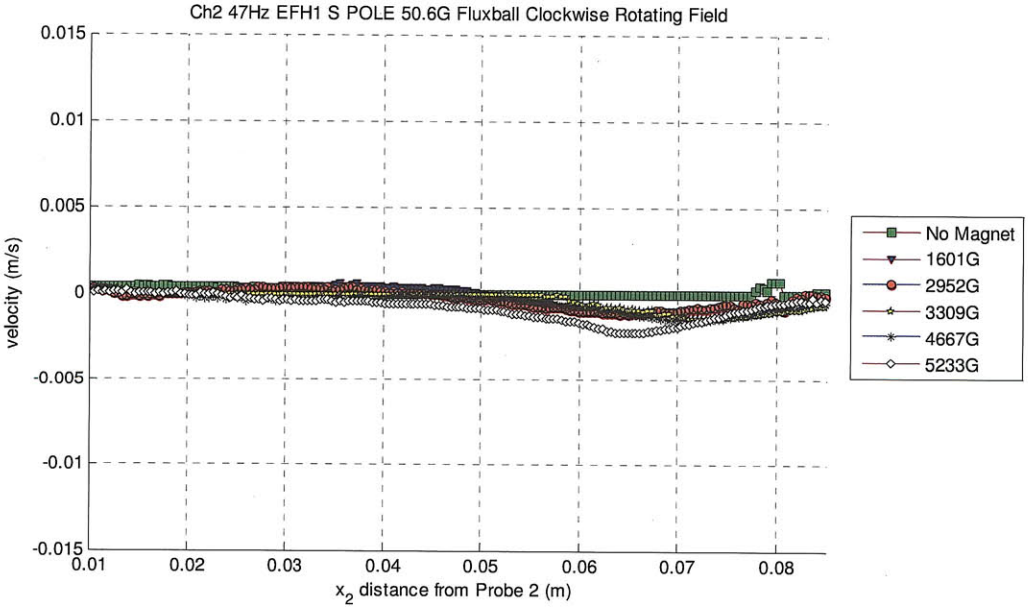
Ch2 47Hz EFH1 S POLE 50.6G Fluxball Clockwise Rotating Field
velocity (m/s)
0.015
0.01
0.005
0
-0.005
-0.01
-0.015
0.01 0.02 0.03 0.04 0.05 0.06 0.07 0.08
x2 distance from Probe 2 (m)
No Magnet
1601G
2952G
3309G
4667G
5233G

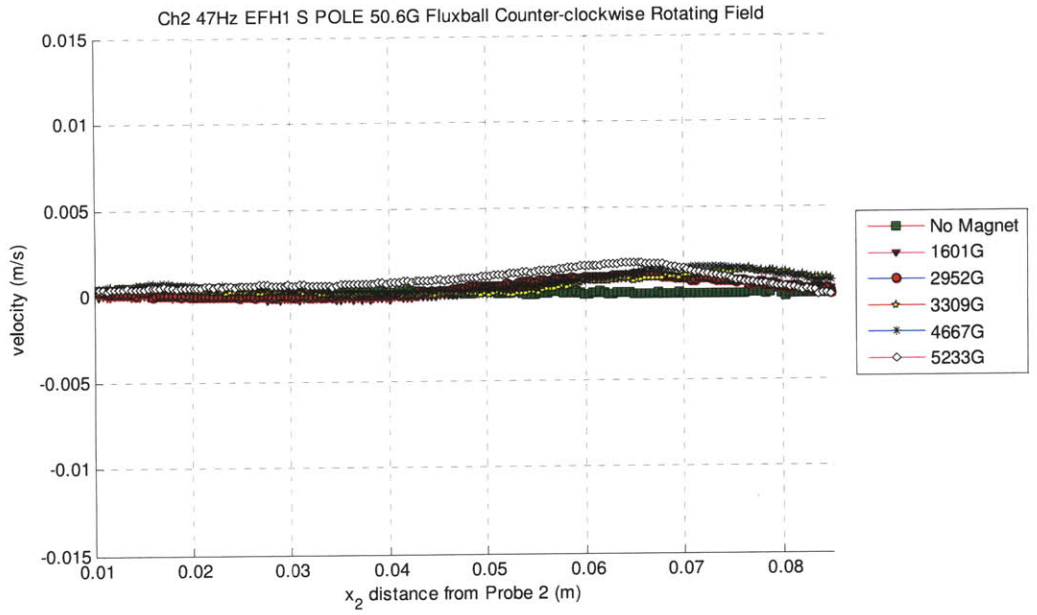
Ch2 47Hz EFH1 S POLE 50.6G Fluxball Counter-clockwise Rotating Field
velocity (m/s)
0.015
0.01
0.005
0
-0.005
-0.01
-0.015
0.01
0.02
0.03
0.04
0.05
0.06
0.07
0.08
x2 distance from Probe 2 (m)
No Magnet
1601G
2952G
3309G
4667G
5233G

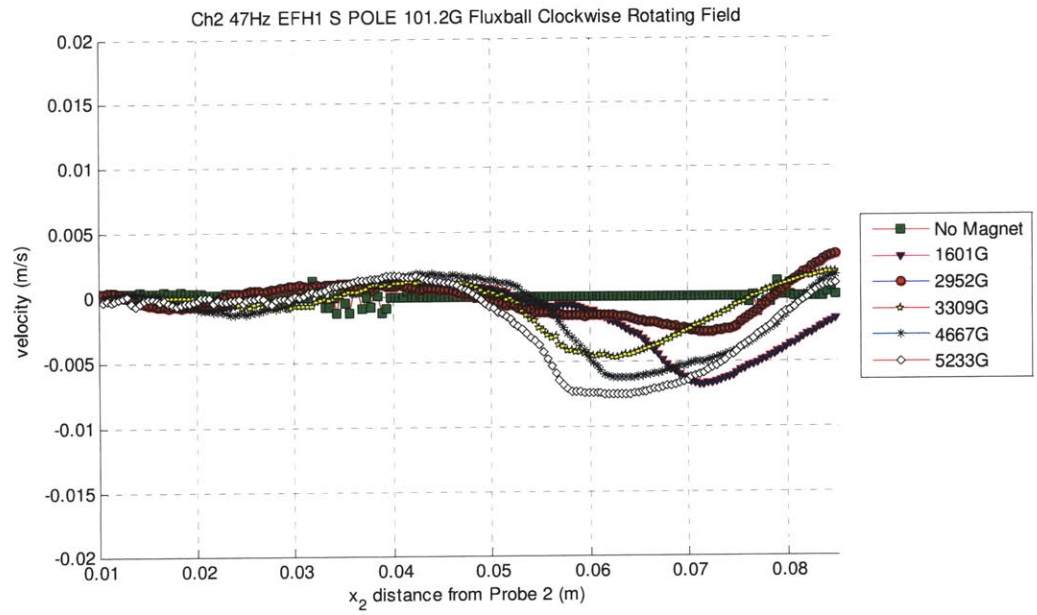
Ch2 47Hz EFH1 S POLE 101.2G Fluxball Clockwise Rotating Field
velocity (m/s)
0.02
0.015
0.01
0.005
0
-0.005
-0.01
-0.015
-0.02
0.01
0.02
0.03
0.04
0.05
0.06
0.07
0.08
x2 distance from Probe 2 (m)
No Magnet
1601G
2952G
3309G
4667G
5233G

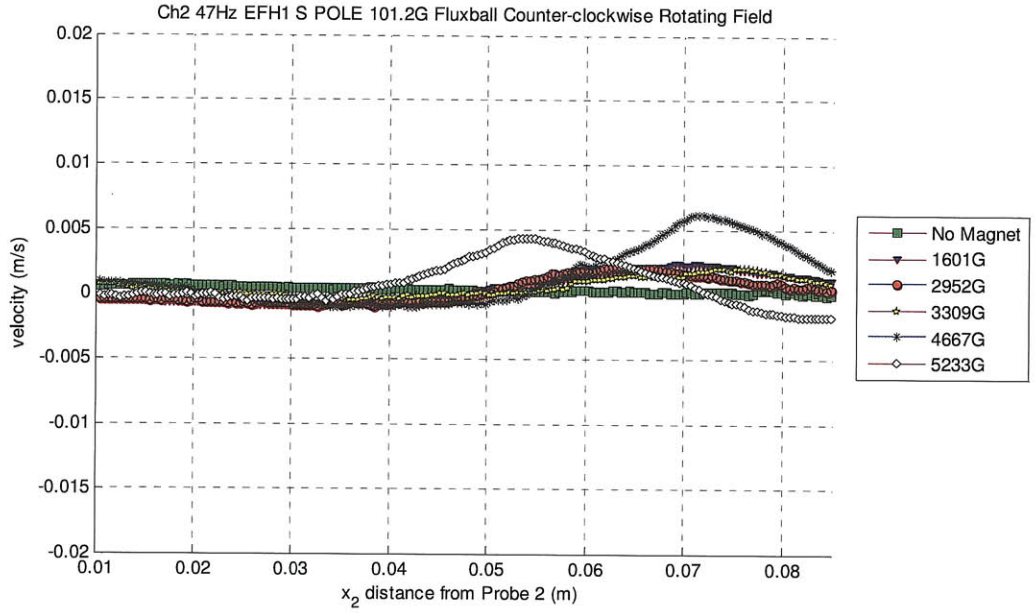
Ch2 47Hz EFH1 S POLE 101.2G Fluxball Counter-clockwise Rotating Field
velocity (m/s)
0.02
0.015
0.01
0.005
0
-0.005
-0.01
-0.015
-0.02
0.01
0.02
0.03
0.04
0.05
0.06
0.07
0.08
x2 distance from Probe 2 (m)
No Magnet
1601G
2952G
3309G
4667G
5233G

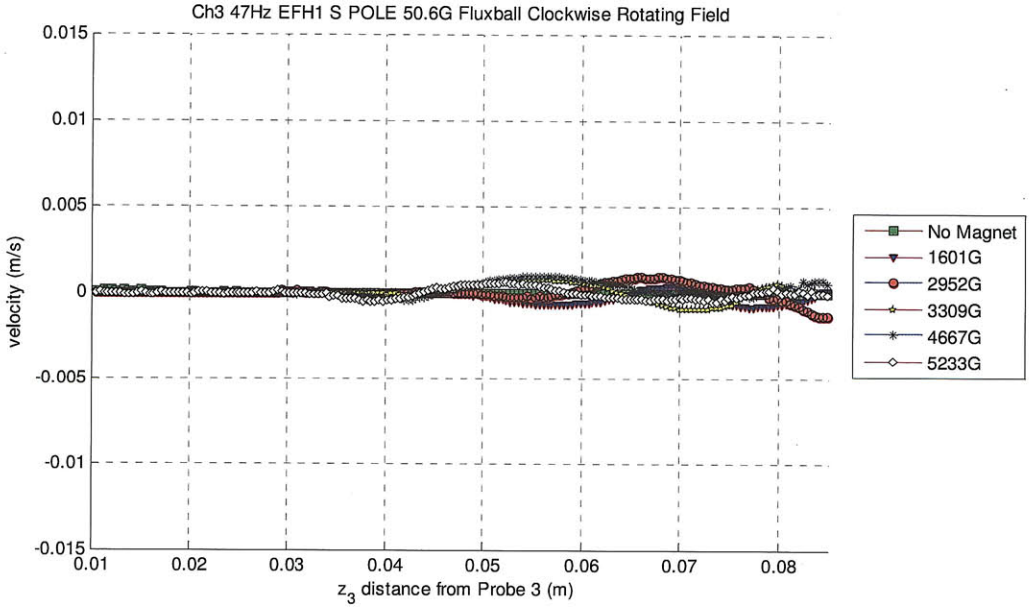
Ch3 47Hz EFH1 S POLE 50.6G Fluxball Clockwise Rotating Field
velocity (m/s)
0.015
0.01
0.005
0
-0.005
-0.01
-0.015
0.01
0.02
0.03
0.04
0.05
0.06
0.07
0.08
z3 distance from Probe 3 (m)
No Magnet
1601G
2952G
3309G
4667G
5233G

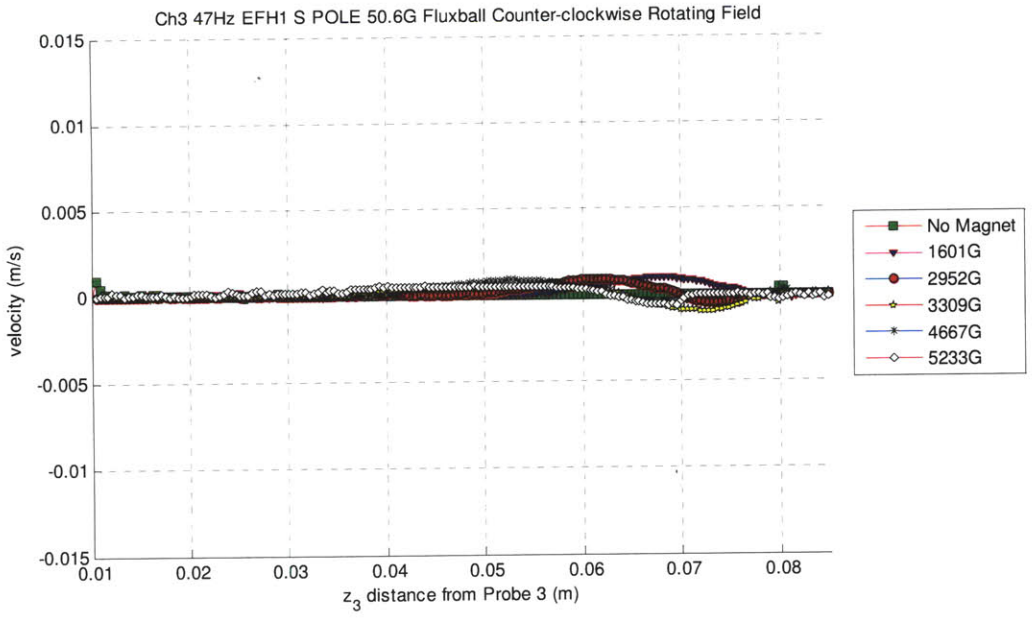
Ch3 47Hz EFH1 S POLE 50.6G Fluxball Counter-clockwise Rotating Field
velocity (m/s)
0.015
0.01
0.005
0
-0.005
-0.01
-0.015
0.01
0.02
0.03
0.04
0.05
0.06
0.07
0.08
z_3 distance from Probe 3 (m)
No Magnet
1601G
2952G
3309G
4667G
5233G

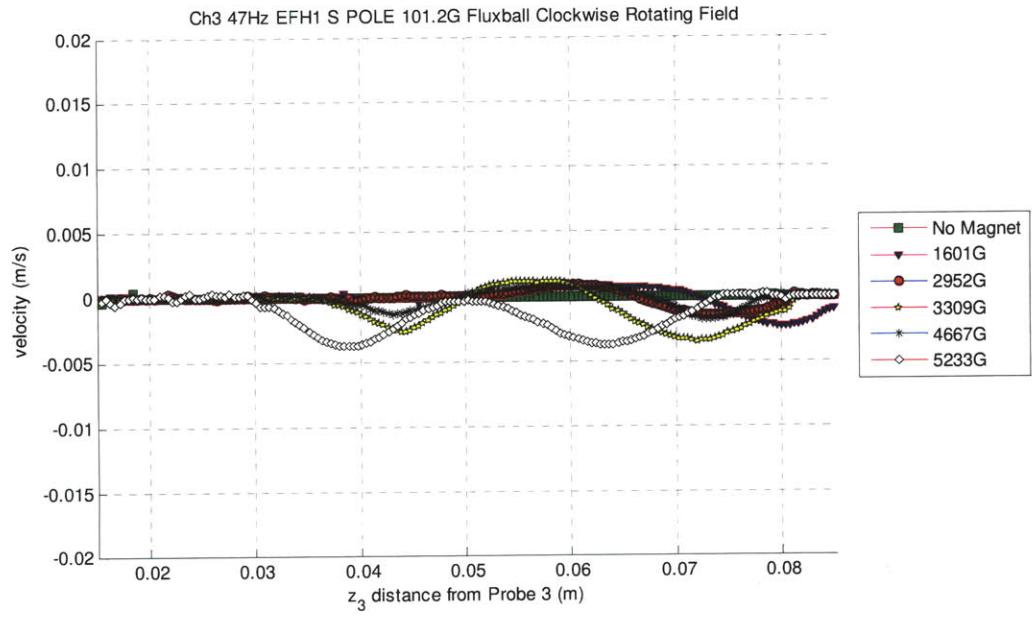
Ch3 47Hz EFH1 S POLE 101.2G Fluxball Clockwise Rotating Field
velocity (m/s)
0.02
0.015
0.01
0.005
0
-0.005
-0.01
-0.015
-0.02
0.02
0.03
0.04
0.05
0.06
0.07
0.08
z_3 distance from Probe 3 (m)
No Magnet
1601G
2952G
3309G
4667G
5233G

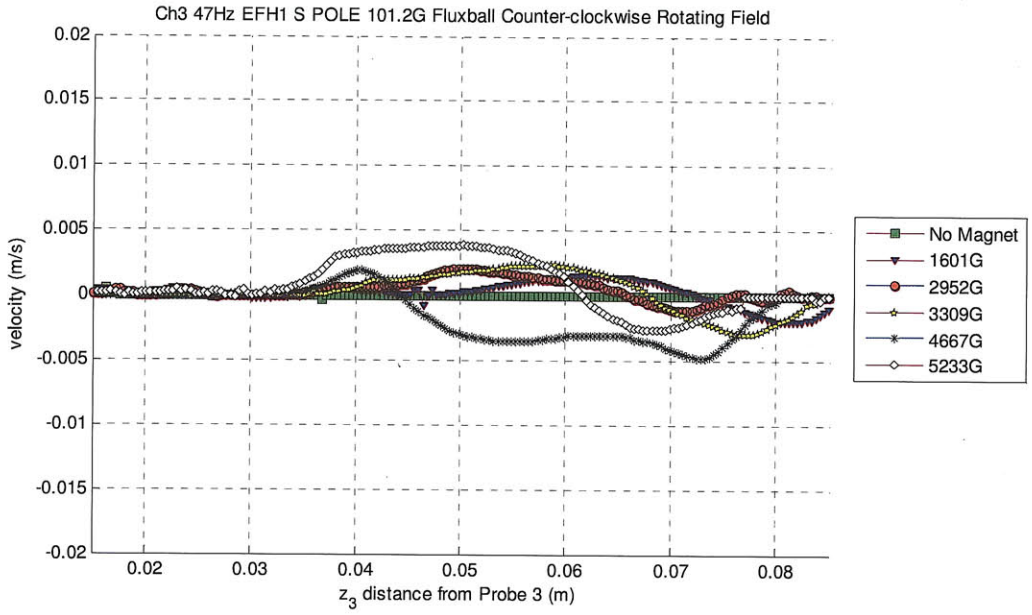
Ch3 47Hz EFH1 S POLE 101.2G Fluxball Counter-clockwise Rotating Field
velocity (m/s)
0.02
0.015
0.01
0.005
0
-0.005
-0.01
-0.015
-0.02
0.02
0.03
0.04
0.05
0.06
0.07
0.08
z_3 distance from Probe 3 (m)
No Magnet
1601G
2952G
3309G
4667G
5233G

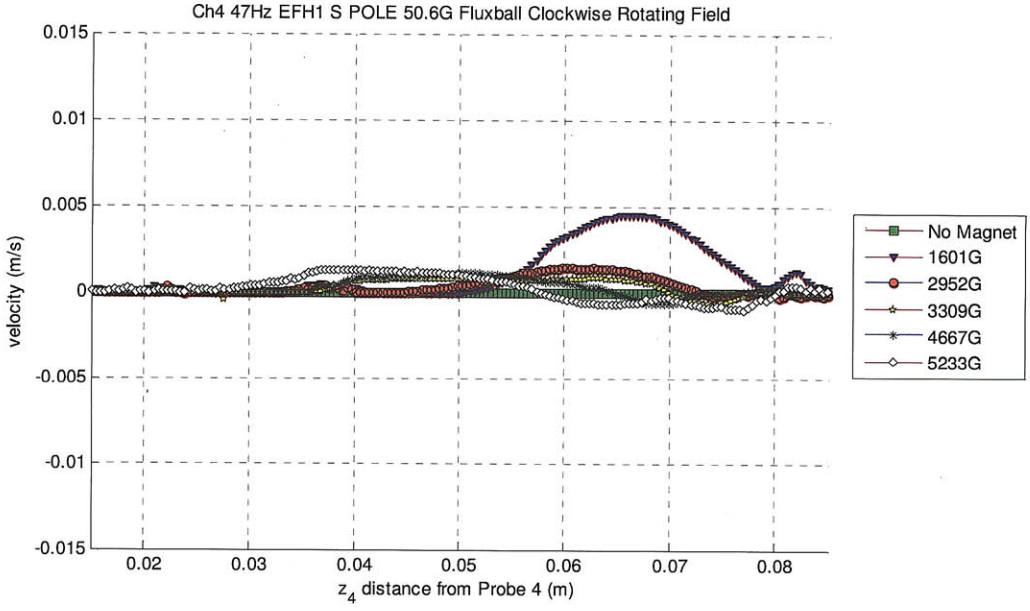
Ch4 47Hz EFH1 S POLE 50.6G Fluxball Clockwise Rotating Field
velocity (m/s)
0.015
0.01
0.005
0
-0.005
-0.01
-0.015
0.02
0.03
0.04
0.05
0.06
0.07
0.08
z_4 distance from Probe 4 (m)
No Magnet
1601G
2952G
3309G
4667G
5233G

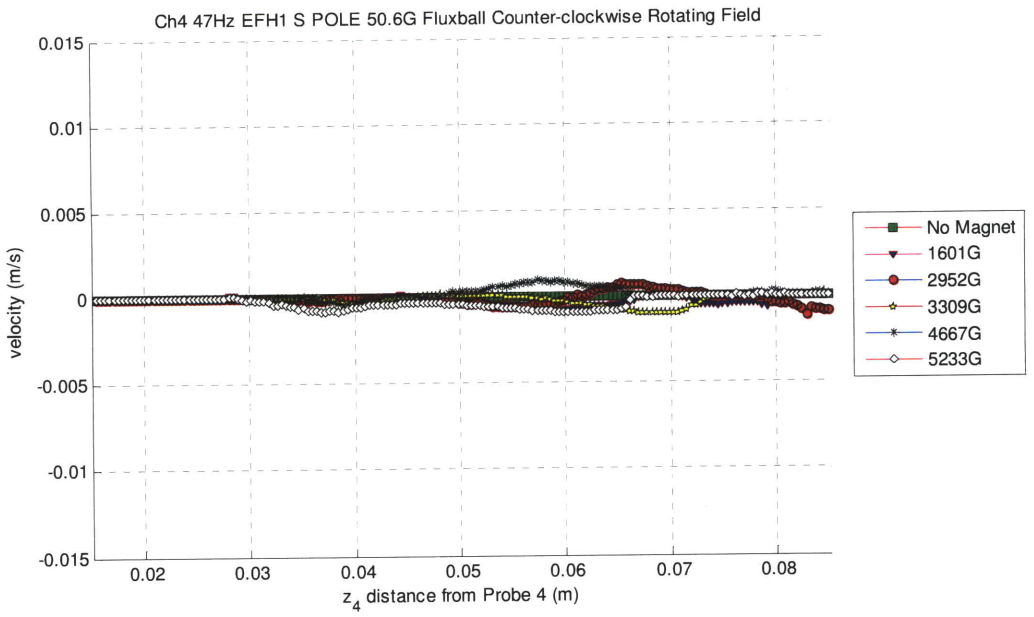
Ch4 47Hz EFH1 S POLE 50.6G Fluxball Counter-clockwise Rotating Field
velocity (m/s)
0.015
0.01
0.005
0
-0.005
-0.01
-0.015
0.02
0.03
0.04
0.05
0.06
0.07
0.08
z4 distance from Probe 4 (m)
No Magnet
1601G
2952G
3309G
4667G
5233G

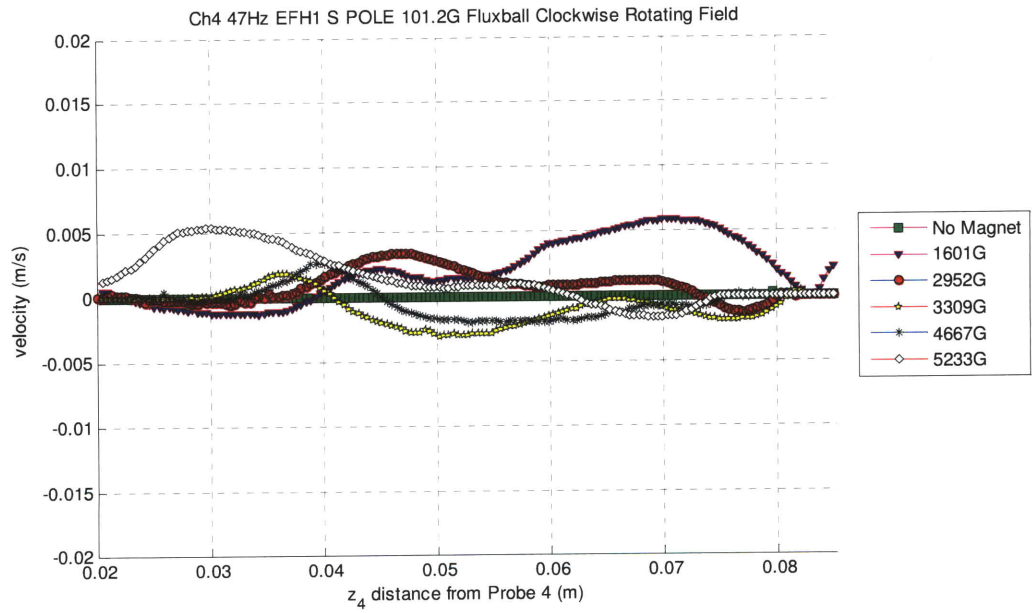
Ch4 47Hz EFH1 S POLE 101.2G Fluxball Clockwise Rotating Field
velocity (m/s)
0.02
0.015
0.01
0.005
0
-0.005
-0.01
-0.015
-0.02
0.02
0.03
0.04
0.05
0.06
0.07
0.08
z4 distance from Probe 4 (m)
No Magnet
1601G
2952G
3309G
4667G
5233G

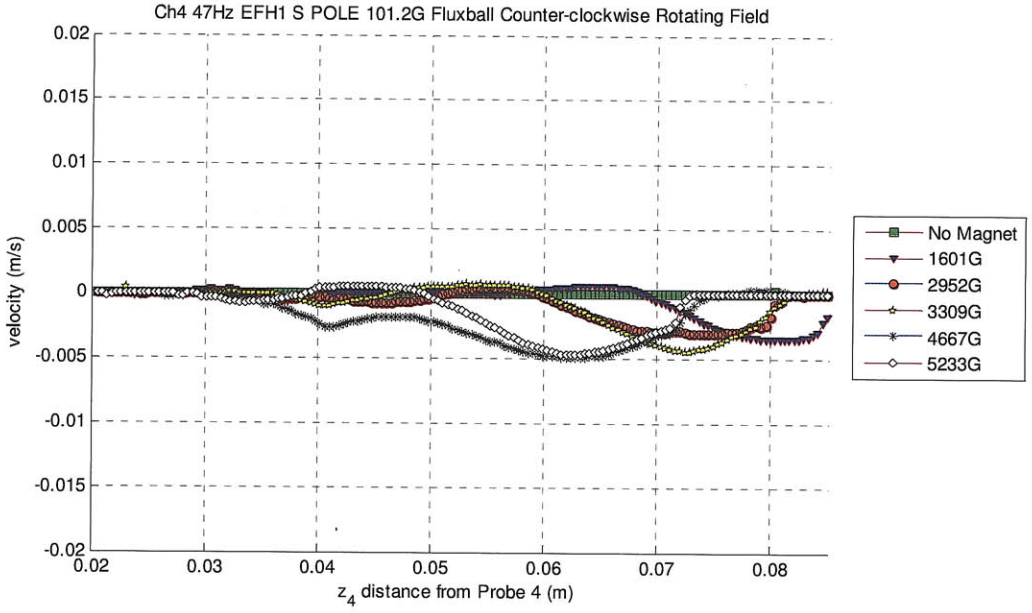
Ch4 47Hz EFH1 S POLE 101.2G Fluxball Counter-clockwise Rotating Field
velocity (m/s)
0.02
0.015
0.01
0.005
0
-0.005
-0.01
-0.015
-0.02
0.02
0.03
0.04
0.05
0.06
0.07
0.08
z4 distance from Probe 4 (m)
No Magnet
1601G
2952G
3309G
4667G
5233G

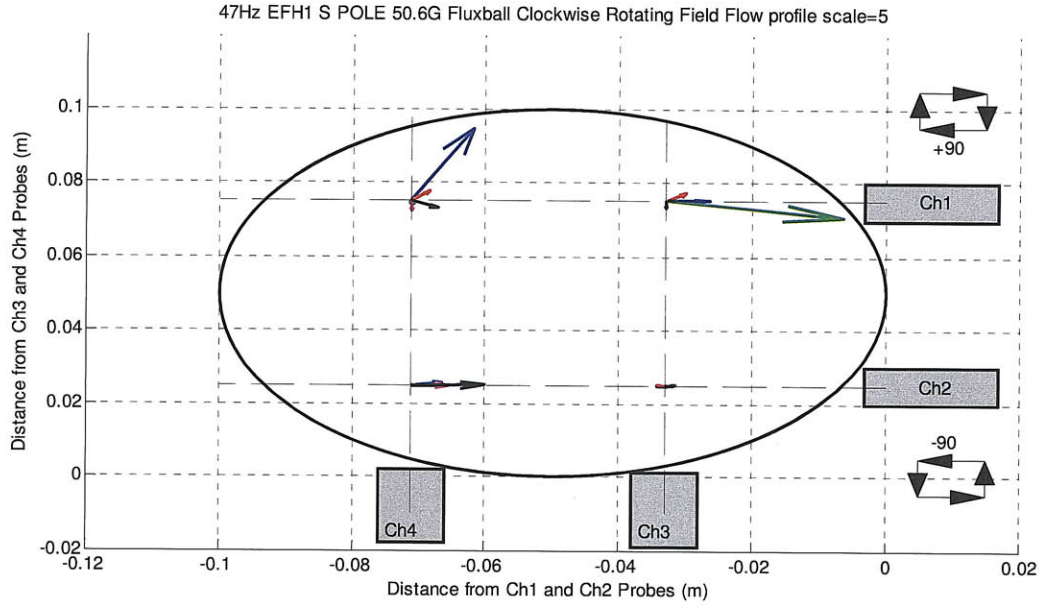
47Hz EFH1 S POLE 50.6G Fluxball Clockwise Rotating Field Flow profile scale=5
Distance from Ch3 and Ch4 Probes (m)
0.1
0.08
0.06
0.04
0.02
0
-0.02
-0.12
-0.1
-0.08
-0.06
-0.04
-0.02
0
0.02
Distance from Ch1 and Ch2 Probes (m)
+90
Ch1
Ch2
-90
Ch4
Ch3

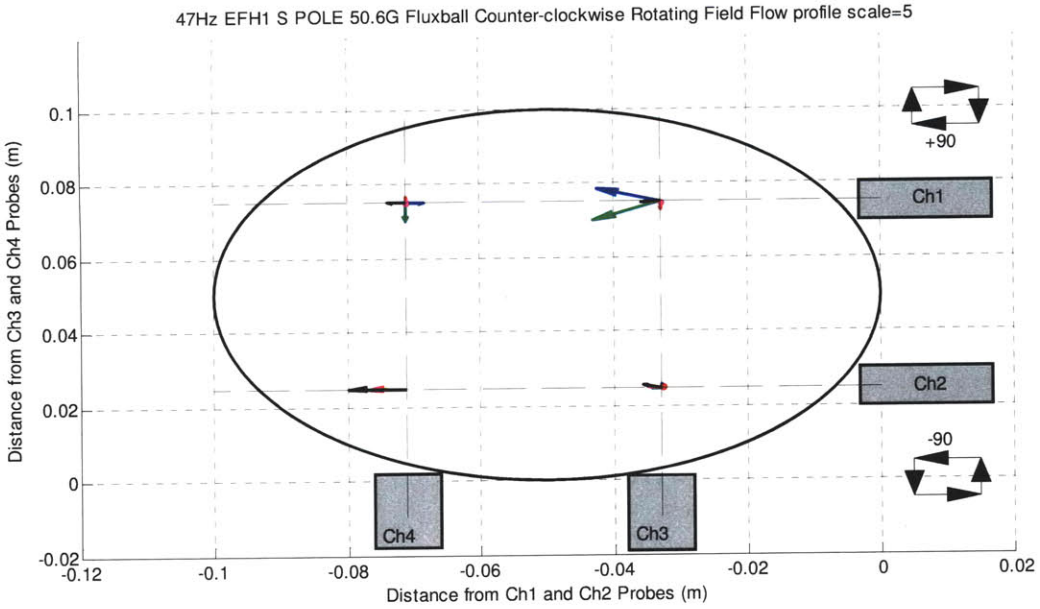
47Hz EFH1 S POLE 50.6G Fluxball Counter-clockwise Rotating Field Flow profile scale=5
Distance from Ch3 and Ch4 Probes (m)
Distance from Ch1 and Ch2 Probes (m)
+90
-90
Ch1
Ch2
Ch3
Ch4
0.1
0.08
0.06
0.04
0.02
0
-0.02
-0.12
-0.1
-0.08
-0.06
-0.04
-0.02
0
0.02

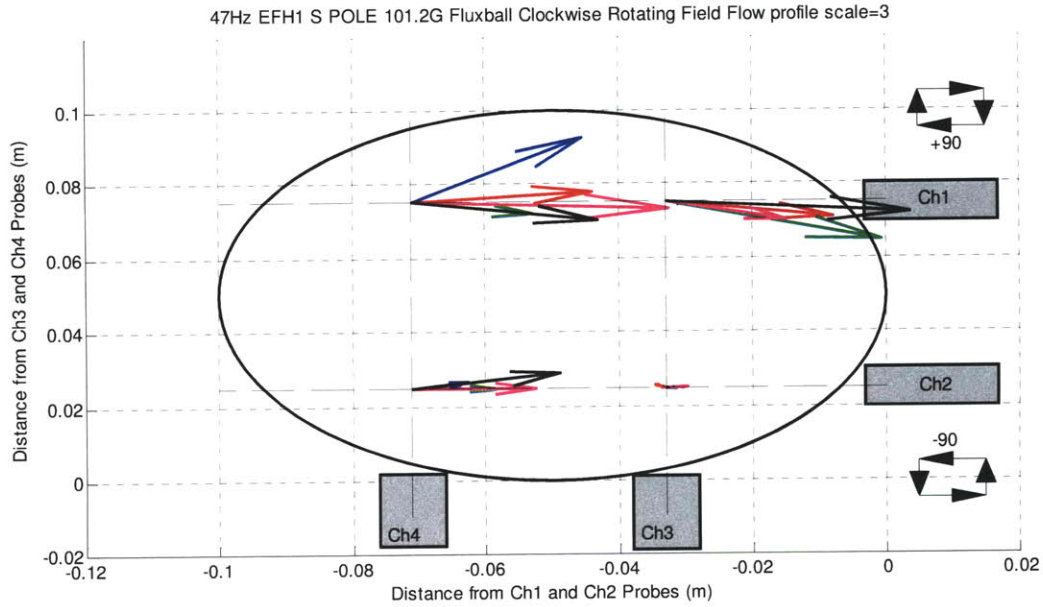
47Hz EFH1 S POLE 101.2G Fluxball Clockwise Rotating Field Flow profile scale=3
Distance from Ch3 and Ch4 Probes (m)
Distance from Ch1 and Ch2 Probes (m)
+90
-90
Ch1
Ch2
Ch3
Ch4
0.1
0.08
0.06
0.04
0.02
0
-0.02
-0.12
-0.1
-0.08
-0.06
-0.04
-0.02
0
0.02

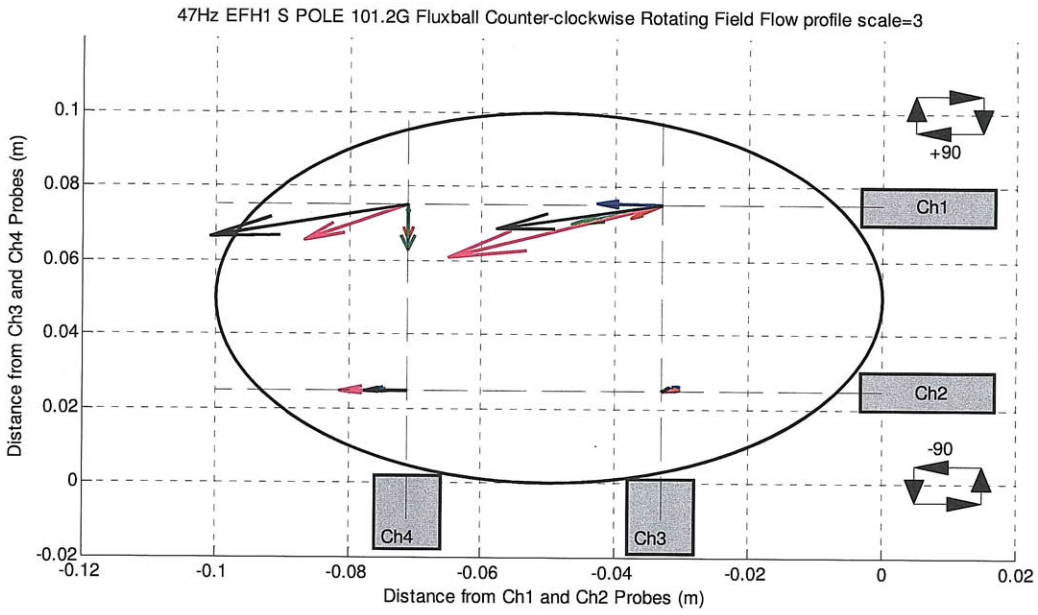
47Hz EFH1 S POLE 101.2G Fluxball Counter-clockwise Rotating Field Flow profile scale=3
Distance from Ch3 and Ch4 Probes (m)
Distance from Ch1 and Ch2 Probes (m)
0.1
0.08
0.06
0.04
0.02
0
-0.02
-0.12
-0.1
-0.08
-0.06
-0.04
-0.02
0
0.02
+90
-90
Ch1
Ch2
Ch3
Ch4

H3. EFH1 Filled Sphere with South Pole Facing Magnets on Top of Sphere at 15Hz

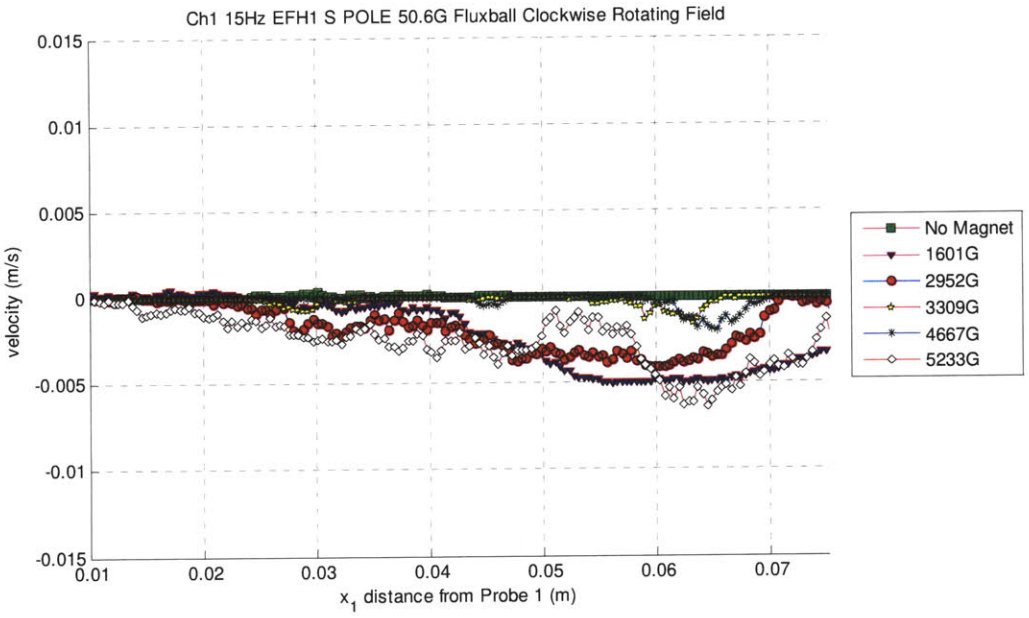

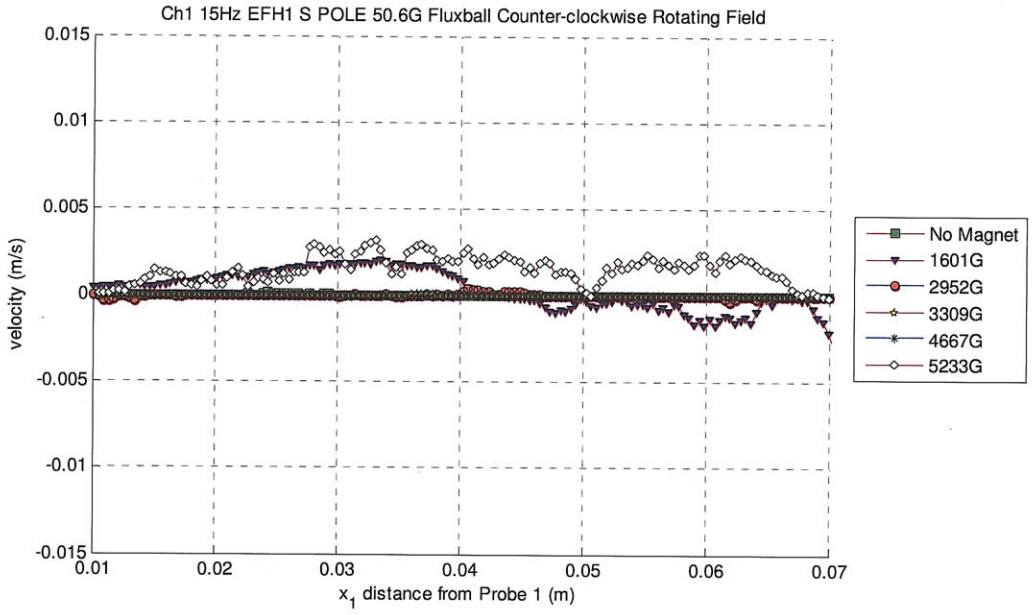
Ch1 15Hz EFH1 S POLE 50.6G Fluxball Counter-clockwise Rotating Field
velocity (m/s)
0.015
0.01
0.005
0
-0.005
-0.01
-0.015
0.01
0.02
0.03
0.04
0.05
0.06
0.07
x1 distance from Probe 1 (m)
No Magnet
1601G
2952G
3309G
4667G
5233G

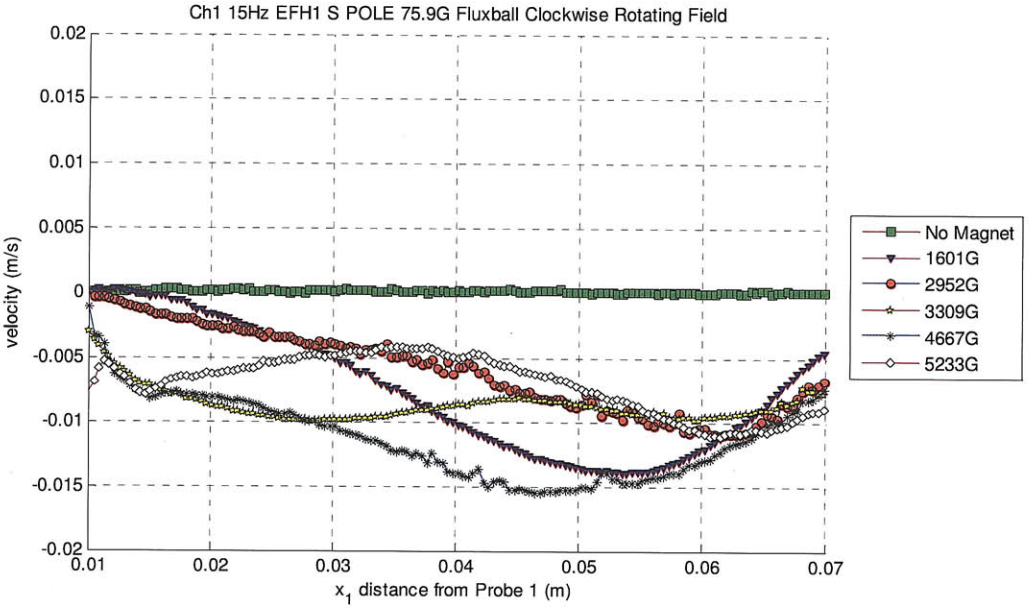
Ch1 15Hz EFH1 S POLE 75.9G Fluxball Clockwise Rotating Field
velocity (m/s)
0.02
0.015
0.01
0.005
0
-0.005
-0.01
-0.015
-0.02
0.01
0.02
0.03
0.04
0.05
0.06
0.07
x1 distance from Probe 1 (m)
No Magnet
1601G
2952G
3309G
4667G
5233G

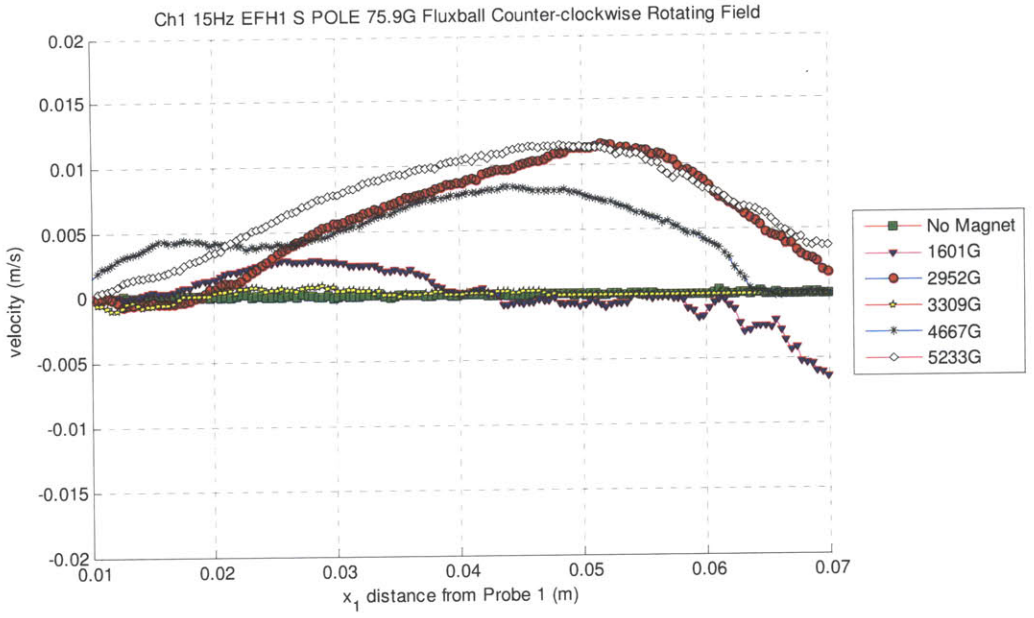
Ch1 15Hz EFH1 S POLE 75.9G Fluxball Counter-clockwise Rotating Field
velocity (m/s)
0.02
0.015
0.01
0.005
0
-0.005
-0.01
-0.015
-0.02
0.01
0.02
0.03
0.04
0.05
0.06
0.07
x1 distance from Probe 1 (m)
No Magnet
1601G
2952G
3309G
4667G
5233G

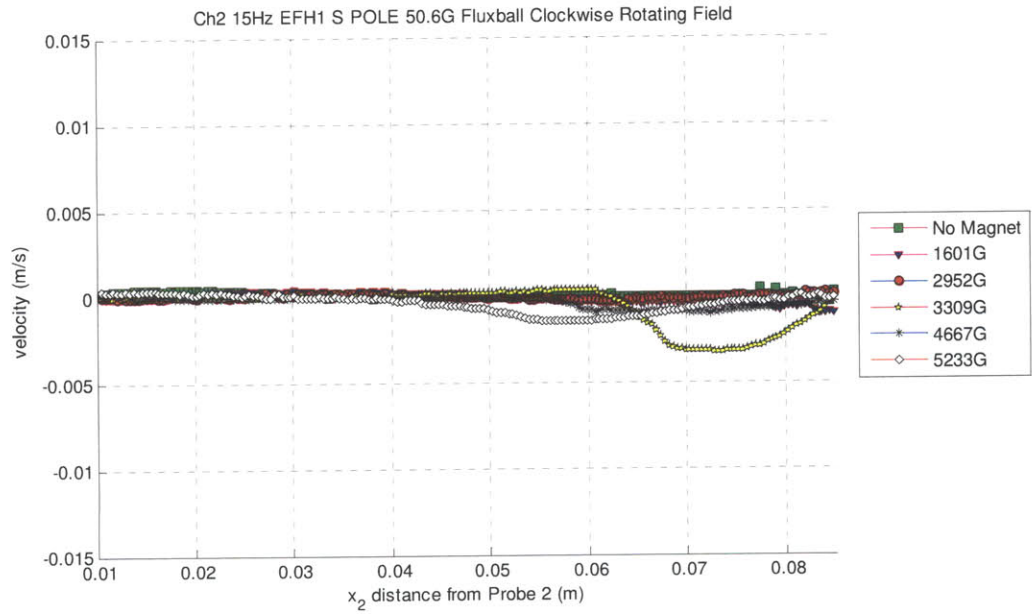
Ch2 15Hz EFH1 S POLE 50.6G Fluxball Clockwise Rotating Field
velocity (m/s)
0.015
0.01
0.005
0
-0.005
-0.01
-0.015
0.01
0.02
0.03
0.04
0.05
0.06
0.07
0.08
x2 distance from Probe 2 (m)
No Magnet
1601G
2952G
3309G
4667G
5233G

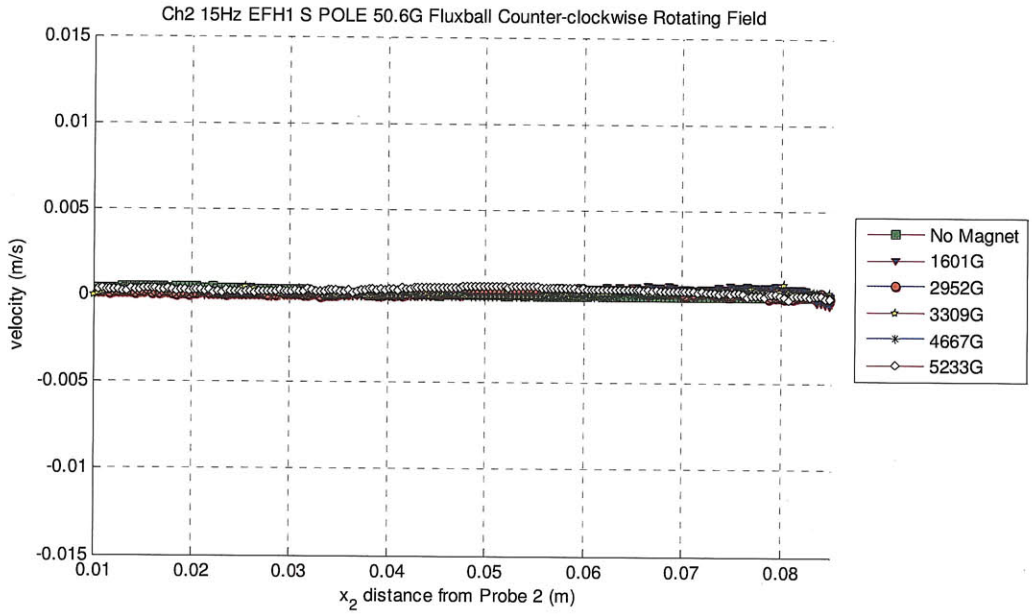
Ch2 15Hz EFH1 S POLE 50.6G Fluxball Counter-clockwise Rotating Field
velocity (m/s)
0.015
0.01
0.005
0
-0.005
-0.01
-0.015
0.01
0.02
0.03
0.04
0.05
0.06
0.07
0.08
x2 distance from Probe 2 (m)
No Magnet
1601G
2952G
3309G
4667G
5233G

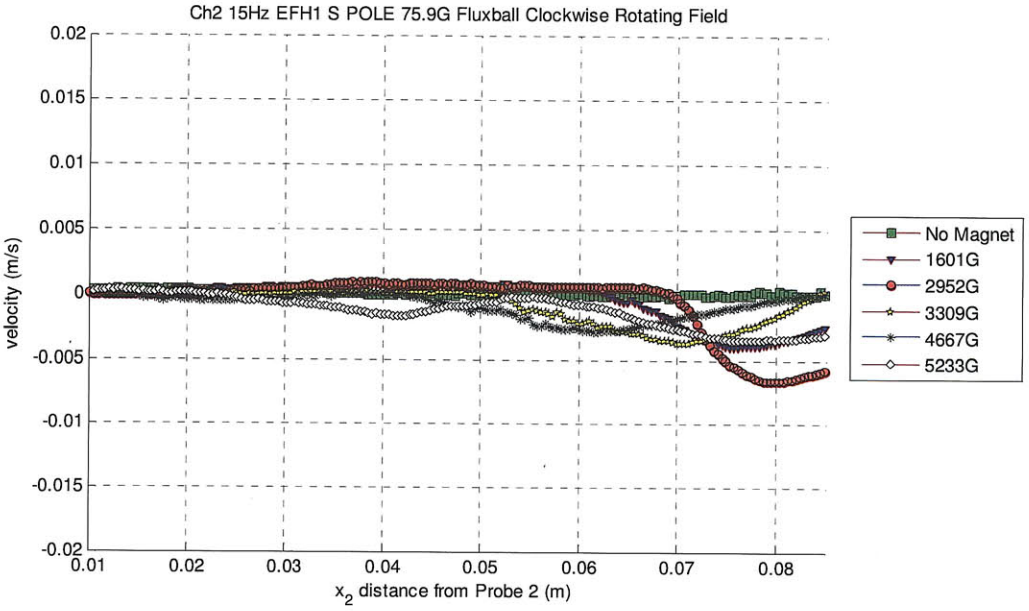
Ch2 15Hz EFH1 S POLE 75.9G Fluxball Clockwise Rotating Field
velocity (m/s)
0.02
0.015
0.01
0.005
0
-0.005
-0.01
-0.015
-0.02
0.01
0.02
0.03
0.04
0.05
0.06
0.07
0.08
x2 distance from Probe 2 (m)
No Magnet
1601G
2952G
3309G
4667G
5233G

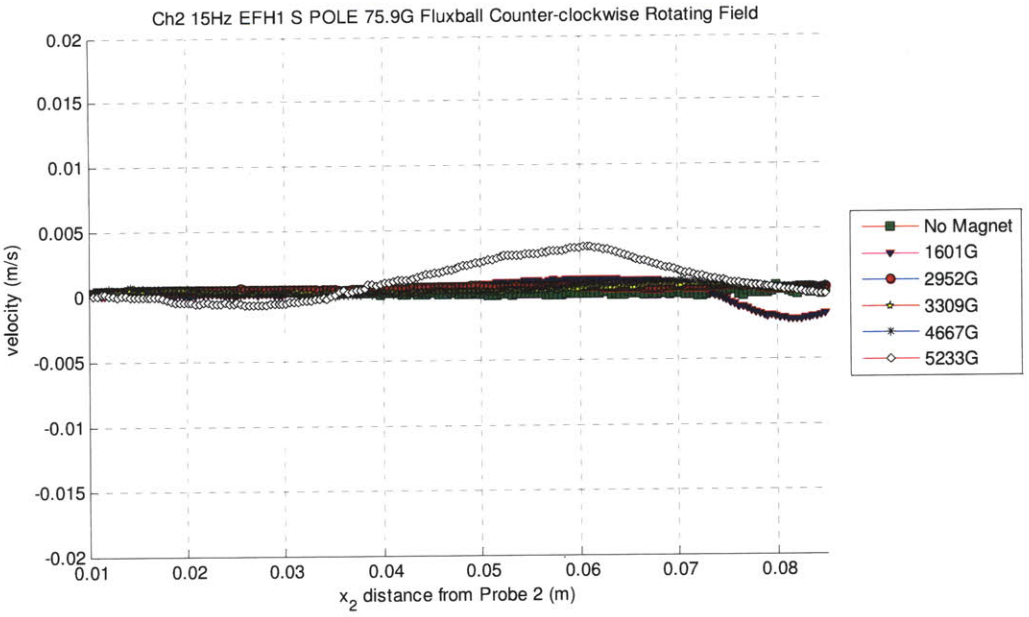
Ch2 15Hz EFH1 S POLE 75.9G Fluxball Counter-clockwise Rotating Field
velocity (m/s)
0.02
0.015
0.01
0.005
0
-0.005
-0.01
-0.015
-0.02
0.01
0.02
0.03
0.04
0.05
0.06
0.07
0.08
x2 distance from Probe 2 (m)
No Magnet
1601G
2952G
3309G
4667G
5233G

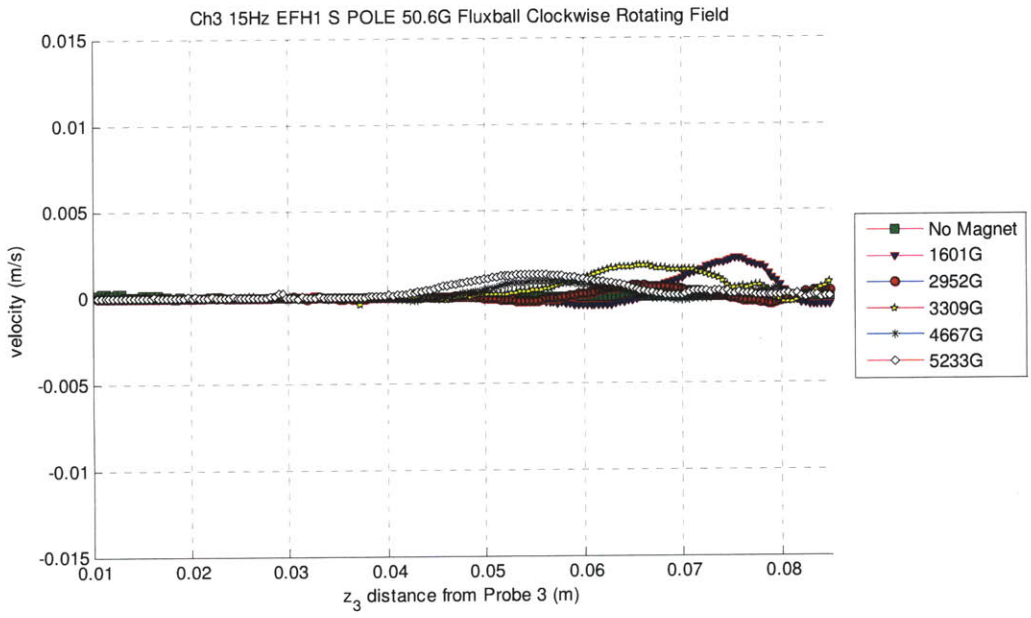
Ch3 15Hz EFH1 S POLE 50.6G Fluxball Clockwise Rotating Field
velocity (m/s)
0.015
0.01
0.005
0
-0.005
-0.01
-0.015
0.01
0.02
0.03
0.04
0.05
0.06
0.07
0.08
z3 distance from Probe 3 (m)
No Magnet
1601G
2952G
3309G
4667G
5233G

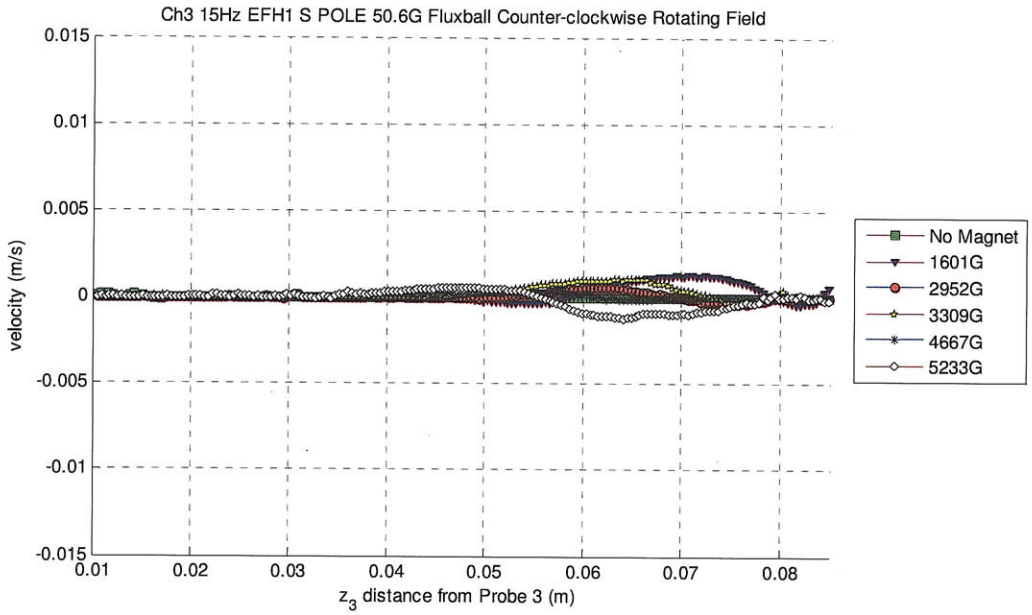
Ch3 15Hz EFH1 S POLE 50.6G Fluxball Counter-clockwise Rotating Field
velocity (m/s)
0.015
0.01
0.005
0
-0.005
-0.01
-0.015
0.01
0.02
0.03
0.04
0.05
0.06
0.07
0.08
z_3 distance from Probe 3 (m)
No Magnet
1601G
2952G
3309G
4667G
5233G

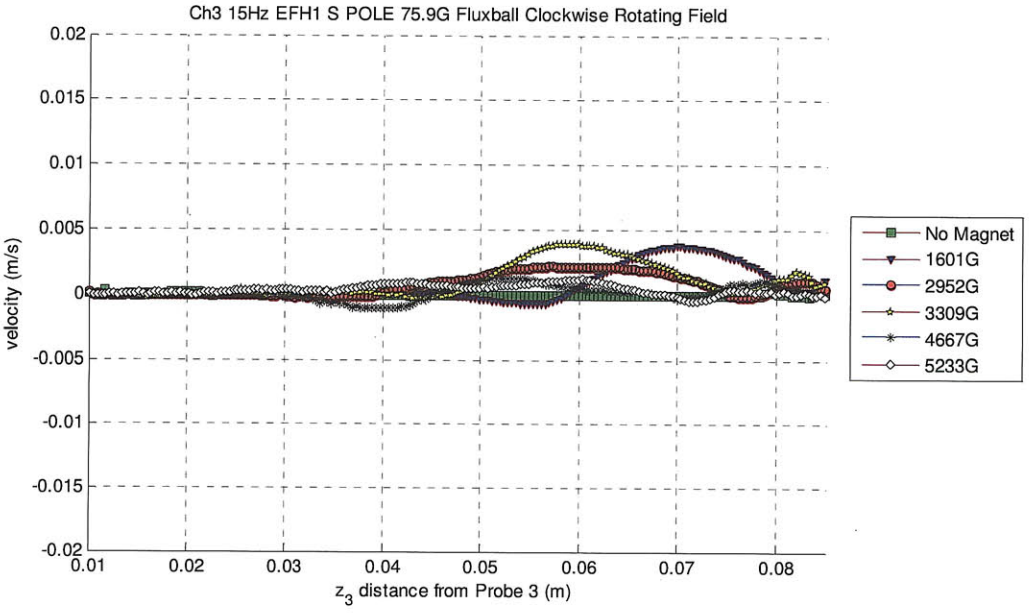
Ch3 15Hz EFH1 S POLE 75.9G Fluxball Clockwise Rotating Field
velocity (m/s)
0.02
0.015
0.01
0.005
0
-0.005
-0.01
-0.015
-0.02
0.01
0.02
0.03
0.04
0.05
0.06
0.07
0.08
z_3 distance from Probe 3 (m)
No Magnet
1601G
2952G
3309G
4667G
5233G

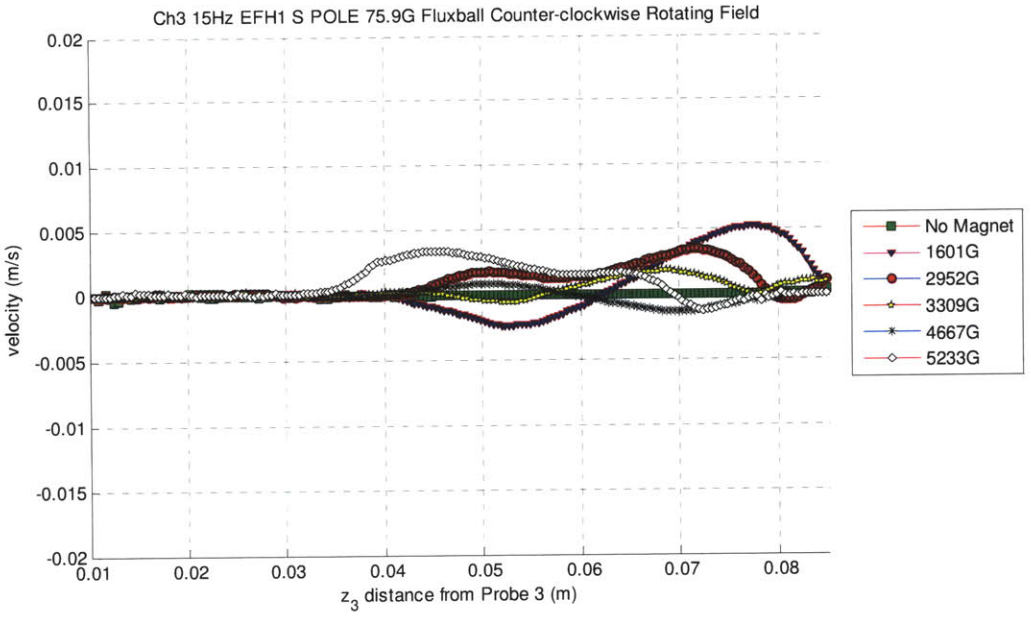
Ch3 15Hz EFH1 S POLE 75.9G Fluxball Counter-clockwise Rotating Field
velocity (m/s)
0.02
0.015
0.01
0.005
0
-0.005
-0.01
-0.015
-0.02
0.01
0.02
0.03
0.04
0.05
0.06
0.07
0.08
z_3 distance from Probe 3 (m)
No Magnet
1601G
2952G
3309G
4667G
5233G

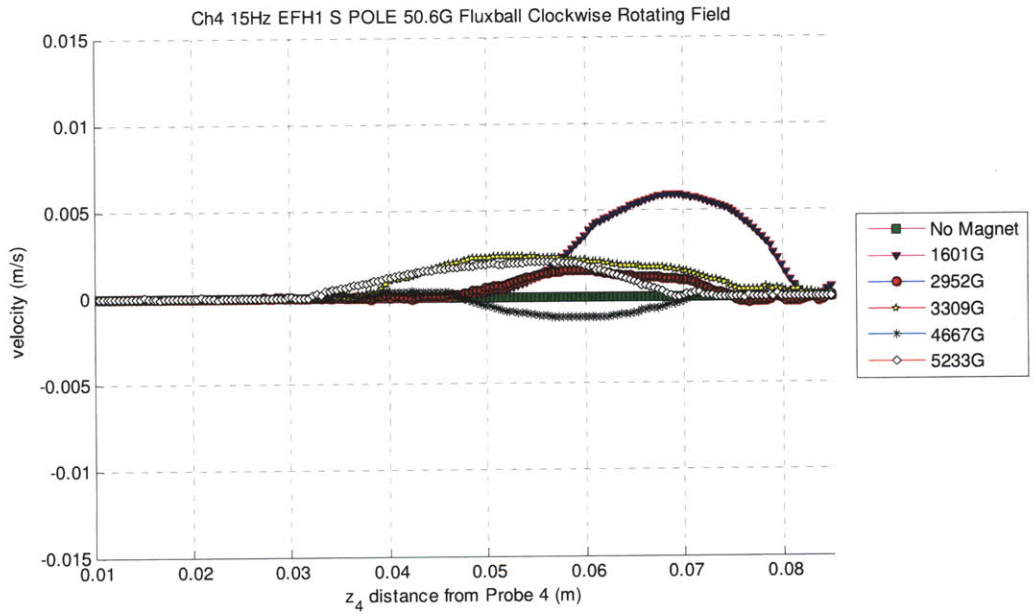
Ch4 15Hz EFH1 S POLE 50.6G Fluxball Clockwise Rotating Field
velocity (m/s)
0.015
0.01
0.005
0
-0.005
-0.01
-0.015
0.01
0.02
0.03
0.04
0.05
0.06
0.07
0.08
z_4 distance from Probe 4 (m)
No Magnet
1601G
2952G
3309G
4667G
5233G

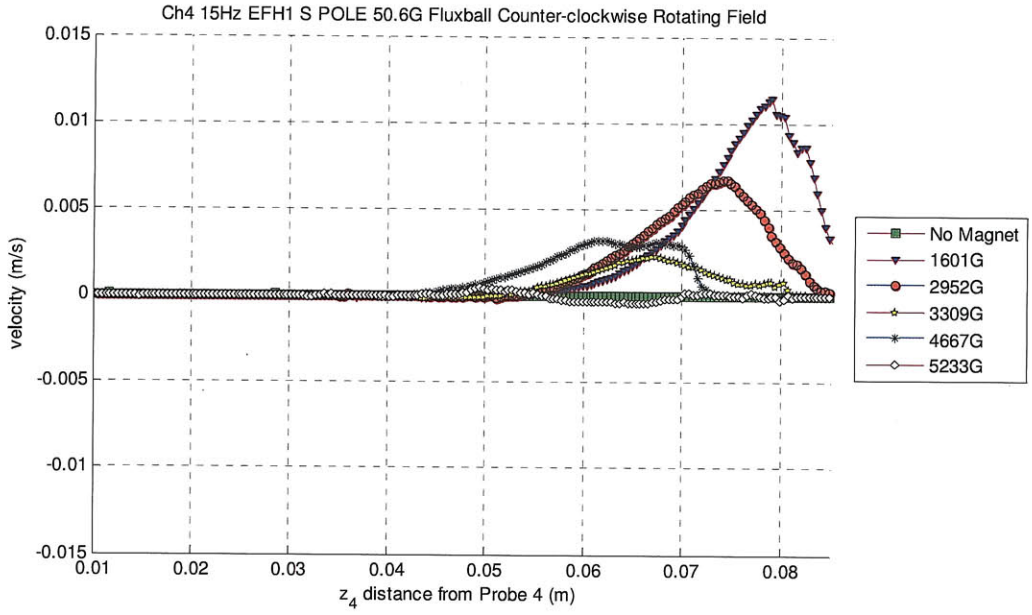
Ch4 15Hz EFH1 S POLE 50.6G Fluxball Counter-clockwise Rotating Field
velocity (m/s)
0.015
0.01
0.005
0
-0.005
-0.01
-0.015
0.01
0.02
0.03
0.04
0.05
0.06
0.07
0.08
z4 distance from Probe 4 (m)
No Magnet
1601G
2952G
3309G
4667G
5233G

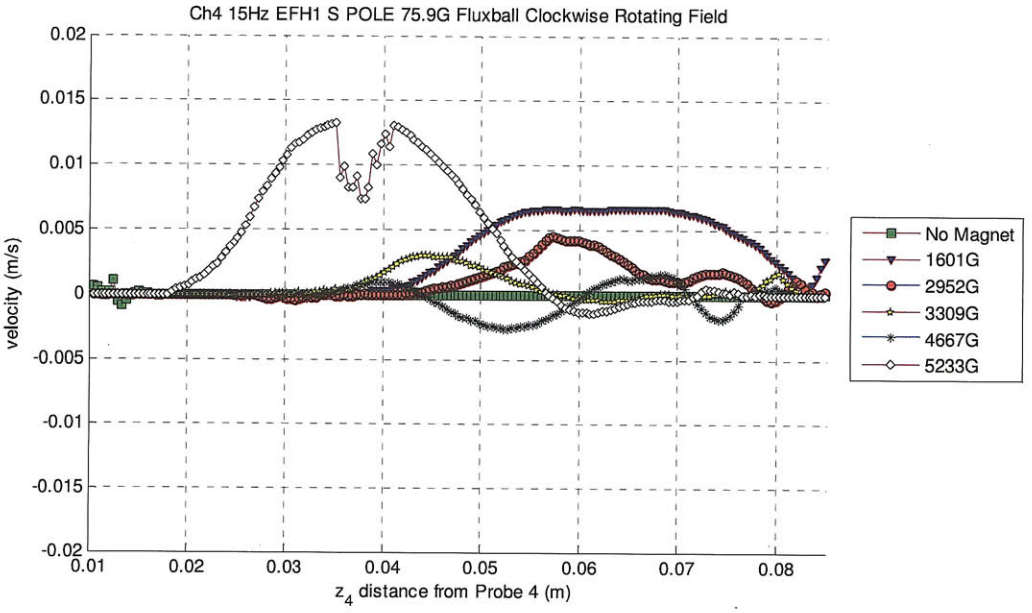
Ch4 15Hz EFH1 S POLE 75.9G Fluxball Clockwise Rotating Field
velocity (m/s)
0.02
0.015
0.01
0.005
0
-0.005
-0.01
-0.015
-0.02
0.01
0.02
0.03
0.04
0.05
0.06
0.07
0.08
z4 distance from Probe 4 (m)
No Magnet
1601G
2952G
3309G
4667G
5233G

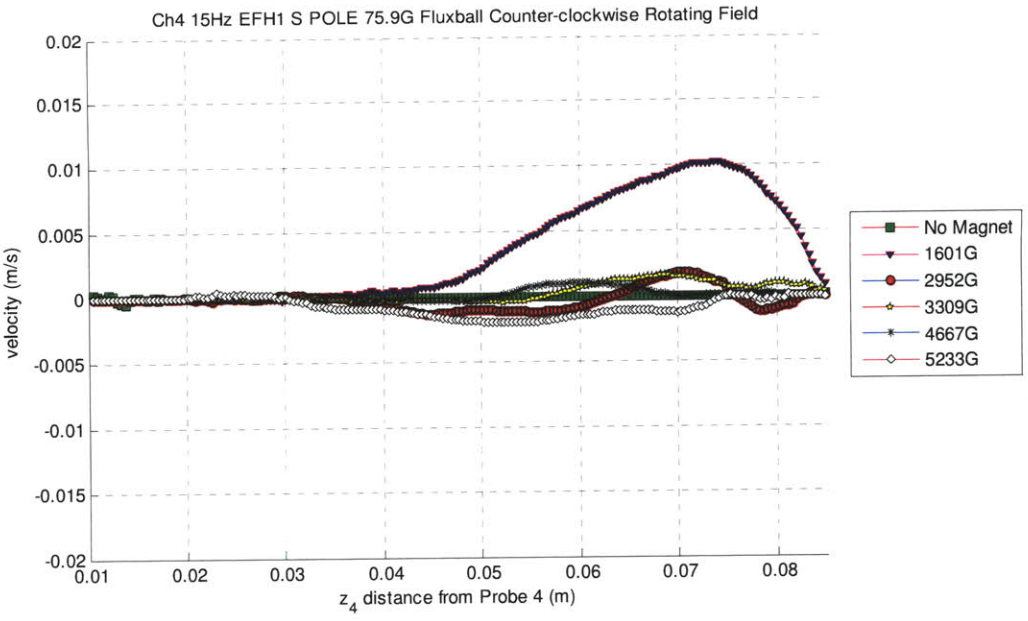
Ch4 15Hz EFH1 S POLE 75.9G Fluxball Counter-clockwise Rotating Field
velocity (m/s)
0.02
0.015
0.01
0.005
0
-0.005
-0.01
-0.015
-0.02
0.01
0.02
0.03
0.04
0.05
0.06
0.07
0.08
z_4 distance from Probe 4 (m)
No Magnet
1601G
2952G
3309G
4667G
5233G

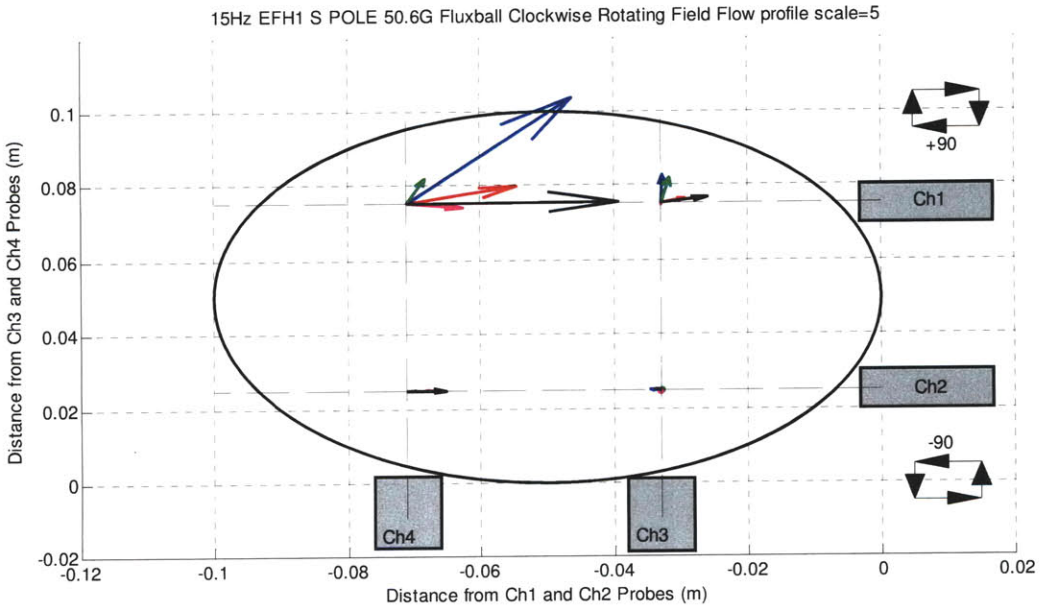
15Hz EFH1 S POLE 50.6G Fluxball Clockwise Rotating Field Flow profile scale=5
Distance from Ch3 and Ch4 Probes (m)
0.1
0.08
0.06
0.04
0.02
0
-0.02
-0.12
-0.1
-0.08
-0.06
-0.04
-0.02
0
0.02
Distance from Ch1 and Ch2 Probes (m)
+90
Ch1
Ch2
-90
Ch4
Ch3

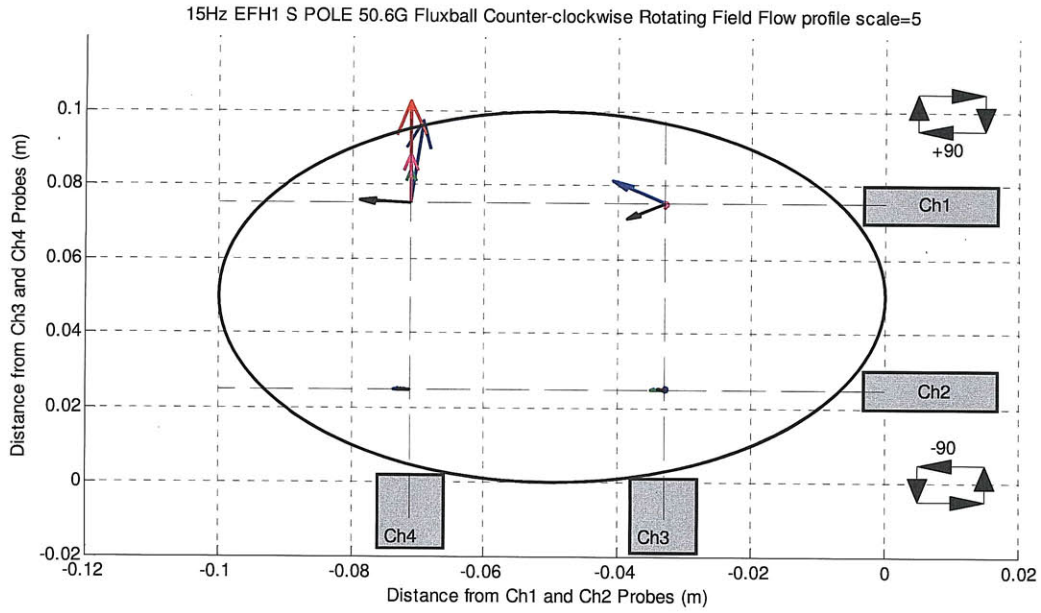
15Hz EFH1 S POLE 50.6G Fluxball Counter-clockwise Rotating Field Flow profile scale=5
Distance from Ch3 and Ch4 Probes (m)
Distance from Ch1 and Ch2 Probes (m)
+90
-90
Ch1
Ch2
Ch3
Ch4
0.1
0.08
0.06
0.04
0.02
0
-0.02
-0.12
-0.1
-0.08
-0.06
-0.04
-0.02
0
0.02

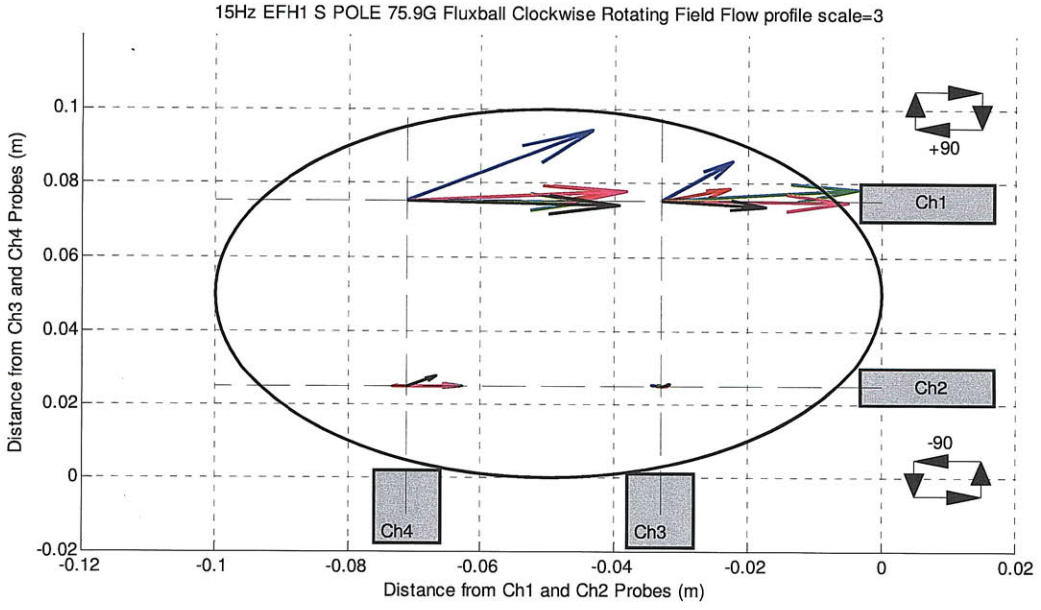
15Hz EFH1 S POLE 75.9G Fluxball Clockwise Rotating Field Flow profile scale=3
Distance from Ch3 and Ch4 Probes (m)
Distance from Ch1 and Ch2 Probes (m)
+90
-90
Ch1
Ch2
Ch3
Ch4
0.1
0.08
0.06
0.04
0.02
0
-0.02
-0.12
-0.1
-0.08
-0.06
-0.04
-0.02
0
0.02

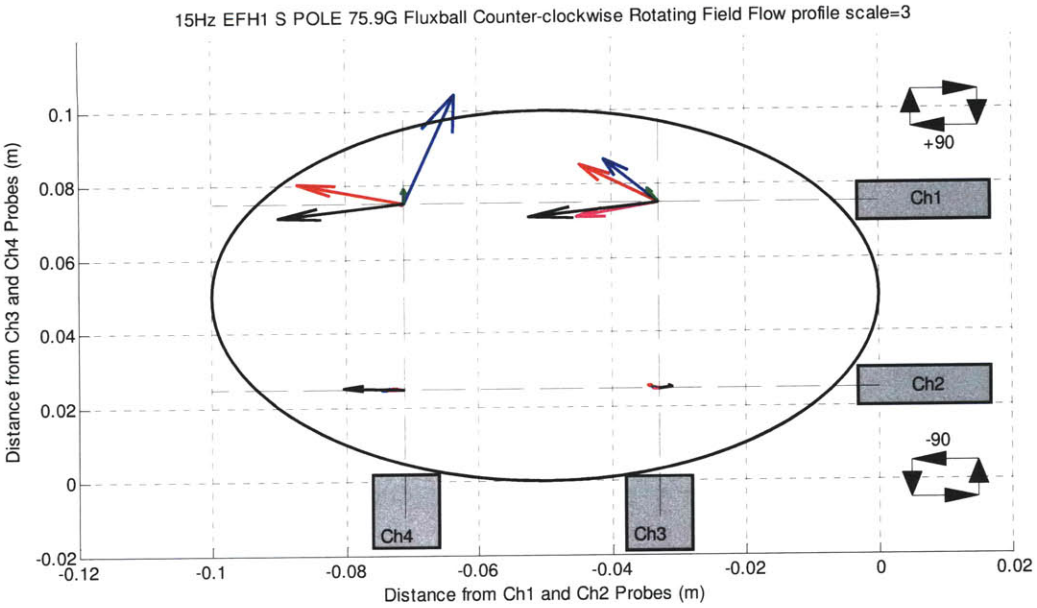
15Hz EFH1 S POLE 75.9G Fluxball Counter-clockwise Rotating Field Flow profile scale=3
Distance from Ch3 and Ch4 Probes (m)
0.1
0.08
0.06
0.04
0.02
0
-0.02
-0.12
-0.1
-0.08
-0.06
-0.04
-0.02
0
0.02
Distance from Ch1 and Ch2 Probes (m)
+90
Ch1
Ch2
-90
Ch4
Ch3

H4. EFH1 Filled Sphere with North Pole Facing Magnets on Top of Sphere at 95Hz

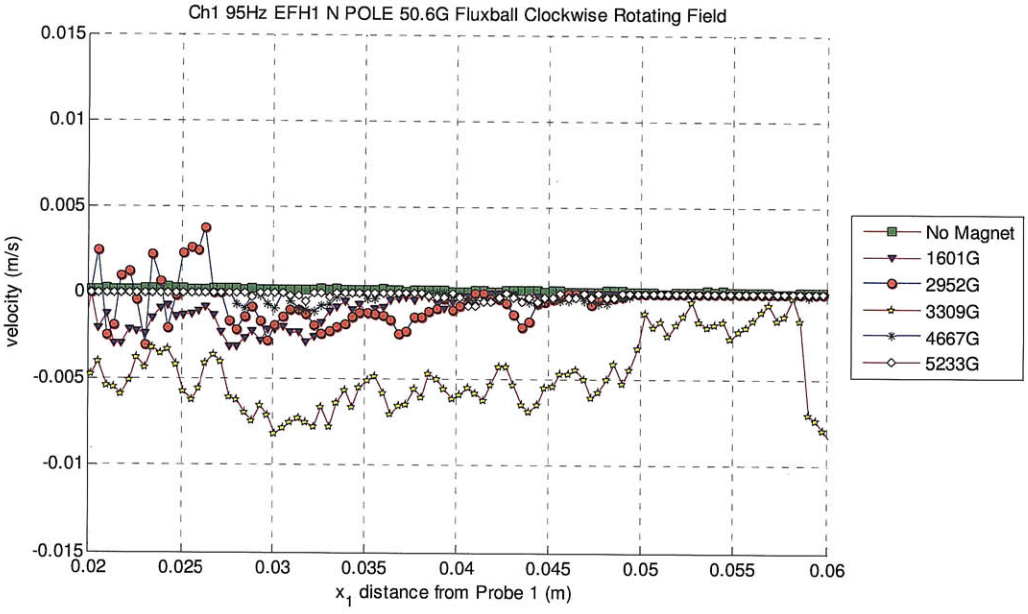

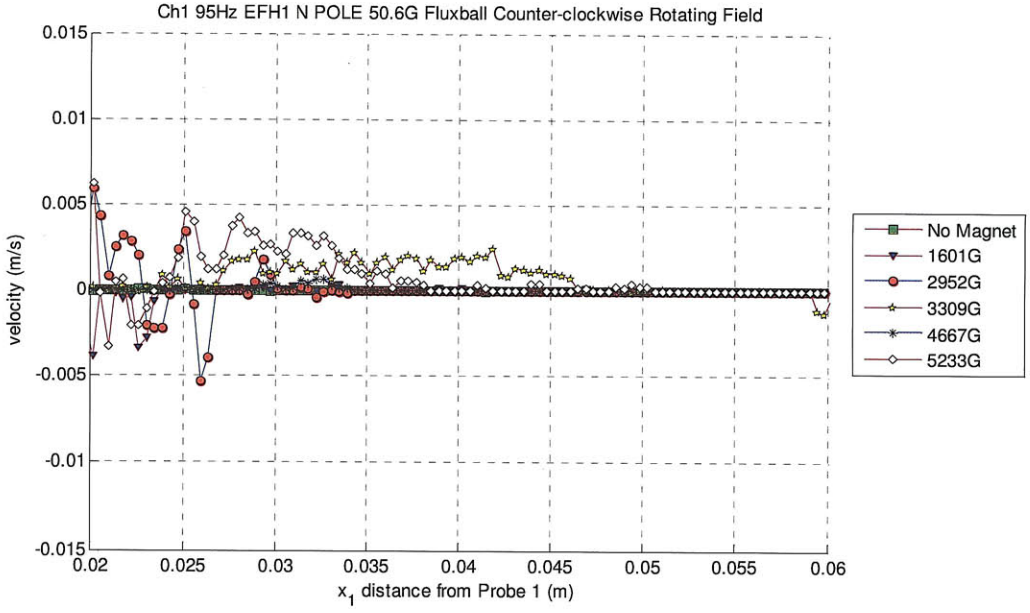

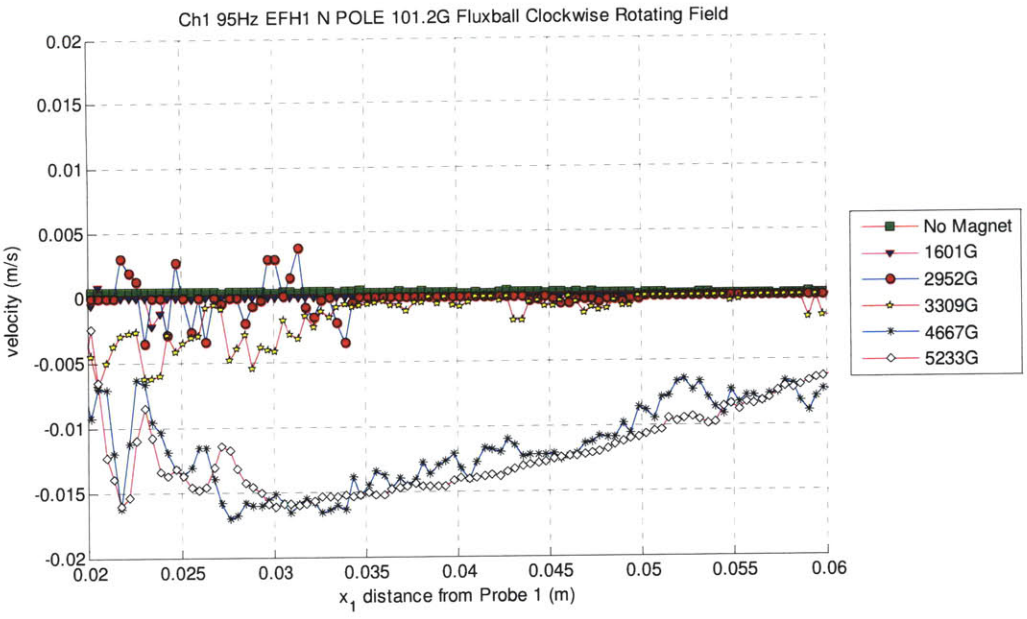
Ch1 95Hz EFH1 N POLE 101.2G Fluxball Clockwise Rotating Field
velocity (m/s)
0.02
0.015
0.01
0.005
0
-0.005
-0.01
-0.015
-0.02
0.02
0.025
0.03
0.035
0.04
0.045
0.05
0.055
0.06
x1 distance from Probe 1 (m)
No Magnet
1601G
2952G
3309G
4667G
5233G

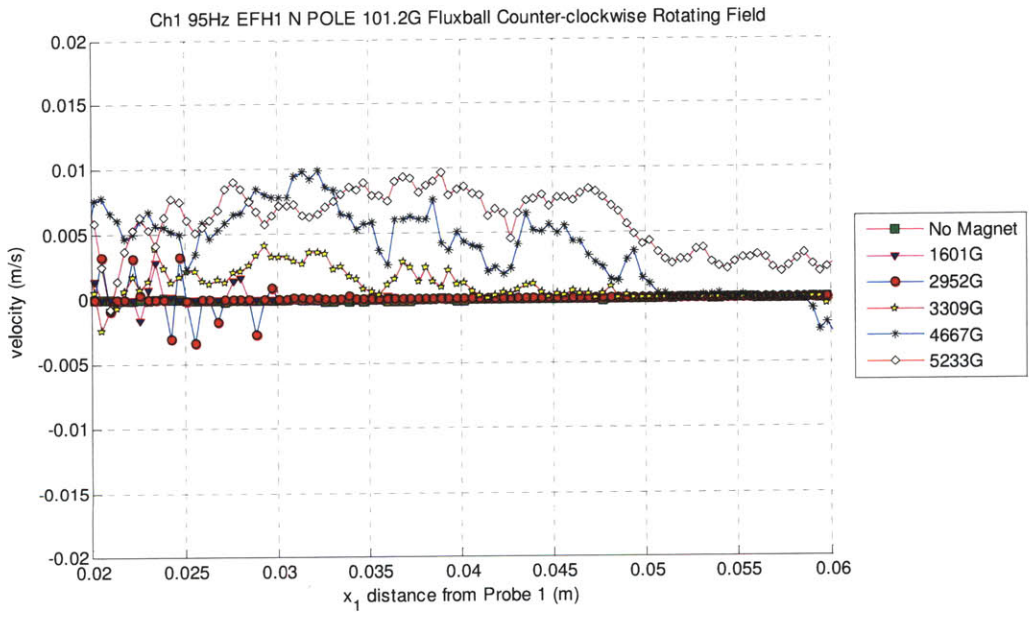
Ch1 95Hz EFH1 N POLE 101.2G Fluxball Counter-clockwise Rotating Field
velocity (m/s)
0.02
0.015
0.01
0.005
0
-0.005
-0.01
-0.015
-0.02
0.02
0.025
0.03
0.035
0.04
0.045
0.05
0.055
0.06
x1 distance from Probe 1 (m)
No Magnet
1601G
2952G
3309G
4667G
5233G

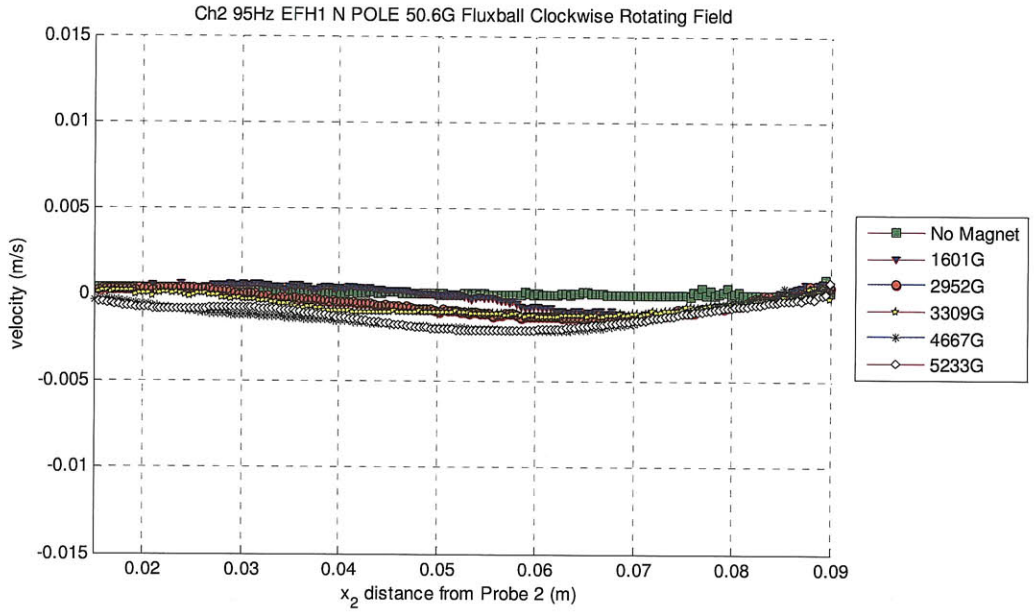
Ch2 95Hz EFH1 N POLE 50.6G Fluxball Clockwise Rotating Field
velocity (m/s)
0.015
0.01
0.005
0
-0.005
-0.01
-0.015
0.02
0.03
0.04
0.05
0.06
0.07
0.08
0.09
x2 distance from Probe 2 (m)
No Magnet
1601G
2952G
3309G
4667G
5233G

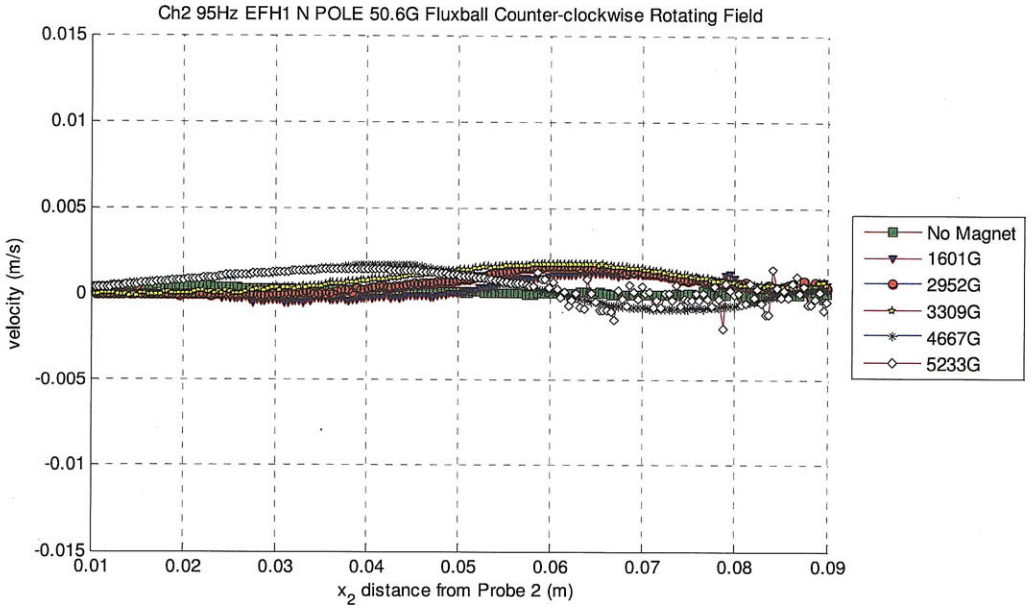
Ch2 95Hz EFH1 N POLE 50.6G Fluxball Counter-clockwise Rotating Field
velocity (m/s)
0.015
0.01
0.005
0
-0.005
-0.01
-0.015
0.01
0.02
0.03
0.04
0.05
0.06
0.07
0.08
0.09
x2 distance from Probe 2 (m)
No Magnet
1601G
2952G
3309G
4667G
5233G

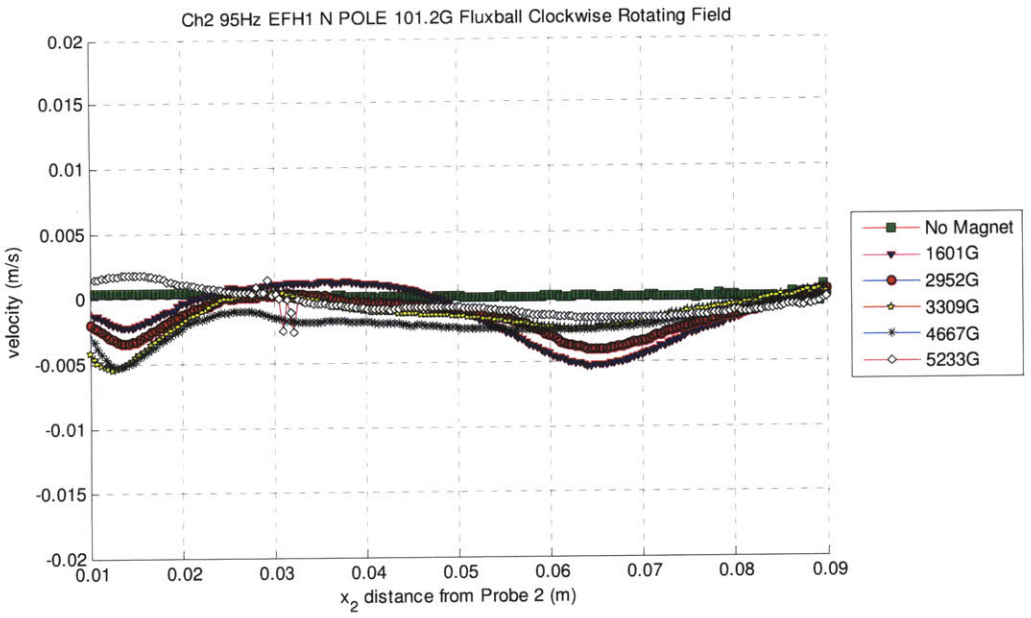
Ch2 95Hz EFH1 N POLE 101.2G Fluxball Clockwise Rotating Field
velocity (m/s)
0.02
0.015
0.01
0.005
0
-0.005
-0.01
-0.015
-0.02
0.01
0.02
0.03
0.04
0.05
0.06
0.07
0.08
0.09
x2 distance from Probe 2 (m)
No Magnet
1601G
2952G
3309G
4667G
5233G

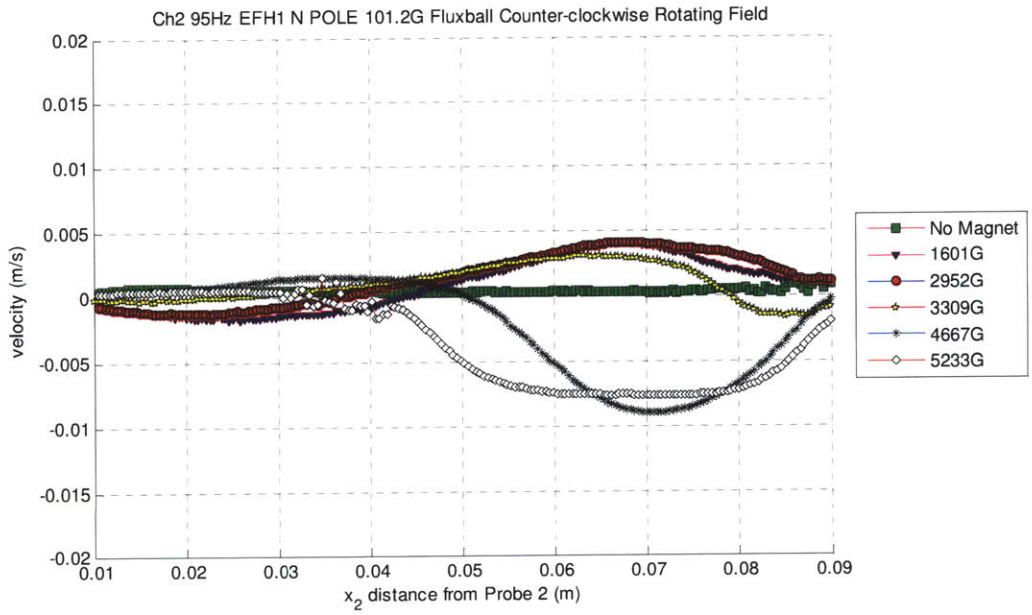
Ch2 95Hz EFH1 N POLE 101.2G Fluxball Counter-clockwise Rotating Field
velocity (m/s)
0.02
0.015
0.01
0.005
0
-0.005
-0.01
-0.015
-0.02
0.01
0.02
0.03
0.04
0.05
0.06
0.07
0.08
0.09
x2 distance from Probe 2 (m)
No Magnet
1601G
2952G
3309G
4667G
5233G

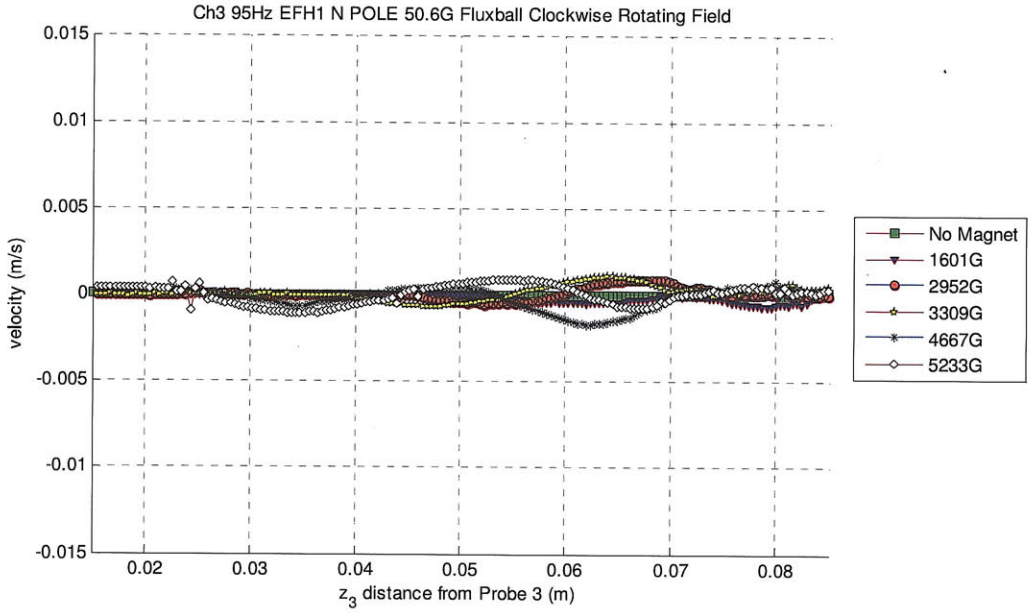
Ch3 95Hz EFH1 N POLE 50.6G Fluxball Clockwise Rotating Field
velocity (m/s)
0.015
0.01
0.005
0
-0.005
-0.01
-0.015
0.02
0.03
0.04
0.05
0.06
0.07
0.08
z_3 distance from Probe 3 (m)
No Magnet
1601G
2952G
3309G
4667G
5233G

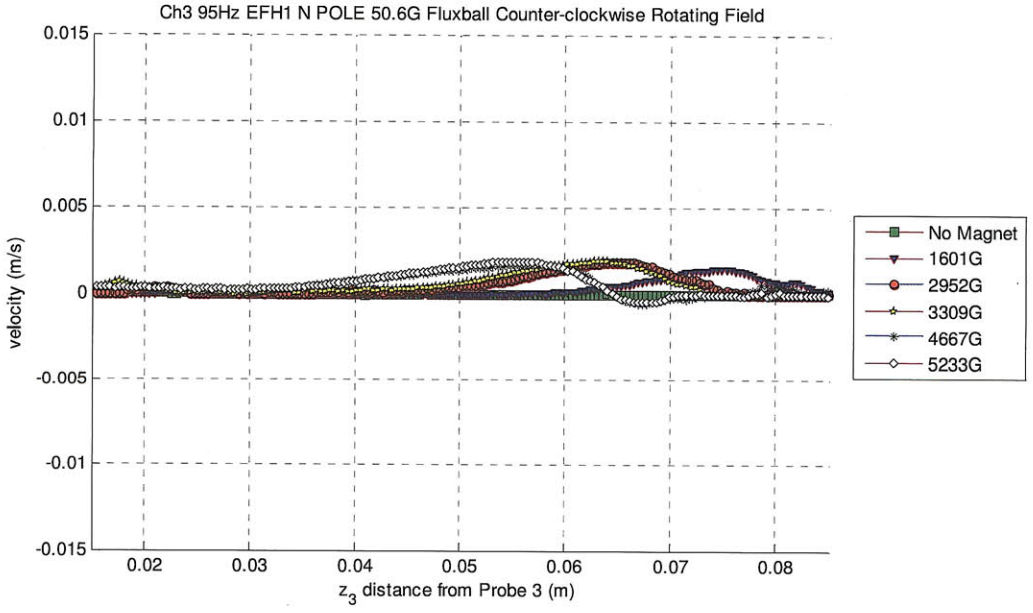
Ch3 95Hz EFH1 N POLE 50.6G Fluxball Counter-clockwise Rotating Field
velocity (m/s)
0.015
0.01
0.005
0
-0.005
-0.01
-0.015
0.02
0.03
0.04
0.05
0.06
0.07
0.08
z_3 distance from Probe 3 (m)
No Magnet
1601G
2952G
3309G
4667G
5233G

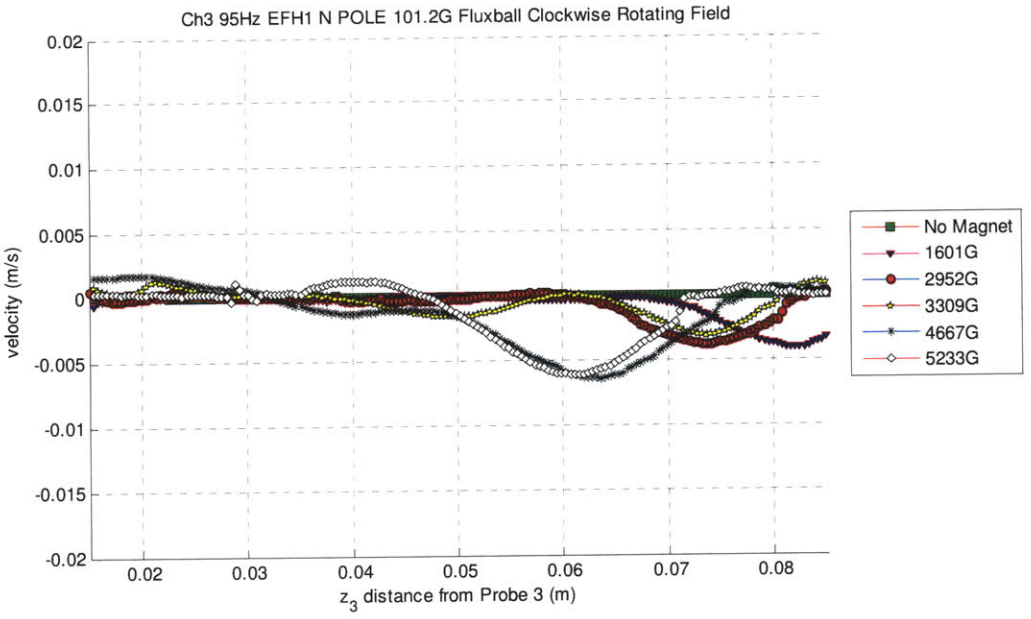
Ch3 95Hz EFH1 N POLE 101.2G Fluxball Clockwise Rotating Field
velocity (m/s)
0.02
0.015
0.01
0.005
0
-0.005
-0.01
-0.015
-0.02
0.02
0.03
0.04
0.05
0.06
0.07
0.08
z_3 distance from Probe 3 (m)
No Magnet
1601G
2952G
3309G
4667G
5233G

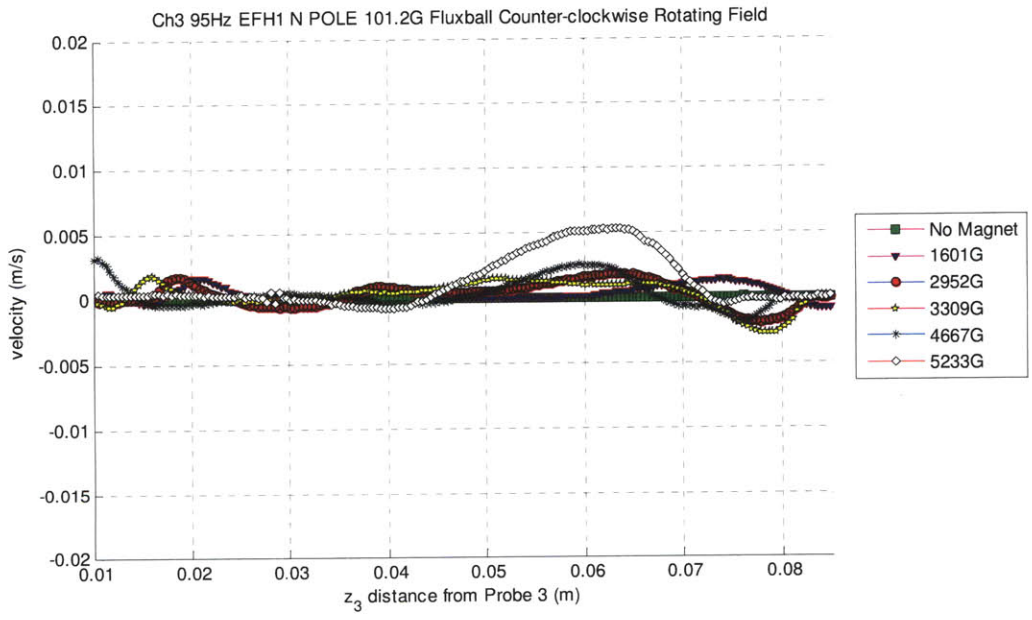
Ch3 95Hz EFH1 N POLE 101.2G Fluxball Counter-clockwise Rotating Field
velocity (m/s)
0.02
0.015
0.01
0.005
0
-0.005
-0.01
-0.015
-0.02
0.01
0.02
0.03
0.04
0.05
0.06
0.07
0.08
z_3 distance from Probe 3 (m)
No Magnet
1601G
2952G
3309G
4667G
5233G

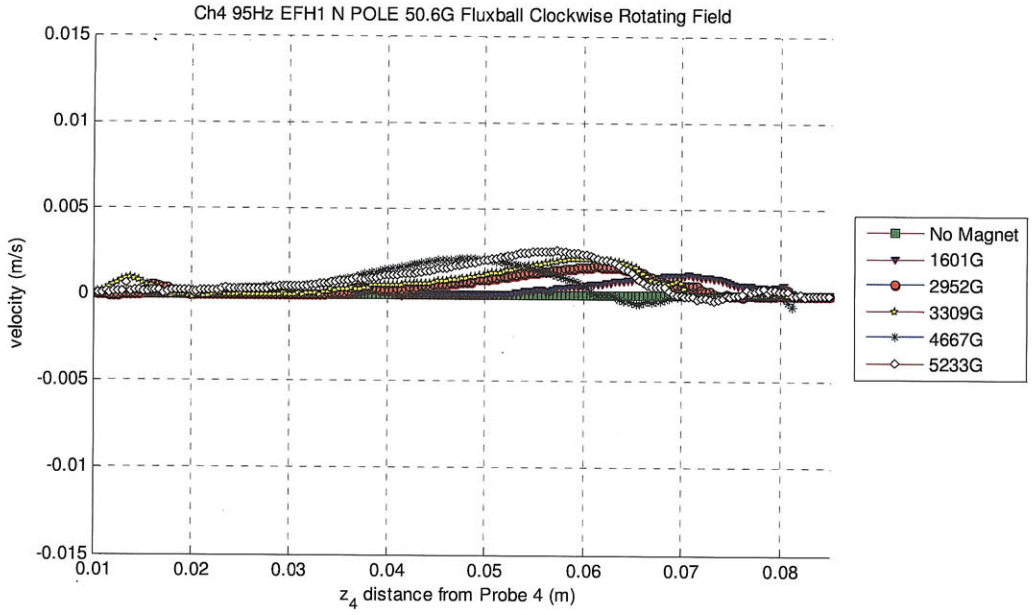
Ch4 95Hz EFH1 N POLE 50.6G Fluxball Clockwise Rotating Field
velocity (m/s)
0.015
0.01
0.005
0
-0.005
-0.01
-0.015
0.01
0.02
0.03
0.04
0.05
0.06
0.07
0.08
z4 distance from Probe 4 (m)
No Magnet
1601G
2952G
3309G
4667G
5233G

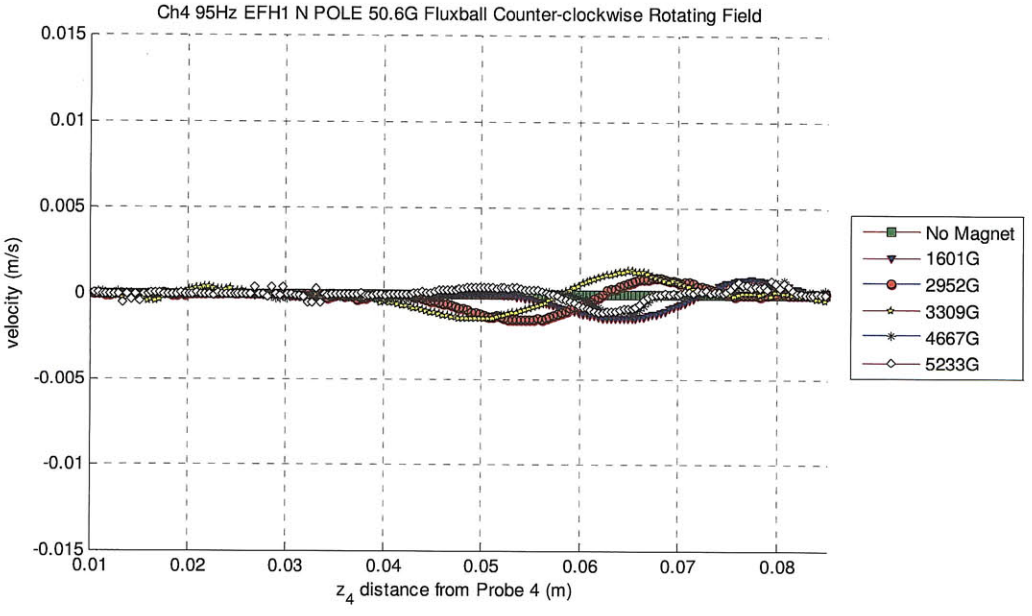
Ch4 95Hz EFH1 N POLE 50.6G Fluxball Counter-clockwise Rotating Field
velocity (m/s)
0.015
0.01
0.005
0
-0.005
-0.01
-0.015
0.01
0.02
0.03
0.04
0.05
0.06
0.07
0.08
z4 distance from Probe 4 (m)
No Magnet
1601G
2952G
3309G
4667G
5233G

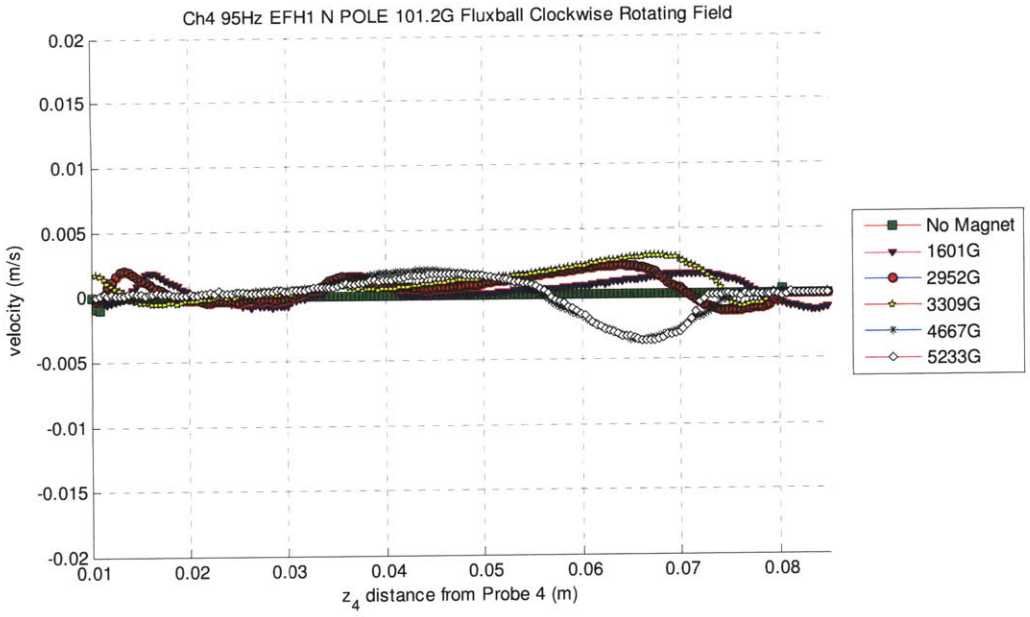
Ch4 95Hz EFH1 N POLE 101.2G Fluxball Clockwise Rotating Field
velocity (m/s)
0.02
0.015
0.01
0.005
0
-0.005
-0.01
-0.015
-0.02
0.01
0.02
0.03
0.04
0.05
0.06
0.07
0.08
z4 distance from Probe 4 (m)
No Magnet
1601G
2952G
3309G
4667G
5233G

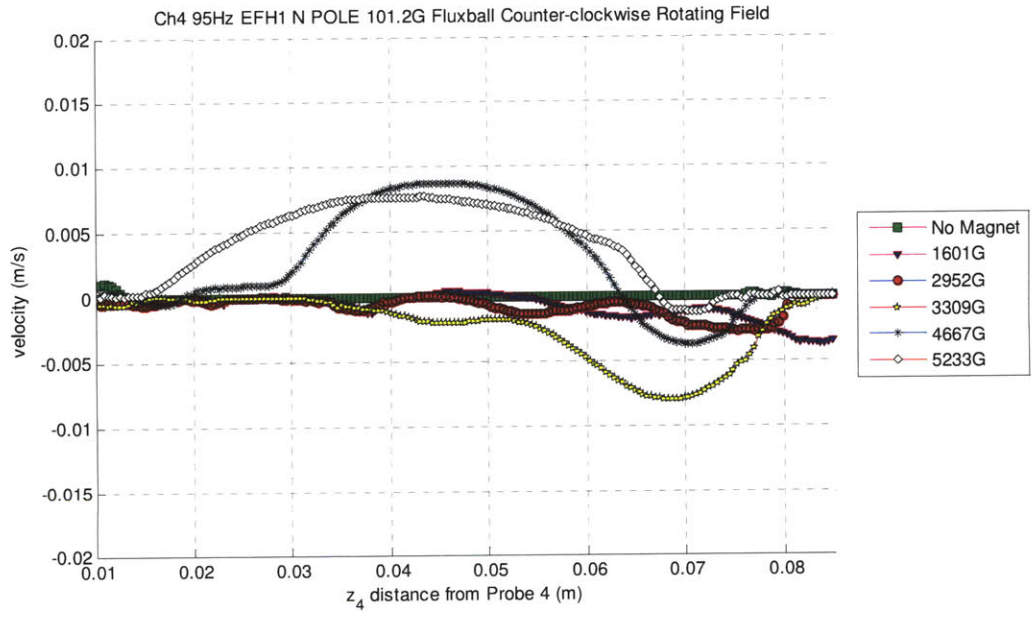
Ch4 95Hz EFH1 N POLE 101.2G Fluxball Counter-clockwise Rotating Field
velocity (m/s)
0.02
0.015
0.01
0.005
0
-0.005
-0.01
-0.015
-0.02
0.01
0.02
0.03
0.04
0.05
0.06
0.07
0.08
z4 distance from Probe 4 (m)
No Magnet
1601G
2952G
3309G
4667G
5233G

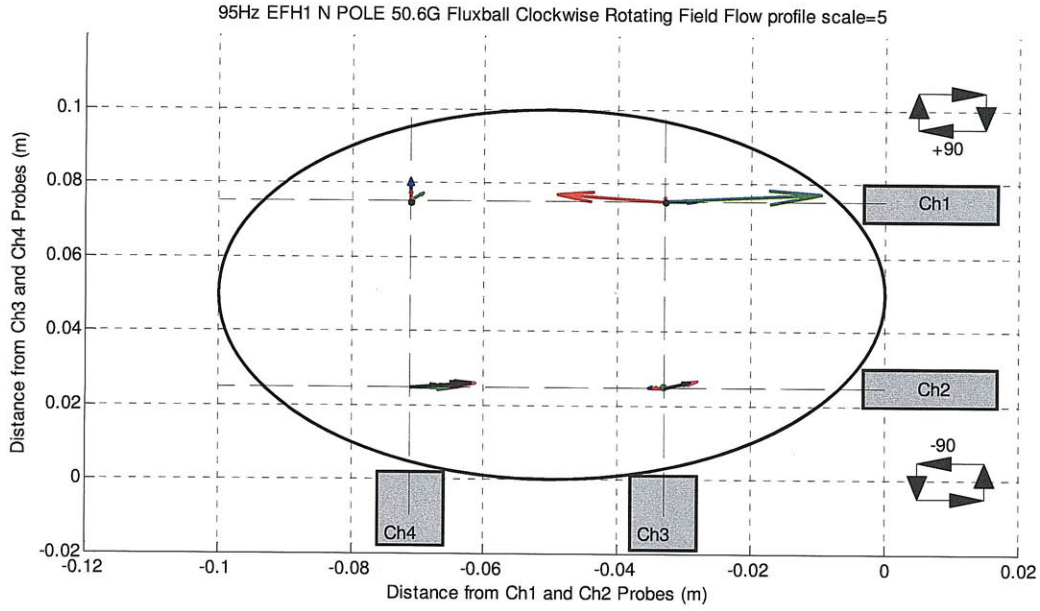
95Hz EFH1 N POLE 50.6G Fluxball Clockwise Rotating Field Flow profile scale=5
Distance from Ch3 and Ch4 Probes (m)
Distance from Ch1 and Ch2 Probes (m)
+90
-90
Ch1
Ch2
Ch3
Ch4
0.1
0.08
0.06
0.04
0.02
0
-0.02
-0.12
-0.1
-0.08
-0.06
-0.04
-0.02
0
0.02

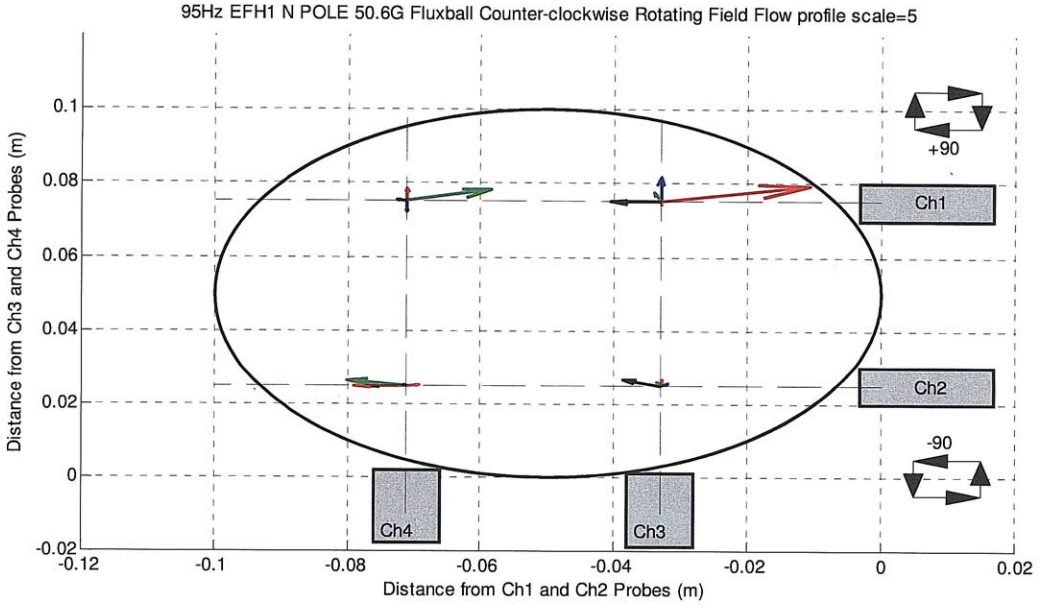
95Hz EFH1 N POLE 50.6G Fluxball Counter-clockwise Rotating Field Flow profile scale=5
Distance from Ch3 and Ch4 Probes (m)
Distance from Ch1 and Ch2 Probes (m)
+90
-90
Ch1
Ch2
Ch3
Ch4
0.1
0.08
0.06
0.04
0.02
0
-0.02
-0.12
-0.1
-0.08
-0.06
-0.04
-0.02
0
0.02

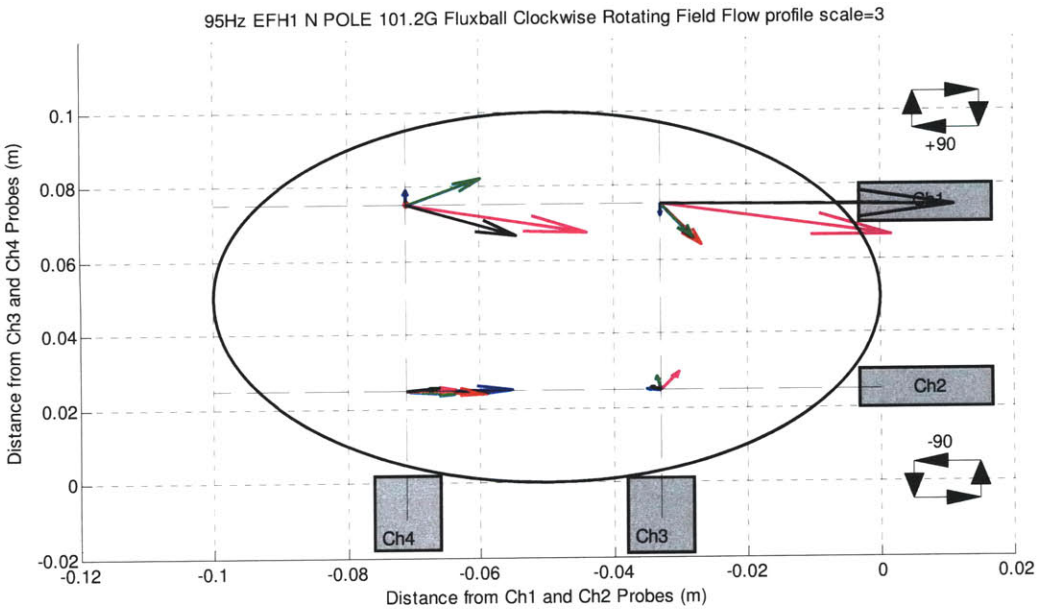
95Hz EFH1 N POLE 101.2G Fluxball Clockwise Rotating Field Flow profile scale=3
Distance from Ch3 and Ch4 Probes (m)
Distance from Ch1 and Ch2 Probes (m)
+90
-90
Ch1
Ch2
Ch3
Ch4
0.1
0.08
0.06
0.04
0.02
0
-0.02
-0.12
-0.1
-0.08
-0.06
-0.04
-0.02
0
0.02

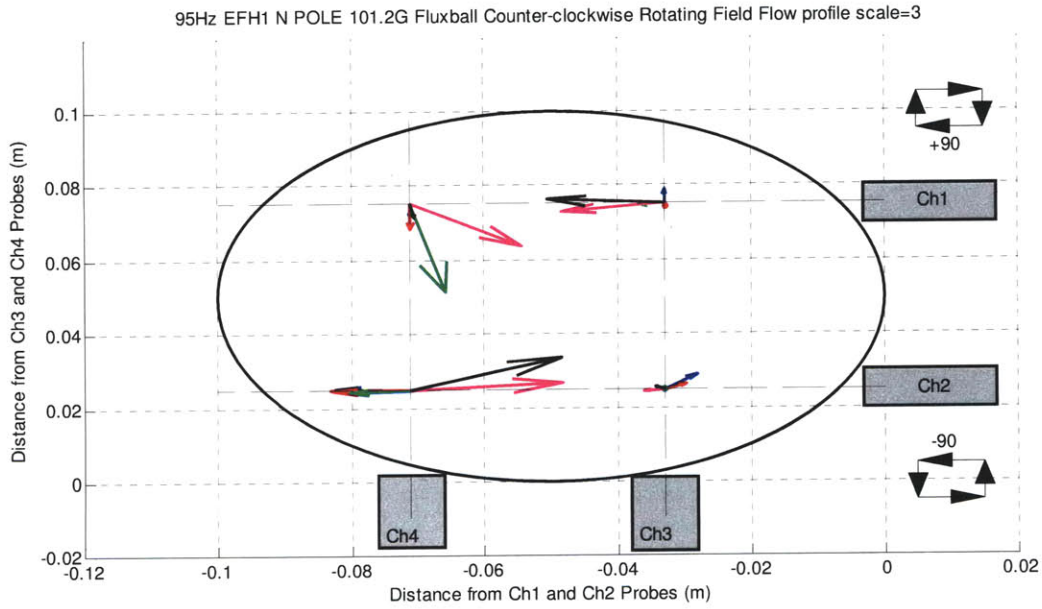
95Hz EFH1 N POLE 101.2G Fluxball Counter-clockwise Rotating Field Flow profile scale=3
Distance from Ch3 and Ch4 Probes (m)
Distance from Ch1 and Ch2 Probes (m)
+90
-90
Ch1
Ch2
Ch3
Ch4
0.1
0.08
0.06
0.04
0.02
0
-0.02
-0.12
-0.1
-0.08
-0.06
-0.04
-0.02
0
0.02

H5. EFH1 Filled Sphere with North Pole Facing Magnets on Top of Sphere at 47Hz

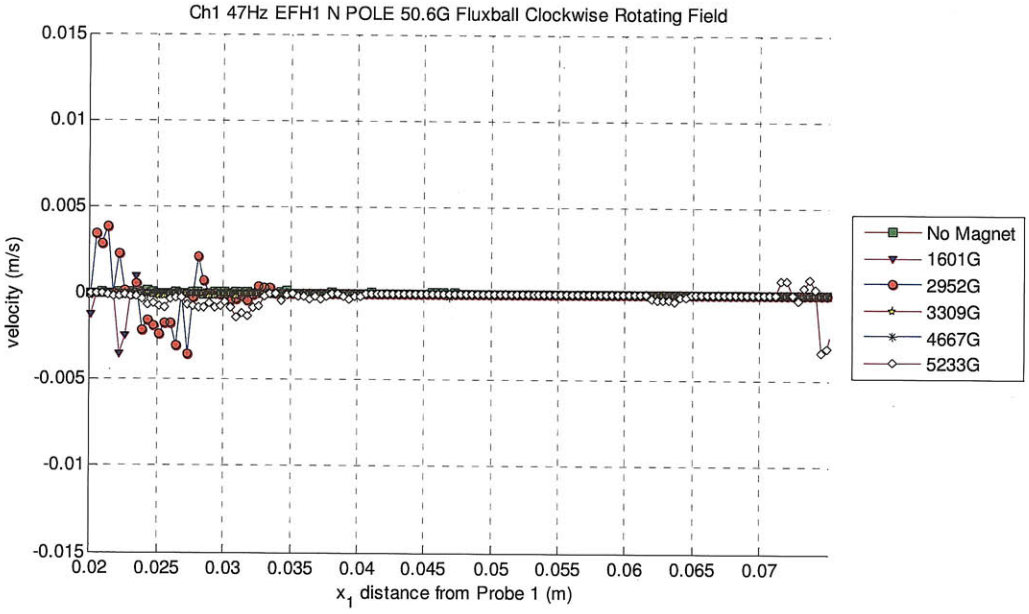

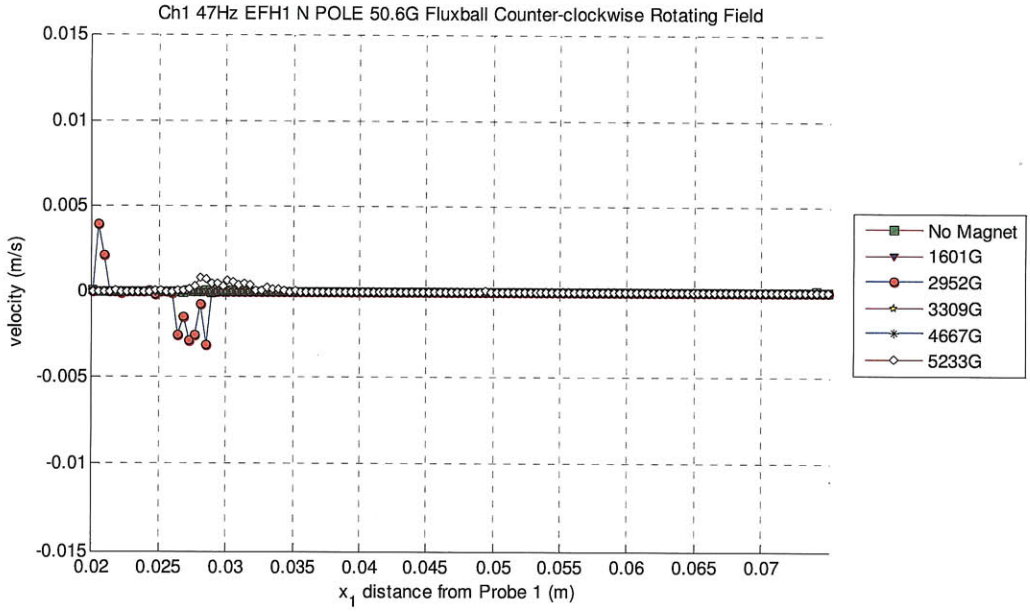

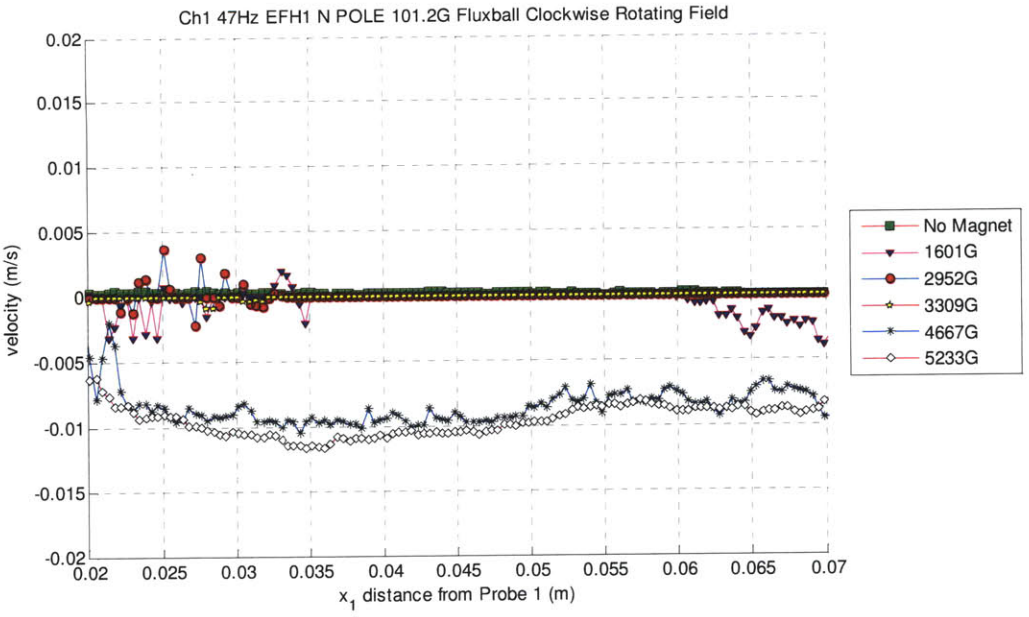
Ch1 47Hz EFH1 N POLE 101.2G Fluxball Clockwise Rotating Field
velocity (m/s)
0.02
0.015
0.01
0.005
0
-0.005
-0.01
-0.015
-0.02
0.02
0.025
0.03
0.035
0.04
0.045
0.05
0.055
0.06
0.065
0.07
x1 distance from Probe 1 (m)
No Magnet
1601G
2952G
3309G
4667G
5233G

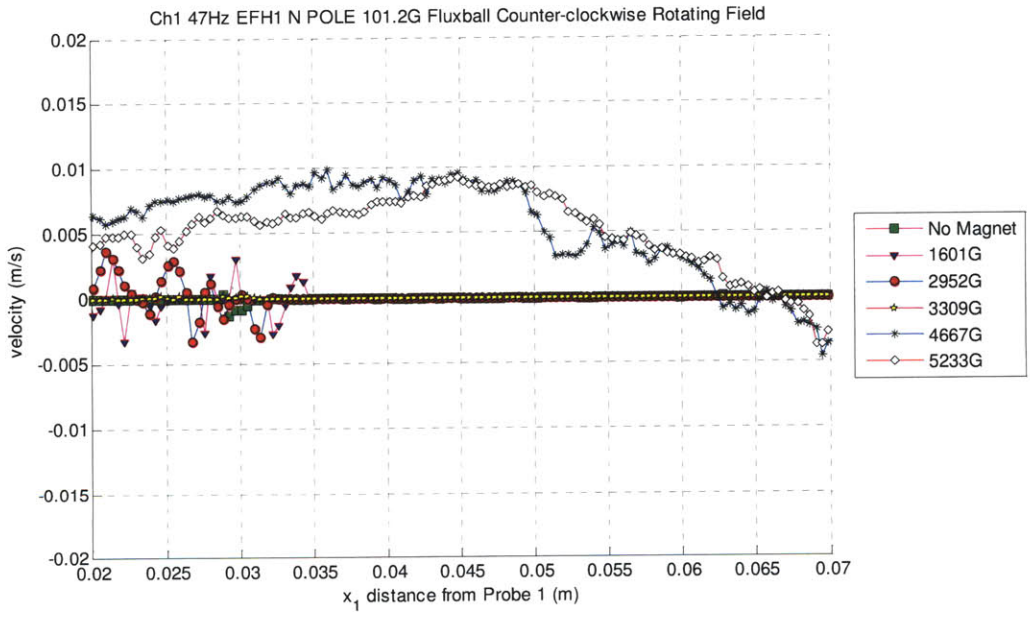
Ch1 47Hz EFH1 N POLE 101.2G Fluxball Counter-clockwise Rotating Field
velocity (m/s)
0.02
0.015
0.01
0.005
0
-0.005
-0.01
-0.015
-0.02
0.02
0.025
0.03
0.035
0.04
0.045
0.05
0.055
0.06
0.065
0.07
x1 distance from Probe 1 (m)
No Magnet
1601G
2952G
3309G
4667G
5233G

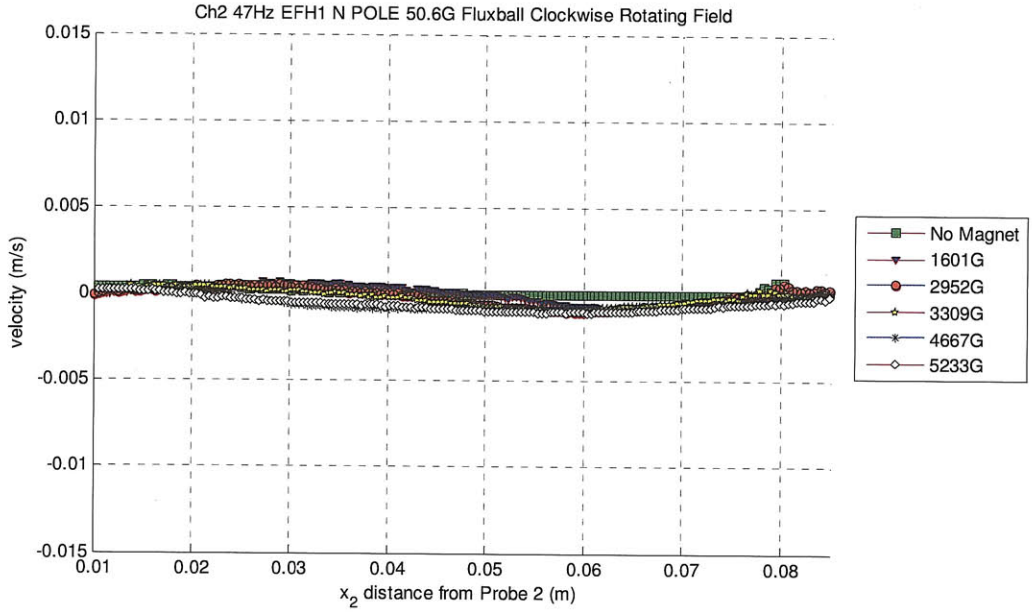
Ch2 47Hz EFH1 N POLE 50.6G Fluxball Clockwise Rotating Field
velocity (m/s)
0.015
0.01
0.005
0
-0.005
-0.01
-0.015
0.01
0.02
0.03
0.04
0.05
0.06
0.07
0.08
x2 distance from Probe 2 (m)
No Magnet
1601G
2952G
3309G
4667G
5233G

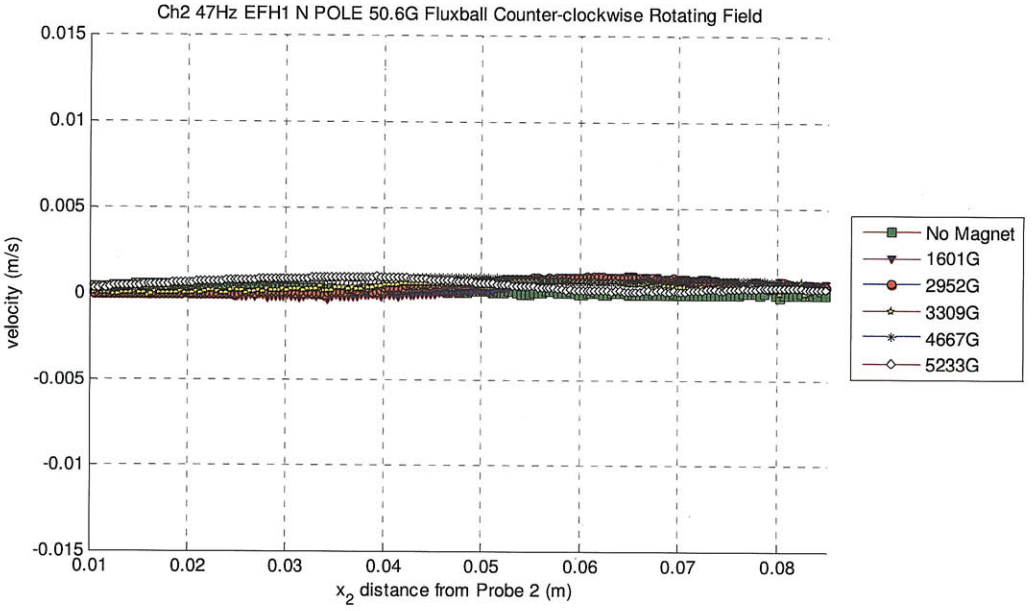
Ch2 47Hz EFH1 N POLE 50.6G Fluxball Counter-clockwise Rotating Field
velocity (m/s)
0.015
0.01
0.005
0
-0.005
-0.01
-0.015
0.01
0.02
0.03
0.04
0.05
0.06
0.07
0.08
x2 distance from Probe 2 (m)
No Magnet
1601G
2952G
3309G
4667G
5233G

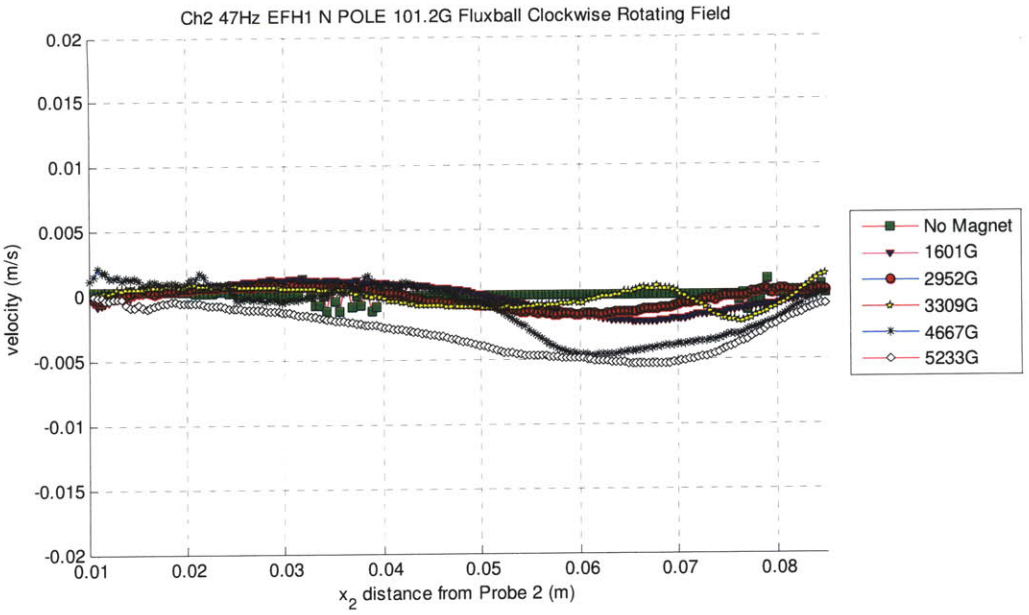
Ch2 47Hz EFH1 N POLE 101.2G Fluxball Clockwise Rotating Field
velocity (m/s)
0.02
0.015
0.01
0.005
0
-0.005
-0.01
-0.015
-0.02
0.01
0.02
0.03
0.04
0.05
0.06
0.07
0.08
x2 distance from Probe 2 (m)
No Magnet
1601G
2952G
3309G
4667G
5233G

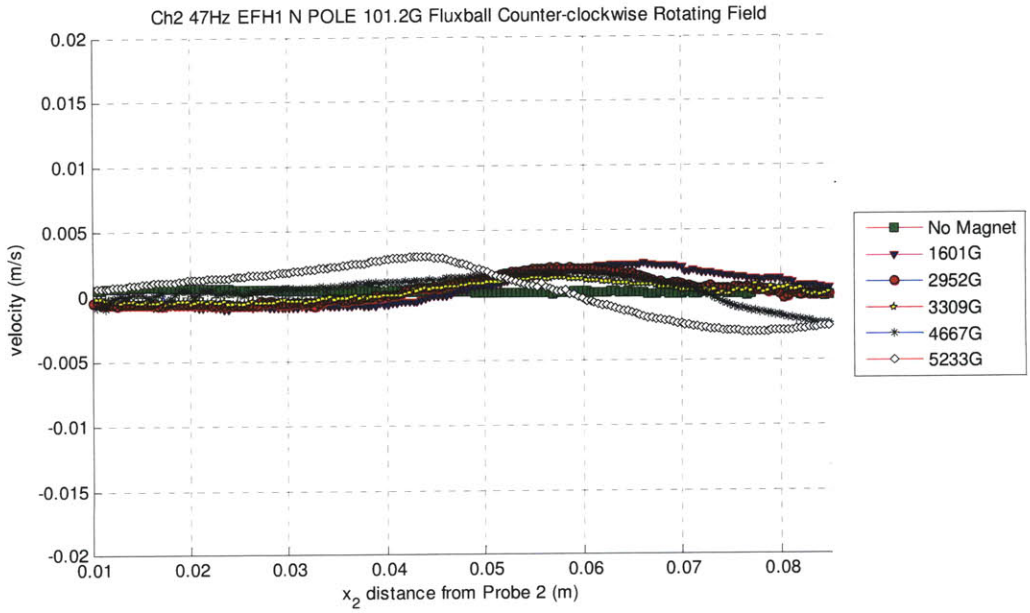
Ch2 47Hz EFH1 N POLE 101.2G Fluxball Counter-clockwise Rotating Field
velocity (m/s)
0.02
0.015
0.01
0.005
0
-0.005
-0.01
-0.015
-0.02
0.01
0.02
0.03
0.04
0.05
0.06
0.07
0.08
x2 distance from Probe 2 (m)
No Magnet
1601G
2952G
3309G
4667G
5233G

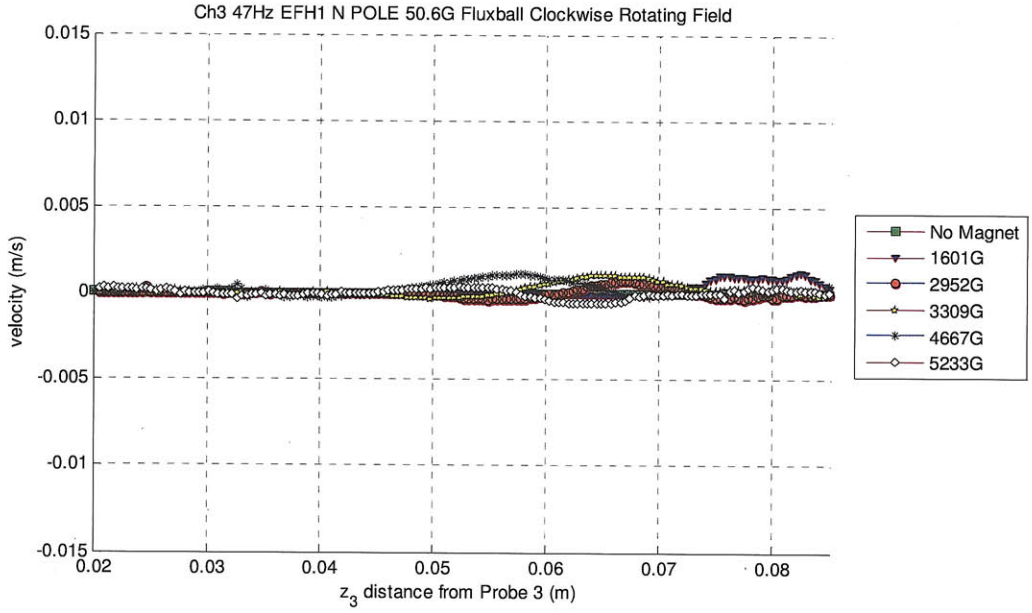
Ch3 47Hz EFH1 N POLE 50.6G Fluxball Clockwise Rotating Field
0.015
0.01
0.005
0
-0.005
-0.01
-0.015
velocity (m/s)
0.02
0.03
0.04
0.05
0.06
0.07
0.08
z3 distance from Probe 3 (m)
No Magnet
1601G
2952G
3309G
4667G
5233G

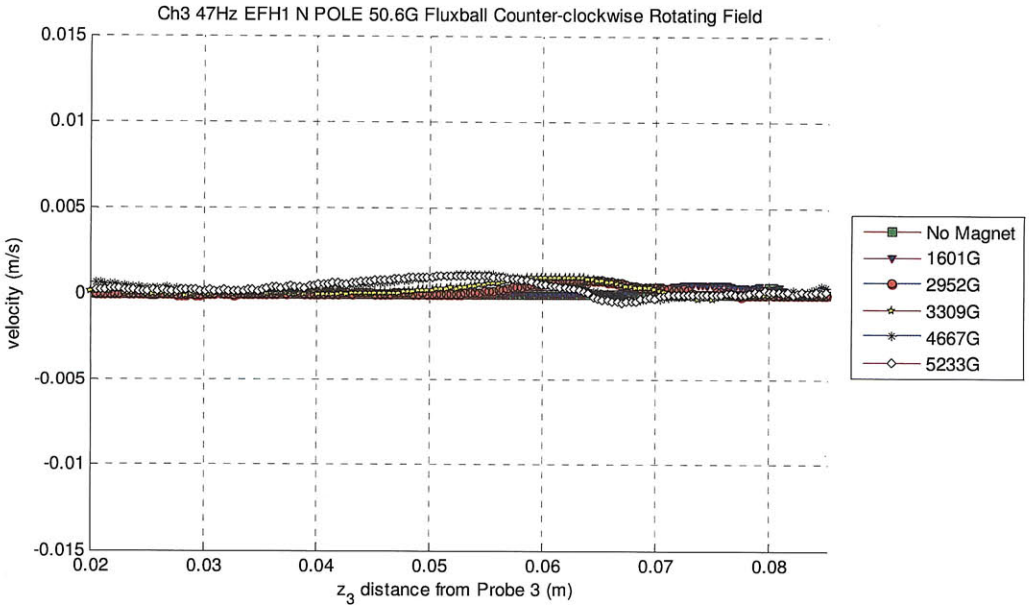
Ch3 47Hz EFH1 N POLE 50.6G Fluxball Counter-clockwise Rotating Field
0.015
0.01
0.005
0
-0.005
-0.01
-0.015
velocity (m/s)
0.02
0.03
0.04
0.05
0.06
0.07
0.08
z3 distance from Probe 3 (m)
No Magnet
1601G
2952G
3309G
4667G
5233G

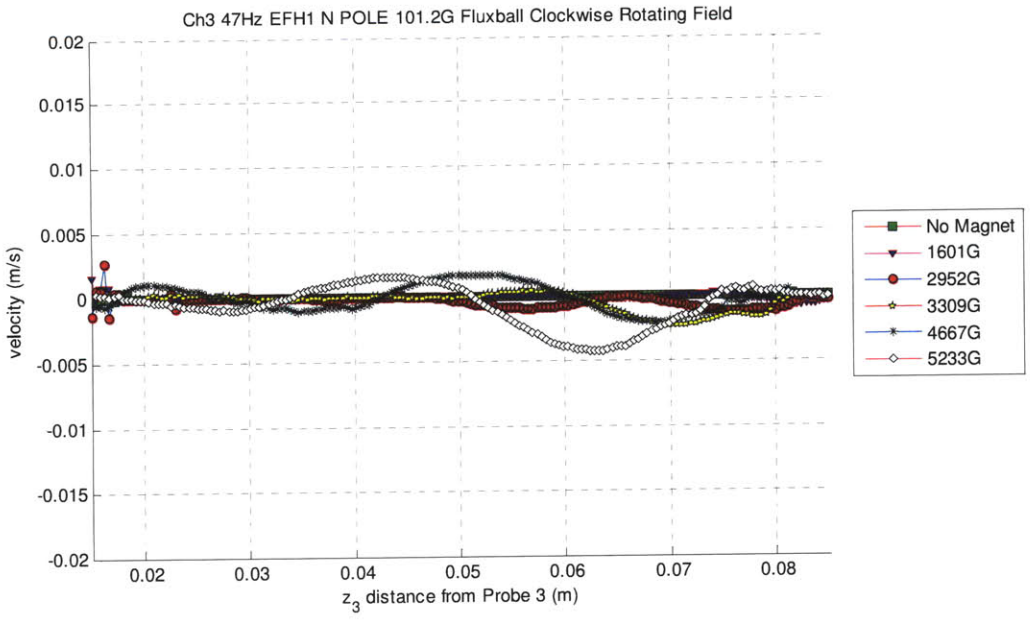
Ch3 47Hz EFH1 N POLE 101.2G Fluxball Clockwise Rotating Field
velocity (m/s)
0.02
0.015
0.01
0.005
0
-0.005
-0.01
-0.015
-0.02
0.02
0.03
0.04
0.05
0.06
0.07
0.08
z_3 distance from Probe 3 (m)
No Magnet
1601G
2952G
3309G
4667G
5233G

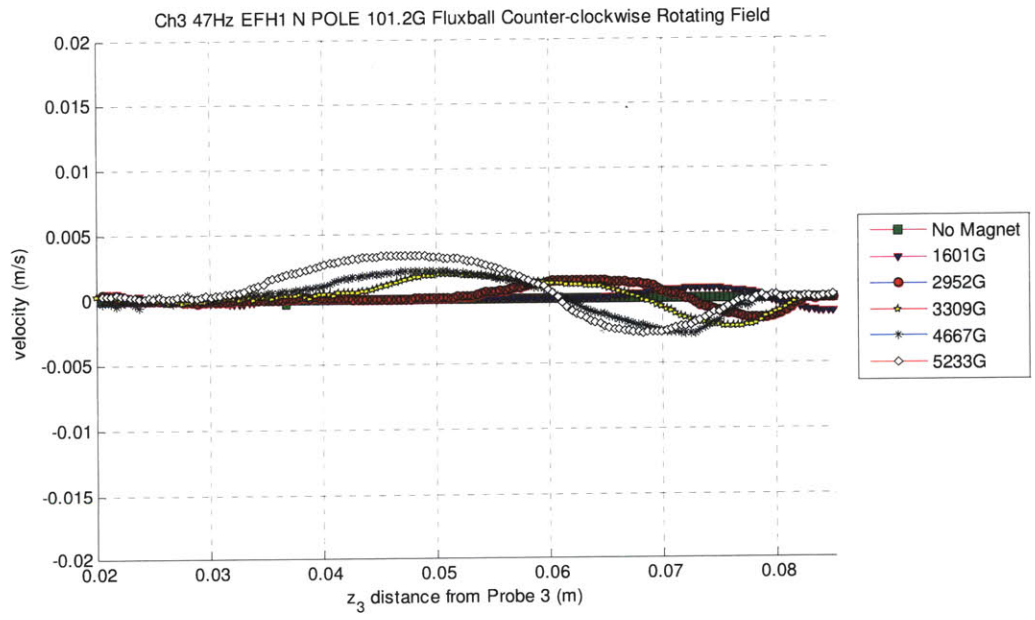
Ch3 47Hz EFH1 N POLE 101.2G Fluxball Counter-clockwise Rotating Field
velocity (m/s)
0.02
0.015
0.01
0.005
0
-0.005
-0.01
-0.015
-0.02
0.02
0.03
0.04
0.05
0.06
0.07
0.08
z_3 distance from Probe 3 (m)
No Magnet
1601G
2952G
3309G
4667G
5233G

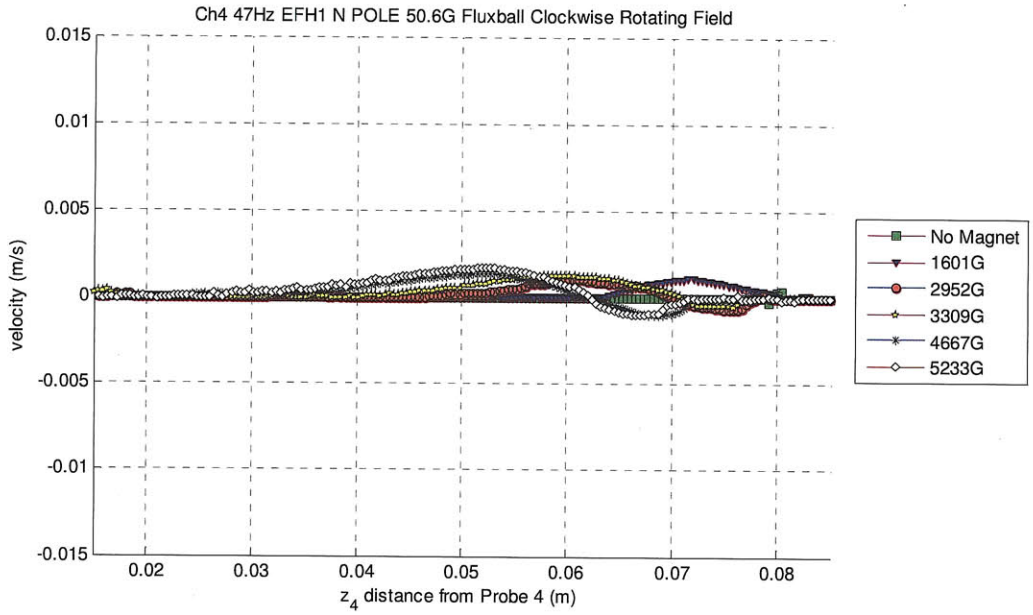
Ch4 47Hz EFH1 N POLE 50.6G Fluxball Clockwise Rotating Field
0.015
0.01
0.005
0
-0.005
-0.01
-0.015
velocity (m/s)
0.02
0.03
0.04
0.05
0.06
0.07
0.08
z4 distance from Probe 4 (m)
No Magnet
1601G
2952G
3309G
4667G
5233G

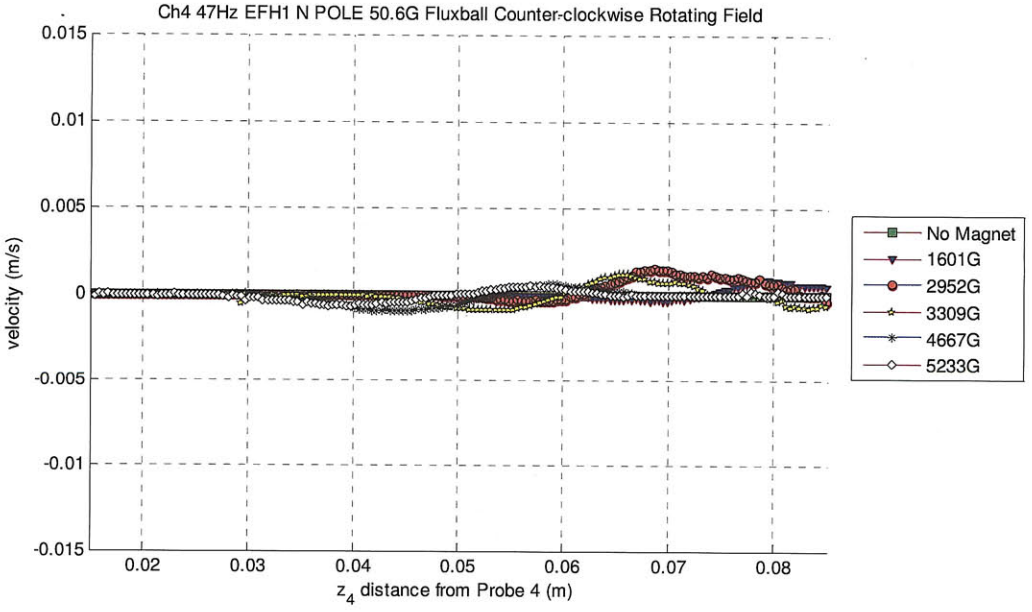
Ch4 47Hz EFH1 N POLE 50.6G Fluxball Counter-clockwise Rotating Field
0.015
0.01
0.005
0
-0.005
-0.01
-0.015
velocity (m/s)
0.02
0.03
0.04
0.05
0.06
0.07
0.08
z4 distance from Probe 4 (m)
No Magnet
1601G
2952G
3309G
4667G
5233G

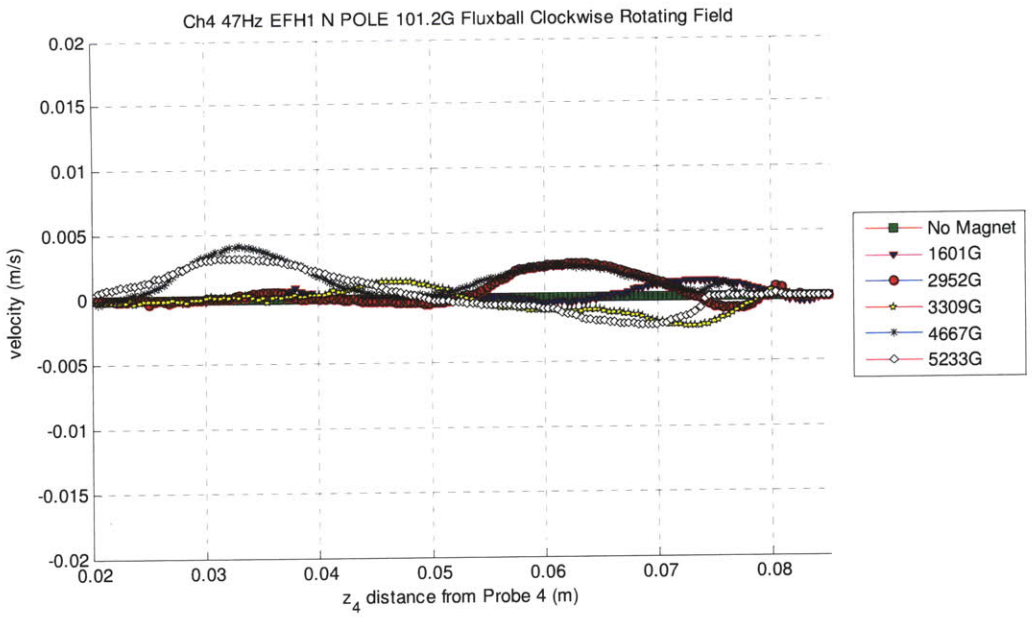
Ch4 47Hz EFH1 N POLE 101.2G Fluxball Clockwise Rotating Field
velocity (m/s)
0.02
0.015
0.01
0.005
0
-0.005
-0.01
-0.015
-0.02
0.02
0.03
0.04
0.05
0.06
0.07
0.08
z4 distance from Probe 4 (m)
No Magnet
1601G
2952G
3309G
4667G
5233G

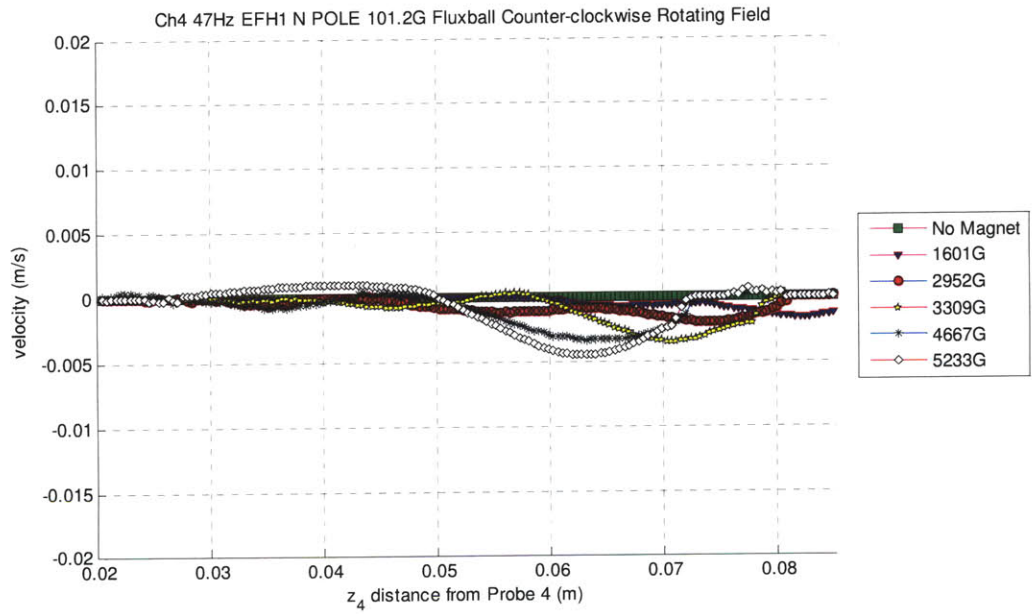
Ch4 47Hz EFH1 N POLE 101.2G Fluxball Counter-clockwise Rotating Field
velocity (m/s)
0.02
0.015
0.01
0.005
0
-0.005
-0.01
-0.015
-0.02
0.02
0.03
0.04
0.05
0.06
0.07
0.08
z4 distance from Probe 4 (m)
No Magnet
1601G
2952G
3309G
4667G
5233G

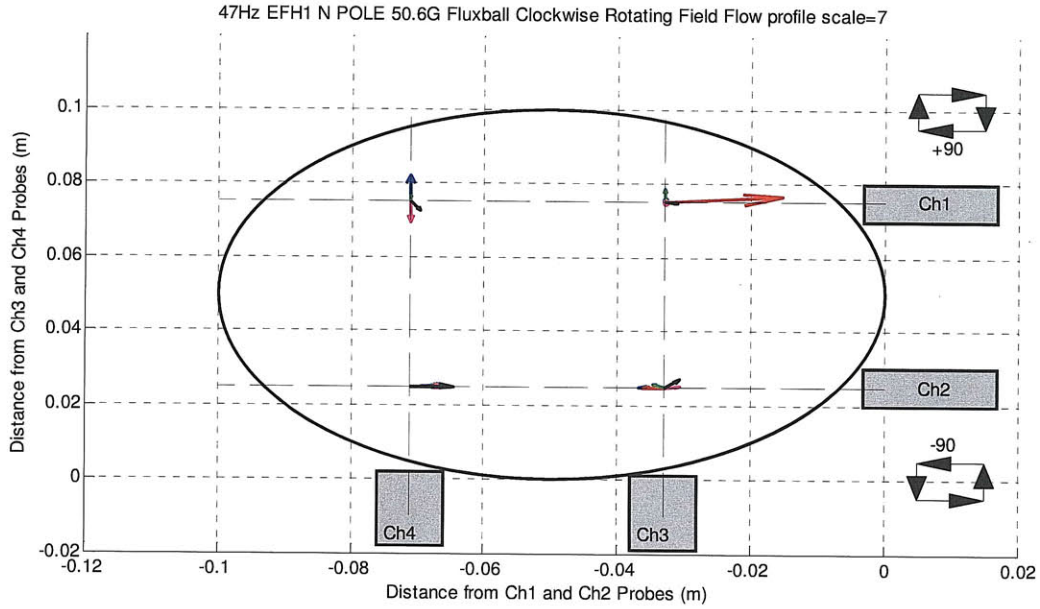
47Hz EFH1 N POLE 50.6G Fluxball Clockwise Rotating Field Flow profile scale=7
Distance from Ch3 and Ch4 Probes (m)
Distance from Ch1 and Ch2 Probes (m)
0.1
0.08
0.06
0.04
0.02
0
-0.02
-0.12
-0.1
-0.08
-0.06
-0.04
-0.02
0
0.02
+90
-90
Ch1
Ch2
Ch3
Ch4

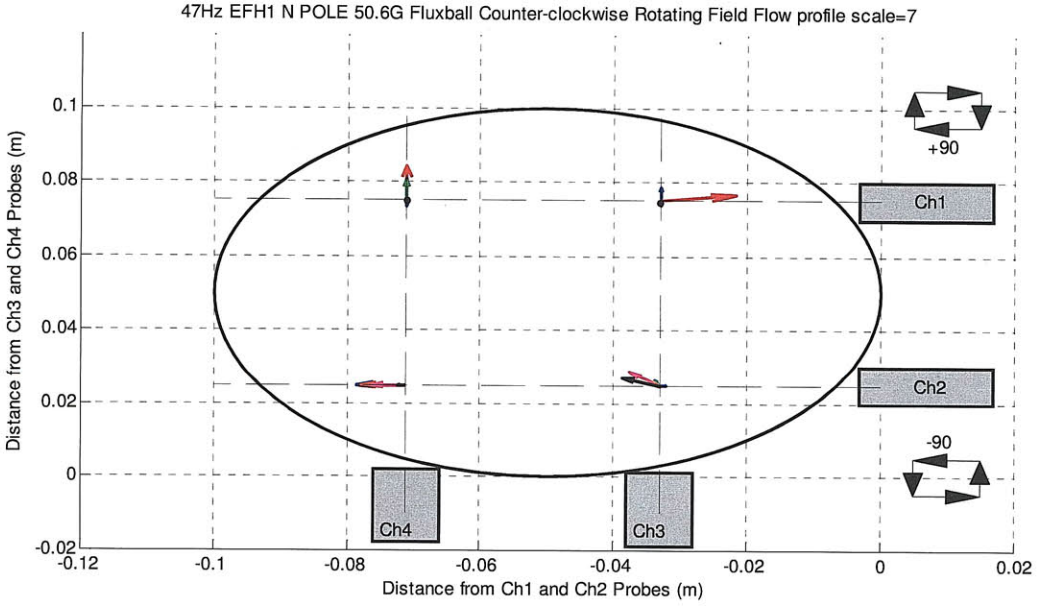
47Hz EFH1 N POLE 50.6G Fluxball Counter-clockwise Rotating Field Flow profile scale=7
Distance from Ch3 and Ch4 Probes (m)
Distance from Ch1 and Ch2 Probes (m)
0.1
0.08
0.06
0.04
0.02
0
-0.02
-0.12
-0.1
-0.08
-0.06
-0.04
-0.02
0
0.02
+90
-90
Ch1
Ch2
Ch3
Ch4

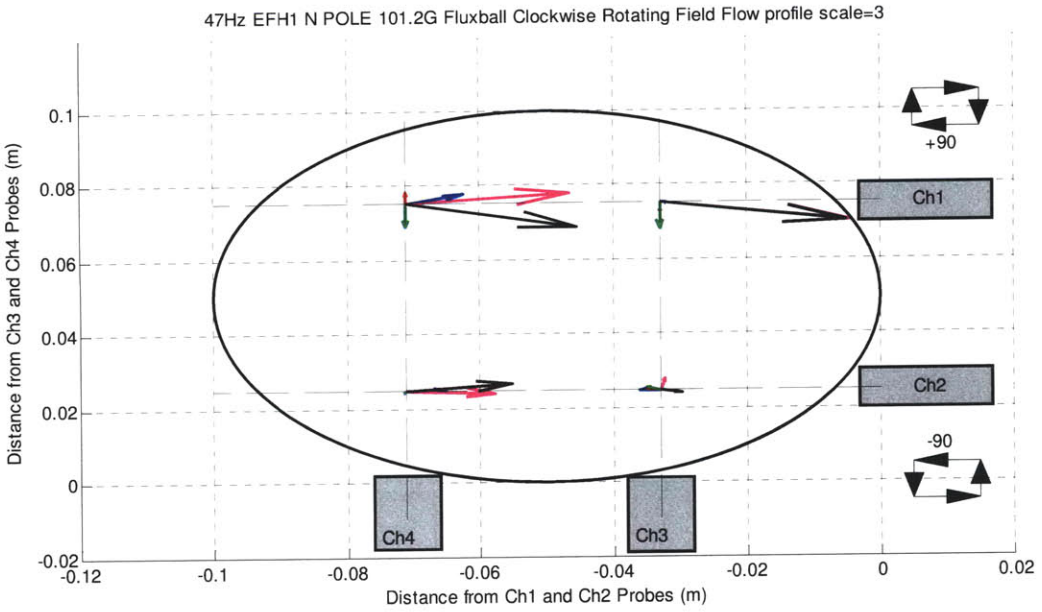
47Hz EFH1 N POLE 101.2G Fluxball Clockwise Rotating Field Flow profile scale=3
Distance from Ch3 and Ch4 Probes (m)
Distance from Ch1 and Ch2 Probes (m)
+90
-90
Ch1
Ch2
Ch3
Ch4
0.1
0.08
0.06
0.04
0.02
0
-0.02
-0.12
-0.1
-0.08
-0.06
-0.04
-0.02
0
0.02

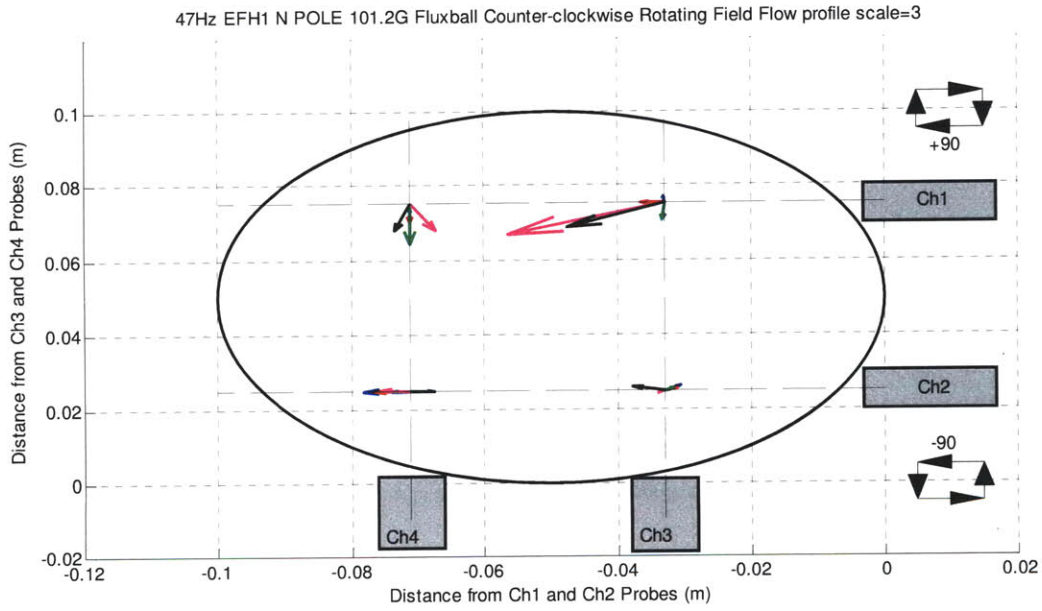
47Hz EFH1 N POLE 101.2G Fluxball Counter-clockwise Rotating Field Flow profile scale=3
Distance from Ch3 and Ch4 Probes (m)
Distance from Ch1 and Ch2 Probes (m)
+90
-90
Ch1
Ch2
Ch3
Ch4
0.1
0.08
0.06
0.04
0.02
0
-0.02
-0.12
-0.1
-0.08
-0.06
-0.04
-0.02
0
0.02

H6. EFH1 Filled Sphere with North Pole Facing Magnets on Top of Sphere at 15Hz

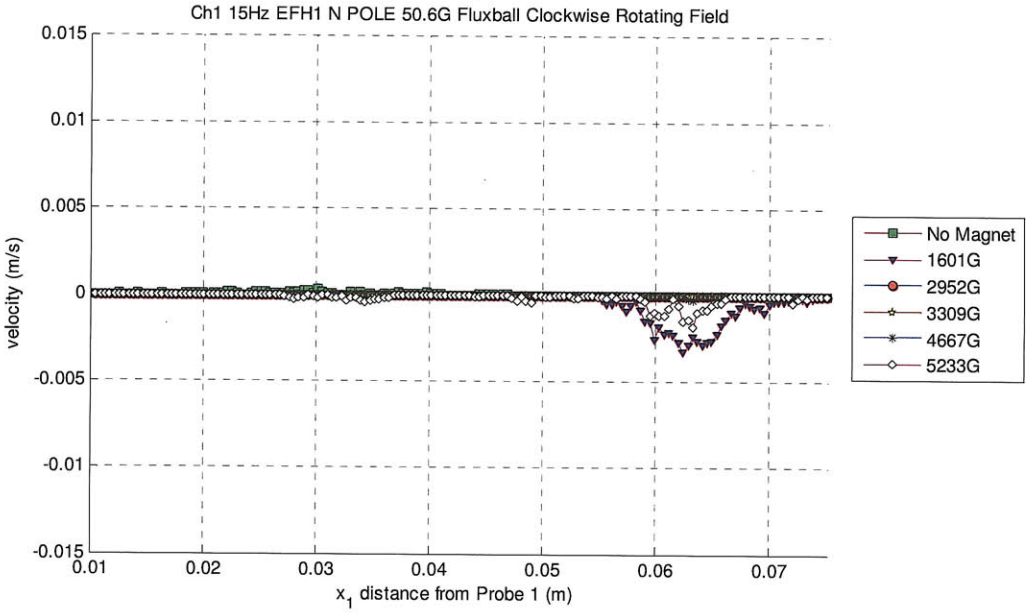

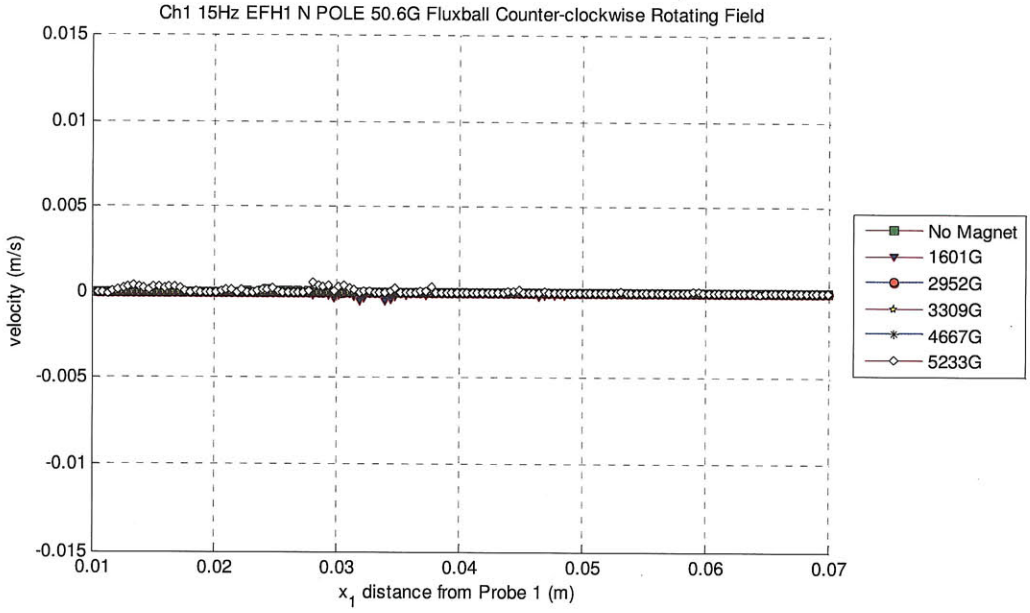

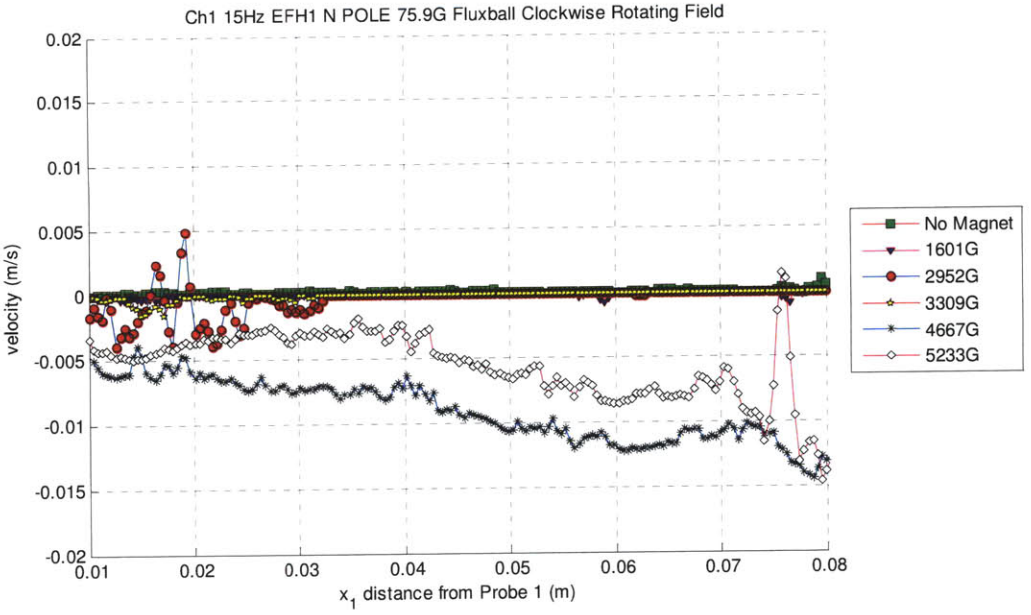
Ch1 15Hz EFH1 N POLE 75.9G Fluxball Clockwise Rotating Field
velocity (m/s)
0.02
0.015
0.01
0.005
0
-0.005
-0.01
-0.015
-0.02
0.01
0.02
0.03
0.04
0.05
0.06
0.07
0.08
x1 distance from Probe 1 (m)
No Magnet
1601G
2952G
3309G
4667G
5233G

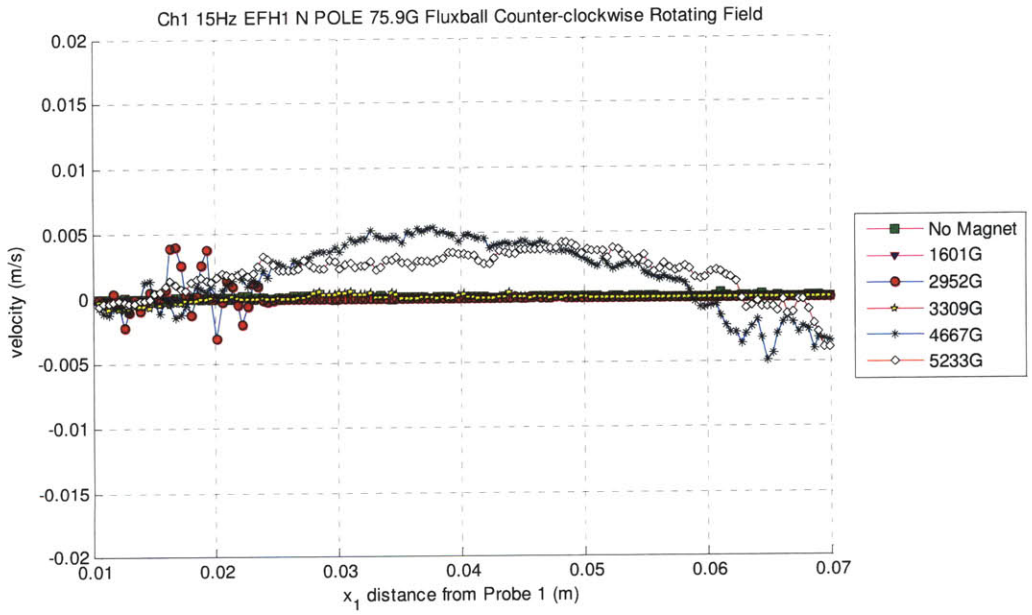
Ch1 15Hz EFH1 N POLE 75.9G Fluxball Counter-clockwise Rotating Field
velocity (m/s)
0.02
0.015
0.01
0.005
0
-0.005
-0.01
-0.015
-0.02
0.01
0.02
0.03
0.04
0.05
0.06
0.07
x1 distance from Probe 1 (m)
No Magnet
1601G
2952G
3309G
4667G
5233G

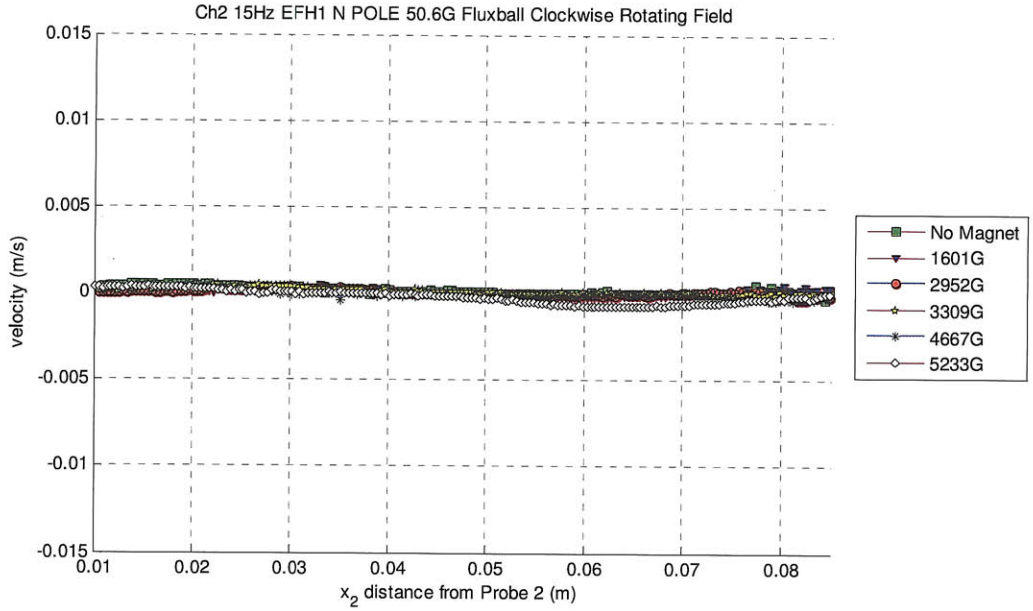
Ch2 15Hz EFH1 N POLE 50.6G Fluxball Clockwise Rotating Field
velocity (m/s)
0.015
0.01
0.005
0
-0.005
-0.01
-0.015
0.01
0.02
0.03
0.04
0.05
0.06
0.07
0.08
x2 distance from Probe 2 (m)
No Magnet
1601G
2952G
3309G
4667G
5233G

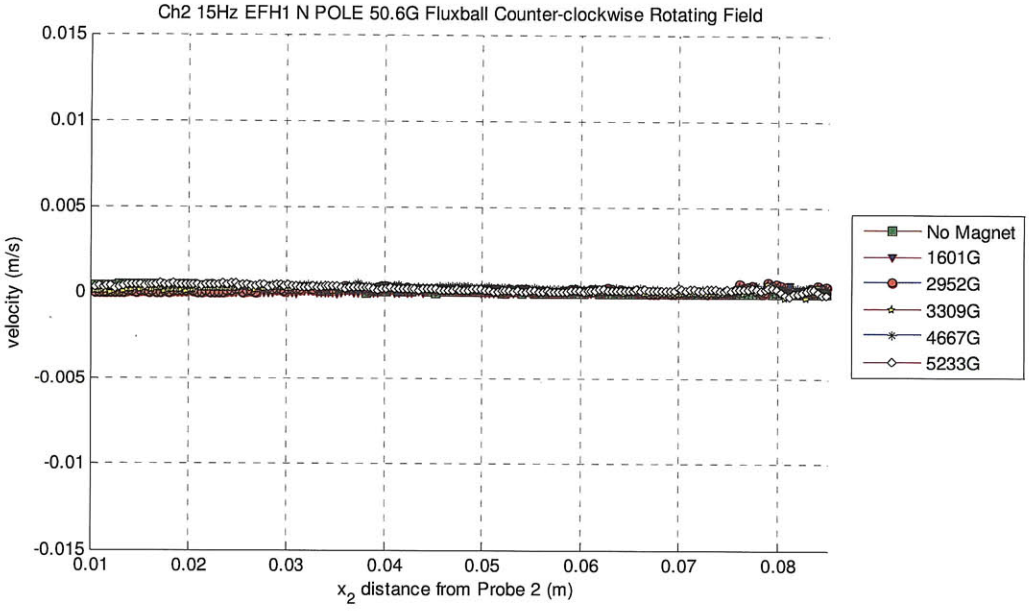
Ch2 15Hz EFH1 N POLE 50.6G Fluxball Counter-clockwise Rotating Field
velocity (m/s)
0.015
0.01
0.005
0
-0.005
-0.01
-0.015
0.01
0.02
0.03
0.04
0.05
0.06
0.07
0.08
x2 distance from Probe 2 (m)
No Magnet
1601G
2952G
3309G
4667G
5233G

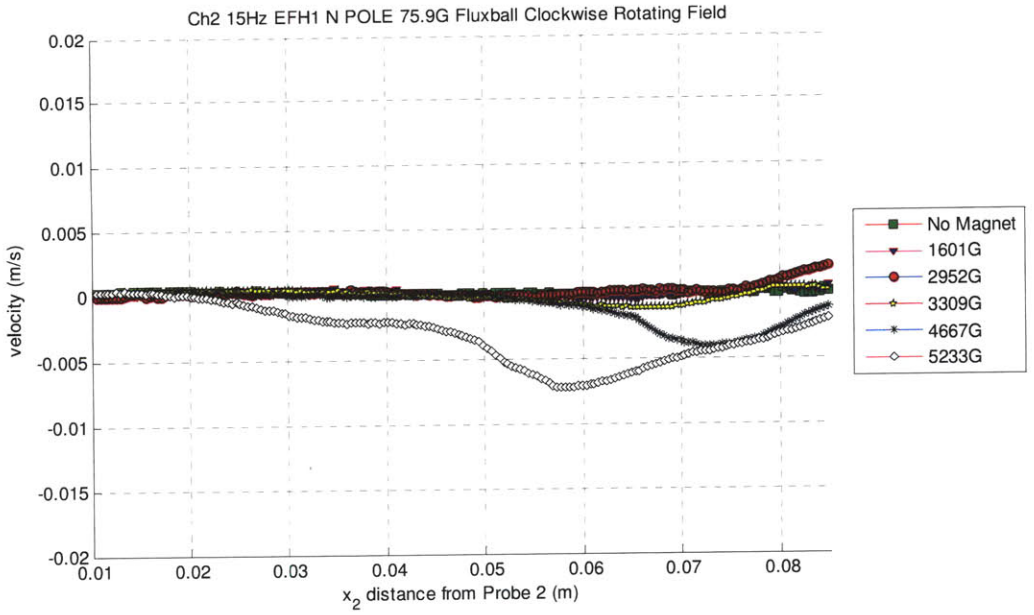
Ch2 15Hz EFH1 N POLE 75.9G Fluxball Clockwise Rotating Field
velocity (m/s)
0.02
0.015
0.01
0.005
0
-0.005
-0.01
-0.015
-0.02
0.01
0.02
0.03
0.04
0.05
0.06
0.07
0.08
x2 distance from Probe 2 (m)
No Magnet
1601G
2952G
3309G
4667G
5233G

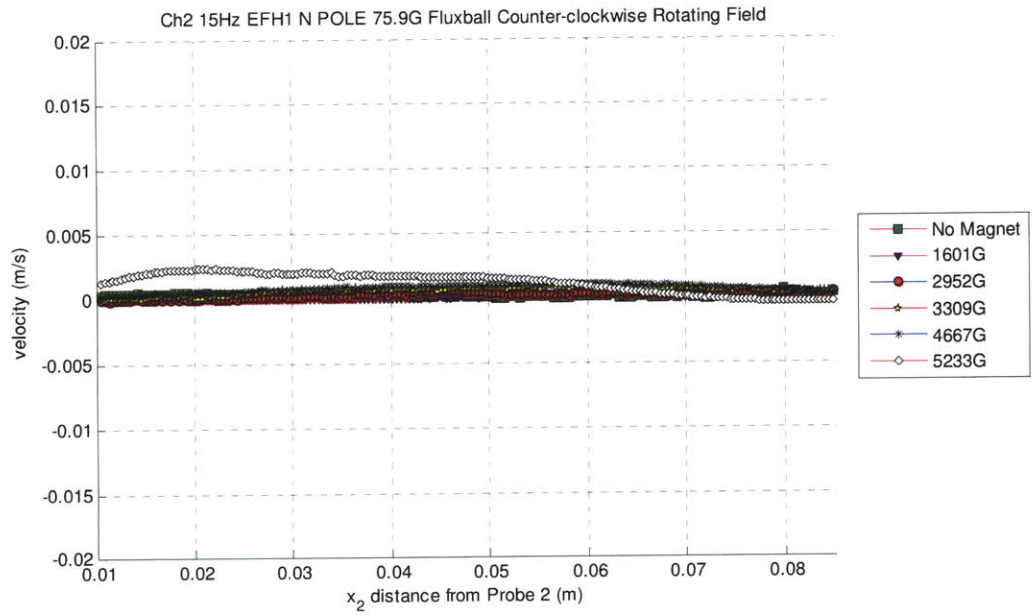
Ch2 15Hz EFH1 N POLE 75.9G Fluxball Counter-clockwise Rotating Field
velocity (m/s)
0.02
0.015
0.01
0.005
0
-0.005
-0.01
-0.015
-0.02
0.01
0.02
0.03
0.04
0.05
0.06
0.07
0.08
x2 distance from Probe 2 (m)
No Magnet
1601G
2952G
3309G
4667G
5233G

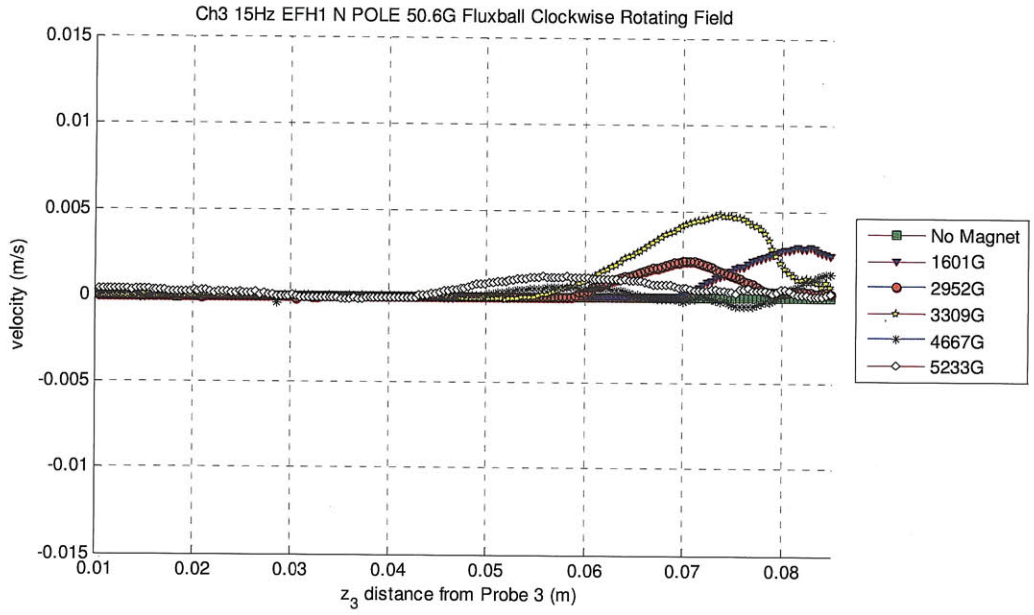
Ch3 15Hz EFH1 N POLE 50.6G Fluxball Clockwise Rotating Field
velocity (m/s)
0.015
0.01
0.005
0
-0.005
-0.01
-0.015
0.01
0.02
0.03
0.04
0.05
0.06
0.07
0.08
z_3 distance from Probe 3 (m)
No Magnet
1601G
2952G
3309G
4667G
5233G

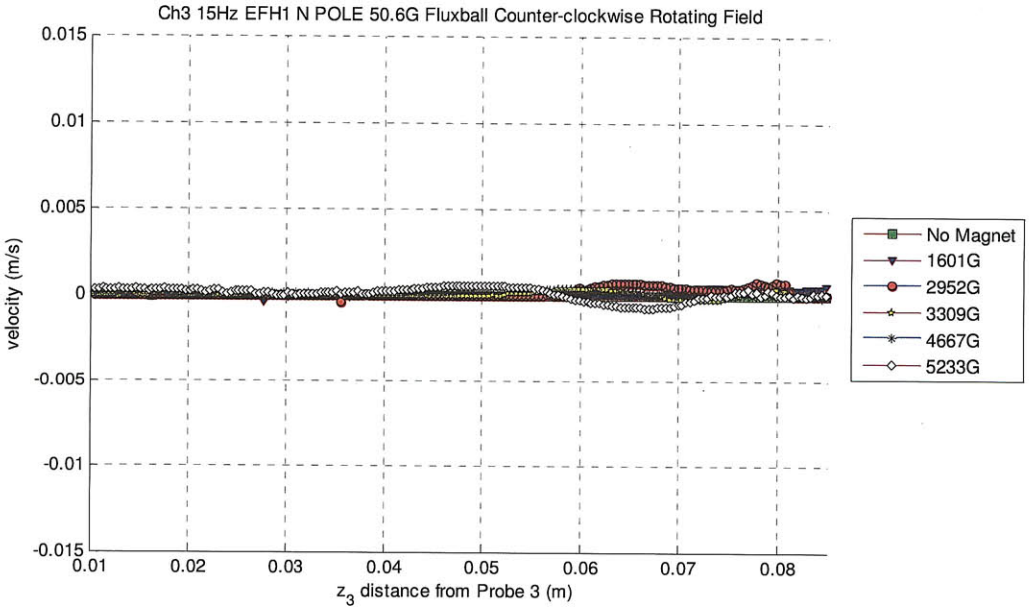
Ch3 15Hz EFH1 N POLE 50.6G Fluxball Counter-clockwise Rotating Field
velocity (m/s)
0.015
0.01
0.005
0
-0.005
-0.01
-0.015
0.01
0.02
0.03
0.04
0.05
0.06
0.07
0.08
z_3 distance from Probe 3 (m)
No Magnet
1601G
2952G
3309G
4667G
5233G

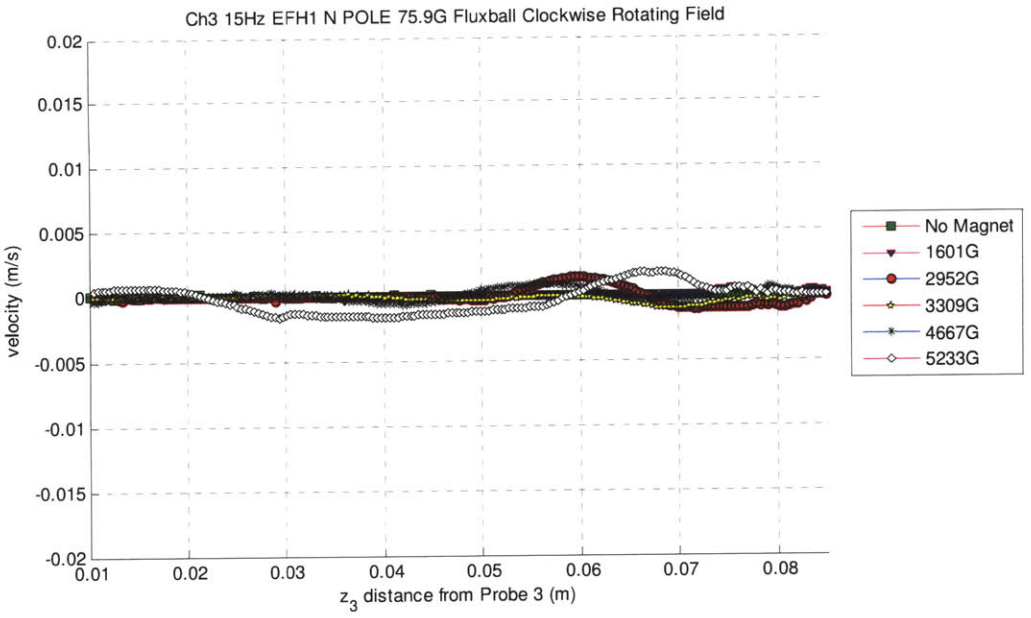
Ch3 15Hz EFH1 N POLE 75.9G Fluxball Clockwise Rotating Field
velocity (m/s)
0.02
0.015
0.01
0.005
0
-0.005
-0.01
-0.015
-0.02
0.01
0.02
0.03
0.04
0.05
0.06
0.07
0.08
z_3 distance from Probe 3 (m)
No Magnet
1601G
2952G
3309G
4667G
5233G

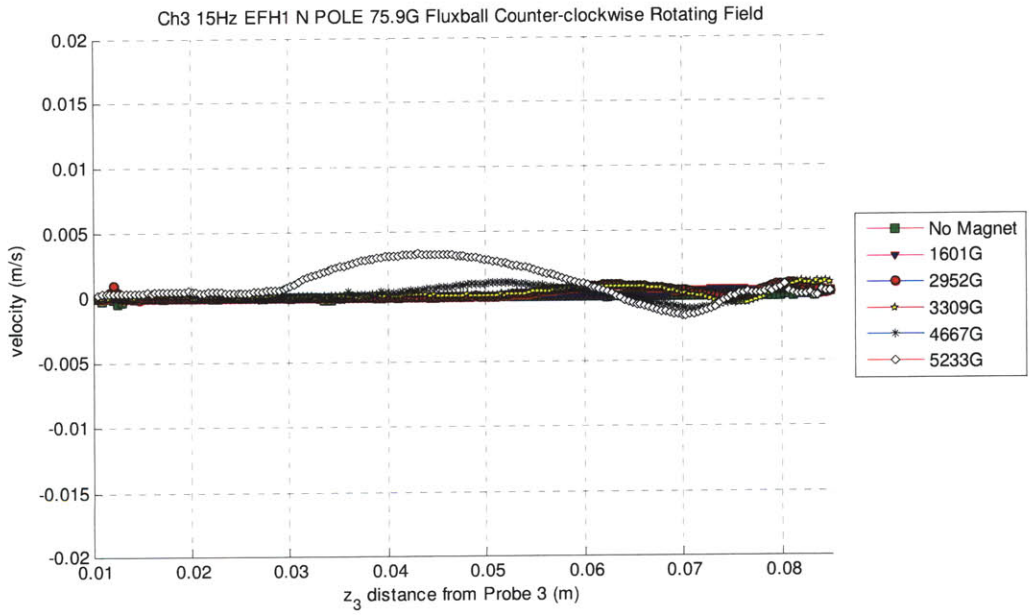
Ch3 15Hz EFH1 N POLE 75.9G Fluxball Counter-clockwise Rotating Field
velocity (m/s)
0.02
0.015
0.01
0.005
0
-0.005
-0.01
-0.015
-0.02
0.01
0.02
0.03
0.04
0.05
0.06
0.07
0.08
z_3 distance from Probe 3 (m)
No Magnet
1601G
2952G
3309G
4667G
5233G

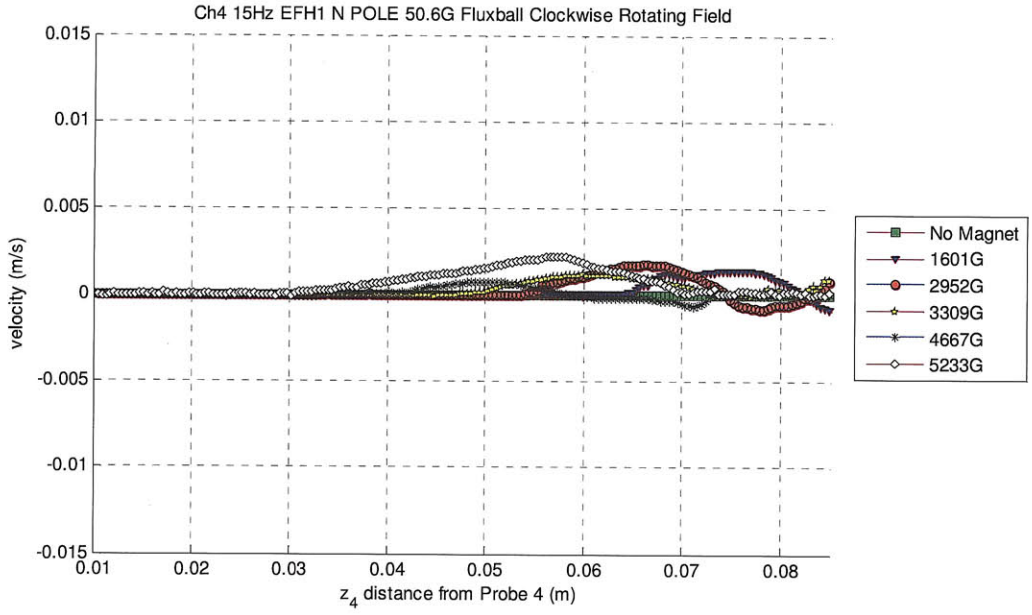
Ch4 15Hz EFH1 N POLE 50.6G Fluxball Clockwise Rotating Field
velocity (m/s)
0.015
0.01
0.005
0
-0.005
-0.01
-0.015
0.01
0.02
0.03
0.04
0.05
0.06
0.07
0.08
z4 distance from Probe 4 (m)
No Magnet
1601G
2952G
3309G
4667G
5233G

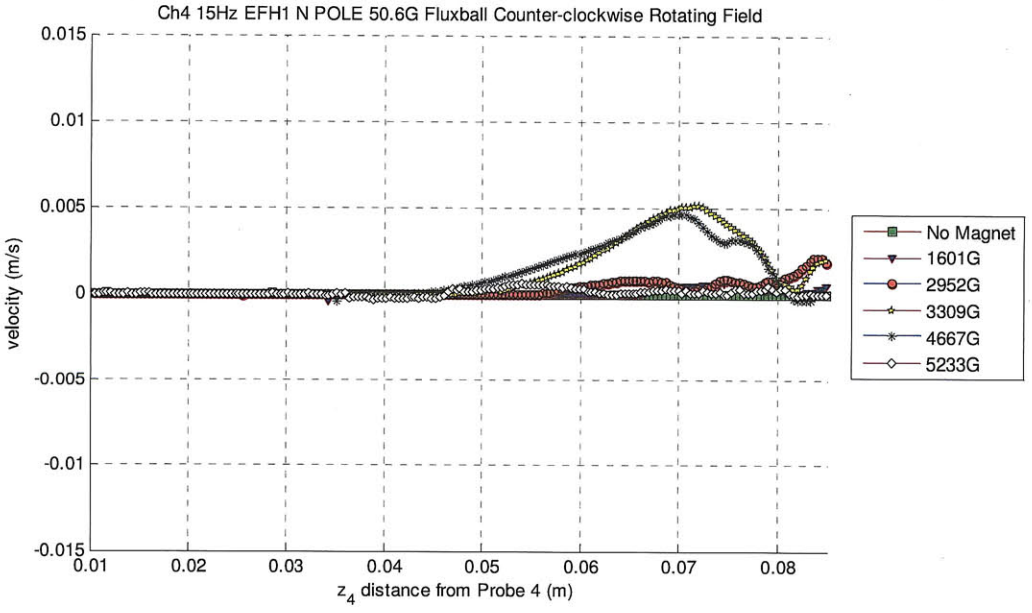
Ch4 15Hz EFH1 N POLE 50.6G Fluxball Counter-clockwise Rotating Field
velocity (m/s)
0.015
0.01
0.005
0
-0.005
-0.01
-0.015
0.01
0.02
0.03
0.04
0.05
0.06
0.07
0.08
z4 distance from Probe 4 (m)
No Magnet
1601G
2952G
3309G
4667G
5233G

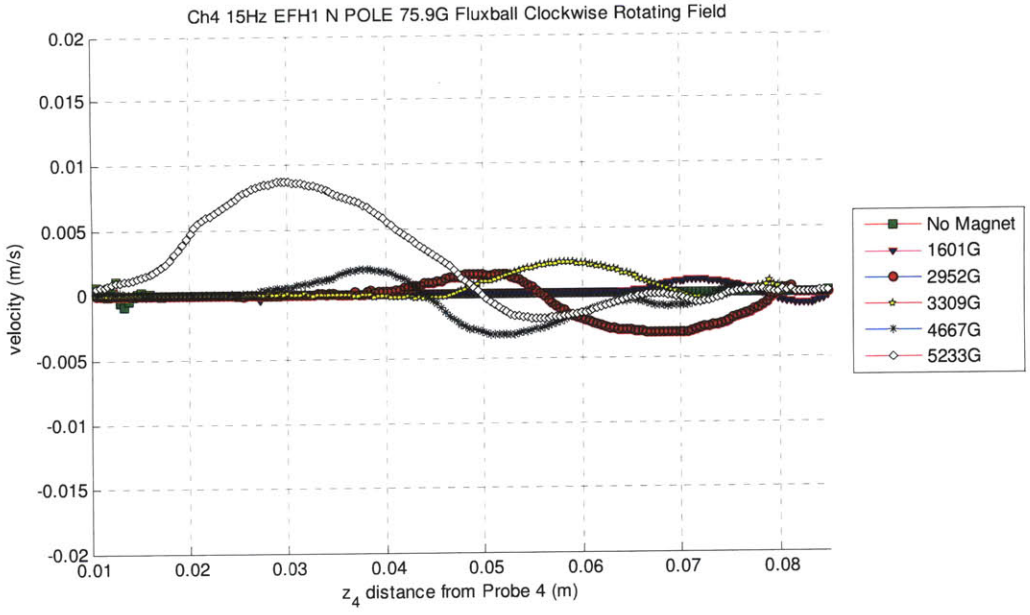
Ch4 15Hz EFH1 N POLE 75.9G Fluxball Clockwise Rotating Field
velocity (m/s)
0.02
0.015
0.01
0.005
0
-0.005
-0.01
-0.015
-0.02
0.01
0.02
0.03
0.04
0.05
0.06
0.07
0.08
z4 distance from Probe 4 (m)
No Magnet
1601G
2952G
3309G
4667G
5233G

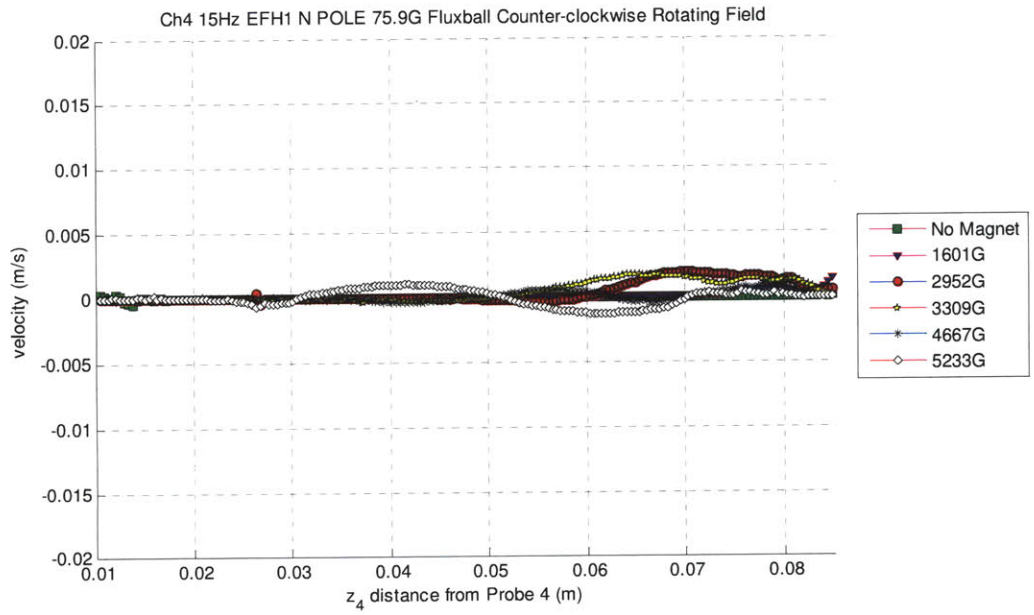
Ch4 15Hz EFH1 N POLE 75.9G Fluxball Counter-clockwise Rotating Field
velocity (m/s)
0.02
0.015
0.01
0.005
0
-0.005
-0.01
-0.015
-0.02
0.01
0.02
0.03
0.04
0.05
0.06
0.07
0.08
z4 distance from Probe 4 (m)
No Magnet
1601G
2952G
3309G
4667G
5233G

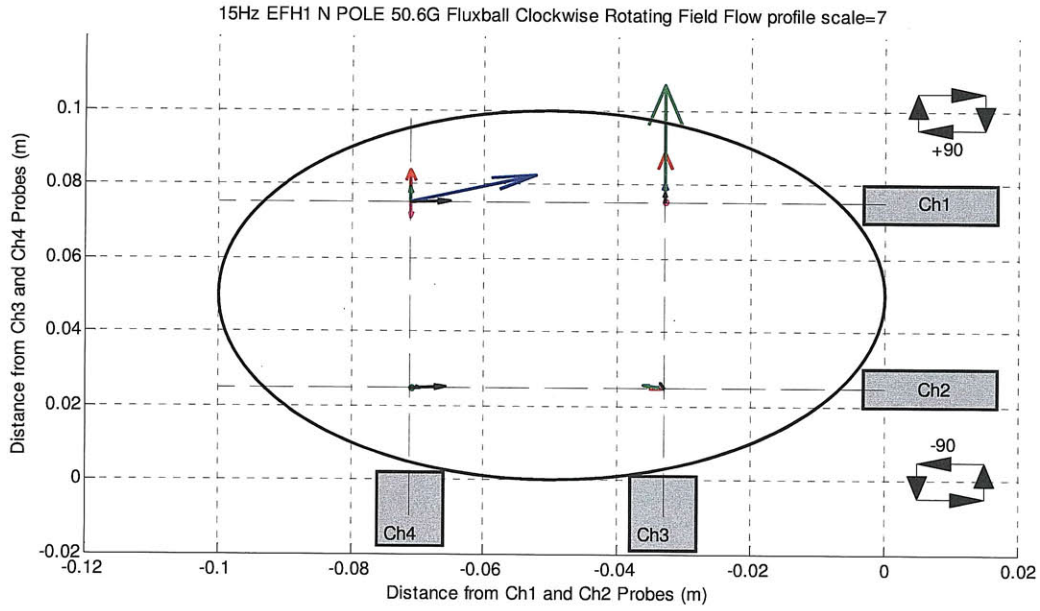
15Hz EFH1 N POLE 50.6G Fluxball Clockwise Rotating Field Flow profile scale=7
Distance from Ch3 and Ch4 Probes (m)
Distance from Ch1 and Ch2 Probes (m)
0.1
0.08
0.06
0.04
0.02
0
-0.02
-0.12
-0.1
-0.08
-0.06
-0.04
-0.02
0
0.02
+90
-90
Ch1
Ch2
Ch3
Ch4

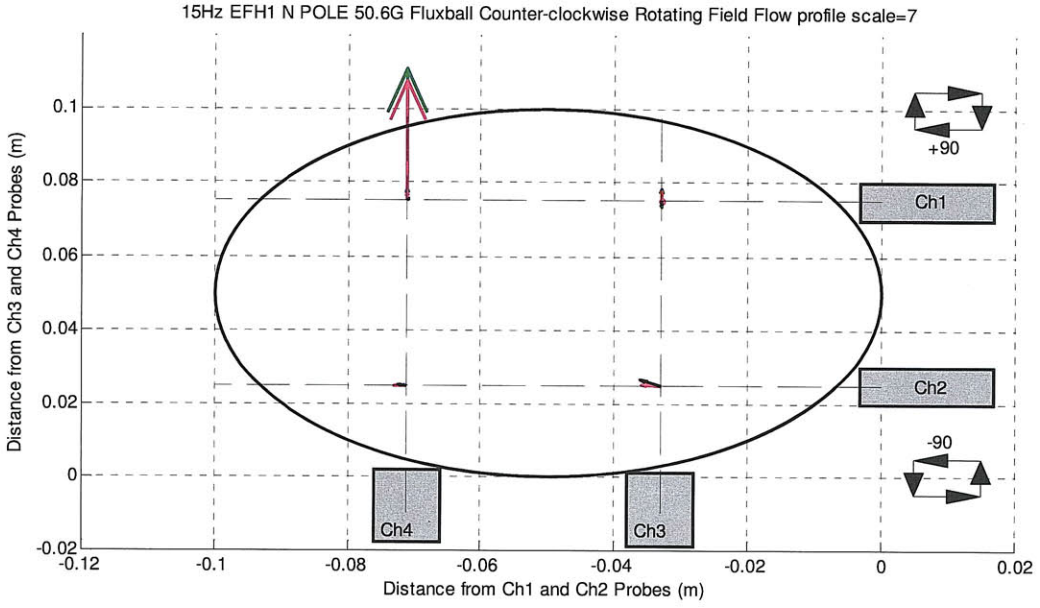
15Hz EFH1 N POLE 50.6G Fluxball Counter-clockwise Rotating Field Flow profile scale=7
Distance from Ch3 and Ch4 Probes (m)
Distance from Ch1 and Ch2 Probes (m)
0.1
0.08
0.06
0.04
0.02
0
-0.02
-0.12
-0.1
-0.08
-0.06
-0.04
-0.02
0
0.02
+90
-90
Ch1
Ch2
Ch3
Ch4

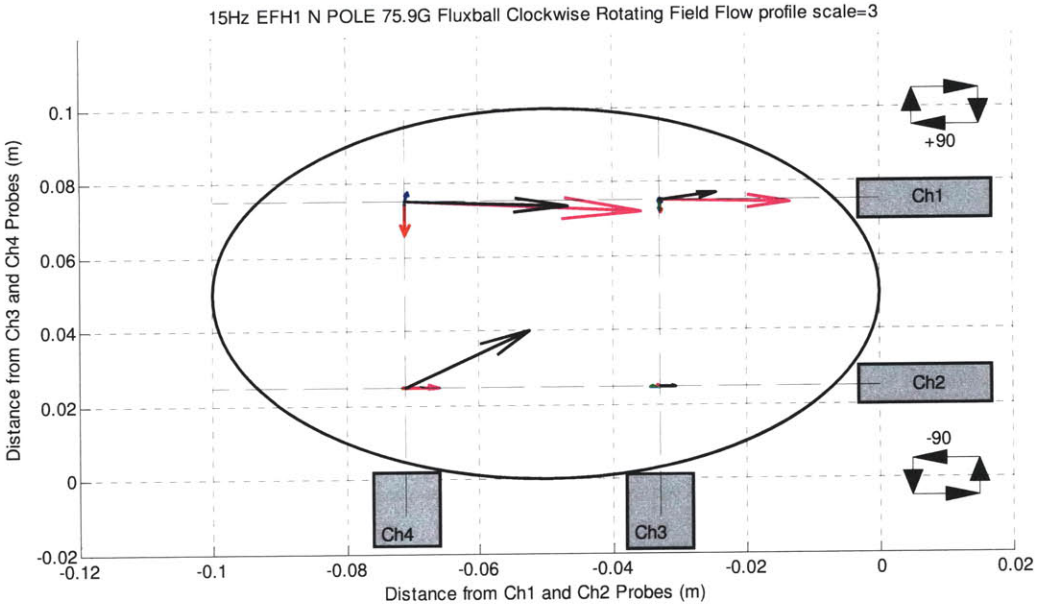
15Hz EFH1 N POLE 75.9G Fluxball Clockwise Rotating Field Flow profile scale=3
Distance from Ch3 and Ch4 Probes (m)
Distance from Ch1 and Ch2 Probes (m)
+90
-90
Ch1
Ch2
Ch3
Ch4
0.1
0.08
0.06
0.04
0.02
0
-0.02
-0.12
-0.1
-0.08
-0.06
-0.04
-0.02
0
0.02

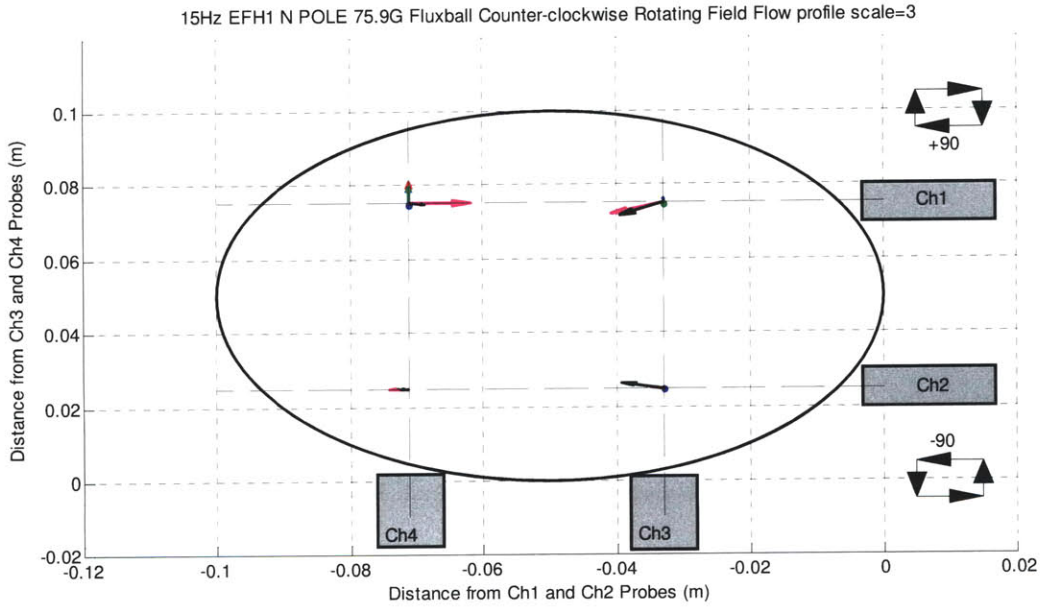
15Hz EFH1 N POLE 75.9G Fluxball Counter-clockwise Rotating Field Flow profile scale=3
Distance from Ch3 and Ch4 Probes (m)
Distance from Ch1 and Ch2 Probes (m)
+90
-90
Ch1
Ch2
Ch3
Ch4
0.1
0.08
0.06
0.04
0.02
0
-0.02
-0.12
-0.1
-0.08
-0.06
-0.04
-0.02
0
0.02

H7. MSGW11 Filled Sphere with South Pole Facing Magnets on Top of Sphere at 95Hz

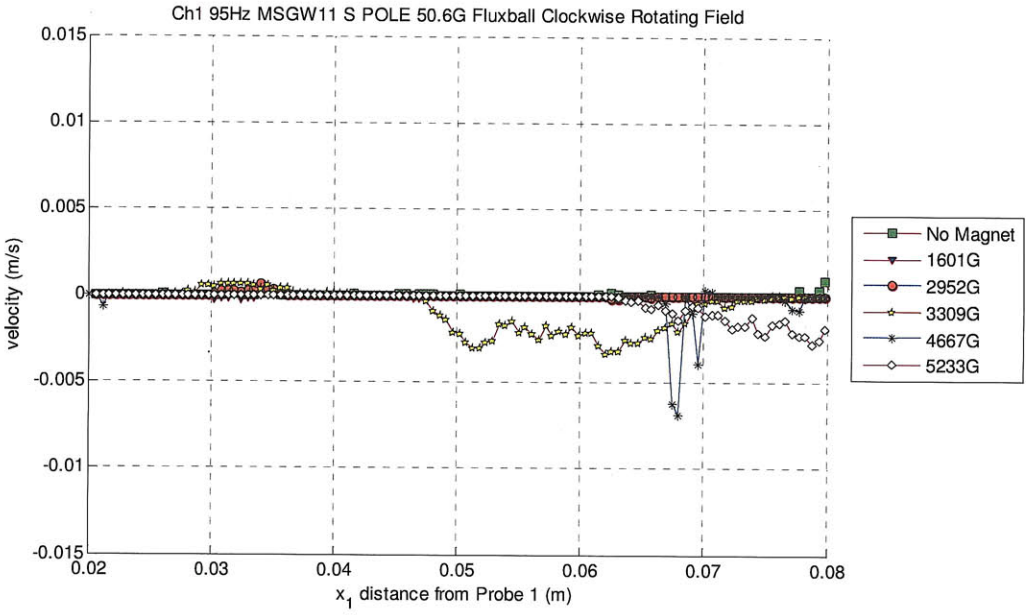

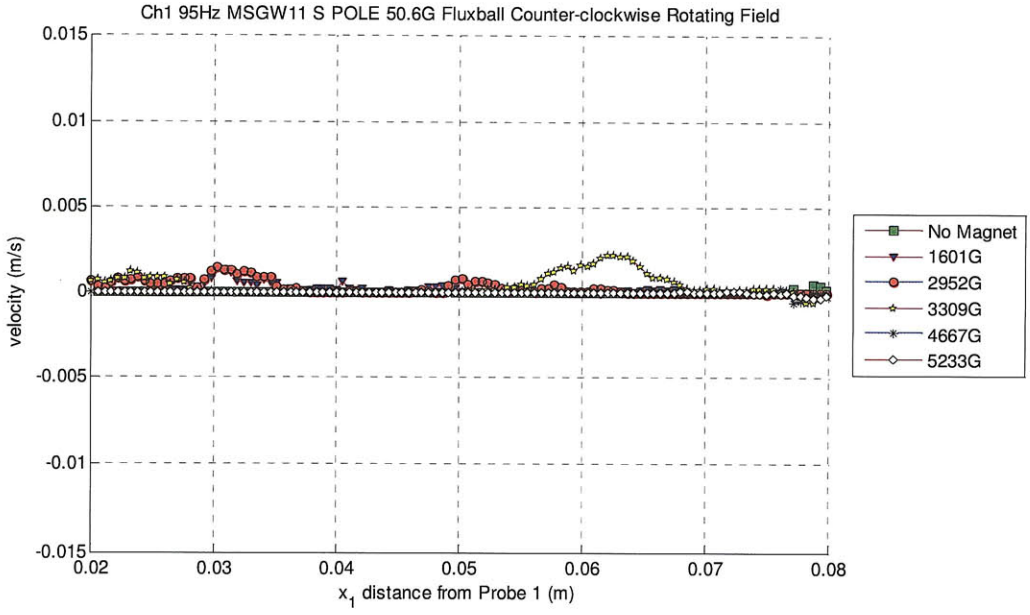

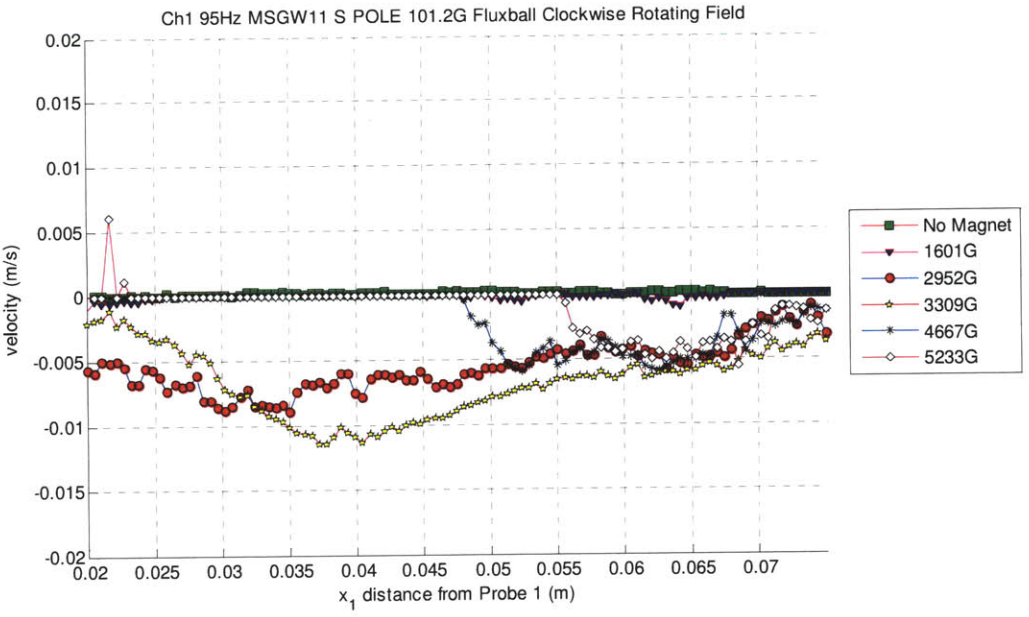
Ch1 95Hz MSGW11 S POLE 101.2G Fluxball Clockwise Rotating Field
velocity (m/s)
0.02
0.015
0.01
0.005
0
-0.005
-0.01
-0.015
-0.02
0.02 0.025 0.03 0.035 0.04 0.045 0.05 0.055 0.06 0.065 0.07
x1 distance from Probe 1 (m)
No Magnet
1601G
2952G
3309G
4667G
5233G

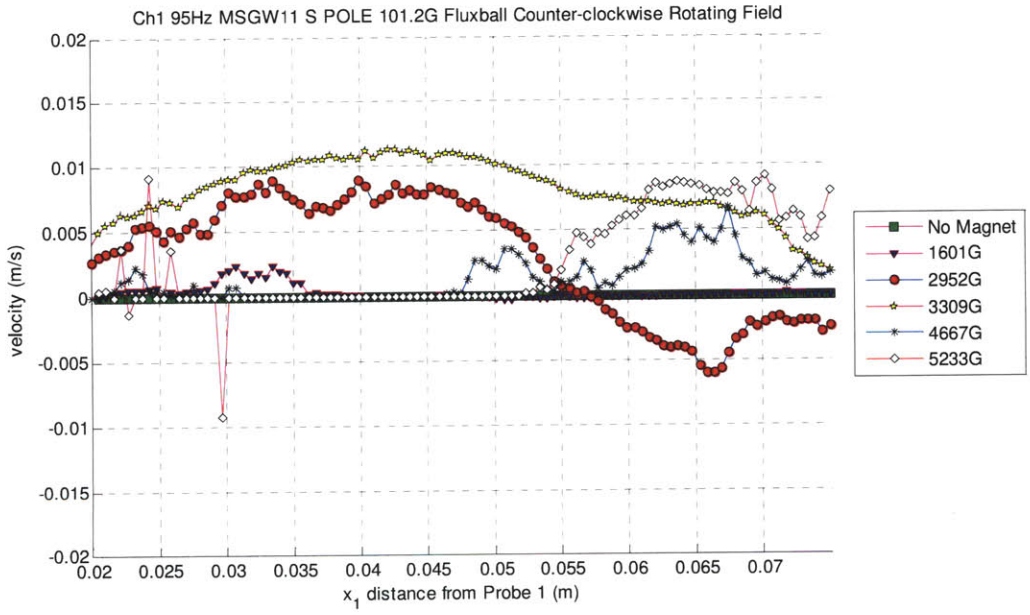
Ch1 95Hz MSGW11 S POLE 101.2G Fluxball Counter-clockwise Rotating Field
velocity (m/s)
0.02
0.015
0.01
0.005
0
-0.005
-0.01
-0.015
-0.02
0.02 0.025 0.03 0.035 0.04 0.045 0.05 0.055 0.06 0.065 0.07
x1 distance from Probe 1 (m)
No Magnet
1601G
2952G
3309G
4667G
5233G

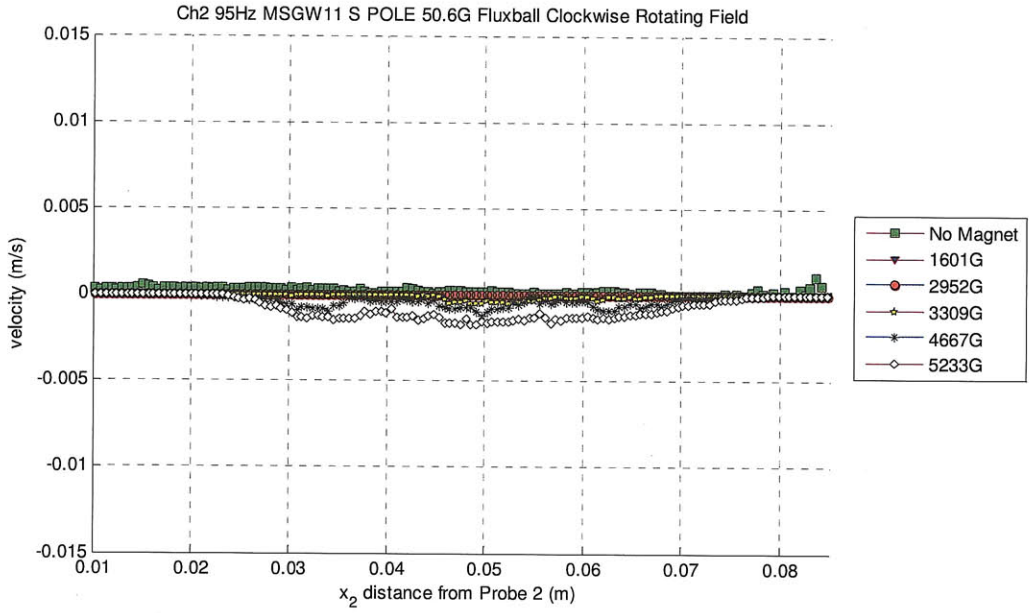
Ch2 95Hz MSGW11 S POLE 50.6G Fluxball Clockwise Rotating Field
velocity (m/s)
0.015
0.01
0.005
0
-0.005
-0.01
-0.015
0.01
0.02
0.03
0.04
0.05
0.06
0.07
0.08
x2 distance from Probe 2 (m)
No Magnet
1601G
2952G
3309G
4667G
5233G

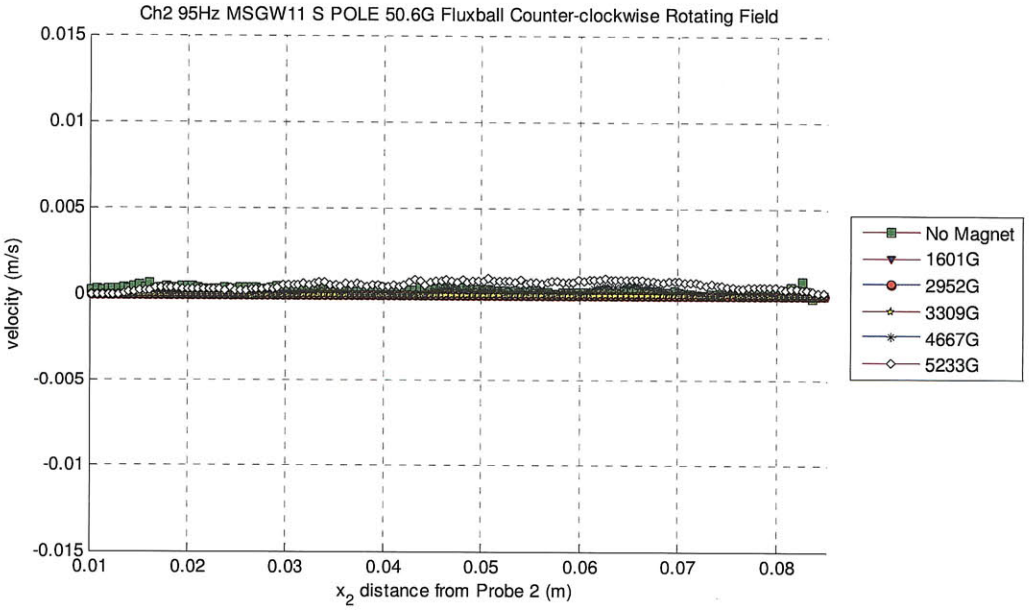
Ch2 95Hz MSGW11 S POLE 50.6G Fluxball Counter-clockwise Rotating Field
velocity (m/s)
0.015
0.01
0.005
0
-0.005
-0.01
-0.015
0.01
0.02
0.03
0.04
0.05
0.06
0.07
0.08
x2 distance from Probe 2 (m)
No Magnet
1601G
2952G
3309G
4667G
5233G

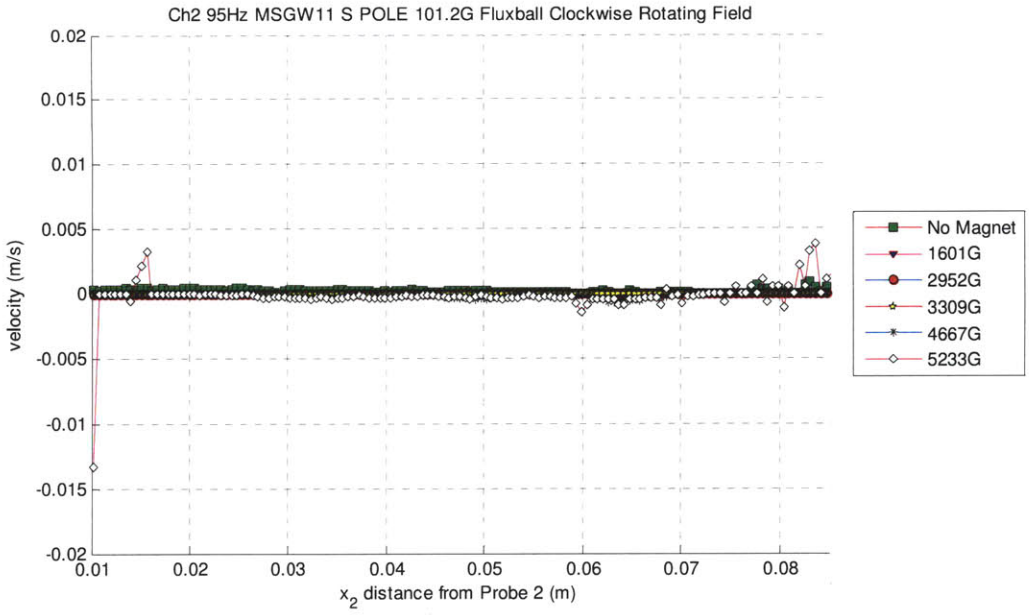
Ch2 95Hz MSGW11 S POLE 101.2G Fluxball Clockwise Rotating Field
velocity (m/s)
0.02
0.015
0.01
0.005
0
-0.005
-0.01
-0.015
-0.02
0.01
0.02
0.03
0.04
0.05
0.06
0.07
0.08
x2 distance from Probe 2 (m)
No Magnet
1601G
2952G
3309G
4667G
5233G

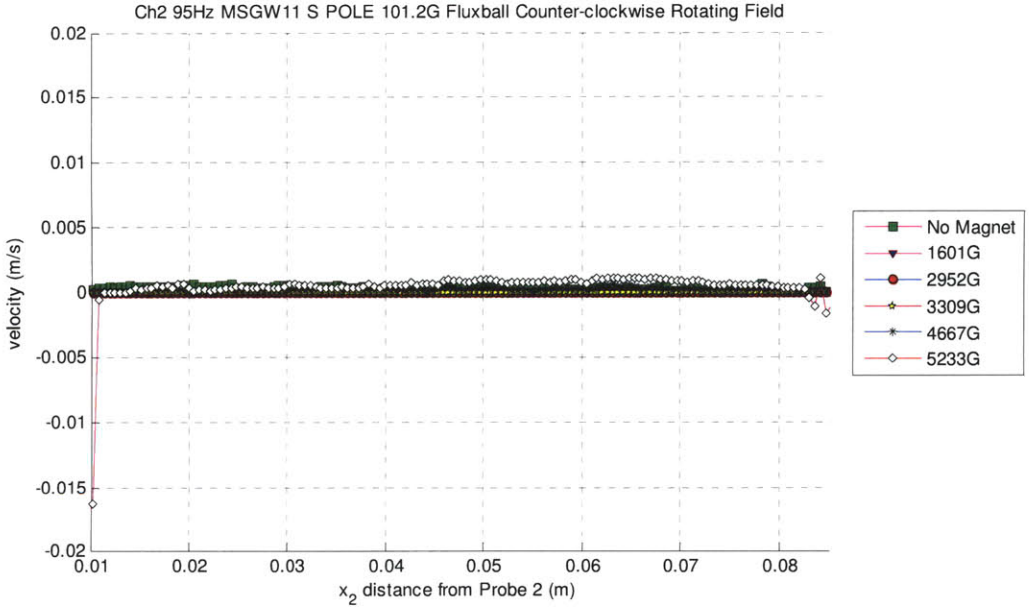
Ch2 95Hz MSGW11 S POLE 101.2G Fluxball Counter-clockwise Rotating Field
velocity (m/s)
0.02
0.015
0.01
0.005
0
-0.005
-0.01
-0.015
-0.02
0.01
0.02
0.03
0.04
0.05
0.06
0.07
0.08
x2 distance from Probe 2 (m)
No Magnet
1601G
2952G
3309G
4667G
5233G

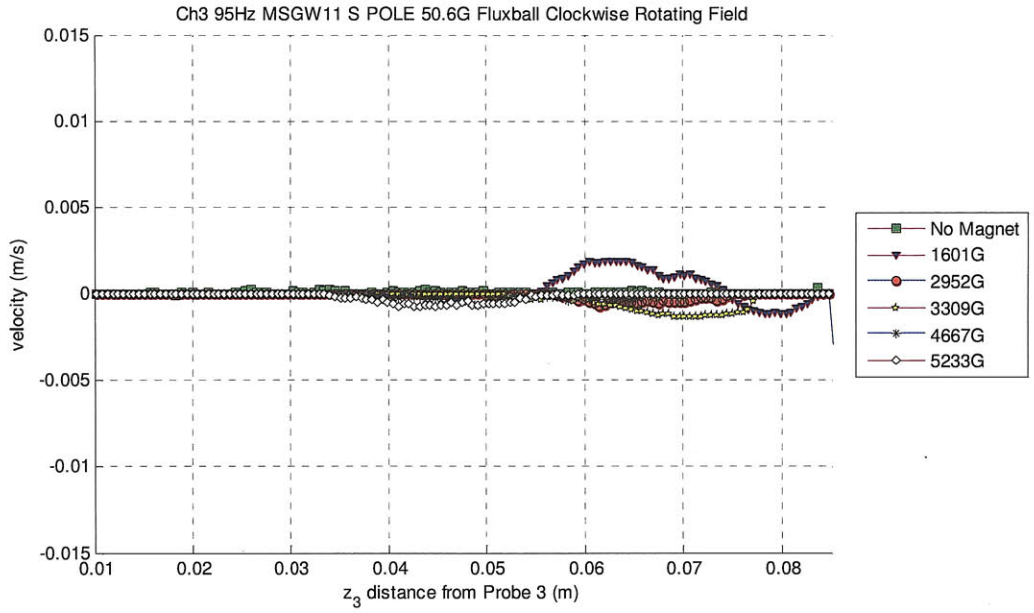
Ch3 95Hz MSGW11 S POLE 50.6G Fluxball Clockwise Rotating Field
velocity (m/s)
0.015
0.01
0.005
0
-0.005
-0.01
-0.015
0.01
0.02
0.03
0.04
0.05
0.06
0.07
0.08
z_3 distance from Probe 3 (m)
No Magnet
1601G
2952G
3309G
4667G
5233G

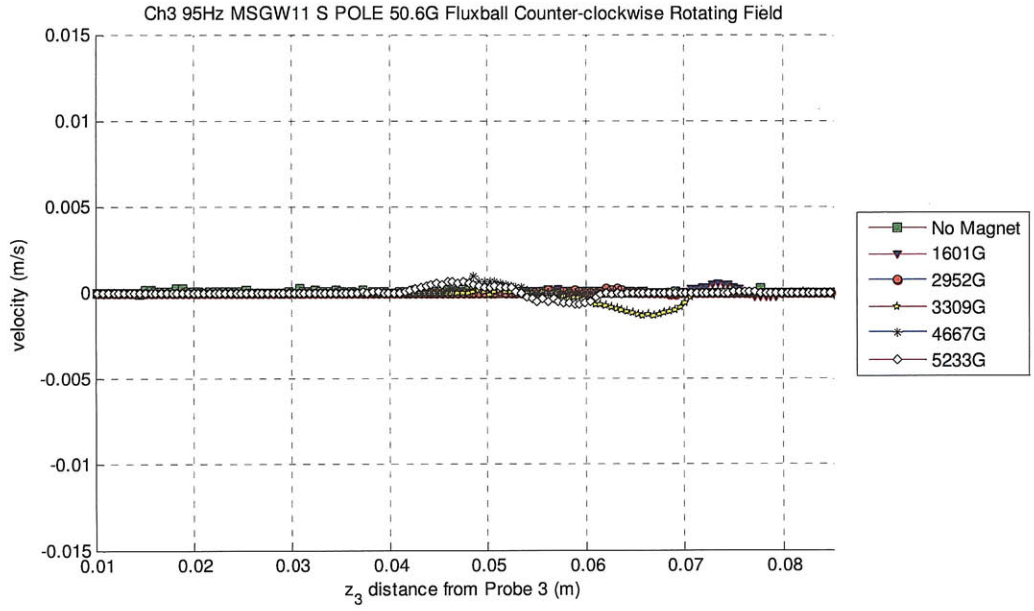
Ch3 95Hz MSGW11 S POLE 50.6G Fluxball Counter-clockwise Rotating Field
velocity (m/s)
0.015
0.01
0.005
0
-0.005
-0.01
-0.015
0.01
0.02
0.03
0.04
0.05
0.06
0.07
0.08
z_3 distance from Probe 3 (m)
No Magnet
1601G
2952G
3309G
4667G
5233G

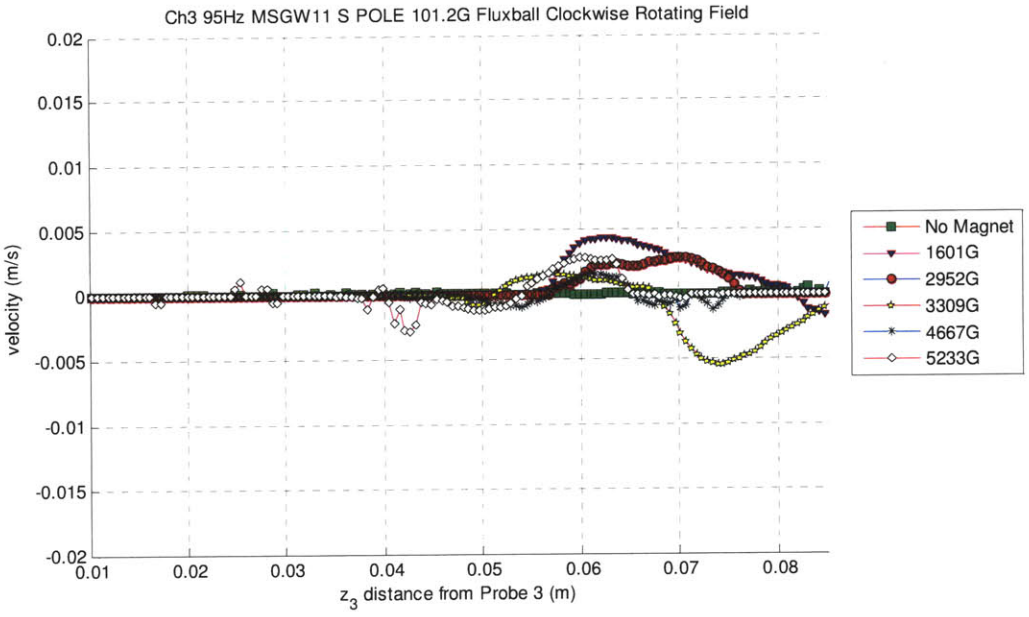
Ch3 95Hz MSGW11 S POLE 101.2G Fluxball Clockwise Rotating Field
velocity (m/s)
0.02
0.015
0.01
0.005
0
-0.005
-0.01
-0.015
-0.02
0.01
0.02
0.03
0.04
0.05
0.06
0.07
0.08
z_3 distance from Probe 3 (m)
No Magnet
1601G
2952G
3309G
4667G
5233G

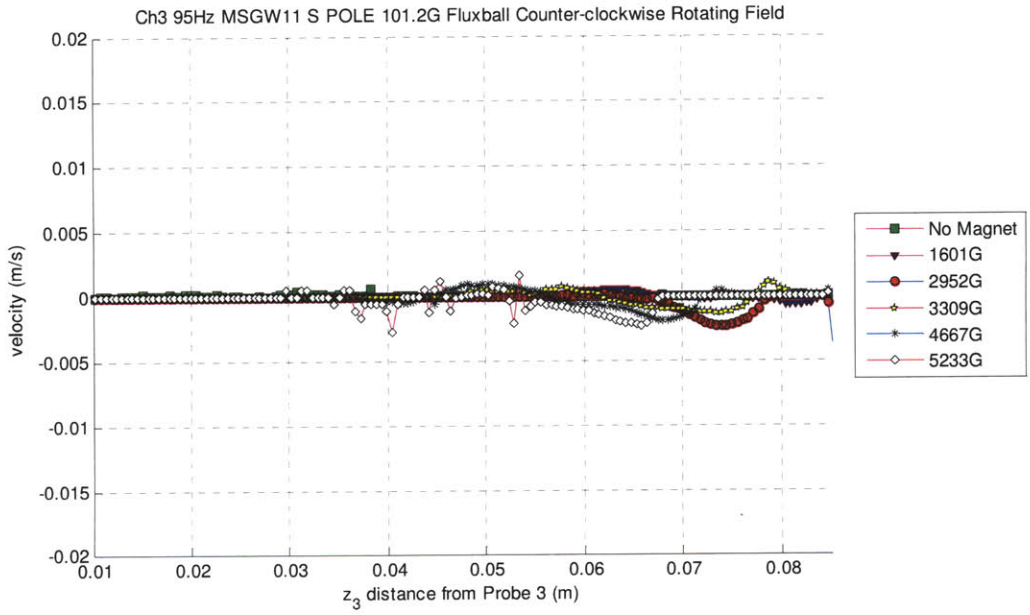
Ch3 95Hz MSGW11 S POLE 101.2G Fluxball Counter-clockwise Rotating Field
velocity (m/s)
0.02
0.015
0.01
0.005
0
-0.005
-0.01
-0.015
-0.02
0.01
0.02
0.03
0.04
0.05
0.06
0.07
0.08
z_3 distance from Probe 3 (m)
No Magnet
1601G
2952G
3309G
4667G
5233G

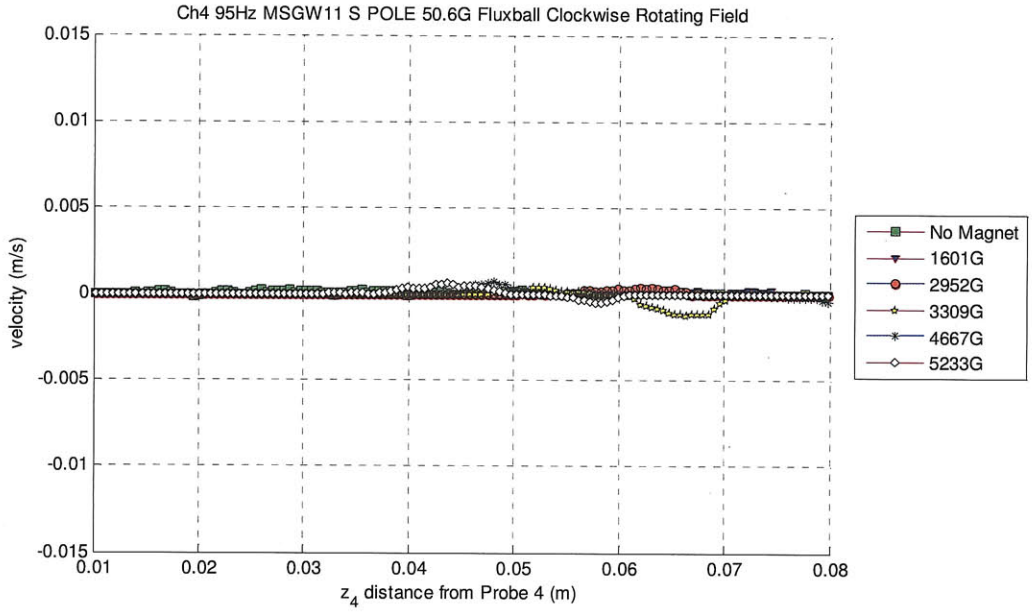
Ch4 95Hz MSGW11 S POLE 50.6G Fluxball Clockwise Rotating Field
velocity (m/s)
0.015
0.01
0.005
0
-0.005
-0.01
-0.015
0.01
0.02
0.03
0.04
0.05
0.06
0.07
0.08
z4 distance from Probe 4 (m)
No Magnet
1601G
2952G
3309G
4667G
5233G

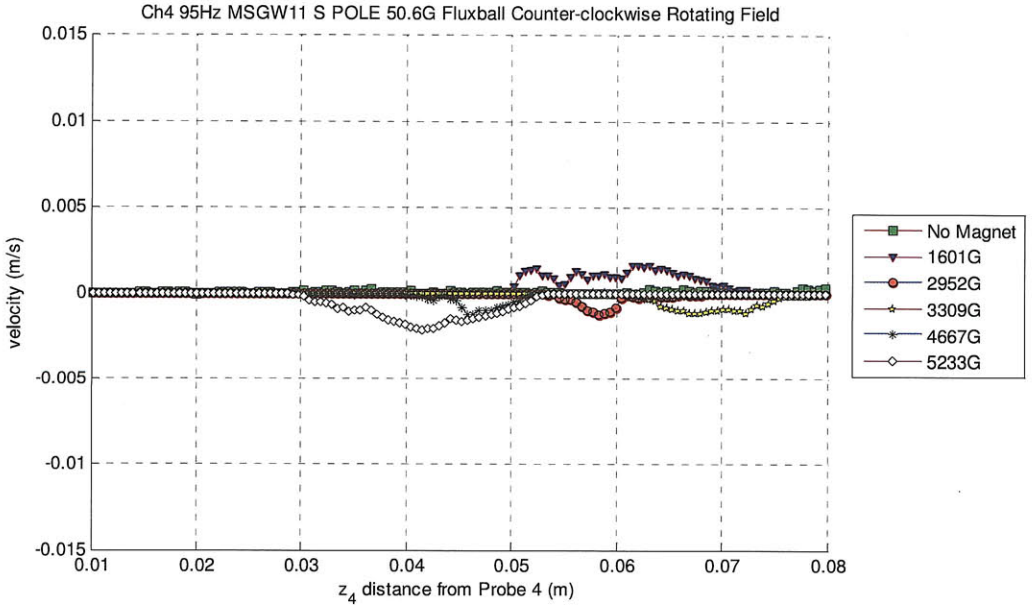
Ch4 95Hz MSGW11 S POLE 50.6G Fluxball Counter-clockwise Rotating Field
velocity (m/s)
0.015
0.01
0.005
0
-0.005
-0.01
-0.015
0.01
0.02
0.03
0.04
0.05
0.06
0.07
0.08
z4 distance from Probe 4 (m)
No Magnet
1601G
2952G
3309G
4667G
5233G

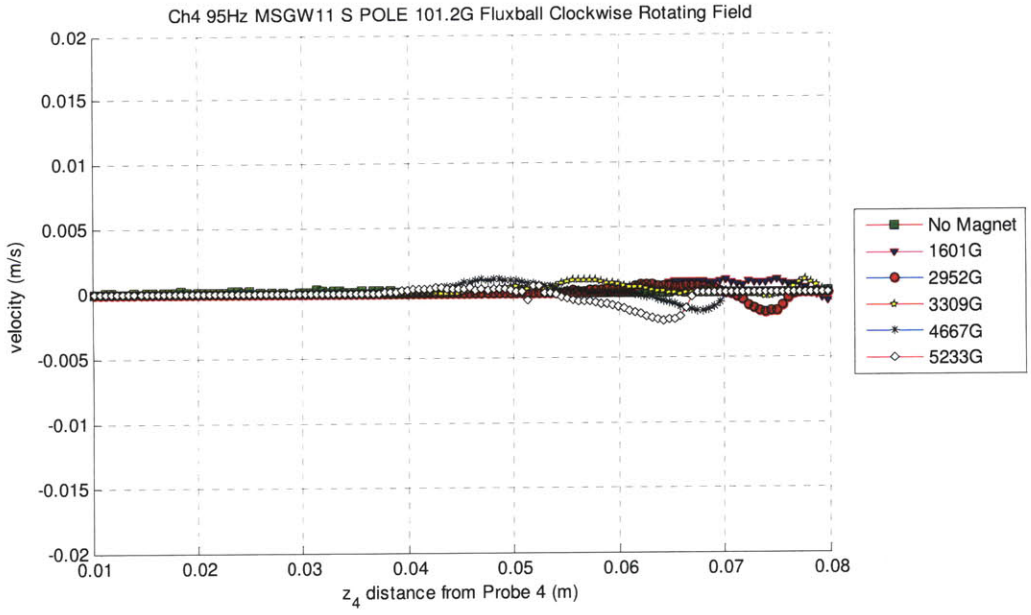
Ch4 95Hz MSGW11 S POLE 101.2G Fluxball Clockwise Rotating Field
velocity (m/s)
0.02
0.015
0.01
0.005
0
-0.005
-0.01
-0.015
-0.02
0.01
0.02
0.03
0.04
0.05
0.06
0.07
0.08
z4 distance from Probe 4 (m)
No Magnet
1601G
2952G
3309G
4667G
5233G

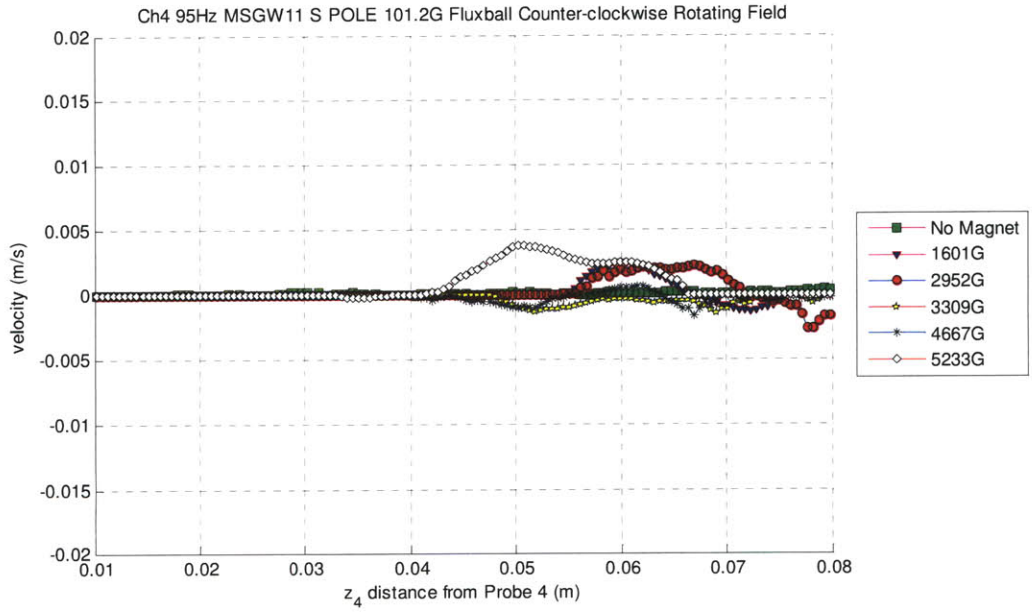
Ch4 95Hz MSGW11 S POLE 101.2G Fluxball Counter-clockwise Rotating Field
velocity (m/s)
0.02
0.015
0.01
0.005
0
-0.005
-0.01
-0.015
-0.02
0.01
0.02
0.03
0.04
0.05
0.06
0.07
0.08
z4 distance from Probe 4 (m)
No Magnet
1601G
2952G
3309G
4667G
5233G

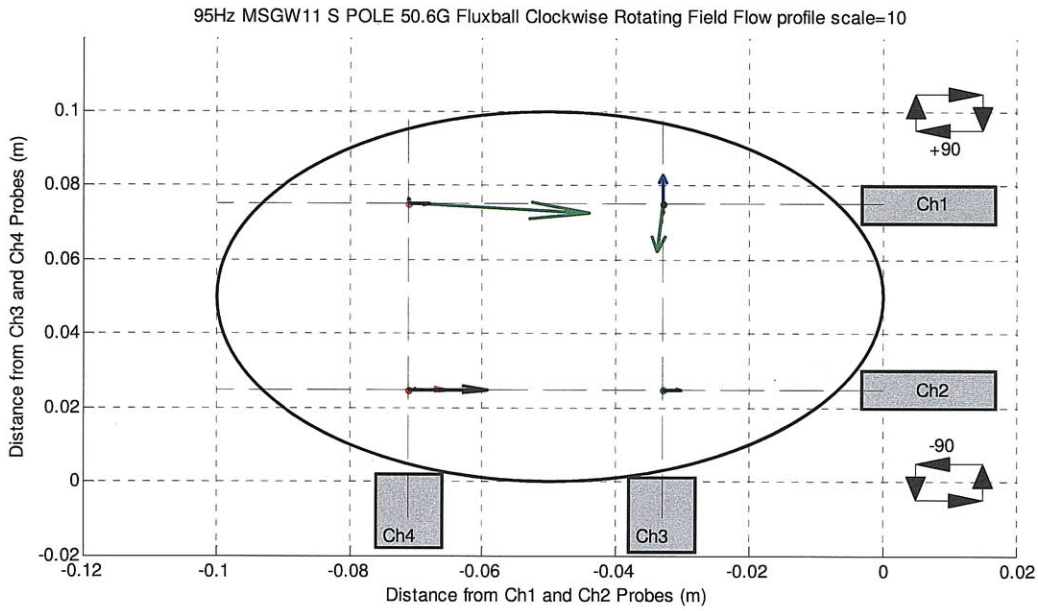
95Hz MSGW11 S POLE 50.6G Fluxball Clockwise Rotating Field Flow profile scale=10
Distance from Ch3 and Ch4 Probes (m)
Distance from Ch1 and Ch2 Probes (m)
+90
-90
Ch1
Ch2
Ch3
Ch4
0.1
0.08
0.06
0.04
0.02
0
-0.02
-0.12
-0.1
-0.08
-0.06
-0.04
-0.02
0
0.02

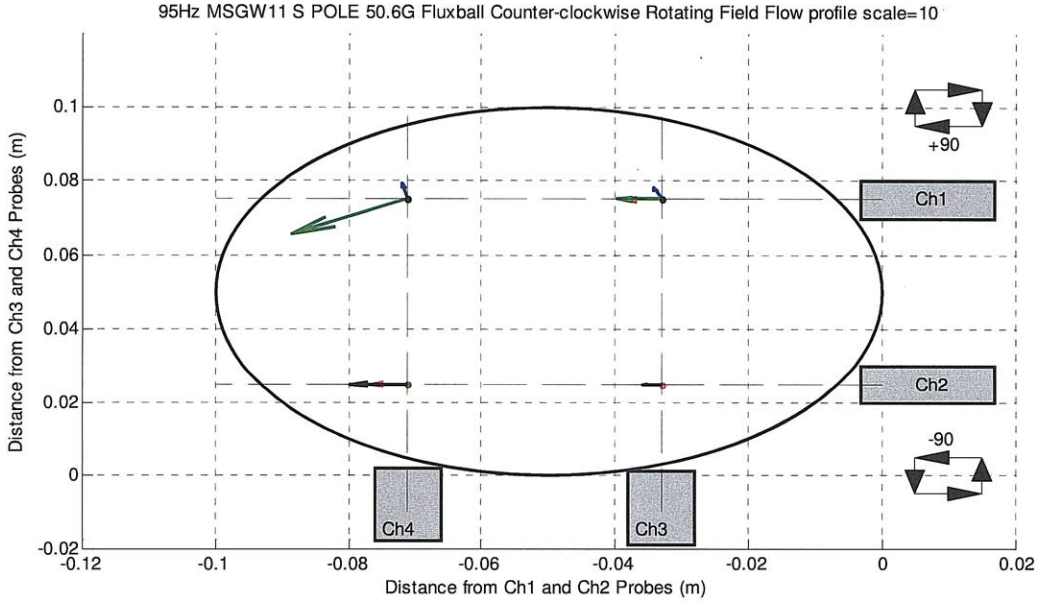
95Hz MSGW11 S POLE 50.6G Fluxball Counter-clockwise Rotating Field Flow profile scale=10
Distance from Ch3 and Ch4 Probes (m)
Distance from Ch1 and Ch2 Probes (m)
+90
-90
Ch1
Ch2
Ch3
Ch4
0.1
0.08
0.06
0.04
0.02
0
-0.02
-0.12
-0.1
-0.08
-0.06
-0.04
-0.02
0
0.02

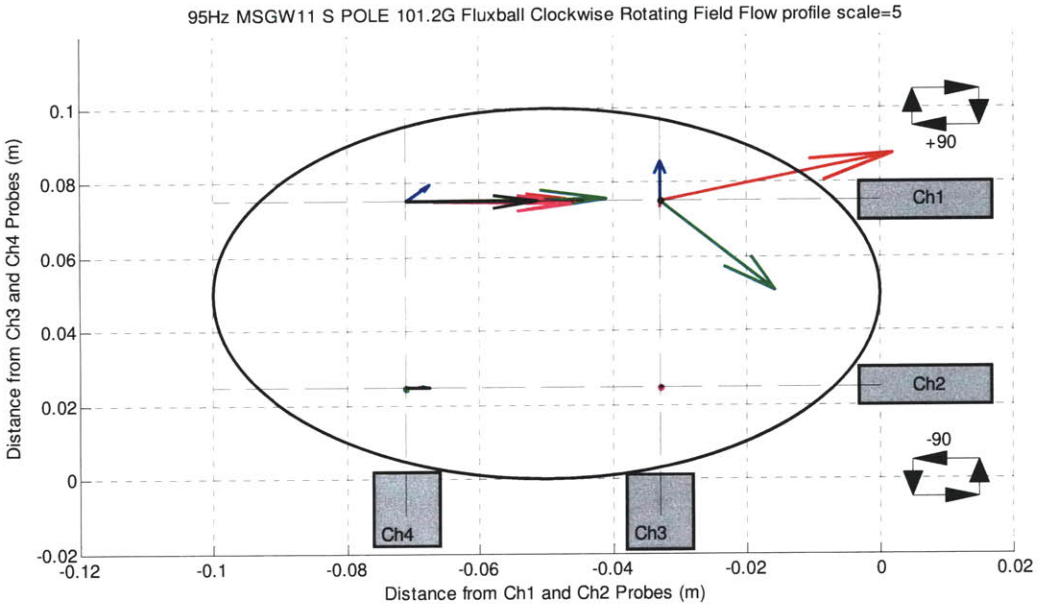
95Hz MSGW11 S POLE 101.2G Fluxball Clockwise Rotating Field Flow profile scale=5
Distance from Ch3 and Ch4 Probes (m)
Distance from Ch1 and Ch2 Probes (m)
+90
-90
Ch1
Ch2
Ch3
Ch4
0.1
0.08
0.06
0.04
0.02
0
-0.02
-0.12
-0.1
-0.08
-0.06
-0.04
-0.02
0
0.02

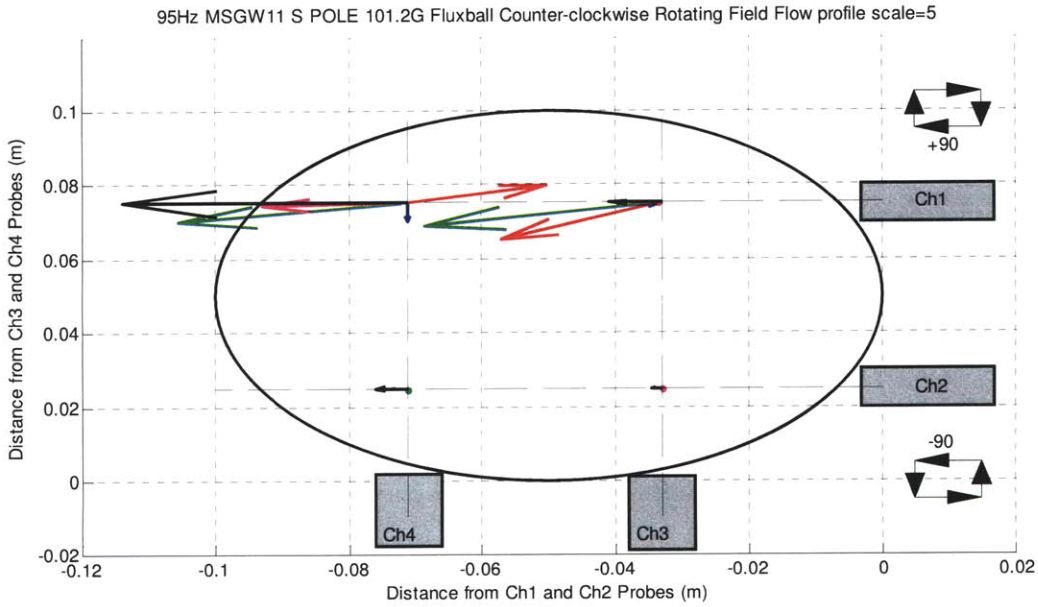
95Hz MSGW11 S POLE 101.2G Fluxball Counter-clockwise Rotating Field Flow profile scale=5
Distance from Ch3 and Ch4 Probes (m)
Distance from Ch1 and Ch2 Probes (m)
+90
-90
Ch1
Ch2
Ch3
Ch4
0.1
0.08
0.06
0.04
0.02
0
-0.02
-0.12
-0.1
-0.08
-0.06
-0.04
-0.02
0
0.02

H8. MSGW11 Filled Sphere with South Pole Facing Magnets on Top of Sphere at 47Hz

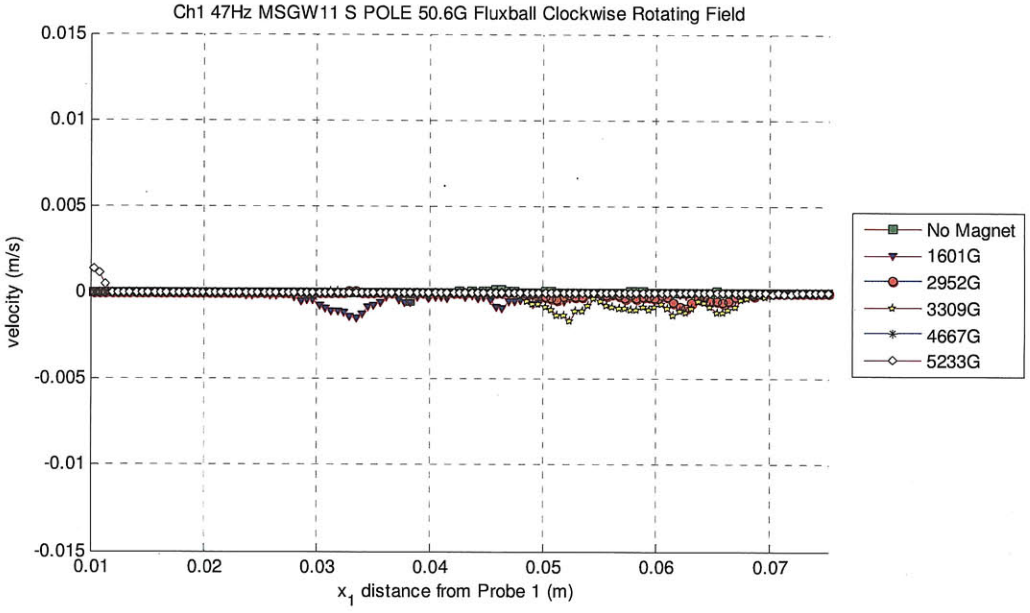

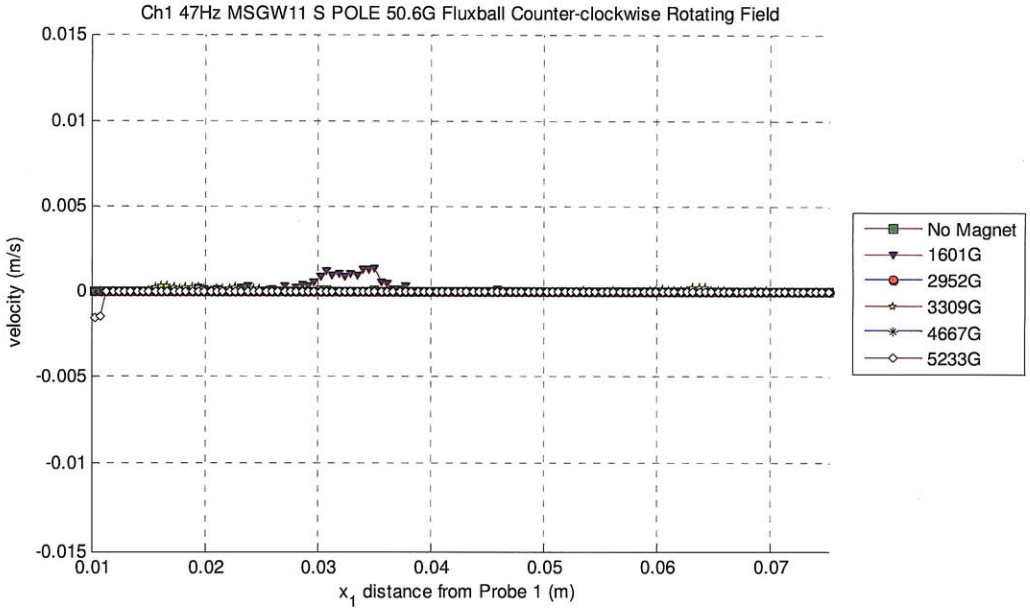

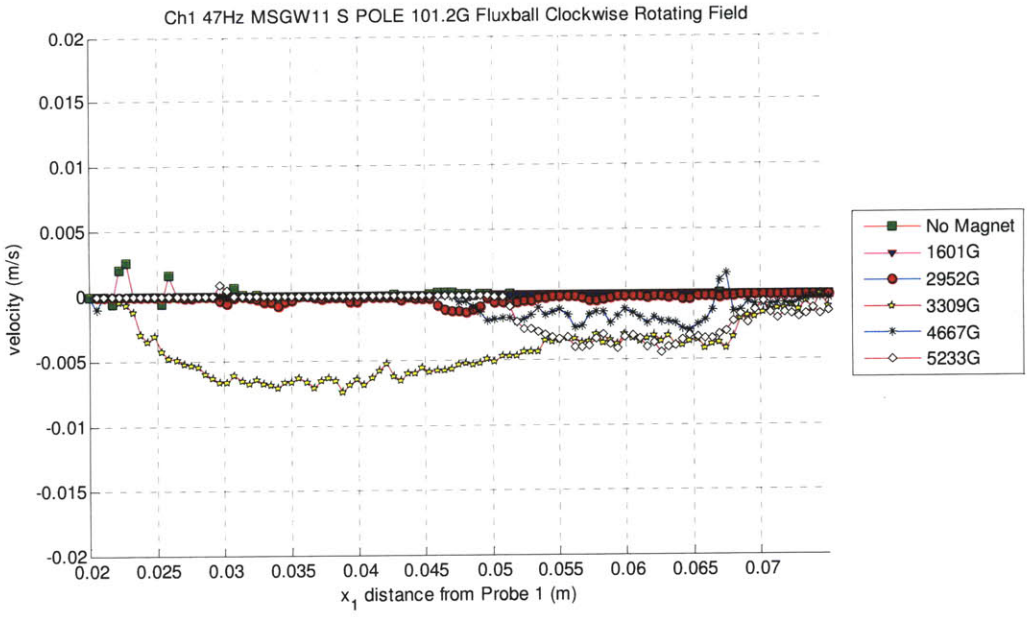
Ch1 47Hz MSGW11 S POLE 101.2G Fluxball Clockwise Rotating Field
velocity (m/s)
0.02
0.015
0.01
0.005
0
-0.005
-0.01
-0.015
-0.02
0.02 0.025 0.03 0.035 0.04 0.045 0.05 0.055 0.06 0.065 0.07
x1 distance from Probe 1 (m)
No Magnet
1601G
2952G
3309G
4667G
5233G

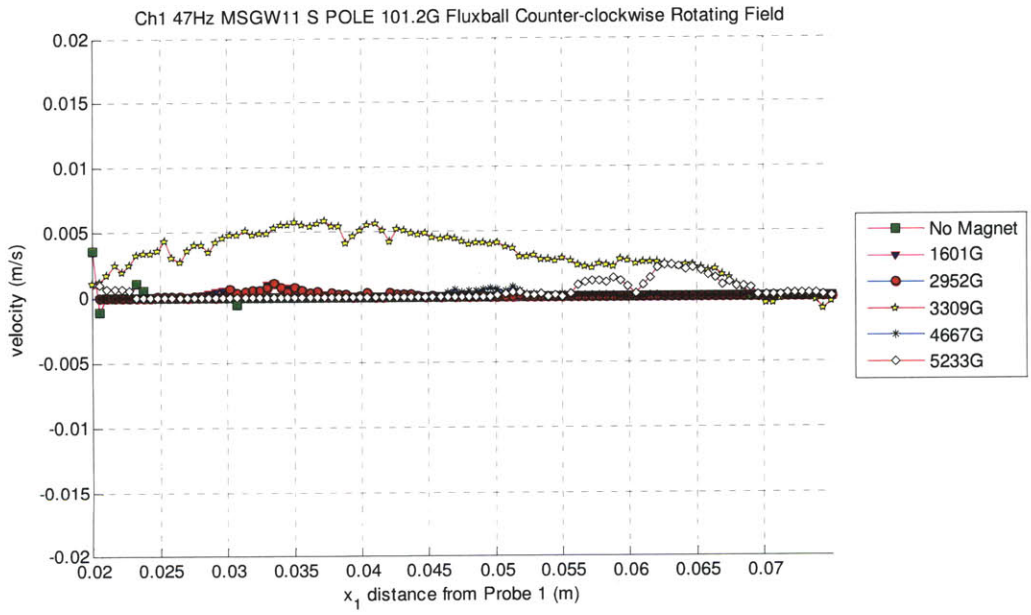
Ch1 47Hz MSGW11 S POLE 101.2G Fluxball Counter-clockwise Rotating Field
velocity (m/s)
0.02
0.015
0.01
0.005
0
-0.005
-0.01
-0.015
-0.02
0.02 0.025 0.03 0.035 0.04 0.045 0.05 0.055 0.06 0.065 0.07
x1 distance from Probe 1 (m)
No Magnet
1601G
2952G
3309G
4667G
5233G

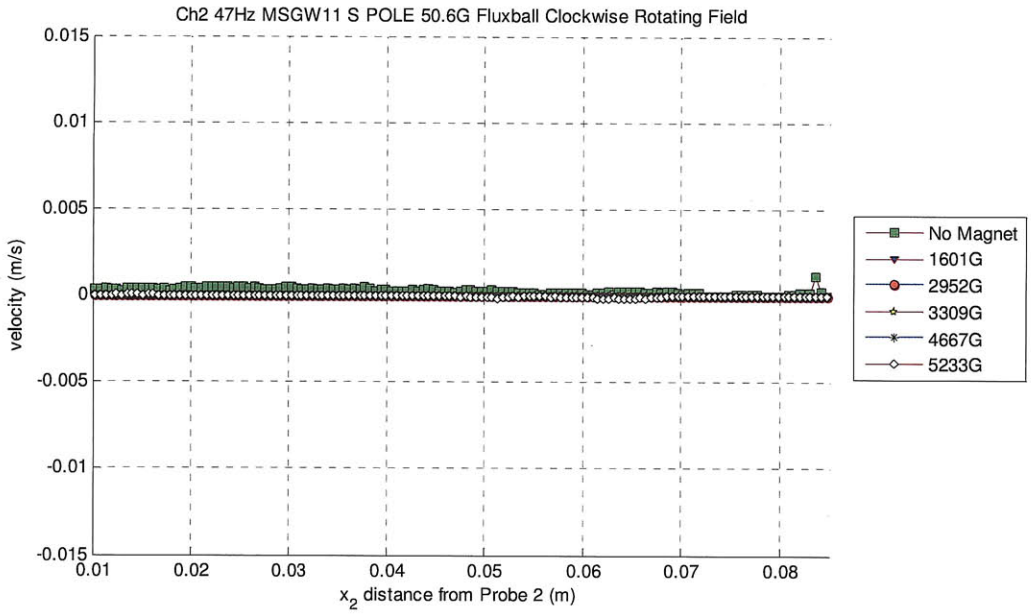
Ch2 47Hz MSGW11 S POLE 50.6G Fluxball Clockwise Rotating Field
velocity (m/s)
0.015
0.01
0.005
0
-0.005
-0.01
-0.015
0.01
0.02
0.03
0.04
0.05
0.06
0.07
0.08
x2 distance from Probe 2 (m)
No Magnet
1601G
2952G
3309G
4667G
5233G

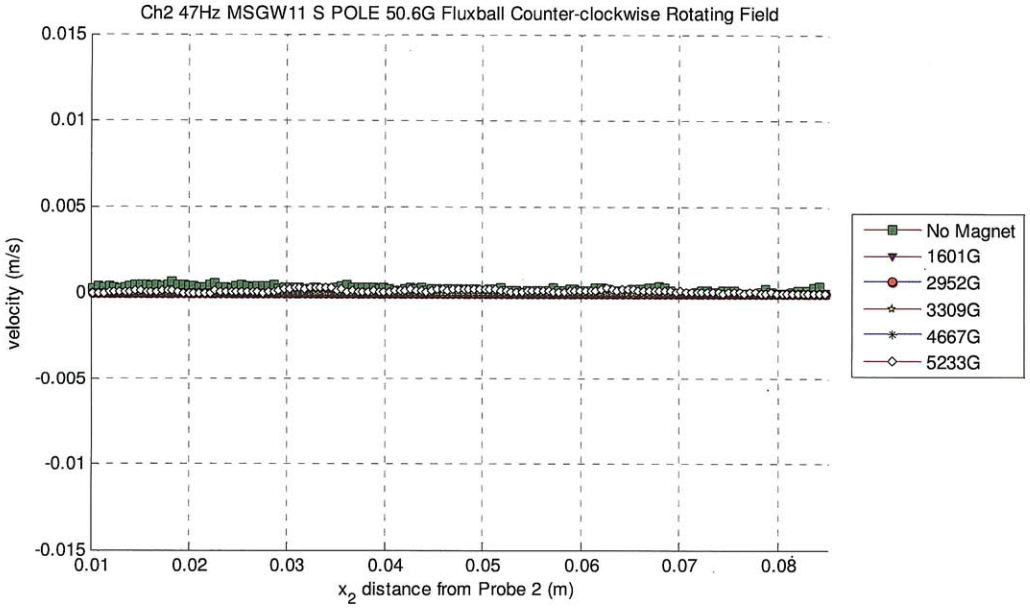
Ch2 47Hz MSGW11 S POLE 50.6G Fluxball Counter-clockwise Rotating Field
velocity (m/s)
0.015
0.01
0.005
0
-0.005
-0.01
-0.015
0.01
0.02
0.03
0.04
0.05
0.06
0.07
0.08
x2 distance from Probe 2 (m)
No Magnet
1601G
2952G
3309G
4667G
5233G

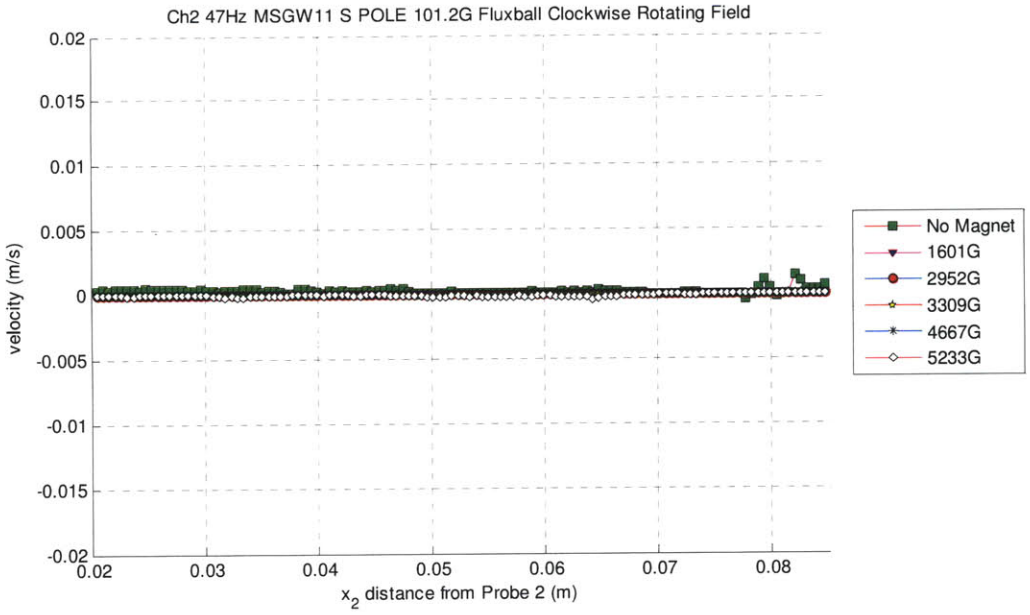
Ch2 47Hz MSGW11 S POLE 101.2G Fluxball Clockwise Rotating Field
velocity (m/s)
0.02
0.015
0.01
0.005
0
-0.005
-0.01
-0.015
-0.02
0.02
0.03
0.04
0.05
0.06
0.07
0.08
x2 distance from Probe 2 (m)
No Magnet
1601G
2952G
3309G
4667G
5233G

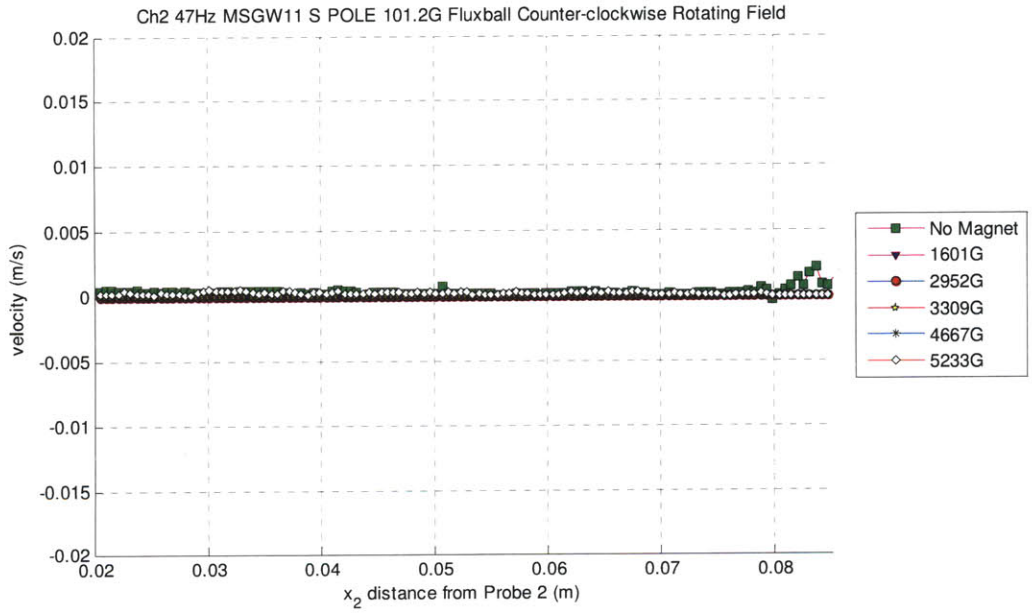
Ch2 47Hz MSGW11 S POLE 101.2G Fluxball Counter-clockwise Rotating Field
velocity (m/s)
0.02
0.015
0.01
0.005
0
-0.005
-0.01
-0.015
-0.02
0.02
0.03
0.04
0.05
0.06
0.07
0.08
x2 distance from Probe 2 (m)
No Magnet
1601G
2952G
3309G
4667G
5233G

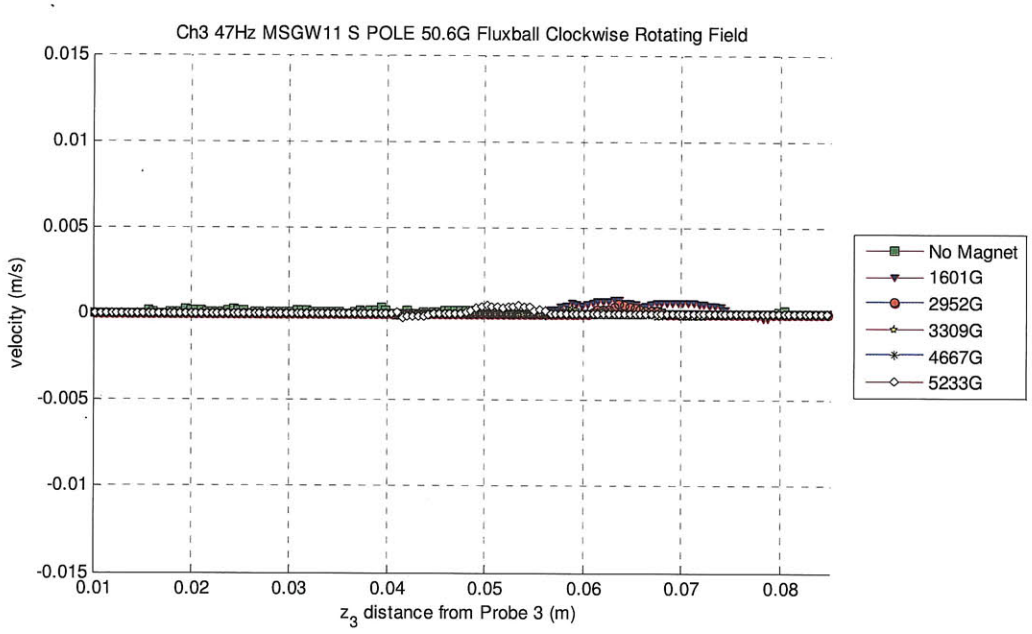
Ch3 47Hz MSGW11 S POLE 50.6G Fluxball Clockwise Rotating Field
velocity (m/s)
0.015
0.01
0.005
0
-0.005
-0.01
-0.015
0.01
0.02
0.03
0.04
0.05
0.06
0.07
0.08
z3 distance from Probe 3 (m)
No Magnet
1601G
2952G
3309G
4667G
5233G

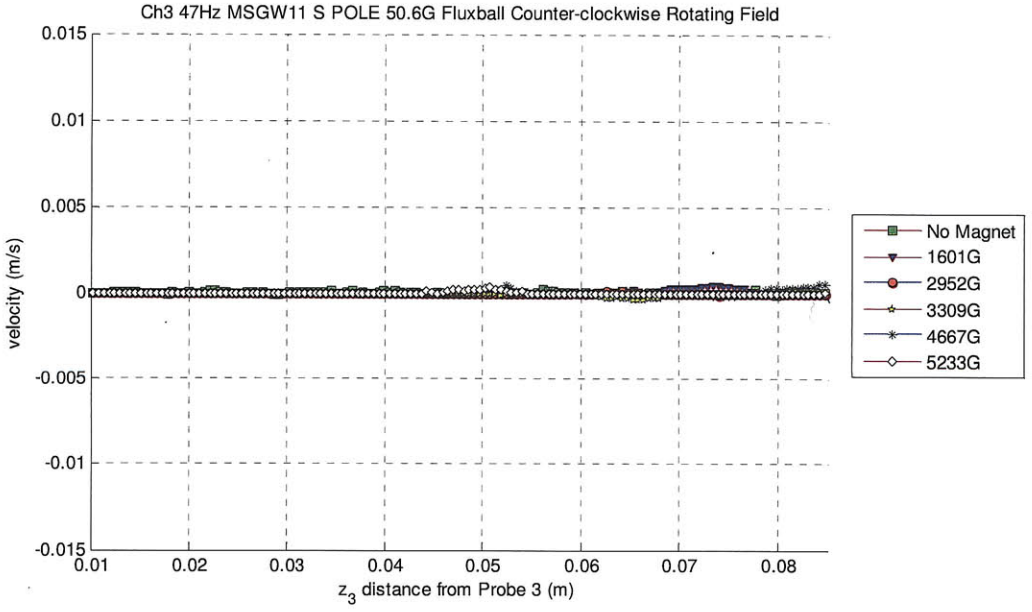
Ch3 47Hz MSGW11 S POLE 50.6G Fluxball Counter-clockwise Rotating Field
velocity (m/s)
0.015
0.01
0.005
0
-0.005
-0.01
-0.015
0.01
0.02
0.03
0.04
0.05
0.06
0.07
0.08
z3 distance from Probe 3 (m)
No Magnet
1601G
2952G
3309G
4667G
5233G

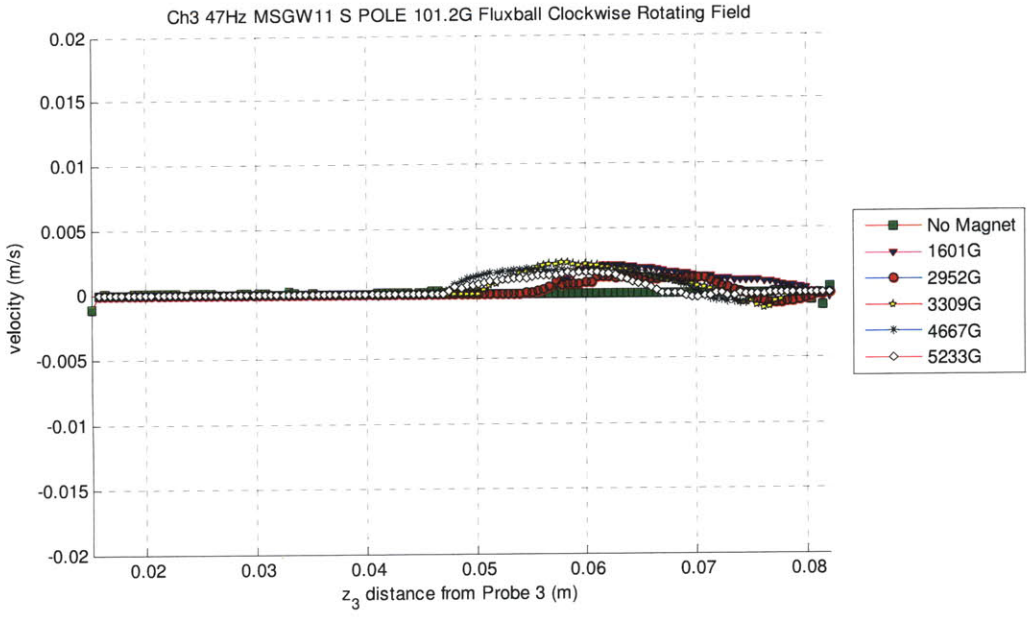
Ch3 47Hz MSGW11 S POLE 101.2G Fluxball Clockwise Rotating Field
velocity (m/s)
0.02
0.015
0.01
0.005
0
-0.005
-0.01
-0.015
-0.02
0.02
0.03
0.04
0.05
0.06
0.07
0.08
z_3 distance from Probe 3 (m)
No Magnet
1601G
2952G
3309G
4667G
5233G

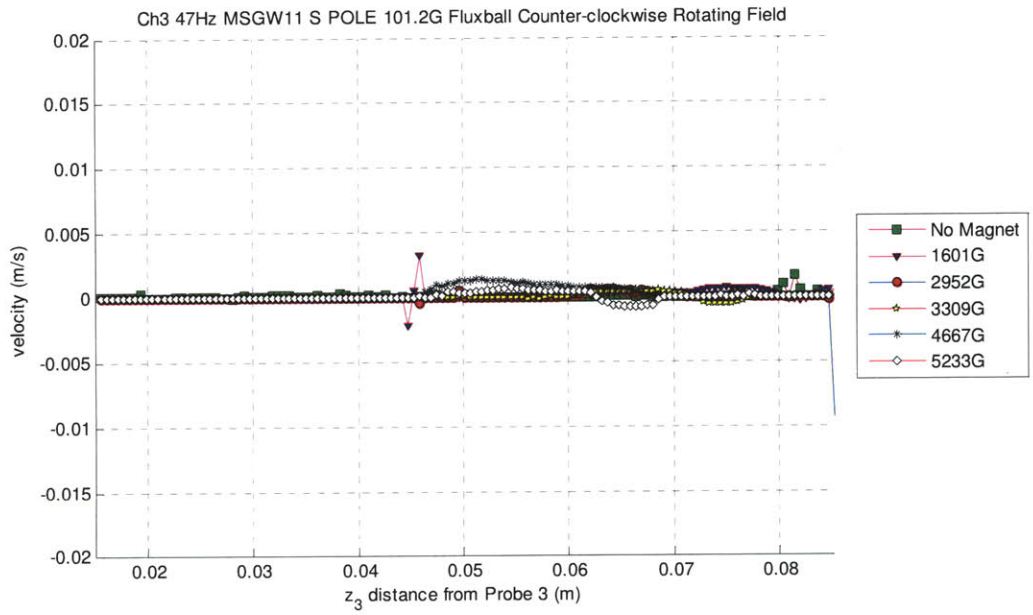
Ch3 47Hz MSGW11 S POLE 101.2G Fluxball Counter-clockwise Rotating Field
velocity (m/s)
0.02
0.015
0.01
0.005
0
-0.005
-0.01
-0.015
-0.02
0.02
0.03
0.04
0.05
0.06
0.07
0.08
z_3 distance from Probe 3 (m)
No Magnet
1601G
2952G
3309G
4667G
5233G

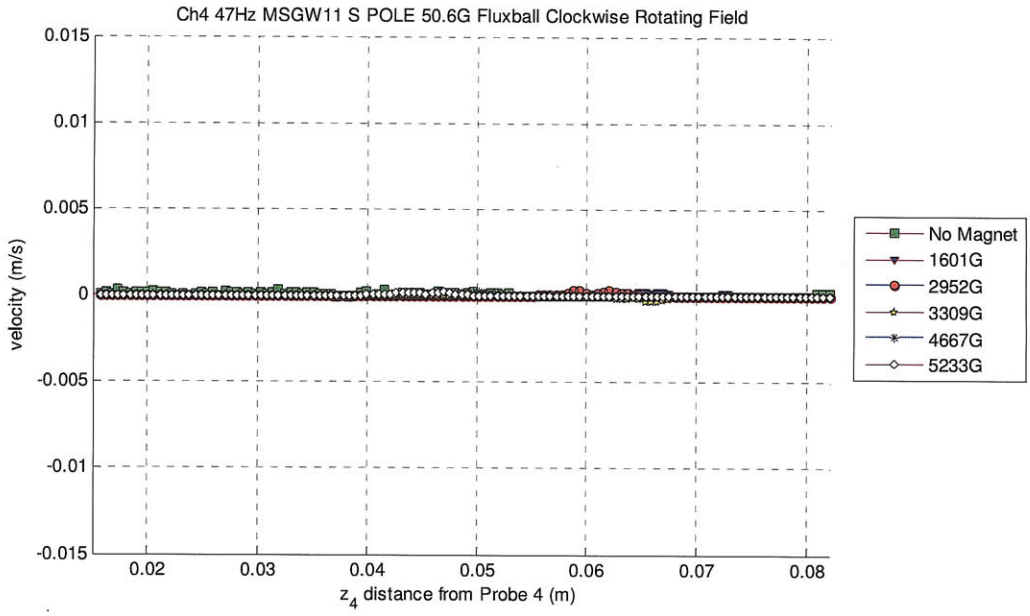
Ch4 47Hz MSGW11 S POLE 50.6G Fluxball Clockwise Rotating Field
0.015
0.01
0.005
0
-0.005
-0.01
-0.015
velocity (m/s)
0.02
0.03
0.04
0.05
0.06
0.07
0.08
z4 distance from Probe 4 (m)
No Magnet
1601G
2952G
3309G
4667G
5233G

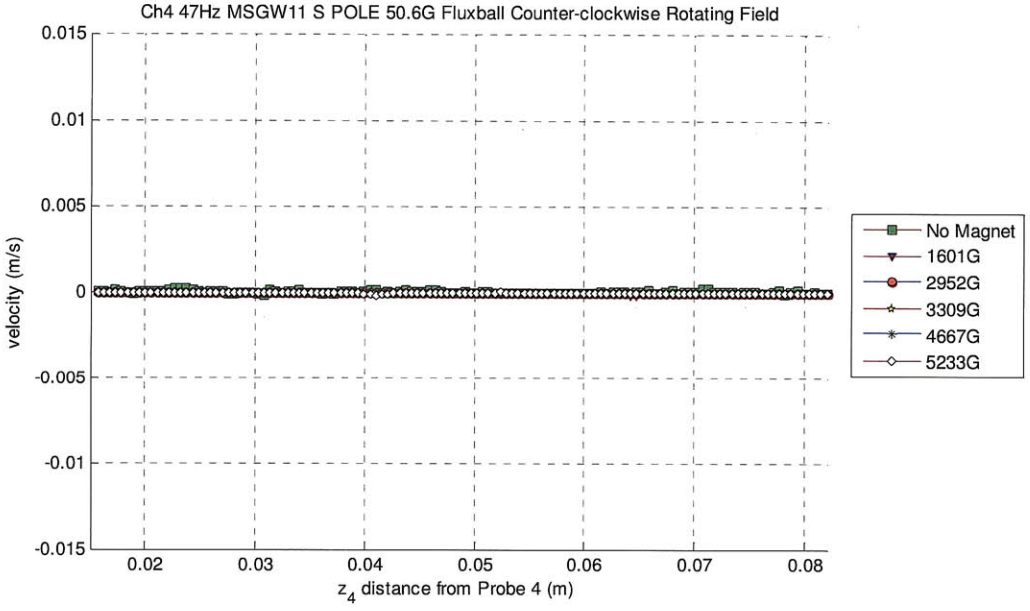
Ch4 47Hz MSGW11 S POLE 50.6G Fluxball Counter-clockwise Rotating Field
0.015
0.01
0.005
0
-0.005
-0.01
-0.015
velocity (m/s)
0.02
0.03
0.04
0.05
0.06
0.07
0.08
z4 distance from Probe 4 (m)
No Magnet
1601G
2952G
3309G
4667G
5233G

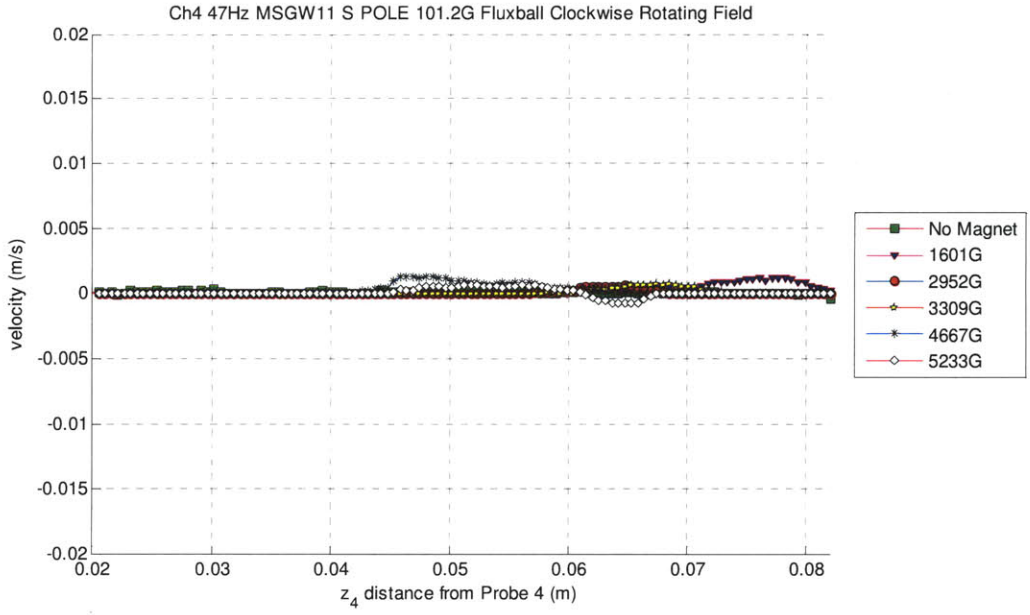
Ch4 47Hz MSGW11 S POLE 101.2G Fluxball Clockwise Rotating Field
velocity (m/s)
0.02
0.015
0.01
0.005
0
-0.005
-0.01
-0.015
-0.02
0.02
0.03
0.04
0.05
0.06
0.07
0.08
z_4 distance from Probe 4 (m)
No Magnet
1601G
2952G
3309G
4667G
5233G

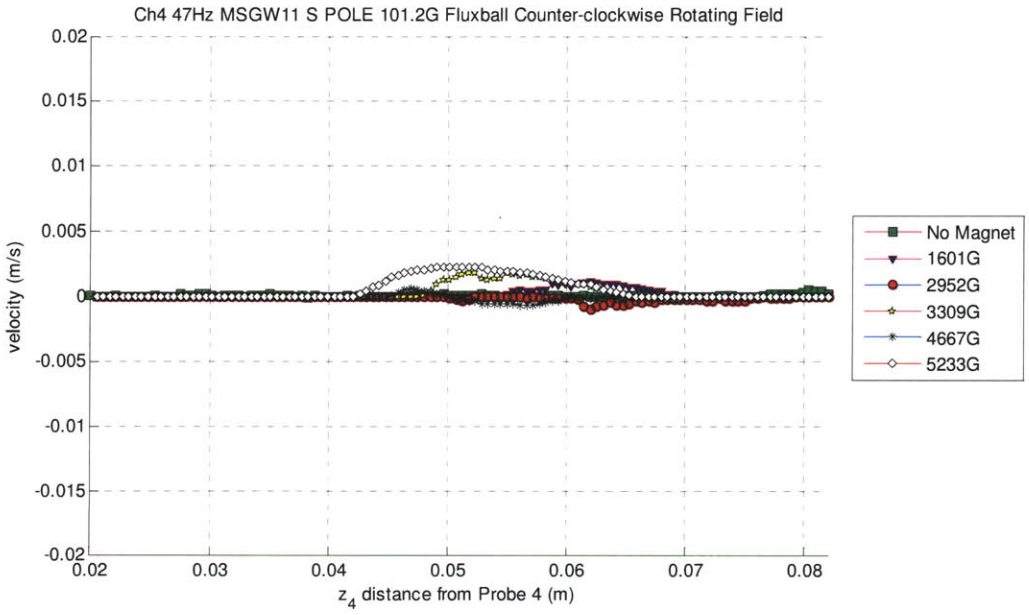
Ch4 47Hz MSGW11 S POLE 101.2G Fluxball Counter-clockwise Rotating Field
velocity (m/s)
0.02
0.015
0.01
0.005
0
-0.005
-0.01
-0.015
-0.02
0.02
0.03
0.04
0.05
0.06
0.07
0.08
z_4 distance from Probe 4 (m)
No Magnet
1601G
2952G
3309G
4667G
5233G

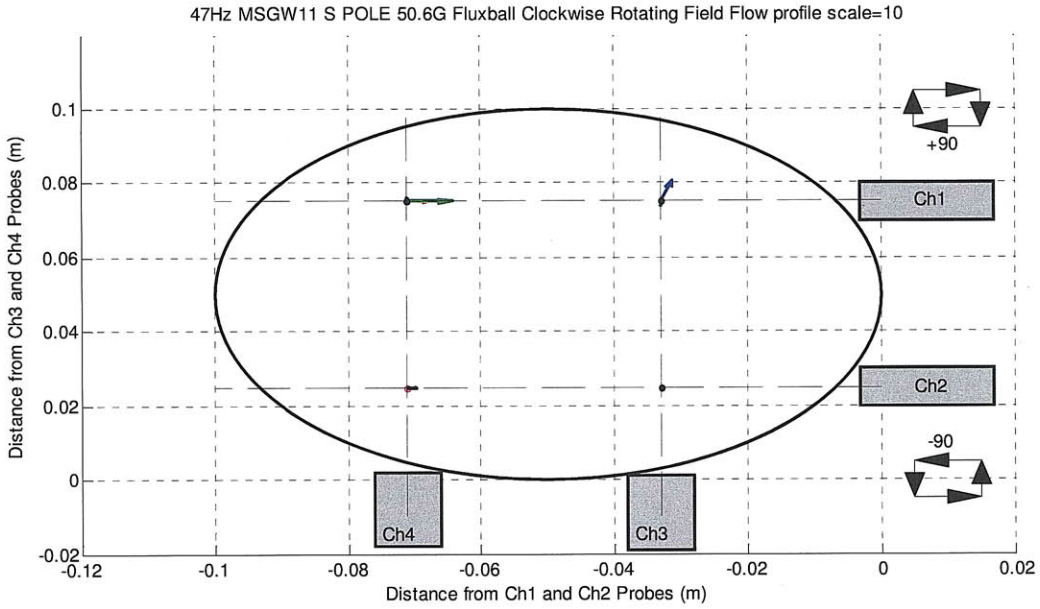
47Hz MSGW11 S POLE 50.6G Fluxball Clockwise Rotating Field Flow profile scale=10
Distance from Ch3 and Ch4 Probes (m)
Distance from Ch1 and Ch2 Probes (m)
+90
-90
Ch1
Ch2
Ch3
Ch4
0.1
0.08
0.06
0.04
0.02
0
-0.02
-0.12
-0.1
-0.08
-0.06
-0.04
-0.02
0
0.02

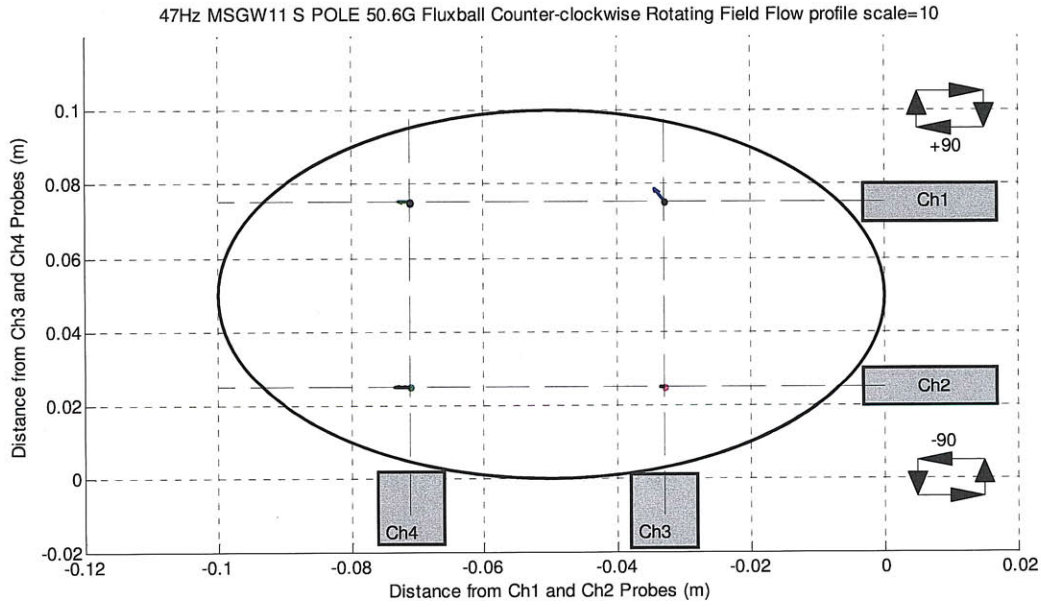
47Hz MSGW11 S POLE 50.6G Fluxball Counter-clockwise Rotating Field Flow profile scale=10
Distance from Ch3 and Ch4 Probes (m)
Distance from Ch1 and Ch2 Probes (m)
+90
-90
Ch1
Ch2
Ch3
Ch4
0.1
0.08
0.06
0.04
0.02
0
-0.02
-0.12
-0.1
-0.08
-0.06
-0.04
-0.02
0
0.02

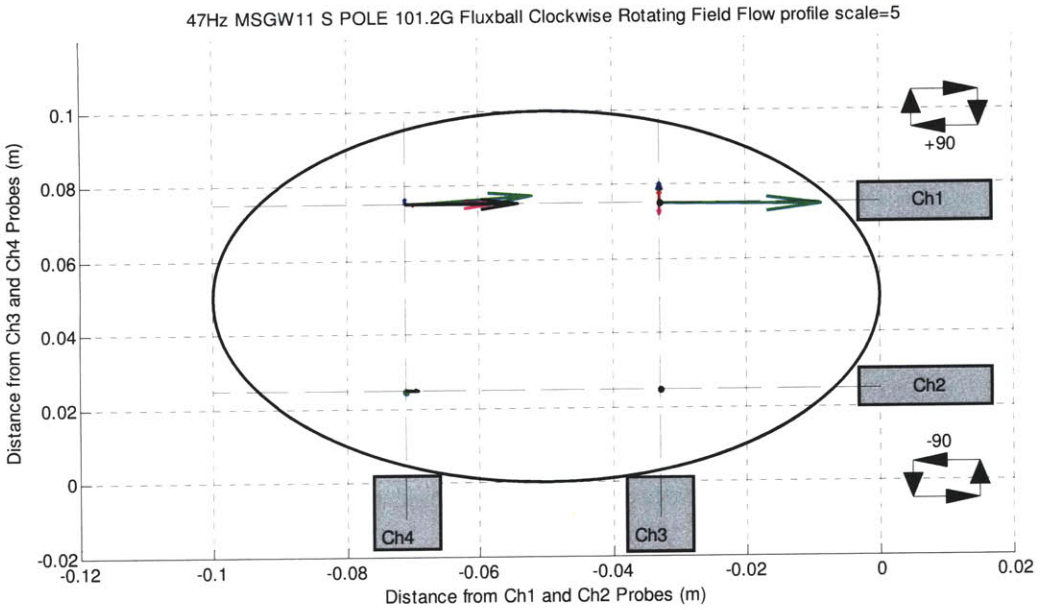
47Hz MSGW11 S POLE 101.2G Fluxball Clockwise Rotating Field Flow profile scale=5
Distance from Ch3 and Ch4 Probes (m)
Distance from Ch1 and Ch2 Probes (m)
0.1
0.08
0.06
0.04
0.02
0
-0.02
-0.12
-0.1
-0.08
-0.06
-0.04
-0.02
0
0.02
+90
-90
Ch1
Ch2
Ch3
Ch4

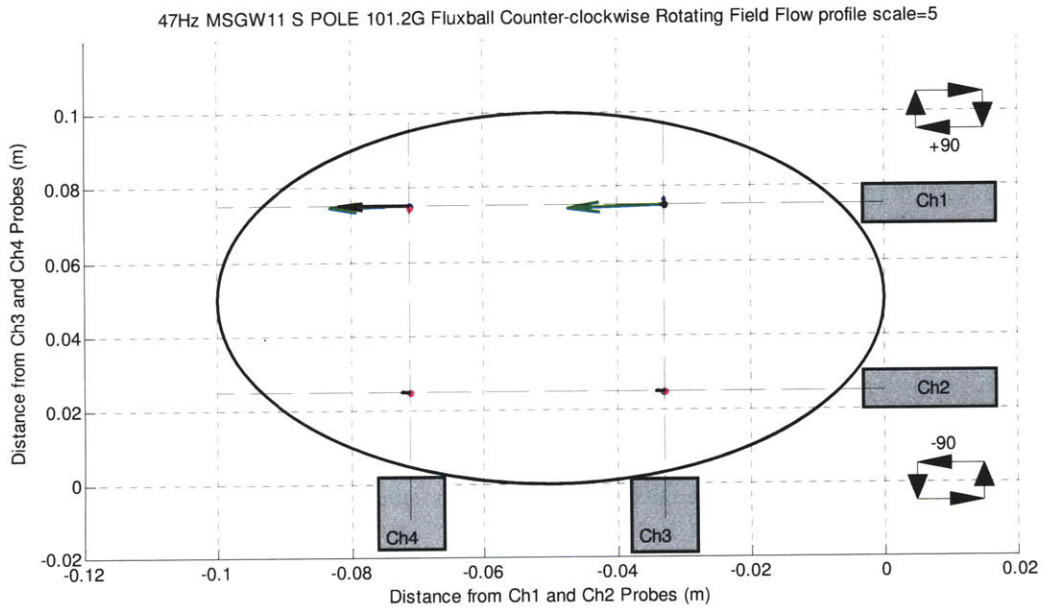
47Hz MSGW11 S POLE 101.2G Fluxball Counter-clockwise Rotating Field Flow profile scale=5
Distance from Ch3 and Ch4 Probes (m)
Distance from Ch1 and Ch2 Probes (m)
0.1
0.08
0.06
0.04
0.02
0
-0.02
-0.12
-0.1
-0.08
-0.06
-0.04
-0.02
0
0.02
+90
-90
Ch1
Ch2
Ch3
Ch4

H9. MSGW11 Filled Sphere with South Pole Facing Magnets on Top of Sphere at 15Hz

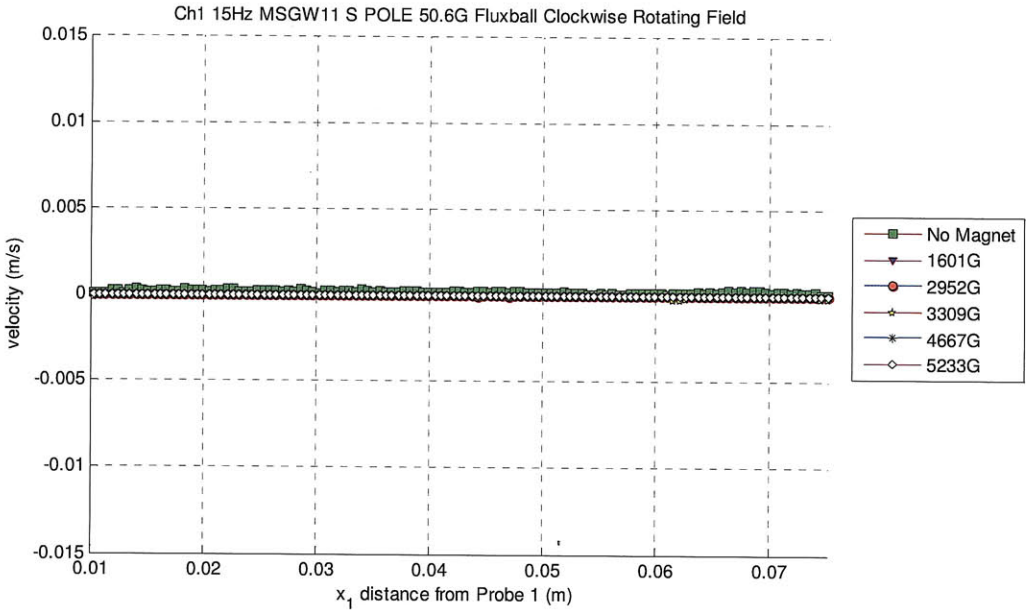

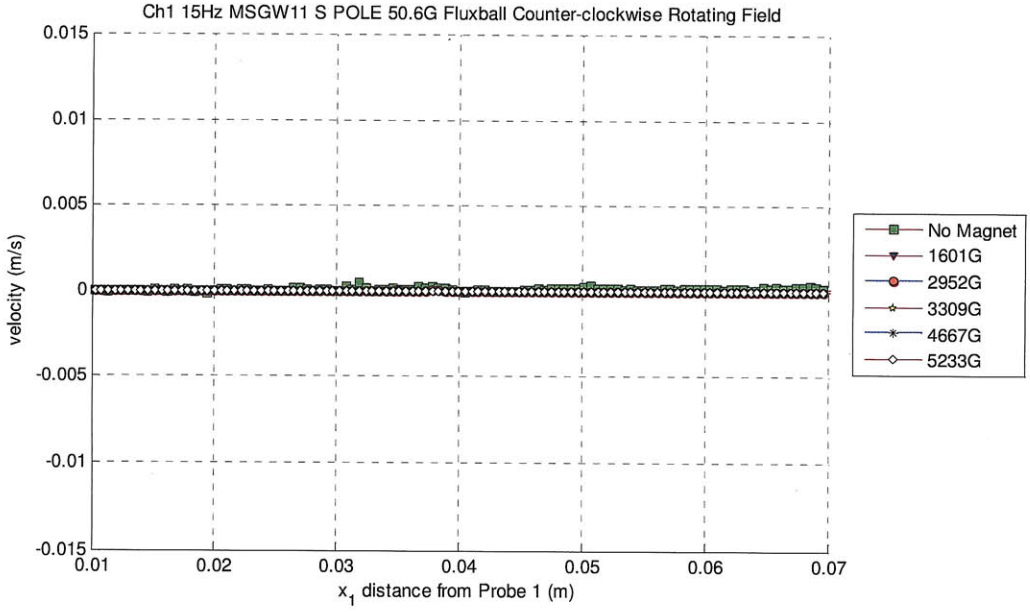

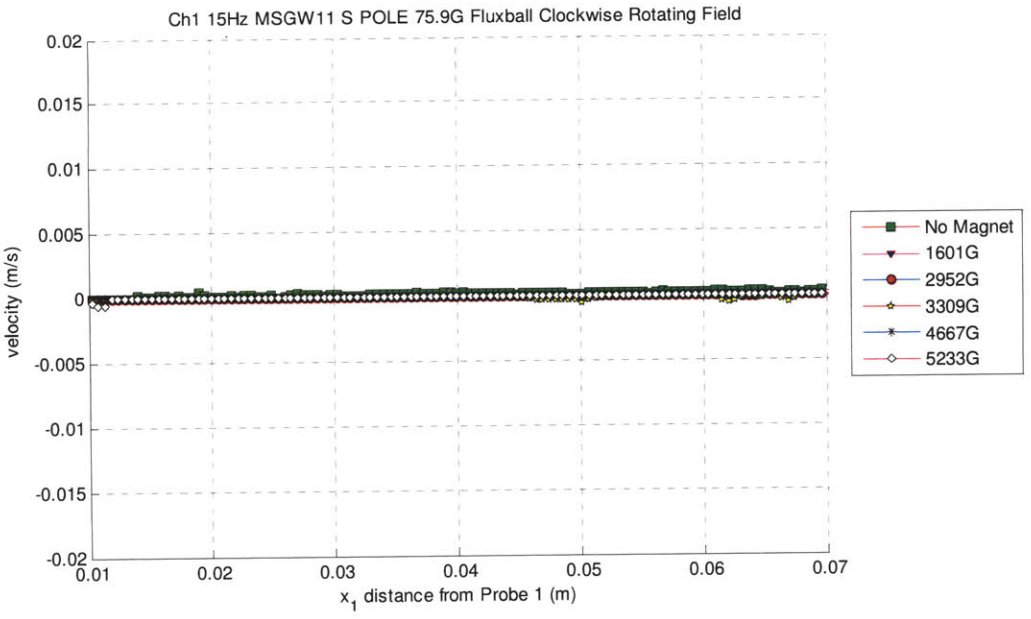
Ch1 15Hz MSGW11 S POLE 75.9G Fluxball Clockwise Rotating Field
velocity (m/s)
0.02
0.015
0.01
0.005
0
-0.005
-0.01
-0.015
-0.02
0.01
0.02
0.03
0.04
0.05
0.06
0.07
x1 distance from Probe 1 (m)
No Magnet
1601G
2952G
3309G
4667G
5233G

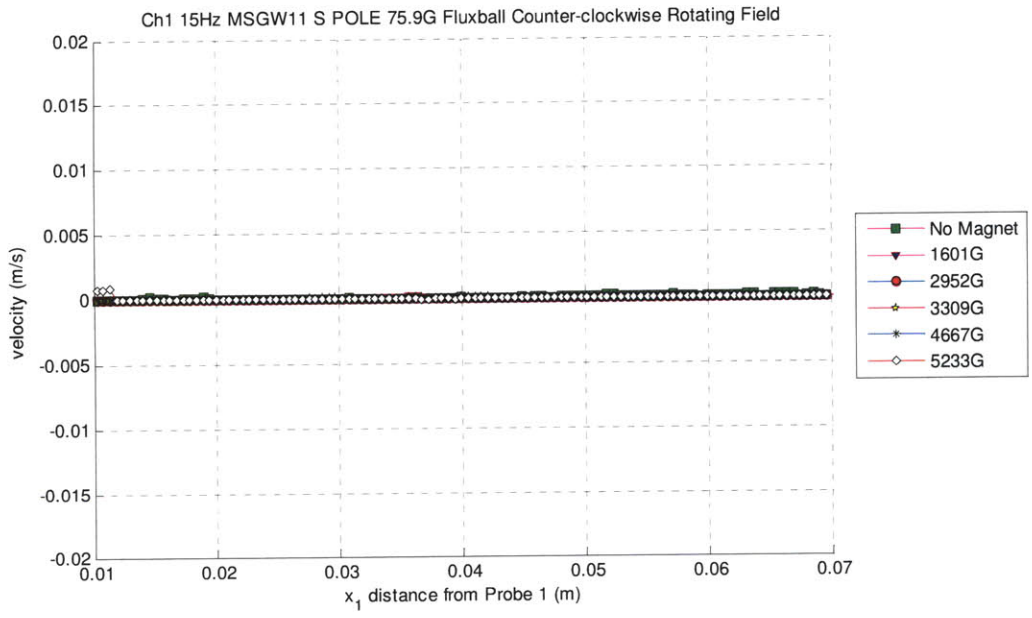
Ch1 15Hz MSGW11 S POLE 75.9G Fluxball Counter-clockwise Rotating Field
velocity (m/s)
0.02
0.015
0.01
0.005
0
-0.005
-0.01
-0.015
-0.02
0.01
0.02
0.03
0.04
0.05
0.06
0.07
x1 distance from Probe 1 (m)
No Magnet
1601G
2952G
3309G
4667G
5233G

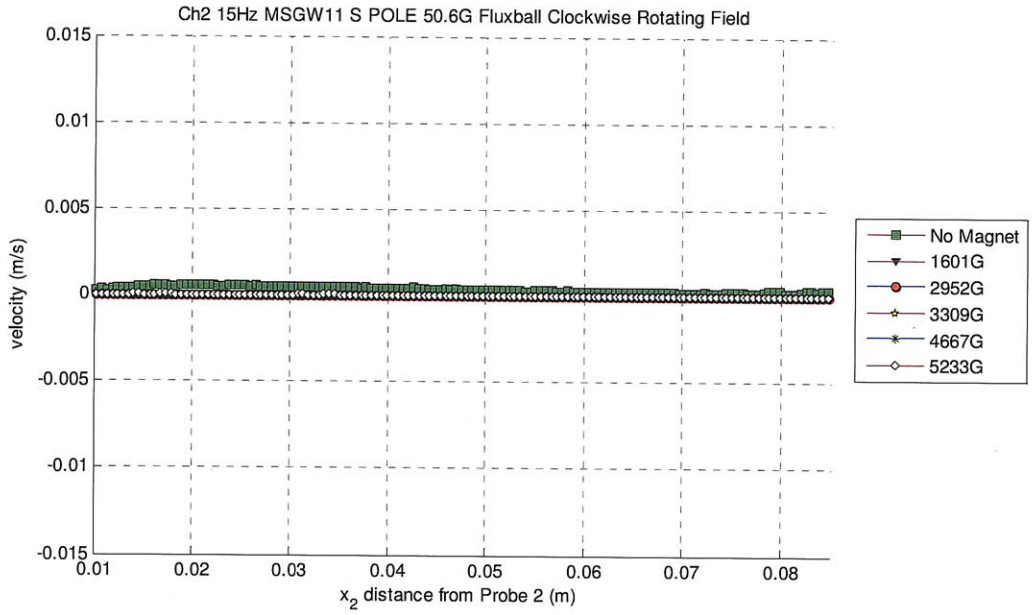
Ch2 15Hz MSGW11 S POLE 50.6G Fluxball Clockwise Rotating Field
velocity (m/s)
0.015
0.01
0.005
0
-0.005
-0.01
-0.015
0.01
0.02
0.03
0.04
0.05
0.06
0.07
0.08
x2 distance from Probe 2 (m)
No Magnet
1601G
2952G
3309G
4667G
5233G

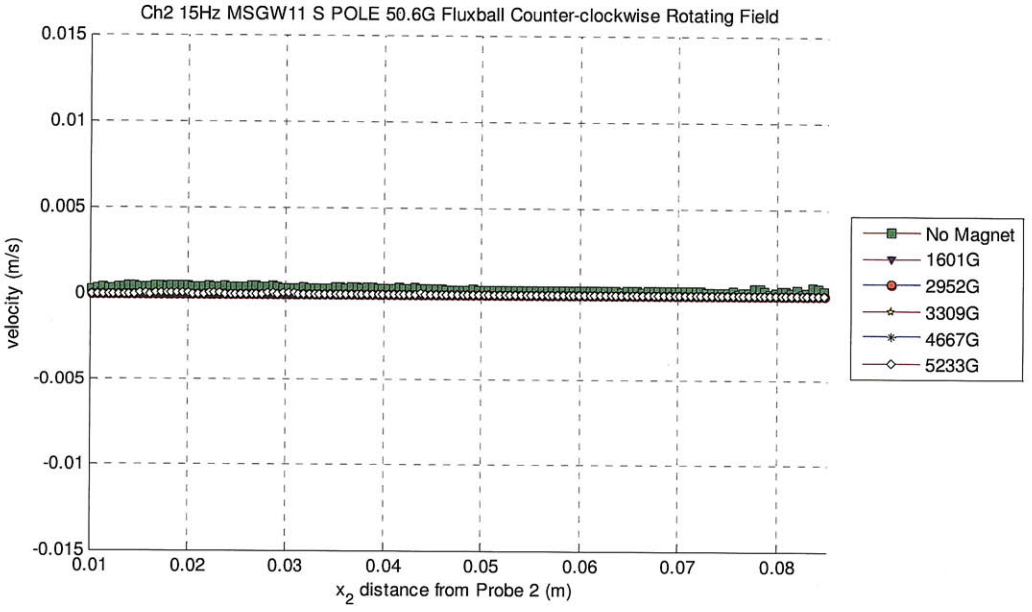
Ch2 15Hz MSGW11 S POLE 50.6G Fluxball Counter-clockwise Rotating Field
velocity (m/s)
0.015
0.01
0.005
0
-0.005
-0.01
-0.015
0.01
0.02
0.03
0.04
0.05
0.06
0.07
0.08
x2 distance from Probe 2 (m)
No Magnet
1601G
2952G
3309G
4667G
5233G

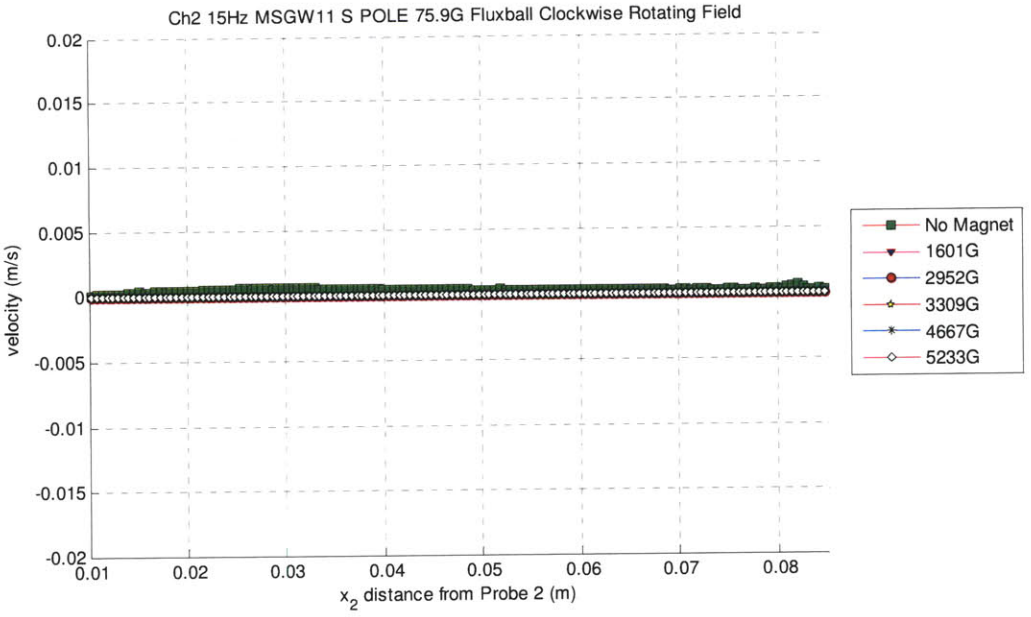
Ch2 15Hz MSGW11 S POLE 75.9G Fluxball Clockwise Rotating Field
velocity (m/s)
0.02
0.015
0.01
0.005
0
-0.005
-0.01
-0.015
-0.02
0.01
0.02
0.03
0.04
0.05
0.06
0.07
0.08
x2 distance from Probe 2 (m)
No Magnet
1601G
2952G
3309G
4667G
5233G

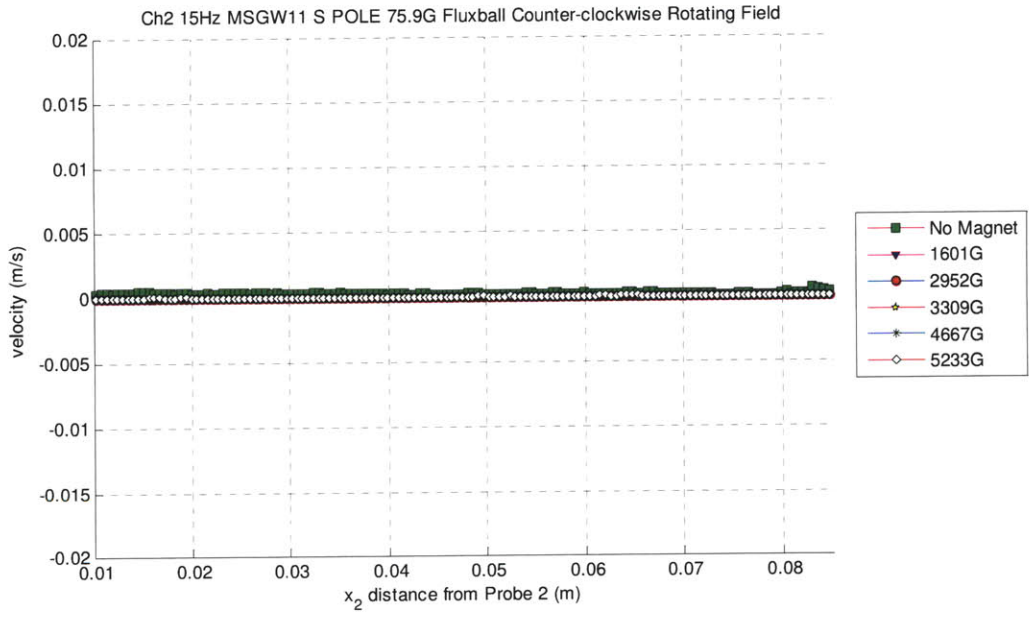
Ch2 15Hz MSGW11 S POLE 75.9G Fluxball Counter-clockwise Rotating Field
velocity (m/s)
0.02
0.015
0.01
0.005
0
-0.005
-0.01
-0.015
-0.02
0.01
0.02
0.03
0.04
0.05
0.06
0.07
0.08
x2 distance from Probe 2 (m)
No Magnet
1601G
2952G
3309G
4667G
5233G

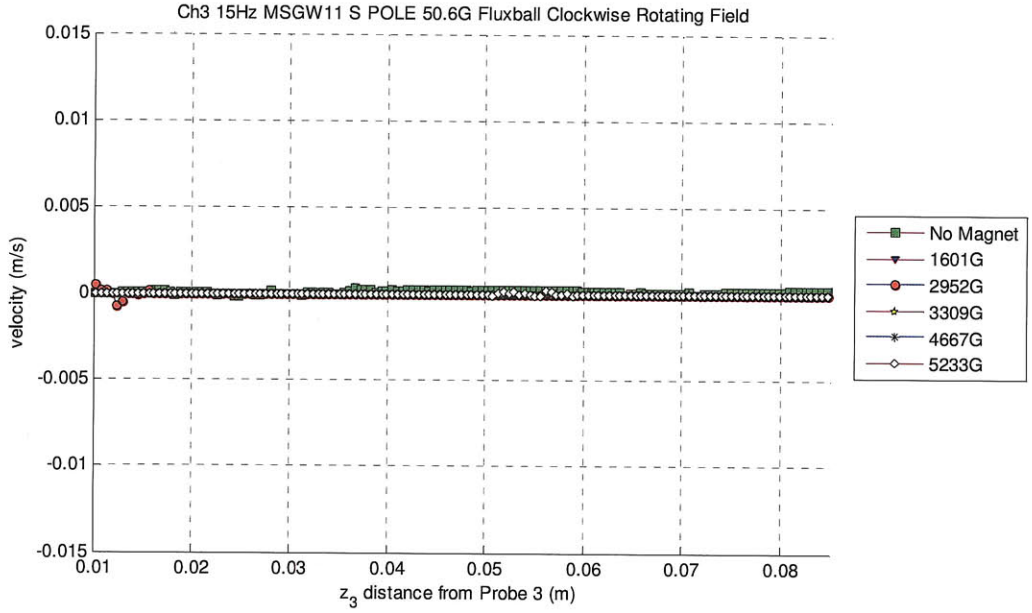
Ch3 15Hz MSGW11 S POLE 50.6G Fluxball Clockwise Rotating Field
velocity (m/s)
0.015
0.01
0.005
0
-0.005
-0.01
-0.015
0.01
0.02
0.03
0.04
0.05
0.06
0.07
0.08
z3 distance from Probe 3 (m)
No Magnet
1601G
2952G
3309G
4667G
5233G

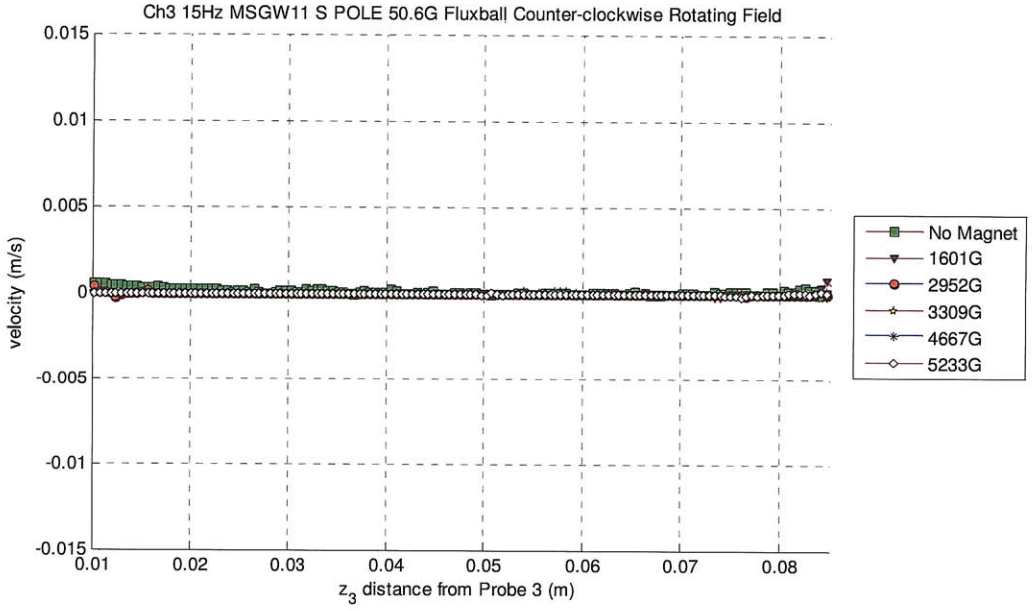
Ch3 15Hz MSGW11 S POLE 50.6G Fluxball Counter-clockwise Rotating Field
velocity (m/s)
0.015
0.01
0.005
0
-0.005
-0.01
-0.015
0.01
0.02
0.03
0.04
0.05
0.06
0.07
0.08
z3 distance from Probe 3 (m)
No Magnet
1601G
2952G
3309G
4667G
5233G

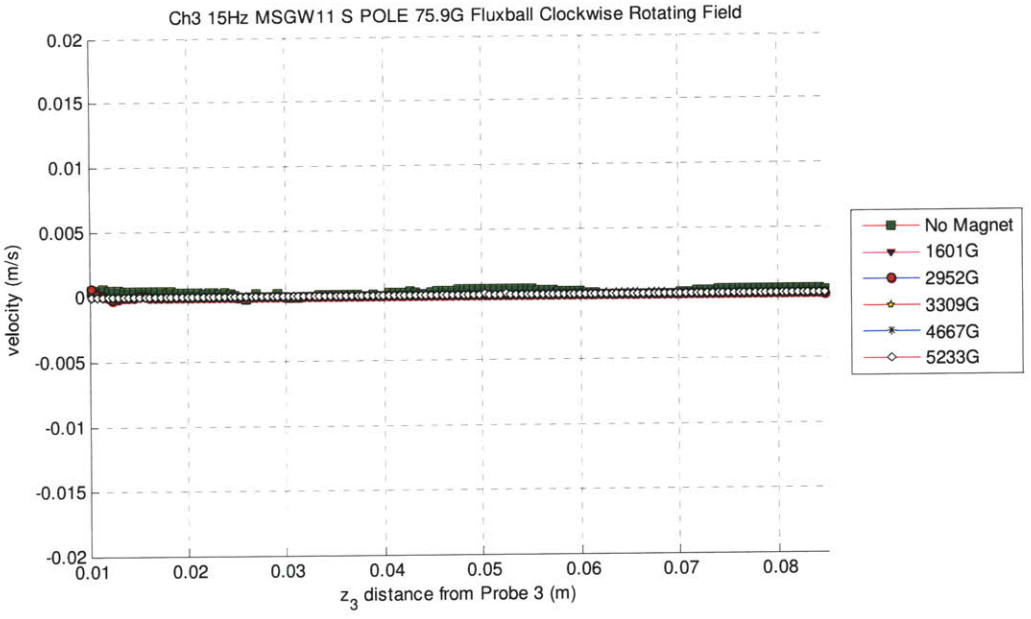
Ch3 15Hz MSGW11 S POLE 75.9G Fluxball Clockwise Rotating Field
velocity (m/s)
0.02
0.015
0.01
0.005
0
-0.005
-0.01
-0.015
-0.02
0.01
0.02
0.03
0.04
0.05
0.06
0.07
0.08
z_3 distance from Probe 3 (m)
No Magnet
1601G
2952G
3309G
4667G
5233G

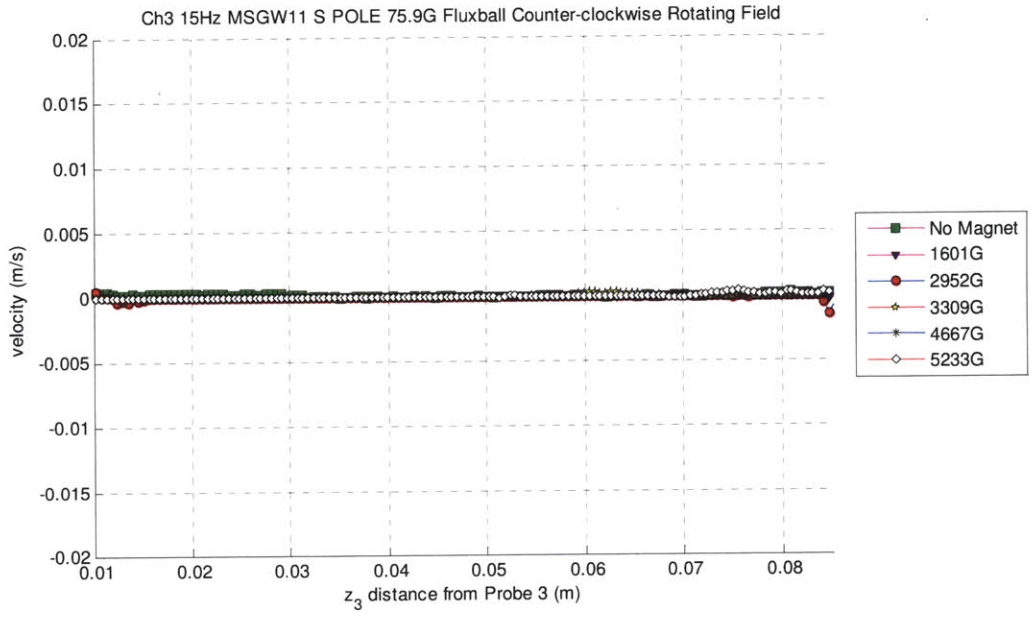
Ch3 15Hz MSGW11 S POLE 75.9G Fluxball Counter-clockwise Rotating Field
velocity (m/s)
0.02
0.015
0.01
0.005
0
-0.005
-0.01
-0.015
-0.02
0.01
0.02
0.03
0.04
0.05
0.06
0.07
0.08
z_3 distance from Probe 3 (m)
No Magnet
1601G
2952G
3309G
4667G
5233G

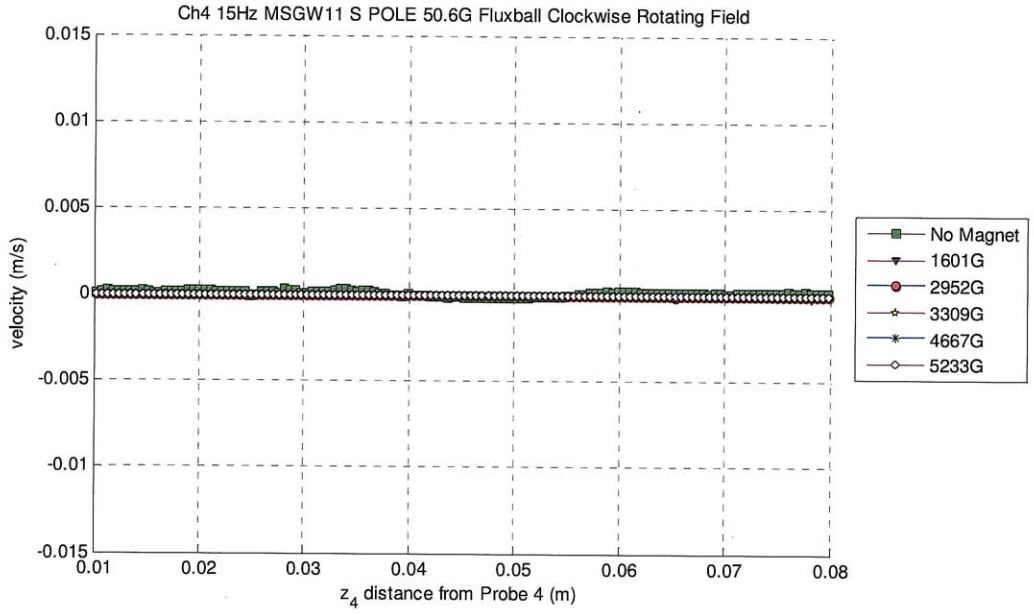
Ch4 15Hz MSGW11 S POLE 50.6G Fluxball Clockwise Rotating Field
velocity (m/s)
0.015
0.01
0.005
0
-0.005
-0.01
-0.015
0.01
0.02
0.03
0.04
0.05
0.06
0.07
0.08
z4 distance from Probe 4 (m)
No Magnet
1601G
2952G
3309G
4667G
5233G

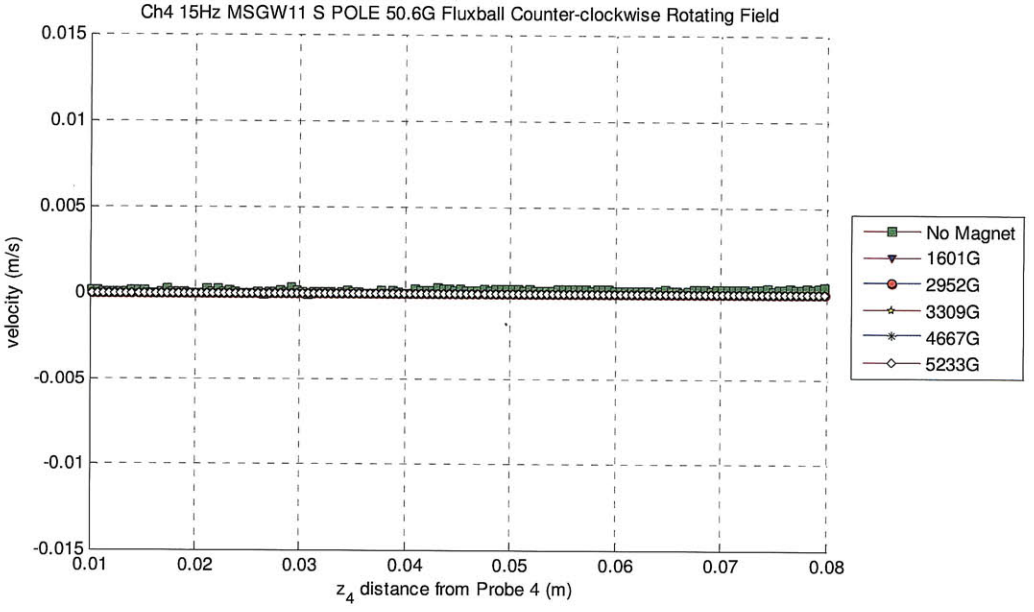
Ch4 15Hz MSGW11 S POLE 50.6G Fluxball Counter-clockwise Rotating Field
velocity (m/s)
0.015
0.01
0.005
0
-0.005
-0.01
-0.015
0.01
0.02
0.03
0.04
0.05
0.06
0.07
0.08
z4 distance from Probe 4 (m)
No Magnet
1601G
2952G
3309G
4667G
5233G

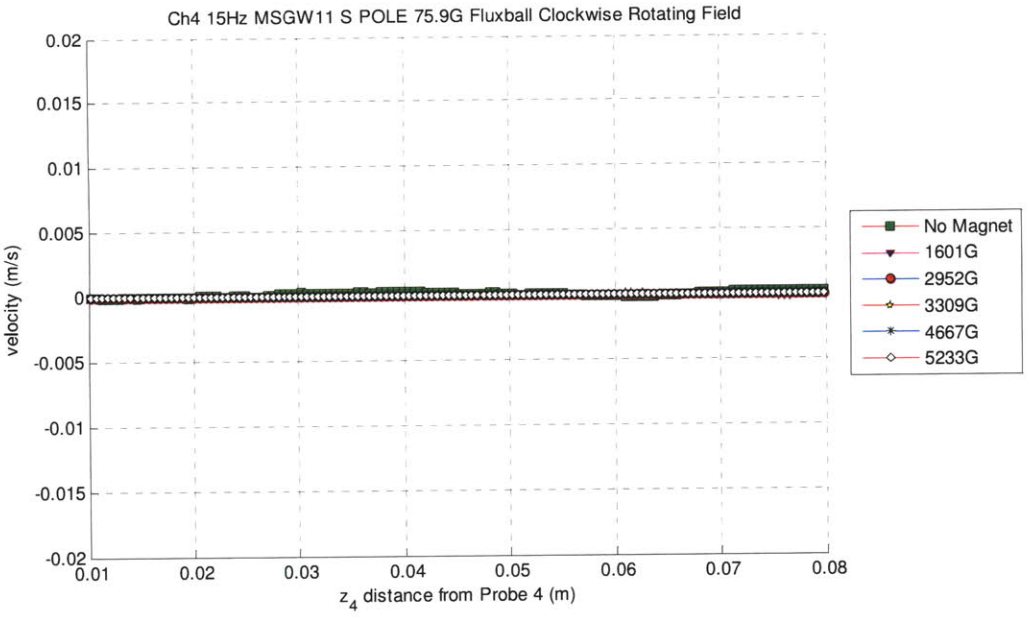
Ch4 15Hz MSGW11 S POLE 75.9G Fluxball Clockwise Rotating Field
velocity (m/s)
0.02
0.015
0.01
0.005
0
-0.005
-0.01
-0.015
-0.02
0.01
0.02
0.03
0.04
0.05
0.06
0.07
0.08
z4 distance from Probe 4 (m)
No Magnet
1601G
2952G
3309G
4667G
5233G

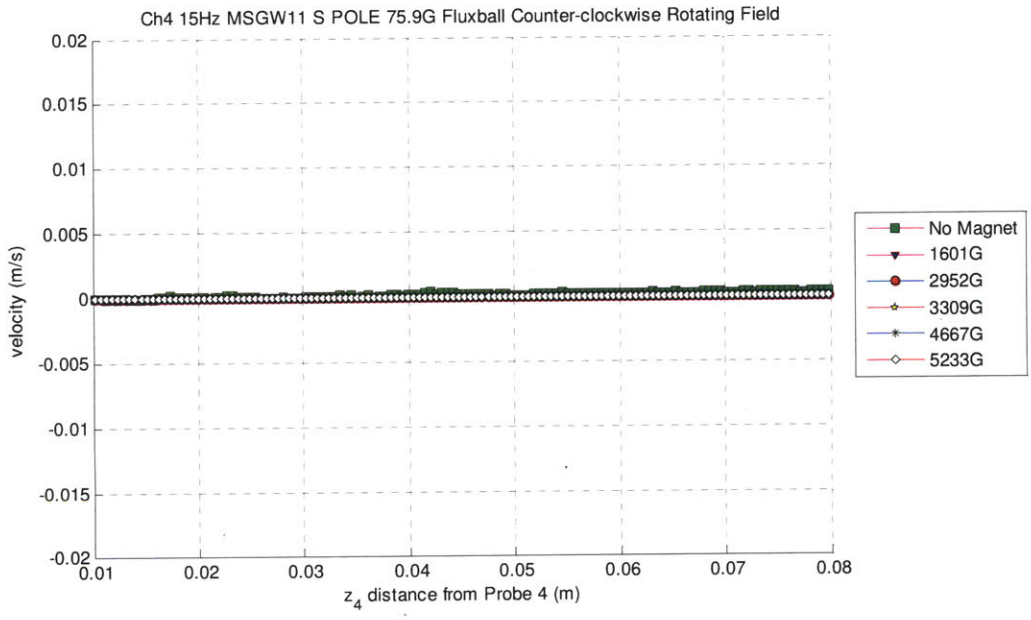
Ch4 15Hz MSGW11 S POLE 75.9G Fluxball Counter-clockwise Rotating Field
velocity (m/s)
0.02
0.015
0.01
0.005
0
-0.005
-0.01
-0.015
-0.02
0.01
0.02
0.03
0.04
0.05
0.06
0.07
0.08
z4 distance from Probe 4 (m)
No Magnet
1601G
2952G
3309G
4667G
5233G

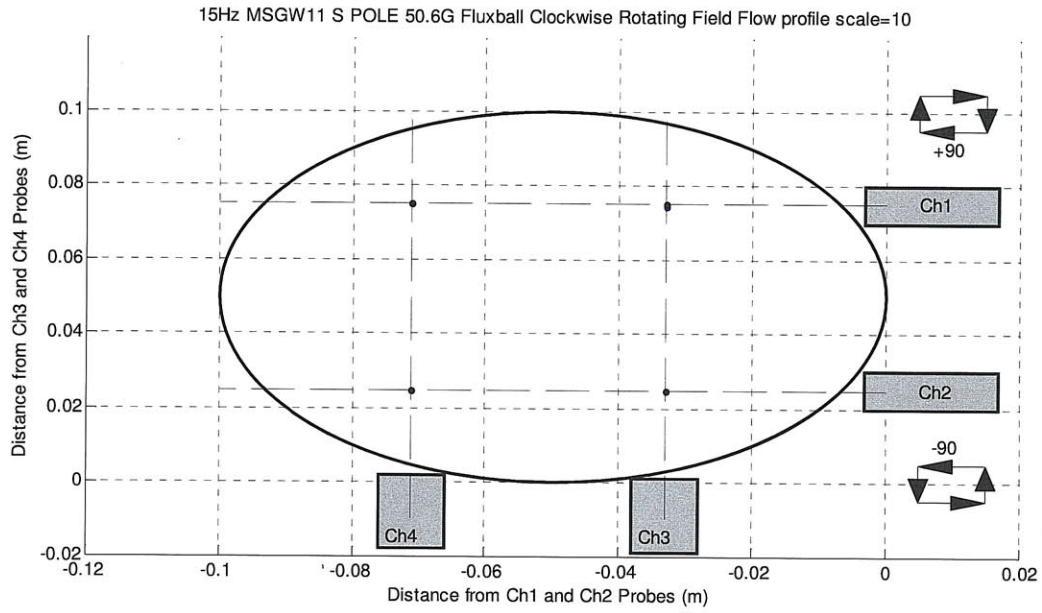
15Hz MSGW11 S POLE 50.6G Fluxball Clockwise Rotating Field Flow profile scale=10
Distance from Ch3 and Ch4 Probes (m)
Distance from Ch1 and Ch2 Probes (m)
0.1
0.08
0.06
0.04
0.02
0
-0.02
-0.12
-0.1
-0.08
-0.06
-0.04
-0.02
0
0.02
+90
Ch1
Ch2
-90
Ch4
Ch3

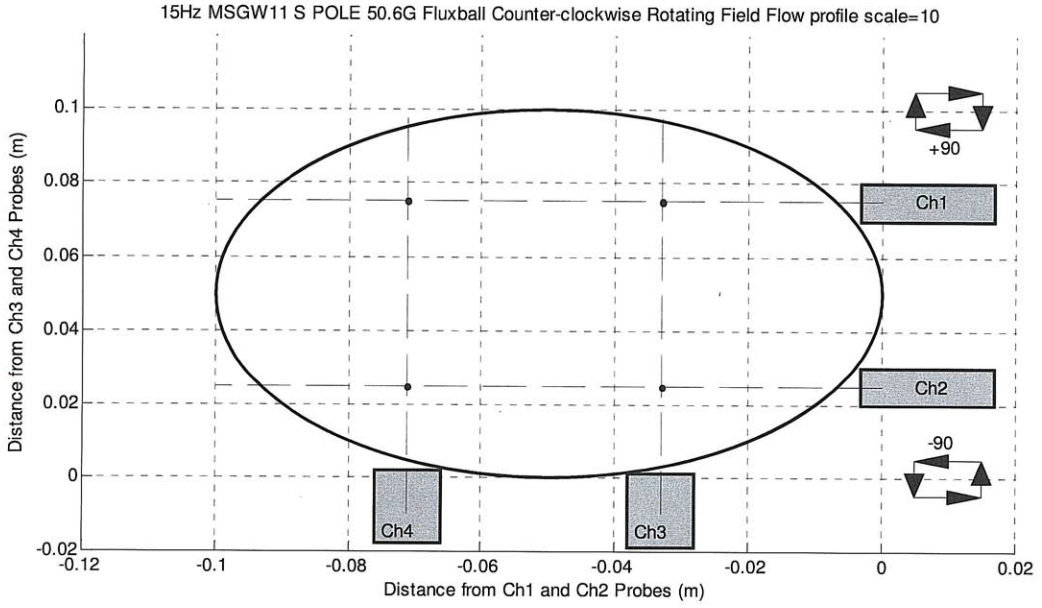
15Hz MSGW11 S POLE 50.6G Fluxball Counter-clockwise Rotating Field Flow profile scale=10
Distance from Ch3 and Ch4 Probes (m)
Distance from Ch1 and Ch2 Probes (m)
0.1
0.08
0.06
0.04
0.02
0
-0.02
-0.12
-0.1
-0.08
-0.06
-0.04
-0.02
0
0.02
+90
Ch1
Ch2
-90
Ch4
Ch3

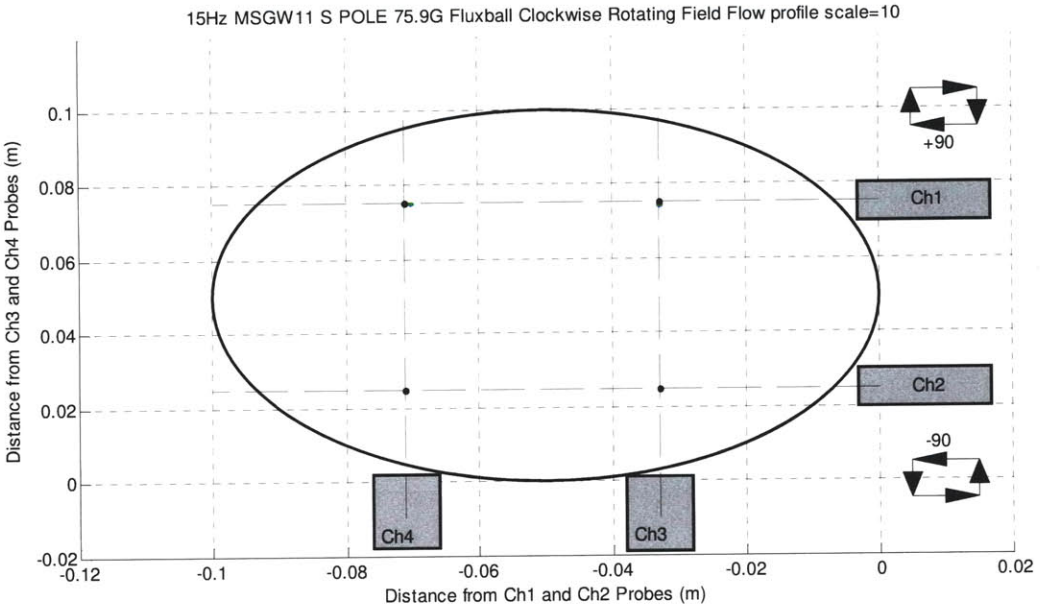
15Hz MSGW11 S POLE 75.9G Fluxball Clockwise Rotating Field Flow profile scale=10
Distance from Ch3 and Ch4 Probes (m)
Distance from Ch1 and Ch2 Probes (m)
+90
-90
Ch1
Ch2
Ch3
Ch4
0.1
0.08
0.06
0.04
0.02
0
-0.02
-0.12
-0.1
-0.08
-0.06
-0.04
-0.02
0
0.02

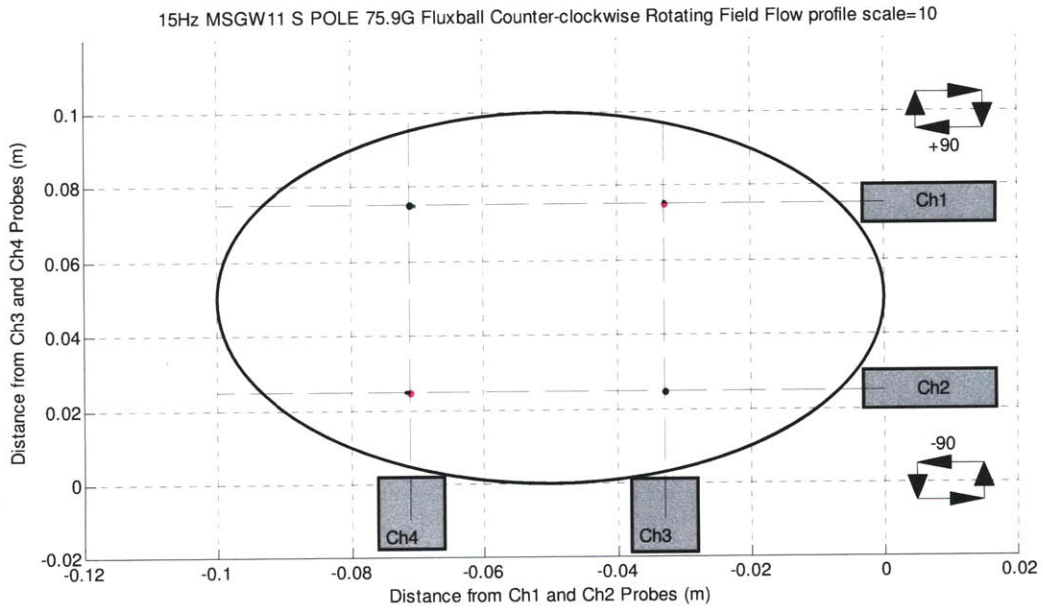
15Hz MSGW11 S POLE 75.9G Fluxball Counter-clockwise Rotating Field Flow profile scale=10
Distance from Ch3 and Ch4 Probes (m)
Distance from Ch1 and Ch2 Probes (m)
+90
-90
Ch1
Ch2
Ch3
Ch4
0.1
0.08
0.06
0.04
0.02
0
-0.02
-0.12
-0.1
-0.08
-0.06
-0.04
-0.02
0
0.02

H10. MSGW11 Filled Sphere with North Pole Facing Magnets on Top of Sphere at 95Hz

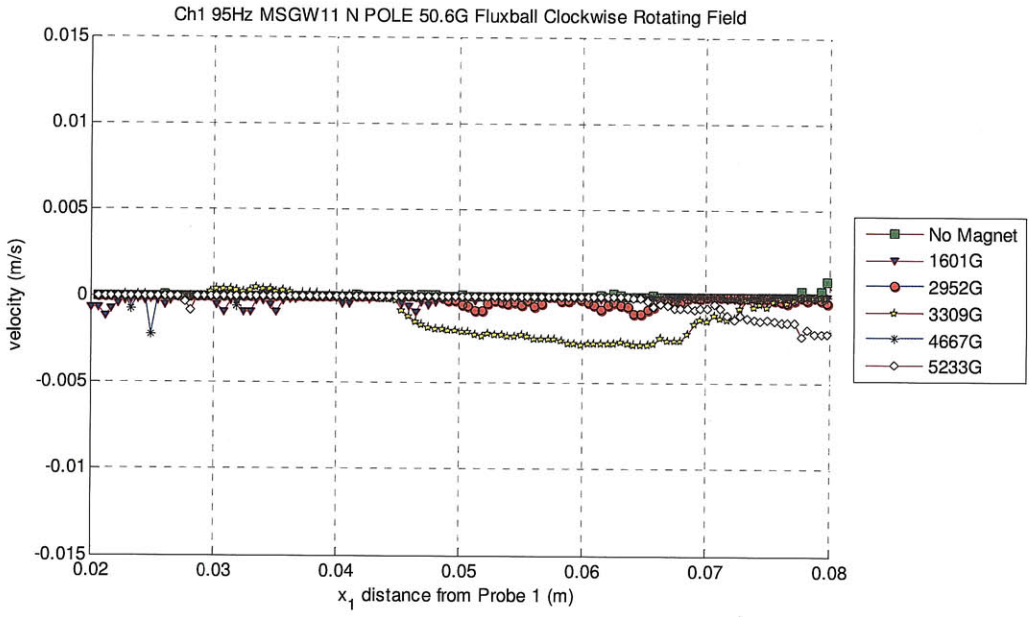

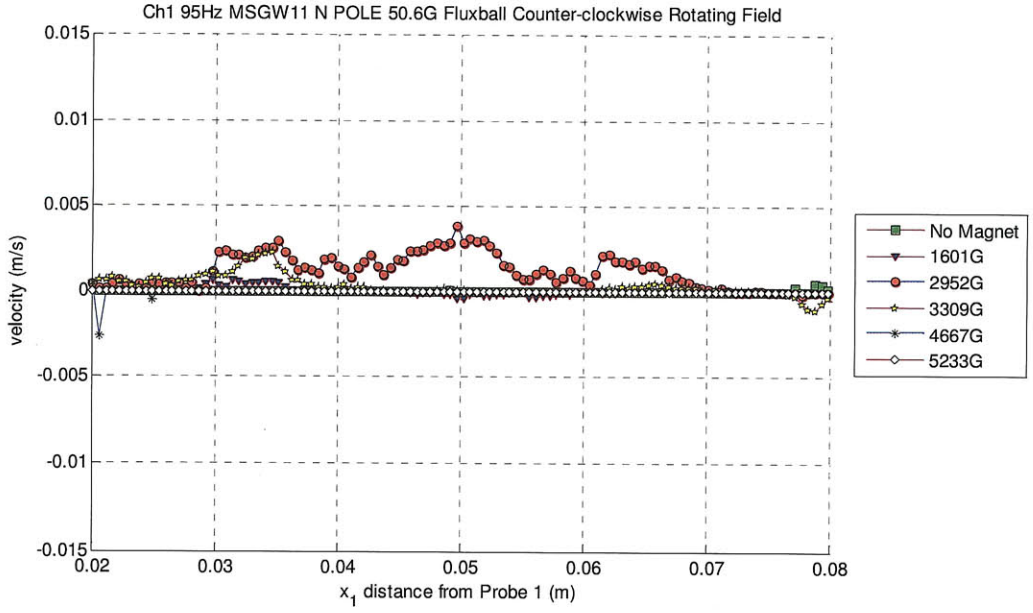

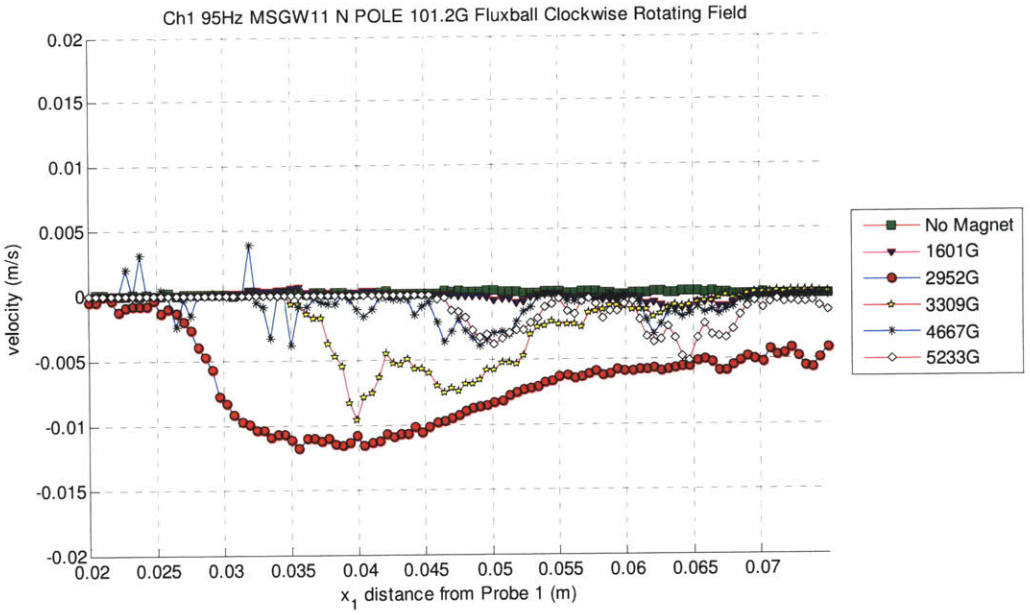
Ch1 95Hz MSGW11 N POLE 101.2G Fluxball Clockwise Rotating Field
velocity (m/s)
0.02
0.015
0.01
0.005
0
-0.005
-0.01
-0.015
-0.02
0.02 0.025 0.03 0.035 0.04 0.045 0.05 0.055 0.06 0.065 0.07
x1 distance from Probe 1 (m)
No Magnet
1601G
2952G
3309G
4667G
5233G

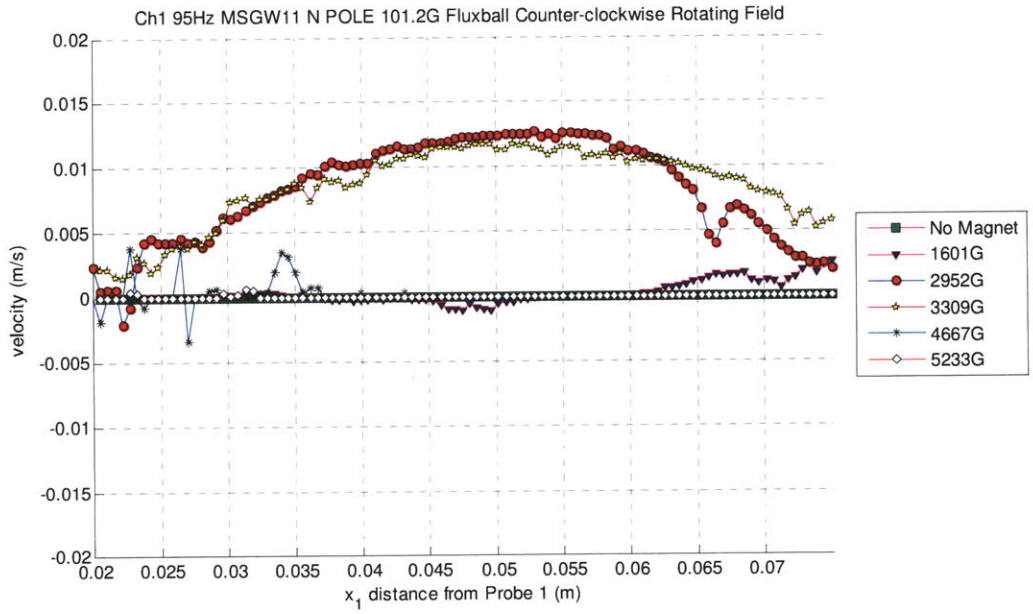
Ch1 95Hz MSGW11 N POLE 101.2G Fluxball Counter-clockwise Rotating Field
velocity (m/s)
0.02
0.015
0.01
0.005
0
-0.005
-0.01
-0.015
-0.02
0.02 0.025 0.03 0.035 0.04 0.045 0.05 0.055 0.06 0.065 0.07
x1 distance from Probe 1 (m)
No Magnet
1601G
2952G
3309G
4667G
5233G

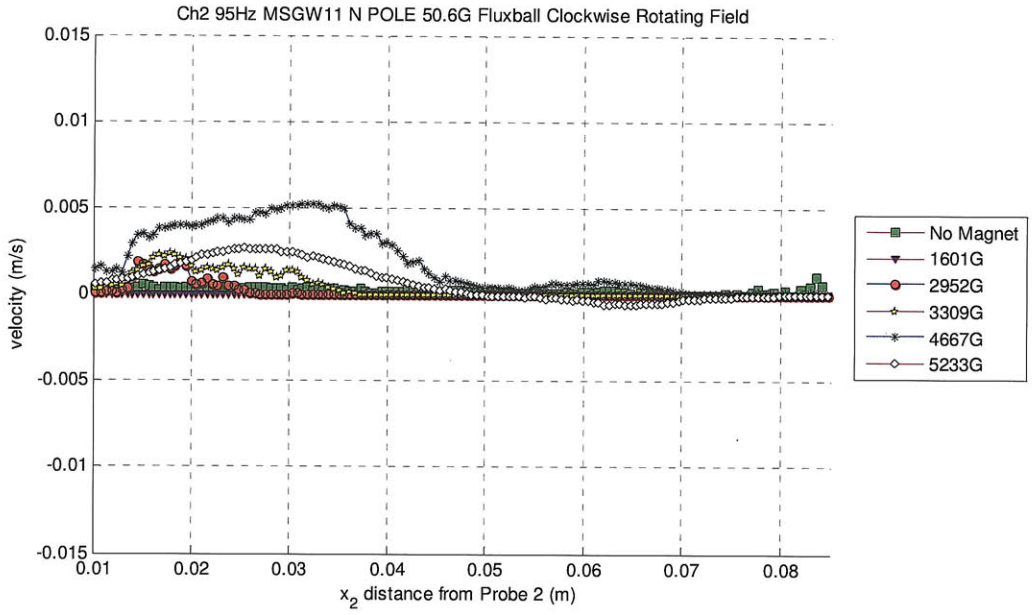
Ch2 95Hz MSGW11 N POLE 50.6G Fluxball Clockwise Rotating Field
velocity (m/s)
0.015
0.01
0.005
0
-0.005
-0.01
-0.015
0.01
0.02
0.03
0.04
0.05
0.06
0.07
0.08
x2 distance from Probe 2 (m)
No Magnet
1601G
2952G
3309G
4667G
5233G

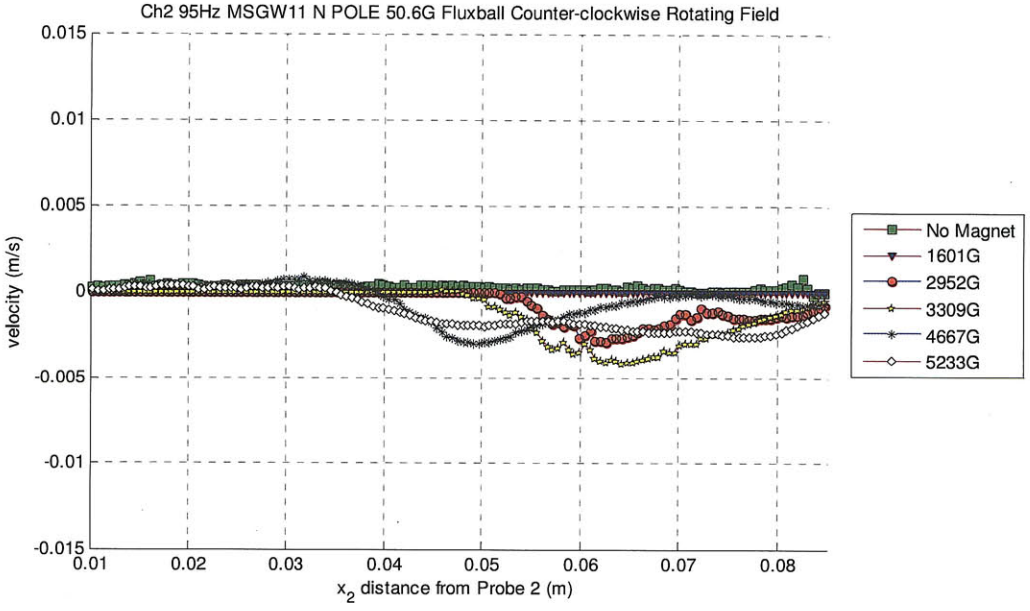
Ch2 95Hz MSGW11 N POLE 50.6G Fluxball Counter-clockwise Rotating Field
velocity (m/s)
0.015
0.01
0.005
0
-0.005
-0.01
-0.015
0.01
0.02
0.03
0.04
0.05
0.06
0.07
0.08
x2 distance from Probe 2 (m)
No Magnet
1601G
2952G
3309G
4667G
5233G

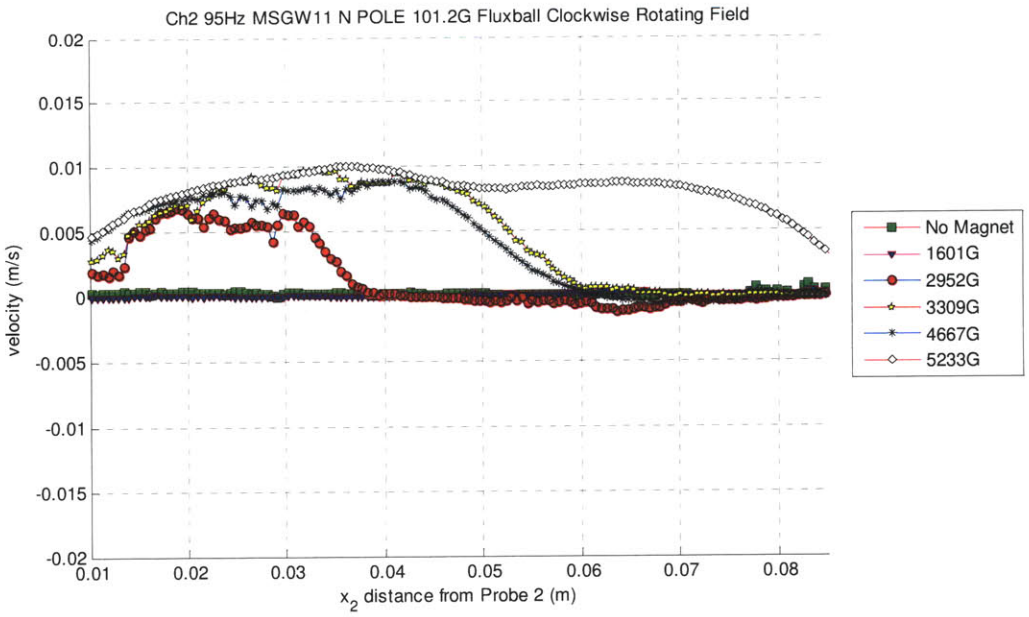
Ch2 95Hz MSGW11 N POLE 101.2G Fluxball Clockwise Rotating Field
velocity (m/s)
0.02
0.015
0.01
0.005
0
-0.005
-0.01
-0.015
-0.02
0.01
0.02
0.03
0.04
0.05
0.06
0.07
0.08
x2 distance from Probe 2 (m)
No Magnet
1601G
2952G
3309G
4667G
5233G

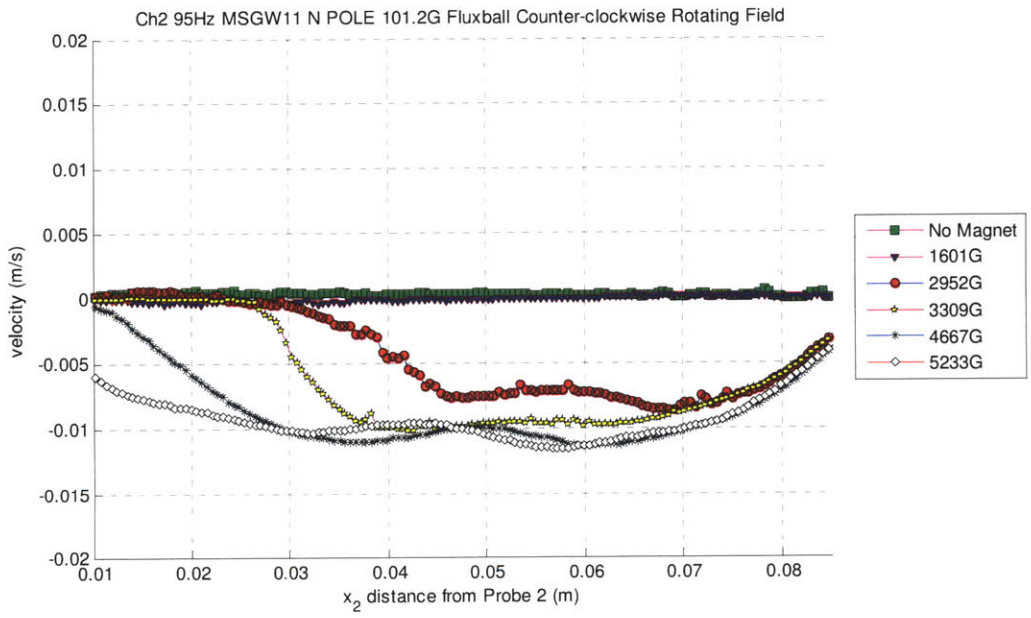
Ch2 95Hz MSGW11 N POLE 101.2G Fluxball Counter-clockwise Rotating Field
velocity (m/s)
0.02
0.015
0.01
0.005
0
-0.005
-0.01
-0.015
-0.02
0.01
0.02
0.03
0.04
0.05
0.06
0.07
0.08
x2 distance from Probe 2 (m)
No Magnet
1601G
2952G
3309G
4667G
5233G

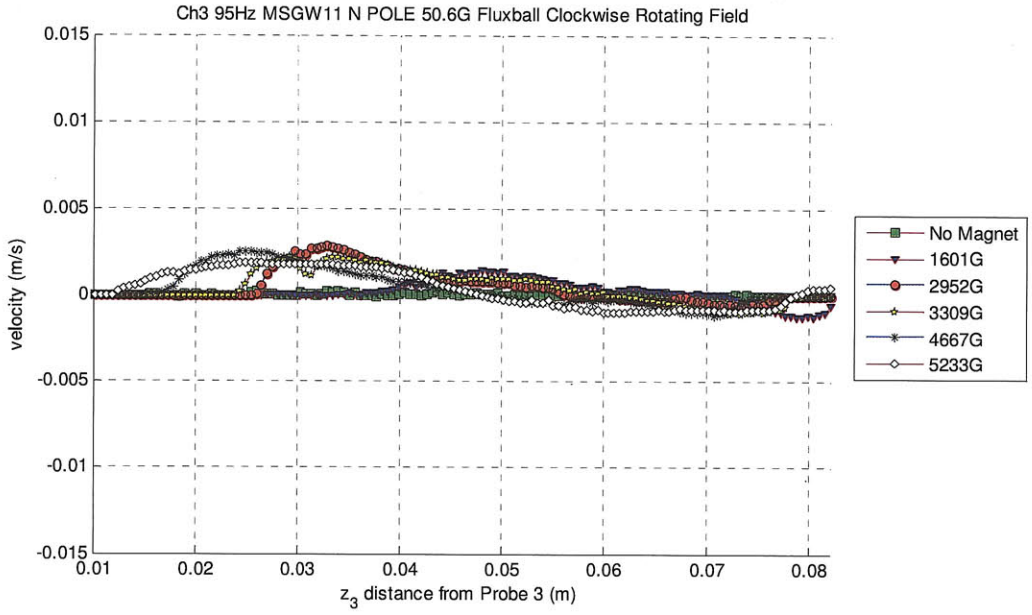
Ch3 95Hz MSGW11 N POLE 50.6G Fluxball Clockwise Rotating Field
velocity (m/s)
0.015
0.01
0.005
0
-0.005
-0.01
-0.015
0.01
0.02
0.03
0.04
0.05
0.06
0.07
0.08
z_3 distance from Probe 3 (m)
No Magnet
1601G
2952G
3309G
4667G
5233G

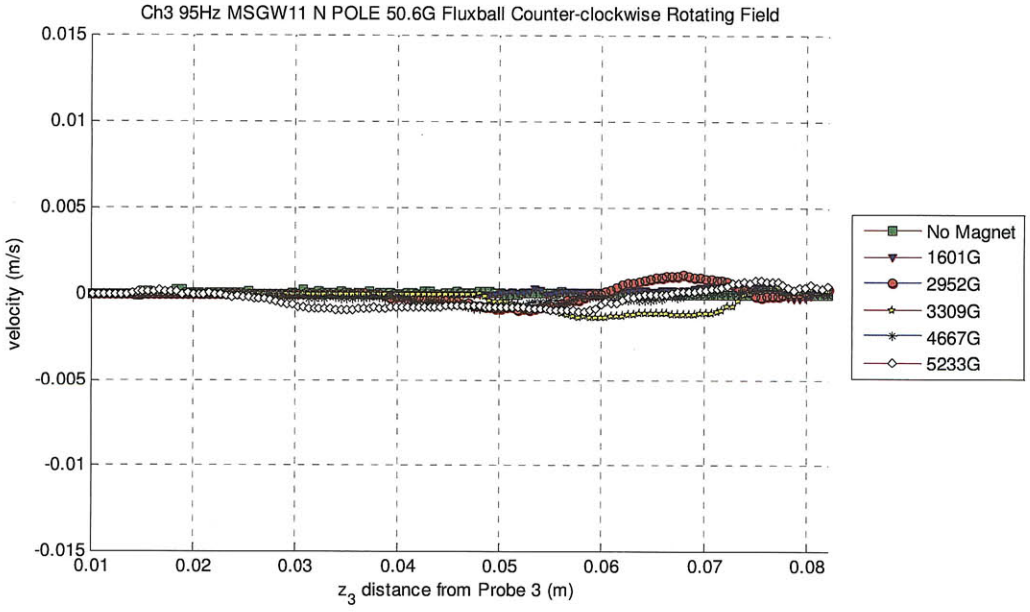
Ch3 95Hz MSGW11 N POLE 50.6G Fluxball Counter-clockwise Rotating Field
velocity (m/s)
0.015
0.01
0.005
0
-0.005
-0.01
-0.015
0.01
0.02
0.03
0.04
0.05
0.06
0.07
0.08
z_3 distance from Probe 3 (m)
No Magnet
1601G
2952G
3309G
4667G
5233G

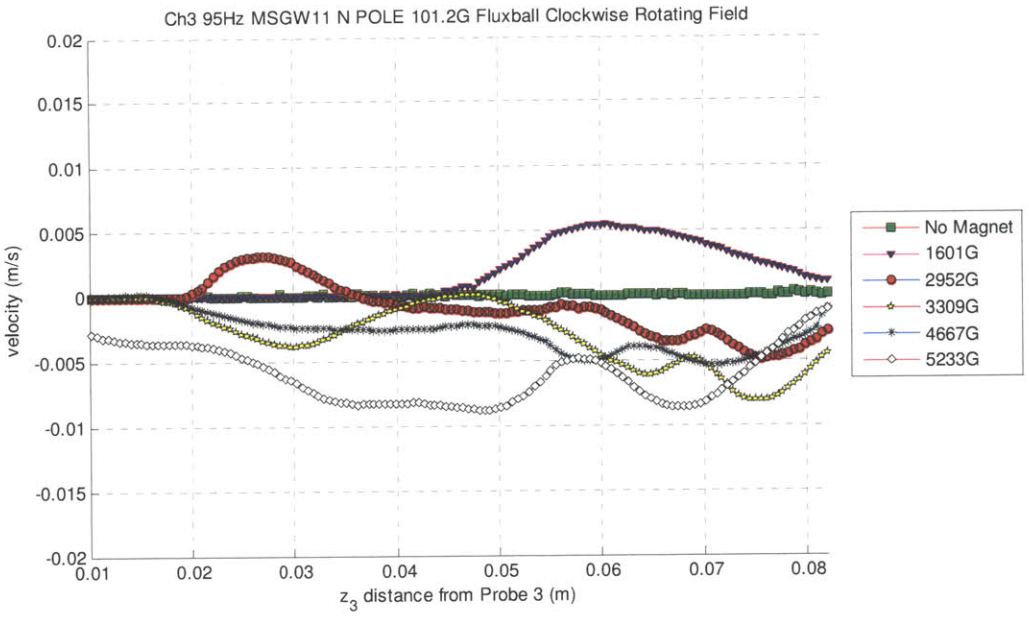
Ch3 95Hz MSGW11 N POLE 101.2G Fluxball Clockwise Rotating Field
velocity (m/s)
0.02
0.015
0.01
0.005
0
-0.005
-0.01
-0.015
-0.02
0.01
0.02
0.03
0.04
0.05
0.06
0.07
0.08
z_3 distance from Probe 3 (m)
No Magnet
1601G
2952G
3309G
4667G
5233G

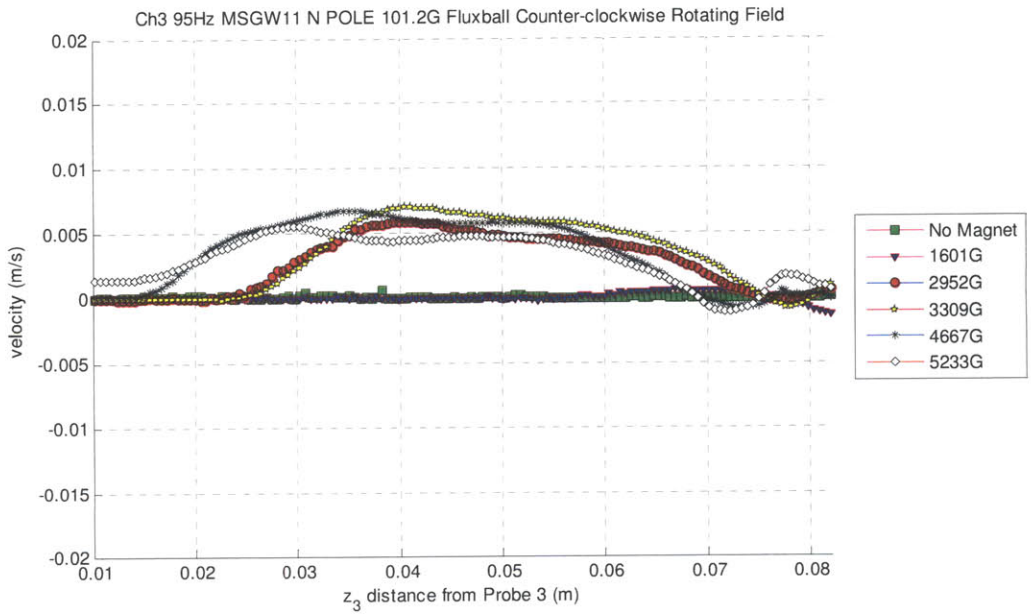
Ch3 95Hz MSGW11 N POLE 101.2G Fluxball Counter-clockwise Rotating Field
velocity (m/s)
0.02
0.015
0.01
0.005
0
-0.005
-0.01
-0.015
-0.02
0.01
0.02
0.03
0.04
0.05
0.06
0.07
0.08
z_3 distance from Probe 3 (m)
No Magnet
1601G
2952G
3309G
4667G
5233G

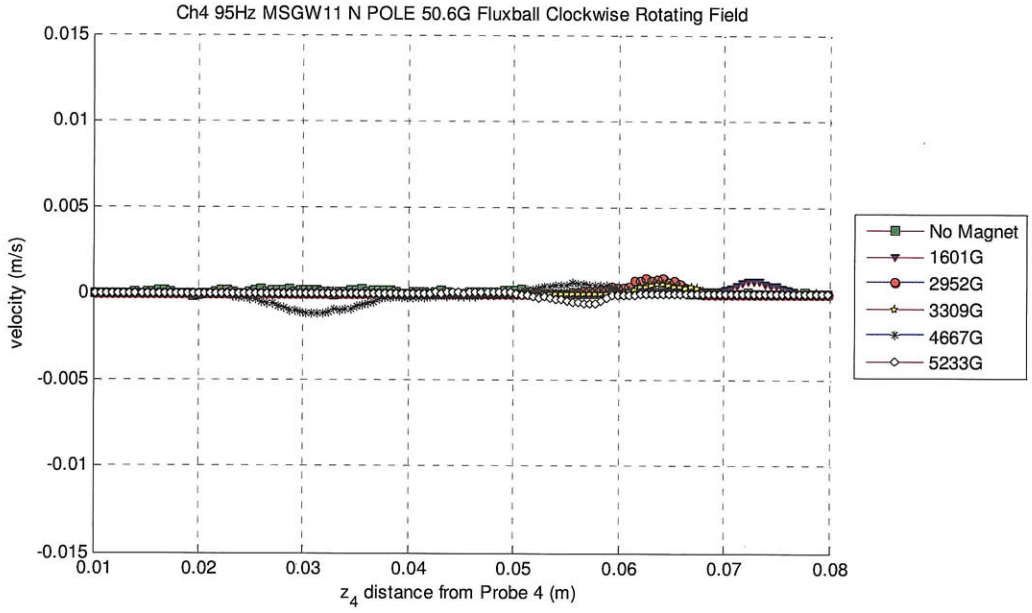
Ch4 95Hz MSGW11 N POLE 50.6G Fluxball Clockwise Rotating Field
velocity (m/s)
0.015
0.01
0.005
0
-0.005
-0.01
-0.015
0.01
0.02
0.03
0.04
0.05
0.06
0.07
0.08
z4 distance from Probe 4 (m)
No Magnet
1601G
2952G
3309G
4667G
5233G

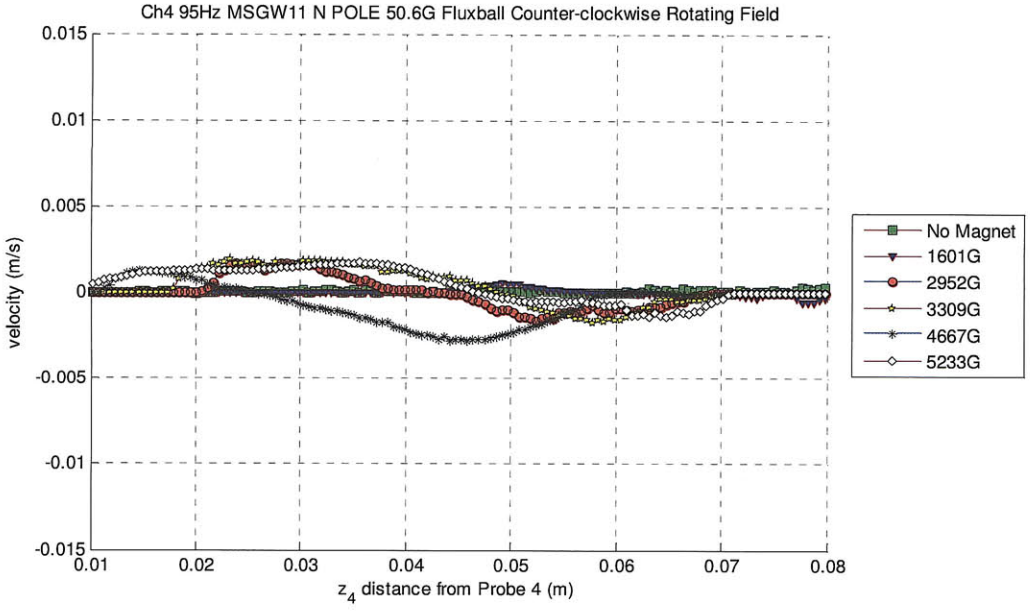
Ch4 95Hz MSGW11 N POLE 50.6G Fluxball Counter-clockwise Rotating Field
velocity (m/s)
0.015
0.01
0.005
0
-0.005
-0.01
-0.015
0.01
0.02
0.03
0.04
0.05
0.06
0.07
0.08
z4 distance from Probe 4 (m)
No Magnet
1601G
2952G
3309G
4667G
5233G

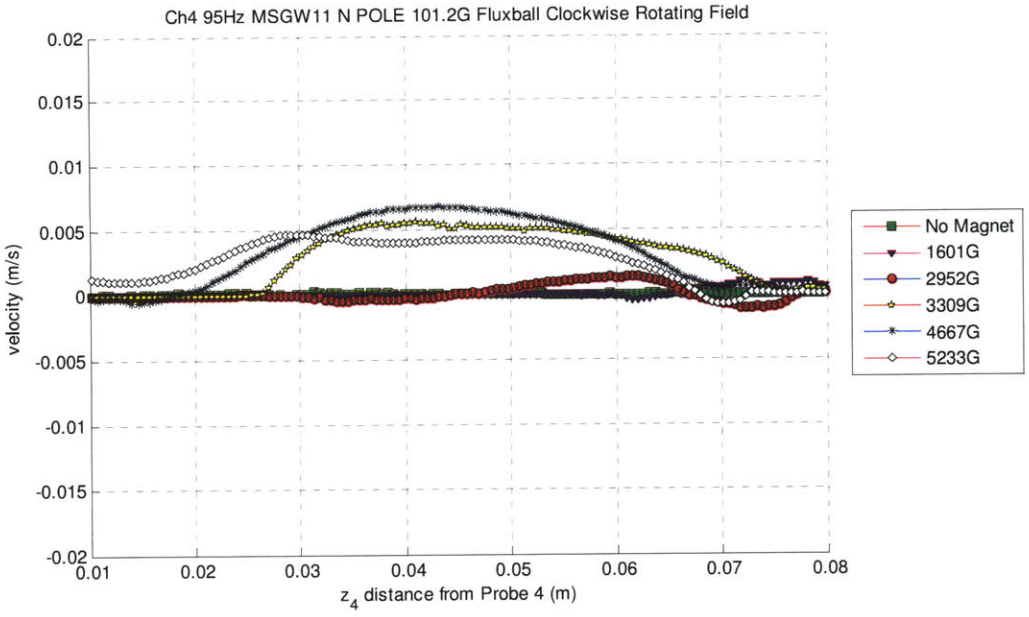
Ch4 95Hz MSGW11 N POLE 101.2G Fluxball Clockwise Rotating Field
velocity (m/s)
0.02
0.015
0.01
0.005
0
-0.005
-0.01
-0.015
-0.02
0.01
0.02
0.03
0.04
0.05
0.06
0.07
0.08
z_4 distance from Probe 4 (m)
No Magnet
1601G
2952G
3309G
4667G
5233G

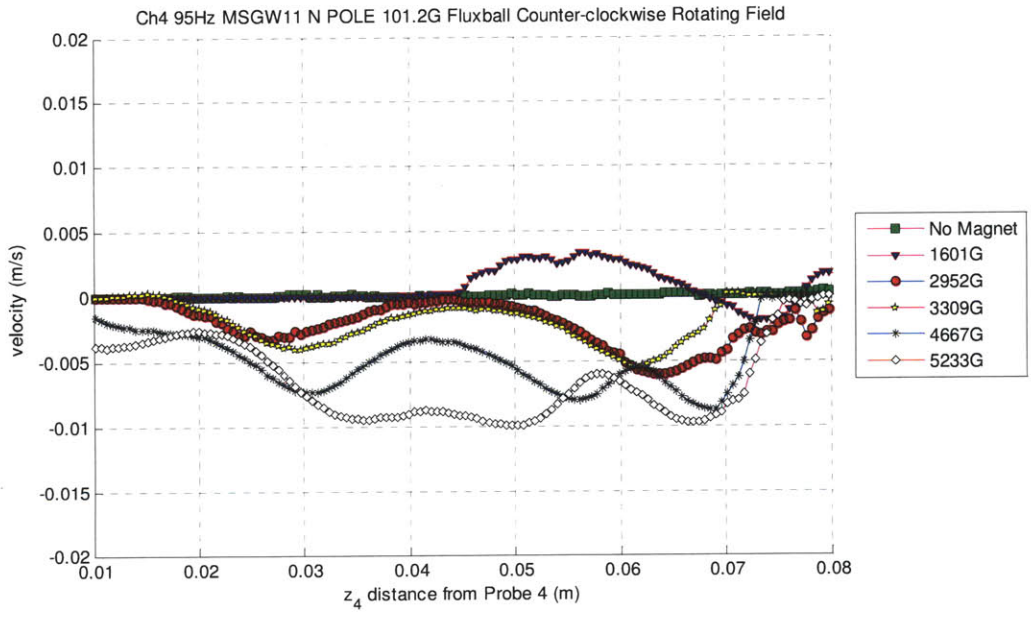
Ch4 95Hz MSGW11 N POLE 101.2G Fluxball Counter-clockwise Rotating Field
velocity (m/s)
0.02
0.015
0.01
0.005
0
-0.005
-0.01
-0.015
-0.02
0.01
0.02
0.03
0.04
0.05
0.06
0.07
0.08
z_4 distance from Probe 4 (m)
No Magnet
1601G
2952G
3309G
4667G
5233G

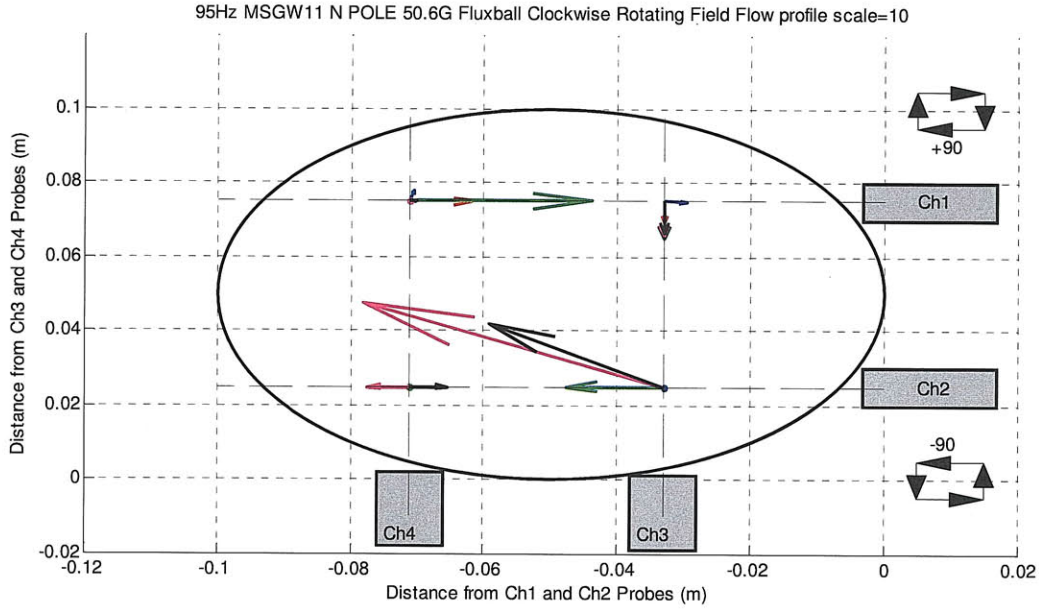
95Hz MSGW11 N POLE 50.6G Fluxball Clockwise Rotating Field Flow profile scale=10
Distance from Ch3 and Ch4 Probes (m)
Distance from Ch1 and Ch2 Probes (m)
+90
-90
Ch1
Ch2
Ch3
Ch4
0.1
0.08
0.06
0.04
0.02
0
-0.02
-0.12
-0.1
-0.08
-0.06
-0.04
-0.02
0
0.02

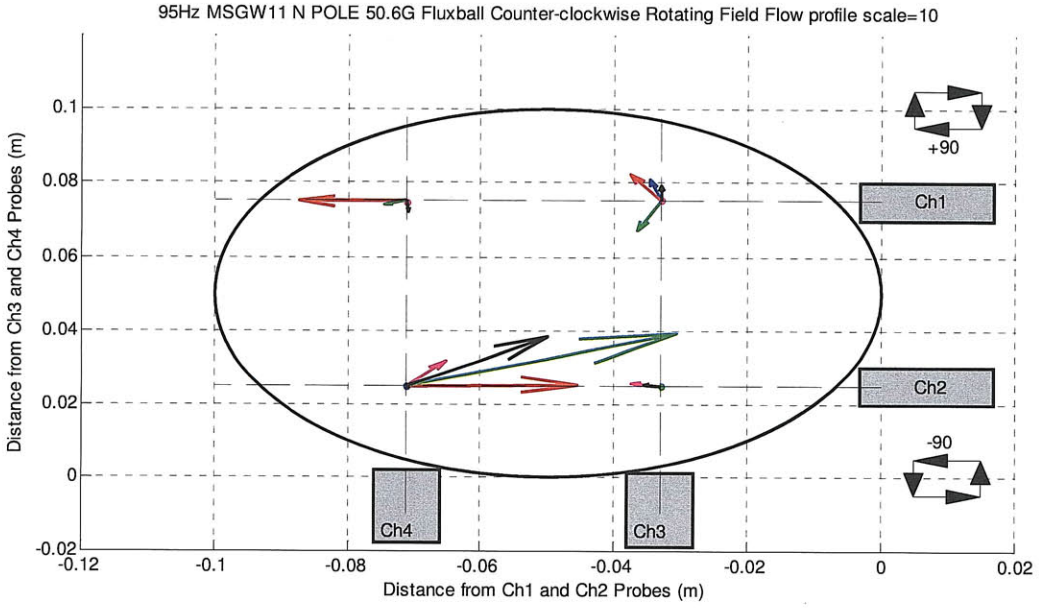
95Hz MSGW11 N POLE 50.6G Fluxball Counter-clockwise Rotating Field Flow profile scale=10
Distance from Ch3 and Ch4 Probes (m)
Distance from Ch1 and Ch2 Probes (m)
+90
-90
Ch1
Ch2
Ch3
Ch4
0.1
0.08
0.06
0.04
0.02
0
-0.02
-0.12
-0.1
-0.08
-0.06
-0.04
-0.02
0
0.02

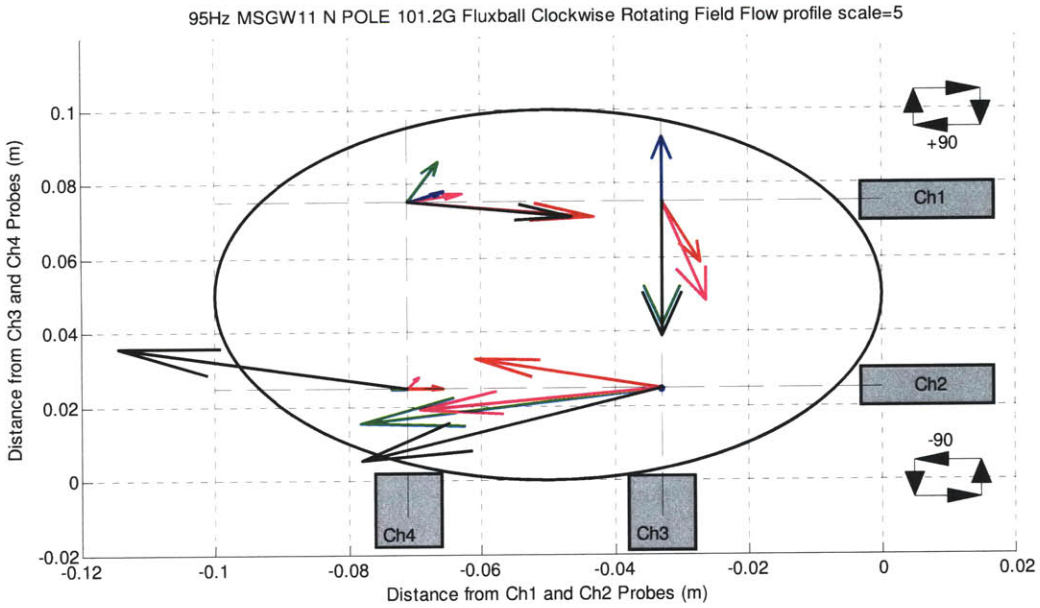
95Hz MSGW11 N POLE 101.2G Fluxball Clockwise Rotating Field Flow profile scale=5
Distance from Ch3 and Ch4 Probes (m)
Distance from Ch1 and Ch2 Probes (m)
+90
-90
Ch1
Ch2
Ch3
Ch4
0.1
0.08
0.06
0.04
0.02
0
-0.02
-0.12
-0.1
-0.08
-0.06
-0.04
-0.02
0
0.02

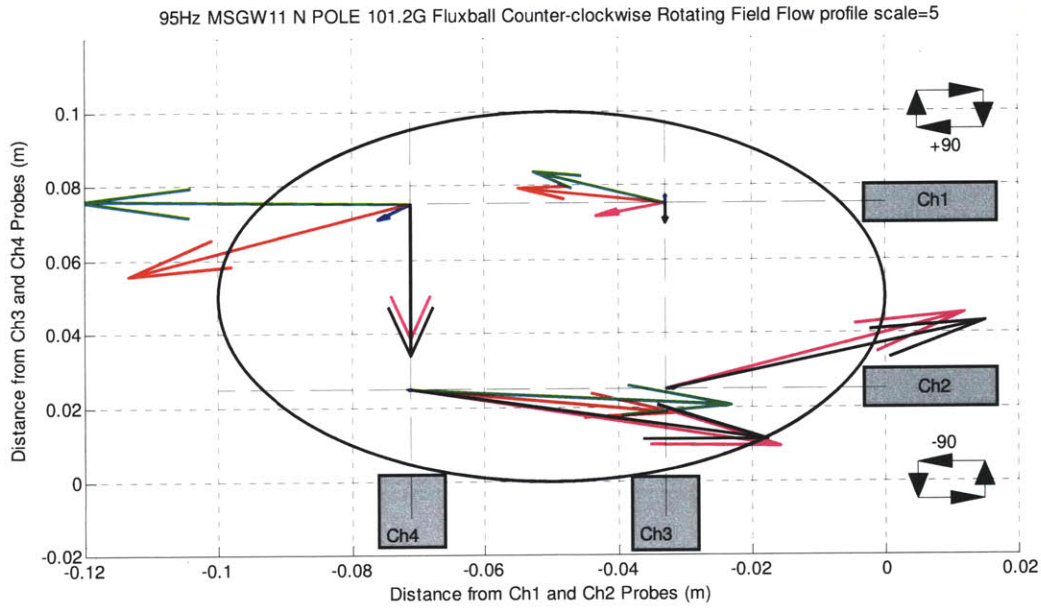
95Hz MSGW11 N POLE 101.2G Fluxball Counter-clockwise Rotating Field Flow profile scale=5
Distance from Ch3 and Ch4 Probes (m)
Distance from Ch1 and Ch2 Probes (m)
+90
-90
Ch1
Ch2
Ch3
Ch4
0.1
0.08
0.06
0.04
0.02
0
-0.02
-0.12
-0.1
-0.08
-0.06
-0.04
-0.02
0
0.02

H11. MSGW11 Filled Sphere with North Pole Facing Magnets on Top of Sphere at 47Hz

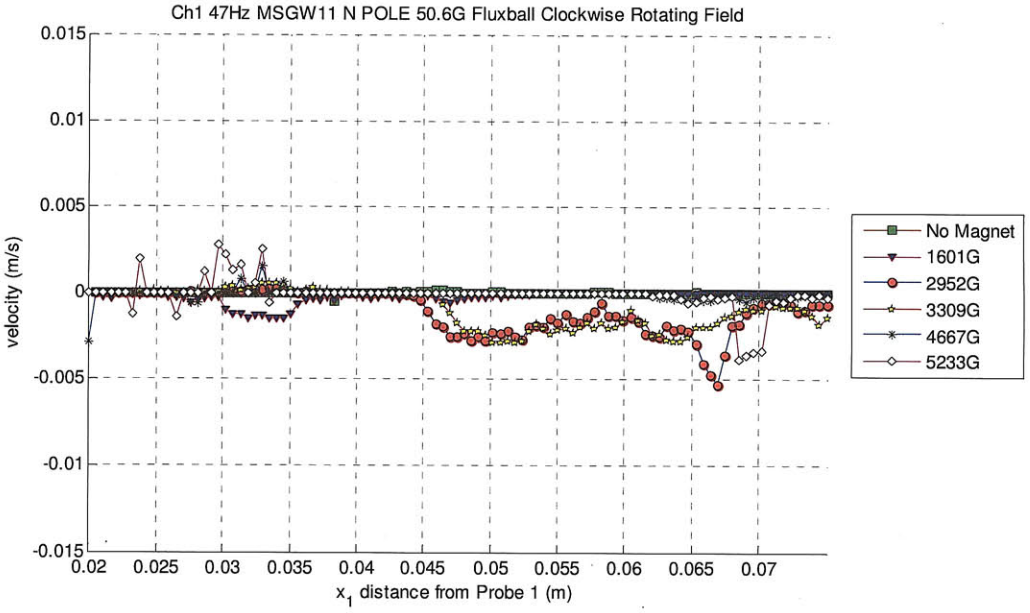

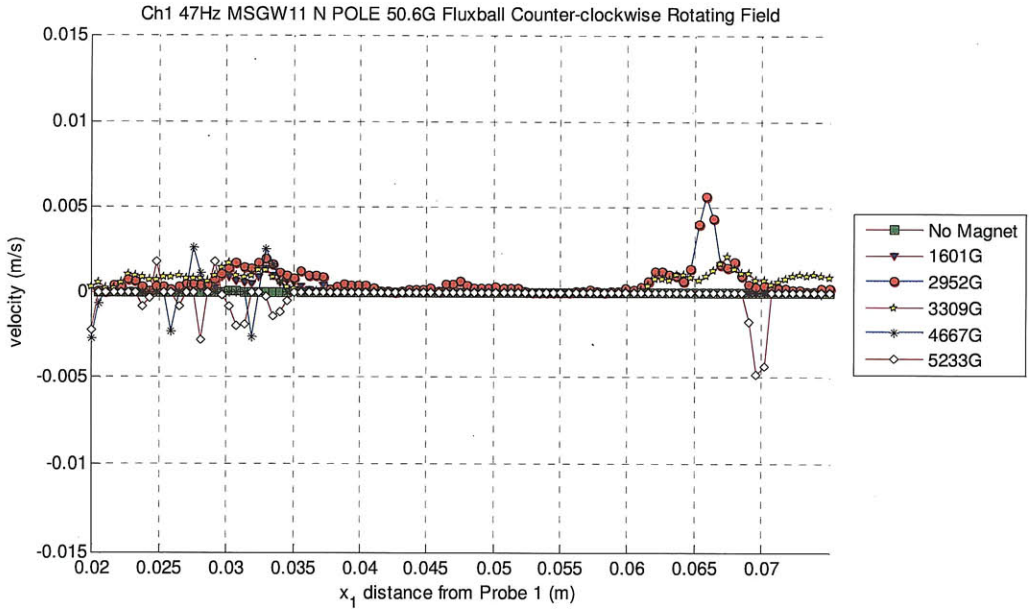

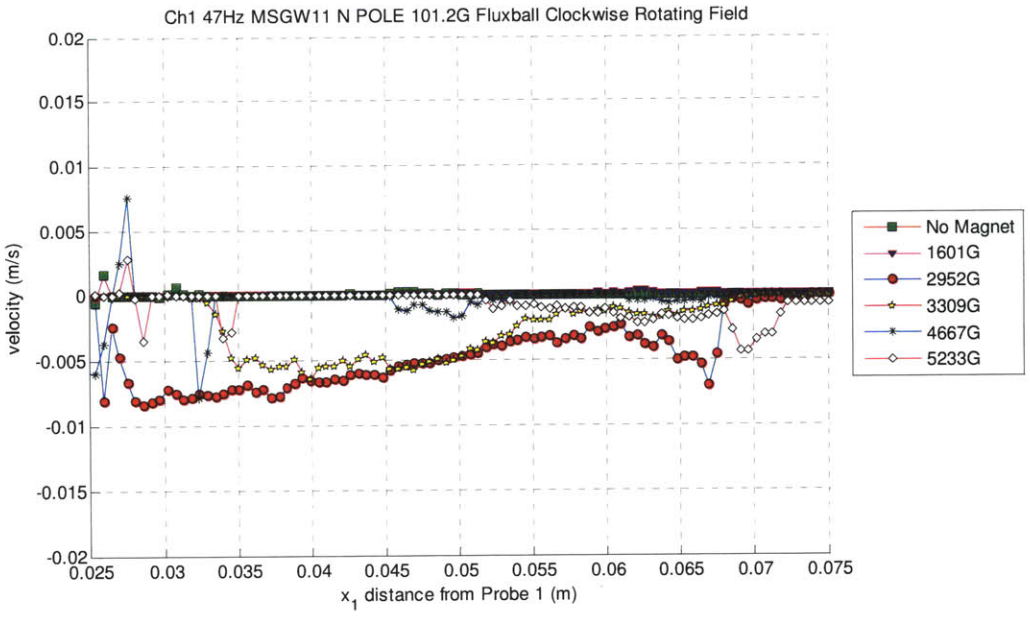
Ch1 47Hz MSGW11 N POLE 101.2G Fluxball Clockwise Rotating Field
velocity (m/s)
0.02
0.015
0.01
0.005
0
-0.005
-0.01
-0.015
-0.02
0.025
0.03
0.035
0.04
0.045
0.05
0.055
0.06
0.065
0.07
0.075
x1 distance from Probe 1 (m)
No Magnet
1601G
2952G
3309G
4667G
5233G

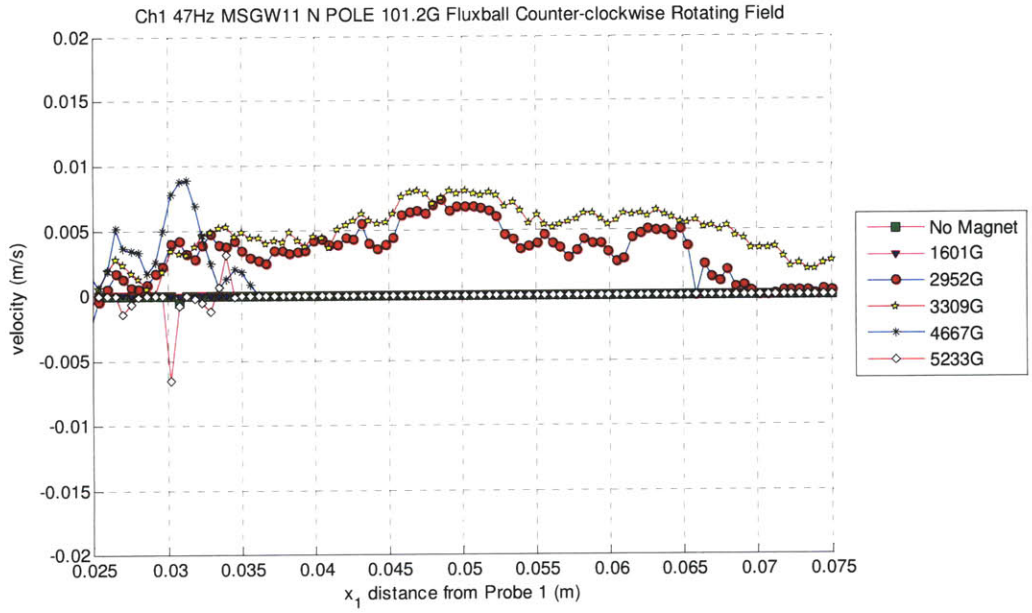
Ch1 47Hz MSGW11 N POLE 101.2G Fluxball Counter-clockwise Rotating Field
velocity (m/s)
0.02
0.015
0.01
0.005
0
-0.005
-0.01
-0.015
-0.02
0.025
0.03
0.035
0.04
0.045
0.05
0.055
0.06
0.065
0.07
0.075
x1 distance from Probe 1 (m)
No Magnet
1601G
2952G
3309G
4667G
5233G

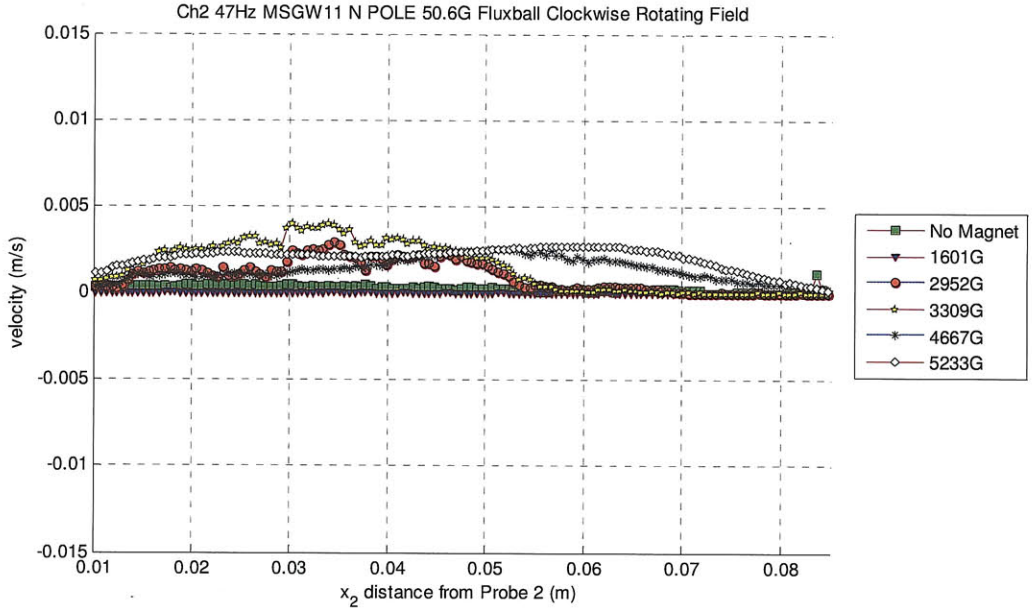
Ch2 47Hz MSGW11 N POLE 50.6G Fluxball Clockwise Rotating Field
velocity (m/s)
0.015
0.01
0.005
0
-0.005
-0.01
-0.015
0.01
0.02
0.03
0.04
0.05
0.06
0.07
0.08
x2 distance from Probe 2 (m)
No Magnet
1601G
2952G
3309G
4667G
5233G

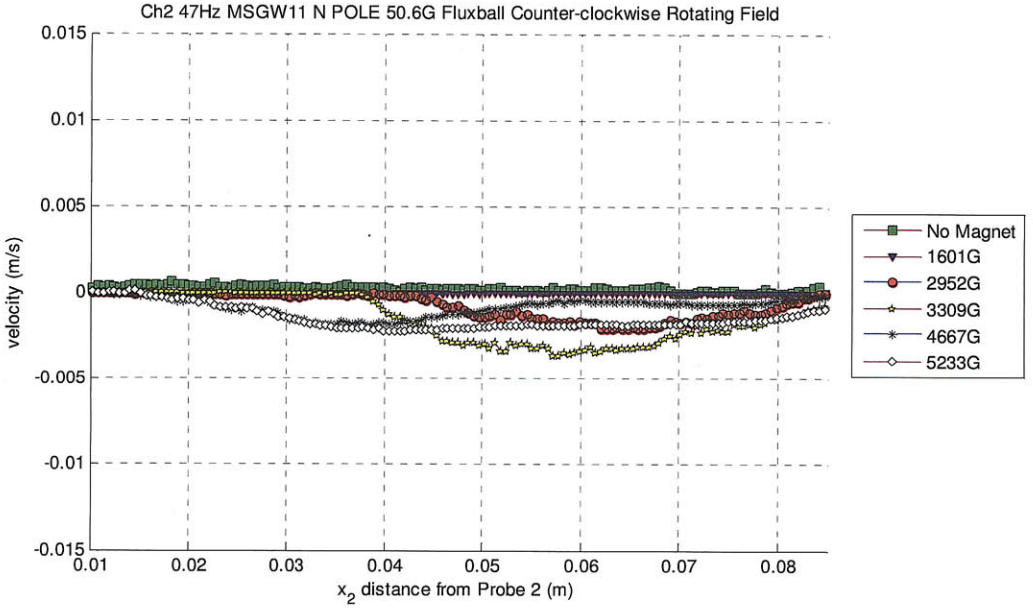
Ch2 47Hz MSGW11 N POLE 50.6G Fluxball Counter-clockwise Rotating Field
velocity (m/s)
0.015
0.01
0.005
0
-0.005
-0.01
-0.015
0.01
0.02
0.03
0.04
0.05
0.06
0.07
0.08
x2 distance from Probe 2 (m)
No Magnet
1601G
2952G
3309G
4667G
5233G

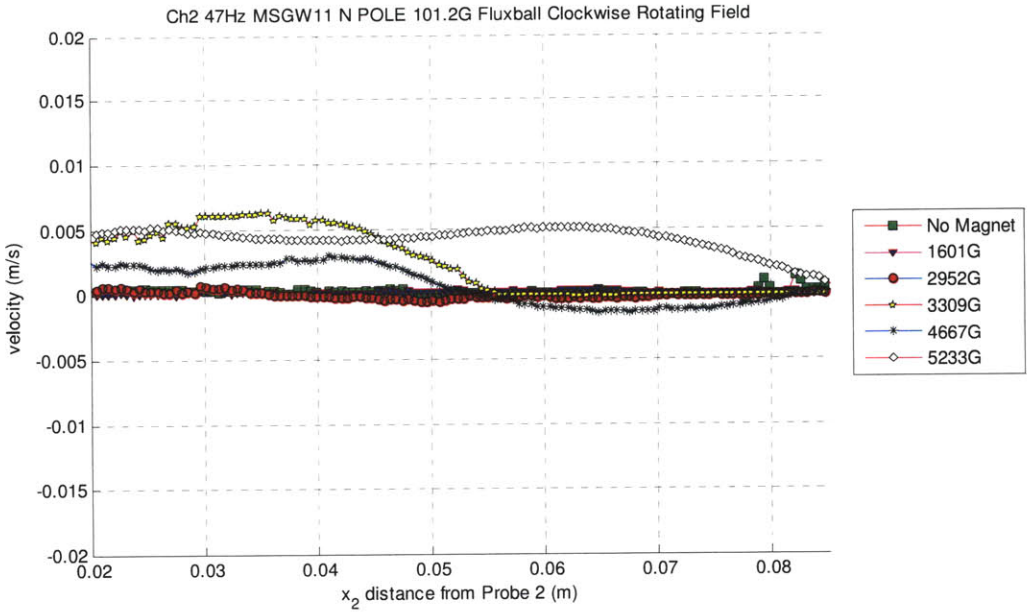
Ch2 47Hz MSGW11 N POLE 101.2G Fluxball Clockwise Rotating Field
velocity (m/s)
0.02
0.015
0.01
0.005
0
-0.005
-0.01
-0.015
-0.02
0.02
0.03
0.04
0.05
0.06
0.07
0.08
x2 distance from Probe 2 (m)
No Magnet
1601G
2952G
3309G
4667G
5233G

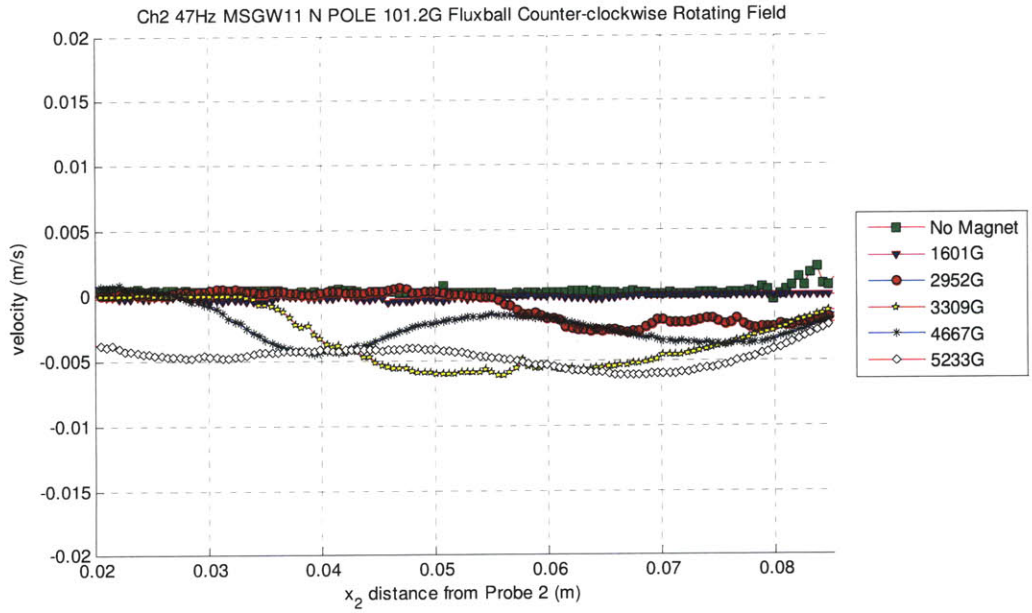
Ch2 47Hz MSGW11 N POLE 101.2G Fluxball Counter-clockwise Rotating Field
velocity (m/s)
0.02
0.015
0.01
0.005
0
-0.005
-0.01
-0.015
-0.02
0.02
0.03
0.04
0.05
0.06
0.07
0.08
x2 distance from Probe 2 (m)
No Magnet
1601G
2952G
3309G
4667G
5233G

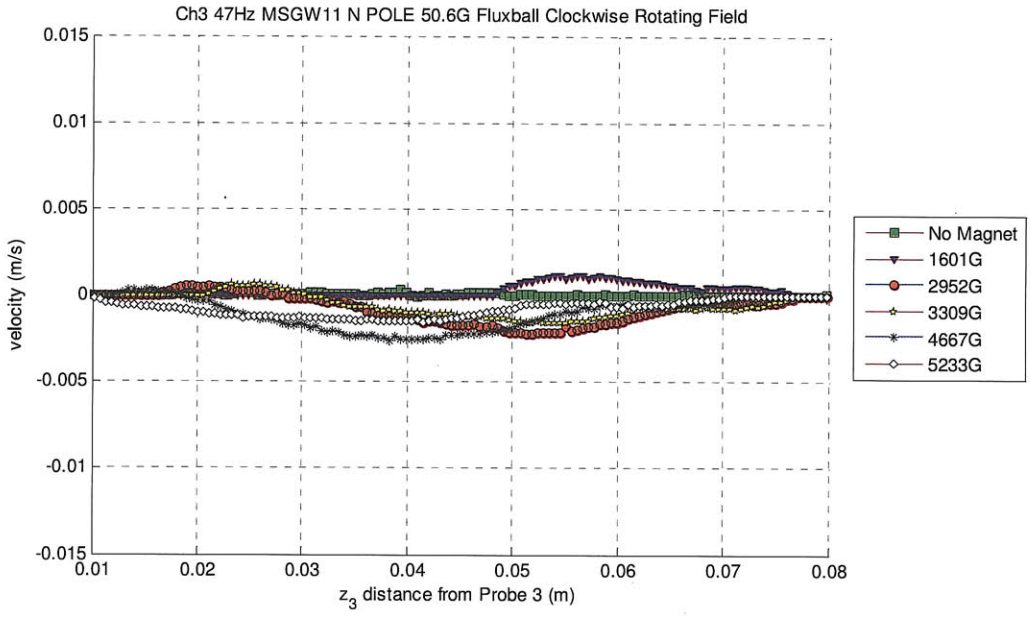
Ch3 47Hz MSGW11 N POLE 50.6G Fluxball Clockwise Rotating Field
velocity (m/s)
0.015
0.01
0.005
0
-0.005
-0.01
-0.015
0.01
0.02
0.03
0.04
0.05
0.06
0.07
0.08
z_3 distance from Probe 3 (m)
No Magnet
1601G
2952G
3309G
4667G
5233G

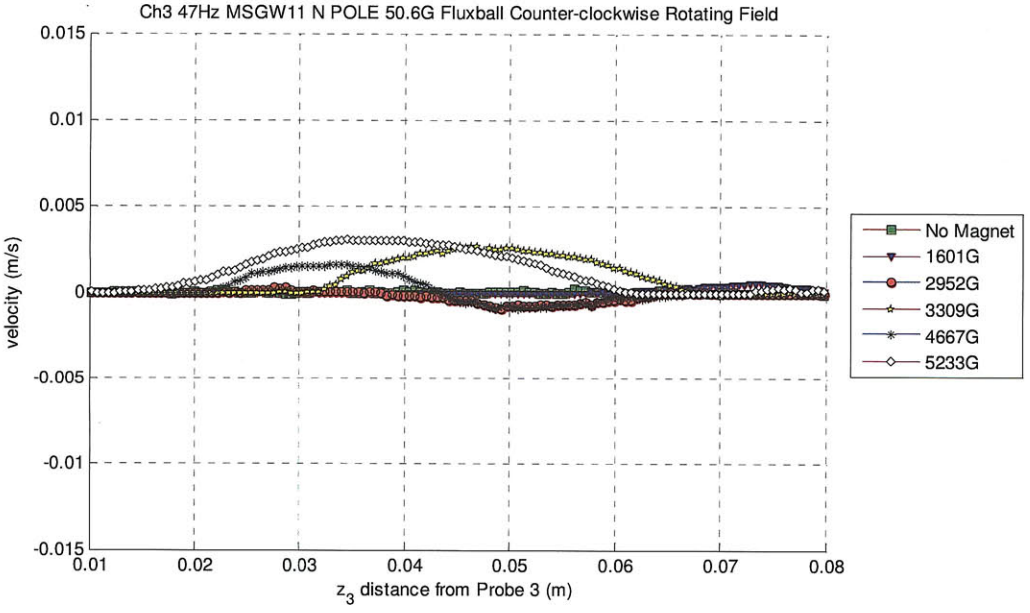
Ch3 47Hz MSGW11 N POLE 50.6G Fluxball Counter-clockwise Rotating Field
velocity (m/s)
0.015
0.01
0.005
0
-0.005
-0.01
-0.015
0.01
0.02
0.03
0.04
0.05
0.06
0.07
0.08
z_3 distance from Probe 3 (m)
No Magnet
1601G
2952G
3309G
4667G
5233G

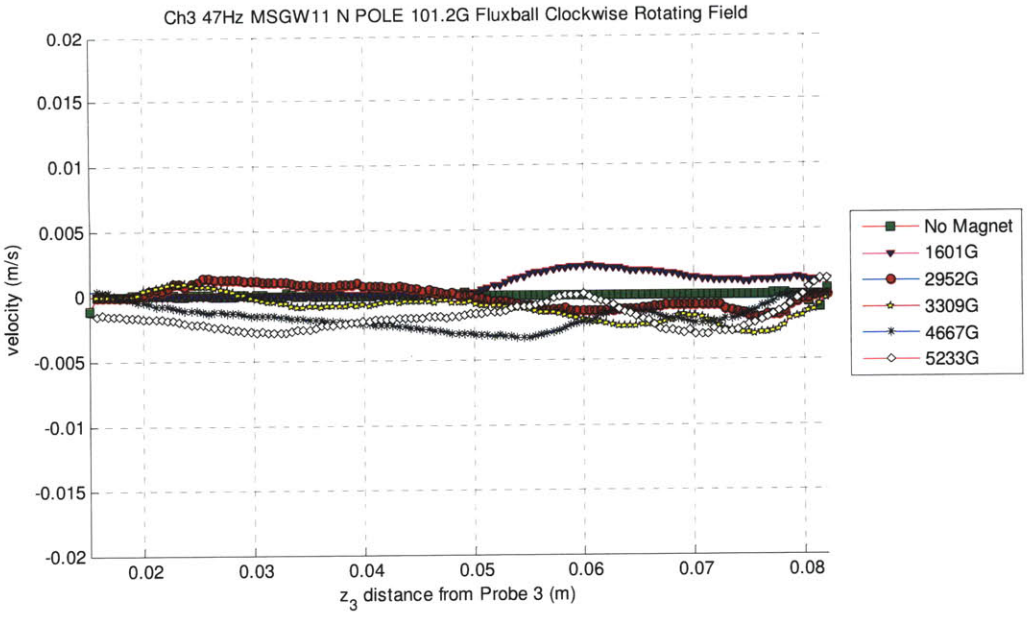
Ch3 47Hz MSGW11 N POLE 101.2G Fluxball Clockwise Rotating Field
velocity (m/s)
0.02
0.015
0.01
0.005
0
-0.005
-0.01
-0.015
-0.02
0.02
0.03
0.04
0.05
0.06
0.07
0.08
z_3 distance from Probe 3 (m)
No Magnet
1601G
2952G
3309G
4667G
5233G

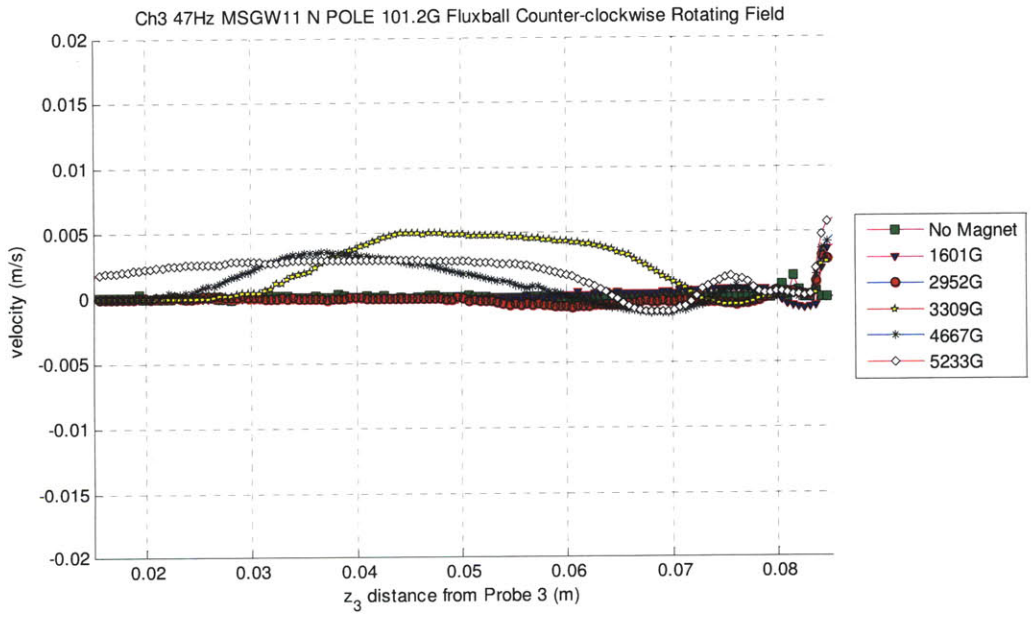
Ch3 47Hz MSGW11 N POLE 101.2G Fluxball Counter-clockwise Rotating Field
velocity (m/s)
0.02
0.015
0.01
0.005
0
-0.005
-0.01
-0.015
-0.02
0.02
0.03
0.04
0.05
0.06
0.07
0.08
z_3 distance from Probe 3 (m)
No Magnet
1601G
2952G
3309G
4667G
5233G

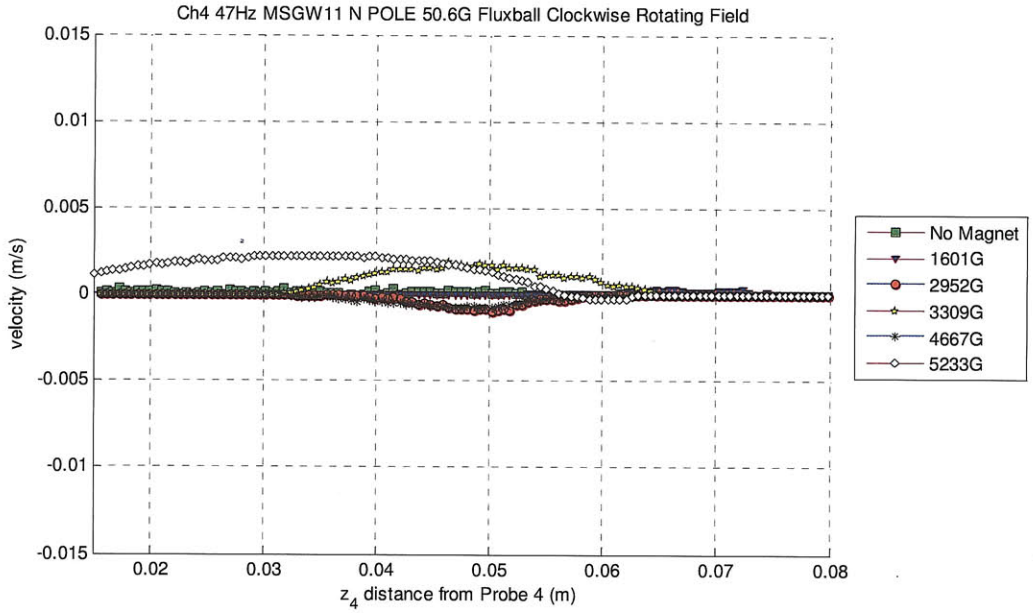
Ch4 47Hz MSGW11 N POLE 50.6G Fluxball Clockwise Rotating Field
velocity (m/s)
0.015
0.01
0.005
0
-0.005
-0.01
-0.015
0.02
0.03
0.04
0.05
0.06
0.07
0.08
z_4 distance from Probe 4 (m)
No Magnet
1601G
2952G
3309G
4667G
5233G

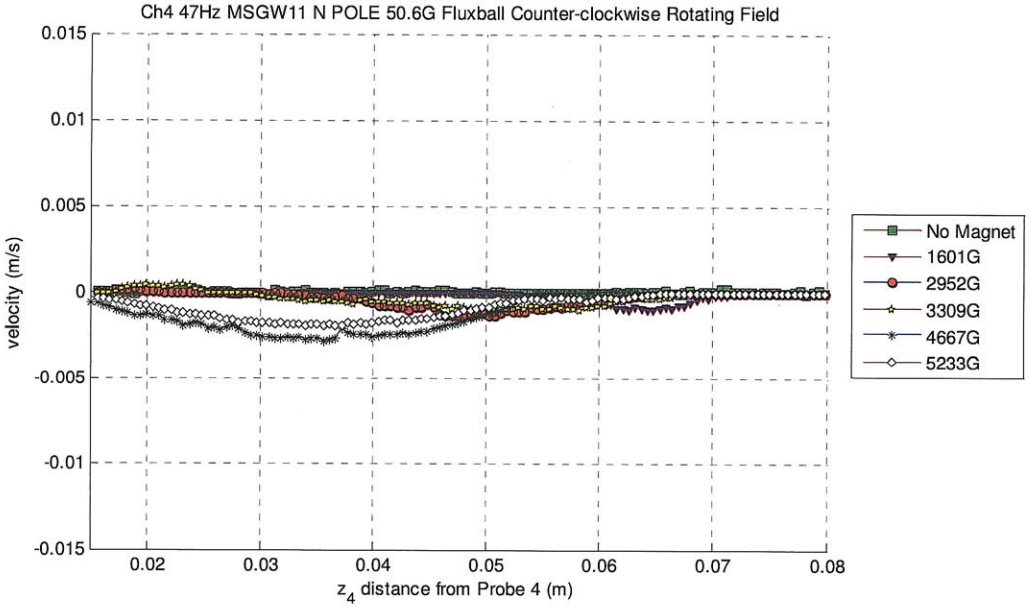
Ch4 47Hz MSGW11 N POLE 50.6G Fluxball Counter-clockwise Rotating Field
velocity (m/s)
0.015
0.01
0.005
0
-0.005
-0.01
-0.015
0.02
0.03
0.04
0.05
0.06
0.07
0.08
z_4 distance from Probe 4 (m)
No Magnet
1601G
2952G
3309G
4667G
5233G

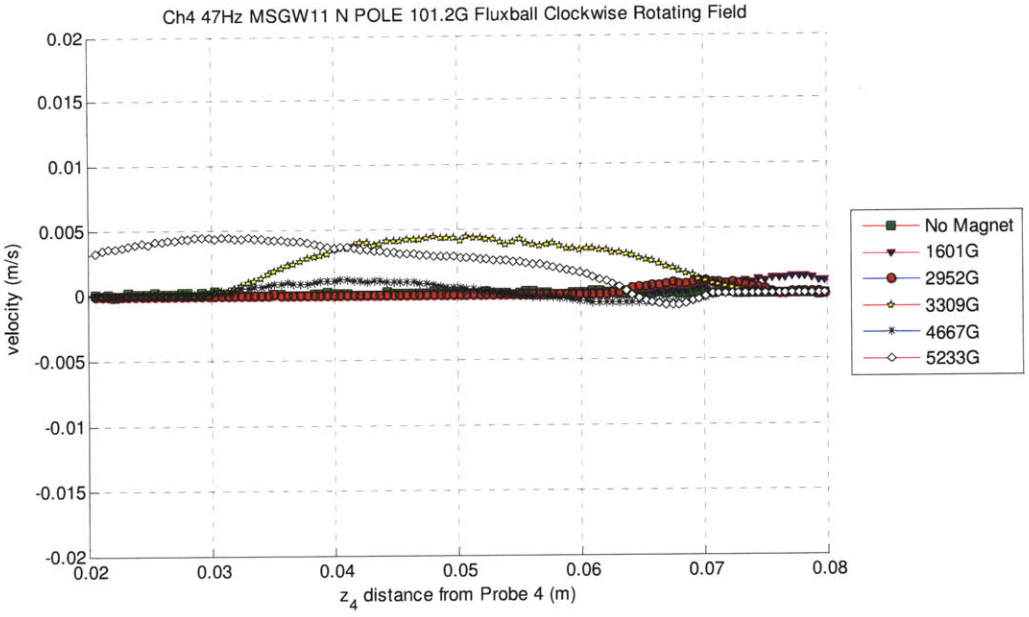
Ch4 47Hz MSGW11 N POLE 101.2G Fluxball Clockwise Rotating Field
velocity (m/s)
0.02
0.015
0.01
0.005
0
-0.005
-0.01
-0.015
-0.02
0.02
0.03
0.04
0.05
0.06
0.07
0.08
z_4 distance from Probe 4 (m)
No Magnet
1601G
2952G
3309G
4667G
5233G

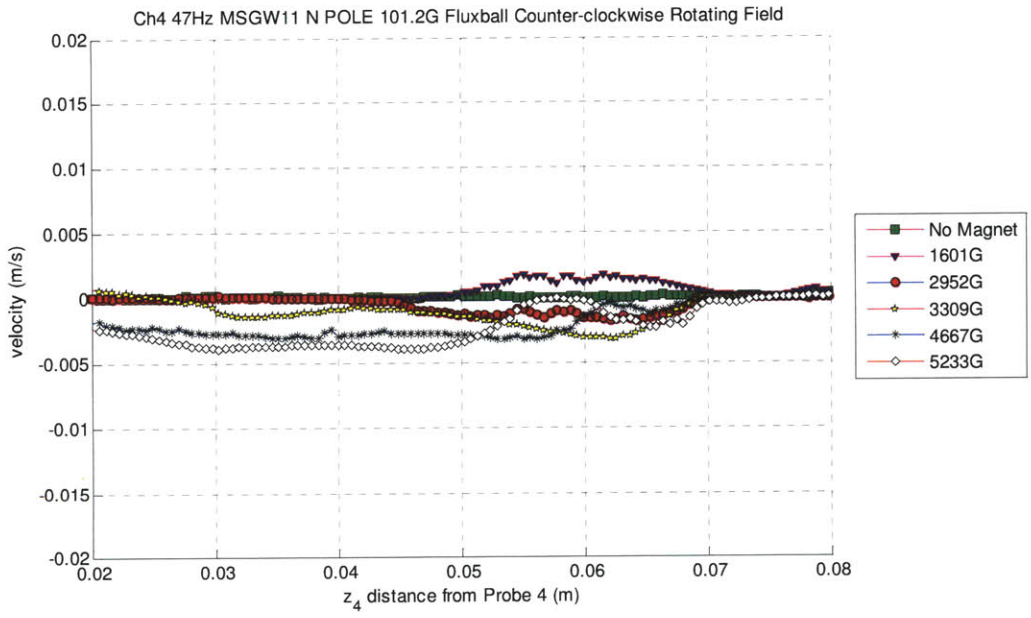
Ch4 47Hz MSGW11 N POLE 101.2G Fluxball Counter-clockwise Rotating Field
velocity (m/s)
0.02
0.015
0.01
0.005
0
-0.005
-0.01
-0.015
-0.02
0.02
0.03
0.04
0.05
0.06
0.07
0.08
z_4 distance from Probe 4 (m)
No Magnet
1601G
2952G
3309G
4667G
5233G

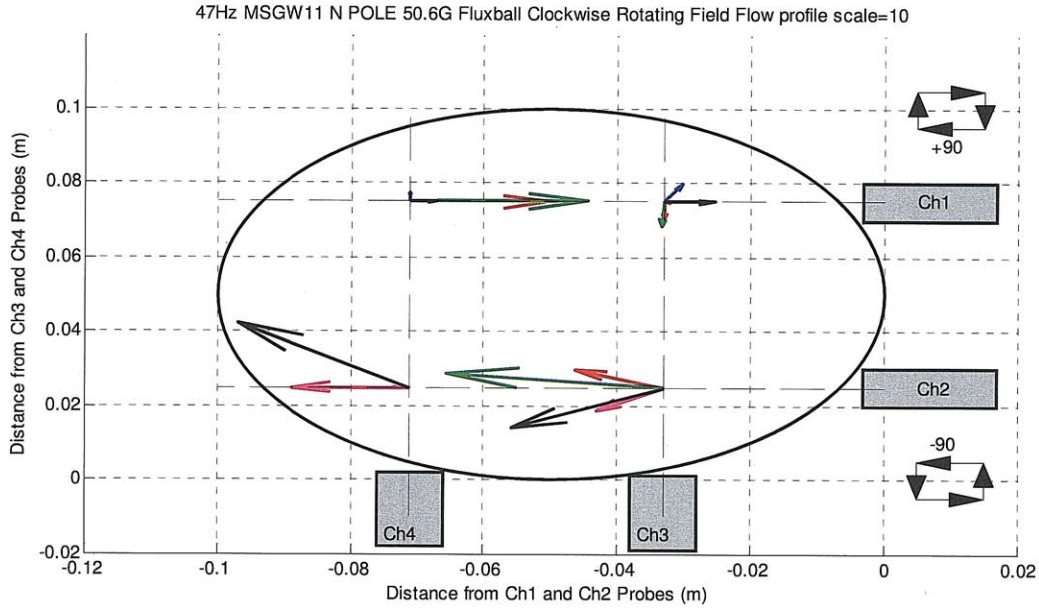
47Hz MSGW11 N POLE 50.6G Fluxball Clockwise Rotating Field Flow profile scale=10
Distance from Ch3 and Ch4 Probes (m)
Distance from Ch1 and Ch2 Probes (m)
+90
-90
Ch1
Ch2
Ch3
Ch4
0.1
0.08
0.06
0.04
0.02
0
-0.02
-0.12
-0.1
-0.08
-0.06
-0.04
-0.02
0
0.02

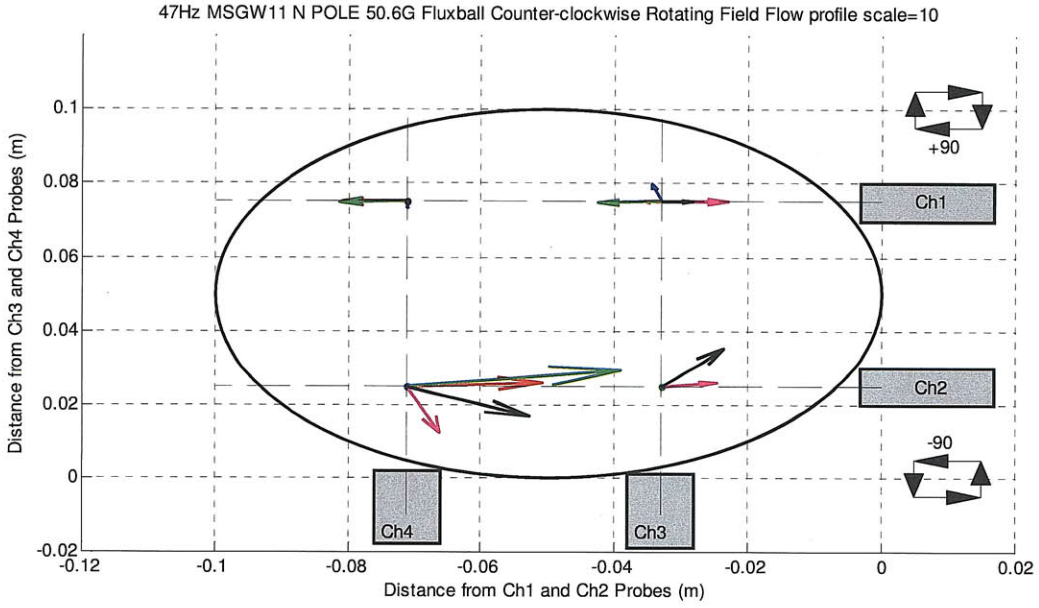
47Hz MSGW11 N POLE 50.6G Fluxball Counter-clockwise Rotating Field Flow profile scale=10
Distance from Ch3 and Ch4 Probes (m)
Distance from Ch1 and Ch2 Probes (m)
+90
-90
Ch1
Ch2
Ch3
Ch4
0.1
0.08
0.06
0.04
0.02
0
-0.02
-0.12
-0.1
-0.08
-0.06
-0.04
-0.02
0
0.02

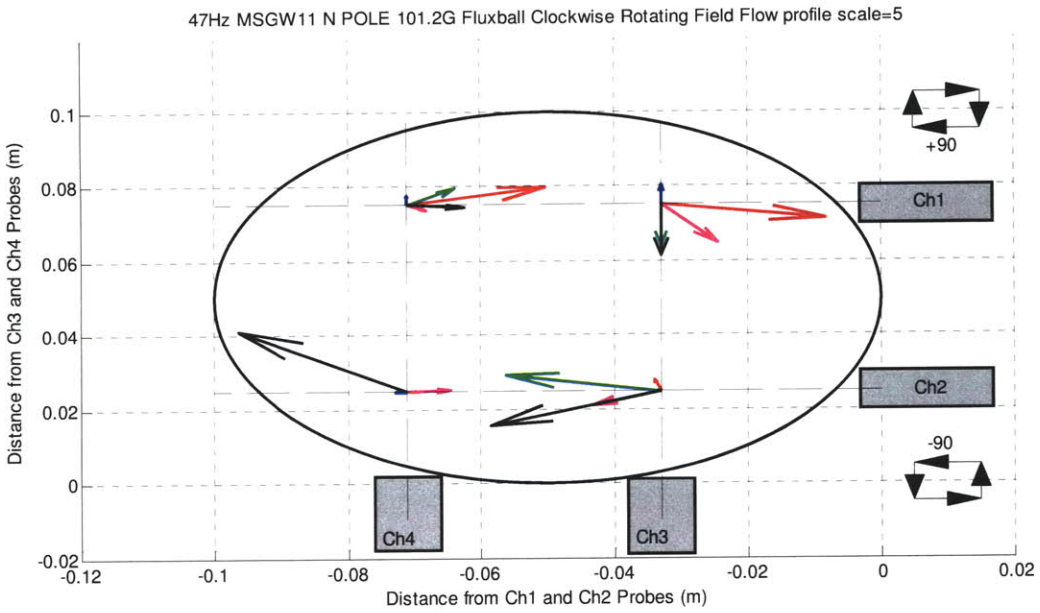
47Hz MSGW11 N POLE 101.2G Fluxball Clockwise Rotating Field Flow profile scale=5
Distance from Ch3 and Ch4 Probes (m)
Distance from Ch1 and Ch2 Probes (m)
+90
-90
Ch1
Ch2
Ch3
Ch4
0.1
0.08
0.06
0.04
0.02
0
-0.02
-0.12
-0.1
-0.08
-0.06
-0.04
-0.02
0
0.02

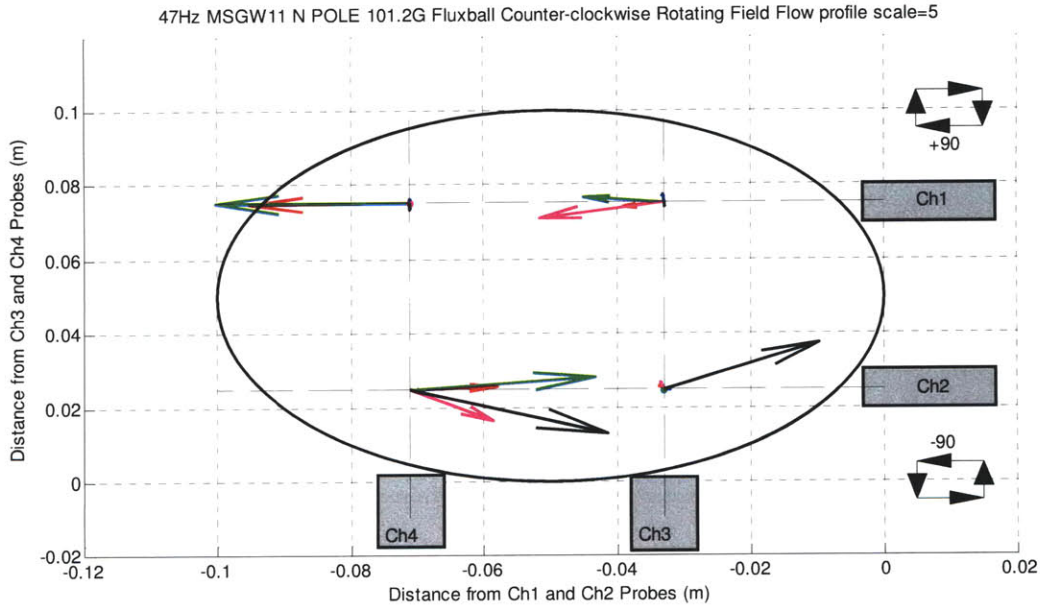
47Hz MSGW11 N POLE 101.2G Fluxball Counter-clockwise Rotating Field Flow profile scale=5
Distance from Ch3 and Ch4 Probes (m)
Distance from Ch1 and Ch2 Probes (m)
+90
-90
Ch1
Ch2
Ch3
Ch4
0.1
0.08
0.06
0.04
0.02
0
-0.02
-0.12
-0.1
-0.08
-0.06
-0.04
-0.02
0
0.02

H12. MSGW11 Filled Sphere with North Pole Facing Magnets on Top of Sphere at 15Hz

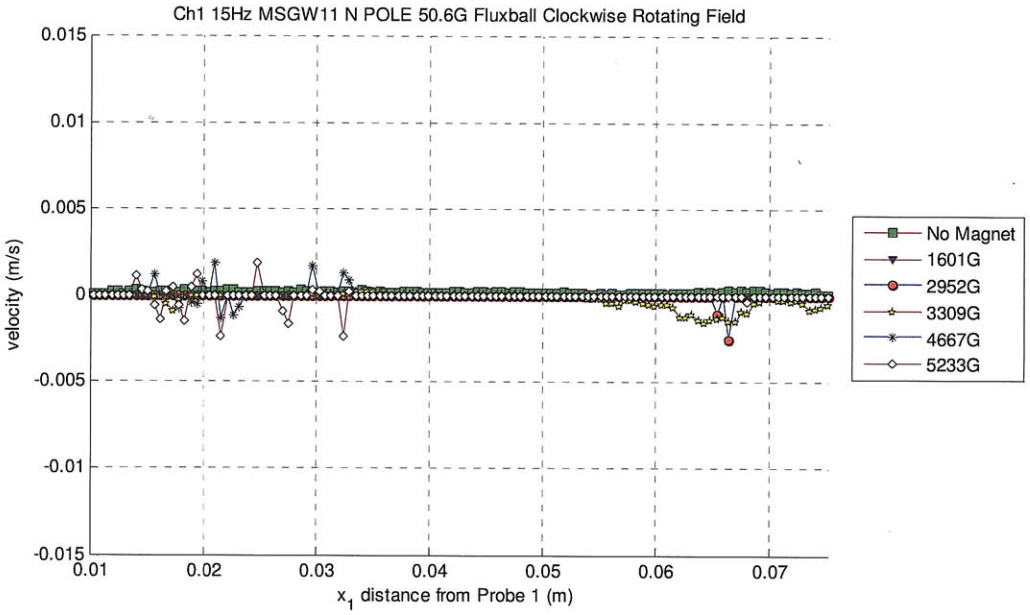

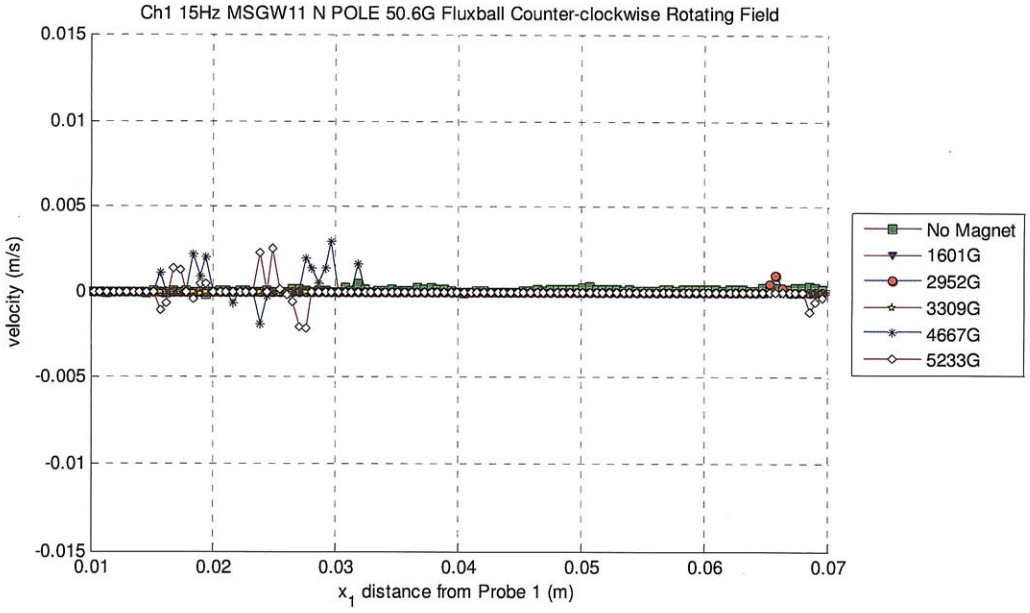

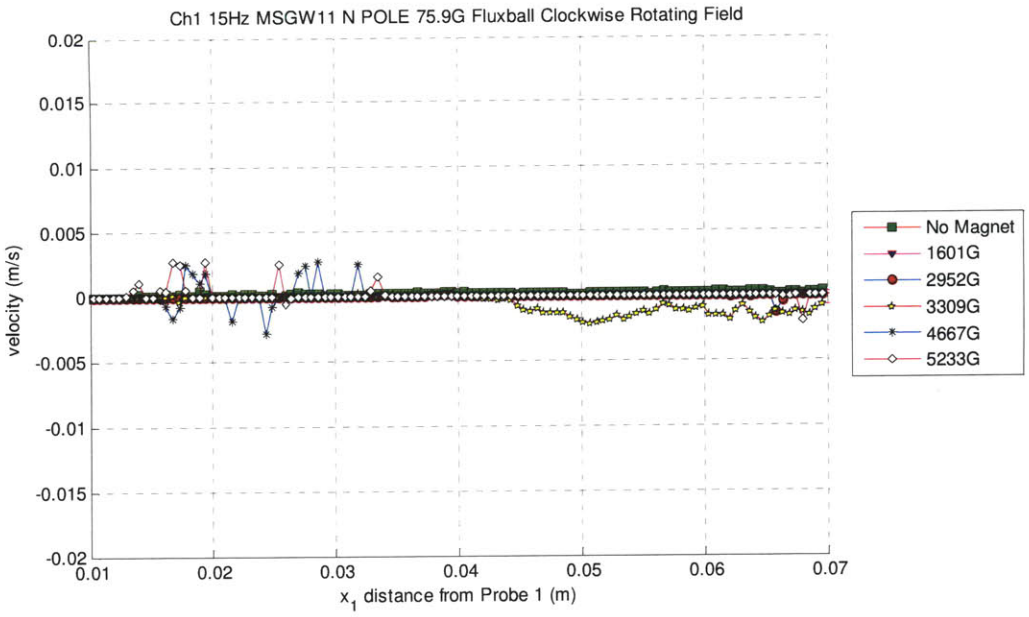
Ch1 15Hz MSGW11 N POLE 75.9G Fluxball Clockwise Rotating Field
velocity (m/s)
0.02
0.015
0.01
0.005
0
-0.005
-0.01
-0.015
-0.02
0.01
0.02
0.03
0.04
0.05
0.06
0.07
x1 distance from Probe 1 (m)
No Magnet
1601G
2952G
3309G
4667G
5233G

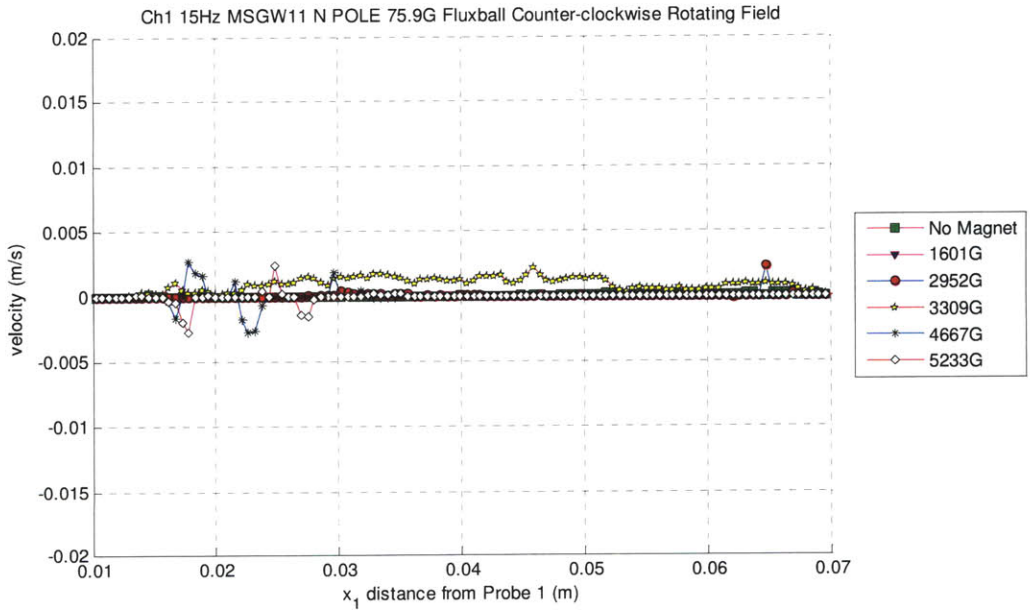
Ch1 15Hz MSGW11 N POLE 75.9G Fluxball Counter-clockwise Rotating Field
velocity (m/s)
0.02
0.015
0.01
0.005
0
-0.005
-0.01
-0.015
-0.02
0.01
0.02
0.03
0.04
0.05
0.06
0.07
x1 distance from Probe 1 (m)
No Magnet
1601G
2952G
3309G
4667G
5233G

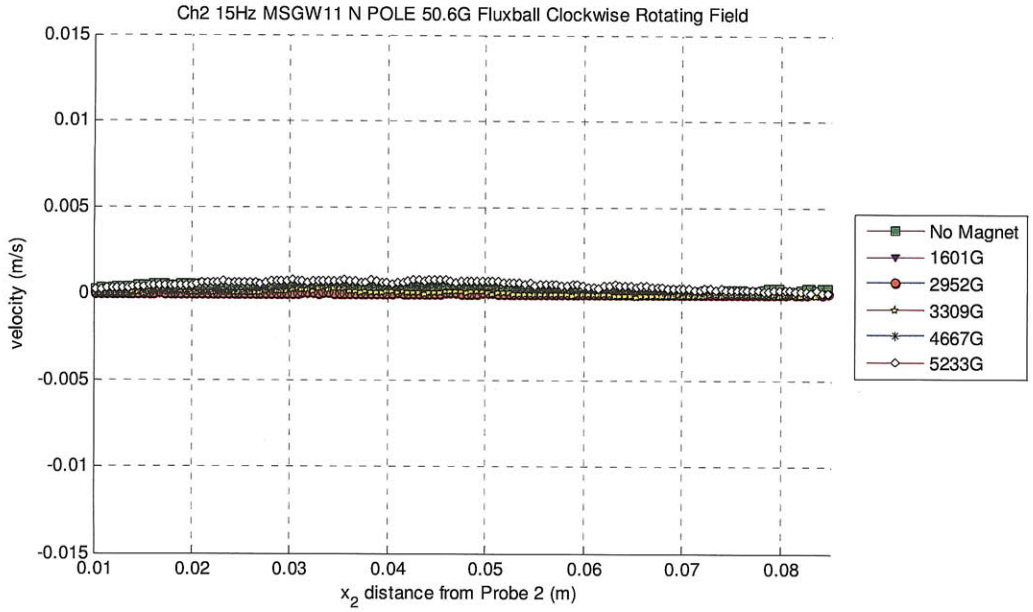
Ch2 15Hz MSGW11 N POLE 50.6G Fluxball Clockwise Rotating Field
velocity (m/s)
0.015
0.01
0.005
0
-0.005
-0.01
-0.015
0.01
0.02
0.03
0.04
0.05
0.06
0.07
0.08
x2 distance from Probe 2 (m)
No Magnet
1601G
2952G
3309G
4667G
5233G

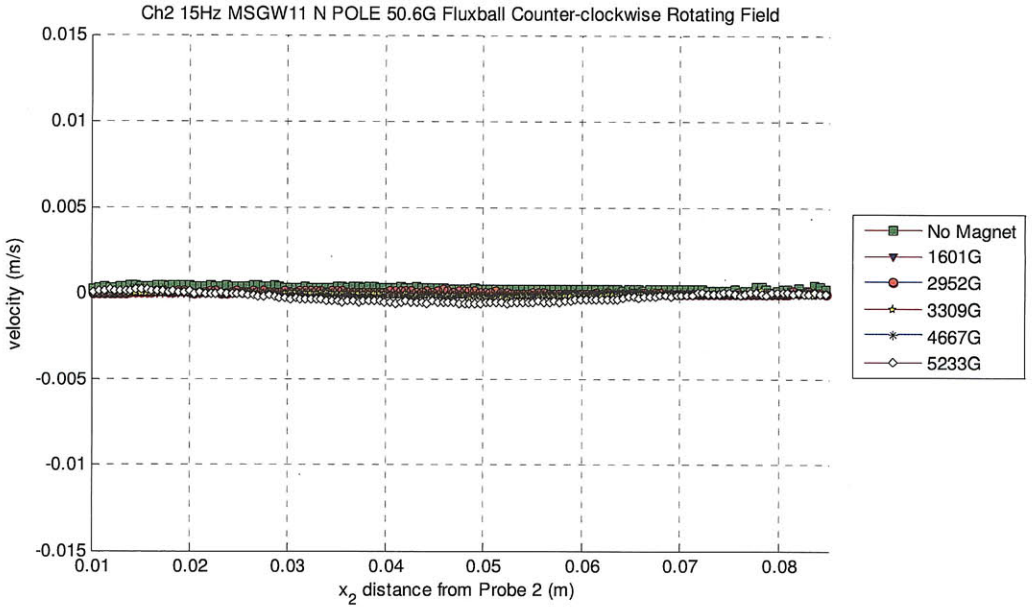
Ch2 15Hz MSGW11 N POLE 50.6G Fluxball Counter-clockwise Rotating Field
velocity (m/s)
0.015
0.01
0.005
0
-0.005
-0.01
-0.015
0.01
0.02
0.03
0.04
0.05
0.06
0.07
0.08
x2 distance from Probe 2 (m)
No Magnet
1601G
2952G
3309G
4667G
5233G

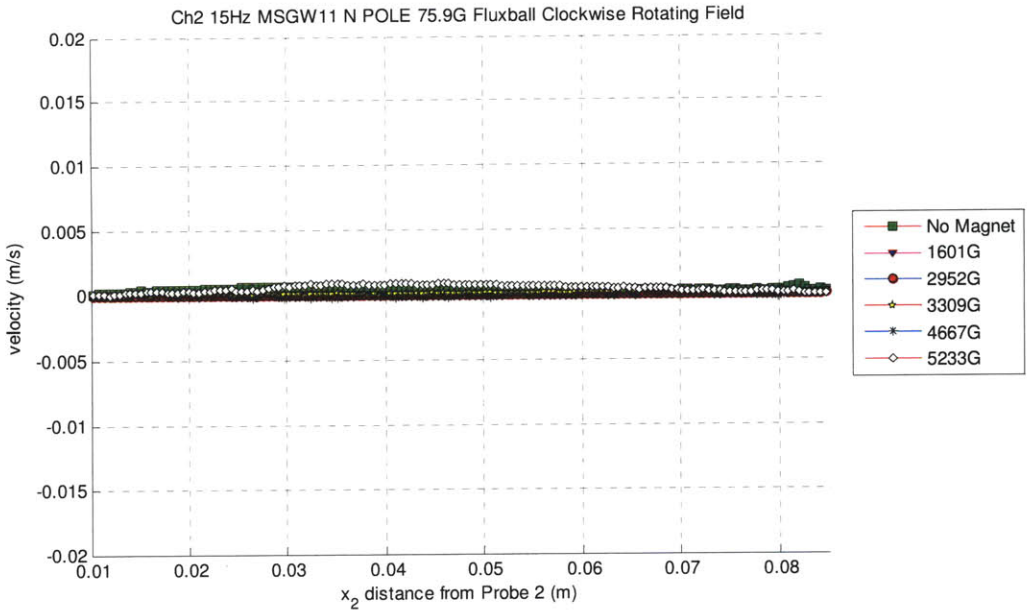
Ch2 15Hz MSGW11 N POLE 75.9G Fluxball Clockwise Rotating Field
velocity (m/s)
0.02
0.015
0.01
0.005
0
-0.005
-0.01
-0.015
-0.02
0.01
0.02
0.03
0.04
0.05
0.06
0.07
0.08
x2 distance from Probe 2 (m)
No Magnet
1601G
2952G
3309G
4667G
5233G

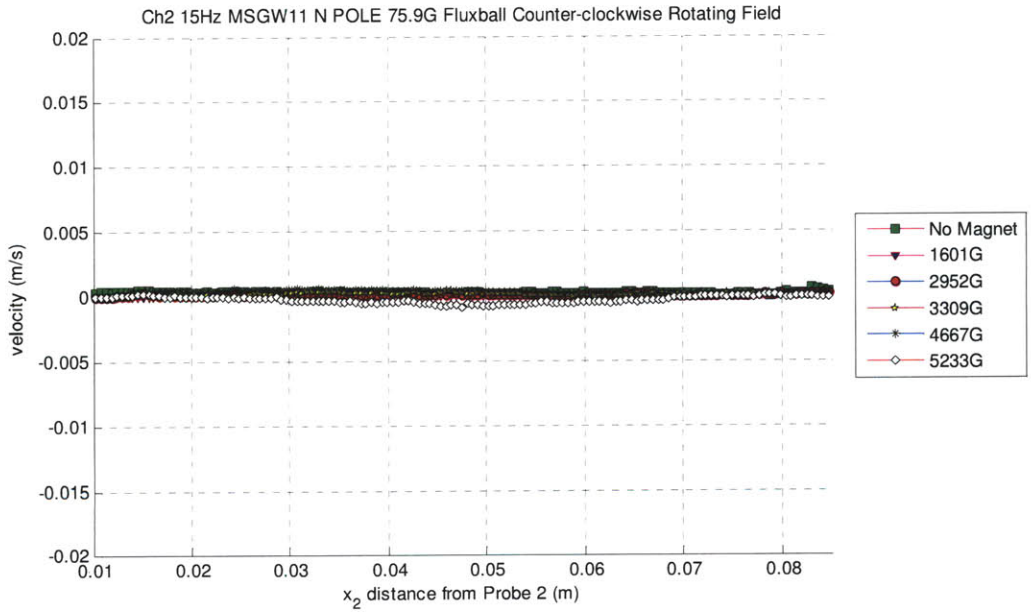
Ch2 15Hz MSGW11 N POLE 75.9G Fluxball Counter-clockwise Rotating Field
velocity (m/s)
0.02
0.015
0.01
0.005
0
-0.005
-0.01
-0.015
-0.02
0.01
0.02
0.03
0.04
0.05
0.06
0.07
0.08
x2 distance from Probe 2 (m)
No Magnet
1601G
2952G
3309G
4667G
5233G

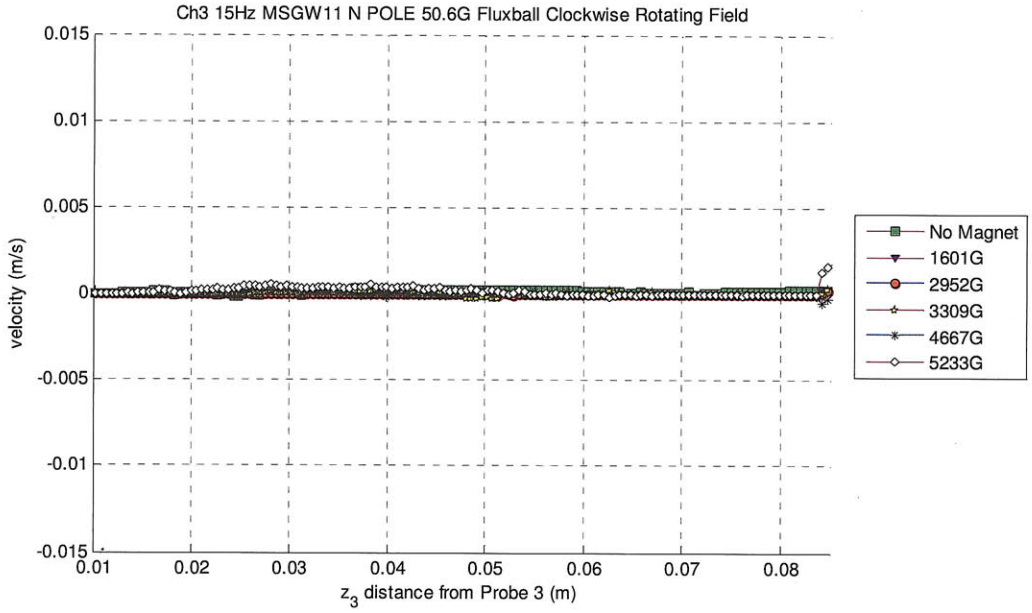
Ch3 15Hz MSGW11 N POLE 50.6G Fluxball Clockwise Rotating Field
velocity (m/s)
0.015
0.01
0.005
0
-0.005
-0.01
-0.015
0.01
0.02
0.03
0.04
0.05
0.06
0.07
0.08
z3 distance from Probe 3 (m)
No Magnet
1601G
2952G
3309G
4667G
5233G

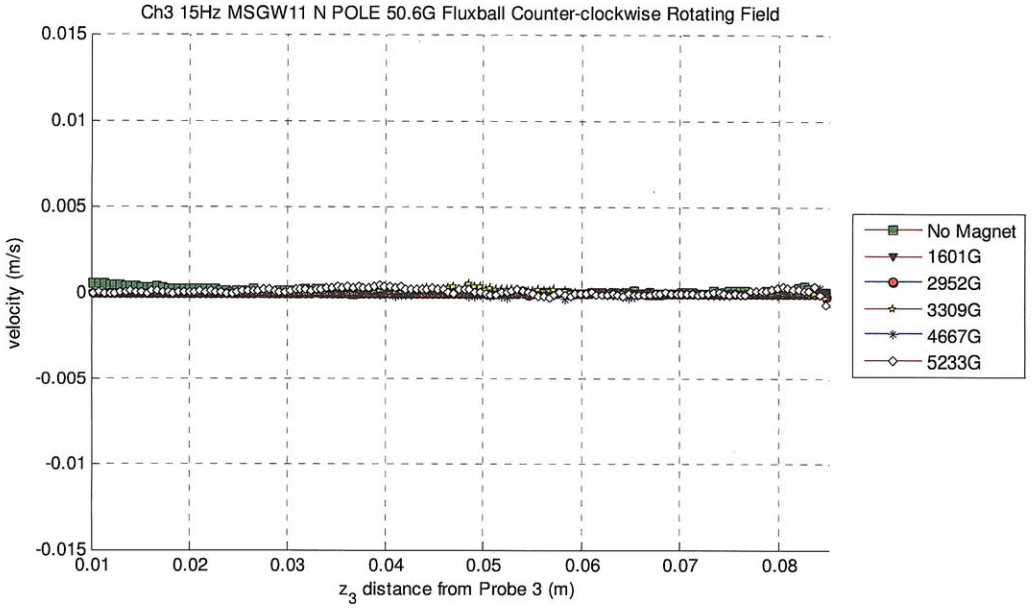
Ch3 15Hz MSGW11 N POLE 50.6G Fluxball Counter-clockwise Rotating Field
velocity (m/s)
0.015
0.01
0.005
0
-0.005
-0.01
-0.015
0.01
0.02
0.03
0.04
0.05
0.06
0.07
0.08
z3 distance from Probe 3 (m)
No Magnet
1601G
2952G
3309G
4667G
5233G

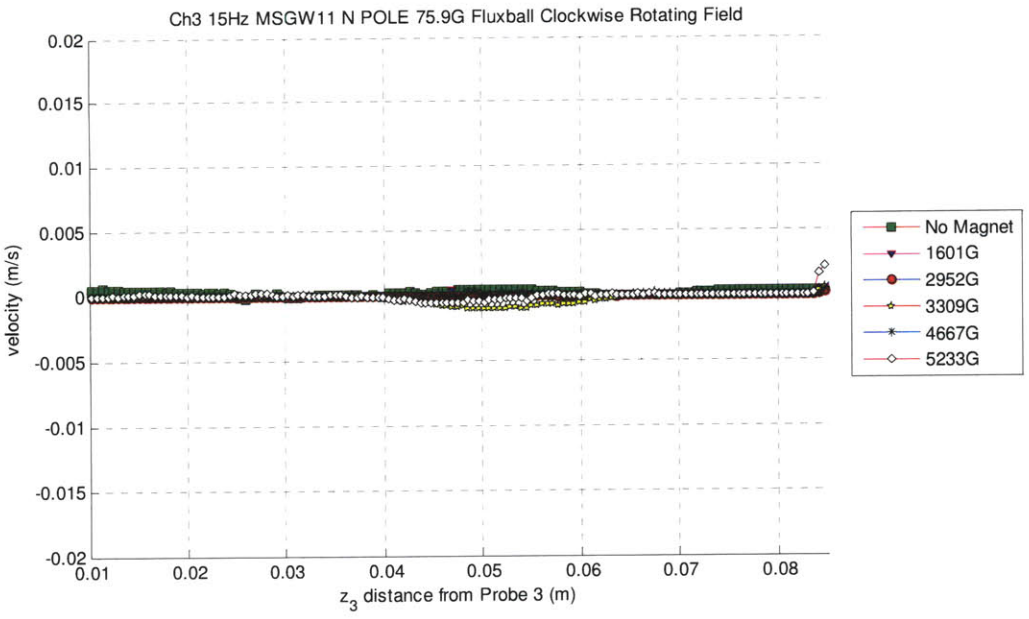
Ch3 15Hz MSGW11 N POLE 75.9G Fluxball Clockwise Rotating Field
velocity (m/s)
0.02
0.015
0.01
0.005
0
-0.005
-0.01
-0.015
-0.02
0.01
0.02
0.03
0.04
0.05
0.06
0.07
0.08
z_3 distance from Probe 3 (m)
No Magnet
1601G
2952G
3309G
4667G
5233G

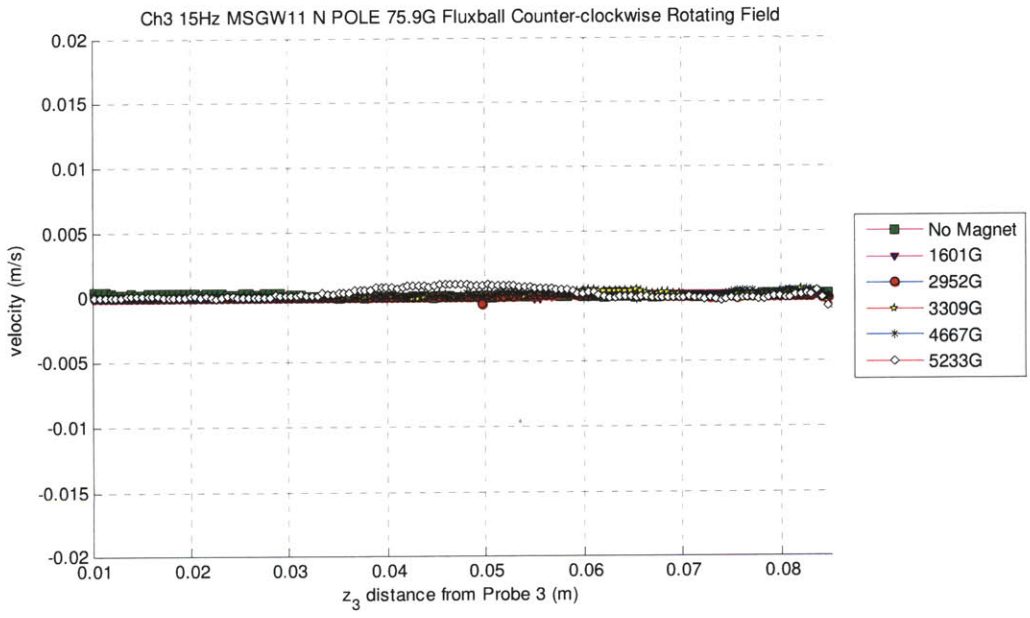
Ch3 15Hz MSGW11 N POLE 75.9G Fluxball Counter-clockwise Rotating Field
velocity (m/s)
0.02
0.015
0.01
0.005
0
-0.005
-0.01
-0.015
-0.02
0.01
0.02
0.03
0.04
0.05
0.06
0.07
0.08
z_3 distance from Probe 3 (m)
No Magnet
1601G
2952G
3309G
4667G
5233G

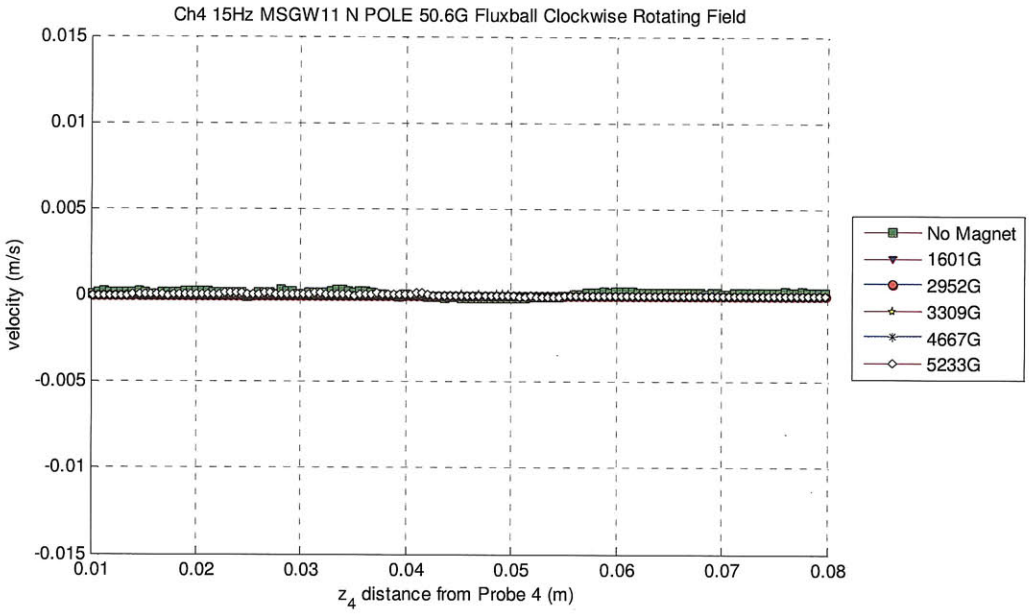
Ch4 15Hz MSGW11 N POLE 50.6G Fluxball Clockwise Rotating Field
velocity (m/s)
0.015
0.01
0.005
0
-0.005
-0.01
-0.015
0.01
0.02
0.03
0.04
0.05
0.06
0.07
0.08
z4 distance from Probe 4 (m)
No Magnet
1601G
2952G
3309G
4667G
5233G

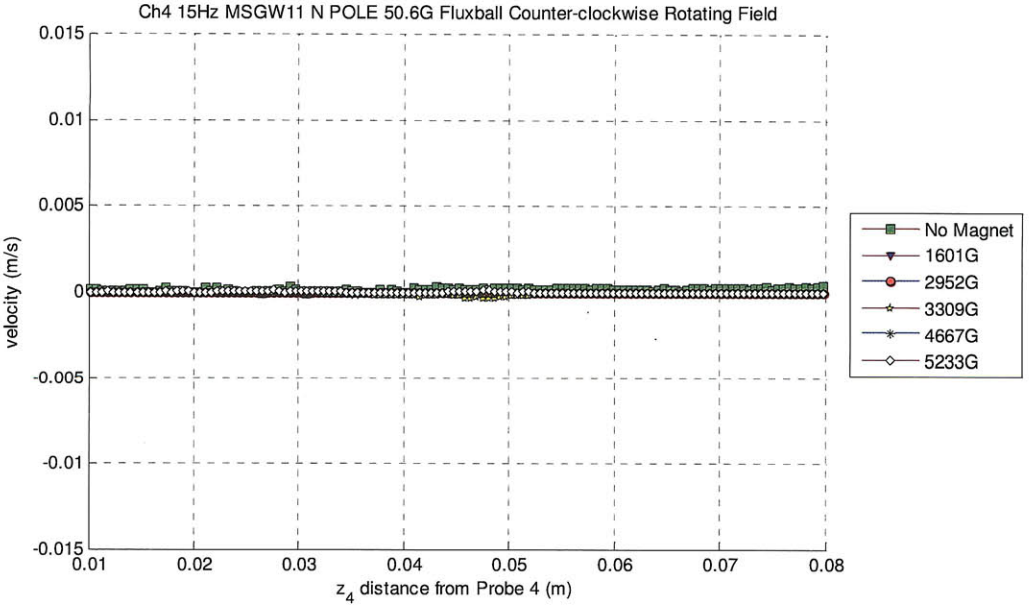
Ch4 15Hz MSGW11 N POLE 50.6G Fluxball Counter-clockwise Rotating Field
velocity (m/s)
0.015
0.01
0.005
0
-0.005
-0.01
-0.015
0.01
0.02
0.03
0.04
0.05
0.06
0.07
0.08
z4 distance from Probe 4 (m)
No Magnet
1601G
2952G
3309G
4667G
5233G

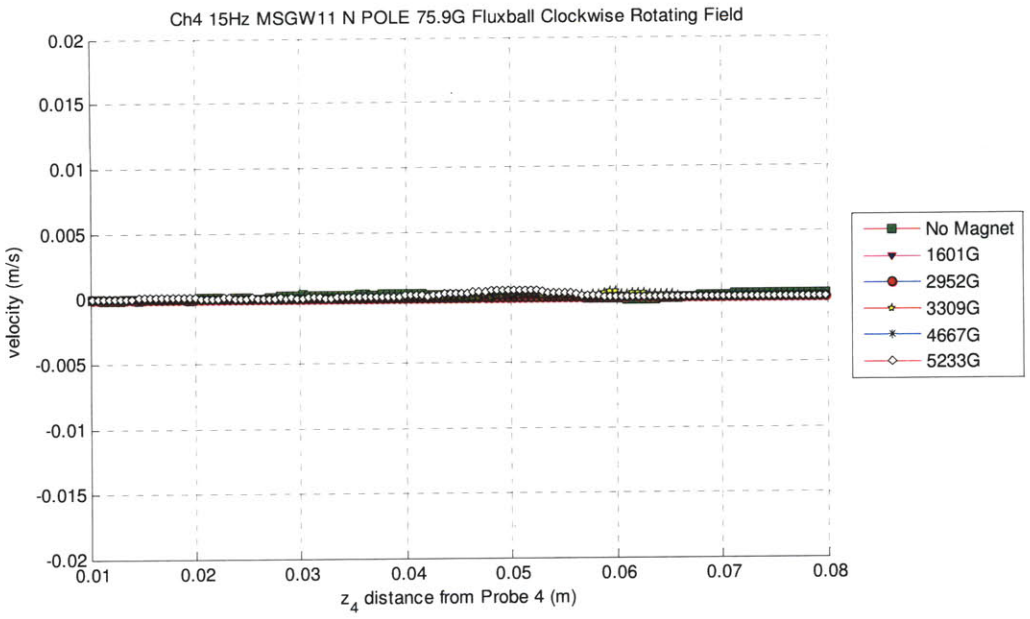
Ch4 15Hz MSGW11 N POLE 75.9G Fluxball Clockwise Rotating Field
velocity (m/s)
0.02
0.015
0.01
0.005
0
-0.005
-0.01
-0.015
-0.02
0.01
0.02
0.03
0.04
0.05
0.06
0.07
0.08
z_4 distance from Probe 4 (m)
No Magnet
1601G
2952G
3309G
4667G
5233G

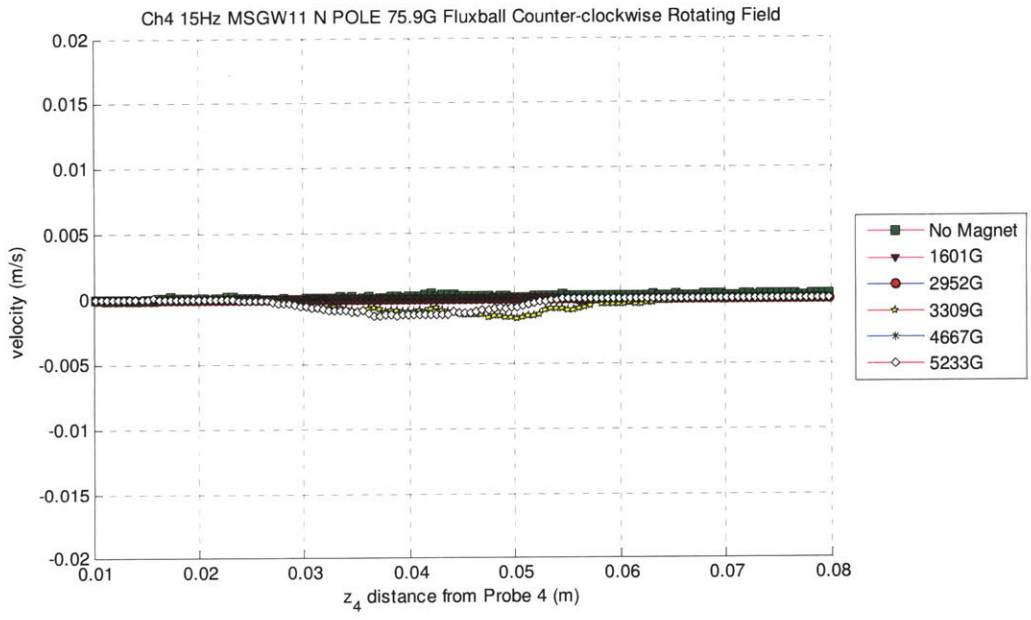
Ch4 15Hz MSGW11 N POLE 75.9G Fluxball Counter-clockwise Rotating Field
velocity (m/s)
0.02
0.015
0.01
0.005
0
-0.005
-0.01
-0.015
-0.02
0.01
0.02
0.03
0.04
0.05
0.06
0.07
0.08
z_4 distance from Probe 4 (m)
No Magnet
1601G
2952G
3309G
4667G
5233G

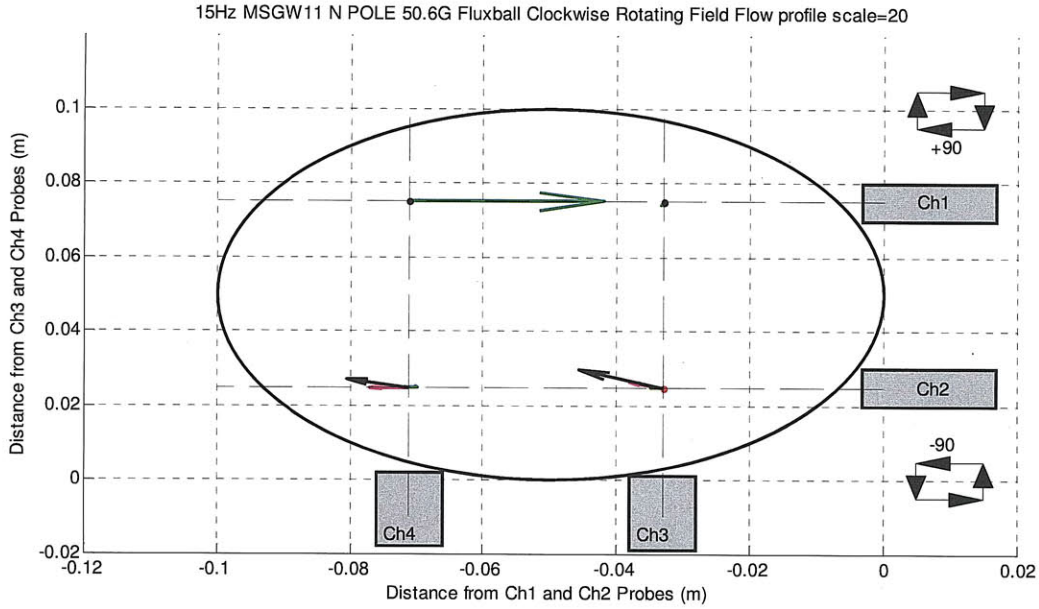
15Hz MSGW11 N POLE 50.6G Fluxball Clockwise Rotating Field Flow profile scale=20
Distance from Ch3 and Ch4 Probes (m)
Distance from Ch1 and Ch2 Probes (m)
+90
-90
Ch1
Ch2
Ch3
Ch4
0.1
0.08
0.06
0.04
0.02
0
-0.02
-0.12
-0.1
-0.08
-0.06
-0.04
-0.02
0
0.02

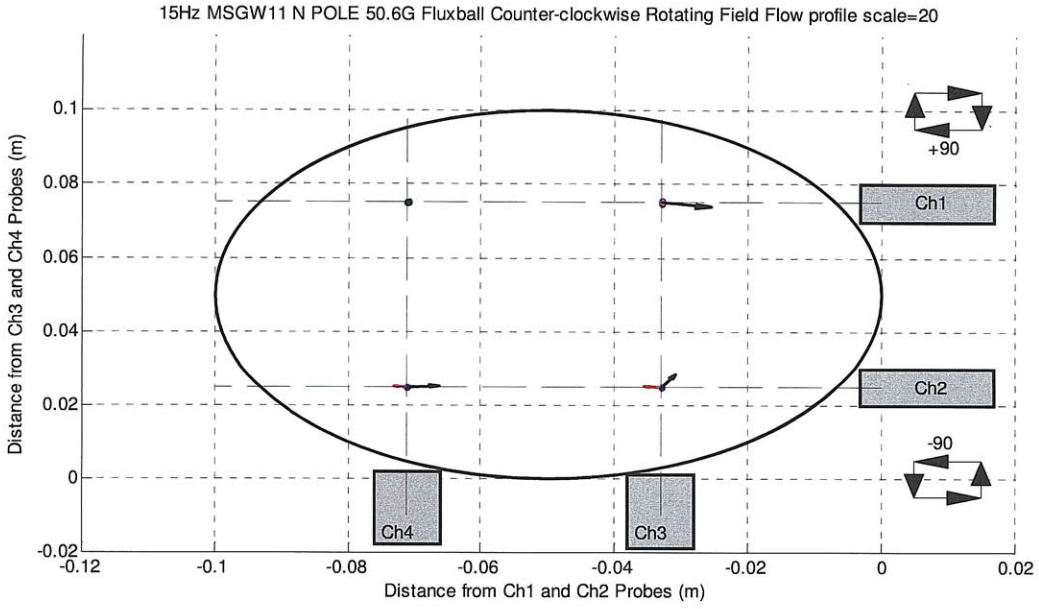
15Hz MSGW11 N POLE 50.6G Fluxball Counter-clockwise Rotating Field Flow profile scale=20
Distance from Ch3 and Ch4 Probes (m)
Distance from Ch1 and Ch2 Probes (m)
+90
-90
Ch1
Ch2
Ch3
Ch4
0.1
0.08
0.06
0.04
0.02
0
-0.02
-0.12
-0.1
-0.08
-0.06
-0.04
-0.02
0
0.02

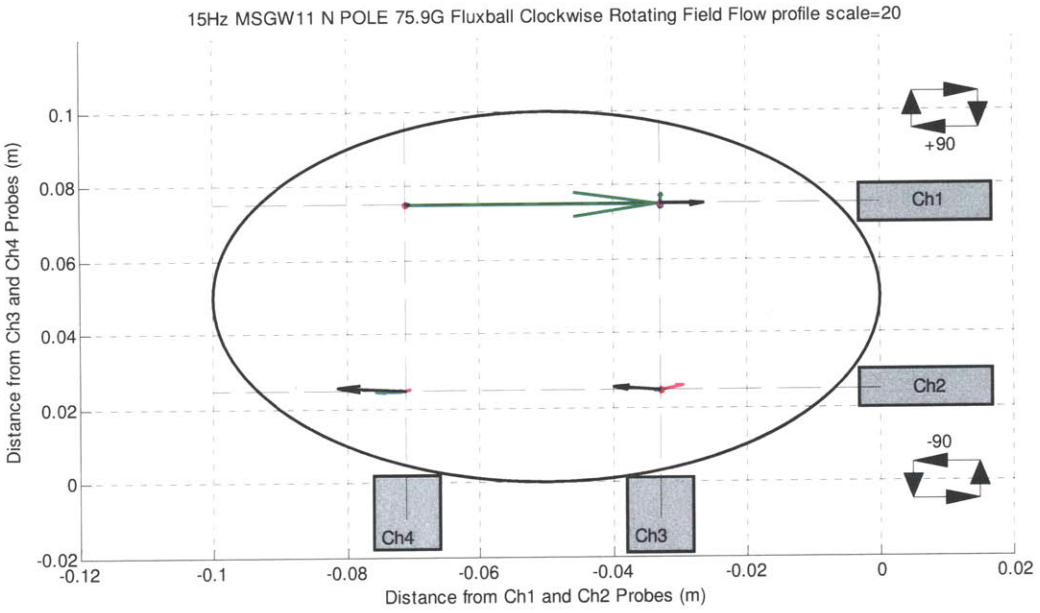
15Hz MSGW11 N POLE 75.9G Fluxball Clockwise Rotating Field Flow profile scale=20
Distance from Ch3 and Ch4 Probes (m)
Distance from Ch1 and Ch2 Probes (m)
+90
-90
Ch1
Ch2
Ch3
Ch4
0.1
0.08
0.06
0.04
0.02
0
-0.02
-0.12
-0.1
-0.08
-0.06
-0.04
-0.02
0
0.02

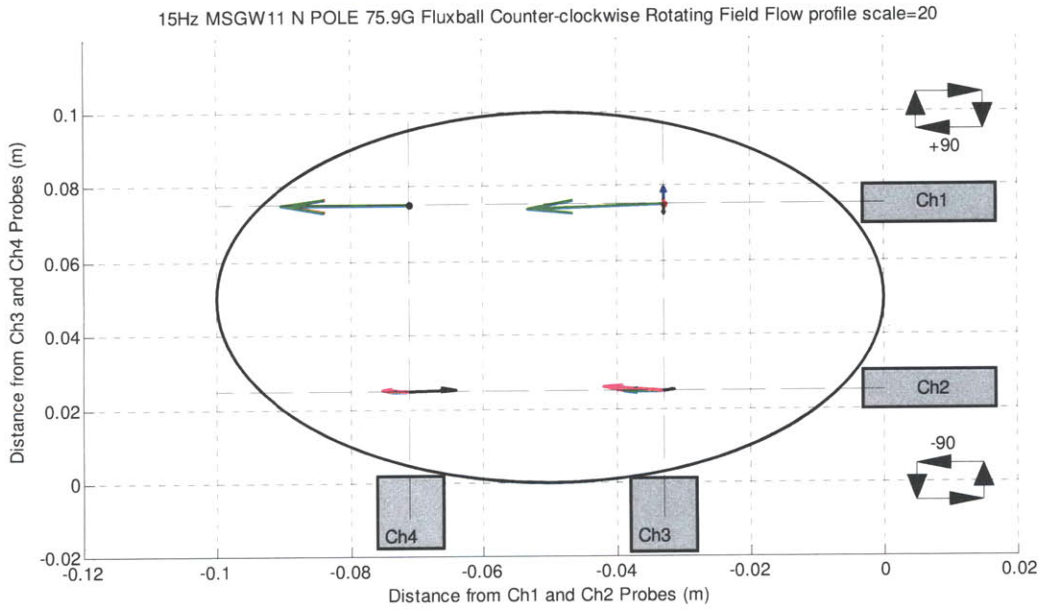
15Hz MSGW11 N POLE 75.9G Fluxball Counter-clockwise Rotating Field Flow profile scale=20
Distance from Ch3 and Ch4 Probes (m)
Distance from Ch1 and Ch2 Probes (m)
+90
-90
Ch1
Ch2
Ch3
Ch4
0.1
0.08
0.06
0.04
0.02
0
-0.02
-0.12
-0.1
-0.08
-0.06
-0.04
-0.02
0
0.02

H13. Comparison of Different Fluids with 1601G Magnet with South Pole Facing Ferrofluid Filled Sphere at Different Frequencies and Field Strengths

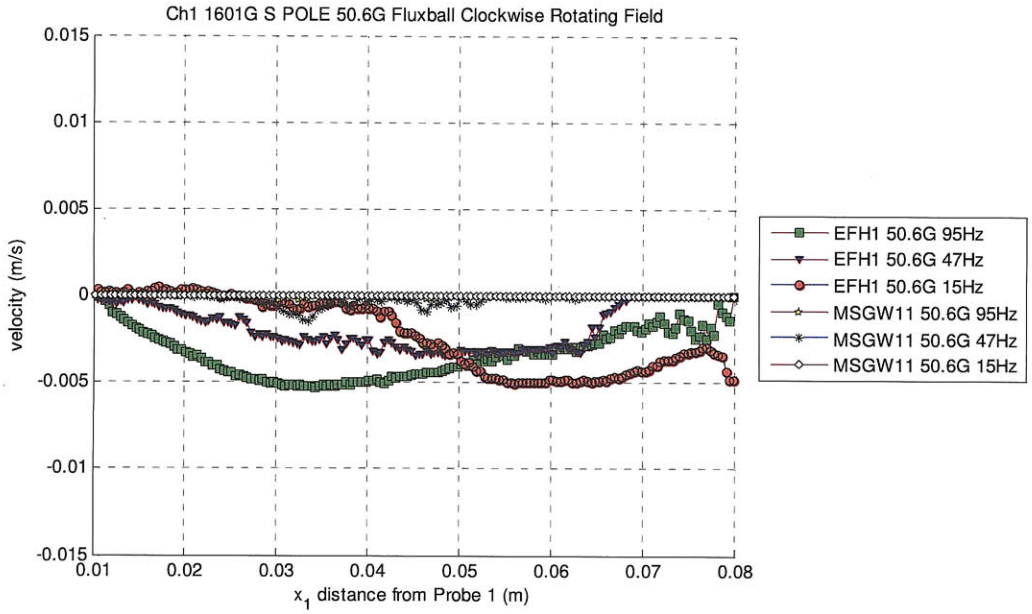

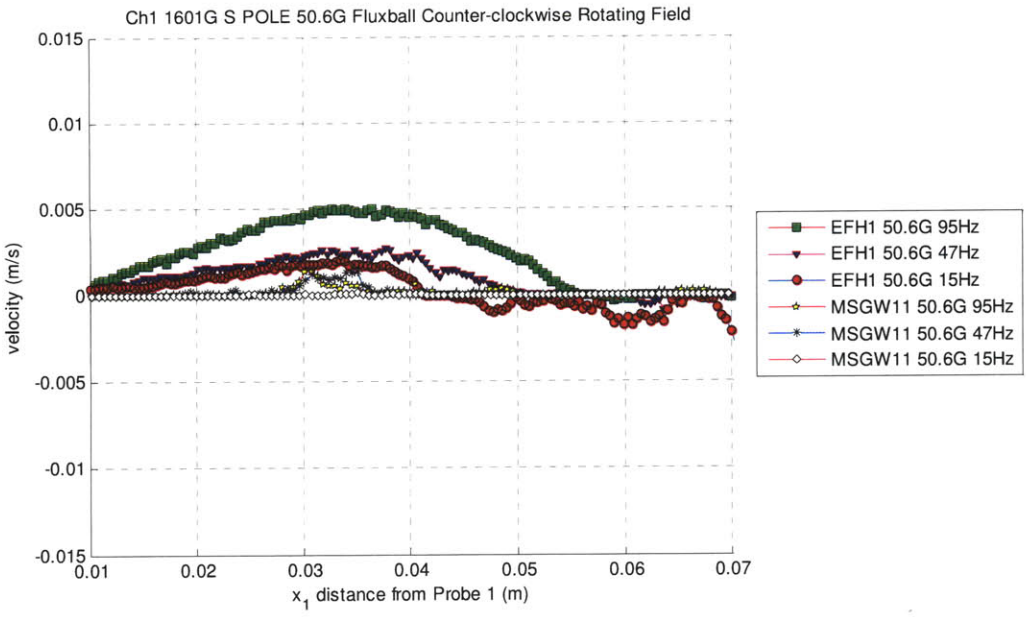
Ch1 1601G S POLE 50.6G Fluxball Counter-clockwise Rotating Field
velocity (m/s)
0.015
0.01
0.005
0
-0.005
-0.01
-0.015
0.01
0.02
0.03
0.04
0.05
0.06
0.07
x1 distance from Probe 1 (m)
EFH1 50.6G 95Hz
EFH1 50.6G 47Hz
EFH1 50.6G 15Hz
MSGW11 50.6G 95Hz
MSGW11 50.6G 47Hz
MSGW11 50.6G 15Hz

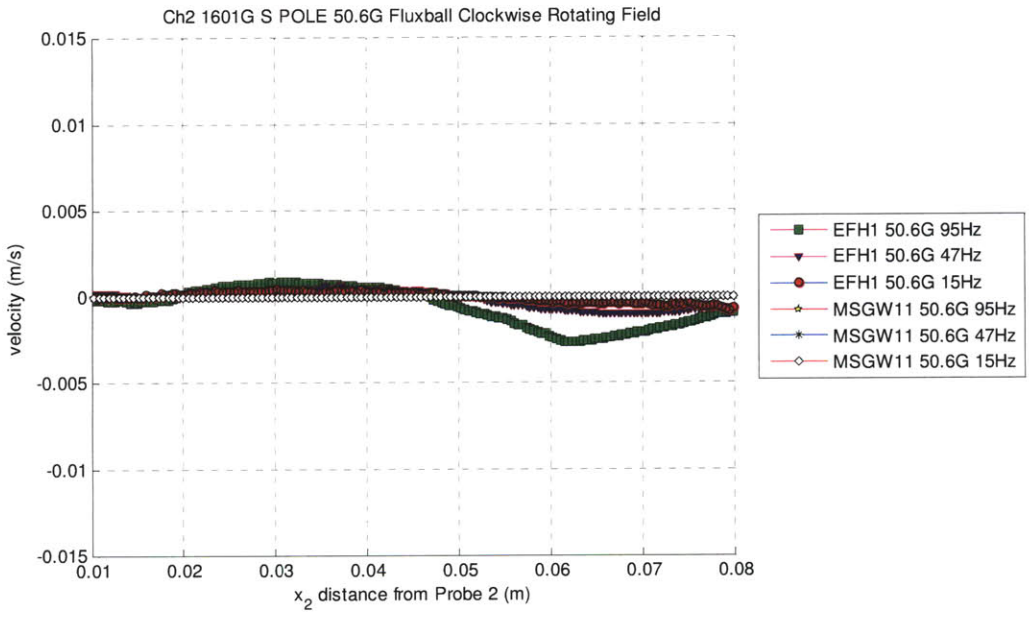
Ch2 1601G S POLE 50.6G Fluxball Clockwise Rotating Field
velocity (m/s)
0.015
0.01
0.005
0
-0.005
-0.01
-0.015
0.01
0.02
0.03
0.04
0.05
0.06
0.07
0.08
x2 distance from Probe 2 (m)
EFH1 50.6G 95Hz
EFH1 50.6G 47Hz
EFH1 50.6G 15Hz
MSGW11 50.6G 95Hz
MSGW11 50.6G 47Hz
MSGW11 50.6G 15Hz

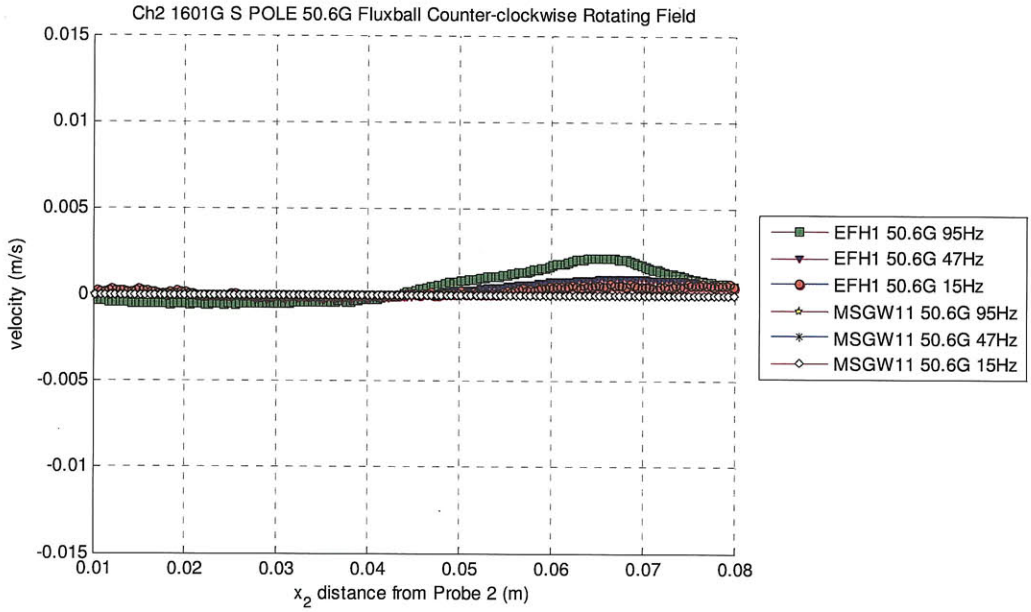
Ch2 1601G S POLE 50.6G Fluxball Counter-clockwise Rotating Field
velocity (m/s)
0.015
0.01
0.005
0
-0.005
-0.01
-0.015
0.01
0.02
0.03
0.04
0.05
0.06
0.07
0.08
x2 distance from Probe 2 (m)
EFH1 50.6G 95Hz
EFH1 50.6G 47Hz
EFH1 50.6G 15Hz
MSGW11 50.6G 95Hz
MSGW11 50.6G 47Hz
MSGW11 50.6G 15Hz

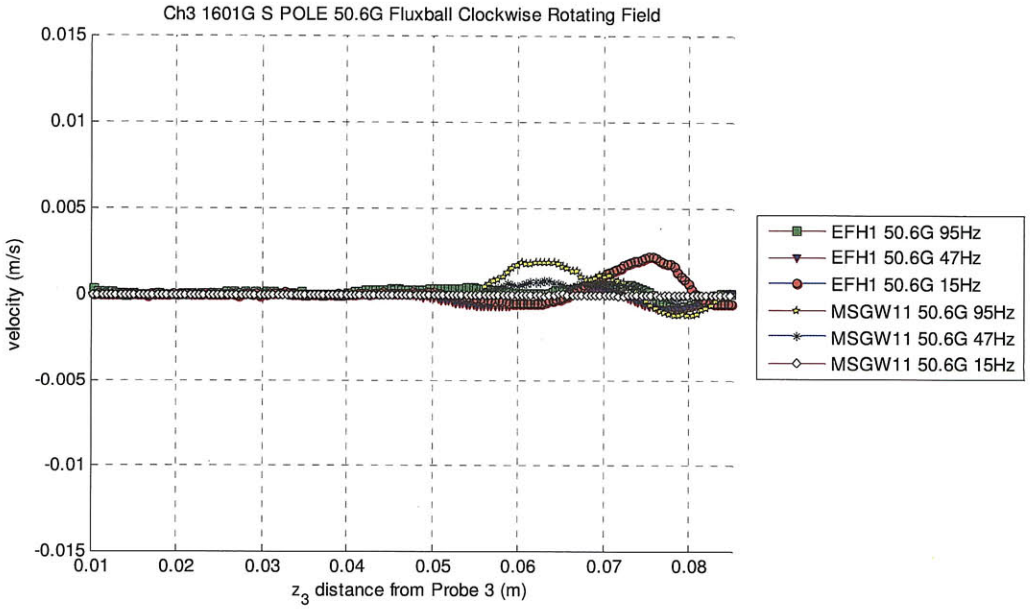
Ch3 1601G S POLE 50.6G Fluxball Clockwise Rotating Field
velocity (m/s)
0.015
0.01
0.005
0
-0.005
-0.01
-0.015
0.01
0.02
0.03
0.04
0.05
0.06
0.07
0.08
z3 distance from Probe 3 (m)
EFH1 50.6G 95Hz
EFH1 50.6G 47Hz
EFH1 50.6G 15Hz
MSGW11 50.6G 95Hz
MSGW11 50.6G 47Hz
MSGW11 50.6G 15Hz

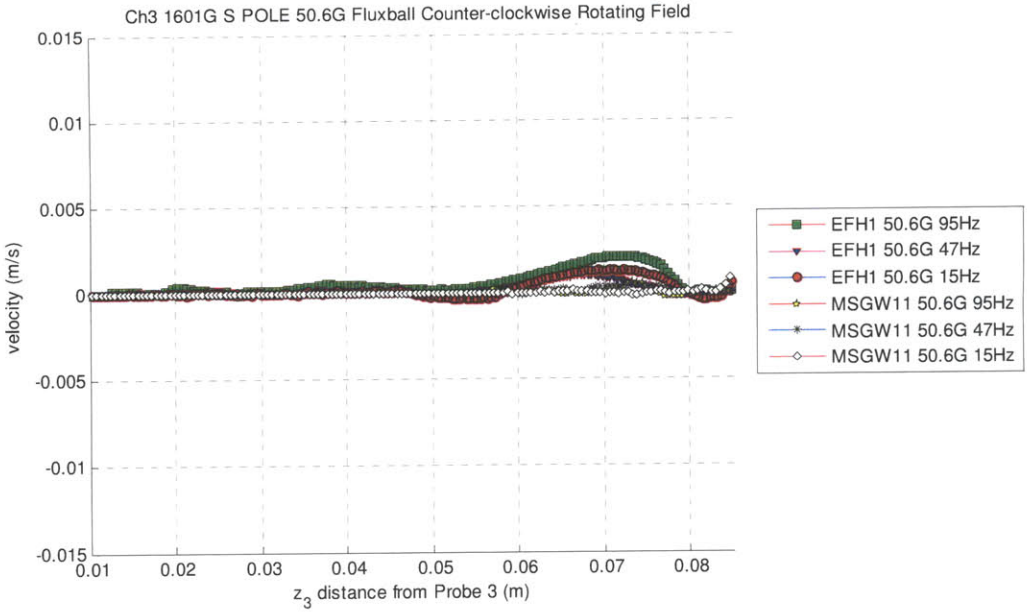
Ch3 1601G S POLE 50.6G Fluxball Counter-clockwise Rotating Field
velocity (m/s)
0.015
0.01
0.005
0
-0.005
-0.01
-0.015
0.01
0.02
0.03
0.04
0.05
0.06
0.07
0.08
z3 distance from Probe 3 (m)
EFH1 50.6G 95Hz
EFH1 50.6G 47Hz
EFH1 50.6G 15Hz
MSGW11 50.6G 95Hz
MSGW11 50.6G 47Hz
MSGW11 50.6G 15Hz

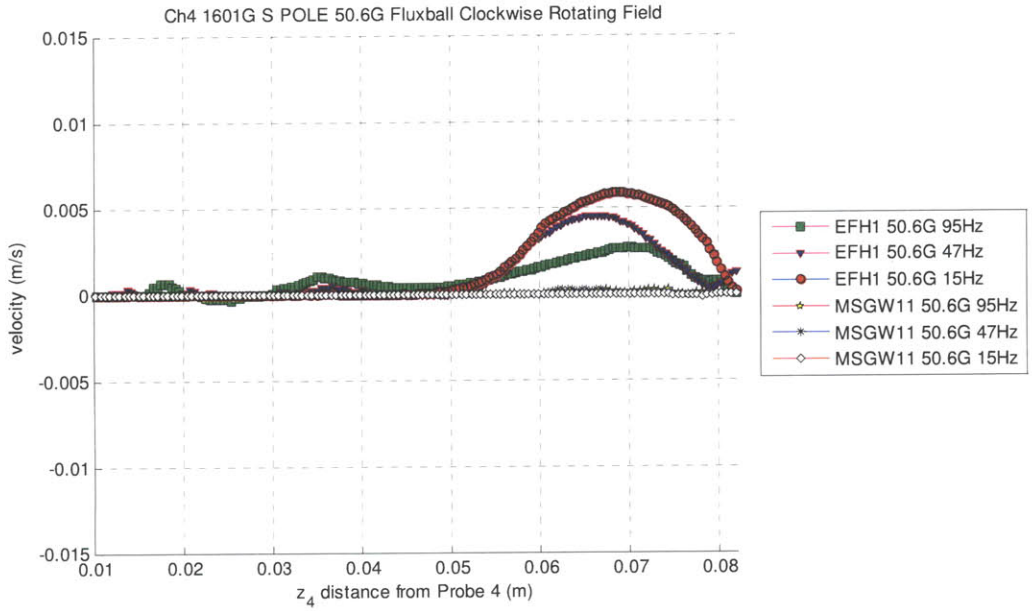
Ch4 1601G S POLE 50.6G Fluxball Clockwise Rotating Field
velocity (m/s)
0.015
0.01
0.005
0
-0.005
-0.01
-0.015
0.01
0.02
0.03
0.04
0.05
0.06
0.07
0.08
z4 distance from Probe 4 (m)
EFH1 50.6G 95Hz
EFH1 50.6G 47Hz
EFH1 50.6G 15Hz
MSGW11 50.6G 95Hz
MSGW11 50.6G 47Hz
MSGW11 50.6G 15Hz

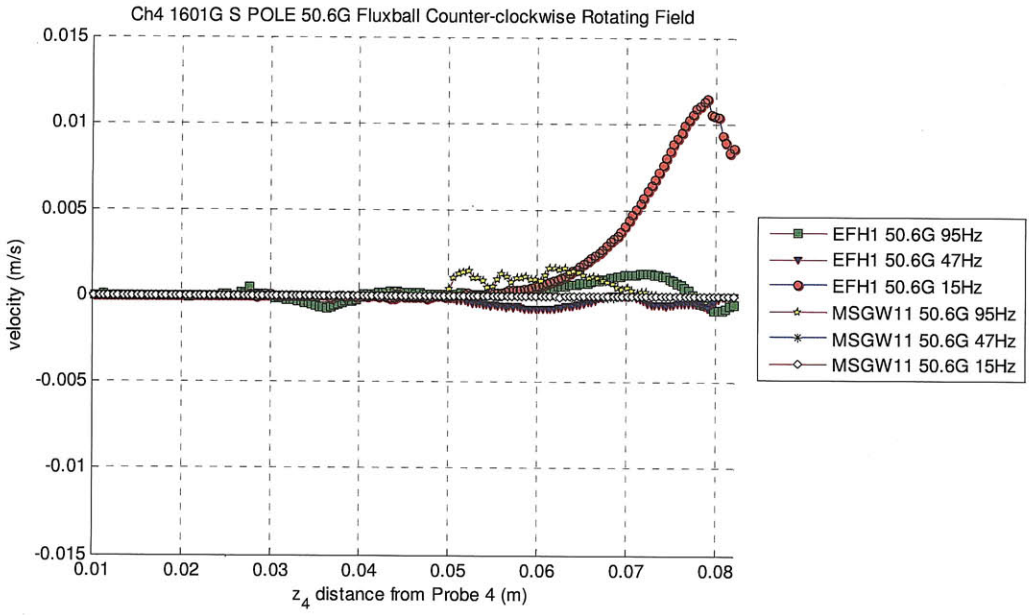
Ch4 1601G S POLE 50.6G Fluxball Counter-clockwise Rotating Field
velocity (m/s)
0.015
0.01
0.005
0
-0.005
-0.01
-0.015
0.01
0.02
0.03
0.04
0.05
0.06
0.07
0.08
z4 distance from Probe 4 (m)
EFH1 50.6G 95Hz
EFH1 50.6G 47Hz
EFH1 50.6G 15Hz
MSGW11 50.6G 95Hz
MSGW11 50.6G 47Hz
MSGW11 50.6G 15Hz

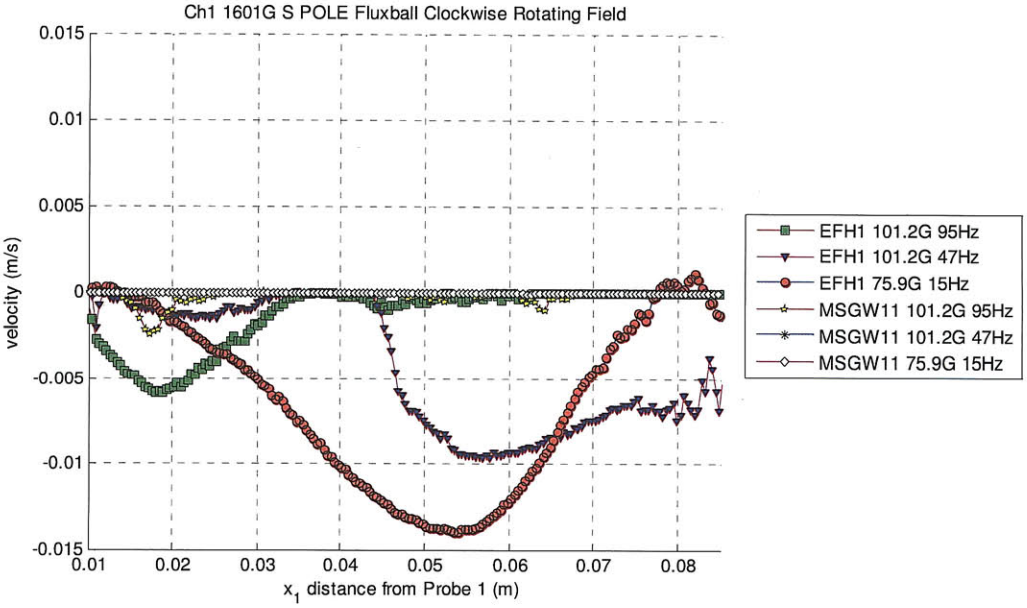
Ch1 1601G S POLE Fluxball Clockwise Rotating Field
velocity (m/s)
0.015
0.01
0.005
0
-0.005
-0.01
-0.015
0.01
0.02
0.03
0.04
0.05
0.06
0.07
0.08
x1 distance from Probe 1 (m)
EFH1 101.2G 95Hz
EFH1 101.2G 47Hz
EFH1 75.9G 15Hz
MSGW11 101.2G 95Hz
MSGW11 101.2G 47Hz
MSGW11 75.9G 15Hz

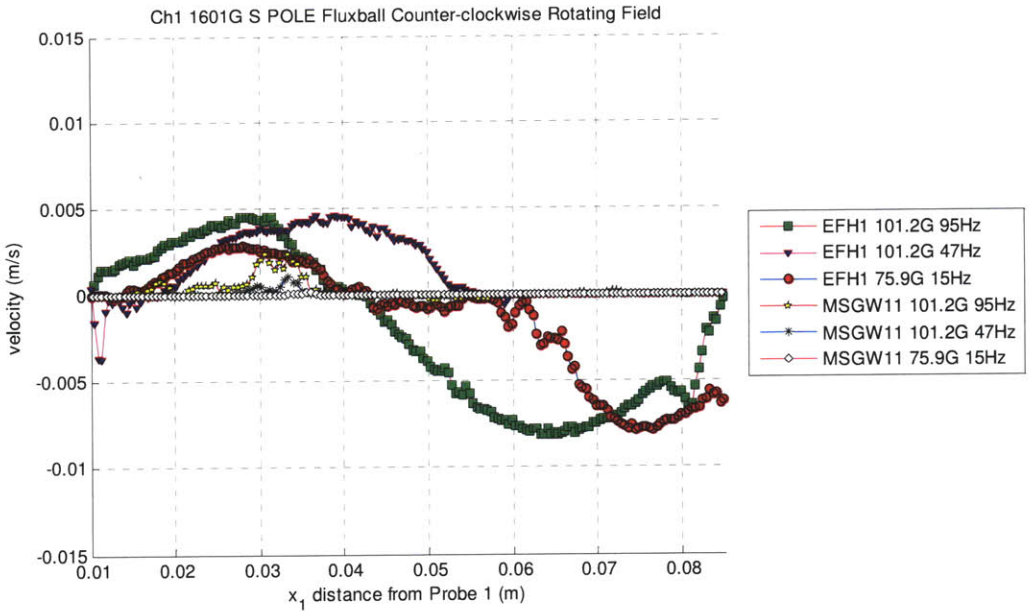
Ch1 1601G S POLE Fluxball Counter-clockwise Rotating Field
velocity (m/s)
0.015
0.01
0.005
0
-0.005
-0.01
-0.015
0.01
0.02
0.03
0.04
0.05
0.06
0.07
0.08
x1 distance from Probe 1 (m)
EFH1 101.2G 95Hz
EFH1 101.2G 47Hz
EFH1 75.9G 15Hz
MSGW11 101.2G 95Hz
MSGW11 101.2G 47Hz
MSGW11 75.9G 15Hz

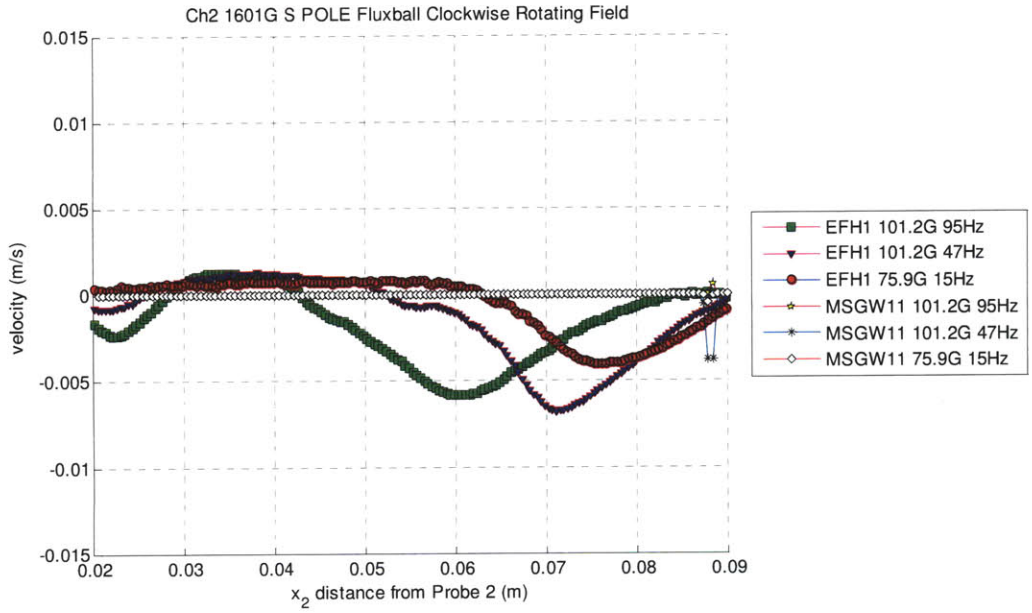
Ch2 1601G S POLE Fluxball Clockwise Rotating Field
velocity (m/s)
0.015
0.01
0.005
0
-0.005
-0.01
-0.015
0.02
0.03
0.04
0.05
0.06
0.07
0.08
0.09
x2 distance from Probe 2 (m)
EFH1 101.2G 95Hz
EFH1 101.2G 47Hz
EFH1 75.9G 15Hz
MSGW11 101.2G 95Hz
MSGW11 101.2G 47Hz
MSGW11 75.9G 15Hz

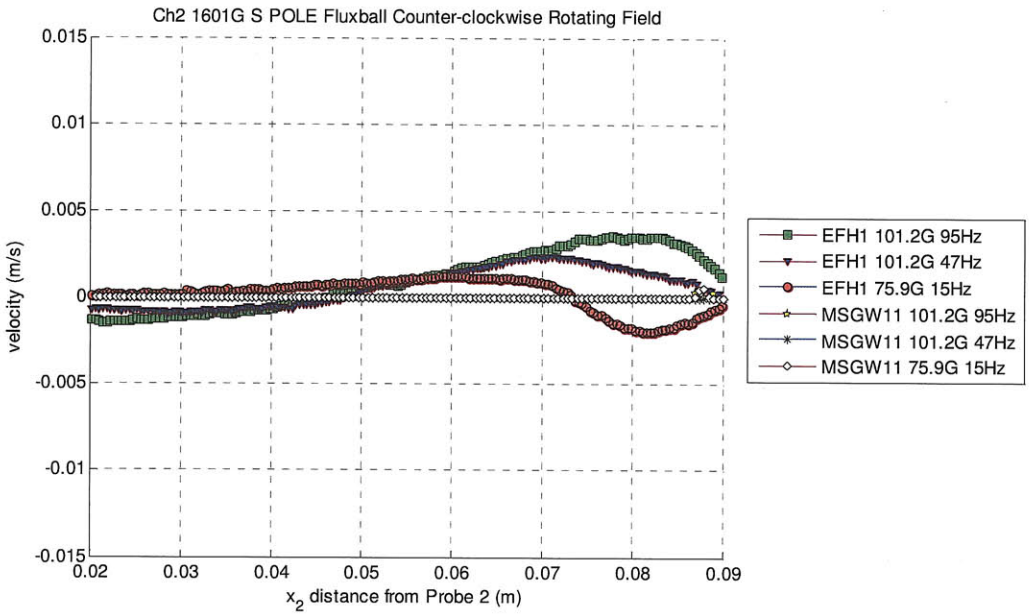
Ch2 1601G S POLE Fluxball Counter-clockwise Rotating Field
velocity (m/s)
0.015
0.01
0.005
0
-0.005
-0.01
-0.015
0.02
0.03
0.04
0.05
0.06
0.07
0.08
0.09
x2 distance from Probe 2 (m)
EFH1 101.2G 95Hz
EFH1 101.2G 47Hz
EFH1 75.9G 15Hz
MSGW11 101.2G 95Hz
MSGW11 101.2G 47Hz
MSGW11 75.9G 15Hz

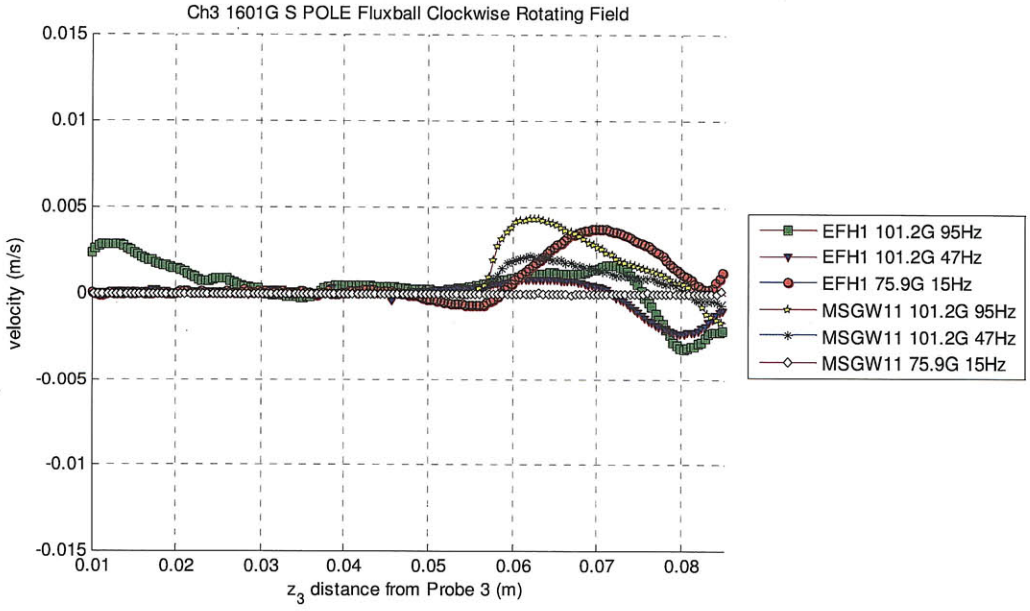
Ch3 1601G S POLE Fluxball Clockwise Rotating Field
velocity (m/s)
0.015
0.01
0.005
0
-0.005
-0.01
-0.015
0.01
0.02
0.03
0.04
0.05
0.06
0.07
0.08
z3 distance from Probe 3 (m)
EFH1 101.2G 95Hz
EFH1 101.2G 47Hz
EFH1 75.9G 15Hz
MSGW11 101.2G 95Hz
MSGW11 101.2G 47Hz
MSGW11 75.9G 15Hz

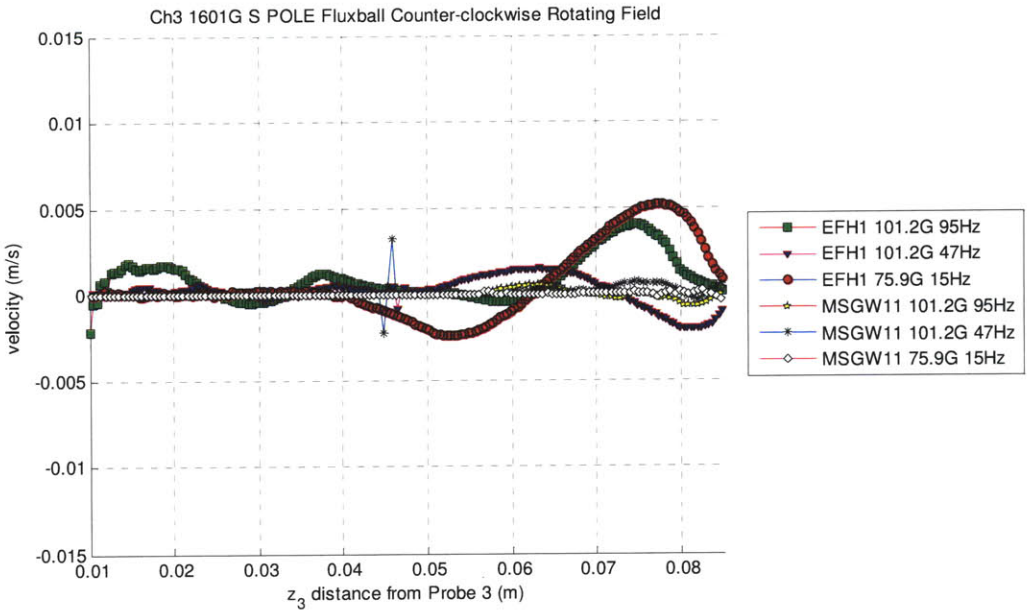
Ch3 1601G S POLE Fluxball Counter-clockwise Rotating Field
velocity (m/s)
0.015
0.01
0.005
0
-0.005
-0.01
-0.015
0.01
0.02
0.03
0.04
0.05
0.06
0.07
0.08
z3 distance from Probe 3 (m)
EFH1 101.2G 95Hz
EFH1 101.2G 47Hz
EFH1 75.9G 15Hz
MSGW11 101.2G 95Hz
MSGW11 101.2G 47Hz
MSGW11 75.9G 15Hz

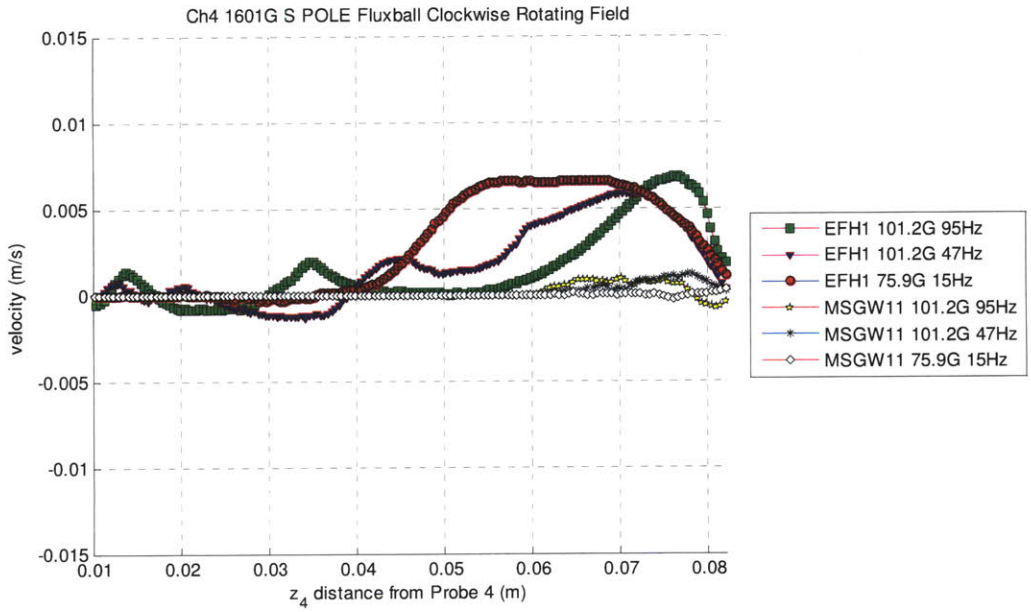
Ch4 1601G S POLE Fluxball Clockwise Rotating Field
velocity (m/s)
0.015
0.01
0.005
0
-0.005
-0.01
-0.015
0.01
0.02
0.03
0.04
0.05
0.06
0.07
0.08
z4 distance from Probe 4 (m)
EFH1 101.2G 95Hz
EFH1 101.2G 47Hz
EFH1 75.9G 15Hz
MSGW11 101.2G 95Hz
MSGW11 101.2G 47Hz
MSGW11 75.9G 15Hz

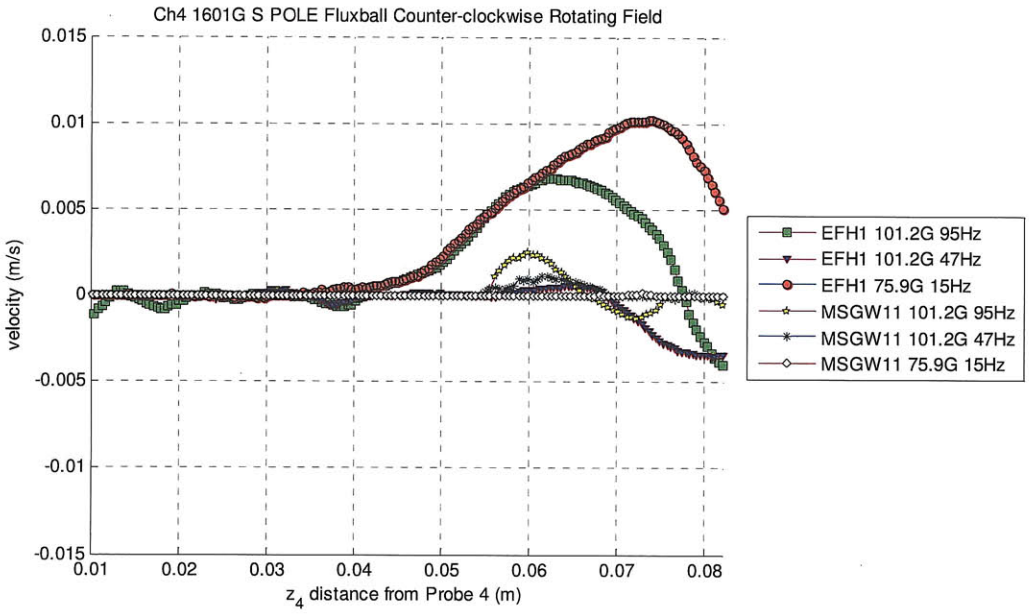
Ch4 1601G S POLE Fluxball Counter-clockwise Rotating Field
velocity (m/s)
0.015
0.01
0.005
0
-0.005
-0.01
-0.015
0.01
0.02
0.03
0.04
0.05
0.06
0.07
0.08
z4 distance from Probe 4 (m)
EFH1 101.2G 95Hz
EFH1 101.2G 47Hz
EFH1 75.9G 15Hz
MSGW11 101.2G 95Hz
MSGW11 101.2G 47Hz
MSGW11 75.9G 15Hz

H14. Comparison of Different Fluids with 1601G Magnet with North Pole Facing Ferrofluid Filled Sphere at Different Frequencies and Field Strengths

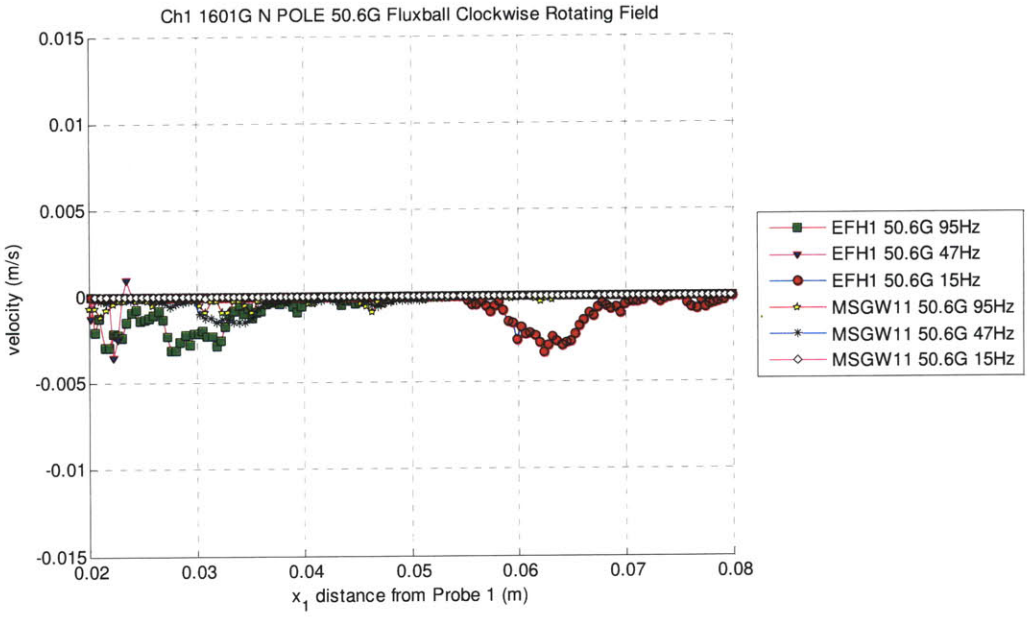

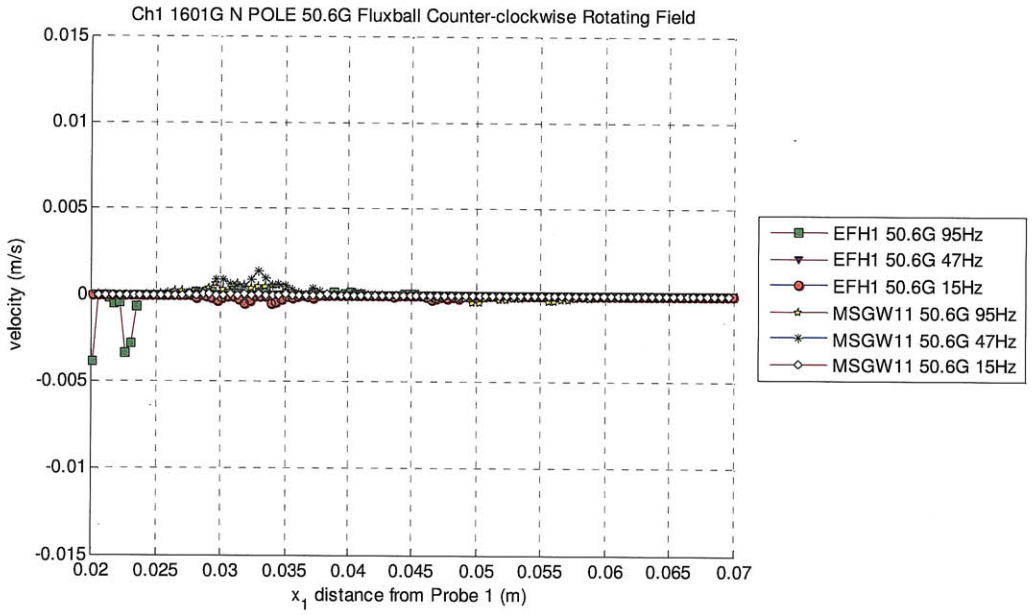
Ch1 1601G N POLE 50.6G Fluxball Counter-clockwise Rotating Field
velocity (m/s)
0.015
0.01
0.005
0
-0.005
-0.01
-0.015
0.02
0.025
0.03
0.035
0.04
0.045
0.05
0.055
0.06
0.065
0.07
x1 distance from Probe 1 (m)
EFH1 50.6G 95Hz
EFH1 50.6G 47Hz
EFH1 50.6G 15Hz
MSGW11 50.6G 95Hz
MSGW11 50.6G 47Hz
MSGW11 50.6G 15Hz

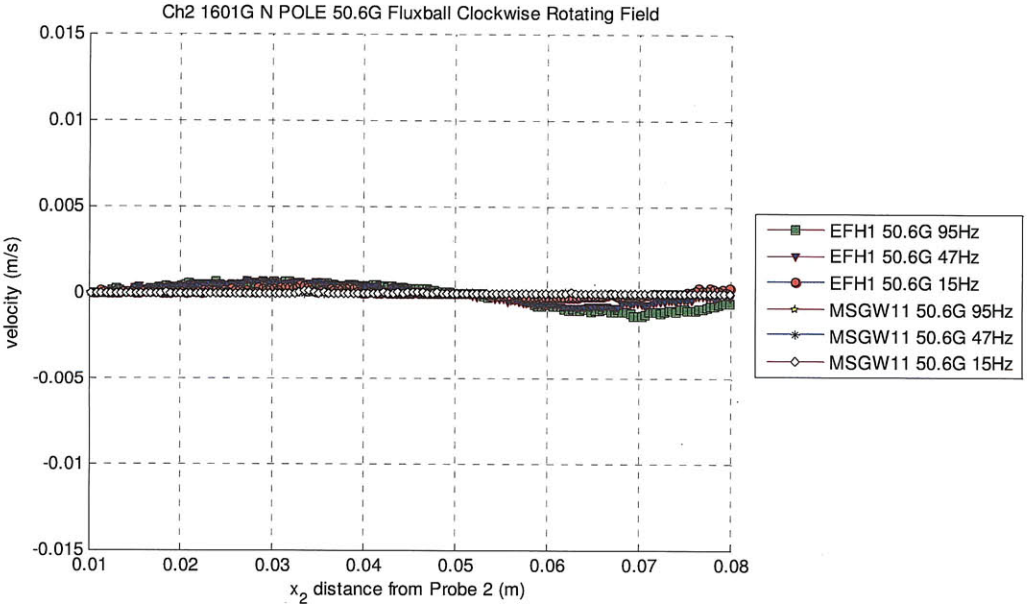
Ch2 1601G N POLE 50.6G Fluxball Clockwise Rotating Field
velocity (m/s)
0.015
0.01
0.005
0
-0.005
-0.01
-0.015
0.01
0.02
0.03
0.04
0.05
0.06
0.07
0.08
x2 distance from Probe 2 (m)
EFH1 50.6G 95Hz
EFH1 50.6G 47Hz
EFH1 50.6G 15Hz
MSGW11 50.6G 95Hz
MSGW11 50.6G 47Hz
MSGW11 50.6G 15Hz

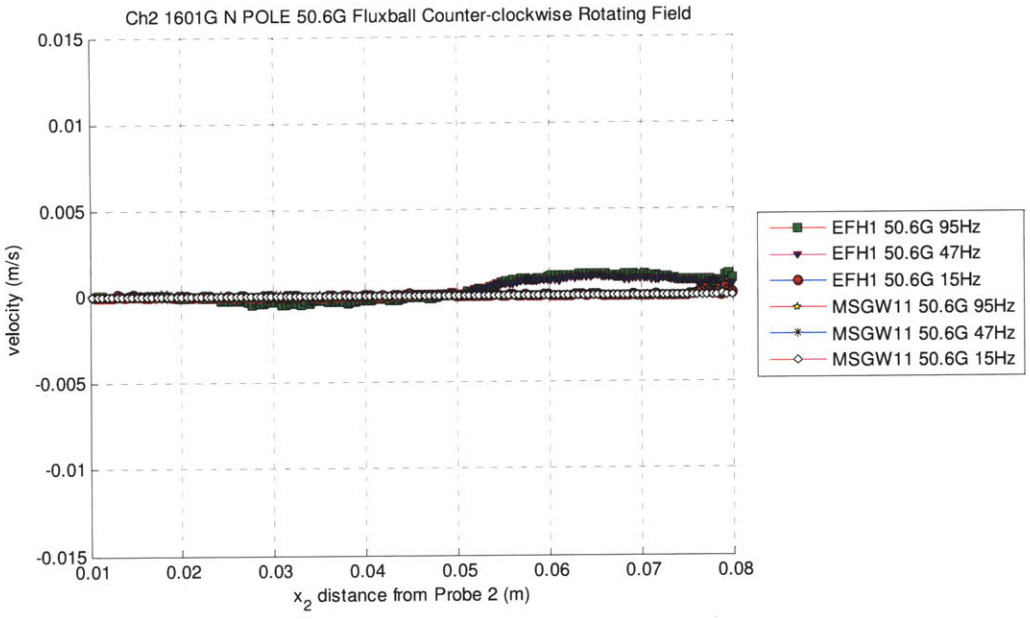
Ch2 1601G N POLE 50.6G Fluxball Counter-clockwise Rotating Field
velocity (m/s)
0.015
0.01
0.005
0
-0.005
-0.01
-0.015
0.01
0.02
0.03
0.04
0.05
0.06
0.07
0.08
x2 distance from Probe 2 (m)
EFH1 50.6G 95Hz
EFH1 50.6G 47Hz
EFH1 50.6G 15Hz
MSGW11 50.6G 95Hz
MSGW11 50.6G 47Hz
MSGW11 50.6G 15Hz

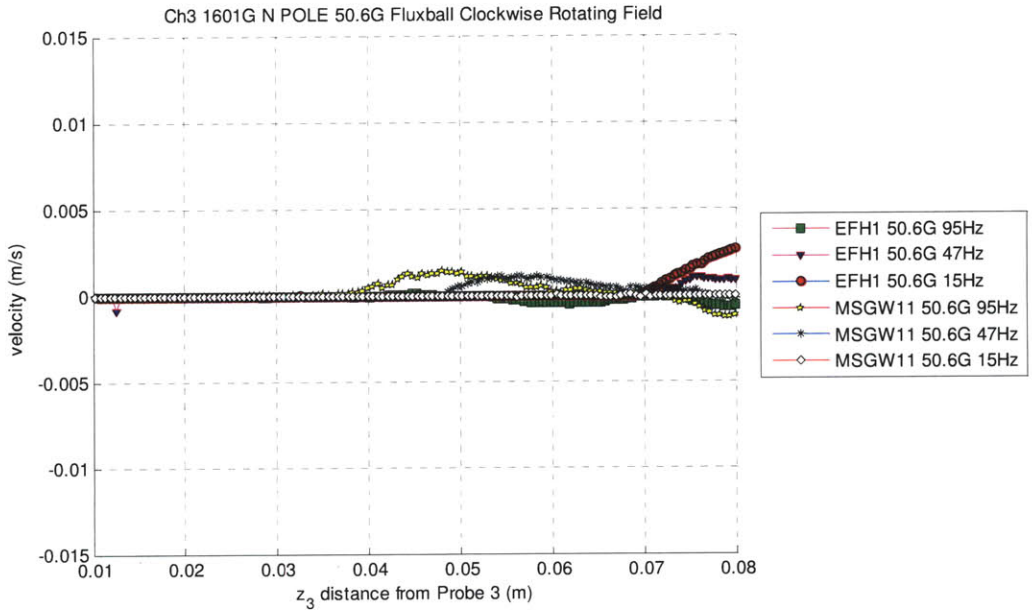
Ch3 1601G N POLE 50.6G Fluxball Clockwise Rotating Field
velocity (m/s)
0.015
0.01
0.005
0
-0.005
-0.01
-0.015
0.01
0.02
0.03
0.04
0.05
0.06
0.07
0.08
z3 distance from Probe 3 (m)
EFH1 50.6G 95Hz
EFH1 50.6G 47Hz
EFH1 50.6G 15Hz
MSGW11 50.6G 95Hz
MSGW11 50.6G 47Hz
MSGW11 50.6G 15Hz

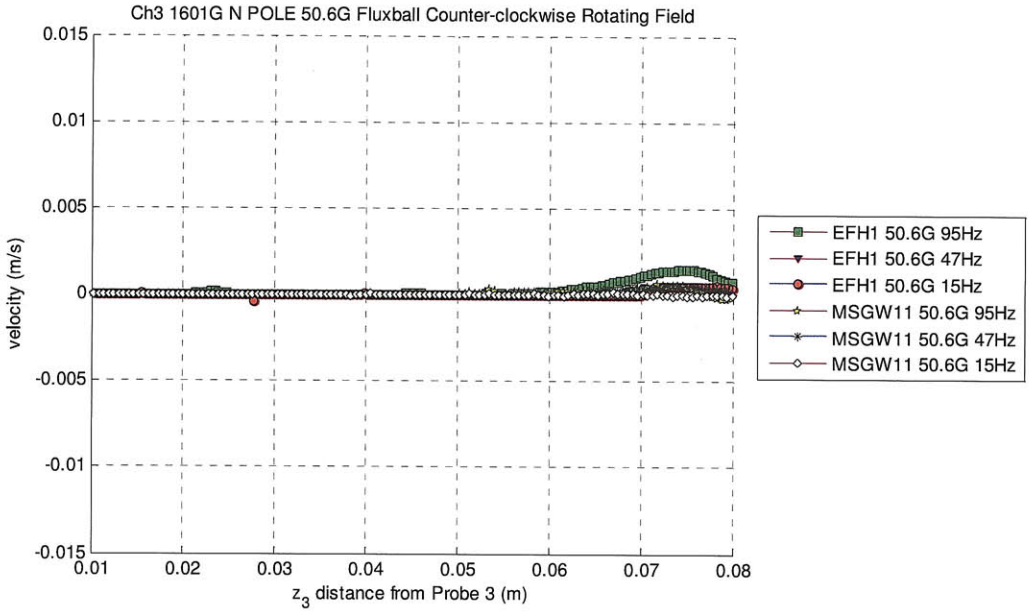
Ch3 1601G N POLE 50.6G Fluxball Counter-clockwise Rotating Field
velocity (m/s)
0.015
0.01
0.005
0
-0.005
-0.01
-0.015
0.01
0.02
0.03
0.04
0.05
0.06
0.07
0.08
z_3 distance from Probe 3 (m)
EFH1 50.6G 95Hz
EFH1 50.6G 47Hz
EFH1 50.6G 15Hz
MSGW11 50.6G 95Hz
MSGW11 50.6G 47Hz
MSGW11 50.6G 15Hz

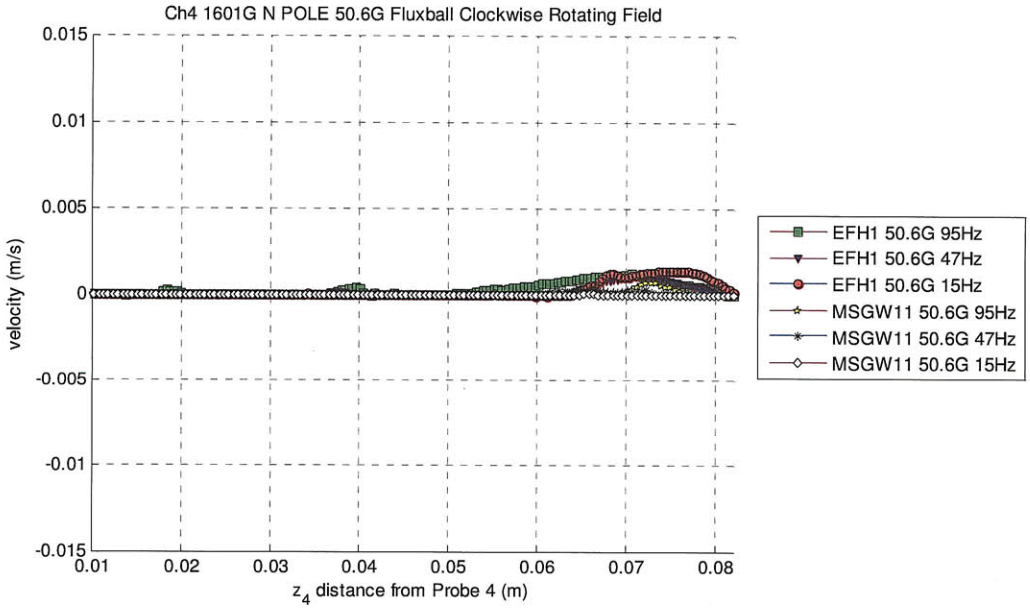
Ch4 1601G N POLE 50.6G Fluxball Clockwise Rotating Field
velocity (m/s)
0.015
0.01
0.005
0
-0.005
-0.01
-0.015
0.01
0.02
0.03
0.04
0.05
0.06
0.07
0.08
z_4 distance from Probe 4 (m)
EFH1 50.6G 95Hz
EFH1 50.6G 47Hz
EFH1 50.6G 15Hz
MSGW11 50.6G 95Hz
MSGW11 50.6G 47Hz
MSGW11 50.6G 15Hz

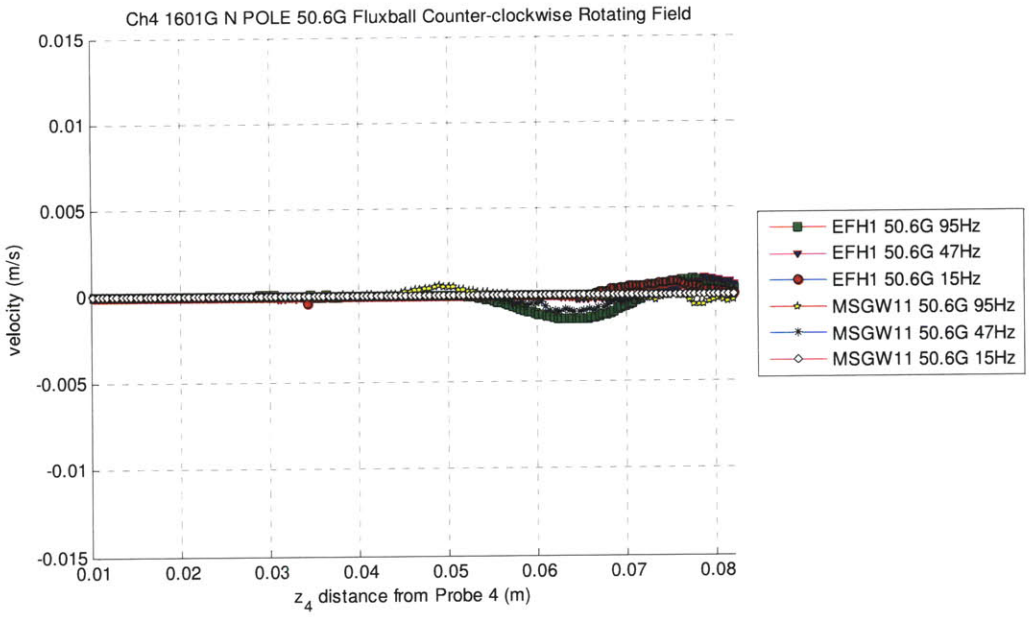
Ch4 1601G N POLE 50.6G Fluxball Counter-clockwise Rotating Field
velocity (m/s)
0.015
0.01
0.005
0
-0.005
-0.01
-0.015
0.01
0.02
0.03
0.04
0.05
0.06
0.07
0.08
z4 distance from Probe 4 (m)
EFH1 50.6G 95Hz
EFH1 50.6G 47Hz
EFH1 50.6G 15Hz
MSGW11 50.6G 95Hz
MSGW11 50.6G 47Hz
MSGW11 50.6G 15Hz

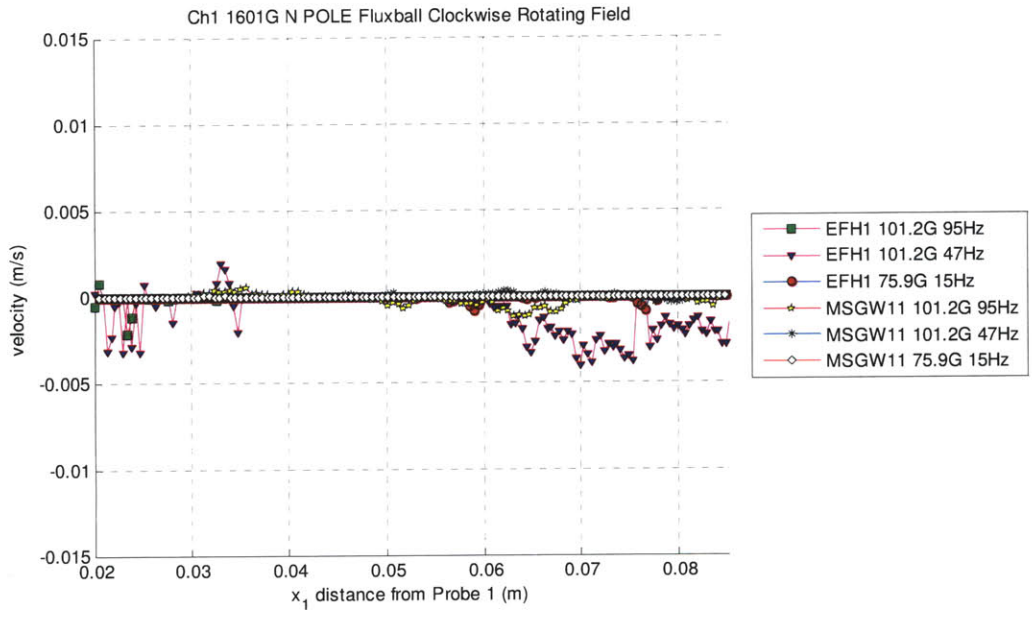
Ch1 1601G N POLE Fluxball Clockwise Rotating Field
velocity (m/s)
0.015
0.01
0.005
0
-0.005
-0.01
-0.015
0.02
0.03
0.04
0.05
0.06
0.07
0.08
x1 distance from Probe 1 (m)
EFH1 101.2G 95Hz
EFH1 101.2G 47Hz
EFH1 75.9G 15Hz
MSGW11 101.2G 95Hz
MSGW11 101.2G 47Hz
MSGW11 75.9G 15Hz

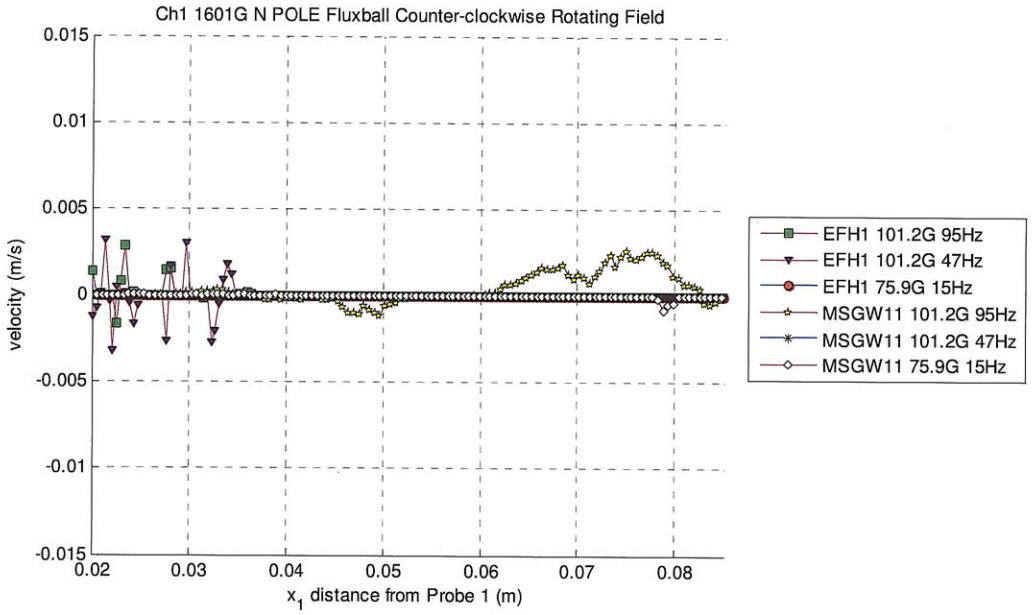
Ch1 1601G N POLE Fluxball Counter-clockwise Rotating Field
velocity (m/s)
0.015
0.01
0.005
0
-0.005
-0.01
-0.015
0.02
0.03
0.04
0.05
0.06
0.07
0.08
x1 distance from Probe 1 (m)
EFH1 101.2G 95Hz
EFH1 101.2G 47Hz
EFH1 75.9G 15Hz
MSGW11 101.2G 95Hz
MSGW11 101.2G 47Hz
MSGW11 75.9G 15Hz

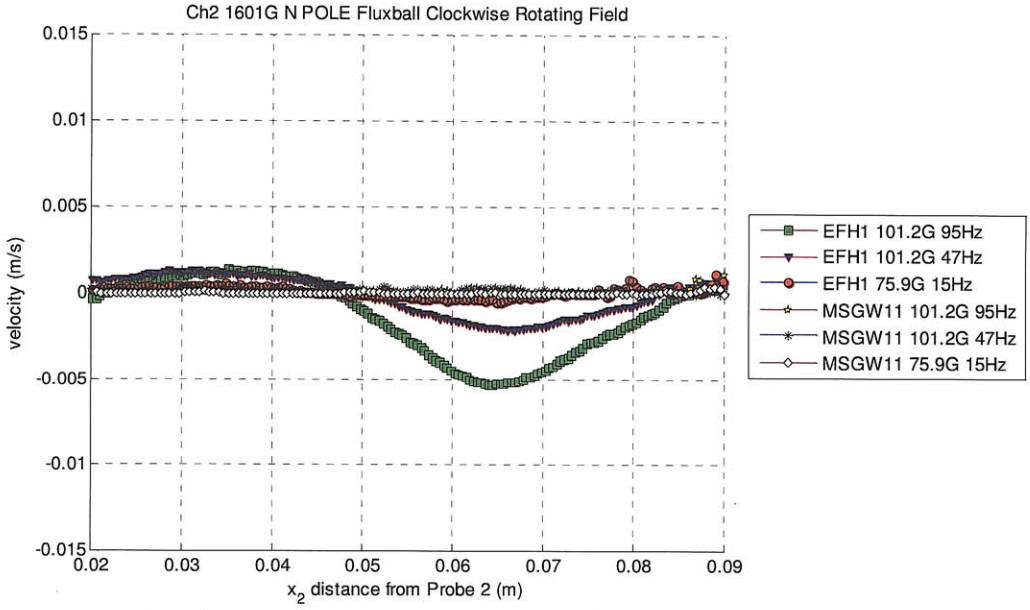
Ch2 1601G N POLE Fluxball Clockwise Rotating Field
velocity (m/s)
0.015
0.01
0.005
0
-0.005
-0.01
-0.015
0.02
0.03
0.04
0.05
0.06
0.07
0.08
0.09
x2 distance from Probe 2 (m)
EFH1 101.2G 95Hz
EFH1 101.2G 47Hz
EFH1 75.9G 15Hz
MSGW11 101.2G 95Hz
MSGW11 101.2G 47Hz
MSGW11 75.9G 15Hz

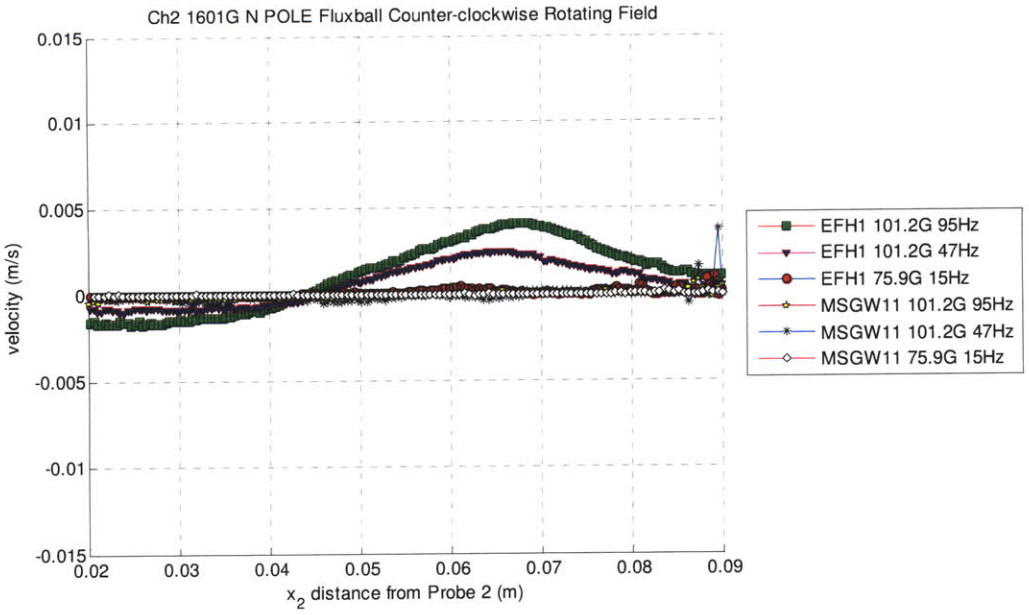
Ch2 1601G N POLE Fluxball Counter-clockwise Rotating Field
velocity (m/s)
0.015
0.01
0.005
0
-0.005
-0.01
-0.015
0.02
0.03
0.04
0.05
0.06
0.07
0.08
0.09
x2 distance from Probe 2 (m)
EFH1 101.2G 95Hz
EFH1 101.2G 47Hz
EFH1 75.9G 15Hz
MSGW11 101.2G 95Hz
MSGW11 101.2G 47Hz
MSGW11 75.9G 15Hz

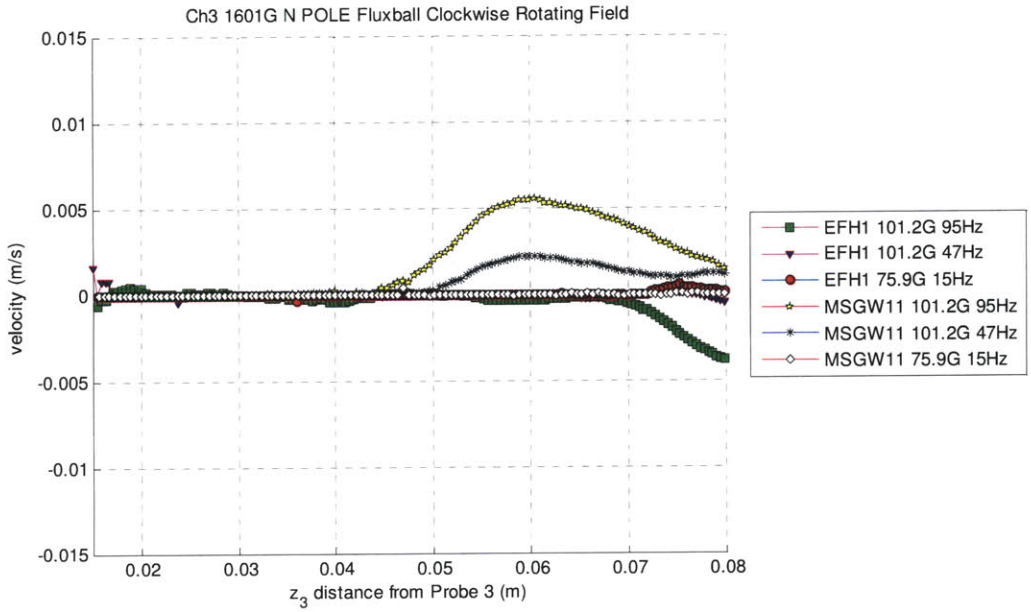
Ch3 1601G N POLE Fluxball Clockwise Rotating Field
velocity (m/s)
0.015
0.01
0.005
0
-0.005
-0.01
-0.015
0.02
0.03
0.04
0.05
0.06
0.07
0.08
z3 distance from Probe 3 (m)
EFH1 101.2G 95Hz
EFH1 101.2G 47Hz
EFH1 75.9G 15Hz
MSGW11 101.2G 95Hz
MSGW11 101.2G 47Hz
MSGW11 75.9G 15Hz

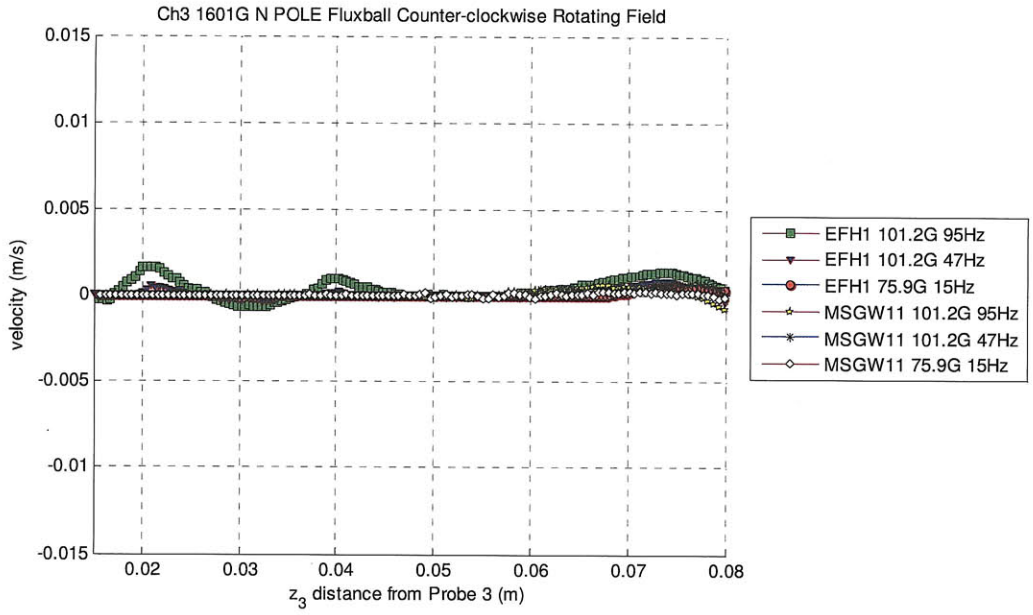
Ch3 1601G N POLE Fluxball Counter-clockwise Rotating Field
velocity (m/s)
0.015
0.01
0.005
0
-0.005
-0.01
-0.015
0.02
0.03
0.04
0.05
0.06
0.07
0.08
z_3 distance from Probe 3 (m)
EFH1 101.2G 95Hz
EFH1 101.2G 47Hz
EFH1 75.9G 15Hz
MSGW11 101.2G 95Hz
MSGW11 101.2G 47Hz
MSGW11 75.9G 15Hz

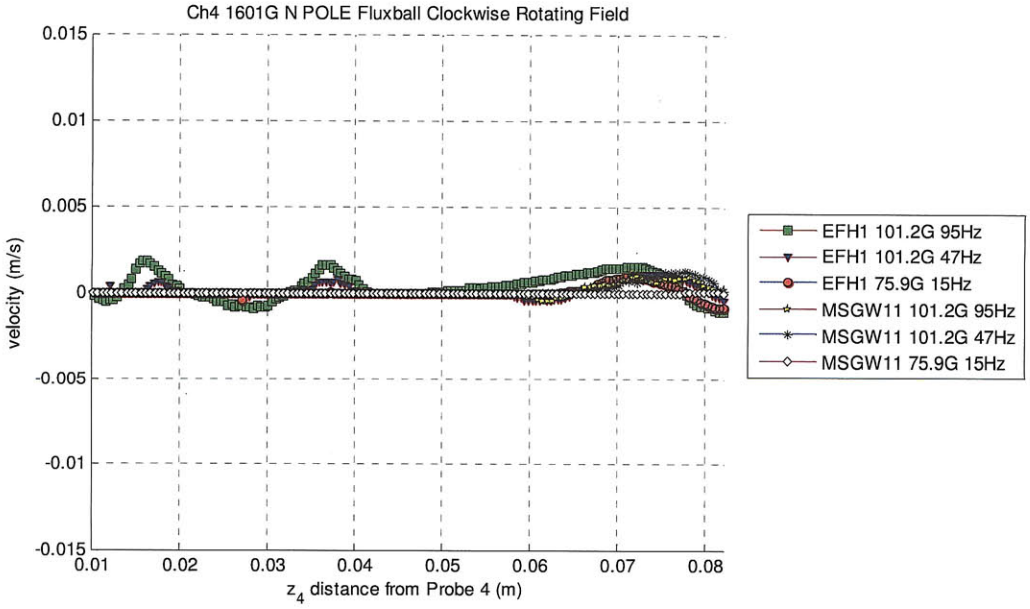
Ch4 1601G N POLE Fluxball Clockwise Rotating Field
velocity (m/s)
0.015
0.01
0.005
0
-0.005
-0.01
-0.015
0.01
0.02
0.03
0.04
0.05
0.06
0.07
0.08
z_4 distance from Probe 4 (m)
EFH1 101.2G 95Hz
EFH1 101.2G 47Hz
EFH1 75.9G 15Hz
MSGW11 101.2G 95Hz
MSGW11 101.2G 47Hz
MSGW11 75.9G 15Hz

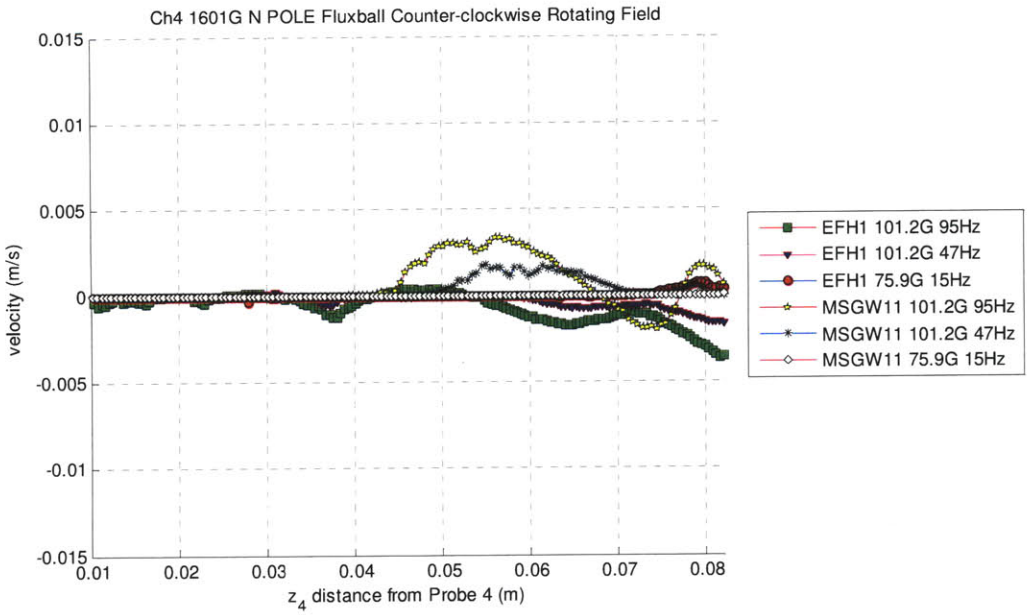
Ch4 1601G N POLE Fluxball Counter-clockwise Rotating Field
0.015
0.01
0.005
0
-0.005
-0.01
-0.015
velocity (m/s)
0.01
0.02
0.03
0.04
0.05
0.06
0.07
0.08
z4 distance from Probe 4 (m)
EFH1 101.2G 95Hz
EFH1 101.2G 47Hz
EFH1 75.9G 15Hz
MSGW11 101.2G 95Hz
MSGW11 101.2G 47Hz
MSGW11 75.9G 15Hz

H15. Comparison of Different Fluids with 2952G Magnet with South Pole Facing Ferrofluid Filled Sphere at Different Frequencies and Field Strengths

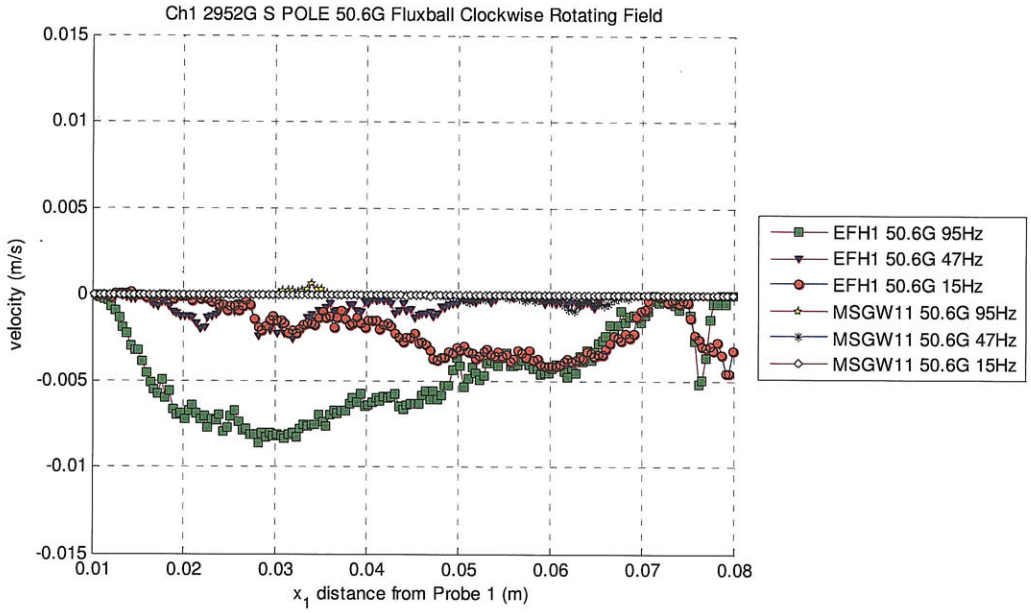

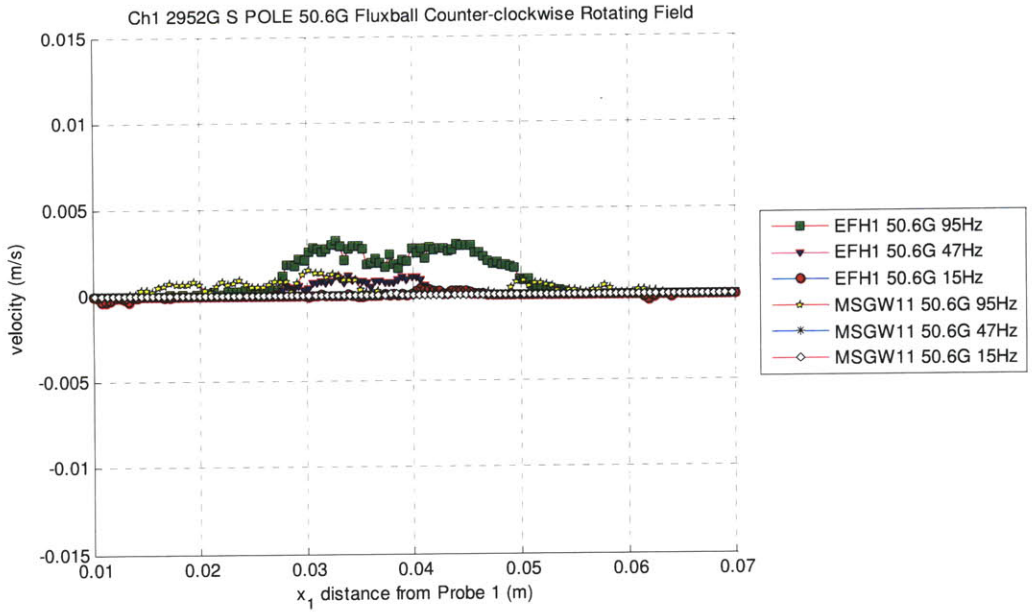
Ch1 2952G S POLE 50.6G Fluxball Counter-clockwise Rotating Field
velocity (m/s)
0.015
0.01
0.005
0
-0.005
-0.01
-0.015
0.01
0.02
0.03
0.04
0.05
0.06
0.07
x1 distance from Probe 1 (m)
EFH1 50.6G 95Hz
EFH1 50.6G 47Hz
EFH1 50.6G 15Hz
MSGW11 50.6G 95Hz
MSGW11 50.6G 47Hz
MSGW11 50.6G 15Hz

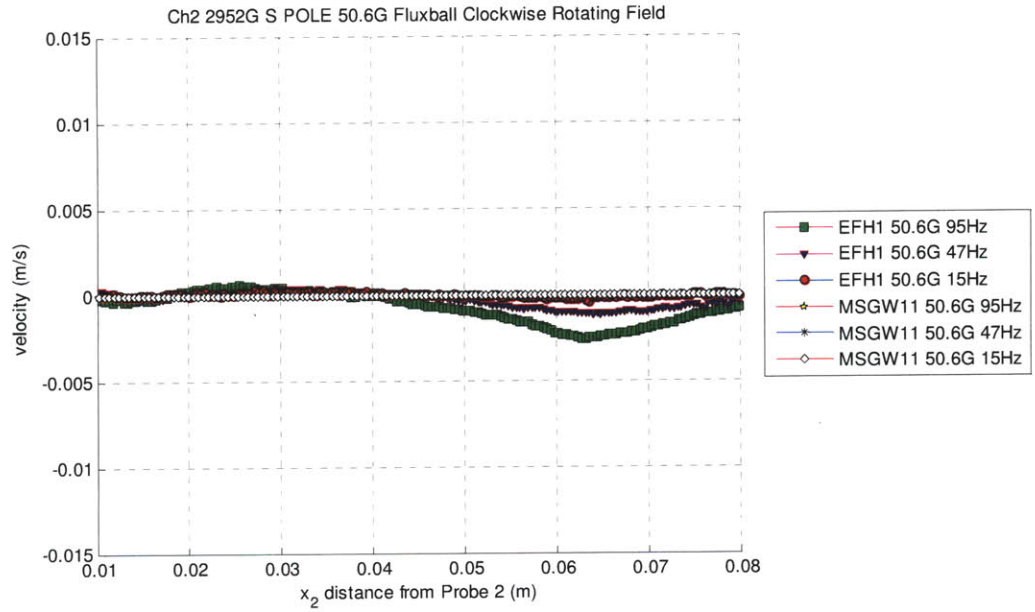
Ch2 2952G S POLE 50.6G Fluxball Clockwise Rotating Field
velocity (m/s)
0.015
0.01
0.005
0
-0.005
-0.01
-0.015
0.01
0.02
0.03
0.04
0.05
0.06
0.07
0.08
x2 distance from Probe 2 (m)
EFH1 50.6G 95Hz
EFH1 50.6G 47Hz
EFH1 50.6G 15Hz
MSGW11 50.6G 95Hz
MSGW11 50.6G 47Hz
MSGW11 50.6G 15Hz

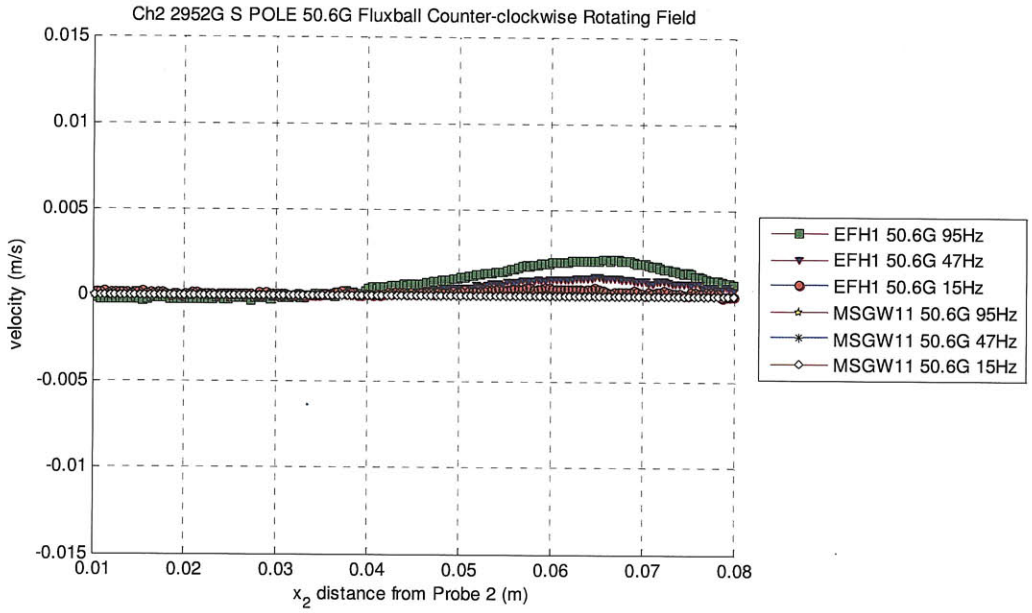
Ch2 2952G S POLE 50.6G Fluxball Counter-clockwise Rotating Field
velocity (m/s)
0.015
0.01
0.005
0
-0.005
-0.01
-0.015
0.01
0.02
0.03
0.04
0.05
0.06
0.07
0.08
x2 distance from Probe 2 (m)
EFH1 50.6G 95Hz
EFH1 50.6G 47Hz
EFH1 50.6G 15Hz
MSGW11 50.6G 95Hz
MSGW11 50.6G 47Hz
MSGW11 50.6G 15Hz

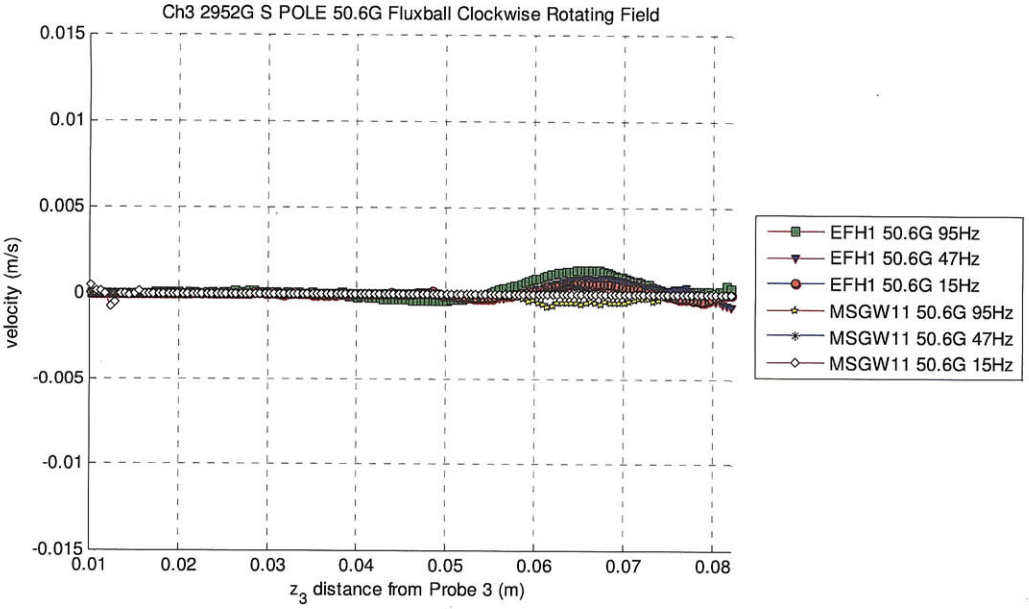
Ch3 2952G S POLE 50.6G Fluxball Clockwise Rotating Field
velocity (m/s)
0.015
0.01
0.005
0
-0.005
-0.01
-0.015
0.01
0.02
0.03
0.04
0.05
0.06
0.07
0.08
z3 distance from Probe 3 (m)
EFH1 50.6G 95Hz
EFH1 50.6G 47Hz
EFH1 50.6G 15Hz
MSGW11 50.6G 95Hz
MSGW11 50.6G 47Hz
MSGW11 50.6G 15Hz

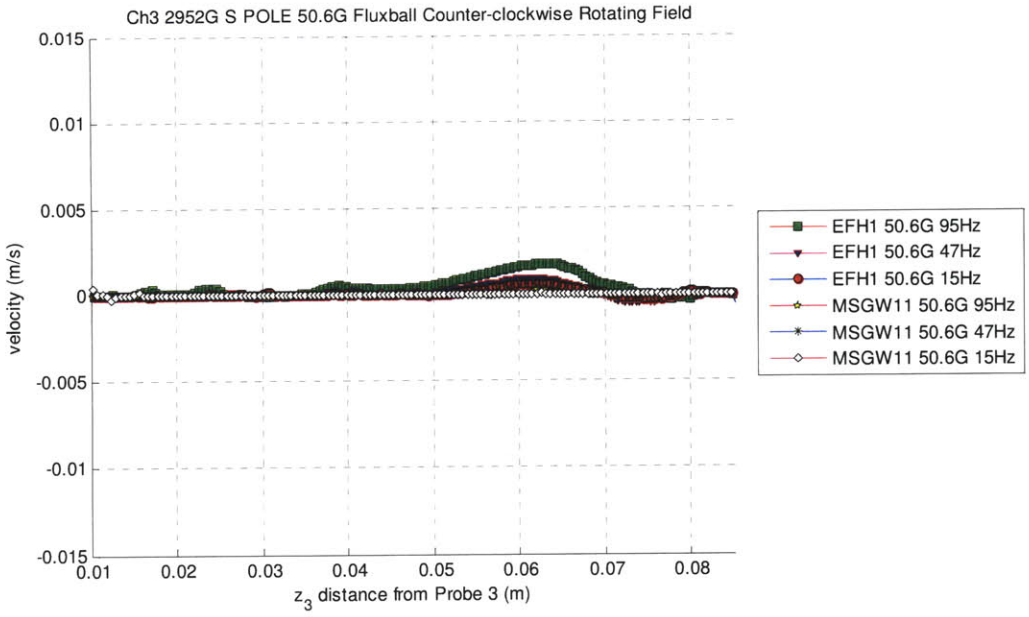
Ch3 2952G S POLE 50.6G Fluxball Counter-clockwise Rotating Field
velocity (m/s)
0.015
0.01
0.005
0
-0.005
-0.01
-0.015
0.01
0.02
0.03
0.04
0.05
0.06
0.07
0.08
z3 distance from Probe 3 (m)
EFH1 50.6G 95Hz
EFH1 50.6G 47Hz
EFH1 50.6G 15Hz
MSGW11 50.6G 95Hz
MSGW11 50.6G 47Hz
MSGW11 50.6G 15Hz

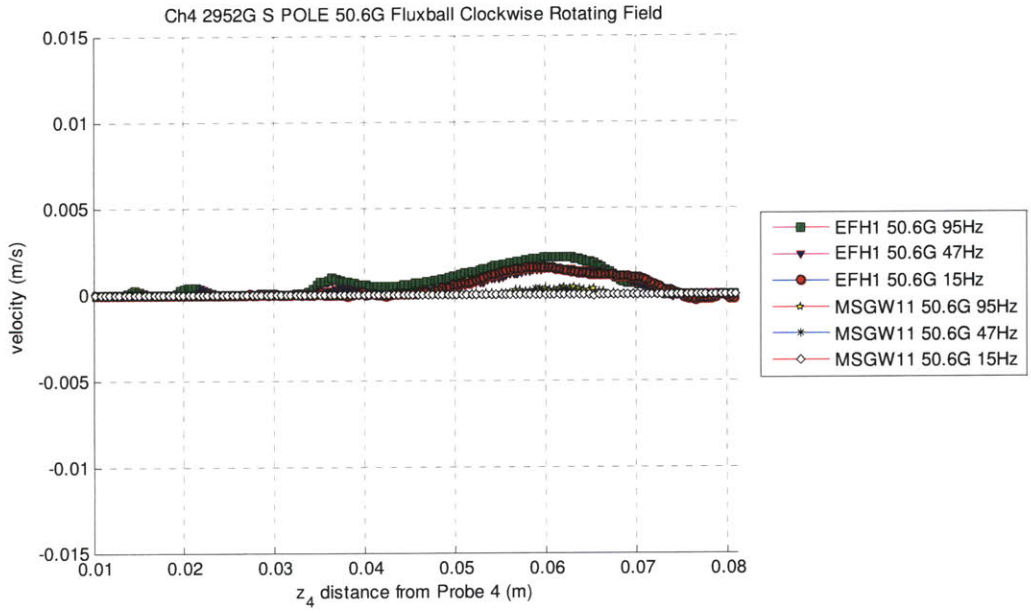
Ch4 2952G S POLE 50.6G Fluxball Clockwise Rotating Field
velocity (m/s)
0.015
0.01
0.005
0
-0.005
-0.01
-0.015
0.01
0.02
0.03
0.04
0.05
0.06
0.07
0.08
z4 distance from Probe 4 (m)
EFH1 50.6G 95Hz
EFH1 50.6G 47Hz
EFH1 50.6G 15Hz
MSGW11 50.6G 95Hz
MSGW11 50.6G 47Hz
MSGW11 50.6G 15Hz

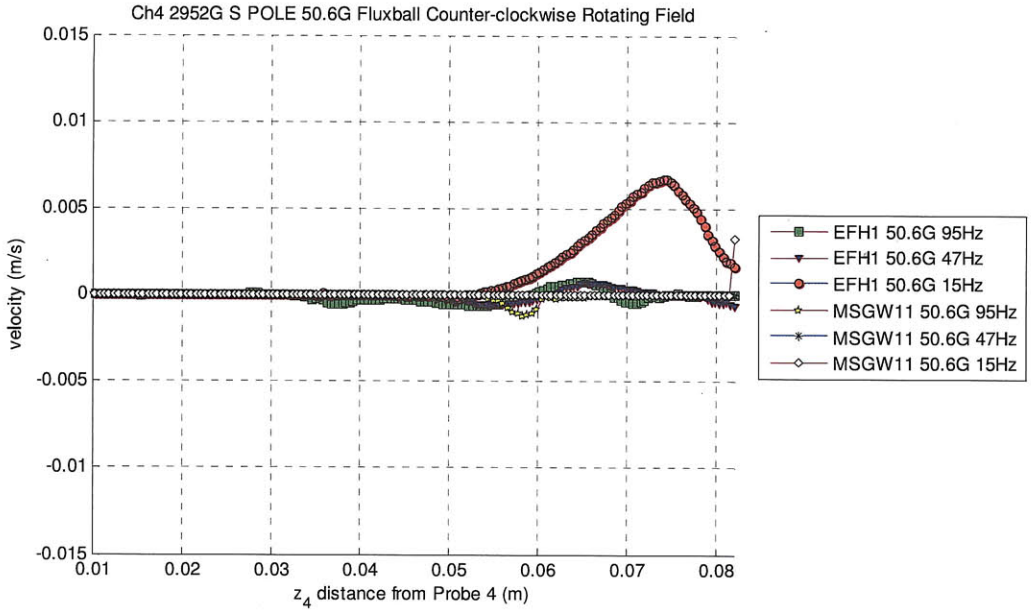
Ch4 2952G S POLE 50.6G Fluxball Counter-clockwise Rotating Field
velocity (m/s)
0.015
0.01
0.005
0
-0.005
-0.01
-0.015
0.01
0.02
0.03
0.04
0.05
0.06
0.07
0.08
z_4 distance from Probe 4 (m)
EFH1 50.6G 95Hz
EFH1 50.6G 47Hz
EFH1 50.6G 15Hz
MSGW11 50.6G 95Hz
MSGW11 50.6G 47Hz
MSGW11 50.6G 15Hz

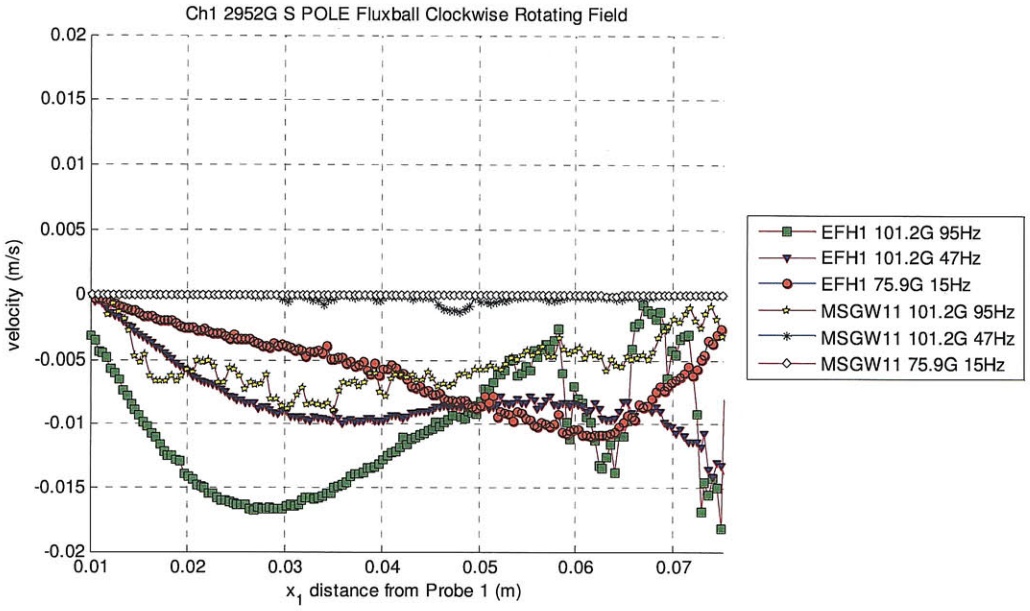
Ch1 2952G S POLE Fluxball Clockwise Rotating Field
velocity (m/s)
0.02
0.015
0.01
0.005
0
-0.005
-0.01
-0.015
-0.02
0.01
0.02
0.03
0.04
0.05
0.06
0.07
x_1 distance from Probe 1 (m)
EFH1 101.2G 95Hz
EFH1 101.2G 47Hz
EFH1 75.9G 15Hz
MSGW11 101.2G 95Hz
MSGW11 101.2G 47Hz
MSGW11 75.9G 15Hz

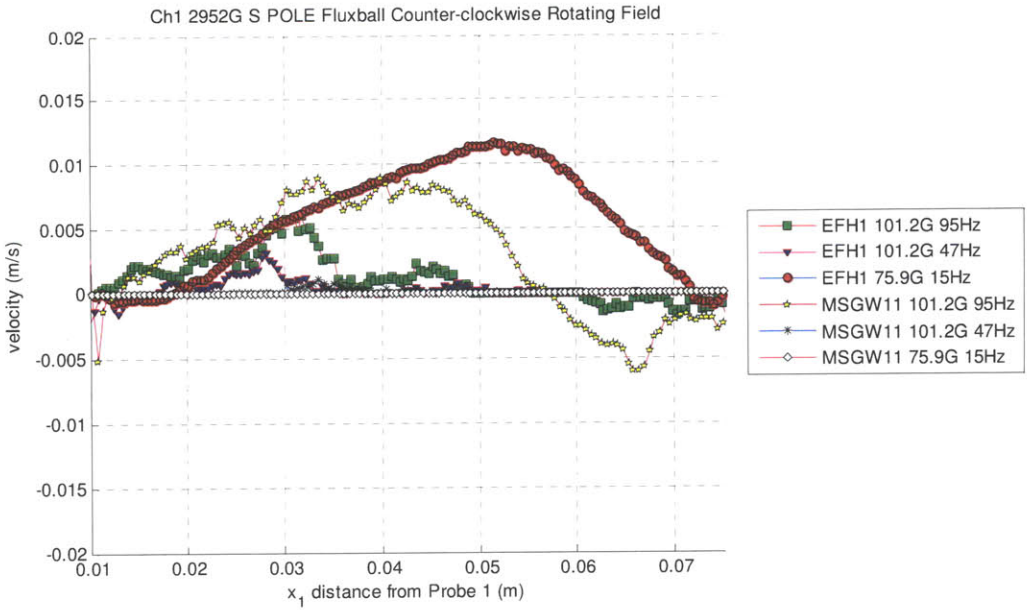
Ch1 2952G S POLE Fluxball Counter-clockwise Rotating Field
velocity (m/s)
0.02
0.015
0.01
0.005
0
-0.005
-0.01
-0.015
-0.02
0.01
0.02
0.03
0.04
0.05
0.06
0.07
x1 distance from Probe 1 (m)
EFH1 101.2G 95Hz
EFH1 101.2G 47Hz
EFH1 75.9G 15Hz
MSGW11 101.2G 95Hz
MSGW11 101.2G 47Hz
MSGW11 75.9G 15Hz

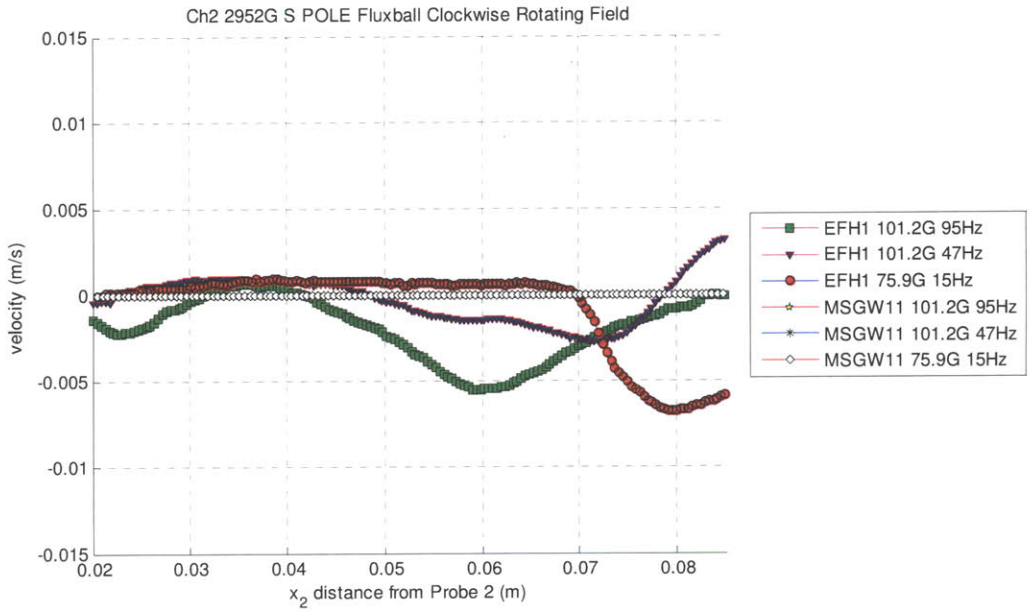
Ch2 2952G S POLE Fluxball Clockwise Rotating Field
velocity (m/s)
0.015
0.01
0.005
0
-0.005
-0.01
-0.015
0.02
0.03
0.04
0.05
0.06
0.07
0.08
x2 distance from Probe 2 (m)
EFH1 101.2G 95Hz
EFH1 101.2G 47Hz
EFH1 75.9G 15Hz
MSGW11 101.2G 95Hz
MSGW11 101.2G 47Hz
MSGW11 75.9G 15Hz

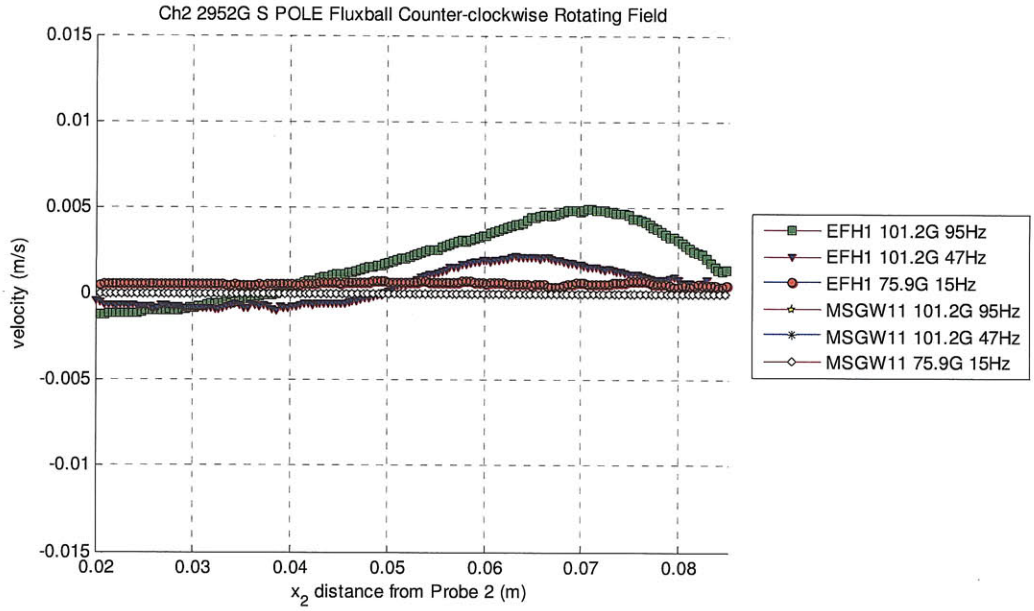
Ch2 2952G S POLE Fluxball Counter-clockwise Rotating Field
0.015
0.01
0.005
0
-0.005
-0.01
-0.015
velocity (m/s)
0.02
0.03
0.04
0.05
0.06
0.07
0.08
x2 distance from Probe 2 (m)
EFH1 101.2G 95Hz
EFH1 101.2G 47Hz
EFH1 75.9G 15Hz
MSGW11 101.2G 95Hz
MSGW11 101.2G 47Hz
MSGW11 75.9G 15Hz

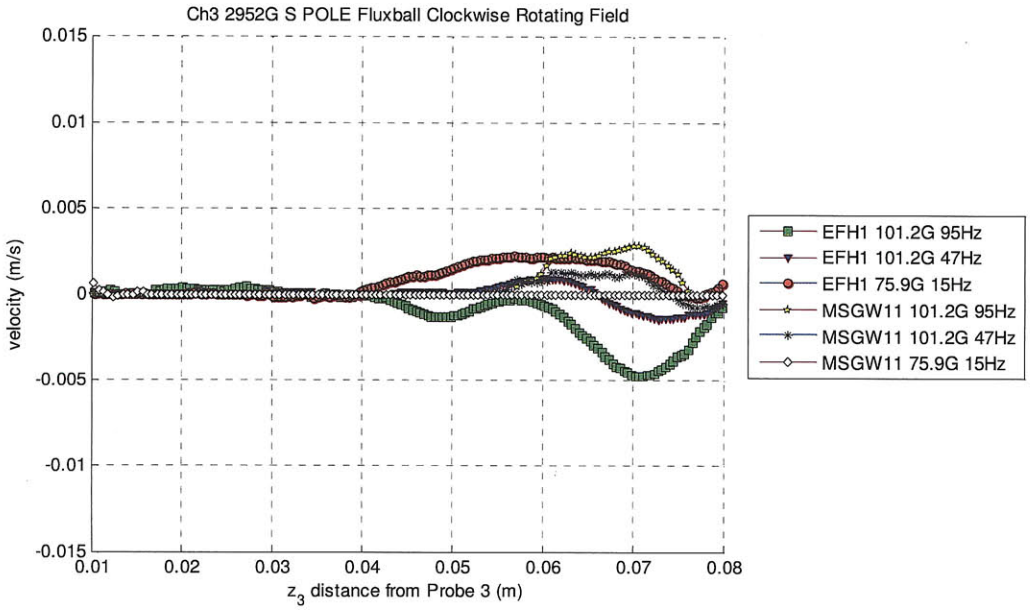
Ch3 2952G S POLE Fluxball Clockwise Rotating Field
0.015
0.01
0.005
0
-0.005
-0.01
-0.015
velocity (m/s)
0.01
0.02
0.03
0.04
0.05
0.06
0.07
0.08
z3 distance from Probe 3 (m)
EFH1 101.2G 95Hz
EFH1 101.2G 47Hz
EFH1 75.9G 15Hz
MSGW11 101.2G 95Hz
MSGW11 101.2G 47Hz
MSGW11 75.9G 15Hz

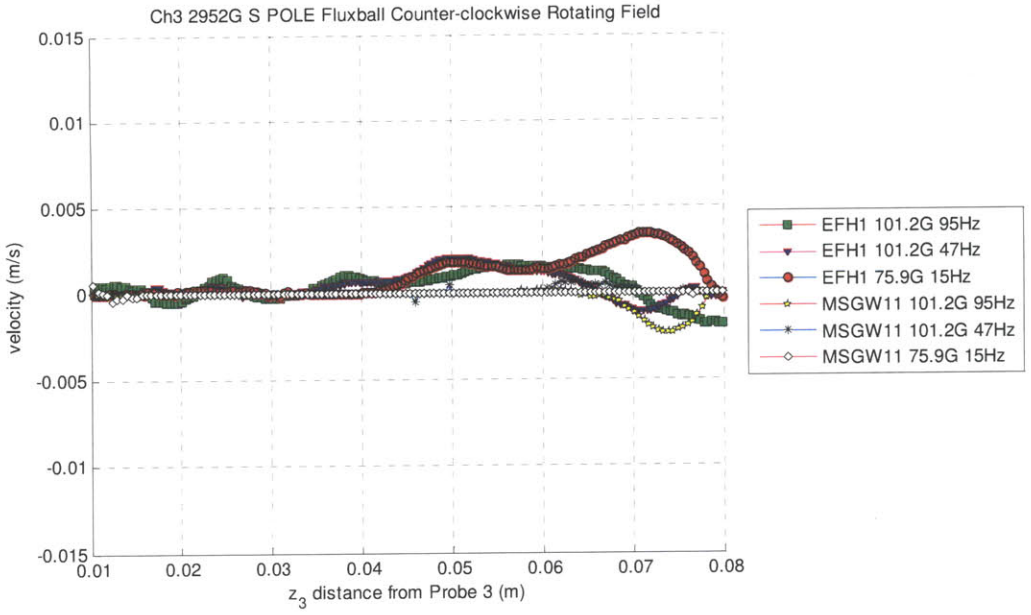
Ch3 2952G S POLE Fluxball Counter-clockwise Rotating Field
velocity (m/s)
0.015
0.01
0.005
0
-0.005
-0.01
-0.015
0.01
0.02
0.03
0.04
0.05
0.06
0.07
0.08
z3 distance from Probe 3 (m)
EFH1 101.2G 95Hz
EFH1 101.2G 47Hz
EFH1 75.9G 15Hz
MSGW11 101.2G 95Hz
MSGW11 101.2G 47Hz
MSGW11 75.9G 15Hz

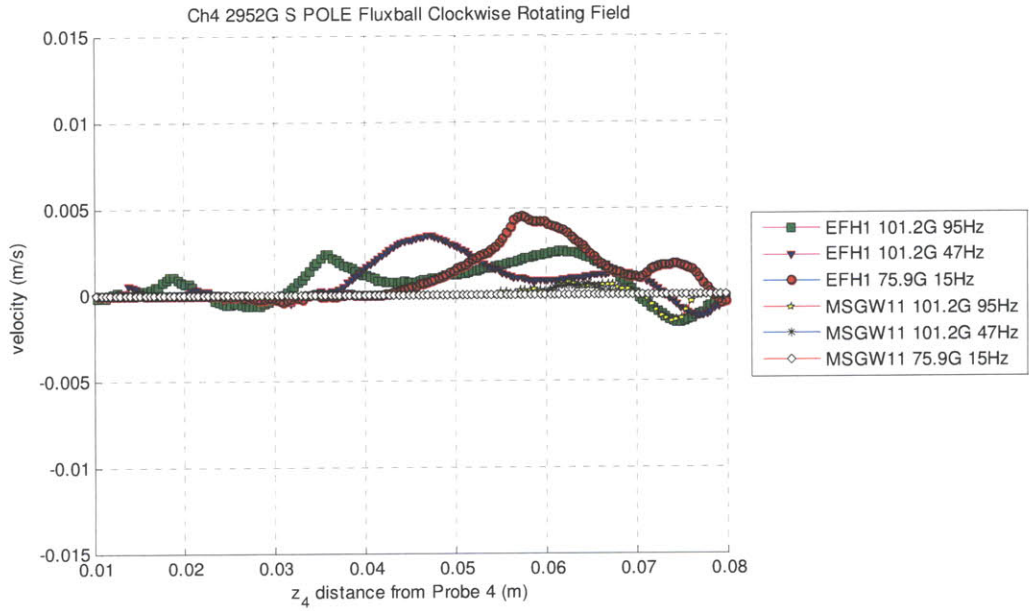
Ch4 2952G S POLE Fluxball Clockwise Rotating Field
velocity (m/s)
0.015
0.01
0.005
0
-0.005
-0.01
-0.015
0.01
0.02
0.03
0.04
0.05
0.06
0.07
0.08
z4 distance from Probe 4 (m)
EFH1 101.2G 95Hz
EFH1 101.2G 47Hz
EFH1 75.9G 15Hz
MSGW11 101.2G 95Hz
MSGW11 101.2G 47Hz
MSGW11 75.9G 15Hz

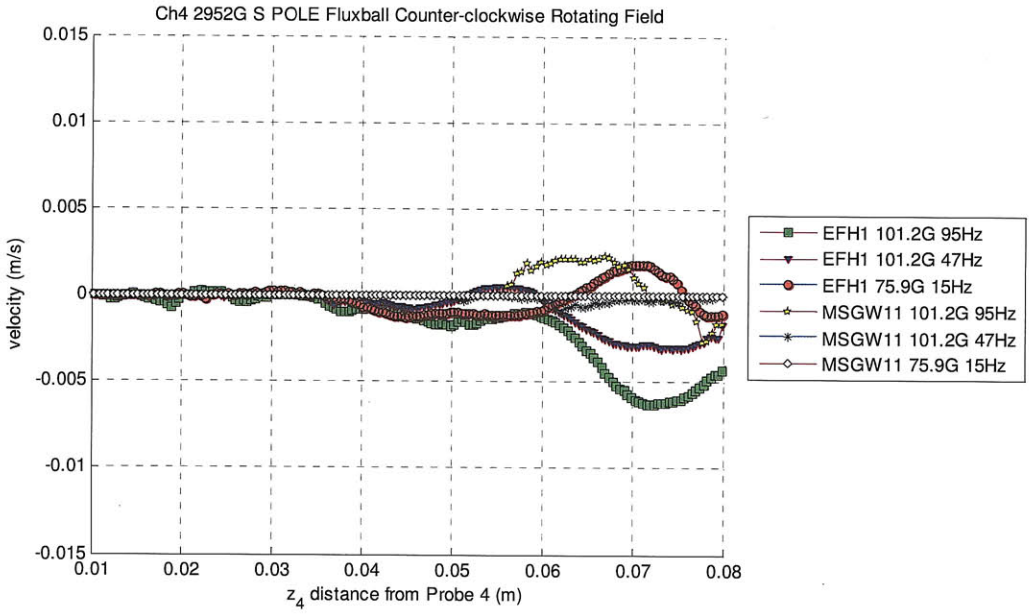
Ch4 2952G S POLE Fluxball Counter-clockwise Rotating Field
0.015
0.01
0.005
0
-0.005
-0.01
-0.015
velocity (m/s)
0.01
0.02
0.03
0.04
0.05
0.06
0.07
0.08
z4 distance from Probe 4 (m)
EFH1 101.2G 95Hz
EFH1 101.2G 47Hz
EFH1 75.9G 15Hz
MSGW11 101.2G 95Hz
MSGW11 101.2G 47Hz
MSGW11 75.9G 15Hz

H16. Comparison of Different Fluids with 2952G Magnet with North Pole Facing Ferrofluid Filled Sphere at Different Frequencies and Field Strengths

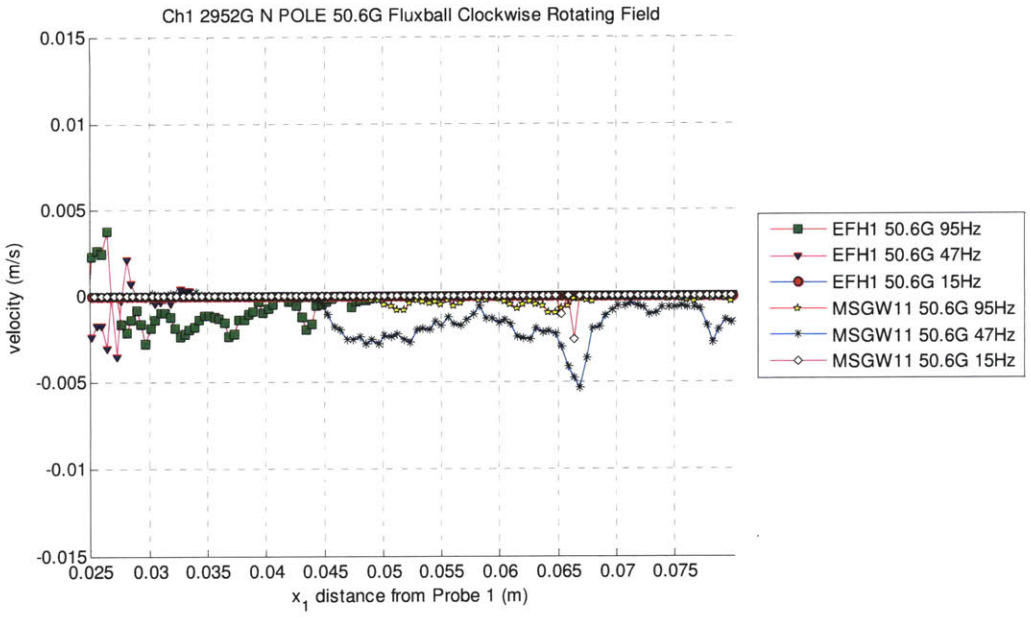

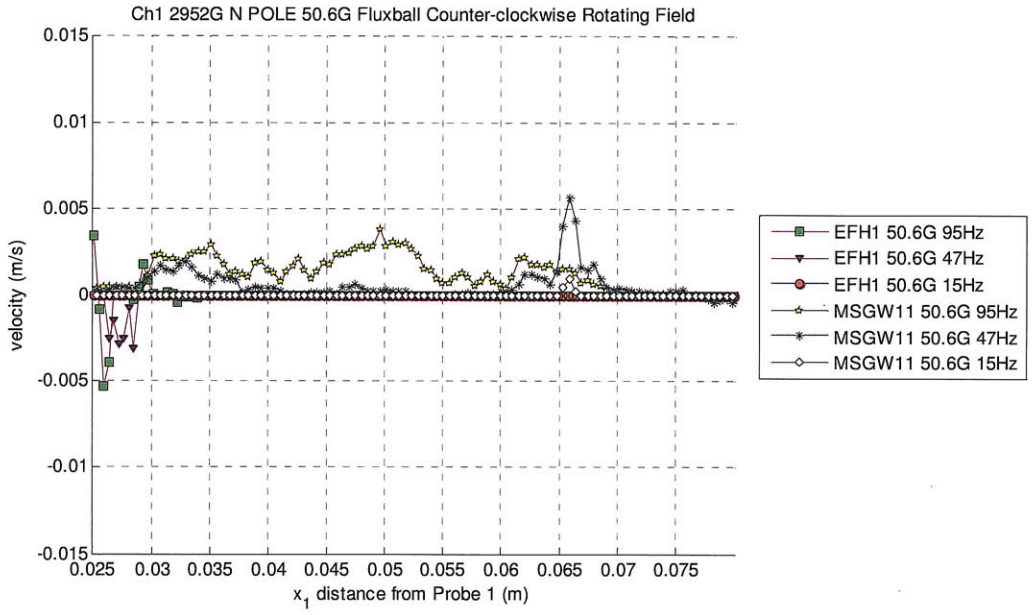
Ch1 2952G N POLE 50.6G Fluxball Counter-clockwise Rotating Field
velocity (m/s)
0.015
0.01
0.005
0
-0.005
-0.01
-0.015
0.025 0.03 0.035 0.04 0.045 0.05 0.055 0.06 0.065 0.07 0.075
x1 distance from Probe 1 (m)
EFH1 50.6G 95Hz
EFH1 50.6G 47Hz
EFH1 50.6G 15Hz
MSGW11 50.6G 95Hz
MSGW11 50.6G 47Hz
MSGW11 50.6G 15Hz

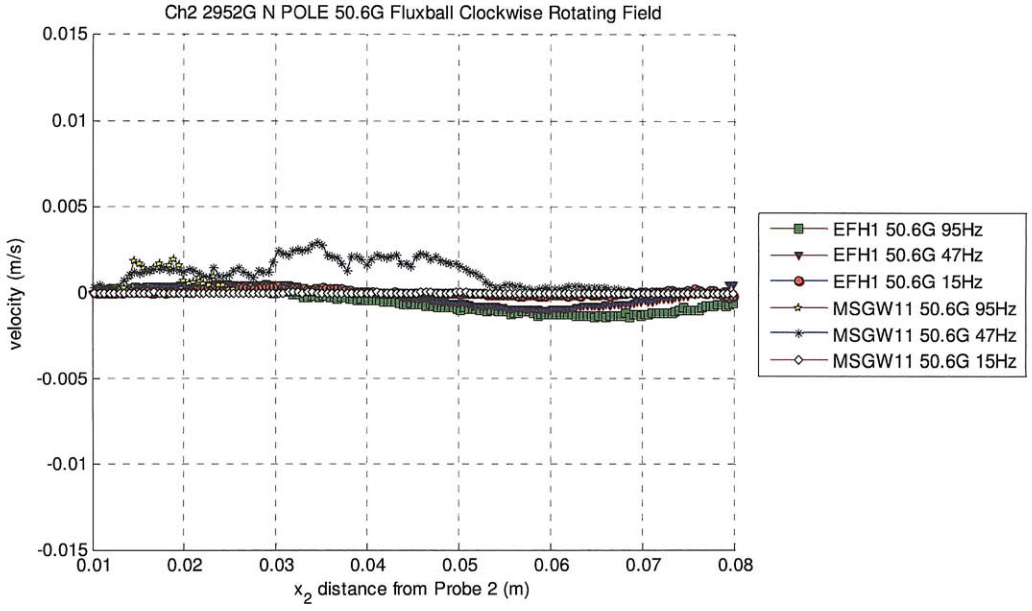
Ch2 2952G N POLE 50.6G Fluxball Clockwise Rotating Field
velocity (m/s)
0.015
0.01
0.005
0
-0.005
-0.01
-0.015
0.01 0.02 0.03 0.04 0.05 0.06 0.07 0.08
x2 distance from Probe 2 (m)
EFH1 50.6G 95Hz
EFH1 50.6G 47Hz
EFH1 50.6G 15Hz
MSGW11 50.6G 95Hz
MSGW11 50.6G 47Hz
MSGW11 50.6G 15Hz

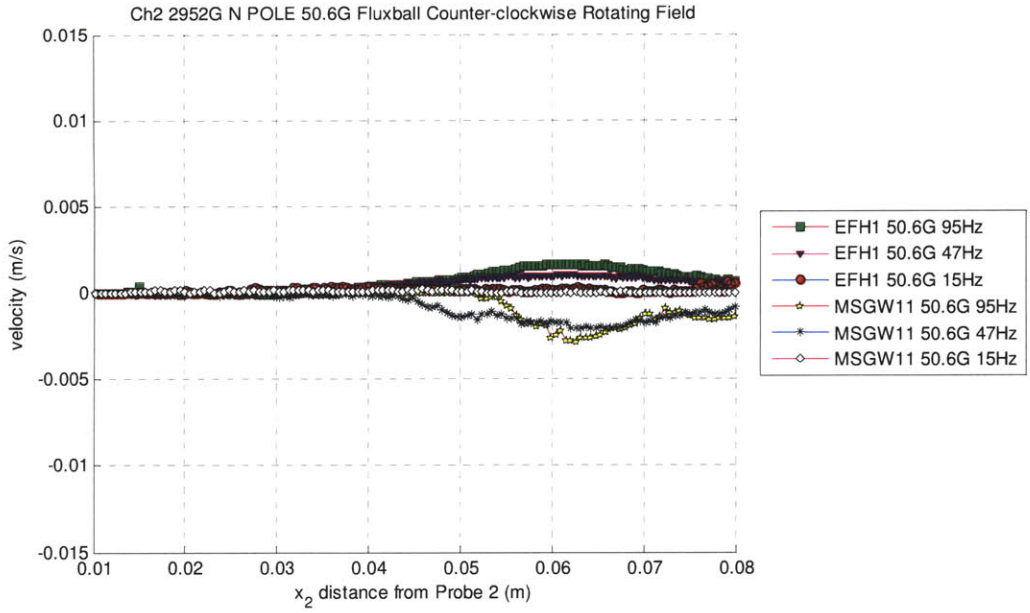
Ch2 2952G N POLE 50.6G Fluxball Counter-clockwise Rotating Field
velocity (m/s)
0.015
0.01
0.005
0
-0.005
-0.01
-0.015
0.01
0.02
0.03
0.04
0.05
0.06
0.07
0.08
x2 distance from Probe 2 (m)
EFH1 50.6G 95Hz
EFH1 50.6G 47Hz
EFH1 50.6G 15Hz
MSGW11 50.6G 95Hz
MSGW11 50.6G 47Hz
MSGW11 50.6G 15Hz

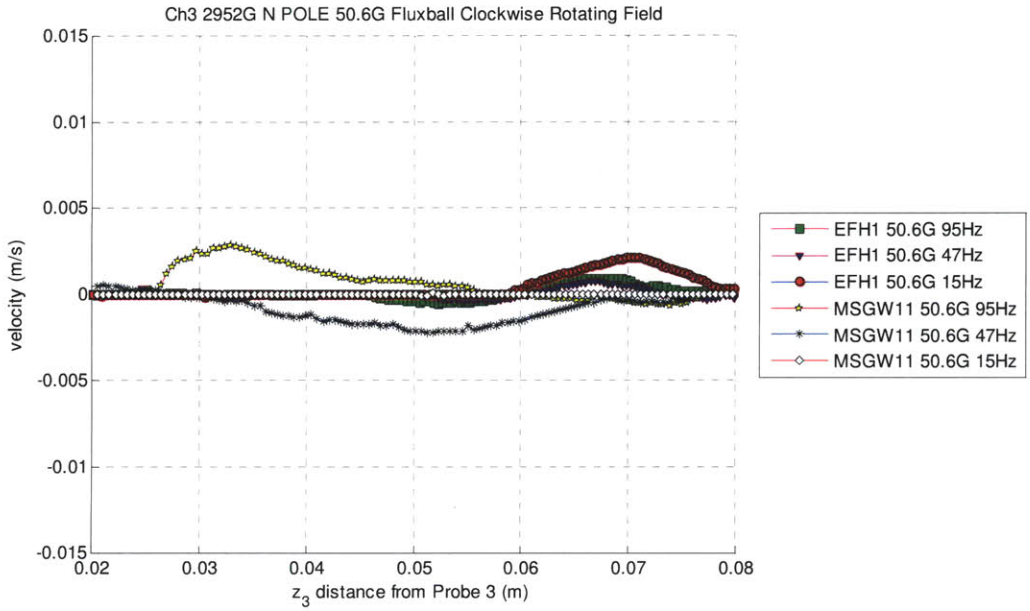
Ch3 2952G N POLE 50.6G Fluxball Clockwise Rotating Field
velocity (m/s)
0.015
0.01
0.005
0
-0.005
-0.01
-0.015
0.02
0.03
0.04
0.05
0.06
0.07
0.08
z3 distance from Probe 3 (m)
EFH1 50.6G 95Hz
EFH1 50.6G 47Hz
EFH1 50.6G 15Hz
MSGW11 50.6G 95Hz
MSGW11 50.6G 47Hz
MSGW11 50.6G 15Hz

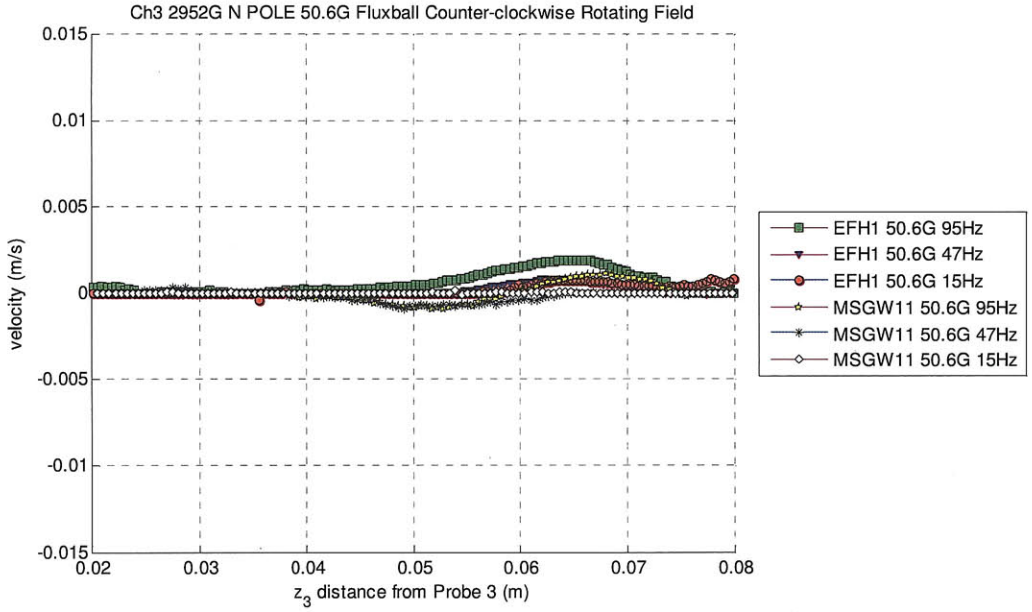
Ch3 2952G N POLE 50.6G Fluxball Counter-clockwise Rotating Field
velocity (m/s)
0.015
0.01
0.005
0
-0.005
-0.01
-0.015
0.02
0.03
0.04
0.05
0.06
0.07
0.08
z_3 distance from Probe 3 (m)
EFH1 50.6G 95Hz
EFH1 50.6G 47Hz
EFH1 50.6G 15Hz
MSGW11 50.6G 95Hz
MSGW11 50.6G 47Hz
MSGW11 50.6G 15Hz

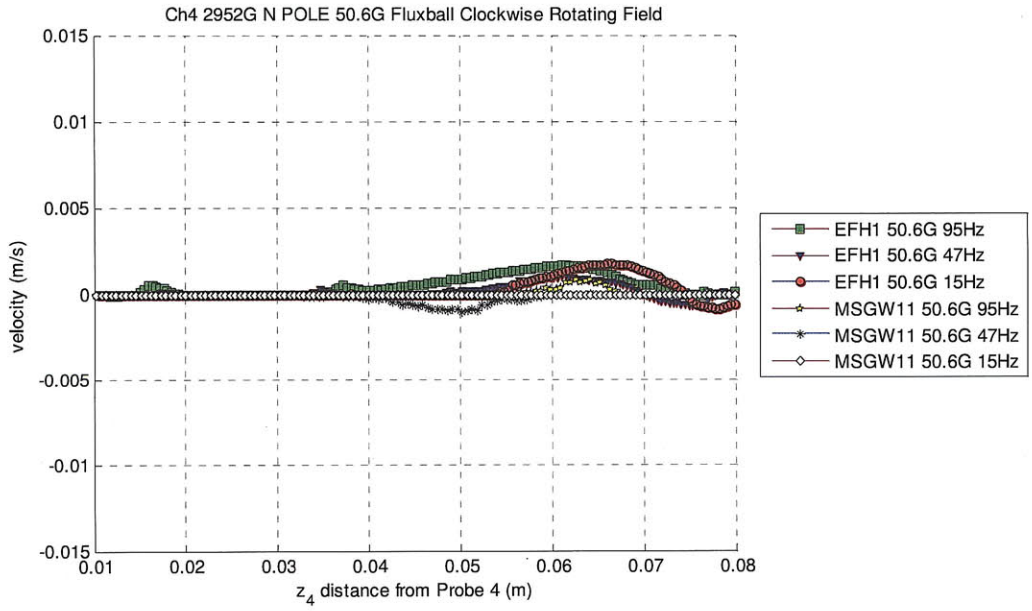
Ch4 2952G N POLE 50.6G Fluxball Clockwise Rotating Field
velocity (m/s)
0.015
0.01
0.005
0
-0.005
-0.01
-0.015
0.01
0.02
0.03
0.04
0.05
0.06
0.07
0.08
z_4 distance from Probe 4 (m)
EFH1 50.6G 95Hz
EFH1 50.6G 47Hz
EFH1 50.6G 15Hz
MSGW11 50.6G 95Hz
MSGW11 50.6G 47Hz
MSGW11 50.6G 15Hz

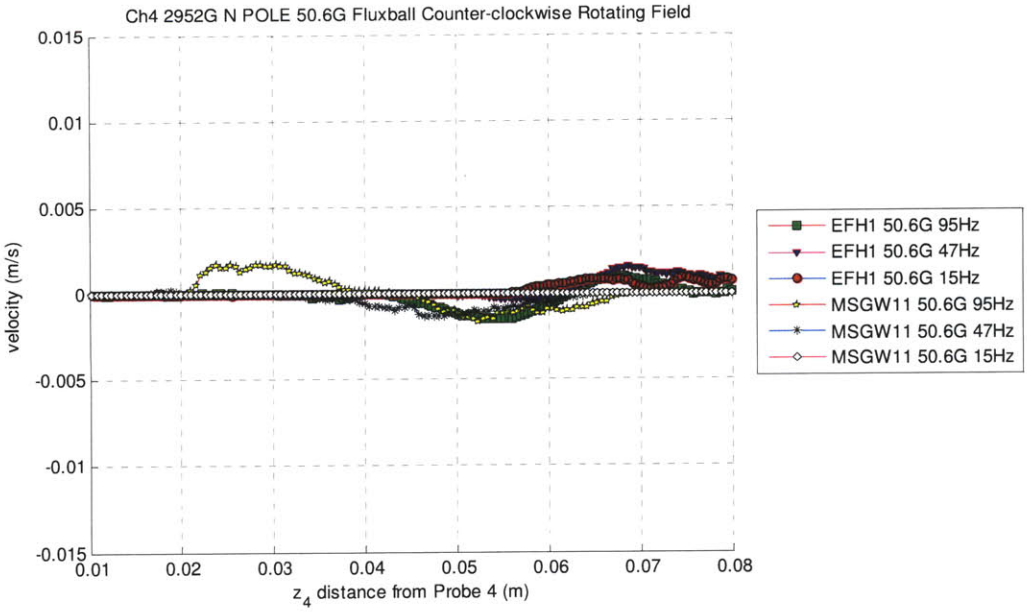
Ch4 2952G N POLE 50.6G Fluxball Counter-clockwise Rotating Field
velocity (m/s)
0.015
0.01
0.005
0
-0.005
-0.01
-0.015
0.01
0.02
0.03
0.04
0.05
0.06
0.07
0.08
z4 distance from Probe 4 (m)
EFH1 50.6G 95Hz
EFH1 50.6G 47Hz
EFH1 50.6G 15Hz
MSGW11 50.6G 95Hz
MSGW11 50.6G 47Hz
MSGW11 50.6G 15Hz

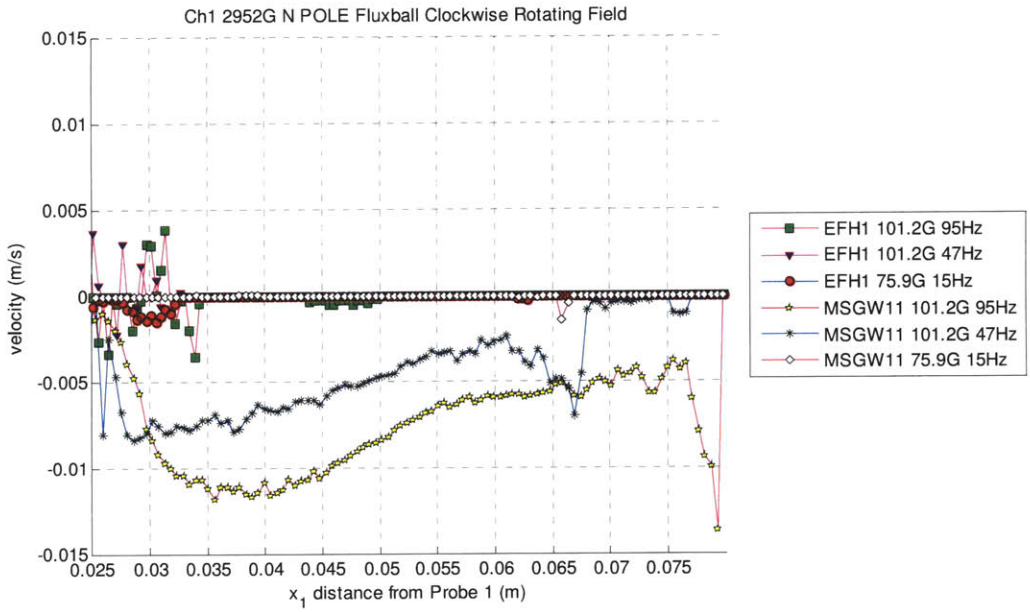
Ch1 2952G N POLE Fluxball Clockwise Rotating Field
velocity (m/s)
0.015
0.01
0.005
0
-0.005
-0.01
-0.015
0.025
0.03
0.035
0.04
0.045
0.05
0.055
0.06
0.065
0.07
0.075
x1 distance from Probe 1 (m)
EFH1 101.2G 95Hz
EFH1 101.2G 47Hz
EFH1 75.9G 15Hz
MSGW11 101.2G 95Hz
MSGW11 101.2G 47Hz
MSGW11 75.9G 15Hz

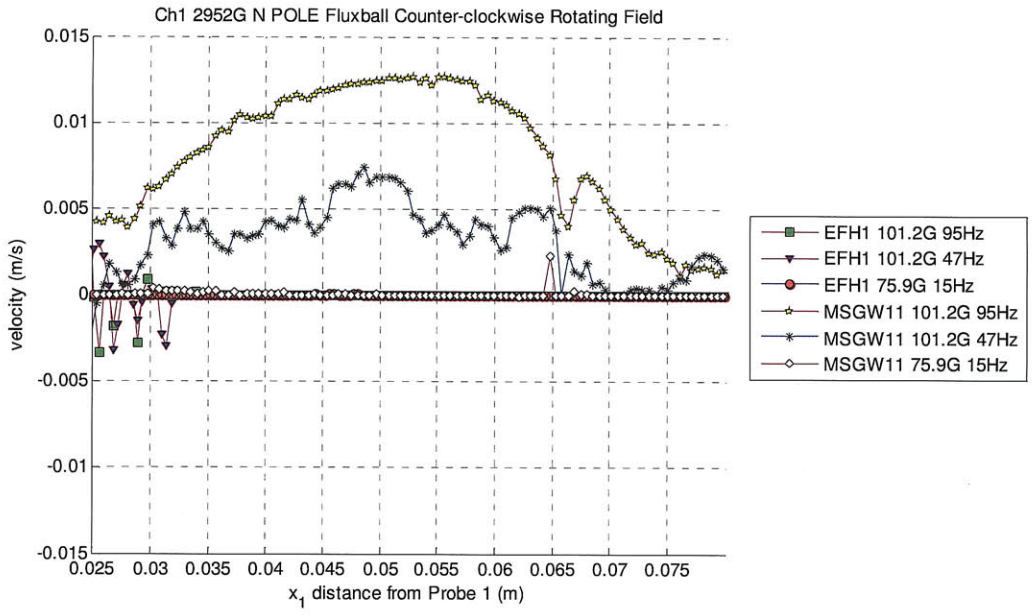
Ch1 2952G N POLE Fluxball Counter-clockwise Rotating Field
velocity (m/s)
0.015
0.01
0.005
0
-0.005
-0.01
-0.015
0.025 0.03 0.035 0.04 0.045 0.05 0.055 0.06 0.065 0.07 0.075
x1 distance from Probe 1 (m)
EFH1 101.2G 95Hz
EFH1 101.2G 47Hz
EFH1 75.9G 15Hz
MSGW11 101.2G 95Hz
MSGW11 101.2G 47Hz
MSGW11 75.9G 15Hz

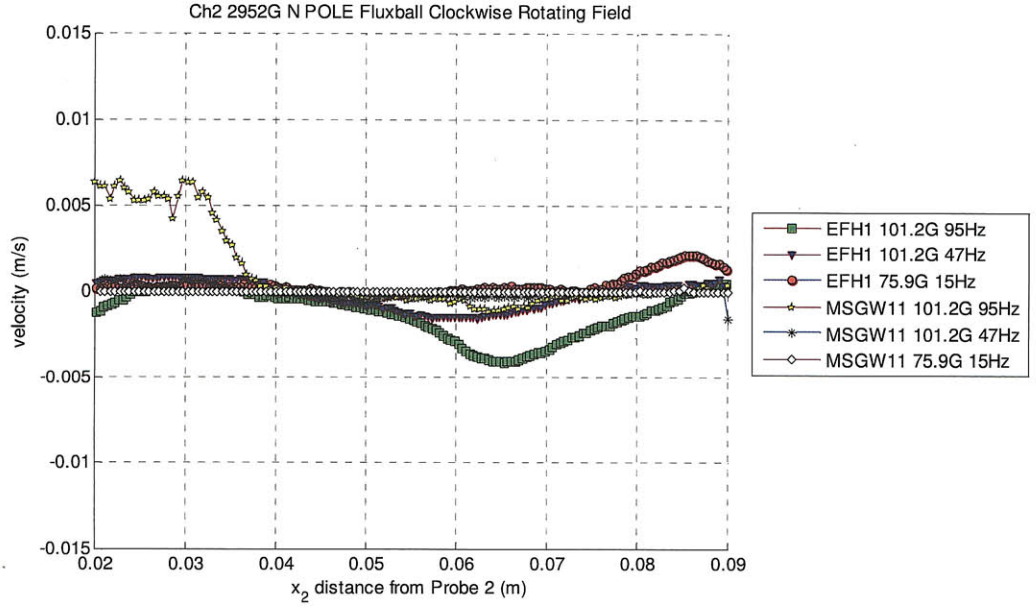
Ch2 2952G N POLE Fluxball Clockwise Rotating Field
velocity (m/s)
0.015
0.01
0.005
0
-0.005
-0.01
-0.015
0.02 0.03 0.04 0.05 0.06 0.07 0.08 0.09
x2 distance from Probe 2 (m)
EFH1 101.2G 95Hz
EFH1 101.2G 47Hz
EFH1 75.9G 15Hz
MSGW11 101.2G 95Hz
MSGW11 101.2G 47Hz
MSGW11 75.9G 15Hz

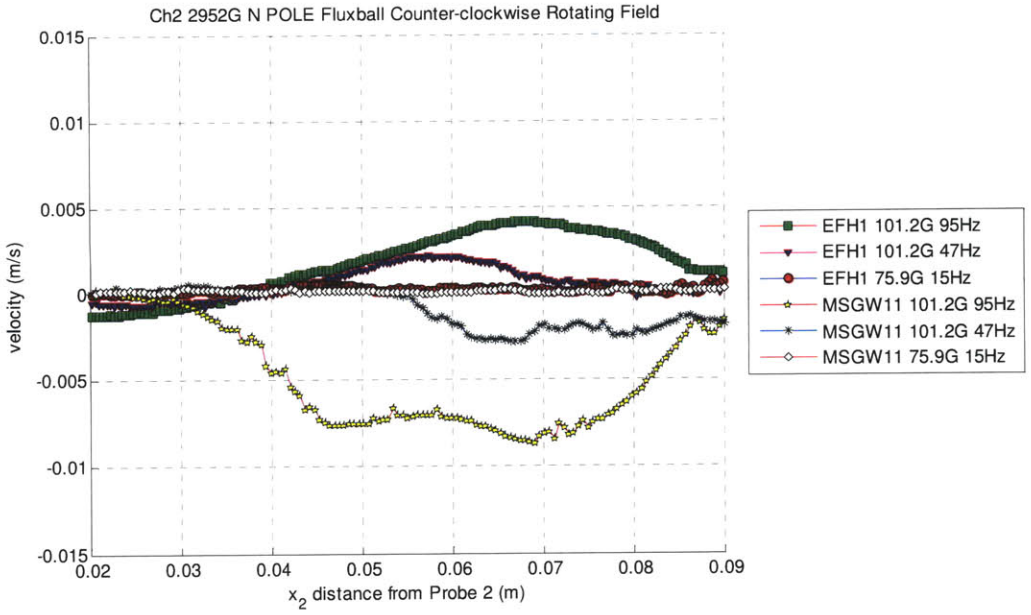
Ch2 2952G N POLE Fluxball Counter-clockwise Rotating Field
velocity (m/s)
0.015
0.01
0.005
0
-0.005
-0.01
-0.015
0.02
0.03
0.04
0.05
0.06
0.07
0.08
0.09
x2 distance from Probe 2 (m)
EFH1 101.2G 95Hz
EFH1 101.2G 47Hz
EFH1 75.9G 15Hz
MSGW11 101.2G 95Hz
MSGW11 101.2G 47Hz
MSGW11 75.9G 15Hz

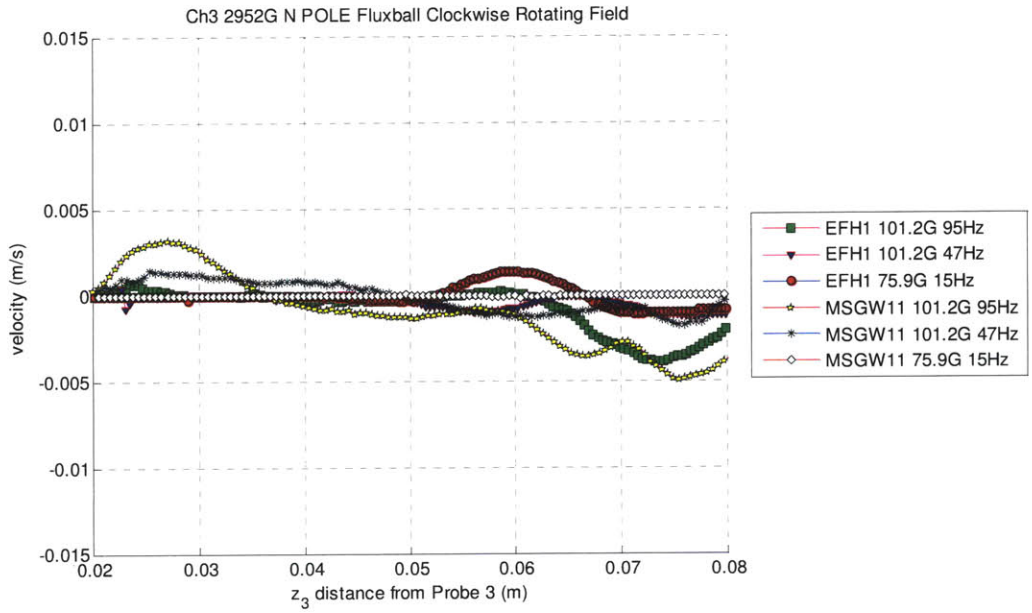
Ch3 2952G N POLE Fluxball Clockwise Rotating Field
velocity (m/s)
0.015
0.01
0.005
0
-0.005
-0.01
-0.015
0.02
0.03
0.04
0.05
0.06
0.07
0.08
z3 distance from Probe 3 (m)
EFH1 101.2G 95Hz
EFH1 101.2G 47Hz
EFH1 75.9G 15Hz
MSGW11 101.2G 95Hz
MSGW11 101.2G 47Hz
MSGW11 75.9G 15Hz

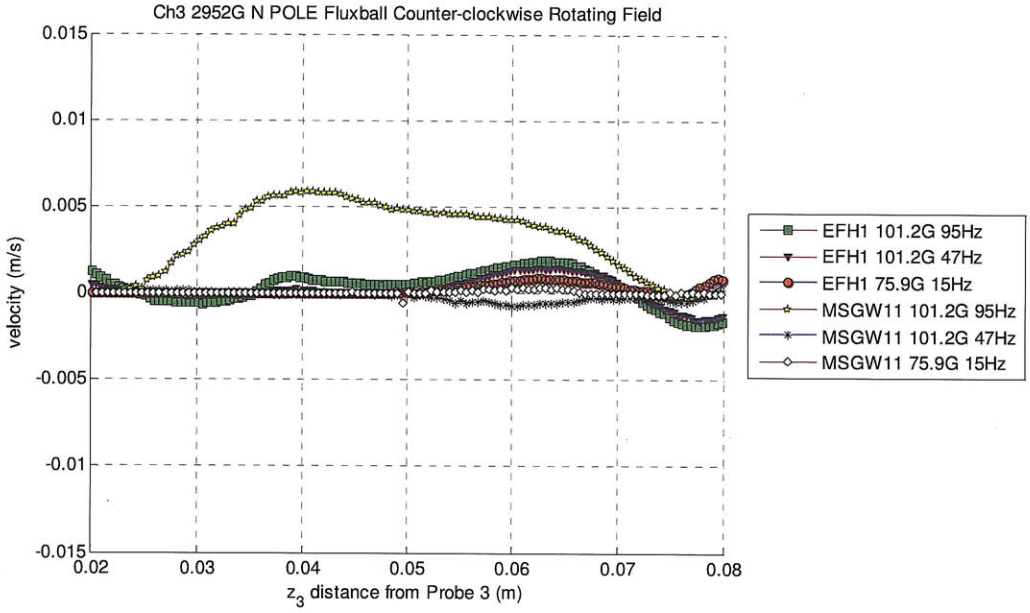
Ch3 2952G N POLE Fluxball Counter-clockwise Rotating Field
velocity (m/s)
0.015
0.01
0.005
0
-0.005
-0.01
-0.015
0.02
0.03
0.04
0.05
0.06
0.07
0.08
z_3 distance from Probe 3 (m)
EFH1 101.2G 95Hz
EFH1 101.2G 47Hz
EFH1 75.9G 15Hz
MSGW11 101.2G 95Hz
MSGW11 101.2G 47Hz
MSGW11 75.9G 15Hz

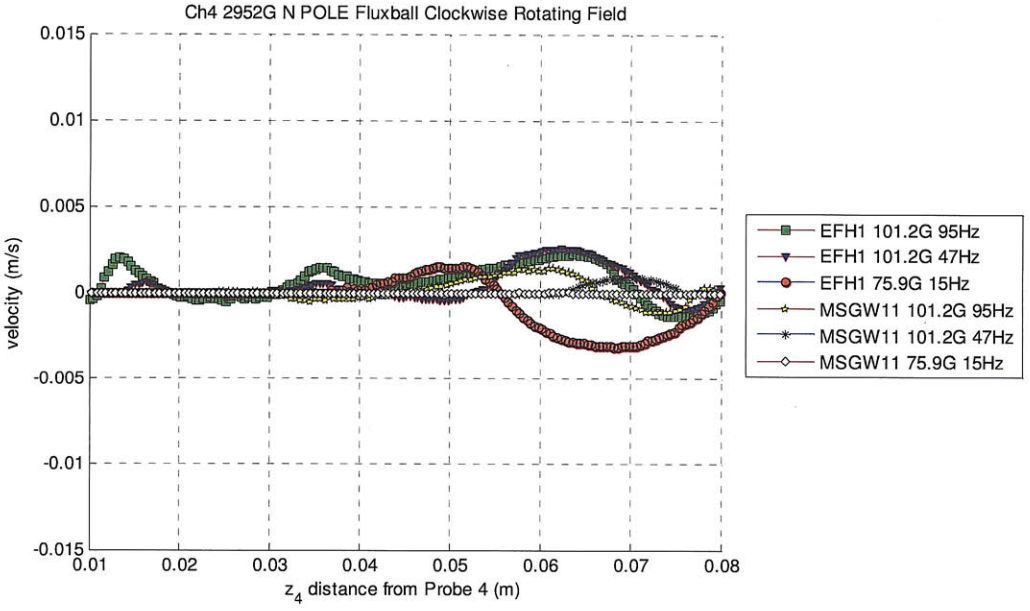
Ch4 2952G N POLE Fluxball Clockwise Rotating Field
velocity (m/s)
0.015
0.01
0.005
0
-0.005
-0.01
-0.015
0.01
0.02
0.03
0.04
0.05
0.06
0.07
0.08
z_4 distance from Probe 4 (m)
EFH1 101.2G 95Hz
EFH1 101.2G 47Hz
EFH1 75.9G 15Hz
MSGW11 101.2G 95Hz
MSGW11 101.2G 47Hz
MSGW11 75.9G 15Hz

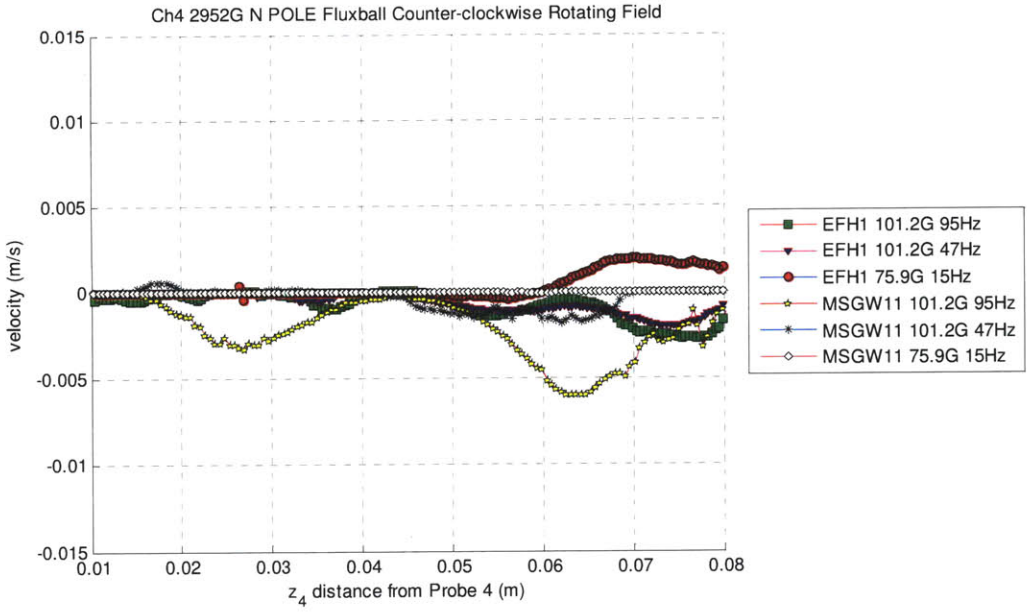
Ch4 2952G N POLE Fluxball Counter-clockwise Rotating Field
velocity (m/s)
0.015
0.01
0.005
0
-0.005
-0.01
-0.015
0.01
0.02
0.03
0.04
0.05
0.06
0.07
0.08
z4 distance from Probe 4 (m)
EFH1 101.2G 95Hz
EFH1 101.2G 47Hz
EFH1 75.9G 15Hz
MSGW11 101.2G 95Hz
MSGW11 101.2G 47Hz
MSGW11 75.9G 15Hz

H17. Comparison of Different Fluids with 3309G Magnet with South Pole Facing Ferrofluid Filled Sphere at Different Frequencies and Field Strengths

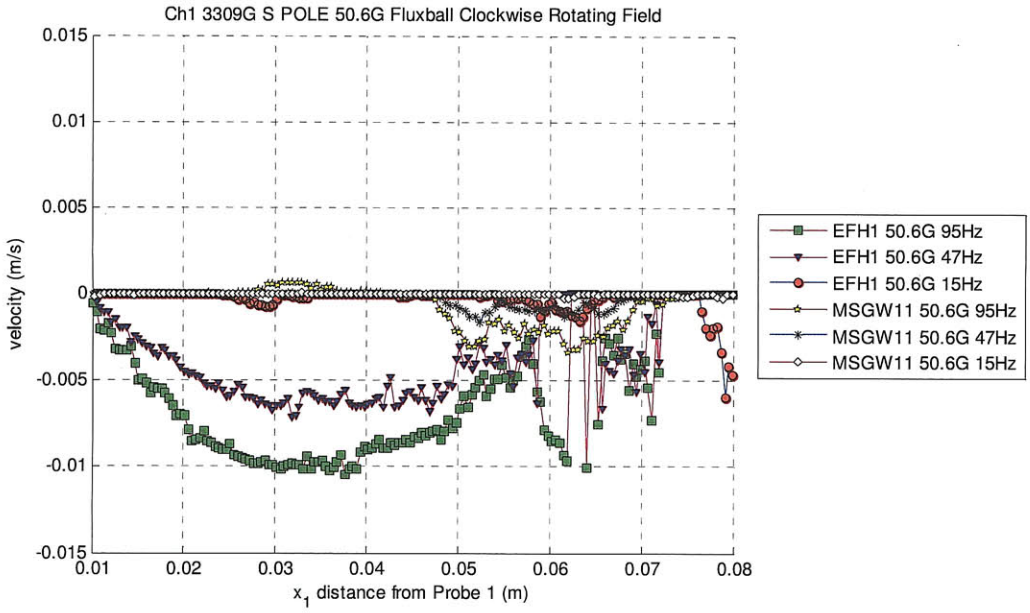

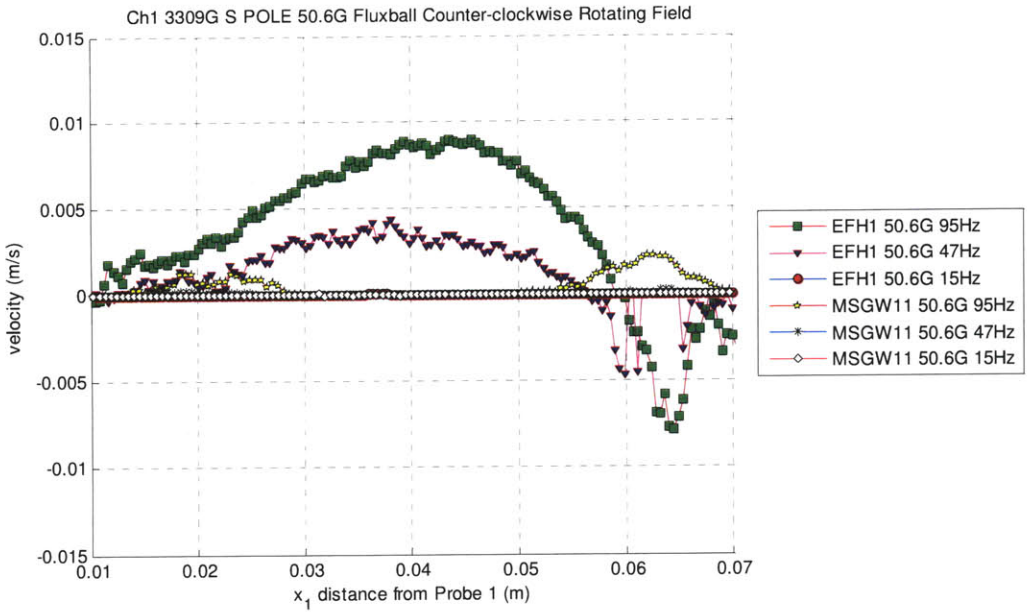
Ch1 3309G S POLE 50.6G Fluxball Counter-clockwise Rotating Field
velocity (m/s)
0.015
0.01
0.005
0
-0.005
-0.01
-0.015
0.01
0.02
0.03
0.04
0.05
0.06
0.07
x1 distance from Probe 1 (m)
EFH1 50.6G 95Hz
EFH1 50.6G 47Hz
EFH1 50.6G 15Hz
MSGW11 50.6G 95Hz
MSGW11 50.6G 47Hz
MSGW11 50.6G 15Hz

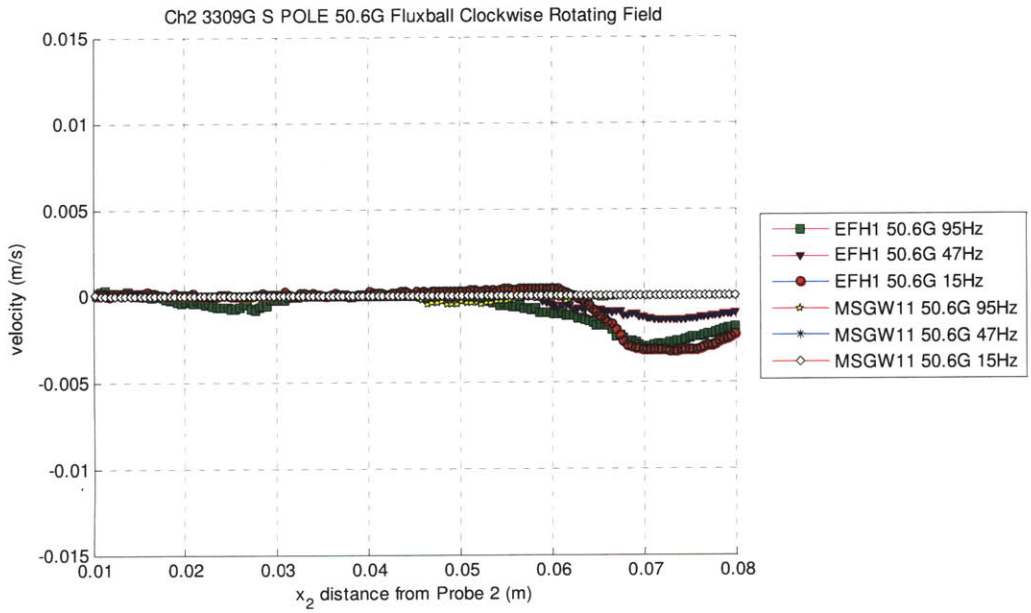
Ch2 3309G S POLE 50.6G Fluxball Clockwise Rotating Field
velocity (m/s)
0.015
0.01
0.005
0
-0.005
-0.01
-0.015
0.01
0.02
0.03
0.04
0.05
0.06
0.07
0.08
x2 distance from Probe 2 (m)
EFH1 50.6G 95Hz
EFH1 50.6G 47Hz
EFH1 50.6G 15Hz
MSGW11 50.6G 95Hz
MSGW11 50.6G 47Hz
MSGW11 50.6G 15Hz

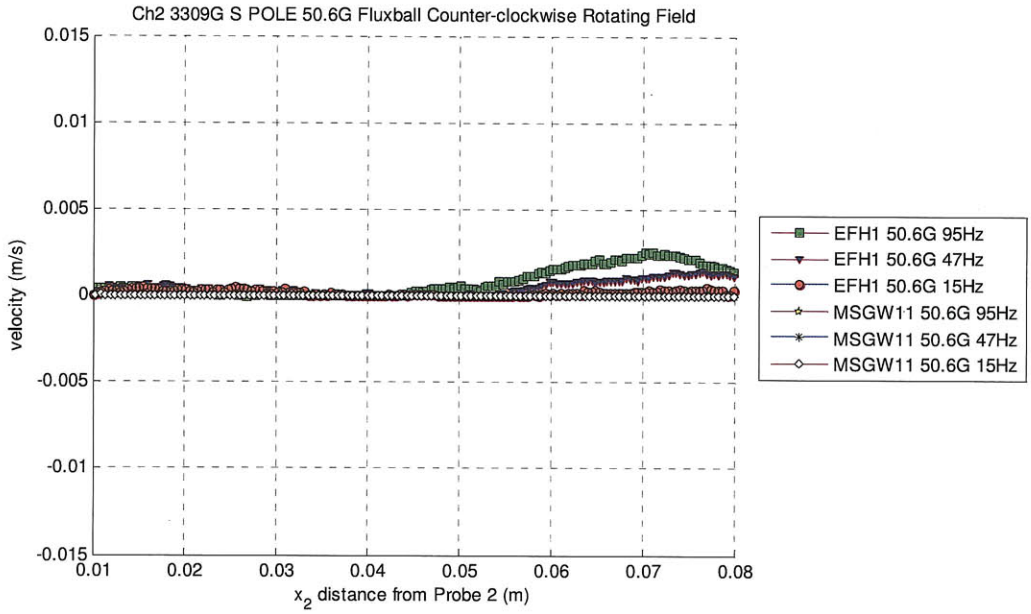
Ch2 3309G S POLE 50.6G Fluxball Counter-clockwise Rotating Field
velocity (m/s)
0.015
0.01
0.005
0
-0.005
-0.01
-0.015
0.01
0.02
0.03
0.04
0.05
0.06
0.07
0.08
x2 distance from Probe 2 (m)
EFH1 50.6G 95Hz
EFH1 50.6G 47Hz
EFH1 50.6G 15Hz
MSGW11 50.6G 95Hz
MSGW11 50.6G 47Hz
MSGW11 50.6G 15Hz

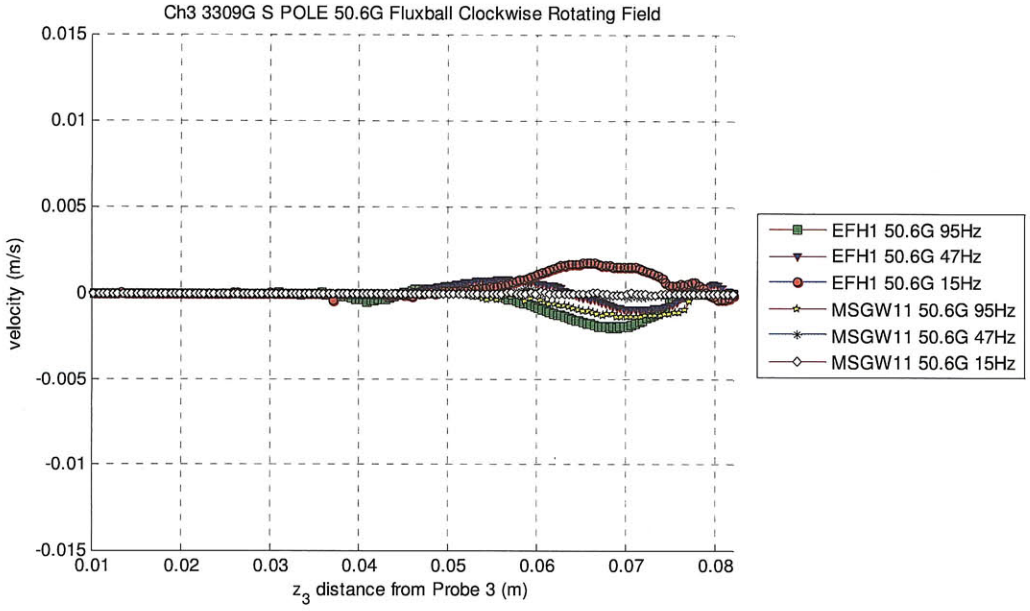
Ch3 3309G S POLE 50.6G Fluxball Clockwise Rotating Field
velocity (m/s)
0.015
0.01
0.005
0
-0.005
-0.01
-0.015
0.01
0.02
0.03
0.04
0.05
0.06
0.07
0.08
z3 distance from Probe 3 (m)
EFH1 50.6G 95Hz
EFH1 50.6G 47Hz
EFH1 50.6G 15Hz
MSGW11 50.6G 95Hz
MSGW11 50.6G 47Hz
MSGW11 50.6G 15Hz

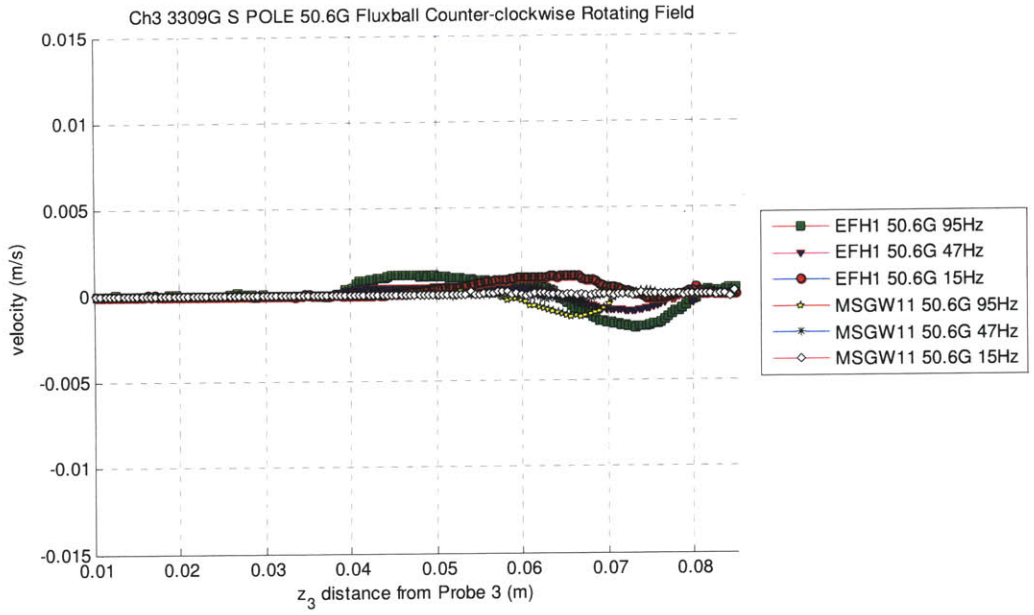
Ch3 3309G S POLE 50.6G Fluxball Counter-clockwise Rotating Field
velocity (m/s)
0.015
0.01
0.005
0
-0.005
-0.01
-0.015
0.01
0.02
0.03
0.04
0.05
0.06
0.07
0.08
z3 distance from Probe 3 (m)
EFH1 50.6G 95Hz
EFH1 50.6G 47Hz
EFH1 50.6G 15Hz
MSGW11 50.6G 95Hz
MSGW11 50.6G 47Hz
MSGW11 50.6G 15Hz

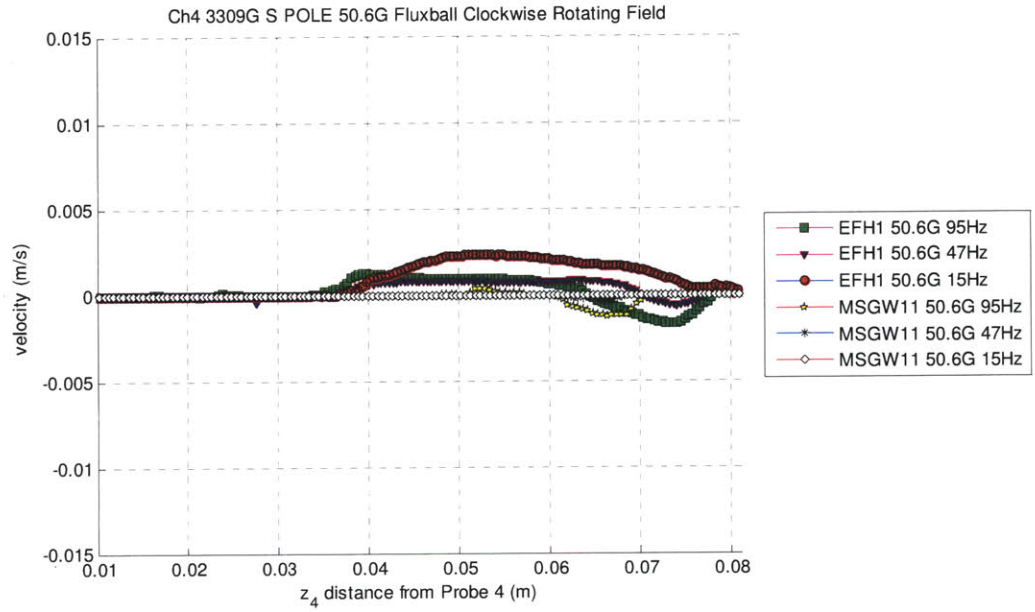
Ch4 3309G S POLE 50.6G Fluxball Clockwise Rotating Field
velocity (m/s)
0.015
0.01
0.005
0
-0.005
-0.01
-0.015
0.01
0.02
0.03
0.04
0.05
0.06
0.07
0.08
z4 distance from Probe 4 (m)
EFH1 50.6G 95Hz
EFH1 50.6G 47Hz
EFH1 50.6G 15Hz
MSGW11 50.6G 95Hz
MSGW11 50.6G 47Hz
MSGW11 50.6G 15Hz

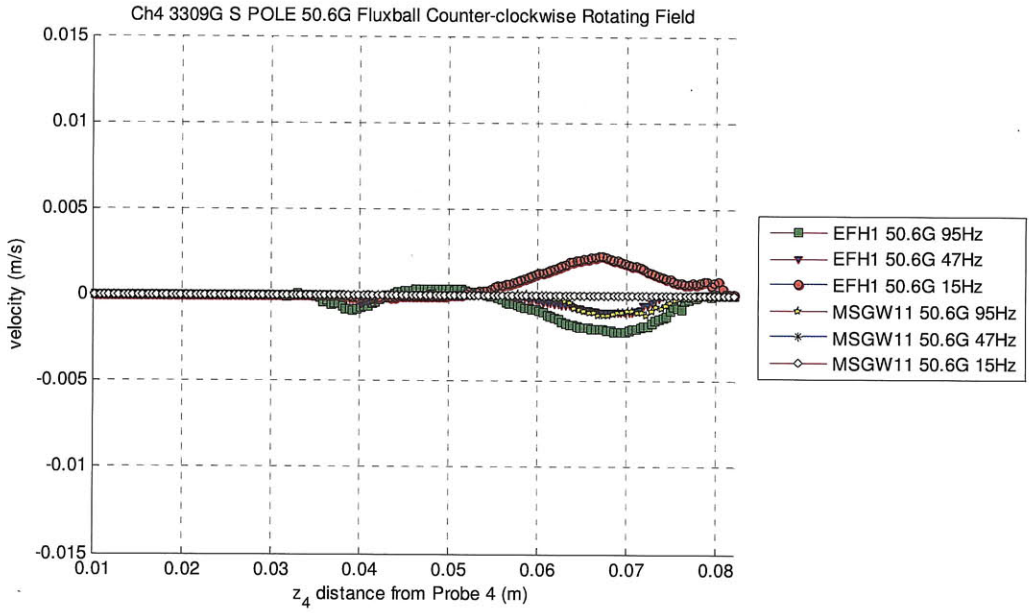
Ch4 3309G S POLE 50.6G Fluxball Counter-clockwise Rotating Field
velocity (m/s)
0.015
0.01
0.005
0
-0.005
-0.01
-0.015
0.01
0.02
0.03
0.04
0.05
0.06
0.07
0.08
z4 distance from Probe 4 (m)
EFH1 50.6G 95Hz
EFH1 50.6G 47Hz
EFH1 50.6G 15Hz
MSGW11 50.6G 95Hz
MSGW11 50.6G 47Hz
MSGW11 50.6G 15Hz

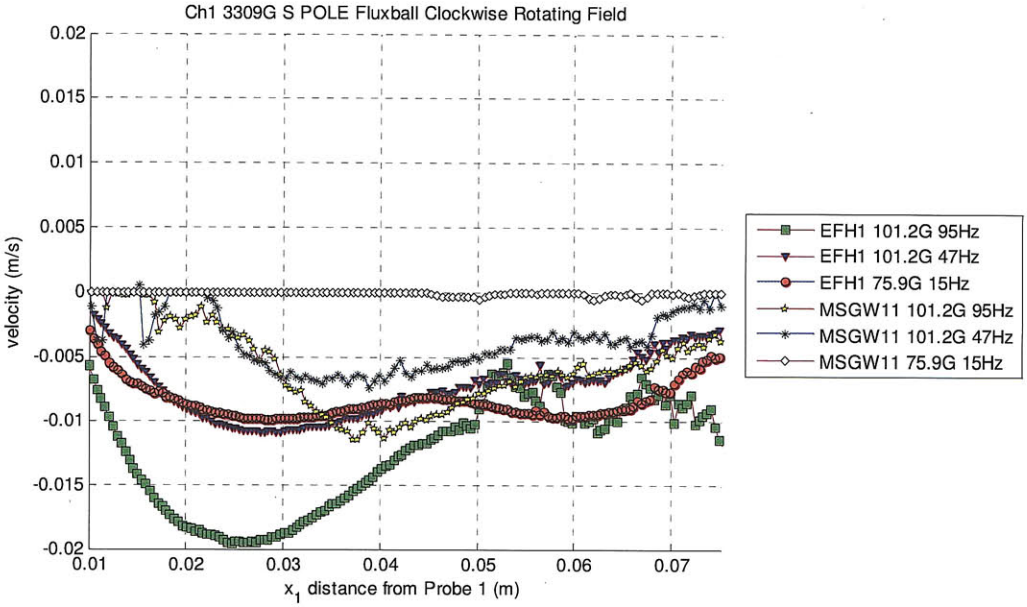
Ch1 3309G S POLE Fluxball Clockwise Rotating Field
velocity (m/s)
0.02
0.015
0.01
0.005
0
-0.005
-0.01
-0.015
-0.02
0.01
0.02
0.03
0.04
0.05
0.06
0.07
x1 distance from Probe 1 (m)
EFH1 101.2G 95Hz
EFH1 101.2G 47Hz
EFH1 75.9G 15Hz
MSGW11 101.2G 95Hz
MSGW11 101.2G 47Hz
MSGW11 75.9G 15Hz

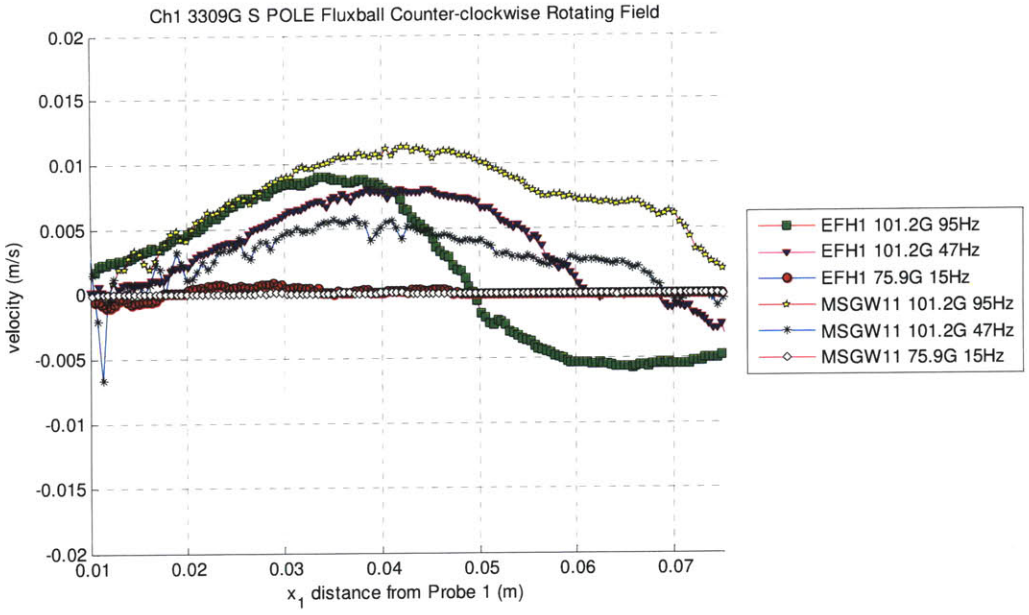
Ch1 3309G S POLE Fluxball Counter-clockwise Rotating Field
velocity (m/s)
0.02
0.015
0.01
0.005
0
-0.005
-0.01
-0.015
-0.02
0.01
0.02
0.03
0.04
0.05
0.06
0.07
x1 distance from Probe 1 (m)
EFH1 101.2G 95Hz
EFH1 101.2G 47Hz
EFH1 75.9G 15Hz
MSGW11 101.2G 95Hz
MSGW11 101.2G 47Hz
MSGW11 75.9G 15Hz

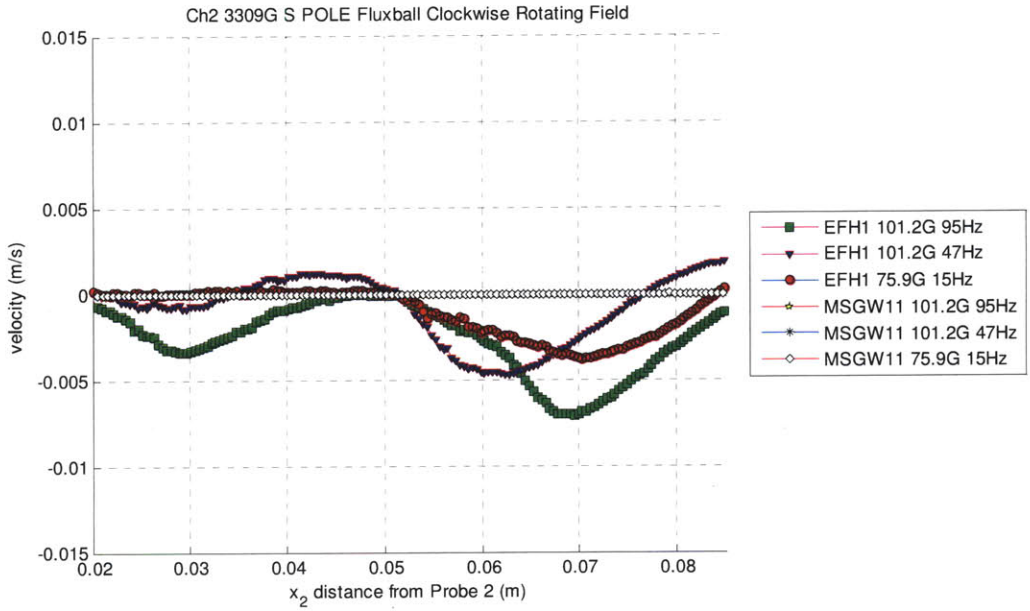
Ch2 3309G S POLE Fluxball Clockwise Rotating Field
velocity (m/s)
0.015
0.01
0.005
0
-0.005
-0.01
-0.015
0.02
0.03
0.04
0.05
0.06
0.07
0.08
x2 distance from Probe 2 (m)
EFH1 101.2G 95Hz
EFH1 101.2G 47Hz
EFH1 75.9G 15Hz
MSGW11 101.2G 95Hz
MSGW11 101.2G 47Hz
MSGW11 75.9G 15Hz

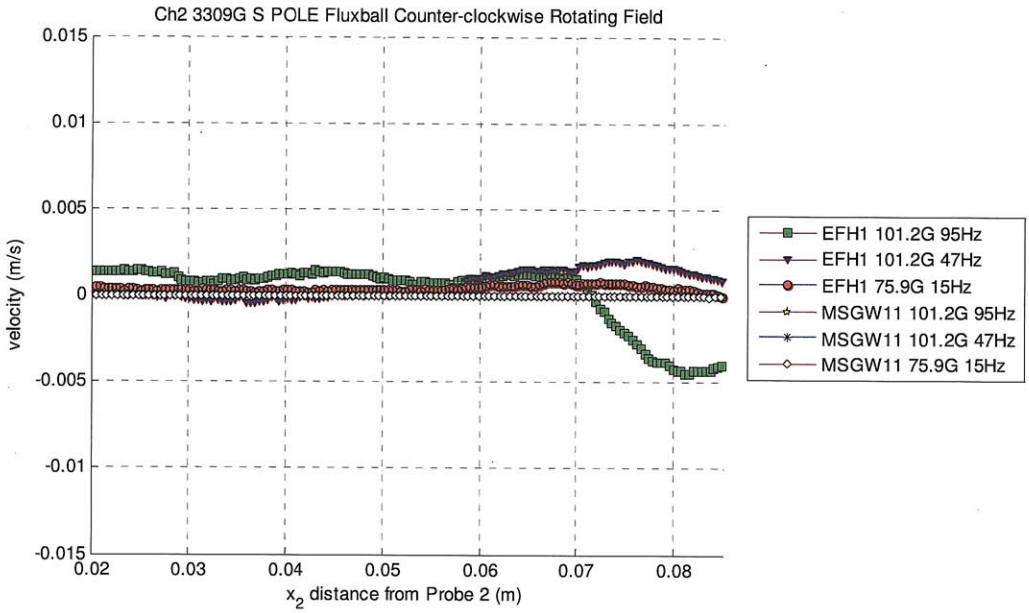
Ch2 3309G S POLE Fluxball Counter-clockwise Rotating Field
velocity (m/s)
0.015
0.01
0.005
0
-0.005
-0.01
-0.015
0.02
0.03
0.04
0.05
0.06
0.07
0.08
x2 distance from Probe 2 (m)
EFH1 101.2G 95Hz
EFH1 101.2G 47Hz
EFH1 75.9G 15Hz
MSGW11 101.2G 95Hz
MSGW11 101.2G 47Hz
MSGW11 75.9G 15Hz

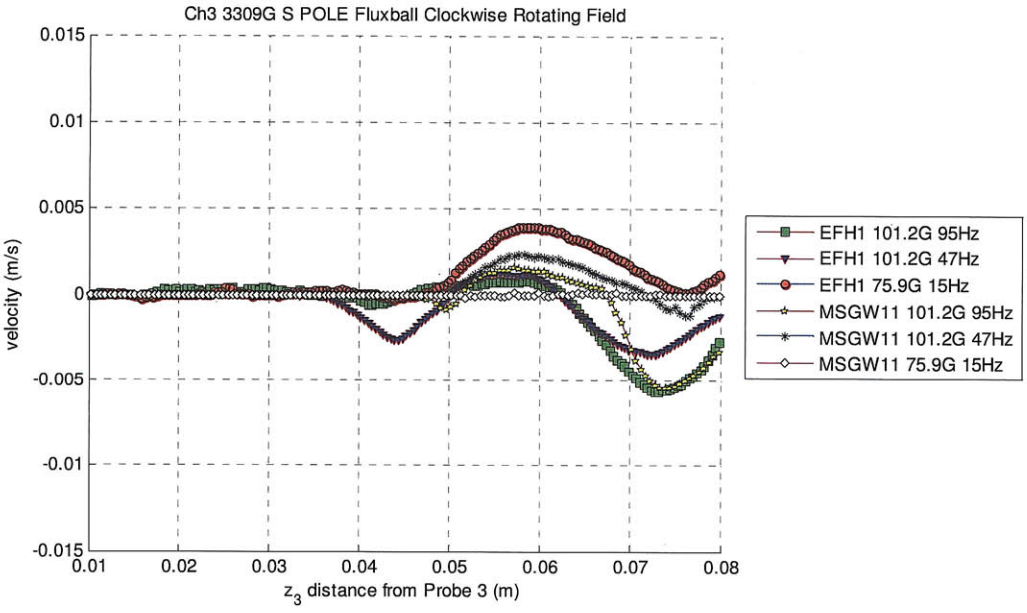
Ch3 3309G S POLE Fluxball Clockwise Rotating Field
velocity (m/s)
0.015
0.01
0.005
0
-0.005
-0.01
-0.015
0.01
0.02
0.03
0.04
0.05
0.06
0.07
0.08
z3 distance from Probe 3 (m)
EFH1 101.2G 95Hz
EFH1 101.2G 47Hz
EFH1 75.9G 15Hz
MSGW11 101.2G 95Hz
MSGW11 101.2G 47Hz
MSGW11 75.9G 15Hz

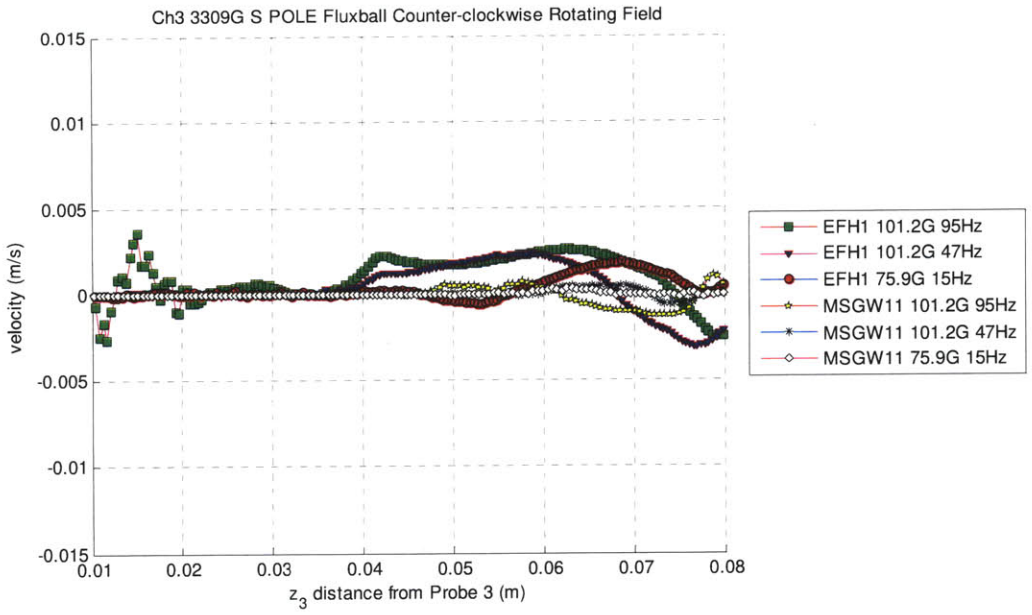
Ch3 3309G S POLE Fluxball Counter-clockwise Rotating Field
velocity (m/s)
0.015
0.01
0.005
0
-0.005
-0.01
-0.015
0.01
0.02
0.03
0.04
0.05
0.06
0.07
0.08
z3 distance from Probe 3 (m)
EFH1 101.2G 95Hz
EFH1 101.2G 47Hz
EFH1 75.9G 15Hz
MSGW11 101.2G 95Hz
MSGW11 101.2G 47Hz
MSGW11 75.9G 15Hz

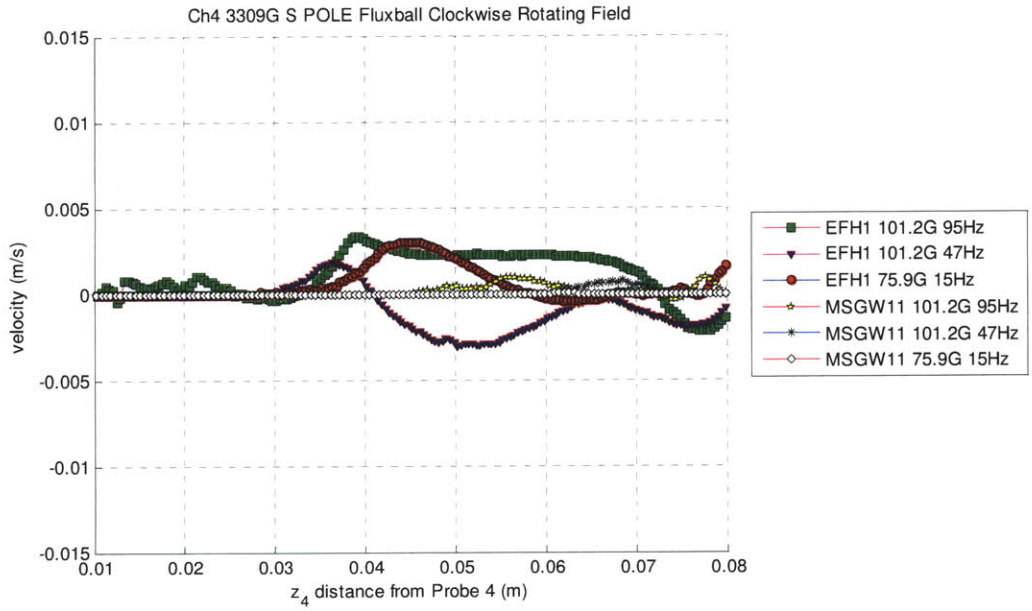
Ch4 3309G S POLE Fluxball Clockwise Rotating Field
velocity (m/s)
0.015
0.01
0.005
0
-0.005
-0.01
-0.015
0.01
0.02
0.03
0.04
0.05
0.06
0.07
0.08
z4 distance from Probe 4 (m)
EFH1 101.2G 95Hz
EFH1 101.2G 47Hz
EFH1 75.9G 15Hz
MSGW11 101.2G 95Hz
MSGW11 101.2G 47Hz
MSGW11 75.9G 15Hz

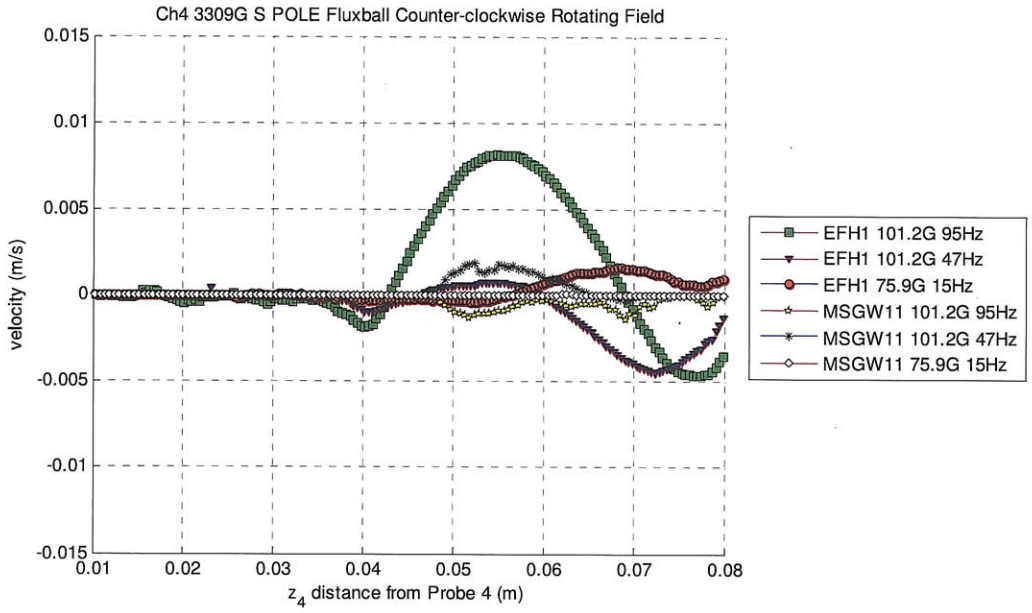
Ch4 3309G S POLE Fluxball Counter-clockwise Rotating Field
0.015
0.01
0.005
0
-0.005
-0.01
-0.015
velocity (m/s)
0.01
0.02
0.03
0.04
0.05
0.06
0.07
0.08
z4 distance from Probe 4 (m)
EFH1 101.2G 95Hz
EFH1 101.2G 47Hz
EFH1 75.9G 15Hz
MSGW11 101.2G 95Hz
MSGW11 101.2G 47Hz
MSGW11 75.9G 15Hz

H18. Comparison of Different Fluids with 3309G Magnet with North Pole Facing Ferrofluid Filled Sphere at Different Frequencies and Field Strengths

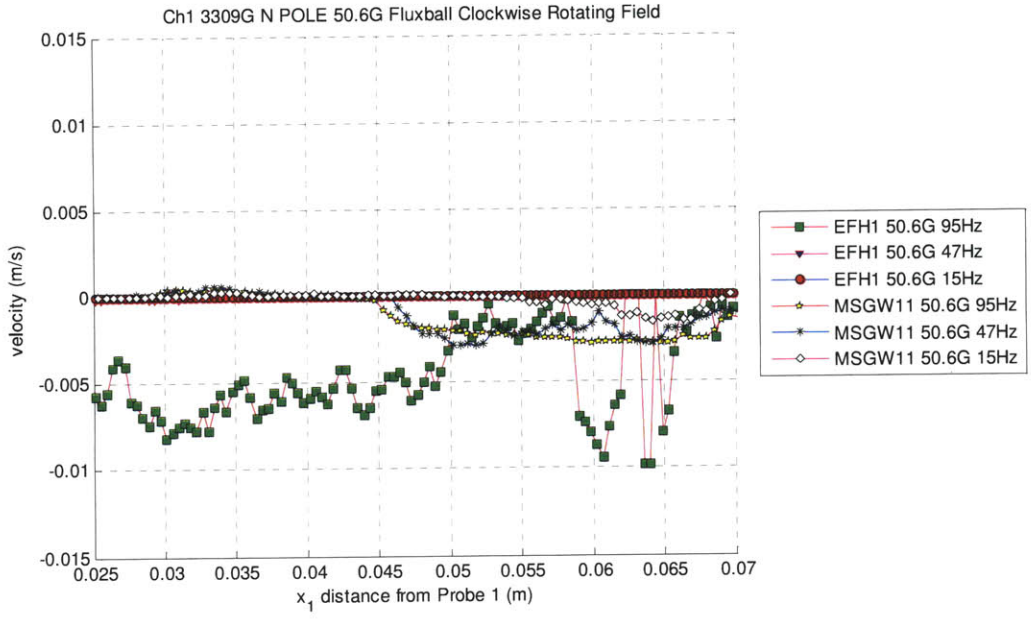

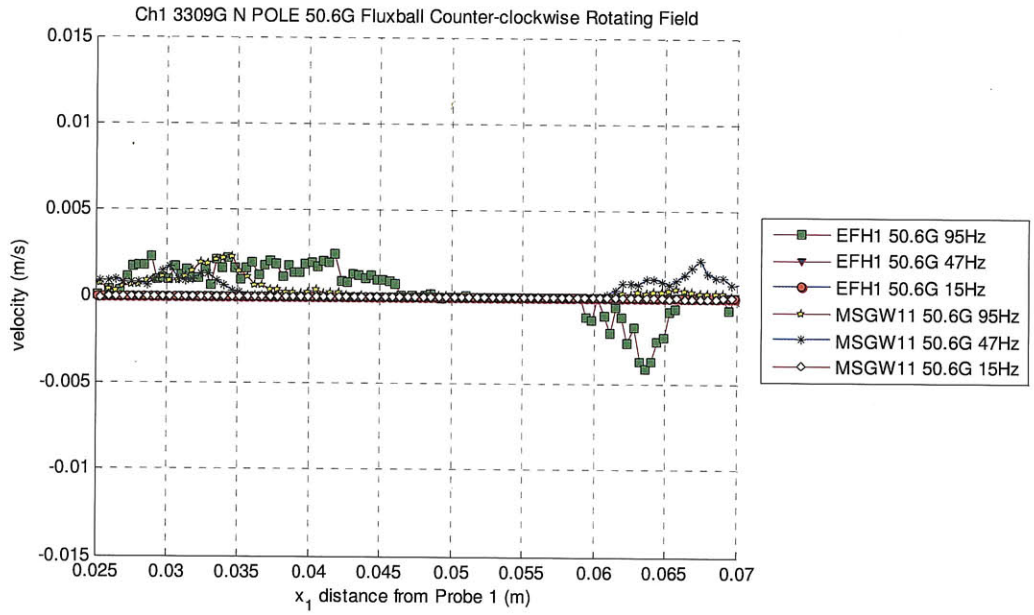
Ch1 3309G N POLE 50.6G Fluxball Counter-clockwise Rotating Field
velocity (m/s)
0.015
0.01
0.005
0
-0.005
-0.01
-0.015
0.025
0.03
0.035
0.04
0.045
0.05
0.055
0.06
0.065
0.07
x1 distance from Probe 1 (m)
EFH1 50.6G 95Hz
EFH1 50.6G 47Hz
EFH1 50.6G 15Hz
MSGW11 50.6G 95Hz
MSGW11 50.6G 47Hz
MSGW11 50.6G 15Hz

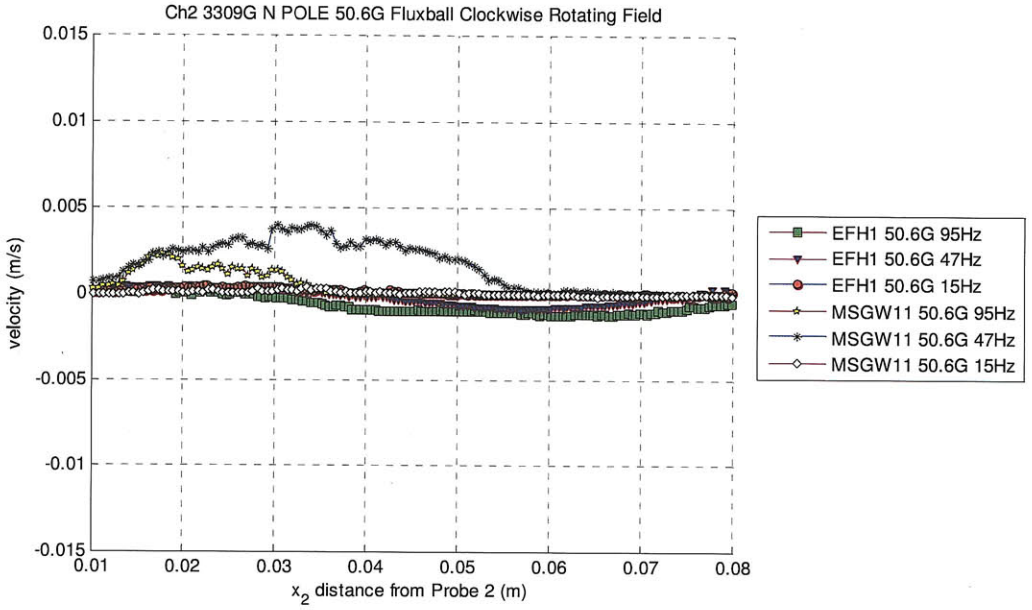
Ch2 3309G N POLE 50.6G Fluxball Clockwise Rotating Field
velocity (m/s)
0.015
0.01
0.005
0
-0.005
-0.01
-0.015
0.01
0.02
0.03
0.04
0.05
0.06
0.07
0.08
x2 distance from Probe 2 (m)
EFH1 50.6G 95Hz
EFH1 50.6G 47Hz
EFH1 50.6G 15Hz
MSGW11 50.6G 95Hz
MSGW11 50.6G 47Hz
MSGW11 50.6G 15Hz

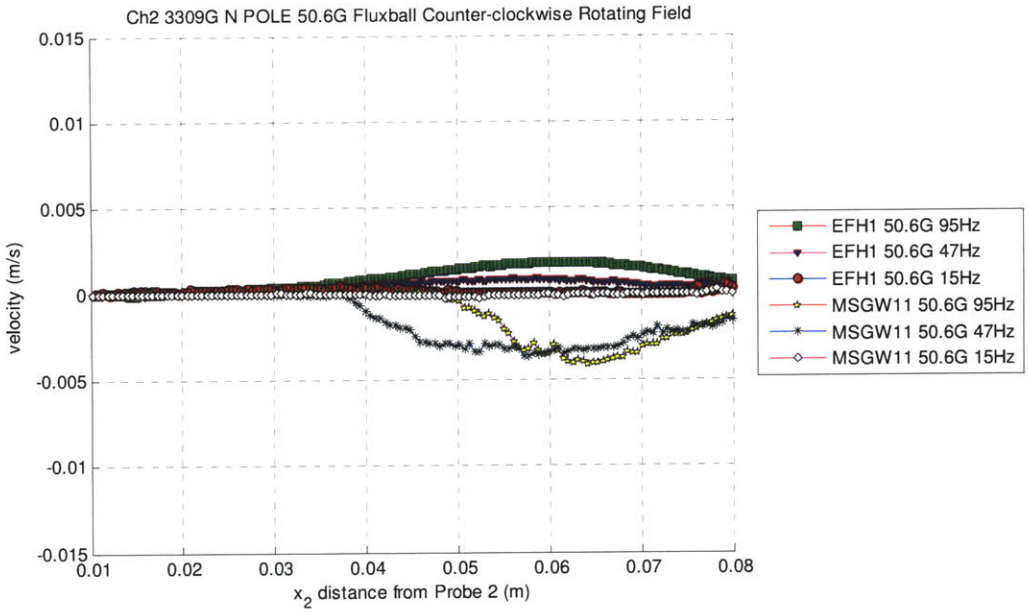
Ch2 3309G N POLE 50.6G Fluxball Counter-clockwise Rotating Field
velocity (m/s)
0.015
0.01
0.005
0
-0.005
-0.01
-0.015
0.01
0.02
0.03
0.04
0.05
0.06
0.07
0.08
x2 distance from Probe 2 (m)
EFH1 50.6G 95Hz
EFH1 50.6G 47Hz
EFH1 50.6G 15Hz
MSGW11 50.6G 95Hz
MSGW11 50.6G 47Hz
MSGW11 50.6G 15Hz

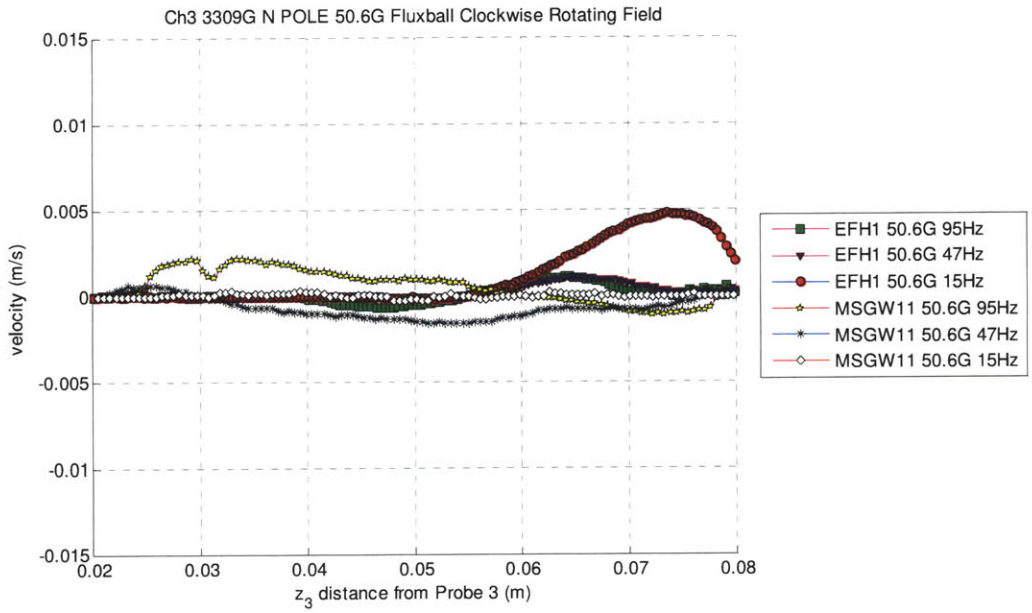
Ch3 3309G N POLE 50.6G Fluxball Clockwise Rotating Field
velocity (m/s)
0.015
0.01
0.005
0
-0.005
-0.01
-0.015
0.02
0.03
0.04
0.05
0.06
0.07
0.08
z3 distance from Probe 3 (m)
EFH1 50.6G 95Hz
EFH1 50.6G 47Hz
EFH1 50.6G 15Hz
MSGW11 50.6G 95Hz
MSGW11 50.6G 47Hz
MSGW11 50.6G 15Hz

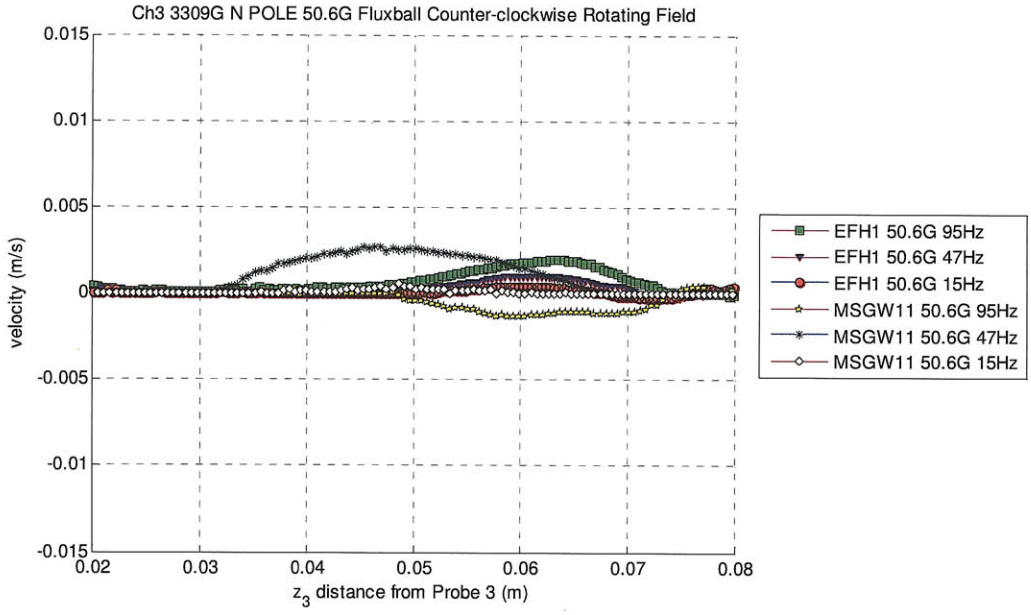
Ch3 3309G N POLE 50.6G Fluxball Counter-clockwise Rotating Field
velocity (m/s)
0.015
0.01
0.005
0
-0.005
-0.01
-0.015
0.02
0.03
0.04
0.05
0.06
0.07
0.08
z3 distance from Probe 3 (m)
EFH1 50.6G 95Hz
EFH1 50.6G 47Hz
EFH1 50.6G 15Hz
MSGW11 50.6G 95Hz
MSGW11 50.6G 47Hz
MSGW11 50.6G 15Hz

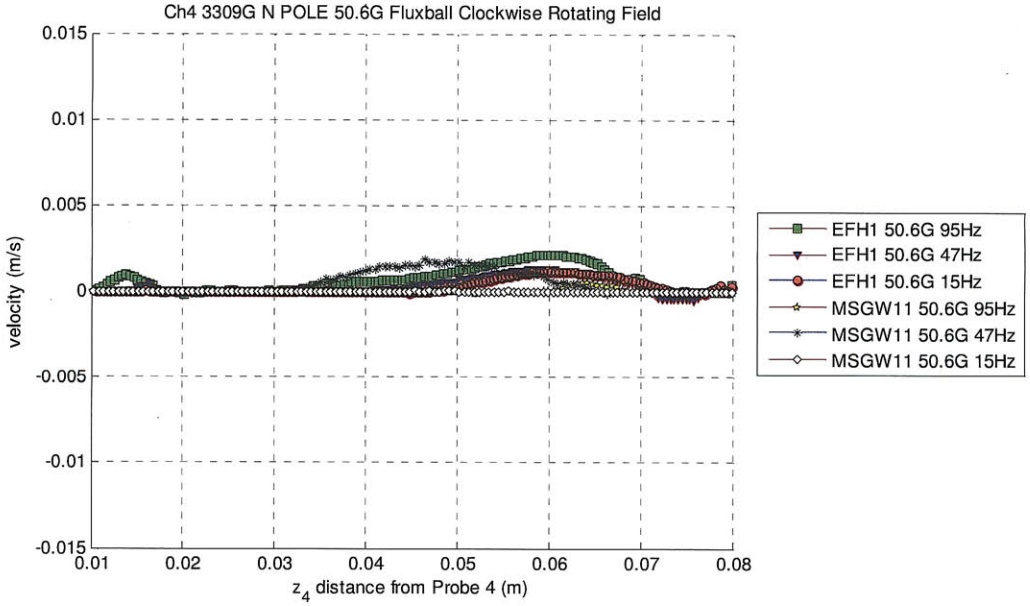
Ch4 3309G N POLE 50.6G Fluxball Clockwise Rotating Field
velocity (m/s)
0.015
0.01
0.005
0
-0.005
-0.01
-0.015
0.01
0.02
0.03
0.04
0.05
0.06
0.07
0.08
z4 distance from Probe 4 (m)
EFH1 50.6G 95Hz
EFH1 50.6G 47Hz
EFH1 50.6G 15Hz
MSGW11 50.6G 95Hz
MSGW11 50.6G 47Hz
MSGW11 50.6G 15Hz

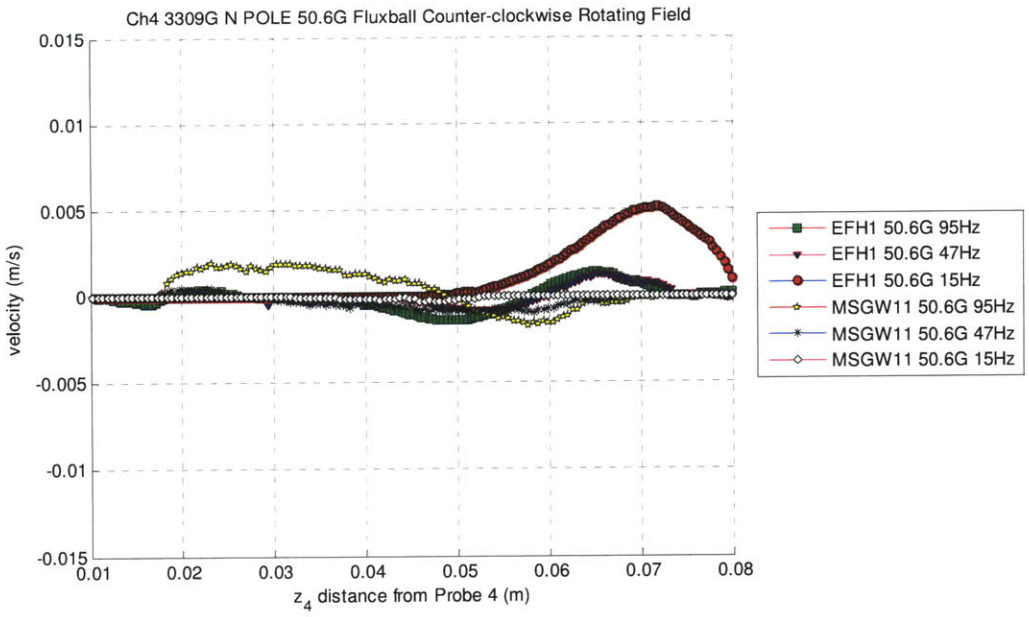
Ch4 3309G N POLE 50.6G Fluxball Counter-clockwise Rotating Field
velocity (m/s)
0.015
0.01
0.005
0
-0.005
-0.01
-0.015
0.01
0.02
0.03
0.04
0.05
0.06
0.07
0.08
z4 distance from Probe 4 (m)
EFH1 50.6G 95Hz
EFH1 50.6G 47Hz
EFH1 50.6G 15Hz
MSGW11 50.6G 95Hz
MSGW11 50.6G 47Hz
MSGW11 50.6G 15Hz

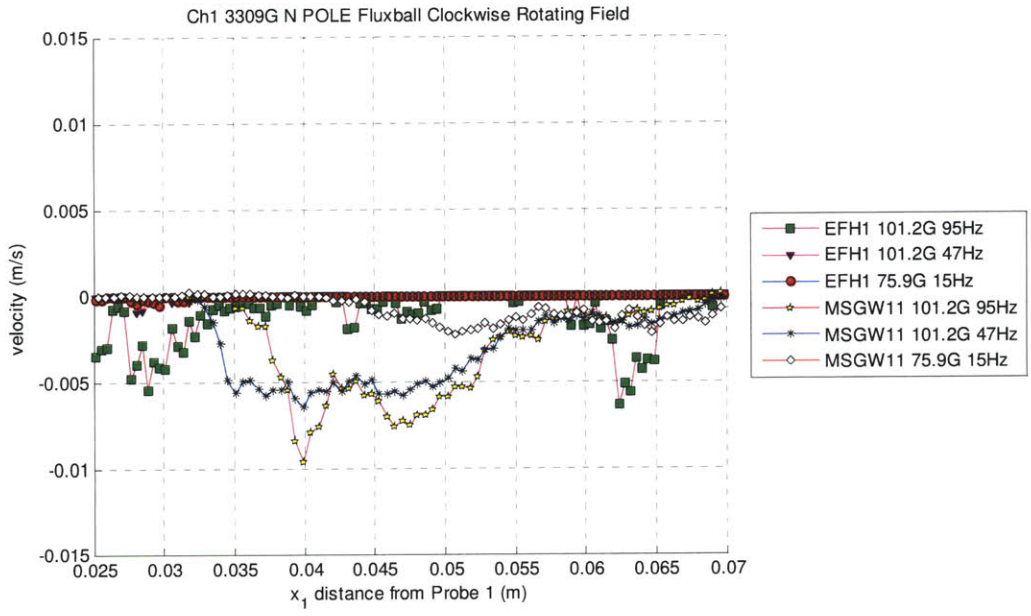
Ch1 3309G N POLE Fluxball Clockwise Rotating Field
velocity (m/s)
0.015
0.01
0.005
0
-0.005
-0.01
-0.015
0.025
0.03
0.035
0.04
0.045
0.05
0.055
0.06
0.065
0.07
x1 distance from Probe 1 (m)
EFH1 101.2G 95Hz
EFH1 101.2G 47Hz
EFH1 75.9G 15Hz
MSGW11 101.2G 95Hz
MSGW11 101.2G 47Hz
MSGW11 75.9G 15Hz

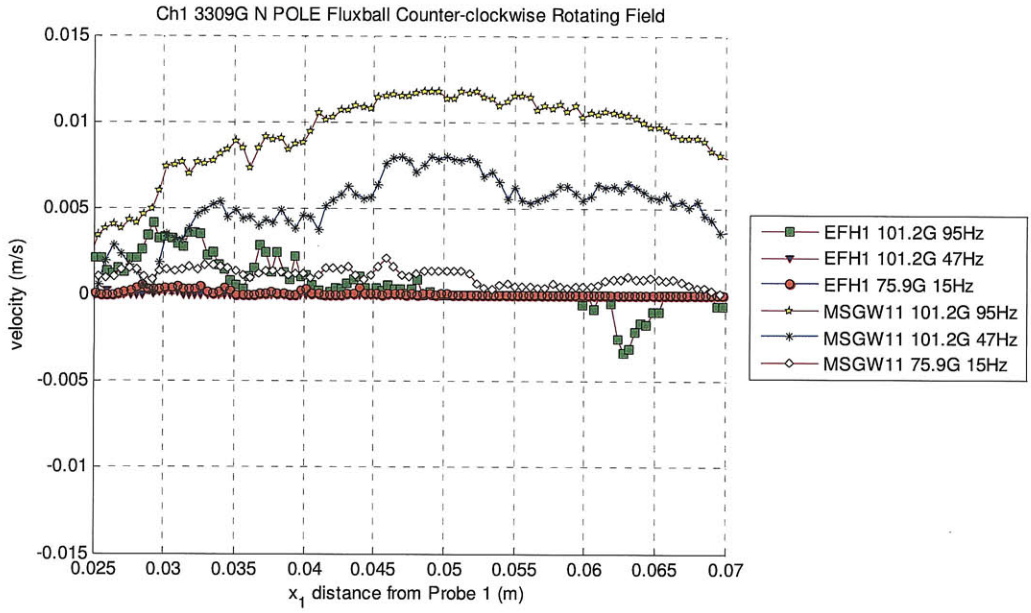
Ch1 3309G N POLE Fluxball Counter-clockwise Rotating Field
velocity (m/s)
0.015
0.01
0.005
0
-0.005
-0.01
-0.015
0.025
0.03
0.035
0.04
0.045
0.05
0.055
0.06
0.065
0.07
x1 distance from Probe 1 (m)
EFH1 101.2G 95Hz
EFH1 101.2G 47Hz
EFH1 75.9G 15Hz
MSGW11 101.2G 95Hz
MSGW11 101.2G 47Hz
MSGW11 75.9G 15Hz

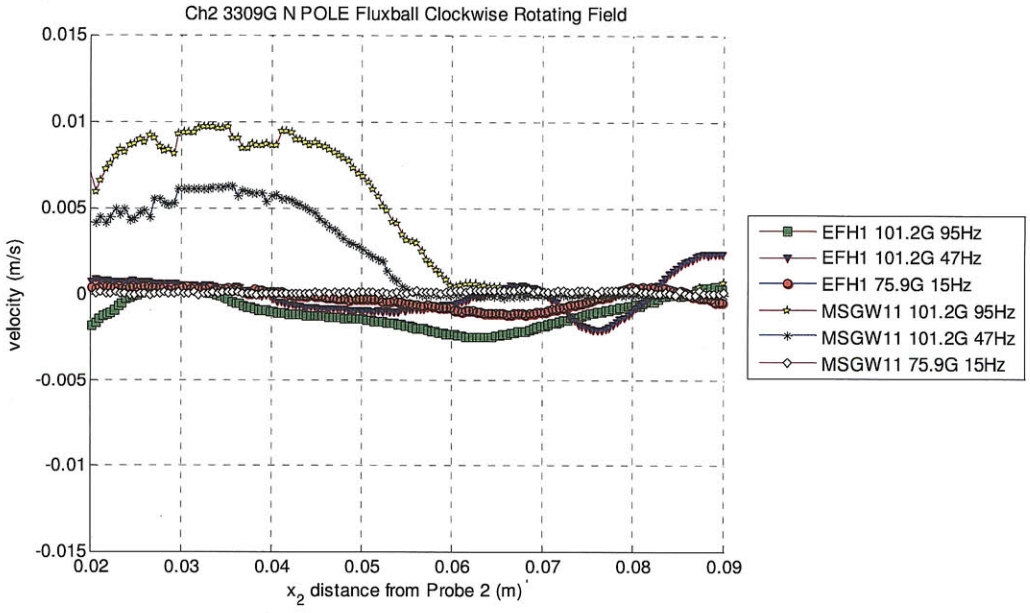
Ch2 3309G N POLE Fluxball Clockwise Rotating Field
velocity (m/s)
0.015
0.01
0.005
0
-0.005
-0.01
-0.015
0.02
0.03
0.04
0.05
0.06
0.07
0.08
0.09
x2 distance from Probe 2 (m)
EFH1 101.2G 95Hz
EFH1 101.2G 47Hz
EFH1 75.9G 15Hz
MSGW11 101.2G 95Hz
MSGW11 101.2G 47Hz
MSGW11 75.9G 15Hz

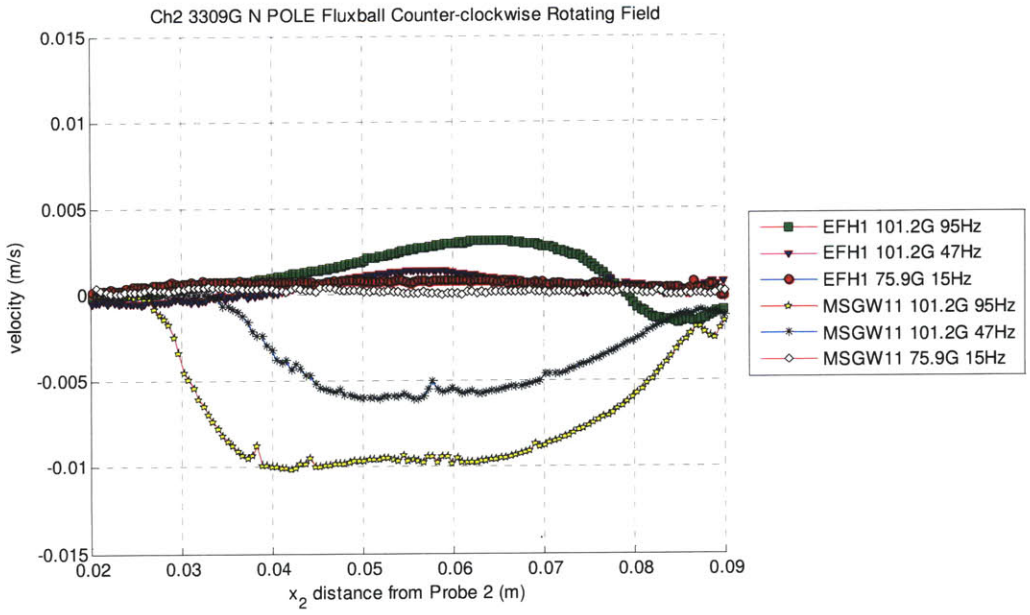
Ch2 3309G N POLE Fluxball Counter-clockwise Rotating Field
velocity (m/s)
0.015
0.01
0.005
0
-0.005
-0.01
-0.015
0.02
0.03
0.04
0.05
0.06
0.07
0.08
0.09
x2 distance from Probe 2 (m)
EFH1 101.2G 95Hz
EFH1 101.2G 47Hz
EFH1 75.9G 15Hz
MSGW11 101.2G 95Hz
MSGW11 101.2G 47Hz
MSGW11 75.9G 15Hz

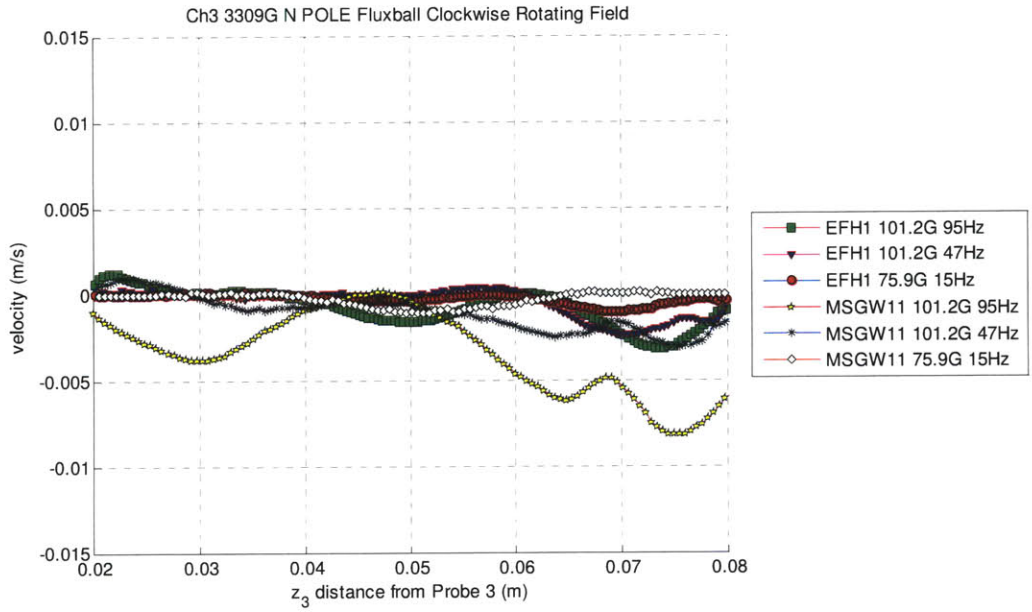
Ch3 3309G N POLE Fluxball Clockwise Rotating Field
velocity (m/s)
0.015
0.01
0.005
0
-0.005
-0.01
-0.015
0.02
0.03
0.04
0.05
0.06
0.07
0.08
z3 distance from Probe 3 (m)
EFH1 101.2G 95Hz
EFH1 101.2G 47Hz
EFH1 75.9G 15Hz
MSGW11 101.2G 95Hz
MSGW11 101.2G 47Hz
MSGW11 75.9G 15Hz

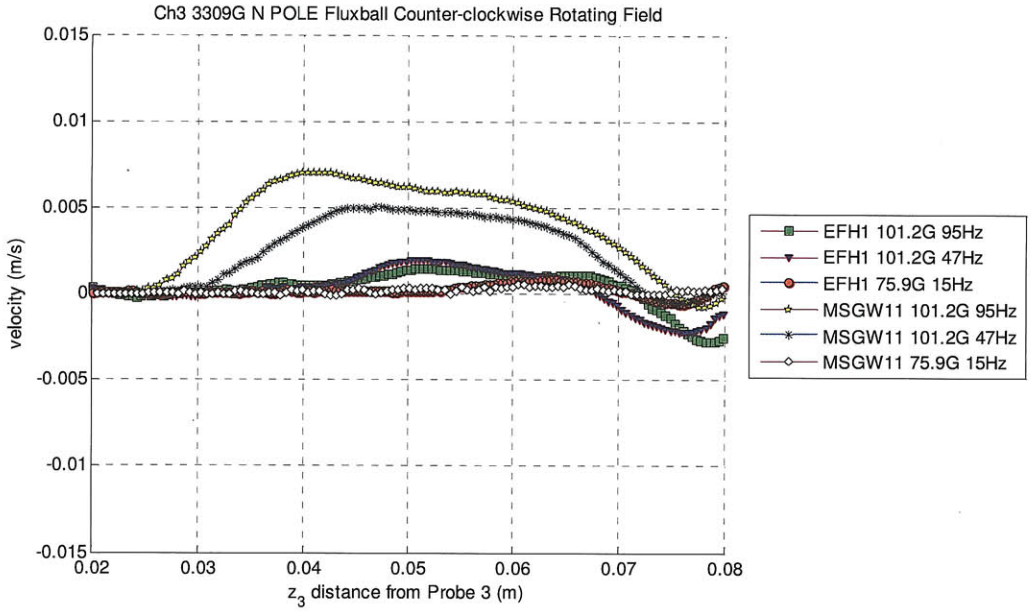
Ch3 3309G N POLE Fluxball Counter-clockwise Rotating Field
velocity (m/s)
0.015
0.01
0.005
0
-0.005
-0.01
-0.015
0.02
0.03
0.04
0.05
0.06
0.07
0.08
z_3 distance from Probe 3 (m)
EFH1 101.2G 95Hz
EFH1 101.2G 47Hz
EFH1 75.9G 15Hz
MSGW11 101.2G 95Hz
MSGW11 101.2G 47Hz
MSGW11 75.9G 15Hz

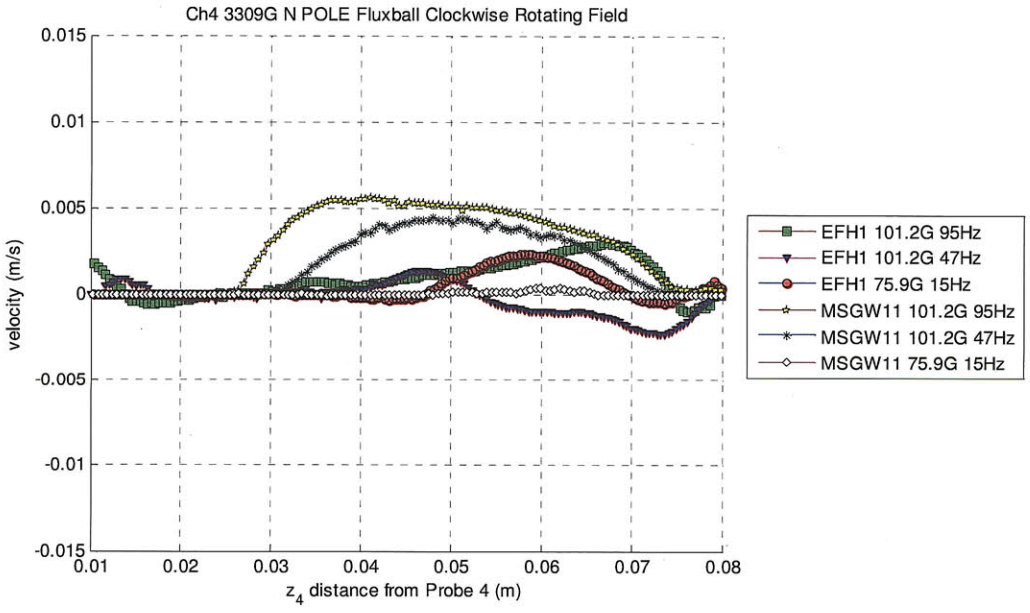
Ch4 3309G N POLE Fluxball Clockwise Rotating Field
velocity (m/s)
0.015
0.01
0.005
0
-0.005
-0.01
-0.015
0.01
0.02
0.03
0.04
0.05
0.06
0.07
0.08
z_4 distance from Probe 4 (m)
EFH1 101.2G 95Hz
EFH1 101.2G 47Hz
EFH1 75.9G 15Hz
MSGW11 101.2G 95Hz
MSGW11 101.2G 47Hz
MSGW11 75.9G 15Hz

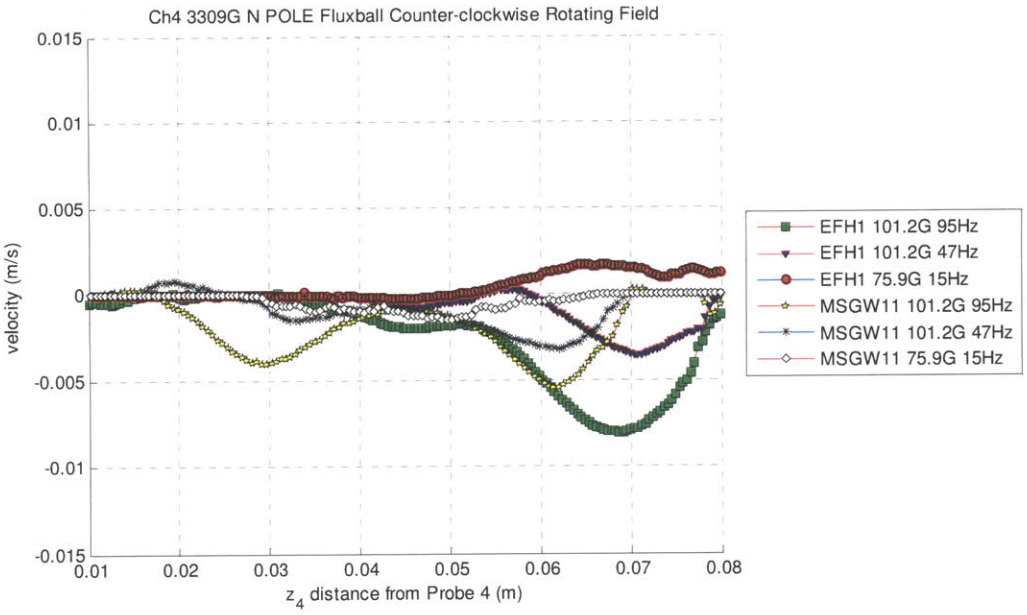
Ch4 3309G N POLE Fluxball Counter-clockwise Rotating Field
0.015
0.01
0.005
0
-0.005
-0.01
-0.015
velocity (m/s)
0.01
0.02
0.03
0.04
0.05
0.06
0.07
0.08
z4 distance from Probe 4 (m)
EFH1 101.2G 95Hz
EFH1 101.2G 47Hz
EFH1 75.9G 15Hz
MSGW11 101.2G 95Hz
MSGW11 101.2G 47Hz
MSGW11 75.9G 15Hz

H19. Comparison of Different Fluids with 4667G Magnet with South Pole Facing Ferrofluid Filled Sphere at Different Frequencies and Field Strengths

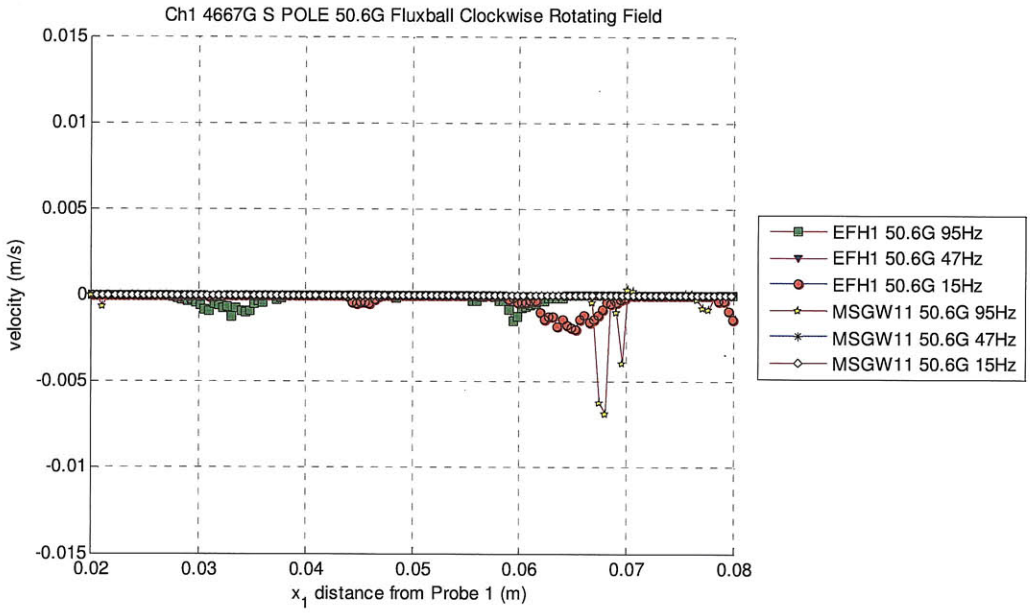

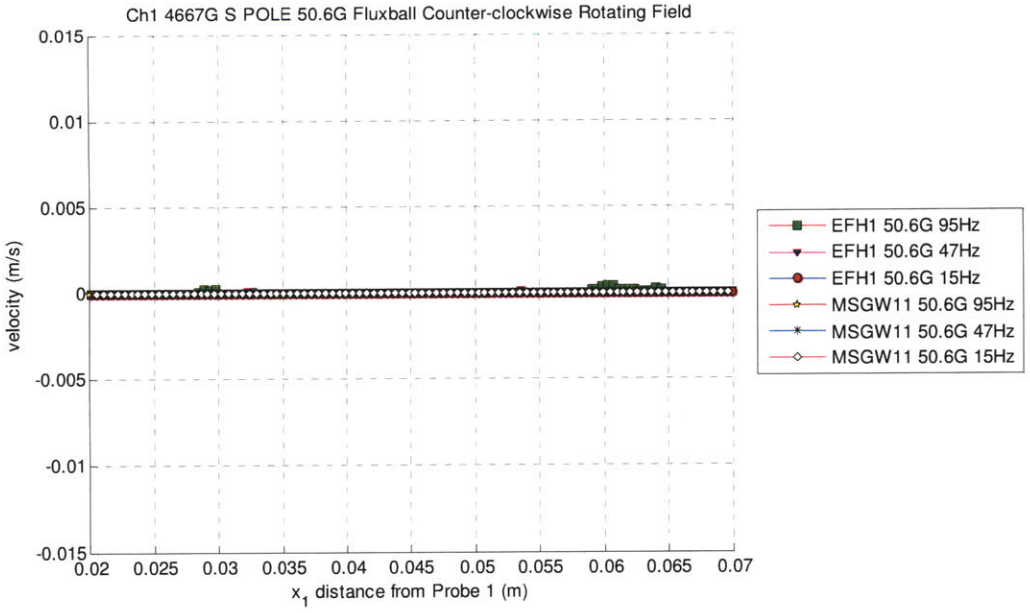
Ch1 4667G S POLE 50.6G Fluxball Counter-clockwise Rotating Field
velocity (m/s)
0.015
0.01
0.005
0
-0.005
-0.01
-0.015
0.02
0.025
0.03
0.035
0.04
0.045
0.05
0.055
0.06
0.065
0.07
x1 distance from Probe 1 (m)
EFH1 50.6G 95Hz
EFH1 50.6G 47Hz
EFH1 50.6G 15Hz
MSGW11 50.6G 95Hz
MSGW11 50.6G 47Hz
MSGW11 50.6G 15Hz

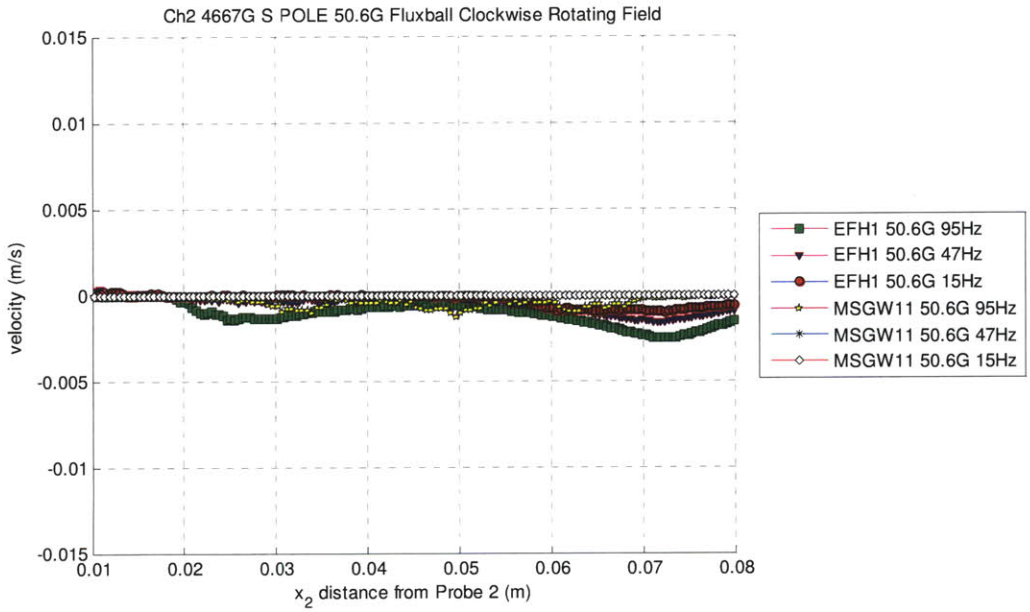
Ch2 4667G S POLE 50.6G Fluxball Clockwise Rotating Field
velocity (m/s)
0.015
0.01
0.005
0
-0.005
-0.01
-0.015
0.01
0.02
0.03
0.04
0.05
0.06
0.07
0.08
x2 distance from Probe 2 (m)
EFH1 50.6G 95Hz
EFH1 50.6G 47Hz
EFH1 50.6G 15Hz
MSGW11 50.6G 95Hz
MSGW11 50.6G 47Hz
MSGW11 50.6G 15Hz

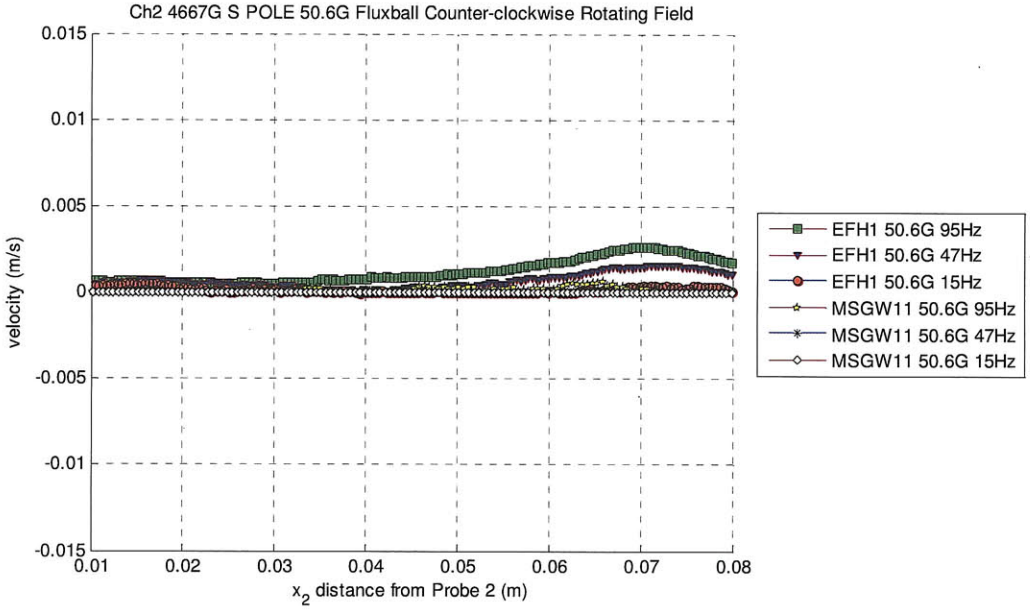
Ch2 4667G S POLE 50.6G Fluxball Counter-clockwise Rotating Field
velocity (m/s)
0.015
0.01
0.005
0
-0.005
-0.01
-0.015
0.01
0.02
0.03
0.04
0.05
0.06
0.07
0.08
x2 distance from Probe 2 (m)
EFH1 50.6G 95Hz
EFH1 50.6G 47Hz
EFH1 50.6G 15Hz
MSGW11 50.6G 95Hz
MSGW11 50.6G 47Hz
MSGW11 50.6G 15Hz

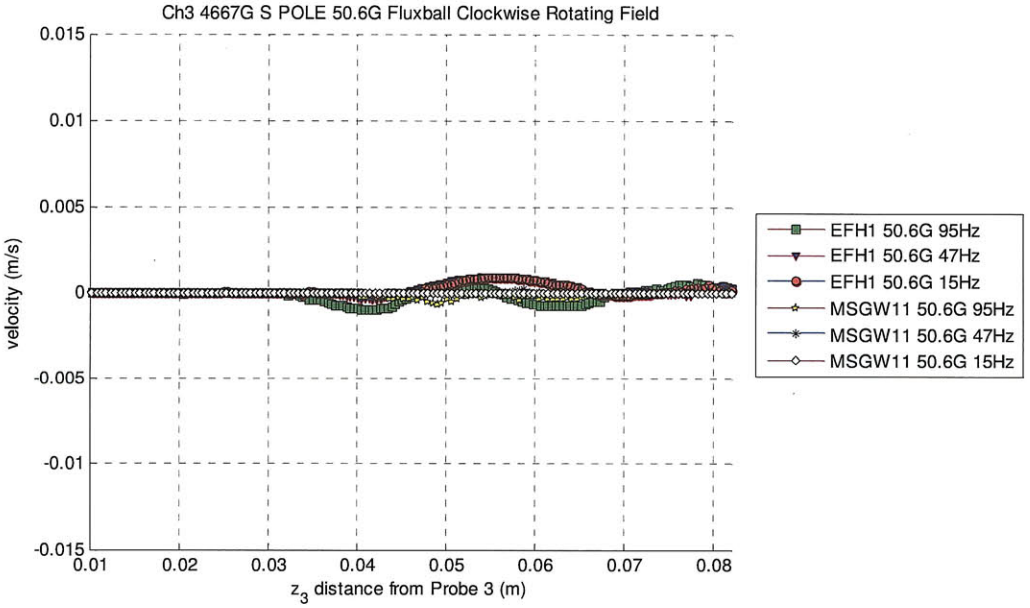
Ch3 4667G S POLE 50.6G Fluxball Clockwise Rotating Field
velocity (m/s)
0.015
0.01
0.005
0
-0.005
-0.01
-0.015
0.01
0.02
0.03
0.04
0.05
0.06
0.07
0.08
z3 distance from Probe 3 (m)
EFH1 50.6G 95Hz
EFH1 50.6G 47Hz
EFH1 50.6G 15Hz
MSGW11 50.6G 95Hz
MSGW11 50.6G 47Hz
MSGW11 50.6G 15Hz

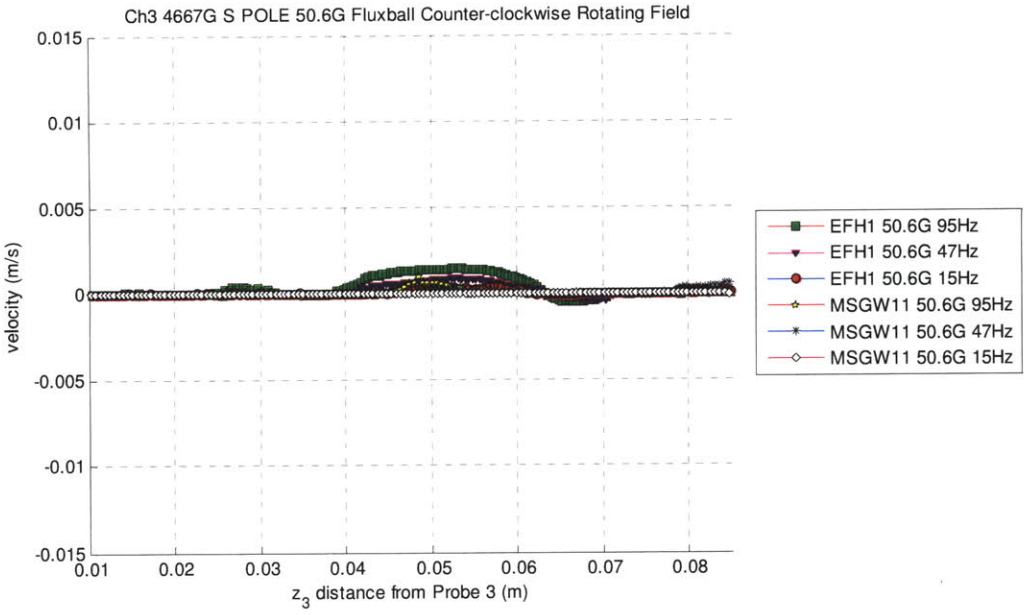
Ch3 4667G S POLE 50.6G Fluxball Counter-clockwise Rotating Field
velocity (m/s)
0.015
0.01
0.005
0
-0.005
-0.01
-0.015
0.01
0.02
0.03
0.04
0.05
0.06
0.07
0.08
z_3 distance from Probe 3 (m)
EFH1 50.6G 95Hz
EFH1 50.6G 47Hz
EFH1 50.6G 15Hz
MSGW11 50.6G 95Hz
MSGW11 50.6G 47Hz
MSGW11 50.6G 15Hz

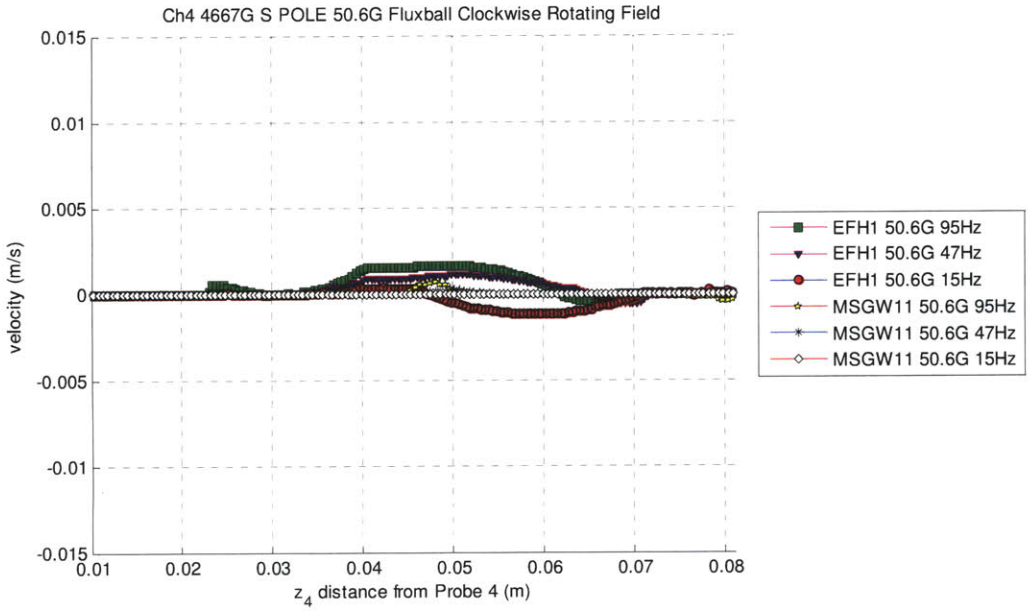
Ch4 4667G S POLE 50.6G Fluxball Clockwise Rotating Field
velocity (m/s)
0.015
0.01
0.005
0
-0.005
-0.01
-0.015
0.01
0.02
0.03
0.04
0.05
0.06
0.07
0.08
z_4 distance from Probe 4 (m)
EFH1 50.6G 95Hz
EFH1 50.6G 47Hz
EFH1 50.6G 15Hz
MSGW11 50.6G 95Hz
MSGW11 50.6G 47Hz
MSGW11 50.6G 15Hz

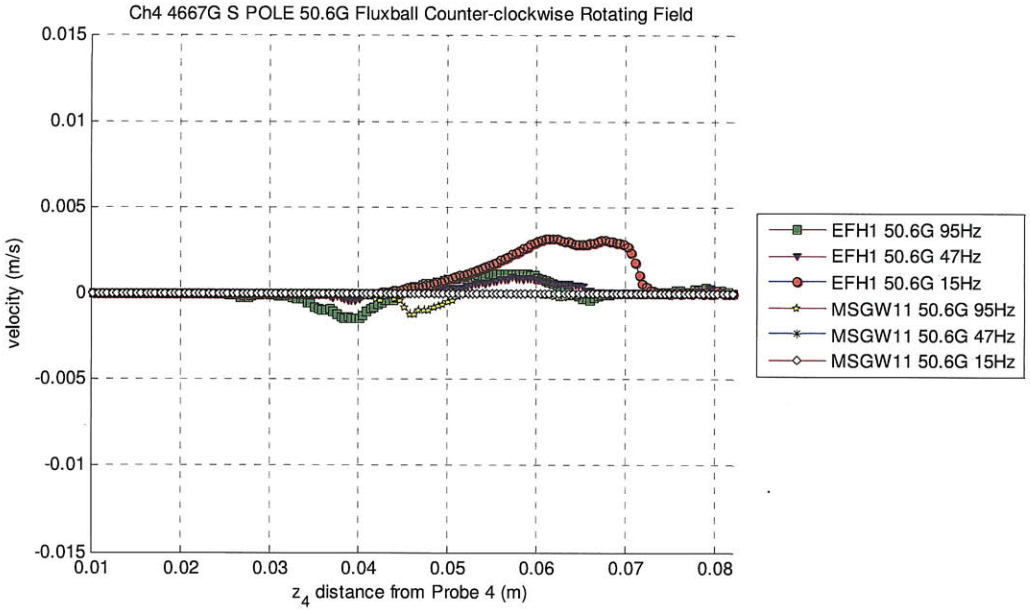
Ch4 4667G S POLE 50.6G Fluxball Counter-clockwise Rotating Field
velocity (m/s)
0.015
0.01
0.005
0
-0.005
-0.01
-0.015
0.01
0.02
0.03
0.04
0.05
0.06
0.07
0.08
z4 distance from Probe 4 (m)
EFH1 50.6G 95Hz
EFH1 50.6G 47Hz
EFH1 50.6G 15Hz
MSGW11 50.6G 95Hz
MSGW11 50.6G 47Hz
MSGW11 50.6G 15Hz

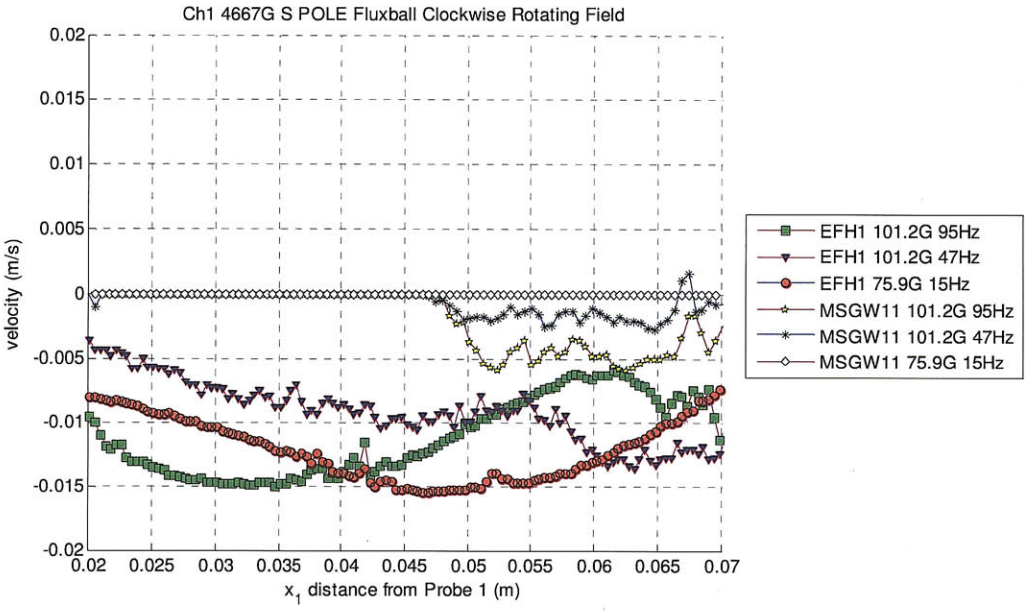
Ch1 4667G S POLE Fluxball Clockwise Rotating Field
velocity (m/s)
0.02
0.015
0.01
0.005
0
-0.005
-0.01
-0.015
-0.02
0.02
0.025
0.03
0.035
0.04
0.045
0.05
0.055
0.06
0.065
0.07
x1 distance from Probe 1 (m)
EFH1 101.2G 95Hz
EFH1 101.2G 47Hz
EFH1 75.9G 15Hz
MSGW11 101.2G 95Hz
MSGW11 101.2G 47Hz
MSGW11 75.9G 15Hz

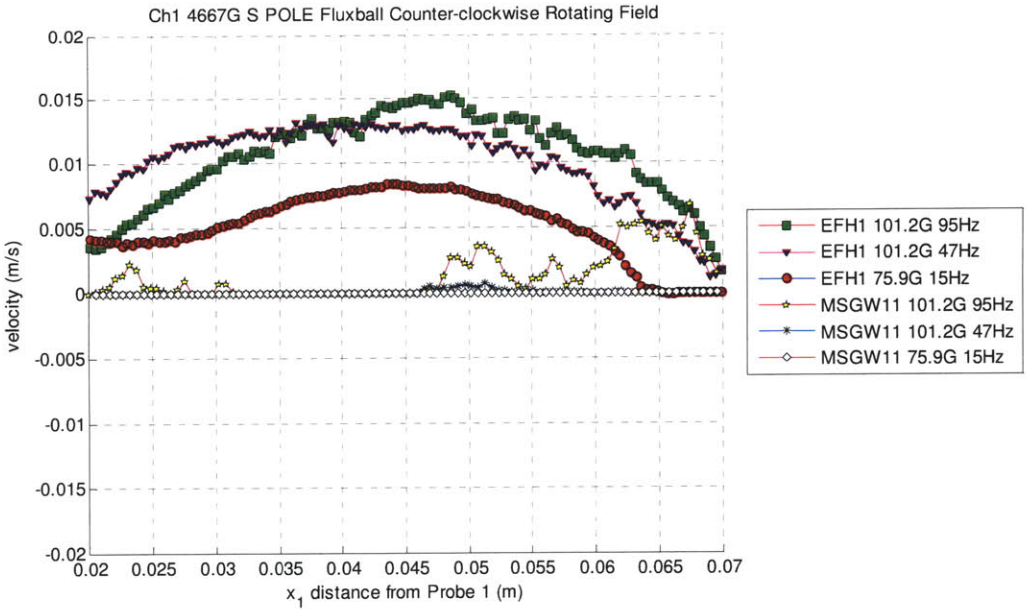
Ch1 4667G S POLE Fluxball Counter-clockwise Rotating Field
velocity (m/s)
0.02
0.015
0.01
0.005
0
-0.005
-0.01
-0.015
-0.02
0.02 0.025 0.03 0.035 0.04 0.045 0.05 0.055 0.06 0.065 0.07
x1 distance from Probe 1 (m)
EFH1 101.2G 95Hz
EFH1 101.2G 47Hz
EFH1 75.9G 15Hz
MSGW11 101.2G 95Hz
MSGW11 101.2G 47Hz
MSGW11 75.9G 15Hz

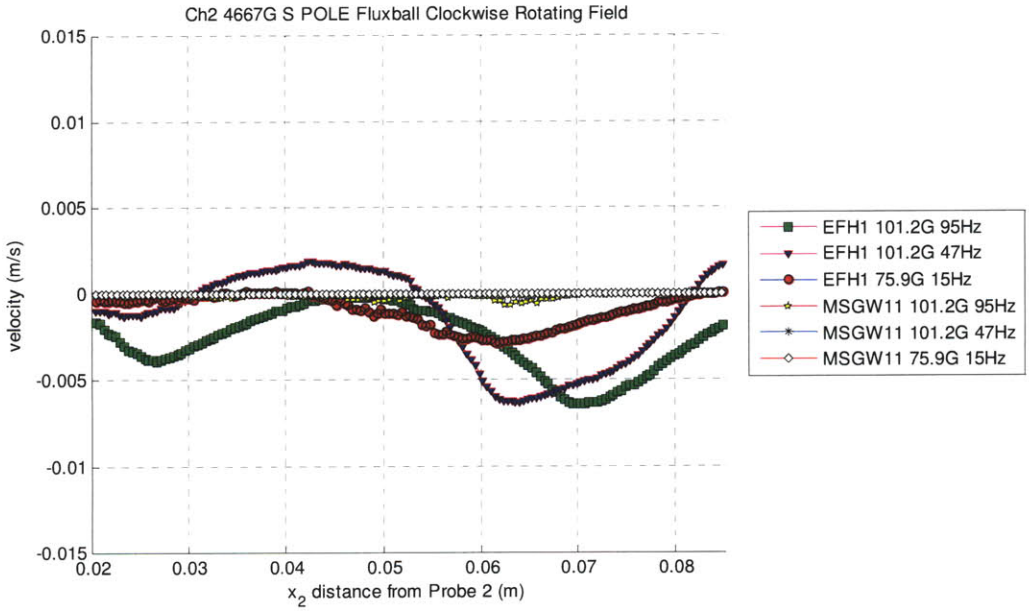
Ch2 4667G S POLE Fluxball Clockwise Rotating Field
velocity (m/s)
0.015
0.01
0.005
0
-0.005
-0.01
-0.015
0.02 0.03 0.04 0.05 0.06 0.07 0.08
x2 distance from Probe 2 (m)
EFH1 101.2G 95Hz
EFH1 101.2G 47Hz
EFH1 75.9G 15Hz
MSGW11 101.2G 95Hz
MSGW11 101.2G 47Hz
MSGW11 75.9G 15Hz

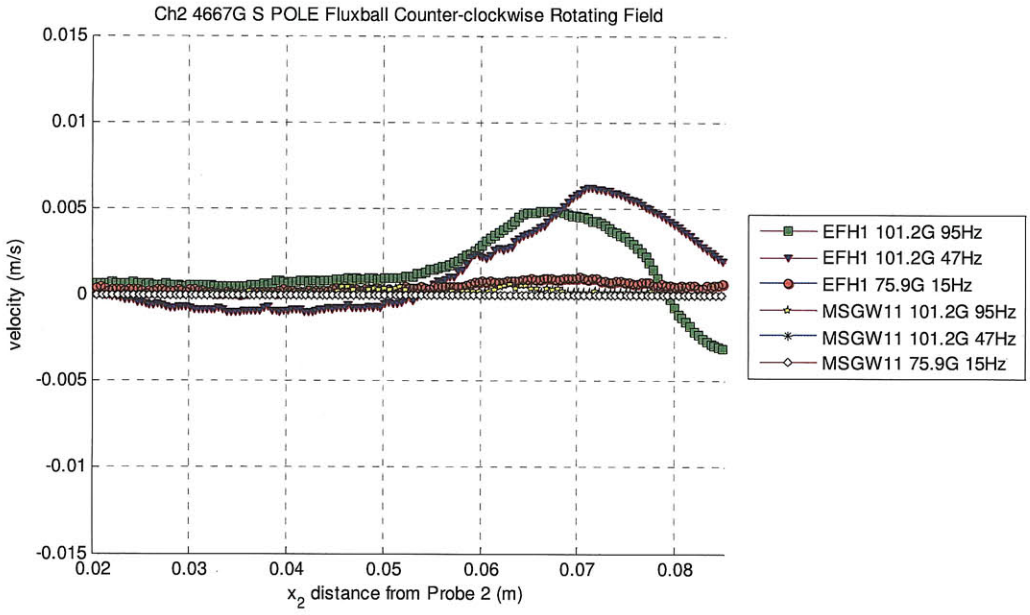
Ch2 4667G S POLE Fluxball Counter-clockwise Rotating Field
velocity (m/s)
0.015
0.01
0.005
0
-0.005
-0.01
-0.015
0.02
0.03
0.04
0.05
0.06
0.07
0.08
x2 distance from Probe 2 (m)
EFH1 101.2G 95Hz
EFH1 101.2G 47Hz
EFH1 75.9G 15Hz
MSGW11 101.2G 95Hz
MSGW11 101.2G 47Hz
MSGW11 75.9G 15Hz

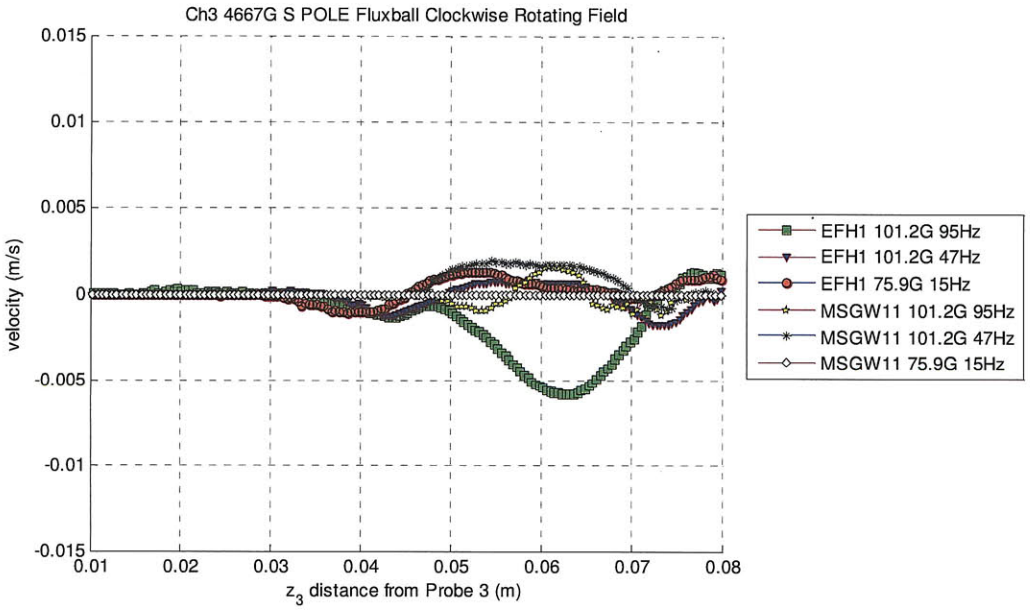
Ch3 4667G S POLE Fluxball Clockwise Rotating Field
velocity (m/s)
0.015
0.01
0.005
0
-0.005
-0.01
-0.015
0.01
0.02
0.03
0.04
0.05
0.06
0.07
0.08
z3 distance from Probe 3 (m)
EFH1 101.2G 95Hz
EFH1 101.2G 47Hz
EFH1 75.9G 15Hz
MSGW11 101.2G 95Hz
MSGW11 101.2G 47Hz
MSGW11 75.9G 15Hz

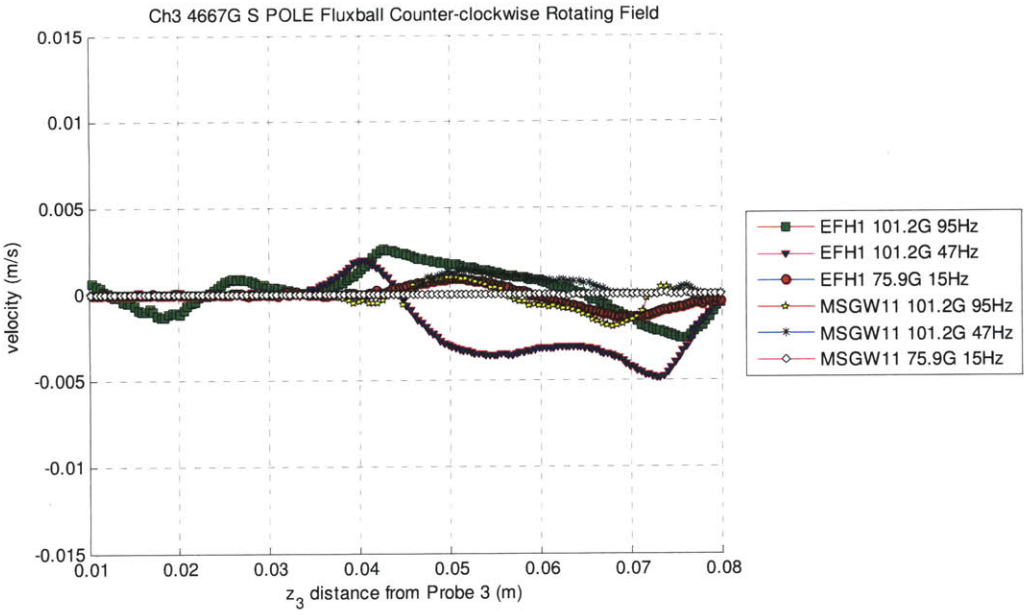
Ch3 4667G S POLE Fluxball Counter-clockwise Rotating Field
velocity (m/s)
0.015
0.01
0.005
0
-0.005
-0.01
-0.015
0.01
0.02
0.03
0.04
0.05
0.06
0.07
0.08
z3 distance from Probe 3 (m)
EFH1 101.2G 95Hz
EFH1 101.2G 47Hz
EFH1 75.9G 15Hz
MSGW11 101.2G 95Hz
MSGW11 101.2G 47Hz
MSGW11 75.9G 15Hz

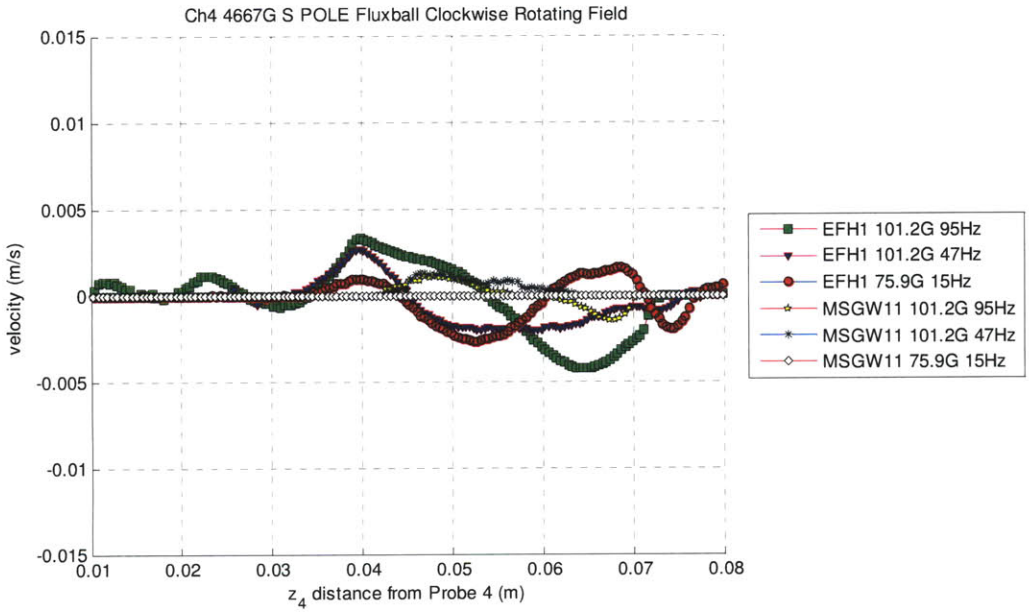
Ch4 4667G S POLE Fluxball Clockwise Rotating Field
velocity (m/s)
0.015
0.01
0.005
0
-0.005
-0.01
-0.015
0.01
0.02
0.03
0.04
0.05
0.06
0.07
0.08
z4 distance from Probe 4 (m)
EFH1 101.2G 95Hz
EFH1 101.2G 47Hz
EFH1 75.9G 15Hz
MSGW11 101.2G 95Hz
MSGW11 101.2G 47Hz
MSGW11 75.9G 15Hz

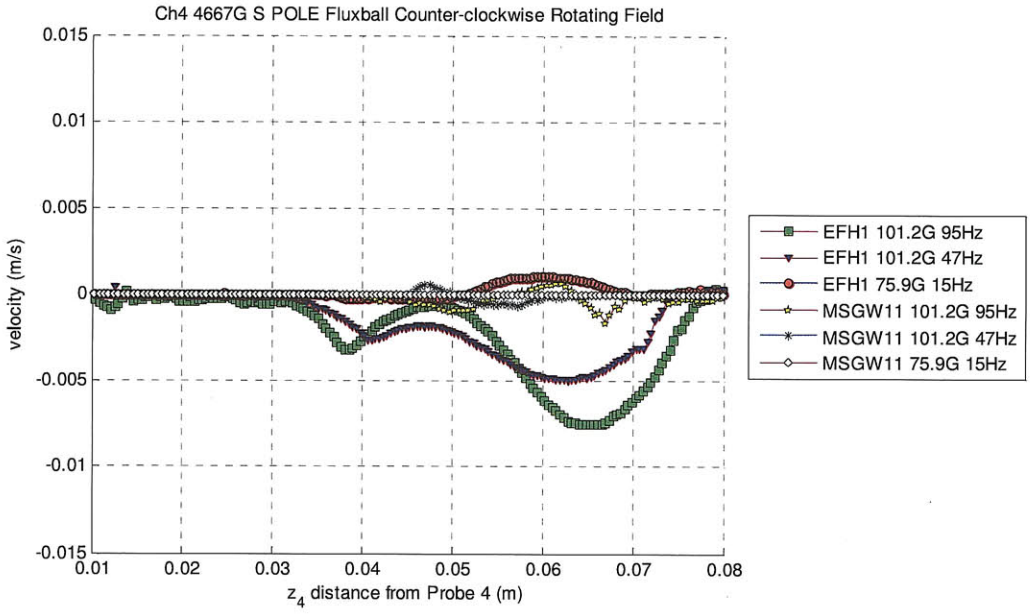
Ch4 4667G S POLE Fluxball Counter-clockwise Rotating Field
0.015
0.01
0.005
0
-0.005
-0.01
-0.015
velocity (m/s)
0.01
0.02
0.03
0.04
0.05
0.06
0.07
0.08
z4 distance from Probe 4 (m)
EFH1 101.2G 95Hz
EFH1 101.2G 47Hz
EFH1 75.9G 15Hz
MSGW11 101.2G 95Hz
MSGW11 101.2G 47Hz
MSGW11 75.9G 15Hz

H20. Comparison of Different Fluids with 4667G Magnet with North Pole Facing Ferrofluid Filled Sphere at Different Frequencies and Field Strengths

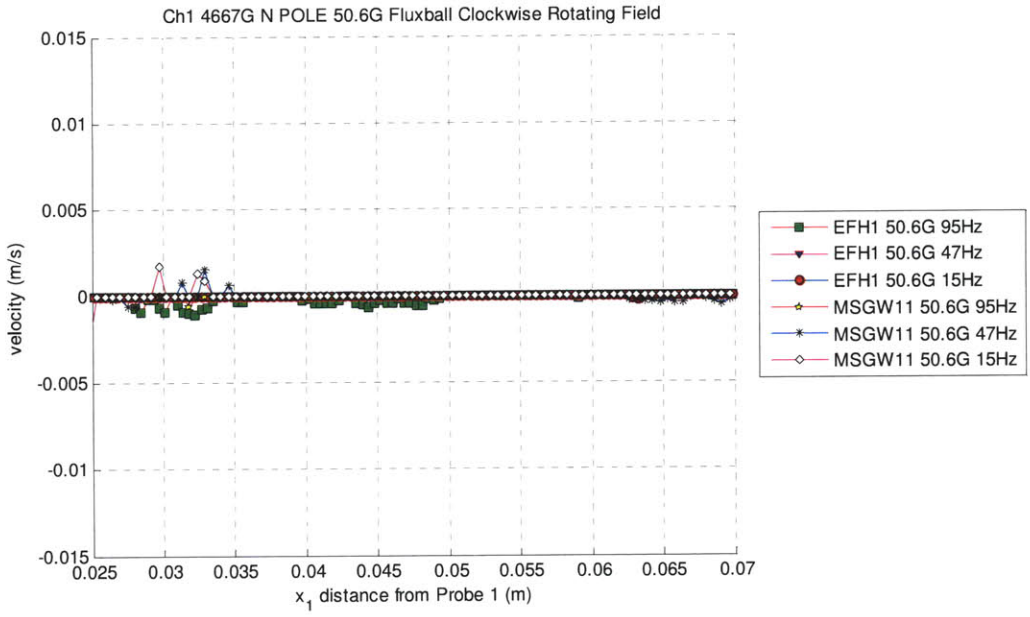

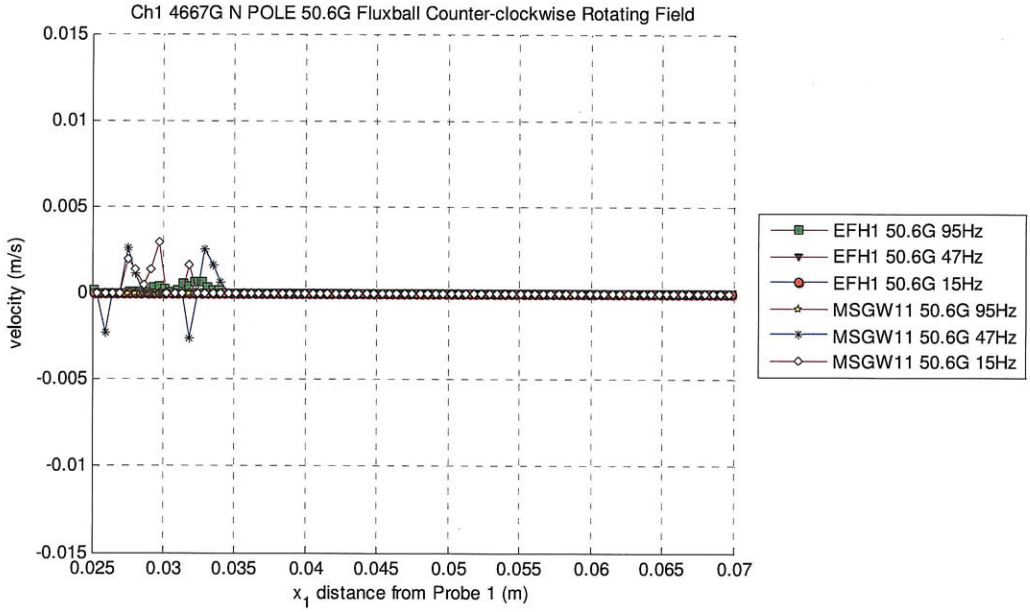
Ch1 4667G N POLE 50.6G Fluxball Counter-clockwise Rotating Field
velocity (m/s)
0.015
0.01
0.005
0
-0.005
-0.01
-0.015
0.025
0.03
0.035
0.04
0.045
0.05
0.055
0.06
0.065
0.07
x1 distance from Probe 1 (m)
EFH1 50.6G 95Hz
EFH1 50.6G 47Hz
EFH1 50.6G 15Hz
MSGW11 50.6G 95Hz
MSGW11 50.6G 47Hz
MSGW11 50.6G 15Hz

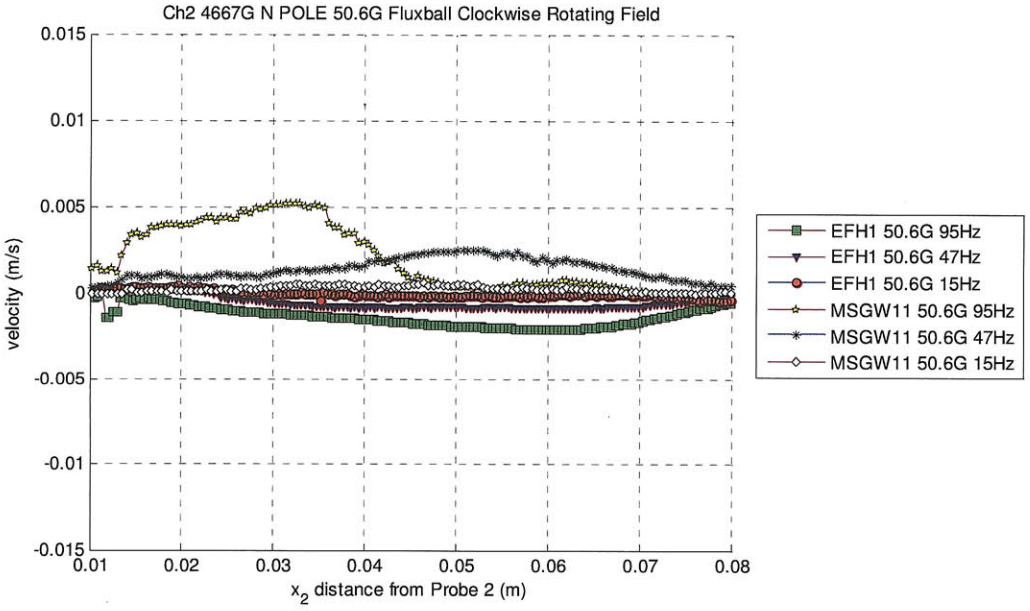
Ch2 4667G N POLE 50.6G Fluxball Clockwise Rotating Field
velocity (m/s)
0.015
0.01
0.005
0
-0.005
-0.01
-0.015
0.01
0.02
0.03
0.04
0.05
0.06
0.07
0.08
x2 distance from Probe 2 (m)
EFH1 50.6G 95Hz
EFH1 50.6G 47Hz
EFH1 50.6G 15Hz
MSGW11 50.6G 95Hz
MSGW11 50.6G 47Hz
MSGW11 50.6G 15Hz

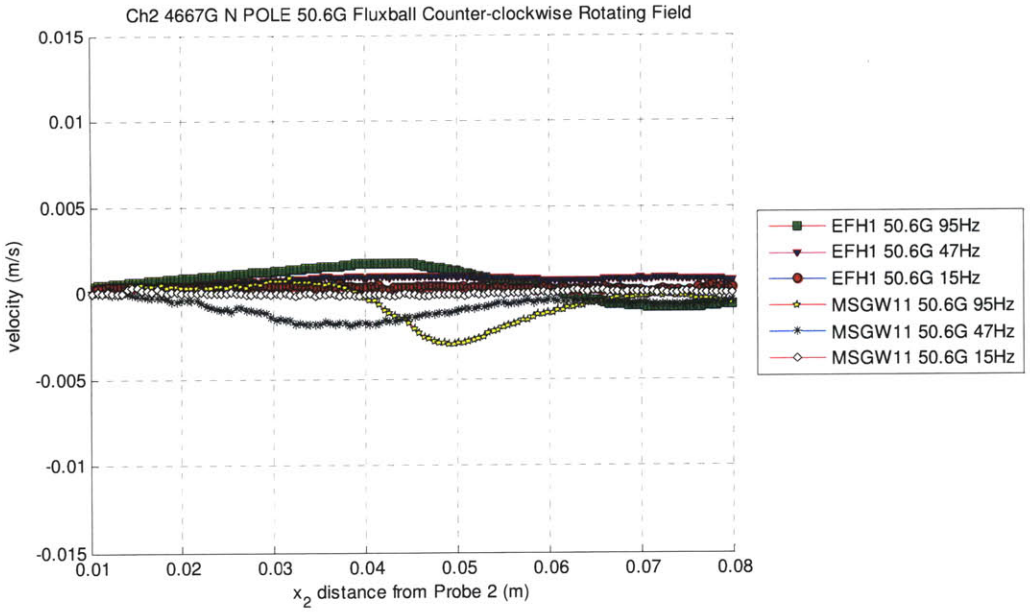
Ch2 4667G N POLE 50.6G Fluxball Counter-clockwise Rotating Field
velocity (m/s)
0.015
0.01
0.005
0
-0.005
-0.01
-0.015
0.01
0.02
0.03
0.04
0.05
0.06
0.07
0.08
x2 distance from Probe 2 (m)
EFH1 50.6G 95Hz
EFH1 50.6G 47Hz
EFH1 50.6G 15Hz
MSGW11 50.6G 95Hz
MSGW11 50.6G 47Hz
MSGW11 50.6G 15Hz

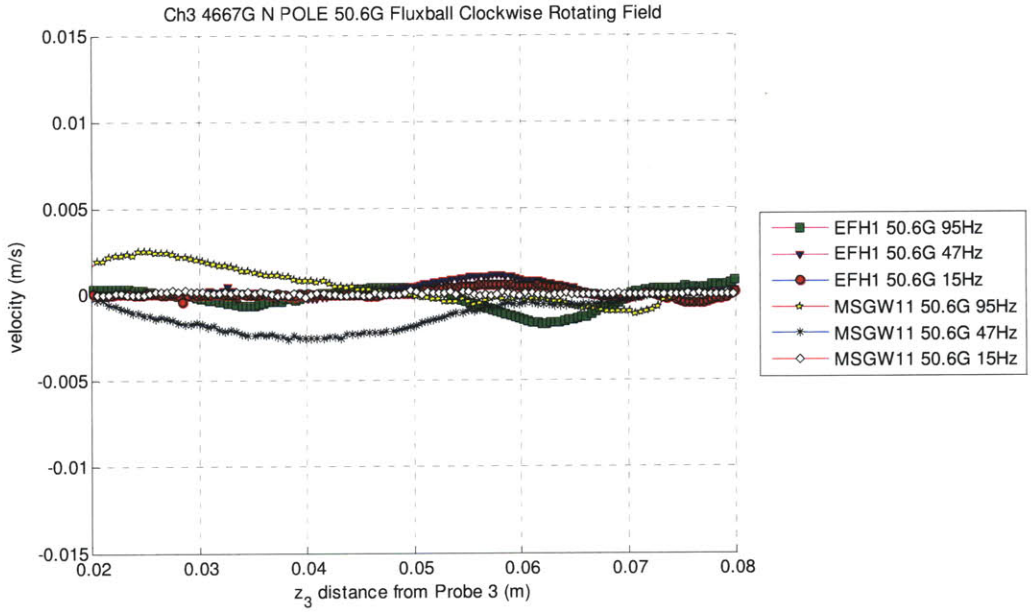
Ch3 4667G N POLE 50.6G Fluxball Clockwise Rotating Field
velocity (m/s)
0.015
0.01
0.005
0
-0.005
-0.01
-0.015
0.02
0.03
0.04
0.05
0.06
0.07
0.08
z3 distance from Probe 3 (m)
EFH1 50.6G 95Hz
EFH1 50.6G 47Hz
EFH1 50.6G 15Hz
MSGW11 50.6G 95Hz
MSGW11 50.6G 47Hz
MSGW11 50.6G 15Hz

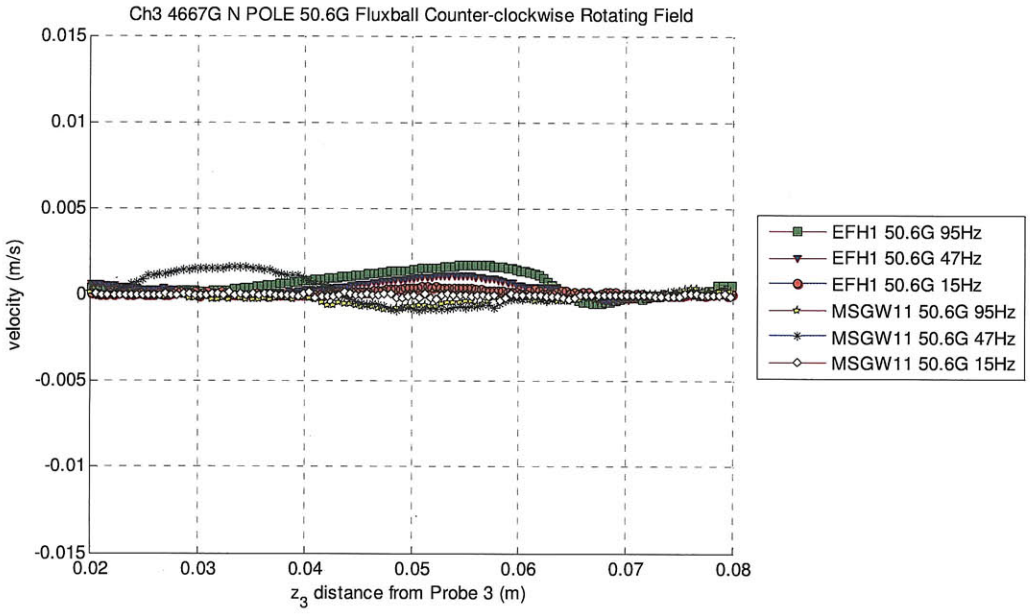
Ch3 4667G N POLE 50.6G Fluxball Counter-clockwise Rotating Field
velocity (m/s)
0.015
0.01
0.005
0
-0.005
-0.01
-0.015
0.02
0.03
0.04
0.05
0.06
0.07
0.08
z_3 distance from Probe 3 (m)
EFH1 50.6G 95Hz
EFH1 50.6G 47Hz
EFH1 50.6G 15Hz
MSGW11 50.6G 95Hz
MSGW11 50.6G 47Hz
MSGW11 50.6G 15Hz

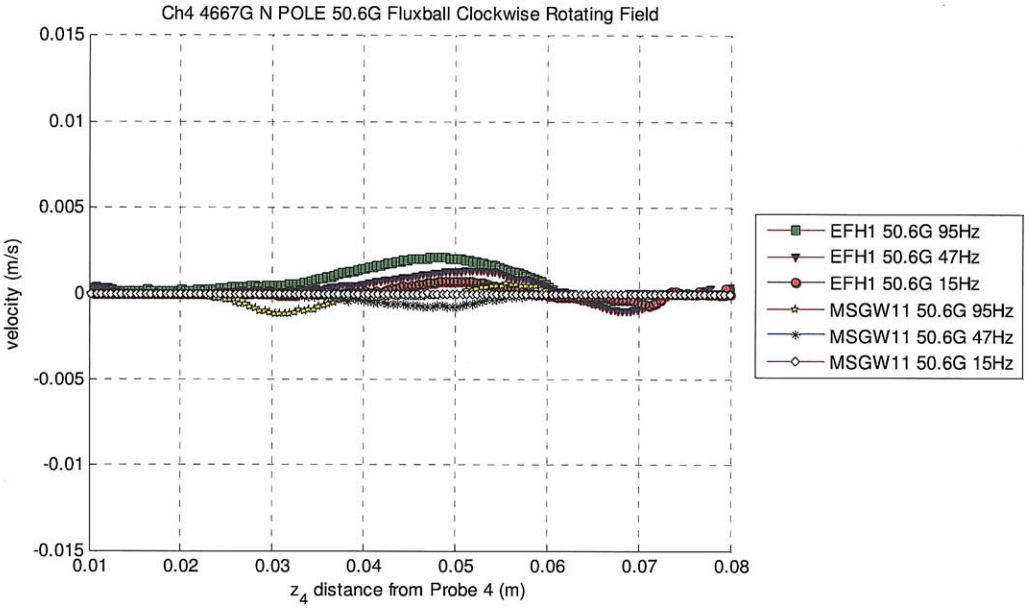
Ch4 4667G N POLE 50.6G Fluxball Clockwise Rotating Field
velocity (m/s)
0.015
0.01
0.005
0
-0.005
-0.01
-0.015
0.01
0.02
0.03
0.04
0.05
0.06
0.07
0.08
z_4 distance from Probe 4 (m)
EFH1 50.6G 95Hz
EFH1 50.6G 47Hz
EFH1 50.6G 15Hz
MSGW11 50.6G 95Hz
MSGW11 50.6G 47Hz
MSGW11 50.6G 15Hz

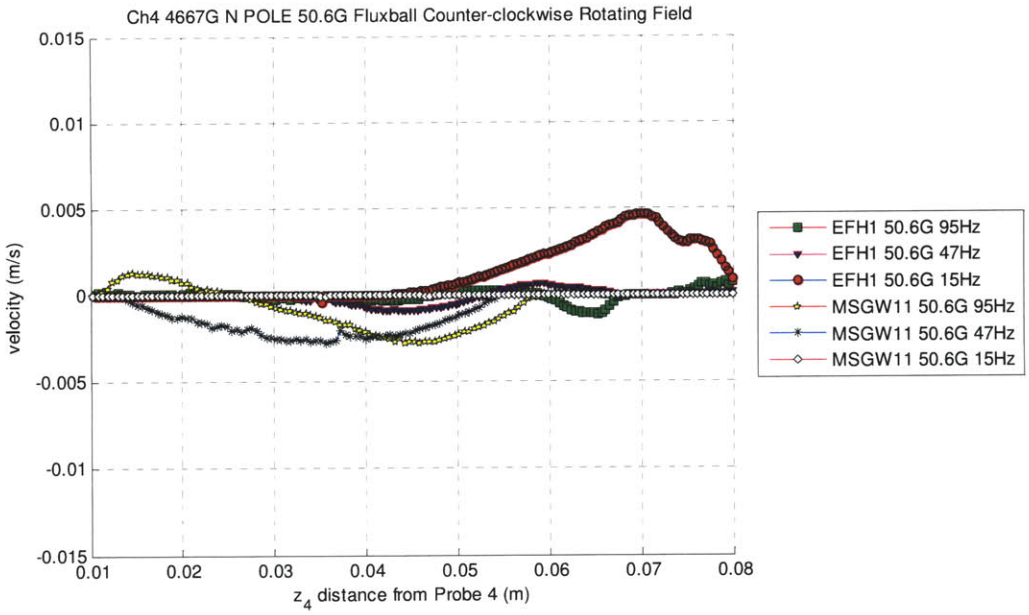
Ch4 4667G N POLE 50.6G Fluxball Counter-clockwise Rotating Field
velocity (m/s)
0.015
0.01
0.005
0
-0.005
-0.01
-0.015
0.01
0.02
0.03
0.04
0.05
0.06
0.07
0.08
z4 distance from Probe 4 (m)
EFH1 50.6G 95Hz
EFH1 50.6G 47Hz
EFH1 50.6G 15Hz
MSGW11 50.6G 95Hz
MSGW11 50.6G 47Hz
MSGW11 50.6G 15Hz

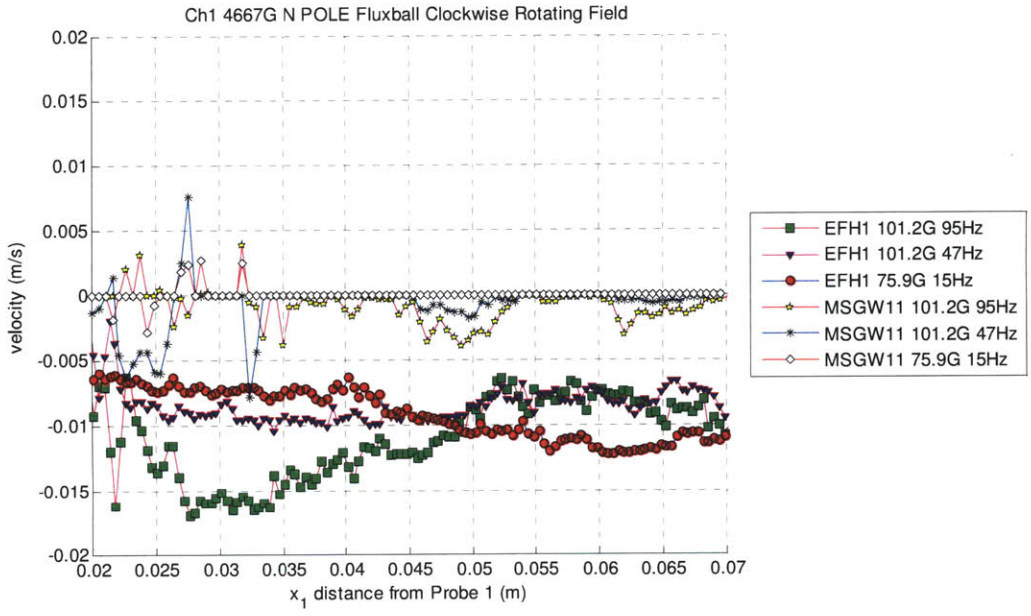
Ch1 4667G N POLE Fluxball Clockwise Rotating Field
velocity (m/s)
0.02
0.015
0.01
0.005
0
-0.005
-0.01
-0.015
-0.02
0.02
0.025
0.03
0.035
0.04
0.045
0.05
0.055
0.06
0.065
0.07
x1 distance from Probe 1 (m)
EFH1 101.2G 95Hz
EFH1 101.2G 47Hz
EFH1 75.9G 15Hz
MSGW11 101.2G 95Hz
MSGW11 101.2G 47Hz
MSGW11 75.9G 15Hz

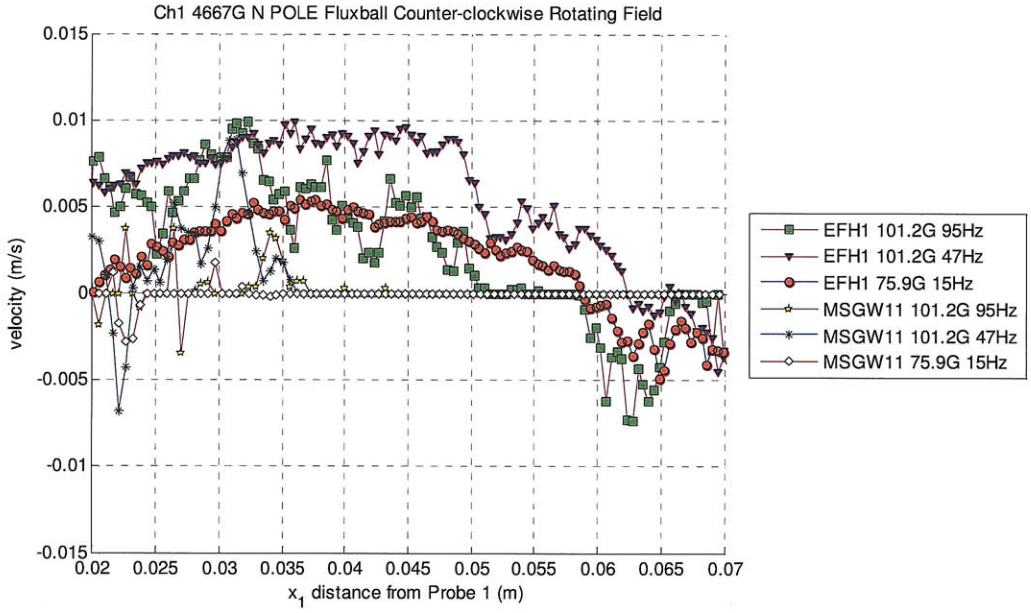
Ch1 4667G N POLE Fluxball Counter-clockwise Rotating Field
velocity (m/s)
0.015
0.01
0.005
0
-0.005
-0.01
-0.015
0.02
0.025
0.03
0.035
0.04
0.045
0.05
0.055
0.06
0.065
0.07
x1 distance from Probe 1 (m)
EFH1 101.2G 95Hz
EFH1 101.2G 47Hz
EFH1 75.9G 15Hz
MSGW11 101.2G 95Hz
MSGW11 101.2G 47Hz
MSGW11 75.9G 15Hz

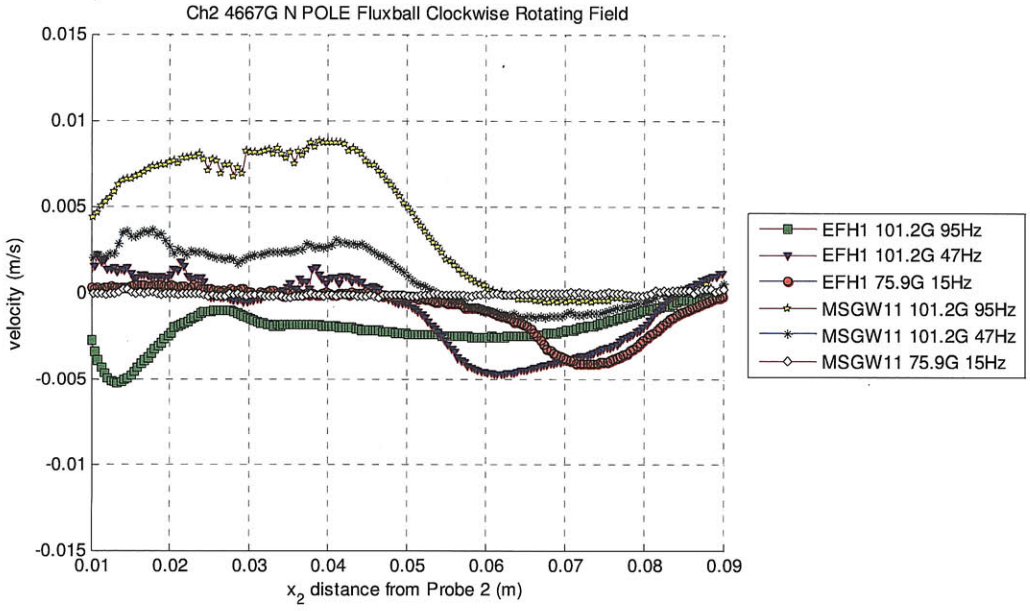
Ch2 4667G N POLE Fluxball Clockwise Rotating Field
velocity (m/s)
0.015
0.01
0.005
0
-0.005
-0.01
-0.015
0.01
0.02
0.03
0.04
0.05
0.06
0.07
0.08
0.09
x2 distance from Probe 2 (m)
EFH1 101.2G 95Hz
EFH1 101.2G 47Hz
EFH1 75.9G 15Hz
MSGW11 101.2G 95Hz
MSGW11 101.2G 47Hz
MSGW11 75.9G 15Hz

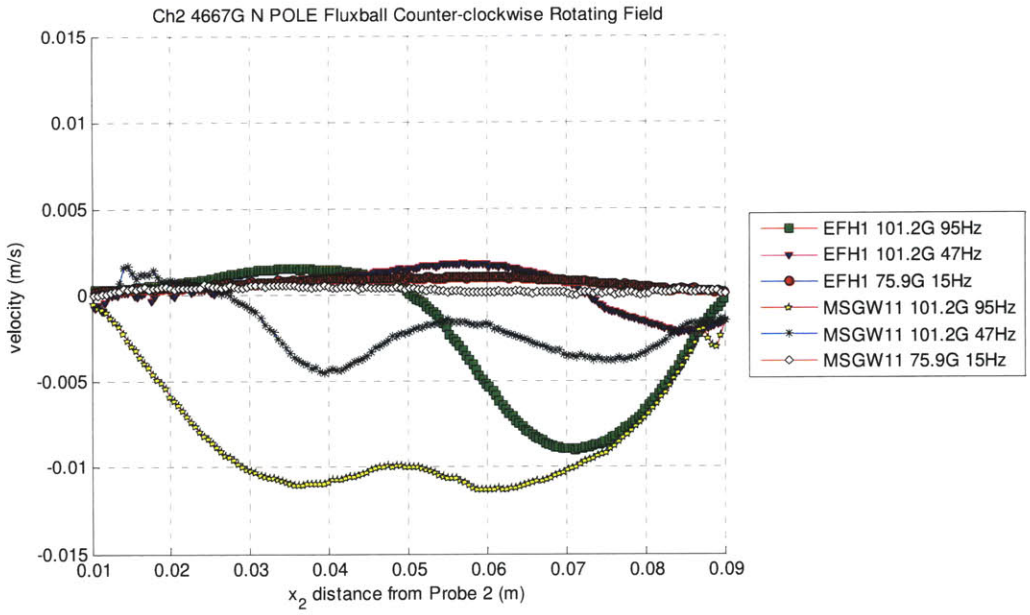
Ch2 4667G N POLE Fluxball Counter-clockwise Rotating Field
velocity (m/s)
0.015
0.01
0.005
0
-0.005
-0.01
-0.015
0.01
0.02
0.03
0.04
0.05
0.06
0.07
0.08
0.09
x2 distance from Probe 2 (m)
EFH1 101.2G 95Hz
EFH1 101.2G 47Hz
EFH1 75.9G 15Hz
MSGW11 101.2G 95Hz
MSGW11 101.2G 47Hz
MSGW11 75.9G 15Hz

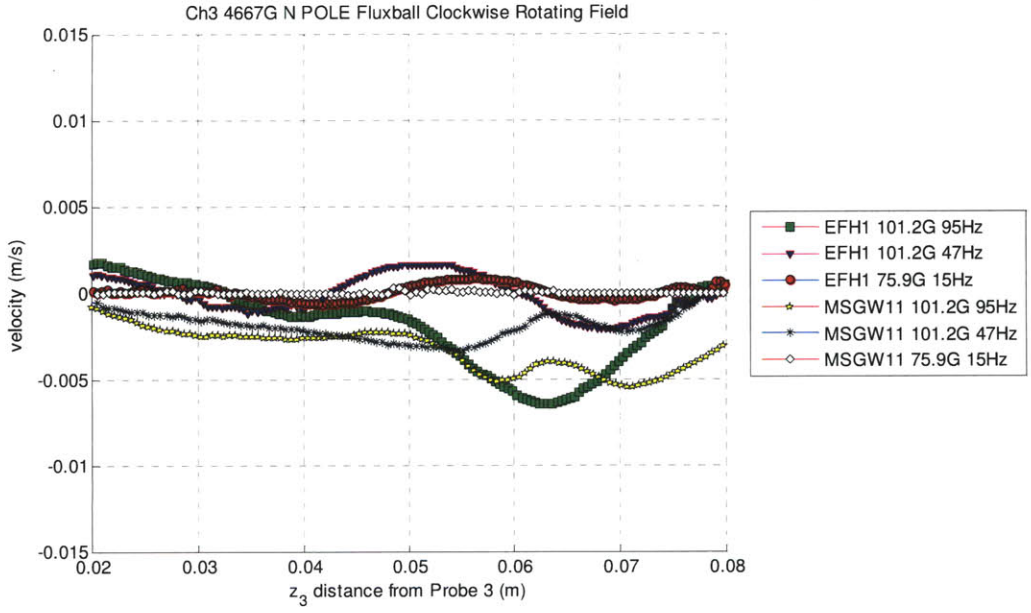
Ch3 4667G N POLE Fluxball Clockwise Rotating Field
velocity (m/s)
0.015
0.01
0.005
0
-0.005
-0.01
-0.015
0.02
0.03
0.04
0.05
0.06
0.07
0.08
z3 distance from Probe 3 (m)
EFH1 101.2G 95Hz
EFH1 101.2G 47Hz
EFH1 75.9G 15Hz
MSGW11 101.2G 95Hz
MSGW11 101.2G 47Hz
MSGW11 75.9G 15Hz

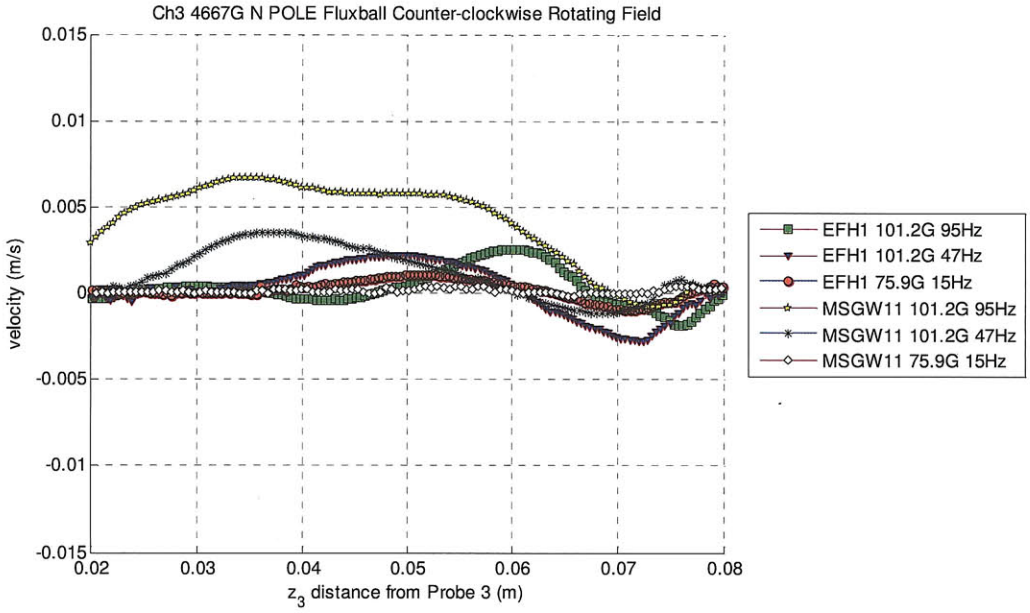
Ch3 4667G N POLE Fluxball Counter-clockwise Rotating Field
velocity (m/s)
0.015
0.01
0.005
0
-0.005
-0.01
-0.015
0.02
0.03
0.04
0.05
0.06
0.07
0.08
z3 distance from Probe 3 (m)
EFH1 101.2G 95Hz
EFH1 101.2G 47Hz
EFH1 75.9G 15Hz
MSGW11 101.2G 95Hz
MSGW11 101.2G 47Hz
MSGW11 75.9G 15Hz

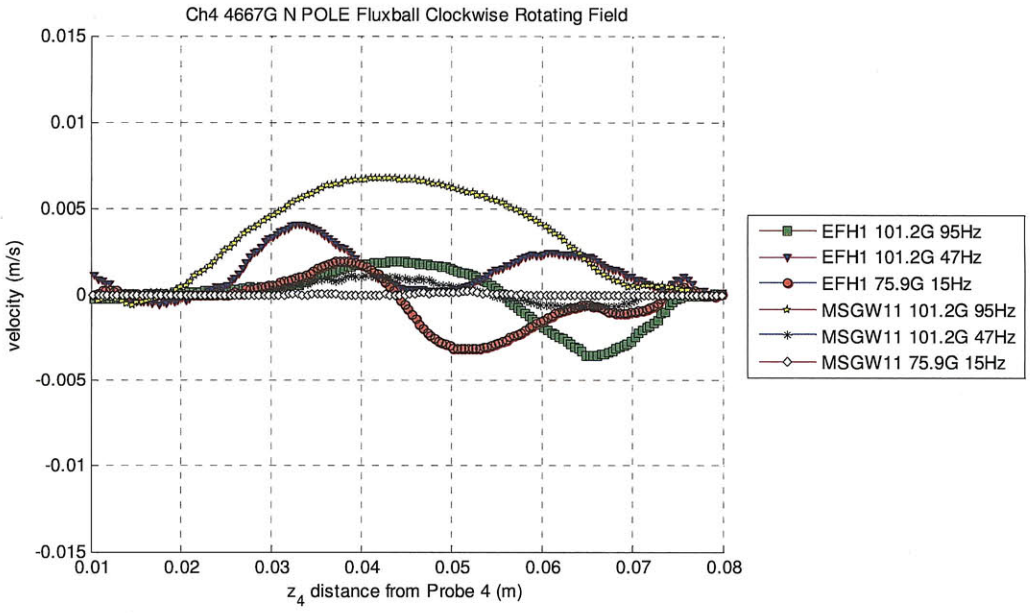
Ch4 4667G N POLE Fluxball Clockwise Rotating Field
velocity (m/s)
0.015
0.01
0.005
0
-0.005
-0.01
-0.015
0.01
0.02
0.03
0.04
0.05
0.06
0.07
0.08
z4 distance from Probe 4 (m)
EFH1 101.2G 95Hz
EFH1 101.2G 47Hz
EFH1 75.9G 15Hz
MSGW11 101.2G 95Hz
MSGW11 101.2G 47Hz
MSGW11 75.9G 15Hz

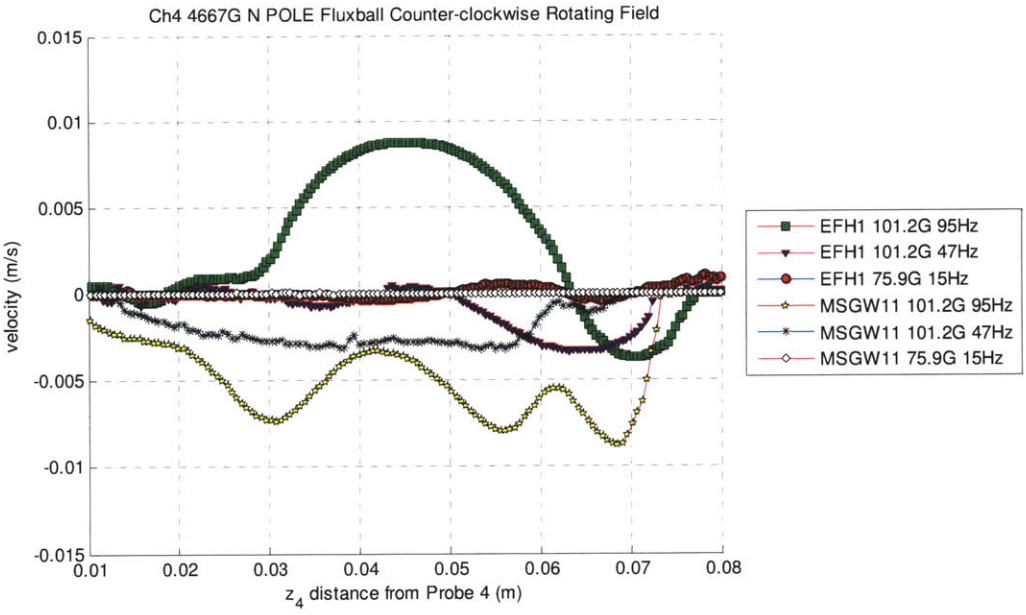
Ch4 4667G N POLE Fluxball Counter-clockwise Rotating Field
velocity (m/s)
0.015
0.01
0.005
0
-0.005
-0.01
-0.015
0.01
0.02
0.03
0.04
0.05
0.06
0.07
0.08
z4 distance from Probe 4 (m)
EFH1 101.2G 95Hz
EFH1 101.2G 47Hz
EFH1 75.9G 15Hz
MSGW11 101.2G 95Hz
MSGW11 101.2G 47Hz
MSGW11 75.9G 15Hz

H21. Comparison of Different Fluids with 5223G Magnet with South Pole Facing Ferrofluid Filled Sphere at Different Frequencies and Field Strengths

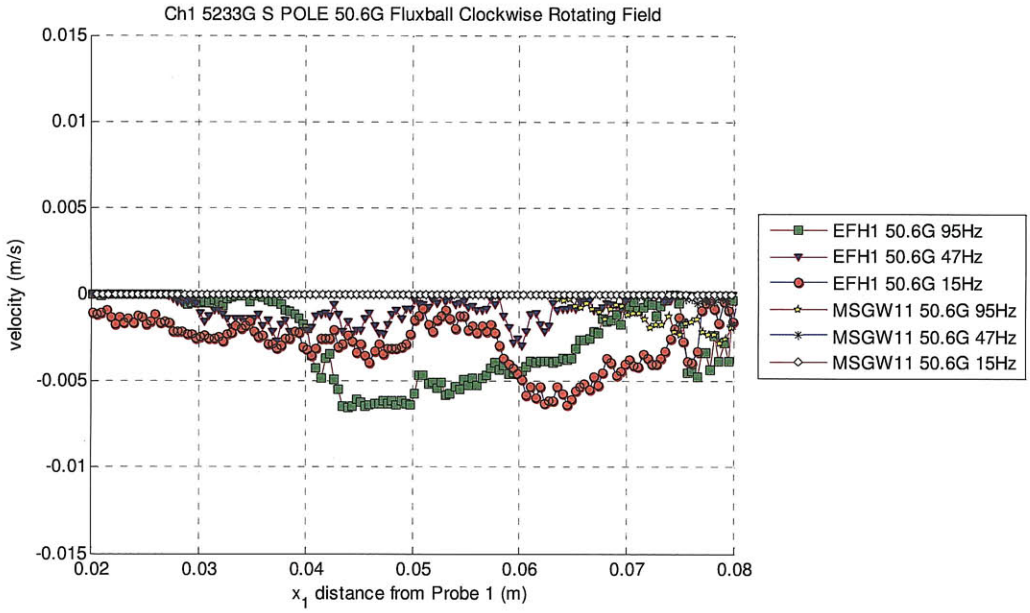

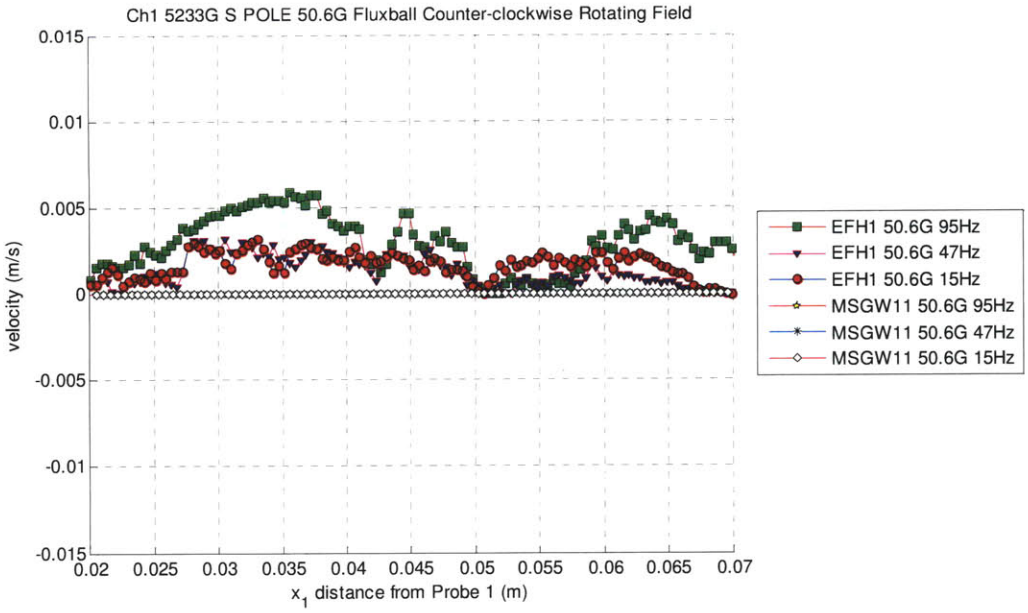
Ch1 5233G S POLE 50.6G Fluxball Counter-clockwise Rotating Field
velocity (m/s)
0.015
0.01
0.005
0
-0.005
-0.01
-0.015
0.02
0.025
0.03
0.035
0.04
0.045
0.05
0.055
0.06
0.065
0.07
x1 distance from Probe 1 (m)
EFH1 50.6G 95Hz
EFH1 50.6G 47Hz
EFH1 50.6G 15Hz
MSGW11 50.6G 95Hz
MSGW11 50.6G 47Hz
MSGW11 50.6G 15Hz

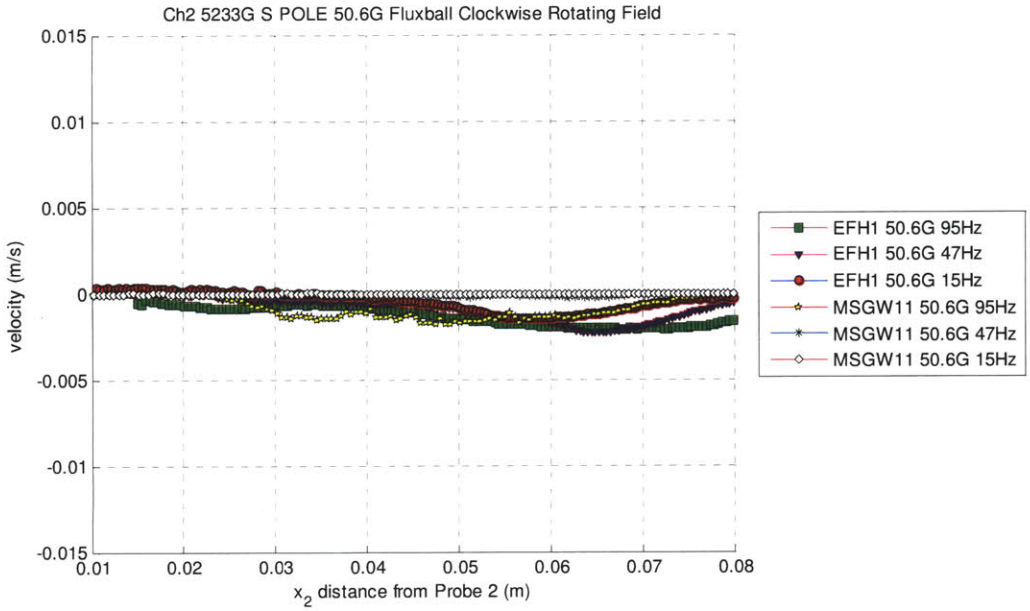
Ch2 5233G S POLE 50.6G Fluxball Clockwise Rotating Field
velocity (m/s)
0.015
0.01
0.005
0
-0.005
-0.01
-0.015
0.01
0.02
0.03
0.04
0.05
0.06
0.07
0.08
x2 distance from Probe 2 (m)
EFH1 50.6G 95Hz
EFH1 50.6G 47Hz
EFH1 50.6G 15Hz
MSGW11 50.6G 95Hz
MSGW11 50.6G 47Hz
MSGW11 50.6G 15Hz

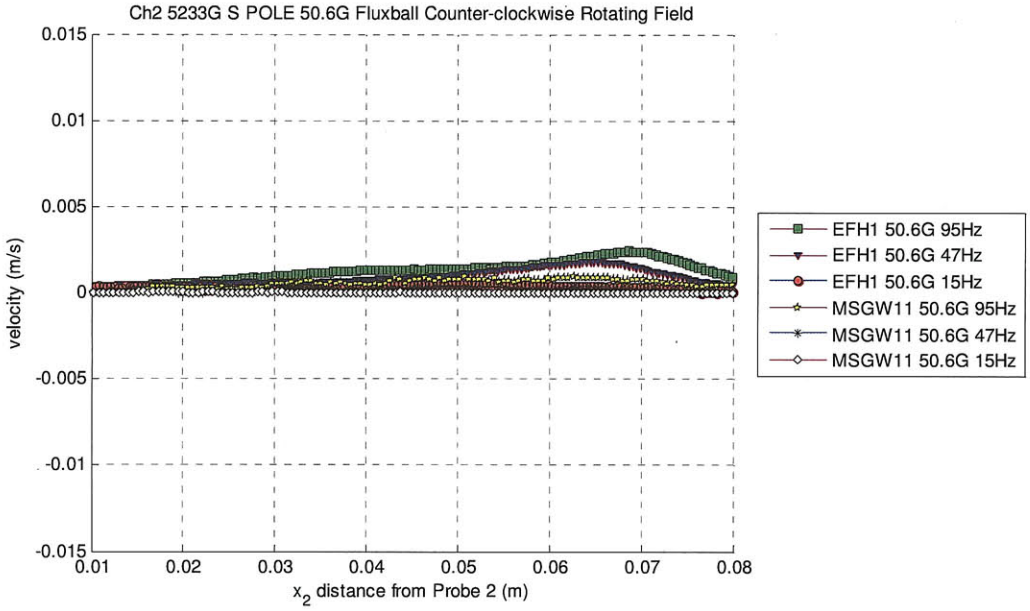
Ch2 5233G S POLE 50.6G Fluxball Counter-clockwise Rotating Field
velocity (m/s)
0.015
0.01
0.005
0
-0.005
-0.01
-0.015
0.01
0.02
0.03
0.04
0.05
0.06
0.07
0.08
x2 distance from Probe 2 (m)
EFH1 50.6G 95Hz
EFH1 50.6G 47Hz
EFH1 50.6G 15Hz
MSGW11 50.6G 95Hz
MSGW11 50.6G 47Hz
MSGW11 50.6G 15Hz

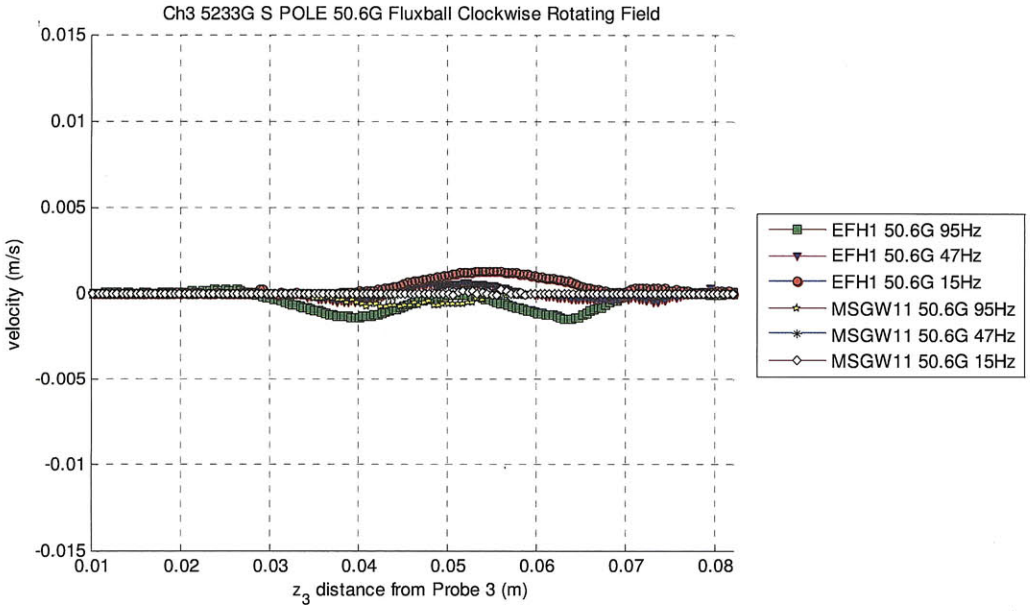
Ch3 5233G S POLE 50.6G Fluxball Clockwise Rotating Field
velocity (m/s)
0.015
0.01
0.005
0
-0.005
-0.01
-0.015
0.01
0.02
0.03
0.04
0.05
0.06
0.07
0.08
z3 distance from Probe 3 (m)
EFH1 50.6G 95Hz
EFH1 50.6G 47Hz
EFH1 50.6G 15Hz
MSGW11 50.6G 95Hz
MSGW11 50.6G 47Hz
MSGW11 50.6G 15Hz

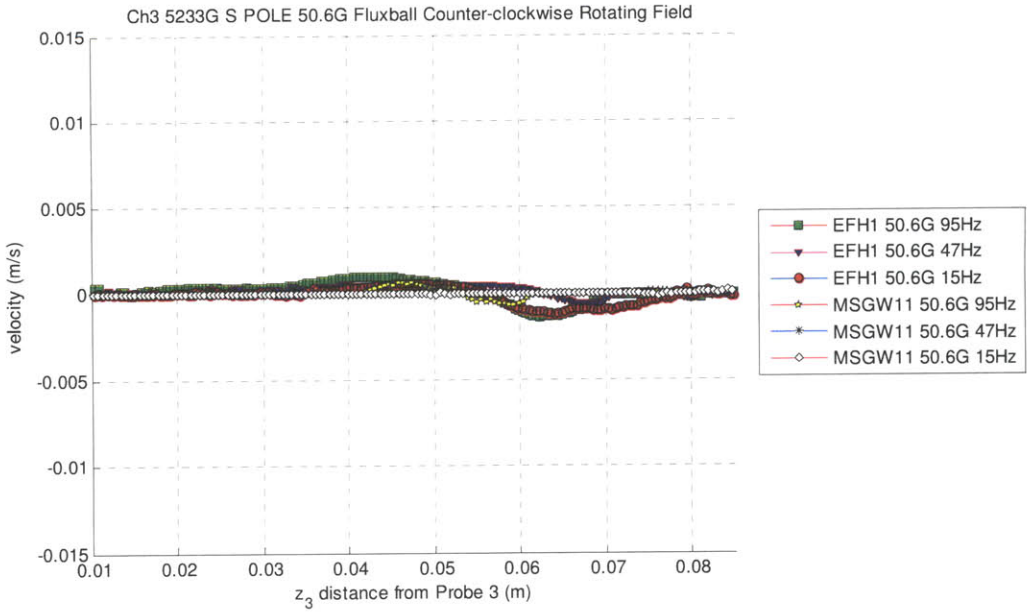
Ch3 5233G S POLE 50.6G Fluxball Counter-clockwise Rotating Field
velocity (m/s)
0.015
0.01
0.005
0
-0.005
-0.01
-0.015
0.01
0.02
0.03
0.04
0.05
0.06
0.07
0.08
z3 distance from Probe 3 (m)
EFH1 50.6G 95Hz
EFH1 50.6G 47Hz
EFH1 50.6G 15Hz
MSGW11 50.6G 95Hz
MSGW11 50.6G 47Hz
MSGW11 50.6G 15Hz

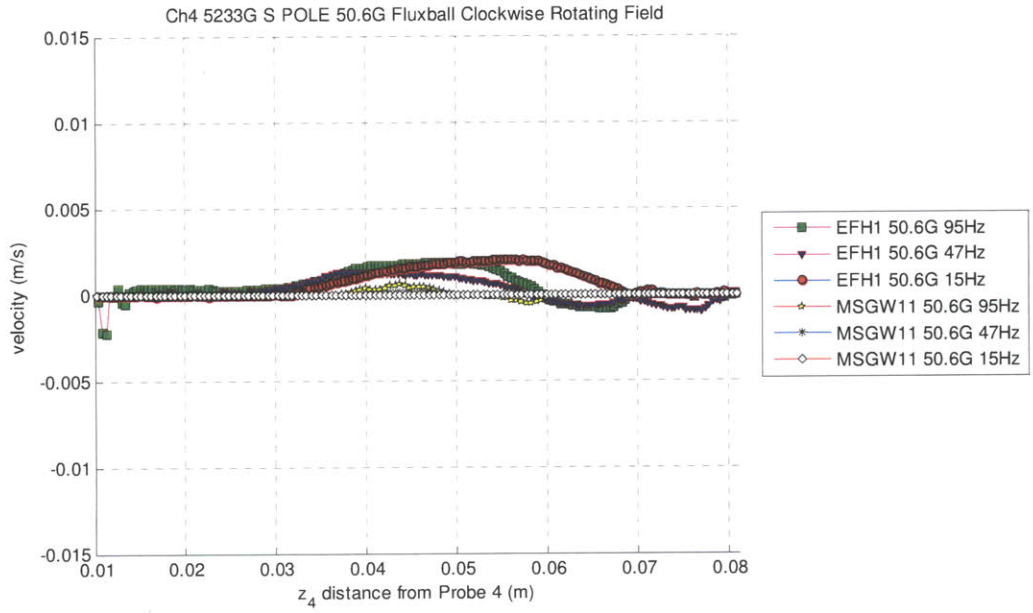
Ch4 5233G S POLE 50.6G Fluxball Clockwise Rotating Field
velocity (m/s)
0.015
0.01
0.005
0
-0.005
-0.01
-0.015
0.01
0.02
0.03
0.04
0.05
0.06
0.07
0.08
z4 distance from Probe 4 (m)
EFH1 50.6G 95Hz
EFH1 50.6G 47Hz
EFH1 50.6G 15Hz
MSGW11 50.6G 95Hz
MSGW11 50.6G 47Hz
MSGW11 50.6G 15Hz

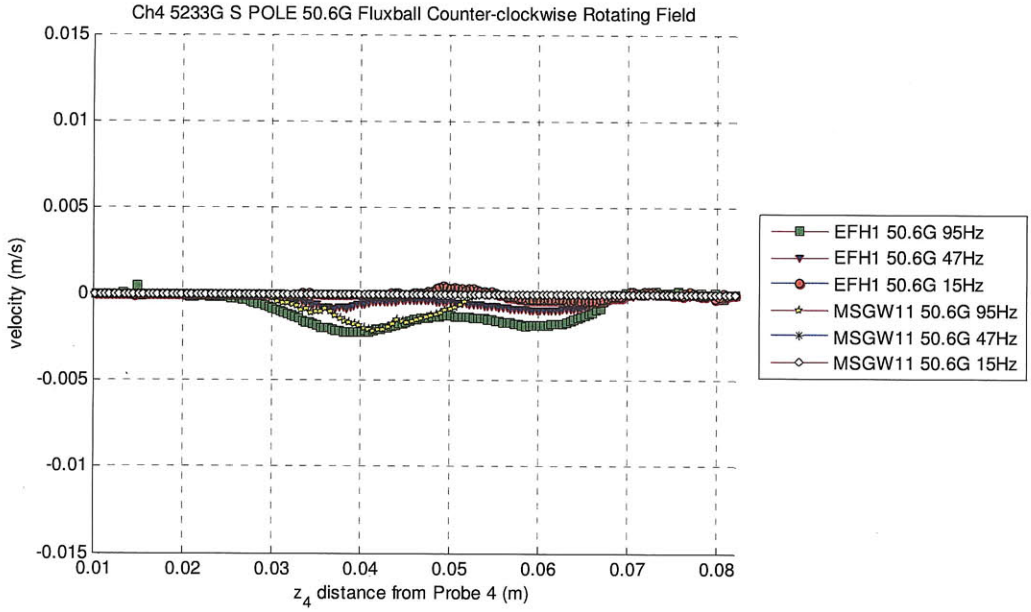
Ch4 5233G S POLE 50.6G Fluxball Counter-clockwise Rotating Field
velocity (m/s)
0.015
0.01
0.005
0
-0.005
-0.01
-0.015
0.01
0.02
0.03
0.04
0.05
0.06
0.07
0.08
z4 distance from Probe 4 (m)
EFH1 50.6G 95Hz
EFH1 50.6G 47Hz
EFH1 50.6G 15Hz
MSGW11 50.6G 95Hz
MSGW11 50.6G 47Hz
MSGW11 50.6G 15Hz

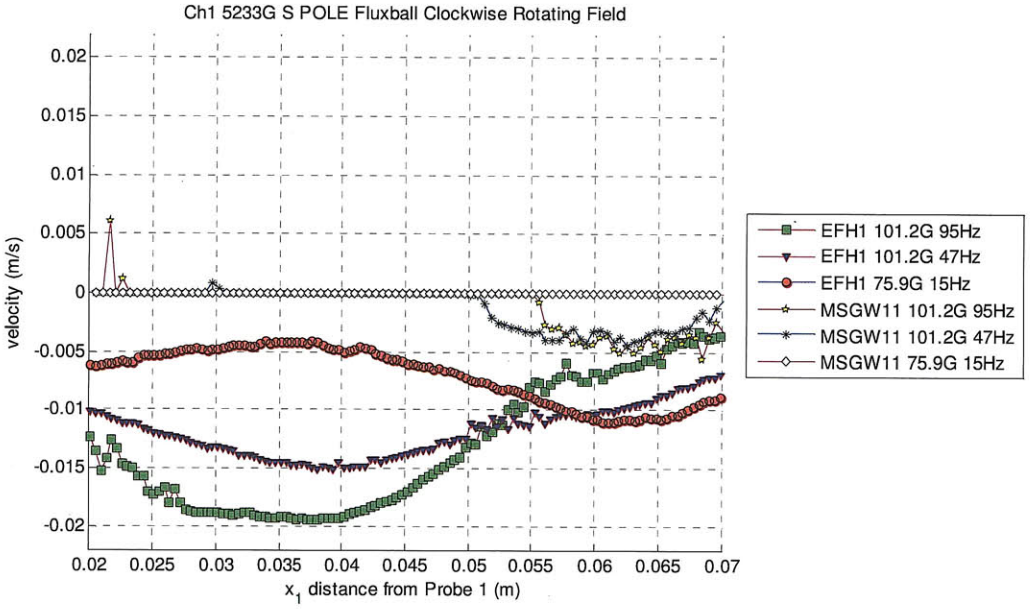
Ch1 5233G S POLE Fluxball Clockwise Rotating Field
velocity (m/s)
0.02
0.015
0.01
0.005
0
-0.005
-0.01
-0.015
-0.02
0.02
0.025
0.03
0.035
0.04
0.045
0.05
0.055
0.06
0.065
0.07
x1 distance from Probe 1 (m)
EFH1 101.2G 95Hz
EFH1 101.2G 47Hz
EFH1 75.9G 15Hz
MSGW11 101.2G 95Hz
MSGW11 101.2G 47Hz
MSGW11 75.9G 15Hz

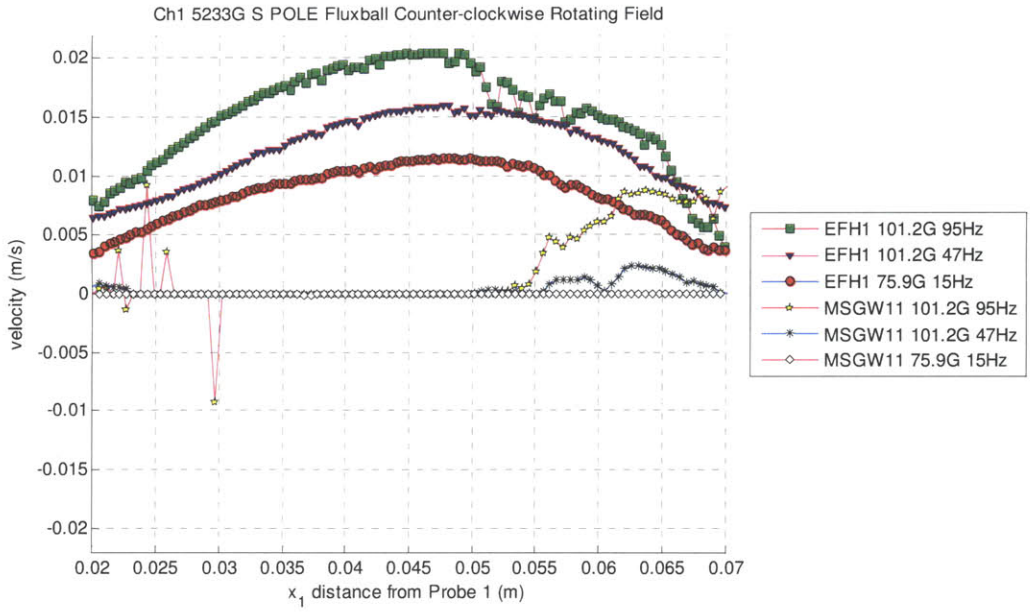
Ch1 5233G S POLE Fluxball Counter-clockwise Rotating Field
velocity (m/s)
0.02
0.015
0.01
0.005
0
-0.005
-0.01
-0.015
-0.02
0.02 0.025 0.03 0.035 0.04 0.045 0.05 0.055 0.06 0.065 0.07
x1 distance from Probe 1 (m)
EFH1 101.2G 95Hz
EFH1 101.2G 47Hz
EFH1 75.9G 15Hz
MSGW11 101.2G 95Hz
MSGW11 101.2G 47Hz
MSGW11 75.9G 15Hz

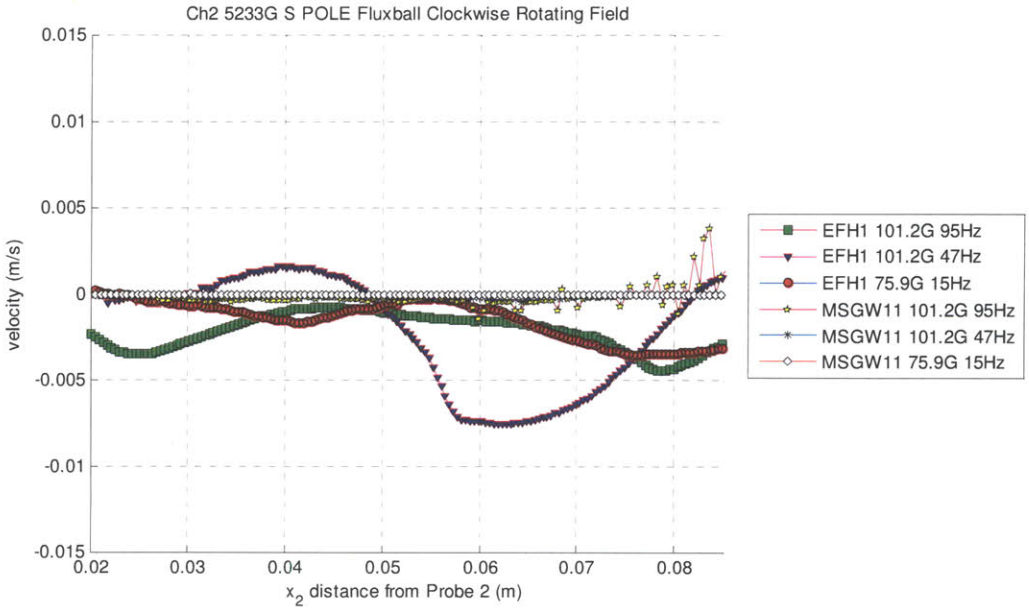
Ch2 5233G S POLE Fluxball Clockwise Rotating Field
velocity (m/s)
0.015
0.01
0.005
0
-0.005
-0.01
-0.015
0.02 0.03 0.04 0.05 0.06 0.07 0.08
x2 distance from Probe 2 (m)
EFH1 101.2G 95Hz
EFH1 101.2G 47Hz
EFH1 75.9G 15Hz
MSGW11 101.2G 95Hz
MSGW11 101.2G 47Hz
MSGW11 75.9G 15Hz

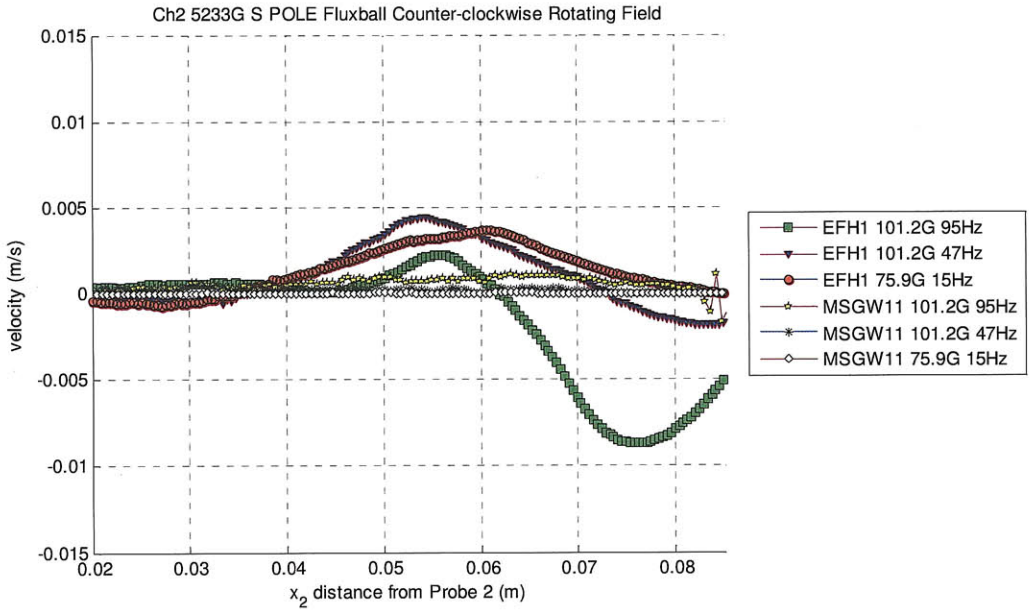
Ch2 5233G S POLE Fluxball Counter-clockwise Rotating Field
velocity (m/s)
0.015
0.01
0.005
0
-0.005
-0.01
-0.015
0.02
0.03
0.04
0.05
0.06
0.07
0.08
x2 distance from Probe 2 (m)
EFH1 101.2G 95Hz
EFH1 101.2G 47Hz
EFH1 75.9G 15Hz
MSGW11 101.2G 95Hz
MSGW11 101.2G 47Hz
MSGW11 75.9G 15Hz

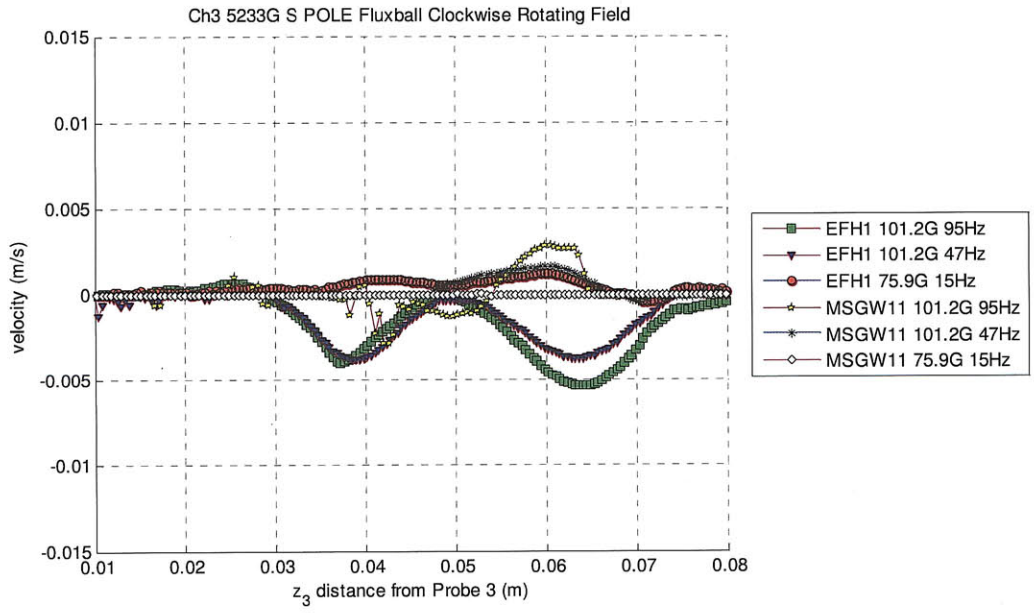
Ch3 5233G S POLE Fluxball Clockwise Rotating Field
velocity (m/s)
0.015
0.01
0.005
0
-0.005
-0.01
-0.015
0.01
0.02
0.03
0.04
0.05
0.06
0.07
0.08
z3 distance from Probe 3 (m)
EFH1 101.2G 95Hz
EFH1 101.2G 47Hz
EFH1 75.9G 15Hz
MSGW11 101.2G 95Hz
MSGW11 101.2G 47Hz
MSGW11 75.9G 15Hz

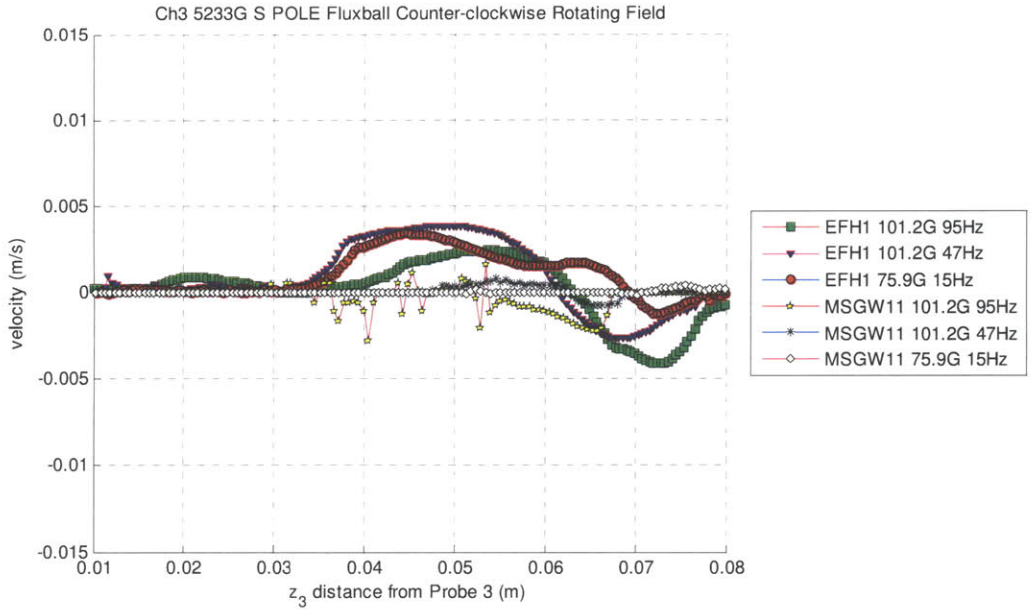
Ch3 5233G S POLE Fluxball Counter-clockwise Rotating Field
velocity (m/s)
0.015
0.01
0.005
0
-0.005
-0.01
-0.015
0.01
0.02
0.03
0.04
0.05
0.06
0.07
0.08
z3 distance from Probe 3 (m)
EFH1 101.2G 95Hz
EFH1 101.2G 47Hz
EFH1 75.9G 15Hz
MSGW11 101.2G 95Hz
MSGW11 101.2G 47Hz
MSGW11 75.9G 15Hz

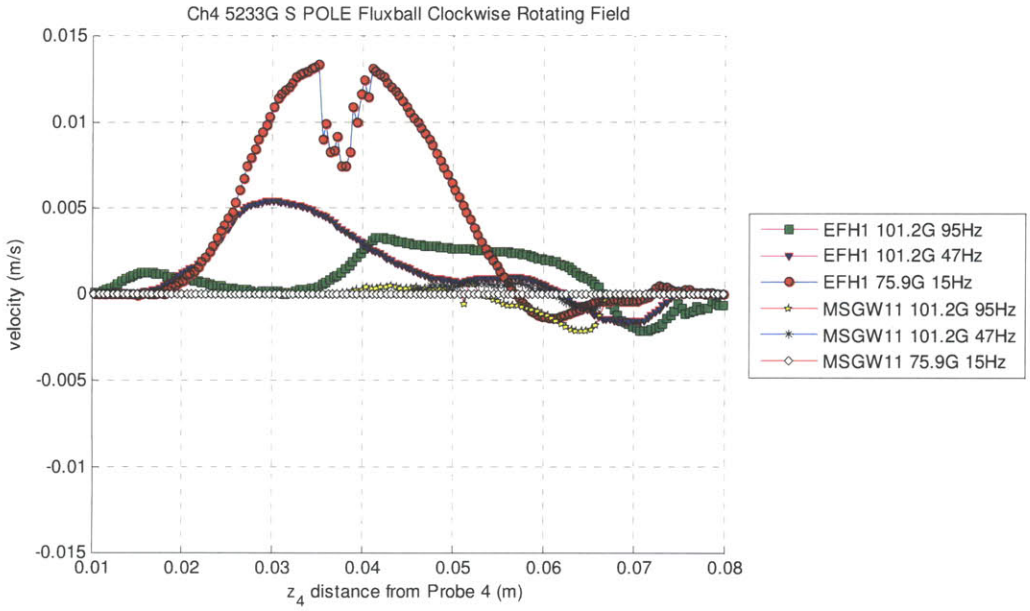
Ch4 5233G S POLE Fluxball Clockwise Rotating Field
velocity (m/s)
0.015
0.01
0.005
0
-0.005
-0.01
-0.015
0.01
0.02
0.03
0.04
0.05
0.06
0.07
0.08
z4 distance from Probe 4 (m)
EFH1 101.2G 95Hz
EFH1 101.2G 47Hz
EFH1 75.9G 15Hz
MSGW11 101.2G 95Hz
MSGW11 101.2G 47Hz
MSGW11 75.9G 15Hz

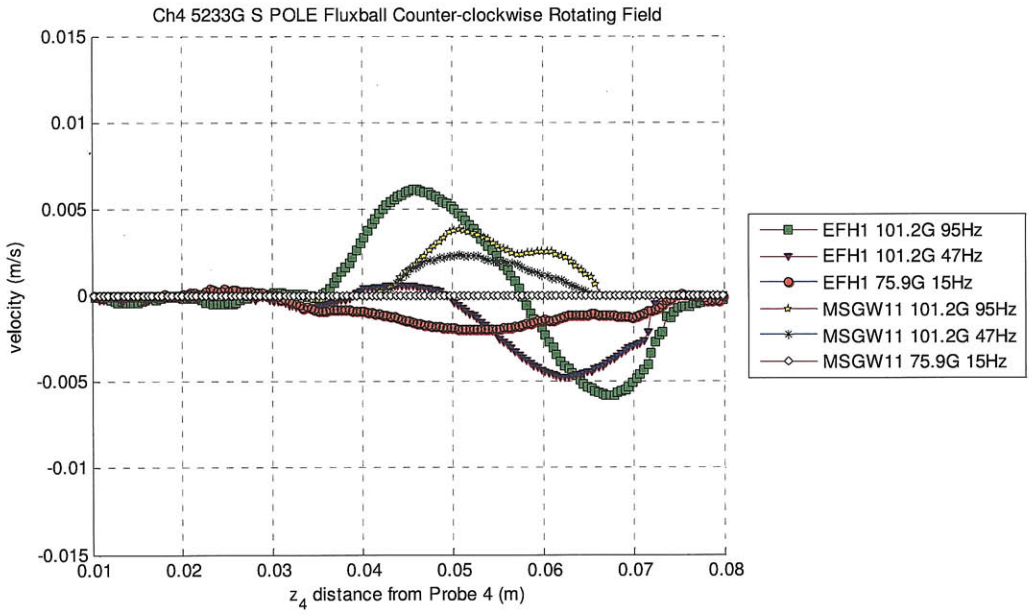
Ch4 5233G S POLE Fluxball Counter-clockwise Rotating Field
0.015
0.01
0.005
0
-0.005
-0.01
-0.015
velocity (m/s)
0.01
0.02
0.03
0.04
0.05
0.06
0.07
0.08
z4 distance from Probe 4 (m)
EFH1 101.2G 95Hz
EFH1 101.2G 47Hz
EFH1 75.9G 15Hz
MSGW11 101.2G 95Hz
MSGW11 101.2G 47Hz
MSGW11 75.9G 15Hz

H22. Comparison of Different Fluids with 5223G Magnet with North Pole Facing Ferrofluid Filled Sphere at Different Frequencies and Field Strengths

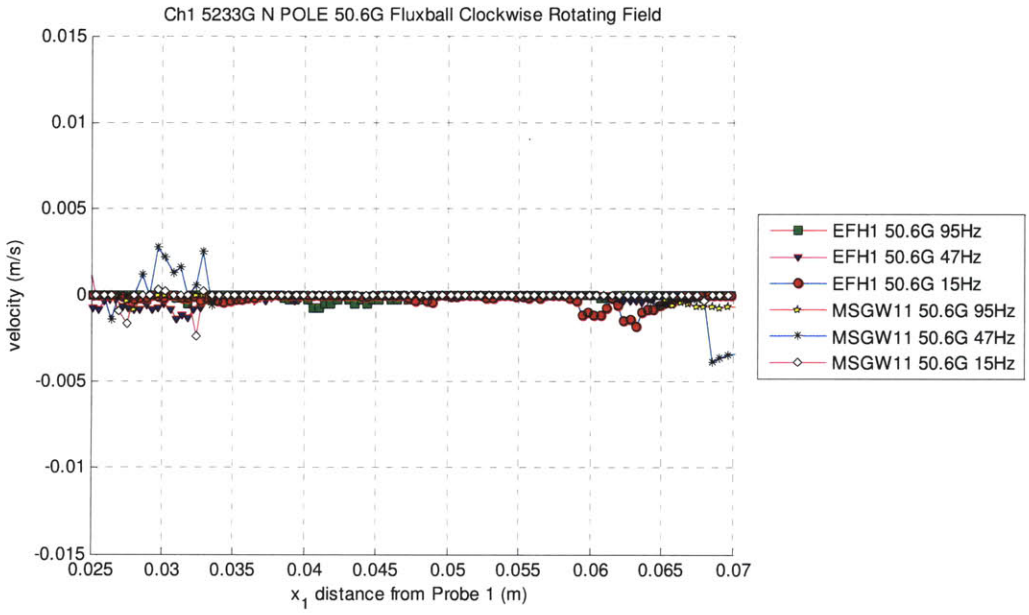

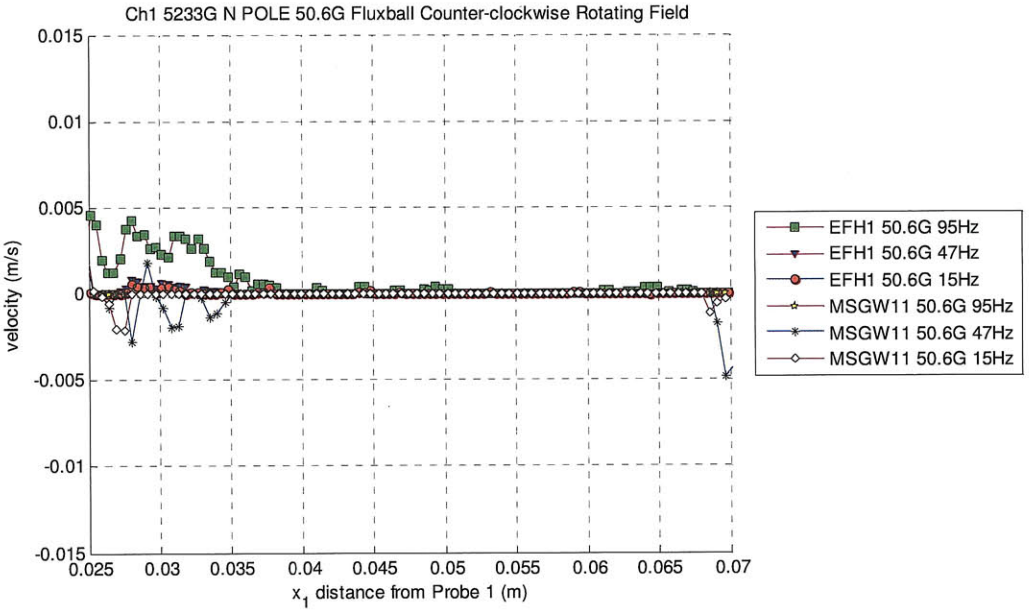
Ch1 5233G N POLE 50.6G Fluxball Counter-clockwise Rotating Field
velocity (m/s)
0.015
0.01
0.005
0
-0.005
-0.01
-0.015
0.025
0.03
0.035
0.04
0.045
0.05
0.055
0.06
0.065
0.07
x1 distance from Probe 1 (m)
EFH1 50.6G 95Hz
EFH1 50.6G 47Hz
EFH1 50.6G 15Hz
MSGW11 50.6G 95Hz
MSGW11 50.6G 47Hz
MSGW11 50.6G 15Hz

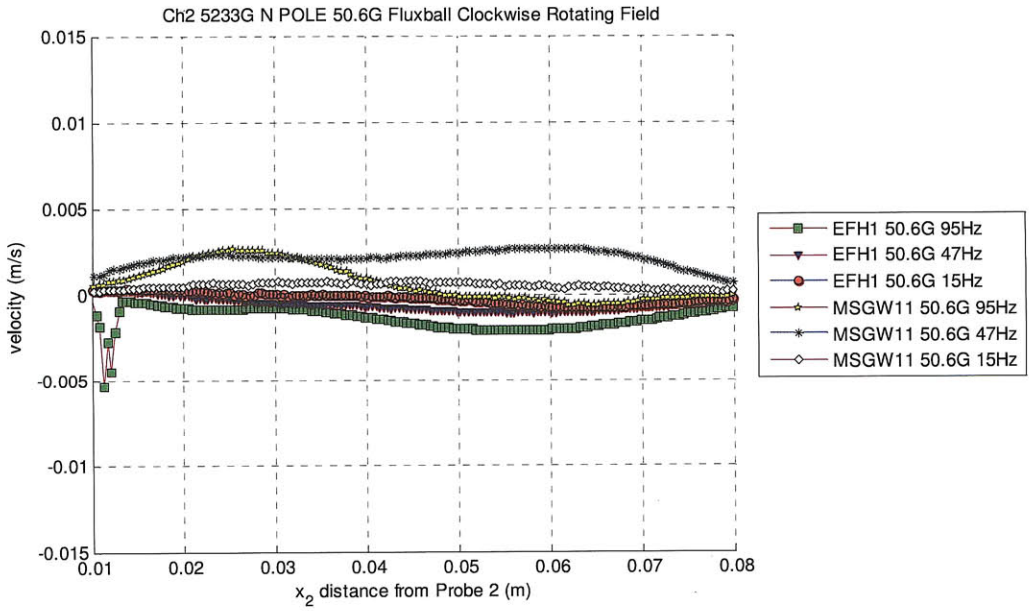
Ch2 5233G N POLE 50.6G Fluxball Clockwise Rotating Field
velocity (m/s)
0.015
0.01
0.005
0
-0.005
-0.01
-0.015
0.01
0.02
0.03
0.04
0.05
0.06
0.07
0.08
x2 distance from Probe 2 (m)
EFH1 50.6G 95Hz
EFH1 50.6G 47Hz
EFH1 50.6G 15Hz
MSGW11 50.6G 95Hz
MSGW11 50.6G 47Hz
MSGW11 50.6G 15Hz

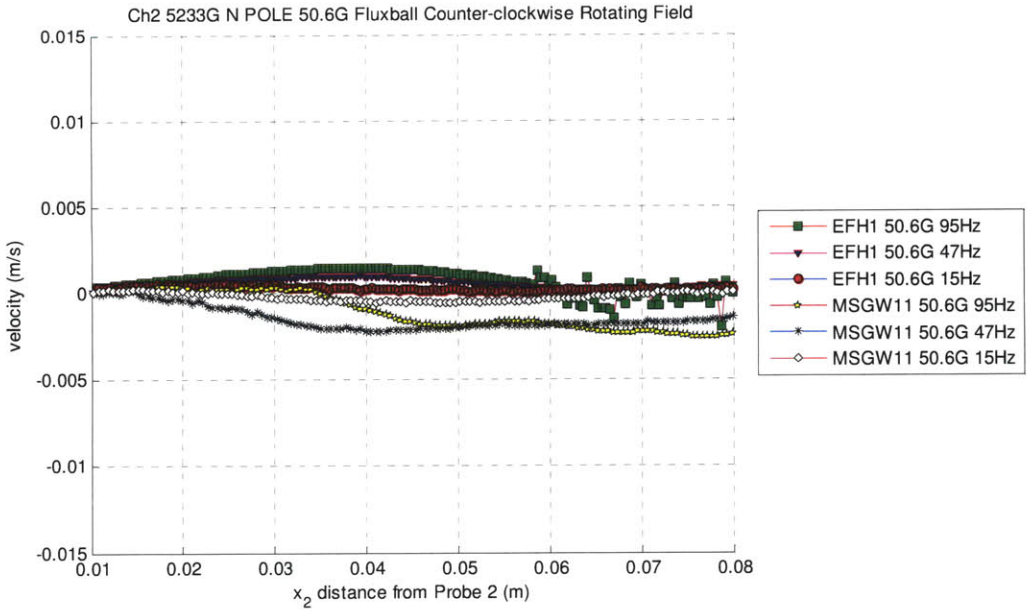
Ch2 5233G N POLE 50.6G Fluxball Counter-clockwise Rotating Field
velocity (m/s)
0.015
0.01
0.005
0
-0.005
-0.01
-0.015
0.01
0.02
0.03
0.04
0.05
0.06
0.07
0.08
x2 distance from Probe 2 (m)
EFH1 50.6G 95Hz
EFH1 50.6G 47Hz
EFH1 50.6G 15Hz
MSGW11 50.6G 95Hz
MSGW11 50.6G 47Hz
MSGW11 50.6G 15Hz

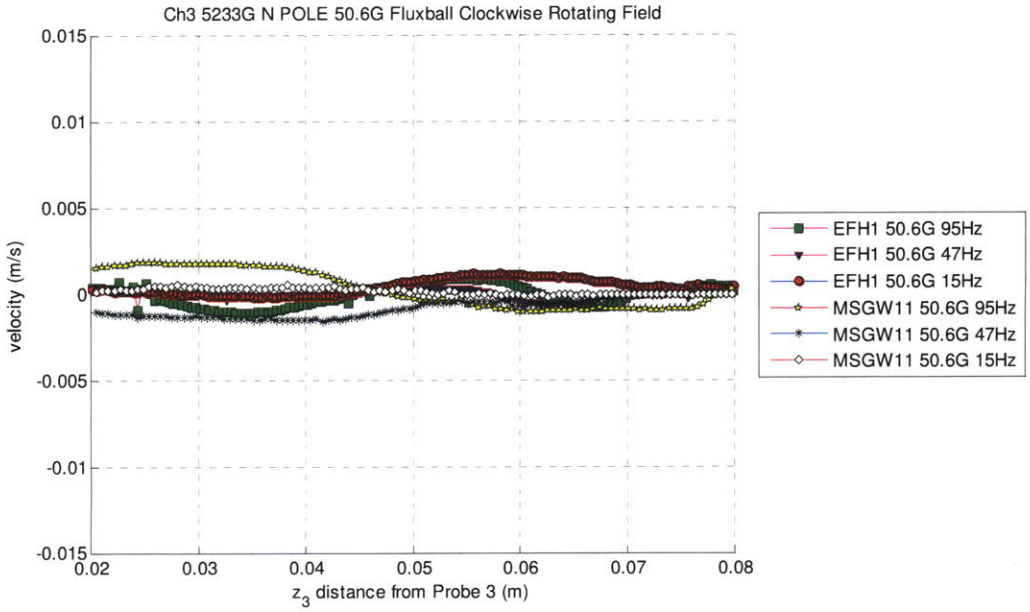
Ch3 5233G N POLE 50.6G Fluxball Clockwise Rotating Field
velocity (m/s)
0.015
0.01
0.005
0
-0.005
-0.01
-0.015
0.02
0.03
0.04
0.05
0.06
0.07
0.08
z3 distance from Probe 3 (m)
EFH1 50.6G 95Hz
EFH1 50.6G 47Hz
EFH1 50.6G 15Hz
MSGW11 50.6G 95Hz
MSGW11 50.6G 47Hz
MSGW11 50.6G 15Hz

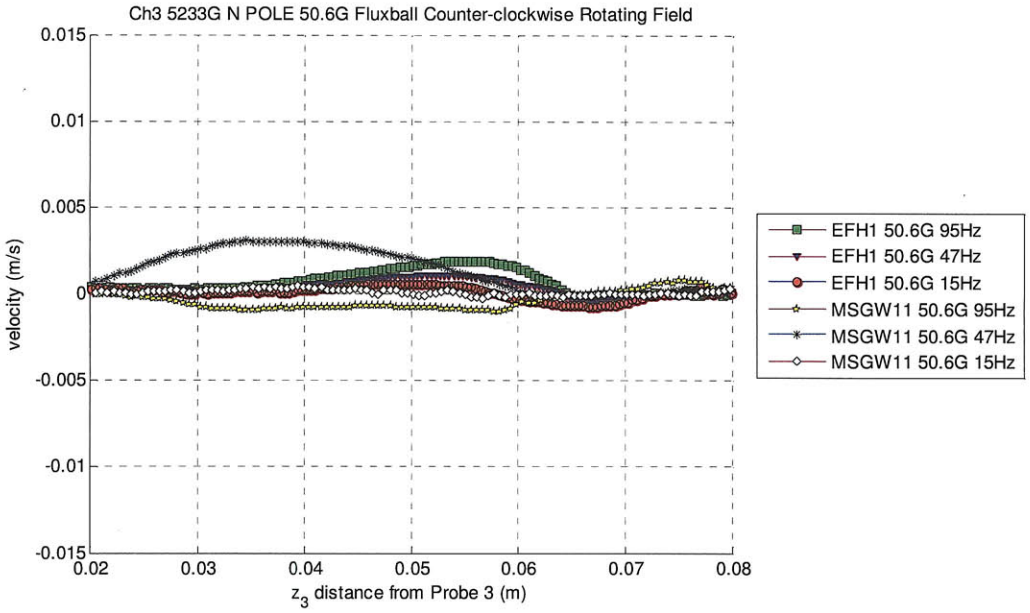
Ch3 5233G N POLE 50.6G Fluxball Counter-clockwise Rotating Field
velocity (m/s)
0.015
0.01
0.005
0
-0.005
-0.01
-0.015
0.02
0.03
0.04
0.05
0.06
0.07
0.08
z_3 distance from Probe 3 (m)
EFH1 50.6G 95Hz
EFH1 50.6G 47Hz
EFH1 50.6G 15Hz
MSGW11 50.6G 95Hz
MSGW11 50.6G 47Hz
MSGW11 50.6G 15Hz

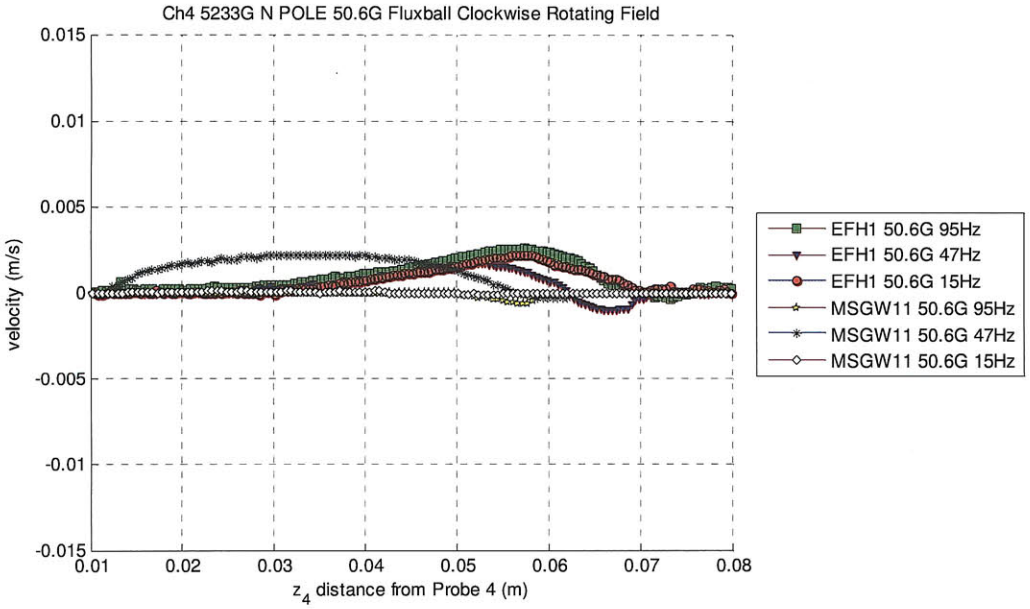
Ch4 5233G N POLE 50.6G Fluxball Clockwise Rotating Field
velocity (m/s)
0.015
0.01
0.005
0
-0.005
-0.01
-0.015
0.01
0.02
0.03
0.04
0.05
0.06
0.07
0.08
z_4 distance from Probe 4 (m)
EFH1 50.6G 95Hz
EFH1 50.6G 47Hz
EFH1 50.6G 15Hz
MSGW11 50.6G 95Hz
MSGW11 50.6G 47Hz
MSGW11 50.6G 15Hz

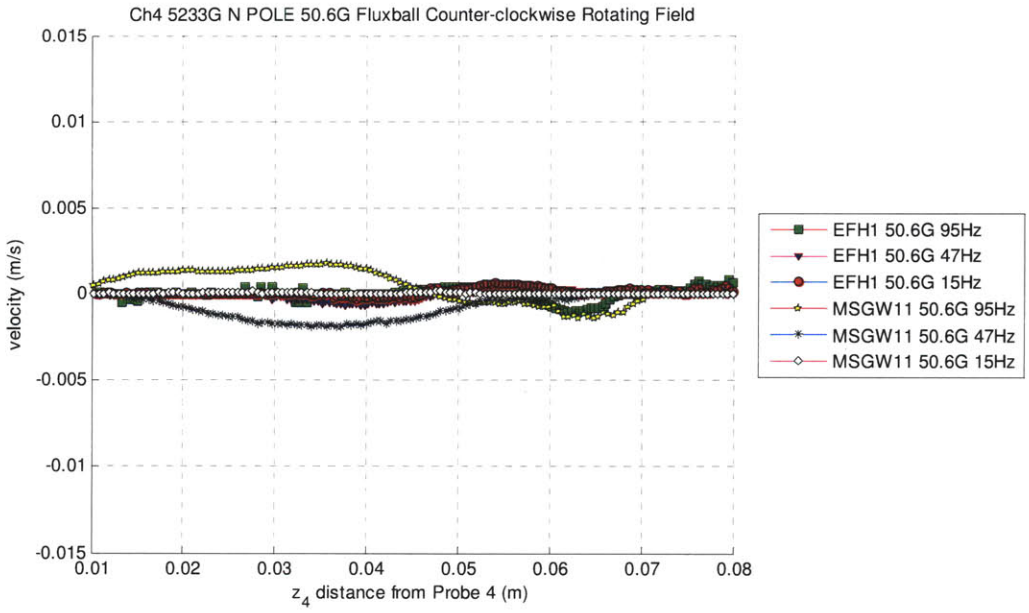
Ch4 5233G N POLE 50.6G Fluxball Counter-clockwise Rotating Field
velocity (m/s)
0.015
0.01
0.005
0
-0.005
-0.01
-0.015
0.01
0.02
0.03
0.04
0.05
0.06
0.07
0.08
z4 distance from Probe 4 (m)
EFH1 50.6G 95Hz
EFH1 50.6G 47Hz
EFH1 50.6G 15Hz
MSGW11 50.6G 95Hz
MSGW11 50.6G 47Hz
MSGW11 50.6G 15Hz

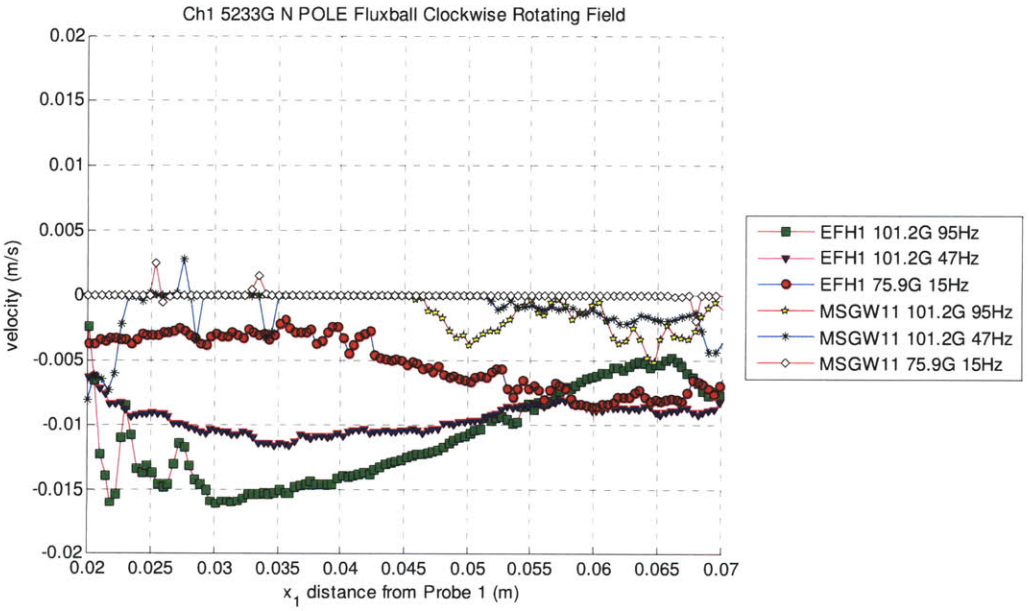
Ch1 5233G N POLE Fluxball Clockwise Rotating Field
velocity (m/s)
0.02
0.015
0.01
0.005
0
-0.005
-0.01
-0.015
-0.02
0.02
0.025
0.03
0.035
0.04
0.045
0.05
0.055
0.06
0.065
0.07
x1 distance from Probe 1 (m)
EFH1 101.2G 95Hz
EFH1 101.2G 47Hz
EFH1 75.9G 15Hz
MSGW11 101.2G 95Hz
MSGW11 101.2G 47Hz
MSGW11 75.9G 15Hz

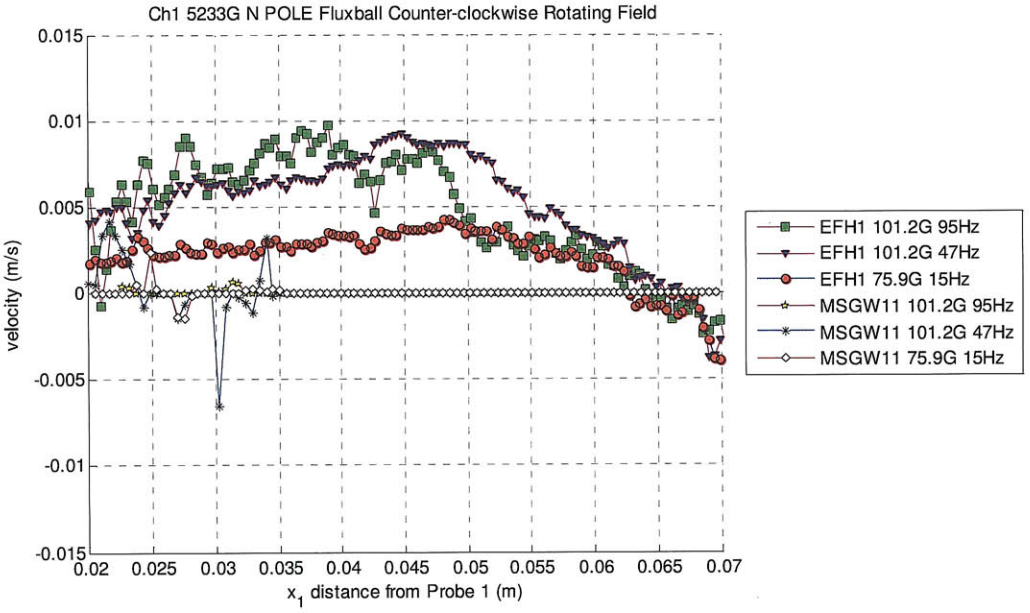
Ch1 5233G N POLE Fluxball Counter-clockwise Rotating Field
velocity (m/s)
0.015
0.01
0.005
0
-0.005
-0.01
-0.015
0.02
0.025
0.03
0.035
0.04
0.045
0.05
0.055
0.06
0.065
0.07
x1 distance from Probe 1 (m)
EFH1 101.2G 95Hz
EFH1 101.2G 47Hz
EFH1 75.9G 15Hz
MSGW11 101.2G 95Hz
MSGW11 101.2G 47Hz
MSGW11 75.9G 15Hz

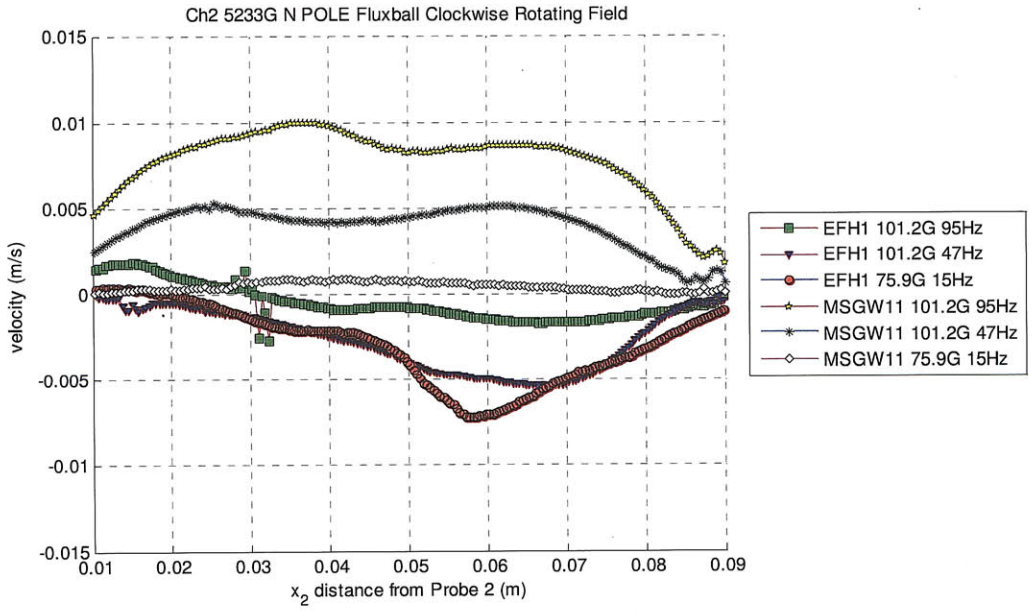
Ch2 5233G N POLE Fluxball Clockwise Rotating Field
velocity (m/s)
0.015
0.01
0.005
0
-0.005
-0.01
-0.015
0.01
0.02
0.03
0.04
0.05
0.06
0.07
0.08
0.09
x2 distance from Probe 2 (m)
EFH1 101.2G 95Hz
EFH1 101.2G 47Hz
EFH1 75.9G 15Hz
MSGW11 101.2G 95Hz
MSGW11 101.2G 47Hz
MSGW11 75.9G 15Hz

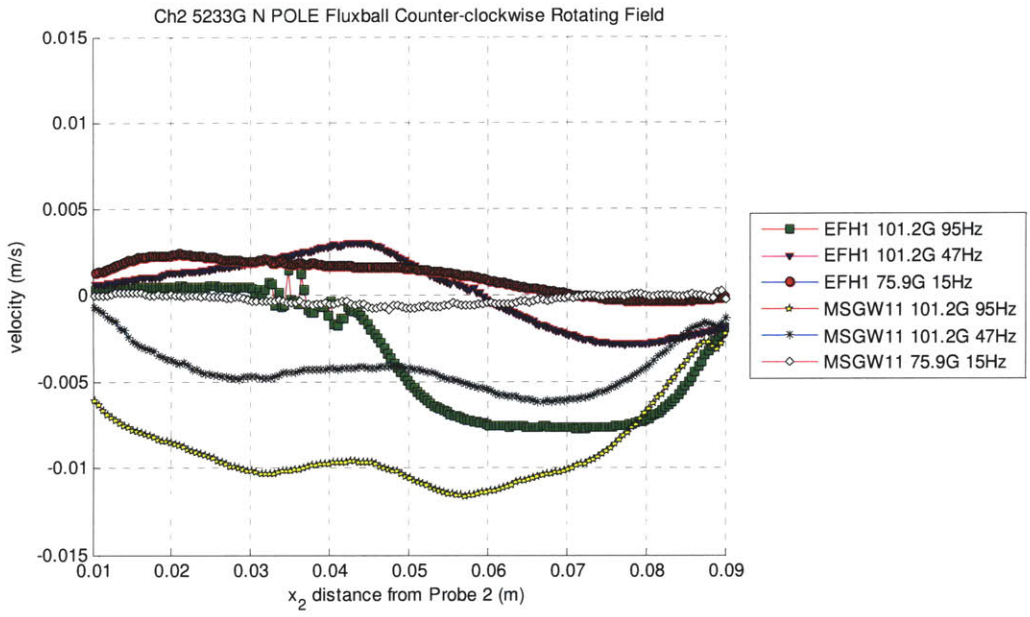
Ch2 5233G N POLE Fluxball Counter-clockwise Rotating Field
velocity (m/s)
0.015
0.01
0.005
0
-0.005
-0.01
-0.015
0.01
0.02
0.03
0.04
0.05
0.06
0.07
0.08
0.09
x2 distance from Probe 2 (m)
EFH1 101.2G 95Hz
EFH1 101.2G 47Hz
EFH1 75.9G 15Hz
MSGW11 101.2G 95Hz
MSGW11 101.2G 47Hz
MSGW11 75.9G 15Hz

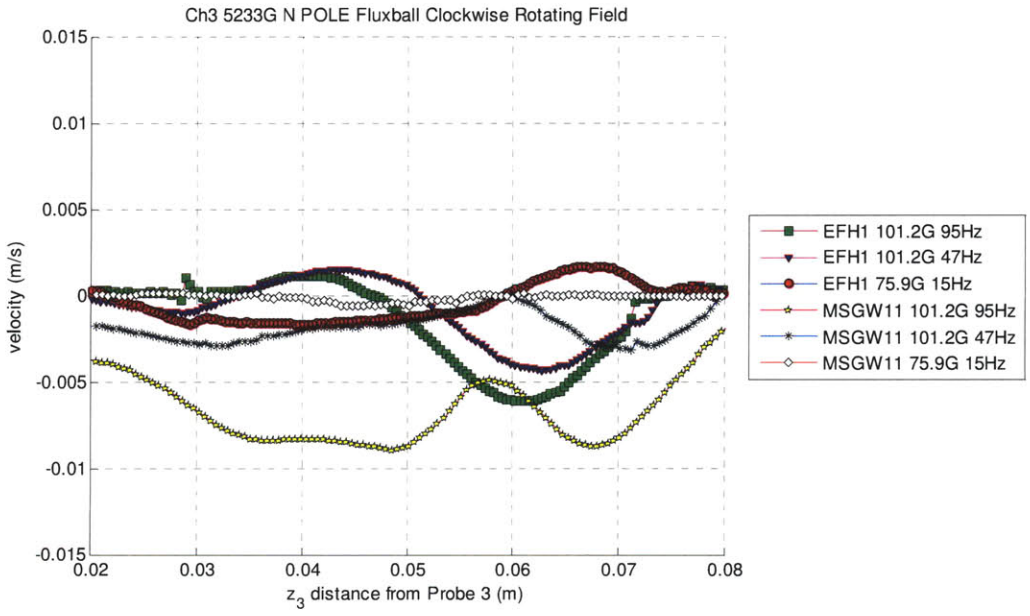
Ch3 5233G N POLE Fluxball Clockwise Rotating Field
velocity (m/s)
0.015
0.01
0.005
0
-0.005
-0.01
-0.015
0.02
0.03
0.04
0.05
0.06
0.07
0.08
z3 distance from Probe 3 (m)
EFH1 101.2G 95Hz
EFH1 101.2G 47Hz
EFH1 75.9G 15Hz
MSGW11 101.2G 95Hz
MSGW11 101.2G 47Hz
MSGW11 75.9G 15Hz

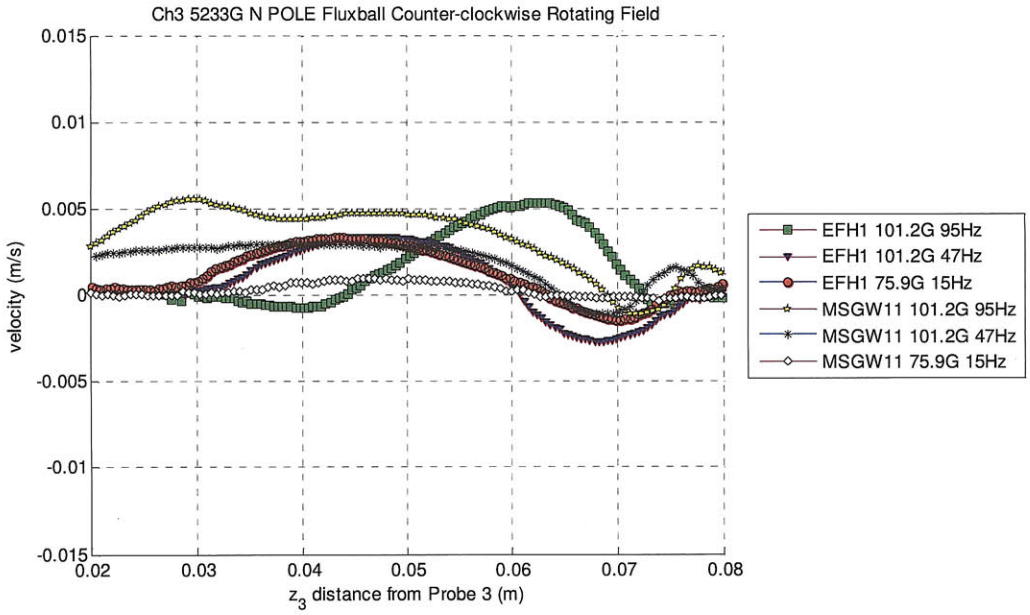
Ch3 5233G N POLE Fluxball Counter-clockwise Rotating Field
velocity (m/s)
0.015
0.01
0.005
0
-0.005
-0.01
-0.015
0.02
0.03
0.04
0.05
0.06
0.07
0.08
z3 distance from Probe 3 (m)
EFH1 101.2G 95Hz
EFH1 101.2G 47Hz
EFH1 75.9G 15Hz
MSGW11 101.2G 95Hz
MSGW11 101.2G 47Hz
MSGW11 75.9G 15Hz

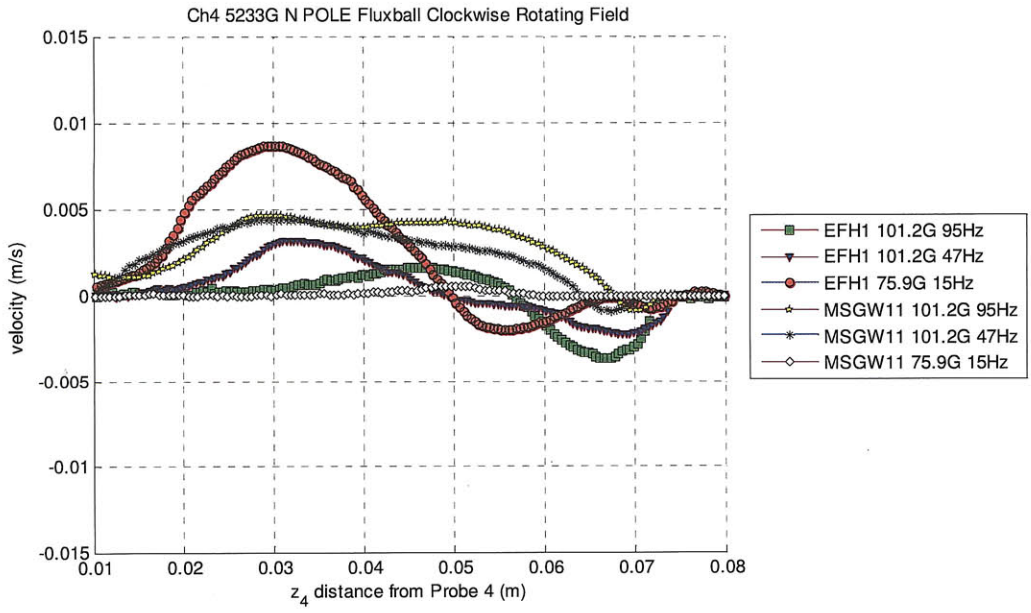
Ch4 5233G N POLE Fluxball Clockwise Rotating Field
velocity (m/s)
0.015
0.01
0.005
0
-0.005
-0.01
-0.015
0.01
0.02
0.03
0.04
0.05
0.06
0.07
0.08
z4 distance from Probe 4 (m)
EFH1 101.2G 95Hz
EFH1 101.2G 47Hz
EFH1 75.9G 15Hz
MSGW11 101.2G 95Hz
MSGW11 101.2G 47Hz
MSGW11 75.9G 15Hz

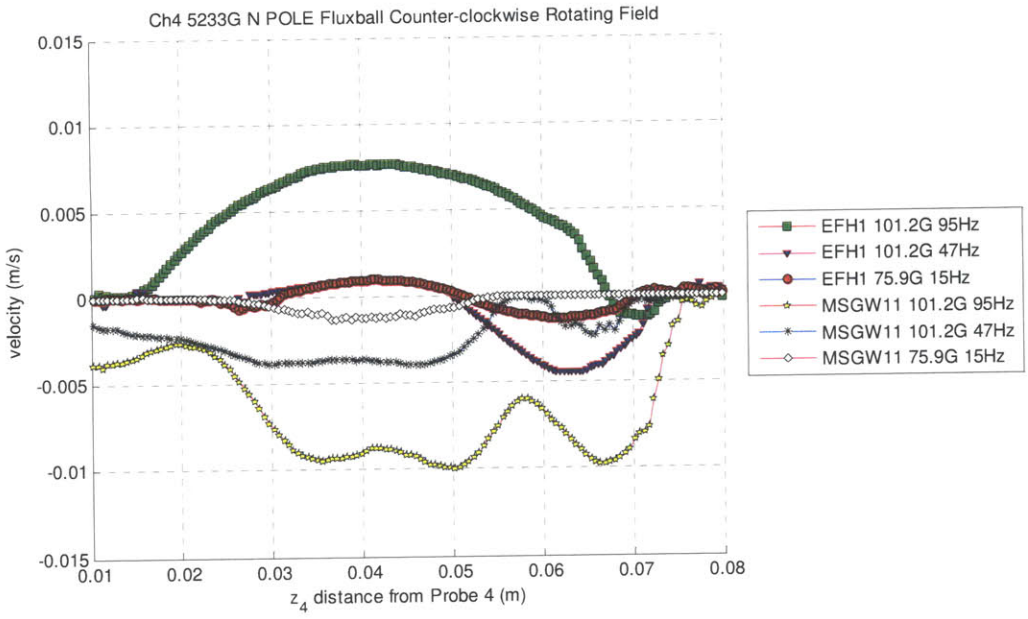
Ch4 5233G N POLE Fluxball Counter-clockwise Rotating Field
0.015
0.01
0.005
0
-0.005
-0.01
-0.015
velocity (m/s)
0.01
0.02
0.03
0.04
0.05
0.06
0.07
0.08
z4 distance from Probe 4 (m)
EFH1 101.2G 95Hz
EFH1 101.2G 47Hz
EFH1 75.9G 15Hz
MSGW11 101.2G 95Hz
MSGW11 101.2G 47Hz
MSGW11 75.9G 15Hz

Appendix I : COMSOL Simulations of Ferrofluid Flows with $\eta'=0$ in Cylindrical Geometry With Non-Uniform Fields (Chapter 7)

I1. EFH1 Filled Cylinder with Magnetic Field Strength of Permanent Magnet 20 Times Stronger than Rotating Field Strength

COMSOL Model Report

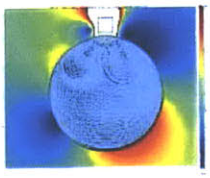

1. Table of Contents

2. Model Properties

Property	Value
Model name	
Author	
Company	
Department	
Reference	
URL	
Saved date	May 12, 2010 11:22:55 PM
Creation date	Sep 19, 2008 9:32:16 PM
COMSOL version	COMSOL 3.5.0.608

File name: D:\My Dropbox\Research Files\Software Data Files\Comsol Files\Good2DMagnetcases\2Dcase_cylinder_surfacecurrent_forceincluded_etaprime0_EFH1_airgap_R10_magnetMz20.mph

Application modes and modules used in this model:

- Geom1 (2D)
  - Incompressible Navier-Stokes
  - Diffusion
  - Convection and Diffusion
  - Convection and Diffusion
  - Perpendicular Induction Currents, Vector Potential (AC/DC Module)

2.1. Model description

Rotation of Ferrofluid in a rotating magnetic field in an infinitely long cylinder with non-uniform field imposed magnet placed on top of cylinder with etaprime=0

Using parameters for EFH1

Excited with surface current on boundary Includes force terms

3. Constants

Name	Expression	Value	Description
Xi	1.59		
omega	2*pi*f		
zeta	0.0031		
eta	0.027		
etaprime	0		
f	95		
tau	7.16e-6		
omegatau	omega*tau		
R0	0.027		
I	2/3		
Ms	4.21		

4. Global Expressions

Name	Expression	Unit	Description
FMx	M_x*(Azyx-M_xx)+M_y*(Azyy-M_xy)		\
FMy	M_x*(-Azxx-M_yx)+M_y*(-Azxy-M_yy)		
T	M_x*Hy-M_y*Hx	A*mol/m^4	
M_eqx	Ms*(coth(alpha)-1/alpha)*Hx/(normH_emqa+1e-20)		
M_eqy	Ms*(coth(alpha)-1/alpha)*Hy/(normH_emqa+1e-20)		
Hx	Hx_emqa	A/m	
Hy	Hy_emqa	A/m	
phi	atan2(y,x)	rad	
alpha	67.182*normH_emqa+1e-20	A/m	

5. Geometry

Number of geometries: 1

5.1. Geom1

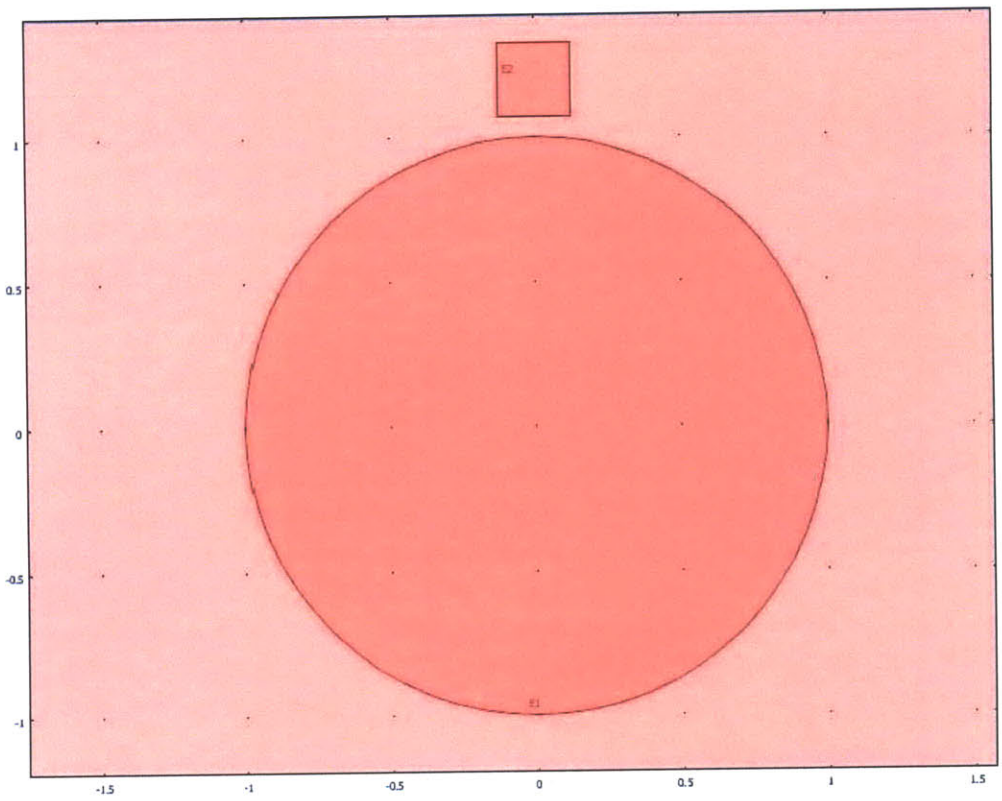

5.1.1. Point mode

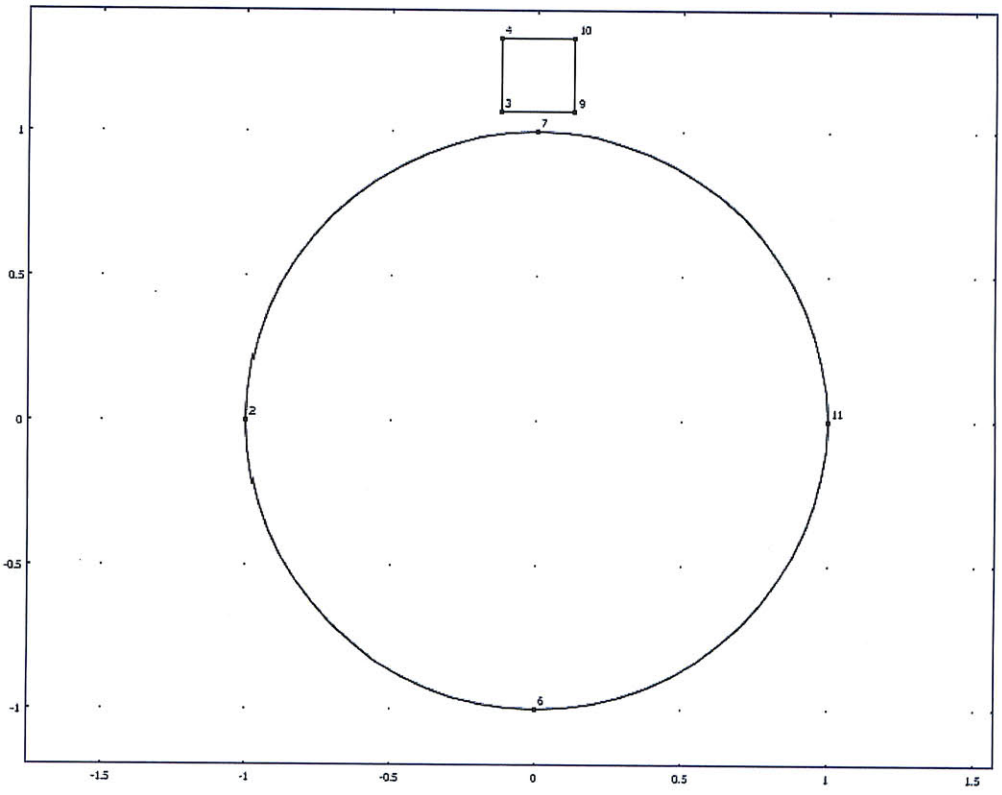

5.1.2. Boundary mode

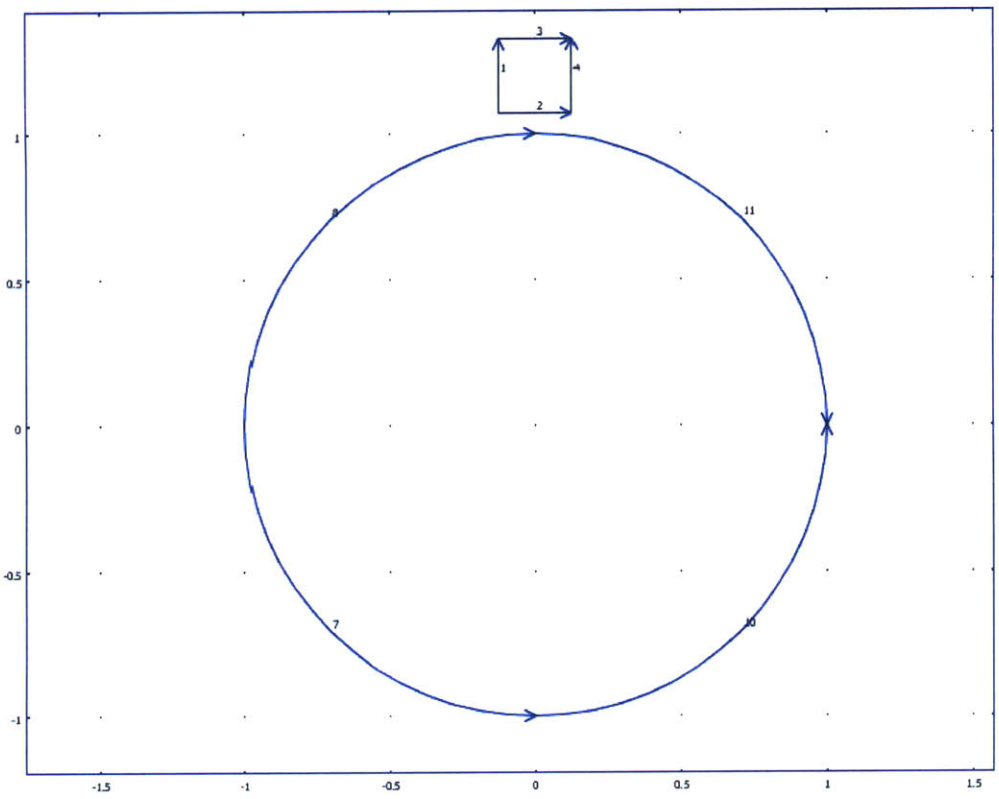

5.1.3. Subdomain mode

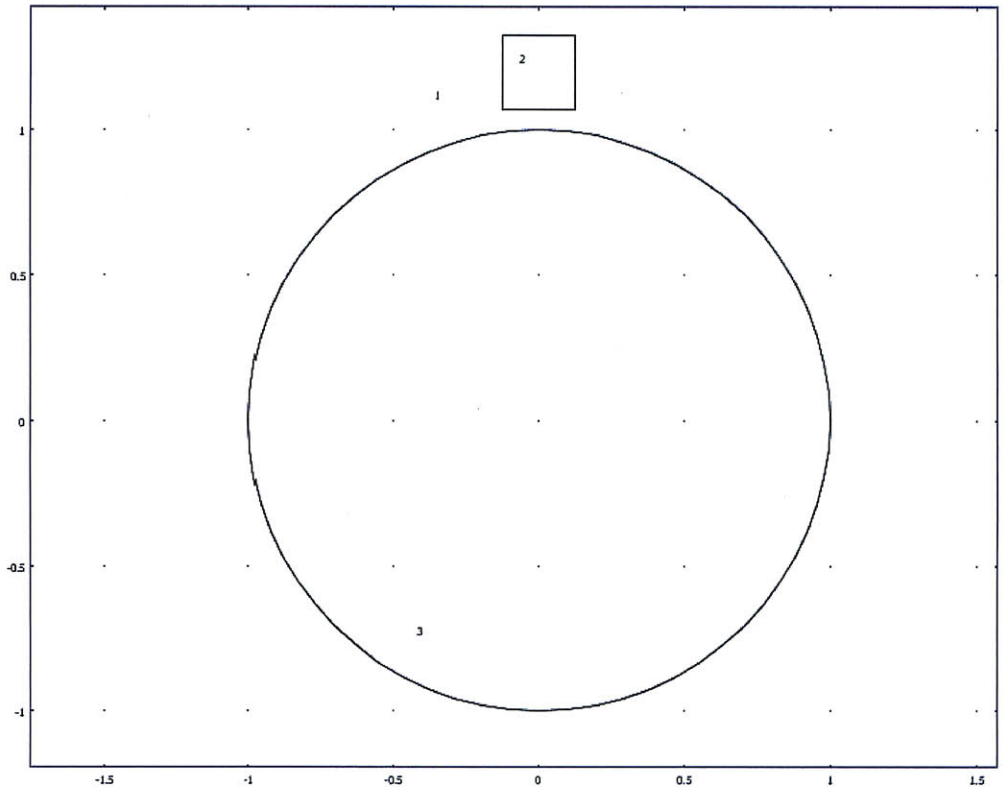

6. Geom1

Space dimensions: 2D

Independent variables: x, y, z

6.1. Mesh

6.1.1. Mesh Statistics

Number of degrees of freedom	275352
Number of mesh points	3898
Number of elements	7734
Triangular	7734
Quadrilateral	0
Number of boundary elements	204
Number of vertex elements	12
Minimum element quality	0.784
Element area ratio	0

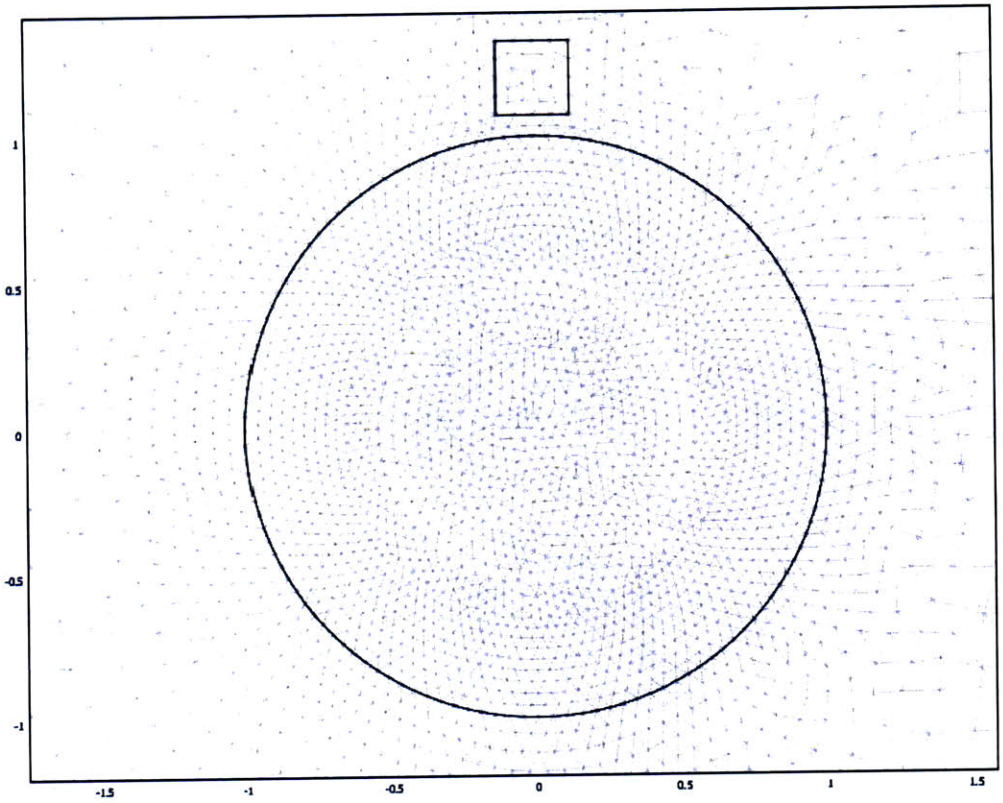

6.2. Application Mode: Incompressible Navier-Stokes (ns)

Application mode type: Incompressible Navier-Stokes

Application mode name: ns

6.2.1. Scalar Variables

Name	Variable	Value	Unit	Description
visc_vel_fact	visc_vel_fact_ns	10	1	Viscous velocity factor

6.2.2. Application Mode Properties

Property	Value
Default element type	Lagrange - P_2 P_1
Analysis type	Transient
Corner smoothing	Off
Frame	Frame (ref)
Weak constraints	Off
Constraint type	Ideal

6.2.3. Variables

Dependent variables: u, v, p, nxw, nyw

Shape functions: shlag(2,'u'), shlag(2,'v'), shlag(1,'p')

Interior boundaries not active

6.2.4. Point Settings

Point		1, 3-12	2
pnton		0	1

6.2.5. Boundary Settings

Boundary		7-8, 10-11
Type		Wall

6.2.6. Subdomain Settings

Subdomain		3
Integration order (gporder)		**4 4 2**
Constraint order (cporder)		**2 2 1**
Density (rho)	kg/m^3	**0**
Dynamic viscosity (eta)	Pa·s	**eta+zeta**
Volume force, x dir. (F_x)	N/m^3	**2*zeta*wy+FMx**
Volume force, y dir. (F_y)	N/m^3	**-2*zeta*wx+FMy**
cdon		**0**

6.3. Application Mode: Diffusion (di)

Application mode type: Diffusion

Application mode name: di

6.3.1. Application Mode Properties

Property	Value
Default element type	Lagrange - Quadratic
Analysis type	Stationary
Frame	Frame (ref)
Weak constraints	Off
Constraint type	Ideal

6.3.2. Variables

Dependent variables: w

Shape functions: shlag(2,'w'), shlag(5,'w')

Interior boundaries not active

6.3.3. Boundary Settings

Boundary	7-8, 10-11
Type	Insulation/Symmetry

6.3.4. Subdomain Settings

Subdomain		3
Shape functions (shape)		**shlag(2,'w') shlag(5,'w')**
Integration order (gporder)		**10**
Constraint order (cporder)		**5**
Diffusion coefficient (D)	m^2/s	**etaprime**
Reaction rate (R)	$mol/(m^3 \cdot s)$	**T+2*zeta*(vx-uy-2*w)**

6.4. Application Mode: Convection and Diffusion (cd3)

Application mode type: Convection and Diffusion

Application mode name: cd3

6.4.1. Application Mode Properties

Property	Value
Default element type	Lagrange - Quadratic
Analysis type	Transient
Equation form	Non-conservative
Frame	Frame (ref)
Weak constraints	Off
Constraint type	Ideal

6.4.2. Variables

Dependent variables: M_x

Shape functions: shlag(2,'M_x'), shlag(5,'M_x')

Interior boundaries not active

6.4.3. Boundary Settings

Boundary	7-8, 10-11
Type	Insulation/Symmetry

6.4.4. Subdomain Settings

Subdomain		3
Shape functions (shape)		**shlag(2,'M_x') shlag(5,'M_x')**

Integration order (gporder)		**10**
Constraint order (cporder)		**5**
Diffusion coefficient (D)	m^2/s	**0**
Reaction rate (R)	$mol/(m^3 \cdot s)$	**-w*M_y-((M_x-M_eqx)/omegatau)**
x-velocity (u)	m/s	**u**
y-velocity (v)	m/s	**v**

6.5. Application Mode: Convection and Diffusion (cd)

Application mode type: Convection and Diffusion

Application mode name: cd

6.5.1. Application Mode Properties

Property	Value
Default element type	Lagrange - Quadratic
Analysis type	Transient
Equation form	Non-conservative
Frame	Frame (ref)
Weak constraints	Off
Constraint type	Ideal

6.5.2. Variables

Dependent variables: M_y

Shape functions: shlag(2,'M_y'), shlag(5,'M_y')

Interior boundaries not active

6.5.3. Boundary Settings

Boundary	7-8, 10-11
Type	Insulation/Symmetry

6.5.4. Subdomain Settings

Subdomain		3
Shape functions (shape)		**shlag(2,'M_y') shlag(5,'M_y')**
Integration order (gporder)		**10**
Constraint order (cporder)		**5**
Diffusion coefficient (D)	m^2/s	**0**
Reaction rate (R)	$mol/(m^3 \cdot s)$	**w*M_x-((M_y-M_eqy)/omegatau)**
x-velocity (u)	m/s	**u**
y-velocity (v)	m/s	**v**

6.6. Application Mode: Perpendicular Induction Currents, Vector Potential (emqa)

Application mode type: Perpendicular Induction Currents, Vector Potential (AC/DC Module)

Application mode name: emqa

6.6.1. Scalar Variables

Name	Variable	Value	Unit	Description
epsilon0	epsilon0_emqa	8.854187817e-12	F/m	Permittivity of vacuum
mu0	mu0_emqa	1	H/m	Permeability of vacuum

6.6.2. Application Mode Properties

Property	Value
Default element type	Lagrange - Quintic
Analysis type	Transient
Bias application mode	None
Solve for	Total potential
Background field	Magnetic vector potential
Frame	Frame (ref)
Weak constraints	Off
Constraint type	Ideal

6.6.3. Variables

Dependent variables: Az, redAz

Shape functions: shlag(5,'Az')

Interior boundaries active

6.6.4. Boundary Settings

Boundary		1-4, 7-8, 10-11	5-6, 9, 12
Type		Continuity	Surface current
Surface current density (Js0z)	A/m	**I*(3/2)*cos(t-phi)*flc2hs(t-1,0.05)**	**I*(3/2)*cos(t-phi)*flc2hs(t-1,0.05)**

6.6.5. Subdomain Settings

Subdomain		1	2	3
magconstrel		**B = $\mu_0\mu_r$H**	**B = μ_0H + μ_0M**	**B = μ_0H + μ_0M**
Magnetization (M)	A/m	{0;0}	**{0;20*flc2hs(t-1,0.05)}**	**{M_x;M_y}**

7. Solver Settings

Solve using a script: off

Analysis type	Transient
Auto select solver	On
Solver	Time dependent
Solution form	Automatic

Symmetric	auto
Adaptive mesh refinement	Off
Optimization/Sensitivity	Off
Plot while solving	Off

7.1. Direct (UMFPACK)

Solver type: Linear system solver

Parameter	Value
Pivot threshold	0.1
Memory allocation factor	0.7

7.2. Time Stepping

Parameter	Value
Times	range(0,0.1,10)
Relative tolerance	0.01
Absolute tolerance	0.0010
Times to store in output	Specified times
Time steps taken by solver	Free
Maximum BDF order	5
Singular mass matrix	Maybe
Consistent initialization of DAE systems	Backward Euler
Error estimation strategy	Include algebraic
Allow complex numbers	On

7.3. Advanced

Parameter	Value
Constraint handling method	Elimination
Null-space function	Automatic
Automatic assembly block size	On
Assembly block size	5000
Use Hermitian transpose of constraint matrix and in symmetry detection	Off
Use complex functions with real input	Off
Stop if error due to undefined operation	On
Store solution on file	Off
Type of scaling	Automatic
Manual scaling	
Row equilibration	On
Manual control of reassembly	Off
Load constant	On
Constraint constant	On
Mass constant	On
Damping (mass) constant	On
Jacobian constant	On
Constraint Jacobian constant	On

8. Postprocessing

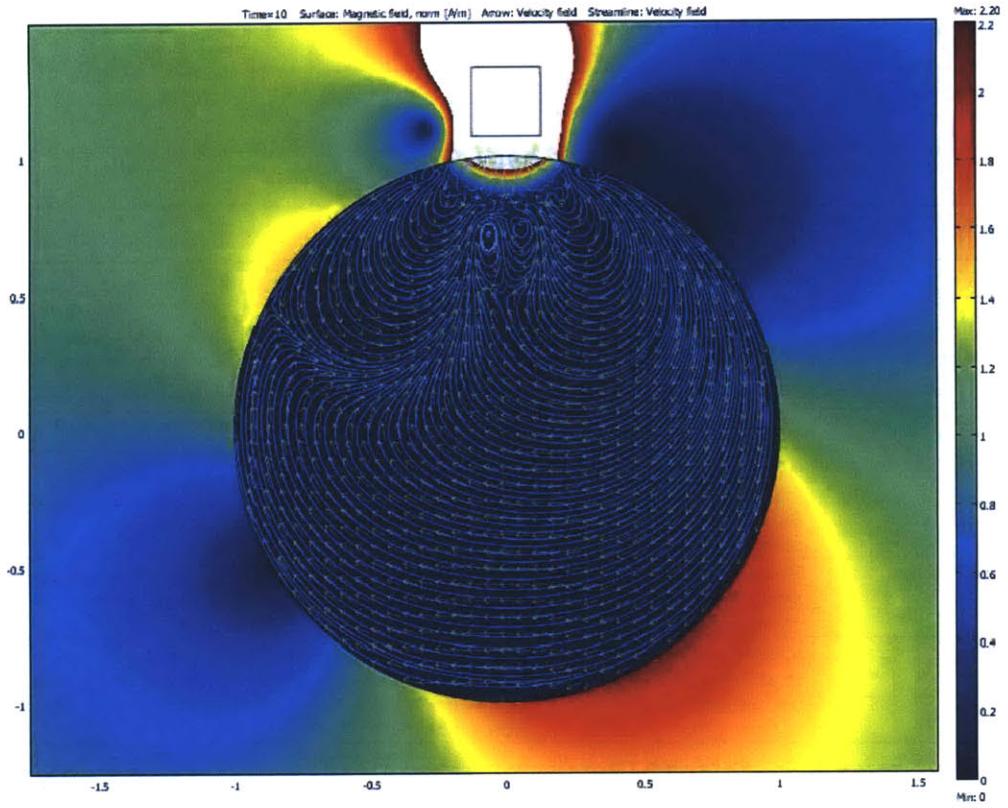

9. Variables

9.1. Boundary

9.1.1. Boundary 1-6, 9, 12

Name	Description	Unit	Expression
K_x_ns	Viscous force per area, x component	Pa	
T_x_ns	Total force per area, x component	Pa	
K_y_ns	Viscous force per area, y component	Pa	
T_y_ns	Total force per area, y component	Pa	

ndflux_w_di	Normal diffusive flux, w	mol/(m^2*s)	
ndflux_M_x_cd3	Normal diffusive flux, M_x	mol/(m^2*s)	
ncflux_M_x_cd3	Normal convective flux, M_x	mol/(m^2*s)	
ntflux_M_x_cd3	Normal total flux, M_x	mol/(m^2*s)	
ndflux_M_y_cd	Normal diffusive flux, M_y	mol/(m^2*s)	
ncflux_M_y_cd	Normal convective flux, M_y	mol/(m^2*s)	
ntflux_M_y_cd	Normal total flux, M_y	mol/(m^2*s)	
dVolbnd_emqa	Area integration contribution	1	1
murbnd_emqa	Relative permeability	1	murbndxx_emqa
Jsz_emqa	Surface current density	A/m	unx * (Hy_emqa_down-Hy_emqa_up)-uny * (Hx_emqa_down-Hx_emqa_up)
unTx_emqa	Maxwell surface stress tensor, x component	Pa	-0.5 * (Bx_emqa_up * Hx_emqa_up+By_emqa_up * Hy_emqa_up) * dnx+(dnx * Hx_emqa_up+dny * Hy_emqa_up) * Bx_emqa_up
dnTx_emqa	Maxwell surface stress tensor, x component	Pa	-0.5 * (Bx_emqa_down * Hx_emqa_down+By_emqa_down * Hy_emqa_down) * unx+(unx * Hx_emqa_down+uny * Hy_emqa_down) * Bx_emqa_down
unTy_emqa	Maxwell surface stress tensor, y component	Pa	-0.5 * (Bx_emqa_up * Hx_emqa_up+By_emqa_up * Hy_emqa_up) * dny+(dnx * Hx_emqa_up+dny * Hy_emqa_up) * By_emqa_up
dnTy_emqa	Maxwell surface stress tensor, y component	Pa	-0.5 * (Bx_emqa_down * Hx_emqa_down+By_emqa_down * Hy_emqa_down) * uny+(unx * Hx_emqa_down+uny * Hy_emqa_down) * By_emqa_down
Qs_emqa	Surface resistive heating	W/m^2	Jsz_emqa * Ez_emqa
nPo_emqa	Power outflow	W/m^2	nx_emqa * Pox_emqa+ny_emqa * Poy_emqa
FsLtzx_emqa	Lorentz surface force contribution, x component	Pa	-Jsz_emqa * By_emqa
FsLtzy_emqa	Lorentz surface force contribution, y component	Pa	Jsz_emqa * Bx_emqa
normFsLtz_emqa	Lorentz surface force contribution, cycle average, norm	Pa	sqrt(abs(FsLtzx_emqa)^2+abs(FsLtzy_emqa)^2)

9.1.2. Boundary 7-8, 10-11

Name	Description	Unit	Expression
K_x_ns	Viscous force per area, x component	Pa	eta_ns * (2 * nx_ns * ux+ny_ns * (uy+vx))
T_x_ns	Total force per area, x component	Pa	-nx_ns * p+2 * nx_ns * eta_ns * ux+ny_ns * eta_ns * (uy+vx)
K_y_ns	Viscous force per area, y component	Pa	eta_ns * (nx_ns * (vx+uy)+2 * ny_ns * vy)
T_y_ns	Total force per area, y component	Pa	-ny_ns * p+nx_ns * eta_ns * (vx+uy)+2 * ny_ns * eta_ns * vy
ndflux_w_di	Normal diffusive flux, w	mol/(m^2*s)	nx_di * dflux_w_x_di+ny_di * dflux_w_y_di
ndflux_M_x_cd3	Normal diffusive flux, M_x	mol/(m^2*s)	nx_cd3 * dflux_M_x_x_cd3+ny_cd3 * dflux_M_x_y_cd3
ncflux_M_x_cd3	Normal convective flux, M_x	mol/(m^2*s)	nx_cd3 * cflux_M_x_x_cd3+ny_cd3 * cflux_M_x_y_cd3
ntflux_M_x_cd3	Normal total flux, M_x	mol/(m^2*s)	nx_cd3 * tflux_M_x_x_cd3+ny_cd3 * tflux_M_x_y_cd3
ndflux_M_y_cd	Normal diffusive flux, M_y	mol/(m^2*s)	nx_cd * dflux_M_y_x_cd+ny_cd * dflux_M_y_y_cd
ncflux_M_y_cd	Normal convective flux, M_y	mol/(m^2*s)	nx_cd * cflux_M_y_x_cd+ny_cd * cflux_M_y_y_cd
ntflux_M_y_cd	Normal total flux, M_y	mol/(m^2*s)	nx_cd * tflux_M_y_x_cd+ny_cd * tflux_M_y_y_cd
dVolbnd_emqa	Area integration contribution	1	1
murbnd_emqa	Relative permeability	1	murbndxx_emqa
Jsz_emqa	Surface current density	A/m	unx * (Hy_emqa_down-Hy_emqa_up)-uny * (Hx_emqa_down-Hx_emqa_up)
unTx_emqa	Maxwell surface stress tensor, x component	Pa	-0.5 * (Bx_emqa_up * Hx_emqa_up+By_emqa_up * Hy_emqa_up) * dnx+(dnx * Hx_emqa_up+dny * Hy_emqa_up) * Bx_emqa_up
dnTx_emqa	Maxwell surface stress tensor, x component	Pa	-0.5 * (Bx_emqa_down * Hx_emqa_down+By_emqa_down * Hy_emqa_down) * unx+(unx * Hx_emqa_down+uny * Hy_emqa_down) * Bx_emqa_down
unTy_emqa	Maxwell surface stress tensor, y component	Pa	-0.5 * (Bx_emqa_up * Hx_emqa_up+By_emqa_up * Hy_emqa_up) * dny+(dnx * Hx_emqa_up+dny * Hy_emqa_up) * By_emqa_up
dnTy_emqa	Maxwell surface stress tensor, y component	Pa	-0.5 * (Bx_emqa_down * Hx_emqa_down+By_emqa_down * Hy_emqa_down) * uny+(unx * Hx_emqa_down+uny * Hy_emqa_down) * By_emqa_down

Qs_emqa	Surface resistive heating	W/m^2	Jsz_emqa * Ez_emqa
nPo_emqa	Power outflow	W/m^2	nx_emqa * Pox_emqa+ny_emqa * Poy_emqa
FsLtzx_emqa	Lorentz surface force contribution, x component	Pa	-Jsz_emqa * By_emqa
FsLtzy_emqa	Lorentz surface force contribution, y component	Pa	Jsz_emqa * Bx_emqa
normFsLtz_emqa	Lorentz surface force contribution, cycle average, norm	Pa	sqrt(abs(FsLtzx_emqa)^2+abs(FsLtzy_emqa)^2)

9.2. Subdomain

9.2.1. Subdomain 1

Name	Description	Unit	Expression
U_ns	Velocity field	m/s	
V_ns	Vorticity	1/s	
divU_ns	Divergence of velocity field	1/s	
cellRe_ns	Cell Reynolds number	1	
res_u_ns	Equation residual for u	N/m^3	
res_v_ns	Equation residual for v	N/m^3	
beta_x_ns	Convective field, x component	kg/(m^2*s)	
beta_y_ns	Convective field, y component	kg/(m^2*s)	
Dm_ns	Mean diffusion coefficient	Pa*s	
da_ns	Total time scale factor	kg/m^3	
taum_ns	GLS time-scale	m^3*s/kg	
tauc_ns	GLS time-scale	m^2/s	
res_p_ns	Equation residual for p	kg/(m^3*s)	
grad_w_x_di	Concentration gradient, w, x component	mol/m^4	
dflux_w_x_di	Diffusive flux, w, x component	mol/(m^2*s)	
grad_w_y_di	Concentration gradient, w, y component	mol/m^4	
dflux_w_y_di	Diffusive flux, w, y component	mol/(m^2*s)	
grad_w_di	Concentration gradient, w	mol/m^4	
dflux_w_di	Diffusive flux, w	mol/(m^2*s)	
grad_M_x_x_cd3	Concentration gradient, M_x, x component	mol/m^4	

dflux_M_x_x_cd3	Diffusive flux, M_x, x component	mol/(m^2*s)	
cflux_M_x_x_cd3	Convective flux, M_x, x component	mol/(m^2*s)	
tflux_M_x_x_cd3	Total flux, M_x, x component	mol/(m^2*s)	
grad_M_x_y_cd3	Concentration gradient, M_x, y component	mol/m^4	
dflux_M_x_y_cd3	Diffusive flux, M_x, y component	mol/(m^2*s)	
cflux_M_x_y_cd3	Convective flux, M_x, y component	mol/(m^2*s)	
tflux_M_x_y_cd3	Total flux, M_x, y component	mol/(m^2*s)	
beta_M_x_x_cd3	Convective field, M_x, x component	m/s	
beta_M_x_y_cd3	Convective field, M_x, y component	m/s	
grad_M_x_cd3	Concentration gradient, M_x	mol/m^4	
dflux_M_x_cd3	Diffusive flux, M_x	mol/(m^2*s)	
cflux_M_x_cd3	Convective flux, M_x	mol/(m^2*s)	
tflux_M_x_cd3	Total flux, M_x	mol/(m^2*s)	
cellPe_M_x_cd3	Cell Peclet number, M_x	1	
Dm_M_x_cd3	Mean diffusion coefficient, M_x	m^2/s	
res_M_x_cd3	Equation residual for M_x	mol/(m^3*s)	
res_sc_M_x_cd3	Shock capturing residual for M_x	mol/(m^3*s)	
da_M_x_cd3	Total time scale factor, M_x	1	
grad_M_y_x_cd	Concentration gradient, M_y, x component	mol/m^4	
dflux_M_y_x_cd	Diffusive flux, M_y, x component	mol/(m^2*s)	
cflux_M_y_x_cd	Convective flux, M_y, x component	mol/(m^2*s)	
tflux_M_y_x_cd	Total flux, M_y, x component	mol/(m^2*s)	
grad_M_y_y_cd	Concentration gradient, M_y, y component	mol/m^4	
dflux_M_y_y_cd	Diffusive flux, M_y, y component	mol/(m^2*s)	
cflux_M_y_y_cd	Convective flux, M_y, y component	mol/(m^2*s)	
tflux_M_y_y_cd	Total flux, M_y, y component	mol/(m^2*s)	
beta_M_y_x_cd	Convective field, M_y, x component	m/s	

beta_M_y_y_cd	Convective field, M_y, y component	m/s	
grad_M_y_cd	Concentration gradient, M_y	mol/m^4	
dflux_M_y_cd	Diffusive flux, M_y	mol/(m^2*s)	
cflux_M_y_cd	Convective flux, M_y	mol/(m^2*s)	
tflux_M_y_cd	Total flux, M_y	mol/(m^2*s)	
cellPe_M_y_cd	Cell Peclet number, M_y	1	
Dm_M_y_cd	Mean diffusion coefficient, M_y	m^2/s	
res_M_y_cd	Equation residual for M_y	mol/(m^3*s)	
res_sc_M_y_cd	Shock capturing residual for M_y	mol/(m^3*s)	
da_M_y_cd	Total time scale factor, M_y	1	
dr_guess_emqa	Width in radial direction default guess	m	0
R0_guess_emqa	Inner radius default guess	m	0
Sx_emqa	Infinite element x coordinate	m	x
S0x_guess_emqa	Inner x coordinate default guess	m	0
Sdx_guess_emqa	Width in x direction default guess	m	0
Sy_emqa	Infinite element y coordinate	m	y
S0y_guess_emqa	Inner y coordinate default guess	m	0
Sdy_guess_emqa	Width in y direction default guess	m	0
curlAx_emqa	Curl of magnetic potential, x component	T	Azy
curlAy_emqa	Curl of magnetic potential, y component	T	-Azx
dVol_emqa	Volume integration contribution	1	detJ_emqa
Bx_emqa	Magnetic flux density, x component	T	curlAx_emqa
By_emqa	Magnetic flux density, y component	T	curlAy_emqa
Hx_emqa	Magnetic field, x component	A/m	Bx_emqa/(mur_emqa * mu0_emqa)
Hy_emqa	Magnetic field, y component	A/m	By_emqa/(mur_emqa * mu0_emqa)
mu_emqa	Permeability	H/m	mu0_emqa * mur_emqa
muxx_emqa	Permeability, xx component	H/m	mu0_emqa * murxx_emqa
muxy_emqa	Permeability, xy component	H/m	mu0_emqa * murxy_emqa

muyx_emqa	Permeability, yx component	H/m	mu0_emqa * muryx_emqa
muyy_emqa	Permeability, yy component	H/m	mu0_emqa * muryy_emqa
Jpz_emqa	Potential current density, z component	A/m^2	sigma_emqa * deltaV_emqa/L_emqa
Ez_emqa	Electric field, z component	V/m	-d(Az,t)
Jz_emqa	Total current density, z component	A/m^2	Jpz_emqa+Jiz_emqa+Jez_emqa
Pox_emqa	Power flow, x component	W/m^2	-Ez_emqa * Hy_emqa
Poy_emqa	Power flow, y component	W/m^2	Ez_emqa * Hx_emqa
normE_emqa	Electric field, norm	V/m	abs(Ez_emqa)
Jiz_emqa	Induced current density, z component	A/m^2	sigma_emqa * Ez_emqa
Q_emqa	Resistive heating	W/m^3	Jz_emqa * (Ez_emqa+deltaV_emqa/L_emqa)
W_emqa	Total energy density	J/m^3	Wm_emqa
dW_emqa	Integrand for total energy	Pa	dVol_emqa * W_emqa
Wm_emqa	Magnetic energy density	J/m^3	0.5 * (Hx_emqa * Bx_emqa+Hy_emqa * By_emqa)
FLtzx_emqa	Lorentz force contribution, x component	N/m^3	-Jz_emqa * By_emqa
FLtzy_emqa	Lorentz force contribution, y component	N/m^3	Jz_emqa * Bx_emqa
normFLtz_emqa	Lorentz force contribution, norm	N/m^3	sqrt(abs(FLtzx_emqa)^2+abs(FLtzy_emqa)^2)
normM_emqa	Magnetization, norm	A/m	sqrt(abs(Mx_emqa)^2+abs(My_emqa)^2)
normBr_emqa	Remanent flux density, norm	T	sqrt(abs(Brx_emqa)^2+abs(Bry_emqa)^2)
normH_emqa	Magnetic field, norm	A/m	sqrt(abs(Hx_emqa)^2+abs(Hy_emqa)^2)
normB_emqa	Magnetic flux density, norm	T	sqrt(abs(Bx_emqa)^2+abs(By_emqa)^2)
normJ_emqa	Total current density, norm	A/m^2	abs(Jz_emqa)
Evz_emqa	Lorentz electric field, z component	V/m	d(x,t) * By_emqa-d(y,t) * Bx_emqa
normEv_emqa	Lorentz electric field, norm	V/m	abs(Evz_emqa)
normPo_emqa	Power flow, time average, norm	W/m^2	sqrt(abs(Pox_emqa)^2+abs(Poy_emqa)^2)

9.2.2. Subdomain 2

Name	Description	Unit	Expression
U_ns	Velocity field	m/s	
V_ns	Vorticity	1/s	
divU_ns	Divergence of velocity field	1/s	

cellRe_ns	Cell Reynolds number	1	
res_u_ns	Equation residual for u	N/m^3	
res_v_ns	Equation residual for v	N/m^3	
beta_x_ns	Convective field, x component	kg/(m^2*s)	
beta_y_ns	Convective field, y component	kg/(m^2*s)	
Dm_ns	Mean diffusion coefficient	Pa*s	
da_ns	Total time scale factor	kg/m^3	
taum_ns	GLS time-scale	m^3*s/kg	
tauc_ns	GLS time-scale	m^2/s	
res_p_ns	Equation residual for p	kg/(m^3*s)	
grad_w_x_di	Concentration gradient, w, x component	mol/m^4	
dflux_w_x_di	Diffusive flux, w, x component	mol/(m^2*s)	
grad_w_y_di	Concentration gradient, w, y component	mol/m^4	
dflux_w_y_di	Diffusive flux, w, y component	mol/(m^2*s)	
grad_w_di	Concentration gradient, w	mol/m^4	
dflux_w_di	Diffusive flux, w	mol/(m^2*s)	
grad_M_x_x_cd3	Concentration gradient, M_x, x component	mol/m^4	
dflux_M_x_x_cd3	Diffusive flux, M_x, x component	mol/(m^2*s)	
cflux_M_x_x_cd3	Convective flux, M_x, x component	mol/(m^2*s)	
tflux_M_x_x_cd3	Total flux, M_x, x component	mol/(m^2*s)	
grad_M_x_y_cd3	Concentration gradient, M_x, y component	mol/m^4	
dflux_M_x_y_cd3	Diffusive flux, M_x, y component	mol/(m^2*s)	
cflux_M_x_y_cd3	Convective flux, M_x, y component	mol/(m^2*s)	
tflux_M_x_y_cd3	Total flux, M_x, y component	mol/(m^2*s)	
beta_M_x_x_cd3	Convective field, M_x, x component	m/s	

beta_M_x_y_cd3	Convective field, M_x, y component	m/s	
grad_M_x_cd3	Concentration gradient, M_x	mol/m^4	
dflux_M_x_cd3	Diffusive flux, M_x	mol/(m^2*s)	
cflux_M_x_cd3	Convective flux, M_x	mol/(m^2*s)	
tflux_M_x_cd3	Total flux, M_x	mol/(m^2*s)	
cellPe_M_x_cd3	Cell Peclet number, M_x	1	
Dm_M_x_cd3	Mean diffusion coefficient, M_x	m^2/s	
res_M_x_cd3	Equation residual for M_x	mol/(m^3*s)	
res_sc_M_x_cd3	Shock capturing residual for M_x	mol/(m^3*s)	
da_M_x_cd3	Total time scale factor, M_x	1	
grad_M_y_x_cd	Concentration gradient, M_y, x component	mol/m^4	
dflux_M_y_x_cd	Diffusive flux, M_y, x component	mol/(m^2*s)	
cflux_M_y_x_cd	Convective flux, M_y, x component	mol/(m^2*s)	
tflux_M_y_x_cd	Total flux, M_y, x component	mol/(m^2*s)	
grad_M_y_y_cd	Concentration gradient, M_y, y component	mol/m^4	
dflux_M_y_y_cd	Diffusive flux, M_y, y component	mol/(m^2*s)	
cflux_M_y_y_cd	Convective flux, M_y, y component	mol/(m^2*s)	
tflux_M_y_y_cd	Total flux, M_y, y component	mol/(m^2*s)	
beta_M_y_x_cd	Convective field, M_y, x component	m/s	
beta_M_y_y_cd	Convective field, M_y, y component	m/s	
grad_M_y_cd	Concentration gradient, M_y	mol/m^4	
dflux_M_y_cd	Diffusive flux, M_y	mol/(m^2*s)	
cflux_M_y_cd	Convective flux, M_y	mol/(m^2*s)	
tflux_M_y_cd	Total flux, M_y	mol/(m^2*s)	
cellPe_M_y_cd	Cell Peclet number, M_y	1	
Dm_M_y_cd	Mean diffusion coefficient, M_y	m^2/s	

res_M_y_cd	Equation residual for M_y	mol/(m^3*s)	
res_sc_M_y_cd	Shock capturing residual for M_y	mol/(m^3*s)	
da_M_y_cd	Total time scale factor, M_y	1	
dr_guess_emqa	Width in radial direction default guess	m	0
R0_guess_emqa	Inner radius default guess	m	0
Sx_emqa	Infinite element x coordinate	m	x
S0x_guess_emqa	Inner x coordinate default guess	m	0
Sdx_guess_emqa	Width in x direction default guess	m	0
Sy_emqa	Infinite element y coordinate	m	y
S0y_guess_emqa	Inner y coordinate default guess	m	0
Sdy_guess_emqa	Width in y direction default guess	m	0
curlAx_emqa	Curl of magnetic potential, x component	T	Azy
curlAy_emqa	Curl of magnetic potential, y component	T	-Azx
dVol_emqa	Volume integration contribution	1	detJ_emqa
Bx_emqa	Magnetic flux density, x component	T	curlAx_emqa
By_emqa	Magnetic flux density, y component	T	curlAy_emqa
Hx_emqa	Magnetic field, x component	A/m	Bx_emqa/mu0_emqa-Mx_emqa
Hy_emqa	Magnetic field, y component	A/m	By_emqa/mu0_emqa-My_emqa
mu_emqa	Permeability	H/m	mu0_emqa * mur_emqa
muxx_emqa	Permeability, xx component	H/m	mu0_emqa * murxx_emqa
muxy_emqa	Permeability, xy component	H/m	mu0_emqa * murxy_emqa
muyx_emqa	Permeability, yx component	H/m	mu0_emqa * muryx_emqa
muyy_emqa	Permeability, yy component	H/m	mu0_emqa * muryy_emqa

Jpz_emqa	Potential current density, z component	A/m^2	sigma_emqa * deltaV_emqa/L_emqa
Ez_emqa	Electric field, z component	V/m	-d(Az,t)
Jz_emqa	Total current density, z component	A/m^2	Jpz_emqa+Jiz_emqa+Jez_emqa
Pox_emqa	Power flow, x component	W/m^2	-Ez_emqa * Hy_emqa
Poy_emqa	Power flow, y component	W/m^2	Ez_emqa * Hx_emqa
normE_emqa	Electric field, norm	V/m	abs(Ez_emqa)
Jiz_emqa	Induced current density, z component	A/m^2	sigma_emqa * Ez_emqa
Q_emqa	Resistive heating	W/m^3	Jz_emqa * (Ez_emqa+deltaV_emqa/L_emqa)
W_emqa	Total energy density	J/m^3	Wm_emqa
dW_emqa	Integrand for total energy	Pa	dVol_emqa * W_emqa
Wm_emqa	Magnetic energy density	J/m^3	0.5 * (Hx_emqa * Bx_emqa+Hy_emqa * By_emqa+Mx_emqa * Bx_emqa+My_emqa * By_emqa)
FLtzx_emqa	Lorentz force contribution, x component	N/m^3	-Jz_emqa * By_emqa
FLtzy_emqa	Lorentz force contribution, y component	N/m^3	Jz_emqa * Bx_emqa
normFLtz_emqa	Lorentz force contribution, norm	N/m^3	sqrt(abs(FLtzx_emqa)^2+abs(FLtzy_emqa)^2)
normM_emqa	Magnetization, norm	A/m	sqrt(abs(Mx_emqa)^2+abs(My_emqa)^2)
normBr_emqa	Remanent flux density, norm	T	sqrt(abs(Brx_emqa)^2+abs(Bry_emqa)^2)
normH_emqa	Magnetic field, norm	A/m	sqrt(abs(Hx_emqa)^2+abs(Hy_emqa)^2)
normB_emqa	Magnetic flux density, norm	T	sqrt(abs(Bx_emqa)^2+abs(By_emqa)^2)
normJ_emqa	Total current density, norm	A/m^2	abs(Jz_emqa)
Evz_emqa	Lorentz electric field, z component	V/m	d(x,t) * By_emqa-d(y,t) * Bx_emqa
normEv_emqa	Lorentz electric field, norm	V/m	abs(Evz_emqa)
normPo_emqa	Power flow, time average, norm	W/m^2	sqrt(abs(Pox_emqa)^2+abs(Poy_emqa)^2)

9.2.3. Subdomain 3

Name	Description	Unit	Expression
U_ns	Velocity field	m/s	sqrt(u^2+v^2)
V_ns	Vorticity	1/s	vx-uy
divU_ns	Divergence of velocity field	1/s	ux+vy
cellRe_ns	Cell Reynolds number	1	rho_ns * U_ns * h/eta_ns
res_u_ns	Equation residual for u	N/m^3	rho_ns * (ut+u * ux+v * uy)+px-F_x_ns-eta_ns * (2 * uxx+uyy+vxy)
res_v_ns	Equation residual for v	N/m^3	rho_ns * (vt+u * vx+v * vy)+py-F_y_ns-eta_ns * (vxx+uyx+2 * vyy)
beta_x_ns	Convective field, x component	kg/(m^2*s)	rho_ns * u
beta_y_ns	Convective field, y component	kg/(m^2*s)	rho_ns * v
Dm_ns	Mean diffusion coefficient	Pa*s	eta_ns
da_ns	Total time scale factor	kg/m^3	rho_ns
taum_ns	GLS time-scale	m^3*s/kg	nojac(1/max(2 * rho_ns * sqrt(emetric(u,v)),48 * eta_ns/h^2))
tauc_ns	GLS time-scale	m^2/s	0.5 * nojac(if(u^2+v^2
res_p_ns	Equation residual for p	kg/(m^3*s)	rho_ns * divU_ns
grad_w_x_di	Concentration gradient, w, x component	mol/m^4	wx
dflux_w_x_di	Diffusive flux, w, x component	mol/(m^2*s)	-Dxx_w_di * wx-Dxy_w_di * wy
grad_w_y_di	Concentration gradient, w, y component	mol/m^4	wy
dflux_w_y_di	Diffusive flux, w, y component	mol/(m^2*s)	-Dyx_w_di * wx-Dyy_w_di * wy
grad_w_di	Concentration gradient, w	mol/m^4	sqrt(grad_w_x_di^2+grad_w_y_di^2)
dflux_w_di	Diffusive flux, w	mol/(m^2*s)	sqrt(dflux_w_x_di^2+dflux_w_y_di^2)
grad_M_x_x_cd3	Concentration gradient, M_x, x component	mol/m^4	M_xx
dflux_M_x_x_cd3	Diffusive flux, M_x, x component	mol/(m^2*s)	-Dxx_M_x_cd3 * M_xx-Dxy_M_x_cd3 * M_xy

cflux_M_x_x_cd3	Convective flux, M_x, x component	mol/(m^2*s)	M_x * u_M_x_cd3
tflux_M_x_x_cd3	Total flux, M_x, x component	mol/(m^2*s)	dflux_M_x_x_cd3+cflux_M_x_x_cd3
grad_M_x_y_cd3	Concentration gradient, M_x, y component	mol/m^4	M_xy
dflux_M_x_y_cd3	Diffusive flux, M_x, y component	mol/(m^2*s)	-Dyx_M_x_cd3 * M_xx-Dyy_M_x_cd3 * M_xy
cflux_M_x_y_cd3	Convective flux, M_x, y component	mol/(m^2*s)	M_x * v_M_x_cd3
tflux_M_x_y_cd3	Total flux, M_x, y component	mol/(m^2*s)	dflux_M_x_y_cd3+cflux_M_x_y_cd3
beta_M_x_x_cd3	Convective field, M_x, x component	m/s	u_M_x_cd3
beta_M_x_y_cd3	Convective field, M_x, y component	m/s	v_M_x_cd3
grad_M_x_cd3	Concentration gradient, M_x	mol/m^4	sqrt(grad_M_x_x_cd3^2+grad_M_x_y_cd3^2)
dflux_M_x_cd3	Diffusive flux, M_x	mol/(m^2*s)	sqrt(dflux_M_x_x_cd3^2+dflux_M_x_y_cd3^2)
cflux_M_x_cd3	Convective flux, M_x	mol/(m^2*s)	sqrt(cflux_M_x_x_cd3^2+cflux_M_x_y_cd3^2)
tflux_M_x_cd3	Total flux, M_x	mol/(m^2*s)	sqrt(tflux_M_x_x_cd3^2+tflux_M_x_y_cd3^2)
cellPe_M_x_cd3	Cell Peclet number, M_x	1	h * sqrt(beta_M_x_x_cd3^2+beta_M_x_y_cd3^2)/Dm_M_x_cd3
Dm_M_x_cd3	Mean diffusion coefficient, M_x	m^2/s	(Dxx_M_x_cd3 * u_M_x_cd3^2+Dxy_M_x_cd3 * u_M_x_cd3 * v_M_x_cd3+Dyx_M_x_cd3 * v_M_x_cd3 * u_M_x_cd3+Dyy_M_x_cd3 * v_M_x_cd3^2)/(u_M_x_cd3^2+v_M_x_cd3^2+eps)
res_M_x_cd3	Equation residual for M_x	mol/(m^3*s)	-Dxx_M_x_cd3 * M_xxx-Dxy_M_x_cd3 * M_xxy+M_xx * u_M_x_cd3-Dyx_M_x_cd3 * M_xyx-Dyy_M_x_cd3 * M_xyy+M_xy * v_M_x_cd3-R_M_x_cd3
res_sc_M_x_cd3	Shock capturing residual for M_x	mol/(m^3*s)	M_xx * u_M_x_cd3+M_xy * v_M_x_cd3-R_M_x_cd3
da_M_x_cd3	Total time scale factor, M_x	1	Dts_M_x_cd3
grad_M_y_x_cd	Concentration gradient, M_y, x component	mol/m^4	M_yx
dflux_M_y_x_cd	Diffusive flux, M_y, x	mol/(m^2*s)	-Dxx_M_y_cd * M_yx-Dxy_M_y_cd * M_yy

	component		
cflux_M_y_x_cd	Convective flux, M_y, x component	mol/(m^2*s)	M_y * u_M_y_cd
tflux_M_y_x_cd	Total flux, M_y, x component	mol/(m^2*s)	dflux_M_y_x_cd+cflux_M_y_x_cd
grad_M_y_y_cd	Concentration gradient, M_y, y component	mol/m^4	M_yy
dflux_M_y_y_cd	Diffusive flux, M_y, y component	mol/(m^2*s)	-Dyx_M_y_cd * M_yx-Dyy_M_y_cd * M_yy
cflux_M_y_y_cd	Convective flux, M_y, y component	mol/(m^2*s)	M_y * v_M_y_cd
tflux_M_y_y_cd	Total flux, M_y, y component	mol/(m^2*s)	dflux_M_y_y_cd+cflux_M_y_y_cd
beta_M_y_x_cd	Convective field, M_y, x component	m/s	u_M_y_cd
beta_M_y_y_cd	Convective field, M_y, y component	m/s	v_M_y_cd
grad_M_y_cd	Concentration gradient, M_y	mol/m^4	sqrt(grad_M_y_x_cd^2+grad_M_y_y_cd^2)
dflux_M_y_cd	Diffusive flux, M_y	mol/(m^2*s)	sqrt(dflux_M_y_x_cd^2+dflux_M_y_y_cd^2)
cflux_M_y_cd	Convective flux, M_y	mol/(m^2*s)	sqrt(cflux_M_y_x_cd^2+cflux_M_y_y_cd^2)
tflux_M_y_cd	Total flux, M_y	mol/(m^2*s)	sqrt(tflux_M_y_x_cd^2+tflux_M_y_y_cd^2)
cellPe_M_y_cd	Cell Peclet number, M_y	1	h * sqrt(beta_M_y_x_cd^2+beta_M_y_y_cd^2)/Dm_M_y_cd
Dm_M_y_cd	Mean diffusion coefficient, M_y	m^2/s	(Dxx_M_y_cd * u_M_y_cd^2+Dxy_M_y_cd * u_M_y_cd * v_M_y_cd+Dyx_M_y_cd * v_M_y_cd * u_M_y_cd+Dyy_M_y_cd * v_M_y_cd^2)/(u_M_y_cd^2+v_M_y_cd^2+eps)
res_M_y_cd	Equation residual for M_y	mol/(m^3*s)	-Dxx_M_y_cd * M_yxx-Dxy_M_y_cd * M_yxy+M_yx * u_M_y_cd-Dyx_M_y_cd * M_yyx-Dyy_M_y_cd * M_yyy+M_yy * v_M_y_cd-R_M_y_cd
res_sc_M_y_cd	Shock capturing residual for M_y	mol/(m^3*s)	M_yx * u_M_y_cd+M_yy * v_M_y_cd-R_M_y_cd
da_M_y_cd	Total time scale factor, M_y	1	Dts_M_y_cd
dr_guess_emqa	Width in radial direction default guess	m	0

R0_guess_emqa	Inner radius default guess	m	0
Sx_emqa	Infinite element x coordinate	m	x
S0x_guess_emqa	Inner x coordinate default guess	m	0
Sdx_guess_emqa	Width in x direction default guess	m	0
Sy_emqa	Infinite element y coordinate	m	y
S0y_guess_emqa	Inner y coordinate default guess	m	0
Sdy_guess_emqa	Width in y direction default guess	m	0
curlAx_emqa	Curl of magnetic potential, x component	T	Azy
curlAy_emqa	Curl of magnetic potential, y component	T	-Azx
dVol_emqa	Volume integration contribution	1	detJ_emqa
Bx_emqa	Magnetic flux density, x component	T	curlAx_emqa
By_emqa	Magnetic flux density, y component	T	curlAy_emqa
Hx_emqa	Magnetic field, x component	A/m	Bx_emqa/mu0_emqa-Mx_emqa
Hy_emqa	Magnetic field, y component	A/m	By_emqa/mu0_emqa-My_emqa
mu_emqa	Permeability	H/m	mu0_emqa * mur_emqa
muxx_emqa	Permeability, xx component	H/m	mu0_emqa * murxx_emqa
muxy_emqa	Permeability, xy component	H/m	mu0_emqa * murxy_emqa
muyx_emqa	Permeability, yx component	H/m	mu0_emqa * muryx_emqa
muyy_emqa	Permeability, yy component	H/m	mu0_emqa * muryy_emqa

Jpz_emqa	Potential current density, z component	A/m^2	sigma_emqa * deltaV_emqa/L_emqa
Ez_emqa	Electric field, z component	V/m	-d(Az,t)
Jz_emqa	Total current density, z component	A/m^2	Jpz_emqa+Jiz_emqa+Jez_emqa
Pox_emqa	Power flow, x component	W/m^2	-Ez_emqa * Hy_emqa
Poy_emqa	Power flow, y component	W/m^2	Ez_emqa * Hx_emqa
normE_emqa	Electric field, norm	V/m	abs(Ez_emqa)
Jiz_emqa	Induced current density, z component	A/m^2	sigma_emqa * Ez_emqa
Q_emqa	Resistive heating	W/m^3	Jz_emqa * (Ez_emqa+deltaV_emqa/L_emqa)
W_emqa	Total energy density	J/m^3	Wm_emqa
dW_emqa	Integrand for total energy	Pa	dVol_emqa * W_emqa
Wm_emqa	Magnetic energy density	J/m^3	0.5 * (Hx_emqa * Bx_emqa+Hy_emqa * By_emqa+Mx_emqa * Bx_emqa+My_emqa * By_emqa)
FLtzx_emqa	Lorentz force contribution, x component	N/m^3	-Jz_emqa * By_emqa
FLtzy_emqa	Lorentz force contribution, y component	N/m^3	Jz_emqa * Bx_emqa
normFLtz_emqa	Lorentz force contribution, norm	N/m^3	sqrt(abs(FLtzx_emqa)^2+abs(FLtzy_emqa)^2)
normM_emqa	Magnetization, norm	A/m	sqrt(abs(Mx_emqa)^2+abs(My_emqa)^2)
normBr_emqa	Remanent flux density, norm	T	sqrt(abs(Brx_emqa)^2+abs(Bry_emqa)^2)
normH_emqa	Magnetic field, norm	A/m	sqrt(abs(Hx_emqa)^2+abs(Hy_emqa)^2)
normB_emqa	Magnetic flux density, norm	T	sqrt(abs(Bx_emqa)^2+abs(By_emqa)^2)
normJ_emqa	Total current density, norm	A/m^2	abs(Jz_emqa)
Evz_emqa	Lorentz electric field, z component	V/m	d(x,t) * By_emqa-d(y,t) * Bx_emqa

normEv_emqa	Lorentz electric field, norm	V/m	abs(Evz_emqa)
normPo_emqa	Power flow, time average, norm	W/m^2	sqrt(abs(Pox_emqa)^2+abs(Poy_emqa)^2)

I2. MSGW11 Filled Cylinder with Magnetic Field Strength of Permanent Magnet 40 Times Stronger than Rotating Field Strength

COMSOL Model Report

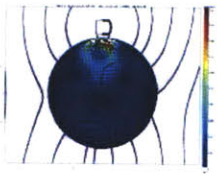

1. Table of Contents

2. Model Properties

Property	Value
Model name	
Author	
Company	
Department	
Reference	
URL	
Saved date	May 13, 2010 10:55:26 PM
Creation date	Sep 19, 2008 9:32:16 PM
COMSOL version	COMSOL 3.5.0.608

File name: F:\Research Files\Software Data Files\Comsol Files\Good2DMagnetcases \2Dcase_cylinder_surfacecurrent_forceincluded_etaprime0_MSGW11_airgap_R10_magnetMz40.mph

Application modes and modules used in this model:

- Geom1 (2D)
  - Incompressible Navier-Stokes
  - Diffusion
  - Convection and Diffusion
  - Convection and Diffusion
  - Perpendicular Induction Currents, Vector Potential (AC/DC Module)

2.1. Model description

Rotation of Ferrofluid in a rotating magnetic field in an infinitely long cylinder with a ferrofluid inner smaller cylinder that has a magnet put on top of it generating a non-uniform field. Etaprime is 0. The magnet is 40 times stronger than the rotating field

MSGW11 is used

Using my normalization scheme outlined in VeryifyingShihabsmethod_081205.doc

Etaprime 0 case

3. Constants

Name	Expression	Value	Description
Xi	0.56		
omega	2*pi*f		
zeta	0.000313		
eta	7.58e-3		
etaprime	0		
f	95		
tau	1.39e-5		
omegatau	omega*tau		
R0	0.027		
I	2/3		
Ms	1.54		

4. Global Expressions

Name	Expression	Unit	Description
FMx	M_x*(Azyx-M_xx)+M_y*(Azyy-M_xy)		\
FMy	M_x*(-Azxx-M_yx)+M_y*(-Azxy-M_yy)		
T	M_x*Hy-M_y*Hx	A*mol/m^4	
M_eqx	Ms*(coth(alpha)-1/alpha)*Hx/(normH_emqa+1e-20)		
M_eqy	Ms*(coth(alpha)-1/alpha)*Hy/(normH_emqa+1e-20)		
Hx	Hx_emqa	A/m	
Hy	Hy_emqa	A/m	
phi	atan2(y,x)	rad	
alpha	27.8*normH_emqa+1e-20	A/m	
divH	d(Hx,x)+d(Hy,y)	A/m^2	
curlM	d(My,x)-d(Mx,y)		
Fx	0.5*(Bx_emqa*divH)-0.5*(Hy*curlM)		
Fy	0.5*(By_emqa*divH)+0.5*(Hx*curlM)		

5. Geometry

Number of geometries: 1

5.1. Geom1

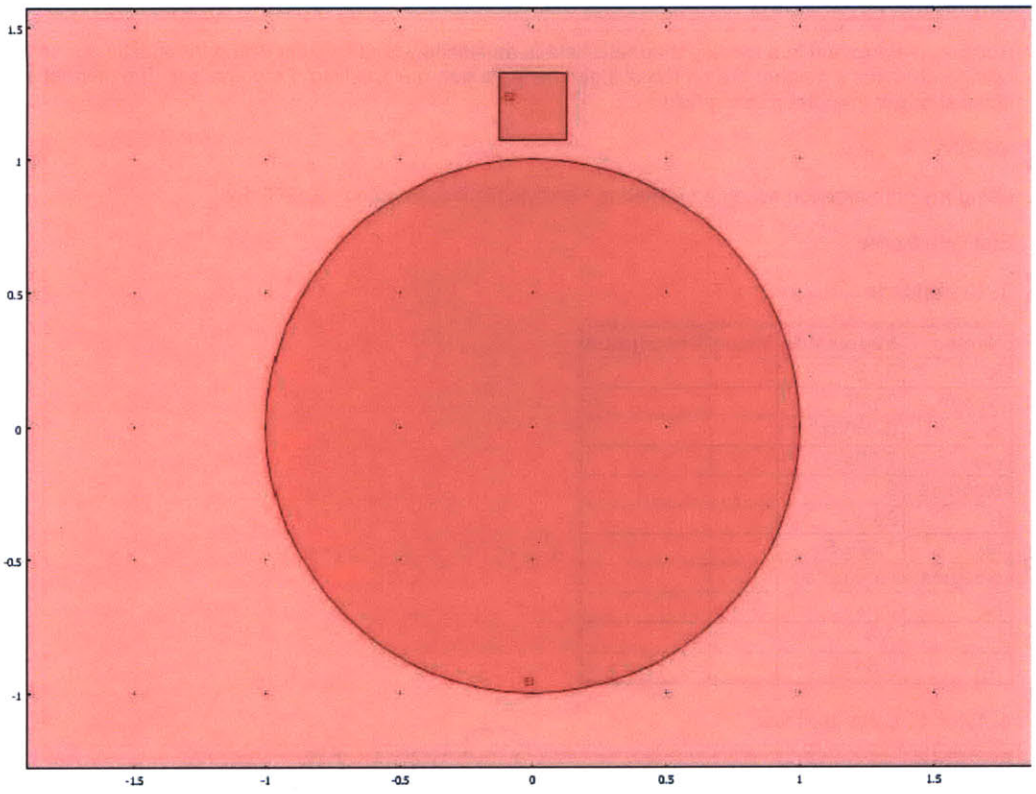

5.1.1. Point mode

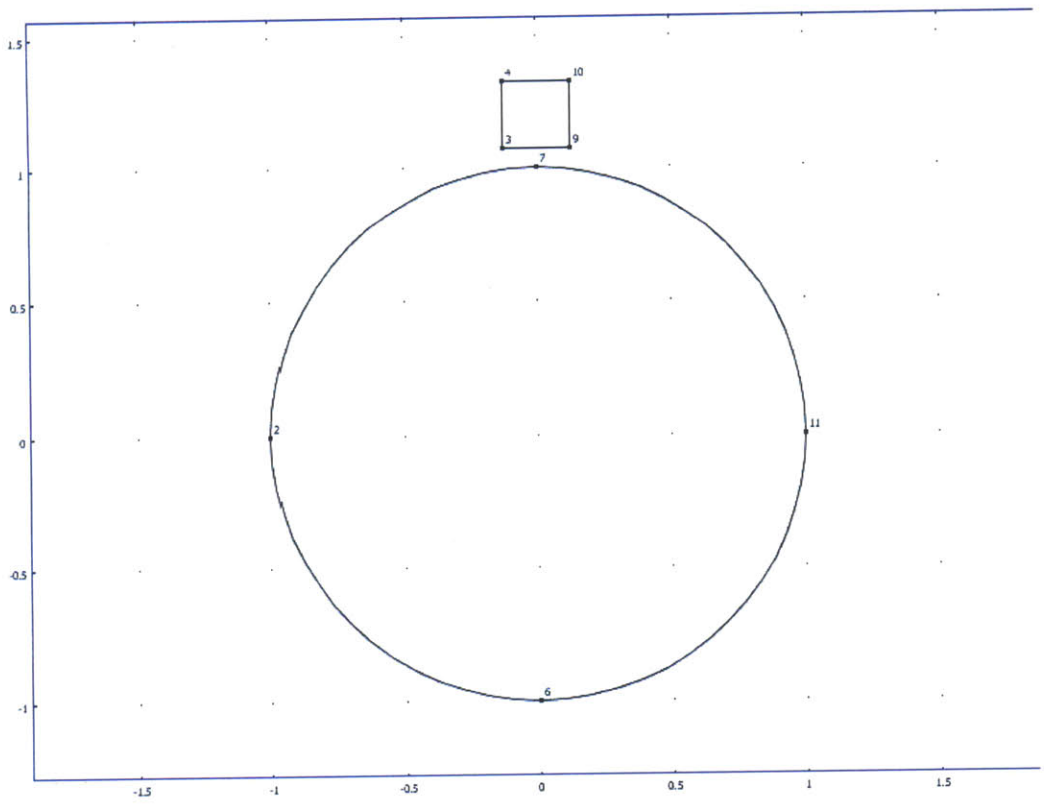

5.1.2. Boundary mode

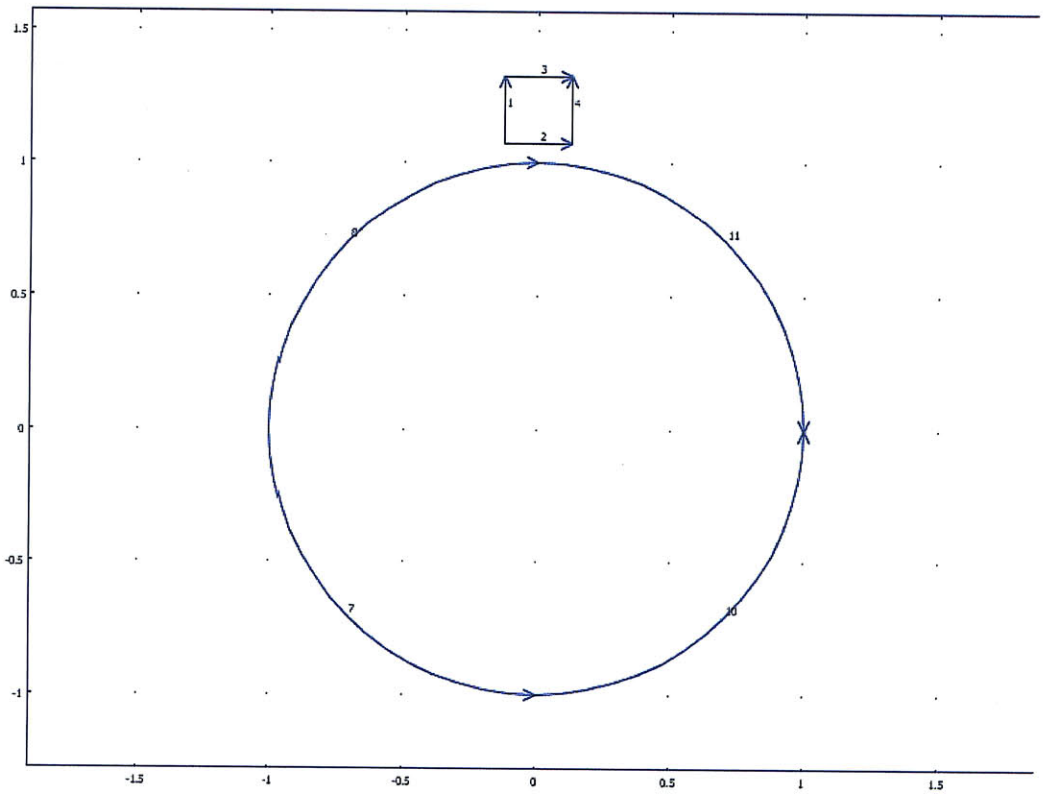

5.1.3. Subdomain mode

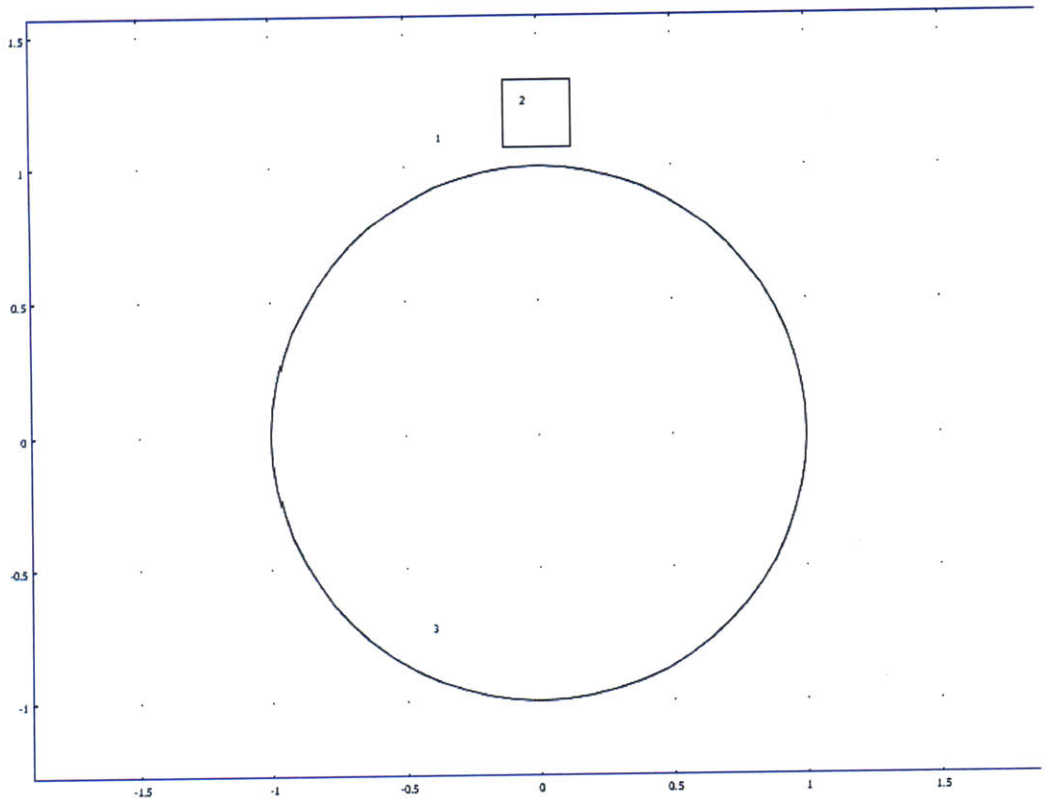

6. Geom1

Space dimensions: 2D

Independent variables: x, y, z

6.1. Mesh

6.1.1. Mesh Statistics

Number of degrees of freedom	275352
Number of mesh points	3898
Number of elements	7734
Triangular	7734
Quadrilateral	0
Number of boundary elements	204
Number of vertex elements	12
Minimum element quality	0.784
Element area ratio	0

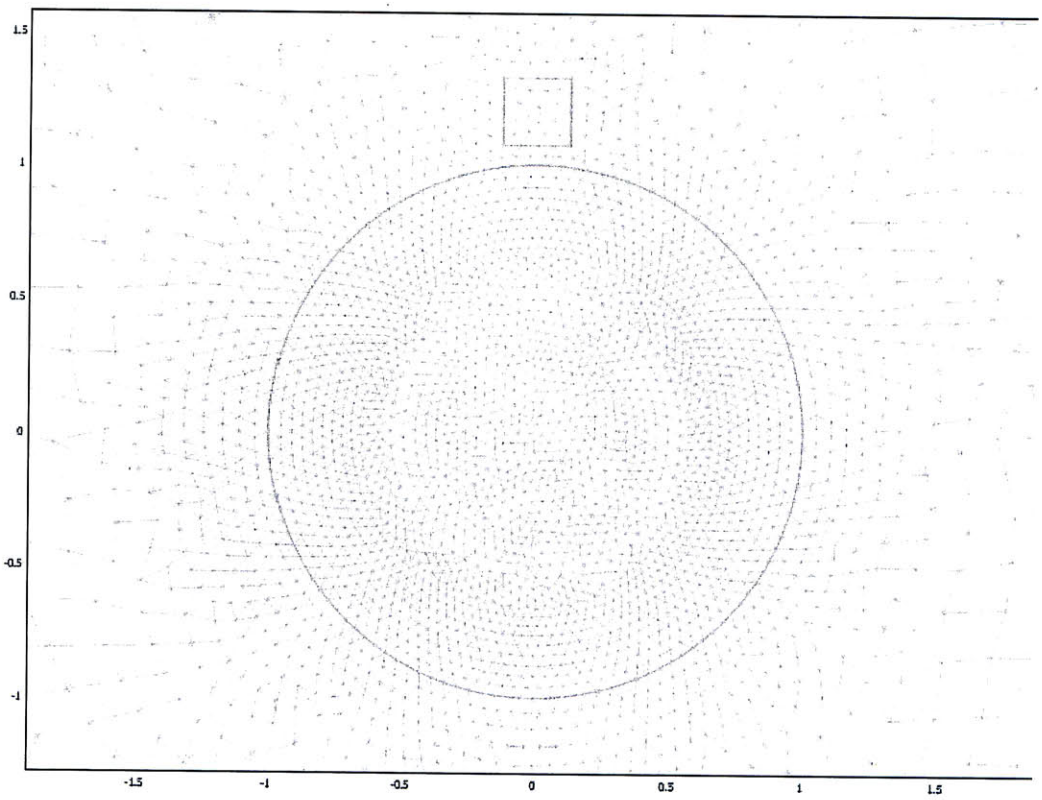

6.2. Application Mode: Incompressible Navier-Stokes (ns)

Application mode type: Incompressible Navier-Stokes

Application mode name: ns

6.2.1. Scalar Variables

Name	Variable	Value	Unit	Description
visc_vel_fact	visc_vel_fact_ns	10	1	Viscous velocity factor

6.2.2. Application Mode Properties

Property	Value
Default element type	Lagrange - P_2 P_1
Analysis type	Transient
Corner smoothing	Off
Frame	Frame (ref)
Weak constraints	Off
Constraint type	Ideal

6.2.3. Variables

Dependent variables: u, v, p, nxw, nyw

Shape functions: shlag(2,'u'), shlag(2,'v'), shlag(1,'p')

Interior boundaries not active

6.2.4. Point Settings

Point	1, 3-12	2
pnton	0	1

6.2.5. Boundary Settings

Boundary	7-8, 10-11
Type	Wall

6.2.6. Subdomain Settings

Subdomain		3
Integration order (gporder)		**4 4 2**
Constraint order (cporder)		**2 2 1**
Density (rho)	kg/m^3	**0**
Dynamic viscosity (eta)	Pa·s	**eta+zeta**
Volume force, x dir. (F_x)	N/m^3	**2*zeta*wy+FMx**
Volume force, y dir. (F_y)	N/m^3	**-2*zeta*wx+FMy**
cdon		**0**

6.3. Application Mode: Diffusion (di)

Application mode type: Diffusion

Application mode name: di

6.3.1. Application Mode Properties

Property	Value
Default element type	Lagrange - Quadratic
Analysis type	Stationary
Frame	Frame (ref)
Weak constraints	Off
Constraint type	Ideal

6.3.2. Variables

Dependent variables: w

Shape functions: shlag(2,'w'), shlag(5,'w')

Interior boundaries not active

6.3.3. Boundary Settings

Boundary	7-8, 10-11
Type	Insulation/Symmetry

6.3.4. Subdomain Settings

Subdomain		3
Shape functions (shape)		**shlag(2,'w') shlag(5,'w')**
Integration order (gporder)		**10**
Constraint order (cporder)		**5**
Diffusion coefficient (D)	m^2/s	**etaprime**
Reaction rate (R)	$mol/(m^3 \cdot s)$	**T+2*zeta*(vx-uy-2*w)**

6.4. Application Mode: Convection and Diffusion (cd3)

Application mode type: Convection and Diffusion

Application mode name: cd3

6.4.1. Application Mode Properties

Property	**Value**
Default element type	Lagrange - Quadratic
Analysis type	Transient
Equation form	Non-conservative
Frame	Frame (ref)
Weak constraints	Off
Constraint type	Ideal

6.4.2. Variables

Dependent variables: M_x

Shape functions: shlag(2,'M_x'), shlag(5,'M_x')

Interior boundaries not active

6.4.3. Boundary Settings

Boundary	7-8, 10-11
Type	Insulation/Symmetry

6.4.4. Subdomain Settings

Subdomain		3
Shape functions (shape)		**shlag(2,'M_x') shlag(5,'M_x')**

Integration order (gporder)		**10**
Constraint order (cporder)		**5**
Diffusion coefficient (D)	m^2/s	**0**
Reaction rate (R)	$mol/(m^3 \cdot s)$	**-w*M_y-((M_x-M_eqx)/omegatau)**
x-velocity (u)	m/s	**u**
y-velocity (v)	m/s	**v**

6.5. Application Mode: Convection and Diffusion (cd)

Application mode type: Convection and Diffusion

Application mode name: cd

6.5.1. Application Mode Properties

Property	Value
Default element type	Lagrange - Quadratic
Analysis type	Transient
Equation form	Non-conservative
Frame	Frame (ref)
Weak constraints	Off
Constraint type	Ideal

6.5.2. Variables

Dependent variables: M_y

Shape functions: shlag(2,'M_y'), shlag(5,'M_y')

Interior boundaries not active

6.5.3. Boundary Settings

Boundary	7-8, 10-11
Type	Insulation/Symmetry

6.5.4. Subdomain Settings

Subdomain		3
Shape functions (shape)		**shlag(2,'M_y') shlag(5,'M_y')**
Integration order (gporder)		**10**
Constraint order (cporder)		**5**
Diffusion coefficient (D)	m^2/s	**0**
Reaction rate (R)	$mol/(m^3 \cdot s)$	**w*M_x-((M_y-M_eqy)/omegatau)**
x-velocity (u)	m/s	**u**
y-velocity (v)	m/s	**v**

6.6. Application Mode: Perpendicular Induction Currents, Vector Potential (emqa)

Application mode type: Perpendicular Induction Currents, Vector Potential (AC/DC Module)

Application mode name: emqa

6.6.1. Scalar Variables

Name	Variable	Value	Unit	Description
epsilon0	epsilon0_emqa	8.854187817e-12	F/m	Permittivity of vacuum
mu0	mu0_emqa	1	H/m	Permeability of vacuum

6.6.2. Application Mode Properties

Property	Value
Default element type	Lagrange - Quintic
Analysis type	Transient
Bias application mode	None
Solve for	Total potential
Background field	Magnetic vector potential
Frame	Frame (ref)
Weak constraints	Off
Constraint type	Ideal

6.6.3. Variables

Dependent variables: Az, redAz

Shape functions: shlag(5,'Az')

Interior boundaries active

6.6.4. Boundary Settings

Boundary		1-4, 7-8, 10-11	5-6, 9, 12
Type		Continuity	Surface current
Surface current density (Js0z)	A/m	**I*(3/2)*cos(t-phi)*flc2hs(t-1,0.05)**	**I*(3/2)*cos(t-phi)*flc2hs(t-1,0.05)**

6.6.5. Subdomain Settings

Subdomain		1	2	3
magconstrel		**B = $\mu_0\mu_r$H**	**B = μ_0H + μ_0M**	**B = μ_0H + μ_0M**
Magnetization (M)	A/m	{0;0}	**{0;40*flc2hs(t-1,0.05)}**	**{M_x;M_y}**

7. Solver Settings

Solve using a script: off

Analysis type	Transient
Auto select solver	On
Solver	Time dependent
Solution form	Automatic

Symmetric	auto
Adaptive mesh refinement	Off
Optimization/Sensitivity	Off
Plot while solving	Off

7.1. Direct (UMFPACK)

Solver type: Linear system solver

Parameter	Value
Pivot threshold	0.1
Memory allocation factor	0.7

7.2. Time Stepping

Parameter	Value
Times	range(0,0.1,10)
Relative tolerance	0.01
Absolute tolerance	0.0010
Times to store in output	Specified times
Time steps taken by solver	Free
Maximum BDF order	5
Singular mass matrix	Maybe
Consistent initialization of DAE systems	Backward Euler
Error estimation strategy	Include algebraic
Allow complex numbers	On

7.3. Advanced

Parameter	Value
Constraint handling method	Elimination
Null-space function	Automatic
Automatic assembly block size	On
Assembly block size	5000
Use Hermitian transpose of constraint matrix and in symmetry detection	Off
Use complex functions with real input	Off
Stop if error due to undefined operation	On
Store solution on file	Off
Type of scaling	Automatic
Manual scaling	
Row equilibration	On
Manual control of reassembly	Off
Load constant	On
Constraint constant	On
Mass constant	On
Damping (mass) constant	On
Jacobian constant	On
Constraint Jacobian constant	On

8. Postprocessing

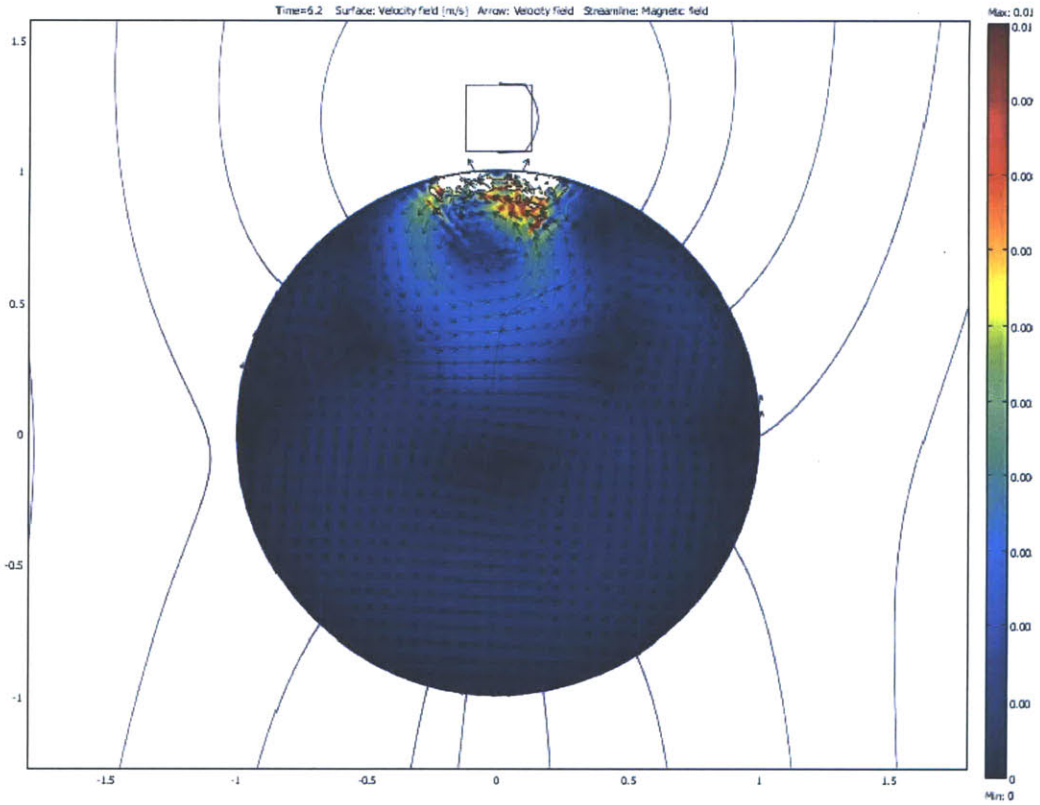

9. Variables

9.1. Boundary

9.1.1. Boundary 1-6, 9, 12

Name	Description	Unit	Expression
K_x_ns	Viscous force per area, x component	Pa	
T_x_ns	Total force per area, x component	Pa	
K_y_ns	Viscous force per area, y component	Pa	
T_y_ns	Total force per area, y component	Pa	

ndflux_w_di	Normal diffusive flux, w	mol/(m^2*s)	
ndflux_M_x_cd3	Normal diffusive flux, M_x	mol/(m^2*s)	
ncflux_M_x_cd3	Normal convective flux, M_x	mol/(m^2*s)	
ntflux_M_x_cd3	Normal total flux, M_x	mol/(m^2*s)	
ndflux_M_y_cd	Normal diffusive flux, M_y	mol/(m^2*s)	
ncflux_M_y_cd	Normal convective flux, M_y	mol/(m^2*s)	
ntflux_M_y_cd	Normal total flux, M_y	mol/(m^2*s)	
dVolbnd_emqa	Area integration contribution	1	1
murbnd_emqa	Relative permeability	1	murbndxx_emqa
Jsz_emqa	Surface current density	A/m	unx * (Hy_emqa_down-Hy_emqa_up)-uny * (Hx_emqa_down-Hx_emqa_up)
unTx_emqa	Maxwell surface stress tensor, x component	Pa	-0.5 * (Bx_emqa_up * Hx_emqa_up+By_emqa_up * Hy_emqa_up) * dnx+(dnx * Hx_emqa_up+dny * Hy_emqa_up) * Bx_emqa_up
dnTx_emqa	Maxwell surface stress tensor, x component	Pa	-0.5 * (Bx_emqa_down * Hx_emqa_down+By_emqa_down * Hy_emqa_down) * unx+(unx * Hx_emqa_down+uny * Hy_emqa_down) * Bx_emqa_down
unTy_emqa	Maxwell surface stress tensor, y component	Pa	-0.5 * (Bx_emqa_up * Hx_emqa_up+By_emqa_up * Hy_emqa_up) * dny+(dnx * Hx_emqa_up+dny * Hy_emqa_up) * By_emqa_up
dnTy_emqa	Maxwell surface stress tensor, y component	Pa	-0.5 * (Bx_emqa_down * Hx_emqa_down+By_emqa_down * Hy_emqa_down) * uny+(unx * Hx_emqa_down+uny * Hy_emqa_down) * By_emqa_down
Qs_emqa	Surface resistive heating	W/m^2	Jsz_emqa * Ez_emqa
nPo_emqa	Power outflow	W/m^2	nx_emqa * Pox_emqa+ny_emqa * Poy_emqa
FsLtzx_emqa	Lorentz surface force contribution, x component	Pa	-Jsz_emqa * By_emqa
FsLtzy_emqa	Lorentz surface force contribution, y component	Pa	Jsz_emqa * Bx_emqa
normFsLtz_emqa	Lorentz surface force contribution, cycle average, norm	Pa	sqrt(abs(FsLtzx_emqa)^2+abs(FsLtzy_emqa)^2)

9.1.2. Boundary 7-8, 10-11

Name	Description	Unit	Expression
K_x_ns	Viscous force per area, x component	Pa	eta_ns * (2 * nx_ns * ux+ny_ns * (uy+vx))
T_x_ns	Total force per area, x component	Pa	-nx_ns * p+2 * nx_ns * eta_ns * ux+ny_ns * eta_ns * (uy+vx)
K_y_ns	Viscous force per area, y component	Pa	eta_ns * (nx_ns * (vx+uy)+2 * ny_ns * vy)
T_y_ns	Total force per area, y component	Pa	-ny_ns * p+nx_ns * eta_ns * (vx+uy)+2 * ny_ns * eta_ns * vy
ndflux_w_di	Normal diffusive flux, w	mol/(m^2*s)	nx_di * dflux_w_x_di+ny_di * dflux_w_y_di
ndflux_M_x_cd3	Normal diffusive flux, M_x	mol/(m^2*s)	nx_cd3 * dflux_M_x_x_cd3+ny_cd3 * dflux_M_x_y_cd3
ncflux_M_x_cd3	Normal convective flux, M_x	mol/(m^2*s)	nx_cd3 * cflux_M_x_x_cd3+ny_cd3 * cflux_M_x_y_cd3
ntflux_M_x_cd3	Normal total flux, M_x	mol/(m^2*s)	nx_cd3 * tflux_M_x_x_cd3+ny_cd3 * tflux_M_x_y_cd3
ndflux_M_y_cd	Normal diffusive flux, M_y	mol/(m^2*s)	nx_cd * dflux_M_y_x_cd+ny_cd * dflux_M_y_y_cd
ncflux_M_y_cd	Normal convective flux, M_y	mol/(m^2*s)	nx_cd * cflux_M_y_x_cd+ny_cd * cflux_M_y_y_cd
ntflux_M_y_cd	Normal total flux, M_y	mol/(m^2*s)	nx_cd * tflux_M_y_x_cd+ny_cd * tflux_M_y_y_cd
dVolbnd_emqa	Area integration contribution	1	1
murbnd_emqa	Relative permeability	1	murbndxx_emqa
Jsz_emqa	Surface current density	A/m	unx * (Hy_emqa_down-Hy_emqa_up)-uny * (Hx_emqa_down-Hx_emqa_up)
unTx_emqa	Maxwell surface stress tensor, x component	Pa	-0.5 * (Bx_emqa_up * Hx_emqa_up+By_emqa_up * Hy_emqa_up) * dnx+(dnx * Hx_emqa_up+dny * Hy_emqa_up) * Bx_emqa_up
dnTx_emqa	Maxwell surface stress tensor, x component	Pa	-0.5 * (Bx_emqa_down * Hx_emqa_down+By_emqa_down * Hy_emqa_down) * unx+(unx * Hx_emqa_down+uny * Hy_emqa_down) * Bx_emqa_down
unTy_emqa	Maxwell surface stress tensor, y component	Pa	-0.5 * (Bx_emqa_up * Hx_emqa_up+By_emqa_up * Hy_emqa_up) * dny+(dnx * Hx_emqa_up+dny * Hy_emqa_up) * By_emqa_up
dnTy_emqa	Maxwell surface stress tensor, y component	Pa	-0.5 * (Bx_emqa_down * Hx_emqa_down+By_emqa_down * Hy_emqa_down) * uny+(unx * Hx_emqa_down+uny * Hy_emqa_down) * By_emqa_down

Qs_emqa	Surface resistive heating	W/m^2	Jsz_emqa * Ez_emqa
nPo_emqa	Power outflow	W/m^2	nx_emqa * Pox_emqa+ny_emqa * Poy_emqa
FsLtzx_emqa	Lorentz surface force contribution, x component	Pa	-Jsz_emqa * By_emqa
FsLtzy_emqa	Lorentz surface force contribution, y component	Pa	Jsz_emqa * Bx_emqa
normFsLtz_emqa	Lorentz surface force contribution, cycle average, norm	Pa	sqrt(abs(FsLtzx_emqa)^2+abs(FsLtzy_emqa)^2)

9.2. Subdomain

9.2.1. Subdomain 1

Name	Description	Unit	Expression
U_ns	Velocity field	m/s	
V_ns	Vorticity	1/s	
divU_ns	Divergence of velocity field	1/s	
cellRe_ns	Cell Reynolds number	1	
res_u_ns	Equation residual for u	N/m^3	
res_v_ns	Equation residual for v	N/m^3	
beta_x_ns	Convective field, x component	kg/(m^2*s)	
beta_y_ns	Convective field, y component	kg/(m^2*s)	
Dm_ns	Mean diffusion coefficient	Pa*s	
da_ns	Total time scale factor	kg/m^3	
taum_ns	GLS time-scale	m^3*s/kg	
tauc_ns	GLS time-scale	m^2/s	
res_p_ns	Equation residual for p	kg/(m^3*s)	
grad_w_x_di	Concentration gradient, w, x component	mol/m^4	
dflux_w_x_di	Diffusive flux, w, x component	mol/(m^2*s)	
grad_w_y_di	Concentration gradient, w, y component	mol/m^4	
dflux_w_y_di	Diffusive flux, w, y component	mol/(m^2*s)	
grad_w_di	Concentration gradient, w	mol/m^4	
dflux_w_di	Diffusive flux, w	mol/(m^2*s)	
grad_M_x_x_cd3	Concentration gradient, M_x, x component	mol/m^4	

dflux_M_x_x_cd3	Diffusive flux, M_x, x component	mol/(m^2*s)	
cflux_M_x_x_cd3	Convective flux, M_x, x component	mol/(m^2*s)	
tflux_M_x_x_cd3	Total flux, M_x, x component	mol/(m^2*s)	
grad_M_x_y_cd3	Concentration gradient, M_x, y component	mol/m^4	
dflux_M_x_y_cd3	Diffusive flux, M_x, y component	mol/(m^2*s)	
cflux_M_x_y_cd3	Convective flux, M_x, y component	mol/(m^2*s)	
tflux_M_x_y_cd3	Total flux, M_x, y component	mol/(m^2*s)	
beta_M_x_x_cd3	Convective field, M_x, x component	m/s	
beta_M_x_y_cd3	Convective field, M_x, y component	m/s	
grad_M_x_cd3	Concentration gradient, M_x	mol/m^4	
dflux_M_x_cd3	Diffusive flux, M_x	mol/(m^2*s)	
cflux_M_x_cd3	Convective flux, M_x	mol/(m^2*s)	
tflux_M_x_cd3	Total flux, M_x	mol/(m^2*s)	
cellPe_M_x_cd3	Cell Peclet number, M_x	1	
Dm_M_x_cd3	Mean diffusion coefficient, M_x	m^2/s	
res_M_x_cd3	Equation residual for M_x	mol/(m^3*s)	
res_sc_M_x_cd3	Shock capturing residual for M_x	mol/(m^3*s)	
da_M_x_cd3	Total time scale factor, M_x	1	
grad_M_y_x_cd	Concentration gradient, M_y, x component	mol/m^4	
dflux_M_y_x_cd	Diffusive flux, M_y, x component	mol/(m^2*s)	
cflux_M_y_x_cd	Convective flux, M_y, x component	mol/(m^2*s)	
tflux_M_y_x_cd	Total flux, M_y, x component	mol/(m^2*s)	
grad_M_y_y_cd	Concentration gradient, M_y, y component	mol/m^4	
dflux_M_y_y_cd	Diffusive flux, M_y, y component	mol/(m^2*s)	
cflux_M_y_y_cd	Convective flux, M_y, y component	mol/(m^2*s)	
tflux_M_y_y_cd	Total flux, M_y, y component	mol/(m^2*s)	
beta_M_y_x_cd	Convective field, M_y, x component	m/s	

beta_M_y_y_cd	Convective field, M_y, y component	m/s	
grad_M_y_cd	Concentration gradient, M_y	mol/m^4	
dflux_M_y_cd	Diffusive flux, M_y	mol/(m^2*s)	
cflux_M_y_cd	Convective flux, M_y	mol/(m^2*s)	
tflux_M_y_cd	Total flux, M_y	mol/(m^2*s)	
cellPe_M_y_cd	Cell Peclet number, M_y	1	
Dm_M_y_cd	Mean diffusion coefficient, M_y	m^2/s	
res_M_y_cd	Equation residual for M_y	mol/(m^3*s)	
res_sc_M_y_cd	Shock capturing residual for M_y	mol/(m^3*s)	
da_M_y_cd	Total time scale factor, M_y	1	
dr_guess_emqa	Width in radial direction default guess	m	0
R0_guess_emqa	Inner radius default guess	m	0
Sx_emqa	Infinite element x coordinate	m	x
S0x_guess_emqa	Inner x coordinate default guess	m	0
Sdx_guess_emqa	Width in x direction default guess	m	0
Sy_emqa	Infinite element y coordinate	m	y
S0y_guess_emqa	Inner y coordinate default guess	m	0
Sdy_guess_emqa	Width in y direction default guess	m	0
curlAx_emqa	Curl of magnetic potential, x component	T	Azy
curlAy_emqa	Curl of magnetic potential, y component	T	-Azx
dVol_emqa	Volume integration contribution	1	detJ_emqa
Bx_emqa	Magnetic flux density, x component	T	curlAx_emqa
By_emqa	Magnetic flux density, y component	T	curlAy_emqa
Hx_emqa	Magnetic field, x component	A/m	Bx_emqa/(mur_emqa * mu0_emqa)
Hy_emqa	Magnetic field, y component	A/m	By_emqa/(mur_emqa * mu0_emqa)
mu_emqa	Permeability	H/m	mu0_emqa * mur_emqa
muxx_emqa	Permeability, xx component	H/m	mu0_emqa * murxx_emqa
muxy_emqa	Permeability, xy component	H/m	mu0_emqa * murxy_emqa

muyx_emqa	Permeability, yx component	H/m	mu0_emqa * muryx_emqa
muyy_emqa	Permeability, yy component	H/m	mu0_emqa * muryy_emqa
Jpz_emqa	Potential current density, z component	A/m^2	sigma_emqa * deltaV_emqa/L_emqa
Ez_emqa	Electric field, z component	V/m	-d(Az,t)
Jz_emqa	Total current density, z component	A/m^2	Jpz_emqa+Jiz_emqa+Jez_emqa
Pox_emqa	Power flow, x component	W/m^2	-Ez_emqa * Hy_emqa
Poy_emqa	Power flow, y component	W/m^2	Ez_emqa * Hx_emqa
normE_emqa	Electric field, norm	V/m	abs(Ez_emqa)
Jiz_emqa	Induced current density, z component	A/m^2	sigma_emqa * Ez_emqa
Q_emqa	Resistive heating	W/m^3	Jz_emqa * (Ez_emqa+deltaV_emqa/L_emqa)
W_emqa	Total energy density	J/m^3	Wm_emqa
dW_emqa	Integrand for total energy	J/m^3	dVol_emqa * W_emqa
Wm_emqa	Magnetic energy density	J/m^3	0.5 * (Hx_emqa * Bx_emqa+Hy_emqa * By_emqa)
FLtzx_emqa	Lorentz force contribution, x component	N/m^3	-Jz_emqa * By_emqa
FLtzy_emqa	Lorentz force contribution, y component	N/m^3	Jz_emqa * Bx_emqa
normFLtz_emqa	Lorentz force contribution, norm	N/m^3	sqrt(abs(FLtzx_emqa)^2+abs(FLtzy_emqa)^2)
normM_emqa	Magnetization, norm	A/m	sqrt(abs(Mx_emqa)^2+abs(My_emqa)^2)
normBr_emqa	Remanent flux density, norm	T	sqrt(abs(Brx_emqa)^2+abs(Bry_emqa)^2)
normH_emqa	Magnetic field, norm	A/m	sqrt(abs(Hx_emqa)^2+abs(Hy_emqa)^2)
normB_emqa	Magnetic flux density, norm	T	sqrt(abs(Bx_emqa)^2+abs(By_emqa)^2)
normJ_emqa	Total current density, norm	A/m^2	abs(Jz_emqa)
Evz_emqa	Lorentz electric field, z component	V/m	d(x,t) * By_emqa-d(y,t) * Bx_emqa
normEv_emqa	Lorentz electric field, norm	V/m	abs(Evz_emqa)
normPo_emqa	Power flow, time average, norm	W/m^2	sqrt(abs(Pox_emqa)^2+abs(Poy_emqa)^2)

9.2.2. Subdomain 2

Name	Description	Unit	Expression
U_ns	Velocity field	m/s	
V_ns	Vorticity	1/s	
divU_ns	Divergence of velocity field	1/s	

cellRe_ns	Cell Reynolds number	1	
res_u_ns	Equation residual for u	N/m^3	
res_v_ns	Equation residual for v	N/m^3	
beta_x_ns	Convective field, x component	kg/(m^2*s)	
beta_y_ns	Convective field, y component	kg/(m^2*s)	
Dm_ns	Mean diffusion coefficient	Pa*s	
da_ns	Total time scale factor	kg/m^3	
taum_ns	GLS time-scale	m^3*s/kg	
tauc_ns	GLS time-scale	m^2/s	
res_p_ns	Equation residual for p	kg/(m^3*s)	
grad_w_x_di	Concentration gradient, w, x component	mol/m^4	
dflux_w_x_di	Diffusive flux, w, x component	mol/(m^2*s)	
grad_w_y_di	Concentration gradient, w, y component	mol/m^4	
dflux_w_y_di	Diffusive flux, w, y component	mol/(m^2*s)	
grad_w_di	Concentration gradient, w	mol/m^4	
dflux_w_di	Diffusive flux, w	mol/(m^2*s)	
grad_M_x_x_cd3	Concentration gradient, M_x, x component	mol/m^4	
dflux_M_x_x_cd3	Diffusive flux, M_x, x component	mol/(m^2*s)	
cflux_M_x_x_cd3	Convective flux, M_x, x component	mol/(m^2*s)	
tflux_M_x_x_cd3	Total flux, M_x, x component	mol/(m^2*s)	
grad_M_x_y_cd3	Concentration gradient, M_x, y component	mol/m^4	
dflux_M_x_y_cd3	Diffusive flux, M_x, y component	mol/(m^2*s)	
cflux_M_x_y_cd3	Convective flux, M_x, y component	mol/(m^2*s)	
tflux_M_x_y_cd3	Total flux, M_x, y component	mol/(m^2*s)	
beta_M_x_x_cd3	Convective field, M_x, x component	m/s	

beta_M_x_y_cd3	Convective field, M_x, y component	m/s	
grad_M_x_cd3	Concentration gradient, M_x	mol/m^4	
dflux_M_x_cd3	Diffusive flux, M_x	mol/(m^2*s)	
cflux_M_x_cd3	Convective flux, M_x	mol/(m^2*s)	
tflux_M_x_cd3	Total flux, M_x	mol/(m^2*s)	
cellPe_M_x_cd3	Cell Peclet number, M_x	1	
Dm_M_x_cd3	Mean diffusion coefficient, M_x	m^2/s	
res_M_x_cd3	Equation residual for M_x	mol/(m^3*s)	
res_sc_M_x_cd3	Shock capturing residual for M_x	mol/(m^3*s)	
da_M_x_cd3	Total time scale factor, M_x	1	
grad_M_y_x_cd	Concentration gradient, M_y, x component	mol/m^4	
dflux_M_y_x_cd	Diffusive flux, M_y, x component	mol/(m^2*s)	
cflux_M_y_x_cd	Convective flux, M_y, x component	mol/(m^2*s)	
tflux_M_y_x_cd	Total flux, M_y, x component	mol/(m^2*s)	
grad_M_y_y_cd	Concentration gradient, M_y, y component	mol/m^4	
dflux_M_y_y_cd	Diffusive flux, M_y, y component	mol/(m^2*s)	
cflux_M_y_y_cd	Convective flux, M_y, y component	mol/(m^2*s)	
tflux_M_y_y_cd	Total flux, M_y, y component	mol/(m^2*s)	
beta_M_y_x_cd	Convective field, M_y, x component	m/s	
beta_M_y_y_cd	Convective field, M_y, y component	m/s	
grad_M_y_cd	Concentration gradient, M_y	mol/m^4	
dflux_M_y_cd	Diffusive flux, M_y	mol/(m^2*s)	
cflux_M_y_cd	Convective flux, M_y	mol/(m^2*s)	
tflux_M_y_cd	Total flux, M_y	mol/(m^2*s)	
cellPe_M_y_cd	Cell Peclet number, M_y	1	
Dm_M_y_cd	Mean diffusion coefficient, M_y	m^2/s	

res_M_y_cd	Equation residual for M_y	mol/(m^3*s)	
res_sc_M_y_cd	Shock capturing residual for M_y	mol/(m^3*s)	
da_M_y_cd	Total time scale factor, M_y	1	
dr_guess_emqa	Width in radial direction default guess	m	0
R0_guess_emqa	Inner radius default guess	m	0
Sx_emqa	Infinite element x coordinate	m	x
S0x_guess_emqa	Inner x coordinate default guess	m	0
Sdx_guess_emqa	Width in x direction default guess	m	0
Sy_emqa	Infinite element y coordinate	m	y
S0y_guess_emqa	Inner y coordinate default guess	m	0
Sdy_guess_emqa	Width in y direction default guess	m	0
curlAx_emqa	Curl of magnetic potential, x component	T	Azy
curlAy_emqa	Curl of magnetic potential, y component	T	-Azx
dVol_emqa	Volume integration contribution	1	detJ_emqa
Bx_emqa	Magnetic flux density, x component	T	curlAx_emqa
By_emqa	Magnetic flux density, y component	T	curlAy_emqa
Hx_emqa	Magnetic field, x component	A/m	Bx_emqa/mu0_emqa-Mx_emqa
Hy_emqa	Magnetic field, y component	A/m	By_emqa/mu0_emqa-My_emqa
mu_emqa	Permeability	H/m	mu0_emqa * mur_emqa
muxx_emqa	Permeability, xx component	H/m	mu0_emqa * murxx_emqa
muxy_emqa	Permeability, xy component	H/m	mu0_emqa * murxy_emqa
muyx_emqa	Permeability, yx component	H/m	mu0_emqa * muryx_emqa
muyy_emqa	Permeability, yy component	H/m	mu0_emqa * muryy_emqa

Jpz_emqa	Potential current density, z component	A/m^2	sigma_emqa * deltaV_emqa/L_emqa
Ez_emqa	Electric field, z component	V/m	-d(Az,t)
Jz_emqa	Total current density, z component	A/m^2	Jpz_emqa+Jiz_emqa+Jez_emqa
Pox_emqa	Power flow, x component	W/m^2	-Ez_emqa * Hy_emqa
Poy_emqa	Power flow, y component	W/m^2	Ez_emqa * Hx_emqa
normE_emqa	Electric field, norm	V/m	abs(Ez_emqa)
Jiz_emqa	Induced current density, z component	A/m^2	sigma_emqa * Ez_emqa
Q_emqa	Resistive heating	W/m^3	Jz_emqa * (Ez_emqa+deltaV_emqa/L_emqa)
W_emqa	Total energy density	J/m^3	Wm_emqa
dW_emqa	Integrand for total energy	Pa	dVol_emqa * W_emqa
Wm_emqa	Magnetic energy density	J/m^3	0.5 * (Hx_emqa * Bx_emqa+Hy_emqa * By_emqa+Mx_emqa * Bx_emqa+My_emqa * By_emqa)
FLtzx_emqa	Lorentz force contribution, x component	N/m^3	-Jz_emqa * By_emqa
FLtzy_emqa	Lorentz force contribution, y component	N/m^3	Jz_emqa * Bx_emqa
normFLtz_emqa	Lorentz force contribution, norm	N/m^3	sqrt(abs(FLtzx_emqa)^2+abs(FLtzy_emqa)^2)
normM_emqa	Magnetization, norm	A/m	sqrt(abs(Mx_emqa)^2+abs(My_emqa)^2)
normBr_emqa	Remanent flux density, norm	T	sqrt(abs(Brx_emqa)^2+abs(Bry_emqa)^2)
normH_emqa	Magnetic field, norm	A/m	sqrt(abs(Hx_emqa)^2+abs(Hy_emqa)^2)
normB_emqa	Magnetic flux density, norm	T	sqrt(abs(Bx_emqa)^2+abs(By_emqa)^2)
normJ_emqa	Total current density, norm	A/m^2	abs(Jz_emqa)
Evz_emqa	Lorentz electric field, z component	V/m	d(x,t) * By_emqa-d(y,t) * Bx_emqa
normEv_emqa	Lorentz electric field, norm	V/m	abs(Evz_emqa)
normPo_emqa	Power flow, time average, norm	W/m^2	sqrt(abs(Pox_emqa)^2+abs(Poy_emqa)^2)

9.2.3. Subdomain 3

Name	Description	Unit	Expression
U_ns	Velocity field	m/s	sqrt(u^2+v^2)
V_ns	Vorticity	1/s	vx-uy
divU_ns	Divergence of velocity field	1/s	ux+vy
cellRe_ns	Cell Reynolds number	1	rho_ns * U_ns * h/eta_ns
res_u_ns	Equation residual for u	N/m^3	rho_ns * (ut+u * ux+v * uy)+px-F_x_ns-eta_ns * (2 * uxx+uyy+vxy)
res_v_ns	Equation residual for v	N/m^3	rho_ns * (vt+u * vx+v * vy)+py-F_y_ns-eta_ns * (vxx+uyx+2 * vyy)
beta_x_ns	Convective field, x component	kg/(m^2*s)	rho_ns * u
beta_y_ns	Convective field, y component	kg/(m^2*s)	rho_ns * v
Dm_ns	Mean diffusion coefficient	Pa*s	eta_ns
da_ns	Total time scale factor	kg/m^3	rho_ns
taum_ns	GLS time-scale	m^3*s/kg	nojac(1/max(2 * rho_ns * sqrt(emetric(u,v)),48 * eta_ns/h^2))
tauc_ns	GLS time-scale	m^2/s	0.5 * nojac(if(u^2+v^2
res_p_ns	Equation residual for p	kg/(m^3*s)	rho_ns * divU_ns
grad_w_x_di	Concentration gradient, w, x component	mol/m^4	wx
dflux_w_x_di	Diffusive flux, w, x component	mol/(m^2*s)	-Dxx_w_di * wx-Dxy_w_di * wy
grad_w_y_di	Concentration gradient, w, y component	mol/m^4	wy
dflux_w_y_di	Diffusive flux, w, y component	mol/(m^2*s)	-Dyx_w_di * wx-Dyy_w_di * wy
grad_w_di	Concentration gradient, w	mol/m^4	sqrt(grad_w_x_di^2+grad_w_y_di^2)
dflux_w_di	Diffusive flux, w	mol/(m^2*s)	sqrt(dflux_w_x_di^2+dflux_w_y_di^2)
grad_M_x_x_cd3	Concentration gradient, M_x, x component	mol/m^4	M_xx
dflux_M_x_x_cd3	Diffusive flux, M_x, x component	mol/(m^2*s)	-Dxx_M_x_cd3 * M_xx-Dxy_M_x_cd3 * M_xy

cflux_M_x_x_cd3	Convective flux, M_x, x component	mol/(m^2*s)	M_x * u_M_x_cd3
tflux_M_x_x_cd3	Total flux, M_x, x component	mol/(m^2*s)	dflux_M_x_x_cd3+cflux_M_x_x_cd3
grad_M_x_y_cd3	Concentration gradient, M_x, y component	mol/m^4	M_xy
dflux_M_x_y_cd3	Diffusive flux, M_x, y component	mol/(m^2*s)	-Dyx_M_x_cd3 * M_xx-Dyy_M_x_cd3 * M_xy
cflux_M_x_y_cd3	Convective flux, M_x, y component	mol/(m^2*s)	M_x * v_M_x_cd3
tflux_M_x_y_cd3	Total flux, M_x, y component	mol/(m^2*s)	dflux_M_x_y_cd3+cflux_M_x_y_cd3
beta_M_x_x_cd3	Convective field, M_x, x component	m/s	u_M_x_cd3
beta_M_x_y_cd3	Convective field, M_x, y component	m/s	v_M_x_cd3
grad_M_x_cd3	Concentration gradient, M_x	mol/m^4	sqrt(grad_M_x_x_cd3^2+grad_M_x_y_cd3^2)
dflux_M_x_cd3	Diffusive flux, M_x	mol/(m^2*s)	sqrt(dflux_M_x_x_cd3^2+dflux_M_x_y_cd3^2)
cflux_M_x_cd3	Convective flux, M_x	mol/(m^2*s)	sqrt(cflux_M_x_x_cd3^2+cflux_M_x_y_cd3^2)
tflux_M_x_cd3	Total flux, M_x	mol/(m^2*s)	sqrt(tflux_M_x_x_cd3^2+tflux_M_x_y_cd3^2)
cellPe_M_x_cd3	Cell Peclet number, M_x	1	h * sqrt(beta_M_x_x_cd3^2+beta_M_x_y_cd3^2)/Dm_M_x_cd3
Dm_M_x_cd3	Mean diffusion coefficient, M_x	m^2/s	(Dxx_M_x_cd3 * u_M_x_cd3^2+Dxy_M_x_cd3 * u_M_x_cd3 * v_M_x_cd3+Dyx_M_x_cd3 * v_M_x_cd3 * u_M_x_cd3+Dyy_M_x_cd3 * v_M_x_cd3^2)/(u_M_x_cd3^2+v_M_x_cd3^2+eps)
res_M_x_cd3	Equation residual for M_x	mol/(m^3*s)	-Dxx_M_x_cd3 * M_xxx-Dxy_M_x_cd3 * M_xxy+M_xx * u_M_x_cd3-Dyx_M_x_cd3 * M_xyx-Dyy_M_x_cd3 * M_xyy+M_xy * v_M_x_cd3-R_M_x_cd3
res_sc_M_x_cd3	Shock capturing residual for M_x	mol/(m^3*s)	M_xx * u_M_x_cd3+M_xy * v_M_x_cd3-R_M_x_cd3
da_M_x_cd3	Total time scale factor, M_x	1	Dts_M_x_cd3
grad_M_y_x_cd	Concentration gradient, M_y, x component	mol/m^4	M_yx
dflux_M_y_x_cd	Diffusive flux, M_y, x	mol/(m^2*s)	-Dxx_M_y_cd * M_yx-Dxy_M_y_cd * M_yy

	component		
cflux_M_y_x_cd	Convective flux, M_y, x component	mol/(m^2*s)	M_y * u_M_y_cd
tflux_M_y_x_cd	Total flux, M_y, x component	mol/(m^2*s)	dflux_M_y_x_cd+cflux_M_y_x_cd
grad_M_y_y_cd	Concentration gradient, M_y, y component	mol/m^4	M_yy
dflux_M_y_y_cd	Diffusive flux, M_y, y component	mol/(m^2*s)	-Dyx_M_y_cd * M_yx-Dyy_M_y_cd * M_yy
cflux_M_y_y_cd	Convective flux, M_y, y component	mol/(m^2*s)	M_y * v_M_y_cd
tflux_M_y_y_cd	Total flux, M_y, y component	mol/(m^2*s)	dflux_M_y_y_cd+cflux_M_y_y_cd
beta_M_y_x_cd	Convective field, M_y, x component	m/s	u_M_y_cd
beta_M_y_y_cd	Convective field, M_y, y component	m/s	v_M_y_cd
grad_M_y_cd	Concentration gradient, M_y	mol/m^4	sqrt(grad_M_y_x_cd^2+grad_M_y_y_cd^2)
dflux_M_y_cd	Diffusive flux, M_y	mol/(m^2*s)	sqrt(dflux_M_y_x_cd^2+dflux_M_y_y_cd^2)
cflux_M_y_cd	Convective flux, M_y	mol/(m^2*s)	sqrt(cflux_M_y_x_cd^2+cflux_M_y_y_cd^2)
tflux_M_y_cd	Total flux, M_y	mol/(m^2*s)	sqrt(tflux_M_y_x_cd^2+tflux_M_y_y_cd^2)
cellPe_M_y_cd	Cell Peclet number, M_y	1	h * sqrt(beta_M_y_x_cd^2+beta_M_y_y_cd^2)/Dm_M_y_cd
Dm_M_y_cd	Mean diffusion coefficient, M_y	m^2/s	(Dxx_M_y_cd * u_M_y_cd^2+Dxy_M_y_cd * u_M_y_cd * v_M_y_cd+Dyx_M_y_cd * v_M_y_cd * u_M_y_cd+Dyy_M_y_cd * v_M_y_cd^2)/(u_M_y_cd^2+v_M_y_cd^2+eps)
res_M_y_cd	Equation residual for M_y	mol/(m^3*s)	-Dxx_M_y_cd * M_yxx-Dxy_M_y_cd * M_yxy+M_yx * u_M_y_cd-Dyx_M_y_cd * M_yyx-Dyy_M_y_cd * M_yyy+M_yy * v_M_y_cd-R_M_y_cd
res_sc_M_y_cd	Shock capturing residual for M_y	mol/(m^3*s)	M_yx * u_M_y_cd+M_yy * v_M_y_cd-R_M_y_cd
da_M_y_cd	Total time scale factor, M_y	1	Dts_M_y_cd
dr_guess_emqa	Width in radial direction default guess	m	0

R0_guess_emqa	Inner radius default guess	m	0
Sx_emqa	Infinite element x coordinate	m	x
S0x_guess_emqa	Inner x coordinate default guess	m	0
Sdx_guess_emqa	Width in x direction default guess	m	0
Sy_emqa	Infinite element y coordinate	m	y
S0y_guess_emqa	Inner y coordinate default guess	m	0
Sdy_guess_emqa	Width in y direction default guess	m	0
curlAx_emqa	Curl of magnetic potential, x component	T	Azy
curlAy_emqa	Curl of magnetic potential, y component	T	-Azx
dVol_emqa	Volume integration contribution	1	detJ_emqa
Bx_emqa	Magnetic flux density, x component	T	curlAx_emqa
By_emqa	Magnetic flux density, y component	T	curlAy_emqa
Hx_emqa	Magnetic field, x component	A/m	Bx_emqa/mu0_emqa-Mx_emqa
Hy_emqa	Magnetic field, y component	A/m	By_emqa/mu0_emqa-My_emqa
mu_emqa	Permeability	H/m	mu0_emqa * mur_emqa
muxx_emqa	Permeability, xx component	H/m	mu0_emqa * murxx_emqa
muxy_emqa	Permeability, xy component	H/m	mu0_emqa * murxy_emqa
muyx_emqa	Permeability, yx component	H/m	mu0_emqa * muryx_emqa
muyy_emqa	Permeability, yy component	H/m	mu0_emqa * muryy_emqa

Jpz_emqa	Potential current density, z component	A/m^2	sigma_emqa * deltaV_emqa/L_emqa
Ez_emqa	Electric field, z component	V/m	-d(Az,t)
Jz_emqa	Total current density, z component	A/m^2	Jpz_emqa+Jiz_emqa+Jez_emqa
Pox_emqa	Power flow, x component	W/m^2	-Ez_emqa * Hy_emqa
Poy_emqa	Power flow, y component	W/m^2	Ez_emqa * Hx_emqa
normE_emqa	Electric field, norm	V/m	abs(Ez_emqa)
Jiz_emqa	Induced current density, z component	A/m^2	sigma_emqa * Ez_emqa
Q_emqa	Resistive heating	W/m^3	Jz_emqa * (Ez_emqa+deltaV_emqa/L_emqa)
W_emqa	Total energy density	J/m^3	Wm_emqa
dW_emqa	Integrand for total energy	Pa	dVol_emqa * W_emqa
Wm_emqa	Magnetic energy density	J/m^3	0.5 * (Hx_emqa * Bx_emqa+Hy_emqa * By_emqa+Mx_emqa * Bx_emqa+My_emqa * By_emqa)
FLtzx_emqa	Lorentz force contribution, x component	N/m^3	-Jz_emqa * By_emqa
FLtzy_emqa	Lorentz force contribution, y component	N/m^3	Jz_emqa * Bx_emqa
normFLtz_emqa	Lorentz force contribution, norm	N/m^3	sqrt(abs(FLtzx_emqa)^2+abs(FLtzy_emqa)^2)
normM_emqa	Magnetization, norm	A/m	sqrt(abs(Mx_emqa)^2+abs(My_emqa)^2)
normBr_emqa	Remanent flux density, norm	T	sqrt(abs(Brx_emqa)^2+abs(Bry_emqa)^2)
normH_emqa	Magnetic field, norm	A/m	sqrt(abs(Hx_emqa)^2+abs(Hy_emqa)^2)
normB_emqa	Magnetic flux density, norm	T	sqrt(abs(Bx_emqa)^2+abs(By_emqa)^2)
normJ_emqa	Total current density, norm	A/m^2	abs(Jz_emqa)
Evz_emqa	Lorentz electric field, z component	V/m	d(x,t) * By_emqa-d(y,t) * Bx_emqa

normEv_emqa	Lorentz electric field, norm	V/m	abs(Evz_emqa)
normPo_emqa	Power flow, time average, norm	W/m^2	sqrt(abs(Pox_emqa)^2+abs(Poy_emqa)^2)

Appendix J : LabVIEW Program Used to Control Fluxball Machine (Chapters 5 & 6)

Switches to turn on/off Inner, Outer Fluxballs and Third Coil

Switching outer fluxball phase from +90 (Clockwise

Front Panel (Inputs)

Voltage outputs from DAQ card for Inner

Voltage outputs from DAQ card for Outer

Voltage outputs from DAQ card for Third

Switches signal to Third Coil to DC from AC

Waveform charts of Inner, Outer and third

Copy Parameters to Text File

B - PID Gains Tuner with displayed values for the various gains to control the phases and magnitudes

Can individually set the RMS current to Inner and Outer Fluxballs (if switch Fluxball and third coil

Setting phase of third coil with respect to phase of

Text to name file that contains parameters

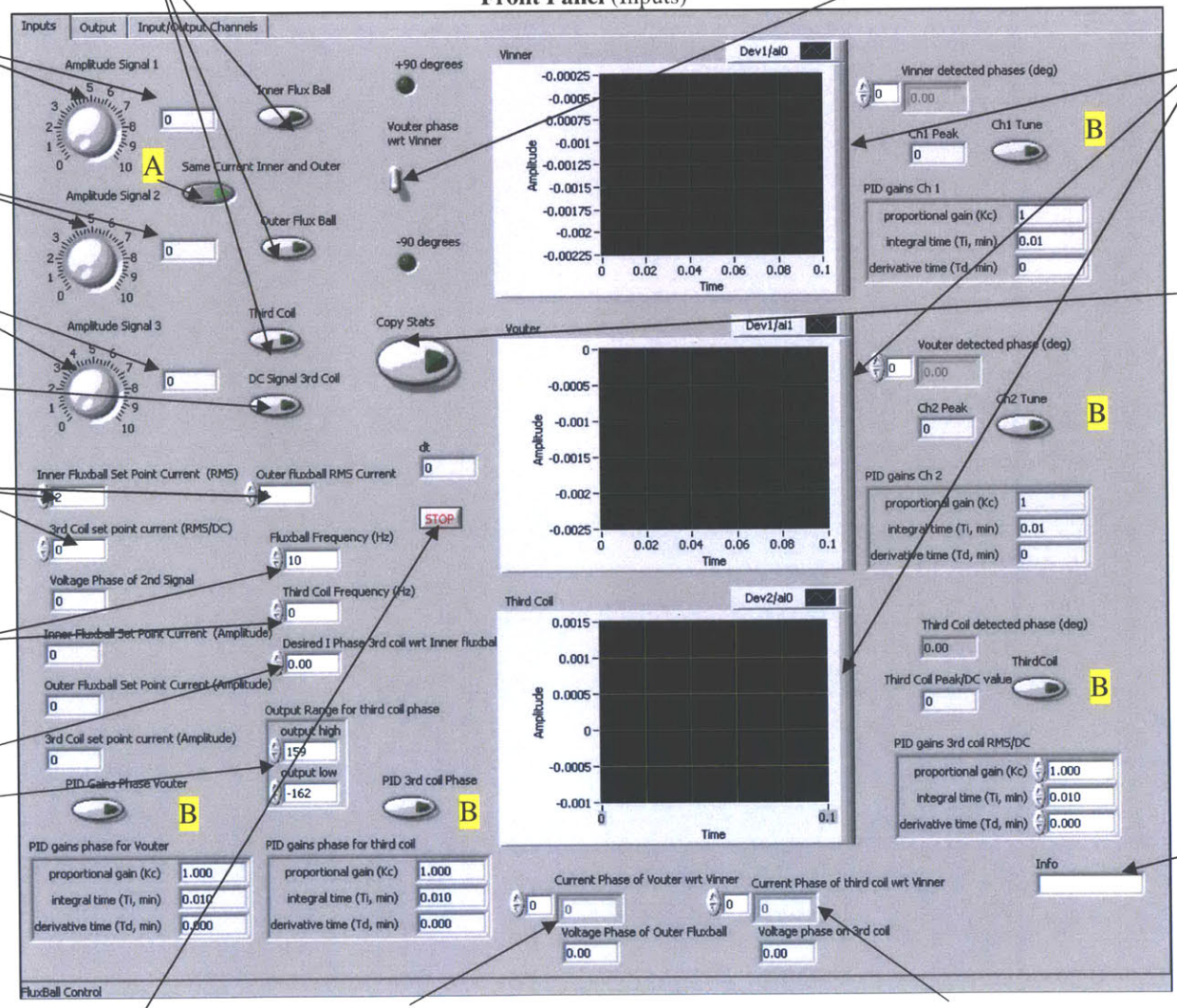

Emergency Stop

Measured phase of current through outer fluxball with

Measured phase of current through third coil with respect

Front Panel (Outputs)

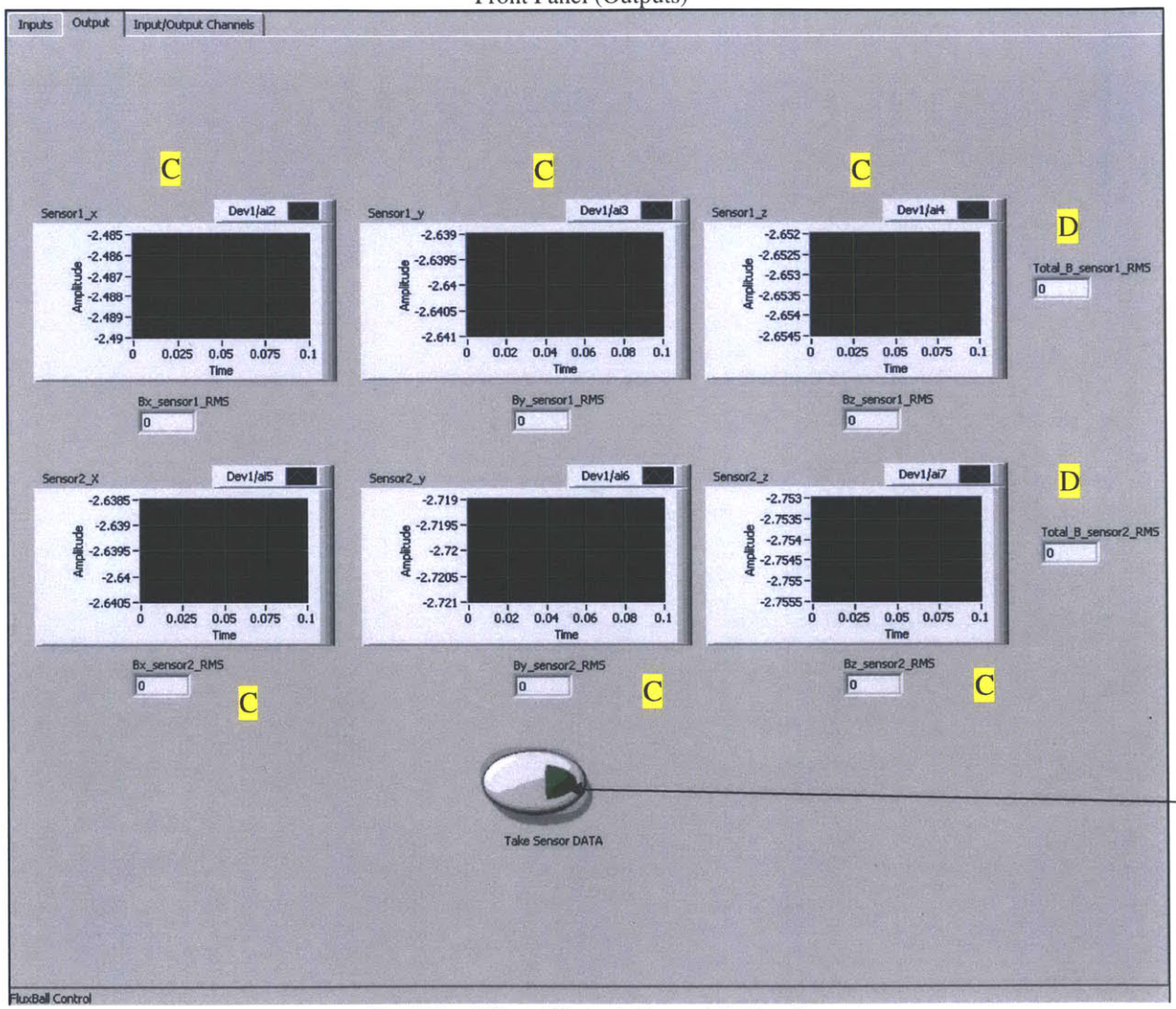

Front Panel (Input/Output Channel Settings)

C - Measured output waveforms from 2 GMW sensors. Each sensor has three axes corresponding to 3 plots each. The RMS magnetic flux is calculated for each sensor along with the RMS magnitude of the

This button saves all the measured RMS sensor values for the magnetic flux density along different axes. It also

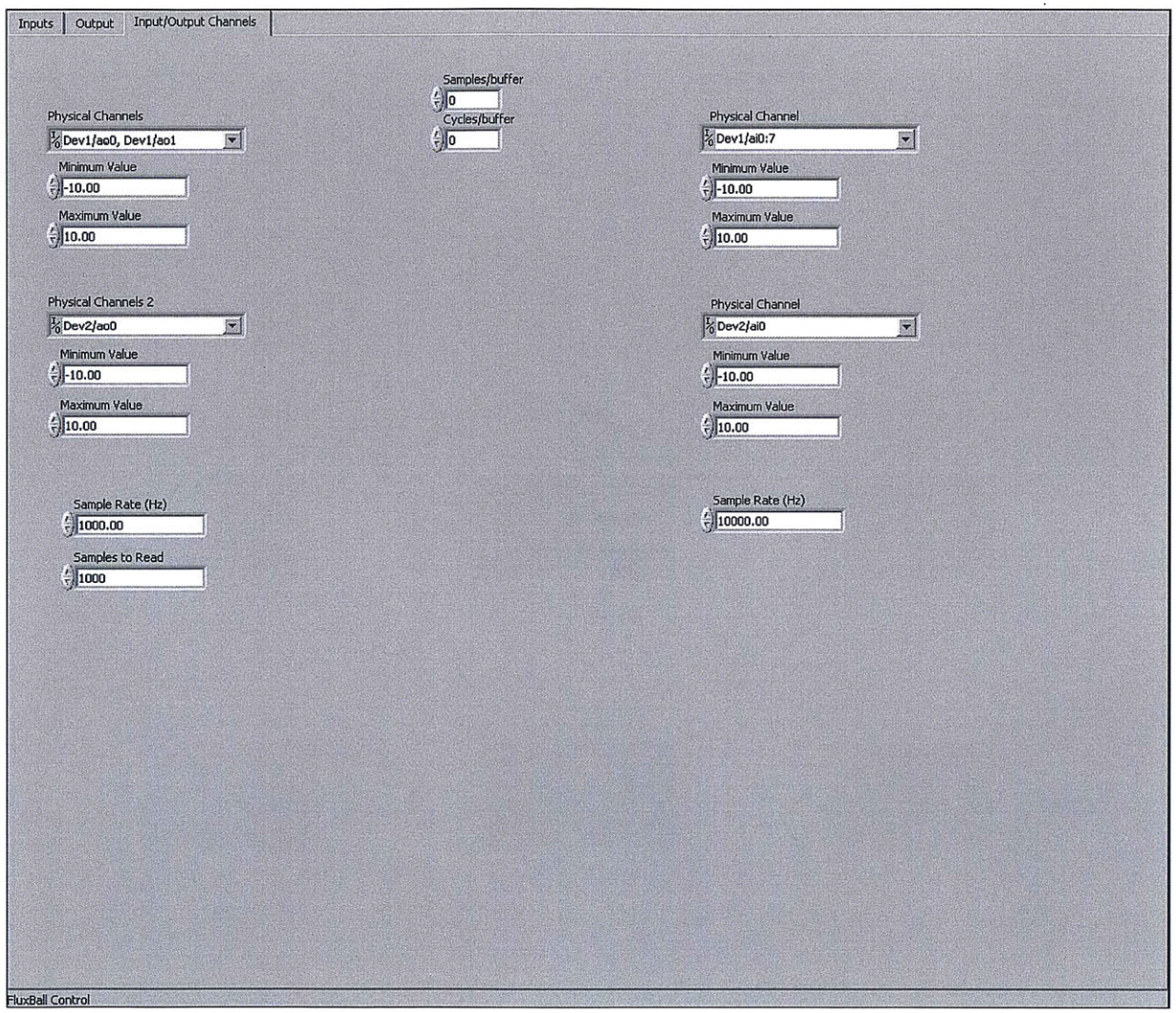

This window sets the devices and the channels necessary for all the measurements taken by the program. The range of voltages measured by the

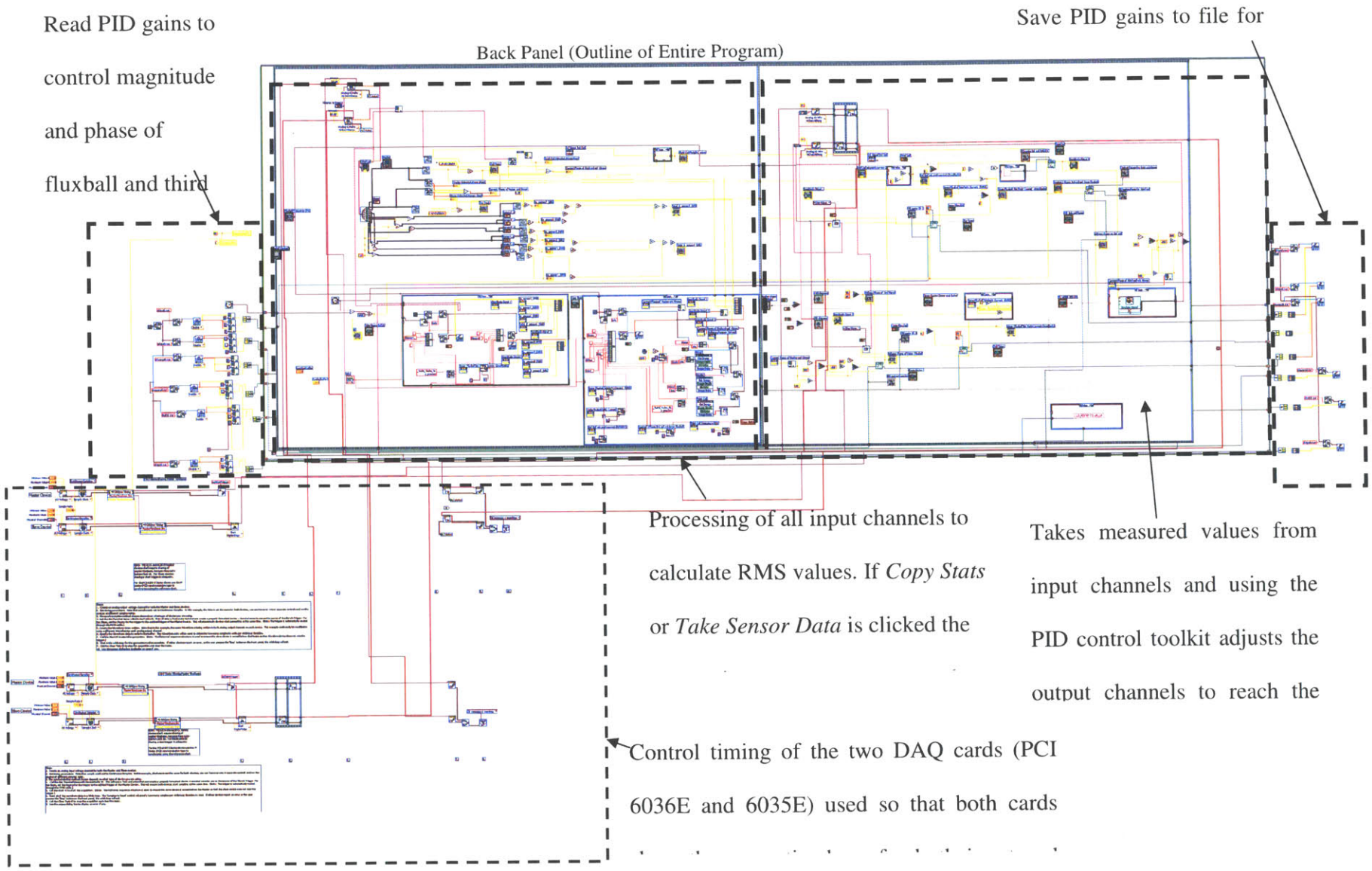
Read PID gains to control magnitude and phase of fluxball and third
Back Panel (Outline of Entire Program)
Save PID gains to file for
Processing of all input channels to calculate RMS values. If *Copy Stats* or *Take Sensor Data* is clicked the
Takes measured values from input channels and using the PID control toolkit adjusts the output channels to reach the
Control timing of the two DAQ cards (PCI 6036E and 6035E) used so that both cards

SECTION A (BLOW UP)

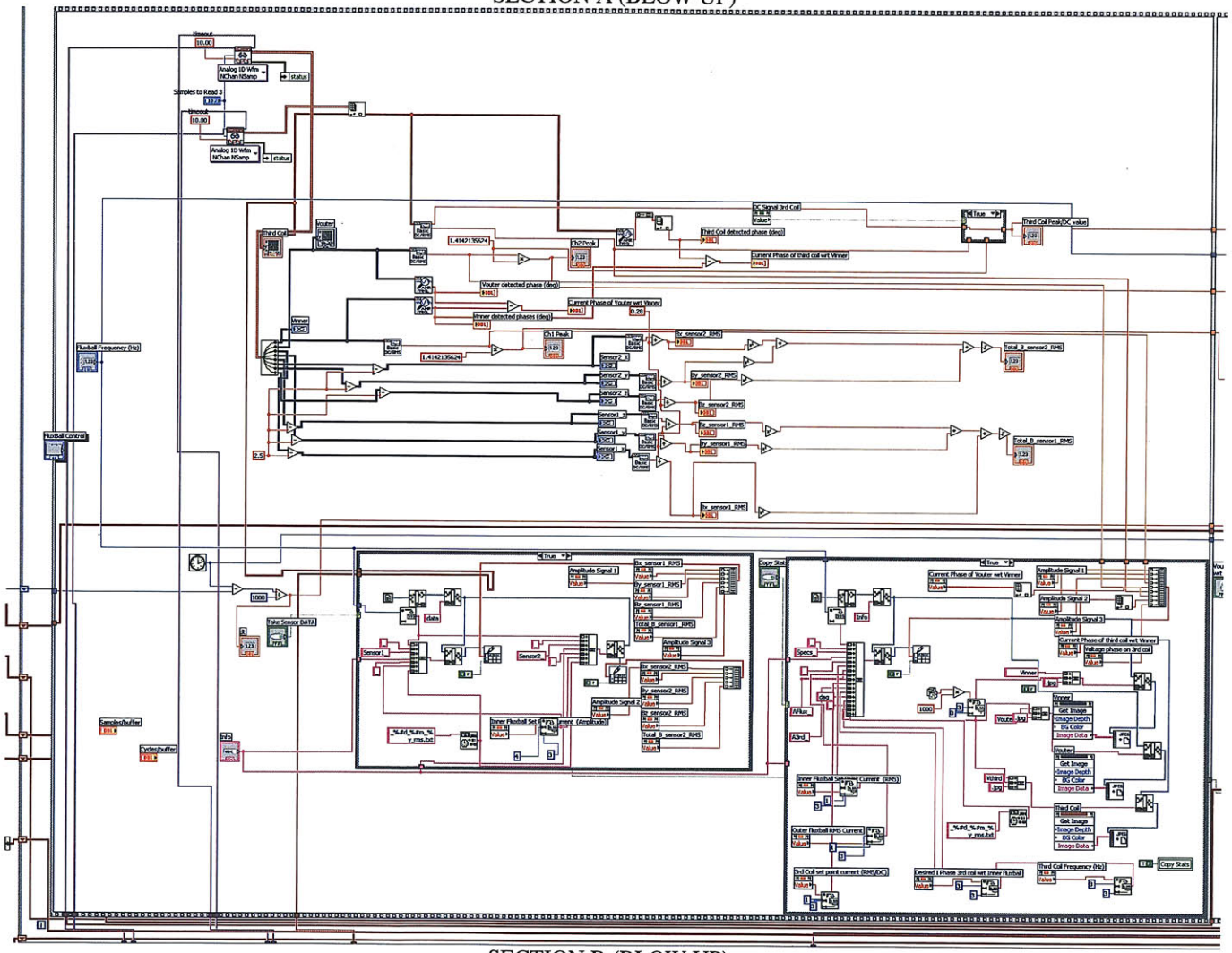

SECTION B (BLOW UP)

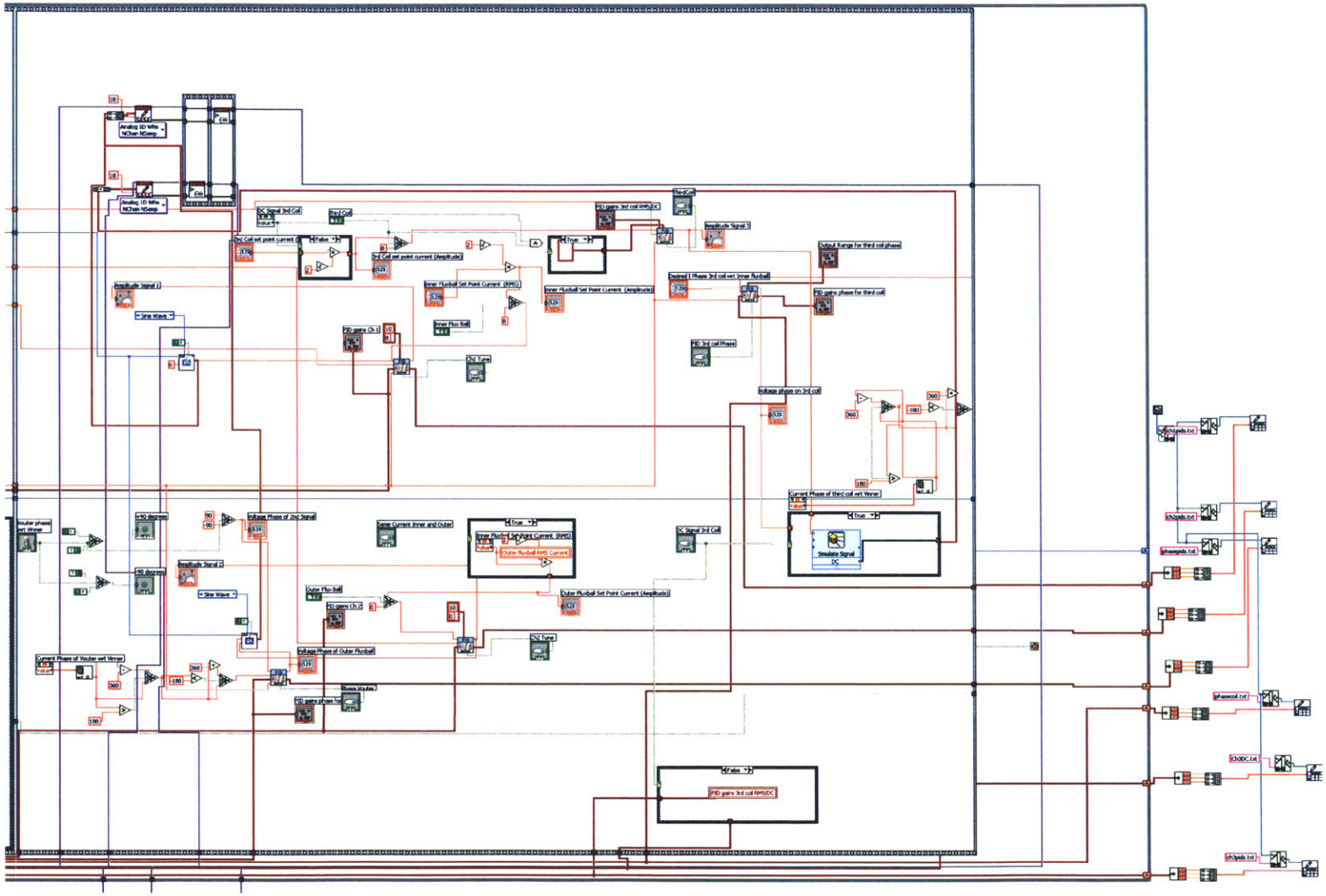

SECTION C (BLOW UP)